MMM2020

Virtual Conference

65th Annual Conference on Magnetism and Magnetic Materials

ABSTRACTS

Jointly sponsored by AIP Publishing LLC, and The IEEE Magnetics Society

Session T1
TUTORIAL: NEUTRON AND X-RAY TECHNIQUES TO STUDY MAGNETISM

Brian Kirby, Chair
NIST, National Institute of Standards and Technology, Gaithersburg, MD, US, govt, Gaithersburg, MD, United States

INVITED PAPERS

9:30

T1-01. Neutron and X-Ray Techniques for Probing Magnetism. *S.G. te Velthuis[1] 1. Materials Science Division, Argonne National Laboratory, Lemont, IL, United States*

Neutron scattering and x-ray techniques play an important role in many scientific fields, including magnetism, as they offer insights into long and short range structures, order parameters, interactions, and dynamics. With the ongoing renewal of high-power spallation neutron, coherent and synchrotron x-ray sources, paired with the continual development of sophisticated instrumentation and data analysis tools, the capabilities are continuously increasing. In this tutorial I will provide an overview, highlighting techniques particularly of interest for the study of magnetism in both bulk and nano-scaled magnetic materials. I will discuss key experiments and achievements that illustrate the strengths and unique capabilities of these techniques that make them important research tools.

10:20

T1-02. Illuminating the Invisible: X-Rays as Probes for Time-Resolved Magnetic Imaging. *S. Wintz[1] 1. Max-Planck-Institut für Intelligente Systeme, Stuttgart, Germany*

125 years after their discovery in 1895 by Wilhelm Konrad Röntgen, x-rays have nowadays become an indispensable tool for magnetism research. This applies to both x-ray magnetic scattering and x-ray magnetic dichroism based techniques. Following a general introduction, the focus of this tutorial will be on utilizing x-rays for advanced time-resolved magnetic microscopy, offering element-specific imaging at a unique spatio-temporal resolution of appx. 10 nm and 10 ps, respectively. Different experimental approaches such as x-ray photo-emission electron microscopy (xPEEM) and transmission x-ray microscopy (TXM) will be presented together with exemplary results on vortex gyration, magnetization switching and spin-wave dynamics. It will be further shown that besides x-ray magnetic circular dichroism (XMCD) as a contrast mechanism for ferromagnetic orientation, also x-ray magnetic linear dichroism (XMLD) - which in principle is sensitive to antiferromagnetic order - can be employed for time-resolved imaging. Recent achievements in time-resolved magnetic x-ray tomography (4D imaging) will be introduced as an outlook.

11:10

T1-03. Oxide Interfaces Studied by Polarized Neutron Reflectometry. *E. Guo[1] 1. Institute of Physics, Chinese Academy of Sciences, Beijing, China*

Novel electric and magnetic properties can be achieved in materials engineered at nanometer dimensions. New functionality stems from the atomic, charge, spin or orbital structure of the interface. With an understanding of interface structure, electric and magnetic degrees of freedom may be controlled, ideally at room temperature, to achieve synthetic magnetoelectric coupling in a nanocomposite or possibly to control spin textures in topological materials. Neutron reflectometry involves measurements of the intensity of a beam of electromagnetic radiation or particle waves reflects by a planar surface or interfaces. The intensity of the reflected radiation is directly related to the depth dependence of the index of reflection averaged over the later dimensions of the surface. Polarized neutron reflectivity (PNR) is the only means so far can directly probe the depth profile of atomic density and magnetization at the same time. Therefore, application of PNR in the low-dimensional functional materials would gain deep insight in better synthesis, engineering and control of their novel properties. In this talk, I will give several examples to use PNR to probe and in-situ control of interfacial magnetism in the quantum oxide heterostructures after a brief introduction of PNR technique.

Session A1
3D MAGNETIC STRUCTURES

Maria Jose Martinez-Perez, Chair
University of Zaragoza, Zaragoza, Spain

INVITED PAPERS

A1-01. Curvature-Driven Chiral Effects in Nanomagnetism. *O. Volkov*[1]
1. Institute of Ion Beam Physics and Materials Research, Helmholtz-Zentrum Dresden-Rossendorf, Dresden, Germany

The structural inversion symmetry plays an important role in low-dimensional nanomagnets, due to its strong influence on magnetic and electrical properties. It can lead to the appearance of chiral effects, such as the topological Hall effect [1], or to the formation of chiral noncollinear magnetic textures, as skyrmions [2] and chiral domain walls (DWs) [3]. These chiral structures can be the key components for realizing novel concepts for magnonics [4], antiferromagnetic spintronics [5], spin-orbitronics [6], and oxitronics [7]. So far, the main chiral symmetry breaking effect considered as being the origin for the presence of chiral noncollinear magnetic textures is the intrinsic Dzyaloshinskii-Moriya interaction (DMI) [8,9], which appears in certain magnetic crystals in which the unit cell lacks inversion symmetry, such as the gyrotropic magnetic crystals, or appear typically in ultrathin films or bilayers due to the inversion symmetry breaking on the film interface [3]. At present, tailoring of DMI is done by optimizing materials, either doping a bulk single crystal or adjusting interface properties of thin films and multilayers. A viable alternative to the conventional material screening approach can be the exploration of the interplay between geometry and topology. This interplay is of fundamental interest throughout many disciplines in condensed matter physics, including thin layers of superconductors [10] and superfluids [11], nematic liquid crystals [12], cell membranes [13], semiconductors [14]. In the emergent field of curvilinear magnetism chiral effects are associated to the geometrically broken inversion symmetries [15]. Those appear in curvilinear architectures of even conventional materials. There are numerous exciting theoretical predictions of exchange- and magnetostatically-driven curvature effects, which do not rely on any specific modification of the intrinsic magnetic properties, but allow to create non-collinear magnetic textures in a controlled manner by tailoring local curvatures and shapes [16,17]. Until now the predicted chiral effects due to curvatures remained a neat theoretical abstraction. Very recently, we provided the very first experimental confirmation of the existence of the curvature-induced chiral interaction with exchange origin in a conventional soft ferromagnetic material. It is experimentally explored the theoretical predictions, that the magnetisation reversal of flat parabolic stripes shows a two step process [18,19]. At the first switching event, a domain wall pinned by the curvature induced exchange-driven DMI is expelled leading to a magnetisation state homogeneous along the parabola's long axis. Measuring the depinning field enables to quantify the effective exchange-driven DMI interaction constant. The magnitude of the effect can be tuned by the parabola's curvature. It is found that the strength of the exchange-induced DMI interaction for the experimentally realised geometries is remarkably strong, namely ~0.4 mJ/m^2, compared the surface induced DMI. The presented study legitimates the predictive power of full-scale micromagnetic simulations to design the properties of ferromagnets through their geometry, thus stabilising chiral textures. We explore these curvilinear magnetic thin films for the realization of novel artificial magnetoelectric materials based on curvilinear helimagnets embedded in piezoelectric matrix [20], to enable the geometrical tuning of the magnetochirality in curvilinear 1D architectures [21], tailoring of magnetic states in flat nanospirals [22] and as components of shapeable magnetoelectronics for interactive wearables [23].

[1] N. Nagaosa, et al., Nature Nanotech. 8, 899 (2013) [2] U. K. Rößler, et al., Nature 442, 797 (2006) [3] A. Fert, et al., Nature Rev. Mat. 2, 17031 (2017) [4] A. V. Chumak, et al., Nature Physics 11, 453 (2015) [5] T. Jungwirth, et al., Nature Nanotech. 11, 231 (2016) [6] I. M. Miron, et al., Nature 476, 189 (2011) [7] V. Garcia, et al., Nature 460, 81 (2009) [8] I. Dzyaloshinsky, J. Phys. Chem. Solids 4, 241 (1958). [9] T. Moriya, Phys. Rev. Lett. 4, 228 (1960). [10] J. Tempere, et al., Phys. Rev. B 79, 134516 (2009) [11] H. Kuratsuji, Phys. Rev. E 85, 031150 (2012) [12] T. Lopez-Leon, et al., Nature Physics 7, 391 (2011) [13] H. T. McMahon, et al., Nature 438, 590 (2005) [14] C. Ortix, Phys. Rev. B 91, 245412 (2015) [15] Y. Gaididei, et al., Phys. Rev. Lett. 112, 257203 (2014) [16] J. A. Otálora, et al., Phys. Rev. Lett. 117, 227203 (2016) [17] V. P. Kravchuk, et al., Phys. Rev. Lett. 120, 067201 (2018) [18] O. Volkov et al., PRL 123, 077201 (2019). [19] O. Volkov et al., PSS-RRL 13, 1800309 (2019). [20] O. Volkov et al., J. Phys. D: Appl. Phys. 52, 345001 (2019). [21] O. Volkov et al., Scientific Reports 8, 866 (2018). [22] M. Nord, et al., Small 1904738 (2019). [23] J. Ge, et al., Nature Comm. 10, 4405 (2019).

A1-02. Creating and Interfacing Chiral Spin Textures Using 3D Geometries. *D. Sanz-Hernandez*[1,2], A. Hierro-Rodriguez[3], C. Donnelly[2], J. Pablo Navarro[4], A. Sorrentino[5], E. Pereiro[5], C. Magen[4,6], S. McVitie[3], J. de Teresa[4,6], S. Ferrer[5], P. Fischer[7,8] and A. Fernandez-Pacheco[2,3]
1. Unité Mixte de Physique, CNRS, Thales, Université Paris-Saclay, Palaiseau, France; 2. Cavendish Laboratory, University of Cambridge, Cambridge, United Kingdom; 3. SUPA, School of Physics and Astronomy, University of Glasgow, Glasgow, United Kingdom; 4. Laboratoria de Microscopias Avanzadas, Instituto de Nanociencia de Aragón, Universidad de Zaragoza, Zaragoza, Spain; 5. ALBA Synchrotron, Cerdanyola del Vallès, Spain; 6. Instituto de Ciencia de Materiales de Aragón, Universidad de Zaragoza-CSIC, Zaragoza, Spain; 7. Materials Sciences Division, Lawrence Berkeley National Laboratory, Berkeley, CA, United States; 8. Physics Department, University of California Santa Cruz, Santa Cruz, CA, United States

The discovery of chiral spin textures such as domain walls, skyrmions, merons and bobbers, with their associated non-trivial topology and superior spintronic properties, is one of the most exciting landmarks in nanomagnetism and spintronics in recent years. Until now, these spin textures have been mostly realised by exploiting symmetry-breaking effects in non-centrosymmetric bulk crystals and synthetic ultra-thin film heterostructures. An emerging alternative route to the generation of chiral spin interactions is geometry [1]. In thin films, for example, curvature can provide the breaking of inversion-symmetry necessary for the generation of localized DMI-like spin interactions [2]. In this work, we employ state of the art 3D nanofabrication [3] to demonstrate the generation of complex chiral spin states using only geometrical effects, with no special material requirements. To do so, we fabricate an artificial magnetic double-helix system (Figure 1a) and perform magnetic X-ray microscopy [4]. This nanostructure is formed by two strongly-interacting strands (Figure 2) with dimensions comparable to fundamental magnetic lengths. By designing geometrical chirality, a wide variety of complex chiral 3D states is imprinted into the internal magnetization vector field. This includes helical magnetic domain walls (Figure 1b), vortex tubes and topologically-induced point-like structures [4]. In this

presentation we will describe in detail how the topological mismatch caused by matching a left-handed and a right-handed double helix (See * in Figure 1a) leads to the generation of a localized Néel defect and the formation of an asymmetric vortex state [4]. These results showcase the power of using geometry for the localized generation of complex spin states, opening new paths for the study of non-trivial spin textures.

[1] Streubel, R. et al. Journal of Physics D: Applied Physics 49.36 (2016): 363001. [2] Kravchuk, V. P., et al. Physical review letters 120.6 (2018): 067201. [3] Skoric, L. et al. Nano Letters 20.1 (2019): 184-191. [4] Sanz-Hernández, D., et al. arXiv:2001.07130 [cond-mat.mes-hall]

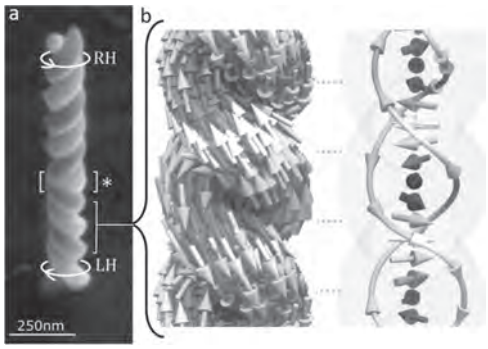

Fig 1. (a) 3D printed pair of double-helices interfaced at point *. (b) Helical domain wall emerging in a double-helix with an anti-parallel arm configuration.

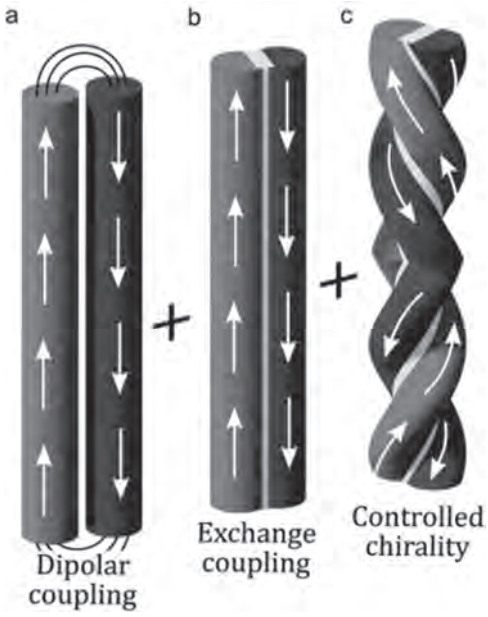

Fig 2. Magnetic interactions in the fabricated artificial double-helices. (a) Dipolar coupling favours an anti-parallel strand configuration. (b) Exchange coupling is induced using strand overlap. (c) Magnetic chirality is controlled through geometry.

CONTRIBUTED PAPERS

A1-03. Control of Vortex Structures in Individual Cylindrical Magnetic Nanowires by Simultaneous Action of Applied Magnetic Field and an Electric Current. *J. Fernandez-Roldan*[1,2], R. Pérez del Real[2], C. Bran[2], M. Vazquez[2] and O. Chubykalo-Fesenko[2] *1. Universidad de Oviedo, Oviedo, Spain; 2. Instituto de Ciencia de Materiales de Madrid, Madrid, Spain*

Cylindrical magnetic nanowires (CNWs) are promising candidates for the building blocks of 3D information technologies such as shift registers, magnetic recording, spintronics and logic gates[1-4]. Spin-polarized-current is an energy efficient way to excite magnetization dynamics in planar nanostructures. However, in CNWs this research is doing its first steps[5]. Magnetization dynamics in a CNW of Permalloy, 100 nm diameter and 1 μm length, is investigated under simultaneous application of electric current and magnetic field by micromagnetic simulations. The magnetization reversal process initiates with the creation of open vortex structures with different rotation senses at the nanowire ends. We conclude that the electric current by itself enlarges or reduces the length of these vortex structures according to the rotational sense of the associated Oersted field. Large enough current densities produce a vortex structure which covers the whole nanowire surface. At the same time, the magnetization in the very core of the nanowire remains the same, i.e. no complete magnetization reversal is possible in the absence of external magnetic field. The simultaneous action of the applied electric current and magnetic field allows the complete control of the vortex structures in terms of setting the polarity and vorticity. The resulting diagram of magnetic states obtained after the application of field and electric current showing the values required for the vorticity and axial magnetization switching is presented in Figure 1. This control is essential for future information technologies based on 3D vertical nanostructures. The presented state diagram will become useful for future experiments on current-induced domain wall dynamics in CNWs.

1. S. Parkin and S.-H. Yang, Nature Nanotechnology., Vol. 10, pp. 195 (2015). 2. F. Nasirpouri, *et al.*, Scientific Reports., Vol. 9, pp. 9010 (2019). 3. S. Ruiz-Gómez *et al.*, Scientific Reports., Vol. 8, pp. 16695 (2018). 4. J. Garcia *et al.*, Journal of Magnetism and Magnetic Materials., Vol. 383, pp. 88 (2015). 5. M. Schöbitz *et al.*, Physical Review Letters Vol. 123, pp. 217201 (2019).

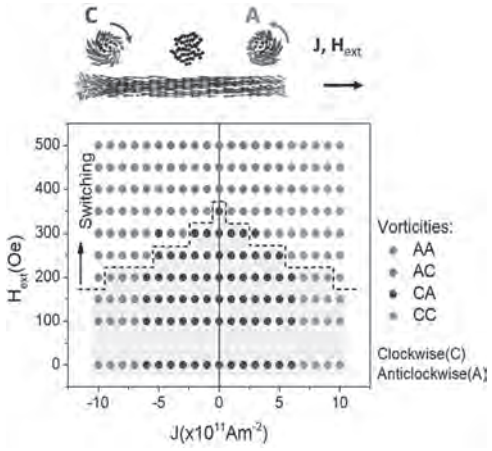

Fig.1. Diagram of magnetization vortex states: Vorticities of the vortex (or curling) structures at the ends of the nanowire in the final state obtained after the application of magnetic field, H_{ext}, and current density, J. C(A) stands for Clockwise (Anticlockwise) vorticity as indicated in the upper sketch. The threshold for the axial component switching field is indicated by the dashed line. No magnetization switching occurs below this line (yellow-shaded region).

A1-04. The Dynamics of Composite Tube-Like Domain Walls.
X. Chen[1], T.J. Hayward[2], W. Liu[1] and M.T. Bryan[1] *1. Electronic Engineering, Royal Holloway University of London, Egham, United Kingdom; 2. Materials Science and Engineering, The University of Sheffield, Sheffield, United Kingdom*

Domain wall (DW) dynamics play an important role in information transmission in spintronic devices[1]. A key factor affecting device performance is the DW velocity. However, the speed of DW motion in planar devices is limited by Walker breakdown, the periodic retrograde motion and rearrangement of magnetization structure experienced by a DW above a critical field[2]. Here we show dipolar interactions across a trilayer structure leads to DW dynamics mimicking those found in tubular structure[3], enhancement of DW velocity and suppression of Walker breakdown. Trilayer wires consisting of two 100 nm wide, 2 nm thick Permalloy (Py, $Ni_{80}Fe_{20}$) layers either side of a non-magnetic spacer of thickness t = 1-2 nm were modelled using OOMMF[4] neglecting interlayer exchange. Due to interlayer dipolar interactions, the transverse DW in the top and bottom Py wires were magnetized opposite to each other, forming a composite DW structure resembling a tubular DW (figs. 1a and 1b)[2]. Compared to a single-layer Py nanowire the average velocity of the 'quasi-tubular' DW was enhanced and Walker breakdown was suppressed over the field range studied (Fig. 2). Similar Walker breakdown suppression also occurs in tubular nanowires. In the trilayers, localized transverse stray fields due to the top DW magnetization are aligned with the magnetization of the bottom DW (and vice versa), resulting in suppression of antivortex nucleation[5]. Therefore, coupling between layers may enable trilayer to reproduce the desirable DW dynamics found in tubular wires without the need for complex 3D fabrication methods.

[1] S.S.P. Parkin and Masamitsu Hayashi, Science. 320, 190 (2008) [2] R.F. Neumann, M. Bahiana, and N.M. Vargas, Appl. Phys. Lett. 102, (2013) [3] M. Yan, C. Andreas, and A. Kákay, Appl. Phys. Lett. 99, 1 (2011) [4] M. Donahue and D. Porter, Interag. Rep. NISTIR 6376, NIST, Gaithersburg, MD (1999) [5] M.T. Bryan, T. Schrefl, D. Atkinson and D.A. Allwood, J. Appl. Phys. 103, 073906 (2008)

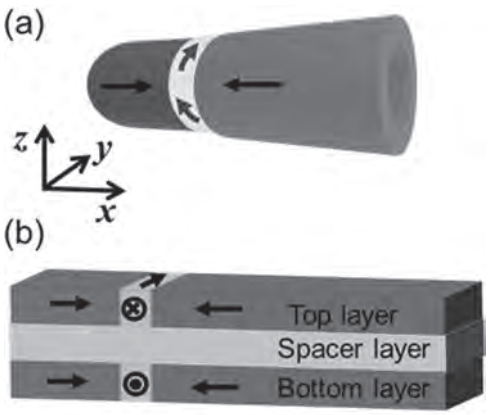

Fig. 1: Schematic of DW structure in (a) a real tube and (b) a trilayer structure.

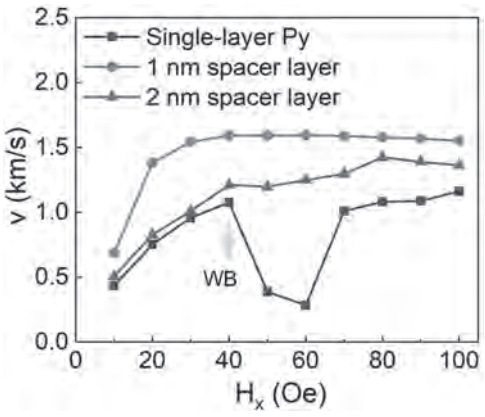

Fig. 2: Field (H_x) dependence of DW average velocity (v) in 2 nm thick single-layer Py nanowire and the trilayer structure. WB: The Walker breakdown field of the single-layer Py wire.

A1-05. Magnetostatics-Induced Symmetry Breaking Effects in Curvilinear Shells.
D. Sheka[1], *O. Pylypovskyi*[2], P. Landeros[3,4], A. Kákay[2] and D. Makarov[2] *1. Taras Shevchenko National University of Kyiv, Kyiv, Ukraine; 2. Helmholtz-Zentrum Dresden-Rossendorf e.V., Dresden, Germany; 3. Universidad Tecnica Federico Santa Maria Departamento de Fisica, Valparaiso, Chile; 4. Center for the Development of Nanoscience and Nanotechnology, Santiago, Chile*

The behavior of any physical system is governed by the order parameter, determined by the geometry of the physical space of the object, namely their dimensionality and curvature. Usually, the effects of curvature are identified using local interactions only, e.g. local spin-orbit- or curvature-induced Rashba and Dzyaloshinskii-Moriya interactions in condensed matter [1]. Lack of the framework, involving both, local and non-local interactions impedes the description of the essentially micromagnetic textures like magnetic domains, skyrmion-bubbles and vortices. Here, we present a micromagnetic theory of curvilinear ferromagnetic shells [2]. New chiral effects, originating from the magnetostatic interaction, can appear in such systems. They manifest themselves even in statics and are essentially nonlocal. This is in contrast to conventional Dzyaloshinskii--Moriya interaction (material intrinsic or curvature-induced, stemming from the exchange). The physical origin is in a non-zero mean curvature of a shell and non-equivalence between the top and bottom surfaces of the shell. To describe the new effects, we split a conventional volume magnetostatic charge into two terms: (i) magnetostatic charge, governed by the tangent to the sample's surface, and (ii) geometrical charge, given by the normal component of magnetization and the mean curvature. We classify the interplay between the symmetry of the shell, its local curvature and magnetic textures and apply the proposed formalism to analyze magnetic textures in corrugated shells with perpendicular anisotropy.

[1] R. Streubel, J. Lee, D. Makarov et al, J. Phys. D, 49, 363001, (2016); [3] O. V. Pylypovskyi, D. D. Sheka, V. P. Kravchuk et al, Sci. Rep. Vol. 6, p. 23316 (2016); O. M. Volkov, D. D. Sheka, Y. Gaididei et al, Sci. Rep. Vol. 8, p. 866 (2018). [2] D. D. Sheka, O. V. Pylypovskyi, P. Landeros et al., Comm. Phys. 3, 128 (2019), DOI:10.1038/s42005-020-0387-2

INVITED PAPER

A1-06. Ferromagnetic Liquid Droplets. *P. Fischer*[1,2], X. Liu[3,1], N. Kent[1,2], A. Ceballos[4], R. Streubel[1], Y. Jiang[1], Y. Chai[1], P. Kim[1], J. Forth[1], F. Hellman[1,4], S. Shi[3], D. Wang[3], B. Helms[1], P. Ashby[1] and T. Russell[1,5] *1. E O Lawrence Berkeley National Laboratory, Berkeley, CA, United States; 2. University of California Santa Cruz, Santa Cruz, CA, United States; 3. Beijing University of Chemical Technology, Beijing, China; 4. University of California Berkeley, Berkeley, CA, United States; 5. University of Massachusetts Amherst, Amherst, MA, United States*

One of the paradigms in condensed matter physics is that ferromagnetic materials are rigid in shape and cannot be reconfigured or reshaped. Ferrofluids, while reconfigurable, are paramagnetic at room temperature and therefore, lose their magnetization when the applied magnetic field is removed. We show a reversible paramagnetic to the ferromagnetic transformation of ferrofluid droplets by the jamming of a monolayer of carboxylated 22-nm-diameter magnetic nanoparticles (Fe3O4-CO2H) assembled at a water-oil interface. These ferromagnetic liquid droplets exhibit a finite coercivity and remanent magnetization, which was measured via vibrating sample magnetometry. The ferromagnetic response is striking since the separation distance between the dispersed nanoparticles is much larger than characteristic distances of ferromagnetic dipolar coupling. The liquid droplets can be easily reconfigured into different shapes while preserving the magnetic properties of solid ferromagnets with classic north- south dipole interactions. We have verified translational and rotational motions that can be actuated remotely and precisely by an external magnetic field. These new class of ferromagnetic materials opens the door to a manifold of applications, including active matter, energy-dissipative assemblies, programmable liquid constructs, dynamic 3D printing of magnetic devices, and biomagnetic applications. This work was funded by the U.S. Department of Energy, Office of Science, Office of Basic Energy Sciences, Materials Sciences and Engineering Division under Contract No. DE-AC02-05-CH11231.

X. Liu, N. Kent, A. Ceballos, R. Streubel, Y. Jiang, Y. Chai, J. Forth, F. Hellman, S. Shi, D. Wang, B.A. Helms, P.D. Ashby, P. Fischer, T.P. Russell, Science 365(6450) 264-267 (2019)

CONTRIBUTED PAPERS

A1-07. Nickel Nanotubes With low Resistivity and Coherent Magnetization Dynamics for 3D Spintronics and Magnonics Prepared by Atomic Layer Deposition. *D. Grundler*[1], M. Giordano[1], K. Baumgaertl[1], S. Escobar-Steinvall[2], J. Gay[1], M. Vuichard[1] and A. Fontcuberta-Morral[2] *1. IMX-LMGN, Ecole Polytechnique Federale de Lausanne Faculte des Sciences et Techniques de l'Ingenieur, Lausanne, Switzerland; 2. IMX-LMSC, Ecole Polytechnique Federale de Lausanne Faculte des Sciences et Techniques de l'Ingenieur, Lausanne, Switzerland*

Ferromagnetic nanotubes generate continuous interest due to non-collinear spin structures which are tailored by the curvature of the ferromagnetic film [1]. If arranged vertically on a chip [2], they allow for high-density arrays and 3D device architectures in spintronics and magnonics. For their realization, coating of filamentary nanotemplates would be advantageous. However, conformal deposition of ferromagnetic metals is still a challenge. We report the fabrication of Ni nanotubes by atomic layer deposition (ALD) applied to single-crystalline semiconductor nanowires. We used nickelocene as a precursor, water as the oxidant agent and an in-cycle plasma enhanced reduction step with hydrogen. The optimized ALD pulse sequence, combined with a post-processing annealing treatment, allowed us to prepare 30 nm thick metallic Ni layers with a low resistivity of 8 μΩcm at room temperature and good conformality both on the planar substrates and nanotemplates [3]. We prepared several micrometer-long Ni nanotubes with diameters ranging from 120 to 330 nm. We report on the correlation between ALD growth and functional properties of individual Ni nanotubes characterized in terms of magneto-transport at room temperature and the confinement of spin wave modes explored by micro-focus Brillouin light scattering. For the relative variation of resistance R of a nanotube in small magnetic fields we find a value of up to 1.3 % which we attribute to the anisotropic magnetoresistance (AMR) effect. This value is larger by about 30 % compared to the best low-field AMR effect of Ni nanotubes studied previously [4,5]. In the ALD process applied to semiconductor nanowires in Refs. [4,5] the plasma enhancement of the hydrogen reduction step was not available. Together with the spin-wave resonances observed in the Ni nanotubes our findings promise Ni-based 3D device architectures for spintronic and magnonic devices prepared by ALD and operated in the GHz frequency regime. Funding by the German Science Foundation DFG via GR1640/5-2 in SPP1538 Spin caloric transport and SNF via grants 163016, BSCGI0157705, and NCCR QSIT is gratefully acknowledged.

[1] R. Streubel, P. Fischer, F. Kronast et al., J. Phys. D: Appl. Phys., Vol. 49, p. 363001 (2016). [2] Y.-P. Wang, Z.-J. Ding, Q.-X. Liu et al, J. Mater. Chem. C, Vol. 4, p. 11059 (2016). [3] M.C. Giordano, K. Baumgaertl, S. Escobar Steinvall et al., ACS Appl. Mater. Interfaces (2020), https://doi.org/10.1021/acsami.0c06879. [4] D. Rüffer, R. Huber, P. Berberich et al., Nanoscale, Vol. 4, p. 4989 (2012). [5] D. Rüffer, M. Slot, R. Huber et al., APL Mater., Vol. 2, p. 076112 (2014).

A1-08. Multimaterial and Flexible 3D Printed Magnets With sub-Millimeter Resolution. *D.K. Patel*[1], C. Velez[1], Z. Fortune[2] and S. Bergbreiter[1] *1. Mechanical Engineering, Carnegie Mellon University, Pittsburgh, PA, United States; 2. Mechanical Engineering, University of Pittsburgh, Pittsburgh, PA, United States*

This work describes a technique for 3D printing of magnetic materials at millimeter and sub-millimeter scales for microrobotic applications using stereolithography. Traditional fabrication techniques to engineer magnetic materials become very challenging at smaller scales. The need for rapid prototyping techniques using materials with tunable magnetic properties is becoming more important [1]. Unfortunately, additive manufacturing of magnets is still in its infancy [2-3]. Most reported techniques that are based on thermoplastic bonded magnets [4-5], filament extrusion [6], binder jetting [7], or laser sintering [8], have limitations for scaling down in size. A better path towards miniaturization is offered by stereolithography [9], as presented in this work. The presented technique combines magnetic particles (NdFeB, Fe or Fe_3O_4) with different mixing ratios to a flexible resin that is made from aliphatic urethane diacrylate, epoxy aliphatic acrylate and a photo-initiator (Irgacure 819 - Irgacure 184) [10]. 3D printed multi-material structures are presented in Fig. 1a. This work is motivated by the need to engineer complex magnetic field patterns for MEMS actuators [11-12] and micro/soft robotics (Fig. 1B) [13]. Magnetic moment was measured to evaluate dependence of saturation magnetization and coercivity with particle material and particle concentration (Fig. 2a). Torques and forces over printed samples were measured in response to external magnetic fields (Fig. 2b), demonstrating an ability to generate highly complex 3D structures for actuation at micro- to meso-scales.

[1] G. Chatzipirpiridis et al., "3D Printing of Thermoplastic Bonded Soft and Hard Magnetic Composites: Magnetically Tuneable Architectures and Functional Devices," Adv. Intell. Syst., vol. 1, no. 6, p. 1900069, 2019. [2] L. Li, B. Post, V. Kunc, A. M. Elliott, and M. P. Paranthaman, "Additive manufacturing of near-net-shape bonded magnets: Prospects and challenges," Scr. Mater., vol. 135, pp. 100–104, Jul. 2017. [3] V. Popov, A. Koptyug, I. Radulov, F. Maccari, and G. Muller, "Prospects of additive manufacturing of rare-earth and non-rare-earth permanent magnets," Procedia Manuf., vol. 21, no. March, pp. 100–108, 2018. [4] L. Pigliaru et al., "3D printing of high performance polymer-bonded PEEK-NdFeB magnetic composite materials," Funct. Compos. Mater., vol. 1, no. 1, p. 4, Dec. 2020. [5] P. P. Wendhausen, C. H. Ahrens, A. B. Baldissera, P. D. Pavez, and J. M. Mascheroni, "Additive manufacturing of bonded NdFeB, process parameters evaluation on magnetic properties," in 2017 IEEE International Magnetics Conference (INTERMAG), 2017, vol. 53, no. 11, pp. 1–1. [6] B. Khatri, K. Lappe, D. Noetzel, K. Pursche, and T. Hanemann, "A 3D-Printable Polymer-Metal

Soft-Magnetic Functional Composite—Development and Characterization," Materials (Basel)., vol. 11, no. 2, p. 189, Jan. 2018. [7] C. L. Cramer et al., "Binder jet additive manufacturing method to fabricate near net shape crack-free highly dense Fe-6.5 wt.% Si soft magnets," Heliyon, vol. 5, no. 11, p. e02804, Nov. 2019. [8] C. V. Mikler et al., "Laser Additive Manufacturing of Magnetic Materials," JOM, vol. 69, no. 3, pp. 532–543, Mar. 2017. [9] L. Lu, P. Guo, and Y. Pan, "Magnetic-Field-Assisted Projection Stereolithography for Three-Dimensional Printing of Smart Structures," J. Manuf. Sci. Eng., vol. 139, no. 7, pp. 1–7, Jul. 2017. [10] D. K. Patel, A. H. Sakhaei, M. Layani, B. Zhang, Q. Ge, and S. Magdassi, "Highly Stretchable and UV Curable Elastomers for Digital Light Processing Based 3D Printing," Adv. Mater., vol. 29, no. 15, p. 1606000, Apr. 2017. [11] A. P. Taylor, C. Velez Cuervo, D. P. Arnold, and L. F. Velasquez-Garcia, "Fully 3D-Printed, Monolithic, Mini Magnetic Actuators for Low-Cost, Compact Systems," J. Microelectromechanical Syst., vol. 28, no. 3, pp. 481–493, Jun. 2019. [12] Y. Kim, G. A. Parada, S. Liu, and X. Zhao, "Ferromagnetic soft continuum robots," Sci. Robot., vol. 4, no. 33, p. eaax7329, Aug. 2019. [13] J. J. Abbott, E. Diller, and A. J. Petruska, "Magnetic Methods in Robotics," Annu. Rev. Control. Robot. Auton. Syst., vol. 3, no. 1, pp. 57–90, May 2020.

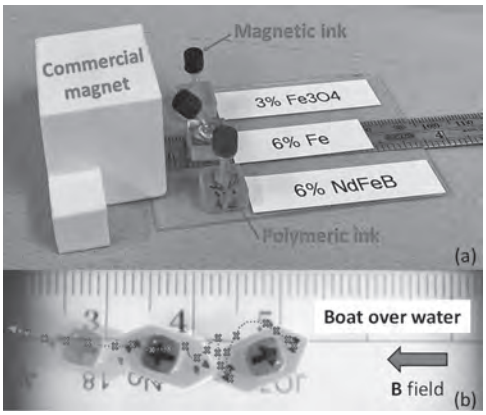

Fig 1: Proof of concept of multi-material 3D printing structure. (a) Center structure responding mechanically to the presence of an external magnetic field. (b) Microrobot boats of different materials were 3D printed and tested on a water pool inside a Helmholtz coil. The magnetic field at the center of the coils is ~33.4 mT (each 12.7 cm diameter coil powered with 5 A and 6.35 V).

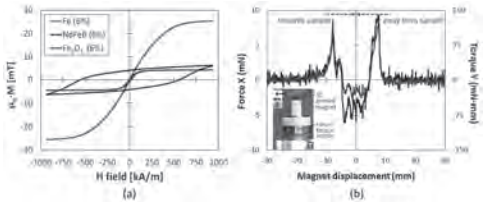

Fig 2: Printed material characterization. (a) Magnetization measured on vibrating sample magnetometer (VSM). Printed materials with different magnetic particles, but same w/w concentration. (b) Pulling Force/Torque experiment Fe_3O_4 printed sample (6% w/w concentration).

A1-09. Advanced Fabrication and Magnetometry of Nanostructures With Complex 3D Geometries. *L. Skoric*[1], D. Sanz-Hernandez[3], C. Donnelly[1], F. Meng[1] and A. Fernandez-Pacheco[2] *1. Physics, University of Cambridge, Cambridge, United Kingdom; 2. School of Physics & Astronomy, University of Glasgow, Glasgow, United Kingdom; 3. UMPhy CNRS-Thales, Univ. Paris-Saclay, Palaiseau, France*

The extension of nanomagnetism to three dimensions is proposed as an exciting route to study new physical effects, such as the emergence of new spin textures and magneto-chiral phenomena, with the prospective of being exploited in future technologies [1,2]. Whereas a significant amount of work has been so far devoted to simulating 3D nanostructures, its fabrication and characterization has proven to be very challenging, and very few of these systems have been experimentally investigated. Our group has been recently developing new fabrication and characterization methods specifically tailored for the study of 3D nanostructures, which made it possible to control the advanced motion of domain walls in 3D straight nanowires [3,4]. Here, we will present recent advances in this realm, which now enable us to create and probe nanomagnets with more complex 3D geometries. First, we will present recent work dedicated to the 3D printing of nanomagnets using Focused Electron Beam Induced Deposition (FEBID). Based on the effective FEBID continuum model [5] and proximity effect corrections, we have developed an algorithm with the capability of modelling the deposition and defining beam scanning patterns for arbitrary 3D geometries [6]. The algorithm performance has been demonstrated in different electron microscopes and precursor gases, allowing us to create 3D nanomagnets with a wide range of geometries directly from CAD files (see Fig. 1). Complementing nanofabrication, we will present a new Kerr magneto-optical setup with the ability to probe 3D magnetic nanostructures, by exploiting the dark-field MOKE (dfMOKE), a technique that we have recently developed [3]. The unprecedented flexibility of the system to characterize these newly accessible 3D geometries will be demonstrated, thanks to the combination of mobile optics and full-3D vector magnetic fields (see Fig. 2).

[1] Fernández-Pacheco, A. *et al. Nat. Commun.* 8, 15756 (2017). [2] Streubel, R. *et al. J. Phys. D. Appl. Phys.* 49, 363001 (2016). [3] Sanz-Hernández, D. *et al. ACS Nano* 11, 11066–11073 (2017). [4] Sanz-Hernández, D. *et al. Nanomaterials* 8, 483 (2018). [5] Toth, M., Lobo, C., Friedli, V., Szkudlarek, A. & Utke, I. *Beilstein J. Nanotechnol.* 6, 1518–1540 (2015). [6] Skoric, L. *et al. Nano Lett.* 20, 184–191 (2020).

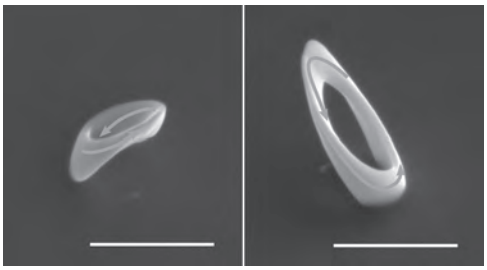

Fig. 1: SEM image of a Cobalt Möbius strip deposited with FEBID. Adapted from [6]. Scale bars are 1μm.

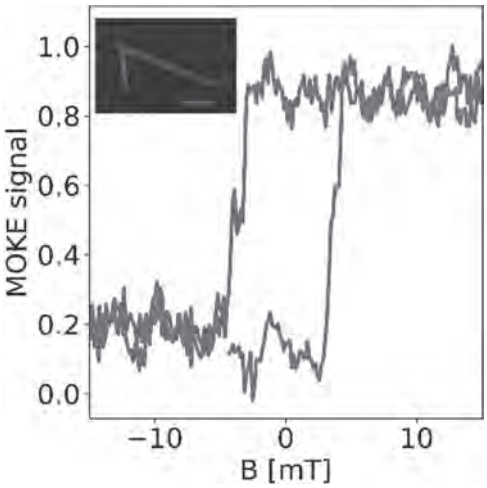

Fig. 2: Dark-field MOKE measurements of a 3D nanowire deposited with FEBID. Scale bar is 1μm.

A1-10. Controlling Magnetic Properties of 3D-Printed Magnetic Elastomer Structures via Fused Deposition Modeling. *T. Calascione*[1], N.A. Fischer[1], T. Lee[1], H. Thatcher[1] and B. Nelson-Cheeseman[1]
1. Mechanical Engineering, University of Saint Thomas, Saint Paul, MN, United States

A magnetic elastomer is a type of magneto-active smart material where a magnetic field induces a mechanical response. Several methods have been used to optimize performance by controlling the microstructure, such as magnetic annealing. Optimization can also be achieved by introducing anisotropy with Fused Deposition Modeling (FDM), a 3D-printing process that extrudes viscous material in 1D lines to create 2D layers which build to a 3D part. Indeed, FDM features have been shown to manipulate the magnetic anisotropy of rigid printed parts.[1] However, printing flexible composite materials presents additional challenges with FDM. Here, FDM structures were printed with thermoplastic polyurethane (TPU) polymer and either 20wt% iron (Fe), 40wt% Fe, 40wt% carbonyl iron (CI), or 40wt% magnetite (Fe_3O_4/Mag). In order to determine the relative effect of different parameters on the magnetic properties, a series of structures were printed combining each material type (Fe-TPU, CI-TPU, Mag-TPU) with different aspect ratios (1:1 / 2:1), infill percentages (60% / 80% / 100%), and infill orientations (parallel/perpendicular to aspect ratio). A Vibrating Sample Magnetometer was used to obtain magnetic hysteresis loops for comparing magnetic susceptibility between samples. Results demonstrated that infill orientation had the largest effect on susceptibility, aspect ratio had the next greatest effect, and infill percentage had a more nuanced effect (Fig.1). This shows that FDM allows the magnetic anisotropy to manifest through mesoscale anisotropy of a part's internal structure. These trends were found to form a continuum of tunable magnetic responses (Fig.2). Additionally, the chosen particulate transfers its unique magnetic signature to the composite material. Overall, the highly customizable and nuanced characteristics of 3D-printed magnetic elastomer structures will allow for its use in emerging magneto-mechanical applications such as magnetic actuation and soft robotics.

1. M. Patton, P. Ryan, T. Calascione, N. Fischer, A. Morgenstern, N. Stenger, and B. Nelson-Cheeseman, Additive Manufacturing, Vol. 27, 482-488 (2019)

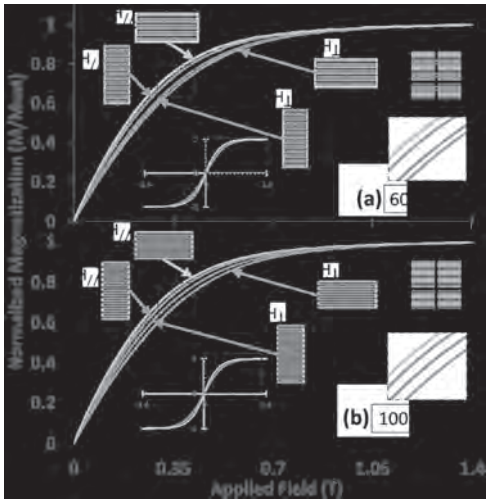

Fig.1: Magnetic susceptibility of printed 40wt% Fe-TPU structures with (a) 60% infill and (b) 100% infill.

Fig.2: Continuum of print structures demonstrating their relative magnetic susceptibilities.

Session A2
FRUSTRATED MAGNETIC SYSTEMS
Shalabh Gupta, Chair
Ames Laboratory, Ames, IA, United States

INVITED PAPER

A2-01. High Magnetic Field Induced Dynamics in the Frustrated Quantum Spin Chain Linarite. L. Heinze[1], *K.C. Rule*[2], M. Le[3], S. Nishimoto[4,5], S. Drechsler[5], U. Roessler[5], R. Mole[2], A. Wolter[4] and S. Suellow[1] *1. Institute for Condensed Matter Physics, TU Braunschweig, Braunschweig, Germany; 2. Australian Centre for Neutron Scattering, Australian Nuclear Science and Technology Organisation - Lucas Heights Campus, Kirrawee, NSW, Australia; 3. Rutherford Appleton Laboratory, Didcot, United Kingdom; 4. Leibniz Institute for Solid State and Materials Research, IFW Dresden, Dresden, Germany; 5. Institute for Solid State Physics, Technische Universitat Dresden, Dresden, Germany*

Linarite, $PbCuSO_4(OH)_2$ is a natural mineral which exhibits one dimensional (1D) frustrated quantum interactions and can be described by the so called J_1 - J_2 model. In this model, competing ferromagnetic nearest-neighbour interactions ($J_1 > 0$) and antiferromagnetic next-nearest-neighbours ($J_2 < 0$) can give rise to novel phenomena such as multipolar and spin nematic phases [1,2]. To date, linarite has been revealed to host a complex applied field phase structure with at least 5 distinct magnetic phases below $T_N = 2.8$K, as seen in Fig. 1 [3-7]. However some controversy exists regarding the phase closest to saturation, phase V [8,9]. We present an inelastic neutron scattering study performed in applied fields up to 8.8T and temperatures as low as 0.5K. These data reveal dispersive modes along each of the principle crystallographic axes that vary between the commensurate phase IV and incommensurate phase V. Linear spin wave theory calculations have been used to model the data and highlight the coupling regime close to saturation resembles that of a modulated moment structure.

[1] S. Furukawa *et al.*, Phys. Rev. Lett., 105, 257205 (2010) [2] J. Sudan *et al.*, Phys. Rev. B, 80 140402(R), (2009) [3] A. U. B. Wolter *et al.*, Phys. Rev. B 85, 014407 (2012). [4] B. Willenberg *et al.*, Phys. Rev. Lett. 108, 117202 (2012). [5] B. Willenberg *et al.*, Phys. Rev. Lett. 116, 047202 (2016). [6] K. C. Rule *et al.*, Phys. Rev. B 95, 024430 (2017). [7] L. Heinze *et al.*, Phys. Rev. B 99, 094436 (2019). [8] E. Cemal *et al.*, Phys. Rev. Lett. 120, 067203 (2018) [9] K. Yu. Povarov, *et al.*, Phys. Rev. B 94, 214409 (2016)

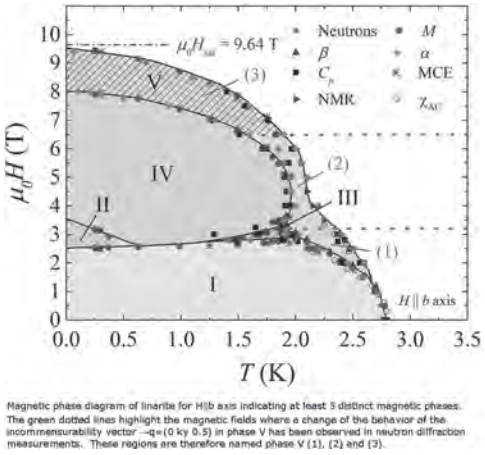

Fig. 1 The magnetic phase diagram of linarite for the H||b axis, indicating at least 5 distinct magnetic phases. The green dotted lines highlight the magnetic fields where a change of the behavior of the incommensurability vector q = (0 ky 0.5) in phase V has been observed in the neutron diffraction measurements.

CONTRIBUTED PAPERS

A2-02. Withdrawn

A2-03. THz Magneto-Optical Investigation of Quadrupolar Spin-Lattice Effects in Magnetically Frustrated $Tb_2Ti_2O_7$. *Y. Alexanian*[1], K. Amelin[2], U. Nagel[2], T. Rõõm[2], E. Constable[3], C. Decorse[4], Z. Wang[5,6], J. Debray[1], V. Simonet[1], J. Robert[1], R. Ballou[1] and S. De Brion[1] *1. Institut NEEL, CNRS-Université Grenoble Alpes, Grenoble, France; 2. Keemilise ja Bioloogilise Fuusika Instituut, Tallinn, Estonia; 3. Technische Universitat Wien Institut fur Festkorperphysik, Wien, Austria; 4. Institut de Chimie Moleculaire et des Materiaux d'Orsay, Université Paris-Sud, Orsay, France; 5. Institut für Strahlenphysik, Helmoltz-Zentrum Dresden-Rossendorf, Dresden, Germany; 6. Universitat zu Koln II Physikalisches Institut, Koln, Germany*

In geometrically frustrated magnetism, the very nature of the ground state of $Tb_2Ti_2O_7$, has remained a long standing conundrum. In this pyrochlore material, no conventional spin-ice or long-range magnetic order is stabilized, even at very low temperatures [1]. Quantum fluctuations are suspected of being at the origin of such an exotic quantum phase, yet so far no complete description is available. Using neutron scattering [2] and synchrotron-based terahertz spectroscopy [3], it has been shown that spin/lattice couplings are present in form of hybrid Tb crystal-field / phonon modes that are present across a broad temperature range from 200 K down to 6 K. This so called vibronic process affects the electronic ground state that can no longer be described solely by electronic wave functions and involve quadrupolar degrees of freedom associated with the rare earth magnetic

element in its local environnement. We present here new magneto-optical investigation of vibronic spin-lattice coupling effects. We apply a static magnetic field along the cubic <111> direction while probing with linearly polarized THz radiation. Through the Zeeman effect, the magnetic field enhances splitting within the low-energy Tb crystal field transitions revealing new details in our THz spectra. Complementary magneto-optical quantum calculations including quadrupolar terms show that indeed vibronic effects are required to describe our observations at 3 K. A further prediction of our theoretical model is the presence of a novel magneto-optical birefringence as a result of this vibronic process. Together, our results [4] reveal the significance of considering quadrupolar spin-lattice effects when describing the spin-liquid ground state of $Tb_2Ti_2O_7$. They also highlight the potential for future magneto-optical investigations to probe complex materials where spin /lattice couplings are present and unravel new magneto-optical activity in the THz range.

[1] J. S. Gardner, B. D. Gaulin, A. J. Berlinsky et al., Phys. Rev. B 64, 224416 (2001) [2] T. Fennell, M. Kenzelmann, B. Roessli et al., Phys. Rev. Lett. 112, 017203 (2014) [3] E. Constable, R. Ballou, J. Robert et al., Phys. Rev. B 95, 020415(R) (2017) [4] K. Amelin, Y. Alexanian, U. Nagel et al, to be published

A2-04. Critical Exponents and Simulation Methods of Frustrated Spin Systems. *D. Kapitan*[1], A. Rybin[1], P. Andriushchenko[2], E. Vasiliev[1], K. Nefedev[1] and V.Y. Kapitan[1] *1. Dal'nevostocnyj federal'nyj universitet, Vladivostok, Russian Federation; 2. Nacional'nyj issledovatel'skij universitet ITMO, Sankt-Peterburg, Russian Federation*

It is well known that critical phenomena occur in condensed matter under certain conditions, when an abrupt change in its properties occurs [1]. Near the critical points, various phenomena may arise. The critical region can be described by a set of state parameters (order parameters), which allow one to obtain information about the anomalous behavior of thermodynamic averages, internal processes, and the nature of the objects of study. The abnormal nonlinear behavior of state parameters is described by critical exponents. In this work, the authors consider two models. The main object of research is the two-dimensional Edwards-Anderson model [2], with the exchange integral J as a random function and the average value of J is zero. In such a system, one half of the spins' interaction is ferromagnetic, and the other is antiferromagnetic. Received results were compared with the values of two-dimensional square Ising model with ferromagnetic interaction between spins. Parallel tempering Monte-Carlo method was used for simulation. Regular Monte-Carlo method suffers from critical slowdown on low temperatures; however, parallel tempering replica exchange is able to eliminate this bottleneck [3]. For the Edwards-Anderson model, the temperature behavior of the average magnetization modulus equals to zero. Because of this fact, we calculated an average size of the percolation cluster, which is defined as the relative size of maximum cluster, which include spins in the ground state, to the total number of spins. The average size of the percolation was chosen as an order parameter [4]. This order parameter, in contrast to other thermodynamic characteristics, makes it possible to describe the behavior of the system with a change in temperature. Using this parameter, we calculated main critical exponents of these two models: correlation length, magnetization, specific heat and susceptibility. This work was supported by the state task of the MSHE of Russia No. 0657-2020-0005.

[1] A. Patashinski, V. Pokrovskii, Pergamon Press (1979) [2] S. Edwards, P. Anderson, Phys. F: Metal Phys., Vol. 5 (5), p. 965 (1975) [3] J. Machta, Phys. Rev. E 80 (2009) [4] P. Andriushchenko, FEFU (2018)

A2-05. Micromagnetic Route Towards the Coulomb Phase Physics of Artificial Frustrated Magnets. V. Schanilec[1,2], O. Brunn[1,3], Y. Perrin[1], V. Uhlir[2], B. Canals[1] and *N. Rougemaille*[1] *1. CNRS - Institut NEEL, Grenoble, France; 2. Stredoevropsky technologicky institut, Brno, Czechia; 3. Inst. Sci. Instruments, Brno, Czechia*

One of the initial motivations of fabricating artificial spin systems was to access, directly in real space, the physics of disordered magnetic states, such as spin liquids. More generally, artificial spin systems offer the appealing opportunity to image, spin by spin, cooperative magnetic phenomena and the complex many-body physics often associated with highly frustrated magnets. Bringing artificial spin systems into their ground state or within a low-energy manifold has been one of the first challenges the community faced. Two main routes have been followed so far: field demagnetization protocols and thermal annealing procedures, either above the Curie point of the constituent material or above the blocking temperature of the nanomagnets. When the spin system orders, both approaches usually allow reaching magnetic states characterized by large patches of the ground state configuration. This is the case for instance in the artificial square ice, in which large patches of the antiferromagnetic ground state are found, regardless of the protocol used. However, for extensively degenerate ice manifolds, all strategies share similar limitations: they hardly bring the system into a correlated liquid phase, although they permitted the visualization of emerging collective phenomena, such as the fragmentation of magnetism in the dipolar kagome ice or the Coulomb phase of the square ice. In this contribution, we will describe a new strategy that greatly improves the efficiency of field demagnetization protocols applied to square [1] and kagome [2,3] arrays of nanomagnets. In particular, we will show how the micromagnetic nature of artificial spin systems can be used to facilitate the access to the degenerate ice manifolds that have so characterized Coulombic spin liquids.

[1] V. Schanilec et al., under review at Nat. Commun. [2] V. Schanilec et al., to be submitted to Appl. Phys. Lett. [3] V. Schanilec et al., under review at Phys. Rev. Lett.

A2-06. Multipolar Degree of Freedom and Metamagnetism of the Quantum Spin Ice Candidate $Pr_2Zr_2O_7$. *N. Tang*[1], A. Sakai[2], K. Kimura[5], M. Fu[1], S. Nakamura[4], Y. Matsumoto[6], T. Sakakibara[1] and S. Nakatsuji[2,3] *1. University of Tokyo, ISSP, Chiba, Japan; 2. Department of Physics, University of Tokyo, Graduate School of Science, Tokyo, Japan; 3. Johns Hopkins University, Baltimore, MD, United States; 4. Department of physics, Nagoya Institute of Technology, Aichi, Japan; 5. Department of advanced materials, University of Tokyo, Graduate school of frontier science, Chiba, Japan; 6. Max-Planck-Institute for solid state research, Stuttgart, Germany*

Frustrated magnets may host novel disordered states even at absolute zero due to the competing exchange interactions. One such example is the "classical spin ice (CSI)" realized in pyrochlore oxides $R_2T_2O_7$, where R and T are a magnetic rare-earth and transitional metal ion, respectively. The competing Ising interaction and dipolar interaction form "2-in, 2-out" spin configurations in the tetrahedra, resulting in macroscopic degeneracy of the ground state [1]. By introducing transverse quantum fluctuations, the massively degenerated CSI state can "melt" into a highly entangled ground state known as the quantum spin ice (QSI). QSI is a specific form of a quantum spin liquid that harbors emergent exotic excitations, such as magnetic and electric monopoles, and gapless photons [2, 3]. Pr-based pyrochlore materials are considered leading candidates of a QSI owing to their signature of a dynamical spin ice state at low temperatures [4, 5]. Their non-Kramers ground state doublet comprises both longitudinal magnetic dipolar and transverse electric quadrupolar moments. The electric quadrupoles are time reversal even, and thus interact linearly with lattice strains. This feature enables the lattice degrees of freedom to act as an effective probe, via magnetostriction and thermal expansion measurements, of the underlying spin correlations. Here, we report low-temperature magnetostriction and thermal expansion

measurements on $Pr_2Zr_2O_7$. We found that the magnetic field tuning of the monopole condensation manifests a much sharper anomaly in lattice response than in magnetization. Around a zero magnetic field, $Pr_2Zr_2O_7$ exhibits no sign of magnetic transition or freezing down to ~ 80 mK. Based on various experimental observations, we show the crucial role of magneto-elastic coupling in shaping the rich magnetic field-temperature (*B*-*T*) phase diagram and pinpoint the evidence for a multipolar-driven spin ice state with emergent low-energy magnetodistortive dynamics.

[1] S.T. Bramwell *et al*., Science 294, 1495-1501 (2001) [2] P.W. Anderson, Mater. Res. Bull. 8, 2 (1973) [3] O. Benton *et al*., PRB 86, 075154 (2012) [4] K. Kimura *et al*., Nat. Commun. 4, 1934 (2013) [5] R. Sibille *et al*., Nat. Phys. 14, 711-715 (2018)

A2-07. Quantum Spin Nematic Liquid in the S=1 Antiferromagnetic Chain With the Biquadratic Interaction. *T. Sakai*[1,2] *1. University of Hyogo, Kamigori, Japan; 2. National Institues for Quantum and Radiological Science and Technology(SPring-8), Sayo, Japan*

The spin nematic phase, which is a kind of multipole phases, has attracted a lot of interest in the field of the strongly correlated electron systems, as well as the quantum spin liquid phase. Using the numerical exact diagonalization, the density matrix renormalization group (DMRG) calculation, and the finite-size scaling analysis, it is found that some spin nematic and spin liquid phases are induced by external magnetic field in the anisotropic and frustrated quantum spin systems. In our previous work[1], it was found that a field-induced nematic phase appears at some critical field in the anisotropic spin ladder. The nematic phase is characterized by the power-law decay in the correlation function of the second-order spin moment. In addition at some higher critical field a quantum phase transition can occur to the conventional field-induced Tomonaga-Luttinger liquid. Several typical magnetization curves calculated by DMRG are presented. Recently the field-induced nematic phase was observed on the frustrated spin ladder system[2]. So we studied on a frustrated spin ladder system[3], using the numerical diagonalization and DMRG. As a result, it was found that several exotic quantum phases, including the spin-nematic liquid phase. We also reported several interesting phase diagrams of this model and some related systems[4,5]. In the present paper, we investigate the S=1 antiferromagnetic chain with the biqadratic interaction, as another candidate that exhibits the field-induced spin nematic liquid pahse. The numerical diagonalization study of finite-size clusters indicates that the spin nematic liquid pahse appears in this model under sufficiently strong magnetic field. The phase diagram in the plane of the magnetic field and the biquadratic interaction is presented.

[1] T. Sakai, T. Tonegawa and K. Okamoto, Physica Status Solidi B 247, 583 (2010). [2] N. Buttgen et al., Phys. Rev B 90, 134401 (2014). [3] T. Hikihara, T. Tonegawa, K. Okamoto and T. Sakai, J. Phys. Soc. Jpn. 86, 054709 (2017). [4] T. Tonegawa, T. Hikihara, K. Okamoto, S. C. Furuya, and T. Sakai, J. Phys. So. Jpn. 87, 104002 (2018). [5] T. Sakai, K. Okamoto and T. Tonegawa, Phys. Rev. B 100, 054407 (2019)

A2-08. Bypassing Dynamical Freezing and Accessing Low-Energy Microstates in Artificial Kagome Ice. *V. Schánilec*[1,2], B. Canals[1], V. Uhlir[2], L. Flajšman[2], J. Sadílek[2], T. Sikola[2,3] and N. Rougemaille[1] *1. CNRS - Institut NEEL, Grenoble, France, Grenoble, France; 2. CEITEC BUT, Brno, Czechia, Brno, Czechia; 3. Brno University of Technology, Institute of Physical Engineering, Brno, Czechia, Brno, Czechia*

Spin liquids are disordered states of matter that still fluctuate at low temperature. In many cases, the ground state of spin liquids is expected to be ordered, for example because the dipolar interaction lifts the (quasi) degeneracy between low-energy spin configurations. However, this is not what is observed experimentally, and many systems dynamically freeze in a liquid phase [1] before the ordering takes place. In spin ice compounds or artificial magnets, ground state configurations are then generally out of reach for practical reasons. In this presentation, we will show how dynamical freezing can be bypassed in an artificial kagome ice. We will illustrate the efficiency of our method by demonstrating that the a priori dynamically inaccessible ordered ground state of the dipolar kagome ice is imaged reproducibly in real space, and at room temperature. The central idea of this work is to replace the spin degree of freedom by a micromagnetic knob, which can be adjusted by a proper design of the vertex geometry. Our strategy is to imprint the desired spin configuration, vertex by vertex, in a kagome array made of connected nanomagnets, with a notch at each vertex site. Each notch locally lifts the energy degeneracy between the six states of a given vertex satisfying the ice rule constraint [2], allowing to reach efficiently any desired spin microstate using a field demagnetization protocol. This concept will be demonstrated both numerically and experimentally, and we will show how we can access all predicted phases of the dipolar kagome ice [3, 4, 5].

[1] I. A. Chioar, B. Canals, D. Lacour, Phys. Rev. B 90, 220407(R) (2014) [2] J. D. Bernal and R. H. Fowler, J. Chem. Phys. 1, 515 (1933) [3] W. R. Branford, S. Ladak, D. E. Read, Science 335, 1597-1600 (2012) [4] B. Canals, I. A. Chioar, V. D. Nguyen, Nature com. 7, 11446 (2016) [5] G.-W. Chern, P. Mellado and O. Tchernyshyov, Phys. Rev. Lett. 106, 207202 (2011).

A2-09. New Approaches to the Nearest Neighbour Ising Antiferromagnet on the Kagome Lattice. *J. Colbois*[1], K. Hofhuis[2,3], Z. Luo[2,3], X. Wang[2,3], A. Hrabec[2,3], L. Heyderman[2,3] and F. Mila[1] *1. Institute of physics, Ecole polytechnique fédérale de Lausanne, 1015 Lausanne, Switzerland; 2. Laboratory for Mesoscopic Systems, Department of Materials, Eidgenossische Technische Hochschule Zurich, 8093 Zurich, Switzerland; 3. Laboratory for Multiscale Materials Experiments, Paul Scherrer Institut, 5232 Villigen PSI, Switzerland*

The nearest neighbour antiferromagnetic Ising model on the kagome lattice is well known for its high frustration and macroscopic ground state degeneracy [1,2]. Recently, new experimental realizations of Ising-like spin systems have been developed - so-called artificial spin systems - based on mesoscopic structures of chirally coupled nanomagnets [3]. On the square lattice, such systems have proven to behave as nearest neighbour Ising antiferromagnets. Because of frustration, realizations of *kagome* lattice Ising antiferromagnets with these mesoscopic structures (Fig.1) are much more challenging to study. From the theoretical side as well, such models still present some difficulties [4,5]. I will describe how to tackle classical frustrated spin systems using Monte Carlo techniques [5] and tensor network methods [4,6,7] (Fig.2), focusing on the kagome lattice nearest neighbour Ising antiferromagnet in an external magnetic field, and I will compare the experimental and numerical results.

[1] K. Kanô and S. Naya, Prog. Theor. Phys., Vol. 10, p. 158 (1953) [2] A. Sütö, Z. Phys. B, Vol. 44, p. 121 (1981) [3] Z. Luo *et. al.*, Science, Vol. 363, p. 1435 (2019) [4] B. Vanhecke, J. Colbois, L. Vanderstraeten, *et. al.*, arXiv:2006.14341 (2020) [5] G. Rakala and K. Damle, Phys. Rev. E Vol. 96, 023304 (2017) [6] V. Zauner-Stauber, L. Vanderstraeten, *et. al*. Phys. Rev. B Vol. 97, 045145 (2018) [7] L. Vanderstraeten, B. Vanhecke, and F. Verstraete, Phys. Rev. E Vol. 98, 042145 (2018)

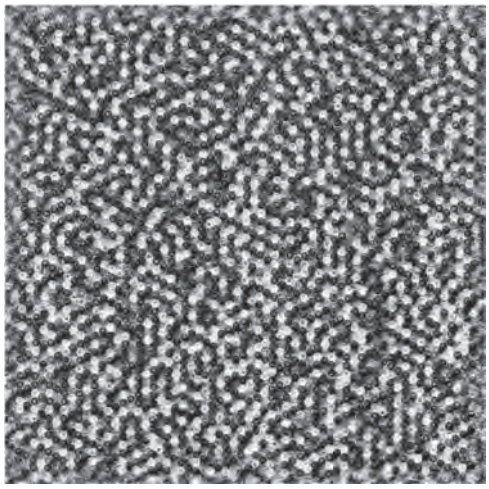

Fig. 1 Magnetic force microscopy image of a kagome lattice structure made of chirally coupled nanomagnets. The out-of-plane Ising spins configuration is the result of a demagnetization protocol applied to the sample. Black and white dots correspond to up or down magnetized islands, and red dots correspond to experimentally unassigned values due to a lack of clear constrast.

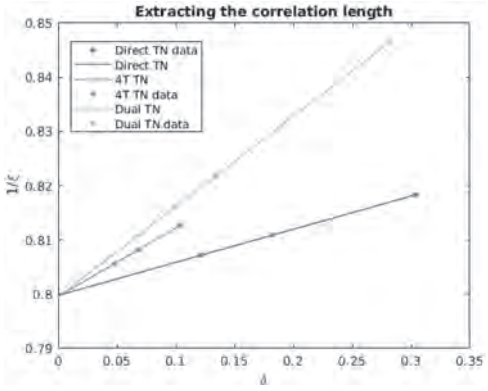

Fig. 2 Using three different tensor network (TN) constructions to compute the correlation length in the ground state of the kagome lattice Ising antiferromagnet. The graph shows the extrapolation of the inverse correlation length as a function of a gap in the transfer matrix eigenvalue spectrum. "Direct" stands for a construction on the triangle level, "dual" stands for a construction using the dice lattice, and "4T" stands for a construction using 4 triangles as a unit cell.

A2-10. Nonequilibrium Quasistationary Spin Disordered State in the Kitaev-Heisenberg Magnet α-$RuCl_3$. *R.B. Versteeg*[1], A. Chiocchetta[2], F. Sekiguchi[1], R. Aldea[1], A. Sahasrabudhe[1], K. Budzinauskas[1], Z. Wang[1], V. Tsurkan[3,4], A. Loidl[3], D. Khomskii[1], S. Diehl[2] and P.H. van Loosdrecht[1] *1. Institute of Physics 2, Universitat zu Koln, Koln, Germany; 2. Institute for Theoretical Physics, Universitat zu Koln, Koln, Germany; 3. Experimental Physics V, Center for Electronic Correlations and Magnetism, Universitat Augsburg, Augsburg, Germany; 4. Institute of Applied Physics Moldova, Chisinau, Moldova (the Republic of)*

Excitation by light pulses enables the manipulation of phases of quantum condensed matter. Here, we photoexcite high-energy holon-doublon pairs as a way to alter the magnetic free energy landscape of the Kitaev-Heisenberg magnet α-$RuCl_3$,[1,2] with the aim to dynamically stabilize a proximate spin liquid phase. The holon-doublon pair recombination through multimagnon emission [3] is tracked through the time-evolution of the magnetic linear dichroism originating from the competing zigzag spin ordered ground state. A small holon-doublon density suffices to reach a spin disordered state. The phase transition is described within a dynamic Ginzburg-Landau framework, corroborating the quasistationary nature of the transient spin disordered phase. Our work provides insight into the coupling between the electronic and magnetic degrees of freedom in α-$RuCl_3$ and suggests a new route to reach a proximate spin liquid phase in Kitaev-Heisenberg magnets.[4]

[1] A. Banerjee *et al.*, Proximate Kitaev quantum spin liquid behaviour in a honeycomb magnet, Nat. Mater. 15, 733-740 (2016). [2] H. Takagi *et al.*, Concept and realization of Kitaev quantum spin liquids, Nat. Rev. Phys. 1, 264-280 (2019). [3] Z. Lenarcic *et al.*, Ultrafast charge recombination in a photoexcited Mott-Hubbard insulator, Phys. Rev. Lett. 111, 016401 (2013). [4] R.B. Versteeg *et al.* Nonequilibrium quasistationary spin disordered state in the Kitaev-Heisenberg magnet α-$RuCl_3$, arXiv:2005.14189 [cond-mat.str-el] (2020)

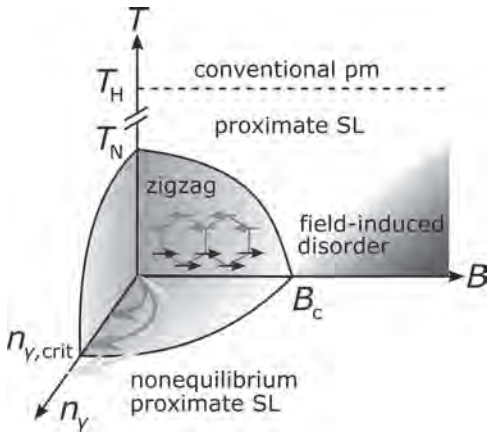

Fig. 1) A nonequilibrium dimension to α-RuCl3's magnetic phase diagram. The (B,T)-plane sketches the equilibrium magnetic phase diagram. Photoexcited holon-doublon pairs n_γ form a new nonequilibrium parameter. For small (red) to intermediate (magenta) quenches the system stays inside the zigzag ordered phase. Above a critical density $n_{\gamma,crit}$ a nonequilibrium proximate spin liquid state may be induced (light blue arrow).

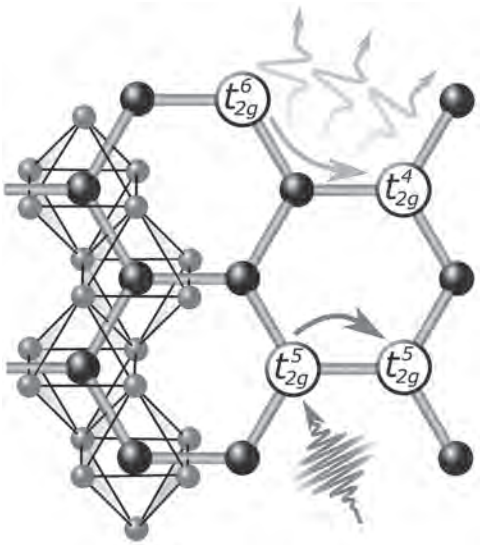

Fig. 2) α-RuCl3's honeycomb lattice. The lower process shows the photogeneration of a holon-doublon pair. The upper process shows the subsequent multimagnon emission by holon-doublon recombination, which drives the system into a nonequilibrium quasistationary spin disordered state.

A2-11. Incipient Antiferromagnetic Order in Metallic Ti_4MnBi_2 Containing Linear Mn Chains of Spin $S = 1/2$. *A. Pandey*[1] *1. School of Physics, University of the Witwatersrand, Johannesburg-Braamfontein, South Africa*

One dimensional spin $S = 1/2$ chain systems provide a perfect platform to explore many of the quantum phenomena and the related excitations. We report here the discovery of a stimulating magnetic ground state in a tetragonal compound Ti_4MnBi_2 that contains perfectly linear chains of Mn-ions with $d_{Mn\text{-}Mn} = 2.49$ Å running along the crystallographic *c*-axis and which are separated from each other by a large interchain distance $d_{chain} \approx 7.4$ Å. Our electrical transport measurements and electronic structure calculations establish that compound is metallic. Curie-Weiss fit to the susceptibility data suggests that Mn moments are in low-spin $S = 1/2$ configuration. The results show that despite the presence of a sizable antiferromagnetic (AFM) interaction [$J_c = 18(6)$ K], the full-moment long range magnetic ordering is not achieved down to 50 mK. Neutron diffraction measurement performed on an assembly of aligned single crystals detect a weak AFM order within the Mn chains, with a further evidence of the reduced-moment ordering coming from heat capacity data. Apparently, strong quantum fluctuations overcome the magnetic order and the material enters into a state at low temperatures which can be best described as a "quantum admixture" of a quantum spin liquid and a long-range magnetically ordered states, resulting into a highly reduced value of the ordered moment $\mu << 1\ \mu_B$.

A. Pandey, P. Miao, M. Klemm, H. He, H. Wang, X. Qian, J. W. Lynn, and M. C. Aronson, Phys. Rev. B in press (2020).

A2-12. Withdrawn

Session A3
MAGNETIZATION DYNAMICS AND DAMPING I: DAMPING AND FERROMAGNETIC RESONANCE

Andreas Ney, Chair
Johannes Kepler Universitat Linz, Linz, Austria

INVITED PAPER

A3-01. Conductivity-Like Gilbert Damping due to Intraband Scattering in Epitaxial Iron. *S. Emori[1] 1. Virginia Polytechnic Institute and State University, Blacksburg, VA, United States*

Confirming the origin of Gilbert damping by experiment has remained a challenge for many decades. This is the case even for some of the simplest and most technologically relevant ferromagnetic metals, such as pure Fe. Here, we experimentally identify intrinsic Gilbert damping that increases with *decreasing* electronic scattering in thin films of BCC Fe [1]. We directly compare the temperature dependence of Gilbert damping and electronic transport in pristine epitaxial films (Figure 1). Our observation of "conductivity-like" damping, which cannot be accounted for by classical eddy current loss, is in excellent quantitative agreement with theoretical predictions of Gilbert damping due to intraband scattering (often understood in terms of the "breathing Fermi surface" model) [2,3], as shown in Figure 2. While this fundamental damping mechanism was originally proposed more than 40 years ago [4], our study is the first to confirm it unambiguously for thin films of a pure ferromagnetic metal. Our results also reveal – somewhat counterintuitively – that disorder can reduce intrinsic damping in ferromagnetic metals particularly at low temperatures. This suggest that optimally disordered films may exhibit enhanced spin coherence required for cryogenic and quantum information devices.

[1] B. Khodadadi, A. Rai, A. Sapkota, et al. Phys. Rev. Lett., Vol. 124, 157201 (2020). [2] K. Gilmore, Y. U. Idzerda, and M.D. Stiles, Phys. Rev. Lett., Vol. 99, 27204 (2007). [3] S. Mankovsky, D. Kodderitzsch, G. Woltersdorf, and H. Ebert, Phys. Rev. B, Vol. 87, 14430 (2013). [3] V. Kamberský and Czechoslov. J. Phys., Vol. 26, 1366 (1976).

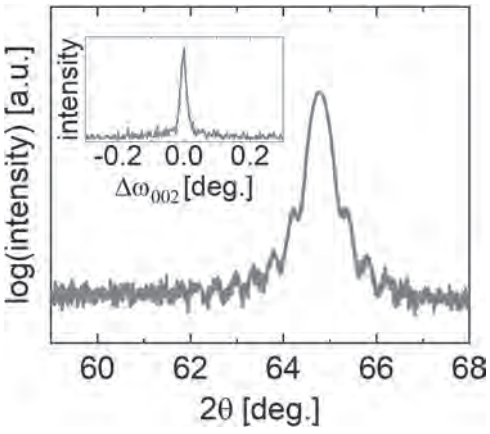

Figure 1. X-ray diffraction scan near the BCC (002) film peak of 25-nm-thick epitaxial Fe grown on a $MgAl_2O_4$ (001) substrate. Laue oscillations indicate smooth film interfaces. Inset: film-peak rocking curve with FWHM of only ~0.02 degrees, indicating minimal mosaic spread.

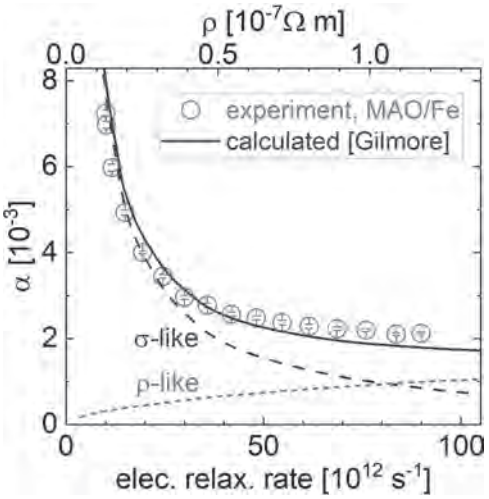

Figure 2. Comparison of the experimentally derived intrinsic Gilbert damping parameter (eddy current contribution subtracted) and the theoretically predicted Gilbert damping parameter (adapted from Ref. [2]) plotted against the electronic relaxation time.

CONTRIBUTED PAPERS

A3-02. Ultra-low Magnetic Damping in Epitaxial $Li_{0.5}Fe_{2.5}O_4$ Thin Films. *X. Zheng[1], L.J. Riddiford[1], J. Wisser[1], S. Emori[2] and Y. Suzuki[1] 1. Applied Physics, Stanford University, Stanford, CA, United States; 2. Physics, Virginia Polytechnic Institute and State University, Blacksburg, VA, United States*

The realization of energy efficient spin-current based electronics relies on the existence of low-loss magnetic insulator thin films capable of generating spin currents without an accompanying charge current. Currently, the number of such materials is extremely limited, with the only candidates being the garnets $Y_3Fe_5O_{12}$ (YIG) [1] and $Lu_3Fe_5O_{12}$ (LuIG) [2] along with the recently discovered spinels $Ni_{0.65}Zn_{0.35}Al_{0.8}Fe_{1.2}O_4$ (NZAFO) [3] and $MgAl_{0.5}Fe_{1.5}O_4$ (MAFO) [4,5]. Bulk phase $Li_{0.5}Fe_{2.5}O_4$ (LFO) is well known to have the lowest Gilbert damping parameter ($\alpha \approx 0.002$) among the spinel ferrites, but thus far LFO thin films have not lived up to these expectations. In this talk, we demonstrate the realization of epitaxial ultra-thin (~3 nm) LFO thin films on $MgAl_2O_4$ substrates with an ultra-low damping parameter of $\alpha \approx 0.0013$ and an FMR linewidth of 1.17 mT at 20.6 GHz. Such a damping value rivals those of YIG and is comparable to the lowest damping previously reported in sub-10-nm magnetic films [2]. LFO also offers distinct advantages over YIG such as smaller external field requirements and thinner interfacial magnetic dead layers due to the low growth temperature, making it ideal for magnetic switching applications. Our results show the promise of LFO as a new candidate for spin-current based spintronics. This work was supported by the U.S. Department of Energy, Director, Office of Science, Office of Basic Energy Sciences, Division of Materials Sciences and Engineering under Contract No. DESC0008505.

[1] B. M. Howe, S. Emori, H. Jeon, IEEE Magnetics Letters., Vol. 6, p. 1-4 (2015) [2] C. L. Jermain, H. Paik, S. V. Aradhya, Applied Physics Letters., Vol. 109, p. 192408 (2016) [3] M. T. Gray, S. Emori, B. A. Gray, Physics Review Applied., Vol. 9, p. 064039 (2018) [4] S. Emori, D. Yi, S. Crossley, Nano Letters., Vol. 18, p. 4273-4278 (2018) [5] J. J. Wisser, S. Emori. L. Riddiford, Applied Physics Letters., Vol. 115, p. 132404 (2019)

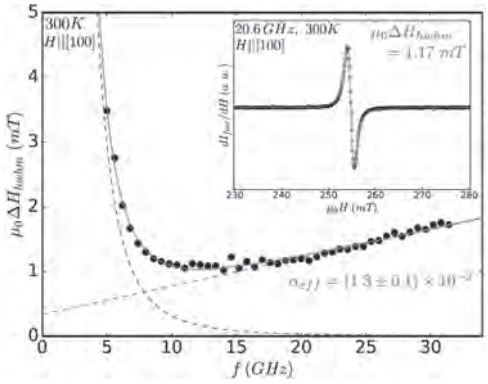

Fig.1 Ferromagnetic resonance (FMR) half-width-half-maximum linewidth plotted against frequency. The solid red line indicates a fit to a funtction with a linear Gilbert component (green dashed line) and a non-linear component (blue dashed line) to account for low-field losses due to incomplete saturation. The inset shows a sample FMR spectrum taken at 20.6 GHz.

A3-03. Low Damping and Linewidth in Magnetostrictive Epitaxial FeGa Thin Films Using Ferromagnetic Resonance. *A. Sapkota*[1], S. Budhathoki[1], B. Nepal[1], K. Law[1], S. Ranjit[1], S. KC[1], A.J. Hauser[1], C. Mewes[1] and T. Mewes[1] *1. Physics and Astronomy, The University of Alabama System, Tuscaloosa, AL, United States*

High magnetostriction and low damping are two crucial properties for voltage tunable high frequency devices using magnetostrictive ferromagnet-piezoelectric hybrid structures to achieve low microwave loss [1, 2]. FeGa is a promising candidate for such devices as it is free of rare earth elements and has a large magnetostriction [3]. We grew epitaxial FeGa films on MgO (100) substrates using off-axis sputtering technique. Broadband ferromagnetic resonance (FMR) is used to investigate the magnetization dynamics of the epitaxial FeGa thin films. The resonance field H_{res} versus frequency f data is fitted using the Kittel equation to extract the reduced gyromagnetic ratio γ', the effective magnetization M_{eff}, and the four-fold magnetic anisotropy H_4. The frequency dependence of the linewidth data is used to extract the effective damping α_{eff} and residual linewidth ΔH_0 due to inhomogeneities in the film. We report ultra-low residual linewidth, $\Delta H_0 = 13\pm1$ [Oe] – indicative of the high quality of the epitaxial films- significantly lower than reported previously [4]. The effective damping parameter α_{eff} is found to be as low as 0.0065(+0.0005 -0.0001), as shown in figure 1, which is one order magnitude lower than previously reported values [5, 6]. In-plane angular dependence of resonance field H_{res} clearly demonstrates a four-fold in-plane anisotropy arising from the crystal symmetry. The four-fold anisotropy extracted from the Kittel plot $H_4 = -786\pm15$ [Oe] is in good agreement with the value determined from fitting of in-plane rotation data $H_4 = -795\pm1$ [Oe] as shown in figure 2.

1) V. Novosad et al., Journal of applied physics 87, 6400 (2000). 2) J. Lou et al., Applied Physics Letters 92, 262502 (2008). 3) A. E. Clark et al., Materials transactions 43, 881 (2002). 4) B. K. Kuanr et al., Journal of Applied Physics 115, 17C112 (2014). 5) D. Parkes et al., Scientific reports 3, 2220 (2013). 6) D. B. Gopman et al., IEEE transactions on magnetics 53, 1 (2017).

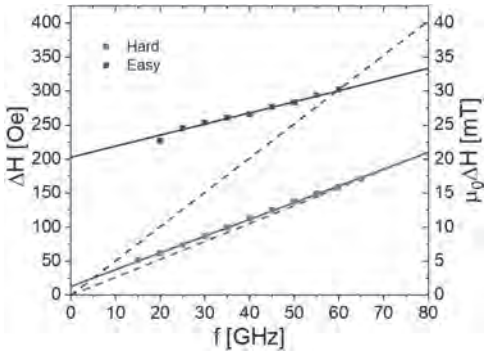

Figure 1: Linewidth as a function of frequency along hard and easy axes of the magnetic anisotropy, fitted using Gilbert damping term (solid lines). Maximum effective damping parameters for our study α_{max} are estimated from a straight line through the origin and the linewidth at the highest frequency (dashed lines).

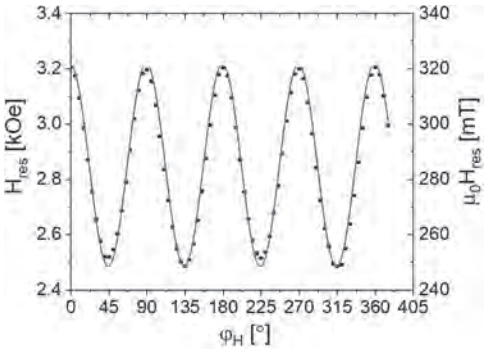

Figure 2: In-plane angular dependence of resonance field H_{res} (black symbols) and fit (red line) used to extract the four-fold magnetic anisotropy H_4.

A3-04. Magnetic Damping in Epitaxial Fe Alloyed With Low-Atomic-Number Elements. *D.A. Smith*[1], A. Rai[2], Y. Lim[1], T. Hartnett[3], A. Sapkota[2], A. Srivastava[2], C. Mewes[2], Z. Jiang[1], M. Clavel[1], M. Hudait[1], D. Viehland[1], J. Heremans[1], P. Balachandran[3], T. Mewes[2] and S. Emori[1] *1. Virginia Polytechnic Institute and State University, Blacksburg, VA, United States; 2. University of Alabama, Tuscaloosa, AL, United States; 3. University of Virginia, Charlottesville, VA, United States*

Recently, there has been an interest in developing ferromagnetic metals that possess both low damping and low saturation magnetization for use in spin-torque devices. While alloying ferromagnetic metals (e.g. Fe, the lowest-damping elemental ferromagnet) with nonmagnetic elements reduces the saturation magnetization, it remains an open question how this impacts damping. Here, we examine whether alloying can lower intrinsic damping through either of the two theoretically-suggested contributions [1]: 1) reduced spin-orbit coupling strength via a lower average atomic number *Z*, or 2) reduced density of states (DOS) at the Fermi level. In particular, we compare magnetic relaxation in epitaxial Fe films alloyed with light nonmagnetic elements of V ($Z = 23$) and Al ($Z = 13$) [2]. If spin-orbit coupling were to dominate, then the lower atomic number of Al would lead to lower Gilbert damping in FeAl than in FeV. Contrary to this expectation, out-of-plane ferromagnetic resonance experiments show a reduction in intrinsic Gilbert damping in FeV alloys, whereas FeAl alloys show an increase (Fig. 1). Additionally, the trend in FeV alloys agrees well with previous theoretical calculations [3] and exhibit an intrinsic Gilbert damping parameter as low as ~0.001, amongst the lowest values reported for ferromagnetic metals. To explain this behavior, we utilized density functional theory calculations to determine the DOS at the Fermi level. As shown in Fig. 2, the reduction (enhancement) in the average DOS for FeV (FeAl) corroborates the trend in intrinsic damping. This leads us to conclude that the DOS, rather than the average atomic number, dominates in governing magnetic relaxation in these Fe-based alloys.

1. K. Gilmore, Y. U. Idzerda, and M. D. Stiles, *J. Appl. Phys*, Vol. 103, 07D303 (2008) 2. D. A. Smith, A. Rai, Y. Lim, *et al.*, *arXiv* 2004.04840 (2020) 3. S. Mankovsky, D. Kodderitzsch, G. Woltersdorf, *et al.*, *Phys. Rev. B,* Vol. 87, 014430 (2013)

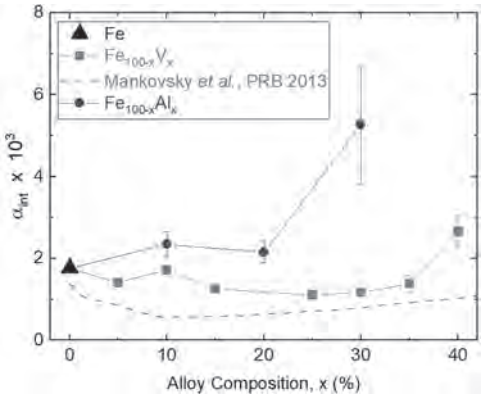

Fig. 1: Intrinsic Gilbert damping parameters for $Fe_{100-x}V_x$ and $Fe_{100-x}Al_x$. The dashed curve shows the theoretically predicted damping parameter computed by Mankovsky *et al.*

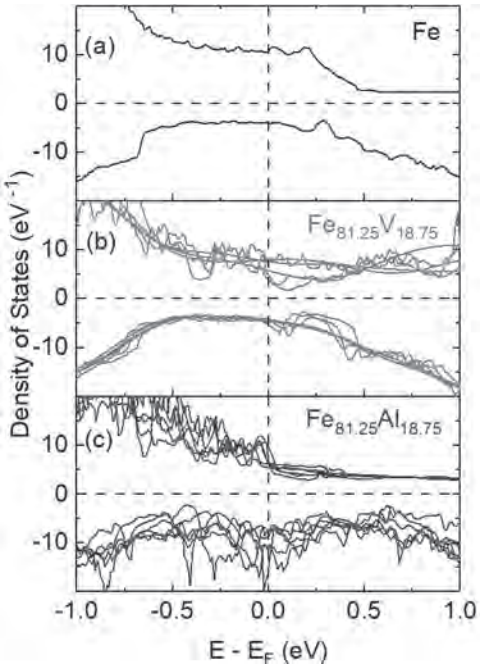

Fig. 2: Calculated density of states for (a) Fe, (b) $Fe_{81.25}V_{18.75}$, and (c) $Fe_{81.25}Al_{18.75}$.

A3-05. Two-Magnon Scattering in Polycrystalline Fe and FeV Alloy Thin Films. *S. Wu*[1], D.A. Smith[1], A. Rai[2], M. Clavel[3], M. Hudait[3], T. Mewes[2] and S. Emori[1] *1. Department of Physics, Virginia Polytechnic Institute and State University, Blacksburg, VA, United States; 2. Department of Physics and Astronomy, The University of Alabama, Tuscaloosa, AL, United States; 3. Department of Electrical and Computer Engineering, Virginia Polytechnic Institute and State University, Blacksburg, VA, United States*

Identifying the origins of ferromagnetic resonance (FMR) linewidth broadening is essential for the fundamental understanding of magnetic relaxation, often discussed in terms of "damping". It is not yet well understood how inhomogeneity and structural disorder contribute to magnetic relaxation in polycrystalline thin films, even though they are widely used in device applications. In this presentation, we systematically examine the impact of inhomogeneity and disorder on the FMR linewidth of sputter-grown polycrystalline Fe and $Fe_{80}V_{20}$ films with thickness 2-25 nm and different seed layers. A highly nonlinear frequency dependence of FMR linewidth is observed for Fe films on Cu/Ti seed layers. As shown in Fig. 1, all linewidth vs frequency data are quantitatively reproduced with a two-magnon scattering model [1, 2, 3] that accounts for a random distribution of the effective anisotropy field among grains in the polycrystalline film. The fit results indicate that a larger grain size is correlated with stronger two-magnon scattering, which – somewhat counterintuitively – may be accompanied by a lower Gilbert damping parameter. Films with the strongest two-magnon scattering contribution (cf. 10-nm-thick Fe/Cu/Ti, Fig. 1) exhibit the highest coercivity, pointing to a connection between magnetic inhomogeneity and the observed non-Gilbert relaxation. In addition, it is found that two-magnon scattering is reduced by changing the seed layer or alloying Fe with V (Fig. 2). We will discuss the possible mechanisms that lead to narrower FMR linewidths in polycrystalline Fe(V) films. The fundamental understanding gained from our study enables a coherent approach to develop low-loss polycrystalline magnetic media for power-efficient spintronic devices.

[1] R. McMichael and P. Krivosik, IEEE Trans. Mag., Vol. 40, p.2 (2004) [2] S. Kalarickal, P. Krivosik and J. Das, Phys. Rev. B, Vol. 77, p.054427 (2008) [3] W. Peria, T. Peterson and A. McFadden, Phys. Rev. B, Vol. 101, p.134430 (2020)

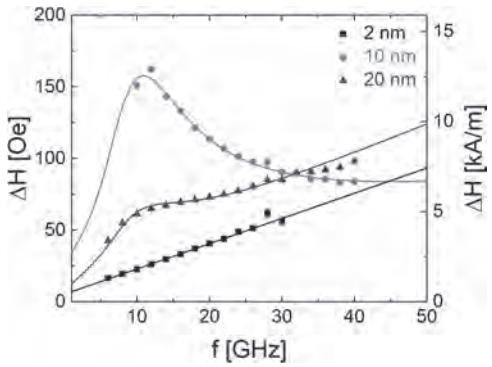

Fig. 1. Linewidth vs. frequency for 2 nm, 10 nm and 20 nm thick Fe/Cu/Ti films. Solid curves correspond to fits to the data.

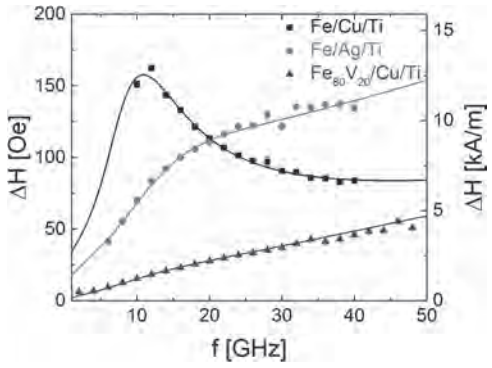

Fig. 2. Linewidth vs. frequency for 10 nm thick Fe/Cu/Ti, Fe/Ag/Ti and $Fe_{80}V_{20}$/Cu/Ti films. Solid curves correspond to fits to the data.

A3-06. Higher-Order Contribution to Perpendicular Anisotropy and Interfacial Damping of Co/Ni Multilayers. *A. Rai*[1], A. Sapkota[1], A. Pokhrel[1], M.P. Li[2], M.D. Graef[2], C. Mewes[1], V. Sokalski[2] and T. Mewes[1] *1. Physics and Astronomy, The University of Alabama, Tuscaloosa, AL, United States; 2. Materials Science and Engineering, Carnegie Mellon University, Pittsburgh, PA, United States*

Magnetic materials showing perpendicular magnetic anisotropy (PMA) and low damping are of great importance in spintronics. Co/Ni multilayers have been known to exhibit large tunable PMA [1], high spin polarization [2] and

relatively low intrinsic damping [3]. In this study we investigated a series of Pt/$[Co/Ni]_N$/Ir multilayers grown on Si/SiO_2 with a Ta/Pt seed adhesion layer and the multilayer stack was capped with an Ir/Pt/Ta capping layer. Broadband ferromagnetic resonance (FMR) and polar angle dependent FMR measurements reveal the presence of a strong fourth-order contribution to the perpendicular anisotropy. Polar angle dependent data are fitted using the Smit-Beljers relation [4] to extract both the second and fourth-order anisotropy constants (shown in Fig.1). This model explains the data qualitatively and we observe systematic deviations for samples near or in the easy cone state of the phase diagram. We find that the effective Gilbert damping scales with the inverse multilayer thickness, indicating a significant interfacial contribution to the damping process.

1. G. Daalderop, P. Kelly and F. D. Broeder, Physical Review Letters., vol 68, p:682-685 (1992) 2. S. Mangin, D. Ravelsona, J. A. Katine, et.al., Nature Materials., vol 5, p:210-215 (2006) 3. J. M. Shaw, H. T. Nembach and T. J. Silva, Journal of Applied Physics., vol 108, p: 093922 (2010) 4. J. Smith and H. Beljers, Philips Research Reports., vol 10, p:113 (1955)

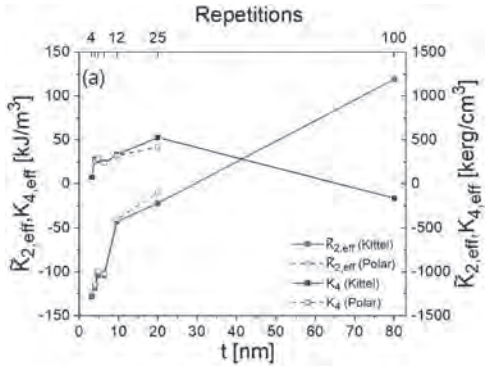

Fig.1 Comparison of second and fourth-order anisotropies using frequency dependent and polar angle dependent measurements.

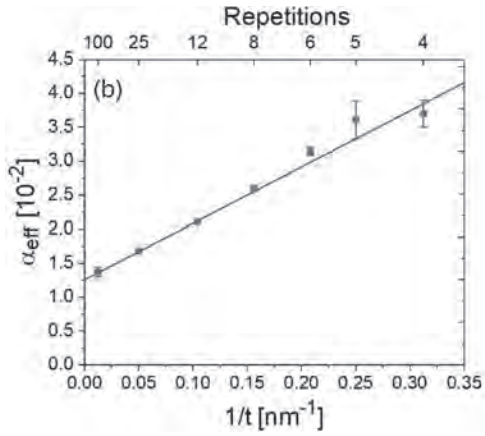

Fig.2 Variation of effective Gilbert damping with the inverse Co/Ni thicknesses.

A3-07. Perpendicular Anisotropy and Damping of MgO/Fe/Au Trilayers With Broken Inversion Symmetry. N. Kamiya[1], *T. Kato*[2], D. Oshima[2] and S. Iwata[2] *1. Department of Electronics, Nagoya University, Nagoya, Japan; 2. Institute of Materials and Systems for Sustainability, Nagoya University, Nagoya, Japan*

Insulator / 3d ferromagnet / 5d metal trilayers with broken inversion symmetry along the film normal direction is of great interest, since the broken symmetry is known to contribute to the perpendicular magnetic anisotropy (PMA) and the conversion of in-plane charge current to perpendicular spin current through the Rashba spin-orbit coupling [1, 2]. Here, we report on the PMA and magnetization dynamics of the MgO/Fe/Au trilayer with the Fe layer thickness from 0.4 nm to 1.2 nm, and compare the results with the Au/Fe/Au system with a symmetric structure along the film normal. These trilayers were grown on MgO(001) substrate by molecular beam epitaxy method. The PMA and dynamics were investigated by the time-resolved magneto-optical Kerr effect (TRMOKE) measurements. Figure 1 shows Fe thickness dependence of (a) effective anisotropy field H_{keff}, (b) g-factor, (c) anisotropy distribution ΔH_{keff}, and (d) damping constant α of MgO/Fe/Au and Au/Fe/Au trilayers. Both MgO/Fe/Au and Au/Fe/Au showed an increase of H_{keff} with decreasing the Fe thickness, and MgO/Fe/Au was confirmed to exhibit slightly larger H_{keff} than Au/Fe/Au due to the Rashba effect. The g-factor of both trilayers decreased from the bulk value with decreasing the Fe thickness. ΔH_{keff} increased at Fe thickness of 0.8 nm for both trilayers which is considered to be due to the relaxation of lattice mismatch around the Fe thickness of 1 nm. The damping constant α of both trilayers increased with decreasing the Fe thickness from 0.8 nm to 0.4 nm due to the effect of spin pumping. The reduction of α at Fe thickness of 0.8 nm is explained by the effect of two-magnon scattering which is enhanced by the increase of ΔH_{keff}. Interestingly, MgO/Fe/Au trilayers show larger damping constant than Au/Fe/Au with the same Fe thickness, which may reflect the Rashba spin-orbit coupling and/or the variation in the density of states at the Fermi level.

[1] S. E. Barnes et. al., Sci. Rep. 4, 4105 (2014). [2] I. M. Miron et al., Nat. Mater. 9, 230 (2010).

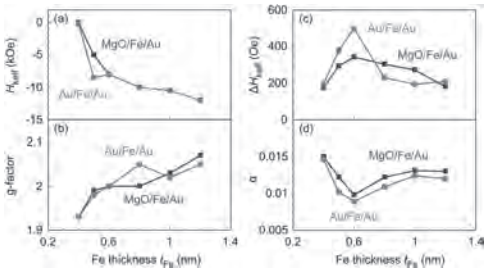

Fig. 1 Fe thickness dependence of (a) effective anisotropy field H_{keff}, (b) g-factor, (c) anisotropy distribution ΔH_{keff}, and (d) damping constant α of MgO/Fe/Au and Au/Fe/Au trilayers.

A3-08. Experimental Realization of Linearly Polarized x-ray Detected Ferromagnetic Resonance. *C. Klewe*[1], S. Emori[2], Q. Li[3], M. Yang[3], B. Gray[5], H. Jeon[4], B.M. Howe[5], Y. Suzuki[6,7], Z.Q. Qiu[3], P. Shafer[1] and E. Arenholz[8] *1. Advanced Light Source, Lawrence Berkeley National Laboratory, Berkeley, CA, United States; 2. Physics, Virgina Tech, Blacksburg, VA, United States; 3. Physics, University of California Berkeley, Berkeley, CA, United States; 4. Sensors Directorate, Air Force Research Lab, Wright Patterson Air Force Base, Dayton, OH, United States; 5. Materials and Manufacturing Directorate, Air Force Research Lab, Wright Patterson Air Force Base, Dayton, OH, United States; 6. Geballe Laboratory for Advanced Materials, Stanford University, Stanford, CA, United States; 7. Applied Physics, Stanford University, Stanford, CA, United States; 8. Cornell High Energy Synchrotron Source, Cornell University, Ithaca, NY, United States*

Recently, antiferromagnetic spintronics have attracted great attention, with extensive research devoted to spin transport between ferromagnetic (FM) and antiferromagnetic (AFM) materials in FM/AFM heterostructures [1-6]. In order to enable a deeper understanding of the mechanisms behind this effect, it would be invaluable to perform time resolved studies of GHz spin dynamics in systems with antiferromagnetic order with sensitivity to each absorber site individually, however, to date experimental techniques that offer these capabilities are lacking. Here, we present the first experimental observation of dynamic X-ray magnetic linear dichroism (XMLD) from GHz spin precessions driven by ferromagnetic resonance (FMR). We explore the capabilities of this new technique in two model systems, a ferromagnetic metal, i.e., $Ni_{80}Fe_{20}$ (Py), and a ferrimagnetic insulator, i.e., $Ni_{0.65}Zn_{0.35}Al_{0.8}Fe_{1.2}O_4$ (NZAFO). Both systems yield dynamic XMLD signals consistent

with our models. Under experimental geometries with oblique x-ray polarization (i.e., when the angle between static magnetization and x-ray polarization is near 45°) the dynamic XMLD response occurs primarily at the fundamental frequency of the driving RF excitation (see Fig. 1). This effect is well suited for in-plane magnetic anisotropy studies conducted in normal incidence geometry. For studies that require complementary geometries (e.g., vertical or horizontal polarization), the dynamic signal can be extracted from the 2nd harmonic response. This also works for grazing incidence measurements that are sensitive to in- vs. out-of-plane magnetic anisotropy. The presented results are a breakthrough achievement in detecting dynamic manifestations of the XMLD effect at technologically relevant, GHz frequencies. By utilizing the sensitivity of XMLD to the spin axis rather than the spin direction, one can expand conventional x-ray detected FMR towards the direct dynamic study of antiferromagnetic order.

[1] C. Hahn *et al.*, EPL 108, 57005 (2014) [2] H. Wang *et al.*, Phys. Rev. Lett. 113, 097202 (2014) [3] W. Lin *et al.*, Phys. Rev. Lett. 116, 186601 (2016) [4] Z. Qiu *et al.*, Nat. Commun. 7, 12670 (2016) [5] Q. Li *et al.*, Nat. Commun. 10, 5265 (2019) [6] M. Dabrowski *et al.*, Phys. Rev. Lett. 124, 217201 (2020)

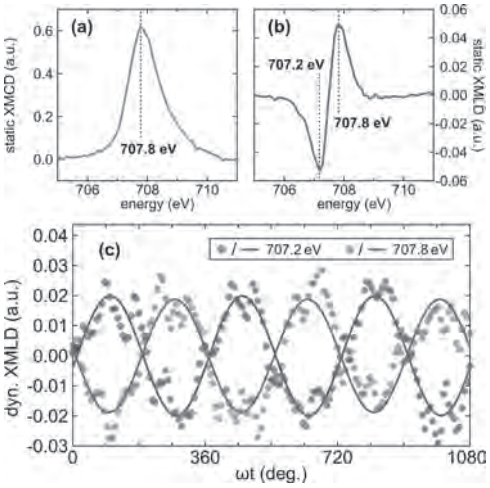

Fig. 1: (a) Static XMCD and (b) static XMLD measurements on Py. (c) The dynamic XMLD measurements for photon energies 707.2eV and 707.8eV show a fundamental response with similar amplitude but opposite sign, analogous to the bipolar lineshape of the static XMLD spectrum.

A3-09. Structural and Magnetic Properties of $Co_{1.5}Ti_{0.5}FeAl$ Heusler Alloy Epitaxial Thin Films. *S. Budhathoki*[1], A. Rai[1], K. Law[1], R. Nahar[1], A. Stewart[1], S. Ranjit[1], S. KC[1], P. LeClair[1], C. Mewes[1], T. Mewes[1] and A.J. Hauser[1] *1. Department of Physics and Astronomy, The University of Alabama, Tuscaloosa, AL, United States*

Heuser alloys present a rich phase diagram to engineer new materials and alter tunability of the desired material properties for potential technological applications in spintronic devices. We investigate the structural, static, and dynamic properties of $Co_{1.5}Ti_{0.5}FeAl$ Heusler alloy thin films, with variable thickness (t = 5 nm, 10 nm, 20 nm, 35 nm, 50 nm, and 70 nm) grown by sputter beam epitaxy on cubic MgO (100), MAO (100) (Fig. 1), and hexagonal Al_2O_3 (110) substrates. By partial substitution of Ti for Co in parent alloy Co_2FeAl i.e $Co_{1.5}Ti_{0.5}FeAl$, we demonstrate a very low total damping parameter of 0.00156 ± 0.00003 and a low linewidth term 17 ±1 Oe (Fig. 2) for 20 nm film grown on MAO (100) substrate using ferromagnetic resonance spectroscopy comparable to elemental Fe[1,2]. A pronounced fourfold anisotropy is consistent with the fourfold crystalline symmetry in the epitaxial thin films grown on cubic substrates. A saturation magnetization of ~ 5.0 μ_B/f.u. (where f.u. represents formula unit) was obtained at room temperature, nearly double the value based on the Slater-Pauling rule. $Co_{1.5}Ti_{0.5}FeAl$ films simultaneously exhibit a very low damping and approximately 40 % lower moment than that of elemental Fe[3]. Taken together, the smaller value of damping, saturation moment, and linewidth for $Co_{1.5}Ti_{0.5}FeAl$ films can significantly improve the efficiency of STT-switching and makes it a promising metallic ferromagnet to engineer low-loss spintronic devices.

1) B. Khodadadi, A. Rai, A. Sapkota, A. Srivastava, B. Nepal, Y. Lim, D.A. Smith, C. Mewes, S. 16 Budhathoki, A.J. Hauser, M. Gao, J.-F. Li, D.D. Viehland, Z. Jiang, J.J. Heremans, P. V Balachandran, T. Mewes, and S. Emori, Phys. Rev. Lett. 124, (2020). 2) M. Oogane, T. Wakitani, S. Yakata, R. Yilgin, Y. Ando, A. Sakuma, and T. Miyazaki, Jpn. J. Appl. Phys. 45, 3889 (2006) 3) J. M. D. Coey, Magnetism and magnetic materials. Cambridge, UK: Cambridge University Press, 2012.

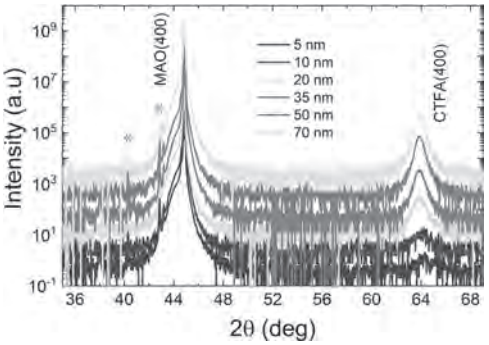

Fig. 1. 2θ-ω XRD (Cu X-ray source) scan of epitaxial $Co_{1.5}Ti_{0.5}FeAl$ thin films (vertically offset for clarity) grown on MAO (100) single crystal substrates. *Asterisks (*) indicate substrate peaks*.

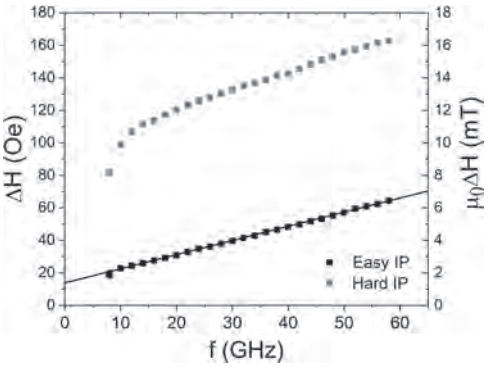

FIG. 2 Frequency-dependent linewidth taken along the magnetic in-plane easy (black) and hard (red) axes for 20 nm thick $Co_{1.5}Ti_{0.5}FeAl$ film grown on MAO substrate.

A3-10. A Systematic Ferromagnetic Resonance Study of Deposition Conditions in NiFe Thin Films for Shielding Applications. *M.R. McMaster*[1], W. Hendren[1], J.N. Scott[1] and R. Bowman[1] *1. Queen's University Belfast, Belfast, United Kingdom*

Tailoring the electromagnetic properties of synthetic magnetic structures is advantageous for high frequency applications, such as engineering shielding materials in magnetic recording where control of properties such as permeability is essential. Design of suitable components requires the characterisation of materials in the gigahertz frequency range to determine the parameters necessary for simulations. We present a systematic study of the dependence of the ferromagnetic resonance (FMR) and spin wave properties of Ni_xFe_{100-x} alloy thin films with varied Ni composition and deposition conditions using a vector network analyser (VNA) and coplanar waveguide [1][2][3][4]. The quality of the FMR response and the effective permeability in single layer films is particularly affected by the NiFe crystal structure, most notably over the fcc-bcc boundary at x=40, Figure 1. The FMR was also improved by proper choice of seed layer and lowering deposition pressure. Increasing

substrate temperature was observed to have an actively detrimental effect on ferromagnetic resonance. The effect on FMR of modulating the composition in NiFe thin films was also studied using repeated bilayer structures with a constant total thickness of the form $n[Ni_xFe_{100-x}/Ni_yFe_{100-y}]$, where n is the number of bilayers and determines the period of modulation. Compared to single layers, the compositionally modulated structures were generally seen to enhance the FMR signal and increase the frequency of resonance, Figure 2.

[1] Y. Ding et al. J. Appl. Phys. 96, 2969 (2004) [2] C. Kittel, Phys Rev 73, 2 (1948) [3] Y.V. Khivintsev. J. Appl. Phys. 108, 023907 (2010) [4] Kalarickal et al. J. Appl. Phys. 99, 093909 (2006)

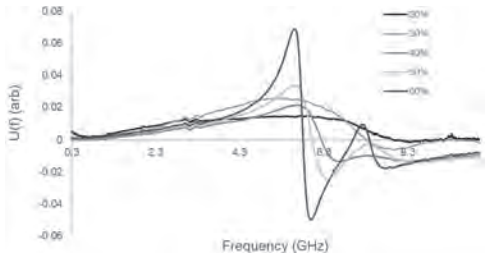

FMR response [4] with frequency for Ni_xFe_{100-x} 100nm thin films. The fcc-bcc boundary at x=40 is accompanied by an abrupt broadening and suppression of the FMR.

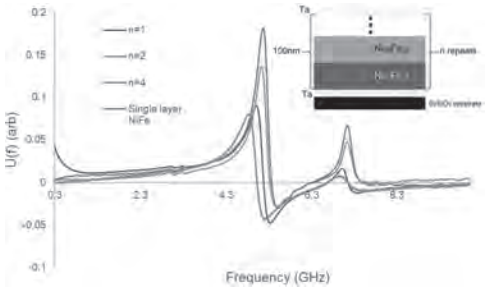

FMR response [4] of a $Ni_{80}Fe_{20}$ single layer film compared to those of repeated bilayer NiFe structures of the form $n[Ni_{82}Fe_{18}/Ni_{78}Fe_{22}]$ and an average composition of $Ni_{80}Fe_{20}$. It can be seen that bilayer structures show an enhanced FMR signal and the resonance frequency increases with increasing n.

A3-11. High-Temperature Ferromagnetic Resonance in FePt Thin Films. *C. Liu*[1], K. Srinivasan[2], A. Ajan[2], E. McCollum[1] and M. Wu[1]
1. Physics department, Colorado State University, Fort Collins, CO, United States; 2. Western Digital Corp, San Jose, CA, United States

Understanding of damping processes in ferromagnetic thin films at temperatures (T) near the Curie temperature (T_c) has significant implications for heat-assisted magnetic recording and magnetic sensors operating at elevated temperatures. Recent ferromagnetic resonance (FMR) studies [PR Applied 10, 054046 (2018)] using out-of-plane fields showed that there are two major relaxation processes in granular $L1_0$-odered FePt thin films at 10-45 K below T_c: two-magnon scattering and spin-flip magnon-electron scattering; with a decrease in T, the FMR linewidth increases due to the enhancement of the two-magnon scattering. This presentation reports high-T FMR studies on continuous FePt thin films with cubic structures, rather than $L1_0$ structures. The films are 6-nm thick and have $T_c \approx 680$ K; the FMR measurements were performed over 300-620 K in out-of-plane fields. As opposed to the $L1_0$ FePt films, the cubic FePt films show an FMR linewidth that decreases with a decrease in T. This T dependence suggests that the spin-flip magnon-electron scattering is dominant over the two-magnon scattering; the two-magnon scattering is weak because it is expected to be absent in continuous films under out-of-plane fields.

A3-12. Two-Magnon Frequency Pulling Effect in Ferromagnetic Resonance. *W. Peria*[2], H. Yu[1], S. Lee[1], I. Takeuchi[1] and P.A. Crowell[2]
1. Department of Materials Science and Engineering, University of Maryland at College Park, College Park, MD, United States; 2. School of Physics and Astronomy, University of Minnesota, Minneapolis, MN, United States

Two-magnon scattering (TMS) is a well-known extrinsic scattering process in ferromagnets, which is usually observed through its broadening effect on ferromagnetic resonance (FMR) lineshapes for in-plane magnetic field [1]. A lesser known effect is frequency pulling on FMR as a result of the hybridization between interacting magnon modes. The frequency pulling is not independent of the linewidth broadening effect and can be calculated if the two-magnon linewidth is known. We present broadband ferromagnetic resonance measurements for in-plane (IP) and perpendicular-to-plane (PP) directions of applied field in order to demonstrate the two-magnon frequency pulling effect in $Fe_{0.7}Ga_{0.3}$ thin films. We first show that a satisfactory fit of the resonance frequencies cannot be obtained when the magnetization is IP, and further, that the fit parameters which are obtained differ greatly from the fit parameters obtained for PP magnetization. We address these problems by first fitting the linewidths (where the two-magnon effect is very pronounced) to a combined two-magnon scattering and Gilbert damping model, and with those fit parameters calculate the corresponding two-magnon resonance line shifts (see figure). The fit to the two-magnon model yields a defect correlation length which we corroborate with structural characterization. We then show that this leads to a much better fit of the IP field-dependent dispersion. In addition, the effective demagnetizing field can be fixed to the value obtained for PP magnetization, and a good fit is still obtained. Thus the inconsistencies between IP and PP dispersions are eliminated by accounting for the frequency pulling effect of two-magnon scattering, and we emphasize the importance of this effect when using FMR to characterize static magnetic properties of thin films. This work was supported by SMART, a center funded by nCORE, a Semiconductor Research Corporation program sponsored by NIST.

[1] R. D. McMichael and P. Krivosik, IEEE Trans. Mag. 40, 2 (2004).

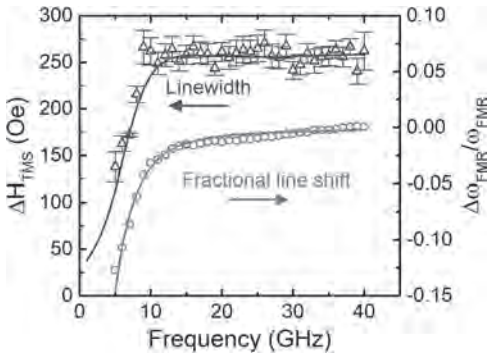

Fig: TMS linewidths and fit (blue points, left ordinate) and fractional line shifts with fit (red points, right ordinate).

A3-13. The Effect of Temporal Evolution of Magnetic Anisotropy Parameters on the Magnetization Precession in Ferromagnetic Films. *P. Gerevenkov*[1], A.W. Rushforth[2], A. Kalashnikova[1] and N. Khokhlov[1]
1. Ioffe Institute, St. Petersburg, Russian Federation; 2. School of Physics and Astronomy, The University of Nottingham, Nottingham, United Kingdom

Recent works demonstrate all-optical excitation of magnetization dynamics (precession and spin waves) due to laser-induced ultrafast changes of the anisotropy field [1, 2]. Owing to ultrafast laser-induced heating, a local change in the material parameters (anisotropy and magnetization) occurs, which leads to a reorientation of the effective field in the sample and thus

triggers the magnetization dynamics [3]. When describing thermal excitation of the laser-induced precession, an instantaneous step-like change in the anisotropy field is often assumed without further change with time. This allows one to simplify the mathematical description of the experiment data. It was experimentally demonstrated for metal films during pulsed laser heating [2], that anisotropy relaxation to its equilibrium value is observed at times of the order of hundreds of picoseconds. If the time is comparable with the life-time of the excited precession it is important to account for the temporal evolution of the anisotropy field after excitation, since it may yield a number of important physical phenomena including magnetization switching [4, 5]. In this work, we pave the way to deriving the temporal evolution of the anisotropy parameters from the experiments on laser-induced magnetization precession and time-dependent hysteresis loops in thin films of a ferromagnet Galfenol. Epitaxial films of Galfenol with the composition $Fe_{0.81}Ga_{0.19}$ and thicknesses of 5-50 nm on GaAs substrates were used. The parameters of laser-induced precession of magnetization in the geometry of the polar Kerr effect were experimentally obtained for various directions of the external magnetic field in the film plane. A theoretical description of the precession parameters was obtained using the Smit-Beljers approach for the case of instantaneous changes in material parameters. Evolution of the anisotropy parameters over the temporal range of 0-3 ns after ultrafast heating were obtained. It is shown that evolution leads to a change in the precession frequency with time, which is seen as a nonsymmetrical shape of the frequency spectrum of the observed precession. Work is supported by RFBR (project 20-32-70149).

1 N.E. Khokhlov, P.I. Gerevenkov, L.A. Shelukhin et al., Phys. Rev. Appl., Vol. 12, p.044044 (2019) 2 E. Carpene, E. Mancini, D. Dazzi et al., Phys. Rev. B., Vol. 81, p.060415 (2010) 3 A. Kirilyuk, A.V. Kimel and T. Rasing, Rev. Mod. Phys., Vol. 82, p.2731 (2010) 4 E. Carpene, C. Piovera, C. Dallera et al., Phys. Rev. B., Vol. 84, p.134425 (2011) 5 A. Stupakiewicz, K. Szerenos, D. Afanasiev et al., Nature., Vol. 42, p.714 (2017)

Session A4
MAGNETO-ELASTIC AND MAGNETO-CALORIC MATERIALS I

Radhika Barua, Co-Chair
Virginia Commonwealth University, Richmond, VA, United States
Suok-Min Na, Co-Chair
Naval Surface Warfare Center Carderock Division, West Bethesda, MD, United States

CONTRIBUTED PAPERS

A4-01. Estimation of Magnetocaloric Effect and Critical Exponents in Fe Doped Mn_5Ge_3 Compound. *S. S*[1], A. K[1], R. U D[1], A. Dzubinska[2], M. Reiffers[3] and N. Ramamoorthi[1] *1. Deaprtment of Physics, National Institute of Technology, Tiruchirappalli, Tiruchirappalli, India; 2. Center for Progressive Materials-Technology and Innovation Park, University of Pavol Jozef Šafárik, Kosice, Slovakia; 3. Faculty of Humanities and Natural Sciences, University of Presov, Presov, Slovakia*

The search for an appropriate magnetocaloric material with reversible room temperature magnetocaloric effect (MCE) has intensified in the past decade and Mn_5Ge_3 family of compounds are found to serve the above need[1]. This abstract briefs the magnetocaloric properties and critical behavior analysis of Fe doped Mn_5Ge_3 compound. We have synthesized $Mn_5Ge_{2.9}Fe_{0.1}$ polycrystalline compound using arc melting technique. It undergoes a ferromagnetic-paramagnetic transition around 299 K and, at 50 K, a minor transition is observed due to orientation of random spins. MCE of this material calculated using Maxwell's equation[2] from *M(B)* data is 4.84 J/kg K for $\Delta B = 5$ T (see *Fig. 1*). However, a substantial relative cooling power of 274.6 J/kg is achieved, as MCE prevails over a wide temperature span of 56.79 K. The second order nature of MCE is demonstrated by plotting the universal curve (see inset of *Fig.1*) which has only 7.07 % dispersion[3]. There are several reports on Mn_5Ge_3 family where the influence of chemical doping on MCE and other properties are lucid. However, to get a clear picture on the magnetic interactions, one has to carry out critical behavior analysis. Using modified Arrott plot and Kouvel-Fischer methods[4,5], the critical exponents were determined and compared with the standard models as shown in *Table. 1*. The exponents of $Mn_5Ge_{2.9}Fe_{0.1}$ compound match well with 3D-Ising model. In addition, using renormalization group theory approach[6], the range of interaction has been estimated and is found to lie in between mean field and Heisenberg model. From the above analyses, we conclude that $Mn_5Ge_{2.9}Fe_{0.1}$ compound exhibits 3D- Ising type short ranged interaction that decays as $r^{-4.97}$. This compound has a modest reversible MCE around room temperature and hence would gain a substantial attention in refrigeration industry.

1. T. Tolinski and K. Synoradzki, Intermetallics 47, 1 (2014). 2. Arun. K, Swathi. S, Remya. U. D, et. al., J. Appl. Phys. 127, 053901 (2020). 3. C. M. Bonilla, J. Herrero-Albillos, F. Bartolomé, et. al., Phys. Rev. B 81, 224424 (2010). 4. J. S. Kouvel and M. E. Fisher, Phys. Rev. 136, A1626 (1964). 5. Stanely H.E., *Introduction to Phase Transitions and Critical Phenonmena* (Oxford Press, London, 1971). 6. M. E. Fisher, S.-k. Ma, and B. G. Nickel, Phys. Rev. Lett. 29, 917 (1972).

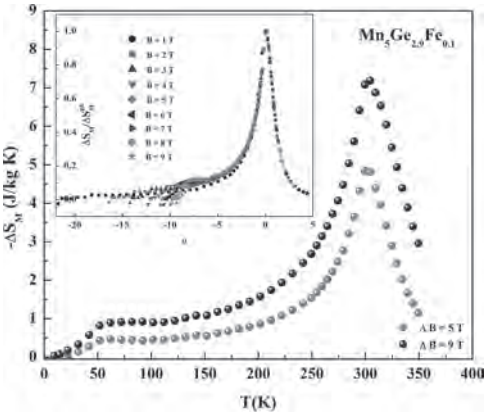

Fig. 1: ***Main Panel:*** **The magnetic entropy change (MCE) of $Mn_5Ge_{2.9}Fe_{0.1}$ compound.** ***Inset:*** **Universal curve demonstrating the second order nature of the compound.**

Table 1. The estimated critical exponents along with those of the standard models.

Sample/Model	Method	β	γ	δ
Mean Field	Theoretical	0.5	1	3
3D Heisenberg	Theoretical	0.365	1.386	4.8
3D XY	Theoretical	0.345	1.316	4.59
3D Ising	**Theoretical**	**0.325**	**1.241**	**4.82**
$Mn_5Ge_{2.9}Fe_{0.1}$	MAP	0.3099(8) T_C=295.4(1) K	1.2152(4) T_C=295.4(7) K	4.9215(9)
$Mn_5Ge_{2.9}Fe_{0.1}$	KF	0.3181(2) T_C=295.8(6) K	1.2144(2) T_C=295.4(7) K	4.8174(9)

Table. 1: **The estimated critical exponents along with those of the standard models.**

A4-02. Effect of Magnetic Proximity on Magnetocaloric Properties of $Ni_{80}Fe_{20}/Ni_xCu_{1-x}/Co_{90}Fe_{10}$ Stacks. M.A. Kuznetsov[1,2], I.Y. Pashenkin[1], *N.I. Polushkin*[1], M.V. Sapozhnikov[1] and A.A. Fraerman[1] *1. Institut fiziki mikrostruktur Rossijskoj akademii nauk, Niznij Novgorod, Russian Federation; 2. Faculty of Physics, Lobachevsky State University of Nizhniy Novgorod, Nizhniy Novgorod, Russian Federation*

Current magnetocaloric materials exhibit large adiabatic changes in temperature (ΔT_{ad}~10 °K) in applied magnetic fields (H) with the strength in several tens of kilo-oersted (kOe). To achieve an appreciable magnetocaloric effect (MCE) with *moderate H*, new magnetic materials with tailored magnetocaloric properties must be synthesized [1]. We explore the MCE in a layered system composed of a ferromagnet, Ni_xCu_{1-x} (x~0.7), with a relatively low Curie temperature (T_C~300 °K), which is sandwiched by stronger ferromagnets, $Ni_{80}Fe_{20}$ and $Co_{90}Fe_{10}$, and exchange coupled to them across the interfaces. Switching of magnetization in the softer ferromagnetic surrounding, $Ni_{80}Fe_{20}$, exposed to H~0.1 kOe provides the isothermal magnetic entropy change (magnetocaloric potential) in the system because of magnetization redistribution in the spacer. In the limit, in which the Ni_xCu_{1-x} spacer can be magnetized at the interfaces up to its saturation magnetization of $4\pi m_s \approx 2.5$ kG, the magnetocaloric potential is [2] $\Delta s = m_s^2/C \approx 10^5$ erg/cm^3/°K (1) with C=0.4 °K being the Curie constant, whereas a separate Ni_xCu_{1-x} film with the same composition x exhibits such an MCE at H~100 kOe only. In real stacks

with the spacer thickness ranging between 5 nm and 20 nm, we have found a significant (up to a factor of ~20) enhancement of MCE by comparison to a separate Ni_xCu_{1-x} film [3, 4]. However, the MCE obtained experimentally is still much lower than that expected in accordance with Eq. (1). To understand a reason for this inconsistency, we have performed simulations of the magnetization distributon across the spacer upon the basis of the phenomenological Landau theory for second-order phase transitions [4]. We find that the results of these simulations are compatible with the experimental data at realistic values of the interfacial exchange coupling constant. To further enhance the MCE in such systems, one should choose a material for the spacer, which would have a higher m_s but still a low T_C not far from room temperatures. This work was supported by the Russian Foundation for Basic Research (Grant No. 20-02-00356) and by the Ministry of Education and Science of Russian Federation (Grant No. 0035-2019-0022-C-01).

[1] T. Mukherjee, *et al*., Magnetocaloric properties of Co/Cr superlattices, Phys. Rev. B, Vol. 79, 144406 (2009) [2] A. A. Fraerman, I. A. Shereshevskii, Magnetocaloric effect in ferromagnet/ paramagnet multilayer structures, JETP Lett., Vol. 101, p.618 (2015) [3] S.N. Vdovichev, *et al.*, High magnetocaloric efficiency of a NiFe/NiCu/CoFe/MnIr multilayer in a small magnetic field, Phys. Rev. B, Vol. 98, 014428 (2018) [4] M.A. Kuznetsov, *et al*., Magnetocaloric effect in exchange-coupled strong/weak/strong ferromagnet stacks, J. Appl. Phys., Vol. 127, 183904 (2020)

A4-03. The Antiferro to Ferrimagnetic Phase Transition in $Mn_2Sb_{1-x}Bi_x$ Compounds. *Q. Shen*[1], I. Batashev[1], N.v. van Dijk[1] and E. Brück[1]
1. Fundamental Aspects of Materials and Energy, Technische Universiteit Delft Faculteit Technische Natuurwetenschappen, Delft, Netherlands

Mn_2Sb is a ferrimagnet with T_C around 550 K crystallizing in the tetragonal Cu_2Sb-type structure[1]. By doping other elements into the system, a Antiferromagnetic-Ferrimagnetic (AFM-FIM) transition can be induced in Mn_2Sb [2,3]. Tunable transition temperature and small thermal hysteresis makes these compounds extremely attractive for heat recovery applications[3]. In this work, the influence of partial substitution of Bi for Sb on the structure, magnetic transition and magnetocaloric effect of $Mn_2Sb_{(1-x)}$ Bi_x (x = 0.02, 0.05, 0.07, 0.09, 0.15) compounds have been investigated. As shown in Fig. 1, the transition temperature from the AFM state to FIM state initially increases with increasing Bi content, then decreases at Bi concentrations exceeding 9%. To clarify which crystallographic positions Bi will occupy, we performed density functional theory calculations. We find the lowest formation energy provided that Bi only occupies Sb sites. Bi substituting on Sb site appears to give for $Mn_2Sb_{0.95}Bi_{0.05}$ an enhanced magnetization jump, in comparison to Cr substituted Mn_2Sb, where Cr substitutes on Mn sites[2]. As we find a larger Mn-Mn interatomic distance for Bi substituted Mn_2Sb, the origin of the AFM-FIM transition in $Mn_2Sb_{(1-x)}$ Bi_x is ascribed to an enhancement of the coefficient of thermal expansion by Bi substitution. A small entropy change of 1.17 J/kgK under 2 T from inverse magnetocaloric effect and strong dependence of the transition temperature on magnetic field ($dT_t/\mu H$) around -5.4 K/T in $Mn_2Sb_{0.95}Bi_{0.05}$ indicate this alloy is promising to be a candidate material for magnetocaloric application.

[1] C. Kittel, Physical Review, Vol. 120, p. 335 (1960). [2] S. Yamamoto, M. Yamamoto, K. Yamaguchi, IEEE transition journal on magnetics, Vol. 3, p. 991 (1990). [3] L. Caron, X. F. Miao, J. C. P. Klaasse, Applied Physics Letters, Vol. 103, p. 112404 (2013).

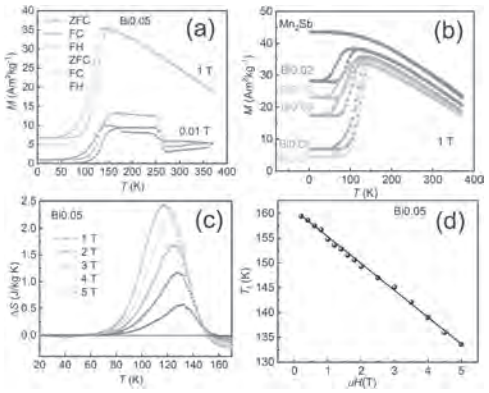

Fig. 1. Temperature dependence of magnetization under the magnetic fields of 0.01 T and 1T (a) for Bi0.05 and (b) for $Mn_2Sb_{(1-x)}$ Bi_x (x = 0.02, 0.05, 0.07, 0.09, 0.15) under 1 T. (c) Temperature dependence of entropy change. (d) The critical temperature T_t of AFM-FI as the function of the magnetic field.

A4-04. Quasi-1D Magnetism in Lanthanide Calcium Oxyborates $Ca_4LnO(BO_3)_3$. *N. Kelly*[1] and S. Dutton[1] *1. Cavendish Laboratory, University of Cambridge, Cambridge, United Kingdom*

Rare-earth calcium oxyborates with the formula $Ca_4LnO(BO_3)_3$, *Ln* = Y, La-Lu, have been extensively investigated for phosphor and display screen applications due to their non-centrosymmetric crystal structure; they also find application as high-temperature piezoelectric materials.[1] The crystal structure[2] contains quasi-1-dimensional chains of Ln^{3+} ions and this arrangement is anticipated to produce unusual magnetic phenomena. We have measured the bulk magnetic properties of several $Ca_4LnO(BO_3)_3$ compounds for the first time. Our results indicate the presence of antiferromagnetic interactions between Ln^{3+} ions, with different spin anisotropy depending on the identity of the lanthanide. No magnetic ordering transitions occur above 4 K and estimates of the exchange and dipolar interaction energies suggest quasi-1D magnetic behaviour. The compounds with *Ln* = Gd and Ho are viable magnetocaloric materials in the liquid helium temperature range, in the high- and low-field regimes respectively.[3]

1. R. Möckel, C. Reuther and J. Götze, *Journal of Crystal Growth*, 371, 70 (2013) 2. R. Norrestam, M. Nygren and J.-O. Bovin, *Chemistry of Materials*, 4, 737 (1992) 3. N. D. Kelly and S. E. Dutton, *Inorganic Chemistry* (2020) https://doi.org/10.1021/acs.inorgchem.0c01098

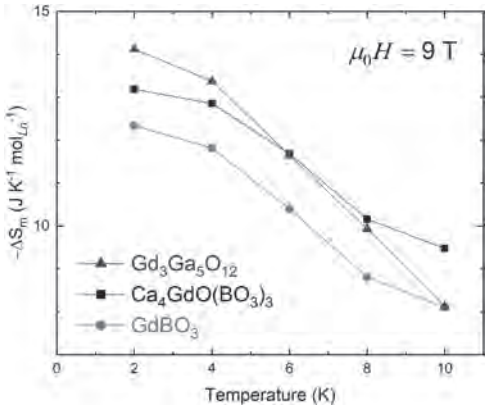

Fig. 1: Magnetic entropy change per mole of lanthanide ion at 9 T: comparison between $Ca_4GdO(BO_3)_3$, $GdBO_3$ and the standard magnetocaloric material $Gd_3Ga_5O_{12}$ (GGG).

A4-05. Fe Addition in six-Element Ferromagnetic Shape Memory Alloys: Paving the way Towards High-Temperature Magnetic Actuation. *J. Porro*[1,2], A. Pérez-Checa[3,1], J.F. feuchtwanger[4], P. Lazpita[1,4], T. Hansen[5], C. Mondelli[6], A. Sozinov[7], J. Barandiarán[4], K. Ullakko[7] and V. Chernenko[1,2] *1. Fundacion BCMaterials - Basque Center for Materials Applications and Nanostructures, Leioa, Spain; 2. Ikerbasque, Basque foundation for science, Bilbao, Spain; 3. TECNALIA, Basque Research and Technology Alliance (BRTA), Donostia-San Sebastián, Spain; 4. Universidad del Pais Vasco, Bilbao, Spain; 5. Institut Laue-Langevin, Grenoble, France; 6. CNR-IOM, Institut Laue-Langevin, Grenoble, France; 7. Material Physics Laboratory, LUT University, Lappeenranta, Finland*

Ni-Mn-Ga ferromagnetic shape memory alloys (FSMAs) are a group of active materials that undergo martensitic transformations (MTs) induced by temperature, stress and/or magnetic fields, resulting in large recoverable mechanical deformations. Their fast response and high energy density make them ideal candidates for implementation in sensors and actuators. Recently, the development of high-temperature FSMAs (HTFSMAs), working at temperatures over 373 K, has become an important task to meet the current requirements of modern technologies. The magnetic and magnetoelastic properties of FSMAs are very sensitive to the interactions between the magnetic moments of atoms that, in turn, depend on the atomic positions within the lattice [1]. Here we investigate a series of the polycrystalline NiMnGaCoCuFe HTFSMAs. Their MT and Curie temperatures, the crystal structures of the martensitic and austenitic phases, the temperature evolutions of the lattice parameters of both phases and the atomic site occupancies have been studied by means of powder neutron diffraction measurements, complemented by standard characterization techniques [2]. Based on the atomic site occupancies and additional measurements of the saturation magnetization, the influence of the structure and atomic ordering on the magnetism in these materials is analysed. A promising candidate for high temperature magnetic actuation is presented, following a combination of the high MT and Curie temperatures, around 370 K and 440 K, respectively, with a low tetragonality ratio, $c/a \approx 1.16$, in the proximity of MT.

[1] P. Lázpita, J.M. Barandiarán, J. Gutiérrez, J. Feuchtwanger, V.A. Chernenko, M.L. Richard, New J. Phys. 13 (2011) 33039 [2] A. Pérez-Checa, J.M. Porro, J. Feuchtwanger, P. Lázpita, T. Hansen, C. Mondelli, A. Sozinov, J.M. Barandiarán, K. Ullakko, V. Chernenko, Acta Materialia 2020, *accepted for publication*

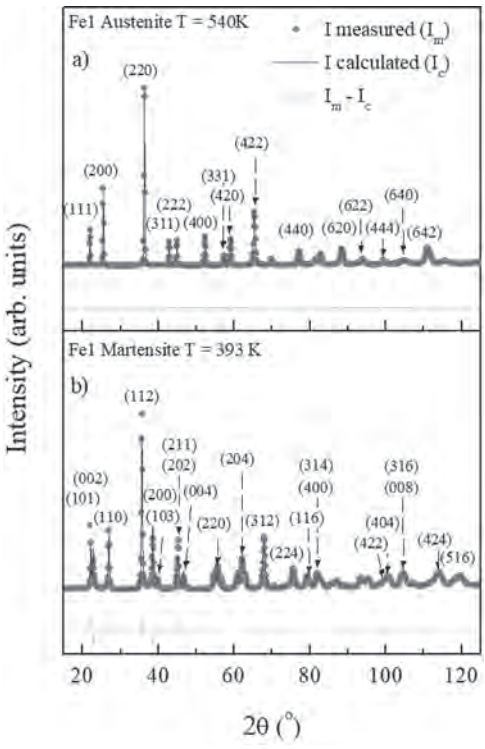

Neutron diffraction patterns and Rietveld refinements for the cubic austenite (a) and tetragonal martensite (b) in one of the alloys. Red dots are experimental points, blue lines are the Rietveld fittings in terms of the I4/mmm structure, and green lines are the difference between experimental data and fittings. The Miller indices corresponding to each reflection are also shown.

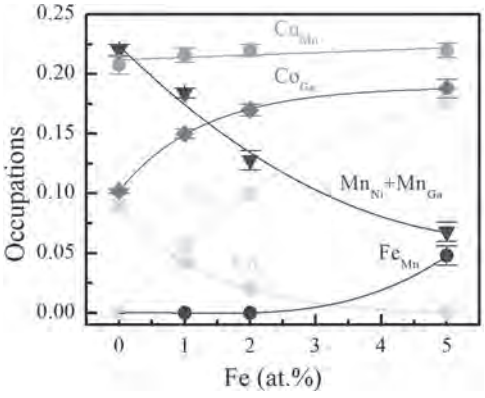

Evolution of the atomic site occupancies as a function of the Fe content. Labels correspond to the elements occupying the positions of the subscripted atom sites in the off-stoichiometric Ni-Mn-Ga $L2_1$ structure. Lines are guides to the eye.

A4-06. Magnetocaloric Effect in the $(Mn,Fe)_2(P,Si)$ System: From Bulk to Nano. *F. Zhang*[1], X. You[1], N.v. van Dijk[1] and E. Brück[1] *1. Faculty of Applied Sciences, Delft University of Technology, Delft, Netherlands*

In the field of nanoscale magnetocaloric materials, some novel concepts have been proposed, including microrefrigerators, thermal switches, microfluidic pumps, energy harvesting devices and biomedical applications[1-3]. However, reports on nano-scale $(Mn,Fe)_2(P,Si)$-based materials, which are one of the most promising bulk materials for solid-state magnetic refrigeration, are rare[4]. In this project we have synthesized nano-scale $(Mn,Fe)_2(P,Si)$-based nanoflakes, and systematically investigated the influence of the grain size

and defect structure on the magnetocaloric effect (MCE). The results show that the decreased saturation magnetization (M_s) is mainly attributed to the introduced defects during synthesis process, and with a decreased particle size, both the thermal hysteresis and T_c are reduced, which can be explained by Heisenberg exchange model. In addition, we find the best heat treatment temperature range (300 - 600 °C) to improve M_s in the $(Mn,Fe)_2(P,Si)$-based nanomaterials. When we annealed our nano-scale materials under N_2 flow at a temperature of 600 °C, the *M-B* curve at 5 K showed that M_s improved from 120 to 148 Am^2kg^{-1} and that the isothermal entropy change (ΔS_T) increased from 0.8 to 1.2 $Jkg^{-1}K^{-1}$ under 1 T. This can be attributed to the synergetic effect with the nitrogen, which recovers disorder defects and releases residual stress, while the grain size obtained from X-ray diffraction only increased by about 13% (27.9 to 31.6 nm). For comparison, in a control experiment under Ar atmosphere M_s slightly improves from 120 to 131 Am^2kg^{-1}, while ΔS_T decreased from 0.8 to 0.5 $Jkg^{-1}K^{-1}$ due to the appearance of an MnP impurity phase. To characterize the introduced defects and the microstructure of our materials, advanced electron microscopy techniques and Mössbauer spectroscopy are applied. Our results provide insight into MCE performance of nanoscale giant magnetocaloric materials.

1. J. Li, Y. Qu, J. Ren, W. Yuan and D. Shi, *Nanotechnology.*, *23* (50), (2012). 2. J. Wu, B. Lu, C. Liu and J. He, *Appl Therm Eng.*, *137*, 836-847 (2018). 3. J. Puga, B. Bordalo, D. Silva, M. Dias, J. Belo, J. Araujo, J. Oliveira, A. Pereira and J. Ventura, *Nano Energy*., *31*, 278-285 (2017). 4. F. Guillou, G. Porcari, H. Yibole, N. van Dijk and E. Brück, *Adv Mater*., *26* (17), 2671-2675 (2014).

A4-07. Calculating the Magnetocaloric Effect in Second-Order-Type Material by Micromagnetic Simulations. *D. Ohmer*[1], M. Yi[2], B. Xu[1], O. Gutfleisch[1] and M. Fries[1] *1. Materials Science, Technische Universität Darmstadt Materialwissenschaft, Darmstadt, Germany; 2. College of Aerospace Engineering, Nanjing University of Aeronautics & Astronautics, Nanjing, China*

Due to the expected increase of the energy consumption related to cooling, finding more energy efficient and environment friendly alternatives is of high interest for researchers. A promising alternative are cooling systems based on the magnetocaloric effect (MCE).[1,2] Since the discovery of the giant MCE,[3] several material systems, e.g. La-Fe-Si-,[4] Fe_2P-,[5] and Heusler alloys,[6] have been studied extensively as their MCE properties are tunable by the elemental composition. However, systematic studies on the effect of microstructure and intrinsic properties, *e.g.* anisotropy, are limited. We propose a methodology for calculating the MCE in the vicinity of T_C in second-order-type materials by combining micromagnetic simulations with the Arrott-Noakes equation (ANE). Firstly, micromagnetic simulations are performed using the Object Oriented MicroMagnetic Framework (OOMMF)[7] in which the microstructure and intrinsic properties can be varied. Secondly, the parameters of the ANE are determined from the simulations. Finally, the parameterized ANE is used to calculate the entropy change ΔS_T around T_C according to the Maxwell relations.[8] We choose Co_2B nanograins as an example system. A simple microstructure of 4x4x4 cube-shaped Co_2B nanograins is generated, for which we vary the grain size and boundary thickness. Fig. 1 shows the calculated ΔS_T in comparison with experimental results on a Co_2B single crystal.[5] It is found that decreasing the grain size results in increased ΔS_T, while the influence of the grain boundary thickness is negligible. The proposed methdology allows for investigating the effect of microstructure and intrinsic properties in micromagnetic simulations and extrapolating them to temperatures above T_C. This allows for more systematic studies on the relation between microstructural and intrinsic properties and the MCE. The authors acknowledge the support from the European Research Council (ERC) under the European Unions Horizon 2020 research and innovation programme (Grant agreement No 743116, project CoolInnov) and from the CRC/TRR 270 HoMMage (DFG).

1. O. Gutfleisch, M. A. Willard, E. Brück, Adv. Mater., 23(7), 821–842, 2011. 2. V. Franco, J.S. S Blázquez, B. Ingale, Annu. Rev. Mater. Res., 42(1), 305–342, 2012. 3. V. K. Pecharsky, K. A. Gschneidner, Phys. Rev. Lett., 78(23):4494–4497, 1997. 4. J. Liu, J. D. Moore, K. P. Skokov, Scr. Mater., 67(6), 584–589, 2012. 5. M. Fries, L. Pfeuffer, E. Bruder, Acta Mater., 132, 222–229, 2017. 6. T. Gottschall, K. P. Skokov, D. Benke, Phys. Rev. B, 93(18), 2–7, 2016. 7. M. J. Donahue, D. G. Porter. OOMMF User Guide. xiii–xxii, 2012. 8. J. C. Maxwell, Phil. Trans. R. Soc., 155, 459–512, 1865.

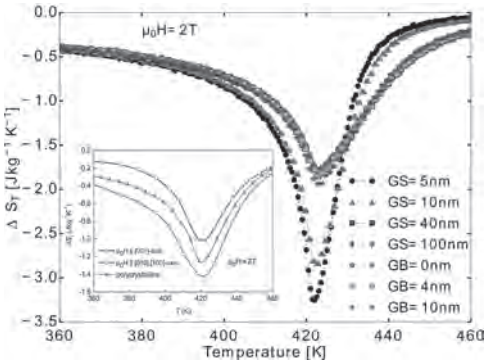

Specific isothermal entropy change ΔS_T calculated via the ANE as a function of grain size and boundary thickness. The inset shows the measured ΔS_T in Ref. 5.

A4-08. Phase Field Model for Ferromagnetic Domain Evolution During Martensitic Transformation of Heusler Alloys. *D. Ohmer*[1], M. Yi[2], B. Xu[1] and O. Gutfleisch[1] *1. Materials Science, Technische Universität Darmstadt Materialwissenschaft, Darmstadt, Germany; 2. College of Aerospace Engineering, Nanjing University of Aeronautics & Astronautics, Nanjing, China*

As the energy consumed by cooling systems is expected to increase over the next decades, magnetocaloric cooling systems are of high interest as a promising more energy efficient alternative to conventional vapor compression refrigerators.[1–3] Heusler alloys show large magnetocaloric effects (MCE) and are therefore of high interest for possible application in magnetocaloric cooling devices.[4,5] They exhibit a magnetostructural transition resulting in larger entropy changes ΔS, thus in larger adiabatic temperature changes ΔT_{ad}. We propose a phase field model based on Landau theory to simulate the magnetic domain evolution during the martensite formation, *e.g.* in Heusler alloys. With our model, we are able to simulate field- and pressure-induced phase transitions, including the martensite and magnetic domain evolution. This is of high interest for a multicaloric cooling cycle as proposed by Gottschall *et al.*[6] In the model, the three order parameters η_1, η_2, and η_3, represent the three martensite variants in a cubic to tetragonal phase transition. The energy of the martensite transformation is described by a Landau-type formulation after Cui *et al.*[7] and is coupled with micromagnetic formulations to take magnetism into account. The 3D finite-element (FE) implementation has been performed within the MOOSE framework.[8] The model is capable of reproducing the formation and evolution of domains in magnetic materials under external magnetic field (Fig. 1) or mechanical loading. Modeling field- and pressure-induced tansformation aims at investigating pressures and fields used in a multicaloric cooling cycle. The FE implementation further allows to investigate the influence of microstructure on the MCE. The authors acknowledge the support from the European Research Council (ERC) under the European Unions Horizon 2020 research and innovation programme (Grant agreement No 743116, project CoolInnov).

1. C. Zimm, A. Jastrab, A. Sternberg, Adv. Cryog. Eng., 1759–1766. Springer US, Boston, MA, 1998. 2. O. Gutfleisch, M. A. Willard, E. Brück, Adv. Mater., 23(7), 821–842, 2011. 3. V. Franco, J.S. S Blázquez, B. Ingale, Annu. Rev. Mater. Res., 42(1), 305–342, 2012. 4. J. Liu, T. Gottschall, K. Skokov, Nat. Mater., 11(7), 620–626, 2012. 5. T. Gottschall, K. Skokov, D. Benke, Phys. Rev. B, 93(18), 2–7, 2016. 6. T. Gottschall, A. Gràcia-Condal, M. Fries, Nat. Mater., 17(10), 929–934, 2018. 7. S. Cui, J. Wan, X. Zuo, Int. J. Solids Struct., 109, 1–11, 2017. 8. D. R. Gaston, C. J. Permann, J. W. Peterson, Ann. Nucl. Energy, 84, 45–54, 2015.

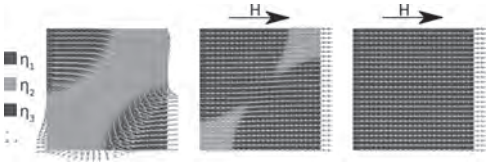

The stable microstructure for the martensite at zero field is shown on the left. Arrows indicate the magnetiztaion, which is parallel to the *x*-axis for martensite variant η_1 and parallel to the *y*-axis for η_2. By the application of an external magnetic field *H*, η_2 starts transforming to η_1 in order to reduce the anisotropy energy.

A4-09. Setting the Basis for the Interpretation of Temperature First Order Reversal Curve (TFORC) Distributions of Magnetocaloric Materials. *L.M. Moreno-Ramírez*[1] and V. Franco[1] *1. Condensed Matter Physics, Sevilla University, Sevilla, Spain*

First Order Reversal Curve (FORC) distributions of magnetic hysteresis is a well-recognized tool to extract information about magnetic interactions or to fingerprint magnetic materials [1, 2]. Their success is based on the extensive modeling that allows to correlate features of the distribution with characteristics of the transition. Recently, magnetocaloric materials are starting to be studied with Temperature-FORC (TFORC) distributions, extending the technique to the analysis of their thermal hysteresis [3,4]. However, the theory supporting the interpretation of the diagrams is still lacking, limiting TFORC to a fingerprinting technique so far. This work is a first approach to correlate the modeling of first-order phase transitions, using the Bean-Rodbell model combined with a phenomenological transformation mechanism, with the features observed in TFORC distributions. The different characteristics of the transformations e.g. transition temperatures, symmetry, temperature range, etc. can be correlated to distinct features of the distributions. Fig. 1 shows some illustrative examples of situations typically found in magnetocaloric materials (magnetization curves plotted in panel (a)): 1) symmetric cooling and heating transformations with the same temperature range produce circular distributions; 2) different temperature ranges for heating and cooling transformations give rise to ellipsoidal distributions; 3) asymmetry in the transformations makes the distribution triangular. This work systematically shows how the different model parameters affect the distributions and prove that the catalogue of figures is be able to explain the experimentally observed distributions. Work supported by AEI/FEDER-UE (grants MAT-2016-77265-R and PID2019-105720RB-I00), US/JUNTA/FEDER-UE (grant US-1260179), Consejería de Economía, Conocimiento, Empresas y Universidad de la Junta de Andalucía (grant P18-RT-746), Army Research Laboratory under Cooperative Agreement Number W911NF-19-2-0212 and Sevilla University under VI PPIT-US program.

[1] I. Mayergoyz, IEEE Transactions on Magnetics., Vol 22(5), p. 603-608 (1986). [2] C. R Pike, A. P. Roberts and K L. Verosub, Journal of Applied Physics., Vol. 85(9) p. 6660-6667 (1999). [3] V. Franco, T. Gottschall, K. P. Skokov et al., IEEE Magnetics Letters., Vol. 7 p. 6602904 (2016). [4] V. Franco, Journal of Applied Physics., Vol. 127 p. 133902 (2020).

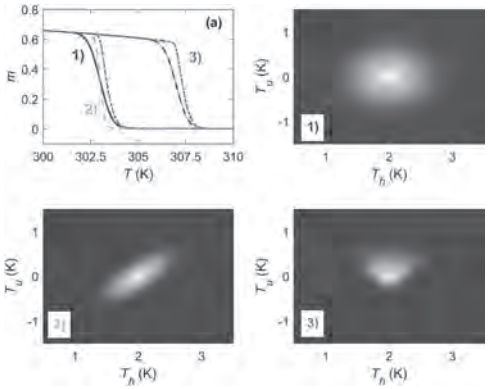

Fig.1. Some illustrative examples of thermal hysteresis curves (a) and their associated TFORC distributions 1), 2) and 3).

A4-10. The Effect of Ionic Radii of the Rare-Earth Ion on the Magnetocaloric Effect of Rare-Earth Chromites. *J. Shi*[1,3] and M. Jain[2,3] *1. Department of Materials Science and Engineering, University of Connecticut, Storrs, CT, United States; 2. Department of Physics, University of Connecticut, Storrs, CT, United States; 3. Institute of Materials Science, University of Connecticut, Storrs, CT, United States*

Magnetic refrigeration based on magnetocaloric effect (MCE) has attracted great attention due to its environmentally friendly nature and potential to improve energy efficiency. In this work, we explore the rare earth chromites ($RCrO_3$) to understand the effect of R-site ionic radii (R= Tb and Er) on their structural and magnetic properties. Bulk powders of $TbCrO_3$ and $ErCrO_3$ were prepared by citrate route and characterized by x-ray diffraction (XRD) and Raman spectroscopy that revealed that both samples crystallized in the orthorhombically distorted perovskite structure (*Pbnm* space group). The structure was found to be more distorted for $ErCrO_3$ (r_{Er}= 1.062Å) as compared to $TbCrO_3$ (r_{Tb}=1.095Å). The dc magnetization measurements revealed that the temperature decreased from 156 K to 131 K with decreasing ionic radii. Interestingly, the maximum MCE was also found to reduce with decreasing ionic radii. The maximum entropy change for $TbCrO_3$ was calculated to be 13.4 J /kg K as compared to 10.7 J/kg K for $ErCrO_3$. The results indicate that the structural distortions induced by the decreasing ionic radii at R-site could be a promising strategy to tune the magnetic and MCE properties in rare earth chromites.

Gschneidner Jr, K. A., and Vitalij K. Pecharsky. *Annual Review of Materials Science* 30, no. 1 (2000): 387-429.

A4-11. Magnon Polarons Induced by a Magnetic Field Gradient. *N. Vidal-Silva*[1], E. Aguilera[2], A. Roldán-Molina[3], R. Duine[4] and A. Nunez[2] *1. Universidad de La Frontera, Temuco, Chile; 2. Universidad de Chile Facultad de Ciencias Fisicas y Matematicas, Santiago, Chile; 3. Universidad de Aysen, Coyhaique, Chile; 4. Institute for Theoretical Physics, Universiteit Utrecht, Utrecht, Netherlands*

Here we report the theoretical possibility of generating magnon polaron excitations through a space-varying magnetic field. The spatial dependence of the magnetic field in the Zeeman interaction gives rise to a magnon-phonon coupling when a magnetic field gradient is applied, and such a coupling depends directly on the strength of the gradient. It is also predicted that the direction of the magnetic field gradient allows control over which phonon polarization couples to the magnons in the material. Here we develop the calculations of the magnon-phonon coupling for an arbitrary (anti)ferromagnet, which are later used to numerically study its consequences. These results are compared to the ones obtained with the phenomenological magnetoelastic coupling in YIG, where we show that the magnon polaron bandgap seen in YIG can also be obtained with a magnetic field gradient of ~0.1T/m which can be achieved with the current experimental techniques. Our results propose a new way of controlling the magnetoelastic coupling in an arbitrary material and open a new route to exploit the magnon-phonon interaction in magnonic and spintronic devices.

A4-12. Effect of Particle Permeability on Macroscopic Behavior of Magnetorheological Elastomers. *W.M. Kiarie*[1] and D.C. Jiles[2,1] *1. Materials Science and Engineering, Iowa State University, Ames, IA, United States; 2. Electrical and Computer Engineering, Iowa State University, Ames, IA, United States*

In this work, we report on an investigation of the effect of the permeability of magnetic particles on the effective macroscopic behavior of magnetorheological elastomers (MREs). MREs are a class of soft active materials known for their tunable deformation [1], [2]. Dispersed with magnetically permeable particles, these polymer-based composites deform under the action of a magnetic field. Such deformational changes in the mechanical properties of these materials are often attributed to the magnetic interaction among the filler particles [3]. Generally, for a maximum possible magnetorheological (MR) effect, particles of high relative permeability μ_r are required [4].

In this study, we determine the effect of the μ_r of the particles on the macroscopic behavior of MREs. Using a finite element simulation method based on continuum field theory, the constitutive and geometric properties on the microscale are considered in order to predict the composite's macroscopic behavior as a function of μ_r by means of a computational homogenization [5]. Additionally, a magnetic flux density B ≤ 0.5T was used, below the saturation magnetization of the filler particles, hence linear constitutive relationships can be utilized. The simulations were performed for isotropic microstructures for different particle permeabilities (μr =1, 100, 10000 and 50000) and volume fractions (φ= ~10, 20 and 27%). The effective magnetic and mechanical properties are calculated as shown in Fig. 1 and Fig. 2. Fig. 1 shows the magnetic flux density distribution for isotropic MRE while Fig.2 shows the average magnetostrictive strain parallel to the direction of the magnetic field as a function of average magnetic flux density for varying permeability of the particles. The results confirmed assumptions stated in the literature whereby higher permeability of the particles caused larger deformation of the MRE (Fig.2). However, for very large permeability values (μr = 10,000 and 50,000), only negligible change in effective MRE deformation is observed.

[1] Y. Han, A. Mohla, and L. E. Faidley *Int. J. Appl. Mech.*, vol. 7, no. 1, pp. 1–16, 2015. [2] K. A. Kalina *et al.*, *Smart Mater. Struct.*, vol. 26, no. 10, 2017. [3] B. Marvalova, "Modelling of Magnetosensitive Elastomers," *Model. Simul.*, 2008. [4] R. Ahamed and S. Choi, "A state of art on magneto-rheological materials and their potential applications," 2018. [5] C. Spieler, M. Kästner, and V. Ulbricht, *Acta Mech.*, vol. 224, no. 11, pp. 2453–2469, 2013.

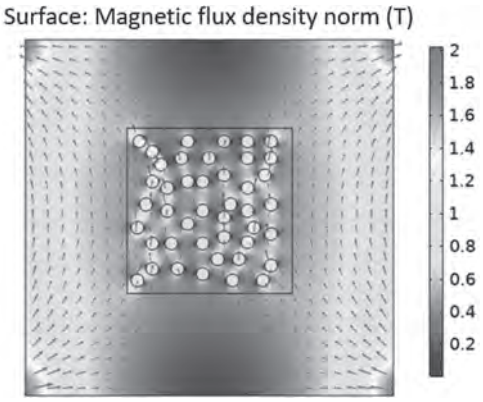

Fig. 1. Magnetic flux density distribution through 2D MRE model

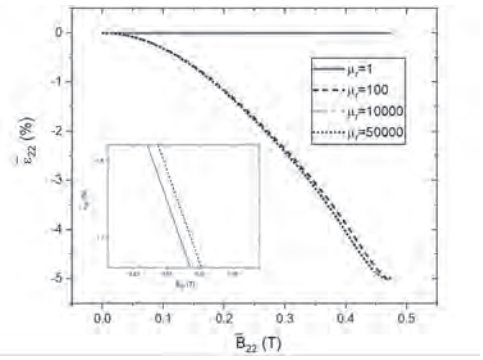

Influence of magnetic flux density on MRE (φ=~20%) magnetostrictive strain for varying permeability (μ_r) (insert: a zoomed in plot)

A4-13. Multiscale Modeling of Magnetorheological Elastomers With a Twist. *D. Marchfield*[1], T. Dang[2,1], A.T. Clark[2], J. Li[2,3], X. Cheng[2] and K. Buchanan[1] *1. Physics, Colorado State University, Fort Collins, CO, United States; 2. Physics, Bryn Mawr College, Bryn Mawr, PA, United States; 3. Physics, Fudan University, Shanghai, China*

Magnetorheological elastomers (MREs) that are made up of micron or submicron ferromagnetic particles embedded in an ultra-soft polymer are a promising platform for studying cell responses to dynamic mechanical changes in their environment, as the shear modulus is tunable via an applied magnetic field *B* [1]. Recent experimental work shows that MREs can deform under applied magnetic fields, and that this deformation can include expansion/contraction as well as twisting of the sample if only one side is fixed to a substrate. In this work, we used a multi-scale approach to model the magnetic reversal and field-dependent deformations. Micron-sized ferromagnetic spheres in the polymer interact via dipolar coupling but may also move. Micromagnetic simulations were used to model the magnetic response of a single sphere, and the balance of the dipolar, elastic, and Zeeman energies, modeled using a point-dipole-based approach similar to that described in [2] but with an additional volume preserving twist, dictates the deformations of the ensemble. Figure 1 shows calculations for a 3x3x10 array of iron spheres with radii of 3 mm arranged on a square lattice with particle center to center separation of 9 mm. Elastic interactions were modeled using a network of springs that connect the nearest neighbors with spring constants *k* ranging from 50 to 6000 J/m^2. When *B* is applied perpendicular to the long axis of the array, the largest particle displacement is seen at fields just below saturation, and the motion involves both deformation and twisting of the lattice (Fig. 1d). The particle displacement and hysteresis increase with decreasing *k*. These results suggest that the incorporation of degrees of freedom beyond simple expansions and contractions may be needed to understand the magnetic responses of MREs.

[1] Corbin, E. A., Vite, A., Peyster, E. G., et al. *ACS Applied Materials and Interfaces*, *11*(23), 20603–20614. (2019). [2] Andriushchenko, P., Nefedev, K., & Stepanov, G. *European Physical Journal B*, *87*(1), 1–6. (2014).

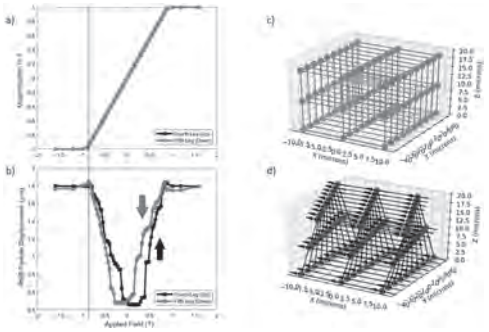

Fig.1: a) Magnetization and b) rms particle displacement versus *B*, applied along the x-direction, shown for the fourth and fifth hysteresis legs. The black line shows the maximum displacement. c) Elastic equilibrium and d) relaxed positions for iron spheres at *B* = -0.87 T on the upward leg of the hysteresis curve shown in b). Significant twisting is observed.

A4-14. Strain Engineered Domain Structure and Their Relaxation in Perpendicularly Magnetized Co/Pt Deposited on Flexible Polyimide. *E. Pandey*[1], B.B. Singh[1], P. Sharangi[1] and S. Bedanta[1] *1. School of Physical Sciences, National Institute of Science Education and Research (NISER), Bhubaneswar, Bhubaneswar, India*

The demand of flexibility in the existing rigid devices has introduced a new field of research 'Flexible Spintronics', which has enormous significance from application viewpoint [1-2]. Flexible device requires all the components of rigid spintronics in a flexible i.e. bendable, foldable, twistable and stretchable mode [3]. The ideal next generation device need to be power efficient as well as flexible. To meet such device requirement stress/strain has proven

to be a potential candidate [4-5]. As magnetic thin films are prime component of every spintronic device hence the flexible counterpart of those are prerequisite. Cobalt/Platinum (Co/Pt) thin films with perpendicular magnetic anisotropy (PMA) are well studied as it has increased magnetic storage density, thermal stability etc. [6]. In our work we have prepared a PMA Co/Pt film on a flexible polyimide substrate by magnetron sputtering. Strain has been generated on the film by fixing it on semi-circular shaped molds of different radius. Here systematically we have measured the effect of both tensile and compressive stresses on the PMA, domain dynamics and relaxation mechanism by MOKE based microscopy. A minimal in-plane tensile strain has increased the coercivity of the film by 34% of its initial value, while a very small change of coercivity has been found under compressive strain (fig. 1) [7]. The size of ferromagnetic domains also decreases under tensile strain, while no change is observed under compressive stress (fig. 2). Due to stress induced anisotropy, Bloch wall formation energy has increased which hindered the domain wall motion and size of bubble domains reduced. Further, magnetization relaxation measured at sub-coercive field values yields a longer relaxation time in the tensile strained state.

1. P. Sheng *et al.,* J. Semicond. 39, 011006 (2018) 2. Z. Bao *et al.,* Adv. Mater. 28, 4177 (2016) 3. K. Harris *et al.,* J. Mater. Sci. 51, 2771–2805 (2016) 4. A. Bukharaev *et al.,* Phys. Uspekhi 61, 1175 (2018) 5. A. K. Biswas *et al.*, Nano letters 17, 3478–3484 (2017) 6. B. Tudu *et al*., Vacuum 146, 329 (2017) 7. E. Pandey *et al.,* Nano Express 1, 010037 (2020)

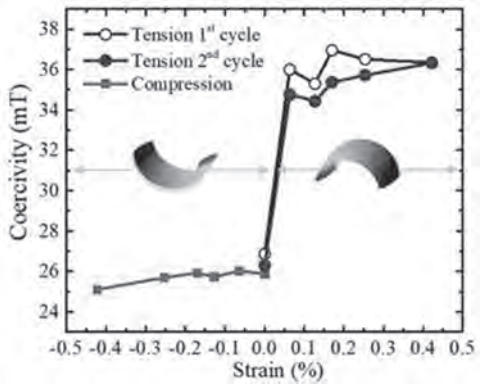

Figure 1. Variation of coercivity of Co/Pt film under tensile\compressive strained state [7]

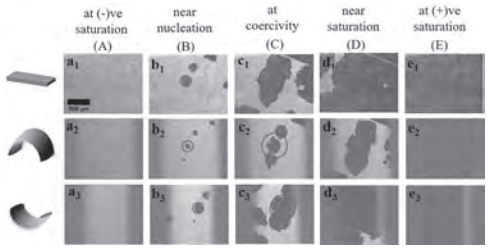

Figure 2. Domain imaging by polar MOKE microscopy at unstrained and different strained state of sample.

A4-15. Magneto-Mechanical Response of Supracolloidal, Magnetic, Polymer-Like Structures. *D. Mostarac*[1], P.A. Sánchez[1,2] and S. Kantorovich[1,2] *1. Computational and Soft Matter Physics, Universitat Wien, Wien, Austria; 2. Ural'skij federal'nyj universitet imeni pervogo Prezidenta Rossii B N El'cina, Ekaterinburg, Russian Federation*

Construction of smart materials with sophisticated magnetic response by incorporating magnetic nanoparticles (MNPs) within permanently crosslinked structures, opens up the possibility for synthesis of more complex, highly magneto-responsive systems.[1] Nanoscopic magnetic filaments (MFs) are magnetic, nano-sized colloids, crosslinked into polymer-like linear chains. They are a promising platform for engineering new magnetically controlled filtering and flow control elements in micro-fluidic devices. Recent advances, advocating an assembly mechanism where the structure building instructions are embedded into nanoparticles via DNA origami frames, finally opened the door towards synthesis of MFs with desirable mechanical properties.[2,3] Using programable DNA origami assembly, we created scaffolds that can serve as blueprints for chain-like assemblies of MNPs (i.e. 20nm, streptavidin coated magnetite NPs), allowing them to assemble in to structures possible only for anisotropic and selective interactions. Using molecular dynamics simulations we have studied MFs with ferromagnetic or super-paramagnetic monomers modeling possible crosslinking scenarios.[4] Magnetic properties of MFs with super-paramagnetic monomers have proven to maintain a desirable magnetic response under various crosslinking approaches, making them a more flexible choice. In strong applied fields, MFs with super-paramagnetic MNPs have similar magnetic properties to ferromagnetic ones, while exhibiting higher susceptibility in low fields. Furthermore, they exhibit an interesting tendency to bend their backbone locally, rather than to fully stretch along the field. In this contribution, we elucidate an interesting phenomenology of MFs with super-paramagnetic monomers, by examining their behavior in implicit solvent representations (i.e, Langevin thermostat) and explicit solvent representations using the Lattice Boltzmann method. Magnetization of super-paramagnetic monomers is taken into account in an accurate manner, inclusive of non-linear contributions. Furthermore, we contrast properties of a free filament suspended in a solvent to the one grafted on to a surface. This comparison enables to fine-tune the properties of filament based brushes.

[1] Sánchez, P. A., et al. Macromolecules 48.20 (2015): 7658-7669. [2] Liu, W., et al. Nature chemistry 8.9 (2016): 867. [3] Tian, Y., et al. Nature materials 15.6 (2016): 654. [4] Mostarac, D., et al. Nanoscale (2020).

A4-16. Theoretical Modelling of Hybrid Magnetic Elastomers. *P.A. Sánchez*[1,2], O. Stolbov[3] and Y. Raikher[3] *1. Ural'skij federal'nyj universitet imeni pervogo Prezidenta Rossii B N El'cina, Ekaterinburg, Russian Federation; 2. Wolfgang Pauli Institute, Universitat Wien, Wien, Austria; 3. FGBUN Institut mehaniki splosnyh sred Ural'skogo otdelenia Rossijskoj akademii nauk, Perm, Russian Federation*

Magnetic elastomers are one of the most important types of magnetoresponsive materials. They are characterized by large changes in their shape and rehological properties as a response to external magnetic fields [1]. Similarly to magnetic fluids and gels, these are hybrid materials that consist of magnetic nano- or microparticles embedded in a magnetically passive carrier material. Magnetic elastomers are candidate materials for many technological applications, like adaptive damping devices, vibrational absorbers, stiffness tunable mounts, soft actuators and micromanipulators, force sensors or artificial muscles, see [2] and references therein. Here, we study theoretically a novel microstructural design for a hybrid magnetic elastomer material that has been synthesized for the first time very recently [3-5]. This design is based on the embedding within the polymer matrix of two types of magnetic particles in different amounts: a low volume fraction of magnetically hard (MH) colloidal particles---typically, ferromagnetic particles of 5-100μm of diameter---and a high volume fraction of smaller, magnetically soft (MS) particles---paramagnetic particles with a diameter typically smaller than 5μm. We study the response of this hybrid magnetic material to external magnetic fields by means of two theoretical approaches. First, we perform extensive computer simulations with a bead-spring model of the system that takes into account the magnetic influence of the MH particles on the MS ones, as well as the mechanical coupling imposed by the polymer matrix on the rearrangements of the particles [6]. Finally, we compare the results obtained from this approach with the ones provided by a continuous magnetomechanical model. In both approaches we focus on a minimal representative volume of the material, consisting of a single MH particle surrounded by a cloud of MS ones and the mechanical coupling between all of them. We analyze the deformations of this elementary volume as a response to the external fields.

[1] S. Odenbach. *Arch. Appl. Mech.*, 86:269–279, (2016). [2] P. Sánchez et al., *Soft Matter,* 15, 175-189 (2018). [3] J.M. Linke, D.Y. Borin, S. Odenbach, *RSC Adv.*, 6, 100407 (2016). [4] M.V. Vaganov, J. Linke, S. Odenbach, Yu.L. Raikher, *J. Mag. Mag. Mat.* 431, 130-133 (2017). [5] P. Sánchez et al., *Soft Matter,* 14, 2170-2183 (2018). [6] P. Sánchez et al., *Soft Matter,* 15, 7145--7158 (2019).

A4-17. Tuning the Magnetocaloric Properties in $(Gd,Tb)_6(Fe,Mn)Bi_2$ Intermetallics. *A. Oleaga*[1], A. Herrero[1], A. Salazar[1], A.V. Garshev[2], V.O. Yapaskurt[3] and A.V. Morozkin[2] *1. Fisica Aplicada I, University of the Basque Country UPV/EHU, Bilbao, Spain; 2. M.N. Department of Chemistry, Moscow State University, Moscow, Russian Federation; 3. Department of Petrology, Moscow State University, Moscow, Russian Federation*

The magnetic and magnetocaloric properties of the intermetallic family $(Gd,Tb)_6(Fe,Mn)Bi_2$ have been studied from 2 K to temperatures above the respective Curie temperatures T_C. The substitution of Gd by Tb (Gd_6FeBi_2, $Gd_3Tb_3FeBi_2$, Tb_6FeBi_2) tunes T_C in the range 350-250 K and favors the apparition of a metamagnetic transition at very low temperature from a magnetic state with a marked antiferromagnetic component to a ferromagnetic one, as well as a spin reorientation transition below T_m = 72 K. An important inverse magnetocaloric effect (IMCE) appears below 20 K and a relevant direct magnetocaloric effect (DMCE) appears over a wide temperature span between T_C and T_m with maxima at those temperatures. The partial substitution of Fe by Mn in $Tb_6Fe_{0.5}Mn_{0.5}Bi_2$ shifts these effects upwards in temperature while expanding the region of the DMCE. Tuning this family allows to locate the magnetocaloric effect in different regions of interest. The critical behavior of the PM-FM transitions has been studied obtaining the critical exponents α, β, γ, δ and checking that the respective magnetocaloric effects also scale with the critical parameters *n* and δ. Universal curves for the magnetocaloric effect were also found for the four cases. The transition in Gd_6FeBi_2 has been found to belong to the Heisenberg universality class with deviations due to magnetocrystalline anisotropies; the critical exponents for $Gd_3Tb_3FeBi_2$ suggest the presence of long range order magnetic interactions, as the critical parameters agree quite well with the Mean Field model, while Tb_6FeBi_2 and $Tb_6Fe_{0.5}Mn_{0.5}Bi_2$ present an unconventional critical behavior aligned with long range order interactions.

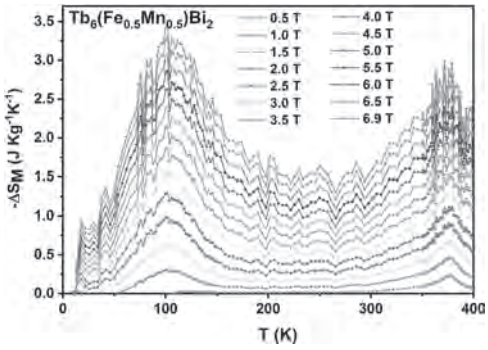

Fig. 1: DMCE for $Tb_6Fe_{0.5}Mn_{0.5}Bi_2$

A4-18. Structure, Magnetocaloric Properties and Critical Behavior in Novel Intermetallic Materials R_3CoNi (R = Tb, Dy, Ho, Er, Tm, Lu). A. Herrero[1], *A. Oleaga*[1], A. Provino[2,3], I.R. Aseguinolaza[1], A. Salazar[1] and P. Manfrinetti[2,4] *1. Fisica Aplicada I, University of the Basque Country UPV/EHU, Bilbao, Spain; 2. Department of Chemistry, University of Genova, Genova, Italy; 3. Rutgers The State University of New Jersey, New Brunswick, NJ, United States; 4. Institute SPIN-CNR, Genova, Italy*

The novel family of rare earth intermetallics R_3CoNi (R = Tb, Dy, Ho, Er, Tm, Lu) has been synthesized. A thorough study of the crystal structure as well as magnetic and magnetocaloric properties has been carried out. The compounds crystallize in the rhombohedral Er_3Ni_2-type [*hR*45, *R*-3h (No. 148), Z = 9]; lattice parameters (*a* and *c*) and unit cell volume well follow the lanthanide-contraction trend, with a linear decrease from Tb down to Lu. Magnetization and *ac*-susceptibility measurements show that from Tb to Tm they present a paramagnetic to ferromagnetic (PM-FM) transition at temperatures in the range 6-96 K, while there are different reorientation transitions below the respective T_C with thermomagnetic irreversibility in most cases. The universality classes to which the PM-FM transitions belong have been found through thermal and magnetic measurements for Tb_3CoNi, Dy_3CoNi, and Ho_3CoNi, obtaining the set of critical exponents α, β, γ, δ. For Tb_3CoNi it is close to the Mean Field model, for Dy_3CoNi it is between the Chiral Heisenberg and the *XY*-Chiral, while for Ho_3CoNi it is close to the *XY*-Chiral model, implying that Dy_3CoNi, and Ho_3CoNi are some kind of frustrated non-collinear ferromagnets. The magnetocaloric measurements in the five members of the family indicate that all of them present highly competitive magnetocaloric properties in their respective temperature ranges, with high magnetic entropy changes (from 12.8 to 18.5 J/Kg.K at $\mu_0\Delta H$ = 5 T) and refrigerant capacities (from 412 to 699 J/Kg at $\mu_0\Delta H$ = 5 T). These results raise the interest in tuning the application range by modifying the rare earth ion. Finally, universal curves for the magnetocaloric properties have been found for Tb_3CoNi, Dy_3CoNi, and Ho_3CoNi and the scaling of the magnetocaloric variables confirms the validity of the universality classes.

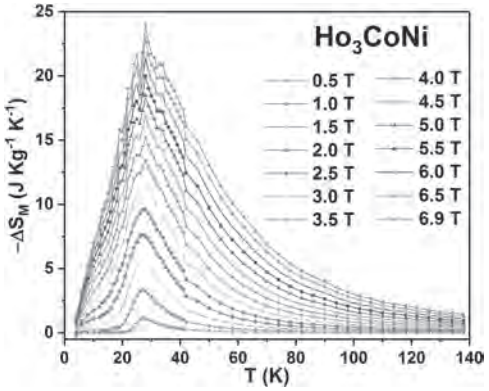

Fig. 1. Magnetic entropy change $-\Delta S_M$ for $\mu_0\Delta H$ from 0.5 T to 6.9 T for Ho_3CoNi

Session A5
NEUROMORPHIC COMPUTING WITH DOMAIN WALLS AND CHIRAL SPIN TEXTURES

Seonghoon Woo, Chair
IBM T. J. Watson Research Center, Yorktown Heights, NY, United States

INVITED PAPER

A5-01. Modeling Biological Behavior in Domain Wall-Magnetic Tunnel Junction Artificial Neurons and Synapses for Energy-Efficient Neuromorphic Computing. *J.C. Incorvia*[2], J.S. Friedman[3], M.J. Marinella[1], O.G. Akinola[2], C. Cui[2], N. Hassan[3], C.H. Bennett[1], X. Hu[3], L. Jiang-Wei[3], W.H. Brigner[3], F. Garcia-Sanchez[4] and M. Pasquale[5] *1. Sandia National Laboratories, Albuquerque, NM, United States; 2. Electrical and Computer Engineering, The University of Texas at Austin, Austin, TX, United States; 3. Electrical and Computer Engineering, The University of Texas at Dallas, Richardson, TX, United States; 4. Universidad de Salamanca, Salamanca, Spain; 5. Istituto Nazionale di Ricerca Metrologica, Torino, Italy*

Modeling computer architecture after the human brain is a promising approach to the ever-increasing demands for real-time processing of massive amounts of data. But, the building blocks of the brain, i.e. neurons and synapses, have more detailed behavior than simply how they are connected, and this behavior is central to their computing efficiency. If we want to capture the energy efficiency of such a neuromorphic architecture, we need devices themselves that can capture the behavior of the biological elements. Magnetic materials and devices have many properties similar to the brain that make them attractive candidates as artificial neurons and synapses. We will present our recent work on designing and modeling three-terminal domain wall-magnetic tunnel junctions (DW-MTJs) that can act as both leaky, integrate, and fire neurons with inherent lateral inhibition [1-2] and as synapses with online learning and spike-timing dependent plasticity behavior [3]. The DW-MTJ neuron consists of a perpendicularly magnetized wire containing a single DW and an MTJ on top of the wire. When current is applied to the wire, the DW propagates through spin transfer torque (STT) or spin orbit torque (SOT). The MTJ defines the firing point of the neuron: when the DW moves past the junction, the MTJ resistance switches to generate a spiking current at the MTJ output terminal. We will show results of integration, firing, and inherent leaking of the device. When assembled into a crossbar array, 1-10 digit identification is simulated by measuring which of ten neurons reach the firing point first. Lateral inhibition (LI) is an important function in neuromorphic computing, modeled after the biological neuron behavior that a neuron prevents its less active neighbors in the same layer from firing. In most neuromorphic hardware platforms, LI is implemented with external circuitry, thereby decreasing the energy efficiency and increasing the area overhead of such systems. We show that the DW-MTJ neuron has inherent LI via magnetic interactions. We will show results from modeling current- and field-driven DW motion in adjacent DW-MTJ neurons. Figure 1 shows that with 90 nm spacing between two 50 nm wide DW-MTJs, the slower device's DW velocity is drastically reduced from 75 m/s to 20 m/s and a LI of 75% is achieved. The results are explained by current-driven DW velocity characteristics in response to external magnetic fields and are quantified by an analytical model based on the Landau-Lifshitz-Gilbert (LLG) equation. We will show results of arrays of DW-MTJs implementing a soft winner-take-all function and application of the effect to image recognition. We will furthermore present simulation results of the DW-MTJ showing synaptic behavior when the MTJ is made long. By constructing a small circuit around the device we implement spike-timing-dependent plasticity (STDP), where the current flowing through the synapse, which will determine its resistive synaptic weight, is determined by the delay between input and output neurons (Fig. 2). We will show that the STDP synapses can process time-dependent input data. The results will be compared with other emerging nonvolatile devices for artificial neural networks. The work presented shows that DW-MTJs can provide a monolithic platform for neuromorphic computing circuits, where both synapses and neurons can be made from the same thin film stack, and motivate further study of magnetic devices for neuromorphic computing. SNL is managed and operated by NTESS under DOE NNSA contract DE-NA0003525.

1. N. Hassan, X. Hu, L. Jiang-Wei, W. H. Brigner, O. G. Akinola, F. Garcia-Sanchez, M. Pasquale, C. H. Bennett, J. A. C. Incorvia & J. S. Friedman. Magnetic domain wall neuron with lateral inhibition. *J. Appl. Phys.* 124, (2018). 2. C. Cui, O. G. Akinola, N. Hassan, H. Christopher, M. J. Marinella, J. S. Friedman & J. A. C. Incorvia. Maximized Lateral Inhibition in Paired Magnetic Domain Wall Racetracks for Neuromorphic Computing. *IOP Nanotechnology* 31, 29 (2020). 3. O. G. Akinola, X. Hu, C. H. Bennett, M. Marinella, J. S. Friedman & J. A. C. Incorvia. Three-terminal magnetic tunnel junction synapse circuits showing spike-timing-dependent plasticity. *J. Phys. D. Appl. Phys.* 52, 49LT01 (2019).

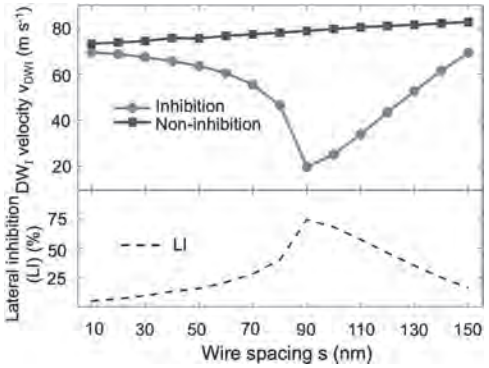

(top) DWI velocity vDWI under inhibition (red circles) and non-inhibition (blue squares) conditions; (bottom) lateral inhibition LI as a function of spacing between DW tracks, s.

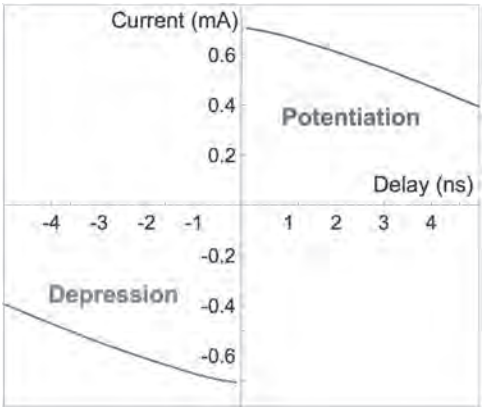

Potentiation and depression currents from SPICE-micromagnetic simulation of DW-MTJ synapse circuit as a function of spiking delay between pre-synaptic and post-synaptic neurons.

CONTRIBUTED PAPERS

A5-02. Online Training of Spiking Neural Networks Using Domain Wall Magnetic Tunnel Junction Synapses. *O.G. Akinola*[1], B. Mendawar[1], C.H. Bennett[2], X. Hu[3], J.S. Friedman[3], M.J. Marinella[2] and J.C. Incorvia[1]
1. Electrical and Computer Engineering, The University of Texas at Austin, Austin, TX, United States; 2. Sandia National Laboratories, Albuquerque, NM, United States; 3. Electrical and Computer Engineering, The University of Texas at Dallas, Richardson, TX, United States

Progress has been made on emulating the neuron and the synapse using magnetic devices [1], [2] especially with three-terminal magnetic tunnel junctions (3T-MTJs) [3], [4]. Increasingly more accurate biological mimics are being developed with the 3T-MTJ like the Leaky-Integrate-Fire (LIF) [5] neuron displaying lateral inhibition, and the 3T-MTJ synapse model showing spike timing dependent plasticity (STDP) [6], [7]. However, more work must be done to achieve real-time machine learning. Using an earlier developed synapse circuit [8] and a 3T-MTJ spice model [9], we show the transient behavior of a 2 by 2 crossbar array (cartoon in Fig 1). There is STDP for different delay conditions between the pre- and post-synaptic neural spikes. The shorter the time difference between the onset of the pre- and post-synaptic neuron spike, the higher the current through the ferromagnet (Fig 2). Higher current leads to higher rate of change of the domain wall (DW) position per neural event and higher DW displacement. At t=0, the initial pair of presynaptic and postsynaptic pulses helps to randomly give the DWs a head start. DW for synapse S2 (red plot) rises faster because it has the least delay of 1 ns between its pre- and post-synaptic pulse despite its pulses lagging that of S1 whose DW had a head start. Scaling this up, the 3T MTJ synapse is robust in more complex systems such as a machine learning clustering task.

[1] S. Lequeux *et al.*, *Sci. Rep.*, vol. 6, no. August, 2016, doi: 10.1038/srep31510. [2] J. Torrejon *et al.*, *Nature*, vol. 547, no. 7664, pp. 428–431 (2017) [3] N. K. Upadhyay, H. Jiang, Z. Wang *et al*, *Adv. Mater. Technol.*, vol. 1800589, pp. 1–13 (2019) [4] N. Hassan *et al.*, *J. Appl. Phys.*, vol. 124, no. 15, p. 152127 (2018) [5] G. Bi and M. Poo, *Annu. Rev. Neurosci.*, vol. 24, no. 1, pp. 139–166 (2002) [6] H. Markram, W. Gerstner, and P. J. Sjöström, *Front. Synaptic Neurosci.*, vol. 4, pp. 2–5 (2012) [7] O. Akinola, X. Hu, C. H. Bennett *et al*, *J. Phys. D. Appl. Phys.*, vol. 52, no. 49 (2019) [8] X. Hu, A. Timm, W. H. Brigner *et al*, *IEEE Trans. Elect. Dev.*, vol. 66, no. 6, pp. 2817–2821 (2019)

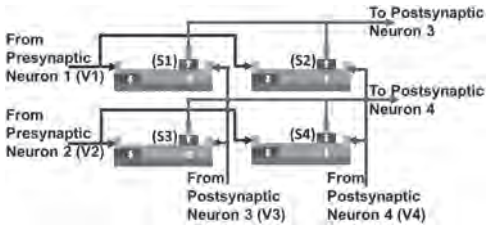

Fig.1: Cartoon showing a 2 x 2 crossbar array of synapses. Synapse modules S1, S2, S3 and S4 are developed from 3T-MTJs. Voltage pulses V1 and V2 feed into the synapses from the presynaptic neuron (blue arrows). Outputs of the synapses feed into the postsynaptic neurons (golden arrows) and the outputs of the postsynaptic neurons feed voltage pulses V3 and V4 back into the third terminals of the synapses (purple arrows).

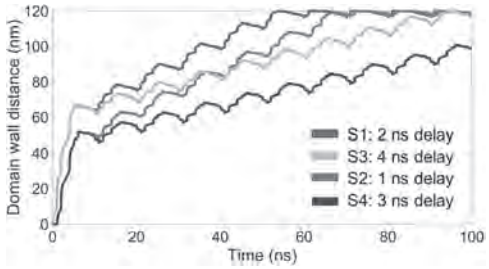

Fig 2. Plots showing domain wall positions of synapses in Fig 1. This is when the neural pulses V1, V2, V3 and V4 (all 1 V in magnitude) come into the synapses with 2 ns, 4 ns, 0 ns and 1 ns delay, respectively corresponding to delays of 2 ns, 1 ns, 4 ns and 3 ns between the pre- and post-synaptic neural pulses in each of synapses S1, S2, S3 and S4, respectively.

A5-03. Purely Spintronic Multilayer Perceptron Enabled by Four-Terminal Domain Wall-Magnetic Tunnel Junction Neuron. *N. Hassan*[1], W.H. Brigner[1], C.H. Bennett[2], A. Velasquez[3], X. Hu[1], O.G. Akinola[4], F. Garcia-Sanchez[5], M.J. Marinella[2], J.C. Incorvia[4] and J.S. Friedman[1]
1. Electrical & Computer Engineering, The University of Texas at Dallas, Richardson, TX, United States; 2. Sandia National Laboratories, Albuquerque, NM, United States; 3. Air Force Research Laboratory, Rome, NY, United States; 4. Electrical & Computer Engineering, The University of Texas at Austin, Austin, TX, United States; 5. Universidad de Salamanca, Salamanca, Spain

Domain wall-magnetic tunnel junction (DW-MTJ) devices intrinsically emulate neuron [1] and synapse [2] functionalities for neuromorphic systems. While these devices efficiently emulate neurobiological components, significant CMOS overhead is required to integrate multiple perceptron layers [3]. This work proposes a four-terminal DW-MTJ neuron [4] that enables purely spintronic multilayer perceptrons that do not require CMOS. The proposed leaky integrate-and-fire neuron [5] in Fig. 1 has a ferromagnetic DW track between terminals T1 and T2 and an MTJ between terminals T3 and T4. The MTJ free layer is coupled to the DW track by an electrically insulated layer. Spin-transfer torque induced by the current through the T1-T2 path moves the DW from right to left to perform integration. DW leaking from left to right intrinsically occurs due to either dipolar magnetic field [1], anisotropy gradient along [6], or shape variation [7]. When the DW passes underneath the electrically-isolated MTJ, the free ferromagnet reorients itself to match the magnetization of the DW track due to dipolar coupling, thereby switching the MTJ between the anti-parallel resistive state and parallel conductive state. A constant voltage applied at the T3 terminal, fires by switching between low and high output currents. Additionally, by exploiting stray magnetic field interactions, these neurons perform lateral inhibition among a group of neighboring neurons [1]. In the multilayer perceptron of Fig. 2, each four-terminal DW-MTJ neuron is connected to the three-terminal analog DW-MTJ input synapses through the T1 terminal and is cascaded to the output synapses through the T4 terminal without any CMOS interface. Finally, an unsupervised learning algorithm results from feedback between the T4 terminals of the neurons and right terminals of the synapses, providing best results of 98.11% accuracy on the Wisconsin breast cancer clustering task [8].

[1] N. Hassan, X. Hu, L. Jiang-Wei, *et al.*, J. Appl. Phys., Vol. 124, no. 15, p. 152127 (2018) [2] O. Akinola, X. Hu, C. H. Bennett, *et al.*, J. Phys. D: Appl. Phys., Vol. 52, no. 49, LT01 (2019) [3] A. Sengupta, Y. Shim, and K. Roy, IEEE TBioCAS, Vol. 10, no. 6, pp. 1152–1160 (2016) [4] W. H. Brigner, N. Hassan, X. Hu, *et al.*, arXiv preprint arXiv: 2002.00862 (2020) [5] A. N. Burkitt, Biol. Cybern., Vol. 95, pp. 97–112 (2006) [6] W. H. Brigner, X. Hu, N. Hassan, *et al.*, IEEE JXCDC, Vol. 5, no. 1, pp. 19–24 (2019) [7] W. H. Brigner, N. Hassan, L. Jiang-Wei, *et al.*, IEEE TED, Vol. 66, no. 11, pp. 4970-4975 (2019) [8] A. Velasquez, C. H. Bennett, N. Hassan, *et al.*, arXiv preprint arXiv: 2003.11120 (2020)

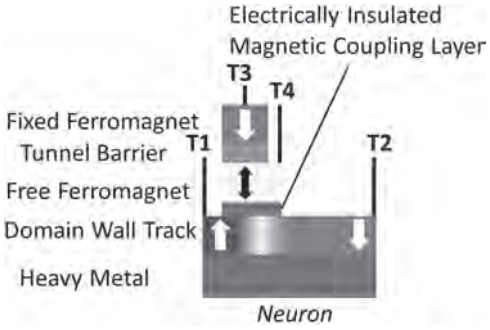

Fig. 1. Four-terminal DW-MTJ neuron.

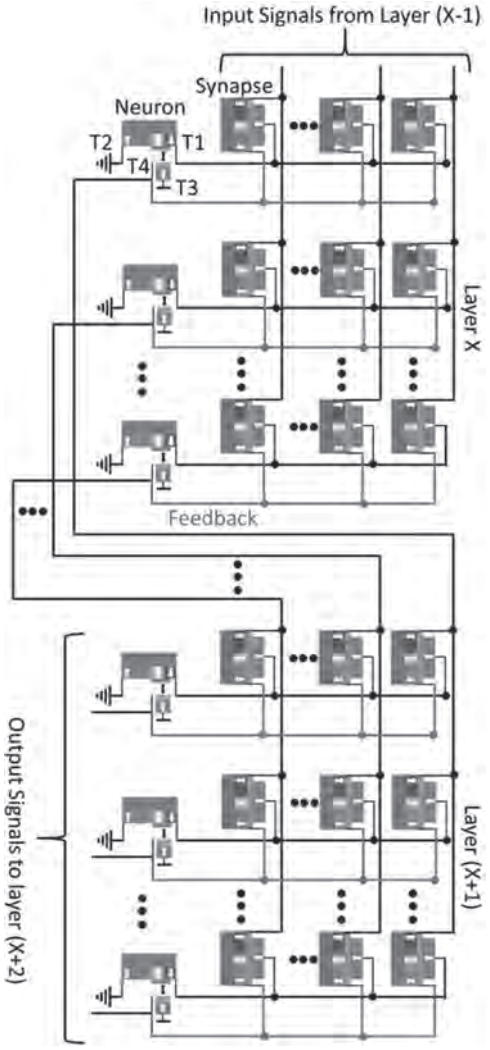

Fig. 2. Purely spintronic multilayer perceptron.

A5-04. Harnessing Stochastic Domain Wall Pinning for Machine Learning. *M.O. Ellis*[1], A. Welbourne[2], S.J. Kyle[2], T.J. Hayward[2], D. Allwood[2] and E. Vasilaki[1] *1. Department of Computer Science, The University of Sheffield, Sheffield, United Kingdom; 2. Department of Material Science and Engineering, The University of Sheffield, Sheffield, United Kingdom*

Magnetic materials are already widely used for long-term data storage, but ongoing work seeks to use them as both working memory and computing architectures. Particularly, devices based on magnetic domain walls (DWs) can perform logic operations and can readily store information [1]. However, the stochasticity of DW pinning limits the feasibility of creating technologically viable devices. Here, we demonstrate how stochasticity can be changed from a technologically inhibitive behaviour into an integral property of machine learning algorithms for specialised neuromorphic devices. We first present experimental measurements that demonstrate the tunability of stochastic processes by applying external stimuli. Focused magneto-optic Kerr effect measurements were used to probe the pinning of DWs at notch-shaped defect sites in 400 nm wide Permalloy nanowires (Fig. 1). DWs were injected into the nanowires and propagated to the defect sites using a field parallel to the nanowire (Hx). The probability of the DWs being pinned at the defect sites was found to depend sigmoidally on the magnitude of a field transverse to the nanowires (Hy). The stochastic behaviour of the nanowire were then integrated into machine learning models. We have developed feedforward neural networks with the nanowires acted as binary stochastic synapses (BSS) that can be sampled by repeating the network. It is found that for a single cycle of the network it can be trained to recognise handwritten digits with an error rate of 19%. Repeated sampling of the network decreases the error rate to 9% for 128 cycles - close to mean field performance (Fig. 2). Adding a hidden layer improves performance with extra pathways for the stochastic behaviour to be averaged over. Our work illustrates how the stochasticity of DW devices can be harnessed to provide tunable bespoke hardware for machine learning tasks.

[1] R. L. Stamps *et al*., J. Phys. D. Appl. Phys. Vol. 47, p. 333001 (2014)

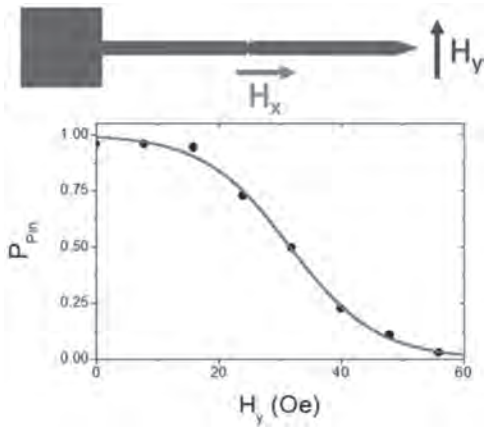

Fig. 1: Schematic of a notched magnetic nanowire for use as a synapse with a parallel driving field (Hx) and a tunable transverse depinning field (Hy) which gives the measured sigmoidal pinning probability.

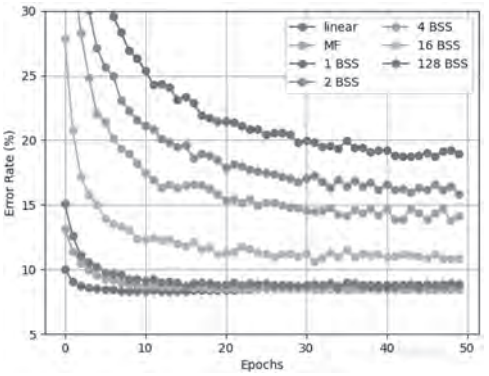

Fig. 2: The classification error rate for handwritten digits using a single layer network with varying number of binary stochastic synapses (BSS).

A5-05. Maximized Lateral Inhibition in Paired Magnetic Domain Wall Racetracks for Neuromorphic Computing. *C. Cui*[1], O.G. Akinola[1], N. Hassan[2], C.H. Bennett[3], M.J. Marinella[3], J.S. Friedman[2] and J.C. Incorvia[1] *1. Electrical and Computer Engineering, The University of Texas at Austin, Austin, TX, United States; 2. Electrical and Computer Engineering, The University of Texas at Dallas, Richardson, TX, United States; 3. Sandia National Laboratory, Albuquerque, NM, United States*

Lateral inhibition (LI) is an important neuromorphic network functionality, modeled after the biological neuron behavior that a firing neuron deactivates its neighbors and prevents their firing. In most neuromorphic hardware platforms LI is implemented by external circuitry, thereby decreasing the energy efficiency and increasing the area overhead. Recently, the domain wall – magnetic tunnel junction (DW-MTJ) neuron is shown in modeling to be intrinsically inhibitory[1]. LI in DW-MTJ neurons results from magnetostatic interaction between adjacent neurons (Fig.1): the two DWs, DW_N and DW_I, are driven by electrical current of densities $J_{eI}<J_{eN}$, so that the DW velocities $v_{DWI}<v_{DWN}$ and the active Neuron N fires first. DW_I falls behind DW_N and is subjected to the stray field of Neuron N in the $-z$ direction. It is demonstrated that such stray field can decrease DW_I velocity and prevent Neuron I from firing, thus emulating LI. However, the LI mechanism in DW-MTJ neurons has not been studied thoroughly, leading to weak inhibition only in very closely spaced devices. In our work[2] we model the current- and field-driven DW motion in two adjacent DW-MTJ neurons to approach these problems. LI is maximized by an optimal magnetic interaction strength, determined by tuning the spacing between the two neurons (Fig.2). The results are explained by the current- and field-driven DW velocity characteristics and are quantified by an analytical model. We further study the influence of device parameters and demonstrate the LI behavior in an array of 1000 neurons, which renders our proposed DW-MTJ array promising for implementing a *k*-winner-take-all layer. With strong LI achieved, a path towards competitive learning algorithms are made possible on the DW-MTJ neurons. This work is funded by Sandia National Lab. *Sandia National Lab (SNL) is managed and operated by NTESS under DOE NNSA contract DE-NA0003525*

1. N. Hassan et al. Journal of Applied Physics, Vol.124, p.152127 (2018) 2. C. Cui et al. *Nanotechnology*, Vol.*31*(29), p.294001 (2020)

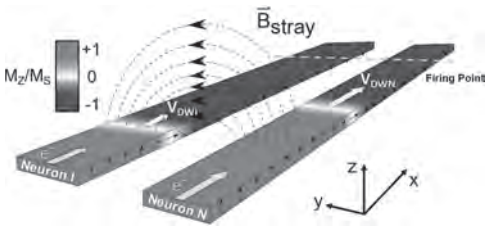

Fig.1 Inhibitory relation between two adjacent DW-MTJ neurons (only the DW racetracks are shown). Yellow dashed line indicates MTJ position (firing point). *Mz*: magnetization in +*z*.

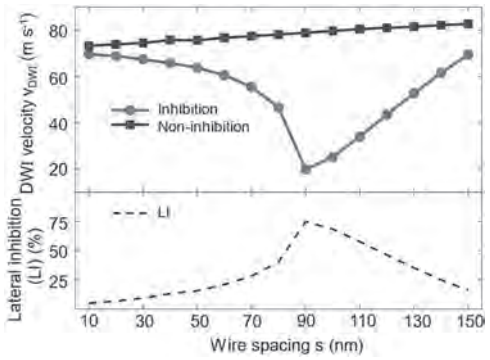

Fig.2 (top) DW_I velocity v_{DWI} under inhibition (red circles) and non-inhibition (blue squares) conditions; (bottom) LI as a function of wire spacing *s*.

A5-06. Linear Intrinsic Leaking in a Domain-Wall Magnetic Tunnel Junction Neuron. *W.H. Brigner*[1], N. Hassan[1], X. Hu[1], C.H. Bennett[2], F. Garcia-Sanchez[3,4], M.J. Marinella[2], J.C. Incorvia[5] and J.S. Friedman[1] *1. Electrical and Computer Engineering, University of Texas at Dallas, Richardson, TX, United States; 2. Sandia National Laboratories, Albuquerque, NM, United States; 3. Department of Applied Physics, University of Salamanca, Salamanca, Spain; 4. Istituto Nazionale di Ricerca Metrologica, Turin, Italy; 5. Electrical and Computer Engineering, University of Texas at Austin, Austin, TX, United States*

Neuromorphic computing attempts to mimic the neurons and synapses in a human brain in order to provide significant improvements in the computation of unstructured, real-world data. In past research, we have proposed three separate leaky integrate-and-fire (LIF) neurons that provide the leaking, integrating, and firing characteristics without the use of any additional circuitry [1]-[3]. These neurons are therefore able to significantly reduce the area and energy overhead of neuromorphic circuits. To increase the biological accuracy of these neurons and to better match the neurons to different neuromorphic schema and algorithms, it is desirable for neuron leaking to implement specific mathematical functions in addition to exhibiting the three basic LIF neuronal functionalities. By varying the shape of the devices, it is possible to implement a variety of leaking characteristics. In this work, we discuss the implementation of linear leaking characteristics. In the neurons of [1]-[3], the leaking DWs accelerate towards the ends of the tracks. To counter this, it is necessary to alter these devices. In fact, by simply introducing slight exponential variations in the sides of the neuron from [3], as in Figure 1, we are capable of constructing neurons with considerably more linear leaking characteristics than those discussed in [1]-[3]. As the exponential variations become more pronounced, the linearity of the neuron's leaking increases as well. Beyond a certain point, however, continued increases in the curvature causes a regression in the leaking functionality's linearity. Figure 2 demonstrates the effect of the curvature of the DW track on the device's leaking functionality, starting with no curvature and progressing to more pronounced curvature.

[1] N. Hassan, X. Hu, L. Jiang-Wei *et al.*, "Magnetic domain wall neuron with lateral inhibition," *J. Appl. Phys.*, vol. 124, no. 15, p. 152127, 2018. [2] W. H. Brigner, X. Hu, N. Hassan, *et al.*, "Graded-Anisotropy-Induced Magnetic Domain Wall Drift for an Artificial Spintronic Leaky Integrate-and-Fire Neuron," *IEEE Journal on Exploratory Solid-State Computational Devices and Circuits*, vol. 5, no. 1, pp. 19–24, 2019. [3] W. H. Brigner, N. Hassan, L. Jiang-Wei, *et al.*, "Shape-Based Magnetic Domain Wall Drift for an Artificial Spintronic Leaky Integrate-and-Fire Neuron," *IEEE Transactions on Electron Devices*, vol. 66, no. 11, pp. 4970-4975, 2019.

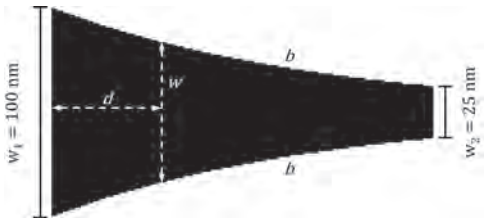

Fig. 1 Structure of the linear neuron, displaying the curvature of the neuron's sides. The curvature is of the following form: $w \propto b^{-d}$, where *b* represents the curvature of the sides and *w* is the cross-sectional width of the device at any distance *d* from the wide end. $b = 1$ represents the neuron from [3].

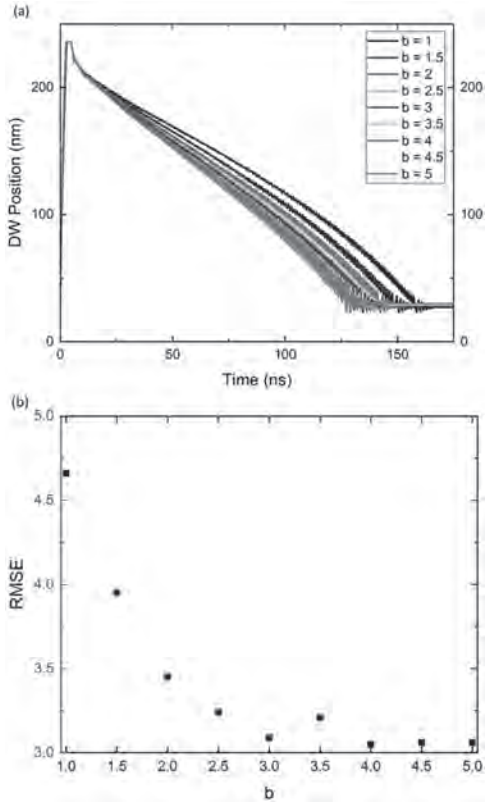

Fig. 2 (a) Leaking characteristics for various values of *b*. (b) Root mean squared error (RMSE) from a linear function.

INVITED PAPER

A5-07. Magnetic Whirls for Unconventional Computing.
K. Everschor-Sitte[1] *1. Institute of Physics, Johannes Gutenberg Universitat Mainz, Mainz, Germany*

Novel computational paradigms in combination with proper hardware solutions are required to overcome the limitations of our state-of-the-art computer technology, in particular regarding energy consumption. Due to the inherent complex and non-linear nature, spintronics offers the possibility towards energy-efficient, non-volatile hardware solutions for various unconventional computing schemes.[1-3] In this talk, I will address the potential of topologically stabilized magnetic whirls – so-called skyrmions – for in particular two unconventional computing schemes – reservoir computing and stochastic computing. Reservoir computing is a computational scheme that allows to drastically simplify spatial-temporal recognition tasks. We have shown that random skyrmion fabrics provide a suitable physical implementation of the reservoir [4,5] and allow to classify patterns via their complex resistance responses either by tracing the signal over time or by a single spatially resolved measurement. [6] Stochastic computing is a computational paradigm that allows to speed up a calculation while trading for numerical precision. Information is encoded in terms of bit-streams as a probability. A key requirement and simultaneously a challenge is that the incoming bitstreams are uncorrelated. The Brownian motion of magnetic skyrmions allows creating a device that reshuffles the bit-streams. [7,8]

[1] J. Grollier, D. Querlioz, K. Y. Camsari, KES, S. Fukami, M. D. Stiles, Nature Electronics (2020) [2] E. Vedmedenko, R. Kawakami, D. Sheka, ..., KES, et al., J. of Phys. D (2020) [3] G. Finocchio, M. Di Ventra, K.Y. Camsari, KES, P. K. Amiri and Z. Zeng, arXiv:1907.04601 [4] D. Prychynenko, M. Sitte, et al, KES, Phys. Rev. Appl. 9, 014034 (2018) [5] G. Bourianoff, D. Pinna, M. Sitte and KES, AIP Adv. 8, 055602 (2018) [6] D. Pinna, G. Bourianoff and KES, arXiv:1811.12623 [7] D. Pinna, F. Abreu Araujo, J.-V. Kim, et al, Phys. Rev. Appl. 9, 064018 (2018) [8] J. Zazvorka, F. Jakobs, D. Heinze, ..., KES, et al., Nat. Nanotech. 14, 658 (2019)

Session B1
ARTIFICIAL SPIN ICE

Jose M. Porro, Chair
BCMaterials, Leioa, Spain

INVITED PAPER

B1-01. Tailoring Spin Wave Channels in a Reconfigurable Artificial Spin Ice. *E. Iacocca*[1], S. Gliga[2] and O. Heinonen[3] *1. Northumbria University, Newcastle upon Tyne, United Kingdom; 2. Paul Scherrer Institut, Villigen, Switzerland; 3. Argonne National Laboratory, Lemont, IL, United States*

Artificial spin ices are superlattices of patterned magnetic nanostructures geometrically arranged to display frustration by design [1]. Recent studies have explored the magnetization dynamics of artificial spin ices, finding band structures [2] that suggest applications as magnonic crystals [3]. An attractive advantage of using artificial spin ices as magnonic crystals is the potential reconfigurability of its long-range magnetic state and associated band structure. While this is not trivial in most spin ice geometries, a recently investigated geometry called "charge ice" can be accurately reconfigured with relatively simple external field protocols [4]. However, this geometry possesses a strict geometrical constraint between the magnetic elements' length and the lattice parameter. This constraint effectively decouples the magnetic elements, leading to identical simulated spectra for both a square and charge ice in Type-I and Type-II configurations. To effectively couple magnetic elements, we propose a hybrid structure where the artificial spin ice is patterned on top of a soft magnetic underlayer [5]. Based on micromagnetic modelling, we find that this strategy allows for both dipolar and spin-wave-mediated coupling between the elements of the artificial spin ice and the soft magnetic underlayer. In this case, the rich spectra shown in Figure 1 are numerically obtained, demonstrating that the proposed system is coupled. Moreover, we find that the low-frequency edge modes in the artificial spin ice give rise to well-defined spin-wave channels in the underlayer. These results open promising pathways for the development of reconfigurable magnonic crystals.

[1] S. H. Skjærvø et al., *Nat. Rev. Phys.* 2 13 – 28 (2020) [2] E. Iacocca et al., *Phys. Rev. B* 93 134420 (2016); S. Gliga et al., APL Materials 8, 040911 (2020) [3] A. V. Chumak et al., *Nat. Phys.* 11, 453 (2015); D. Grundler, *Nat. Phys.* 11 438 (2015) [4] Wang et al., *Science* 352 962 (2016) [5] E. Iacocca et al., *Phys. Rev. Applied* 13, 044047 (2020)

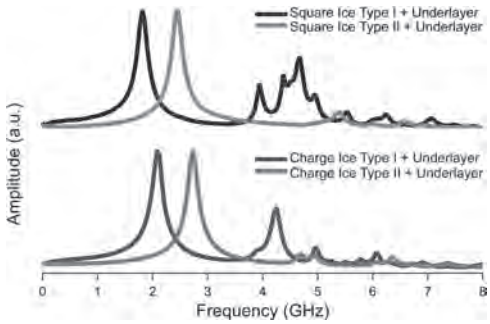

Figure 1. Simulated spectra for square and charge ice on a soft magnetic underlayer.

CONTRIBUTED PAPERS

B1-02. Switching Barriers in Artificial Square ice. *N. Leo*[1], S. Koraltan[2], M. Pancaldi[3], P. Villalba[1], C. Abert[2], C. Vogler[2], K. Hofhuis[4,5], F. Slanovc[2], F. Bruckner[2], P. Heistracher[2], M. Menniti[1], D. Suess[2] and P. Vavassori[1,6] *1. CIC nanoGUNE, Donostia - San Sebastián, Spain; 2. Universitat Wien, Wien, Austria; 3. Stockholms Universitet, Stockholm, Sweden; 4. Paul Scherrer Institut, Villigen, Switzerland; 5. Eidgenossische Technische Hochschule Zurich, Zurich, Switzerland; 6. Ikerbasque, Bilbao, Spain*

The relaxation kinetics and emerging correlations of arrays of interacting Ising-like nanomagnets are governed by the switching rates of the individual magnets. These rates depend, via the Arrhenius law, on the energy barrier for moment reversal in the nanomagnets. In this work, we consider how the switching behaviour of a nanomagnet in archetypical artificial square ice is modified by the interaction with its six nearest neighbours. We find that due to two effects the transition barriers can be significantly lowered compared to an approximation commonly used for kinetic Monte Carlo simulations: (1) Based on a simplified point-dipole model, we find that the barriers for clockwise and counter-clockwise uniform rotation can differ significantly due to the interactions with neighbours. For a subset of environmental microstates this leads to a significant enhancement of the switching rate, which is especially marked in the limit of rare events. (2) Micromagnetic simulations employing the string method to model the moment reversal in an extended nanomagnets reveal that, in addition to the clockwise/counter-clockwise splitting, the environments promote non-uniform reversal leading to further reductions of the switching barriers. These results highlight that local microstates can significantly enhance moment reversals already in ideal systems, without defects or additional anisotropies, and are particularly pronounced for fully-magnetised configurations. Thus, we expect that the initial stages of demagnetisation will proceed faster than assumed from previous models. These findings are of integral importance to achieve realistic kinetic Monte Carlo simulations of emergent correlations in extended artificial spin systems or the evolution of small-scale nanomagnetic logic circuits.

B1-03. Role of Higher-Order Magnetostatic Interactions for the Directional Injection of Monopole Currents. *E.Y. Vedmedenko*[1] *1. Universitat Hamburg, Hamburg, Germany*

The dynamics involving directed separation of a monopole-antimonopole pair in two- or three-dimensional spin ices is conventionally defined as magnetic current or magnetricity. While the feasibility of magnetricity in artificial spin ices has been shown theoretically and experimentally [1,2], the controllability of magnetic currents is still under debate. Particularly, it has been theoretically shown that maximization of Dirac string's tension is a necessary condition for stabilization of directed magnetic currents [1]. Experimentally, however, magnetic currents are often of only short duration, because magnetic monopoles created at one sample edge do not reach the other sample edge, but rather stick in the middle of the sample. Here, we explore theoretically the role of the termination of arrays and the higher order magnetic interactions for the directionality of magnetic currents in two-dimensional artificial spin-ice. Our Monte-Carlo calculations show that arrays of point dipoles and identical array with realistic multipole moments give qualitatively similar results with respect to the end states and with respect to the averaged propagation of the monopoles. However, the

Monte-Carlo calculations using the higher order contributions reflect much better formation of domains with phase shifted Dirac strings, found in recent experiments [3]. Our calculations permit us to elaborate a phase diagram predicting the probability of directed propagation of monopole current as a function of termination type of a realistic artificial spin-ice array.

[1] E. Y. Vedmedenko, Dynamics of Bound Monopoles in Artificial Spin Ice: How to Store Energy in Dirac Strings. Physical Review Letters 116, 077202 (2016). [2] A. Farhan et al., Direct Observation of Thermal Relaxation in Artificial Spin Ice. Phys. Rev. Lett. 111, 057204 (2013). [3] A. Hanu, E. Y. Vedmedenko, J. Cuia, J. Vijayakumard, A. Kleibertd, L.J. Heyderman, Control of emergent magnetic monopole currents in artificial spin ice, submitted.

B1-04. A Magnon Approach to Thermal Fluctuations in Ising-Like Mesospins. *S. Slöetjes*[1], B. Hjörvarsson[1] and V. Kapaklis[1] *1. Physics and Astronomy, Uppsala Universitet, Uppsala, Sweden*

1D and 2D arrays of coupled magnetic nanoislands, also known as mesospins, have recently attracted much attention for offering the possibility to mimic exotic physical systems [1]. In analyzing these coupled mesospin arrays, the individual building blocks are often assumed to consist of simple dipoles, where any inner structure is ignored. Such an approximation of a mesospin however, leads to discrepancies when temperature becomes an important parameter [2]. Temperature excites thermal magnons in a ferromagnet, which is the basis for temperature dependence of the magnetization as expressed by the Bloch law. Here, we present a framework for studying temperature induced magnetization fluctuations in terms of magnonic excitations. We use MuMax3 to numerically subject a single stadium shaped mesospin (450 nm x 150 nm x 5 nm) to a highly inhomogeneous stochastic thermal field [3], and study the emerging spectrum by Fourier transforming the magnetization. The length, width and thickness of the mesospin element are varied to study the resulting effect of size variation on the spectra. The spectra are found to be gapped, and the spectral peaks pertain to specific edge- and center oscillation modes. Finally, we study the effect of temperature variation and we find that the magnon density of states plays an important role on the overall shape of the spectra. The results of this study are not only useful from the perspective of thermal switching of nanoislands, but also for the design of magnonic crystals based on mesospins.

1. S. H. Skjærvø, et al., *Nature Reviews Physics*, Vol. 2, p. 13–28 (2020) 2. M. Pohlit, G. Muscas, I. A. Chioar, et al., *Physical Review B*, Vol. 101, p. 134404 (2020) 3. J. Leliaert, J. Mulkers, J. De Clercq, et al., *AIP Advances*, Vol. 7, p. 125010 (2017)

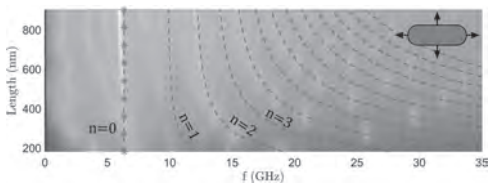

Thermal spectra upon size variation of the mesospin, where the aspect ratio is kept constant.

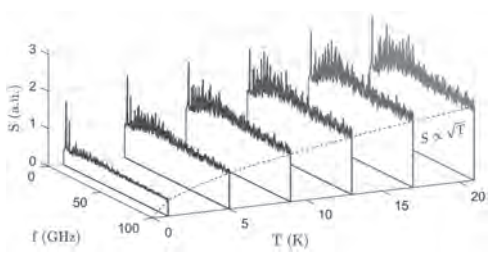

The effect of temperature variation on the thermal spectra.

B1-05. Long-Range Magnetic Ordering in Artificial Kagome Spin Ice. *K. Hofhuis*[1,2], A. Hrabec[1,2], H. Arava[1,2], N. Leo[2,3], S.H. Skjærvø[1,2], Y. Huang[4], R.V. Chopdekar[5], S. Parchenko[1,2], A. Kleibert[6], S. Koraltan[7], C. Abert[7], C. Vogler[7], D. Suess[7], P. Derlet[8,1] and L. Heyderman[1,2] *1. Department of Materials, ETH Zurich, Zurich, Switzerland; 2. Laboratory for Multiscale Materials Experiments, Paul Scherrer Institute, Villigen, Switzerland; 3. CIC nanoGUNE, San Sebastian, Spain; 4. Department of Materials Science and Engineering, University of California Berkeley, Berkeley, CA, United States; 5. Advanced Light Source, Lawrence Berkeley National Laboratory, Berkeley, CA, United States; 6. Swiss Light Source, Paul Scherrer Institute, Villigen, Switzerland; 7. Christian Doppler Laboratory, Advanced Magnetic Sensing and Materials, University of Vienna, Wien, Austria; 8. Condensed Matter Theory Group, Paul Scherrer Institute, Villigen, Switzerland*

The extent of magnetic ordering in highly-frustrated thermally-active artificial kagome spin ice is limited by the lowest achievable blocking temperature, as the moments freeze in before ordering is achieved [1]. A more substantial degree of magnetic ordering can be achieved by lowering the blocking temperature of the individual nanomagnets or by increasing the critical transition temperature for the system. We pursue an original approach of introducing interfacial Dzyaloshinskii-Moriya interactions, which lowers the blocking temperature while keeping the transition temperature unchanged [2]. Using this approach, we demonstrate that a seven-ring kagome structure consisting of 30 nanomagnets can be thermally annealed into its ground state. Furthermore, the spin-ice correlations extracted from extended kagome lattices are found to exhibit the quantitative signatures of long-range charge-order, thereby giving experimental evidence for the theoretically predicted continuous transition to a charge-ordered state. We also find that slight modifications of the nanomagnets at a vertex in the artificial kagome ice lead to an increase in the critical temperatures, and allow us to control the energy landscape. Our results provide the foundations for the tuning of magnetic ordering in several different artificial spin systems.

[1] S.H. Skjærvø, C.H. Marrows, R.L. Stamps, L.J. Heyderman. *"Advances in artificial spin ice."* Nature Reviews Physics 2, 13-28 (2020). [2] K. Hofhuis *et al.*, *under review*.

B1-06. The Formation of Complex Spin Textures in $La_{0.7}Sr_{0.3}MnO_3$ Artificial Spin Ice Arrays. *D.Y. Sasaki*[1], R.V. Chopdekar[2], S. Retterer[3], D.Y. Jiang[4], J. Mason[1], M.S. Lee[1] and Y. Takamura[1] *1. Department of Materials Science and Engineering, University of California Davis, Davis, CA, United States; 2. Advanced Light Source, E O Lawrence Berkeley National Laboratory, Berkeley, CA, United States; 3. Center for Nanophase Materials Sciences, Oak Ridge National Laboratory, Oak Ridge, TN, United States; 4. Department of Chemical Engineering, University of California Davis, Davis, CA, United States*

Artificial spin ices (ASIs) are lithographically patterned arrays of single domain magnetic nanoislands where the dipolar interactions between these Ising-like macrospins have served as the basis for investigating phenomena such as geometric frustration and emergent magnetic monopoles [1]. While the majority of ASI studies have utilized nanoislands composed of soft magnetic metals (e.g. permalloy), the use of complex oxides, such as $La_{0.7}Sr_{0.3}MnO_3$ (LSMO), could permit room temperature studies of thermally-active ASIs (T_C ~ 360 K) and serve as a platform for coupling the rich physics of both complex oxide heterostructures and ASI structures. In this work, we utilize x-ray photoemission electron microscopy (X-PEEM) to image LSMO-based brickwork ASI structures where a breakdown of the Ising model of individual nanoislands occurs at a critical coupling strength which balances intra- and inter-island magnetic interactions. For ASI structures with nanoislands of identical dimensions, the ASI lattice parameter controls the inter-island coupling strength, resulting in systems composed solely of single-domain magnetic nanoislands, or a mixture of single-domain and complex spin textures (CST, i.e. single and double vortex states). Analysis of magnetic ordering in X-PEEM images reveals that nucleation of CST in frustrated nanoislands is accompanied by a disruption in long-range

ordering. While it is generally assumed that inter-island interactions in ASI systems only influence the ordering of the nanomagnetic ensemble, in this LSMO-based ASI system inter-island coupling can dictate both the spin texture within individual nanoislands and long-range magnetic ordering. These results suggest the potential to create tunable nanoisland domain states, providing a new direction in developing ASI systems with exotic phase transitions as well as novel nanomagnetic logic architectures.

1. Skjærvø, S.H., et al., Nature Reviews Physics., Vol. 2, p.13 (2020)

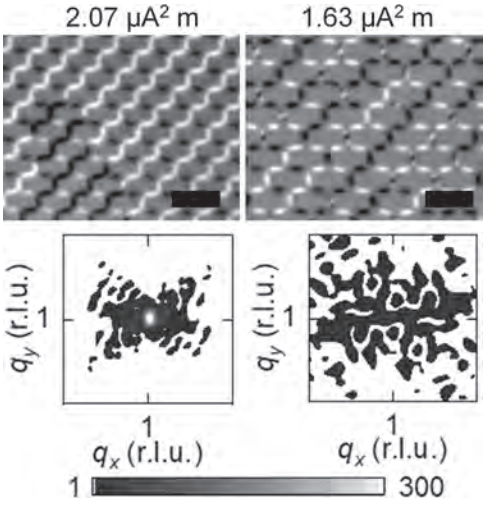

Fig. 1: XMCD-PEEM images (top) and corresponding magnetic structure factors (bottom) of brickwork ASI at coupling strengths of 2.07 μA² m and 1.63 μA² m. Scale bar is 2 μm.

B1-07. Withdrawn

B1-08. Ferromagnetic Antidot Arrays With Complex Geometries. *D. Navas*[1], D.G. Trabada[1] and M. Vazquez[1] *1. Instituto de Ciencia de Materiales de Madrid (ICMM-CSIC), Madrid, Spain*

The magnetic behaviour of ferromagnetic antidot thin films can be tuned by engineering their geometry, such as the hole diameter, inter-hole distance and film thickness [1,2]. Although antidot patterned nanostructures are grown by template-assisted methods mostly using lithographical techniques [1,2], the use of anodic alumina templates has also been checked successfully [3]. However, this latter alternative shows some challenging aspects for the patterning of large areas with sufficiently high ordering and/or complex antidot geometries. These limitations are partly overcome by performing a mechanical nanoimprinting process before a single anodization process [4-6]. This work introduces an easy and less-expensive route to synthesize highly ordered nanoporous alumina templates in large areas and subsequently magnetic antidot arrays with different and complex geometries. The procedure is based on large-scale nanoimprint using patterned commercial disks as a 1-D grating stamp (e.g., CD, DVD and BR disks) followed by single anodization process which allows obtaining 1-D anodic alumina templates (Figure 1a). In addition, complex 2-D patterned nanoporous alumina templates, with square or triangular ordering (Figures 1b and c), were generated using the 1-D grating stamp by multiple imprinting steps at different angles. Afterwards, Co antidot thin films were sputtered onto these templates with different thickness (from 20 to 100 nm) and symmetries. Magnetic studies confirm the presence of in-plane anisotropy with easy axis parallel to the nanostripes in Co antidot films, while a modest in-plane bi-axial magnetic anisotropy with perpendicular magnetization easy axes is concluded in Co squared nanodot arrays. In summary, a non-expensive methodology, combining soft-imprint and single anodization, is introduced for massive mould production and complex pattern generation, avoiding standard lithographical techniques. The magnetic response of the final sputtered antidot films can be engineered by the appropriate nanoimprinted processes.

1. R. P. Cowburn, A. O. Adeyeye, and J. A. C. Bland, Appl. Phys. Lett. 70, 2309 (1997). 2. N. G. Deshpande, M. S. Seo, X. R. Jin, S. J. Lee, Y. P. Lee, J. Y. Rhee and K. W. Kim, Appl. Phys. Lett. 96, 122503 (2010). 3. K. J. Merazzo, C. Castán-Guerrero, J. Herrero-Albillos, F. Kronast, F. Bartolomé, J. Sesé, R.P. Del Real, L. M. García and M. Vázquez, Phys. Rev. B. 85, 184427 (2012). 4. W. Lee, R. Ji, C. A. Ross, U. Gosele and K. Nielsch, Small, 2, 978 (2006). 5. J. Choi, R.B. Wehrspohn, and A. Gösele, Adv. Mater., 15, 1531 (2003). 6. J. Um, M. R. Z. Kouhpanji, S. Liu, Z. N. Porshokouh, S.-Y. Sung, J. Kosel and B. Stadler, IEEE Trans. Magn. 56, 6701006 (2020).

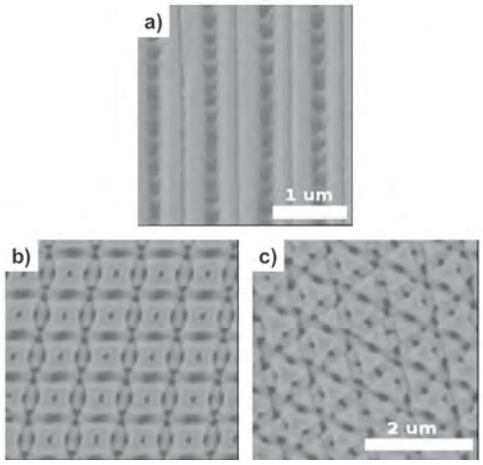

Figure 1. SEM images of alumina templates with line (a), square (b) and triangular configurations (c) imprinted using DVD-ML molds and an anodization step.

B1-09. Magnetic Properties of Novel 3D Antidot Matrix Created by Stepwise Nanosphere Lithography. *B. Myint*[1] and V. Ng[1] *1. Electrical and Computer Engineering, National University of Singapore, Singapore*

Recently, there has been increased interest in 3D nanostructures arising from the extra degree of freedom in magnetic spins at the third dimension [1,2]. Work has been limited to simulation [3] due to substantial nanoscale alignment challenges in 3D fabrication. We report here a new self-assembly based lithography technique to create 3D nanostructures and study their magnetic properties experimentally. In *stepwise nanosphere lithography,* nanospheres are first self-assembled by tilted assembly [4] to form a mask and then etched using O_2 plasma to reduce their size. Permalloy is then deposited through the mask at 0° to create an antidot layer, followed by a second deposition at 45° to form an array of nanowires over the former antidot matrix (Fig 1a). Unlike the conventional 2D antidot layer with three easy and hard magnetization axes [5-6], the hysteresis of the fabricated 3D antidot matrix measured by magneto-opto Kerr Effect shows only one easy and hard axis. Its easy axis lies along the length of the nanowire, while the hard axis is perpendicular to it. Hard axis magnetization reversal of 3D antidot matrix shows that magnetic moments reverse their direction via coherent rotation of magnetic domains (Fig 1). This rotational reversal behavior is stimulated mainly by the interconnected bottom antidot layer. In contrast, when magnetization is along the easy axis, reversal takes place via domain wall propagation (Fig 2). Domain walls nucleate from a single nanowire and then propagate towards the neighboring nanowires. This process indicates that the easy axis reversal process in the 3D antidot matrix is dominated by the top-nanowire layer. Magnetization changes with applied field along each axis will be reported in detail. The effect of size and location of the nanowires on the 3D antidot matrix will be investigated. Results will be verified using OOMMF simulations [7].

[1] A. Fernández-Pacheco, R. Streubel and O. Fruchart, Nature Communications, vol. 8 (2017). [2] G. Gubbiotti, M. Kostylev and S. Tacchi,

Journal of Physics D: Applied Physics, vol. 47, p. 105003 (2014). [3] G. Chern, C. Reichhardt and C. Nisoli, Applied Physics Letters, vol. 104, p. 013101 (2014). [4] V. Ng, Y. V. Lee, B. T. Chen and A. O. Adeyeye, Nanotechnology. vol 13, p 554 (2002) [5] U. Wiedwald, J. Gräfe, and K. M. Lebecki, et al., Beilstein Journal of Nanotechnology, vol. 7, p 733 (2016). [6] B. Summers, Y. Chen, A. Dahal and D. Singh, Scientific Reports, vol. 7 (2017). [7] M. J. Donahue and D. G. Porter, OOMMF User's Guide, Version 1.0 Interagency Report NISTIR 6376

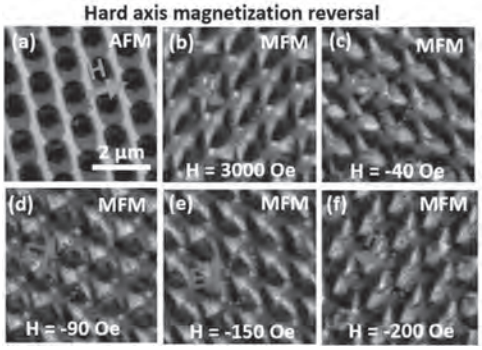

Fig. 1 (a) AFM and (b-f) MFM images of 3D antidot matrix during hard axis reversal process. Red arrows show the magnetic moment directions. Blue arrow shows the field direction.

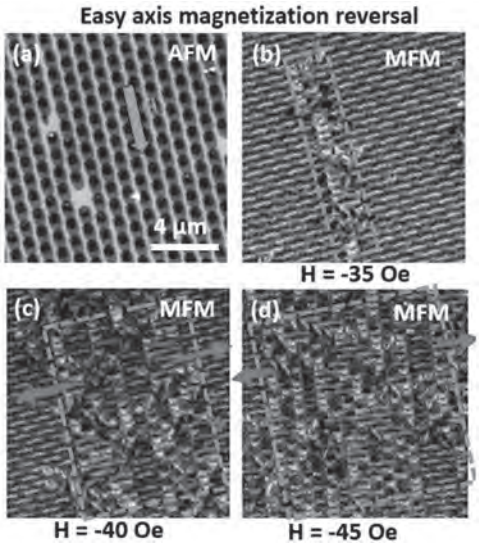

Fig. 2 (a) AFM and (b-d) MFM images of 3D antidot matrix during easy axis reversal process. Blue boxes show the domain walls. Red arrows show their propagation direction.

B1-10. Magnetic Tunability of Permalloy Artificial Spin Ice Structures.
A. Talapatra[1], N. Singh[2] and A. Adeyeye[1,3] *1. Department of Electrical and Computer Engineering, National University of Singapore - Kent Ridge Campus, Singapore, Singapore; 2. Institute of Microelectronics, Singapore, Singapore; 3. Physics, Durham University, Durham, United Kingdom*

Artificial spin ice (ASI) structures, consisting of arrays of interacting, single domain nanomagnets (NMs) are promising model systems to explore microscopic features of geometrical frustration [1]. While the structural geometry is responsible for tuning the shape anisotropy and the configurational anisotropy of the system, the strength of dipolar coupling can be modified by the film thickness. In the present work, we achieved magnetic tunability for $Ni_{80}Fe_{20}$ (Py) ASI structures by three distinct methods namely, the geometrical arrangements of the nanomagnets, the variation in film thickness (20 nm, 30 nm and 50 nm) for each geometry and the applied field orientation [2]. The different ASI geometries such as square spin ice (SSI), kagome spin ice (KSI) and comparatively newer triangular spin ice (TSI) structures are shown in Fig. 1 (a), (b) and (c) respectively. The corresponding hysteresis loops in Fig. 1 (d) depict a marked difference in magnetization reversal mechanism with the variation in film thickness which indicates a possible transition from single domain nanostructure to the formation of vortex states with increasing thickness. The ferromagnetic resonance (FMR) spectra, shown in Fig. 2 explain the dependence of various spin wave modes and their spatial localization on the structural symmetry, film thickness and applied field (H_{app}) orientation. Micromagnetic simulations are in good agreement with the experimental data and shows the space-frequency resolved localization of the spin wave modes. The results show a great potential towards designing reconfigurable magnonic crystals for microwave filter applications.

[1] R. F. Wang, C. Nisoli, R. S. Freitas, J. Li, W. McConville, B. J. Cooley, M. S. Lund, N. Samarth, C. Leighton, V. H. Crespi and P. Schiffer, *Nature* 439, 303-306 (2006). [2] A. Talapatra, N. Singh and A. O. Adeyeye, *Physical Review Applied* 13, 014034 (2020).

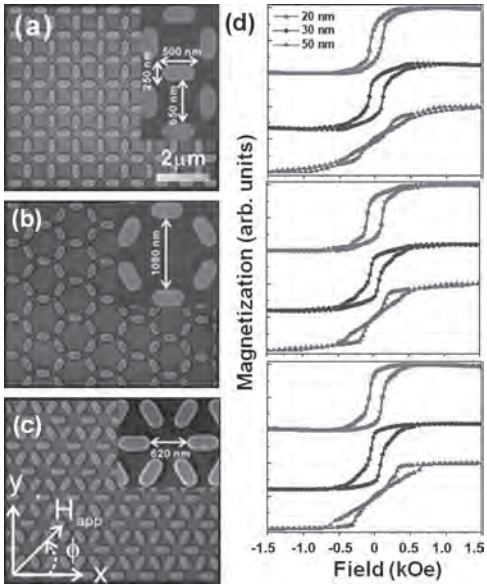

Different geometries of the ASI lattices, (a) SSI, (b) KSI, (c) TSI and (d) the corresponding hysteresis loops with H_{app} along 0°.

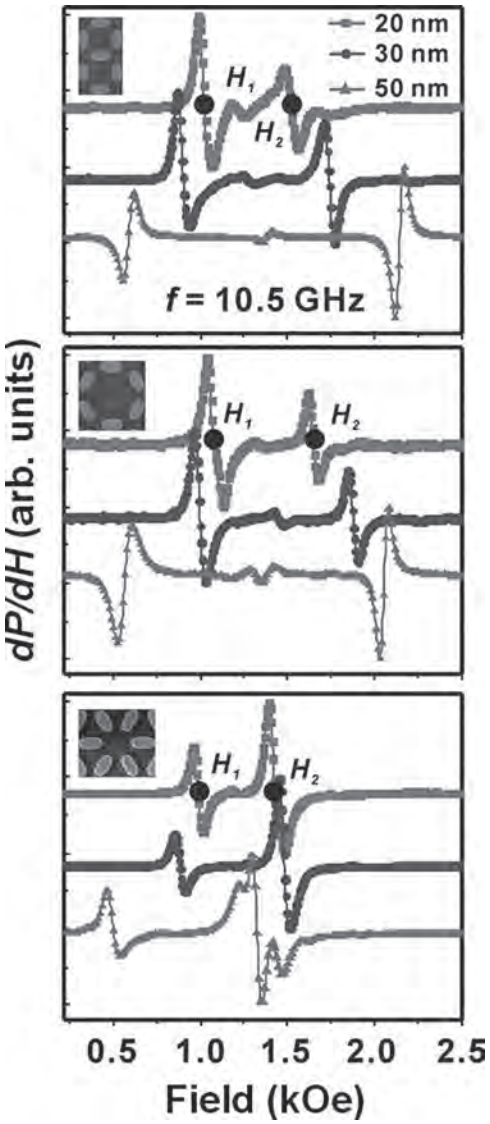

Thickness-dependent FMR spectra for different ASI structures (shown as insets) with H_{app} along 0°.

B1-11. Tunability in the Dynamics of a Bicomponent Artificial Spin Ice. *S. Lendinez*[1], M. Taghipour Kaffash[1] and M. Jungfleisch[1]
1. Department of Physics and Astronomy, University of Delaware, Newark, DE, United States

Artificial spin ices (ASI) are magnetic metamaterials initially designed to mimic the frustrated behavior of crystalline spin ice systems such as pyrochlore crystals. They show complex magnetic ordering and can exhibit exotic phase diagrams. Unlike their crystalline counterparts, the ASI geometry can be designed and the state of their constituent elements can be directly probed. Recent studies have focused on their dynamic behavior at high frequencies (in the GHz and tens of GHz range), as they can be used as magnonic metamaterials to modify the spin-wave properties by creating band gaps in the resonance spectra [1]. Previous works have shown that different geometries produce unique dynamic spectra. Here, we performed angular-dependent broadband ferromagnetic resonance measurements on a square ASI composed of different materials for each sublattice (NiFe and CoFe). Our experiments show that the interaction between the sublattices results in unique resonance spectra attributed to the two sublattices (see Fig. 1). By performing micromagnetic simulations, we identify the modes observed in the experiment. Our results show that the interaction in the ASI can be tuned not only by the geometry of the lattice, but also by the proper choice of the materials.

[1] S Lendinez, MB Jungfleisch, Journal of Physics: Condensed Matter, Vol. 32, p. 013001 (2019)

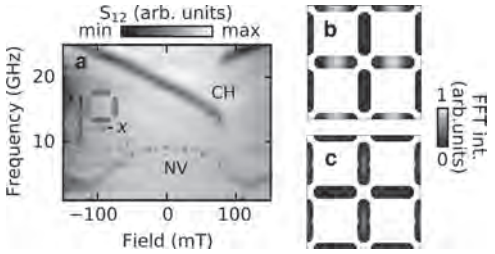

(a) Absorption spectra at magnetic fields applied parallel to the horizontal CoFe islands (represented in blue color in the inset). The vertical NiFe islands are represented in red. Two main modes, corresponding to the horizontal CoFe islands (blue dashed curve, CH) and to the vertical NiFe islands (red dotted curve, NV) have been fitted according to their analytical expression. Micromagnetic simulations show the localization of each mode in (b) the horizontal islands (CoFe) and (c) the vertical islands (NiFe).

B1-12. Collective Magnetic Dynamics in Artificial Spin Ice Probed by AC Susceptibility. *M. Pohlit*[1], G. Muscas[1], I. Chioar[1], H. Stopfel[1], A. Ciuciulkaite[1], E. Östman[1], S.D. Pappas[1], A. Stein[2], B. Hjörvarsson[1], P.E. Jönsson[1] and V. Kapaklis[1] *1. Physics and Astronomy (Material Physics), Uppsala University, Uppsala, Sweden; 2. Center of Functional Nanomaterials, Brookhaven National Laboratory, Upton, NY, United States*

Collective behaviour of interacting single-domain magnetic nanoparticles has been a matter of considerable interest[1,2]. Nanofabricated arrays of magnetostatically coupled ferromagnetic islands acting as mesoscopic spins, like Artificial Spin Ice (ASI), can serve as model systems exhibiting also collective phenomena[3] where the geometry and interaction strength can be tailored at will[4-7]. Appropriate material choice can facilitate thermally induced magnetization reversal, allowing for the investigation of thermal dynamics and transitions in such systems[4,8-10]. Up till now, studies of thermally induced transitions in mesospin systems are still scarce due to the limited availability of large facility-based techniques and accessible timescales. Recently, we adapted AC susceptibility based on the magneto-optical Kerr effect, to explore the collective freezing of thermally active square ASI on a laboratory scale[11]. Three ASI arrays with the identical mesospin but different gaps between the islands were selected to study their freezing dynamics and the influence of inter-island coupling (Fig 1). A broad peak in the AC susceptibility marks the freezing of the mesospin dynamics well below the materials Curie temperature (T_C = 410K, comp. Fig 1). Besides the influence of coupling a systematic frequency dependence of the freezing transition was observed. In an attempt to extract the energy barrier and interaction energy the data was fitted with a Vogel-Fulcher-Tammann (VFT) law[12], which had only recently been applied to ASI[13,14]. We scrutinize the validity of this simple approach and discuss substantial discrepancies of the obtained interaction energies from theoretical predictions. We conclude that AC susceptibility is a promising tool that allows for temperature and frequency dependent studies of mesospin behaviour on a laboratory scale, while for the quantitative extraction of microscopic variables a multi-length-scale theoretical description has to be developed.

1) C. Djurberg et al., Phys. Rev. Lett. 79, 5154 (1997). 2) P. E. Jönsson et al., Adv. Chem. Phys. 128, 191 (2004). 3) E. Östman et al., J. Phys. Condens. Matter 30, 365301 (2018). 4) V. Kapaklis et al., Nat. Nanotechnol. 9, 514519 (2014). 5) E. Östman et al., Nature Physics 14, 375 (2018). 6) C. Nisoli et al., Rev. Mod. Phys. 85, 1473 (2013). 7) R. F. Wang et al., Nature 439, 303 (2006). 8) V. Kapaklis et al., New J. Phys. 14, 035009 (2012). 9) A. Farhan et al., Nature Physics 9, 375 (2013). 10) J. M. Porro et al., New

J. Phys. 15, 055012 (2013). 11) M. Pohlit et al., Phys. Rev. B 101, 134404 (2020) 12) S. Shtrikman and E. Wohlfarth, Phys. Lett. A 85, 467 (1981). 13) M. S. Andersson et al., Scientific Reports 6, 37097 (2016). 14) S. A. Morley et al., Phys. Rev. B 95, 104422 (2017).

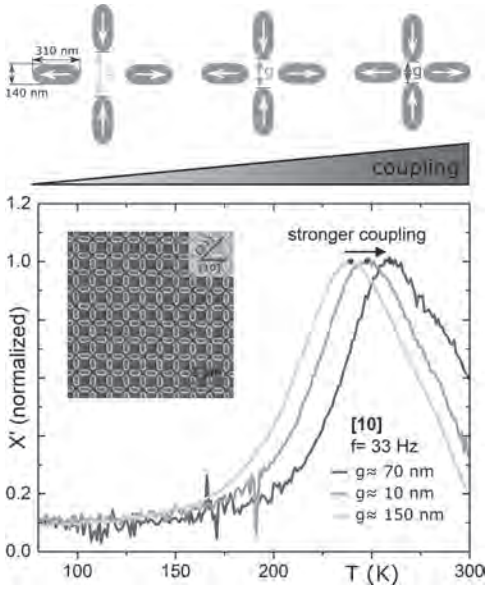

Fig 1: Temperature dependence of the in-phase component of the AC susceptibility χ′ for three thermally active ASI-lattices. An increased inter-island coupling shifts the peak towards higher temperatures corresponding to a higher collective freezing temperature.

B1-13. FORC Investigations of Large-Scale NiFe Nano-Ellipses Arrays. *H. Brueckl*[1], A. Shoshi[1], L. Breth[1], J. Fischbacher[1], T. Schrefl[1], M.J. Haslinger[2], T. Mitteramskogler[2], S. Schrittwieser[3] and J. Schotter[3]
1. Department for Integrated Sensor Systems, Donau-Universitat Krems, Wiener Neustadt, Austria; 2. Profactor GmbH, Steyr-Gleink, Austria; 3. Austrian Institute of Technology GmbH, Wien, Austria

Magnetic nanoparticles operating in the magnetic vortex configuration are of interest in magnetic field sensors [1] and as magnetic nanoprobes for immunoassay diagnostics [2]. In both applications, vortex states are found to be more advantageous compared to single-/multi-domain magnetization states. We use thin film technologies and nanoimprint lithography to reliably produce and controllably stabilize magnetic spin-textures in large-area nanoparticle arrays. The periodically arranged nanoparticles are monodisperse, elliptically shaped cylinders (fig. 1). The ellipses have a size of 400 nm x 200 nm with a periodicity of 600 nm x 400 nm. The very narrow size distribution within 3% standard deviation results in highly uniform magnetic properties. The total number of ellipses is more than 10^8 on 1 cm^2. We use this well-defined system as a model to study magnetic vortex behavior by first-order-reversal-curves (FORC). By increasing the film thickness of the Permalloy (Ni80Fe20) ellipses from 5 to 50 nm, the magnetization state changes from quasi-single domain to the vortex state. The system is anisotropic. FORC measurements provide insight into the relative proportions of reversible and irreversible magnetization processes. We interpret the FORC diagrams by a kind of Hysteron model (fig. 2) and micromagnetic simulations. From these, we can relate the FORC features to vortex properties like critical field distributions of nucleation and annihilation and interaction fields. This work helps to better interpret former FORC publications.

[1] D. Suess, A. Bachleitner-Hofmann, A. Satz, H. Weitensfelder, C. Vogler, F. Bruckner, C. Abert, K. Prügl, J. Zimmer, C. Huber, S. Luber, W. Raberg, T. Schrefl, H. Brückl, Nature Electronics 1, 362–370 (2018) [2] S. Schrittwieser, F. Ludwig, J. Dieckhoff, K. Soulantica, G. Viau, L.-M. Lacroix, S.M. Lentijo, R. Boubekri, J. Maynadié, A. Huetten, H. Brueckl, J. Schotter, ACS Nano 6, 791 (2012)

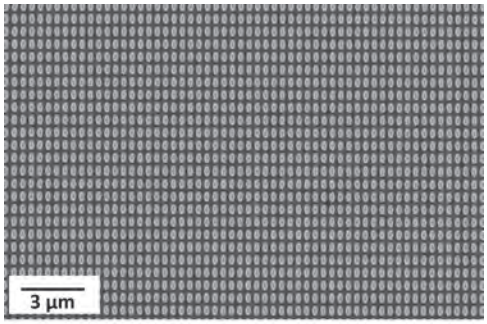

Fig. 1. Scanning electron microscope image of an array section of NiFe nano-ellipses.

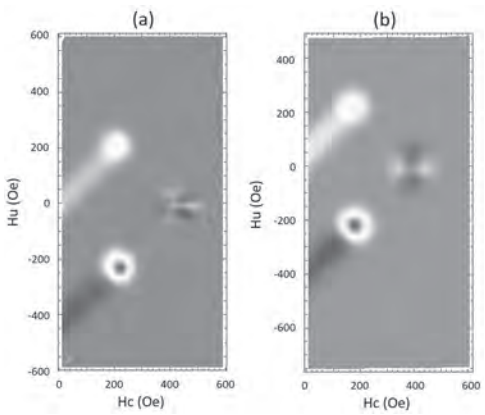

Fig. 2. Experimental (a) and model (b) FORC diagrams.

B1-14. Magnetization Reversal Studies of Building Blocks of Square Artificial Spin Ice Probed by 2-DEG Based Micro-Hall Magnetometry. *N. Keswani*[1], Y. Nakajima[2], N. Chauhan[2], T. Ukai[2], H. Chakraborti[3], K. Das Gupta[3], T. Hanajiri[2], S. Kumar[2], Y. Ohno[4], H. Ohno[5] and P. Das[1]
1. Physics, Indian Institute of Technology Delhi, New Delhi, India; 2. Bio Nano Electronics Research Centre, Toyo University, Saitama, Kawagoe, Saitama, Japan; 3. Physics, Indian Institute of Technology Bombay, Mumbai, India; 4. Tsukuba Daigaku Daigakuin Suri Busshitsu Kagaku Kenkyuka, Tsukuba, Japan; 5. Tohoku Daigaku, Sendai, Japan

In recent years, a great deal of interest has been attracted by the physics of designer materials called 'Artificial Spin Ice' (ASI) systems [1-2]. One of the most promising aspects of ASI system is their high tunability of the array geometry, which has opened new avenues [2]. While most efforts have focused on study of array of artificial spin ice structures [3-4], little work has been done on understanding the switching behavior of individual nanoislands coupled by dipolar interactions in ASI systems [5-6]. These strong shape anisotropic nanomagnets exhibits Ising spin-like behavior and may get affected by the unintentional defects introduced during fabrication. Thus, it is essential to investigate how such defects modify the local magnetic behavior which in turn may play a significant role in the overall switching behavior of the corresponding nanostructures [7]. In this work, we have investigated the magnetization reversal of a special geometry of dipolar coupled system of $Ti/Ni_{80}Fe_{20}/Al$ arranged in double square-ring geometry, which represents the building block of square ASI system. We employed two-dimensional electron gas (2-DEG) based micro-Hall magnetometry technique to measure the nanoislands' stray field and study their switching behavior. Fig. 1(a) shows the SEM image of fabricated structure on top of GaAs/AlGaAs based Hall sensors. The changes in the Hall voltage reflect the changes in the magnetic state of the dipolarly coupled nanomagnets. We observe that although magnetic force microscopy images exhibit single domain like magnetic states for the nanostructures (shown in Fig. 1(b)), their reversal processes undergo complex behavior. The results suggest that local

irregularities may play critical role in defining the exact micromagnetic state of the otherwise single domain nanomagnets leading to complex switching behavior, which is discussed in this work.

[1] R. Wang, *et al.*, Nature 439, 303 (2006). [2] N. Rougemaille and B. Canals, Eur. Phys. J. B 92, 62 (2019). [3] A. Farhan, *et al.*, Science Adv. 5, eaav6380 (2019). [4] E. Östman, *et al.,* Nature Phys. 14, 375 (2018). [5] F. Montoncello, *et al.,* Phys. Rev. B 97, 014421 (2018). [6] N. Keswani and P. Das, J. Appl. Phys. 126, 214304 (2019). [7] N. Keswani, *et al.,* Appl. Phys. Lett. 116, 102401 (2020).

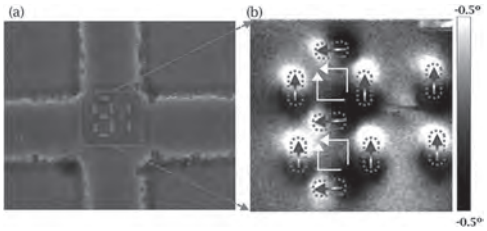

Fig. 1 (a) SEM image of nanomagnets grown on GaAs/AlGaAs Hall sensor and (b) MFM image of nanomagnetic system as shown by dotted arrows in (a)

B1-15. Magnetic Charge Propagation Upon a 3D Artificial Spin-ice.

M.O. Hunt[1], *A. May*[1], M.D. Saccone[2], J. Askey[1], A. van den Berg[1] and S. Ladak[1] *1. School of Physics and Engineering, Cardiff University College of Physical Sciences and Engineering, Cardiff, United Kingdom; 2. Physics Department, University of California, Santa Cruz, Santa Cruz, CA, United States*

Magnetic charge propagation[1-3] in the bulk frustrated materials known as spin-ice has yielded a paradigm shift in science, allowing the symmetry between electricity and magnetism to be studied in condensed matter systems. Artificial spin-ice materials[4], arrays of frustrated nanostructured magnetic islands, have been produced in a range of sophisticated geometries[5]. These systems provide a powerful insight into the physics of frustration but do not capture the exact 3D geometry of the spin-ice lattice, meaning it is not possible to explore monopole transport upon the surface, where the lattice symmetry is broken. In this talk we will detail the direct imaging of magnetic charge propagation upon a 3D nanostructured diamond-bond lattice (Fig 1), capturing the geometry of bulk systems. Vastly different magnetic charge dynamics are observed along two principle lattice directions. Applying a field along the [110] direction leads to a small number of distant magnetic charges within the measured area. In contrast, a field along [-110] leads to a larger number of closely spaced monopole-antimonopole pairs. We will discuss these results by referring to detailed Monte-Carlo simulations and calculations which illuminate the importance of the surface coordination in determining the monopole effective chemical potential.

1. Castelnovo, C., Moessner, R. & Sondhi, *Nature* 451, 42-45 (2008) 2. Jaubert, L. D. C. & Holdsworth, P. C. W., *Nat Phys* 5, 258-261 (2009) 3. Morris, D. *et al.*, *Science* 326, 411-414 (2009) 4. Wang, R. F. *et al., Nature* 446, 102-102 (2007) 5. S. H. Skjærvø, C. M., R. L. Stamps and L.J. Heyderman, *Nature Physics Reviews* 2, 13-28 (2020)

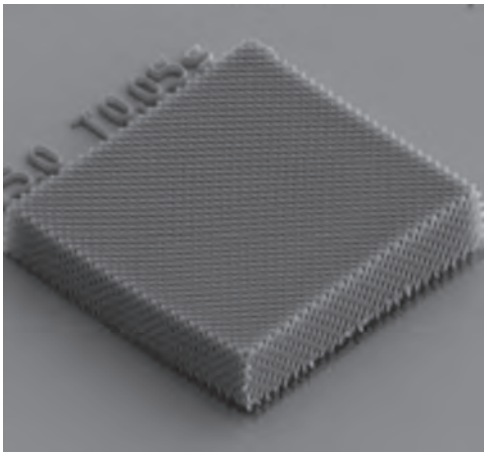

Figure 1: A 3D artificial spin-ice system.

Session B2
INTERDISCIPLINARY APPLICATIONS I

Michalis Charilaou, Co-Chair
University of Louisiana at Lafayette, Lafayette, LA, United States
Yuko Ichiyanagi, Co-Chair
Yokohama National University, Yokohama, Japan

INVITED PAPERS

B2-01. Magnetic-Based Tactile Sensors for Dexterous Robotic Manipulation. *L. Jamone[1] 1. Queen Mary University of London, London, United Kingdom*

A robotic sense of touch would increase the capabilities of robots in a variety of tasks and applications; in particular, it will permit safe and robust handling of different kinds of objects in several scenarios: industrial manufacturing, precision agriculture, food processing, healthcare, public spaces and challenging environments such as nuclear sites or space missions. In the talk I will present a novel concept for the realization of tactile sensors, based on magentic technology. Using this idea, we have developed different types of tactile sensors with different sensing characteristics, that can be used in different robotic applications, from safe object grasping to texture analysis of fruits. Our early work on tactile robot fingertips [1,2], which at the time of publication had the best performance in terms of sensitivity, initiated a world-wide trend of using magnetics-based sensor solutions for embedded tactile/force sensing. The latest advances include: a multi-curved robot fingertip covered with a soft electronic skin that can measure 3D contact forces on multiple distributed contact points, at high spatial resolution and sensitivity [3], a soft miniaturized electronic cilia (200 microns diameter) that can measure contact forces as small as 333 micronewtons [4], a highly-robust and highly-sensitive flat tactile sensor that can be easily integrated on industrial robotic grippers and has become a commercial product [5].

[1] L. Jamone, G. Metta, F. Nori and G. Sandini, James: A Humanoid Robot Acting over an Unstructured World. IEEE-RAS International Conference on Humanoid Robots (Humanoids). Genova, Italy., 2006. [2] L. Jamone, L. Natale, G. Metta and G. Sandini, Highly sensitive soft tactile sensors for an anthropomorphic robotic hand. IEEE Sensors Journal 15(8):4226-4233, 2015. [3] T. P. Tomo, S. Schmitz, W. Wong, H. Kristanto, S. Somlor, J. Hwang, L. Jamone and S. Sugano, Covering a Robot Fingertip with uSkin: a Soft Electronic Skin with Distributed 3-axis Force Sensitive Elements for Robot Hands. IEEE Robotics and Automation Letters 3(1):124-131, 2018. [4] P. Ribeiro, M. A. Khan, A. Alfadhel, J. Kosel, F. Franco, S. Cardoso, A. Bernardino, A. Schmitz, J. Santos-Victor and L. Jamone, Bio-inspired ciliary force sensor for robotic platforms. IEEE Robotics and Automation Letters 2(2):971-976, 2017. [5] T. P. Tomo, M. Regoli, A. Schmitz, L. Natale, H. Kristanto, S. Somlor, L. Jamone, G. Metta, S. Sugano, A New Silicone Structure for uSkin-a Soft, Distributed, Digital 3-axis Skin Sensor-and its Integration on the Humanoid Robot iCub, IEEE Robotics and Automation Letters 3(3): 2584-2591, 2018.

B2-02. Storage and Retrieval of Microwave Pulses With Molecular Spin Ensembles. *C. Bonizzoni[1,2], A. Ghirri[1] and M. Affronte[2,1] 1. Istituto Nanoscienze Consiglio Nazionale delle Ricerche Sede secondaria di Modena, Modena, Italy; 2. Physics, Informatics and Mathematics, Università di Modena e Reggio Emilia, Modena, Italy*

Electronic spin degrees of freedom provided by spin ensembles have been efficiently exploited into circuit quantum electrodynamics architectures based on microwave devices and resonators at low temperature. Molecular spins have recently emerged as a new class of quantum systems whose electronic and nuclear spin states and their related quantum features can be tailored synthetically. Different strategies for encoding quantum information with molecular ensembles or single molecules have been developed and experimentally proved. Moreover, the coherent coupling with microwave photons have been recently successfully achieved with transition metal-based oxovanadium(IV) complexes [1,2] as well as with organic radicals [3,2] embedded into planar resonant geometries, paving the way for the integration of molecular spin ensembles into microwave quantum architectures. However, along this line, optimal experimental conditions and protocols (i.e. pulse sequences) to efficiently address the molecular spins still need to be found. In this work we test single crystals and solid dispersions of diluted oxovanadium tetraphenyl porphyrin (VO(TPP)) as prototypical molecular spin ensembles for the storage and retrieval of microwave pulses when embedded into planar superconducting microwave resonators (Fig. 1) at low temperature (2K) [4]. We first measure the (Hahn-echo) memory time and the Rabi Oscillations of the samples. We then test two Dynamical Decoupling sequences: the Carr-Purcell-Meiboom-Gill and the Uhrig Dynamical Decoupling. Both the sequences are found to enhance the memory time of the crystal samples up to three times after the application of a low number (3,4) of π pulses, reaching up to 3 μs. We then successfully store and retrieve into the ensembles trains of up to 5 small pulses and we show that individual control on such excitations can be achieved. Our proof-of-principle results demonstrate the memory capabilities of molecular spins when embedded into quantum circuits [4].

[1] C. Bonizzoni, A. Ghirri, ... and M. Affronte, Scientific Reports, Vol. 7, p. 13096 (2017). [2] C. Bonizzoni, A. Ghirri and M. Affronte, Advances on Physics X, Vol. 3, p. 435305 (2018). [3] A. Ghirri, C. Bonizzoni, ... and M. Affronte, Physical Review A, Vol. 93, p. 063855 (2016). [4] C. Bonizzoni, A. Ghirri, ... and M. Affronte, NPJ Quantum Information, Vol. 6, p. 68 (2020).

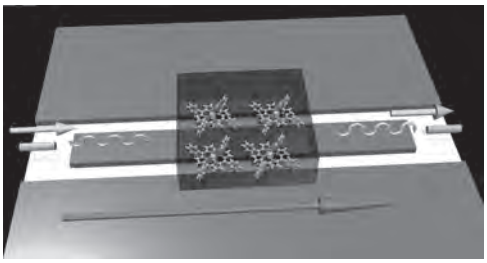

Fig. 1: Pictorial sketch of the coplanar resonator with a VO(TPP) crystal on it. Green arrows represent the microwave pulses, while the red arrow represents the applied static magnetic field. Yellow cylinders are the tunable coupling antennas.

CONTRIBUTED PAPERS

B2-03. Inelastic Neutron Scattering Spectrum of a Cr_{10} Molecular Ring Compound With Unusual $S = 9$ Ground State. *J. Rubín*[1,6], E. Bartolome[2], T. Guidi[3], J. Bartolome[1,7], A. Arauzo[1,7], F. Sedona[4], M. Rancan[4], M. Sambi[4], E. Garlatti[5], S. Carretta[5] and F. Bartolome[1,7] *1. Instituto de Ciencia de Materiales de Aragón (CSIC-Universidad de Zaragoza), Zaragoza, Spain; 2. Escola Universitaria Salesiana de Sarria, Barcelona, Spain; 3. ISIS Facility, Rutherford Appleton Laboratory, Chilton, United Kingdom; 4. Dipartimento di Scienze Chimiche, Università di Padova, Padova, Italy; 5. Dipartimento di Science Matematiche, Fisiche e Informatiche, Università di Parma, Parma, Italy; 6. Dpto. Ciencia y Tecnología de Materiales y Fluidos, Universidad de Zaragoza, Zaragoza, Spain; 7. Dpto. de Física de la Materia Condensada, Universidad de Zaragoza, Zaragoza, Spain*

The molecular compounds $[Cr_{10}(OR)_{20}(O_2CR')_{10}]$, (R, R' = Me, Et or CMe_3) contain Cr_{10} rings where the interaction between spin-3/2 Cr^{3+} ions can be ferromagnetic or antiferromagnetic [1]. Although most of the compounds show a total spin $S = 15$ or $S = 0$, *i.e.*, all interactions within a ring are ferromagnetic or antiferromagnetic, the case of R = Me, R'= CMe_3 displays an unusual $S = 9$ spin ground state [1,2] and a single molecule magnet (SMM) behavior [2]. The macroscopic magnetic properties are partially accounted for by a model with ferromagnetic interactions except those of two opposite Cr^{3+} ions, which would show antiferromagnetic interaction with their nearest neighbours [3]. Inelastic neutron scattering (INS) spectra have been collected at the cold neutron multi-chopper spectrometer LET at ISIS in order to study the structure of the low-lying magnetic states and clarify the intra-ring interactions. The analysis of the spectra at 1.8 K and 5 K shows the magnetic anisotropy splitting of the $S = 9$ ground state in agreement with previous EPR results, but the next INS multiplet is consistent with $S = 8$ excited state, instead of a previously claimed $S = 10$. The INS results are compared to calculations of a spin Hamiltonian with both next-neighbour ferro- and antiferromagnetic interactions within the ring and single ion magnetic anisotropy.

1. D. Low *et al*., *Chem.-A Eur. J.,* 12, 1385-1396 (2006). 2. S. Sharmin *et al*., *App. Phys. Lett*., 86, 032507 (2005). 3. F. Bartolomé *et al.*, *21*th *International Conference on Magnetism* 2018, July 15th-20th, San Francisco, USA

B2-04. Structure and Magnetism of FePc/Ag(110) Monolayer Phases Under Oxygen Dosing. *E. Bartolome*[1], J. Bartolome[2], F. Sedona[3], J. Lobo-Checa[2], D. Forrer[3], J. Herrero-Albillos[4], M. Piantek[2,5], J. Herrero-Martin[6], D. Betto[7], E. Velez-Fort[7], L.M. Garcia[2], J. Rubín[2], M. Panighel[8], A. Mugarza[9,10], M. Sambi[3] and F. Bartolome[2] *1. Escola Universitària Salesiana de Sarrià (EUSS), Barcelona, Spain; 2. ICMA, CSIC, Consejo Superior de Investigaciones Cientificas, Zaragoza, Spain; 3. CNR-ICMATE, Department of Chemical Sciences, University of Padova, Padova, Italy; 4. Centro Universitario de la Defensa, Academia General Militar, Zaragoza, Spain; 5. Instituto de Nanociencia de Aragón, Universidad de Zaragoza, Zaragoza, Spain; 6. ALBA Synchrotron, Barcelona, Spain; 7. ESRF, Grenoble, France; 8. Laboratorio TASC, CNR-IOM, Trieste, Italy; 9. Catalan Institute of Nanoscience and Nanotechnology, CSIC + BIST, Barcelona, Spain; 10. ICREA, Institucio Catalana de Recerca i Estudis Avancats, Barcelona, Spain*

Iron-phtalocyanines (FePc) adsorbed onto a Ag(110) substrate self-assemble into different monolayer phases going from rectangular to different oblique phases, with increasing molecular density. We have investigated the oxygen uptake capability of the different phases and their associated magneto-structural changes [1,2,3]. Our study combines scanning tunneling microscopy and spectroscopy (STM/STS), X-ray magnetic circular dichroism (XMCD), and density functional theory (DFT) calculations. STM measurements reveal that the oxygenation reaction of the FePc/Ag(110) generally involves a displacement and a rotation of the molecules, which affects the electronic state of the Fe centers. The oxygen intercalation between FePc and the substrate is greatly obstructed by the steric hindrance in the high-density phases, to the point that a fraction of oblique phase molecules cannot change their position after oxydizing. Depending on the oxidation state and adsorption geometry, the STS spectra evidence clear differences in the Fe local density of states, which are mirrored in the XAS and XMCD experiments. Particularly, XMCD spectra of the oxidized phases reflect the distribution of FePc species (non-oxygenated, oxygenated-rotated and oxygenated-unrotated) in the different cases. Sum rule analysis yields the effective spin and orbital magnetic moments of Fe in the different FePc species. Upon oxygenation, the magnetic moment of FePc molecules increases about an order of magnitude, reaching $m_{TOT} \sim 2.2\ \mu_B$ per Fe atom.

1: F. Sedona, M. Di Marino, D. Forrer et al., Nature Materials 11, 970 (2012) 2: J. Bartolome, F. Bartolome, F. Sedona, et al., J. Phys. Chem. C 119, 12488 (2015) 3: E. Bartolomé, J. Bartolome, F. Bartolome, et al., J. Phys. Chem. C 124, 13993 (2020)

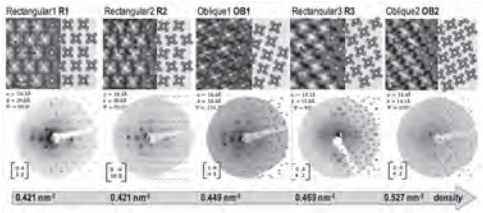

Figure 1: FePc/Ag(110) sub-ML phases with increasing molecular density (from left to right). Each column identifies a phase containing an STM image acquired at room temperature, the unit cell model, the matrix notation and the LEED pattern

B2-05. Tuning the Magnetic Properties of Oleic Acid Coated Co Ferrite Nanoparticles by Varying the Surfactant Coverage: a Multiscale Numerical Approach. *K.N. Trohidou*[1], N. Ntallis[1] and M. Vasilakaki[1] *1. Institute of Nanoscience and Nanotechnology, Ethniko Kentro Ereunas Physikon Epistemon Demokritos, Athens, Greece*

Recent studies have demonstrated that organic coatings modify the magnetic properties of nanoparticles. Their effect on the magnetic behaviour depends on the type of the magnetic nanoparticle, of the type of coating and the percentage of surface coverage [1- 4]. In the latter case, experimental studies have shown that the effect on the magnetic behaviour depends on the amount of the coverage, i.e. the number of capping molecules attached onto the particle surface [3,4]. In this study, we investigate numerically for the first time how the oleic acid (OA) concentration on the surface of single Co ferrite nanoparticles affects their magnetic behavior, using a combined DFT and Monte Carlo simulation approach. We have calculated the magnetic exchange coupling constants, magnetocrystalline anisotropies and magnetic moments for $CoFe_2O_4$ nanoparticle of ~2 nm size with inverse spinel structure for different oleic acid concentrations. Our results demonstrate that the increase in the OA surface coverage results to a monotonic decrease of the mean magnetocrystalline anisotropy, reduction of the magnetic moments and the exchange coupling constants. This is attributed to the partial recovery of the spinel structure at the coated surface as the OA coverage increases. This behavior is verified by our MC simulation results which show an increase of the coercive field with the increase in the percentage of the surface coverage (e.g. reaching to 20% for 20% surface coverage) in agreement with the experimental results of ref [4]. Importantly, these results suggest the possibility of tailoring Co ferrite nanoparticles for high performance biomedical and magneto/thermoelectric applications by varying the coating concentration.

[1] J. Salafranca, J. Gazquez, N. Perez, A. Labarta, S. T. Pantelides, S. J. Pennycook, X. Batlle, M. Varela, Nano Lett., 12, 2499–2503 (2012) [2] M. Vasilakaki, N. Ntallis, N. Yaacoub, G. Muscas, D. Peddis, K. N. Trohidou, Nanoscale, 10, 21244 (2018) [3] S. Jovanovic, M. Spreitzer, M. Tramsek, Z. Trontelj, D. Suvorov, J. Phys. Chem. C, 118, 13844 (2014) [4] M. V.

Limaye, S. B. Singh, S. K. Date, D. Kothari, V. R Reddy, A. Gupta, V. Sathe, R. J. Choudhary, S. K. Kulkarni, J. Phys. Chem. B, 113, 9070 (2009)

B2-06. Synthesis of Magneto-Responsive Micro Swimmers for Biomedical Applications. *H.A. Alshammari*[1], N. Gunduz Akdogan[2] and O. Akdogan[1] *1. Engineering and Natural Sciences, Bahcesehir University, Istanbul, Turkey; 2. Piri Reis University, Istanbul, Turkey*

Interest in micro robotics and swimmers has showed a significant increase lately, especially magnetic micro swimmers. In this study, using an extrusion-based 3D printer, magnetic micro swimmers were synthesized, dropwise, with different types of incorporated magnetic materials; Fe micro flakes and nanoparticles, and Nd-Fe-B micro flakes. Particles were encapsulated in alginate matrix. Next, these micro swimmers were stirred along a path via the magnetic gradient created by an electromagnetic system. The base of the electromagnetic system was designed using a CAD computer program and 3d printed. Consisting of four independent solenoids, each two controlling the movement on an axis, the system was designed to move the micro swimmers in a certain path as shown in Figure 1. The solenoids were controlled by Arduino microcontroller board. The electrical current applied to the electromagnetic device in all the trials was 2 amperes which generates a magnetic field in between 100 to 485 Gauss throughout the experiment area (Figure 1 B); as a result a magnetic gradient from the center to the pole of the solenoid was established. The magnetic and chemical behavior of these materials were compared based on their magnetic responsiveness and 3d printability. The comparison showed the high responsiveness of iron flakes relatively to the other materials as shown in Figure 2. Applications of magnetic micro swimmers include biomedical robotics and drug delivery.

This work was supported by BAP.2019-03.11

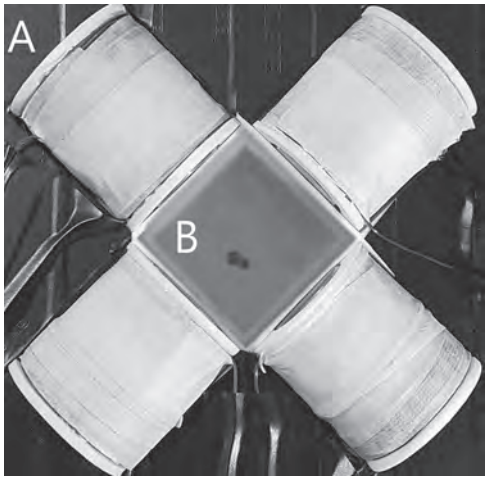

Figure 1: (A) The electromagnetic system layout. (B) The experiment container bracket. Inside it is an example of the magnetic swimmer going around the path.

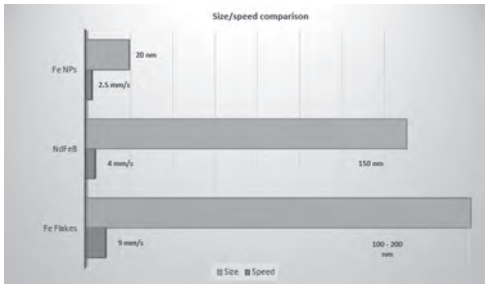

Figure 2: Comparison between the size of the materials and the speed of the swimmer in the path.

B2-07. Self-Propelled Dipolar Nanocubes. *M. Kaiser*[1], S. Kantorovich[1,2], Y. Martinez[3] and A. Schmidt[3] *1. Universitat Wien Fakultat fur Physik, Wien, Austria; 2. Ural'skij federal'nyj universitet imeni pervogo Prezidenta Rossii B N El'cina, Ekaterinburg, Russian Federation; 3. Universitat zu Koln, Koln, Germany*

Using molecular dynamics simulations and transmission electron microscopy, we investigate the bulk behaviour of new magnetically controllable nanomotors. Each of these nanomotors consists of two units: one is a magnetic cube that can be directed by an externally applied magnetic field due to Zeeman coupling: the second is a non-magnetic active particle attached to the corner of the cube with a propulsion force directed into the cubes centre of mass. In the experiment, magnetic cubes are made of CoFe and the active particle is Pt. In simulations, we use a previously developed approach to model magnetic nanocubes [1], whereas the active particle is simulated in the frame work of Active Brownian Particle model [2]. Previously, we investigated the diffusion of a single cubic nanomotor and discovered that the anisotropy of the diffusion caused by the application of an external magnetic field strongly depends on the cube crystallographic anisotropy and the intrinsic orientation of the cube magnetisation [3]. Here, we discuss the self-assembly of cubic nanomoters in a broad range of system parameters in order to understand the influence of particle concentration, cube magnetic anisotropy with respect to the propulsion direction, field and dipolar strength. Due to competing propulsion and magnetic forces, we investigate the differences in cluster size distribution and topology if compared to the self-assembly of non-active magnetic cubes [1].

[1] J. Donaldson et al. (2017), ACS nano 11.8: 8153-8166. [2] C. Bechinger et al. (2016), Rev. Mod. Phys. 88, 045006 [3] Kaiser, Martin, et al. (2020), *Journal of Molecular Liquids* 304: 112688

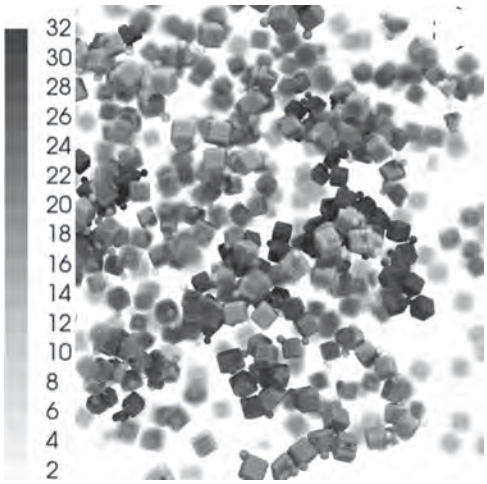

Simulation snapshot of nanocube system (clusters are coloured according to their size, as indicated in the colour bar on the left)

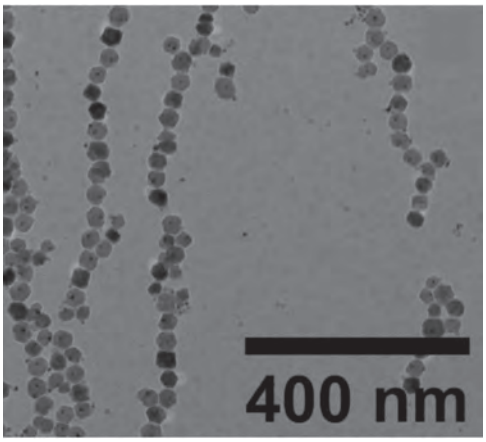

Experimental image of active dipolar nanocube system with chain formation, active particles are seen as dark spots.

B2-08. Withdrawn

B2-09. Alignment of Magnetic Particles in Functionalized Magnetic 3D Printer. *A. Sarkar*[1], P. Paranthaman[2] and I.C. Nlebedim[1] *1. Critical Materials Institute, Ames Laboratory, Ames, IA, United States; 2. Oak Ridge National Laboratory, Oak Ridge, TN, United States*

Additive manufacturing via 3-D printing technologies have become a frontier in materials research, including its application in the development and recycling of permanent magnets[1,2]. I*n-situ* alignment during 3D printing of magnetic materials has opened new horizons for manufacturing of complex permanent magnets[3,4]. Based on our former work[3], we will present a multiphysics model that couples fluid dynamics and electromagnetic interactions, to predict the degree of alignment (DoA) of a polymer bonded magnet printed under applied field. We have developed a mathematical model which predicts the flow of magnetic particles in a viscous fluid through a nozzle under applied magnetic field. A particle-fluid interactive fluid flow simulation is performed to model the flow regime of molten bonded magnet. The interactions between the drag, inertial, and magnetophoretic forces are analyzed to predict the particle trajectory. Torque balance is performed between the drag torque, magnetic torque on particles from the applied field, and torque from particle-particle interactions. The torque balance is coupled with the flow simulation to predict the degree of rotation of magnetic particles during printing. Experimental validation of the DoA predictions (exp = 0.62 and theory = 0.634) was performed using 65vol.% NdFeB+SmFeN in Nylon12 3D printed samples with variable alignment field (Fig.1a). The model is parameterized to predict the impact design and operating parameters including alignment field, magnetic loading fraction, and particle size. The results demonstrate an increasing alignment field with higher loading fraction magnets (Fig.1b). This work is supported by the Critical Materials Institute (CMI), an Energy Innovation Hub funded by the U.S. Department of Energy (DOE), Office of Energy Efficiency and Renewable Energy, Advanced Manufacturing Office. Ames Laboratory is operated for the U.S. Department of Energy by Iowa State University of Science and Technology under Contract No. DE-AC02-07CH11358. Figure 1. a) DoA prediction for 65vol.% NdFeB+SmFeN in Nylon12 before and after printing with 0.15[T] field, and b) DoA vs. field for NdFeB+SmFeN in Nylon12 with different magnetic loading fractions.

[1] C. Huber, C. Abert, F. Bruckner, M. Groenefeld, O. Muthsam, S. Schuschnigg, K. Sirak, R. Thanhoffer, I. Teliban, C. Vogler, R. Windl, and D. Suess, Appl. Phys. Lett. 109, 162401 (2016). [2] L. Li, B. Post, V. Kunc, A.M. Elliott, and M.P. Paranthaman, Scr. Mater. (2017). [3] A. Sarkar, M.A. Somashekara, M.P. Paranthaman, M. Kramer, C. Haase, and I.C. Nlebedim, Addit. Manuf. 34, 101289 (2020). [4] Y. Kim, H. Yuk, R. Zhao, S.A. Chester, and X. Zhao, Nature 558, 274 (2018).

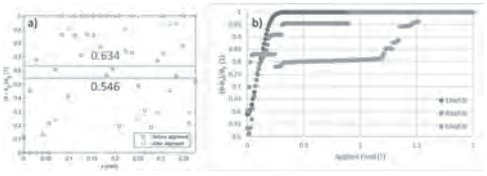

B2-10. Ferrofluid Thermomagnetic Convection Based Magnetic Cooling Devices for Large Scale Cooling. M.S. Pattanaik[1,2], V.B. Varma[1,2], S.K. Cheekati[1,2] and *R. Ramanujan*[1,2] *1. School of Materials Science & Engineering, Nanyang Technological University, Singapore 639798, Singapore; 2. Singapore-HUJ Alliance for Research and Enterprise (SHARE), Nanomaterials for Energy and Energy-Water Nexus (NEW), Campus for Research Excellence And Technological Enterprise, Singapore 138602, Singapore*

Current technology demands effective heat transfer to enhance the reliability and life span of many industrial, domestic, and electronic devices [1]. Magnetic cooling (MC) devices, governed by ferrofluid thermomagnetic convection (TMC), can be effective in removing the waste heat from such systems [2]. Previous reports of MC focused on the development of miniaturized devices and small-scale applications [2-5]. Instead, we have developed a multi-torus MC device [1] and an 8 m long MC device for large-scale applications e.g., to cool industrial systems, battery cabinets, solar panels, and data servers. The thermomagnetic (TM) cooling performance of a multi-torus MC device for kW level heat loads was determined, a heat load temperature drop by up to 214°C was achieved. The thermal resistance of our device was 0.26°C/W, comparable to the conventional heat pipe thermal resistance. An 8 m long racetrack-shaped MC device was also developed and its cooling performance investigated. This device transported heat from systems with heat flux values of up to 8.85 kW/m^2. The drop in temperature is up to 41°C for a heat load temperature of 197 °C. The heat load cooling performance was also modeled and simulated. The effect of ferrofluid properties, such as saturation magnetization, Curie temperature, and the pyro-magnetic coefficient were studied. Soft-ferrite based ferrofluids of $CoFe_2O_4$, Fe_3O_4, and γ-Fe_2O_3 exhibited superior cooling performance for a range of heat load powers. Metal based ferrofluids, e.g., Fe, Fe-Ni, and Fe-Co exhibited cooling by more than 140°C for an initial heat load temperature of 200°C. *Acknowledgement* This research is supported by grants from the National Research Foundation, Prime Ministers Office, Singapore under its Campus of Research Excellence and Technological Enterprise (CREATE) programme.

[1] Pattanaik, M. S., Varma, V. B., & Ramanujan, R. V. (2019). *Energy Conversion and Management*, *198*, 111819. [2] Chaudhary, V., Wang, Z., & Ramanujan, R. V. (2016). *Journal of Physics D: Applied Physics*, *50*(3), 03LT03. [3] Chaudhary, V., & Ramanujan, R. V. (2016). *Scientific reports*, *6*(1), 1-9. [4] Sharma, V., Pattanaik, & Ramanujan, R. V. (2018). *MRS Communications*, *8*(3), 988-994. [5] Lian, W., Xuan, Y., & Li, Q. (2009). *Energy Conversion and Management*, *50*(1), 35-42.

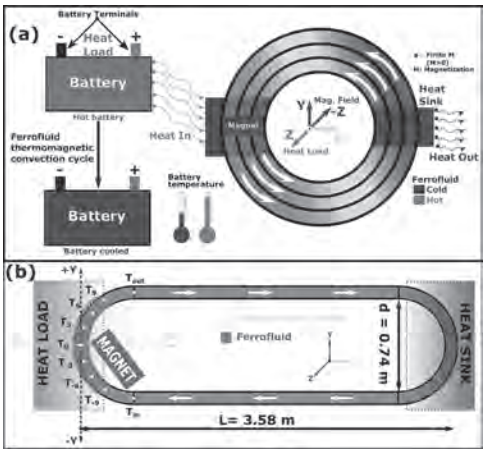

Schematics of the (a) multi-torus magnetic cooling device *[1]*, and (b) 8 m long racetrack magnetic cooling device.

B2-11. Withdrawn

B2-12. Spin-Torque-Induced Chaos in Antiferromagnets.
A. Parthasarathy[1] and S. Rakheja[2] *1. Electrical and Computer Engineering, New York University, New York, NY, United States; 2. Holonyak Micro and Nanotechnology Laboratory, University of Illinois at Urbana-Champaign, Urbana, IL, United States*

When a spin current is injected into an antiferromagnet, above a certain value of current, the Néel order precesses in a circular orbit about an axis oriented at an angle from the spin-polarization direction [1]. But below this value, for moderate values of damping, the motion evolves into chaos (aperiodic long-term behavior) for a small window of current, before settling down to equilibrium. We theoretically study the chaotic dynamics and emphasize its potential application in secure communication. Consider a uniaxial antiferromagnet whose easy axis is along z. Let the spin polarization make an angle ρ from the easy axis in the z-x plane. If at an instant, the Néel order n makes a polar angle θ from z and azimuthal angle φ from x, the equation of motion in the characteristic timescale of antiferromagnet for effective damping β and spin-current drive Γ is [1] $\theta'' + \beta\theta' - (\varphi'^2 - 1)\sin\theta\cos\theta = -(\Gamma/2)\sin\varphi\sin\rho$, $\varphi'' + \beta\varphi' + 2\varphi'\theta'\cot\theta = (\Gamma/2)(\cos\rho - \cot\theta\cos\varphi\sin\rho)$. The chaotic dynamics arises from the nonlinear structure of the flow in the four-dimensional phase space $(\theta, \varphi, \theta', \varphi')$ from the initial condition $(\pi/2, 0, 0, 0)$. For $\rho = \pi/4$ and $\beta = 0.2$ in specific, the steady-state behavior is static for $\Gamma < 0.43$, periodic for $0.43 < \Gamma < 0.44$, chaotic for $0.44 < \Gamma < 0.5$ and periodic for $\Gamma > 0.5$ as shown in Fig. 1. For other values of ρ and β, the chaos would occur for different values of Γ. The dynamics of Néel order in the antiferromagnet can reciprocally pump spin current into an adjacent conductor, proportional to the angular velocity $\omega = n \times n'$ shown in Fig. 2. This phenomenon may be exploited to detect and generate a chaotic electric signal at terahertz frequency, which may be used for communication via synchronized chaos. In this scheme, a louder chaos signal is used to mask the information-bearing signal and transmitted. The decryption utilizes the intended receiver's ability to reproduce the chaos and subtract it from the mask.

[1] A. Parthasarathy et al., arXiv:1911.00445 (2019).

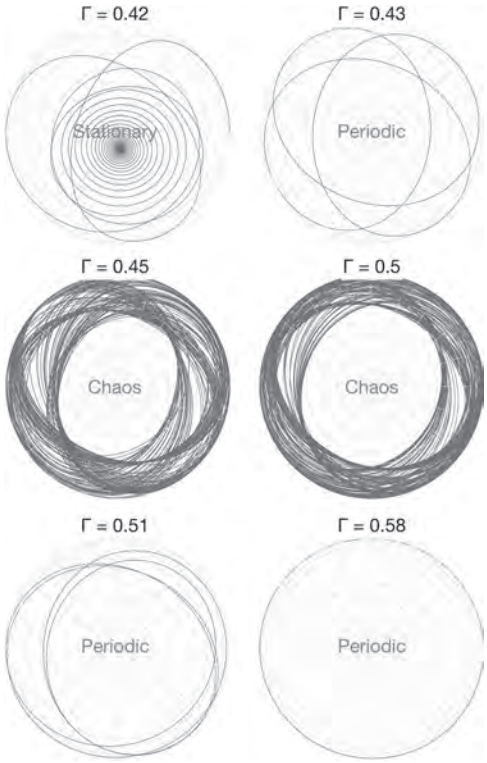

Long-term behavior of the Néel-order trajectory on unit sphere viewed from z axis as the spin-current drive Γ is varied.

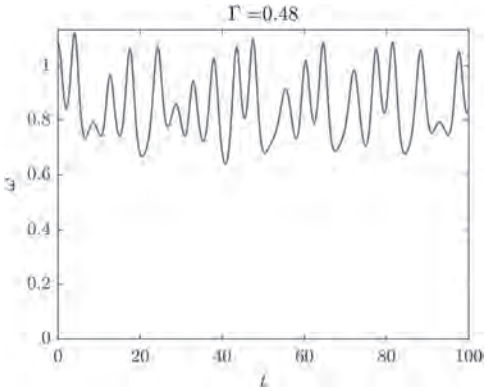

Magnitude of angular velocity ω of the Néel order, which is proportional to the spin-pumping signal. The peaks and valleys of the signal appear with no pattern.

B2-13. Optimizing the Thermoelectric Behavior of Ferrofluid Based Nanomaterials: a Theoretical Study.
M. Vasilakaki[1], I. Chikina[2], V.S. Shikin[3], N. Ntallis[1], D. Peddis[4,5], A.A. Varlamov[6] and K.N. Trohidou[1] *1. Institute of Nanoscience and Nanotechnology, Ethniko Kentro Ereunas Physikon Epistemon Demokritos, Athens, Greece; 2. CEA-CNRS, IRAMIS, LIONS, CEA-Saclay, France; 3. Institute of Solid State Physics, Chernogolovka, Moscow, Russian Federation; 4. Dipartimento di Chimica e Chimica Industriale, Università di Genova, Genova, Italy; 5. Istituto di Struttura della Materia-CNR, Rome, Italy; 6. CNR-SPIN, Rome, Italy*

Recent studies have demonstrated that magnetic nanoparticles (MNPs), ionically stabilized and dispersed in aqueous electrolytes, show enhanced thermo-power, characterized by the so called Seebeck coefficient [1]. We have addressed this issue by deriving an analytic expression that relates the Seebeck coefficient to the system's chemical potential and its temperature derivative taking into account the nanoparticles intrinsic characteristics, i.e.

magnetization and magnetic anisotropy [2]. We study the particles' heating contribution to the Seebeck coefficient by using a mesoscopic scale model of diluted assemblies of γ-Fe_2O_3 and $CoFe_2O_4$ nanoparticles - commonly used ferrofluid materials with different magnetic anisotropies and particle concentrations. Monte Carlo simulations are performed employing the Metropolis algorithm to calculate the particle Seebeck coefficient at different temperatures. Importantly, our numerical results show enhancement of the Seebeck coefficient with the increase of the magnetic particle anisotropy and particle concentrations with a maximum that shifts to higher temperatures as the anisotropy increases. Our findings suggest that enhanced thermoelectric signal can be achieved in ferrofluid based thermoelectric materials by tailoring the magnetic particle anisotropy. Our approach provides a new insight into the nanoscale phenomena that govern the properties of complex thermo-electro-magnetic nanomaterials.

[1] T.J. Salez, B.T. Huang, M. Rietjens, M. Bonetti, C. Wiertel-Gasquet, M. Roger, C.L. Filomeno, E. Dubois, R. Perzynski, S. Nakamae, Phys. Chem. Chem. Phys., 19, 9409–9416 (2017) [2] M. Vasilakaki, I. Chikina, V. B. Shikin, N. Ntallis, D. Peddis, A. A. Varlamov, K. N. Trohidou, Applied Materials Today, 19, 100587 (2020)

B2-14. Wastewater and Leachate Treatment Using Magnetic Particles and Magnetic Separation. *P.A. Augusto*[1,2], T. Castelo-Grande[2], J. Rico[1], R. Iglesias[1], J. Marcos[1], L. Merchán[1], L. Hernández[1] and D. Barbosa[2]
1. Universidad de Salamanca, Salamanca, Spain; 2. Faculty of Engineering, University of Porto, Porto, Portugal

1. Introduction The treatment of leachates as pollutant concentrated wastewaters, is still an open issue, and although several different methods are applied for this goal, we are still far way from obtaining low-cost and at the same time efficient processes. Even for wastewater and water, removal of specific contaminants is far from being economical. Magnetic particles (nano or micron-sized), namely those based on iron oxides, have shown good sorption capabilities, which may be useful for removal/concentration of pollutants/nutrients. Joining this sorption capabilities with their magnetic properties, and with potential functionalization, makes the application of these particles for wastewater or leachate treatment very interesting, especially as we may use magnetic separation methods to further remove, recover and reuse these particles. 2. Methods In this work we have tested three different kind of magnetic particles, in order to remove/concentrate organic matter (DQO reduction), Nitrogen (Total Nitrogen) and Phosporous (Total Phosporous), during several time periods, being successful in removing between 4 and 65 % of them, depending on the controlled parameter, sorption time and type of particle. We have applied the same particles in three different water streams with different degrees of pollution, so we would be able to analyze the pollutant concentration influence: these being water, wastewater and leachate. 3. Results and discussion In Figure 1 we present as example the case of removal for wastewater resultant from sludge centrifugation, by one of the three different magnetic particle systems we have used. Figure 1. Treatment results 4. Conclusions Efficient removal of contaminants/nutrients from water have been achieved from real wastewaters and leachates. Particles used in the sorption/Fenton process were able to be recovered and regenerated for further re-use.

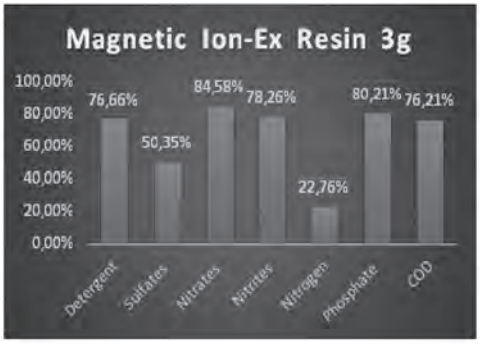

Session B3
SPIN-TORQUE OSCILLATORS

Christopher Safranski, Chair
IBM T. J. Watson Research Center, Yorktown Heights, NY, United States

CONTRIBUTED PAPERS

B3-01. Precession Coupled Spin Current in Spin-Torque Driven Magnetic Tunnel Junctions. *J. Sun[1] 1. IBM Research, Yorktown Heights, NY, United States*

Precession coupled spin current in spin-torque driven magnetic tunnel junctions J. Z. Sun IBM T. J. Watson Research Center Yorktown Heights, NY 10598, USA A spin-torque switchable magnetic tunnel junction is formed with two ferromagnetic electrodes across a barrier that supports spin-polarized tunnel current. The spin-torque induced magnetic switching of its more agile, or "free" layer provides the "write" mechanism. Often the dynamics of the stable "reference" layer is also important. Here, we model one such dynamics involving both the free and the reference layers using a two-moment, exchange-coupled macrospin approximation. This model system is analyzed numerically, with a Landau-Lifshitz-Gilbert equation set, including damping-like spin-transfer torque acting between the two moments, and a Langevin-field for finite temperature. The coupled precession dynamics is shown to reduce effective spin-current due to what we call a "precessional resonant spin-current back flow". This back-flow of spin current preferentially affects the parallel state dynamics more, due to the chiral nature of rotational field excitation. The resonance effect can be significant and is not directly related to the reference layer's thermal stability, nor its spin-torque switching threshold, determined by the total anisotropy energy and magnetic volume. These results suggest that a desirable materials choice is to avoid anisotropy fields giving the free and the reference layer similar dynamic frequencies, and to prevent such resonance-related spin-current loss.

B3-02. Bipolar Spin Hall Nano-Oscillators. *T. Hache[1,2], Y. Li[3], T. Weinhold[4], B. Scheumann[1], F.J. Gonçalves[1], O. Hellwig[1,2], J. Fassbender[1,4] and H. Schultheiss[1,4] 1. Helmholtz-Zentrum Dresden-Rossendorf, Dresden, Germany; 2. Technische Universitat Chemnitz, Chemnitz, Germany; 3. Johns Hopkins University, Baltimore, MD, United States; 4. Technische Universitat Dresden, Dresden, Germany*

Spin Hall nano-oscillators (SHNO) convert dc currents in microwave oscillations of the magnetization[1]. The frequency can be tuned by external magnetic fields, the applied dc current or by injection locking[2,3] if an additional microwave field is applied to the SHNO. Here, we demonstrate a new approach to extend the frequency range of a SHNO by adding an additional ferromagnetic layer[4]. Moreover, the auto-oscillations can be switched from one to the other ferromagnetic layer by switching the current direction. A constriction-based SHNO consisting of a Py(5nm)/Pt(7nm)/CoFeB(5nm) layer stack with 2 nm Ta as seed and capping layer was used. If a dc current is applied to the structure, a pure spin current is generated by the spin Hall effect in the Pt layer[5]. For a fixed current direction the spin polarization of the pure spin currents entering in the Py and CoFeB layers have opposite directions. Therefore, only one of both ferromagnetic layers experiences a decrease of damping due to the spin orbit torque and can show auto-oscillations of the magnetization. To change the frequency of the SHNO, the dc current direction has to be switched in order to switch the auto-oscillations to the other material with a different frequency range. The Figure demonstrates the generation of auto-oscillations in different current ranges at opposite current polarities at a fixed magnetic field. Figure (a) reveals the generation of auto-oscillations for negative current polarity in CoFeB at higher frequencies due to larger saturation magnetization. Figure (b) shows the auto-oscillations signal within the Py layer at lower frequencies at positive direct current polarity. This is in contrast to SHNOs with only one ferromagnetic layer, which show microwave oscillations only for one current polarity for a fixed magnetic field direction. The authors acknowledge financial support from the Deutsche Forschungsgemeinschaft within programme SCHU 2922/1-1.

[1] Demidov, V., Urazhdin, S., Ulrichs, H. *et al.* Magnetic nano-oscillator driven by pure spin current. *Nature Mater* 11, 1028–1031 (2012). [2] Demidov, V., Ulrichs, H., Gurevich, S. *et al.* Synchronization of spin Hall nano-oscillators to external microwave signals. *Nat Commun* 5, 3179 (2014). [3] T. Hache, T. Weinhold, K. Schultheiss *et al.*Combined frequency and time domain measurements on injection-locked, constriction-based spin Hall nano-oscillators. *Appl. Phys. Lett.* 114, 102403 (2019). [4] T. Hache, Y. Li, T. Weinhold *et al.* Bipolar spin Hall nano-oscillators. *Appl. Phys. Lett.* 116, 192405 (2020). [5] A. Hoffmann, Spin Hall Effects in Metals. *IEEE Transactions on Magnetics*, vol. 49, no. 10, pp. 5172-5193 (2013).

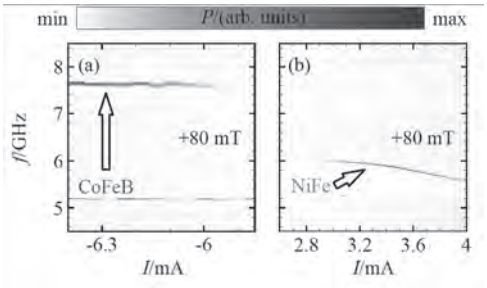

B3-03. Programmable Two Channel Frequency Detector Based on a Vortex Nano-Oscillator. *L. Martins[2,1], J. Borme[2], A. Jenkins[2], J. Ventura[1] and R. Ferreira[2] 1. Institute of Physics for Advanced Materials, Nanotechnology and Photonics (IFIMUP), Porto, Portugal; 2. International Iberian Nanotechnology Laboratory, Braga, Portugal*

Magnetization dynamics induced by spin-polarized currents have enabled a new class of spin-torque nano-oscillators (STNOs) including frequency detectors. Frequency detection in vortex STNOs has been demonstrated using several different mechanisms that include the spin diode effect[1], resonant core expulsion[2,3] and frequency to resistance transduction[4]. The DC voltage output generated by an RF current injected in a vortex STNO has been shown to exceed the sensitivities of Schottky diodes[5]. In this work we propose the possibility of adding non-volatility to the functionalities associated with vortex STNOs and we demonstrate that the frequency detection channel can be changed upon fabrication by means of electrical signals. Figure 1(a) shows the stack used for the measured devices. The experiment starts with an initialization (INIT) step where an in-plane field (H_{in}) applied by a DC current passing through an integrated field line saturates

the free layer. Finally, its removal leads to the vortex renucleation. After, an RF signal with a sweeping frequency is applied to the STNO while the DC voltage is monitored [Fig. 1(b)]. Figure 2 shows two spin diode results, where the difference relies on I_{DC} applied to the STNO during INIT. After INIT, with I_{DC} = +5mA (-5mA), the device operates at a gyrotropic frequency of 58.8MHz (60.2MHz). We discuss the relation of these two modes with the four possible combinations of polarity (out-of-plane vortex magnetization component) and chirality (in-plane vortex magnetization circulation). For $H_{in} = I_{DC} = 0$, the different frequencies associated with two different states can only be caused by an intrinsic break of symmetry[6] that we attribute to the stray magnetic field produced by an uncompensated SAF. In summary, we present a device that acts as a two-channel vortex-based STNO detector with a full electrical and non-volatile control of the selected channel and demonstrate that vortex STNOs can be used to implement programmable frequency RF detectors with potential interest for a wide range of applications.

[1] Jenkins, A. S. *et al.,* Appl. Phys. Lett. 105, 172403 (2014). [2] Jenkins, A. S. *et al.,* Nat. Nanotechnol. 11, 360–364 (2016). [3] Menshawy, S. *et al.,* AIP Adv. 7, 056608 (2017). [4] Jenkins, A. S. *et al.*, Phys. Rev. Appl. 13, 014046 (2020). [5] Tsunegi, S. *et al.*, Appl. Phys. Express 11, 053001 (2018). [6] Uhlír, V. *et al.*, Nat. Nanotechnol. 8, 341–346 (2013).

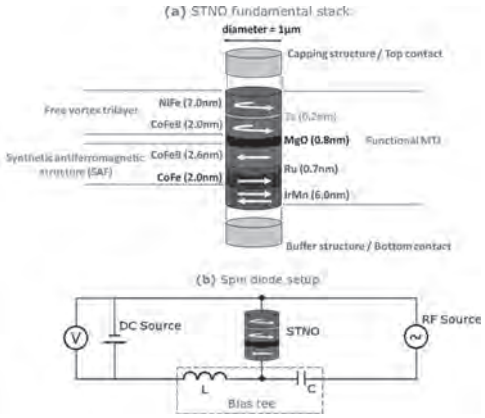

(a) Magnetic tunnel junction stack used for the measured devices. (b) Experimental setup used for spin diode.

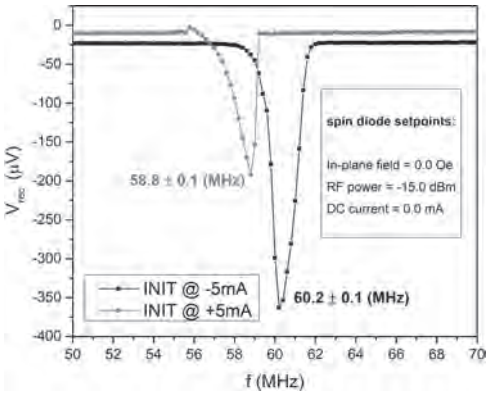

Spin diode detections obtained for different INIT conditions.

B3-04. Vortex Dynamics in Magnetic Tunnel Junctions as the Basis of a Novel Modulation and Demodulation Transmission Scheme.

A. Jenkins[1], L. San Emeterio Alvarez[1], P. Freitas[1] and R. Ferreira[1]
1. Spintronics, International Iberian Nanotechnology Laboratory, Braga, Portugal

The magnetisation dynamics associated with the free layer of a magnetic tunnel junction (MTJ) have been intensely studied over recent years, giving rise to the idea of a spin-torque nano-oscillator (STNO). Whilst these devices have been shown to have clear technological advantages in terms of tunability, agility, scalability and integration. However, the very advantages that make STNOs exciting in terms of tunability make them unlikely to be integrated with conventional wireless communication paradigms, which operate over very narrow frequency bands. In order for STNOs to have a role to play in data transfer, a new paradigm for the data transmission scheme must be envisaged. In this presentation we focus on using the magnetization dynamics of a vortex-based MTJ specifically as a wideband radio-frequency detector. We will present a thorough investigation of the novel dynamic behaviour in such systems, where the in-plane magnetic field induced by an integrated field line induces the constant nucleation and expulsion of the vortex core. Furthermore, we will show how this behaviour can lead to a strong MTJ resistance dependence on the incoming radio-frequency power and frequency, a behaviour which is well recreated with micromagnetic simulations. The frequency and power dependence of the vortex-based MTJs makes them exciting candidates as wide-band analogue dynamic sensors, which are particularly well suited to the demodulation of information encoded by STNOs. In conclusion we present an STNO-based modulation and demodulation scheme, which can encoded and alphabet of M characters, which has the potential for highly efficient data transfer for use in on-chip communications and autonomous sensor networks.

A. S. Jenkins *et al.*, "Nanoscale true random bit generator based on magnetic state transitions in magnetic tunnel junctions" Scientific Reports vol. 9, p. 15661 (2019) A. S Jenkins *et al.,* "Wideband High-Resolution Frequency-to-Resistance Converter Based on Nonhomogeneous Magnetic-State Transitions", Phys. Rev. Applied 13, 014046, (2020) A. S. Jenkins *et al.*, "Digital and analogue modulation and demodulation scheme using vortex-based spin torque nano-oscillators", Scientific Reports, (Accepted, published July 7th)

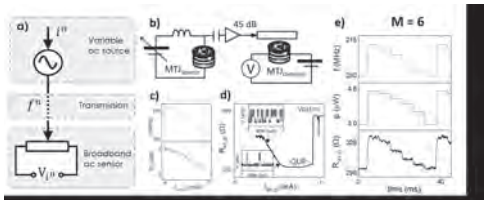

Figure 1. – a) STNO transmission scheme b) experimental set-up and c) dynamic output of MTJ_{source} and d) resultant resistance of $MTJ_{detector}$, and e) example of transmission of M=6 dynamic states/characters.

B3-05. Enhanced Amplitude Noise in Synchronized Spin Torque Nano Oscillators. *S. Wittrock*[1], S. Tsunegi[2], K. Yakushiji[2], A. Fukushima[2], H. Kubota[2], P. Bortolotti[1], U. Ebels[3], R. Ferreira[4], S. Yuasa[2], G. Cibiel[5], S. Galliou[6], E. Rubiola[6] and V. Cros[1] *1. Unité Mixte de Physique CNRS, Thales, Palaiseau, France; 2. National Institute of Advanced Industrial Science and Technology (AIST), Tsukuba, Japan; 3. Univ. Grenoble Alpes, CEA, INAC-SPINTEC, CNRS, SPINTEC, Grenoble, France; 4. International Iberian Nanotechnology Laboratory (INL), Braga, Portugal; 5. Centre National d'Etudes Spatiales (CNES), Toulouse, France; 6. FEMTO-ST Institute, CNRS, Univ. Bourgogne Franche Comté, Besancon, France*

Mutual synchronization of spin torque nano oscillators (STNOs) has become a very useful technique in order to improve the rf emission characteristics of STNOs since the experimental demonstration of a nonlocal coupling scheme in 2017 [1]. Beyond the improvement of the oscillator's oscillation coherence, synchronization is furthermore essential for the "bioinspired" mimicking of neural networks that are capable of performing complex tasks, such as pattern recognition [2]. In order to efficiently achieve this, it will be necessary to experimentally increase the synchronized number of STNOs to larger arrays, which has so far been experimentally demonstrated for up to 8 STNOs [3]. Here, we investigate the noise characteristics of the synchronized system of, first, two synchronized vortex based STNOs. Indeed, we experimentally find an improvement of the phase coherence of the synchronized signal and thus, a decrease of phase noise (see figure). However, we simultaneously observe a significantly increased amplitude noise compared to the emitted signal of one STNO alone. In order to understand the measurements, we study different potential origins and find that the enhanced amplitude noise is caused by, first, the nature of the synchronization potential and occurring phase slips and, second, intrinsic noise cross-conversion effects in the coupled nonlinear Langevin equations [4] describing the mutual system. Subsequently reanalyzing experimental data of 8 synchronized STNOs [3], we deduce that the mechanism apparently scales with the size of the synchronized array: While the phase noise decreases with the number of STNOs, the amplitude noise further increases. Thus, the described behavior might become particularly important for large arrays of STNOs. S.W. acknowledges financial support from Labex FIRST-TF. The French ANR project "SPINNET" ANR-18-CE24-0012 is acknowledged.

[1] Lebrun et al., Nat. Commun. 8, 15825 (2017). [2] Romera et al., Nature 563, 230–234 (2018). [3] Tsunegi et al., Sci. Rep. 8, 13475 (2018). [4] A. Slavin and V. Tiberkevich, IEEE Transactions on Magnetics 45, 1875 (2009).

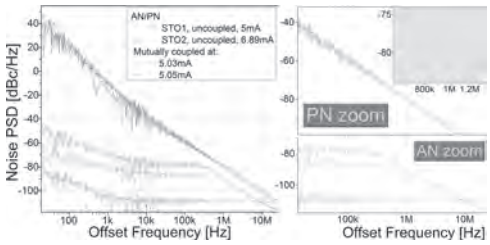

(a) Noise power spectral density of two vortex based spin torque nano oscillators alone (green, blue) and synchronized at different conditions (gray, reddish): The coherence improvement at synchronization leads to a decreased phase noise (PN). However, a significantly increased amplitude noise (AN) is observed.

B3-06. Dynamic C-State Beyond the Gyrotropic Motion in the Vortex Dynamics of a Spin Torque Nano Oscillator. *S. Wittrock*[1], P. Talatchian[1,2], M. Romera[1,3], M. Jotta Garcia[1], R. Ferreira[4], R. Lebrun[1], P. Bortolotti[1], U. Ebels[5], J. Grollier[1] and V. Cros[1] *1. Unite Mixte de Physique CNRS/Thales, Palaiseau, France; 2. Institute for Research in Electronics and Applied Physics, Univ. of Maryland, College Park, MD, United States; 3. NGFMC, Departomento de Fisica de Materiales, Univ. Complutense de Madrid, Madrid, Spain; 4. International Iberian Nanotechnology Laboratory (INL), Braga, Portugal; 5. Univ. Grenoble Alpes, CEA, INAC-SPINTEC, CNRS, SPINTEC, Grenoble, France*

Magnetic vortices represent a model system for the study of spin transfer induced magnetic dynamics [1] and are moreover commonly exploited in spin torque nano oscillators in order to generate coherent, large amplitude rf electrical signals [2]. However, mainly the fundamental gyrotropic (G) motion of the vortex core has so far been in the focus of investigations along with specifically higher order modes corresponding to radial or orthoradial spin wave modes in the vortex tail [3]. Here, we present a lower order dynamical mode in a confined magnetic disk of a nano-pillar spin torque nano oscillator beyond the G-state. It is characterized by the in-plane circular precession of a C-shaped magnetization distribution. The mode is closely related to the G motion and can be triggered from it by external parameters such as the magnetic field or the applied dc current. Moreover, the transition between G- and C-state is found to be purely stochastic, such that the dynamics is for instance precessing in the G- or C-state for a couple of periods before randomly switching the mode (see fig. 1). In order to study the characteristics, we also perform micromagnetic simulations and compare with experimental data, particularly focusing on the noise and coherence characteristics of the two modes and the stochastics in the transition. We believe that the vicinity of the two dynamic modes exhibiting rather different dynamic properties and their relatively easy control through external parameters might be interesting also from an applicational perspective handling spin torque oscillators. Furthermore, the stochastic regime might provide exploitation in random bit generators or neuromorphic computing schemes. S.W. acknowledges financial support from Labex FIRST-TF. The French ANR project "SPINNET" ANR-18-CE24-0012 is acknowledged.

[1] S. Wittrock et al., Phys. Rev. B 99, 235135 (2019). [2] N. Locatelli, V. Cros, J. Grollier, Nature Mater 13, 11 (2014). [3] K. Guslienko et al., PRB 71, 144407 (2005); B. Ivanov et al., PRL 94, 027205 (2005); B. Taurel et al., PRB 93, 184427 (2016).

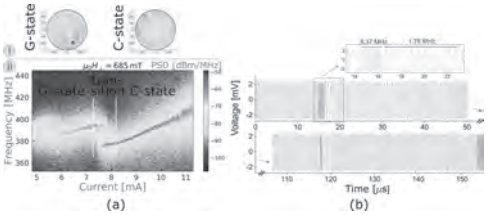

Micromagnetic representation of gyrotropic and C-state with and without vortex core inside the nanodisk, resp (a.i). A C-shaped in-plane magnetization characterizes the C-state. (a.ii) Measurement of the two distinct states: The transition is triggered by the applied dc current. (b) Measurement of the transition between the two states via a heterodyne technique: Switching between the states is stochastic.

B3-07. Withdrawn

B3-08. Origin of Nonlinear Damping due to Mode Coupling in Auto-Oscillatory Modes Strongly Driven by Spin-Orbit Torque. *I. Lee*[1], C. Zhang[1], S. Singh[1], B. McCullian[1] and P. Hammel[1] *1. Ohio State University, Columbus, OH, United States*

We investigate the physical origin of nonlinear damping due to mode coupling between several auto-oscillatory modes driven by spin-orbit torque in constricted Py/Pt heterostructures by examining the dependence of auto-oscillation on temperature and applied field angle. We observe a transition in the nonlinear damping of the auto-oscillation modes extracted from the total oscillation power as a function of drive current, which coincides with the onset of power redistribution amongst several modes and the crossover to linewidth broadening of all individual modes, as opposed to linewidth narrowing expected from the larger anti-damping current. This indicates the activation of a new relaxation process by nonlinear magnon-magnon scattering within the modes. We also find that both nonlinear damping and threshold current in the mode interaction damping regime at high drive current after transition are temperature independent, suggesting that the mode coupling occurs dominantly through a non-thermal magnon scattering process via a dipole or exchange interaction rather than thermally excited magnon-mediated scattering.

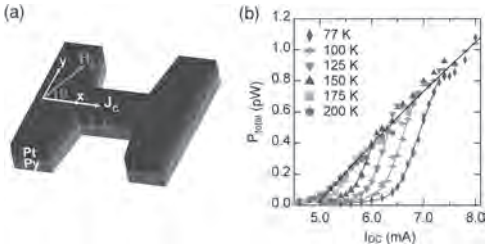

Fig. 1 (a) Schematic of spin-orbit torque driven auto-oscillation in 2D constricted Pt(5nm)/Py(5nm) bilayer structure. (b) Total power P_{total} of the auto-oscillations for θ=65° as a function of DC charge current I_{DC} at various temperature T. In the damping regime (a black line) due to mode-mode interaction at high I_{DC} after transition, both damping and threshold current extracted from the relationship with P_{total} are temperature independent, while in the single mode dominant regime (color lines) at low I_{DC}, they vary with temperature.

B3-09. Ultra-Fast Spectrum Analysis at GHz Frequencies Using Spin-Torque Nano-Oscillators. *A. Litvinenko*[1], A. Sidi El Valli[1], V. Iurchuk[1], P. Sethi[1], S. Louis[2], V. Tyberkevych[2], A. Jenkins[3], R. Ferreira[3], R. Sousa[1], L. Vila[1], S. Auffret[1], L. Prejbeanu[1], B. Dieny[1], A.N. Slavin[2] and U. Ebels[1] *1. Spintec, University Grenoble Alpes, CEA, CNRS, IRIG, Grenoble, France; 2. Oakland University, Rochester, MI, United States; 3. International Iberian Nanotechnology Laboratory, Braga, Portugal*

In modern radar and communication systems it is important to determine the frequency composition of complex external signals on the μs time scale and faster [1]. Common swept-tuned spectrum analyzers (SA) are limited to sweep times of 10-100 ms determined by the characteristic times of macroscopic VCOs and YIG-tuned reference oscillators. In contrast, recent progress in spintronics has led to the development of spin-torque nano-oscillators (STNO) generating in the GHz frequency range, and naturally having time constants of the order of several nanoseconds determined by the intrinsic properties of magnetization dynamics at nano-scale [2]. In [3] it was proposed theoretically and in [4] demonstrated experimentally for a vortex-state configuration that STNOs can be used as a central element of an ultra-fast spectrum analyzer. A fastest sweep rate of 0.67us was achieved for spectral analysis in the range of 25MHz around center frequency of 300MHz. Here we demonstrate that an ultra-fast sweep-tuned spectrum analysis can be performed at a central frequency of 3 GHz using uniform-state STNOs. The obtained SA performances sufficiently exceed the results obtained with a vortex-state STNO with a reduced sweep time of T =0.1μs, sweep range of 400 MHz (limited by the STNO power and not by tuning range capabilities) keeping the RBW (resolution bandwidth) close to the theoretical limit (14 MHz). This GHz-frequency technique of spectrum analysis was implemented as shown in Fig.1. The STNO was used as a local oscillator whose frequency was sweep-tuned by injecting a saw-tooth sweep signal. The STNO output (a) is, then, mixed with the input signal (b), digitized (c), and processed with a matched filter, resulting in a narrow output peak (d) whose temporal position corresponds to the input frequency while the width determines the RBW. Financial support is acknowledged from the EC program ERC MAGICAL 669204, from the NSF of the USA (Grants # EFMA-1641989 and "ECCS-1708982), and by the US AFOSR (MURI grant # FA9550-19-1-0307). The EC program GREAT is acknowledged for provision of perpendicular MTJ devices operating at GHz frequencies.

[1] Chen, V.C. and Miceli, W.J., "Time-varying spectral analysis for radar imaging of manoeuvring targets", IEEE Proceedings - Radar, Sonar and Navigation 145, 262-268 (1998). [2] Tingsu Chen, *et al.*, "Spin-Torque and Spin-Hall Nano-Oscillators", IEEE Proceedings, 104, 1919-1945 (2016). [3] Louis, S. *et al.*, "Ultra-fast wide band spectrum analyzer based on a rapidly tuned spin-torque nano-oscillator", *Applied Physics Letters* 113, 112401 (2018). [4] A. Litvinenko, et al., "Experimental demonstration of a rapid sweep-tuned spectrum analyzer with temporal resolution based on a spin-torque nano-oscillator," arXiv preprint arXiv:2004.03508, (2020).

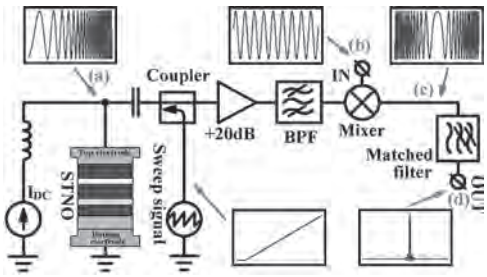

Fig. 1. Ultra-fast GHz STNO-based spectrum analyzer.

B3-10. Physical Reservoir Computing by Spin-Torque Oscillator at the Edge of Chaos. *A. Kamimaki*[1], S. Tsunegi[1], T. Taniguchi[1], N. Akashi[2], K. Nakajima[2], A. Fukushima[1], S. Yuasa[1], V. Cros[3], J. Grollier[3] and H. Kubota[1] *1. Spintronics Research Center, AIST, Tsukuba, Japan; 2. Graduate School of Information Science and Technology, University of Tokyo, Tokyo, Japan; 3. Unité Mixte de Physique, CNRS/Thales, Palaiseau, France*

Physical reservoir computing by magnetic devices is becoming an exciting topic in spintronics [1]. Recent studies on physical reservoir computing reveal that high-computation performance is achieved by physical systems at the edge of chaos [2], which is a boundary between chaos and the other dynamical states. An excitation of chaos in spin-torque oscillator (STO) by the delayed feedback was predicted recently [3,4]. Therefore, it becomes of great interest to perform the physical reservoir computing by STOs with the feedback circuit. Although an enhancement of the computation performance of the STO by the feedback was reported in 2019 [5], chaos in the STO was not identified. Since the intensity of the feedback effect in the experiments was weak, only ordered dynamics, such as self-synchronization, had been reported previously [6,7]. In this work, we investigate the edge of chaos in a vortex-type STO by enhancing feedback efficiency. Figure 1 is a schematic view of the STO with the feedback circuit. Spin-transfer torque by direct current excites an autooscillation of the vortex core. The output signal generated from the STO was gained of 40 dB, and was applied to the STO as microwave field with time delay of 150 ns. The magnitude of the feedback signal was toned by an attenuator. Figure 2 summarizes power spectra of the STO with various attenuation rate r_{Att}. The number of the peaks increases with decreasing the attenuation, as shown in Figs. 2(a) and 2(b), which was

typically found in the feedback system [6]. The linewidth of the main peak in Fig. 2(b) is narrow compared with that in Fig. 2(a), indicating the stabilization of the oscillation by the feedback. A further reduction of r_{Att}, however, results in a broad linewidth with a low power at the main peak shown in Fig. 2(c), which implies an appearance of chaos [8]. The performance of the reservoir computing at this state will be presented at the meeting. This work was supported by NEDO.

[1] J. Torrejon *et al*., Nature 547, 428 (2017). [2] J. Nakayama *et al*., Opt. Exp. 24, 8679 (2016). [3] J. Williame *et al*., Appl. Phys. Lett. 114, 232405 (2019). [4] T. Taniguchi *et al*., Phys. Rev. B. 100, 174425 (2019). [5] M. Riou *et al*., Phys. Rev. Appl. 12, 024049 (2019). [6] S. Tsunegi *et al*., Sci. Rep. 6, 26849 (2016). [7] D. Kumar *et al*., Sci. Rep. 6, 30747 (2016). [8] A. Uchida, "Optical communication with chaotic Lasers: Applications of Nonlinear Dynamics and Synchronization", Wiley (2012).

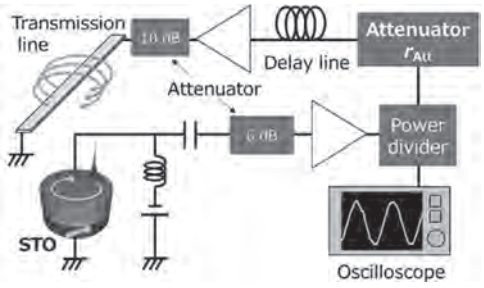

Fig. 1 Schematic illustration of self-feedback circuit. An attenuator (r_{Att}) controls the magnitude of the microwave field generated from the feedback current.

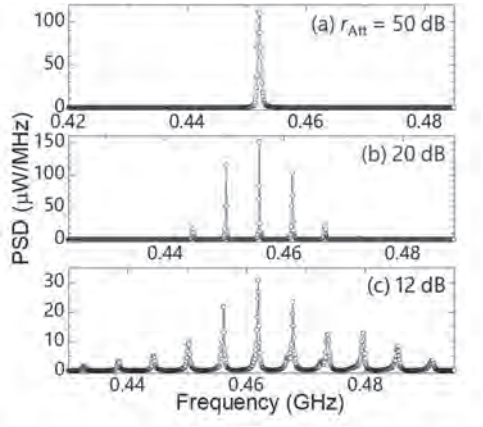

Fig. 2 Power spectrum density (PSD) of the STO for attenuation rate r_{Att} of (a)50, (b)20, and (c)12 dB, respectively.

Session B4
COMPLEX OXIDE, HEUSLER ALLOY, AND 2D SYSTEMS
(Poster Session)

Christianne Beekman, Chair
Florida State University/NHMFL, Tallahassee, FL, United States

B4-01. Bose-Einstein Condensation of Triplons Close to the Quantum Critical Point in the Quasi-One-Dimensional Spin-1/2 Antiferromagnet $NaVOPO_4$. *P.K. Mukharjee*[1], K. Ranjith[2], B. Koo[2], J. Sichelschmidt[2], M. Baenitz[2], Y. Skourski[3], Y. Inagaki[4,5], Y. Furukawa[5], A. Tsirlin[6] and R. Nath[1] *1. Physics, Indian Institute of Science Education Research Thiruvananthapuram, Thiruvananthapuram, India; 2. Physics of Quantum Materials, Max-Planck-Institut fur Chemische Physik fester Stoffe, Dresden, Germany; 3. Dresden High Magnetic Field laboratory, Dresden, Germany; 4. Department of Applied Quantum Physics, Faculty Of Engineering, Kyushu Daigaku, Fukuoka, Japan; 5. Ames Laboratory, Iowa State University, Ames, IA, United States; 6. Experimental physics VI, Centre for Electronic Correlations and Magnetism, Institute of Physics, University Of Augsberg, Augsberg, Germany*

Structural and magnetic properties of a quasi-one-dimensional spin-1/2 compound $NaVOPO_4$ are explored by x-ray diffraction, magnetic susceptibility, high-field magnetization, specific heat, electron spin resonance, and ^{31}P nuclear magnetic resonance measurements, as well as complementary ab initio calculations. Whereas magnetic susceptibility of $NaVOPO_4$ may be compatible with the gapless uniform spin chain model, a detailed examination of the crystal structure reveals a weak alternation of the exchange couplings with the alternation ratio $\alpha \sim 0.98$ and the ensuing zero-field spin gap $\Delta_0/k_B \sim 2.4$ K directly probed by field-dependent magnetization measurements. No long-range order is observed down to 50 mK in zero-field. However, applied fields above the critical field $H_{c1} \sim 1.6$ T give rise to a magnetic ordering transition with the phase boundary $T_N \propto (H - H_{c1})^{1/\varphi}$, where $\varphi \sim 1.8$ is close to the value expected for Bose-Einstein condensation of triplons. With its weak alternation of the exchange couplings and small spin gap, $NaVOPO_4$ lies close to the quantum critical point.

[1] P. K. Mukharjee *et. al.,* Phys. Rev. B 100, 144433 (2019) [2] S. Sachdev, Nat. Phys. 4, 173 (2008) [3] Mukhopadhyay *et. al*, Phys. Rev. Lett. 109, 177206 (2012) [4] Zapf *et. al*., Rev. Mod. Phys. 84, (2014)

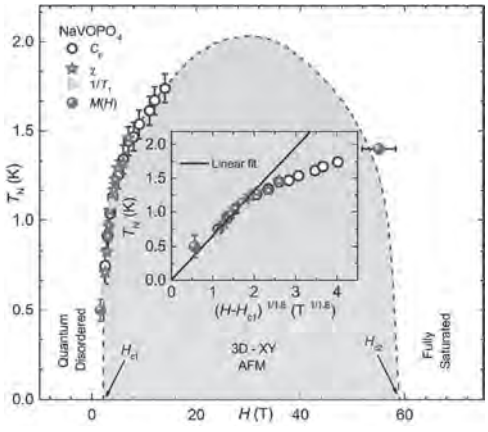

***H-T* phase diagram of $NaVOPO_4$ obtained using the data points from $\chi(T)$, $C_p(T)$, and $1/T_1(T)$ measurements.**

B4-02. First-Principles Studies of Quantum Magnetism in Mo_3O_8 Cluster Systems. *S.A. Nikolaev*[2], I. Solovyev[1] and S. Streltsov[3] *1. Busshitsu Zairyo Kenkyu Kiko Kokusai Nanoarchitectonics Kenkyu Kyoten, Tsukuba, Japan; 2. Tokyo Kogyo Daigaku, Meguro-ku, Japan; 3. Institut fiziki metallov imeni M N Miheeva Ural'skogo otdelenia Rossijskoj akademii nauk, Ekaterinburg, Russian Federation*

During the past few years, the Mo_3O_8 quantum magnets with kagome layers formed by Mo atoms have attracted a great deal of attention as a new candidate to realise quantum spin liquid states. The magnetic susceptibility of $LiZn_2Mo_3O_8$ has been experimentally shown to follow a Curie-Weiss law with the low- and high-temperature regimes whose Curie constants are related as $C_L \sim 1/3 C_H$. Originally, the disappearance of 2/3 of the paramagnetic spins at low temperatures in $LiZn_2Mo_3O_8$ was attributed to valence bond condensation on the trimerized lattice of the Mo_3O_{13} clusters [1], and several possible scenarios have been proposed to describe this unusual behaviour [2,3]. However, their adequacy was questioned by recently synthesized $Li_2InMo_3O_8$, that shows a conventional Neel 120° magnetic order, and its counterpart $Li_2ScMo_3O_8$, where no magnetic order has been observed down to 0.5 K [4]. Motivated by these studies, we combine rigorous first-principles calculations and effective low-energy models to study the microscopic origin of magnetism in $LiZn_2Mo_3O_8$, $Li_2InMo_3O_8$, and $Li_2ScMo_3O_8$. Considering the extended Hubbard model constructed in the basis of Wannier functions for the Mo *d* states on the anisotropic kagome lattice, we argue that the magnetic properties of these systems can be described by two different regimes of electron localization defined by the competition of kinetic energy and intersite Coulomb interactions. Being in the strong interaction limit, $LiZn_2Mo_3O_8$ will be proposed to reveal a plaquette charge order due to the correlated collective motion of electrons, where the partial spin pairing decoupling 2/3 of the spin originates from the asymmetry of tunneling processes. On the other hand, $Li_2InMo_3O_8$ and $Li_2ScMo_3O_8$ will be shown to fall into a cluster Mott insulator regime with the electrons localized at the Mo_3O_{13} clusters, where the former exhibits long-range antiferromagnetic order and the latter is more likely to reveal short-range order with quantum spin liquid-like excitations.

[1] J. P. Sheckelton, J. R. Neilson, D. G. Soltan, T. M. McQueen, Nat. Mater., Vol. 11, p. 493 (2012). [2] Rebecca Flint and Patric A. Lee, Phys. Rev. Lett., Vol. 111, p. 217201 (2013). [3] Gang Chen, Hae-Young Kee, and Yong Baek Kim, Phys. Rev. B, Vol. 93, p. 245134 (2016). [4] Yuya Haraguchi, Chishiro Michioka, Masaki Imai et. al, Phys. Rev. B, Vol. 92, p. 014409 (2015).

B4-03. Withdrawn

B4-04. Study of Structural, Transport and Magneto-Crystalline Anisotropic Properties in $La_{1-x}Sr_xMnO_3$ ($0.30 \leq x \leq 0.40$) Perovskite Manganite. *G. Channagoudra*[1], S. Gupta[2], V.K. Pecharsky[2] and V. Dayal[1] *1. Department of Physics, Maharaja Institute of Technology Mysore, Mandya, India; 2. Division of Materials Science and Engineering, Ames Laboratory, US Dept. of Energy, Ames, IA, United States*

Perovskite manganites $La_{1-x}Sr_xMnO_3$ (LSMO) ($0.30 \leq x \leq 0.40$) exhibits interesting physical properties such as; colossal magnetoresistance, high spin-polarized current (~90%), Curie temperature (~370K) due to coupling between the charge, spin and orbital degrees of freedom, making it potential

candidate for research for decades and application [1-3]. Additionally, a material with high magneto-crystalline anisotropy (MCA), which also depends on temperature, is largely influenced by crystal structure and spin-orbital coupling. In this abstract, we present structural, transport, magnetic and magneto-crystalline anisotropy in $La_{1-x}Sr_xMnO_3$ (x=0.30, 0.33, 0.36, 0.40) synthesized using solid-state reaction method. X-ray diffraction patterns of all the samples were well indexed by a rhombohedral structure with R3c space group. It is observed that lattice parameters and unit cell volume decrease monotonically upon increasing Sr concentration. X-ray photoelectron spectroscopy confirms the presence of Mn^{4+} and Mn^{3+}, the ratio which from 1.37-1.54 % as increasing Sr^{2+} concentration. From the ρ(T) and M(T) data analysis we observe that T_{MI} and M_S is larger for x=0.33 composition, which suggest weakening of the double-exchange interaction and Jahn-Teller distortion in x=0.30, 0.36 and 0.40 [4]. We have calculated MCA constant (K_1) fitting the law of approach [5-6] to saturation magnetisation data at higher magnetic field, well fitted with the equation, $M=M_S[1-a/H-b/H^2]-\chi$ with $K_1^2= (105/8)\times b$. The obtained K_1 in order of ~10^5 erg/cm^3, slightly decreased as Sr^{2+} increases which is understood due to reduction of crystal volume. In all samples, the value of K_1 at 100 K is higher than that at 300 K, suggesting that the samples at 100 K are more magnetically ordered than at 300 K. This work is supported by SERB-DST, New Delhi (EMR/2016/005424), Ames Lab and MRF (MITM)

1. J.B. Goodenough, Phys. Rev. 100 564-573 (1955) 2. C.N.R. Rao, J. Phys. Chem. B. 104 (2000) 5877-5889. 3. Ganesha Channagoudra, Ajay Kumar Saw and Vijaylakshmi Dayal, Thin Solid Films, 709, 138132 (2020) 4. A. Urushibara, Y. Moritomo, Y. Tokura, Phys. Rev. B. 51 (1995) 14103-14109. 5. A. D. Souza, P.D. Babu, Mamatha Daivajna, J. Alloys Compd. 797 (2019) 874-882 6. M. Suliga, K. Chwastek, Acta Phys. Pol. A. 135 (2019) 243–245.

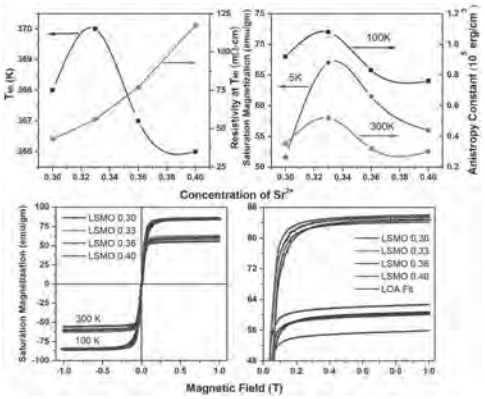

Fig 1 (a). Variation of T_{MI}, resistivity at T_{MI},(b). M_S with respect to the concentration of Sr^{2+}, (c). Field dependent magnetization at 100 K and 300 K, (d). Law of approach fitting to saturation. Magnetisation at high field.

B4-05. Withdrawn

B4-06. Effect of the Y Element on the Structural, Electronic and Magnetic Properties of Heusler Compounds Co_2YIn (Y=Nb, Ti). an a*b Initio* Study. *Z.W. Muthui*[1], R.J. Musembi[2], J.M. Mwabora[2] and A. Kashyap[3] *1. Physical Sciences, Chuka University, Chuka, Kenya; 2. Physics, University of Nairobi, Nairobi, Kenya; 3. Basis Sciences, Indian Institute of Technology, Mandi, Mandi, India*

We report on the effect of varying the Y element on the structural, electronic and magnetic properties of Co_2YIn (Y=Nb, Ti) Heusler compounds using Density Functional Theory (DFT). The effect of the lattice parameter and total number of valence electrons on spin polarization and the magnetic properties of the Heusler compounds is revealed by comparing with Co_2VIn Heusler compound, which has the same number of valence electrons as Co_2NbIn, Nb and V being from the same group in the periodic table, whereas it has almost the same lattice constant as Co_2TiIn, but differing in the total number of valence electrons by one, Ti and V being next neighbors in the same period of the periodic table. The optimized lattice parameters for Co_2NbIn and Co_2TiIn are found to be 6.20 Å and 6.05 Å respectively, while that of Co_2VIn has been reported to be 6.00 Å. Co_2NbIn is half metallic with an energy band gap of 0.1 eV in the minority states and has total magnetic moments of 2.02 μ_B/f.u. very close to the 2.00 μ_B/f.u. predicted by the Slater-Pauling rule, while Co_2TiIn is not half metallic but has a highly spin polarized electronic structure having a spin polarization of 89.59% and total magnetic moments of 1.04μ_B/f.u. While reducing the number of the valence electrons by one in Co_2TIIn has a significant effect on the magnetic moments and spin polarization, an increase in the lattice parameter while maintaining the same number of valence electrons in Co_2NbIn does not result in the destruction of the half metallic gap.

[1] T. Graf, C. Felser, and S. S. P. Parkin, "Heusler Compounds: Applications in Spintronics," in *Handbook of Spintronics*, Y. Xu, D. D. Awschalom, and J. Nitta, Eds. Springer Netherlands, 2016, pp. 335–364. [2] A. Birsan and P. Palade, "Band structure calculations of Ti2FeSn: A new half-metallic compound," *Intermetallics*, vol. 36, pp. 86–89, May 2013. [3] C. Felser, L. Wollmann, S. Chadov, G. H. Fecher, and S. S. P. Parkin, "Basics and prospective of magnetic Heusler compounds," *APL Mater.*, vol. 3, no. 4, p. 41518, Apr. 2015. [4] J. Ma *et al.*, "Computational investigation of half-Heusler compounds for spintronics applications," *Phys. Rev. B*, vol. 95, no. 2, p. 24411, Jan. 2017. [5] S. Mizukami and A. A. Serga, "Advancement in Heusler compounds and other spintronics material designs and applications," *J. Phys. Appl. Phys.*, vol. 48, no. 16, p. 160301, 2015. [6] X. Xu *et al.*, "Electronic structures of Heusler alloy Co2FeAl1−xSix surface," *Rare Met.*, vol. 31, no. 2, pp. 107–111, Apr. 2012. [7] T. Graf, C. Felser, and S. S. P. Parkin, "Simple rules for the understanding of Heusler compounds," *Prog. Solid State Chem.*, vol. 39, no. 1, pp. 1–50, May 2011. [8] T. Graf, S. S. P. Parkin, and C. Felser, "Heusler Compounds—A Material Class With Exceptional Properties," *IEEE Trans. Magn.*, vol. 47, no. 2, pp. 367–373, Feb. 2011. [9] E. Sasioglu, L. M. Sandratskii, and P. Bruno, "Role of conduction electrons in mediating exchange interactions in Mn-based Heusler alloys," Quanten-Theorie der Materialien, PreJuSER-754, 2008. [10] I. Galanakis and P. Mavropoulos, "Spin-polarization and electronic properties of half-metallic Heusler alloys calculated from first principles," *J. Phys. Condens. Matter*, vol. 19, no. 31, p. 315213, 2007. [11] H. Luo *et al.*, "Prediction of half-metallic properties for the Heusler alloys Mn2CrZ (Z=Al, Ga, Si, Ge, Sb): A first-principles study," *J. Magn. Magn. Mater.*, vol. 320, no. 3, pp. 421–428, Feb. 2008. [12] I. Galanakis, "Orbital magnetism in the half-metallic Heusler alloys," *Phys Rev B*, vol. 71, no. 1, p. 12413, Jan. 2005. [13] I. Galanakis, P. H. Dederichs, and N. Papanikolaou, "Origin and properties of the gap in the half-ferromagnetic Heusler alloys," *Phys. Rev. B*, vol. 66, no. 13, p. 134428, Oct. 2002. [14] M. Zipporah, R. Pathak, M. Robinson, J. Mwabora, R. Skomski, and A. Kashyap, "First-principle investigation of structural, electronic and magnetic properties of Co2VIn and CoVIn Heusler compounds," *AIP Adv.*, vol. 7, no. 5, p. 55705, Jan. 2017. [15] S. Khenchoul, A. Guibadj, B. Lagoun, A. Chadli, and S. Maabed, "First-Principles Prediction of Structural, Magnetic, Electronic, and Elastic Properties of Full-Heusler Compounds Co2YIn (Y = Ti, V)," *J. Supercond. Nov. Magn.*, vol. 29, no. 9, pp. 2225–2233, Sep. 2016. [16] Enamullah *et al.*, "Electronic structure, magnetism, and antisite disorder in CoFeCrGe and CoMnCrAl quaternary Heusler alloys," *Phys Rev B*, vol. 92, no. 22, p. 224413, Dec. 2015. [17] I. Galanakis, P. H. Dederichs, and N. Papanikolaou, "Slater-Pauling behavior and origin of the half-metallicity of the full-Heusler alloys," *Phys Rev B*, vol. 66, no. 17, p. 174429, Nov. 2002. [18] L. Wollmann, S. Chadov, J. Kübler, and C. Felser, "Magnetism in cubic manganese-rich Heusler compounds," *Phys. Rev. B*, vol. 90, no. 214420, Dec. 2014.

B4-07. Evidence for Slow Magnetic Relaxation and Memory Effects in the Spin Glass Phase of a $BiFeO_3$-Based Multiferroic Solid Solution System Having Aquasi-2D Magnetic Correlations. *P. Singh*[1] and D. Pandey[1] *1. School of Materials Science and Technology, Indian Institute of Technology Banaras Hindu University, Varanasi, India*

Study of spin glass phase transitions in disordered magnetic systems have been one of the most attractive areas of research in magnetism since decades because of the fascinating physics involved behind these transitions [1]. The physics of these transitions gains more significance when the 'dimensionality' aspect is taken into account since there is still no clear picture regarding lowest possible dimensionality of the spin glass systems [2-3]. By taking care of the dimensionality of the magnetic system, the validity of different theoretical models proposed for spin glass transitions explaining their characteristic features can also be verified. In the present work, we have reported a finite temperature spin glass transition in a $BiFeO_3$-based multiferroic solid solution system having quasi-2D magnetic correlations via analysis of both macroscopic and microscopic magnetic features of the system. Using different magnetization measurement protocols, we have verified the existence of key features observed in canonical spin glass systems like the bifurcation of the zero field cooled and field cooled magnetization curves, the signature slow magnetic relaxation and the memory effects (Figs. 1 and 2). The memory effect of the magnetic relaxation was tested using both cooling and heating cycles in order to check the validity of the hierarchical and droplet models [4]. For our system, the memory effect was observed only during cooling cycle, not in the heating cycle which supports the hierarchical model constituting of infinitely many possible energy states arranged hierarchically separated by finite energy barriers proposed for the spin glass phase, not the droplet model [4]. All these features establish the spin glass transition in the quasi-2D magnetic system unambiguously along with providing an understanding of the microscopic picture of the spin glass phase.

[1] K. Binder and A. P. Young, Rev. Mod. Phys. 58, 801 (1986). [2] J. A. Mydosh, Spin glasses: an experimental introduction. CRC Press, 2014 [3] K. H. Fischer and J. A. Hertz, Spin glasses. Vol. 1. Cambridge University Press, 1993. [4] Y. Sun et al., Phys. Rev. Lett. 91, 167206 (2003).

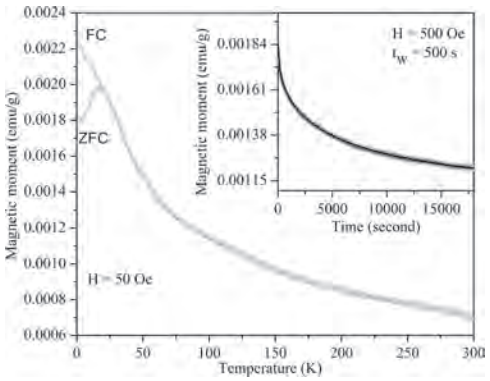

Zero field cooled (ZFC) and field cooled (FC) magnetization showing bifurcation as a function of temperature at an applied magnetic field of 50 Oe. The inset shows thermoremanent magnetization as a function of time.

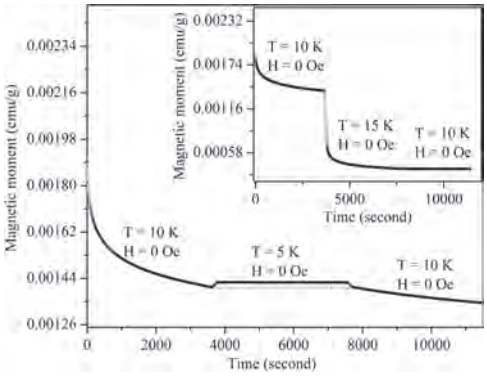

Thermoremanent magnetization as a function of time during cooling (main graph) and heating (inset) cycles.

B4-08. Magnetic and Structural Properties of MnCoNiSn. *Y. Khatri*[1], R. Skomski[2], D.J. Sellmyer[2] and A. Kashyap[1] *1. Indian Institute of Technology Mandi, Mandi, India; 2. Department of Physics and Astronomy & NCMN, University of Nebraska, Lincoln, NE, United States*

Manganese-containing Heusler compounds have recently attracted renewed attention as shape- memory alloys [1, 2], but is difficult to simultaneously satisfy the criteria for a good shape-memory alloy, such as a double-well potential as a function of c/a ratio, as high magnetization, and a Curie temperature above room temperature. Our focus is on the structures, magnetizations, and Curie temperatures of Mn_2NiSn [3] and MnCoNiSn. Ongoing experimental work [4] indicates that the substitution of Co for Mn enhances magnetization, Curie temperature, and degree of chemical order, but the mechanisms behind these changes are poorly understood. We have performed density- functional theory (DFT) using the Vienna ab-initio simulation package (VASP) to investigate the atomic positions, magnetic moments, and exchange couplings in the alloy. The physics of the system is characterized by a close competition between different crystal structures (inverse cubic Heusler, quaternary Y structure, tetragonal Heuslers), and spin structures (ferromagnetism and several types of ferrimagnetism). Structurally, the main distinction is the site occupancy of the Co atoms. In the notation of Ref. 3, the Co can replace Mn_{III} atoms, which form an NaCl sublattice with the Sn atoms, or the Mn_I atoms, which form an NaCl sublattice with the Ni atoms. A common feature of the structures is that Mn atoms one site have moments of the order of 3 μ_B. The Ni moments are much smaller, about 0.5 μ_B or less, whereas the Co moments are intermediate, varying around 2 μ_B. The Curie temperature reflects several inter- and intra-atomic exchange couplings, which are investigated by comparing the total energies for a variety of spin configurations. We have also investigated lattice-parameter effects, especially the substitution-induced reduction of the cubic lattice parameter a, which has a pronounced effect on the spin structure, and the c/a ratio. — The research in Nebraska is supported by DE-FG02-04ER46152 and NCMN.

[1] Y. N. Duan, X. X. Fan, A. Kutluk, X. J. Du, Z. W. Zhang, and Y. L. Song, J. Magn. Magn. Mater. 386, 1026 (2015). [2] L.Wollmann, S. Chadov, J. Kübler, and C. Felser, Phys. Rev. B 92, 064417 (2015). [3] S. Paul, B. Sanyal, and S. Ghosh, J. Phys.: Condens. Matter 25, 236005 (2013). [4] W. Zhang et al., in preparation (2020).

B4-09. Withdrawn

Session C1
FERRITES AND GARNETS I

Tianxiang Nan, Chair
Institute of Microelectronics, Tsinghua University, Beijing, China

CONTRIBUTED PAPERS

C1-01. A new way to Determine the Magneto-Crystalline Anisotropy of Li-Zn Ferrites. *J. Saied*[1,2], R. Lebourgeois[1] and V. Laur[2] *1. Thales Research and Technology France, Palaiseau, France; 2. LABSTICC, Universite de Bretagne Occidentale, Brest, France*

Lithium based spinel ferrites have been widely studied for their attractive electromagnetic properties. They exhibit a high magnetization up to 5000G, a high Curie temperature up to 650°C, and square hysteresis loop[1] which is essential for latched devices like switches and phase shifters for space applications [2]. Today, the strong demand of new ferrite devices operating at high frequency and high power level encouraged us to reconsider polycrystalline lithium ferrites properties, and specifically to determine their magneto-crystalline anisotropy. The determination of the magneto-crystalline anisotropy of spinel ferrites remains an ambitious challenge. The best accurate techniques require having monocrystalline samples [3]. Unfortunately, the preparation of ferrite single crystals is limited to a short range of chemical compositions and most of the time it is not possible to characterize the desired formulation which implements specific cationic substitutions. Therefore, it is crucial to be able to quantify the magneto-crystalline anisotropy of complex formulations, in order to design the ferrite devices. The aim of this work is to obtain experimentally the value of magneto-crystalline anisotropy field by measuring the ferrite's complex permeability $\mu(f) = \mu'(f) - j\,\mu''(f)$ between 1 MHz to 3 GHz. The complex permeability of a ferrite can be described by two magnetization mechanisms [4]: - The domain wall displacement which accounts for the permeability at low frequency (< 100 MHz). - The spins rotation which accounts for the permeability at high frequency (> 100 MHz) Most of the time, it is impossible to distinguish the two latter resonances because the two phenomena are too close and overlap (figure 1, sample F900) [5]. Thanks to controlled experimental conditions based on a conventional ceramic route, we have been able to prepare materials in which the two resonances are separated (figure 1, sample F940). Thus, we have determined the field anisotropy of Li-Zn ferrites using the spin rotation resonance frequency (f_r) according to the formula $H_A = f_r/\gamma$ (in which γ is the gyromagnetic ratio). The resulting anisotropy fields are in good agreement with previous results obtained with FMR experiments [6].

[1] G. M. Argentina et P. D. Baba, *IEEE,* Vol. 1,16, pp. 652-658, (1974) [2] T. Collins et A. E. Brown, *Journal of applied physics,* vol. 42, pp. 3451-3454, (1971) [3] C. J. Brower et C. E. Patton, *Journal of applied physics,* vol. 53,12104, (1982) [4] R. Lebourgeois, C. Le Fur, M. Labeyrie, M. Paté et J.-P. Ganne, *Journal of magnetism and magnetic materials,* vol. 160, pp. 329-332, (1996) [5] T. Tsutaoka, *Journal of applied physics,* vol. 82,13068, (1997) [6] R. Bozorth, E. Tilden et A. Williams, *Physical review,* vol. 99, 16, pp. 1788-1799, (1955)

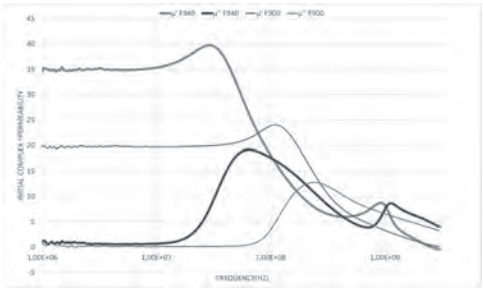

C1-02. Low Damping BiYIG and BiYIG/TmIG Heterostructures for Spintronics. *T. Fakhrul*[1], G.A. Riley[2], E. Rosenberg[1], S. Huang[1], L.M. Caretta[1], J. M. Shaw[2], G. Beach[1], H. Nembach[2] and C. Ross[1] *1. Massachusetts Institute of Technology, Cambridge, MA, United States; 2. National Institute of Standards and Technology, Gaithersburg, MD, United States*

Ferrimagnetic rare earth iron garnets with perpendicular magnetic anisotropy (PMA) have recently attracted a great deal of attention for spintronic applications. However, a major drawback for most rare earth iron garnets is their large Gilbert damping. Bi-substituted yttrium iron garnet (BiYIG) has been shown to have both large PMA and low damping,[1] and spin-orbit torque-driven domain wall velocities of 4.5 km/s have been observed. In this work we report the growth, magnetic and spintronic transport properties of single layers and heterostructures consisting of PMA BiYIG and thulium iron garnet (TmIG) grown epitaxially on substituted $Gd_3Ga_5O_{12}$ (GSGG, SGGG) and $Nd_3Fe_5O_{12}$ (NGG) by pulsed laser deposition. BiYIG films with thickness as low as 2.4 nm (2 unit cells) give magnetic hysteresis loops, and magnetization vs. thickness shows a non-magnetic layer of only 1.4 nm at the BiYIG/substrate interface, attributed to interdiffusion, and a magnetization of 115 kA/m. The PMA in these films can be fine-tuned by the lattice mismatch between the film and garnet substrate, varying from an anisotropy energy, K_u , of 2.95 kJ/m^3 for BiYIG on GSGG, 1.12 kJ/m^3 for BiYIG on NGG and 0.6 kJ/m^3 for BiYIG on SGGG. Ferromagnetic Resonance (FMR) measurements in the out-of-plane configuration demonstrate the BiYIG films have Gilbert damping as low as 9.7×10^{-5} while introduction of a TmIG layer raises the damping to 5.6×10^{-3} as shown in Fig.2. Brillouin Light Scattering (BLS) measurements reveal the absence of Dzyaloshinskii-Moriya interaction in the pure BiYIG films, whereas TmIG/GGG exhibits DMI[2]. Furthermore, Spin Hall magnetoresistance (SMR) measurements were also performed to study the efficiency of spin transport in Pt/(Bi,Tm) YIG heterostructures.

[1] Soumah, L., Beaulieu, N., Qassym, L., Carrétéro, C., Jacquet, E., Lebourgeois, R., Youssef, J.B., Bortolotti, P., Cros, V. and Anane, A., Nat. Commun. 9, 3355 2018 [2] Caretta, L., Rosenberg, E., Büttner, F., Fakhrul, T., Gargiani, P., Valvidares, M., Chen, Z., Reddy, P., Muller, D.A., Ross, C.A. and Beach, G.S., Nat. Commun. 11, 1090 2020

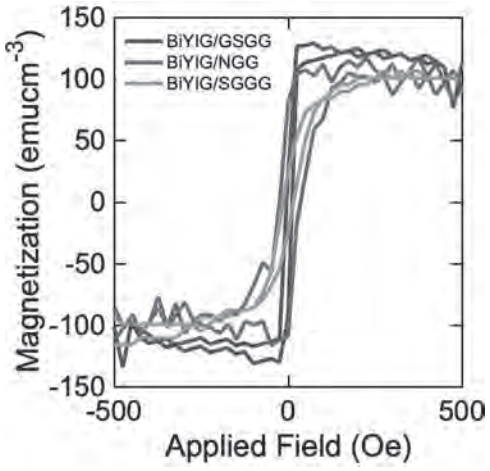

Figure 2. Out-of-plane hysteresis loops for (22.6nm) BiYIG/GSGG, (15nm)BiYIG/NGG and (25nm) BiYIG/SGGG

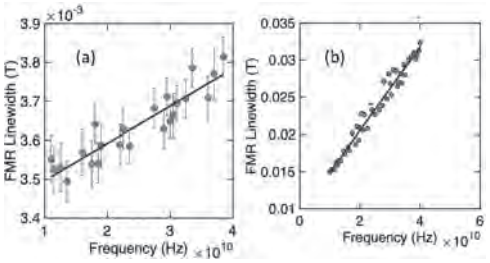

Figure 2. Out-of-plane FMR linewidth versus frequency for (a) (25nm) BiYIG/SGGG (b)BiYIG (15.5nm)/TmIG(5.6nm)/NGG film

INVITED PAPER

C1-03. Nanoscale U-Type Hexaferrites as Microwave Absorbers.
R. Chatterjee[1] and S. Kumar[2] *1. Physics, Indian Institute of Technology Delhi, New Delhi, India; 2. Physics, University of Delhi, New Delhi, India*

With the unprecedented surge in wireless communication systems, microwave (MW) absorbers are becoming increasingly important for civil as well as military applications. When a MW signal is incident on a surface, the signal energy is divided into three parts: (i) reflected, (ii) transmitted and (iii) absorbed energies. For the usual metal-backed MW absorbing coating, transmitted energy=0; thus, minimizing reflection is the key for good absorbers. The reflection of EM energy can be curtailed by two methods: (i) an increase in absorption, and (ii) the quarter wavelength cancellation [1,2]. The loss of EM energy may originate from a number of processes within the absorber such as conduction, resonances, and relaxations etc. MW signal, on passing through an absorber dissipates its energy in the form of heat through interactions with the dielectric and magnetic structures of a material. Hence, in terms of two characteristic material parameters: relative permeability (μ^*) and relative permittivity (ε^*) in the absorbing medium are to be tailored for attaining a strong and broadband MW absorption. For MW absorbing applications, U-type hexaferrite phase with chemical formula $Ba_4Me_2Fe_{36}O_{60}$ (Me_2U, Me: divalent transition-metal cation) has most complicated crystal structure and is least studied [3-11]. In present work, we investigate the preparation and MW absorbing properties of the nanoscale U-type hexaferrites (NANO-U) for development of a broadband MW absorber. The nano-powders are prepared using two different methods: (1) mechanical jet-milling of bulk U-type hexaferrite prepared by the standard solid-state reaction route at ~1250 °C, designated here as $(NANO\text{-}U)_{JM}$ and (2) a novel one-pot chemical route, designated here as $(NANO\text{-}U)_C$. In the first method, average particle size ~20–50 nm powders were achieved; whereas, the $(NANO\text{-}U)_C$ powders of controlled particle sizes (~65 to ~170 nm) were prepared by changing the holding time (4, 6, 8 and 10 h) at a constant optimized working temperature of ~900 °C. Four samples of $(NANO\text{-}U)_C$ were prepared that are designated as per their holding time as- $(NANO\text{-}U)_{C4}$, $(NANO\text{-}U)_{C6}$, $(NANO\text{-}U)_{C8}$, $(NANO\text{-}U)_{C10}$. A blend of all powders in equi-proportion, is designated as $(NANO\text{-}U)_{CMIX}$, The advantage of one-pot chemical method is attainability of comparable particles sizes of a few tens of nm, at much lower working temperatures. We compare the EM parameters and MW absorbing properties of $(NANO\text{-}U)_{JM}$, $(NANO\text{-}U)_C$ and bulk U-type hexaferrite powders. It is interesting to note that the $(NANO\text{-}U)_{JM}$ demonstrates excellent reflection loss (R_L) of ~ -43.8 dB (99.99% MW absorption) at ~11.3 GHz frequency with a broad bandwidth of 8.6 GHz (8.9 $\leq f \leq$ 17.5 GHz) for 90% or more MW absorption. The values for $(NANO\text{-}U)_C$ too are comparable, with R_L of -44.2 dB (99.99% MW absorption) at 11.6 GHz frequency for $(NANO\text{-}U)_{C8}$ and a broadband MW absorption with an excellent bandwidth of 8.4 GHz (9.3 $\leq f \leq$ 17.7 GHz) for $(NANO\text{-}U)_{CMIX}$. Significantly improved MW absorption performance are demonstrated in NANO-U hexaferrites, in comparison to the previously reported nanoscale spinel ferrites (-38.9 dB or 99.8% MW absorption along with a bandwidth of ~3.7 GHz only). We believe that nanoscale particle sizes in U-type hexaferrites result in synergistic enhancements of the dielectric and magnetic losses. A self-explanatory schematic representation of the various possible loss mechanisms in NANO-U absorbers is shown in Fig. 1. Easy tunability, large magnetic anisotropy, presence of disordered surface spin states, defect polarization centres, greater magnetic and dielectric losses and large hopping conduction are responsible for large and broad-band MW absorption in NANO-U hexaferrites. These economical and easily processed U-type hexaferrite ultrafine particles can be used in the paints and sheets for wide-band and strong MW absorbing coating applications.

(1) Y. Huang, H. Zhang, G. Zeng, Z. Li, D. Zhang, H. Zhu, R. Xie, L. Zheng, J. Zhu, J. Alloys Compd., 682 (2016) 138-143. (2) L. Wan, J. Zhang, Y. Chen, H. Wang, W. Hu, L. Liu, Y. Deng, J. Phys. D: Appl. Phys., 48 (2015) 355302-355310. (3) D. Lisjak, M. Drofenik, J. Appl. Phys., 93 (2003) 8011-8013. (4) M.N. Afsar, D. Lisjak, A. Bahadoor, Y. Wang, IEEE Trans. Magn., 41 (2005) 3472–3474. (5) D. Lisjak, V.B. Bregar, M. Drofenik, J. Magn. Magn. Mater., 310 (2007) 2558-2560. (6) R.S. Meena, S. Bhattacharya, R. Chatterjee, J. Magn. Magn. Mater., 322 (2010) 2908-2914. (7) R.S. Meena, S. Bhattacharya, R. Chatterjee, Mater. Sci. Eng., B, 171 (2010) 133-138. (8) R.S. Meena, S. Bhattacharya, R. Chatterjee, J. Magn. Magn. Mater., 322 (2010) 1923-1928. (9) R.S. Meena, S. Bhattacharya, R. Chatterjee, Mater. Des., 31 (2010) 3220–3226. (10) S. Padhy, S. Sanyal, R.S. Meena, R. Chatterjee, A. Bose, Journal of Electromagnetic Waves and Applications, 27 (2013) 191-204. (11) S. Padhy, S. Sanyal, R.S. Meena, R. Chatterjee, A. Bose, IET Microw. Antennas Propag., 8 (2014) 165–170.

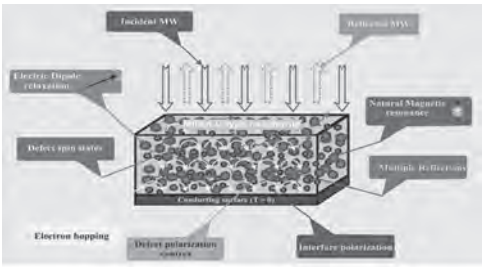

Fig. 1: Schematic representation of various loss mechanisms in prepared U-type hexaferrites.

CONTRIBUTED PAPERS

C1-04. Permeability Spectra of Planar M-Type Barium Hexaferrites With High Snoek's Product by Two-Step Sintering. *Q. Li*[1], Y. Chen[2], C. Yu[1], K. Qian[1] and V. Harris[1] *1. Department of Electrical and Computer Engineering, Northeastern University, Boston, MA, United States; 2. Innovation Center, Rogers Corporation, Burlington, MA, United States*

High-frequency ferrite ceramics exhibiting high permeability and low magnetic loss have been recently attracting more and more attention owing to the rapid development of modern communication technologies.[1-3] It is known that the magnetic performance of ferrites is strongly associated with the morphology of their polycrystalline structure.[4] During the final-stage sintering, densification is typically accompanied by rapid grain growth.[5] In this work, we focus on the control of grain growth and densification process for planar Co-Ti doped M-type barium hexaferrites, $BaCo_{1.2}Ti_{1.2}Fe_{9.6}O_{19}$, by one-step sintering (OSS) and two-step sintering (TSS) techniques. Experimental results in Fig. 1. indicate that the microstructure of the samples prepared by TSS shows visibly finer and more uniformity compared to that of the samples prepared by conventional OSS, evidence in that the grain growth during the second-step sintering of TSS is successfully suppressed while the density continues to increase. More importantly, the TSS technique shifts the resonant frequency to a higher value as shown in Fig. 2. In addition, the uniformity of the microstructure contributes to a narrower resonant peak. The reshaping of the magnetic spectra leads to a significant reduction of magnetic loss below 300 MHz. The ferrites prepared by TSS demonstrate high permeability ($\mu' = 18$-20), low magnetic loss ($\tan\delta_m = 0.1$-0.3), and high Snoek's product (>25 GHz) in the frequency range of 100-400 MHz. By fitting experimental data, we have determined that low magnetic loss is derived from the small damping coefficient of spin rotation in terms of Kittel's theory. Therefore, the TSS technique provides an effective and efficient approach to prepare planar BaM hexaferrite materials for ultra-high frequency (UHF) communication devices requiring low loss and high Snoek's product.

[1] V. G. Harris, Z. Chen, Y. Chen *et al*., J. Appl. Phys., Vol. 99, p. 08M911 (2006). [2] V. G. Harris, A. Geiler, Y. Chen *et al*., J. Magn. Magn. Mater., Vol. 321, p. 2035 (2009). [3] V. G. Harris, IEEE Trans. Magn., Vol. 48, p. 1075 (2012). [4] Q. Li, Y. Chen, and V. G. Harris, J. Magn. Magn. Mater., Vol. 453, p. 44 (2018). [5] I. W. Chen and X. H. Wang, Nature, Vol. 404, p. 168 (2000).

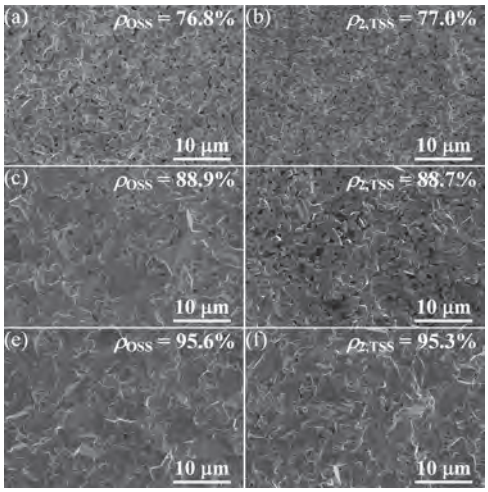

Fig. 1. Scanning electron microscopy micrographs of $BaCo_{1.2}Ti_{1.2}Fe_{9.6}O_{19}$ samples sintered by one-step sintering ((a), (c) and (e)) and two-step sintering ((b), (d) and (f)) to similar densities.

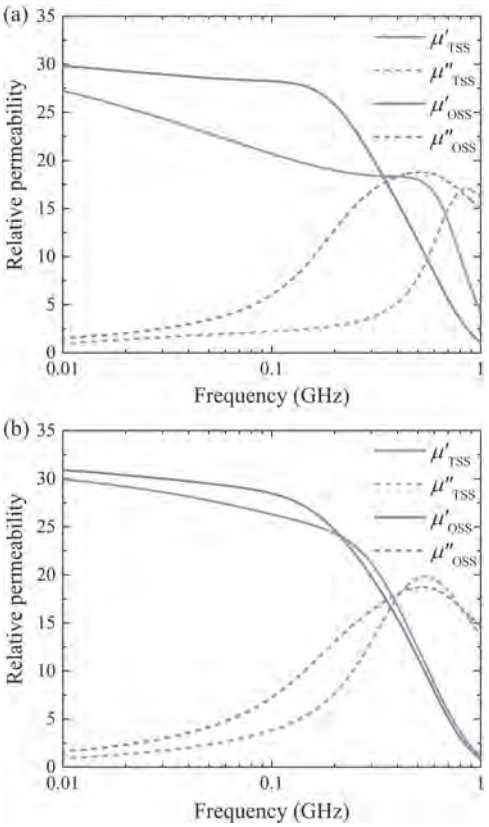

Fig. 2. Relative permeability spectra of $BaCo_{1.2}Ti_{1.2}Fe_{9.6}O_{19}$ samples sintered by one-step sintering and two-step sintering with different densities of (a) 88.8% and (b) 95.4%.

C1-05. Epsilon Iron Oxide Based Nanomagnets Exhibiting Large Magnetic Hysteresis Loop. *M. Yoshikiyo*[1], A. Namai[1] and S. Ohkoshi[1] *1. Department of Chemistry, The University of Tokyo, Tokyo, Japan*

ε-Fe_2O_3 is one of the polymorphs of Fe_2O_3, which was first discovered by our group as a pure phase. This material exhibits a large coercive field over 20 kOe at room temperature [1]. Due to its strong magnetic anisotropy, ε-Fe_2O_3 also exhibits high-frequency electromagnetic wave absorption in the millimeter wave region, and the physical properties could be widely controlled by metal substitution [2,3]. In this work, we report a highly oriented magnetic film of metal-substituted ε-Fe_2O_3 nanoparticles dispersed in resin [4,5]. An oriented film was prepared by dispersing ε-$Ga_{0.45}Fe_{1.55}O_3$ nanoparticles into vehicle resin and drying under an applied external magnetic field. ε-$Ga_{0.45}Fe_{1.55}O_3$ exhibits millimeter wave absorption at 79 GHz, which is a common frequency used for car radars. X-ray diffraction (XRD) pattern of the oriented film shows a strong single peak from the 200 reflection, indicating that the crystallographic *a*-axis of the orthorhombic crystal structure is oriented along the out-of-plane direction of the film (Fig. 1b). The degree of orientation is very high with a Lotgering factor of $F = 0.94$. The angular dependence of the magnetic hysteresis loops at room temperature (Fig. 1c) shows a rectangular hysteresis loop with a coercive field of 9.7 kOe and a magnetization value of 30.4 emu g^{-1} at 7 T when the external field is along the out-of-plane direction with respect to the plane of the film, indicating that the easy axis corresponds to the crystallographic *a*-axis. To understand the origin of the high degree of orientation, we calculated the magnitude of the magnetic coupling between the ε-$Ga_{0.45}Fe_{1.55}O_3$ magnetic nanoparticles based on the magnetic dipole-dipole interaction. The theoretical model considering uniaxial magnetic anisotropy reproduces the angular dependence of the magnetic loops well.

[1] J. Jin, S. Ohkoshi, K. Hashimoto, *Adv. Mater.*, 16, 48 (2004). [2] M. Yoshikiyo, K. Yamada, A. Namai, and S. Ohkoshi, *J. Phys. Chem. C*, 116, 8688 (2012). [3] A. Namai, M. Yoshikiyo, K. Yamada, S. Sakurai, T. Goto, T. Yoshida, T. Miyazaki, M. Nakajima, T. Suemoto, H. Tokoro, S. Ohkoshi, *Nature Communications*, 3, 1035 (2012). [4] S. Ohkoshi, K. Imoto, A. Namai, S. Anan, M. Yoshikiyo, H. Tokoro, *J. Am. Chem. Soc.*, 139, 13268 (2017). [5] M. Yoshikiyo, A. Namai, K. Imoto, H. Tokoro, S. Ohkoshi, *Eur. J. Inorg. Chem.*, 2018, 847 (2018).

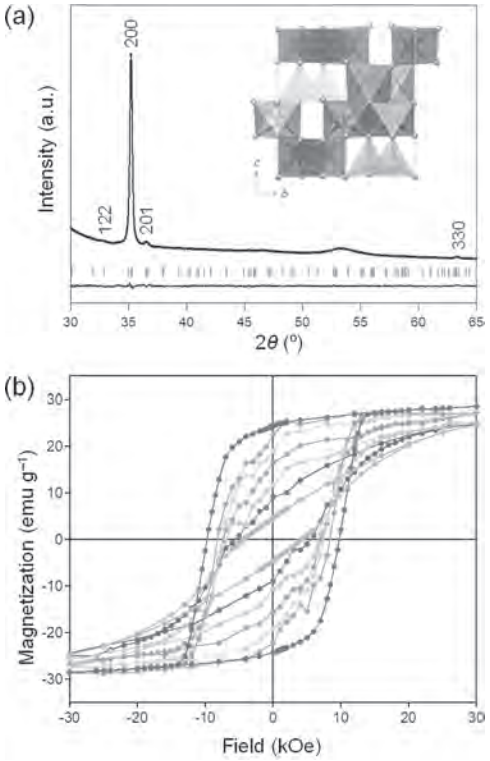

Figure 1. (a) XRD pattern and (b) angular dependence of the magnetic hysteresis loop at 300 K of ε-$Ga_{0.45}Fe_{1.55}O_3$ oriented film. Inset of (a) is the crystal structure of ε-Fe_2O_3.

C1-06. Hexagonal Nano-Ferrites Used on a v-Band Self-Bias on-Chip Circulator for CMOS. W. Quan[1], *M.N. Afsar*[1] and V. Koomson[1] *1. Tufts University, Medford, MA, United States*

Hexagonal ferrite materials such as $BaFe_{12}O_{19}$ and $SrFe_{12}O_{19}$ have strong anisotropic magnetic field and strong remnant magnetism. These properties enable the working frequency of devices such as phase shifter, isolator and circulator, move up to tens of GHz without a strong external bias field and even achieve self-biasing. Other features such as large saturation magnetization, large anisotropy, and low dielectric loss and most importantly, its potential of achieving self-bias, paves the way to fabrication of planar ferrite device that can play a crucial role in a next generation wireless system. The advantage of ferrite devices are their low insertion loss, high isolation, broad bandwidth and high power handling ability compared to their active counterparts. If the fabrication process of aforementioned devices can be integrated into the mature CMOS process flow as an option, it will gain great competiveness as regards the cost. In this work, thin film ferrite material was deposited by employing spin-casting method [Liu 2013] and patterned with the help of Chemical-Mechanical Polishing (CMP). The spin-casting is a low-temperature process: the nano-sized barium ferrite materials can be processed into composite and spin-casted into thin film layer. This method requires only 120°C baking under external biasing filed. In this research, we present the design, simulation, fabrication and measured results of a self-bias micro-strip line Barium hexagonal Nano-ferrite (BaM) circulator on silicon wafer as Fig. 1. This planar Y-junction circulator is 2mm by 2mm by 0.5mm in size, which is capable of future integration with the top three layers of 180nm CMOS technology. Ferrite thin film is deposited and patterned employing composite spin-casting method. Typical characterization techniques are employed together with free-space quasi-optical spectrometry to study complex permittivity and permeability of deposited film up to 120GHz. S parameters of fabricated circulators are characterized by a set of on wafer probes up to 67GHz as Fig. 2. We observed over 15dB non-reciprocal phenomenon at 55GHz.

Liu C, Sholiyi O, Afsar M N and Williams J D (2013), "Characterization of micro-structured ferrite materials: course and fine barium, and photoresist composite," Magnetic, IEEE Transactions on, vol. 49, pp.4319-4322, July 2013.

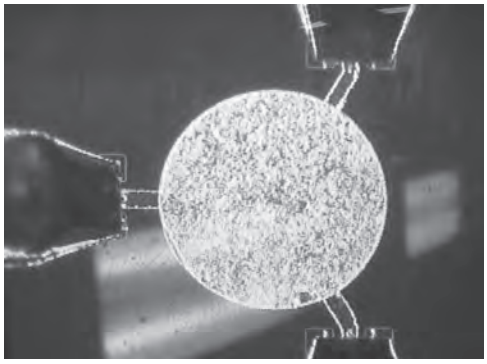

Fig. 1. Three ports probing of fabricated circulator

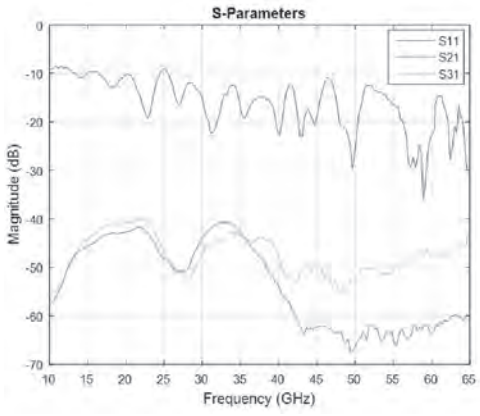

Fig. 2. Measured S-parameter of fabricated ferrite circulator

C1-07. Origin of Magnetic Anistropy and Damping in Spinel Ferrites. *J. Lumetzberger*[1], M. Buchner[1], S. Pile[1], V. Ney[1], W. Gaderbauer[2], N. Daffe[3], M.V. Moro[4], D. Primetzhofer[4], K. Lenz[5] and A. Ney[1] *1. Institute of Semiconductor and Solid State Physics, Johannes Kepler University Linz, Linz, Austria; 2. Center for Surface and Nanoanalytics, Christian Doppler Laboratory for Nanoscale Phase Transformations, Johannes Kepler University Linz, Linz, Austria; 3. Paul Scherrer Institut, Swiss Light Source (SLS), Villigen, Switzerland; 4. Department of Physics and Astronomy, Angström Laboratory, Uppsala University, Uppsala, Sweden; 5. Institute of Ion Beam Physics and Materials Research, Helmholtz-Zentrum Dresden-Rossendorf, Dresden, Germany*

In spintronics one aims to obtain pure spin currents as an additional degree of freedom. To ensure pure spin currents and exclude charge currents, ferromagnetic insulators are the material of choice. However, ferromagnetic insulators with low intrinsic damping are sparse. Promising results are obtained by spinel ferrites, i.e. cubic NiZnAl ferrite (NiZAF) and $MgAl_{0.5}Fe_{1.5}O_4$ (MAFO), grown as a thin film on spinel $MgAl_2O_4$ [1,2]. In this contribution reactive magnetron sputtering was used a preparation method. NiZAF

samples are analysed with X-ray diffractometry for their crystallographic properties. Furthermore, the angular and frequency dependence of the resonance position is measured by ferromagnetic resonance (FMR) and fitted to quantify the anisotropy fields, g-factor and magnetic damping. Additionally, transmission electron microscopy is performed to investigate the interface on an atomic scale and the chemical composition is studied by means of ion beam analysis. The doping percentage of Zn and Al are of special interest, since they reportedly have a significant influence on damping according to the single ion model of ferrite magnetism [3]. Tuning these components, enables the control of strain and cation distribution in this material system. In a last step X-ray magnetic circular dichroism (XMCD) at the $L_{3,2}$ edge of Ni and Fe are performed to identify the different oxidation states as well as occupied lattice sites of Ni and Fe. A comparison between similarly strained materials revealed the importance of site occupancy as a major tuning factor for the magnetic properties [4]. First results on MAFO thin films are presented in this contribution, studying the correlation between strain, structure and magnetic anisotropy and damping.

[1] S. Emori et. al., Adv. Mater., Vol. 29, p. 1701130 (2017) [2] J. J. Wisser et al., Appl. Phys. Lett., Vol. 116, p. 142406 (2020) [3] G.F. Dionne, IEEE: Transactions on Magnetics, Vol. 47, p. 2 (2011) [4] J. Lumetzberger, arXiv:1908.08257 (2019)

C1-08. Switching Field, Orientation and Shape Anisotropy Contribution on the Magnetic Heating of Fe_3O_4 Nanodisc.

G. Niraula[1], J.A. Antonio Coaquira[3], F.H. Aragon[3], F. Garcia[2], A. Mello[2], A.F. Bakuzis[4], D. Muraca[5] and S.K. Sharma[1] *1. Physics, Federal University of Maranhao, Sao Luiz, Brazil; 2. Brazilian Center for Physics Research, Rio de Janerio, Brazil; 3. Physics, University of Brasilia, Brasília, Brazil; 4. Physics, Federal University of Goais, Goiania, Brazil; 5. Institute of Physics "Gleb Wataghin" (IFGW), Physics, University of Campinas, Campinas, Brazil*

The present work reports the synthesis of Fe_3O_4 nanotubes (NTs), nanorods (NRs), and nanodiscs (NDs) prepared by microwave-hydrothermal route with varying ratio of sodium phosphate/sodium sulfate ions. The Rietveld refinement analysis of the X-ray diffraction patterns divulges the presence of a metallic iron phase decreasing gradually from NTs ~16 %, NRs ~11 % to NDs ~ 0% with increasing concentration of phosphate ions as confirmed later by Mossbauer data. A sharp drop in the coercive field from NTs (~252 Oe) to NDs (~182 Oe) indicates clearly a magnetic vortex state in NDs as also reported by Lorenz microscopy and micromagnetic simulation [1]. Further, a reduction in Verwey transition temperature (NTs to NDs) is observed in zero fields cooled magnetization measurement (Figure 1(a)) related to a gradual loss of stoichiometry for Fe_3O_4 nanostructures. The obtained results are understood based upon a core-shell structure consist of stoichiometric Fe_3O_4 surrounded by a non-stoichiometric one. The magnetic vortex NDs are further analyzed for their utilization in magnetic hyperthermia applications [2,3]. The specific absorption rate (SAR) for NDs is calculated by orientation-dependent hysteresis loss through micromagnetic simulation and found to be 16 % higher at $\theta = 15^o$ as compared to randomly oriented NDs, where q is the angle between magnetization (M) and applied field (H). Interestingly, the switching field (H_S) of magnetic vortex NDs is responsible for a larger hysteresis loss at $\theta = 15^o$ which is understood by developing a relationship with anisotropy constant (K). The theoretical SAR (~ 182 W/g_{NPs}) of NDs is almost constant for aspect ratio β (= t/d) ≤ 0.13 whereas it is dramatically enhanced by ~5 times (~ 862 W/g_{NPs}) at β = ~ 0.26, which is assigned due to the contribution of shape anisotropy. Our results indicate the implication of switching field (H_S), orientation, anisotropy (K), and geometrical parameters (d & t) for improving the heating performance of Fe_3O_4 nanodiscs.

1. H. M. Fan, J. B. Yi, Y. Yang. ACS Nano 3:2798–2808 (2009). DOI: 10.1021/nn9006797 2 Y. Yang, X. Liu, and Y. Lv, Adv Funct Mater 25:812–820(2015). DOI: 10.1002/adfm.201402764 3. D. H. Kim, E.A. Rozhkova, and I. V. Ulasov. Nat Mater 9:165–171(2010). DOI: 10.1038/nmat2591

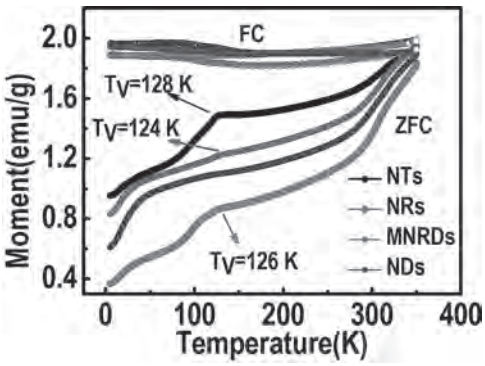

Fig. 1: Magnetization versus temperature for NTs, NRs, MNRDs, and NDs

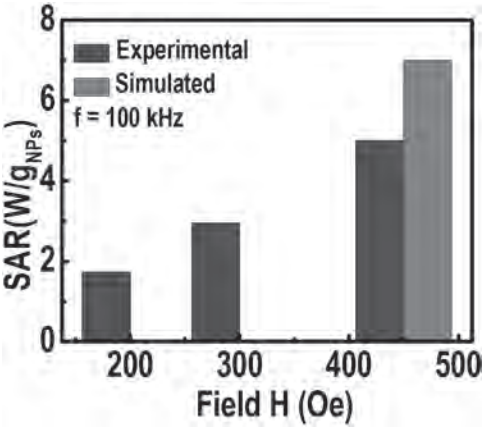

Fig. 2: Experimental and simulated SAR value for NDs at clinical relevant conditions.

C1-09. Improved Residual Flux Measurement Method Based on Transient Current Characteristics Used in Single-Phase Power Transformer.

S. Wu[1], Y. Wang[1], H. Cailing[1] and C. Liu[1] *1. Hebei University of Technology, Tianjin, China*

With the development of AC/DC UHV grid, large capacity transformer is widely used in power grid. After DC resistance measurement, no-load test and other operations of power transformer, mainly due to hysteresis phenomenon of ferromagnetic materials, a certain magnetic flux is left in the core, which is called residual flux. When transformer switching on without load, residual flux will lead to inrush current which is several times of the rated current. Inrush current endangers the mechanical stability and insulation strength of power transformer windings, and affects the normal operation of power system, resulting in many adverse effects. In this paper, an improved method is proposed to establish the relationship between residual flux and transient current characteristics by analyzing the transient current waveform of winding under different residual flux with different polarity DC voltage. DC voltage amplitude is determined by a criterion that the residual flux in the core should not change over 10% after the DC voltage unloaded. Based on the previous studies on positive and negative transient current, the relationship between transient characteristics and residual flux is further studied and analyzed. Combined with theory and experiment, the form of empirical formula and parameter calculation flow are determined. Compared with directly using transient current amplitude at a certain moment to calculate, using waveform characteristics to calculate residual flux is more accurate and less susceptible to measurement error and noise.

C. Huo, Y. Wang, S. Wu, Y. Yang, and Z. Zhao, "Residual Flux Density Measurement Method for Transformer Core Considering Relative Differential Permeability," IEEE Trans. Magn., pp. 1-1, 2020. G. Wenqi, W. Youhua, Z. Zhenghan, Y. Xiaoguang, and L. Yongjian, "Residual Flux in

the Closed Magnetic Core of a Power Transformer," IEEE Trans. Appl. Supercond., vol. 24, no. 3, pp. 1-4, 2014. W. Ge, J. Zhao, and Y. Wang, "Analysis of the residual flux influence on inrush current and electromagnetic force in large power transformer," The Journal of Engineering, vol. 2019, no. 16, pp. 2426-2429, 2019.

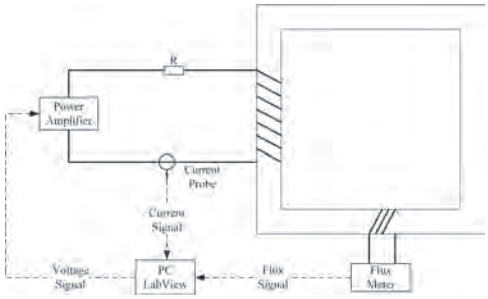

Fig.1 Experimental schematic for measuring residual flux.

C1-10. Narrow Ferromagnetic Resonance Linewidth in Perpendicularly Magnetized $Tm_3Fe_5O_{12}$ Thin Films Grown by Pulsed Laser Deposition. *D. Gouéré*[1], H. Merbouche[1], C. Carrétero[1], R. Lebrun[1], P. Bortolotti[1], V. Cros[1] and A. Anane[1] *1. Unité Mixte de Physique CNRS, Thales, Université Paris-Saclay, 91767 Palaiseau, France., Palaiseau, France*

Spintronic with garnets materials is an emerging field that promises the use of pure spin currents to realize low power electronics thanks to the insulating character and low Gilbert dampings of this family of materials. The recent demonstration of the possibility to control the magnetization dynamics with a DC current through spin-orbit-torques (SOT) provides some great perspectives in tunable spin wave devices for magnonic applications. An example illustrating these opportunities is the auto-oscillations that can be induced in YIG/Pt bilayers using SOT [1] or compensate the damping of propagating spin-waves [2]. In Bi doped YIG/Pt that shows a perpendicular anisotropy, coherent spin-waves emission can be generated by SOT [3]. However, SOT induced irreversible switching of magnetization has only been observed so far in $Tm_3Fe_5O_{12}$ (TmIG) thin films covered with Pt, with the disadvantage that TmIG has a much larger Gilbert damping than YIG and BiYIG [4], which limits the scope of applications. In this study, we grew some series of epitaxial TmIG with different thicknesses (from 6 to 50nm) by pulsed laser deposition (PLD) on sGGG(111)-oriented substrate. Their structural characterization demonstrated the high epitaxial strain of the films up to a thickness of 25nm. Epitaxial strain could be maintained up to films thickness of 50 nm as shown in the XRD pattern in Figure 1. Kerr microscopy was used to image the magnetics domains of the samples and their hysteresis loops. The results attest the strong perpendicular magnetic anisotropy of these TmIG samples as depicted in Figure 2. Magnetic dynamical properties were probed by broadband ferromagnetic resonance with a coplanar waveguide. We hence found that the Gilbert damping of TmIG can still be improved for very thin films by tailoring the growth parameter to achieve a ferromagnetic linewidth of 72 Oe at 12 GHz, narrower than recent results in literature [5,6]. This work has been funded by the European Union's Horizon 2020 research and innovation program within the FET-OPEN project CHIRON under grant agreement No. 801055.

[1] V. E. Demidov, S. Urazhdin, G. De Loubens, *et al.*, Physics Reports, 673, 1-31 (2017) [2] V. E. Demidov, S. Urazhdin, A. Anane, *et al.*, Journal of Applied Physics, 127, 170901 (2020) [3] M. Evelt, L. Soumah, A. B. Rinkevich, *et al.*, Physical Review Applied, 10 (4), 041002 (2018) [4] L. Soumah, N. Beaulieu, L. Qassym, *et al.*, Nature Communications, 9, 3355 (2018) [5] C. Tang, P. Sellappan, Y. Liu *et al*., Physical Review B, 94, 140403(R) (2016) [6] O. Ciubotariu, A. Semisalova, K. Lenz *et al.,* Scientific Reports, 9, 17474 (2019)

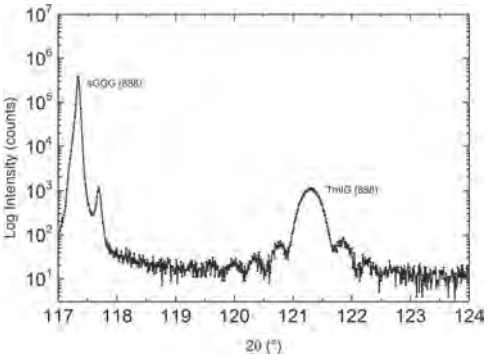

Figure 1 ***XRD pattern of the (888) plane for the 50nm TmIG sample***

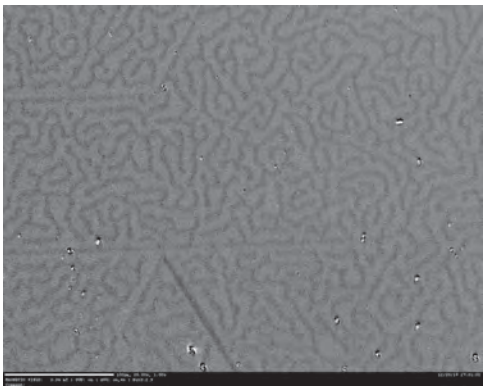

Figure 2 ***MOKE domains imaging of the 50nm TmIG sample***

C1-11. Cation-Specific Magnetic Depth Profiles of Ultrathin Fe_3O_4 Films Obtained by X-Ray Resonant Magnetic Reflectivity (XRMR). T. Pohlmann[1,2], T. Kuschel[3], J. Rodewald[1], J. Thien[1], K. Ruwisch[1], F. Bertram[2], E. Weschke[4], P. Shafer[5], J. Wollschläger[1] and *K. Küpper*[1] *1. Physics, University of Osnabruck, Osnabruck, Germany; 2. Photon Science, DESY, Deutsches Elektronen-Synchrotron, Hamburg, Germany; 3. Center for Spintronic Materials and Devices, Department of Physics, Universitat Bielefeld, Bielefeld, Germany; 4. Wilhelm-Conrad-Röntgen-Campus BESSY II, Helmholtz-Zentrum Berlin fur Materialien und Energie, Berlin, Germany; 5. Lawrence Berkeley National Laboratory, Berkeley, CA, US, Berkeley, CA, United States*

Magnetite, Fe_3O_4, is a frequently studied magnetic oxide growing in the inverse spinel structure Fe_3O_4 exhibits a ferrimagnetic ground state which stems from the interplay of its three cation species due to super exchange and double exchange depending on site and oxidation state: Octahedrally coordinated Fe^{2+} and Fe^{3+} ions, and tetrahedrally coordinated Fe^{3+} ions. The coupling among octahedral sites is ferromagnetic, while tetrahedral and octahedral sites couple antiferromagnetically. One of the most successful ways to discriminate between the magnetic contributions of these cations are X-Ray Magnetic Circular Dichroism (XMCD) experiments across the Fe $L_{2,3}$ edges, making use of a slight difference of their L edge energies and the easily resolvable antiferromagnetic coupling between the tetrahedral and the octahedral sites (c.f. Fig. 1). On the other side, X-Ray Resonant Magnetic Reflectivity(XRMR) is a technique combining the depth resolution of X-Ray Reflectivity and the site- and magnetism-sensitivity of XMCD. This enables us to determine the magnetooptical depth profiles at the energies characteristic for Fe^{2+}_{oct}, Fe^{3+}_{tet}, and Fe^{3+}_{oct} in the XMCD of Fe_3O_4/MgO(100) ultrathin films (c.f. Fig. 2). We find a ~3.9Å layer of enhanced magnetooptical absorption at the surface for both Fe^{3+} species but not for Fe^{2+} [1]. The magnetically enhanced Fe^{3+}_{tet} layer is additionally shifted about 3±1.5 Å into the sample compared to the Fe^{3+}_{oct} layer. We attribute this to the first unit cell from the surface containing an excess to Fe^{3+} cations.

[1] T. Pohlmann et al., arXiv:2005.01657 [2] S. Macke and E. Goering, J. Phys.: Cond. Matter 26, 363201 (2014).

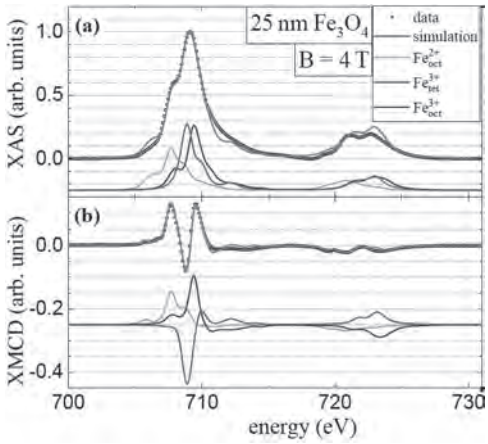

Fig. 1: (a) XAS and (b) XMCD spectrum at the Fe L2,3 edge for a 25nm Fe_3O_4 thin film, taken at 4T external magnetic field, at room temperature and in TEY mode. Black dots are data points; green, red and blue spectra are multiplet calculations for the three cation species of Fe3O4, the grey line is their sum.

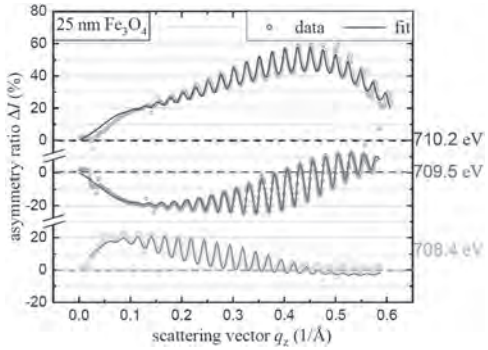

Fig. 2: XRMR data (open circles) and corresponding fits based on the algorithm introduced in [2] (solid lines) from the 25nm thin film, recorded at the three resonant energies of the XMCD L_3 edge. Data were recorded with a magnetic field of 200mT along the Fe_3O_4[001] direction at room temperature.

C1-12. Magnetic Properties of PLD-Grown TmYIG Thin Films.

E.R. Rosenberg[1], J. M. Shaw[2], G.A. Riley[2], S. Ngo[1], H. Nembach[2] and C. Ross[1] *1. Massachusetts Institute of Technology, Cambridge, MA, United States; 2. National Institute of Standards and Technology, Boulder, CO, United States*

Rare earth iron garnets (REIG) can be grown as thin films with strain-induced perpendicular magnetic anisotropy (PMA), and their spintronic applications have been studied intensively in recent years. The magnetic properties of REIGs have been manipulated via RE composition [1], strain engineering [2], and via substitutions such as Bi on the c-site to lower magnetic damping [3]. Thulium iron garnet (TmIG) in particular has excited great interest due to record-breaking spin orbit torque-driven domain wall velocities over 2 km/s and the presence of the Dzyaloshinskii-Moriya interaction, which stabilizes chiral Néel domain walls [4]. In this study we describe the static and dynamic magnetic properties of yttrium-substituted TmIG (TmYIG) thin films with a variety of Y:Tm ratios grown by pulsed laser deposition. We find that, by varying the Y:Tm ratio over a range of 0-0.67, we can tune the anisotropy energy of the film over three orders of magnitude and observe a transition from PMA to in-plane anisotropy with little change in room temperature magnetization. We relate the anisotropy to the changes in both magnetostriction and strain state vs. composition. Films with intermediate yttrium concentrations and low PMA display highly sheared easy axis loops with zero remanance which, based on micromagnetic simulations, is consistent with the spontaneous formation of stripe domains. Through broadband FMR measurements, we find that the g-factor of these thin films depends strongly on the yttrium content, varying from 1.56 for TmIG to 2.0 for YIG which gives an excellent agreement with Kittel's theoretical model for bulk garnet crystals (see figure 2) [5]. The widely tunable anisotropy in TmYIG is useful for spintronic device applications.

1. E.R. Rosenberg, L. Beran, C.O. Avci, *et al*., Phys. Rev. Materials, Vol. 2 no. 9 (2018) 2. G. Vilela, H. Chi, G. Stephen, *et al.* J. Appl. Phys., Vol. 127 no. 11, p. 115302 (2020) 3. L. Souman, N. Beaulieu, L. Qassym, *et al.*, Nature Communications, Vol. 9 no. 1, p.1 (2018) 4. L. Caretta, E.R. Rosenberg, F. Büttner *et al,* Nature communications, Vol. 11 no. 1, p.1 (2020) 5. C. Kittel, Physical Review, Vol.115 no. 6, p.1587 (1959)

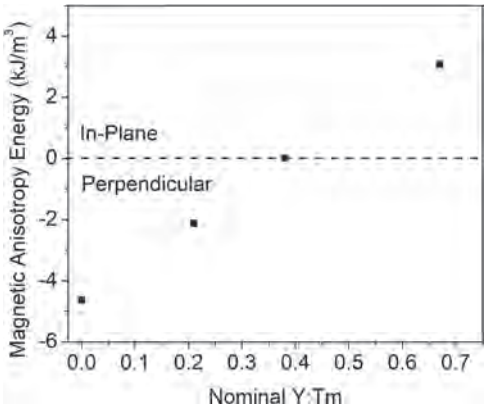

Fig. 1: Magnetic anisotropy energies of TmYIG thin films with different Y:Tm ratios

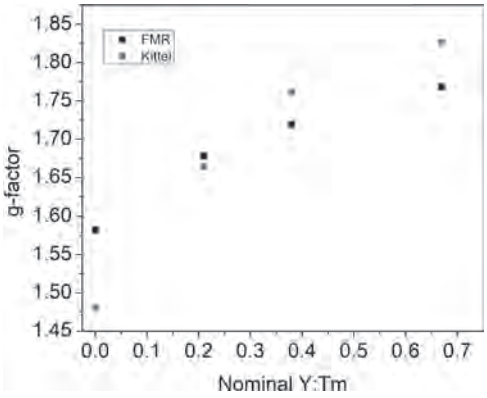

Fig. 2: Landé g-factors of TmYIG thin films with different Y:Tm ratios. There is good agreement between values obtained from FMR and from Kittel's model for bulk garnets.

C1-13. The Impact of the Solvent tanδ on the Magnetic Characteristics of Nanostructured NiZn-Ferrite Film Deposited by Microwave-Assisted Solvothermal Technique.

R.R. Kahmei[1], S. Arackal[1], S. Shivashankar[1], N. Bhat[1] and R. Sai[1] *1. Centre for Nanoscience and Engineering, Indian Institute of Science, Bangalore, India*

Nanostructured Ni-Zn ferrite (NZF) thin film, deposited by a CMOS-compatible microwave-assisted solvothermal (MAS) process, exhibits 'far-from-equilibrium' arrangement of cations in the spinel structure with significant anisotropy, thus promising for miniaturized passive devices in GHz regime [1, 2]. Achieving extreme cationic distribution at sub-200°C is the hallmark of this process [3] where, selected metal precursors dissolved in a solvent transform into metal oxide and nucleate on an immersed substrate under microwave heating at 2.45 GHz interacting with solvents of high loss-tangent (tanδ). The objective here is to study the impact of the solvent tanδ on the film's magnetic property, especially the surface spin-canting

layer and interparticular dipolar interaction. NZF films were deposited on Si(100) substrates using various ratios of ethanol (tanδ≈0.941), 1-decanol (tanδ≈0.1), and benzyl alcohol (tanδ≈0.667). The best characteristics were for ethanol:benzyl alcohol ratio (vol.) of 3:5. A smooth, densely packed NZF film (~ 200 nm) composed of highly crystalline nanoparticles (8.6 nm) resulted. Raman analysis of A_{1g} mode shows a degree of inversion for Fe^{3+} ions x = 0.21 corresponding to 89% population of Fe^{3+} in octahedral site which led to a net magnetic moment enhancement (M_s of 79 emu/cc@300K), much higher than with 1-decanol [1]. The magnetic size deduced from the Langevin function (D_L:9.4 nm) is consistent with that of Scherrer's crystallite size with surface spin canting layer of 0.5 nm at 300 K. Temperature-dependent magnetization at different dc fields shows strong inter-particle dipolar interaction, estimated as $E_{Dipole} \approx 1.9\times10^{-17}$ J (300 K); 1.3×10^{-16} J (5 K). The blocking process shows individual 2-level energy system replaced by a multi-valley energy system. Thus, T_B distribution and anisotropy energy barrier were ascertained from the derivative of thermoremnant magnetization with temperature. A close association between the anisotropy constants and strength of dipolar interaction is realized, driven by the influence of high microwave absorbing solvents.

[1] R.R. Kahmei, R. Sai, S. Arackal, S.A. Shivashankar, and N. Bhat, IEEE Magn. Lett. 10, 1 (2019). [2] R. Sai, S.D. Kulkarni, M. Yamaguchi, N. Bhat, and S.A. Shivashankar, IEEE Magn. Lett. 8, 3 (2017). [3] I. Bilecka and M. Niederberger, Nanoscale 2, 1358 (2010).

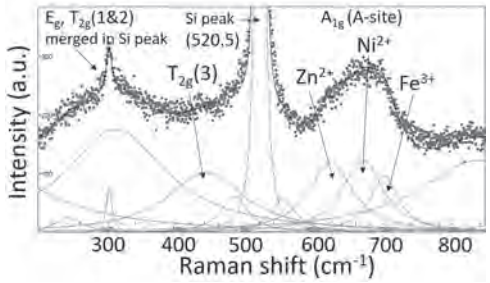

Deconvoluted A_{1g} mode of Raman spectra

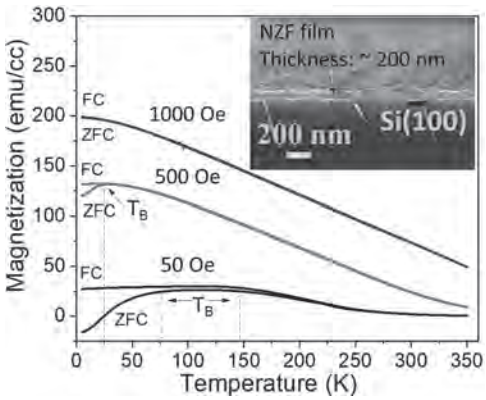

Temperature/field dependent magnetization(inset:FESEM image)

Session C2
RARE EARTH TRANSITION METAL BORIDES I

Tanjore V Jayaraman, Chair
University of Michigan, Dearborn, MI, United States

INVITED PAPER

C2-01. Finite-Temperature Dynamical and Static Properties of the Nd Magnet Studied by an Atomistic Modeling. *M. Nishino*[1,2], I.E. Uysal[2], T. Hinokihara[3,2] and S. Miyashita[3,2] *1. Research Center for Advanced Measurement and Characterization, National Institute for Materials Science, Tsukuba, Japan; 2. Elements Strategy Initiative Center for Magnetic Materials, National Institute for Materials Science, Tsukuba, Japan; 3. Institute for Solid State Physics, the University of Tokyo, Kashiwanoha, Japan*

Nd–Fe–B permanent magnets are indispensable materials for high-technology commercial products such as motors, electronic devices, etc., because of their high coercive force. However, the mechanism of the coercive force has not been well understood [1]. For the understanding of the microscopic mechanisms, atomistic modeling, which is a new trend of permanent-magnet modeling, is important. We have studied dynamical and static properties of the Nd magnet, $Nd_2Fe_{14}B$, by applying the stochastic LLG equation [2] and Monte Carlo methods to an atomistic model, in which microscopic parameters were introduced by first-principles calculations [2-7]. We have shown the temperature dependencies of the magnetization, domain-wall profiles, dipolar-interaction effect, ferromagnetic resonance, inhomogeneity effect, surface Nd anisotropy effect, etc. [2-7] In this presentation, we mainly show dynamical aspects of the magnet, focusing on the effect of the interface between grains and grain boundaries. There exist difficulties to estimate long relaxation times of barrier-crossing magnetization reversal quantitatively due to the limitation of simulation time and the dependence on the damping factor. Here we propose a statistical method to estimate precisely long relaxation times in the stochastic region, by which one can identify an initial transient process and a long-time regularly relaxation process. We show an estimation of the coercive force of a single grain using this method [6]. Local environments around rare-earth ions at the interfaces of rare-earth magnets may be different from those in the bulk. First-principles studies have suggested that the magnetocrystalline anisotropies of the Nd atoms at the (001) surface of grains in the Nd magnet have in-plane (c-plane) anisotropy, while those in the bulk have out-of-plane anisotropy. Thus, we investigated the effect of the surface magnetic anisotropy of the Nd atoms on the coercivity in the Nd magnet (Fig. 1). We analyzed the coercive force in three cases, in which the Nd atoms in surface layers have (I) no anisotropy, (II) in-plane anisotropy, and (III) doubly reinforced anisotropy for not only the (001) surface but also (100) surface, with the layer-depth dependence [6]. We find that at zero temperature the modification of the anisotropy of the Nd atoms at the first-surface layer reduces the coercive force in cases I and II and enhances the force in case III, but at room temperature, this modification does not affect the coercive force, and the modification at several surface layers is necessary to reduce or enhance the coercivity at room temperature. We also present the nucleation and pinning fields of the Nd magnet as a function of the strength of the anisotropy energy of the soft magnet and also as a function of the thickness of the soft magnet (Fig. 2) [7]. In the Nd magnet, reflecting the lattice structure, the properties of domain walls (DWs) depend on their moving directions. Bloch and Néel DWs move along the a (or b) and c axes, respectively. We show the difference in the nucleation and pinning fields between the Bloch and Néel DWs. We find that the thermal fluctuation effect affects the threshold fields in the Nd magnet significantly. We also find that the strength of the anisotropy energies of the soft magnet phase is not so important for the pinning field, while it is essential for the nucleation field, etc.

[1] S. Hirosawa et al., Adv. Nat. Sci.: Nanosci. Nanotechnol. 8, 013002 (2017). [2] M. Nishino and S. Miyashita, Phys. Rev. B 91, 134411 (2015); 100, 020403(R) (2019). [3] M. Nishino et al., Phys. Rev. B 95, 094429 (2017). [4] S. Miyashita et al., Scr. Mater. 154, 259 (2018). [5] T. Hinokihara et al., Phys. Rev. B. 97, 104427 (2018). [6] M. Nishino et al., submitted. [7] I. E. Uysal et al., Phys. Rev. B 101, 094421 (2020).

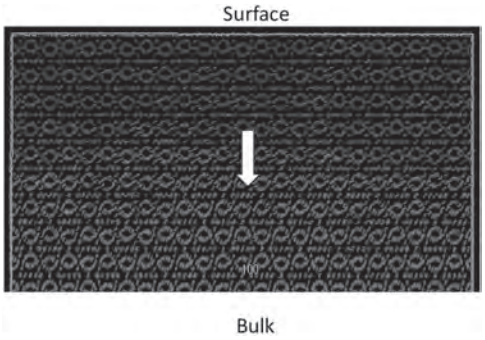

Magnetization reversal process affected by the effect of the surface magnetic anisotropy of the Nd atoms. Surface nucleation and domain growth along the c axis in the Nd magnet model.

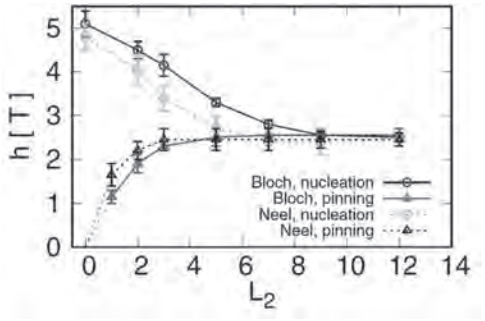

L2 (the thickness of the soft magnet) dependence of the nucleation and pinning fields of the Nd magnet model.

CONTRIBUTED PAPERS

C2-02. Revisiting, Understanding, and Predicting Magnetism and Magnetic Anisotropy of $RE_2Fe_{14}B$ (RE = Rare Earth) From Electronic Structure. H. Ucar[1], R. Choudhary[2] and *D. Paudyal*[2] *1. Chemical and Materials Engineering, California State Polytechnic University Pomona, Pomona, CA, United States; 2. Ames Laboratory, Ames, IA, United States*

We report here the developments in the predictions of the hard-magnetic properties of the $RE_2Fe_{14}B$ (R = rare earth) compounds from the state-of-the-art first principles Density Functional Theory (DFT) methods including spin orbit coupling. We focus primarily on three important materials owing to their potential use in permanent magnet applications: (i) $(Nd\text{-}RE)_2(Fe\text{-}TM)_{14}B$

(where TM = transition metal), because it is still the best performing magnet with its largest $(BH)_{max}$ among all rare-earth based magnets; (ii) $(Y\text{-}RE)_2(Fe\text{-}TM)_{14}B$ because, in addition to having reasonable hard-magnetic properties, it serves as a test-bed for the advancement of our understanding of the complex interplay between distinct iron sites in this structure; and (iii) $(Ce\text{-}RE)_2(Fe\text{-}TM)_{14}B$ because cerium, being the most abundant RE, is currently remerging as a candidate element - when alloyed with TM, for magnetic performance due to its prospects for providing anisotropic properties. A common underlying theme in the iron sublattice of all these compounds is that, high symmetric iron sites, most notably the $8j_1$, provide large magnetization, and they drive the magnetic polarizations of other iron sites. These distinguishable sites bring about interesting site substitution ideas with tremendous possibilities of achieving better magnetic properties with reduced cost. We also highlight the influence of boron for the stability of the tetragonal structure in these class of materials. The last but not the least, Ce's complex electronic structure associated with its mixed valency raise several questions that call for further exploration [1,2]. To help address the lack of understanding about Ce, we report electronic structure calculations of the $(La\text{-}Ce)_2Fe_{14}B$ system. We reveal that doping La with Ce at the 4f RE-site increases the magnetic anisotropy compared to the doping at the 4g RE-site. These changes in magnetocrystalline anisotropy energy (MAE) are linked to the orbital magnetic moments as well as the valence state of Ce at these two distinct RE sites.

[1] A. Alam, M. Khan, R. W. McCallum, and D. D. Johnson, Appl. Phys. Lett. 102, 042402, (2013). [2] T. W. Capehart, R. K. Mishra, G. P. Meisner, C. D. Fuerst, and J. F. Herbst, Appl. Phys. Lett. 63, 3642 (1993)

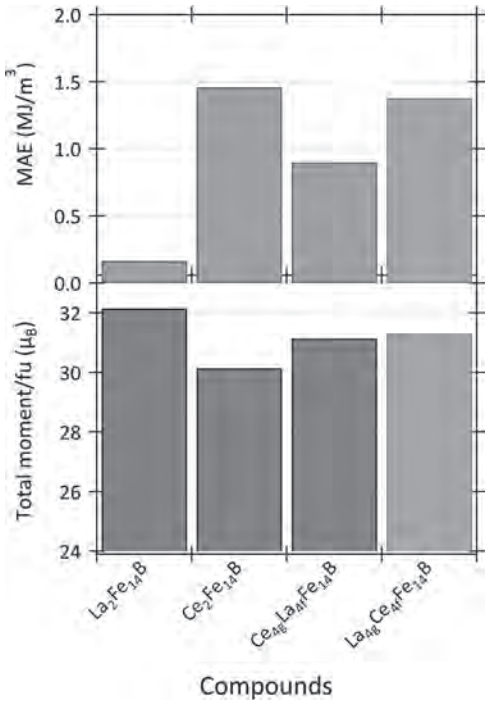

Fig 1: MAE and total magnetic moment/f.u. in four compounds investigated in this study: $La_2Fe_{14}B$, $Ce_2Fe_{14}B$, $Ce_{4g}La_{4f}Fe_{14}B$ and $La_{4g}Ce_{4f}Fe_{14}B$.

C2-03. Application of Systems Level Modeling for Addressing Criticality in Rare Earth Permanent Magnets. *I.C. Nlebedim*[1], X. Liu[1] and A. Sarkar[1] *1. Critical Materials Institute, Ames Laboratory, Ames, IA, United States*

In this talk, we will present how system levels modeling is being used to define critical paths for addressing challenges associated with the supply of rare earth elements for permanent magnets. Permanent magnets enable many applications including energy, national security, transportation, industrial automation and personal devices. However, the geographical distribution of rare earth elements poses a challenge for sustainable development and use of permanent magnets. This challenge can be addressed by systems level modeling which provides understanding of how suitable a permanent magnet is for an application, beyond BH_{max} and other properties typically measured in the laboratory. It provides a virtual testbed for determining when large demagnetization resistance is more important than flux or when high mechanical robustness is more crucial than Curie temperature. An example of tools for systems level modeling is finite element analysis (FEA). Such tools can be used to couple different physics that manifest in a given application in order to gain insight into actual contribution of a permanent magnet when used with other materials in a system. Via such approach, we have predicted and also experimentally validated that the magnetic field strength needed to align magnet powders in bonded magnets can be significantly reduced ($m_0H < 1T$). As shown in the figure for a surface mounted permanent motor, the torque generated at low alignment field of 0.25 T is comparable to those generated at higher alignment fields. We have also quantified the effect of using anisotropic bonded magnets, compared to isotropic bonded magnets. We have shown the economic impact of using Sm-Co magnets, compared to Nd-Fe-B for wind energy applications. This talk will cover different applications of systems level modeling which is a powerful tool for addressing criticality in the supply of rare earth elements for permanent magnet technologies.

INVITED PAPER

C2-04. Nucleation and Coercivity Analyses on the Atomistic Spin Model of Permanent Magnets. *Y. Toga*[1,2] *1. Institute for Solid State Physics, The University of Tokyo, Kashiwa, Japan; 2. Elements Strategy Initiative Center for Magnetic Materials (ESICMM), Tsukuba, Japan*

For the improvement of efficiency for cars, robots, and aerogenerators, etc., amelioration of high-performance permanent magnets is a key point to save energy. Especially the performance at high temperature (room temperature+100K) is a primary target. The coercivity mechanism of the permanent magnets is an unresolved issue for over half a century because magnetization reversal is multi-scale and multi-time physics. The multi-scale means the size from atomic-scale to reversal nucleation and crystal grains, the multi-time means the time from thermal fluctuations (~ps) of magnetic moments to the nucleation (~1second). The rare-earth permanent magnets (e.g., Nd-Fe-B) are composed of polycrystalline. The interfaces have been considered to play critical roles in the formation of magnetic nucleation and the inhibition of domain wall propagation. Therefore, the first step was to carry out multi-scale simulations [1-3], connecting first-principles calculation, spin model, and continuum models to reflect atomic-scale properties in the coercivity analysis. This approach successfully produced static properties, i.e., temperature dependences of the magnetic anisotropy constants and the exchange stiffness constant for the Nd-Fe-B magnet. However, in magnetization reversal processes, this approach hardly considers the effects caused by the non-uniformity near the interfaces/surfaces. As a next stage for the coercivity analysis, we propose an approach based on free-energy landscape simulations for the magnetization [4]. Here, we combined the replica-exchange Wang-Landau method and other some methods and then applied it to large size atomistic spin models. Figure 1 shows the quantitatively correct (not schematic) form of the free-energy landscape. From the shapes of the free energy with the reverse magnetic field $\mu_0 H_z$, we can determine the coercivity for the nucleation process with the thermal fluctuations. For the Nd-Fe-B spin model of isolated grains, we observed in Fig. 2 that the thermal fluctuations (i.e., surface effects and thermal activation) lead to a

downward convexity in the coercivity concerning the temperature. And also, we discover the nucleation volume is insensitive to a magnetic field around the coercivity. The proposed approach is complementary to conventional methods for the time evolution of atomistic spin models [5, 6], so we expect it to provide a breakthrough in the long-lived problem of the coercivity.

[1] Y. Toga, et. al., Phys. Rev. B 94, 174433 (2016). [2] S. Miyashita, M. Nishino, Y. Toga et al., Scripta Mater. 154, 259 (2018). [3] Y. Toga, et al., Phys. Rev. B 98, 054418 (2018). [4] Y. Toga, S. Miyashita, A. Sakuma, T. Miyake, Npj Comput Mater 6, 67 (2020). [5] S. C. Westmoreland, et al., J. Appl. Phys. 127, 133901 (2020). [6] I. E. Uysal, M. Nishino, and S. Miyashita, Phys. Rev. B 101, 094421 (2020).

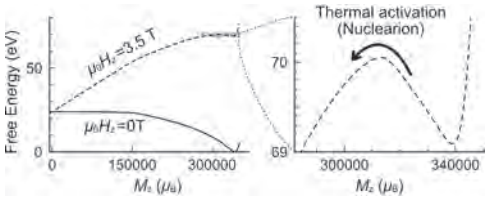

Free energy as a function of the magnetization M_z for the Nd-Fe-B isolated grain at 0.46T_C. The dashed line is obtained by applying a magnetic field to the free energy under the non-magnetic field (the solid line).

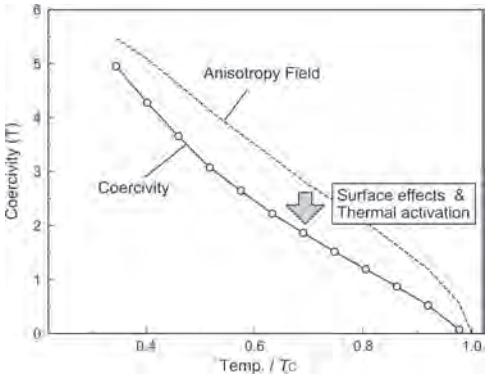

The circle line is the temperature dependence of the coercivity, and the dashed line is the one of the magnetic anisotropy field. Surface effects and thermal activation cause the difference between the two lines.

CONTRIBUTED PAPERS

C2-05. Cold Spray Additive Manufacturing of Permanent Magnets. *A. Baker*[1], R. Thuss[2], N. Woollett[1], E. Stavrou[1], S. Mccall[1] and H. Radousky[1] *1. Lawrence Livermore National Laboratory, Livermore, CA, United States; 2. TTEC LLC, Berryville, VA, United States*

Additive manufacturing (AM) techniques are well suited to the fabrication of structural materials in novel form factors, but struggle when applied to functional materials such as magnets where controlled microstructure is of paramount importance. The careful work optimizing composition and grain structure is lost in high energy AM processes. Binder-jetting techniques [1, 2] have had success when mixing NdFeB formulations with shear-thinning inks, but limitations on density and operating temperature may preclude these from competing in the high-performance space. Cold-spray AM offers an unconventional approach to circumvent this limitation [3], entraining NdFeB powders in a supersonic gas stream to direct high-density deposition on substrates ranging from aluminum to quartz, in multiple form factors. A survey of recent progress will be presented, focusing on the influence of powder preparation and spray conditions on the final magnetic properties. The as-sprayed material has a random microstructure with nucleation-limited magnetic reversal, and a parasitic soft phase that can be eliminated through proper choice of spray conditions.

[1] Li *et al*, *Sci Rep* 6, 36212 (2016), https://doi.org/10.1038/srep36212 [2] Huber, C *et al. Sci Rep* 7, 9419 (2017). https://doi.org/10.1038/s41598-017-09864-0 [3] Baker *et al*, JOM (2020) https://doi.org/10.1007/s11837-020-04151-2

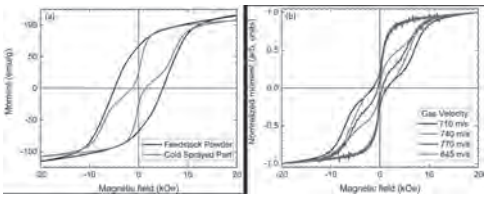

Figure 1: (a) Room temperature M-H loops for NdFeB, showing formation of a secondary phase due to particle damage. (b) Analysis of link between gas velocity in particle damage shows that reducing kinetic energy improves magnetic performance.

C2-06. Upscaling of the Novel 2 Powder Method for the Manufacturing of Heavy Rare Earth-Lean Permanent Magnets. *K. Opelt*[1], T. Ahmad[1], O. Diehl[1], M. Schönfeldt[1], E. Brouwer[1], J.D. Rossa[1], J. Gassmann[1] and O. Gutfleisch[1,2] *1. Magnetic Materials, Fraunhofer-Einrichtung fur Wertstoffkreislaufe und Ressourcenstrategie IWKS, Hanau, Germany; 2. Functional Materials, Technische Universität Darmstadt Fachbereich Material- und Geowissenschaften, Darmstadt, Germany*

The 2 powder method for the production of high performance Nd/Pr-Fe-B sintered magnets with low content of critical elements is investigated. Therefore, two starting powders, a coarse heavy rare-earth (HRE) free main phase powder (D_{50} = 5.5 μm) and a fine HRE contending anisotropy powder (D_{50} = 2.1 μm), were produced by the conventional powder metallurgical magnet production process. For each alloy, about 20 kg raw materials were strip-casted, as well as FeB pre-alloys. The nominal composition in wt.% was $[(Nd_{22.7}Pr_{7.5}])_{30.2-x}Dy_xFe_{bal}Co_{1.9}TM_{0.32}B_{0.91}$ for both alloys. Thereby TM means transition metals, which are Cu, Ga and Al. In the case of the starting alloy for the main phase powder (MP) the Dy content was set to 0 wt.% and in the case of the starting alloy for the anisotropy powder (AP) the Dy content was set to 10.0 wt.%, whereby the ratio of Nd/Pr was fixed. Afterwards the strip-cast alloys were been hydrogen decrepitated and jet milled. The powders were blended in different concentrations to reach a HRE content of 0, 1, 2, and 3 wt.% in the magnets. Fig.1 shows the demagnetization curves of the magnets produced by using the 2 powder. Coercivity in the magnets was increased about 750 kA/m for the samples with 3 wt.% Dy, while remanence stays almost constant. The core shell structure of HREs enclosing the 2-14-1 grains could been observed within the whole magnet independent of its size or the position in the magnets containing 2 and 3 wt.% Dy with secondary electron microscopy (Fig.2). In order to demonstrate the advantage of the 2 powder process that magnets independent of their dimension can be produced, it was compared with the well-known grain boundary diffusion process (GBDP). Thereby magnets with 10 mm thickness were manufactured once by the 2 powder method and once by the GBDP, showing that using the GBDP for such large magnet dimensions is not useful any more, whereas the 2 powder method is.

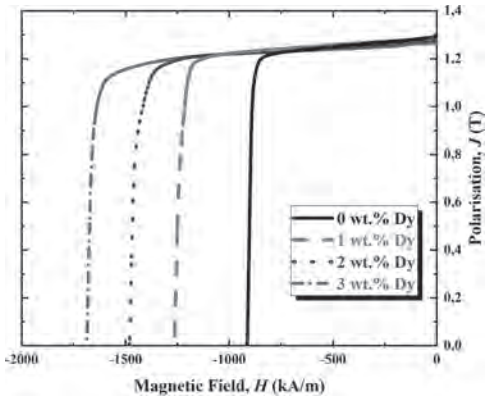

Fig.1: Demagnetization curves of the magnets produced by using the 2 powder method.

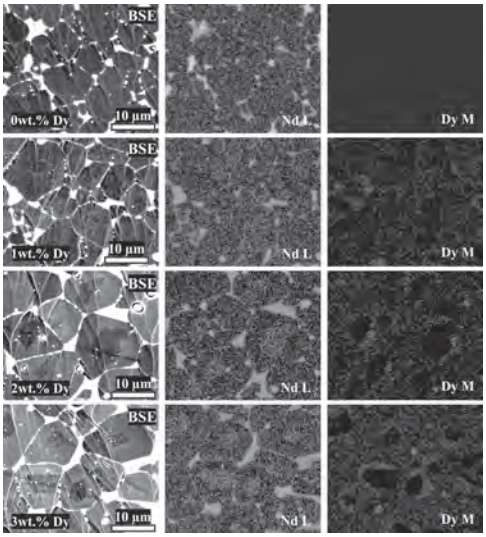

Fig.2: Microstructure investigation of the magnets produced by using the novel 2 powder method. The left column show the SEM BSE images and the other columns show the corresponding EDX maps for Nd and Dy for the very same regions.

C2-07. Nd-Fe-B Based Permanent Magnetic Materials Design for Additive Manufacturing: 3DREMAG. *S. Riegg*[1], J. Reijonen[2], O. Tosoni[3], J. Gassmann[4], K. Skokov[1] and O. Gutfleisch[1] *1. Material and Geo science, Functional Materials, Technische Universität Darmstadt Fachbereich Material- und Geowissenschaften, Darmstadt, Germany; 2. VTT Technical Research Centre of Finland Ltd, Espoo, Finland; 3. Commissariat a l'energie atomique et aux energies alternatives Laboratoire d'Innovation pour les Technologies des Energies Nouvelles et les Nanomateri, Grenoble, France; 4. Fraunhofer-Einrichtung fur Wertstoffkreislaufe und Ressourcenstrategie IWKS, Hanau, Germany*

Recently, additive manufacturing (AM) of functional materials started integrating an additional physical property available besides the mechanical stability in printed parts. This additional property can be an increased electrical conductivity or as addressed here a specific magnetic stray field. AM allows near-net-shape manufacturing of complex magnet shapes, avoiding significant machining waste during conventional manufacture of the final shape from sintered magnet blocks. However, the development of the AM process in general requires a qualified starting material for each process such as powder bed fusion [1], binder jetting or material extrusion. Since the supply of metal powders for AM is limited in general, and there is no Nd-Fe-B based powder designed for use in AM, the development of a Nd-Fe-B-based starting material for commercial production is the goal of the EIT Raw Materials funded project 3DREMAG [2]. Commercial powders designed for injection molding are already used for different AM techniques in combination with different polymers and binders [3 and references therein]. E.g. self-produced Mn-Al powders were used in electron beam melting to produce polymer (and rare-earth element) free hard magnetic fully dense bodies [4]. The printing process was followed by a heat treatment to achieve 90% of the hard ferromagnetic tau-phase in the samples. It is very challenging to obtain fully dense Nd-Fe-B magnets by AM due to the specific microstructure of uniform micrometer sized Nd2Fe14B grains separated by a rare-earth rich grain boundary phase that has to be established to achieve high remanence and coercivity. To obtain sufficient amounts of powders that can be processed by powder bed fusion, Nd-Fe-B strip cast flakes are milled and further plasma spheroidized. First results of lab scale production of the powders and first AM tests will be presented and discussed.

[1] Mateusz Skalon, Michael Görtler, Benjamin Meier, Siegfried Arneitz, Nikolaus Urban, Stefan Mitsche, Christian Huber, Joerg Franke and Christof Sommitsch, Influence of Melt-Pool Stability in 3D Printing of NdFeB Magnets on Density and Magnetic Properties, Materials 13 (2020), 139. [2] http://3dremag.eu [3] Christian Huber, Gerald Mitteralmskogler, Michael Goertler, Iulian Teliban, Martin Groenefeld, Dieter Suess, Additive manufactured isotropic NdFeB magnets by stereolithography, fused filament fabrication, and selective laser sintering, arXiv:1911.02881 [4] I. Radulov, V. Popov Jr, A. Koptyug, F. Maccari, A. Kovalevsky, S. Essel, J. Gassmann, K. Skokov, M. Bamberger, Production of net-shape Mn-Al permanent magnets by electron beam melting, Additive Manufacturing 30 (2019) 100787.

C2-08. Understanding the Enhancement in Hard Magnetic Properties of Rapidly Solidified (Nd, Pr)-Fe-B Melt-Spun Ribbons. *K. Gandha*[1], X. Liu[1], W. Tang[2] and I.C. Nlebedim[1] *1. Critical Materials Institute, Ames Laboratory, Ames, IA, United States; 2. Ames Laboratory, Ames, IA, United States*

The coercivity of $RE_2Fe_{14}B$-type permanent magnet is strongly influenced by the microstructural features such as grain boundary phases as well as grain size. Micromagnetic simulations are powerful tools for revealing the correlation between microstructure and the evolution of hard magnetic properties, including the effects of grain size and grain boundary phases. We have combined micromagnetic simulations and experiments to elucidate the role of excess RE (Nd/Pr) in determining the resulting hard magnetic properties of Nd-Pr-Fe-B melt-spun ribbons. Also, the effect of non-magnetic grain refining refractory carbide (TiC) on both the microstructure and magnetic hardening was studied. For the simulated polycrystalline microstructure of Nd-Pr-Fe-B magnets (Fig. 1(a)) with a mean grain size of 40 nm, the coercivity increases with decreasing inter-grain magnetic exchange interaction Fig. 1(b). The increasing trend in magnetic coercivity of measured melt-spun (Nd, Pr)–Fe–B alloys is ascribed to weak inter-grain exchange coupling due to non-magnetic RE-rich grain boundary phase (Fig. 1(c)) and/or TiC at grain boundary (Fig. 1(d)). This work provides useful information on the role of non-magnetic grain boundary phase to improve the coercivity in Nd-Pr-Fe-B magnets. Combined with experimental and modeling results, we will discuss the mechanism responsible for the enhancements in coercivity and the suitability of the alloys for high performance permanent magnet development. This research was supported by the Critical Materials Institute, an Energy Innovation Hub funded by the U.S. Department of Energy, Office of Energy Efficiency and Renewable Energy, Advanced Manufacturing Office.

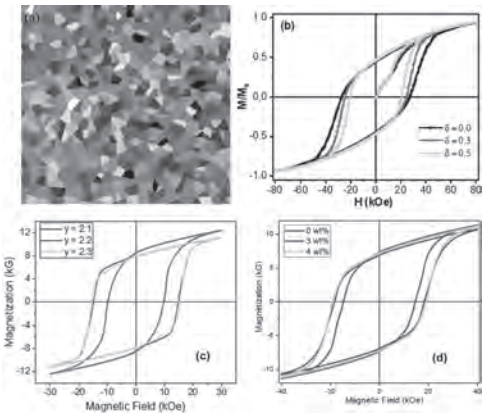

Fig. 1: (a) A polycrystalline microstructure model of Nd-Pr-Fe-B magnets created by the Voronoi tessellation method (mean grain size of 40 nm based on the experimental values); (b) Calculated magnetic hysteresis loops of Nd-Fe-Fe-B with different inter-grain exchange interaction of δ=0, 0.3 and 0.5, mimicked the role of non-magnetic grain boundary phase; (c-d) Measured magnetic hysteresis loops of thermally treated $(Nd_{0.80}Pr_{0.20})_yFe_{14}B$ (y = 2.1, 2.2, 2.3) and $(Nd_{0.65}Pr_{0.35})_{2.6}Fe_{14}B+(TiC)_x$ (x = 0, 3, 4) melt-spun ribbon measured at 300 K.

C2-09. Magnetic Properties of $R_2Fe_{14}B$ Sintered Magnets Substituted 50 at Substitution of Nd With Y and Ce. *Y. Enokido*[1], A. Koda[1], Y. Umeda[1], D. Tanaka[2] and Y. Kitamoto[3] *1. Technology and Intellectual Property HQ, TDK Corportion, Chiba, Japan; 2. Production Engineering HQ, TDK Corportion, Chiba, Japan; 3. Department of Materials Science and Engineering, Tokyo Institute of Technology, Yokohama, Japan*

Sintered $R_2Fe_{14}B$ (R: rare earth element) magnets with 50 at substitution of Nd by Y and Ce were studied in order to reduce the amount of precious rare earth elements used and to make effective use of the surplus rare earth elements. Nd was substituted with Y for larger magnetization and Ce for higher coercivity. By substituting 50 at% of Nd by Y and Ce with an equi-atomic composition, a maximum energy density of 355 kJ/m^3 was achieved with the residual flux density of 1.38 T and the coercivity of 533 kA/m as shown in Fig. 1. In order to increase the coercivity, the introduction of $R_6Fe_{13}Ga$ grain boundary phase to lead the magnetic separation between grains, which is commonly used for $Nd_2Fe_{14}B$, was studied, however the coercivity was not improved due to a large magnetization of $R_6Fe_{13}Ga$, 0.3 to 0.5 T. By introducing the RFe_2 grain boundary phase, the coercivity of 1063 kA/m with the residual flux density of 1.22 T was achieved at the composition of Ce of 40% in the total rare earth elements in $R_2Fe_{14}B$ sintered magnet. The magnetization of the RFe_2 phase was estimated to be about 0.3 T and was not sufficiently low. Since the RFe_2 boundary phase improved the covering of the grains, the magnetic separation was enhanced to increase the coercivity.

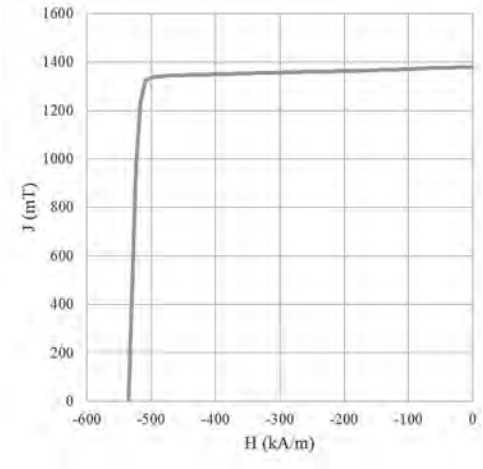

Demagnetization curve of 50 at% Nd substituted $R_2Fe_{14}B$ sintered magnet.

C2-10. Manifestation of Initial Crystallization and c-Axis Texture in Pr-Fe-B Thin Films Grown on Glass Substrates. L.T. Tran[1], *C. Chang*[1] and A. Sun[1] *1. Yuan Ze University, Chung-Li, Taiwan*

$Pr_2Fe_{14}B$-based thin films are the useful nano-material for the high-tech performance of the magnetic devices. With its studied outstanding magnetic property such as high uniaxial magnetocrystalline anisotropy (K_u), high coercivity (H_c), high saturation magnetization (M_s), large energy products (BH_{max}), excellent anisotropic behavior, and super low spin-reorientation at temperature about 4.2 K, $Pr_2Fe_{14}B$ magnetic thin films become an alternative candidate for the $Nd_2Fe_{14}B$-based magnetic thin films. In this study, the perpendicular magnetic anisotropy (PMA) Pr-Fe-B films were deposited on corning glass substrate at 600 °C with Si_3N_4 cover layer and underlayer from $Pr_{25}Fe_{65}B_{10}$ alloy target by RF magnetron sputtering technique. VSM, XRD, SEM, TEM, and EDS measurements were applied to investigate the relationship between thickness and the microscopic magnetization structures of the PrFeB layer which initiated and propagated crystallization of PMA $Pr_2Fe_{14}B$ phase. The magnetic properties of sputtered Pr-Fe-B film was also investigated in terms of the micro-texture evolution. The structure with thickness 50 nm showed the initial point of crystalline characteristic. The initial appearance signal of c-axis orientation of $Pr_2Fe_{14}B$ phase and the perpendicular coercive force in the film were comparable at 50 nm, and were alternatively evolved on glass substrates. SEM, TEM, and EDS results revealed that localized grains occurred at the initial stages of growth, and developed non-uniform grain networks across the substrate. The highly c-axis oriented films have a special microstructure which $Pr_2Fe_{14}B$ phase showed blossom surface morphology. The exchange coupling was mainly explained for the two-phase nanostructure formed from hard magnetic phase and soft magnetic phase. The texture with the c-axis perpendicular to the film plane had finely signal of development after in-situ annealing at 600 °C. The magnetization irregularity of the thin film was strongly affected by the underlayer and the substrate. The magnetic analysis assuming that the value of film was composed of the correlation between microstructures and magnetic properties on underlayer and substrates.

Session C3
INTERDISCIPLINARY APPLICATIONS II
(Poster Session)

Feodor Ogrin, Chair
University of Exeter, Exeter, United Kingdom

C3-01. Intrinsic Magnetic Properties of Individual Magnetite Nanoparticles With Different Sizes and Shapes. *H. Mamiya*[2], H. Fukumoto[1], J. Cuya Huaman[1], K. Suzuki[1], H. Miyamura[1] and B. Jeyadevan[1] *1. Shiga Kenritsu Daigaku Kobakugu Daigakuin Kogaku Kenkyuka, Hikone, Japan; 2. National Institute for Materials Science, Tsukuba, Japan*

Understanding the magnetic properties of magnetite nanoparticles (MNPs) is a key to advance biomedical applications of magnetic nanomaterials. In prior studies, shape-controlled MNPs have been synthesized for studying surface effects on the magnetic properties, while nonmagnetic-layer thickness-controlled MNPs have been prepared for investigating dipolar interaction effects on those properties. Little has been, however, clarified due to confusion of the surface and dipolar effects that can rarely be controlled simultaneously. In this study, spherical, cubic and octahedral-shaped MNPs with average sizes ranging from 7.6 nm to 23.4 nm were synthesized using solution techniques. Then, these nanoparticles were coated with appropriate shell thicknesses of silica to prepare magnetic interaction-free samples and their non-interactive nature was confirmed through first-order reversal curve (FORC) diagrams (Fig. 1). For these well-isolated nanoparticles, remanent magnetizations of the hysteresis loops are just equal to half of the saturation magnetizations. This result indicates that uniaxial magnetic anisotropy is predominant in each nanoparticle. To clarify the origin of the uniaxial magnetic anisotropy, the analysis of blocking temperature - switching field distribution diagrams are constructed based on thermal decay curves of isothermal remanent magnetization under various applied fields. The obtained effective magnetic anisotropy constants are distributed around 10-20 kJ/m and have insignificant size dependence. This result seems inconsistent with the inverse proportional relationship between magnetic anisotropy and the size predicted from surface magnetic anisotropy contribution. The theoretical calculation suggested that the crystalline magnetic anisotropy plays a major role in magnetic properties of the magnetite nanoparticles at lower temperatures. However, it should be noted that effective magnetic anisotropy seems slightly different for MNPs with different shapes. The mechanism is discussed from the viewpoints of the shape, surface and crystalline anisotropy contributions [1].

[1] H. Mamiya, H. Fukumoto, J. L. Cuya Huaman et al., ACS nano, in press.

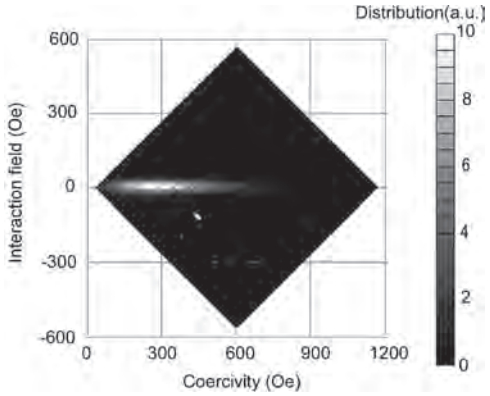

Fig. 1 FORC diagram for magnetite particles with a mean diameter of 13.1 nm

C3-02. Ab Initio Calculation of Hubbard Parameter (U) for Alpha-MnO_2. *R. Mahajan*[1] and A. Kashyap[1] *1. Indian Institute of Technology Mandi, Mandi, India*

On-site Coulomb repulsion energy represented as Hubbard corrections (U), is needed to predict the properties of materials containing partially filled d and/or f shells. Timrov et al. [1] has developed a first-principles approach for the calculation of Hubbard parameters from linear-response theory-based (using density-functional perturbation theory for primitive cells with monochromatic perturbations). Following this approach, we present here the first-principles computation of U for α-MnO^2. This material is an active catalyst for oxygen reduction and evolution reactions [2]. The most common oxidation state of Mn is +4 in Alpha-MnO_2 but it also shows a large range of Mn oxidation states (+2 to +6) and hence, it combines with many elements. It has a wide range of applications e.g as a cathode for lithium-air batteries [3], to name a few. α-MnO_2 shows semiconducting behavior with an indirect experimental bandgap of 1.3eV [4]. In this work, electronic structure and magnetic properties of α-MnO_2 have been studied using the ab initio value of U. Hubbard parameter U is reported here. For Mn, we set the U value to 3.9eV. This is an empirical approach but not predictive. The calculated value of U is 4.70eV from density functional perturbation theory calculation [1]. For this value of U, the bandgap for the material is predicted correctly. The computed magnetic structure is found to be antiferromagnetic as known experimentally [5] and theoretically [6].

References [1]. Iurii Timrov, Nicola Marzari, and Matteo Cococcioni. Hubbard parameters from density-functional perturbation theory. *Physical Review B,* 98(8):085127, 2018. [2]. Ankita Mathur and Aditi Halder, *Catalysis Science and Technology*, 9,5, 1245--1254 (2019). [3]. Crespo, Yanier and Seriani, Nicola, *Journal of Materials Chemistry A*, 2,39 16538--16546 (2014). [4]. Gao, Tao, et al. "Microstructures and spectroscopic properties of cryptomelane-type manganese dioxide nanofibers." *The Journal of Physical Chemistry C* 112.34 (2008): 13134-13140. [5]. N. Yamamoto, T. Endo, M. Shimada, and T. Takada, Jpn. *J. Appl Phys*. 13, 723 (1974). [6]. Crespo, Y, and Seriani, *Physical Review B*, 88,14,144428 (2013).

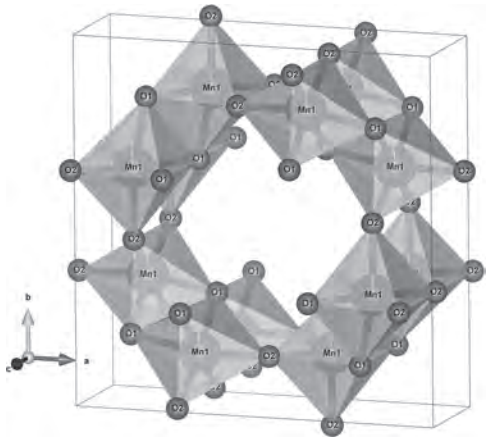

Fig 1. Crystal Structure of α-MnO_2

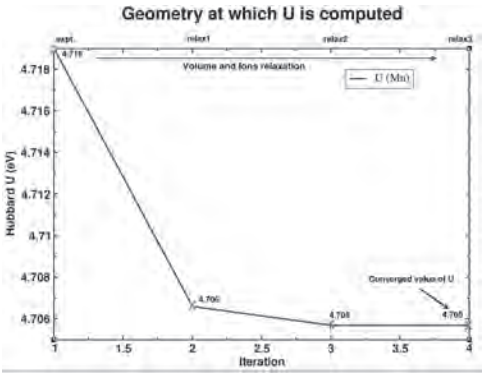

Fig 2. Self Consistent calculation of U_{eff}

C3-03. Oleic Acid Functionalized Fe_3O_4 Magnetic Nanoparticles and its Adsorption Capability of oil for Potential Biomedical Applications. *G.C. Hermosa*[1], K. Chen[1] and A. Sun[1] *1. Yuan Ze University, Chung-Li, Taiwan*

Hypertension is caused by excessive oils present in the blood vessels and is a global epidemic at present. Though the conventional method such as different drug blockers are available, they still face challenges regarding adverse effects which can greatly limit their efficacies. Oleic acid (OA) is a good lipophilic material, which already widely used in nanoparticle synthesis since it can form a protective layer and can strongly be bonded to the nanoparticles. In recent years, Fe_3O_4 (commonly known as magnetite) is the choice of researchers because of their, high moment at low magnetic field, superparamagnetic property, stability at physiological conditions, biocompatibility and excellent adsorption capacity. In order for the OA suitable to be controlled *in vivo* applications and for an easy recovery from aqueous solutions, they are coated with magnetite nanoparticles. Henceforth, in this work, magnetite was synthesized via co-precipitation method and modified with different amounts for oleic acid (x=0.5, 1, 2 mL) with the evaluation of the synthesis process parameters (temperature, H_2O amount and pH), in seeking to understand the adsorption capability of oil for potential biomedical usage. The morphology and chemical structure of the OA coated Fe_3O_4 nanoadsorbents were characterized by FT-IR, XRD, SEM, VSM and MTT assay for the cytotoxicity test. Successful coating was confirmed by FTIR and showed COO- groups within the spectra. The results indicated that the adsorption capacity was 588, 833 and 1000 mg/g for x= 0.5, 1 and 2 mL respectively. An increase in the amount of OA leads to the decrease in magnetization but still demonstrated a superparamagnetic property for an easy recovery. Grain size was evaluated, and was found out to be in the range of 8nm-10nm. The adsorbent is well fitted on the Langmuir model suggesting a monolayer adsorption. Regarding the adsorption kinetics, the adsorbent follows the pseudo second order with high $R^2 = 0.98$. The nanoadsorbent exhibited a high cell viability rate signifying low toxicity. Therefore, the synthesized nanoparticle is a good candidate for biomedical applications as such for hypertension treatment, as shown in this study.

N. Jović Orsini, B. Babić-Stojić, and G. F. Goya, *Journal of Magnetism and Magnetic Materials,* vol. 449, pp. 286-296, (2018). X. Wang, Y. Shi, R. W. Graff, D. Lee, and H. Gao, *Polymer,* vol. 72, no. Supplement C, pp. 361-367, (2015). H.-C. Roth, S. P. Schwaminger, M. Schindler, F. E. Wagner, and S. Berensmeier, *Journal of Magnetism and Magnetic Materials,* vol. 377, pp. 81-89, (2015). M.-J. Chen, H. Shen, X. Li, J. Ruan, and W.-Q. Yuan, *Chemical Papers,* vol. 70, no. 12, pp. 1642-1648, (2016). L. Zhang, R. He, and H.-C. Gu, *Applied Surface Science,* vol. 253, no. 5, pp. 2611-2617, (2006).

C3-04. Weak Magnetic Anomaly Signal Detection Based on Entropy of Coherent Differential Signal. *Z. Wang*[1], J. Qiu[1], D. Xie[1], J. Ou[1] and Q. Xu[1] *1. Key Laboratory of Optoelectronic Technology & System of Ministry of Education, College of Optoelectronic Engineering, Chongqing University, Chongqing, China, Chongqing, China*

Magnetic anomaly detection (MAD) can hide self-information better than acoustic detection, due to the passive detection performance. It is of great research significance in the detection, positioning and tracking of underwater targets. However, MAD is not ideal for weak target signals for its interference of geomagnetic background noise [1]. We proposed a coherent differential minimum entropy (CDME) method, which used the coherence of the background noise between the two detection signals, and performed a difference operation in the frequency domain to reduce the interference of the practical background noise. The low spatial stability of geomagnetic noise at frequencies produced high-frequency noise [2], which interferes with the detection of weak magnetic anomaly signals. Compared to adding a low-pass filter, we used entropy to describe the information of the ferromagnetic target on the surrounding magnetic field, highlight the existence of target signals and improve the ability to detect weak magnetic anomaly signals. The simulated magnetic anomaly signal and the detected background noise signals constituted the simulated detection signals. According to the Neyman-Pearson criterion, the relationship between detection capability and the signal-to-noise ratio of the three methods was calculated (Fig. 1). Compared with the adaptive coherent noise suppression (ACNS) method, CDME could achieve an incremental detection probability of about 53.9%, and it improves about 16.8% than the method of adding a low-pass filter method. The processing effect of the actual detection data shows that the CDME method is more advantageous for weak magnetic anomaly signals detection (Fig. 2).

[1] B. Tan, J. B. Guo and G. Chang, Journal of Intelligent & Fuzzy Systems., Vol. 36, p.6669(2019). [2] D. Liu, X. Xu and C. Huang, Measurement Science and Technology., Vol. 26, p.015008(2015).

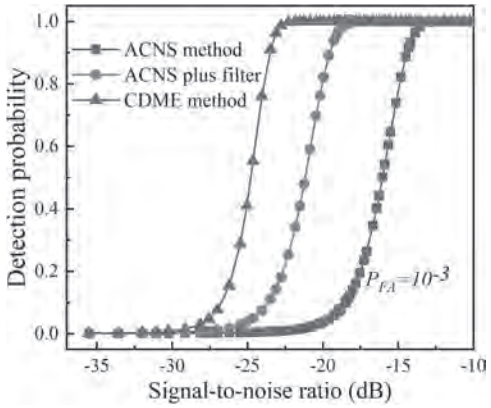

Fig. 1: The detection probabilities of three methods. We have used a target characteristic time in 1.6s. The threshold value was set using the Neyman-Pearson criterion for false alarm rate less than 0.1%.

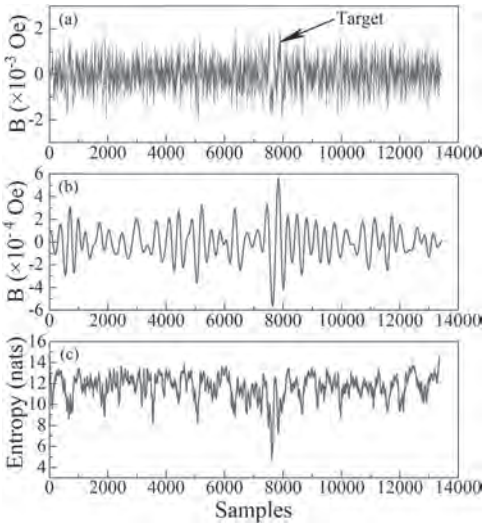

Fig. 2: A signal of an Iron target aligned with the Earth magnetic field, contaminated by real-world magnetic noise. The target moved along a straight line toward the sensor, reaching a CPA of 1.5m. (a) Signal output by the ACNS method. (b) Signal output by the method of ACNS plus a low pass filter. (c) Signal output by the CDME method.

C3-05. Conceptual Design of Magnetic Force Control System Using Wedge Mechanism. A. Wang[1], S. Park[1], M. Noh[1] and *Y. Park[1] 1. Chungnam National University, Daejeon, The Republic of Korea*

This paper presents a conceptual design and a proof-of-concept to control a magnetic force using a wedge mechanism. The concept starts with the general knowledge that magnetic force is inversely proportional to distance. A magnetic model is created, which consists of a permanent magnet (PM), two magnetic flux paths, two wheels, and a steel plate (Fig. 1). This model is subjected to formulate a mathematical relationship between the PM position and a magnetic force exerted on the steel plate. A 3D simulation is conducted to verify the effectiveness of the developed mathematical model. The comparison between the mathematical and simulation models is likely to be fair. The next is to design a wedge mechanism, which is composed of two wedges, a trenching plate, and a stepping motor (Fig. 2). Finally, the proof-of-concept is place on a magnetic force measurement, and subjected to the experiments. The result shows that the magnetic force change according to the PM movements is 84.5 percent with simulation and 80.1 percent with the experiments, respectively. It can be concluded that the proposed concept is effective to control the magnetic force reasonably.

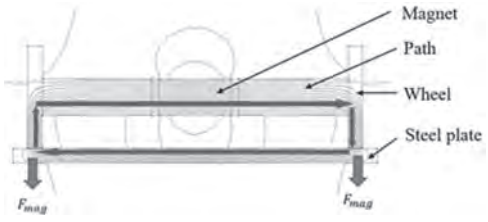

Fig. 1 A Schematic of magnetic model

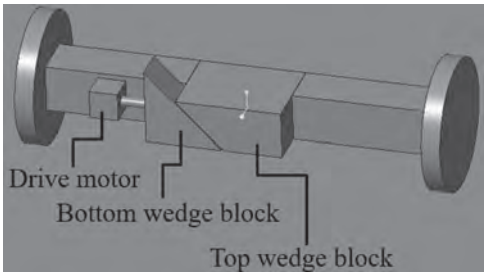

Fig. 2 A 3D model of Proof-of-Concept

C3-06. Investigation of the Graphitization Process of a Highly Oriented Graphite Precursor by a Magnetic Field. *A. Hamasaki*[1], A. Sadohara[1], Y. Takeuchi[3], A. Katsuki[2] and S. Ozeki[1] *1. Faculty of Science, Shinshu University, Matsumoto, Japan; 2. School of General Education, Shinshu University, Matsumoto, Japan; 3. Muroran Institute of Technology, Muroran, Japan*

Graphite consists of stacked layers of a two-dimensional carbon hexagonal lattice (i.e., graphene). The higher the heat treatment temperature, the larger the size of the graphene sheets. Previously, we reported that when carbon pitch was carbonized under a strong magnetic field to prepare a graphite precursor, a macroscopic oriented structure formed due to large diamagnetic susceptibility anisotropy [1]. Because the final orientation of the carbon material occurs during the graphitization process [2], we investigated the effects of precursor structure on graphitization. Graphite precursors prepared from coal tar pitch in the absence and presence of a magnetic field of 6 T, which are denoted as general carbonized pitch (GCP) and highly oriented carbonized pitch (HOCP), respectively, were formed into pellets with 20% coal pitch as a binder and then carbonized at more high temperature as shown in Fig. 1. The Raman spectra of carbon materials are characterized by a G band around 1600 cm^{-1} derived from the growth of the graphene plane and D band around 1350 cm^{-1} originating from defects in the graphene plane. The dependence of the D-to-G-band intensity ratio (I_D/I_G) of the carbon materials on treatment temperature is plotted in Fig. 2(a). I_D/I_G of graphite produced from HOCP decreased faster above 1300 K than was the case using GCP. Figure 2(b) shows the (002) lattice spacing of the carbon hexagonal layer obtained from X-ray diffraction (XRD) measurements. The interplanar spacing of graphite obtained from HOCP is narrower than that from GCP. Therefore, if the precursor is previously oriented, rearranging the crystallites during graphitization becomes relatively easy. As a result, energy was effectively used for crystal growth during the rearrangement process, and graphitization was accelerated.

[1] Atom Hamasaki, et al., scientific reports, Vol. 9, 7489 (2019)
[2] H. Marsh and F. R. Reinoso, Activated carbon.1st ed. p.26–50 (Elsevier, 2006).

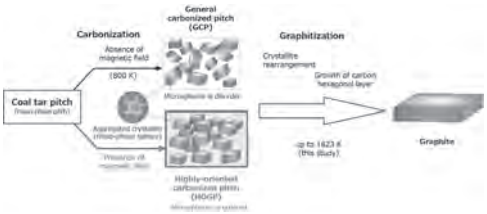

Fig. 1. Preparation processes of graphite.

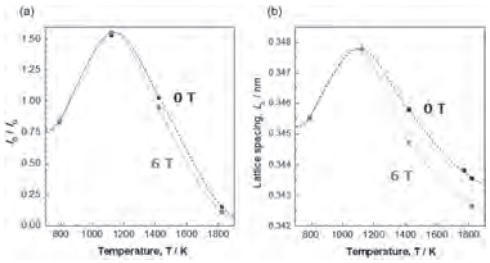

Fig. 2. Evaluation of the temperature dependence of graphitization degree by (a) Raman spectroscopy and (b) XRD.

C3-07. Withdrawn

C3-08. Sensorless Control Scheme for PMSM Based on High-Frequency Square-Wave Voltage Injection Considering Non-Linear Change of Inductance in D-Q Axis. W. Cui[1], *S. Zhang*[1] and Y. Feng[1] *1. Department of Automation, Shanghai University, Shanghai, China*

High-Frequency Signal injection (HFSW)method is a technology to obtain the rotor position information from the high-frequency response of the injected voltage or current signal. While this method is quite sensitive to the motor parameters, the correct parameter decides the rotor position estimation accuracy. In traditional scheme, the d-q axis inductance is set as a constant value under the rated conditions in the high-frequency mathematical models, while the d-q axis inductance varies in different operating conditions exactly. Even in the same operating conditions, the d-q axis inductance also changes due to the magnetic field saturation caused by phase current. JMAG simulation verifies the assumption, as shown in Fig.1. However, very little about that has been discussed in the published papers corresponding to HFSW method. Inspired by current linkage harmonics and torque ripple [1], a modified motor model considering non-linear change of inductance is proposed in this paper, where motor parameter is changing with magnetic field saturation. With the adoption of new model, the traditional HFSW injection equation is also modified in the paper. Compared with the traditional scheme, the modified model takes the dynamic change of d-q axis inductance into consideration and reduced the influence of the induction variation. Simulation in matlab Simulink shows a good performance in rotor error suppression and steady state error depression. The proposed method has also been employed in a 4p-24s permanent magnet synchronous motor. Fig.2 exhibits the high frequency incremental current in α-β axis while Fig.2 shows the incremental current with the modified high frequency square wave injection equation. (The variation of inductance is reflected as 5th and 7th current harmonics in α-β axis). It can be verified that the proposed method can not only compensate the HFI current harmonics caused by non-linear changes in d-q axis inductance but also maintain the good steady-state and dynamic performance of traditional systems.

[1] Ponomarev, P., Petrov, I., & Pyrhonen, J. (2014). Influence of travelling current linkage harmonics on inductance variation, torque ripple and sensorless capability of tooth-coil permanent-magnet synchronous machines. IEEE Transactions on Magnetics, 50(1), 1-8.

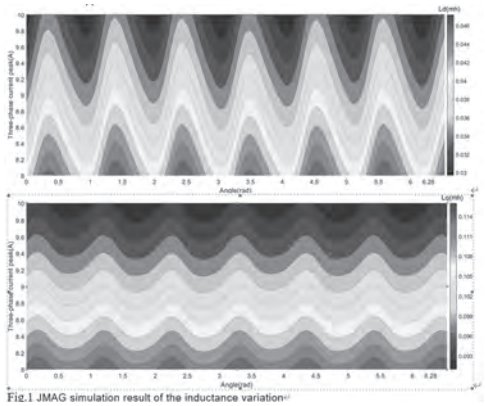

Fig.1 JMAG simulation result of the inductance variation

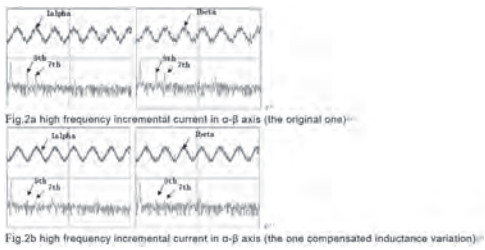

Fig.2a high frequency incremental current in α-β axis (the original one)

Fig.2b high frequency incremental current in α-β axis (the one compensated inductance variation)

C3-09. Regeneration and Reuse of Magnetic Particles for Wastewater Treatment. *L. Hernández García*[2], P.A. Augusto[2], T. Castelo-Grande[1] and D. Barbosa[1] *1. Laboratory for Process Engineering, Environment, Biotechnology and Energy, Universidade de Porto, Faculdade de Engenharia, Porto, Portugal; 2. Ingeniería Química y Textil, Universidad de Salamanca, Facultad de Ciencias Químicas, Salamanca, Spain*

The presence in wastewater of complex organic compounds, pharmaceuticals, etc, is a problem due to the difficulty of removing these compounds in traditional water treatment plants. The current available processes, like reverse osmosis, are costly and complicated, so new materials and processes for the removal of these compounds are necessary. Iron-based magnetic particles are one of the materials most studied recently for the elimination of contaminants, both through physical and chemical processes. The manufacture of these particles is cheap and simple, and their magnetic properties make their recovery for reuse one of their main advantages. The Fenton reaction is an oxidation process capable of degrading organic compounds through hydroxyl radicals. Iron-based magnetic particles can be a catalyst for heterogeneous Fenton processes, but they present the problem of electronic depletion, as the iron ions of the surface become oxidized, reducing the efficiency of catalysis, and adsorption of the particles reducing the available surface further. In our study, we developed Fenton process to degrade colorant content of waters, achieving a very good efficiency. We have also studied the kinetics of the process. To solve the problem of spent particles by regenerating the magnetic particles used we have used reducing agents, so that the efficiency of the particles for catalysing the Fenton reaction is maintained or increased after repeated uses. Efficiency is obtained by measuring the relative degradation of methylene blue, an organic dye. We have tested two different agents and compared with non-regenerated particles. The relative degradation of non-regenerated particles has reduced to less than 20% after the 2nd use, while particles regenerated one of the reducing agents had the degradation reduced to less than 20% after 8 re-uses, and particles regenerated with another reducing agent maintained relative degradation above 70% for all 10 re-uses that were tested.

Paulo A. Augusto, Teresa Castelo-Grande, Diana Vargas, Lorenzo Hernández, Leticia Merchán, Angel M. Estevez, Juan Gómez, José M. Compaña, Domingos Barbosa, 2020. Water Decontamination with Magnetic Particles by Adsorption and Chemical Degradation. Influence of the Manufacturing Parameters. Materials, Volume 13, Issue 10 (2020)

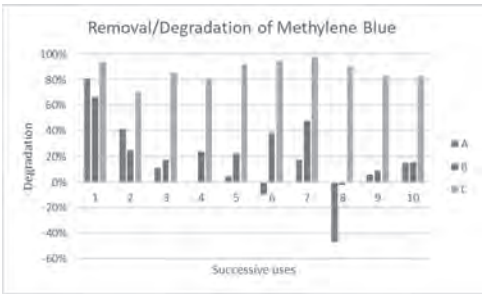

Fig.1: Degradation (in % reduction of methylene blue concentration) vs number of uses of A: non-regenerated particles; B: regenerated with reagent 1; C: regenerated with reagent 2

C3-10. Micromagnetic Analysis of Exchange-Coupled $Nd_2Fe_{14}B/\alpha$-Fe Multilayers and Their Applications in Micro-Scale Devices. *P. Pathak*[1], V.K. Yadav[1] and D. Mallick[1] *1. Department of Electrical Engineering, Indian Institute of Technology Delhi, New Delhi, India*

The difficulty in the development and integration of the high-performance Permanent Magnets in micro-scale devices has stimulated a significant amount of research[1]. Nano-composite magnets combining soft and hard magnetic materials via exchange coupling are feasible solutions, but their potential is yet to be explored for MEMS/microfluidics applications. In this work, micromagnetic FEM analysis is used to optimize the maximum energy product [$(BH)_{max}$] of exchange-coupled $Nd_2Fe_{14}B/\alpha$-Fe multilayer system which is ideal for integration at micro-scale. By varying the relative geometric dimensions of the soft and hard phases, the magnetic properties can be tuned significantly (Fig. 1). The dependence is due to the change of exchange-coupling between the successive layers with change of the thickness. Maximum energy product is obtained when α-Fe thickness lies between 5-20 nm. In addition, dependences of the magnetic properties on the geometric anisotropy and magneto-crystalline anisotropy have been studied. Magnetic field intensity (for micro-energy harvesting) and gradient (for lab-on-a-chip devices) are critical parameters for device applications[2,3]. It is equally important to design the integrated magnetic structures efficiently as the thin films only produce stray fields at their edges due to high demagnetizing factor[4]. To produce high flux density with micro-scale resolution over large areas, patterning the magnetic surface is required. An integration strategy incorporating optimized micro-patterns (Fig. 2) of simulated exchange-coupled magnets is shown. The co-simulation at material and device level, provides an effective design methodology for developing highly efficient micro-magnetic flux sources for numerous applications.

[1] D. P. Arnold, N. Wang, J. Microelectromechanical Syst., 18.6:1255-1266 (2009). [2] D. Mallick, A. Amann, S. Roy, J. Microelectromechanical Syst., 26:273–282 (2016). [3] Y. Y. Huang, P. Chen, C. H. Wu, K. Hoshino, K. Sokolov, N. Lane, J. X. Zhang, Sci. Rep., 5:16047 (2015). [4] D. Mallick, T. Maity, K. Paul, S. Roy, J. Appl. Phys., 125(2):023092 (2019).

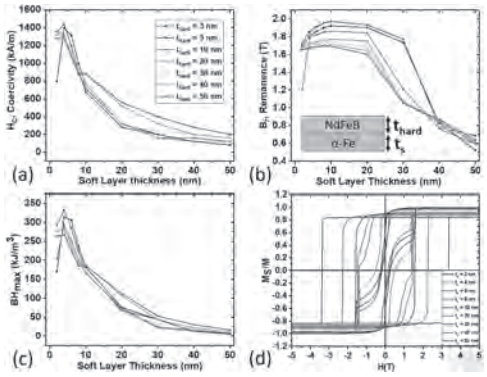

Fig. 1: Change of (a) H_C, (b) B_r, (c) $(BH)_{max}$ with α-Fe layer thickness t_s for different $Nd_2Fe_{14}B$ layer thickness t_{hard}. (d) M-H hysteresis loops for t_{hard} = 10 nm with varying soft layer thickness.

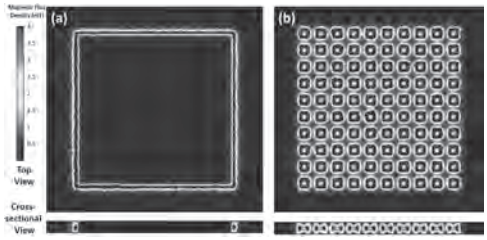

Fig. 2: Proposed permanent magnet integration strategy. A thin film (a) produces magnetic field only at the edges whereas the flux density (or gradient) can be significantly improved by micro-patterning (b) of the magnet. Magnetic flux intensity variation is shown by the color distribution.

C3-11. Effect of Direct Exchange Coupling via the Insulator on the Magnetic Tunnel Junction Based Molecular Spintronics Devices With Pre-Existing Strong Molecule Induced Antiferromagnetic Coupling. *H. Brown*[1], A. Grizzle[1], C. DAngelo[1] and P. Tyagi[1,2] *1. Center for Nanotechnology Research and Education, University of the District of Columbia, Washington, DC, United States; 2. Mechanical Engineering, University of the District of Columbia, Washington, DC, United States*

The magnetic tunnel junction(MTJ) based molecular spintronics device (MTJMSD) approach provides solutions to decades-old fabrication difficulties in mass-producing molecular spintronics-based computer devices. To producing MTJMSD, molecular channels are bridged across the insulator of an MTJ with exposed side edges. In an MTJMSD, two ferromagnets (FMs) are simultaneously connected by an insulator film and the molecular channels along the exposed sides. In our prior experimental studies, we observed that paramagnetic molecules connected to ferromagnet produced unprecedented antiferromagnetic coupling when the competing coupling via insulator was minimized[1]. In this paper, our Monte Carlo Simulation (MCS) study the effect of varying coupling via insulator (Ji) on the magnetic properties of an MTJMSD. To complement our prior work[1], we assumed molecules produced strong antiferromagnetic coupling. The nature (ferromagnetic or antiferromagnetic) and magnitude of Ji determined the resultant effect. Antiferromagnetic Ji enhanced the pre-existing antiferromagnetic molecular coupling effect. Ferromagnetic Ji competed with molecular coupling. Ferromagnetic Ji/kT~0.4 coupling made two FM electrodes parallel by overcoming the molecular coupling effect (Fig.1). We also studied the impact of thermal energy on the Ji ability to impact the MTJMSD properties. The Ji variation critically impacted the temporal evolution of the equilibrium MTJMSD magnetic moment. For the Ji's intermediate values, ferromagnetic electrodes exhibited different phases around the junction area (Fig 2). Our MCS intends to consider the impact of defects and even intentional insemination of nanostructure within insulator thickness to producing direct coupling that competes with molecular coupling.

[1] P. Tyagi, C. Baker, C. D'Angelo, *Nanotechnology* 2015, *26*, 305602.

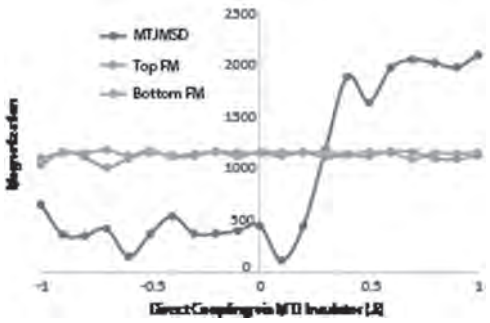

Effect of variation Ji.causing transition from antiferromagnetic to the ferromagnetic coupling on MTJMSD.

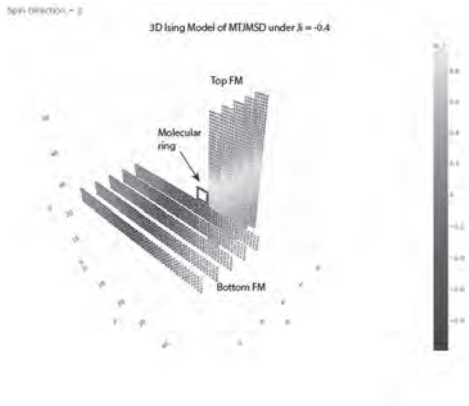

C3-12. Monte Carlo Simulation Study of the Effect of Inter-Molecular Coupling on the Magnetic Properties of Magnetic Tunnel Junction Based Molecular Spintronics Devices. *P. Suh*[1] and P. Tyagi[1] *1. Center for Nanoscale Research and Education (CNRE), University of the District of Columbia, Washington, DC, United States*

Paramagnetic molecules, with a net spin state, can tailor magnetic exchange coupling strength between two ferromagnetic electrodes in a magnetic tunnel junction based molecular spintronics devices (MTJMSD). The MTJMSD approach provides solutions to fabrication difficulties in the mass production of molecular-based computer devices. MTJMSD is produced by bridging the molecular channels across the insulator of an MTJ with exposed side edges. Our prior experimental and Monte Carlo Simulations(MCS) studies showed that paramagnetic molecules produced unprecedented strong antiferromagnetic coupling between two ferromagnets[1]. The overall antiferromagnetic coupling occurred when a paramagnetic molecule made antiferromagnetic coupling to the first electrode and ferromagnetic coupling to the second electrode. In this paper, we report the study on the effect of coupling among molecules (Jm) on the MTJMSD. This study is critical because prior work in the MTJMSD area focused on the coupling between molecules and ferromagnets. For the first time, we studied the effect of Jm (coupling between molecules) using the Ising Model of MTJMSD. MTJMSD used in this study was 11x 10 x 50 size, with 11 being the thickness of the MTJMSD, and 5x10x50 being the size of each electrode. In this study, while other parameters were kept constant, we varied Jm between -1 to 1, using a step size of 0.2, at simulation counts varying from 10,000 to 500M. It was observed at the various simulation counts that the molecules were settling in the same spin direction for Jm=-1, 0, 1. The only anomaly occurred at 200M simulation counts, where the two ferromagnetic electrodes had spins in opposite directions, which gives room for more investigations for the future. A general observation of the spin states shows that at lower simulation counts, that is at 10million, 1million, and 100,000, the spin states become more random without a clear spin direction. Investigating the effect of coupling on the magnetic properties of the MTJMSD, with smaller step sizes of about 0.1, using the MCS could produce more revealing results, as we couple the Jm with both ferromagnetic electrodes.

Tyagi, P.; Baker, C.; D'Angelo, C., *Nanotechnology* 2015, *26*, 305602.

C3-13. Influence of Cerium Dioxide Content on Degradation Efficiency and Iron Oxide Transformations in CeO_2/Fe_2O_3 Sorbents. *O. Zivotsky*[1], J. Lunacek[1], Y. Jiraskova[2], J. Ederer[3], P. Janos[3] and K. Cabanova[4] *1. Department of Physics, Vysoka skola banska-Technicka univerzita Ostrava Fakulta elektrotechniky a informatiky, Ostrava, Czechia; 2. Ustav fyziky materialu Akademie ved Ceske republiky, Brno, Czechia; 3. Univerzita Jana Evangelisty Purkyne v Usti nad Labem Fakulta zivotniho prostredi, Usti nad Labem, Czechia; 4. Vysoka skola banska-Technicka univerzita Ostrava, Ostrava, Czechia*

Magnetically separable sorbents and catalysts have great potential in environmental applications [1]. Currently incurred separable sorbents, formed by grains of iron oxide decorated by cerium dioxide (CeO_2) nanocrystallites, were successfully applied for a decomposition of organophosphorus pesticides and chemical warfare agents [2]. In this work, several series of the similar sorbents were prepared, consisting of ferrimagnetic iron oxide serving as a magnetically separable core or carrier, and cerium oxide serving as active constituent capable to destroy dangerous chemicals. The magnetite (maghemite) core was synthesized by the co-precipitation of the Fe^{2+} and Fe^{3+} salts from cheap and commercially available raw materials. Subsequently, it was re-dispersed in the solution containing various doses of cerium (III) nitrate, and the cerium (III) carbonate was prepared by precipitation with ammonium hydrogen carbonate. The cerous carbonate/magnetite precursor were annealed in a muffle furnace at various temperatures ranging from 200 to 800°C for 2 h to obtain the CeO_2/Fe_2O_3 – type reactive sorbents. Their structural and physical properties were investigated by X-ray diffraction, first-order reversal curves (FORC), low-temperature magnetic measurements, and Raman and Mössbauer spectroscopy. Samples with the CeO_2 content ≤ 20 wt.% exhibited an increase in coercivity from 0.2 kA/m to 27 kA/m and a decrease of saturation magnetization from 50 Am^2/kg to 1 Am^2/kg after annealing at 600°C. This deterioration of magnetic properties was caused by transformation of magnetite and maghemite into weak ferromagnetic hematite with a typical peak at FORC diagram (see Figure 1) and Morin transition about 200 K. At sorbents with higher CeO_2 contents the hematite dominates at calcination temperatures above 600°C. Degradation efficiency, Figure 2, studied by application of the paraoxon methyl pesticide was found to increase with CeO_2 content and reached optimal values at samples treated between 300°C and 500°C.

[1] K. A. Abd-Elsalam, M. A. Mohamed, R. Prasad, (Eds.) Magnetic Nanostructures – Environmental and Agricultural Applications, Springer Nature, Switzerland (2019) [2] P. Janoš et al., Chemical Engineering Journal, Vol. 262, p. 747 (2015)

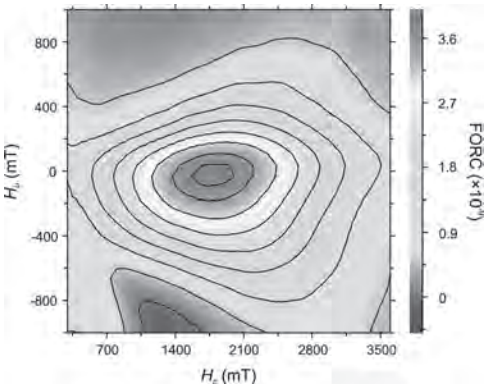

Fig. 1 FORC diagram of sorbent with 5% CeO_2 calcined at 800°C.

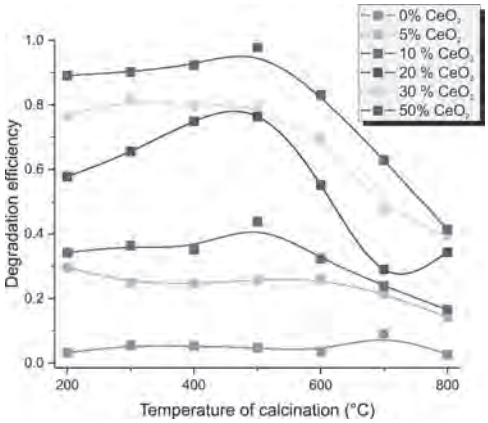

Fig. 2 Degradation efficiency of CeO_2/Fe_2O_3 sorbents against paraoxon methyl in dependence on calcination temperature and content of cerium dioxide.

C3-14. Magneto-Elastic Coupling in Multiferroic Metal-Organic Framework $[(CH_3)_2NH_2]Co(HCOO)_3$ Complex. *K. Thirunavukkuarasu*[1,2], R. Richardson[1], Z. Lu[2], N. Huang[3], D. Smirnov[2] and D. Mandrus[3]
1. Department of Physics, Florida Agricultural and Mechanical University, Tallahassee, FL, United States; 2. National High Magnetic Field Laboratory, Tallahassee, FL, United States; 3. University of Tennessee Knoxville, TN, US, Knoxville, TN, United States

Metal-organic frameworks (MOFs) are a class of nanoporous compounds where organic groups are used in combination with transition metal ions to obtain multifunctional materials. The family of MOFs comprised of methylammonum (A= $(CH_3)_2NH_2$) and metal (B=Co, Cu, Fe, Mn, Ni) cations with a formate (X=$HCOO_3$) anion are very interesting because of their multiferroic properties [1]. Therefore, several efforts have been made to understand the exchange interactions in these materials including magnetization at high magnetic fields up to 60 T and infrared spectroscopy at magnetic fields up to 35 T [2,3]. In the infrared studies under applied magnetic fields, it was concluded that Co complex adopts a different mechanism involving formate stretching distortions unlike other complexes in the family that use the formate bending mode [3]. Concurrently, we performed Raman spectroscopy on $[(CH_3)_2NH_2]Co(HCOO)_3$ at magnetic fields up to 31T to probe the magneto-elastic coupling. We find that a weak Raman active vibrational mode at about 798 cm^{-1} corresponding to symmetric bending of the formate ion does exhibit magnetic-field-induced frequency shifts. The results of our investigations and its implications will be discussed in detail in the presentation. Funding Acknowledgement: This work has been performed at the user facilities in the National High Magnetic Field Laboratory (NHMFL), Tallahassee. The NHMFL is supported by the National Science Foundation through NSF/DMR-1644779 and the state of Florida. The project is also funded by DoN HBCU/MI program award # N000141713061.

[1] P. Jain, V. Ramachandran and R. J. Clark et al., Journal of American Chemical Society, Vol.131, p.13625 (2009) [2] B. Pato-Dolda, L. C. Gomez-Aguirre and A. P. Hansen *et al*., Journal of Materials Chemistry C, Vol. 4, p.11164 (2016) [3] K. D. Hughey, A. J. Clune and M. O. Yokosuk *et al*., Inorganic Chemistry, Vol. 57, p.11569 (2018)

Session C4
MAGNETIC NANOSTRUCTURED MATERIALS
(Poster Session)

Karine Chesnel, Chair
Brigham Young University, Provo, UT, United States

C4-01. Subharmonic Return Point Memory in Artificial Spin Ice.
A. Vanstone[1], J.C. Gartside[1], K. Stenning[1], D. Arroo[2] and W. Branford[1]
1. Imperial College London, Imperial College London, London, London, GB, London, United Kingdom; 2. University College London, London, United Kingdom

Many hysteretic systems exhibit an effect where the system traverses the exact same loop through microstate space when cycled through repeated minor field loops. This behaviour, termed 'return point memory' (RPM) has been observed in a diverse set of physical systems, from superfluid Helium condensation in capillaries [1] to the domain structure in thin magnetic films [2]. However, in these systems RPM is inferred from macroscopic measurements rather than full microstate imaging. Artificial spin ice (ASI) is an array of frustrated magnetic nanoislands, allowing observation of the precise microstate throughout the minor loop, and has previously been seen to exhibit RPM [3, 4]. Using a dipolar needle model we examine the behaviour of square-based ASI geometries subjected to repeated minor field loops for a broad range of parameter space. We show that subsets of spins within the lattice no longer return to the same microstate after a single minor loop, instead taking several minor loops to return to the same microstate, exhibiting subharmonic behaviour. This subharmonic RPM is highly sensitive to interaction strength between neighbouring nanoislands and occurs within a finely-tuned pocket of parameter space. Exploring this in different square-based ASI geometries shows that this form of subharmonic RPM can be more generally applied to other hysteretic systems.

[1] Lilly, M. P. et al. (1993). Memory, congruency, and avalanche events in hysteretic capillary condensation. *Physical Review Letters*, *71* (4186). [2] Pierce, M. S. et al. (2003). Quasistatic X-Ray speckle metrology of microscopic magnetic return-point memory. *Physical Review Letters*, *90* (175502). [3] Libál, A. et al. (2012). Hysteresis and return-point memory in colloidal artificial spin ice systems. *Physical Review E*, *86* (2). [4] Gilbert, I. et al. (2015). Direct visualization of memory effects in artificial spin ice. *Physical Review B*, *92* (10).

C4-02. Magnetic Hysteresis of Blocked Ferrihydrite Nanoparticles.
S. Komogortsev[1], D. Balaev[1], A. Krasikov[1], S. Stolyar[1], R. Yaroslavtsev[1], V. Ladygina[1] and R. Iskhakov[1] *1. Kirensky Institute of Physics, Federal Research Center KSC SB RAS, Krasnoyarsk, Russian Federation*

An experimental study of the hysteresis in magnetic nanoparticles is a tool for studying the potential relief controlling reversible and irreversible processes of their magnetization. Such a study should be carried out at low temperatures for nanoparticles in a blocked state. A well known feature of hysteresis in ferrihydrite nanoparticles, that is common for nanoparticles with negative exchange interactions, is extremely high field of the closing of major hysteresis loop, up to several hundred kOe. This field provides an upper limit of the potential barrier height for the magnetization. Here, we report on some new findings in the study of minor hysteresis loops of ferrihydrite nanoparticles. For the particles with zero exchange bias, starting from state with a zero average magnetic moment, a series of minor loops were measured with progressively increasing magnitude of the maximum field from 0.1 to 70 kOe. Both biogenic and chemically synthesized ferrihydrite nanoparticles were studied. At low field amplitude, a reversible magnetic response is observed. With increasing the field amplitude, the minor loops became open and then they approach the major loop. Since this resembles the behavior of single-domain particles in the Stoner-Wohlfarth model, we tested this model to describe the dependence of the coercive force of a minor loop versus the field amplitude. Such a description is successful when the dispersion of the anisotropy field is taken into account. The description makes it possible to estimate the distribution parameters of the anisotropy field and to reveal correlation between the field of opening of the minor loop and the value of coercivity. It turned out that this correlation is significantly different from the predictions of the Stoner-Wohlfarth model with different symmetries of the magnetic anisotropy. We also compared the anisotropy field obtained from this description with the estimate from the value of the blocking temperature. This makes it possible to evaluate the applicability framework of the simplest models of coherent rotation of magnetization in the description of the magnetic hysteresis of ferrihydrite.

C4-03. Evidence of Two Dimensional Dilute Antiferromagnet Mediated Exchange Bias and Giant Vertical Shift in $LaFeO_3$ - NiO Nanocomposite.
P. Sharma[1] and R. Chatterjee[1] *1. Physics, Indian Institute of Technology, Delhi, Hauz Khas, India*

In magnetic core-shell nanoparticles, an interesting consequence is the exchange coupling across the core-shell interface that is frequently seen in the form of exchange bias, a horizontal shift in the hysteresis loop accompanied by an increase in coercivity after cooling in a magnetic field[1]. Formation of nanocomposites is an efficient way of fabricating interface by dispersing one magnetic phase into another, leading to enhanced interface effects. In addition to ferromagnetic (FM)/antiferromagnetic (AFM) interfaces, exchange bias and related effects have also been observed in other types of interfaces, e.g. involving ferrimagnet (FI) (e.g. FI/FM or FI/AFM), spin-glass (SG) (e.g. AFM/SG, FM/SG, FI/SG) and AFM/AFM systems. Recently, antiferromagnetic (AFM) nanoparticles have been the subject of renewed attention, due to their surface and interface effects giving rise to exchange anisotropy[2]. In this report, we have investigated the observation of exchange bias in nanocomposites composed of two AFM nanoparticles namely $LaFeO_3$ (LFO) and NiO. Owing to high Néel temperature (T_N) of $LaFeO_3$ and NiO, significant exchange bias and vertical magnetization shift is observed at room temperature. Both, the exchange bias and the vertical magnetization shift shows the strong dependence on temperature (Fig. 1) as well as cooling field. Using Benik's model we have interpreted the observed training effect in $LaFeO_3$/NiO nanocomposite. The thermoremanent magnetization (TRM) and isothermoremanent magnetization (IRM) analyses (Fig. 2) identify the behavior of surface shell of nanoparticles in nanocomposite as two-dimensional diluted antiferromagnet (2D-DAFF) [3].

1) Nogués, J., et al., Physics Reports, 2005. 422(3): p. 65-117. 2) Winkler, E., et al., Physical Review B, 2005. 72(13): p. 132409. 3) Benitez, M., et al., Physical Review B, 2011. 83(13): p. 134424.

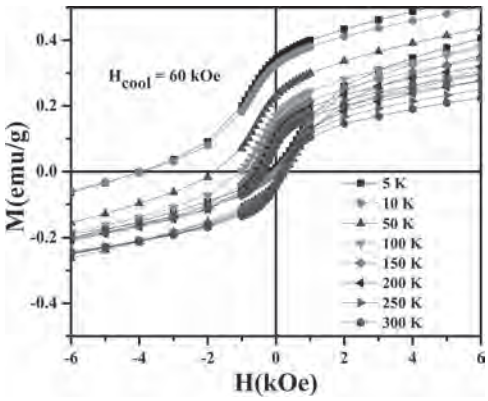

Hysteresis loop of LFO/NiO nanocomposite measured at different target temperatures in presence of 60 kOe cooling field.

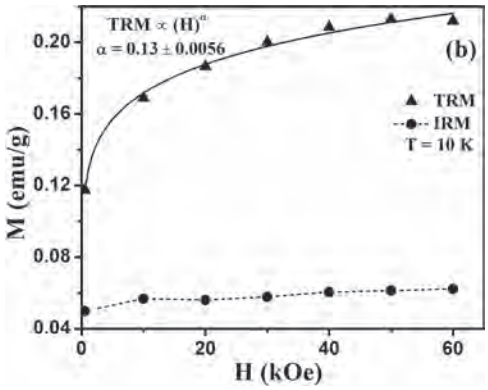

TRM & IRM vs magnetic field (H) at 10 K in order to understand magnetic behavior of nanocomposite.

C4-04. Withdrawn

C4-05. Magnetic Hysteresis Scaling of Fe_3O_4 Nanoparticles With Controlled Interparticle Distance. *K. Oyanagi*[1], S. Kobayashi[1] and J. Choi[2]
1. Faculty of Science and Engineering, Iwate University, Morioka, Japan; 2. Hanbat National University, Daejeon, The Republic of Korea

The magnetic hysteresis scaling of minor loops has been widely studied for evaluating material's quality and microstructures. This scaling law with an exponent of 1.3-1.5 universally holds true for ferromagnets with size down to ~50 nm, where magnetization rotation mechanism starts to dominate [1]. In this paper, we report results of the scaling analysis of minor hysteresis loops for 12-nm size Fe_3O_4 nanoparticles where only single-domain reversal takes place. The obtained scaling behaviors for variable interparticle distance were compared, along with results of first-order reversal curves (FORCs). We used Fe_3O_4 spherical nanoparticles with 12 nm size, whose surface was polymer-or SiO_2-coated to control interparticle distance; d = 12, 18 and 34 nm (inset in Fig. 2(a)). Minor loops and FORCs were measured in the temperature range of 10 – 300 K using a SQUID magnetometer. As shown in Fig. 1, we found that the relation between hysteresis loss and remanence of minor loops follows a power law and the exponent was ~ 1.3 for all the samples. The results strongly indicate that the power-law scaling is universally valid even for single domain nanoparticles. Figure 2 shows coercivity and minor-loop coefficient as a function of temperature. Although coercivity for d=34 nm has a larger value at T=10 K and steeply decreases with increasing temperature due to an enhanced superparamagnetic behavior, the coefficient for d=34 nm is nearly one-third the value for d=12 and d=18 nm at all measuring temperatures. The observed higher coefficient for smaller d samples can be attributed to dipolar interparticle interactions, which effectively reduce the remanence magnetization. The coefficient can be therefore a sensitive indicator of the interparticle distance, as similarly observed for local interaction field in the FORC measurements.

[1] S. Kobayashi, T. Sato, Z. Li, X. Dong. AIP Advances, 8 (2018) 056301.

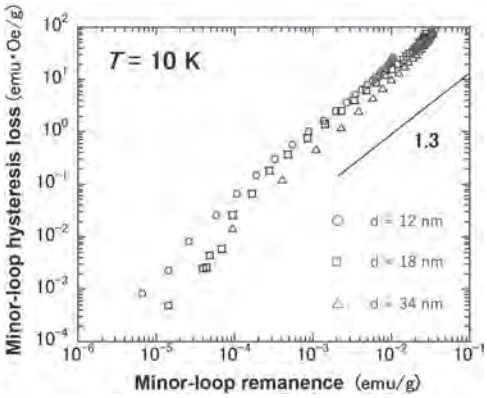

Double logarithmic plot of a relation between hysteresis loss and remanence of minor loops at 10 K. The slope of 1.3 is shown for comparison.

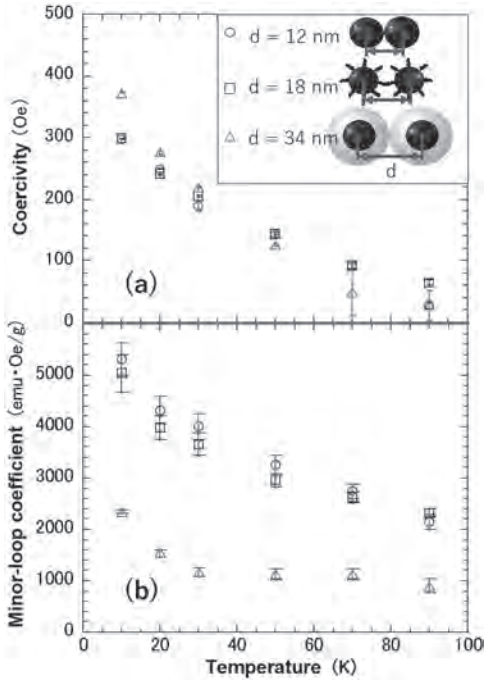

(a) Coercivity and (b) minor-loop coefficient, as a function of temperature. The inset in (a) shows a schematic diagram of each sample.

C4-06. Directional Dependence of Magnetic Nanodiscs Placed on a Square Lattice. *N. Strandqvist*[1], B. Skovdal[1], H. Stopfel[2], R. Rowan-Robinson[3], V. Kapaklis[1] and B. Hjörvarsson[1] *1. Physics and Astronomy, Uppsala Universitet, Uppsala, Sweden; 2. Engineering Sciences, Uppsala Universitet, Uppsala, Sweden; 3. Materials Science and Engineering, The University of Sheffield, Sheffield, United Kingdom*

The possibility to tailor the geometry, influencing the energy scales, allows one to investigate magnetic ordering and other emergent phenomena such as correlations [1] in artificial arrays. The symmetry of nano-sized elements with a circular shape are one of the factors setting the magnetic ground state of a system, which can either be collinear or vortex [1,2]. The dimensionality, size and spacing between the islands are all influencing the interaction energy and the strength of the intra-disk coupling and therefore impact the

magnetic state. Here we realize three set of samples with magnetic nano discs composed of a FePd alloy placed in on a square lattice. The disc diameter ranges from 250 to 450 nm, where the element spacing has been kept at 20 nm in order to promote interactions. Synchrotron-based Photoemission Electron Microscopy employing the X-ray Magnetic Circular Dichroism was used to determine a vortex ground state of our system. Thus, by use of Magneto Optical Kerr Effect at lower temperatures, a static collinear-like state can be observed after reducing the magnetic field to zero. At higher temperatures, thermal fluctuations become prominent and overcome the magnetostatic coupling and the vortex state become dominant. We will demonstrate that the transition from the collinear-like state along [10] direction occur at lower temperatures in contrary to [11] direction. Furthermore, discussions will be made regarding results obtained from micromagnetic simulations which tells that the distinctive magnetic texture within the islands along [10] and [11] is influencing the thermal behaviour.

[1] R. Streubel, et al. Nano Lett. 18 7428-7434 (2018) [2] N. Leo, et al. Nat. Commun. 9 2850 (2018) [3] E. Östman, et al. New J. Phys. 16 053002 (2016)

C4-07. Magnetization Reversal Mechanism of Magnetic Ring Nanostructures With Varying Widths Under Different Magnetic Field Directions. *T. Huang*[1], K. Wu[1], Y. Lin[1], W. Peng[1], P. Chen[1] and M. Chen[1]
1. National Applied Research Laboratories, Hsinchu, Taiwan

The purpose of this study is to investigate the magnetization reversal process of magnetic ring nanostructures with varying widths in different magnetic field directions. The outer edge of the ring is circular, and the diameter Do is 500 nm. The inner edge of the ring is elliptical, the short axis Db is 300 nm, and there are five dimensions of 300, 400, 450, 480, and 500 nm in the long axis Da. The structure presents a gradual change in width along the circular direction and the material of the structure is Permalloy. The angle between the magnetic field and the long axis is θ, as shown in Fig. 1. Figure 1 shows the hysteresis loop of the Permalloy nanostructure with an angle of 30 degrees, a long axis of 400 nm, and a short axis of 300 nm. Figure 2 presents the switching fields of abnormal rings with different magnetic field angles. Preliminary results show that the varying widths bring on different anisotropies along the ring, and a narrow region of the ring pins magnetic moments. When we apply magnetic fields to the ring nanostructure in various angles, the mechanisms of the magnetization reversal process change due to the pinning effects of the narrow regions in the varying positions. This results in the variations of the switching fields and the shape of hysteresis loops.

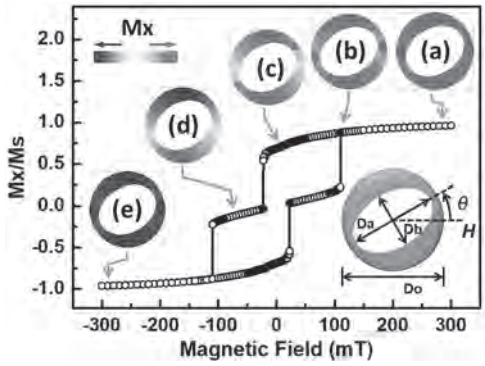

Fig. 1. A hysteresis loop of a Permalloy ring nanostructure. Do, Da, and Db are 500, 400, and 300 nm, respectively. The thickness of the magnetic structure is 30 nm. The magnetic field is applied in the horizontal direction. The angle θ between the long axis of the ellipse and the magnetic field is 30 degrees. The inserted Figs. (a)-(e) are the magnetization states of the ring nanostructures under different magnetic fields. The magnetic moments are shown in red and blue color toward the right and left. Up and down are shown in white color. The lighter red or lighter blue means the small component in the horizontal direction.

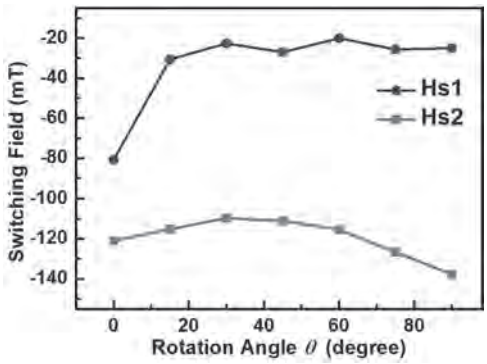

Fig. 2. The relationship between the first Hs1 and second Hs2 switching fields under different angles of magnetic fields.

C4-08. Magnetic Configurations in Nanoscale Epitaxial Iron Cuboids. *S. Guo*[1], M. Henschel[1], V. Neu[1], T. Blon[2] and K. Leistner[1] *1. Leibniz IFW Dresden, Dresden, Germany; 2. Laboratoire de Physique et Chimie des Nano-Objets, UMR 5215 INSA, CNRS, UPS, Université de Toulouse, Toulouse, France*

The magnetic configuration in nanoscale ferromagnetic elements is of central importance for their functionality in modern spintronic devices, such as in magnetic random access memory (MRAM).[1,2] Magnetic properties of nanopatterned polycrystalline magnetic films of different shape and sub-50 nm nanoparticles with cubic shape[1] were intensively investigated during the last few years. Still, very little information is available about the magnetization behavior of nanoscale magnetic elements with intermediate lateral size of 0.1-1 μm.[3] Micromagnetic simulations predict that for iron nanocuboids, the stabilization of different magnetization configurations, such as single domain flower and vortex states, strongly depends on the size and aspect ratio.[4] Here, aligned, isolated iron nanocuboids [Fig. 1 (a)] have been fabricated by taking advantage of epitaxial, three-dimensional-island growth on GaAs(001) during electrodeposition at low deposition rates.[5] The nanoparticles exhibit lateral size between 10 and 250 nm and heights below 80 nm. Surface {100} facets predominate with a thin crystalline oxide shell that protects the nanoparticles during prolonged storage in air. The magnetic configurations inside the cuboids are systematically investigated by combining quantitative magnetic force microscopy (MFM) [Fig. 1 (b)] with micromagnetic simulation. Micromagnetic simulation results give evidence for a transition from single-domain state to vortex state with increasing the size of cuboids, demonstrating the key importance of nanometric size control of magnetic nanoparticles. Such a measurement opens the door to fine tuning the magnetic configuration of nano-objects that will find applications in fields of sensor, magnetic recording, and biomedicine.

1. C. Gatel, F. J. Bonilla, A. Meffre, et al. Nano Lett. 2015, 15, 6952−6957. 2. M. Bode, A. Wachowiak, J. Wiebe, et al. Appl. Phys. Lett. 2004, 84, 948−950. 3. L. A. Fomin, I. V. Malikov, S. V. Pyatkin, et al. J. Magn. Magn. Mater. 2010, *322*, 851−857. 4. F. J. Bonilla, L.-M. Lacroix, T. Blon, J. Magn. Magn. Mater. 2017, *428,* 394−400. 5. K. Leistner, M. Yang, C. Damm, et al. Nanoscale, 2017, 9, 5315–5322.

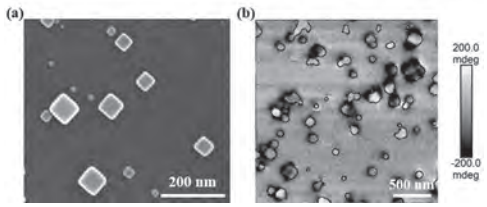

Fig.1 (a) SEM image showing isolated iron nanocuboids with different size, (b) MFM scan of the as-grown sample with contour of cuboids superimposed

C4-09. Effects of Infill Orientation and Percentage on the Mechanical and Magnetoactive Properties of 3D-Printed Magnetorheological Elastomer Structures. *H. Thatcher*[1], T. Calascione[1], N.A. Fischer[1], A. Robinson[1] and B. Nelson-Cheeseman[1] *1. Mechanical Engineering, University of Saint Thomas, Saint Paul, MN, United States*

Magnetorheological elastomers (MREs) consist of magnetic particles dispersed in an elastomeric matrix, allowing the material to be mechanically deformed by applying an external magnetic field. Often, these materials are made with thermoset elastomers to control curing and particle alignment, but using thermoplastic elastomers allows the material to be used for a type of 3D printing called fused deposition modeling (FDM) through which complex three-dimensional parts can be created. The interior of these parts, containing a layer-by-layer buildup of extruded filament (infill) in a specified pattern, creates intrinsic anisotropy, much like curing thermoset MREs with all magnetic particles aligned with an external field would do, but with the possibility of greater complexity. It has already been shown that magnetic properties vary based on print parameters during the FDM process, but it is yet to be seen how the mechanical and magnetoactive properties of MREs are affected by these variables. In order to determine the effects of infill orientation and infill percentage on MREs, we use thermoplastic polyurethane (TPU) as the matrix and 40 wt.% carbonyl iron as the dispersed magnetic particles, with a control group of non-filled TPU. We print samples in triplicate with different infill orientations (0°, 45°, 90°) (Fig. 1) and with different infill percentages (60%, 80%, 100%) for a total of 54 samples. Tensile tests and 3-point bend tests are conducted in order to determine effects of infill orientation and infill percentage on the elastic modulus and tensile strength of the printed samples. Additionally, custom magnetoactive tests are conducted where a transverse magnetic field at varying strengths up to 0.4 T is applied, in order to determine how the structural print variables affect both the degree and orientation of magnetoactive deformation. Understanding the mechanical and magnetoactive properties of these 3D-printed magnetorheological elastomers provides insight into how the magnetoactive response of MREs can be controlled by the underlying FDM structures.

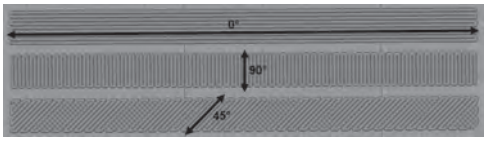

Fig. 1. 3D printer slicer (Simplify3D) image of 100% infill samples with infill orientations of 0°, 90°, and 45° relative to the longitudinal sample axis.

C4-10. Use of two-Photon Lithography With a Negative Resist and Processing to Realise Cylindrical Magnetic Nanowires. *J. Askey*[1], M.O. Hunt[1], W. Langbein[1] and S. Ladak[1] *1. School of Physics and Astronomy, Cardiff University, Cardiff, United Kingdom*

Cylindrical magnetic nanowires have been shown to exhibit a vast array of fascinating spin textures, including chiral domains [1], skyrmion tubes [2], and topologically protected domain walls that harbour Bloch points [3]. In this presentation we will outline a novel methodology for the fabrication of cylindrical magnetic nanowires (NWs) combining standard UV lithography, two photon lithography (TPL), electrodeposition and further processing. Custom electrodes fabricated with UV lithography are patterned with porous templates fabricated through TPL, electrodeposition is then used to fill the pores with Nickel and finally plasma ashing is used to liberate the encased NWs, leaving free standing magnetic nanowires. We demonstrate first proof-of-principle of this methodology by realising larger dimension nanowires, with length of order 3μm and diameter of 420nm. Magnetic force microscopy under an external field shows a complex spiralling magnetisation state, which demagnetises through the production of vortices of alternating chirality. Finite-difference micro-magnetic simulations are used in conjunction with experimental MFM and give qualitative agreement with respect to the switching mechanism. Surprisingly, we also observe a meta-stable Bloch point state in simulations during the switching process. Our work may provide new model systems for studying these fascinating singularities in magnetization texture. Finally, we show that with optimization of TPL write parameters, one can realise smaller cylindrical nanowires, with diameter approximately 180nm, providing new opportunities for study of Bloch point domain walls within complex 3D geometries.

[1] Fernandez-Roldan, J., et al., Nanoscale, 10(13), p.5923-5927, 2018. [2] Charilaou, M., H. Braun, and J. Loffler, Physical Review Letters, 121(9), p.097202, 2018. [3] Da Col, S., et al., Physical Review B, 89(18), p.180405 2014.

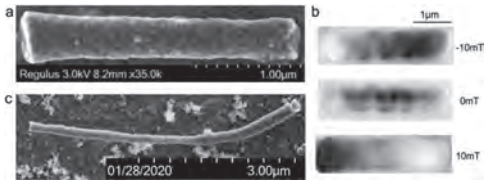

Figure 1 a) SEM image of 420nm diameter Nickel NW. b) MFM images of the 420nm diameter NW at saturation and remanence. c) SEM of a NW with a reduced diameter of 180nm.

C4-11. Fabrication of 3D Magnetic Nanocomposite Materials Using Inkjet Printing. *M. Cannamela*[1,2], J. Stasiak[3] and P. Dhagat[4] *1. School of Mechanical, Industrial and Manufacturing Engineering, Oregon State University, Corvallis, OR, United States; 2. HP, Inc., Corvallis, OR, United States; 3. HP Labs, HP, Inc., Corvallis, OR, United States; 4. School of Electrical Engineering and Computer Science, Oregon State University, Corvallis, OR, United States*

This work reports on the fabrication of 3D magnetic nanocomposites using a novel inkjet printing process as illustrated in Fig. 1a. Magnetic nanoparticle containing ink is dispensed, via a thermal inkjet printhead, into a heat-fusible polymer powder layer, spread in a given thickness over a translatable stage [1]. The ink infiltrates the powder, transporting the magnetic nanoparticles into the volume of the porous layer [2]. The polymer/particle matrix is then fused to form a composite in the desired shape by jetting a heat absorbing ink over the requisite regions and exposing the matrix to infrared radiation. A new powder layer is spread atop the just fused material and the printing process repeated to achieve the desired build thickness. The printhead print parameters are computer-controlled allowing for 3D composites with spatial control of magnetic susceptibility to be fabricated predictably. Such metamaterials are of interest for electromagnetic wave shaping in microwave communication systems. Samples with varying volume fractions of magnetic nanoparticles are printed and characterized for physical and magnetic properties. Scanning electron microscope (SEM) images of cross-sections of the samples confirm the homogeneous distribution of the particles in the composite (see example image in Fig. 1b). The volume fraction of the particles is calculated from their mass obtained by thermogravimetric analysis of the samples. Magnetic properties are determined via magnetometry and frequency-dependent susceptometry measurements. The saturation magnetization and susceptibility, as expected, increase with the volume fraction of the magnetic particles in the composite (Fig. 2). Given a volume fraction of particles, the susceptibility decreases at higher frequencies (Fig. 2b). The presentation will compare the experimental susceptibility data to effective medium theory-based models for magnetic composites and discuss advancements in materials and printing technology necessary to realize practical devices.

[1] HP Inc., "HP Multi Jet Fusion technology: Technical white paper," HPI, 2018. Accessed: Sept. 1, 2019. [Online]. Available: https://www8.hp.com/us/en/printers/3d-printers/products/multi-jet-technology.html. [2] K. Donovan, "Microfluidic Investigations of Capillary Flow and Surface Phenomena in Porous Polymeric Media for 3D Printing," Ph.D. dissertation, Oregon State Univ., Corvallis, OR, USA, 2019.

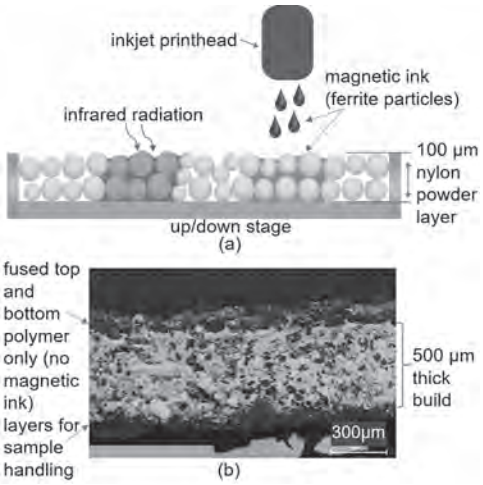

Fig. 1. (a) Illustration of printing process. (b) SEM image of composite with 15.3 vol% of magnetic particles.

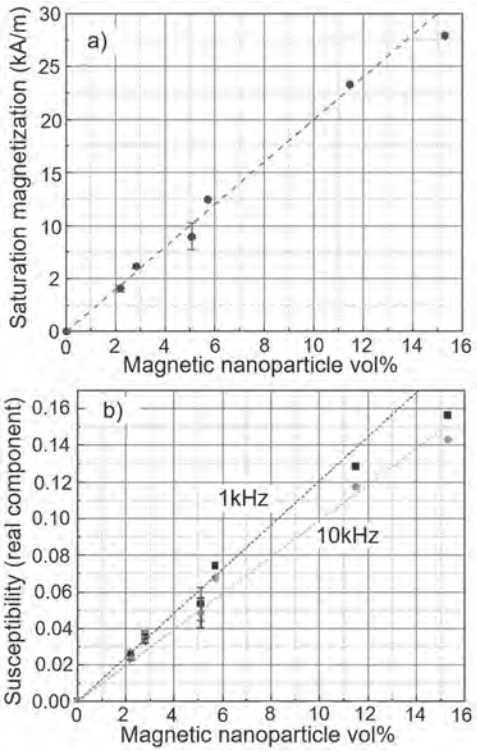

Fig. 2. (a) Saturation magnetization and (b) Susceptibility vs. vol% of magnetic particles in composite.

C4-12. Fabrication of Hydroelectric Cells Using Ferrites and Stannic Oxide for the Production of Green Energy. *P. Kumar*[1,2] and V.K. Verma[2] *1. Department of Physics and Astrophysics, University of Delhi, New Delhi, India; 2. Department of Physics, Hindu College New Delhi, New Delhi, India*

In modern technology, magnetic materials like ferrites play significant role. It is thorny to dream a world without magnetic materials and they are becoming more significant in the progress of modern society. In the area of modern sensors, electrical engineering, memory devices, medical field, water treatment many more, magnetic materials especially ferrites played very important role. Recently, it has been observed that ferrites and other oxide materials can generate electricity by water dissociation without any harmful effect to environment. We have fabricated hydroelectric cells (HECs) using ferrites and stannic oxide for the production of green energy. The working of HECs is based on the adsorption of water molecules on the surface of materials and dissociation (H_3O^+ and OH^-). Lithium doped magnesium ferrites and stannic oxide samples have been synthesized by solid-state sintering method. X-ray Diffraction pattern of the MLFO sample confirms the spinel phase formation and pattern of SnO_2 sample confirms the rutile structure. Scanning Electron Microscopy images confirms the porous nature of the samples with randomly oriented crystalline nature. Hydroelectric cell of 2 inch diameter was used to investigate hydroelectric properties for both the samples. As few milliliter water is sprayed on the MLFO cell it produces 17.0 mA of peak current and 950 mV voltage with a maximum output power of 16.15 mW whereas SnO_2 cell produces a peak current of 72.1 mA and 981 mV voltage with maximum output power of 70.7 mW. These results show a promising future oxide based HECs which offers an eco friendly, cost effective source of green energy production.

[1]. P. Kharbanda, T. Madaan, I. Sharma, S. Vashishtha, P. Kumar, A. Chauhan, S. Mittal, J. S. Bangruwa, V. Verma, Heliyon, 5, e01151, (2019).
[2] R. K. Kotnala, R. Gupta, A. Shukla, S. Jain, A. Gaur, J. Shah, J. Phys. Chem. C,122, 18841-18849, (2018).

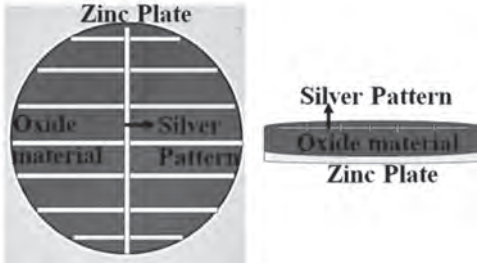

Hydroelectric cell of oxide material with zinc and silver electrodes.

S.No.	Sample	Minimum Voltage (mV)	Maximum Current (mA)	Maximum Power (mW)
1.	$MgFe_2O_4$	1000	2.47	2.46
2.	$Mg_{0.9}Li_{0.1}Fe_2O_4$	883	8.18	6.94
3.	$Mg_{0.9}Li_{0.2}Fe_2O_4$	950	17.0	16.15
4.	$Mg_{0.9}Li_{0.3}Fe_2O_4$	939	16.67	15.7
5.	SnO_2	981	72.1	70.7

Voltage, Current and Power values for MLFO and SnO_2 samples.

Session C5
SPIN INJECTION AND NEUROMORPHIC COMPUTING
(Poster Session)

Rahul Mishra, Chair
National University of Singapore, Singapore

C5-01. Spin Injection Characteristics of Py/Graphene/Pt by Means of THz Measurement and Spin Pumping. *H. Idzuchi*[1,2], S. Iihama[1], M. Shimura[1], A. Kumatani[1,3], S. Mizukami[1] and Y.P. Chen[2,1] *1. Tohoku University, Sendai, Japan; 2. Purude University, West Lafayette, IN, United States; 3. National Institute for Material Science, Tsukuba, Japan*

Recently, two-dimensional (2d) material has attracted considerable attention, providing easy access on highly crystalline thin sample, and offering new spintronics research direction. So far, the spin transport is widely studied in in-plane direction in 2d material [1-3]. In three dimensional material (such as Pt), spin transport in out-of-plane direction is often studied with spin Hall effect: the spin polarization, the spin current direction and detection voltage needs to be all perpendicular. This geometrical constraint, with the thickness of 2d material in interest extremely thin, makes one difficult to study spin transport through *c*-axis of 2d material thus unexplored. Here, we study spin injection characteristics in *c*-axis of graphene(Gr) by using THz measurement as well as spin pumping. Monolayer Gr film was prepared by a standard CVD method. Raman microscopy was used to characterize the number of layers in Gr. We prepared Pt/Gr/Py and Pt/Py (as a reference). We sputtered for Pt (3 nm in thick), Py and MgO capping films. The static magnetization process of the film was examined by magneto optical Kerr effect. All measurement was conducted at room temperature. Ultrafast spin current was optically generated in Py, and terahertz charge current and electric field is generated via inverse spin-Hall effect in nonmagnetic layer. In our bilayer Pt/Py, we observed clear THz signal and its signal is systematically inverted with different bias field, as shown in inset of Fig. 1. Interestingly, on Pt/Gr/Py, the THz signal was significantly decreased and the characteristic oscillation disappeared (Fig.1). This implies strong suppression of spin injection from Py to Pt by Gr monolayer. We also employed spin pumping (using ultrafast laser heating and demagnetization process). We have observed significantly different field dependence of the lifetime in Pt/Py and Pt/Gr/Py as shown in Fig.2, yielding the damping parameter of 0.015 and 0.011, respectively. This indicates strong suppression of spin current with Gr. With these two different characterization methods, we conclude Gr effectively blocks spin current even as thin as monolayer.

[1] Y. Liu et al Appl. Phys. Lett. Vol. 102 p.033105 (2013). [2] H. Idzuchi et al Phys. Rev. B Vol. 91 p.241407 (2015) [3] J. Tian et al, Sci. Adv. vol. 3 p.e1602531 (2017).

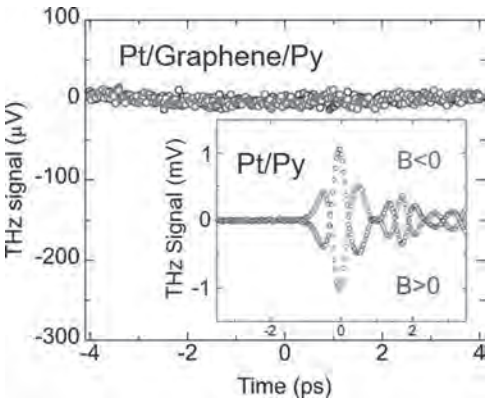

THz signal for Pt/Graphene/Py (inset for Pt/Py).

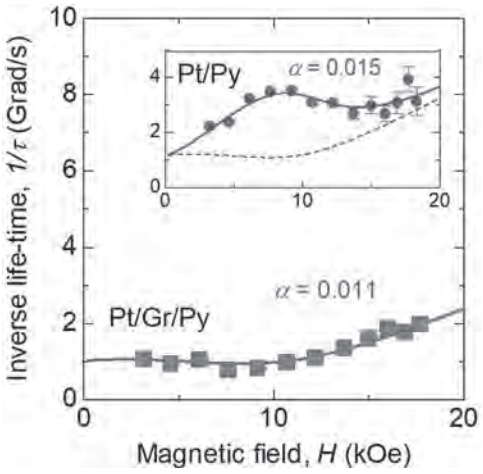

Spin lifetime extracted from spin pumping.

C5-02. Efficient Control of Magnon Population by Injecting Spin Current Generated Using Naturally-Oxidized Copper Film. *G. Okano*[1] and Y. Nozaki[2] *1. CEMS, RIKEN, Wako, Japan; 2. Dept. of Physics, Keio University, Yokohama, Japan*

In recent years, magnon spintronics [1] has attracted much attention as a promising research field for integrating magnonic and electric circuits via spin current. Although the spin current generated using spin Hall effect in heavy metals (HMs) has been widely utilized to control magnetization dynamics [2], the HMs also lead to an increase of magnetization damping in an adjacent ferromagnet. Such conflicting effects are attributable to a large spin orbit interaction in HMs. In this study, we demonstrated an efficient control of magnon population in ferromagentic NiFe film by injecting a spin current generated using a naturally oxidized copper (Cu*) whose SOI is much weaker than in HMs. Very recently, we found that Cu* could generate spin current as large as Pt, although NiFe/Cu* bilayer showed negligible spin pumping effect [3,4]. Figure 1(a) shows our schematic experimental setup. Magnon excitations, caused by a parallel pumping as schematically shown in Fig.1 (b), were quantitatively compared between NiFe(5)/Cu*(10) and NiFe(5)/Pt(10) bilayers. The bilayers were patterned in the Hall bar structure followed by fabricating a coplanar waveguide (CPW). The magnon population can be measured by using the anisotropic magnetoresistance (AMR) because the increase of precession angle owing to the magnon excitation leads to an increases of the electric resistance ΔR. Figure 2(a) show the AMR curves under the microwave with frequency and amplitude of12 GHz and 20 dBm, respectively, by injecting electric current (*J*) with −9 mA. Figure 2(b) shows the *J* dependence of Δ*R* for the NiFe/Cu* bilayer. The Δ*R* decreases monotonically with *J*, which is caused by the spin current injection from the Cu* layer. Moreover, we confirmed that the interface of NiFe/Cu* bilayer shows negligible spin pumping effect. Namely, unlike large SOI materials, Cu* can solve a competition between anti-damping effect of spin transfer torque and spin pumping effect which leads to a serious problem for successful excitation of nonlinear spin dynamics.

[1] A. V. Chumak et al., Nat. Phys. 11, 452-461 (2015) [2] Lin Xue et al., Phys. Rev. Lett. 108, 147201 (2012) [3] H. An et al., Nat. Commun. 7, 13069 (2016) [4] G. Okano et al., Phys. Rev. Lett. 122, 217701 (2019)

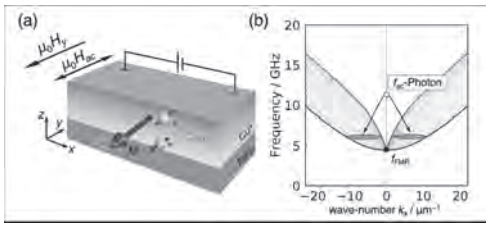

Fig.1 Schematic illustrations of (a) experimental setup and (b) magnon band configuration for parallel pumping.

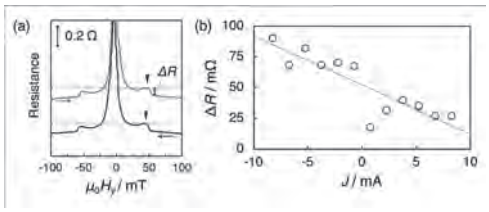

Fig.2 (a) AMR curves under the application of microwave with $J = -9$ mA. (b) J-dependence of ΔR.

C5-03. Sensing Stray Fields From Magnetic Nanocircuits With Nitrogen-Vacancy Defects. *A. Solyom*[1], M. Caouette-Mansour[1], B. Ruffolo[1], P.M. Braganca[2], M. Pioro-Ladrière[3,4], L. Childress[1] and J. Sankey[1] *1. Physics, McGill University, Montreal, QC, Canada; 2. Western Digital Corp, San Jose, CA, United States; 3. Institut Quantique and Département de Physique, Universite de Sherbrooke, Sherbrooke, QC, Canada; 4. Quantum Information Science Program, Canadian Institute for Advanced Research, Toronto, ON, Canada*

We discuss our latest efforts toward using a single, optically active nitrogen-vacancy (NV) spin sensor (implanted in a single-crystal diamond substrate) to measure magnetic thermal noise modified by spin Hall torques [1] in a Py/Pt nanowire [2]. In this poster, we first present our subtractive method for fabricating magnetic nanocircuits on diamond, and initial characterization of working Py(5 nm)/Pt(5 nm) nanowires. We reliably achieve contacts with few-ohms of resistance and 200 nm of overlap at each end of the 2-μm-long, 400-nm-wide wire, and we observe an anisotropic magnetoresistance of 0.4%. Importantly, we observe that the subtractive patterning process (masked ion milling) used to define the devices reduces the NV spin resonance contrast by a factor of ~5, but that subsequent exposure to an oxygen plasma returned the contrast to its nominal level without affecting the nanowire behavior. Finally, we present progress toward using transport measurements to estimate thermal time scales in these systems (while calibrating the RF current in the nanowire), as well as preliminary NV readout of spin-transfer-controlled magnetic thermal noise.

[1] C. Du, T. van der Sar, et al., Science, 357, 195-198 (2017) [2] A. Solyom, Z. Flansberry, et al., Nano Lett., 18, 6494-6499 (2018)

C5-04. The Structure and Dynamics of Magnetic Vortices and Solitons in Multilayer Ferromagnetic Nanostructures. *K. Samsonov*[1], S. Stepanov[3], G. Antonov[5], A. Ekomasov[3], R. Kudryavtsev[2], A. Gumerov[3], K. Zvezdin[4] and E. Ekomasov[3,1] *1. Department of Physical Processes and Systems Modeling, University of Tyumen, Tyumen, Russian Federation; 2. Institute of Molecule and Crystal Physics UFRC RAS, Ufa, Russian Federation; 3. Department of theoretical physics, Baskirskij Gosudarstvennyj Universitet, Ufa, Russian Federation; 4. Institut obsej fiziki imeni A M Prohorova RAN, Moskva, Russian Federation; 5. Baskirskij Gosudarstvennyj Universitet, Ufa, Russian Federation*

The structure and dynamics of magnetization in a vortex spin-transfer nanooscillator, which is a three-layer spin-valve magnetic nanopillar with a small diameter, is studied during the passage of a spin-polarized current. Using micromagnetic simulation [1,2], we studied the dynamic change in the vortices structure, the formation of the C-structure vortex state and edge vortices, the trajectory of movement and the time it takes to reach different dynamic modes. The time needed for the vortices to reach different dynamic modes was found. The possibility of the dynamic generation of radial edge vortices without the presence of a Dzyaloshinsky field or an external inhomogeneous magnetic field is shown. We demonstrate that a vortex in a thick magnetic layer can be a generator of spin waves in a thin magnetic layer with an adjustable oscillation frequency. We consider also multilayer magnetic structures, which are periodically alternating layers of two materials with different physical properties. In such systems it is possible to generate localized magnetization waves (LMW) of the magnetic solitons and breathers type [3]. Special interest in magnetic solitons and breathers is currently associated with the appearance of new experimental techniques that allow to study formation and propagation of localized magnetization waves of nanometer dimensions and their interaction with domain walls (DW). The possibility of controlling the structure and dynamic parameters of magnetic solitons and breathers using an external magnetic field is shown [4]. Dependences of the center of the DW and amplitudes of the LMW on time are constructed and analyzed in the presence of three, five and seven layers. It is shown that the LMW vibrations for the case of five layers can be described by two harmonic oscillators, for the case of seven layers, three harmonic oscillators. This work was supported by RFBR, project No19-02-00316\19 and No20-31-90048.

1. A.E. Ekomasov et al., Journal of Magnetism and Magnetic Materials, 471, 2019, 513-520; 2. E.G. Ekomasov et al., Chelyabinsk Physical and Mathematical Journal. 2020. Vol. 5, iss. 2. P. 161–173; 3. A.M. Gumerov et al., Journal of Physics: Conference Series. VII Euro-Asian Symposium "Trends in Magnetism". 2019. V. 1389. p. 012004: 1–6; 4. E.G. Ekomasov et al., Letters on Materials 10 (2), 2020 pp. 141-146.

C5-05. Mutual Synchronization of Spin-Torque Oscillators With a Perpendicular Polarizer. *M. Castro*[1,2], D. Mancilla[1], N. Strelkov[2], A. Litvinenko[2], M. Ibarra[2], S. Allende[1], B. Dieny[2], U. Ebels[2] and L. Buda-Prejbeanu[2] *1. Universidad de Santiago de Chile, Santiago de Chile, Chile; 2. Univ. Grenoble Alpes, CEA, CNRS, Grenoble INP, IRIG-SPINTEC, 38000, Grenoble, France*

The implementation of Spin-torque nano-oscillators (STNOs) in wireless communication [1] and neuromorphic computing [2] requires the use of a large array of coupled STNOs. While most of the theoretical [3] and experimental studies considered single STNO devices, mutual synchronization of several oscillators [4, 5] remains a challenging task. As a first step in this direction, we apply the analytical approach based on the spin-wave formalism [3] to the mutual synchronization of two STNOs, consisting of a perpendicular polarizer and an in-plane free layer, see Fig. 1. This STNO configuration can be realized experimentally, and leads under a strong out-of-plane field to symmetric out-plane precession modes generating strong dynamic dipolar coupling fields. We derived analytical expressions for the phase difference, as well as the oscillation amplitudes and the locking range for the general case of non-identical oscillators, differing in their

radius R, anisotropies and/or current densities. For the mutual synchronization of two STNOs different degrees of approximations for the expression of the dipolar coupling field were considered: 0, 1st and 2nd order in power. Analytical results agree perfectly with numerical solutions of the Landau-Lifshitz-Gilbert equation for small frequency mismatch Δ for all three approximations. However, it is found that for large Δ the 2nd order approximation in the interaction is needed for best agreement. The Arnold tongue illustrates these results, see Fig. 2, that is defined by the maximum current difference in the two STNOs (defining Δ) as a function of their separation D (defining the coupling strength). The analytical description will provide a guide for analyzing and optimizing the mutual synchronization of more than two STNO devices. We acknowledge financial support in Chile from FONDECYT 1200867, and Financiamiento Basal para Centros Científicos y Tecnológicos de Excelencia AFB 180001. D. M.-A. acknowledges Postdoctorado FONDECYT 2018, 318041. M. A. Castro acknowledges Conicyt-PCHA/Doctorado Nacional/2017-21171016. The project was supported in by ERC Advanced Grant MAGICAL No. 669204

[1] T. Chen, et al. Proceedings of the IEEE., 104, 1919-1945(2016). [2] P. Talatchian, et al., Phys. Rev. Applied., 13, 024073(2020). [3] A. Slavin and V. Tiberkevich, IEEE Trans. Magn., 45,1875(2009). [4] S. Tsunegi, et al., Scientific Reports., 8, 13475(2018). [5] R. Lebrun et al., Nat. Commun., 8, 15825(2017).

Fig.1. Illustration of the interaction of two STNO

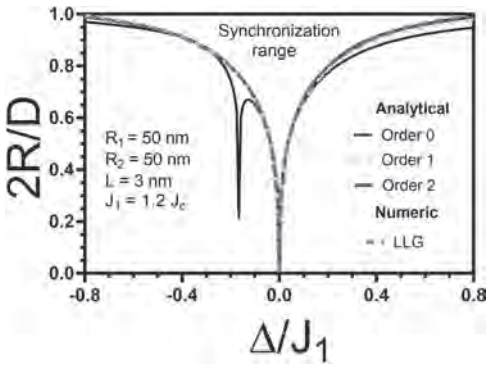

Fig. 2. Arnold tongue

C5-06. Numerical Simulation of Artificial Spin ice for Reservoir Computing. *K. Hon*[1], Y. Kuwabiraki[2], M. Goto[1,3], H. Nomura[1,3], R. NAKATANI[2] and Y. Suzuki[1,3] *1. Graduate School of Engineering Science, Osaka University, Toyonaka, Japan; 2. Department of Materials Science and Engineering, Graduate School of Engineering, Osaka University, Suita, Japan; 3. Center for Spintronics Research Network (CSRN), Osaka University, Toyonaka, Japan*

Reservoir computing (RC) is a framework with a simple training process to minimize the computation cost, which is suitable for temporal data processing. In the field of spintronics, it has been demonstrated that RC based on spin torque oscillators can perform speech recognition tasks [1]. Other proposed spintronics-based RC candidates include magnetic skyrmions [2], spin wave [3] and coupled nanomagnets [4]. Artificial spin ices (ASI) are arrays of interacting Ising-type nanomagnets causing geometrical frustration which provides a large number of accessible states for computation [5]. In this study, we propose ASI as a reservoir for RC and evaluate its performance from simulation results. Numerical simulation based on the macrospin model is performed to configure honeycomb arrays of nanomagnets at temperature of 0 K. In this design, the central nanomagnets act as the input layer of the RC, and the binary input is defined by the magnetization of the central nanomagnets as shown in Fig. 1. External magnetic fields in various direction are successively applied to the nanomagnets to update the reservoir. The ASI reservoir is evaluated from its short-term memory capacity and non-linear computation capacity, which are determined from the correlation between the teacher data and the trained output. Fig. 2. shows an example of a well-trained ASI reservoir which predicts the teacher data perfectly. This study shows that artificial spin ices would be a potential candidate for reservoir computing. This research and development work was supported by the Ministry of Internal Affairs and Communications, JAPAN. Part of this work was supported by JSPS KAKENHI Grant Number JP19H00860.

[1] J. Torrejon, et al., Nature., 547, 428 (2017) [2] D. Prychynenko, et al., Phys. Rev. Appl., 9, 014034 (2018) [3] R. Nakane, et al., IEEE Access., 6, 4462 (2018) [4] H. Nomura, et al., Jpn. J. Appl. Phys., 58, 070901 (2019) [5] H. Arava, et al., Phys. Rev. Appl., 11, 054086 (2019)

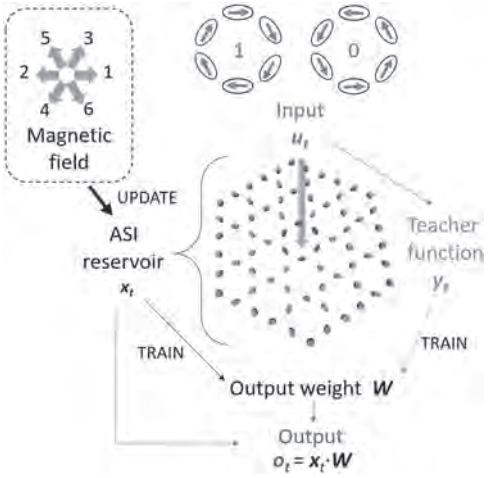

Fig. 1 Schematic design of artifical spin ices for reservoir computing.

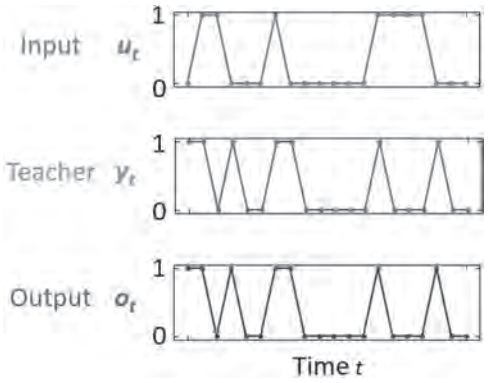

Fig. 2 An example of input, teacher and output after training. The teacher function is parity check with a time delay = 1 for checking the non-linear computation capacity of the reservoir.

C5-07. A Spintronic Neuron Based on Spin-Orbit Torque Induced Stochastic Switching of a Nanomagnet. *S. Zhang*[1], J. Zhang[1], S. Li[1], J. Hong[1] and L. You[1] *1. School of Optical and Electronic Information, Huazhong University of Science and Technology, Wuhan, China*

Spintronic devices have been investigated for the basic units of neuromorphic computation: synapses and neurons. Stochastic units based on nanomagnets have shown a high energy-efficient pathway to imitate neurons[1–4].

We propose a magnetic field-controlled artificial neuron based on spin-orbit torque (SOT) induced stochastic switching of a nanomagnet with perpendicular magnetic anisotropy. The stochastic behavior is dependent on the applied in-plane magnetic field and the switching probability is well fitted by a sigmoid function. The result provides an alternative way for building spintronic neuromorphic computing systems. Our deposited film stack is comprised of the following layers: thermally oxidized Si substrate/Ta (10 nm)/CoFeB (1 nm)/MgO (1 nm)/Ta (2 nm). A scanning electron microscope image of a typical Hall bar structure with a magnetic device (200 × 200 nm^2) at the cross-section is shown in Fig. 1. To harness the random magnetization orientations, the Hall resistance (R_H) due to the anomalous Hall effect is detected. Here, we chose a write current of 12 MA/cm^2 to observe the stochastic switching. A read current of 0.5 MA/cm^2 is followed by the write current to detect the magnetization orientation in every cycle. We performed 100 cycles under different in-plane magnetic fields and the resulted upward states are counted as N_{up} that can reveal the switching probability, as shown in Fig. 2. One can see that $N_{up} = 3$ at $H_x = -50$ Oe and $N_{up} = 93$ at $H_x = +50$ Oe. Such bipolar switching behavior also indicates that SOT, instead of *Joule* heating, is dominant during the current-induced magnetization switching. Furthermore, the switching probability could be fitted with a sigmoid function (green line in Fig. 2) that is an activation function of the artificial neurons[1–4], implying that our device has the potential to be used to implement neuromorphic computing.

1. A. Sengupta, et al. IEEE Trans. Electron Dev. Vol. 63, p. 2963 (2016). 2. R. Zand, et al. In Proc. 2018 Great Lakes Symposium on VLSI 15–20 (ACM, 2018). 3. J. Cai, et al. Phys. Rev. Appl. Vol. 11, p. 034015 (2019). 4. A. Jaiswal, et al. In 2019 IEEE International Joint Conference on Neural Networks (IJCNN) 1-6 (2019).

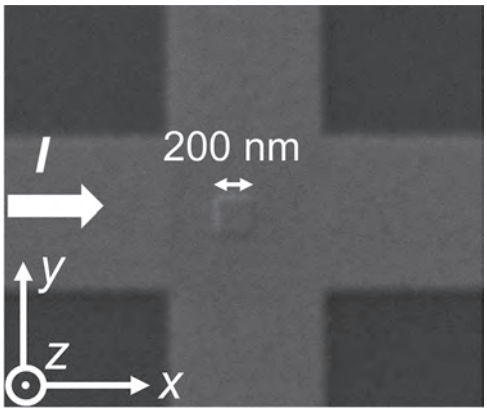

Fig.1 Scanning electron microscope image of the nanomagnet.

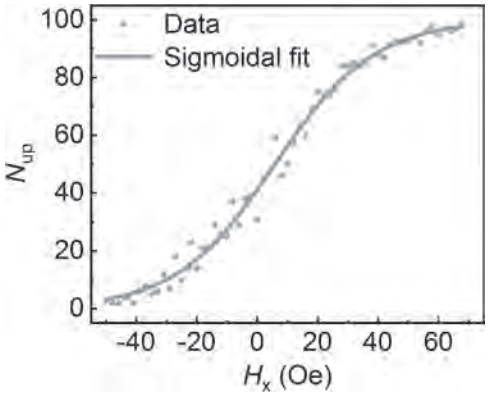

Fig.2 Counts of upward states in 100 cycles under various H_x (orange dots). The data is fitted by a sigmoid function (green line).

C5-08. Spike Time Dependent Plasticity Based Spin-Neuromorphic Computing for Pattern Recognition Application. *A. Lone*[1], S. Amara[1] and H. Fariborzi[1] *1. Computer, Electrical and Mathematical Science and Engineering Division, King Abdullah University of Science and Technology, Thuwal, Saudi Arabia*

Due to non-volatile behavior, stochastic switching for low thermal stability, and lower switching power requirements, spintronic devices are being used as synapses and neurons for energy-efficient neuromorphic computing [1][2]. In this work, we propose a spin-orbit torque-driven neuromorphic device-circuit co-design to implement the Hebbian learning algorithm. Using spike time-dependent plasticity (STDP)-based updating of synaptic weights, 8-bit, dynamic pattern recognition is illustrated. The artificial synapse we propose is based on the steady-state domain-wall motion in the MTJ free layer, driven by spin-orbit torque (SOT). The schematic of the neuromorphic circuit is presented in Fig.1(a). While Fig. 1(b) shows the time evolution of synaptic resistance during the learning phase of the circuit to recognize the pattern "A". At the end of the training phase, we observe that all synapses connected to pre-neurons corresponding to the pattern (A) have been configured into the lowest MTJ resistance state while background synapses are in the highest resistance state. The leaky-integrate and fire mechanism of post-neuron are computed using *Landau-Lifshitz-Gilbert* (LLG) equation and shown in Fig. 2(a). Fig. 2(b) shows the neurons resetting by a negative current pulse. Post-neuron output voltage pulse generated by firing and resetting of the neuron is shown in Fig. 2(c). The parameters of 3T-MTJ are optimized such that its critical current is (75-80) % of the total current. This ensures that after the training phase, the neuromorphic circuit easily recognizes the incomplete/noisy images of only those patterns which it has been trained for. In this work, spintronics-based neuromorphic device-circuit co-design is proposed to solve some basic pattern recognition task using the STDP algorithm.

[1]. Deming Zhang, Weisheng Zhao et. al, "All spin neural networks based on compound spintronic synapses and neurons," *IEEE Advances in Biomedical Circuits and Systems*, vol. 10, no.4, August-2016. [2]. Chamika M. Liyanagedera, Kaushik Roy et. al, "Stochastic spiking neural networks enabled by magnetic tunnel junction: From non-telegraphic to telegraphic switching regimes," *Physical Review Applied,* 8, 064017,2017.

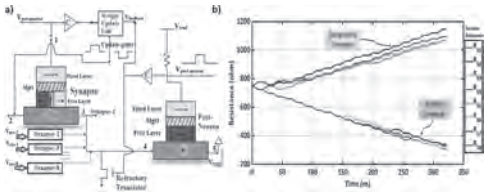

Fig. 1 (a) complete schematic description of an 8-bit spin-neuromorphic circuit. (b) Time evolution of the synaptic resistance.

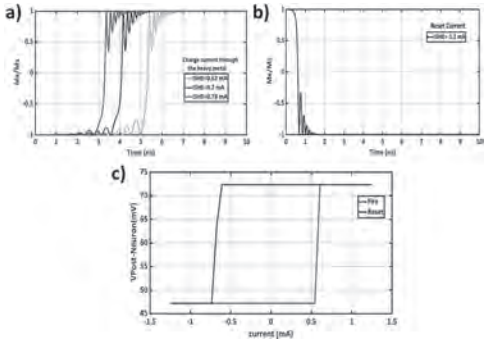

Fig. 2(a) Magnetization dynamics of the 3T-MTJ neuron. (b) Resetting of neuron (c) Post-neuron output voltage pulse vs charge current density in heavy metal computed using coupled-SHE-LLG and MTJ spin transport formalism.

Session D1
EXCHANGE BIAS AND OTHER NOVEL EXCHANGE IN THIN FILMS

Patrick Quarterman, Chair
NIST Center for Neutron Research, Gaithersburg, MD, United States

INVITED PAPER

D1-01. Exchange Bias due to Dipolar Interactions in Heterostructures. *F. Torres*[1,2], I. Montoya[4], C. Redondo[4], M. Kiwi[1], R. Morales[4] and I.K. Schuller[3] *1. Physics, Universidad de Chile, Santiago de Chile, Chile; 2. CEDENNA, Centro para el Desarrollo de la Nanociencia y la Nanotecnología CEDENNA, Santiago, Chile; 3. Physics, University of California San Diego, La Jolla, CA, United States; 4. Department of Physical-Chemistry, Universidad del Pais Vasco, Bilbao, Spain*

Exchange bias (EB) was discovered more than 60 years ago by Meiklejohn and Bean [1-2]. The origin of EB is the magnetic interaction between two differently ordered magnetic materials that are in close contact. Its fingerprint is the off-center shift of the hysteresis loop [3-4]. Some features of EB can be explained based on this type of model, but many open questions remain [4-8]. In this talk, we present the discovery of exchange bias (EB) switching, from negative to positive sign, in a dipole-induced coupling system where the antiferromagnet (AFM) and the ferromagnet (FM) are separated by a metallic paramagnetic (PM) spacer (AFM-PM-FM); and the EB enhancement in an AFM/FM bilayer coupling across an ultra-thin diluted spacer layer, as shown in the above figure. The results provide a new approach and exciting findings to design novel interacting heterostructures, control localized spin structures at the nanoscale, and create layered structures with novel spin textures.

[1] W. P. Meiklejohn and C. P. Bean, Phys. Rev., vol. 102, no. 5, pp. 1413–1414 (1956). [2] W. P. Meiklejohn and C. P. Bean, Phys. Rev., vol. 105, no. 3, pp. 904–913 (1957). [3] J. Nogués and I. K. Schuller, J. Magn. Magn. Mater., 192, 203–232 (1999). [4] J. Nogués, J. Sort, V. Langlais, V. Skumryev, S. Suriñach, J. Muñoz and M. Baró, Phys. Rep., 422, 65–117 (2005). [5] B. Dieny, V. S. Speriosu, S. Metin, S. S. P. Parkin, B. A. Gurney, P. Baumgart and D. R. Wilhoit, J. Appl. Phys., 69, 4774–4779 (1991). [6] B. Negulescu, D. Lacour, F. Montaigne, A. Gerken, J. Paul, V. Spetter, J. Marien, C. Duret and M. Hehn, Appl. Phys. Lett., 95, 112502 (2009). [7] M. Kiwi, J. Magn. Magn. Mater., 234, 584–595 (2001). [8] J. Nogués, D. Lederman, T. Moran and I. K. Schuller, Phys. Rev. Lett.,76, 4624 (1996). [9] F. Torres, R. Morales, Ivan K. Schuller, and M. Kiwi, Nanoscale 9, 17074 (2017). [10] F. Torres, and M. Kiwi, IEEE Transactions on Magnetics, 50, 4 (2014).

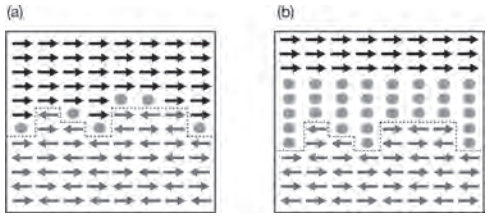

Schematic illustration of the EB coupled heterostructures in a compensated AFM surface. (a) AFM/FM dusted interface, (b) AFM/PM/FM trilayer. Legend: PM atoms (green dots), FM spins (black arrows), AFM spins (blue and red arrows illustrate the sublattice structure).

CONTRIBUTED PAPERS

D1-02. Exchange Bias in Fe/$Ir_{20}Mn_{80}$ Bilayers: Role of Spin-Glass Like Interface and 'Bulk' Antiferromagnet Spins. *S. Nayak*[1], P.K. Manna[1], V. Thiruvengadam[1], B.B. Singh[1], J.A. Chelvane[2] and S. Bedanta[1] *1. National Institute of Science Education and Research, Bhubaneswar, India; 2. Advanced Magnetics Group, Defence Metallurgical Research Laboratory (DMRL), Hyderabad, India*

Modern spintronic based devices, such as magnetic random-access memories and magnetic read head sensors have been designed on the principles of exchange bias effect [1]. A unidirectional interfacial exchange coupling between a ferromagnet (FM) and an antiferromagnet (AFM) is the primary reason for the shift of field-cooled hysteresis loop leading to the exchange bias effect [2]. Other prominent signatures of exchange bias are enhancement of coercivity and observation of training effect. This phenomenon is generally interfacial in origin, however sometimes spins from the 'bulk' part of the AFM can also contribute to exchange bias [3]. Besides, the interface can be ferromagnetic, antiferromagnetic or spin-glass in nature. Interestingly, all the above features are system dependent and can vary with the thickness of the films. We have investigated the role of 'bulk' spins of the AFM and also explored the magnetic nature of interface in exchange coupled Fe/IrMn bilayers by varying the thickness of the IrMn layer. In contrast with the conventional FM/AFM exchange bias systems [4], the exchange bias field (H_{EB}) was found to decrease with increasing cooling field (H_{FC}) due to random interface effect [2, 5]. The analysis of the training effect data indicates the presence of frozen and rotatable interfacial spins that contributed to the observed loop shift and coercivity enhancement, respectively.

[1] K. O'Grady, S. J. Greaves, S. M. Thompson, J. Magn. Magn. Mater., 322, 883 (2010) [2] K. D. Usadel, U. Nowak, Phys. Rev. B, 80, 014418 (2009) [3] A. C. Basaran, T. Saerbeck, J. de la Venta, H. Huckfeldt, A. Ehresmann, Ivan K. Schuller Appl. Phys. Lett., 105, 072403 (2014) [4] L. D. Bianco, F.Spizzo, M.Tamisari, S.Laureti, Solid State Commun., 151, 351 (2011) [5] S. Nayak, P. K. Manna, V. Thiruvengadam, B. B. Singh, S. Bedanta, J. Magn. Magn. Mater., 499, 166267 (2020)

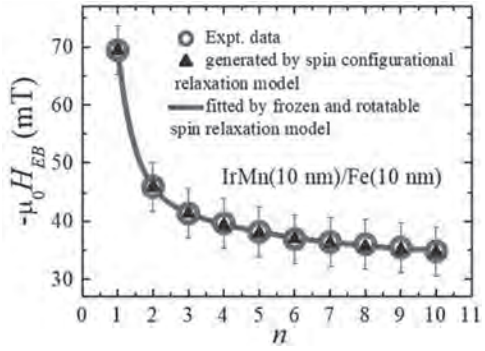

Fig. 1 Variation of exchange bias field (H_{EB}) with loop number (n) of the IrMn (10 nm)/Fe (10 nm) thin film.

D1-03. Demonstration and Characterization of Effective Random Exchange Fields in Ferromagnet/Antiferromagnet Bilayers. *G. Chen*[1], D. Collette[1] and S. Urazhdin[1] *1. physics, Emory University, Atlanta, GA, United States*

It was conjectured more than 30 years ago that frustrated exchange interactions at the F/AF interfaces act as an effective random field *h* exerted on both F and AF at their interfaces [1], profoundly affecting the magnetic properties of the system. However, until now this hypothesis has not been tested. We utilize magnetoelectronic measurements of anisotropic magnetoresistance in F/AF=Py/CoO bilayers to experimentally confirm and to quantify the predicted random-field effects [2]. Our approach is based on the dependence of the magnetization state on the relationship between the magnetic correlation length l_M determined by the thickness t of F, and the correlation length l_h of the effective field [Fig. 1]. The response of a magnetic system to external field is thus expected to exhibit a crossover at thickness yielding $l_M=l_h$. For uncorrelated field, we determined the thickness-dependent response by using scaling arguments and simulations [Fig.2(a)]. Fitting of the magnetoelectronic data with these relations yields the magnitudes of random field that are nearly independent of t [Fig.2(b)], confirming the uncorrelated random-field hypothesis. The presented approach opens a route for the analysis of effective fields and anisotropies in magnetic heterostructures for memory, sensing and computing applications.

[1] A. Malozemoff, Phys. Rev. B 37, 7673 (1988). [2] G.X. Chen, D. Collette, S. Urazhdin, Phys. Rev. B 101, 144427 (2020)

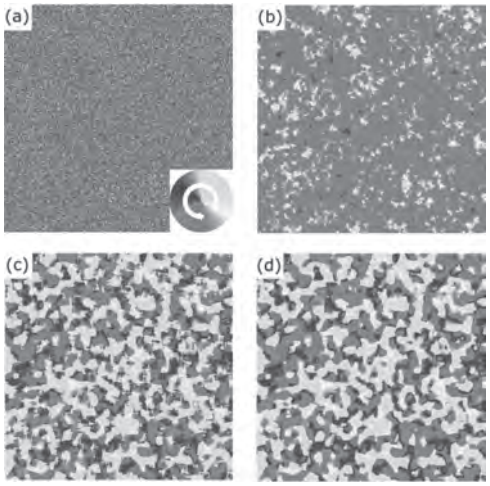

Fig.1 Distributions of random field with $l_h << l_m$ (a) and $l_h >> l_m$ (c), and the resulting magnetization distributions (b),(d), calculated using the MUMAX3 micromagnetic simulations.

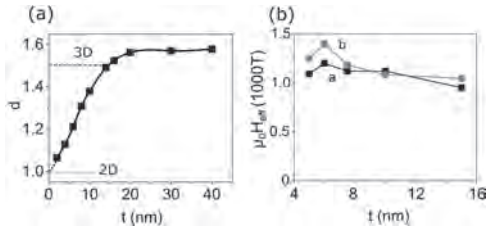

Fig.2 (a) Power law exponent *d* in the dependence $<\varphi^2>=CH^{d-2}$ of the average square of the angle between the magnetization and external field, vs Py film thickness, determined from micromagnetic simulations. Dashed lines show the analytical results for 2D and 3D systems. (b) Magnitude of the effective random exchange field in Py/CoO bilayer vs Py thickness, determined from the two branches of the hysteresis loop for the field aligned with the cooling field.

D1-04. Microscopic Origin of Magnetization Reversal in Exchange-Coupled Ferro-/Ferrimagnetic Bilayers. *M. Heigl*[1], C. Vogler[2], A. Mandru[3], X. Zhao[3], H.J. Hug[3,4], D. Suess[2] and M. Albrecht[1] *1. Institute of Physics, University of Augsburg, Augsburg, Germany; 2. Faculty of Physics, University of Vienna, Vienna, Austria; 3. Empa-Swiss Federal Laboratories for Materials Science and Technology, Dübendorf, Switzerland; 4. Department of Physics, University of Basel, Basel, Switzerland*

Exchange-coupled systems employing ferrimagnets (FI) provide high tunability, interfacial exchange interaction, and zero magnetic moment at the compensation temperature [1], which is highly beneficial for many applications such as spin valves [2] and magnetic tunnel junction devices [3]. Micromagnetic simulations showed that a partial domain wall is formed at the FI/ferromagnet(FM) interface layer during the reversal of the FM. The minor loop becomes fully reversible if this domain wall generates a hard-axis field that overcomes the anisotropy field of the FM [4]. In this study, the magnetic reversal process of exchange-coupled bilayer systems, consisting of a FI TbFeCo alloy layer and a FM $[Co/Ni/Pt]_N$ multilayer (ML), was investigated [5]. In particular, minor loop studies, probing solely the reversal characteristics of the softer FM layer, reveal two distinct reversal mechanisms, which depend strongly on the thickness of the FM layer. For thick layers (*N*=9, 10.8 nm), irreversible switching of the macroscopic minor loop is observed. The underlying microscopic origin of this reversal process was studied in detail by high-resolution magnetic force microscopy, showing that the reversal is triggered by in-plane domain walls propagating through the FM layer. In contrast, thin FM layers (*N*=5, 6.0 nm) show a hysteresis-free reversal, which was already reported in previous work [6] and is nucleation-dominated due to grain-to-grain variations in magnetic anisotropy of the Co/Ni/Pt ML and an inhomogeneous exchange coupling with the magnetically hard TbFeCo layer. The results were confirmed by micromagnetic simulations.

[1] B. Hebler, S. Böttger, M. Albrecht et al., Phys. Rev. B93, 184423 (2016) [2] F. Radu, R. Abrudan, H. Zabel et al., Nat. Commun. 3, 715 (2012) [3] J. S. Moodera, L. R. Kinder, R. Meservey et al., Phys. Rev. Lett. 74, 3273 (1995) [4] C. Vogler, M. Heigl, D. Suess et al., arXiv:2004.04419 (2020) [5] M. Heigl, C. Vogler, M. Albrecht et al., arXiv:2007.00333 (2020) [6] X. Zhao, A.-O. Mandru, H. J. Hug et al., ACS Appl. Nano Mater. 2, 12, 7478 (2019)

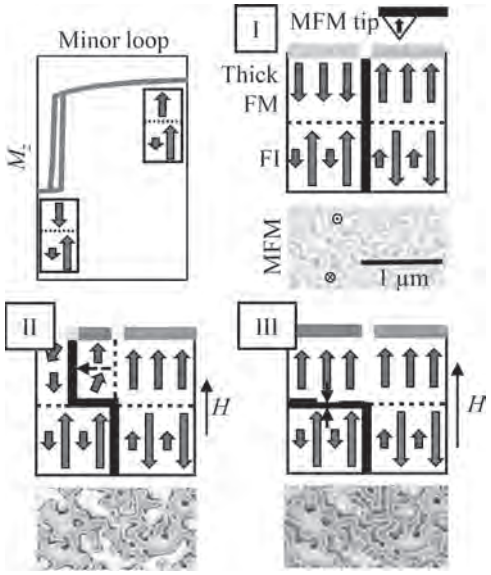

The thicker FM layer switches irreversibly as indicated by the presence of hysteresis in the *M-H* minor loop. I-III show schematically the reversal process starting from the demagnetized state. The corresponding in-field MFM images are displayed underneath.

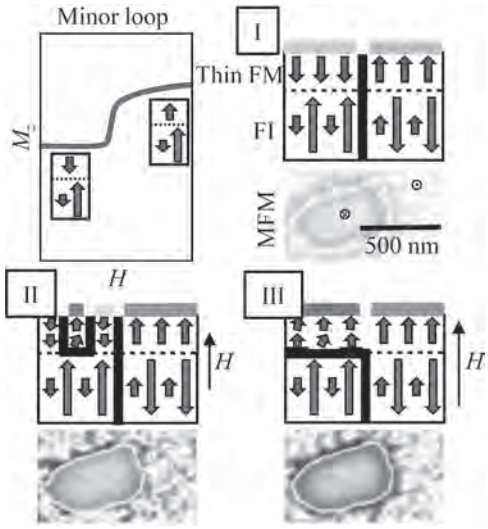

The thinner FM layer exhibits a fully reversible switching in the minor loop. I-III show schematically three magnetic states of the nucleation driven reversal process starting from the demagnetized state. Corresponding in-field MFM images are displayed underneath.

D1-05. Tuning of the Magnetization Direction in Cr_2O_3-Based Exchange-Coupled Systems. I. Hontecillas[1] and *R. Ranchal*[1,2] *1. Universidad Complutense de Madrid, Madrid, Spain; 2. Universidad Complutense de Madrid Instituto de Magnetismo Aplicado, Madrid, Spain*

Materials with out-of-plane magnetization are desirable to increase magnetic storage density or for new spintronic devices [1]. We have used an antiferromagnet with magnetic moments perpendicular to the plane, Cr_2O_3, to exchange-coupled with a Fe-based alloy with magnetization mostly in the sample plane, $Fe_{72}Ga_{28}$. Cr_2O_3 was synthesized from the oxidation of Cr thin films in oxygen atmosphere. Then, we have sputtered $Fe_{72}Ga_{28}$ layers that were capped with Mo. We have not found traces of oxidation in the $Fe_{72}Ga_{28}$ within the resolution technique of x-ray diffractometry in the Bragg-Brentano configuration when the Cr_2O_3 roughness is low. We have analyzed the evolution of the magnetic behavior varying the $Fe_{72}Ga_{28}$ thickness from 240 to 20 nm keeping fixed Cr_2O_3 thickness (30 nm). Magnetic force microscopy (MFM) reveals the enhancement of the out of plane component of the $Fe_{72}Ga_{28}$ magnetization as its thickness is reduced. Although a uniaxial in-plane magnetic anisotropy is expected in the $Fe_{72}Ga_{28}$ layers [2], it is completely vanished because of the coupling with Cr_2O_3. The comparison between perpendicular and in-plane hysteresis loops measured by vibrating sample magnetometry (VSM) also indicates the gradual reversal of the magnetization from in-plane to out-of-plane as the $Fe_{72}Ga_{28}$ thickness decreases. Combining MFM and VSM results, we have inferred a perpendicular magnetic anisotropy constant of 3×10^6 erg/cm^3. A field-cooling process from 343 K with an applied magnetic field of just 90 Oe makes possible to obtain at room temperature an exchange-bias field of -100 Oe in the perpendicular direction when the $Fe_{72}Ga_{28}$ thickness is 20 nm.

[1] B. Dieny, and M. Chshiev, Rev. Mod. Phys., Vol. 89, p. 025008 (2017).
[2] P. Bartolomé, A. Begué, A. Muñoz-Noval, M. Ciria, and R. Ranchal. J. Phys. Chem C, Vol. 124, p. 4717 (2020).

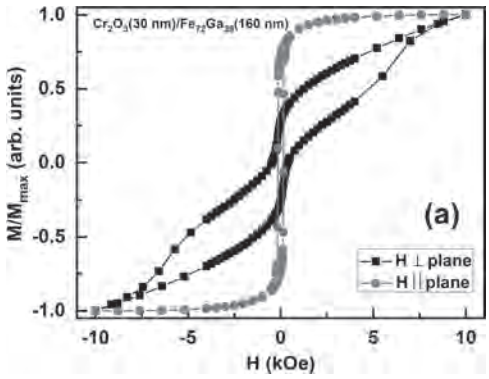

(a) Perpendicular (■) and in-plane (●) room temperature hysteresis loops recorded after a field-cooling process with the applied magnetic field perpendicular to the sample plane of 90 Oe (a) Cr_2O_3(30 nm)/ $Fe_{72}Ga_{28}$(160 nm).

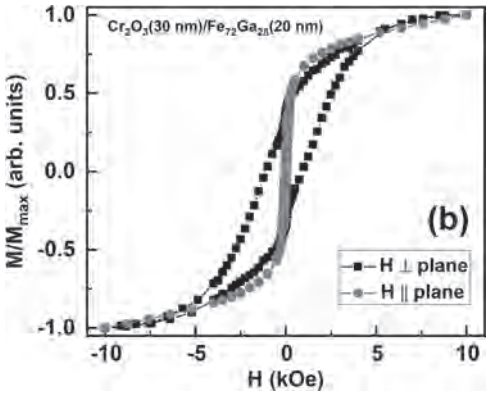

(b) Cr_2O_3(30 nm)/$Fe_{72}Ga_{28}$(20 nm).

D1-06. Atomistic Spin Dynamics Simulations of Exchange Bias in Polygranular IrMn/CoFe Bilayers and the Origin of the Athermal Training Effect. *S. Jenkins*[1], R.F. Evans[1] and R. Chantrell[1] *1. Department of Physics, University of York, York, United Kingdom*

Exchange bias is essential to the operation of magnetic read sensors. Recently it has been discovered that in single grain Co/$IrMn_3$ bilayers the exchange bias is caused by a small statistical imbalance in the number of Mn atoms in each sublattice [1]. In realistic devices the IrMn is split into multiple non interacting grains, each of which contributes separately to the exchange bias. Here, we have developed a model of a multigranular IrMn/CoFe bilayer using an atomistic spin model [2]. The properties of the disordered γ-$IrMn_3$ AFM are modelled including localized magnetocrystalline anisotropies and Heisenberg exchange, reproducing key experimental results including the Néel temperature and magnetic ground state. For an atomically flat interface the polygranular system qualitatively reproduces the experimentally observed temperature and grain size dependence of the exchange bias. A problem in maximising the exchange bias is the training effect. There are two known contributions to training: thermal and athermal. Thermal training arises due to the AFM spins undergoing thermally activated transitions during the magnetization reversal process of the FM layer [3]. However, the origin of athermal training is still a widely disputed problem due to the difficulty in experimentally probing the rearrangement of AFM spins. For an atomically flat interface no athermal training was found as the switching of the interfacial spins was found to be completely reversible. By increasing the intermixing between the ferromagnetic and antiferromagnetic layers at the interface we found the appearance of thermal training due to metastable spin states in the interfacial Mn spins which reorient during the first hysteresis cycle. We find a strong dependence on the amount of training on the

interface mixing as shown in Fig. 1. These results represent a significant step towards a full understanding of the exchange bias effect in nanoscale devices.

[1] S. Jenkins, W. J. Fan, R. Gaina, R. Chantrell, T. Klemmer, and R.F.L. Evans. Uncovering the mystery of delocalised pinned interface spins responsible for exchange bias. arXiv:1610.08236 [2] R. F.L. Evans, et al, J Phys Cond. Matter, 26, (2014) [3] X. P. Qiu et al, Phys. Rev. Lett., 101:147207 (2008).

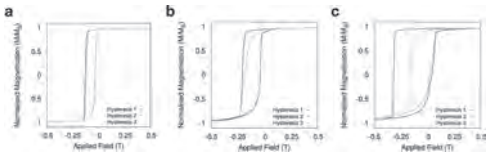

Figure 1. The first three simulated hysteresis loops for different intermixing widths, showing an increase in athermal training.

D1-07. π – Anisotropy: a Magneto-Electric Explanation for Molecular Exchange Bias. *T. Moorsom*[3,1], S. Alghamdi[1,2], S. Stansill[1], E. Poli[4], G. Teobaldi[4,5], M. Beg[6], H. Fangohr[6], M.D. Rogers[1], Z. Aslam[1], M. Ali[1], B. Hickey[1] and O. Cespedes[1] *1. University of Leeds, Leeds, United Kingdom; 2. Taibah University, Madinah, Saudi Arabia; 3. University of Glasgow College of Science and Engineering, Glasgow, United Kingdom; 4. Science and Technology Facilities Council, Swindon, United Kingdom; 5. University of Liverpool, Liverpool, United Kingdom; 6. European XFEL GmbH, Schenefeld, Germany*

Exchange bias is usually the product of an uncompensated spin plane at the interface between an anti-ferromagnet and a ferromagnet. First discovered in 1956, the effect is one of the most studied phenomena in magnetism. [1] However, in the past ten years, numerous observations have been made of exchange bias at molecule-metal interfaces. [2,3] This is unusual, since van der Waals crystals of organic molecules are not expected to exhibit robust magnetic order or strong exchange interactions. There is not yet a universally accepted mechanism for molecular exchange bias, and debate has raged about whether these effects are truly exchange bias, or simply the result of increased interfacial anisotropy.[4] Furthermore, it is not yet clear whether molecular exchange bias occurs only in anti-ferromagnetic stacks of molecular magnets, or whether hybridization and charge transfer also play a role. Here, we present a detailed study of molecular exchange bias at the interface between Co and the non-magnetic molecule C60.[5] We observe the largest bias field and magnetic hardening ever observed in a hybrid molecular system, and provide density functional theory and micro-magnetic models which strongly suggest an exchange spring like mechanism arising from broken interfacial symmetry. We provide a formalism for a new form of interfacial anisotropy, dubbed π-anisotropy, which we explain as the result of asymmetric p-d hybrid interfacial dipoles. While this effect is still confined to low temperature, we explain a development pathway towards a room temperature manifestation of the effect.

[1] W H Meiklejohn and C P Bean, Phys. Rev. 102, 1413, 1956. [2] M Gruber et al, Nat Mat, 14, 981-984, 2015. [3] J Jo et al, ACS Nano, 13, 1, 894-903, 2019. [4] S Boukari et al, Nano Lett. 18, 8, 4659 – 4663, 2018. [5] T Moorsom et al, Phys Rev B. 101, 060408(R), 2020.

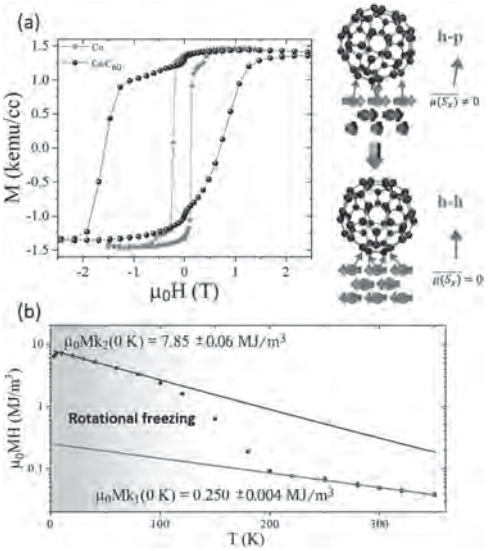

Fig 1. a. Hysteresis loop at 3 K for a Co/C_{60} bilayer in comparison to a Co thin film. The right panel shows the expected configuration of the surface spins and surface dipoles during the negative and positive field sweeps. b. Dependence of the MH product on temperature, showing the transition from a low to high coercivity region.

D1-08. Is Exchange Bias at the Hybrid Organic/Ferromagnet Interface an Intrinsic Effect? *G. Avedissian*[1], J. Arabski[1], J. Wytko[2], J. Weiss[2], V. Papaefthimiou[3], E. Beaurepaire[1] and C. Meny[1] *1. Institut de Physique et Chimie des Materiaux de Strasbourg, Strasbourg, France; 2. Institut de Chimie de Strasbourg, Strasbourg, France; 3. Institut de Chimie et Procedes pour l'Energie, l'Environnement et la Sante, Université De Strasbourg, Strasbourg, France*

Exchange bias (EB) plays an important role in spintronic devices. It has been thoroughly studied between inorganic anti-ferromagnets and metallic ferromagnetic (FM) layers but rather surprisingly, similar EB effects have been reported between metallic ferromagnets and organic molecular (OM) layers. In this case, EB is considered "spinterface" induced magnetic effect and could play big role in the next generation of environment-friendly electronic devices. Molecular EB effect has been first observed in 2015 [1] between cobalt films and manganese phthalocyanine, then expanded and reproduced with different metal (Zn, Fe, Co) phthalocyanine [2] and metal octa-ethyl porphyrin molecules [3]. However, fundamentals of molecular EB and its origins is still not understood and stays controversial. In this work, we investigate the possibility of molecular EB in cobalt/metal tetra-phenyl porphyrin (M=Zn and Ni) hybrid structures. Careful SQUID magnetometer measurements show the absence of EB in "freshly deposited" hybrid samples. Surprisingly, EB appears within few hours and gradually increases with time. Additionally, new, and similar "freshly deposited" samples kept under ultra-high vacuum (UHV) for the same time span did not show EB when measured directly after removal from the UHV chamber. This indicates that EB effect has its origin from the exposure of samples to air. In the light of these unexpected results, atomic force microscopy and X-ray photoelectron spectroscopy have been performed to identify and understand the reasons of our observations. The experimental evidences strongly suggest that EB in FM/OM systems is not an intrinsic effect and originates from air-driven oxidation of cobalt films transforming part of the metallic cobalt into CoO_x that is well known to produce EB effects.

[1] M. Gruber, F. Ibrahim, S. Boukary et al. Nature Materials., Vol 14, p. 981 (2015). [2] S. Boukary, H. Jabbar, F. Schleicher et al. Nano Letters., Vol 18, p. 4659 (2018). [3] J.Jo, J. Byun, I. Oh et al. ACS Nano., Vol 13, p. 894 (2019).

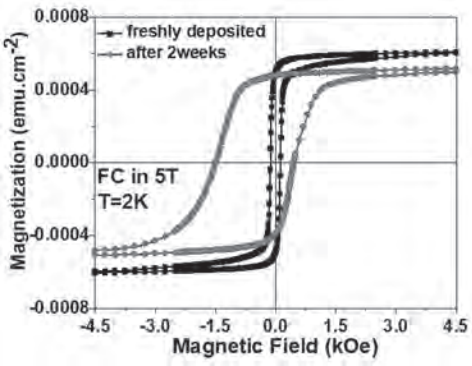

Fig. 1 Magnetization loops of 50 nm Au capped "freshly deposited" Co (6nm)/ZnTPP (10nm) sample (black loop) and of same sample measured after 2 weeks (red loop). Loops acquired at 2K after FC in +5T magnetic field

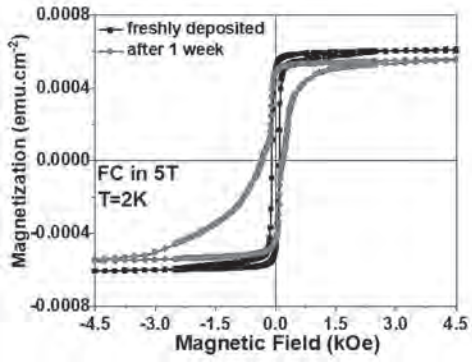

Fig. 2 Magnetization loops of 50 nm Au capped "freshly deposited" Co (6nm)/NiTPP (10nm) sample (black loop) and of same sample measured after 2 weeks (red loop). Loops acquired at 2K after FC in +5T magnetic field

D1-09. Emrgence and Disappearance of Exchange Bias in Ni-Mn/ Fe-Ni Thin Films Due to Structural Transformations. *M. Moskalev*[1], E. Kudyukov[1], E. Kravtsov[2,1], V. Lepalovskij[1] and V. Vas'kovskiy[1,2]
1. Department of magnetism and magnetic nanomaterials, Ural'skij federal'nyj universitet imeni pervogo Prezidenta Rossii B N El'cina, Ekaterinburg, Russian Federation; 2. Institut fiziki metallov imeni M N Miheeva Ural'skogo otdelenia Rossijskoj akademii nauk, Ekaterinburg, Russian Federation

The exchange bias effect, which manifests itself as a shift of the hysteresis loop of a ferromagnet when it is adjacent to an antiferromagnet, is a key feature used in such technological spheres as magnetic recording and storage as well as magnetic sensorics [1]. However, technological applications require materials whose performance is sustainable in a broad temperature range. A perfect candidate for this role is the antiferromagnetic Ni-Mn, multilayered structures based on which are capable of exhibiting exchange bias up to temperatures of above 700 K [2]. It is also a much more affordable option when compared to currently used Ir-Mn and Pt-Mn, since it doesn't consist precious metals. Although very promising, formation of the ordered q-NiMn requires post-deposition annealing. In this work we show how the emergence of this phase leads to the emergence of exchange bias, depending on the initial condition of the Ni-Mn layer. Moreover, we show that the irreversible disappearance of exchange bias is associated with structural transformations occurring in the films at higher temperatures. In this work we study magnetron-sputtered Ni-Mn (20 nm) and Ni-Mn (20 nm)/ Fe-Ni (40 nm) films with and without a 5 nm thick buffer Fe-Ni layer. Films were deposited on Corning glass substrates; 5 nm thick Ta layers were used as seed and capping layers. The composition of the Ni-Mn layer was varied from 10 to 50 at. % of Ni. Structural and magnetic properties of the films were studied by means of X-ray diffractometry (XRD) and vibrating sample magnetometry, accordingly. XRD measurements included a variety of geometries, such as grazing incidence (GIXRD), θ-2θ, and rocking curves (ω-scans). Structural and magnetic studies were executed in a high-temperature chamber, which allowed in-situ observation of corresponding evolution of structural and magnetic properties of films. This work was financially supported by the Russian Science Foundation, project No. 18-72-10044.

1. F. Radu, H. Zabel, Magnetic heterostructures, Springer, 97 (2008). 2. V.O. Vas'kovskiy et al., J. Alloys Compd., 777, 264 (2019).

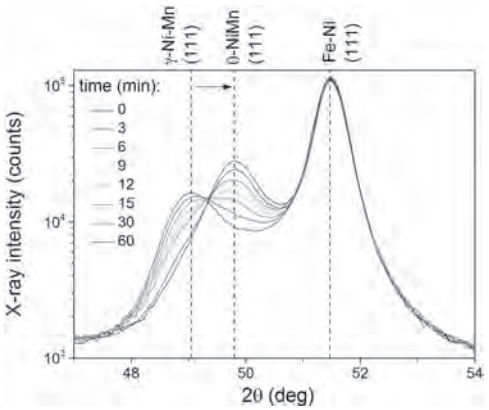

Fig. 1. Time evolution of XRD θ-2θ spectra of a Fe-Ni (5 nm)/$Ni_{30}Mn_{70}$ (20 nm)/Fe-Ni (40 nm) film when heated up to 300 °C. The initial γ-Ni-Mn under annealing transforms into θ-NiMn, which is indicated by the shift of the (111)-peak.

D1-10. Mini Magnetic Propellers: Stability Considerations in Twisted Magnetic Structures. *B.R. McGrath*[1], K. Livesey[1,2] and R. Camley[1]
1. Physics, University of Colorado at Colorado Springs, Colorado Springs, CO, United States; 2. School of Mathematical and Physical Sciences, The University of Newcastle, Callaghan, NSW, Australia

Rubber bands can be found in many children's toys. For example, one winds up a rubber band and when released it drives an airplane or a racing car. If instead we wind up a tiny magnetic structure, where the magnetization twists and stores energy, then that energy will be released upon unwinding. In this theoretical work we consider a very soft, low-exchange film (80-400 atomic layers of Cu-doped Permalloy [1]), which is pinned at the bottom and coupled to a high-exchange ferromagnetic film on top. We apply a magnetic field which is rotated in the plane of the film. This generates a slow twisting of the soft material with the high-exchange ferromagnet acting as a handle as is seen in Fig. 1. We use both a local self-consistent mean-field theory [2] as well as a dynamic approach with the Landau-Lifshitz equation, with results matching well for both. With these models we have been able to generate multiple twists (over 10) in these films. At some point an instability occurs that prevents additional twists. Often the instability causes one or more twists to be released from the structure. The tightness of the twists as well as how many twists are formed before snapping depends on the length of the structure, the strength of the applied field, the size of the of the ferromagnetic cap, the exchange coupling strength, and the saturation magnetization. For example, increasing the exchange coupling decreases the number of twists that are stable in a given structure. The number of allowed twists also increases linearly with the length of the sample. Analytic energy minimization calculations, using a constant turn angle approximation, also allow us to estimate how many twists will fit into a given structure, matching reasonably well with numerical outcomes. The more twists in a given structure, the more energy it can hold. Once the twist is released or snapped, the system will unwind with frequencies in the gigahertz range. We study the frequency distribution as a function of the number of twists. Based on energy storage and this frequency generation we discuss potential applications.

[1] N. Sorensen, R. E. Camley and Z. Celinski, *J.Magn Magn Mat,* vol. 477, p. 344, (2019). [2] R. E. Camley, *Phys Rev B,* vol. 35, p. 3608, (1987).

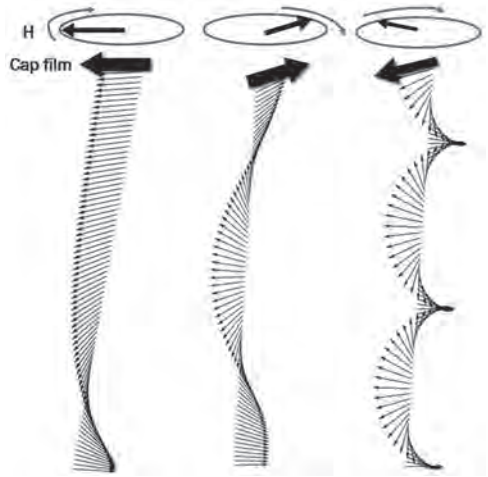

Fig. 1 Illustrations of the spin configurations in various twisted states. The magnitude of the applied field is 500 Oe.

D1-11. Ferromagnetic SmN/GdN Superlattices. *E.M. Anton*[1], W. Holmes-Hewett[1], J. McNulty[1], F. Natali[1], S. Granville[2], F. Bramley[1], B. Ruck[1] and H. Trodahl[1] *1. School of Chemical and Physical Sciences, Victoria University of Wellington, Wellington, New Zealand; 2. Robinson Research Institute, Victoria University of Wellington, Lower Hutt, New Zealand*

The rare-earth mononitrides, LN (L one of the fourteen lanthanide elements), are mostly intrinsic ferromagnetic semiconductors, though with strongly contrasting magnetic responses that reside in their variously-filled L^{3+} cations. Their magnetic order is at most weakly influenced by doping, in clear contrast with the diluted magnetic semiconductors, which then presents the potential for developing even active controlled-conductivity devices. Their simple rock-salt structure, with only two ions in the primitive cell, is further promising for the development of such devices.[1] GdN, the most heavily investigated of the series, harbours a conventional spin-only ferromagnetic order. In contrast SmN features a nearly zero orbital-dominated magnetisation in which the spin magnetic moment is aligned in opposition to an applied magnetic field. Their magnetic responses thus contrast strongly in homogeneous films, but an even richer magnetic state is found in SmN/GdN superlattices, where the exchange interaction across a GdN/SmN interface competes with the Zeeman interaction. The balance between the two interactions is then a complex function of the applied field, shifting from interface exchange-dominated behaviour in low fields to an increasingly Zeeman-interaction dominance as the field is increased. In this presentation we report magnetisation, XMCD, magnetoresistance and both the ordinary and anomalous Hall effect that reveal details of the magnetic and transport channels in superlattices: (i) depth-dependent spin and orbital alignment in SmN layers, (ii) SmN-mediated GdN/GdN magnetism, (iii) mix of transport in the two layer classes. The results highlight the influence of the interface exchange/Zeeman conflict on the magnetic alignment and the coupled magnetic/electronic responses.

[1] F. Natali et al., Prog. Mat. Sci. 58, 1316 (2013)

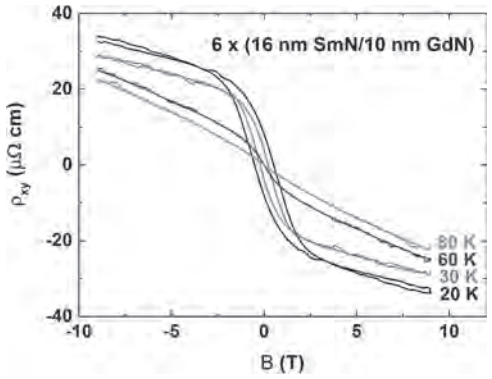

Hall effect of a 6x(16 nm SmN/10 nm GdN) superlattice. The shape anisotropy in this field-normal orientation determines that the magnetisation does not saturate until the applied field is 0.8 T. Above 0.8 T the Hall resistivity is linear with field as is typical of the ordinary Hall effect. The offset across zero field is a measure of the anomalous Hall effect. The coercive field rises dramatically below the 30 K Curie temperature of SmN.

D1-12. Critical Magnetic Behavior in $[Ag_8/Co_{0.5}]x64$, $[Ag_{16}/Co_1]x32$ and $[Ag_8/Co_1]x32$ Epitaxial Multilayers. E. Navarro[2], M. Alonso[2], A. Ruiz[2], C. Magen[3], U. Urdiroz[2], F. Cebollada[1], L. Balcells[4], B. Martínez[4], *J.M. González*[2] and F. Palomares[2] *1. Universidad Politécnica de Madrid, Madrid, Spain; 2. Instituto de Ciencia de Materiales de Madrid - CSIC, Madrid, Spain; 3. Instituto de Ciencia de Materiales de Aragón - CSIC, Zaragoza, Spain; 4. Instituto de Ciencia de Materiales de Barcelona - CSIC, Barcelona, Spain*

We analyze in this work the low temperature magnetic behavior of a series of Co/Ag multilayers formed by samples having reduced Co content per period (either one monolayer or half a monolayer) separated by several Ag monolayers (either 8 or 16). The multilayers were grown by molecular beam epitaxy on a clean MgO (001) surface, alternating Ag and Co deposition up to complete either 32 or 64 periods (in order to maintain constant in the series the nominal number of Co atoms per unit surface of the sample) and protected by a 3nm Ag cap layer. The samples were studied by X-ray reflectivity and diffraction, TEM, SQUID magnetometry, and ac susceptometry. From the results of our measurements we identified the following facts: 1) the occurrence in all the samples of stacking sequences corresponding to the nominal ones 2) the spatial discontinuity of the Co layers that corresponded to a quasi-monodisperse in-plane distribution of Co particles embedded in a Ag(001) matrix; 3) the observation of hysteresis at temperatures (always below 20 K) that depended on both the number of Co and Ag monolayers per period; 4) an ac field frequency dependence of the real part of the susceptibility, χ', maxima temperatures corresponding to a Vogel-Fulcher behavior with a frequency shift parameter of the order in all the samples of 4×10^{-2}; 5) the collapse (Figure 1), for each sample, of the experimental data corresponding to the ac field frequency, f, and temperature, T, variations of the imaginary part of the ac susceptibility, χ'', in a single curve, G(x) with $x = f[(T/T_g) - 1]^{-Z\nu}$ (where T_g and $Z\nu$ are the critical temperature and exponent, respectively), and verifying $T\chi''(f, T) = [(T/T_g) - 1]^{\beta} G(x)$ [1]. Taken together, these results allow us to conclude that our three multilayers experience a phase transition (of the paramagnetic to superspin glass type) at the corresponding critical temperature and that the exponent β in the universal dynamic scaling law takes values dependent on the number of Co monolayers per period.

[1] P. Beauvillain, C. Dupas, J.P. Renard, and P. Veillet, Physical Review B 29 (7), 4086 (1984).

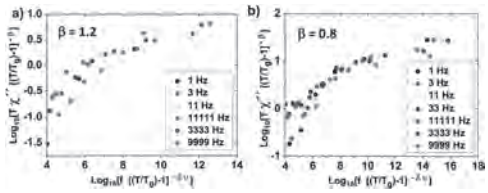

Figure 1. Collapse of the χ″ data to the universal dynamic scaling law; a) Co 0.5/Ag 8 sample; b) Co 1/Ag 8 sample

D1-13. Investigation of the Spin Glass Density of States Using a Combination of Monte Carlo Method and Neural Network.
A.O. Korol[1], K. Makarova[1,2], D. Kapitan[1,2], A. Rybin[1,2], E. Vasiliev[1,2], A. Makarov[1,2], K. Soldatov[1,2], Y. Shevchenko[1,2] and V.Y. Kapitan[1,2]
1. Computer Systems, Dal'nevostocnyj federal'nyj universitet, Vladivostok, Russian Federation; 2. Institut prikladnoj matematiki DVO RAN, Vladivostok, Russian Federation

The study of magnetic systems, spin glasses, and their states, is an actively developed field of statistical physics. Spin glass models are studied in various scientific contexts, including experimental physics, condensed matter physics, theoretical physics, mathematical statistical physics and, more recently, probability theory [1 - 3]. The problem of finding the ground states (GS), i.e. states with the lowest energy is a very difficult task due to the macroscopic degeneracy and frustrations that are exist in various realistic spin glass models. In fact, it's well known that finding the GS, of a spin glass in a three-dimensional lattice is an NP-complete problem, which means that this challenge is at least as difficult as the hardest problems of practical interest. The system of interest is the Edwards-Anderson (EA) spin glass model [4] in two-dimensional (2D) lattice, with bimodal distribution of bonds. In present work, for simulation we used a combination of our Hybrid Multispin Method (HMM) [5] and Long Short-Term Memory (LSTM) - an artificial recurrent neural network (RNN) architecture [6] with Boltzmann distribution. HMM's advantages are the ability to increase the number of simultaneously gathered statistical-thermodynamic parameters without noticeable speed and efficiency loss, and the ability to search for configurations of the ground and low-energy states. The usage of machine learning in statistical physics began relatively recently but is developing rapidly. Neural networks have become popular tool due to the high speed of their training and accuracy of predictions. LSTM with Boltzmann distribution is useful for certain types of prediction that require the network to retain information for longer periods of time that traditional RNNs encounter. In our research, MC algorithm generated a training data set which is configurations of SG system. The trained predicted system configurations, which are using for the next computing cycle for HMM. Such iterative approach allows us to efficiently simulate the spin-glass systems even in the low-temperature regime, avoiding the critical slowing down that plague of usual MC simulation. This work was supported by the state task of the MSHE of Russia No. 0657-2020-0005.

[1] A. Callison et al., New J. Phys., Vol. 21, 123022 (2019) [2] B. McNaughton et al., Phys. Rev. E, Vol. 101, 053312 (2020) [3] L. A. Fernandez, E. Marinari, V. Martin-Mayor, I. Paga, and J. J. Ruiz-Lorenzo, Phys. Rev. Vol. 100, 184412 (2019) [4] S. Edwards, P. Anderson, Phys. F: Metal Phys., Vol. 5 (5), p. 965 (1975) [5] A.G. Makarov et al., JETP Letters., Vol. 110 (10), pp. 702-706 (2019) [6] S. Hochreiter, J. Schmidhuber, Neural computation., Vol. 9(8), pp. 1735-1780 (1997)

D1-14. The Effect of x-ray Illumination on Magnetic Domain Memory in [Co/Pd] / IrMn Multilayers.
C.S. Walker[1], M. Parkes[1], D. Keavney[2], E. Fullerton[3] and K. Chesnel[1] *1. Physics, Brigham Young University, Provo, UT, United States; 2. Argonne National Laboratory Advanced Photon Source, Lemont, IL, United States; 3. Center for Memory and Recording Research, UCSD, San Diego, CA, United States*

We are studying the effect that illumination by coherent resonant x-rays may have on magnetic domain memory (MDM) in a [Co / Pd] / IrMn multilayers [1-3]. MDM is the ability of the magnetic domains to retain their exact same domain topology upon field cycling. Earlier studies have suggested that under higher doses of x-ray illumination, the material may lose its existing MDM. To investigate this possible effect we have used both x-ray resonant magnetic scattering (XRMS) along with magneto-transport measurements [4,5] to track the exchange bias while the sample is illuminated with x-rays, as illustrated in Figure 1. Fig.1a shows magneto-transport data collected on the [Co/Pd] / IrMn multilayer from which we hope to extract information about exchange bias. A loss of exchange bias would indicate that the x-rays illumination dose may alter the strength of the internal exchange couplings between the ferromagnetic and antiferromagnetic layers. Ultimately it would alter the amount of MDM, which is measured via XRMS as illustrated in Fig. 1b, and represented in a correlation map such as Fig.1c.

[1] K. Chesnel, A. Safsten, M. Rytting, and E.E. Fullerton, Nature Communications 7, (2016). [2] K. Chesnel, B. Wilcken, M. Rytting, S.D. Kevan, and E.E. Fullerton, New Journal of Physics 15, 023016 (2013). [3] K. Chesnel, J. Nelson, B. Wilcken, and S.D. Kevan, Journal of Synchrotron Radiation 19, 293 (2012). [4] C. Hurd, *Hall Effect in Metals and Alloys* (Springer, 2012). [5] L.J. van der Pauw, A Method of Measuring Specific Resistivity and Hall Effect of Discs of Arbitrary Shape (1958).

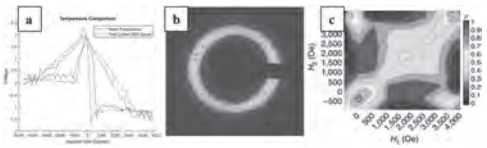

Figure 1: a) Magneto-transport measurement taken while [Co/Pd] / IrMn multilayers was illuminated with x-rays. b) XRMS speckle pattern from the [Co/Pd] / IrMn film, measured at the Co L_3 edge. c) correlation map between speckle patterns collected throughout the magnetization loop.

Session D2
MAGNETIC INTERACTIONS AND STRUCTURES

Kirrily C Rule, Chair
Australian Nuclear Science and Technology Organisation, Kirrawee DC, NSW, Australia

CONTRIBUTED PAPERS

D2-01. Unveiling Phonons in a Molecular Qubit With Four-Dimensional Inelastic Neutron Scattering and Density Functional Theory. *E. Garlatti*[1,2], L. Tesi[3,4], A. Lunghi[5], M. Atzori[3,6], D. Voneshen[7], P. Santini[1,2], S. Sanvito[5], T. Guidi[7], R. Sessoli[3,2] and S. Carretta[1,2] *1. Department of Mathematical, Physical and Computer Sciences, Universita degli Studi di Parma, Parma, Italy; 2. Consorzio Interuniversitario Nazionale per la Scienza e Tecnologia dei Materiali, Firenze, Italy; 3. Department of Chemistry U. Schiff, Universita degli Studi di Firenze, Firenze, Italy; 4. Institute of Physical Chemistry, Universitat Stuttgart, Stuttgart, Germany; 5. School of Physics, CRANN and AMBER, University of Dublin Trinity College, Dublin, Ireland; 6. Laboratoire National des Champs Magnétiques Intenses, Grenoble, France; 7. ISIS Neutron and Muon Source, Science and Technology Facilities Council, Didcot, United Kingdom*

One of the most important goals in the current research in molecular magnetism is to reach a deep understanding of the relaxation dynamics of Molecular NanoMagnets (MNMs), being this aspect of paramount importance in the design of new systems acting as classical [1, 2] or quantum bits [3]. Despite being the main source of relaxation in MNMs, very limited experimental investigations on their phonons have been done so far, yielding no information about their dispersions. Indeed, the key to construct a reliable model of phonon-induced relaxation dynamics in MNMs is to have access to phonon dispersions and eigenvectors, which are necessary for a quantitative evaluation of spin-phonon coupling coefficients. Here we exploit the four-Dimensional Inelastic Neutron Scattering (4D-INS) technique [4] to directly measure for the first time phonon dispersions in a prototypical molecular qubit, $[VO(acac)_2]$. Vanadyl-based molecules are in fact currently emerging as archetypes of a new generation of molecular qubits with long coherence times even at high temperatures [3]. 4D-INS is a very powerful technique to study phonons, because it enables a direct access to phonon eigenvalues and eigenvectors, by measuring the four-dimensional scattering function in large portions of the reciprocal space. We detected both acoustic and optical branches in single crystals of $[VO(acac)_2]$ along different directions in the reciprocal space and we compared the results of this challenging experiment with state-of-the-art density functional theory (DFT) calculations (Fig.1). Simulations reproduce important features of the 4D-INS data, such as the presence of low-lying optical modes and anti-crossings between acoustic and optical phonons, providing insights on their effect on spin-phonon couplings [5].

[1] C.A.P. Goodwin, F. Ortu, D. Reta, *et al.*, Nature Vol. 548, p. 439, (2017). [2] F.-S. Guo, B. M. Day, Y.-C. Chen, *et al.*, Science Vol. 362, p. 1400, (2018). [3] M. Atzori, L. Tesi, E. Morra, *et al.*, J. Am. Chem. Soc. Vol. 138, p. 2154, (2016). [4] E. Garlatti, A. Chiesa, T. Guidi, *et al.*, Eur. J. Inorg. Chem., p. 1106, (2019). [5] E. Garlatti, L. Tesi, A. Lunghi, *et al.*, Nat. Commun. Vol. 11, p. 1751 (2020).

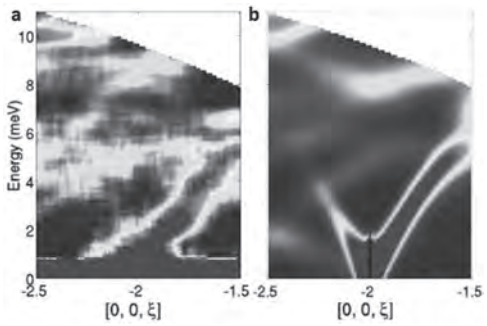

Fig.1: $[VO(acac)_2]$ phonon dispersions measured on LET (panel a) and simulated with phonon energies and polarisation vectors obtained from DFT calculations (panel b), showing longitudinal acoustic modes and low-lying optical ones along the symmetry direction Γ–Z.

D2-02. Molecular Nanomagnets as Qubits With Embedded Quantum-Error Correction. *A. Chiesa*[1,2], E. Macaluso[1], F. Petiziol[1,2], S. Wimberger[1,3], P. Santini[1,2] and S. Carretta[1,2] *1. Universita degli Studi di Parma, Parma, Italy; 2. UdR Parma, INSTM, Parma, Italy; 3. Istituto Nazionale di Fisica Nucleare Sezione di Trieste, Sezione Milano Bicocca, Gruppo Collegato di Parma, Italy*

Protecting qubits from errors is mandatory to realize scalable quantum computing platforms able to implement complex algorithms. However, standard quantum error correction (QEC) codes based on multi-qubit encoding yield a large increase in the number of physical qubits and operations, thus making the control of such a platform very demanding for current technologies. Here we show [1] that Molecular Nanomagnets can be used to easily overcome this limitation, by naturally embedding quantum error corrected units in a single multi-level molecule [2]. This is made possible by the rich and chemically tunable spectrum of these systems, characterized by many accessible levels with long coherence times [3]. We perform a perturbative expansion of the Lindbald equation [4] to design a scheme, based on such molecular qudits, which efficiently protects them from real errors, induced by pure dephasing. We then derive the sequence of pulses actually implementing QEC on a real spin system and demonstrate the effectiveness of our approach by numerical simulations. We already get a remarkable gain (up to an order of magnitude compared to an uncorrected S=1/2, see Fig. 1) in the final error with a simple existing molecule consisting of a nuclear qudit coupled to an electronic ancilla, used for error detection. This gain is further improved by scaling to larger spins, as we quantitatively analyze, and is found to be resistant to measurement errors (Fig. 1). Finally, the single-object nature of the error-protected qubits allows two-qubit gates to be easily implemented, without needing non-local interactions as in many multi-qubit encodings. Hence, this proposal opens a new avenue towards the actual realization of a scalable error-corrected quantum computing architecture.

[1] A. Chiesa, E. Macaluso, F. Petiziol, S. Wimberger, P. Santini and S. Carretta, submitted. [2] R. Hussain, G. Allodi, A. Chiesa, E. Garlatti, D. Mitcov, A. Konstantatos, K. S. Pedersen, R. De Renzi, S. Piligkos and S. Carretta, J. Am. Chem. Soc., 140, 9814 (2018). [3] J. M. Zadrozny, J.

Niklas, O. G. Poluektov, and D. E. Freedman, ACS Cent. Sci., 1, 488 (2015).
[4] M. H. Michael, M. Silveri, R. T. Brierley, V. V. Albert, J. Salmilehto, L. Jiang, and S. M. Girvin, Phys. Rev. X, 6, 031006 (2016).

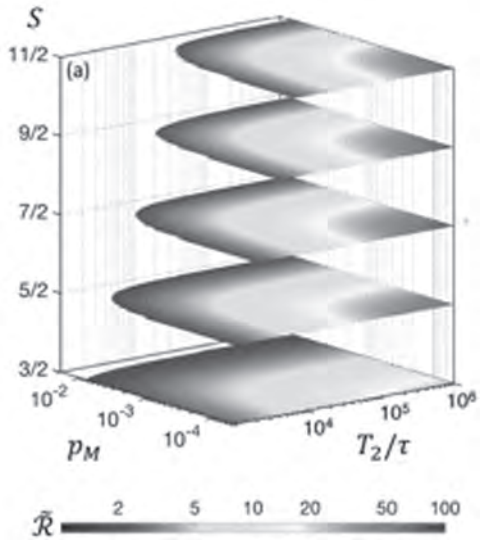

Ratio between the error on the qudit after QEC and that on an uncorrected spin ½, subject to pure dephasing, as a function of the qudit spin *S*, the qudit coherence time T_2 (in units of the elementary gate time τ) and the measurement error p_M.

D2-03. A Heterometallic [LnLn'Ln] Lanthanide Complex as a Qubit With Embedded Quantum Error Correction. *E. Macaluso*[3,4], M. Rubin[1,2], D. Aguilà[5,6], A. Chiesa[3,4], L. Barrios[5,6], J. Martínez[1,2], P. Alonso[1,2], O. Roubeau[1,2], F. Luis[1,2], G. Aromì[5,6] and S. Carretta[3,4]
1. Instituto de Ciencia de Materiales de Aragón (ICMA), CSIC and Universidad de Zaragoza, Zaragoza, Spain; 2. Departament de Física de la Materia Condensada, Universidad de Zaragoza, Zaragoza, Spain; 3. Dipartimento di Scienze Matematiche, Fisiche e Informatiche, Universita degli Studi di Parma, Parma, Italy; 4. UdR Parma, INSTM, Consorzio Interuniversitario Nazionale per la Scienza e Tecnologia dei Materiali, Parma, Italy; 5. Departament de Química Inorgànica, Universitat de Barcelona, Barcelona, Spain; 6. Institute of Nanoscience and Nanotechnology of the University of Barcelona (IN2UB), Barcelona, Spain

The achievement of quantum error correction is a fundamental step towards the implementation of a scalable platform for quantum computation, in which logical units are made robust against errors. Here we show that magnetic molecules consisting of weakly interacting and individually addressable spins ½ centers are a very promising platform to implement repetition codes for quantum error-correction, where several spins ½ are used to encode an error protected logical qubit. In particular, we demonstrate that these challenging requirements can be fulfilled by the [Er-Ce-Er] molecular trinuclear coordination compound. We show that this complex can be exploited to efficiently implement the three-qubit quantum error correction code protecting against pure dephasing, the most important error in magnetic molecules [1]. The system is characterized by combining magnetometry, low-temperature specific heat and electron paramagnetic resonance measurements on both the trimer and the properly synthesized [LuCeLu] and [ErLaEr] analogues, which contain only one of the two types of magnetic ions. The resulting large and distinct g values, together with weak but non-negligible dipolar interactions, enable us to selectively address different transitions by a proper sequence of microwave pulses, implementing the three-qubit repetition code. The parameters obtained from the experimental characterization are finally used to perform thorough numerical simulations of the system dynamics, including the effect of pure dephasing in a Lindblad formalism. These show a remarkable gain of the quantum error correction procedure, thus proving the efficiency of the device in suppressing pure dephasing.

[1] E. Macaluso, M. Rubin, D. Aguilà, A. Chiesa, L. Barrios, J. I. Martínez, P. J. Alonso, O. Roubeau, F. Luis, G. Aromí and S. Carretta, submitted.

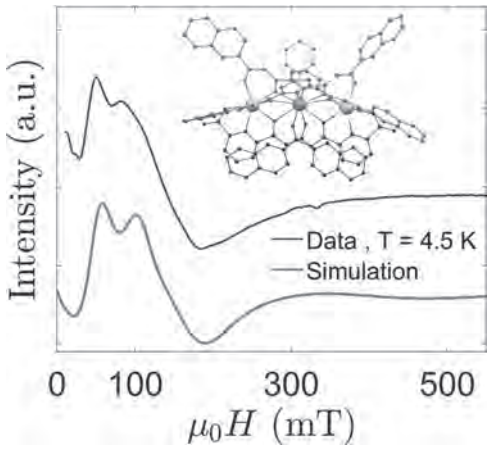

Fig. 1: Characterization by CW-electron paramagnetic resonance. Molecular structure of [ErCeEr] complex is reported as inset.

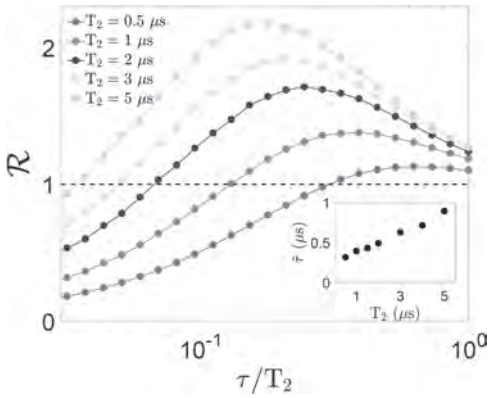

Fig. 2: Efficiency of the code in suppressing pure dephasing, quantified by the ratio between the error on an uncorrected qubit and on the logical [ErCeEr] unit subject to quantum error correction.

D2-04. Observation of a Superparamagnetic Breakdown in Gadolinium Chloride Filled Double-Walled Carbon Nanotubes. *S. Ncube*[1], C. Coleman[2], E. Flahaut[3], S. Bhattacharrya[2], A. Prinsloo[1] and C. Sheppard[1] *1. Physics, University of Johannesburg, Auckland Park, South Africa; 2. Physics, University of the Witwatersrand, Johannesburg-Braamfontein, South Africa; 3. Materials Science and Engineering, Universite Paul Sabatier Toulouse III Faculte de Chirurgie Dentaire, Toulouse, France*

In this work, we explored the magnetic properties of gadolinium chloride-filled double-walled carbon nanotubes ($GdCl_3$@DWNTs) in the 2 - 300 K range. The temperature-dependent phonon frequencies of the G-band were studied from 77 - 300 K to investigate the effect of temperature on the magnetic ordering. Temperature-dependent susceptibility measurements shown that the $GdCl_3$@DWNTs had a pronounced superparamagnetic phase from 100 K. The temperature dependence of the G-band frequency for filled tubes exhibited a distinct difference compared to pristine nanotubes, where a sharp phonon hardening at low temperatures was observed. We evidenced a correlation between the onset temperature of superparamagnetism and the abrupt G-band phonon hardening in the filled tubes. $GdCl_3$@ DWNTs were characterized by a finite remnant magnetization at 300 K which decreased as the temperature was lowered due to the presence of

the discontinuous magnetic nanoparticles providing a superparamagnetic contribution [1], characterized by a zero-remnant magnetization at 50 K. As seen in the susceptibility data, superparamagnetism could be verified in the filled DWNTs through the bifurcation of zero-field cooled (ZFC) and field cooled (FC) measurements, which occurred at approximately 100 K. The blocking temperature for the superparamagnetic phase was determined to be 23 K, characterized by a sharp turn in the FC data. Remarkably, the onset of superparamagnetism marked by the bifurcation point occurred at roughly the same temperature where the G-band phonon frequency showed a pronounced hardening ~ 100 K, indicating a close correlation between phonon modes and spin clusters. This is particularly interesting when considering the spin relaxation mechanisms known for the superparamagnetic breakdown [1,2,3]. At higher temperatures the spin relaxation is considered to be dominated by phonon interference and characterized by an Arrhenius type dependence, however at lower temperatures in the superparamagnetic phase, spin relaxation occurs through quantum mechanical tunneling of the magnetic moment.

1. S. Ncube, C. Coleman, A. S. de Sousa et al J. Appl. Phys. 123, 213901(2018). 2. H.D. Pfannes, Hyperfine Interactions 110, 127 (1997). 3. H.D. Pfannes, A. Mijovilovich, R. Magalhães-Paniago and R. Paniago Phys. Rev. B 62, 3372 (2000) 4. Q. C. Sun, C. S. Birkel, J. Cao, W. Tremel, and J. L. Musfeldt, ACS Nano 6, 4876 (2012).

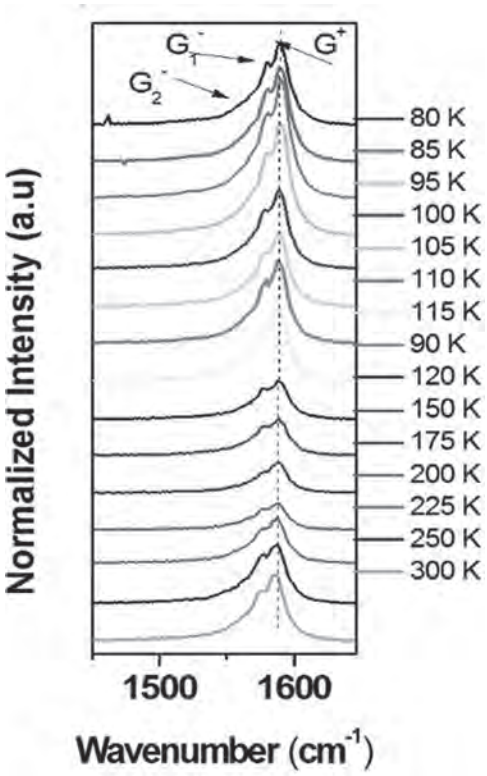

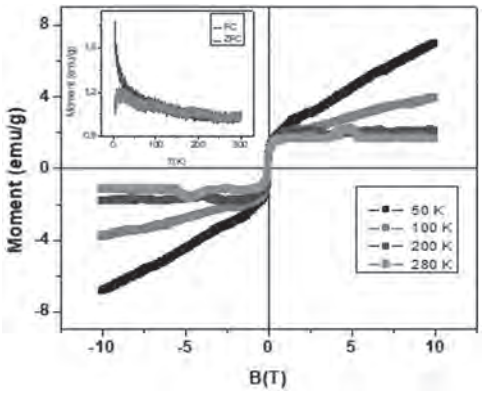

D2-05. Coupling Nanostructured CsNiCr Prussian Blue Analogue to Resonant Microwave Fields. *A. Ghirri*[1], T. Mallah[3] and M. Affronte[2,1]
1. Istituto Nanoscienze - Consiglio Nazionale delle Ricerche, Modena, Italy; 2. Dipartimento di Scienze Fisiche, Informatica e Matematica, Universita di Modena e Reggio Emilia, Modena, Italy; 3. Institut de Chimie Moleculaire et des Materiaux d'Orsay CNRS, Universite Paris Sud, Universite Paris Saclay, Orsay, France

Collective spin excitations in magnetically ordered materials are exploited for advanced applications in magnonics and spintronics. In these contexts, conditions for minimizing dissipative effects are sought in order to obtain long living excitations that can be coherently manipulated. Organic and coordination materials may offer alternative options for their flexibility and low spin–orbit effects. Likewise, ferromagnetic nanostructures provide a versatile platform for hybrid architectures, yet downsizing affects the spin dynamics and needs to be controlled. Here, a systematic investigation on insulating $CsNiCr(CN)_6$ Prussian blue analogue, including isolated nanoparticles dispersed in polyvinylpyrrolidone (PVP), mutually interacting nanoparticles embedded in cetyltrimethylammonium (CTA^+), and bulk samples, is reported [1]. Ferromagnetic resonance spectroscopy is performed in a wide temperature range across the bulk ferromagnetic transition occurring at 90 K. This allows us to monitor coupling and linewidth parameters through different types of nanostructured samples. It is found that the Gilbert damping parameter of 10 nm nanoparticles compares well (10^{-3}) with values reported for prototypical yttrium iron garnet $Y_3Fe_5O_{12}$ nanoparticles. Strong coupling with confined microwave field of a microstrip resonator is then observed for bulk $CsNiCr(CN)_6$ as well as for interacting nanoparticles. These results clarify conditions for the coherent manipulation of collective spin degrees of freedom in nanostructured coordination materials.

[1] A. Ghirri, C. Herrero, S. Mazerat, T. Mallah, O. Moze and M. Affronte, Adv. Quantum Technol. 3, 1900101 (2020).

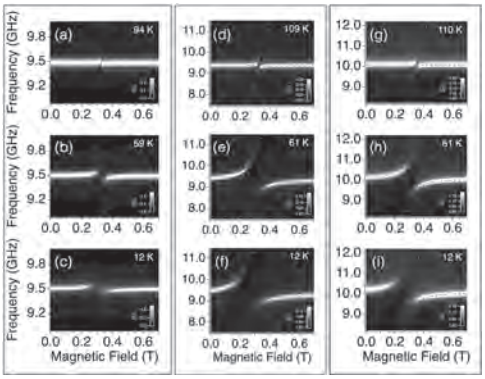

Fig. 1. Transmission maps obtained at different temperature for (a–c) 10 nm NPs in PVP; (d–f) 8.6 nm NPs in CTA+; (g–i) bulk sample. Dashed lines show the calculated frequency dependence of the polariton branches. For each temperature, data are normalized to the maximum transmission.

D2-06. Realization of Random Exchange Interactions and Spin on a Square Lattice With Entropy Stabilization Synthesis. *A.R. Mazza*[1], E. Skoropata[1], T.R. Charlton[1] and T.Z. Ward[1] *1. Oak Ridge National Laboratory, Oak Ridge, TN, United States*

Pure materials, free of disorder and defects, are often the goal for the study of magnetic materials. However, this often can stunt the ability to manipulate material properties and study fundamental subjects such as magnetic frustration. Materials in the chaotic or disordered limit open the door to a number of physical phenomena. One such example is the random spin/exchange model on a square lattice, where a degenerate ground state can lead to spin liquid-like behaviors, spinons, or magnetic critical points. While this concept has been limited primarily to theoretical work, we have synthesized such a system where 15 atomic pairs with different exchange interactions and 5 possible spin states can be studied as a single crystal. We present our recent stabilization of single crystal epitaxial films of the ABO_3 perovskite $La(Cr_{0.2}Mn_{0.2}Fe_{0.2}Co_{0.2}Ni_{0.2})O_3$. XRD and STEM-EELS studies confirm crystallinity, epitaxy, and full site mixing of the 5 B-site elements (no single element clustering). Experimental results from neutron studies, XMCD, and SQUID magnetometry demonstrate unexpected long-range magnetic ordering arising from the highly frustrated local environment. The near degeneracy of macroscopic magnetic phase percolation between antiferromagnetic and ferromagnetic states will also be addressed as a promising route to designing phase metastability.

D2-07. Withdrawn

D2-08. Orbital Magnetization in Magnetic Neutron Scattering. *H. Chen*[1,2] *1. Physics, Colorado State University, Fort Collins, CO, United States; 2. School of Advanced Materials Discovery, Colorado State University, Fort Collins, CO, United States*

Magnetic neutron scattering has been a powerful tool to reveal the microscopic magnetic structures of ordered and disordered magnetic systems. For magnetically ordered crystalline systems it has been a common practice to fit the elastic neutron cross-section to models of periodically arranged localized magnetic moments. However, it is unclear how the orbital magnetization which has an itinerant nature manifests in neutron scattering. The question is relevant to, e.g., metallic antiferromagnets and 4d/5d transition metal materials. We show that magnetic neutron scattering in general maps out the equilibrium electric current distribution inside the material but leaves the magnetization density unfixed because of a gauge freedom. We discuss the connection between the equilibrium current density and the modern theory of orbital magnetization, and provide examples on calculating the orbital contribution to elastic neutron cross-section using models and first-principles methods.

D2-09. Antiferromagnetic Fluctuations in One-Dimensional Hubbard Model. *V. Janiš*[1], A. Klíč[1] and J. Yan[1] *1. Institute of Physics, The Czech Academy of Sciences, Praha, Czechia*

Low-dimensional (d=1,2) metallic systems with electron-hole symmetry are dominated at low temperatures by spin-flip fluctuations and enhanced antiferromagnetic interaction. They show, however, no long-range order at non-zero temperatures. The electronic structure is nevertheless substantially altered by the antiferromagnetic fluctuations and significantly deviates from the Fermi liquid. These changes are difficult to capture by the standard theoretical many-body techniques. We show that only many-body approaches including renormalizations of the interaction strength can successfully describe the low-temperature behavior of low-dimensional metals. We use the standard many-body perturbation expansion within which we resort to the reduced parquet equations introducing a two-particle self-consistency suppressing spurious phase transitions. They were introduced by the authors to describe quantum criticality in strongly correlated electron systems, Refs. [1-3]. We choose the one-dimensional Hubbard model and show that the solution at zero temperature and at half-filling contains an antiferromagnetic quantum critical point even if there is no long-range antiferromagnetic order at non-zero temperatures. Antiferromagnetic fluctuations open an energy gap in the spectral function that is proportional to the bare interaction strength. This behavior can be derived only if the quantum critical point and the renormalization of the interaction strength are treated consistently in both the thermodynamic response and spectral functions. That is, a balance between quantum and thermal fluctuations is maintained and consistency between one-particle and two-particle functions is accomplished.

[1] V. Janiš, P. Zalom, V. Pokorný, and A. Klíč, Phys. Rev. B 100, 195114 (2019). [2] V. Janiš and A. Klíč, JPS Conference Proceedings 30, 011124 (2020). [3] V. Janiš, A. Klíč, and J. Yan, preprint arXiv:2006.08492 (2020).

D2-10. Theoretical Framework for Calculating Heisenberg Exchange and Dzyaloshinskii-Moriya Interaction in Correlated Magnetic Materials With Significant Spin-Orbit Coupling. *V. Borisov*[1], Y. Kvashnin[1], D. Thonig[2], P. Thunström[1], M. Pereiro[1], A. Bergman[1], E. Sjöqvist[1], A. Delin[1,3], L. Nordström[1] and O. Eriksson[1,2] *1. Department of Physics and Astronomy, Uppsala University, Box 516, SE-75120 Uppsala, Sweden; 2. School of Science and Technology, Örebro University, SE-70182 Örebro, Sweden; 3. Department of Applied Physics, School of Engineering Sciences, KTH Royal Institute of Technology, Electrum 229, SE-16440 Kista, Sweden*

Low-dimensional skyrmionic magnetic systems attract a lot of attention due to their possible applications in spintronics, for example, in new types of memory and logic devices. The microscopic mechanism of skyrmion formation in such systems relies on the presence of the Dzyaloshinskii-Moriya (DM) interaction which requires a crystal structure with a broken space-inversion symmetry and a substantial spin-orbit coupling [1]. So far skyrmions have been observed in relatively few systems, for example, the B20 compounds MnSi [2] and FeGe [3] and thin bilayers made from combinations of light and heavy transition metals (e.g. Fe/Ir(111) [4]). This motivates a search for further potential skyrmionic systems with larger spin-orbit coupling effects and higher skyrmion stability. Such a study requires a detailed knowledge of magnetic interactions, including the isotropic Heisenberg and anisotropic DM interactions. State-of-the-art theoretical methods allow to calculate accurately the Heisenberg interactions in correlated systems and determine reliably many measurable magnetic properties [5]. However, the effect of dynamical electronic correlations on the character and size of the DM interactions has not been studied in detail. We propose a theoretical framework which allows to address this issue from first principles using a combination of density functional (DFT) [6] and dynamical

mean-field theories (DMFT) [7] as well as the relativistic generalization of the magnetic force theorem [8]. Using this framework, we study the Heisenberg and DM interactions in a few representative cases, including bulk systems with broken space-inversion symmetry (the B20 compounds MnSi and FeGe and the artificial alloys CoPt and FePt) and the low-dimensional systems Co/Pt(111) and Mn/W(001). The dynamical correlations are included on the level of the fluctuation-exchange approximation, but more advanced DMFT solvers can be incorporated in the calculations as well. We find that, in some of these systems, e.g. in the B20 compounds and Co/Pt(111), the electronic correlations can produce non-trivial variations of the dominating magnetic exchange parameters, which may significantly influence the resulting magnetic properties.

1. I. Dzyaloshinsky, Journal of Physics and Chemistry of Solids, Vol. 4, p.241 (1958). 2. S. Mühlbauer, B. Binz, F. Jonietz *et al.*, Science, Vol. 323, p.915 (2009). 3. X. Z. Yu, N. Kanazawa, Y. Onose *et al.*, Nature Materials, Vol. 10, p.106 (2011). 4. S. Heinze, K. v. Bergmann, M. Menzel *et al.*, Nature Physics, Vol. 7, p.713 (2011). 5. C. Etz, L. Bergqvist, A. Bergman, A. Taroni and O. Eriksson, Journal of Physics: Condensed Matter, Vol. 27 (24), p.243202 (2015). 6. P. Hohenberg and W. Kohn, Phys. Rev., Vol. 136, p.B864 (1964). 7. G. Kotliar, S. Y. Savrasov, K. Haule *et al.*, Rev. Mod. Phys., Vol. 78, p.865 (2006). 8. A. Liechtenstein, M. Katsnelson, V. Antropov, and V. Gubanov, Journal of Magnetism and Magnetic Materials, Vol. 67, p.65 (1987).

D2-11. Atomic Cooperation in Enhancing Magnetism: (Fe, Cu)-Doped CeCo5. R. Choudhary[1] and *D. Paudyal*[1] *1. Iowa State University, Ames Laboratory, Ames, IA, United States*

Developing permanent magnet alloys with decreased critical elements (e.g., Nd, Dy, and Co) requires identifying compositions and structures with uniaxial magneto-crystalline anisotropy energy (MAE), large magnetization, and a high ferromagnetic transition temperature (Curie temperature - TC). One approach to minimizing the critical elements in potential permanent magnet alloys is to use overly produced Ce, which is less critical. Furthermore, reducing Co content in RCo5 (R = Rare Earth) alloys is necessary since Co is also a critical element. An obvious choice for decreasing Co content is a substitution with non-critical Fe. However, the Fe is not stable in the lattice due to the reduced number of d-electrons. Concomitant substitution of Cu stabilizes Fe substitution. Employing first-principles electronic structure theory, we identify the weakly localized nature of cobalt in CeCo5, which causes high uniaxial magnetic anisotropy of ~ 10 MJ/m3. In contrast, substituted Cu delocalizes the Co's 3d-states, resulting in lower anisotropy. Calculations show that 10% Cu can stabilize 20% Fe replaced for the Co, which significantly enhances magnetic moment in the Ce (Co, Fe, Cu)5. This prediction is in good agreement with a single-crystal experiment in which the best optimal composition was identified to be 15% of Fe and 12% Cu. The competitive non-equivalent Co sites preferred by Cu and Fe, a unique electronic structure including exchange and crystal field splitting, and rigid band shift variation are borne by 3d states of Co, Fe, and Cu around the Fermi level, all play an essential role in tuning the magnetic properties. This work is supported by the Critical Materials Institute, an Energy Innovation Hub, funded by the U. S. Department of Energy, Office of Energy Efficiency and Renewable Energy, Advanced Manufacturing Office.

R. Choudhary et al., J. Alloys and Compounds 839, 155549 (2020).

D2-12. Withdrawn

D2-13. Is it Time to Sideline the Renowned Heisenberg Hamiltonian? *N. Bykovetz*[1] *1. Physics, Temple University, Philadelphia, PA, United States*

For nearly 100 years the localized-exchange-interaction, as represented by the Heisenberg Hamiltonian $H = \Sigma J(r) S_i \cdot S_j$, has been viewed as the primary underlying cause of magnetism in magnetic materials. An inescapable consequence of the Heisenberg Hamiltonian is that the magnetic dispersion relation at small k must go as $\omega \propto k^2$ (for sufficiently short-range J(r)). Empirical evidence over the past 60 years has persistently given indications, however, that the measured dispersion-relation exponents in various ferromagnetic systems were invariably smaller than 2. The empirical evidence thus appears to be in direct conflict with the applicability of the Heisenberg Hamiltonian to explain spin ordering in real ferromagnets. The very first attempt to determine ω(k) at small k, using Spin Wave Resonance (SWR) showed near linear dependence,[1] but the belief in the validity of theory was so strong that a way was always found to force agreement (e.g., by renumbering[1,2] the resonances so as to obtain the expected $\omega \propto k^2$ dependence). Such *ad hoc* renumbering, as well as postulation of magnetization and anisotropy variations within the films, etc., have been used to this day to insist that ω *must* be $\propto k^2$. Neutron scattering (NS) has not been precise enough until recently to measure $\omega \propto k^d$ at small k. But a recent measurement[3] on $CrSiTe_3$ showed that d is indeed <2, despite the authors' attempt to fit the data to $\omega \propto k^2$. Indirect evidence from precision NMR measurements had previously shown that empirically[4] only $\omega \propto k$; $k^{1.5}$; and $k^{1.75}$ for 3D ferromagnets, and $\propto k$ and $k^{1.5}$ for 2D ferromagnets, appear to characterize simple ferromagnets. These behaviors may be understood as resulting from the exchange interaction being a collective-exchange effect, instead of an interatomic-exchange effect. If d<2, then 2D magnets can order spontaneously (the Mermin-Wagner theorem no longer applies). This is consonant with the existence of high Tc magnetic monolayers and quasi-2D magnets, no matter the strength of the anisotropy fields. A full replacement model Hamiltonian is yet to be discovered. However, a simple spin-wave scheme can already be formulated from just the small-k approximations and is in excellent agreement with experimental evidence.

1. M.H. Seavey and P.E.Tannenwald, Phys Rev Lett 1, 168 (1958); J Appl Phys, 30, S227 (1959) - SWR in permalloy 2. P.K. Schwob and G.E. Everett, J Phys Colloque C1, 1066 (1971). Also, P.K. Schwob et al, PR B 10, 165 (1974) - SWR in EuS - 3. T.J. Williams et al, PR B 92, 144404 (2015) - NS in $CrSiTe_3$ - 4. N. Bykovetz, J Appl Phys 55, 2062 (1984). Please note the obvious typographical error in the abstract, where n=0 should be replaced by n=∞

INVITED PAPER

D2-14. Helimagnetic Correlations Close to the Quantum Critical Points of MnSi Under Mechanical and Chemical Pressure. *C. Pappas*[1], A.O. Leonov[2], L.J. Bannenberg[1], R. Sadykov[3], R.M. Dalgliesh[4], C. Goodway[4], D.L. Schlagel[5], T.A. Lograsso[5], E. Lelièvre-Berna[6], P. Falus[6], P. Fouquet[6], T. Wolf[7] and F. Weber[7] *1. Technische Universiteit Delft Faculteit Technische Natuurwetenschappen, Delft, Netherlands; 2. Chiral Research Center, Hiroshima Daigaku, Higashihiroshima, Japan; 3. Institut adernyh issledovanij RAN, Moskva, Russian Federation; 4. ISIS, Rutherford Appleton Laboratory, Didcot, United Kingdom; 5. Ames Laboratory, Iowa State University, Ames, IA, United States; 6. Institut Laue-Langevin, Grenoble, France; 7. Karlsruher Institut fur Technologie, Karlsruhe, Germany*

The physics of the chiral magnet MnSi touches onto several fundamental questions in condensed-matter physics, from the stabilisation of exotic states like chiral skyrmions [1] to the interplay between localised and itinerant magnetism. Under mechanical pressure, or chemical pressure in the form

of Fe doping in $Mn_{1-x}Fe_xSi$, a non-Fermi liquid behaviour sets-in which has been attributed to a chiral spin liquid and quantum fluctuations [2]. The origin and nature of these phenomena are still an open question, which we address by combining small angle neutron scattering and neutron spin echo spectroscopy [3-5]. Our results show that the destabilisation of the long range helical periodicity, close to the quantum critical points, is driven by the modification of the electronic state but with different microscopic mechanisms for mechanical and chemical pressure. Mechanical pressure enhances the itinerant electron character of MnSi leading to a softening of the magnetic moment. On the other hand, chemical doping increases the weight of achiral RKKY interactions. The resulting frustration explains both the destabilisation of long range helical periodicity and the enhancement of the precursor region with increasing doping.

1. S. Mühlbauer et al., Science 323, 915 (2009). 2. C. Pfleiderer, et al., Nature 414, 427 (2001) 3. L. J. Bannenberg et al., Phys. Rev B 100, 054447 (2019). 4. L. J. Bannenberg, et al., Phys. Rev. B 98, 184431 (2018). 5. C. Pappas, et al., in preparation

CONTRIBUTED PAPERS

D2-15. Withdrawn

D2-16. Ab Initio Study of Magnetocrystalline Anisotropy in Antiferromagnetic Fe_2As. *K. Kang*[1], K. Yang[2], D. Cahill[1] and A. Schleife[1]
1. Department of Materials Science and Engineering, University of Illinois at Urbana-Champaign College of Engineering, Urbana, IL, United States; 2. Department of Physics, University of Illinois at Urbana-Champaign College of Engineering, Urbana, IL, United States

Ferromagnetic materials have played a significant role in magnetic memory devices. However, due to inherent limitations associated with stray field generation and vulnerability to external stimulation, antiferromagnetic materials are increasingly investigated as alternatives. Specifically, metallic tetragonal antiferromagnets with easy-plane magnetism are appealing because of the degenerate domains with 90° difference of Néel vector for binary information storage and the possibility of electrical switching. To understand the switching process, the magnetocrystalline anisotropy is essential, acting as an energy barrier between two degenerate states. In this study, we used density functional theory (DFT) to unravel the origin of the magnetocrystalline anisotropy in Fe_2As, one of the metallic tetragonal antiferromagnets with easy-plane magnetism. The tetragonal structure allows two possible anisotropies out-of-plane and in-plane. Here, we calculate the spin-orbit interaction (SOI) in a DFT framework and the magnetic dipole-dipole interaction (MDD) based on the DFT ground state structure using a classical model. The computed out-of-plane $|K_1|$ anisotropy coefficient is 830 kJ/m^3, composed to one-third of MDD and two-thirds of SOI, both of which exhibit the same two-fold symmetry. Conversely, the MDD contribution for in-plane anisotropy is almost imperceptible, leading to an in-plane $|K_{22}|$ anisotropy coefficient of 280 J/m^3 with four-fold symmetry, due to SOI. The lowest frequency of a spin-wave is calculated using our anisotropy result, and it is predicted as 0.64 THz. Based on the frequency and anisotropy, the fast dynamics and high speed of switching are anticipated. However, low thermal stability might be observed due to the small in-plane anisotropy barrier. ** The Illinois Materials Research Science and Engineering Center is supported by the National Science Foundation MRSEC program under NSF Award Number DMR-1720633.

Session D3
APPLIED AND POWER MAGNETICS
(Poster Session)

Christopher Olson, Chair
NVE Corporation, Eden Prairie, MN, United States

D3-01. Cryogenic Motor With Two Radial AMBs in Liquid Nitrogen. *M. Komori*[1], H. Kato[1], K. Asami[1] and N. Sakai[1] *1. Electrical and Electronic Engineering, Kyushu Institute of Technology, Kitakyushu, Japan*

1. Introduction This paper discusses the basic study on a cryogenic motor with active magnetic bearings (AMBs) which works in liquid nitrogen (-200C). The cryogenic motor is very interesting and special, because conditions in liquid nitrogen are very different from those at room temperature [1, 2]. 2. Structure of Cryogenic Motor Fig. 1(a) shows an illustration of the cryogenic motor which works in liquid nitrogen. The cryogenic motor is composed of two radial AMBs, four displacement sensors, a permanent magnet (PM) motor, etc. The stator of the AMB has eight electromagnets with 250 turns. The displacement sensors are inductance-type sensors based on detecting the inductance difference between two sensing coils. A passive magnetic bearing composed of PMs facing each other is set at the bottom of the rotor. Thus, the rotor is levitated completely without any mechanical contacts. Fig. 1(b) shows the photo of the cryogenic motor. The black parts at the upper and lower parts are the same AMBs. The PM motor is set in the center of the cryogenic motor. 3. Experiments and discussions Fig. 2(a) shows the relationship between sensor output and displacement. In the figure, black and white circles represent the output voltages at room temperature and that in liquid nitrogen, respectively. The result shows that the relationship between output voltage and displacement is almost linear. However the difference between output voltages at room temperature and that in liquid nitrogen is observed. This shows that the output voltage depends on the temperature. Fig. 2(b) shows the relationship between rotor displacement and rotation speed working in liquid nitrogen. x1 and y1 represent the displacements in the x and y directions at the upper part of rotor. x2 and y2 represent the displacements in the x and y directions at the lower part of rotor, respectively. The rotor displacements are measured in the range lower than 4,500 rpm. The result shows that each displacement is smaller than 0.2 mm, which is very small.

[1] K. Kajikawa, H. Kuga et al., TEION KOGAKU (in Japanese), Vol. 47, p. 674 (2012) [2] M. Komori and K. Uchino, IEEE Trans. on Applied Superconductivity, Vol. 14, p. 1659 (2004)

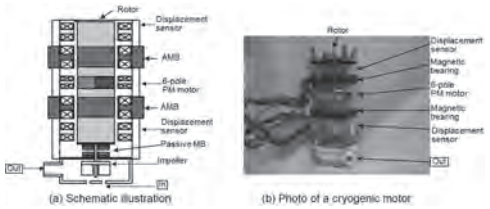

Fig.1 Cryogenic motor with two radial magnetic bearings working in liquid nitrogen

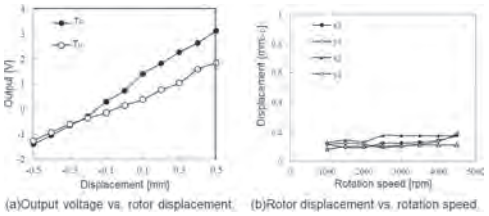

Fig.2 Experimental results in liquid nitrogen

D3-02. Withdrawn

D3-03. Detailed Analytical Technique for Characteristic Analysis of Actively Shielded Superconducting Machine. K. Shin[1], *T. Bang*[2], H. Cho[2], J. Choi[2] and K.S. Haran[3] *1. Chonnam National University, Yeosu, The Republic of Korea; 2. Chungnam National University, Daejeon, The Republic of Korea; 3. University of Illinois at Urbana-Champaign, Urbana, IL, United States*

The application of superconducting (SC) technology with high power and low losses has emerged as a suitable alternative to next-generation electrical systems such as electric propulsion aircraft, ships, and more [1], [2]. These advantages make it possible to reduce the size and weight of the electric machine and achieve high energy efficiency in the electrical system. To satisfy the required goals such as high power density and efficiency, it is necessary to consider numerous parameters and optimize the whole system. Therefore, the focus of this paper is to predict the magnetic field quantities and performances in actively shielded SC machines. The analytical technique using the Fourier series is employed to calculate the magnetic field by using SC main field coil and shielding coils. Figs. 1(a) and 1(b) show the configuration and analytical model of the SC machines. As shown in Fig. 1 (a), the entire domain of the field problem is divided into seven domains. By using the separation of variables technique, the analytical solutions can be obtained to Poisson's equations in the armature, field, and shield domains, and Laplace's equation in the air core and air-gap domains. The governing equation in all subdomains can be solved, and the field distribution can be obtained by applying the boundary conditions on the interfaces between each domain. Based on these solutions, the electromagnetic performance can also be determined analytically. The distribution of the magnetic field over the whole area is shown in fig 1 (c) and 1 (d). Both analyzes were calculated from the finite element (FE) and analytical methods, respectively. Except for the difference of graphics, the two analysis results have an error within 5% of the whole area, so the reliability of the proposed method is verified. The magnetic field and the electromagnetic performances obtained using the analytical method were compared with those obtained using the FE analysis, and the comparison validates the analytical methods presented in this paper, as shown in Fig. 2. Specific illustrations of the analyses and the results will be presented later on in the full paper.

[1] K. S. Haran, T. O. Deppen, and L. Zheng, IEEE Trans. Appl. Supercond. Vol. 26, Art. no. 5202508 (2016). [2] Y. Terao, W. Kong, H. Ohsaki, H. Oyori, and N. Morioka, IEEE Trans. Appl. Supercond., Vol. 28, Art. no. 5208005 (2018).

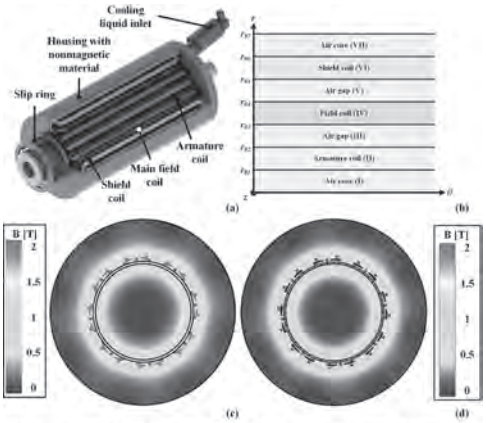

Fig. 1. Actively shielded superconducting machine: (a) structure; (b) analytical model; flux density distribution; (c) FE; and (d) analytical model.

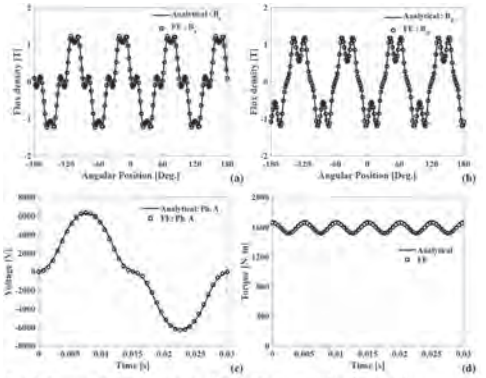

Fig. 2. Comparison between analytical and FE results: (a) radial flux density at the center of the armature coil; (b) tangential flux density at the center of the armature coil; (c) back EMF at rated speed; and (d) electromagnetic torque under load condition.

D3-04. Analysis and Comparison of Magnetic Planetary Gear With Halbach Permanent Magnet Arrays. L. Quan[1], *K. Zhang*[1], Y. Du[1] and X. Zhu[1] *1. School of Electrical and Information Engineering, Jiangsu University, Zhenjiang, China*

Due to the advantages of noise-free, maintenance-free and physically isolated overload protection, magnetic gears (MGs) are widely concerned [1][2]. However, compared with traditional mechanical gears, the practical application of MGs is limited due to the issues of stability, torque density, and so on. The purpose of this paper is to present a high torque density magnetic planetary gear (MPG) with Halbach permanent magnet (PM) arrays. Fig. 1 shows the configurations of the proposed MPG compared with an existing MPG with radial magnetized PMs. The Halbach PM arrays can produce an approximately sinusoidal airgap magnetic flux density distribution, with strong magnetic field intensity and good self-shielding performance. In the case of the same PM usage and topological structure, simulation and experiment results prove that the proposed MPG has higher torque transmission density, lower torque ripple, and lower iron loss than the existing counterpart. As shown in Fig. 2, the maximum transmission torque and torque ripple of the ring gear are increased and reduced by 19.5% and 36.8%, respectively. More information, such as parameters design and loss analysis, will be presented in the full paper.

[1] L. Jing, Z. Huang, et al, "An asymmetric pole coaxial magnetic gear with unequal Halbach arrays and spoke structure," *IEEE Trans. App Super.*, Vol. 30, No. 4, pp. 1-4, Oct. 2020 [2] L. Jian, K. T. Chau, Yu Gong, "Comparison of coaxial magnetic gears with different topologies," *IEEE Trans. Magn.*, vol. 45, no. 10, pp. 4526-4529, Oct. 2009.

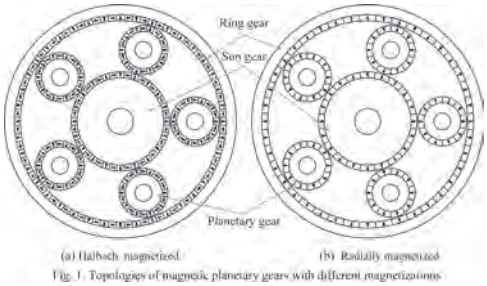

Fig. 1. Topologies of magnetic planetary gears with different magnetizations.

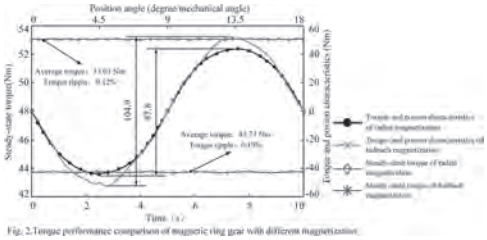

Fig. 2.Torque performance comparison of magnetic ring gear with different magnetization.

D3-05. An Improved Jiles-Atherton Hysteresis Model With a Sixth Parameter to Represent the Frequency-Dependent Characteristics. *S. He*[1], J. Li[1] and J. Zhu[2] *1. electrical engineering, xian jiaotong university, XIAN, China; 2. School of Electrical and Information Engineering, University of Sydney, Sydney, NSW, Australia*

Grain-oriented silicon sheet steel has been widely used in the manufacture of iron core of large power transformer, due to its excellent magnetization properties with high magnetic permeability and low losses. Modeling of its magnetization characteristics is of great significance to the modeling of the devices with iron core such as transformer and motors. The ferromagnetic resonance, inrush current and other low-frequency electromagnetic transient characteristics are closely related to the hysteresis characteristics of transformer core. At present, the most representative models proposed for representation of hysteresis charecteristics are Preisach model, Jiles-Atherton(JA)model, E&S model and Stoner-Wolhfarth (SW) model. Each model has its specific application scope, so the most suitable hysteresis model should be selected according to different application scenarios. However, the existing models only represent the characteristics of a single hysteresis loop, and cannot reflect the influence of alternating electromagnetic field frequency on the hysteresis loop. Moreover, with the development of science and technology, the application environment of electromagnetic equipment is becoming more and more complex, owing to an increasing probability of suffering from multi frequency resonance transient or even pulse transient with rich frequency content. In order to accurately characterize the hysteresis characteristics under different frequency excitation, a model with which frequency dependent parameters is needed to ensure the accuracy of modeling and calculation. Considering that JA hysteresis model parameters can be obtained from the measured hysteresis loops [1], an improved JA model is proposed. In this paper, according to the hysteresis loops of silicon steel sheet at different frequencies obtained from previous work [2], an improved JA model with six parameters is proposed, and the sixth parameter (γ) represent the influence of frequency on other 5 parameters. This paper provides a wide-band modeling method of ferromagnetic material magnetic properties for broadband or pulsed application scenarios.

1. D. Sedira, Y. Gabi, A. Kedous-Lebouc, K. Jacob, B. Wolter and B. Strass, J. Magn. Magn. Mater. 505, 6 (2020). 2. S. He, D. D. Huang, X. Feng, J. Deng, J. T. Li and J. G. Zhu, AIP Adv. 10 (1), 5 (2020).

D3-06. Withdrawn

D3-07. A Study on Leakage Magnetic Field Reduction Configuration for High Power Contactless Power Transfer for Industrial Moving Systems. *T. Abe*[1], M. Yokosawa[1], S. Miyahara[1], f. sato[1], H. Matsuki[2] and K. Inada[3] *1. Electrical Engineering, Tohoku gakuin University, Tagajo, Japan; 2. Tohoku University, Sendai, Japan; 3. NITTOKU Co., Ltd., Saitama, Japan*

In recent years, it has been proposed to use wireless power supply for industrial products in terms of convenience, safety and cost [1]. However, there is a problem that the system in the current industrial products becomes power supply in a limited situation where the power transmission and reception system is stopped. As a system to solve this problem, we propose a high-power wireless power transfer system for moving systems. As a result, further improvement in productivity can be expected. In this study, we constructed a coil configuration that can reduce the leakage magnetic field while supplying a large amount of power. The power supply to the moving system is much larger in the transmitting coil than in the receiving coil. Even in this state, we constructed a system that can supply large power of 600W while reducing the leakage magnetic field. Figure 1 shows an image of wireless power transfer for a moving system. In this study, we consider contactless power transfer using the electromagnetic induction method [2]. The coil shape when feeding 600W is as follows. The power transmission coil is 2 m long and 20 cm wide. The power receiving side has a booster coil with a coil length of 35 cm and a width of 20 cm including pickup coils of the same size. This fits the size of the AGV to be implemented. Using the above coil configuration, it was confirmed whether 600 W of electric power could be supplied to each gap and the leakage magnetic field was confirmed. It was possible to confirm the power supply of 600 W at the gap between the coils of 2 cm to 4 cm. Figure 2 shows the comparison results of the leakage magnetic field when the noise reduction coil and the standard coil with a gap of 3 cm were fed with 600 W. This shows that the leakage magnetic field can be reduced compared to the conventional standard coil. We have constructed a system that can supply large power of 600W while reducing the leakage magnetic field. It was shown that the leakage magnetic field could be reduced compared to the conventional standard coil.

[1] KAMEDA Atsushi : “Factory Automation with Wireless Power Technology, and Products Progress for the Future”, The Journal of the Institute of Electrical Installation Engineers of Japan 38(7), pp.369-372(2018)
[2]MATSUZAKI, and MATSUKI : “Transcutaneous Energy-Transmitting Coils for FES.”, Journal of the Magnetics Society of Japan 18(2), pp.663-666(1994)

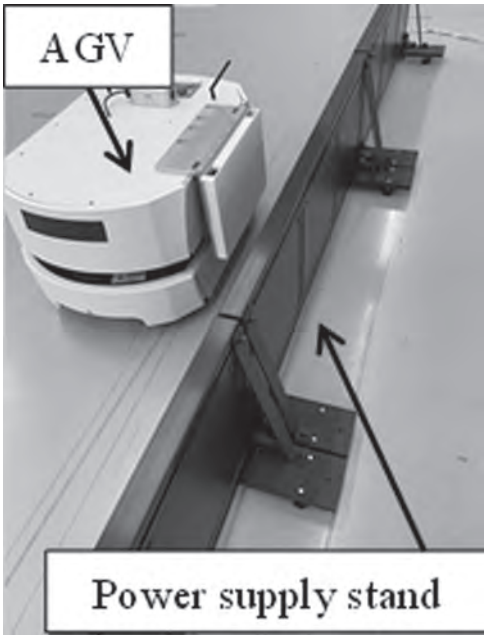

Fig. 1. Image of power supply to operating AGV

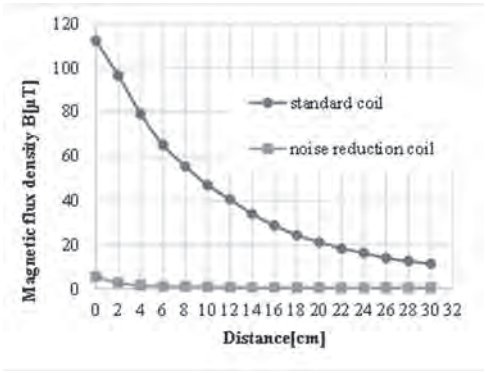

Fig. 2. Comparison of leakage magnetic field at 600W power supply

D3-08. Development of a Position-Based Precise Magnetic Torque and Force Generation Method Using a Triad of Electromagnetic Coils for Biomedical Magnetic Robot Applications. *H. Lee*[1], B. Kim[1], J. Shin[1] and S. Jeon[1] *1. Kongju National University, Gongju, The Republic of Korea*

Magnetic navigation systems (MNSs) capable of generating various types of magnetic fields have been widely studied for the effective manipulation of biomedical magnetic robots [1-4]. Previous researchers proposed a geometrically and electrically efficient MNS comprised of a simple triad of electromagnetic coils (TEC) that can generate two-dimensional (2D) magnetic robot motions [3]. However, the TEC suffered from the restricted working area of the magnetic robot due to the nonlinearly distributed magnetic field throughout the system. In this research, we propose a method to precisely generate 2D magnetic torque and force of a magnetic robot regarding the robot’s current position inside the TEC. Since the TEC is composed of three identical circular coils located at the vertices of an equilateral triangle, the magnetic field at a certain position inside the TEC can be expressed in terms of the three coils’ currents and a position vector by using Jacobian and transformation matrices [4]. From this expression, we established several constraint equations to optimally manipulate the magnetic robot’s 2D motions at any position within the TEC. Fig. 1 shows several simulated magnetic fields of the TEC to propel a magnetic robot (red dots) in the direction of the x-axis. It shows that the TEC can generate a relatively uniform magnetic force within the nearby area of a magnetic robot, making it possible to move the magnetic robot in the desired direction (Fig. 2).

We then constructed the TEC and a closed-loop visual tracking system to demonstrate that the TEC can manipulate a magnetic robot inside the TEC in a closed-loop manner. The results showed that the proposed method and system can improve the magnetic robot's admissible working area in the TEC effectively and precisely.

[1] M. Kummer, J. Abbott, and B. E. Kratochvil et al., IEEE Transactions on Robotics, Vol. 26, pp. 1006-1017, 2010. [2] Q. Cao, X. Han, B. Zhang, and L. Li et al., IEEE Transactions on Applied Superconductivity, Vol. 22, 2012. [3] H. Lee and S. Jeon, AIP Advances. Vol. 10, 2020. [4] G. Go, H. Choi, and S. Jeong et al., Sensors and Actuators, Vol. 205, P. 215-223, 2014.

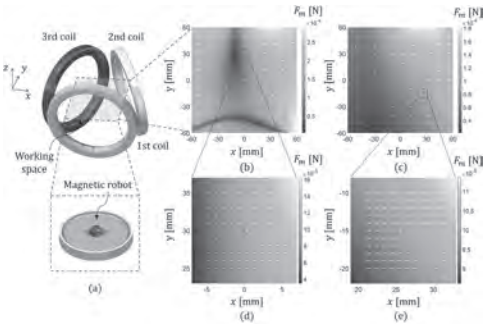

Fig. 1 (a) Schematic view of the TEC. Simulation results of magnetic force (F_m) generated by the TEC with respect to different positions (red dots) of a magnetic robot

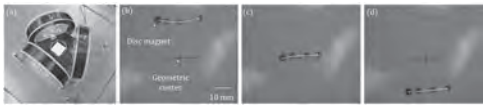

Fig. 2 (a) Experimental setup of the TEC. (b)-(d) Overlapped images of the translational motion of a disc-type robot in different starting positions. The red and yellow lines are respectively the reference line and a trajectory of the robot when the proposed method is applied.

D3-09. Magnetization and Thickness Dependent Microwave Attenuation Behavior of Ferrite-PANI Composites and Embedded Composite-Fabrics Prepared by in-Situ Polymerization. *S. Kumar*[1], V. Verma[2] and R. Walia[3] *1. Department of Physics and Astrophysics, University of Delhi, New Delhi, India; 2. Department of Physics, Hindu College, University of Delhi, New Delhi, India; 3. Department of Physics, Deen Dayal Upadhyaya Gorakhpur University, Gorakhpur, India*

Ultrahigh efficient and effective electromagnetic-interference (EMI) shielding composites have been fabricated with the combination of Polyaniline and zinc-cobalt ferrites ($Co_{1-x}Zn_xFe_2O_4$, $0.1 \leq x \leq 0.4$). Ferrite nanoparticles synthesized via the sol-gel method were functionalized to polyaniline via in-situ polymerization. Average crystallite sizes of the nanoparticles were estimated using Debye–Scherrer and Reitveld method and found to be in between 20-30 nm. FTIR spectra revealed to the formation of interactions between the PANI molecules and the ferrite nanoparticles. Substitution of the nonmagnetic Zn^{2+} ions considerably changes the magnetic properties of cobalt ferrites as observed from the M-H loops recorded by VSM at room temperature. The EMI-shielding performance of the fabricated composites was examined at various thicknesses with the polymer filler ratio of 1:1 in X-band frequency region using vector network analyzer. The EMI shielding performance of composites was found to be increasing with the thickness of composites where thickness of 3.0 mm achieved an SE of ~ 100 dB for the $Co_{0.7}Zn_{0.3}Fe_2O_4$-PANI composite. Composite absorbers were deposited on cotton fabrics for protective clothing by in situ incorporation during the synthesis of composites which displayed relatively high EMI shielding effectiveness (SE) (40-45 dB) at a thickness of only 0.30 mm for the fabrics. The PANI-Ferrite nanocomposites can be established as promising high capacity electromagnetic shielding materials because of the dipole polarizations and the magnetic losses with low cost, light weight, high durability and good flexibility.

D3-10. Construction of Wireless Power Transfer System Assuming Drone Operation and Examination of Booster Coil Size. *T. Sawa*[1], f. sato[1], S. Miyahara[1], H. Matsuki[2] and S. Sasaki[3] *1. Division of Engineering, Program in Electrical Engineering, Tohoku Gakuin University, Tagajo, Japan; 2. Tohoku University, Sendai, Japan; 3. Hikaridenshi Corporation, Osaki, Japan*

In recent years, it is expected that the drone industry will develop rapidly according to the report of the research company which is the business intelligence of the commercial drone industry. However, the problem with industrial drones is that they have a short operating time. The operating time of an industrial drone is about 30 minutes, and it will decrease to less than half depending on the conditions. In order to solve the problem of operating time, we propose a drone capable of bidirectional power transfer of wireless power transfer using electromagnetic resonance. Therefore, there is a possibility that the drone may be lost due to the power being cut off or that the range of activities may be limited. By enabling not only charging of themselves but also power supply between drones, a power network will be formed and problem will be solved. In this research, we will confirm and verify the basic configuration of bidirectional power supply, and show the superiority of each size from the positional deviation characteristics due to the difference in booster coil size, which will lead to the realization of bidirectional power supply of drone. As shown in Fig.1, in the demonstration of the basic configuration of bidirectional power supply, power was transmitted between two devices that had both power transmission and power reception. In the research of booster coil size, in order to improve the positional displacement characteristics of Fig. 2 that occur when wireless charging is performed, we show the superiority of characteristics in the same size and the large and small sizes as the power transmitting receiving coil. The difference between the analysis and the actual measurement was clarified by comparing the value obtained by circuit analysis with the actually measured value. This makes it possible to quantitatively predict the difference between analysis and actual measurement due to the influence of various geometrical parameters.

[1] M. Radovic, H Bodecker, "The Commercial Drone Market 2019-2024", Drone Industry Insights (2019) [2] S. Takahashi, "Trend and Forefront of Magnetic Wireless Power Supply Technology for EV", The Magnetic Society of Japan, Vol.9, pp96-104, (2014) [3] Y. Ota, "Research into Design Methods for Electromagnetic Induction Type Contactless Power Transmission Systems", Tohoku University Doctoral Dissertation (2015)

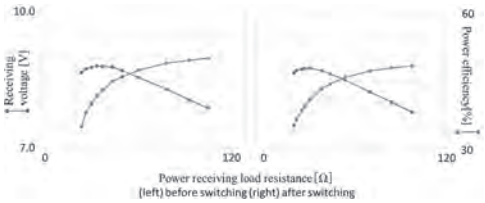

Fig.1 Power receiving load characteristics (left) before switching (right) after switching

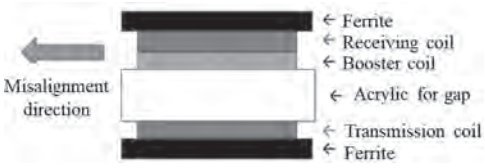

Fig.2 Coil position and displacement direction

Session D4
HARD MAGNETIC MATERIALS: NANOSTRUCTURES AND OTHERS (Poster Session)

Bin Ma, Chair
University of Minnesota, Minneapolis, MN, United States

D4-01. Magnetic Properties of Ternary $Fe_{49}Ni_{49}X_2$ (X = Ti, Al) Alloys After Severe Plastic Deformation. *M.N. Ulyanov*[1,2], S.V. Taskaev[2], M.Y. Bogush[2] and M.A. Gavrilova[2] *1. Immanuel Kant Baltic Federal University, Baltijskij federal'nyj universitet imeni Immanuila Kanta, Kaliningrad, Russian Federation; 2. Chelyabinsk State University, Chelyabinsk, Russian Federation*

An $L1_0$-ordered FeNi phase called tetrataenite is a natural rare earth free permanent magnet but the magnetic properties are comparable to the properties of the most modern permanent magnets based on $Nd_2Fe_{14}B$ [1-2]. The task of significantly increasing the kinetics of formation of the $L1_0$ phase in the Fe-Ni system can be solved by applying severe plastic deformation (SPD). In recent years, a large amount of research on the influence of high pressure torsion (HPT), which is a representative SPD technique [3], is promising for the production of bulk $L1_0$-FeNi [4-7]. The aim of this work is to study the magnetic properties and microstructure of $Fe_{49}Ni_{49}X_2$ (X = Ti, Al) alloys after SPD by HPT technique and low temperature annealing. The saturation magnetization M_S for bulk samples is expected to decrease up to 10 %. As a result of SPD, a slight decrease in the saturation magnetization, caused by an increase in the concentration of defects after plastic deformation, was found for $Fe_{49}Ni_{49}X_2$ (X = Ti, Al) samples. As compared with the saturation magnetization of the bulk samples, this value is 10 % smaller for HPT samples. Also a decrease in the coercive force of the plastically deformed material with compared to the bulk samples, by more than an order of magnitude was found. Such behavior most likely indicates the formation of superparamagnetic clusters within a plastically deformed material. In a single-domain state, as the particle size decreases, the coercive force falls and a super-paramagnetic state is formed in which the coercive force is zero. The superparamagnetic state is interesting in that the magnetization loss is almost zero due to the absence of magnetic hysteresis. Our research (Fig. 1) shows that low-temperature annealing at T = 573 K for t = 1300 hours of plastically deformed $Fe_{49}Ni_{49}X_2$ (X = Ti, Al) samples leads to an increase in saturation magnetization M_S by 3-10 % for different compositions. The authors gratefully acknowledge the financial support of Russian Science Foundation–Helmholtz project #18-42-06201 and of Russian Science Foundation project #19-72-00047. This work is supported by 5 top 100 Russian Academic Excellence Project at the Immanuel Kant Baltic Federal University.

[1] L.H. Lewis, F.E. Pinkerton, N. Bordeaux, *IEEE Magn. Lett*., vol. 5, pp. 1-4 (2014). [2] J.F. Albertsen, J.M. Knudsen, G.B. Jensen, *Nature*, vol. 273, pp. 453-454 (1978). [3] R.Z. Valiev, Y. Estrin, Z. Horita, *JOM*, vol. 58, No. 4, pp. 33-39 (2006). [4] M. Kolodziej, Z. Sniadecki, A. Musiala, *Journal of Magnetism and Magnetic Materials*, vol. 502, pp. 166577 (2020). [5] S. Lee, K. Edalati, H. Iwaoka, Horita, *Philosophical Magazine Letters*, vol. 94, No. 10, pp. 639-646 (2014). [6] T. Ohtsuki, M., Kotsugi T. Ohkochi, *Journal of Applied Physics*, vol. 114, pp. 143905 (2013). [7] S. Taskaev, K. Skokov, V. Khovaylo, *Physics Procedia*, vol. 75, pp. 1404-1409 (2015).

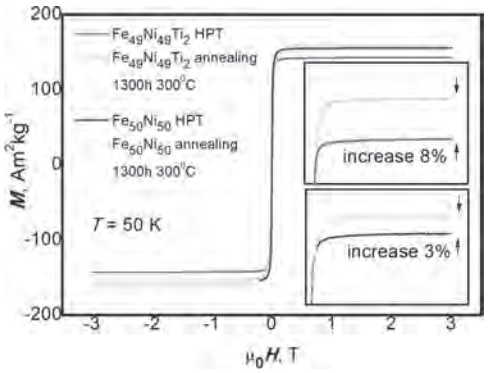

D4-02. Structural and Magnetic Properties of Iodide-Mediated Chemically Synthesized $FePt_3$ Nanoparticles. *V. Deepchand*[1], V. Tzitzios[2] and G.C. Hadjipanayis[1] *1. Physics and Astronomy, University of Delaware, Newark, DE, United States; 2. Institute of Nanoscience and Nanotechnology National Centre for Scientific Research Demokritos, Athens, Greece*

The structural and magnetic properties $Fe_{1-x}Pt_x$ nanoparticles are highly dependent on the composition x, which can be tailored to suit potential applications such as ultrahigh density storage media, biomedicine and catalysis. [1, 2] Most of the studies so far have been focused on equiatomic Fe-Pt with the highly anisotropic $L1_0$ structure. In bulk, $FePt_3$ in the $L1_2$ structure is paramagnetic at room temperature and shows two coexisting antiferromagnetic transitions at T_{N1}~160 K and T_{N2}~120 K. [3] Recently, $L1_0$ FePt nanoparticles have been chemically synthesized through a halide mediated route without requiring any post annealing. [4, 5]. In this work, we studied the effect of elemental iodine as our halide intermediary in the synthesis of FePt nanoparticles using a co-reduction of $Fe(acac)_3$ and $(NH_4)_2PtCl_2$ with 1,2-hexadecanediol in trioctylamine and oleylamine. Our study showed that the elemental iodine facilitated primarily the formation of $FePt_3$. When iodine was not used, the as-made nanoparticles had mostly the disordered fcc in structure (Figure 1). Annealing all of the as-made nanoparticles led to an increased particle size and transformation to the $L1_2$ ordered structure. The longer the annealing time, the greater the atomic ordering (Figure 1). Thermomagnetic data showed that the magnetic properties depend strongly on the degree of atomic ordering. The as-made particles with the disordered fcc structure are ferromagnetic with an ordering temperature of 380 K. The samples annealed at 700°C for 30 minutes showed a lower ordering temperature of ~250 K and another magnetic transition at 135 K possibly due to an antiferromagnetic structure. Room temperature hysteresis loops showed that the coercivity of our samples increased with annealing at 700°C up to 0.23 kOe. Future work is focused on finding the optimum conditions to obtain a highly ordered and monodispersed $L1_2$ $FePt_3$ nanoparticles without the need for any additional heat treatment. This work was supported by DOE Grant FG02-90ER45413.

[1] Sun, S., Adv. Mater., 18, 393 (2006) [2] Zhu, K., Ju, Y., Yang, Z., Acc. Chem. Res., 51, 404-413 (2018) [3] A.T. Heitsch, D.C. Lee, B.A. Korgel, J. Phys. Chem. C 114, 2512–2518 (2010) [4] W. Lei et al., Nano Lett., 18, 7839-7844 (2018) [5] W. Lei et al., Nanoscale, 9, 12855 (2017)

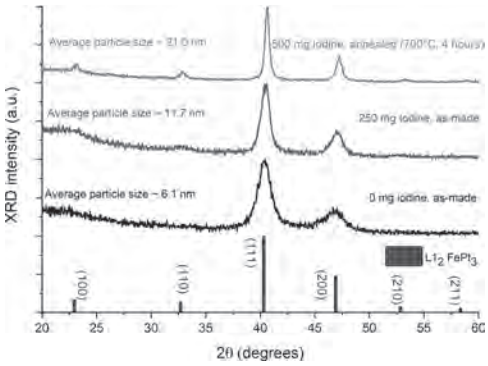

FIG. 1. XRD comparison of nanoparticles synthesized with and without iodine

D4-03. Withdrawn

D4-04. Critical Particle Size of α″-$Fe_{16}N_2$ Nanoparticles Prepared by Low-Temperature Nitriding. *B. Ma*[1], J. Liu[1], G. Guo[1] and J. Wang[1] *1. University of Minnesota, Minneapolis, MN, United States*

α″-$Fe_{16}N_2$ is expected to be the most-potential next generation permanent magnet, which greatly reduce the environment pollution. Among the methods to prepare the α″-$Fe_{16}N_2$ phase, nanoparticle approach is the best one so far for high purity phase. However, how to select the precursor is still a challenge. In this paper, the mechanism of α″-$Fe_{16}N_2$ phase formation during the low-temperature nitriding process (≤ 180 °C) was investigated. Both α-Fe and γ-Fe_2O_3 nanoparticles with different sizes were used to prepare α″-$Fe_{16}N_2$ by using the low-temperature nitriding, and nearly pure α″-$Fe_{16}N_2$ particles (93 %) were made. According to the experimental results, he formation of α″-$Fe_{16}N_2$ phase includes three stages: (1) the nucleation of α″-$Fe_{16}N_2$ phase, (2) the growth of metastable α″-$Fe_{16}N_2$, and (3) the nucleation of other stable Fe-N phases (ε-Fe_3N or γ′-Fe_4N). Nucleation of α″-$Fe_{16}N_2$ is a chemical reaction following the decomposition of NH_3, and it occurs at the high-energy surface sites with defects and strain. The growth of α″-$Fe_{16}N_2$ is in the frame of electric field modified diffusion, whose electric field established by the migration of Fe ions and electron. In order to obtain α″-$Fe_{16}N_2$ phase, the critical thickness and the crucial particle size should be within the range of 10-15 nm and 20-30 nm, respectively. Finally, the nucleation of Fe-N stable phase will cease the further growth of α″-$Fe_{16}N_2$ layer, and slowly encroach the α″-$Fe_{16}N_2$ layer.

D4-05. Magnetocrystalline Anisotropy of $Fe_{16}N_2$ Under Various DFT Approaches. *P. Stoeckl*[1], P. Swatek[2] and J. Wang[2] *1. Department of Physics, University of Minnesota Twin Cities, Minneapolis, MN, United States; 2. Department of Electrical and Computer Engineering, University of Minnesota Twin Cities, Minneapolis, MN, United States*

The magnetocrystalline anisotropy (MCA) energy of the giant saturation magnetization candidate material α″–$Fe_{16}N_2$ was investigated using first-principles electronic-structure calculations. The plane-wave density-functional theory (DFT) code Quantum ESPRESSO was employed to study the effect of different DFT approaches on the system, particularly the influence of exchange-correlation functionals and pseudopotential methods. The MCA energies obtained this way are within the range of previous theoretical and experimental results, while exhibiting significant variation between the different approaches. The role and limitations of these approaches in the view of $Fe_{16}N_2$ band structure will be discussed in detail.

N. Ji, X. Liu, and J.-P. Wang, New J. Phys. 12, 063032 (2010). N. Ji, M. S. Osofsky, [...], and J.-P. Wang, Phys. Rev. B 84, 245310 (2011).

D4-06. Withdrawn

D4-07. Size-Dependent Magnetic Properties of Barium Hexaferrite Platelets Synthesized Using a Salt Assisted Sol-Gel Technique. *N. Joseph*[1] and S. Thomas[1] *1. Department of Physics, Cochin University of Science and Technology, Kochi, India*

The magnetic properties of hexaferrite nanoparticles critically depend on the intrinsic anisotropy induced by its size as well as the morphology. This study demonstrates the controllable growth of barium hexaferrite ($BaFe_{12}O_{19}$) platelets using a salt-assisted sol-gel method. We employed salts like KBr, KCl, KI, and K_2CO_3 as a matrix to assist the formation of $BaFe_{12}O_{19}$ nanoplatelets from its precursor mixture gamma-Fe_2O_3 and $BaCO_3$. Within the detection limit of the x-ray diffraction technique, pure barium hexaferrite phases are obtained through the salt-assisted sol-gel process. The reaction of pre-calcined precursors in the presence of potassium-based salts favors a template mechanism, resulting in platelet-shaped barium hexaferrite (fig 1). The salt matrix acts as a barrier, preventing possible particle coarsening at high-temperature treatments and promotes the evolution of the hard magnetic phase. The width and thickness of the plates decrease with the addition of high melting point potassium halide salts. The magnetization and coercivity at 300 K of the barium hexaferrite particles were also systematically analyzed as a function of the dimension of platelets. Barium hexaferrite platelets of 0.20 μm width and 0.07 μm thickness yielded coercivity of the order of 4.6 kOe and saturation magnetization, close to 71 emu/g. Plate-shaped hexaferrite particles could be stacked and aligned by applying an external magnetic field and pressure, which could result in high-performance bulk hexaferrite magnets.

[1] W. Yongfei, L. Qiaoling, Z. Cunrui, and J. Hongxia, J. Alloys Compd. Vol.467, p.284 (2009). [2] A. Z. Eikeland, M. Stingaciu, A. H. Mamakhel, M. Saura-Múzquiz, and M. Christensen, Sci. Rep. Vol.8, p.7325 (2018).

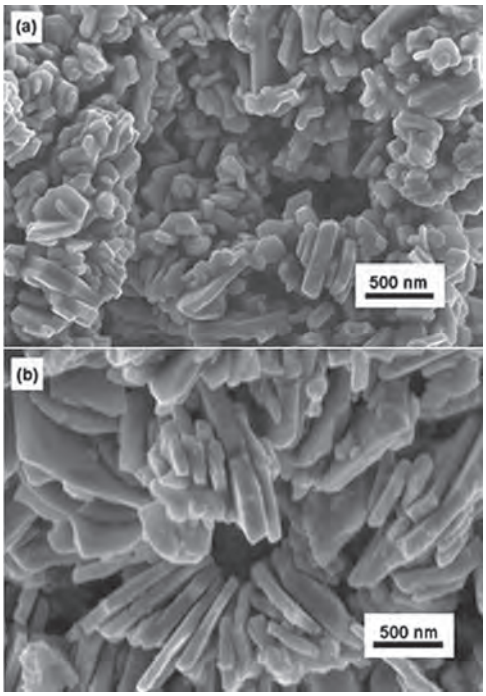

Fig.1. Scanning electron micrographs of barium hexaferrite platelets synthesized in the presence of (a) KBr and (b) K_2CO_3

D4-08. Local Inspection of Magnetic Properties in GdMnIn by Measuring Hyperfine Interactions. G. Cabrera-Pasca[1], J.F. Magno[1], W. Ferreira[2], A.C. Campos[2], *B. Bosch-Santos*[3], T.S. Sales[2], L.F. Pereira[2], A. Burimova[2], R.N. Saxena[2], R.S. Freitas[4] and A.W. Carbonari[2] *1. Faculdade de Ciências Exatas e Tecnologia (FACET), Universidade Federal do Para, Abaetetuba, Brazil; 2. CERPQ, Instituto de Pesquisas Energeticas e Nucleares - IPEN-CNEN/SP, Sao Paulo, Brazil; 3. Material Measurement Laboratory, National Institute of Standards and Technology, Gaithersburg, MD, United States; 4. Instituto de Fisica, Universidade de Sao Paulo, Sao Paulo, Brazil*

$GdMn_2$ is a member of a series of Laves phase containing a rare-earth element and a magnetic 3*d*-transition metal with very peculiar magnetic properties[1]. Doping with a non-magnetic element such as indium affects these properties[2,3]. GdMnIn is reported to crystalize in the hexagonal $MgNi_2$-type structure presenting a spin-glass behavior with no magnetic order attributed to the triangular spin frustration of magnetic ions[3]. The observed absence of long-range interactions by magnetization measurements along with the almost impossible measurements with neutron diffraction due to the presence of Gd with very high neutron absorption cross section makes the investigation of local exchange interactions in this compound very difficult. In the present work, measurements of hyperfine interactions at In sites using ^{111}In(^{111}Cd) probe nuclei were carried out by perturbed angular correlations (PAC) technique to investigate the local magnetic exchange in GdMnIn compound. Results displayed in Fig. 1 for the behavior of the major component (V_{zz}) of the electric field gradient (efg) tensor and the distribution of electric quadrupole frequency (δ) show a strong instability of the electronic environment of In sites when temperature decreases indicating a Mn-In disorder. The weak magnetic hyperfine field at In sites also shown in Fig.1 with an anomalous temperature dependence below around 140 K along with the increase in the angle between B_{hf} and V_{zz} directions suggest a weak long-range exchange interaction.

[1] K. Krop, *Physica B* 319, 9–16 (2002). [2] S.K. Dhar, C. Mitra, P. Manfrinetti, R. Palenzona, and A. Palenzona, *J. Phase Equilibria* 23, 79-82 (2002). [3] S. De Negri, D. Kaczorowski, A. Grytsiv, E. Alleno, M. Giovannini, R. Gorzelniak, P. Rogl, C. Godart, A. Saccone, and R. Ferro, *J. Alloys Compounds* 365, 58–67 (2004).

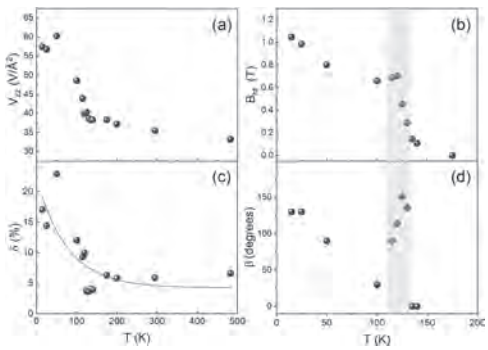

Fig. 1. Temperature dependence of the hyperfine parameters measured at In sites: (a) the major component of the efg tensor; (b) the magnetic hyperfine field; (c) the electric quadrupole frequency distribution; (d) the angle between the V_{zz} and B_{hf} directions.

D4-09. Crystallographic Texture and Magnetic Anisotropy of $CeCo_5$ Nanomagnets With Functional Gradient Prepared *via* a Simple Melt-Spinning Route. *L. Zha*[1], F. Wang[1], Z. Lin[1] and J. Yang[1] *1. Department of Physics, Peking University, Beijing, China*

The family of Co-based rare-earth (RE) intermetallic compounds of the form $RECo_5$ is known for its extremely large uniaxial magnetocrystalline anisotropy and high magnetic transition temperatures [1]. The most well-known and well-studied examples are $SmCo_5$ (K_u, 11-20 MJ/m^3, T_c, 1000 K) and $PrCo_5$ (K_u, 8.1 MJ/m^3, T_c, 893 K) [2]. However, due to the technical difficulties in achieving the appropriate microstructure previously, it is hard to obtain high enough coercivity in $RECo_5$ compounds composed of the light rare-earth element (La, Ce, Y). Fortunately, with the development of metallurgy technique recently, to modify the microstructure further for improving the magnetic performances of these compounds has again drawn considerable attention. In the course of the attempts, the preferential orientation of the 1:5 grains have been found with the *c*-axis preferentially aligned parallel to the ribbon plane by using the melt-spinning technique. While a buffer-free and highly textured (0 0 1) oriented $CeCo_5$ thin films exhibiting perpendicular magnetic anisotropy were synthesized on (0 0 1) Al_2O_3 substrates by molecular beam epitaxy. And single crystals of $CeCo_5$ with Ta-, Cu-, and/or Fe-substitution to improve the magnetic properties were fabricated by using the self-flux technique. In this study, $CeCo_5$ nanomagnets with strong crystallographic texture were prepared directly by high-speed melt-spinning. The *c*-axis texture of the $CeCo_5$ crystals is predominantly parallel to the ribbon plane direction only on the wheel side, while it exhibits isotropic orientation on the wheel side. The whole magnets show strong magnetic anisotropy between in and out of the ribbon planes. A remanence ratio of 0.71 parallel to the ribbon plane direction, higher than that of 0.58 perpendicular to the ribbon plane was observed in the magnets prepared at a wheel speed of 60 m/s.

[1] G.H.O. Daalderop, P.J. Kelly, M.F.H. Schuurmans, J. Magn. Magn. Mater. 104–107, p.737–738(1992) [2] K.H.J. Buschow, A.M. van Diepen, H.W. de Wijn, Solid State Commun. 15, p.903–906(1974)

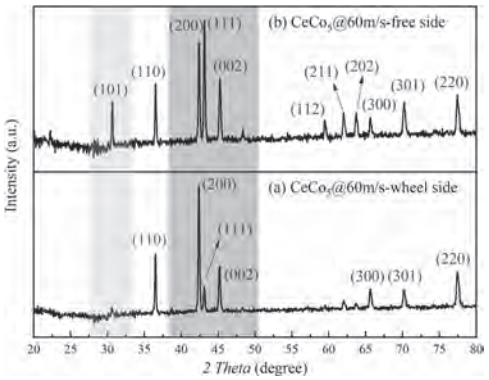

Fig. 1. XRD patterns of the wheel side (a), and free side (b) for $CeCo_5$ ribbons under 60 m/s.

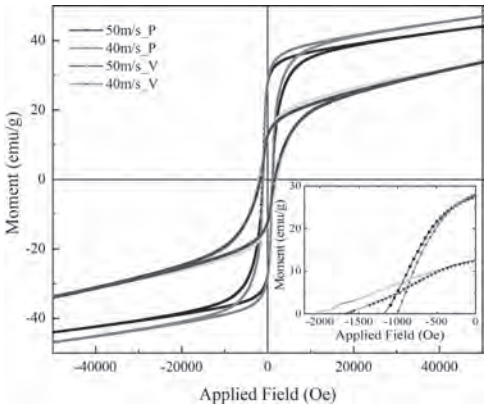

Fig. 2. Hysteresis loops for the $CeCo_5$ ribbons with applied field parallel and perpendicular to the ribbon plane.

D4-10. First-Principles Prediction of the Enhanced Uniaxial Magnetic Anisotropy and Thermal Stability in α″-$Fe_{16}N_2$. *T. Ochirkhuyag*[1], S. Cheol Hong[2] and D. Odkhuu[1] *1. Department of Physics, Incheon National University, Incheon, The Republic of Korea; 2. Department of Physics, University of Ulsan, Ulsan, The Republic of Korea*

Herein, employing first-principles prediction and rigid-band analysis, we have demonstrated an extremely large uniaxial magnetic anisotropy (K_u) up to 3 MJ m^{-3} in rare-earth (RE) free magnet α"-phase $Fe_{16}N_2$ by replacing Fe

with more valence electron elements, Co to Zn in the periodic table, which is more than 60% of K_u (4.9 MJ m^{-3}) attained for RE-included permanent magnet $Nd_2Fe_{14}B$, while improving thermal stability. Such a supreme K_u can be attributed to the mutual mechanisms of the Jahn-Teller orbital splitting and excess electron-induced energy level changes in the rigid-band selection rule. Moreover, we reveal that the replacement by Ti in addition to the above replacements can improve the thermal stability further by an order of magnitude in terms of the formation enthalpy without much suppressing K_u. These results provide an instructive guideline for simultaneous improvements of the thermal stability and energy product in 3d-only permanent magnets without RE or heavy-metal elements. Keywords: Rare-earth free permanent magnets, First-principle calculations, Uniaxial magnetic anisotropy E-mail: ochirkhuyag.t@inu.ac.kr, *schong@ulsan.ac.kr, †odkhuu@inu.ac.kr This work is supported by Future Materials Discovery Program through the National Research Foundation of Korea (NRF) funded by the Ministry of Science and ICT (2016M3D1A1027835) and by the Korea Institute of Energy Technology Evaluation and Planning (KETEP) grant funded by the Korean government (MOTIE) (20192010106850, development of magnetic materials for IE4 class motor).

D4-11. Improved Stability and Magnetic Anisotropy in $L1_0$ -FeNi by Interstitial Doping: a First-Principles Prediction. *T. Dorjsuren*[1], S. Cheol Hong[2] and D. Odkhuu[1] *1. Department of Physics, Incheon National University, Incheon, The Republic of Korea; 2. Department of Physics, University of Ulsan, Ulsan, The Republic of Korea*

Due to remarkable success in many uses today such as motors in an electric vehicle and memory devices, there have been intensive research interests centered at synthesizing a rare earth (RE)-free permanent magnetic material that has a cheap cost for mass production and various methods to improve a uniaxial magnetic anisotropy (K_u), saturation magnetization ($\mu_0 M_s$) as well as thermal stability of the previously known materials. RE-free $L1_0$ ordered FeNi alloys boast with affordable cost, large $\mu_0 M_s$ and also notable K_u owing to their tetragonal structure but has very low stability and degree of ordering. Herein, through first-principles electronic structure calculations, we have studied possible improvements of the structural stability and magnetic properties of $L1_0$-FeNi by an interstitial doping with 2p-electron elements (B, C, and N). It is found that the additions of 12.5 at.% B and N enhance K_u up to 0.9 and 1.8 MJ/m^3, respectively, which are 35% and about 3 times larger than that (0.66 MJ/m^3) of FeNi. More importantly, unlike the C and N dopants, the B greatly improves the stability and reaches K_u of 2.8 MJ/m^3 at 25 at.%. These results demonstrate the feasibility of possible enhancements on the magnetic anisotropy and energy product of 3*d*-only metals for RE-free permanent magnet applications.

D4-12. Artificially Produced Rare Earth Free $L1_0$-FeNi Phase Through Annealing of the FeNiPC Amorphous Alloy. *J. Han*[1] and H.C. Yim[1] *1. Physics, Sookmyung Women's University, Yongsan-gu, The Republic of Korea*

With the expansion of the necessity for electrical application such as motors, automobiles and renewable energy, the demand for high-specific permanent magnets is rapidly increasing [1-4]. However, the problem of resource strategicization due to supply and demand imbalance are emerging [5]. In addition, critical environmental pollution caused by securing rare earth resources [6]. Therefore, it is essential to develop new rare-earth-free permanent magnets that can solve these problems and reduce dependence on rare earths resources. The rare-earth-free hard magnetic L10-FeNi phase found in cosmic meteorites demonstrates potential as a next generation permanent materials [7]. However, it is very difficult to produce a bulk-shaped magnet by artificially forming the $L1_0$-FeNi phase as a previous process method due to the low atomic diffusion coefficients of Fe and Ni near the order-disorder transition temperature (~320°C) [8]. Therefore, to solve these process problems, $[Fe_{0.5}Ni_{0.5}]_x[P_{0.65}C_{0.35}]_{100-x}$ amorphous alloy systems exhibiting crystallization temperature (T_x) near the transition temperature were investigated by melt spinning technique. The amorphous alloys were annealed at T_x, resulting in high atomic diffusion. The structural and microstructural characterizations of annealed ribbons revealed the formation of $L1_0$-FeNi phase through observation of the superlattice peak. The magnetic property, such as coercivity (H_c), also indicated the formation of $L1_0$-FeNi phase, because the maximum H_c value is about of 700 Oe after the annealing process.

[1] R. Skomski, J.M.D. Coey, Permanent Magnetism, Institute of Physics, Bristol (1999) [2] S. Chikazumi, Physics of Magnetism, Wiley, New York (1964) [3] R. Skomski, J.M.D. Coey, "Magnetic anisotropy — How much is enough for a permanent magnet?," Scripta Mater. 112 (2016) [4] J.M.D. Coey, "Permanent magnet applications," J. Magn. Magn. Mater. 248 (2002) [5] T. Dutta, K. Kim, M. Uchimiya, and E.E. Kwon, "Global demand for rare earth resources and strategies for green mining," Environ. Res. 150 (2016) [6] S. Massari, M. Ruberti, "Rare earth elements as critical raw materials: Focus on international markets and future strategies," Resour. Policy 38 (2013) [7] L. Néel, J. Pauleve, and R. Pauthenet, "Magnetic properties of an iron—Nickel single crystal ordered by neutron bombardment," J. Appl. Phys. 35 (1964) [8] A. Makino, P. Sharma, and K. Sato, "Artificially produced rare-earth free cosmic magnet," Sci. Rep. 5 (2015)

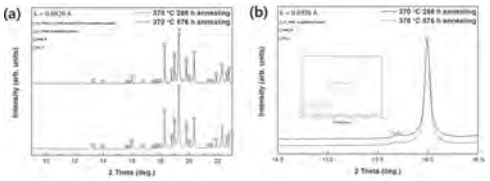

Fig. 1. (a), (b) Synchrotron X-ray diffraction patterns of the annealed $[Fe_{0.5}Ni_{0.5}]_x[P_{0.65}C_{0.35}]_{100-x}$ ribbons.

	H_c (Oe)			
	FeNiPC_1	FeNiPC_2	FeNiPC_3	FeNiPC_4
Degree	285h annealing			
0 (in-plane)	293	274	306	238
10	299	276	330	245
20	312	284	326	262
30	336	305	347	300
40	375	330	360	338
50	435	385	441	386
60	524	465	547	502
70	633	585	709	664
80	641	708	698	586
90 (out-of-plane)	540	360	472	503

Table 1. Magnetic property (H_c) of annealed $[Fe_{0.5}Ni_{0.5}]_x[P_{0.65}C_{0.35}]_{100-x}$ ribbons.

D4-13. Magnetic Properties of (Sm,Zr)Fe_5 Alloys and Their Nitrides. *T. Saito*[1] *1. Chiba Institute of Technology, Narashino, Japan*

The $SmFe_5$ phase is a metastable phase and its formation has been reported only in sputtered films. It has been reported that the $SmFe_5$ phase can be stabilized by the addition of zirconium or titanium [1–3]. The magnetic properties of the $SmFe_5$ phase may be improved by the nitrogenation. In this study, (Sm,Zr)Fe_5 powders were prepared by melt-spinning and subsequent nitrogenation. The relationship between the structures and magnetic properties of the (Sm,Zr)Fe_5 melt-spun ribbons and their nitrides is discussed. (Sm,Zr)Fe_5 alloy ingots were prepared by induction melting under an argon atmosphere. The molten alloy ingots were then ejected through an orifice with argon onto a copper wheel rotating at a surface velocity of 40 ms^{-1}. The melt-spun ribbon annealed at 973-1073 K for 1 h was subsequently nitrogenated under a nitrogen atmosphere at temperatures between 673 K and 773 K for 20 h. The specimens were examined by an X-ray diffraction (XRD) system, deferential thermal analysis (DTA), and vibrating sample magnetometer (VSM). Figure 1 shows the hysteresis loops of the (Sm,Zr)Fe_5 melt-spun ribbon and that nitrogenated specimen. Although the coercivity of the (Sm,Zr)Fe_5 melt-spun ribbon was low, the nitrogenated specimen exhibited a high coercivity over 10 kOe. This indicates that the nitrogenation of the (Sm,Zr)Fe_5 melt-spun ribbon resulted in a drastic increase in coercivity.

[1] F. Cadieu, et al. J. Appl. Phys. 55, 2611 (1984). [2] C. Lin, et al. J. Appl. Phys. 63, 3592 (1988). [3] Q. F. Xiao, et al. J. Appl. Phys. 82, 6170 (1997).

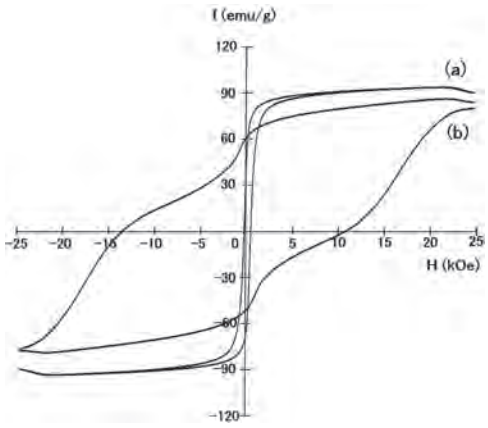

Fig.1 Hysteresis loops of (a) the (Sm,Zr)Fe_5 melt-spun ribbon and (b) that nitrogenated specimen.

D4-14. In-Situ Crystallization and Magnetic Measurement of Hexaferrite Glass-Ceramics. *A.J. Lere-Adams*[1], M. Ahmadzadeh[1], N. Smith-Gray[1] and J. McCloy[1] *1. Washington State University, Pullman, WA, United States*

Glass-ceramic (GC) materials have formability advantages of glasses controlled crystallization of functional ceramic phases. Here, we obtain GCs containing the hard magnetic phases Ba- or Sr-hexaferrite from a borate glass. Twelve compositions were explored, varying B_2O_3 and Ba/Fe or Sr/Fe ratio. Selected compositions were heat treated from 30°C to 700-900°C. Resulting phases were identified using X-ray diffraction (XRD) as α-Fe_2O_3 plus SrB_2O_4 and $SrFe_{12}O_{19}$ or their Ba equivalents. Vibrating sample magnetometry (VSM) also identified Fe_3O_4. The best compositions for hexaferrite GCs contained 40-42 mol% B_2O_3 and Fe/(Sr,Ba) ratios of 0.5-1. Heat treatments for one Sr glass were performed at 625°C or 675°C to assess phase development at the peak crystallization temperatures determined by thermal analysis, but both treatments yielded only SrB_2O_4 by XRD; however, coercivity increased from the quenched glass (395 Oe) to 625°C (460 Oe) to 675°C treatment (520 Oe). Selected glasses were studied with in-situ crystallization, measuring magnetic properties during heating to 800°C in the VSM. Hysteresis measurements on initial heating showed predominantly paramagnetism. After cooling and reheating, wasp-waisted loops were observed with H_c > 650 Oe, dropping to 0 at 650°C, with changes occurring 290°C, 490°C (T_C of $SrFe_{12}O_{19}$) and 550°C (T_C of Fe_3O_4 suggesting oxidation despite Ar heating gas). First order reversal curve (FORC) measurements confirmed low and high coercivity phases. These results suggest that crystallization of magnetic phases is most significant on cooling, and that this glass might allow alignment of the anisotropic hexaferrite crystals while heating and cooling with an applied field.

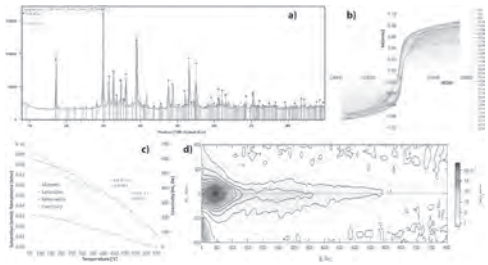

Fig. 1. 42B_2O_3-43SrO-15Fe_2O_3 (mol%) (A) XRD pattern, 800°C heat treat. (B) In-situ temperature-dependent VSM hysteresis loops, on reheating from 30°C to 650°C after heating glass to 700°C and cooling to crystallize. (C) Moment, saturation, remanence, and coercivity from data in B). (D) FORC plot (SF = 5) showing main coercivity ~500 Oe from softer magnetic material (likely magnetite), but with higher field component ~2500-3000 Oe due to hexaferrite or hematite, with their interaction causing the wasp-waisted loops.

Session S1
WEYL SEMIMETALS FOR SPINTRONICS

Axel Hoffmann, Chair
University of Illinois at Urbana-Champaign, Urbana, IL, United States

INVITED PAPERS

8:00

S1-01. Fermi-arc Diversity on Surface Terminations of the Magnetic Weyl Semimetal $Co_3Sn_2S_2$. *N. Avraham*[1], N. Morali[1], R. Batabyal[1], P. Kumar Nag[1], E. Liu[2], Q. Xu[2], Y. Sun[2], B. yan[1], C. Felser[2] and H. Beidenkopf[1] *1. Condensed matter physics, The Weizmann Institute of Science, Rehovot, Israel; 2. Max Planck Institute for Chemical Physics of Solids, Dresden, Germany*

Weyl semimetals are gapless topological materials, breaking either spatial inversion or time reversal symmetry, that host Weyl fermions in the bulk and topological Fermi arcs states on their surface. The time reversal symmetry broken Weyl semimetals are particularly attractive since they allow us to study the interplay between magnetism, electron correlations, and topology. While several inversion symmetry broken Weyl semimetals have been identified and verified experimentally, showing unambiguously that a material is a time reversal symmetry breaking Weyl semimetal is quite challenging. We used scanning tunneling spectroscopy to study the ferromagnetic semimetal $Co_3Sn_2S_2$ and verified spectroscopically its classification as a time-reversal symmetry-broken Weyl semimetal [1]. In my talk I will describe how we visualize the topological "Fermi arc" states using quasiparticle interference measurements and show that the emergent band structure of $Co_3Sn_2S_2$ exhibits direct signature of time reversal symmetry breaking, induced by the magnetic order of the Co atoms. By investigating three distinct surface terminations of the sample we examined complementary aspects of the surface and bulk band structure. I will describe the various surface and bulk electronic properties we extracted from each of the terminations. In particular I will demonstrate that the three different terminations of $Co_3Sn_2S_2$ exhibit not only distinct Fermi-arc contours, but also distinct connectivity between the Weyl nodes. The observed Weyl node connectivity changes from intra Brillouin zone connectivity on the Sn termination to a cross Brillouin-zones on the Co termination. This has significant implication on the magneto-transport properties of the Weyl electrons; finally, the S termination allowed us to extract the extent of the Weyl gap by following the surface state dispersion. This provides a clear demonstration of the surface bulk correspondence in Weyl semimetals.

[1] Morali et. al. Science 365, pp 1286, (2019).

8:36

S1-02. Spin-to-Charge Conversion in Magnetic Weyl Semimetals. *S. Zhang*[1,3], A. Burkov[2], I. Martin[1] and O. Heinonen[1] *1. Argonne National Laboratory Materials Science Division, Lemont, IL, United States; 2. Deptartment of Physics and Astronomy, University of Waterloo, Waterloo, ON, Canada; 3. Department of Physics, Case Western Reserve University, Cleveland, OH, United States*

Weyl semimetals (WSM) are a newly discovered class of quantum materials which can host a number of exotic bulk transport properties, such as the chiral magnetic effect, negative magnetoresistance, and a novel anomalous Hall effect [1,2]. In this work [3], we theoretically investigated spin-to-charge conversion in magnetic WSMs with a single pair of Weyl nodes. We found that a charge current can be induced by injecting a pure spin current into a magnetic WSM layer from an adjacent nonmagnetic metal layer. Formally, the induced charge current was calculated by solving for the scattering wave functions and the nonequilibrium distribution functions in each layer. Interestingly, we found the spin-to-charge conversion in magnetic WSMs exhibits remarkable features that are distinctly different from that arising from either the Rashba or Dirac surface state in various magnetic heterostructures studied previously [4]. For one thing, the induced charge current depends on spin and flowing directions of the injected spin current with respect to the crystallographic axes of the magnetic WSM; in particular, it vanishes along the direction parallel to the line connecting the two Weyl nodes, regardless of the direction of the injected spin. In addition, we showed that there exists a strong dependence of the induced charge current on the position of the Fermi level as well as on the separation between the two Weyl nodes. Therefore, the spin-to-charge conversion may not only serve as experimental probes of magnetic WSMs but may also provide extra knobs for controlling the spin-charge conversion in these topological materials. Work by S.S.-L.Z., A.A.B. and O.G.H. was supported as part of the Center for the Advancement of Topological Materials, an Energy Frontier Research Center funded by the U.S. Department of Energy (DOE), Office of Science; work by I.M. was supported by the U.S. DOE, Office of Science, Basic Energy Sciences, Materials Science and Engineering Division.

[1] A. Burkov, Nat. Mater. Vol. 15, p. 1145 (2016). [2] N. P. Armitage, E. J. Mele, and A. Vishwanath, Rev. Mod. Phys. Vol. 90, p. 015001(2018). [3] S. S-.L Zhang, A. Burkov, I. Martin, and O. Heinonen, Phys. Rev. Lett. 123, 187201(2019). [4] W. Han, Y. Otani, S. Maekawa, npj Quantum Materials Vol. 3, p. 27 (2018).

9:12

S1-03. Evidence for Pseudogravitational Fields in Antiferromagnetic FeRh. *J. Sklenar*[1], J.S. Shim[2], H. Saglam[3], J. Oh[2], A. Hoffmann[2], B. Bradlyn[2], N. Mason[2] and M. Gilbert[2] *1. Wayne State University, Detroit, MI, United States; 2. University of Illinois at Urbana-Champaign, Urbana, IL, United States; 3. Yale University, New Haven, CT, United States*

In this work, we provide experimental evidence that antiferromagnetic order and topology can be linked through theoretically predicted "pseudogravitational" interactions [1,2,3]. As the name suggests, pseudogravity is not a true gravitational field. In the case of antiferromagnetic Weyl semimetals, pseudogravity means that chiral fermions, in motion within an antiferromagnetic ordered system, are formally equivalent fermions in motion within a space-time containing a classical gravitational background. To make an observable connection to pseudogravity, experiments on FeRh were performed and compared to a tight-binding model of thin and strained FeRh. The model, which indicates that FeRh is a Weyl semimetal, predicts a sign change in the FeRh anisotropic magnetoresistance (AMR) when a field-induced magnetization is generated [see Figure 1 (a)] within the antiferromagnetic ordered phase. We experimentally observe this sign change, which is a distinct signature of both topology and pseudogravity in FeRh. Our samples are thin FeRh films, between 7.5 nm and 20 nm, grown on MgO using magnetron sputtering. The experimental AMR was obtained by applying a fixed in-plane external field (1 – 12 T), and by measuring the longitudinal magnetoresistance as a function of the relative orientation

between the field and the current [see Figure 1 (b)]. As the magnitude of the external field increases, the measured antiferromagnetic AMR exhibits a strong field-dependence that evolves from a two-fold, to a four-fold, and back to a two-fold angular signal. At the highest field strengths, the two-fold AMR has the opposite sign of the low field AMR, in agreement with pseudo-gravity theory. Because thin and strained FeRh films are known to have a residual ferromagnetic moment, we performed additional magnetic and electrical characterizations of our films to exclude ferromagnetic effects from explaining the unusual AMR. Our results demonstrate how an anomaly in the AMR of antiferromagnetic FeRh is consistent with the presence of a pseudogravitational background, providing better understanding of AMR in topological antiferromagnets. This invites a new way to design the next generation of antiferromagnetic spintronic devices, especially in antiferromagnetic Weyl semimetals where the anomalous Hall effect [4] has already been used to read out magnetic memory [5]. On a fundamental level, our results highlight how antiferromagnetic Weyl semimetals are a unique testbed for fundamental physics in solid state systems where exotic effects, such as gravitational phenomena can be examined.

[1] A. Cortijo and M. A. Zubkov. Annals of Physics 366, 45-56 (2016). [2] L. Liang and T. Ojanen. Phys. Rev. Res. 1, 032006(R) (2019). [3] B. Bradlyn and M. J. Gilbert. Submitted (2020). [4] S. Nakatsuji, N. Kiyohara, and T. Higo. Nature 527, 212–215 (2015). [5] H. Tsai, T. Higo, K. Kondou et. al. Nature 580, 608-613 (2020).

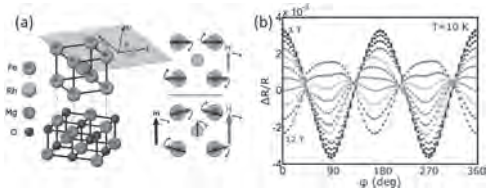

(a) Schematic of FeRh grown on MgO. In our main results, the current is aligned along the [100] direction as indicated and the external field is allowed to rotate in the plane of the FeRh. The right schematic shows how increasing the external induces magnetization (m) in the FeRh from by tilting the magnetic moments. The curved arrows give a sense of how the moment structure and the external field rotate within the plane. (b) The AMR is shown as a function of the in-plane angle for applied fields between 1 T and 12 T. At low fields, the AMR is mainly two-fold but a four-fold structure becomes apparent as the field increases. At the highest fields (10-12 T) the two-fold AMR signal clearly changes sign.

9:48

S1-04. Large and Robust Charge-to-Spin Conversion in Sputtered Disordered WTe_x. *X. Li*[1], P. Li[1], V.D. Hou[2], M. DC[1], C. Nien[2], F. Xue[1], D. Yi[1], C. Bi[1], C. Lee[2], S. Lin[2], W. Tsai[2], Y. Suzuki[1] and S. Wang[1] *1. Stanford University, Stanford, CA, United States; 2. Taiwan Semiconductor Manufacturing Co Ltd, Hsinchu, Taiwan*

Topological insulators have recently shown great promise for ultralow-power spin-orbit torque (SOT) devices thanks to their large charge-to-spin conversion efficiency originating from the spin-momentum-locked surface states. Recently, Weyl semimetals emerge as an alternative SOT source with spin-polarized surface as well as bulk states, robustness against magnetic and structural disorder, and higher electrical conductivity for integration in metallic magnetic tunnel junctions. Here, we report that long-range disordered sputtered WTe_x thin films exhibit local chemical and structural order as those of Weyl semimetal WTe_2 and conduction behavior that is consistent with semi-metallic Weyl fermion.[4] We find large charge-to-spin conversion properties in thermally annealed sputtered WTe_x films that are comparable with those in crystalline WTe_2 flakes.[5, 6] Besides, the strength of unidirectional spin Hall magnetoresistance in annealed WTe_x/Mo/CoFeB heterostructure is 5 to 20 times larger than typical SOT/ferromagnet bilayers reported at room temperature. We further demonstrate room temperature field-free magnetization switching at a current density of 1 – 2 MA/cm^2. These large charge-to-spin conversion properties that are robust in the presence of long-range disorder and thermal annealing pave the way for industrial integration of such topological materials. Our results open a new class of sputtered semimetals for memory and computing based on magnetic tunnel junctions as well as broader planar heterostructures consisting of SOT layer/ferromagnet interfaces. This research was supported in part by ASCENT, one of six centers in JUMP, a Semiconductor Research Corporation (SRC) program sponsored by DARPA. Part of this work was performed at the Stanford Nano Shared Facilities (SNSF)/Stanford Nanofabrication Facility (SNF), supported by the National Science Foundation under award ECCS-1542152. The Stanford authors wish to thank NSF Center for Energy Efficient Electronics Science (E3S) and TSMC for additional financial support.

[1] B. Feng *et al.*, *Physical Review B,* vol. 94, no. 19, Nov 18 2016. [2] A. A. Zyuzin, S. Wu, and A. A. Burkov, *Physical Review B,* vol. 85, no. 16, p. 165110, 04/06/ 2012. [3] A. A. Soluyanov *et al.*, *Nature,* vol. 527, p. 495, 11/25/online 2015. [4] X. Li *et al.*, *arXiv preprint arXiv:.04054,* 2020. [5] S. Shi *et al.*, *Nat Nanotechnol,* vol. 14, no. 10, pp. 945-949, Oct 2019. [6] B. Zhao *et al.*, *Physical Review Research,* vol. 2, no. 1, p. 013286, 03/10/ 2020.

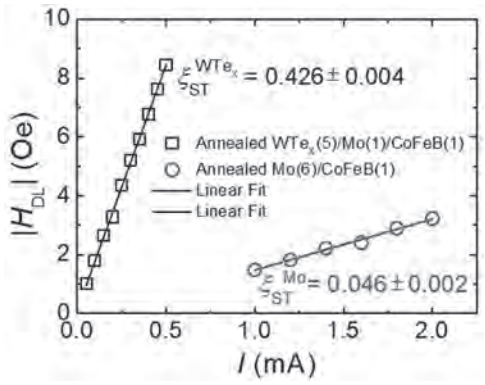

Damping-like field as a function of AC current amplitude for WTe_x(5)/Mo(1)/CoFeB(1)/MgO(2)/Ta(2) and Mo(6)/CoFeB(1)/MgO(2)/Ta(2) heterostructure, both annealed at 300°C for 30 minutes.

10:24

S1-05. Electrical Manipulation of a Topological Weyl Antiferromagnet. *S. Nakatsuji*[1,2] *1. Department of Physics, University of Tokyo, Tokyo, Japan; 2. Trans-scale Quantum Science Institute, University of Tokyo, Tokyo, Japan*

Electrical manipulation of emergent phenomena due to nontrivial band topology is a key to realize next-generation technology using topological protection. Recent discovery of the magnetic Weyl fermions in the antiferromagnet Mn_3Sn has attracted significant attention [1], as the magnetic Weyl semimetal exhibits various exotic phenomena such as chiral anomaly [1], large anomalous Hall effect (AHE)[2], anomalous Nernst effect [3,4], magneto-optical effects [5], and magnetic spin Hall effect [6], which have robust properties due to the topologically protected Weyl nodes. Given the prospects of antiferromagnetic (AF) spintronics for realizing high-density devices with ultrafast operation, it would be ideal if one could electrically manipulate an AF Weyl semimetal. Here we demonstrate the electrical switching of a topological AF state and its detection by AHE at room temperature [7]. In particular, we employ a polycrystalline thin film of the AF Weyl metal Mn_3Sn, which exhibits zero-field AHE. Using the bilayer device of Mn_3Sn and nonmagnetic metals (NMs), we find that an electrical current density of ~10^{10}-10^{11} A/m^2 in NMs induces the magnetic switching with a large change in Hall voltage, and besides, the current polarity along

a bias field and the sign of the spin Hall angle of NMs determines the sign of the Hall voltage. Notably, the electrical switching in the antiferromagnet is made using the same protocol as the one used for ferromagnetic metals. Our observation may well lead to another leap in science and technology for topological magnetism and AF spintronics. This is the work in collaboration with Hanshen Tsai, Tomoya Higo, Kouta Kondou, Takuya Nomoto, Akito Sakai, Ayuko Kobayashi, Takafumi Nakano, Kay Yakushiji, T. Koretsune, M. Suzuki, Ryotaro Arita, Shinji Miwa, YoshiChika Otani, Muhammad Ikhlas, Tahahiro Tomita, Hua Chen, Allan MacDonald.

[1] K. Kuroda, T. Tomita et al., Nature materials 16, 1090-1095 (2017). [2] S. Nakatsuji, N. Kiyohara, T. Higo, Nature 527, 212-215 (2015). [3] M. Ikhlas, T. Tomita, T. Koretsune, M.-T. Suzuki, D. Nishio-Hamane, R. Arita, Y. Otani and S. Nakatsuji, Nature Physics 13, 1085-1090 (2017). [4] A. Sakai, Y. P. Mizuta, A. A. Nugroho, R. Sihombing, T. Koretsune, M.-T. Suzuki, N. Takemori, R. Ishii, D. N.-Hamane, R. Arita, P. Goswami and S. Nakatsuji, Nature Physics, 14, 1119–1124 (2018). [5] T. Higo et al., Nature Photonics 12, 73-78 (2018); T. Matsuda et al., Nature Communications 11, 2863 (2020). [6] M. Kimata et al., Nature 565, 627–630 (2019). [7] Hanshen Tsai, Tomoya Higo, Kouta Kondou, Takuya Nomoto, Akito Sakai, Ayuko Kobayashi, Takafumi Nakano, Kay Yakushiji, Ryotaro Arita, Shinji Miwa, YoshiChika Otani, and Satoru Nakatsuji, Nature 580, 608–613(2020).

Session S2
ADVANCED STATIC AND DYNAMIC SPIN DEPTH PROFILING

Timo Kuschel, Co-Chair
Bielefeld University, Bielefeld, Germany
Christoph Klewe, Co-Chair
Lawrence Berkeley National Laboratory, Berkeley, CA, United States

INVITED PAPERS

9:00

S2-01. Surface Versus Bulk Characterization of 3D Skyrmion Lattices in Chiral Magnets. *G. van der Laan*[1], S. Zhang[2] and T. Hesjedal[3]
1. Diamond Light Source Ltd, Didcot, United Kingdom; 2. ShanghaiTech University, Shanghai, China; 3. University of Oxford, Oxford, United Kingdom

It is commonly assumed that surfaces modify the properties of stable materials within the top few atomic layers of a bulk specimen only. Exploiting the polarization dependence of resonant elastic x-ray scattering (REXS) to go beyond conventional diffraction and imaging techniques, we have determined the depth dependence of the full 3D spin structure of skyrmions—that is, topologically nontrivial whirls of the magnetization—below the surface of a bulk sample of Cu_2OSeO_3. It was found that the skyrmions change exponentially from pure Néel- to pure Bloch-twisting over a distance of several hundred nanometers between the surface and the bulk, respectively (see Fig. 1). The exact surface helicity angles of twisted skyrmions for both left- and right-handed chiral bulk Cu_2OSeO_3, in the single as well as in the multidomain skyrmion lattice state, are determined, revealing their detailed internal structure. The experimental results are compared with different theoretical models [1,2]. The findings suggest that a skyrmion surface reconstruction is a universal phenomenon, stemming from the breaking of translational symmetry at the interface. Fig. 1. Illustration of skyrmion order ranging from Néel- to Bloch-twisting with increasing depth below a surface. (*A1–A4*) Hedgehog spin configuration on the surface of a sphere for skyrmions with winding number $N = 1$ varying between pure Néel-twisting (*A1*) and pure Bloch-twisting (*A4*). (*B1–B4*) Real-space planar spin configuration varying between pure Néel-twisting (*B1*) and pure Bloch-twisting (*B4*). A stereographic projection connects the planar patterns shown in *B1–B4* with the hedgehog configurations shown in *A1–A4*, respectively. (*C1–C4*) Calculated dichroic REXS diffraction pattern associated with a hexagonal lattice composed of the spin configurations shown in *B1–B4*. The orientation of the extinction line marked by a white arrow corresponds to the helicity angle denoted on the right-hand side of the panels. Consequently, the chirality of the skyrmions can be straightforwardly determined.

[1] S.L. Zhang, G. van der Laan, W.W. Wang, A.A. Haghighirad, T. Hesjedal. Phys. Rev. Lett. 120, 227202 (2018). [2] S.L. Zhang, G. van der Laan, J. Müller, L. Heinen, M. Garst, A. Bauer, H. Berger, C. Pfleiderer, T. Hesjedal. Proc. Natl. Acad. Sci. U.S.A. (PNAS) 115, 6386 (2018).

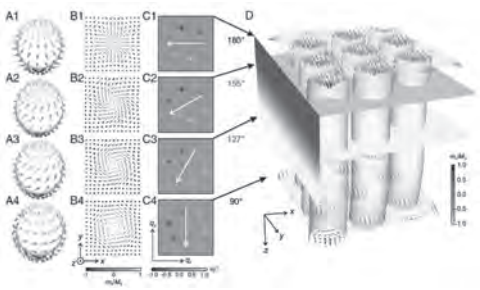

9:36

S2-02. Coherent AC Spin Transport Across Antiferromagnetic Insulators Detected by Element-Resolved and Time-Resolved x-ray Magnetic Dichroism. *Z.Q. Qiu*[1] *1. Physics, Univ. of California at Berkeley, Berkeley, CA, United States*

One mystery surrounding the subject of spin current in antiferromagnetic (AF) insulators is the frequency mismatch between the THz AF magnons and the GHz spin current. Specifically, it is a fundamental and critical issue that whether a GHz ac spin-current can ever keep its coherence inside an antiferromagnetic insulator and so drive the spin precession of another ferromagnet layer coherently? In this talk, I will report our study of ac spin current using element-resolved and time-resolved x-ray magnetic dichroism measurement at the Advanced Light Source of Lawrence Berkeley National Laboratory. By direct probing of spin dynamics of Py and $Fe_{75}Co_{25}$ seperatively in Py/Ag/CoO/Ag/$Fe_{75}Co_{25}$/MgO(001) heterostructures, we demonstrate that GHz ac spin current pumped by the Py ferromagnetic resonance can transmit coherently across the antiferromagnetic CoO insulating layer and drive a coherent spin precession of the $Fe_{75}Co_{25}$ layer [1].

[1]. Q. Li, M. Yang, C. Klewe, P. Shafer, A. T. N'Diaye, D. Hou, T. Y. Wang, N. Gao, E. Saitoh, C. Hwang, R. J. Hicken, J. Li, E. Arenholz, and Z. Q. Qiu, "Coherent ac spin current transmission across an antiferromagnetic CoO insulator", Nat. Commn. 10, 5265 (2019).

10:12

S2-03. Scaling of Proximity Induced Magnetism in Pt With Magnetism of Ferromagnet Using Pt/CoFeTaB/Pt. *O.A. Inyang*[1,2], L. Bouchenoire[3,4], M. Tokac[1], R. Rowan-Robinson[1], B. Nicholson[1], C. Kinane[5] and A. Hindmarch[1] *1. Department of Physics, Durham University, Durham, United Kingdom; 2. Department of Physics, Akwa Ibom State University, Mkpat Enin, Nigeria; 3. XMaS beam line, ESRF, Grenoble, France; 4. Department of Physics, University of Liverpool, Liverpool, United Kingdom; 5. ISIS Neutron Facility, Rutherford Appleton Laboratory, Didcot, United Kingdom*

Proximity induced magnetism (PIM) has been inferred in several Spintronic phenomena, despite limited understanding of the underlying mechanism governing how PIM arises. Since PIM is an interfacial effect, it has an impact on spin current transport, spin-orbit torque and other transport phenomena [1]. Here, we used two complementary reflectivity techniques of polarized neutron reflectivity (PNR) and X-ray resonance magnetic reflectivity (XRMR) to shed light on the phenomenology of PIM. Modelling temperature-dependent data taken using these techniques demonstrated that, contrary to the widely accepted theory that PIM scales linearly with FM magnetism as a function of temperature [2, 3], a threshold FM interface magnetism is required to induce PIM as shown in Fig 1a [4]. The FM magnetization was obtained from the depth dependence profile from PNR (see Fig 1b) while the Pt induced magnetization was from scattering length density (SLD) profile

from XRMR data turned to Pt L_3 absorption edge of 11.56 keV (see Fig 1c). XRMR is an element sensitive technique with sensitivity to Pt polarized magnetic moment only [5]. In addition, the magnitude of Pt magnetization at the top interface was larger than the buffer Pt interface, indicating a difference in the magnetic susceptibility at these interfaces and explaining the frequently observed asymmetry in PIM [6].

[1] Huang et al., *Phys. Rev. Lett.* 109, 107204 (2012). [2] L. Weng et al., *Appl. Phys. Lett.* 102, 162404 (2013). [3] T. Hase et al., *Phys. Rev*. B 90, 104403 (2014). [4] O. Inyang et al., *Phys. Rev. B* 100, 174418 (2019). [5] P. Bougiatioti et al., arXiv:1807.09032v2 (2018). [6] D.-O. Kim et al., *Sci. Rep.* 6, 25391 (2016).

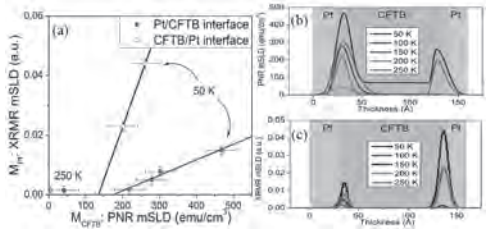

Fig 1: (a) Linear scaling of PIM to FM interface magnetism as a function of temperature (b) SLD profile from PNR and (c) SLD profile from XRMR

10:48

S2-04. Probing Quantum Materials and Devices With Next-Generation Neutron Reflectometry. *A.J. Grutter*[1] *1. NIST Center for Neutron Research, Gaithersburg, MD, United States*

Whether it originates in crystallinity, magnetism, or electronic structure, interfacial symmetry breaking represents one of the most powerful tools for the realization of new quantum materials with advanced functionality. Mismatches in band topology and time reversal symmetry across interfaces have been harnessed to open gaps in the surface states of topological insulators or to induce topological transitions. Heterostructures interfacing superconductors with a quantum anomalous hall insulator (QAHI) have been reported to exhibit signatures of Majorana fermions[1], while two-dimensional systems with strong spin-orbit interactions have long been suspected of harboring skyrmions at interfaces with perpendicular magnetic materials[2]. In all of these cases, our understanding of the underlying physics has hinged critically on the ability to precisely understand and isolate the properties of the interface from the bulk of the system. By decomposing the magnetic and electronic properties on a layer-by-layer and element-resolved basis, new quantum material systems may be robustly understood and designed. In this talk, I will discuss our recent progress in combining depth-resolved information from polarized neutron reflectometry with element-specific information from soft X-ray spectroscopy to design and control magnetic interfaces in topologically nontrivial systems such as SnTe, $(Bi,Sb)_2Te_3$/antiferromagnet and Bi_2Se_3/oxide heterostructures.[3-7] I will focus in particular on the new capabilities enabled by CANDOR, the new polychromatic neutron reflectometer at the NIST Center for Neutron Research. A highly intensity-limited technique, the application of neutron reflectometry has been critically hampered by the long measurement times necessary to probe the trace magnetic signal in systems such as superconductors and QAHIs. By implementing a polychromatic beam with multiplexed energy analyzing detectors, CANDOR allows for multiple orders of magnitude intensity gains, allowing even more sensitive measurements to be performed in hours instead of days.

[1] Q. L. He et al., Science 357, 294 (2017) [2] Q. Shao et al., Nature Electronics 2, 182 (2019) [3] Q. L. He et al., Nature Materials 16, 94 (2017) [4] Q. L. He et al., Physical Review Letters 121, 096802 (2018) [5] Q. L. He et al., Nature Communications 9, 2767 (2018) [6] L. Pan et al., Submitted (2020) [7] C.-Y. Yang et al., Submitted (2020)

11:24

S2-05. Enabling Atomic Resolution in Electron Magnetic Circular Dichroism (EMCD) Measurements. *J. Rusz*[1], D. Negi[2], E. Rotunno[3], P. Zeiger[1], L. Jones[4], M. Zanfrognini[3], J. Idrobo[5], V. Grillo[3] and P. van Aken[2] *1. Department of Physics and Astronomy, Uppsala Universitet, Uppsala, Sweden; 2. Max Planck Institute for Solid State Research, Stuttgart, Germany; 3. CNR-NANO, Modena, Italy; 4. University of Dublin Trinity College, Dublin, Ireland; 5. Oak Ridge National Laboratory, Oak Ridge, TN, United States*

Progress in nanotechnology requires modern characterization tools with sufficient spatial resolution. Transmission electron microscopy (TEM) is a natural method of choice, routinely allowing measurements at nanometer scale or even at atomic lateral resolution – thanks to the aberration correctors, which allow to focus electron beams to areas with diameter smaller than an Ångström. Within the field of magnetic studies, one typically applies Lorentz microscopy and holographic methods. An alternative measurement method in development is electron magnetic circular dichroism (EMCD; [1]), which is an electron microscopy analogue of the well-established method utilizing circularly polarized x-rays, the x-ray magnetic circular dichroism (XMCD). While XMCD is limited by the beam size to spatial resolutions of approximately 10nm, EMCD has a potential to reach atomic resolution. EMCD has been proposed in 2003 and for the first time experimentally realized in 2006 [1]. Since then the method went through a rapid development at both fronts – experimental and theoretical. Dynamical diffraction effects severely complicate EMCD detection and often reduce its strength. To circumvent this, numerous ways of acquiring EMCD have been proposed and many of them were experimentally tested. Recently, EMCD was detected using astigmatic electron beams on antiferromagnets [2], or with convergent probes [3], resolving magnetic signals from areas smaller than a square nanometer [4]. In high-resolution TEM setting, EMCD signal from individual atomic planes was detected using the PICO instrument [5], where a crucial role was played by chromatic aberration corrector. Theory predicts that electron vortex beams should be efficient probes of EMCD at atomic resolution [6]. Successful realization of this experiment could be extended further to probe the third dimension by means of magnetic depth sectioning [7], see Fig. 1. Alternative methods of reaching atomic resolution include filtering the transmitted electron beam in terms of both energy loss and orbital angular momentum (OAM; [8]), see Fig. 2. An overview of the current state of the art in EMCD will be presented. We will discuss ongoing projects and challenges, such as improved experiments with the astigmatic electron beams and path toward an OAM- and energy-filtered detection of EMCD. We will also discuss the modern statistical data processing methods, which are a great aid in extraction of the magnetic signal from typically large datasets, typically consisting of multiple three-dimensional data structures called spectrum images. We acknowledge funding from Swedish Research Council, STINT and Carl Tryggers foundation. Calculations utilized resources of the Swedish National Infrastructure for Computing at NSC Center. L. J. is supported by Science Foundation Ireland (URF/RI/191637). This work is supported projects funded by the European Union's Horizon 2020 Research and Innovation Program under grant agreements No. 766970 - Q-SORT and No. 823717 - ESTEEM3.

1. P. Schattschneider et al., Nature, Vol. 441, p.486 (2006). 2. J. C. Idrobo et al., Advanced Chemical and Structural Imaging, Vol. 2, p.5 (2016). 3. T. Thersleff et al., Physical Review B, Vol. 94, p.134430 (2016). 4. J. Rusz et al., Nature Communications, Vol. 7, p.12672 (2016). 5. Z. Wang et al., Nature Materials, Vol. 17, p.221 (2018). 6. D. Negi, J.-C. Idrobo, J. Rusz, Sci. Rep., Vol. 8, p.4019 (2018). 7. D. Negi et al., Phys. Rev. B, Vol. 98, p.174409 (2018); D. Negi et al., Phys. Rev. B, Vol.100, p.104434 (2019). 8. E. Rotunno et al., Phys. Rev. B, Vol. 100, p.224409 (2019).

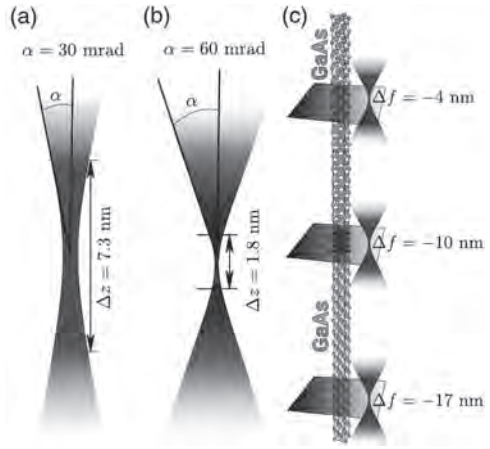

Fig.1: Illustration of magnetic depth sectioning with convergent electron vortex beams. Larger convergence semi-angle α leads to a smaller depth of focus Δz. Compare panels a) and b) with schematically illustrating beam profiles and depths of foci for convergence semi-angles of 15mrad and 30mrad, respectively. By moving the focal plane through the thickness of the sample, as is shown in c), it will be possible to extract depth-dependent magnetic infomration. Figure taken from Ref. [7].

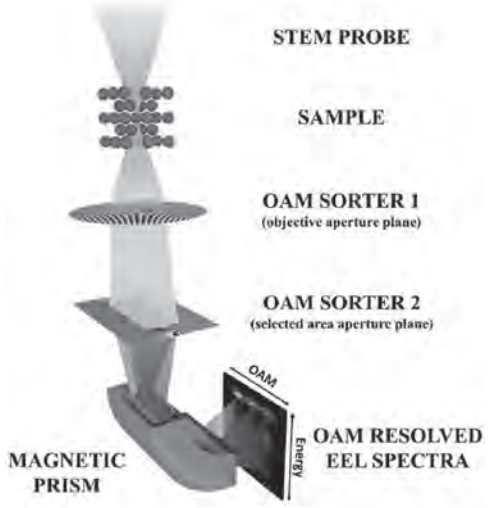

Fig. 2: Schematic illustration of the atomic resolution EMCD experiment with filtering the exit wave by energy loss and OAM. OAM sorter consists of two phase elements (OAM sorter 1 and 2). Spectrometer then disperses the outgoing beam as a function of the electron energies. CCD records a two-dimensional image with vertical axis corresponding to electron energies and horizontal axis to individual discrete values of OAM. Figure taken from Ref. [8].

Session E1
HALF-METALLIC MATERIALS

Peter Wadley, Co-Chair
University of Nottingham, Nottingham, United Kingdom
Arjun K Pathak, Co-Chair
Ames National Laboratory, Ames, IA, United States

INVITED PAPER

E1-01. Magneto-Thermal Transport in Weyl Semimetal Co_2MnGa Thin Films. *H. Reichlova*[1], G. Park[3], P. Ritzinger[1], A. Markou[2], R. Schlitz[1], M. Lammel[3], K. Vyborny[4], D. Kriegner[2,4], P. Swekis[2], J. Noky[2], Y. Sun[2], J. Gayles[2], A. Thomas[3], C. Felser[2] and S. Goennenwein[1]
1. Technische Universitat Dresden, Dresden, Germany; 2. MPI Dresden, Dresden, Germany; 3. Leibniz-Institut fur Festkorper- und Werkstoffforschung Dresden eV, Dresden, Germany; 4. FZU, Academy of Science, Prague, Czechia

The ferromagnetic Heusler compound Co_2MnGa is a promising Weyl semimetal with the Fermi energy in the vicinity of the Weyl nodes. Bulk Co_2MnGa recently attracted attention because of an exceptionally large anomalous Nernst effect [1,2] and exotic surface states [3]. Simultaneously, Co_2MnGa thin films were successfully prepared and showed interesting transport properties [4]. Beside others, the non-trivial topology of the band structure of Weyl semimetals leads to unexpected magneto-thermoelectic transport phenomena which will be discussed in this talk. We report on our observation of a record large anomalous Nernst coefficient in Co_2MnGa thin films - up to -3μV/K [5, 6], and discuss the procedure for the quantitative determination of the anomalous Nernst coefficient. Several samples with comparable saturated magnetization were studied, yielding significantly different anomalous Nernst responses. We conclude that the microscopic origin of the anomalous Nernst effect in Co_2MnGa is complex and contains contributions from the intrinsic Berry phase and surface states. We further employ a series of Co_2MnGa thin films to study the validity of the Mott relation by measuring all four transport coefficients - the longitudinal resistivity, anomalous Hall, Seebeck and anomalous Nernst coefficients [6]. We show that the measured anomalous Nernst signal can be connected to the remaining three magneto-thermal transport coefficients in the whole sample series. This is strong evidence that the Mott relation holds also in Weyl semimetals, where the intrinsic Berry curvature dominates the transport. In the last part of the talk we focus on another magneto-transport phenomena and its thermal counterpart – anisotropic magnetoresistance and anisotropic magneto-thermopower. We show that due to high epitaxial quality of the Co_2MnGa films both non-crystalline and crystalline contributions to the anisotropic magnetoresistance can be measured. Interestingly, we do not observe the same crystalline contributions in the magneto-thermopower measurements [7].

[1] S. N. Guin et al., NPG Asia Materials 11, 16 (2019) [2] A. Sakai et al., Nat. Phys. 13, 1119-1124 (2018) [3] I. Belopolski et al., Science 365, 1278-1281 (2019) [4] A. Markou et al., PRB 100, 054422 (2019) [5] H. Reichlova et al., APL 113, 212405 (2018) [6] G. H. Park, H.R. et al. PRB 101, 060406(R) (2020) [7] P. Ritzinger, H.R. et al., in preparation

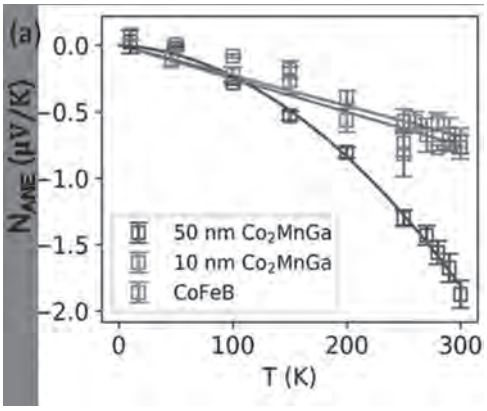

The measured anomalous Nernst coefficient in three samples with the same saturated magnetization is significantly different, suggesting that Berry curvature contributes to the anomalous Nernst signal.

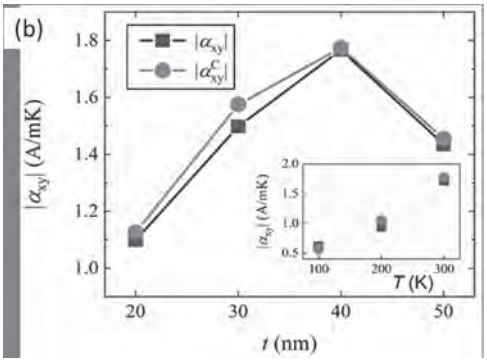

The measured and calculated anomalous Nernst conductivity is in excellent agreement in the whole sample series suggesting that the Mott relation is applicable to the Co_2MnGa Weyl semimetal.

CONTRIBUTED PAPERS

E1-02. Investigation of non-Collinearity in Mn_2Ru_xGa Compensated Ferrimagnetic Half-Metallic Thin Films. *K.E. Siewierska*[1], D. Betto[2], N. Teichert[1], Z. Gercsi[1], G. Atcheson[1], N.B. Brookes[3], M. Coey[1] and K. Rode[1] *1. Physics, University of Dublin Trinity College, Dublin, Ireland; 2. Max Planck Institute for Solid State Research, Stuttgart, Germany; 3. ESRF, Grenoble, France*

Mn_2Ru_xGa (MRG) is a half-metallic compensated ferrimagnet crystallising in a cubic inverse Heusler structure (*XA*) with a substrate-induced biaxial strain of about 1% leading to perpendicular magnetic anisotropy of the net moment. The Mn atoms occupy two different crystallographic sites, Wyckoff positions 4*a* and 4*c*. [1] From band structure calculations we find that the states originating from the Mn4*c* sites dominate the transport. Anomalous Hall

effect (AHE) resistance is proportional to the z-component of the magnetisation of the Mn4*c* sublattice. [2] The AHE measurements show loops with high remanence and only one magnetic phase, with coercivity diverging close to compensation. SQUID magnetometry measures the net moment, i.e. the sum of Mn4*a* and Mn4*c* sublattice moments. SQUID-measured magnetisation, in the same geometry as AHE, exhibits a combination of an apparent soft magnetic response in addition to a component with the coercivity observed by AHE. We infer that the net magnetic moment is canted due to non-collinearity of the sublattice moments. Our DFT calculations suggest that the non-collinearity may be due to competing exchange on the Mn4*c* sites as bulk antisymmetric exchange averages to zero in the -43m point group [3]. The Mn4*c* sublattice and net magnetisations differ by an order of magnitude, so a small canting of the Mn4*c* moment can result in a large canting of the net moment. X-ray magnetic circular dichroism measurements were performed to map sublattice magnetisations in the z-x plane. Both sublattices can be distinguished by L-edge absorption due to charge-transfer separation of the Mn absorption edges at the two sites by ≈ 1 eV. [2] Analysis of the m_z-m_x moments shows that they are indeed non-collinear (Fig.1). From balancing of torques, anisotropy fields at the Mn4*a* and Mn4*c* sublattices were found to be easy-plane -1.8 T and easy-axis 3 T, respectively (Fig.2.).

[1] H. Kurt, K. Rode, P. Stamenov, *et al.*, "Cubic Mn_2Ga thin films: crossing the spin gap with ruthenium", Phys. Rev. Lett., 112, p. 27201, 2014. [2] D. Betto, N. Thiyagarajah, Y.-C. Lau, *et al.*, "Site-specific magnetism of half-metallic Mn_2Ru_xGa thin films determined by x-ray absorption spectroscopy", Phys. Rev. B, 91, p. 094410, 2015. [3] O. Meshcheriakova, S. Chadov, A.K. Nayak, *et al*. "Large Noncollinearity and Spin Reorientation in the Novel Mn_2RhSn Heusler Magnet", Phys. Rev. Lett. 113, p. 087203, 2014.

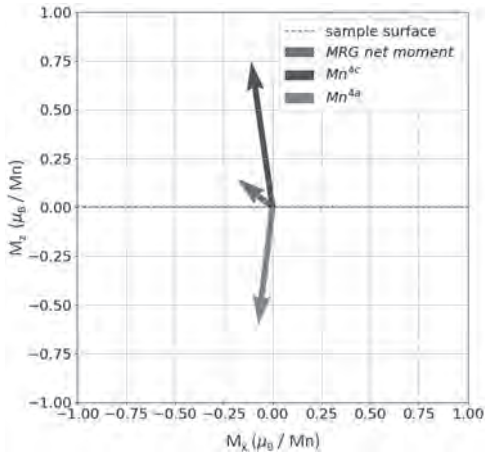

Net (green), Mn4*a* sublattice (red) & Mn4*c* sublattice (blue) magnetisation projections onto the x-z plane at 200 K from XMCD in 0 T.

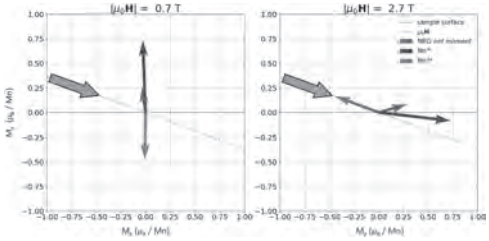

Mn4*a* (red) & Mn4*c* (blue) sublattice magnetisation projections onto the x-*z* plane at 200 K from XMCD. The large green arrow indicates the field direction. Data used for torque balancing.

E1-03. Possible Half-Metallic Behavior of $Co_{2-x}Cr_xFeGe$ Heusler Alloys: Theory and Experiment. *R. Mahat*[1], S. KC[1], D. Wines[2], S. Regmi[1], U. Karki[1], F. Ersan[2,3], J. Law[4], C. Ataca[2], V. Franco[4], A. Gupta[5] and P. LeClair[1] *1. Physics and Astronomy, The University of Alabama, Tuscaloosa, AL, United States; 2. Physics, University of Maryland Baltimore County, Baltimore, MD, United States; 3. Physics, Aydin Adnan Menderes University, Aydin, Turkey; 4. Dpto. Física de la Materia Condensada ICMSE-CSIC, Universidad de Sevilla, Sevilla, Spain; 5. Chemistry and Biochemistry, The University of Alabama, Tuscaloosa, AL, United States*

Co_2- based intermetallic Heusler alloys are among the most attractive half-metallic systems due to their high Curie temperatures, high spin polarization and the structural similarity to binary semiconductors [1,2]. The Co_2FeGe system is one such candidate of interest for spintronic applications, but experimentally it does not form a single phase in bulk form [3,4,5]. In this work, we have introduced Cr doping to stabilize the Co_2FeGe system, and examined the structural, magnetic, transport, and mechanical properties of quaternary Heusler alloys $Co_{2-x}Cr_xFeGe$ with $0 \le x \le 1$, both experimentally and theoretically. Single phase microstructures are observed for Cr compositions from x = 0.25 to x = 1. The samples with Cr concentrations below x = 0.25 are multi-phase. XRD patterns at room temperature show the presence of ordered Y structure (space group F-43m, # 216) for all single-phase samples. The low-temperature saturation magnetic moments agree fairly well with our theoretical results and also obey the Slater-Pauling rule, a noted prerequisite for half metallicity. The Density functional theory calculations performed using VASP code with projector augmented wave method (PAW) and the Perdew-Burke-Enzerhof (PBE) functional predict half-metallic character in the alloys after Cr substitution. All alloys are observed to have high Curie temperatures, and show a linear dependence with the saturation magnetic moment which is expected in half metallic Co-based Heusler alloys [6]. Transport measurements were performed to explain the electronic structure of the alloys. High mechanical hardness values are also observed which makes these materials suitable for industrial applications requiring repetitive thermal cycling and resist cracking from vibrations.

1. I. Galanakis, P. Dederichs, and N. Papanikolaou, Physical Review B 66, 174429 (2002). 2. C. Felser, G. H. Fecher, and B. Balke, Angewandte Chemie International Edition 46, 668(2007). 3. K. R. Kumar, K. K. Bharathi, J. A. Chelvane, IEEE Transactionson Magnetics 45, 3997 (2009). 4. S. KC, R. Mahat, P. LeClair, Phys. Rev. Materials 3 (2019) 114406. 5. R. Mahat, S. KC, D. Wines, P. LeClair, Bulletin of the American Physical Society (2020). 6. G. H. Fecher, H. C. Kandpal, S. Wurmehl, C. Felser, Journal of applied Physics 99, 08J106 (2006).

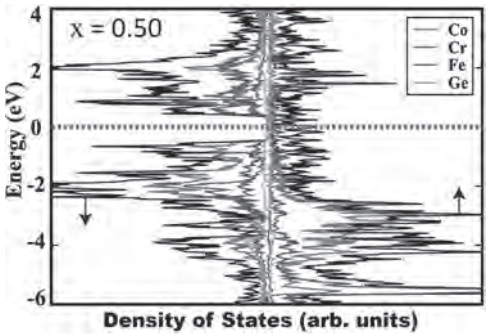

FIG. 1. The DOS plot for the lowest energy structure of $Co_{1.5}Cr_{0.5}FeGe$, showing Half-metallic behavior.

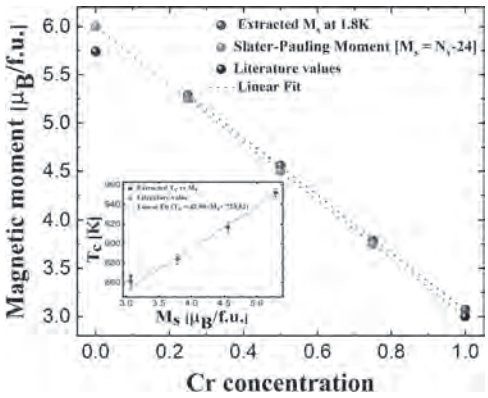

FIG. 2. The variation of saturation magnetic moment with Cr concentration, both experimental and expected from Slater Pauling rule. The insert shows the linear dependence of Curie temperature with saturation magnetic moment.

E1-04. Manipulation of Gilbert Damping in Ultrathin Half-Metallic Co_2FeAl_{1+x} by Composition-Deficiency-Compensation. Y. Xu[1], *Q. Gao*[1], X. Lu[1] and L. He[1] *1. York-Nanjing Joint Center, Nanjing University, Nanjing, China*

The current density required for current induced magnetization switching in magnetic devices such as Magnetoresistive Random Access Memory (MRAM) is proportional to Gilbert damping constant. The lower damping would enable more energy-efficient excitations and thus less current needed. The Gilbert damping constant of the Co_2FeAl film, a half-metal material important for spintronics with its 100% spin polarization at Fermi level, has shown the lowest Gilbert damping constant among the Heusler alloys. However, the increased Gilbert damping constant in ultra-thin Co_2FeAl films is undesirable for low power consumption applications such as STT-MRAM. Being able to manipulate the Gilbert damping on demand is crucial for spintronic device engineering and optimization. Here, we report that the Gilbert damping of ultra-thin Co_2FeAl_{1+x} films of nanometer thicknesses can be effectively tuned by delicately controlling the stoichiometric ratio during the growth. The Gilbert damping has been found to be the lowest of 0.065 in $Co_2FeAl_{1+0.1}$, which is deduced by ~50% compared to that in Co_2FeAl. We have further found that the damping constant of the ultra-thin $Co_2FeAl_{1+0.1}$ film is restored to the value of 0.062 of the nominal stoichiometric Co_2FeAl by compensating the Al composition-deficiency- as supported by the 10.37% of composition change from the scanning transmission electron microscope energy-dispersive-spectroscopy. This work offers a unique path to manipulate the Gilbert damping constant in ultra-thin Co_2FeAl films by Al concentration control.

E1-05. Prediction of Structural, Electronic and Magnetic Properties of Full Heusler Alloys Ir_2YSi (Y= Sc, Ti, v, Cr, Mn, Fe, Co & Ni) via First -Principles Calculation. *R. Prakash*[1] and G. Kalpana[1] *1. Physics, Anna University Chennai, Chennai, India*

First principles electronic structural calculation of full Heusler [1] alloys Ir_2YSi (Y= Sc to Ni) in the $L2_1$ and X_a structures have been studied using full-potential linearized augmented plane wave method as implemented in WIEN2k code [2]. From the total energy calculations, it has been observed that all these alloys are stable in $L2_1$ than X_a structure and also it is found that the alloys Ir_2YSi (Y =V to Co) are ferromagnetically stable whereas the other alloys are non-magnetic in their stable $L2_1$ structure. From spin polarized band structure calculations it is observed that in Ir_2YSi (Y= V to Co) alloys that there is spin splitting of energy states around the Fermi level (E_F) and moreover in Ir_2YSi (Y= V, Cr & Mn) alloys majority electrons have metallic behavior while minority electrons have semiconducting nature exhibiting half metallic ferromagnetism (HMF) nature. HMF [3] property of the alloys Ir_2YSi (Y= V, Cr & Mn) have been confirmed from the integer value of total magnetic moment of 3.0 μ_B, 4.0 μ_B and 5.0 μ_B per formula unit and this is also agreement with earlier results on Ir_2MnSi [4]. Spin polarization mainly arises from the interaction between 3*d* electrons of V/ Cr/ Mn atom and 5*d* electrons Ir atom. This strong d-d hybridization between the transition atoms like Ir and V/Cr/Mn composing Heusler alloys is essential for the formation of the gap at the E_F between the valence and conduction bands. Our results show that Ir_2YSi (Y= V, Cr & Mn) will be suitable for ferromagnetic and spintronics applications [5].

1. F. Heusler, W. Starck, E. Haupt, Verh DPG 5 (1903) 2. P. Blaha, KSchwartz, wien2k users guide. Vienna University of technology, Vienna (2013) 3. De Groot, R.A. Mueller, F.M., New Class of Materials: Half-metallic Ferromagnets. Phys. Rev. Lett. 1983, 50, 2024. 4. E.G. Ozdemir, E. Eser, Investigation of Structural, Half-Metallic and Elastic Properties of a New full-Heusler Compound - Ir2MnSi, Chinese Journal of Physics (2018). 5. Zutic, I, Fabian, J. Sama, SD: Spintronics fundamentals and applications. Rev.Mod.Phys.76 323-410(2004)

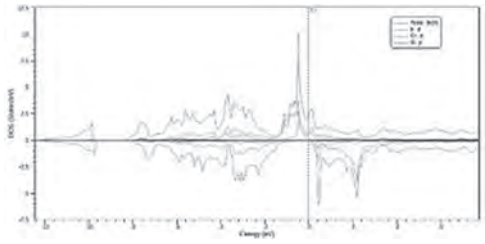

Fig 1. Total density of states of Ir_2CrSi alloy

E1-06. Interplay Between Mn, Fe, and Co in the Co_2FeGe Alloy to Design Novel Singe-Phase Compounds With Potential Spintronic Application. *S. KC*[1], R. Mahat[1], S. Budhathoki[1], J. Law[2], V. Franco[2], W.H. Butler[1], A. Gupta[3] and P. LeClair[1] *1. Physics and Astronomy, The University of Alabama, Tuscaloosa, AL, United States; 2. Departmento de Fisica de la Materia Condensada ICMSE-CSIC, Universidad de Sevilla, Sevilla, Spain; 3. Department of Chemistry and Biochemistry, The University of Alabama, Tuscaloosa, AL, United States*

While the half-metallic Heusler alloys are considered ideal materials to be used in magnetic tunnel junctions, spin-filters, and spin valves, the search for new candidate half-metal remains an active field of research [1]. One of the ways of rational material design is by doping, which is useful not only to tailor the electric and magnetic properties but also to stabilize a single-phase compound [2, 3]. In this work, we show how the introduction of Mn helps to stabilize a single-phase compound and to tune half-metallic character in the Co_2FeGe alloy, which otherwise is a multi-phased normal ferromagnet. We have investigated three substitutional series viz; $(Co_{2-\alpha}Mn_\alpha)FeGe$, $(Co_{2-\alpha}Fe_\alpha)MnGe$, $Co_2(Fe_\alpha Mn_{1-\alpha})Ge$, that can be generated from the intermixing of Mn, Fe, and Co by keeping the Ge content constant in the Co_2FeGe alloy. These series cover all possible site doping that can be made for a magnetic atom in a full Heusler alloy and allow us to directly compare their magnetic and electric properties. First principles calculations performed using the generalized gradient approximation (GGA) predict that a half-metal is obtained in $Co_2(Fe_\alpha Mn_{1-\alpha})Ge$ series while the other two series generate "near half-metallic" alloys. The experimental investigation of bulk samples of the $(Co_{2-\alpha}Mn_\alpha)FeGe$ series shows that a single-phase compound can be achieved up to $\alpha = 1.25$. For all the single-phase compounds, the magnetic moment agrees reasonably well with the Slater-Pauling moment and a very high Curie temperature (~ 1000 K) is measured for low α. The experimental investigation of other series is currently underway; however, the preliminary results show that these series also generate single-phase compounds. Hence by doping Mn, Fe, and Co for one another, many single-phase compounds can be designed from Co_2FeGe, with potential half-metallic behavior that can have actual use in spintronic devices

1. Z. Bai, L. Shen, G. Han, Spin, Vol. 02, No. 04, 1230006 (2012) 2. R. Umetsu, K. Kobayashi, A. Fujita, Phys. Rev. B, 72, 214412 (2005) 3. S. KC, R. Mahat, S. Regmi, Phys. Rev. Materials, 03, 114406 (2019)

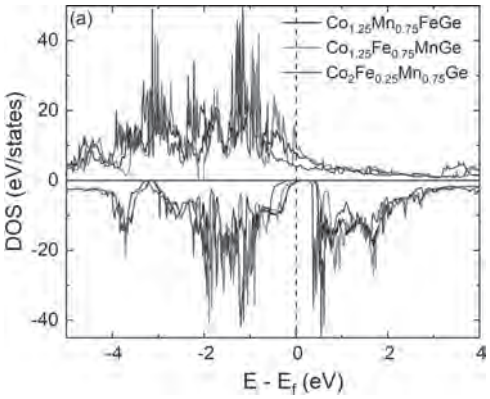

(a) Density of states plot for α = 0.75.

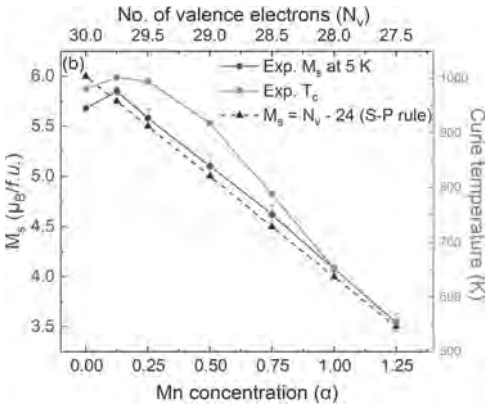

(b) Magnetic moment and Curie temperature variation with Mn concentration in $(Co_{2-\alpha}Mn_{\alpha})FeGe$ series.

INVITED PAPER

E1-07. Direct Light–Induced Spin Transfer Between Different Elements in a Spintronic Heusler Material via Femtosecond Laser Excitation. *P.M. Tengdin*[2,1], C. Gentry[2], D. Zusin[2], M. Gerrity[2], L. Hellbrück[3], M. Hofherr[3], J. M. Shaw[4], Y. Kvashnin[5], E.K. Delczeg-Czirjak[5], H. Nembach[4], T. Silva[4], S. Mathias[3], M. Aeschlimann[3], H. Kapteyn[2], D. Thonig[5], K. Kompouras[5], O. Eriksson[5] and M. Murnane[2] *1. Ecole Polytechnique Federale de Lausanne, Lausanne, Switzerland; 2. University of Colorado Boulder, Boulder, CO, United States; 3. Research Center OPTIMAS, University of Kaiserslautern, Kaiserslautern, Germany; 4. Quantum Electromagnetics Division, National Institute of Standards and Technology, Boulder, CO, United States; 5. Uppsala Universitet, Uppsala, Sweden*

Heusler compounds are exciting materials for future spintronics applications because they display a wide range of tunable electronic and magnetic interactions. Here, we use a femtosecond laser to directly transfer spin polarization from one element to another in a half-metallic Heusler material, Co_2MnGe. This spin transfer initiates as soon as light is incident on the material, demonstrating spatial transfer of angular momentum between neighboring atomic sites on time scales < 10 fs. Using ultrafast high harmonic pulses to simultaneously and independently probe the magnetic state of two elements during laser excitation, we find that the magnetization of Co is enhanced, while that of Mn rapidly quenches. Density functional theory calculations show that the optical excitation directly transfers spin from one magnetic sublattice to another through preferred spin-polarized excitation pathways. This direct manipulation of spins via light provides a path toward spintronic devices that can operate on few-femtosecond or faster time scales.

CONTRIBUTED PAPERS

E1-08. Probing Dynamic Magnetization in Ferrimagnetic Sr_2FeMoO_6 With a Lock-in Broadband Spectrometer. R. Das[1], U. Chaudhuri[1] and *R. Mahendiran*[1] *1. Physics, National University of Singapore, Singapore*

Sr_2FeMoO_6 is a ferrimagnetic double perovskite with a Curie temperature of 420 K. It received a lot of attention due to tunneling magnetoresistance exhibited in the polycrystalline form [1]. The Curie temperature and saturation magnetization of this sample are sensitive to oxygen stoichiometry, antisite defects, and grain size [2]. While static magnetization of samples prepared by different methods has been extensively reported, there is a lack of investigation on dynamic magnetic properties[3] over a broad frequency range. This work reports ferromagnetic resonance (FMR) properties of double perovskite, Sr_2FeMoO_6 synthesized via sol-gel technique in an inert atmosphere of H_2/Ar gas. The nanostructured Sr_2FeMoO_6 exhibits ferromagnetic Curie temperature of 325K and low-field magnetoresistance of ~ 12% at 10K. Microwave absorption at room temperature was investigated in the frequency range of 2–15 GHz using the lock-in broadband ferromagnetic resonance technique in a field up to 1500 Oe. In the magnetic field sweep mode, the field-derivative of microwave power absorption (*dP/dH*) exhibits a peak and a dip feature at a critical field H_{res}, which we attribute to the occurrence of ferromagnetic resonance. With increasing microwave frequency, the resonance field H_{res} and linewidth (ΔH) increase. The intensity of the *dP/dH* spectra is a single Lorentzian type. H_{res}, ΔH *was* estimated from the fitting of the spectra to a linear combination of symmetric and antisymmetric Lorentzian function. $f_{res}(H_{dc})$ curve fitted with the Kittel's expression for in-plane FMR, corresponds to a *g* factor of 2.02 in the sample. Gilbert damping parameter is estimated and compared with other ferrimagnetic conducting oxides. R.M. acknowledges the Ministry of Education, Singapore for supporting this work through Grant no. R144-0004-404-114 and R144-000-381-112.

[1] K. Kobayashi et al., *Nature* 395, 6703 (1998); D. Serrate et al., *J. Phys. Condens. Matter*. 19, 023201 (2007). [2]M. García-Hernández *et al*., *Phys. Rev. Lett.* 86, 2443 (2001); J. L. Alonso *et al. Phys. Rev. B.* 67, 214423 (2003). [3] A.G. Flores *et al*., *J. Appl. Phys.* 93, 8068 (2003); T. Nosach., *J. Appl. Phys.* 103, 07E311 (2008).

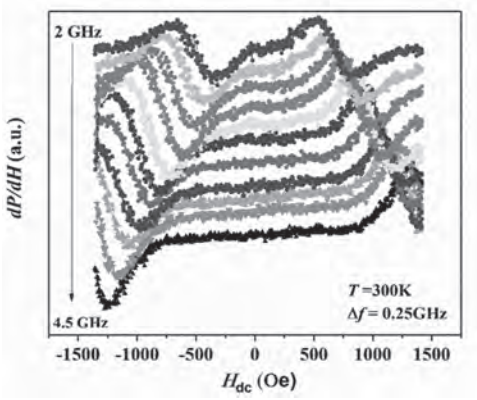

FIG 1: Room temperature magnetic resonance spectra in Sr_2FeMoO_6 as a function of dc magnetic field for different frequencies of microwave excitation (*f* = 2-4.55 GHz).

E1-09. Creating Half-Metallicity in two-Dimensional Magnetoelectric Materials. *C. Gong*[1], S. Gong[2,3], A. Rappe[4] and X. Zhang[5,6] *1. University of Maryland, College Park, College Park, MD, United States; 2. East China Normal University, Shanghai, China; 3. Fudan University, Shanghai, China; 4. University of Pennsylvania, Philadelphia, PA, United States; 5. University of California, Berkeley, Berkeley, CA, United States; 6. University of Hong Kong, Hong Kong, China*

Magnetic two-dimensional (2D) materials [1, 2] opened unprecedented opportunities for nanoscale spintronic devices in miniaturized form factor. With the aggressive pursuit for dimensional scaling is another paramount endeavor, persistently ongoing for high power efficiency [3]. Under this energy consumption umbrella, high spin polarization is one critical prerequisite. In this talk, I will introduce two schemes [4, 5] to create half-metallicity in layered material systems. In scheme I [4], electric field will be applied across the bilayer A-type antiferromagnetic 2D materials. By electrostatically changing the relative energy levels of the two spin-polarized bands in the two layers, one spin-polarized band from both layers will be merged whereas the other spin-polarized band will be opened with a gap, leading to half-metallicity (i.e., 100% spin polarized conductive electrons). In scheme II [5], a multiferroic superlattice consisting of alternative ferroelectrics and A-type antiferromagnets is constructed. In ferroelectric phase, the two interfaces on the opposite sides of the ferroelectric layer will be made half metallic, with 2D electron gas and 2D hole gas of the same pure spin polarization created at the alternative interfaces. With the opposite ferroelectric polarization, the half metallicity of the opposite spin polarization will be produced, leading to ferroelectric switching of the interfacial half metallicity. Both schemes are generic and experimentally practical, and will provide valuable contributions to the developments of miniaturized, high-efficiency spintronics.

[1] C. Gong *et al.*, Discovery of intrinsic ferromagnetism in two-dimensional van der Waals crystals, Nature 546, 265-269 (2017). [2] C. Gong, X. Zhang, Two-dimensional magnetic crystals and emergent heterostructure devices, Science 363, eaav4450 (2019). [3] C. Gong *et al.*, Multiferroicity in atomic van der Waals heterostructures, Nat. Commun. 10, 2657 (2019). [4] S.-J. Gong, *et al.*, Electrically induced 2D half-metallic antiferromagnets and spin field effect transistors, Proc. Natl. Acad. Sci. 115, 8511-8516 (2018). [5] E.-W. Du, *et al.*, Ferroelectric switching of pure spin polarization in two-dimensional electron gas, (2020, unpublished).

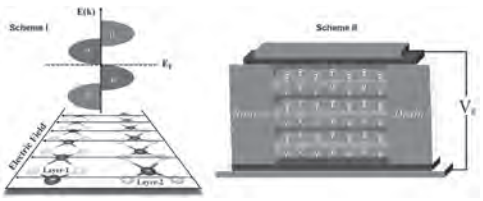

Figure 1. Two schemes to create half metallicity in layered materials systems. Scheme I is based on bilayer A-type antiferromagnetic 2D materials [4]. Scheme II is based on multiferroic superlattices consisting of alternative ferroelectrics and A-type antiferromagets [5].

E1-10. Anomalous Nernst Effect in Co_2MnSi Thin Films. *C. Cox*[1], A. Caruana[2], m. cropper[1] and K. Morrison[1] *1. Physics, Loughborough University, Loughborough, United Kingdom; 2. ISIS Neutron and Muon Source, Didcot, United Kingdom*

The Anomalous Nernst Effect (ANE) is defined as the generation of a transverse electric current (J_e) when an in plane magnetised material is subjected to an out of plane temperature gradient (ΔT) (Figure 1). Over recent years a vast number of materials have been shown to exhibit an ANE response to a temperature gradient. From thin films to bulk single crystals, dilute magnetic semiconductors to topological insulators, the landscape has been reenergised by the enhancement of the ANE, intrinsically derived from the exotic band structures of materials which exhibit Weyl-like transport phenomena [1,2]. The family of Heusler alloys contain proposed (and confirmed) magnetic Weyl semimetals most notably Co_2MnGa. However, another Heusler which is of interest, particularly in the magnetic recording field is Co_2MnSi, identified for its 100% spin polarisation[3] and high magnetisation and Curie temperature. We present a series of Co_2MnSi thin films where there is dependence of the lattice ordering upon annealing temperature (T_{Ann}) (Figure 2)[4]. We show that polycrystalline thin films of Co_2MnSi exhibit ANE of the order of $S = 0.114\ \mu VK^{-1}$ for a fully ordered $L2_1$ phase and $S = 0.662\ \mu VK^{-1}$ for a disordered A2 phase. A similar trend with the disorder is seen in the anomalous Hall resistivity (which is expected to scale with the ANE). Whilst Co_2MnSi in the $L2_1$ phase does not exhibit any form of non-trivial band structure (and hence the low ANE), the increase in the ANE and AHE counter to the decrease in magnetisation with increasing disorder is suggestive of an intrinsic difference in the band structures between the two phases.

[1] H. Reichlova, R. Schlitz, S. Beckert et. al., Appl. Phys. Lett. 113, (2018). [2] S.N. Guin, P. Vir, Y. Zhang et. al., Adv. Mater. 1806622, 1806622 (2019). [3] M. Jourdan, J. Minár, J. Braun et. al., Nat. Commun. 5, 3974 (2014). [4] C.D.W. Cox, A.J. Caruana, M.D. Cropper et. al., J. Phys. D. Appl. Phys. 53, 035005 (2020).

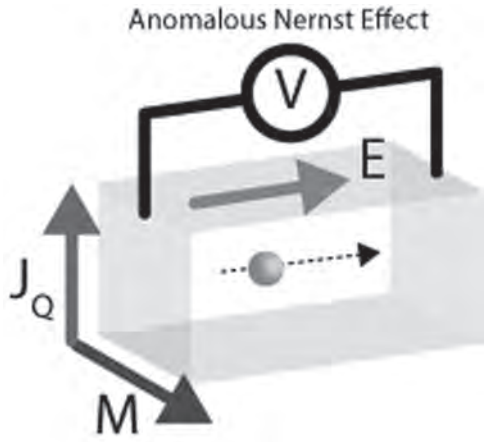

Fig.1 Anomalous Nernst Effect.

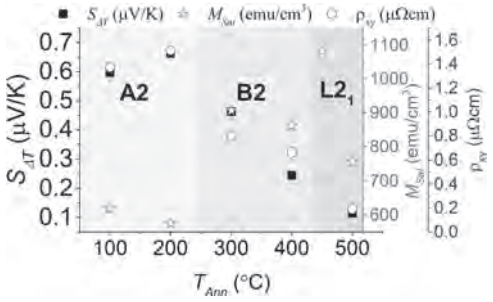

Fig.2 Dependence of ANE ($S_{\Delta T}$), magnetisation (M_{Sat}) and Anomalous Hall resistivity (ρ_{xy}) on the ordering of Co_2MnSi thin films.

E1-11. Scaling of Quadratic and Linear Magneto-Optic Kerr Effect Spectra With $L2_1$ Ordering of Co_2MnSi Heusler Compound. *R. Silber*[2,1], D. Král[3], O. Stejskal[3], T. Kubota[4], Y. Ando[6], J. Pištora[2,1], M. Veis[3], J. Hamrle[3] and T. Kuschel[5] *1. IT4Innovations, VSB-Technical University of Ostrava, Ostrava, Czechia; 2. Nanotechnology Centre, VSB-Technical University of Ostrava, Ostrava, Czechia; 3. Faculty of Mathematics and Physics, Charles University, Praha, Czechia; 4. Institute for Materials Research, Tohoku University, Sendai, Japan; 5. Center for Spinelectronic Materials and Devices, Department of Physics, Bielefeld University, Bielefeld, Germany; 6. Department of Applied Physics, Tohoku University, Sendai, Japan*

The Heusler compound Co_2MnSi provides a crystallographic transition from B2 to $L2_1$ structure with increasing annealing temperature T_a [1-3], being a model system for investigating the influence of crystallographic ordering

on structural, magnetic, optic, and magnetooptic (MO) properties. Here, we present quadratic magnetooptic Kerr effect (QMOKE) spectra [4] depending on M^2 in addition to the linear magnetooptic Kerr effect (LinMOKE) spectra being proportional to M, both in the extended visible spectral range of light from 0.8 eV to 5.5 eV. We investigated a set of Co_2MnSi thin films deposited on MgO(001) substrates and annealed from 300°C to 500°C. The amplitude of LinMOKE and QMOKE spectra scales linearly with T_a, and this effect is well pronounced at the resonant peaks below 2.0 eV of the QMOKE spectra. Furthermore, the spectra of the MO parameters, which fully describe the MO response of Co_2MnSi up to the second order in M, are obtained dependend on T_a. Finally, the spectra are compared to ab-initio calculations of a purely $L2_1$ ordered Co_2MnSi Heusler compound [5].

[1] O. Gaier, J. Hamrle, Y. Ando, J. Appl. Phys. 103, 103910 (2008). [2] S. Trudel, O. Gaier, B. Hillebrands, J. Phys. D 43, 193001 (2010). [3] G. Wolf, J. Hamrle B. Hillebrands, J. Appl. Phys. 110, 043904 (2011). [4] R. Silber, T. Kuschel, J. Hamrle, Phys. Rev. B 100, 064403 (2019). [5] R. Silber, J. Hamrle, T. Kuschel, Appl. Phys. Lett. 116, 262401 (2020);

E1-12. Giant Enhancement of Perpendicular Magnetic Anisotropy and Induced Quantum Anomalous Hall Effect in the Graphene/ NiI_2 Heterostructure via Tuning the van der Waals Interlayer Distance. *Q. Cui*[1,2], J. liang[1] and H. Yang[1] *1. Ningbo Institute of Materials Technology and Engineering, Ningbo, China; 2. University of Nottingham Ningbo China, Ningbo, China*

Using first-principles calculations, we demonstrated that the perpendicular magnetic anisotropy (PMA) of NiI_2 monolayer can be effectively enhanced by decreasing interlayer distance of graphene/NiI_2 (Gr/NiI_2) heterostructure. Furthermore, by analyzing atomic-resolved magnetocrystalline anisotropy energy (MAE), orbital-hybridization-resolved MAE and density of states, we clarify that the magnetic anisotropy enhancement originates from the electronic states of interfacial I atoms. At the same time, the NiI_2 substrate induces magnetic proximity effects on graphene, which can lead to the quantum anomalous hall effect (QAHE). Our findings demonstrate the enhancement of PMA via tuning interlayer distance of vdW heterostructure and provides a possible vdW system for realizing QAHE.

Q. Cui, J. Liang, B. Yang, Z. Wang, P. Li, P. Cui, and H. Yang, Phys. Rev. B 101, 214439 (2020)

E1-13. Co_2Mn-Based Heusler Compounds in Thin Films for Spintronic Applications. C. Guillemard[1,2], S. Petit-Watelot[1], P. Le Fevre[2], F. Bertran[2] and *S. Andrieu*[1] *1. institut jean lamour, universite de lorraine, Nancy, France; 2. synchrotron SOLEIL, Gif-sur-Yvette, France*

Heusler magnetic alloys offer a wide variety of electronic properties very promising for spintronics. Some alloys in particular exhibit a spin gap in their band structure at the Fermi energy, the so-called Half-Metal Magnetic behavior. This particular property leads to two very interesting properties for spintronics, i.e. the possibility to get fully polarized current together with ultra-low magnetic damping, two key-points for spin-torque based devices. We focus here on the electronic properties of Co_2MnZ compounds with Z=Al, Si, Ga, Ge, Sn, Sb grown as thin film by using Molecular Beam Epitaxy [1,2]. We will first show how to control the stoichiometry as best as possible, and some methods are presented to test it. The chemical ordering within the lattice was examined by using electron diffraction during growth, regular x-ray diffraction and scanning transmission electron microscopy. The electronic properties like magnetic moments spin polarization and magnetic damping were reviewed and discussed according to the quality of the films and also theoretical predictions. Polycrystalline films were also analyzed and we show that the peculiar HMM properties are not destroyed, a good news for applications [3]. A clear correlation between the spin polarization at Fermi energy and the magnetic damping is experimentally demonstrated. At least, our study highlights the major role of stoichiometry on the expected properties. Finally some issues are given for preparing the best material as possible to fully use the remarkable properties of these Heusler compounds in spintronic devices.

[1] S. Andrieu *et al*, Phys. Rev. B 93, 094417 (2016) [2] C. Guillemard *et al*, Phys. Rev. Appl. 11, 064009 (2019) [3] C. Guillemard *et al*, Appl. Phys. Lett. 115, 172401 (2019

Session E2
NANOPARTICLE AND NANOWIRE ARRAYS AND SELF-ASSEMBLY

Dedalo Sanz-Hernandez, Chair
Unité Mixte de Physique CNRS/Thales, Palaiseau, France

INVITED PAPER

E2-01. Multi-Shaped Individual Nanoparticles Investigated by NanoSQUID Magnetometry at Variable Temperature. *M. Martinez-Perez*[1,2], J. Pablo Navarro[1], B. Mueller[3,4], J. Lin[3,4], R. Kleiner[3,4], C. Magen[1], J. de Teresa[1], J. Sese[1] and D. Koelle[3,4] *1. ICMA, CSIC - Universidad de Zaragoza, Zaragoza, Spain; 2. ARAID foundation, Zaragoza, Spain; 3. Physikalisches Institut, Universität Tübingen, Tübingen, Germany; 4. LISA+, Universität Tübingen, Tübingen, Germany*

Performing magnetization studies on individual nanoparticles is a highly demanding task, especially when measurements need to be carried out under large sweeping magnetic fields or variable temperature. Yet, characterization under varying ambient conditions is paramount in order to fully understand the magnetic behavior of these objects, e.g., the formation of non-uniform states, the mechanisms leading to magnetization reversal, thermal stability or damping processes. This, in turn, is necessary for the integration of magnetic nanoparticles and nanowires into useful devices, e.g., spin-valves, racetrack memories or magnetic tip probes. Here we show that $YBa_2Cu_3O_7$ nano Superconducting QUantum Interference Devices (YBCO nanoSQUIDs, see Fig.) are particularly well suited for this task. We have successfully characterized a number of individual nanoparticles of soft magnetic materials with different shapes (nanodots, nanodiscs and nanowires, see Figure). Samples are transported to the surface of the sensor with nanometric resolution, achieving sufficiently strong particle-SQUID coupling. Magnetization measurements (see Figure) performed under sweeping magnetic fields (up to ~ 500 mT) and variable temperature (1.4 - 80 K) underscore the intrinsic differences between samples owing to their shape and the presence (or absence) of magnetocrystalline anisotropy. Our measurements also allow us to distinguish the mechanisms leading to magnetization reversal mediated by, i.e., nucleation/propagation of domain walls or nucleation/annihilation of magnetic vortices. These studies serve to shed light on the nature and magnitude of the energy barriers separating different magnetic states, nucleation/annihilation fields and switching times.

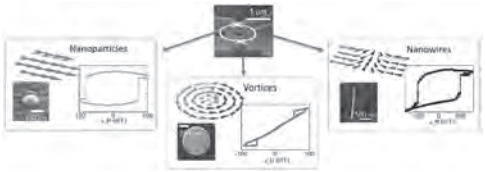

CONTRIBUTED PAPERS

E2-02. Spin Ordering in Bi-Magnetic (Core / Shell) Nanoparticles With Varying Anisotropy. *C. Kons*[1], K.L. Krycka[2], J.A. Borchers[2], N. Ntallis[3], M. Pereiro[3], E. Sjöqvist[3], A. Delin[4], D. Thonig[5], O. Eriksson[3], A. Bergman[3], J. Robles[1], M. Phan[1], H. Srikanth[1] and D.A. Arena[1] *1. Univ. of South Florida, Tampa, FL, United States; 2. National Institute of Standards and Technology, Gaithersburg, MD, United States; 3. Uppsala University, Uppsala, Sweden; 4. KTH Royal Institute of Technology, Stockholm, Sweden; 5. Örebro Universitet, Orebro, Sweden*

Chemically-synthesized magnetic nanoparticles (MNPs) consisting of different combinations of spinel ferrites (γ-Fe_2O_3, Fe_3O_4, $MnFe_2O_4$, $CoFe_2O_4$) provide a platform for developing ensembles of nanostructures whose magnetic properties are distinct from their bulk counterparts. We report on studies of MNPs composed of high-anisotropy $CoFe_2O_4$ combined with relatively high-moment, low anisotropy Fe_3O_4. We examined two variations of MNPs: a $CoFe_2O_4$ core with a Fe_3O_4 shell and the inverted structure (Fe_3O_4 core / $CoFe_2O_4$ shell). Both variants had a core diameter of 3-3.5 nm and an overall diameter of ~10 nm and we investigated their properties using magnetometry, small-angle neutron scattering (SANS), and Monte Carlo simulations. The magnetometry indicates that both MNP variants are superparamagnetic at room temperature with a considerable coercivity enhancement below the blocking temperature (~250 K) accompanied by a multi-step path towards magnetization reversal (Fig 1-b). Fully spin-polarized SANS measurements show that magnetic order perpendicular to the applied field direction is strong at remanence; this spin configuration is quenched upon application of a small field (Fig. 1-a). Spin alignment parallel to the field develops at higher fields. Monte Carlo simulations indicate that the emergence of dipolar-coupled long range order may be associated with the steps observed in the field hysteresis loops. Modelling of the SANS distributions, informed by the Monte Carlo simulations, to investigate the spin alignment in the core and shell, as demonstrated for metallic Fe core / Fe oxide shell MNPs [1], for both MNP variants is currently underway. The results demonstrate the value of combining modeling of fully-spin polarized SANS data with numerical simulations of ensembles of macrospins to illuminate the complex spin ordering across a range of length scales. The authors acknowledge the support of Univ. of South Florida Nexus Initiative (UNI) Award, US Department of Energy, Office of Basic Energy Sciences (Award DE-FG02-07ER46438) and the Knut and Alice Wallenberg Foundation (Grant 2018.0060). Access to spin filters on NG-7 SANS was provided by CHRNS, a partnership between NIST and the NSF (No. DMR-1508249).

[1] C. Kons, D. A. Arena, *et al.*, "Investigating spin coupling across a three-dimensional interface in core/shell magnetic nanoparticles," *Phys. Rev. Mater.*, 4 034408 (2020).

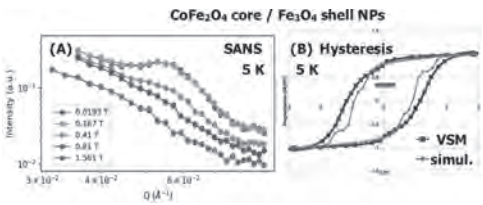

Fig. 1

E2-03. Quantitative Understanding of Superparamagnetism in Ni Nanoparticle Assemblies. *B. Das*[1], J. Batley[1], C. Korostynski[1], M. Nguyen[1], I. Kamboj[1], E.S. Aydil[1,2] and C. Leighton[1] *1. Chemical Engineering and Materials Science, University of Minnesota, Minneapolis, MN, United States; 2. Department of Chemical and Bimolecular Engineering, New York University Tandon School of Engineering, Brooklyn, NY, United States*

Thanks to advances in synthesis that enable control over size, structure, and properties, magnetic nanoparticles (NPs) present opportunities in data storage, cancer treatment, biomedical imaging, *etc.* While superparamagnetism (SP) dominates the properties of magnetic NPs, *quantitative* understanding of SP blocking in NP assemblies remains elusive. We address this here *via* comprehensive magnetic characterization and analysis of soft ferromagnetic Ni NP ensembles. NPs were synthesized by hot injection of a Ni-oleylamine (OAm) complex into trioctylphosphine (TOP), with size control achieved *via* TOP:OAm ratio, reaction time, and differential centrifugation.[1] X-ray diffraction, transmission electron microscopy (TEM), and various spectroscopies reveal polycrystalline/twinned FCC Ni NPs with mean diameters $\langle D \rangle$ from 4 to 22 nm, dispersity down to 10%, and TOP/OAm ligands.[1] SP blocking temperatures (T_B) are carefully determined, quantitatively accounting for the substantial yet frequently ignored effects of dispersity, yielding mean T_B ($\langle T_B \rangle$) from 5 to 300 K.[1] *Quantitative* understanding of the size-dependent $\langle T_B \rangle$ is achieved (Fig. 1), *with no adjustable parameters*, but only by accounting for the size distribution, effective ferromagnetic volume (V_{mag}), temperature-dependent magnetocrystalline anisotropy (MCA), and average shape anisotropy due to random deviations from spherical.[1] The reduced saturation magnetization (M_s) and V_{mag} deduced from magnetometry were investigated by small-angle neutron scattering (SANS) (Fig. 2) and high-resolution TEM, evidencing a thin Ni-P shell arising from reactions with TOP. We thus achieve fully quantitative understanding of SP blocking in model NP assemblies. Work supported by 3M and DOE Center for Quantum Materials.

[1] J.T. Batley, M. Nguyen, I. Kamboj, C. Korostynski, E.S. Aydil and C. Leighton, submitted (2020).

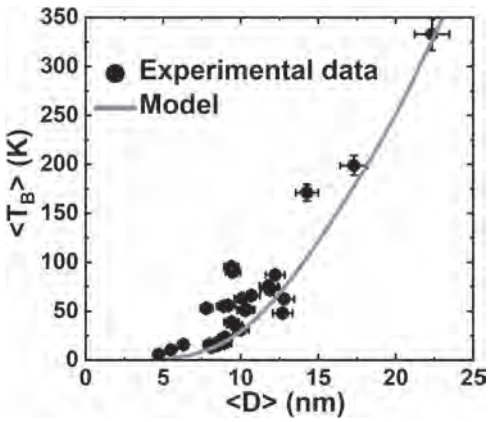

Figure 1. Points are experimental data and the green line is a parameter-free model considering *T*-dependent MCA, V_{mag}, and shape anisotropy due to random deviations from spherical.

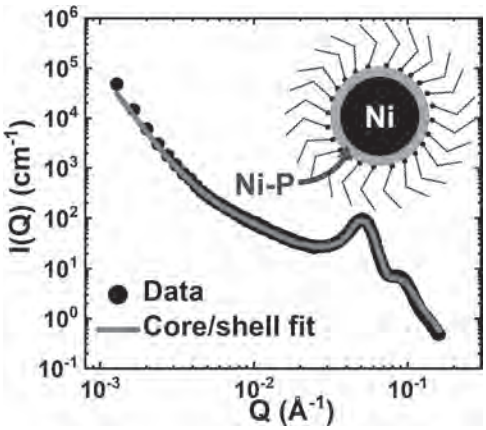

Figure 2. Points show intensity *vs*. scattering vector for unpolarized SANS from a Ni NP assembly with TEM $\langle D \rangle$ = 11.5 nm. The red line is a fit to a core-shell model (see inset) yielding a Ni core with radius 5.2 nm and a 1.4 nm Ni-P shell.

E2-04. Magnetic Correlations and Time Fluctuations in Assemblies of Fe_3O_4 Nanoparticles. *K. Chesnel*[1], J. Rackham[1], D. McPhearson[1], B. Newbold[1], D. Griner[1], M. Transtrum[1], R. Harrison[1], A. Reid[2] and J. Kortright[3] *1. Brigham Young University, Provo, UT, United States; 2. SLAC, SIMES, Menlo Park, CA, United States; 3. E O Lawrence Berkeley National Laboratory, Berkeley, CA, United States*

Magnetic nanoparticles are increasingly used in biomedical applications such as drug-delivery, gene delivery, hyperthermia, or contrast agents for MRI. Magnetite (Fe3O4) nanoparticles are good candidates for these applications due to their non-toxicity and long-life in the bloodstream. While the structural and magnetic properties of bulk Fe3O4 has been widely studied [1], knowledge is still lacking regarding the magnetic behaviour of collections of Fe3O4 nanoparticles. In particular, when the particles are small and the assembly is superparamagnetic, it is useful to understand the nature of the magnetic correlations within the assemblies. Here we show how inter-particle magnetic correlations can be probed at the nanoscale via x-ray resonant magnetic scattering (XRMS) [2] as illustrated in Figure 1. By tuning the energy of the x-rays to resonant edges of Fe and comparing opposite polarization helicities, we extract information about the local inter-particle magnetic orders within the nanoparticle assemblies. We show the dependence on particle size, varying from 5 to 11 nm, suggesting an enhancement of magnetic couplings for bigger particles. [3] Additionally, we show a model based on chains of nanoparticles, which we use to fit the XRMS data. The data fitting suggests the occurrence of ferromagnetic ordering when an external magnetic field is applied, but when the external field is brought to zero (remanence), the fit suggest a mix of antiferromagnetic ordering and randomness. [4]

[1] Verwey, *Nature* 144, 327 (1939); Fleet, *Acta Cryst. B* 37, 919-929 (1981) [2] Kortright *et al.*, *Phys. Rev. B* 71, 012402 (2005) [3] Chesnel *et al.*, *Magnetochemistry* 4, 42-58 (2018) [4] J. Rackham et al, AIP Advances 9, 035033 (2019)

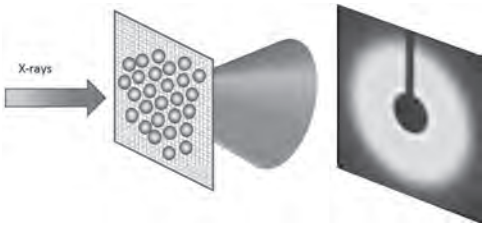

Figure 1: Layout for the x-ray resonant magnetic scattering (XRMS) measurement of a nanoparticle assembly

E2-05. Modeling Magnetic Correlations in Magnetite Nanoparticle Assemblies Using x-ray Magnetic Scattering Data. *J. Rackham*[1], B. Newbold[1], S. Kotter[1], D. Smith[1], D. Griner[1], A. Reid[3], R. Harrison[2], M. Transtrum[1] and K. Chesnel[1] *1. Physics and Astronomy, Brigham Young University, Provo, UT, United States; 2. Chemistry and Biochemistry, Brigham Young University, Provo, UT, United States; 3. SIMES, SLAC National Accelerator Laboratory, Menlo Park, CA, United States*

Magnetic nanoparticles are increasingly used in nanotechnologies and biomedical applications, such as drug targeting, MRI, bio-separation [1-3]. Magnetite (Fe_3O_4) nanoparticles stand to be effective in these roles due to the non-toxic nature of magnetite and its ease of manufacture [4]. To be more effective in these applications, a greater understanding of the magnetic behavior of the individual magnetite nanoparticles is needed when a collection of them is used. This research seeks to discover the local magnetic ordering of ensembles of magnetite nanoparticles occurring at various stages of the magnetization process at temperatures above and below their blocking temperature and at various particle sizes [5]. To complete this study, we use x-ray circular dichroism [6] and x-ray resonant magnetic scattering (XRMS) [7], which provides information about the magnetic orders in the material. Here we discuss the modeling of the magnetic scattering data using a one-dimensional chain of nanoparticles in real space and an empirical gaussian packet model in q-space [8]. By fitting the models to the experimental data, we extract information about the magnetic correlations in the nanoparticle assembly.

[1] Frey N.A.; Peng S.; Cheng K.; Sun S. Chem. Soc. Rev. 38, 2532-2542 (2009) [2] S. Mornet et al., J. Mater. Chem. 14, 2161 (2004) [3] E. Duguet et al., Nanomedicine 1(2), 157 (2006) [4] A. Ito et al., J. Biosci. Bioeng. 100, 1 (2005) [5] K. Chesnel et al, Journal of Physics: Conference Series, Volume 521, 8th International Conference on Fine Particle Magnetism (ICFPM2013) 24–27 June 2013, Perpignan, France [6] Y. P. Cai et al, J. Appl. Phys. 115 (17), 17B537 (2014) [7] K. Chesnel, et al., Magnetochemistry 4 (4), 42 (2018) [8] J. Rackham et al, AIP Advances 9, 035033 (2019)

E2-06. Berry Curvature and Topological Hall Effect in Quasi-Coherent Nanoparticles. *A. Ullah*[1], B. Balasubramanian[1], R. Pahari[1], D.J. Sellmyer[1] and R. Skomski[1] *1. Physics and Astronomy, University of Nebraska-Lincoln, Lincoln, NE, United States*

Magnetization states in conducting nanostructures have attracted renewed attention because they give rise to a Berry phase and to an anomalous Hall contribution commonly known as topological Hall effect (THE). The effect requires spin configurations that are not only noncollinear but also noncoplanar, while spins in small spherical Stoner-Wohlfarth particles are parallel and the THE is therefore zero. However, metallic nanoparticles are never perfectly spherical, which creates magnetization inhomogeneities. Examples are stray-field effects near corners and edges, such as the flower state in cubes [1] and the spin configuration shown in Fig. 1(a). When the particles form in conducting thin films or granular nanostructures, then these inhomogeneities yield skyrmionic magnetization features [2] and THE contributions [3]. Our focus is on nanoparticles whose radius R is smaller than the coherence radius R_{coh} above which a reverse magnetic field causes magnetization curling. We estimate the Berry curvature Φ by considering the triple product $M_1.(M_2 \times M_3)$, which describes the degree of noncoplanarity. When the three vectors are symmetrically arranged and form an angle θ with the symmetry axis, then the triple product is equal to $(27/4)^{1/2} \sin^2\theta\cos\theta\, M_s^3$. The angle θ depends on the radius of the nanoparticles and on the external magnetic field. In very small nanoparticles, the exchange energy $\sim A/R^2$ dominates, and θ approaches zero. Figure 1(b) shows the zero-field Berry curvature as a function of R. An external magnetic field reduces Φ, and the THE is obtained by areal integration. For very small nanoparticles, Φ decreases as R^4. This research is supported by DOE BES (DE-FG02-04ER46152).

[1] E. Pinilla-Cienfuegos, S. Mannas-Valero, A. Forment-Aliaga, and E. Coronado, ACS Nano 10, 1764 (2016). [2] B. Das, B. Balasubramanian, R. Skomski, P. Mukherjee, S. R. Valloppilly, G. C. Hadjipanayis, and D. J. Sellmyer, Nanoscale 10, 9504 (2018). [3] W. Zhang, B. Balasubramanian, A. Ullah, R. Pahari, X. Li, L. Yue, S. R. Valloppilly, A. Sokolov, R. Skomski, and D. J. Sellmyer, Appl. Phys. Lett. 115, 172404 (2019).

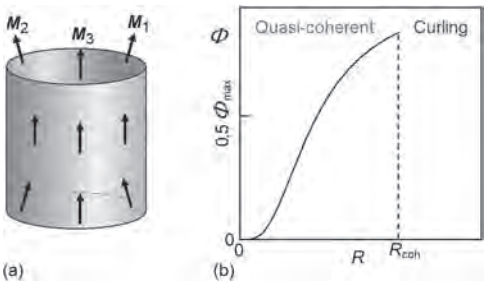

Fig. 1. Berry curvature Φ and THE in quasi-coherent nanoparticles: (a) schematic spin configuration and (b) Φ as a function of particle radius *R*. The dashed line shows the transition to magnetization curling, where THE behavior changes qualitatively.

E2-07. Grain Growth Study in Sequentially-Sputtered Co-HfO_2 Granular Films. *A.K. Toh*[1] and V. Ng[1] *1. Electrical and Computer Engineering, National University of Singapore, Singapore*

Magnetic granular films (GFs) have potential sensor applications due to superparamagnetism and magnetoresistance (MR) properties [1-2]. However, a major challenge faced is fabricating GFs with uniform sized nanoparticles (NPs) [3]. Sequential-sputtering of alternating discontinuous metal and oxide layers can control NP sizes by stopping grain growth via the sequential oxide layer [4]. We study the grain growth in sequentially-sputtered Co-HfO_2 GFs as a function of deposition conditions. m(H) was measured by SQUID magnetometer, MR by probing, and nanostructure imaged by conductive atomic force microscopy (CAFM) [5]. Fig.1(a) shows the m(H) of four samples with 20 bilayers of varying Co and HfO_2 content, fabricated at a nominal sputter rate of 0.0214 and 0.0125 nm s^{-1}, respectively. Eg, sample labelled 17/70 was fabricated with 17 s Co sputter-time and 70 s HfO_2 sputter-time per bilayer. It can be seen that the two samples fabricated with the larger Co content (samples 35/(70, 140)) had larger $m_{7\,T}$ than the other two samples (samples 17/(70, 140)), and $m_{7\,T}$ decreased as HfO_2 content increases. The m(H) loops in fig.1(b) show that samples 35/(70, 140) were ferromagnetic and samples 17/(70, 140) were superparamagnetic. The two superparamagnetic samples showed MR% which decreased due to the increase in HfO_2 content, as shown in fig.1(c). Fig.2 shows the CAFM results of the four samples, and it can be seen that NP sizes increased as Co content increases, which is congruent with the m(H) results. However, insignificant NP size change was observed with HfO_2 content. To investigate the inconsistency of the CAFM results with the properties of the samples, a novel technique we call CAFM tomography was performed. 3D reconstructed images show that the HfO_2 suppressed NP growth in the vertical profile. We will present results showing that the sequential-sputter technique can control the growth of the NPs in the lateral and vertical axes as a function of deposition conditions.

[1] H. Kijima-Aoki, et al., IEEE Magnetics Letters, Vol. 9, p. 5, (2018) [2] M. Huth, Journal of Applied Physics, Vol. 107, p. 7 (2010) [3] K. Yakushiji, et al. Physics Reports, Vol. 451, p. 1-35 (2007) [4] M. Chadha and V. Ng, Journal of Magnetism and Magnetic Materials, 426, 302-309 (2017) [5] A. Toh and V. Ng, 2019 Joint MMM-Intermag Conference, Poster, DQ-04 (2019)

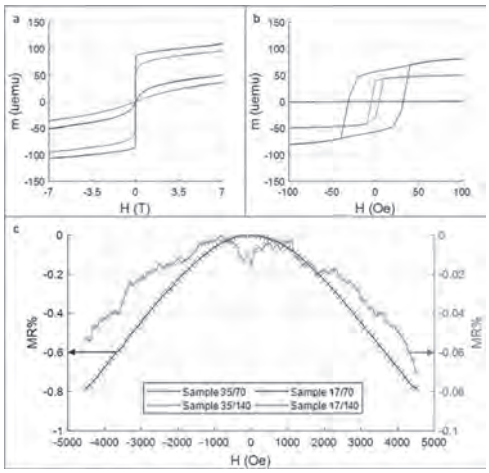

Fig.1: (a) m(H) at H = ±7 T, (b) m(H) at H = ±100 Oe, (c) MR% of Sample 17/70 & 17/140

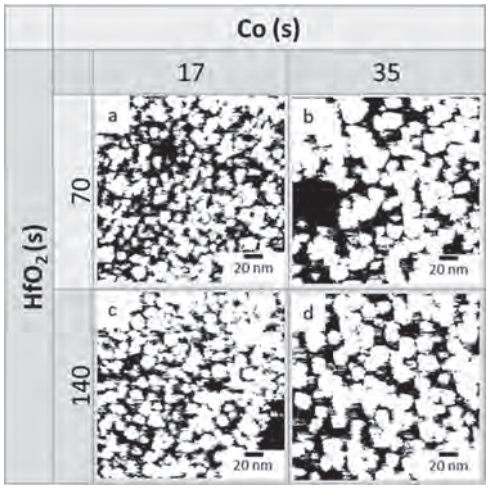

Fig.2: CAFM images with Co and HfO2 sputter-time per bilayer for four 20 bilayers samples: (a) Sample 17/70, (b) Sample 35/70, (c) Sample 17/140, (d) Sample 17/140

E2-08. Fabrication of Thick and Stable Nanoparticle Films via Electrophoretic Deposition on Substrates Functionalized With Chelating Agents. *S.C. Mills*[1], N.E. Starr[1], N.J. Bohannon[1] and J. Andrew[1] *1. University of Florida, Gainesville, FL, United States*

In applications that utilize films of nanoparticles, there is a need to develop methods to fabricate stable thick films to improve materials for energy storage, sensing, or flexible electronics. [1-3]. This work seeks to increase film thickness and stability by increasing film-substrate interactions by functionalizing conductive substrates with various chelating agents. These nanoparticles are deposited via electrophoretic deposition (EPD), a method that deposits charged particles in colloidal suspensions via electrophoresis. Here, we will demonstrate the efficacy of this approach by depositing iron oxide nanoparticles onto conductive substrates functionalized with three chelating agents with different functional moieties and therefore differing chelating strengths [4]. We show that increasing chelating strength can increase film-substrate interactions, resulting in thicker films when compared to traditional EPD. Results will also be presented on how the effect of the chelating strength relates to film formation as a function of deposition conditions. Yield for EPD is influenced by deposition conditions including applied electric field, particle concentration, and deposition time. Substrates functionalized with chelating agents were used with three different sets of deposition parameters, varying the applied electric field and particle concentration. This work shows that the functionalization of substrates with chelating agents that coordinate strongly with nanoparticles used for deposition overcome parameters that traditionally hinder the deposition of thicker and more stable films. Further, films that suffer instability and low quality from high applied electric field and high particle concentration were more stable when deposited on substrates functionalized with phosphonic acid and dopamine.

[1] C. Mahender, T. Sumangala, R. Ade, Ceram. Int., Vol. 45, p. 4316-4321 (2019) [2] E. Cao, Z. Chu, H. Wang, Ceram. Int., Vol. 44, p. 7180-7185 (2018) [3] L. Ming, H. Yang, W. Zhang, J. Mater. Chem., Vol. 2, p. 4566-4573 (2014) [4] A. Walter, A. Garofalo, A. Parat, Nanotechnol. Rev., Vol. 4, p. 581-593 (2015)

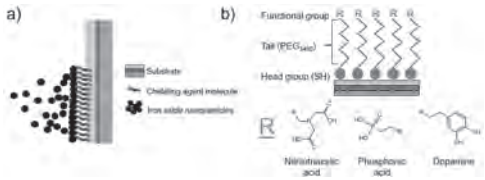

Fig. 1. (a) Illustration of the substrate functionalized with chelating agent molecules for use during the electrophoretic deposition of iron oxide nanoparticles. b) Expected structure of the chelating agent molecules functionalized on an Au/Ti/Si substrate.

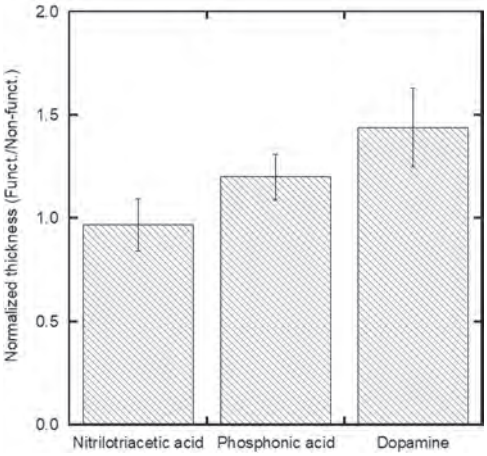

Fig. 2. Plot of the comparison of the normalized film thickness between each chelating agent for the low particle concentration and moderate field condition.

E2-09. Withdrawn

E2-10. Atomic-Level Analysis of Oxidation Pathways in Fe/Fe Oxide Magnetic Nanoparticles. *T. Bird*[1], S. Aktas[2,1], S. Alotaibi[1], L. Lari[3,1], D. Kepaptsoglou[4,1], R. Kröger[1] and A. Pratt[1] *1. Department of Physics, University of York, York, United Kingdom; 2. Mechanical Engineering, Giresun Universitesi, Giresun, Turkey; 3. York JEOL Nanocentre, University of York, York, United Kingdom; 4. SuperSTEM, Warrington, United Kingdom*

Magnetic nanoparticles continue to attract a great deal of attention relating to their potential use in biomedical, environmental, and data storage applications [1,2]. Pure Fe nanoparticles (zero-valent iron) have higher magnetic moments than their Fe oxide counterparts but their reactivity currently precludes use in these applications. Hence, a deeper understanding of oxidation at the nanoscale is required and how this differs from the well-understood theory of bulk metal oxidation [3]. In particular, the roles of grain boundary and lattice diffusion, and the effects of size and shape on reactivity

need elucidating before these factors can be engineered. In this study, Fe/Fe oxide nanoparticles were produced under ultrahigh vacuum conditions in a gas-aggregation cluster source and size-selected using a quadrupole mass filter. As well as being cleaner than typical methods of chemical synthesis, this physical approach allows control over geometry with cubic, cuboctahedral, and spherical shapes possible under different source conditions [4]. Results from aberration corrected environmental transmission electron microscopy (TEM) imaging of Fe/Fe_xO_y nanoparticles of different shapes will be presented correlating the balance between grain boundary and lattice diffusion to particle oxidation. Analysis of high-resolution STEM data, combined with electron energy loss spectroscopy and energy dispersive X-ray spectroscopy, allows the extraction of quantitative information on the atomic-level organisation of the oxide shell and the core/shell structure. From our data, we deduce that the oxidation process sensitively depends on the particle size, shape and composition. As we will show, the particles were found to oxidise through a process that differs from the accepted theories of bulk oxidation of Cabrera-Mott [5] and Wagner [6] suggesting that nanoscale effects such as geometry and confinement will be key to engineering magnetic nanoparticle structures with bespoke magnetic and reactive properties.

[1] M. Walker, I. Will, A. Pratt *et al*., ACS Appl. Nano Mater. 3, 5008 (2020). [2] A. Pratt, *Environmental Applications of Magnetic Nanoparticles*, in: Frontiers of Nanoscience (Ed.: C. Binns) Vol. 6, pp.259-307 (2014). [3] A. Pratt, L. Lari, O. Hovorka *et al.*, Nature Mater. 13, 26 (2014). [4] S. Aktas, S. C. Thornton, C. Binns *et al*. Mater. Res. Exp. 2, 035002 (2015). [5] N. Cabrera and N.F. Mott, Rep. Prog. Phys. 12, pp.163-184 (1949). [6] C. Wagner, Z. Phys. Chem. 21, pp. 25-41 (1933).

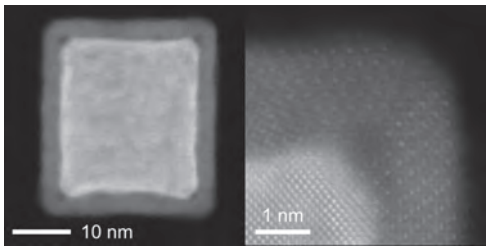

Aberration-corrected STEM images of a cubic Fe/Fe_xO_y core-shell nanoparticle. The high magnification image (right) shows the oxide-oxide domain boundary formed at a nanoparticle vertex and the nucleation of a Kirkendall void.

E2-11. Withdrawn

E2-12. Size-Dependent Magnetism and Skyrmionic Properties in CoSi Nanoclusters. *R. Pahari*[1], B. Balasubramanian[1], P. Manchanda[2], A. Ullah[1], P. Dev[2], R. Skomski[1] and D.J. Sellmyer[1] *1. Department of Physics and Astronomy and Nebraska Center for Materials and Nanoscience, University of Nebraska, Lincoln, NE, United States; 2. Department of Physics and Astronomy, Howard University, Washington DC, DC, United States*

Magnetic transition-metal silicides and germanides, crystallizing in the B20 cubic structure with broken inversion symmetry, have attracted much attention in the context of Dzyaloshinskii-Moriya interactions, helical spin structures, and magnetic skyrmions [1, 2]. Finding skyrmions in confined geometries such as nanoparticles and nanowires is particularly intriguing from the viewpoints of fundamental science and practical applications [3]. Such low-dimensional structures also often show size-induced magnetic properties as compared to corresponding bulk alloys [4]. We have used density-functional-theory (DFT) calculations and cluster-deposition experiments to investigate the size dependence of magnetic properties in equiatomic CoSi; the average particle size *d* of the clusters varies from about 0.6 nm to 11.6 nm. In sharp contrast to bulk CoSi, which is nonmagnetic down to liquid helium temperature, the nanoclusters order magnetically with a net low-temperature magnetic moment from 0.69 to 0.21 μ_B/Co as *d* varies from 0.6 to 11.6 nm. The fast Fourier transform (FFT) of the HRTEM image (Fig. 1a) and x-ray diffraction pattern (not shown here) of the sample having $d = 11.6$ nm confirm the cubic B20 structure. The corresponding DC susceptibility curves display anomalies in limited field (about 20 – 200 Oe) and temperature (100 K – 300 K) ranges (Fig. 1b), which are similar to the signature of helical or skyrmion-like spin structures. DC susceptibility and anomalous Hall resistivity data are used to determine a field-temperature magnetic phase diagram that includes a skyrmionic region and to discuss the confinement effect on skyrmions within the small diameter of CoSi nanoclusters. This research is supported by the US DOE/BES (DE-FG02-04ER46152) and performed in part in the Nebraska Nanoscale Facility and the NCMN, which are supported by the U.S. NSF (NNCI -1542182), and the Nebraska Research Initiative (NRI).

[1] N. Nagaosa and Y. Tokura, *Nature Nanotech*. 8, 899 (2013). [2] B. Balasubramanian, P. Manchanda, R. Pahari, Z. Chen, W. Zhang, S.R. Valloppilly, X. Li, A. Sarella, L. Yue, A. Ullah, P. Dev, D. A. Muller, R. Skomski, G. C. Hadjipanayis, and D.J. Sellmyer, *Phys. Rev. Lett.* 124, 057201 (2020). [3] B. Das, B. Balasubramanian, R. Skomski, P. Mukherjee, S.R. Valloppilly, G.C. Hadjipanayis, and D.J. Sellmyer, *Nanoscale*. 10, 9504 (2018). [4] B. Balasubramanian, M. Sakurai, C.-Z. Wang, X. Xu, K.-M. Ho, J. R. Chelikowsky and D. J. Sellmyer, *Mol. Syst. Des. Eng*. DOI: 10.1039/d0me00050g (2020).

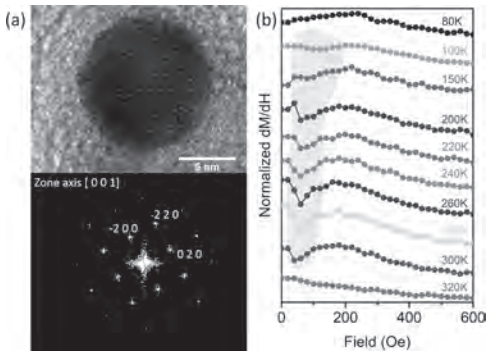

Fig. 1 (a) A HRTEM image (top) and the corresponding FFT image (bottom) and field-dependent susceptibility data $\chi = d\mathit{M}/d\mathit{H}$ at different temperatures from a CoSi nanocluster sample. The anomalies correspond to skyrmionic phase and its temperature-dependence are highlighted using a green-shaded region in (b).

E2-13. Colossal Heating Efficiency for Nearly Zero Magnetostrictive Amorphous Microwires via Eddy Currents at Radiofrequency Fields. I. Morales[1], D. Archilla[1], *P. de la Presa*[1,3], A. Hernando[1,2] and P. Marin[1,3] *1. Instituto de Magnetismo Aplicado, Universidad Complutense de Madrid, Madrid, Spain; 2. Nanoscience, Instituto Madrileno de Estudios Avanzados, Madrid, Spain; 3. Materials Physics, Universidad Complutense de Madrid, Madrid, Spain*

This work shows that Co-rich microwires (MWs) with nearly zero magnetostriction have colossal heating efficiency under radiofrequency fields.[1] MWs of 31 μm diameter and 5 mm length show a specific loss power (SLP) of 3000 W/g at 36 Oe and 625 kHz. The SLP varies with the MWs length and number. The role of length lies on the magnetic domains that change from radial to axial when the length is reduced, as deduced from the hysteresis curve shapes, and makes SLP to decrease by a factor of 10 when the length switch from 5 to 15 mm, see Fig. 1. The number of MWs sets side by side determine the magnetostatic interactions which affect to the remanence (M_r) and susceptibility: Mr = 80% for 2 to 6 MWs and then decreases to Mr = 50% for 10 MWs, suggesting the formation of closure domains that diminish the magnetostatic energy. This change of the hysteresis loop shapes also influences the SLP. In this work, it is assumed that this colossal heating efficiency is dominated by the eddy-currents, although a small contribution

from hysteresis losses cannot be ruled out. The eddy currents are generated by electromagnetic induction and lead to Joule heating of the material. The eddy–currents in Co-rich MWs are enhanced by the magnetization reversal and, thus, the magnetic susceptibility becomes a key factor for the heating efficiency. This magnetic susceptibility is given by the change of the magnetic domain with the length, with the circumferential domains playing probable the main role at high frequency. Therefore, short MWs with nearly zero magnetostriction are key candidates to show colossal heating efficiency

[1] I. Morales, D. Archilla, P. de la Presa, et al., Sc. Report 10, 602 (2020).

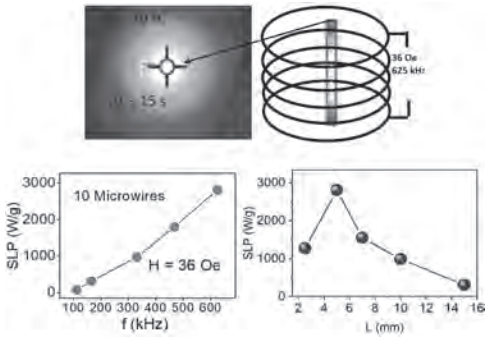

Fig. 1: ***SLP as a function of frequency for H=36 Oe and as a function of MWs length.***

E2-14. Insights on the Heating Characteristics of Mn and Co-Doped Fe_3O_4. *S. J*[1] and R.J. Joseyphus[1] *1. Deaprtment of Physics, National Institute of Technology Tiruchirappalli, Tiruchirappalli, India*

Fe_3O_4 (FeF), $Mn_xFe_{3-x}O_4$ (Mn1, Mn3, Mn5 for x = 0.1, 0.3, 0.5) and $Co_xFe_{3-x}O_4$ (Co1, Co3, Co5 for x = 0.1, 0.3, 0.5) nanoparticles (NPs) were synthesized using co-precipitation technique to study the effect of factors that influence the effective specific absorption rate (ESAR). The samples were characterized using XRD, TEM, VSM, TMA and ESR. The heating efficiency was probed employing infrared thermography at ac field of 4 kA/m and frequency 500 kHz [1, 2]. The particle sizes are in the range of 10-13 nm, except Co5 which is 40 nm. The saturation magnetization (M_s) of the samples at 300 K is between 55-66 emu/g. The coercivity (H_c) of the Mn-doped samples is below 33 Oe where it increased up to 548 Oe with Co-doping. The low-temperature (15 K) hysteresis show a decrease in H_c with Mn-doping and enhancement with Co from 326 to 180 and 4345 Oe, respectively. Fig. 1 shows the ESR spectra from which the effective magnetic anisotropy (K_{eff}) was computed. While the values are between 15.3-16.5 kJ/m^3 for the Mn-doped samples, an increase in K_{eff} of 20.9 (Co1) and 31.3 kJ/m^3 (Co3) is observed with Co-doping reflecting the effect of particle size and doping. ESAR vs. magnetic anisotropy energy ($K_{eff}V$) was theoretically and experimentally estimated (Fig. 2), where V is the volume of the particle. The highest and lowest ESAR (theoretical) of 1124 and 89 × 10^{-9} $Wg^{-1}Oe^{-2}Hz^{-1}$ was obtained for Mn5 and Mn3, respectively. In contrast, the experimental ESAR (right axis) was the highest for Mn3 with a value of 21 × 10^{-9} $Wg^{-1}Oe^{-2}Hz^{-1}$ and decreased with $K_{eff}V$. The ESAR of FeF is 20 × 10^{-9} $Wg^{-1}Oe^{-2}Hz^{-1}$. The deviation in the experimental from the theoretical values of the Mn-doped samples is mainly due to the distribution in particle sizes, whereas the decrease in ESAR with Co-doping from 20 to 18 × 10^{-9} $Wg^{-1}Oe^{-2}Hz^{1}$ was as per the linear response theory (LRT) [3]. Our superparamagnetic NPs produce heat in accordance with LRT. The decreasing trend in ESAR with Co-doping in Fe_3O_4 is correlated with anisotropy, whereas with Mn-doping, particle size distribution plays a significant role rather than anisotropy.

[1] J.S. Anandhi, G.A. Jacob and R.J. Joseyphus, *Mater. Res. Express*, 6, 015045 (2019) [2] J.S. Anandhi, G.A. Jacob and R.J. Joseyphus, *J. Magn. Magn. Mater.*, 512, 166992 (2020) [3] J. Carrey, B. Mehdaoui and M. Respaud, *J. Appl. Phys.*, 109, 083921 (2011)

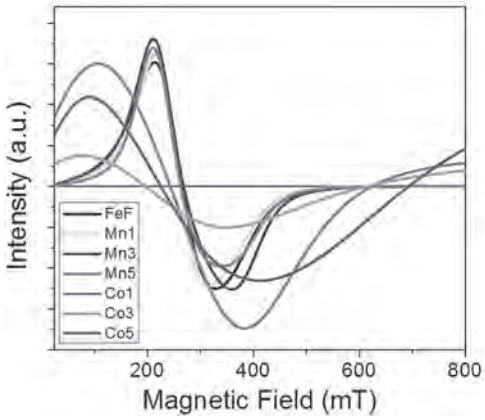

Fig. 1. ESR spectra of Mn and Co-doped Fe_3O_4.

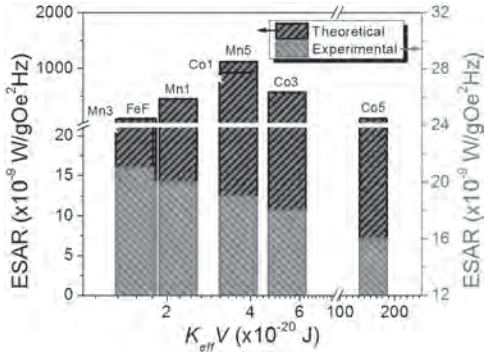

Fig. 2. ESAR of Mn and Co-doped Fe_3O_4 as a function of magnetic anisotropy energy.

Session E3
NEW PROBING TECHNIQUES FOR SPIN TORQUES

Shawn Pollard, Chair
University of Memphis, Memphis, TN, United States

INVITED PAPER

E3-01. Real-Time Measurements of Field-Free Spin-Orbit Torque Switching in 3-Terminal Magnetic Tunnel Junctions. *V. Krizakova*[1], E. Grimaldi[1], G. Sala[1], F. Yasin[2], S. Couet[2], G.S. Kar[2], K. Garello[2] and P. Gambardella[1] *1. ETH Zurich, Zurich, Switzerland; 2. imec, Leuven, Belgium*

Current-induced spin-orbit torques (SOT) have attracted great attention for their unique ability to manipulate the magnetization of ferromagnets and antiferromagnets [1]. SOT-induced switching offers speed and reliability comparable to or better than spin transfer torque (STT) switching, as was shown in nanodots [2,3] and magnetic tunnel junctions (MTJ) [4,5]. However, whereas the STT-driven switching dynamics of MTJs has been extensively studied [6-8], less is known about the transient dynamics and actual speed of the magnetization reversal induced by SOT. In this study we investigate the reversal dynamics of SOT switching in 3-terminal MTJs and show how the interplay of voltage control of magnetic anisotropy (VCMA) and STT can be used to optimize the switching efficiency [9,10]. We report real-time measurements of in-field and field-free SOT switching and disentangle the combined impact of SOT, STT, and VCMA on the switching speed and efficiency. We show that the combination of these effects leads to reproducible sub-ns switching with an extremely narrow distribution of the switching times without the aid of an external field. Our 3-terminal devices are fabricated using a fully compatible CMOS process [11] and are based on CoFeB/MgO/CoFeB MTJs grown on a b-W SOT-injection line and patterned into 80 nm pillars (Fig. 1a). The field-free switching functionality is enabled by an in-plane magnet embedded into a hard-mask [12], which provides a symmetry-breaking magnetic field to the magnetization of the free layer (Fig. 1b). Our electrical setup combines after-pulse and real-time detection [13] allowing for the exploration of individual SOT switching events in the time domain as well as of their statistical distributions. The voltage time traces of individual switching events exhibit a finite incubation delay followed by a single-jump reversal, after which the magnetization remains quiescent in the final state (Fig. 1c,d) [13]. Whereas complete magnetization reversal occurs within ≈1 ns, the incubation delay can take a substantial part of the total switching time in close-to-critical conditions. This incubation time, which is not expected for the "instant-on" SOT in perpendicular MTJs, can be minimized by a moderate increase of the SOT current (compare Figs. 1c and 1d), resulting in a very narrow distribution of the switching latency (Fig. 1e) [14]. A similar effect is achieved by increasing the external magnetic field strength or by biasing the MTJ. We attribute the two-steps switching process to the nucleation of a reversed domain and propagation of a domain-wall across the free layer, as supported by micromagnetic simulations (Fig. 1f). The model reveals that a key element to the observed dynamics is the reduction of magnetic anisotropy of the free layer related to the current-induced temperature rise [13]. The results further evidence a significant dependence of the switching speed and reversal onset on the MTJ bias. In Fig. 1g, averaged time traces obtained for different bias conditions clearly show that the bias accelerates the switching process. Finally, from symmetry considerations, we show that the contributions of STT and VCMA can be separated, unraveling their distinct impact on the magnetization dynamics.

[1] A. Manchon, J. Železný, I. M. Miron, et al. Rev. Mod. Phys. 91, 035004 (2019) | [2] K. Garello, C. O. Avci, I. M. Miron, et al. Appl. Phys Lett. 105, 212402 (2014) | [3] M. Baumgartner, K. Garello, J. Mendil, et al. Nat. Nanotech. 12, 980-986 (2017) | [4] S. V. Aradhya, G. E. Rowlands, J. Oh, et al. Nano Lett, 16, 5987-5992 (2016) | [5] M. Cubukcu, O. Boulle, N. Mikuszeit, et al. IEEE Trans. Magn. 54, 9300204 (2018) | [6] Y.-T. Cui, G. Finocchio, C. Wang, et al. Phys. Rev. Lett. 104, 097201 (2010) | [7] C. Hahn, G. Wolf, B. Kardasz, et al. Phys. Rev. B 94, 214432 (2016) | [8] T. Devolder, J.-V. Kim, F. Garcia-Sanchez, et al. Phys Rev. B 93, 024420 (2016) | [9] H. Yoda, H. Sugiyama, T. Inokuchi, et al. IEEE Int. Mem. Wkshp. (2017) | [10] A. van den Brink, S. Cosemans, S. Cornelissen, et al. Apply. Phys. Lett. 104, 012403 (2014) | [11] K. Garello, F. Yasin, S. Couet, et al. IEEE Symp. VLSI Circ., 81-82 (2018) | [12] K. Garello, F. Yasin, H. Hody, et al. IEEE Symp. VLSI Circ., T194-195 (2019) |[13] E. Grimaldi, V. Krizakova, G. Sala, et al. Nat. Nanotech. 15, 111-117 (2020) | [14] V. Krizakova, K. Garello, E. Grimaldi, et al. Appl. Phys. Lett. 116, 232406 (2020)

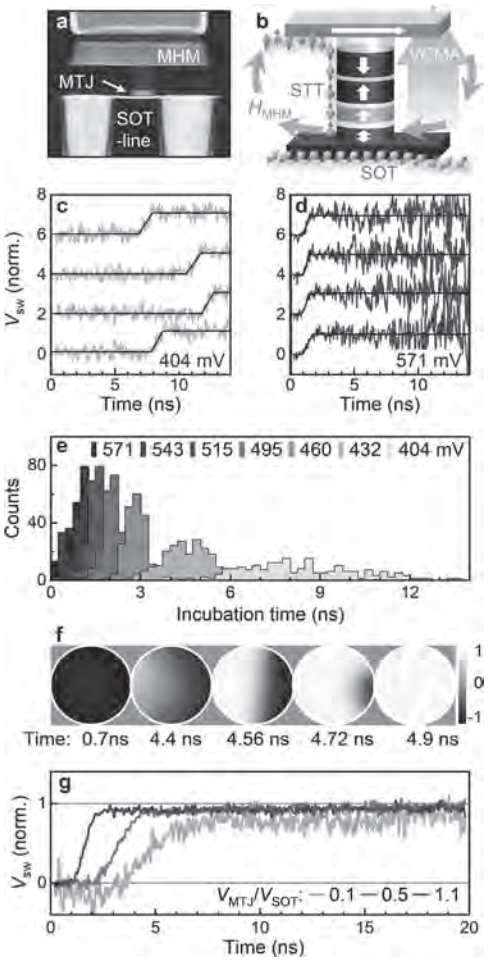

CONTRIBUTED PAPERS

E3-02. All-Optical Probe of Magnetization Precession Frequency Modulated by Spin-Orbit Torque. *K. Ishibashi*[1,2], S. Iihama[3,4], Y. Takeuchi[5], K. Furuya[5], S. Kanai[5,4], S. Fukami[5,4] and S. Mizukami[2,4]
1. Department of Applied Physics, Graduate School of Engineering, Tohoku University, Sendai, Japan; 2. WPI Advanced Institute for Materials Research, Tohoku University, Sendai, Japan; 3. Frontier Research Institute for Interdisciplinary Sciences, Tohoku University, Sendai, Japan; 4. Center for Spintronics Research Network, Tohoku University, Sendai, Japan; 5. Labratory for Nanoelectronics and Spintronics, Research Institute of Electrical Communication, Tohoku University, Sendai, Japan

Spin-orbit torque (SOT) has drawn significant attention as a technique to control magnetization. SOT is conventionally investigated using spin-torque ferromagnetic resonance and second harmonic Hall effect measurements. However, it is known that the parasitic electrical voltages arisen by spin-charge conversion and thermoelectric effect overlap with the signal [1,2]. All-optical measurement can directly investigate the magnetization precession modulated by the SOT and is free from such effects; thus it is a promising way. The change in the life-time of the magnetization precession was previously reported [3,4]. In general, the evaluation of frequency change is more precise than that of the precession life-time. Here we report the observation of the modulation of the precession frequency due to the SOT. The stack, $Si/SiO_2/W(5)/CoFeB(2.4)/MgO(1.3)/Ta(1)$ (thickness in nm), was fabricated by a DC/RF magnetron sputtering [5]. The film was patterned into a rectangular stripe (10×40 μm^2). The magnetization precession modulated by SOT was investigated by an all-optical time-resolved magneto-optical Kerr effect (TRMOKE) microscope, in which an external field H_{ext} was applied at an out-of-plane angle θ_H and a direct current I was applied parallel to y-axis [Fig. 1(a)]. This geometry is different from that previously reported [3,4] and the modulation of the precession frequency induced by the direct current was distinctly observed. This change was well explained by the change in angle of precessional axis of magnetization θ induced by SOT. The generation efficiency of the SOT was estimated as ~−0.35, which was reasonably independent of the external field [Fig. 1(b)] [6]. The result indicated that all-optical TRMOKE measurements of the precession frequency shift induced by the SOT would be one of the powerful tools to evaluate the SOT.

[1] K. Kondou, *et al*., Appl. Phys. Exp. 9, 023002 (2016). [2] C. O. Avci, *et al*., Phys. Rev. B 90, 224427 (2014). [3] A. Ganguly, *et al*., Appl. Phys. Lett. 105, 112409 (2014). [4] S. Mondal, *et al*., Phys. Rev. B 96, 054414 (2017). [5] Y. Takeuchi *et al.*, Appl. Phys. Lett. 112, 192408 (2018). [6] K. Ishibashi *et al*. manuscript in preparation.

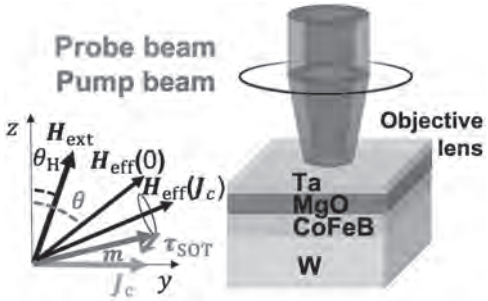

Fig. 1 Schematic of the optical setup and experimental geometry.

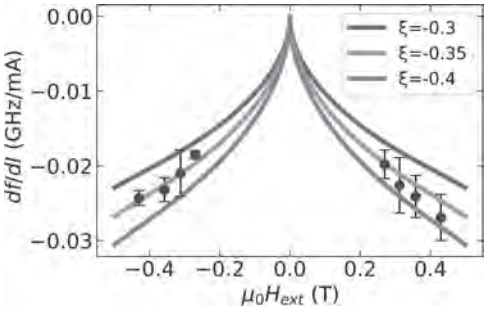

Fig. 2 The external field dependence of the slope of frequency f vs current ($I \parallel y$). Curves are the calculated data with different generation efficieny of SOT.

E3-03. Optical Spin-Torque in FeCo / Pt Bilayer Thin Films. *S. Iihama*[1,2] and S. Mizukami[3,2] *1. Frontier Research Institute for Interdisciplinary Sciences (FRIS), Tohoku University, Sendai, Japan; 2. Center for Spintronics Research Network (CSRN), Tohoku University, Sendai, Japan; 3. Advanced Institute for Materials Research (AIMR), Tohoku University, Sendai, Japan*

Manipulation of magnetization precession, namely magnon, with circularly-polarized light has attracted much attention. Many of relevant studies have focused on magnon driven by the inverse Faraday effect in magnetic insulators or semiconductors. However, there have been few reports on metals. Recently Choi *et al.* reported magnetization precession driven by the circularly-polarized light in ferromagnet/heavy metals bilayers [1]. They proposed new physics, optical spin-torque which is distinct from the traditional inverse Faraday effect. However, the physics of optical spin-torque is not clearly understood yet; thus, it is demanded to deeply understand the physics toward photo-spintronic applications. Here, we observed light-helicity induced magnetization precession in FeCo / Pt bilayers, which is found to be explained by the optical spin-torque. MgO / FeCo / Pt thin film were deposited on thermally oxidized Si substrate by a magnetron sputtering. The pulse width and wavelength of the femtosecond laser pulse used were 120 fs and 800 nm. Figure 1 shows the magnetization precession in FeCo / Pt bilayer with different light helicities, where 2 T in-plane magnetic field is applied. The solid curves in Fig. 1 show the fitting of sinusoidal function to the data. The phase of the magnetization precession has an information of a torque direction. Optical spin-torque is believed to be regarded as a damping-like torque, which is induced by a current of the spin-angular momentum in a nonmagnetic layer transferred from the circularly-polarized light and makes magnetization initailly tilt away from the film surface as shown in Fig. 2. It was found that the magnetization precession is mainly induced by the damping like-torque, however, we also observed field-like torque as a phase shift of the magnetization precession. The detailed discussion of field-like torque as well as its thickness dependence will be discussed in the presentation. This work was partially supported by KAKENHI (19K15430), Advanced Technology Institute Research Grants, and CSRN.

[1] G. -M. Choi *et al*. Nat. Commun. 8, 15085 (2017), G. -M. Choi *et al*. Nat. Commun. 11, 1482 (2020). [2] S. Iihama and S. Mizukami, in-preparation.

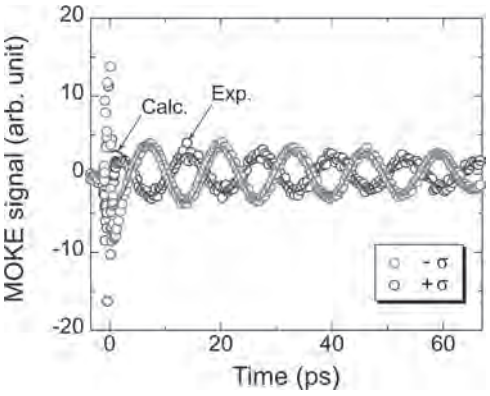

Magnetization precession in FeCo/Pt bilayer excited by left and right circularly polarized laser pulses.

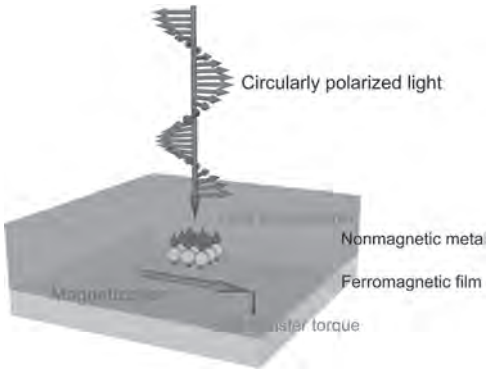

Schematic illustration of optical spin-torque in metallic bilayer thin films.

E3-04. Magneto-Optical Detection of Spin-Orbit Torque Phenomena Using Sagnac Interferometer Microscope. *Z. Huang*[1], E. Vetter[1,2], Y. Xiong[3], W. Zhang[3] and D. Sun[1,4] *1. Department of Physics, North Carolina State University, Raleigh, NC, United States; 2. Department of Materials Science and Engineering, North Carolina State University, Raleigh, NC, United States; 3. Department of Physics, Oakland University, Rochester, MI, United States; 4. Organic and Carbon Electronics Lab (ORaCEL), North Carolina State University, Raleigh, NC, United States*

An important aspect of spin-orbitronics is to electrically manipulate the spin degree of freedom in order to achieve spin-based logic and memory functionalities. Spin-orbit torques (SOTs), direct control of the magnetization via spin-orbit interaction of materials by passing an electric current, have been demonstrated in a variety of metallic and insulating ferromagnetic/non-magnetic heavy metal bilayers utilizing both magneto-transport and magneto-optical Kerr effect (MOKE) measurements. Whereas the conventional MOKE measurement successfully expands the detectability of SOTs, an AC current modulation in the SOT devices is required to achieve the desired sensitivity. Here, we show that instead of using the AC current modulation, the SOT-induced effect can be studied by observing static magnetization switching under a DC current excitation taking advantage of the ultrahigh sensitivity of a Sagnac interferometer microscope. Upon the DC current excitation, spatially resolved static magnetization switching in a prototypical SOT device, i.e., NiFe/Pt bilayer is directly measured, by which a current-induced Oersted field, joule-heating, and other parasite artifacts can be well-separated. Our work provides a promising continuous-wave magneto-optical approach to optically characterize the static spin Hall angle in a range of SOT devices without the need for the AC current modulation. This work was supported by NSF-ECCS under grants No. 1933301 and 1933297.

INVITED PAPER

E3-05. Sensing Stray Fields From Spin-Hall-Controlled Magnetic Nanowires With Nitrogen-Vacancy Centers in Diamond. *J. Sankey*[1], A. Solyom[1], M. Caouette-Mansour[1], B. Ruffolo[1] and L. Childress[1] *1. Physics, McGill University, Montreal, QC, Canada*

The individual spins associated with nitrogen-vacancy (NV) centers in diamond can serve as exquisite nanoscale magnetic field sensors, enabling (among other things) the measurement of stray fields near YIG [1] and Py [2] films influenced by spin transfer torques. This presentation provides an overview of our latest efforts to (i) reliably fabricate high-quality Py/Pt nanowires on a single-crystal diamond substrate while maintaining the performance of NVs implanted 10's of nanometers below the surface, (ii) develop a Bayesian protocol for optimal estimation of NV spin relaxation, and (iii) estimate thermal time scales in these (and other) nanocircuits while calibrating the applied microwave current. Time permitting, I will also discuss preliminary measurements (microwave transport and NV magnetometry) of driven and thermally populated spin wave modes controlled by spin Hall torques.

[1] C. Du, T. van der Sar, et al., Science, 357, 195-198 (2017) [2] A. Solyom, Z. Flansberry, et al., Nano Lett., 18, 6494-6499 (2018)

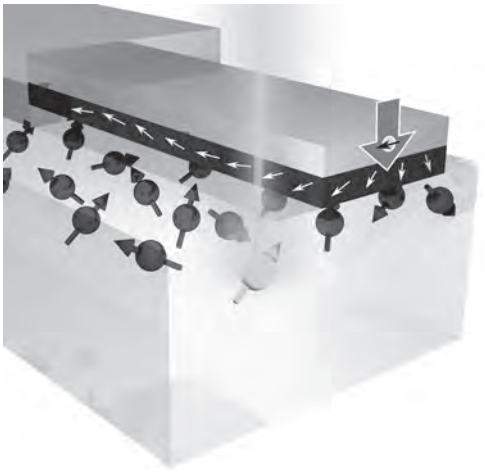

Sensing geometry, comprising a Py/Pt nanowire deposited on a single-crystal diamond substrate with optically active nitrogen-vacancy spins residing 10's of nanometers below the surface (not to scale).

CONTRIBUTED PAPERS

E3-06. Withdrawn

E3-07. Spin-Orbit Torque in a Low Moment Ferrimagnet at High Current Density. *A. Jha*[1], S. Lenne[1], G. Atcheson[1], K. Rode[1] and P.S. Stamenov[1] *1. School of Physics and CRANN, University of Dublin Trinity College, Dublin, Ireland*

Recently, candidate zero moment half metallic materials in the Mn_2RuGa system, have attracted attention, due to a unique blend of properties – low M_{net} in a broad temperature range, close to T_{comp} for these ferrimagnets [1], high resonance frequencies [2] and high Fermi level spin polarisation and spontaneous Hall effect [3]. Potential applications include MTJs for CPP transport [4] and CIP Hall bar type structures [5] for the exploitation of either STT or SOT. Here, we focus on the EHE and SOT in Hall bar structures out

of single layer of MnRuGa (MRG), close to T_{comp}, at high current density. MRG films of thickness 40 nm has been grown on MgO (001) substrates using a DC magnetron sputtering. A set $U_{Hall}(3\omega)$ curves at $\mu_0|H| = 0.4$ T are displayed on Fig. 1. The $|I|$ dependence is strong, with notable angular hysteresis. To gain clarity, the ~I^3 dependence can be subtracted, as shown on Fig 1. At close to the maximal Joule dissipation, the order of the non-linearity is > I^3 and ~ I^5. Background-corrected, the data is visualized on Fig. 2. Only the angular-dependent non-linearity persists, due to the current-non-linear part of the spin-orbit torque. The calibration of the effective torques is shown on Fig. 2. The magnitude of the resulting inductance L_{eff}(10 mA) > 70 pH, with a notable rotational hysteresis. The geometrical L of the Hall bar structure is ~ 30-35 pH, which would suggest that resonators and oscillators could be created out of single active layers of Mn_2RuGa. As f_{FMR} > 250 – 300 GHz has already been shown, a tantalizing prospect emerges to create on-chip tuneable spintronic oscillators, with no critical tunnel barriers, which can bridge the THz gap of availability of compact sources and local heterodyne oscillators.

[1] H. Kurt, K. Rode, P. Stamenov, M. Venkatesan, et. al., Phys. Rev. Lett., 112, 027201 (2014) [2] R. E. Troncoso, K. Rode, P. Stamenov, J. M. D. Coey and Arne Brataas, Phys. Rev. B, 99, 054433 (2019) [3] N. Thiyagarajah, Y.-C. Lau, D. Betto, K. Borisov, J. M. D. Coey, P. Stamenov and K. Rode, Appl. Phys. Lett., 106, 12402 (2015) [4] A. Titova, C. Fowley, E. Clifford, et. al., Sci. Reports, 9, 4020 (2019)

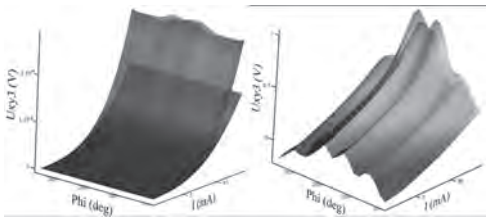

Current dependence of the third harmonic Hall voltage as a function of the direction of the in-plane applied field of 0.4 T (left). The same current and angular field ependence with background subtracted (right).

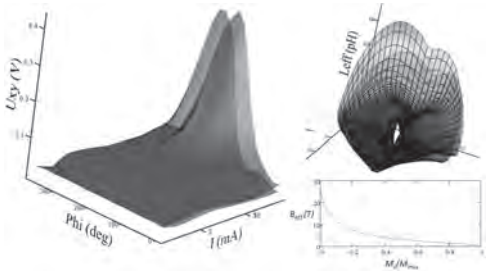

Scaled third harmonic Hall voltage as a function of current and the inplane orientation of $\mu_0|H| = 0.4$ T, with background subtracted (left). Spin-orbit torque induction for various in-plane applied field directions and various currents (top right). $B_{eff}(m_z/m)$ (bottom right).

E3-08. Helium Ion Microscopy for Reduced Spin Orbit Torque Switching Currents. P. Dunne[1,2], C. Fowley[3], G. Hlawacek[3], *J. Kurian*[1], G. Atcheson[4], S. Colis[1], N. Teichert[4], B. Kundys[1], M. Venkatesan[4], J. Lindner[3], A. Deac[3], T.M. Hermans[2], M. Coey[4] and B. Doudin[1]
1. Université de Strasbourg, CNRS, IPCMS UMR 7504, Strasbourg, France; 2. Université de Strasbourg, CNRS, ISIS, Strasbourg, France; 3. Institute of Ion Beam Physics and Materials Research, Helmholtz-Zentrum Dresden, Dresden, Germany; 4. AMBER and School of Physics, Trinity College, Dublin, Ireland

Spin Orbit Torque (SOT) is an efficient way to electrically manipulate nanoscale magnetic objects for high-speed, high-density and low power spintronic devices[1]. However, the high critical current density, j_c, required to switch the magnetization of a film is a major bottleneck that limits the practical application of SOT in memory devices[2] In this work, we achieve an order of magnitude reduction in j_c by irradiating magnetic thin films using a focused helium ion beam. These films consist of Pt(2.0)/Co(1.0)/W(1.5) sandwiches (numbers in nm), chosen to have heavy metals with opposite spin Hall angles (Pt, W)[3], and they are sufficiently thin to exhibit perpendicular magnetic anisotropy. The critical current required to switch the magnetic state ($\pm M_z$) depends on several parameters including saturation magnetization and magnetic anisotropy, all of which are interface dependent, and can be altered using He^+ irradiation[4]. Our key advance is *in-situ* monitoring of the evolution of the out-of-plane magnetization under local ion irradiation using the anomalous Hall effect (Fig. 1a). In principle, this allows both precise control of the anisotropy and <~10 nm spatial resolution, while avoiding additional lithography steps needed for patterned broad-beam irradiation. The reduction of the j_c is determined via Sot switching experiments (Fig. 1b). This work demonstrates a promising and practical approach for the reduced power consumption in SOT-based spintronic devices which opens the prospect of preferential current driven magnetization switching of predetermined sample areas, limited by the resolution of the ion beam microscope, down to the nanometer scale, while preserving the flat topography of the initial magnetic stack.

[1] I.M. Miron, K. Garello and G. Gaudin, Nature 476, 189 (2011). [2] R. Ramaswamy, J.M. Lee and K. Cai, Appl. Phys. Rev. 5, 031107 (2018). [3] S. Woo, M. Mann and A.J. Tan, Appl. Phys. Lett. 105, 212404 (2014). [4] C. Chappert, H. Bernas and J. Ferré, Science 280, 1919 (1998).

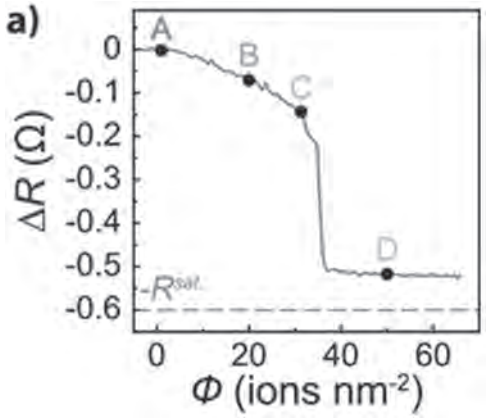

Fig. 1*a) in-situ* Hall resistance measurement as a function of ion dose

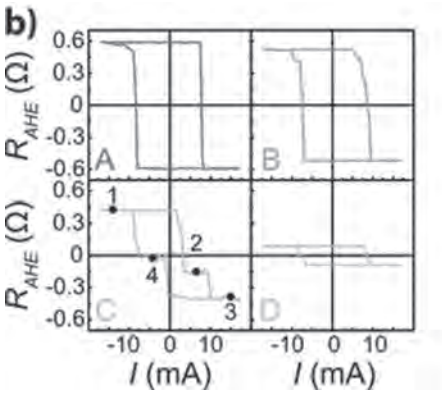

Fig. 1b) Current driven SOT switching curves at specific doses chose from a) under a bias field of $\mu_0 H_x = 150$ mT.

Session E4
SPIN WAVE I: SPATIAL AND NONLINEAR BEHAVIOR

Stefano Bonetti, Co-Chair
Stockholm University, Stockholm, Sweden
Giovanni Finocchio, Co-Chair
University of Messina, Messina, Italy

INVITED PAPER

E4-01. Magnetization Dynamics in Topological Spin Structures Revealed by Diffractive Ferromagnetic Resonance (DFMR). *D. Burn*[1], S. Zhang[3,2], G. van der Laan[1] and T. Hesjedal[2] *1. Magnetic Spectroscopy Group, Diamond Light Source, Didcot, United Kingdom; 2. Department of Physics, University of Oxford, Oxford, United Kingdom; 3. ShanghaiTech University School of Physical Science and Technology, Shanghai, China*

The understanding and ability to manipulate collective spin excitation modes in topologically ordered magnetic structures offers great potential for the development of novel devices. At present, the understanding of these dynamic magnetization modes is based on ferromagnetic resonance (FMR) studies, probing the bulk of the material system, in conjunction with micromagnetic and theoretical modelling. On the other hand, experimental tools to directly probe complex magnetization dynamics in such spin systems are lacking. Here, we will present a novel diffractive ferromagnetic resonance (DFMR) technique with the ability to uniquely resolve the dynamic behavior of individual resonance modes tied to topological spin structures [1]. This new technique brings together the power of two synchrotron x-ray based techniques: Firstly, x-ray detected ferromagnetic resonance (XFMR) provides a chemical- and time-resolved probe to explore the magnetization dynamics [2,3]. Secondly, resonant elastic x-ray scattering (REXS) selectively probes periodic spin structures within the magnetic material [4]. In combination, DFMR reveals new and unique insights into the dynamics of ordered spin systems.

[1] D.M. Burn *et.al. Nano Lett.* 20, 345 (2020). [2] G. van der Laan, *J. of Electron Spectrosc. Relat. Phenom.* 220, 137 (2017). [3] C. Klewe, *et. al. Sync. Rad. News* 33, 12 (2020). [4] G. van der Laan. *C. R. Phys*. 9, 570 (2008).

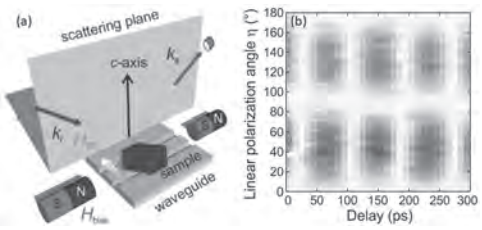

Fig. 1 (a) Experimental DFMR schematic where x-rays are scattered from magnetic structures within the sample with magnetization dynamics driven by a RF magnetic field. (b) Example data showing the variation of the dynamic signal with linear polarization angle and pump-probe delay for Y-type hexaferrite.

CONTRIBUTED PAPERS

E4-02. Demonstration of *k*-Vector Selective Microscopy for Nanoscale Mapping of Higher Order Spin Wave Modes. *N. Träger*[1], P. Gruszecki[2,3], F. Lisiecki[3], F. Gross[1], J. Förster[1], M. Weigand[4], H. Glowinski[3], P. Kuswik[3], J. Dubowik[3], M. Krawczyk[2] and J. Gräfe[1] *1. Modern Magnetic Systems, Max Planck Institute for Intelligent Systems, Stuttgart, Germany; 2. Faculty of Physics, Adam Mickiewicz University, Poznan, Poland; 3. Institute of Molecular Physics, Polish Academy of Sciences, Poznan, Poland; 4. Helmholtz-Zentrum Berlin, Berlin, Germany*

Magnonic waveguides and their potential for both miniaturization and new fundamental wave physics at the nanoscale are becoming increasingly important for future data communication [1,2]. Especially multimode propagation and multiplexing techniques, which are already omnipresent in modern photonic appliciations, are highly interesting regarding enhanced data rates. Here, we use scanning transmission x-ray microscopy (STXM) with magnetic contrast and spatial and temporal resolution of 20 nm and 50 ps respectively to investigate the dynamics of spin wave propagation in magnonic Py waveguides. A global continuous wave (CW) excitation causes spin wave emission from the short edges forming a periodic magnetization pattern which shows symmetric and antisymmetric higher order spin wave modes (n=1,2,3). Due to the physical confinement of the width of the waveguide, standing spin waves also exist in lateral dimension as schematically shown in the dispersion relation in Fig. 1(a) [3,4]. Non-reciprocity of these lateral waves and the overlapping of excited backward-volume waves from the short edges cause the formation of symmetric and antisymmetric modes [4]. Furthermore, we introduce an evaluation technique, which permits mode selective imaging with both amplitude and phase information at the nanoscale. In doing so, we observe characteristic nodes with a phase shift of the standing wave pattern. Fig. 1(b) illustrates the *k*-space during CW excitation of the waveguide. Three different peaks indicate the excitation of multiple modes, which can be selectively imaged in real space (Fig. 1(c)). Micromagnetic simulations and analytical theory complement these experimental results. *k*-selective imaging and higher order mode excitation could pave the way for future multimode propagation and multiplexing in magnonic applications [4].

[1] Chumak, A.V. et al., Nat. Phys., Vol. 11(6), p.453-461 (2015) [2] Kruglyak, V.V. et al., J. Phys. D., Vol. 43(26), p.246001 (2010) [3] Brächer, T. et al., Phys. Rep., Vol. 699, p.1-34 (2017) [4] Träger, N. et al., Nanoscale. (2020), DOI: 10.1039/d0nr02132f

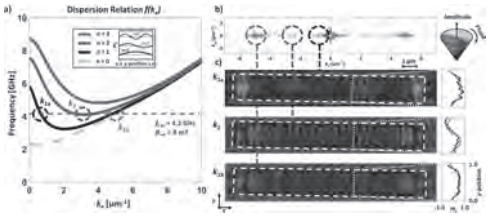

Fig. 1: (a) Dispersion relation $f(k_x)$. The excitation frequency f_{CW} intersects with higher order modes (n=1,2,3) leading to multimode excitation. The inset schematically shows lateral mode profiles. (b) k-space of the magnonic waveguide during CW excitation. (c) k-selective imaging of higher order modes. The insets show the cross-sections revealing the predicted lateral standing spin wave distribution.

E4-03. Non-Standing Spin-Waves in Confined Micron-Sized Structures Imaged With Time-Resolved STXM. *S. Pile*[1], T. Schaffers[1,2], S. Stienen[3], M. Buchner[1], S. Wintz[4], S. Mayr[5], J. Förster[4], V. Ney[1], R. Narkowicz[3], K. Lenz[3], M. Weigand[6], J. Lindner[3] and A. Ney[1] *1. Johannes Kepler Universitat Linz, Linz, Austria; 2. Aalto-yliopisto Perustieteiden korkeakoulu, Aalto, Finland; 3. Helmholtz-Zentrum Dresden-Rossendorf, Dresden, Germany; 4. Max-Planck-Institut fur Intelligente Systeme, Stuttgart, Germany; 5. Paul Scherrer Institut, Villigen, Switzerland; 6. Helmholtz-Zentrum Berlin fur Materialien und Energie GmbH, Berlin, Germany*

For the development of novel spintronic devices, it is important to understand the dynamic magnetic processes on the micro- and nanoscale [1]. By using lithographically fabricated planar micro-resonators it became possible to measure ferromagnetic resonance (FMR) of small samples with a detection sensitivity of down to 10^6 atoms [2]. These microresonators allow combining scanning transmission x-ray microscopy (STXM) using x-ray magnetic circular dichroism (XMCD) as contrast mechanism with FMR (STXM-FMR). STXM-FMR enables the visualization of high frequency magnetization dynamics in the GHz regime with a high lateral resolution of nominally below 50 nm and a stroboscopic time resolution of below 50 ps [3]. In this contribution we present microresonator based FMR and STXM-FMR results for thin magnetic Py ($Ni_{80}Fe_{20}$) microstrips of 5x1 μm^2 lateral size in comparison to respective micromagnetic simulations. Two types of samples were investigated: single Py microstrips and a pair of perpendicularly arranged strips of the same size. For FMR and STXM-FMR measurements a static magnetic field was applied in the plane of the strips. Both FMR and STXM-FMR measurements confirm that quasi-uniform and finite wavelength spin-wave modes can be excited in the Py microstrips. The results show, that by increasing the static magnetic field it is possible to observe the transition from one spin-wave resonance to another. Additionally, we demonstrate that the pair sample geometry allows us to modify the magnetic field distribution within one of the strips, thus leading to a change in the spin-wave dynamics [4]. Financial support by the Austrian Science Fund (FWF), Project No. I-3050 is gratefully acknowledged.

[1] H. Stoll et al., Front. in Phys. 3, 26 (2015). [2] R. Narkowicz et al., J. Magn. Reson. 175, 275 (2005). [3] S. Bonetti et al., Rev. Sci. Instrum. 86, 093703 (2015). [4] S. Pile et.al., Appl. Phys. Lett. 116, 072401 (2020).

E4-04. Nonreciprocal Behavior in Ferromagnets With Spatially Varying Exchange. *R. Macedo*[3], A.S. Kudinoor[1,2], K. Livesey[4,1] and R. Camley[1] *1. Physics, University of Colorado at Colorado Springs, Colorado Springs, CO, United States; 2. Physics, Columbia University, New York, NY, United States; 3. James Watt School of Engineering, University of Glasgow, Glasgow, United Kingdom; 4. School of Mathematical and Physical Sciences, The University of Newcastle, Callaghan, NSW, Australia*

Recently ferromagnets with antisymmetric exchange (e.g. DMI) interactions have been actively investigated, in part because of the nonreciprocal propagation of spin waves where the frequency for positive and negative wavevectors, i.e. +k or -k, is not the same. This occurs because the DMI interaction leads to an effective field which is proportional to the wavevector k. In contrast, we study a system without DMI, but where the exchange interaction varies linearly as a function of position as shown in Fig. 1. Such a structure could be created by nonuniform lateral doping of Cu into Permalloy for example. [1] We also find an effective field which is linear in k, but the directions of the effective field are different from those found in the DMI systems. Using a simple one-dimensional model and a set of coupled Landau-Lifshitz equations, we set the exchange on the right side to be the value for iron, and it is decreased linearly by a factor of three at the left side. A field of 100 mT is applied perpendicular to the chain. The length of the system is 1 micron, but larger lengths give similar results. We demonstrate a number of interesting features: (1) The eigenstates are strongly asymmetric and can be localized on one side of the sample or the other [2]; (2) Depending on the frequency of excitation, there can be a huge asymmetry in propagation amplitudes for waves going in opposite directions as seen in Fig. 2, and (3) If a wave is excited at the center of a sample, there is a large asymmetry in propagation speed for waves travelling in different directions, where waves travelling in the region where the exchange is larger propagate at a higher speed than waves travelling where the exchange is smaller. We compare our results with analytic calculations, with reasonable agreement. We discuss the potential for applications such as isolators at the end.

[1] N. Sorensen, R. E. Camley, and Z. Celinski, J. Magn and Magn. Mat. Vol. 477, p 344 (2019) [2] K L Livesey, D C Crew, R L Stamps, Phys. Rev. B Vol. 73, p. 184432 (2006)

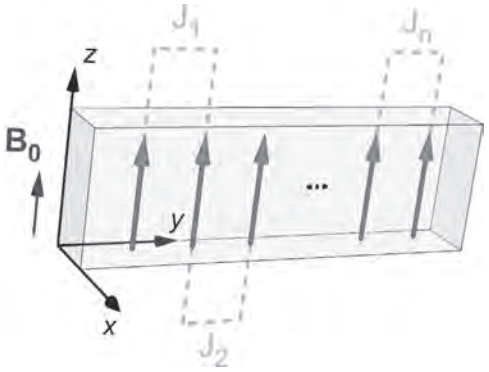

Fig. 1 Illustration of the geometry. The value of the exchange coupling constant increases as one moves to the right.

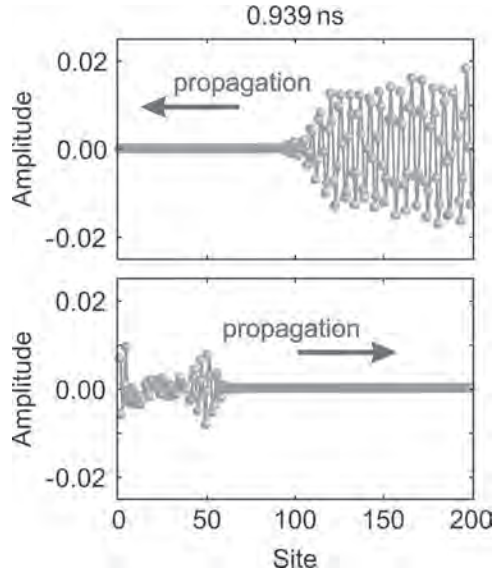

Fig. 2 Nonreciprocal propagation resulting from a oscillating field, at a frequency of 12 GHz, applied at the right (top panel) or left (bottom panel). The wave propagating to the left has a much larger amplitude.

INVITED PAPER

E4-05. Spatially Resolved Magnon Modes in Kagome Artificial Spin Ice With Topological Defects. *V.S. Bhat*[1,2], S. Watanabe[1], K. Baumgaertl[1] and D. Grundler[1,3] *1. Institute of Materials, Laboratory of Nanoscale Magnetic Materials and Magnonics, School of Engineering, Ecole Polytechnique Fédérale de Lausanne, Lausanne, Switzerland; 2. International Research Centre MagTop, Institute of Physics, Polish Academy of Sciences, Warsaw, Poland; 3. Institute of Microengineering, Laboratory of Nanoscale Magnetic Materials and Magnonics, School of Engineering, Ecole Polytechnique Fédérale de Lausanne, Lausanne, Switzerland*

Kagome artificial spin ice (KASI) is a network of Ising type nanobars on a kagome lattice [1-3]. The magnetodynamic study of disordered states has been restricted to global magnetodynamic (e.g. broadband spin wave spectroscopy) and micromagnetic simulations [4]. The experimental studies of microstates in KASIs are key towards their usage as a new type of microwave filter [5], reprogrammable magnonic crystal [6], and a new way to introduce Dirac strings interior to KASI. We investigate spin dynamics of a KASI consisting of $Ni_{81}Fe_{19}$ nanomagnets arranged on an interconnected kagome lattice using broadband ferromagnetic resonance (FMR) (Fig. a,b), magnetic force microscopy (MFM) (Fig. c,d), and micro-focus Brillouin light scattering (BLS) microscopy (Fig. e-f). Micro-focus BLS performed on magnetically disordered states exhibit a series of magnon resonances that depend on topological defect configurations that we image by MFM. Nanomagnets on a Dirac string and between a monopole-antimonopole pair show pronounced modifications in magnon frequencies both in experiments and simulations. Our work is key for the creation and annihilation of Dirac strings via microwave assisted switching and reprogrammable magnonics based on ASIs. Acknowledgment: The research was supported by the Swiss National Science Foundation via Grant No. 163016. V.S. Bhat acknowledges support from the foundation for Polish Science through the IRA Programme financed by EU within SG OP Programme.

1) S. Ladak, D. Read, G. Perkins, L. Cohen, and W. Branford, Nature Physics 6, 359 (2010). 2) R. Wang, C. Nisoli, R. Freitas, J. Li, W. McConville, B. Cooley, M. Lund, N. Samarth, C. Leighton, V. Crespi, *et al.*, Nature 439, 303 (2006). 3) E. Mengotti, L. J. Heyderman, A. F. Rodrguez, F. Nolting, R. V. Hugli, and H.-B. Braun, Nat. Phys. 7, 68 (2011). 4) V. Bhat, F. Heimbach, I. Stasinopoulos, and D. Grundler, Physical Review B 93, 140401 (2016). 5) X. Zhou, G.-L. Chua, N. Singh, and A. O. Adeyeye, Advanced Functional Materials 26, 1437 (2016). 6) M. Krawczyk and D. Grundler, J. Phys.: Condens. Matter 26, 123202 (2014).

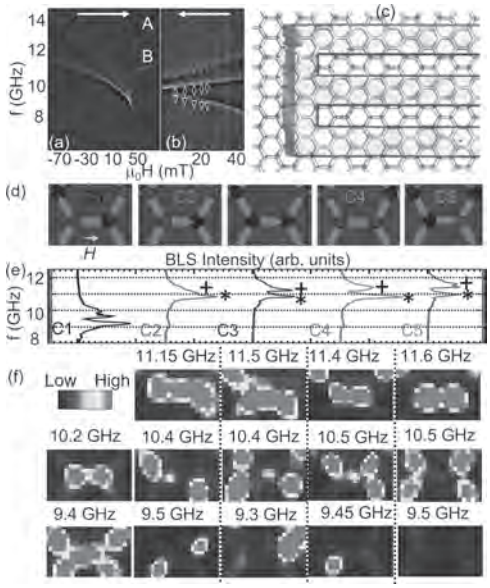

Gray scale FMR derivative spectra of KASI for a field protocol of (a) -90 mT → +90 mT and (b) -90 mT → +45 mT → 0 mT. (c) MFM image of KASI after a field protocol of –100 mT → +45 mT → 0 mT. Stray fields detected by MFM are colored in blue and red consistent with charges $Q = +q$ and $Q = -q$, respectively. (d) Sketches of charge configurations (blue and red spheres) and magnetization vectors M (arrows) for configurations C1 to C5. (e) BLS intensities measured at the central position on horizontal nanobars belonging to the configurations displayed above the spectra at $\mu_0 H = 25$ mT. (f) Spatially resolved BLS intensity maps at 25 mT for fixed frequencies in configurations C1 to C5 displayed above.

CONTRIBUTED PAPERS

E4-06. Nonlocal Stimulation of Three-Magnon Splitting in a Magnetic Vortex. *L. Körber*[1,2], K. Schultheiss[1], T. Hula[1,3], R.V. Verba[4], J. Fassbender[1,2], A. Kákay[1] and H. Schultheiss[1,2] *1. Institute of Ion Beam Physics and Materials Research, Helmholtz-Zentrum Dresden-Rossendorf, Dresden, Germany; 2. Fakultät Physik, Technische Universitat Dresden, Dresden, Germany; 3. Institut für Physik, Technische Universitat Chemnitz, Chemnitz, Germany; 4. Institute of Magnetism, Kyiv, Ukraine*

Spin waves (or magnons) in a micrometer-sized disk magnetized in the vortex state offer an ideal playground to investigate nonlinear magnetization dynamics. In the past, we demonstrated that the radial spin waves in a vortex, once excited above their instability threshold decay into secondary azimuthal modes due to highly efficient spontaneous three-magnon splitting in a rich variety of scattering channels [1]. Here, we present a combined numerical, theoretical and experimental study on nonlocal stimulated splitting in a magnetic vortex disk. We show that three-magnon splitting can be triggered below the threshold of spontaneous splitting by coupling the magnetic vortex to magnons propagating in an adjacent waveguide. Furthermore, using nonlinear spin-wave theory and time-resolved Brillouin-light-scattering experiments we demonstrate that stimulated scattering can be used to manipulate the time scales of nonlinear magnetization dynamics. We believe that the possibility to actively control three-magnon splitting in confined magnetic elements could provide a way to use magnon-based

nonlinear networks as hardware e.g. for neuromorphic computing. Financial support by the Deutsche Forschungsgemeinschaft within programmes SCHU 2922/1-1 and KA 5069/1-1 is gratefully acknowledged.

[1] K. Schultheiss, et al. PRL 122, 097202 (2019) [2] L. Körber, et al. arXiv:2005.12663 (submitted)

E4-07. Emission and Conversion of Ultra-Short Spin Waves. *F. Gross*[1], M. Zelent[3], N. Träger[1], U. Sanli[1], R. Sauter[1], J. Förster[1], M. Weigand[2], K. Keskinbora[1], M. Krawczyk[3] and J. Gräfe[1] *1. Max Planck Institute for Intelligent Systems, Stuttgart, Germany; 2. Helmholtz-Zentrum Berlin fur Materialien und Energie, Berlin, Germany; 3. Adam Mickiewicz University, Poznan, Poland*

Over the last decade, magnonics [1] has proven to be a powerful candidate for wave-based computing. Their complex dispersion relation enriches them for applications by allowing for the coexistence of multiple wave modes with different wavelengths at the same excitation frequency [2]. However, the excitation and steering of spin waves with wavelengths relevant for nanoscale applications remains a challenge, which needs to be overcome to unlock their full potential. In this work, we present an antidot structure acting as a versatile spin wave converter or emitter while also revealing the full complexity of the spin wave dispersion. Figure 1a) displays the sample structure consisting of a 50 nm permalloy ($Fe_{20}Ni_{80}$) layer and two antidots. Running an rf-current through the antenna results in spin wave generation by the emitter antidot via the Schlömann effect [3] while the converter transforms long range Damon-Eshbach [4] waves into short backward volume waves. Usually, the wavelength is limited by the size of the smallest underlying exciting element, may it be magnetic or structural. Here, the emission and conversion is mediated by demagnetizing structures close to the antidots (<< 100 nm). Therefore, the emission and conversion method is able to generate spin waves of approximately 100 nm. Figure 1b) displays the experimental comparison between emitter and converter spectrum in reciprocal space. Using simulations [5] we propose a spin wave converter for the generation of a coherent spin wave beam while simultaneously utilizing its redirection capabilities for spin wave steering. Figure 2 displays two different points in time after the beginning of the rf-excitation. It can be seen that short wavelength spin wave propagate away from the antidot filling the entire channel at 45 ns. In summary, we presented a lithographically easily accessible system, which provides full knowledge about the complex magnon dispersion relation. The system is not only able to generate 100 nm spin waves but also provides utilities for spin wave steering.

[1] V. V. Kruglyak, S. O. Demokritov, and D. Grundler, J. Phys. D, 43, 260301 (2010). [2] H. Yu, G. Duerr, R. Huber, et al., Nat. Commun., 4, 2702 (2013). [3] E. Schlömann, J. Appl. Phys., 35, 159 (1964). [4] R. W. Damon and J. R. Eshbach, J. Phys. Chem. Solids, 19, 308 (1961). [5] A. Vansteenkiste, J. Leliaert, M. Dvornik, et al., AIP Adv., 4, 107133 (2014).

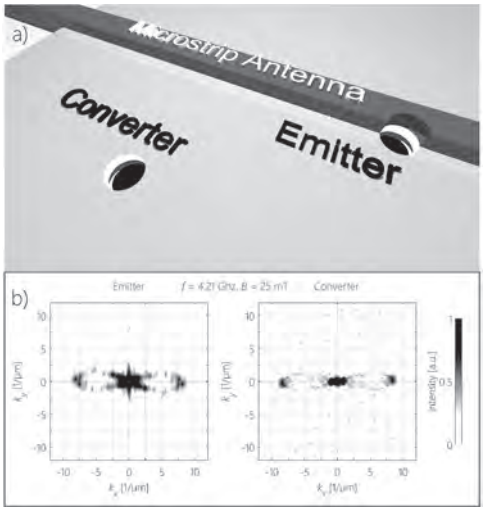

Figure 1: Experimental comparison of converter and emitter: a) Sample illustration (not to scale). b) Experimental reciprocal space.

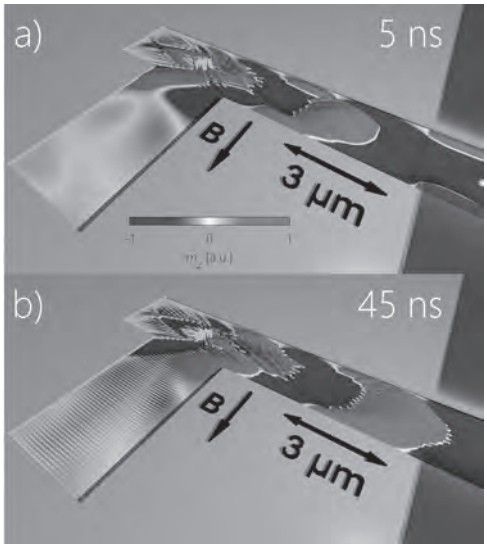

Simulation of a short wavelength spin wave channel.

E4-08. Nonreciprocal Propagation of Spin Waves in a Ni Film Excited Using Shear Strain Component of Rayleigh-Type Surface Acoustic Wave. *S. Tateno*[1] and Y. Nozaki[1,2] *1. Physics, Keio University, Yokohama, Japan; 2. Center for Spintronics Research Network, Keio University, Yokohama, Japan*

Surface acoustic wave (SAW) device has been widely utilized for radio-frequency filters and sensors with the high quality factor and low dissipation. Moreover, the dependence of the SAW amplitude on the propagation direction is applicable for both acoustic rectifier and isolator. In this study, we demonstrate the nonreciprocal SAW propagation in the SAW filter device with a ferromagnetic Ni waveguide [1]. Similar to the early work [2], a spin wave (SW) was excited magnetoelastically in the Ni waveguide on a piezoelectric LiNbO3 (LNO) substrate. In a Rayleigh-type SAW, there are two strain components, i.e. longitudinal and shear strains. The former is symmetric with respect to the SAW propagating direction (k), but the latter changes its sign when $-k$. It was reported that the shear strain lead to the nonreciprocal SAW attenuation via SW excitation [3]. We found that a huge nonreciprocity of the SW excitation could be realized by deeply embedding the Ni waveguide from the free surface. This is attributable to the relative increase in the shear strain. Figure 1 shows the schematic experimental

setup. Our SAW device consists of Ni(20 nm)/Si(400 nm) bilayered waveguide deposited between a pair of interdigital transducers (IDTs) on a LNO substrate. The amplitude of the SW excitation was evaluated from the SAW attenuation measured by a vector network analyzer. An in-plane external field ($\mu_0 H$) was applied at an angle θ from k. Figure 2 shows the reduced SAW attenuation ΔP^{norm} as functions of amplitude and angle of $\mu_0 H$. The SAW attenuation owing to the SW excitation was clearly asymmetric with respect to the polarity of $\mu_0 H$. The nonreciprocity of SW excitation was approximately 10 times larger than the case of single Ni waveguide [3], where a longitudinal shear strain was dominantly excited the SW.

[1] S. Tateno and Y. Nozaki, Phys. Rev. Applied 13, 034074 (2020). [2] M. Weiler, L. Dreher, C. Heeg, R. Gross, M. S. Brandt and S. T. B. Goennenwein, Phys. Rev. Lett. 106, 117601 (2011). [3] R. Sasaki, Y. Nii, Y. Iguchi and Y. Onose, Phys. Rev. B 95, 020407 (R) (2017).

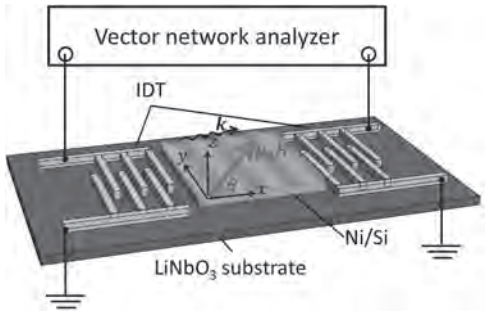

Schematic illustration of experimental setup. Ni/Si bilayer was deposited between a pair of IDTs on a LNO substrate. $\mu_0 H$ is applied at θ from x axis which corresponds to k.

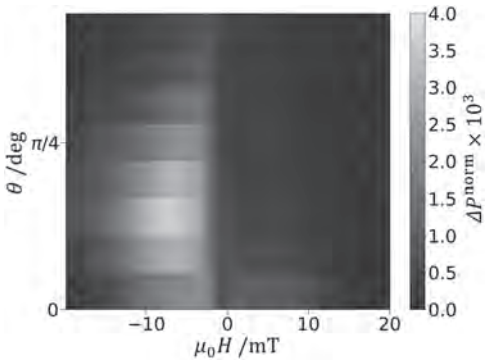

Color plot of ΔP^{norm} in H-θ plane. The magnitude of ΔP^{norm} is asymmetric with the polarity of $\mu_0 H$. The nonreciprocal ratio is reached up to 1200%, 10 times larger than in the previous report using a single Ni waveguide [3].

E4-09. Non-Linearities Induced by Surface Acoustic Waves in Magnetization Dynamics. *L. Thevenard*[1,2], M. Kraimia[3,1], P. Kuszewski[1,2], A. Lemaître[4,5], F. Margaillan[1,2], J. Duquesne[1,2] and C. Gourdon[1,2] *1. Institut des Nanosciences de Paris, Sorbonne Université, Paris, France; 2. Centre National de la Recherche Scientifique, Paris, France; 3. LR01ES15 Laboratoire de Physique des Matériaux, Faculté des Sciences de Bizerte, Bizerte, Tunisia; 4. Centre de Nanosciences et de Nanotechnologies, CNRS, Palaiseau, France; 5. Université Paris-Saclay, Palaiseau, France*

Spin waves can be excited by a radio-frequency (rf) real magnetic field or an effective one generated e.g. by a surface acoustic wave (SAW) using magneto-elasticity [1,2]. Thanks to their low attenuation, SAWs in the GHz frequency range are an ideal tool to address remotely magnetic structures and generate or actuate on spin waves quasi-resonantly, which could be implemented in magnonic devices. Although the dynamic strain created by the SAW remains weak (10^{-5}-10^{-3}), non-linear magnetization dynamics is acoustically induced even in moderately magnetostrictive ferromagnetic layers. In order to become of technological interest these non-linearities must be carefully characterized and modeled. Using a time- and spatially-resolved magneto-optical Kerr setup with laser detection synchronized to the SAW rf bursts [3], we evidence clear non-linear effects (frequency and wavevector doubling: f/2f and k/2k components, respectively) in the magnetization dynamics of a GaMnAs ferromagnetic layer [4]. Tuning the spin-wave frequency close to the SAW frequency by magnetic field and temperature the resonance behavior of both the f and 2f dynamical components are obtained. The dependence on these components on the strain amplitude reveals two regimes. In the low-strain regime the f (2f) component has a linear (quadratic) behavior with the SAW amplitude. We show that this regime is well accounted for by an all-analytical perturbative model of two coupled parametric oscillators [5] with SAW-dependent frequency, damping, coupling and force terms while the intrinsic magnetic non-linearities of the Landau-Lifschitz-Gilbert equation can be neglected. With increasing SAW amplitude, the f-component becomes sublinear and the peak of the SAW-induced ferromagnetic resonance curve shifts to lower magnetic field, which are signatures of the rising importance of intrinsic magnetic nonlinearities as shown by our numerical simulations. We thus reach a comprehensive description of the acoustically-driven magnetization dynamics, enabling further development of this magnon-phonon coupling.

[1] L. Dreher, M. Weiler, M. Pernpeintner et al., Phys. Rev. B 86, 134415 (2012). [2] L. Thevenard, C. Gourdon et al., Phys. Rev. B 90, 094401 (2014). [3] P. Kuszewski, J.-Y. Duquesne, L. Becerra et. al., Phys. Rev. Appl. 10, 034036 (2018). [4] M. Kraimia, P. Kuszewski, J.-Y. Duquesne et al., Phys. Rev. B 101, 144425 (2020). [5] C. L. Chang, A. M. Lomonosov, J. Janusonis et al., Phys. Rev. B 95, 060409 (2017).

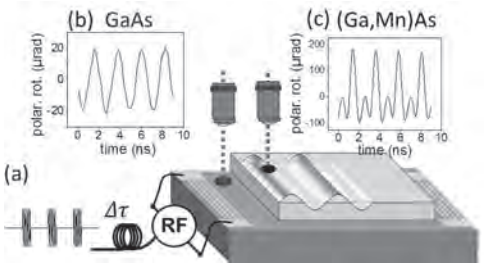

(a) Schematics of the experimental setup, (b) photo-elastic and (c) magneto-optical signals

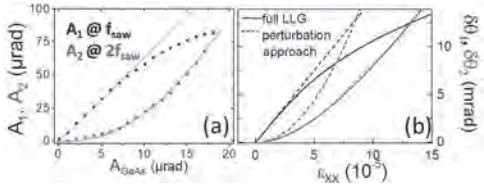

(a) Magneto-optical vs photo-elastic signal at f and 2f and (b) models

E4-10. Generation and Tuning of a Spin Wave Frequency Comb. *T. Hula*[1], L. Flacke[2,3], M. Copus[4], L. Liensberger[2,3], K. Schultheiss[1], A. Buzdakov[1], F.J. Gonçalves[1], A. Kákay[1], M. Weiler[2,3], R. Camley[4] and H. Schultheiss[1] *1. Helmholtz-Zentrum Dresden-Rossendorf, Dresden, Germany; 2. Walther-Meißner-Institute, Bayerische Akademie der Wissenschaften, Garching, Germany; 3. Physik-Department, Technische Universität München, Munich, Germany; 4. Center for Magnetism and Magnetic Nanostructures, University of Colorado, Colorado Springs, CO, United States*

Optical frequency combs are powerful tools used for synchronization, stabilization and frequency conversion in both fundamental science and technical applications. In this work, we present experimental observations on the generation of a spin wave frequency comb in a low damping $Co_{25}Fe_{75}$ conduit measured using Brillouin light scattering microscopy. By driving

the magnetization to large precession angles, nonlinear interactions such as four magnon scattering can be observed. When applying two RF signals with independently tunable frequencies and amplitudes to our microstructure, we can actively control the final states that will be populated by these scattering processes. Our results show the generation of a frequency comb, consisting of several spin waves with adjustable frequency spacing and amplitude. We demonstrate that the known effect of frequency mixing for k=0 modes [1] can be extended towards propagating spin waves. This enables simultaneous information transport and processing. This behaviour is studied for different sample geometries, which allow mixing of co-propagating as well as counter-propagating spin waves. Our observations are in qualitative agreement with micro magnetic simulations. The presented data encourage a deeper understanding of the interaction of propagating spin waves in the nonlinear regime and propose utilization of spin wave frequency combs as broadband tunable clocks for information processing. The authors acknowledge financial support from the Deutsche Forschungsgemeinschaft within programs SCHU 2922/1-1, WE5386/4-1 and WE5386/5-1. K. S. acknowledges funding within the Helmholtz Postdoc Programme.

[1] Marsh, J., & Camley, R. E., Physical Review B - Condensed Matter and Materials Physics, 86(22), 224405 (2012)

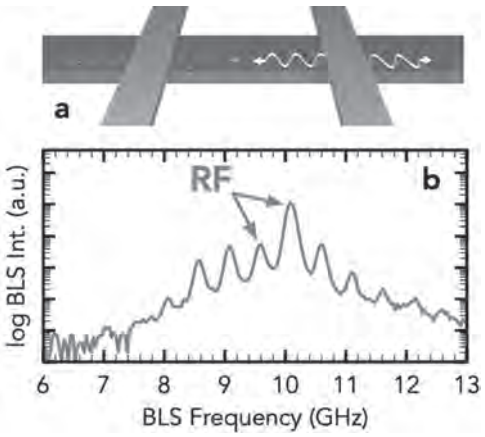

E4-11. Electrical Spectroscopy of Forward Volume Spin Waves in Perpendicularly Magnetized Materials. M. Sushruth[1], M.G. Grassi[2], K. Ait-Oukaci[3,4], D. Stoeffler[2], Y. Henry[2], D. Lacour[3], M. Hehn[3], U. Bhaskar[1], M. Bailleul[2], T. Devolder[1] and *J. Adam*[1] *1. Universite Paris-Saclay, Saint-Aubin, France; 2. Universite de Strasbourg, Strasbourg, France; 3. Institut Jean Lamour, Nancy, France; 4. Synchrotron SOLEIL, Gif-sur-Yvette, France*

Spin waves (SWs) are attractive for future wave-based-computing applications since they have easy-to-tune wavelengths from the macroscopic scale to the sub-micron scale at GHz frequencies. Information can be stored in the amplitude and phase of the SWs and transported through a thin magnetic material conduit. Isotropic SWs like the forward volume spin waves (FVSW) enable for SW based transmission, and processing of information in any arbitrary direction such as logic operations [1]. And, materials with both a perpendicular magnetic anisotropy (PMA) and a large magnetization-thickness product would be much preferred for FVSW applications [2]. We study the potential of all-electrical inductive techniques for the spectroscopy of propagating FVSW and we apply this to the case of perpendicularly magnetized Co/Ni multilayers. We develop a one-dimensional model to account for the electrical signature of spin-wave reflection and transmission between inductive antennas and validate it with experiments. We describe the influence of the antennae geometry and of the material parameters on the lineshape of the inductive signals. For a finite damping, the broadband character of the antenna emission in the wave vector space imposes to take into account the growing decoherence of the magnetisation waves upon their spatial propagation. The transmission signal results from two contributions: (i) from propagating spin-waves leading to an oscillatory phase of the broadband transmission coefficient, and (ii) from the distant induction of ferromagnetic resonance because of the long-range stray fields of realistic antennas. Depending on the ratio of these two contributions, the transmitted signal decay may not be exponential with the propagation distance and the oscillatory character of the spin-wave phase may be hidden. Our model and its experimental validation (Fig. 1) allow to define geometrical and material specifications to be met to enable the use of forward volume spin waves as efficient information carriers.

[1] S. Klingler *et al.*, Applied Physics Letters, Vol. 106, p. 212406 (2015)
[2] J. Han *et al.*, Science, Vol. 366, p. 1121-1125 (2019)

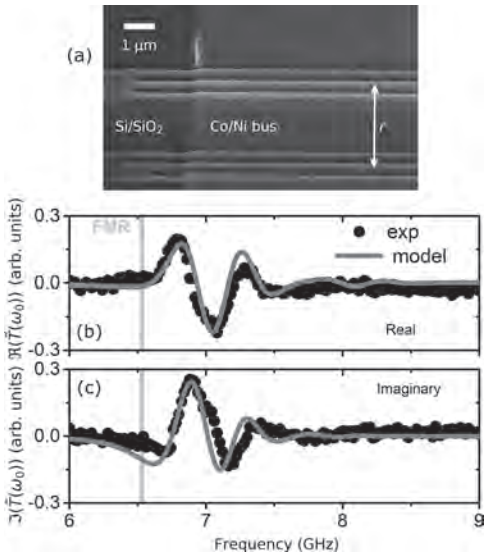

Fig. 1: (a) Colorised scanning electron micrograph of a device with CPW antennas on a Co/Ni multilayer. The scale bar is 1µm. (b) Real and (c) imaginary parts of the experimental transmission parameter and fits.

E4-12. Amplification of Propagating Spin Waves by Rapid Cooling. *M. Schneider*[1], D. Breitbach[1], B. Lägel[1], C. Dubs[2], H. Musiienko-Shmarova[1], D.A. Bozhko[5], A.A. Serga[1], A.N. Slavin[3], V. Tyberkevych[3], P. Pirro[1], B. Hillebrands[1] and A. Chumak[4] *1. Fachbereich Physik and Landesforschungszentrum OPTIMAS, TU Kaiserslautern, Kaiserslautern, Germany; 2. Innovent e.V. Technologieentwicklung, Jena, Germany; 3. Department of Physics, Oakland University, Rochester, MI, United States; 4. Faculty of Physics, University of Vienna, Vienna, Austria; 5. Department of Physics and Energy Science, University of Colorado at Colorado Springs, Colorado Springs, CO, United States*

Recently, the formation of a magnon Bose-Einstein Condensate (BEC) triggered by the rapid cooling of magnonic nano-structures was reported [1]. A rapid decrease in the phonon temperature achieved by the application of DC pulses to a nano-sized YIG/Pt sample leads to a non-equilibrium between the phononic and the magnonic system. This results in a redistribution of magnons to the lowest frequencies of the spectrum. Here we report on the application of such a non-equilibrium, showing the possibiltiy to amplify coherently excited spin waves. The structures under investigation (see Fig. 1) consist of a 34 nm thin and 2 µm broad YIG-waveguide. A 3 µm long area is covered with a 7 nm thin layer of platinum, and an antenna allows for the excitation of a propagating spin-wave packet. The magnetization dynamics is investigated using time-resolved micro-focussed Brillouin light scattering spectroscopy. After the applied DC pulse is switched off, a spin wave pulse excited by the antenna is propagating in the waveguide region below the Pt covered area during rapid cooling. Depending on the time-delay between the DC-pulse and the spin-wave package, an amplification of the propagating spin wave is observed (see Fig. 2). This research does not only show the applicability of the phenomenon of rapid cooling to compensate the intrinsic damping in spintronic devices [2], but also gives insight to new

physics, namely the interaction of a prepared coherent state with the rapid cooling induced quantum state of the magnon BEC. This research has been supported by ERC StG 678309 MagnonCircuits, ERC ADG 694709 SuperMagnonics and DFU Grant DU 1427/2-1.

[1] M. Schneider, T. Brächer, D. Breitbach, et. al., Bose-Einstein Condensation of Quasi-Particles by Rapid Cooling, Nat. Nanotechnol. 15, 457–461 (2020) [2] Q. Wang, M. Kewenig, M. Schneider, et. al., Realization of a nanoscale magnonic directional coupler for all-magnon circuits, arXiv:1905.12353

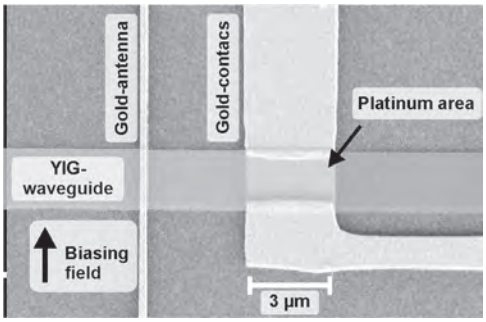

Colored SEM-image of the structure under investigation. The purple parts indicate the 2 µm broad YIG-waveguide. On top there is a gold-antenna (left side) to excite spin waves and a Pt-covered area (blue) allows for the application of DC-pulses.

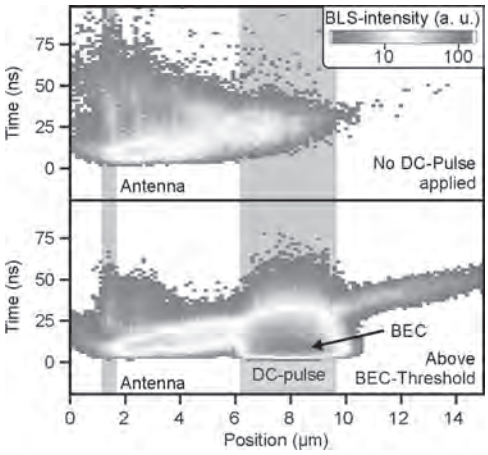

BLS intensity on a logarithmic scale over the time (y-axis) along the waveguide (x-axis). Upper panel: No DC-current is applied to the Pt-area. Lower panel: A DC-current above the threshold of BEC is applied. BEC is visible in the large intensity below the Pt-area after the pulse. Propagation distance of the spin wave packet is substantially increased.

E4-13. Investigation of Spin Wave - Skyrmion Interactions for Magnonic Information Processing. *Z. Hu*[1], Y. Shao[1], V. Lopez Dominguez[1] and P. Khalili Amiri[1] *1. Northwestern University, Evanston, IL, United States*

Magnonic computing (MC) architectures based on spin waves are increasingly of interest for special-purpose computing applications [1]. MC offers advantages over conventional charge-based computing [2-5], including low power dissipation (magnon propagation does not require charge transfer), and incorporation of phase information in addition to amplitude, reducing the component count needed for certain logic operations [6]. One of the challenges in the realization of most MC concepts is that they require an efficient means for routing magnons in complex networks. In particular, a scalable, nonvolatile, and reconfigurable mechanism to do so is currently lacking [6,7]. Here we address this challenge by utilizing a Néel skyrmion as a programmable scattering center to route magnons. The skyrmion is stabilized by the interfacial Dzyaloshinskii-Moriya Interaction (DMI) and perpendicular magnetic anisotropy (PMA), which itself can be controlled by electric fields via the voltage-controlled magnetic anisotropy (VCMA) effect, making the magnon-skyrmion interaction tunable by voltage. We investigate the interaction of exchange spin waves with wavelength of 26 to 190 nm, with skyrmions having diameters from 9 to 74 nm. Our micromagnetic simulations show that the propagation, scattering angle, and energy transmission of spin waves can be effectively controlled by tuning the ratio of magnon wavelength to the skyrmion diameter, which depends strongly on PMA and DMI. Based on this approach, we propose a new skyrmionic magnon switch (SMS) device, which provides voltage-controlled routing of spin waves in a magnetic wire and can be applied to build basic logic circuits. We simulate the SMS performance using typical material parameters for thin ferromagnetic films supporting skyrmions, and assess the requirements for its experimental realization.

[1]. Khalili P, Wang K L. IEEE Spectrum, Vol.52(7), p.30-56(2015) [2]. Wang, K.L. and P. Khalili Amiri, SPIN, Vol.02(02), p.1250009(2012) [3]. Khitun, A., D.E. Nikonov, and K.L. Wang, Journal of Applied Physics, Vol.106(12), p.123909(2009) [4]. Dutta, S., et al., Scientific Reports, Vol.5, p.9861(2015) [5]. Cherepov, S., et al., Applied Physics Letters, Vol.104(8), p.082403(2014) [6]. Shabadi, P., et al., SPIN, Vol.02(03), p.1240006(2012) [7]. Vogt, K., et al., Applied Physics Letters, Vol.101(4), p.042410(2012)

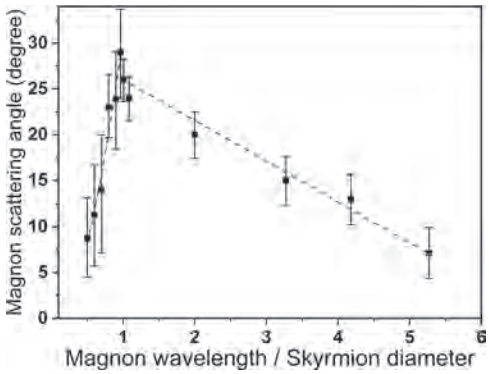

Figure 1. Magnon scattering angle as a function of the ratio of magnon wavelength to skyrmion diameter. The scattering angle is maximized when the wavelength and skyrmion diameter are comparable in size.

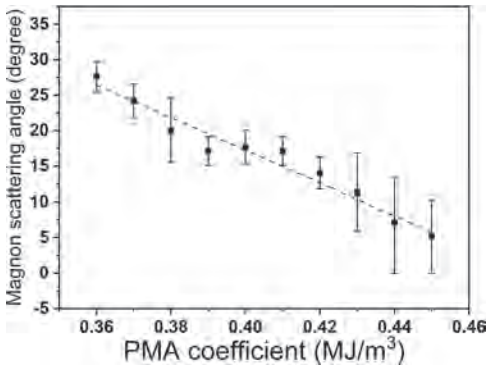

Figure 2. Dependence of magnon scattering angle on PMA coefficient. Larger PMA reduces the skyrmion size relative to the magnon wavelength, reducing the scattering angle.

E4-14. Magnon Diffusion Lengths in Bulk and Thin Film Fe_3O_4 for Spin Seebeck Applications. *K. Morrison*[1], G. Venkat[1,2], C. Cox[1], D. Voneshen[3], A. Caruana[3], A. Piovano[4] and m. cropper[1] *1. Physics, Loughborough University, Loughborough, United Kingdom; 2. Materials Science and Engineering, The University of Sheffield, Sheffield, United Kingdom; 3. ISIS Neutron and Muon Source, Didcot, United Kingdom; 4. Institut Laue-Langevin, Grenoble, France*

The spin Seebeck effect (SSE) is defined as the generation of a pure spin current (J_s) when a magnetised material is subjected to a temperature gradient. [1] To detect J_s, a thin non-magnetic [NM] layer such as Pt, is deposited on top of the material of interest. This converts J_s into an observable thermoelectric voltage (V_{SSE}) by way of the Inverse Spin Hall Effect (ISHE). It is of interest for thermoelectric and spintronic applications where it could be used to harvest electricity, or produce a pure spin current, respectively. The spin Seebeck effect can be phonon or magnon driven, therefore investigating the thermomagnetic voltage V_{SSE} as a function of temperature can enable separation of these contributions – particularly in non-insulating materials such as Fe_3O_4 which undergoes a semiconductor-insulator phase transition at approximately 120 K.[2],[3] We have developed a measurement of V_{SSE} as a function of temperature using the heat flux method [4][5], which enables accurate measurement of thin film samples. We will show how this technique can be used to investigate subtle changes in the SSE as a function of temperature and correlate this with measurement of the magnon dispersion in single crystal Fe_3O_4 using time of flight (TOF) inelastic neutron scattering (INS). We find an upper limit of the magnon diffusion length (MDL) of 34 ± 7 nm determined from bulk INS (Figure 1). Corresponding SSE measurements of Fe_3O_4 thin films as a function of thickness indicate an MDL of 19 ± 2 nm, which does not change significantly between 300 and 50 K.[6] We also find that the low energy magnon modes are steeper than previously reported[7] and broaden with increasing temperature (Figure 2).

[1] K. Uchida *et al.*, *Nature*, 455, 778 (2008) [2] A. Caruana *et al.*, *Phys. Status Solidi: RRL*, 10, 613-617 (2016) [3] E. J. W. Verwey, *Nature*, 144, 327 (1939) [4] A. Sola *et al.*, *Sci. Rep.* 7 46752 (2017) [5] G. Venkat *et al.*, arXiv:2003.07925, submitted to *Rev. Sci. Instrum.* [6] G. Venkat *et al.*, arXiv:2001.03738, accepted to *Phys. Rev. Mat.* (2020) [7] R. J. McQueeney *et al.*, *Phys. Rev. B* 73 174409 (2006)

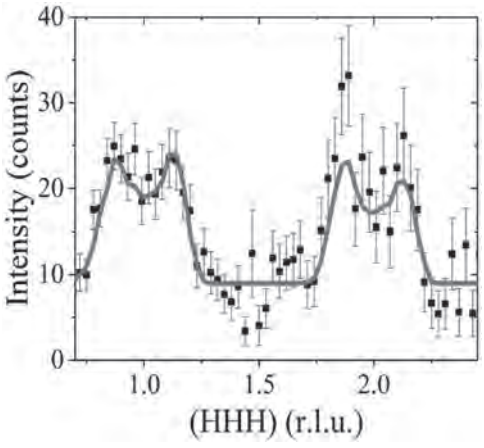

Figure 1 - Representative line cut along q and integrated in energy from 20-30 meV, fit (shown in red) to the simulated neutron intensity for the Fe_3O_4 magnetic structure.

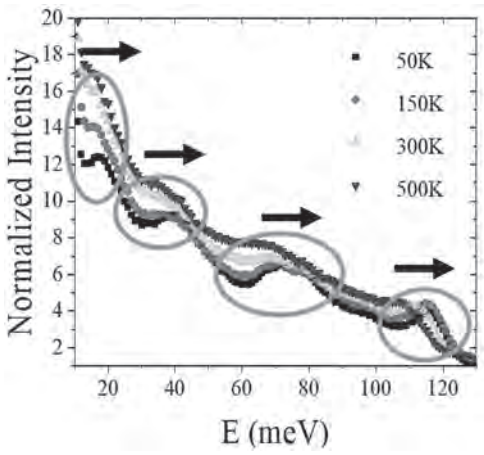

Figure 2 - Energy variation of scattered neutron intensity, integrated over all reciprocal space directions. arrows indicate the blue shift of magnon modes with decreasing temperature.

Session E5
DOMAIN WALLS AND THE DZYALOSHINSKII-MORIYA INTERACTION I (Poster Session)

Jun-young Kim, Co-Chair
Johannes Gutenberg University of Mainz, Mainz, Germany
Luis Lopez-Diaz, Co-Chair
University of Salamanca, Salamanca, Spain

E5-01. Ultrafast Domain Wall Propagation due to the Interfacial Dzyaloshinskii-Moriya Interaction. *D. Mancilla*[1], R. Jaeschke-Ubiergo[2], A. Núñez[2] and S. Allende[1] *1. Universidad de Santiago de Chile, Santiago de Chile, Chile; 2. Universidad de Chile, Santiago de Chile, Chile*

The study of the dynamical properties of curved ferromagnetic systems has become fertile ground for potential applications in spintronic devices, such as memory devices and microwave technologies, among others [1]. In particular, ferromagnetic nanotubes present a Dzyaloshinskii-Moriya-like interaction that arises from their curvature. This induces a chiral symmetry breaking in the domain walls (DW) dynamics [2]. In this way, an interesting competition is expected if the system is engineered to display an actual Dzyaloshinskii– Moriya interaction (DMI) as well. While the effect of the volumetric DMI has been studied in ferromagnetic nanotubes [3], the behaviour when an interfacial DMI is present has not been fully studied yet. In this work, we theoretically study the effect that interfacial DMI has on the average velocity of a vortex DW in thin ferromagnetic nanotubes grown around a core composed of heavy atoms. It is observed that by delaying the Walker breakdown instability, the DW average velocity is of the order of 10^3 m/s [4], which is greater than usual values for these systems. The remarkable velocities achieved through this configuration could greatly benefit the development of spintronic devices. We acknowledge financial support in Chile from FONDECYT 1161018, 1190324, and Financiamiento Basal para Centros Científicos y Tecnológicos de Excelencia FB 0807. D. M.-A. acknowledges Postdoctorado FONDECYT 2018 3180416.

[1] R. Streubel, et al., J. Phys. D: Appl. Phys. 49, 363001 (2016). [2] J. A. Otálora, et al., J. Magn. Magn. Mater. 341, 86-92 (2013). [3] A. Goussev A, et al., Phys. Rev. B 93, 054418 (2016). [4] D. Mancilla-Almonacid, et al., Nanotechnology 31, 125707 (2020).

E5-02. Ta/CoFeB/MgO Analysis for Low Power Nanomagnetic Devices. *F. Riente*[2], S. Mendisch[1], L. Gnoli[2], V. Ahrens[1], M. Ruo Roch[2] and M. Becherer[1] *1. Technische Universitat Munchen, Munchen, Germany; 2. Politecnico di Torino, Torino, Italy*

Magnetic materials with perpendicular magnetic anisotropy, such as thin films based on CoFeB alloys, are gaining interest and have accelerated the development of high-density non-volatile memories. The requirement of high memory bandwidth for next-generation computing systems moved the attention to the development of devices that can combine storage and logic capabilities. The High Bandwidth Memory interface for 3D-stacks DRAM chips is just one example. Domain wall-based spintronic devices intrinsically combine both these requirements making them suitable both for non-volatile storage and computation. Among all the proposed logics, perpendicular nanomagnetic logic (pNML) takes advantage of magnetic dipole coupling to propagate and elaborate information. The materials explored in literature for its realization such as Co/Pt and Co/Ni were the technology drivers [1], but for power constraints and depinning fields, novel CoFeB/MgO layers are investigated for low power and high-density computing devices. Ta/CoFeB/MgO ultrathin films show significantly lower coercivities, even with high perpendicular anisotropy (PMA) [2], thus becoming very promising candidates for low power pNML devices. In this paper, we investigate different Ta/CoFeB/MgO stacks at the simulation and experimental level, to show their potential for the next generation of magnetic logic devices. The micromagnetic simulations are used to support the experiments. We focus, first, on the magnetostatic analysis of magnetic islands quantifying the stray field that can be achieved with different layout topologies. Then, at the experimental level, we measure the coercivity of films with different thicknesses, Ms from SQUID measurements to estimate the coupling strength achievable between neighboring magnetic islands and measure the domain wall speed on magnetic nanowires. Our results show that the achieved coupling is strong enough to realize logic computation with magnetic islands, moving a step forward in the direction of low power perpendicularly magnetized logic devices.

[1] S. Breitkreutz et al., in IEEE Transactions on Magnetics, vol. 49, no. 7, pp. 4464-4467 (2013) [2] T Devolder et al., Journal of Applied Physics, 113(20):203912, (2013).

E5-03. Phase Transitions Induced by Concentration and Thermodynamic Magnetic Fluctuations in Chiral Ferromagnets $Fe_{1-x}Co_xSi$. A. Povzner[1], A. Volkov[1], T. Nogovitsyna[1] and *S. Bessonov*[1] *1. Ural'skij federal'nyj universitet imeni pervogo Prezidenta Rossii B N El'cina, Ekaterinburg, Russian Federation*

The fluctuation theory of concentration and thermodynamic magnetic phase transitions in chiral helicoidal ferromagnetic binary and quasi-binary alloys with the Dzyaloshinsky-Moriya interaction is being developed. The ground state is described based on the LDA+U+SO approximation with additional allowance for concentration fluctuations associated with the difference in the potentials of intra-atomic Hubbard interaction at the sites. The functional of free energy of electronic and magnetic subsystems with thermodynamic and concentration spin fluctuations is constructed. The equations of magnetic state obtained from the conditions of the saddle point allow us to consider the conditions for the realization of the phases of the helicoidal long-range and short-range orders with right and left magnetic chirality. Solutions of the equations of magnetic state are considered on the example of quasi-binary alloys $Fe_{1-x}Co_xSi$, which are the main prototypes of materials of modern spintronics. h-T diagrams of spin phases arising due to the concentration shift of the chemical potential and concentration magnetic fluctuations with a change in the concentration x were constructed. It was found that, in the concentration range $0.05<x<0.2$, the left-chiral helicoidal order is realized, and concentration fluctuations increase, and the Fermi level remains near the edge of the zone. At $0.2<x<0.5$, the Fermi level is in the region of the local minimum of DOS and a crossover of the thermodynamic and concentration magnetic phase transition occurs, accompanied by a change in the mode-mode parameter sign and the formation of skyrmion microstructures. A further increase in the cobalt concentration leads to a weakening of concentration fluctuations, and for $0.5<x<0.65$, the left-chiral long-range order is again realized. At $x=0.65$, the chemical potential appears at the DOS maximum and a topological transition to the right chiral helicoid is realized. Calculations show that such a magnetic order is maintained up to $x=0.8$, after which a region of paramagnetic compositions arises.

E5-04. Withdrawn

E5-05. Design of Giant DMI and its Microscopic Origin in Magnetic Bilayers. *P. Jadaun*[1], L.F. Register[1] and S.K. Banerjee[1] *1. Electrical and Computer Engineering, The University of Texas at Austin, Austin, TX, United States*

Magnetic skyrmions are compact spin textures that show remarkably unique, particle-like properties. They are widely regarded as promising candidates for emergent magnetic devices as they are small in size and easily maneuverable [1]. The Dzyaloshinskii-Moriya interaction (DMI) is often critical to the generation and manipulation of skyrmions. However, there has been a fundamental lack of understanding of the microscopic origin of DMI or the mechanisms by which DMI stabilizes skyrmions in magnetic bilayers. Little has been known of the material parameters that determine the value of DMI. This knowledge is critical for rational design of skyrmion-hosting materials and further development of skyrmion technology [2]. Here, we address this knowledge gap and present a model to explain the microscopic origin of DMI in heavy metal/ferromagnet (HM/FM) bilayers. We calculate the DMI values in a series of HM/FM bilayers and explain the trend of DMI values observed [3]. We present a new theoretical model that explains the microscopic origin of DMI in these bilayers. We show that the value of DMI depends on two parameters, namely, interfacial hybridization and orbital contributions of the heavy metal. Using these parameters, we explain the experimentally observed DMI trends. Additionally, we report four new materials systems predicted to demonstrate giant DMI. In HM/FM bilayers, the size and stability of DMI-stabilized-skyrmions is decided by the interplay between the DMI, the exchange constant, the out-of-plane anisotropy and dipolar fields. Due to their giant DMI, our newly discovered materials are promising for hosting small sized skyrmions at room-temperature, enabling ultra-dense, ultra-low power skyrmion devices. Together, our results put forth a new understanding of DMI, discover promising materials and suggest pathways for the controlled generation of skyrmions.

1. A. Fert, V. Cros, and J. Sampaio, Nature nanotechnology, Vol. 8, p. 152 (2013) 2. W. Jiang et al., Physics Reports, Vol. 704, p. 1-49 (2017). 3. P. Jadaun, L. F. Register and S. K. Banerjee, npj Computational Materials, Vol. 6, p.88 (2020)

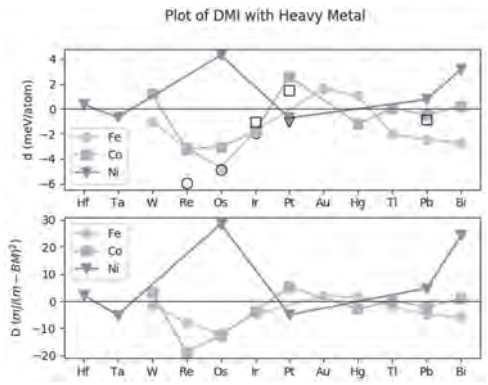

Plots of Dzyaloshinskii-Moriya interaction (DMI) for a series of HM/FM bilayers. Our DMI results are plotted with filled markers, whereas corresponding DMI values in literature are plotted using unfilled black markers. Circles represent Fe, squares represent Co and triangles represent Ni. The unit of D is mJ/(m-BM)^2, where BM is the Bohr magneton.

E5-06. Density Functional Theory and Machine Learning Aided Design of Novel B20 Alloys. *P. Balachandran*[1,2] *1. Materials Science and Engineering, University of Virginia, Charlottesville, VA, United States; 2. Mechanical and Aerospace Engineering, University of Virginia, Charlottesville, VA, United States*

Chiral magnets in the B20 crystal structure host a peculiar spin texture in the form of a topologically stable skyrmion lattice. However, the helical transition temperature (T_C) of these compounds is below room temperature, which limits their potential in spintronics applications. Here, a data-driven approach is demonstrated, which integrates density functional theory (DFT) calculations with machine learning (ML) in search of alloying elements that will enhance the T_C of known B20 compounds. Initial DFT screening led to the identification of chromium (Cr) and tin (Sn) as potential substituents for alloy design. Then, trained ML models predict Sn substitution to be more promising than Cr-substitution for tuning the T_C of FeGe. The magnetic exchange energy calculated from DFT validates the promise of Sn as an effective alloying element for enhancing the T_C in Fe(Ge,Sn) compounds. New B20 chiral magnets are recommended for experimental investigation.

1. P.V. Balachandran, Journal of Materials Research., Vol. 35, p.890-897 (2020)

E5-07. Effect of the Temperature Annealing-Driven Structural Modification on the Interfacial Dzyaloshinskii-Moriya Interaction in Ru/Co/W/Ru Films. *A. Samardak*[1], A. Kolesnikov[1], M. Stebliy[1], A. Gerasimenko[2], A. Sadovnikov[3], S. Nikitov[4], A. Ognev[1] and A.S. Samardak[1] *1. Far Eastern Federal University, Vladivostok, Russian Federation; 2. Institute of Chemistry, Far Eastern Branch of Russian Academy of Sciences, Vladivostok, Russian Federation; 3. Laboratory "Metamaterials", Saratov State University, Saratov, Russian Federation; 4. Kotel'nikov Institute of Radioengineering and Electronics, Russian Academy of Sciences, Moscow, Russian Federation*

Ultrathin magnetic films sandwiched between to heavy metals are a source of intriguing spin-related phenomena such as spin Hall effect, spin-orbit torques, antisymmetric exchange due to the interfacial Dzyaloshinskii-Moriya interaction (DMI), chiral damping and non-trivial spin textures, namely, skyrmions, skyrmioniums, merons and bimerons [1]. In this work we study the structural transformation of interfaces in a series of Ru/Co/W/Ru films sputtered by magnetron [2] and annealed in the temperature range from 100 to 250°C. Ru and W are used as heavy metals with the opposite signs of DMI: it is negative for Ru/Co and positive for W/Co. As a result, we observe additive effect of the negative DMI from the bottom Ru/Co and the top Co/W interfaces [3]. We vary the thickness of W in the range from 0 to 0.3 nm with the step of 0.01 nm. We define the maximum effective DMI (D_{eff}=-3.1 mJ/m^2) for t_W=0.23 nm. We demonstrate the significant increase of DMI after annealing of all samples at T_{an} ranging from 200 to 240°C and the sequential decrease after the thermal treatment at T_{an}=250°C. The changes of DMI is explained by the structural modification of layers affecting the interface quality, which was estimated by x-ray reflectometry. The degree of atom intermixing at Ru/Co and Co/W interfaces changes with increasing annealing temperature up to 240°C promoting an enhancement of perpendicular magnetic anisotropy and the interfacial Dzyaloshinskii-Moriya interaction. Further annealing at 250°C brings the interface deterioration and, consequently, a drastic degradation of magnetic properties. The Ru/Co/W/Ru films are the decent counterpart of the widely-used Pt/Co-based systems, because they possess the large PMA and DMI and can be used for realization of skyrmion-based devices. Moreover, the modified

Ru/Co/Ru/W films are interesting for SOT-induced magnetization switching [4]. This work was supported by the Russian Ministry of Science and Higher Education (the state task 0657-2020-0013).

[1] F. Hellman, A. Hoffmann, Y. Tserkovnyak, et al. Reviews of Modern Physics, 89, 025006 (2017). [2] A.G. Kolesnikov, A.V. Ognev, M.E. Stebliy, et al. Journal of Magnetism and Magnetic Materials, 454, 78-84 (2018). [3] A.S. Samardak, A.G. Kolesnikov, M.E. Stebliy, et al. Applied Physics Letters, 112,192406 (2018). [4] M.E. Stebliy, A.G. Kolesnikov, A.V. Ognev, et al. Physical Review Applied, 11, 054047 (2019).

E5-08. Experimental Correlation of Interfacial Dzyaloshinskii-Moriya Interaction Amplitude and Work Function in Magnetic Multilayers.
F. Ajejas[1], W. Legrand[1], Y. Sassi[1], S. Collin[1], A. Vecchiola[1], K. Bouzehouane[1], S. Pizzini[2], N. Reyren[1], V. Cros[1] and A. Fert[1] *1. Unite Mixte de Physique CNRS/Thales, Palaiseau, France; 2. Institut NEEL, Grenoble, France*

Magnetic multilayers (MML) with large perpendicular magnetic anisotropy (PMA) and Dzyaloshinskii-Moriya interaction (DMI) have attracted great attention in recent years owing to the possibility of stabilizing non-collinear magnetic textures such as chiral domain walls (DW) [1], spin spirals [2] or skyrmions [3-4] with Neeel chiral spin rotation. The latter are promising candidates as carriers of information for next-generation race-track magnetic memories or logic devices. To this aim, the accurate experimental determination of DMI is an important challenge allowing the engineering of future devices with tailored properties. The determination of the effective DMI amplitude D in MML is still a current subject of research, in particular for metallic multilayers with a high number of repetitions. In this study, we have performed a series of measurements to determine DMI values by two different techniques: domain size periodicity (λ) [5] of aligned-stripe domains after in-plane (IP) demagnetization by magnetic force microscopy (MFM), and asymmetric expansion of domains in the presence of an in-plane magnetic field, by Kerr microscopy [6-7]. For this purpose, we selected different materials to build asymmetric trilayers, with the general structure is $[Pt/Co/M]_{xN}$ with M = Ru, Ni, Pd, Al, Al/Ta and N = 2, 3, 4, 5, 6 the number of repetitions. We observe a correlation between $D_s = D/t$ (t is the Co thickness), the interfacial DMI obtained in the previous methods and intrinsic material parameters such as atomic number (Z), Pauling electronegativity (χ) [8] work function (Wf) [9] of Co/M interfaces. We find a clear linear behaviour between D_s and Wf. This correlation points to Rashba-like interfacial fields, leading to the modulation of the effective interfacial DMI. French ANR grant TOPSky TOPSKY (ANR-17-CE24-0025) and DARPA TEE program grant (MIPR#HR0011831554) and EU grant SKYTOP (H2020 FET Proactive 824123) are acknowledged for their financial support.

[1] A. Thiaville *et al.* EuroPhys. Lett, 100, 57002 (2012) [2] P. Ferriani *et al*. Phys. Rev. Lett. 101, 27201 (2008). [3] A. Fert, N. Reyren, V. Cros, Nat. Rev. Mat. 2, 17031 (2017). [4] C. Moreau-Luchaire *et al*. Nature Nanotechnology 11, 444 (2016) [5] I. Lemesh *et al.* Physical Review B 95, 174423 (2017) [6] F. Ajejas *et al.* Appl. Phys. Lett. 111, 202402 (2017); [7] T. Ha Pham *et al EPL* 113 67001 (2016) [8] H. Jia *et al.* Phys. Rev. M 4, 024405 (2020) [9] Y.-K. Park *et al.* NPG Asia Materials 10*,* 995 (2018)

E5-09. Withdrawn

E5-10. Investigation of Interfacial Dzyaloshinskii-Moriya Interaction and Ferromagnetic Resonance of MBE Grown W/Co/Pt Heterostructures.
S.K. Jena[1], R. Islam[2], E. Milinska[1], M. Jakubowski[1], A. Pietruczik[1], R. Minikayev[1], W. Paszkowicz[1], S. Lewinska[1], A. Lynnyk[1], R. Puzniak[1], I. Sveklo[3], P. Aleshkevych[1], C. Autieri[2], A. Maziewski[3] and A. Wawro[1]
1. Institute of Physics, Polish Academy of Sciences, Warsaw, Poland; 2. International Research Centre MagTop, Institute of Physics, Polish Academy of Sciences, Warsaw, Poland; 3. Faculty of Physics, University of Bialystok, Bialystok, Poland

The interfacial Dzyaloshinskii-Moriya interaction (iDMI) [1,2] is responsible for the chiral magnetic spin structure creating like vortex or skyrmions which are potential candidates for data storage in thin film technology. Here, we show the value of iDMI at the interface of heavy metal (Pt and W) and magnetic material (Co) in epitaxial $[W(10A)/Co(6A)/Pt(10A)]_{20}$ heterostructure. The iDMI strength has been calculated which approximately equals to 2.55 mJ/m^2 by K_{eff} method with considering magnetic exchange constant A=13pJ/m [3]. Apart from this, the strength of iDMI 2.56 mJ/m^2 has been calculated by first principle calculation with fcc lattice structure of W/Co/Pt which agrees to our experimental value of iDMI. Further, the micromagnetic simulation has been performed to calculate the domain wall width. Results of simulations correspond to the MFM image of labyrinth domains at remanence. Estimated from micromagnetic simulation iDMI value agrees with the results obtained by other methods. The investigations of magnetic dynamics have been performed by VNA-FMR and cavity FMR. We observed different types of resonances by exciting the sample in the presence of GHz frequency and static magnetic field. The gilbert damping has been calculated which is equal to 0.027 for the particular frequency of 9.387 GHz. With increasing the magnetic field, from lower to higher, the two types of resonance occur which are interpreted as Kittle resonance and labyrinth domains resonance (Fig-1). Whereas, with the decreasing field the three types of resonance are observed i.e. Kittle and labyrinth domains resonance and we are expecting the third kind of resonance is due to the presence of iDMI which gives the chiral structure e.g. skyrmions which recently have been studied in the reference paper[4,5]. We also observe the dependence of resonance due to labyrinth domains upon the history of the magnetic field, whereas for other resonances such dependence is not seen.

1. I.E. Dzyaloshinskii, JETP Lett., 5, 259-1262 (1957). 2. T. Moriya, Phys. Rev., 91,10 (1960). 3. W. Legrand, J Chauleau, D Maccariello, *et al.,* 4, eaat0415 (2018). 4. B. Satywali, F. Ma, S. He, *et al.,* arxiv:1802.03979(2018). 5. T. Schwarze, J. Waizner, M. Garst, *et al., Nat. Mater.* 14, 478 (2015).

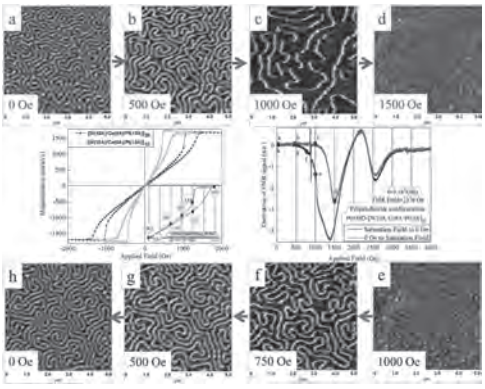

Fig.1 shows the magnetisation reversal and its corresponding magnetic domain at the different applied magnetic fields. The MFM images in Fig.1. a,b,c,d,e,f,g and h are the corresponding domain structure at different field as mentiond the points in Hysteresis loop and FMR-spectra.

E5-11. Withdrawn

E5-12. Magneto-Transport Studies in Gd-Fe Thin Films. *H.N. Mohanty*[1], A.K. Sahoo[1], J.A. Chelvane[2] and J.R. Mohanty[1] *1. Physics, Nanomagnetism and Microscopy Laboratory, Department of Physics, Indian Institute of Technology Hyderabad, Kandi, Sangareddy 502285, Telangana, India, Hyderabad, India; 2. Defence Metallurgical Research Laboratory, Hyderabad 500058, India, Hyderabad, India*

Tuning the perpendicular magnetic anisotropy (PMA) in magnetic thin films has been an interest for several decades owing to its potential in magnetic recording applications. For device-level applications, it is preferable to employ a single film layer with PMA instead of a multilayer to evade the complicated fabrication process. Therefore, there is a search for materials exhibiting strong PMA in a single layer. Of the several materials exhibiting PMA, rare-earth transition metal-based Gd-Fe thin films have attracted special attention from both the fundamental and technological viewpoints. Gd-Fe films exhibit tunable magnetic anisotropy that can be tailored by modifying the composition, thickness, ion-irradiation and annealing conditions, etc.[1]. Although substantial work has been carried out in understanding the magnetic anisotropy of these films, studies on magnetic transport are still elusive. In the present study, we have grown 150 nm thick Gd-Fe thin film capped with 5nm Cr on Si and Si/SiO_2 substrates by electron-beam evaporation under vacuum. Films were found to be amorphous in nature due to the large difference between the atomic radius of Gd and Fe atoms and high cooling rate attained during the deposition process. Magnetization measurements and domain imaging studies indicated the anisotropy axis is tilted in between in-plane and out-of-plane direction. This inherent tilt anisotropy makes it a unique material for sensing vector fields. Magneto-transport measurement on this film showed positive magneto-resistance along both in-plane (IP) and out-of-plane (OOP) directions. This resistance change was mainly contributed by the scattering at domain walls [2].

[1] A. Talaptra, J. Arout Chelvane and J. Mohanty, AIP Advances., Vol. 8, p. 056327 (2018) [2] M. Tofizur Rahman, et al, Journal of applied physics., Vol. 97, p. 10C515 (2005)

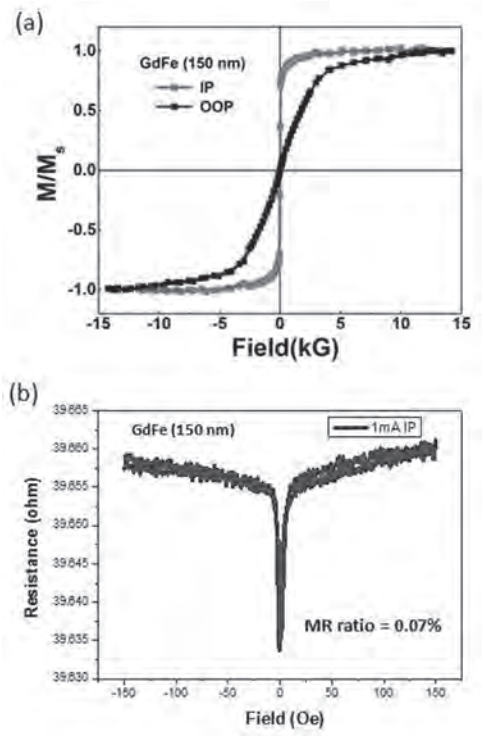

Fig. 1: (a) Hysteresis loop and (b) anisotropic magneto-resistance (AMR) curve in IP configuration for the 150 nm GdFe thin film at room temperature.

E5-13. FORC-Based Study of the Magnetization Reversal in Synthetic Antiferromagnets With the Interfacial Dzyaloshinskii-Moriya Interaction. A. Ognev[1], *A. Kolesnikov*[1], M. Stebliy[1], I. Soldatov[2] and A.S. Samardak[1] *1. School of Natural Sciences, Far Eastern Federal University, Vladivostok, Russian Federation; 2. Leibniz Institute for Solid State and Materials Research, Dresden, Germany*

Synthetic antiferromagnetic (SAF) with perpendicular magnetic anisotropy are promising for the development of magnetic storage with high-speed magnetization reversal [1]. Asymmetric interfacial Dzyaloshinskii-Moriya interaction (DMI) induced on interfaces between heavy metal and a ferromagnet allows to control the chirality of the Neel domain walls in the layers, and also promotes nucleation of skyrmions. In SAF the magnetization orientation of domains in the adjacent layers is aligned in opposite directions, which leads to the disappearance of long-range dipolar interaction. At the same time between the domain walls or spin textures, the local dipolar interaction arises, because the layers are separated by an interspace. In this paper, we show the influence of the indirect exchange coupling and the interfacial DMI on magnetization reversal processes using the first-order reversal curves (FORC) diagram method. We estimate the local dipolar interaction, induced by the magnetic structure in SAF such as Ru/Co/Ru/Co/Ru and Ru/Co/W/Ru/Co/W/Ru. We use W, because of its insertion between Ru and Co increases the DMI value up to -2.71 erg/cm^2 [2]. Experimental studies of magnetization reversal processes are supported by micromagnetic simulations. This work has been supported by the Russian Foundation for Basic Research (grant #19-02-00530) and the Russian Ministry of Science and Higher Education (the state task 0657-2020-0013).

[1] S. Yang, K. Ryu, S. Parkin, Nature Nanotechnology, 10, p. 221–226 (2015) [2] A.S. Samardak et al., Applied Physics Letters, 112 (19), 192406 (2018).

E5-14. Magnetic Properties of Intercalated Transition Metal Dichalcogenides: $v_{1/3}NbS_2$ and $Cr_{1/3}NbS_2$. *A. Hall*[1], D. Mayoh[1], S.J. Holt[1], M. Lees[1], O. Petrenko[1] and G. Balakrishnan[1] *1. Department of Physics, University of Warwick, Coventry, United Kingdom*

Chiral helimagnetism is an incommensurate form of magnetism that arises from competition between the antisymmetric Dzyaloshinskii-Moriya interaction and the symmetric ferromagnetic exchange interaction in noncentrosymmetric materials. These magnets can host several interesting magnetic phenomena, including skyrmions and chiral soliton lattices. The intercalated transition metal dichalcogenides (TMDCs) of the form $M_{1/3}XS_2$, where M is the intercalate and X = Ta, Nb, are a family that crystallises in the chiral hexagonal noncentrosymmetric *P6₃22* space group. The TMDCs are layered materials that show a diverse range of magnetic behaviours [1]. Of this family, $Cr_{1/3}NbS_2$ has been shown to host a chiral soliton lattice (CSL) when a magnetic field is applied perpendicular to the *c*-axis [2]. Magnetic solitons can be described as magnetic domain walls surrounded by regions of forced ferromagnetism. In $Cr_{1/3}NbS_2$, they are fast-moving and robust against perturbation, and so have great potential for spintronic device applications [2]. Our research aims to discover whether any other members of this family are capable of hosting chiral soliton lattices and other interesting phenomena. We have successfully prepared polycrystalline samples of several members of this family and single crystals by the chemical vapour transport technique using iodine as the transport agent. We present a comparison of the magnetic properties of several members of this family, including $V_{1/3}NbS_2$ and $Cr_{1/3}NbS_2$ [Fig.1].

[1] S. S. P. Parkin and R. H. Friend, Phil. Mag. B., 41 65-93 (1980) [2] Y. Togawa, T. Koyama, and K. Takayanagi *et al*., PRL, 108 107202 (2012)

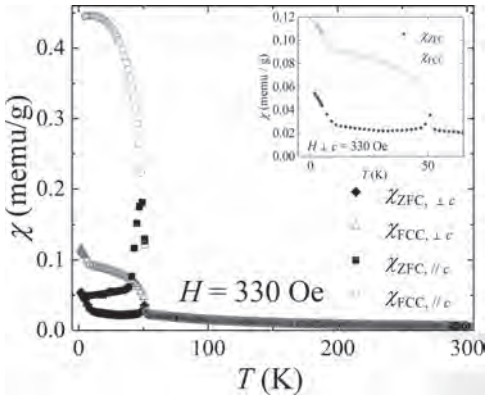

Fig.1: The dc susceptibility of $V_{1/3}NbS_2$ for H = 330 Oe applied both perpendicular and parallel to the c-axis. The inset shows the data for $H \perp c$ in the temperature range of interest.

Session F1
DMI & PROXIMITY EFFECTS IN THIN FILMS

Andoni Lasheras, Chair
University of the Basque Country (UPV/EHU), Bilbao, Spain

INVITED PAPER

F1-01. Large Dzyaloshinskii–Moriya Interaction Induced by Chemisorbed Species on Ferromagnets. *G. Chen*[1], A. Mascaraque[3], H. Jia[2], B. Zimmermann[2], M. Robertson[1], R. Lo Conte[4,5], C. Ophus[6], A. Fernandes Cauduro[6], M. Hoffmann[2], M.A. Barrio[3], H. Ding[7], R. Wiesendanger[5], E.G. Michel[8], S. Bluegel[2], A.K. Schmid[6] and K. Liu[9,1]
1. Physics Department, University of California, Davis, Davis, CA, United States; 2. Peter Grünberg Institute, Julich, Germany; 3. Depto. Física de Materiales, Universidad Complutense de Madrid, Madrid, Spain; 4. Department of Materials Science & Engineering, University of California, Berkeley, Berkeley, CA, United States; 5. Department of Physics, University of Hamburg, Hamburg, Germany; 6. Molecular Foundry, Lawrence Berkeley National Laboratory, Berkeley, CA, United States; 7. Department of Physics, Nanjing University, Nanjing, China; 8. Depto. de Física de la Materia Condensada, Universidad Autónoma de Madrid, Madrid, Spain; 9. Physics Department, Georgetown University, Washington, DC, United States

Chiral spin textures lead to a host of fascinating phenomena due to their topologically protected spin configurations and emergent electromagnetic field, offering great potential for novel concepts in low dissipation magnetic information storage [1-3]. The most common mechanism to stabilize magnetic chirality is the Dzyaloshinskii–Moriya interaction (DMI), originating from broken inversion symmetry. To date, sufficiently large DMI has been found in a limited set of bulk materials with chiral lattice, and in magnetic thin films adjacent to heavy metals or oxides. Using spin-polarized low energy electron microscopy (SPLEEM), we have previously discovered that chiral spin textures are induced at graphene/ferromagnet interfaces due to a Rashba-type DMI [4]. More recently, we have found that chemisorbed species such as oxygen [5] (which are different from the ionic oxygen in oxide systems) and hydrogen [6] on the surface of ferromagnetic films can induce significant DMI, despite their low atomic number. Using a model system of Ni/Co/Pd/W(110) multilayers, where the effective DMI can be tuned by precisely controlling the Pd spacer layer thickness, we have observed a chemisorbed oxygen / hydrogen coverage dependent evolution of domain wall chirality. A systematic measurement of the chirality evolution has allowed us to quantify the DMI induced by chemisorption. We find that the DMI at the oxygen/ferromagnet interface is comparable to those at ferromagnet/transition-metal interfaces. This large induced DMI has enabled direct tailoring of skyrmions winding number as well as domain wall type at room temperature via oxygen chemisorption (Fig. 1). We have also demonstrated a sensitive and reversible chirality switching of magnetic domain walls via hydrogen chemisorption/desorption [6]. These results extend the understanding of the DMI induced by light elements and support chemisorption-related design of spin-orbitronics and magneto-ionic devices. This work has been supported by the NSF (DMR-1610060 and DMR-1905468), UCOP-MRPI (MRP-17-454963), the nCORE-SMART Center (2018-NE-2861) through SRC/NIST, DOE (DE-AC02-05CH11231) and other agencies.

[1] R. Wiesendanger, *Nat. Rev. Mater.* 1, 16044 (2016). [2] A. Fert, N. Reyren, V. Cros, *Nat. Rev. Mater.* 2, 17031 (2017). [3] W. Jiang, *et al. Phys. Rep.* 704, 1 (2017). [4] H. Yang, G. Chen, *et al. Nat. Mater.* 17, 605 (2018). [5] G. Chen, et al. *Sci. Adv.* DOI: 10.1126/sciadv.aba4924 (2020). [6] G. Chen, et al. *submitted*.

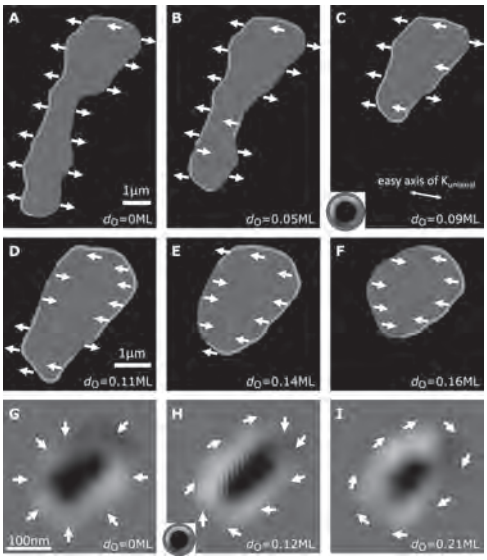

Figure 1 Oxygen-assisted chirality modification at room temperature. (A-F) SPLEEM images of a magnetic bubble in perpendicularly magnetized thin films with increasing oxygen coverage (labeled in each panel), showing a complete chirality transition from left-handed (panel A) to achiral (panel D) to right-handed (panel F). Color wheel and white arrows show in-plane magnetization directions. Grey/black regions show out-of-plane components of the magnetization pointing down (-z) or up (+z). (G) Compound SPLEEM image of a left-handed Néel-type skyrmion in a perpendicularly magnetized thin film system. (H-I) The Néel-type skyrmion in panel G evolves into a skyrmion with tilted wall and finally a Bloch-type skyrmion upon oxygen chemisorption.

CONTRIBUTED PAPERS

F1-02. Temperature Dependence of the Dzyaloshinskii-Moriya Interaction in Ultrathin Films. *Y. Zhou*[1], R. Mansell[1], S. Valencia[2], F. Kronast[2] and S. van Dijken[1] *1. NanoSpin, Department of Applied Physics, Aalto University School of Science, P.O. Box 15100, FI-00076 Aalto, Finland; 2. Helmholtz-Zentrum Berlin für Materialien und Energie, Albert-Einstein Str. 15, 12489, Berlin, Germany*

The temperature dependence of magnetic properties in thin films are important for understanding the underlying physics and enabling the creation of novel devices. Whilst the temperature dependence of saturation magnetization *Ms*, exchange stiffness *A* and anisotropy *K* have been widely investigated [1, 2, 3], research on the interfacial Dzyaloshinskii–Moriya interaction (DMI) remains limited [4]. The DMI exists in perpendicularly magnetized ultrathin films with interfaces to heavy metals and is critical to the formation of magnetic skyrmions. We present a study of the temperature dependence of DMI in a Ta/Pt/CoFeB/Ru/Pt/CoFeb/Ru/Pt heterostructure hosting skyrmions, based on extensive characterization by bulk magnetometry and x-ray magnetic circular dichroism photoemission electron microscopy (XMCD-PEEM). *Ms*, anisotropy field *Hk*, zero-field domain width *W* and skyrmion

radius *R* are extracted directly from the measurements. Through *Ms* and *Hk*, the strength of uniaxial anisotropy *Ku* is determined. Then, we adapt the bulk Bloch law to the thin film geometry to extract *A* from the temperature dependence of *Ms* (Fig. 1). Furthermore, we combine *Ms*, *W*, *R*, *Ku* and *A* in the static multilayer domain energy model [5] and the static skyrmion size model [6], where the DMI values are calculated at different temperatures (Fig. 2). We find a large spatial variation of the DMI strength between the one derived by the spatial domains and that at skyrmion sites. Besides, the DMI value shows a linear correlation with *A* and *Ku*. The possible physical origins are discussed. Finally, according to our results, we argue that the skyrmion size should remain constant over an extensive temperature range [7].

[1] Atxitia, U., et al., Phys. Rev. B 82, 134440 (2010) [2] Moreno, R., et al., Phys. Rev. B 94, 104433 (2016) [3] Sato, H., et al., Phys. Rev. B 98, 214428 (2018) [4] Schlotter, Sarah, Parnika Agrawal, and Geoffrey SD Beach, Appl. Phys. Lett. 113, 092402 (2018) [5] Lemesh, Ivan, Felix Büttner, and Geoffrey SD Beach, Phys. Rev. B 95, 174423 (2017) [6] Wang, X. S., H. Y. Yuan, and X. R. Wang, Commun Phys 1, 31 (2018) [7] Zhou, Yifan, et al., Phys. Rev. B 101, 054433 (2020)

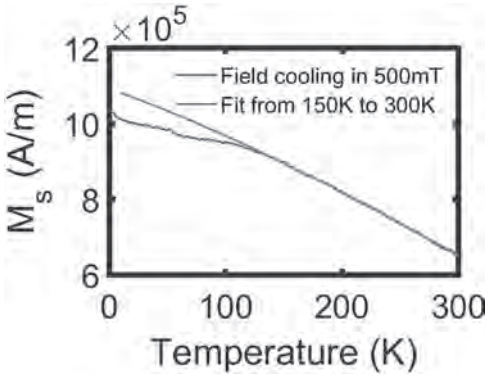

Fig. 1: Fit the thin film Bloch law to field cooling data taken at 500 mT in-plane applied field.

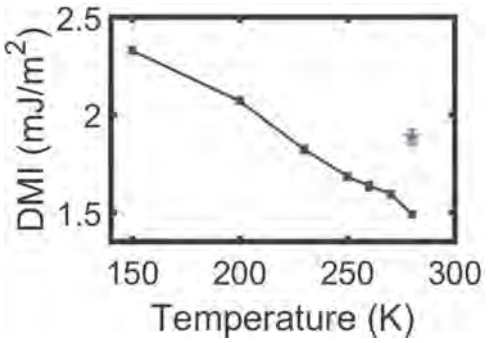

Fig. 2: The DMI value from stripe domain model for 150 K to 280 K. The DMI value from the Skyrmion model is marked as red dot.

F1-03. Experimental Observation of Interlayer Dzyaloshinskii-Moriya Interaction in Synthetic Antiferromagnets. *A. Fernandez-Pacheco*[2,5], E.Y. Vedmedenko[1], F. Ummelen[3], R. Mansell[4], M. Cascales Sandoval[2], N. Jaouen[6], S. Stanescu[6], D. Petit[5] and R. Cowburn[5] *1. Universitat Hamburg, Hamburg, Germany; 2. University of Glasgow, Glasgow, United Kingdom; 3. Technische Universiteit Eindhoven, Eindhoven, Netherlands; 4. Aalto-yliopisto, Aalto, Finland; 5. University of Cambridge, Cambridge, United Kingdom; 6. Synchrotron SOLEIL, Gif-sur-Yvette, France*

The interfacial Dzyaloshinskii-Moriya Interaction (DMI) is a magnetic chiral interaction emerging in ultra-thin film magnetic systems lacking inversion symmetry. This interaction is an essential ingredient to create and stabilize complex spin textures such as magnetic skyrmions, chiral domain walls and spin spirals, which are under intense investigation in the field of spintronics, due to their great technological potential. Until quite recently, DMI had been observed only as an intralayer interaction, providing chiral coupling in between spins within the same ferromagnetic layer, mediated by a neighboring paramagnetic layer (Fig. 1a). In this contribution, we will present recent experimental work [1], where we have observed that DMI can also be an interlayer interaction, leading to the chiral coupling of spins located at two different ferromagnetic layers separated by a paramagnetic spacer (Fig. 1b), an effect that has been simultaneously reported by others [2]. Our samples are synthetic antiferromagnets (SAFs) with canted magnetization states [3], where a delicate balance between competing magnetic energies enables to observe interlayer-DMI. This interaction breaks the symmetry of the magnetization reversal process, leading to room-temperature chiral exchange biased hysteresis loops (Fig. 2). In this presentation, we will show how this type of chiral bias is observed in multiple magnetic systems, and how these results can be understood using atomistic spin simulations based on the standard DMI formalism, recently extended to SAFs [4, 5]. We will also outline challenges, as welll as exciting opportunities, in order to exploit this effect to create and manipulate three-dimensional magnetic states [6].

[1] A. Fernández-Pacheco at al, Nature Mater., Vol. 18, p.679 (2019). [2] D.-S. Han et al, Nature Mater. Vol. 18, p.703 (2019). [3] F. Ummelen et al, Appl. Phys. Lett. Vol 110, p.102405 (2017). [4] E. Vedmedenko et al, Phys. Rev. Lett. 122, 257202 (2019). [5] E. Vedmedenko et al, J. Phys. D (Appl. Phys.), in press. [6] A. Fernández-Pacheco, Nature Comm. Vol. 8, p.15756 (2017).

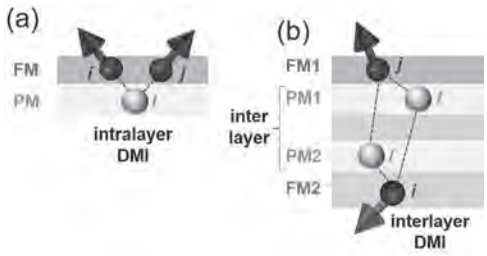

Schematic representation of intra- (a) and inter- (b) interfacial DMI effects.

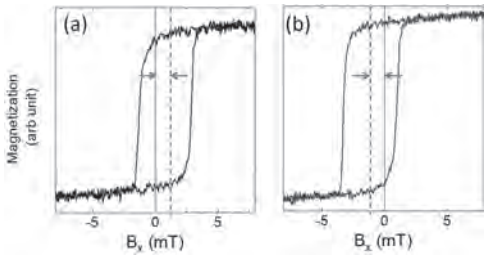

In-plane hysteresis loops of canted SAFs showing a chiral exchange bias of different signs, depending on the direction of the initial out-of-plane saturating field, either negative (a) or positive (b).

F1-04. Temperature Dependence of the Magnetic Proximity Effect in Magnetic Insulator/Platinum Heterostructures by Polarized Neutron Reflectometry. *J. Bauer*[1], P. Quarterman[2], A.J. Grutter[2], B. Kirby[2], J.A. Borchers[2] and C. Ross[1] *1. Materials Science and Engineering, Massachusetts Institute of Technology, Cambridge, MA, United States; 2. NIST Center for Neutron Research, National Institute of Standards and Technology, Gaithersburg, MD, United States*

The magnetic proximity effect (MPE) in nonmagnetic heavy metal/magnetic heterostructures has received much recent attention. The MPE is believed to play a role in the spin Hall magnetoresistance (SMR) and may also be leveraged to control the emerging phenomena associated with topological insulators. Pt is most commonly used due to its vicinity to the Stoner criterion, and its use as a source of spin-orbit torques in spintronic measurements.

However, much is still unknown about the properties of the MPE, such as the temperature dependence and the coupling to magnetic layers when multiple magnetic sublattices are present. To explore this, we examined pulsed laser deposited 25 nm thick dysprosium iron garnet (DyIG)/sputtered 10 nm Pt heterostructures using polarized neutron reflectometry (PNR), above (200K) and below (15 K) the magnetic compensation temperature (T_{comp} = 190 K)[1]. Below T_{comp}, the Dy^{3+} sublattice dominates the net moment, and above T_{comp}, the net Fe^{3+} dominates. The MPE magnetization has only small effects on the fit to the data, but the results are consistent with a small Pt moment antiparallel to the net DyIG moment at 15 K, i.e. the Pt moment is parallel to the net Fe^{3+} moment, whereas at 200 K the Pt magnetization is negligible. The M_S obtained from the PNR fits is 605 kA/m at 15 K (literature value = 622 kA/m) and 10 kA/m at 200 K (VSM value = 10 kA/m) [1]. The scattering length density profile suggests interdiffusion at the GGG substrate interface over a 2-3 nm region, consistent with previous studies. This is accounted for with a layer of composition intermediate between DyIG and GGG. A dip in density at the DyIG/Pt interface is also present, indicating the presence of surface contamination due to the *ex situ* Pt deposition, or a translational growth region.

J.J. Bauer, E.R. Rosenberg, S. Kundu, K.A. Mkhoyan, P. Quarterman, A.J. Grutter, B.J. Kirby, J.A. Borchers, and C.A. Ross, Adv. Electron. Mater., Vol. 6, 1900820 (2020).

F1-05. Quantitative Determination of the Pt Magnetic Moment in Proximity to Ferromagnetic Material. *T. Kuschel*[1] *1. Bielefeld University, Bielefeld, Germany*

The magnetic proximity effect (MPE) enhances the exchange interaction of nominally non-ferromagnetic materials overcoming the Stoner limit in close contact to ferromagnetic (FM) materials. The paramagnet Pt is a famous example and gets spin polarized by the MPE in Pt/FM bilayers which is of huge importance when studying spin transport phenomena at interfaces such as for the spin Seebeck effect [1], the spin Hall magnetoresistance [2], or spin-orbit torque effects [3]. However, the exact quantitative values for the induced magnetic moment per Pt atom cannot be determined by standard x-ray magnetic circular dichroism (XMCD) experiments on a single thin-film system due to the depth-insensitivity of the XMCD technique at buried interfaces of the sample. Within this contribution, we present the quantitative determination of the Pt magnetic moment induced by the MPE utilizing x-ray resonant magnetic reflectivity (XRMR) [4-6], a favored synchrotron-based technique for spin-depth profiling. Thus, element selectivity and depth resolution can be combined. A detailed data analysis based on asymmetry ratio fits and mapping the goodness of fit parameter X^2 (see Fig. 1) [3,7] together with an ab-initio factor (conversion from magnetooptic constant $\Delta\beta$ to Pt magnetic moment) [4] provides quantitative reliable results. The obtained quantitative XRMR values are in very good agreement to vibrating sample magnetometry results [3] and XMCD analyses [8] which take the effective magnetic Pt thickness determined by XRMR into account. Therefore, XRMR is a powerful technique to study spin distributions with depth resolution, element selectively and quantitative reliability.

[1] P. Bougiatioti et al., Phys. Rev. Lett. 119, 227205 (2017) [2] M. Althammer et al., Phys. Rev. B 87, 224401 (2013) [3] A. Moskaltsova et al., AIP Advances 10, 015154 (2020) [4] T. Kuschel et al., Phys. Rev. Lett. 115, 097401 (2015) [5] C. Klewe et al., Phys. Rev. B 93, 214440 (2016) [6] T. Kuschel et al., IEEE Trans. Magn. 52, 4500104 (2016) [7] J. Krieft et al., J. Phys. D: Appl. Phys. 53, 375004 (2020) [8] D. Graulich et al., in preparation

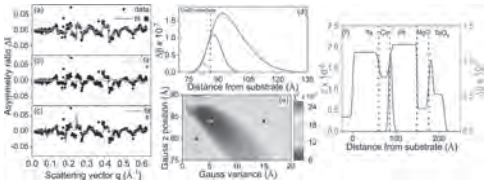

(a), (b), (c) Asymmetry ratios and fits for a Ta/Co/Pt trilayer. (d) Corresponding magnetooptic Pt depth profiles. (e) X^2 map plot of the Gauss variance vs. the Gauss z position of the magnetic Pt depth profile. The +, * and x symbols identify the respective asymmetry ratios. (f) Optic δ depth profile (solid blue line) and magnetooptic Δβ depth profile (solid red line) from (d). Figure taken from Ref. [3].

F1-06. Microscopic Study of Magnetic Anisotropy Modification in Nanoscale Heavy Metal/Ferromagnetic Insulator Heterostructures. *G. Wu*[1], S. White[1], W. Ruane[1], Y. Cheng[1], J. Brangham[1], D. Pelekhov[1], F. Yang[1] and P. Hammel[1] *1. physics, The Ohio State University, Columbus, OH, United States*

Enhancement of ferromagnetic resonance damping due to spin pumping from a ferromagnetic insulator (FI) into adjacent heavy metal (HM) is well-known. The less known phenomenon of a substantial magnetic anisotropy induced in FI at the interface with an HM overlay has not been fully studied. Here, we report a microscopic study of the HF/FI interfacial spin interaction in thin films using scanned ferromagnetic resonance force microscopy (sFMRFM). HM nanostructures, such as 5nm-thick Au pads, are patterned onto 20nm-thick $Y_3Fe_5O_{12}$ (YIG) grown on $Gd_3Ga_5O_{12}$ substrate using off-axis sputtering technique. Scanning the sFMRFM probe across the boundary separating the bare YIG and YIG/Au bilayer reveals a substantial, 32 Gauss, change of resonance field in the magnetic field out-of-plane geometry. Detailed micromagnetic simulation accurately reproduces the experimental result, demonstrating that a sharp change of uniaxial anisotropy across the boundary induces the observed resonance field shift in YIG/Au. This sharp variation of magnetic anisotropy creates a drastic change of internal field over a short spatial distance, can be highly useful in designing nanoscale spintronic devices. The modification of magnetic properties at the nanoscale is usually achieved by modifying the shape or crystal structure of the FI thin film, such as etching or ion irradiation. Notably, we achieve this modification of magnetic anisotropy by a heavy metal pattern overlayer, thus opening a novel path to fabricate nanoscale magnetic structure with minimal disturbance to the material properties of the FI thin film. Utilizing the ability to vary the magnetic anisotropy in nanometer scale, we propose spintronic devices based on the integration of heavy metal nanostructures on YIG thin films.

G. Wu, S. P. White, W. T. Ruane *Physical Review B*, *101*(18), 184409. (2020)

F1-07. Withdrawn

F1-08. Detection of Interfacial Effects in Rare Earth Metal Doped Ferrimagnet Layer / Heavy Metal Layer Using Magneto-Optical Kerr Effect. *K. Matsumoto*[1], S. Sumi[1], K. Tanabe[1] and H. Awano[1] *1. Toyota Kogyo Daigaku, Nagoya, Japan*

Dzyaloshinskii-Moriya Interaction (DMI) generated at the interface between the magnetic layer and heavy metal layer plays an important role in studies on current-induced magnetic domain wall motion[1-2]. However, since it is difficult to estimate DMI with existing methods, a simple estimation method is required. Although the magneto-optical Kerr effect (MOKE) measurement is one of the simplified measurement methods, the signal of the MOKE is not high. Recently, Sumi et al. have reported that the MOKE can be enhanced by using multiple interference[3] in thin films. In this study, we have applied the

multiple interference effect to MOKE measurement in the magnetic layer / heavy metal layer hetero-structure to enhance the signal from the interface and discuss the contribution of the DMI. Thin films with structures of Pt(5 nm)/GdFeCo(6 nm)/SiN_x(10 nm), was deposited on silicon substrates with thermally oxidized SiO_2 layer (100 nm). Kerr rotation angle and ellipticity spectra of the samples were measured in an energy range of 1.77–4.13 eV (wavelength range of 300-700 nm) by home-made MOKE spectroscopy[3]. Figure 1 shows MOKE spectra of (a)Pt/GdFeCo. Measured spectra are different from calculated ones in the low photon energy region. This result is quite similar to our previous result of (b)Pt(3 nm)/TbCo(6 nm)/SiN_x(10 nm)[4]. Such differences are attributable to the interfacial effect of the DMI at Pt/GdFeCo and Pt/TbCo. We can confirm the differences remain when the ferrimagnet layer was changed. Focuses on ellipticity spectra, the peak of the measured spectrum is in a similar position in the photon energy region as calculated one for (b)Pt/TbCo. On the other hand, the peak of the measured spectrum is located in a larger photon energy region than the calculated one for (a)Pt/GdFeCo. MOKE spectra may have the information of not only the interface effect originated from large DMI of heavy metal, but also the interfacial magnetic structure of ferrimagnet material. This research was supported by JSPS Grant-in-Aids for Scientific Research (20H02185).

[1] K. Ryu et al., Nature Nanotech. 8, 527 (2013). [2] Yang, S.-H. et al., Nat. Nanotech. 10, 221 (2015). [3] Sumi, S. et al., Sci. Rep. 8, 776 (2018). [4] Iemoto, S. et al., crystals 8, 377 (2018).

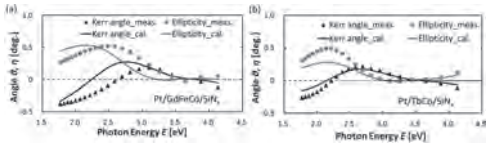

Fig. 1 Polar MOKE rotation and ellipticity spectra for (a)Pt/GdFeCo/SiN_x and (b)Pt/TbCo/SiN_x[4]. Solid and dot lines represent simulated and experimented data, respectively.

F1-09. Transport and Magnetic Properties of TiN Thin Films. *M. Roy*[1], N. Mucha[1] and D. Kumar[1] *1. Mechanical Engineering, North Carolina Agricultural and Technical State University, Greensboro, NC, United States*

This research reports a fundamental study of transport and magnetic properties of pulsed laser deposited metallic (film thickness ≈ 25-100 nm) and semiconducting (film thickness ≈ 25 – 10 nm) titanium nitride (TiN) thin films. The study is motivated to discern the critical thickness at which the properties of TiN films digress from bulk-like (3D) to 2D thin films. The study showed that while the crystal structure remains rock salt in the entire thickness range, the films undergo a metal-to-insulator (MI) transition around ~15 nm. The thickness (dimensionality) dependent MI transition, which is free from a structural phase transition, is attributed to a the localization of $3d^1$ electrons in the valence band, which takes place due to the separation in the energy states larger than the gaps between the valence and conduction bands. Analysis of transport resistivity data in different temperature regions indicated that while the Arrhenius law governs the transport properties for all the TiN films in 300 – 350 K range, the transport properties are governed by a thickness-dependent variable range hopping mechanism below 300 K. The magnetic properties of metallic and semiconducting TiN films were also found to be interesting. A room temperature ferromagnetic behavior was observed for both metallic and semiconducting TiN films, there was a marked correlation between coercivity (H_c) and saturation magnetization (M_s) with TiN film thickness. At room temperature, H_c increased from 66 to134 Oe as the thickness decreased from 100 to 9 nm. Similarly, the M_s (2.8 emu/g) at room temperature for the 9 nm sample was the highest. The maximum values of H_c and M_s are among the best values reported for TiN thin films in the literature. Contrary to previous reported causes of ferromagnetism in TiN due to nitrogen vacancies or oxygen doping, we have attributed the observed magnetic behavior of TiN films to the localized $3d^1$ electrons in TiN which become more localized with the decrease in film thickness due to the size-dependent enhanced separation of energy states. Thickness dependent ferromagnetism study of TiN thin films can add a new dimension to their current applications and tune the magnetic nature of low dimensional TiN films.

F1-10. Revealing the Morphology and Magnetic Properties of Single Hybrid Interfaces Embedded in Co/ZnTPP and ZnTPP/Co by FNR. *G. Avedissian*[1], J. Arabski[1], J. Wytko[2], J. Weiss[2] and C. Meny[1] *1. Institut de Physique et Chimie des Materiaux de Strasbourg, Strasbourg, France; 2. Institut de Chimie de Strasbourg, Strasbourg, France*

The deeply buried, yet most important part of any spintronic device is the interface. This is even more interesting and much more complex when soft, light materials like organic molecules are in contact with an inorganic metallic electrode. Hence, exceptional care is required to better understand the phenomena driven by this type of hybrid organic-inorganic interfaces. To this end, ferromagnetic nuclear resonance (FNR) spectroscopy [1] studies were performed to investigate the morphology and magnetic properties of the hybrid organic-inorganic interfaces when zinc tetra-phenyl porphyrin (ZnTPP) molecules are at the vicinity of ferromagnetic metallic cobalt (Co) electrodes. With unique sample architectures, the experimental results of FNR suggest that Co/ZnTPP and ZnTPP/Co interfaces are governed by weak van der Waals interactions in the absence of strong chemical bonds between interfacial ZnTPP molecules and Co atoms. Nevertheless, when ZnTPP is deposited on top of Co the resulting interface (Co/ZnTPP) consists of around 0.3 nm of Co leading to smooth and quite sharp interface morphology. On the contrary, the interface obtained for deposition of Co on top of ZnTPP (ZnTPP/Co) involves much larger amount of Co (0.8nm) resulting in wide and diffusive type of interface. These observations suggest that the two type of interfaces are highly asymmetrical, and that a minimum of 5 nm of Co is required to complete the interface formation. Finally, and more importantly, through the so-called site dependent restoring fields [1] of FNR, the experimental evidence showed that Co/ZnTPP and ZnTPP/Co interfaces are magnetically softer than the bulk of Co of the sample, demonstrating the absence any magnetic hardening effect that is generally present in other organic/inorganic hybrid systems [2,3].

[1] P. Panissod and C. Meny, Applied Magnetic Resonance, Vol 19, p. 447 (2000) [2] T. Moorsom, M. Wheeler, T. Mohd Khan et al, Physical Review B, Vol 90, p. 125311 (2014) [3] M. Callsen, V. Caciuc, N. Kiselev et al. Physical Review Letters, Vol 111, p. 106805 (2013)

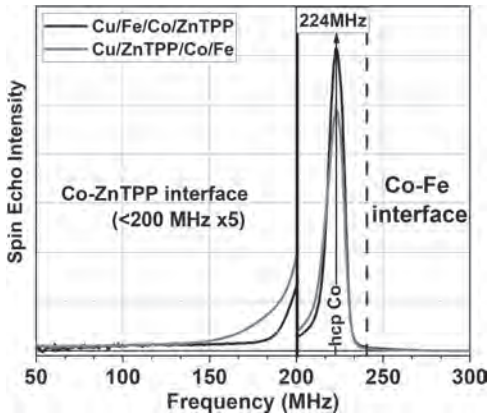

Fig. 1 FNR spectra of Cu/Fe/Co/ZnTPP (black) and Cu/ZnTPP/Co/Fe (red) heterostructures. The low frequency spectral region is magnified by a factor of 5.

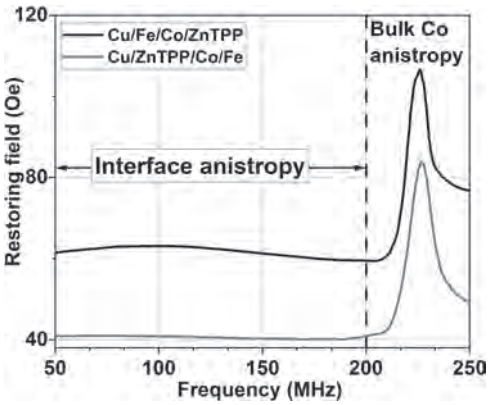

Fig. 2 Frequency dependent restoring field. Graph shows the magnetic softness of the interfaces (< 200 MHz) and the magnetically stiffer cobalt in the bulk part of the cobalt films (> 200 MHz).

F1-11. Magnetic Domain Patterns of Multilayered [Co/Pt] Thin Films.

A. Gentillon[1], C. Richards[1], H. McGhie[1] and O. Hellwig[2] *1. Brigham Young University, Provo, UT, United States; 2. Helmholtz Zentrum Dresden Rossendorf, Dresden, Germany*

Understanding the formation of magnetic domain patterns in ferromagnetic thin films and their evolution under a magnetic field is useful for application in nanotechnologies such as magnetic storage. We are specifically studying domains patterns in multilayered [Co/Pt]_N thin films with perpendicular magnetic anisotropy (PMA). We are imaging the domain patterns via Atomic and Magnetic Force Microscopy (AFM/MFM) at remanence as well as in the presence of a magnetic field applied in-situ. The films consist of 3 nm thick Co layers and 0.7 nm thick Pt layers, with a number of repeats N, varying from 6 to 20. We are investigating how the number of layers N affects the domain size and therefore the domain density but also the degree of PMA exhibited by the films. We will show images of magnetic domain patterns collected at remanence as well as over a range of field values from about 0.10 T to 0.60 T. The data shows the evolution of the magnetic domain morphology from a maze-like state at remanence and low field values, toward a bubble state at higher field values. The bubble-like domains then disappear as the sample reaches saturation, occurring at about 1 T. When the field is released, the magnetic pattern may remain in a bubble state. This study provides with a unique view of how the thin films react to external magnetic fields and how to optimize domain density.

Session F2
MAGNETO-ELASTIC AND MAGNETO-CALORIC MATERIALS II

Jia Yan Law, Co-Chair
Sevilla University, Sevilla, Spain
Nirmala R, Co-Chair
Indian Institute of Technology Madras, Chennai, India

CONTRIBUTED PAPERS

F2-01. Giant Anisotropic Magnetocaloric Effect in all-Sputtered Epitaxial Terbium Thin Films. *M. El Hadri*[1], V. Polewczyk[2], Y. Xiao[1], S. Mangin[2] and E. Fullerton[1] *1. Center for Memory and Recording Research, University of California San Diego, La Jolla, CA, United States; 2. Institut Jean Lamour, Universite de Lorraine, Nancy, France*

We report on the anisotropic magnetocaloric effects in epitaxial Tb films. The investigation of the magnetocaloric effect in Tb has attracted increasing interest, since it combines a large magnetic moment, a relatively high Curie temperature, and a strong magnetic anisotropy [1]. Initial experimental work by Nikitin and Tishin has shown that bulk single-crystal Tb exhibits a large maximum magnetic entropy change of 15.7 $J.kg^{-1}.K^{-1}$ at a Néel temperature of 230 K and for a magnetic field change ΔH = 60.2 kOe [2]. More recently, Tb-based films have been the focus of intense research interest from both experimental [3,4] and theoretical [5,6] viewpoints, revealing the role of size effects in tailoring their magnetocaloric properties. To further elucidate the magnetocaloric effect in Tb thin films, we present an experimental investigation of both the magnetic and magnetocaloric properties of sputtered epitaxial and amorphous Tb thin films. We successfully grow epitaxial Nb (50 nm)/Tb (100 nm) bilayer thin films on Al_2O_3(11-20) substrate using DC magnetron sputtering at high temperature, with excellent crystalline quality of the hcp Tb(0001) layer as evidenced by X-ray diffraction measurements. More importantly, we show that the studied epitaxial Tb thin film displays giant anisotropic magnetocaloric properties, with a large maximum magnetic entropy change of 6.25 $J.kg^{-1}.K^{-1}$ at the Néel temperature with a magnetic field change ΔH = 20 kOe applied along the in-plane direction (Fig.1). Our findings open up new routes for the growth of epitaxial rare-earth thin films using sputtering technique and demonstrate a novel approach to study the magnetocaloric effect in Tb thin films.

[1] Ed. R.J. Elliott, Magnetic Properties of the Rare-Earth Metals (Plenum, New York, 1972). [2] S. A. Nikitin, and A. M. Tishin, *Sov. Tech. Phys. Lett. 14, 327*–328 (1988). [3] C. H. Lambert, M. S. El Hadri, M. Hamedoun, *et al*., *J. Magn. Magn. Mater*. 443, 1–3 (2017). [4] M. Tadout, C.-H. Lambert, M. S. El Hadri, *et al*., *J. Appl. Phys*. 123, 053902 (2018). [5] V. D. Mello, D. H. A. L. Anselmo, M. S. Vasconcelos, *et al*., *Solid State Commun*. 268, 56–60 (2017). [6] R. R. Gimaev, V. I. Zverev, and V. D. Mello, *J. Magn. Magn. Mater*. 505, 166781 (2020).

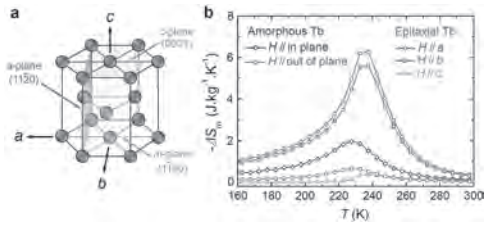

Fig.1: (a) Schematic representation of the Tb hcp lattice structure. The *c*-, *a*- and *b*-axes are parallel to the [0001], [11-20] and [1-100] crystallographic directions, respectively. (b) Temperature dependence of the magnetic entropy change $-\Delta S_m$ for the studied epitaxial and amorphous Tb thin films measured under an applied field change interval of 20 kOe.

F2-02. Giant Anisotropy of the Magnetocaloric Effect in the Orthovanadate $TbVO_4$ Single Crystals. *M. Balli*[3,5], S. Mansouri[5], D. Dimitrov[1,2], P. Fournier[5,4], S. Jandl[5] and J. Juang[2] *1. Institute of Solid State Physics, Bulgarian Academy of Science, Sofia, Bulgaria; 2. Department of Electrophysics, National Chiao Tung University, Hsinchu, Taiwan; 3. LERMA, ESIE, International University of Rabat, Rabat, Morocco; 4. Canadian Institute for Advanced Research, Toronto, ON, Canada; 5. Institut quantique, Université de Sherbrooke, Sherbrooke, QC, Canada*

In this work, we demonstrate that the $TbVO_4$ compound can be used as magnetic refrigerant in efficient and ecofriendly magnetic cryocoolers due to its giant magnetocaloric effect (MCE) at low temperature regime. The application of a relatively low magnetic field of 2 T along the easy magnetization plane (ab) gives rise to a maximum entropy change of about 20 J/kg K at 4 K. More interestingly, under sufficiently high magnetic fields, the entropy change (-ΔS) remains approximately constant over a wide temperature range which is highly appreciated from a practical point of view. For example, in the magnetic field change of 7 T, -ΔS that reaches roughly 22 J/kg K remains practically unchanged over about 34 K, leading to an outstanding refrigerant capacity of 823 J/kg. On the other hand, the change in the crystallographic symmetry from the tetragonal to the orthorhombic structure occurring close to 33 K as confirmed by Raman scattering data (Figure 1), results in a strong magnetocrystalline anisotropy. Accordingly, giant thermal effects are obtained simply by spinning the $TbVO_4$ single crystals between the hard (c axis) and easy (ab plane) orientations (Figure 1) in constant magnetic fields. The rotation of $TbVO_4$ crystals between their easy and hard magnetization directions in a constant magnetic field of 2 T, enables to generate entropy changes of about 18 J/kg K around the liquid helium temperature. Such rotating MCEs would open the way for the implementation of $TbVO_4$ in more efficient and compact magnetocaloric coolig systems with a simplified design that could be dedicated to the hydrogen and helium liquefaction.

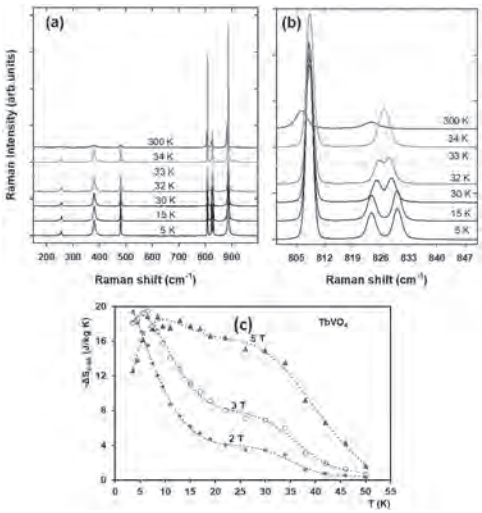

Figure 1: (a, b) Micro-Raman spectra of $TbVO_4$ at some selected temperatures. (c) Entropy changes related to the rotation of $TbVO_4$ between the c axis and the ab plane by 90 ° in different constant magnetic fields, with magnetic field initially parallel to the c-axis.

F2-03. Tailoring Magnetocaloric Effect in all-d-Metal Ni-Co-Mn-Ti Heusler Alloys: a Combined Experimental and Theoretical Study.
A. Taubel[1], B. Beckmann[1], L. Pfeuffer[1], N. Fortunato[1], F. Scheibel[1], S. Ener[1], T. Gottschall[2], K. Skokov[1], H. Zhang[1] and O. Gutfleisch[1]
1. Materials Sciences, Technical University of Darmstadt, Darmstadt, Germany; 2. Dresden High Magnetic Field Laboratory, Helmholtz-Zentrum Dresden-Rossendorf, Dresden, Germany

The family of Ni(-Co)-Mn-X Heusler alloys with X = Al, Sn, Ga, In shows a first-order magnetostructural phase transition and has been studied intensively in terms of magnetocaloric properties [1]. Recently, the principle of all-d metal Heusler alloys has been demonstrated for X=Ti in these alloys [2]. The Ni-Co-Mn-Ti alloy system is a promising material for multicaloric applications due to its large magnetization and volume change, good tunability of the phase transition and enhanced mechanical properties. The good mechanical stability and the high pressure sensitivity make this material system very suitable for the novel approach of multicaloric cooling cycles, using both magnetic field and mechanical pressure as stimuli [3]. By optimizing the processing route of this system, we improved the inverse magnetostructural phase transition from high magnetic austenite to low magnetic martensite in terms of sharpness and magnetization change. Microstructural investigations reveal differences in grain sizes and stoichiometric homogeneity that lead to large differences in the transition width for different heat treatments. A large isothermal entropy change of up to 38 $Jkg^{-1}K^{-1}$ in 2 T has been measured in isofield protocol for $Ni_{37}Co_{13}Mn_{34}Ti_{16}$. However, the adiabatic temperature change in magnetic field changes below 2 T is significantly lower compared to Ni-Mn-In alloys because of a lower magnetic-field sensitivity of the phase transition temperature. Maximum adiabatic temperature changes of 3.5 K are measured directly for a magnetic field change of 2T. In order to design an efficiently working magnetocaloric material, the magnetic-field sensitivity needs to be adjusted to induce a completed phase transition. For this purpose, we produced sample series of different Co and Ti contents in order to study the influences of stoichiometry on the maximum achievable magnetocaloric effect in low and high magnetic fields. The experimental data are in good agreement with DFT calculations, which correlate a strong influence of the e/a ratio on the Curie temperature with the strong d-d hybridization and a preferred B2 disorder. This work is supported by ERC Advanced Grant "CoolInnov", and CRC/TRR 270 "HoMMage".

[1] A. Taubel et. al, Phys. Status Solidi B, Vol. 255, p. 1700331 (2018) [2] Z. Wei et al., Applied Physics Letters, Vol. 107, p. 022406 (2015) [3] T. Gottschall et al., Nature Materials, Vol. 17, p. 929-934 (2018)

F2-04. Influence of the Martensite Transformation Dynamics on the Magnetocaloric Effect in NiMn-Based Heusler Compounds.
L. Pfeuffer[1], T. Gottschall[2], T. Faske[1], A. Taubel[1], F. Scheibel[1], A.Y. Karpenkov[1,3], K. Skokov[1] and O. Gutfleisch[1] *1. Department of Materials Sciences, Technical University of Darmstadt, Darmstadt, Germany; 2. High Magnetic Field Laboratory, Helmholtz-Zentrum Dresden-Rossendorf, Dresden, Germany; 3. National Research South Ural State University, Chelyabinsk, Russian Federation*

NiMn-based Heusler compounds display excellent magnetocaloric properties - high adiabatic temperature changes ΔT_{ad} and isothermal entropy changes Δs_T - upon the field-induced phase transformation from non-magnetic martensite to ferromagnetic austenite [1]. However, in cyclic operation ΔT_{ad} and Δs_T are drastically reduced by the compounds' large intrinsic thermal hysteresis. For that reason, we recently presented a new magnetic cooling concept, which exploits the thermal hysteresis and enables the utilization of the materials outstanding magnetocaloric potential [2]. In this so-called exploiting hysteresis cycle the amount of permanent magnets can be significantly reduced and higher, as more focused, fields can be applied compared to conventional magnetic refrigeration. Furthermore, a decoupling of the heat transfer and the field step allows utilizing larger magnetic field-sweep rates. To analyze the materials response to high magnetic fields and field-sweep rates, we performed simultaneous ΔT_{ad} and strain $\Delta l/l_0$ measurements in pulsed magnetic fields up to 10 T with a Ni-Mn-In prototype compound. A large ΔT_{ad} of -10 K and a $\Delta l/l_0$ of 0.22 % was observed when the phase transition is completed. By varying sweeping speeds from 316 Ts^{-1} to 1850 Ts^{-1}, dynamic effects of the reverse martensitic transformation were clearly noticeable. At field rates higher than 865 Ts^{-1} the austenite growth couldn't follow the magnetic field anymore, which results in an increasing field hysteresis and higher saturation fields. Thereby, the kinetic information was only accessible by the combined measurement of ΔT_{ad} and $\Delta l/l_0$. Complementary, isofield XRD and simultaneous magnetization and $\Delta l/l_0$ measurements were performed. Our data give a new detailed insight in the magnetostructural transformation process in NiMn-based Heusler compounds and demonstrate the necessity to consider kinetical effects for magnetic refrigeration with high sweeping speeds. The results are submitted to Physical Review Materials. We acknowledge the ERC "CoolInnov" and the CRC/TRR 270 "HoMMage" for funding this work.

[1] J. Liu, T. Gottschall, K. P. Skokov1, J. D. Moore and O. Gutfleisch; Giant magnetocaloric effect driven by structural transitions; *Nat. Mat. 11 (2012)* [2] T. Gottschall, A. Gràcia-Condal, M. Fries, A. Taubel, L. Pfeuffer, L. Mañosa, A. Planes, K. P. Skokov and O. Gutfleisch; A multicaloric cooling cycle that exploits thermal Hysteresis; *Nat. Mat. 17 (2018)*

F2-05. Magneto-Transport and Magnetocaloric Properties of $Al_{1.1}Fe_{2-x}M_xB_2$ (M=Mn, Cr, Co) Intermetallic Compounds.
D. Malaviya[1], A.K. Pathak[2], M. Himel[3] and M. Khan[3] *1. Department of Computer Information System, SUNY Buffalo State College, Buffalo, NY, United States; 2. Department of Physics, SUNY Buffalo State College, Buffalo, NY, United States; 3. Department of Physics, Miami University, Oxford, OH, United States*

Materials that exhibit ferromagnetic/antiferromagnetic to paramagnetic phase transition around room temperature also demonstrate interesting functionalities, including magnetocaloric effects, a property that can be exploited in a magnetic refrigerator. $AlFe_2B_2$ is one such material that was initially reported by Jeitschko *et al.* (Acta Crystallogr., Sect. B: Struct. Sci, 25 (1969) 163). Recently, a large magnetocaloric effect near room temperature (Tan *et al*. JACS 135 (2013) 9553) was reported for the material. While $AlFe_2B_2$ is a ferromagnet with T_C ~282 K, analogous AlM_2B_2 alloys with M = Mn or Cr do not show long-range magnetic ordering up to 400 K (Chai *et al*., J. Solid. State. Chem., 224, (2015) 52). Recent neutron powder diffraction study shows $AlMn_2B_2$ order antiferromagnetically near room temperature (Potashnikov *et al*. JMMM 471, (2019) 468). It is, therefore, interesting to explore the magneto-transport and magnetocaloric properties of partially M doped $AlFe_{2-x}M_xB_2$ system. We have observed a previously unreported unusual

electrical transport phenomena with distinct behavior above and below the phase transition for $Al_{1.1}Fe_{2-x}M_x B_2$. In this presentation, we focus on the detailed study of magneto-transport phenomena along with the magnetic and magnetocaloric properties of $AlFe_{2-x}M_xB_2$ that will provide valuable information for the intermetallic community. A part of the work is supported by the Buffalo State Incentive Award and Undergraduate Research office, EURO Award, Buffalo State College.

F2-06. Enhanced Magnetic and Magnetocaloric Properties of Fe Nanoparticles in TiN Thin Film Matrix. *S. Shaji*[1], N. Mucha[1] and D. Kumar[1] *1. Mechanical Engineering, North Carolina Agricultural and Technical State University, Greensboro, NC, United States*

Fe nanoparticles are grown in a TiN/Fe/TiN heterostructure using a pulsed laser deposition (PLD) system. TiN/Fe/TiN multilayers are made by altering the average interlayer distance between two Fe nanoparticles and varying Fe nanoparticle sizes by changing the number of laser pulses impinging on a commercial Fe target. Crystallographic studies carried out using x-ray diffraction (XRD) have indicated crystalline nature of the film with an FWHM of 0.13°. By controlling the nanoparticle size in the confined layers, a superparamagnetic to ferromagnetic phase transition is observed during zero field cooled (ZFC) temperature (T) dependent magnetization (M) measurements and thereby tuned magnetocaloric properties in a controlled manner. A maximum magnetization of ~3.6 × 10^5 A/m which is 2 order of magnitude higher than our previously reported Fe_2Ta thin films is obtained at 0.075 T. Applying the Maxwell relation to the MT curves at various fields, we have calculated vs H the integration of which provides quantitative information about the isothermal entropy change. We have observed a positive MCE with maximum entropy change of ~ 600 J/K-m^3 for the magnetic field changing from 0.002 - 0.075 T in TiN/Fe/TiN system. A coexistence of positive and negative ΔS is observed below and above blocking temperature respectively.

1. V. Franco, J. Blázquez, B. Ingale and A. Conde, Annual Review of Materials Research., 42, pp. 305-342 (2012). 2. C. W. Miller, D. D. Belyea and B. J. Kirby, Journal of Vacuum Science & Technology A., 32(4), p. 040802 (2014). 3. O. Tegus, E. Brück and K. H. J. Buschow, Nature, 415(6868), pp. 150-152 (2002).

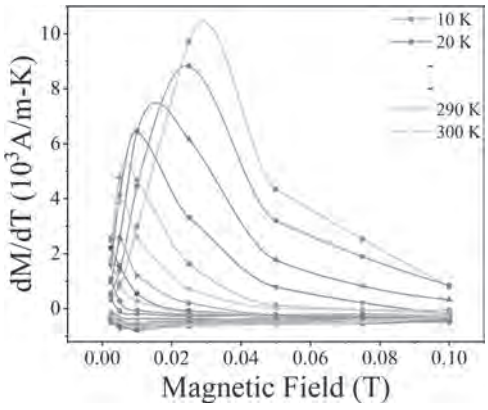

Fig. 1. δM/δT plots as a function of applied field (μ_0H) for a TiN/Fe/TiN thin film matrix.

F2-07. Combined Pressure and Magnetic Field Induced Caloric Effects in Fe_7Se_8 Single Crystals. *Y. Konopelnyk*[1], I. Radelytskyi[1], P. Iwanowski[1], D. Gawryluk[1], M. Berkowski[1], R. Diduszko[2,1], J. Fink-Finowicki[1], R. Puzniak[1] and H. Szymczak[1] *1. Institute of Physics, Polish Academy of Sciences, Warsaw, Poland; 2. Tele and Radio Research Institute, Warszawa, Poland*

The effect of hydrostatic pressure on magnetic entropy change in Fe_7Se_8 single crystals is determined. The combined magnetic entropy change, due to both magnetic field and pressure application is analyzed experimentally and theoretically. The studied material is a ferrimagnetic metal with Néel temperature (T_N) equal 450 K. The first-order spin reorientation transition (SRT) from easy *c*-axis to easy *c*-plane is observed in this material at the temperature $T_r \approx 125$ K [1]. This effect was shown to originate from the specific dependence of the magnetocrystalline energy on temperature and can be induced by applied hydrostatic pressure and/or by a magnetic field. Under applied hydrostatic pressure, T_r is shifting to the lower temperatures, while the effect of the magnetic field depends on the direction to the *c*-axis. Magnetic measurements show the decrease of Fe_7Se_8 magnetization under applied hydrostatic pressure. It is a consequence of iron vacancies redistribution induced by pressure. It has been observed that the entropy change ΔS_{mag} and refrigeration capacity RC, are in strong dependence on T_r and magnetization. Indirect methods, based on magnetization measurements, were used to calculate ΔS_{mag} (Fig.1). It has been shown that the combined application of the magnetic field and hydrostatic pressure can significantly affect entropy change. The sign of the ΔS_{mag} is determined on the direction of the magnetic field *H*. In conclusion, we have shown, that entropy change in magnetic materials such as Fe_7Se_8, subjected to simultaneous variation of magnetic field and pressure, reach large values in a wide range of temperatures in the vicinity of T_r. This study was partly financed by the National Centre for Research and Development, Research Project no. PBS2/A5/36/2013

[1] I. Radelytskyi *et al*., J. Appl. Phys. 124, 143902 (2018).

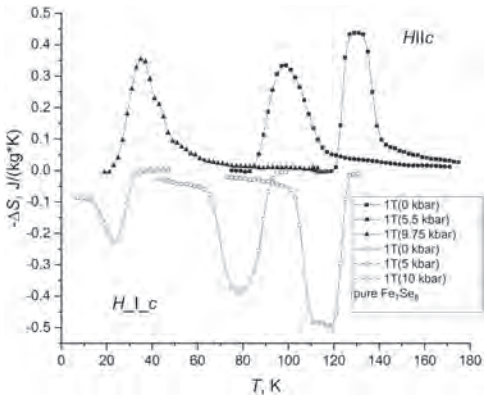

Fig.1. Entropy change vs temperature for various magnitudes of hydrostatic pressure

F2-08. Use of the Scaling Laws of the Magnetocaloric Effect to Deconvolute Overlapping Phase Transitions in Biphasic Composites. *Á. Díaz-García*[1], J. Law[1], P. Gebara[2] and V. Franco[1] *1. Condensed Matter Physics, Universidad de Sevilla, Sevilla, Spain; 2. Physics, Czestochowa University of Technology, Czestochowa, Poland*

Scaling laws have been widely applied for the study of second-order phase transition (SOPT) magnetocaloric materials as their magnetic entropy change, ΔS_M, collapses onto a single universal curve [1]. However, for non-single phase SOPT cases, distortions in the scaled curves prevent good collapse. These distortions get more evident when the ratio of the different phases and the proximity of their transitions increase [2]. Based on scaling laws, a procedure is proposed and successfully applied to deconvolute the

magnetocaloric responses of biphasic $Gd_{80}Pd_{20}$ composite (formed by Gd and Gd_7Pd_3 with Curie temperatures separated by ~45 K) [3, 4]. The global ΔS_M curves of the composite were firstly rescaled by the typical universal scaling procedure considering separately each phase (i=1, 2), i.e. temperature rescaling using one reference temperature, $T_{r,i}$, *as* $\theta_i = (T-T_{pk,i})/(T_{r,i}-T_{pk,i})$ and normalizing the ΔS_M with respect to the corresponding peak values, $\Delta S_M^{pk,i}$. In this case of highly overlapped phase transitions, the typical power law behavior for SOPT ($\Delta S_M^{pk} \propto H^n$ and $T_r \propto H^{\zeta}$) is not fulfilled. An iterative procedure is then followed to account for the phase overlap, leading to a good agreement between experimental and calculated phase fractions and reconstruction of the experimental ΔS_M curves (Fig. 2). This procedure can be applied to extract the response of a pure phase even in cases where the synthesis procedure gives rise to impurity phases, providing a tool to gauge the potential applicability of a material without dedicating large efforts for optimizing its synthesis. Work supported by AEI/FEDER-UE (grants MAT-2016-77265-R and PID2019-105720RB-I00), US/JUNTA/FEDER-UE (grant US-1260179), Consejería de Economía, Conocimiento, Empresas y Universidad de la Junta de Andalucía (grant P18-RT-746), Army Research Laboratory under Cooperative Agreement Number W911NF-19-2-0212 and Polish National Science Centre (Project 2019/03/X/ST5/00066).

[1] V. Franco et al., Int. J. Refrig., 33 465–473 (2010). [2] V. Franco et al., J. Magn. Magn. Mater., 321 1115–1120 (2009). [3] Á. Díaz-García et al., JOM, (2020). https://doi.org/10.1007/s11837-020-04251-z. [4] P. Gebara et al., J. Magn. Magn. Mater., 500 166175 (2020).

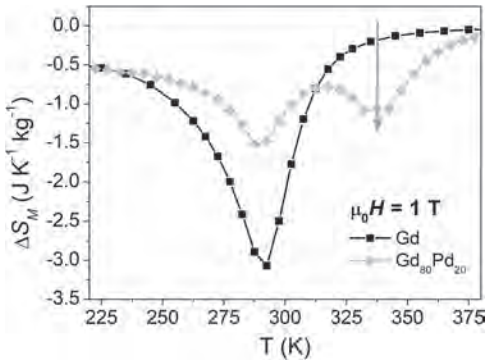

Fig. 1. Temperature dependence for 1 T of ΔS_M for pure Gd and for the composite sample.

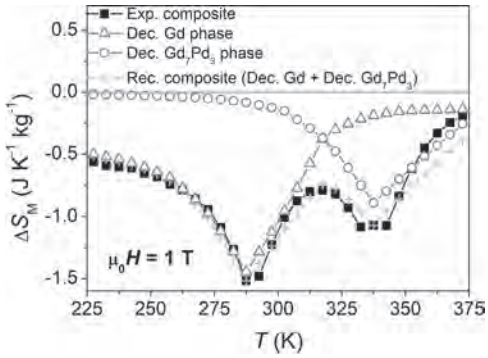

Fig. 2. ΔS_M of the composite sample as function of temperature. Squares: experimental curve; +: reconstructed responses from the deconvoluted responses (triangles and circles).

F2-09. Withdrawn

F2-10. Applying Materials Informatics Insights to Magnetocaloric Materials Screening and Discovery. *A.N. Tantillo*[1,2] and K.G. Sandeman[1,2] *1. Physics, The Graduate Center at CUNY, New York, NY, United States; 2. Physics, Brooklyn College, Brooklyn, NY, United States*

It is over twenty years since the discovery of a giant magnetocaloric effect (GMCE) in Gd-Si-Ge [1], and in that time two low-cost GMCE materials systems have been pursued towards commercialization: Mn-Fe-P-Si [2] and La-Fe-Si [3]. This relatively small number of target room temperature magnetic refrigerants underscores the need for time- and cost-effective magnetocaloric materials discovery projects. The ideal material candidates for magnetocaloric applications must be non-toxic, inexpensive, and readily manufacturable [4]. High- throughput workflows, guided by machine learning and other statistical methods in material informatics, are essential to streamlining the process of screening new possible materials, making the experimental process as targeted and efficient as possible. This presentation describes two approaches to materials screening based on simulated data. The first approach is a modification of the screening method of Bocarsly et al. [5], wherein lattice deformation across the magnetic phase transition (magnetic deformation) was computed based on the difference between unit cell dimension lengths with and without magnetic interactions in models based on density function theory (DFT). We add a phenomenological parameter calculated from the electronic density of states available from the Materials Project [6]. The addition of this new parameter can enhance the prediction of magnetic field-induced entropy change, ΔS_M, with nearly 60% better correlation than using magnetic deformation alone. The second approach is motivated by the relative scarcity of consistent magnetic entropy data for stoichiometric compounds, which limits the ability of researchers to cross-check predicted ΔS_M with experiment. We describe a method of scraping the Materials Project database for DFT results on magnetically ordered compounds [7] using the Pymatgen open-source Python library [8]. By analyzing the electronic density of states, computed unit cell volume and other parameters obtained through the Materials Project database for over 20,000 materials, we compile a data subset which we use to propose directions for magnetocaloric material research.

[1] V. Pecharsky et al. 1997 Phys. Rev. Let. 78 4494 [2] N. H. Dung et al. 2011 Adv. Energy Mater 1 1215-1219. [3] M. Katter et al. US Patent Application No. 2012/0043497 A1 (23 Feb. 2012) [4] N. A. Zarkevich et al. 2018 J. Phys. D: Appl. Phys. 51 024002 [5] J. Bocarsly, et al. 2017 Chem. Mat. 29 (4), 1613-1622 [6] A. Jain, S.P. Ong et al. 2013 APL Materials, 2013, 1(1), 011002 [7] S. P. Ong et al. 2015 Comp. Mat. Sci. 97 209–215 [8] S. P. Ong et al. 2013 Comp. Mat. Sci. 68 314–319

F2-11. Withdrawn

F2-12. Bulk-Like First-Order Phase Transition in Mechanochemically Fabricated FeRh Particles. *D. Clifford*[1], S. Gupta[2], R. Barua[1], A. Biswas[2], R.L. Hadimani[1], Y. Mudryk[2] and V.K. Pecharsky[2,3] *1. Mechanical and Nuclear Eng., Virginia Commonwealth University, Richmond, VA, United States; 2. Division of Materials Science, Ames Laboratory, Ames, IA, United States; 3. Dept. of Materials Science and Engineering, Iowa State University, Ames, IA, United States*

Near-equiatomic iron-rhodium (FeRh) is a fundamentally and technologically interesting material exhibiting giant inverse magnetocaloric effect (MCE), potentially suitable for applications at the diminutive scale such as microcooling and medical diagnostic imaging, which require sharp first-order magnetic phase transitions (FOMPTs). Reports on FeRh having a sharp FOMPT in its bulk form are common,[1] however the transition broadens considerably

in some non-bulk forms, particularly thin-films (thickness < 50nm) and fine particles.[2] In this work, an abrupt, bulk-like FOMPT has been demonstrated for the first time in FeRh particles produced using a solvent-free, reactive mechanochemical co-reduction of $FeCl_2$ and $RhCl_3$ precursors. Characterization using structural and magnetic probes indicates that annealing at temperatures ranging from 600°C to 800°C and subsequent quenching enables tuning of composition, microstructure, and physical properties of the particles. Depending upon the heat treatment condition, the fraction of *fcc* paramagnetic FeRh and *B*2 FeRh (both ferromagnetic (FM) α' and antiferromagnetic (AFM) α'') phases can be controlled. The M-T analysis indicates that the first-order magnetostructural transition temperature, T_t, can be tailored between 380K and 325K, and both the ΔM between the AFM and FM states and the thermal hysteresis can be manipulated as well (Fig. 1). A maximum magnetic entropy change of ΔS_{mag} ~10 J/kgK at μH=2T was noted in FeRh particles annealed at 800°C. These results will be discussed in the context of the compositional phase diagram and strain accommodation mechanism. Implications of this study on emerging biomedical applications, mainly thermal magnetic resonance imaging and magnetic hyperthermia therapy, will be presented. Acknowledgement: Research at VCU supported by VCU College of Engineering start-up funds and NSF-MRI Grant (1726617). Research in Ames (AL) supported by the M.S.E.D., Office of Basic Energy Sciences of the US DOE. AL is operated for the US DOE by Iowa State University under Contract No. DE-AC02-07CH11358.

°[1] L. H. Lewis et. al., *J. Phys. D: Appl. Phys.* vol. 49. 323002 (2016) [2] R. Barua, "Pathways for tailoring the magnetostructural response of FeRh-based systems." Ph.D. Dissertation (2014).

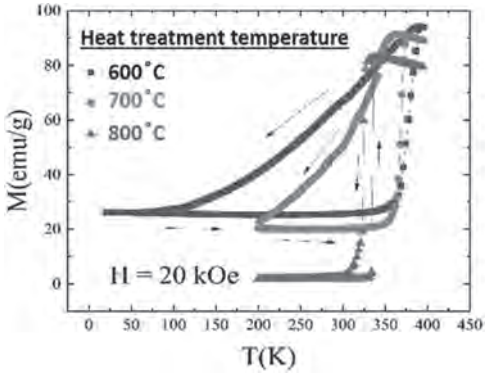

Fig. 1 Magnetothermal curves (heating and cooling cycles) for mechanochemically synthesized FeRh particles subjected to heat treatment at 600°C, 700°C and 800°C.

F2-13. Withdrawn

F2-14. Dysprosium-Yttrium Solid Solutions as Magnetocaloric Materials for Nitrogen gas Liquefaction. S.V. Taskaev[1,3], K. Skokov[4], *V. Khovaylo*[2], M.N. Ulyanov[1], D. Bataev[1], D. Plakhotskiy[1], M. Kononova[1,2] and Z. Hu[5] *1. Chelyabinsk State University, Chelyabinsk, Russian Federation; 2. National University of Science and Technology "MISIS", Moscow, Russian Federation; 3. National Research South Ural State University, Chelyabinsk, Russian Federation; 4. Material Science, Technische Universität Darmstadt, Darmstadt, Germany; 5. University of Science and Technology Beijing, Beijing, China*

During the last two decades, there has been significant interest in the investigation of the magnetocaloric effect (MCE) due to its potential advantage in magnetic cooling, both for near room temperature application ("magnetic" fridge) and for cryogenic gas liquefaction [1]. In this respect, attention has been given to alloys and compounds undergoing magnetic phase transitions of 1st- and 2nd order [2–5]. Considering engineering aspects of MCE cooling, it is evident that the heat exchange between MCE materials of a refrigerator and the surroundings is a critical issue for developing efficient magnetic refrigerators. Therefore, research also focused on the study of MCE materials with "reduced" dimensions, i.e., having the form of thin films, foils or microwires. Because of their technological significance in cryogenic gas liquefaction, MCE in ribbons of rare-earth (RE) alloys and compounds has been reported for several systems [6]. Alongside with this, magnetic and MCE properties of elemental rare-earths in different structural states have been characterized as well [7-8]. It has been shown that magnetic properties of RE materials in submicrocrystalline and large-grain structural states differ, sometimes significantly. Among the RE elements, Dy possesses the highest magnetic moment and demonstrates a rich magnetic phase diagram [9]. Under zero magnetic field and pressure, bulk Dy is paramagnetic at room temperature and undergoes a sequence of magnetic and structural phase transition upon cooling. Moreover, several intermediate magnetic phases have been reported to emerge in non-zero magnetic field. Evidently, such a delicate balance of magnetic interactions in Dy should be sensitive not only to external pressure or magnetic field, but to the structural state and alloying as well. In present research we discuss the thermodynamic properties of Dy-Y solid solutions as perspective materials for N_2 gas liquefaction using AMR scheme of magnetic cooling. It is shown that the dilution of magnetic system of Dy by Y atoms allows one to flexibly tune T_c in final solid solution in a wide temperature range as well as to preserve the magnitude of the MCE near initial one. Acknowledgement: RSF-Helmholtz project # 18-42-06201.

[1] A.M. Tishin, Y.I. Spichkin, The Magnetocaloric Effect and its Applications, IoP Publishing, Bristol and Philadelphia, 2003. [2] F. Scheibel, T. Gottschall, A. Taubel, M. Fries, K.P. Skokov, A. Terwey, W. Keune, K. Ollefs, H. Wende, M. Farle, M. Acet, O. Gutfleisch, M.E. Gruner, Hysteresis design of novel magnetocaloric materials – from basic mechanisms to applications, Energy Technol. 6 (2018) 1397. [3] O. Gutfleisch, T. Gottschall, M. Fries, D. Benke, I. Radulov, K.P. Skokov, H. Wende, M. Gruner, M. Acet, P. Entel, M. Farle, Mastering hysteresis in magnetocaloric materials, Phil. Trans. R. Soc. A 374 (2016) 20150308. [4] O. Gutfleisch, J.P. Liu, M. Willard, E. Brück, C. Chen, S.G. Shankar, Magnetic materials and devices for the 21st century: stronger, lighter, and more energy efficient (review), Adv. Mater. 23 (2011) 821. [5] S. Taskaev, K. Skokov, V. Khovaylo, V. Buchelnikov, A. Pellenen, D. Karpenkov, M. Ulyanov, D. Bataev, A. Usenko, M. Lyange, O. Gutfleisch, J. Appl. Phys. 117 (2015) 123914. [6] S. Taskaev, V. Khovaylo, D. Karpenkov, I. Radulov, M. Ulyanov, D. Bataev, A. Dyakonov, D. Gunderov, K. Skokov, O. Gutfleisch, J. Alloys Comp. 754 (2018) 207. [7] S.V. Taskaev, M.D. Kuz'min, K.P. Skokov, D.Yu. Karpenkov, A.P. Pellenen, V.D. Buchelnikov, O. Gutfleisch, J. Magn. Magn. Mater. 331 (2013) 33. [8] S.V. Taskaev, K.P. Skokov, V.V. Khovaylo, M.V. Gorshenkov, A.N. Vasiliev, O.S. Volkova, V.D. Buchelnikov, A.P. Pellenen, O. Gutfleisch, I.E.E.E. Magn, Lett. 7 (2016) 5203104. [9] A.S. Chernyshov, Ya. Mudryk, V.K. Pecharsky, K.A. Gschneidner Jr., Phys. Rev. B 77J. Yu, P.R. LeClair, G.J. Mankey, J.L. Robertson, M.L. Crow, W. Tian, Phys. Rev. B 91 (2015) 014404.

F2-15. Decoupling of Magnetic Sublattices in NiMn-Based Heusler Compounds. *F. Cugini*[1,2], S. Chicco[1], G. Cavazzini[1,2], F. Orlandi[3], G. Allodi[1], V. Vezzoni[1], M. Gruner[4], L. Righi[5], S. Fabbrici[2], F. Albertini[2] and M. Solzi[1,2] *1. SMFI Department, Universita degli Studi di Parma, Parma, Italy; 2. IMEM-CNR Institute, Parma, Italy; 3. ISIS Facility STFC, Didcot, United Kingdom; 4. Department of Physics, Universitat Duisburg-Essen, Duisburg, Germany; 5. SCVSA department, Universita degli Studi di Parma, Parma, Italy*

The complex interplay between structural, electronic and magnetic degrees of freedom in Mn-based magnetic Heusler compounds gives rise to a great variety of functional properties suitable for sustainable technological applications (energy conversion devices, sensors, actuators, spintronic components…) [1]. The adaptive lattice allows, by changing composition, the development of different crystallographic and magnetic structures, thus offering the possibility to tune properties and effects. Great efforts have been devoted in the last decades to investigate these materials by combining various experimental techniques and first-principles calculations, nonetheless a comprehensive and

coherent description, able to drive the full control of Heusler properties, it is far from being achieved. In this work, we combine bulk-sensitive magnetometry, neutron diffraction and ^{55}Mn nuclear magnetic resonance experiments with first-principles calculations to decouple and clarify the different contributions that define the ferromagnetic structure of off-stoichiometric NiMn-based Heusler compounds. We selected, as test material, the $Ni_{48}Mn_{36}In_{16-x}Sn_x$ series [2], showing a stable cubic austenitic phase down to 5 K, with a Curie transition slightly above room temperature. The replacement of In with Sn leads to a decrease of the saturation magnetization whereas the Curie temperature is featured by a non-monotonic variation (Fig. 1). First-principles calculations suggested the intrinsic nature of the behaviours of the critical temperature, which turns out to be related to the electronic properties. On the contrary, neutron diffraction and NMR experiments revealed that the decrease of magnetization by increasing the Sn content is caused by the disordering of the Mn magnetic moments sited in the mixed sublattice. The progressive replacement of In by Sn leads to a decrease of ordering temperature of Mn in the mixed site (Fig. 2), due to the destabilization of the complex magnetic interactions.

[1] T. Graf, C. Felser and S. S. Parkin, Prog. Solid. State Ch., 39, 1-50 (2011). [2] G. Cavazzini, F. Cugini, M. E. Gruner, et al., Scripta Mater., 170, 48–51 (2019).

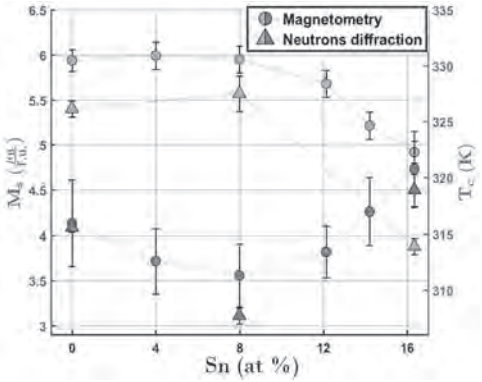

Fig. 1: Dependence of magnetization and Curie temperature versus Sn at.% content obtained by magnetometry and neutron diffraction.

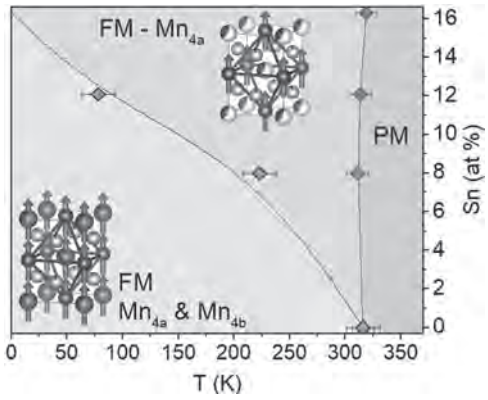

Fig. 2: Magnetic phase diagram of $Ni_{48}Mn_{36}In_{16-x}Sn_x$ compounds.

F2-16. Designing Multicaloric Materials for Novel Multi-Stimuli Cooling Cycle. *F. Scheibel*[1], A. Taubel[1], L. Pfeuffer[1], B. Beckmann[1], W. Liu[1], T. Gottschall[2], K. Skokov[1] and O. Gutfleisch[1] *1. Materials Sciences, Technical University of Darmstadt, Darmstadt, Germany; 2. Dresden High Magnetic Field Laboratory, elmholtz-Zentrum Dresden-Rossendorf, Dresden, Germany*

Magnetocaloric (MC) refrigeration can be more energy efficient and environmentally friendly than current vapor compression technology [1]. It is based on a solid-state magnetic material exhibiting large magnetocaloric effects (MCE) at a first-order magnetostructural phase transition (FOMST). A major challenge in materials with a FOMST is the thermal hysteresis, which deteriorates the cyclic performance for MC refrigeration [2]. Instead to reducing the hysteresis an alternative solution has been proposed, which benefits from the hysteresis by using two stimuli to trigger the FOMST [3]. A magnetic field induces the high magnetization state while the hysteresis prevents the back transformation after field removing. For the back transformation an external pressure is used as a second stimulus. The use of two stimuli enable a complete FOMST under cyclic conduction and overcomes the drawback of the hysteresis. Furthermore, the amount of permanent magnets can be reduced because the material needs to be magnetized only for a short time. Ni-(Co)-Mn-X (X:In, Sn, Ti) Heusler alloy show a large MCE and tailorable FOMST. We performed constant-stress thermal cycling experiments to investigate the sensitivity of the FOMST towards both stimuli and the mechanical stability required for the multistimuli cooling. The MC response is investigated in high magnetic fields and fast field-sweep rates. Especially the influence of grain refinement on the mechanical properties and the thermal hysteresis has been investigated for designing well-performing and durable multicaloric materials. The presence of secondary phases in Gd-doped Ni-(Co)-Mn-In improves the mechanical stability and preserve the good MC properties. All-d-metal Heusler Ni-Co-Mn-Ti are also investigated intensively because of their large MCE [4]. In addition, they show a large volume change during FOMST leading to a large elastocaloric effect ECE [5] as well as enhanced mechanical stability. This work is supported by ERC Advanced Grant “CoolInnov”, and CRC/TRR 270 “HoMMage”.

[1] O. Gutfleisch et al., Adv. Mater. 23, 821-842 (2011) [2] F. Scheibel et al., Energy Technol. 6, 1397-1428 (2018) [3] T. Gottschall et al., Nature Mat. 17, 929–934 (2018) [4] Z. Y. Wei et al., Appl. Phys. Lett. 107, 022406 (2015) [5] Z- Y. Wei et al., Appl. Phys. Lett. 114, 101903 (2019)

F2-17. Withdrawn

F2-18. Temperature Dependence of the Magnetic Interactions Taking Place in Monodisperse Magnetite Nanoparticles Having Different Morphologies. E. Navarro[1], Y. Luengo[1], S. Veintemillas-Verdaguer[1], M.P. Morales[1], F. Palomares[1], U. Urdiroz[1], F. Cebollada[2] and *J.M. González*[1] *1. Instituto de Ciencia de Materiales de Madrid - CSIC, Madrid, Spain; 2. Universidad Politécnica de Madrid, Madrid, Spain*

In a recent paper [1], the authors have evidenced how the thermally activated demagnetization processes taking place in magnetite nanoparticles (NPs) play a major role on deteriorating the dc coercivity values measured in these samples at temperatures above ca. 150 K. The mechanisms for that deterioration are the increase with the temperature of both the fluctuation field and the activation volume, the latter reaching at room temperature values of up more than 40 times the average particle volume value. We aim here at the quantitative evaluation of the inter-particles interactions underlying that phenomenology and, particularly, at the identification of the role played by the nanoparticles morphology. For that purpose, we have measured magnetite NPs prepared via oxidative precipitation by controlling their size through the nature of the base and nitrate salt and the ethanol content in the media, and their morphology (either octahedral or spherical) by changing the final base concentration [2]. Particle size, shape and crystal structure were determined by transmission electron microscopy (TEM), high-resolution electron microscopy (HRTEM), and X-rays diffraction (XRD), respectively. The magnetic properties of were measured by means of a vibrating sample magnetometer, working in the temperature range from 5 K up to 290 K by applying a maximum field of 9 T. Figure 1 displays the temperature dependence of the reduced saturation remanence (M_r/M_S) clearly showing that in both morphologies, but to a larger extent in the spherical NPs, the measured isotropic powder exhibits reduced remanences below 0.5, which suggests the occurrence of demagnetizing interactions. The actual occurrence of that type of interactions was confirmed from the measurement (at 5 K, 125 K and 200 K) of the field dependencies of the isothermal and demagnetization

remanences of the samples and the evaluation of the associated Henkel plots. The differences identified in those plots between the spherical and octahedral NPs are discussed in terms of the particle aggregation into close-flux structures.

[1] E. Navarro, Y. Luengo, S. Veintemillas, M. P. Morales, F. Javier Palomares, U. Urdiroz, F. Cebollada, and J. M. González; AIP Advances 9, 125143 (2019) [2] Y. Luengo, M. P. Morales, L. Gutiérrez, S. Veintemillas-Verdaguer, J. Mater. Chem. C, 4, 9482-9488 (2016)

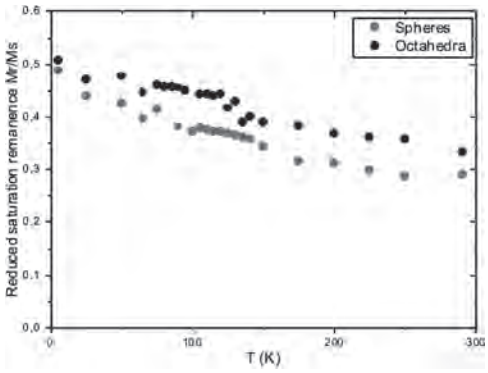

Figure 1. Temperature dependence of the reduced saturation remanence measured in the spherical and octahedral NPs

Session F3
NOVEL SENSORS I

Hendrik Ohldag, Co-Chair
Lawrence Berkeley National Laboratory, Berkeley, CA, United States
Tom Thomson, Co-Chair
University of Manchester, Manchester, United Kingdom

INVITED PAPER

F3-01. Magnetic Domain Behavior up to the GHz Regime in Magnetic Sensors With PicoTesla Sensitivity – Magnetic Noise and Domain Optimization. *J. McCord*[1], C. Müller[1], M. Jovičević Klug[1], E. Golubeva[1], N. Urs[1] and D. Schiewitz[1] *1. Institute for Materials Science, Kiel University, Kiel, Germany*

The role of magnetic domain formation and reorientation processes reveals fascinating physics and is of great relevance for technological applications. Recent advances in thin film devices adopting magnetic films as sensing layers, involving magnetoelectric (ME) cantilever sensors, surface acoustic wave (SAW) devices, and giant magnetoimpedance (GMI) devices offer a promising route for sensing ultra-low magnetic signals. These kinds of sensors are typically operated by external stimuli from the kHz to the GHz regime. Therefore, understanding and controlling the complex physics of magnetic domain activity at the relevant modulation frequencies are the most important factors that determine the performance of the magnetic field sensors as the signal-to-noise ratios of the sensors are dominated by magnetic domain and domain wall activity. In-operando time-resolved magnetic domain observation sheds light on the irreversible and hysteretic magnetization changes due to domain nucleation, domain wall resonances, precessional magnetization effects, and spin-wave phenomena, determining the various sensors' performances at different frequencies of operation. Using time-resolved magneto-optical Kerr effect microscopy with time resolutions from nanoseconds to picoseconds, we show the impact of spatial magnetization distribution, especially of magnetic domains and domain walls on ME, ΔE-effect, SAW and GMI sensor performance. The domain activity in operating devices is studied and compared at a broad temporal range from a few hundred Hz up to GHz. With the spatial and temporal analysis together with complementary electrical measurements, the physical origin of the various effects is determined. From this, strategies for sensor improvement are provided, some of which are already implemented in various sensor designs. The role and impact of static and dynamic magnetic domain and domain wall activity and their influence on the magnetic sensor response will be discussed in detail. The aspects will be discussed on ferromagnetic single layer systems as well as on multilayer systems, demonstrating unique magnetization coupling phenomena. Magnetic noise density originating from magnetic domain activity and not sensitivity is the main figure-of-merit for optimizing sensor performance. Even minimal magnetic domain activity is restricting magnetic sensor performance. Localized magnetostrictive effects are central to the magnetic domain behavior. Understanding the magnetic domain physics and controlling magnetic domain behavior is a key to improved sensor performance. The data proves the importance of micromagnetic processes for real-world applications. We highly acknowledge cooperation and funding through DFG CRC 1261 "Magnetoelectric Sensors: From Composite Materials to Biomagnetic Diagnostics" and cooperation with the group of Nian X. Sun from Northeastern University Boston. We highly acknowledge cooperation within and funding through DFG CRC 1261 "Magnetoelectric Sensors: From Composite Materials to Biomagnetic Diagnostics" and cooperation with the group of Nian X. Sun from Northeastern University Boston.

N.O. Urs, E. Golubeva, V. Röbisch, S. Toxværd, S. Deldar, R. Knöchel, M. Höft, E. Quandt, D. Meyners and J. McCord, Physical Review Applied Vol. 13, p.024018 (2020) P. Hayes, M. Jovičević Klug, S. Toxværd, P. Durdaut, V. Schell, A. Teplyuk, D. Burdin, A. Winkler, R. Weser, Y. Fetisov, M. Höft, R. Knöchel, J. McCord, and E Quandt, Scientific Reports Vol. 9, p.16355 (2019) M. Jovičević Klug, L. Thormählen, V. Röbisch, S. Salzer, M. Höft, E. Quandt D. Meyners and J. McCord, Applied Physics Letters Vol. 114, p.192410 (2019) A. Kittmann, P. Durdaut, S. Zabel, J. Reermann, J. Schmalz, B. Spetzler, D. Meyners, N.X. Sun, J. McCord, M. Gerken, G. Schmidt, M. Höft, R. Knöchel, F. Faupel and E. Quandt, Scientific Reports Vol. 8, p.278 (2018) R.B. Holländer, C. Müller, M. Lohmann, B. Mozooni and J. McCord, Journal of Magnetism and Magnetic Materials Vol. 432, p.283 (2017) N.O. Urs, B. Mozooni, P. Mazalski, M. Kustov, P. Hayes, S. Deldar, E. Quandt and J. McCord, AIP Advances Vol. 6, p.055605 (2016) J. McCord, Journal of Physics D: Applied Physics Vol. 48, p.333001 (2015)

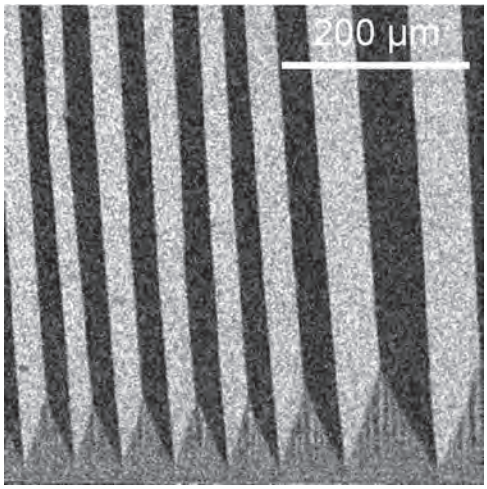

Fig. 1 Snapshot of a characteristic magnetic domain process in a magnetic modulated ME cantilever sensor (the frequency of operation is 876 Hz).

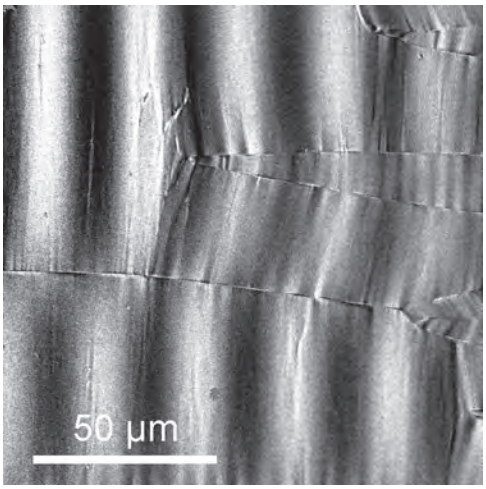

Fig. 2 Dynamic magnetic response imaging in a SAW sensor device showing propagating Love waves together with induced domain wall actvity (the frequency of operation is 150 MHz).

CONTRIBUTED PAPERS

F3-02. Detection Limit Normalization and Study of TMR Magnetic Field Sensors. *E. Monteblanco*[1], C. Chopin[1], J. Moulin[1], P. Belliot[2], N. Belin[2], C. Fermon[1], M. pannetier-lecoeur[1] and A. Solignac[1] *1. SPEC, Commissariat a l'energie atomique et aux energies alternatives Institut rayonnement-matiere de Saclay, Gif-sur-Yvette, France; 2. CrivaSense Technologies SAS, 91190 Saint Aubin, France, Saint Aubin, France*

Magnetic tunnel junction (MTJ) is a promising candidate for the development of ultrasensitive magnetic field sensor (TMR sensor) capable to detect extremely weak magnetic fields (<nT/Hz$^{0.5}$) opening the possibilities for biomedical applications[1]. The performance of these type of sensors is limited by the high low-frequency noise (1/f) which appears due to the presence of magnetic domain fluctuations or by defects inside the insulator barrier[2]. In this work, we study the normalization and voltage bias effect on the detection limit in TMR sensors based in MTJs. The multilayer stack is Ta(5)/ SyF_1/MgO/SyF_2/Ta(10), where the synthetic ferrimagnet structures are SyF_1: PtMn(25)/CoFe(2.3)/Ru(0.83)/CoFe(1)/Ta(0.1)/CoFeB(1.5) and SyF_2: CoFeB(1.5)/Ta(0.1)/CoFe(1)/Ru(2.6)/CoFe(2)/PtMn(16) (nanometers). Samples were processes using optical UV lithography to define the diameter (D) and number of MTJs circular pillars in serie (N) inside the sensor. The RA product was typically around 13-20kΩµm^2 at 0 mT and the TMR 200 % at room temperature. In order to provide a good interpretation of the results we propose a theoretical model to extract the real output voltage noise from standard electronic circuits. This model was used on a ¼ Wheatstone bridge setup, where the resistive elements were modelled as fluctuating resistances. Our TMR sensors show a sensitivity of 4 %/mT (<0.1%/mT) at 0mT (P state at -100mT)[3]. The 1/f noise was quantified by the Hooge-like parameter, which allow to compare the 1/f noise of different types of TMR sensors. We observed that well known equation works only below a threshold voltage, due to the non-linearity of the I-V curve related maybe to different symmetry conduction bands. At low bias voltage, devices show higher values at 0 mT (3.10^{-8}µm^2) than in the P state ($2–4.10^{-9}$µm^2). An interesting feature for applications is the almost constant detectivity (100nT/Hz$^{0.5}$ at 10Hz) as a function of the bias voltage. This is a result of the compromise between the output noise voltage and the sensitivity. The subsequent output power and detection limit normalization allow us to design new TMR sensors with optimal conditions.

[1] S. Cardoso, D. C. Leitao, T. M. Dias, J. Valadeiro, M. D. Silva, A. Chicharo, V. Silverio, J. Gaspar, and P. P. Freitas, J. Phys. D: Appl. Phys. 50, 213001 (2017). [2] J. Scola, H. Polovy, C. Fermon, M. P. Lecoeur, G. Feng, K. Fahy, and J. M. D. Coey. Appl., Phys. Lett., vol. 90, p. 252501, 2007 [3] J. M. Almeida, P. Wisniowski, and P. P. Freitas IEEE Trans Mag, VOL. 44, NO. 11, (2008)

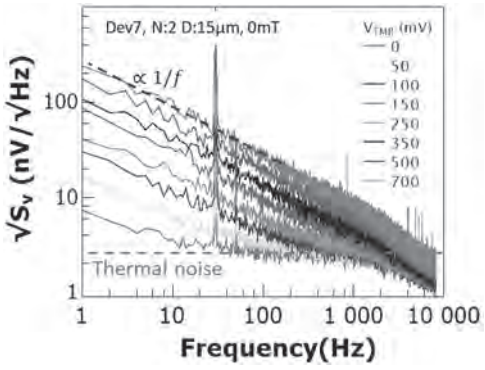

Output voltage noise vs. frequency

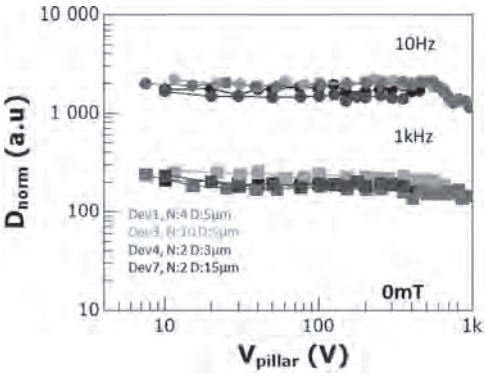

Detectivity vs. applied voltage by pillar

F3-03. Withdrawn

F3-04. Withdrawn

INVITED PAPER

F3-05. Magnetic Noise due to Asymmetric Oscillations in Magnetic Tunneling Readers. *A. Stankiewicz*[1] *1. Seagate Recording Head Operations, Bloomington, MN, United States*

Magnetic noise is a major contributor to the signal-to-noise ratio (SNR) of readback channels in magnetoresistive readers, where all noise sources can be divided into two groups, which call for very different analysis tools: 1. Thermal noise, in which the system remains in a stable equilibrium configuration. Here, noise is generated by thermal excitation of the system around this stable state. 2. Instability, in which the system supports more than one equilibrium configuration, separated by energy barriers, which are low enough to allow for switching due to thermal excitation. Here we will focus on the first, concerning thermal noise in stable devices. Thermal noise analysis in magnetoresistive readers has been traditionally done by micromagnetic modeling with random fields, which simulates thermal excitation. This approach is very time consuming, and provides limited understanding of the noise sources. However, the mode structure (including amplitude and phase) can be derived from simulation data by phase sensitive detection in every pixel. The frequency of all modes is larger than ~4 GHz in typical

readers. Then, the extracted modes can be analyzed separately for their impact on the noise in the device operation frequency band (*NDOB*), which is typically below 2 GHz. Recent studies report [1] that an oscillation mode impact on *NDOB* strongly depends on its symmetry. The noise remains very small while the mode is symmetric, and grows rapidly with emerging asymmetry. In magnetic readers the asymmetry may be caused by a presence of anisotropy (including shape anisotropy). Fig. 1 illustrates the effect using a simple macrospin model of a typical readers with different shape anisotropy. It has been shown that asymmetric oscillations lead to strong noise tails, which may look similar to random telegraph noise or 1/f noise profiles. This is a new effect, first observed in magnetoresistive readers. The ultimate test for asymmetric oscillation noise is a correlation between *NDOB* and instantaneous amplitude of resonant mode fluctuations (*CorFL2G*). It can only be detected in the time domain data (waveforms). This analysis can be applied to modeled [1] and experimental [2] results, and consists of the following steps: 1. Generate/collect a high bandwidth (0-20 GHz) thermal noise waveform. 2. Filter out *NDOB* and resonant mode waveforms using band-pass digital filters. 3. Calculate envelope of the resonance waveform (*ERW*), which estimates fluctuations of the oscillation amplitude. 4. Calculate a correlation coefficient between *NDOB* and *ERW*. Fig.2 shows *NDOB* and *CorFL2G* as a function of an external transverse field in a noisy reader, where larger noise corresponds to a larger magnitude of the correlation, indicating that asymmetric oscillations are the primary source of noise. There is also a direct correspondence to the M-shape noise profile obtained in the model (Fig.1). The presented results led to development of a patented method of asymmetric oscillation noise correction, which can improve the SNR by several dB in readers with large asymmetric oscillation noise [3]. The introduced concepts and techniques are very general, and can be applied to other dynamical systems.

[1] T. Pipathanapoompron, A. Stankiewicz, K. Subramanian, A. Grier, A. Kaewrawang, "Modeling of Magnetic Thermal Noise in Stable Magnetic Sensors," *Journal of Applied Physics,* Vol. 127 p. 073902 (2020). [2] T. Pipathanapoompron, A. Stankiewicz, J. Wang, K. Subramanian, A. Kaewrawang, "Magnetic reader testing for asymmetric oscillation noise," *Journal of Magnetism and Magnetic Materials*, Vol. 514, p. 167064 (2020). [2] A. Stankiewicz, S. Stokes, K. Subramanian, "Mitigation of noise generated by random excitation of asymmetric oscillation modes," *US Patent* 10,615,887 (2020).

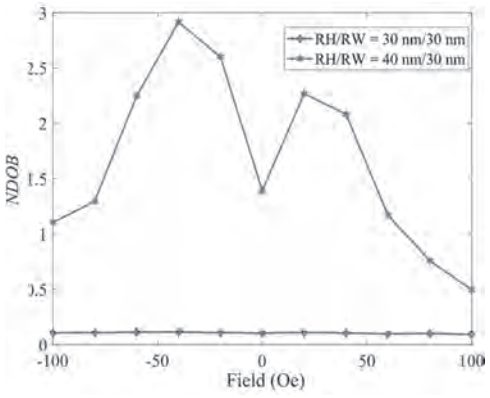

Fig. 1 Macrospin model: noise in the device operationy band (*NDOB*) vs. the external field - comparison between no shape anisotropy and high shape anisotropy readers with the same bias field (= 800 Oe). The model does not include shields, so the external field magnitude is much lower than in the experiment (Fig. 2).

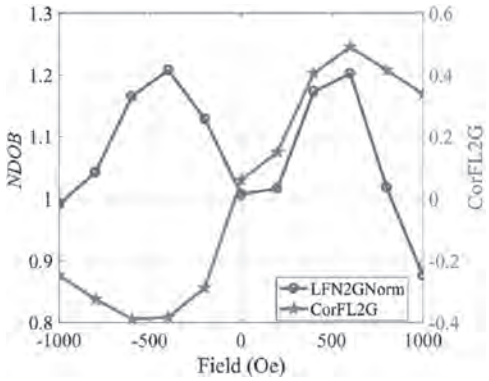

Fig. 2 Experiment: Noise in the device operation frequency band (*NDOB*) and correlation coeficient (*CorFL2G*) between low frequency noise and instantaneous amplitude of the free layer resonance vs. external field for a noisy reader with width-height product equal to 28x35 nm².

CONTRIBUTED PAPERS

F3-06. FeAlSi Thin Films With low Magnetic Anisotropy for the Free Layer of Magnetic Tunnel Junction Based Sensors. *S. Akamatsu*[1], M. Oogane[1], M. Tsunoda[1] and Y. Ando[1] *1. Engineering, Tohoku Daigaku, Sendai, Japan*

Soft magnetic materials showing a high tunnel magnetoresistance (TMR) effect are needed for improving the sensitivity of magnetic tunnel junction (MTJ) based sensors. We focused the Sendust alloy ($Fe_{85}Al_{5.4}Si_{9.6}$ wt.%, hereinafter, this is called "FeAlSi"), which has soft magnetic property in $D0_3$-ordered structure. FeAlSi electrode is also expected to show a high TMR ratio by Δ_1 electron coherent tunneling through MgO barriers as well as Fe electrodes with similar crystal structure to FeAlSi [1]. In previous work [2], we firstly succeeded to fabricate epitaxial $D0_3$-FeAlSi films with thickness of 30 nm on MgO substrates. Additionally, we observed good soft magnetic properties comparable to other free layer materials such as NiFe [3]. The purpose of this study is fabrication of MTJs using FeAlSi free layer and investigation of their TMR properties. All films were deposited on Si/SiO_2 substrates using magnetron sputtering. The stacking structure for the characterization of magnetic and structural properties was Si/SiO_2/Ta(5)/CoFeB(5)/MgO(20)/FeAlSi(30)/Ta(5)(in nm). TMR properties were investigated in the MTJs with stacking structure of Si/SiO_2/Ta(5)/CoFeB(5)/MgO(20)/FeAlSi(30)/MgO(2)/CoFeB(3)/Ru(0.85)/CoFe(5)/IrMn(10)/Ta(5)/Ru(10). Crystal structure, magnetic properties, and TMR properties were measured by X-ray diffraction (XRD), vibrating sample magnetometer (VSM), and 4-probe DC measurement. Fig. 1 shows the XRD patterns for FeAlSi films prepared by optimal condition. A fundamental peak of FeAlSi (004) and superlattice peak of FeAlSi (002) from B2-ordered structure were clearly observed. The XRD result indicates that the FeAlSi film grown on SiO_2 substrates with an MgO underlayer has (001)-orientation and contains B2-ordered structure. Fig. 2 shows magnetoresistance curve for MTJs with FeAlSi bottom electrode. We firstly observed TMR effect of 18.1% at RT using FeAlSi electrode with relatively small switching field. Although the further improvement of TMR effect is needed, the prepared FeAlSi thin film with soft magnetic property is a promising candidate for the free layer of MTJ based sensors with high sensitivity.

[1] W. H. Butler *et al.*, Phys. Rev. B, Vol. 63, p.054416 (2001). [2] S. Akamatsu *et al.*, AIP Advances 10, 0 15302 (2020). [3] K. Fujiwara *et al.*, Jpn. J. Appl. Phys., Vol. 52, p.04CM07 (2013).

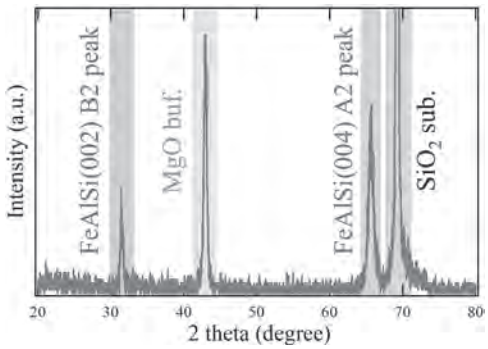

Fig. 1 XRD patterns for FeAlSi free layer

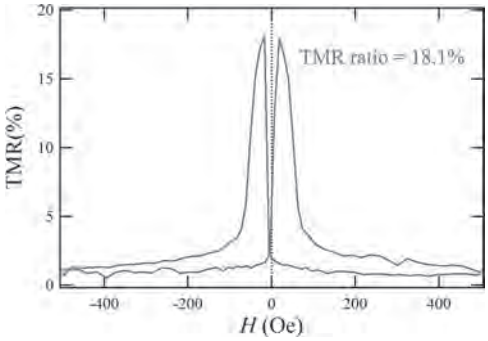

Fig. 2 TMR curve in MTJ with FeAlSi electrode

F3-07. Highly Sensitive Magnetic Sensor for Detecting Magnetic Nanoparticles Based on Magnetic Tunnel Junctions at a Static Field. *Z. Jin*[1], T. Koo[2], M. Kim[5], M. Al-Mahdawi[3,4], M. Oogane[1,3], Y. Ando[1,4] and Y. Kim[2,5] *1. Department of Applied Physics, Tohoku University, Sendai, Japan; 2. Department of Materials Science and Engineering, Korea University, Seoul, The Republic of Korea; 3. Center for Science and Innovation in Spintronics (Core Research Cluster) Organization for Advanced Studies, Tohoku University, Sendai, Japan; 4. Center for Spintronics Research Network, Tohoku University, Sendai, Japan; 5. The Institute for High Technology Materials and Devices, Korea University, Seoul, The Republic of Korea*

Magnetic nanoparticles (MNPs) with surface functionalization are promising for lab-on-chip applications, especially for immunoassay and biomarker detection [1]. Tunnel magnetoresistance (TMR) sensors are suitable to detect MNPs, because of their high sensitivity and excellent scalability [2]. In a previous study, TMR sensors based on arrays of magnetic tunnel junctions (MTJs) can detect ultra-small biomagnetic fields (<0.5 nT) [3]. In this study, we demonstrate that high-sensitivity TMR sensors can detect small amounts (< 500 ng) of MNPs, at a small constant bias magnetic field. Herein, we use a magnetite (Fe_3O_4) mesocrystal as an MNP and synthesize them via a modified polyol method. The MNPs are consisted of hundreds of small crystallites by modulating precursor and reaction time, and, therefore, the MNPs show a superparamagnetic-like behavior with high saturation magnetization (74.4 emu/g) and low coercivity (3.70 Oe). We use MTJ structures with synthetic antiferromagnetic free layers (SAF) with a double-annealing process for linearizing the transfer curve [4]. After fabrication, the 500-element based TMR transfer curve and noise property are measured. Figure 1 presents the schematic view of the TMR sensor for the detection of MNPs. The solvent containing MNPs (2 μg/μL concentration) is overlayed on the Au-electrode surface of the sensor. The external field aligns the average magnetic moments of MNPs and increases the stray field sensed by the TMR sensors. Figure 2(a) shows the change in MR transfer curves after the attachment of MNPs. As more MNPs are added, the response saturates at a smaller field, due to an increase in MNPs stray field. Figure 2(b) shows the TMR ratio shows a large increase at low amounts of MNPs, then it saturates as the number of MNP increases. Therefore, this TMR sensor clearly shows a high-sensitivity ability, under a practical static field, for quantitative analysis of MNPs in biomedical applications.

[1] M. S. Kim, B. C. Park, Y. J. Kim, et al., *Small*, vol. 16, no. 20, p. 2001103, (2020) [2] D. Su, K. Wu, R. Saha, et al., *Micromachines*, vol. 11, no. 1, p. 34, (2019) [3] K. Fujiwara, M. Oogane, A. Kanno, et al., *Applied Physics Express*, vol. 11, no. 2, p. 023001, (2018) [4] K. Fujiwara, M. Oogane, T. Nishikawa, et al., *Japanese Journal of Applied Physics*, vol. 52, no. 4, pp. 04CM07, (2013)

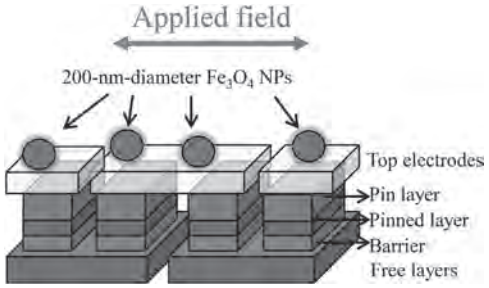

Fig. 1. Schematic view of MNP detection with a TMR sensor.

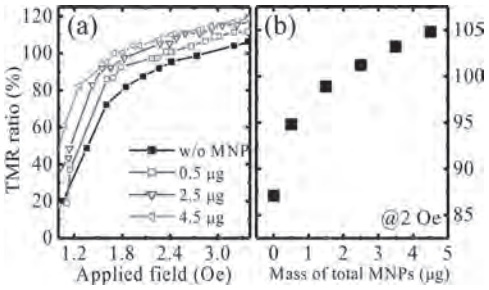

Fig. 2. (a) TMR transfer curves for a varying mass of MNPs. (b) Output response to mass of MNPs at an applied bias of 2 Oe.

F3-08. Analysis of 1/f Low-Frequency Noise in Vortex-Based Spin-Torque Nano-Oscillators for Magnetic Sensing Applications. *M. Jotta Garcia*[1], J. Moulin[2], S. Wittrock[1], S. Tsunegi[3], K. Yakushiji[3], H. Kubota[3], S. Yuasa[3], U. Ebels[4], M. pannetier-lecoeur[2], C. Fermon[2], P. Bortolotti[1], A. Solignac[2] and V. Cros[1] *1. Unité Mixte de Physique, CNRS, Thales, Université Paris-Saclay, 91767 Palaiseau, France; 2. SPEC, CEA-Saclay, CNRS, Université Paris-Saclay, 91191 Gif-sur-Yvette, France; 3. National Institute of Advanced Industrial Science and Technology, Spintronics Research Center, Tsukuba, Ibaraki 305-8568, Japan; 4. SPINTEC, CEA-Grenoble, CNRS and Université Grenoble Alpes, 38054 Grenoble, France*

Spin-torque nano-oscillators (STNOs) are spintronic devices operating in frequencies ranging from less than 100 MHz up to a few GHz [1]. Vortex-based STNOs have a distinct configuration exhibiting a vortex magnetization distribution of the free layer in the equilibrium state. STNOs are promising candidates for future-generation implementations, such as rf generation [2], detection [3] or bio-inspired computing [4]. However, their use as magnetic field sensors remains understudied. Vortex-based devices provide a large linear range for magnetic field detection [5] and their nanometric size allows for improved spatial resolution. Such advantages motivate the study of vortex STNOs for sensing applications. One of the main limiting factors for magnetic sensors, notably vortex-based ones, is their intrinsic 1/f noise, which inhibits the device's detection capabilities at low-frequencies. Here, we study the low-frequency noise of vortex-based STNOs. We determine the Hooge parameter α [6] - a figure of merit used to characterize sensor's noise properties. In the uniform states, α is in the same order of magnitude as those measured in state-of-the-art TMR sensors with similar RA product, $\alpha = 10^{-11}$ - 10^{-10} μm^2. In the vortex state, the measured noise level is around one order of magnitude greater than in the parallel state (Fig. 1), due to the

increased probability of pinning of the vortex core due to material defects and/or inhomogeneities at the free layer. Furthermore, we examine the impact of the vortex dynamics in the low-frequency noise. Above a certain critical current, the spin transfer torques surpass the intrinsic damping of the free layer resulting in self-sustained oscillations of the vortex core [7]. We find that these dynamics strongly modify the characteristics of the STNOs and, in consequence, the achievable performances of magnetic field sensors relying on magnetic vortex dynamics. We present a detailed analysis of these characteristics and how they relate to the device's noise properties. The work is supported by the French ANR project "SPINNET" ANR-18-CE24-0012.

[1] S. Kiselev et al., Nature Vol. 425, 380 (2003) [2] S. Wittrock et al., Phys. Rev. B Vol. 99, 235135 (2019) [3] A. S. Jenkins et al., Nat. Nanotech., Vol. 11, 360 (2016) [4] M. Romera et al., Nature Vol. 563, 230–234 (2018); J. Torrejon et al., Nature, Vol. 547, 428-431 (2017) [5] D. Suess et al., Nature Electronics volume 1, pages 362–370 (2018) [6] F. Hooge and A. Hoppenbrouwers, Physica 45, 386-392 (1969) [7] A. Dussaux et al., Nat. Comm., Vol. 1, 8 (2010)

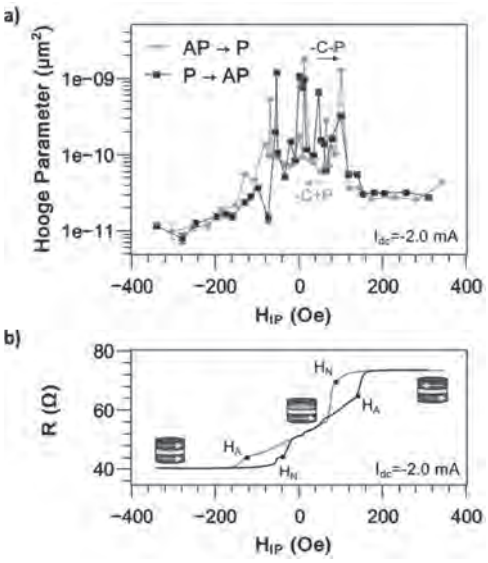

a) Hooge parameter and b) device resistance as an in-plane magnetic field is swept from the parallel to the anti-parallel state and reverse.

F3-09. 2D Magnetrode for Local Neuronal Magnetic Recording.
C. Chopin[1], E. Paul[1], C. Fermon[1], A. Solignac[1] and M. pannetier-lecoeur[1]
1. Service de Physique de l'Etat Condense, Gif Sur Yvette, France

Ionic flows circulating inside and outside neurons create a magnetic signal with an amplitude estimated from 10 to 100 pT. We designed a probe to record this local magnetic signal *in-vivo* in close vicinity of neurons for direct neuronal imaging[1]. This probe has two Giant magnetoresistive (GMR) sensors based on spintronic principle that provide highly sensitive and miniaturized sensor. This probe is called magnetrode. First, we worked on mastering Deep RIE for thinning the magnetrode's tip by using Silicon On Insulator (SOI) substrate to decrease damage during probe insertion in the brain and to be as close as possible of neurons as the magnetic field decrease quickly with distance. We succeed by thinning our magnetrode's tip down from 270μm to 25μm without loss of sensitivity or increasing sensor's noise for a resulting limit of detection around 1nT. Then we implemented two GMR sensors with orthogonal axis of sensitivity (Fig.1) on the same magnetrode for mapping neuronal current in 2 dimensions. GMR axis of sensitivity is determined by two parameters: free and reference layer magnetization. Here the sensors shape defines free layer magnetization so the two sensors have a shape designed with an angle of 90° and to set both reference layer magnetization two steps are required. A global annealing set both sensors magnetization in the same direction and a local repining has to set reference layer magnetization of only one sensor at 90°. This probe is called 2D magnetrode. Here we present the thinning process of a 2D magnetrode, the characterization of both sensors at 0° and 90° with a phantom and our conclusion towards *in-vivo* application

[1] L. Caruso *et al.* Neuron, Volume 95, Issue 6, 1283 - 1291.e4 (2017).

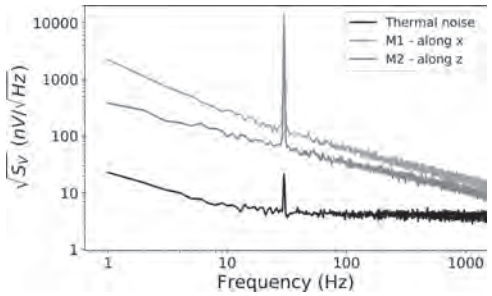

Fig.1: Output voltage noise vs. frequency of two GMR sensors (M1 and M2) on the same probe. M1 and M2 have orthogonal axis of sensitivity (respectively along x and along z). A magnetic signal with a frequency of 30 Hz is used to estimate the sensitivity of the sensors.

F3-10. Anomalous Hall Sensors With High Sensitivity and Stability for Microsensing.
K. Wang[1], Y. Zhang[1] and G. Xiao[1] *1. Brown University, Providence, RI, United States*

Magnetic sensors have great potential in magnetic imaging, microscopy and biomedical applications. However, most magnetic sensors suffer from the trade-off between the sensor size, sensing capability and stability, restricting their applications in microsensing that may be exposed to harsh environments. In this presentation, we will show that the interlayer exchange-coupled magnetic thin films can be employed to fabricate ultrasensitive and thermally stable magnetic sensors, taking advantage of the linear anomalous Hall effect (AHE) *via* tuning the interlayer exchange coupling and magnetic anisotropy. After a brief introduction of AHE sensors, we will present magnetotransport and noise properties of the interlayer exchange-coupled magnetic thin-film-based AHE sensors. At room temperature, the magnetic field detectability reaches 126.1 nT/√Hz at 1 Hz and 4.5 nT/√Hz at 1 kHz. Meanwhile, the achieved dynamic reserve is 103.0 dB. Within the temperature range from 200 to 300 K, the sensor has a low temperature coefficient of sensitivity (530 ppm/K). The high temperature stability is a result of the interlayer exchange coupling between ferromagnetic layers that also improves the stability against orthogonal magnetic fields, beneficial for perpendicular magnetic field sensing. Finally, we will discuss comparisons between our AHE sensors and other magnetic sensors. We would conclude that if the same microsensing area is used, one expects that our AHE sensor performs comparably or even outperforms magentoresistive sensors in microsensing. In addition, our AHE sensor is a complementary to magnetoresistive sensors for three-dimensional magnetic field sensing with high field resolution.

K. Wang, Y. Zhang, and G. Xiao, Phys. Rev. Appl. 13, 064009 (2020).

F3-11. Curvature Effects on Magnetic Field Sensitivity of Magnetoelectric Nano-Plate Resonators.
A. Matyushov[1,2], B. Spetzler[3], M. Zaeimbashi[1], J. Zhou[1], Z. Qian[1], E. Golubeva[3], C. Tu[1], Y. Guo[1], B. Chen[1], D. Wang[1], A. Will-Cole[1], H. Chen[1], M. Rinaldi[1], J. McCord[3], F. Faupel[3] and N.X. Sun[1] *1. ECE, Northeastern University, Boston, MA, United States; 2. Physics, Northeastern University, Boston, MA, United States; 3. Institute of Material Science, Kiel University, Christian-Albrechts-Universitat zu Kiel, Kiel, Schleswig-Holstein, DE, Kiel, Germany*

We present nanoscale, resonator-based piezoelectric/magnetostrictive magnetometers that operate on the delta-E effect and are capable of detecting weak magnetic fields at low frequency or DC. As these devices are just hundreds of nanometers thick, and on the order of a hundred microns

laterally, they can be produced by lithographic microfabrication techniques. This results in sensors that offer high portability, low cost, low power consumption, and the potential for high spatial resolution in magnetic sensor arrays. However, no prior study exists of a systematic examination of the properties that affect sensing performance in such magnetic sensors. Here, we report on how the deformation of the resonator plate, quantified as curvature, affects the total frequency response of these delta-E effect-based magnetometers. It was found that frequency response changed by as much as two orders of magnitude based on this parameter in devices that are otherwise identical and fabricated on the same Si wafer. Ultimately, a sensor with low curvature was fabricated and a record-high sensitivity to DC magnetic fields, of 4.98 Hz/nT, was achieved. To study this phenomenon in more detail, we measured the Q factor, imaged the magnetic domains using the magneto-optical Kerr effect (MOKE), and performed simulations to shed light on the internal stress distribution. From the Q factor data, we observed a loss mechanism dominated by magnetic loss. Informed by the MOKE images and simulation results, we then tested a simple magnetic model with fitting parameters of active volume fraction, mean easy axis, and effective anisotropy energy density. The model was found to fit the data quite well with low volume fraction but a large easy axis tilt and anisotropy energy.

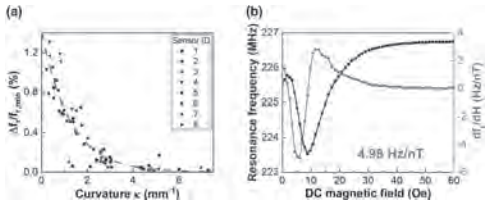

(a) Ensemble of all delta-E effect-based sensors that were fabricated on the same wafer and with the same thin film layer structure. (b) The frequency response curve of the best performing sensor.

F3-12. Flexible Highly Compliant Magnetoelectronics. G. Canon Bermudez[1], J. Ge[1], M. Kaltenbrunner[2], J. Fassbender[1] and *D. Makarov*[1]
1. Helmholtz-Zentrum Dresden-Rossendorf, Dresden, Germany;
2. Johannes Kepler Universitat Linz, Linz, Austria

Mechanical flexibility and even stretchability of functional elements is a key enabler of numerous applications including wearable electronics, healthcare and medical appliances. The magnetism community developed the family of high-performance shapeable magnetoelectronics [1], which contain flexible [2-4], printable [5-7], stretchable [8-11] and even mechanically imperceptible [12-16] magnetic field sensorics. The technology relies on a smart combination of thin inorganic functional elements prepared directly on flexible or elastomeric supports. The concept of shapeable magnetoelectronics is explored for various applications ranging from automotive [17] through consumer electronics and point of care [2,18] to virtual and augmented reality [14-16] applications. Here, we will focus on the use of compliant magnetosensitive skins [14-16] for augmented reality systems. We demonstrate that e-skin compasses [14] allow humans to orient with respect to earth's magnetic field ubiquitously. The biomagnetic orientation enables the realization of a touchless control of virtual units in a game engine using omnidirectional magnetosensitive skins (Fig. 1). This concept was further extended by demonstrating a compliant magnetic microelectromechanical platform (m-MEMS), which is able to transduce both tactile (via mechanical pressure) and touchless (via magnetic field) stimulations simultaneously and discriminate them in real time [16] (Fig. 2). We demonstrate data selection and manipulation with our m-MEMS e-skins leading to the realization of a multi-choice menu for augmented reality through three dimensional (3D) touch. Beyond the field of augmented reality, our m-MEMS will bring great benefits for healthcare, e.g. to ease surgery operations and manipulation of medical equipment, as well as for humanoid robots to overcome the challenging task of grasping.

[1] D. Makarov et al., Appl. Phys. Rev. (Review) 3, 011101 (2016). [2] G. Lin, D. Makarov et al., Lab Chip 14, 4050 (2014). [3] N. Münzenrieder, D. Makarov et al., Adv. Electron. Mater. 2, 1600188 (2016). [4] M. Melzer, D. Makarov et al., Adv. Mater. 27, 1274 (2015). [5] D. Makarov et al., ChemPhysChem (Review) 14, 1771 (2013). [6] D. Karnaushenko, D. Makarov et al., Adv. Mater. 24, 4518 (2012). [7] D. Karnaushenko, D. Makarov et al., Adv. Mater. 27, 880 (2015). [8] M. Melzer, D. Makarov et al., J. Phys. D: Appl. Phys. (Review) 53, 083002 (2020). [9] M. Melzer, D. Makarov et al., Nano Lett. 11, 2522 (2011). [10] M. Melzer, D. Makarov et al., Adv. Mater. 24, 6468 (2012). [11] M. Melzer, D. Makarov et al., Adv. Mater. 27, 1333 (2015). [12] M. Melzer, D. Makarov et al., Nat. Commun. 6, 6080 (2015). [13] P. N. Granell, D. Makarov et al., npj Flexible Electronics 3, 3 (2019). [14] G. S. Cañón Bermúdez, D. Makarov et al., Nature Electronics 1, 589 (2018). [15] G. S. Cañón Bermúdez, D. Makarov et al., Science Advances 4, eaao2623 (2018). [16] J. Ge, D. Makarov et al., Nature Communications 10, 4405 (2019). [17] M. Melzer, D. Makarov et al., Adv. Mater. 27, 1274 (2015). [18] G. Lin, D. Makarov et al., Lab Chip (Review) 17, 1884 (2017).

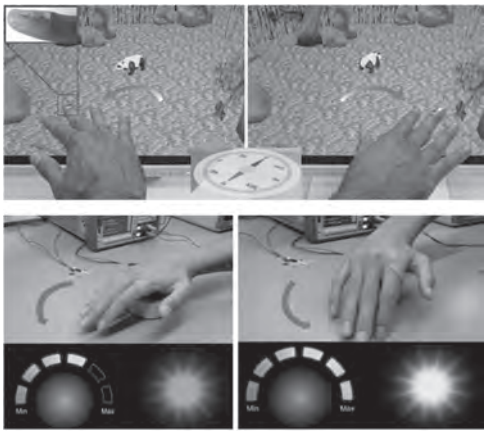

Fig. 1. Magnetosensitive skins for touchless interactive electronics. (top) Control of the trajectory of a virtual character (panda) by hand motion in the geomagnetic field [14]. (bottom) Dimming the light intensity upon the hand motion in the field of a permanent magnet [15].

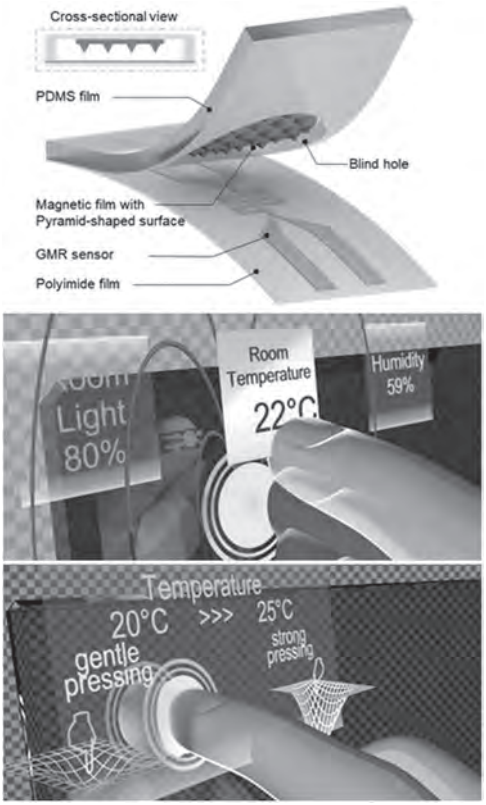

Fig. 2. Schematics of the m-MEMS platform and its use for interactive electronics [16].

Session F4
INTERDISCIPLINARY APPLICATIONS III
(Poster Session)

Claudio Bonizzoni, Chair
Istituto Nanoscienze Consiglio Nazionale delle Ricerche Sede secondaria di Modena, Modena, Italy

F4-01. Monte Carlo Simulation to Study the Effect of Molecular Spin State on the Spatio-Temporal Evolution of Equilibrium Magnetic Properties of Magnetic Tunnel Junction Based Molecular Spintronics Devices. *A. Grizzle*[1] and P. Tyagi[1] *1. Center for Nanoscale Research and Education (CNRE), University of the District of Columbia, Washington, DC, United States*

Magnetic tunnel junction based molecular spintronic devices (MTJMSDs) approach can incorporate molecules with variable spin states. MTJMSD approach typically uses an exposed side magnetic tunnel junction (MTJ) as the testbed. Along the exposed sides of the MTJ, the molecular channels with the variable spin state can be bridged between the two ferromagnetic electrodes. In our prior study[1-4], we found the paramagnetic molecules, such as single molecular magnets(S=+/-10) and octa-metallic clusters (S=+/-6), produced strong antiferromagnetic coupling between the two ferromagnetic electrodes. However, due to experimental challenges, we were unable to investigate the properties of cross-junction MTJMSDs with the variation in the molecular spin state. This paper reports our Monte Carlo Simulation (MCS), focusing on the effect of variable molecular spin state on the cross-junction shape MTJMSD properties. We designed the MCS study to maintain a close agreement with the prior experimental observations; a magnetic molecule was ferromagnetically coupled with the top ferromagnet and antiferromagnetically coupled with the bottom ferromagnet. We varied the molecular spin state from 0 to 4 at increments of 0.5. For S=0 molecular spin, two magnetic electrodes aligned independently and validated the MCS approach. MCS study showed that for the molecular spin states S=0.5, 1,1.5,2, 2.5, 3,3.5, and 4, the ferromagnetic electrodes of the MTJMSD settled in the antiparallel state. Our MCS result agrees with the experimental observation on MTJMSD with two different types of magnetic molecules possessing different spin states. According to the time vs. magnetization study, all the molecular spin states lead to the equilibrium MTJMSD state in a similar manner. This study suggests that under strong coupling regime variation in molecular spin state does not produce a significant change in the magnetic properties of the MTJMSD.

1. Tyagi, P.; Riso, C.; Amir, U.; Rojas-Dotti, C.; Martínez-Lillo, J., *RSC Advances* 2020, *10* (22), 13006-13015. 2. Tyagi, P.; Riso, C.; Friebe, E., *Organic Electronics* 2019, *64*, 188-194. 3. Tyagi, P.; Riso, C., *Organic Electronics* 2019, *75*, 105421. 4. Tyagi, P.; Baker, C.; D'Angelo, C., *Nanotechnology* 2015, *26*, 305602.

F4-02. Optimization of Cobalt Concentration & Cation Distribution for Improved Magnetic Characteristics and Stability of $Co_xFe_{3-x}O_4$ Mixed Ferrite Magnetic Fluids. *P. Kumar*[1,3], S. Pathak[1,4], A. Singh[1,2], K. Singh[1,3], H. Khanduri[1], G. Basheed[1,3] and R. Pant[1,3] *1. Indian Reference Materials Division, National Physical Laboratory CSIR, New Delhi, India; 2. Indian Institute of Technology Jammu, Jammu, India; 3. Academy of Scientific and Innovative Research, Ghaziabad, India; 4. RMIT University College of Science Engineering and Health, Melbourne, VIC, Australia*

The $Co_xFe_{3-x}O_4$ ($0.8 \le x \le 0$) ferrites based magnetic nanoparticle with single domain nature have potential applications in the development ofthe high-density memory devices, magnetic fluid hyperthermia and biomedicine. The present work deals with the experimental investigation of oleic acid coated $Co_xFe_{3-x}O_4$ ($0.8 \le x \le 0$) nano ferrite based ferrofluids synthesized by the wet chemical co-precipitation method and oleic acid used as surfactant to prevent the agglomeration of magnetic nanoparticles. Structural and magnetic properties of these ferrofluids have been investigated using different characterization techniques. The structural, cations distribution and Rietveld refinement was carried out by the XRD data and the result confirms that single cubic spinel phase belongs to Fd3m space group and the average crystallite size calculated from the XRD data varies from 11 to 14 nm. The Transmission Electron Microscopy (TEM) studies revealed that the particles are spherical in nature and mean particle size varies from 10 to 15 nm and all samples are polycrystalline in nature. The SEM result were also demonstrate the surface morphology of magnetic particle are spherical in shape nanoparticle with least agglomeration. FTIR spectroscopy showed the molecular dynamics and the formation of cubic spinel phase of frequency bands at 545 cm^{-1} and 404 cm^{-1} respectively. The UV-Visible measurement we have estimate the band gap of the materials lies between(2.2 to 2.8& 3.1 to 3.8 e V) of the all the sample form optical absorption spectra fitting by Tauc plot method. The room temperature Vibrating Sample Magnetometer(VSM) analysis revealed that the saturation magnetization and coercivity value varies from 26.18 to 61.78 emu/g and 31.45 to 128.36 Oe, respectively by the increasing the Co concentration. These magnetic properties can be enhanced by the distribution of cations on both A-site and B-site.

1. Clara Pereira et al., *J. Phys. Chem. C* 2016, 120, 2, 1328-1341. 2. R. Tackett et al., JMMM (2008), 320 2755– 2759.

F4-03. Equilibrium Configurations in a Magnetic Fluid-Based Mapping System for Designing MagLev Devices: Experiment and Simulations. *P. Ryapolov*[1], V. Bashtovoi[2], A. Reks[2], E. Sokolov[1] and E. Postnikov[3] *1. Natural science faculty, Southwest State University, Kursk, Russian Federation; 2. UNESCO Chair, Belarusian National Technical University, Kursk, Russian Federation; 3. Theoretical Physics, Kursk State University, Kursk, Russian Federation*

Recently, we proposed an experimental setup, which allows 3D mapping the magnetic field created by a ring magnet in the configuration discussed as promised for modern single-magnet magnetic levitation systems (MagLev) [1]. The premises for creating such a device are based on the effect of capturing a gas inclusion by the magnetic fluid placed in a magnetic field [2]. This work presents further investigations of this approach aimed at the enhancement of efficiency of such a device as well as the development of a numerical simulation procedure, should allow for designing more sophisticated object-capturing fields configurations, possibility to use a spatial area extended into the far-field region, etc. The latter takes into account the balance of surface tension components originated from capillary, magnetic and gravitational forces in the case when neither is a leading one. Within the experimental part of this work, new experimental data are obtained for several ring magnets, which have different configurations. We explored the influence of the magnetic liquid's parameters and the scanning protocol on the efficiency of determination of the size and topology of the region best adjusted to the magnetic levitation purposes. The results obtained during the work could be used to develop devices for manipulation by non-magnetic inclusions and their separation, 3D bioprinting and controlled self-assembling in liquid magnetic media. The investigation was carried out with the support of the grant of the President of the RF MK-1393.2019.8 and part of the implementation of the state task for 2020 (No 0851-2020-0035). Belarusian co-authors are grateful to the Belarusian Republican Foundation for Fundamental Research for financial support (project T20MC-015).

P.A. Ryapolov, V.G. Bashtovoi, A.G. Reks, E.A. Sokolov, E.B. Postnikov, Study of the working area of a ring magnet MagLev system using a thin layer of magnetic fluid (submitted). P.A. Ryapolov, V.M. Polunin, E.B. Postnikov, V.G. Bashtovoi, A.G. Reks, E.A. Sokolov, The behaviour of gas inclusions in a magnetic fluid in a non-uniform magnetic field. Journal of Magnetism and Magnetic Materials, 497 (2020) 165925.

F4-04. Passive Piezomagnetic Monitoring of Structures Subjected to in-Service Cyclic Loading: Application to the Detection of Fatigue Crack Initiation and Propagation. *A. Ouaddi*[1,2], O. Hubert[1], J. Furtado[2], D. Gary[2] and S. He[3] *1. Laboratoire de Mecanique et Technologie, Cachan, France; 2. Air Liquide Centre de Recherche Paris-Saclay, Jouy-en-Josas, France; 3. Groupe Leonard de Vinci, Paris, France*

The application of a mechanical stress to a demagnetized ferromagnetic material can modify the magnetic microstructure of the material without macroscopic magnetization [1]. If the material is initially magnetized, even weakly - which is the general rule in industrial parts -, a stress can lead to a variation of the magnetization. This is the so-called "Villari effect" or "piezomagnetic effect" [2][3]. The magnetization variations depend on stress level, multiaxiality and rate, but also on the prior metallurgical-mechanical state of the material and its evolution in use. Its measurement can be done via a secondary coiling by measuring the induced voltage or via external magnetic flux gates, referred as leakage method in previous studies [4][5]. Indeed, the magnetic flux leakage methods use the natural magnetization and its time evolution to investigate and characterize the structural integrity of structures. The piezomagnetic technique can on the other hand be used for the purpose of passive monitoring of structures subjected to in-service cyclic loading (e.g. cyclic pressure), which constitutes a first originality of the work. The principle is based on measuring the Villari's signal evolution. The development, the implementation and the generalization of such techniques involve innovative experiments for identification of mechanisms, innovative modeling methods and their validation. In this study, the principle of passive monitoring by piezomagnetic variation of magnetic flux leakage in structures is first detailed. It is applied to the monitoring of fatigue crack in a ferritic-pearlitic steel commonly used for pressure vessel construction. Results show a sensitivity of the Villari signal to the crack initiation and a clear relationship between the crack size, the local stress level and the magnetization variations, indicating a weak influence of metallurgical defects comparing to the stress influence, and joining the results of other authors [6]. Results are then interpreted using a simplified magneto-elastic hysteresis model [7]. This aspect constitutes a second originality of the work.

[1] R. M. Bozorth, New York: Ed. Van Nostrand, 1951. [2] L. Lollioz, S. Pattofatto and O. Hubert, J. of Electrical Engineering, 57 8 (2006) 15-20. [3] O. Hubert, K. J. Rizzo, J. of Magnetism and Magnetic Materials, 320 20 2008, 979-982. [4] S. Bao, T. Erber, S.A. Guralnick, W.L. Jin, Strain 47(4): 372–381 (2011). [5] S. A. Guralnick, S. Bao, T. Erber, J. of Physics D: Applied Physics, 2008, 41 115006 (p11). [6] M.I.M Ahmad., A. Arifin, S. Abdullah, Steel and Composites Structures, Vol. 19, No. 6(2015) 1549-1560. [7] A. Ouaddi, O. Hubert, J. Furtado, D. Gary, Mechanics & Industry, (2020), in press, - DOI:10.1016/10.1051/meca/2020050.

F4-05. Development of Sub-mm Period Undulator With $L1_0$ Phase FePt Micromagnet Array. *B.D. Gürel*[1,2], N. Gunduz Akdogan[3] and O. Akdogan[1] *1. Bahcesehir Universitesi, Istanbul, Turkey; 2. Sabanci Universitesi, Istanbul, Turkey; 3. Piri Reis Universitesi, Istanbul, Turkey*

An undulator is a device including two parallel arrays of magnets (separated by a gap) with a polarity in an alternating manner (↑↓↑↓↑↓…). The undulator is an essential part of a Free Electron Laser (FEL) upon which a large body of literature has expressed interest for the applications on various areas such as defence industry, material science and medicine. Also, sub-millimeter period undulators are another interesting approach. The current state of the art of X-FEL uses undulator period down to 3 cm which creates an output radiation wavelength down to 1.5 A using ~14GeV e- beam, ergo big and costly e-beam source is needed. By developing a sub-mm period undulator (i.e. a period of 300μm), it is possible to obtain the same output radiation wavelength with a much less e-beam energy of ~1.4 GeV which could be revolutionary since much smaller FELs could be constructed. Undulators are constructed using either electromagnets or permanent magnets. The latter is the choice due to the fact that no additional power supply is needed. On the other hand, there is a growing interest on $L1_0$ phase FePt thin films on the magnetic applications due to their high magnetic anisotropy. In this work, FePt thin films and micro magnets were synthesized by sputtering technique and their magnetic properties were extensively studied. FePt micromagnets could be utilized in next generation sub-mm period undulators. This work was supported by TUBITAK project: 118F319

F4-06. Study of Thermo-Magnetoconvection of a Magnetofluidic Cooling Device. *V.B. Varma*[1,2], M.S. Pattanaik[1,2], S.K. Cheekati[1,2] and R. Ramanujan[1,2] *1. School of Materials Science and Engineering, Nanyang Technological University, Singapore, Singapore; 2. Singapore-HUJ Alliance for Research and Enterprise (SHARE), Nanomaterials for Energy and Energy-Water Nexus (NEW), Campus for Research Excellence And Technological Enterprise (CREATE), Singapore, Singapore*

Magnetofluidic cooling (MFC, Figure 1a) is a passive heat transfer technique governed by the principle of thermomagnetic convection (TMC)[1, 2]. Under the effect of a thermal and magnetic field gradient, the magnetic fluid's temperature-dependent response leads to TMC[3]. However, practical applications require specific device design and materials, mainly determined by the flow behavior of the magnetic fluid. However, the opaque nature of the magnetic fluid limits the experimental flow investigations. We addressed this challenge by a range of experimental setups to measure velocity profiles, vorticity, and temperature profiles. We developed a hybrid PIV method to measure velocity profiles by fabricating a bonding-free 3D PDMS device and analyzed by a MATLAB based image analysis code. The results of the PIV analysis are summarized in Figure 1. We utilized the experimental findings to develop a simulation model and studied the effect of magnetic and hydrodynamic properties of the fluid on the MFC process (Figure 2). Simulation-driven system design was performed[4]. A ferrofluid was developed and integrated with our MFC system, significantly enhancing device performance. We found that the MFC flow velocity, vorticity increases with increasing HL power, resulting in higher cooling at higher HL powers (Figure 2). Experiments and simulations demonstrated the role of magnetoconvection on device performance. The new device showed enhanced performance viz. cooling up to 200°C at a heat load of 10 W. Our superior device performance is attributed to increased fluid mixing and mass transfer during MFC. Acknowledgments This research is supported by grants from the National Research Foundation, Prime Minister's Office, Singapore under its Campus of Research Excellence and Technological Enterprise (CREATE) programme.

1. V. B. Varma, Energy Efficient Green Magnetic Cooling, 2019. https://youtu.be/caInO_IxnHQ. CREATE Symp.- Climate Change, Singapore 2. R. V. Ramanujan, Pushing Frontiers, Issue 14, 32 (2018). 3. M. S. Pattanaik, V. B. Varma, S. K. Cheekati, G. Prasanna, N. M. Sudharsan and R. V. Ramanujan, Energy Conversion and Management, vol. 198, p. 111819 (2019). 4. V. B. Varma, M. S. Pattanaik, S. K. Cheekati and R. V. Ramanujan, Applied Energy, (2020- in Communication).

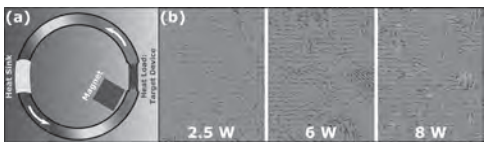

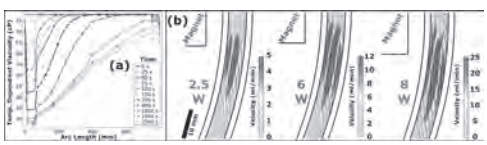

F4-07. Full Scale Localization of Underwater Magnetic Sensors Using Natural Computing Algorithms. R. Alimi[1], *E. Fisher*[1,2], K. Nahir[1] and E. Weiss[1] *1. Soreq NRC, Soreq Nuclear Research Center, Yavne, IL, Yavne, Israel; 2. Jerusalem College of Technology, Yerushalayim, Israel*

Underwater sensors arrays have been widely used for various applications such as scientific exploration, sea disaster investigation and military purposes. Either acoustic, optical or RF sensing technologies are commonly used. The challenging task is the estimating of the precise location of the deployed sensors due to the special and extreme underwater environment, as well as the lack of GPS data. This is critical to enable the system to provide an accurate description of the investigated phenomenon. Unfortunately, common localization solutions do not provide a satisfactory response to this crucial issue. In the shallow water regime, several positioning methods using magnetic technologies have been investigated. The magnetic fields generated at the sensors location, given a well determined ferromagnetic object trajectory, define a so-called inverse problem in which the precise positions of the sensors are the variables of the equations to be solved. These studies are based on either computer simulations or downscaled laboratory experiments. Also, only one type of algorithm is generally considered. In this work we address this issue within a full scale experimental setup of eight magnetometers arranged according to a 2.5x2.5 m grid. Six meters above, a known ferromagnetic object is moving according to a well-defined path, velocity and direction. The magnetic field recorded by the sensors network is then analyzed by the algorithms. We have implemented two natural computing algorithms: A Genetic Algorithm (GA) and a Particle Swarm Optimizer (PSO). For both methods, single and multi-objective versions have been run and compared. Also, in order to optimize the performance of the locating algorithms we have tested cross-correlations and Hausdorff metrics in the fitness calculations. The results show that all tested methods performed very well and were able to determine the location of the sensors within a relative error between 1-3%. The absolute error in the position lies between 20-35 cm for the close and far sensor respectively. In most cases the multi-objective versions perform better than the single ones. No significant differences could be noted between the Hausdorff and the cross correlation approaches.

Z.Yu, C.Xiao, and G.Zhou, Multi Objectivization Based Localization of Underwater Sensors Using Magnetometers, IEEE SENSORS JOURNAL, VOL. 14, NO. 4, 2014 J. Callmer, M. Skoglund, and F. Gustafsson, Silent Localization of Underwater Sensors Using Magnetometers, EURASIP J. Adv. SignalProcess., vol. 2010, pp. 1–8, 2010.

F4-08. Enhancement for Magnetic Field Strength of a Magnetohydrodynamic Thruster Consisting of Permanent Magnets. *Y. Li*[1], C. Zeng[1] and Y. Chen[1] *1. Mechanical and Aerospace Engineering, National Defense University Chung Cheng Institute of Technology, Taoyuan, Taiwan*

This work aims at designing a closed-loop magnetic circuit to enhance the uniformity and intensity of the magnetic field based on an internal conductive square Magnetohydrodynamics (MHD) thruster. Figure 1(a) shows the diagram of the square MHD thruster consisting of a pair of NdFeB magnets and electrodes. Figure 1(b) shows the design of the permanent magnet set comprising two permanent magnet pieces and an iron shell. The magnetization of the magnet pair is along the +z axis, and the iron shell formed a closed-loop magnetic circuit which reduces the magnetic leakage and enhances the magnetic field at the central region i.e. z=0 mm. Theoretically, the field strength decreases when the distance from the magnet is increased. The accurate measured magnetic flux density along the y-axis on the central cross-section shown in figure 1(c) reveals that the maximum field strength increases from 0.116 T to 0.142 T after installing the 2-mm thick iron shell, which reduces the magnetic leakage and increases the uniformity of the field. We performed a systematic experiment to measure the field distribution under various width and thickness of iron casing in this work. It is noticed the thicker shell results in stronger magnetic strength inside the thruster, and the field strength becomes stronger as the width of the iron shell decreases. The thruster with an iron shell is fully submerged in the saline water and hanged on a sliding track with negligible friction to verify its performance, as shown in figure 1(d). The moving speed is increased from 0.0826m/s to 0.12 m/s when the iron shell is installed. In this paper, the effect of the material of the shell is also investigated to evaluate the optimal design to enhance the uniformity and strength of the magnetic field at the central region of square MHD thruster.

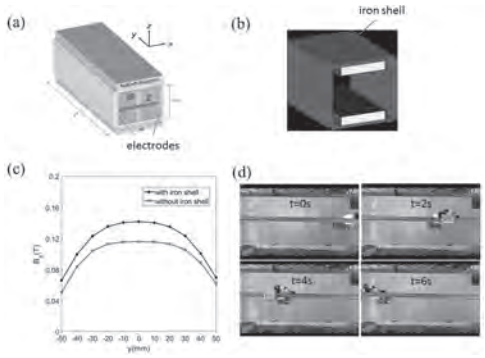

Fig.1 (a) Sketch of the square MHD thruster consisting of magnets and electrodes. (b) Design of the permanent magnets set with a 2-mm thick iron shell. (c) Comparison of the measured field strength along the y-axis on central cross-section (x=0 and z=0) of the thruster with and without the iron shell. (d) Sequential images of experimental tests of MHD thruster with iron shell hanged on a sliding track.

F4-09. Electro-Permanent Magnetic Actuator for Miniaturized Well Logging Tool. *H.R. Seren*[1], E. Buzi[1] and M. Deffenbaugh[1] *1. Aramco Research Center - Houston, Aramco Services Company, Houston, TX, United States*

We present the design and tests of a magnetic actuator that switches between holding and releasing a ballast by electronically repolarizing a permanent magnet. A low-coercivity AlNiCo magnet is placed in parallel with a high-coercivity NIB magnet. An electrical pulse to a coil around the magnets reverses the polarization of the AlNiCo magnet while not affecting the NIB magnet [1]. When the two magnets are polarized in the same direction, their field extends outside the actuator and holds a steel weight. When the magnets are polarized in the opposite direction, their field is contained within the actuator and the weight is released (Fig. 1). This actuator is used in a palm-sized well logging tool where it releases a ballast weight as the tool approaches the bottom of the well, causing the tool to float back toward the surface [2]. The magnetic assembly occupies less than 2 cm^3 and provides 2 kg-f of pull force. The driver circuit charges a capacitor to 48 V from two lithium coin cells using a boost converter and discharges the capacitor through the coil. The circuit can provide ~1 kW instantaneous power for a few tens of microseconds for the polarization reversal. We found that a 1 mF capacitor is needed to repolarize with a single discharge with the target voltage rating. A 0.1 mF capacitor was shown to produce similar repolarization after five discharge cycles, which saves space and energy. Nonlinear circuit analysis showed that the applied current was primarily limited by the inductance during repolarization due to large permeability of AlNiCo core. In minor magnetization curves and close to saturation, inductance becomes smaller and coil resistance becomes the limiting factor. Pulse currents were measured experimentally and showed good agreement with the numerical model (Fig. 2).

[1] A.N. Knaian, PhD diss., Massachusetts Institute of Technology (2010)
[2] H.R. Seren, E. Buzi, L. Al-Maghrabi, et al., IEEE T. Instrum. Meas., Vol. 67(4), p. 798-803 (2018)

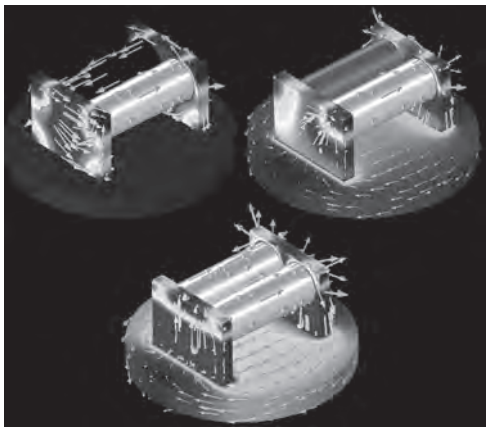

Finite element analysis showing the B-field distribution on poles and the ballast for the AlNiCo magnet is (a) polarized in opposite direction to NIB; (b) depolarized; (c) polarized parallel to NIB.

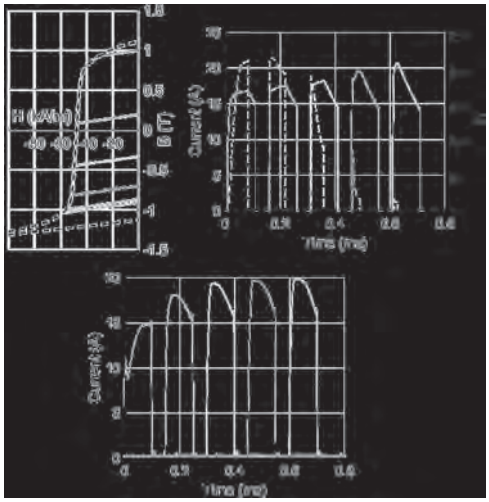

Nonlinear circuit analysis (a) Repolarization of AlNiCo magnet by applying 5 discharge pulses using 0.1 mF capacitor; (b) Corresponding currents (solid) and relative permeabilities (dashed) during the pulses; (c) Measured currents.

F4-10. The Underwater Ferromagnetic Target Location System Based on Gauss Meter Array. *D. Xie*[1] and J. Qiu[1] *1. Chongqing University, Chongqing, China*

Magnetic gradient tensor is a significant method for locating ferromagnetic target. According to the data that has been processed, the position of the target can be calculate. However, it will work only in ideal condition. Magnetic sensor, ambient ocean magnetic noise, the relative position of the unknown ferromagnetic target and the detection point will seriously impact the detection accuracy. Aiming at the problem of detection blind area and detection array arrangement optimization for underwater ferromagnetic target location based on magnetic gradient tensor, a underwater ferromagnetic target location system based on gauss meter array is introduced. Through improved particle swarm optimization, the layout of the sensor in specific area can be determined by making the overall coverage and the cross coverage maximum. In the light of the reliability assessment for location in joint detection system, the relationship between the direction of the magnetic moment of target and the detection reference coordinate axes is studied, so that the detection reliability can be determined. In order to verify the feasibility, the simulation test and the experimental verification of the system are made. The results show that the system can be used to detect and locate the magnetic anomaly target in specific area, and the error rate of the detection compared with the traditional system is significantly improved. Fig. 1 shows the distribution of sensors under simulated specific water surface conditions, in which the red rectangle represents the overall detection range. In the case of setting the blue circle as the obstacle range, the distribution position of sensors is optimized to maximize the overall coverage within the red rectangle. And the coverage fitness function is shown in Fig. 2(a). In order to count the relationship between the gradient measurement matrix of magnetic sensor and detection reliability, the corresponding data are obtained by simulation software. The fitting curve drawn with the obtained data has been shown in Fig. 2(b)

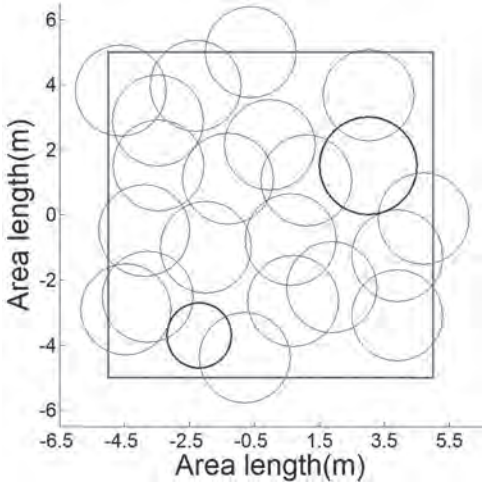

Fig.1 Sensor distribution

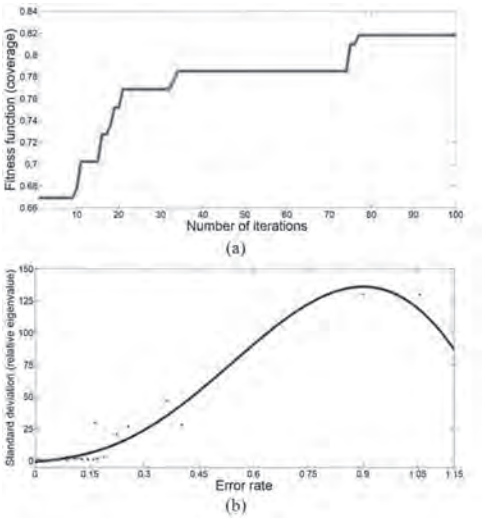

Fig.2 (a)Fitness function (coverage) (b)Relation between relative eigenvalue standard deviation and error rate

F4-11. Withdrawn

F4-12. γ-Irradiation Synthesis and Characterization of Iron Oxide Nanomaterials. *I. Marić*[3], M. Gotić[1], G. Štefanić[1], J. Grenèche[2], A. Pustak[3] and T. Jurkin[3] *1. Laboratory for molecular physics and synthesis of new materials, Institut Ruder Boskovic, Zagreb, Croatia; 2. Institut des Molecules et Materiaux du Mans, Le Mans, France; 3. Radiation chemistry and dosimetry laboratory, Institut Ruder Boskovic, Zagreb, Croatia*

γ-irradiation is an attractive and ecologically friendly technique for the synthesis of magnetic nanoparticles (MNPs) at room temperature. It has the advantage of inducing electrons and other reducing species homogeneously throughout the reaction vessel. Unlike radiolytic synthesis of noble metal NPs, the radiolytic synthesis of iron oxide NPs is much less

investigated. One of the reasons is a very complex iron oxide chemistry that produces numerous phases. Furthermore, MNPs have a high tendency for agglomeration and due to these reasons, various polymers are used that act as dispersants and stabilizers of MNPs in suspensions as well as growth and surface modifiers. We investigated the effect of 3 different polymers (DEAE-dextran, dextran sulfate and poly(ethylene oxide)), as well as the effect of absorbed dose of γ-irradiation on the synthesis of iron oxide MNPs. The results have shown that dextran polymers, especially DEAE-dextran, completely stabilize the precursor particles forming colloidal precursor solutions before irradiation. Irradiation of such colloidal solutions resulted in the synthesis of stable magnetic suspensions. In the case of DEAE-dextran, the phase composition of formed NPs was predominantly magnetite or δ-FeOOH depending on the absorbed dose [1]. In the case of dextran sulfate, a multiphasic system was obtained in all cases [2]. On the other hand, on irradiation in the presence of PEO a completely different kind of product forms - PEO/Fe-oxide magnetic nanocomposite hydrogel. Due to the nature of the PEO polymer, a simultaneous crosslinking of the polymer and reduction of precursor NPs to single-phase iron oxide nanoparticles (magnetite in most cases) occurred. Mössbauer spectroscopy was used to investigate the hyperfine interactions of the materials. Samples generally exhibited superparamagnetic relaxation phenomena, and in some cases, samples were not completely magnetically blocked even at 77 K (Fig. 1). *Acknowledgments: This work has been supported by the Croatian Science Foundation under the project UIP-2017-05-7337 (POLRADNANOP).*

[1] I. Marić, G. Drazić, G. Štefanić, K. Zadro, M. Gotić, T. Jurkin, Materials Characterization, Vol. 159, 110038 (2020) [2] I. Marić, G. Štefanić, M. Gotić, T. Jurkin, Journal of Molecular Structure, Vol. 1183, p. 126 (2019)

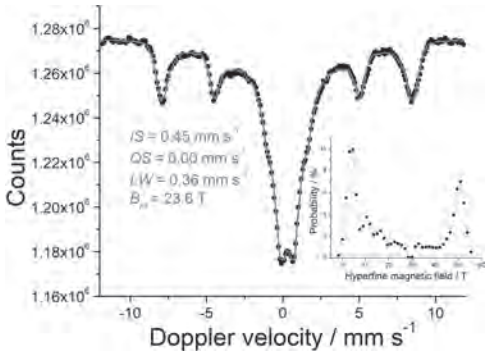

Fig. 1 77 K Mössbauer spectrum of a magnetic nanocomposite gel obtained in one-step by γ-irradiation with the absorbed dose of 300 kGy in the presence of PEO.

F4-13. Eddy Current Loss Analysis in Permanent Magnet Linear Gear Using Analytical Method. *G. Jang*[1], S. Seo[1], J. Nah[1], J. Bird[2] and J. Choi[1]
1. Chungnam National University, Daejeon, The Republic of Korea;
2. Portland State University, Portland, OR, United States

This paper describes an analytical method to calculate the eddy current loss of a permanent magnet linear gear. Owing to the high energy densities of Nd–Fe–B permanent magnets, they can be miniaturized to enable production of relatively lightweight, high-efficiency permanent magnet linear machines. Among these, linear magnetic gears have been introduced and used in addition to the linear machine systems. Equipment using permanent magnets with conductivity inevitably generate eddy currents in the magnets, which cause eddy current losses. In particular, the magnetic gear uses a magnetic flux modulating pole between the primary and secondary magnets to act as a gear[1-2]. Consequently, the waveform of the air-gap magnetic flux density of the magnetic gear is not sinusoidal but distorted. The air-gap flux densities of time-varying distorted waveforms create eddy currents in the permanent magnets, which lead to increased losses. Eddy current analysis has been performed widely using both the finite element method (FEM) and analytical methods. It is often advantageous to use an analytical method in the initial design as it can yield results quickly[3-4]. Therefore, a method to analyze the eddy currents generated in the permanent magnets of linear magnetic gears and to calculate the eddy current losses is proposed herein. Based on this, it is possible to calculate the eddy current loss generated in the linear magnetic gear. Fig.1 shows the structure and analysis model of the magnetic gear used in this paper. Fig. 2 shows the results of eddy current density and eddy current loss analysis. Based on these results, it can be confirmed that the loss prediction is accurate according to the design variable changes in the early stages of design. More detailed discussions and analyses will be presented in the final paper.

[1] T. Okitsu, D. Matsuhashi, Y. Gao and K. Muramatsu, "Coupled 2-D and 3-D Eddy Current Analyses for Evaluating Eddy Current Loss of a Permanent Magnet in Surface PM Motors," *IEEE Trans. Magn.*, vol. 48, no. 11, pp. 3100-3103, Nov. 2012. [2] Liang Chen, Jiabin Wang, and Sreeju S. Nair, "An Analytical Method for Predicting 3-D Eddy Current Loss in Permanent Magnet Machines Based on Generalized Image Theory," *IEEE Trans. Magn.*, vol. 52, no. 6, June. 2016, Art. ID 8103311. [3] J. Y. Choi, J. H. Choi, S. M. Jang, H. W. Cho, S. H. Lee, "Eddy-Current Loss Analysis in Rotor of Surface-Mounted Permanent Magnet Machines Using Analytical Method," *KIEE*, vol. 61, no. 8, pp. 1115-1122, Aug. 2012 [4]O. de la Barriere, S. Hlioui, H. Ben Ahmed, and M. Gabsi, "An Analytical Model for the Computation of No-load Eddy-Current Losses in the Rotor of a Permanent Magnet Synchronous Machine," *IEEE Trans. Magn.*, vol. 52, no. 6, June. 2016.

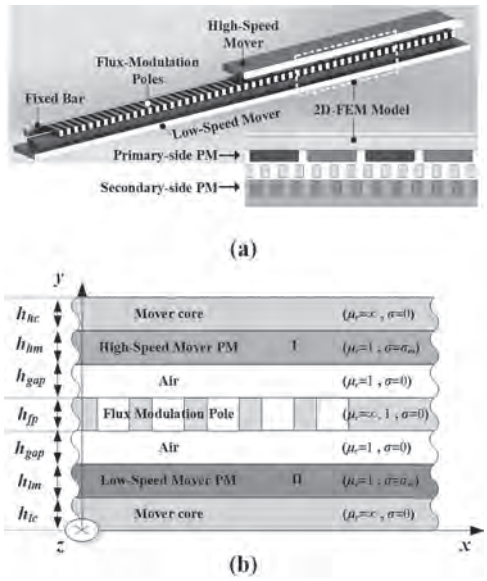

Fig. 1. (a) Linear magnetic gear structure, (b) Linear magnetic gear analysis model.

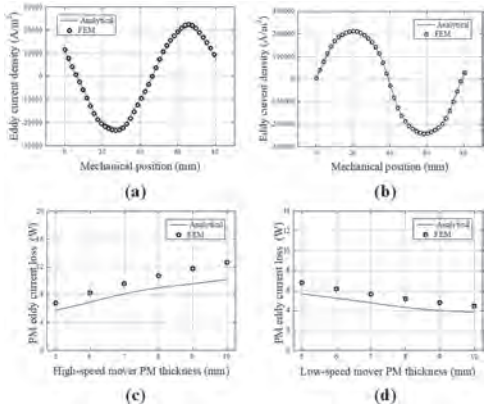

Fig. 2. Analysis of the eddy current density distribution of the permanent magnet on (a) the high-speed mover and (b) the low-speed mover; and the results of eddy current loss analysis according to the thickness of (c) the high-speed mover's permanent magnet and (d) low-speed mover's permanent magnet.

Session F5
MAGNETISM AND SUPERCONDUCTIVITY
(Poster Session)

Rolando Valdes Aguilar, Chair
The Ohio State University, Columbus, OH, United States

F5-01. Influence of Single-ion Anisotropy on the Phase States of two-Sublattice non-Heisenberg Magnet. *E. Yarigina*[1], P. Klevets[1] and Y. Fridman[1] *1. V.I. Vernadsky Crimean federal university, Simferopol, Russian Federation*

It is a well-known fact that the non-Heisenberg magnets exhibit rather interesting physical properties absent for the Heisenberg magnets. We studied the phase states and dynamic properties of an anisotropic spin-1 non-Heisenberg magnet. The results of the study allow to state that the account of the easy-axis, or the easy-plane single-ion anisotropy preserves the phase states found for an isotropic spin-1 non-Heisenberg magnet [1]. However, both the type of phase transitions and the phase diagram of the system substantially depend on the symmetry of single-ion anisotropy. In addition, the account of the single-ion anisotropy substantially changes the dynamic properties of a magnetically ordered system. Thus, in case of the easy-axis anisotropy, the phase diagram completely coincides with the phase diagram of the isotropic non-Heisenberg magnet with S=1, and the phase transitions are the degenerate first-order phase transitions. And in this case, the SU(3) point is retained, as in the isotropic system. However, the spectra of elementary excitations in the easy-axis magnetic differ significantly from the isotropic case. In the easy-plane non-Heisenberg magnet, the situation is fundamentally different. Although the same phase states are realized in the system as in the isotropic and the easy-axis cases, the phase transitions between the dipole (ferromagnetic and antiferromagnetic) and the nematic and orthogonal nematic phases are the first-order phase transitions, while in isotropic and easy-axis models these transitions are degenerate transitions of the first order. Besides, in the easy-plane anisotropy case, the first-order transition occurs between the spin nematic and the orthogonal nematic phases, while the direct transition between these states is absent in the isotropic model. Instead of it, the so-called SU(3) point, in which the energies of all four phases coincide, realizes in the isotropic case.

[1] Yu.A. Fridman, O.A. Kosmachev, Ph.N. Klevets, Spin nematic and orthogonal nematic states in S=1 non-Heisenberg magnet, JMMM 325 (2013) 125

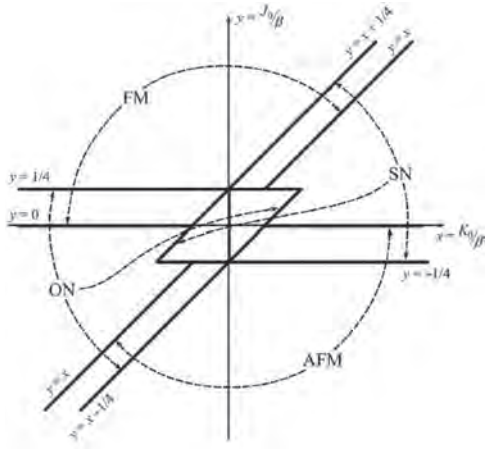

Fig. 1. Phase diagram of the non-Heisenberg easy-plane magnet.

F5-02. MöSsbauer Studies on Magnetism in FeSe. *H. Choi*[1], J. Seo[1], Y. Uhm[2], G. Sun[2] and C. Kim[1] *1. Department of Physics, Kookmin University, Seoul, The Republic of Korea; 2. HANARO Operation and Utilization, Korea Atomic Energy Research Institute, Daejeon, The Republic of Korea*

Iron selenide has a complicated with several structures phase diagram in existing only in very narrow compositional ranges. The structure and magnetic properties of this phase diagram depend sensitively on the relative ratio of Fe and Se. In this paper, we have investigated the magnetism of FeSe by focusing on Mössbauer spectroscopy measurement. The crystal structure of FeSe was characterized by powder X-ray diffraction. The FeSe contains a mixture of tetragonal (*P*4/*nmm* space group) and hexagonal (*P*63/*mmc* space group) peak. Magnetization measurements were performed with vibrating sample magnetometer (VSM) and Mössbauer spectroscopy. The magnetic hysteresis curve of FeSe measured at 295 K. The saturation magnetization and coercivity were found to be 8.03 emu/g and 357.40 Oe. Temperature dependence of magnetization was measured using VSM at H = 100 Oe. The Mössbauer spectra were taken at various temperatures ranging from 4.2 to 295 K. Fig. 1 shows the spectra at 4.2 and 295 K. Theses spectra have been fitted one-doublet (tetragonal) and three sets (hexagonal) of six Lorentzian assigned to three magnetically nonequivalent A, B, and C-sites. The isomer shift (δ) values at temperatures from 4.2 to 295 K were confirmed Fe^{2+} state at all sites. The magnetic hyperfine field (H_{hf}) and electric quadrupole splitting (ΔE_Q) values of FeSe at 295 K were determined to be 241.0, 193.2, and 105.8 kOe for A, B, and C-sites, 0.01, 0.02, and 0.02 mm/s for A, B, and C-sites. The ΔE_Q and δ values of one-doublet at 295 K were analyzed 0.29 and 0.31 mm/s, respectively. The H_{hf} and ΔE_Q values at 4.2 K were determined to be 283.2, 230.1, and 128.7 kOe for A, B, and C-sites, 0.0, -0.04, and 0.01 mm/s for A, B, and C-sites. The ΔE_Q and δ values of one-doublet at 4.2 K were analyzed 0.33 and 0.41 mm/s, respectively. It can be seen that as the temperature decreases, the ratio of doublet (tetragonal) decreases and the ratio of sextet (hexagonal) increases relatively.

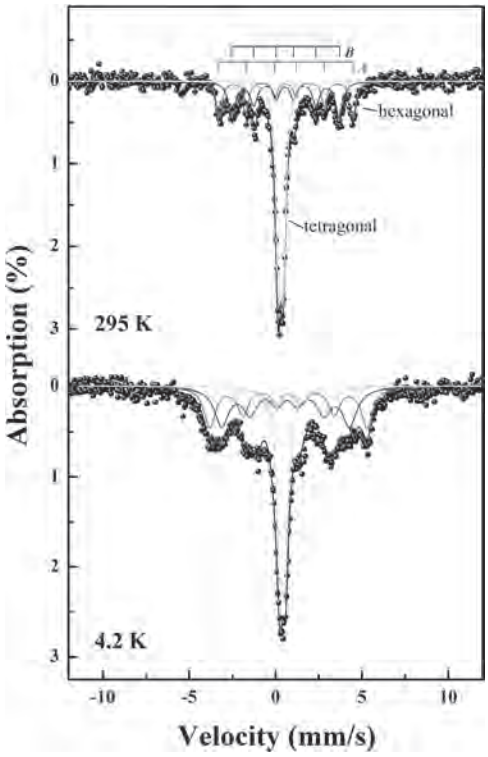

Fig. 1. Mössbauer spectra of FeSe at 4.2 and 295 K.

F5-03. Low-Dimensional Antiferromagnets Near SU(N) Symmetry.
A. Kolezhuk[1,2] and *T. Zavertanyi*[1] *1. Taras Shevchenko National University of Kyiv, Kyiv, Ukraine; 2. Institute of Magnetism NAS and MES of Ukraine, Kyiv, Ukraine*

During the last several decades, SU(N) antiferromagnets have attracted attention due to their possible exhibition of unconventional spin states [1-2] and realization in optical lattices of ultracold alkaline atoms [3]. It has been shown [2] that in spin-1 antiferromagnetic systems under a perturbation that breaks SU(3) symmetry down to SU(2), unit-charge topological excitations (skyrmions, hedgehogs) bind into doublets. Here we study a spin-3/2 system on a bipartite optical lattice in the vicinity of the antiferromagnetic SU(4)-symmetric point under the perturbation that breaks the symmetry down to SU(2). Starting from the effective low-energy continuum theory for such type antiferromagnet, described by CP^3 model, we derive an effective field theory for the perturbed system. We show that due to the dynamic generation of the third inertia momentum, caused by fluctuations of massive scalar fields, the perturbed theory is not described by the usual O(3) nonlinear sigma model (NLSM), but rather the O(3)×O(2) NLSM. Also, the perturbation from SU(4) to SU(2) effects unit-charge skyrmions of the CP^3 model by making them bind into triplets. Moreover, we derive the general relation between CP^{2S} and O(3) charges for arbitrary spin S systems under symmetry breaking from SU(2S+1) to SU(2) that shows 2S-multiplet binding of topological excitations.

[1] Read N., Sachdev S., Nuclear Physics B, 316.3, 609 – 640 (1989) [2] Ivanov B.A., Khymyn R.S., Kolezhuk A.K., Phys. Rev. Lett., 100, 047203 (2008) [3] Scazza, Francesco, et al., Nature Physics, 10.10, 779–784 (2014)

F5-04. Quantum-Classical Crossover in Nanomagnets Embedded in the Josephson φ_0 Junction.
G. Kim[1] *1. Physics and Astronomy, Sejong University College of Natural Sciences, Gwangjin-gu, The Republic of Korea*

Investigations of the macroscopic quantum tunneling in nanospin systems have been a topical issue of intensive theoretical and experimental studies over the past few years. One good subject is a quantum-classical crossover in magnetic nanoparticles with the magnetization (M) whose direction is subject to the magnetocrystalline anisotropy. At sufficiently high temperature the direction of M is changed by thermal activation and its rate obeys the Arrhenius law rate with being the height of the energy barrier, whereas at temperature close to absolute zero, pure quantum tunneling is relevant and, with the WKB exponent. Hence the crossover temperature is expected to exist between the thermal activation and quantum tunneling. Many studies have focused on whether the two regimes smoothly [first-order crossover (FC)] join or not [second-order crossover (SC)] around Tc in nanomagnetic systems. In recent years special interest has emerged in the quantum tunneling rate manipulated by a Josephson current. As is well known, an influence of ferromagnetism on superconductivity is much stronger than the opposite one of the superconductivity on the ferromagnetism because the exchange interaction for ferromagnet is much larger than the order parameter for conventional superconductor. However, relativistic interactions responsible for the direction of M in nanomagnets are expected to be of the same order as the superconducting order parameter. Such a possibility was recently studied by Chudnovsky[1] who investigated the tunneling rate of M in the Josephson φ_0 junction based on Buzdin's work[2]. In this work we argue that such Josephson junction is ideally suited for the study of quantum-classical crossover of the escape rate of M in nanomagnetic systems. Employing nonlinear perturbation near the top of the barrier based on the spin-coherent-state path integral method[3], we present the crossover boundary between FC and SC in nanomagnets with several crystal symmetries, and demonstrate that the junction is a good device to control such a boundary by applying the current as well as the external magnetic field.

[1] E. M. Chudnovsky, Phys. Rev. B 93, 144422 (2016). [2] A. Buzdin, Phys. Rev. Lett. 101, 107005 (2008); F. Konschelle and A. Buzdin, *ibid.* 102, 017001 (2009). [3] G.-H. Kim, Phys. Rev. B 77, 104405 (2008); J. Magn. Magn. Mater. 491, 165535 (2019).

F5-05. Fabrication and Characterization of NbN Magnetic Josephson Junctions Using non-Collinear Antiferromagnet Mn_3GaN.
H. Kato[1], S. Nakamura[1], K. Matsuura[1], B. Qiang[1], T. Hajiri[1] and H. Asano[1] *1. Nagoya Daigaku Kogakubu Daigakuin Kogaku Kenkyuka, Nagoya, Japan*

Magnetic Josephson junctions, where a magnetic material is sandwiched by superconductors, show peculiar phenomena such as π junction and spin triplet due to the exchange energy of the magnetic material. Among the magnetic Josephson junctions, ferromagnetic materials have been commonly used, and the π state has been reported in ferromagnetic CuNi[1)]. However, ferromagnet has stray field, which would affect to superconductivity. To avoid the effect of stray field, we focus on antiferromagnet Mn_3GaN (MGN). MGN is a non-collinear antiferromagnetic material in which magnetic moments cancel each other out noncollinearly and has characteristic properties not found in collinear antiferromagnetic materials.[2)] By using MGN in the Josephson junction, not only suppress the deterioration of the superconducting characteristics, but also unconventional magnetic junction characteristics is expected. In this study, we fabricated NbN/MGN/NbN hetero-stacked structures and evaluated the crystal structure and junction characteristics. NbN and MGN layers were deposited on a MgO(001) substrate by reactive magnetron sputtering. Figure 1 shows the out-of-plane XRD pattern of NbN/MGN bilayers. Both NbN and MGN(002) and (004) peaks were observed, indicating that (001)-oriented NbN/MGN bilayers grow on the MgO(001) substrates. Square mesa junctions of NbN/MGN/NbN with in-plane size L = 20 - 100 μm were fabricated by a conventional photolithographic and liftoff process. Figure 2 shows the current-voltage properties of the junction with 2.5 nm MGN layer. Thanks to the suppression of deterioration of superconducting properties at the junction interface, I_cR_N is as high as 3.1 mV, which is on the same order as the theoretical value, indicating that the Josephson junctions using the non-collinear antiferromagnetic material MGN are feasible and good junction characteristics can be obtained. Our results show the possible further improvement of the magnetic junction characteristics by using non-collinear antiferromagnet and potential of non-collinear antiferromagnetic Josephson junctions.

1) T. Yamashita *et al*., Phys. Rev. Appl. 8, 054028 (2017) 2) T. Hajiri *et al*., Appl. Phys. Lett. 115, 052403 (2019)

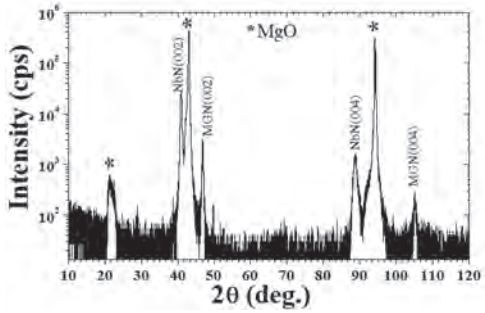

Fig. 1 XRD 2θ-θ pattern of a MgO//NbN/MGN film.

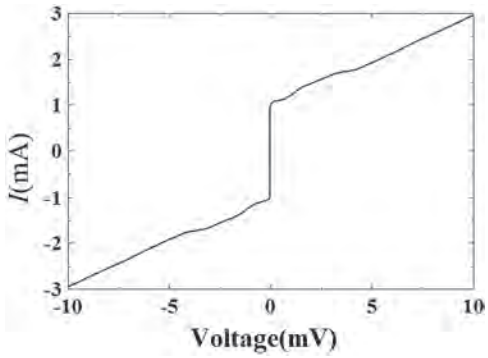

Fig. 2 Current vs Voltage curve for a NbN/MGN (2.5 nm)/NbN junction.

F5-06. DFT-Based Calculations of the Magnetic Hyperfine Interactions at Cd Sites in RECd Compounds With the FP-LAPW ELK Code. *L. Scalise*[1], A. Burimova[1], L.F. Pereira[1], W. Ferreira[1], T.S. Sales[1], V. Gonçalves[1], G. Cabrera-Pasca[2], R.N. Saxena[1] and A.W. Carbonari[1]
1. Instituto de Pesquisas Energeticas e Nucleares, Sao Paulo, Brazil;
2. Universidade Federal do Para - Campus Abaetetuba, Abaetetuba, Brazil

In this work we tested the methodology to map magnetic hyperfine interactions in strongly correlated materials using a free open-source all-electron FP-LAPW code ELK. The RECd (RE = Ce, Pr, Nd, Pm, Sm, Eu, Gd, Tb, Dy, Ho, Er, Tm, Yb) series was chosen as a laboratory system, since an almost complete set of experimental data on the hyperfine parameters at Cd sites in these compounds was acquired previously with an extremely sensitive TDPAC technique [1]. Moreover, these TDPAC results were complemented with WIEN2k DFT calculations that allow a qualitative comparison of the two codes. The ELK calculations were performed with PBE96 GGA-type exchange-correlation functional, the cases of scalar relativistic approximation and fully relativistic relaxation of the states were treated separately. A dense *k*-mesh and adequate $R_{MT}K_{max}$ were chosen in both cases to comply with the sensitivity of magnetic hyperfine parameters. We emphasize that the exploited version of ELK accounted for the contact field only. Yet, as it is the only contribution expected for Cd site in RECd, the values of B_{hf}, albeit generally overestimated, have shown reasonable agreement with the experiment (Fig. 1). Spin-orbit coupling taken into account led to a decrease in deviation from experimental data. An addition of the Hubbard-like term was essential to reach a tolerable result for CeCd. This behavior may be associated with a weaker localization of the 4f electron of Ce. Concerning the potential sources of discrepancy between our ELK results and those previously obtained with WIEN2k, (i) a different way of accounting for relativistic corrections, (ii) the use of GGA (our ELK study) versus LDA (previous WIEN2k study) and other details are discussed.

[1] F. H. M. Cavalcante et al. Phys. Rev. B, Vol. 94, 064417 (2016)

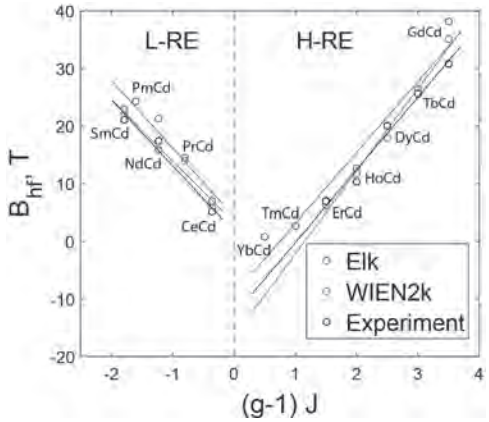

Fig. 1: Spin dependence of hyperfine magnetic field at Cd sites obtained with the ELK and WIEN2k codes and in the TDPAC experiment, and their linear fits.

F5-07. Coherent Manipulation of a Vanadium-Based Molecular Qubit Coupled to a Nuclear Qudit. *S. Chicco*[1,2], E. Garlatti[1,2], G. Allodi[1], M. Atzori[4], A. Chiesa[1,2], A. Albino[3], L. Sorace[3,2], R. De Renzi[1], R. Sessoli[3,2] and S. Carretta[1,2] *1. Mathematical, Physical and Computer sciences, Universita degli Studi di Parma, Parma, Italy; 2. Consorzio Interuniversitario Nazionale per la Scienza e Tecnologia dei Materiali, Firenze, Italy; 3. Universita degli Studi di Firenze, Firenze, Italy; 4. Laboratoire National des Champs Magnétiques Intenses, Grenoble, France*

VCp_2Cl_2 belongs to the S = 1/2 class of magnetic molecules characterized by an almost isotropic spin state and a relative long spin-spin relaxation time T_2 [1]. These systems have been proposed as attractive candidates for qubits realization, because of their capability to be placed in states of coherent superposition by easy manipulations through pulsed fields, even at high temperature [2]. Moreover, the V atom provides a nuclear spin I = 7/2, that can be rapidly manipulated because of its strong hyperfine interaction with the effective electronic spin [3]. Thus, the V atom of VCp_2Cl_2 can be considered as a coupled electronic qubit-nuclear qudit. Here we use "unconventional" Nuclear Magnetic Resonance [3] on the ^{51}V nuclei to determine the spectra evolution as a function of the static applied field and spin-coherence times of VCp_2Cl_2 (Cp = η^5-cyclopentadienyl). Measurements were performed at T = 4 K on a single crystal, diluted at 1% into the Ti isostructural diamagnetic host ($TiCp_2Cl_2$), in order to reduce dipolar interactions. Spectra for three orthogonal configurations of the applied static field with respect to the two inequivalent molecules in the primitive cell were successfully fitted by a model Hamiltonian composed by a hyperfine coupling, an axial quadrupolar term and nuclear and electronic Zeeman interactions. To investigate the coherence times, the decay of the transverse nuclear magnetization after a $\pi/2$-pulse perturbation was measured for each intense spectral resonance and fitted by a single-exponential function. The resulting T_2 relaxation rates (~10 μs) were observed to increase with the static magnetic field, as a consequence of the decrease of the electron-nuclear mixing that ruled these relaxation mechanisms. The possibility to coherently manipulate the VCp_2Cl_2 qubit-qudit system by radio frequency pulses is demonstrated by the induction of Rabi oscillations in various field configurations by sequences of pulses with different durations, refocused by a final π-pulse.

[1] J. M. Zadrozny, J. Niklas, O. G. Poluektov, et al., *ACS Cent. Sci.*, 1, 9, 488–492(2015). [2] M. Atzori, L. Tesi, E. Morra, et al., *J. Am. Chem. Soc.*, 138, 2154–2157, (2016). [3] R. Hussain, G. Allodi, A. Chiesa, *et al.*, *J. Am. Chem. Soc.*, 140, 31, 9814–9818, (2018).

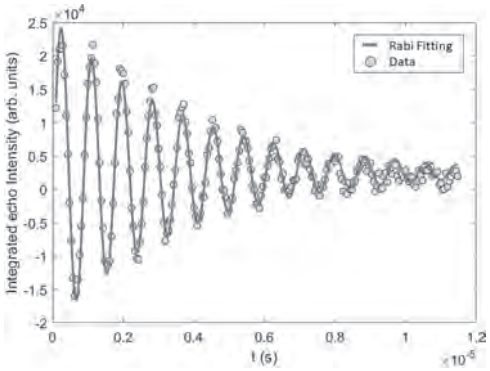

Fig.1 Rabi Oscillation induced by spin-echo NMR sequences of pulses with increasing durations.

F5-08. Crystalline Structure and Magnetic Properties of Pyrite FeS_2. *H. Choi*[1], J. Seo[1], Y. Uhm[2], G. Sun[2] and C. Kim[1] *1. Department of Physics, Kookmin University, Seoul, The Republic of Korea; 2. HANARO Operation and Utilization, Korea Atomic Energy Research Institute, Daejeon, The Republic of Korea*

Iron pyrite (FeS_2) are recognized significant attention as promising inorganic materials applications, such as electrode materials for high-energy batteries, medical diagnostics, semiconductor materials, and photovoltaic solar cells. In this paper, we provide that the crystalline structure and magnetic properties of pyrite FeS_2 were characterized with X-ray diffraction (XRD), vibrating sample magnetometer (VSM), and Mössbauer spectroscopy. From the refined XRD patterns, it was confirmed that the crystalline structure of FeS_2 was cubic pyrite (P*a-3* space group) with the lattice constants of a_0 = 5.4176 Å. The hysteresis loops of FeS_2 were measured by VSM in the maximum applied field of 10 kOe at 4.2 and 295 K. As shown in Fig. 1, the saturation magnetization at 4.2 and 295 K was 0.123 and 0.035 emu/g, respectively. Mössbauer data were collected in the temperature range of 4.2-500 K. The spectra at all temperature were fitted one-doublet. The Mössbauer spectra of FeS_2 at 4.2 and 295 K are shown in the inset of Fig. 1. The electric quadrupole splitting (ΔE_Q) values are 0.63 and 0.60 mm/s for 4.2 and 295 K, respectively. The ΔE_Q values with decreasing temperatures increases slightly due to changes in the Fe-S distance. The isomer shift (δ) values are 0.28 and 0.18 mm/s for 4.2 and 295 K, indicating the Fe^{3+} state. The temperature dependence of δ values is due to the second order doppler shift.

[1] Z. Meng, F. Wei, W. Ma, etc., Adv. Funct. Mater., Vol. 26, p.8231 (2016).

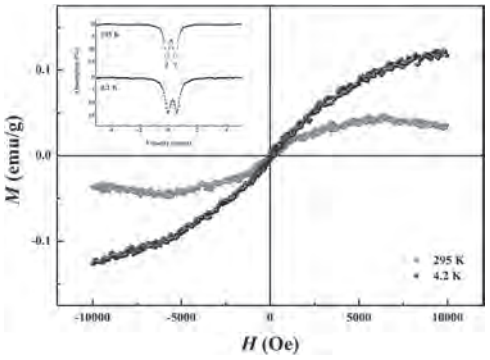

Fig. 1. Hysteresis loops and Mössbauer spectra of FeS_2 at 4.2 and 295 K.

F5-09. Nonequilibrium Critical Behavior of the 3D Isotropic and Anisotropic Heisenberg Models. *A.S. Lyakh*[1], P.V. Prudnikov[1] and V.V. Prudnikov[1] *1. Theoretical Physics, Dostoevsky Omsk State University, Omsk, Russian Federation*

We present results of Monte Carlo study of non-equilibrium critical behavior in three-dimensional Heisenberg model in isotropic case and with anisotropy of easy axis type. We investigate relaxation Glauber-like dynamics of these models with evolution from different initial states. Usually, we can distinguish the high-temperature initial states created at temperatures $T_0 > T_c$ with initial magnetization $m_0 = 0$ and low-temperature initial states with $T_0 < T_c$ and $m_0 \neq 0$. Initial states with $m_0 \neq 0$ give rise to a new time scale $t_m \sim m_0^{-k}$ with the exponent $k > 0$. This time scale produces a pronounced effect on the temporal behavior of magnetization, autocorrelation function and response function [1-4]. Study of influence of initial states with $0 < m_0 \leq 1$ on dynamical properties of model has been carried out. It is established realization of scaling relation for time dependence of magnetization. We calculated critical exponents for isotropic and anisotropic models with values $\beta/z\nu$= 0.2565(4) and z=2.035(4) for the anisotropic Heisenberg model which agree well with the exponents for the 3D Ising model. Aging has been revealed during study of two-time dependence of the autocorrelation function and dynamical susceptibility on different initial states which are characterized by the slowing down with growth of its age t_w. We show that the slowing down of the correlation function during evolution from high-temperature initial state is considerably slower than in case of low-temperature initial state. Analysis of parametrical dependence of the dynamical susceptibility on the correlation function gave possibility to determine asymptotical values of the fluctuation-dissipation ratio (FDR) for isotropic X^∞=0.383(6) and anisotropic X^∞=0.392(7) Heisenberg models with evolution from high-temperature initial states. The obtained value of FDO for anisotropic model agrees very well with X^∞=0.391(12) for the 3D Ising model calculated in [4] by the same method. This study is supported by RFBR (projects 18-42-550003, 20-32-70189), the Ministry of Education and Science of Russian Federation (state assignment 0741-2020-0002) and grant MD-2229.2020.2 of the President of the Russian Federation.

1. *V.V. Prudnikov, P.V. Prudnikov and M.V. Mamonova*, Phys. Usp., 60, 762 (2017). 2. *V.V. Prudnikov, P.V. Prudnikov and E.A. Pospelov,* J. Stat. Mech., 2016, 043303 (2016). 3. *V.V. Prudnikov, P.V. Prudnikov, E.A. Pospelov and A N. Vakilov,* Phys. Lett. A 379, 774 (2015). 4. *P.V. Prudnikov, V.V. Prudnikov, E.A. Pospelov and P.N. Malyarenko*, PTEP, 2015, 053A01 (2015).

F5-10. Probing Majorana Fermion in Two Dimensional Noncentrosymmetric Superconductors by Using Equal-Spin Andreev Reflections. H. Lai[1], *M. Wang*[1] and C. Chang[1] *1. Physics, National Taiwan University, Taipei, Taiwan*

So far, finding Majorana fermion is one of the important research in condensed matter physics. In theory, zero energy Majorana modes resides on the edge or vortex core in topological superconductor, characterizing the topological phase of matter protected by particle hole symmetry. Zero bias conductance peak is one of the phenomena from Andreev reflection process in normal metal/topological interface. In this work, we use the non-equilibrium Green's function method to study the interface between the normal metal and two dimensional noncentrosymmetric superconductor which lack a center of inversion symmetry and exhibit spin orbital coupling. The tight binding hamiltonian[1] for noncentrosymmetric superconductor is used. Then, we simulate the selective equal spin Andreev reflection[2]. Equal spin Andreev reflection means if the electrons in normal metal has the same spin polarization with the electrons on the edge state of superconductor, they are reflected as holes with the same spin. Moreover, with opposite spin polarization between electrons in normal metal and electrons in the edge of superconductor, they are reflected as electrons with same spin. As the result, we can get the conductance as the function of the spin polarized angle of electron in normal metal to realize the properties of Majoranana edge state. In addition, the spin current can be injected to the noncentrosymmetric superconductor which allow both singlet and triplet cooper pairs, generating the new spintronic device.

1. M. Biderang, H.Yavari, Mohammad-Hossein Zare, PHYSICAL REVIEW B 98, 014524(2018) 2. PA. Lee, PHYSICAL REVIEW LETTERS 112, 037001(2014)

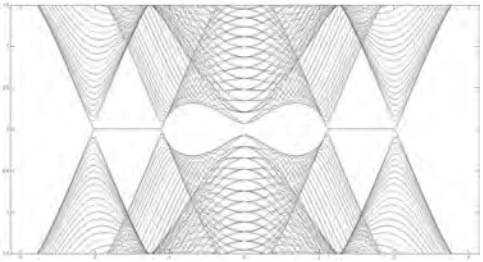

band structure of d+p wave superconductor

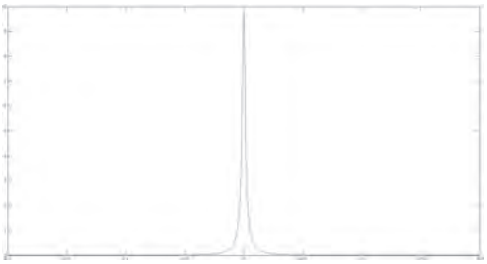

zero bias Andreev conductance in metal-d+p wave superconductor systems

F5-11. Annealing Effect on the Structural and Local Magnetic Properties of Nickel Ferrite Nanoparticles Studied by Hyperfine Interaction Measurements. *P.S. Rodrigues*[1], I.T. Matos[1], T.S. Sales[1], A. Burimova[1], G. Cabrera-Pasca[2], L.F. Pereira[1], R.N. Saxena[1], L. Otubo[1] and A.W. Carbonari[1] *1. Instituto de Pesquisas Energeticas e Nucleares, Sao Paulo, Brazil; 2. Universidade Federal do Para, Belem, Brazil*

Nickel ferrite in the form of nanoparticles is a technologically important material that can be applied for the production of biosensors, catalysts, drug delivery, and magnetic resonance contrast agents. In this work $NiFe_2O_4$ samples comprising spherical nanoparticles of ~6 nm in diameter have been synthesized via a thermal decomposition route. The quality control of the samples was carried out with conventional techniques including X-ray diffraction and transmission electron microscopy. Post-synthesis XRD pattern revealed textured spinel $NiFe_2O_4$. Local magnetic properties were examined with Time Differential Perturbed Angular Correlation (TDPAC) spectroscopy within the 12 - 773K temperature range. TDPAC probes were introduced into the samples at synthesis. Quasi-static magnetic properties were observed (including above room temperature), as expected due to the small time window of TDPAC. The TDPAC results shown in Fig. 1 were analyzed using a model with combined electric quadrupole and magnetic dipole interactions. An expressive dynamic interaction was observed upon heating after synthesis. A theoretical model based on the Brillouin function for different ionic moments was applied to study the evolution of the hyperfine magnetic field with temperature (see Fig. 1-2) and allowed to attribute the magnetic interaction to the probe location at Fe^{3+} site. Site occupancy and the interplay between magnetic and structural properties are discussed with respect to application perspectives.

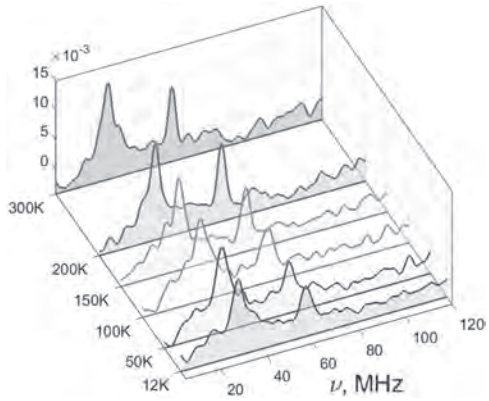

Fig. 1: Fourier transform of TDPAC perturbation factors taken in the range 12 - 300K on cooling

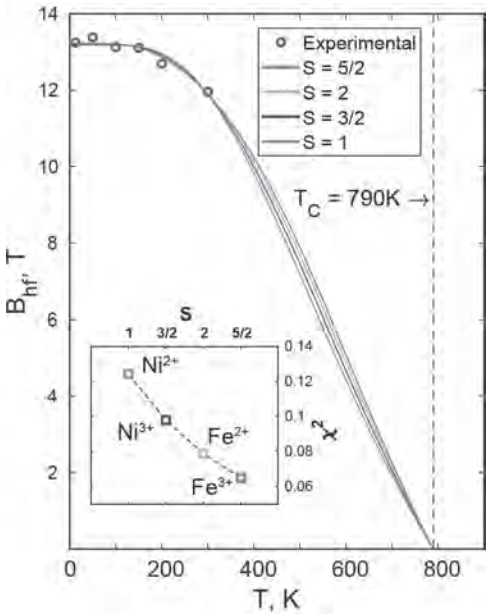

Fig. 2: The evolution of magnetic hyperfine field with temperature and fits for selected ion moments

F5-12. Field-Induced Phase Transitions of Tetramer-Singlet States in Synthetic SU(4) Magnets. *Y. Miyazaki*[1], D. Yamamoto[1] and N. Furukawa[1] *1. Department of Physics, Aoyama Gakuin University, Sagamihara, Japan*

Quantum dimer magnets such as $TlCuCl_3$ [1,2], which have a non-magnetic spin-singlet ground state, are a prototypical example for studying exotic phases of matter provided by quantum entanglement [Fig. 1]. When a magnetic field is applied, the energy gap in the triplet excitations decreases and eventually closes at a certain critical value of the field strength, resulting in Bose-Einstein condensation of magnons (or triplons). In the field of atomic, molecular, and optical physics, a great deal of effort is being made to simulate quantum magnetism using alternative systems based on ultracold atomic gases loaded in an optical lattice. Besides conventional SU(2) systems, it has also been succeeded in realizing SU(N>2) symmetric Mott insulators with alkaline-earth(-like) atoms such as ^{173}Yb [3,4]. Quantum magnetism with a high SU(N) symmetry has great potential to explore exotic phase transition phenomena associated with a rich variety of spontaneous symmetry breaking. In this work, we study the field-induced phase transition phenomena of the SU(4) Heisenberg model on the tetramerized square lattice [5] shown in Fig. 2. For an isolated tetramer (J>0, J'=0), the lowest energy state is the singlet state obtained by antisymmetrizing the four-flavor states (plaquette-singlet state). Using an extended flavor-wave theory in the

presence of weak couplings $J' << J$, we calculate the excitation spectra from the direct-product ground state of local SU(4) singlets, and discuss the gap closing induced by applying magnetic fields. In contrast to the SU(2)-dimer case, the field term has three degrees of freedom, reflecting how one tunes the differences among the chemical potentials of four different flavors. We investigate several forms of "magnetic field," supposing different experimental implementation in cold atoms. We also perform the cluster mean-field analysis to discuss the whole magnetization process with multiple quantum phase transitions up to the magnetic saturation.

[1] T. Nikuni *et al*., Phys. Rev. Lett. 84, 5868 (2000). [2] F. Yamada *et al*., J. Phys. Soc. Jpn. 77, 013701 (2008). [3] S. Taie *et al*., Nat. Phys. 8, 825 (2012). [4] C. Hofrichter *et al*., Phys. Rev. X 6, 021030 (2016). [5] S. Fölling *et al*., Nature 448, 1029 (2007).

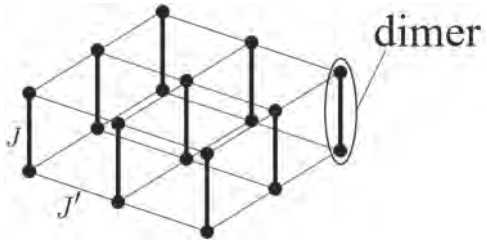

Fig. 1: Quantum dimer magnet.

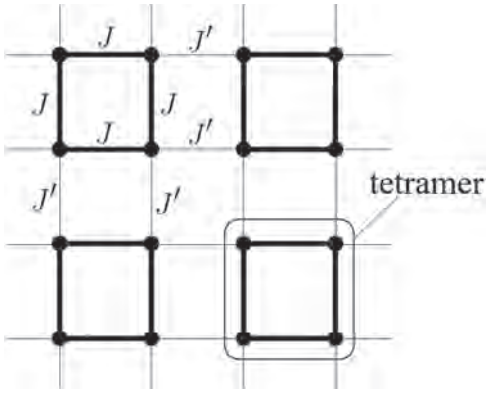

Fig. 2: SU(4) artificial magnet on a tetramerized square lattice.

F5-13. Withdrawn

Session F6
RARE EARTH TRANSITION METAL BORIDES II
(Poster Session)

Hossein Sepehri Amin, Chair
National Institute for Materials Science, Tsukuba, Japan, Tsukuba, Japan

F6-01. Withdrawn

F6-02. Microstructure and Magnetic Properties of Novel Cu-Containing Sintered Nd-Fe-B Magnet. *D. Shi*[1], Q. Lan[1], Q. Huang[2], D. Chen[2] and Y. Shi[1] *1. Institute of rare earth magnetic material, Xiamen Tungsten Co. Ltd., Xiamen, China; 2. Fujian Changting Golden Dragon Rare-Earth Co. Ltd., Longyan, China*

Sintered Nd-Fe-B magnet has been widely applied as rotor magnet in various motors of energy-saving household appliances and hybrid or electric vehicles (HEV or EV). Recently, increasing interest has been paid to the investigation of Ga-doped Nd-Fe-B magnet. Coercivities of the magnet can be enhanced significantly with the formation of extra non-ferromagnetic $Nd_6Fe_{13}Ga$ phase after optimal post-sinter annealing treatment [1, 2]. Since Ga is expensive and scarce, it is important to investigate whether or not similar effects can be achieved with the addition of other abundant elements. Studies on $Re_6Fe_{13-x}M_{1+x}$ (M=Au, Ag, Cu, Si and Ga)have been carried out since 1985 [3, 4]. However, their influences on the properties of materials as second phase in NdFeB-permanent magnets are still unclear. In this work, we report a study on microstructure and magnetic properties of novel high Cu-containing Nd-Fe-B magnet. Nominal composition of the sintered magnet was $Pr_{7.62}Nd_{22.88}Tb_{0.8}Fe_{65.2}Co_{2.0}Cu_{0.4}Al_{0.2}B_{0.9}$ in wt%, which was rich in Cu and low in B compared to that of standard commercial magnets. Effects of annealing temperature and time on microstructure evolution of casting strips were systematically investigated. Distinct $Re_6Fe_{13}Cu$ phase was observed both in casting strips and magnet after optimally annealing. Ultrafine random equiaxed matrix grains were completely eliminated in annealed casting strips. Columnar grains increased from 3.7 μm to 5.8 μm with volume fraction of Nd rich phases increased by 1.6%. In contrast to poor squareness and low coercivity of the sintered magnet fabricated by casting strips without annealing, magnetic properties were significantly improved for final magnet made from annealed strips. After Dy grain boundary diffusion (GBD) treatment, coercivity increased drastically from 14.87 kOe to 25.39 kOe in the magnet with presence of $Re_6Fe_{13}Cu$ grain boundary phases. These results indicate the formation of $Re_6Fe_{13}Cu$ phase might correlate strongly with coercivity enhancement of the magnet.

1) T. T. Sasaki, T. Ohkubo and K. Hono *et al*., *Scripta Mater.* Vol. 113, p. 218 (2016) 2) X.D. Xu, T. T. Sasaki and K. Hono *et al.*, *Acta Mater.* Vol. 156, p.146 (2018) 3) O. M. Sichevich, R. V. Lapunova and Ya. P. Yarmulek *et al.*, *Sov. Phys. Crystallogr.* Vol. 30, p. 627, (1985) 4) C. H. de Groot, K. H. J. Buschow and F. R. de Boer, *Phys. Rev. B*, Vol. 57, p. 11472 (1998)

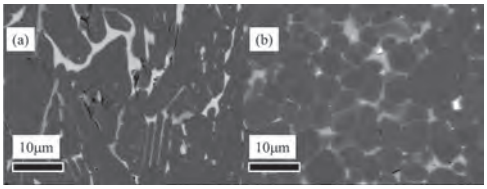

Fig.1 BSE-SEM images showing the microstructure of annealed casting strips and post-sinter annealed magnet

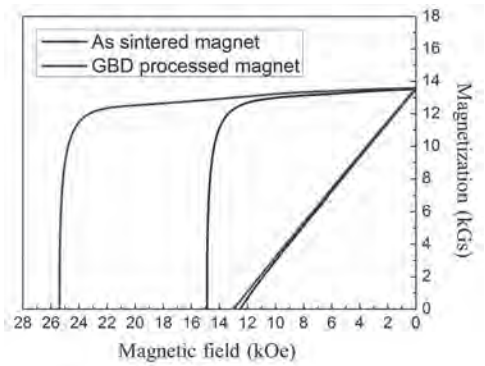

Fig.2 Demagnetization curves of as sintered magnet and GBD processed magnet

F6-03. Effect of Mo Monoatomic Interlayer on Magnetic Properties of in-Plane Anisotropic Nd-Fe-B/Mo/FeCo Nanocomposite Multilayered Films. *K. Koike*[1], K. Ohashi[2], T. Suzuki[2], C. Okita[2], N. Inaba[2], H. Kato[1], M. Itakura[3], S. Hara[4], Y. Saito[4], S. Okubo[4] and H. Ohta[4] *1. Applied Mathematics and Physics, Yamagata University, Yonezawa, Japan; 2. Informatics and Electronics, Yamagata University, Yonezawa, Japan; 3. Interdisciplinary Graduate School of Engineering Sciences, Kyushu University, Kasuga, Japan; 4. Molecular Photoscience Research Center, Kobe University, Kobe, Japan*

Exchange-coupled nanocomposite magnets consisting of nano-sized hard/soft magnetic particles are known as a method of increasing the $(BH)_{max}$ of NdFeB magnets [1, 2]. Although many reports on perpendicular anisotropic NdFeB/Fe based nanocomposite magnet films have been published so far [3-5], there have been no reports on in-plane anisotropic Nd-Fe-B magnet films with an easy axis of magnetization in the in-plane direction. Therefore, in this study, we report the in-plane magnetic anisotropy and magnetic interaction of NdFeB/Mo/FeCo multilayers with a monatomic Mo interlayer. The [NdFeB(30 nm)/Mo(0, 0.3 nm)/FeCo(5 nm)/Mo(0, 0.3 nm)]$_5$ multilayered films were deposited on an Mo(001)/MgO(001) heated at 300°C using UHV sputtering. Annealing was carried out in the range of 400°C to 800°C. Fig.1 shows typical demagnetization curves for as-deposited NdFeB/Mo/FeCo multilayered film and annealed at 800°C. The as-deposited film showed soft magnetic property with weak perpendicular magnetic anisotropy, while the films annealed above 650°C exhibited hard magnetic property with in-plane magnetic anisotropy, well squareness, and high coercivity about 10 kOe. The (220) peak of $Nd_2Fe_{14}B$ was identified in the XRD pattern after annealing of the film, which means that the *c*-axis, which is the easy axis of magnetization, points in the plane of the film, consistent with the measurement of the magnetization curve. The positive peak of ΔM plot of in-plane direction of the film annealed at 800°C is shown as Fig. 2. These results indicate existence of positive exchange coupling interaction between the Nd-Fe-B and FeCo layers in the in-plane anisotropic multilayered film with monoatomic Mo interlayer.

References [1] E. F. Kneller and R. Hawig: IEEE Trans. Magn. 27 (1991) 3588-3560. [2] R. Skomski and J. M. D. Coey: Phys. Rev. B, 48, (1993) 15812. [3] H. Kato, H. Kubota, K. Koyama, and T. Miyazaki: J. Alloys

Comp. (2006), 408–412, 1368. [4] W-B. Cui, Y. K. Takahashi, and K. Hono: Adv. Mater. (2012) 1-6. [5] K. Kobayashi, et al.: J. Phys., Conf. Seri. 903 (2017) 012015-1-3.

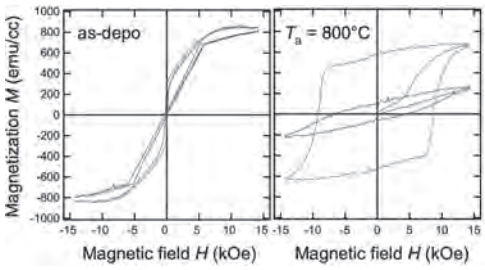

Fig.1 Demagnetization curves for as-deposited Nd-Fe-B/Mo/FeCo multilayered film and annealed at 800°C. Direction of external magnetic field; in-plane (red) and out of plane (blue).

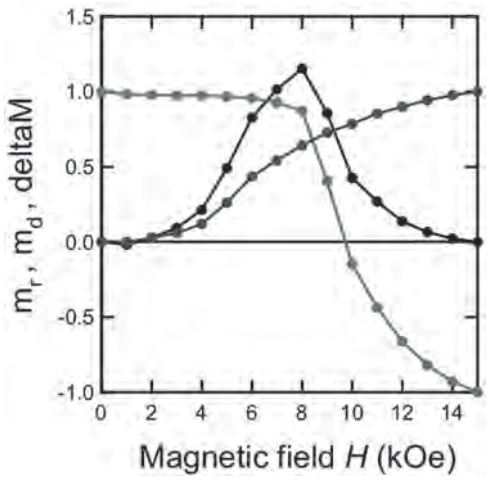

Fig.2 ΔM plot (black) and M_r (blue) and M_d (red) curves of in-plane direction of Nd-Fe-B/Mo/FeCo multilayered film annealed at 800°C.

F6-04. Reduction of Nd Moments and Local Magnetic Anisotropy in $Nd_2Fe_{14}B$ Single Crystals. *H. Sato*[1], Y. Kubo[1], T. Yoshioka[2], H. Tsuchiura[2], Y. Mizuno[1], K. Koike[1], K. Takahashi[3] and H. Kato[1] *1. Graduate School of Science and Engineering, Yamagata University, Yonezawa, Japan; 2. Department of Applied Physics, Tohoku University, Sendai, Japan; 3. Institute for Materials Research, Tohoku University, Sendai, Japan*

In relation to the origin of relatively small coercivity in Nd-Fe-B magnets, degraded magnetic anisotropy (MA) of the Nd moment at the 4*f* site of the main $Nd_2Fe_{14}B$ phase was discussed both experimentally[1] and theoretically[2]. In this work, we pay attention to the Nd-moment reduction estimated from the difference in saturation magnetization (M_s) between easy and hard directions, since the reduction rate would be different in inequivalent Nd sites reflecting the difference in the local MA. We measured the magnetization curves in $Nd_2Fe_{14}B$ single crystals between 300 K and 600 K, and the paramagnetic susceptibility χ up to 900 K. As a result, we found that M_s [100] is 3%~4% smaller than M_s [001], not only at 300 K but also up to the Curie temperature T_c (Fig. 1). Moreover, we observed a significant anisotropy in χ for $T > T_c$ (Figs. 1 & 2). First-principles calculations were performed to obtain crystalline electric field parameters for $Nd_2Fe_{14}B$ and the magnetization was calculated by using an effective spin model[2,3]. As shown in Fig. 2, calculated anisotropy in M_s was found to be finite up to T_c, although the M_s reduction rate ΔM was slightly smaller than the experiment. Calculated anisotropy $\Delta\chi$ in paramagnetic phase was also finite, in good agreement with the experiment. It is possible now to estimate the reduction rate for Nd moments in inequivalent sites $\Delta m_{Nd}(f)$ and $\Delta m_{Nd}(g)$. Fig. 2 suggests that the former is much smaller than the latter. In general, a magnetic moment with a larger local MA tends to shrink more significantly when forced to align along the hard direction. This result thus suggests a significant deterioration of MA at the Nd(*f*) site even at elevated temperatures.

[1] D. Haskel, J. C. Lang, Z. Islam, et al., Phys. Rev. Lett. 95, 217207 (2005). [2] T. Yoshioka and H. Tsuchiura, Appl. Phys. Lett. 112, 162405 (2018). [3] M. Yamada, H. Kato, et al, Phys. Rev. B 38, 620 (1988).

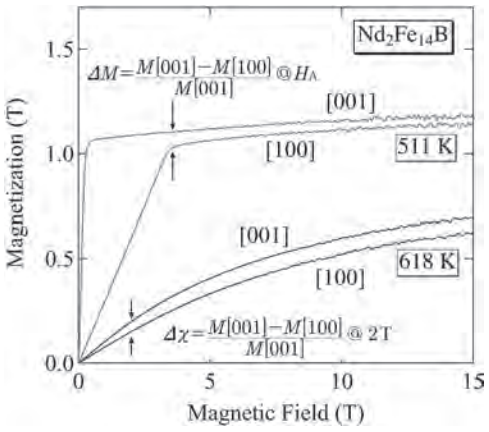

Fig. 1 Magnetization curves in $Nd_2Fe_{14}B$ single crystals at 511 K and 618 K. Definition of the reduction rates ΔM and $\Delta\chi$ is indicated.

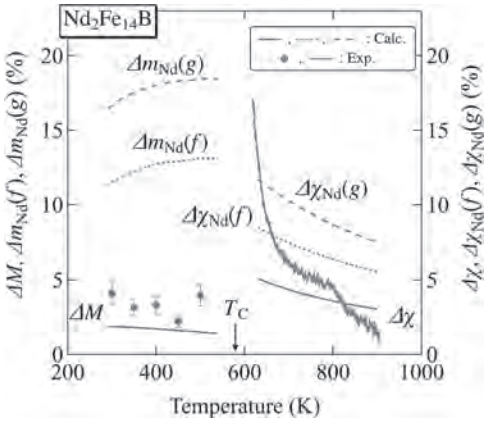

Fig. 2 Temperature dependence of the reduction rate parameters ΔM and $\Delta\chi$, together with those for Nd moments at *f* and *g* sites.

F6-05. Coercivity Enhancement of hot-Deformed NdFeB Magnet by Doping $R_{80}Al_{20}$ (R= La, Ce, Dy, Tb) Alloy Powders. *Y. Wong*[1], G. Lin[1], H.W. Chang[1] and W. Chang[1] *1. National Chung Cheng University, Minhsiung, Taiwan*

Since the discovery of the NdFeB magnet, it has been widely used due to the outstanding magnetic properties at room temperature. Because of finer and platelet $Nd_2Fe_{14}B$ grains, the hot-deformed Nd-Fe-B magnets generally exhibit superior coercivity ($_iH_c$) to the sintered magnets. In order to widen the applications at high temperature, coercivity enhancement in hot-deformed Nd-Fe-B magnets is critical. Addition of heavy rare earth (HRE) element, such as Dy or Tb, into NdFeB magnet is effective in enhancing coercivity, nevertheless, the rare abundance and rapidly increasing cost for HRE elements hinders the application. In contrast, doping non- or low-magnetic alloys, i.e. RCu (R=La, Ce or misch-metals) into NdFeB magnets could lower the melting points of the grain boundary (GB) phase, reduce the magnetization of GB phase and strengthen the decoupling effect between grains. In this work, magnetic properties of hot deformed NdFeB magnets made from the commercial MQU-F powder doped with $R_{80}Al_{20}$ (R= La, Ce, Dy, Tb) alloy powders are reported. By doping $R_{80}Al_{20}$ powders, the coercivity of hot deformed NdFeB magnets is significantly increased from 15.0 kOe to 19.4 kOe, 20.1 kOe, 21.8 kOe, and 23.8 kOe for R = La, Ce, Dy, and Tb, respectively, while $(BH)_{max}$ is slightly decreased from 40.5 MGOe

to 35.7-39.2 MGOe. Coercivity enhancement of the magnets doped with $R_{80}Al_{20}$ powders in this work is superior to that with RCu powders, reported previously[1]. Microstructure analysis shows that Ce or La and Al prefer to distribute mostly at grain boundary, while Dy or Tb distributes over grain interior and boundary. The magnetic isolation effect due to R-rich phase containing Nd, Ce or La, Al at the grain boundary attributes to coercivity enhancement with the samples with R = La and Ce. In additional to magnetic isolation, the strengthened magnetocrystalline anisotropy field of 2:14:1 phase due to Dy or Tb substitution gives rise to the significant enhancement of coercivity for those with RAl (R = Dy and Tb). This study provides a useful way to enhance coercivity of hot deformed NdFeB magnets under the conservation of the rare earth resources.

[1] Y. I. Lee, H. W. Chang, G. Y. Huang, C. W. Shih, W. C. Chang, IEEE Transactions on Magnetics, 53, 2100704 (2017).

F6-06. Effect of Shape and Crystallinity of $Tb_{70}Co_{15}Cu_{15}$ Powders on the Coercivity Enhancement of the Sintered NdFeB Magnet by Grain Boundary Diffusion. *Y. Wong*[1], W. Hsu[1], H.W. Chang[1], Y. Lee[1], W. Chang[1], C. Chiu[2] and C. Mo[3] *1. National Chung Cheng University, Minhsiung, Taiwan; 2. China Steel Corp., Kaohsiung, Taiwan, Kaohsiung, Taiwan; 3. Himag Magnetic Corporation, Pingtung, Taiwan, Pingtung, Taiwan*

NdFeB sintered magnet shows the highest energy product ($(BH)_{max}$) of all studied hard magnetic materials originated from its outstanding magnetically intrinsic properties of $Nd_2Fe_{14}B$ unit cell at room temperature. Traditionally, Dy or Tb is generally added to the Nd-Fe-B magnets to enhance the coercivity ($_iH_c$) for the applications at higher temperature. Since the price surge of above critical RE elements, how to reduce the usage of Dy or Tb in the magnets while keeping high coercivity is a crucial issue. The grain boundary diffusion (GBD) technique is considered as an effective method to meet this goal. Several kinds of Tb or Dy-based powders or films have been adopted as diffusion sources for improving the coercivity of the NdFeB magnets. In this work, $Tb_{70}Co_{15}Cu_{15}$ alloy powders are adopted as the GBD source. They are prepared by melt spinning, and then milled to form the powders by high-energy ball milling (HEBM) and low-energy rolling ball milling (LEBM). Two kinds of powders exhibit two different shape and crystalline state, that is, granular amorphous-like for HEBM and platelet crystalline-like for LEBM, respectively. The particle size of the powders made by HEBM is finer than that made by LEBM. The commercial NdFeB sintered magnets with the magnetic properties of B_r=14.0 kG, $_iH_c$= 17.5 kOe and $(BH)_{max}$= 48.4 MGOe are chosen as original magnets. The coercivity increment of the NdFeB magnets is 7.6 kOe and 9.4 kOe after GBD with the alloy powders made by HEBM and LEBM, respectively. Due to the better crystallinity and the platelet shape of the powders made by LEBM, the higher coercivity increment can be obtained. The magnetic properties of the magnet GBD with $Tb_{70}Co_{15}Cu_{15}$ alloy powders made by LEBM are B_r=13.6 kG, $_iH_c$= 25.1 kOe and $(BH)_{max}$= 46.1 MGOe. The platelet shape powders represent the bigger contact area between the powders and the surface of the magnets which are beneficial for Tb to diffuse into the NdFeB magnet. In the meantime, higher crystallinity powders need not to absorb energy for crystallization prior to diffusion, which is also helpful for improving diffusion efficiency.

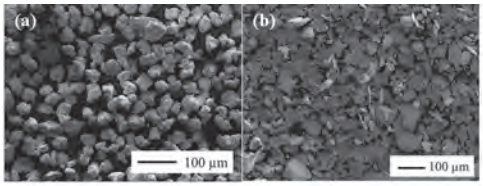

SEM images of the alloy powders made by (a) HEBM and (b) LEBM.

F6-07. Enhanced Magnetic Properties of Chemically Prepared NdFeB Particles by Reduction-Diffusion Method Through Optimization of Heat Treatment. *S. Kim*[1,3], R. Kuchi[1,2] and D. Kim[1,2] *1. Korea Institute of Materials Science, Changwon, The Republic of Korea; 2. Korea Institute of Geoscience and Mineral Resources, Daejeon, The Republic of Korea; 3. Chungnam National University, Daejeon, The Republic of Korea*

NdFeB magnets are widely used in advanced electric vehicles, electric motors for power generators, wind turbine generators, energy conversion systems and many other novel applications. However, the high energy density (BHmax) magnets are needed to utilise them. For this purpose, the NdFeB magnetic particles should prepare with higher magnetic properties (high coercivity and remenance) which could mainly depends on the $Nd_2Fe_{14}B$ phase purity, crystallinity and microstructure. To wards this direction, we report the cost effective and a facile chemical synthesis including spray drying and reduction-diffusion (RD) process with some modefications [1, 2]. Importantly, we invesigated the heat treatments for RD pcocess because it is very importane to control the particles nucleation and growth process during RD. Different heating rates include 5, 10, 20 and 30 °C per minute to reach 1000 °C for RD propcess were used. Among them, the 20 °C heating rate results the NdFeB particles with improved magnetic and structural properties. The prepared NdFeB particles shows the corcivity (Hc) of 2580 Oe, remanence (Mr) of 139 emu/g, saturation magnetization (Ms) of 156 emu/g (Ms value was close to the bulk NdFeB (168 emu/g) [3]) and BHmax of 12.48 MGOe. This is attributed to the shape uniformity of NdFeB particles and phase purity with high crystallinity.

1. Chen C.Q, Kim D, Chuljin C (2014) Influence of Ca amount on the synthesis of $Nd_2Fe_{14}B$ particles in reduction–diffusion process. J. Mag. Mag. Mater 355:180–183. 2. Wang Y, Ahn J, Kim D, Ren W.J, Liu W, Zhang Z.D, Choi C.J (2017) Effect of washing process on the magnetic properties of Nd-Fe-B nanoparticles prepared by reduction-diffusion method. J. Mag. Mag. Mater 439:91–94. 3. Hirotaka Y, Hiroaki W (2017) Magnetic properties of hard magnetic nanoparticles of Nd2Fe14B synthesized using self-assembled block copolymers. Intermetallica 85:125–129.

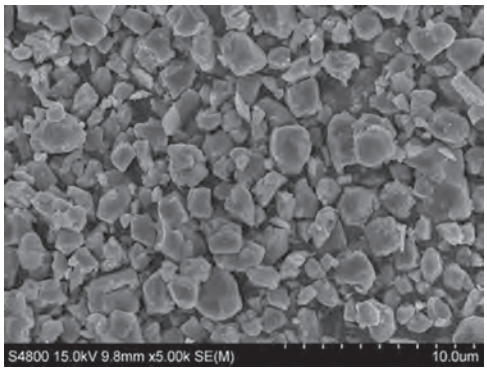

F6-08. Coercivity Mechanism of Ce-Fe-B Melt-Spinning Ribbons Crystallized by Electron Beam Exposure. *L. Zha*[1], Z. Lin[1], F. Wang[1] and J. Yang[1] *1. Department of Physics, Peking University, Beijing, China*

$Ce_2Fe_{14}B$ nanostructured magnetic materials were crystallized by electron beam exposure with a greatly reduced annealing time of 0.1 s. This is by far the most effective method due to the extremely high heating rate with rapid heat treatment [1][2]. The mechanism of the coercivity in Ce-Fe-B ribbons with the measuring field perpendicular and vertical to the ribbon's surface were discussed in details. It was speculated that the discrepancy of remanence ratio with different measuring direction was related to the different intergranular interaction. The intergranular exchange coupling was strengthened in the direction parallel to the ribbon compared to the full magnetostatic interaction in the vertical direction. This work suggests that electron beam exposure is effective to fabricate nanostructured Ce-Fe-B magnets.

[1] M. Sagawa, S. Fujimura, N. Togawa, H. Yamamoto, Y. Matsuura, New material for permanent magnets on a base of Nd and Fe (invited), J. Appl. Phys. 55, p. 083–2087(1984) 2 [2] L. Zha, Y. Han, L. Pi, Y. Luo, D. Yu, L. Han, J. Xu, W. Yang, S. Liu, J. Han, C. Wang, H. Du, Y. Yang, Y. Hou, P. Liu, W. Xia, J. Yang, Acta Mater. 195, p.282–291(2020)

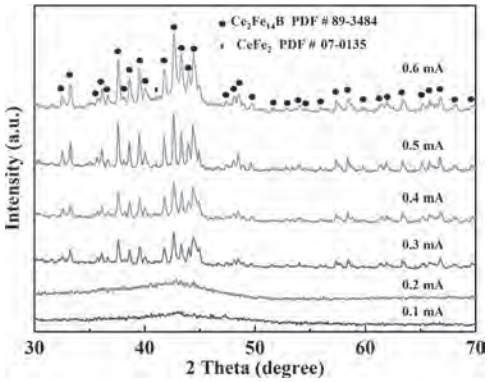

Fig. 1. XRD patterns of the $Ce_{12.2}Fe_{81.6}B_{6.2}$ free side under different electron beam currents with a focus beam at 200 mA and accelerating voltage at 10 kV for 0.1 s.

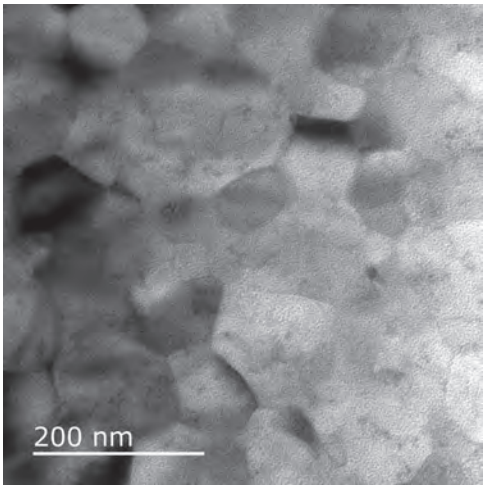

Fig. 2. TEM image of $Ce_{12.2}Fe_{81.6}B_{6.2}$ ribbon udner I_B = 0.3 mA.

Session S3
MAGNETIC NANOPARTICLES FOR BIOMEDICAL DIAGNOSTICS AND IMAGING: RECENT ADVANCES AND PERSPECTIVES

Frank Wiekhorst, Chair
Physikalisch-Technische Bundesanstalt, Berlin, Germany

INVITED PAPERS

3:00

S3-01. Technology Development for Monitoring of Immune Response Signaling in Primary Brain Tumors With Magnetic Nanoparticles. *S. Diamond*[1,2], C. Spatarelu[1,2], C. Knopke[2] and A.B. Gaur[3] *1. Thayer School of Engineering, Dartmouth College, Hanover, NH, United States; 2. Lodestone Biomedical LLC, Lebanon, NH, United States; 3. Geisel School of Medicine, Dartmouth College, Hanover, NH, United States*

Glioblastomas are primary brain tumors that present as a highly heterogeneous group of neoplasms and are among the most aggressive, and refractory to therapy, of all cancers. In the United States, nearly 700,000 people live with a brain tumor and face an abysmal 35% 5-year survival. The overarching goal of this technology development project is to develop an "Immunotherapy Response Indication System" (IRIS) as a platform technology for use in profiling various biomarker expression patterns in the tumor-immune microenvironment (TIME) using practical and deployable imaging devices to significantly improve patient outcomes by getting the right medicine to the right patients efficiently. This project uses implantable biosensor probes for monitoring of therapeutic responses in the TIME (Figure 1); the probes contain functionalized magnetic nanoparticles whose binding state to a biomarker target can be monitored by spectroscopic AC susceptibility imaging (sASI) systems (Figure 2). Preliminary studies are being conducted on the sASI/fMNPs monitoring system in a murine xenograft model of the most aggressive human primary brain tumor, glioblastoma multiforme (GBM). We will review progress on in vitro qualifications of fMNPs and singleplex biosensor probes for monitoring biomarker targets associated with various immune signaling factors. We will also review preliminary findings from in vivo preclinical experiments using the IRIS technology. The long-term objective of this project is to provide an early indicator of patient responsiveness to combination immunotherapies in GBM and other malignancies. Fundamentally, we believe that non-invasive, longitudinal, near real-time IRIS monitoring of signaling factors in TIME holds the potential to enable true precision medicine in cancer.

Figure 1. Left: Closeup of nanoparticle biosensor. Right: Subcutaneously implanted nanoparticle biosensor in mouse model (right).

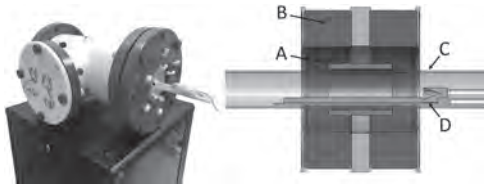

Figure 2. Left: Small-animal nanoparticle spectrometer. Right: Schematic cross-section of the coil assembly and specimen positioning system. The pickup coil gradiometer (A) is centered within the two AC drive coils (B). The open warm bore (C) contains the specimen bed with anesthesia nose cone (D).

3:36

S3-02. Hard Magnetic Microparticles in 3D-Nanoprinted Hybrid Micro-Robots for Biological Applications. *T. Devillers*[1], V. Vieille[1,2], R. Pétrot[1,2], O. Stephan[3], G. Delattre[3], F. Marchi[1], M. Verdier[4] and O. Cugat[2] *1. Univ. Grenoble Alpes, CNRS, Grenoble INP, Institut Néel, Grenoble, France; 2. Univ. Grenoble Alpes, CNRS, Grenoble INP, G2ELab, Grenoble, France; 3. Univ. Grenoble Alpes, CNRS, Grenoble INP, LIPhy, Grenoble, France; 4. Univ. Grenoble Alpes, CNRS, Grenoble INP, SIMAP, Grenoble, France*

Magnetically actuated micro-robots are extremely promising for biomedical applications such as microsurgery, drug delivery, micro-assembling or local mechanical stimulation(Ceylan et al., 2017). However, the fabrication of magnetic structures which are deformable or articulated and can perform functional actions as well as locomotion is still particularly challenging at the submillimeter scale. The potential of the recently developed 3D nano-printing by two-photon polymerization(Kawata et al., 2001) was already demonstrated for photonic structures, cell scaffolds or microfluidic components, and this technique is very well suited to design complex and 3D polymer micro-systems at the micron scale. However, the controlled incorporation of a magnetic material in the printed structure, which is a prerequisite for magnetic actuation, is still a major bottleneck to achieve versatile micro-actuators(Hu et al., 2018). In addition, to make micro-robots capable of dexterous actuation, it is important to be able to program locally the magnetization in order to induce heterogeneous forces and torques and thus control the deformation of the robot. In this work, we demonstrate the fabrication and actuation of hybrid micro-robots composed of polymer structures built by 3D nanoprinting and hard magnetic particles. The structure of the robot itself is built in Ormocomp®. NdFeB spherical gas-atomized particles were chosen for their high coercivity and remanence, in order to have a magnetic response that is fully independent of the geometry of the robot, contrary to systems using superparamagnetic nanoparticles or physical deposition of a soft ferromagnetic metal on top of the structure. In addition, thanks to the application of an external variable magnetic field during fabrication, the technique that we developed allows for the precise positioning of the NdFeB particles and control of their magnetization direction. This fine control over the printed structure, localization and orientation of magnetic moments gives access to degrees of freedom in the fabrication that were

never before accessible at this scale. To demonstrate the potential of this technique, we designed a 100 μm micro-gripper containing three NdFeB microparticles of different magnetization directions, inspired by the work of Diller & Sitti(Diller and Sitti, 2014). The actuation of the micro-gripper is performed through the application of a variable external magnetic field. Combining magnetic forces induced by the gradient of the external magnetic field and magnetic torques, the micro-robot can be actuated in various ways: (i) the application of a magnetic field gradient will induce a translation of the micro-robot; (ii) the rotation of the applied magnetic field will generate a rotational motion of the robot which can result in a "walking motion" thanks to friction with the substrate; (iii) because of the magnetization direction of particles in the arms, an increase of the magnetic field magnitude results in the opening of the gripper arms of the robot. This high dexterity allows for complex tasks at the microscale. In particular, we demonstrated the possibility to use such a micro-gripper to manipulate spheres of diameter below 40μm, a size comparable to certain cells. The forces applied by the micro-gripper are in the pN-nN range, which are physiologically relevant. We believe that similar micro-tools based on hard magnetic microparticles incorporated in complex 3D nano-printed structures may pave the way to a new generation of micro-robotic tools for life science studies.

H. Ceylan, J. Giltinan, K. Kozielski, M. Sitti, Lab Chip 17, 1705–1724 (2017) E. Diller, M. Sitti, Adv. Funct. Mater. 24, 4397–4404 (2014) C. Hu, S. Pané, B.J. Nelson, Annual Review of Control, Robotics, and Autonomous Systems 1, 53–75 (2018) S. Kawata, H.-B. Sun, T. Tanaka, K. Takada, Nature 412, 697–698 (2001)

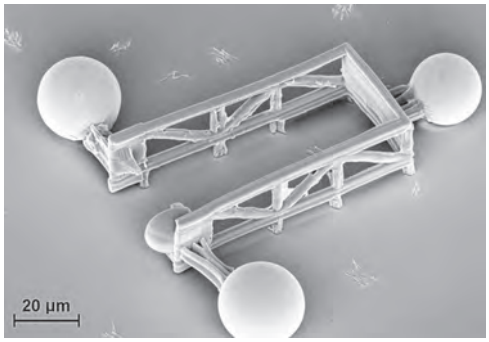

Fig.1: Magnetic Microgripper: magnetic micro-particles are made of gas-atomized NdFeB, and the body is built with the polymer Ormocomp®

4:12

S3-03. Quantitative Magnetorelaxometry Imaging of Magnetic Nanoparticles for Monitoring Human Cancer Therapies.
D. Baumgarten[1], M. Liebl[2], P. Schier[1], A. Jaufenthaler[1], U. Steinhoff[2] and F. Wiekhorst[2] *1. Institute of Electrical and Biomedical Engineering, UMIT - Private University for Health Sciences, Medical Informatics and Technology, Hall in Tirol, Austria; 2. Metrology for Magnetic Nanoparticles, Physikalisch-Technische Bundesanstalt, Berlin, Germany*

Magnetic nanoparticles (MNP) are a key element in a number of novel cancer therapy modalities in which their location and/or physical state is noninvasively controlled by magnetic fields, e.g. for the identification of sentinel lymph nodes in surgical tumor removal, as remotely controlled drug carriers in magnetic drug targeting, as heat generators in magnetic hyperthermia or as scout particles to predict the tumoral uptake of non-magnetic therapeutic nanoparticles. However, all these approaches require detailed knowledge of the MNP distribution inside a body for their successful development and clinical acceptance. Any information on location and quantity of MNP makes physiological transport phenomena transparent and is useful for local drug enrichment and heat production. Quantitative imaging of the MNP distribution before, during and after magnetic therapy can improve therapy efficiency and reduce unwanted side effects. At present, quantitative imaging of magnetic nanoparticles over larger volumes or the whole body is not established in a clinical environment. Magnetic relaxometry (MRX) is based on the measurement of the magnetic moment of MNPs in response to changes of an applied magnetic field (Wiekhorst 2012). It has already demonstrated its fundamental suitability for the sensitive and specific detection of MNP in tissue in pre-clinical applications. The quantitative detection of MNP distributions by magnetic relaxometry imaging (MRXI) has been experimentally demonstrated for small animal sized fields of view (Liebl 2015). In this case, the MNP distribution is estimated from the relaxation signals by solving an ill-posed inverse problem (Föcke 2018). MRXI yields information about the interaction of the MNP with the biological matrix, enabling specific quantification of MNP and their functional behavior in the molecular environment for therapy assessment (Coene 2017). Since MRXI employs moderate magnetic excitation fields, no unwanted side effects like tissue heating or peripheral nerve stimulation are expected. Finally, MRXI does not require MNP particularly optimized for imaging, but in most cases is capable to detect those MNP employed in the intended magnetic therapy. Whereas MRX measurements have been conducted using highly-sensitive superconducting quantum interference devices (SQUIDs), it could be recently shown that MRX employing novel optically pumped magnetometers (OPMs) is able to quantify MNP with a similar sensitivity (Jaufenthaler 2020, Baffa 2019). These sensors would allow for more flexible setups and reduced sensor-to-source distances. We aim at establishing MRXI for monitoring of magnetic nanoparticles in human cancer therapies. For this purpose, novel imaging setups and procedures are developed to detect MNP distributions in specific human body regions. This comprises novel excitation coil design, flexible and application specific fields of view and handling individually sized objects. In this respect, we presented approaches for employing random excitation sequences (Haltmeier 2019) and for optimizing excitation coil currents by minimizing the Frobenius condition number of the system matrix describing the measurement setup (Schier 2019). It was shown that the optimization approach yields improved reconstructions with fewer activation sequences compared to non-optimized measurements. Additionally, the potential of multi-channel OPM systems for MRXI is assessed with respect to the flexible positioning of OPMs around the volume of interest and reduced sensor-source and sensor-coil distances. Recently, we recently demonstrated quantification, quantitative 1D reconstruction and quantitative 2D imaging of MNP by exploiting OPMs. Finally, realistic body phantoms modeling physical and physiological aspects of relevant MNP therapy scenarios are developed for the evaluation of the technology.

F. Wiekhorst, U. Steinhoff, D. Eberbeck, et al., Pharmaceutical Research, Vol. 29, p.1189-1202 (2012) M. Liebl, F. Wiekhorst, D. Eberbeck, et al., Biomedical Engineering / Biomedizinische Technik, Vol. 60(5), p.427-43 (2015) J. Föcke, D. Baumgarten, M. Burger, Inverse Problems Vol. 34(11) (2018) A. Coene, J. Leliaert, M. Liebl, et al., Physics in Medicine & Biology, Vol. 62, p.3139-3157 (2017) A. Jaufenthaler, P. Schier, T. Middelmann, et al., Vol. Sensors, 20(3), p.753-764 (2020) O. Baffa, R.H. Matsuda, S. Arsalani, et al., Journal of Magnetism and Magnetic Materials, Vol. 475, p.533-538 (2018) M. Haltmeier, G. Zangerl, P. Schier, et al. International Journal of Applied Electromagnetics and Mechanics, Vol. 60(S1), p.63-78 (2019) P. Schier, M. Liebl, U. Steinhoff, et al. Journal of Mathematical Imaging and Vision, Vol. 62, p.238-252 (2019)

4:48

S3-04. Advances and Perspectives in Theranostic Monitoring Using Magnetic Nanoparticles.
J. Leliaert[1], A. Coene[2], P. Radon[3], U. Steinhoff[3] and F. Wiekhorst[3] *1. Dept. of Solid State Sciences, Universiteit Gent, Ghent, Belgium; 2. Department of Electronic Systems, Universiteit Gent, Ghent, Belgium; 3. Metrology of Magnetic Nanoparticles, Physikalisch-Technische Bundesanstalt, Berlin, Germany*

Magnetic nanoparticles (MNP) are already widely employed in diagnostic and therapeutic applications in biomedicine[1]. For example, in magnetic hyperthermia the particles are used as heat sources to increase the temperature of the surrounding tissue in order to damage tumor cells. Another application

is the detection of diseases by tracking MNP attached to biomolecular targets. Research has focused on developing an optimized MNP type for each application, e.g. to achieve a fine resolution in disease detection, or high heating rates in magnetic hyperthermia. An imaging tool that is capable of reconstructing the spatial distribution of multiple MNP types simultaneously would allow to combine diagnosis and therapy into one theranostic platform, fully based on MNP. Moreover, the same platform could be used during therapy to monitor parameters such as MNP clustering, tissue viscosity and tissue temperature to enable the necessary performance enhancement of biomedical applications. Indeed, as soon as the MNP are immersed in a biological environment, the performance of even well-optimized MNP often drastically decreases[2]. As a specific example of how such a theranostic platform could function, we present an implementation using the promising MNP imaging technique called magnetorelaxometry (MRX) imaging. All information about the MNP types, tissue viscosity, tissue temperature and particle interactions is encoded in the MRX relaxation curves. In a first step we successfully employed MRX imaging to distinguish between various particle types and allow their simultaneous imaging[3]. Further advancing, the MRX imaging procedure was adapted to include tissue information from other imaging modalities, significantly increasing image quality. Additionally, by using Kaczmarz' algorithm, the prerequisite of a priori MRX reference curves for different MNP types and environments could be omitted. Finally, the feasibility of extracting temperature information, tissue properties, and even live monitoring of particle aggregation using MRX imaging was investigated. Thus, using the example of MRX imaging, we prove the feasibility of a smart MNP-based theranostic platform.

[1] Q. Pankhurst, et al., Journal of Physics D: Applied Physics, 42 224001 (2009) [2] D. Cabrera, et al., ACS Nano. 12 2741-2752 (2018) [3] A. Coene, et al., Physics in Medicine and Biology 62 3139 (2017)

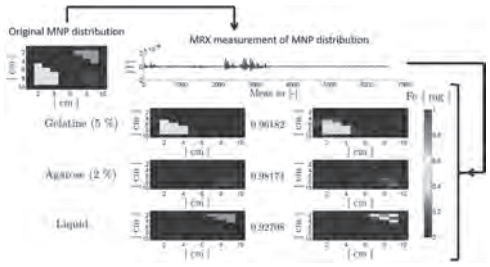

Reconstruction of the spatial distribution of MNP suspended in different environments using MRX imaging. The three numbers indicate the correspondence between the actual MNP distribution in a given environment and the reconstructed MNP distribution over the complete sample with 1 representing a 'perfect' reconstruction.

5:24

S3-05. Whither Magnetic Nanoparticles in Translational Cancer Research? *D. Ortega*[1,2], A. Santana[2], J. Ortega[2] and I. Rubia-Rodríguez[2]
1. Condensed Matter Physics, Universidad de Cadiz, Campus de Puerto Real, Universidad de Cadiz Campus de Rio San Pedro, Puerto Real, Andalucía, ES, Puerto Real, Spain; 2. IMDEA Nanociencia, Madrid, Spain

Nanomedicine has been regarded as the big hope for a range of long-standing health challenges. Millions of lives will be at stake if urgent improvements in fighting the biggest killers - mainly cancer, cardiovascular diseases and respiratory diseases - are not made soon. The needs vary from upper- to low-income countries, but nanomedicine is already making a difference in terms of preventing and treating these ailments. Magnetic nanoparticles represent a significant portion of the nanomaterials intended for diagnostic and therapeutic applications, and the range of new potential uses is continuously increasing. The present talk will deal with all the aspects around the design and use of magnetic nanoparticles for cancer research, with special emphasis on diagnosis, showcasing present and future research results. One of the covered topics will be the development of dual imaging contrasts for MRI based on single phase magnetic nanoparticles, with the possibility of tuning relaxivity through the manipulation of shape anisotropy. These agents are expected to overcome the ambiguity of single agents in some tissues under either T1 or T2 imaging conditions, perhaps focusing more on versatility and speed during diagnostic screenings rather than on resolution. Other field of activity within the topic is around more accurate in vitro diagnostics (IVD) tests based on functionalized magnetic nanoparticles. During the last years, the quantification of cell-free DNA (cfDNA) from liquid biopsies – involving extraction of bodily fluids, mainly peripheral blood - is gaining traction as a candidate for early diagnosis of cancer [1], especially in metastatic cases. This is exemplified by the recent approval of the first point-of-care PSA test for prostate cancer detection [2] by the FDA. In this regard, magnetic nanoparticles enable new dedicated sensing techniques that may bring substantial improvements in sensitivity, which is the main challenge – along with representativeness- given the low concentration of cfDNA in liquid biopsies. Another much awaited innovation expected in cancer theranostics is the possibility of having a reliable clinical nanothermometry option. Recently, we demonstrated experimentally and theoretically an innovative thermal transient thermometry technique based on luminescent and magnetic nanoparticles as a simple, fast, sensitive and reliable tool for advanced diagnosis of tumour development in small animal models [3]. In addition, the introduction of in silico testing for pre-clinical assessment of methodologies based on magnetic nanoparticles will be discussed. Finally, an overview of regulatory issues involving magnetic nanoparticles as medical devices and some exemplary clinical trials will be given.

[1] J. D. Cohen et al., Science, Vol. 359, p.926 (2018) [2] A. R. Meyer and M. A. Gorin, Nature Reviews Urology, Vol. 16, p. 331 (2019) [3] H. Santos, E. Ximendes, M. C. Iglesias de la Cruz, I. Chaves-Coira, B. del Rosal, C. Jacinto, L. Monge, I. Rubia-Rodríguez, D. Ortega, S. Mateos, J. García Solé, D. Jaque and N. Fernández, Advanced Functional Materials, Vol. 28, p.1803924 (2018)

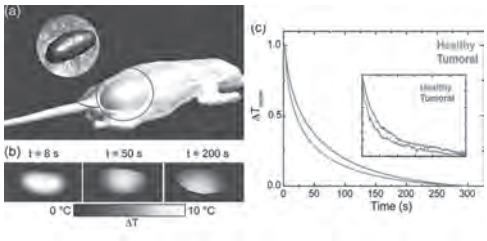

a) Computable mouse virtual phantom used for in silico testing. b) Temperature maps of a melanoma corresponding to different times after starting thermal relaxation. c) Time evolution of temperature extracted from the analysis of the thermal maps in (b) for an advanced-stage tumor and a healthy tissue. Adapted from ref. [3].

Session G1
ANTIFERROMAGNETIC SPINTRONICS I

Takahiro Moriyama, Chair
Kyoto University, Uji, Japan

INVITED PAPER

G1-01. Unconventional Dynamics of Ferrimagnets in the Vicinity of Compensation Points. *S. Kim[1] 1. Physics, Korea Advanced Institute of Science and Technology, Daejeon, The Republic of Korea*

Ferrimagnets have recently emerged as versatile platforms for spintronics owing to their unique tunability of material parameters. In particular, they offer the independent control of the spin density and the magnetization, which are impossible to achieve in more conventional magnets such as ferromagnets and antiferromagnets and thereby offer unprecedented opportunity to discover novel spin physics and realize highly tunable spintronic devices [1-8]. Ferrimagnets typified by rare-earth transition-metal alloys such as GdFeCo or GdCo possess two special temperatures. The first is the angular momentum compensation point, where the spin density vanishes and thus the nature of the magnetic dynamics is antiferromagnetic, but the magnetization is finite. The second is the magnetization compensation point, where the magnetization is absent but the spin density is finite and thus the nature of the dynamics is close to those of ferromagnets. In particular, the angular momentum compensation point has been attracting a great attention recently since, at the compensation point, the motions of topological solitons such as domain walls (that can be used as topological information carriers in racetrack memory) can exhibit much higher speeds than those in ferromagnets reaching a few km/s due to the realization of the antiferromagnetic dynamics at the compensation point as demonstrated theoretically and experimentally [1-3]. Also, it has been theoretically [4] and experimentally [5] shown that the deviation of skyrmion motion from the direction of an applied force, which is known as the skyrmion Hall effect that has been hampering the practical utilization of skyrmions for spintronic devices, can be completely suppressed in ferrimagnets at their angular momentum compensation points. In addition to the aforementioned peculiar dynamics of topological solitons, ferrimagnets can exhibit novel phenomena associated with spin waves or their quanta, magnons [6,7]. For example, we theoretically study magnons in a ferrimagnetic skyrmion crystal and show that they exhibit the magnonic Landau levels induced by the emergent magnetic field from the skyrmion crystal, which leads us to identify a ferrimagnetic skyrmion crystal as a magnonic topological insulator. We propose the thermal Hall effect as its experimental probe, which is expected to change the sign across the angular momentum compensation point [7]. Despite recent intensive research, the interaction of the charge current and the magnetic dynamics of ferrimagnets are largely unexplored [8], calling for further and deeper research into the non-equilibrium properties of ferrimagnets. * This work was supported by Brain Pool Plus Program through the National Research Foundation of Korea funded by the Ministry of Science and ICT (2020H1D3A2A03099291).

[1] K.-J. Kim, S. K. Kim, T. Tono et al., *Fast domain wall motion in the vicinity of the angular momentum compensation temperature of ferrimagnets,* Nat. Mater. 16, 1187 (2017) [2] S.-H. Oh, S. K. Kim, D.-K. Lee et al., *Coherent terahertz spin-wave emission associated with ferrimagnetic domain wall dynamics,* Phys. Rev. B 96, 100407(R) (2017) [3] H.-A. Zhou, Y. Dong, T. Xu et al., *Compensated magnetic insulators for extremely fast spin-orbitronics,* arXiv:1912.01775 [4] S. K. Kim, K.-J. Lee, Y. Tserkovnyak, *Self-focusing skyrmion racetracks in ferrimagnets,* Phys. Rev. B 95, 140404(R) (2017) [5] Y. Hirata, D.-H. Kim, S. K. Kim et al., *Vanishing skyrmion Hall effect at the angular momentum compensation temperature of a ferrimagnet,* Nat. Nanotechnol. 14, 232 (2019) [6] C. Kim, S. Lee, H.-G. Kim et al., *Distinct handedness of spin wave across the compensation temperatures of ferrimagnets,* Nat. Mater. (2020) [7] S. K. Kim, K. Nakata, D. Loss et al., *Tunable Magnonic Thermal Hall Effect in Skyrmion Crystal Phases of Ferrimagnets,* Phys. Rev. Lett. 122, 057204 (2019) [8] T. Okuno, D.-H. Kim, S.-H. Oh et al., *Spin-transfer torques for domain wall motion in antiferromagnetically coupled ferrimagnets,* Nat. Electron. 2, 389 (2019)

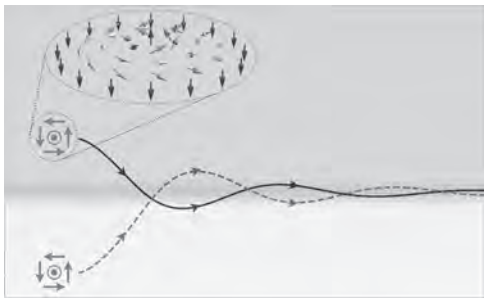

Ferrimagnetic skyrmions can exhibit snake trajectories along the line of the vanishing spin density, analogous to the snake orbits of electrons in a nonuniform magnetic field. This can be utilized as dynamically self-focusing racetracks for skyrmions, paving the way for skyrmion-based memory devices [4].

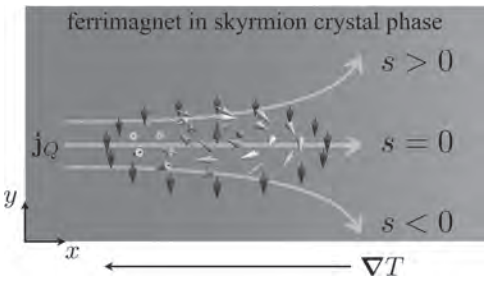

Schematic illustration of the magnonic heat flux j_Q through a ferrimagnet in its skyrmion crystal phase subjected to a temperature gradient ∇T. The colored small arrows depict a single skyrmion texture of the magnetization. Magnons can exhibit the thermal Hall effect since the skyrmion crystal gives rise to the fictitious magnetic field, which magnons of left and right circular polarization (with respect to the order parameter) experience as if they carry the positive and the negative charge, respectively [7]. The induced transverse heat flux changes its direction as the net spin density s along the magnetization varies across 0.

CONTRIBUTED PAPERS

G1-02. Current-Induced Magnetotransport in Epitaxial Antiferromagnetic Insulator/Heavy-Metal Heterostructures.

A. Churikova[1], A. Wittmann[1], N.O. Birge[3], L. Scipioni[2], A. Shepard[2], T. Newhouse-Illige[2], J.A. Greer[2] and G. Beach[1] *1. Materials Science and Engineering, Massachusetts Institute of Technology, Cambridge, MA, United States; 2. PVD Products, Inc, Wilmington, MA, United States; 3. Michigan State University, East Lansing, MI, United States*

We examine the origins of current-induced spin Hall magnetoresistance (SMR)[1] signals in epitaxial antiferromagnetic (AF) insulators. We show that transverse resistance R_{xy} signals consistent with toggle switching of the Néel order *n* in Pt/NiO on Al_2O_3 are also present in Pt/Al_2O_3 in which the NiO layer is absent. This R_{xy} has a thermal origin and arises from transient changes in the current distribution due to nonuniform Joule heating and electromigration.[2] Our results suggest that switching measurements in AFMs must be supplemented by in-situ magnetic control of *n*. Thus, we study the unambiguous effect of writing current on *n* in α-Fe_2O_3 (hematite), with a low spin-flop transition. Figure 1 shows current-induced switching in α-Fe_2O_3(10nm)/Pt(5nm), in which the write current direction was alternated from the easy axis E1 to E2 every 5 pulses. To ascertain the AF origin of the transverse signal, a magnetic field H_{IP} (=600 mT) is set $\perp$E1, E2, and E3 axes, as shown (so that $n \perp H$) while continuing to pulse along E1 and E2. The $n \| E1$, $n \| E2$, and $n \| E3$ directions of *n* are the medium, low, and high R_{xy} states respectively. When H was set to zero, alternating series of pulses along E1 and E2 continue to be applied and a switching signal is observed. The average switching amplitude ΔR_{xy} is approximately 5% of the maximal ΔR_{xy} between the $n \| E1$ and $n \| E2$ states obtained from angle-dependent SMR, indicating that a relaxation process occurred between the pulse and the probe measurement. A small fraction of the re-oriented domains retains their Néel order after a current pulse is turned off and the rest of the domains relax toward an equilibrium state. The orientation of *n* following each pulse is consistent with the thermo-magnetoelastic mechanism of domain wall motion.[3-4] This study advances understanding of current-induced effects in AF materials with low anisotropy and high magnetostriction, where magnetoelastic effects dominate switching processes.

[1] J. Fischer, O. Gomonay, R. Schlitz, K. Ganzhorn, N. Vlietstra, M. Althammer, H. Huebl, M. Opel, R. Gross, S. T. B. Goennenwein, and S. Geprägs, Phys. Rev. B 97, 014417 (2018). [2] A. Churikova, D. Bono, B. Neltner, A. Wittmann, L. Scipioni, A. Shepard, T. Newhouse-Illige, J. Greer, and G.S.D. Beach, Appl. Phys. Lett. 116, 022410 (2020). [3] P. Zhang, J. Finley, T. Safi, and L. Liu, Phys. Rev. Lett. 123, 247206 (2019). [4] L. Baldrati, C. Schmitt, O. Gomonay, R. Lebrun, R. Ramos, E. Saitoh, J. Sinova, and M. Kläui, ArXiv:2003.05923 [Cond-Mat] (2020).

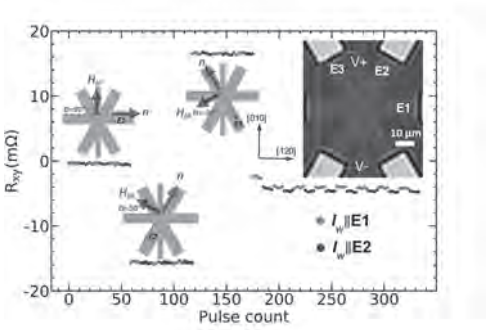

The R_{xy} signal during current pulsing along the hematite E1 (red) and E2 (blue) easy axes at H_{IP} which rotates *n* along the easy axes, and corresponding orientations of *n* indicated on the device schematic. Device micrograph and pulsing directions are shown in the inset.

G1-03. Withdrawn

G1-04. X-ray Magnetic Linear Dichroism Studies of Electrical Switching of Antiferromagnetic Order in α-Fe2O3 Epitaxial Films.

E. Cogulu[1], N.N. Statuto[1], Y. Cheng[2], S. Yu[2], F. Yang[2], R.V. Chopdekar[3], H. Ohldag[3] and A.D. Kent[1] *1. Physics Department, Center for Quantum Phenomena, New York University, New York, NY, United States; 2. Department of Physics, The Ohio State University, Columbus, OH, United States; 3. Advanced Light Source, Lawrence Berkeley National Laboratory, Berkeley, CA, United States*

Recently manipulation of antiferromagnetic (AFM) order has been gaining the attention of the spintronics community [1]. Magnetic switching has been reported in AFM thin films based on electronic transport methods, which provide only spatially averaged information on AFM states. Other techniques, such as x- ray magnetic linear dichroism (XMLD) microscopy, can provide local information on AFM domains. In this study, we report the direct observation of spin reorientation in response to current pulses in (0001)-oriented α-Fe2O3 films [2,3]. Our experiment combines the application of current pulses and spatially resolved photoemission electron microscopy (PEEM) with XMLD to detect AFM contrast. Pulses were applied in two different configurations A and B (Fig. 1a), which results in resistance changes (Fig. 1b), and XMLD images were taken before and after the application of a current pulse to reveal changes in the AFM domains (Fig. 1c). Our analysis shows that electrical pulses do not only reorient the Néel vector within the easy plane as previous work indicates [2,3]. Instead, we conclude that most of the change associated with the Néel vector is out of the film plane and different pulse directions can bring the AFM order in and out of the plane deterministically. This work is supported in part by the Air Force Office of Scientific Research under Grant FA9550- 19-1-0307.

[1] V. Baltz et al., Rev. Mod. Phys. 90, 015005 (2018) [2] Y. Cheng et al., Phys. Rev. Lett. 124, 027202 (2020) [3] P. Zhang et al., Phys. Rev. Lett. 123, 247206 (2019)

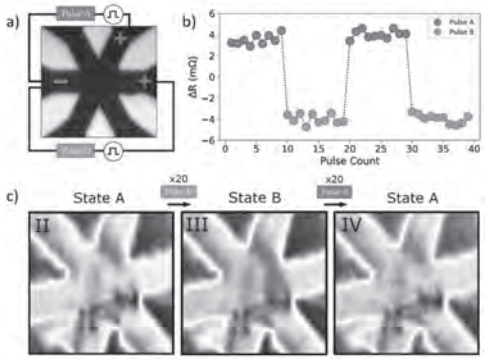

FIG1. (a) PEEM image of the 6-legged Hall cross with schematic representation of the circuit. Bright regions correspond to α-Fe2O3 (30 nm thickness) and dark regions correspond to Pt (2 nm thickness). The Pt leads are aligned with the 3 in-plane easy axes of Fe2O3. Plus and minus signs represent the connections to the two pulse generator outputs, where the minus sign indicates a connection to ground. (b) Resistance data showing switching between two states after sequential current pulses applied along either current path shown in panel a. (c) XMLD-PEEM images (4 μm field of view) before and after a 4 mA current pulse along the pulse A & B configurations.

G1-05. Importance of the Ferromagnetic Moment Induced by Dzyaloshinskii-Moriya Interaction in a Canted Antiferromagnet for Electrical and Magnetic Field Control of the Néel Order. *A. Wittmann*[1], A. Churikova[1], L. Scipioni[2], A. Shepard[2], T. Newhouse-Illige[2], J.A. Greer[2], N.O. Birge[3] and G. Beach[1] *1. Massachusetts Institute of Technology, Cambridge, MA, United States; 2. PVD Products, Wilmington, MA, United States; 3. Michigan State University, East Lansing, MI, United States*

In this work, we study the canted antiferromagnet α-Fe_2O_3. At room temperature, the Dzyaloshinskii-Moriya interaction (DMI) induces canting of the two magnetic sublattices M_A and M_B giving rise to a weak ferromagnetic (FM) moment m. We employ spin Hall magnetoresistance (SMR) measurements to study electrical and magnetic field control of the Néel order in α-Fe_2O_3/Pt bilayers. The angle-dependent magnetoresistance (ADMR) shows the characteristic saturated negative SMR signal of AFMs (red curve in figure 1) agreeing with previous findings[1–4]. We note that the FM moment lifts the degeneracy of the sublattices and consequently the orientation of the Néel vector with respect to the applied magnetic field. The blue curve in figure 1 shows the remanent resistance as a function of the angle of the preceding saturating magnetic field. The data shows a simple scaling between the saturated ADMR signal and the remanent resistance. The lack of signatures of anisotropy in the remanent signal implies that the relaxation of the SMR signal is dominated by destressing effects favoring an equilibrium state with multiple domains distributing the orientation of the Néel vector along different directions. Applying the insights from investigating the remanence of α-Fe_2O_3 with an external magnetic field on our current-induced switching experiments, we find that the fundamental limit of the switching efficiency is given by the magnitude of the remanence Furthermore, we observe hysteresis in the SMR signal. The irreversibility upon switching the direction of the magnetic field in combination with investigating the transient effects of current-induced changes in the domain structure allows us to study the nature and formation of domain walls at low magnetic fields. Our work emphasizes the importance of the FM moment induced by DMI and the relaxation effects for the equilibrium domain structure in α-Fe_2O_3.

1. Lebrun, R. *et al.* Anisotropies and magnetic phase transitions in insulating antiferromagnets determined by a Spin-Hall magnetoresistance probe. *Commun. Phys.* 2, 50 (2019). 2. Cheng, Y., Yu, S., Zhu, M., Hwang, J. & Yang, F. Electrical Switching of Tristate Antiferromagnetic Néel Order in a-Fe2O3 Epitaxial Films. *Phys. Rev. Lett.* 124, 027202 (2020). 3. Fischer, J. *et al.* Large Spin Hall Magnetoresistance in Antiferromagnetic a-Fe2O3/Pt Heterostructures. *Phys. Rev. Appl.* 13, 014019 (2020). 4. Zhang, P., Finley, J., Safi, T. & Liu, L. Quantitative Study on Current-Induced Effect in an Antiferromagnet Insulator/Pt Bilayer Film. *Phys. Rev. Lett.* 123, 247206 (2019).

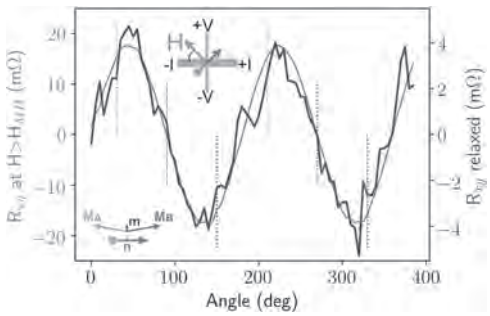

Figure 1: Transverse resistance (blue) after H has been relaxed from a saturated state (red) to zero field as a function of angle of the applied magnetic field. The inset in the bottom left corner shows a schematic of the canting of the sublattice magnetization M_A and M_B due to DMI giving rise to the ferromagnetic moment m.

G1-06. Competing Magnetic Ordering in Thin Films of $SrMnO_3$ Studied by Spin Transport. A. Das[1], *E. Vallabhaneni*[1], a. watson[1] and T. Banerjee[1] *1. faculty of science and engineering, Rijksuniversiteit Groningen Zernike Institute for Advanced Materials, Groningen, Netherlands*

The ability to tune the magnetic ordering via precise control of strain gradient and oxygen vacancies in strongly correlated rare-earth manganites, exhibiting rich magnetic phase diagram has remained largely unexplored. Here we show how different competing magnetic phases can be induced in nominally antiferromagnetic (AFM) $SrMnO_3$ (SMO) thin films by tailoring the strain quotient while adopting careful growth strategies. We find tensile strain-induced coexistence of a wide range of magnetic ordering, as established from the temperature dependence of the spin Hall magnetoresistance (SMR) and spin Seebeck effect (SSE) studies complemented by structural and bulk magnetization measurements. The temperature dependence of the SMR, SSE and bulk magnetization studies, fingerprints the competition between different magnetic domains across the manganite film thickness and hints at magnon-phonon interaction as a possible candidate for the decrease of SSE signals with increasing temperature. Our work is a first attempt to understand the complex magnetic structure in such multiferroic materials and for investigating magnon spin transport by controlling the AFM order parameter via Neel vector manipulation. Tailoring different competing magnetic phases in SMO thin films via strain quotient is an important platform for designing and stabilizing diverse magnetic phases useful for the development of AFM oxide-based spintronics.

G1-07. Reversible Hydrogen-ion Control of Room Temperature Antiferromagnetic State in α-Fe_2O_3. *H. Jani*[1] and T. Venkatesan[2] *1. Physics, National University of Singapore, Singapore; 2. ECE, National University of Singapore, Singapore*

Antiferromagnetic insulators are a ubiquitous class of magnetic materials, holding the promise of low-dissipation spin-based computing devices that can display ultra-fast switching and are robust against stray fields. However, their imperviousness to magnetic fields also makes them difficult to control in a reversible and scalable manner. Here we demonstrate a novel ionic pathway to drive a 90° spin-reorientation reversibly in the most common antiferromagnetic insulator α-Fe_2O_3 (hematite) – now an emerging spintronic material that has recently been shown to host topological AFM textures (eg: half-skyrmions and bimerons) and long magnon-diffusion lengths. Our low-temperature catalytic-spillover process involves the incorporation (or removal) of hydrogen from α-Fe_2O_3, post-growth, driving pronounced changes in its magnetic anisotropy, Néel-vector orientation and canted magnetism via electron injection and localized strains. We explain these effects with a detailed magnetic anisotropy model and first-principles calculations. Tailoring our work for future applications, we demonstrate control of the spin-state at room-temperature by reversibly doping hydrogen in Rh-substituted α-Fe_2O_3 and suggest pathways to build electric-field-controlled antiferromagnetic devices by deploying ionotronics.

G1-08. Observation of Magnon-Polarons in a Uniaxial Antiferromagnetic Insulator Cr_2O_3. *J. Li*[1], H.T. Simensen[2], D. Reitz[3], Q. Sun[4], C. Li[4], y. Tserkovnyak[3], A. Brataas[2] and J. Shi[1] *1. Department of Physics and Astronomy, University of California Riverside, Riverside, CA, United States; 2. Department of Physics, Norwegian University of Science and Technology, Trondheim, Norway; 3. Department of Physics and Astronomy, University of California Los Angeles, Los Angeles, CA, United States; 4. Department of Mechanical Engineering, University of California Riverside, Riverside, CA, United States*

Magnons and phonons are two elementary excitations associated with spin waves and lattice vibrations in solids. In the presence of magneto-elastic interactions, the coupling of the spin and lattice degrees of freedom leads to the formation of a new type of hybridized excitation, i.e., magnon-polarons. Manifested as anomalies in the spin Seebeck effect (SSE) in a ferrimagnet

YIG, magnon-polarons have profound consequences in modifying the magnon and phonon dispersion relations and affecting spin transport properties in ferrimagnetic insulators. In antiferromagnetic insulators, the magnon spectrum is distinctly different due to the existence of two equivalent, antiferromagnetically coupled spin sub-lattices. Here we report an observation of antiferromagnetic magnon-polarons in Cr_2O_3, a prototypical uniaxial antiferromagnet, featured as anomalies in the SSE signals of Cr_2O_3/heavy metal heterostructures. Despite the relatively high magnon energy in the absence of an external magnetic field, near the spin-flop transition of ~ 6 T, the left-handed magnon spectrum shifts downward to intersect those of acoustic phonons (both longitudinal and transverse) to cause hybridization. We have measured the temperature dependence of the SSE magnon-polaron anomalies in Cr_2O_3 and revealed the strength of the magneto-elastic coupling. Our study indicates that the hybridized excitations can be employed to manipulate spin transport in antiferromagnetic systems. This work was supported as part of the SHINES, an Energy Frontier Research Center funded by the US Department of Energy, Office of Science, Basic Energy Sciences under Award No. SC0012670.

G1-09. Domain Walls in Antiferromagnets With Strong Magnetoelastic Coupling. *O. Gomonay*[1] *1. Johannes Gutenberg Universitat Mainz, Mainz, Germany*

Searching for the efficient manipulation of antiferromagnets for spintronic applications, we study the properties of the magnetic domain walls with due account of magnetoleastic effects. We show that magnetoelastic coupling induces anisotropy of the domain wall orientation which affects the shape and distribution of the domain walls in a sample. In case of non-180° domains such anisotropy favours formation of the plane walls oriented along or perpendicular the hard magnetic axis. We study the pinning effects caused by magnetoelasticity and calculate the frequency of the localized oscillations and depinning field for an easy-plane antiferromagnet. We further consider dynamics of excitations of magnetoelastic domain wall and show that such a wall effectively scatters the long-wave magnons. The scattering and pinning effects are more pronounced in case of non-180° domains, due to the strain-induced anisotropy inside domains. However, 180° domain wall can also scatter the magnons due to the magnetoelastic strains inside the wall. To illustrate possible applications of our results we discuss the magnon propagation in multidomain hematite and NiO.

G1-10. Electrical Control of Antiferromagnetic Domain Walls. *O.J. Amin*[1], K.W. Edmonds[1], P. Wadley[1], A.W. Rushforth[1], R.P. Campion[1], S. Reimers[1,2], L.X. Barton[1], V. Novák[3], F. Krizek[3], S.S. Dhesi[2] and F. Maccherozzi[2] *1. Physics and Astronomy, University of Nottingham, Nottingham, United Kingdom; 2. Diamond Light Source Ltd, Didcot, United Kingdom; 3. Institute of Physics, Academy of Sciences of the Czech Republic, Praha, Czechia*

The prospect of using antiferromagnets as the main component in logic devices has gained a lot of interest. Antiferromagnets offer many benefits over their ferromagnetic counterparts: terahertz dynamics, no device cross-talk, and robustness to external fields. However, the latter property makes them difficult to control and has hindered their potential for use in spintronics devices. Recently, electrical switching of antiferromagnets has been demonstrated using current-induced spin-orbit torques due to bulk crystal symmetry[1,2,3], or spin-transfer torque from a neighbouring heavy metal layer[4,5,6]. Changes to the magnetic state are typically detected electrically in the transverse anisotropic magnetoresistance, which depends on the angle between the antiferromagnetic Néel vector and the direction of the probe current. This method is effective for measuring the average Néel vector orientation, but provides limited information on the microscopic magnetic texture. We study current-induced modification of the antiferromagnetic domain structure in CuMnAs microdevices using X-ray photoemission electron microscopy (XPEEM). Magnetic contrast is obtained due to X-ray magnetic linear dichroism, i.e. dependence on the angle between the magnetic moments and the incident X-ray polarisation. Our results show a current-induced motion of both 90° and 180° domain walls, in a direction which depends on the polarity of the current pulse (Fig.1). This is an important step towards the development of low power antiferromagnetic domain wall memory devices. Furthermore, 180° domain walls are topologically protected making them particularly good candidates for non-volatile applications.

[1] P. Wadley et al. Electrical switching of an antiferromagnet. Science, 2016. [2] J. Godinho et al. Electrically induced and detected Néel vector reversal in a collinear antiferromagnet. Nature Communications, 2018. [3] S. Yu. Bodnar et al. Writing and reading antiferromagnetic Mn_2Au by Néel spin-orbit torques and large anisotropic magnetoresistance. Nature Communications, 2018. [4] X. Z. Chen et al. Antidamping-torque-induced switching in biaxial antiferromagnetic insulators. Physical Review Letters, 2018. [5] M. Dunz et al. Spin-orbit torque induced electrical switching of antiferromagnetic MnN. Physical Review Research, 2020. [6] P. Zhang et al. Quantitative study on current-induced effect in an antiferromagnet Insulator/Pt bilayer film. Physical Review Letters, 2019.

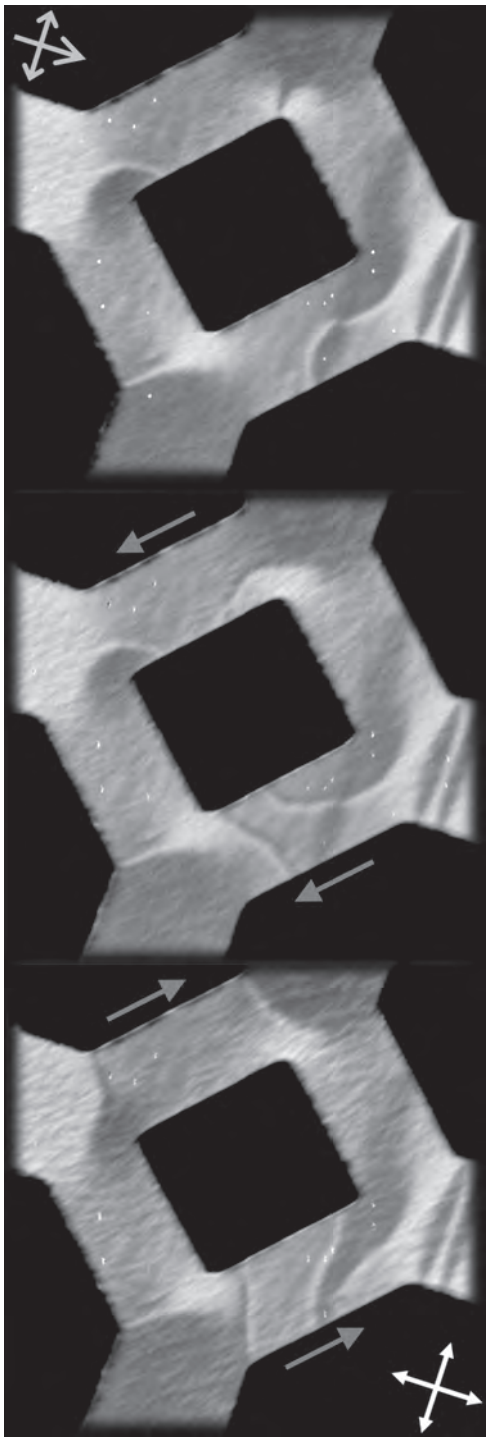

Fig.1. XPEEM images of the magnetic domain structure in a Wheatstone bridge device with 3 µm arm widths. The incident linearly polarised X-rays direction is shown by the blue arrow with polarisation perpendicular. Magnetic domains along the easy axes (white arrows) show maximum contrast. Shown are three stages of domain wall movements; top) before applying current pulse, middle) after 1 ms, 17 MA/cm^2 current pulse in direction (red arrows), and bottom) after the same current pulse with opposite polarity.

G1-11. Efficient Magnon Transport in Insulating Antiferromagnets Governed by Domain Structures and Doping. *A. Ross*[1,2], R. Lebrun[3], O. Gomonay[1], D. Grave[4], A. Kay[4], L. Baldrati[1], S. Becker[1], A. Qaiumzadeh[6], C. Ulloa[5], G. Jakob[1,2], F. Kronast[7], J. Sinova[1,2], R. Duine[5,6], A. Brataas[6], A. Rothschild[4] and M. Klaui[1,2] *1. Johannes Gutenberg Universitat Mainz, Mainz, Germany; 2. Johannes Gutenberg University Mainz Graduate School of Excellence Materials Science in Mainz, Mainz, Germany; 3. Unite Mixte de Physique CNRS/Thales, Palaiseau, France; 4. Technion Israel Institute of Technology, Haifa, Israel; 5. Universiteit Utrecht Departement Natuur- en Sterrenkunde, Utrecht, Netherlands; 6. Norges teknisk-naturvitenskapelige universitet, Trondheim, Norway; 7. Helmholtz-Zentrum Berlin fur Materialien und Energie GmbH, Berlin, Germany*

With high frequency spin dynamics, stability in the presence of external magnetic fields, and a lack of stray fields, antiferromagnetic materials are positioned to become key in future low power spintronic devices [1]. Here, we study the spin transport in high quality thin films of hematite (α-Fe_2O_3) (< 500 nm) of different orientations. Through measurements of the spin Hall magnetoresistance in hematite/Pt bilayers, the magnetic anisotropies of the thin films can be extracted, and the critical temperature of the Morin transition from the easy plane to the easy axis antiferromagnetic phase is electrically observed [2]. We find that the strain introduced by the growth process tilts the antiferromagnetic anisotropy axis, leading to complex signals across the full temperature range investigated [3]. Whilst a key part of antiferromagnetic spintronics is to encode and read information in the Néel vector, the efficient transfer of information is crucial for integration of antiferromagnets into devices. Recently, we demonstrated that a diffusive magnon current can be carried over micrometres in antiferromagnetic single crystals, but such crystals are not suitable for spintronic devices [4]. While mechanisms for the long-distance propagation of pure spin currents carried by the antiferromagnetic order [5, 6] have been developed for thin film antiferromagnets, experimentally the long distance transport of angular momentum by magnons has previoulsy not been achieved [7]. Making use of hematite thin films, a robust magnon current can propagate with intrinsic diffusion lengths of hundreds of nanometres [8]. The efficiency of the transport mechanisms can be tuned by the domain structure, the growth orientation, and the relative orientations of the magnetic field and magnetic anisotropies. Finally, we achieve room temperature magnon transport, where the films present an easy plane anisotropy, by dilute substitution of the ferric ions in order to alters the magnetic anisotropy axes of the thin films.

[1] T. Jungwirth, J. Sinova, A. Manchon *et al.*, *Nat. Phys.* 14, 200-203 (2018) [2] R. Lebrun, A. Ross, O. Gomonay *et al.*, *Comm. Physics* 2 50 (2019) [3] A. Ross, R. Lebrun, C. Ulloa *et al.*, *arXiv:2001.03117* (2020) [4] R. Lebrun, A. Ross, S. Bender *et al.*, *Nature* 561, 222-225 (2018) [5] S. Takei, B. Halperin, A. Yacoby *et al.*, *Phys. Rev. B*, 90, 94408 (2014) [6] S. Bender, H. Skarsvåg, A. Brataas *et al.*, *Phys. Rev. Lett.* 19, 056804 (2017) [7] H. Wang, C. Du, P. C. Hammel *et al.*, *Phys. Rev. B* 91, 220410 (2015) [8] A. Ross, R. Lebrun, O. Gomonay *et al.*, *Nano Letters* 20 1, 306-313 (2020)

G1-12. Birefringence-Like Spin Transport via Linearly Polarized Antiferromagnetic Magnons. *J. Han*[1*], P. Zhang[1], Z. Bi[1], Y. Fan[1], T.S. Safi[1], J. Xiang[1], J. Finley[1], L. Fu[1], R. Cheng[2] and L. Liu[1] *1. Massachusetts Institute of Technology, Cambridge, MA, United States; 2. University of California Riverside, Riverside, CA, United States*

Antiferromagnets (AFMs) possess great potential in spintronics because of their immunity to external magnetic disturbance, the absence of a stray field, or the resonance in the terahertz range. The coupling of insulating AFMs to spin-orbit materials enables spin transport via AFM magnons. Particularly, spin transmission over several micrometers occurs in some AFMs with easy-axis anisotropy [1]. Easy-plane AFMs with two orthogonal, linearly polarized magnon eigenmodes own unique advantages for low-energy control of ultrafast magnetic dynamics. However, it is commonly conceived that these magnon modes are less likely to transmit spins because of their vanishing angular momentum. In this work, we report experimental evidence that an

** - Best student presentation award finalist*

easy-plane insulating AFM, a α-Fe_2O_3 thin film, can efficiently transmit spins over micrometer distances (Fig. 1) [2]. Using nonlocal transport device geometry, we find that the spin transmission reaches maximum (zero) when the injected spin polarization is collinear with (perpendicular to) the Néel vector of the AFM, indicating that spins are carried by the excitations of the Néel vector rather than the residual magnetic moment. The spin decay length measured by varying the injector-detector distances shows an unconventional temperature dependence which cannot be captured considering solely thermal magnon scatterings. We interpret our observations in terms of an interference of two linearly polarized, propagating magnons in analogy to the birefringence effect in optics. Furthermore, our devices can realize a bi-stable spin-current switch with a 100% on/off ratio under zero remnant magnetic field. These findings provide additional tools for nonvolatile, low-field control of spin transport in AFM systems.

1. Lebrun, R. et al. Tunable long-distance spin transport in a crystalline antiferromagnetic iron oxide. Nature 561, 222 (2018). 2. Han, J. et al. Birefringence-like spin transport via linearly polarized antiferromagnetic magnons. Nat. Nanotechnol. https://doi.org/10.1038/s41565-020-0703-8 (2020).

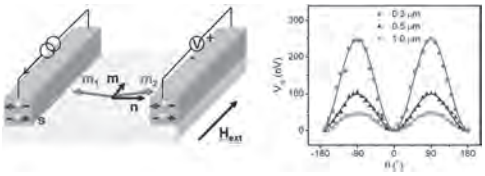

Fig. 1. Left: schematic of the nonlocal transport device. The external magnetic field direction corresponds to the angle of 90 degree. Right: nonlocal voltage as a function of the external field direction, measured in devices with different injector-detector distances.

G1-13. Voltage Control of Magnon Spin Currents in an Antiferromagnetic Insulator. *C. Liu*[1], Y. Luo[1,2], D. Hong[1], S. Zhang[3], F. Brandon[1], J. Pearson[1], S. Jiang[1], A. Hoffmann[1,4] and A. Bhattacharya[1]
1. Argonne National Laboratory, Lemont, IL, United States; 2. Hangzhou Dianzi University, Hangzhou, China; 3. Case Western Reserve University, Cleveland, OH, United States; 4. University of Illinois at Urbana-Champaign, Urbana, IL, United States

Voltage-controlled spintronic devices utilizing the spin degree of freedom are desirable for future applications, and may allow energy-efficient information processing. A pure spin current can be created by thermal excitations in magnetic systems via the spin Seebeck effect (SSE). However, controlling such spin currents, by purely electrical means, has been a fundamental challenge. Here, we investigate voltage control of the SSE in an antiferromagnetic insulator. We demonstrate that the SSE response generated in this material can be effectively controlled by applying a bias voltage, owing to the sensitivity of the SSE to the orientation of the magnetic sublattices as well as the existence of magnetoelectric couplings in the present system. Our experimental results on the voltage-controlled switching of magnetic sublattices are explained using a model based on the magnetoelectric effect. Acknowledgments: all work at Argonne was supported by the US Department of Energy, Office of Science, Basic Energy Sciences, Materials Sciences and Engineering Division. The use of facilities at the Center for Nanoscale Materials, an Office of Science user facility, was supported by the US Department of Energy, Basic Energy Sciences under Contract No. DE-AC02-06CH11357.

Session G2
INSTRUMENTATION AND MEASUREMENT TECHNIQUES I

Valerio Scagnoli, Chair
Paul Scherrer Institut, Villigen, Switzerland

INVITED PAPER

G2-01. Spin Dynamics of Molecular Nanomagnets With Four-Dimensional Inelastic Neutron Scattering. *T. Guidi*[1], E. Garlatti[2], S. Carretta[2], A. Chiesa[2], P. Santini[2], G. Timco[3] and R.E. Winpenny[3]
1. ISIS, STFC, Science and Technology Facilities Council, Didcot, United Kingdom; 2. Dipartimento di Scienze Matematiche, Fisiche e Informatiche, Universita degli Studi di Parma, Parma, Italy; 3. School of Chemistry and Photon Science Institute, University of Manchester, Manchester, United Kingdom

Molecular nanomagnets (MNMs) are clusters made of a finite number of magnetic ions coupled by a strong exchange interaction within the clusters and with a negligible magnetic interaction between adjacent clusters in the crystal lattice. They are promising systems for technological applications in the fields of high-density magnetic memory devices, quantum information processing and spintronics. They are also model systems to study the fundaments of quantum mechanics as they display quantum mechanics effects at the macroscopic level. The advances in the chemical engineering of these molecules have allowed the synthesis of tailor-made systems displaying several interesting quantum phenomena and to improve their properties to bring them closer to technological applications. Neutron scattering techniques have been intensively and successfully used to study the microscopic properties of molecular magnets and have enabled to reveal the signatures of their quantum behaviour. I will show how advanced neutron scattering experiments have been pivotal for the understanding of the magnetic properties and quantum behaviour of a selection of molecular magnets model systems. The new generation of neutron instruments equipped with position sensitive detectors together with the availability of large single crystals has allowed us to reveal the microscopic details of prototypical MNMs unambiguously characterising their Spin Hamiltonian [1,2], to detect the entanglement between complex spin systems [3] and to understand the relaxation dynamics in molecular qubits [4].

[1] M.L. Baker, T. Guidi *et al.*, Nature Physics, vol. 8, p 906 (2012). [2] A. Chiesa, T. Guidi, *et al.*, Phys. Rev. Lett. 119, 217202 (2017). [3] E. Garlatti, T Guidi *et al*., Nat. Comm. 8, 14543 (2017). [4] E. Garlatti *et al*., Nat. Comm. 11, 1751 (2020).

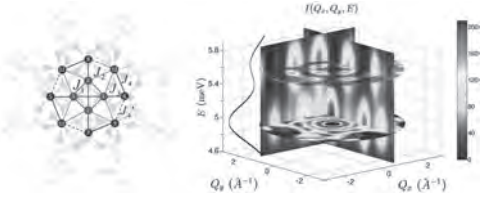

Molecular structure of the Mn_{12} cluster with the relevant magnetic exchange interactions and INS magnetic excitations from the single crystal measurements [2].

CONTRIBUTED PAPERS

G2-02. X-ray Magnetic Circular Dichroism (XMCD) Study of FeCoMnCrSi Multi-Principal Element Alloy. *R. Jangid*[1], J. Mehta[1], J. Li[1], A.T. N'Diaye[2] and R. Kukreja[1] *1. Materials Science and Engineering, University of California, Davis, Davis, CA, United States; 2. Advanced Light Source, Lawrence Berkeley National Laboratory, Berkeley, CA, United States*

High entropy alloys (HEA) or multi-principal element alloys (MPEAs) have recently gained interest due to their unique properties such as high-temperature strength, exceptional ductility, and potential applications in permanent magnets. [1, 2] However, the magnetic behavior of MPEA thin films as a function of temperature is still not well understood as most of the studies have focused on bulk magnetic properties and thus have not been able to identify the behavior of individual elements in this complex multi-dimensional compositional space. [3-6] We have recently shown that FeCoMnCrSi MPEA thin films exhibit four orders of magnitude increase in saturation magnetization compared to the bulk. [7] Magnetization as a function of temperature shows a spin-glass phase transition at 390 K and a ferromagnetic transition near 150 K, which increases to 250 K for films with lower thickness. Consequently, film thickness can be used to tailor the ferromagnetic transition and the magnetization of MPEAs. Our X-ray magnetic circular dichroism (XMCD) studies at Advanced Light Source (ALS) show that Fe and Co are ferromagnetically aligned throughout the measured temperature range, while Cr is antiferromagnetically coupled to Fe and Co. These studies provide a detailed characterization of magnetic and structural properties of FeCoMnCrSi HEA which is critically needed to guide the design and development of MPEA based soft magnetic systems.

[1] Zhiming Li, et. al. Nature, 534(7606):227–230, 2016. [2] Yong Zhang, et. al. Progress in Materials Science, 61(October 2013):1–93, 2014. [3] Oldich Schneeweiss, et. al. Physical Review B, 96(1):014437, 2017. [4] M. S. Lucas, et. al. Journal of Applied Physics, 109(7):107–110, 2011. [5] Shuo Huang, et. al. Intermetallics, 95(February):80–84, 2018. [6] Ming Hung Tsai, Entropy, 15(12):5338–5345, 2013. [7] Rahul Jangid, et. al. Journal of Materials Research, pages 1–9, 2020.

G2-03. Magnetization Configuration of Bi and Ga Substituted $Tm_3Fe_5O_{12}$ Probed by Proximate Anomalous Hall Effect and x-ray Magnetic Circular Dichroism. *Y. Wang*[1], A.T. Clark[2], H. Chen[1], X. Wang[2], X. Cheng[2], J.W. Freeland[3] and J.Q. Xiao[1] *1. University of Delaware, Newark, DE, United States, Newark, DE, United States; 2. Bryn Mawr College, Bryn Mawr, PA, United States, Bryn Mawr, PA, United States; 3. Argonne National Laboratory, Lemont, IL, United States, Lemont, IL, United States*

Ferrimagnetic thulium iron garnet ($Tm_3Fe_5O_{12}$ or TIG) grown on GGG substrate is known to have perpendicular magnetic anisotropy and magnetic compensation [1,2]. We investigated magnetization configuration of bismuth and gallium substituted $Tm_3Fe_5O_{12}$ films by anomalous Hall effect (AHE) induced in a proximately coupled Pt film, and by x-ray magnetic circular dichroism (XMCD) between 10-200 K. In the TIG/Pt heterostructure, anomalous Hall hysteresis changes sign first at 135 K and then at around 60 K. Besides, above 135K, three hysteresis loops are formed under small (less

than 1T) field sweep and in a wide temperature range (135-200K). XMCD measurement confirms 135 K as the compensation temperature, and shows that there is no magnetic moment flip around 60 K. Hence the sign change of AHE at 60 K is attributed to competition between spin Hall effect and magnetic proximity effect contributions. XMCD result also demonstrates that above compensation point, both Fe and Tm sublattice moment flips three times under field sweep at a fixed temperature, while their magnitude remains unchanged. This behavior is not likely from canted spin phase in ferrimagnet [3] since spin canting typically requires a field much larger than 1 T. The reason for this field-induced sublattice moment reorientation is unclear yet.

[1] C. Tang *et al*., Phys. Rev. B 94, 140403 (2016). [2] Q. Shao *et al*., Phys. Rev. B 99, 104401 (2019). [3] J. Bernasconi and D. Kuse, Phys. Rev. B 3, 811 (1971).

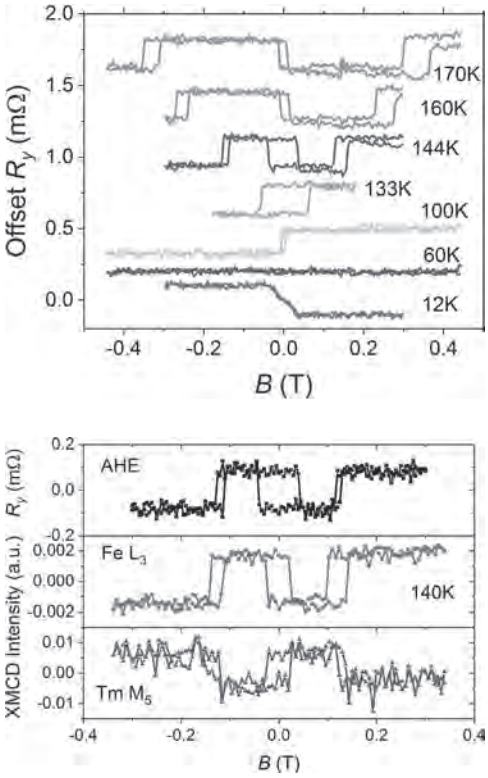

G2-04. Non-Standard Imaging in Magnetic Force Microscopy.
M. Jaafar[1,2], E. Berganza[2] and A. Asenjo[2] *1. Condensed Matter, Universidad Autonoma de Madrid, Madrid, Spain; 2. ICMM, Consejo Superior de Investigaciones Cientificas, Madrid, Spain*

Despite decades of advances in magnetic imaging, obtaining direct, quantitative information with high spatial resolution remains an outstanding challenge. The imaging technique most widely used for local characterization of magnetic nanostructures is the Magnetic Force Microscope (MFM), which is indeed a very active topic of investigation [1]. Advantages of MFM include relatively high spatial resolution, simplicity in operation as well as sample preparation, and the capability to applied in situ magnetic fields to study magnetization process [2]. Recently we have also demonstrate the possibility of operate in different environments including liquid media that allow us to investigate biological samples [3, 4]. In the present work, we try to approach some of the challenges of MFM, spatial resolution, sensitivity and quantitative measurements, by following different routes. One route is the development of high-performance MFM probes with sub-10 nm (sub-25 nm) topographic (magnetic) lateral resolution by following different easy and quick low-cost approaches [5]. This allows one to not only customize the tip stray field, avoiding tip-induced changes in the sample magnetization [6], but also to optimize MFM imaging in vacuum (or liquid media) by choosing tips mounted on hard (or soft) cantilevers, a technology that is currently not available on the market.

[1] O. Kazakova, et al. Journal of Applied Physics 125, 060901 (2019). [2] E. Berganza, M. Jaafar, et al. Sci Rep 7, 11576 (2017) [3] M.Jaafar et al. ACS Appl. Mater. Interfaces 2014, 6, 20936 [4] P. Ares, M. Jaafar et al. Small 11,36, 4731-4736 (2015) [5] M.Jaafar et al, Nanoscale, 2020,12, 10090 –1009 [6] E. Berganza, M. Jaafar, et al. Nanoscale, 2020 https://doi.org/10.1039/D0NR02173C

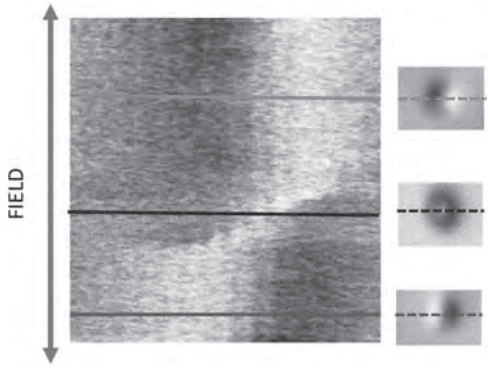

Nonstandard MFM image of a Py nanodot (height ~30 nm). With this method, we can study the magnetization process of a single particle.

G2-05. A Position-Independent Approach to Accurate Measurement of Broadband Electromagnetic Constitutive Parameters of Magneto-Dielectric Materials.
Q. Li[1], Y. Chen[2], C. Caisse[3], A. Horn[3] and V. Harris[1] *1. Department of Electrical and Computer Engineering, Northeastern University, Boston, MA, United States; 2. Innovation Center, Rogers Corporation, Burlington, MA, United States; 3. Lurie R&D Center, Rogers Corporation, Rogers, CT, United States*

Magneto-dielectric materials have been recently attracting great attention owing to their significant advantages for miniaturization of antennas.[1,2] Precise measurement of permeability and permittivity over a wide frequency range is crucial to develop and evaluate advanced magneto-dielectric materials.[3,4] The Nicolson-Ross-Weir (NRW) method is widely used to extract electromagnetic constitutive parameters from measured scattering parameters.[5] One of the drawbacks of this method is requiring direct measurement of the actual sample position in the measurement fixture, which leads to uncertainty in the measured permeability and permittivity. In this work, we improve the standard NRW method by removing the need for prior knowledge of sample position. For any isotropic material, the sample position in the measurement fixture can be precisely determined by matching the phasor angles of the reflection coefficients at the sample surfaces. The phasor matching algorithm is verified by two kinds of magneto-dielectric materials, ferrite ceramics and ferrite/polymer composites, measured in two sets of test fixtures of different geometries. The uncertainty is independent of the actual sample position along the measurement cell as shown in Fig. 1. The measured permeability and permittivity spectra of the ferrite sample are plotted in Fig. 2, showing quite small and stable standard deviations at lower frequencies. The experimental results indicate that the improved NRW method reduces the errors in calculated permeability and permittivity by one order of magnitude compared to those obtained by the conventional NRW method. Therefore, the proposed position-independent NRW method is a precise, efficient and statistically robust technique to characterize the electromagnetic properties of magneto-dielectric materials over a wide frequency range.

[1] R. C. Hansen and M. Burke, Microw. Opt. Technol. Lett., Vol. 26, no. 2, p. 75 (2000). [2] K. Buell, H. Mosallaei, and K. Sarabandi, IEEE Trans. Microw. Theory Tech., Vol. 54, p. 135 (2006). [3] Q. Li, Y. Chen, C. Yu *et al*., J. Am. Ceram. Soc., Vol. 105, (2020). [4] Q. Li, Y. Chen, and V. G. Harris, J. Appl. Phys., Vol. 125, p. 185107 (2019). [5] J. R. Baker-Jarvis, Nat. Inst. Stands. Tech. Tech. Note 1341, (1990).

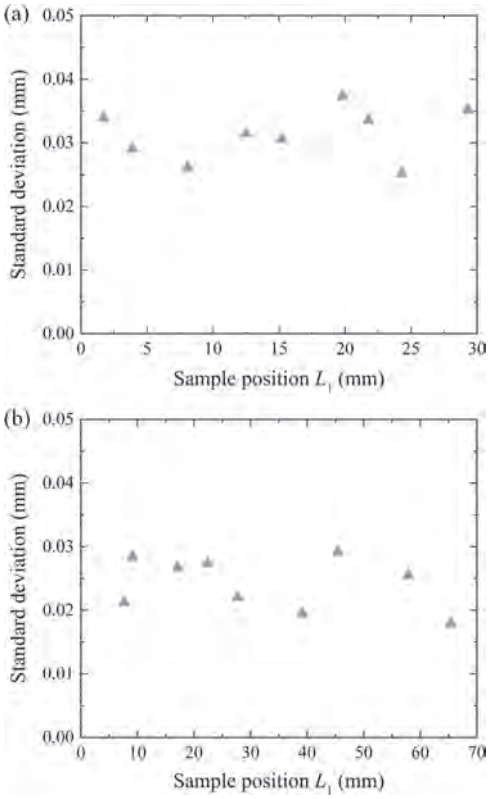

Fig. 1. Standard deviation of the sample position determined by the phasor matching algorithm using two reference frequencies at different sample positions in (a) the 7.00-mm coaxial air line and (b) the 25.40-mm coaxial air line.

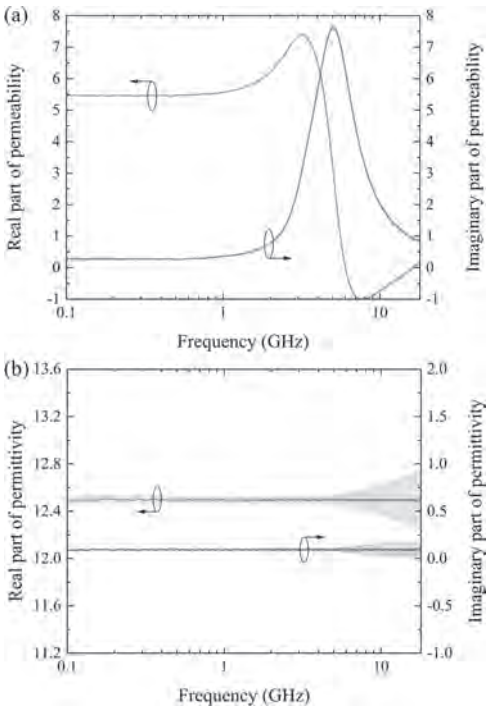

Fig. 2. (a) Magnetic spectra and (b) dielectric spectra of the ferrite sample calculated by the position-independent NRW method.

G2-06. Withdrawn

INVITED PAPER

G2-07. Laser-Free GHz Stroboscopic TEM: Deployment, Benchmarking, and Applications. *J.W. Lau*[1], K.B. Schliep[1], M.B. Katz[1], V.J. Gokhale[1], J.J. Gorman[1], A. Liu[2], Y. Zhao[2], C. Jing[2], A. Kanareykin[2], X. Fu[3] and Y. Zhu[3] *1. National Institute of Standards and Technology, Gaithersburg, MD, United States; 2. Euclid TechLabs, Bolingbrook, IL, United States; 3. Brookhaven National Laboratory, Upton, NY, United States*

In the previous two decades, important technological advancements have expanded the range of temporal resolution in transmission electron microscopes (TEM). Commercial direct-counting and single-electron detectors have revealed dynamics in the ms-timescale. Laser-actuated photoemission microscopes [1, 2] combined with beam scanning, spatially-parsed large area detectors [3], and sparse-sensing algorithms [4], can now unlock phenomena at the ms to sub-ps timescales. Further optimization of the photoemission stage [5] and beam bunching technologies could potentially extend the temporal resolution into the deep fs-regime. Following our earlier concept paper [6], we now present the modifications to a pair of commercial instruments – one Schottky (200 keV) [7] and one thermionic (300 keV) [8] that can confer temporal information spanning the ns and ps range with MHz to GHz repetition rates, in the stroboscopic mode without an excitation laser. The key enabling technology is a pair of broadband phase-matched modulating and demodulating RF pulsers. We have demonstrated 11 ps and 30 ps on the 200 keV and 300 keV microscopes respectively. The placement of the pulsers, mounted immediately below the gun, allows for the preservation of all optical configurations otherwise available to the unmodified instrument, and therefore makes these instruments dual-mode, both stroboscopic time-resolved (strobe) mode and conventional continuous waveform (CW) mode. To show that the modifications preserved imaging and diffraction functionalities of the instrument, we obtained Au images and diffraction patterns using both a continuous and a strobed beam. We will also show the first proof-of-principle demonstration of these new instruments through images of RF waves moving though an interdigitated MEMS device.

[1] VA Lobastov, R Srinivasan, AH. Zewail, Proc. Natl. Acad. Sci. 102 (2005) 7069–7073. [3] T LaGrange, et. al., Appl. Phys. Lett. 89 (2006) 044105 [3] T LaGrange, BW Reed, DJ. Masiel, MRS Bulletin 40 (2015) 22-28 [4] A Stevens, et al., Advanced Structural and Chemical Imaging 1 (2015). [5] DA Plemmons and DJ Flannigan, Chemical Physics Letters 683 (2017) 186–192 [6] J Qiu, et. al., Ultramicroscopy 161 (2016) 130. [7] C Jing, et al., Ultramicroscopy, 207 (2019) 112829. [8] JW Lau, et. al., Review of Scientific Instruments, 91 (2020) 021301. https://doi.org/10.1063/1.5131758 [*] We are grateful for the invaluable assistance from JEOL USA. This work was supported by DOE BES SBIR program Grant no. DE-SC0013121 and NIST award SB1341-16-CN-0035. During this work, K. Schliep was supported by the Research Associateship Program of the National Research Council and M. Katz was partially supported by the Professional Research Experience Program at the University of Maryland. Work at BNL was supported by the US DOE-BES, MSED, under Contract No. DESC0012704.

CONTRIBUTED PAPERS

G2-08. Magnetic Characterization and Quantification of Magnetic Nanoparticle Endocytosis Mechanisms by Particle Tracking Velocimetry. *A. Sannidhi*[1], P. Todd[2] and T. Hanley[1] *1. Chemical Engineering, Auburn University, Auburn, AL, United States; 2. Magnaquant, Louisville, KY, United States*

Magnetic nanoparticles (MNPs) with varied surface modifications are widely used in cell labeling, biochemical micro assays, drug delivery, endocytosis, endosome research, cell separation, and in vivo diagnostics. The Hyperflux™ velocimeter uses particle tracking velocimetry to measure magnetophoretic mobility, size and other morphological parameters of magnetic particles and magnetically labeled cells. Particle tracking velocimetry records the motion of thousands of magnetically labeled mammalian cells in an applied isodynamic magnetic field thereby estimating the magnetophoretic mobility (Fig. 1), which is proportional to the number of particles ingested per cell. The instrument facilitates cellular uptake quantification and kinetic studies in less time than any other existing technique[1]. The receptor-independent uptake by cultured CHO (Chinese Hamster Ovary) cells of 100 nm iron oxide nanoparticles with surface coatings of starch and amino groups was studied to reveal the role of nanoparticle endocytosis mechanisms. Caveolae-mediated and clathrin-coated endocytosis mechanisms are revealed by using specific mechanism-based inhibitors such as genistein and chlorpromazine hydrochloride. Uptake inhibition has been investigated at different inhibitor dosages during endocytosis by evaluating the cellular viability, toxicity, and uptake of nanoparticles with different surface coatings. Characterization of labeled cells and magnetic particles by magnetic velocimetry facilitates the rapid estimation of intrinsic magnetic properties[2], the optimization of MNP coatings, a better understanding of cell labeling, and the evaluation of the role of different cellular endocytosis mechanisms.

[1] C. Zhou, Z. Qian, Y.S. Choi, Journal of Magnetism and Magnetic Materials., Vol. 427, pp.25-28 (2017) [2] A. Sannidhi, P.W. Todd, T.R. Hanley, IEEE Magnetics Letters., Vol. 10, pp.1-5 (2019)

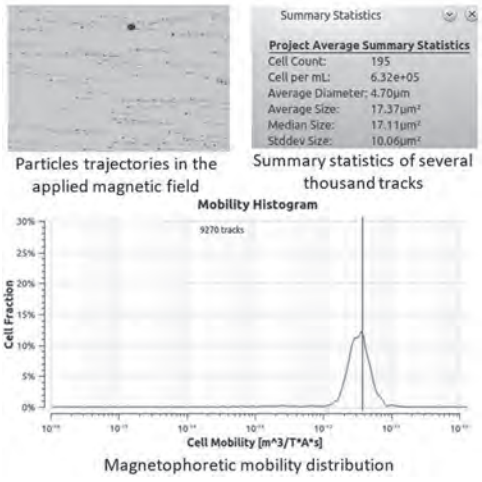

Fig. 1. Trajectories of magnetically labeled cells, summary statistics and the magnetophoretic mobility distribution of CHO-K1 cells labeled with starch coated 100 nm particles given by the Hyperflux instrument

G2-09. Withdrawn

G2-10. Electromagnetic Modelling of the Magnetic Needle Probe Method From Parallel Domain Structure by FD Approximation. *Y. Tene Deffo*[2,1], P. Tsafack[2] and B. Ducharne[1] *1. Laboratoire de Génie Electrique et Ferroélectricité, INSA de Lyon, 69100, Villeurbanne, France; 2. Faculty of Engineering and Technology, University of Buea, Buea, Cameroon*

Magnetic characterization is an undeniable scheme for the identification of magnetic and mechanical properties of materials [1] [2]. More pertinent is the unavoidable urge for localized magnetic monitoring schemes in line with the current growing industrial expectations [3] [4]. Herein, the adequacy and consistency of the magnetic needle probe (MNP) method over the conventional search coil method were concealed by the instrumentation prerequisite coupled to very weak levels of the sensor signals and the limited theoretical investigation on the method, generally considered quite blurry. The first hindrance taken care of by technological upgrades, studies on the basis of the electromagnetic theory from eddy-current distribution in magnetic materials has advanced the interpretation of the MNP method for local magnetic measurements [5] [6]. The objectives of this paper are twofold; it presents an electromagnetic modelling of the MNP method in a rectangular bar from a micro-magnetic perspective and exploits the model to derive the magnetic anhysteretic behaviour of the ferromagnetic materials. In the first objective, the advance theoretical background of the MNP method is modelled for anti-parallel domain structure using Finite Difference (FD) approach and compared to the analytical approach in [5]. Then, the model is used to simulate the reversible stochastic motion of domain walls for a hysteresis free magnetic material. The dependence of the anhysteretic model on the domain width (d) and the ratio of domain width to the thickness (d/c) of a Fe-3%Si sheet tells of the sensitivity of the magnetic microstructure on the magnetic signature. Noticeable hysteresis losses were however observed at smaller domain width translating to a state of high magneto-crystallographic anisotropy where closure domain effects add the resultant magnetization in the magnetic material. A complete account of the domain constituency is envisaged for future studies.

[1] Y. A. Tene, P. Tsafack, B. Ducharne and al, IEEE Trans. Mag., vol. 55, no. 7, 2019. [2] B. Ducharne, B. Gupta and al, IEEE Trans. on Mag., vol. 54, no. 11, 6202606, Nov. 2018. [3] A. Pulnikov, V. Permiakov and al, J. Magn. Magn. Mater., vol. 47, no. 9, p. 254–255, 2003. [4] K. S. H. Nguedjang, D. Y. A. Tene and al, J. Magn. Magn. Mater., pp. 1-10, 505, 166767, March 2020. [5] T. Yamaguchi, K. Senda and al, J. Physique IV, vol. 8, p. 717–20, 1998. [6] K. Senda, M. Ishida and al, Electr. Eng. Japan, vol. 126, p. 942–9, 1999.

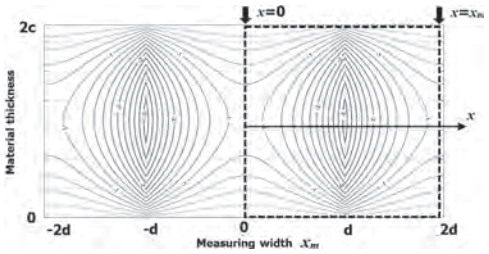

Eddy-current distribution in the magnetic material

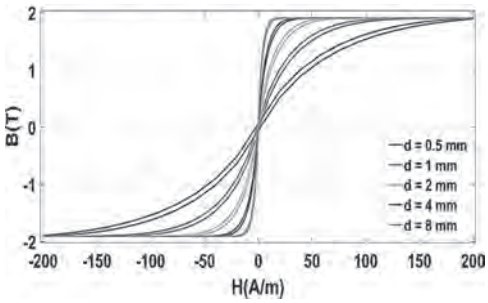

Magnetic anhysteretic dependence on the domain width (d)

G2-11. Mechanical Torque Vector Measurements for Micromagnets. *K. Fast*[1], J. Thibault[1], V. Sauer[1,4], M. Dunsmore[1], A. Kav[1], J.E. Losby[1,5], Z. Diao[1,6], E. Luber[2], M. Belov[3] and M.R. Freeman[1] *1. Physics, University of Alberta, Edmonton, AB, Canada; 2. Chemistry, University of Alberta, Edmonton, AB, Canada; 3. National Research Council Canada Nanotechnology Research Centre, Edmonton, AB, Canada; 4. Wyvern Space, Edmonton, AB, Canada; 5. Physics and Astronomy, University of Calgary, Calgary, AB, Canada; 6. Physics, Florida Agricultural and Mechanical University, Tallahassee, FL, United States*

A technique to measure the full magnetic torque vector (three orthogonal torque components) on micro- and nano-scale magnetic materials is introduced. Measurements of a single axis or component of torque are most common and are very useful for hysteresis measurements of thin film structures in particular, where high shape anisotropy yields a near-proportionality of in-plane magnetic moment and the magnetic torque along the perpendicular in-plane axis. More generally, any component of cross-product torque involves a linear combination of perpendicular moment and magnetic susceptibility, yielding the rotational magnetic anisotropy or stiffness of the spin texture in response to torque. The method is demonstrated using a modified, single-paddle silicon-on-insulator resonant torque sensor [1]. The torsion mechanical susceptibilities to *x*- and *z*-torques are maximized by clamping the sensor at a single point. Figure 1 shows a completed device supporting a permalloy / cobalt oxide bilayer disk, deposited on a silicon paddle which is supported by a single beam. Mechanically-resonant AC torques are driven by an RF field containing a frequency component for each fundamental torsional mode of the device, and the resulting displacements read out through optical position-sensitive detection. A typical hysteresis measurement obtained as an in-plane DC bias field is swept is shown in Figure 2. The measurements are compared with micromagnetic simulations of the mechanical torque to verify the interpretation of the signals. As an application example, simultaneous observations of hysteresis in the net magnetization along with the field-dependent in-plane anisotropy is highly beneficial for studies of exchange bias.

[1] Z. Diao *et al.*, J. Vac. Sci. Technol. B., Vol. 31, p.051805 (2013)

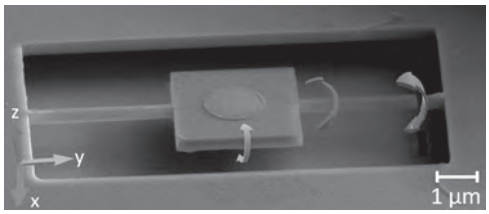

Fig. 1. Electron micrograph of a micromechanical device used for demonstration of the three-axis torque measurement technique. The arrows indicate the three orthogonal torsional displacements.

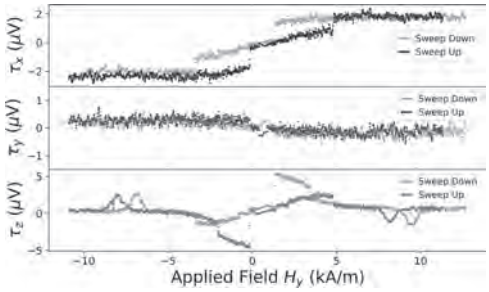

Fig. 2. Simultaneous hysteresis measurements of orthogonal AC torques from a permalloy / cobalt oxide bilayer disk at room temperature. The in-plane bias field direction here is rotated -15° from *y* towards *x*.

G2-12. Effect of Field Orientation and Infill Percentage on the VSM Calibration Factor of FFM 3D Printed Samples. *K. Dieckow*[1], C.Q. Howlader[2], T.N. Ahmed[2], M.C. Belduque[3], J. Tate[3,2] and W.J. Geerts[1,2] *1. Physics, Texas State University, San Marcos, TX, United States; 2. MSEC, Texas State University, San Marcos, TX, United States; 3. Engineering, Texas State University, San Marcos, TX, United States*

Among several advantageous, additive manufacturing facilitates rapid prototyping and the realization of objects that cannot be made with traditional manufacturing methods. Recently, additive manufacturing of magnetic structures is being investigated including the inkjet [1], Fused Filament Modelling (FFM) [2], and UV Assisted Direct Write methods [3]. Soft or hard magnetic particles are included in polymer binder to realize objects interesting for magnetic shielding, magnetic flux guiding, or for their permanent magnetic properties. Magnetic characterization of 3D printed samples with a Vibrating Sample Magnetometer (VSM) however is not straightforward, particularly when larger samples are characterized that have a non-zero infill percentage. Determination of the saturation magnetization is difficult because of the lack of calibration standards for such inhomogeneous samples. Therefore, we modeled the sensitivity of a biaxial VSM for different 3D printed samples produced by FFM. The magnetic potential of a distributed coil with finite dimensions was approximated from the first 3 Legendre polynomial terms and used to determine the point dipole sensitivity of a MicroSense VSM employing a Mallinson pickup coil set using an approach similar as described in [4]. The obtained point sensitivity function was used to calculate the sample signal of various 3D printed samples with different infill orientations and infill percentages using Mathematica. The calculations show that the measured signal is strongly affected by the infill percentage and orientation. For 2D shaped samples (1x1x0.05 cm^3) with low infill percentages, the signal differs by up to a factor 2 depending on the sample orientation. The calculated signal of cubed samples (1x1x1 cm^3) can vary as much as 30% with infill percentage. A Mathematica spreadsheet was developed that allows one to calculate the signal produced by any specific 3D printed sample in a biaxial VSM that employs a Mallinson coil set configuration. This work was supported in part by NSF through an DMR-MRI Grant under Award 1726970.

[1] M.P. Paranthaman, C.S. Shafer, M. Elliot, JOM 68 (2017) 1978. [2] C. Huber, C. Abert, F. Bruckner, et al., App. Phys. Lett. 109 (2016) 162401. [3] Alan Shen, Xiaoguang Peng, Callum P. Bailey et al., Mater. and Des.183 (2019) 108133. [4] Co-Cr layers for perpendicular magnetic recording, J.P.C. Bernard, C.P.G. Schrauwen, PhD. Thesis University of Twente, ISBN 90-9003454-4.

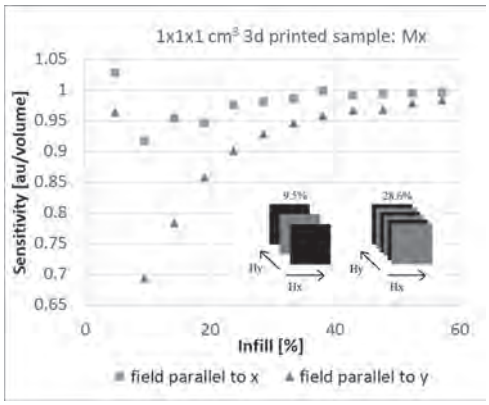

Fig. 1: Calculated sensitivity of 3D printed sample as function of infil percentage for two field orientations.

G2-13. Prediction of Magnetic Shield Plate Performance Using Permeability in Alternating Micromagnetic Fields. *M. Sakakibara*[2,1], G. Uehara[1], Y. Adachi[1] and T. Shinnoh[2] *1. Kanazawa Institute of Technology, Kanazawa, Japan; 2. Ohtama Co., Ltd., Tokyo, Japan*

High-performance mu-metal magnetically shielded rooms (MSRs) are used for highly sensitive machines such as magnetoencephalographs (MEGs). The magnetic properties of the material are important to ensure its magnetic shield performance. Precisely predicting the shielding factor via permeability measurement of the material may be beneficial. As the first step in the study of the real model of an MSR, we compare the permeability measured with a ring-shaped mu-metal and the shielding factor of a plate-shaped mu-metal. Considering that a typical MEG signal has an amplitude of 1 mA/m and a frequency of approximately 1–10 Hz, we propose using permeability in alternating low-frequency micromagnetic fields [1]. For the experiment, a ring-shaped test piece and plate were manufactured from the same lot of mu-metal material and annealed in the same batch. As shown in Fig. 1(a), the permeabilities of the test piece are calculated from V, I, and other parameters. The amplitude of the magnetic field excited by current I was changed in the range from 1 mA/m to 1.35 A/m. As shown in Fig. 1(b), the magnetic shielding factor of the mu-metal plates is measured in a uniform magnetic field, as a ratio of B_z with mu-metal plate to B_z without mu-metal plate, and the amplitude magnetic field H was changed in the range from 2 mA/m to 80 A/m. A nonlinear magnetic field analysis is performed for the configuration in Fig.1(b) based on the permeabilities obtained in Fig. 1(a), and the results are compared with the experimental data obtained in Fig. 1(b). As can be seen in Fig. 2, the analysis results are consistent with the experimental data across a wide range of magnetic fields. This implies the MSR performance can be predicted using permeability in an alternating micromagnetic field. In the future, we plan to extend this study to other magnetic shield shapes.

[1] M. Sakakibara, S. Muto, M. Okuda, Y. Adachi, G. Uehara, "Evaluation Method for Magnetic Shield Material using Incremental Permeability against Very Low Frequency Micro Magnetic Field Fluctuation, " IEEJ Trans. Fundamental and Materials, Vol.140, No. 6, pp. 331-337, Jun. 2020.

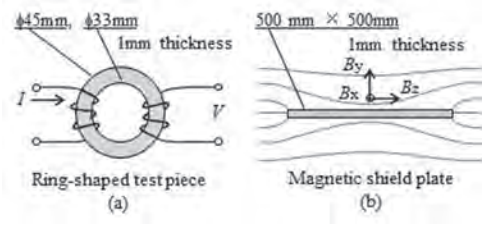

Fig.1(a) A sinusoidal 1 Hz current I was applied, and the induced voltage V was measured. (b) The magnetic flux density B_z beside the plate was measured using a flux gate sensor in a uniform magnetic field H.

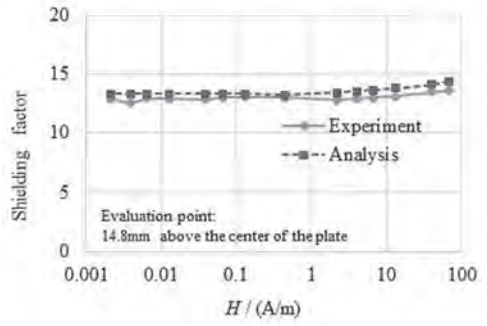

Fig.2 Comparison of the experiment results and analysis of shielding factors.

G2-14. An Algorithm for Radial Offset Systematic Error Correction in Second-Order Gradiometer-Based Vibrating Sample Magnetometers. *P.S. Stamenov*[1] *1. School of Physics and CRANN, University of Dublin Trinity College, Dublin, Ireland*

Modern inductive magnetometry is very widely used for bulk samples and thin films alike. SQUID-based, superconducting second-order gradiometer magnetometry has become the *de facto* standard, worldwide. While a decade ago, it was dominated by primarily extraction-style systems, where the sample is moved at relatively long distances (~ base of the gradiometer) and at low frequencies (~ 1 Hz); nowadays, higher frequency (many 10ns of Hz), shorter translation length systems, rapidly gain popularity. The benefits of faster measurements must be paid by a compromise of capability elsewhere: increased sample geometry- and position-dependent systematic errors are two just two examples. Here, the influence of the dominating radial sample offset and radial projection systematic uncertainties is analysed [1] and a new data processing algorithm is advised, which allows for the determination of the radial sample offset, minimizing its impact. The normalized point spread functions (PSF) of the MPMS3 and its predecessor, the MPMS system [2], are shown on Fig. 1. The PSF of the MPMS3 is sharper, larger in amplitude. [3] The change of shape and magnitude of the PSF of the MPMS3 as a function of radial sample offset is also shown on Fig. 1. There is a pronounced amplitude increment and a narrowing of the z-axis carrier, with radial offset. [4] The normalized response as a function of oscillation amplitude is shown on Fig. 2. With our algorithm, it is possible to fit it and extract the radial offset, by means of generalized non-linear least squares regression, with an uncertainty of about 10 %, as illustrated using Monte-Carlo simulated data, on Fig. 2. [5] It is hoped that this algorithm will be utilized by the magnetic community and will help reduce the spread of data in very many experimental situations.

[1] Based on a direct quadrature integration approach for the computation of the coupled flux. [2] Quantum Design, San Diego, CA, USA. [3] The MPMS3 gradiometer is more sensitive to radial offsets or spread of the moment distribution. [4] This results in a very substantial increase in the second harmonic pickup, > 200 % in the worse case scenario: millimetric radial

errors result in systematic errors of 10ns of percent. [5] This leads to a relative uncertainty of about 2-3 % in a general experimental scenario – a rather substantial and welcome error containment.

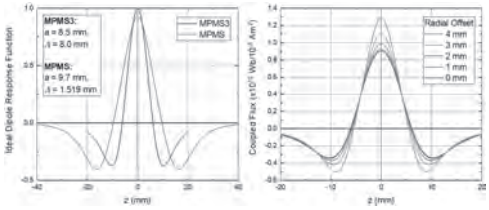

Point dipole response for the MPMS3 and MPMS magnetometer systems (left). PSF for various offsets away from the central axis of the MPMS3 system (right).

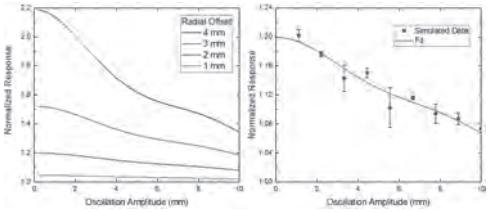

Oscillation amplitude scans, for different radial offsets away from the central axis of the MPMS3 system (left). Monte-Carlo simulated amplitude scan data for a radial offset of 2 mm, and a fit to it (right). The extracted offset is 2.1(2) mm.

Session G3
MAGNETIZATION DYNAMICS AND DAMPING II: ULTRAFAST DEMAGNETIZATION AND MAGNETO-OPTICS

André Philippi-Kobs, Chair
Deutsches Elektronen-Synchrotron, Hamburg, Germany

CONTRIBUTED PAPERS

G3-01. Effects of CoFe Alloy Composition on Magnetization Dynamics and Magnetic Thermal Transport. *R. Mohan*[1], V.H. Ortiz[2], Y. Sun[2], S. Mathaudhu[2], S. Coh[2] and R. B. Wilson[1,2] *1. Material Science & Engineering, University of California, Riverside, Riverside, CA, United States; 2. Mechanical Engineering, University of California, Riverside, Riverside, CA, United States*

The lifetime of magnetic excitations in metals is governed by scattering rates between magnons and electrons. Recent investigations [1, 2] document how magnetization dynamics vary with composition in magnetic metal alloys due to changes in their electronic band structures; e.g. $Co_{0.25}Fe_{0.75}$ thin-films display low magnetic damping ($\alpha \sim 10^{-4}$). In my talk, I will present experimental measurements of magnetic damping, ultrafast magnetization dynamics, and thermal transport properties of CoFe magnetic alloys, varying with alloy composition. To explore the magnetization dynamics, I use a time-resolved MOKE set-up to observe ultrafast demagnetization in a few hundred femtoseconds followed by precessional dynamics. Through TDTR measurements, I check if lower electron-magnon scattering rates lead to improved thermal transport. My investigation sheds light on how magnon-electron scattering rates govern dynamics on femtosecond (ultrafast demagnetization), nanosecond (magnetic precession and damping), and microsecond time-scales (thermal transport of energy). *This work was supported by the U.S. Army Research Laboratory and the U.S. Army Research Office under grant # W911NF-18-1-0364.

[1] Qin, H. J., et al. *Nature communications* 6 (2015): 6126. [2] Schoen, Martin AW, et al. *Nature Physics* 12.9 (2016): 839.

G3-02. Engineering $Co_2MnAl_xSi_{1-x}$ Heusler Compounds as a Model System to Correlate Spin Polarization, Intrinsic Gilbert Damping and Ultrafast Demagnetization. *W. Zhang*[1], C. Guillemard[1,2], C. de Melo[1], G. Malinowski[1], S. Petit-Watelot[1], J. Gorchon[1], S. Mangin[1], F. Bertran[2] and S. Andrieu[1] *1. institut jean lamour, lorraine unviersity, Nancy, France; 2. synchrotron SOLEIL, Gif-sur-Yvette, France*

Engineering of magnetic materials for developing better spintronic applications relies on the control of two key parameters: the spin polarization and the Gilbert damping responsible for the spin angular momentum dissipation. Both of them are expected to affect the ultrafast magnetization dynamics occurring on the femtosecond time scale. Here, we use engineered $Co_2MnAl_xSi_{1-x}$ Heusler compounds grown by molecular beam epitaxy to adjust the degree of spin polarization at the Fermi energy P and investigate how it correlates with the damping. We first demonstrate experimentally that substituting Si by Al in $Co_2MnAl_xSi_{1-x}$ Heusler compounds allows us to get a tunable spin polarization at E_F from ~60% in Co_2MnAl to 100% in Co_2MnSi, indicating the transition from metallic to half metallic behaviors. Second, a strong correlation between the spin polarization and the Gilbert magnetic damping is established in these films. The damping decreases when increasing the spin polarization from 1.1 10^{-3} for Co_2MnAl (with 63% spin polarization) to an ultra-low value of 4.10^{-4} for the half-metallic ferromagnet Co_2MnSi [1]. This allows us investigating the relation between these two parameters and the ultrafast demagnetization time characterizing the loss of magnetization occurring after femtosecond laser pulse excitation. The demagnetization time is observed to be inversely proportional to 1-P and as a consequence to the magnetic damping, which can be attributed to the similarity of the spin angular momentum dissipation processes responsible for these two effects. Altogether, our high quality Heusler compounds allow controlling the band structure and therefore the channel for spin angular momentum dissipation [2].

[1] C. Guillemard et al, Phys. Rev. Appl. 11, 064009 (2019) [2], W. Zhang, C. Guillemard, et al, Advanced Materials, 1908357 (2020)

G3-03. Photon Energy Dependent fs-Demagnetization Dynamics of Thin Nickel Films. *M. Stiehl*[1], C. Seibel[1], M. Weber[1], J. Hoefer[1], S. Ashok[1], S. Weber[1], B. Stadtmüller[1], H. Schneider[1], B. Rethfeld[1] and M. Aeschlimann[1] *1. Physics, Technische Universitat Kaiserslautern, Kaiserslautern, Germany*

After the first observation of the ultrafast demagnetization process, a huge experimental and theoretical effort was devoted to reveal the microscopic mechanism governing the ultrafast optically induced loss of magnetic order in ferromagnetic materials. Almost all experimental fs-demagnetization studies so far employed fs light pulses of 1.55 eV to trigger the magnetization-dynamics. Hence, the role of the photon energy of the exciting light pulse has been largely neglected so far. Therefore, we have implemented an all-optical time-resolved MOKE setup with variable pump photon energy in the range of 1.55 to 3.10 eV. As prototypical system, we investigated the ultrafast demagnetization dynamics of thin Ni films on insulating and conducting substrates. The characteristic parameters of the demagnetization process, i.e., the demagnetization time for various excitation photon energies are compared with simulations applying a temperature-based model. These simulations consider the density of states of Nickel and interface effects to describe the non-equilibrium dynamics of the spin-carrying excited electrons. For metallic substrates, we further discuss the magnitude and timescale of the optically injected spin carriers across the magnetic/non-magnetic interface.

M. Hofherr, et al., Physical Review B 96, 100403 (2017) U. Bierbrauer, et al., J. Phys.: Condens. Matter 29, 244002 (2017) B.Y. Mueller and B. Rethfeld, Phys. Rev. B 90, 144420 (2014)

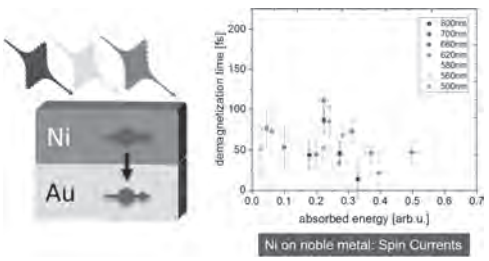

INVITED PAPER

G3-04. Ultrafast Optically Induced Spin Transfer (OISTR) in Ferromagnetic Alloys. *M. Aeschlimann[1] 1. Department of Physics and Research Center OPTIMAS, Technische Universitat Kaiserslautern, Kaiserslautern, Germany*

A thorough understanding of femtosecond magnetism will address the important questions of how fast the magnetization can be reoriented in a material and what physical processes present fundamental limits to this speed. Ultimately, light represents the fastest means to alter the state of a material since laser pulses can now be generated with extremely short temporal duration down to a few tens of attoseconds. One particularly interesting and novel scheme for the ultrafast manipulation of spins using light takes advantage of the optically-induced spin transfer (OISTR), which was recently introduced by Dewhurst et al. [1]. This microscopic mechanism is driven by a spin-selective direct optical excitation from one magnetic sublattice to another. Guided by time dependent density functional theory calculations, we are able to monitor the optically induced transient changes in the model systems FeNi in real time by time-resolved magneto-optical Kerr spectroscopy using high-harmonic generation (HHG TMOKE) [2]. Exploiting the spectral sensitivity of this measurement technique we are able to follow the ultrafast spin transfer from Fe to Ni during the optical excitation. OISTR, therefore, opens up a new avenue towards manipulating solids on timescales only limited by the duration of the exciting light pulse, which forecasts a control of the spin dynamics on the attosecond time scale. How far this spin manipulation via OISTR is a general phenomenon or restricted to a subset of materials with specific properties is an open experimental and theoretical question. In order to opens up a systematic path for coherent manipulation of spin dynamics by direct light-matter interaction we started to investigate OISTR in a variety of different compounds with higher complexity [3]. We reveal for example that the half-Heusler materials NiMnSb and CoMnSb exhibit strong signatures of OISTR, whereas this is less pronounced in the full-Heusler compounds Co_2MnSi, Co_2FeSi, and Co_2FeAl in agreement with *ab initio* calculations [4].

[1] J.K. Dewhurst et al, Nano Lett. 18 1842 (2018) [2] M. Hofherr et al. Sci. Adv. 6 eaay8717 (2020) [3] P. Tengdin et al, Sci. Adv. 6 eaaz1100 (2020) [4] D. Steil et al, Phys. Rev. Research 2, 023199 (2020)

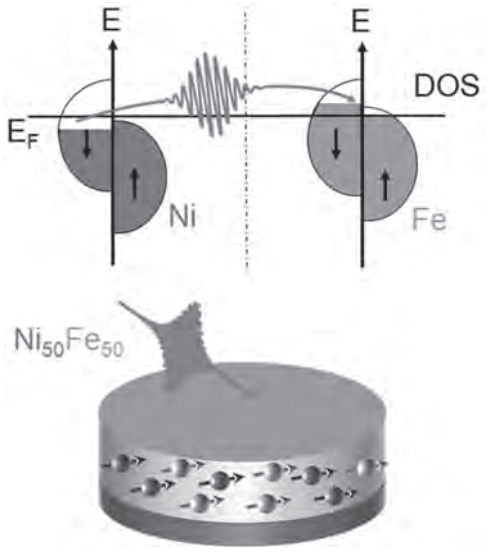

Illustration of the optically induced spin transfer process in a Fe-Ni alloy

CONTRIBUTED PAPERS

G3-05. Ultrafast Demagnetization Excited by Extreme Ultraviolet Light From a Free-Electron Laser. *A. Philippi-Kobs[1,2], L. Müller[1,2], M. Berntsen[1,3], W. Roseker[1], M. Riepp[1], K. Bagschik[1,2], J. Wagner[2], R. Frömter[2], M. Danailov[4], F. Capotondi[4], E. Pedersoli[4], M. Manfredda[4], M. Kiskinova[4], M. Stransky[5], V. Lipp[6], A. Scherz[7], B. Ziaja[6,8], H. Oepen[2] and G. Grübel[1] 1. Deutsches Elektronen-Synchrotron DESY, Hamburg, Germany; 2. Universitat Hamburg, Hamburg, Germany; 3. KTH Royal Institute of Technology, Stockholm, Sweden; 4. Elettra Sincrotrone Trieste, Trieste, Italy; 5. Academy of Sciences of the Czech Republic, Praha, Czechia; 6. Center for Free Electron Laser Science, Hamburg, Germany; 7. European XFEL GmbH, Schenefeld, Germany; 8. Polish Academy of Sciences, Krakow, Poland*

Free-electron lasers (FELs) enable the study of dynamics in matter on combined femtosecond time and nanometer length scales [1]. One of the most intriguing topics within contemporary research on magnetism, ultrafast near-infrared (IR) laser-induced demagnetization [2,3], has greatly benefited from the advent of FELs [4] as it was shown that optically generated super-diffusive spin currents [5] contribute to that phenomenon [6]. Following a previous campaign [7], here we report on the observation of a quenching of the magnetic scattering cross section of Co/Pt multilayers using 70-fs-long pulses with a photon energy tuned to the $M_{3,5}$-edge of Co ($2p$-$3d$ transitions) from the extreme ultraviolet (XUV) free-electron laser FERMI for fluences >1 mJ/cm^2 defining the threshold fluence for FEL experiments where the FEL is meant to be a non-invasive probe. Utilizing single and double-pulse schemes, XUV-radiation-induced demagnetization is identified as the underlying mechanism behind the quenching. The analysis indicates that the demagnetization proceeds on an unprecedented sub-20-fs timescale, which is significantly faster than reported for the near-infrared radiation regime. The shorter timescale can be explained by the sub-femtosecond lifetime of hot electrons with energies of a few 10eV that are generated by the XUV radiation. Further, we performed calculations that additionally prove that light-induced transient changes in the population and energy level of the $3p$-shell cannot explain the experimental data.

[1] E. A. Seddon et al., Rep. Prog. Phys. 80, 115901 (2017), [2] E. Beaurepaire et al., Phys. Rev. Lett. 76, 4250 (1996), [3] D. Sander et al., J. Phys. D: Appl. Phys. 50, 363001 (2017), [4] M. Malvestuto, J. Phys. Cond. Mat. 30, 053002 (2018), [5] M. Battiato et al., Phys. Rev. Lett. 105, 027203 (2010), [6] B. Pfau et al., Nat. Commun. 3, 1100 (2012), [7] L. Müller et al., Phys. Rev. Lett. 110, 234801 (2013).

G3-06. Probing the Laser-Driven Antiferromagnetic to Ferromagnetic Phase Transition of FeRh With Femtosecond Time-Resolved Small Angle X-ray Scattering (tr-SAXS) and X-ray Absorption Spectroscopy (tr-XAS). *N. Agarwal[1,2], R. Carley[1], J. Ander Arregi Uribeetxebarria[3], A. Yaroslavtsev[1], V. Valmispild[2,1], L. Le Guyader[1], I. Vaskivskyi[4], R. Kurta[1], M. Izquierdo[1], L. Mercadier[1], G. Mercurio[1], R. Gort[1], N. Gerasimova[1], J. Schlappa[1], B. E. Van Kuiken[1], M. Teichmann[1], S. Molodtsov[1], D. Turenne[5], V. Uhlir[3], C. Back[6], H. Durr[5], A. Lichtenstein[2,1] and A. Scherz[1] 1. European XFEL GmbH, Schenefeld, Germany; 2. University of Hamburg, Hamburg, Germany; 3. Brno University of Technology, Brno, Czechia; 4. Jozef Stefan Institute, Ljubljana, Slovenia; 5. Uppsala University, Uppsala, Sweden; 6. Technical University of Munich, Munchen, Germany*

The observation of ultrafast manipulation and coherent control of spins in magnetic materials at room temperature [1-2] has prompted the intense experimental and theoretical efforts to understand the underlying microscopic mechanisms and relevant interactions (exchange, spin-lattice, electron-phonon, coulomb etc.) driving such magnetic phenomena at sub-picosecond timescales. Stoichiometric B2 ordered epitaxial (001) FeRh undergoes a first order magnetic phase transition from antiferromagnetic (AFM) to ferromagnetic (FM) at ≈ 380K. In the AFM phase of FeRh, only Fe has net magnetic

moment, whereas in the FM phase both Fe and Rh carry net moments. The phase transition is also accompanied by a ≈ 1% isotropic lattice expansion in the bulk BCC structure, and changes in electronic structure, see [3-5] and refs. therein. Since magnetic and structural dynamics occur at different timescales, it makes FeRh an ideal candidate for disentangling relevant interaction mechanisms at different timescales. The phase transition has been extensively studied theoretically and experimentally[6-8], in thermal equilibrium and in the time domain, but a precise understanding of the roles of the electronic, phononic and spin sub-systems remains elusive. We have studied the laser-driven AFM to FM phase transition in FeRh with small angle X-ray scattering (tr-SAXS) and X-ray absorption spectroscopy (tr-XAS) around the Fe L3 edge. The experiments were performed at the SCS Instrument of the European XFEL. We also performed the time-dependent density functional theory(TD-DFT) calculations to simulate the XAS spectra at different time delays. In this contribution, we will discuss the changes of the electronic structure of FeRh on the femto- and picosecond timescales, derived from the XAS and scattering measurements at the Fe L3 absorption edge performed at European XFEL, and compare them with the theoretical simulations (see the figure), in order to show the relation between them and the first order AFM-FM phase transition in FeRh.

[1] E. Beaurepaire et al., Phys. Rev. Lett. 76, 4250 (1996) [2] J.-Y. Bigot et al., Nature Physics 5, 515 (2009) [3] J.-U. Thiele et al. Appl. Phys. Lett. 82, 2859 (2003) [4] A.X. Gray et al., Phys. Rev. Lett. 108, 257208 (2012). [5] C. Baldasseroni et al., Appl. Phys. Lett. 100, 262401 (2012). [6] J.-U. Thiele, M. Buess, C.H. Back, Appl. Phys. Lett 85, 2857 (2004). [7] G. Ju et al., Phys. Rev. Lett. 93, 197403 (2004) [8] I. Radu et al., PRB 81, 104415 (2010)

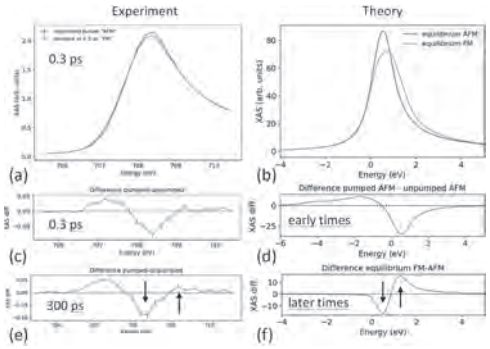

Experimental (a, c, e) and calculated (b, d, f) XAS and dXAS of FeRh at the Fe L3 edge. Before laser excitation (AFM phase, blue line) and after (orange line) laser excitation.

G3-07. Ultrafast Laser Induced Precessional Dynamics in Antiferromagnetically Coupled Ferromagnetic Films. *J. Zhou*[1,2], S. Saha[1,2], Z. Luo[1,2], E. Kirk[1,2], V. Scagnoli[1,2] and L. Heyderman[1,2]
1. ETH Zürich, Eidgenossische Technische Hochschule Zurich, Zurich, Switzerland; 2. Paul Scherrer Institut, Villigen, Switzerland

Antiferromagnetically coupled ferromagnetic thin films have recently attracted significant attention in magnonics because of the possibility to tune the spin-wave dispersion by altering the interlayer exchange coupling, which would help to achieve the spin-wave nonreciprocity [1]. To implement such coupled films in magnonic devices, a detailed understanding of the precessional dynamics of magnetization in such systems is required. Here, we present a systematic characterization of the precessional dynamics for systems with the layer magnetization going from nearly antiparallel to parallel alignment on application of a magnetic field. Experimentally, we have measured the ultrafast-laser-induced magnetization precession in samples with different interlayer exchange coupling strengths using the time-resolved magneto-optical Kerr effect. In addition to the acoustic and optical modes, an extra mode is observed that is due to the laser-induced decoupling of the two ferromagnetic layers. The observed precessional dynamics is in good agreement with our theoretical model based on the Landau-Lifshitz-Gilbert equation, and can be separated into three different field regions determined by the relationship between the Zeeman energy and the energy associated with the interlayer exchange coupling, as shown in Fig. 1 [2]. This work gives a detailed insigth of how the interlayer exchange coupling and Zeeman energy influence the precessional dynamics, and provides an important guide to implement antiferromagnetically coupled films in functional magnonic devices.

[1] R. A. Gallardo, et al. Phys. Rev. Appl. 12, 034012 (2019) [2] J. Zhou, et al. Phys. Rev. B, 101, 214434 (2020)

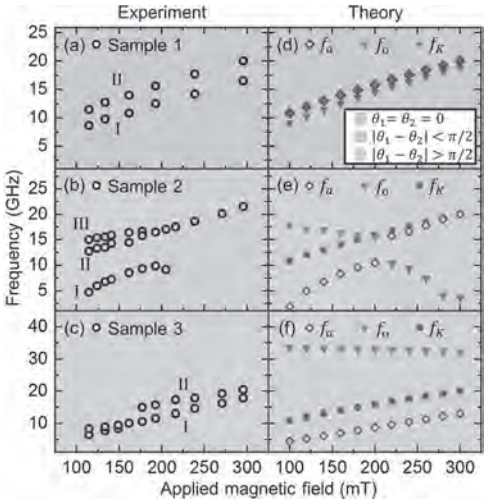

Fig.1. Dependence of the frequency on the applied magnetic field for the different modes. (a)-(c) Experimental data: the different precessional modes are indicated with Roman numbers. (d)-(f) Theoretical data: fa, fo and fK are the frequency of the acoustic mode, optical mode, and the FMR mode for a 7.5 nm CoFeB film. The three different background colors indicate the three field regions given in the inset of (d).

G3-08. Chiral Versus Collinear Magnetic Order Dynamics: Faster Chiral Recovery After Optical Excitation Revealed by Femtosecond XUV Scattering. *N. Kerber*[1,2], D. Ksenzov[3], F. Freimuth[4], F. Capotondi[5], E. Pedersoli[5], I. Lopez-Quintas[5], B. Seng[1,6], J. Cramer[1], K. Litzius[1], D. Lacour[6], H. Zabel[1,7], Y. Mokrousov[1,4], M. Klaui[1,2] and C. Gutt[3]
1. Institut für Physik, Johannes Gutenberg-Universität Mainz, Mainz, Germany; 2. Graduate School of Excellence Materials Science in Mainz, Mainz, Germany; 3. Department Physik, Universität Siegen, Siegen, Germany; 4. Peter Grünberg Institute and Institute for Advanced Simulation, Forschungszentrum Jülich and JARA, Jülich, Germany; 5. Elettra-Sincrotrone Trieste, Trieste, Italy; 6. Institut Jean Lamour, UMR CNRS 7198, Université de Lorraine, Nancy, France; 7. Department of Physics, Ruhr-University Bochum, Bochum, Germany

While chiral spin structures stabilized by Dzyaloshinskii-Moriya interaction (DMI) are candidates as novel information carriers, their dynamics on the fs-ps timescale is little known [1-4]. Since with the bulk Heisenberg exchange and the interfacial DMI two distinct exchange mechanisms are at play, the ultra-fast dynamics of the chiral order needs to be ascertained and compared to the dynamics of the conventional collinear order. Using an XUV free-electron laser we determine the fs-ps temporal evolution of the chiral order in domain walls in a magnetic thin film sample by an IR pump - X-ray magnetic scattering probe experiment. Upon demagnetisation we observe that the dichroic (CL-CR) signal connected with the chiral order correlator $m_z m_x$ in the domain walls recovers significantly faster than the (CL+CR) sum signal representing the average collinear domain magnetisation $m_z^2+m_x^2$ [5]. We explore possible explanations based on spin structure dynamics and reduced transversal magnetisation fluctuations inside the domain walls and find that the latter can explain the experimental data leading to distinctly different dynamics for collinear magnetic order and chiral magnetic order.

[1] Beaurepaire, E. et al., Phys. Rev. Lett. 76, 4250–4253 (1996). [2] Koopmans, B. et al., Nat. Mater. 9, 259–265 (2010). [3] Battiato, M. et al., Phys. Rev. Lett. 105, 027203 (2010). [4] Pfau, B. et al., Nat. Commun. 3, 1100 (2012). [5] Kerber N. et al., arXiv:2002.03971 (2020).

G3-09. Thermal Coupling Parameters Between Electron, Phonon, and Magnon of Nickel. *K. Kang*[1] and G. Choi[1,2] *1. Department of Energy Science, Sungkyunkwan University, Suwon city, The Republic of Korea; 2. Center for Integrated Nanostructure Physics, Institute for Basic Science (IBS), Suwon city, The Republic of Korea*

Thermal coupling parameters between different baths (electron, phonon, and magnon) in a nanoscale ferromagnetic Ni layer is investigated. To observe the local thermal interactions, we use time-resolved pump-probe spectroscopy. We collect both thermoreflectance and magneto-optical Kerr rotation, which represent the phonon temperature and magnon temperature, respectively, in a picosecond time scale. To analyze the experimental data, we employ the three-temperature thermal model including a spatial diffusion and local coupling mechanisms. We determine the thermal coupling parameters of Ni and find that the coupling parameter between phonon and magnon baths has a comparable magnitude to that between electron and magnon. The phonon-magnon coupling is responsible for the fast restoration of magnetization right after the ultrafast demagnetization (Fig. 1). In addition, we compare the coupling parameters with direct heating of Ni and in-direct heating of Ni via Au (Fig. 1). The in-direct heating suppresses the non-thermal electrons that reach to Ni, so that we can investigate the effect of thermal electrons on the ultrafast demagnetization. Both direct and in-direct heating situations lead to similar values of the coupling parameters, and the discrepancy is less than 30 %. We conclude that the thermalized electrons play the major role in the ultrafast demagnetization of Ni.

Kyuhwe Kang and Gyung-Min Choi, J. Magn. Magn. Mater., Vol. 514, p.167156 (2020)

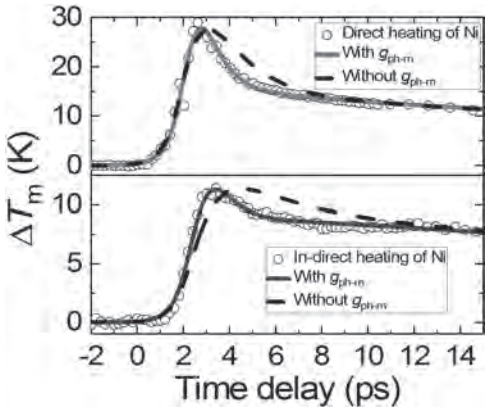

Fig. 1. Magnon temperature (T_m) excursions of Ni in the Ni (20 nm)/ Au (100 nm) bilayer. The upper/lower panel represents the direct/in-direct heating. The circle symbols are experimental data. The red and blue solid lines are analytic results with a phonon-magnon coupling (g_{ph-m}), and the black dashed lines are that without g_{ph-m}.

G3-10. Unification of Ultrafast Demagnetization and Switching. *G. Zhang*[1], M. Murakami[1], Y. Bai[1], T.F. George[2] and X. Wu[3] *1. Indiana State University, Terre Haute, IN, United States; 2. University of Missouri-St Louis, St Louis, MO, United States; 3. Nanjing University, Nanjing, China*

All-optical spin switching and demagnetization are two sides of the same physics. We find a way to unify them through the same model that takes into account the Heisenberg exchange between spins and spin-orbit coupling. To have efficient spin switching, the electron initial momentum direction must closely follow the spin's orientation, so that the orbital angular momentum is transverse to the spin, and consequently the spin–orbit torque lies in the same direction as the spin. The demagnetization can be understood from the spin-orbit coupling-mediated spin-wave excitation. The efficiency of laser-induced demagnetization is very high. We also observe the collapse of the spin-spin correlation length within 20 fs, consistent with the experimental findings [2]. Upon laser excitation there is a massive spin wave generated. The wave starts at the center of the laser beam and propagates outwards. Figure 1(b) shows the effect of the linearly polarized light at 123 fs after laser excitation. The spins close to the center bend strongly to the –z-axis. The situation is quite different with a right-circularly polarized laser (see Fig. 1(c)), where the spins are much more strongly affected. For left-circularly polarized light, the effect is much weaker. The demagnetization results from spin misalignment across the sample. This is similar to the traditional spin wave theory, with the low-energy spin wave excitation across several hundred lattice sites, which is far beyond the capability of the time-dependent density functional theory. Our simulation shows that the spin-spin correlation is reduced within 20 fs [3], consistent with the experimental results.

[1] G. P. Zhang and M. Murakami, Journal of Physics: Condensed Matter 31, 345802 (2019). [2] P. Tengdin et al., Science Advances 4, eaap9744 (2018). [3] G. P. Zhang, M. Murakami, Y. H. Bai, Thomas F. George, and X. S. Wu, J. Appl. Phys. 126, 103906 (2019).

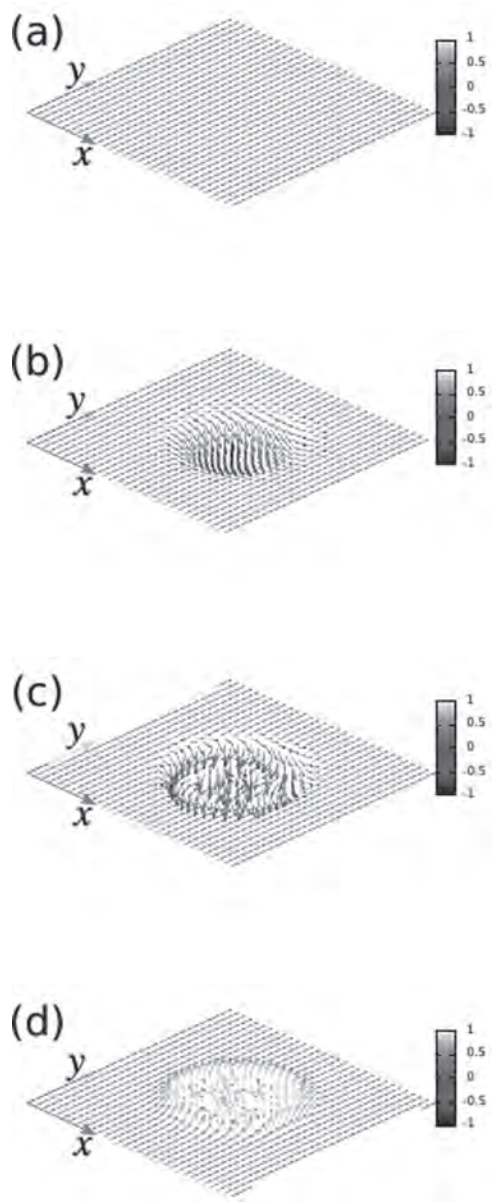

Spin reversal in a uniform magnetized slab. (a) Initial spin configuration. All the spins are in-plane and along the y axis. There are 501 spins along both the x and y axes. To reduce the huge amount ofdata, we only show one out of every ten spins. (b)-(d) Snapshot of spins at 123 fs under linearly-, right- and left-circularly polarized light, respectively.

G3-11. Role of Spin-Resolved Charge and Heat Transport in Ultrafast Demagnetization Dynamics. *S. Ashok*[1,2], J. Hoefer[1,2], S. Weber[1,2], M. Stiehl[1,2], C. Seibel[1,2], J. Briones[1,2], B. Rethfeld[1,2], M. Aeschlimann[1,2] and B. Stadtmüller[1,2] *1. Technische Universitat Kaiserslautern Staatliches Forschungszentrum fur Optik und Materialwissenschaften, Kaiserslautern, Germany; 2. Department of Physics, Technische Universitat Kaiserslautern, Kaiserslautern, Germany*

Ultrafast Demagnetization of metallic ferromagnets due to excitation with a femtosecond laser pulse was discovered by Beaurepaire et al. in thin Nickel films [1]. In case of metallic magnets with thickness lesser than penetration depth of the laser, the film is heated homogeneously. Therefore, due to absence of temperature and density gradients within the material there would be no heat- or charge-currents. For thicker magnets, the heating is not uniform and therefore one needs to distinguish the resulting role of heat and spin-resolved charge transport in ultrafast de- and re-magnetization. This is a pivotal issue owing to rich possibilities in its applications. Therefore, in this contribution, we theoretically and experimentally study the role of transport in ultrafast magnetization dynamics. It has been shown that ultrafast demagnetization can be interpreted as being driven by an equilibration of chemical potentials of up- and down-electrons [2]. Starting from itinerant picture of metallic magnetism [3] and the ultrafast reduction of exchange-splitting the Thermodynamic μT-model [4] traces ultrafast quenching of magnetization. This is accomplished by tracing the equilibration of chemical potentials and temperatures of up-, down-electrons and temperature of lattice separately. Magnetization dynamics in thick magnetic films can be experimentally studied by measuring the changes in Kerr-rotation and Ellipticity using Complex-MOKE technique [5]. Magneto-optic signal of a thick magnetic film is due to sum of partial-contributions of effectively thin layers at various depths of the film [6]. By integrating the depth sensitivity function [7] weighted by spatially resolved magnetization at various time instances we obtain the changes in Magneto-optic signal on a femtosecond timescale. In this work we study the role of spin-resolved charge and heat transport in ultrafast demagnetization of thick magnetic metal using Thermodynamic μT-model and obtain spatial and temporal evolution of magnetization. This is translated to temporal dynamics of Magneto-optic signal. The theoretical predictions are then compared with the experimentally measured changes in Kerr-rotation and Ellipticity for a 100 nm thick Nickel film.

[1] E. Beaurepaire, J.-C. Merle, A. Daunois and J.-Y. Bigot, Phys. Lett. 76, 4250 (1996). [2] B. Y. Mueller et al., Phys. Rev. Lett. 111, 167204 (2013). [3] W. Nolting and A. Ramakanth, ISBN: 978-3-540-85416-6 (2009). [4] B. Y. Mueller and B. Rethfeld, Phys. Rev. B 90, 144420 (2014). [5] Y. Liu et al., J. Magn. Magn. Mat. 502, 166477 (2020). [6] G. Traeger, L. Wenzel and A. Hubert, Phys. Status Solidi A 131, 201 (1992). [7] W. Kuch, R. Schaefer, P. Fischer and F. Hillebrecht, ISBN: 978-3-662-44532-7 (2015).

G3-12. A Simulation Study of RKKY Exchange Mediated Ultrafast all-Optical Switching of GdCo/[Co/Pt] Heterostructures. *D. Polley*[1,2], H. Jang[2], J. Chatterjee[2] and J. Bokor[1,2] *1. Material Science, E O Lawrence Berkeley National Laboratory, Berkeley, CA, United States; 2. EECS, University of California Berkeley, Berkeley, CA, United States*

Helicity-independent all-optical switching (HI-AOS) of rare-earth/transition metal ferrimagnets is being intensively studied [1-6] for the last few years due to its potential applications towards faster read-write spintronic devices. The underlying magnetization dynamics has been discussed using two different approaches; i) atomistic Landau-Lifshitz-Gilbert model [3-4] and ii) microscopic three temperature model (M3TM) [5]. Recently, the ultrafast switching (< 10 ps) of ferromagnetic Co/Pt stack (exchange coupled with GdFeCo ferrimagnet) has been demonstrated showing a greater potential for technological applications [6]. We have extended the M3TM approach, to investigate similar systems by including a RKKY exchange (J_{RKKY}) coupled ferromagnetic (Co/Pt) layer along with a ferrimagnet (GdCo) alloy. J_{RKKY}, estimated as a fraction of CoPt exchange ($J_{CoPt} = 1.26X10^{-21}$ J), depends on the thickness of the Pt spacer layer separating Co/Pt from GdCo. Positive and negative sign of J_{RKKY} means ferromagnetic and anti-ferromagnetic type coupling respectively. The dynamics for each of the magnetic sub-lattices have been plotted in Fig. 1. M_{Co} crosses zero in < 1 ps while M_{Gd} is still in its demagnetized state and thereby forming a transient ferromagnetic state which is a necessary condition for HI-AOS [4-5]. Co/Pt remains demagnetized and its switching depends on the strength and sign of J_{RKKY}. The white and dark region in Fig. 2 depicts relaxed and randomly demagnetized state of the material. The light green denotes switching of both the Co/Pt and $Gd_{23}Co_{77}$, while the dark green region denotes switching of only $Gd_{23}Co_{77}$. We found that the switching time of Co/Pt significantly depends on the composition of the GdCo alloy, absorbed power and the strength of J_{RKKY}. Our simulation qualitatively explains the switching of Co/Pt in < 10 ps as experimentally observed by Gorchon et al. [6] and establishes the role of indirect exchange coupling in such switching.

1. I. Radu, K. Vahaplar, C. Stamm et al., Nature 472, 205 (2011) 2. A. Ceballos, A. Pattabi, A. El-Ghazaly et al., arXiv:1911.09803 3. U. Atxitia,

P. Nieves and O. Chubykalo-Fesenko, Phys. Rev. B 86, 104414 (2012) 4. F. Jakobs, T. Ostler, C. H. Lambert et al., arXiv:2004.14844 5. M. Beens, M. L. M. Lalieu, A. J. M. Deenen et al., Phys. Rev. B. 100, 220409(R) (2019) 6. J. Gorchon, C. H. Lambert, Y. Yang, et al., Appl. Phys. Lett. 111, 042401 (2017)

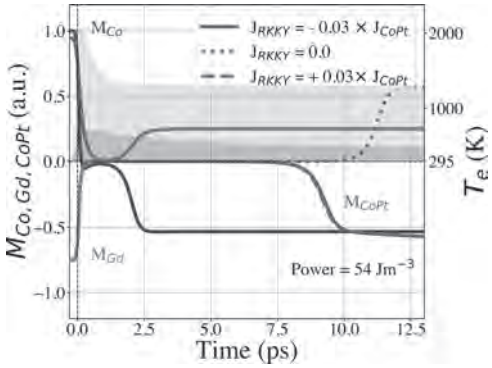

Fig. 1. Magnetization dynamics of the Co, Gd and Co/Pt sub-lattices. The blue and magenta filled region shows the electronic temperature of the $Gd_{23}Co_{77}$ and Co/Pt sub-system respectively.

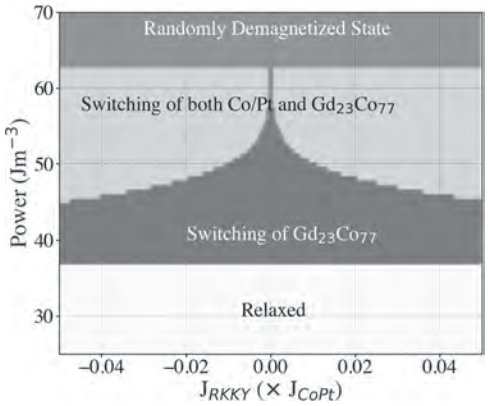

Fig. 2. A phase-plot of switching as a function of RKKY coupling and absorbed power.

G3-13. Advanced Atomistic Modelling of Magnetisation Dynamics With Spin and Lattice Degrees of Freedom. *M.S. Strungaru*[1], M.O. Ellis[2], S. Ruta[1], O. Chubykalo-Fesenko[3], R.F. Evans[1] and R. Chantrell[1] *1. Physics, University of York, York, United Kingdom; 2. Computer Science, The University of Sheffield, Sheffield, United Kingdom; 3. Instituto de Ciencia de Materiales de Madrid, Madrid, Spain*

The relaxation of the magnetisation in magnetic materials is of great importance from both an applied and fundamental point of view. Conventional modelling of magnetisation dynamics employs the Landau-Lifshitz-Gilbert (LLG) equation[1] where the damping is included phenomenologically by a term that describes the coupling of the magnetic modes (given primarily by the atomic spin) to the non-magnetic modes (lattice vibrations and electron orbits) which are assumed to be in equilibrium. Recent studies of the dynamics induced by THz laser pulses has highlighted the necessity of understanding magnetisation relaxation beyond this assumption. In reality the spin and lattice dynamics mutually influence one another, hence it is necessary to employ a unified model of molecular and spin dynamics [2], Spin-Lattice dynamics (SLD). The transfer of energy and angular momentum between the lattice and the spin system is realised by the pseudo-dipolar coupling [3], which arises from the spin-orbit interaction and can be parameterised by magneto-elastic experiments. Our results show that the equilibrium magnetisation is independent of the thermostat used and by coupling the spin system only to the lattice vibrations the magnetisation temperature dependence can be reproduced without the need of a phenomenological spin damping. The autocorrelation of the coupling field (which acts as an induced noise on the spin systems) shows well defined excitation peaks at nonzero frequencies corresponding to both phonon and magnon modes, proving a successful coupling between the two subsystems (Fig.1). The magnon-phonon damping is evaluated within this framework (Fig. 2) and agrees well with the damping measured in magnetic insulators where it depends more on magnon-phonon coupling than electronic effects. Our model opens the possibility to describe the distinct dynamics of spins and phonons, necessary for the understanding of ultrafast magnetisation dynamics experiments.

[1] T. L. Gilbert, IEEE Trans. Magn. 40, 3443 (2004). [2] P.-W. Ma, C. Woo, and S. Dudarev, "Large-scale simulation of the spin-lattice dynamics in ferromagnetic iron," *Phys. Rev. B*, vol. 78, no. 2, p. 024434, Jul. 2008. [3] Aßmann, Matthias, and Ulrich Nowak. "Spin-lattice relaxation beyond Gilbert damping." *Journal of Magnetism and Magnetic Materials* 469 (2019): 217-223.

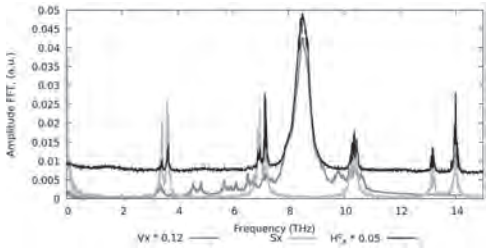

The magnon, phonon and coupling field autocorrelation from SLD simulations at T=300K calculated using the Fourier transform.

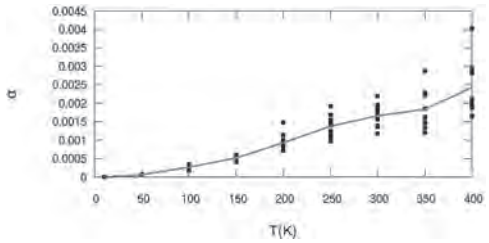

Temperature dependence of magnon-phonon induced damping within the SLD framework.

Session G4
NEUROMORPHIC COMPUTING WITH NANOMAGNETS
Alice Mizrahi, Chair

CONTRIBUTED PAPERS

G4-01. Experimental Demonstration of Probabilistic Spin Logic by Magnetic Tunnel Junctions. *Y. Lv*[1], R.P. Bloom[1] and J. Wang[1]
1. Department of Electrical and Computer Engineering, University of Minnesota, Minneapolis, MN, United States

The recently proposed probabilistic spin logic (PSL) offers promising solutions to novel computing applications[1], including some that have previously been covered by quantum computing. The PSL's basic element is probabilistic bit (p-bit). A p-bit outputs random signals continuously while the mean of the output signal is input-dependent. When multiple p-bits are coupled through a network, a PSL is built. So far, several task implementations of PSL, including invertible logic gate, have been simulated numerically. Here, we report an experimental demonstration of a magnetic tunnel junction (MTJ) based hardware implementation of PSL[2]. Differently from the original p-bit proposals, we propose using two biasing methods, magnetic field and voltage, on the MTJ to excite and fine tune the random fluctuation of MTJ[3]. Therefore, our proposed hardware implementation of p-bit carries the benefit of extra tunability of random signal properties, which are eventually used to compensate the variations of mean and rate of random signals due to the intrinsic device-to-device variations of MTJs. As a result, multiple p-bits are tuned to exhibit similar properties even they are built with highly varied MTJs. Another benefit of the proposed p-bit design is that the similar principle could work for not only thermally-unstable MTJs but also thermally-stable MTJs, which are matured for STT-MRAM technologies and are more ready for integration. Then three p-bits are connected by a coupling network so that a PSL of an invertible logic gate is experimentally demonstrated (Fig. 1). As shown in Fig. 2, the invertible AND gate hops between all possible combinations under the AND logic constraint, C=AB. Along with more results from the demonstration, the PSL of an invertible AND logic gate is shown to function as intended. And thanks to the proposed p-bit hardware design that offers high tunability, the entire PSL system does not suffer from the slowest of the system, and shows much greater performance and potential for further scaling.

[1] K. Y. Camsari, B. M. Sutton, and S. Datta, "P-bits for probabilistic spin logic," *Applied Physics Reviews*, vol. 6, no. 1. AIP Publishing LLC, p. 011305, 11-Mar-2019. [2] Y. Lv, R. P. Bloom, and J. P. Wang, "Experimental Demonstration of Probabilistic Spin Logic by Magnetic Tunnel Junctions," *IEEE Magn. Lett.*, vol. 10, 2019. [3] B. R. Zink, Y. Lv, and J.-P. Wang, "Independent Control of Antiparallel- and Parallel-State Thermal Stability Factors in Magnetic Tunnel Junctions for Telegraphic Signals With Two Degrees of Tunability," *IEEE Trans. Electron Devices*, vol. 66, no. 12, pp. 5353–5359, Dec. 2019.

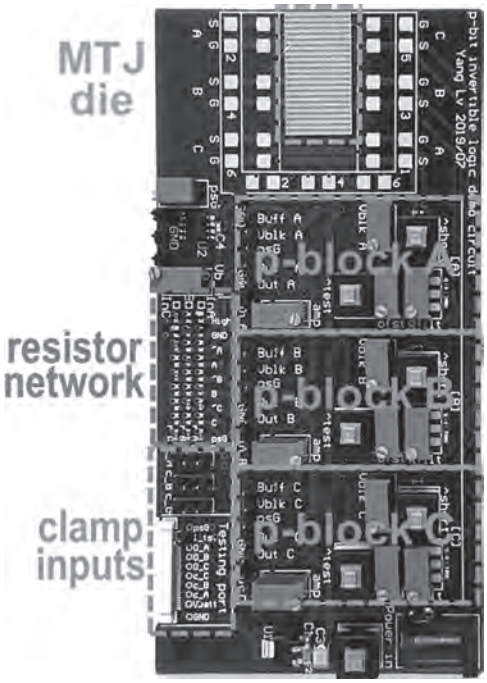

Fig. 1. Photograph of p-bit and PSL demonstration hardware. Note that a 'p-block' refers to a specific hardware implementation of a p-bit.

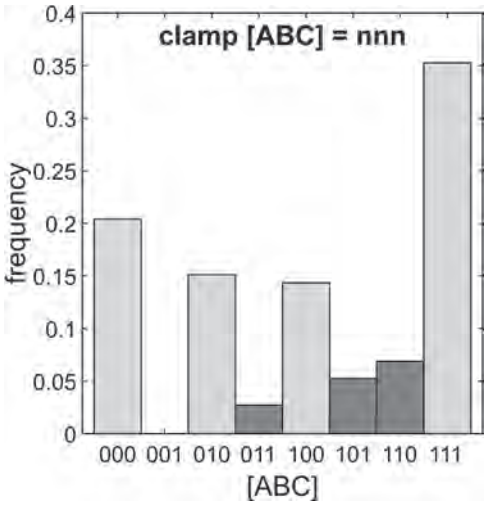

Fig. 2. p-bits state relative histogram with all p-bits left free.

G4-02. Spintronic Memristor Based on the Angular Variation of TMR.
M. Mansueto[1], A. Chavent[1], S. Auffret[1], I. Joumard[1], L. Vila[1], R. Sousa[1], *L. Buda-Prejbeanu*[1], L. Prejbeanu[1] and B. Dieny[1] *1. SPINtronique et Technologie des Composants, Grenoble, France*

In the development of dedicated hardware for neuromorphic applications, the realization of suitable memristive devices as synaptic elements is a key factor. The main drawback of the existing devices is the reliability of the intermediate states and their scalability. In this study we propose a memristive device based on magnetic tunnel junctions (MTJ) and whose functionalities do not depend directly on the size of the device. The state of the memristor relates to the tunnel magnetoresistance (TMR) variation with the relative angle between the two in-plane magnetizations. The specificity of our concept consists in the integration of an isotropically coercive medium as magnetic free layer able to stabilize its magnetization along whatever in-plane direction. Here the current driven rotation of the magnetization is investigated on devices of 100nm of diameter. The spin transfer torque (STT) of the in-plane MTJ is considered together with the contribution of the additional perpendicularly magnetized polarizer. For a proper ratio of the two STT contributions, the magnetization switches from the parallel to the anti-parallel state following a circular out-of-plane trajectory as for the precessional switching [4]. We prove experimentally that by properly designing the voltage pulses we can discretely rotate and stabilize the magnetization along different in-plane directions, reaching an almost continuous range of intermediate resistances. The resistance variation turns out to be monotonous with the voltage polarity confirming the memristive behavior of the device under a train of pulses. A study on the thermal stability of the intermediate states shows a resistance variation below 2% for a 3min timescale. Moreover, the Joule effect, occurring during the application of pulses, adds a random contribution to the resistance jumps. The observed resistance noise is associated to the thermally activated switching of small magnetic areas of the samples, probably due to the granular nature of the sputtered samples. The larger the diameter, the lower the noise due to the increased number of grains.

1. Mansueto, M. *et al*. *Phys. Rev. Appl.* 12, 044029 (2019). 2. Mansueto, M. *et al. 2020 IEEE International Memory Workshop (IMW)* 1–4 (2020). 3. Mansueto, M. *et al.* in preparation 4. Vaysset, A. *et al. Appl. Phys. Lett*. 98, 242511 (2011)

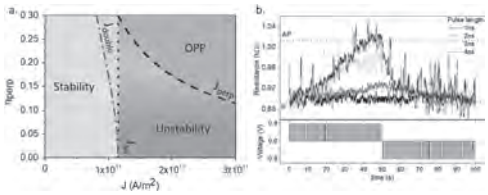

Fig. 1 a. STT efficiency dependence of the working regions. b. Resistance variation due to a train of pulses as in the bottom panel.

G4-03. Reservoir Computing With Planar Nanomagnet Arrays.
P. Zhou[1], A.J. Edwards[1], N.R. McDonald[2], L. Loomis[2], C.D. Thiem[2] and J.S. Friedman[1] *1. Department of Electrical and Computer Engineering, The University of Texas at Dallas, Richardson, TX, United States; 2. Air Force Research Laboratory Information Directorate, Rome, NY, United States*

Reservoir computing (RC) [1] is a subset type of recurrent neural network, where only the weights of the output layer are altered during training. This training scheme does not require multi-layer backpropagation and gradient descent, making RC simple to train. This technique is therefore well suited for resource constrained hardware environments, since expensive circuitry for updating internal reservoir weights is unnecessary. Some spintronic devices can exhibit highly nonlinear behavior that is extremely well-suited for implementing RC in hardware. We have proposed a novel reservoir comprising a planar arrangement of nanomagnets each having perpendicular magnetic anisotropy (PMA) [2]. Our solution differs from [3], which uses voltage pulses to move information within the reservoir, whereas ours uses the natural relaxation of the nanomagnets. Fig. 1(a) shows an example layout of nanomagnets with two input nanomagnets (A and B). The effect of nanomagnet magnetic fields upon adjacent nanomagnets exhibits two features: non-linear interaction and variable interaction strength, making the proposed implementation well-suited for RC. Information is input by stimulating individual nanomagnets or portions of the nanomagnet reservoir with external magnetic fields. The magnetizations of various nanomagnets are read electrically via magnetic tunnel junctions. A complementary single layer circuit is used to perform vector-matrix multiplication on the magnetization values and the trained output weights to obtain the output vector. Micromagnetic simulations are performed with MuMax3 for the nanomagnet network pictured in Fig. 1(a). The nanomagnet reservoir was simulated with an input stream comprising triangle or square waves. Fig. 1(b-d) shows various snapshots of the network during the simulation; colors indicate magnetization directions. Fig. 1(e) shows the reservoir inputs and outputs, and Fig. 1(f) tracks the magnetization over time for three nanomagnets. The reservoir successfully identified the waveforms with 100% accuracy for both the training and testing data.

[1] H. Jaeger, Bonn, Germany: German National Research Center for Information Technology GMD Technical Report., Vol. 148, p.13 (2001) [2] P. Zhou, N. McDonald, A. Edwards, L. Loomis, C. Thiem, and J. Friedman. arXiv:cs.NE/2003.10948 (2020) [3] H. Nomura, T. Furuta, K. Tsujimoto, Y. Kuwabiraki, F. Peper, E. Tamura, S. Miwa, M. Goto, R. Nakatani, and Y. Suzuki. 2019, Japanese Journal of Applied Physics., Vol. 58, p.070901 (2019)

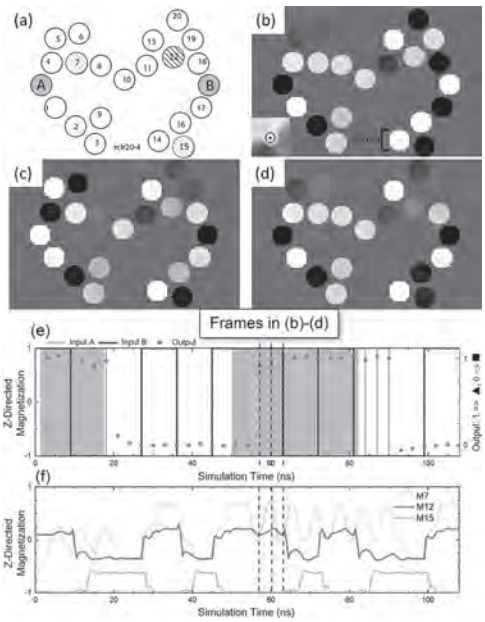

Fig. 1. Nanomagnet RC Simulations: (a) reservoir layout, (b-d) simulation snapshots, (e) trained output, and (f) selected traces.

INVITED PAPER

G4-04. Superparamagnets for Stochastic Computing. *S. Majetich*[1] *1. Physics, Carnegie Mellon University, Pittsburgh, PA, United States*

Interacting nanomagnets with low thermal stability have been proposed for probabilistic computing, which has potential uses in low power sensing and logic, as well as in encryption and decryption [1]. Superparamagnetic tunnel junctions (SP-MTJs) are an ideal type of nanomagnet because their time-averaged magnetization of the free layer can be programmed with a voltage or current (Figure 1). We have previously used SP-MTJs for random number generation (RNG), and analog multiplication [2]. While voltage-controlled

magnetic anisotropy (VCMA) has advantages for RNG due to ultra-low power consumption, spin transfer torque (STT) or spin orbit torque (SOT) is superior for logic devices due to the wider tuning range. For small sizes, magnetic tunnel junctions can be superparamagnetic near zero bias voltage, and the average retention time can be as short as a few hundred nanoseconds, so GHz speeds are feasible [3]. Pairs of superparamagnetic tunnel junctions fluctuate independently when isolated (Figure 2, top), but when coupled, the output of one is the NOT of the other (Figure 2, bottom). For AND and NAND gates the coupling between three SP-MTJs is optimized by Boltzmann machine simulations to statistically favor the set of microstates consistent with the truth table. Experimental results show that fast operation can be achieved with a hybrid SP-MTJ – CMOS circuit and without the need for a separate microprocessor. Prospects for optimizing the speed and performance of these devices will be discussed, and benchmarked with non-magnetic stochastic computing technologies.

1. K. Y. Camsari, et al., Phys. Rev. X 7, 031014 (2017). 2. M. Bapna and Sara A. Majetich, Appl. Phys. Lett. 111, 243107 (2017). 3. B. Parks, A. Abdelgawad, T. Wong, R.F. L. Evans, and S. A. Majetich, Phys. Rev. Applied 13, 014163 (2020).

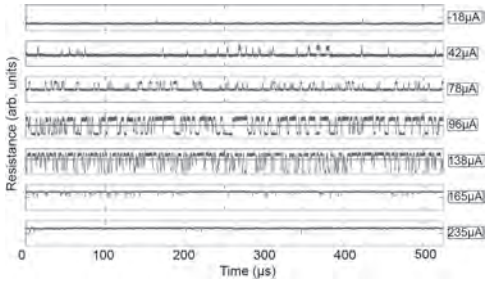

Fig. 1. Resistance fluctuations as a function of the current through a superparamagnetic MTJ, as a function of current.

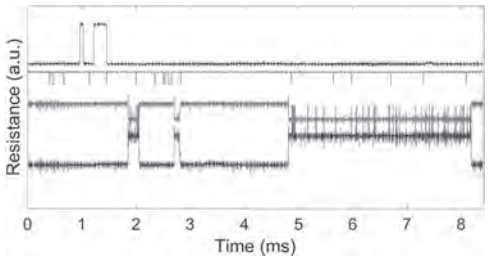

Fig. 2. Top: When isolated, MTJ #1 (blue) is mostly in the P state and MTJ #2 is mostly in the AP state. Their switching events are uncorrelated. Bottom: When coupled together, the switching events are almost perfectly anti-correlated, as expected for a logical NOT gate.

CONTRIBUTED PAPERS

G4-05. Implementation of Artificial Neural Networks Using Stochastic Computing Units Based on Magnetic Tunnel Junctions. *Y. Shao*[1], S. Sinaga[1], I. Sunmola[1], A. Borland[1], M. Carey[2], J. Katine[2], V. Lopez Dominguez[1] and P. Khalili Amiri[1] *1. Electrical and Computer Engineering, Northwestern University, Evanston, IL, United States; 2. Western Digital Corp, San Jose, CA, United States*

Hardware implementation of Artificial Neural Networks (ANNs) using conventional binary arithmetic units requires large area and energy, due to the massive multiplication and addition operations in the inference process, limiting their use in portable systems and the emerging Internet of Things. Stochastic computing (SC) [1-3] has been proposed as an alternative for compact and low-energy arithmetic hardware. SC uses the probability of 1s or 0s in a randomly generated bit-stream to represent a decimal number. This allows SC to implement basic arithmetic operations using far fewer logic gates than binary operations. To realize SC in hardware, a key requirement are tunable true random number generators (TRNGs) which cannot be efficiently realized using existing CMOS technology. Here we address this challenge by using a series of magnetic tunnel junctions (MTJs) as TRNGs, and demonstrate a SC-based ANN using these MTJ-TRNGs that performs handwritten digit recognition with excellent accuracy. The TRNG operation is based on the thermal fluctuations at room temperature of the MTJ free layer [4-6]. The stochasticity of this process can be tuned by electric current via spin-transfer torque (STT) [7], to generate tunable stochastic bit-streams representing the range of numbers from 0 to 1. We used 6 MTJs with 50 nm diameter to generate the bit-streams. The training process of the ANN results in bias voltages that are applied to tune the probability of 1s and 0s in bit-streams generated by each MTJ. Tunability from > 95% antiparallel (AP) to > 95% parallel (P) was experimentally achieved by a voltage < 1V (Fig. 1), corresponding to an ultralow current of < 5 μA (= 0.25 MA cm^{-2}). To achieve deeper number resolution, the product (XNOR) of two MTJs was used to generate stochastic bit-streams corresponding to the values of inputs and weights in different layers. The resulting spintronic SC-based ANNs (Fig. 2) achieved 94% accuracy for handwritten digit classification on the MNIST database.

[1] Gaines, B.R., *Advances in information systems science*. Springer. p. 37-172 (1969). [2] Brown, B.D. and H.C. Card, *IEEE Transactions on computers*, Vol. 50(9): p. 891-905 (2001). [3] Wang, S., Pal, S., Li, T., *Design, Automation & Test in Europe Conference & Exhibition* (DATE), 2017, pp. 1438-1443. IEEE, (2017). [4] Camsari, K.Y., S. Salahuddin, and S. Datta, *IEEE Electron Device Letters*, Vol. 38(12): p. 1767-1770 (2017). [5] Brown Jr, W.F., *Physical review*, Vol. 130(5): p. 1677 (1963). [6] Fukushima, A., Seki, T., Yakushiji, K., *Applied Physics Express*, Vol. 7(8): p. 083001 (2014). [7] Fuchs, G.D., Emley, N.C., Krivorotov, I.N., *Applied Physics Letters*, Vol. 85(7): p. 1205-1207 (2004).

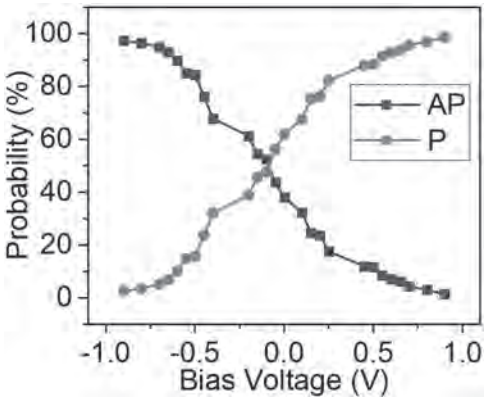

Fig. 1 Probabilities of 1s and 0s (parallel and antiparallel state) generated by an MTJ under different bias voltages.

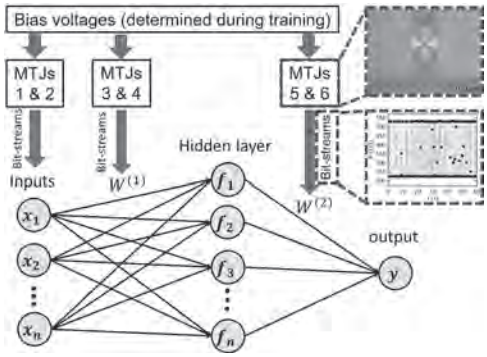

Fig. 2 Structure of the ANN in this work, using MTJ pairs for stochastic bit-stream generation.

G4-06. Superparamagnetic Tunnel Junctions for Invertible Stochastic Logic Gates. *B. Parks*[1], H. Chen[1], H. Pan[2] and S. Majetich[1] *1. Physics, Carnegie Mellon University, Pittsburgh, PA, United States; 2. University of Science and Technology of China, Hefei, China*

We experimentally demonstrate the application of superparamagnetic magnetic tunnel junctions (MTJs) in stochastic logic operations. The two resistance states of an MTJ are used as logical 1 and 0. When the energy barrier to magnetization reversal is low compared to the thermal energy, the MTJ switches between the 1 and 0 states stochastically. The MTJ resistance is instantaneously digital yet analog in time average. Spin transfer torque (STT) enables electronic control of the time averaged resistance [1]. Three 60 x 90 nm CoFeB MTJs were connected to the logical circuit, and their resistances were measured simultaneously (Figure 1(a)). The probabilities P of the eight possible microstates (x_1,x_2,y) were analyzed pairwise. We denote by (0,0) the state 000 that is consistent with the truth table of an AND gate together with 001 that is not. The preference for 001 relative to 000, C(x_1=0,x_2=0), was defined as the normalized difference between the probabilities P(001) and P(000). After connecting feedback, when, P(000) will increase and P(001) will become smaller, effectively decreasing C(0,0). The condition will be the same for C(0,1) and C(1,0) but not C(1,1), since P(111) increases but P(110) decreases. Figure 1(b) shows experimental results with the feedback connected, showing a statistical preference for valid AND gate states. Invertibility is based on what happens when the output is pinned to a particular value. Pinning y to 1 increases the probabilities for all the states with y = 1 (Figure 1(c)), while pinning y to 0 increases the probability for all the states with y = 0 (Figure 1(d)). This is qualitatively consistent with the energies of the different states.

Bapna, M., & Majetich, S. A. (2017). Current control of time-averaged magnetization in superparamagnetic tunnel junctions. *Applied Physics Letters*, *111*(24), 243107.

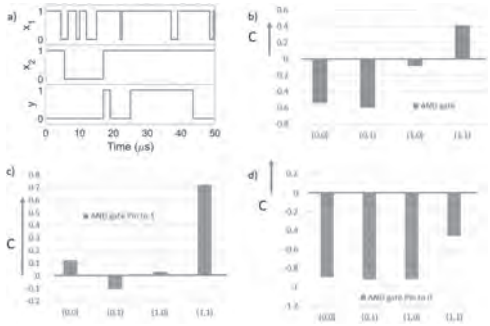

The binary outputs of three superparamagnetic MTJs connected to a logical circuit are read simultaneously (a). The relative probabilities when the output bit, y, can fluctuate (b), when y is pinned to 1 (c) and when y is pinned to 0 (d) are consistent with the expected behavior of a stochastic AND gate.

G4-07. Neuromorphic Computation Using Emergent Magnetisation Dynamics. *I.T. Vidamour*[1], R. Dawidek[1], S. Kyle[1], P.W. Fry[2], F. Maccherozzi[3], S.S. Dhesi[3], N. Steinke[4], J.F. Cooper[4], E. Vasilaki[2], D. Allwood[1] and T.J. Hayward[1] *1. Materials Science and Engineering, The University of Sheffield, Sheffield, United Kingdom; 2. The University of Sheffield, Sheffield, United Kingdom; 3. Diamond Light Source Ltd, Didcot, United Kingdom; 4. Isis Neutron and Muon Source, Didcot, United Kingdom*

Emergent behaviours in complex systems arise from simple interactions between individual components that lead to global complexity [1]. Emergence is found in nature as a mechanism behind intelligent biological processes [2], but thus far, little has been done to exploit the computational power that emergence could offer for machine learning hardware. Here we demonstrate how the emergent properties of a magnetic system can be exploited to perform meaningful computation *in materio*. Using a combination of X-ray photoemission electron (X-PEEM) microscopy and polarised neuron reflectivity (PNR), we show that arrays of interconnected magnetic nanowire rings demonstrate emergence as a result of complex domain wall (DW) pinning events. The stochasticity associated with DW pinning produces emergent, dynamic equilibria in DW population and array magnetisation [3]. We then present a phenomenological model of these stochastic pinning events and show that the model provides excellent agreement to our experimental data (Fig. 2). The system's nonlinear response and its inherent memory allowed us to implement a machine learning paradigm called 'reservoir computing' (RC). In RC, artificial neural networks are replaced by time-dependent 'reservoirs' which capture the advantages of recurrent neural networks (RNNs), without the associated difficulty of training RNNs [4]. Using the model, we demonstrated the feasibility of the ring arrays performing machine learning tasks, including speech processing and signal classification. We believe the sub-millimetre size and ability to solve complex tasks makes the arrays exciting candidates for microprocessors, with parallel computation and memory capability, enabling more energy efficient data processing tasks due to the reduced computational expense.

[1] - P. Curseu, *J. Inf. Technol.*, 21, (2006), [2] - B. Lindsey et al, *Comprehensive Physiology*, 2, (2012). [3] - R. Dawidek et al. [Under Review], [4] - M. Lukoševičius and H. Jaeger, *Comput. Sci. Rev.*, 3, (2009).

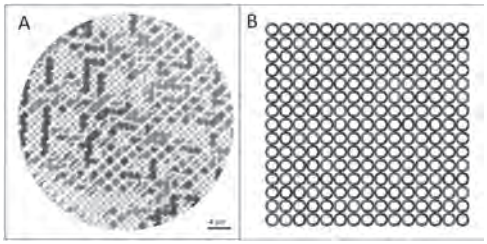

A) X-PEEM image representing domain configuration of 25x25 ring array after 30 successive rotations of 31 Oe field. B) Phenomenological simulation of 15x15 ring array after 30 successive rotations of 31 Oe field.

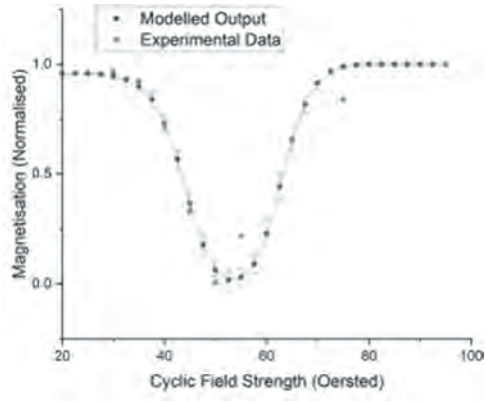

Comparison between experimental PNR data and modelled arrays of 25x25 rings after 50 rotations of a range of magnetic fields. Error bars represent maximum/minimum values during 100 repetitions, plotted points represent mean values

Session G5
2D MAGNETIC MATERIALS: FUNDAMENTAL PROPERTIES (Poster Session)

Amber McCreary, Chair
National Institute of Standards and Technology, Gaithersburg, MD, United States

G5-01. Observation of Semimetallic Behaviour and Resolution of Rashba Split Bands Through Shubnikov de Haas Effect in Topological Insulator Sb_2Te_3. *J. Gretton*[1] and S. Sasaki[1] *1. Condensed Matter Physics, University of Leeds Faculty of Mathematics and Physical Sciences, Leeds, United Kingdom*

We investigate single crystal Sb_2Te_3 grown with a range of super-stoichiometric Te content used to tune the defect density and electronic transport properties, motivated by huge surface-carrier mobility (25'000 cm^2/Vs) [1] and the functional opportunities afforded by both the topological Dirac surface state and a so far electrically uncharacterised Rashba spin-split surface state [2][3]. We find a non-linear Hall resistivity (ρ_{yx}) and large, saturating MR (ρ_{xx}) across the composition range (Figure 1), and find that both are well described by a two-band model comprised of both bulk electron and hole carriers in the material. Fitting to such a model finds reduced carrier densities (~10^{19} cm^{-3}) and increased mobilities (~6000 cm^2/Vs) for a super-stoichiometric Te concentration compared to nominally stoichiometric samples. The high carrier mobilities allow us to observe large Shubnikov de Haas oscillations (SdHO) in ρ_{xx} and ρ_{yx} up to an applied field of 8T (Figure 1) where the different carrier densities for each composition allow us to probe different electronic states at the chemical potential: for some carrier concentrations we expect the Rashba like states to contribute to the transport, and we find strong beating patterns in the SdH envelopes (Figure 2) reminiscent of spin-splitting effects in 2DEG structures [4]. Detailed analysis of the oscillations show that for the lowest carrier density samples the SdH beating is a result of closely matched cross-sectional area (CSA) bulk Fermi pockets rather than a Rashba spin-split Fermi surface, but in higher carrier density samples we resolve a momentum splitting in agreement with the predicted Rashba splitting [3], and extract a non-zero Berry phase with opposing sign for each oscillatory branch in agreement with previous observations of Rashba split bands in BiTeI [5]. Despite this, linearly dispersive bulk states with closely matched CSA are likely causing the beating and non-trivial phase, highlighting the need for surface dominant samples of Sb_2Te_3 with 2-8x10^{19} cm^{-3} carriers.

[1] L. Zhao, H. Deng and I. Korzhovska, Nat. Comms., Vol. 6, p.8279 (2015) [2] L. Plucinski, A. Herdt and S. Fahrendorf, J. Appl. Phys., Vol. 113, p.053706 (2013) [3] C. Pauly, G. Bihlmayer and M. Liebmann, Phys. Rev. B, Vol. 86, p.235106 (2012) [4] K. Tsubaki, N. Maeda, T. Saitoh and N. Kobayashi, Appl. Phys. Lett., Vol. 80, p.3126 (2002) [5] H. Murakawa, M. S. Bahramy and M. Tokunaga, Science, Vol. 342, p.1490-93 (2013)

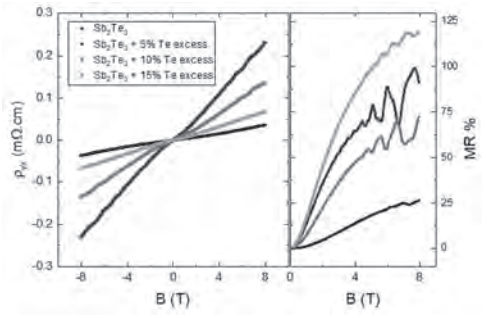

Non-linear Hall resistivity and large saturating MR are well described by a 2 band model, enhanced SdHO are observed for higher mobility samples.

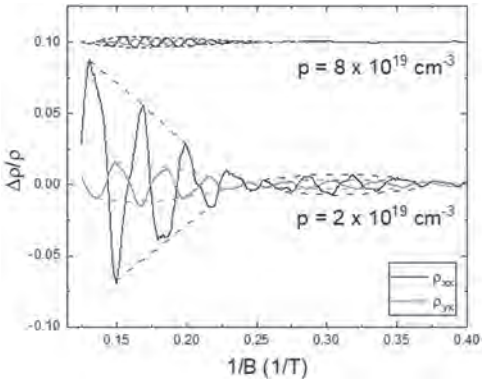

Clear beating patterns are observed in the SdHO, whose origins stem from trivial bulk and Rashba states for the lower and higher carrier densities respectively.

G5-02. A First Principles Study for X-ray Spectra of 2-Dimensional Materials - Fe_3GeTe_2, CrI_3, and $CrGeTe_3$. *Y. Lee*[1], B. Harmon[1] and L. Ke[1] *1. Ames Laboratory, Ames, IA, United States*

Using first-principles methods, we calculated X-ray absorption spectra (XAS) and X-ray circular dichroism spectra (XMCD) of transition metal atom (Cr, Fe) L_3/L_2 edges for 2-dimensional magnetic materials - Fe_3GeTe_2, CrI_3, and $CrGeTe_3$. We applied density functional theory (DFT)+*U* methods to handle better the correlation effects of 3*d* electrons of transition metal atoms in the semi-conductors. For Fe_3GeTe_2, as shown in Fig. 1, the calculated XAS and XMCD spectra within DFT show reasonable agreement with experiments [1] except for the intensity ratio between the first and the second peaks in XAS spectra, which can be explained by the overestimation of the magnetic moment in PBE. For CrI_3, as shown in Fig. 2, although the calculated spectra with PBE show all fine structures of experimental spectra [2], the agreement between the calculated and measured spectra can be improved with a rather higher Hubbard *U* value. However, unlike XAS, XMCD spectra showed some discrepancies for peak positions. For $CrGeTe_3$, the calculated spectra with PBE show fine structures of measured spectra. The Cr *d*-state in $CrGeTe_3$ has a broader bandwidth than in CrI_3, and it

suggests that the Cr atom is involved in stronger hybridization than in CrI_3. Overall, the PBE+*U* method is not effective for improving the agreement between the theoretical and experimental spectra, compared to the CrI_3 case, since the Cr atom in $CrGeTe_3$ is less localized than in CrI_3. In summary, we discuss relations between x-ray spectra, the density of states, and *U* values of Fe_3GeTe_2, CrI_3, and $CrGeTe_3$. By comparing the calculated spectra with the experimental measurements, we evaluate the reliability of DFT+*U* method to describe these materials [3]. We find that FGT and CrI_3 can be described reasonably well using DFT and DFT+*U*, respectively, while CGT requires more sophisticated methods.

[1] Jian-Xin Zhu, Marc Janoschek, D. S. Chaves, Phys. Rev. B 93, 144404 (2016) [2] Andreas Frisk, Liam B. Duffy, Shilei Zhang, Materials Letters 232 (2018) 5-7 [3] Y. Lee, T. Kotani, L. Ke, Phys. Rev. B 101, 241409 (2020)

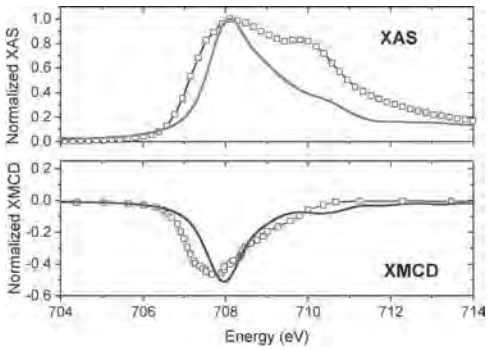

Fig.1 Comparison between calculated and experimental X-ray spectra of Fe_3GeTe_2. The top (bottom) panel shows XAS (XMCD) of Fe L_3 edge. Experimental data were obtained from Zhu *et al.* [1]

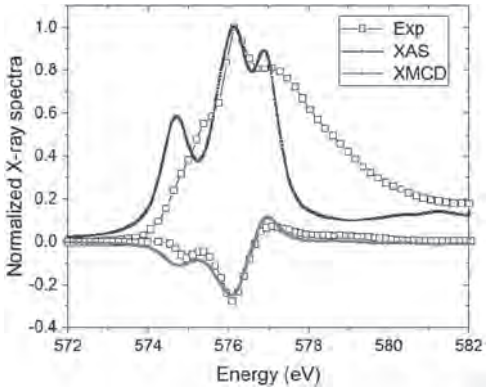

Fig.2 Comparison between calculated and experimental X-ray spectra of CrI_3. The blue (red) line shows XAS (XMCD) of Cr L_3 edge. Experimental data were obtained from Frisk *et al.* [2]

G5-03. Using Atomic Hydrogen to Activate Graphene on SiC.
P. Bentley[1], T. Bird[1], K. Chan[2,1], A. Graham[1], J.C. Zhang[1], A. Ferreira[1] and A. Pratt[1] *1. Department of Physics, University of York, York, United Kingdom; 2. Department of Physics, Imperial College London, London, United Kingdom*

Graphene's large spin-relaxation length at room temperature makes it a potential candidate for the channel material of a spin-based transistor such as that proposed by Datta and Das [1]. However, to tailor graphene for spintronic applications, its spin-orbit coupling (SOC) must be enhanced. Weakly hydrogenated graphene has been reported to enhance the SOC in graphene by 2.5 meV [1, 2] and therefore such a system could be a route towards 2D spintronic devices. Fabrication of high-quality 2D monolayers continues to be a challenge though with several different methods routinely used to produce graphene. One of these involves annealing the six- and four-hexagonal polymorphs of silicon carbide in ultrahigh vacuum leading to the desorption of silicon atoms and the formation of high-quality epitaxial graphene [3]. Such a system is of interest due to silicon carbide's large bandgap of 3.02 eV (6H polytype) and the ability to change both the face polarity and the cutoff angle of the substrate [4]. However, single-layer graphene on the Si-terminated surface of SiC(0001) features back-bonds to surface Si atoms which inhibits linear dispersion around the Dirac point of the electronic density of states. These back-bonds can be saturated through the intercalation of atomic hydrogen to leave a quasi-free-standing layer of graphene, but this process is still not fully understood [3, 4]. Here, we report on the reversible transformation of the surface density of states (SDOS) as a consequence of hydrogenation of the Si back-bond state for the 6H-SiC(0001) system. We use ultraviolet and X-ray photoemission spectroscopy to analyse the transformation of states due to hydrogenation and additionally, for the first time with this system, the extremely surface sensitive technique of metastable de-excitation spectroscopy (MDS) to probe the SDOS of the hydrogen intercalated and decorated buffer layer [5]. Significant changes to the MDS spectra are observed as a result of hydrogenation (see Figure). Supporting density functional theory calculations are presented and compared to the experimental data.

[1] A. Avsar *et al*., Rev. Mod. Phys. 92, 1 (2020). [2] J. Blakrishnan *et al*., Nat. Phys. 9, 284 (2013). [3] C. Riedl *et al*., J. Phys. D: Appl. Phys. 43, 374009 (2010). [4] I. Shtepliuk *et al*., Semicond. Sci. Technol. 31, 113004 (2016). [5] A. Pratt *et al*., Phys. Rev. B 85, 180409(R) (2012).

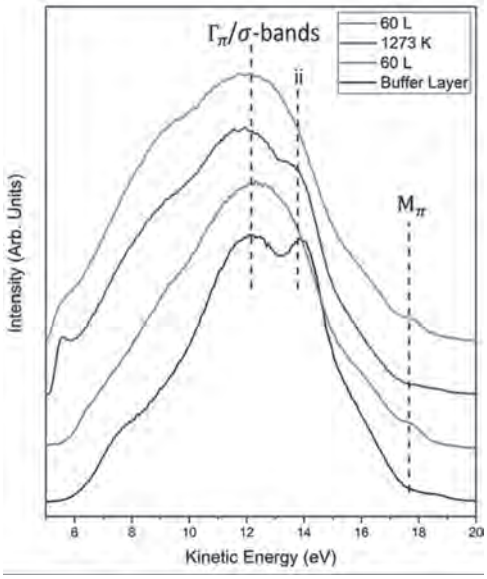

MDS spectra of the back-bonded carbon (buffer) layer before and after exposure to 60 Langmuir (L) of atomic hydrogen.

G5-04. Effect of Magnetic and Electric Fields Work on Cr-Doped $Mo_{1-x}Cr_xSe_2$ (x=0, 0.5) Nanosheet.
Y. Lee[1], T. Tsai[1], Y. Tung[1], C. Kao[1], T. Hsu[1], W. Wu[1], *C. Yang*[1] and K. Lin[2] *1. Department of Physics, Chung Yuan Christian University, Chung Li, Taiwan; 2. Department of Chemical Engineering and Materials Science, Yuan Ze University, Chung-Li, Taiwan*

Two-dimensional MoSe is a multipurpose material that can be made into valleytronics and spintronic devices, quantum dots led, hydrogen evolution reaction catalyst, and ion-batteries. All the above functions are sensitive in any structural variation. The Cr-doped effect turns the $MoSe_2$ from diamagnetism to paramagnetism. Room temperature Raman spectra show different behaviors between pure (x=0) and half Cr-doped (x=0.5) samples. The out-of-phase A_{1g} vibration mode along c-axis of the crystal, shows an enhancement in the Crdoped $MoSe_2$ but weaken in pure one. Both of two samples will return to their original status as magnetic field removed. In contrast, the applying external electric field broadening the FWHM of A_{1g} mode in both samples and will not narrow down again as electric field removed. Furthermore, the Cr-doped $MoSe_2$ also shows less influenced by

the electric field. Varied-temperature x-ray diffraction (xrd) and Raman spectroscopy were studied. The temperature profile of xrd {002} peak position is associated with that's of the FWHM of A_{1g} mode of Raman spectra. This observation shows how the $MoSe_2$ interlayer's spacing influent the phonon softening behavior. The varied-temperature Raman spectra of $MoSe_2$ sample display two peak broadening maxima of the A mode at T_a =150 K and T_b =220 K. Similar phenomena also appeared in Cr-doped one, but the T_a' and T_b' shifted to the higher temperature of 180 K and 260 K, respectively. This observation refers to both phonon softening temperatures are influent by Crdoped effect. As the 200 mT magnetic field applied, all of T_a, T_b, T_a', and T_b' disappeared in both samples. The magnetic field reduces the phonon softening no matter Cr-doped or not. This study can be a reference for how the lattice and energy gap be affected under electric and magnetic filed as these materials are made as and electronic devices.

1. John R. Schaibley, Hongyi Yu, Genevieve Clark, Pasqual Rivera, Jason S. Ross, Kyle L. Seyler, Wang Yao & Xiaodong Xu, Nature Reviews Materials 1, 16055 (2016). 2. Wenwu Guo, Quyet Van Le, Amirhossein Hasani, Tae Hyung Lee, Ho Won Jang, Zhengtang Luo, and Soo Young Kim, Polymers 10, 1309 (2018). 3. Philipp Tonndorf, Robert Schmidt, Philipp Boettger, Rudolf Bratschitsch, Optics Express 21, 4908-4916 (2013). 4. Dahyun Nam, Jae-Ung Lee, and Hyeonsik Cheong, Scientific Reports 5, 17113 (2015).

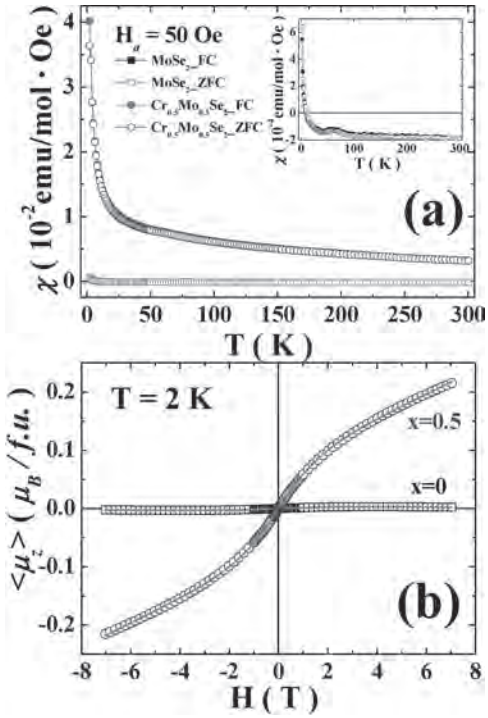

Figure 1. (a) ZFC and FC curves of magnetic susceptibility of x=0 and 0.5 samples. The inset displays the enlarge scale result of x=0 sample. (b) M-H curves of x=0 and 0.5 samples at 2 K.

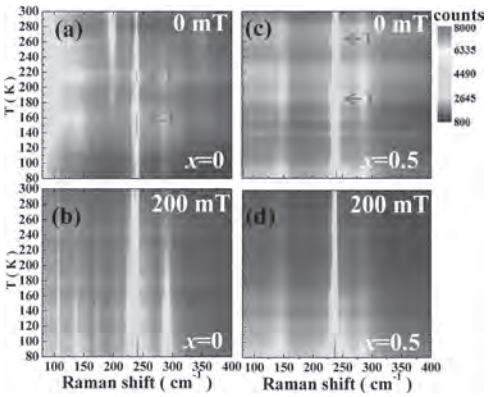

Figure 2. Varied-temperature Raman spectra with applying magnetic fields (H_a) of (a) x=0 and H_a=0 mT, (b) x=0 and Ha=200 mT, (c) x=0.5 and Ha=0 mT, (d) x=0.5 and H_a=200 mT.

G5-05. Enhancement of Coercive Field in van der Waals Ferromagnet Fe_5GeTe_2. *T. Ohta*[1], K. Sakai[1], H. Taniguchi[1], B. Driesen[4], Y. Okada[4], K. Kobayashi[1,2] and Y. Niimi[1,3] *1. Department of Physics, Osaka University, Toyonaka, Japan; 2. Institute for Physics of Intelligence, University of Tokyo, Bunkyo-ku, Japan; 3. Center for Spintronics Research Network, Osaka University, Toyonaka, Japan; 4. Okinawa Institute of Science and Technology Graduate University, Kunigami-gun, Japan*

Since the discovery of graphene, researches on two-dimensional (2D) materials have attracted much attention because of the good controllability of material properties. In 2018, 2D ferromagnetic metal Fe_3GeTe_2 devices have been developed [1], where the Curie temperature T_C is originally 220 K and enhanced above room temperature by gating. In the next year, a cleavable ferromagnetic metal Fe_5GeTe_2 with T_C = 310 K has been synthesized [2]. Although this material could be useful for future van der Waals (vdW) spintronic devices, magnetic properties of the thin Fe_5GeTe_2 films are not well established yet. In this work, we have fabricated thin film devices of both quenched (Q) and non-quenched (NQ) Fe_5GeTe_2 with various thicknesses and measured the Hall resistivities in a wide temperature range [3]. Figure 1 shows typical anomalous Hall effect (AHE) curves measured with both Q- and NQ- Fe_5GeTe_2 thin film (less than 10 atomic layer (L)) devices at T = 50 K. While any significant differences between Q and NQ devices have not been observed for thicker film (more than 10 L) devices (not shown here), the coercive field H_c of 5L Q-Fe_5GeTe_2 is about two times larger than that of 6L NQ-Fe_5GeTe_2. To investigate more details, we have plotted H_c as a function of temperature with both Q- and NQ-Fe_5GeTe_2 in Fig. 2. For comparison, H_c of thicker Q- and NQ-Fe_5GeTe_2 are also plotted. For all the devices, H_c starts to increase below 200 K, but the enhancement of H_c for thinner Q-Fe_5GeTe_2 can be clearly seen below 120 K, where one of the Fe atoms would be ferrimagnetically ordered. This work has demonstrated that the coercive field can be controlled by the film thickness and the synthesis method, and such a controllability of the perpendicular magnetic anisotropy should be useful for future vdW spintronic devices.

[1] Y. Deng *et al*., Nature 563, 94 (2018). [2] A. F. May *et al*., ACS Nano 13, 4436 (2019). [3] T. Ohta *et al*., Appl. Phys. Express 13, 043005 (2020).

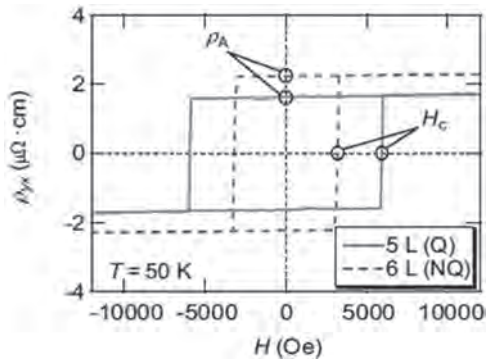

Fig. 1: Hall resistivity of thin Q- and NQ-Fe_5GeTe_2 devices measured at T = 50 K. ρ_A and H_c means the anomalous Hall resistivity and the coercive field, respectively. L indicates the number of unit-cell layer.

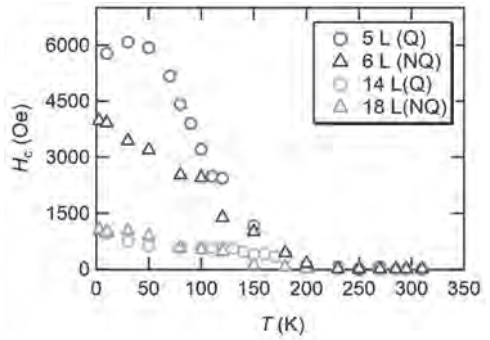

Fig. 2: Temperature dependence of H_c for Q- and NQ-Fe_5GeTe_2 devices with different numbers of L.

G5-06. Self-Hybridization of Optical and Acoustic Magnon Modes in van der Waals Magnets. *J. Sklenar*[1] and W. Zhang[2] *1. Wayne State University, Detroit, MI, United States; 2. Oakland University, Rochester, MI, United States*

Van der Waals magnetic materials are uniquely positioned at the intersection between two-dimensional (2D) materials and antiferromagnetic spintronics. Recent experiments have demonstrated that both optical and acoustic antiferromagnetic resonance in these materials, namely $CrCl_3$, can exist at GHz frequencies [1]. The ability to access antiferromagnetic magnons at GHz frequencies creates new applications for antiferromagnetic spintronics. Chromium trihalides [2] should be considered as candidate materials for hybrid quantum magnonics devices [3]. Here, we present analytical calculations and micromagnetic simulations of the optical and acoustic magnon modes in layered antiferromagnetic structures incorporating both a modified macrospin model and micromagnetic simulations using Mumax3 [4]. We find that the number of optical and acoustic magnon modes, as well as the mode frequencies, are quite sensitive to the number of layers in each structure. Specifically, we have considered layered films in the ultrathin limit, i.e. bilayers, tetralayers, and hexlayers. Within these layered structures, we find that for four and six layers, a magnon self-hybridization effect arises where pairs of optical or acoustic magnons interact and hybridize. This leads to the characteristic avoided energy level crossings in the energy spectra that are seen by both the macrospin model and micromagnetic simulations. We will conclude by computationally demonstrating that if the damping of surface layers is controlled with spin-torques, both the strength and number of avoided energy level crossings in the magnon spectra can be electrically controlled. These results offer a direct interpretation to the experimentally-observed spin dynamics phenomena in 2D magnet layers and also offer new insight connecting 2D materials with quantum magnonics [5].

[1] D. MacNeill, J. T. Hou, D. Klein, et al. Phys. Rev. Lett. 123, 047204 (2019). [2] H. H. Kim, B. Yang, S. Li, et al. PNAS 116, 11131 (2019). [3] Y. Li, W. Cao, V. P. Amin, et al. Phys. Rev. Lett. 124, 117202 (2020). [4] A. Vansteenkiste, J. Leilaert, M. Dvornik, et al. AIP Advance 4, 107133 (2014). [5] Y. Li, W. Zhang, V. Tyberkevych, et. al., ArXiv: 2006.16158.

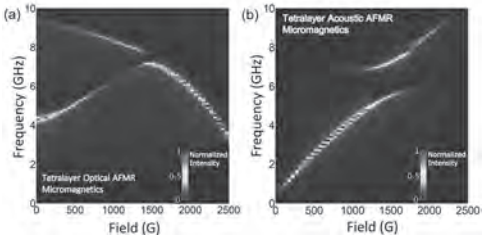

The optical and acoustic antiferromagnetic resonance spectra are calculated for a $CrCl_3$ tetralayer. Note that there are two optical and two acoustic branches. Both optical magnons branches and acoustic magnon branches have an avoided energy level crossing as the field increases.

G5-07. Extended Bloch's law Description of two-Dimensional Dilute Magnetic Semiconductors. *Y. Pham*[1], V. Ortiz Jimenez[1], V. Kalappattil[1], B. Muchharla[1], F. Zhang[2], M. Liu[2], M. Terrones[2] and M. Phan[1] *1. University of South Florida, Tampa, FL, United States; 2. The Pennsylvania State University, University Park, PA, United States*

The recent discoveries of intrinsic ferromagnetism (FM) in two-dimensional (2D) dilute magnetic semiconductors with high Curie temperature (> 300 K) capable of spintronic applications are among the most impressive *tour de force* achieved by theoretical and experimental physicists in the field [1,2]. However, the origin of FM in these systems has remained an open issue. The power function proposed by Bloch, $M(T) = M(0)[1 - (T/T_C)^{\alpha}]$ with $\alpha = 3/2$, has successfully described the temperature dependence of saturation magnetization $M_S(T)$ for bulk ferromagnetic materials [3]. The extended Bloch's law for ferromagnetic nanoparticles (α-Fe) embedded in a non-magnetic matrix (SiO_2) has yielded higher values of α associated with the reduced dimensionality effect [4]. In this study, we demonstrate that V doping into WS_2 monolayer induces ferromagnetic couplings between the vanadium and its tungsten neighbors, forming nanosized ferromagnetic clusters that behave like ferromagnetic nanoparticles. The $M_S(T)$ dependence of the nanoclusters in V-WS_2 monolayer samples with different V concentrations (0, 0.4, 2, and 8 at.%) is well described by the modified Bloch's law at temperatures higher than the blocking temperature. Relative to the Bloch coefficient ($\alpha = 3/2$), the higher values of α (up to 5.96) and its dopant concentration dependence reveal the dimensional effect and the magnetic interaction between the nanoclusters. This method has been successfully applied to describe the M(T) dependence of other 2D magnetic systems such as VSe_2 monolayers that exhibit similar magnetic behavior. Our findings also offer a new way to predict the Curie temperatures of low-dimensional magnetic materials that may not be measured experimentally.

1. S. J. Yun, D. L. Duong, D. M. Ha, K. Singh, T. L. Phan, W. Choi, Y. M. Kim, Y. H. Lee, *Adv. Sci.* 7, 1903076 (2020). 2. F. Zhang, B. Y. Zheng, A. Sebastian, H. Olson, M. Z. Liu, K. Fujisawa, Y. T. H. Pham, V. J. Ortiz, V. Kalappattil, T. Zhang, R. Pendurthi, Y. Lei, A. Laura Elias, Y. Wang, P. E. Hopkins, S. Das, V. H Crespi, M. H. Phan, M. Terrones, *Adv. Sci.* 2020 (https://arxiv.org/abs/2005.01965) 3. F. Bloch, *Z. Phys.* 61, 206 (1930). 4. G. Xiao, C.L. Chien, *J. Appl. Phys,* 61, 8 (1987).

G5-08. Moir'e Magnons in Twisted Bilayer Magnets With Collinear Order. *Y. Li*[1] and R. Cheng[1] *1. University of California, Riverside, Riverside, CA, United States*

We explore the magnonic moir'e bands of twisted bilayer magnets in the presence of next-nearest neighboring Dzyaloshinskii-Moriya interaction, assuming collinear magnetic orders that are preserved under weak interlayer coupling. By calculating comparatively the band structures and the topological Chern numbers for four representative cases, we find: (i) the valley moir'e bands are extremely flat over a wide range of continuous twist angles; (ii) the lowest few bands in valleys can be topological flat-bands, entailing

nontrivial transverse thermal spin transport; (iii) the Chern numbers of these flat bands vary significantly with the twist angle. These properties make twisted bilayer magnets an ideal platform to study the magnonic counterparts of moir'e electrons in twisted two-dimensional materials, where the statistical distinction between magnons and electrons leads to fundamentally new physical behavior.

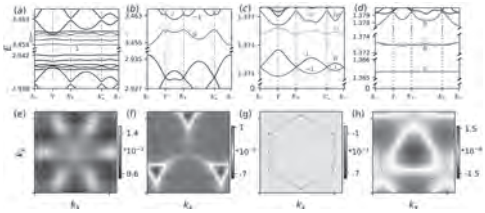

(a), (b), (c) and (d) are the moir'e band structures of the four cases shrunk from K point. The band Chern numbers are labeled on the top of each band. Note that the band Chern number is not well defined if two bands intersect with each other. The DMIs are 0.05 in (a) and (b), while 0.35 in (c) and (d). The twist angle here is $\theta=1.0^{\degree}$. (e), (f), (g) and (h) are the corresponding Berry curvatures of the band i.

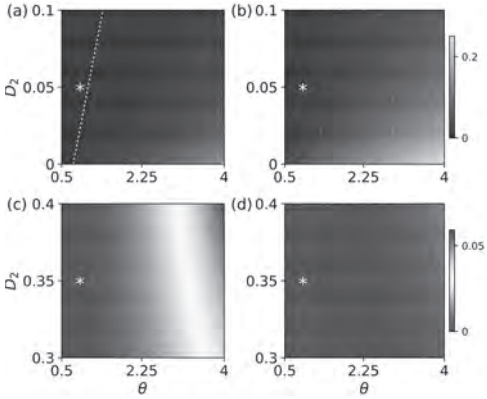

Bandwidth δ of the lowest flat bands (see red curves in Fig.~\ref{Band_Curvature}) as a function of the twist angle θ and the DMI D_{2} for $J_p=0.1$. The white dashed line in (a) indicates the local minimum of δ, or The white star marks where parameters in Fig.~\ref{Band_Curvature} are chosen: $\theta=1^{\degree}$ and $D_{2}=0.05$ (0.35) for cases I and II (III and IV).

G5-09. Valley Polarization, Magnetic Anisotropy and Dzyaloshinskii-Moriya Interaction in Ferromagnetic Janus 2H-VSe*X* (*X* = S, Te) Monolayers.

S. Qi[1], J. Jiang[1] and W. Mi[1] *1. Tianjin University, Tianjin, China*

Two-dimensional (2D) Janus materials are a novel kind of 2D materials, which has potential applications in the nanoelectronics, optoelectronics and catalysts[1]. Here, the electronic structure and magnetic properties of 2D intrinsic ferromagnetic Janus 2H-VSe*X* (*X* = S, Te) monolayers are investigated by density-functional theory. The Janus 2H-VSe*X* (*X* = S, Te) monolayers are intrinsic ferromagnetic semiconductor with an in-plane magnetic anisotropy. The valley splitting of Janus 2H-VSe*X* (*X* = S, Te) monolayers appears by considering the spin-orbit coupling and out of plane magnetization. Additionally, the spontaneous vertical electric dipole moment and large DMI are also found in Janus 2H-VSe*X* (*X* = S, Te) monolayers due to the broken inversion symmetry. Moreover, the valley splitting and DMI can be significantly increased by the in-plane biaxial strain. This work is supported by the National Natural Science Foundation of China (51871161). It is also supported by the High Performance Computing Center of Tianjin University, China.

[1] A. C. Riis-Jensen, T. Deilmann, T. Olsen and K. S. Thygesen, Classifying the electronic and optical properties of Janus monolayers. *ACS Nano* 13, 13354 (2019).

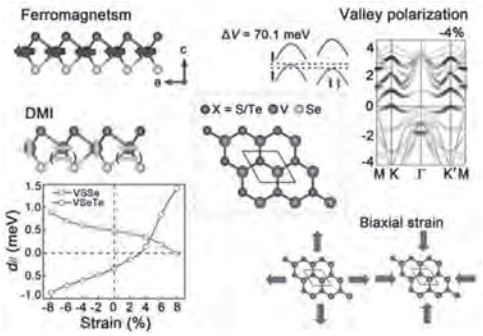

Valley polarization and DMI of 2D intrinsic ferromagnetic Janus 2H-VSe*X* (*X* = S, Te) monolayers.

G5-10. Increased Curie Temperature and Enhanced Perpendicular Magneto Anisotropy of Cr_2Ge_2Te6/NiO Heterostructures.

H. Idzuchi[1,2], A.E. Llacsahuanga Allcca[2], X. Pan[1], K. Tanigaki[1] and Y.P. Chen[2,1] *1. Tohoku University, Sendai, Japan; 2. Purdue University, West Lafayette, IN, United States*

Recently, magnetism in layered van der Waals (vdW) materials has attracted great attention because of their unique magnetic properties, an opportunity to fabricate heterostructures free from constraints in conventional film growth, and the capability of the electric field and crystalline symmetry effect. One of the major issues in vdW ferromagnets is that Curie temperature is relatively low. CrI_3 and $Cr_2Ge_2Te_6$ (CGT) were reported as atomically thin-form ferromagnets in 2017, where the Curie temperature ranges from 30 K (bilayer CGT) to 45K (monolayer CrI_3), being intriguingly low compared to the bulk values of 61 K (bulk CrI_3) and 66K (bulk CGT) [1]. Only a few approaches have been implemented and reported so far, such as electric gating [2]. Therefore, it is important to search for other effective approaches to enhance the Curie temperature. Here, we study magnetic properties in heterostructures between antiferromagnet NiO and vdW ferromagnet CGT. We will report magneto-optical Kerr effects (MOKEs) and detect hysteresis arising from ferromagnetism [3]. We observe a notable increase in both Curie temperature and magnetic perpendicular anisotropy in CGT/NiO heterostructures compared to those in CGT. Measurements on the same exfoliated $Cr_2Ge_2Te_6$ flake (on a SiO_2/Si substrate) before and after depositing NiO show that the hysteresis loop can change into a square shape with larger coercive field for CGT /NiO. The maximum Curie temperature (T_C) observed for CGT /NiO reaches ~120 K, is nearly twice the maximum T_C ~ 60 K reported for CGT alone (Fig.1). Both enhanced perpendicular anisotropy and increased Curie temperature are observed for CGT flakes with a variety of thicknesses ranging from ~5 nm to ~200 nm. We further studied thickness dependences of both CGT and NiO. As shown in Fig.2, CGT/NiO clearly shows increase of Curie temperature for a variety of $Cr_2Ge_2Te_6$ thickness indicates intrinsic in origin. The results indicate that magnetic properties of two-dimensional van der Waals magnets can be engineered and controlled by using the heterostructure interface with other materials.

[1] C. Gong et al Nat. Vol. 546 p.265 (2017). [2] Z. Wang et al Nat. Nanotech. Vol. 13 p.554 (2018). [3] H. Idzuchi et al, Appl. Phys. Lett. vol. 115 p.232403 (2019).

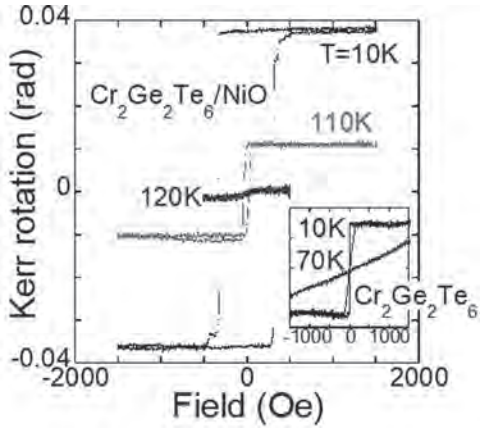

MOKE hysteresis for $Cr_2Ge_2Te_6$/NiO (and $Cr_2Ge_2Te_6$: inset).

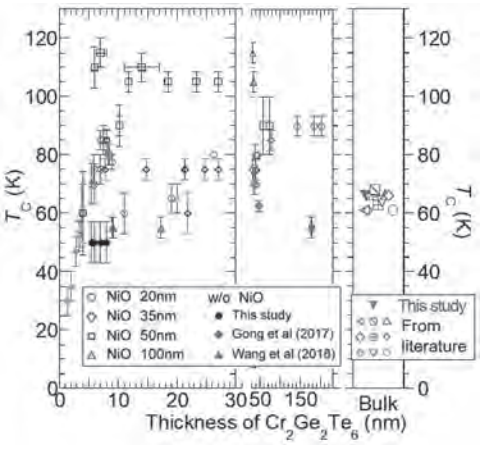

Thickness dependence of Curie temperature for $Cr_2Ge_2Te_6$/NiO and $Cr_2Ge_2Te_6$.

G5-11. Magnon-Phonon Hybridization in a 2D Antiferromagnet.

T.T. Mai[1], K. Garrity[2], A. McCreary[1], J. Argo[3], J. Simpson[4], V. Doan-Nguyen[3], R. Valdes Aguilar[5] and A. Hight Walker[1] *1. PML, National Institute of Standards and Technology, Gaithersburg, MD, United States; 2. MML, National Institute of Standards and Technology, Gaithersburg, MD, United States; 3. Materials Science and Engineering, The Ohio State University, Columbus, OH, United States; 4. Physics, Astronomy, and Geosciences, Towson University, Towson, MD, United States; 5. Physics, The Ohio State University, Columbus, OH, United States*

Low dimensional, van der Waal (vdW) materials, from graphene to 2D magnets such as Fe_3GeTe_2 and CrI_3, show exotic behaviors at the single and few atomic layers limit, including superconductivity, long range magnetism and topological edge states. Their "stackability" further creates new opportunities to explore quantum phenomena, previously studied only in 3D crystals. Here we demonstrate that magneto-Raman spectroscopy is a unique measurement capability, exceptionally well suited to study these exotic 2D materials. Specifically, in the MPX_n (M=Fe, Mn, Ni, X =S, Se) compounds, inter-layer antiferromagnetic ordering has been suggested to survive in the monolayer limit through the measurement of spin-phonon coupling. Using temperature-, polarization-, and wavelength-dependent Raman scattering, we studied the Neel-type antiferromagnet $MnPSe_3$ through its ordering temperature, and as a function of applied magnetic field. Surprisingly, the previously assigned one-magnon scattering peak showed no change in frequency with an increasing in-plane magnetic field. Instead, the Raman data revealed a more surprising story. Due to magnetic ordering, the optical band gap changes in such a way that $MnPSe_3$ resonantly absorbs the 515 nm (2.4 eV) laser, giving rise to resonant Raman scattering and increased signal -to-noise. Furthermore, a broad 2-magnon scattering continuum is observed below T_N that red shifts over 10 cm^{-1} as a function of temperature. We track the hybridization of the closest E_g phonons with this continuum and observe a minimum in lifetime showing the maximum interaction is far below T_N. Combining these data with first-principle calculations, we analyze the Raman features and their interactions.

G5-12. Withdrawn

G5-13. Robust Ferromagnetism in 2D α-Fe_2O_3 Nanosheets.

J. Mohapatra[1], A. Ramos[1], M. Xing[1], J. Elkins[1], J. Beatty[1] and P. Liu[1] *1. Department of Physics, The University of Texas at Arlington, Arlington, TX, United States*

Despite the success in the development of single-atom-layer semiconductors, insulators, and superconductors from a broad range of compounds, there is one category of 2D materials that has received far less attention: 2D magnetic materials. Here, we have synthesized 2D α-Fe_2O_3 nanosheets with exceptionally high coercivity up to 7 kOe (see Figure 1) via a soft-chemical exfoliation process. The remarkably high coercivity observed correlates with the enhanced uncompensated spin canting.[1] The spins on the surface of the 2D sheets contribute to ferromagnetic behavior, while the bulk materials exhibit antiferromagnetic ordering.[2] In addition to the Morin transition, a spin glass-like transition with a rapid increase in saturation magnetization and an increase in anisotropy is observed in the ultra-thin α-Fe_2O_3 nanosheets at a temperature below 50 K. The presence of spin-glass behavior is settled by the observed exchange bias and the frequency-dependent ac susceptibility anomaly.

[1] K. Gandha, J. Mohapatra, N. Poudyal, K. Elkins, J.P. Liu, AIP Adv., 7 (2017) 056324. [2] K. Gandha, J. Mohapatra, M.K. Hossain, K. Elkins, N. Poudyal, K. Rajeshwar, J.P. Liu, RSC Adv., 6 (2016) 90537-90546.

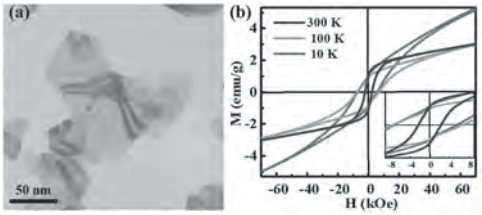

Figure 1. (a) TEM micrograph of 2D layered structures of hematite and (b) the corresponding temperature dependence hysteresis loops.

Session G6
SPECIAL MAGNETIC MATERIALS
(Poster Session)

Takayuki Ishibashi, Chair
Nagaoka University of Technology, Nagaoka, Japan

G6-01. A Typology for Magnetic Field Generator Technologies.
N. Bouda[1], N. Prabhu Gaunkar[1], W. Theh[1] and M. Mina[1] *1. Electrical and Computer Engineering, Iowa State University, Ames, IA, United States*

Abstract This paper identifies different methodologies used to design and enhance suitable magnetic field generator (MFG) with adjustable pulse width. Variations in parameters, such as pulse frequency and amplitude elicit distinct responses. Assessing the differences between functional and experimental parameters of magnetic field generator is essential for application and comparison of results. The use of MFG based techniques is first studied in applications related to optical transmission, transcranial magnetic stimulation devices and magnetic resonances. The paper presents a future framework and design considerations where new (MFG) are expected to play key role in the future. Introduction Magnetic field generator (MFG) systems are ubiquitously used in a wide variety of applications. Some applications areas include magnetic/optical switching, power converters, radar, and medical therapy [1-4]. The ubiquitous nature of such system implies that several attributes may be shared though there might be application-specific variations. In this work, we aim to examine the similarities and dissimilarities (Fig.1)that may exist in MFG systems and identify unifying factors. Design framework The design of new magnetic field generators and the expansion of existing magnetic field generator technologies are required for future innovations. This research/paper highlights the major issues associated with these designs and provides an understanding of the types of issues that must be addressed during the design process. Each magnetic field generator has a related type of functionality to perform and for each functionality a type of response. Results Appropriate signals were applied to the gate drivers and output the desired output was achieved. For the NMOS driver circuit, applying 10V to the gate driver results in an output pulse with 200us. A load resistance of 50mΩ was used, so the output corresponds to a coil current of 25A(Fig. 2). Conclusion In this paper, a new method/classification for Magnetic Field Generator with adjustable pulse width for nuclear magnetic resonance, optical switching and medical therapy applications was presented. Design framework in functionality of the system were introduced and demonstrated

[1] N. P. Gaunkar, J. Selvaraj, W.-S. Theh, R. Weber, and M. Mina, "Pulsed magnetic field generation suited for low-field unilateral nuclear magnetic resonance systems," AIP Advances, vol. 8, no. 5, p. 056814, 2018. [2] J. Selvaraj, P. Rastogi, N. P. Gaunkar, R. L. Hadimani, and M. Mina, "Transcranial magnetic stimulation: Design of a stimulator and a focused coil for the application of small animals," IEEE Transactions on Magnetics, no. 99, pp. 1–5, 2018. [3] N. R. Bouda, M. Mina, and R. J. Weber, "High-current magnetic field generator for transcranial magnetic stimulation applications," IEEE. Transactions on Magnetics, vol. 50, no. 11, pp. 1–4, 2014. [4] N. Prabhu Gaunkar, J. Selvaraj, L. Bauer, M. Mina, R. Weber and D. Jiles, "Design and Experimental Implementation of a Low Frequency Pulsed Magnetic Field Generator," in IEEE Transactions on Magnetics, vol. 53, no. 11, pp. 1-4, Nov. 2017

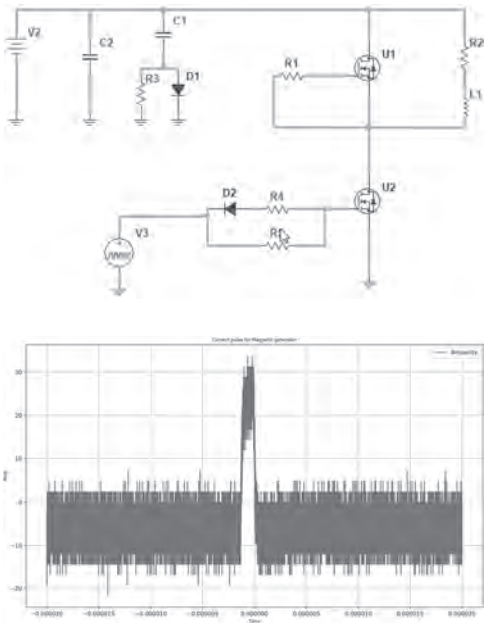

G6-02. Enhancing Magnetic and Magneto-Optical Properties of Praseodymium Substituted Bi-YIG Thin Film on the Glass Substrate by MOD Method. T. Thi[1], V. Dongquoc[1], C. Phuoc[1], D. Viet[1], H. Ahn[1] and *J. Jeong*[1] *1. Department of Materials Science and Engineering, Chungnam National University, Daejeon, The Republic of Korea*

Magneto-optical (MO) thin films can be used for applications in various ways such as MO microscopy, optical isolaters, and information storage devices. Although it is widely investigated, growth of high Faraday rotation magnetic thin films on glass substrate is still considered as a primary issue in MO thin films. Here, we have investigated enhancement of MO properties in praseodymium-substituted bismuth yttrium iron garnet ($Pr_xBi_1Y_{2-x}Fe_5O_{12}$) thin film on a glass substrate by using a metallo-organic decomposition (MOD) method. To improve the MO performance of the as-prepared $Pr_xBi_1Y_{2-x}Fe_5O_{12}$ thin film, different concentrations of Pr-substituted bismuth yttrium iron garnet were prepared. It shows that $Pr_xBi_1Y_{2-x}Fe_5O_{12}$ thin film with an optimal concentration of x=1 exhibited high crystallinity, high saturation magnetization and the highest Faraday rotation (FR) angle of $-6.5^0/\mu m$ at a wavelength of 510 nm as shown in figure below. The $Pr_1Bi_1Y_1Fe_5O_{12}$ thin film fabricated by the modified MOD method displayed excellent MO performance and is a potential candidate for application in optical devices.

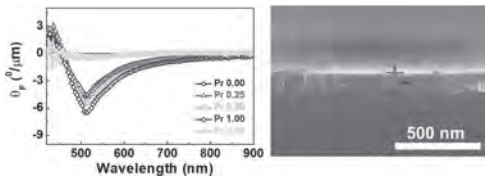

Figure 1. Faraday roation spectrra and SEM image of Pr substituted Bi-YIG thin film.

G6-03. Withdrawn

G6-04. Withdrawn

G6-05. Prospects for Efficient Microwave Energy Harvesting by Thermoelectric Elements Based on the Tunnel Magneto-Seebeck Effect in Magnetic Tunnel Junctions. *G.D. Demin*[1] and N.A. Djuzhev[1] *1. R&D Center "MEMSEC", National Research University of Electronic Technology (MIET), Moscow, Russian Federation*

In the context of the modern development of the Internet of Things (IoT) market, which consists of a billion interacting smart devices, an important task is the search for new technologies for creating energy-efficient power sources that can ensure their long-term autonomous operation [1]. Today, conventional battery cells are not able to overcome this issue, since they have a limited supply of energy and cannot be used to deploy a large-scale IoT network. One of the promising ways to solve the above problem is wireless energy harvesting from the ambient environment [2]. The tunnel magneto-Seebeck (TMS) effect in magnetic tunnel junction (MTJ) seems especially attractive for the conversion of thermal energy resulting from the asymmetric electromagnetic heating of the MTJ [3]. In [4] the record value of the Seebeck coefficient in IrMn-based MTJ was obtained, varying from 0.39 to 1.1 mV/K, which opens the real prospects for the practical implementation of thermoelectric elements based on a set of series-connected MTJs. However, the thermovoltage in MTJ remains relatively small compared to the rectified voltage generated by the spin-torque diode effect, providing sensitivity up to 210000 mV/mW [5]. In order to increase the efficiency of thermal energy conversion in the MTJ, we propose the original concept of MTJ-based thermoelectric element with a thin-film coating of metal-dielectric-metal metamaterial (MM) absorber (Fig. 1). The simulation of a such coating demonstrates close-to-unity absorption of electromagnetic energy in a wide frequency range, which leads to a high temperature gradient (up to several mK) through the MTJ during its electromagnetic heating [6]. It was shown that the inclusion of thermal barrier layers on both sides of the tunnel layer allows one to increase the temperature difference by an order of magnitude (Fig. 2), which ensures enhancement of the thermovoltage. The results obtained can be useful for developing a new class of thermoelectric elements based on the TMS in MTJ, that can provide efficient charging of low-power IoT devices in energy-harvesting powered wireless sensor systems. The work is supported by RF President Grant (#075-15-2019-1139).

[1] W.Z. Khan et al., Computers & Electrical Engineering 81, 106522 (2020); doi: 10.1016/j.compeleceng.2019.106522. [2] M. Gholikhani et al., Applied Energy 261, 114388 (2020); doi: 10.1016/j.apenergy.2019.114388. [3] G.D. Demin et al., Adv. Cond. Matter Phys., article ID 5109765 (2019); doi: 10.1155/2019/5109765. [4] S. Tu et al., Nature Communications 11, 1 (2020); doi: 10.1038/s41467-020-15797-6. [5] L. Zhang et al., Appl. Phys. Lett. 113, 102401 (2018); doi: 10.1063/1.5047547. [6] G. Demin et al., Proceedings of 19th International Conference on Micro and Nanotechnology for Power Generation and Energy Conversion Applications (PowerMEMS) (IEEE, Krakow, Poland, 2019), pp. 1–5; doi: 10.1109/PowerMEMS49317.2019.61547409666.

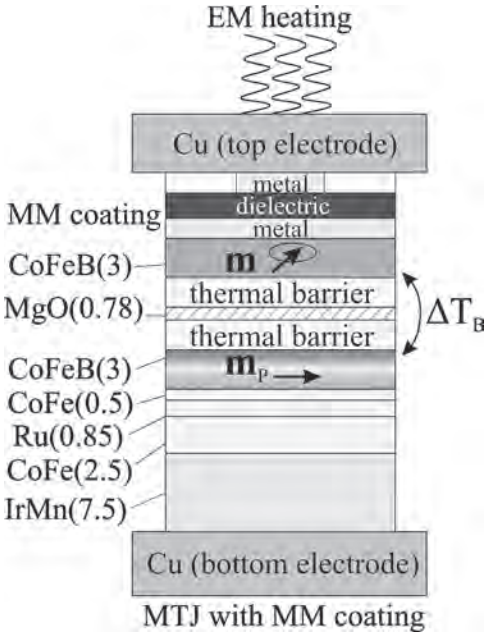

Fig.1. MTJ.

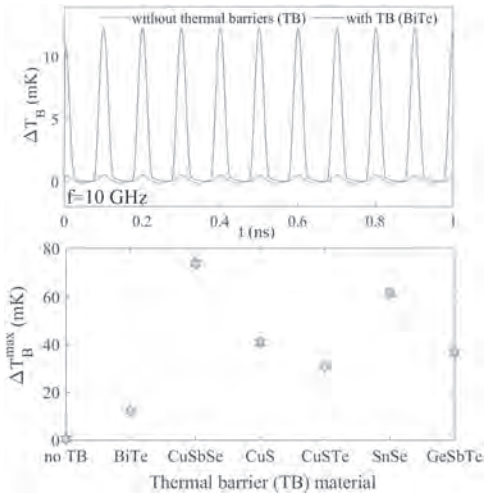

Fig.2. ΔT_B vs TB material.

G6-06. Design of High-Speed Permanent-Magnet Synchronous Machines Considering Thermal and Mechanical Characteristics of Permanent Magnet. *T. Bang*[1], K. Shin[3], J. Woo[1], J. Lee[1], H. Cho[1], J. Bird[2] and J. Choi[1] *1. Chungnam National University, Daejeon, The Republic of Korea; 2. Portland State University, Portland, OR, United States; 3. Chonnam National University, Yeosu, The Republic of Korea*

Through the development of the manufacturing technology of the Permanent Magnet (PM), efficiency and output power of the permanent-magnet synchronous machines have dramatically increased, and various industries are replacing the conventional mechanical gear transmission system by the direct-drive type high-speed permanent-magnet synchronous machine. Previously, various researchers studied design methods for the rotor structure of high-speed PM synchronous machines. For instance, Hong et al. studied a design method considering rotor dynamics, and Ede et al. considered the natural frequency and bending mode of the rotor in the design process. Moreover, Ahn et al. designed the rotor structure considering PM and sleeve material stress by employing an analytical method, and Kim et al. optimized the PM considering the demagnetization. However, these studies did not consider the characteristics change of the rotor structure depending

on the operating temperature. Besides, the electromagnetic properties generally change following the B-H characteristic curve according to the operating temperature. This produces irreversible magnetization during on operation, causing not only the output decrease, but also changing the electromagnetic characteristics. Thus, thermal characteristics of rotor structure materials have to be considered. In this study, the rotor structure is designed considering the stress distribution and the demagnetization characteristics that vary with the materials and operating temperature. Figure 1 shows the analytical model and the prototype built for the verification of the analytical method. Figure 2 (a) shows the results of the stress characteristics analysis and the design range, which vary with temperature. Furthermore, Figure 2 (b) shows the B-H curve analysis results during operation.

[1]C. L. Jeong, J. Hur, "Optimization Design of PMSM With Hybrid-Type Permanent Magnet Considering Irreversible Demagnetization," IEEE Trans. Magn., IEEE Trans. Magn., vol. 53, no. 11, 2017, ID 8110904 [2] M. R. Park, H. J. Kim, Y. Y. Choi, J. P. Hong, J. J. Lee, "Characteristics of IPMSM According to Rotor Design Considering Nonlinearity of Permanent Magnet," IEEE Trans. Magn., vol. 52, no. 3, 2016, ID 8101904 [3] J. H. Ahn, C. Han, C. W. Kim, and J. Y. Choi, "Rotor Design of High-Speed Permanent Magnet Synchronous Motors Considering Rotor Magnet and Sleeve Materials," IEEE Trans. Appl. Superconduct., vol. 28, no. 3, 2018, ID 5201504 [4] K. C. Kim, S. B. Lim, D. H. Koo and J. Lee, "The Shape Design of Permanent Magnet for Permanent Magnet Synchronous Motor Considering Partial Demagnetization," IEEE Trans. Magn., vol. 42, no. 10, pp. 3485-3487, 2006

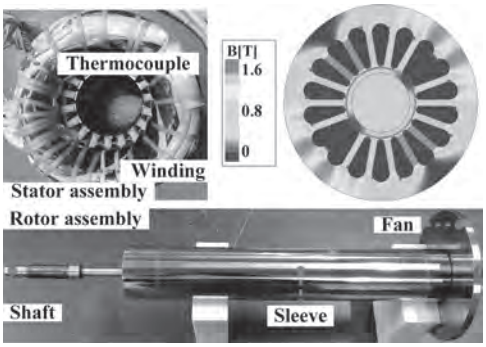

Fig. 1. Analysis model and proto type model

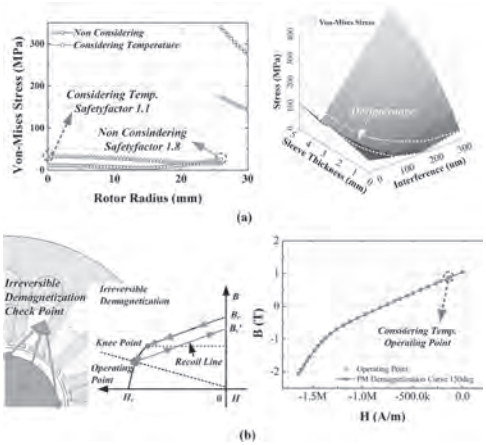

Fig. 2. (a) Analysis results of stress considering temperature (b) Analysis results of PM Demagnetization curve considering temperature

G6-07. Withdrawn

G6-08. The Microwave Absorption Properties of $Y_2Fe_{16}Si$@MOF and $Y_2Fe_{16}Si$@GO Composites. *Y. Wang*[1] and J. Yang[1] *1. Peking University, Beijing, China*

With the development in communication technology, serious electromagnetic wave radiation pollution have been created, resulting in electromagnetic interference and health hazards. Thus, materials with excellent microwave absorbing properties have become an urgent need. Magnetic particles with core-shell structure are widely used as microwave absorbers due to their high magnetic loss, high surface anisotropy and low skin effect. The rare earth-Fe intermetallic compounds with planar magnetocrystalline anisotropy were considered to be promising candidates as microwave absorbing materials due to their higher Snoek's limit as compared to the cubic spinel-type ferrites. In this work, $Y_2Fe_{16}Si$ alloy was massively produced through strip casting technique. The $Y_2Fe_{16}Si$ alloy exhibits a single phase of hexagonal Th_2Ni_{17}-type structure with a planar magnetocrystalline anisotropy and a saturation magnetization of 121 emu/g. Metal Organic Framework(MOF) and Graphene Oxide(GO) are used to coat the $Y_2Fe_{16}Si$(YFeSi) magnetic powder. Their microwave absorption properties of $Y_2Fe_{16}Si$-MOF/GO-paraffin composites were investigated. The reflection loss of YFeSi@MOF-paraffin and YFeSi@GO-paraffin could reach -19.2dB@3.3GHz and -18.3dB@16.2GHz with qualified bandwidth (QB, RL < -10 dB) over 1GHz and 4GHz, respectively. It was found that impedance matching and the attenuation capability of the composites can be easily tuned by varying the mass ratios of $Y_2Fe_{16}Si$ to paraffin. Full covers of QB on the Ku-band can be achieved for $Y_2Fe_{16}Si$-GO-paraffin composite when the thickness is less than 2.0 mm. Hence, $Y_2Fe_{16}Si$-GO-paraffin composites exhibit great potential as a high-performance microwave absorber.

Yang, W.Y., et al., Acta Materialia., Vol. 145, p.331-336(2018) Green, M., et al., Materials Today Chemistry., Vol. 9, p.140-148(2018)

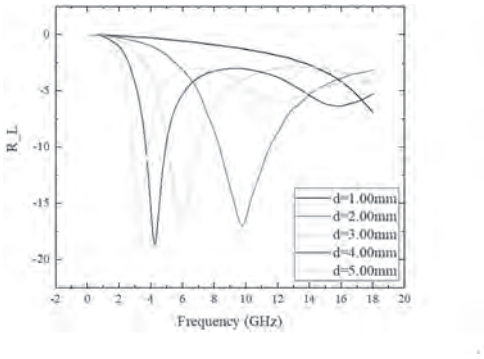

The reflection loss of YFeSi@MOF/paraffin composites.

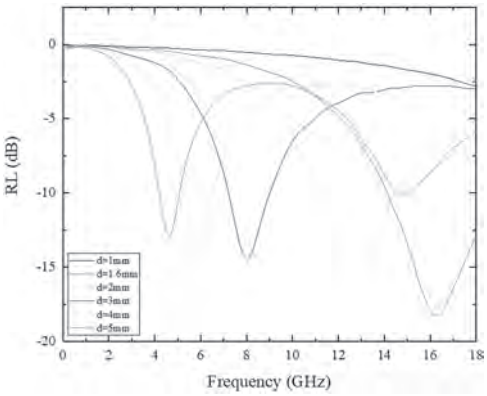

The reflection loss of YFeSi@GO/paraffin composites.

G6-09. Superconducting Ferromagnet Based on Ni_2NbSn Heusler Alloy. *S. Nalevanko*[1,2], L. Galdun[1], T. Ryba[3], M. Reiffers[4], J. Kačmarčík[5] and R. Varga[1] *1. CPM-TIP, UPJS, Trieda SNP 1, 040 11 Kosice, Slovakia, Kosice, Slovakia; 2. UFV, PF UPJS, Kosice, Park Angelinum 9, 040 01 Kosice, Kosice, Slovakia; 3. RVmagnetics, a.s., Nemcovej 30, 04001 Kosice, Slovakia, Kosice, Slovakia; 4. Inst. Phys., Fac. Hum. and Nat. Sci., UNIPO, Ul. 17. Novembra 1, 080 01 Presov, Slovakia, Presov, Slovakia; 5. UEF SAV, Watsonova 47, 04001 Kosice, Slovakia, Kosice, Slovakia*

Heusler alloys are well-known materials with different magnetic and electrical transport properties like shape memory effect, magnetocaloric effect, etc. Additionally, in Heusler alloy with the chemical composition Ni_2NbSn, a superconducting state can be observed [1]. Under the critical temperature, superconductors show strong diamagnetic behavior and lead current without resistance. Even though superconductivity and ferromagnetism are antagonistic, the coexistence of ferromagnetism and superconductivity has been observed. One example of such an alloy is Ni_2NbSn [2]. In this work, we present structural, magnetic, and electrical properties of Ni_2NbSn Heusler alloy prepared in the form of an ingot. The structural analysis has revealed a B2 disordered phase. The coexistence of ferromagnetism and strong diamagnetism has been observed using magnetic measurements. Moreover, transport measurements show superconducting behavior at the temperature below 3.39K. To increase the homogeneity and to improve the structural disorder of the alloy, annealing has been performed. The subsequent magnetic measurement showed improvement in the magnetic properties of the bulk sample. The Ni_2NbSn Heusler alloy has also been prepared in the form of a glass-coated microwire. In contrast to the bulk sample, the glass-coated microwire exhibits only superconducting behavior. This research was supported by the projects APVV-16-0079 and Slovak VEGA grant. No. 1/0053/19.

[1] T. Klimczuk, C.H. Wang, et al., Physical Review B 85, 174505, (2012) [2] P. Kanuch, T. Ryba, et al., Acta Physica Polonica A 131, 1057-1059, (2017)

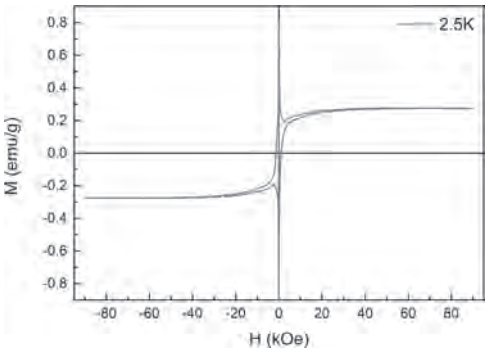

Fig. 1: Hysteresis loop of annealed Ni_2NbSn Heusler alloy at 2.5K

G6-10. Study on Structure and Magnetic Properties of $Y_2(Fe,Co)_{14}B$ Melt-Spun Ribbons. X. Zhang[1], *J. Han*[1], P. Liu[1], S. Liu[1], C. Wang[1], X. Zhang[1], Q. Xu[1] and Y. Yang[1] *1. School of Physics, Peking University, Beijing, China*

In recent years, the adjustable anisotropy of rare earth transition metal intermetallic compounds has attracted more and more attention. This is because the compounds can not only be used as hard magnetic materials by taking advantage of their strong uniaxial anisotropy, but also can be used as soft magnetic materials by using their plane or cone anisotropy. $Re_2Fe_{14}B$ (Re is rare earth element) is one of the compounds. Previous studies have shown that $Re_2Fe_{14}B$ compounds may have high saturation magnetization. When Re is Nd or Pr element, $Nd_2Fe_{14}B$ or $Pr_2Fe_{14}B$ materials exhibit strong uniaxial anisotropy, and the coercivity is very high. Thus, the materials can be used as hard magnetic materials. However, if Re is high-abundance Y element, and Fe is partly replaced by Co, the anisotropy of $Y_2Fe_{14-x}Co_xB$ can be changed from c-axis to ab-plane, and the anisotropy can be continuously adjusted. This means that $Y_2Fe_{14-x}Co_xB$ material may be used as soft magnetic materials. However, in the past, more attention has been focused on develop high-performance $Re_2Fe_{14}B$ hard magnetic materials, while ignoring the possibility of $Re_2Fe_{14}B$ as soft magnetic materials. Therefore, in order to develop a usable $Y_2Fe_{14-x}Co_xB$ soft magnetic material, it is necessary to systematically investigate its structure and magnetic properties to obtain high saturation magnetization and low coercivity. In this study, $Y_2Fe_{14-x}Co_xB$ melt-spun ribbons were prepared by adjusting alloy composition and optimizing melt-spinning technique. It is found that Y2Fe4.5Co9.5B ribbons with saturation magnetization of 120 emu/ g and coercivity less than 1 Oe can be prepared at x = 9.5 and wheel speed of 55 m / s (see Fig.1). TEM investigations exhibit that the ribbons were composed of $Y_2(Fe,Co)_{14}B$ nanocrystals with a grain size of 2-4 nm and an amorphous matrix. The high energy ball milling technology was used to crush the ribbons and the flake particles with the size of ~30 um and the thickness of ~250 nm were obtained (see Fig.2), which shows the potential for high frequency soft magnetic materials. It is found that the magnetic ring composed of the flake particles and paraffin wax in the mass ratio of 2:1 has good microwave absorbing properties near 1-2 GHz.

1. M. Sagawa, S. Fujimura and N. Togawa. Journal of Applied Physics. Vol. 55, P. 2083 (1984). 2. T. Ukai, K. Yamaki and H. Takahashi. Journal of Applied Physics. Vol. 69, P. 4662 (1991). 3. Yingchang Yang, Jinbo Yang and Jingzhi Han. IEEE transactions on magnetics. Vol. 51, P. 2103806(2015).

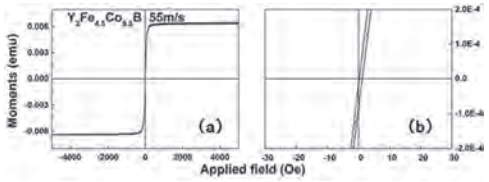

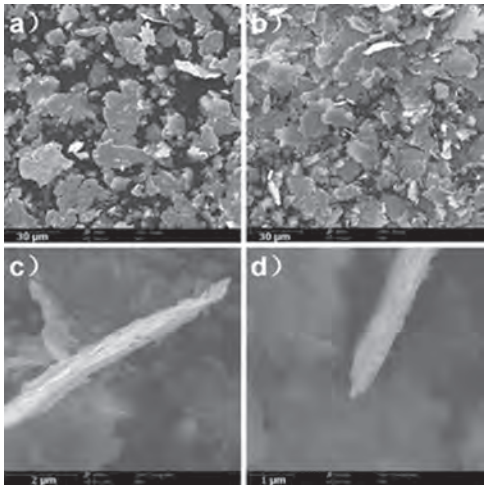

G6-11. High Frequency Magnetic Properties of Nanostructured $YFe_8Ni_{0.4}B_{0.6}$/Ferrits/Paraffin Composites. *S. Liu*[1], C. Meng[2,1], W. Chang-Sheng[1] and J. Yang[1] *1. Physics, Peking University, Beijing, China; 2. School of Physical Science and Technology, Inner Mongolia University, Hohhot, China*

With the rapid development of electronic communication device and radar detection system, the microwave absorption materials (MAMs) with a thin thickness, lightweight, wide bandwidth and strong absorption are urgently desired to cope with electromagnetic wave pollution and threats of military radar. Ferrites are considered to be the best candidate for MAMs due to its unusual combination of magnetic and insulating properties. However, the permeabilities of spinel ferrites decline dramatically in high-frequency regions, such as the GHz region. The rare-earth transition-metal (R-T) intermetallic compounds show planar anisotropy and high saturation

magnetization and are found to be promising candidates as MAMs. However, their resistivities are in the millions of parts of the ferrite. By embedding the conductive metallic magnetic particles in an insulating matrix such as ferrits, the resistivity of the composites increases from 10^{-6} to 10^{-4} Ω*m, which can reduce the eddy current losses. In this work, nanostructured $YFe_8Ni_{0.4}B_{0.6}$ ribbons with $TbCu_7$-type structure were synthesized using melting spinning technique. It exhibits a planar magnetocrystalline anisotropy and high magnetization. The $YFe_8Ni_{0.4}B_{0.6}$ powders were mixed with ferrite ($NiFe_2O_4$ nanopowders), to form a composite with high resistivity. The high-frequency properties of $YFe_8Ni_{0.4}B_{0.6}$-ferrits-paraffin composites were investigated. It was found that the introduction of the ferrits can dramatically increase the qualified bandwith(*QB*, *RL* < -10 dB)) of the $YFe_8Ni_{0.4}B_{0.6}$. These composites exhibit excellent microwave absorption properties with an average value of reflection loss (*RL*) being below -10 dB at 6 - 18 GHz. The composite with mass ratio of 3:0.45:1(wt%) among $YFe_8Ni_{0.4}B_{0.6}$:ferrits:paraffin exhibits microwave absorption performance with minimum reflection loss (*RL*) of -20 dB with the thickness of 2.0 mm and a QB of 4 GHz. The qualified bandwidth (*QB*, *RL* < -10 dB) could fully cover the S, X, and Ku-band with a thickness of 2.5, 2.0 and 1.8mm, respectively,which can be one of the promising microwave absorbing materials.

1. E.A. Périgo, B. Weidenfeller, P. Kollár, J. Füzer, Past, present, and future of soft magnetic composites, Applied Physics Reviews, 5 (2018) 031301. 2. F.M. Idris, M. Hashim, Z. Abbas, I. Ismail, R. Nazlan, I.R. Ibrahim, Recent developments of smart electromagnetic absorbers based polymer-composites at gigahertz frequencies, Journal of Magnetism and Magnetic Materials, 405 (2016) 197-208. 3. S.P. Pawar, S. Biswas, G.P. Kar, S. Bose, High frequency millimetre wave absorbers derived from polymeric nanocomposites, Polymer, 84 (2016) 398-419. 4. I. Kong, S. Hj Ahmad, M. Hj Abdullah, D. Hui, A. Nazlim Yusoff, D. Puryanti, Magnetic and microwave absorbing properties of magnetite–thermoplastic natural rubber nanocomposites, Journal of Magnetism and Magnetic Materials, 322 (2010) 3401-3409.

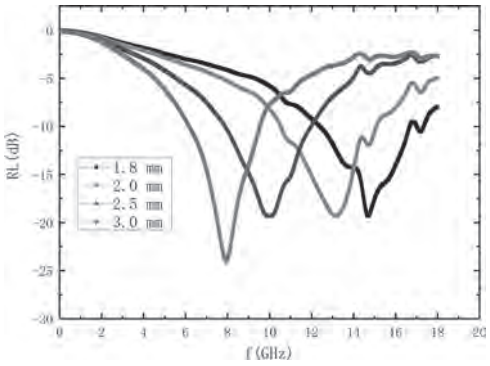

The microwave absorption performance of the composite with mass ratio of 3:0.45:1(wt%) among $YFe_8Ni_{0.4}B_{0.6}$:ferrits:paraffin

G6-12. Composition Graded Materials With Different Spatial Distribution of Nanograin: Synthesis and Magnetic Properties. *E. Denisova*[1,2], L. Chekanova[1], I. Nemtsev[1], R. Iskhakov[1], N. Shepeta[2] and L. Kuzovnikova[3]
1. Kirensky Institute of Physics, Federal Research Center KSC SB RAS, Krasnoyarsk, Russian Federation; 2. Siberian Federal University, Krasnoarsk, Russian Federation; 3. Krasnoyarsk Institute of Railways Transport, Krasnoyarsk, Russian Federation

Functionally graded materials are some of the most promising materials, whose compositions and microstructures are varied continuously from place to place. Magnetization-graded ferromagnetic materials have recently emerged as the magnetic counterparts of compositionally doped semiconductors, with internal magnetostatic potentials determined by the magnitude and direction of their magnetization gradients [1-2]. These gradients are introduced intentionally and are controlled in order to optimize materials properties. This work focuses on the comparison between the magnetic properties of compositionally graded and uniform materials with different spatial distribution of nanograin, such as composite particles, multisegmented and gradient nanostructured rods and multilayer films. The CoNi, Ni/Co particles, multisegmented CoNi/FeNi rods, Co-Ni and Fe-Ni rods with gradient Ni content along rod, multilayer Co/CoNi films were synthesized by electroless deposition. The magnetic and structural properties are characterized by electron microscopy, X-ray diffraction, ferromagnetic resonance spectroscopy and vibrating sample magnetometer. The FMR spectrum for gradient CoNi rods consists of a single absorption line. The presence of graded Ni content could give rise to graded anisotropy effects (that is, local variations of the effective magnetic anisotropy field H_a along the rod axis). Such variations in H_a values manifests in variations of resonance fields for different rod segments and increases linewidth of gradient rods. In case of multisegmented Ni/Co and Co-Ni/Fe-Ni rods the FMR spectrum consists of two wide absorption lines corresponding to different segments. For multilayer Co/CoNi films the range of Co layer thickness covers both the case where the thickness is smaller than t_L=30 Å, we observe a single absorption line, and the case where the thickness is comparable or bigger t_L, the FMR spectrum consists of two absorption lines corresponding to Co and CoNi layers. The coercivity magnitudes for composite particles Ni/Co (700 Oe) are larger than that CoNi (200 Oe) particles with the same composition. Therefore it would be possible to tune the magnetic properties of the particles by their structural architecture.

1. C. Sudakar, R. Naik, G. Lawes and J. V. Mantese, Appl. Phys. Lett. Vol.90, p.062502 (2007) F.A. Chyad, A.R. Jabur, S.A. Sabreen, Energy Procedia, Vol. 119, p. 52-60 (2017)

Session H1
AMORPHOUS AND NANOCRYSTALLINE SOFT MAGNETS

Song Lan, Chair
Chongqing Jiaotong University, Chongqing, China

CONTRIBUTED PAPERS

H1-01. Fe-ETM-Nb-B (ETM = Cr, Mn) Glassy Alloys for Energy Recovery. M. Lostun[1], M. Grigoras[1], G. Ababei[1], G. Stoian[1], H. Chiriac[1] and *N. Lupu*[1] *1. Magnetic Materials and Devices, National Institute of Research and Development for Technical Physics, Iasi, Romania*

The increasing demand of energy is requiring the continuous diversification of the production sources and the consideration of alternative potential resources such as the waste heat from industrial processes or residential heating systems. New devices and materials must be designed to recover efficiently the waste heat and among them, the thermomagnetic materials are an interesting alternative. The ideal thermomagnetic materials for energy harvesting devices should have a sharp ferro-paramagnetic phase transition, with minimal hysteresis and minimal latent heat and be accurately tuned to the available waste-heat temperature. The main objective of this work is to thoroughly investigate the thermomagnetic characteristics and their connection with the microstructural features for $Fe_{79.7-x}ETM_xNb_{0.3}B_{20}$ (ETM = Cr, Mn; x = 11.5÷20 at.%) rapidly quenched alloys, depending on the ETM content. The possibility to tailor T_C around room temperature and their minimal hysteresis recommends these glassy alloys for energy conversion applications. UHR-TEM studies indicate glassy structures with clusters of 2-3 nm embedded within an amorphous matrix. Mn additions double the saturation magnetization (80 emu/g) compared with Cr compositions (40 emu/g). The larger the ETM content (up to 20 at.%), the more reduced the Curie temperature is (from +45°C down to -100°C). However, the Curie temperature is strongly dependent on the addition element. Mn is antiferromagnetic and behaves in a similar way as Cr does. Thus, the larger the Mn content the more numerous the antiferromagnetic interactions are, suggesting a transition temperature evolving more towards a Néel temperature for Mn contents over 16 at.%. Our aim is to study the complex interrelation among structure, mechanical, magnetic and thermal properties and, subsequently, to design new energy conversion devices with enhanced efficiency. *Work supported by the Nucleu Programme (Project PN 19 28 01 01) and Contract No. 11PFE/16.10.2018 financed by the Romanian Ministry of Education and Research.*

H1-02. Investigating Hidden Devitrification Pathways in the Fe-Si-B System Without Alloying Additions. *X. Zhang*[1], A. Jimenez[2], J. Mesa[1], R. Pérez del Real[3], M. Vazquez[3] and L. Lewis[1,2] *1. Mechanical and Industrial Engineering, Northeastern University, Boston, MA, United States; 2. Chemical Engineering, Northeastern University, Boston, MA, United States; 3. Instituto de Ciencia de Materiales de Madrid, CSIC, Madrid, Spain*

The performance of advanced soft ferromagnets relies on achievement of an optimized nanocrystalline structure through controlled devitrification from amorphous precursors. While small additions of early/late transition metal elements (Nb, Cu, etc.) assist in structural refinement through tuning of devitrification kinetics[1], they also reduce the alloys' saturation magnetization. In this study, we present new results that the devitrification kinetics of FeSiB metallic glasses can also be tailored by the quenching conditions delivered by different rapid solidification treatments. Metallic glasses of composition $Fe_{79}Si_{11}B_{10}$ were fabricated into two distinct forms: 1) melt-spun ribbons of ~25 μm in thickness and 2) water-quenched microwires of ~150 μm in diameter. The structural, calorimetric, and magnetic behavior of these alloys were probed. The samples are confirmed to undergo a two-stage devitrification, with the devitrification kinetics assessed using the Johnson-Mehl-Avrami model[1]. While it is confirmed that both as-quenched samples have a nominally identical chemical composition and amorphous structure, they show distinctly different devitrification behaviors. As revealed by the calorimetric data (Fig. 1), the primary devitrification of the wires occurs at a lower temperature (by ~80 K) with a slower heat release, while the secondary devitrification stage is consistent between the two samples. Kinetics analysis reveals that the wires exhibit a reduction in activation energy for devitrification by ~50%, and a smaller value of the Avrami exponent, relative to the ribbons. These results suggest that the water-quenched wires show devitrification kinetics that mimics the Finemet-type nanocrystalline alloys[1]. These differences in the samples' devitrification are attributed to the condition of the initial glassy state, which is subtly affected by the specifics of the rapid solidification process. The results from this work are anticipated to allow tuning of rapid solidification conditions to achieve high-moment, high-performance alloys without alloying additions. Acknowledgments: Northeastern University, Fulbright Scholar Program, and ICMM/CSIC, Spain

1. M.E. McHenry et al., Scripta Materialia, vol.48, p.881–887(2003)

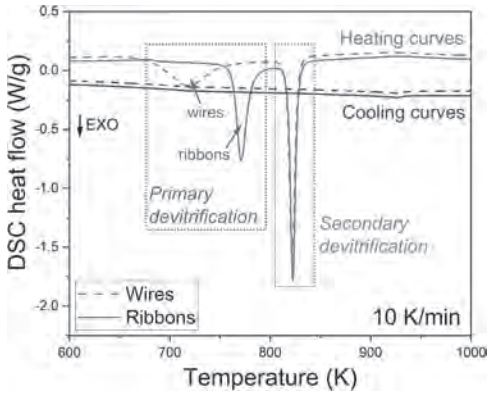

Fig.1. Calorimetric results for the as-quenched ribbons and wires

H1-03. Effects of Magnetostriction on Domain Wall Dynamics Inside Multi-Grains Soft Magnet Revealed by Micromagnetic Simulations. *H. Tsukahara*[1,2], H. Imamura[2] and K. Ono[1] *1. Daigaku Kyodo Riyo Kikan Hojin Ko Energy Kasokuki Kenkyu Kiko, Tsukuba, Japan; 2. National Institute of Advanced Industrial Science and Technology Tsukuba Center Tsukuba Central, Tsukuba, Japan*

Magnetostriction plays a key role in magnetization dynamics inside soft magnetic materials, which are widely used in electronic devices for inductor cores. In general, the performance of the soft magnetic device is governed by magnetization dynamics such as domain-wall motions. Thus, it is indispensable to understand how magnetostriction affects the magnetization dynamics. We performed micromagnetic simulations in order to clarify the effects of the magnetostriction. To simulate the magnetostriction, we have

to solve the elastic equations of the crystal structure.[1,2] The magnetization generates strains of the crystal structure, and deformations of the crystal are affected by the distant magnetization. We solved equations of motions for the strains, and we obtained the magnetostrictive field. We parallelized simulations using Message Passing Interface.[3] Figure 1 shows a simulation model containing two grains. Inside the grains, we consider strip-shape magnetic domains. The crystal axes are rotated -20 and 20 degrees from the x-direction in the grain A and B, respectively. We applied AC magnetic field along the x-direction. The frequency of the AC magnetic field is 100MHz. We also applied static external stress parallel to the crystal axis of the grain A. The magnetic material is Fe. Figure 2 shows energy losses as a function of the external stress using the simulation results. When the tensile strain is 20 MPa, the energy loss is 1.8 times larger than that without stress. The results of this work show that the energy loss strongly depends on the stress and the microstructure of the soft magnetic materials.

[1] J.X. Zhang, and L.Q. Chen, Acta Materialia 53, 2845 (2005). [2] S. Bhattacharyya, T.W. Heo, K. Chang, and L.-Q. Chen, Modelling Simul. Mater. Sci. Eng. 19 035002 (2011). [3] H. Tsukahara, K. Iwano, C. Mitsumata, T. Ishikawa, K. Ono, Comput. Phys. Commun, 207, 217 (2016).

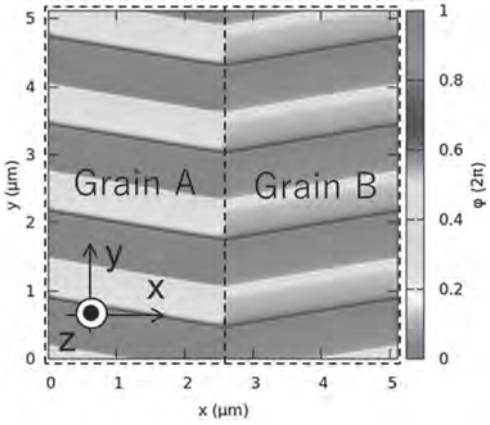

FIG.1 Illustration of the simulation model constructed by two grains.

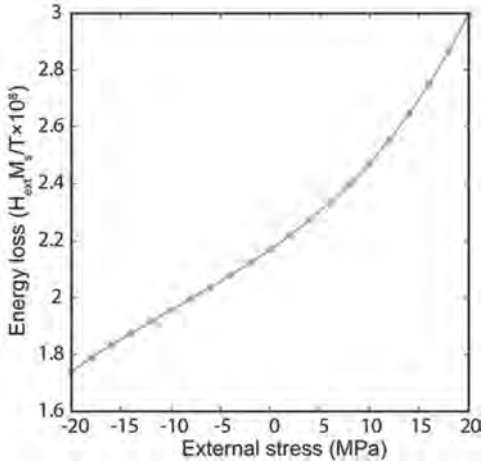

FIG.2 Energy losses as a function of the external stress.

H1-04. Iron Loss and Magnetic Properties of Amorphous and Nanocrystalline Ring Core Under Inverter Excitation on the Order of MHz. *A. Yao*[1], F. Kato[1] and H. Sato[1] *1. Advanced Power Electronics Research Center, National Institute of Advanced Industrial Science and Technology (AIST), Tsukuba, Japan*

In high speed (HS) motor systems, a pulse width modulation (PWM) inverter is often used[1~8]. To realize low loss HS motor systems, it is important to understand iron loss characteristics of amorphous and nanocrystalline magnetic materials (AMM and NMM), which have low iron loss properties[3,4], fed by PWM inverter. However, there has been no report on magnetic properties of AMM and NMM under PWM inverter excitation at high-carrier frequencies (HCF). This study focuses on the determination of iron losses and *B*-*H* loop properties of AMM and NMM under inverter excitation at HCF on the order of MHz. Fig. 1 shows a schematic of the ring test under PWM inverter excitation at HCF. Here, the iron loss W is calculated by $W=\int H dB/\rho$, where f(=50Hz) is the fundamental frequency, ρ is the density, H is the magnetic field intensity, and B is the magnetic flux density. The maximum magnetic flux density is set to 0.5T. The carrier frequency f_c and dead time D are varied from 400kHz to 1MHz and 0 to 10ns. The ratio η of the loss at D=0ns to that at D=10ns is defined by W_{10ns}/W_{0ns}. See Ref.8 for details of the method. Figs. 2 (a) and (b) show *B*-*H* curves of AMM and NMM under PWM inverter excitation. The variation of the minor loop of AMM (3 A/m) is larger than that of NMM (0.2 A/m). Fig. 2(c) and (d) show W and η under inverter excitation. Due to the skin effect and the distortion of voltage[16], the W decreases with the increase in f_c and then increase. In addition, we for the first time found that η of NMM is smaller than that of AMM because the variation in H of the minor loop of AMM enlarges. The NMM is expected to be suitable for use in large dead time of HS motor compared to the AMM. These results open the way to further research in HS motor system based on studies of magnetic properties at HCF.

[1] A. Boglietti, *et al.*, IEEE Transactions on Magnetics, 27 (6), 5334–5336 (1991). [2] M. Kawabe, *et al.*, IEEE Transactions on Magnetics, 48 (11), 3458–3461 (2012). [3] A. Yao, *et al.*, AIP Advances, 8 (5), 056804 (2018). [4] A. Yao, *et al.*, IEEE Transactions on Magnetics, 54 (11), 1–5 (2018). [5] A. Yao, *et al.*, IEEJ Journal of Industry Applications, 7 (4), 321–328 (2018). [6] A. Yao, *et al.*, Journal of the Magnetics Society of Japan, 43 (6), 105–108 (2019). [7] A. Yao, *et al.*, Journal of the Magnetics Society of Japan, 44 (3), 52–55 (2020). [8] A. Yao, *et al.*, Journal of the Magnetics Society of Japan (accepted), (2020).

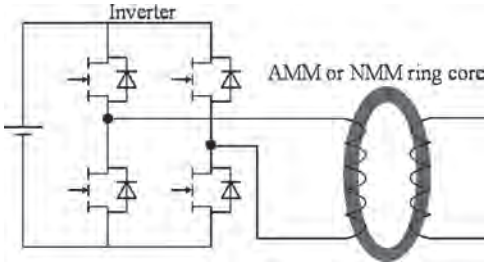

Schematic of ring test under PWM inverter excitation.

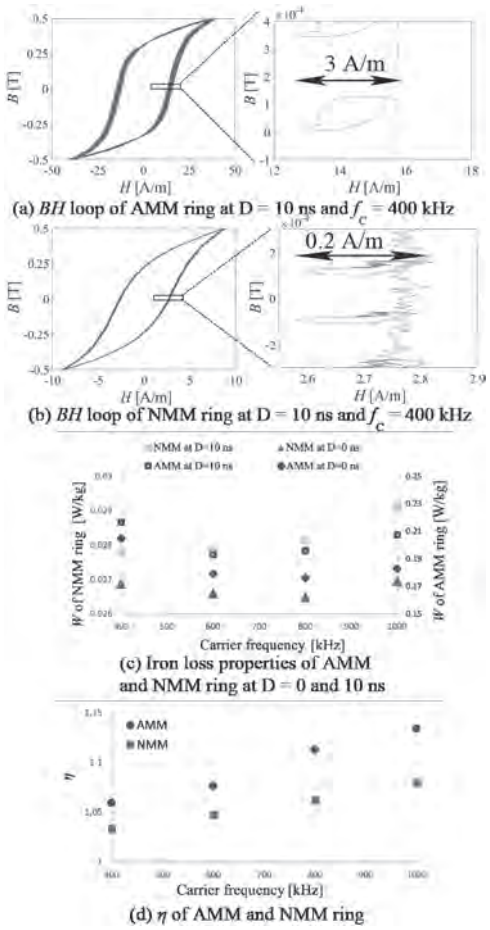

Loss and hysteresis properties.

H1-05. Local Coercivity at X-Rays Nanobeam Irradiated Regions in Amorphous $Fe_{80}B_{20}$ Stripes. U. Urdiroz[2], E. Navarro[2], M. Sánchez-Agudo[1], F. Cebollada[1], *F. Palomares*[2], G. Martínez Criado[2] and J.M. González[2] *1. Universidad Politécnica de Madrid, Madrid, Spain; 2. Instituto de Ciencia de Materiales de Madrid - CSIC, Madrid, Spain*

The modification in magnetic films of the local magnetic properties is a fruitful strategy to achieve or optimize application required functionalities as it was shown on the development of spin waves phase shifters [1] and that of magnetic field sensors [2]. This work focuses on the use of synchrotron nanobeams to explore the possibility of modifying, at length scale of the beam size, the magnetic anisotropy of materials suitable for implementing spin waves guides. Our samples were amorphous $Fe_{80}B_{20}$ stripes (15 nm thick, 700 μm long and 15 μm wide) that were prepared using UV lithography from films grown by using pulsed laser ablation deposition. Irradiation, at the ID16B-ESRF, was performed by using a 56 nm x 56 nm spot size, an energy maximum at E = 17.5 keV and a flux of 2.21 x 10^{11} photons/s. Our characterization of the irradiation outcome, Figure 1, revealed that the local coercive force, measured by means of a Kerr effect device at points in between different irradiated regions (IR), in the same stripe and separated by 100 μm, increased with the IR width (varied by scanning in different areas the nanobeam). That increase can be understood by recalling that the reversal mechanisms of our stripes corresponds to the wall propagation/pinning type [3]. The wall involved in the reversal gets pinned when it finds a region at which it lowers its energy (as, for instance, a reduced anisotropy region). The depinning field (that is, the local coercivity) is related both to the local anisotropy decrease and to the domain wall width that is, approximately, 350 nm [3]. When the width of the IR is lower than that of the domain wall the local coercivity can be approximated to the local anisotropy reduction induced by the irradiation (local amorphous relaxation) multiplied by the ratio of the IR width to the wall one. Differently, when the wall is narrower than the IR the coercivity gets almost constant and measures, to a first approach, the difference in anisotropy energy between the irradiated and non-irradiated zones. We conclude about the need of implementing IR widths larger than ca. 500 nm in order to adequately stabilize a propagating wall.

[1] R. Hertel, W. Wulfhekel, and J. Kirschner, "Domain-wall induced phase shifts in spin waves", Physical Review Letters, vol. 93, no. 25, p. 257202 (2004) [2] Isaac Koh and Lee Josephson, "Magnetic Nanoparticle Sensors", Sensors, vol. 9, p. 8130-8145 (2009) [3] U. Urdiroz et al., "Antiphase resonance at x-ray irradiated microregions in amorphous $Fe_{80}B_{20}$ stripes," Journal of Magnetism and Magnetic Materials, https://doi.org/10.1016/j.jmmm.2020.167017

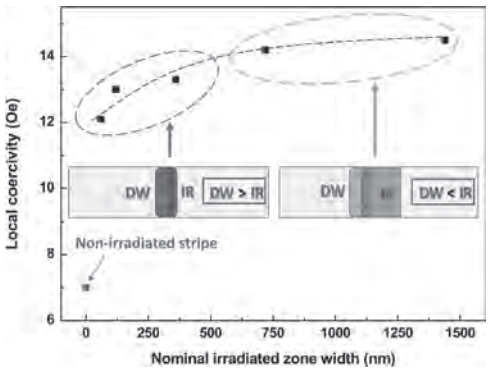

Figure 1. Local coercivity dependence on the IR width

H1-06. Soft Magnetic Properties of Co-Based Supersaturated Solid Solutions by Severe Plastic Deformation. *M. Stückler*[1], J. Zálešák[1], H. Krenn[2], L. Weissitsch[1], S. Wurster[1], C. Gammer[1] and A. Bachmaier[1] *1. Erich Schmid Institute of Materials Science, Austrian Academy of Sciences, Leoben, Austria; 2. Institute of Physics, Karl-Franzens-Universitat Graz, Graz, Austria*

Severe plastic deformation (SPD) can be used to obtain grain sizes in the nanocrystalline regime while the material retains its shape. High-pressure torsion (HPT) in particular, exhibits the advantage of continuously applying a desired amount of strain [1]. Another advantage of SPD by HPT is, that conventional powders can be used as starting materials, making large compositional ranges accessible. In this study, the thermodynamically non-miscible Co-Cu system is investigated [2]. The as-deformed state shows the presence of a nanocrystalline, single-phase microstructure. Transmission electron microscopy investigations reveal a highly homogeneous supersaturated state (Fig.1). Various annealed states are investigated to study the materials' thermal stability, showing a spinodal-like decomposition, but maintaining nanocrystallinity up to a homologous temperature of 0.6 (Fig.2). SQUID-magnetometry reveals soft magnetic properties persisting in a wide temperature range of annealing treatments. To optimize the soft magnetic properties, Co is partially substituted by Fe, causing an enhanced magnetic moment as well as a diminishing coercivity. The magnetic hysteresis of the ternary Fe-Co-Cu sample is also monitored as a function of annealing temperature and compared to the binary Co-Cu system. A strong focus is on the correlation between the magnetic properties and the microstructure, which is further investigated with electron microscopy and X-ray diffraction. This project has received funding from the European Research Council (ERC) under the European Union's Horizon 2020 research and innovation programme (grant agreement No 757333). A part of this work was carried out with the support of CEITEC Nano Research Infrastructure (ID LM2015041, MEYS CR, 2016).

[1] Valiev, R. Z., Islamgaliev, R. K., & Alexandrov, I. V. (2000). Bulk nanostructured materials from severe plastic deformation. Progress in materials science, 45(2), 103-189. [2] Stückler, M., Krenn, H., Pippan, R., Weissitsch, L., Wurster, S., & Bachmaier, A. (2019). Magnetic Binary Supersaturated Solid Solutions Processed by Severe Plastic Deformation. *Nanomaterials*, *9*(1), 6.

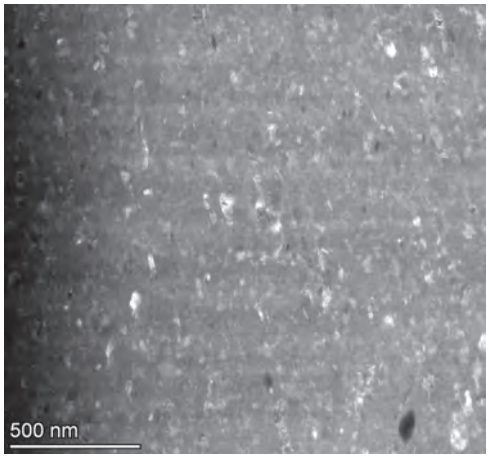

HAADF micrograph of Co72wt.%-Cu in as-deformed state showing nanocrystallinity

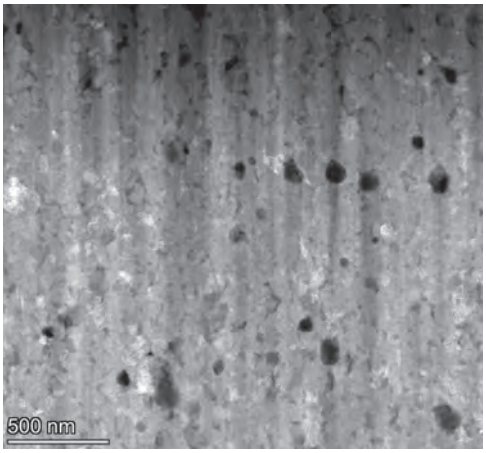

HAADF micrographs of Co72wt.%-Cu in annealed state (1h@600°C) showing persisting nanocrystallinity

INVITED PAPER

H1-07. Tunable Magnetic Anisotropy in Amorphous-Fiber-Based Structures for Multiferroic Applications. *V. Rodionova*[1] *1. Laboratory of Novel Magnetic Materials, Immanuel Kant Baltic Federal University, Kaliningrad, Russian Federation*

Magnetization reversal in 1D structures attracts increasing interest due to its connection with the development of novel spintronics, logic devices, actuators and manipulators for nano-sized objects. Amorphous micro-scale objects (stripes, films, rods) are attractive as materials with an extremely high magnetic softness, but difficult to be studied because of amorphous state and macro scale. Magnetic domain structure and magnetization reversal mechanism in amorphous fibers are defined by magnetoelastic energy, which leads to (i) very sensitive tunability of magnetic anisotropy and (ii) unusually fast domain wall propagation when reversing the magnetization. The role of relaxation processes under current annealing and conventional annealing in initially stressed amorphous materials is considered as a part of the complex process involving both magnetostriction constant change and stress components redistribution [1, 2]: a sign of the magnetostriction can be changed through annealing, which leads to the change of a type of magnetic domain structure. Moreover, the relationships between anisotropy constant and characteristics of domain wall dynamics are established: anisotropy value at the fiber axis enters the expressions for domain wall width, length, slope, velocity and mobility, whereas rate of anisotropy radial variation influences only on the length of domain wall [3]. Configuration of the head-to-head domain wall is visualized as a particular solution of Landau-Lifshitz-Gilbert equation. 1D amorphous fibers are considered as prospective magnetic materials suitable for multiferroic applications especially when they are incorporated into piezo-polymer matrices [4]. Due to the sensitivity of soft magnetic materials to low magnetic field, this approach can be used for the design of new self-biased magnetoelectric composites that provide large ME coupling under an external AC magnetic field in the absence of a DC magnetic field.

1. K. Chichay, V. Rodionova et al., Journal of Alloys and Compounds 835 (2020) 154843; 2. G. Nematov, I. Baraban et al., Journal of Alloys and Compounds 837 (2020) 155584; 3. M. Vereshchagin, I. Baraban et al., Journal of Magnetism and Magnetic Materials 504 (2020) 166646; 4. A. Amirov, V. Rodionova et al., Materials, 13, 916 (2020).

CONTRIBUTED PAPERS

H1-08. Exceptional Magnetomechanical Response of Glass-Coated Amorphous Microwires. *B. Lejeune*[1], P. Gueye[2], D. Archilla[2], E. Navarro[2], M. Vazquez[3,4], R. Pérez del Real[3,4], P. Marin[2] and L. Lewis[1,3] *1. Chemical Engineering, Northeastern University, Boston, MA, United States; 2. Departamento de Física de Materiales, Instituto de Magnetismo Aplicado, UCM-ADIF-CSIC, UCM, P.O. Box 155, Las Rozas, Madrid 28230, Spain; 3. Instituto de Ciencia de Materiales de Madrid, CSIC, Sor Juana Inés de la Cruz 3, 28049 Madrid, Spain; 4. Instituto de Magnetismo Aplicado (UCM), Unidad Asociada (CSIC), Madrid, Spain*

The interesting magnetic behavior of chemically resistant and biologically inert glass-coated amorphous magnetic microwires has been of enduring interest since the mid-1980's. However, their response under different mechanical loading conditions, of great interest for numerous sensor applications, has not been thoroughly explored. Here we present data connecting the magnetoelastic response of glass-coated amorphous ferromagnetic microwires with mechanical loading, revealing an exceptional magnetomechanical response. A selection of amorphous glass-coated $Fe_{73}Si_{11}B_{13}Nb_3$ microwire samples (100-110 μm outer diameter, 4 cm in length) were evenly covered with a thin layer of electrically conducting silver paint (Coating 1), electrically insulating nitrocellulose (Coating 2), or were left uncoated. The magnetomechanical response (resonant frequency and amplitude) of the wires was probed in the frequency range 30-100 kHz using a wireless pickup coil set-up of fixed 1.5 V voltage and a modulated current. It was found that the microwire resonant frequency systematically decreased on the order of ~3 kHz/mg, Fig. 1(a), independent of coating type, Fig. 1(b). These data confirm a shift in the magnetoelastic resonant frequency response of microwires that is approximately 100 times greater than that reported for Metglass amorphous magnetic ribbons (ref = Grimes *et al.*). These findings quantify the lower detection limits of mass loading in glass-coated amorphous magnetic microwires, where microgram differences in mass can be detected wirelessly and with no applied bias field. This exceptional responsiveness to mass loading, along with their small diameter, highlights the promise of magnetic microwires for a variety of sensor applications, including as biosensors, for civil infrastructure monitoring, and for anti-counterfeit measures. Acknowledgements – Fulbright España, I-Link A20074 (CSIC), Spanish Ministry of Science and Innovation RTI2018-095856-B-C21 and Comunidad de Madrid NANOMAGCOST S2018/NMT-4321

[1] C.A. Grimes, S.C. Roy, S. Rani, Q. Cai, Theory, Instrumentation and Applications of Magnetoelastic Resonance Sensors: A Review, 18 (2011) 2809–2844. doi:10.3390/s110302809.

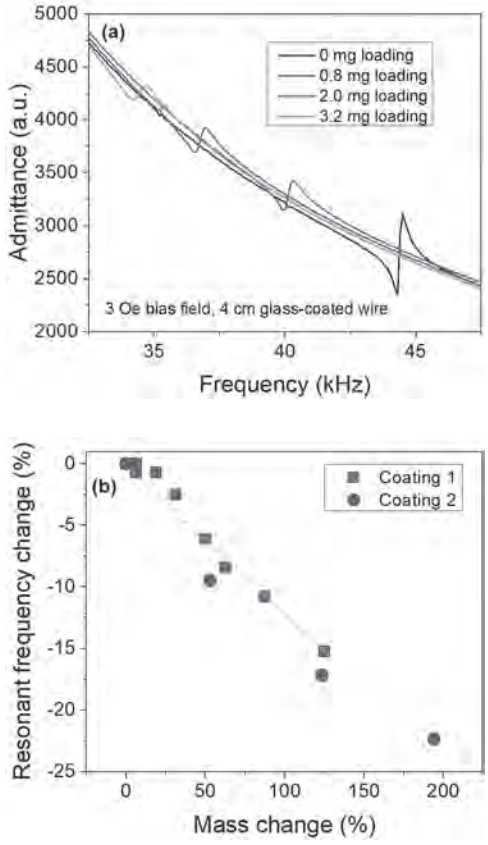

Fig 1. (a) The resonant frequency response of magnetic microwire decreases with increased mass loading. (b) The linear response in resonant frequency with mass loading in glass-coated microwires, irrespective of coating material.

H1-09. Control of the Length of $Fe_{73.5}Si_{13.5}Nb_3Cu_1B_9$ Microwires to be Used for Magnetic and Microwave Absorbing Purposes. *P. Gueye*[1], J. Sanchez[1], E. Navarro[1], A. Serrano[2] and P. Marin[1] *1. Universidad Complutense de Madrid Instituto de Magnetismo Aplicado, Madrid, Spain; 2. Instituto de Ceramica y Vidrio, Madrid, Spain*

A combination of high energy ball milling, vacuum filtering and sedimentation processes has been demonstrated to be a useful approach to reduce, in a controlled way, the length of as-cast Fe73.5Si13.5Nb3Cu1B9 amorphous magnetic microwires (MWs) and annealed material at 550 C in nitrogen condidions. Homogeneous compositional microstructures with fairly narrow size distributions between 1300 μm and 11.7 μm are achieved exhibiting tunable response as a soft magnetic material and as a microwave absorber. From the magnetic perspective, the soft magnetic character is increased with smaller length of the MWs whereas the remanence has the opposite behavior mainly due to the structural defects and the loss of the shape anisotropy. From the microwave absorption perspective, a novel potential applicability is tested in these refined microstructures. This innovation consists of coatings based on commercial paints with a filling percentage of 0.55% of MWs with different lengths deposited on metallic sheets. Large attenuation values around -40 dB are obtained in narrow spectral windows located in the GHz range and their position can be varied by combining different optimized lengths of MW. As an example of this powerful mechanism for absorbing microwaves at specific frequencies, MW lengths of 2 mm and 50 μm are chosen, where a precise tailoring of the minimum reflection loss (RL) is obtained in a range between 8.85 GHz and 13.25 GHz. To confirm these experimental results an effective medium standard model proposed for electrical permittivity is used. Experimental and theoretical results are consistent and these novel composites are also proposed as a feasible candidate for designing frequency selective microwave absorbers on demand, with low filling percentages and high absorption intensity values.

1. P. G. B. Gueye, J. López-Sánchez, P. Marín, ACS Applied Materials, March 2020 2. Joseph A. Beardslee, and Nathan S. Lewis, ACS Nano, VOL. 6 ′ NO. 11 ′ 10303–10310 (2012)

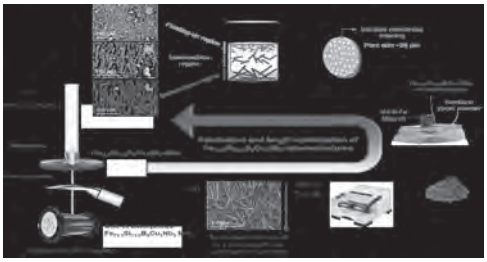

Fig.1: Schematic diagram of fabrication and length optimization processes to obtain the final powders amorphous and annealed $Fe_{73.5}Si_{13.5}B_9Cu_1Nb_3$ MWs with different lengths.

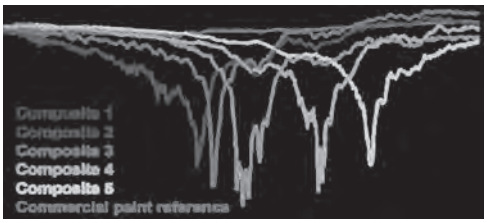

Fig.2: Tunability of MWs as absorber microwave materials: R_L curves as a function of the frequency (4-16 GHz) obtained from composites prepared with different $V_{f,2mm}$ and $V_{f,50\mu m}$ mixed with commercial paint (added as a reference in dark yellow color).

H1-10. Withdrawn

H1-11. Depth Profiling Study of Magnetic CoFeB Thin Film. *J. Dwivedi*[2], M. Gupta[1], V. Reddy[1], A. Mishra[2], G. Das[4] and A. Gupta[3] *1. University Grants Commission Department of Atomic Energy Consortium for Scientific Research, Indore, India; 2. School of Physics, Devi Ahilya Vishwavidyalaya, Indore, India; 3. Amity University, Noida, India; 4. KEK-High Energy Accelerator Research Organization, Tsukuba, Japan*

Magnetic Tunnel Junction (MTJ) consisting of two ferromagnetic electrodes separated by thin oxide layer are used as magnetic field sensors in read-write heads as well as in spintronic logic devices. High tunnel magnetoresistance, of the order of 1000 percent is a prerequisite for such applications. Till date highest tunnel magnetoresistance is observed in MTJs consisting of CoFeB as magnetic electrode with thin MgO tunnel barrier. Post-deposition thermal annealing is an important step in which amorphous CoFeB is partially crystallized to form bcc-CoFe phase, resulting in enhancement of TMR by several orders of magnitude. In recent years buffer layers of refractory metals (W, Mo, Hf) have been used to induce perpendicular magnetic anisotropy in CoFeB films [1]. Since in a MTJ multilayer, we would like to

obtain depth-resolved information about structural changes occurring in CoFeB layer with temperature. X-ray diffraction understanding wave conditions were used for this purpose. X-ray standing waves are generated using total external reflection (TER) of X-rays by the W, Mo & Hf buffer layer. We used an x-ray waveguide structure: substrate/W(30nm)/CoFeB(25nm)/ W(2nm). Various waveguide modes (TE0, TE1 etc.) can be excited in the multilayer by varying the angle of incidence of x-rays. TE0 and TE1 provide information about the center of sample and both the interfaces, respectively. In this view, GIXRD measurements were performed at PF, KEK, JAPAN, at various grazing angles to see the transformation of amorphous matrix into nano-crystalline phase. Crystallization starts from the center of film. Also, there is one additional peaks present near CoFe(110) peak at the interface. In addition, one can see that the samples have uniaxial magnetic anisotropy at its as-deposited state and show a large increase in the coercivity. Also, 250°C annealed film shows the different behavior at hard axis(figure 1).

[1] S. Ikeda, K. Miura, H. Yamamoto, K. Mizunuma, H. D. Gan, M. Endo, S. Kanai, J. Hayakawa, F. Matsukura, and H. Ohno, Nature Mater. 9, 721 (2010).

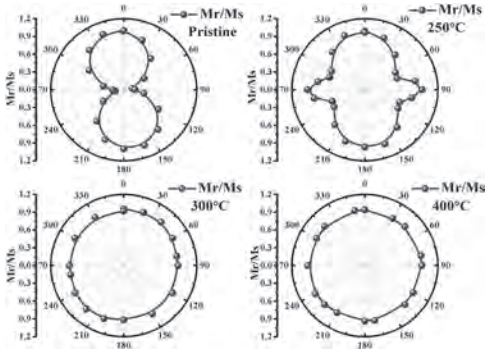

Figure1: ***MOKE hysteresis loops taken as a function of azimuthal angle, of the film in pristine state and annealing at different temperatures.***

H1-12. Magnetism and Transport Signatures in Amorphous Transition Metal Silicide and Transitional Metal Germanide Thin Films. D. Bouma[1,2], J. Karel[3,4], C. Fuchs[1], P. Corbae[5], *N.D. Reynolds*[2,1] and F. Hellman[1,2] *1. Physics, University of California Berkeley, Berkeley, CA, United States; 2. Materials Science Division, E O Lawrence Berkeley National Laboratory, Berkeley, CA, United States; 3. Materials Science and Engineering, Monash University, Clayton, VIC, Australia; 4. ARC Centre of Excellence in Future Low-Energy Electronics Technologies, Clayton, VIC, Australia; 5. Materials Science and Engineering, University of California Berkeley, Berkeley, CA, United States*

Exotic massless fermions have been predicted in a family of transition metal silicides and germanides, and experiments have provided evidence for these chiral fermions and their associated long Fermi-arc surface states.[1,2] Additionally, a recent report has predicted that the topological properties in the electronic structure may be preserved even in the presence of complete structural disorder (e.g. amorphous materials).[3] In this talk, we will discuss studies of the magnetism and transport signatures in a series of amorphous transition metal silicide and germanide thin films, M_xZ_{1-x} (M=Fe, Co; Z=Si, Ge; x=0.45-0.71). In the amorphous Co_xZ_{1-x} thin films, we will show a positive magnetoresistance at low temperature which crosses from a quadratic dependence at low field to a non-saturating linear dependence at high field (up to 14T). We will suggest these results may be an indication of Abrikosov's quantum magnetoresistance. We will also show that not only do the amorphous thin films of Fe_xZ_{1-x} exhibit Stoner model-type itinerant ferromagnetism over the whole range of x studied, the equiatomic films have a larger moment per Fe than their crystalline counterparts.[4,5] In contrast, the Co_xZ_{1-x} amorphous thin films only become weakly magnetic at x=0.6 and the moment per Co atom in these films scales non-linearly with Co concentration, unlike in the case of Fe. The origin of this difference between M=Fe, Co as well as the differences between Z=Si,Ge on the ferromagnetic properties will be discussed. Ultimately we show that these amorphous M_xZ_{1-x} alloys are highly tunable magnetic materials which have potential for the development of novel magnetic memory technologies. This work was supported primarily by the Department of Energy, Materials Sciences and Engineering Division Contract DE-AC02-05-CH11231 within the LBNL magnetism (NEMM) program, and in part through the Australian Research Council Centre of Excellence in Future Low Energy Electronics Technologies CE170100039 and the Australian Research Council Discovery Project DP200102477, using the Melbourne Centre for Nanofabrication of the Australian National Fabrication Facility.

[1] P. Tang *et al.*, *Phys. Rev. Lett.* 119, 206402 (2017) [2] D. Takane *et al.*, *Phys. Rev. Lett.* 122, 076402 (2019) [3] Y.B. Yang *et al., Phys Rev Lett* 123 076401 (2019) [4] D.S. Bouma *et al.*, *Phys Rev B* 101 014402 (2020) [5] J. Karel *et al.*, in preparation

H1-13. The Improvement of the CoZrTaB Thin Films on Different Substrates for Flexible Device Applications. *Y. Wu*[1], I. Yeng[2] and H. Yu[1] *1. Electrical, Computer and Energy Engineering, Arizona State University, Tempe, AZ, United States; 2. Materials Science and Engineering, Arizona State University, Tempe, AZ, United States*

Magnetic core has been widely used in integrated inductor as it can provide a high inductance and reduce the device size due to its high permeability [1]. At the same time, the relatively high loss tangent and saturation current will diminish the performance enhancement in the high frequency and high current applications, respectively [2]. The dilemma has resulted in the investigation of magnetic core materials, among which CoZrTaB demonstrated a low Hk, high resistivity and low loss tangent below 500 MHz, which is compatible with most of the integrated voltage regulators' working frequency [3]. Here we fabricated CoZrTaB thin films with sputtering on different substrates and characterized them comprehensively. The CoZrTaB thin films have been fabricated in single layer and multi-layer structures (Fig. 1(a)), of which the VSM results, shown in Fig. 2, suggest that the Hk change of the multi-layer structure can be neglected while it can suppress the eddy current at high working frequency. Compared with the continuously sputtered 400nm CoZrTaB thin film, the multi-layer thin film shows a more desirable hysteresis loop with a single domain. The surface roughness of the Si and two kinds polyimide was extracted with the AFM, followed by the VSM characterization to verify the performance degradation. In addition, the material characterization such as XRD and RBS have been conducted to acquire the information of phase and element ratio of the CoZrTaB thin film, as shown in Fig.1 (b)(c). A comparison is made with the previous reported results from Gardner [4] and Koh [5] to see the successful implantation of the CoZrTaB thin film on different substrates.

[1] Xu, Wei, et al. "Performance enhancement of on-chip inductors with permalloy magnetic rings." *IEEE Electron Device Letters* 32.1 (2010): 69-71. [2] Bechir, M. H., et al. "Magnetic inductor model which take into account permeability and loss tangent of the magnetic material." *2015 Symposium on Design, Test, Integration and Packaging of MEMS/ MOEMS (DTIP)*. IEEE, 2015. [3] Burton, Edward A., et al. "FIVR—Fully integrated voltage regulators on 4th generation Intel® Core™ SoCs." *2014 IEEE Applied Power Electronics Conference and Exposition-APEC 2014*. IEEE, 2014. [4] Gardner, Donald S., et al. "Integrated on-chip inductors with magnetic films." *2006 International Electron Devices Meeting*. IEEE, 2006. [5] Koh, Kisik, et al. "High frequency microwave on-chip inductors using increased ferromagnetic resonance frequency of magnetic films." *2015 28th IEEE International Conference on Micro Electro Mechanical Systems (MEMS)*. IEEE, 2015.

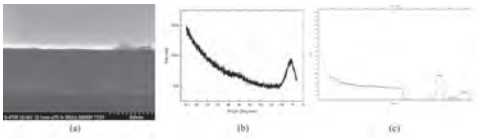

Fig.1–(a)The SEM image of the cross section of the 4*100nm CoZrTaB thin film on Si substrate. The (b)XRD and (c)RBS results of the 100nm CoZrTaB thin film on Si substrate. In the RBS result, the red line is the experimental data and the blue line is the simulated data. The atomic ratio of Co, Zr, Ta, and B is 69.8%, 2.5%, 3.4%, and 24.2%, respectively.

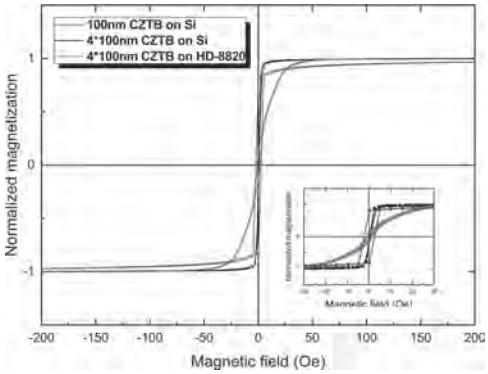

Fig.2 –The VSM result of the 100nm CoZrTaB thin film on Si substrate.

H1-14. Magnetic Metal Oxide Nanoparticles for a Remote 3D Thermometry Platform. *A.J. Biacchi*[1], T.Q. Bui[1], B. Correa[1], C. Dennis[1], S. Woods[1] and A.R. Hight Walker[1] *1. National Institute of Standards and Technology (NIST), Gaithersburg, MD, United States*

Colloidal magnetic nanoparticles (MNPs) of metal oxides have found use in biomedical imaging, sensing, drug delivery, and hyperthermia. These applications exploit the softness of the magnetism in oxide MNPs, often ferrites, which yields a strong collective response to dynamic applied magnetic fields while simultaneously remaining dispersed in a medium. Their synthesis relies on reproducible, scalable, solution chemistry routes. Further, the size, shape, structure, and composition are tunable, which serve as levers to design and manipulate the magnetic behavior of the particles. Magnetic nanothermometry is an emerging application of MNPs currently being explored as a technique to measure temperature remotely with high spatial resolution throughout a volume. This metrology is based on the temperature-dependent nature of the particles' magnetization. Although progress has been made in the development of magnetic nanothermometry,[1] commercially available MNPs lack the particle-to-particle consistency and magnetic thermosensitivity necessary for widespread application. Here, we report colloidal MNPs specifically designed for remote nanoscale 3D thermometry. A series of shape- and size-controlled colloidal MNPs based on ferrites were synthesized *via* the thermal decomposition of organometallic precursors. Further, we exploited compositional doping of transition metal elements (Co,Mn,Zn) and exchange coupling between core-shell magnetic heterostructures[2,3] as means of generating improved temperature-dependent magnetization in the particles (200-400 K at 0.01 T applied field). Extensive characterization using X-ray diffraction, Raman spectroscopy, and high-resolution electron microscopies revealed correlations between particles' nanoscale structure and their magnetic response. Finally, we used a home-built AC magnetic particle spectrometer to measure the magnetization-dependence of these nanothermometers as a function of temperature in their local environment. Collectively, we show that carefully designed complex metal oxide MNPs display tunable thermosensitivity and AC field signal response, which represents a potential pathway to the implementation of a practical 3D thermal imaging platform based on magnetometry.

[1] J. Weaver, A. Rauwerdink, and E. Hansen, Med. Phys., 36, 1822-1829 (2009). [2] R. Evans, R. Chantrell, and O. Chubykalo-Fesenko, MRS Bull., 38, 909-914 (2013). [3] K. Zhu, Y. Ju, J. Xu, Z. Yang, S. Gao, and Y. Hou, Acc. Chem. Res., 51, 404–413 (2018).

H1-15. Temperature Dependence of the Dzyaloshinskii-Moriya Constant in Ultrathin Pt/Co(Fe)B/Ir Films. *K.N. Alshammari*[1], L. Benito[1], R. Temple[1], M. Alyami[1], M. Ali[1], P.S. Keatley[2], T. Forrest[3], F. Maccherozzi[3], S. Cavill[4] and T. Moore[1] *1. Uinversity of Leeds, Leeds, United Kingdom; 2. Uinversity of Exeter, Exeter, United Kingdom; 3. Diamond Light Source Ltd, Diamond Light Source Ltd, Harwell, Harwell, United Kingdom; 4. University of York, York, United Kingdom*

It is well known that both the anisotropy K and the exchange stiffness A in magnetic materials decrease as the temperature increases [1]. The temperature dependence of these parameters is often expressed as a power law in the reduced magnetization (m), e.g. calculations for Co indicate that the Callen-Callen law $K(m) \sim m^3$ is a very good approximation for the anisotropy, while for the exchange stiffness, $A(m) \sim m^{1.8}$ [1]. Since the domain wall width is proportional to the square root of A/K, it increases with temperature, as does the domain wall energy. However, in thin films with an interfacial Dzyaloshinskii-Moriya interaction (DMI), the DMI constant (D) also enters in the expression for the domain wall energy. As the DMI leads to chiral domain walls and skyrmions, determining the temperature dependence of D and hence the domain wall energy is important from both fundamental and applied points of view. We report on our study of multilayers of Pt/$Co_{68}Fe_{22}B_{10}$/Ir and Pt/$Co_{68}B_{32}$/Ir multilayers, deposited by dc magnetron sputtering onto a silicon oxide substrate. Wide-field Kerr microscopy was used to image the domains in the demagnetised state. We measured the domain period in the temperature range from -264 to 17 °C [Fig.1], enabling a calculation of D following the approach of Woo et al [2] as shown in [Fig.2]. In a second study, we deposited the same multilayers onto $BaTiO_3$ (BTO) (100), which undergoes structural phase transitions close to 0 and -100 °C and thus exerts a strain on the multilayers. Images of domains in a [Pt/CoB/Ir]x10 superlattice were obtained using X-ray magnetic circular dichroism - photoemission electron microscopy (XMCD-PEEM). It was found that the domain period increases as the temperature increases as shown in [Fig.1]. However the DMI for all the samples decreases when the temperature increases as shown in [Fig.1].

[1] Moreno et al., Phys. Rev. B 94, 104433 (2016) [2] Woo et al., Nat. Mater. 15, 501 (2016) [3]Bennett, et al., Scientific reports, 6, p.22708 (2016).

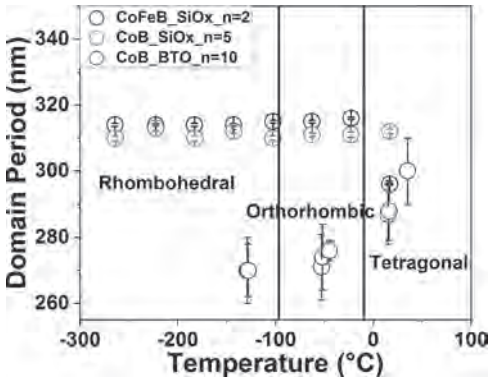

Fig.1. Temperature dependence of the magnetic domain period for the multilayer Pt/Co(Fe)B/Ir n=2,5,10 grown on SiOx and BTO substrates. The labels 'Rhombohedral' etc [3]. refer to the structure of the BTO substrate at the given temperature.

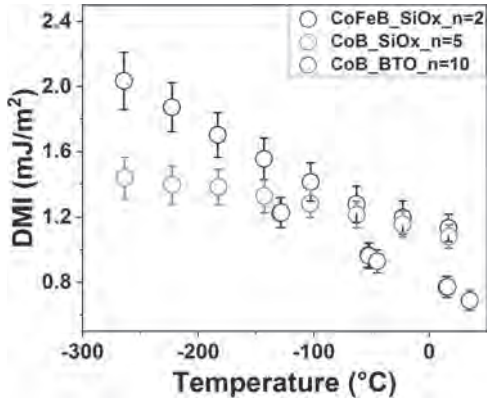

Fig. 2. Dzyaloshinskii-Moriya constant D vs. temperature calculated from (Fig.1).

Session H2
EMERGENT PHENOMENA IN COMPLEX OXIDES AND NITRIDES

Catherine Pappas, Chair
Delft University of technology, Delft, Netherlands

CONTRIBUTED PAPERS

H2-01. Colossal Acoustoelectric Effect in $La_{0.7}Sr_{0.3}MnO_3$. *P.N. Lapa*[1], M. Lee[1], I. Chiu[2], Y. Takamura[3] and I.K. Schuller[1] *1. Department of Physics, University of California San Diego, La Jolla, CA, United States; 2. Department of Chemical Engineering, University of California Davis, Davis, CA, United States; 3. Department of Materials Science and Engineering, University of California Davis, Davis, CA, United States*

The acoustoelectric (AE) effect, i.e. the generation of a DC current by a propagating acoustic wave, may provide crucial information on the relationship between the structural and electronic properties of strongly correlated oxides. We discovered that acoustic waves may couple not only to electronic but also to magnonic state of these materials. To investigate the magnetic effects, we compared the AE effect in non-magnetic VO_2 and ferromagnetic $La_{0.7}Sr_{0.3}MnO_3$ wires grown on top of piezoelectric $LiNbO_3$ substrates. According to the phenomenological model for the AE effect [1], its magnitude depends non-linearly on the wire resistance. Due to the large resistance change with temperature, the AE voltage generated in the VO_2 wire is greatly enhanced at the metal-insulator transition. The significant colossal magnetoresistance change of the $La_{0.7}Sr_{0.3}MnO_3$ wire with an external magnetic field [Fig. 1(b)] is only slightly dependent on the field orientation. On the other hand, the field dependences of the AE voltage are very different when the field is parallel and perpendicular to the wire [Fig. 1(a)]. This finding has no explanation within standard AE phenomenological models. We propose a new mechanism which explains this unusual dependence of the AE effect on the colossal magnetoresistance of the $La_{0.7}Sr_{0.3}MnO_3$ wire. This research was supported by the Office of Basic Energy Science, U.S. Department of Energy, BES-DMS funded by the Department of Energy's Office of Basic Energy Science, DMR under grant DE FG02 87ER-45332.

[1] V. I. Fal'ko, S. V. Meshkov, and S. V. Iordanskii, Phys. Rev. B 47, 9910 (1993).

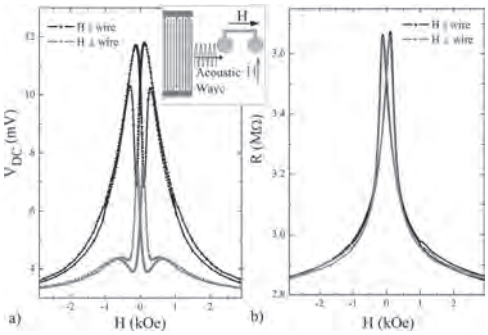

Fig. 1 Magnetic field dependences of the AE voltage (a) and resistance (b) in the $La_{0.7}Sr_{0.3}MnO_3$ wire. The inset in fig a) shows the geometry of the measurement including the relationship between the interdigitated electrodes, the microwire, the propagation of acoustic waves and the magnetic field direction, H.

H2-02. Rashba-Like Spin-Orbit Coupling in the Strained Ferroelectric $PbTiO_3$. *J. Gosteau*[1], R. Arras[1], C. Paillard[2], H. Zhao[3] and L. Bellaiche[3] *1. CEMES, Centre d'Elaboration de Materiaux et d'Etudes Structurales, Toulouse, France; 2. Laboratoire SPMS, CentraleSupélec/CNRS UMR8580, Université Paris-Saclay, Gif-sur-Yvette, France; 3. Physics Department and Institute for Nanoscience and Engineering University of Arkansas, Fayetteville, AR, United States*

Understanding and manipulating the spin degree of freedom in materials is a hot topic due to the potential applications to develop new computing systems or low-consumption-operating electronic devices. First well-known in semiconductor heterostructures and heavy metal, and now in other materials such as transition-metal oxides, the Rashba spin-orbit effect, which appears as a result of the surface inversion asymmetry, has recently motivated lots of research due to its role in transport processes and its ability to be tuned by an external electric field. In 2013, the Rashba effect has been predicted theoretically,[1] and later confirmed experimentally,[2] in ferroelectric materials. The link between the reversible spin textures resulting from the spin-orbit interaction and the electric polarization is very promising to design devices based on non-volatile magneto-electric states. We will present our recent results based on *ab initio* calculations applied to the Rashba spin-orbit effect in the well-known ferroelectric perovskite $PbTiO_3$.[3] We propose to detail the spin-texture differences linked to the Ti-d and Pb-p bands of $PbTiO_3$, which can exhibit a *cubic* and *linear* Rashba spin-splitting (RSS) variation as a function of the wave vector *k*. We will discuss the effect of epitaxial strain and crystallographic phase transitions as a route to modify the RSS and the spin textures. This study has been partially supported through the EUR Grant NanoX No. ANR-17-EURE-0009. H.J. and L.B. thank the Department of Energy, Office of Basic Energy Sciences, under Award No. DE-SC0002220. C.P. acknowledges ARO Grant No. W911NF-16-1-0227. This work was granted access to the HPC resources of CALMIP (Allocation No. 2020/P1229).

[1] D. Di Sante, *et al.,* Adv. Mater. 25, 509 (2013). [2] C. Rinaldi, *et al.,* Nano Lett. 18, 2751 (2018). [3] R. Arras, *et al.,* Phys. Rev. B 100, 174415 (2019).

H2-03. Structural and Magnetic Properties of Perovskite $LaCo_{0.5}Fe_{0.5}O_3$ Nanostructures Sintered at Various Temperatures. *E. Sert*[1,2], M. Kaynar[2,3], C. Ünlü[4], B. Kalkan[5] and S. Özcan[2,3] *1. Physics, Cankiri Karatekin Universitesi, Cankiri, Turkey; 2. Nanotechnology and Nanomedicine, Hacettepe Universitesi, Graduate School of Science and Engineering, Ankara, Turkey; 3. Physics Engineering, SNTG Lab. Hacettepe University, Ankara, Turkey; 4. Biomedical Engineering, Pamukkale Universitesi Muhendislik Fakultesi, Denizli, Turkey; 5. Physics Engineering, Hacettepe Universitesi, Mühendislik Fakültesi, Ankara, Turkey*

In this work, we present the effect of sintering temperature on the perovskite $LaCo_{0.5}Fe_{0.5}O_3$ synthesized by sol-gel method. Stoichiometric amounts of Nitrate salts of La, Co and Fe were dissolved in water and were mixed with ethanol and citric acid solution. The stirred mixture was heated up to about 200°C until becoming a gel and the gel form was kept in a box oven for 12 hours at 600°C to remove the organic molecules. The powder form was then sintered for 24 hours at 700°C, 800°C, 900°C and 1100°C. Structural and

magnetic properties were investigated by XRD and Quantum Design PPMS. The effect of the sintering temperature on the properties of the samples could be observed by comparing in between and with the non-sintered sample. According to the XRD measurements, an orthorhombic form is observed for the non-sintered sample and the samples sintered at low-temperatures. On the other hand, high temperatures induce the formation of rhombohedral structure. As been expected, the temperature-dependent magnetic measurements verified the effect of this structural change on the magnetic properties. Graphs of the samples sintered at higher temperatures revealed a second phase and moreover a negative magnetization under a critical temperature for the 1100°C sample which can be attributed to an antiferromagnetic interaction between two sub-lattices.

[1] L. Bedel, A. C. Roger, C. Estournes, and A. Kiennemann, "Co0 from partial reduction of La(Co,Fe)O3 perovskites for Fischer-Tropsch synthesis," Catal. Today, vol. 85, no. 2–4, pp. 207–218 (2003) [2] A. Kumar ve S. M. Yusuf, "The phenomenon of negative magnetization and its implications", Phys. Rep., c. 556, ss. 1–34 (2015) [3] C. Li et al., "Negative magnetization and the sign reversal of exchange bias field in Co(Cr1-xMnx)2O4 ($0 \le x \le 0.6$)," J. Appl. Phys., vol. 123, no. 9, pp. 1–8 (2018) [4] L. Néel, *Ann. de Phys.*, 3, pp. 137 (1948) [5] T. Nagata, Rock Magnetism, second ed., Maruzen, Tokyo (1961)

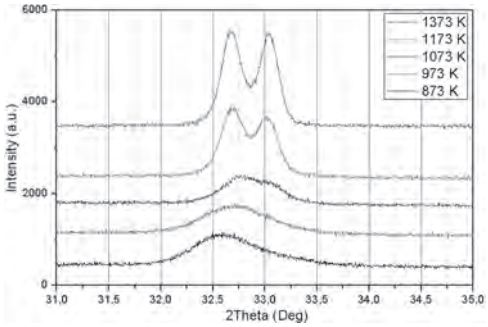

Fig.1. The variation of the main XRD peak of $LaCo_{0.5}Fe_{0.5}O_3$ with varying sintering temperature.

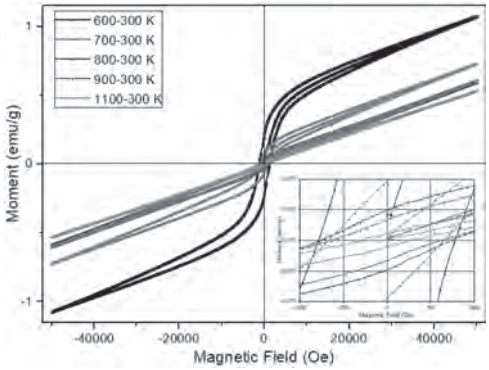

Fig.2. Room temperature measurements of magnetization vs magnetic field for $LaCo_{0.5}Fe_{0.5}O_3$ sintered at different temperatures.

H2-04. Electronic Structure and Magnetism of Half-Metallic Quadruple Perovskite $ACu_3Fe_2Re_2O_{12}$(a=Ca, Sr, Ba, Pb, Sc, Y, La) by First Principles Theory. *D. Wang*[1], M. Shaikh[2], S. Ghosh[2] and B. Sanyal[1]
1. Physics and Astronomy, Uppsala Universitet, Uppsala, Sweden;
2. Department of Physics and Nanotechnology & SRM Research Institute, SRM University, SRM Institute of Science and Technology, Kattankulathur, India

A- and B-site ordered quadruple perovskites with the chemical formula $AA'_3B_2B'_2O_{12}$ can form with a 1:3 ratio at the A site. A unique feature for this specially ordered perovskite is that three different atomic sites (A′, B, and B' sites) can all accommodate magnetic transition metals. As a consequence, multiple magnetic interactions can occur at A′, B and/or B' sites, giving rise to a series of intriguing physical phenomena. $CaCu_3Fe_2Re_2O_{12}$ is a good example, which shows the half-metallic electronic structure, large magnetization, and very high Curie temperature [1]. Here we have investigated a series of ferrimagnetic compounds $ACu_3Fe_2Re_2O_{12}$(A=Ca, Sr, Ba, Pb, Sc, Y, La) by using density functional theory and Monte Carlo simulations. We found that all compounds with A^{2+} ions exhibit high Curie temperatures (above 405 K), and the compounds with A^{3+} substitution yield even higher T_c (above 502 K). By examining interatomic exchange parameters, we found that the antiferromagnetic exchange couplings between Re and Cu as well as Re and Fe are responsible for this very high Curie temperature. For the compounds with A^{3+} substitution, an electron doping at the band around the Fermi level dominated by the Re ions strengthen the Re-Cu, Re-Fe and Re-Re exchange interactions, which cause an increase in the critical temperatures. In summary, this work demonstrates a design strategy of enhancing spin ordering temperatures by replacing A-site non-magnetic ions.

1. Chen, Wei-tin, Masaichiro Mizumaki, Hayato Seki, Mark S. Senn, Takashi Saito, Daisuke Kan, J. Paul Attfield, and Yuichi Shimakawa. "A half-metallic A-and B-site-ordered quadruple perovskite oxide CaCu3Fe2Re2O12 with large magnetization and a high transition temperature." Nature Communications 5, no. 1 (2014): 1-7.

H2-05. Thermal Decomposition of $GdCrO_4$ to $GdCrO_3$: Structure and Magnetism. *P. Mohanty*[1], S. Jacobs[1], A. Prinsloo[1] and C. Sheppard[1]
1. Physics, University of Johannesburg, Johannesburg, South Africa

Rare-earth orthochromites ($RCrO_3$) with orthorhombically distorted perovskite (ABO_3) structure exhibit a wealth of magnetic phenomena such as temperature-induced magnetization reversal (TMR), spin-reorientation (SR), spin-flipping (SF), and exchange-bias (EB). These occur as a result of magnetic interactions among the cations such as Cr^{3+}–Cr^{3+}, Cr^{3+}–R^{3+} and R^{3+}–R^{3+}, where R is the rare earth element, such as Gd, Sm, Tm [1]. Rare-earth orthochromites also form a class of magnetoelectric multiferroics which exhibit the coexistence of ferroelectric and magnetic orders [1]. Single crystalline $GdCrO_3$, exhibit a giant magnetic entropy change (ΔSm) at a reasonable magnetic field, making it a potential candidate for the application in magnetic refrigeration [2]. TMR and EB have been reported in several $RCrO_3$ compounds due to the competition between the R^{3+} moment and the canted weak ferromagnetic (FM) component of Cr^{3+} ions [3]. In the present work, $GdCrO_4$ samples were obtained using sol-gel technique [4]. X-ray diffraction and Raman techniques were used to identify the phase of the samples. Calcination of the samples at 600 °C led to $GdCrO_4$ phase formation [5]. Further calcination of the samples at 1000 °C led to the decomposition of $GdCrO_4$ into $GdCrO_3$. Upon heat treatment, the Cr^{5+} oxidation state in the $GdCrO_4$-zircon phase reduces to the relatively stable Cr^{3+} together with oxygen loss to stabilize the $GdCrO_3$ perovskite-structure [5]. The role of thermal decomposition of $GdCrO_4$ to $GdCrO_3$ on crystal structure and magnetic transitions, studied using XRD and vibrating sample magnetometer (VSM), will be discussed. Magnetization measurements as a function of temperature (*M-T*) with different probing magnetic fields were carried out to locate the various magnetic transitions in the samples under different measurement protocols such as zero field cooled (ZFC), field cool cooling (FCC) and field cool warming (FCW). Anomalies in the *M-T* curves observed at $T \approx 10$ K and $T \approx 170$ K correspond to spin - flip and Néel transitions, respectively. This is in agreement with previously reported values [1]. The hysteresis loops measured across the transition temperatures validate the magnetic transitions as observed in the *M-T* curves.

[1] S. Mahana, U. Manju and D. Topwal, *J. Phys. D: Appl. Phys.* 51 (2018) 305002. [2] L. Yin, J. Yang, X. Kan, W. Song, J. Dai and Y. Sun, *J. Appl. Phys.* 117 (2015)133901. [3] B.B. Dash and S. Ravi, *Solid State Sciences* 83 (2018) 192. [4] P. Mohanty, A.R.E. Prinsloo, B.P. Doyle, E. Carleschi, C.J. Sheppard, *AIP Advances* 8 (2018) 056424. [5] A.J. Dossantos-Garcia, E. Climent-Pascual, J.M. Gallardo-Amores, M.G. Rabie, Y. Doi, J. Romero de Paz, B. Beuneu, R. Saez-Puche, *Journal of Solid State Chemistry* 194 (2012) 119.

H2-06. Withdrawn

H2-07. Hidden Multipolar Orders in 5d^1 Ba_2MgReO_6. *A. Mansouri Tehrani*[1] and N.A. Spaldin[1] *1. Eidgenossische Technische Hochschule Zurich - Campus Honggerberg, Zurich, Switzerland*

We present the results of density functional calculations of the proposed low temperature charge quadrupolar ordering in Ba_2MgReO_6. Ba_2MgReO_6 is a spin-orbit-driven Mott insulator with a symmetry-lowering structural phase transition at 33 K and a canted antiferromagnetic ordering of the small (around 0.25 μ_B) Re magnetic moments at 18 K. The goal of our calculations is to test the existence of the quadrupolar order, and to understand its relationship to the structural and magnetic orders, which we achieve by separately isolating the ordering of the charge, spins, orbital moments, and structure. We find that the charge quadrupole ordering exists, and can be realized in the absence of magnetic ordering. In addition to shedding light on the detailed behavior of Ba_2MgReO_6, our work provides insight into the intriguing physics of 5d^1 double perovskites in general, and illustrates a method for the analysis of magnetic ordering interactions combined with higher orders such as charge quadrupoles.

H2-08. Clinching Experimental Evidence of "Room Temperature Ferromagnetic Behavior" in 5 mol% Mn Doped $SrTiO_3$. *P. K R S*[1], P. Janolin[2], U. Luders[3] and K. Varma[4] *1. Materials Science, Central University of Tamil Nadu, Tiruvarur, India; 2. SPMS, CentraleSupelec Bibliotheques, Gif-sur-Yvette, France; 3. Materials Science, Laboratoire de Cristallographie et Sciences des Materiaux, Caen, France; 4. Materials Science, Indian Institute of Science, Bangalore, India*

Theoretical prediction and rare experimental observation of room temperature ferromagnetism in transition metal doped semiconductors/insulators such as ZnO, TiO_2, $SrTiO_3$ and $BaTiO_3$ has been of key fundamental interest in understanding materials [1-3]. In this work, 5 mol% of Mn doped $SrTiO_3$ was synthesized by chemical coprecipitation [4]. This synthesis technique has been adopted specifically to ensure the most homogeneous doping of Mn in $SrTiO_3$ lattice thus largely preventing the formation of any other impurity phases. Analysis of high resolution XRD data collected for the sample sintered at 1150°C revealed that the phase was of high purity. Magnetization measurements were carried out on the same sample where the variation of Magnetization (M) with temperature under both zero field cooled (ZFC) and field cooled conditions (FC) were measured under an applied magnetic field (H) of 100 Oe. The trend in ZFC is quite contrary to the expected paramagnetic nature in this system. The increase in ZFC magnetization values when the temperature was increased beyond 150 K has to be taken into consideration [Fig. 1]. Also the dispersion in the ZFC and FC curves is quite significant near room temperature and there is a difference of an order in the ZFC and the FC magnetization values around 300 K unlike conventional paramagnetic systems. Therefore the temperature dependent magnetization data (>150 K) clearly exhibits the sign for an impending ferromagnetic behavior around RT. The M versus H behavior was studied in the -1.5 T to 1.5 T range at three different temperatures - 10 K, 150 K and 300 K. Saturated hysteresis loop observed at RT corroborates our observation of the bifurcation observed in ZFC/FC behavior around 300 K [Fig.2]. At 10 K, hysteresis loop turns to look more paramagnetic-like indicating the presence of only a weak ferromagnetic ordering with a strong paramagnetic matrix. A suitable mechanism based on defects induced by Mn doping in $SrTiO_3$ will be discussed to explain this observation of RT Ferromagnetic behavior [5].

K. Ueda, H. Tabata and T. Kawai, Appl. Phys. Lett. 79, 988 (2001) J.-Y. Kim, J.-H. Park, H.-J. Noh, Phys. Rev.Lett. 90, 017401 (2003) M. Valant, T. Kolodiazhnyi, I. Arčon, Adv. Funct. Mater. 22, 2114 (2012) Preethi Meher K.R.S, Christine B, Pierre-Eymeric Janolin and K.B.R. Varma, Journal of Solid state Chemistry, 192, 296 (2012) R. Ishikawa, Y. Shimbo, I. Sugiyama, Phys Rev B, 96, 024440 (2017)

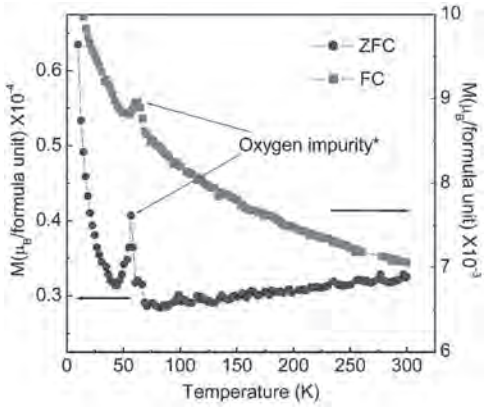

Magnetization versus temperature curve obtained under ZFC and FC conditions

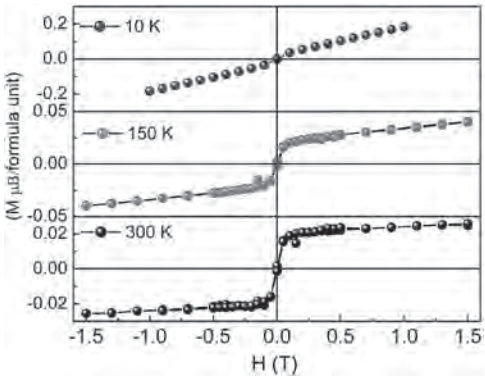

Magnetization versus magnetic field curves at 10K, 150 K and 300 K

INVITED PAPER

H2-09. Interfacial Tuning of Chiral Magnetic Interactions for Large Topological Hall Effects in $LaMnO_3/SrIrO_3$ Heterostructures. *E. Skoropata*[1], J. Nichols[1], J. Ok[1], R.V. Chopdekar[2], E. Choi[3], A. Rastogi[1], C. Sohn[1], X. Gao[1], T. Farmer[1], R. Desautels[1], Y. Choi[4], D. Haskel[4], J.W. Freeland[4], S. Okamoto[1], M. Brahlek[1] and H. Lee[1] *1. Oak Ridge National Laboratory, Oak Ridge, TN, United States; 2. E O Lawrence Berkeley National Laboratory, Berkeley, CA, United States; 3. National High Magnetic Field Laboratory, Tallahassee, FL, United States; 4. Argonne National Laboratory Advanced Photon Source, Lemont, IL, United States*

One of the most intriguing outcomes of symmetry breaking and spin-obit interactions in magnetic systems is the possibility to create non-collinear and chiral spin textures. The Dzyaloshinskii-Moriya interaction (DMI) results from strong spin-orbit coupling and broken inversion symmetry to generate magnetization rotations with fixed chirality. The discovery of magnetic skyrmions originating from strong DMI in metal thin films has led to an explosion of efforts to manipulate magnetic phases originating from interfaces. We have studied interface-induced magnetism in epitaxial 3*d*/5*d* iridate/manganite superlattices. In $LaMnO_3/SrIrO_3$ superlattices, we find a large additional topological Hall effect arising from the interaction of charge carriers with a noncoplanar chiral spin texture induced by interfacial DMI [1]. I will describe how the interfacial atomic layer stacking and symmetry enabled by the nonmagnetic A-sites determine the competition between collinear and chiral magnetic interactions originating from the oxide interface. Our findings [2] provide insight to the manipulation of chiral magnetism from atomic-scale control of exchange interactions at oxide interfaces.

[1] P. Bruno *et al.*, *Phys. Rev. Lett.* 93, 096806 (2004). [2] E. Skoropata *et al.*, *Sci. Adv.*, 6, eeaz3902 (2020).

CONTRIBUTED PAPERS

H2-10. Withdrawn

H2-11. Withdrawn

H2-12. Nuclear Magnetic Resonance and Relaxation in Uranium Mononitride. *A.Y. Germov*[1], V.V. Ogloblichev[1], S.V. Verkhovskii[1], A.M. Potapov[2] and A.V. Andreev[3] *1. M N Mikheev Insititute of metal physics of the Ural Branch of the Russian Academy of Sciences, Yekaterinburg, Russian Federation; 2. The Institute of High Temperature Electrochemistry of the Ural Branch of the Russian Academy of Sciences, Yekaterinburg, Russian Federation; 3. FZU Institute of Physics, Czech Academy of Sciences, Prague, Czechia*

Uranium pnictide compounds are promising for various branches of energy industry, because they are relatively simple magnetic systems with low resistivity and high thermal conductivity. Properties of actinide compounds significantly depend on the degree of localization of 5*f*-electrons, which is usually characterized by the Hill's criterion [1] proposed in 1970. The criterion is determined by the ratio of the average radius of the 5*f*-shell of atom to half the distance between the actinide atoms. Uranium mononitride (UN) is a representative of actinide compounds with metallic conductivity, in which Hill's criterion is close to critical value and 5*f*-electrons demonstrate local and band magnetism. For half a century, experimental and theoretical studies of actinide materials have focused on such behavior of 5*f*-electrons [2,3]. The UN powder and single crystalline samples has been studied in a wide temperature range from 10 K to 800 K. The ^{14}N NMR spectra and nuclear relaxation have been measured at the external magnetic field H_0 = 92.8 kOe. X-ray analysis (cubic NaCl-type lattice, space group *Fm3m*) and magnetic susceptibility data are in agreement with previous study [4]. Temperature-dependent spin contribution to the ^{14}N NMR line shift is connected with the magnetism of 5*f*-electrons of uranium at the paramagnetic phase of UN. Magnetic susceptibility, χ, and line shift, K, are well described by Curie-Weiss law at $T > T_N$ (T_N = 52±1 K). The linear approximation of the $K(\chi)$ diagram gives an estimate of the constant value of the hyperfine field H_{hf} = 2.6±0.2 kOe/μ_B induced on the nitrogen nucleus. The ^{14}N NMR spin-lattice relaxation data indicate that the localization of 5*f*-shell electrons of uranium takes place. The Korringa contribution in the spin-lattice relaxation is higher than for the most of metals [5,6,7]. In antiferromagnetic state, the ^{14}N NMR spectra of single crystal split into 3 lines corresponding to parallel and perpendicular orientations of magnetic domains and metallic-like Korringa temperature dependence of spin-lattice relaxation take place below 30 K. This study was supported by the Russian Science Foundation (project # 18-72-10022).

1. H. H. Hill, in Plutonium and Other Actinides, ed. by W. N. Miner, AIME, New York, p. 2 (1970). 2. A.Z. Solontsov, V.P. Silin, *The Physics of Metals and Metallography*, Vol. 97, p.35 (2004). 3. R. Troć, Pnictides and chalcogenides III (Actinide monopnictides), ed. by H. P. J. Wijn, Landolt-Börnstein, New Series, Group III, Vol. 27 Springer-Verlag, Berlin (2006). 4. Staun Olsen J, Gerward L, Benedict U*, J. Appl. Cryst.*, Vol. 18, p. 37 (1985). 5. D. L. Cox, N.E. Bickers, and J.W. Wilkins, *J. Appl. Phys.,* Vol. 57, p. 3166 (1985). 6. V.V. Oglobichev et al., *JETP Letters,* Vol. 108, p. 650 (2018). 7. V.V. Ogloblichev et al., *Journal of Physics: Conference Series*, Vol. 1389, p.12082 (2019).

Session H3
HARD MAGNETIC MATERIALS: SM-BASED INTERMETALLICS AND OTHERS

Yanglong Hou, Chair
Peking University, Beijing, China

INVITED PAPER

H3-01. Intrinsic and Extrinsic Properties of $Sm(FeCo)_{12}$ With $ThMn_{12}$ Structure. *Y. Takahashi[1] 1. Busshitsu Zairyo Kenkyu Kiko, Tsukuba, Japan*

The Sm-Fe-based $ThMn_{12}$-type rare-earth transition-metal compounds have drawn considerable attention because their rare earth content is the lowest among all known iron rare earth compounds, and they show large uniaxial magnetocrystalline anisotropy and large magnetizations [1,2]. However, most of the RFe_{12} binary compounds are not thermodynamically stable. In order to obtain the RFe_{12} phase in a bulk form, the substitution of Fe with a stabilizing element M, such as Al, Cr, V, Ti, Mo, W, Si and Nb, is required, where the reduction of $\mu_0 M_S$ occurs as M increases. Recently, we have demonstrated that the $Sm(Fe_{0.8}Co_{0.2})_{12}$ compound has the excellent intrinsic properties of $\mu_0 M_s \sim 1.78$ T, $\mu_0 H_a \sim 8$ T and $T_c \sim 859$ K using a single crystalline thin film [3]. These intrinsic hard magnetic properties surpass those of $Nd_2Fe_{14}B$. Mossbauer measurement shows that the each site of Fe increases with Co. One drawback of the $Sm(Fe,Co)_{12}$ compounds is the low coercivity which is due to the lack of suitable secondary phases that can decouple hard magnetic grains. To decouple the exchange coupling in $Sm(Fe,Co)_{12}$ grains, we have investigated the diffusion process with various non-magnetic materials. Cu-Ga diffused $Sm(Fe_{0.8}Co_{0.2})_{12}$ shows highest coercivity of 0.84 T [4]. EDS analysis shows that Cu atoms are enriched in the grain boundary of $Sm(Fe_{0.8}Co_{0.2})_{12}$ grains which causes the enhancement of the coercivity of $Sm(Fe_{0.8}Co_{0.2})_{12}$ thin film. Recently, we obtained very high Hc of 1.2 T by the addition of B. It has granular type microstructure with 40nm grain of 1-12 and B rich grain boundary phase. [5] In addition to the enhancement of coercivity, we found that Zr addition increases the magnetization of $Sm(Fe_{0.8}Co_{0.2})_{12}$. The increase of Zr substitution for Sm from $x = 0$ to 0.26 for $(Sm_{1-x}\ Zr_x)(Fe_{0.8}Co_{0.2})_{12}$ increases saturation magnetization ($\mu_0 M_s$) from 1.78 T to 1.90 T, the highest value reported for hard magnetic compounds[6]. The largest $\mu_0 H_a$ and T_c for Zr-doped samples were found to be 9.8 T and 671 K for $x = 0.18$ which is superior to those for Nd2Fe14B. In this presentation, I will discuss the possibility of $Sm(FeCo)_{12}$ as the permanent magnet by comparing with Nd2Fe14B.

[1] K. Ohashi, T. Yoneyama, R. Osugi, and Y. Tawara, IEEE Trans. Magn., vol. MAG-23, No.5, 3101 (1987). [2] K. H. J. Buschow, J. Magn. Magn. Mater. 100, 79 (1991). [3] Y. Hirayama *et al*., *Scripta Mater*.138, 62 (2017). [4] D. Ogawa *et al*., *Scripta Mater*., 164, 140 (2019) [5] H. Sepehri-Amin *et al. Acta Mater.* 194 337 (2020). [6] P. Tozman *et al*., *Acta Mater*., 178, 114 (2019)

CONTRIBUTED PAPERS

H3-02. Study on Phase Relations of Sm-Fe,Co-Ti-(Ga) System Towards Development of $SmFe_{12}$-Based Permanent Magnets. *S. Ashok Krishnaswamy[1,2], H. Sepehri Amin[1], X. Tang[1], P. Tozman[1], S. Kobayashi[3], T. Ohkubo[1] and K. Hono[1,2] 1. Research Center for Magnetic and Spintronic Materials, National Institute for Materials Science, Tsukuba, Japan; 2. Graduate School of Pure and Applied Sciences, University of Tsukuba, Tsukuba, Japan; 3. Japan Synchrotron Radiation Research Institute (JASRI), Sayo, Japan*

Rare earth permanent magnets are important industrial materials that are essential to build energy efficient motors and generators. Recent studies showed that $Sm(Fe,Co,Ti)_{12}$ (1:12) based compounds of the tetragonal $ThMn_{12}$-type crystal structure, have a superior combination of intrinsic magnetic properties compared to the widely used $Nd_2Fe_{14}B$ magnets (as shown in Fig. 1) [1]. Desirable extrinsic properties needed for practical applications, can be achieved by controlling various microstructural features via effective processing [2]. In particular, the formation of a suitable low-melting and non-ferromagnetic intergranular (IG) phase is important for realizing coercivity in these compounds, as it can facilitate liquid phase sintering needed for controlled grain growth and enable exchange decoupling of the hard magnetic grains. Recently, Ogawa *et al.* studied the effect of diffusing various non-ferromagnetic sources in $Sm(Fe_{0.8}Co_{0.2})_{12}$ thin films, among which the Cu-Ga source shows a potential to realize an IG network and resulted in a high coercivity of 0.84 T [3]. It has also been shown that Ga substitution in rapidly quenched $SmFe_{10}TiV$ ribbons leads to enhancement in the coercivity [4]. Hence, it is important to understand the influence of Ga on the phase relations of the 1:12 compound with a goal to identify a suitable IG phase. The present work extensively investigates the Sm-Fe,Co-Ti-(Ga) system, demonstrating that addition of Ga in Sm-rich $Sm(Fe,Co,Ti)_{12}$ alloys, leads to formation of Sm-Ga based non-ferromagnetic intergranular phases, such as Ba_5Si_3-type Sm_5Ga_3 and TlI-type SmGa (as shown in Fig. 2). Further, melt-spinning of these alloys leads to grain refinement up to 0.5 – 2 μm, while retaining the IG network at low quenching rates. However, the coercivity was limited to ~0.5 T (only ~5% of H_A), due to the presence of defects and fluctuation of Co content at the surface of the 1:12 grains, according to high resolution TEM observations.

[1] G. C. Hadjipanayis et al, Engineering, Vol. 7, p. 141 (2020). [2] D. Goll, Kronmuller, S. Parkin, USA:Wiley, Handbook of Magnetism and Advanced Magnetic Materials, Vol. 2, p. 1 (2007). [3] D. Ogawa et al, Scripta Mater., Vol. 164, p. 140 (2019). [4] Y. Wang et al, J. Appl. Phys.,Vol. 67, p. 4954 (1990).

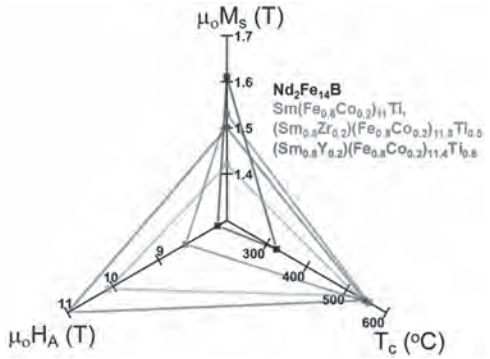

Fig. 1 Intrinsic magnetic properties: saturation magnetization (μ_oM_s), anisotropy field (μ_oH_A) and Curie temperature (T_c)

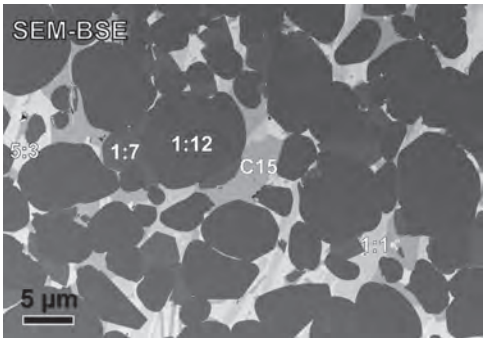

Fig. 2 BSE-SEM micrograph of Sm-rich Ga-containing alloy showing Sm_5Ga_3 (5:3), SmGa (1:1) and $Sm(Fe,Co,Ga)_2$ (C15) intergranular phases in bright contrast.

H3-03. Combinatorial Study of Sm-Co-Ti Amorphous Hard Magnet Thin Films. *P. Rani*[1], E. Carneiro[1], G. Muscas[1], H. Stopfel[1], D. Primetzhofer[1], P.E. Jönsson[1] and G. Andersson[1] *1. Uppsala University, Uppsala, Sweden*

Rare-earth-lean permanent magnetic materials play a key role in many technology sectors like spintronics, energy transport, aerospace, and biomedicine. Structure and composition are likely to control material properties such as magnetic moment and coercivity. Here, we study thin-film libraries of Sm-Co-Ti, fabricated on Si wafer by combinatorial DC magnetron sputtering, with a focus on magnetic and structural properties over wide ranges of composition and thickness. The samples had a thickness ranging from 370 to 450 Å and $Sm_xCo_yTi_{100-x-y}$ alloy compositions with x = 10-25 at% and y = 65-86 at%, as estimated by MATLAB theoretical calculations and subsequently confirmed by Rutherford backscattering spectroscopy. Structural properties were investigated by GIXRD, confirming all samples to be amorphous. MOKE, VSM, and SQUID magnetometry were used to investigate the magnetic properties. In-plane magnetic hysteresis loops show a coercive field of 10-250 mT and a saturation magnetization of approximately 800 kA/m in the full thin libraries. RT-MOKE measurements confirmed that the addition of Ti to the SmCo alloy makes it likely to obtain greater coercivity (~180 mT) as compared to SmCo (~100 mT) [1] while reducing the necessity for a high Sm content. Fig 1 shows representative in-plane and out-of-plane hysteresis loop measured with VSM and In-plane coercivity measurement along the center stipe of the libraries. The Sm-Co gradient is along this stripe, and the Ti content is roughly constant (~7 at%).

[1] Magnus, F.*, et al* (2013). Tunable giant magnetic anisotropy in amorphous SmCo thin films. *Applied Physics Letters*, *102*(16), 162 402.

H3-04. Micromagnetic Simulation Study on Coercivity in $CeCo_5$ Magnet. *X. Liu*[1] and I.C. Nlebedim[1] *1. Ames Laboratory, Ames, IA, United States*

High-performance permanent magnets require critical chemical elements such as Pr, Nd, Sm, and Dy. To reduce the use of these critical elements, Ce-based magnets attract renewed research interest. Depending on chemical composition and microstructure, there are three types of Ce-Co type magnet: single phase $CeCo_5$, precipitated $Ce(Co, Cu, Fe)_5$ and $Ce(Co,Cu,Fe,Ti)_{6-7}$ magnet [1]. However, single phase $CeCo_5$ sintered magnet shows typical coercivity less than 4 kOe while it has a magnetic anisotropic field up to 210 kOe [1]. Proper understanding of the coercivity mechanism is necessary to improve coercivity of single phase $CeCo_5$ magnet. Since the sintered $CeCo_5$ has nearly featureless single-phase microstructures, most of the structural defects are Ce-deficient structural imperfection at grain boundaries due to the sensitivity of Ce to oxygen. We have studied the correlation between the structural imperfection of grain boundary (GB) and demagnetization process using micromagnetic simulation (MS). The single crystal grain of $CeCo_5$ was modelled with a cube with edge length of 1 micron including a defect layer with varied thickness. Three types of structure are selected to mimic the defect layers at GB: (1) 1:5-type with the magneto-crystalline anisotropy (MCA) parameter reduced by 90%, relative to $CeCo_5$; (2) 2:17-type with intrinsic magnetic properties of Ce_2Co_{17}; (3) Co-type with intrinsic magnetic properties of pure cobalt metal. It was found from the MS that coercivity of an ideal $CeCo_5$ has a value of about 81 kOe. For the same $CeCo_5$ cube, including a defect layer with a thickness of 6nm, coercivity values are 2.8 kOe, 5.0 kOe and 11.8 kOe for the 2:17-type, Co-type and 1:5-type structure layers, respectively (Fig. 1). The results indicate that the formation of 2:17-type or Co-type defects can abruptly reduce the coercivity of $CeCo_5$, which is ascribed to weak magnetic anisotropy and relative high magnetization of the 2:17-type or Co-type structures. The 2:17 type structure are the most possible defects due to the Ce oxidation during processing, which is responsible for the low coercivity of $CeCo_5$ magnet.

[1] Karl J. Strnat, and Reinhold M.W. Strnat, Journal of Magnetism and Magnetic Materials 100 (1991) 38-56

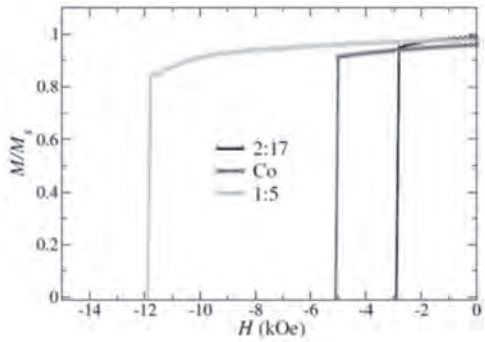

Fig.1 M-H curves of $CeCo_5$ with defect layer of 1:5-, Co- and 2:17-type, respectively (see detail in main text).

H3-05. Design of Sm-Fe-N Magnets. *T. Saito*[1] *1. Chiba Institute of Technology, Narashino, Japan*

Sm-Fe-N magnets are a possible alternative to Nd-Fe-B permanent magnets, due to its high saturation magnetization with a high anisotropy field and high Curie temperature. The $Sm_2Fe_{17}N_3$ phase has been obtained in powder form by the nitrogenation of Sm_2Fe_{17} alloy powder [1]. Unlike the case of Nd-Fe-B magnets, which are widely used as high-performance permanent magnets, conventional sintering techniques cannot be applied to the production of Sm-Fe-N magnets because the $Sm_2Fe_{17}N_3$ phase lacks stability at high temperatures and decomposes into a-Fe and SmN above 873 K. It is therefore essential to develop a new technique for the production of Sm-Fe-N bulk magnets. One of the most promising techniques to obtain bulk Sm-Fe-N magnets is the spark plasma sintering (SPS) method [2].

It has been demonstrated that Sm-Fe-N powder can be consolidated into a bulk material by the spark plasma sintering (SPS) method [3]. However, the reported magnetic properties of Sm-Fe-N magnets were not yet comparable to the original Sm-Fe-N powder. The purpose of this study was to improve the magnetic properties of Sm-Fe-N magnets by optimizing the SPS conditions. Here the structures and magnetic properties of Sm-Fe-N bulk magnets are discussed. Sm-Fe-N powder was blended with Zn powder and additive before the consolidation. The Sm-Fe-N powder was placed in a carbon die and then magnetically aligned before the consolidation by the SPS method. The Sm-Fe-N powder was sintered by the SPS method. The Sm-Fe-N magnets were successfully produced by the SPS method. The magnetic properties of the resultant Sm-Fe-N magnets deeply depended on the processing condition. Figure 1 shows the Sm-Fe-N magnets produced by the SPS method with and without the Zn powder and additive. It was found that the coercivity and remanence of the Sm-Fe-N magnets were improved by the small amounts of Zn powder and additive. The Sm-Fe-N magnets with the Zn powder and additive were found to be the anisotropic Sm-Fe-N magnets.

[1] J. M. D. Coey and H. Sun, J Magn. Magn. Mater. 87, L251 (1990). [2] M. Tokita, J. Soc. Powder Technol. Jpn, 30, 790 (1993). [3] T. Saito, J. Magn. Magn. Mater. 320, 1893 (2008).

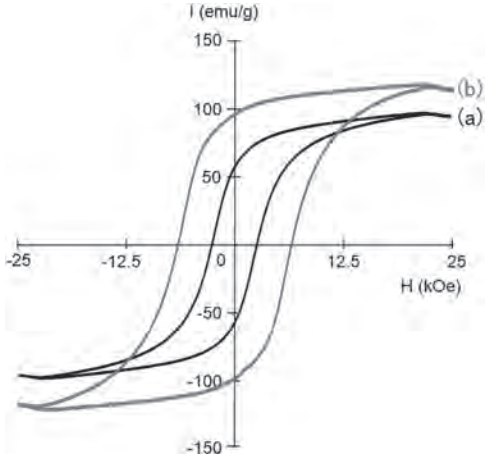

Fig.1 Sm-Fe-N magnets produced by the SPS method: (a) Sm-Fe-N powderr and (b) Sm-Fe-N powder with small amounts of Zn powder and additive.

H3-06. Withdrawn

H3-07. Nitrided $ThMn_{12}$-Type Compounds for Sustainable Advanced Manufacturing. *D. Salazar*[1] *1. BCMaterials, Basque Center for Materials Applications and Nanostructures, Leioa, Spain*

The revisited interest in permanent magnets based in the $ThMn_{12}$-type compounds is driven by their reduced content of critical elements and the current availability of advanced processing techniques scalable to the industry. The nitride $Nd_{1.1}Fe_{10.5}Mo_{1.5}N_x$ (NdFeMoN) compound shows not only promising intrinsic but extrinsic properties after a defined powder processing. This system has a high anisotropy field (>10T) and high saturation polarization (>1T). By means of a nitrogenation process of melt-spun ribbons, high coercivity powders suitable for bonded and printed magnets are obtained. The development of sustainable advanced manufacturing by the fabrication of composite materials should be based on renewable polymeric matrices and magnetic fillers, combining the processability and natural availability of polymers, with the suitable performance of magnetic materials. This work proposes the use of both silk and hydroxypropyl cellulose (HCP) as matrixes, natural materials obtained from silkworm cocoons and from water-soluble cellulose derivatives, respectively, because of their natural abundance, biodegradability, thermal stability and biocompatibility. Films of HPC/NdFeMoN and Silk/NdFeMoN composites with particle concentrations from 75 to 95 wt. % were fabricated by a doctor blade technique. Nitride powders with Curie point of 370C, coercive field of 0.5 T and saturation polarization of 1 T were used as filler material. The influence of an external magnetic field on the printed material during evaporation is studied. Magnetic inks for screen-printing/stencils were prepared following the same method using solutions of a 90 wt. % of NdFeMoN.

H3-08. Production of $Sm(Fe,Ti)_{12}$ Magnets by hot Deformation. T. Saito[1], *Y. Ogawa*[1] and D. Nishio-Hamane[2] *1. Chiba Institute of Technology, Narashino, Japan; 2. Institute for Solid State Physics, The University of Tokyo, Kashiwa, Japan*

In recent years, the search for new permanent magnet materials has focused on the RFe_{12} (R = rare earth) intermetallic compounds. Although the binary RFe_{12} intermetallic compounds with the $ThMn_{12}$-type structure are not thermodynamically stable and do not exist in bulk form, it has been found that the substitution of T (T = Ti, V, Cr, Mo) for Fe in the RFe_{12} intermetallic compound stabilizes the $ThMn_{12}$-type structure [1–6]. The objective of the present study was to produce anisotropic $Sm(Fe,Ti)_{12}$ magnets. In the case of Nd-Fe-B magnets, anisotropic Nd-Fe-B magnets have been produced by either the sintering of Nd-Fe-B powder or hot deformation of hot-pressed Nd-Fe-B magnets. In this study, we attempted to produce anisotropic $Sm(Fe,Ti)_{12}$ magnets by the hot deformation of hot-pressed $Sm(Fe,Ti)_{12}$ magnets. The structures and magnetic properties of the hot-pressed and hot-deformed $Sm(Fe,Ti)_{12}$ magnets are discussed. $Sm(Fe,Ti)_{12}$ alloy ingots were prepared by induction melting in an argon atmosphere. The alloy ingots were induction melted and then ejected through an orifice with argon onto a copper wheel. The resultant melt-spun ribbons were comminuted into powders and then hot-pressed by the spark plasma sintering (SPS) method. Hot deformation of the hot-pressed $Sm(Fe,Ti)_{12}$ magnets was performed in a vacuum at 973–1173 K under a pressure of ~200 MPa by the SPS method. Figure 1 shows the hysteresis loops of the hot-deformed $Sm(Fe,Ti)_{12}$ magnets, measured parallel and perpendicularly to the pressing direction. The magnetic anisotropy of the hot-deformed $Sm(Fe,Ti)_{12}$ magnets was confirmed by the existence of a higher remanence in the parallel direction than in the perpendicular direction. This indicates that anisotropic $Sm(Fe,Ti)_{12}$ magnets were successfully produced by the hot deformation of hot-pressed $Sm(Fe,Ti)_{12}$ magnets.

[1] F. R. De. Boer, et al. J. Less-Common Met. 135, 199 (1987). [2] L. X. Liao, et al. J. Appl. Phys. 70, 6006 (1991). [3] L. Shultz and J. Wecker, J. Appl. Phys. 64, 5711 (1988). [4] Y. Wang, et al. J. Appl. Phys. 67, 4954 (1990). [5] Y. Otani, et al. IEEE Trans. Magn. 26,2658 (1990). [5] J. Yang, et al. J. Appl. Phys. 88, 988 (2000). [6] E. Tomey, et al. J. Alloys Compd. 231, 195 (1995).

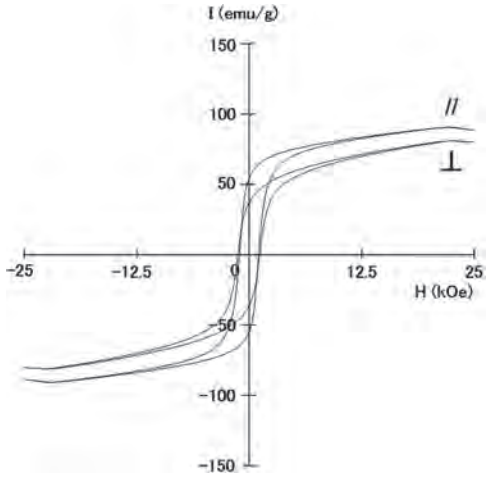

Fig.1 Hysteresis loops of the hot-deformed $Sm(Fe,Ti)_{12}$ magnets.

H3-09. Grain Boundary Segregation, Phase Formation, and Their Influence on the Coercivity of Rapidly Solidified $SmFe_{11}Ti$ Hard Magnetic Alloys. *S. Ener*[1], F. Maccari[1], D. Palanisamy[2], L. Schaefer[1], K. Skokov[1], D. Raabe[2], B. Gault[2] and O. Gutfleisch[1] *1. Functional Materials, Technische Universitat Darmstadt Fachbereich Material- und Geowissenschaften, Darmstadt, Germany; 2. Max-Planck-Institut fur Eisenforschung GmbH, Dusseldorf, Germany*

The rare-earth (RE) supply crisis around 2010/2011 led to a drastic increase in prices and revealed the dependency on critical RE elements [1] for the production of high-performance permanent magnets. Significant efforts have been made since in the search for new material systems which present magnetic properties similar or superior to those of benchmark $Nd_2Fe_{14}B$, but which contain less critical elements [2]. One of such alternatives are Nd- and Sm-based intermetallic compounds with a tetragonal $ThMn_{12}$-type crystal structure, exhibiting intrinsic magnetic properties comparable to $Nd_2Fe_{14}B$ [3-6]. In this study, we carried out advanced characterization of grain boundaries of polycrystalline bulk $SmFe_{11}Ti$ samples. Detailed microstructural analysis was carried out using HR-SEM coupled with TEM and APT. Additionally, for the determination of the magnetic properties room-temperature isothermal magnetization measurements were carried out. To get a better understanding of the demagnetization behavior of the samples, in-situ demagnetization measurements were done using MOKE microscopy. The EDX analysis results indicate that the chemical composition of the suction casted and annealed sample is slightly off-stoichiometric $SmFe_{11.1}Ti_{0.9}$. The APT measurements revealed a distinct composition of grain boundaries compared to the adjoining 1:12 matrix grains where a grain boundary composition with more than 75 at. % of iron was measured. Additionally, three different phases, namely, monoclinic $Sm_3(Fe,Ti)_{29}$, cubic $SmFe_2$-, and Fe_2Ti-Laves phases, all form preferably at the grain boundaries and at triple junctions. The MOKE measurements reveal a strong ferromagnetic coupling of the 1:12 grains across the grain boundaries. Based on these results, we assume that the grain boundaries, with more than 75 at% of iron, behave like ferromagnetic regions and therefore no magnetic isolation is observed at the grain boundaries. Financial support of the future pioneering program Development of Magnetic Material Technology for High-Efficiency Motors (MagHEM) commissioned by the New Energy and Industrial Technology Development Organization (NEDO) of Japan and the DFG – Project-ID 405553726 – TRR 270 are gratefully acknowledged.

[1] O. Gutfleisch et al., Adv. Mat. 23 (2011) 821. [2] K.P. Skokov and O. Gutfleisch, Scr. Mat. 154 (2018) 289. [3] K.H.J. Buschow, Journal of Appl. Phys. 63 (1988) 3130. [4] D.B. De Mooij and K.H.J. Buschow, J. Less Common Met. 136 (1988) 207. [5] F. Maccari et al., Acta Mat. 180 (2019) 15-23. [6] D. Palanisamy et al., Phys. Rev. Mat. 4 (2020) 054404.

INVITED PAPER

H3-10. Recent Advances in SmFe12-Based Hard Magnetic Materials. *H. Sepehri Amin*[1], Y. Tamazawa[2], M. Kambayashi[2], G. Saito[2], Y. Takahashi[1], D. Ogawa[1], T. Ohkubo[1], S. Hirosawa[1], M. Doi[2], T. Shima[2] and K. Hono[1] *1. Busshitsu Zairyo Kenkyu Kiko, Tsukuba, Japan; 2. Tohoku Gakuin Daigaku, Sendai, Japan*

$SmFe_{12}$-based compounds have been considered as promising candidates for next-generation permanent magnet materials because of their excellent intrinsic hard magnetic properties with minimum usage of rare earth elements [1]. However, realizing high coercivity in anisotropic microstructure is a big challenge, which hinders their practical applications [2]. In this work, we first review our recent progress on realizing coercivity in bulk SmFe12-based alloys. It was found that the main challenge in realizing coercivity in SmFe12-based magnets is to realize a grain boundary phase which can magnetically isolate SmFe12-based grains. We have investigated the possibility of such a microstructure in a modelled thin films. A novel anisotropic granular microstructure of $Sm(Fe_{0.8}Co_{0.2})_{12}$ with a sufficiently large coercivity ($\mu_0 H_c$) of 1.2 T and with a high remanent magnetization of 1.50 T is demonstrated in thin films prepared by co-sputtering $Sm(Fe,Co)_{12}$ with boron [3]. We prepared magnetic $Sm(Fe_{0.8}Co_{0.2})_{12}B_x$ films with a varied B content (0£x£1.5) by co-sputtering Sm, Fe, $Fe_{50}Co_{50}$, and $Fe_{80}B_{20}$ (at.%) targets, and investigated their magnetic properties. $Sm(Fe_{0.8}Co_{0.2})_{12}$ film showed the perpendicular coercivity of only 0.1 T, which causes demagnetization at the remanent state, resulting in a very low remanent magnetization of only 0.2 T. Coercivity in the $Sm(Fe_{0.8}Co_{0.2})_{12}B_{0.5}$ film increased to 1.2 T with a remanent magnetization of 1.50 T. Detailed microstructure characterization showed the B-free film has no distinct intergranular phase and $Sm(Fe_{0.8}Co_{0.2})_{12}$ grains with slight orientation changes are in direct contact (Fig. 1 a,c). In the case of $Sm(Fe_{0.8}Co_{0.2})_{12}B_{0.5}$ film, columnar-shaped $Sm(Fe_{0.8}Co_{0.2})_{12}$ grains with a size of ~40 nm was observed which are surrounded by ~3-nm-thick B-enriched amorphous intergranular phase (Fig. 1 ((b,d)). Domain wall pinning at the amorphous grain boundary phase is attributed to the high coercivity. Furthermore, we found excellent thermal stability of coercivity in the B-doped $Sm(Fe_{0.8}Co_{0.2})_{12}B_{0.5}$ film, i.e., the temperature coefficient of coercivity, $\beta = -0.22\%/°C$ in the temperature range of 27-227°C [3]. This work provides a guiding principle for realizing high-coercivity anisotropic $SmFe_{12}$-based permanent magnets, which can outperform Nd-Fe-B magnets and could be used as the next-generation high-performance permanent magnets in various applications. This work was supported by Elements Strategy Initiative Center for Magnetic Materials (ESICMM), Grant Number JPMXP0112101004, through the Ministry of Education, Culture, Sports, Science and Technology (MEXT).

[1] P. Tozman, H. Sepehri-Amin, Y.K. Takahashi, S. Hirosawa, K. Hono, Acta Mater. 153 (2018) 354. [2] I. Dirba, Y. Harashima, H. Sepehri-Amin, T. Ohkubo, T. Miyake, S. Hirosawa, K. Hono, J. All. Comp. 813 (2020) 152224. [3] H. Sepehri-Amin *et al.* Acta Mater. 194 (2020) 337.

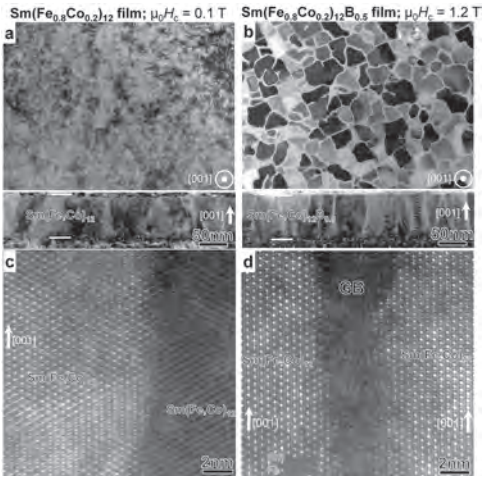

Fig. 1. Plane-view (top) and cross-sectional (bottom) BF-TEM images of (a) $Sm(Fe_{0.8}Co_{0.2})_{12}$ and (b) $Sm(Fe_{0.8}Co_{0.2})_{12}B_{0.5}$ films. HAADF-STEM images obtained from the cross-sectional view of (c) $Sm(Fe_{0.8}Co_{0.2})_{12}$ and (d) $Sm(Fe_{0.8}Co_{0.2})_{12}B_{0.5}$ films.

CONTRIBUTED PAPERS

H3-11. Withdrawn

H3-12. Withdrawn

H3-13. The Influence of Grain Size on the Internal Oxidation of Sm_2Co_{17} Sintered Magnets. *A.R. Campbell*[1] and R.S. Sheridan[1] *1. School of Metallurgy and Materials, University of Birmingham, Birmingham, United Kingdom*

The drive towards electrification of propulsion systems previously dominated by fossil fuel combustion, has resulted in a rapid increase in the use of rare-earth permanent magnets. The high energy density of NdFeB based magnets has seen them dominate in the automotive sectors, but the high Curie temperature, magnetic stability over broad temperature ranges, and resistance to corrosion without a surface coating of Sm_2Co_{17} type magnets means they are likely to be the material of choice in the electrification of aerospace. Work into improving the high temperature performance of Sm(Co,Fe,Cu,Zr) magnets has resulted in some compositions having useful magnetic behaviour up to 500°C [1,2]. However, it has been shown that at these temperatures, an internal oxidation zone (IOZ) forms via the transformation of the hard magnetic Sm_2Co_{17} matrix to a soft magnetic Fe(Co) solid solution, impacting magnetic performance [3,4]. Coatings have been shown to be effective [5,6] but may not be applicable when the magnets are used in electrical machines, where they are often built into complex arrays that require a final surface grind. This work has investigated the influence of grain size on the growth-rate of the IOZ at 500°C in two commercial sintered magnets with similar composition and magnetic properties. It was found that smaller grain size may be beneficial to minimize IOZ growth and the resultant loss in remanence (B_r). It is suggested that the rate control mechanism for oxygen diffusion differs depending upon IOZ growth direction. Reducing grain size was most effective at reducing IOZ growth in the direction perpendicular to the crystallographic c-axis (Fig1), as here thick grain boundary precipitates form, retarding oxygen diffusion. As the loss in B_r is proportional to the volume consumed by the IOZ, thin magnets will suffer greater magnetic losses than bulk magnets. When using uncoated Sm_2Co_{17} magnets in high temperatures, one must therefore consider their morphology and the crystallographic orientation of exposed faces, in addition to microstructure and composition, in order to minimize induction loss from oxidation.

1. C. H. Chen et al. *J. Appl. Phys.*, vol. 83, no. 11, p. 6706, (1998) 2. J. F. Liu et al *J. Appl. Phys.*, vol. 85, no. 8, p. 5660, (1999) 3. W. M. Pragnell et al. *J. Alloys Compd.*, vol. 487, no. 1–2, p. 69–75, (2009) 4. Z. Yang, et al *Corros. Sci.*, vol. 61, p. 72–82, (2012) 5. Q. Wang et al *J. Magn. Magn. Mater.*, vol. 331, p. 245–249,(2013) 6. W. M. Pragnell et al *J. Alloys Compd.*, vol. 517, p. 92–97, (2012)

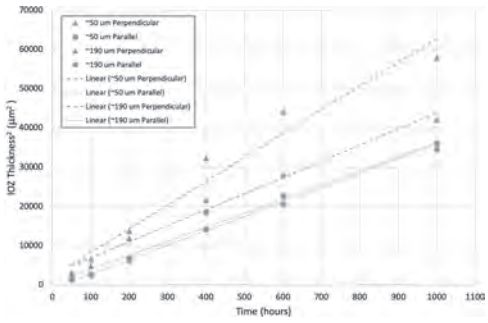

Fig.1 IOZ growth at 500°C, varying with growth direction in respect to crystallographic c-axis and grain size

H3-14. Epitaxy Induced Controlled Phase Separation in Y-Co and Sm-Co Thin Films. *S. Sharma*[1], D. Ohmer[1], A. Zintler[1], D. Guenzing[2], M. Major[1], I. Radulov[1], P. Komissinskiy[1], B. Xu[1], H. Zhang[1], K. Ollefs[2], K. Skokov[1], L. Molina-Luna[1] and L. Alff[1] *1. Institute of Materials Science, Technische Universität Darmstadt, Darmstadt, Germany; 2. Universität Duisburg-Essen, Duisburg, Germany*

Thin-film fabrication methods provide a non-equilibrium means to control and design magnetic materials at the nanoscale and validate novel hardening mechanisms. Utilizing the technique of molecular beam epitaxy, a nanoscale magnet of R_2Co_{17} and RCo_5 (R = Y and Sm) phases with a perfect *c*-axis growth texture, is stabilized. While typically in bulk rare-earth cobalt systems, only by addition of further elements like Cu, Fe, and Zr, and complex heat treatments, a phase decomposition can be obtained, here we directly induce phase separation by the film growth kinetics. The resulting nanoscale architecture is revealed by cross-sectional scanning transmission electron microscopy. The Y-Co nanocomposite film (Fig. 1) is made up of a network of coherently interlinked Y_2Co_{17} and YCo_5 building blocks with *c*-axis oriented growth texture. [1,2] As a result of favourable exchange-interaction, the nanocomposite film exhibits the desired perpendicular anisotropy. The observed pinning mechanism in combination with the increased total magnetization due to the Y_2Co_{17} phase, yields an enhanced energy product of the nanocomposite. The nanoscale architecture of the Sm-Co film comprises of *c* - axis oriented Sm_2Co_{17} and $SmCo_5$ phases with an atomically smooth interface (Fig. 2). A detailed analysis of the extended X-ray absorption fine structure of the film confirmed the co-existence of Sm_2Co_{17} and $SmCo_5$ phases with about 35% of $SmCo_5$. [3] The analysis shows a novel method to quantify these phases in a reliable way. The formation of coherent precipitations in these *R*-Co systems is facilitated by the perfectly matching lattice constants, atomic species, and crystal symmetry of the two phases. The knowledge significantly contributes to establish new theoretical and experimental concepts to engineer the microstructure for beyond state-of-the-art magnets.

[1] S. Sharma, D. Ohmer, A. Zintler, M. Major, I. Radulov, U. Kunz, P. Komissinskiy, B. Xu, H. Zhang, L. Molina-Luna, K. P. Skokov, and L. Alff, (Manuscript under Review in Phys. Rev. B) [2] S. Sharma, E. Hildebrandt, S. U. Sharath, I. Radulov, and L. Alff, J. Magn. Magn. Mater. 432, 382 (2017) [3] S. Sharma, I. Radulov, M. Major, and L. Alff, IEEE Trans. Magn. 54, 1 (2018)

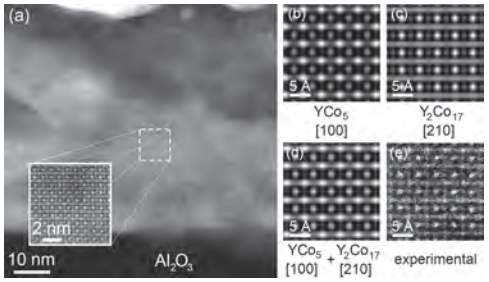

Fig. 1: Thin film nanocomposite of Y-Co system made up of YCo_5 and Y_2Co_{17} phases.

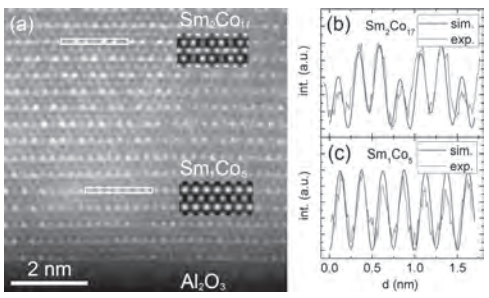

Fig. 2: Thin film nanocomposite of Sm-Co system comprising of $SmCo_5$ and Sm_2Co_{17} phases.

Session H4
FERRITES AND GARNETS II
(Poster Session)

Feng Xu, Chair
Nanjing University of Science and Technology, Nanjing, China

H4-01. Influence of Size and Shape on key Performance Metrics in Spin-Torque Oscillators. *B.R. Zink*[1], Y. Lv[1] and J. Wang[1] *1. Electrical and Computer Engineering, University of Minnesota, Minneapolis, MN, United States*

Spin Torque Oscillators (STOs) are promising solutions in a wide variety of next generation technologies from read-head sensors in high-density magnetic recording arrays [1] to neural oscillator units for neuromorphic computing [2-3]. There are several metrics that can be used to quantify the performance of an STO such as power, quality factor, frequency tunability, etc., most of which are dependent on the design of the STO device itself. Furthermore, determining the most important metric will be contingent on its desired application, meaning that it is crucial to understand how the STOs design parameters influence all aspects of its performance so that its design can be optimized to perform the desired function. Our previous studies have investigated the influence of STO size [4] and shape anisotropy [5] on precession frequency and linewidth. In this work, we expand on our previous research and study the influence of device size and shape on several STO performance metrics and use correlation coefficients to quantify relative magnitude of these effects. This was done by analyzing spin torque oscillations generated from 20 magnetic tunnel junctions with in-plane anisotropy and patterned into elliptical nano-pillars with a wide range of sizes and aspect ratios. For each device, we acquired 20 to 50 data sets at various bias fields and currents and obtained power spectral density (PSD) plots for each set, examples of which are shown in Fig. 1a. Each PSD plot was used to measure frequency and linewidth (as illustrated in Fig. 1b) as well as output power. From these measurements, we then calculated quality factor and power-to-linewidth ratio for each set. We also analyzed each STOs performance in terms of the bias fields and bias currents required to maximize output power and signal quality as well as the frequency tunability with both field and current. All of these performance metrics were compared between all 20 STOs tested.

[1] H. Suto *et al.*, "Real-Time Measurement of Temporal Response of a Spin-Torque Oscillator to Magnetic Pulses", *Appl. Phys. Express*, vol. 4, p. 013003, Dec. 2010, doi: 10.1143/APEX.4.013003. [2] D. E. Nikonov *et al.*, "Coupled-Oscillator Associative Memory Array Operation for Pattern Recognition", *IEEE J. Explor. Solid-State Comput. Devices Circuits*, vol. 1, pp. 85–93, Nov. 2015, doi: 10.1109/JXCDC.2015.2504049. [3] M. R. Pufall *et al.*, "Physical Implementatin of Coherently Coupled Oscillator Networks", *IEEE J. Explor. Solid-State Comput. Devices Circuits*, vol. 1, pp. 76-84, Aug. 2015, doi: 10.1109/JXCDC.2015.2468070. [4] X. Chao, M. Jamali, and J.-P. Wang, "Scaling effect of spin-torque nano-oscillators", *AIP Advances*, vol. 7, issue 5, p. 056624 Jan. 2017, doi: 10.1063/1.4974014. [5] X. Chao, M. Jamali, and J.-P. Wang, "Shape anisotropy effects on spin-torque oscillators", *AIP Advances*, vol. 10, issue 4, p. 045101, Mar. 2020, doi: 10.1063/1.5130480.

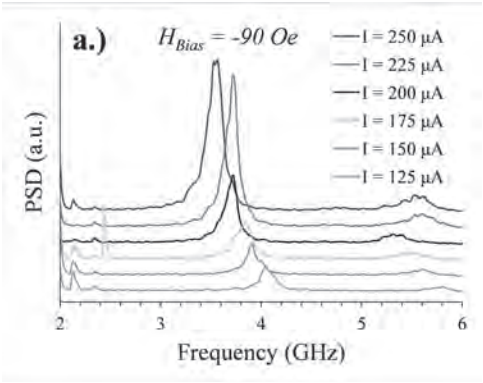

Fig. 1. a.) Example of power spectral density plots at a bias field of -90 Oe and various bias currents (I_{bias}).

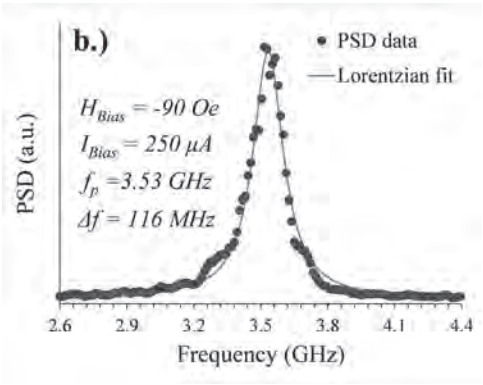

b.) Lorentzian fit on the I_{bias} = 250 μA data set, from which, frequency (f_p) and linewidth (Δf) can be obtained.

H4-02. Characterization of NiFe and Silicon Dioxide Multilayers for on-Wafer Inductors Operating at Radio and Low GHz Frequencies. *S. Goldman*[1] and Z. Celinski[1] *1. Physics, University of Colorado at Colorado Springs, Colorado Springs, CO, United States*

The concept of magnetic layers surrounding copper core inductors is proposed for use in circuits operating at radio and low GHz frequency ranges, in order to address performance issues and quality losses normally observed in miniaturized inductors at high frequency. Coating an inductor core in a magnetic material has the potential to increase the inductance proportional to the magnetic permeability of the coating. The objective of this research is to identify and construct an appropriate magnetic coating to improve the inductance (L) and quality (Q-factor) of high frequency inductors. An alloy of 81% nickel and 19% iron (NiFe), was selected for these experiments due to its high relative permeability. NiFe layers are sputter deposited, from 10nm to 1μm thick, on silicon wafers for characterization. A specific issue we address is that inductor coatings have the potential to decrease the Q-factor due to eddy currents during high frequency operation. A method to reduce eddy current losses is to reduce layer thickness. Therefore, in addition to individual layers, multilayer coatings are developed:

depositing 5 to 50 identical layers of NiFe (for totals from 150nm to 1.5μm) separated with 5nm layers of silicon dioxide. This allows for thin individual layers, while maintaining a large total thickness. We present the characteristics of the individual and multilayer coatings to determine their suitability for high frequency inductor operations.

H4-03. Simultaneous Measurement of Permeability and Permittivity Using a Flexible Microstrip Line-Type Probe up to 67 GHz. *S. Yabukami*[1,2], K. Nozawa[2], L. Ton That[2] and K. Okita[1] *1. Graduate School of Biomedical Engineering, Tohoku University, Sendai, Japan; 2. Graduate School of Engineering, Tohoku University, Sendai, Japan*

High frequency permeability and permittivity measurement is important for radio wave absorber and electromagnetic shielding materials. Usually, in order to measure the magnetic permeability and the permittivity simultaneously, the sample had to be processed into a solenoid [1]. Further, when the dielectric constant and the magnetic permeability are separately measured, it is necessary to process the sample into a thin shape or a needle shape, and the method using the waveguide has problems such as discontinuous frequency. In our previous work, we developed a flexible microstrip line-type probe, and present permeability measurement [2]. In this research, this probe is applied to the simultaneous evaluation of permittivity and permeability of electromagnetic materials without restriction on sample size. As shown in in Fig. 1, the probe was composed of a straight microstrip conductor on a flexible substrate, a ground plane, lead lines, and two connectors. The microstrip line sloped to meet the lead line at either end, and had slopes to maintain a characteristic impedance of around 50 Ω and to allow close contact of a large samples. In permeability and permittivity measurement, firstly, S_{21} is calibrated without sample. Secondly, $S_{21}^{(sat)}$ is measured by applying of a strong dc field (around 20 kOe) to saturate the magnetic film. Thirdly, $S_{21}^{(sample)}$ is measured by removing the strong dc field, and then the complex permeability is optimized by $S_{21}^{(sample)}$-$S_{21}^{(sat)}$ using FEM analysis [2]. Then the complex permittivity also optimized by $S_{21}^{(sat)}$ using FEM analysis, because magnetic signal was removed in $S_{21}^{(sat)}$, therefore dielectric signal mainly can be obtained. Fig. 2 shows the complex permittivity of PTFE (polytetrafluoroethylene,25 mm x 25 mm, 0.79 mm in thickness) to demonstrate accurate permittivity measurement. The relative permittivity of this sample was measured to be about 2.1, which almost matched the manufacturer's specifications [3]. Relative permeability was also measured, but cannot be posted due to the limited number of graphs. The permeability graph will be presented at the conference.

[1] https://www.keysight.com/jp/ja/assets/7018-03896/brochures/5991-2171.pdf [2] S. Yabukami, K. Nozawa, L Tonthat, and K. Okita, IEEE Trans. Magn. Vol. 56 (2020, in press) [3] https://www.meilhaus.de/en/u2941a-201.htm

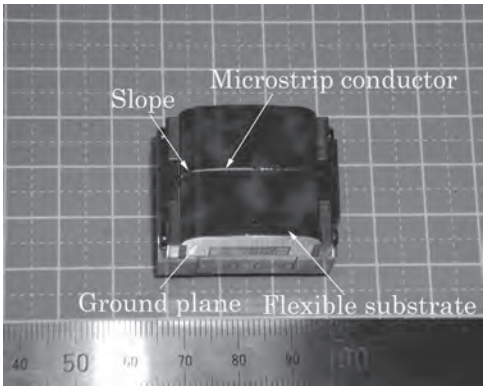

Fig. 1 Schematic view of probe.

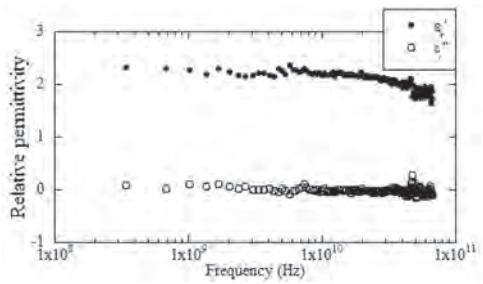

Fig. 2 The complex permittivity of PTFE.

H4-04. Consideration on Lowering Loss Design of Skin Effect Suppressed Multi-Layer Transmission Line With Positive/Negative (Cu/NiFe) Permeability Materials for High Data-Rate and Low Delay-Time I/O Interface Board. *K.H. Kubomura*[1], Y. Aizawa[1], H. Nakayama[2], R. Hara[2] and H. Tanaka[2] *1. Advanced Course of Production and Environment System, National Institute of Technology (KOSEN), Nagano College, Nagano, Japan; 2. Department of Electronics and Control Engineering, National Institute of Technology (KOSEN), Nagano College, Nagano, Japan*

INTRODUCTION - This paper proposes a new application of skin effect suppression technology [1]-[5] for long wiring on high-speed & low-delay I/O board. In previous research [6], a lower loss structure of electroplated conductor/magnetic multilayer was clarified by changing thickness of each layer with an electromagnetic field calculation theory for rectangular multilayer transmission line. A challenge in this paper is to clarify the structure with the lowest loss by the method of changing each layer's thickness. Also an electroplated conductor/magnetic multilayer transmission line will be able to used as a band pass filter, utilizing characteristics of the magnetic material. VERIFICATION - Cu and NiFe were selected as metal conductor material and negative permeability magnetic material, respectively. Permeability and Q factor of NiFe were estimated by the L.L.G. equation. The Cu and NiFe films are alternately stacked to form the multilayer, as shown in Fig. 1. An electromagnetic field distribution, which considers the skin effect in a rectangular multilayer transmission line, is derived based on Maxwell's equation. The current density of each layer and the total loss can be obtained by the equations (1) and (2) in Fig. 1. The loss of transmission line whose total thickness is 12.67 μm was compared under the following conditions. 1) A 33 layered structure by a constant ratio, Cu t_N = 0.51 μm and NiFe t_F = 0.25 μm. 2) A 33 layered optimal design we proposed at 16 GHz. 3) A 17 layered optimal design we proposed at 16 GHz. RESULTS AND DISCUSSION - Fig. 2 shows the frequency characteristics of loss in each model. At 16 GHz, where NiFe has the best Q value, compared to conventional thickness by a constant ratio, it was estimated that the loss is 80% in optimal thickness of 33 layers. In the structure we proposed, the loss increases compared to the conventional one in the outside band of optimal frequency. It can be expected to obtain a steeper filter function utilizing the frequency characteristics of the magnetic material by designing a transmission line we proposed.

[1] B. Rejaei and M. Vroubel, J. Appl. Phys., Vol. 96, p.6863 (2004) [2] Y. Zhuang, B. Rejaei and H. Schellevis, IEEE Electron Device Lett., Vol. 29, pp.319–321 (2008) [3] M. Yamaguchi, N. Sato and Y. Endo, Proc. 40th Eur. Microw. Conf., pp.1182-1185 (2010) [4] N. Sato, Y. Endo and M. Yamaguchi, J. Appl. Phys., Vol. 111, pp.07A501-1-07501-3 (2012) [5] M. Yamaguchi, T. Yanai and H. Nakayama, IEEE Trans. Magn., Vol. 54, pp.1-5 (2018) [6] Y. Aizawa, H. Nakayama, K. Kubomura, R. Nakamura, and H. Tanaka, AIP Advance, Vol. 10, p.015124 (2020)

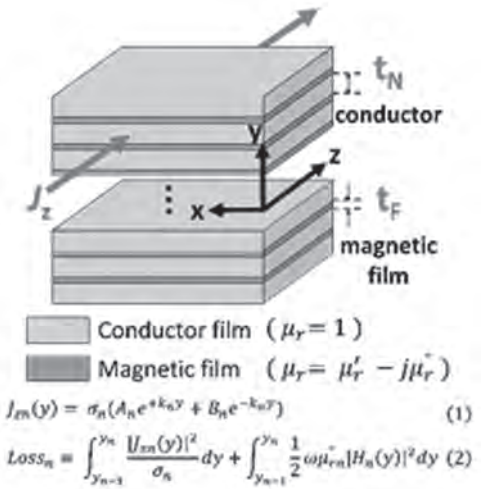

Fig. 1. Structure of conductor/magnetic film multilayer.

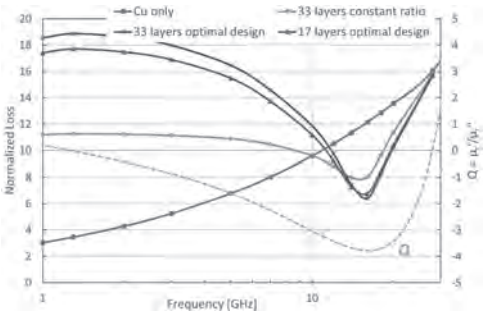

Fig. 2. Result calculation: Frequency characteristics of loss

H4-05. The Effect of Praseodymium and Samarium Substitution in Inverse Spinel Nickel Ferrite: Structural, Magnetic, and Mossbauer Study. *D. Guragain*[1], S.R. Mishra[1], T.P. Poudel[1], B.K. Rai[2] and S. Yoon[3] *1. Department of Physics and Material Science, The University of Memphis, Memphis, TN, United States; 2. Materials Science and Technology Division, Oak Ridge National Laboratory, Oak Ridge, TN, United States; 3. Department of Physics, Kunsan National University, Gunsan, The Democratic People's Republic of Korea*

Influence of Praseodymium (Pr) and Samarium (Sm) on the structural and magnetic properties of nickel ferrite is observed in this report. $NiRE_xFe_{2-x}O_4$ (RE=Pr, Sm) ($0<x<1$) ferrites nanoparticles were successfully synthesized by using sol-gel method. The effect due to the substitution of praseodymium and Samarium were studied by using X-ray diffraction (XRD). Studies show the formation of single-phase cubic spinel structure with the rising trend in lattice parameter, x-ray density and decreasing trend in crystallite size with increase content of Pr^{3+} and Sm^{3+} were observed. ^{57}Fe Mössbauer spectra were recorded to determine the Pr^{3+} and Sm^{3+} content dependent variation in the line width, isomer shift, quadrupole splitting, and hyperfine magnetic fields. Furthermore, the magnetic parameters of the prepared nanoparticles (NPs) were investigated by using vibrating sample magnetometer (VSM) via hysteresis loops, and magneto-crystalline anisotropy determined from the Law of Approach.

H4-06. Withdrawn

H4-07. Synthesis of Reduced Graphene Oxide/$CoFe_2O_4$ Composite Particles and Their Magnetorheological Characteristics. *Y. Dong*[1] and H. Choi[1] *1. Polymer Science and Engineering, Inha University, Incheon, The Republic of Korea*

Magnetorheological (MR) fluids are considered as a class of promising smart materials because of their rapid transformation between a liquid-like and a solid-like state under the stimulation of a magnetic field [1, 2]. MR fluids are usually composed of magnetic particles dispersed in a non-magnetic carrier liquid. Concurrently, graphene is a kind of two-dimensional carbon layer structure materials, possessing potential applications in many fields. [3] Moreover, graphene oxide (GO) obtained by oxidation of natural graphite has been known as a low cost method to realize industrial scale production of graphene. Amount of reactive oxygen-based functional groups, such as carbonyl, epoxide, carboxyl groups on the basal planes and edges of graphene-derived layers increases the distance between the layers [4]. In this work, reduced(r)GO/$CoFe_2O_4$ composite was fabricated and adopted as an MR material, where the presence of rGO reduces the density of the material and serves as a matrix to prevent excessive agglomeration of $CoFe_2O_4$ nanoparticles [5]. The SEM images of synthesized GO and rGO/$CoFe_2O_4$ are shown in Fig. 1(a) and Fig. 1(b), respectively. As shown in Fig. 1(a), GO exhibits a sheet morphology with smooth surface. However, the surface of rGO/$CoFe_2O_4$ is obviously rougher than GO and the inset shows that there are many nanoparticles on the surface of rGO/$CoFe_2O_4$, indicating the presence of $CoFe_2O_4$. Figure 2 shows the shear stress of rGO/$CoFe_2O_4$ based MR fluid as a function of shear rate under various magnetic field strengths. Compared with the absence of a magnetic field, the value of the shear stress under the action of the magnetic field increases significantly and increases with applied magnetic field strengths. This is because the particles are magnetized under a magnetic field, and the magnetostatic force between the particles causes the particles to be arranged in chain-like structures. Additional MR tests were performed for further analysis.

[1] Y.P. Seo, S. Han, J. Choi, A. Takahara, H.J. Choi, and Y. Seo, *Adv. Mater.* 30, 1704769 (2018). [2] S.G. Sherman and N.M. Wereley, *IEEE Trans. Magn.* 49, 3430 (2013). [3] Y. Zhou, H. Guo, Y. Yong, Z. Wang, X. Li, and R. Zhou, *Mater. Lett*. 195, 164 (2017). [4] M. Seredych, A. V. Tamashausky, and T. J. Bandosz, *Adv. Funct. Mater.* 20, 1670 (2010). [5] Y. Huang, X. Ding, S. Li, N. Zhang, and J. Wang, *Ceram. Int.* 42, 17116 (2016).

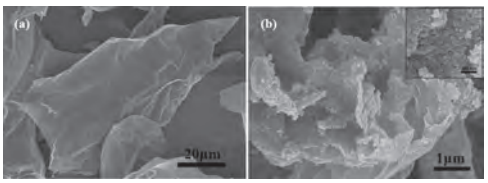

Figure 1. SEM images of (a) GO and (b) rGO/$CoFe_2O_4$. Inset shows the partial enlargement of rGO/$CoFe_2O_4$ surface

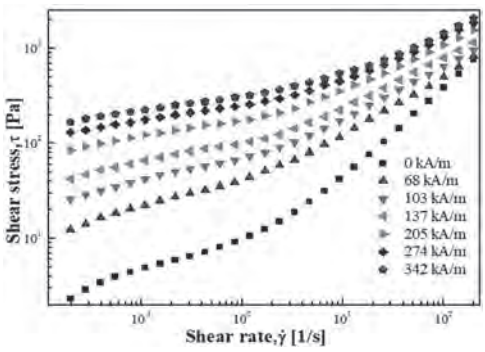

Figure 2. Shear stress and of rGO/$CoFe_2O_4$ based MR fluid as a function of shear rate under various magnetic field strengths

H4-08. Magnetic Performance Improvement Caused by Tensile Stress in Equivalent Iron Core Fabricated by High-Strength Non-Oriented Electrical Steel. *L. Gao*[1], H. ZHANG[2] and R. Pei[3] *1. Suzhou Inn-mag New Energy Ltd., Suzhou, China; 2. Universite de Technologie de Troyes, Troyes, France; 3. Shenyang University of Technology, Shenyang, China*

Permanent Magnet Synchronous Machines (PMSM) have gradually become the mainstream solution for drive motors. One main trend for advanced PMSM optimization is focused on new material application. Conventional PMSM iron core is fabricated by Non Grain-Oriented (NGO) silicon steel sheet lamination, based on traditional technic, the high-strength NGO silicon steel uses solid solution strengthening and precipitation strengthening methods to enhance mechanical strength [1]. As mentioned in [2-3], due to the increase in mechanical strength of high-strength NGO steel, a narrower magnetic bridge design can be applied in the rotor design. Thereby reducing the leakage flux to increase the output torque and the overall efficiency. Even though the high-strength NGO had higher iron loss, counting the reduction in the rotor bridge width, the overall performance can be significantly enhanced. The maximum speed of advanced PMSM is mostly greater than 12000rpm, thus the rotor sustains significant tensile stress due to centrifugal force. It's easier to form the striped 180° domain with higher permeability under tensile stress [4]. While the frequency influence and thermal condition has not been discussed in [4]. In this paper, we designed an equivalent sample to simulate the condition of an iron core, similarly in [5], with different excitation and manufacture parameter such as laminated number and thermal condition. Three types of high-strength NGO (SW35YS600\SW35YS900\B35AHS500) and a controlled group (conventional NGO B35A270) has been tested. Magnetic performance of equivalent sample is measured by ring sample method. Two narrow sides of the sample are subjected to large tensile stress concentration, the lamination number is 5, 10, and 20. At high excitation frequencies, the level of iron loss improvement caused by tensile stress is significant. Four materials have also been annealed respectively at 720°C for 10 hours under argon atmosphere. After annealing, the tensile stress has lower effect on the magnetic properties for B35AHS500 and B35A270, but is significant for SW35YS600 and SW35YS900. Therefore, it is speculated that a large proportion of heat treatment process has been adopted during SW35YS600 and SW35YS900.

[1] GONG, Jian, and Hai-wen LUO. "Progress on the research of high-strength non-oriented silicon steel sheets in traction motors of hybrid/electrical vehicles." Journal of Materials Engineering 43.6 (2015): 102-112. [2] Tietz, Marco, et al. "Effects and advantages of high-strength non grain oriented (NGO) electrical steel for traction drives." 2013 3rd International Electric Drives Production Conference (EDPC). IEEE, 2013. [3] Tanaka, Ichiro, et al. "Application of high-strength nonoriented electrical steel to interior permanent magnet synchronous motor." IEEE transactions on magnetics 49.6 (2012): 2997-3001. [4] Senda, Kunihiro, et al. "Magnetic properties and domain structure of non-oriented electrical steel under stress." IJTFM 131.10 (2011): 884-890. [5] Gao, Lingyu, et al. "Application of grain-oriented electrical steel used in super-high speed electric machines." AIP Advances 10.1 (2020): 015127.

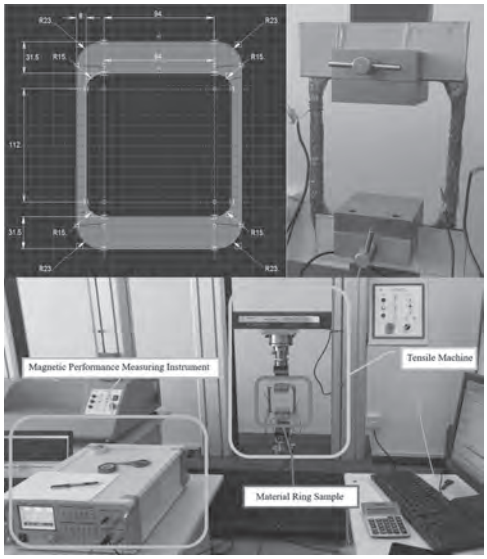

Fig.1

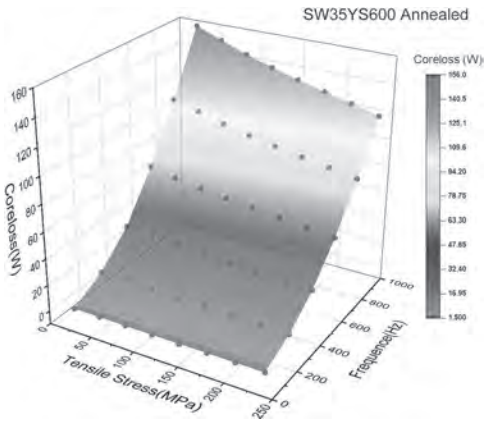

Fig.2

H4-09. Withdrawn

H4-10. Withdrawn

H4-11. Withdrawn

H4-12. Withdrawn

Session H5
HALF-METALLIC MATERIALS AND MAGNETIC SEMICONDUCTORS (Poster Session)

Simon Granville, Chair
Victoria University of Wellington, Lower Hutt, New Zealand

H5-01. Synthesis and Characterization of ScPtBi Thin Films.
Ö. Polat[1,2], I. Mohelsky[1,2], J. Polčak[1,2], J. Ander Arregi Uribeetxebarria[1] and T. Sikola[1,2] *1. Stredoevropsky technologicky institut, Brno, Czechia; 2. Vysoke uceni technicke v Brne, Brno, Czechia*

In the contribution we will report on preparation of ScPtBi thin films grown on different substrates such as Si, Al_2O_3 and MgO at 200° C and 300° C by dc magnetron co-sputtering. It has been carried out by three magnetron guns equipped with Sc, Pt, and Bi targets, respectively. X-ray diffraction (XRD) studies have revealed the films exhibit polycrystalline structures. Scanning electron microscope (SEM) examinations have revealed that films have different nanostructures on the surface depending upon deposition temperature. Furthermore, X-ray photoelectron spectroscopy (XPS) analysis have exhibited the stoichiometry of the films Sc:Pt:Bi is 32.5:33.0:34.5, which is close to ideal 1:1:1 ideal ratio. Magneto-transport measurements were conducted by a conventional four-probe method in a temperature range of 5–300 K and at fields up to 9 T. Even though a small low-field positive magnetoresistance values are obtained at all temperatures and magnetic fields, the weak antilocalization (WAL) effect, considered as one of signatures of topological insulator property, has been observed for the examined samples. The response of magnetoconductance has been studied with the Hikami-Larkin-Nagaoka (HLN) relation and the phase coherence length, l_φ, decreases as the operating temperature raises. The sheet resistance, carrier type, mobility and density at the temperature 5 K and 300 K at 1 T magnetic field have been investigated by the Hall measurements.

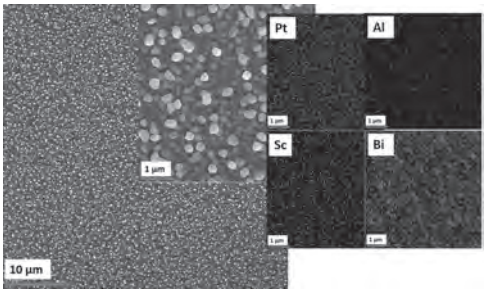

SEM and EDX images for ScPtBi thin film grown on Si substrate at 200°C.

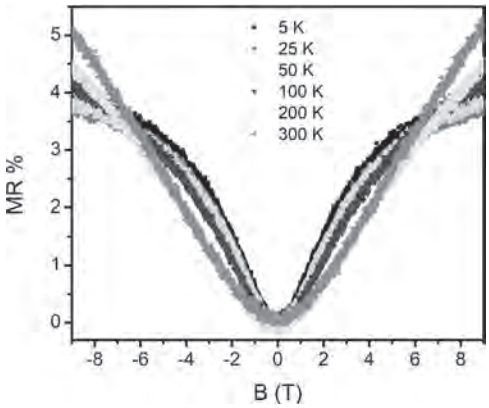

Magnetoresistance (MR) % data for ScPtBi deposited on Si substrate at 200°C.

H5-02. Electroresistivity, Magnetic and Galvanomagnetic Properties of Co-Based Heusler Alloys in the States of Half-Metallic Ferromagnet and Spin Gapless Semiconductor.
A. Semiannikova[1], V. Irkhin[1], Y.A. Perevozchikova[1], P. Korenistov[1] and V. Marchenkov[1,2] *1. M N Mikheev Institute of Metal Physics of the Ural Branch of the Russian Academy of Sciences, Ekaterinburg, Russian Federation; 2. Ural Federal University named after the first President of Russia B N Yeltsin, Ekaterinburg, Russian Federation*

Half-metallic ferromagnets (HMFs) and spin gapless semiconductors (SGSs) are promising materials for spintronics with almost 100% spin polarization of charge carriers. They possess a gap near the Fermi energy for the current carriers with spin down. However, for the opposite spin projection, these materials have a difference: the energy gap is absent in HFMs [1], while it is zero in SGSs. Parameters of the energy gap and, consequently, physical properties can vary quite strongly in different X_2YZ Heusler alloys [2, 3, 4], where *Y*-elements are 3d-transition metals and *Z*-components are s- and p-elements. Thus, the aim of the work is to follow the changes in the electrical, magnetic and galvanomagnetic properties and to establish their interconnection and basic behavior patterns of the Co_2*Y*Si (*Y* = Ti, V, Cr, Mn, Fe, Co, Ni) and Co_2Mn*Z* Heusler alloys (*Z* = Si, Al, Ge, Sb) in the HMF and/or SGS states. The electrical resistivity was measured in a wide temperature range from 4.2 to 300 K, the field and temperature dependences of magnetic and galvanomagnetic properties being studied too. Significant changes in the values of the coefficients of the normal and anomalous Hall Effect, magnetization, residual resistivity, type, and concentration of current carriers and their mobility were found. At the same time, the correlation between the changes in these electronic and magnetic characteristics depending on the number of valence electrons are observed. The work was performed within the framework of the state assignment of the Ministry of Science and High Education of Russia (the themes “Spin”, No. AAAA-A18-118020290104-2-2 and “Quantum” No. AAAA-A18-118020190095-4) with partial support from the RFBR (project No. 18-02-00739 and 20-32-90065) and the Government of the Russian Federation (Decree No. 211, Contract No. 02.A03.21.0006).

[1] M.I. Katsnelson, V.Yu. Irkhin, L. Chioncel et al., Rev. Mod. Phys., Vol. 80, p. 315 (2008). [2] V.V. Marchenkov, Yu.A. Perevozchikova, N.I. Kourov et al., J. Magn. Magn. Mat., Vol. 459, p. 211 (2018). [3] Yu.A. Perevozchikova, A.A. Semiannikova, A.N. Domozhirova, P.B. Terentyev, E.B. Marchenkova, E.I. Patrakov, M. Eisterer, P.S. Korenistov and V.V. Marchenkov, Low Temp. Phys., Vol. 45, p. 789 (2019). [4] Yu.A. Perevozchikova, A.A. Semiannikova, P.B. Terentyev, M. Eisterer, P.S. Korenistov and V.V. Marchenkov, Journal of Physics: Conf. Series, Vol. 1389, p. 012110 (2019).

H5-03. Co_2FeSn Heusler Nanowires With High Spin Polarization.

L. Galdun[1,3], P. Szabo[2], V. Vega[3], E. Barriga-Castro[4], R. Mendoza-Reséndez[5], C. Luna[5], J. Kovac[2], O. Milkovic[6,2], R. Varga[1] and V.M. Prida[3]
1. Center for Progressive Materials, TIP, UPJS, Kosice, Slovakia; 2. Institute of Experimental Physics, Slovak Academy of Sciences, Kosice, Slovakia; 3. Departamento de Física, Facultad de Ciencias, Universidad de Oviedo, Oviedo, Spain; 4. Centro de Investigación en Química Aplicada, Coahuila, Mexico; 5. Universidad Autónoma de Nuevo León, Nuevo León, Mexico; 6. Institute of Materials Research, Slovak Academy of Sciences, Kosice, Slovakia

Spin transfer electronics or spintronics offers the possibility of enhancement of regular electronic devices [1]. Because of that, the demand for materials that acquire high values of spin polarization is growing. From several groups of materials, half-metallic Co_2-based Heusler alloys are well appropriate materials for spintronic devices due to their high Curie temperature, high magnetic moment, and low Gilbert dumping [2]. The majority of Heusler alloys are usually prepared in the form of ribbons, bulk, or thin films. However, due to technological progress, Heusler alloys face a new production challenge in the nano-scale regime. Several publications deal with the preparation of Heusler nanowires, but with the lack of the spin polarization measurements [3]. Magnetic nanowires prepared in the form of dense array offer the possibility for the development of next-level 3D magnetic "racetrack" memory. Here, the information is stored in the domain wall pattern and shift with spin-polarized current [4]. Therefore, it is essential to determine the spin polarization of the material, which is considered for possible spintronic applications. In the present work, Co_2FeSn nanowires have been prepared using template-assisted electrochemical deposition. The nanowires have been grown in the pores of Anodic Alumna Oxide membranes. The spin polarization values have been determined using Point-Contact Andreev Reflection spectroscopy. We show that the spin polarization is preserved in the nanoscale, and by creating a contact with the fresh surface, it is possible to achieve high spin polarization values up to 100 %. This research was supported by Slovak Grant Agency VEGA 1/0053/19, Slovak Grant Agency grant number APVV-16-0079 and VVGS-2019-1231.

[1] J. P. DeGrave, A. L. Schmitt, R.S. Selinsky, *Nano Lett.*, *11*, 4431-4437(2011). [2] M. Jourdan, J. Minár, J. Braun, *Nat. Commun., 5*, 3974 (2014). [3] L. Galdun, V. Vega, Z. Vargova, *ACS Appl. Nano Mater*., *1*, 7066-7074 (2018). [4] S. S. P. Parkin, M. Hayashi, L.Thomas, Magnetic Domain-Wall Racetrack Memory. *Science*, *320*, 190-194 (2008).

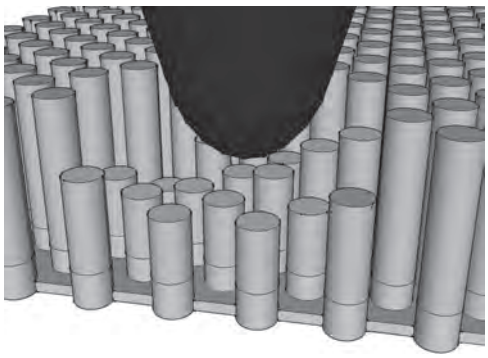

Fig. 1, Visualization of Nb/Co_2FeSn array point-contact.

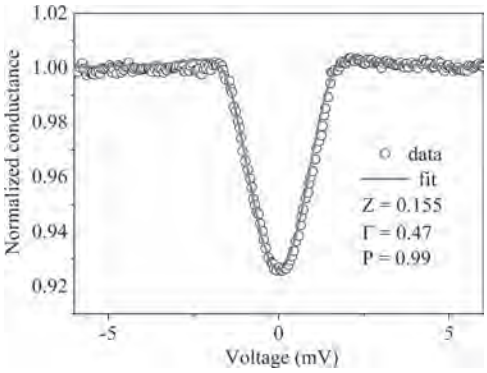

Fig. 2, Point-Contact Andreev Reflection spectrum measured on an Nb/Co_2FeSn array point-contact with 99% spin polarization.

H5-04. Preparation and Thermoelectric Properties of Mn_2CoAl Inverse Full-Heusler Alloy.

H. Li[1], Y. Nagashima[1], K. Hayashi[1] and Y. Miyazaki[1] *1. Tohoku Daigaku Daigakuin Kogaku Kenkyuka Kogakubu, Sendai, Japan*

Recently, thermoelectric materials that can convert thermal energy into electricity have attracted much attention as clean energy harvesting materials. The efficiency of a thermoelectric material is evaluated by the dimensionless figure of merit, $zT = S^2\sigma T/\kappa$, where S, σ, T, and κ are the Seebeck coefficient, electrical conductivity, absolute temperature, and thermal conductivity, respectively. In order to achieve a high zT, a high PF ($=S^2\sigma$) is desired. The Inverse full-Heusler alloy Mn_2CoAl has been considered to be a spin gapless semiconductor from first principles calculations and experiments[1]. Our preliminarily calculation predicted that the thermoelectric properties of spin gapless semiconductor Mn_2CoAl can be improved through component adjustment or partial substitution. In this study, we have prepared a single phase samples of Mn_2CoAl and evaluated the thermoelectric properties. Mn_2CoAl polycrystalline samples were prepared by the three different method (1)arc-melting,(2)spark plasma sintering (SPS) after arc-melting, (3) SPS after ball-milling. The crystal structure of the samples was characterized by powder X-ray diffraction (XRD). The S and σ were simultaneously measured from 300 K to 1050 K. Figure 1 shows the powder XRD patterns of the samples prepared by the methods 1 ~ 3. It was found that the sample 1 was a single phase of Mn_2CoAl. On the other hand, the samples 2 and 3 contained Mn-Al alloy as a secondary phase. Figure 2 showed the temperature dependence of the σ, S, and PF of the samples 1 ~ 3. Sample 1 shows the lowest σ value, since the absences of metallic Mn-Al secondary phase in the samples 2 and 3. Regarding the S, negative value was achieved, which means that Mn_2CoAl has an n-type behavior. The maximum absolute value of S was obtained for the single-phase sample 1, which was -22.5 μV/K at 760 K. The sample 1 showed the highest PF, and the highest value reached 0.198 mW/mK^2 at 764 K. It is expected that the thermoelectric properties of Mn_2CoAl can be improved by the partial substitution, which will be exhibited on the day of the meeting.

[1] S. Ouardi *et al., Phys. Rev. Lett.,* 122 (2019) 059901.

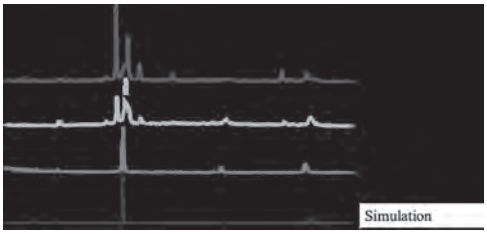

Fig. 1: XRD patterns of samples prepared by different methods.

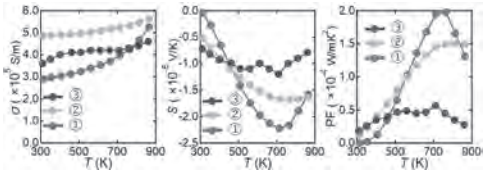

Fig. 2: Thermoelectric properties of samples prepared by different methods.

H5-05. Magnetic Properties of Co_2MeSi and Co_2MeAl (Me = Ti, v, Cr, Mn, Fe, Co, Ni) Half-Metallic Heusler Alloys. *Y.A. Perevozchikova*[1], A. Semiannikova[1], V. Irkhin[1] and V. Marchenkov[1,2] *1. IMP UB RAS, Ekaterinburg, Russian Federation; 2. UrFU, Ekaterinburg, Russian Federation*

The search, development, and study of new magnetic materials for spintronics is an important and actual task of magnetic phenomena physics and material science. Half-metallic ferromagnets (HMF) and spin gapless semiconductors (SGS) belong to this class of materials. Their electronic spectra demonstrate a wide energy gap at the Fermi level E_F for one spin projection of current carriers, and absence of gap (HMF) or a zero energy gap (SGS) for opposite spin direction. This can lead to 100% spin polarization. Probably, some of Co_2MeAl and Co_2MeSi Heusler alloys with Me = Ti, V, Cr, Mn, Fe, Co, Ni are such materials. They have as a rule high Curie temperatures and can possess high spin polarization at room temperature. Thus, we investigated magnetic properties of these Co_2MeAl and Co_2MeSi Heusler alloys. The alloys were prepared in an induction furnace in a purified argon atmosphere, and then annealed at different temperatures with subsequent cooling to room temperature. Elemental and X-ray analyses show that deviation from the stoichiometric composition in all the samples is insignificant and crystal structure is $L2_1$. The field dependences of the magnetization $M(H)$ were measured at T = 4.2 K and 300 K in magnetic fields up to 70 kOe. Magnetization of all samples goes to saturation at fields above 20 kOe (except Co_2VSi and Co_2CrSi). The saturation moment values of Co_2MeAl (Me = Ti, V, Cr, Mn, Fe) and Co_2MeSi (Me = Ti, Mn, Co, Ni) observed at 4.2 K are close to calculated one [1-4]. The obtained results indicate that the materials studied, in particular of Co_2MeSi system, can find practical application in spintronics devices. This work was partly supported by the state assignment of Minobrnauki of Russia (themes "Spin" No. AAAA-A18-118020290104-2 and "Quantum" No. AAAA-A18-118020190095-4), RFBR (grants No. 18-02-00739 and 20-32-90065) and the Government of the Russian Federation (state contract No. 02.A03.21.0006).

1. H.C. Kandpal, G.H. Fecher and C. Felser, J Phys D: Appl Phys, Vol. 40, p. 1507 (2007) 2. S.V. Faleev *et. al.*, Phys. Rev. Mater., Vol. 1, p. 024402 (2017) 3. B. Pradines *et. al.*, Phys. Rev. B, Vol. 95, p. 094425 (2017) 4. M.K. Zayed, A.A. Elabbar and O.A. Yassin, J. Alloys Comp., Vol. 737, p. 790 (2018)

H5-06. Magnetotransport Properties of Ru Doped Cobalt Ferrite Thin Film With Perpendicular Magnetic Anisotropy. *M. P*[1] and A.K. P S[1] *1. Physics, Indian Institute of Science, Bangalore, India*

Room temperature magnetic semiconductors have drawn significant attention due to their potential application in spintronic devices. Cobalt ferrite with large magneto-crystalline anisotropy is an alternative candidate for such applications. However, its insulating nature restricts the realization of spin polarized electron transport even at room temperature. Ruthenium doping in cobalt ferrite essentially increases the conductivity while retaining its magnetic properties. Ru^{4+} doped cobalt ferrite can be a tunable magnetic semiconductor. Epitaxial thin films of $(Co,Ru)Fe_2O_4$ (CRFO)were grown on MgO (001) substrate using pulsed laser ablation technique. The magnetization measurement reveals an easy axis perpendicular to the film surface. We investigated the magnetic, electrical and magneto-transport properties of the film having Perpendicular Magnetic Anisotropy (PMA). Temperature dependent resistivity indicates about electronic conduction mechanism. Electron conduction follows Arrhenius type thermal conduction as well as small polaron hopping model at higher temperature. However, at lower temperature, it follows variable range hopping model [1]. Room temperature Hall measurement confirms 'n' type carriers with a carrier concentration of $10^{21}/cm^3$. The R_{Hall}-H loop overlaps with out of plane M-H loop especially at lower field, thus indicating an Anomalous Hall effect (AHE) [2]. Magnetoresistance (MR) measurement is done with a perpendicular magnetic field at different temperatures. It manifests a negative and linear relationship with the applied field [3]. However, the value is higher at lower temperature. So CRFO film is a promising magnetic semiconductor with PMA, having greater potential for spintronics application.

[1] M. Takahashi, T. Ohshima and H. Tabata, Journal of Applied Physics., Vol. 116, p.213907 (2014) [2] M. Seki, M. Takahashi and H. Tabata, Applied Physics Letters., Vol. 103, p.212404 (2013) [3] N.Jedrecy, C. Hebert and E. Millon, Journal of Applied Physics., Vol. 116, p.213903 (2014)

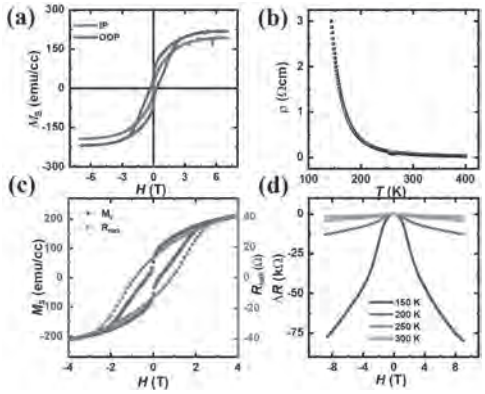

Fig 1 (a) In-plane (IP) and out of plane (OOP) MH loop (b) variation of ρ with T (c) Hall resistance and OOP Magnetization variation with H (d) MR at different temperatures.

H5-07. Magnetic and Electronic Properties of Transition Metal Doped Aluminium Nitride: Haldane's Approach Combined With ab Initio Results. *P. Harikumar*[1] *1. materials science group, Indira Gandhi Centre for Atomic Research, Kalpakkam, India*

The dilute magnetic semiconductors (DMSs) have time again proved to be promising candidates for spintronics applications mostly owing to their unique magnetic behavior. Aluminium Nitride (AlN) containing TM elements such as Mn, Cr etc. belongs to this interesting class of semiconductors and has been studied extensively ever since. Ab initio calculations using results of Density functional theory (DFT) (1,3) were able to partially describe the phenomenon of the rising local moment. Yet a complete description in terms of orbital hybridisation and Coulomb Correlation strength (U) requires a theoretical approach to the problem. This paper combines the model extended by Haldane in his paper (2) with the Bloch energies obtained from DFT calculations of AlN in the wurtzite structure. We investigate the magnetic moment of some of the TM elements with a doping concentration of 6.25% and also the effect of U on the magnetic properties of the system. The Anderson Hamiltonian for semiconductors (2) was solved in the unrestricted Hartree- Fock approximation (HFA), using a Green's function method. The electronic band structure of the host semiconductor AlN was obtained using the generalized gradient approximation (GGA) based on Perdew, Burke and Ernzerhof (PBE) in VASP. Assuming contribution to hybridisation only from the bands lying around the Fermi energy (E_F) the value of p-d hybridisation was taken as 1.5 eV. The electronic self energies $\sum(\omega)$ for complex energies were calculated by applying the Neville's algorithm. The assumed values of U for Mn and Cr are 4.0 & 2.6 in eV resp.(3). The spin resolved density of states from Mn d states for AlN:Mn is given in fig.1. Fig.2 shows values of magnetic moment obtained for Cr and Mn impurities in AlN using the method described. These values are in excellent agreement with earlier studies on the system using different methods(1,3). Moreover, Mn almost exhibits an integral value of magnetic moment showing half metallic behavior. The U/W ratio where W is the band

width plays a major role in deciding the magnetic behavior of a DMS.The advantage of this approach is the flexibility of handling the parameters and see what happens to the system under physical conditions pertaining to them.

1. Hassan Ahmoum et.al.,Journal of Superconductivity and Novel Magnetism, vol.32,pg. 3691-3697,2019 2. F. D. M. Haldane, P. W. Anderson, Phys. Rev. B.,vol.13,no.6,1976 3. J. Kaczkowski and A. Jezierski, Acta Physica Polonica Series a, 116(5), 2009

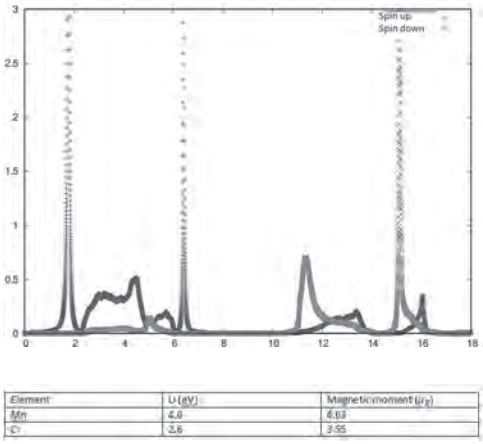

H5-08. Temperature Controlled Anomalous Hall Voltage Switching in Co/Gd Ferrimagnet Near Compensation. *L.A. Hernandez*[1], R.W. Greening[1], M. Roos[1], X. Fan[1] and B.L. Zink[1] *1. Physics and Astronomy, University of Denver, Denver, CO, United States*

Interest in ferrimagnetic metals as active elements in spintronic devices is growing due to their intriguing magnetization effects close to compensation [1]. Mostly studied in alloys, the SOTs that arise from the negative exchange interaction attribute to interesting Hall measurements and can be manipulated through control of temperature [1, 2]. Here we demonstrate another unique feature of these systems: temperature-driven switching. We measured the anomalous Hall effect (AHE) in a van der Pauw geometry on a Ta(3nm)/Pt(3nm)/Co(.5nm)/Gd(1.8nm)/Pt(3nm) synthetic ferrimagnet stack, where the antiferromagnetic exchange coupling between the Co and Gd layers forms the ferrimagnet [3]. The observed compensation temperature is between 150 and 155 K as seen in the diverging coercivity of the sample when measuring AHE vs. perpendicular external field (Figure 1). At 115 K, the AHE displays an external field dependent hysteresis with a coercivity around 300, and 1200 Oe at 150 K (Figure 1). Because this is beneath the compensation temperature, the saturation voltage at 1500 Oe is more negative than at -1500 Oe, creating two anomalous Hall voltage states influenced by the net Gd moment. At 155 and 165 K the coercivities are 850 and 250 Oe respectively, yet the saturation voltages are reversed (Figure 1). This indicates the influence of the net Co moment above the compensation temperature, and the divergence of the coercivity between 150 and 155 K. By then applying a static external field, the AHE state can be switched as the temperature of the sample is lowered or raised above the compensation temperature. In Figure 2, a constant external magnetic field of 450 Oe is applied, and the AHE shows temperature dependent coercivity and hysteresis. This confirms that temperature can be used to write a magnetization state of a ferrimagnet, with a memory window between 145 and 156 K in the case of this sample.

[1] X. Jiang, L. Gao, J. Z. Sun, and S. S. P. Parkin, Phys. Rev. Lett. 97, 217202 (2006). [2] R. Mishra, J. Yu, X. Qiu, Phys. Rev. Lett. 118, 167201 (2017). [3] P. Hansen, C. Clausen, G. Much, J. Appl. Phys. 66, 756 (1989).
Funding acknowledgements: B. L. Zink Group: NSF DMR 1709646

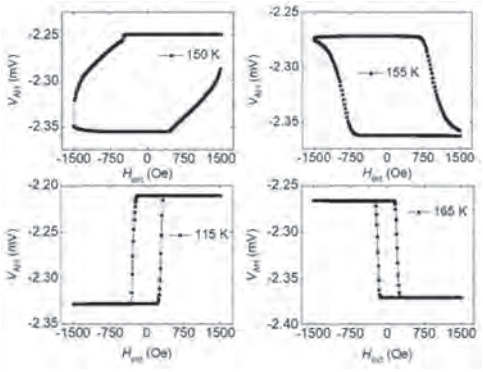

AHE vs. external field at temperatures below and above compensation. Switching of saturation voltage states occurs across the compensation temperature.

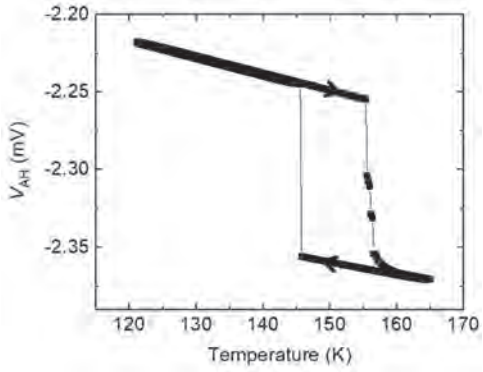

Temperature dependent hysteresis of Ta/Pt/Co/Gd/Pt with a constant external field of 450 Oe. Hysteresis indicates temperature-controlled memory of AHE states.

Session S4
ANTIFERROMAGNETIC SPINTRONICS: TRANSPORT AND DYNAMICS IN METALS, INSULATORS AND MAGNETIC TUNNEL JUNCTIONS

Xin Fan, Chair
University of Denver, Denver, CO, United States

INVITED PAPERS

9:00

S4-01. Theory of Spin Transport and Torque in Non-Collinear Antiferromagnets. *A. Manchon[1] 1. Aix-Marseille Universite, Marseille, France*

Antiferromagnets have long remained an intriguing and exotic state of matter whose application has been restricted to interfacial exchange bias in spin-valves. In recent years, theoretical and experimental progress has brought the attention on *non-collinear* antiferromagnets (see Figure), which can display anomalous Hall effect under certain conditions [1] and widens the horizon of spintronics research. In this presentation, I will explore the ability of non-collinear antiferromagnets for spintronics operation. I will first discuss new results on electron- and magnon-mediated transport in non-collinear magnetic textures and show that they can support (possibly quantum) spin and anomalous Hall effects [2,3]. I will then discuss the nature of the spin-orbit torques obtained in heterostructures involving (both coplanar and non-coplanar) non-collinear antiferromagnets, as well as the expected dynamics (*unpublished*). Afterwards, I will discuss the conditions under which non-collinear antiferromagnets can convey spin information through either diffusive or superfluid spin currents [4].

[1] Chen and MacDonald, Phys. Rev. Lett. 112, 017205 (2014); Nakatsuji et al., Nature 527, 212 (2015). [2] Ndiaye et al., Physical Review B 100, 144440 (2019). [3] Varga and Manchon, arXiv:2005.04678 [4] Goli and Manchon, arXiv:2005.13481

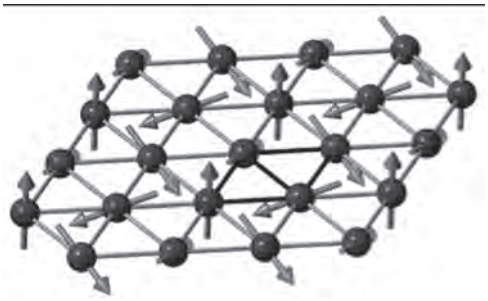

Example of a non-collinear antiferromagnet.

9:36

S4-02. Sub-Terahertz Antiferromagnetic Spin Pumping in Cr_2O_3. *J. Shi[1], J. Li[1], C. Wilson[2], M. Lohmann[1], R. Cheng[1], M. Kavand[2], W. Yuan[1], M. Aldosary[1], N. Agladze[2], P. Wei[1] and M. Sherwin[2]*
1. University of California Riverside, Riverside, CA, United States;
2. University of California Santa Barbara, Santa Barbara, CA, United States

Similar to coherently generated spin currents in ferromagnets, spin currents in antiferromagnets can also be generated by spin pumping with a coherent drive and electrically detected via the inverse spin Hall effect using heavy metals. In uniaxial antiferromagnets, spin currents are carried by the two eigen-modes of the systems, i.e., left- and right-handed magnon modes, with the frequencies typically in the terahertz regime. Cr_2O_3, a uniaxial antiferromagnet, has the Neel temperature of 308 K and the easy axis directed along the c-axis of the corundum lattice. At zero magnetic field, the resonance frequency is 165 GHz for both modes. With the microwave excitation frequency of 240 GHz, the antiferromagnetic resonance occurs only for the right-handed mode at the easy-axis magnetic field of ~ 2.7 T. In our antiferrimagnetic spin pumping experiments (1), we have successfully demonstrated spin current generation in both Cr_2O_3/Pt and Cr_2O_3/Ta heterostructure devices at this antiferromagnetic resonance condition. The opposite polarity in the inverse spin Hall voltages detected by Pt and Ta, two heavy metals with opposite spin Hall angles, confirms the pure spin current nature. In addition to the antiferromagnetic resonance for the righ-handed mode, we have observed another resonance peak at the spin-flop transition (~ 6 T) and yet another resonance for the net induced magnetic moment at higher field (~ 10.5 T). At the antiferromagnetic resonance, we observed a sign change in the inverse spin Hall voltage at about 45 K as the temperature is varied. Discussions of the peculiar temperature dependence of the spin pumping responses will be presented in the context of the coherent and incoherent magnon thermalization process.

(1) J.X. Li *et al.*, Nature 578, 70 (2020).

10:12

S4-03. Voltage-Controlled Antiferromagnetism in Magnetic Tunnel Junctions. *W. Wang[1] 1. Physics, University of Arizona, Tucson, AZ, United States*

Although antiferromagnets (AFs) have routinely been used in magnetic tunnel junctions (MTJs) to provide exchange bias (EB), incorporation of an active AF layer that can be electrically controlled in an MTJ remains to be challenging. It has been shown that an energy efficient current-induced switching can be potentially achieved in MTJs with AF barriers[1]. On the other hand, it is more desirable if the AFs can be controlled by voltage directly. Here we demonstrate a voltage-controlled antiferromagnetism effect in the CoFeB/MgO/CoFeB magnetic tunnel junctions, which represents a model spintronics system with interesting phenomena such as coherent tunneling of electrons, perpendicular magnetic anisotropy and voltage-controlled magnetic anisotropy. It has been shown that a voltage-controlled exchange bias effect exists in this system, which is related to the interfacial oxide formed between the CoFeB electrodes and the MgO barrier. The unique combination of interfacial antiferromagnetism, giant tunneling magnetoresistance, and sharp switching of the perpendicularly-magnetized CoFeB layers allows sensitive detection of the exchange bias. It is found that the exchange bias field can be isothermally controlled by magnetic fields at low temperatures. More importantly, the exchange bias can also be effectively manipulated by the electric field applied to the MgO barrier due to the voltage-controlled antiferromagnetic anisotropy in this system [2]. These results represent a new method towards energy-efficient control of future

antiferromagnetic spintronics devices and open a new window to investigate voltage-controlled antiferromagnetism in other systems.

[1] Y Cheng et. Al, *"Amplification of spin-transfer torque in magnetic tunnel junctions with an antiferromagnetic barrier"*, Phys. Rev. B, 99, 104417 (2019) [2] M. Xu et al, "*Voltage-Controlled Antiferromagnetism in Magnetic Tunnel Junctions*", Phys. Rev. Lett., 124, 187701 (2020)

10:48

S4-04. Antiferromagnetic Insulatronics: Spintronics Without Magnetic Fields and Moving Charges. *P. Kläui[1] 1. Physics, Johannes Gutenberg-Universitat Mainz Fachbereich Physik Mathematik und Informatik, Mainz, Germany*

While known for a long time, antiferromagnetically ordered systems have previously been considered, as expressed by Louis Néel in his Nobel Prize Lecture, to be "interesting but useless". However, since antiferromagnets potentially promises faster operation, enhanced stability with respect to interfering magnetic fields and higher integration due to the absence of dipolar coupling, they could potentially become a game changer for new spintronic devices. The zero net moment makes manipulation using conventional magnetic fields challenging. However recently, these materials have received renewed attention due to possible manipulation based on new approaches such as photons [1] or spin-orbit torques [2]. In this introductory talk, we will present an overview of the key features of antiferromagnets to potentially functionalize their unique properties. This includes writing, reading and transporting information using antiferromagnets. We recently realized switching in the metallic antiferromagnet Mn_2Au [3] by intrinsic staggered spin-orbit torques [4] and characterize the switching properties by direct imaging. While switching by staggered intrinsic spin-orbit torques in metallic AFMs requires special structural asymmetry, interfacial non-staggered spin-orbit torques can switch multilayers of many insulating AFMs capped with heavy metal layers. We probe switching and spin transport in selected collinear insulating antiferromagnets, such as NiO [5-7], CoO [8,9] and hematite [10,11]. In NiO and CoO we find that there are multiple switching mechanisms that result in the reorientation of the Néel vector and additionally effects related to electromigration of the heavy metal layer can obscure the magnetic switching [5,7,9]. For the spin transport, spin currents are generated by heating as resulting from the spin Seebeck effect and by spin pumping measurements and we find in vertical transport short (few nm) spin diffusion lengths [6,8]. For hematite, however, we find in a non-local geometry that spin transport of tens of micrometers is possible [10,11]. We detect a first harmonic signal, related to the spin conductance, that exhibits a maximum at the spin-flop reorientation, while the second harmonic signal, related to the Spin Seebeck conductance, is linear in the amplitude of the applied magnetic field [10]. The first signal is dependent on the direction of the Néel vector and the second one depends on the induced magnetic moment due to the field. We identify the domain structure as the limiting factor for the spin transport [11]. We recently also achieved transport in the easy plane phased [12], which allows us to obtain long distance spin transport in hematite even at room temperature [12]. From the power and distance dependence, we unambiguously distinguish long-distance transport based on diffusion [10,11] from predicted spin superfluidity that can potentially be used for logic [13]. Note that a number of excellent reviews are available for further information on recent developments in the field [14]. *This work is supported by the IEEE Magnetics Society as part of the Distinguished Lecturer Program.

[1] A. Kimel et al., Nature 429, 850 (2004). [2] J. Zelezny et al., Phys. Rev. Lett. 113, 157201 (2014); P. Wadley et al., Science 351, 587 (2016). [3] M. Jourdan et al., J. Phys. D: Appl. Phys. 48, 385001 (2015). [4] S. Bodnar et al., Nature Commun. 9, 348 (2018) [5] L. Baldrati et al., Phys. Rev. Lett. 123, 177201 (2019) [6] L. Baldrati et al., Phys. Rev. B 98, 024422 (2018); L. Baldrati et al. Phys. Rev. B 98, 014409 (2018) [7] F. Schreiber et al., arxiv:2004.13374 (2020) [8] J. Cramer et al., Nature Commun. 9, 1089 (2018) [9] L. Baldrati et al., arxiv:2003.05923 (2020) [10] R. Lebrun et al., Nature 561, 222 (2018). [11] A. Ross et al., Nano Lett. 20, 306 (2020). [12] R. Lebrun et al., arxiv:2005.14414 (2020). [13] Y. Tserkovnyak et al., Phys. Rev. Lett. 119, 187705 (2017). [14] Rev. Mod. Phys. 90, 15005 (2018); Nat. Phys. 14, 200-242 (2018); Adv. Mater. 32, 1905603 (2020)

11:24

S4-05. Magnetic Spin Hall Effects in Topological Chiral Antiferromagnets. *Y. Otani[1,2] 1. Institute for Solid State Physics, Tokyo Daigaku, Bunkyo-ku, Japan; 2. Center for Emergent Matter Science, Rikagaku Kenkyujo, Wako, Japan*

A chiral antiferromagnet Mn_3Sn exhibits a substantial anomalous Hall effect (AHE) at room temperature, the magnitude of which reaches almost the same order of magnitude as in ferromagnetic metals irrespective of a small spontaneous magnetization of about 1 mT [1]. This large AHE originates from a significantly enhanced Berry curvature associated with the formation of Weyl points near Fermi energy [2]. A detailed comparison between angle-resolved photoemission spectroscopy measurements and density functional theory calculations revealed significant bandwidth renormalization and damping effects due to the strong correlation among Mn 3d electrons. Magnetotransport measurements provide strong evidence for the chiral anomaly of Weyl fermions[3]. All the above characteristic electronic properties of Mn_3Sn imply that the spin Hall effect could also take place in the Mn_3Sn. Our SHE experiments showed that the non-collinear antiferromagnet Mn_3Sn has richer spin Hall properties than non-magnetic materials, that is, the SHE has an unusual sign change when its triangularly ordered moments switch orientation. Our observations demonstrate that a novel type of contribution to the SHE (magnetic SHE) and the inverse SHE (MISHE) can dominate in some magnetic materials, including antiferromagnets. We attribute this magnetic mechanism in Mn_3Sn to the momentum-dependent spin splitting produced by the non-collinear magnetic order [4]. This discovery further expands the horizons of antiferromagnet spintronics and motivates a universal outlook on spin-charge coupling mechanisms in spintronics.

[1] S. Nakatsuji, N. Kiyohara, and T. Higo, Nature 527, 212–215 (2015). [2] J. Kuebler, and C. Felser, EPL 108, 67001 (2014). [3] K. Kuroda et al. Nat Mater. 16, 1090 (2017) [4] M. Kimata et al. Nature 565, 627 (2019).

Session I1
INNOVATIVE MAGNETICS DESIGN AND APPLICATIONS

Joe E. Davies, Chair
NVE Corporation, Eden Prairie, MN, United States

INVITED PAPER

I1-01. Thermomagnetic Harvesting of low Temperature Waste Heat.
S. Fähler[1] 1. IMW, Leibniz IFW Dresden, Dresden, Germany

Thermomagnetic materials are a new type of magnetic energy materials, which enable the conversion of low temperature waste heat to electricity by three routes: Thermomagnetic motors, oscillators, and generators. Taking our recent work on thermomagnetic generators with different magnetic field topologies (TMG, Fig. 1 and 2) [1] as a starting point, in this talk we also analyse the material requirements for a more energy and economic efficient conversion. We present experiments of our TMG using different thermomagnetic materials (La-Fe-Si-Co with different transition temperatures and Gd). We compare the suitability of these materials and from this derive a generalized approach to evaluate the suitability of different thermomagnetic materials, which is different compared to magnetocaloric materials. We show that the thermodynamic efficiency of the best thermomagnetic materials outperforms thermoelectric materials when harvesting low temperature waste heat. Furthermore, the low raw materials cost results in a price per watt more than one order of magnitude lower than today's power plants and thermoelectrics, which makes them also economically competitive. As summary, we present a materials library, which allows selecting the best available thermomagnetic materials in two Ashby plots as figures of merit and gives guidelines for future development of this material class [2]. At the end of this talk, approaches towards micro systems for harvesting low temperature waste heat are described.

[1] A. Waske et al. Nature Energy 4, 68 (2019) [2] D. Dzekan et al, arXiv: 2001.03375 (2020)

Photo of our thermomagnetic generator (TMG), which converts low temperature waste heat to electric energy. As active material a thermomagnetic material based on La-Fe-Co-Si is used, which exhibits a steep and sharp change of magnetization just above room temperature. The thermomagnetic material is alternatingly subjected to hot and cold water.

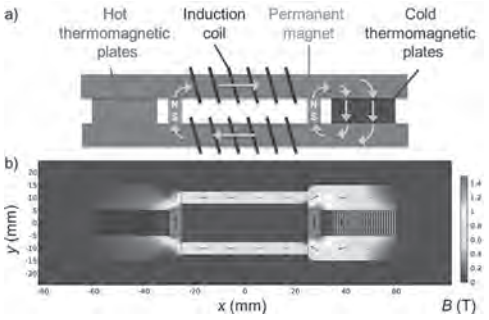

Thermomagnetic generator with genus = 3 (3 holes within the magnetic circuit). a) The setup consists of two permanent magnets which create the magnetic flux, two soft magnetic yokes which conduct the flux and two sets of thermomagnetic plates which switch the flux. Each time the temperatures of the thermomagnetic plates on both sides is exchanged between hot and cold, the direction of the magnetic flux is reversed, which induces a voltage in the coils. b) shows the result of finite element calculations of the magnetic flux density *B* for the same setup.

CONTRIBUTED PAPERS

I1-02. On-Chip Thin-Film Microtransformer With Improved Coupling Factor for High Frequency Data Transmission.
D. Dinulovic[1], M. Shousha[1] and M. Haug[1] 1. MagI3C R&D Division, Wuerth Elektronik eiSos GmbH & Co. KG, Garching, Germany

The miniaturization and integration is important market requirements for emerging electronic devices. Magnetic passive components are one of the most bulky components on the electronic boards. Therefore, a significant challenge for magnetic devices is miniaturization and integration towards system in package (SiP) and system on chip (SoC) [1]. Increasing the switching frequency in the applications is a way for miniaturization of magnetic components. On-chip inductors and transformers with magnetic materials fabricated on silicon are potential candidates for high switching frequency applications [2-4]. Developments of thin-film magnetic components in the last years show significant improvement in integration technology. In many works, newely developed microinductors and microtransformers were implemented in different electrical applications [5-10]. This paper will show the improved microtransformer on silicon with a bar magnetic core for data transmission applications [11]. The microtransformer can be used for higher frequencies data transmission application up to 25 MHz. The size of microtransformer device is 1.6 mm x 0.8 mm. The microtransformer consists of a bar magnetic core and interleaved primary and secondary windings Both windings feature 12 turns each. One turn has a length of 640 μm, width of 40 μm and thickness of 1 μm. A copper was applied for the windings. For magnetic core, a $Co_{60}Fe_{20}B_{20}$ alloy is used. The magnetic core consists of two magnetic layers with dimensions 1400 μm x 500 μm x 0.4 μm. As insulating material SiO_2 and Si_3N_4.are implemented. The inductance of the device is about 40 nH. The breakdown voltage is in the range of 1.5 kV. Using sputtering deposition a copper layer with only 1 μm is deposited, therefore the microtransformer device shows high electrical

resistance of about 7 Ω. The coupling factor of the transformer has a value of over 0.6. For this reason, the microtransformer is suitable for data transmission applications. Fig. 1 shows a completed device.

[1] C. O'Mathuna et al., IEEE Trans. Power Electron., 27(11), 4799–4816 (2012). [2] D. S. Gardner et al., IEEE Trans. on Magnetics, vol. 45, no. 10, pp. 4760-4766, 2009. [3] D. S. Gardner et al., IEEE Trans. on Magnetics, vol. 43, no. 6, pp. 2615-2617, 2007. [4] P. R. Morrow et al., IEEE Trans. on Magnetics, vol. 47, no. 6, pp. 1678-1686, 2011. [5] H. Wu et al., IEEE Trans. on Magnetics, vol. 52, no. 7, pp. 1-4, June 2016, Art. No. 8401204. [6] D. Dinulovic et al., IEEE Trans. on Magnetics, vol. 53, no. 11, pp. 1-7, Nov. 2017, Art no. 4700107. [7] H. T. Le et al., IEEE Trans. on Power Electronics, vol. 34, no. 1, pp. 74-85, 2019. [8] D. V. Harburg et al., IEEE Journal of Emerging and Selected Topics in Power Electronics, vol. 6, no. 3, pp. 1280-1294, 2018. [9] J. Michel et al., IEEE Trans. on Magnetics, vol. 55, no. 7, pp. 1-7, 2019, Art no. 8401207. [10] Z. Yue et al., 2019 IEEE Int. Solid- State Circuits Conference - (ISSCC), San Francisco, CA, USA, 2019, pp. 244-246. [11] D. Dinulovic et al., AIP Advance, vol. 10, no. 1, 2020, p. 015206.

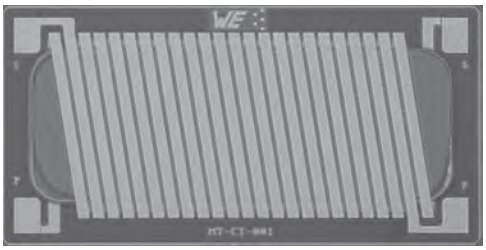

Fig.1: Fabricated microtransformer device

I1-03. Power Conversion Efficiency Prioritized AC Filter Inductor Design for Three-Phase PWM Inverter. *H. Matsumori*[1], D. Mizutani[1], T. Kosaka[1], N. Matsui[1], T. Miyazaki[2] and Y. Okawauchi[2] *1. Nagoya Kogyo Daigaku, Nagoya, Japan; 2. ROHM Co., Ltd, Kyoto, Japan*

A power electronics converter is required the high power density. Recently put to practical use the SiC power device helps to increase the switching frequency and the power density. It is generally known that enhancing the switching frequency reduces the volume of the passive components although it increases the switching device loss. However, as far as the author knows, there is no practical paper on the design method of the PWM inverter including the AC filter inductor because the copper loss and core loss of the inductor are complicatedly changed such as switching ripple current, DC-bias excitation, as shown in Fig.1 [1-4]. Therefore, the authors study loss minimized AC filter inductor design used in a three-phase PWM inverter with related to switching frequency. The inductance value of the filter inductor in each phase is designed so that the inductor current ripple at the maximum load is 20% of the fundamental wave. The magnetic material of the inductor uses an iron powder provided by Toho Zinc. Corp. Two inductor design methods are examined. As the base inductor design, turn number of windings, wire thickness, and magnetics pass length keep constant, but the inductance value is adjusted by changing core surface area as the required inductance value for switching frequency. On the other hand, in the proposed design, the core parameters other than the magnetic material, such as the aspect ratio of the core and the winding thickness, are changed. As the inverter efficiency and inductor loss calculation, the device loss is calculated by Ref. [5], and iron loss of inductor is calculated by Steinmetz equation [3] and loss map method [2]. Fig. 2 shows the simulated and measured result for efficiency and power density at 835 W output. The efficiency difference in base design is less than 0.4%. The accuracy of the design method is validated. Furthermore, in the proposed design, efficiency can enhance up to 0.7%. Even with the same material, a large efficiency gain can be expected. The more experimental result in the proposed design will site in the final paper.

[1] J. W. Kolar, U. Drofenik, and J. Biela, IEE Japan Trans. Ind. Appl., vol. 128, no. 4, pp.468-480, (2008). [2] H. Matsumori, T. Shimizu, and K. Takano, IEEE Trans. Power Electronics., vol. 31, no. 4, pp. 3080–3095, (2016) [3] A. Krings and J. Soulard, 5th International Conference and Exhibition on Ecological Vehicles and Renewable Energies (EVER 10), Monte-Carlo, MONACO, MAR 25-28, (2010). [4] C. A. Baguley, U. K. Madawala, and B. Carsten, IEEE Trans. Magn., vol. 47, no. 8, pp. 2022–2028, (2011). [5] K. Berringer, J. Marvin, and P. Perruchoud, IEEE IAS Annual Meeting, pp. 341-345 (1995)

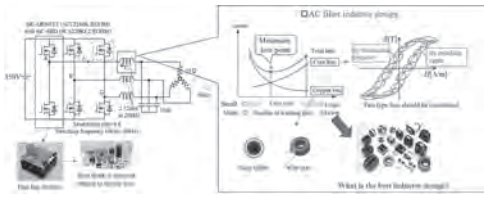

Fig. 1 Overview of AC filter inductor design for three-phase inverter.

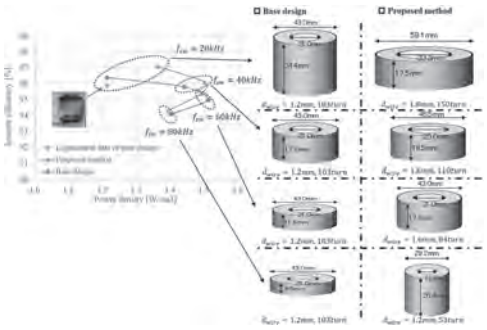

Fig. 2 Simulated and measured results for efficiency and power density.

I1-04. Fast and in Situ Remanent Flux Detection Method for a Protection Current Transformer Based on the Fluxgate Theory. T. Zheng[1] and *Y. Wang*[1] *1. College of Electrical Engineering, Zhejiang University, Hangzhou, China*

The performance of protection current transformers (CTs), which are one of the key components of the measurement chain for any protection device, have a significant impact on the performance of power system protection. The demagnetization of protection CTs is vital to ensuring the proper performance of power system protection [1]. However, the most difficulty of demagnetization is how to detect the remanent flux. This paper proposes a fluxgate theory based remanent flux detection method for protection CTs. The proposed circuit for remanent flux detection is shown in Fig. 1. The high-frequency square-wave voltage source, composed by a DC voltage source (V_{DC}) and a full-bridge DC/AC converter, is connected to a resistor (R_1) at the secondary side of the CT, and causes the core of the CT saturated slightly in the positive or negative direction. The polarity of the remanent flux is determined by the sign of integration of the voltage across R_1. The level of the remanent flux is calculated with the linear relationship between the remanent flux and the second harmonic of the high-frequency component of the voltage across R_1, as seen in Fig. 2. The linear relationship can be obtained in advance considering the fluxgate theory. The proposed method is tested for different hysteresis characteristics, different levels of remanent flux, with and without primary current, and errors in the assumed element parameters using EMTP-RV simulations. The results indicate that the proposed method can quickly and effectively detect the remanent flux of a protection CT in situ. The CT is not required to be disconnected from the substation, which means that the remanent flux can be detected in situ. The maximum detection time in all cases is smaller than 20ms. In addition, it is also confirmed that the slight distortion of the secondary current can be clearly filtered by a low pass filter, which consequently insure any protection device against maloperation.

[1] T. Zheng, E. Hu, H. Yang, R. Zhao, Y. C. Kang, P. Wall and V. Terzija, "Fast, in Situ Demagnetization Method for Protection Current Transformers," *IEEE Trans. on Magnetics*, Vol. 52, No. 7, July 2016, pp. 1-4.

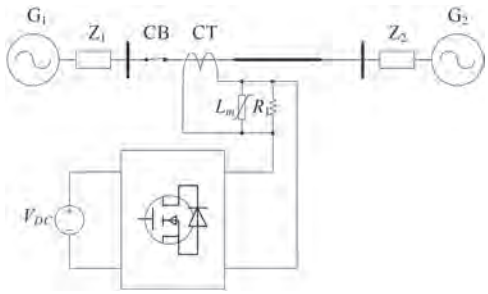

Fig. 1. Proposed circuit for remanent flux detection

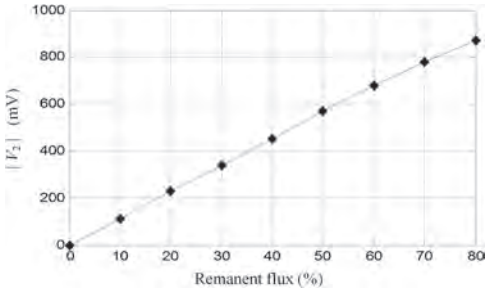

Fig. 2. Linear relationship between the remanent flux and the second harmonic of the high-frequency component of the voltage

I1-05. Optically Powered Diamagnetically Levitated Robots for Biomedical Applications. *M. Beauchamp*[1], S. Yee[1] and H. ElBidweihy[1]
1. Electrical and Computer Engineering, United States Naval Academy, Annapolis, MD, United States

Parallel control of milli-scale robots (milli-robots) is important for biomedical applications because it can improve fluidic delivery systems, which interface with cells and tissues. Systems based on diamagnetic levitation are advantageous because of frictionless transport around the workspace. The most common technique for contactless actuation in these systems is achieved through current traces in printed circuit boards or electromagnets to drive a milli-scale permanent magnet array levitated on graphite [1, 2]. Such systems have segmented work surfaces, limited motion in close proximity, and require extensive changes to expand the workspace. Automated optical actuation of diamagnetic pyrolytic graphite (PyG) levitating over permanent magnet arrays has been previously demonstrated using single laser sources for individual control [3, 4] and commercial projectors for parallel control [5]. Optical actuation allows accurate control of multiple PyG milli-robots that are able to move within close proximity to each other throughout an unsegmented work surface. Parallel control is demonstrated using three 17mmΦ levitating PyG milli-robots, which were simultaneously controlled using spotlights moving along pre-programmed paths forming the letters 'U', 'S', and 'N' as shown in Fig. 1. In this work, we demonstrate the potential use of multiple diamagnetically levitated milli-robots for delivering biological samples. As a proof of concept, we demonstrate loading, transporting, and releasing water into agar gel with microscale precision. End effectors, in the form of micropipettes, are placed on top of the PyG milli-robots. The fluid sample loads into the micropipette, which behaves as a horizontal capillary, through the aid of capillary action. The dimesions of the micropipettes and the properties of the fluid use dictate the time to fully load the capillary. A micropipette resting on top of a PyG milli-robot is shown in Fig. 2.

[1] E. E. Hunter, et al., IEEE Robotics and Automation Letters 4.2 (2019): 997-1004. [2] A. Hsu, et al., IEEE Robotics and Automation Letters 5.2 (2020): 2913-2920. [3] M. Ewall-Wice, et al., IEEE Transactions on Magnetics 55.7 (2019): 1-6. [4] J. Young, et al. AIP Advances 9.12 (2019): 125038. [5] J. Young, et al. MOEMS and Miniaturized Systems XIX, 2020.

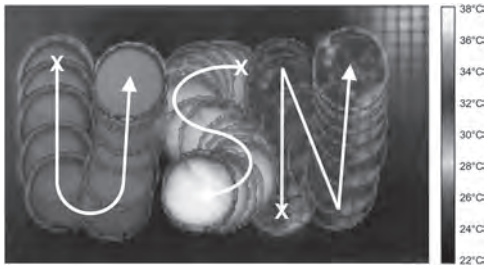

Fig. 1. Overlaid frames of three 17mmΦ PyG milli-robots maneuvered in paths forming 'U', 'S', and 'N' under spotlight actuation

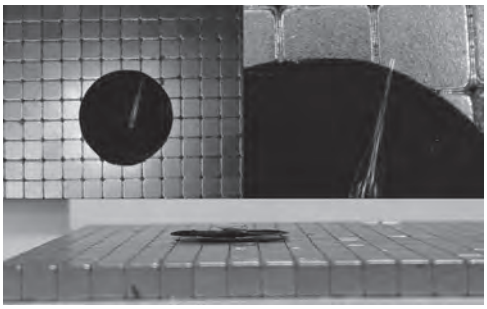

Fig. 2. Photographs of a micropipette resting on top of a diamagentically levitated 15mmΦ PyG sample.

I1-06. Permanent Magnet Dipole Design With Strong in-Plane Magnetic Field. *C. Li*[1], D. Adeyemo[1], B. Zhang[1] and A. Radomski[2]
1. R&D Engineering, dexter magnetic technologies, Elk Grove Village, IL, United States; 2. manufacturing, Dexter Magnetic Technologies inc, Elk Grove Village, IL, United States

Permanent magnet dipole can generate magnetic field higher than the Br of the material with structures such as the Halbach array [1] and Stelter array [2]. These arrays usually generate magnetic field inside a cavity. And the magnetic field is perpendicular to the axis of the cavity. For applications such as Faraday Effect and erasing hard disks perpendicular media, a strong in-plane magnetic field is required. In the case of erasing hard disks, the disk needs to rotate in the air gap with magnetic field perpendicular to the surface of the disks. This requires that the dipole must open along the field direction. And it is often difficult to generate strong magnetic field when magnets can only be placed around the path of the magnetic flux. This paper presents a permanent magnet dipole design for strong in-plane magnetic field. The design starts with a Halbach structure that generates strong magnetic field in the cavity. To create access to the cavity from the in-plane field direction, a pair of magnets with orientation opposite to the magnetic field of the Halbach dipole are substituted along the field direction. The magnetic field from the substitute magnets is analyzed using current sheet equivalent method. This field is then subtracted from the Halbach magnet to generate the magnetic field from the new structure. We then used Bound Analysis software to simulate the structure. For the prototype, we choose an 8-segment Halbach magnet as the basic structure and used triangular magnets so that the magnets fit inside a rectangular steel housing. The magnetic material is NdFeB 48 MGOe with Br of 13600 G. Fig 1 shows the prototype dipole and the magnetic field in the air gap. In conclusion, this paper proposes a permanent magnet dipole with strong in-plane magnetic field. The prototype dipole generates strong in-plane magnetic field that is in line with the predictions from the analytical equation as well as our BEA analysis. This strong dipole can be used in many applications such as Faraday Effect and hard disk erase. The design is granted with US patent 10529362 [3]

[1] K.Halbach, “Design of permanent multipole magnets with oriented rare earth cobalt materials”, *Nucl. Instru. and Methods,* Vol.169, pp 1-10 (1980) [2] Richard E. Stelter, US patent 5635889, 1997 [3] Chun Li, US patent 10,529,362, 2020

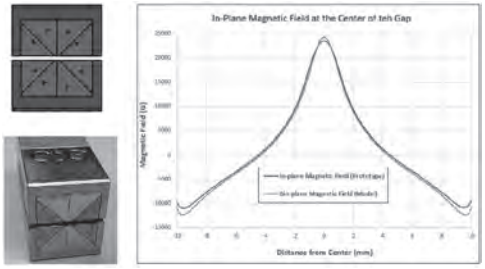

Fig.1, Structure of the prototype dipole and the measured magnetic field

I1-07. Iron Loss and Hysteresis Properties of Magnetic Materials Excited by Multi Level PWM Inverter. *A. Yao*[1], F. Kato[1] and H. Sato[1]
1. Advanced Power Electronics Research Center, National Institute of Advanced Industrial Science and Technology (AIST), Tsukuba, Japan

Multi level pulse width modulation-(MLPWM)inverter is used for control in motor drive system[1,2]. Many studies have shown that the high frequency components caused by PWM waveforms and ON-voltages of semiconductors induce complex dynamic hysteretic magnetic loops in soft magnetic materials (used as a motor core)[3–8]. To design the high-efficiency motor system, it is necessary to numerically represent the dynamic hysteretic loops of soft magnetic materials under PWM inverter excitation. Previous studies have shown only experimental properties of magnetic materials excited by MLPWM-inverter[2]. However, there has been no report on a coupling analysis to express numerical hysteretic loops under MLPWM-inverter. In this study, we focus on clarifying numerical magnetic properties under MLPWM-inverter excitation using the coupling analysis. In addition, we address the effect of ON-voltages of semiconductors on iron loss of magnetic materials. Fig. 1 shows schematic of the strong coupling analysis with the MLPWM-inverter circuit and the hysteresis model (the play model with the Cauer circuit[7]). In our study, we apply the model to the circuit simulator to realize the numerical calculation of magnetic hysteresis properties under MLPWM-inverter excitation. See Ref.7 for details of numerical methods. Fig. 2(a) and (b) show the magnetic hysteresis loops of magnetic materials under MLPWM-inverter excitation with a carrier frequency of 1 and 20kHz. Here, we for the first time realized the numerical expression for magnetic hysteresis properties under MLPWM-inverter excitation using the coupling analysis. Fig. 2(c) and (d) shows iron loss and η as a function of carrier frequency at 1T. Here, η is defined by the ratio of loss caused by ON-voltages to the total loss. We for the first time showed that the maximum proportion of loss caused by ON-voltages have about 2.4% within the parameter range of this study. These results open the way to further research in low loss motor system based on coupled studies of magnetic and semiconductor properties under MLPWM-inverter excitation.

[1] A. Radan, *et al.*, IEEE International Symposium on Industrial Electronics, 389–394 (2007). [2] H. Obara, *et al.*, (in japanese), IEEJ Industry Applications Society Conference, 1-82 (2013). [3] M. Kawabe, *et al.*, IEEE Transactions on Magnetics, 48 (11), 3458–3461 (2012). [4] A. Yao, *et al.*, AIP Advances, 7 (5), 056618 (2017). [5] A. Yao, *et al.*, IEEE Transactions on Magnetics, 54 (11), 1–5 (2018). [6] A. Yao, *et al.*, Journal of the Magnetics Society of Japan, 43 (3), 46–49 (2019). [7] A. Yao, *et al.*, Journal of the Magnetics Society of Japan, 43 (6), 105–108 (2019). [8] A. Yao, *et al.*, Journal of the Magnetics Society of Japan (accepted), (2020).

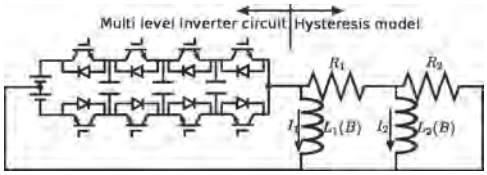

Schematic of coupling analysis with MLPWM-inverter circuit and hysteresis model.

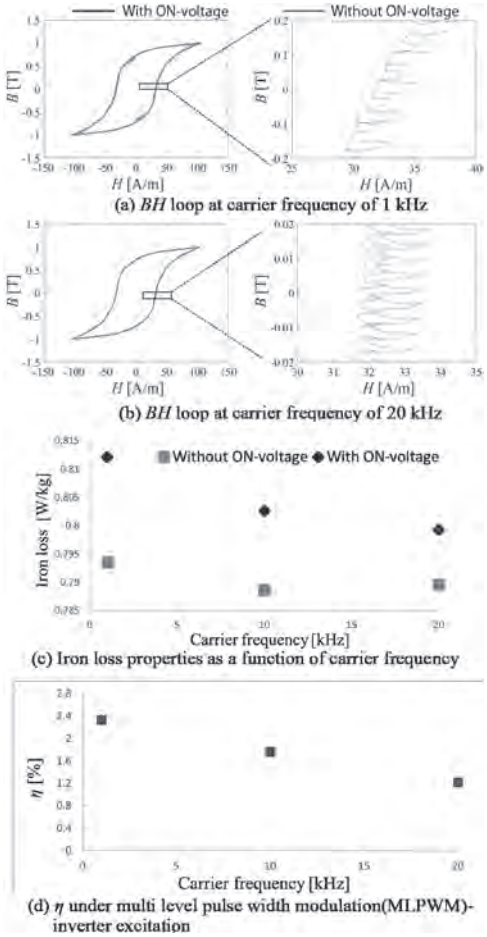

Magnetic properties under MLPWM-inverter excitation.

I1-08. Withdrawn

I1-09. Parameter Identification of Preisach Model Based on Velocity-Controlled Particle Swarm Optimization Method. *L. Chen*[1,2], Q. Yi[1], T. Ben[1], H. Xiong[1] and Y. Wang[2] *1. China Three Gorges University, Yichang, China; 2. Hebei University of Technology, Tianjin, China*

I Introduction Accurate modeling of the hysteresis characteristics of magnetic materials is of great significance to analysis the electromagnetic performance of electrical equipment[1]. The Preisach model is widely used in the simulation of the magnetic characteristic of transformers through the FEM calculation, while its parameter identification problem is still a complicated task[2]. This paper proposed a new parameter identification method based on an intelligent optimization algorithm with the explicit-form Everett function, which can speed the identification process. II Method and Discussion Firstly, the hysteresis loops of the B30P105 steel under quasi-static conditions are measured according to the IEC60404-2; Secondly, the Preisach

model is built through the explicit-form Everett function. The explicit-form Everett function transformed the integral on the Preisach plane into the sum of a series of exponential functions which gives an explicit expression of the Everett function. To simulate the hysteresis loops of the material by the proposed method, the parameters identification problems of the explicit function need to be fully investigated. The optimization process of calculating the Everett function is shown in Figure 1 (where *a, b, c,* γ*, Hs, Ms* are the parameters of the proposed model); Finally, a Velocity-Controlled Particle Swarm (VCPSO) algorithm, which only needs the limiting hysteresis loop of the experimental data is developed and implemented to find the optimal parameters of the model. The simulation results are in good agreement with the experimental data as shown in Figure 2. III Conclusion A new parameter identification method of the Preisach model with explicit Everett function is proposed. By using the VCPSO algorithm, a fast parameter identification process, which only needs the limiting loop of the experimental data is developed. The proposed method are proved to be very efficient and accurate to construct the Preisach model, which has great significance on fast simulating magnetic performance of the transformer when considering hysteresis properties.

[1] X. Zhao, X. Liu, Z. Zhao, X. Zou, Y. Xiao, and G. Li, "Measurement and modeling of hysteresis characteristics in ferromagnetic materials under DC magnetizations," Aip Advances, vol. 9, no. 2, Feb 2019, Art no. 025111, doi: 10.1063/1.5054948. [2] S. Hussain and D. A. Lowther, "An Efficient Implementation of the Classical Preisach Model," IEEE Trans. Magn., vol. 54, no. 3, Mar 2018, Art no. 7300204, doi: 10.1109/tmag.2017.2748100.

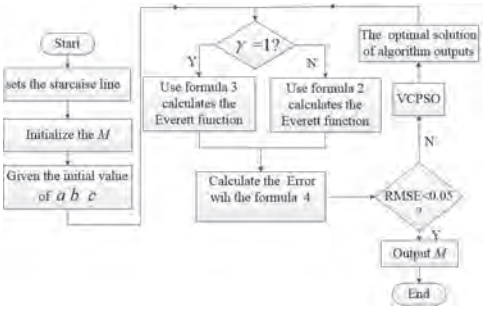

Fig.1. Optimizing process of the explicit-form Everett function with VCPSO

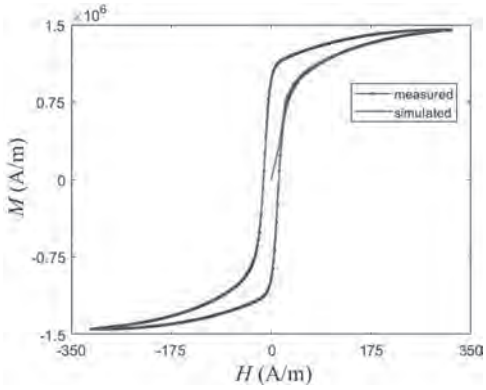

Fig.2. Comparison of the measured and simulated hysteresis loop

Session I2
MICROWAVE AND OPTICAL MAGNETIC MATERIALS

Xinjun Wang, Chair
University of Maryland, Boston, MA, United States

CONTRIBUTED PAPER

I2-01. Development of Magnetic Core/Shell Nanostructures for 5G mm Wave Absorbers. *J. Han*[1], A. Baker[1], A. Troksa[1], d. Qu[1] and S. Mccall[1]
1. Lawrence Livermore National Laboratory, Livermore, CA, United States

Millimeter-wave electronics are crucial for next-generation (5G) electronic communication systems. However, the development of desirable millimeter (mm) wave absorbers remains an ongoing challenge due to the difficulties of fabricating suitable magnetic absorbers in mm regimes. For ideal mm wave magnetic absorbers, materials should have 1) large anisotropy field (H_A) and 2) saturation magnetization (M_s). The resonance frequency is proportional to H_A and thus materials must have a large H_A are essential for their resonance frequency to be located in mm wave range (20-100 *GHz*)[1]. However, the permeability decreases with increasing resonance frequency according to Snoek's limit[2]. Thus, materials with larger M_s, are also required to mitigate this challenge. Combing both properties will enable us to achieve enhanced absorption intensity and broaden the bandwidth at mm waves. Rather than focusing on optimization of a single material, here we employ exchange coupled core/shell strategies to generate composite structures with both large M_s and H_A. Here, we have fabricated novel magnetic core/shell nanostructures with the goal to realize a highly efficient mm wave absorber. Specifically, we have successfully synthesized ε-Fe_2O_3 core particles and ε-Fe_2O_3/Co core/shell nanoparticles using wet-chemistry methods specifically via sol-gel and thermal decomposition of metal precursors. The structural analysis of core and core/shell structures was performed by TEM, HRTEM and EDX, revealing well-defined interfaces and good crystal structure. Furthermore, the coercivity of resulting ε-Fe_2O_3 core particles is in the range of 2 – 18 *kOe*, which is significantly affected by the synthetic conditions. Details of the magnetic and the frequency response from the mm wave range of ε-Fe_2O_3 core and ε-Fe_2O_3/Co core/shell nanostructures performed by DC-magnetometry, X-ray magnetic circular dichroism and custom built vector network analyzer system will be discussed in the presentation. Prepared by LLNL under Contract DE-AC52-07NA27344.

1. S. Ohkoshi, S. Kuroki, S. Sakurai, K. Masumoto, K. Sato, S. Sasaki, Angew. Chem. 119, 8544-8547 (2007). 2. J. V. I. Timonen, R. H. A. Ras, O. Ikkala, M. Oksanen, E. Seppälä, K. Chalapat, J. Li, G.S. Poraoanu, Magnetic Nanocomposites at Microwave Frequencies. In Trends in Nanophysics: Theory, Experiment and Technology; Bârsan, V., Aldea, A., Eds.; Springer Berlin Heidelberg: Berlin, Heidelberg, pp 257-285 (2010).

INVITED PAPER

I2-02. Giant Nonreciprocity in Magnetoacoustic Devices. P.J. Shah[1,2], D.A. Bas[1], I. Lisenkov[3], A. Matyushov[4], N.X. Sun[4] and *M. Page*[1] *1. Air Force Research Laboratory, Wright-Patterson AFB, OH, Wright-Patterson AFB, OH, United States; 2. Apex Microdevices, West Chester, OH, United States; 3. Independent Researher, Newton Upper Falls, MA, United States; 4. Northeastern University, Northeastern University, Boston, MA, Boston, MA, United States*

Nonreciprocity, the property of merit for a variety of RF components such as isolators and circulators, is typically difficult to achieve with the magnitude required for applications. Many systems which demonstrate non-reciprocity are not suitable for scaling to the size, weight, and power required for applications, or do not exhibit a sufficient intensity of the effect for applications relevance. One such physical system which generally does not exhibit non-reciprocity is that of acoustic waves. Acoustic waves are an important medium for information transport, but they are inherently symmetric in time. By achieving non-reciprocity in an acoustic system, the decades of industrial research in this relatively mature field can be leveraged for new applications. The most promising route to accomplish this is by incorporating magnetic materials into surface acoustic wave (SAW) devices, as in the field of acoustically driven ferromagnetic resonance. While this field remained relatively small since the initial discovery, in the past year, many new reports investigating magnetic materials in SAW devices have been published. Motivated by this expanding field, I will discuss our recent work at the Air Force Research Laboratory on the discovery of giant nonreciprocity in the transmission of surface acoustic waves (SAWs) on a lithium niobate substrate coated with ferromagnet/insulator/ferromagnet (FeGaB/Al_2O_3/FeGaB) multilayer structure[1]. I will discuss how this structure, with a unique asymmetric band diagram, can be exploited for very large non-reciprocal behavior. I will expand on magnetoelastic coupling theory to show how the magnetic bands couple with acoustic waves only in a single direction. In our devices, we measure 48.4 dB (ratio of 1:100,000) isolation which outperforms current state of the art microwave isolator devices in a novel acoustic wave system that facilitates unprecedented size, weight, and power reduction. Finally, I will discuss how these results offer a promising platform to study nonreciprocal SAW devices and other such magnetoacoustic devices.

[1] P. J. Shah, D. A. Bas, I. Lisenkov, arXiv:2004.14190 [physics.app-ph] (2020)

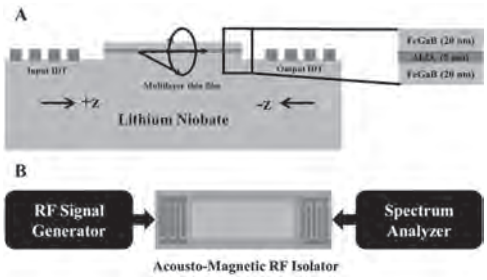

Schematic of device design and experimental setup for measurement. (A) Schematic cross-section representation of the magnetoelastic isolator device. The geometry of the device is similar to the standard ADFMR device. The multilayer thin film stack in this study is FeGaB/Al_2O_3/FeGaB thin film. L is the thickness of magnetic film and ds is the thickness of dielectric (spacer) film (B) Schematic top view representation of the isolator device including measurement setup[1].

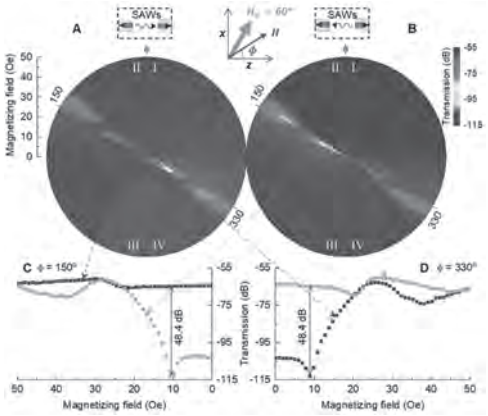

Nonreciprocal SAW transmission in a multilayer stack. ADFMR plot with 1435-MHz SAWs traveling in (A) +z-direction (forward) and (B) -z-direction (reverse). Absorption (blue on color scale) occurs at ADFMR resonance, which we observe in directions perpendicular to the growth field. (C) Field sweeps at phi = 150 degrees for forward (blue) and reverse (orange) SAW propagation. (D) Field sweeps at phi = 330 degrees for forward (blue) and reverse (orange) SAW propagation. The difference between forward and reverse sweeps at a common static field condition is the isolation[1].

CONTRIBUTED PAPERS

I2-03. Multiferroic Lamb Wave Antenna With Energy Reflecting Components. *R. Zheng*[1], V.M. Estrada[1] and A. Sepulveda[1] *1. MAR, University of California Los Angeles, Los Angeles, CA, United States*

Conventionally, antennas such as dipoles and loops rely on an electromagnetic (EM) wave resonance, therefore the sizes of such antennas are within the same order of free-space wavelength. Electrically small antennas (i.e. size < λ/10) at ultra-high frequency hold promises for reducing the antenna system's size, weight, and volume, yet state-of-the-art electrically small antennas confront a daunting challenge. So far, electrically small antennas radiate poorly when placed near a conducting surface because of platform effects. Recently, induced strain-mediated multiferroic composites interconvert between alternating magnetization and mechanical strain wave with ultra-high energy efficiency due to negligible current and Ohmic loss. Several reports of such devices, modified from thin-film bulk acoustic resonator (FBAR), have demonstrated a new concept on an electrically small antenna. However, until now, fabrication challenges hindered attempts at forming large scale antenna arrays to improve the signal strength. This work demonstrates a new strain-mediated multiferroic antenna that relies on shear (d15) mode resonance of piezoelectrical substrate such as Aluminum Nitride (AlN). Oscillation of Ni microelements excited by free space EM wave is detected by comb-shaped arrays of metallic electrodes through the out-of-plane electrical field. Surrounding the Ni microelements and comb-shaped electrodes there are acoustic gratings and Bragg acoustic mirrors to reflect the acoustic energy to form a standing wave and prevent energy dissipation. A 4 kV/m electrical field through the piezoelectrical material corresponded by several micro strain's deformation is predicted under the EM wave environment in the numerical finite element model. Reversely, at least -40dBm radiation power is expected according to a 10dBm's energy be input to a 2cm*2cm antenna. Based on the model and optimized structure, we designed the system and we are currently fabricating a device to make preliminary tests on it. This work demonstrates the feasibility of shear mode strain-mediated multiferroic antenna, which shows promising potential for the next-generation electrically small antenna at ultra-high frequency.

M. Lakin, K. T. McCarron, and R. Rose, Proc. - IEEE Ultrason. Symp., pp. 905–908, 1995. E. Godshalk and G. Bouche, "Bragg Mirror Optimized for Shear Waves," 2010. A. Mourachkine, O. V. Yazyev, C. Ducati, and J. P. Ansermet, Nano Lett., vol. 8, no. 11, pp. 3683–3687, 2008.

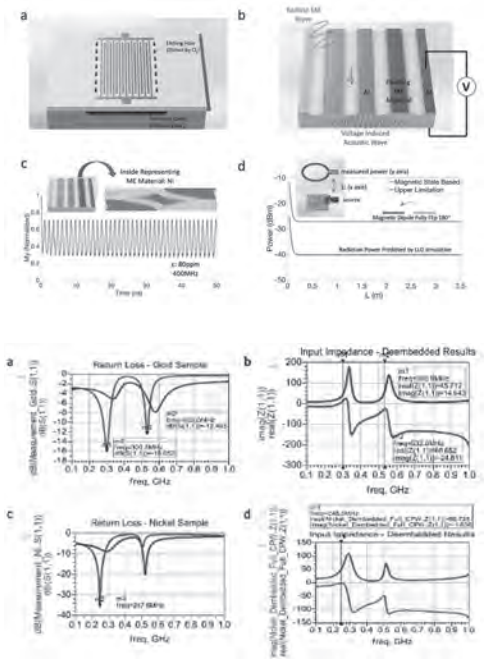

I2-04. Hexagonal Ferrite Composite and Sintered Slab Noise Suppressor Embedded in-Between IC Chip and Interposer. A. Takahashi[1], Y. Miyazawa[1], *M. Yamaguchi*[1,2], R. Sai[4], S. Tanaka[3], K. Jike[3], K. Watanabe[3] and M. Nagatana[3] *1. New Industry Creation Hachery Center, Tohoku Unversity, Sendai, Japan; 2. Department of Electrical Engineering, Tohoku Gakuin Daigaku, Sendai, Japan; 3. Graduate School of Science, Technology and Innovation, Kobe University, Kobe, Japan; 4. Centre for Nano Science and Engineering, Indian Institute of Science, Bengaluru, India*

The glowing 5G telecom system needs new low noise technology for high reliability and low latency in a smaller volume in and beyond 3 - 6 GHz range [1]. This paper suggests a solution to this challenge by using RF magnetic noise suppressor integrated into narrow gap in-between IC die and its interposer that routes wires between one socket or connection to another socket or connection [2]. In Fig. 1, circuits on an IC die faces downside and noise-carrying on-chip wires face the noise suppressor very closely. Narrower space is preferred for better noise suppression. The noise in the on-chip wires will be dissipated into heat by means of FMR losses of magnetic material [3], [4]. Referring high frequency properties of hexaferrites [5], two types of composite sheet samples were prepared[4]; Zn-substituted Y-type barium hexaferrite (Ba2Zn2Fe12O22, μr" = 1.9 @ FMR=2.4 GHz, FoM [6]: ω x μr"=23.8 @ 6 GHz, same hereafter) and Co/Zn-substituted Z-type barium hexaferrite (Ba3Co1.25Zn0.75Fe24O41, 0.9, 2.1 GHz, 26.7) particles mixed respectively with polyurethane resin as magnetic inclusions with ~50 vol.%, and about 50 μm thickness. Another 50 μm thick sintered slab is prepared; Ni-Cu-Zn spinel ferrite (10.0, 1.0 GHz, 60.3) [6]. The test IC chips were driven at 100 MHz clock while magnetic near field emission from was analyzed by a coil type probe (Langer XF-R 3-1) at 4.8 GHz (even harmonic, 48th), as a measure of conduction noise suppression in the chip (note that magnetic material is located beneath the IC die). In Fig. 2, it is clear that the Y-type hexaferrite composite and Ni-Cu-Zn spinel slab successfully suppressed the radiated emission by 10 dB in average while level of the emission fluctuate chip by chip. The suggested method offers low temperature process and more material selectiveness for further high-frequency application. Part of this work is supported by the Development of Technical Examination Services Concerning Frequency Crowding, MIC, Japan (JPJ000254). The authors are grateful to the help of Takaaki Okidono for packaging technology.

[1] 3GPP, "Release 14: TR 38.913, 2016. [2] A. Usman, E. Shah, N. B. Satishprasad, et al, IEEE Trans. CPMT, vol. 7, pp. 819-828, 2017 [3] K. Kondo, T. Chiba, H. Ono, et al, J. Appl. Phys., vol. 93, pp. 7130-7133, 2003. [4] M. Yamaguchi, S. Tanaka, Y. Endo et al, APEMC 2015, SS10-5, 2015. [5] V. G. Harris, A. Geiler, Y. Chen, et al, J. Magn. Magn. Mater., vol. 321, pp. 2035–2047, 2009. [6] M. Yamaguchi, Y. Miyazawa, J. Ma, et al, Proc. EMC Europe 2018, pp. 608 - 612, 2018.

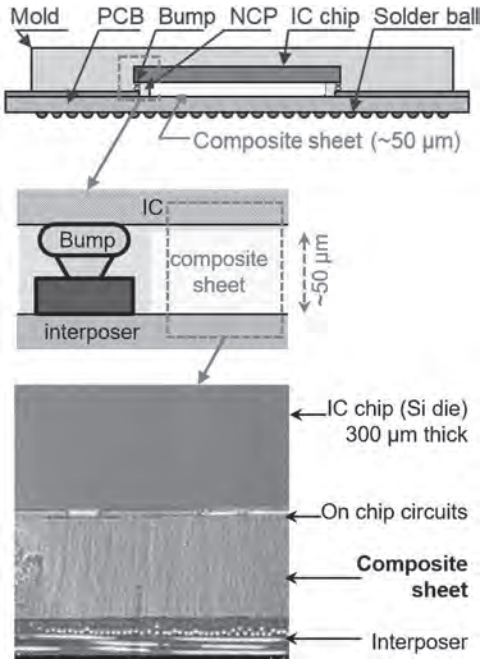

Fig. 1 Magnetic powder composite implementation to IC chip interposer.

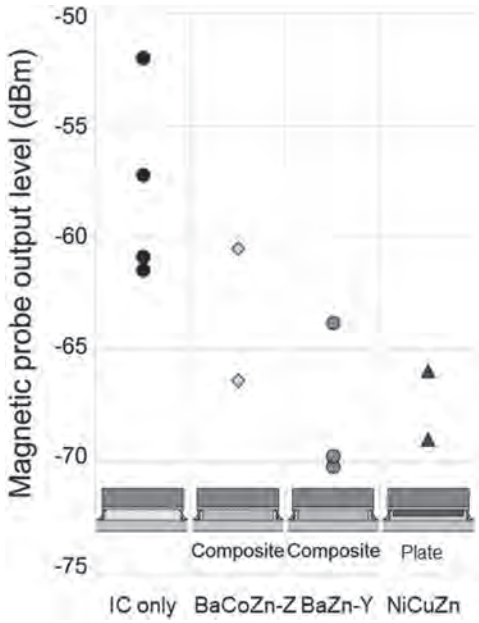

Fig. 2 Magnetic near field suppression by magnetic powder composite integrated to IC chip interposer.

I2-05. Broadband-Millimeter-Wave Absorber Based on Ti-Co Substituted ε-Iron Oxide. *A. Namai*[1], K. Ogata[1], M. Yoshikiyo[1] and S. Ohkoshi[1] *1. Department of Chemistry, School of Science, The University of Tokyo, Bunkyo-ku, Japan*

High-speed wireless communication plays a significant role in the Internet of Things era. 120-GHz and 140-GHz band millimeter waves have potential in broadcasting wireless communications, wireless data transmissions between cellular base stations, and traffic monitoring sensors in intersection areas for advanced driver assistance systems. As millimeter wave applications become more common, millimeter wave absorbing materials become necessary. ε-Fe_2O_3 is reported to show millimeter wave absorption at 182 GHz due to natural resonance, which is achieved by its large magnetic anisotropy [1]. For tuning millimeter wave absorption properties, Co^{II} is attractive because it is a magnetic ion with strong single-ion anisotropy. In the present paper, we report the synthesis and millimeter wave absorption property of Ti-Co substituted ε-iron oxide, ε-$(Ti^{IV}Co^{II})_xFe^{III}_{2-2x}O_3$ (x = 0 (1), 0.014 (2), 0.033 (3), and 0.048 (4)) [2]. The samples were synthesized by the sol-gel method. The X-ray diffraction patterns show that the ε-phase is the main product. Transmission electron microscope images indicate that the samples are composed of nanoparticles. The particle sizes are 20-30 nm. The samples possess spontaneous magnetization at room temperature and show magnetic hysteresis loops. The coercive field value monotonously decreases as the x value increases from 20.0 kOe (1) to 8.4 kOe (4). The millimeter wave absorption spectra measured by terahertz time domain spectroscopy show absorption peaks. The resonance frequency (f_r) decreased, and the full width at half maximum (Δf) increased as the x value increased as follows: (f_r, Δf) = (181 GHz, 6 GHz) for 1, (162 GHz, 9 GHz) for 2, (140 GHz, 15 GHz) for 3, and (121 GHz, 24 GHz) for 4. In addition, we demonstrated a sheet shaped 140 GHz band millimeter wave absorber composed of 3. The sheet with the thickness of 612±8 μm shows a reflection loss at 140 GHz is −9 dB. This material has potential as a millimeter wave absorber especially for 140-GHz or 120-GHz usages.

[1] A. Namai, M. Yoshikiyo, K. Yamada, S. Sakurai, T. Goto, T. Yoshida, T Miyazaki, M. Nakajima, T. Suemoto, H. Tokoro, and S. Ohkoshi, *Nature Communications*, 3, 1035 (2012). [2] A. Namai, K. Ogata, M. Yoshikiyo, and S. Ohkoshi, *Bull. Chem. Soc. Jpn.*, 93, 20 (2020).

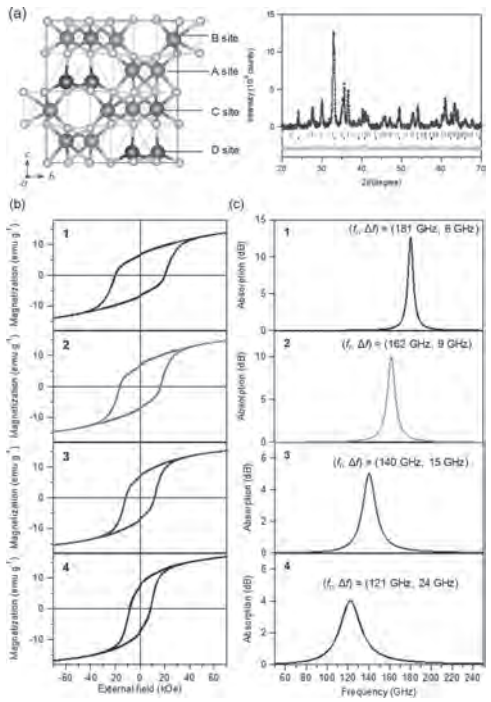

Figure 1. (a) Crystal structure of ε-$(TiCo)_{0.033}Fe_{1.934}O_3$ and XRD pattern of 3. (b) M-H curves at 300 K and (c) millimetre wave absorption spectra.

INVITED PAPER

I2-06. Single-Pulse all-Optical Toggle Switching of Magnetization Without a Rare Earth. *J. Besbas*[1], C. Banerjee[1], K.E. Siewierska[1], G. Atcheson[1], N. Teichert[1], P.S. Stamenov[1], K. Rode[1] and M. Coey[1]
1. School of Physics, Trinity College Dublin, Dublin, Ireland

Ten years ago, it was shown that ultrafast laser-induced heating of a thin film of amorphous $Gd(FeCo)_3$ can magnetically switch the irradiated area [1-2]. A train of light pulses toggles the magnetization between two equivalent directions perpendicular to the film. Since then an intense research effort, both experimental and theoretical, has sought to unravel the underlying mechanisms of this single-pulse, all-optical switching (SP-AOS). Empirically it was established that the material needs to be ferrimagnetic with two magnetic lattices that demagnetize at different rates. As the initial, purely thermal demagnetisation rate is proportional to the local atomic moments on the sublattices, efforts were therefore focused on the gadolinium/transition metal alloys where the moments differs by a factor of almost four. It is therefore surprising that a second material, where we recently discovered SP-AOS [3], was the XA-ordered ferrimagnetic Heusler alloy Mn_2Ru_xGa (MRG) where both magnetic sublattices are composed of manganese, with similar atomic moments. In this talk, we discuss how ~200 femtosecond light pulses toggle the magnetization of MRG.[3]. MRG is a half-metallic ferrimagnet with two antiparallel sublattices made up of manganese occupying inequivalent 4*a* and 4c positions in the F-43m space group[4]. On account of its unusual electronic structure, 4*c* electrons at the Fermi level dominate both magneto-optic and magneto-transport properties [5-6]. The sublattice moments compensate at a temperature T_{comp} that depends on x and the thin film preparation conditions. Usually, at low temperatures the moment of the 4*c* sublattice is bigger than that of the 4a sublattice, but as the temperature rises, it falls off faster than 4a, and the two cross at T_{comp} where they are equal but opposite. Unlike $Gd(FeCo)_3$, which exhibits toggle switching for a range of initial temperatures ranging from 100 K below to 100 K above its compensation temperature, because the difference in atomic moments ensures the TM sublattice is demagnetised before the RE one, MRG will only switch when the initial temperature lies below T_{comp}. This suggests that exchange relaxation plays a much more important role in the switching of MRG. MRG is a versatile material magnetic material. Its compensation temperature can easily be tuned and it is impervious to high magnetic fields in the vicinity of T_{comp}, where the coercive field rises to 10 T. Furthermore, it possesses a large anomalous Hall effect and a very high intrinsic spin-orbit torque that may be useful for spintronic applications [7-8]. The observation of SP-AOS in a material with these properties opens both new technological prospects, and new challenges for understanding the fundamental non-equilibrium electronic processes involved.

1. Radu *et al.*, Nature, Vol. 472, p. 205 (2011) 2. Ostler *at al.*, Nature Communications, Vol. 3, p. 666 (2020) 3. C. Banerjee *et al.*, arXiv, Vol. 1909, p. 09085 (2020) 4. H. Kurt *et al.*, Physical Review Letters, Vol. 112, p. 027201 (2014) 5. K. Fleisher *et al.*, Physical Review B, Vol. 98, p. 134445 (2018) 6. K. E. Siewierska *et al.*, IEEE Transactions on Magnetics, Vol. 55, p. 2 (2019) 7. N. Thiyagarajah *et al.*, Applied Physics Letters, Vol. 106, p. 122402 (2015) 8. S. Lenne *et al.*, arXiv, Vol 1903, p. 04432 (2019)

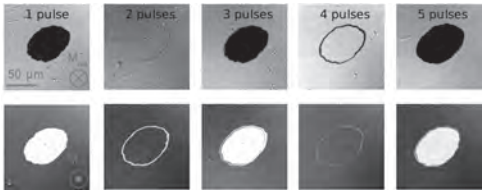

Toggling of magnetization in MRG following the irradiation by 200 fs light pulses.

CONTRIBUTED PAPERS

I2-07. Linear Chains of Nanomagnets: Engineering the Effective Magnetic Anisotropy. *A. Talapatra*[1] and A. Adeyeye[1,2] *1. Department of Electrical and Computer Engineering, National University of Singapore - Kent Ridge Campus, Singapore, Singapore; 2. Physics, Durham University, Durham, United Kingdom*

We have investigated the control of effective magnetic anisotropy in Permalloy ($Ni_{80}Fe_{20}$) linear chain arrays by tuning the symmetry arrangements of the ellipsoidal nanomagnets and the film thickness. The coupled ellipsoidal nanomagnets are arranged in two distinct configurations (Fig. 1 (a) and (b)), namely: type-I, where elements are arranged along the major axis of the ellipsoid, and type-II, in which the neighboring elements are coupled along the minor axis of the ellipsoid [1, 2]. Hence, the shape anisotropy of each nanomagnet and the configurational anisotropy due to the lattice arrangements favor the same direction of magnetization for type-I arrays while competition exists between the shape and configurational anisotropy for type-II arrays. The hysteresis loops depicted in Fig. 2 (a) and (c) clearly show the variation of the effective anisotropy with thickness which is also supported by the ferromagnetic resonance (FMR) spectra, shown in Fig. 2 (b) and (d) for type-I and type-II arrays respectively. A clear transition from a single domain states to a combination of complex flux closure states such as vortex, double vortices are observed at different applied field angles (φ) when the film thickness is varied in the range from 20 nm to 100 nm. Tunable microwave absorption spectra established the complex interplay between the shape anisotropy and magnetostatic interactions at different film thicknesses and applied field angles. Micromagnetic simulations are in good agreement with the experimental results. Our results demonstrate the possible ways of manipulating the effective magnetic anisotropy in the arrays of nanomagnets for magnonics and microwave applications.

[1] S. Jain, A. O. Adeyeye, N. Singh, *Nanotechnology* 2010, *21* (28), 285702. [2] A. Talapatra, A. O. Adeyeye, Linear Chains of Nanomagnets: Engineering the Effective Magnetic Anisotropy (submitted).

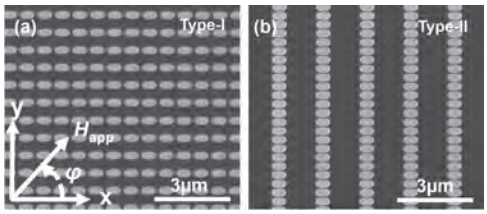

Scanning electron microscope images of (a) type-I and (b) type-II arrays of nanostructures over large area. The inset shows the geometry of the applied field (H_{app}) with respect to the nanoelements.

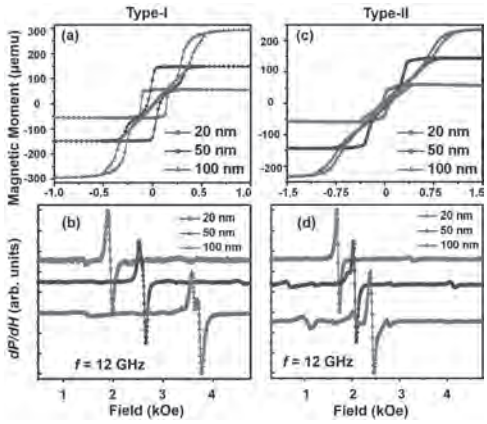

The thickness-dependent hysteresis loops (at φ = 0°) for (a) type-I, (c) type-II arrays and FMR spectra for (b) type-I, (d) type-II arrays of nanomagnets.

I2-08. Withdrawn

I2-09. Controlling Magnetic Properties of the van der Waals Crystal $MnPS_3$ via the Absorption Spectrum. *M. Birowska*[1] and J. Kunstmann[2]
1. Faculty of Physics, University of Warsaw, Warsaw, Poland;
2. Theoretical Chemistry, Department of Chemistry and Food Chemistry TU Dresden, Dresden, Germany

Atomically thin, magnetic materials have gained a lot of attention since 2017, when the first 2D ferromagnet was reported [1]. This breakthrough has triggered research on 2D magnetic materials [2]. They are not only important from a fundamental point of view -to understand the theory of magnetism in reduced dimensions-, but also for technological applications. However, probing the magnetic order of the 2D systems by conventional magnetic experimental setups is very challenging. On the other hand, it is well known, that even in the single layer limit, semiconducting two-dimensional materials strongly absorb light. Therefore, optical spectroscopy is a good method for their characterization. In order to shed light on the intriguing phenomena of 2D magnetism, we present comprehensive theoretical investigations of the optical properties of the van der Waals layered material $MnPS_3$, which is one important example from the large family of transition metal phosphorus trisulfide (MPS_3) [3]. Our study reveals, that the interband absorption spectrum, which is proportional to the imaginary part of the dielectric function, is very similar for different possible magnetic states of $MnPS_3$. On the other hand, the calculated effective masses of electrons and holes exhibit an anisotropic behaviour and they strongly depend on the magnetic order. Aforementioned properties are reflected in the binding energy of excitons in the studied systems. The impact of the magnetic order on electronic band gap is also revealed, and indirect character of electronic band gap is confirmed as the groundstate of bulk system. Our results demonstrate that the magnetic order of 2D materials can be indirectly inferred via optical measurements. The study was accomplished thanks to the funds allotted by the National Science Centre, Poland within the framework of the research project 'SONATA12' no. UMO-2016/23/D/ST3/03446. Access to computing facilities of TU Dresden ZIH for the project "TransPheMat", PL-Grid Polish Infrastructure for Supporting Computational Science in the European Research Space, and of the Interdisciplinary Center of Modeling (ICM), University of Warsaw are gratefully acknowledged

[1] B. Huan *et al.*, Nature 546, p. 270-273 (2017) [2] M. Gibertini *et al.*, Nat. Nanot. vol. 14, p. 408 (2019). [3] R. Brec, Solid State Ionics vol. 22, p. 3-30 (1986).

I2-10. Enhanced Magneto-Optical Effect in Ce:YIG Based All Dielectric Metasurfaces. *X. Shuang*[1], Q. Liu[2], J. Qin[1], Y. Chen[2], H. Duan[2], L. Deng[1] and L. Bi[1] *1. National Engineering Research Center of Electromagnetic Radiation Control Materials, University of Electronic Science and Technology of China, Chengdu, China; 2. College of Mechanical and Vehicle Engineering National Engineering Research Center for High Efficiency Grinding, Hunan University, Changsha, China*

Magneto-optical (MO) devices based on the Faraday effect are widely used for optical communication and optical sensing. Due to their weak MO effect in the optical frequency range, the size of MO devices is typically in the range of 10~1000 wavelengths, limiting their application in integrated photonic systems. Currently, most studies for enhancing the Faraday effect are based on surface plasmon resonance.[1, 2] However, due to the Ohmic loss of metals, these structures are optically lossy. Therefore, all dielectric nanostructures provide an alternative route to achieve high Faraday rotation and high transparency simultaneously.[3,4] Here, we report theoretical and experimental study on enhanced Faraday effect in all dielectric MO metasurfaces based on Si/Ce:YIG nanostructures. The device is composed of a 2D periodic array of amorphous Si nanodisks patterned on Ce:YIG/YIG oxide thin film stacks grown on silica. By adjusting the geometric parameters, magnetic dipole and electric dipole Mie resonance modes can be excited in the Si disks. Thanks to the high refractive index of Ce:YIG/YIG, the modes are also strongly confined in the Ce:YIG/YIG layers. The transmission spectrum is simulated using the finite element time-domain difference method, which agrees excellently with experimental results. The Faraday rotation spectrum of the sample was measured using a home-made microscale Faraday rotation characterization set-up, which shows obvious enhancement peaks in the vicinity of each resonance. The MO response of the Ce:YIG thin film deposited on the same silica substrate is also presented as a reference. With the transmission close to 40%, we achieved 2.3-fold Faraday rotation enhancement compared to bare Ce:YIG thin films. Our device shows effective MO enhancement in the sub-wavelength scale, which is promising for applications such as free space non-reciprocal photonic devices and MO imaging.

1. Liu, M. and Zhang, X., Nature Photonics., Vol. 7, p.430-431 (2013) 2. Armelles, G. and Cebollada, A., Advanced Optical Materials., Vol. 1, p.10-35 (2013) 3. Christofi, A., Kawaguchi, Y. and Alu, A., Optics Letters, Vol. 43, p.1838-1841 (2018) 4. Royer, F., Varghese, B. and Gamet, E., ACS omega, Vol. 5, p.2886-2892 (2020)

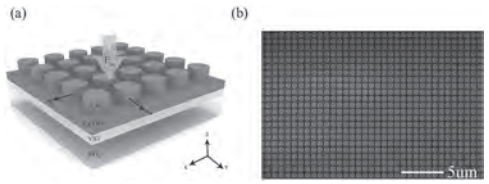

Fig. 1 (a) Schematic diagram of the metasurface (b) Scanning electron microscope image of a fabricated device

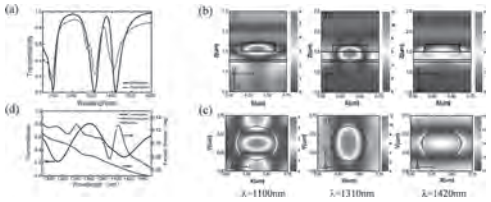

Fig. 2 (a) The measured and simulated transmission spectrum of the device(b) (c) Simulated near-field maps in the X-Z and X-Y plane(d) The experimental measured MO response of the metasurface compared with a Ce:YIG thin film

I2-11. Design of Tb_xCo_{100-x} for All Optical Switching of Magnetization. *A. Ciuciulkaite*[1], K. Mishra[2], M.V. Moro[1], I. Chioar[1], R. Rowan-Robinson[3], S. Parchenko[4], A. Kleibert[4], B. Lindgren[1], G. Andersson[1], C. Davies[5], A. Kimel[2], M. Beritta[1], P.M. Oppeneer[1], A. Kirilyuk[5] and V. Kapaklis[1]
1. Physics and Astronomy, Uppsala Universitet, Uppsala, Sweden;
2. Radboud Universiteit Institute for Molecules and Materials, Nijmegen, Netherlands; 3. Department of Material Science and Engineering, The University of Sheffield, Sheffield, United Kingdom; 4. Swiss Light Source, Paul Scherrer Institut, Villigen, Switzerland; 5. FELIX laboratory, Radboud Universiteit, Nijmegen, Netherlands

Observation of All-Optical Switching (AOS) of magnetization in ferrimagnetic GdFeCo alloys, using ultrashort circularly polarized laser pulses [1], triggered a renewed interest in ferrimagnetic rare Earth-transition metal (RE-TM) alloys [1-5]. Tb-containing ferrimagnetic alloys exhibit all-optical helicity-dependent switching (AO-HDS), and have strong perpendicular magnetic anisotropy, a result of a high spin-orbit coupling in Tb [6]. In this work we study the magnetic properties and AOS performance of amorphous TbCo alloys, prepared by a DC magnetron sputtering (for more details see [7]). We measured $\mu_0 H_c$ using polar magneto-optical Kerr effect (MOKE), and investigated the AOS behaviour using a pump-probe based static magneto-optical imaging setup. We show that AO-HDS is possible in Tb_xCo_{100-x} for certain compositions (x=24-30 at.%) and thicknesses (Fig. 1), if the laser pulse parameters such as pump fluence, are optimized, and the

number of pulses in one burst is at least 50-100. Samples with the compositions out of this range show only helicity-independent thermal demagnetization. We also performed *ab initio* calculations of the inverse Faraday effect to explain the cumulative nature of the multi-shot AO-HDS switching. It is triggered by circularly polarized laser light, inducing a helicity dependent magnetic moment in the Co atoms of the alloys (Fig. 2). This study shows that ferrimagnetic TbCo films can exhibit AO-HDS in a certain compositional range and laser pulse parameters, with a minimal amount of shots.

1. C. D. Stanciu et al Phys. Rev. Lett. 99, 047601 (2007) 2. B. Hebler et al, Frontiers in Materials 3, 8 (2016). 3. S. Alebrand et al Applied Physics Letters101,162408 (2012). 4. S. Mangin et al, Nature Materials 13, 286 (2014). 5. C. H. Lambert et al, Science 345, 1337 (2014) 6. R. Moreno et al, Phys. Rev. B 96, 014409 (2017). 7. A. Ciuciulkaite et al. arXiv:2002.07544

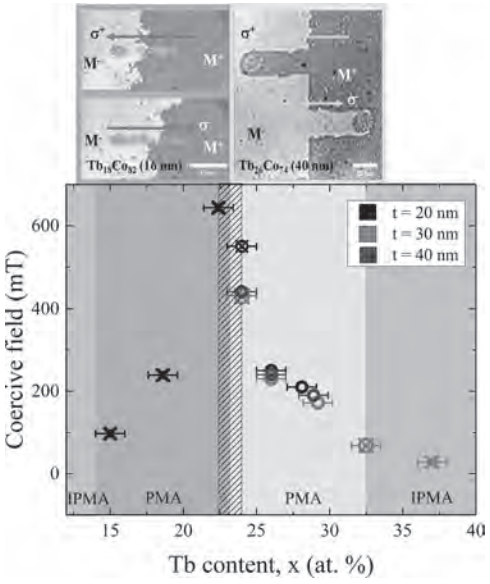

Fig.1. Diagram showing the switching behavior as a function of coercive field $\mu_0 H_c$ and composition for samples of different thickness. The red (× symbols) and green (o symbols) regions denote areas where pure helicity-independent thermal demagnetization (top left image) and multi-shot AO-HDS (top right image), are observed, respectively. Grey regions correspond to samples with in-plane magnetic anisotropy.

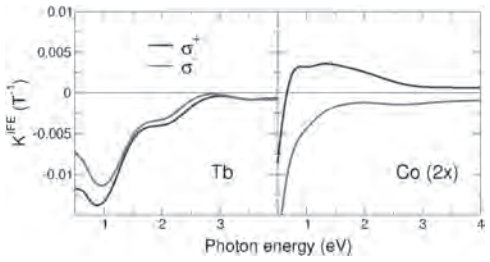

Fig. 2. *Ab initio* computed helicity- and frequency-dependent IFE constants for Tb and Co atoms in $TbCo_2$. Note that the values for Co are multiplied by a factor of two.

I2-12. Waveguide Integrated Broadband Magneto-Optical Isolators on Silicon Nitride Platforms. *W. Yan*[1,2], Y. Yang[1,2], S. Liu[1,2], J. Qin[1,2], L. Deng[1,2] and L. Bi[1,2] *1. National Engineering Research Center of Electromagnetic Radiation Control Materials, University of Electronic Science and Technology of China, Chengdu, China; 2. State Key Laboratory of Electronic Thin-Films and Integrated Devices, University of Electronic Science and Technology of China, Chengdu, China*

On-chip optical isolators are key components in photonic integrated circuits (PICs). In recent years, passive magneto-optical (MO) isolators based on nonreciprocal phase shift (NRPS) have been widely studied [1]. Micro-ring and Mach-Zehnder interferometer (MZI) isolators have achieved considerable progress on silicon on insulator (SOI) platforms [2, 3]. As a different material platform, silicon nitride (SiN) based PICs show much lower propagation loss, which are highly promising for telecommunication, data communication and sensing applications [4, 5]. However, high performance MO isolators have not been demonstrated on SiN, which is fundamentally limited by the low Faraday rotation and weak NRPS for MO thin films grown on SiN waveguides. Here, we report high-performance integrated MO isolators on SiN platforms for both TM and TE polarizations using cerium doped yttrium iron garnet (Ce: YIG) thin films deposited by pulsed laser deposition (PLD). By increasing the Ce solubility up to 40% [6], Ce:YIG thin films grown on SiN show high Faraday rotation up to -5500 deg/cm at 1550 nm wavelength, which is 83% higher than previously reported $Ce_1Y_2Fe_5O_{12}$ thin films [7, 8]. Based on these materials, broadband SiN MZI isolators are designed and fabricated. The TM isolators show 24 dB isolation and 4 dB insertion loss around 1567 nm wavelength, with a footprint of 0.9×0.25 mm^2. For TE isolators, a maximum isolation ratio of 28 dB with insertion loss of 7.5 dB is observed at 1565 nm wavelength. These devices have exceeded the performance of their counterparts on SOI [7]. Our work demonstrates that high performance MO thin films and optical isolators can be monolithically integrated on SiN PICs.

[1] Bi L, H.J. and Jiang P, Nature Photonics., Vol. 5, p.758 (2011) [2] Shoji Y, F.A. and M. T, IEEE Journal of Selected Topics in Quantum Electronics., Vol. 22, p.264-270 (2016) [3] Pintus P, H.D. and Morton P A, Journal of Lightwave Technology., Vol. 37, p.1463-1473 (2019) [4] Baets R, S.A.Z and Clemmen S, Optical Fiber Communication Conference., p. Th3J-1 (2016) [5] Gaeta A L, Lipson M and Kippenberg T J, Nature Photonics., Vol. 13, p.158-169 (2019) [6] Zhang Y, Wang C T and Liang X, Journal of Alloys and Compounds., Vol. 703, p.591-599 (2017) [7] Zhang Y, Du Q and Wang C, Optica., Vol. 6, pp.473-478 (2019) [8] Du Q, Wang C and Zhang Y, ACS Photonics., Vol. 5, p.5010-5016 (2018)

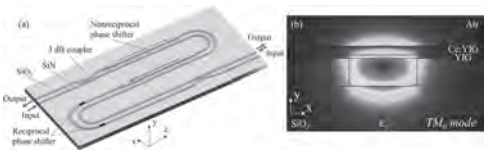

Fig. 1. (a) Layout of TM MO isolators on SiN substrates. (b) Simulated Ey field distribution of TM_0 mode for SiN MO waveguides.

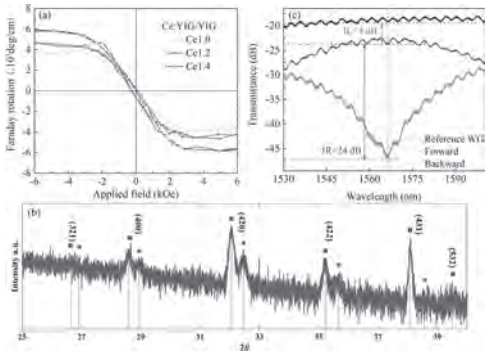

Fig. 2. (a) Faraday rotation of yttrium iron garnet doped with different cerium solubilities on silicon substrates. (b) X-ray diffraction patterns of Ce1.4Y1.6Fe5O12, where red squares and blue dots represent garnet peaks originating from Ce: YIG and YIG resperctively. (c) Transmission spectra of the TM MO isolator.

I2-13. Magneto-Optical Detection of Photoinduced Magnetism *via* Chirality Induced Spin Selectivity in 2D Chiral Hybrid Organic-Inorganic Perovskites. *Z. Huang*[1], B. Bloom[2], X. Ni[3], Z. Georgieva[2], M. Marciesky[2], E. Vetter[1], f. liu[3], D. Waldeck[2] and D. Sun[1] *1. Physics, North Carolina State University, Raleigh, NC, United States; 2. Chemistry, University of Pittsburgh, Pittsburgh, PA, United States; 3. Material Science and Engineering, Univeristy of Utah, Salt Lake City, UT, United States*

The recent convergence of chiral molecules with metal halide perovskite frameworks gives rise to an interesting family of chiral systems: two-dimensional, chiral hybrid organic-inorganic perovskites (2D-chiral-HOIPs). While possessing photovoltaic properties of traditional HOIPs, this class of materials is endowed with chirality through its organic ligands in which the degeneracy of the electron spin in charge transport is broken, *i.e.*, the Chirality-Induced Spin Selectivity (CISS) effect manifests, making it a promising platform to bridge opto-spintronic studies and the CISS effect. In this work, 2D-chiral-HOIP/NiFe heterostructures are studied by means of the magneto-optical Kerr effect using a Sagnac interferometer. Upon illumination of the HOIPs, the Kerr signal at the HOIP / NiFe interface changes, and a linear dependence of the response on the magnetic field is observed. The sign of the slope was found to depend on the chirality of the HOIPs. The results demonstrate the utility of chiral HOIP materials for chiral Opto-spintronic applications. D.S. acknowledges the support from National Science Foundation ECCS 1936527. D.H.W. acknowledges the support of the Department of Energy (Grant No. ER46430). Work at Utah is supported by US Department of Energy (Grant No. DE-FG02-04ER46148). F.L. acknowledges NERSC and CHPC at the University of Utah for providing the computing resources.

I2-14. Interfacial and Bulk Magnetic Properties of Stoichiometric Cerium Doped Terbium Iron Garnet Polycrystalline Thin Films. *K. Srinivasan*[1], C. Radu[2], D. Bilardello[3], P. Solheid[3] and B. Stadler[1] *1. Electrical and Computer Engineering, University of Minnesota, Minneapolis, MN, United States; 2. Lake Shore Cryotronics Inc., Westerville, OH, United States; 3. Institute for Rock Magnetism, Department of Earth and Environmental Sciences, University of Minnesota, Minneapolis, MN, United States*

High-gyrotropy rare-earth iron garnets with low losses enable the realization of integrated optical isolators for laser-on-chip silicon photonics [1]. However, integrated isolators with magneto-optical materials have always required an external magnetic field. Novel waveguide isolator designs with Ce:TbIG can operate in the remnant magnetization state and overcome the magnetic field requirement [2,3]. Further magnetless design optimizations and device downscaling require a deeper understanding of the magnetic properties of the material in the bulk and at the interface. Here, sputter-deposited Ce:TbIG thin films with large Faraday rotation (~-3500°/cm) are shown to have a near-ideal stoichiometry of $Ce_{0.5}Tb_{2.5}Fe_{4.75}O_{12}$ with a rare-earth to iron ratio (Ce+Tb/Fe) of 0.57. Magnetometry revealed a 44nm magnetic dead layer (MDL) at the garnet-silicon interface that can be detrimental to waveguide photonics relying on evanescent tail interaction. However, the large Faraday rotation (independent of film thickness) compensates for gyrotropy loss due to the MDL, Figure 1(a). The effective anisotropy of Ce:TbIG on Si is also important, but calculations using bulk thermal mismatch overestimate the effective anisotropy. X-ray diffraction measurements yield highly accurate measurements of strain that show anisotropy favors an in-plane magnetization in agreement with the positive magnetostriction of Ce:TbIG, Figure 1(b). Upon doping TbIG with Ce, a slight decrease in compensation temperature occurs which points to preferential rare-earth occupation in dodecahedral sites and an absence of cation redistribution between different lattice sites [4]. The high Faraday rotation, large remanent ratio, large coercivity, and preferential in-plane magnetization enable Ce:TbIG to be an in-plane latched garnet, immune to stray fields with magnetization collinear to the direction of light propagation.

[1] K. Srinivasan and B. J. H. Stadler, *Opt. Mater. Express*, Vol. 8, p. 3307 (2018). [2] K. Srinivasan *et al.*, *ACS Photonics*, Vol. 6, pp. 2455–2461 (2019). [3] C. Zhang *et al.*, *Sci. Rep.*, Vol. 7, pp. 1–8 (2017). [4] K. Srinivasan *et al.*, *Adv. Funct. Mater.*, Vol. 30, p. 2000409 (2020).

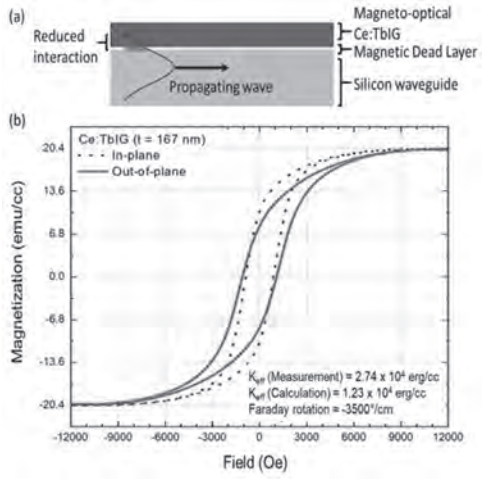

I2-15. Optical Vortex and Ferrocell: a Comparative Study. *A. Tufaile*[2], T.A. Vanderelli[1], M. Snyder[3] and A.P. Tufaile[2] *1. Ferrocell USA, Ligonier, PA, United States; 2. Soft Matter Lab/EACH, Universidade de Sao Paulo, Sao Paulo, Brazil; 3. Morehead State University, Morehead, KY, United States*

We are presenting some results of our experiments image of formation using a device in which light is scattered by a thin film of ferrofluid subjected to an external magnetic field and comparing them with the effect of optical vortex [1-7]. When the light passes through this thin layer of ferrofluid, we can observe directly, with the naked eye, the formation of interesting luminous patterns. In addition to this, we can also observe the effects of light polarization in this system using a polariscope. Some interesting applications of this type of device include optical switches, or the simulation of atmospheric optics known as jumping laser dogs, just to cite few of them. Another potential application is characterizing and controlling the quality of compound magnets observing the patterns formed in this type of Hele-Shaw cell filled with ferrofluids, known as Ferrocell. Using polarized light, the pattern formation curiously resembles the nodal lines of the transverse electric and magnetic modes observed in optical resonant cavities, associated with the hypergeometric polynomials [6], such as Hermite-Gauss, Laguerre-Gauss, and Ince-Gauss polynomials. In this analogy, the magnetic field has an equivalent role of the Gaussian irradiance distribution, and the light source

is a very flat lamp normal to z, which nearly corresponds to a plane wave with constant flux set up to the z-axis, analogous to a standing wave in the optical cavity. In this work, we are exploring the analogy between our experiment with the mode conversion in a laser cavity with our system, because mode convergion requires Hermite-Gaussian (HG) modes, which can easily be made inside the laser cavity and in our experiment using polarized light.

1) A. Tufaile, T. A. Vanderelli, A. P. B. Tufaile, Journal of Applied Mathematics and Physics 4, 1977-1988 (2016). 2) A. Tufaile, T. A. Vanderelli, A. P. B. Tufaile, Advances in Condensed Matter Physics 2017, Article ID 2583717 (2017). 3) Y. Shen, X. Wang, Z. Xie, C. Min, X. Fu, Q. Liu, M. Gong and X. Yuan, Light Science & Applications 8, 90 (2019). 4) A. Tufaile, A. P. B. Tufaile, T. A. Vanderelli, M. Snyder, *Proceedings of Frontiers in Optics/Laser Science,* JTu3A.17 (2019) 5) A.P.B Tufaile, T.A. Vanderelli, R. Amorim, A. Tufaile, Proceedings of the 12th Conference on Light and Color in Nature, 24–25 (2016). 6) A. Tufaile, T. A. Vanderelli, M. Snyder, A. P. B. Tufaile, *Condens. Matter* 2019, *4*, 35. 7) A. Tufaile, T. A. Vanderelli, M. Snyder, A. P. B. Tufaile, *Controlling Light Diffraction with Magnetic Nanostructures*; TechConnect Briefs: Boston, MA, USA; ISBN 978-009988782-8-7, (2019).

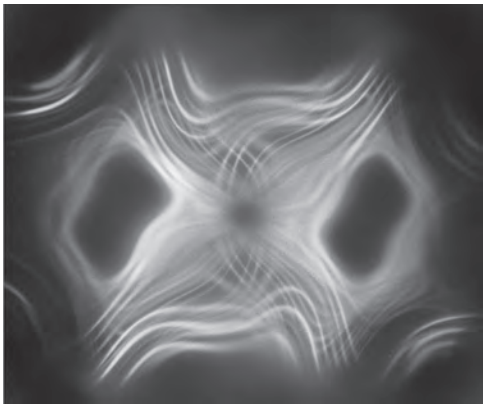

Light pattern obtained with a thin film of ferrofluid (Ferrocell) subjected to an external magnetic field.

I2-16. GaN Based High Strength Magnetic Field Pulser. *W. Theh*[1], N. Prabhu Gaunkar[1] and M. Mina[1] *1. Electrical and Computer Engineering, Iowa State University, Ames, IA, United States*

Magnetic field pulser generates magnetic field by driving current through an inductor. These pulsers have numerous applications based on the output magnetic field intensity and switching time. For communication systems, the pulser is central for an all-optical switching platform employing the theory of Faraday rotation [1]. In medical field, the pulser is used to perform transcranial magnetic stimulation to provide safer, noninvasive treatment for certain mental disorders [2]. Another application area is portable magnetic resonance systems where the pulser initiates magnetic resonance [3]. These are just some of the many fields where magnetic field pulsers have found applicability over the years. Recent developments in transistor technologies have enabled production of transistors with higher power and superfast switching. Among these is the introduction of gallium nitride (GaN) based transistors. Compared to silicon-based transistors, GaN transistors have higher electron mobility, a property which allows smaller size for a given on-resistance and breakdown voltage. GaN transistor also offers high drain current and extremely fast switching speed [4]. These are all desirable properties for a switch in the magnetic field pulser design. This investigation will explore the application of GaN transistor in a pulser design. Based on the advantages of GaN transistor, the investigation looks towards creating a pulser capable of producing magnetic field of 500 Gauss with a rise/fall time of less than 500 nanoseconds. This investigation will surpass findings from prior studies to build a pulser targeted for magneto-optic switching [5] applications. A preliminary result as seen in Figure 1 shows that at the same maximum current level, the GaN transistor displays steeper rise and fall when compared to a Si transistor. This result further highlights the potential of GaN transistor as the switching device where rapid switching is preferable.

[1] J. W. Tioh, M. Mina, and R. J. Weber, "All-optical integrated switch utilizing Faraday rotation," IEEE Trans. Magn., vol. 46, no. 6, pp. 2474–2477, Jun. 2010. [2] J. Selvaraj, P. Rastogi, N. P. Gaunkar, R. L. Hadimani, and M. Mina, "Transcranial magnetic stimulation: Design of a stimulator and a focused coil for the application of small animals," IEEE Transactions on Magnetics, no. 99, pp. 1–5, 2018. [3] N. P. Gaunkar, J. Selvaraj, W.-S. Theh, R. Weber, and M. Mina, "Pulsed magnetic field generation suited for low-field unilateral nuclear magnetic resonance systems," AIP Advances, vol. 8, no. 5, p. 056814, 2018. [4] L. F. Eastman and U. K. Mishra, "The toughest transistor yet [GaN transistors]," IEEE Spectrum, vol. 39, no. 5, pp. 28-33, May 2002, doi: 10.1109/6.999791. [5] J.W. Pritchard, M. Mina, and R.J. Weber, "Magnetic Field Generator Design for Magneto-Optic Switching Applications," IEEE Transactions on Magnetics, Vol. 49, No. 7, pp. 4242-4244, 2013.

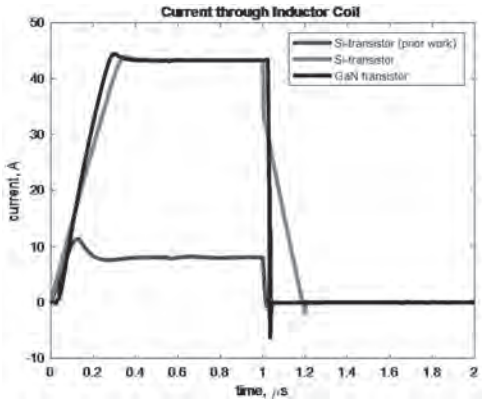

Figure 1: Comparison of current across resistor in series with inductor coil.

Session I3
SKYRMION IMAGING
David Burn, Chair
Diamond Light Source Ltd, Didcot, United Kingdom

INVITED PAPER

I3-01. Real-Space Imaging of Confined Magnetic Skyrmion Tubes. *M.T. Birch*[1,2], D. Cortés-Ortuño[3], L. Turnbull[1], M. Wilson[1], F. Gross[4], N. Träger[4], A. Laurenson[5], N. Bukin[5], S. Moody[1], M. Weigand[6], G. Schütz[4], H. Popescu[7], R. Fan[2], P. Steadman[2], J. Verezhak[8], G. Balakrishnan[8], J. Loudon[9], A. Twitchett-Harrison[9], O. Hovorka[3], H. Fangohr[3,10], F. Ogrin[5], J. Gräfe[4] and P. Hatton[1] *1. Durham University, Durham, United Kingdom; 2. Diamond Light Source Ltd, Didcot, United Kingdom; 3. University of Southampton, Southampton, United Kingdom; 4. Max Planck Institute for Intelligent Systems, Stuttgart, Germany; 5. University of Exeter, Exeter, United Kingdom; 6. Helmholtz-Zentrum Berlin fur Materialien und Energie GmbH, Berlin, Germany; 7. Synchrotron SOLEIL, Gif-sur-Yvette, France; 8. University of Warwick, Coventry, United Kingdom; 9. Cambridge University, Cambridge, United Kingdom; 10. European XFEL GmbH, Schenefeld, Germany*

Magnetic skyrmions are topologically nontrivial particles with a potential application as information elements in future spintronic device architectures [1, 2]. While they are commonly portrayed as two dimensional objects, in reality magnetic skyrmions are thought to exist as elongated, tube-like objects extending through the thickness of the host material, as seen in Fig. 1 [3]. These structures are theorised to exhibit Bloch points, responsible for the topological unwinding of skyrmions [4]. The study of this skyrmion tube state (SkT) is vital for furthering the understanding of skyrmion formation and dynamics for future applications. However, direct experimental imaging of skyrmion tubes has yet to be reported. Here, we demonstrate the real-space observation of skyrmion tubes in a lamella of FeGe using resonant magnetic x-ray imaging and comparative micromagnetic simulations, the horizontal stripes seen in Fig. 2, confirming their extended structure [5]. The formation of these structures at the edge of the sample highlights the importance of confinement and edge effects in the stabilisation of the SkT state, opening the door to further investigation into this unexplored dimension of the skyrmion spin texture.

[1] Rößler, U. K., Bogdanov, A. N. & Pfleiderer, C. Spontaneous skyrmion ground states in magnetic metals. *Nature* 442, 797 (2006). [2] Nagaosa, N. & Tokura, Y. Topological properties and dynamics of magnetic skyrmions. *Nat. Nanotechnol.* 8, 899 (2013). [3] Seki, S. et al. Propagation dynamics of spin excitations along skyrmion strings. *Nat. Commun.* 11, 256 (2020). [4] Milde, P. et al. Unwinding of a skyrmion lattice by magnetic monopoles. *Science* 340, 1076 (2013). [5] Birch, M. et al. Real-space imaging of confined magnetic skyrmion tubes. *Nat. Commun.* 11, 1726 (2020).

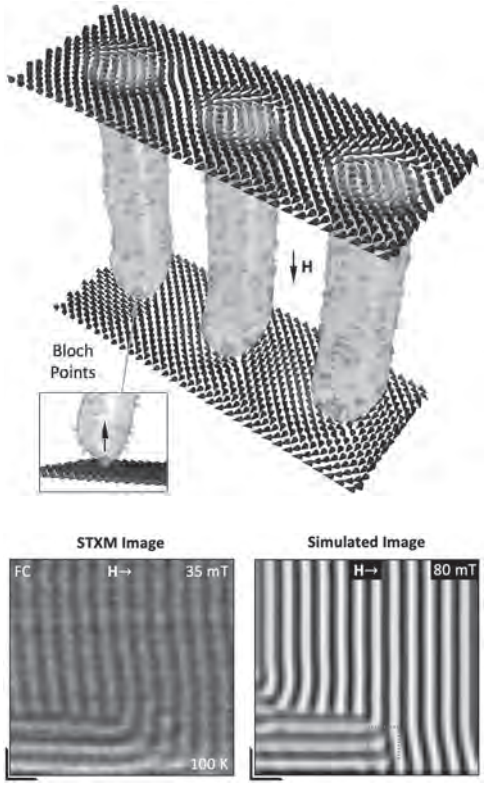

CONTRIBUTED PAPERS

I3-02. Fractal Analysis of Magnetic Domain From Ferromagnetic to Skyrmion States in MgO/Mn_2CoAl/Pd Ultrathin Films. *G. Dubuis*[1,2], Y. Zhang[1,2], T.J. Butler[1,2] and S. Granville[1,2] *1. Robinson Research Institute, Victoria University of Wellington, Wellington, New Zealand; 2. MacDiarmid Institute for Advanced Materials and Nanotechnology, Wellington, New Zealand*

Magnetic skyrmions are topologically protected whirling spin textures nucleated from other ferromagnetic states, which have great potential applications for nanoscale devices. Finding a method to quantitatively study the transition in a film from uniform ferromagnetic domain or labyrinth domain to skyrmions will allow to better understand them. Here, we experimentally generated skyrmions in MgO/Mn2CoAl/Pd ultrathin films and investigated the fractal dimension of various magnetic phases using MOKE imaging. These ultrathin films exhibit perpendicular magnetic anisotropy with labyrinth domains at out-of-plane field. However, skyrmions can be generated from labyrinth domains or uniformly ferromagnetic phase by applying an in-plane field (Fig.2). By employing fractal analysis, we obtain a magnetic phase diagram (Fig.1) related to fractal dimension which can quantitatively describe the evolution of magnetic states and the origin of skyrmions. Moreover, we also observe that the skyrmion density increases at small in-plane fields, but reaches a plateau at higher in-plane field. Thus indicating that it is

determined not only by critical material parameter κ but also by the repulsive skyrmion-skyrmion interaction at high field. We thus establish a reliable and powerful method to quantitatively analyze the evolution of magnetic domains and origin of skyrmions.

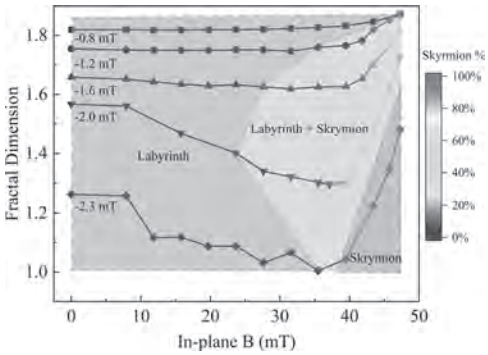

Fractal dimension (D_f) extracted from MOKE imaging *vs* the in-plane magnetic field (B‖). With proportion of Skyrmions indicated by the colour scale. For each curve, we start with different initial out-of-plane magnetic fields ($B_\perp$), and then ramp B‖ from 0 *mT* to 47.3 *mT*.

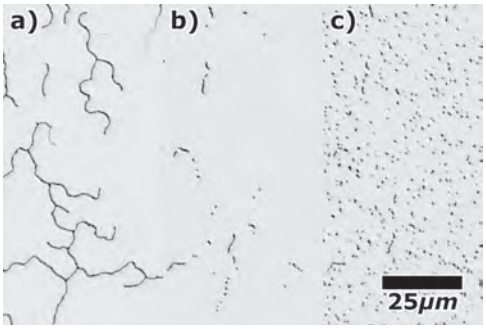

MOKE image showing the evolution of the domain morphology from labyrinth domain to skyrmions under increasing in-plane magnetic field, associated with change in fractal dimension. $B_\perp$ = -2.0 *mT*. a) $B\| = 0$ *mT*, $D_f = 1.56$; b) $B\| = 39.5$ *mT*, $D_f = 1.30$; c) $B\| = 47.3$ *mT*, $D_f = 1.73$.

I3-03. Domain Wall Skyrmions: Examining Domain Wall Substructures in $[Pt/(Co/Ni)_M/Ir]_N$ Multi-Layers. *M.P. Li*[1], A. Sapkota[2], A. Rai[2], A. Pokhrel[2], T. Mewes[2], D. Xiao[3,1], C. Mewes[2], M. De Graef[1] and V. Sokalski[1] *1. Materials Science & Engineering, Carnegie Mellon University, Pittsburgh, PA, United States; 2. Department of Physics and Astronomy/MINT Center, The University of Alabama, Tuscaloosa, AL, United States; 3. Department of Physics, Carnegie Mellon University, Pittsburgh, PA, United States*

Magnetic domain wall (DW) Skyrmions are 360° transitions of the internal magnetization in a Dzyaloshinskii DW. These structures are analogous to vertical Bloch lines (VBLs), which were once considered for magnetic memory storage. Although they have been predicted theoretically [1], DW skyrmions have only recently been observed experimentally [2]. Here we performed a systematic study of multiple iterations of $[Pt/(Co/Ni)_M/Ir]_N$ multi-layers to formulate a phase diagram of magnetic excitations related to domain wall substructures, including DW skyrmions, via Lorentz transmission electron microscopy (LTEM). $[Pt/(Co/Ni)_M/Ir]_N$ multi-layers were deposited by magnetron sputtering onto Si_3N_4 TEM membranes [3]. LTEM was performed using an aberration-corrected FEI Titan G2 80-300. In low DMI samples, VBLs are formed over all thicknesses, but are only seen to form pile-ups (i.e. n-π VBLs) in the case of ultrathin samples. We attribute this to the formation of hybrid DWs in thicker samples where the magnetization varies along the z-axis, thereby, creating low energy paths to annihilation of 2π VBLs. Likewise, only pure Dzyaloshinskii DWs are observed in thicker samples with high DMI. It is only for lower thicknesses in this strong DMI regime that DW skyrmions are observed. Like their VBL counterparts, DW Skyrmions are found to have a pinning effect on the domain wall as seen through the in-situ application of a perpendicular magnetic field. The stability and dynamic response of DW skyrmions are examined further via micromagnetics. The energy barrier to annihilation was calculated using M[3] [4] and a GNEB method and is observed to decrease with increased DMI strength. Most notably an energy barrier to annihilation of >60 k_{BT} was found for D<1.0 mJ/m^2 at room temperature giving confidence in the stability of DW Skyrmions for use in magnetic memory devices. Details regarding their dynamic response to electric current will be discussed. [5]

[1] R. Cheng, M. Li, A. Sapkota, A. Rai, et al., *Phys. Rev. B*, Vol. 99, p. 184412 (2019). [2] M. Li, A. Sapkota, A. Rai, et al., ArXiV: 2004.07888 (2020). [3] M. Li, D. Lau, M. De Graef, and V. Sokalski, *Phys. Rev. Mater*., Vol. 3, p. 064409, (2019). [4] Micromagnetic Code M[3]: http://magneticslab.ua.edu/micromagnetics-code.html. [5] This research is supported by the Defense Advanced Research Project Agency (DARPA) program on Topological Excitations in Electronics (TEE) under grant number D18AP00011. The authors also acknowledge use of the Materials Characterization Facility at Carnegie Mellon University supported by grant MCF-677785.

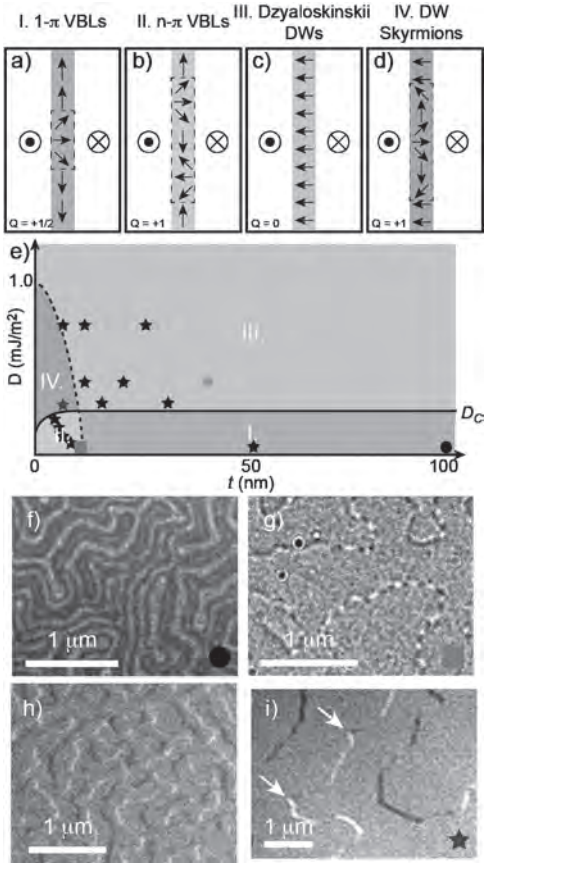

Schematics of the magnetic profiles of a a) Bloch DW, b) VBL, c) Dzyaloshinskii DW, and d) DW skyrmion. e) Magnetic phase diagram of domain wall substructures with respect to film thickness and DMI strength. f-i) Representative LTEM images of aforementioned DW substructures a-d, respectively.

INVITED PAPER

I3-04. Utilizing Vacuum States Above Surfaces for Imaging and Manipulation of Atomic-Scale Magnetism. *A. Schlenhoff*[1] *1. Department of Physics, University of Hamburg, Hamburg, Germany*

Imaging and manipulation of atomic-scale magnetism for future spintronic applications demands for a spin-sensitive technique with ultimate lateral resolution. Exploiting the tunneling effect between magnetic electrodes, as between a magnetic probe tip and a magnetic sample in a spin-polarized scanning tunneling microscopy (SP-STM) set up, has proven to be capable of resolving and switching magnetic structures down to the single atomic level. However, this approach disqualifies for many technical applications, since it requires tip-sample distances in the order of a few angstroms. For practical applications, technical feasible distances, like flying distances of read-write heads in current data storage devices, are in the range of a few nanometers. Electron tunneling over this distance is very unlikely and therefor not detectable. Spin-polarized vacuum states are unoccupied electronic states located nanometers apart from the underlying magnetic surface in vacuum [1]. In an SP-STM setup, these states can be addressed by spin-polarized electrons that tunnel resonantly from the magnetic tip via a vacuum state into the surface, resulting in a magnetic image [2]. As I will show in this talk, these states exhibit the same local spin quantization axis as the spin texture of the underlying sample surface, even when the spins are rotating on the atomic-scale [2]. Our SP-STM experiments at low temperatures on ultrathin films with non-collinear spin textures demonstrate that the spin-polarized resonant tunneling via the vacuum states allows for atomic-scale spin-sensitive imaging in real space at tip-sample distances of up to 8 nm [3]. Acting as mediators for the spin contrast across the nm-spaced vacuum gap, the vacuum states provide thereby a loophole from the hitherto existing dilemma of losing spatial resolution when increasing the tip-sample distance in a scanning probe setup. Experimental results will be presented and discussed in terms of the vacuum states' spin-splitting and the magnetic contrast as a function of bias and tip-sample distance, as well as in terms of the atomic-scale nature of the resonant tunneling condition between the probe tip and the sample. While spin-polarized resonant tunnel currents in the low nA regime are used for non-perturbative imaging, injecting high spin-polarized resonant tunnel currents (~100 nA) via vacuum states considerably affect the underlying magnetism. As I will demonstrate in this talk, atomic-scale ferromagnets can be efficiently switched via these states, with the underlying current-induced mechanism being based on thermally-assisted spin-transfer torque mediated by the vacuum states [4]. Consequently, spin-polarized vacuum states can be utilized for the readout and manipulation of atomic-scale magnetic objects from nanometer distances. Spin-polarized resonant tunneling qualifies for a spin-sensitive read-write technique with ultimate lateral resolution, potentially opening a pathway towards future technical applications.

[1] M. Donath, C. Math, M. Pickel, A.B. Schmidt, and M. Weinelt, Surf. Sci. 601, 5701 (2007). [2] A. Schlenhoff, S. Kovarik, S. Krause, and R. Wiesendanger, Phys. Rev. Lett. 123, 087202 (2019). [3] A. Schlenhoff, S. Kovarik, S. Krause, and R. Wiesendanger, Appl. Phys. Lett. 116, 122406 (2020). [4] A. Schlenhoff, S. Krause, A. Sonntag, and R. Wiesendanger, Phys. Rev. Lett. 109, 097602 (2012).

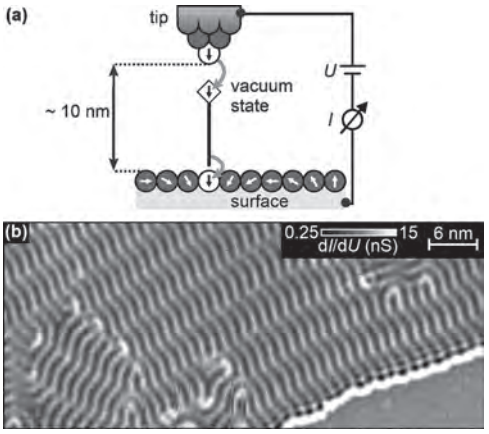

Figure: (a) Schematic sketch of the experimental approach. The net spin-polarized tunnel current flowing from the scanning probe tip via the vacuum states to the sample is recorded and analyzed. Achievable tip-sample distances are indicated. (b) Magnetic map of an ultrathin Fe film grown on Ir(111) exhibiting spin spirals, imaged via spin-polarized resonant tunnelling.

CONTRIBUTED PAPERS

I3-05. Antiferromagnetically-Coupled Skyrmion Lattices in Topological Insulator/Ferrimagnet Heterostructures. *H. Wu*[1], F. Gross[2], B. Dai[1], D. Lujan[3], S. Razavi[1], P. Zhang[1], X. Li[3], J. Gräfe[2] and K. Wang[1] *1. University of California Los Angeles, Los Angeles, CA, United States; 2. Max Planck Institute for Intelligent Systems, Stuttgart, Germany; 3. The University of Texas at Austin, Austin, TX, United States*

Magnetic skyrmions, which are chiral geometric spin textures with a non-trivial topology [1, 2], are shown to have the advantages of small size, low driven current density and robustness against external perturbations for potential applications in the next-generation spintronic devices. Generally, skyrmions are stabilized by the non-collinear Dzyaloshinskii–Moriya interaction (DMI), originates from the strong spin-orbit coupling (SOC) combined with the inversion symmetry breaking, the latter of which may be implemented with a heterostructure. We report the use of the heterostructure consisting of a high SOC topological insulator (TI) (BiSbTe) and the ferrimagnet (GdFeCo) to create the DMI and demonstrate the presence of skyrmions [3]. A sizable interfacial DMI coefficient (D = 35.5±0.25 μJ m^{-2}) is obtained by the Brillouin-Light-Scattering spectrum from the topological surface states, as shown in Figure 1. Small sizes of skyrmions under 100 nm are observed by the scanning transmission X-ray microscopy (STXM) at room temperature, and the Néel-type spin spiral transition is verified by the line-scan spin profile of the single skyrmion. Furthermore, the ferrimagnet is shown to create the antiferromagnetic (AFM) skyrmions, for which the element-resolved STXM identifies the AFM-coupled Gd and FeCo skyrmion lattices, as shown in Figure 2, which promises the potential of vanishing skyrmion Hall effect and ultrafast skyrmion dynamics. This work demonstrates the Néel-type skyrmions at the topological interface, where small skyrmions combined the giant spin-orbit toque have potential applications for high-density and energy-efficient spintronic devices [4].

[1] A. Fert, N. Reyren and V. Cros, Nature Reviews Materials 2 (7), 17031 (2017). [2] W. Jiang, G. Chen, K. Liu, J. Zang, S. G. E. te Velthuis and A. Hoffmann, Physics Reports 704, 1-49 (2017). [3] H. Wu, F. Groß, B. Dai, D. Lujan, S. A. Razavi, P. Zhang, Y. Liu, K. Sobotkiewich, J. Förster, M. Weigand, G. Schütz, X. Li, J. Gräfe, and K. L. Wang, Advanced Materials 2003380 (2020). [4] H. Wu, Y. Xu, P. Deng, Q. Pan, S. A. Razavi, K. Wong, L. Huang, B. Dai, Q. Shao, G. Yu, X. Han, J.-C. Rojas-Sánchez, S. Mangin and K. L. Wang, Advanced Materials 31 (35), 1901681 (2019).

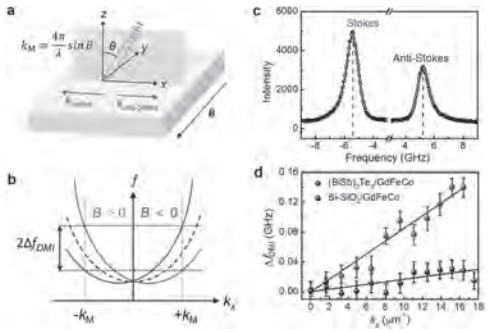

Figure 1. (a) Schematic of the Brillouin light scattering (BLS) measurement. (b) Spin wave dispersion in the presence of Dzyaloshinskii–Moriya interaction (DMI). (c) Typical BLS spectra, where the frequency shift between Stokes and anti-Stokes peaks originates from the DMI. (d) DMI-induced frequency shift as a function of wave vector.

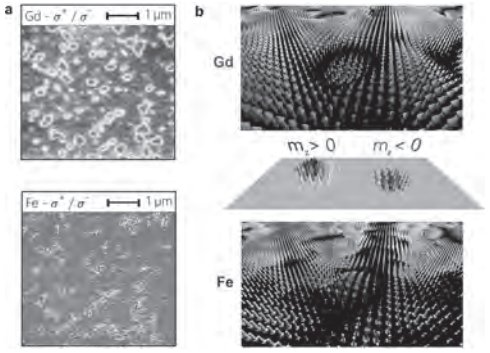

Figure 2. (a) 2-dimentional (2D) skyrmions for Gd and Fe elements measured by the element-resolved scanning transmission X-ray microscope. (b) 3-dimentional (3D) skyrmions for Gd and Fe elements.

I3-06. Room-Temperature Skyrmions at Zero Field in Exchange-Biased Ultrathin Films. *F. Fabre*[1], K. Rana[2], A. Finco[1], S. Chouaieb[1], A. Haykal[1], L. Buda-Prejbeanu[2], O. Fruchart[2], S. Le Denmat[3], P. David[3], M. Belmeguenai[4], T. Denneulin[5], R. Dunin-Borkowski[5], G. Gaudin[2], O. Boulle[2] and V. Jacques[1] *1. Laboratoire Charles Coulomb, Montpellier, France; 2. SPINtronique et Technologie des Composants, Grenoble, France; 3. Institut NEEL, Grenoble, France; 4. Laboratoire des Sciences des Procedes et des Materiaux, Villetaneuse, France; 5. Ernst Ruska-Centre for Microscopy and Spectroscopy with Electrons and Peter Grünberg Institute, Jülich, Germany*

Magnetic skyrmions are topologically stable configuration with particle-like properties. Due to their efficient current-induced manipulation, they could act as carrier of information in futur devices. They where initially observed at low temperature and by applying an intense magnetic field in bulk materials exhibiting broken inversion symmetry[1-2] and in epitaxial ultrathin films with interfacial Dzyaloshinskii-Moriya interaction[3-4]. An intense research effort during the past few years has led to their stabilization at room temperature[5] but still by applying an external magnetic field. A promising strategy to overcome this last obstacle is to exploit the interlayer exchange coupling in magnetic heterostructure to produce an internal effective magnetic field B_{int}[6-7]. Here, we demonstrate that magnetic skyrmions with a mean diameter around 60 nm can be stabilized at room temperature and zero external magnetic field in an exchange-biased $Pt/Co/Ni_{80}Fe_{20}/Ir_{20}Mn_{80}$ multilayerstack[8]. This is achieved through an advanced optimization of the multilayer-stack composition in order to balance the different magnetic energies controlling the skyrmion size and stability. Magnetic imaging is performed both with magnetic force microscopy and scanning nitrogen-vacancy magnetometry, the latter providing unambiguous measurements at zero external magnetic field. Simulation of the PL quenching image are also achieved and the results, in agreement with experimental data, allows us to extract informations such as skyrmion's size. These results establish exchange-biased multilayer stacks as a promising platform toward the effective realization of memory and logic devices based on magnetic skyrmions.

[1] S. Mühlbauer et al., Science323, 915 (2009) [2] X. Z. Yu et al., Nature (London) 465, 901 (2010) [3] S. Heinze et al., Nature Phys.7, 713 (2011) [4] N. Romming et al., Science341, 636 (2013) [5] W. Jiang et al., Science349, 283 (2015) [6] G. Chen et al., Appl. Phys. Lett.106, 242404 (2015) [7] Y. Guang et al., Nat. Commun.11, 949 (2020) [8] K. Gaurav Rana et al., Phys. Rev. Applied 13, 044079 (2020)

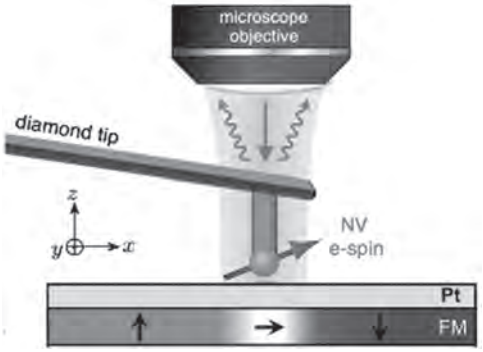

Principle of a scanning-NV magnetometer operating in PL quenching mode.

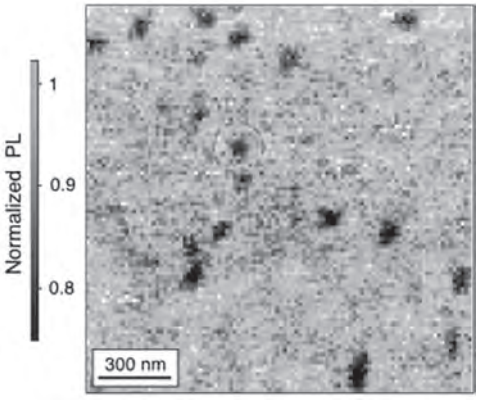

A N-V magnetometry image recorded inphotoluminescence-quenching mode above the optimizedexchange-biased multilayer stack at room temperature and zero external magnetic field. In these experiments, the distance between the N-Vsensor and the ferromagnetic layer is approximately 65 nm.

I3-07. Magnetic Skyrmions in Epitaxial Thin Films of a_2Mo_3N With the Filled β-Mn-Type Structure. *B. Qiang*[1], N. Togashi[1], S. Wada[1], S. Momose[1], T. Hajiri[1], M. Kuwahara[1] and H. Asano[1] *1. Nagoya Daigaku, Nagoya, Japan*

Skyrmions induced by the Dzyaloshinskii–Moriya (DM) interaction have the great potential for spintronic applications, owing to emergent electromagnetic phenomena, and ultra-low current driven motion. Although near room temperature skyrmions were reported for B20-type FeGe (ferromagnetic Curie temperature T_C = 278 K)[1], β-Mn type $Co_xZn_yMn_z$ (T_C = 420 K)[2] and tetragonal Heusler $Mn_{1.4}Pt_{1-y}Rh_ySn$ (T_C = 390 K)[3], their skyrmion size were found to be relatively large around 100 nm. It is of particular importance to develop new materials that exhibited skyrmions with small skyrmion sizes at and above room temperature. In this study, we focused on β-Mn type nitride A_2Mo_3N, because skyrmion phase was observed at 100 K by Lorenz transmission electron microscopy (LTEM) in $Fe_xCo_{1.5-x}Rh_{0.5}Mo_3N$ (x = 0.3 and 0.5)[4]. We prepared the epitaxial A_2Mo_3N films and investigated the effects

of multi doping of A site on magnetic properties as well as the appearance of skyrmion phases. A series of A_2Mo_3N (A = Fe, Pd, Ni, Pt,) epitaxial thin films was fabricated on *c*-plane sapphire substrates with the (110) orientation by reactive magnetron sputtering. The skyrmion phase in a 50 nm thick film with $Fe_{1.68}Pd_{0.32}Mo_3N$ was determined by topological Hall effect (THE) and LTEM imaging. Topological Hall resistivity ρ_{TH} induced by skyrmions at 4 K and 300 K are shown in Fig. 1 as a function of applied magnetic field. Enormous ρ_{TH} at 4 K indicates the dense skyrmion phase, and reduced ρ_{TH} at 300 K indicates the isolated skyrmion phase with sign reversal, which is considered to be induced by the temperature-dependent electronic state. LTEM images of single skyrmion at 90 K and 300 K are shown in Fig. 2. Small size skyrmion (ca. 60 nm) was observed unaffected by the temperature. These results indicate that β-Mn-type A_2Mo_3N has a great potential and is a candidate as a host of new kind of skyrmion, which may help us to understand the fundamental mechanisms of DM interaction in the skyrmion.

[1] P. Upadhyaya *et al*., Phys. Rev. B 92, 134411 (2015). [2] Y. Tokunaga *et al*., Nat. Commun. 6, 7638 (2015). [3] V. Kumar *et al*., Phys. Rev. B 101, 014424 (2020). [4] W. Li et al. Phys. Rev. B 93, 060409(R) (2016).

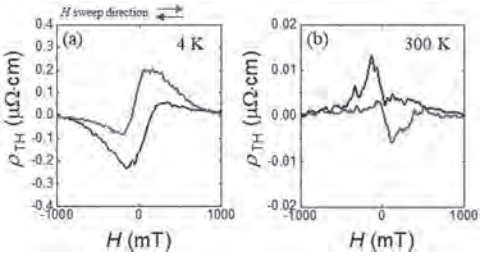

Fig.1 Topological Hall resistivities of $Fe_{1.68}Pd_{0.32}Mo_3N$ films. (a) at 4 K (b) at 300 K.

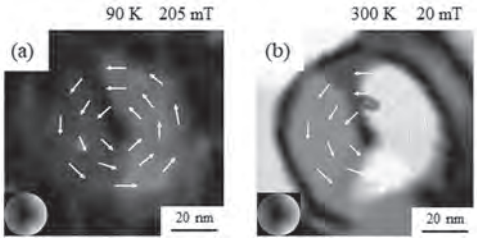

Fig.2 LTEM images of single skyrmions of $Fe_{1.68}Pd_{0.32}Mo_3N$ films. (a) at 90 K (b) at 300 K.

I3-08. Significant Anisotropy and Creation of Skyrmions Induced by Chemisorbed Hydrogen. *G. Chen*[1], A. Quintana[2], A.K. Schmid[3] and K. Liu[2,1] *1. Physics Department, University of California, Davis, Davis, CA, United States; 2. Physics Department, Georgetown University, Washington, DC, United States; 3. Molecular Foundry, Lawrence Berkeley National Laboratory, Berkeley, CA, United States*

Hydrogenation has been found to greatly alter magnetic anisotropy in thin films, e.g., perpendicular magnetic anisotropy (PMA) was observed via hydrogen-induced distortion of the Ni lattice in the Ni/Cu(001) system [1], and in-plane magnetic anisotropy was found when hydrogen adsorbs on the surface of the Co/Ru(0001) [2]. Recently, H^+-based reversible magneto-ionic switching has been demonstrated, where electric field-controlled hydrogenation at the buried Co/GdO_x interface can be used to toggle the PMA [3]. We have investigated chemisorbed hydrogen induced magnetic anisotropy on Ni/Co bilayers using spin-polarized low energy electron microscopy [4], by tracking the evolution of stripe domain near spin reorientation transition. We find that either in-plane magnetic anisotropy or PMA could be induced depending on the surface materials. We also demonstrated the reversible writing/deleting of magnetic skyrmions via hydrogen chemisorption/desorption at room temperature (Fig. 1). This work may help to better understand the role of chemisorbed hydrogen on ferromagnet surfaces. This work has been supported by the NSF (DMR-1905468), UCOP MRPI (MRP-17-454963), the nCORE-SMART Center (2018-NE-2861) through SRC/NIST, and DOE (DE-AC02-05CH11231).

[1] D. Sander, *et al. Phys. Rev. Lett.* 93, 247203 (2004) [2] B. Santos, *et al. Phys. Rev. B* 85, 134409 (2012). [3] A. J. Tan, *et al. Nat. Mater.* 18, 35 (2019). [4] G. Chen, *et al. Adv. Mater.* 27, 5738 (2015).

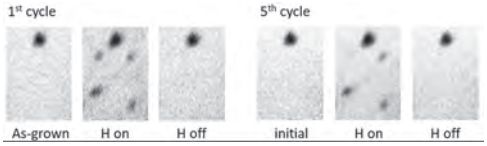

Figure 1 Spin-polarized low energy electron microscopy image sequence of magnetic Ni/Co bilayer with out-of-plane sensitivity (black $+M_z$, white $-M_z$), capturing the reversible creation/ annihilation of skyrmions during cycles of hydrogen chemisorption/desorption, which is attributed to the hydrogen-induced magnetic anisotropy. The field of view is 1.5 μm × 2.1 μm.

I3-09. Room-Temperature Magnetic Imaging of Antiferromagnetic Skyrmions in Multi-Repeats Synthetic Antiferromagnets. *Y. Sassi*[1], W. Legrand[1], F. Ajejas[1], S. Collin[1], K. Bouzehouane[1], A. Vecchiola[1], N. Reyren[1], V. Cros[1] and A. Fert[1] *1. Unité Mixte de Physique, CNRS, Thales, Univ. Paris-Sud, Université Paris-Saclay, 91767 Palaiseau, France*

Magnetic skyrmions are localized magnetic textures in magnetic films, behaving as particles and topologically different from the uniform ferromagnetic state, which have been identified to be extremely promising for applications, as well as of fundamental interest [1]. The magnetism community has provided a great effort in the last years to stabilize them at room temperature, most often by designing magnetic and heavy-metal multilayers combining perpendicular magnetic anisotropy and Dzyaloshinskii-Moriya interaction (DMI) [2]. The DMI promotes a unique chirality of the skyrmionic spin textures and, combined with spin-orbit torques generated in the heavy-metal layer(s), allows efficient current-induced motion of skyrmions [3]. However, recent observations have revealed that multilayered skyrmions are prone to present a hybrid chirality, due to the competition between dipolar interaction and DMI, which can negatively influence their current-induced motion [4] and also their size and stability [6]. We will discuss how those effects can be reduce thanks to synthetic antiferromagnets (SAF) based systems that allow the stabilisation of smaller antiferromagnetic skyrmions, due to the cancellation of the long range dipolar effects [7]. We will mainly focus on Pt/Co/Ru and Pt/CoFeB/Ru based systems and present the optimization process that has been done on the thicknesses of the different layer in order to maximize the antiferromagnetic RKKY coupling without cancelling the perpendicular magnetic anisotropy, needed to stabilize skyrmions. Those optimizations enabled for example the observation at room temperature of spin spiral, predicted by micromagnetic simulations, by reaching an effective anisotropy close to zero. We will then describe how, combined to a bias layer structure, multi-repeats SAF can host antiferromagnetic skyrmions and present their observation by MFM techniques without needs to go under vacuum. Those observations will also be completed by NV center microscopy images. The ANR grant TOPSky TOPSKY (ANR-17-CE24-0025), the SESAME Ile de France IMAGeSPIN (EX039175), the DARPA TEE program grant (MIPR#HR0011831554) and EU grant SKYTOP (H2020 FET Proactive 824123) are acknowledged for their financial support.

[1] A. Fert, N. Reyren, V. Cros, Nat. Rev. Mat. 2 (2017), 17031. [2] C. Moreau-Luchaire *et al*, Nat. Nanotech, 11 (2016), 444 ; S. Woo *et al*, Nat. Mater. 15 (2016), 501 ; A. Soumyanarayanan *et al*, Nat. Mater. 16 (2017), 898 ; A. Hrabec *et al*, Nat. Comm. 8 (2017), 15765. [3] K. Litzius *et al*, Nat. Phys. 13 (2017), 170 ; S. Woo *et al*, Nat. Comm. 8 (2017), 15573. [4] W. Legrand *et al*, Sci. Adv. 4 (2018), eaat0415 ; Y. Dovzhenko *et al*, Nat. Comm. 9 (2018), 2712. [5] F. Büttner *et al*, Sci. Rep., 8 (2018), 4464 ; A. Bernand-Mantel *et al*, SciPost Phys. 4 (2018), 027. [6] W. Legrand *et al*, Phys. Rev. Applied 10 (2018), 064042. [7] W. Legrand *et al*, Nat. Mater. 19 (2019), 34–42.

I3-10. Zero-Field Room Temperature Skyrmion Lattice Stabilized by Interlayer Electronic Coupled Bias Layer. *F. Ajejas*[1], Y. Sassi[1], W. Legrand[1], S. Collin[1], K. Bouzehouane[1], N. Reyren[1], V. Cros[1] and A. Fert[1] *1. Unite Mixte de Physique CNRS/Thales, Palaiseau, France*

Magnetic skyrmions are non-collinear chiral spin textures stabilized in magnetic materials by interfacial Dzyaloshinskii-Moriya interaction (DMI). Room-temperature skyrmions has been presented as potential candidates for encoding information bits in new computing technologies [1]. There have been many recent progresses stabilizing skyrmions in ferromagnetic thick layers or in thin magnetic multilayers (MML) under an external out-of-plane magnetic field or current-induced nucleation [2-3]; however, this mechanism is not fully understood or is mostly due to thermal effects. The stabilization of zero-field isolated skyrmions or skyrmion lattices is an important step towards application. There are recent works demonstrating isolated zero-field skyrmions stabilized due to interlayer exchange in polycrystalline [4], epitaxial [5] or exchange biased [6] trilayers. Here we demonstrate a new approach showing that room-temperature zero-field skyrmion lattices can be stabilized in MML. We developed a system in which perpendicular magnetic anisotropy, chiral order and bias field strength, through a non-magnetic spacer, can be adjusted simultaneously. Typical stacking sequence is schematically presented in Figure 1 (a). The samples have been characterized first by standard magnetometry (see Fig. 1b). Relying on the interlayer electronic coupling to an adjacent bias magnetic layer with strong PMA (uniform configuration), we demonstrate by Magnetic Force Microscopy that the remnant wormy-stripe "as-grown" domains (panel d) is turned into skyrmion lattice phase (See Fig. 1c). Interestingly, the skyrmion density and size can be modified by finely tuning the thicknesses of the layers. Finally, these MFM observations of sub 80 nm skyrmions has been compared to images using scanning NV microscopy in which the potential perturbation from the tip are not existing. French ANR grant TOPSky TOPSKY (ANR-17-CE24-0025), the SESAME Ile de France IMAGeSPIN (EX039175), the DARPA TEE program grant (MIPR#HR0011831554) and EU grant SKYTOP (H2020 FET Proactive 824123) are acknowledged for their financial support.

[1] A. Fert, N. Reyren, V. Cros, Nat. Rev. Mat. 2, 17031 (2017) [2] C. Moreau-Luchaire *et al.*, Nat. Nanotechnol. 11, 444 (2016) [3] W. Legrand *et al.,* Nano Letters 17, 2703 (2017) [4] G. Chen et al., Appl. Phys. Lett. 106, 242404 (2015) [5] R. Loconte et al., doi : 10.1021/acs.nanolett.0c00137 [6] K. G. Rana et al., Phys. Rev. Applied 13, 044079 (2020)

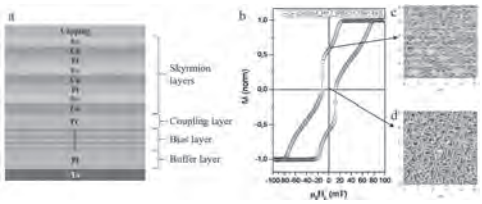

I3-11. Chirality Switch of Magnetic Skyrmion in Ta/FeCoB/TaOx Trilayers. *C. Fillion*[1], R. Kumar[1], B. Lovery[1], I. Benguettat-El Mokhtari[3], I. Joumard[1], S. Auffret[1], L. Ranno[2], Y. Roussigné[3], S. Chérif[3], A. Stashkevich[3], M. Belmeguenai[3], C. Baraduc[1] and H. Béa[1] *1. SPINtronique et Technologie des Composants, Grenoble, France; 2. CNRS, Néél Institute, Grenoble, France; 3. Université Sorbonne Paris Nord, LPSM, CNRS, UPR 3407, F-93430 Villetaneuse, France*

Magnetic skyrmions [1] are promising candidates for next-generation spintronic devices. Their solitonic and chiral nature allows an efficient current-induced motion up to high velocities [2]. A fine tuning of their chirality would enable highly-manipulable magnetic skyrmions, which paves the way for new functionalities in spintronic memory, logic and neuromorphic devices [3,4]. This gives great importance to the control of the interfacial Dzyaloshinskii-Moriya interaction (iDMI) [5,6] strength and sign, at the origin of magnetic skyrmions and their chirality. In this study, we directly demonstrate magnetic skyrmion's chirality switching in a Ta/FeCoB/TaOx trilayer. In fact, by varying the thickness of FeCoB and the oxidation state at the FeCoB/TaOx interface, we are able to obtain different regions in which magnetic skyrmions are right-handed (iDMI>0) or left-handed (iDMI<0) (resp. regions #4 and #2 on Fig.1). This material-dependent chirality switching brings a new degree of freedom to the exciting physics of magnetic skyrmions. For the first time, we show that the iDMI sign crossover in the different regions, as measured by Brillouin-Light-Scattering (BLS), is accompanied by a change of skyrmion chirality, as confirmed by the opposite direction of current-induced motion of magnetic skyrmions (See Fig. 2). Notably, between the two regions of opposite iDMI sign we have found, as expected, a region where iDMI~0. In this region, the control of the iDMI with an electric field [7] may lead to a voltage-induced chirality switching, which hasn't been observed yet. This all-electrical control of magnetic skyrmions represents a cornerstone towards power efficient spintronic devices and multidirectional logic functionnalities.

[1] A. N. Bogdanov and D. A. Yablonskii, *J. Exp. Theor. Phys.*, Vol. 95, p101–103 (1989) [2] W. Jiang, P. Upadhyaya and W. Zhang et al., *Science*, Vol. 349 (2015) [3] X. Zhang, Y. Zhou and K. M. Song et al., *J. Phys.: Condens. Matter*, Vol. 32 (2020) [4] A. Fert, N. Reyren and V. Cros et al., *Nat. Rev. Mater.*, Vol. 2 (2017) [5] I. E. Dzyaloshinskii, *Sov. Phys. JETP*, Vol. 5 (1957) [6] T. Moriya, *Phys. Rev.*, Vol. 120 (1960) [7] T. Srivastava, M. Schott and R. Juge et al., *Nano. Lett*, Vol. 18 (2018)

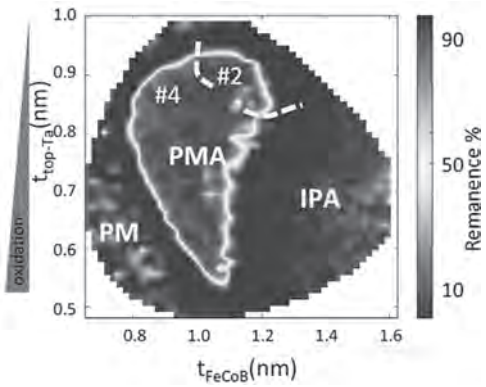

Perpendicular remanence map of the Ta(3)/FeCoB(0.6-1.6)/Ta(0.5-1) Ox/Al(0.5) double wedge showing perpendicular magnetic anisotropy (PMA), in-plane anisotropy (IPA) and paramagnetic (PM) regions. Yellow line corresponds to the transition between the regions of opposite iDMI

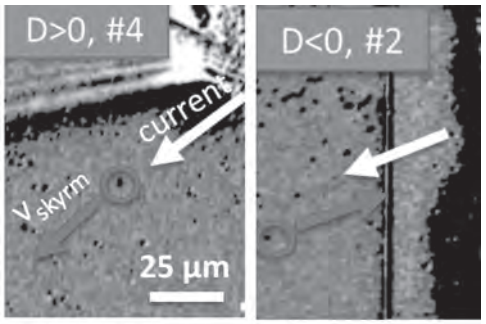

In the two regions on the sample, the current induced motion of magnetic skyrmions, encircled in red, is of opposite direction, which is a signature of a chirality switch.

Session I4
STRAIN & DOPING EFFECTS IN THIN FILMS

Daniel Salazar, Chair
BCMaterials, Derio, Spain

INVITED PAPER

I4-01. Curvilinear Magnetism: Fundamentals and Applications.
D. Makarov[1] *1. Intelligent Materials and Systems, Helmholtz-Zentrum Dresden-Rossendorf, Dresden, Germany*

There is one aspect, which is in common to the majority of fundamentally appealing and technologically relevant novel magnetic materials, namely their non-collinear magnetic textures like spin spirals, chiral domain walls or skyrmions [1]. These textures are typically driven by the Dzyaloshinskii-Moriya interaction (DMI). Recently, curvature effects emerged as a novel mean to design chiral magnetic properties by relying on extrinsic parameters, e.g. geometry of thin films [2]. In particular, novel effects occur when the magnetization is modulated by curvature leading to new magnetization configurations and is implications on the spin dynamics due to topological constraints. Advances in this novel field solely rely on the understanding of the fundamentals behind the modifications of magnetic responses of 3D-curved magnetic thin films [3-5] and nanowires [6,7]. The lack of an inversion symmetry and the emergence of a curvature induced effective anisotropy and DMI are characteristic of curved surfaces, leading to curvature-driven magnetochiral effects and topologically induced magnetization patterning [8,9]. The application potential of 3D-shaped objects is currently being explored as mechanically reshapeable magnetic field sensorics [10] for flexible interactive electronics [11-13], magnetic field sensors [14-18], curvilinear magnetoelectrics for memory devices [19], spin-wave filters and high-speed racetrack memory devices [20]. To advance in this research field, novel theoretical methods and fabrication/characterization techniques [21-24]. The fundamentals as well as application relevant aspects of curvilinear nanomagnets will be covered in this presentation.

[1] D. Sander, DM et al., "The 2017 Magnetism Roadmap", J. Phys. D 50, 363001 (2017). [2] R. Streubel, DM et al., "Magnetism in curved geometries", J. Phys. D 49, 363001 (2016). [3] Y. Gaididei et al., "Curvature Effects in Thin Magnetic Shells", Phys. Rev. Lett. 112, 257203 (2014). [4] V. Kravchuk, DM et al., "Multiplet of Skyrmion States on a Curvilinear Defect: Reconfigurable Skyrmion Lattices", Phys. Rev. Lett. 120, 067201 (2018). [5] O. V. Pylypovskyi, DM et al., "Chiral Skyrmion and Skyrmionium States Engineered by the Gradient of Curvature", Phys. Rev. Appl. 10, 064057 (2018). [6] O. M. Volkov, DM et al., "Mesoscale Dzyaloshinskii-Moriya interaction: geometrical tailoring of the magnetochirality", Scientific Reports 8, 866 (2018). [7] O. M. Volkov, DM et al., "Experimental observation of exchange-driven chiral effects in curvilinear magnetism", Phys. Rev. Lett. 123, 077201 (2019). [8] O. V. Pylypovskyi, DM et al., "Coupling of Chiralities in Spin and Physical Spaces: The Möbius Ring as a Case Study", Phys. Rev. Lett. 114, 197204 (2015). [9] J. A. Otalora et al., "Curvature-Induced Asymmetric Spin-Wave Dispersion", Phys. Rev. Lett. 117, 227203 (2016). [10] D. Makarov et al., "Shapeable magnetoelectronics", Appl. Phys. Rev. 3, 011101 (2016). [11] S. Canon Bermudez, DM et al., "Magnetosensitive e-skins with directional perception for augmented reality", Science Advances 4, eaao2623 (2018). [12] S. Canon Bermudez, DM et al., "Electronic-skin compasses for geomagnetic field driven artificial magnetoreception and interactive electronics", Nature Electronics 1, 589 (2018). [13] J. Ge, DM et al., "A bimodal soft electronic skin for tactile and touchless interaction in real time", Nature Comm. 10, 4405 (2019). [14] D. Karnaushenko, DM et al., "Self-assemled on-chip integrated giant magneto-impedance sensorics", Adv. Mater. 27, 6582 (2015). [15] G. Lin, DM et al., "A highly flexible and compact magnetoresistive analytic device", Lab Chip 14, 4050 (2014). [16] N. Münzenrieder, DM et al., "Entirely flexible on-site conditioned magnetic sensorics", Adv. Electron. Mater. 2, 1600188 (2016). [17] C. Becker et al., "Self-assembly of highly sensitive 3D magnetic field vector angular encoders", Science Advances 5, eaay7459 (2019). [18] M. Kondo et al., "Imperceptible magnetic sensor matrix system integrated with organic driver and amplifier circuits", Science Advances 6, eaay6094 (2020) [19] O. M. Volkov, DM et al., "Concept of artificial magnetoelectric materials via geometrically controlling curvilinear helimagnets", J. Phys. D: Appl. Phys. 52, 345001 (2019). [20] M. Yan et al., "Beating the Walker Limit with Massless Domain Walls in Cylindrical Nanowires", Phys. Rev. Lett. 104, 057201 (2010). [21] R. Streubel, DM et al., "Retrieving spin textures on curved magnetic thin films with full-field soft X-ray microscopies", Nature Comm. 6, 7612 (2015). [22] T. Kosub, DM et al., "Purely antiferromagnetic magnetoelectric random access memory", Nature Comm. 8, 13985 (2017). [23] M. Huth et al., "Focused electron beam induced deposition meets materials science", Microelectron. Engineering 185-186, 9 (2018). [24] M. Nord, DM et al., "Strain Anisotropy and Magnetic Domains in Embedded Nanomagnets", Small 15, 1904738 (2019).

CONTRIBUTED PAPERS

I4-02. Magnetic and Electronic Transport Properties of Reactively Facing-Target Sputtered Fe_4N/Muscovite Flexible Heterostructures.
X. Shi[1] and W. Mi[1] *1. Tianjin University, Tianjin, China*

Bending strain is an effective strategy to modulate the magnetic and electronic transport properties of flexible ferromagnetic films for stretchable spintronic devices[1]. Here, the flexible epitaxial Fe_4N/mica films are fabricated by facing-target reactive sputtering. At a tensile strain with a radius of curvature (ROC) of 3 mm, the saturation magnetization (M_s) of Fe_4N/mica film is tailored significantly with a maximal variation of 210%. Meanwhile, the magnetic anisotropy was broadly tunable at different strains, where the out-of-plane M_r/M_s at a tensile strain of ROC=2 mm is 6 times larger than that at unbent state. Besides, the strain-tailored longitudinal resistance R_{xx} and anomalous Hall resistivity ρ_{xy} appear, where the drop of R_{xx} (ρ_{xy}) reaches 5% (22%) at a tensile strain of ROC=3 mm. The shift of nitrogen position in Fe_4N unit cell at different bending strains plays a key role on the strain-tailored magnetic and electronic transport properties. This work is supported by National Natural Science Foundation of China (51871161 and 51671142).

[1] Z.N. Bao and X.D. Chen, Flexible and Stretchable Devices. *Adv. Mater*. 28, 4177 (2016).

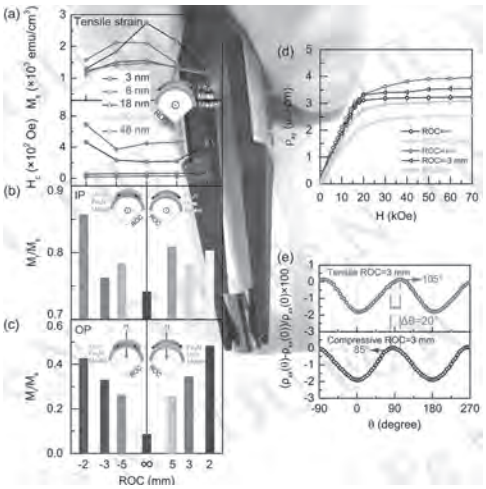

(a) Saturation magnetization (M_S) and coercivity (H_C), (b) in-plane squareness M_r/M_S, (c) out-of-plane squareness M_r/M_S, (d) anomalous Hall resistivity ρ_{xy} and (e) anisotropy magnetoresistance (AMR) of Fe_4N/mica film at different radius of curvatures (ROCs).

I4-03. Strengthen the Magnetic Properties of Pr-Fe-B Thin Films by Biased Substrate. *L.T. Tran*[1], C. Chang[1], M. Kuo[1] and A. Sun[1] *1. Yuan Ze University, Chung-Li, Taiwan*

Praseodymium Iron Boron (PrFeB) thin film has recently attracted considerable attention for the potential magnetic property, which can alternate for currently NdFeB magnetic materials. The super low spin-reorientation temperature (about 4.2 K), huge uniaxial magnetocrystalline anisotropy (K_u), large coercivity (H_c), high saturation magnetization (M_s), and large energy products (BH_{max}) are the great properties that make PrFeB become a promising candidate in application of magnetic recording media nowadays. It is known that there is the body-centered tetragonal (BCT) structure of $Pr_2Fe_{14}B$ phase mainly existing in PrFeB thin films to strengthen perpendicular magnetic anisotropy (PMA). The small lattice mismatch (δ) between $Pr_2Fe_{14}B$ (00*l*) texture with [100] direction and BCC(110) texture underlayer with [110] and [001] directions makes the easy axis [001] perpendicular to the film plane. In this study, the Pr-Fe-B films with PMA were fabricated without underlayer on biased substrate by $Pr_{25}Fe_{65}B_{10}$ alloy target. The substrate temperature was kept at 650°C and the bias was adjusted from -150 V to +100 V during sputtering hard magnetic Pr-Fe-B films. Then, Si_3N_4 cover layer was deposited at room temperature (RT). The deposited films were characterized for structural and magnetic properties by employing appropriate techniques. Effect of the substrate bias voltage on physical properties of thin film was systematically investigated. From our results, the squareness of the Pr-Fe-B film was enhanced significantly, because an epitaxial growth was initiated from applying substrate bias continuously through the Pr-Fe-B magnetic layer with the range of voltage from -50 to +50 V. Applying positive substrate bias changed atomic mobility, the Pr, Fe, and B atoms may diffuse chaotically in the magnetic layer. Consequently, an epitaxial barrier of the Pr-Fe-B alloy was broken among the elements in the magnetic layer, affected the deposition rates, improved the magnetic performance, and epitaxial growth of Pr-Fe-B thin films.

I4-04. Temperature Dependence of the Anisotropic Magnetoresistance of Compressively Strained Thin Films of $La_{2/3}Sr_{1/3}MnO_3$ on $LaAlO_3$. *A. Burema*[1], J.J. van Rijn[1] and T. Banerjee[1] *1. Rijksuniversiteit Groningen, Groningen, Netherlands*

We report on magnetoresistance studies in $La_{0.67}Sr_{0.33}MnO_3$ (LSMO) thin film on $LaAlO_3$ by strain engineering at the interface. For this we investigate the magnetization and transport properties of compressively strained ferromagnetic LSMO films. We patterned Hall bars of the LSMO films and measure the longitudinal resistance in a 4-probe configuration applying a dc current bias. We systematically characterize the magnetic anisotropy of the thin films by varying temperature, applied magnetic field and the angle between current and field. The temperature and angular dependence of the longitudinal magnetoresistance for an in plane magnetic configuration explicitly shows three distinctly different magnetic phases. We observe a fourfold symmetry in the angular dependence of the magnetoresistance, for the temperature range between 10 to 125 K, indicating a biaxial anisotropy in the plane parallel to the (110) and (1-10) directions of thin film. Increasing the temperature further shows the presence of a second magnetic phase between 125 K to 250 K characterized by a twofold in-plane angle dependent magnetoresistance signal. We postulate that the fourfold symmetry is driven by magneto crystalline anisotropy whereas the twofold symmetry arises due to conventional anisotropic magnetoresistance. On increasing the temperature further, the thin film transit to a paramagnetic insulating phase. We show that the temperature variation of the angular dependence of the magnetoresistance is an important approach to study the different anisotropy induced in such strained thin oxide films and can complement torque based magnetometry studies.

I4-05. Resistance Minimum in Pd Induced by Hydrogen Absorption. *T. Ozawa*[1], R. Shimizu[2], T. Hitosugi[2] and K. Fukutani[1,3] *1. Institute of Industrial Science, The University of Tokyo, Meguro, Japan; 2. School of Materials and Chemical Technology, Tokyo Institute of Technology, Meguro, Japan; 3. Advanced Science Research Center, Japan Atomic Energy Agency, Tokai, Japan*

Absorbed hydrogen has ability to modulate electrical and/or magnetic properties [1,2]. Palladium, known as a hydrogen-absorbing metal, reveals drastic changes in electrical properties by hydrogen absorption. Palladium hydride (PdH_x) shows superconductivity below 10 K and a resistance anomaly around 50 K [3,4]. In the present study, we systematically investigated temperature dependence of the electrical resistance for nm-thick PdH_x films and discovered a resistance minimum depending on the hydrogen concentration x at low temperature. We demonstrate the possibility for absorbed hydrogen to induce the Kondo effect in Pd. The samples were polycrystalline Pd films deposited by sputtering at room temperature. Hydrogenation was performed by H_2 gas exposure at 200 K, and x was derived by thermal desorption spectroscopy. Fig. 1 shows the temperature dependence of the resistance for PdH_x with a thickness of 50 nm. A resistance minimum was observed at about 25 K for x larger than 0.3, whitch shifts to higher temperature with increasing x. The resistance $R(T)$ was described well by the equation of $R(T) = R_0 + R_1T^5 - R_3\ln T$, where the last term represents the Kondo effect. These results suggest the existence of localized spins induced by hydrogen absorption. We speculate the spin originates from either a hydrogen atom itself or a palladium atom bonded with hydrogen atoms. On the other hand, a 2-nm-thick PdH_x film revealed two bending points in the resistance as shown in Fig. 2. We discuss manifestation of the Anderson localization as a two-dimensional system coexistent with the Kondo effect. We also report the hydrogen concentration dependence of such resistance minimum for Pd films with various thicknesses and isotope effect.

[1] A. León et al, Journal of Magnetism and Magnetic Materials 498 (2020) 166147. [2] M. D'Angelo, Physical Review Letters 108 (2012) 116802. [3] T. Skoskiewicz et al., Physica Status Solidi (b) 30 (1968) K33. [4] T. Skokiewicz, Phys. stat. sol., (a)11 (1972) K123.

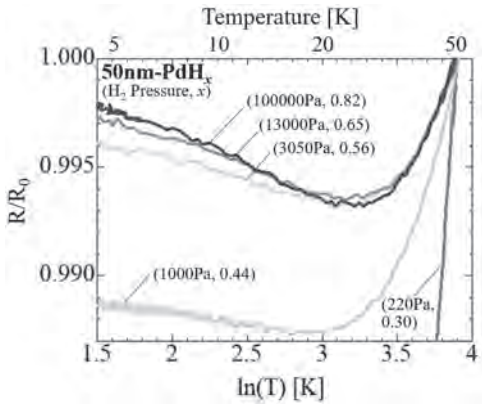

Fig. 1 Temperature dependence of resistance for 50-nm-thick PdH*x*.

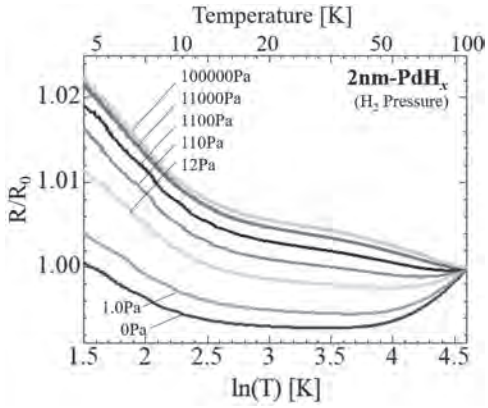

Fig. 2 Temperature dependence of resistance for 2-nm-thick PdH*x*.

I4-06. Strain-Modulated Helimagnetism and Magnetic Phase Diagram in a Film of Highly Crystalline MnP Nanorods. *R. Pokharel Madhogaria*[1], C. Hung[1], E. Clements[1], A. Duong[2], R. Das[2], P. Huy[2], S. Cho[3], M. Phan[1] and H. Srikanth[1] *1. University of South Florida, Tampa, FL, United States; 2. Phenikaa University, Hanoi, Vietnam; 3. University of Ulsan, Ulsan, The Republic of Korea*

Manganese phosphide (MnP), a classical metallic helimagnet, is known to host interesting and complex magnetic properties such as multiple metamagnetic phase transition, Lifshitz critical behavior and the magnetocaloric effect [1]. The modulation of spin structure caused by Dzyaloshinskii-Moriya interaction gives rise to the non-trivial Hall effect in the fan phase of MnP [2]. Recently, MnP has been established as an unconventional superconductor in which the application of pressure allows the tuning of antiferromagnetically to ferromagnetically mediated superconductivity [3]. Mostly recently, study has shown the control of spin helicity via electric and magnetic fields in MnP [4]. The presence of exotic magnetic phases and magnetic tunability makes MnP an excellent model to probe dimensional and strain effects in helimagnetic systems. In this study, we explore strain-modulated helimagnetism in highly crystalline MnP nanorod films grown on Si (100) substrates using molecular beam epitaxy. While a bulk-like paramagnetic-ferromagnetic (FM) phase transition at T_C = 276 K is observed for the MnP film, the FM-helical phase change occurs at T_N = 117 K and 101 K for the corresponding in-plane and out-of-plane field directions. These values of T_N are much higher than T_N = 47 K for the single crystal [1], indicating strong strain-modulated helimagnetic states. The presence of significant thermal hysteresis in the helical phase indicates a coexistence of competing magnetic interactions, leading to the first order metamagnetic transition. The evolution of screw (SCR) to CONE and FAN phase is precisely tracked from magnetization versus magnetic field/temperature measurements. Unfolding of the different helical phases at T < 120 K is analyzed by the temperature- and field-dependent magnetic entropy change. The comprehensive magnetic phase diagrams for both in-plane and out-of-plane magnetic measurements are established in the MnP film, revealing emergent features that are absent in the magnetic phase diagram of the single crystal.

[1] Teruo Yamazaki, Yoshikazu Tabata, Takeshi Waki, Taku J. Sato, Masato Matsuura, Kenji Ohoyama, Makoto Yokoyama, and Hiroyuki Nakamura, *Journal of the Physical Society of Japan* 83, 054711 (2014). [2] Y. Shiomi, S. Iguchi and Y. Tokura, Phys. Rev.B 86,180404 (2012). [3] Yishu Wang, Yejun Feng, J.-G. Cheng, W.Wu, J.L. Luo and T.F. Rosenbaum, Nature Communications 7, 113037 (2016). [4] N. Jiang, Y. Nii, H. Arisawa, E. Saitoh and Y. Onose, Nature Communications 11, 1601 (2020).

I4-07. Strain Induced Magnetic Transition in $CaMnO_3$ Ultrathin Films. M.A. Barral[1], A.M. Llois[1] and *S.M. Di Napoli*[1] *1. CNEA-CONICET, Instituto de Nanociencia y Nanotecnologia, San Martin, Argentina*

The effect of high tensile strain and low dimensionality on the magnetic and electronic properties of $CaMnO_3$ ultrathin films, epitaxially grown on $SrTiO_3$ substrates, are theoretically analyzed (Fig. 1). By means of *ab initio* calculations, we find that, both, the high strain produced by the substrate and the presence of the free surface contribute to the stabilization of an in-plane ferromagnetic coupling, giving rise to a non-zero net magnetic moment in the ultrathin films. Remarkably, the FM component of the magnetic structure is stabilized, not as a consequence of a direct electron doping, as it happens when substituting the divalent Ca by trivalent elements or in the presence of O vacancies, as reported in the past, but rather because of a self-doping charge redistribution due to, both, the strain and the absence of apical oxygens. A deeper analysis of this charge redistribution can be obtained from the partial densities of states (pDOS) depicted in Fig. 2, where we separate the contributions of different MnO_2 planes. From the total density of states projected onto each layer, we can see that the oxygens located at the surface are the ones which loose part of their charge, and this charge is redistributed in the Mn atoms located in inner layers, and begin to occupy the $d_{x^2-y^2}$ orbitals. The self-doping electrons of this e_g states, allow the presence of the FM double exchange and the AAF magnetic structure with more FM pairs becomes more stable. As it can also be seen from Fig.2, coupled with this change in the magnetic order we find an insulator-metal transition triggered by the quantum confinement and the tensile epitaxial strain.

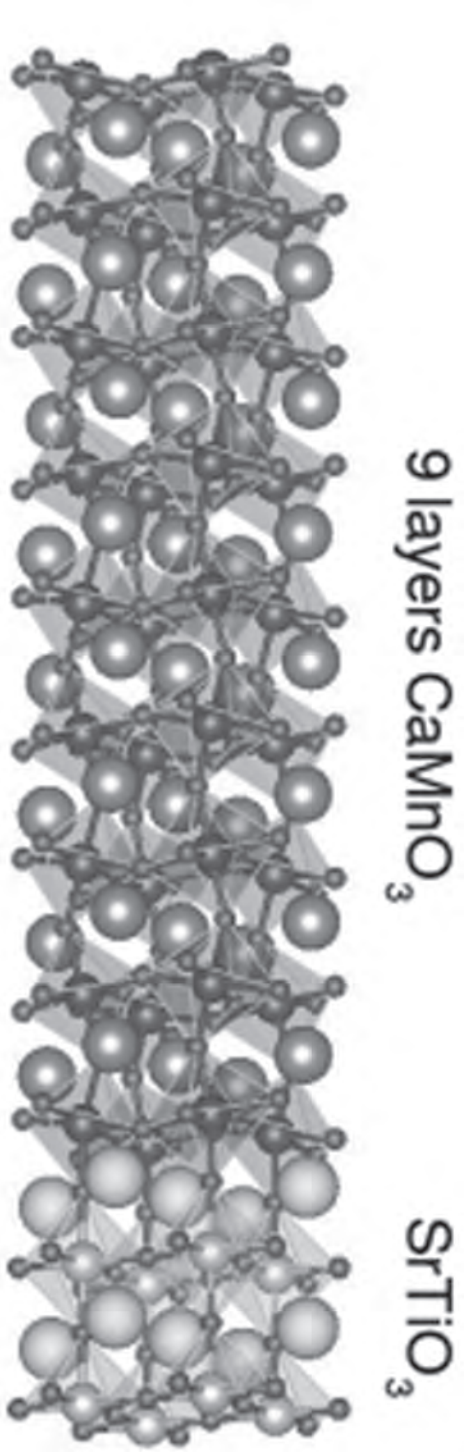

Schematic representation of the $CaMnO_3/SrTiO_3$ ultrathin films

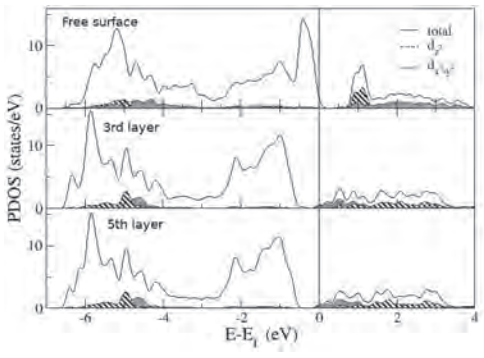

PDOS of the surface (top), third (middle) and central (bot-tom) MnO_2layers. Black lines: total DOS of each layer, dashed blue lines: PDOS of each layer projectedonto thed_{x2-y2}-symmetry and red lines: PDOS of each layer projected onto the d_{z2}-symmetry. The occupied t_{2g}-orbitals are localized in the range of energies between -6.5 and -3.5eV.

I4-08. Magnetic Anisotropy and Electrical Property of CoZrTaB Thin Films Deposited by Oblique Sputtering. S. Tummalapalli[1] and *H. Yu*[1]
1. School of Electrical, Computer and Energy Engineering, Arizona State University, Tempe, AZ, United States

Soft magnetic materials have been studied extensively in the recent years due to their applications in micro-transformers, micro-inductors, spin dependent memories etc. The unique features of these materials are the high frequency operability and high magnetic anisotropy. High uniaxial anisotropy is one of the most important properties for these materials. There are many methods to achieve high anisotropy field (H_k) which include sputtering with presence of magnetic field, exchange bias and oblique angle sputtering without the presence of the magnetic field, etc. There are multiple ways to increase the ferromagnetic resonance frequency which is proportional to coercivity H_k and magnetic saturation M_s. The ferromagnetic resonance depends on softness of the magnetic material to the applied field. With a highly soft magnetic material, one can operate the devices made out of these films at giga hertz regions without loss of efficiency. of the magnetic films is also highly desirable for many applications, such as power conversion and radio frequency (RF) devices operating at high frequencies. This work focuses on analyzing different growth conditions of thin films of CoZrTaB and the resulting magnetic and electrical properties of the films. Thin films are grown by oblique-angle sputtering method, where the sputtering gun forms an angle with respect to the sample substrate normal, ranging from 0 to 75 degrees. External magnetic field normally applied in order to form magnetic anisotropy is not used during film sputtering process. Using vibrating sample magnetometer, it was observed that films resulting from small oblique angles have no clear magnetic anisotropy developed; whereas in samples deposited at large angles close to 60 degree, there is clear magnetic anisotropy observed. Scanning electron microscopy imaging of the cross-section views of such film suggests the formation of tilted columns, which is likely to be the reason for magnetic anisotropy. Resistivity of the films was measured systematically and found to increase as the magnitude of oblique angle during sputtering increased.

1. M. Yamaguchi, K. H. Kim and S. Ikedaa, J. Magn. Magn. Mater. 304 (2), 208-213 (2006). 2. H. Wu, D. S. Gardner, W. Xu and H. B. Yu, IEEE Trans. Magn. 48 (11), 4123-4126 (2012). 3. H. Wu, D. S. Gardner, S. R. Zhao, H. Huang and H. B. Yu, J. Appl. Phys. 115 (17) (2014).

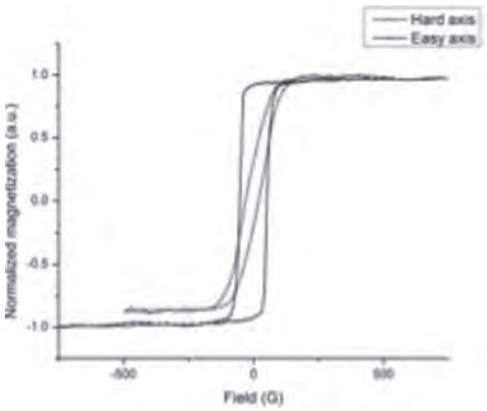

Hysteresis loop of sputtering magnetic film

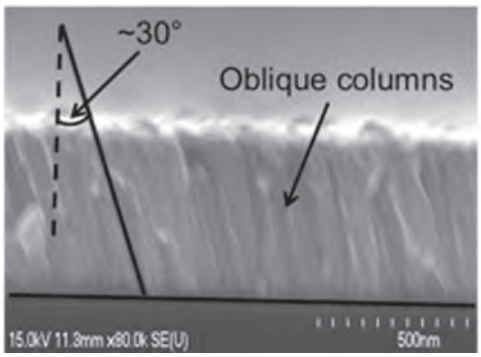

SEM image of film showing tilted columnar structure.

I4-09. Two Magnetic Phases in Mn-Bi_2Te_3 Superlattice. *S. Bac*[1], X. Liu[1], J. Wang[1], M. Dobrowolska[1], J. Furdyna[1] and B. Assaf[1] *1. Physics, University of Notre Dame, Notre Dame, IN, United States*

Mn-doped Bi_2Te_3 is a promising platform for exploring the Majorana fermion, topological magneto-electric coupling, and axion electrodynamics in condensed matter because of the self-organized superlattice. Recently, many groups reported that Mn-doped Bi_2Te_3 naturally forms a superlattice with $MnBi_2Te_4$ septuple-layers interspersed between quintuple-layer of Bi_2Te_3. The spins below Curie temperature couple ferromagnetically in each magnetic layer with an out-of-plane easy axis, but adjacent magnetic layer coupled antiparallel to each other. Thus, $MnBi_2Te_4$ becomes either antiferromagnet or ferromagnet, depending on the number of magnetic layers. Here we investigate magnetic properties of $MnBi_2Te_4$ superlattice grown by MBE with various Mn contents. Hall measurements clearly indicate that a single step in the lightly doped systems (less than ~6 %), which evidence of a ferromagnetic phase. However, three steps were measured in the systems with heavily doped Mn, which indicate an antiferromagnetic phase. These results show that the $MnBi_2Te_4$ with a remarkable crystal quality could be realized by MBE growth. And both ferromagnetic and antiferromagnetic phases were achieved by controlling the Mn concentration. Moreover, it shows the possibility of making a superlattice of $MnBi_2Te_4$ by MBE to fulfill those exotic phenomena.

I4-10. Ordered Occupancy of Interstitial Voids in Mn_5Ge_3 Lattice by the Carbon Dopant. *R. Kalvig*[1], E. Jedryka[1], M. Wojcik[1], M. Petit[2] and L. Michez[2] *1. Polska Akademia Nauk Instytut Fizyki, Warszawa, Poland; 2. Aix-Marseille Universite, Marseille, France*

Epitaxial films of Mn_5Ge_3/Ge<111> are interesting as a potential source of highly spin polarized electrons directly into Ge. Moreover, the high out-of-plane anisotropy of Mn_5Ge_3 opens up prospect for combining spintronics with data storage. The ferromagnetic Mn_5Ge_3 compound crystallizes in the hexagonal $D8_8$ structure; Mn atoms occupy two magnetically and structurally nonequivalent positions: 4d (Mn_I) and 6g (Mn_{II}). The Curie temperature of 296 K can be increased up to 445 K by doping with carbon [1]. Recent ^{55}Mn NMR studies have shown that the magnetocrystalline anisotropy in Mn_5Ge_3 originates from the unquenched orbital moment of Mn in both crystallographic positions [2]. Furthermore, the ^{55}Mn NMR study in $Mn_5Ge_3C_{0.2}$/Ge(111) film has shown that carbon enters interstitially occupying the 2(*b*) octahedral voids and reduces the magnetic moment of the Mn_{II} atoms in the corners of a host octahedron [3]. To achieve further understanding of the role that carbon plays in this system, we carried out a systematic FMR and ^{55}Mn NMR study on a series of epitaxial 30 nm thick $Mn_5Ge_3C_x$/Ge(111) films with the nominal carbon content x varying between 0 and 0.8. The FMR experiment shows that the uniaxial anisotropy constant K_u measured at 4.2 K systematically drops from $5{,}69\times10^6$ erg/cm^3 to $8{,}06\times10^5$ erg/cm^3 for the nominal concentration of $x \approx 0.6$. The ^{55}Mn NMR shows that in the concentration range up to x=0.5 the Mn_{II} atoms are found in two distinctly different magnetic states, identified as Mn_{II} (no carbon nearest neighbor) and Mn_{II_C} (one carbon nn). With increasing carbon concentration the NMR signal intensity is systematically transferred from Mn_{II} to Mn_{II_C}, and at x=0.5 no Mn_{II} NMR signal is observed anymore. On the other hand, no second satellite line is observed in the vicinity of the Mn_{II} signal in the entire concentration range, even though there are two available 2(*b*) positions around the Mn_{II} atoms. These two observations implicate that carbon does not enter statistically in the 2(*b*) voids, but shows a strong preference towards ordering, occupying every second 2(*b*) void along the hexagonal c-direction. This sets the limit for the uptake of the carbon atoms in the Mn_5Ge_3 lattice to x=0.5.

[1] M. Gajdzik et al., J. Magn. Magn. Mater., Vol. 221 p. 248 (2000) [2] R. Kalvig et al., Phys. Rev. B, Vol. 97 p. 174428 (2018) [3] R. Kalvig et al., Phys. Rev. B, Vol. 101 p. 094401 (2020)

I4-11. Evolution of Structural and Magnetic Properties of Ar^{2+} Ion Irradiated TiO_2 Thin Films Annealed Under Argon Atmosphere. *B. Bharati*[1] and C. RATH[1] *1. SCHOOL OF MATERIALS SCIENCE AND TECHNOLOGY, Indian Institute of Technology BHU Varanasi, Varanasi, India*

TiO_2 crystallizes in three different structures such as anatase, brookite and rutile [1-3]. In addition, Magneli phase is a titanium sub oxide (Ti_nO2_{n-1}, $4 \le n \le 10$) have been explored as a promising candidate because of their high electrical conductivity, chemical inertness and corrosion resistance [4]. Among the Magneli phase compounds, Ti_4O_7 is important for its high electrical conductivity. In general, Ti_4O_7 is synthesised by thermal reduction of TiO_2 [5]. These Magneli phases can easily accommodate oxygen deficiency through anionic vacancies, which leads to the partial reduction of Ti^{4+} to Ti^{3+}. This Ti^{3+} gives local ferromagnetism in the material through hopping of the single 3*d* electron [6]. In this work, ion irradiation is used as a unique tool for the material modification depending upon the projectile ion, energy and the nature of the target. Ion irradiation has been found to amorphize, recrystallise and induce crystalline to crystalline phase transition or defects in various materials. In our earlier studies, we have used 500 keV Ar^{2+} ions to irradiate on the TiO_2 thin films grown on Si substrate by e-beam evaporation technique and subsequently annealed under O_2 environment at 500 C [7-8]. However, we have observed phase transformation from anatase to brookite through amorphisation and room temperature ferromagnetism (RTFM) in the films attribute to oxygen vacancies [7-8]. Hence, in the present study we have explored the role of 500 keV Ar^{2+} ion irradiation on the structural and magnetic properties of TiO_2 thin films annealed under Ar at 900 C. The annealed films show Ti_4O_7 phase which transform to anatase phase upon irradiation with fluence 1×10^{14} ions.cm^{-2} as observed from the glancing angle x-ray diffraction (GAXRD). Further, irradiation with fluence 5×10^{16} ions.cm^{-2} recrystallizes to Ti_4O_7 phase. Raman spectroscopic studies also support the changes in phase. AFM show small change of surface morphology upon ion irradiation with roughness, 0.060, 0.062, 0.079 nm and grain size, 28, 28, 29 nm for the pristine film, films irradiated with ion fluenece 1×10^{14} and 5×10^{16} ions.cm^{-2}, respectively. The origin of RTFM is coined with the oxygen vacancies concentration in the films.

[1] C. Rath, P. Mohanty, A.C. Pandey, N. C. Mishra, J. Phys, D: Appl. Phys 47 315001 (2009). [2] P. Mohanty, V. P. Singh, N. C. Mishra, S. Ojha, D. Kanjilal, C. Rath, J. Phys, D: Appl. Phys 47 315001 (2014). [3] B. Bharati, N. C. Mishra, A. S. K. Sinha, C. Rath, Materials Research Bulletin 123 110710 (2020). [4] P. Geng, J. Su, C. Miles, C. Comninellis, G. Chen, Electrochimica Acta 153 316–324. (2015) [5] G. Wang, Y. Liu, J. Ye, W. Qiu, Journal of Alloys and Compounds 704 18 (2017). [6] M. Parras, A. Varela, R. C. Gil, K. Boulahya, A Hernando, J. M. G. Calbet, J. Phys. Chem. Lett. 4 2171 (2013). [7] B. Bharati, N. C. Mishra, D. Kanjilal, C. Rath, Applied Surface Science 428 723 (2018). [8] B. Bharati, N. C. Mishra, C. Rath, Applied Surface Science 455 717 (2018).

I4-12. Study of Magnetization Behaviour of Co-Doped TiO_2.

R. Gupta[3], *S. Kumar*[1], A. Gupta[2], D. Phase[3] and A. Pandey[4] *1. School of Instrumentation, Devi Ahilya University, Indore, India; 2. Center for Spintronics, Amity University, Noida, India; 3. UGC DAE Consortium for Scientific Research, Indore, India; 4. Inter-University Accelerator Center, New Delhi, New Delhi, India*

For the development of spintronic and optoelectronic devices, oxide-based dilute magnetic semiconductors are the potential candidate. From the practical problems, the material should possess the magnetic properties at room temperature along with its optical and magnetic properties, which can be easily tailored to the desired level. In device fabrication, ion-implantation plays a significant role, thus the study of ion-implantation on these materials is very important from the fabrication point of view. In the present work, we have studied the effect of ion-implantation on Co-doped TiO2 thin films, prepared by ion beam sputtering using RF ion source. The as-prepared thin film shows ferromagnetism at room temperature and the Curie Temperature of the film is above 300 K. The total thickness of the film was 73.5 nm. The magnetization curve at room temperature shows a typical hard-axis behavior and isotropic in nature. Ion irradiation induces magnetic softness in the film and it shows magnetic anisotropy in the film. The as-deposited film gives a finite XMCD signal, mainly around L3 edge of Co. The broad XMCD signals of as-deposited specimens suggest the formation of a diffused magnetic moment. Fig. 1 shows the XMCD plot of the as-deposited thin film along with the simulated graph. It shows that the film contains Co2+ and Co3+. After ion-irradiation, the XMCD signal becomes weaker compared to the as-deposited specimen. Detailed analysis of magnetization with its electronic structure will be discussed.

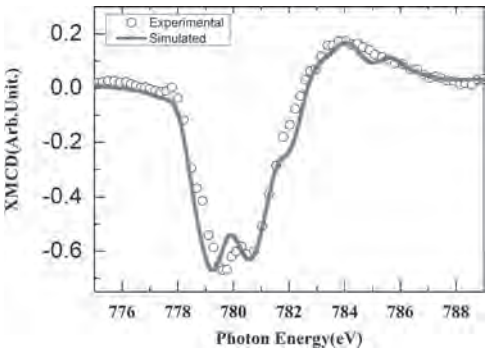

Fig. 1 shows the XMCD signal of as-deposited specimen.

I4-13. Spin Ordering and Precessional Damping in Ferrimagnetic Thin Film Structures Near Compensation.

J. Shoup[1], H. Liu[1], D. Khadka[2], T.R. Thapaliya[2], S. Huang[2], D. Karaiskaj[1] and D.A. Arena[1] *1. University of South Florida, Tampa, FL, United States; 2. University of Miami, Coral Gables, FL, United States*

Metallic ferrimagnets consisting of rare earth (RE) / transition metal (TM) alloys exhibit an intriguing magnetic compensation of the RE/TM magnetic sublattices as a function of composition and temperature. We examine two types of metallic ferrimagnets: $Fe_{1-x}Gd_x$ and $(FeCo)_{1-x}Gd_x$ thin films where the composition and structure of the film are modified systematically. Static magneto-optic Kerr effect (MOKE, see Fig. 1-a) and magneto-transport measurements, both sensitive to the spin polarization at the Fermi level, confirm the room-temperature (RT) composition that exhibits magnetic compensation while temperature-dependent magnetometry reveals the onset of magnetic compensation below RT for specific Gd concentrations. In the ~50nm thick $Fe_{1-x}Gd_x$ films, static MOKE measurements confirm RT compensation at a nominal Gd concentration of 29%. Below (above) this Gd concentration, the MOKE response is aligned (anti-aligned) with the external field. A similar reversal is seen in the time-resolved MOKE (tr-MOKE) studies of the $(FeCo)_{1-x}Gd_x$ samples (RT compensation ~26% Gd). We observe a clear reversal of the tr-MOKE signal between samples with 23% and 27% Gd content. The tr-MOKE signals from both samples share some features, including a rapid demagnetization on ps timescales, accompanied by strong precession oscillations that are superposed on a long recovery time (> 1 ns). The demagnetization timescale, precessional dynamics, and damping will be discussed along with the influence of structural variations of sample composition. The authors acknowledge the support of Univ. of South Florida Nexus Initiative (UNI) Award. This material is based upon work supported by the National Science Foundation under Grant No. ECCS-1952957.

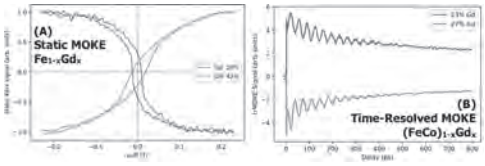

Fig. 1 (A) MOKE measurements of representative $Fe_{1-x}Gd_x$ samples. The reversal of the MOKE signal for the different Gd concentrations illustrates the change from Fe-dominated to Gd-dominated net moment. (B) time-resolved MOKE measurements of $(FeCo)_{1-x}Gd_x$ samples. The reversal of the magneto-optical signal again depicts the changeover from Fe- to Gd-dominated net moment, along with ultrafast demagnetization, followed by the onset of precession oscillations and a return to equilibrium.

I4-14. Effect of the N_2/RE Ratio During Growth on the Properties of Rare Earth Nitrides.

A. Shaib[1,2], J. Chan[1,2], W. Holmes-Hewett[1,2], F. Ullstad[1,2], J. Miller[1,2], B. Ruck[1,2], H. Trodahl[1,2] and F. Natali[1,2] *1. School of Chemical and Physical Sciences, Victoria University of Wellington, Wellington, New Zealand; 2. The MacDiarmid Institute for Advanced Materials and Nanotechnology, Wellington, New Zealand*

The rare earth nitride (REN) series is a promising candidate for spintronics applications. It is the only epitaxy-compatible series of intrinsic ferromagnetic semiconductors, with members possessing complementary and contrasting magnetic properties.[1] It is established that REN properties display high sensitivity to native defects, mainly the nitrogen vacancies (V_N). V_N form at the level of a few percent or less during thin film growth even in the most nearly stoichiometric films. The vacancies act as dopants and introduce n-type conductivity. The literature reports on more V_N-induced effects in the REN such as the enhanced Curie temperature in GdN (from 50K to 70K) due to the formation of magnetic polarons at V_N sites, and superconductivity below 4K in heavily V_N-doped ferromagnetic semiconducting SmN thin films [2,3] Here, we show that the rate of N_2 flow during growth and thin film properties are intimately linked, suggesting that the growth stoichiometry is key for understanding the structural, transport, and magnetic properties of the REN. X-ray diffraction, magnetic, Hall-effect, and transport measurements are carried out on a series of polycrystalline REN (GdN, SmN, and DyN) thin films. We show remarkable changes to the properties of the films: SmN film resistivity can be controlled over six orders of magnitude by less than one order of magnitude change of the N_2/RE growth ratio. Hall-effect measurements correlate this increase in resistivity to a drop in the V_N concentration. We also observe the signature of a

secondary structural phase of GdN associated with N-deficient regions that develops as the N_2 pressure decreases during the growth and has a smaller lattice parameter than stoichiometric GdN. We also observe an enhanced T_C (up to 90 K) for the films grown with the lowest N_2/Gd ratio.

[1]F. Natali et al, Prog. Mater. Sci. 58, 1316 (2013). [2]F. Natali, et al, Phys. Rev. B 87, 035202 (2013). [3]E. M. Anton et al, Phys. Rev. B 94, 024106 (2016).

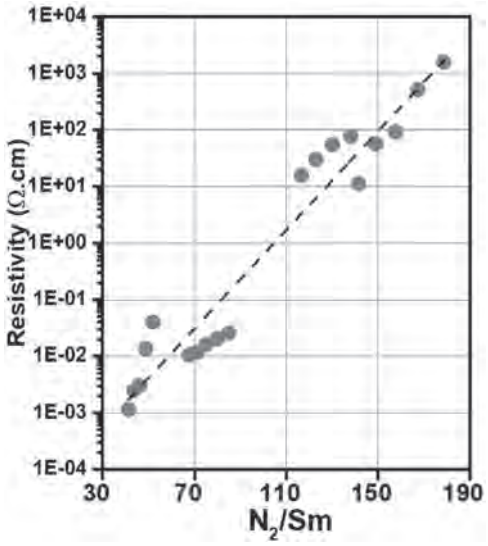

Fig.1 SmN ambient temperature resistivity as a function of the N_2/Sm ratio during film growth. The dashed line is a linear fit. Over six orders of magnitude increase is observed for a ~4-fold increase of the N_2/Sm ratio.

I4-15. High Degree of Order and Uniaxial Magnetic Anisotropy of $L1_0$-FeNi Films Fabricated by Denitriding Epitaxial FeNiN Films. *K. Ito*[1,2], M. Hayashida[1], T. Ichimura[1], T. Nishio[3], S. Goto[3], H. Kura[3], T. Koganezawa[4], M. Mizuguchi[5], Y. Shimada[1], T. J. Konno[1], H. Yanagihara[6] and K. Takanashi[1,2] *1. Institute for Materials Research, Tohoku University, Sendai, Japan; 2. Center for Spintronics Research Network, Tohoku University, Sendai, Japan; 3. Advanced Research and Innovation Center, DENSO CORPORATION, Nisshin, Japan; 4. Japan Synchrotron Radiation Research Institute, Sayo, Japan; 5. Department of Materials Process Engineering, Nagoya University, Nagoya, Japan; 6. Department of Applied Physics, University of Tsukuba, Tsukuba, Japan*

An $L1_0$-ordered FeNi alloy has been focused as a rare-earth free high uniaxial magnetic anisotropy energy (K_u) material [1]. Recently, the synthesis of polycrystalline $L1_0$-FeNi powder by denitriding FeNiN powder was reported, and a degree of order (S) of 0.71 was achieved [2]. However, the exact K_u value of $L1_0$-FeNi formed by the denitriding method is still unclear, and the evaluation of K_u using a single-crystal $L1_0$-FeNi is required. In this study, we grew epitaxial FeNiN films by molecular beam epitaxy and fabricated $L1_0$-FeNi films by nitrogen topotactic extraction, and characterized their S and K_u values. 20 nm-thick FeNiN films were grown on $SrTiO_3$(001) substrates at 200, 250, and 350 °C by supplying Fe, Ni, and RF N_2 plasma, simultaneously [3]. Denitriding was performed by *ex-situ* furnace annealing at 300 °C for 4 h under an H_2 gas flow rate of 1 L/min at ambient pressure. Structure of the samples was characterized by x-ray diffraction measurements using Cu-$K\alpha$ radiation and synchrotron radiation ($h\nu$ = 7.11 keV), and cross-sectional scanning transmission electron microscope (STEM) measurements. The saturation magnetization (M_S) and the K_u were estimated by magnetic torque measurements. The epitaxial $L1_0$-FeNi films oriented with the *a*-axis perpendicular to the film plane having two variants with the orthogonal in-plane *c*-axes are fabricated. Figure 1 shows the growth temperature dependences of M_S and K_u of the samples. For the sample grown at 350 °C, the S and K_u values are evaluated to be 0.87 and 5.9×10^5 J/m^3, respectively. In spite of the large S value exceeding those reported previously [1,2], the K_u value is modestly high. The exchange length of $L1_0$-FeNi (3.2 nm) is comparable to the variant sizes of our samples estimated by the STEM measurements. This strongly suggests that the obtained macroscopic K_u value is smaller than the actual K_u of each variant [4]. This work was supported by the Future Pioneering Program "Development of magnetic material technology for high-efficiency motors" (JPNP14015) commissioned by the NEDO, Japan. The synchrotron radiation XRD was conducted at the BL46XU of SPring-8 with the approval of JASRI (2019A1802).

[1] K. Takanashi *et al*., J. Phys. D: Appl. Phys. 50, 483002 (2017). [2] S. Goto *et al*., Sci. Rep. 7, 13216 (2017). [3] K. Ito *et al*., J. Magn. Soc. Jpn. 43, 79 (2019). [4] K. Ito *et al*., Appl. Phys. Lett. 116, 242404 (2020).

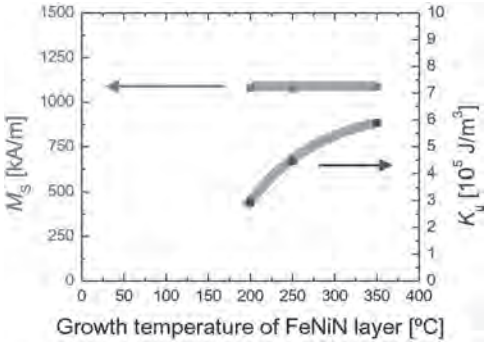

Fig. 1 Growth temperature dependences of M_S and K_u of the samples.

Session I5
INSTRUMENTATION AND MEASUREMENT TECHNIQUES II
(Poster Session)

Tatiana Guidi, Chair
Science and Technology Facilities Council, Didcot, United Kingdom

I5-01. Withdrawn

I5-02. Magnetic Properties Measurement and Simulation of Electrical Steel Sheet Under Cutting Influence. Y. Li[1], *Y. Fu*[1], Y. Dou[1] and K. zhang[1] *1. State Key Laboratory of Reliability and Intelligence of Electrical Equipment, Hebei University of Technology, Tianjin, China*

Abstract – Cutting is a necessary manufacturing technique when using silicon steel to produce electrical devices. Different cutting methods have different effects on the internal structure and magnetic properties of electrical steel sheets[1]. Laser cutting will produce thermal stress during processing, while mechanical cutting will produce plastic deformation near the cutting edge, which both lead to deterioration in the magnetic properties of the material. Therefore, studying the effect of different cutting techniques on magnetic properties is of great significance to accurately simulate and predict the iron losses of electrical equipment. The existing research methods cut the same sample into the different number of strips along the rolling direction, and these methods conclude that the cutting has a certain influence on the magnetic properties of the electrical steel sheet. But they cannot systematically compare the differences in magnetic properties and degraded range of the three cutting methods[2]. In this paper, the influence of cutting methods, such as wire cutting, laser cutting, and shear cutting on the local magnetic properties of the silicon steel sheet is studied and analyzed. The magnetic properties measurement system is shown in Fig. 1. A mobile *B-H* composite sensor is designed to sense the distribution of local magnetic properties near the cutting edges. The results show that different cutting methods have different effects on the spatial distribution of magnetic flux and the corresponding *B-H* curves. With the increase of the distance from the cutting edge, the degree of magnetic degradation decreases gradually. Two mathematical models used to simulate the cutting edge effect by the finite element simulation can also better describe the magnetization curve of the electrical steel sheet damage trend, thus providing a model basis for the application of electrical equipment under actual working conditions.

[1] G. Loisos, A. J, Moses, Journal of Materials Processing Tech., vol. 161, p. 151-155(2005) [2] A. Saleem, N. Alatawneh, R. R. Chromik and D. A. Lowther, IEEE Transactions on Magnetics., vol. 52, no. 5, p. 1-4(2016)

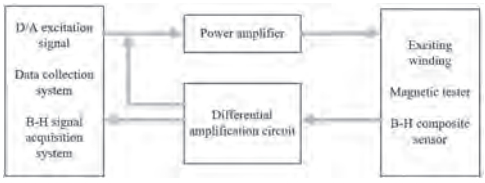

Fig. 1 The magnetic properties measurement system.

I5-03. Effect of Plastic Straining on the Remanent Magnetization of Ferrite-Pearlitic Steel: Experimental and Modeling Aspects. Z. Maazaz[1,2], *O. Hubert*[1] and E.A. Fnaiech[2] *1. LMT - Laboratoire de Mécanique et Technologie, Université Paris-Saclay/ENS Paris-Saclay/ CNRS, Gif-sur-Yvette, France; 2. SKIPPER - NDT, Paris, France*

Some recent nondestructive testing methods have been developed to detect very small variations in the magnetic field surrounding a massive ferromagnetic structure, such as a tank or pipe [1]. In particular, the detection of sinking in buried pipelines becomes possible [2]. The sinking is characterized by local plastic deformation and the creation of long range residual stresses. These two elements are known to have a considerable influence on the magnetic behavior [3,4,5]. One of the keys to detection is the substantial modification of the remanent magnetization of the material. The study material is a two-phase ferrito-pearlitic steel. Strips are subjected to an incremental tensile plastic deformation interspersed with elastic unloading. The magnetic behavior is carried out along the tensile direction at different levels of applied stress after deformation. The figure below shows the typical evolution of the remanent magnetization. The figure highlights: (i) that the remanent magnetization increases with the applied stress to a maximum value then decreases; (ii) that the plastic strain at zero stress considerably reduces the remanent magnetization in a highly non-linear manner; (iii) that the behavior of the deformed material seems to be able to be obtained by a simple translation in the stress space of the behavior at the undeformed state. These results join some former results [6] and the interpretation of the effect of plastic deformations by Hubert & Lazreg [7]. Following this work, a magneto-elastic two-phase modeling of the magnetization is proposed. Plasticity is introduced as an internal stress state inherent with the plastic deformation of the two-phase material (so-called kinematic hardening). The associated mechanical state being multiaxial, an equivalent uniaxial state can be calculated, requiring the use of a new material coefficient making it possible to consider the effect of the pearlitic phase on the average behavior of the medium. It is shown that the translation in the stress space predicted by the model is consistent with the experimental values.

[1] international patent CA2998095A1 [2] E. A. Fnaiech, M.Munschy, S. Corbineau, M. Marzin, P. Rohart, S. Takillah, “Large stand-off magnetometry (LSM) for buried pipeline inspection: Influence of dent depth on residual magnetic signal “, Pipeline Technology Conference, Berlin (2020) [3] R.M. Bozorth, Ferromagnetism, Wiley-IEEE press, (1993) [4] J.M. Makar, B.K. Tanner, J. Magn. Magn. Mater. 184, p.193 (1998) [5] O. Hubert, M. Clavel, I. Guillot, E. Hug, Jal Phys. IV, 9, p.207 (1999) [6] V.E. Iordache, E. Hug, N. Buiron, Mater. Sci. Eng. A 359, p.62 (2003) [7] O. Hubert, S. Lazreg, Journal of Magnetism and Magnetic Materials, 424 2, p.421 (2017)

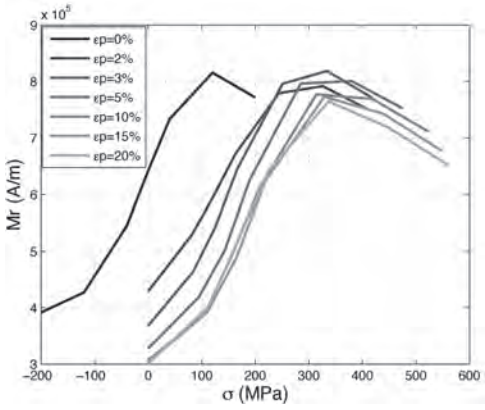

Figure: remanent magnetization Mr as function of stress σ for different plastic strain levels εp.

I5-04. Withdrawn

I5-05. Ferromagnetic Resonance Studies of Composite EMF Shielding Materials. *P. Couture*[1], R. Camley[1], K. Livesey[1], T. Robinson[2], D. Meyers[2], S. Maat[2] and Z. Celinski[1] *1. Physics, University of Colorado at Colorado Springs, Colorado Springs, CO, United States; 2. YTC America Inc, Camarillo, CA, United States*

We characterize MnZn ferrite particles, and Ni-coated carbon fibers (Ni CCF), embedded in a polymer for use in low frequency EMF emissions shielding. The ferrites particles are approximately 1.2 μm in diameter and embedded in PVC resin in various concentrations: 10% - 70% by weight. The composite undergoes an extrusion process which creates a 0.6 mm thick slab and orders some of the particles along the extrusion direction. This creates an easy axis along the extrusion direction with an associated anisotropy. We characterized the ferromagnetic resonance absorption peaks for the ferrites with broad-band FMR, 1-30 GHz, and cavity based FMR systems. Comparing the experimental results to the expected FMR peaks position for measurements along the easy and hard axes in-plane, as well as normal to the slab, using the Landau-Lifshitz-Gilbert (LLG) equation provides insight into occurring rf absorption dependent on the ferrite concentrations. For samples with high ferrite concentrations, shown in Fig. 1, a typical solution for a thin film resonance condition (Kittel's eq. [1-3]) can be used, with demagnetizing factor D z =1, to describe the FMR frequency vs. field dependence. For lower ferrite concentrations, however, the resonance conditions have to be modified to account for an effective sample thickness beyond using a normal filling factor correction associated with presence of matrix [4], shown in Fig. 2. These results indicate that the effective demagnetizing factors, determined by the spatial extend of the rf fields, can properly describe the observed FMR absorption.

[1] *C. Kittel, Phys. Rev., Vol. 73.2, p.155-161 (1948)* [2] *J. Dubowik, Phys. Rev. B, Vol. 54.2, p.1088-1091 (1996)* [3] *G.N. Kakazei et al., J. Appl. Phys., Vol. 85.8, p.5654 (1999)* [4] *A. Aharoni, J. Appl. Phys., Vol. 83, p. 3432 (1998)*

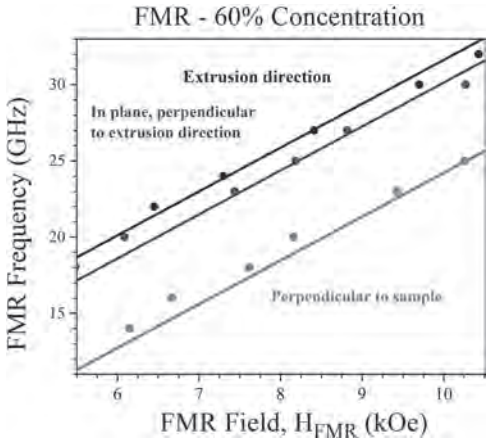

Fig. 1. FMR plot of applied field vs frequency for the 60% ferrite concentration composite material showing experimental (dots) and calculated (lines) results. The theoretical values assume $D_z = 1$.

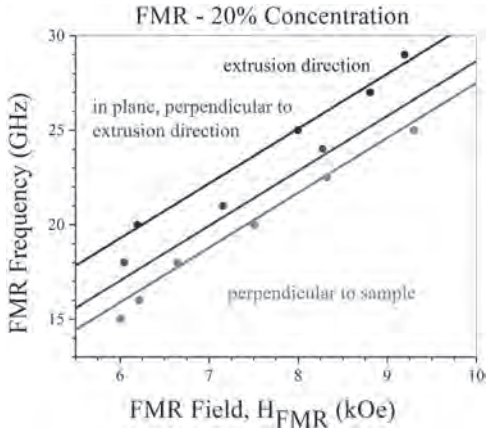

Fig. 2. FMR plot of applied field vs frequency for the 20% ferrite concentration composite material showing experimental (dots) and calculated (lines) results. The theoretical calculation accounts for the modified demagnetizing factors where D_z is no longer equal to 1.

I5-06. Magnetic Field Spectra and Sizing of Defects in Magnetic Flux Leakage Inspection. *M. Aziz*[1], R. Abdulla[2] and M. Al-Dujaili[2] *1. Engineering, University of Exeter, Exeter, United Kingdom; 2. MEDCO Ltd, Surrey, United Kingdom*

Magnetic flux leakage (MFL) is a widely used non-destructive method for the detection of defects and abnormalities in magnetic structures such as oil and gas steel tubes for health and condition monitoring [1]. MFL involves the application of a magnetizing field in close proximity to the inspected magnetic medium and measuring the resulting leakage magnetic fields from defects, which are key for the detection and characterization of defects. To understand the correlation between the measured fields and physical defects dimensions, leakage fields are conventionally modeled for simple defect shapes (such as rectangles [2] or cylinders [3,4]) using magnetic charge sheets representing the inner surfaces of the defect. This approach assumes uniform magnetic charges through the defect and ignores nonlinear saturation effects in the corners which makes characterization and sizing of defects from measured field distributions difficult and inaccurate. Frequency domain analysis of leakage fields in MFL provide an alternative and less explored method for characterization of defects. The spectrum of the leakage magnetic fields in MFL was recently derived for rectangular defects based on magnetic charge sheets [5,6]. This approach revealed spectral features that potentially enable more accurate sizing of defects from measured MFL signals compared to direct analysis of spatial field distributions. In this work the Fourier transforms of the leakage magnetic fields from rectangular and

tilted two-dimensional defects are analytically derived using scalar magnetic potential theory and superposition [7,8]. This approach does not assume uniform magnetic charges through the defect surfaces. The scalar magnetic potential approach yielded closer agreement to more detailed finite-element calculations and published measurements, and used to assess the sensitivity and feasibility of the spectral sizing method for different defect geometries.

[1] D. E. Bray and R. K. Stanley, Nondestructive Evaluation, Part IV: Magnetic Flux Leakage Techniques in Nondestructive Evaluation, Florida: CRC Press (1997). [2] N. Zatsepin and V. Shcherbinin, Defektoskopiya 5, 50 (1966). [3] C. Mandache and L. Clapham, J. Phys. D: Appl. Phys. 36, 2427 (2003). [4] S. M. Dutta, F. H. Ghorbel, and R. K. Stanley, IEEE Trans. Magn. 45, 1959 (2009). [5] Li E, Kang Y, Tang J, Wu J, and Yan X, IEEE Trans. Magn. 54, 1 (2018). [6] M. M. Aziz, R. Abdulla, and M. Al-Dujaili, IEEE Mag. Lett. 10, 2102404 (2019). [7] M. M. Aziz, A. Edress, and C. D. Wright, IEEE Trans. Magn. 52, 3300712 (2016). [8] D. A. Lindholm, IEEE Trans. Magn. 12, 710 (1976).

I5-07. Study of Mechanical Resonance Induced by Magnetostriction in Closed Structures Based on Fe-Si. *J. Li*[1], G. Li[1], D. Zhang[1] and K. Yu[2]
1. Dalian University of Technology, Dalian, China; 2. Waseda University, Tokyo, Japan

ABSTRACT: The noise produced by power transformers and electrical machines is harmful and its reduction is the hot subject in continuous research. Such systems are likely to be in resonance and become more vociferous, and the resonance may be mechanical or magnetic forces. The interaction between deformation due to magnetostriction and mechanical resonance of a structure made up of laminated steel sheets is investigated in this paper. The resonance phenomena are generally studied and analyzed by considering that frequency and spatial distribution of electromagnetic forces coincide with natural frequency and modes shapes of the corresponding structure. It is observed that magnetostriction may induce a resonance without the need to combine these two conditions. Two closed sheets structures of frame shape and ring shape consisting of cold-rolled grain-oriented (GO) and non-grain oriented (NO) electrical steels are used to confirm this assumption. Finite element (FE) calculations and measurements are made and compared with vibration displacements. Results of mechanical resonance induced by the magnetostrictive strain from ferromagnetic materials are shown, as well as the corresponding vibration spectrums. *CONTENT:* This paper presents a complete study on magnetostriction induced resonance from mechanical study to resonance detection. In Section II, the studied structure is described. In Section III, a comparison between Maxwell stresses and magnetostrictive strains is introduced and results of simulation are discussed. In Section IV, a complete study of mechanical properties of structure is presented and comparison between experimental and modeling results is described. In Section V, the summary of mechanical resonance due to magnetostriction is detailed. *CONCLUSION:* This paper has demonstrated that magnetostriction deformation can be implicated in mechanical resonance of a laminated structure and should be considered at the design stage for cold-rolled GO and NO electrical materials or any magnetostrictive materials grade.

[1] K. Fonteyn, A. Belahcen, R. Kouhia, *et al*, "FEM for directly coupled magneto-mechanical phenomena in electrical machines," *IEEE Trans. Magn.,* vol. 46, no. 8, pp. 2923-2926, Aug. 2010. [2] U. Aydin, *et al.*, "Magneto-mechanical modeling of electrical steel sheets," *J. Magn. Magn. Mater.,* vol. 439, pp. 82-90, Oct. 2017. [3] M. Liu, *et al.*, "Reduction of power transformer core noise generation due to magnetostriction-induced deformations using fully coupled finite element modeling optimization procedures," *IEEE Trans. Magn.,* vol. 53, no. 8, Aug. 2017, Art. no. 8400511. [4] S. Somkun, A. J. Moses, and P. I. Anderson, "Mechanical resonance in nonoriented electrical steels induced by magnetostriction under PWM voltage excitation," *IEEE Trans. Magn.,* vol. 44, no. 11, pp. 4062-4065, Nov. 2008.

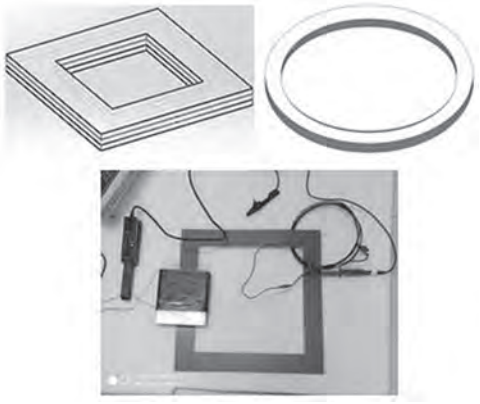

Fig. 1. Test verification models for magnetostriction based on two closed sheets structures of frame and ring shapes.

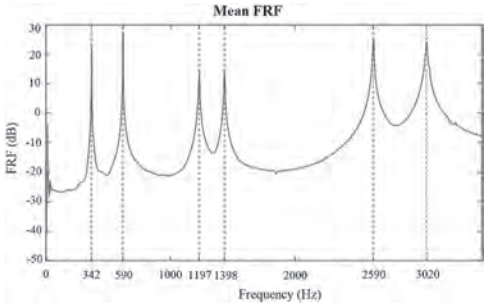

Fig. 2. Experimental mean frequency response functions (FRF) for in-plane modes.

I5-08. Magnetic Measurement and Analysis of C-Type Amorphous by an Improved Adjustable Air Gap Tester. Y. Li[1], *Z. Wan*[1], H. Sun[1] and H. Liu[1] *1. State Key Laboratory of Reliability and Intelligence of Electrical Equipment, Hebei University of Technology, Tianjin, China*

In order to increase the saturation current and the ability of energy storage, an air-gap C-type core is usually used in the inductor or high-frequency transformer. The effect of air gap on the magnetic characteristics of C-type core can not be ignored[1]. Accurate magnetic properties of the air-gap core is of great significance for the optimal design of magnetic components. At present, the PCB board or other nonferromagnetic material is usually used as the interlayer to determine the length of the air gap[2,3]. Interlayer of different thicknesses is needed when the size of the core or the air gap is changed. This is not convenient to operate. In this paper, a device is designed. The device can be easier and more accurate to change the length of the air gap. As shown in Fig.1, this device can fix the position of the core firmly through the slider in six directions. And it is suitable for various types of cores, leg length from 34 to 110 mm and the height less than 50 mm. A spiral micrometer ritual is adopted to adjust the air gap length with an accuracy of 0.02 mm. The excitation coil is wound on the coil frame, which can change the position of the coil relative to the air gap. Finally, the dynamic magnetic characteristics of the amorphous core (AMCC016B) under different air gap lengths by this device. The hysteresis loop and core loss of the core under the different air gap length is shown in Fig. 2. It can be found that the magnetic permeability of the core changes significantly as the length of the air gap increases. The hysteresis loop gradually slopes as well. While the change of core loss is not obvious in the case of a small air gap. This paper analyzes the experimental data and summarizes the influence of the air gap length on the core loss. This is of great significance for the optimization of high-frequency devices. More details will be shown in the full text.

[1]W. Shen, F. Wang, D. Boroyevich and C. W. Tipton, IEEE Transactions on Power Electronics, Vol. 23, p. 475-484(2008) [2]G. Calderon-Lopez, Y. Wang and A. J. Forsyth, IEEE Transactions on Power Electronics,

Vol. 34, p. 4656-4664(2019) [3]Y. Wang, G. Calderon-Lopez and A. J. Forsyth, IEEE Transactions on Power Electronics, Vol. 32, p. 4683-4690(2017)

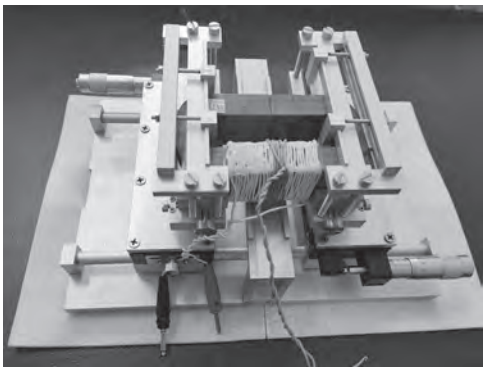

Fig.1 Adjustable air gap tester.

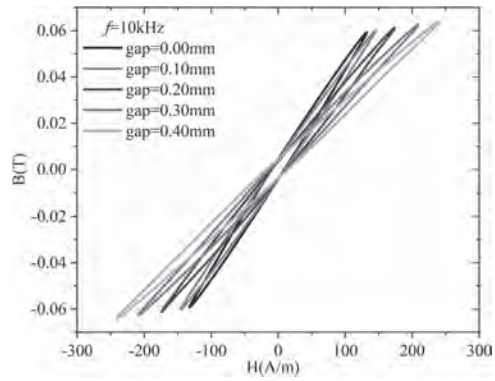

Fig.2. The hysteresis loops and core loss under different conditions.

I5-09. Frequency Characteristics of an air-Cored Coil and its Application to Conductivity Examination. *W. Cheng*[1,2] and H. Hashizume[2]
1. NDE Center, Japan Power Engineering and Inspection Corp., Yokohama, Japan; 2. Department of Quantum Science and Energy Engineering, Tohoku University, Sendai, Japan

In the eddy current testing (ECT), a coil carrying alternating current is used to induce eddy current in the test object and/or collect signals. The resistance and reactance of the coil change with frequency because of skin and proximity effects in the winding. There is also stray capacitance between the wires. The coil resonates at a particular frequency. For conventional ECT, the coil normally operates far below its self-resonant frequency, the capacitance is negligible; the resistance and reactance are considered to be frequency-invariant. An ECT coil is practically modelled by a serially connected resistance and reactance without taking into account the eddy current effect in the coil itself. In last decades, the range of ECT application is expanded, together with widening of operating frequency. Probes working at extremely high and low frequencies have been developed. On the other hand, the conventional ECT coil is explored anew in 'unconventional' frequency range. Nevertheless, in-depth understanding of a coil's frequency characteristic is essential. As the first trial, we studied a simple air-cored coil's frequency characteristics and apply it to exam conductivity change. The signals were attained from sweep frequency eddy current testing [1], analyzed based on lumped element circuit model, together with simplified analytical and numerical analysis. Fig. 1 shows the impedances of the coil itself, the coil on test pieces of conductivity AISC 100.98%, 57.71% and 19.70%, respectively. Different resonant frequency and impedance-at-resonant correspond to different conductivity. For signals taken far below the resonant frequency, the local minimum of normalized resistance [1] (enclosed by ellipse in Fig. 2) also indicates conductivity change. All the indicators appear at frequencies that the effect of the test piece's thickness is cut to minimum.

Acknowledgement: This work was partially supported by JSPS KAKENHI Grant Number JP20k05000.

Weiying Cheng, Thickness Measurement of Metal Plates Using Swept-Frequency Eddy Current Testing and Impedance Normalization, IEEE Sensors Journal, July 15, 2017, Vol.17, No.14, pp.4558-4569, DOI: 10.1109/JSEN.2017.2710356

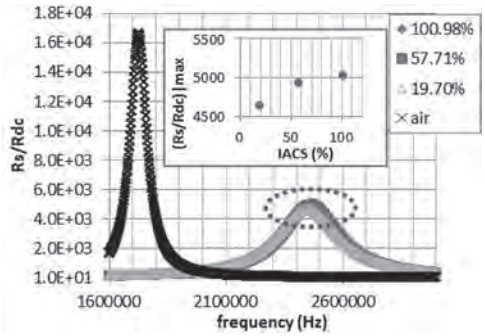

The coil at resonance and the characteristic feature indicating conductivity change

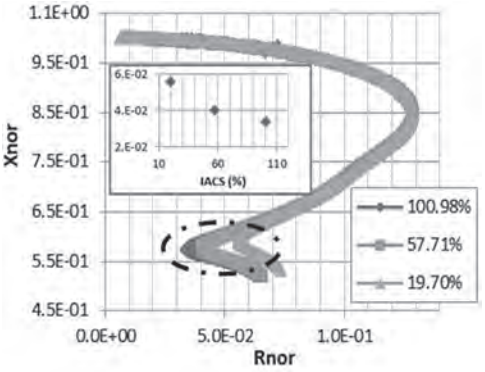

Normalized impedance and the indicator of conductivity change

I5-10. Withdrawn

I5-11. Withdrawn

Session J1
BIOMEDICAL APPLICATIONS I - THERAPEUTIC APPLICATIONS

Anirudh Sharma, Co-Chair
University of Minnesota, Minneapolis, MN, United States
Daniel Ortega, Co-Chair
University of Cádiz, Cádiz, Spain

INVITED PAPER

J1-01. Effect of Cortex-Coil Distance on Resting Motor Threshold in Schizophrenia Patients During Transcranial Magnetic Stimulation.
E. Cheng[1], U.M. Mehta[2], A.K. Pandurangi[3] and *R.L. Hadimani*[4,1]
1. Department of Biomedical Engineering, Virginia Commonwealth University, Richmond, VA, United States; 2. Department of Psychiatry, National Institute of Mental Health & Neurosciences, Bangalore, India; 3. Department of Psychiatry, Virginia Commonwealth University, Richmond, VA, United States; 4. Department of Mechanical and Nuclear Engineering, Virginia Commonwealth University, Richmond, VA, United States

Patients with schizophrenia often receive rTMS treatment, in which the dorsolateral prefrontal cortex or the primary auditory cortex and the Tempo-ro-Parietal Junction are stimulated in order to treat negative symptoms and cognitive deficits or auditory hallucinations, respectively [1], [2]. Finite element (FE) simulations of TMS on heterogeneous head models have been conducted to mimic what might be happening electromagnetically within the brain, a comparison between clinical resting motor threshold (RMT) data and simulation data has not been published [3]. In this study, we used individualized finite element models derived from patients' MRIs to investigate the correlation between RMT and brain anatomy. We first developed anatomically accurate head and brain models of 20 schizophrenia patient MRIs using SimNIBS pipeline. We then utilized FE analysis software to compute induced electric fields using patient's clinical parameters during their investigational procedure as shown in Fig. 1. In this way, the simulations were based on real patient data and completely customized to each subject. The electric field induced in the brain was recorded and compared with variables such as cortex-coil distance (CCD), age, and RMT as shown in Fig 2 (a) and (b) respectively. Our results show that there is little to no correlation between the measured CCD at M1 and the clinically-reported RMT or the maximum electric field recorded in the brain after TMS was simulated using Sim4Life. Thus, we hypothesize that the lack of clear correlation between the CCD at M1 and the measured RMT suggests that there are many other variables which may be influencing an individual's RMT, beyond the CCD. We hope the results of this study highlight key considerations that may be useful to future researchers designing methodology for studying RMT in TMS FE simulations. *This project was partially funded by NSF (#1357565) and Wellcome Trust / DBT India Alliance Early Career Fellowship to U. M. Mehta (IA/E/12/1/500755)*

[1] E. Poulet, J. Brunelin, B. Bediou, R. Bation, L. Forgeard, and J. Dalery, "Slow Transcranial Magnetic Stimulation Can Rapidly Schizophrenia," *Soc. Biol. Psychiatry*, pp. 95–98, 2005, doi: 10.1016/j.biopsych.2004.10.007. [2] H. He, J. Lu, L. Yang, J. Zheng, F. Gao, Y. Zhai, J. Feng, Y. Fan, and X. Ma, "Repetitive transcranial magnetic stimulation for treating the symptoms of schizophrenia: A PRISMA compliant meta-analysis," *Clin. Neurophysiol.*, vol. 128, no. 5, pp. 716–724, 2017, doi: 10.1016/j.clinph.2017.02.007. [3] E. G. Lee, P. Rastogi, R. L. Hadimani, D. C. Jiles, and J. A. Camprodon, "Impact of non-brain anatomy and coil orientation on inter- and intra-subject variability in TMS at midline," *Clin. Neurophysiol.*, vol. 0, no. 0, doi: 10.1016/J.CLINPH.2018.04.749.

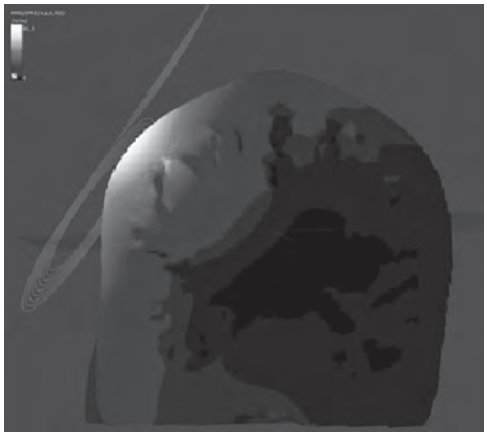

Fig.1. **Slice of schizophrenia patient head model with resultant electric field and TMS on M1 region.**

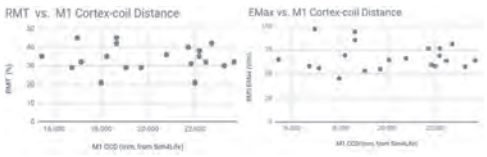

Figure 2 (a). **A comparison of reported RMT and measured CCD *(b).* calculated E_{max} and measured CCD.**

CONTRIBUTED PAPERS

J1-02. Quadruple Silicon Steel Core Coil for Highly Focused Transcranial Magnetic Stimulation in Small Animals.
I.C. Carmona[1], D. Kumbhare[2], M.S. Baron[3,4] and R.L. Hadimani[1,5] *1. Dept. of Mechanical and Nuclear Engineering, Virginia Commonwealth University, College of Engineering, Richmond, VA, United States; 2. Department of Neurosurgery, Virginia Commonwealth University Health System, Richmond, VA, United States; 3. McGuire Research Institute, Hunter Holmes McGuire Veterans Affairs Medical Center, Richmond, VA, United States; 4. Southeast Parkinson's Disease Research, Education and Clinical Center (PADRECC), Hunter Holmes McGuire Veterans Affairs Medical Center, Richmond, VA, United States; 5. Dept. of Biomedical Engineering, Virginia Commonwealth University, Richmond, VA, United States*

Transcranial magnetic stimulation (TMS) is a non-invasive technique used to regulate the synaptic activity of neurons in the brain, improving the functionality of connecting regions and bringing effective treatment to different neurological and psychiatric disorders. Treatment of many of these conditions requires application of external time-varying magnetic fields on a small cortical region to precisely alter connecting pathological sub-networks. The TMS induced field needs to be focused enough to avoid unwanted side effects caused by stimulation of the adjacent regions. Attempts at TMS in small animals[1] like rodents are highly constrained[2,3,4], since most of these

studies use commercial equipment intended for humans, with power and coil geometries not intended for small animals. The present work shows the design and evaluation of customized arrays of two and four double-winding coils with a silicon steel core to restrict the stimulation to areas as small as 1 mm^2, using finite element analysis with ANSYS Maxwell software. The coil is made with 50 turns of a wire with thickness = 1 *mm*, I.D. = 0.7 *mm*, O.D. = 4.5 *mm* and height = 25.4 *mm*. The cylindrical cores were designed with V-shape tip sharpening. The core material is silicon steel of 1.75 *T* of saturation flux density at 800 *A/m* and initial relative permeability of 500. The B-field was calculated 4.25 *mm* below the coil (vertical distance from the top of the scalp to the cortical layer 5/6 in adult rats) with currents of 1,000 *A* in short single (non-repetitive) pulses (≤ 4 *msec*) and showed values of up to 270 *mT* in 1 mm^2. The very small area achieved supports the utility of the coil to perform in-vivo experimentation on rodents. Future works will seek to improve the duration of pulses for repetitive TMS (rTMS) with refrigeration and pulse conformation techniques and to validate the novel TMS device with in-vivo experiments in rat models. This study was partially funded by the Dept. of VA Biomedical Lab Research and Development 2I01BX001147-05A2 merit review award (M. Baron, PI).

[1] J. Boonzaier, P. I. Petrov, W. M. Otte, N. Smirnov, S. F. W. Neggers, and R. M. Dijkhuizen, "Design and Evaluation of a Rodent Specific Transcranial Magnetic Stimulation Coil: An *In Silico* and *In Vivo* Validation Study," *Neuromodulation Technol. Neural Interface*, p. ner.13025, Jul. 2019, doi: 10.1111/ner.13025. [2] J. Selvaraj, P. Rastogi, N. P. Gaunkar, R. L. Hadimani, and M. Mina, "Transcranial Magnetic Stimulation: Design of a Stimulator and a Focused Coil for the Application of Small Animals," *IEEE Trans. Magn.*, vol. 54, no. 11, Nov. 2018, doi: 10.1109/TMAG.2018.2846521. [3] M. T. Wilson, A. D. Tang, K. Iyer, H. McKee, J. Waas, and J. Rodger, "The challenges of producing effective small coils for transcranial magnetic stimulation of mice," Biomed. Phys. Eng. Express, vol. 4, no. 3, Apr. 2018, doi: 10.1088/2057-1976/aab525. [4] I. P. de Sousa, C. R. H. Barbosa, and E. C. Monteiro, "Safe exposure distances for transcranial magnetic stimulation based on computer simulations," PeerJ, vol. 2018, no. 6, 2018.

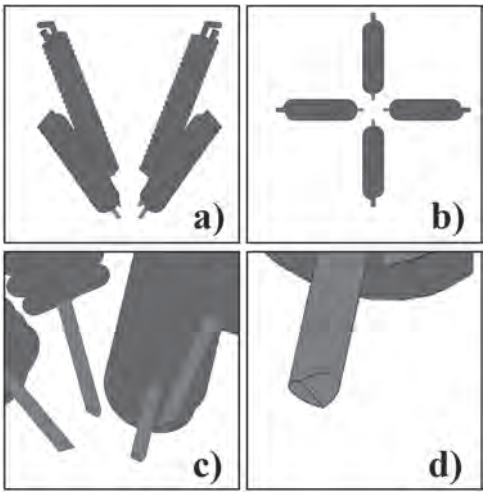

Fig. 1) Quadruple core array of coils. a) Isometric view. b) Top view. c) Bottom view. d) Tip sharpening details.

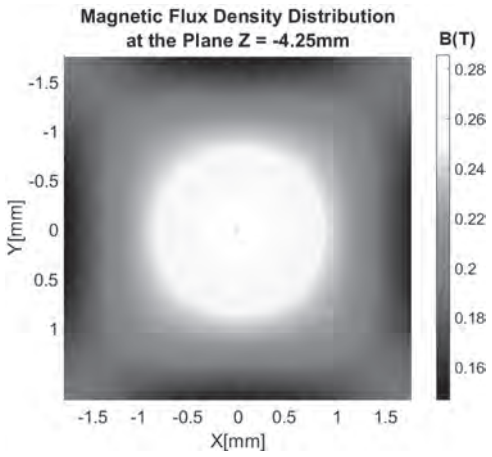

Fig. 2) B-field Magnitude at the plane z = -4.25 *mm* below the coils.

J1-03. Contacless Sensing of Spinal Cord Temperature Using Magnetically Bistable Microwires. J. Gamcova[1,2], M. Bacova[3], I. Sulla[4], L. Slovinska[5], J. Galik[3] and *R. Varga[1,6] 1. RVmagnetics a.s., Kosice, Slovakia; 2. Institute of Material Science, Slovak Academy of Sciences, Kosice, Slovakia; 3. Institute of Neurobiology, Slovak Academy of Sciences, Kosice, Slovakia; 4. Department of Anatomy, Histology and Physiology, University of Veterinary Medicine and Pharmacy, Kosice, Slovakia; 5. Associated Tissue Bank of Faculty of Medicine, University of Pavol Jozef Safarik in Kosice, Kosice, Slovakia; 6. Center of Progressive Materials TIP, University Pavol Jozef Safarik in Kosice, Kosice, Slovakia*

Temperature and pressure monitoring is one of the key factor in medicine. Therefore, there is an increasing demand for contactless and battery-less in vivo sensing. There are different approaches how to solve it using e.g. RF powering [1]. Glass-coated magnetic microwires are ideal materials for in-vivo medical applications [2]. They offer biocompatibility due to the Pyrex-glass coating and contactless sensing due to magnetic nature within the range of small magnetic field of low frequency and amplitude ($f \sim 100$ Hz, $H \sim 3$ Oe). Due to their small size (diameter cca. 10 μm), they are able to be implemented inside the living tissue. Having high and positive magnetostriction, they offer monodomain structure and magnetically bistable behaviour (there are only two possible magnetic states - positive or negative saturation), which is sensitive to temperature and allows to sense the temperature contactless, playing the single wire the role of passive element for in-vivo sensing. In the given contribution, we show the possibility to employ microwires as an in-vivo contactless temperature sensor for spinal cord monitoring. After correct adjustment of the system, it is possible to get sensitivity down to 0.01°C. Apart from showing the technique for temperature sensing, we have also performed histology study that confirms that microwire does not influence the living tissue of the spinal cord in rats even after 10 months. This research was supported by Slovak Grant Agency VEGA 1/0053/19, Slovak Grant Agency grant number APVV-16-0079.

[1] N. Chaimanonart and D. J. Young, *TRANSDUCERS 2009 - 2009 International Solid-State Sensors, Actuators and Microsystems Conference*, Denver, CO, pp. 1473-1476, 2009, [2] D. Kozejova et al., J. Magn. Magn. Mater. 470, pp. 2-5, (2019).

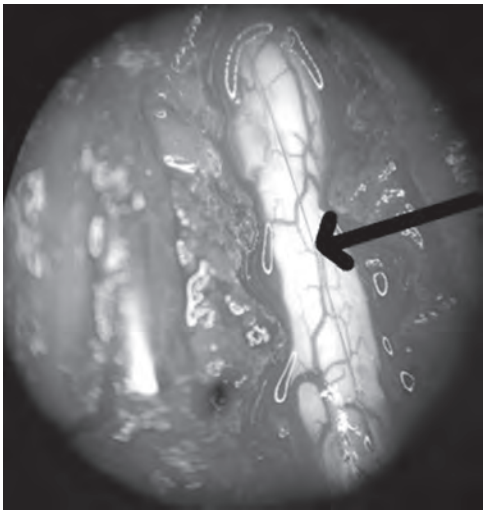

Spinal cord of rat with microwires included. Arrow show the position of microwire

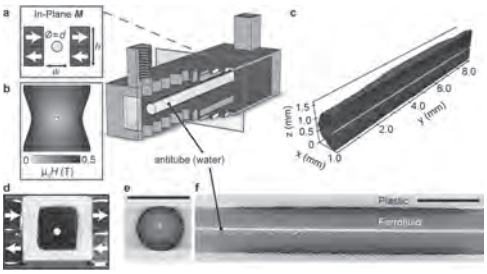

Wall-less magnetic confinement in a fluidic channel. *Centre*: exploded view, where permanent magnets (red, blue) in an in-plane quadrupolar configuration create a low-field zone at the centre *a*, where an antitube of water (yellow) is stabilized inside an immiscible magnetic liquid; *b* contour plot of the magnetic field; *c* synchrotron X-ray tomographic reconstruction of a water antitube (yellow) with diameter 81 μm surrounded by ferrofluid (blue); *d* optical end-view of a water antitube in ferrofluid; *e* X-ray end-view cross-section from tomographic data at *y* = 4 mm; and *f* X-ray side-view cross-section from tomographic data at *x* = 1 mm. Scale bars (black/white) are 2 mm.

INVITED PAPERS

J1-04. Liquid Flow and Control Without Solid Walls. *P. Dunne*[1,2], T. Adachi[2,3], A.A. Dev[1], A. Sorrenti[2,4], L. Giacchetti[2,5], A. Bonnin[6], C. Bourdon[7], P. Mangin[7], M. Coey[8], B. Doudin[1] and T.M. Hermans[2]
1. Institut de Physique et Chimie des Materiaux de Strasbourg, Strasbourg, France; 2. Institut de Science et d'Ingenierie Supramoleculaires, Strasbourg, France; 3. Universite de Geneve, Geneva, Switzerland; 4. Eidgenossische Technische Hochschule Zurich, Zurich, Switzerland; 5. Qfluidics, Strasbourg, France; 6. Paul Scherrer Institut, Villigen, Switzerland; 7. INSERM, EFS Grand-Est, BPPS UMR-S1255, FMTS, Strasbourg, France; 8. University of Dublin Trinity College, Dublin, Ireland

Solid walls become increasingly important when miniaturizing fluidic circuitry. They limit flow-rates achievable for a given pressure drop, and are plagued by fouling[1]. Approaches to reduce the wall interactions include hydrophobic coatings[2], liquid-infused porous surfaces[3], changing the surface electronic structure[4], electrowetting[5], and surface tension pinning[6]. A better solution may be to avoid the solid walls altogether[7]. Droplet microfluidics or sheath flow achieves this, but require continuous flow of both the liquid transported and the outer carrier liquid. Here we present a new approach[8], where wall-less aqueous liquid channels are surrounded by an immiscible magnetic liquid, both being stabilised by a quadrupolar magnetic field. This creates self-healing, uncloggable, anti-fouling, and near-frictionless liquid-in-liquid fluidic channels with millimetre effective slip lengths, with diameters of order 10 cm, or as small as 10 μm. Pumping is achieved by moving permanent magnets that have no physical contact with the liquid channel. We show that this magnetostaltic pumping method can be used to transport whole human blood with very little damage due to shear forces; haemolysis is reduced by an order of magnitude compared to traditional peristaltic pumping. Our liquid-in-liquid approach provides new avenues to transport delicate liquids, particularly when scaling channels down to the micron scale with no need for high pressures, while retaining basic microfluidic circuitry functionalities.

1. R. Mukhopadhyay, *Anal. Chem.* 77, 429 A-432 A (2005). 2. B. Zhao, *et al.*, *Science* 291, 1023–1026 (2001). 3. W. Wang, *et al., Nature* 559, 77 (2018). 4. E. Secchi, *et al., Nature* 537, 210–213 (2016). 5. K. Choi, *et al., Annu. Rev. Anal. Chem.* 5, 413–440 (2012). 6. E. J. Walsh, *et al.,* Microfluidics with fluid walls. *Nat. Commun.* 8, 816 (2017). 7. J. M. D. Coey, *et al.,* Proc. Natl. Acad. Sci. U.S.A. 106, 8811 (2009) 8. P. Dunne *et al.*, Nature, 581, 58 (2020)

J1-05. 2D Nanodisks for Magnetic Hyperthermia: Role of Hysteresis Losses. *P. Tiberto*[1], G. Barrera[1], F. Celegato[1] and M. Coïsson[1] *1. Advance materials and life science, Istituto Nazionale di Ricerca Metrologica, Torino, Italy*

Size, shape and aspect ratio play a very important role influencing circulation time, biodistribution and the processes of cellular phagocytosis and internalization. In the last decade, the advantages provided by the discoidal shape were combined with the magnetic functionality in order to synthesize multifunctional magnetic nanodisks (NDs) [1,2]. The cellular uptake of sub-micron Au-coated Py nanodisks has been recently observed and their presence on the tumor cells verified [2]. Pancreatic tumor cells have been found to uptake and retain Au-coated $Ni_{80}Fe_{20}$ NDs prepared by means of a bottom-up self-assembling nanolithography technique. The chosen geometrical parameters, i.e. diameter (650 nm) and thickness (30 nm), give rise to magnetic domain patterns arranged in vortex state at the magnetic remanence. Tumor cell lines were cultured in presence of different concentrations of Au-coated $Ni_{80}Fe_{20}$ nanodisks (NDs) and NDs biocompatibility was evaluated by viability and proliferation tests [2]. Among the open issues preventing NPs and NDs full exploitation as therapeutic agents, reliable and reproducible methods of measuring the functional capability have to be established. In case of magnetic hyperthermia, traceability of specific absorption rate (SAR) is far to be gained. In particular, a careful characterization of the magnetic properties regarding both the fundamental properties of the studied particles (magnetization curves, hysteresis losses) and their thermal properties during hyperthermia treatments is required. Magnetic hysteresis loops areas and their role on the heat released have been studied with the aim of providing reliable and reproducible methods to measure the specific absorption rate (SAR) or Specific Loss Power (SLP) [3]. Specific loss power (SLP) has been measured on a water solution containing a known concentration of free-standing nanodisks through a calibrated non-adiabatic setup [3]. The water solution is exposed to an alternating electromagnetic field (frequency 100 kHz) having a peak amplitude in the range 30 – 60 mT (for its magnetic component), which is compatible with exposure of biological tissues. A suitable thermodynamic model is exploited to fit the experimental data and determine the SLP, by properly taking into account self-heating of water and heat exchanges among the different components of the setup. SLP values much larger than those achieved with conventional magnetite or ferrite nanoparticles are achieved. Such a method has been tested in $Fe_{70}Pd_{30}$ nanodisks obtained by nanosphere lithography following a process described in [1,2]. NDs have different geometrical parameters (thickness = 30 nm, diameter ranging from 250 nm to 500 nm). SEM images of the attached nanodisks together with the corresponding hysteresis loops measured by Alternating Gradient Field Magnetometer are shown in Fig. 1. The magnetisation process of all samples displays a vortex-like behavior,

although fainter in the sample having 250 nm diameter (see Fig. 1a). To evaluate the role of hysteresis losses, minor loops at selected applied field have been measured and the losses calculated. SAR values obtained from hyperthermia measurements will then be directly compared with the ones obtained by the hysteresis losses from the area of the minor loops measured at the same maximum magnetic field (gray area in Fig. 2). By this comparison, the role of magnetic losses on the hyperthermia treatment will be discussed.

[1] M. Campanini at al., Small (2018) doi.org/10.1002/smll.201803027 [2] C. Divieto, G. Barrera et al. Front. Nanotechnol. doi: 10.3389/fnano.2020.00002 [3] M. Coisson et al. Biochem. Biophys. Acta 1861 (2017) 1545

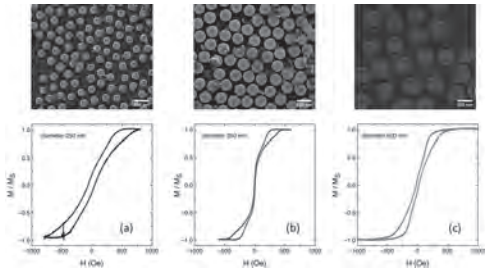

SEM images (upper panel) together with corresponding hysteresis loops (lower panel) for $Fe_{70}Pd_{30}$ nanodisks having 30 nm thickness and diameter: (a) 250 nm; (b) 350 nm and (c) 500 nm.

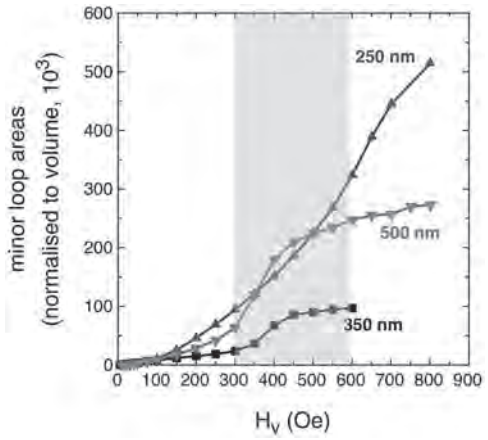

Minor loops area as a function of maximum applied field for all nanodisks diameters

J1-06. Janus Magnetic-Plasmonic Nanoparticles for Magnetically Targeted and Thermally Activated Cancer Therapy. *A. Espinosa*[1,2], J. Reguera[3,5], A. Curcio[2], A. Muñoz-Noval[6], C. Kuttner[4], A. Van de Walle[2], L. Liz-Marzán[4,5] and C. Wilhelm[2] *1. IMDEA Nanociencia, Madrid, Spain; 2. Laboratoire Matière et Systèmes Complexes (MSC), Université Paris Diderot, Paris, France; 3. BCMaterials, Basque Center for Materials, Applications and Nanostructures, Bilbao, Spain; 4. CIC biomaGUNE and Ciber-BBN, Donostia-San Sebastián, Spain; 5. Ikerbasque, Basque Foundation for Science, Bilbao, Spain; 6. Dpto. Física Materiales, Facultad CC. Físicas, Universidad Complutense de Madrid, Madrid, Spain*

Treatments based on multifunctional thermal-activated nanomaterials have emerged as a promising biomedical strategy [1]. One of the major limitations in nanoparticles-mediated thermal therapies to be translated to the clinics is to achieve sufficient nanoparticles concentration at tumor site to elicit a therapeutic action after systemic administration [2]. In this work, we have tested the use of double-faced gold-iron oxide Janus nanoparticles as efficient therapeutic nanoheaters when subjected to magneto- and photo-thermal heating, whose combination into a magneto-photo-thermal treatment led to a synergistic effect in tumour cells [3,4]. The on-site delivery of these nanoparticles to the tumour was improved thanks to their high potential for magnetic guiding. This nanoparticle concentration at the tumor site was sufficient to achieve a therapeutic temperature elevation under photothermal therapy at moderate laser power in animal models This magnetic-targeted photothermal therapy *in vivo* resulted in a successful tumor growth inhibition after only 1-day shot exposure.

[1] A. Curcio, A. K. Silva, S. Cabana *et al.*, Theranostics 9, 1288 (2019). [2] S. Wilhelm, A. J. Tavares, Q. Dai *et al.*, Nature Reviews Materials 1, 16014 (2016). [3] J. Reguera, D. Jiménez De Aberasturi, M. Henriksen-Lacey *et al.*, Nanoscale 9, 9467 (2017). [4] A. Espinosa, J. Reguera, A. Curcio *et al.*, Small, 1904960 (2020).

J1-07. Functional Magnetic Ferrogels: From Biosensors to Regenerative Medicine. *G.V. Kurlyandskaya*[1,5], F.A. Blyakhman[5,3], N.A. Buznikov[2], A.P. Safronov[5,4] and S.V. Shcherbinin[5,4] *1. Electricity and Electronics, University of Basque Country UPV-EHU, Leioa, Spain; 2. Scientific and Research Institute of Natural Gases and Gas Technologies, Moscow, Moscow, Russian Federation; 3. Biophysics, Ural State Medical University, Ekaterinburg, Ekaterinburg, Russian Federation; 4. Institute of Electrophysics, UD RAS, Ekaterinburg, Russian Federation; 5. Institute of Natural Sci. and Math., Ural Federal University, Ekaterinburg, Russian Federation*

In-tissue embedded magnetic nanoparticle (MNPs) detection is one of the most requested cases for biomedical applications. We propose to use synthetic hydrogel with certain amount of MNPs. Natural tissue requires tight protocol of storage and testing but synthetic hydrogels mimic many functional properties being less demanding to test conditions. In order to make functional ferrogels (FG) widely available there is a need in the development of synthesis techniques with enhanced size of a batch: electrophysical techniques of electric explosion of the wire or laser target evaporation (LTE)). We have developed magnetic biosensor prototype for the detection of mesoscopic distributions of nanoparticles using magnetimpedance (MI). Prototype with FeNi-based multilayered structures was designed and tested. MI responses were measured with and without polyacrylamide FG layer in order to evaluate stray fields of embedded MNPs. A model for MI response based on a solution of Maxwell equations with Landau-Lifshitz equation was developed. LTE MNPs were used for synthesis of polyacrylamide ferrogels. Their adhesive and proliferative potentials were studied. We discussed the possibility of creation of a new generation of drug delivery systems for multifunctional devices. We discussed the possibility of creation of a new generation of drug delivery systems for magnetic field assisted delivery and biosensing. This research was funded by the Russian Science Foundation, grant number 18-19-00090.

1. Beketov I.V. et al. AIP Adv., 2 (2012) 022154. 2. Safronov A.P. et al. AIP Adv. 3(5) (2013) 052135. 3. Kurlyandskaya G.V. et al. Appl. Phys. Lett., 106 (19) (2015) 193702. 4. Buznikov N.A. et al. Bios. Bioelectr. 117 (2018) 366. 5. Blyakhman F.A. et al. Nanomater. 9 (2019) 232.

CONTRIBUTED PAPERS

J1-08. Using Dipolar Interactions to Improve Magnetic-Hyperthermia Performance of Low-Anisotropy Nanoparticles: Theoretical Study of Chain-Like Structures. *D.P. Valdés*[1,2], E. Lima Jr.[1], R.D. Zysler[1,2] and E. De Biasi[1,2] *1. Instituto de Nanociencia y Nanotecnología, CNEA-CONICET, S.C. de Bariloche, Argentina; 2. Instituto Balseiro, Universidad Nacional de Cuyo, S.C. de Bariloche, Argentina*

Improvement of the Specific Power Absorption (SPA) is a key factor for future use of magnetic nanoparticles (NPs) in magnetic-fluid-hyperthermia (MFH) protocols, since it allows working with low concentration of NPs, avoiding toxic effects and simplifying the task of localizing a great amount of NPs in a tumour. *In vitro* and *in vivo* experiments generally lead to

interacting NP systems due to agglomeration inside cells. For linear aggregates, the impact of dipolar interactions on the SPA of the system is still an open discussion: there are reports of beneficial [1] and detrimental [2] effects. In this work, we analyzed dipolar interactions in 1D chains of NPs with low uniaxial anisotropy along the chain. Starting from a previously reported non-linear probabilistic model [3], interactions were taken into account by adding a dipolar contribution in the local field felt by each NP [4]. The main focus was done in the repercussion on the enclosed area of the hysteresis loops, that can be translated into the SPA in a MFH experiment. Chains with different orientation Φ_n (regarding the external field H) were simulated. We confirmed that interactions in these kind of low-anisotropy systems help to increase de area of the loops, both for individual orientations and randomly oriented chains (see Figure). We interpreted this increment as a consequence of an effective shift between the local field felt by a NP and the external field. We decomposed the dipolar field in the parallel ($H_{dip}^{\parallel}$) and perpendicular ($H_{dip}^{\perp}$) components (with respect to H) and obtained that both of them exhibit hysteresis, as does the magnetization. The relative area contribution was evaluated and it was seen that for the parallel (perpendicular) spatial configuration, $H_{dip}^{\parallel}$ ($H_{dip}^{\perp}$) is the most relevant component. This means that, when simulating a chain with Φ_n close to $\pi/2$, the system cannot be modeled with a dipolar field parallel to H, as usually done. In conclusion, low-anisotropy linear arrangements help to significantly enhance MFH in NP systems, obtaining a better heating performance, with the parallel configuration being the most favored one.

[1] B. Mehdaoui, R.P. Tan and A. Meffre, Physical Review B, Vol. 87, p. 174419 (2013). [2] L.C. Branquinho, M.S. Carrião, A.S. Costa, Scientific Reports, Vol. 3, p. 2887 (2013). [3] E. De Biasi, R.D. Zysler and C.A. Ramos, Journal of Magnetism and Magnetic Materials, Vol. 320, p. 312 (2008). [4] D. P. Valdés, E. Lima Jr. and R.D. Zysler, Physical Review Applied, Vol.14, p. 014023 (2020).

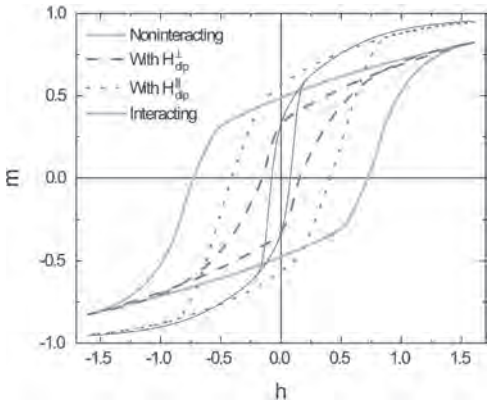

Normalized magnetization vs. normalized external field for a system of randomly oriented chains.

J1-09. Fundamental Study on Cancer Therapy by Blocking Newborn Blood Vessels With Surface Modified Magnetite Particles.

M. Kirimura[1], Y. Akiyama[1] and F. Sato[1] *1. Graduate School of Engineering, Osaka Daigaku, Suita, Japan*

In this study, we proposed a novel cancer treatment by blocking newborn blood vessels around the diseased part, which has low side effect and less invasiveness. In the therapy, ferromagnetic particles administered into the body are accumulated in the newborn blood vessels using a rotating magnetic field[1], and then are aggregated by a uniform magnetic field to block the blood vessels. The blockage prevents the cancer from growth and metastasis. In order to block the newborn blood vessels, it is necessary to aggregate submicron-sized ferromagnetic particles to the size of the inner diameter of the blood vessels as large as 10-40 μm. In addition, irreversible aggregation ire necessary to keep the blockage. In the previous studies[2], we prepared stearic acid modified magnetite particles that form irreversible aggregation under the magnetic field, and found that the aggregates could maintain a blockage of flow channel even after application of magnetic field. In this study, in order to design the particles for practical use, we simulated the aggregation process of particles in a flow channel and calculated the pressure loss. According to the simulation results of the aggregation process under a uniform magnetic field of 0.40 T, it was found that chain aggregation were formed in the flow channel. The pressure loss calculated by Kozeny-Carman equation showed that a decrease in the void ratio causes a pressure loss higher than the blood pressure of 4.0×10^3 Pa. Based on the result, we experimented the blockage of the flow channel using these particles under the uniform magnetic field. A 25 wt% PVA (Polyvinyl alcohol) solution (4.7 mPa●s) that simulated the viscosity of blood was flowed into a channel, branched into four capillary tubes with inner diameter 500 μm, simulating the vessels at a flow rate of 1.8 mm/s. While introducing the PVA solution, a uniform magnetic field of 0.45 T was applied only to one channel, and then 25 mL of 500 ppm suspension of polyacrylic acid-modified particle was introduced. As a result, chain aggregation were formed as shown in Fig. 1, and only the flow path under magnetic field was blocked.

[1]Makoto Kirimura, Yoko Akiyama, "Fundamental Study on Cancer Therapy by Blocking Newborn Blood Vessels Using a Rotating Magnetic Field", *Journal of Physics: Conference Series*, vol. 1293, pp. 1-10, 2019 [2]Makoto Kirimura, Yoko Akiyama, Shigehiro Nishijima, "Fundamental Study on Cancer Therapy by Blocking Newborn Blood Vessels by Magnetic Force Control", *Progress in Superconductivity and Cryogenics*, vol. 20, No. 2, pp.11-15, 2018

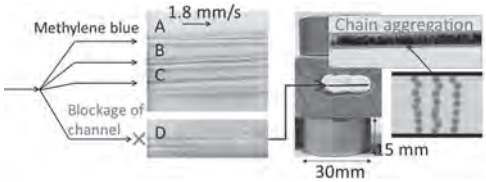

Fig. 1 Blockage of flow channel caused by chain aggregation under homogeneous magnetic field.

Session J2
CRYSTALLINE SOFT MAGNETIC MATERIALS

Alex Leary, Chair
NASA Glenn Research Center, Sandusky, OH, United States

CONTRIBUTED PAPERS

J2-01. An Improved Magnetostriction Model of Silicon Steel Considering the Saturated Magnetic Domain Wall Movement. *T. Ben*[1], F. Chen[1], L. Chen[1,2] and R. Yan[2] *1. China Three Gorges University, Yichang, China; 2. Hebei University of Technology, Tianjin, China*

I Introduction In order to obtain the deformation characteristic of silicon steel with yoke clamping applied under alternating magnetic field, a stress-dependent magnetostriction model of silicon steel must be construct. Due to the rotation of magnetic domain and the movement of magnetic domain wall with stress applied, the magnetostrictive deformation of the material will reverse and saturate in both magnitude and direction [1-3]. Therefore, the saturated magnetic domain wall movement effect must be considered in stress-dependent magnetostriction model. II The hysteresis stress-dependent magnetostriction model of silicon steel Based on the comparison of the measured magnetostrictive strain curves and hysteresis loops, the hysteresis effect of magnetostrictive curve is obvious even the area of hysteresis loop is small [2]. Therefore, this paper constructs the magnetization model based on the J-A hysteresis model. Then, based on the macroscopic thermodynamics and Gibbs free energy expansion, the stress-dependent magnetostriction model in the excitation state is constructed. Meanwhile, due to the pinning effect, the magnetostrictive curve of silicon steel in demagnetization process cannot return along the original path and reach the initial state. Therefore, the magnetostrictive parameter λws which express the magnetic domain wall movement under varying stress in saturated magnetization was introduced into the magnetostriction model in the demagnetization case. The parameters of the model which control the saturated magnetic domain wall movement are extracted from the measured magnetic curves of non-oriented silicon steel sheet, which are shown in Fig. 1. III Results and discussion The simulated results are shown in Fig. 2. As shown, the time when magnetostriction reaches the maximum in the simulation is consistent with the experimental results, which shows that influence of saturated magnetic domain wall movement on magnetostrictive deformation is accurately simulated in the model.

[1] Zhu L, Li J, Yang Q, et al. An Improved Magnetostriction Model for Electrical Steel sheet Based on Jiles-Atherton Model[J]. IEEE Transactions on Magneics, 2020, 56(3):7514604. [2] Zhang Y, Zhou H, Zhou Y. Vibration suppression of cantilever laminated composite plate with nonlinear giant magnetostrictive material layers[J]. Acta Mechanica Solida Sinica, 2015, 28(1):50-61. [3] Wang Z, Zhang Y, Ren Z, et al. Modeling of Anisotropic Magnetostriction Under DC Bias Based on an Optimized BP Neural Network[J]. IEEE Transactions on Magnetics, 2020, 56(3): 7512204

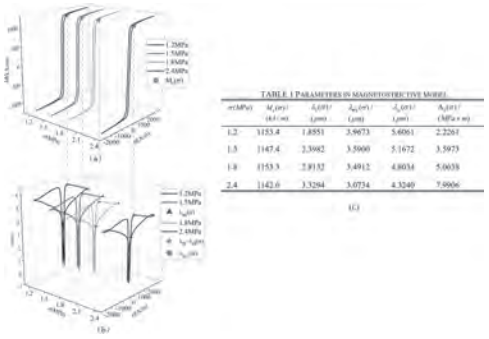

TABLE I PARAMETERS IN MAGNETOSTRICTIVE MODEL

σ(MPa)	M_s(σ)/(kA/m)	k_1(σ)/(μm)	λ_{ws}(σ)/(μm)	c_1(σ)/(μm)	A_1(σ)/(MPa·m)
1.2	1153.4	1.8551	3.9673	5.6061	2.2261
1.5	1147.4	2.3982	3.5900	5.1672	3.5973
1.8	1153.3	2.8152	3.4912	4.8034	5.0038
2.4	1142.6	3.3294	3.0734	4.3249	7.9906

Fig.1. The extraction method of magnetic domain movement parameters : (a) magnetization; (b) magnetostriction; (c) parameters.

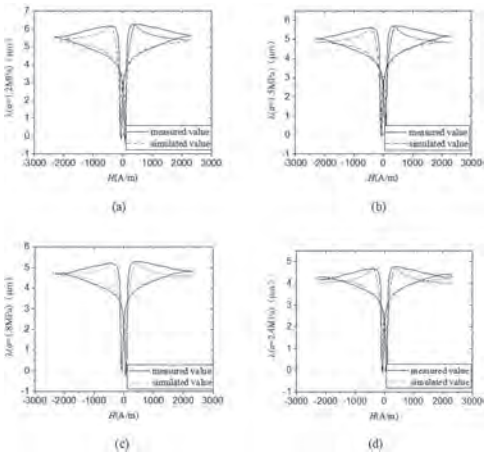

Fig.2. Magnetostrictive loops under different stresses: (a) 1.2MPa, (b) 1.5MPa, (c) 1.8MPa, (d) 2.4MPa

J2-02. Withdrawn

J2-03. Domain Structure and Energy Losses up to 10 kHz in Grain-Oriented Fe-Si Sheets. A. Magni[1], A. Sola[1], O. de la Barrière[2], E. Ferrara[1], L. Martino[1], *C. Ragusa*[3], C. Appino[1] and F. Fiorillo[1] *1. Istituto Nazionale di Ricerca Metrologica, Torino, Italy; 2. Lab. SATIE, CNRS–ENS, Saclay, France; 3. Department of Energy, Politecnico di Torino, Torino, Italy*

Recent trends in the distribution of electrical energy through medium- and low-voltage grids, involving a variety of sources and smart infrastructures, call for extensive use of medium frequency transformers, as required for conversion steps and bidirectional power transfers. The employed grain-oriented (GO) cores are subjected to kHz frequencies and harmonics-rich voltages. These are scarcely assessed working regimes, regarding both loss behavior and dynamics of the domain structure. We perform in this work a thorough investigation on

the energy loss dependence on frequency f (DC – 10 kHz) and peak polarization J_p (0.25 T – 1.7 T) of high-permeability 0.29 mm thick GO steel sheets, combined with the magneto-optical Kerr analysis of the dynamics of the domain walls and the evolution of the domain structure in well-oriented grains. The predicting model starts with the determination of the induction profile across the sheet thickness at any instant of time, according to the Maxwell's diffusion equation, which is applied using the experimental normal/anhysteretic curves as magnetic constitutive equations. The classical energy loss component W_{cl} is calculated versus f and J_p, together with the evolution of the hysteresis loss W_h. This, although increasing with f, is observed to provide negligible contribution in the kHz range. The Kerr images show that the regular antiparallel domain wall (dw) structure is initially preserved under increasing f, at the cost of bowing and dw densification, while the excess loss W_{exc} follows a regular power law. However, at sufficiently high f and J_p values, the dws meet and annihilate at the surface, while remaining stuck as cylindrical domains at the sheet midplane. It turns out that in the high (f, J_p) corner the magnetization process occurs by penetration towards the midplane of extended dws parallel to the sheet surface, with W_{exc} and W_h dwarfed by the classical loss component.

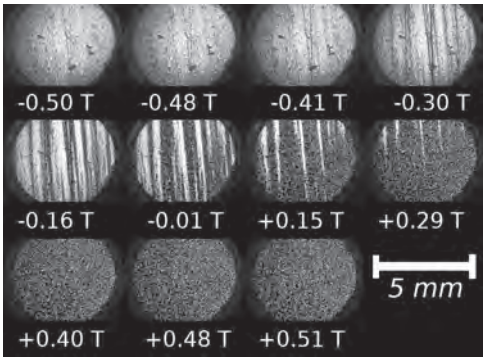

Fig. 1. Domain structure evolving between J_p = ± 0.5 T at 10 kHz. Saturation at the surface occurs for J slightly larger than ± 0.30 T.

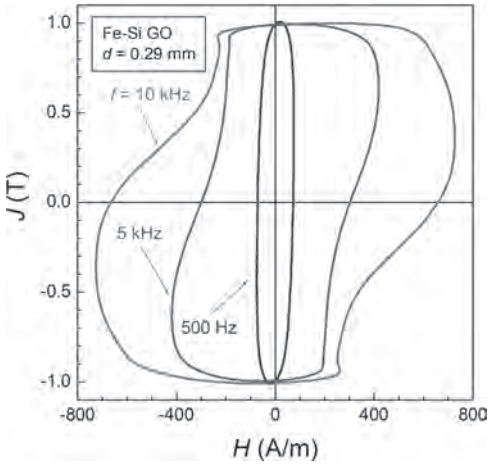

Fig. 2. J_p = 1 T. The hysteresis loop shape evolution with f points to a transition towards inward penetration of the saturated surface state.

J2-04. Secondary Recrystallization Behavior in Magnetostrictive Fe-Ga Thin Sheets Induced by Nano-Sized Composite Precipitates. *Z. He*[1,2], Y. Sha[2], G. Zhou[1], F. Zhang[2] and L. Zuo[2] *1. School of Materials Science and Engineering, Shenyang University of Technology, Shenyang, China; 2. Key Laboratory for Anisotropy and Texture of Materials (Ministry of Education), Northeastern University, Shenyang, China*

Fe-Ga alloy is an advanced magnetostrictive material for actuators and sensors in terms of combining excellent mechanical and magnetostrictive properties. It is desirable to produce η(<100>//RD) textured Fe-Ga sheets due to the magnetostriction anisotropy with the largest coefficient along <100> direction and the serious eddy current loss in high-frequency use [1,2]. The secondary recrystallization Goss ({110}<001>) texture and large magnetostriction coefficient were mainly achieved by the combination of micron-sized NbC particles and surface energy effect in high-temperature annealing [3,4], as well as the initial sharp <100>-oriented columnar grains by directional solidification [5,6]. However, nano-sized MnS and AlN precipitates are used to induce the secondarily recrystallized Goss grains with an average deviation angle of 3° in grain-orientated silicon steel by conventional rolling and annealing method [7]. Therefore, the characteristic of precipitates has not been well solved in Fe-Ga alloy sheet, so that the application of surface energy and unconventional processing method is still necessary. In the present study, the composite inhibitor composed of nanometer-sized sulfide and carbonitride are dispersedly precipitated in hot rolling and subsequent annealing. The gradually dissipated inhibition force during high-temperature annealing promotes a few exact Goss grains to grow abnormally by consuming primary recrystallized matrix grains textured by γ-fiber. Centimeter-sized secondary recrystallization Goss grains with smaller average deviation angle and large magnetostriction coefficient as high as 307 ppm is obtained without surface energy effect. The result indicates that complete secondary recrystallization can be realized based on the precise design and control of nano-sized composite precipitates and primary recrystallization microstructure/texture in Fe-Ga alloy by conventional rolling and annealing methods.

[1] E. M. Summers, R. Meloy and S. M. Na, J Appl Phys., Vol. 105, p.07A922 (2009). [2] S. M. Na and A. B. Flatau, J Appl Phys., Vol. 101, p.09N518 (2007). [3] S. M. Na, K. M. Atwater and A. B. Flatau, Scripta Mater., Vol. 100, p.1 (2015). [4] S. M. Na and A. B. Flatau, Scripta Mater., Vol. 66, p.307 (2012). [5] C. Yuan, J. H. Li, W. L. Zhang, J Magn Magn Mater., Vol. 391, p.145 (2015). [6] Y. Y. Liu, J. H. Li, X. Mu, J Magn Magn Mater., Vol. 444, p.364 (2017). [7] Z. S. Xia, Y. L. Kang and Q. L. Wang, J Magn Magn Mater., Vol. 320, p.3229 (2008).

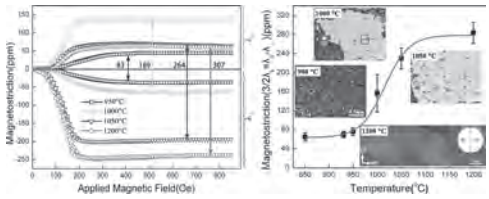

Fig.1 Magnetostriction curves functioned with magnetic fields and magnetostriction values functioned with heating temperatures of the Fe Ga sheets, Insets figures present the texture of sheets

J2-05. Domain Observation in Electrodeposited Permalloy Thin Films. *K. Dev*[1], G. VASHISHT[1], V.R. Reddy[2] and A. Subramanian[1] *1. Department of Physics and Astrophysics, University of Delhi, New Delhi, India; 2. UGC-DAE Consortium for Scientific Research, Indore, India*

Ni-rich FeNi alloy (permalloy) thin films possess high permeability, low anisotropy and low damping constant. These unique set of properties mark their importance in high frequency micro-devices. The synthesis of $Fe_{20}Ni_{80}$ films using cost-effective simple technique without involving high vacuum conditions and investigation of their magnetic behavior is of great importance for such technical applications. $Fe_{20}Ni_{80}$ films were deposited on Indium Tin Oxide (ITO) coated glass substrates by electrochemical deposition technique in potentiostatic mode using three-electrode cell. I-V characteristics measured using cyclic voltammetry revealed oxidation-reduction states and potential for onset of film deposition onto the substrate. The desired composition of $Fe_{20}Ni_{80}$ films, were prepared using calculated concentration of solutions in electrolyte. The elemental composition was confirmed by EDAX. FESEM images depict uniformly dispersed nanocubes all over the substrate. Bulk hysteresis measurement by VSM confirms low coercivity (H_c) ~ 42 Oe, high saturation magnetization (M_s) ~ 760 emu/cm^3 and high remanence (M_r), with the ratio of M_r/M_s ~ 0.7 in-plane geometry *(Fig.1)*. Reduced M_r/M_s ~ 0.2 was observed in out-plane configuration.

The M_r/M_s ratio increased to 0.8 after annealing at 400 °C in Ar+H_2 atmosphere while retaining low H_c for in-plane configuration. The out-plane M-H curves shows increased H_c~560 Oe attributed to pinning and M_r/M_s ~ 0.26. The surface magnetic properties observed using L-MOKE revealed similar H_c and enhanced remanence after annealing. The in-plane hysteresis curves recorded at azimuthal angles of 0°, 45°, and 90° do not show significant changes, indicating random distribution of easy axis along film plane. The magnetization reversal is directed by stripe-like domains *(Fig. 2)* originating due to slight perpendicular component of magnetization evidenced by non-zero remarkable remanence in out-plane hysteresis. Such domain configuration along with low H_c and high M_s makes the presented highly permeable $Fe_{20}Ni_{80}$ useful for high frequency device applications.

1. Cao, D., Pan, L., Liu, Q. *Journal of Physics D: Applied Physics*, *51*(2), 025001 (2017). 2. Vashisht, G., Kumar, V., Annapoorni, S. *Journal of Magnetism and Magnetic Materials*, *497*,166064 (2020). 3. Hubert, Alex, and Rudolf Schäfer. Springer Science & and Business Media, (2008). 4. Kainuma, S., Tsuya, N., *Journal of Applied Physics*, *34.* 795-799 (1963). 5. Bhatia, E., Hussain, Z., Reddy, V. R., *arXiv preprint arXiv:1903.08106* (2019).

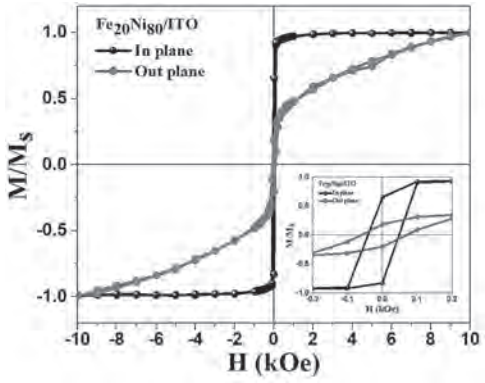

Fig.1 M-H curve for in-plane and out-plane geometry for as synthesized sample

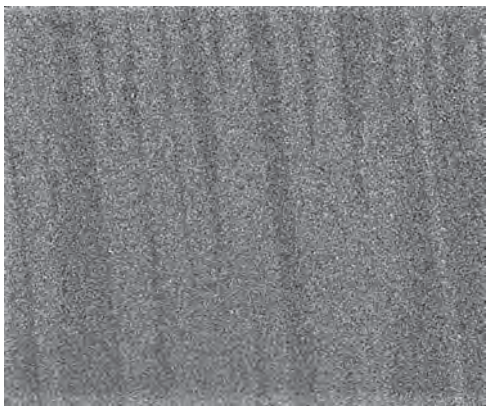

Fig.2 MOKE microscopy image showing domain structure with 180° reversal.

J2-06. New Pathways to Iron Nitride Soft Magnets. *T. Monson*[1], T. Stevens[1], C. Pearce[1], M. Hoyt[1], E. Vreeland[1], R. Delaney[1], S. Atcitty[1], B. Zheng[2], C. Belcher[2], Y. Zhou[2], E. Lavernia[2] and T. Rupert[2] *1. Sandia National Laboratories, Albuquerque, NM, United States; 2. University of California, Irvine, Irvine, CA, United States*

The magnetic properties of the iron-nitrogen system have only been explored on a very limited basis. Theoretical predictions of the magnetic behavior of the different phases of iron nitride are limited and experimental data is quite sparse. By employing several different techniques which include solution based nanoparticle nitridation, electrochemical methods, and metathesis based reactions we have synthesized several different phases of iron nitride: FeN, Fe_2N, Fe_3N, Fe_4N, and $Fe_{24}N_{10}$. Additionally, we have demonstrated a path for consolidating raw powders of iron nitride into bulk material, enabling integration into devices such as inductors, transformers, and motors. Our difficulties and successes in synthesizing and processing these different phases of iron nitride will be described. Additionally, the magnetic properties of these seldom explored iron-nitrogen compounds will be summarized. Sandia National Laboratories is a multimission laboratory managed and operated by National Technology and Engineering Solutions of Sandia, LLC., a wholly owned subsidiary of Honeywell International, Inc., for the U.S. Department of Energy's National Nuclear Security Administration under contract DE-NA0003525.

J2-07. Accelerated Soft Magnetic Materials Development.
V. Chaudhary[1], M.S. Nartu[2], S. Dasari[2], R. Banerjee[2] and R. Ramanujan[1] *1. School of Materials Science and Engineering, Nanyang Technological University, Singapore, Singapore; 2. Department of Materials Science and Engineering, University of North Texas, Denton, TX, United States*

Developing a new magnetic material from laboratory to real applications often requires long timelines and high cost. The accelerated development of soft magnetic materials is vital for addressing the challenges associated with improving the performance of electrical machines, transformer cores, electric vehicles, etc[1]. We used a direct energy deposition based additive manufacturing technique, i.e., Laser Engineering Net Shaping (LENS) to produce compositionally graded magnetic materials. There[1, 2] are two advantages; i) rapid mapping of a vast composition space and ii) functionally graded magnetic alloys necessary for the next generation of electric machines. A combinatorial assessment of the structural and magnetic properties of a range of soft magnetic materials such as Fe-xNi, Co-xFe, Fe-xNi-yMo, Co-xFe-yNi, AlxCoFeNi, etc. has been carried out. As an example, the change in saturation magnetization (M_s) and coercivity (H_c) of Co-xFe and Ni-xFe samples are shown in Figure 1. The most promising composition, structure and properties are rapidly identified, enabling accelerated materials development of soft magnetic materials. Studies on the use of computational approaches and their integration with these experiments[3] will also be elucidated. This work is supported by the AME Programmatic Fund by the Agency for Science, Technology and Research, Singapore under Grant No. A1898b0043.

1. V. Chaudhary, S. A. Mantri, R. V. Ramanujan, and R. Banerjee, Progress in Materials Science 114, 100688 (2020). 2. V. Chaudhary, N. M. S. K. K. Yadav, S. A. Mantri, S. Dasari, A. Jagetia, R. V. Ramanujan, and R. Banerjee, Journal of Alloys and Compounds 823, 153817 (2020). 3. S. Dasari, V. Chaudhary, B. Gwalani, A. Jagetia, V. Soni, S. Gorsse, R. V. Ramanujan, and R. Banerjee, Materialia 12, 100755 (2020).

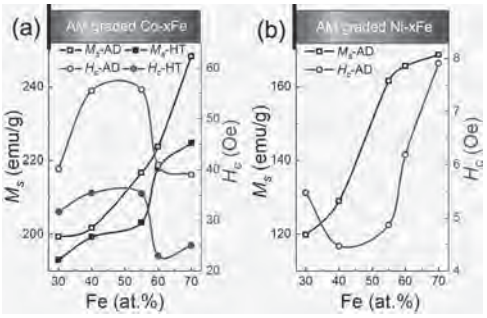

Fig. 1 (a) Saturation magnetization (left axis, black curve) and coercivity (right axis, blue curve) of (a) Co-xFe and (b) Ni-xFe as a function of iron concentration. AD and HT denote the results for the samples of as deposited and after heat treatment, respectively.

J2-08. Evaluation of Medium-Entropy $Fe_xCo_yNi_z$ Alloys as Precursors for FeCoNi-Based High-Entropy Soft-Magnetic Alloys. A.A. Paul[1] and *T.V. Jayaraman*[1] *1. Mechanical Engineering, University of Michigan Dearborn, Dearborn, MI, United States*

High-entropy magnetic alloys present an excellent combination of functional and structural properties that broadens the space for developing high-performance soft-magnetic magnetic alloys for several energy conversion applications [1-2]. We evaluated the suitability of several $Fe_xCo_yNi_z$ medium-entropy alloy compositions, whose configurational entropy (ΔS_{config}) is higher than ~9 J/mol K [3], as a precursor for FeCoNi-based high-entropy soft-magnetic alloys. We examined and compared the magnetic properties and structure of $Fe_xCo_yNi_z$, synthesized by mechanical alloying, over a range of temperatures. We characterized the structure by electron microscopy and x-ray diffraction, and the magnetic properties by vibrating sample magnetometry. Most compositions comprised the γ phase and the rest γ + α phase. The magnetic saturation (M_s) was as high as ~150 Am^2/kg and coercivity (H_c) as high as ~4 kA/m. The magnetic anisotropy (K) was on the order of 10^6 J/m^3. M_s and H_c incremented at cryogenic temperatures. Increment in thermal-treatment temperature increased M_S and decreased H_c. We applied multiple attribute decision making and advanced analyses to rank and select suitable $Fe_xCo_yNi_z$ alloy compositions, as a precursor to fabricate high-entropy soft-magnetic alloys.

[1] E.P. George, R. Raabe, R.O. Ritchie, High-entropy alloys, Nat. Rev. Mater., vol. 4, p. 5151 (2019) [2] D.B. Miracle, O.N. Senkov, A critical review of high-entropy alloys and related concepts, Acta Mater., vol. 122, p. 448 (2017) [3] Y. Zhiu, D. Zhou, X. Jin, L. Zhang, X. Du, B. Li, Design of non-equiatomic medium-entropy alloys, Sci. Rep., vol. 8, p. 1 (2018)

Session J3
MAGNETIC PHASE TRANSITION AND SUPERCONDUCTIVITY

Elizabeth Skoropata, Chair
Oak Ridge National Laboratory, Knoxville, TN, United States

CONTRIBUTED PAPER

J3-01. Withdrawn

INVITED PAPER

J3-02. Photoinduced Spin-Density and Charge-Density Wave Dynamics in Cr. *S.K. Patel*[1,2] *1. Center for Memory and Recording Research, University of California, San Diego, La Jolla, CA, United States; 2. Physics Department, University of California, San Diego, La Jolla, CA, United States*

In strongly correlated systems, the coupling between spin, charge, and lattice degrees of freedom results in the emergence of complex order such as antiferromagnetism and density wave systems. One example is single-crystal chromium, which exhibits an incommensurate spin-density wave (SDW) below its Néel temperature of 311 K and a commensurate charge-density wave (CDW) that appears as a second harmonic of the SDW ordering. The CDW can be measured by X-ray diffraction as satellite peaks around the (002) Bragg peak (see Fig. 1). In this talk I will describe measurements of the ultrafast CDW dynamics to a photoexcitation pump with an X-ray Free-Electron Laser (XFEL) probe of a epitaxial Cr film.[3-5] In Cr[001] films, the SDW and CDW are directed normal to the film surface and are pinned at the interfaces such that the number of wavelengths of the SDW and CDW is quantized and jumps hysteretically as the temperature is varied.[1] By analyzing the amplitude and position of the CDW satellite peaks, we are able to directly measure the CDW order and, indirectly, the SDW order following ultrafast photoexcitation. [3-5] Immediately following this photoexcitation, the magnetic order in Cr is suppressed and the static CDW becomes a dynamic coherent phonon (see Fig. 2). With weak excitation, we observe a transient enhancement of the CDW order by up to 30%.[3] A second weak excitation can dampen the phonon oscillation or can further enhance the CDW order and sustain the oscillation longer.[5] Stronger photoexcitation suppresses the SDW and CDW order in the system primarily through heating above the its Néel temperature and after the phonon is damped, there is no lattice distortion remaining in the system. The recovery of this order is assumed to be consistent with cooling times, however we see that the recovery slows by orders of magnitude as the sample is excited from temperatures that approach the hysteretic region where there is a change in the number of wavelengths of the CDW in the sample. These observations provide insight into the magnetization dynamics of systems with coupled degrees of freedom. The work is done in collaboration with Andrej Singer, Roopali Kukreja, Vojtech Uhlir, Sven Festersen, Devin Cela, Stjepan Hrkac, Nelson Hua, Rajasekhar Medapalli, Joshua Ruby, Anatoly Shabalin, James Wingert, Diling Zhu, Mike Kozina, Mike Glownia, Henrik Lemke, Silke Nelson, Michael Bauer, Kai Rossnagel, Bridget Murphy, Olaf Magnussen, Oleg Shpyrko, and Eric Fullerton. Work at UCSD was supported by the U.S. Department of Energy, Office of Science, Office of Basic Energy Sciences, under Contracts No. DE-SC0018237 and DE-SC0001805.

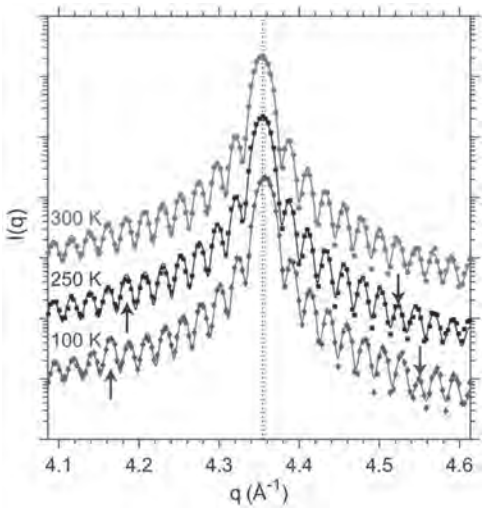

Fig. 1: X-ray diffraction of the (002) Bragg peak of a 28 nm Cr film showing Laue fringes due to the finite sample thickness. Satellite peaks due to the charge density wave ordering appear below the Néel temperature and result in constructive interference at low q and destructive interference at high q.

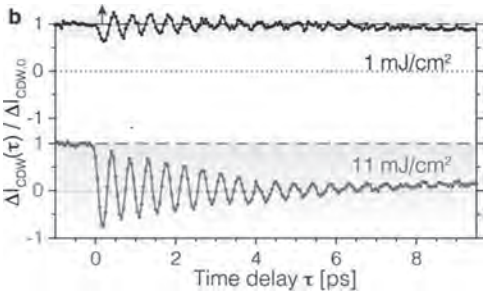

Fig. 2: Normalized CDW satellite peak amplitude following photoexcitation. Immediately following the pulse, the static CDW becomes a dynamic coherent phonon. At low fluence, the CDW order is transiently enhanced. At high fluence, the magnetic and electronic order are suppressed and the lattice distortion disappears after the phonon is damped.

CONTRIBUTED PAPERS

J3-03. Magnetism and Magnetotransport Around the Curie Temperature in the Dilute Ferromagnetic Semiconductor (Ga,Mn)as. *M. Wang*[1], B. Howells[1], R.A. Marshall[1], J.M. Taylor[1], K.W. Edmonds[1], A.W. Rushforth[1], R.P. Campion[1] and B.L. Gallagher[1] *1. School of Physics and Astronomy, University of Nottingham, Nottingham, United Kingdom*

We present detailed experiment and simulation studies of behavior of field-dependent magnetization and magnetoresistance in the vicinity of the Curie temperature in the highly disordered dilute ferromagnetic semiconductor

(Ga,Mn) As system. (Ga,Mn) As has a low saturation magnetization and relatively strong magnetocrystalline anisotropy, which inhibits domain formation. The critical behavior of (Ga,Mn) As is shown to be consistent with the three-dimensional Heisenberg model, despite the very strong disorder present in this system [1]. Clear correspondence of the magnetization and magnetoresistance is observed in the critical region. We found large anisotropy of the magnetoresistance within the critical region in our high Curie temperature (Ga,Mn) As system.

1. M. Wang, et.al., *Phys. Rev. B* 93, 184417 (2016).

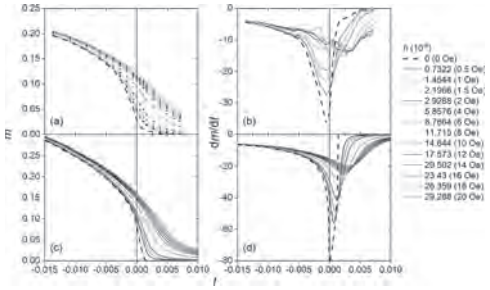

Figure 1. (a,b) Plots of *m vs. t* and *dm*/*dt vs. t* obtained from magnetometry measurement, where *m* and *t* are the reduced magnetization and temperature; (c,d) Three-dimensional Heisenberg simulation for an inhomogeneous sample with 0.5K rectangular broadening of Curie temperature.

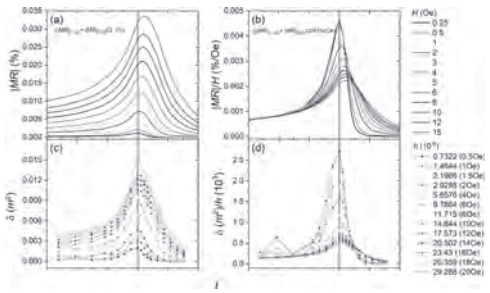

Figure 2. (a,b) The magnetoresistance versus reduced temperature *t*, with magnetic field *H* applied along the magnetic easy axis [1-10]; (c,d) Plots of $\delta(m^2)$ *vs. t* and $\delta(m^2)/h$ *vs. t* obtained from magnetometry measurement, where $\delta(m^2)=m^2(h)-m^2(0)$ *m* is the reduced magnetization and *h* is the reduced field.

J3-04. Observed Effects of Magnetism on the Calculated Stacking Fault Energies of FCC Co. *K. Cole-Piepke*[1], A. Srivastava[1], A. Koenig[2], D. Tweddle[2], C. Mewes[1], T. Mewes[1], G. Thompson[2], R. Noebe[3] and A. Leary[3] *1. Department of Physics and Astronomy, The University of Alabama, Tuscaloosa, AL, United States; 2. Department of Metallurgy and Materials Engineering, The University of Alabama, Tuscaloosa, AL, United States; 3. Materials and Structures Division, NASA John H Glenn Research Center, Cleveland, OH, United States*

An *ab initio* study of the stacking fault energy (SFE) curve of pure FCC Co was performed. This system was considered in order to determine a baseline for similar SFE curves calculated for Co-based alloys, particularly alloys containing Mn, Fe, or a combination of the two. The calculated SFE is normalized with respect to the number of atoms, number of faults, and interfacial area of the unit cell. All unit cells were allowed to relax to a high degree to ensure SFE calculations were performed at the lowest energy state. In addition, all cells utilized the same relaxation method to ensure uniformity. The results varied from previous results published in literature [1], which were not taking the magnetic state of the system into account. Upon investigation, it was determined that there is a strong magnetic effect on the SFE of Co, similar to results calculated for FCC Fe [2]. Subsequent calculations were performed assuming a nonmagnetic system, and results yielded the previous obtained results found in literature. Additionally, it was determined that FCC Co undergoes a magnetic phase transition, where it has the potential to become non-magnetic [3]. Analysis of the magnetic system revealed changes in the total moment of the system depending on the fault state (Fig. 1). Acknowledgements: This work was supported by NASA CAN 80NSSC18M0023. Computational support was provided by the University of Alabama High Performance Computing facilities and staff.

[1] L.-Y. Tian, R. Lizárraga, and H. Larsson, Acta Mater., Vol. 136, p.215 (2017) [2] I. Bleskov, T. Hickel, and J. Neugebauer, Phys. Rev. B, Vol. 93 (2016) [3] V. L. Moruzzi, P. M. Marcus, and K. Schwarz, Phys. Rev. B, Vol. 34, p.1784 (1986)

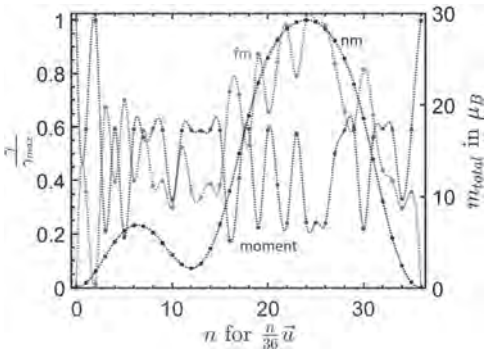

Fig. 1: A plot showing the normalized SFE for magnetic Co (red curve), nonmagnetic Co (black curve), and the moment of the magnetic Co (blue curve). The nonmagnetic system demonstrates the typical curve for SFE, with peaks in locations where close-packed stacking is violated, and troughs where it is maintained. The moment curve mirrors the magnetic system's SFE, such that increases in moment indicate decreases in SFE.

J3-05. Magnetic Phase Diagram and Exchange Bias Effect of $TbFe_xMn_{12-x}$ (x=6.0 -9.0) Intermetallic Compounds. Y. Xia[1], Z. Lin[1] and *J. Yang*[1] *1. physics, Peking University, Beijing, China*

$ThMn_{12}$ type $R(Fe, M)_{12}$ (M=Mo, V, Cr, Ti, etc.) compound has a high transition metal to rare earth ratio, and its Curie temperature and magnetocrystalline anisotropy are adjustable to display interesting magnetic phenomenon. The composition and content of M in the $R(Fe, M)_{12}$ compound have a wide distribution range, and the magnetic properties of the compound can be sensitively adjusted by changing the composition and content of M, so that it is possible to perform appropriate magnetic regulation on such compounds as needed. By optimizing the composition of $TbFe_xMn_{12-x}$ alloy, single-phase $TbFe_xMn_{12-x}$ (x=6.0 -9.0) alloys were prepared, and the magnetic properties and phase diagram of these samples were investiagted. It was found that there are many kinds of magnetic phase transitions in these samples. All samples have the characteristics of traditional spin glass state at low temperature, and the spin freezing temperature is slightly lower than the Curie temperature, depending on the Fe content. The magnetization decreases with temperature and even reaches a negative value, which is due to the magnetic moments of Tb sublattice and the Fe/Mn lattice reversely arranged and the absoulte values of the two varies with temperature; when T=10 K, as the Fe content decreases, the hysteresis loop of the sample changes from elongated to rectangular, and the decrease in the coercive force field indicates that the negative exchange interaction between the Tb lattice and the Fe/Mn lattice becomes weaker as the Fe content decreases. The sample has a large negative inter-atomic exchange effect at low temperature, resulting in a large coercive force field at low temperature, and an exchange-like bias effect was also observed in the $TbFe_8Mn_4$ alloy.

1. K. H. J. Buschow, Structure and properties of some novel ternary Fe-rich rare-earth intermeallics, J. Appl. Phys., 1988, 63, 3130. 2. J. B. Yang, W. B. Yelon, W. J. James, Q. S. Cai, D. Eckert, A. Handstein, K. H. Muller and Y. C. Yang, Structural and magnetic properties of RFe_xMn_{12-x}, (R=Ho,Y), Phys. Rev. B, 2002, 65, 064444.

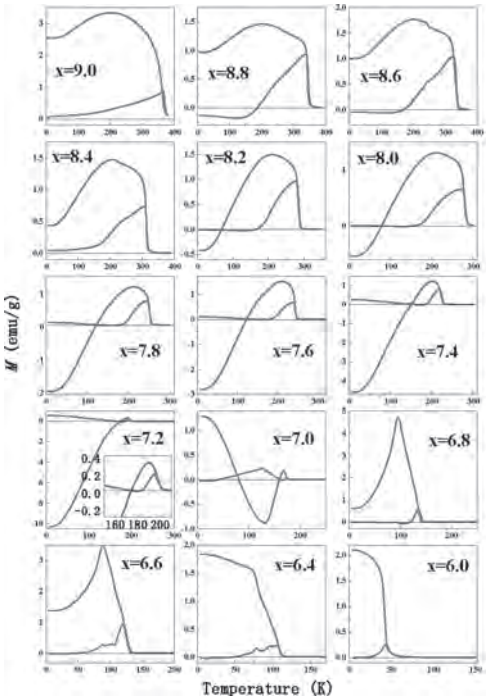

M-T curves of $TbFe_xMn_{12-x}$ under field and zero field cooling.

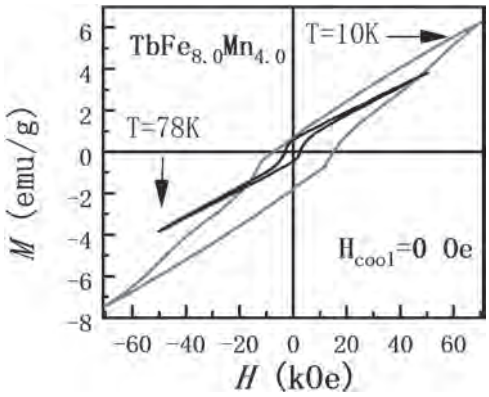

Exchange bias effect in $TbFe_8Mn_4$ compound

J3-06. Withdrawn

J3-07. Withdrawn

J3-08. Interplay Between Magnetism and Superconductivity in Iron Substituted $FeSr_2YCu_2O_{7+\delta}$ Cuprates Studied by μSR. *S.A. López Paz*[1], D. Sari[3,4], A. Hillier[2] and M. Alario-Franco[1] *1. Inorganic Chemistry Department, Universidad Complutense de Madrid, Avda. Complutense s/n, 28040, Madrid, Spain; 2. ISIS facility, Rutherford Appleton Laboratory, Chilton, United Kingdom; 3. College of Engineering, Shibaura Institute of Technology, 307 Fukasaku, Minuma-ku, Saitama City, Saitama 337-8570, Japan; 4. Meson Science Laboratory, RIKEN, 2-1 Hirosawa, Wako, Saitama 351-0198, Japan*

Substitution of copper by iron in the charge reservoir block of the YSCO cuprate superconductor brings out an appealing insight on the interplay between superconductivity and magnetism. In the resulting $FeSr_2YCu_2O_{7+\delta}$ compounds, $[FeO_{1+\delta}]$ layers and CuO_2 bi-layers are alternated along the stacking direction (*Figure 1a*), in close analogy to the $RuSr_2GdCu_2O_8$ ferromagnetic superconductor[1]. By modifying the hole doping level through different reducing-oxidizing treatments, we have explored the evolution from a non-superconducting phase with an AFM ordered Cu^{2+} sublattice for δ=0.08, to a superconducting sample with Tc= 70 K for δ=0.85, in which superconductivity *coexist* with Fe^{4+} long-range magnetic ordering (T_N=110 K > Tc)[2]. An intermediate-doped sample, with δ=0.56, present a mixed valent $Fe^{3.5+}$ state and superconductivity at a lower Tc= 30K (*Figure 1b*), but with no evidence of magnetic interactions in the magnetization data. However, zero-field muon spin rotation spectroscopy (ZF-μSR) reveals, for the two superconducting samples, the presence of magnetic interactions involving the copper sublattice at T<Tc (*Figure 1c*), as previously found in YBCO by means of the same technique[3]. For the here described $FeSr_2YCu_2O_{7+\delta}$ system, there is a clear enhancement of the magnetic interactions starting at the superconducting transition (*Figure 1d*). This suggests a complex interplay between, the normally exclusive phenomena, of magnetism and superconductivity[4]. The analysis of the μSR data will be described and the eventual interplay between the magnetic and superconducting properties discussed.

(1) C. Bernhard, J. L. Tallon, C. Niedermayer, Phys. Rev. B, 59 (21), 14099 (1999) (2) S. A. López-Paz, X. Martínez De Irujo-Labalde, M. A. Alario-Franco, Inorg. Chem., 58 (19), 12809 (2019) (3) S. Sanna, A. D. Hillier, R. De Renzi, Phys. Rev. Lett. 12, 207001 (2004) (4) J. Chakhalian, C. Bernhard, G. Cristiani, Nat. Phys., 2 (4), 244 (2006)

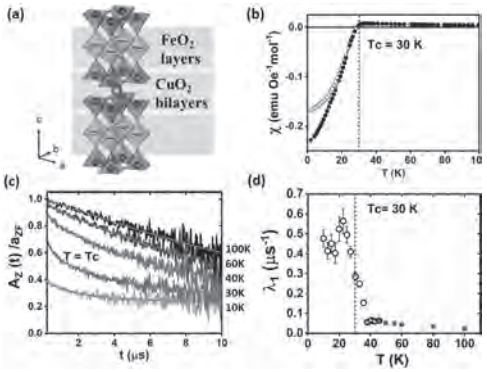

Figure 1. (a) Crystal structure of the $FeSr_2YCu_2O_{7+d}$ compounds, comprising CuO_2-Y-CuO_2 bilayers stacked between SrO-$FeO_{1+\delta}$-SrO blocks. (b) Magnetic susceptibility for the $FeSr_2YCu_2O_{7.56}$ sample showing the superconducting transition at Tc= 30K. (c) ZF-μSR spectra and (d) the derived temperature dependence of the relaxation rate for the same sample, evidencing the onset of the magnetic interactions at T ~Tc.

J3-09. Magnetic Phases in Superconducting, Polycrystalline Bulk FeSe Samples. Q. Nouailhetas[1,2], A. Koblischka-Veneva[1,3], *M.R. Koblischka*[1,3], K. Berger[2], B. Douine[2], Y. Slimani[4] and E. Hannachi[5] *1. Experimental Physics, Universitat des Saarlandes Naturwissenschaftlich-Technische Fakultat, Saarbrucken, Germany; 2. GREEN, University of Lorraine, Nancy, France; 3. Materials Science, Shibaura Institute of Technology, Tokyo, Japan; 4. Biophysics, Imam AbdulRahman Bin Faisal University, Dammam, Saudi Arabia; 5. Material Physics, Universite de Carthage, Tunis, Tunisia*

For possible applications as trapped field (TF) magnets, it is essential to fabricate large, polycrystalline bulk samples from the FeSe compound, the simplest high-T_c superconductor (HTSc) possible. FeSe is relatively cheap to prepare, and does not contain any rare-earth material. The grain boundaries in this compound are not acting as weak links as it is the case for the YBCO compound. Although the transition temperature, T_c, is just below 10 K, the upper critical fields are comparable with other HTSc. Preparing the FeSe samples using solid-state sintering yields samples exhibiting strong magnetic

hysteresis loops (MHLs), and the superconducting contribution is only visible after subtracting MHLs from above T_c. Due to the complicated phase diagram [1], the samples are a mixture of several phases, α-FeSe, β-FeSe, δ-FeSe (Fe_7Se_8) and metallic α-Fe [2]. The amount of the latter two phases depends directly on the Se loss during the sintering process. The δ-FeSe is antiferromagnetic, and α-Fe is ferromagnetic [3]. In the present contribution, we show MHLs of a variety of samples measured up to ±7 T and determine the magnetic characteristics, together with the amount of superconductivity determined from $M(T)$ measurements. We performed a thorough analysis of the microstructures using polarization microscopy, Kerr effect, MFM, SEM, EBSD and TEM in order to establish a relation between microstructure and sample properties. To prepare good superconducting samples, the presence of the (anti)ferromagnetic phases must be reduced by carefully adjusting the Se content using Ti foils as getter materials. Measuring magnetoresistance of these samples [4] implies that the samples are always cooled in the own local field, and thus, the analysis of the resistance data calculating the fluctuation-induced conductivity above T_c [5] is strongly affected by this local magnetic field. We demonstrate the importance of preparing phase-pure FeSe samples, which are essential for the various applications envisaged. This work is part of the SUPERFOAM international project funded by ANR and DFG under the references ANR-17-CE05-0030 and DFG-ANR Ko2323-10, respectively.

[1] H. Okamoto, J. Phase Equilibria 12, 383 (1991). [2] P. Diko et al., Physica C 476, 29 (2012). [3] A. J. Williams, T. M. McQueen, R. J. Cava, Solid State Commun.149, 1507 (2009). [4] T- Karwoth et al., J. Phys. Conf. Ser. 1054, 012018 (2018). [5] A. Almessiere et al., Mat. Chem. Phys. 243, 122665 (2020).

INVITED PAPER

J3-10. Enhanced Superconductivity in Single Layer FeTeSe/$SrTiO_3$ Heterostructures. *L. Li*[1] *1. Physics and Astronomy, West Virginia University, Morgantown, WV, United States*

Bulk FeTe exhibits a bicollinear (BCL) antiferromagnetic (AFM) ordering that can be suppressed by Se alloying, where superconductivity emerges with T_C=10K at 30% Se. We explore reduced dimensionality on AFM ordering & superconductivity in nanoribbons of single layer $FeTe_{1-x}Se_x$ grown on $SrTiO_3$ by MBE. Using scanning tunneling microscopy, we find 1D superconducting channel at ribbon edge with a T_C of 42K for x<0.1, coexisting with BCL AFM ordered interior. Calculations indicate Se incorporation and presence of the edge destabilize the BCL magnetic order, resulting in a paramagnetic region near the edge with local checkerboard fluctuations conducive to superconductivity. These results show an effective route towards stabilizing superconductivity in Fe-based superconductors at reduced dimensions.[1] Furthermore, we show the Tc of single layer FeSe/$SrTiO_3$ can be enhanced by UV light, attributed to a metastable polar distortion at the interface. The enhancement is also nonvolatile and persists even when the light is removed, and is reversible with a voltage pulse (Fig.1),[2] paving a path towards high-speed superconducting switches with infinite on/off ratio.

1. "Superconductivity on edge: Evidence of one-dimensional superconducting channel on the edges of antiferromagnetic single layer FeTeSe nanoribbons", ACS Nano, DOI:10.1021/acsnano.9b08726. 2. "Light induced non-volatile switching of superconductivity in single layer FeSe on $SrTiO_3$ substrate", *Nat. Commun*. 10, 85 (2019).

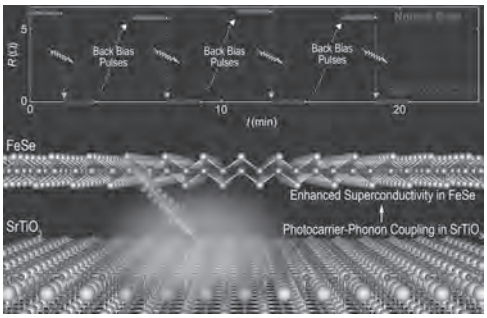

Fig. 1 Light induced non-volatile switching of superconductivity in single layer FeSe on SrTiO3 substrate.

CONTRIBUTED PAPER

J3-11. Predicting Long- and Short-Range Order With Restricted Boltzmann Machine. *M. Timirgazin*[1] and A. Arzhnikov[1] *1. Physical-Technical Institute, UdmFRC UB RAS, Izhevsk, Russian Federation*

Nowadays machine learning is becoming more and more popular and powerful tool for scientific research. Carrasquilla and Melko have demonstrated how neural networks can be used for classifying phases in solids [1]. Restricted Boltzmann machine (RBM), a simple stochastic neural network, is shown to reproduce ferromagnetic Ising model results if trained on the dataset obtained by Monte-Carlo (MC) method [2]. The authors calculate observable physical properties with RBMs trained at different temperatures and find good agreement with MC results for corresponding temperatures. We show that RBM is able not only to reproduce observable physical properties calculated earlier, but also to predict them. First of all, we study short-range order in binary alloys. In the simplest case, this problem can be reduced to the Ising model with spins up and down corresponding to atoms of types A and B. The dataset of 10^6 samples of 10x10 square matrices is calculated using the Metropolis algorithm for the alloy concentration equal to one half. We propose an algorithm which allows RBM trained on this dataset to generate new samples for any alloy concentration. In Fig. 1 the Warren-Cowley short-range order parameter is presented. It can be seen that RBM trained at one concentration can correctly predict short-range order in the full concentration range. Moreover, long range magnetic order can also be successfully predicted. Fig. 2 shows the magnetization for the 2D ferromagnetic Ising model. RBM result is obtained by training the machine for T=2.5, which is close to the critical temperature, and then scaling the weights and biases to generate data for all other temperatures. We see that RBM, based on data for only one temperature, reproduces the thermodynamic properties for the entire temperature range and correctly predicts critical temperature.

[1] J. Carrasquilla and R.G. Melko, Nat. Phys., Vol. 13, p. 431 (2017) [2] G. Torlai and R.G. Melko, Phys. Rev. B, Vol. 94, p. 165134 (2016)

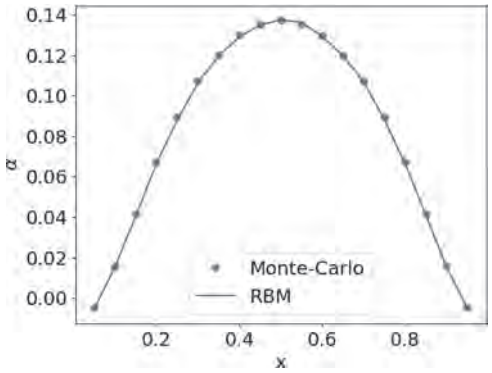

Fig. 1. Warren-Cowley parameter for binary alloy.

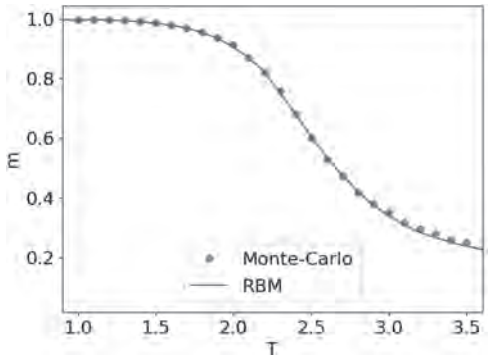

Fig. 2. Magnetization in 2D ferromagnetic Ising model

Session J4
SPIN CURRENTS I

Satoru Emori, Co-Chair
Virginia Tech, Blacksburg, VA, United States
Aurelien Manchon, Co-Chair
Aix-Marseille Universite, Marseille, France

CONTRIBUTED PAPERS

J4-01. Efficient Spin-Orbit Torque in vdW Heterostructure of 2D Itinerant Ferromagnet and Weyl Semimetal. *I. Kao*[1], J. Gobbo[1], R. Muzzio[1], J. yan[2], J. Goldberger[3], J. Katoch[1] and S. Singh[1] *1. Department of Physics, Carnegie Mellon University, Pittsburgh, PA, United States; 2. Oak Ridge National Laboratory, Oak Ridge, TN, United States; 3. Department of Chemistry, The Ohio State University, Columbus, OH, United States*

Manipulation of the magnetization state of spintronic devices can be achieved by spin-orbit torque (SOT). SOT can be induced by Rashba effect[1] or Spin Hall effect[2], which are both originated from the spin-orbit (SO) coupling. Therefore, to enhance SOT, materials with strong SO coupling are favored. Weyl semimetals are predicted to be a good candidate for achieving an efficient charge to spin interconversion driven by spin-galvanic effect[3]. Crystalline Weyl semimetals (e.g., WTe_2) also provide an exciting possibility of generating out-of-plane (OOP) anti-damping SOT. The presence of strong OOP anti-damping SOT in WTe_2/Py heterostructure, originated from the broken 2-fold rotational symmetry at the interface of WTe_2, has been demonstrated by spin-torque ferromagnetic resonance[4]. Unlike conventional heavy metals such as Pt and Ta that only allow in-plane AD SOT, WTe_2 can be more efficient for perpendicular magnetization switching. The 2D ferromagnet Fe_3GeTe_2 (FGT) has been reported to possess strong perpendicular anisotropy at temperatures below $T_C \sim 230$ K[5]. Anomalous Hall effect can be utilized to monitor the magnetization state of FGT flake during the switching measurements. SOT switching of perpendicular magnetization has been realized in Pt/FGT semi van der Waals (vdW) heterostructure[6-7]. However, SOT switching in a complete vdW heterostructure still needs to be demonstrated to fill the gap. As shown in Fig.1, we demonstrated SOT switching of perpendicular magnetization in WTe_2/FGT vdW heterostructure, and the chirality of SOT switching was found to switch with the direction of the in-plane field. The current density threshold is plotted in Fig.2 as a function of temperature, where the magnitude required for switching is one order smaller than the previously reported value in conventional heavy metal system Pt/FGT[6].

1. I. M. Miron, G. Gaudin and S. Auffret, Nat. Mater., Vol. 9, p.230 (2010) 2. K. Ando, S. Takahashi and K. Harii, Phys. Rev. Lett., Vol. 101, p.036601 (2008) 3. A. Johansson, J. Henk and I. Mertig, Phys. Rev. B, Vol. 97, p. 085417 (2018) 4. J. Jiang, F. Tang and X. C. Pan, Phys. Rev. Lett., Vol. 115, p.166601 (2015) 5. D. MacNeill, G. M. Stiehl and M. H. D. Guimarães, Nat. Phys., Vol. 13, p. 300 (2017) 6. M. Alghamdi, M. Lohmann and J. Li, Nano Lett., Vol. 19, p.4400 (2019) 7. X. Wang, J. Tang and X. Xia, Sci. Adv., Vol. 5, p.eaaw8904 (2019)

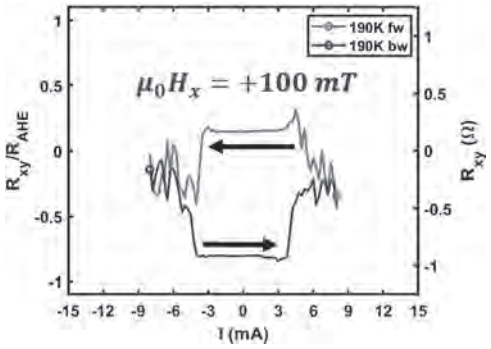

Fig.1. SOT switching in WTe_2/FGT at 190 K with an in-plane magnetic field applied parallel to the in-plane charge current.

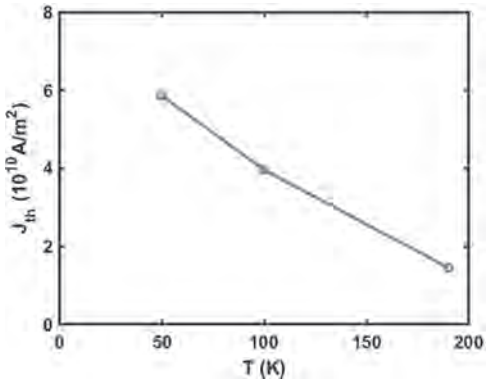

Fig.2. The temperature dependence of the current density threshold.

J4-02. Composition Dependence of Spin Anomalous Hall Effect in a Ferromagnetic Fe-Co Alloy. *Y. Koike*[1,2], S. Iihama[3,4] and S. Mizukami[2,4] *1. Department of Applied Physics, Tohoku University, Sendai, Japan; 2. WPI-AIMR, Tohoku University, Sendai, Japan; 3. FRIS, Tohoku University, Sendai, Japan; 4. CSRN, Tohoku University, Sendai, Japan*

Manipulation of magnetization utilizing spin-orbit torque (SOT) has attracted much attention for recent spintronics device. For case of the spin-Hall effect (SHE) in non-magnetic heavy metals, SOT vector lies in film plane; thus it is unfavorable to manipulate an out-of-plane magnetization. On the other hand, a spin-anomalous Hall effect (SAHE) is a promising way to overcome this restriction [1-2]. However, its detailed physic is not yet clear. In particular, the magnitude and sign of SAHE were not known yet even in elemental ferromagnets, such as Fe or Co. In this study, we investigated SAHE in Fe-Co binary alloys with different compositions to deeply understand the physics behind. Stacking structure of the samples was Si / SiO_2 sub. / $Fe_{100-x}Co_x$ (5) / Ti (3) / NiFe (Py) (4) / MgO (3) / Ta (2) (thickness is in nm, x=0, 15, 35, 50, 65, 100). Here, a Ti layer was used to

reduce an interlayer exchange coupling between Fe-Co alloy and Py layer. The samples were patterned into micron-sized strips to measure the spin-torque ferromagnetic resonance (ST-FMR). The spin-torque efficiencies due to SAHE of Fe-Co ξ_{SAHE} were evaluated from the change in the FMR linewidth of the Py layer induced by the dc current application. Figure 1 shows the composition dependence of the values for ξ_{SAHE} in $Fe_{100-x}Co_x$. Pure Fe shows small positive value, and the value significantly increased at *x* of 15%. Interestingly, ξ_{SAHE} changes its sign as Co composition further increases. We will discuss the origin of this dependence in detail. This study was supported in part by KAKENHI (K19K154300).

[1] T. Taniguchi *et al*., Phys. Rev. Appl. 3, 044001 (2015) [2] S. Iihama *et al*., Nat. Electro. 1, 120 (2018) [3] Y. Koike *et al.*, in preparation.

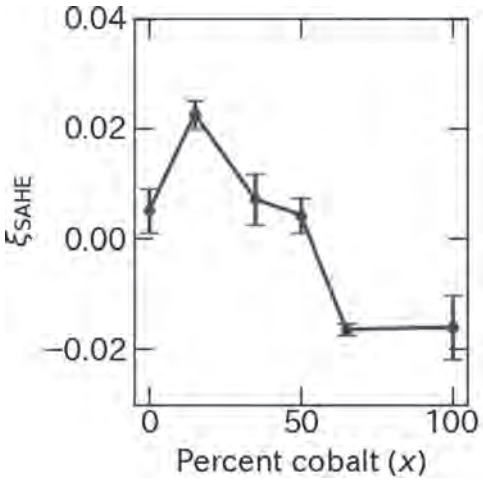

Fig. 1 The composition dependence of the spin-torque efficiencies due to SAHE of Fe-Co alloys ξ_{SAHE}, which were evaluated with the ST-FMR linewidth modulation.

J4-03. Amorphous Transition Metal Thin Films for Spin Current Generation. *J. Karel*[1,2], C. Hsu[3], D. Bouma[4], C. Fuchs[4], P. Corbae[5], N. Roschewsky[3], S. Salahuddin[3,6] and F. Hellman[4,6] *1. Materials Science and Engineering, Monash University, Clayton, VIC, Australia; 2. ARC Centre of Excellence in Future Low-Energy Electronics Technologies, Clayton, VIC, Australia; 3. Department of Electrical Engineering and Computer Science, University of California Berkeley, Berkeley, CA, United States; 4. Physics, University of California Berkeley, Berkeley, CA, United States; 5. Materials Science and Engineering, University of California Berkeley, Berkeley, CA, United States; 6. Materials Science Division, E O Lawrence Berkeley National Laboratory, Berkeley, CA, United States*

The efficient generation of spin currents is critical to numerous low-energy electronic devices, including the attojoule logic gate and spin orbit torque magnetoresistive random access memory (SOT-MRAM). Efforts to identify materials that act as good spin current sources have focused primarily on crystalline systems. In this talk, it will be shown that amorphous materials are potential candidates to generate spin currents. First, the talk will examine the anomalous Hall angle (AHA) in a series of ferromagnetic amorphous transition metal thin films M_xY_{1-x} (M=Fe, Co; Y=Si, Ge; x=0.40-0.71). It will be shown that the AHA ($=\sigma_{xy}/\sigma_{xx}$) is as large as 5%, which is substantial even for crystalline systems.[1,2] These results will be compared with the AHAs reported in a broad range of crystalline and amorphous materials. It will be shown that the AHA increases with increasing Hall conductivity (σ_{xy}) in the amorphous systems. This trend, which is opposite to that which occurs in crystalline systems, is attributed to low σ_{xx}, while σ_{xy} and M remain high. The talk will then report observation of a spin-orbit torque in an amorphous non-magnetic Fe_xSi_{1-x}/cobalt bilayer via spin-torque ferromagnetic resonance and harmonic Hall measurements. Both techniques provide a consistent spin Hall angle of about 3%.[3] The origins of this SOT will be discussed.

[1]D.S. Bouma *et al.*, *Phys Rev B* 101 014402 (2020) [2]J. Karel *et al.*, in preparation [3]C.-H. Hsu, J. Karel *et al.*, https://arxiv.org/abs/2006.07786

INVITED PAPER

J4-04. Optical Spin-Orbit Torque in Heavy Metal-Ferromagnet Heterostructures. *G. Choi*[1], J. Oh[2], D. Lee[2], s. lee[2], K. Kim[3], M. Lim[4], B. Min[5], K. Lee[2] and H. Lee[4] *1. Department of Energy Science, Sungkyunkwan University - Natural Sciences Campus, Suwon, The Republic of Korea; 2. Department of Materials Science and Engineering, Korea University, Seongbuk-gu, The Republic of Korea; 3. Center for theoretical physics of complex system, Institute for Basic Science, Daejeon, The Republic of Korea; 4. Department of physics, Pohang University of Science and Technology, Pohang, The Republic of Korea; 5. Center for spintronics, Korea Institute of Science and Technology, Seongbuk-gu, The Republic of Korea*

Spin current generation through the spin-orbit interaction in non-magnetic materials lies at the heart of spintronics. When the generated spin current is injected to a ferromagnet, it produces spin-orbit torque and manipulates magnetization efficiently, and the electrical generation of a spin-orbit torque through the spin Hall effect in heavy metals is intensively studied [1,2]. For the fast magnetization dynamics, however, the optical generation of a spin-orbit torque is more promising than its electrical counterpart. A prerequisite for the optical generation is the photo-spin conversion, which has been intensively studied for semiconductors such as GaAs. A well-known mechanism of the conversion is the optical orientation [3]; photo-excitation by a circularly polarized light with angular momentum along the direction σ can generate excited electrons that are spin-polarized along the direction σ. Such optically generated spins have been used to generate a spin torque in a ferromagnetic semiconductor MnGaAs [4]. In this work, we report optical spin-orbit torques in heavy metal/ferromagnet heterostructures [5]. The strong spin-orbit coupling of heavy metals induces photo-excited carriers to be spin-polarized, and their transport from heavy metals to ferromagnets induces a torque on magnetization. These results resemble, in many ways, the electrically generated spin-orbit torque that also utilizes the strong spin-orbit coupling of heavy metals. We thus call the optically generated damping-like torque in heavy metal/ferromagnet heterostructures. as optical spin-orbit torque [5].

1. I. M. Miron, G. Gaudin, S. Auffret, B. Rodmacq, A. Schuhl, S. Pizzini, J. Vogel, and P. Gambardella, *Nature Mater,* Vol. 9, p. 230 (2010). 2. L. Liu, C.-F. Pai, Y. Li, H. W. Tseng, D. C. Ralph, R. A. Buhrman, *Science*, Vol. 336, p. 555 (2012). 3. F. Meier and B. P. Zakharchnya, *Optical Orientation* (North-Holland, Amsterdam, 1984). 4. P. Němec, E. Rozkotová, N. Tesařová, F. Trojánek, E. De Ranieri, K. Olejník, J. Zemen, V. Novák, M. Cukr, P. Malý, and T. Jungwirth, *Nature Phys.* Vol. 8, p. 411 (2012). 5. G.-M. Choi, J. H. Oh, D.-K. Lee, S.-W. Lee, K. W. Kim, M. Lim, B.-C. Min, K.-J. Lee, and H.-W. Lee, *Nature Commun.* Vol. 11, p. 1482 (2020).

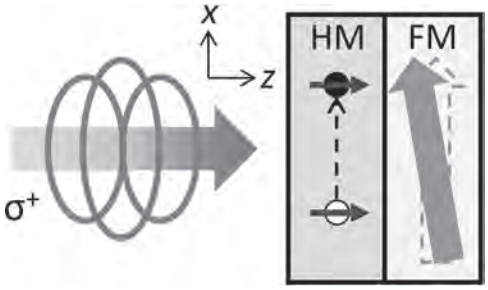

Figure 1: Schematics for mechanism. A right circularly polarized light (σ^+) generates a spin-polarized electron (filled circle) and hole (empty circle) excitations in HM (Blue arrows indicate the spin angular momentum). A spin transport from HM to FM induces a damping-like torque on the magnetization of FM (green arrow). A light propagates to the *z*-direction, and initial magnetization lies along the *x*-direction [5].

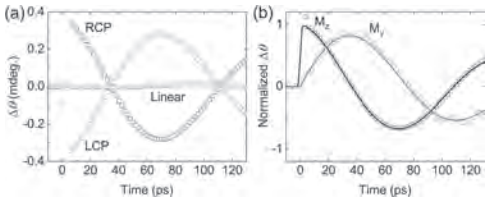

Figure 2: Optical spin-orbit torque. (a) The measured dynamics of the *z*-component of Co magnetization in the sap/Pt(5)/Co(3)/MgO(3) sample driven by pump pulse, incident on the substrate side, with right circular polarization (RCP) (black squares), left circular polarization (LCP) (red circles), and linear polarization (blue triangles). Given the negative value of the static Kerr rotation of Co (Supplementary Note 6), positive/negative Δθ of (a) indicates –*z*/+*z* tilting of magnetization. (b) The comparison of the M_z (black squares) and M_y (red circles) dynamics of Co in the sap/Pt(5)/Co(3)/MgO(3) sample. The black and red lines are fitting with cosine and sine functions, respectively [5].

CONTRIBUTED PAPERS

J4-05. Piezoelectric Strain Control of Spin-Orbit Torques in Perpendicularly Magnetized CoFeB Thin Films. *M. Filianina*[1,2], J. Hanke[1,3], K. Lee[1], D. Han[1,5], S. Jaiswal[1,4], A. Rajan[1], G. Jakob[1,2], Y. Mokrousov[1,3] and M. Klaui[1,2] *1. Johannes Gutenberg Universitat Mainz, Mainz, Germany; 2. Graduate School of Excellence Materials Science in Mainz, Mainz, Germany; 3. Forschungszentrum Julich Peter Grunberg Institut, Julich, Germany; 4. Singulus Technology AG, Kahl am Mainz, Germany, Kahl am Main, Germany; 5. Korea Advanced Institute of Science and Technology, Seoul, The Republic of Korea*

Energy-efficient control of magnetization in nanoscale is fundamental for designing future generation spintronic devices. Current-induced magnetization switching via spin-orbit torques (SOTs), realized in ferromagnet/heavy metal bilayers, has emerged as one of the most promising approaches [1]. The magnitude and the sign of the SOT can be adjusted by optimizing the parameters of the system such as the thickness and the composition of the layers [2]. In this case, however, the SOTs are fixed once the multilayer is fabricated. However, for complex switching concepts, i.e. to selectively switch parts of the ferromagnet using single pulse lines, which may lead to drastically simplified device architectures, it is necessary to locally and dynamically tune the SOTs in a system. Here we demonstrate the possible dynamic control of SOTs in perpendicularly magnetized W/$Co_{20}Fe_{60}B_{20}$/MgO multilayers by piezoelectric strain [3]. We find that modulated by an electric field, tensile strain increases the damping-like torque by a factor of two, while the compressive strain leads to a decrease. On the contrary, the field-like torque remains largely unaffected by strain. We explain our experimental results with the help of theoretical *ab initio* calculations revealing the difference in the response of the SOTs to the strain.

1. I.M. Miron et al., *Nat. Mater.* 9, 230 (2010). 2. A. Manchon et al., *Rev. Mod. Phys.* 91, 035004 (2019). 3. M. Filianina et al., *Phys. Rev. Lett.* 124, 217701 (2020).

J4-06. Probing Spin-Orbit Torques in Heterostructures With in-Plane Magnetic Anisotropy via Spin Hall Effective Field. *Y. Liu*[2], T. Chen[2], T. Lo[2], T. Tsai[2], S. Yang[1], Y. Chang[1], J. Wei[1] and C. Pai[2,3] *1. Electronic and Optoelectronic System Research Laboratories, Industrial Technology Research Institute, Hsinchu, Taiwan; 2. Department of Materials Science and Engineering, National Taiwan University, Taipei, Taiwan; 3. Center of Atomic Initiative for New Materials, National Taiwan University, Taipei, Taiwan*

The spin Hall effect from 5d transition metals can generate sufficient spin-orbit torque (SOT) and further produce current-induced SOT-driven magnetization switching in the adjacent ferromagnetic layer. However, for the ferromagnetic layer with in-plane magnetic anisotropy (IMA), probing such switching phenomenon typically relies on tunneling magnetoresistance measurement of nano-sized three-terminal devices[1-3], differential planar Hall effect measurement in Hall-bar devices[4], or Kerr effect imaging approaches[5]. In this work, we present a reliable and all-electrical strategy to characterize the damping-like SOT (DL-SOT) and field-like SOT (FL-SOT) in micron-sized magnetic heterostructures with IMA. Firstly, we show that in magnetic heterostructures with spin Hall metals, there exist current-induced in-plane spin Hall effective fields (H^y_{eff}) and unidirectional magnetoresistance (UMR) that will modify their anisotropic magnetoresistance (AMR) behavior (Fig.1). The electrical detection of current-induced SOT-driven magnetization switching (Fig. 2(b) and (d)) in a W/CoFeB device is demonstrated by means of AMR measurement under such influences. From switching measurements, Effective DL-SOT efficiency $|\xi^{eff}_{DL}|=0.32$ is estimated for Hall-bar devices with $2.0nm \leq t_{CoFeB} \leq 3.5nm$, which is fairly consistent with the values for thin W layer obtained by other approaches[3, 6-8]. Effective FL-SOT efficiency ($|\xi^{eff}_{FL}| \leq 0.05$) can be obtained by AMR measurement. Moreover, we demonstrate that for heterostructures with an in-plane easy axis, as prepared from an 8-inch CMOS-compatible fabrication facility, the probing of SOT switching can also be achieved by the UMR readouts. Our findings suggest that this pump (DL-SOT)-probe (AMR or UMR) method can be able to determine key parameters of SOT switching from IMA heterostructures without length device fabrication processes and complicated measurement protocol.

[1] M. Cubukcu, O. Boulle, M. Drouard, et al., Appl. Phys. Lett., Vol. 104, 042406 (2014). [2] L. Liu, C.-F. Pai, Y. Li, et al., Science, Vol. 336, 555 (2012). [3] C.-F. Pai, L. Liu, Y. Li, et al., Appl. Phys. Lett., Vol. 101, 122404 (2012). [4] G. Mihajlović, O. Mosendz, L. Wan, et al., Appl. Phys. Lett., Vol. 109, 192404 (2016). [5] S. Shi, S. Liang, Z. Zhu, et al., Nat. Nanotechnol., Vol. 14, 945-949 (2019). [6] R. Bansal, G. Nirala, A. Kumar, et al., Spin, Vol. 08, 1850018 (2019). [7] Q. Hao, G. Xiao, Phys. Rev. Appl., Vol. 3, 034009 (2015). [8] S. Mondal, S. Choudhury, N. Jha, et al., Phys. Rev. B, Vol. 96, 054414 (2017).

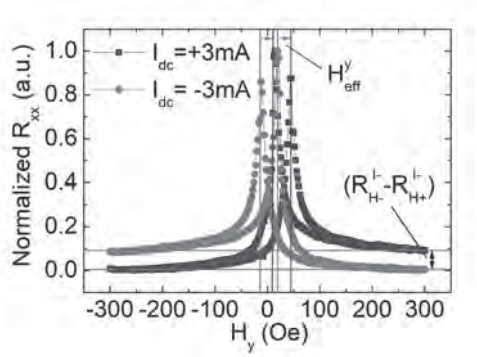

Figure 1. Representative shifted AMR loops measured from a W(3)/CoFeB(1.8) sample with dc current I_{dc} = ± 3mA.

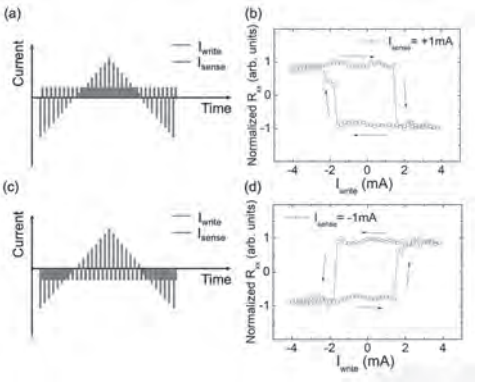

Figure 2. (a,c) Measurement sequence for the switching experiment and (b,d) Current-induced DL-SOT switching results of a W(3)/CoFeB(1.8) Hall-bar sample with opposite sense currents I_{sense} = +1mA and I_{sense} = -1mA.

J4-07. Spin to Charge Conversion of ac Spin Current in Si Detected by Inductive Measurements. *E. Shigematsu*[1], L. Liensberger[2,3], M. Weiler[2,3], R. Ohshima[1], Y. Ando[1], T. Shinjo[1], H. Huebl[2,3] and M. Shiraishi[1]
1. Department of Electronics Science and Engineering, Kyoto University, Kyoto, Japan; 2. Walther-Meißner-Institut, Bayerische Akademie der Wissenschaften, Garching, Germany; 3. Physik-Department, Technische Universität München, Garching, Germany

An ac spin current is generated along with a dc spin current in the spin pumping scheme in ferromagnetic/nonmagnetic systems. In 2018, Berger and co-workers made use of the ac component of the injected spin current to inductively detect spin to charge conversion in Pt and Cu [1]. Here, this inductive method is applied to quantify ac spin to charge conversion in Si, as a typical industry friendly semiconductor [2]. Our experimental method is immune to the electric and thermal rectification effects peculiar to the dc spin pumping scheme. The used samples have a layered structure consisting of a 7-nm-thick $Ni_{80}Fe_{20}$ layer, a 3-nm-thick Cu interlayer, and a 100-nm-thick Si layer. In the experiment, the layered structure is placed closed to the coplanar wave-guide connected to a vector network analyzer as shown in Fig. 1. By sweeping the external magnetic field applied perpendicular to the sample's face, the complex transmission spectra were obtained at each fixed frequency. The spectra reflect the inductance caused by the magnetic precession and the inductive response caused by the ac spin to charge conversion. The model analysis yielded the complex spin-orbit torque conductivity, the imaginary part of which represents the conversion from the magnetic dynamics to the ac current via the inverse spin Hall effect. We performed the measurement with a set of samples with systemically modulated doping configurations. In Fig.2, the doping dependence of the imaginary part of the spin-orbit torque conductivity is shown. A monotonous decrease in a transition from n-type to p-type doping of Si was observed. Considering the common bias level originated from the spin to charge conversion in the $Ni_{80}Fe_{20}$ and Cu layers, the trend suggests switching of the sign of spin Hall angle of Si by changing the doping type. The detailed picture of the spin to charge conversion in the bulk Si and at the Si/metal interface will be discussed in the presentation.

[1] A. J. Berger, E. R. J. Edwards, H. T. Nembach, A. D. Karenowska, M. Weiler, and T. J. Silva, Phys. Rev. B Vol.97, p.094407 (2018). [2] E. Shigematsu, L. Liensberger, M. Weiler, R. Ohshima, Y. Ando, T. Shinjo, H. Huebl, and M. Shiraishi, submitted.

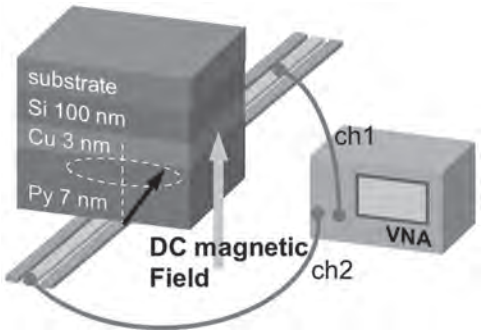

Schematic of the measurement setup and the sample structure.

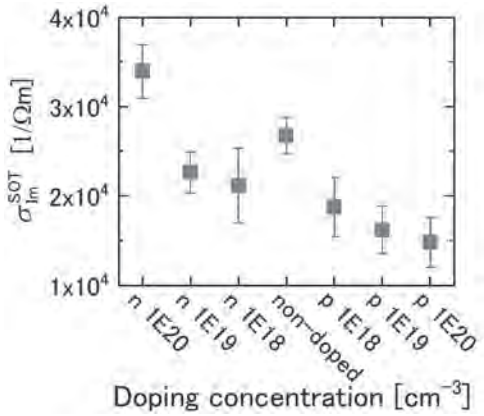

Doping dependence of the imaginary part of the measured spin-orbit conductivity.

J4-08. Bias-Field-Free Spin Hall Oscillator With an out-of-Plane Precession Mode. *T. Shirokura*[1] and H.N. Pham[1,2] *1. Electrical and Electronic Engineering, Tokyo Institute of Technology, Meguro-ku, Japan; 2. Center for Spintronics Research Network (CSRN), The University of Tokyo, Bunkyo-ku, Japan*

Spin Hall oscillator (SHO) is a promising spin torque oscillator (STO) having high durability due to a small driving current. However, conventional SHOs with in-plane precession (IPP) mode require bias-fields for stable oscillations [1-4], which are not favored in certain applications such as a neuromorphic computing [5]. Here, we propose and theoretically analyze a bias-field-free SHO with an in-plane hard axis and out-of-plane precession (OPP) mode by solving the macrospin Landau-Lifshitz-Gilbert-Slonczewski equation analytically and numerically. Fig. 1 shows the schematic structure of our two-terminal bias-field-free SHO. The SHO consists of a magnetic tunnel junction, a spin source layer, and a shunting resistance. Materials with a small spin Hall angle are also available for the spin source because the shunting resistance provides an in-plane charge current path for a spin current generation by the spin Hall effect. A bias-field-free OPP mode can be obtained by controlling a magnetic hard axis of free layer in the same direction of a spin polarization. In our simulations, the magnetic anisotropy was controlled by demagnetization coefficients without the loss of generality.

Fig. 2 shows the typical simulation result of the magnetization dynamics in our SHOs. Bias-field-free oscillations were successfully observed. We also derived formulas for a critical current, a driving current and an oscillation frequency by using the saddle and constant energy approximations [6], and they were in good agreement with numerical simulation results. Furthermore, the drive current of our SHOs were almost ten times smaller than that of conventional bias-field-free STOs.

[1]L. Liu, C. -F. Pai and D. C. Ralph, Phys. Rev. Lett., Vol. 109, p.186602 (2012) [2]Z. Duan, A. Smith and L. Yang, Nat. Commun., Vol. 5, p.5616 (2014) [3]V. E. Demidov, S. Urazhdin and H. Ulrichs, Nat. Mater., Vol. 11, p.1028 (2012) [4]V. E. Demidov, S. Urazhdin and A. Zholud, Appl. Phys. Lett., Vol. 105, p.172410 (2014) [5]J. Torrejon, M. Riou and F. A. Araujo, Nature, Vol. 547, p.428 (2017) [6]T. Taniguchi and H. Kubota, Phys. Rev. B, Vol. 93, p.174401 (2016)

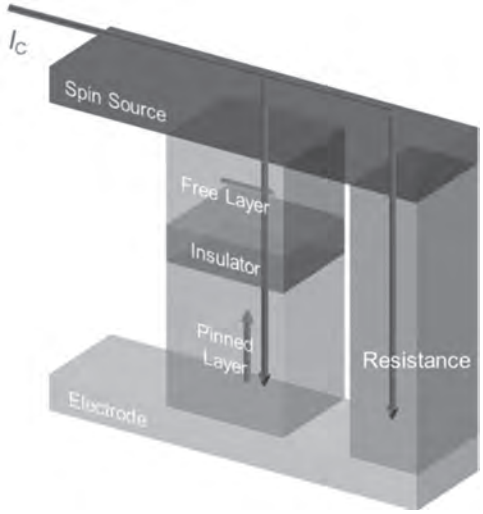

Fig. 1 Schematic structure of our two-terminal bias-field-free SHO. The SHO consists of a magnetic tunnel junction, a spin source layer, and a shunting resistance. The orange and red arrows show the magnetization of the free and pinned layer, respectively. The blue arrows show the current flow paths.

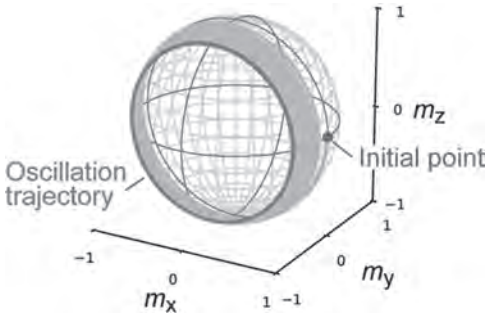

Fig. 2 Typical oscillation dynamics of the magnetization unit vector in our SHO. The orange and red solid lines show the transient and oscillation trajectory in a self-oscillation state. The green point shows the initial state.

J4-09. Controllable Orientations of Spin Polarization Beyond the Spin Hall Effect. *T. Chuang*[1], D. Qu[2], S. Huang[1] and S. Lee[2] *1. Department of Physics, National Taiwan University, Taipei, Taiwan; 2. Institute of Physics, Academia Sinica, Taipei, Taiwan*

In the spin Hall effect (SHE), a longitudinal charge-current induced transverse pure spin current has been extensively studied for the application of magnetization switching by spin-orbit torque. However, due to the strict right-hand rule among charge current, spin current, and spin polarization, this highly attractive switching scheme is not efficient and often accompanied by an unfavorable external magnetic field in a heterostructure with perpendicular magnetization (PM). In this work, we lift the restriction by demonstrating the magnetization-dependent spin Hall effect (MDSHE) in YIG/PM heterostructure, as shown in Fig. 1. Unlike the conventional SHE with the locked orientation of spin polarization, the spin current induced by the MDSHE can be arbitrarily and independently controlled by the magnetization direction of the magnetic layer. We reported about 3.6% of injected spins experience the effective spin rotation in PM layer of Pt(2)/Co(0.5)/Pt(2). Our approach provides an explicit route in exploring the spin-to-charge conversion with controllable orientations of spin polarization, which offers significant advantages in developing energy-efficient spintronic devices.

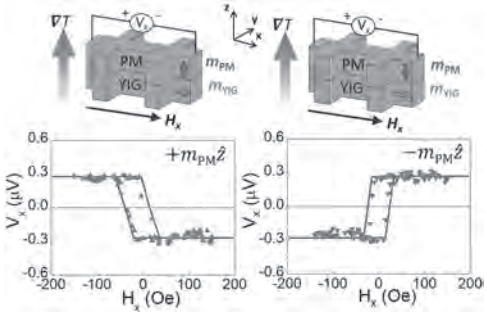

J4-10. Transverse and Longitudinal Spin-Torque Ferromagnetic Resonance for Improved Measurements of Spin-Orbit Torques. *S. Karimeddiny*[1], J.A. Mittelstaedt[1], R. Buhrman[2,1] and D. Ralph[1,3] *1. Physics, Cornell University, Ithaca, NY, United States; 2. Applied and Engineering Physics, Cornell University, Ithaca, NY, United States; 3. Physics, Kavli Institute at Cornell for Nanoscale Science, Ithaca, NY, United States*

Spin-torque ferromagnetic resonance (ST-FMR) is a common method used to measure spin-orbit torques (SOTs) in heavy metal/ferromagnet bilayer structures. In the course of a measurement, other resonant processes such as spin pumping (SP) and heating can cause spin current or heat flows between the layers, inducing additional resonant voltage signals via the inverse spin Hall effect (ISHE) and Nernst effects (NE). In the standard ST-FMR geometry, these extra artifacts exhibit a dependence on the angle of an in-plane magnetic field that is identical to the rectification signal from the SOTs. We show experimentally that the rectification and artifact voltages can be quantified separately by measuring the ST-FMR signal transverse to the applied current (i.e., in a Hall geometry) in addition to the usual longitudinal geometry. We find that in Pt (6 nm)/CoFeB samples the contribution from the artifacts is small compared to the SOT rectification signal for CoFeB layers thinner than 6 nm, but can be significant for thicker magnetic layers. We observe a sign change in the artifact voltage as a function of CoFeB thickness that we suggest may be due to a competition between a resonant heating effect and the SP/ISHE contribution.

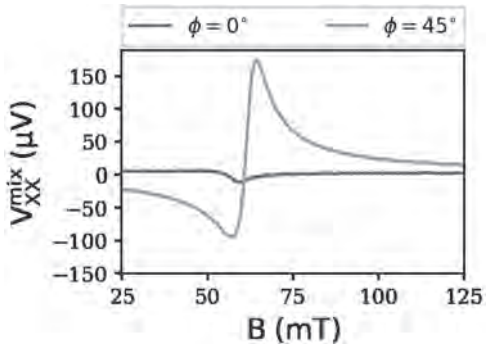

A conventional ST-FMR signal for an in-plane-magnetized sample with the strength of the external magnetic field swept: along the direction of microwave current (φ = 0, grey) and at 45-degrees to the microwave current (φ = 45, orange).

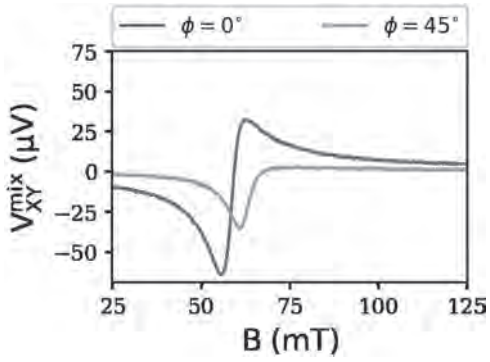

A *transverse* (Hall) ST-FMR signal for an in-plane-magnetized sample with the strength of the external magnetic field swept: along the direction of microwave current (φ = 0, grey) and at 45-degrees to the microwave current (φ = 45, orange).

J4-11. Spin-Orbit Interaction in Fe_xSi_{1-x}/Co Bi-Layers. *C. Hsu*[1], J. Karel[2], N. Roschewsky[3], S. Cheema[4], D. Bouma[3], S. Sayed[1], F. Hellman[3] and S. Salahuddin[1] *1. Electrical Engineering and Computer Science, University of California Berkeley, Berkeley, CA, United States; 2. Materials Science and Engineering, Monash University, Clayton, VIC, Australia; 3. Physics, University of California Berkeley, Berkeley, CA, United States; 4. Materials Science and Engineering, University of California Berkeley, Berkeley, CA, United States*

Current-induced magnetization switching via spin-orbit torque (SOT) has been an active field of research for the past few years as it serves as a potential candidate for next generation magnetic random access memory (MRAM) technology [1]. As a result, extensive effort has been put into understanding SOT and spin current generation in multiple polycrystalline and single crystalline material systems including heavy metals [2,3], topological insulators [4], semiconductors [5], two-dimensional materials [6] and three-dimensional semi-metals [7]. However, questions on the origin of the underlying physics still remain, often stemming from the challenge in differentiating between spin currents generated from the bulk bandstructure due to the associated crystallinity and other sources such as inversion symmetry breaking at the interface [3] and or scattering [8]. On the other hand, SOT generated through fully amorphous non-magnetic system composed of light weight elements is a great candidate for addressing this question. Here we report the observation of spin-orbit torque under room temperature in fully amorphous non-ferromagnetic Fe_xSi_{1-x}/cobalt bilayer with harmonic Hall measurement and spin-torque ferromagnetic resonance. Both techniques provide a minimum spin torque efficiency of about 3%, comparable to prototypical heavy metals such as Pt [2]. According to the conventional theory of spin Hall effect, a spin current generated through a fully amorphous material is not expected to have any contribution from the bandstructure since no crystallinity of any sort is present in a fully amorphous material. This, combined with the fact that Fe_xSi_{1-x} does not contain any heavy element, paves a new way for understanding the underlying physics of spin-orbit interaction and spin current generation.

[1] Salahuddin, S., Ni, K., & Datta, S., *Nature Electronics*, Vol. 1(8), p.442–450 (2018). [2] Liu, L., *et al*., *Science.*, Vol. 336, p.555–558 (2012). [3] Miron, I. M., *et al.*, *Nature*, Vol. 476, p.189–193 (2011). [4] Mellnik, A. R., *et al*., *Nature*, Vol. 511(7510), p.449–451 (2014). [5] Skinner, T. D., *et al*, *Nature Communications*, Vol. 6(1), 6730 (2015). [6] MacNeill, D., *et al.*, *Nature Physics,* Vol. 13(3), p.300–305 (2017). [7] Nan, T., *et al.*, *Proceedings of the National Academy of Sciences*, Vol. 116(33), p. 16186–16191 (2019). [8] Saidaoui, H. B. M., & Manchon, A., *Physical Review Letters*, Vol. 117(3), 036601 (2016).

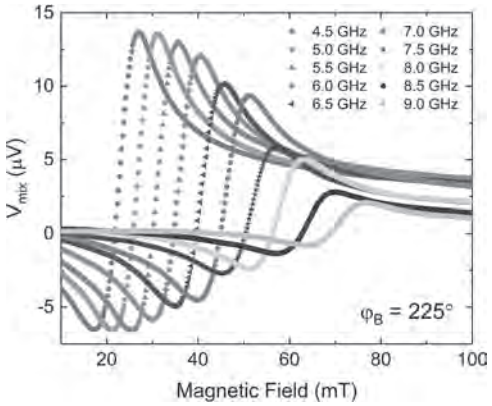

ST-FMR spectrum of Fe(x)Si(1-x) (x=45%)/cobalt bilayer shows strong signature of spin-orbit torque.

J4-12. Effect of Interfacial Intermixing on Spin-Orbit Torque in Co/Pt Bilayers. *G.G. Baez Flores*[1] and K. Belashchenko[1] *1. Physics and Astronomy, University of Nebraska-Lincoln, Lincoln, NE, United States*

Using the first-principles non-equilibrium Green's function technique [1] with supercell disorder averaging, we study the influence of interfacial intermixing on the spin-orbit torque in Co/Pt (111) bilayers. The interlayer distances are optimized, several models of intermixing are considered, and atomic potentials in the intermixed layers are obtained using the coherent potential approximation. The magnitude and thickness dependence of the damping-like torque are similar to earlier results for the Co/Pt (001) interface [1,2] and rather insensitive to intermixing. In contrast, the field-like torque, which is small in the case of an ideal interface, is strongly enhanced by intermixing.

[1] K. D. Belashchenko, A. A. Kovalev, and M. van Schilfgaarde, Phys. Rev. Mater. 3, 011401 (2019). [2] K. D. Belashchenko, A. A. Kovalev, and M. van Schilfgaarde, arXiv:1908.02680.

Session J5
WEYL AND TOPOLOGICAL MATERIALS

Ralph Skomski, Chair
University of Nebraska-Lincoln, Lincoln, NE, United States

CONTRIBUTED PAPERS

J5-01. Correlating Magnetic Structure and Magnetotransport in Thin Films of the Weyl Semimetal $Eu_{1-x}Sm_xTiO_3$. *R. Need*[1], Z. Porter[2], K. Ahadi[3], B. Kirby[4], S. Stemmer[2] and S. Wilson[2] *1. University of Florida, Gainesville, FL, United States; 2. University of California Santa Barbara, Santa Barbara, CA, United States; 3. North Carolina State University, Raleigh, NC, United States; 4. National Institute of Standards and Technology, Gaithersburg, MD, United States*

Weyl semimetals (WSMs) are an intriguing class of topological materials in which the bulk band structure generates linearly dispersive surface states near the Fermi energy. In the case of magnetic WSMs, broken time reversal symmetry results in electronic properties that are strongly dependent on the magnetic structure. In this talk, we describe recent work using a combination of neutron diffraction and reflectometry to quantify the magnetic structure of thin $Eu_{1-x}Sm_xTiO_3$ films, in order to better understand recent magnetotransport results that suggest $EuTiO_3$ is a WSM and that Sm doping can drive the Fermi level across the Weyl node. Specifically, we report the evolution of the average and depth-dependent magnetic order in thin film samples of biaxially strained and electron-doped $EuTiO_3$ for samples across a doping range <0.1 to 7.8 $\times 10^{20}$ cm^{-3}. Under an applied in-plane field, the G-type antiferromagnetic ground state undergoes a continuous phase transition to in-plane field-polarized ferromagnetism. The critical field for ferromagnetism decreases with itinerant carriers, yet the field evolution is qualitatively similar across the doping range. Unexpectedly, we observe interfacial ferromagnetism with saturated Eu moments at low fields that precedes ferromagnetic saturation throughout the bulk of the film. We bring these results together to paint a complete picture of the materials magnetic structure evolution with doping and field and discuss its connections to the unusual magnetotransport observed, including anisotropic magnetoresistance and the topological Hall effect.

Z. Porter, R.F. Need, K. Ahadi, Y. Zhao, Z. Xu, B.J. Kirby, J.W. Lynn, S. Stemmer, and S.D. Wilson. “Correlating magnetic structure and magnetotransport in semimetal thin films of $Eu_{(1-x)}Sm_{(x)}TiO_3$”, *Physical Review Materials* 4, 054411 (2020).

J5-02. Grain Size Dependence of Transverse Thermomagnetic Transport in the Weyl Semimetal NbP. *E. Scott*[1], C. Fu[2], S. Guin[2], C. Felser[2] and S. Watzman[1] *1. University of Cincinnati College of Engineering and Applied Science, Cincinnati, OH, United States; 2. Max Planck Institute for Chemical Physics of Solids, Dresden, Germany*

Weyl semimetals combine both topological and semimetallic effects in their transport of fermions through both bulk and surface states, making them excellent candidates for transverse thermomagnetic transport via the Nernst effect. The Nernst effect is a thermoelectric phenomenon requiring a magnetic field. A temperature gradient is applied to a sample, and the sample is placed in an external magnetic field orthogonal to the temperature gradient. The charge carriers, moving parallel to the temperature gradient, now experience a Lorentz force due to the cross product of the magnetic field and the temperature gradient. An electric field is produced in the mutually perpendicular direction. Single-crystal NbP has shown an unprecedentedly large Nernst thermopower at high magnetic fields, exceeding 800 $\mu V\ K^{-1}$ at 109 K and 9 T [1]. Bulk polycrystalline NbP maintains a large Nernst thermopower, although its magnitude is decreased by approximately a factor of 8 under similar circumstances. Due to the high electrical conductivity of the material, polycrystalline NbP’s Nernst power factor is determined to be 35 x 10^{-4} W m^{-1} K^{-2} at 9 T and 136 K, which is comparable to that of state-of-the-art thermoelectric materials [2]. This high conversion of thermal-to-electrical energy in NbP has been determined as due to the chemical potential’s location near linear, Dirac band crossing points (called Weyl points), giving access to many mobile holes and electrons. These initial results of transverse thermomagnetic transport in both single-crystal and polycrystalline NbP motivate further study to elucidate Weyl fermion transport and the length scales over which it is effective and dominant. Here, we present a grain size study on bulk polycrystalline samples of NbP, where different annealing times result in different grain sizes. Via microstructural characterization and thermomagnetic transport measurements, we can begin to determine the effects of grain size on transport in Weyl semimetals.

[1] S. J. Watzman et al. Phys. Rev. B 97(16), 161404(R) (2018). [2] C. Fu et al. Energy Environ. Sci. 11(10), 2813-2830 (2018).

J5-03. Chiral-Anomaly-Induced Nonlinear Hall Effect in Tilted Weyl Semimetals. *R. Li*[1], S. Zhang[1], A. Burkov[2] and O. Heinonen[3] *1. Physics, Case Western Reserve University, Cleveland, OH, United States; 2. Physics, University of Waterloo, Waterloo, ON, Canada; 3. Argonne National Laboratory Materials Science Division, Lemont, IL, United States*

Weyl semimetals (WSMs) are a newly discovered class of quantum materials which can host a number of massless quasiparticles called Weyl fermions. One of the most unique properties of WSMs is the chiral anomaly – a pair of Weyl nodes of opposite chirality acts as source and drain of electrons in the presence of non-perpendicular electric and magnetic fields. To date, the most remarkable phenomenon induced by the chiral anomaly is the longitudinal negative magnetoresistance, which is a linear response effect. In this work, we theoretically investigate the transport properties of WSMs in the nonlinear regime and predict a novel nonlinear Hall effect in tilted noncentrosymmetric Weyl semimetals. Intuitively, a steady-state density difference between a pair of Weyl nodes is established when the chiral pumping and internode relaxation reach a balance, which conspires with the anomalous velocity to give rise to this nonlinear Hall effect. Taking the semiclassical Boltzmann approach, we find that the nonlinear Hall conductivity scales linearly with both the electric and magnetic fields, and depends critically on the tilting of the Weyl cones in both type-I and type-II WSMs. For a pair of Weyl cones that are un-tilted or oppositely tilted, the chiral-anomaly-induced nonlinear Hall current vanishes because it is forbidden by a mirror symmetry. We also show that this effect does not rely on a finite Berry curvature dipole, in contrast to the intrinsic quantum nonlinear Hall effect that was proposed to occur in time-reversal invariant materials [1].

[1] I. Sodemann and L. Fu, Phys. Rev. Lett. 115, 216806 (2015).

J5-04. Anomalous Planar Hall Effect in Predicted Type II Weyl Fe_3Sn_2. *N. Kumar*[1], Y. Soh[1], Y. Wang[2], J. Li[2] and Y. Xiong[2] *1. Neutrons and Muons, Paul Scherrer Institut, Villigen, Switzerland; 2. Anhui Province Key Laboratory of Condensed Matter Physics at Extreme Conditions, High Magnetic Field Laboratory of the Chinese Academy of Sciences, Hefei, China*

We have investigated various electronic transport properties such as the anisotropic magnetoresistance, planar Hall effect, and anomalous Hall effect in kagome Fe_3Sn_2, which has been predicted to be a type II Weyl metal. Based on magnetortransport, we determine the spin reorientation transition to peak at 120 K and coexistence of both out of plane and in plane phases at temperatures around the spin reorientation, indicative of a first order phase transition. In planar Hall effect, we discover a field antisymmetric contribution in addition to the standard field symmetric contribution. This field antisymmetric planar Hall effect has an in-plane 3-fold rotational symmetry, which is distinctively different from the symmetric counterpart. Furthermore, the temperature and field dependence of the field antisymmetric contribution is different from both the symmetric planar Hall effect and anomalous Hall effect, pointing to a different origin. A linear and antisymmetric planar Hall effect is predicted to be present in the case of non-magnetic Weyl semimetals. The experimental signatures in our case fit well with the prediction in addition to reflecting contributions from its ferromagnetism. As the magnetization of Fe_3Sn_2 has a 3-fold rotational degeneracy, the associated band structure and Weyl nodes determined by the magnetization direction owing to the spin-orbit coupling will have accordingly a 3-fold rotational degeneracy giving rise to the 3-fold antisymmetric PHE. We thus propose that the antisymmetric PHE that we discovered is the realization of an antisymmetric and linear planar Hall effect due to the presence of Weyl nodes near the Fermi level in a time reversal symmetry broken system. Our finding offers a promising route for macroscopically probing Weyl systems.

[1] Neeraj Kumar, Y. Soh, Yihao Wang, et al., Anomalous planar Hall effect in a kagome ferromagnet, arXiv:2005.14237 (2020). [2] Nandy, S., G. Sharma, A. Taraphder, et al., Chiral Anomaly as the Origin of the Planar Hall Effect in Weyl Semimetals. Phys Rev Lett, 119(17): p. 176804 (2017). [3] M. Yao, H. Lee, N. Xu, et al., Switchable Weyl nodes in topological Kagome ferromagnet Fe3Sn2, arXiv:1810.01514 (2018).

J5-05. Epitaxial Growth of the Weyl Semimetal YbPtBi (111) on C-Plane Sapphire by Co-Sputtering. *M. Vaughan*[1], M. Dearg[1], M. Ali[1], C.H. Marrows[1] and G. Burnell[1] *1. University of Leeds, Leeds, United Kingdom*

YbPtBi is a half Heusler alloy with claimed properties of topological Weyl nodes and chiral anomaly; antiferromagnetism from the RKKY coupling of localized Yb f-electrons at low temperatures; and heavy fermion behaviour as those localized f-electrons interact with the conduction bands [1,2]. So far only bulk crystals have been grown of YbPtBi with no published work on thin films. By using c-plane sapphire the half Heusler alloy has an epitaxially relationship of YbPtBi(111)||Al_2O_3(0001) and YbPtBi(110)||Al_2O_3(1100). With thin films we could have to option of induced strain, device fabrication and many other thin films manipulation techniques. In this work, we present a study of epitaxially grown YbPtBi thin films that grew as triangular islands with matched faceted edge orientations. The structure is confirmed to be epitaxial from x-ray diffraction and cross-sectional transmission electron microscopy. We also measure the electrical transport properties and find a non-metallic ρ(T) similar to other semimetals RePtBi (Re=Gd, Ce, Sm) half Heusler Alloy, although different from bulk YbPtBi. We measured a negative longitudinal magnetoresistance and the temperature dependence of an apparent chiral anomaly (Fig: a,b). Both of which are indicators of a possible Weyl semimetal state. We also obversed a large hysteretic MR at very low temperatures, 250 mK, not previously seen in YbPtBi.

[1] C. Y. Guo, F. Wu, Z. Z. Wu, M. Smidman, C. Cao, A. Bostwick, C. Jozwiak, E. Rotenberg, Y. Liu, F. Steglich, and H. Q. Yuan, Nature Communications. 9, 4622 (2018) [2] B. G. Ueland, A. Kreyssig, E. D. Mun, J. W. Lynn, L. W. Harriger, D. K. Pratt, K. Prokeš, Z. Hüsges, R. Toft-Petersen, S. Sauerbrei, S. M. Saunders, Y. Furukawa, S. L. Bud'ko, R. J.McQueeney, P. C. Canfield, and A. I. Goldman, Phys. Rev. B. 99, 184431 (2019)

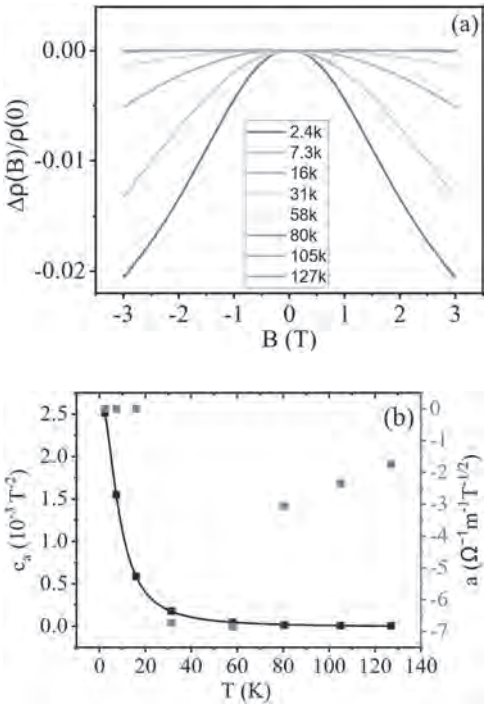

INVITED PAPER

J5-06. Weyl-Kondo Semimetals: Correlated Topology and Control of Nodes. *S.E. Grefe*[1], H. Lai[1], S. Paschen[2] and Q. Si[1] *1. Rice University, Houston, TX, United States; 2. Technische Universitat Wien, Wien, Austria*

How strong correlations drive quantum states of matter with nontrivial topology is an outstanding issue in contemporary condensed matter physics. This talk will provide an overview and discuss the latest development on Weyl-Kondo semimetal, which has been concurrently advanced by theoretical [1,2] and experimental [3,4,5] studies. The theoretical work addressed a nonsymmorphic Anderson lattice model that breaks the inversion symmetry while preserving the time-reversal symmetry, whereas the experimental effort focused on the non-magnetic non-centrosymmetric and non-symmorphic heavy fermion semimetal $Ce_3Bi_4Pd_3$. The salient signatures of the Weyl-Kondo semimetal include a correlation enhanced specific heat $C=\Gamma T^3$ [3], and a giant zero-magnetic-field Hall response and even-in-field Hall effects [4]. The latest high magnetic field experiments observed a two-stage topological phase transition, from Weyl-Kondo semimetal to Kondo insulator to heavy-fermion metal [5]. To bridge the latest experiments and our theoretical work, we investigated the aforementioned Anderson lattice model in the presence of a Zeeman coupling. Tuning both the Zeeman coupling and the inversion-symmetry-breaking potential controls the position and number of Weyl nodes in the Brillouin zone, and several topologically distinct phases emerge in this model.

[1] H.-H. Lai, S. E. Grefe, S. Paschen, and Q. Si, Proc. Natl. Acad. Sci. U.S.A. 115, 93 (2018). [2] S. E. Grefe, H.-H. Lai, S. Paschen, and Q. Si, Phys. Rev. B, 101, 075138 (2020). [3] S. Dzsaber, L. Prochaska, A. Sidorenko, G. Eguchi, R. Svagera, M. Waas, A. Prokofiev, Q. Si, and S. Paschen, Phys. Rev. Lett. 118, 246601 (2017). [4] S. Dzsaber, X. Yan, G. Eguchi, A. Prokofiev, T. Shiroka, P. Blaha, O. Rubel, S. E. Grefe, H.-H. Lai, Q. Si, and S. Paschen., arXiv preprint arXiv:1811.02819, (2018). [5] S. Dzsaber, D. A.

Zocco, A. McCollam, F. Weickert, R. McDonald, M. Taupin, X. Yan, A. Prokofiev, L. M. K. Tang, B. Vlaar, et al., arXiv preprint arXiv:1906.01182 (2019).

CONTRIBUTED PAPERS

J5-07. Meta-Magnetism of Weakly-Coupled Antiferromagnetic Topological Insulators. *A. Tan*[1,3], V. Labracherie[1,3], N. Kunchur[1], A. Wolter[1], J. Dufouleur[1], B. Büchner[1,2], A. Isaeva[1,2] and R. Giraud[1,3]
1. Leibniz-Institut fur Festkorper- und Werkstoffforschung Dresden eV, Dresden, Germany; 2. Technische Universitat Dresden, Dresden, Germany; 3. Universite Grenoble Alpes, Grenoble, France

The magnetic properties of van der Waals magnetic topological insulators $MnBi_2Te_4$ and $MnBi_4Te_7$ are investigated by magneto-transport measurements. We evidence that the relative strength of the inter-layer exchange coupling J to the uniaxial anisotropy K controls a transition from an A-type antiferromagnetic order to a ferromagnetic-like metamagnetic state. A bi-layer Stoner-Wohlfarth model allows us to describe this evolution, as well as the typical angular dependence of specific signatures, such as the spin-flop transition of the uniaxial antiferromagnet and the switching field of the metamagnet. In micron-size magnets, the single-domain switching-field astroid are however partly truncated by the nucleation of domain walls along the easy-axis direction.

A. Tan, V. Labracherie, N. Kunchur, A. U. B. Wolter, J. Cornejo, J. Dufouleur, B. Büchner, A. Isaeva and R. Giraud Metamagnetism of Weakly Coupled Antiferromagnetic Topological Insulators. *Phys. Rev. Lett.* 124, 197201. (2020)

J5-08. Peculiarities of the Electro- and Magnetoresistivity of WTe_2 and $MoTe_2$ Single Crystals. *A. Domozhirova*[1], S.V. Naumov[1], S.M. Podgornykh[1], V. Chistyakov[1], J.A. Huang[2] and V. Marchenkov[1,3]
1. M.N. Mikheev Institute of Metal Physics, UB RAS, Ekaterinburg, Russian Federation; 2. National Cheng Kung University, Tainan, Taiwan; 3. Ural Federal University, Ekaterinburg, Russian Federation

Topological Weyl semimetals (TWSs) based on transition metal dichalcogenides (TMDs) are of great interest both from fundamental and applied points of view. Such materials have promising prospects for use in spintronics and micro- and nanoelectronics due to unusual electronic and magnetic properties owing to their unique band structure, such as extremely large magnetoresistance, high charge carrier mobility, and spin-polarized transport. TMD WTe_2 and $MoTe_2$ were found to exhibit the TWS features. Moreover, the physical properties of $MoTe_2$ are known to strongly depend on the type of crystal structure that can be tuned by heat treatment [1, 2]. $MoTe_2$ undergoes a transition from the diamagnetic semiconductor phase to the paramagnetic metal one under certain conditions. Therefore, in this work, we studied the electro- and magnetoresistivity of WTe_2 and $MoTe_2$ before and after quenching in temperature range from 1.8 to 300 K and in magnetic fields of up to 9 T. The type of the temperature dependence of the electroresistivity of WTe_2 is shown to be "metallic", and the resistivity value is $(0.02\text{-}0.86)\times10^{-3}$ Ohm×cm. The magnetoresistivity of WTe_2 reaches ~1700% at T = 2 K in a field of 9 T. Quenching leads to the dramatic changes in the electroresistivity of $MoTe_2$. The resistivity value of quenched $MoTe_2$ decreases up to 8 orders of magnitude (!) from ~10^5 Ohm×cm to ~10^{-3} Ohm×cm at low temperatures and the type of its temperature dependence changes from "semiconductor" to "metallic". The magnetoresistivity of $MoTe_2$ is also modified from 7% to 15% at T = 12 K in a field of 9 T, although these changes are not so huge as in the case of the electroresistivity. The research was carried out within the state assignment of the Ministry of Education and Science of the Russian Federation (theme "Spin", No. AAAA-A18-118020290104-2), supported in part by RFBR (projects nos.. 17-52-52008 and 20-32-90069) and the Government of Russian Federation (Decree No. 211, Contract No. 02.A03.21.0006).

1. Y.-Y. Lv, L. Cao, X. Li et al., Scientific Reports, Vol. 7, p. 44587 (2017).
2. V.V. Marchenkov, A.N. Domozhirova, R.A. Parulin et al., Journal of Physics: Conference Series, Vol. 1482, p. 012004 (2020).

J5-09. Anomalous Hall Effects in Rare Earth Nitrides. *W. Holmes-Hewett*[1,2], B. Ruck[1,2], R.G. Buckley[1,3] and H. Trodahl[1,2]
1. The MacDiarmid Institute for Advanced Materials and Nanotechnology, Wellington, New Zealand; 2. School of Chemical and Physical Sciences, Victoria University of Wellington, Wellington, New Zealand; 3. Robinson Research Institute, Victoria University of Wellington, Wellington, New Zealand

The rare earth nitride series of intrinsic ferromagnetic semiconductors offers a rich selection of spin-orbit systems in which to study electrical transport and magnetic phenomenon, the various Hall effects being one of the many meeting places of these[1,2]. The central member of the series GdN ($^8S_{7/2}$) has a strong spin only magnetisation and relatively simple band structure, dominated by the Gd 5d conduction band and N 2p valence band. Electron doping is routinely achieved via the inclusion of nitrogen vacancies. Here we report on 'anomalous' Hall effect data in heavily doped GdN, which show an apparent change of sign of the dominant charge carrier as the sample is cooled through the ferromagnetic transition, while the anomalous Hall effect retains the negative sign of electron doped GdN. We will discuss these in the context of the calculated band structures of stoichiometric and heavily doped GdN.

[1] W. F. Holmes-Hewett, R. G. Buckley, B. J. Ruck, F. Natali and H. J. Trodahl, 4f conduction in the magnetic semiconductor NdN, Phys. Rev. B. 100, 195119 (2019) [2] W. F. Holmes-Hewett, F. H. Ullstad, B. J. Ruck, F. Natali and H. J. Trodahl, Anomalous Hall effect in SmN: Influence of orbital magnetism and 4f band conduction, Phys. Rev. B. 98, 235201 (2018)

J5-10. Direct Observation of Hidden Spin Polarization in 2H-$MoTe_2$. Y. Xu[1], *J. Tu*[1] and X. Ruan[1] *1. York-Nanjing Joint Center, Nanjing University, Nanjing, China*

Spin polarization in nonmagnetic materials originates from the break of inversion crystalline symmetry that could occur globally or locally. Centrosymmetric (CS) nonmagnetic materials with hidden spin polarization induced by non-CS site symmetries and spin-orbit coupling are promising candidates for spintronic applications, in light of the zero net spin polarization and modulatable spin effects hidden in the local structures. There is, however, an open issue regarding the possible spin splitting induced by broken inversion symmetry at the sample surface. Therefore, it is critical to perform combined experimental and theoretical studies on centrosymmetric TMDC materials such as 2H-$MoTe_2$ to explore the mechanism of the hidden spin polarization. 2H-$MoTe_2$ crystallizes in a trigonal prismatic arrangement with an in-plane lattice constant of 3.517 Å and an out-of-plane lattice constant of 13.962 Å. The unit cell of it is centrosymmetry, but the monolayer has non-centrosymmetric structure. With the virtue of low detection depth of spin-ARPES (<6 Å with He-I), a large spin splitting of 236 meV and opposite spin polarizations up to 80% along out-of-plane direction (z axis) in K and K′ valleys were observed, consist with the density functional theory (DFT) calculations. We further found from the DFT calculations that a medium dipole field mimicked the surface symmetry breaking in ARPES measurements induces negligible variation of spin polarization, confirming that the measured spin effects originate from the intrinsic hidden spin polarization in 2H-$MoTe_2$. The large spin splitting and net spin polarization found in spin-ARPES experiments also suggest that the hidden spin effects in inversion symmetric layered compounds can be used to generate large spin splitting on the surfaces in the absence of strong dipole field. Our combinatorial experimental and theoretical studies clarify the existence of hidden spin polarization in the centrosymmetric materials and opens the way of designing novel functional materials with coexisting hidden spin polarization and other hidden effects, such as hidden orbital polarization and hidden Berry curvature, for the energy efficient spintronics applications.

J5-11. Rotational Currents Around Lanthanide Dopants in Simple Metals. *A.O. Leon*[4], A. Cahaya[2], M. Rahimi[3] and G. Bauer[1] *1. Institute for Materials Research, Tohoku University, Sendai, Japan; 2. Department of Physics, Universitas Indonesia, Depok, Indonesia; 3. Nano-Structured Coatings Institute, Yazd Payame Noor University, Yazd, The Islamic Republic of Iran; 4. Department of Physics, Metropolitan University of Technology, Santiago, Chile*

Magnetic impurities in metals spin polarize their surroundings. This Ruderman-Kittel-Kasuya-Yosida (RKKY) polarization has been fundamental in the understanding of interactions in magnetic atoms and layers. When the impurity is heavy and magnetic, its large atomic spin-orbit coupling unquenches the orbital momentum. This is the case of lanthanide atoms, which have a significant orbital momentum responsible for their strong magnetocrystalline anisotropy. Recent utilization of this atomic spin-orbit coupling in spintronics include the perpendicular magnetic anisotropy of thulium iron garnet (TIG) films [1-4], the voltage-controlled magnetic anisotropy of interfacial rare-earth ions [5-6], and double compensation points of ferrimagnets [7]. In this presentation, we study lanthanide impurities in simple metals. The lanthanide orbital momentum couples to conduction electrons via the so-called skew scattering and induces a rotational current [8]. The predicted current has an orbital momentum density very similar to the RKKY one, with an algebraic decay and oscillations at twice the Fermi wavenumber. In addition to the charge density profile, we compute the observable effects, namely the Oersted magnetic field and Knight shift.

[1] M. Kubota, A. Tsukazaki, F. Kagawa, K. Shibuya, Y. Tokunaga, M. Kawasaki, and Y. Tokura, APEX 5, 103002 (2012). [2] C. Tang, P. Sellappan, Y. Liu, Y. Xu, J. E. Garay, and J. Shi, Phys. Rev. B 94, 140403(R) (2016). [3] C. N. Wu, C. C. Tseng, Y. T. Fanchiang, C. K. Cheng, K. Y. Lin, S. L. Yeh, S. R. Yang, C. T. Wu, T. Liu, M. Wu, M. Hong, and J. Kwo, Sci. Rep. 8, 11087 (2018). [4] C. O. Avci, A. Quindeau, C.-F. Pai, M. Mann, L. Caretta, A. S. Tang, M. C. Onbasli, C. A. Ross, and G. S. D. Beach, Nat. Mat. 16, 309 (2017). [5] A. O. Leon, A. B. Cahaya, and G. E. W. Bauer, Phys. Rev. Lett. 120, 027201 (2018). [6] AO Leon, GEW Bauer, accepted by Journal of Physics: Condensed Matter. [7] M. Imai, H. Chudo, M. Ono, K. Harii, M. Matsuo, Y. Ohnuma, S. Maekawa, and E. Saitoh, Appl. Phys. Lett. 114, 162402 (2019). [8] A. B. Cahaya, A. O. Leon, M. Rahimi Aliabad, G. E. W. Bauer, arXiv:2006.13024

J5-12. Quantifying Induced Moment in non-Magnetic Cu – C_{60} Interfaces via x-ray Magnetic Circular Dichroism. *P. Sharangi*[1], P. Gargiani[2], M. Valvidares[2] and S. Bedanta[1] *1. School of Physical Science, National Institute of Science Education and Research (NISER), Bhubaneswar, India; 2. Alba Synchrotron Light Source, Barcelona, Spain*

The signature of magnetism without having a ferromagnet in the sample stack is both novel and fascinating from fundamental research point of view. It is possible to alter the electronic states of non-ferromagnetic materials (Cu, Mn, Sc, Pt) to overcome the Stoner criterion and make them ferromagnetic at room temperature[1,2]. In this context it is desired to quantify the magnetic moment at the interface of such non-FM/OSC. We have studied the Cu/C_{60} heterostructure and quantified the magnetic moment induced in Cu using X-ray magnetic circular dichroism (XMCD) sum rules. The multilayer of Cu/C_{60} were prepared on Si (100) substrate without breaking the vacuum using DC magnetron sputtering and thermal evaporation for Cu and C_{60}, respectively. SQUID magnetometry on sample S1:(Si(100)/Ta(5nm)/C_{60}(8nm)/Cu(1.8nm)/C_{60}(4nm)/Ta(2nm)) and S2:(Si(100)/Ta(5nm)/C_{60}(16nm)/[Cu(1.8nm)/C_{60}(8nm)]x2/Ta(2nm)) exhibit a clear ferromagnetic hysteresis even in the absence of any ferromagnetic element in the sample stack. The induced magnetic moment in the samples is corroborated to the charge transfer and the molecular coupling between the metal (Cu) and carbon. The origin of the charge state of C_{60} to a reconstructed interface is due to (4 4) 7-atom vacancy holes in the surface[3]. The possible reason of this induced magnetic moment is hybridization between d_{cu} and p_{C60} orbitals[1]. In order to evaluate the spinterfacial magnetic moment, XMCD has been performed on the samples. Figure1 shows the XAS and XMCD spectra of the samples. The XAS spectra do not exactly match with Cu. The reason behind such misalignment is the hybridization between Cu and C_{60}. Due to the charge transfer at the reconstructed Cu/C_{60} interface the density of state of Cu has been modified and exhibits ~ 0.01 μ_B /atom magnetic moment[4]. Our understanding of the interface between the NM/OSC heterostructures may bring the new insights to the field of organic spintronics.

1. F. Al Ma'Mari *et.al., Nature* 524, 69 (2015). 2. F. Al Ma'Mari *et al*., *PNAS*, 1620216114 (2017). 3. W.W.Pai *et.al., PRL* 104, 036103 (2010). 4. P. Sharangi *et al*., (unpublished)

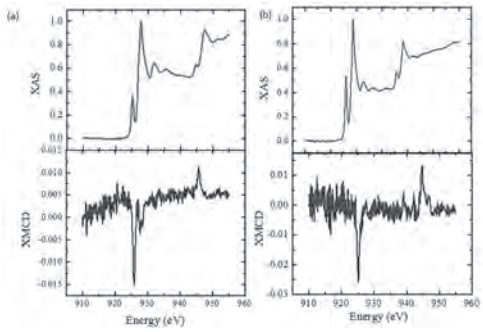

Figure 1. XAS and XMCD spectra of (a) sample S1 and (b) sample S2 at Cu L2,3 edges. All the measurements were performed at 1.7 K under 6 T magnetic field.

J5-13. Density Functional Theory and Machine Learning Guided Study of Mn-Ga Alloys With Targeted Magnetic Properties. *T. Hartnett*[1], P. Balachandran[1,2] and S. Gangopadhyay[1] *1. Materials Scinece Engineering, University of Virginia, Charlottesville, VA, United States; 2. Mechanical Engineering, University of Virginia, Charlottesville, VA, United States*

Mn-Ga alloys show promise for spintronic applications based on their tunable saturation magnetization (Ms) and goldilocks region perpendicular magnetic anisotropy (Ku).[1] Thin films with perpendicular magnetic anisotropy have potential as low-dimensional highly reliable spintronic devises.[2-5] The task remains to optimize magnetic properties for applications as a function of composition and dimensionality. In this study we attempt to understand the impact of composition on magnetic properties of Mn-Ga systems in the $D0_{22}$ structure. Density Functional Theory (DFT) calculations are used to study the role of vacancies on M_s and K_u of Mn-Ga family of alloys. While the DFT calculations capture the general trends seen in experiments, they are unable to quantitatively predict M_s and K_u with sufficient accuracy. This is attributed to the inherent complexities in the thin film growth of Mn-Ga systems, where the variations in M_s and K_u show a strong dependence on the growth variables. Machine Learning (ML) is implemented as a low-cost alternative to DFT, where we train and validate data-driven models based on M_s and K_u data compiled from surveying experimental literature. The ML models enable rapid predictions of M_s and K_u for previously unexplored compositions. New compositions are identified with implications in emerging spintronics applications.

1) H. Kurt, K. Rode, M. Venkatesan, P. Stamenov, PHYSICAL REVIEW B 83, 020405(R) (2011) 2) S. Iwasaki and K. Ouchi, IEEE Trans. Magn. 14, 849 (1978) 3) P. F. Carcia, J. Appl. Phys. 63, 5066 (1988) 4) T. Seki, T. Shima, K. Takanashi, Y. Takanashi, E. 82, 2461 (2003) 5) S. N. Piramanayagam, J. Appl. Phys. 102, 011301 (2007).

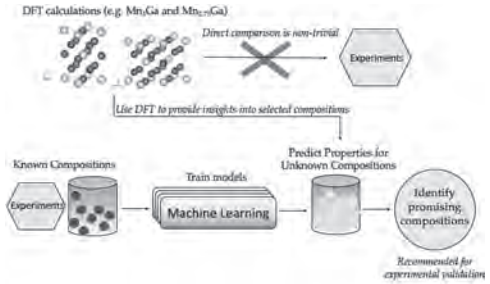

Fig.1 shows the general flowchart of the study.

J5-14. Unusual Magnetic and Transport Properties of PrScGe-GdScGe Solid Solution. *T. Del Rose*[1,2], A.K. Pathak[3], Y. Mudryk[2] and V.K. Pecharsky[1,2] *1. Materials Science and Engineering, Iowa State University, Ames, IA, United States; 2. Ames Laboratory, Ames, IA, United States; 3. University at Buffalo - The State University of New York, Buffalo, NY, United States*

Ternary RTX intermetallics, where R = rare earth element, T = transition metal, and X = *p*-block element, exhibit a wide range of structures and intriguing physical phenomena, and, therefore, are among the most interesting families of intermetallic compounds to explore [1, 2]. Among them are the diverse RScX compounds which for X = Ge and R = La-Eu crystallize in a CeScSi-type (*I*4/*mmm*) structure [3]. Specifically, for R = Gd a ferromagnetic to paramagnetic (PM) transition occurs at T_C = 350 K [4], and for R = Pr, a series of magnetic transformations is as follows: PM to antiferromagnetic (AFM) at T_N = 140 K, AFM to ferrimagnetic (FiM-I) at T_C = 82 K, and a spin reorientation from FiM-I to FiM-II at T_C = 62 K [5]. In this work, we study the pseudo-binary solid solution $Pr_{1-x}Gd_xScGe$. The series exhibits a plethora of interesting physics, such as spontaneous and conventional exchange bias, magnetic memory effects, and unconventional thermal conductivity. We show how small impurities, namely Al in ~0.5 at.% concentration influence the magnetic properties and substantially increase the spontaneous exchange bias. Furthermore we examine differences between the powder and bulk x = 0.25 composition, in particular the unique shape dependent mechanism of magnetic compensation. This work was supported by the Office of Science of the U.S. Department of Energy (DOE), Division of Materials Sciences and Engineering, Office of Basic Energy Sciences. The Ames Laboratory is operated for the U.S. Department of Energy (DOE) by Iowa State University of Science and Technology under contract No. DE-AC02-07CH11358.

[1] S. Gupta and K. G. Suresh, *J. Alloys Compd.*, Vol. 618, p.562–606 (2015). [2] R. Pöttgen, O. Janka, and B. Chevalier, *Zeitschrift für Naturforsch. B.*, Vol. 71, p.165–191 (2016). [3] O. I. Bodak and Z. M. Kokhan, *Inorg. Mater.*, Vol. 19, p.987–989 (1983). [4] F. Guillou *et al.*, *J. Phys. Condens. Matter.*, Vol. 29, p.485802 (2017). [5] P. Manfrinetti *et al.*, *J. Alloys Compd.*, Vol. 450, p.86–91 (2008).

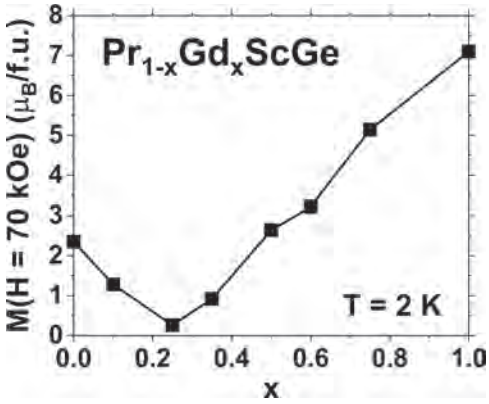

Figure 1: Maximum magnetization of the $Pr_{1-x}Gd_xScGe$ series of compounds at H = 70 kOe and T = 2 K.

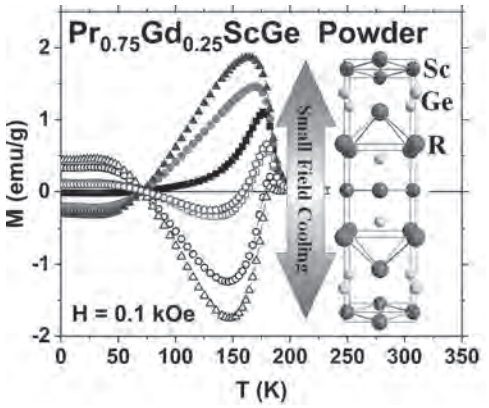

Figure 2: Unusual magnetic memory effect in x = 0.25.

Session J6
ANTIFERROMAGNETIC SPINTRONICS II (Poster Session)

Angela Wittmann, Chair
Massachusetts Institute of Technology, Cambridge, MA, United States

J6-01. Withdrawn

J6-02. Growth of non-Collinear Antiferromagnet Thin Films for Spintronics. *B. Rimmler*[1] and S.S. Parkin[1] *1. Nano-Systems from ions, spins and electrons, Max Planck Institute of Microstructure Physics, Halle (Saale), Germany*

Antiferromagnetic spintronics attempts to control the spin state of electrons in spintronic devices in which the active materials possess antiferromagnetic order. These materials are promising because of their robustness against magnetic fields, the absence of magnetic stray fields, ultrafast dynamics and large magnetotransport effects[1,2]. In recent years, antiferromagnets with non-collinear magnetic order have received much attention due to interesting effects resulting from Berry curvature in crystal momentum space and the presence of non-trivial topological states[3]. Amongst these materials are the Heusler alloys Mn_3X (X = Ge, Sn, Ir, Pt) as well as nitrides with antiperovskite structure Mn_3AN (A = Ni, Ga, Sn). However, relatively few compounds have thus far been grown as thin films and used in spintronic devices. Therefore, in this work we show the growth of epitaxial thin films of non-collinear antiferromagnetic antiperovskite nitrides and investigations of their magnetic and magnetotransport properties. A better understanding of the physics of these materials will help in incorporating them into next-generation spintronic devices.

[1] V. Baltz et al., Rev. Mod. Phys., 90, 015005 (2018) [2] T. Jungwirth et al., Nat. Nanotechnol., 11, 231-241 (2016) [3] L. Šmejkal et al., Nat. Phys., 14, 242-251 (2018)

J6-03. Diffusive Spin Nernst Effect of Antiferromagnetic Magnons. *H. Zhang*[1] and R. Cheng[1,2] *1. Department of Electrical and Computer Engineering, University of California Riverside, Riverside, CA, United States; 2. Department of Physics and Astronomy, University of California Riverside, Riverside, CA, United States*

Magnon spin Nernst effect (SNE) has recently been proposed as a bulk effect in antiferromagnetic insulators without considering diffusions and boundaries[1,2]. However, real experiments[3] deal with situations far from the ideal bulk picture in that: 1) the system is finite and shares imperfect boundaries with the detecting leads; 2) both the electrons in the leads and the magnons are diffusive; 3) the thermal power rather than the temperature gradient is calibrated. To properly accommodate these complexities, we formulate a diffusive theory of the SNE of antiferromagnetic magnons under a realistic device geometry. By solving the coupled spin diffusion equations of magnons and electrons with a finite spin transmission across the boundaries, we find that the detectable signal can be much larger than that predicted by the bulk picture. The diffusive effects also lead to a different phase diagram of the SNE compared to the bulk theory without diffusion. Counterintuitively, we also find that the diffusive magnon SNE exhibits an even symmetry with respect to a perpendicular magnetic field.

1. R. Cheng, S. Okamoto and D. Xiao, Phys. Rev. Lett., Vol. 117, 217202 (2016) 2. V. A. Zyuzin and A. A. Kovalev, Phys. Rev. Lett., Vol. 117, 217203 (2016) 3. Y. Shiomi, R. Takashima and E. Saitoh, Phys. Rev. B, Vol. 96, 134425 (2017)

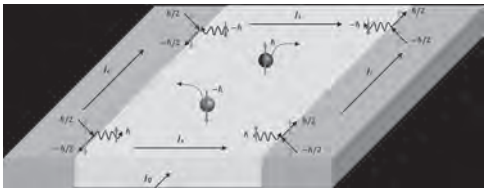

Fig 1. Illustration of system geometry and spin transmission processes at boundaries.

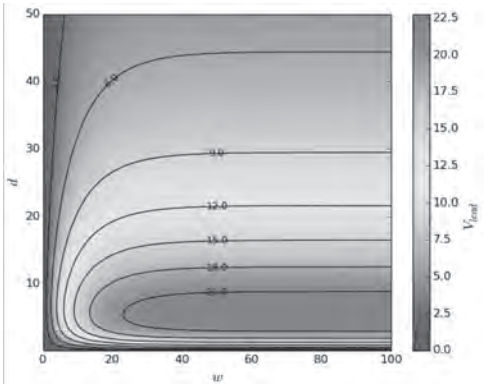

Fig 2. Inverse spin Hall voltage V_{lead} in the leads as a function of the width w of antiferromagnet and the width d of lead. All quantities have arbitrary unit.

J6-04. Evidence of Topological Hall Effect in Pt/Antiferromagnetic-Insulator Bilayers. *Y. Cheng*[1], S. Yu[1], M. Zhu[2], J. Hwang[2] and F. Yang[1] *1. Physics, The Ohio State University, Columbus, OH, United States; 2. Materials Science and Engineering, The Ohio State University, Columbus, OH, United States*

Topological spin textures, such as skyrmions, have attracted intense interest in recent years. Magnetic skyrmions have been studied almost exclusively in bulk ferromagnets (FM) or FM multilayers. Antiferromagnets (AF) have also been predicted to harbor topological spin textures such as AF skyrmions. Topological Hall effect has been a primary indicator of spin textures in magnetic materials. We observe unambiguous evidence of topological Hall effect in Pt/Cr_2O_3 bilayers grown on $Al_2O_3(0001)$ and $Al_2O_3(11\text{-}20)$, where Cr_2O_3 epitaxial film is an antiferromagnetic insulator[1]. Although Cr_2O_3 is insulating, the topological magnetic textures can be detected through a novel phenomenon: "spin-Hall topological Hall effect" (SH-THE), similar to what recently observed topological Hall effect in $Pt/Tm_3Fe_5O_{12}$ bilayers[2]. The Pt/Cr_2O_3 bilayers exhibit clear topological Hall resistivity for Cr_2O_3 thicknesses below 6 nm near and above room temperature, which is above the Néel temperature of Cr_2O_3, revealing the key role of thermal fluctuations in the formation of spin textures[3]. The similarity of topological Hall signals in (0001) and (11-20)-oriented Cr_2O_3 films indicates that the emergence of spin textures is insensitive to crystalline orientation. This first observational evidence of topological Hall effect in HM/AFI bilayers significantly expands our materials base to include the large family of AF insulators for the exploration of AF-based skyrmion technology.

[1]. Yang Cheng, Sisheng Yu, Menglin Zhu, Jinwoo Hwang and Fengyuan Yang, "Evidence of Topological Hall Effect in Pt/Antiferromagnetic-Insulator Bilayers," *Phys. Rev. Lett.* 123, 237206. [2]. A. S. Ahmed, A. J. Lee, N. Bagués, B. A. McCullian, A. M. A. Thabt, A. Perrine, P.-K. Wu, J. R. Rowland, M. Randeria, P. C. Hammel, D. W. McComb, and F.. Y. Yang, "Spin-Hall topological Hall effect in highly tunable Pt/ferrimagnetic-insulator bilayers," *Nano Lett.*, 19, 5683 (2019). [3]. Wenbo Wang, Matthew W Daniels, Zhaoliang Liao, Yifan Zhao, Jun Wang, Gertjan Koster, Guus Rijnders, Cui-Zu Chang, Di Xiao and Weida Wu, "Spin chirality fluctuation in two-dimensional ferromagnets with perpendicular magnetic anisotropy" *Nat. Mater.* 2019, 18, 1054.

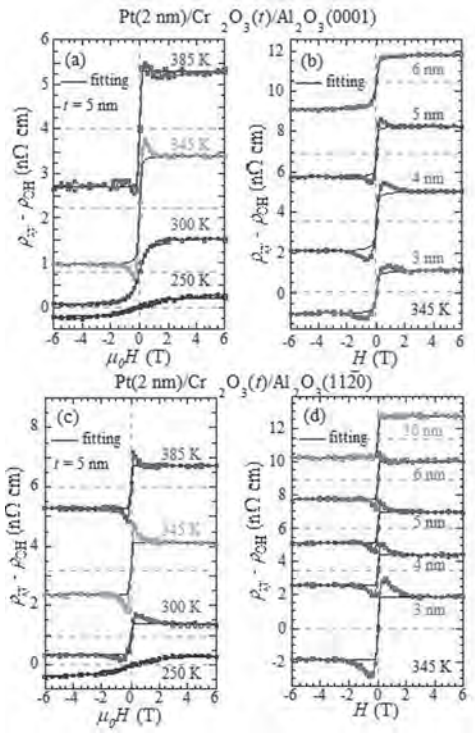

Figure 1 (a) and (c) Hall measurements of a Pt(2 nm)/Cr_2O_3(*t* = 5 nm) bilayer on Al_2O_3(0001) and Al_2O_3(11-20), respectively. ρ_{xy} - ρ_{OH} measured at various temperatures from 250 to 385 K, where the black curves are the fitting for ρ_{AH} with Langevin function. The clear bumps indicate the shown up of topological hall (TH) signal. (b) and (d) Hall resistivity ρ_{xy} - ρ_{OH} of Pt(2 nm)/Cr_2O_3(*t*) bilayers at 345 K with different thickness (*t*) of Cr_2O_3 on Al_2O_3(0001) and Al_2O_3(11-20), respectively.

J6-05. Effects of Geometry on Curvilinear Spin Chains. D. Kononenko[1,2], *O. Pylypovskyi*[3], K. Yershov[2,4], U. Roessler[2], A. Tomilo[1], J. Fassbender[3], J. van den Brink[2,5], D. Makarov[3] and D. Sheka[1] *1. Taras Shevchenko National University of Kyiv, Kyiv, Ukraine; 2. Leibniz-Institut fur Festkorper- und Werkstoffforschung Dresden eV, Dresden, Germany; 3. Helmholtz-Zentrum Dresden-Rossendorf, Dresden, Germany; 4. Institut teoreticnoi fiziki imeni M M Bogolubova Nacional'na akademia nauk Ukraini, Kyiv, Ukraine; 5. Institute for Theoretical Physics, TU Dresden, Dresden, Germany*

Curvilinear magnetism is of great fundamental and practical interest whose rapid development is inspired by novel experimental technologies and wide potential applications [1]. A general approach for description of curvilinear ferromagnets [2] has been recently developed and used for thin wires and shells uncovering magnetochiral effects in statics and dynamics [1,3]. Besides intensive research of ferromagnetic materials, their antiferromagnetically ordered (AFM) counterparts are promising candidates for spintronics applications by their low sensitivity to external fields and ultra high eigenfrequencies [4]. Here, we present a general approach for description of AFM textures in curvilinear spin chains [5]. We show that the magnetic dipole-dipole interaction in these systems can be reduced to a hard-axis anisotropy along the chain. Lagrangian of the curvilinear AFM spin chain in continuum limit corresponds to the biaxial chiral helimagnet. Helix geometry shows existence of two equilibrium magnetic states depending on values of curvature and torsion: (i) homogeneous state in the local reference frame, it is typical for helices with the curvature larger than torsion; and (ii) periodic state is quasi-homogeneous in the laboratory reference frame. For specific case of the AFM flat chain there is the only ground state, with the order parameter being oriented perpendicular to the chain plane. We show that in curvilinear system transverse and longitudinal magnon modes in the AFM helix and ring are coupled due to geometry-induced Dzyaloshinskii–Moriya interaction.

[1] R. Streubel, J. Lee, D. Makarov et al, J. Phys. D, 49, 363001, (2016); A. Fernández-Pacheco et al, Nat. Comm., Vol. 8, p. 15756 (2017). [2] Y. Gaididei, V. P. Kravchuk, D. D. Sheka, Phys. Rev. Lett. 112, 257203 (2014); D. D. Sheka, V. P. Kravchuk, Y. Gaididei, J. Phys. A, Vol. 48, p. 125202 (2015). [3] O. V. Pylypovskyi, D. D. Sheka, V. P. Kravchuk et al, Sci. Rep. Vol. 6, p. 23316 (2016); O. V. Pylypovskyi, D. Makarov, V. P. Kravchuk et al, Phys. Rev. Applied, Vol. 10, p. 064057 (2018) [4] V. Balz, A. Manchon, M. Tsoi et al, Rev. Mod. Phys., Vol. 90, p. 015005 (2018) [5] D. Y. Kononenko, O. V. Pylypovskyi, K. V. Yershov et al., arXiv:2005.05835 (2020)

J6-06. Withdrawn

J6-07. Antiferromagnetic Domain Structure in CuMnAs Devices. *S. Reimers*[1,2], O.J. Amin[1], R.P. Campion[1], O. Gomonay[6], F. Maccherozzi[2], F. Krizek[4], V. Novák[4], T. Jungwirth[4,1], D. Kriegner[5,4], A. Björling[3], D. Carbone[3], K.W. Edmonds[1], P. Wadley[1] and S.S. Dhesi[2] *1. School of Physics and Astronomy, The University of Nottingham, Nottingham, United Kingdom; 2. Diamond Light Source, Didcot, United Kingdom; 3. MAX IV Laboratory, Lund, Sweden; 4. Department of Spintronics and Nanoelectronics, Institute of Physics ASCR, FZU, Prague, Czechia; 5. Institute for Solid State and Materials Physics, Technical University Dresden, Dresden, Germany; 6. Johannes Gutenberg Universitat Mainz, Mainz, Germany*

The demonstration of efficient manipulation of the antiferromagnetic (AF) order parameter has highlighted its highly attractive properties for spintronics, including lack of magnetic stray fields, robustness against magnetic field perturbations and intrinsic dynamics in the THz regime [1, 2, 3]. Specific functionalities often depend sensitively on the magnetic domain structure [4]. In fully compensated AFs with no demagnetizing fields, magnetoelastic effects are expected to dominate [5,6]. We report direct imaging and analysis of AF domains in patterned epitaxial CuMnAs thin films. A pronounced effect of patterned edges on the domain orientation and domain wall width is demonstrated, which extends over several microns. A local alignment of the Néel vector with microtwin line defects is observed, which, combined with the edge effect, leads to the formation of lens-shaped domains oriented perpendicular to the patterned edges. We observe magneto-structural reconfigurations in which defect lines and surrounding AF domains grow together over the timescale of weeks at room temperature and over minutes 30K above room temperature.

[1] P. Wadley, B. Howells, J. Zelezny et al., Science., Vol. 351, p. 587 (2016) [2] X.Z. Chen, R. Zarzuela, J. Zhang et al., Physics Review Letters., Vol. 120, p. 207204 (2018) [3] P. Nemec, M. Fiebig, T. Kampfrath and A.V. Kimel, Nature Physics., Vol. 14, p. 229 (2018) [4] A.L. Ross et al., Nano Letters, Vol. 20(1), p. 306 (2020) [5] O. Gomonay and V. Loktev, Journal of Magnetism and Magnetic Materials., Vol. 242(2), p. 1418 (2002) [6] O. Gomonay, V. Baltz, A. Brataas and Y. Tserkovnyak, Nature Physics., Vol. 14, p. 213 (2018)

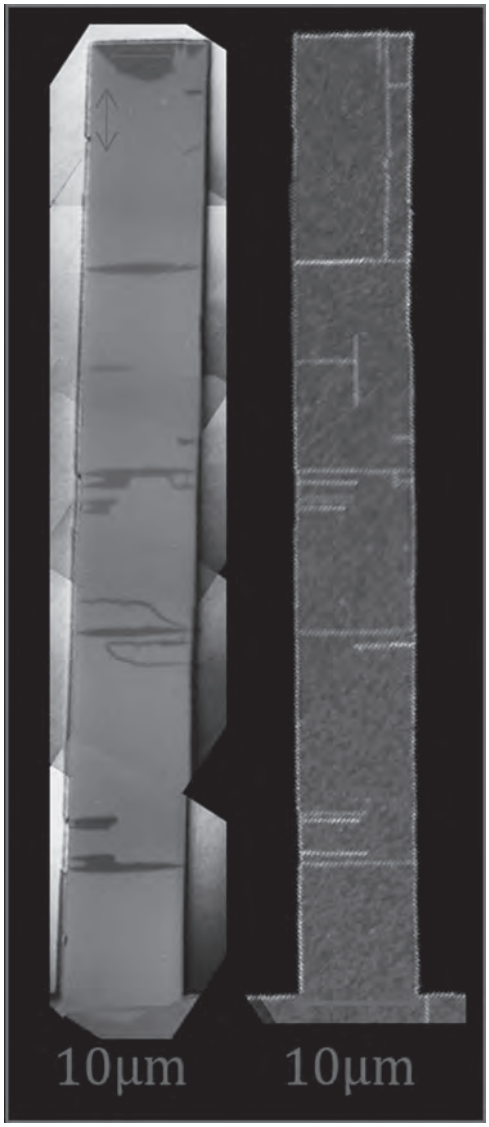

Fig. 1: AF domain structure and correlation to microtwin defects in a patterned 80μm x 10μm sized CuMnAs stripe. Left: AF domain structure imaged in XMLD-PEEM. The double-headed red arrows indicate the local spin axes. Right: Scanning X-ray diffraction map of the same bar showing the distribution of line-defects. The image axes are aligned with the CuMnAs [110] and [1-10] crystalline axes.

J6-08. Withdrawn

J6-09. Anomalous Hall Effect in Mn-Sn Thin Films - Correlation With Crystal Structure. *J. Yoon*[1], Y. Takeuchi[1], Y. Yamane[1,2], S. Kanai[1,3], J. Ieda[1,4], H. Ohno[1,5] and S. Fukami[1,6] *1. Lab. for Nanoelectronics and Spintronics, RIEC, Tohoku University, Sendai, Japan; 2. FRIS, Tohoku Univiersity, Sendai, Japan; 3. FRiD, Tohoku University, Sendai, Japan; 4. ASRC, Japan Atomic Energy Agency, Tokai, Japan; 5. CSIS, Tohoku University, Sendai, Japan; 6. WPI-AIMR, Tohoku University, Sendai, Japan*

Non-collinear antiferromagnets such as $D0_{19}$-Mn_3Sn have attracted much attention owing to their large anomalous Hall effect (AHE) originating from non-vanishing Berry curvature [1-5]. We recently reported a growth of epitaxial $D0_{19}$-Mn_3Sn thin films with various orientations by sputtering, where anisotropic AHE was observed [5]. To realize functional devices harnessing the unique features of this material system, it is necessary to clarify the correlation of the physical properties with various factors of thin film. Here, we study the correlation between AHE and crystal structure of Mn-Sn alloy film by changing post-annealing temperature (T_a) and Mn-Sn composition. We prepare two series of $Mn_{3+x}Sn_{1-x}$ thin films which are deposited on MgO(110) substrate by sputtering. The first series have a fixed x = +0.06 and T_a is changed from 300 to 600°C. The second series have various x (-0.35 ~ +0.32) with a fixed T_a = 500°C. Crystal structures are characterized by X-ray diffraction (XRD). Transport measurement is performed for microfabricated Hall devices. From XRD measurement, we find that dominant phase of Mn-Sn changes from $Mn_{1.75}Sn$ to $D0_{19}$-Mn_3Sn as T_a increases (series 1), and changes from Mn_3Sn_2 to $D0_{19}$-Mn_3Sn as x increases (series 2) in the studied range. Transport measurement for the series 1 reveals that appearance of AHE coincides with the formation of $D0_{19}$-Mn_3Sn and the magnitude increases with T_a [Fig. 1]. Meanwhile, for the series 2, the largest AHE is obtained at around the stoichiometric composition [Fig. 2]. We here note that the two series are prepared at different times, leading to different magnitude of AHE. From a comparison with XRD results, we find that magnitude of AHE is well explained by multiple factors of crystalline structure including proportion of $D0_{19}$-Mn_3Sn crystallite, crystalline orientation, and the order parameter. The obtained results provide an important insight to deepen the physics of non-collinear antiferromagnet and to realize new-functional devices. This work is partly supported by JSPS Kakenhi No. 19H05622 and No. 19J13405.

[1] S. Nakastuji, N. Kiyohara and T. Higo, Nature, Vol. 527, p.212 (2015). [2] A. K. Nayak, J. E. Fischer and S. S. P. Parkin, Sci. Adv., Vol. 15, p.e1501870 (2016). [3] T. Higo, D. Qu and S. Nakatsuji, Appl. Phys. Lett., Vol. 113, p.202402 (2018). [4] T. Ikeda, M. Tsunoda and Y. Ando, Appl. Phys. Lett., Vol. 113, p.222405 (2018). [5] J. Yoon, Y. Takeuchi and H. Ohno, Appl. Phys. Express, Vol. 13, p.013001 (2020).

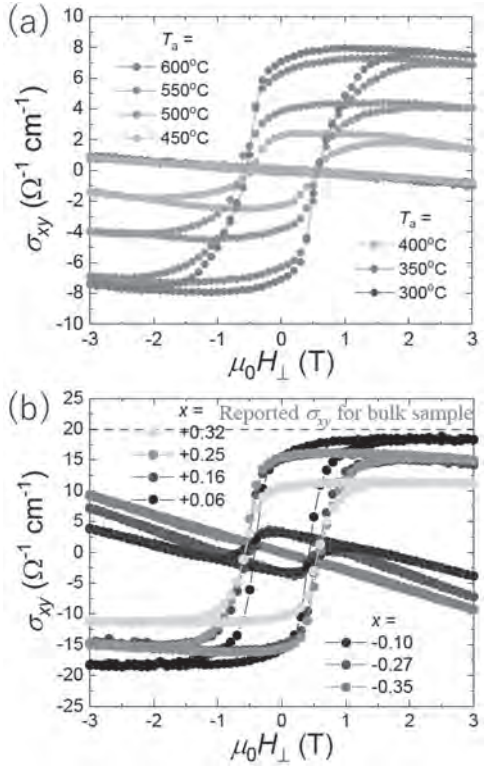

Fig. 1 Hall conductance σ_{xy} vs. out-of-plane magnetic field for various (a) annealing temperature T_a and (b) Mn-Sn composition x.

J6-10. Withdrawn

J6-11. Terahertz Emission From an Exchange-Coupled Synthetic Antiferromagnet. *Q. Zhang*[1,2], Y. Yang[1], Z. Luo[1], Y. Xu[1], R. Nie[1], X. Zhang[2] and Y. Wu[1] *1. National University of Singapore, Singapore; 2. Southern University of Science and Technology, Shenzhen, China*

In this work, we report on THz emission from FeMnPt-based synthetic antiferromagnetic structures (SAF), originating from the anomalous Hall effect (AHE) [1][2]. The peak amplitude of the THz emission is almost doubled as compared to the respective single layer with the same equivalent thickness. In addition, we demonstrate by both simulation and experiment that the THz emission provides a powerful tool to probe the magnetization reversal process of individual ferromagnetic layers in the SAF structure – an important building block for all types of spintronic devices. By measuring the polarization of the THz wave, we are able to determine the magnetization directions of the individual magnetic layers which are not possible or difficult to obtain by using other magnetic characterization techniques. Fig. 1 shows the shematic of the FeMnPt SAF structure under an in-plane external field. A femtosecond laser pulse is used to excite the sample, thereby generating the THz emission. Fig. 2 shows the temperoal profile of the THz emmission from both the FeMnPt SAF (solide-line: 0 Oe; dashed-line: 200 Oe) and a single layer FeMnPt (dotted-line). At zero field, The AHE in both layers of the SAF contributes to the THz emission, leading to a larger THz amplitude, which is almost doubled that of the single layer. By correalting the simulated and experimental results, the direction of magnetizaion in each FM layer during field sweeping can be determined becasue the THz emission is propotional to the dedection of mangetization in each FM layer. Our results show that THz emission provides a powerful tool to understand the magnetic reversal of SAFs.

[1] Q. Zhang, Z. Luo, H. Li, et al., Physical Review Applied, vol.12, p.054027, (2019) [2] Q. Zhang, Y. Yang, Z. Luo, et al., Physical Review Applied, vol.13, p.054016, (2020)

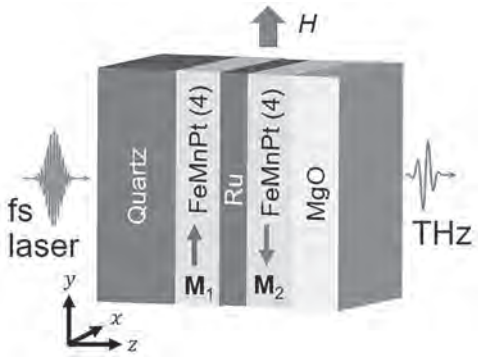

Fig. 1. Schematic of the FeMnPt SAF

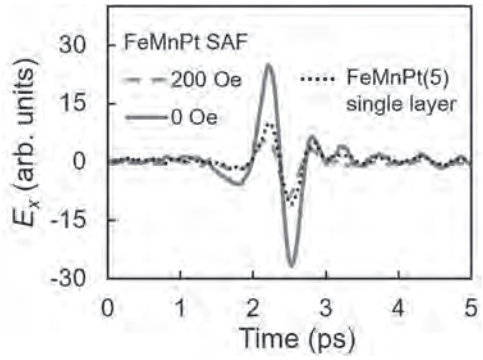

Fig. 2. THz waveforms of the (4, 4) FeMnPt SAF at 200 Oe (dashed-line) and 0 Oe (solid-line), and FeMnPt (5) single layer emitter (dotted-line) at a positive magnetic field.

J6-12. Temperature-Dependent Exotic Spin Torques in Antiferromagnetic FeRh. *J. Gibbons*[1], T. Dohi[2], H. Saglam[3], J. Pearson[4], S. Fukami[2] and A. Hoffmann[1] *1. Materials Science and Engineering, University of Illinois at Urbana-Champaign, Urbana, IL, United States; 2. Laboratory for Nanoelectronics and Spintronics, Research Institute of Electrical Communication, Tohoku Daigaku Denki Tsushin Kenkyujo, Sendai, Japan; 3. Applied Physics, Yale University, New Haven, CT, United States; 4. Materials Science Division, Argonne National Laboratory, Lemont, IL, United States*

Exotic spin torques resulting from reduced symmetry in quantum materials stand out as strong possibilities for advancing the future of MRAM and spin-torque based neuromorphic computing. Magnetic ordering can reduce the symmetry of a material in a manipulatable way, generating customizable spin torques, and is thus an attractive trait in spin source materials. Antiferromagnets are particularly attractive due to the robustness of their magnetic ordering, which can be prepared into a state and remain stable in that state in a wide range of device setups. Iron rhodium (FeRh) exhibits a transition between a low-temperature antiferromagnetic state and a high-temperature ferromagnetic state. For appropriately grown thin film FeRh, this transition can be found close to room temperature, making both of its magnetic states easily accessible. We report large exotic spin torques generated in an antiferromagnetic FeRh spin source layer and investigate the role of magnetic ordering on the size and geometry of generated spin torques. We also show strong temperature dependence of the spin torque efficiency in the antiferromagnetic phase of FeRh. This work was supported as part of Quantum Materials for Energy Efficient Neuromorphic Computing, an Energy Frontier Research Center funded by the U.S. DOE, Office of Science.

Session K1
MULTIFERROIC MATERIALS AND HETERO-STRUCTURES I

Rajesh Vilas Chopdekar, Chair
Lawrence Berkeley National Laboratory, Berkeley, CA, United States

INVITED PAPER

K1-01. Magnetoelectric Behavior via a Spin State Transition.
S. Chikara[1,5], J. Gu[2], X. Zhang[2], H. Cheng[2], N. Smythe[3], J. Singleton[1], B. Scott[3], E. Krenkel[4], J. Eckert[4] and V. Zapf[1] *1. Pulsed Field Facility, Los Alamos National Laboratory, Los Alamos, NM, United States; 2. University of Florida, Gainesville, FL, United States; 3. Los Alamos National Laboratory, Los Alamos, NM, United States; 4. Harvey Mudd College, Claremont, CA, United States; 5. National High Magnetic Field Laboratory, Tallahassee, FL, United States*

Magnetoelectric and multiferroic materials exhibit more than one ferroic order, usually ferromagnetism and ferroelectricity. This definition has extended to encompass magnetic behavior beyond ferromagnetism. Magnetoelectrics are especially attractive as they allow manipulation of magnetic properties by electric field and vice versa. This coupling could enable lower power consumption and new functionalities in devices such as sensors, memories and transducers. We explore a different approach to magnetoelectric coupling. We use the ordering of the magnetic spin state instead of the traditional ferro or antiferromagnetic ordering of spins. In our molecular compound, magnetic field induces a spin crossover which generates molecular distortions and electric dipoles. These dipoles couple to the magnetic easy axis and form different polar phases with magnetic field and temperature. Spin crossover compounds are a large class of materials where the spin state can modify the structure, and here we demonstrate that this is a route to magnetoelectric behavior.

S. Chikara et. al. Nat. Comm. 10, 4043 (2019) V. Jakobsen et. al. Angew. Chem. 2, 59 (2020)

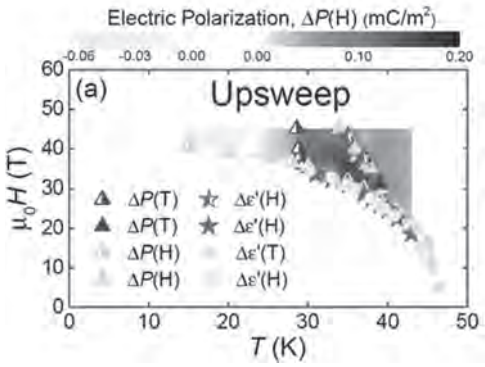

CONTRIBUTED PAPERS

K1-02. Electric-Field-Modulated Magnetism in All-Oxide Multiferroic Heterostructures.
P. Wang[1], C. Jin[1] and H. Bai[1] *1. Tianjin Key Laboratory of Low Dimensional Materials Physics and Processing Technology, School of Science, Tianjin University, Tianjin, China*

Electric field modulated magnetism provides a promising method to achieve low-power and high-speed memory devices.[1] The magnetic properties of single ferro(i)magnetic layer on the $Pb(Mg_{1/3}Nb_{2/3})_{1-x}Ti_xO_3$ (PMN-PT) substrates under electric fields have been investigated widely. Recently, the modulation of the ferro(i)magnetic bilayers/PMN-PT heterostructures has attracted much attention, which probably achieves electric-field-modulated tunnel magnetoresistance (TMR). The $La_{0.67}Sr_{0.33}MnO_3$ (LSMO) films are always used as ferromagnetic electrode and the spinel ferrite $CoFe_2O_4$ (CFO) films can be chosen as the spin-filter ferromagnetic insulator.[2,3] Moreover, the magnetism of the CFO films with large magnetic anisotropy can be mediated by electric fields significantly.[4] Hence, we investigated electric-field-mediated magnetism of the (011)-CFO/LSMO/PMN-PT hetero- structures. The coercivity along in-plane [01-1] direction is reduced by ~50% under the electric field of 10 kV/cm [Fig. 1], which is due to the strain effect of PMN-PT substrate and the large magnetic anisotropy of CFO layer.[5] The results indicate that the electric-field-controlled TMR can be further achieved in the CFO/LSMO/PMN-PT heterostructures.

[1] A. Chen, Y. Wen and B. Fang, Nat. Commun., Vol. 10, p.243 (2019). [2] J. B. Moussy, J. Phys. D: Appl. Phys., Vol. 46, p.143001 (2013). [3] Y. F. Chen and M. Ziese, Phys. Rev. B, Vol. 76, p.014426 (2007). [4] J. J. Yang, Y. G. Zhao and H. F. Tian, Appl. Phys. Lett., Vol. 94, p.212504 (2009). [5] P. Wang, C. Jin and D. Li, Phys. Chem. Chem. Phys., Vol. 22, p.12651 (2020).

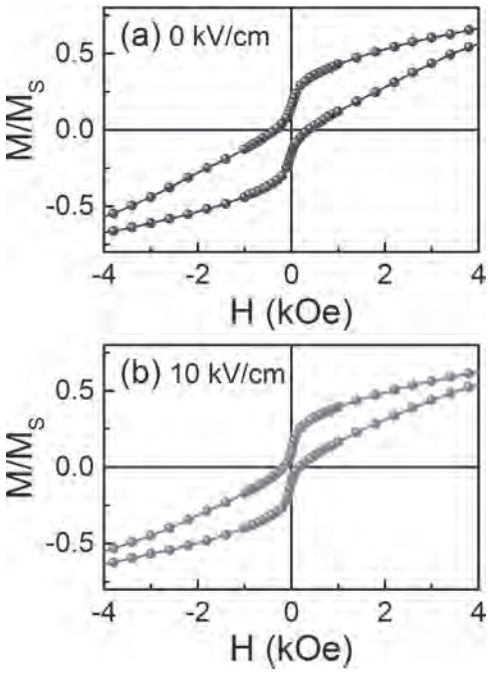

Fig. 1 Magnetization curves of the CFO/LSMO/PMN-PT heterostructures measured with electric fields of (a) 0 kV/cm and (b) 10 kV/cm along in-plane [01-1] direction at 300 K.

K1-03. Voltage Control of Néel Wall Interaction in Thin Films With Uniaxial in-Plane Anisotropy. *J. Zehner*[1], I. Soldatov[1], S. Schneider[1], S. Fähler[1], K. Nielsch[1], R. Schäfer[1] and K. Leistner[1] *1. Leibniz-Institut fur Festkorper- und Werkstoffforschung Dresden eV, Dresden, Germany*

Ionic modulations of magnetic properties, controlled by a low voltage, are attractive for future energy efficient magnetic devices. [1,2] We study the magneto-ionic control of thin iron films with uniaxial in-plane anisotropy, which is induced by oblique sputtering. The polycrystalline iron films are natively oxidized to yield iron oxide/iron films suitable for magneto-ionic manipulation by electrolytic gating in alkaline electrolyte. [3] Angle resolved magnetic measurements reveal a uniaxial anisotropy (Fig.1). In the pristine state (Fig. 1a, b, black curves), the remanence and coercivity along the hard axis are enhanced, due to the formation of a blocked magnetic state resulting from interactions of the charged Néel walls. [4] A voltage-controlled transformation of the FeO_x layer into metallic Fe upon electrolytic gating leads to a drastic decrease in coercivity in all directions (Fig. 1a, blue curve). At the same time, the remanence remains unchanged for angles close to the easy axis but almost vanishes in the vicinity of the hard axis upon the reduction process (Fig. 1b, blue curve). Anhysteretic measurements along the hard axis revealed that the anisotropy increases upon voltage application. The unexpected finding of an inverse anisotropy-coercivity relationship is further studied by investigating the magnetic microstructure by in-situ Kerr microscopy. We find a significant increase in domain size by 60% upon reduction. We attribute the observed coarsening of the magnetic microstructure to the anisotropy-related increase in the domain wall energy. At the same time, the anisotropy increase causes a decrease of the Néel wall tails. Both effects will result in a weakening of the Néel wall interactions during voltage application, which can explain the observed magnetic de-blocking, and thus, the collapse of remanence and coercivity. [5]

[1] C. Navarro-Senent, A. Quintana, E. Menéndez, E. Pellicer, and J. Sort, APL Materials 7, 030701 (2019). [2] A. Molinari, H. Hahn, and R. Kruk, Advanced Materials 31, 1806662 (2019). [3] K. Duschek, M. Uhlemann, H. Schlörb, K. Nielsch, and K. Leistner, Electrochemistry Communications 72, 153 (2016). [4] A. Hubert and R. Schäfer, *Magnetic Domains* (Springer Berlin Heidelberg, Berlin, Heidelberg, 1998). [5] J. Zehner, I. Soldatov, S. Schneider, R. Heller, N. B. Khojasteh, S. Schiemenz, S. Fähler, K. Nielsch, R. Schäfer, K. Leistner, *submitted*

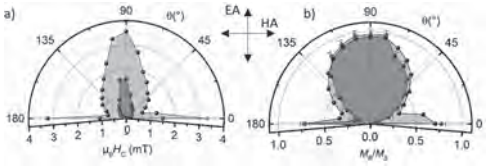

Fig. 1.: Comparison of angle resolved in-plane measurement of coercivity (a) and remanence ratio (b) before (black) and during (blue) the voltage-controlled transformation from FeO_x to metallic Fe in FeO_x/Fe thin films. EA and HA refer to easy and hard axis, respectively.

K1-04. Withdrawn

K1-05. Oxidation Effect on the Interface Magnetoelectric Coupling in Co/Pb(Zr,Ti)O_3(001). *R. Arras*[1] and S. Cherifi-Hertel[2] *1. Centre d'Elaboration de Materiaux et d'Etudes Structurales, Toulouse, France; 2. Institut de Physique et Chimie des Materiaux de Strasbourg, Strasbourg, France*

Recent research on spin electronics has been strongly influenced by the discovery of alternative means to control the magnetization other than by applying a magnetic field. Rapidly, the electric control of magnetism has appeared as the method of choice for this purpose due to its promising potential for spintronic applications with thrifty energy consumption. In this framework, artificial multiferroic materials such as ferromagnetic/ferroelectric bilayers, represent a natural pathway towards the efficient electric control of the magnetization, owing to the magnetoelectric coupling (MEC). The voltage control of magnetism through electronic processes is particularly promising for spintronic applications due to, *e.g.*, the possibility to electrically control two non-volatile magnetization states, the ultra-low energy consumption of the device, and the intrinsically fast response of the magnetization resulting from changes in the electronic structure. Therefore, electronically-driven interface MEC has attracted much attention lately. In particular, great efforts are being made to improve the functionality of magnetoelectric interfaces by searching for new mechanisms leading to enhanced coupling constants [1,2]. Based on first-principles calculations, we have recently predicted the polarization control of the interfacial magnetic phase and a giant electronically-driven magnetoelectric coupling (MEC) in $Co/PbZr_{0.25}Ti_{0.75}O_3(001)$ (Co/PZT) due to the oxidation of Co at the interface [3]. The magnetic phase of the oxidized Co interface is electrically switched from the ferromagnetic to the antiferromagnetic state by reversing the PZT polarization from upward to downward, respectively. A surface MEC constant $\alpha_S \approx 2 \times 10^{-10}$ G cm^2 V^{-1} is derived from our calculations in unoxidized Co/PZT bilayers, in agreement with previously reported experimental results [4], and a giant surface MEC constant $\alpha_S \approx 12 \times 10^{-10}$ G cm^2 V^{-1} is obtained in the case of oxidized Co/PZT interfaces. In this talk, I will discuss in details the changes of the electronic and magnetic properties occurring at the Co/PZT interface as a function of the polarization state, the Co thickness, and its oxidation state.

[1] G. Radaelli, D. Petti, E. Plekhanov, et al., Nature Commun., Vol. 5, p. 3404 (2014) [2] I. R. Reddy, P. M. Oppeneer and K. Tarafder, Phys. Rev. B, Vol. 98, p. 140401(R) (2018) [3] R. Arras and S. Cherifi-Hertel, ACS Appl. Mater. Interfaces, Vol. 11, p. 34399 (2019) [4] O. Vlasin, R. Jarrier, R. Arras, et al., ACS Appl. Mater. Interfaces, Vol. 8, p. 7553 (2016)

K1-06. Influence of Size on the Magnetization Switching of Strain-Mediated FeGaB/PMN-PT Magnetoelectric Heterostructure: a Micromagnetic Study. *P. Pathak*[1] and D. Mallick[1] *1. Department of Electrical Engineering, Indian Institute of Technology Delhi, New Delhi, India*

Recently, electric field controlled magnetization switching in strain-mediated magnetoelectric devices has gained major attention for nanomagnetic memory and logic applications due to their low-power consumption and low switching current [1-3]. In this work, micromagnetic analysis is performed to study the voltage controlled magnetization switching of FeGaB nanomagnets as a function of elliptical disk-shaped geometry having different Aspect Ratios (AR-major axis: minor axis) keeping the thickness fixed. For larger AR nanomagnet (Fig.1(a)), magnetization rotation begins at higher voltage and intermediate incoherent states are observed in each step. There is larger variation of the demagnetisation energy with the applied voltage compared to the pre-stress equilibrium state, signifying that higher voltage is required to overcome the demagnetisation energy. Upon the voltage removal, the elliptical nanomagnets rotate back to the initial pre-stress equilibrium state showing the volatile nature. As the nanomagnet AR is reduced, the critical stress for the switching is observed at relatively lower voltage and the magnetization rotates in a coherent manner. The circular nanomagnet (Fig.1(b)) does not rotate to pre-stress equilibrium state when the voltage is removed and tries to remain at the immediately previous state showing non-volatility. The pre-stress total energy (Fig.2) rises as the AR is lowered, showing the stability of higher AR shapes under pre-stress condition. As negative voltage is applied to create critical stress, the total energy reduces with the AR.The interplay between the stress, magnetization, and demagnetization energies is analysed further to explain the underlying physics including coherent/incoherent flipping, flipping energies, the required voltage, the dissipation energy, and the switching time.

[1] Dhritiman Bhattacharya et. al., Multifunct. Mater., 2:032001 (2019). [2] M-J. Zhou et. al., J. Phys. D: Appl. Phys., 53.2:024002 (2019). [3] H.Cui et. al., J. Phys. D: Appl. Phys. 50:285001 (2017).

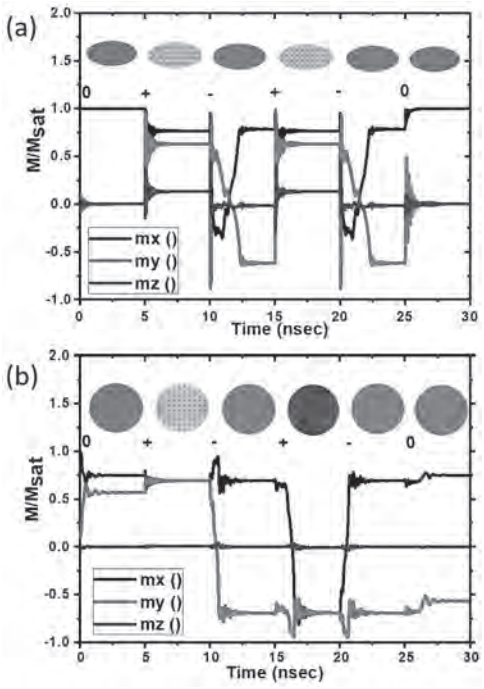

Fig. 1: Magnetization switching of (a) elliptical disk of AR 2:1 (500nm: 250nm: 15nm) and (b) circular disk of AR 1:1 (500nm: 500nm: 15nm). State 0, + and – shows the magnetization at zero, +ve and -ve voltage at the start of each cycle. Magnetization distribution at the end of each cycle are shown at the top.

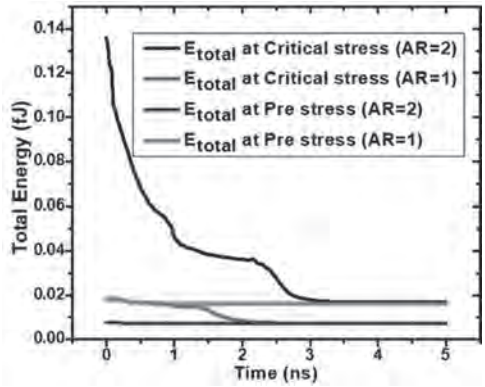

Fig. 2: Total energy change as a function of time for pre-stress and critical stress conditions.

K1-07. Reconfigurable Magnonic Crystal Based on Multiferroic-Ferromagnetic Heterostructures. *I. Boventer*[1], H. Merbouche[1], V. haspot[1], C. Carrétero[1], S. Fusil[1], V. Garcia[1], A. Barthelemy[1] and A. Anane[1] *1. Unité Mixte de Physique CNRS/Thalès, Palaiseau, France*

To date, magnonics is a promising paradigm for digital and analogue information processing overcoming current limitations such as increasing self-heating of CMOS chips. Magnons - the associated quasiparticles of collective spin excitations, known as spin waves – serve as the fundamental information carrier. Magnonic circuits would gain efficiency and functionality if their characteristics could be reconfigurable. Despite recent progress [1, 2], the realization of reconfigurable magnonic devices is still lacking a robust and efficient paradigm that could for example allow for tuneable frequency filtering. In magnonics filters are most often based on magnonic crystals (MC) where a periodic modulation of the spin wave's energy landscape results in frequency bandgaps in the magnon spectrum [3]. Here, we employ a heterostructure of multiferroic bismuth ferrite $BiFeO_3$ (BFO)-lanthanum strontium manganite $La_{2/3}Sr_{1/3}MnO_3$ (LSMO). The LSMO layer has a Gilbert damping of $6x10^{-3}$. Instead of modulating the sample shape, we create a MC by a spatial variation of the ferroelectric (FE) domain configuration in the BFO (c.f. Fig. 1) via direct voltage polling using piezoresponse force microscopy. Propagating spin-wave spectroscopy is used to study the frequency response of the filter [4]. We show that a periodic FE domain pattern in BFO results in a bandgap in the spin wave dispersion spectrum (c.f. Fig. 1). The written FE domains are long-lived and can be reliably switched back and forth. Hence, we present a non-volatile, voltage controlled, reconfigurable magnonic filter. It is for the moment unclear if the origin of the effect is related to multiferroic effects [5] or a ferroelectric modulation of the interfacial electronic density of LSMO. Nevertheless, our results open a new path for the transduction and configurable filtering of spin waves within a single micron-scale magnonic device.

[1] T. Schneider *et al.,* Appl. Phys. Lett. 92, 022505 (2008) [2] T. Fischer *et al.* Appl. Phys. Lett. 110, 152401 (2017) [3] A. V. Chumak, A. A. Serga and B. Hillebrands, *J. Phys. D* 50, 24 (2017) [4] M. Collet *et al*., Appl. Phys. Lett. 110, 092408 (2017) [5] N. Spaldin and R. Ramesh, Nat. Mat. 18, 203-212 (2019)

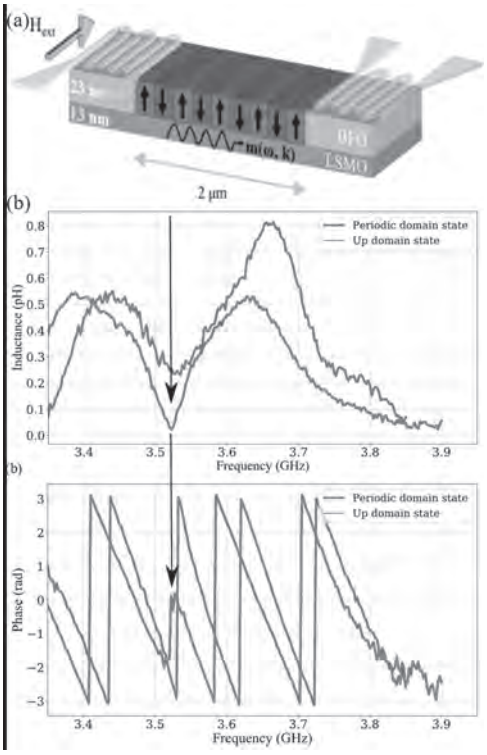

Fig. 1: (a) Experimental setup with periodic BFO domains (b) Evidence for the bandgap for the BFO/LSMO heterostructure with periodic domains in the BFO for the transmission amplitude of the inductance (top) and the corresponding phase response (bottom)

K1-08. Withdrawn

K1-09. Elastic Properties of the Multiferroic BiFeO3 by Time Resolved Acoustic Measurements. *P. Hemme*[1], P. Djemia[2], Y. Galais[1], A. Sacuto[1], D. Colson[3], P. Rovillain[4], B. Perrin[4], L. Belliard[4] and M. Cazayous[1]
1. Laboratoire Materiaux et Phenomenes Quantiques, Paris, France; 2. Laboratoire des Sciences des Procedes et des Materiaux, Villetaneuse, France; 3. Service de Physique de l'Etat Condense, Gif Sur Yvette, France; 4. Institut des NanoSciences de Paris, Paris, France

Multiferroics that show coupling between electric and magnetic properties are promising materials for devices that transform information from one state into another, such as spin excitations into charge, phonons or photons. Among them, $BiFeO_3$ (BFO) is one of the very few compound displaying room temperature multiferroicity. BFO leads for example to spectacular THz electromagnetic wave generation and photostriction properties. The prospects for applications in this area such as optically triggered piezotransducers require a perfect knowledge of the elastic properties of materials. Combining Time Resolved Acoustic Measurements (TRAM) with density functional theory (DFT) calculations and volumic and surface mode propagations simulations, we have studied the elastic properties of $BiFeO_3$. Using TRAM, we have measured wave propagation along 3 differents directions in the (110) plane of BFO. Then, we determined three modes speeds : one longitudinal mode, one fast and one slow transverse modes. With DFT, we calculated a set of elastic constants for $BiFeO_3$. We used these elastic constants to simulate the propagation of volumic and surface modes. The comparison between the calculated and measured speeds enables to ajust the elastic constants. In conclusion, we have been able to fully determine the elastic constant of $BiFeO_3$ that are essential for future integration of BFO in acoustic micro/nano-devices.

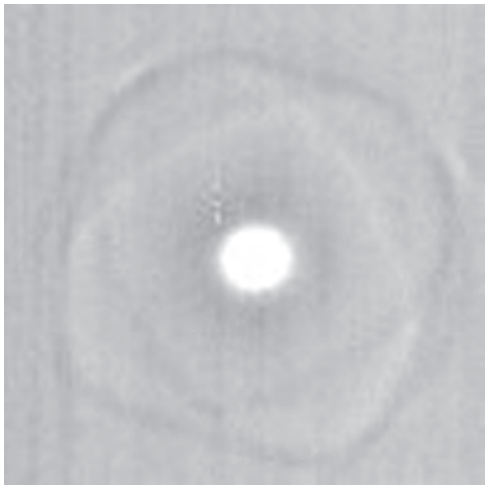

Fig. 1: Observation of waves in the (110) plan of $BiFeO_3$

K1-10. Magneto-Ionic Effect in Piezo-Ionic/Magnetostrictive Composites for Energy Generation Applications. *A. Lasheras*[1], P. G.Saiz[2,1], J. Gutierrez[1,2] and A. Lopes[2] *1. University of the Basque Country, Leioa, Spain; 2. Fundacion BCMaterials - Basque Center for Materials Applications and Nanostructures, Leioa, Spain*

We present novel piezo-ionic/magnetostrictive bi-layer composites for energy generation systems. These structures, fabricated with Metglas® 2826MB ferromagnetic alloys and ionic liquid based PVDF-HFP polymer composites, show an induced electric response as a consequence of the coupling between the magnetostrictive properties of the Metglas® 2826MB and the piezo-ionic ones of the ionic liquid based PVDF-HFP polymer composites. These flexible, simple and low cost structures do not need to be polarized to exhibit an electric response, and show an increased induced voltage as the percentage of the ionic liquid in the PVDF-HFP matrix does. This response is a consequence of the asymmetric deformation caused by the magnetostrictive material on the piezo-ionic composite, which induces a non-uniform distribution of the cations and anions in the polymer matrix. The laminates present a maximum response under the application of a low magnetic fields of 9 Oe, and a normalized magneto-ionic coefficient values up to 130 mV/cm.Oe at 60 kHz for the structure with an ionic liquid content of 30 %. These values are even higher than others obtained with piezoelectric materials based ME composites [1][2]. The simple fabrication process and potentiality of these new piezo-ionic/magnetostrictive laminates contributes to broaden and improve the state of the art of the energy generation systems. [1] P. Galizia, M. Algueró, N. Bernier, N. Gambacorti, E. Aza, A. Lappas, M. Venet and C. Galassi, J. Alloys Compd., vol. 783, p.237–45 (2019) [2] Y. Kumar, K.L. Yadav, J. Shah and R.K. Kotnala, J. Adv. Ceram., vol. 8, p.333–44 (2019)

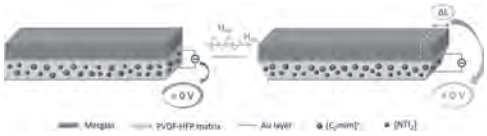

Scheme of the detection of the induced MI response in the fabricated structures

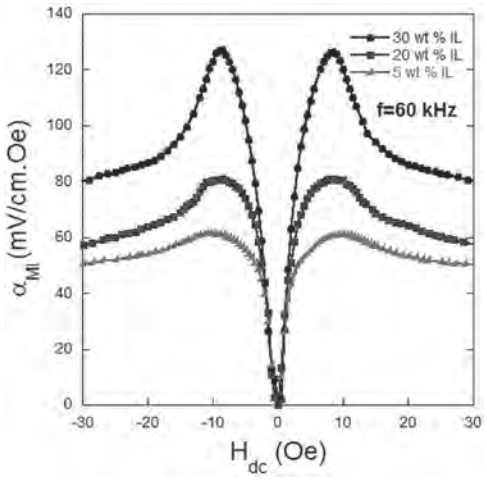

MI coefficients of the fabricated structures as a function of the applied DC magnetic field at 60 kHz

K1-11. Formation of Spiral Ordering by Magnetic Field in Frustrated Anisotropic Antiferromagnets. *O.I. Utesov*[1,2] and A.V. Syromyatnikov[1,2]
1. Theory Division, National Research Center "Kurchatov Institute" B.P. Konstantinov Petersburg Nuclear Physics Institute, Gatcina, Russian Federation; 2. Physics Department, Sankt-Peterburgskij gosudarstvennyj universitet, Sankt-Peterburg, Russian Federation

Multiferroics attracts great attention in the present time due to their very promising technological applications. In the so-called multiferroics of spin origin [1] phenomenon of giant magnetoelectric response was observed [2,3]. Two mechanisms of magnetic ordering induced ferroelectricity, namely inverse Dzyaloshinskii-Moriya and spin-dependent p-d hybridization, imply noncollinear magnetic structure [1], which can appear for example due to the frustration of exchange interaction. This makes research on such incommensurate spin structures as helicoids very important since their properties determine electric polarization. Recently we propose a theoretical description of spiral plane flops in anisotropic frustrated helimagnets [4]. Using smallness of anisotropic interactions in comparison with the exchange one, energies of competing spin textures were described perturbatively and simple equations for the flop fields were derived. Notably, formulas have a similar form with

the spin-flop field in uniaxial antiferromagnets. Moreover, the theory was successfully applied to the experimental data on several magnets. In the present research, we further proceed with the theoretical study of anisotropic frustrated antiferromagnets [5]. We show, that if there is competing commensurate spin ordering along with two conventional phase transitions at small magnetic fields (spin-flop and spiral pane flop, see Fig.1 (a) and (b)) there appears a possibility to induce helical ordering using an external magnetic field (see Fig.1 (c), (d) and (e)). We propose and describe theoretically three sequences of phase transitions, where at zero field conventional antiferromagnetic ordering is the ground state. We successfully apply our approach for the description of phase transitions in $MnWO_4$ [6] (scenario shown in Fig. 1 (c)). Furthermore, the scenario shown in Fig. 1 (e) was observed experimentally in Ref. [7] after our research was published. To the best of our knowledge, scenario Fig. 1 (d) has not been found yet and it seems to be an interesting experimental problem.

[1] Y. Tokura, S. Seki, and N. Nagaosa, Rep. Prog. Phys. 77, 076501 (2014), and references therein [2] S.-W. Cheong and M. Mostovoy, Nat. Mater. 6, 13 (2007), and references therein. [3] Y. Tokura and S. Seki, Adv. Mater. 22, 1554 (2009). [4] O. I. Utesov and A. V. Syromyatnikov, Phys. Rev. B 98, 184406 (2018). [5] O. I. Utesov and A. V. Syromyatnikov, Phys. Rev. B 100, 054439 (2019). [6] M. V. Gvozdikova, T. Ziman, and M. E. Zhitomirsky, Phys. Rev. B 94, 020406(R) (2016). [7] J. Lass, et. al., Phys. Rev. B 101, 054415 (2020).

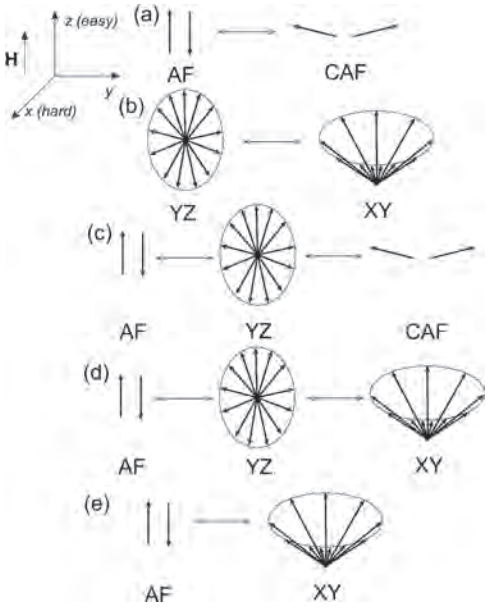

Fig. 1. Possible scenarios of phase transitions in frustrated anisotropic antiferromagnets in external magnetic field oriented along easy z-axis and zero temperature.

K1-12. Ho Doping Induced Spin Reorientation in O- $Lu_{1-x}Ho_xFeO_3$ (x = 0 to 1). *L. S*[1], B. P.D[2], S. Kaul[1] and S. S[1] *1. School of Physics, University of Hyderabad, Hyderabad, India; 2. UGC-DAE Consortium for Scientific Research, Mumbai Center, Mumbai, India*

$LuFeO_3$ (LFO) a member of the orthoferrite ($RFeO_3$) family, holds the promise of replacing the well-known room temperature multiferroic, $BiFeO_3$ [1]. LFO nanoparticles with and without Ho doping (i.e., $Lu_{1-x}Ho_xFeO_3$ with $0 \le x \le 1$) were synthesized using the hydrothermal method [2]. Rietveld refinement of the XRD data (Fig.1) for x = 0 (0.05) reveal the presence of both the hexagonal (h) $P6_3cm$ and orthorhombic (o) Pnma phase fractions as 96% (6%) and 4% (94%), respectively. Further Ho doping resulted in pure o- structure. The lattice parameters (*a, b, c*) follow Vegard's law ensuring the replacement of Lu atoms by Ho atoms. The common characteristics of o- $RFeO_3$ are i) negligible ferroelectric polarization, ii) ordering of Fe^{3+} moments antiferromagnetically via Fe^{3+}-O^{2-}-Fe^{3+} super-exchange interaction in *ac* plane and net magnetic moment along *b* direction for $T < T_{N1} \approx 600$ K, iii) ordering of R^{3+} moments at $T < T_{N2} \approx 10$ K, iv) possible re-orientation of spins (SR) from b to c direction between T_{N1} and T_{N2} owing to the R^{3+}-O^{2-}-Fe^{3+} interaction [3, 4]. To understand the effect of Ho doping on the magnetic properties of $Lu_{1-x}Ho_xFeO_3$ with $0 \le x \le 1$, the magnetization (M) has been measured as a function of temperature at a magnetic field of 100 Oe in both the zero-field-cooled (ZFC) and field-cooled (FC) modes (Fig.2). For $x = 0$, the SR is observed at 120 K. In this case, the SR is attributed to h- LFO since in o- LFO, no SR has been reported [5, 6]. For $x = 0.05$, SR could not be observed even at the lowest measurement temperature of 3 K presumably due to the weak R^{3+}-O^{2-}-Fe^{3+} interaction. Further increase in Ho concentration progressively strengthens the R^{3+}-O^{2-}-Fe^{3+} interaction and hence T_{SR} shifts to higher temperatures with increasing x, as shown in Fig.2. When the M due to Fe^{3+} moments is equal and opposite to M due to Ho^{3+} moments, compensation (comp) occurs and the net M goes to zero. For $x = 0.3$ to 0.6, T_{comp} is found to increase with Ho concentration. This study establishes that the Ho doping stabilizes O-structure beyond $x > 0.05$ and increases the T_{SR} from 0 in o-LFO to 57.8 ± 0.2 K in o-HFO.

1. Chowdhury, U. *et al.* 1–12 (2017). 2. Leelashree, S *et al.*. *J. Supercond. Nov. Magn.* (2019) doi:10.1007/s10948-019-5114-4. 3. Zhou, Z *et al.*. *J. Alloys Compd.* 583, 21–31 (2014). 4. Yamaguchi, T. *J. Phys. Chem. Solids* 35, 479–500 (1974). 5. Liu, J. *et al. Adv. Funct. Mater.* 28, 1–7 (2018). 6. Zhu, W, *et al.*. *Appl. Phys. Lett.* 100, 4–8 (2012).

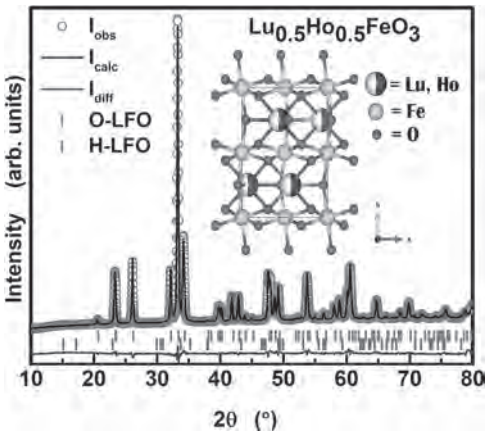

XRD pattern and Rietveld refinement. Inset: crystal structure

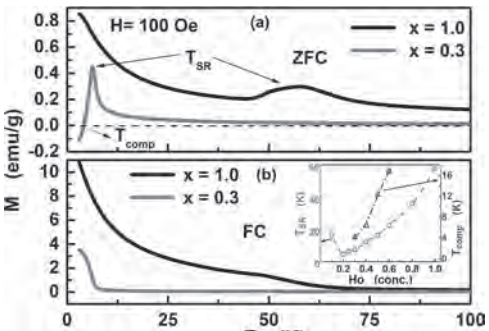

(a) M_{ZFC} (T), (b) M_{FC} (T). Inset in (b): T_{SR} (x), T_{comp} (x)

K1-13. Withdrawn

K1-14. On the Correlation of the Magnetic Properties With the Structural Parameters in Fe-Doped Europium Chromite.
D.R. Ratkovski[1], E. França[1], J.M. Marin[2], A. Franco Jr[3] and *F. Machado*[1]
1. Departamento de Física, Universidade Federal de Pernambuco, Recife, Brazil; 2. Instituto de Fisica, Universidad de Antioquia, Medellin, Colombia; 3. Instituto de Física, Universidade Federal de Goiás, Goiânia, Brazil

Europium chromite ($EuCrO_3$) is a multifunctional material presenting physical and chemical properties that are strongly influenced by the rare-earth ion lying on the A-site of an orthorhombic distorted perovskite structure [1]. $EuCrO_3$ does also present a variety of spin interactions that are highly dependent on temperature (T), leading to a spin-canting antiferromagnetic phase with a Néel temperature (T_N) close to about 170 K [2]. In the present work, the dynamics of the spins and the structural parameters of as prepared and thermal treated (T = 1073 K, time = 24 h) samples of $Eu_{1-x}Fe_xCrO_3$ (x = 0, 0.10 and 0.20) were investigated. The ac-magnetic susceptibility (χ_{ac}) was measured near T_N for frequencies (f) in the range 10-10^4 Hz, magnitude of the ac magnetic field of 10 Oe and for 5 ≤ T ≤ 300 K. X-ray diffraction data were used for measuring the lattice parameters (a, b and c) and the bonding angle θ_B (Cr^{3+}–O(2)–Cr^{3+}), for 100 ≤ T ≤ 300 K. The maximum in χ_{ac} was found to shift to higher values of T for increasing values of f. The Voguel-Fulcher law was used for analyzing χ_{ac} yielding values for the characteristic relaxation time τ_0, activation energy E_a/k_B and T_G, respectively, in the ranges 1.1 - 4.2 ns (3.1 - 3.6 ps), 29.4 - 45.5 K (46.5 - 47.2 K) and 159 - 166 K (170 -173 K) for the as prepared (thermal treated) samples. The super-exchange parameter $J \sim \cos^4[(180-\theta_B)/2]/d^7$, where d is the length of the Cr-O(2) bound [3], was also obtained for both as prepared and thermal treated samples yielding a good correlation of the values of J with the corresponding ones of T_G. Work partially supported by CNPq, CAPES, FACEPE and FINEP (Brazilian Agencies).

1 - J. M. Marín Ramírez, H. V. S. Pessoni, A. Franco Jr. and F.L.A. Machado, J. Alloys Compd., Vol. 690, p.315 (2017). 2 - D. R. Ratkovski, J. M. Marín Ramírez, P. R. T. Ribeiro et all., J. Alloys Compd., Vol. 724, p.501 (2017). 3 - J. S. Zhou and J. B. Goodenough, Phys. Rev. B, Vol. 77, p.132104 (2008).

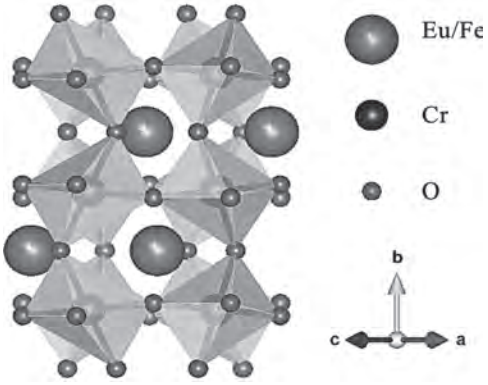

Orthorhombic distorted perovskite structure for Fe-doped europium chromite.

K1-15. Evaluation of Structural Transformation, Magnetization Reversal Along With Magnetic Switching Effect in $GdMn_{1-x}Cr_xO_3$ Perovskite.
P. Tiwari[1] *1. Materials Science, Indian Institute of Technology BHU Varanasi, Varanasi, India*

Due to their enthralling fundamental physics along with potential application in the field of multiferrocity, rare earth manganites have received a lot of attention within research communities [1]. Here we have investigated the effect of Cr in structural as well as in different magnetic transitions in GdMn1-xCrxO_3. As we have increased the Cr concentration from 0 to 0.5, Rietveld refinement of X-ray diffraction patterns demonstrates that an O' type orthorhombic structure transforms to O type, manifesting a reduction in lattice volume. The reduction in lattice volume is correlated to smaller ionic radii of Cr^{3+} in comparison to Mn^{3+}. The structural transformation is accompanied with a considerable decrease in the Jahn–Teller distortion factor evaluated from XRD, Raman and photoluminescence measurements. An enhancement in Neel temperature (T_N) from 42 K to 150 K is confessed from Magnetic. Along with increase in T_N, interestingly, we inspect magnetization reversal (MR) with spin reorientation (T_{SR}) for Cr doped sample. On the basis of competition between Mn, Cr and Gd the mechanism for such a magnetic behavior is discussed. The incorporation of Cr not only constructively modifies the crystal structure but also evokes the magnetic reversal phenomenon. The promising structure and magnetic properties of $GdMn_{1-x}Cr_xO_3$ offer potential pathways for spintronics and magnetic switching devices

Priyanka Tiwari, Sandeep Kumar, and Chandana Rath, J. Appl. Phys. 126, 045102 (2019).

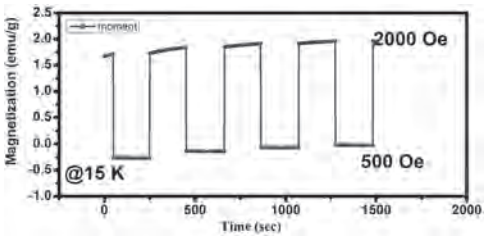

Fig.1 **Magnetic switching behaviorof $GdMn_{1-x}Cr_xO_3$ perovskite**

Session K2
NEW MAGNETIC MATERIALS

Ziyao Zhou, Co-Chair
Xi'an Jiaotong University, Xi'an, China
Chuanpu Liu, Co-Chair
Colorado State University, Fort Collins, CO, United States

CONTRIBUTED PAPERS

K2-01. Withdrawn

K2-02. Cluster Glass Magnetism in Z_2XY Type Heusler Alloy.

T. Samanta[1] and P. Bhobe[2] *1. Metallurgy Engineering and Materials Science, Indian Institute of Technology Indore, Indore, India; 2. Discipline of Physics, Indian Institute of Technology Indore, Indore, India*

Heusler alloys are intermetallic systems with the chemical formula X_2YZ, with X, Y being the 3d transition metals, and Z the sp element. A rock salt type frame is formed by Y, Z atoms, and X atoms occupy the body-centered positions of the sub-cells, thus creating a cubic $L2_1$ structure. Unlike this standard form, the Z_2XY compositions have sp element in excess and reversed chemical built-up, yet the cubic structure is maintained. To date, very few such Z_2-based systems exist [1, 2], with a limited study about their structure and physical properties. An increased hybridization between the sp electrons of Z and the d electrons of X, Y, should play a crucial role in deciding the electronic and magnetic ground state of these systems, resulting in exotic properties. Our study of Ga_2MnCo [3] has revealed a re-entrant cluster glass ground state with unusual magneto-structural coupling at the glass transition temperature. Using neutron diffraction and synchrotron x-ray diffraction experiments, we demonstrated that the site disorder between Mn-Co brings about a competing antiferro coupling that prevents the long-range ferromagnetic order. We now extend our study to new compositions, Al_2MnCo, Ga_2MnPd, and Al_2MnPd. Measurement of the ac susceptibility (χ'(T)) presented in Fig.1-2, indicates a re-entrant cluster glass phase in all the systems. However, the heat-capacity measurements show the absence of any first-order phase transition associated with the cluster glass transition. Magnetism in Heusler systems being driven by RKKY interactions, we investigate the local structure using temperature-dependent EXAFS measurements to understand the interplay between the structure and different correlations at the atomic level. The various bond distances between nearest-neighbor atoms provide a connection with its unconventional magnetic state.

1. G.J. Li, E.K. Liu and Y.J. Zhang, J. Appl. Phys., 113, 103903 (2013). 2. S.R. Barman, A. Chakrabarti and S. Singh, Phys. Rev. B, 78, 134406 (2008) 3. T. Samanta, P. A. Bhobe and A. Das, Phys. Rev. B, 97, 184421 (2018)

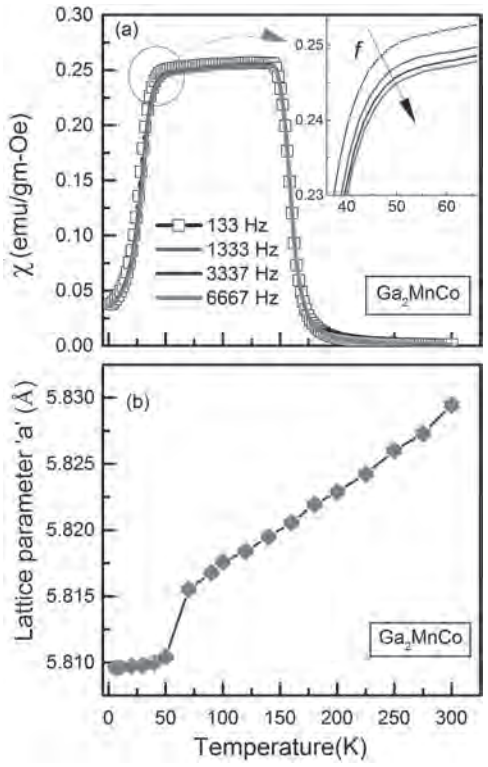

Fig.1 (a) Temperature response of $\chi'(T)$ recorded at different frequencies for Ga_2MnCo. Inset: Magnified view around the freezing temperature. (b) The lattice parameter variation with the temperature of Ga_2MnCo.

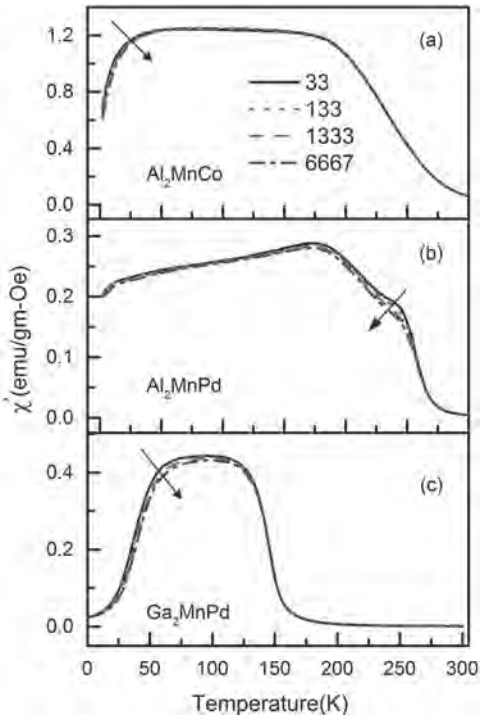

Fig.2 Temperature dependence of χ'(T) obtained for (a) Al_2MnCo, (b) Al_2MnPd, and (c) Ga_2MnPd at different frequencies.

INVITED PAPERS

K2-03. Tunable Room-Temperature Ferromagnetism and Emergent Phenomena in Atomically Thin Transition Metal Dichalcogenide Semiconductors. *M. Phan[1] 1. Department of Physics, University of South Florida, Tampa, FL, United States*

Our recent discovery of room-temperature ferromagnetism (FM) in transition metal dichalcogenide (TMD) monolayers of VSe_2 has triggered intense research efforts by the scientific community [1,2]. However, the VSe_2 monolayers are metallic which may not access the rich electronic and optical phenomena open to semiconductors. In this talk, we present a novel approach to induce long-range FM in TMDs through introducing magnetic dopants to form a dilute magnetic semiconductor. We demonstrate the tunability of room temperature FM in semiconducting TMD monolayers (V-doped WS_2 and WSe_2) [3,4]. Ferromagnetism peaks at an intermediate vanadium concentration of a few atomic percent (2-4 at.% V) and decreases for higher concentrations, which is consistent with quenching due to orbital hybridization at closer vanadium-vanadium distances. We discover a novel thermally induced spin flipping phenomenon in the V-doped WSe_2 monolayers [4], and demonstrate the light-mediated FM in the V-WS_2 monolayers at room temperature [5]. These findings pave a new pathway for the development of novel spintronic and valleytronic nanodevices based on atomically thin van der Waals magnetic semiconductors and stimulate further studies in this rapidly expanding research field of 2D magnetism.

[1] M. Bonilla, M.H. Phan, *et al.*, Strong Room Temperature Ferromagnetism in VSe_2 Monolayers on van der Waals substrates*, Nature Nanotechnology* 13, 289 (2018) [2] V.O. Jimenez, M.H. Phan, *et al.*, A magnetic sensor using a 2D van der Waals ferromagnetic material, *Scientific Reports* 10, 4789 (2020) [3] F. Zhang, M.H. Phan, *et al.*, Monolayer Vanadium-doped Tungsten Disulfide: An Emerging Room-Temperature Diluted Magnetic Semiconductor, *Advanced Science*: https://arxiv.org/abs/2005.01965 [4] Y.T.H. Pham, M.H. Phan, *et al.*, Tunable Ferromagnetism and Thermally Induced Spin Flip in Vanadium-doped Tungsten Diselenide Monolayers at Room Temperature, https://arxiv.org/abs/2005.00493 [5] V.O. Jimenez, M.H. Phan, *et al.,* Light-controlled room temperature ferromagnetism in vanadium-doped tungsten diselenide semiconducting monolayers, *Nature Communications* (submitted).

K2-04. Probing Hidden Interfacial Magnetism in Magnetic Insulator Hybrid Structures. *P. Quarterman[1], Y. Fan[2], J. Bauer[2], Y. Lv[3], J. Wang[3], C. Ross[2], L. Liu[2], J.A. Borchers[1] and A.J. Grutter[1] 1. NIST Center for Neutron Research, Gaithersburg, MD, United States; 2. Massachusetts Institute of Technology, Cambridge, MA, United States; 3. University of Minnesota, Minneapolis, MN, United States*

Hybrid structures containing magnetic insulators show exciting potential for energy-efficient spintronic memories and logic devices—especially for controlling spin torques, magnon information transmission, and magneto-optical isolators. In particular, the ferrimagnetic garnet class of materials are of interest due to their low damping, long magnon propagation length, and tunable properties. When hybrid structures are made by combining garnets with metallic ferromagnets, heavy metals, or topological materials, unique interfacial magnetic effects have been shown to arise and are highly relevant for both fundamental understanding of magnetism and enhanced spintronic functionalities. Polarized neutron reflectometry (PNR) is sensitive to both chemical composition and in-plane magnetization as a function of depth with sub-nanometer resolution, and so provides unique capability to directly probe buried interfacial magnetism in thin films. I will show PNR studies for interfacial magnetic effects that occur in these garnet heterostructures, which cannot be thoroughly understood with laboratory benchtop techniques alone. In particular, I will focus on Si-based Pt / yttrium iron garnet / metallic-ferromagnet hybrid structures, where we observed emergence of unexpected antiparallel coupling and demonstrated such a structure can serve as the building block for a highly efficient magnon spin valve [1]. I will also discuss substrate-induced interfacial coupling, inhomogeneous magnetizations [2], and proximity magnetism in garnet/heavy metal and garnet/topological insulator heterostructures [3]—understanding of these phenomena are essential for interpreting exotic spin-based magnetoresistances.

[1] Fan *et al*, Phys. Rev. Appl. 13, 061002 (2020) [2] Bauer *et al*, Adv. Elect. Mat. 6 1900820 (2020) [3] Lv *et al*, in preparation (2020)

CONTRIBUTED PAPERS

K2-05. Green Synthesis of Magnetic Fe_3O_4, $CoFe_2O_4$ and $NiFe_2O_4$ From Aloe Vera Extract for Future Biomedical Applications. *G.C. Hermosa[1], H. Wu[1], C. Liao[1], S. Wang[2], Y. Chen[1,3], Y. Tsai[1,3] and A. Sun[1] 1. Chemical Engineering and Materials Science, Yuan Ze University, Chung-Li, Taiwan; 2. Materials and Mineral Resources Engineering, National Taipei University of Technology, Taipei, Taiwan; 3. Far Eastern Memorial Hospital, New Taipei City, Taiwan*

A variety of chemical and physical procedures could be used for synthesis of magnetic nanoparticles. However, these methods are fraught with many problems with the use of toxic solvents, generation of hazardous by-products, and high energy consumption. Accordingly, there is a vital need to develop environmentally benign procedures for the synthesis of nanoferrites. A promising approach to achieve this objective is to exploit the array of biological resources in nature. Indeed, over the past several years, plants, have been used for production of low-cost, energy-efficient, and nontoxic metallic nanoferrites. Plant-mediated synthesis of nanoparticles is a green chemistry approach that connects nanotechnology with plants. This innovation is particularly compensating as far as decreasing the poisonous quality caused by the conventionally integrated NPs. Aloe Vera leaf extract is a medicinal agent with multiple properties including an antibacterial effect. Moreover, the constituents of Aloe Vera leaves include lignin, hemicellulose, and pectins which can be used in the reduction of nanoferrites. The magnetic nanoferrites (Fe, Co, Ni) were prepared by an eco-friendly

hydrothermal method using an Aloe Vera plant extract solution as both a reducing and stabilizing agent. Magnetic nanoferrites were characterized using FTIR, XRD, VSM and SEM. Cytotoxicity were obtained using the MTT assay. X-ray diffraction analysis also demonstrated that the size range of the nanoferrites exhibited average diameters of 7- 19 nm. Results showed that all the metallic nanoparticles are magnetic with values Fe= 52 emu/g, Co= 33 emu/g and Ni=7.1 emu/g. The magnetic nanoferrites exhibited high cell viability rate at high concentrations signifying their non-toxic property. The magnetic nanoferrites produced in this study by green synthesis methodology from leaf extract of *Aloe Vera* needs to be further evaluated and could find greater biomedical application.

K. Schulze, A. Koch, B. Schopf and A. Petri, *Journal of Magnetism and Magnetic Materials*, Vol. 293, pp. 419-432, (2005). S. Das, C. Dickinson, F. Lafir and D. Brougham, *Green Chemistry*, Vol. 14, pp. 1322–1334, (2012). M. Ferrari, Nature Reviews Cancer, Vol. 5, pp.161-171, (2005). M. Venkatachalam, G. Parthasarathy and P. Gowthaman, *Imperial Journal of Interdisciplinary Research (IJIR)*, Vol. 2, pp. 1570-1575, (2016). T. Neuberger, B. Schopf and H. Hofmann, *Journal of Magnetism and Magnetic Materials,* Vol. 293, pp. 483–496, (2005).

K2-06. Twisted Magnetism in Ultra-Short 1D Iron Chains With Hybridized Boundaries. *N.M. Vargas*[1], F. Torres[2], A. Baker[3], J.R. Lee[3], M. Kiwi[2], T.M. Willey[3], C. Monton[4] and I.K. Schuller[1] *1. Physics, University of California San Diego, La Jolla, CA, United States; 2. Physics, Universidad de Chile Facultad de Ciencias Fisicas y Matematicas, Santiago, Chile; 3. Materials Science Division, Lawrence Livermore National Laboratory, Livermore, CA, United States; 4. General Atomics, San Diego, CA, United States*

Magnetic order at the atomic scale has received considerable attention due to its potential application in spin transistors[1-2], quantum computing[3-4], and ultra-dense memories[5-6]. Although one dimensional (1D) magnetic systems have been intensely studied theoretically, the experimental determination of the extent and persistence of short- and long-range magnetic interactions, and how these interactions are affected by boundary conditions induced at the end of the chains remain unknown. We report structural and magnetic properties of ultra-short 1D iron chains subject to controlled boundary conditions. These iron chains are grown using iron phthalocyanine (FePc) thin films and FePc/ metal-free-phthalocyanine (H_2Pc) superlattices (SLs), in which their length is precisely controlled by the thickness of the deposited FePc layers, and boundary conditions by electronic hybridization at the end of the chains. The electronic hybridization and local bonding environment is observable by element selective X-ray absorption spectroscopy (XAS). Ultra-short 1D iron chains between 7 and 200 atoms long become ferromagnetic below 5 K, and their magnetic response is strongly dependent on the boundary conditions imposed on the end atoms. The coercive field increases with the iron chain length with hybridized boundaries, whereas in chains not subject to hybridization the coercive field remains constant. A quantitative, semi-classical model based on the Dzyaloshinski-Moriya interaction, provides an understanding of these observations, in good agreement with experimental results. Work supported by the National Science Foundation under grants No. 1804414 and 1805585. Prepared by LLNL under Contract DE-AC52-07NA27344.

1. S. Datta, B. Das, *Appl Phys Lett 56* (7), 665-667 (1990) 2. I, Zutic, J. Fabian, S. Das Sarma, *Rev Mod Phys 76* (2), 323-410 (2004) 3. V. A. Dediu, L. E. Hueso, I. Bergenti, C. Taliani, *Nat Mater 8* (9), 707-716 (2009) 4. A. J. Leggett, S. Chakravarty, A. T. Dorsey, M. P. A. Fisher, A. Garg, W. Zwerger, *Rev Mod Phys 59* (1), 1-85, (1987) 5. Sinitskii, A.; Fursina, A. A.; Kosynkin, D. V.; Higginbotham, A. L.; Natelson, D.; Tour, J. M., *Appl Phys Lett 95* (25), 253108 (2009) 6. Sinitskii, A.; Tour, J. M., *ACS Nano 3* (9), 2760-2766 (2009)

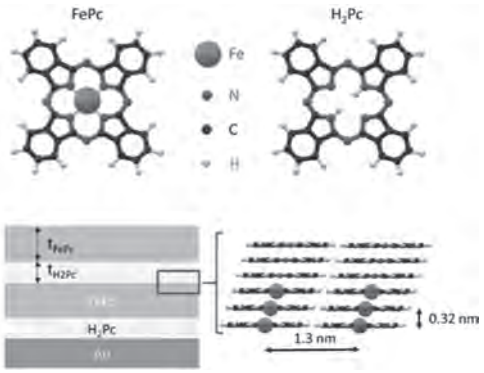

1D Fe chains based in Organic superlattices, and their molecular orientation. Magnetic Iron (II) phthalocyanine ($FeC_{32}H_{16}N_8$) and week diamagnetic H_2-phthalocyanine ($H_2C_{32}H_{16}N_8$) molecules

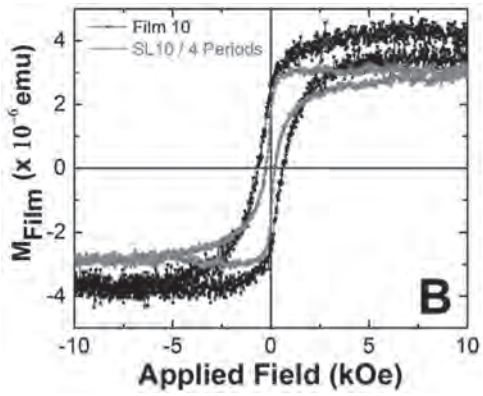

Magnetic hysteresis loops at 1.8 K shows a different magnetic response of 1D iron chains based in FePc films and FePc/H_2Pc SLs

K2-07. Light-Mediated Magnetism in Atomically Thin Vanadium-Doped Tungsten Disulfide Semiconductors. *V. Ortiz Jimenez*[1], Y. Pham[1], M. Liu[2], F. Zhang[2], V. Kalappattil[1], B. Muchharla[1], T. Eggers[1], D. Duong[3], M. Terrones[2] and M. Phan[1] *1. University of South Florida, Tampa, FL, United States; 2. The Pennsylvania State University, University Park, PA, United States; 3. Sungkyunkwan University, Suwon, The Republic of Korea*

Atomically thin transition metal dichalcogenides (TMD) semiconductors hold enormous potential for modern optoelectronic and ultra-low powered devices. By inducing long-range ferromagnetism (FM) in these semiconductors through the introduction of small amounts of a magnetic dopant, it is possible to extend their potential in emerging spintronic applications [1,2]. Our recent study showed that room temperature magnetism is achieved in V-doped WS_2 monolayers [3], while still maintaining its characteristic optical properties. In this work we demonstrate light-mediated, room temperature FM, in V-doped WS_2 monolayers. We probe this effect using the principle of magnetic LC resonance [4], which employs a soft ferromagnetic Co-based microwire coil driven near resonance in the radio frequency regime. Combining LC resonance, with an outstanding giant magneto-impedance effect, renders the coil highly sensitive to changes in the magnetic flux through its core. The V-doped WS_2 monolayer is placed at the core of the coil where it is excited with a laser, while its magnetic permeability is probed by the coil. We found that the magnetic permeability of the monolayers is dependent on laser intensity, confirming light control of room temperature magnetism in this two-dimension material. Density functional theory calculations lead us to understand that this phenomenon is a consequence of an accumulation of excess holes in the conduction and valence bands, as well as carriers trapped in the magnetic doping states, which in turn mediates the magnetization of V-WS_2 monolayers. These findings provide a promising route to exploit light-controlled FM in two-dimensional TMD based spintronic devices.

[1] Dietl, T. A ten-year perspective on dilute magnetic semiconductors and oxides. *Nat. Mater.* 9, 965-974 (2010) [2] Dietl, T., Bonanni, A. & Ohno, H. Families of magnetic semiconductors – an overview. *Journal of Semiconductors* 40, 8 (2019) [3] Zhang, F., et. al. Monolayer Vanadium-doped Tungsten Disulfide: A Room-Temperature Dilute Magnetic Semiconductor. https://arxiv.org/abs/2005.01965 [4] Ortiz Jimenez, V., et. al. A magnetic sensor using a 2D van der Waals ferromagnetic material. *Sci. Rep.* 10, 4789 (2020)

K2-08. Magnetic Doping of Graphene With Substitutional Manganese Atoms. *P. Lin*[1], R. Villarreal[1], H. Bana[1], S. Brems[2], S. Achilli[3], G. Fratesi[3], M.N. Nair[4] and L.M. Pereira[1] *1. Quantum Solid State Physics, KU Leuven, Leuven, Belgium; 2. Interuniversitair Micro-electronica Centrum (imec), Leuven, Belgium; 3. ETSF and Dipartimento di Fisica, Università degli Studi di Milano, Milan, Italy; 4. CUNY Advanced Science Research Centre, New York, NY, United States*

Inducing magnetism in graphene has been an important challenge since its discovery. In the dilute regime, magnetic impurities are expected to couple to the Dirac electrons via the Kondo effect in a paramagnetic phase. In the less dilute regime, magnetic impurities in graphene may develop long-range magnetic order mediated by the conduction electrons via the Ruderman-Kittel-Kasuya-Yoshida (RKKY) interaction. Today, the Kondo and RKKY-exchange physics of Dirac electrons in graphene is still elusive while theory predicts competition between a non-trivial Kondo unscreened phase against a RKKY-coupled phase. Considerable experimental efforts have been devoted in this context, with the local magnetic moments originating from carbon vacancies, from adsorption and intercalation (of atoms, clusters or molecules), and from substitutional foreign atoms. Here, we report the incorporation of substitutional manganese (Mn) atoms into graphene as a model case of magnetic doping with transition metals. Ultra-low energy (ULE) ion implantation allows us to precisely tune the kinetic energy of Mn ions, providing control over the form of incorporation and concentration while preserving the structural and electronic properties of graphene [1]. Using low-temperature scanning tunneling microscopy (LT-STM) together with density functional theory (DFT), we identified and characterized point defects that are associated with substitutional-Mn in a carbon single vacancy (Fig.1). These results are complemented by synchrotron-based X-ray photoelectron spectroscopy (XPS), angle-resolved photoemission spectroscopy (ARPES), Raman spectroscopy, X-ray magnetic circular dichroism (XMCD), among others. The new insights provided by our work establish a framework for the controlled incorporation of magnetic dopants in graphene and other 2D materials, using ULE ion implantation.

[1] P. Willke *et al.*, Appl. Phys. Lett. 105, (2014), 111605

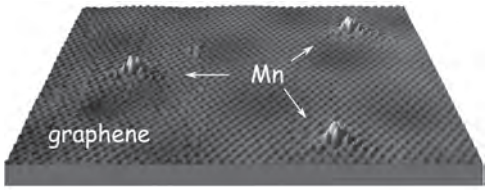

STM micrograph of graphene with substitutional Mn atoms incorporated by ultra-low energy ion implantation.

K2-09. Withdrawn

K2-10. Properties of Quaternary-Alloy Ferromagnetic Semiconductor (in,Ga,Fe)Sb. *T. Hotta*[1], K. Takase[1], K. Takiguchi[1], S. Karumuri[1], L. Anh[2,3] and M. Tanaka[1,4] *1. Department of Electrical Engineering and Information Systems, The University of Tokyo, Bunkyo-ku, Japan; 2. Institute of Engineering Innovation, The University of Tokyo, Bunkyo-ku, Japan; 3. PRESTO, JST, Tokyo, Japan; 4. Center for Spintronics Research Network, The University of Tokyo, Bunkyo-ku, Japan*

Ferromagnetic semiconductors (FMSs) are promising materials for spintronics applications because they are compatible with the highly established semiconductor technology. Although the prototypical FMS (Ga,Mn)As was intensively investigated, it shows low Curie Temperature ($T_C \leq 200$ K) with only p-type conduction [1]. Recently we have successfully grown Fe-doped III-V FMSs with high T_C and both n-type and p-type conduction; p-type (Ga,Fe)Sb ($T_C = 400$ K) [2] and n-type (In,Fe)Sb ($T_C = 385$ K) [3]. In this work, we extend our study to a quaternary-alloy FMS, $(In_{1-x-y},Ga_x,Fe_y)Sb$. This new FMS allows us to widen the degree of freedom in designing the material properties, including lattice constant, band structure, carrier type and magnetic anisotropy. We investigate the epitaxial growth, transport and magnetic properties of $(In_{1-x-y},Ga_x,Fe_y)Sb$ thin films with different Fe concentration y and Ga concentration x. The sample structure consists of (from top to bottom) InSb (2 nm) / $(In_{1-x-y},Ga_x,Fe_y)Sb$ (15 nm) / AlSb (100 nm) / AlAs (6 nm) / GaAs (100 nm) on a semi-insulating GaAs(001) substrate, grown by low-temperature molecular-beam epitaxy (LT-MBE). Fig.1 shows an X-ray diffraction (XRD) spectrum of the $(In_{0.74},Ga_{0.1},Fe_{0.16})Sb$ sample. The XRD and other characterizations including scanning transmission electron microscopy and magnetic circular dichroism (MCD) indicate that the (In,Ga,Fe)Sb layers grown by LT-MBE maintain the zinc-blende crystal and band structure without any other second phases. Carrier concentrations and T_C are estimated from Hall measurements and Arrott plots of the MCD intensity *vs*. magnetic field (MCD - *H*) curves, respectively. In $(In_{0.84-x},Ga_x,Fe_{0.16})Sb$ samples (x = 2, 6, 8, 10%), the carrier type can be changed between p-type and n-type by changing x while high $T_C > 300$ K is maintained [Fig.2]. These materials are promising for device applications such as spin diodes and spin transistors. This work was partly supported by Grants-in-Aid for Scientific Research (Nos. 16H02095, 18H05345), the CREST Program (JPMJCR1777) and PRESTO Program (JPMJPR19LB) of JST, and the Spin-RNJ.

[1] L. Chen *et al*, Nano Lett., Vol. 11, p.2584 (2011). [2] S. Goel *et al*, PRB., Vol. 99, p.014431 (2019). [3] N. T. Tu *et al*, APEX., Vol.12, p.103004 (2019).

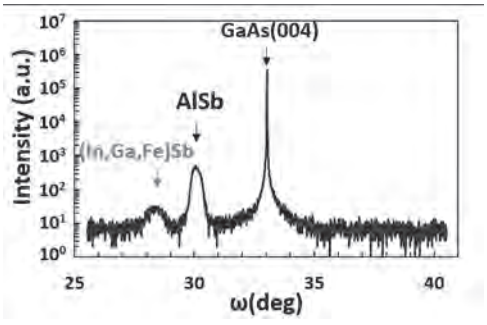

Fig.1 XRD spectrum of $(In_{0.74},Ga_{0.1},Fe_{0.16})Sb$.

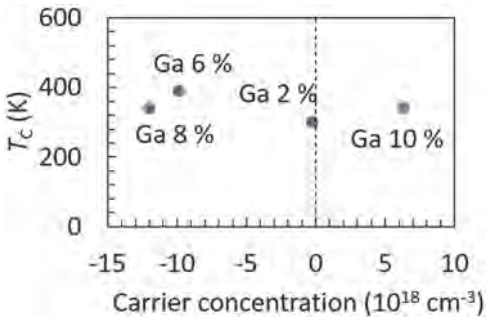

Fig.2 T_C *vs.* carrier concentration of $(In_{0.84-x},Ga_x,Fe_{0.16})Sb$ (x = 2, 6, 8, 10 %).

K2-11. Withdrawn

K2-12. Phase Behavior of Charged Magnetic Nanoplatelets. *M. Rosenberg*[1] and S. Kantorovich[1,2] *1. Universitat Wien, Wien, Austria; 2. Ural'skij federal'nyj universitet imeni pervogo Prezidenta Rossii B N El'cina, Ekaterinburg, Russian Federation*

Recent decades have seen the emergence of a new branch of science, magnetic soft matter, fueled by the advances in synthesis techniques, which have also made a wide variety of anisotropic magnetic colloidal nanoparticles available. Colloidal anisometry can be used as an effec- tive control parameter to tune both self-assembly scenarios and ther- modynamic, rheological and phase behavior of dipolar (magnetic) soft matter. For instance, magnetic nanoplatelets can form macroscopic ferromagnetic phases at room temperature. Although the phase behavior of a system hard-core platelets is well known, this novel ferromagnetic phase is not yet well-understood. In particular, we study the the influence of the magnetic dipole moment and electrostatic repulsion on suspensions of magnetic platelets is not yet fully understood. We use MD simulations to recreate such a system. The colloidal particles are modelled by charged soft spheres, with a central dipole possessing a magnetic moment of a constant length, permanently oriented perpendicular to the platelet surface. In order to investigate the structural properties of the platelets, we vary the amplitude of an applied magnetic field and the magnetic dipole. We analyze at which electrostatic conditions the system exhibits self-assembly or/and field alignment, based on RDFs, structure factors parallel and perpendicular to the field and extensive cluster analysis.

K2-13. Room-Temperature Ferromagnetism and Strain-Dependent Magnetic Anisotropy in 2D MnGaN. Y. Ma[1], D. Hunt[2,3], K. Meng[4], T. Erickson[1], F. Yang[4], M. Barral[2,3], V. Ferrari[2,3] and *A.R. Smith*[1] *1. Ohio University Nanoscale and Quantum Phenomena Institute, Department of Physics and Astronomy, Athens, OH, United States; 2. Departamento de Física de la Materia Condensada, GIyA, CAC, Comisión Nacional de Energía Atómica, Buenos Aires, Argentina; 3. Instituto de Nanociencia y Nanotecnología INN (CNEA-CONICET), Buenos Aires, Argentina; 4. The Ohio State University Department of Physics, Columbus, OH, United States*

Two-dimensional magnetic materials are of great interest for fundamental science and advanced applications while dilute magnetic semiconductors captured worldwide interest by combining magnetism with electronics. MnGaN-2D is an ultimately-thin, 2D-DMS material, consisting of a dense, well-ordered layer of Mn, Ga, and N atoms. MnGaN-2D shows room-temperature ferromagnetism as previously demonstrated with spin-polarized scanning tunneling microscopy as a function of applied magnetic field. This was also predicted by first-principles theoretical calculations which reveal the origins of the ferromagnetism through its highly spin-split and spin-polarized electronic structure.[1] The SP-STM results are recently confirmed by SQUID magnetometry which reveals perpendicular magnetic anisotropy and a high spin-polarization of ~79% at room temperature.[2] New results for this novel system also suggest the possibility of magneto-elasticity. Theoretical calculations reveal sensitivity of the spin polarization to lattice strain. Spin-orbit coupling is included in the calculations, which indicate either *out-of-plane* or *in-plane* anisotropy, dependent on the type of strain whether compressive or tensile. Clear evidence for both compressive and tensile local lattice strains is found by detailed analysis of atomic resolution STM images which reveal a wide, non-Gaussian range of lattice spacings (-18% to + 18% variations), unlike normal materials. Furthermore, scanning tunneling spectroscopy measurements, showing the spin-polarized filled states manganese peak, find fluctuations in the electronic position of the peak from spectrum to spectrum. The FSMP position is also found to fluctuate, depending on lattice strain, in the theoretical calculations, thus indicating a connection between electronic states and magnetic anisotropy in this RT ferromagnetic 2D layer.

[1] Yingqiao Ma, Abhijit V. Chinchore, Arthur R. Smith, María Andrea Barral, and Valeria Ferrari, A Two-Dimensional Manganese Gallium Nitride Surface Structure Showing Ferromagnetism at Room Temperature, Nano Letters, Vol. 18, p. 158 (2018) [2] Yingqiao Ma, Diego Hunt, Kengyuan Meng, Tyler Erickson, Fengyuan Yang, María Andrea Barral, Valeria Ferrari, and Arthur R. Smith, Local strain-dependent electronic structure and perpendicular magnetic anisotropy of a MnGaN 2D magnetic monolayer, Physical Review Materials, Vol. 4, p. 064006 (2020)

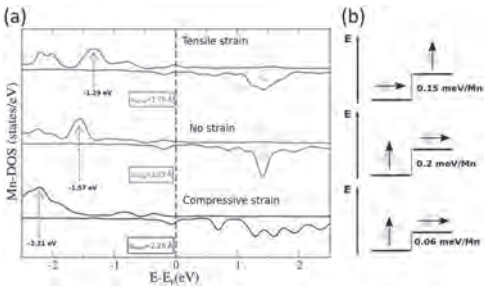

FIG. 1. Lateral isotropic strain effect on the MnGaN-2D electronic structure. (a) The calculated spin-polarized, Mn PDOS for lateral expansion, no strain, and lateral compression are shown in the top, middle, and bottom panels, respectively. (b) Magnetic anisotropic energy (MAE) obtained with first-principles spin-orbit calculations. (Ref. 2)

K2-14. Withdrawn

Session K3
SPIN INJECTION AND TRANSPORT IN NANOSCALE DEVICES

Dong-Soo Han, Chair
Korea Institute of Science and Technology, Seoul, The Republic of Korea

CONTRIBUTED PAPERS

K3-01. Energy and Momentum Conservation in Spin Transfer.
A. Mitrofanov[1] and S. Urazhdin[1] *1. Emory University, Atlanta, GA, United States*

Spin transfer (ST) effect is a consequence of angular momentum conservation [1-3], one of the three fundamental conservation laws in nature. We use fully quantum simulations of scattering of spin-polarized electron wavepacket by a ferromagnet modelled as a 1d spin-1/2 chain [4], as illustrated in Fig.1, to show that energy and momentum conservation laws impose strong restrictions on the characteristics of magnetic excitations generated by spin transfer. We found that two groups of magnons are generated by ST in this 1d system, forward-propagating magnons with large energy E_f, and backward-propagating magnons with small energy E_b. Analysis shows that the backward-propagating magnons are generated by the reflected electron component, while the forward-propagating magnons -by the transmitted electron component, with the values of energy and momenta of the generated magnons determined by the changes of the corresponding characteristics of the electron wave [Fig.2]. We also show a converse effect – dependence of the scattered electron's characteristics on the dynamical characteristics of the magnetic system. In particular, variations of magnetic anisotropy result in the variations of energy of the scattered electrons, and of the probability of electron reflection. For large anisotropy, electron reflection is completely suppressed, and only one group of magnons is generated. Our results demonstrate that quantum magnetism plays an important role in magnetoelectronic phenomena. This work was supported by the U.S. Department of Energy, Office of Science, Basic Energy Sciences, under Award # DE-SC0018976.

1. J. Slonczewski, J. Magn. Magn. Mater. 159, L1 (1996). 2. L. Berger, Phys. Rev. B 54, 9353 (1996). 3. D. Ralph and M. Stiles, J. Magn. Magn. Mater. 320, 1190 (2008). 4. P. Mondal, et al, Phys. Rev. B 99, 094431 (2019).

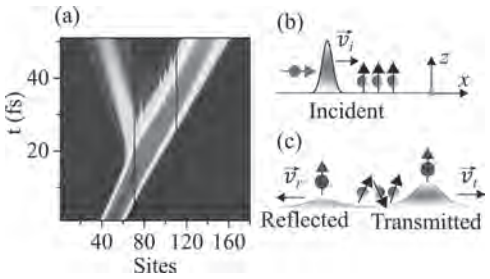

Fig.1 ST due to scattering of electron wavepacket by the chain of 40 spins (a) Pseudocolor map of wavepacket intensity in the position-time coordinates, for the initial wavepacket polarization along the x-axis. Schematics: the wavepacket and the spin chain before (b) and after (c) scattering with v_i, v_t and v_r – velocity of the incident, transmitted and reflected electron.

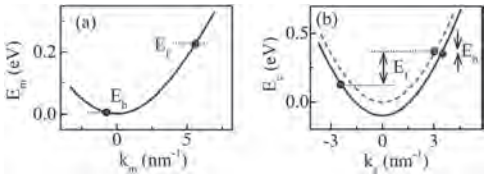

Fig.2 (a) Magnon dispersion (b) Electron dispersion outside the spin chain (dashed curve) and majority spin dispersion in the spin chain (solid curve). The energies E_f, E_b of forward- and the backward-propagating magnon groups are indicated.

K3-02. Far out-of-Equilibrium Spin Populations Trigger Giant Spin Injection Into Atomically Thin MoS_2.
M. Battiato[1], K. Held[2], L. Cheng[1], X. Wang[1], J. Chai[3], W. Yang[3], M. Yang[3], M. Cheng[4], Y. Wu[4], X. Cheng[1], D. Chi[3], K. Goh[3], J. Zhu[5], H. Sun[1], S. Wang[3], J. Song[1], H. Yang[4] and E. Chia[1] *1. Nanyang Technological University, Singapore, Singapore; 2. Technische Universitat Wien, Wien, Austria; 3. Agency for Science Technology and Research, Singapore, Singapore; 4. National University Singapore Faculty of Science, Singapore, Singapore; 5. Los Alamos National Laboratory, Los Alamos, NM, United States*

Efficient spin injection into semiconductors remains a formidable and elusive challenge even after almost three decades of major scientific effort, studded by obstacles and only partial workarounds. Few years ago, I predicted the possibility of injecting massive ultrashort spin current pulses across a ferromagnetic metal/semiconductor interface [1-2]. We have now proved experimentally the prediction [3]. By injecting strongly out-of-equilibrium sub-picosecond spin current pulses across a bare ferromagnet/semiconductor interface, we have overcome the crippling problem of impedance mismatch and obtained a massive spin transfer. We demonstrated this by producing ultrashort spin current pulses into cobalt and injecting them into monolayer MoS_2. The semiconducting MoS_2 layer also acts as a selective converter of the spin current into a charge current, whose THz emission is then measured. As predicted, we measured a giant spin current, orders of magnitude larger than typical injected spin current densities in modern devices.

[1] M. Battiato, K. Held, *Phys. Rev. Lett.* 116, 196601 (2016) [2] M. Battiato *J. Phys. Condens. Matter* 29, 174001 (2017). [3] L. Cheng et al., *Nature Physics* 15, 347 (2019).

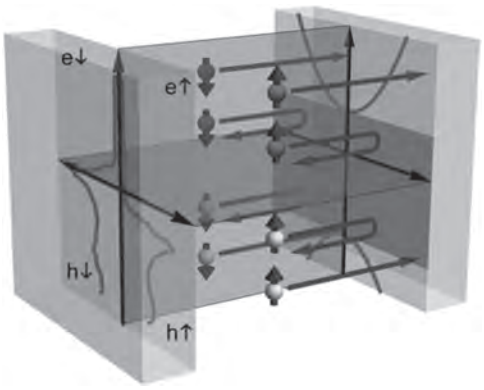

Fig. 1 - Sketch of strongly out of equilibrium spin injection in semiconductors.

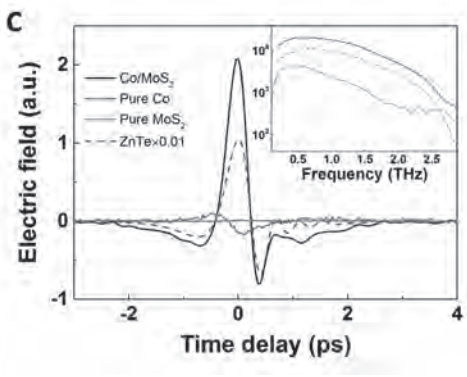

Fig.2 - Comparison of THz emissions from samples, in the absence and presence of spin injection.

K3-03. Spin Injection Enhancement via Ultra-Thin Oxide Barriers Into Molecularly Functionalized Graphene. *J.C. Toscano Figueroa*[1,2], N. Natera Cordero[1,2], D. Bandurin[1], C.R. Anderson[1], V. Guarochico Moreira[1], I. Grigorieva[1] and I.J. Vera-Marun[1] *1. Physics and Astronomy, The University of Manchester, Manchester, United Kingdom; 2. Consejo Nacional de Ciencia y Tecnologia, Mexico City, Mexico*

Tunneling spin injection on graphene is possible by using different materials as barriers[1–3]. However, the growth of ultra-thin tunnel barriers leads to the creation of pinholes, which in turn causes direct ohmic contact and a large suppression of spin polarization. This occurs due to a fundamental limitation known as the *resistance mismatch problem*[4], which limits spin injection when the resistance of an injector contact, is lower than the spin resistance of the graphene channel,. This is the result of contact-induced spin relaxation, which greatly decreases the measured spin signals[5]. In this work, we demonstrate an alternative approach to grow ultra-thin tunnel barrier contacts made by oxidizing aluminium on top of previously functionalized graphene. We show that molecular functionalization of graphene allows the growth of smooth, high quality tunnel barriers, leading to contacts with increased spin injection efficiency and enhanced spin signals by one order of magnitude. The functionalization process consists on the laser activated physisorbtion of benzoyl peroxide (BPO) molecules on graphene. This laser controlled photoreaction enables us to control both the spatial location and the degree of functionalization, as visualized by Raman spectroscopy maps via the intensity ratio of and peaks (I_D/I_G). We assess the quality of the oxide barriers using atomic force microscopy, charge transport and spin transport measurements. These results open the path towards engineering spintronic devices with spatially controlled functionalization and efficient tunnel contacts.

Tombros, N. *et al*, *Nature* 448, 571–574 (2007). Tombros, N. *et al, Phys. Rev. Lett.* 101, 2–5 (2008). Han, W. *et al, Phys. Rev. Lett.* 105, 167202 (2010). Schmidt, G. *et al*, *Phys. Rev. B* 62, R4790–R4793 (2000). Maassen, T. et al, *Phys. Rev. B* 86, 235408 (2012).

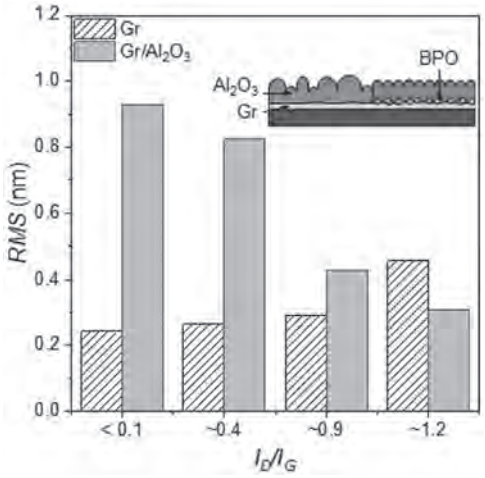

Roughness of graphene before (hatched) and after (grey) Al evaporation, creating an Al_2O_3 layer, versus I_D/I_G ratio. Inset: Schematic of roughness difference with and without molecules on top of graphene.

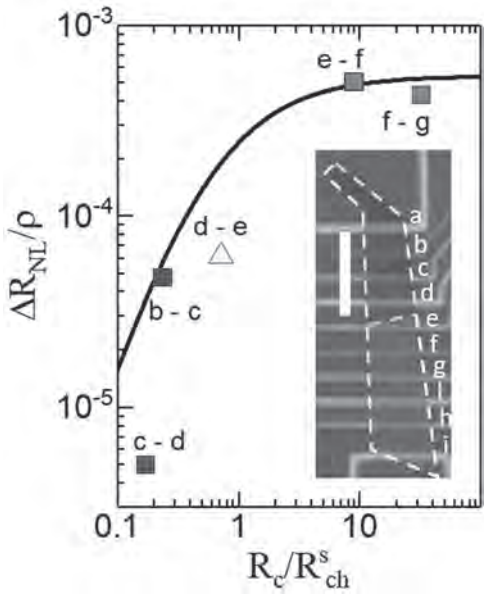

Scaled non-local spin signal as a function of the ratio R_c/R_{ch}^s. Inset: Optical image of a device with two levels of functionalization, grey and red regions have I_D/I_G ratios of 0.1 and 1.9 respectively. Scale bar is 5 μm.

INVITED PAPER

K3-04. Spin Transport in two-Terminal Lateral Devices. *A.M. Spiesser*[2], H. Saito[2], Y. Fujita[3], S. Yamada[3,1], K. Hamaya[3,1], S. Yuasa[2] and R. Jansen[2]
1. Center for Spintronics Research Network, Osaka University Graduate School of Engineering Science, Osaka, Japan; 2. Spintronics Research Center, National Institute of Advanced Industrial Science and Technology (AIST), Tsukuba, Japan; 3. Department of Systems Innovation, Osaka University Graduate School of Engineering Science, Osaka, Japan

A two-terminal (2T) lateral spin-transport device, which consists of a nonmagnetic (NM) channel with two ferromagnetic contacts, is one of the most simple and relevant spintronic devices. Its operation is based on the injection, transport, manipulation and detection of spin-polarized carriers in the NM channel. Typically, the creation of a spin-polarized current is achieved by electrical transfer of spins from the ferromagnetic metal (FM). This method efficiently induces a non-equilibrium spin density (i.e. a spin accumulation) in the NM channel due to spin-polarized tunneling. During the last decade, remarkable progress has been made in the demonstration of spin transport in such lateral devices. In particular, spin transport is now well-understood in the nonlocal four-terminal configuration, enabling a precise determination of all the relevant spin-transport parameters [1]. However, in 2T-devices in which the spin detector contact is biased, the observed spin signals are, without exception, surprising and puzzling, and the spin transport has remained poorly understood. Moreover, when existing theories are applied, the conclusions are inconsistent with those obtained from analysis of nonlocal spin transport devices, even if the same structure is used for the different measurement configurations. Thus, to advance spintronics technology, it is indispensable to develop a thorough understanding of the process of spin injection, transport and conversion in 2T devices. Recently, we have reported the creation of a giant spin accumulation in Si-based lateral devices using the nonlocal geometry [1], which was enabled by the growth of high-quality Fe/MgO contacts with a tunnel spin polarization of up to 90% [2]. This opened the way to a series of remarkable advances in the understanding of spin transport in 2T devices. Here, I will discuss three crucial aspects observed in 2T Si-based spin transport devices with Fe/MgO tunnel contacts: (i) the role of the nonlinearity of spin-to-charge conversion [3], (ii) how to consistently describe 2T spin-valve and Hanle spin signals [4] and (iii) how to accurately quantify spin drift due to electric fields [5]. We first present compelling data that all the inexplicable spin signals in the various 2T devices with a biased detector have, in fact, a single common origin. This common origin is the nonlinearity of the spin conversion at a biased ferromagnetic tunnel contact [3]. The nonlinearity of spin detection can be understood using a simple tunnel transport model and provide a unified description of electrical spin signals in devices with and without biased detector. In a second part, we show that spin voltages in 2T devices contain not only the expected contributions due to spin transport from one electrode to the other, but also local contributions from the spin accumulation in the Si created and detected at each of the two contacts separately [4]. The salient features of the 2T spin signals therefore differ from those in nonlocal devices. The local and transport contributions to the 2T spin signal can be disentangled and described by the same set of device parameters as the nonlocal spin signals measured in the same devices [4]. Finally, we demonstrate how a drift electric field in a heavily doped Si channel changes the spin transport. In particular, we provide a simple, general and accurate method that uses nonlocal devices to quantify spin drift [5]. Such experimental quantification is important for a correct assessment of the role of spin drift in devices in which there is an electric field in the channel. Through these milestones we provide a coherent picture of spin transport in 2T-devices that will be of general interest to those working on devices based on semiconductors, metals, or two-dimensional materials such as graphene and van der Waals crystals. Acknowledgements: This work was supported by Grant-in-Aid for Scientific Research (Grant No. 18K13807).

[1] A. Spiesser *et al.*, Phys. Rev. Appl. 8, 064023 (2017). [2] A. Spiesser *et al.*, Phys. Rev. B 99, 224427 (2019). [3] R. Jansen, A. Spiesser *et al.*, Phys. Rev. Appl. 10, 064050 (2018). [4] A. Spiesser *et al.*, Appl. Phys. Lett. 114, 242401 (2019). [5] A. Spiesser *et al.*, Phys. Rev. Appl. 11, 044020 (2019).

CONTRIBUTED PAPERS

K3-05. Origin of the Magnetic Field Enhancement of the Spin Signal in Metallic Non-Local Spin Transport Devices. *A.J. Wright*[1], M.J. Erickson[2,3], D. Bromley[1], P.A. Crowell[2], C. Leighton[3] and L. O'Brien[1]
1. Physics, University of Liverpool, Liverpool, United Kingdom; 2. Physics and Astronomy, University of Minnesota, Minneapolis, MN, United States; 3. Chemical Engineering and Materials Science, University of Minnesota, Minneapolis, MN, United States

The non-local spin valve (NLSV) is an important tool in spintronics, primarily due to its ability to isolate pure spin currents[1]. As such, NLSVs have been instrumental in spin transport measurements of a wide range of materials[2]. Yet, even in relatively simple systems, questions remain on the impact of interfaces, defects and impurities[3–5]. Of particular interest is an increase in the "spin-signal", ΔR_{NL}, under large magnetic fields (up to 9 T) in all-metallic NLSVs[6], in stark contrast to the key tenet that ΔR_{NL} is invariant under a magnetic field. This effect, which appears only for certain combinations of FM and normal metals, has been a long-standing mystery and, thus far, has been a challenge to describe with existing models. Our earlier works on similar materials have shown that a low temperature upturn in spin-relaxation rate, $1/\tau_s$, originates from magnetic impurity (MI) scattering near the NLSV interfaces[5,7], underlining the importance of the Kondo effect in determining spin-relaxation, particularly in Cu devices. In this study we demonstrate MI scattering as the origin of the field enhancement of ΔR_{NL}, and we provide a theoretical framework. By correlating the magnitude of the field enhancement, δR_{NL}, with the NLSV material pairings, we ascertain that δR_{NL} is only present in those materials that can host MI moments (Figure 1). Next, focusing on Cu/Fe NLSVs, we extract spin-transport parameters from the field-enhanced ΔR_{NL}. Under zero-field, we observe the same increase in $1/\tau_s$ at low temperatures (Figure 2), due to Kondo scattering from MIs, in agreement with our previous work[5]. Importantly, we show that this mechanism is quenched by a magnetic field and we successfully model the data using a magnetic-field-modified Kondo expression[8]. This work not only highlights a systematic overestimation of $1/\tau_s$ in materials containing MIs, including a clear impact on Hanle spin relaxation measurements, but also provides a simple means to quantify and suppress this scattering mechanism.

[1] F.J. Jedema, M.S. Nijboer, A.T. Filip, and B.J. van Wees, Phys. Rev. B 67, 085319 (2003). [2] I. Zutić, J. Fabian, and S. Das Sarma, Rev. Mod. Phys. 76, 323 (2004). [3] H. Idzuchi, Y. Fukuma, L. Wang, and Y. Otani, Appl. Phys. Lett. 101, 022415 (2012). [4] E. Villamor, M. Isasa, L.E. Hueso, and F. Casanova, Phys. Rev. B 87, 094417 (2013). [5] L. O'Brien, M.J. Erickson, D. Spivak, et al., Nat. Commun. 5, 3927 (2014). [6] K. Výborný, G. Mihajlović, A. Hoffmann, and S.I. Erlingsson, J. Phys. Condens. Matter 25, (2013). [7] J.D. Watts, L. O'Brien, J.S. Jeong, et al., Phys. Rev. Mater. 3, 124409 (2019). [8] V.I. Litvinov, Phys. Status Solidi 77, 71 (1976).

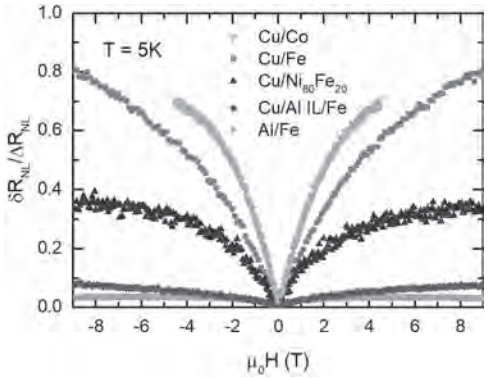

Fig 1. Magnetic field response of δR_{NL}, for different material combinations, normalised to the zero-field ΔR_{NL}.

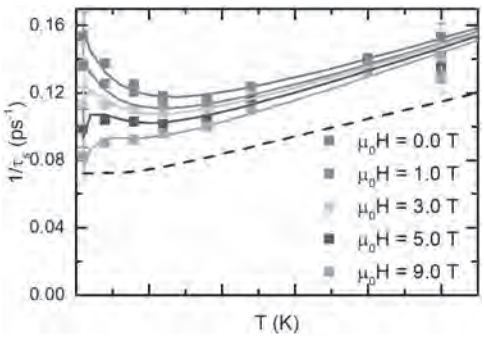

Fig. 2. $1/\tau_s$ as a function of temperature, for different magnetic fields. The dashed line is an MI-free estimate of $1/\tau_s$

K3-06. Ballistic Spin Transport in InSb Nanowires With Strong Rashba Spin-Orbital Interaction. *Z. Yang*[1], B. Heischmidt[1], S. Gazibegovic[2], G. Badawy[2], D. Car[2], P.A. Crowell[1], E.P. Bakkers[2] and V.S. Pribiag[1] *1. School of Physics and Astronomy, University of Minnesota, Minneapolis, MN, United States; 2. Eindhoven University of Technology, Eindhoven, Netherlands*

Semiconductors nanowires (NWs) with strong spin-orbital interaction, like InSb and InAs nanowires, are a leading platform for realizing future computing devices, such as Datta-Das spin-transistor[1] and topological-superconductor quantum computing devices[2] using Majorana zero modes. Coupling nanowires to electrical spin-selective contacts, therefore, is an important step as it can, on the one hand, provide a setting to study spin transport in quantum wires, and on the other hand could enable the realization of Majorana devices that do not require an applied magnetic field, by taking advantage of the magnetic exchange interaction or spin accumulation. Here, we will discuss our measurements on InSb NW devices with iron (Fe) electrical contacts[3] (see Figure 1, scanning electron microscopy picture). Conductance measurements show conductance quantization and Fabry–Pérot interference, clearly demonstrating phase-coherent and ballistic electronic transport with spin-polarized currents. Our magnetoconductance study clearly demonstrates spin injection/ transport across the NWs by the observation of hysteretic spin-valve signals (Figure 2a). Moreover, we show that electrostatic gating tunes the observed hysteretic signal and reveals a transport regime where the device acts as a spin filter (Figure 2b). *Supported primarily by the Department of Energy under Award No. DE-SC-0019274. Nanowire growth was supported by the European Research Council (ERC HELENA 617256), and the Dutch Organization for Scientific Research (NWO).

1. Datta, S. & Das, B. Electronic analog of the electro-optic modulator. *Appl. Phys. Lett.,* Vol.56, p.665–667 (2016) 2. Mourik, V. *et al.* Signatures of Majorana Fermions in Hybrid Superconductor-Semiconductor Nanowire Devices. *Science.,* Vol.336, p.1003–1007 (2012) 3. Yang, Z. *et al.* Spin Transport in Ferromagnet-InSb Nanowire Quantum Devices. *Nano Lett.*, Vol 20, p.3232-3239 (2020)

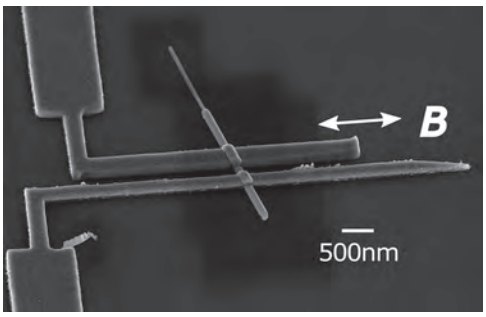

Fig.1 Scanning Electron Microscopy (SEM) picture of the device.

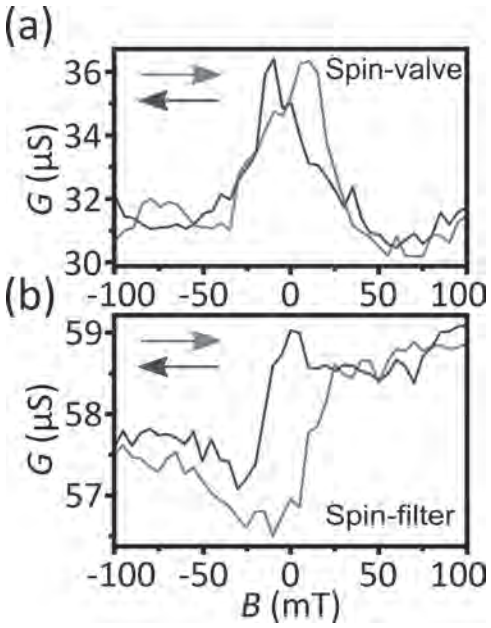

Fig.2. (a) Spin-valve magnetoconductance. (b) Spin-filter magnetoconductance.

K3-07. Unusual Scaling of Kondo Spin Relaxation. *X. Shen*[1] and Y. Ji[1] *1. University of Delaware, Newark, DE, United States*

It has been demonstrated that the Kondo effect from iron impurities substantially enhances the spin relaxation rate at low temperature in submicron copper channels of nonlocal spin valves (NLSV) [1,2]. In this work, we explore a long standing question about the physical existence of Kondo screening clouds [3] by examining the relationship between Kondo spin relaxation rate and Kondo resistivity. A systematic method is utilized to extract spin and charge transport parameters from each of the 20 NLSV devices investigated. Figure 1 (a) shows that the spin relaxation length of a NLSV reaches its maximum of 3.0 microns at 30K. Low temperature upturns are clearly observed in the spin relaxation rate versus temperature (Figure 1 (b)) and the Cu resistivity versus temperature (inset of Figure 1 (b)) plots. Both upturns are attributed to the Kondo effect from Fe impurities of several ppm. The Kondo spin relaxation rate and Kondo resistivity are extracted by fitting and plotted in Figure 1 (c) for all 20 NLSVs. Surprisingly, the Kondo spin relaxation rate remains almost constant, while the Kondo resistivity varies by nearly a factor of 10. This is significantly different from the linear relationship predicted by the Elliott-Yafet model. The effective Kondo spin flip probability, shown in Figure 1 (d), is greatly suppressed as the Kondo resistivity (proportional to impurity density) increases. The data can be explained by considering the spin dephasing processes through the Kondo screening clouds around Fe impurities, and support the physical existence of Kondo screening clouds.

[1] L. O'Brien, et.al, Nat. Commun. 5, 3927 (2014). [2] J. T. Batley, et.al, Phys. Rev. B 92, 220420(R) (2015). [3] V. Borzenets, et.al, Nature 579, 210–213 (2020).

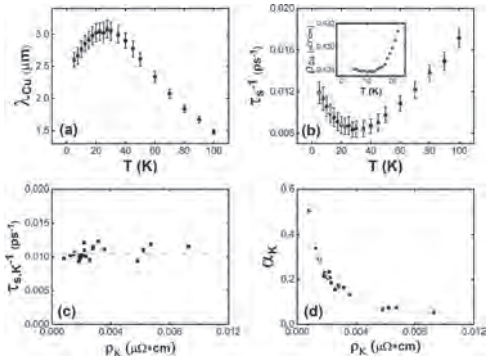

Fig. 1: (a) Spin relaxation length versus temperature; (b) Spin relaxation rate and Cu resistivity (inset) versus temperature; (c) Kondo spin relaxation rate versus Kondo resistivity; (d) Effective Kondo spin-flip probability versus Kondo resistivity.

K3-08. Magnetotransport Effect in Magnetic Heterojunctions: Combined First-Principles With NEGF and Spin Dynamics. *B. Huang*[1], C. Chao[1], Y. Tang[1] and C. Kaun[2] *1. Physics, National Central University, Chung-Li, Taiwan; 2. Research Center for Applied Sciences Academia Sinica, Taipei, Taiwan*

Recently, we have successfully employed the single-band tight-binding (SBTB) model to predict the noncollinear spin torque effect in FM/I/FM and FM/I/SF/I/FM [1] magnetic tunnel junctions, where I and SF represent insulting and spin-filter barriers, respectively. However, for real complex heterojunctions, the injected spin-polarized electrons from FM electrode can be strongly influenced by the complicated interfacial spin-polarized charge transfer, which is ignored in the SBTB model. In this study, our newly developed "JunPy" [2] package has successfully combined the self-consistent Hamiltonian by using the first-principles calculation with the non-equilibrium Green's function (NEGF) method to obtain the noncollinear spin torque effect in nm-scale magnetic heterojunctions. In addition, the generalized Landau-Lifshitz-Gilbert (LLG) equation implemented by our calculated spin transfer torque (STT) effect is developed to simulate the magnetization switching in Fe/MgO/Fe MTJ in the presence of external magnetic field and current-induced STT. The resistance as a function of the magnetic field (R-H loop) and of bias (R-V loop) are thus obtained and well comparable with experimental results [3]. We further employed it to predict the giant field-like spin torque (FLST) effect in the amine-ended single-molecule magnetic junction [4], which may open a new avenue for multifunctional manipulation in next-generation organic FLST-MRAMs with lower power consumption. We believe that this newly developed calculation process not only can efficiently resolve current self-consistent difficulties in the first-principles calculation for non-collinear cases but also may inspire future experimental explorations in novel magnetic heterojunctions for future spintronics applications. This work is supported by the Ministry of Science and Technology of Taiwan (MOST 107-2633-M-008-004 and 108-2628-M-008-004-MY3).

[1] Y. –H. Tang et al., Phys. Rev. Lett. 103, 057206 (2009); Sci. Rep. 5, 11341 (2015). [2] https://labstt.phy.ncu.edu.tw/junpy [3] H. Kubota et al., Nature Phys. 4, 37 (2008). [4] Y. –H. Tang and B. –H. Huang, J. Phys. Chem. C 122, 20500 (2018).

Session K4
2D MAGNETIC MATERIALS: TRANSPORT PROPERTIES (Poster Session)

Yong-Chang Lau, Chair
Tohoku University, Sendai, Japan

K4-01. Ultrahigh Efficient Spin-Orbit-Torque Magnetization Switching in Sputtered Topological Insulator BiSb and $(Co/Pt)_2$ Multilayers.
F. Tuo[1], H. Nguyen[1,2], S. Nakano[1] and H.N. Pham[1,3] *1. Department of Electrical and Electronic Engineering, Tokyo Institute of Technology, Tokyo, Japan; 2. Department of Physics, Ho Chi Minh City University of Education, Ho Chi Minh City, Vietnam; 3. Center for Spintronics Research Network, The University of Tokyo, Tokyo, Japan*

Topological insulator BiSb is a promising candidate for spin-orbit-torque (SOT) magnetoresistive random-access memory (MRAM), due to its giant spin Hall effect (spin Hall angle $\theta_{SH} \sim 52$ for BiSb(012) surface) [1] and high electrical conductivity ($\sigma \sim 2.5 \times 10^5\ \Omega^{-1}m^{-1}$) [2] at room temperature. Recently, we demonstrated that high-quality BiSb thin films with quasi single crystal structure could be grown by sputtering deposition, underlying its potential for mass production of SOT-MRAM [3]. In this work, we show that in all-sputtered BiSb-$(Co/Pt)_n$ multilayers structure, the BiSb layer with (110) surface has large $\theta_{SH} = 12.3$ and high $\sigma \sim 1.5 \times 10^5\ \Omega^{-1}m^{-1}$, which lead to ultrahigh efficient SOT magnetization switching of $(Co/Pt)_n$ multilayers. We deposited (0.4 nm Co/0.4 nm $Pt)_2$ - 10 nm BiSb multilayers on *c*-plane sapphire (0001) substrate at room temperature (Fig. 1a). The $(Co/Pt)_2$ multilayers are perpendicularly magnetized with a large anisotropy field, as shown in Fig. 1b. We employed the second harmonic Hall measurement to evaluate θ_{SH} in 50 μm × 25 μm Hall bars. A representative 2nd harmonic Hall resistance ($R_2\omega$) is plotted as a function of in-plane magnetic field (H) in Fig. 1c, and the antidamping-like field H_{AD} is evaluated by fitting to $R_2\omega$ at high field. Fig. 1d shows the H_{AD} at various current density J^{BiSb}, from which we obtained $\theta_{SH} = 12.3$. Thanks to the large θ_{SH}, the magnetization of $(Co/Pt)_2$ can be efficiently switched by a small DC threshold current density $J_{th}^{BiSb} = 1.5 \times 10^6$ Acm^{-2} at $H = \pm 2.75$ kOe (Fig. 2a and 2b). Fig. 2c shows robust switching by 75 consecutive pulses at ±1.83 kOe ($J^{BiSb} = 4.4 \times 10^6$ Acm^{-2}, $t_{pulse} = 100$ μs). Our results demonstrate the feasibility of BiSb for ultralow power SOT-MRAM and other SOT-based spintronics devices.

[1] N. H. D. Khang, Y. Ueda and P. N. Hai, Nat. Mater. 17, 808-813 (2018). [2] Y. Ueda et al., Appl. Phys. Lett. 110, 062401 (2017). [3] T. Fan et al., Jpn. J. Appl. Phys. 59, 063001 (2020).

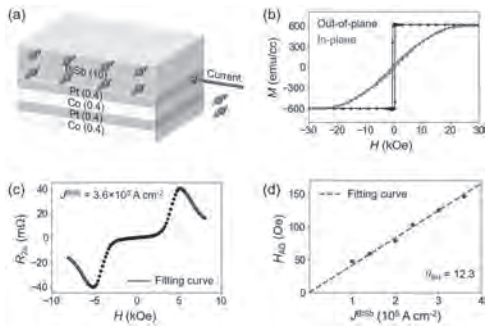

Fig. 1 (a) Sample structure. (b) Magnetization curves of the $(Co/Pt)_2$ multilayers. (c) Represenative 2nd harmonic Hall resistance. (d) Antidamping-like field H_{AD} as a function of J^{BiSb}.

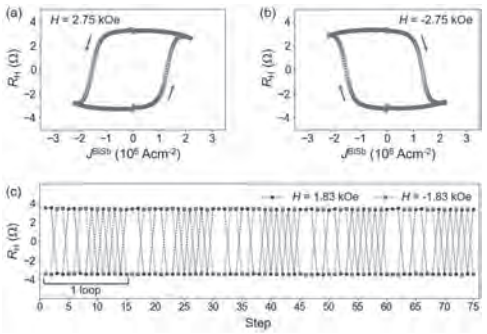

Fig. 2 (a) (b) SOT switching by DC currents at +2.75 kOe and -2.75 kOe, respectively. (c) Robust switching by 75 consecutive pulses at ±1.83 kOe ($J^{BiSb} = 4.4 \times 10^6$ Acm^{-2}, $t_{pulse} = 100$ μs).

K4-02. Withdrawn

K4-03. Band-Structure Spin-Filtering in Vertical Spin Valves Based on CVD Grown WS_2.
V. Zatko[1], M. Galbiati[1], S. Dubois[2], M. Och[3], C. Mattevi[3], P. Brus[4], B. Servet[4], M. Martin[1], F. Godel[1], J. Charlier[2], F. Petroff[1], B. Dlubak[1] and P. Seneor[1] *1. Unité Mixte de Physique, CNRS, Thales, Université Paris-Saclay, Palaiseau, France; 2. Institute of Condensed Matter and Nanosciences, Université catholique de Louvain, Louvain- La-Neuve, Belgium; 3. Department of Materials, Imperial College, London, United Kingdom; 4. Thales Research and Technology, Palaiseau, France*

Spintronics has opened a new paradigm through the use of the spin variable as the vector of information and has been largely applied from hard drives read-heads to the STT-MRAMs. While very recent, the introduction of 2D materials in Magnetic Tunnel Junctions (MTJs) has already shown some promising properties[1]. Graphene and the 2D insulator h-BN have been the first 2D materials to show strong impact on spin transport in MTJs. The recent advent of the wide TMDC family of 2D semiconductors opened new opportunities for further tailoring of spintronics properties. We will present results on the scarcely studied WS_2. We will detail a protocol using laser lithography technology to fabricate spin valves based on CVD grown WS_2, with step by step characterizations in support (Raman spectroscopy, photoluminescence, and AFM measurements). We will finally show our first spin transport measurements obtained in a CVD WS_2 based MTJ. Our measured MR signals, above state of the art for 2D semiconductor based MTJs, validates our integration approach. We observe that the spin signal extracted from a ferromagnetic electrode can be tuned by placing atomically thin WS_2 on top of it. Furthermore the thickness of WS_2 significantly affects the extracted spin polarization of the 2D/FM interface. We discuss that trend using the peculiar band structure of WS_2, supported by DFT calculations, leading to thickness dependent spin filtering. Our work opens the way to the integration of different members of the very large TMDCs family, in order to reveal their spin transport properties in MTJs[2].

[1] M. Piquemal-Banci, R. Galceran, M-B. Martin et al. J. Phys. D: Appl. Phys., 50, 203002 (2017). [2] V. Zatko, M. Galbiati, S-M-M. Dubois et al. ACS Nano., 13, 14468 (2019).

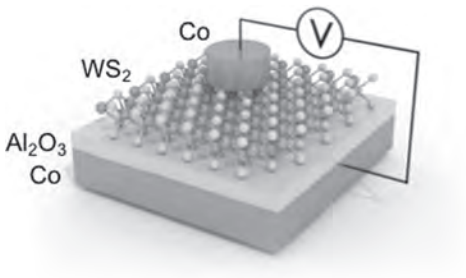

Schematic of a 2D tungsten disulfide based magnetic tunnel junction.

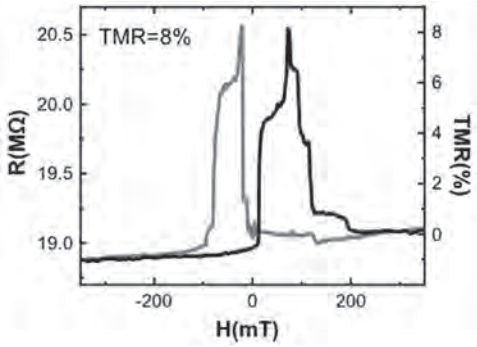

State of the art tunneling magnetoresistance measured on our 2D-tungsten disulfide based magnetic tunnel junction.

K4-04. Magnetotransport Characteristics in Second-Order Weyl Semimetals. *S. Komori*[1] and K. Kondo[1] *1. Research Institute for Electronic Science, Hokkaido University, Sapporo, Japan*

Topological materials have received considerable attention among theoretical and experimental researchers for the last few decades. Among them, Weyl semimetals (WSMs) attract attention in the spintronics field because they exhibit negative magnetoresistance due to chiral anomaly. Recently, new kinds of topological insulators whose gapless modes localize at 1-dimensional hinges were discovered by Schindler et al. They are called "second-order topological insulators" and investigated intensively. Also, second-order Weyl semimetals (SOWSMs), which have Fermi-arc-like energy levels corresponding to 1-dimensional hinge states, have been recently proposed. The transport properties of SOWSMs have not yet been investigated to our knowledge while those of first-order Weyl semimetals are studied in detail. In this study, we propose an effective model of SOWSMs with a tilt parameter γ. Our model becomes Type-I or Type-II SOWSMs depending on γ. Moreover, utilizing the Boltzmann equation including Berry curvature, we examine the magnetotransport of SOWSMs. Figure 1 shows the Fermi-arc-like energy levels emerging in a SOWSM when γ = 0.2. It is confirmed that the system is classified as a Type-II SOWSM by the existence of electron pockets and hole pockets. Figure 2 shows angle dependence of magnetoconductivity σ_{xx} of SOWSMs under the application of external magnetic field. Here, the magnetic field is applied in the direction tilted from the *x* axis by an angle φ inside the *xy* plane perpendicular to the node separation. We can observe that the magnetoconductivity σ_{xx} behaves as $\cos^2\varphi$. SOWSMs exhibit the negative magnetoresistance as the same case of conventional ones. Therefore, SOWSMs are expected to be candidates for novel switching devices in the spintronics field. At the conference, we are going to discuss planer Hall conductivity σ_{xy}.

Frank Schindler et al., Sci. Adv. 4, eaat0346 (2018) K. Das and A. Agarwal, Phys. Rev. B 99, 085405 (2019) Bitan Roy, Phys. Rev. Research 1, 032048(R) (2019) S. Komori and K. Kondo, 64th Annual Conference on Magnetism and Magnetic Materials, (Las Vegas, America) 2019

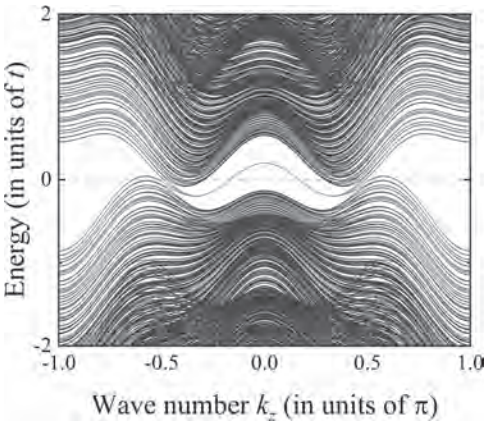

Fig. 1. Fermi-arc-like energy levels of a Type-II second-order Weyl semimetal (γ = 0.2).

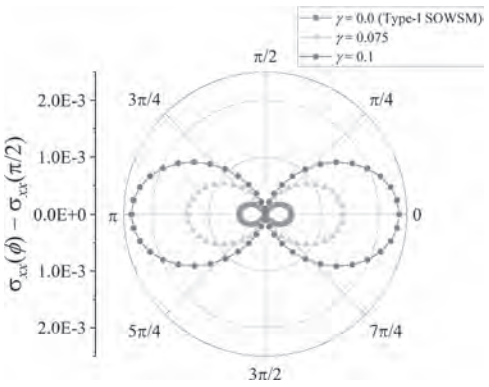

Fig. 2. Field angle dependence of magnetoconductivity σ_{xx} of second-order Weyl semimetals.

K4-05. α-Sn Magnetotransport Devices. *O. Vail*[1], A. Chang[2], S. Harrington[2], P. Folkes[1], P. Taylor[1], G. de Coster[1] and C. Palmstrom[2] *1. RLS-EE, US Army Research Laboratory, Adelphi, MD, United States; 2. Electrical & Computing Engineering and Materials, University of California Santa Barbara, Santa Barbara, CA, United States*

The large spin-orbit coupling of diamond-cubic α-Sn shows great promise for magnetic memory devices along with its topological band structure and single-element nature. As such, consistent high-quality growth on insulating CdTe opens the doors to unconventional electronics using a widely available source material. After verifying epitaxial growth of our films, we perform transport measurements to characterize the electronic carriers in the material. We identify two-channel transport and semimetallic behavior in thicker samples, while thinner samples that approach the topological insulator regime are dominated by impurities resulting from the particulars of growth on the CdTe substrate. We apply a field effect gate voltage in order to modulate the channel between majority n-type and majority p-type carriers and further characterize its behavior under large magnetic fields. Careful preparation of the CdTe surface before growth is considered crucial to attain a low residual density and accessible topological states on an insulating substrate. This work readily lends itself to the development of topologically enabled devices for fieldable applications such as low power magnetoelectronics.

K4-06. Withdrawn

K4-07. Withdrawn

K4-08. Spin Caloritronic Device Based on Asymmetric Surfaces of Magnetic Topological Insulators. *T. Chiba*[1], S. Takahashi[2] and T. Komine[3] *1. National Institute of Technology, Fukushima College, Iwaki, Japan; 2. Advanced Institute for Materials Research, Tohoku University, Sendai, Japan; 3. Faculty of Engineering, Ibaraki University, Hitachi, Japan*

Recently, possible applications for thermoelectrics and spin caloritronics utilizing topological materials have been studied. Thermoelectric (TE) conversion that can convert heat into electricity has been attracting attention as a clean power generation technology without greenhouse gases in energy harvesting. The conversion efficiency is evaluated by the dimensionless figure of merit *ZT*, which is needed to be larger than 1 (energy conversion efficiency is 10%) in practice. Recently, a bismuth chalcogenide which shows the best TE conversion on the nanoscale has been also known as a three-dimensional topological insulator (3D TI). TI has a linear electronic dispersion on the surface. In the presence of a surface gap induced by magnetic dopants, the surface electronic transport strongly depends on the chemical potential, promising very large TE conversion efficiency [1]. Here, we propose a TE energy conversion device based on the surface of 3D TIs that is magnetically gap-opened and ionically disordered [2]. This device can achieve the thermocouple p-n junction by a single TI film, in which a pair of top and bottom surfaces of a 3D TI takes a role of the vertical p-n junction, which can be considered a thermocouple consisting of two dissimilar TE materials (see Fig. 1). Based on the Boltzmann theory at finite temperatures, we compute TE transport coefficients taking into account electron scattering by screened disorder potentials on the surface. By tuning the surface carrier screening by means of electric gating, we find that *ZT* of the present device achieves more than 1 in the wide temperature-regime from 100 K to 300 K.

[1] T. Chiba and S. Takahashi, J. Appl. Phys. 126, 245704 (2019). [2] T. Chiba, S. Takahashi, and T. Komine, Appl. Phys. Lett. 115, 083107 (2019).

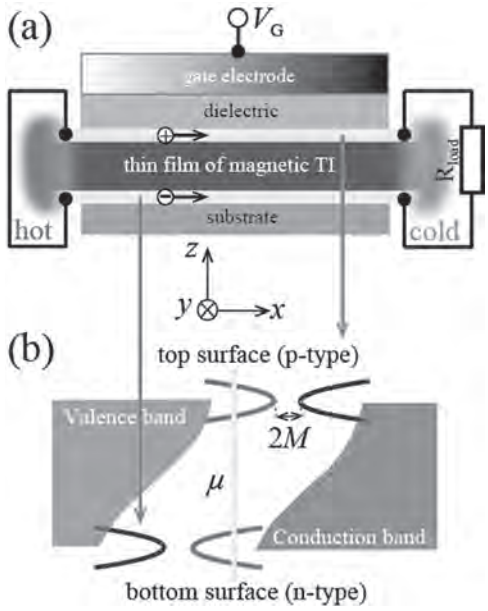

FIG. 1. (a) Schematic geometry (side view) of the TE power generation device, which consists of a magnetic TI film. (b) Corresponding *k*-dependent surface band dispersions.

K4-09. Large Multi-Directional Spin-to-Charge Conversion in low Symmetry Semimetal $MoTe_2$ at Room Temperature. *N. Ontoso*[1], C. Safeer[1], J. Ingla-Aynés[1], F. Herling[1], V. Pham[2,1], A. Kurzmann[3], K. Ensslin[3], A. Chuvilin[1,6], I. Robredo[4,7], M. Vergniory[4,6], F. de Juan[4,6], L.E. Hueso[1,6], M. Calvo[1,5] and F. Casanova[1,6] *1. CIC nanoGUNE, San Sebastian, Spain; 2. SPINtronique et Technologie des Composants, Grenoble, France; 3. Department of Physics, ETH Zurich Campus Honggerberg, Eidgenossische Technische Hochschule Zurich - Campus Honggerberg, Zurich, Switzerland; 4. Donostia International Physics Center, San Sebastian, Spain; 5. Departamento de Física Aplicada, Universitat d'Alacant, Alacant, Spain; 6. Ikerbasque, Bilbao, Spain; 7. Department of Condensed Matter Physics, Universidad del Pais Vasco, Bilbao, Spain*

Efficient and versatile spin-to-charge current conversion is crucial for the development of spintronic applications, which strongly rely on the ability to electrically generate and detect spin currents. In this context, the spin Hall effect has been widely studied in heavy metals with strong spin-orbit coupling. While the high crystal symmetry in these materials limits the conversion to the orthogonal configuration [1], unusual configurations are expected in low symmetry transition metal dichalcogenide semimetals [2], which could add flexibility to the electrical injection and detection of pure spin currents. Here, we report the observation of spin-to-charge conversion in $MoTe_2$ flakes, which are stacked in graphene lateral spin valves [3]. We detect two distinct contributions arising from the conversion of two different spin orientations. In addition to the conventional conversion where the spin polarization is orthogonal to the charge current, we also detect a conversion where the spin polarization and the charge current are parallel. Both contributions, which could arise either from bulk spin Hall effect or surface Edelstein effect, show large efficiencies comparable to the best spin Hall metals and topological insulators. Our finding enables the simultaneous conversion of spin currents with any in-plane spin polarization in one single experimental configuration [3].

[1] Sinova, J.; Valenzuela, S. O.; Wunderlich, *et al*., *Rev. Mod. Phys.*, Vol. 87, p.1213-1260 (2015) [2] MacNeill, D.; Stiehl, G. M.; Guimaraes, *et al*., *Nat. Phys.* Vol. 13, p.300-305 (2017) [3] Safeer, C. K.; Ontoso, N.; Ingla-Aynés, *et al., Nano Lett*., Vol.19, p8758-8766 (2019)

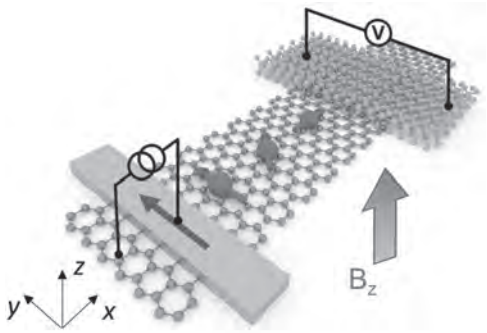

Fig.1.- Schematic of the measurement configuration showing the spin precession by applying an out-of-plane magnetic field.

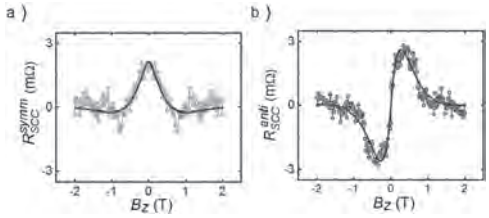

Fig.2.-(a-b)Symmetric and antisymmetric components of the spin-to-charge conversion signal fitted to the Bloch equation (solid black line) corresponding to the spin to charge conversion of the spin component along y and x directions respectively.

K4-10. Electrical Bandgap Tuning and Spin Transport in Fully Encapsulated Bilayer Graphene Devices: Steps Towards 2D Spin Logic. *C.R. Anderson*[1], V.H. Guarochico-Moreira[1,2], N. Natera Cordero[1,3], J.C. Toscano Figueroa[1,3], I. Grigorieva[1] and I.J. Vera-Marun[1] *1. Physics and Astronomy, The University of Manchester, Faculty of Science and Engineering, Manchester, United Kingdom; 2. Departmento de Física, Escuela Superior Politécnica del Litoral, Guayaquil, Ecuador; 3. CONACyT, Consejo Nacional de Ciencia y Tecnologia, Mexico City, Mexico*

The state variable in digital devices has been realised, to date, by measurement of charge. Spintronics offers a new paradigm to improve performance, whereby the quantum spin states of one or more electrons could be used as an alternative state variable. Improvements in transport and control of spin information are necessary for spin logic to be fully realised in graphene devices. Bilayer graphene (BLG) offers the opportunity to electrically control its bandgap[1][2][7] (Figure 1) and, as a result, the spin transport in the channel; thereby potentially enabling fabrication of a graphene based spin field effect transistor. BLG spin transport measurements are conventionally made[3][4][7] using invasive 2D contacts which interface over the width of the graphene channel and, as such, modify the properties of the channel. This type of contact has been shown to cause spin relaxation[5] and inhomogeneous doping[6]. In contrast, our devices incorporate fully encapsulated, high quality BLG with non-invasive contacts, enabled by 1D edge contact technology (Figure 2). These only make contact with the edge of the graphene, preserving the channel's electronic properties. Figure 1 shows the resistivity change at low temperature, afforded by a perpendicular electric field (D) applied via a top gate, thus revealing the bandgap opening. Spin transport in a non-local spin valve arrangement, has been achieved in the same device and measured as a function of carrier density, revealing signals (DR_{nl}) of the order of an ohm at low temperature. Similar measurements at room temperature have also been achieved. The status of our research is presented, along with an outline of future steps paving the way to electrical control of spin transport in a high quality, 1D edge contacted BLG device.

[1] Y.B. Zhang et al, Nature, Vol. 459, p.820-823 (2009). [2] T. Taychatanapat, P. Jarillo-Herrero, PRL, Vol. 105, p.166601 (2010). [3] A. Avsar, I.J. Vera-Marun et al, NPG Asia Materials, Vol. 8, p.274 (2016). [4] J. Ingla-Aynés, B.J. van Wees, PRB, Vol. 92, p.201410 (2015). [5] T. Maassen, I.J. Vera-Marun, B.J. van Wees et al, PRB, Vol. 86, p.235408 (2012). [6] F. Volmer et al, Synthetic Metals, Vol. 210, p.42 (2015). [7] J. Xu et al, PRL, Vol. 121, p.127703 (2018).

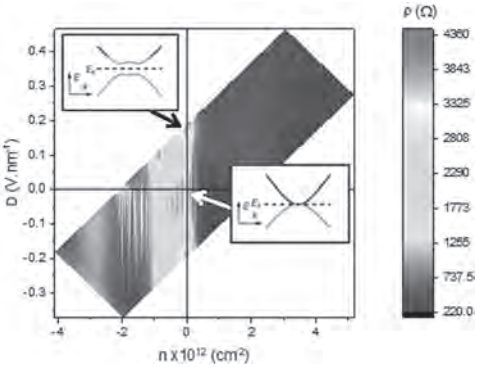

Fig. 1 Graphene channel resistivity as a function of carrier density and perpendicular electric field, at low temperature. Insets adapted from [1].

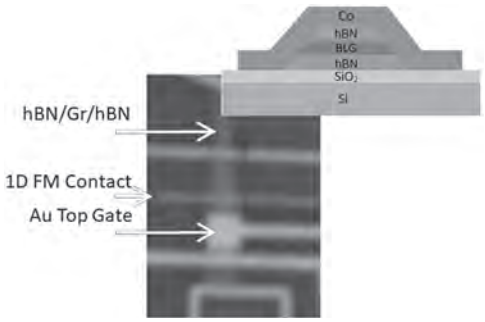

Fig. 2 Optical Image of the BLG device and schematic of its cross-section

K4-11. Withdrawn

K4-12. A Study of Magnetoresistance in Type-I and Type-II Weyl Semimetals. *K. Morishima*[1] and K. Kondo[1] *1. Research Institute for Electronic Science, Hokkaido University, Sapporo, Japan*

Weyl semimetals (WSMs) are characterized by having even pairs of Weyl points with opposite chirality. Depending on the existence of electron pockets and hole pockets, they are classified into two types: Type-I WSMs and Type-II WSMs. In both cases, an interesting phenomenon manifests itself, which originates from "chiral anomaly". The chiral anomaly results in a negative magnetoresistance when an electric field is applied along the direction of the magnetic field. Moreover, the negative magnetoresistance gives rise to planar Hall effect. Because of these transport properties, WSMs attract much attention in the spintronics field. In 2017, a time reversal symmetry broken WSM model was proposed by McCormick et al., which can realize both the Type-I WSMs and the Type-II WSMs by tuning parameters. The transport properties of this model have not yet been well investigated. In this study, we utilize this model to perform numerical calculations of the negative longitudinal magnetoresistance and the planar Hall effect of Type-II WSMs. Furthermore, we compare the above results with those of the Type-I WSMs. Both the Type-I WSMs and the Type-II WSMs exhibit negative magnetoresistance as shown in Fig. 1 and planar Hall effect as shown in Fig. 2. In both cases, magnetic field B [T] = (0, 3cosθ, 3sinθ) is applied. The solid curves represent the positive values and the dotted curves represent the negative ones. Therefore, both types of WSMs are expected to be candidates for novel switching devices. In our presentation, we are going to discuss the differences in numerical results between the Type-I WSMs and the Type-II WSMs. Moreover, we are going to discuss the origins of the difference in detail.

[1] Timothy M. McCormick, Itamar Kimchi, and Nandini Trivedi, *Phys. Rev.* B 95, 075133 (2017). [2] Kamal Das and Amit Agarwal, *Phys. Rev.* B 99, 085405 (2019). [3] K. Morishima, S. Komori and K. Kondo, The 80th JSAP Autumn Meeting, Hokkaido University (2019).

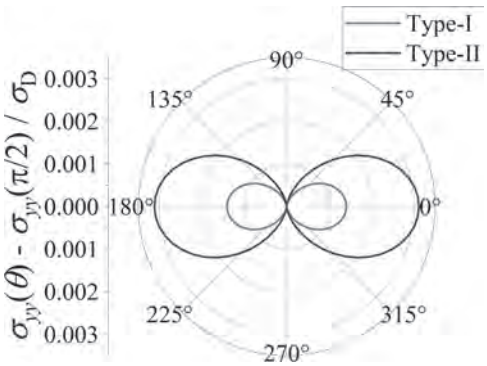

Fig. 1. Longitudinal magnetoconductivities of Type-I and Type-II Weyl semimetals.

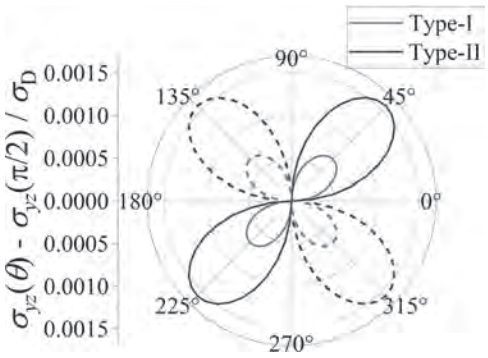

Fig. 2. Transverse magnetoconductivities of Type-I and Type-II Weyl semimetals.

K4-13. Size Effect in the Kinetic Properties in Thin Films of Bi_2Se_3 Topological Insulator. *V. Chistyakov*[1], A. Domozhirova[1], J.A. Huang[3] and V. Marchenkov[1,2] *1. M.N. Mikheev Institute of Metal Physics UB RAS, Ekaterinburg, Russian Federation; 2. Ural Federal University, Ekaterinburg, Russian Federation; 3. National Cheng Kung University, Tainan, Taiwan*

In recent years new quantum materials with a topologically nontrivial band structure resulting from strong spin-orbit interaction have been predicted theoretically and discovered experimentally. First of all, these are topological insulators (TI). In these compounds there is an energy gap in the bulk of the material, characteristic of an insulator, and protected gapless conducting states on its surface. Since TIs of conductivity in its bulk and near the surface differ significantly, TI can be represented as a system of two parallel-connected conductors: a "metal" surface and a "semiconductor" bulk (see e.g. [1-4] and references therein). As was shown in [1-3], the conductivity σ of such a system can be represented as: $\sigma = f(d^{-1})$. In this paper we talk about the size effect in the magnetoconductivity and Hall coefficient of the topological insulator Bi_2Se_3. The Hall resistivity and magnetoresistivity were measured by the conventional 4-points method at dc-current in the temperature range from 4.2 to 80 K and in magnetic fields of up to 10 T. As a result of the experiments performed, a size effect was observed, i.e. the dependence of the kinetic coefficients (magnetoconductivity, Hall coefficient) on the inverse film thickness. The results of this work allow to experimentally "separate" the bulk and surface contributions. It was found that the value of the surface contribution by almost an order of magnitude exceeds the value of the bulk. The obtained results can be used for "separation" and evaluation of the values of surface and bulk contributions in kinetic coefficients also in other TIs and systems with non-uniform distribution of direct current over the cross section of the sample. The research was carried out within the state assignment of the Ministry of Education and Science of the Russian Federation (theme "Spin", No. AAAA-A18-118020290104-2), supported in part by RFBR (project No. 17-52-52008) and the Government of Russian Federation (Decree No. 211, Contract No. 02.A03.21.0006).

[1] V.V. Marchenkov, V.V. Chistyakov, J.C.A. Huang at al., EPJ Web of Conferences., Vol. 185, p. 01002 (2018) [2] V.V. Chistyakov, A.N. Domozhirova, J.C.A. Huang at al., Bulletin of the Russian Academy of Sciences: Physics, Vol. 83, p. 838 (2019) [3] V.V. Chistyakov, A.N. Domozhirova, J.C.A. Huang at al., Journal of Physics: Conference Series, Vol. 1389, p. 12051 (2019) [4] V.V. Chistyakov, A.N. Domozhirova, J.C.A. Huang at al., Journal of Physics: Conference Series, Vol. 1410, p. 12199 (2019)

K4-14. Charge Trapping Analysis in Sputtered Bi_xSe_{1-x} Based Accumulation-Mode FETs - Part 2. *P. Sahu*[1], J. Chen[2,3] and J. Wang[3] *1. School of Physics and Astronomy, University of Minnesota, Minneapolis, MN, United States; 2. HFC Semiconductor, Fishkill, NY, United States; 3. Electrical and Computer Engineering, University of Minnesota, Minneapolis, MN, United States*

In the first part of this publication, we analyzed the basic experimental data for sputtered Bi_xSe_{1-x} - based accumulation mode FETs [1]. These devices hold key to several spintronic devices. A major chunk of the new physics comes from the interplay of the transport properties between surface and bulk states. The unique ability of these devices allows us to manipulate the surface and bulk transport properties (carrier density, mobility etc.) via a third terminal (gate voltage). In this part, we analyze the effects of gate voltage and charge trapping on various device transport properties and paramenters. We start by analyzing the carrier concentration of the thin films at various gate voltages. This is derived by combining a semi-empirical model between carrier density and mobility with Drude's transport model [2]. This allows us to calculate the effective carrier density contributing to the transport behavior. However, this changes in transport properties is limited to the Bi_xSe_{1-x} / SiO_2 interface. This means that there is major contribution from this interface towards the gate-output characteristics. We calculate the zero-point voltage of this system from the analysis of the gate-voltage hysteresis curve. This zero-point voltage is a combination of the effects of flat-band voltage as well as the presence of trapped charges due to fabrication process. Based on that, we calculated the effective carrier profile inside the film, contributing to the transport. This shows that the interfacial conduction increases under the accumulation and depletion mode. This increase in interfacial conduction exponentially decays into the bulk of the film. We also calculated the effective sheet carrier density at the interface. This can be understood as an effective capacitance per unit area at the Bi_xSe_{1-x} / SiO_2 interface generated by the transport electrons at various gate voltages.

[1] P. Sahu, JY Chen, JP Wang AIP Advances, 10, 1, 015315 [2] P. Sahu, JY Chen, JC Myers, JP wang et al. APL, 112, 12, 122402

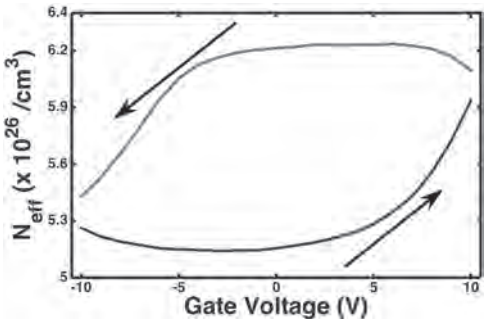

Effective carrier concentration with respect to gate voltage

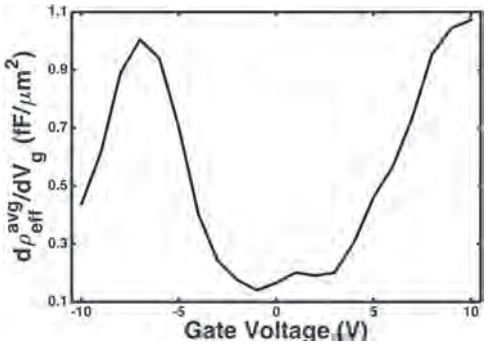

Change in effective surface charge with respect to gate voltage

Session K5
BIOMEDICAL APPLICATIONS II
(Poster Session)

Gaspare Varvaro, Chair
Consiglio Nazionale delle Ricerche, Monterotondo Scalo (RM), Italy

K5-01. Advancements in the Receive Hardware for the Single Sided Magnetic Particle Imaging Scanner. J.D. Pagan[1], C. McDonough[1], J. Lin[2] and *A. Tonyushkin*[1] *1. Physics Department, University of Massachusetts Boston, Boston, MA, United States; 2. Engineering Department, University of Massachusetts Boston, Boston, MA, United States*

Magnetic Particle Imaging (MPI) is an emerging tracer-based biomedical imaging modality[1]. MPI is a sensitive technique for imaging the distribution of superparamagnetic iron oxide nanoparticles (SPIO) without use of ionizing radiation, which makes it very promising in certain clinical applications, such as an angiography and cancer screening. Most MPI scanners employ a cylindrical geometry, enclosing the small subject, however such a geometry has prevented extending this technology to humans. Our single-sided device[2] utilizes a unilateral geometry allowing imaging of small animals or a region of interest in humans, e.g., breast imaging. In our device, a field-free line for mapping the distribution of the SPIO is generated by two elongated selection coils, a strong excitation magnetic field is generated by an elongated transmission coil, and the SPIO response is simultaneously detected by a surface receive coil. Traditionally, solenoid gradiometer is used to effectively reject excitation feedthrough voltage in the receive coil. However, solenoid geometry cannot be readily accommodated in the single-sided design. Thus, feedthrough saturation persists, concealing the small SPIO response, impinging potential sensitivity gain. Here we present the first implementation of gradiometer receive coil configurations in a single-sided MPI device with the purpose of removing feedthrough, whilst preserving the SPIO signal. Experimental data of the first order gradiometer effect, by means of polarity reversal exploitation, indicate a decrease in feedthrough by an order of 2 compared to the collinear receive coil configuration. Further implementation of the second-order gradiometer, by means of dual coil cancelation, result in a 4-fold increase in receive sensitivity over the first-order gradiometer. Numerical simulations and experimental data indicate higher sensitivity of the device over previous receive coil designs as well as a new SPIO limit of detection for our device.

1. B. Gleich and J. Weizenecker, "Tomographic imaging using the nonlinear response of magnetic particles," *Nature*, vol. 435, no. 7046, pp. 1214–1217, 2005. 2. A. Tonyushkin, "Single-Sided Field-Free Line Generator Magnet for Multi-Dimensional Magnetic Particle Imaging," *IEEE Transactions on Magnetics*, vol. 53, no. 9, 2017.

K5-02. Effects of PEGylated Fe/Fe3O4 Core Shell Nanoparticles on Cancer Cells. *B.H. Domac*[1], S. Alkhatib[1], O. Zirhli[2], N. Gunduz Akdogan[3], G. Bulut[1] and O. Akdogan[1] *1. Bahcesehir Universitesi Muhendislik ve Doga Bilimleri Fakultesi, Istanbul, Turkey; 2. Sabanci Universitesi Muhendislik ve Doga Bilimleri Fakultesi, Istanbul, Turkey; 3. Piri Reis Universitesi, Istanbul, Turkey*

Metallic-based nanoparticles have been investigated extensively for their robustness, effectiveness and the potential functionalization of their surface. Especially, magnetic nanoparticles with their distinctive characteristics are widely used in bioassays and magnetic drug delivery systems in biomedical applications as an anti-cancer agent. In this study, Fe/Fe3O4 core-shell nanoparticles (13-20nm) (Figure 1), coated with PEG, have been successfully synthesized by Y-junction flow tube technique. The room temperature coercivity was found to be 350 Oe. A549 non-small cell lung cancer and NIH3T3 mouse embryonic fibroblast cell lines were used to monitor cellular toxicity (IC50) and proliferation effects of PEG-ylated Fe/Fe3O4 nanoparticles. The inhibitory potential on the cell motility of A549 cancer cells were higher than NIH3T3 cells. The results showed that the toxic effect of particles was higher on cancer cells. Upon examination, IC50 values were found to be 27.5 μg/ml and 1 μg/ml for NIH3T3 cell and A549 cell, respectively. (Figure 1 a and b) The nanoparticles were found to be 100 times more toxic on cells when compared to the previous studies. According to the results, PEG-ylated Fe/Fe3O4 nanoparticles not only have significantly lower IC50 values compared to similar research but also they could be used in diagnosis, magnetic hyperthermia and various drug systems as a treatment method against cancer. This work was supported by BAP.2018-2.05

Domac, B. H., AlKhatib, S., Zirhli, O., Akdogan, N. G., Öcal Dirican, S. C., Bulut, G., & Akdogan, O., *Effects of PEGylated Fe–Fe3O4 core-shell nanoparticles on NIH3T3 and A549 cell lines. Heliyon, 6(1),* (2020).

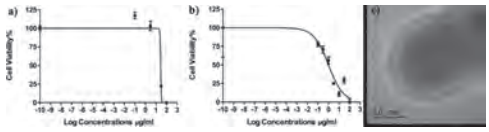

Fig. 1. Cell viability versus concentration plots of the nanoparticles at 0, 100 ng/ml, 300 ng/ml, 1 μg/ml, 3 μg/ml, 10 μg/ml, 30 μg/ml and 100 μg/ml concentrations on (a) NIH3T3 cells and, (b) A549 cells respectively, (c) TEM bright field image of the core-shell nanoparticle.

K5-03. Effect of Applied Magnetic Field on Permeability and Heating Efficiency of Multifunctional Micro/Nano-Magnetic Particles for Hyperthermia Therapy. *L. Ton That*[1], Y. Yamamoto[2], K. Mitobe[3] and S. Yabukami[1] *1. Department of Electrical Engineering, Tohoku University, Sendai, Japan; 2. Department of Systems Design Engineering, Akita University, Akita, Japan; 3. Department of Mathematical Science and Electrical-Electronic-Computer Engineering, Akita University, Akita, Japan*

Magnetic hyperthermia is a promising cancer therapy utilizing heat generation from magnetic particles subjected to a high-frequency magnetic field to kill cancer cells. In previous studies, we succeeded in developing a multifunctional mixture of micro/nano-magnetic particles with high heating efficiency for hyperthermia treatment and considerable permeability change around a therapeutic temperature of 40-45°C for wireless temperature measurement [1]. It is well reported that the specific absorption rate (SAR) of superparamagnetic nanoparticles which is mainly ascribed to relaxation loss is linearly proportional to the square of magnetic field amplitude H^2 and frequency f, but little is known about the mixture of micro/nano-magnetic particles. For this reason, in this study, we examined its heating efficiency as well as permeability when there was a change in the magnetic field amplitude and frequency used for hyperthermia using the experimental setup in Fig. 1. The change in magnetic flux density around the sample resulting from its permeability was measured by a pickup coil (i.e. pickup voltage V_P). The samples used were the mixture consisted of 0.7 g of the previously-developed ferromagnetic implant with low Curie temperature (FILCT, the average particle size of 83.6 μm and Curie point of 45°C) which was mixed with 0.3 mL of Resovist® (average particle size of 3.6 nm) at a preferred mixing rate (volume fraction of nanoparticles of 0.5%), 0.7 g of FILCT, and 0.3 mL of Resovist®. In Fig. 2, the intensity of magnetization ($\mu_0 M$) calculated from pickup voltage (at 20°C) was linearly proportional to the amplitude,

whereas it remained almost unchanged with the frequency. The SARs of the mixture, FILCT, and Resovist® were dependent on the amplitude with the power factor of 1.68, 1.78, 2.09, whereas they were linearly proportional to the frequency. The results obtained here may enable us to find the optimal conditions of the applied magnetic field or the dosage of particles required for hyperthermia under the specific condition of the applied magnetic field.

[1] L. Tonthat *et al*., *IEEE Trans. Magn.*, Vol. 54, No. 7, p. 5400506 (2018)

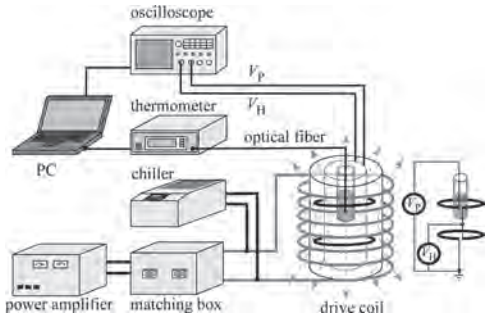

Fig. 1 Experimental setup.

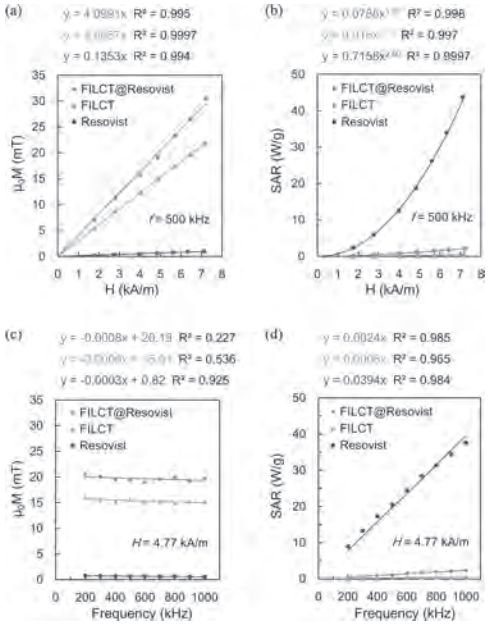

Fig. 2 Magnetic field dependence of magnetization resulting from the samples at 20°C, and the specific absorption rate of the samples.

K5-04. Iron Carbide Nanoparticles for Multimodal Hyperthermia Heating. M. Xing[1], *J. Mohapatra*[1], J. Beatty[1], J. Elkins[1], A. Chalise[1], W. Chen[1], M. Jin[1] and P. Liu[1] *1. Department of Physics, The University of Texas at Arlington, Arlington, TX, United States*

Localized induction heating using magnetic nanoparticles under an alternating magnetic field and photothermal therapy based on gold or silver plasmonic nanostructures are becoming very promising supplementary techniques to the well-established cancer treatments such as radiotherapy and chemotherapy.[1, 2] The efficiency of both techniques for cancer treatment has been studied separately by making their respective nanostructures. As singular thermal therapy showed some limitations, there have been tremendous efforts to synthesize homogeneous nanocrystals with synergistic heat contributions from photothermal effects and magnetic hyperthermia. Here, we demonstrate that iron carbide (Fe_5C_2) nanoparticles with a thin carbon shell (see Figure 1a) have the collective inductive heating and photothermal effects based on the magnetic and photonic properties. In accordance with the linear response theory, the inductive heating properties reveal a specific absorption rate (SAR) maximum of about 30 W/g at concertation of 4 mg/ml.[3] In addition, exposure of Fe_5C_2 nanoparticle suspension to near-infrared laser irradiation (808 nm) yields an unprecedented SAR up to 166 W/g (see Figure 1b), which is 5 folds higher than that obtained by magnetic induction alone. More importantly, the SAR values observed for the magnetite nanoparticles of equivalent size are lower than those of the Fe_5C_2 nanoparticles. The enhanced heating efficiencies in Fe_5C_2 nanoparticles are attributed to the high saturation magnetization and surface-enhanced IR absorption resulted from the carbon coating.

[1] J. Mohapatra, M. Xing, J.P. Liu, Materials, 12 (2019) 3208. [2] J. Mohapatra, M. Xing, J. Beatty, J. Elkins, T. Seda, S.R. Mishra, J.P. Liu, Nanotechnology, 31 (2020) 275706. [3] J. Mohapatra, F. Zeng, K. Elkins, M. Xing, M. Ghimire, S. Yoon, S.R. Mishra, J.P. Liu, Phys. Chem. Chem. Phys., 20 (2018) 12879-12887.

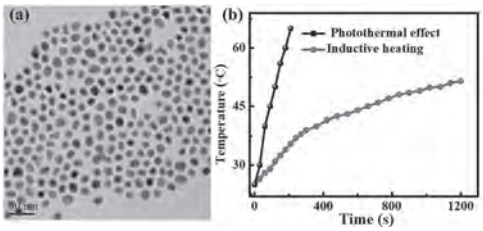

Figure 1. (a) TEM micrograph of Fe_5C_2 nanoparticles synthesized via thermal decomposition of iron pentacarbonyl. (b) Temperature changes of Fe_5C_2 nanoparticles suspension under NIR irradiation (808 nm, 0.8 W/cm^2) and AC magnetic field (amplitude of 184 Oe and frequency of 265 kHz).

K5-05. Core-Shell ZnO@Fe_3O_4 Nanostructure for Magnetic Hyperthermia and Bio-Imaging Applications. *J. Gupta*[1], P. Hassan[1] and k. Barick[1] *1. Chemistry, Bhabha Atomic Research Centre, Mumbai, India*

Combining two materials having different functional properties has become a current research area for biomedical applications. The progress of nanoplatforms brings a new non-invasive imaging and therapeutic tools for cancer. Here, biocompatible and multifunctional magnetic Fe_3O_4-ZnO core–shell nanostructure has been developed by using a soft chemical approach. Fe_3O_4-ZnO core–shell is well characterized by various sophisticated characterization techniques such as X-ray diffraction (XRD), Transmission electron microscopy (TEM), X-ray photoelectron spectroscopy (XPS), UV-visible absorption, photo-luminescent spectroscopy and physical properties measurement system (PPMS). X-ray diffraction (XRD) confirms the presence of both Fe_3O_4 and ZnO phases. XPS analysis confirms the magnetite phase of Fe_3O_4 nanodots in the core-shell structures. TEM micrograph clearly reveals that 5 nm Fe_3O_4 nanodots are well decorated with ZnO nanoparticles shell. This multi-functional approach will facilitate magnetic targeting and generation of reactive species under an external AC magnetic field, providing therapy a smart therapeutic agent for cancer. Fe_3O_4-ZnO core–shell conserves the intrinsic superparamagnetic behaviour of its constituent Fe_3O_4 with a magnetization value of ~ 36.5 emu/g. The aqueous colloidal stability, optimal magnetization, and good specific absorption rate (under external AC magnetic field) of Fe_3O_4-ZnO core–shell particles perform as an effective heating source for thermal therapy. Cytotoxicity studies exhibit the reduction of cellular viability for human cervical cancer cells (HeLa). Further, A combined effect of thermo-therapy and generation of reactive oxygen species under AC magnetic field results in a synergistic effect on the cancer cell death. Therefore, these results indicate that core–shell is sufficient materials for magnetic hyperthermia and bio-imaging.

1. J. Wan, H. Li, and K. Chen, Materials Chemistry and Physics, 114, 2009, 30-32. 2. H. Zhang, L. Guo, S. Ding, J. Xiong, and B. Chen, Oncotarget. 7, 2016, 36602–36613. 3. K. Patel, B. S. Raj, Y. Chen, and X.Lou, Colloids and Surfaces B: Biointerfaces, 150, 2017, 317–325.

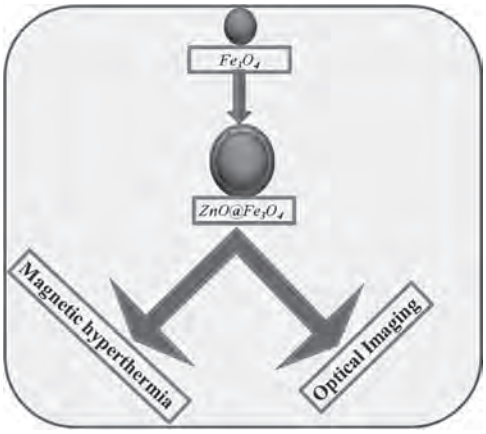

K5-06. Effect of Coil Positioning and Orientation of the Quadruple Butterfly Coil During Transcranial Magnetic Stimulation.
O.F. Afuwape[1,2], P. Rastogi[1] and D.C. Jiles[1] *1. Department of Electrical and Computer Engineering, Iowa State University, Ames, IA, United States; 2. Department of Mechanical Engineering, Iowa State University, Ames, IA, United States*

Transcranial Magnetic Stimulation (TMS) is a non-invasive technique of modulating the neurons of the brain that functions on the principle of electromagnetic induction to treat disorders.[1] TMS, which has been employed in research and clinically, has proven to be a useful tool for the treatment for certain neurological and psychiatric disorders.[2] The modulation of the neurons of the brain is dependent on the magnitude and direction of the electric field (E-Field) induced from the time-varying magnetic field generated from TMS coils. The coil geometry and orientation are known to define the E-Field magnitude and direction and to achieve high effectiveness, and these parameters are required to be optimized.[3] In recent years, researchers have proposed several coil designs for TMS with the aim of achieving focality and deep penetration.[4] Amongst this design is the commercially available Figure-of-Eight Coil and the novel Quadruple Butterfly Coil (QBC).[5] The QBC consists of two sets of coils that are inclined at an angle of 45° to the vertical axis.[6] In this research, the QBC orientation in steps of 15° within a range of ± 60° over the vertex location was modeled using a finite element tool, Sim4life, the maximum electric field intensity (E-Max) and stimulated volume of the brain (V-Half) were computed and compared to determine the optimal coil orientation. Fig. 1 shows the different QBC orientation and the E-Max distribution in the grey matter of the brain.

[1]Zhong, X., Rastogi, P., Wang, Y., Lee, E. G., & Jiles, D. C. (2019). *IEEE Transactions on Magnetics*, *55*(7), 1–5. https://doi.org/10.1109/TMAG.2018.2890069 [2]Chail, A., Saini, R. K., Bhat, P. S., Srivastava, K., & Chauhan, V. (2018). *Industrial Psychiatry Journal*, *27*(2), 172–180. https://doi.org/10.4103/ipj.ipj_88_18 [3]Reijonen, J., Säisänen, L., Könönen, M., Mohammadi, A., & Julkunen, P. (2020). *Journal of Neuroscience Methods*, *331*, 108521. https://doi.org/10.1016/j.jneumeth.2019.108521 [4]Deng, Z.-D., Lisanby, S. H., & Peterchev, A. V. (2013). *Brain Stimulation*, *6*(1), 1–13. https://doi.org/10.1016/j.brs.2012.02.005 [5]Rastogi, P., Lee, E. G., Hadimani, R. L., & Jiles, D. C. (2017). *AIP Advances*, *7*(5), 056705. https://doi.org/10.1063/1.4973604 [6]Rastogi, Priyam (2019), *Iowa State University, Ames, IA, USA,* https://lib.dr.iastate.edu/etd/17547

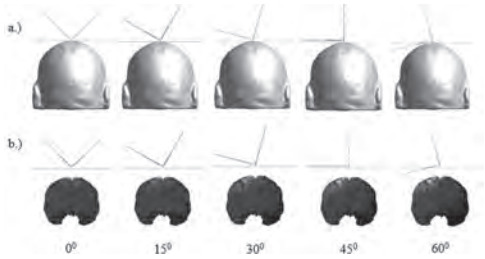

Fig. 1. a.) Quadruple Butterfly Coil (QBC) Orientation over the vertex of the head. b.) Maximum induced electric field intensity (E-Max) in the grey matter of the head model.

K5-07. Coil Design for Simultaneous Dual-Site Transcranial Magnetic Stimulation to Effectively Modulate the Motor Cortex.
J. Boldrey[1], G. Goss[1], A. Boes[2] and D.C. Jiles[1] *1. Electrical and Computer Engineering, Iowa State University, Ames, IA, United States; 2. Departments of Neurology, Psychiatry, and Pediatrics, University of Iowa Carver College of Medicine, Iowa City, IA, United States*

Transcranial Magnetic Stimulation (TMS) is a neuromodulation technique that non-invasively activates neurons in the brain. During TMS, a pulse (or multiple pulses) of a time-varying magnetic field is delivered to the brain. The time-dependent H field induces an electric field in the brain which, at sufficient levels, causes neurons to depolarize. One of the persistent challenges in the development of TMS therapy is avoiding the unnecessarily stimulation of surrounding areas while delivering a sufficiently strong H field to the target area. Dual-site paired-pulse TMS (dsppTMS) is a method of stimulating two locations of the brain simultaneously or with a slight delay of a few milliseconds between the paired stimulations. Multiple studies have used dsppTMS to investigate the interconnectivity between different parts of the brain [1][2]. Additionally, researchers have used dsppTMS to explore therapies for Parkinson's disease, and recovery after stroke [3][4]. We have developed six novel TMS coils that can be used to target small, localized areas of the brain within proximity of, and with minimal interference between, one another (Fig. 1). Each coil targets an area of 2 cm^2 to 4 cm^2 with less stimulation of surrounding regions. This improves the ability to deliver dsppTMS using a personalized network of nodes using an individuals' own fMRI results. This will result in more effective modulation, specifically of the motor cortex, than present methods provide.

[1] L.P. Lafleur et al, "Assessment of Effective Connectivity and Plasticity With Dual-Coil Transcranial Magnetic Stimulation," Brain Stimul., vol. 9, no. 3, pp. 347–355, 2016, doi: 10.1016/j.brs.2016.02.010. [2] S. Schintu et al., "Paired-pulse parietal-motor stimulation differentially modulates corticospinal excitability across hemispheres when combined with prism adaptation," Neural Plast., vol. 2016, 2016, doi: 10.1155/2016/5716179. [3] C. Fricke et al., "Dual-Site Transcranial Magnetic Stimulation for the Treatment of Parkinson's Disease," Front. Neurol., vol. 10, no. March, pp. 1–9, 2019, doi: 10.3389/fneur.2019.00174. [4] J. Lee et al., "Modulating brain connectivity by simultaneous dual-mode stimulation over bilateral primary motor cortices in subacute stroke patients," Neural Plast., vol. 2018, 2018, doi: 10.1155/2018/1458061.

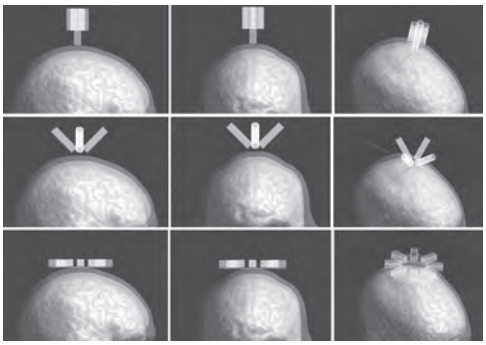

Fig. 1. Three examples of coil designs and a simulation head model in Sim4Life software. Different views of three designs show the side view (left in column), frontal view (center column), and one-quarter top view (right column).

K5-08. Modification of Thiol Groups on Magnetic Nanoparticles for Theranostics. H. Katayanagi[1], S. Hamada[1], A. Usui[3], Y. Hosokai[4] and *Y. Ichiyanagi[1,2] 1. Physics, Yokohama National University, Yokohama, Japan; 2. Research Center for Thermal and Entropic Science, Osaka University, Toyonaka, Japan; 3. School of Medicine, Tohoku University, Sendai, Japan; 4. International University. of Health and Welfare, Otawara, Japan*

$Co_{1-x}Mg_xFe_2O_4$(x = 0.0, 0.2, 0.4, 0.6, 0.8, 1.0)nanoparticles surrounded by amorphous SiO_2 with particle sizes around 5 nm were prepared by an original wet chemical method. Furthermore, in order to develop the particles for conjugation with proteins, thiol group was modified. These particles were further confirmed as an agent for hyperthermia treatment. The heat dissipation characteristics of the particles were investigated by measuring AC magnetic susceptibility and the relationship between the imaginary part of AC magnetic susceptibility χ'' and the increase in temperature in the AC field was estimated. We have carried out spin echo MRI measurements for $Co_{1-x}Mg_xFe_2O_4$ nanoparticles using a 0.3-T MRI system. The particles showed drastic T_2 shortening effect comparing to agarose as background depending on the composition. All the particles showed effective relaxivity, R_2 values and significant contrast was observed in the phantom image. These particles are expected for future agents for theranostics.

[1] T. Kondo, K. Mori, M. Hachisu, T. Yamazaki, D. Okamoto, M. Watanabe, K. Gonda, H. Tada, Y. Hamada, M. Takano, N. Ohuchi, and Y. Ichiyanagi, *J. Appl. Phys*. 11717D157 (2015). [2] D. Shigeoka, T. Yamazaki, T. Ishikawa, K. Miike, K. Fujiwara, T. Ide, A. Usui, Y. Hosokai, H. Saito and Y. Ichiyanagi, *IEEE Trans. Magn.*, 54 6100707 (2018).

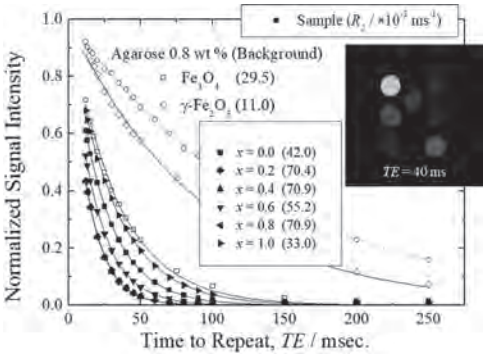

K5-09. Withdrawn

K5-10. An Experimental View on Retinal Receptivity of ELF-Inducing Blindsight-Like Phosphenes. *H. Nakagawa*[1], M. Sugai[1], S. Fujiwara[2] and S. Ueno[3] *1. Tokyo Denki University, Tokyo, Japan; 2. CPCC, Tokyo, Japan; 3. Kyushu University, Fukuoka, Japan*

Background Up to the present, not a few reports have shown the peculiarity that hemispherectomized subjects with blindsight do not receive any input from retinal short (S)-cone (blue-sensitive, 430 nm) photoreceptor cells [1]–[3]. As far as previous information is concerned, considerations for details in the retinal receptivity of the extremely low frequency (ELF)-inducing blindsight-like phosphenes are of great importance. For the expression of S-cone-dependent blindsight, the ELF stimulus specific to the S-cone [4] is expected to take full advantage of the specificity as a significant result of going through the superior colliculus, which is a shortcut route without passing through the V1 (Fig. 1). In this research, a further detailed verification of human reliabilities during the ELF stimuli was carried out. Methodology Human reliability measurements during ELF stimuli were carried out according to the previous method [5]. A small spot was presented randomly within the flicker-perception area into subjects' visual fields. Consequently, the error rates for the spot-detections were recorded on an original form. Hemodynamic changes at the occipital regions were measured using an fNIRS instrument equipped with 4×5 probes (31 ch) which were separated from each other by 30 mm. Results Judging from the results of our fNIRS measurements during the ELF stimuli, the occipital hemodynamics corresponding to the spot-detections were enhanced noticeably when compared with a control ($P < 0.05$). Next, as a proof-of-concept proposal, we performed the observations in the visual fields for the perception. In the results of our analysis using signal detection theory, we did discovered that the supraliminal effect had a certain amount of persistence for the flicker in the central part of the visual fields. Conclusion Our experimental results undoubtedly revealed invaluable findings about a virtual control of retinal activities with ELF-inducing blindsight-like phosphenes, which may be able to provide preventive solutions for serious human errors and/or artificial mistakes.

1) N. Hall and C. Colby, J. Cogn. Neurosci. 26, 1234 (2014). 2) J. Jayakumar *et al.*, Clin. Exp. Optom. 96, 259 (2013). 3) I. Alexander and A. Cowey, Exp. Brain Res. 225, 147 (2013). 4) H. Nakagawa and S. Ueno, IEEE Trans. Magn. 53, 5000604 (2017). 5) H. Nakagawa and S. Ueno, AIP Advances 9, 035216 (2019).

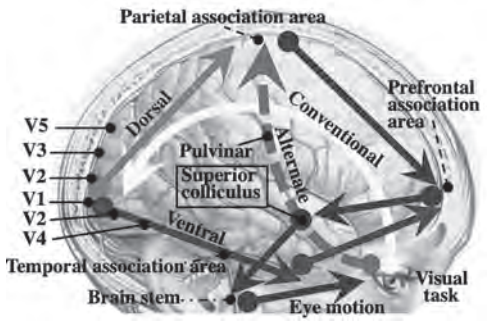

Fig. 1. Integration of visual information with and without primary visual cortex.

K5-11. Methodology for Focality Homogenization in Magnetic Stimulation of Biological Tissues. *I.C. Carmona*[1] and R.L. Hadimani[1,2] *1. Dept. of Mechanical and Nuclear Engineering, Virginia Commonwealth University, Richmond, VA, United States; 2. Dept. of Biomedical Engineering, Virginia Commonwealth University, Richmond, VA, United States*

Transcranial Magnetic Stimulation (TMS) regulates the synaptic activity of neurons to treat several neurological and psychiatric disorders. E-fields are induced by exposing the brain cortex to time-varying B-fields using coils

from outside the head. Different coil geometries are proposed in the literature to increase the focality and minimize the overstimulation beyond the targeted region[1][2][3][4]. However, the most of them differ in measurement methodologies with lack of homogeneity in the focality definition. Some definitions do not consider certain critical factors that influence the coil's capacity to be focal. For instance, many authors define focality in TMS as the cortical area in which the electric field exceeds its 50%. Since the E-field distribution depends on its interaction with the matter (tissue), given by its relative electric permittivity, this variable cannot provide data about intrinsic properties of a coil. Nevertheless, biological tissues show relative magnetic permeabilities close to 1, which do not affect the original magnitude, hence the B-field is more appropriate for this purpose. Another common problem is definitions of "focality" without a focal point or target. Furthermore, to evaluate the degree of magnetic stimulation, a criterion indicating how well the stimulated area overlaps the targeted area is needed. This work proposes a generalized function and methodology for the focality quantification (fig. 1 & 2) considering target area, focal distance, maximum magnitude and stimulation threshold. New definitions are introduced, such as: "specific focal distance" (Z_{fd}); "focality form factor (d_n)"; stimulation threshold (*th) and* "specific focality (*sf*)". They seek to describe the suitability of coils for specific stimulation applications and offer a general framework to compare coils under homogeneous methodology, parameters and nomenclature, with potential impact in the magnetic stimulation standardization.

[1] M. T. Wilson, A. D. Tang, K. Iyer, H. McKee, J. Waas, and J. Rodger, "The challenges of producing effective small coils for transcranial magnetic stimulation of mice," Biomed. Phys. Eng. Express, vol. 4, no. 3, Apr. 2018, doi: 10.1088/2057-1976/aab525. [2] P. Rastogi, E. G. Lee, R. L. Hadimani, and D. C. Jiles, "Transcranial Magnetic Stimulation-coil design with improved focality," AIP Adv., vol. 7, no. 5, May 2017, doi: 10.1063/1.4973604. [3] Z.-D. Deng, S. H. Lisanby, and A. V Peterchev, "Electric field depth-focality tradeoff in transcranial magnetic stimulation: simulation comparison of 50 coil designs.," Brain Stimul., [4] I. P. de Sousa, C. R. H. Barbosa, and E. C. Monteiro, "Safe exposure distances for transcranial magnetic stimulation based on computer simulations," PeerJ, vol. 2018, no. 6, 2018.

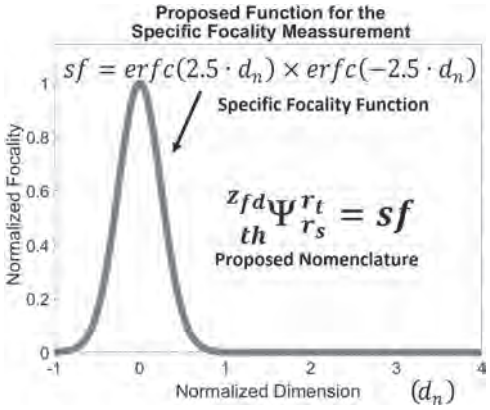

Fig. 1) Specific focality (sf) vs the normalized difference between the targeted and stimulated areas (focality form factor, d_n).

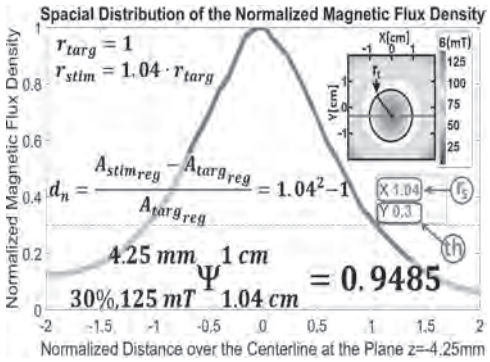

Fig. 2) Normalized B-field of a customized TMS coil for small animals used as an example for the methodology to obtain the stimulated area.

K5-12. Withdrawn

Session L1
MAGNETIC MICROSCOPY AND IMAGING I

Sophie A Morley, Chair
Lawrence Berkeley National Laboratory, Berkeley, CA, United States

INVITED PAPER

L1-01. Frontiers of Magnetic Force Microscopy. *O. Kazakova*[1], R. Puttock[1], C. Barton[1], H. Corte-León[1], M. Jaafar[2], V. Neu[3] and A. Asenjo[2] *1. Quantum Technology, NPL, London, United Kingdom; 2. Consejo Superior de Investigaciones Cientificas, Madrid, Spain; 3. IFW, Dresden, Germany*

Since it was first demonstrated in 1987, magnetic force microscopy (MFM) has become a truly widespread and commonly used characterization technique that has been applied to a variety of research and industrial applications. Some of the main advantages of the method includes its high spatial resolution (typically ~50 nm), ability to work in variable temperature and applied magnetic fields, versatility, and simplicity in operation, all without almost any need for sample preparation. However, the technique has historically provided only qualitative information, and the number of available modes was typically limited, thus not reflecting the experimental demands. We present the recent progress and development of MFM as well as a summary of the current state-of-the-art techniques and objects for study. Aspects including quantitative MFM, the accurate interpretation of the MFM images, new instrumentation, probe-engineering alternatives, and applications of MFM to new (often interdisciplinary) areas of the materials science, physics, and biology are discussed. We outline the importance of the technique in emerging fields including skyrmions, 2D-materials, and topological insulators.

O. Kazakova, et al., 'Frontiers of Magnetic Force Microscopy' J Appl. Phys. 125, 060901 (2019) H. Corte-León, et al., 'Magnetic imaging using geometrically constrained nano-domain walls' Nanoscale 11, 4478 (2019) V. Panchal, et al., 'Calibration of multilayered magnetic force microscopy probes' Sci Reports 7, 7224 (2017) F. Moro, et al., 'Room temperature uniaxial magnetic anisotropy induced by Fe-islands in the InSe semiconductor van der Waals crystal', Advanced Science, 5, 1800257 (2018) H. Corte-León, et al., 'Comparison and validation of different magnetic force microscopy calibration schemes' Small 20, 1906144 (2020) X. Hu, et al., 'Round Robin Comparison on Quantitative Nanometer Scale Magnetic Field Measurements by Magnetic Force Microscopy' J. Magn. Magn Mater. 511, 166947 (2020)

CONTRIBUTED PAPERS

L1-02. New Vortex Core Probe for Magnetic Force Microscopy. J. Soltys[1], I. Vetrova[1], J. Feilhauer[1], *J. Tobik*[1], K. Bublikov[1], V. Cambel[1] and J. Fedor[1] *1. Elektrotechnicky ustav SAV, Bratislava, Slovakia*

We present successful fabrication and demonstration of magnetic vortex core tip (VC) for magnetic force microscopy (MFM). The design of VC probe is based on permalloy disk with diameter of 330nm and thickness of 55nm fabricated on intentionaly blunted tip (see the Fig.1). The ground state of this permalloy disk is the magnetic vortex state with out-of-plane magnetic moment determined by well spatially localized vortex core. The novelty of this design is creation of spatially well localized magnetic out-of-plane field in mechanically blunt tip. This design offers two advantages: First, due to large area of the disk, VC probe has higher wear resistance and longer lifetime than sharp commercial MFM probes. Second, it has very good stability of the out-of-plane magnetic moment, because vortex core is almost independent on the edge imperfections. However, VC probe has also some limitations: the sample should be flat and it should not produce quasi-uniform field in large volume nearby the tip, because the polarization affects vortex core position. We analyze the permalloy tip polarization effect by micromagnetic calculations of MFM images of periodic magnetic strips. By this approach we identify the limits on samples for this new kind of MFM probe.

J. Soltys, J. Feilhauer, I. Vetrova, J. Tobik, K. Bublikov, T. Scepka, J. Fedor, J. Derer, and V. Cambel, Appl. Phys. Lett. 116, 242406 (2020).

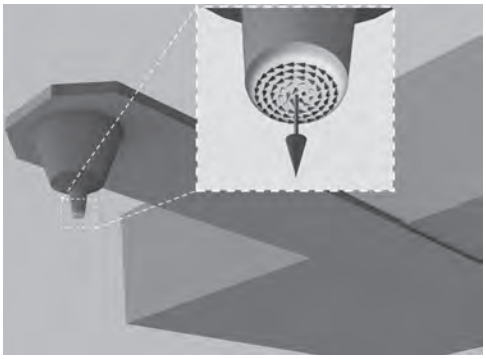

Schematic sketch of VC MFM tip. The magnetically soft disk from permalloy is deposited on the apex of Si tip. In the center of the disk, small vortex core is formed creating well localized out-of-plane magnetic moment (shown as big red arrow).

L1-03. Magnetic Field Induced Half-Hedgehog Spin-Textures in Soft Hemispherical Nanodots. E. Berganza[1,2], M. Jaafar[1,3], J.A. Fernandez- Roldan[1,4], M. Goiriena-Goikoetxea[5,6], J. Pablo-Navarro[7], A. García-Arribas[5,8], K.Y. Guslienko[9], C. Magén[7,10], J. de Teresa[7,10], O. Chubykalo-Fesenko[1] and *A. Asenjo*[1] *1. ICMM-CSIC, Madrid, Spain; 2. Institute of Nanotechnology, KIT, Eggenstein-Leopoldshafen, Germany; 3. Departamento de Física de la Materia Condensada, UAM, Madrid, Spain; 4. Departamento de Física, Universidad de Oviedo, Oviedo, Spain; 5. Departamento de Electricidad y Electrónica, UPV/EHU, Leioa, Spain; 6. Department of Electrical Engineering and Computer Science, University of California Berkeley, Berkeley, CA, United States; 7. Instituto de Nanociencia de Aragon, Zaragoza, Spain; 8. Fundacion BCMaterials - Basque Center for Materials Applications and Nanostructures, Leioa, Spain; 9. Department of Materials Physics, UPV/EHU, Donostia, Spain; 10. ICMA-CSIC, Zaragoza, Spain*

Topologically non-trivial structures such as magnetic skyrmions[1] are nanometric spin textures of outstanding potential for spintronic applications due to their unique features.[2] Néel skyrmions of definite chirality are stabilized in the presence of Dzyaloshinskii-Moriya exchange interaction (DMI) in bulk non-centrosymmetric materials or ultrathin films with strong spin-orbit coupling at the interface. [3,4] In this work, we report the nucleation of a complex three dimentional spin texture, with a half hedgehog skyrmion in the planar base, on a soft magnetic hemispherical-shaped nanodot.[5] As a matter of fact, curvature has been proven to be an element which can

favour the stability of skyrmionic configurations and introduce chirality.[6] The half hedgehog spin-textures are observed at room temperature, in absence of DMI interaction and can be induced and further stabilized by the magnetic field arising from the Magnetic Force Microscopy probe.[7] The half-hedgehog configuration behaves as theoretically predicted under the presence of magnetic field, i.e. Variable Field-Magnetic Force Microscopy measurements show that the core moves parallel or antiparallel to the in-situ applied field, depending on the sign of the radial component of the magnetization. The results are supported by micromagnetic simulations and the 2D topological charge is assessed as a function of the nanodot thickness. Our work implies the existence of a new degree of freedom to create and manipulate complex 3D spin-textures in soft magnetic nanodots and opens up future possibilities to explore their magnetization dynamics.

[1] T. H. R. Skyrme, Nucl. Phys. 31, 556–569 (1962) [2] A. Fert, V. Cros, J. Sampaio, Nature Nanotechnology 8, 152–156 (2013) [3] O. Boulle, J. Vogel, H. Yang, et al. Nat. Nanotechnol., 11 (5), 449–454 (2016) [4] C. Moreau-Luchaire, C. Moutafis, N. Reyren, et al., Nat. Nanotechnol., 11 (5), 444–448 (2016) [5] M. Goiriena-Goikoetxea, A. García-Arribas, M. Rouco, et al., Nanotechnology, 27, 175302 (2016). [6] E. Berganza, J. A. Fernandez- Roldan, M. Jaafar, K. Guslienko, A. Asenjo, O. Chubykalo-Fesenko. In preparation. [7] E. Berganza, M. Jaafar J. A. Fernandez- Roldan, M. Goiriena-Goikoetxea, J. Pablo-Navarro, A. García-Arribas, K. Guslienko, C. Magén, J. M. De Teresa, O. Chubykalo-Fesenko, Agustina Asenjo. Nanoscale, DOI: 10.1039/D0NR02173C (2020)

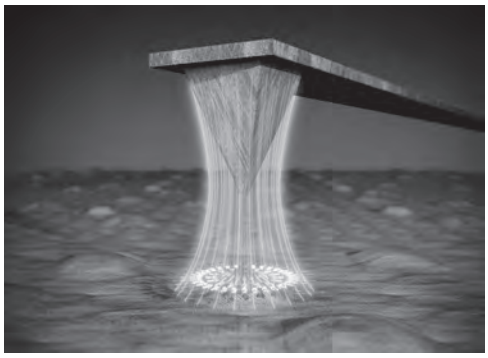

Figure 1: Magnetic Force Microscopy tip inducing a half-skyrmion spin texture in soft magnetic hemispherical nanoparticles.

L1-04. Magnetic Texture Evolution Within Uniaxial Kagome Ferromagnets at Constant Heating/Cooling Rates. *A. Sugawara*[1], T. Akashi[1], M. Kassem[2,3], Y. Tabata[2], T. Waki[2] and H. Nakamura[2]
1. Center for Exploratory Laboratory, Hitachi Ltd, Hatoyama, Japan; 2. Department of Materials Science and Engineering, Kyoto University, Kyoto, Japan; 3. Assiut University Faculty of Science, Assiut, Egypt

Rich variation of magnetic texture attracts attention in connection with topology of electronic structures. The temperature range slightly below Curie temperature (T_c) is interesting, because the contributing micromagnetic energies (demagtization, exchange, Dzyaloshinsky-moriya and anisotropy) change rapidly with temperature. Recently we reported bubble domain formation immediately below T_c within a kagome ferromagnet $Co_3Sn_2S_2$ (T_c=176 K) in which anomalous high-temperature, low-field magnetic phase occurred [1]. Self-reorganization of domain walls (DWs) occurred even at zero field, and the domain evolution was dependent not only on temperature and field but also on temperature variation rate [2]. To examine such domain evolution associated with slow spin dynamics, we developed a method to record Lorentz images continuously at a fixed time interval when a specimen is heated/cooled at a constant rate, not like an usual manner to wait until thermal drift settles down. We applied it to examine domain evolution within another uniaxial kagome magnet, Fe_3Sn_2 (T_c= 657 K), in the temperature range at 303-673 K under no external field. A psuedo-three-dimensional (x-y-time (temperature)) image was constructed from a series of drift-corrected Lorentz images. Fig. 1 shows a cross-section image including time-axis, exhibiting time(temperature) evolution of the magnetic domains. The stripe domain stricture was very stable between room temperature (RT) and 620 K at which DW contrast disappeared due to reduced magnetization both on heating and cooling across T_c, although interesting temperature-dependent texture such as skyrmionic bubble was observed for the alloy below RT. It was also found that the domain structure was nearly independent of cooling/heating rate. The differece in domain evolution between Fe_3Sn_2 and $Co_3Sn_2S_2$ is explained in terms of DW creep associated with thermal depinning in $Co_3Sn_2S_2$.

[1] M. A. Kassem et al., Phys. Rev. B 96, 014429 (2017). [2] Akira Sugawara et al., Phys. Rev. Mater. 3, 104421 (2019)

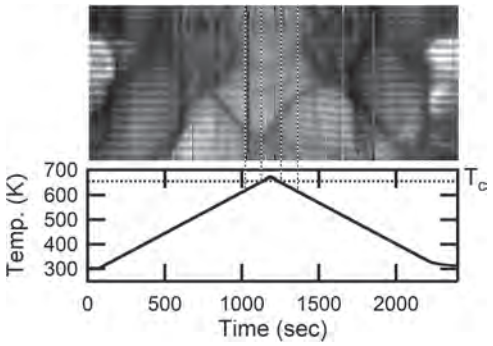

Fig.1 (top) A Y-time slice of a pseudo 3D image exhibiting temperature-dependent domain structure and (bottom) a temperature-time profile. Horizontal black and white stripes with a constant period are DW images, while the broad black bands bending along time axis are non-magnetic contrast (bend contours).

L1-05. Using Time-Resolved SEMPA Imaging to Reveal the Dynamics of Multiple Competing Switching Pathways Using Just a Single Measurement. *R.M. Reeve*[1], D. Schönke[1], H. Stoll[2,1] and M. Klaui[1]
1. Johannes Gutenberg Universitat Mainz, Mainz, Germany; 2. Max-Planck-Institut fur Intelligente Systeme, Stuttgart, Germany

Functional reliability is a major issue when determining whether spintronic devices based e.g. on domain wall motion will be ready for the market. This includes the requirement for stable magnetic states and reproducible switching between those states. In general, it is difficult to understand stochastic processes experimentally and detect rare events that might lead to errors. Pump-probe techniques are frequently employed for dynamic magnetic imaging based on billions of repetitions with the resulting images showing an average of all events that occurred, but conventionally no quantitative information concerning the reliability of the observed pathways for the switching is determined. In this work, we employ a recently developed scanning electron microscopy with polarization analysis system that offers pump-probe imaging with ns temporal resolution [1] to demonstrate a novel approach to determine details of competing magnetic states and dynamic switching pathways [2]. The experiments are supported by micromagnetic simulations. We investigate domain wall based switching [3] and chirality control in asymmetric Py half-ring pairs via temperature dependent dynamic imaging. Understanding and controlling the switching behavior of such elements is vital for reliable operation of possible devices such as data storage, logic elements and sensors [4-6]. The demonstrated reliability of chirality control by curvature could be of used for chirality-encoded DW logic [7]. The results allow us to extract details of stochastic pathways and determine the probabilities of the various processes occurring, as well as the effectiveness of the DW chirality protection in the system. Our results reveal details of the rare thermally activated processes that lead to different dynamic switching events. Furthermore, the attraction of vortex DWs in adjacent wires is found to play an important role in stabilizing the switching pathways. With this approach, we are able to overcome some of the limitations

of conventional pump-probe imaging and establish a tool to additionally reveal the dynamics of systems that exhibit multiple switching pathways using just a single measurement.

[1] D. Schönke, R. Reeve and M. Kläui, Rev. Sci. Instrum., Vol. 89, p. 083703 (2018) [2] D. Schönke, R. Reeve and M. Kläui, https://arxiv.org/abs/2006.11271 [3] M.-A. Mawass, R. Reeve and M. Kläui, Phys. Rev. Applied, Vol. 7, p. 044009 (2017) [4] M. Diegel, R. Mattheis and E. Halder, Sens. Lett., Vol. 5, p. 118 (2007) [5] D. Allwood, G, Xiong and R. P. Cowburn, Science, Vol. 309, p. 1688 (2005) [6] X. Han, Z. C. Wen and D. P. Liu, IEEE Trans. Magn. Vol. 47, p. 2957 (2011) [7] K. Omari, R. C. Bradley and T. J. Hayward, Appl. Phys. Lett. Vol. 107, p. 222403 (2015)

L1-06. Imaging Magnetic Domains at the Surface of Fe_3O_4(001) Using a Spin-Polarised Metastable Helium Beam. *P. Bentley*[1,2], R.F. Evans[1], X. Sun[3], M. Kurahashi[2], A. Pratt[1] and Y. Yamauchi[2] *1. Department of Physics, University of York, York, United Kingdom; 2. National Institute for Materials Science, Tsukuba, Japan; 3. University of Science and Technology of China, Hefei, China*

Here we present the first results from a new method of imaging surface magnetic spin structures based on the use of a spin-polarised beam of metastable helium atoms. As we demonstrate, spin-polarised metastable emission electron microscopy (SPMEEM) offers unrivalled surface sensitivity in mapping surface magnetic domains so that it provides a novel and timely addition to other electron emission microscopy techniques based on low-energy electrons (SPLEEM) and photoemission (X-PEEM) [1]. Magnetic domains form to minimise the magnetic free energy of a material determined by a balance of competing exchange interactions, anisotropies, and stray fields. The broken symmetry at the surface of a material introduces sub-coordinated atoms and lower-order magnetocrystalline anisotropy terms meaning that surface anisotropies are often very different to the bulk. Weak surface anisotropy can lead to out-of-plane magnetization (spin canting) whilst a stronger surface anisotropy, often arising from confinement and spin-orbit effects, can lead to perpendicular magnetic anisotropy. With such a variety of magnetic phenomena, imaging domains and domain walls is essential in order to understand and control spin structures. SPMEEM achieves this by using a beam of spin-polarized metastable helium 2^3S atoms which de-excite at the topmost region of a surface through one of two Auger processes emitting an electron from the atom-surface system. To probe magnetic domains, images are obtained for He 2^3S spins aligned parallel and antiparallel to a specified magnetization direction [2]. A pixel-by-pixel asymmetry signal is calculated that is proportional to the scalar product of the surface magnetization and the He 2^3S spin polarization vectors producing bright and dark regions (see Figure). We demonstrate SPMEEM by investigating surface anisotropy at the surface of Fe_3O_4(001) [3-5], highlighting the effectiveness of this new technique and how it shows potential for the study of other exotic spin textures, proximity effects, and spin canting in key magnetic materials and nanostructures.

[1] E. Bauer, *LEEM, SPLEEM, and SPELEEM*, in *Springer Handbook of Microscopy*, P. W. Hawkes and J. C. H. Spence (Eds)., Springer 2019. [2] A. Pratt, M. Kurahashi, X. Sun *et al*., Phys. Rev. B 85, 180409R (2012). [3] L. Martin-Garcia, G. Chen, Y. Montana *et al*., Sci. Rep. 8, 5991 (2018). [4] Z. Y. Li, M. Jibran, X. Sun *et al*., Phys. Chem. Chem. Phys. 20, 15871 (2018). [5] X. Sun, A. Pratt, and Y. Yamauchi, Phys. Chem. Chem. Phys. 17, 15386 (2015).

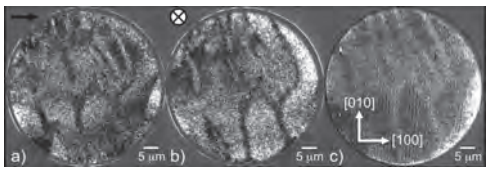

(a) In-plane SPMEEM, (b) out-of-plane SPMEEM, and (c) ultraviolet magnetic circular dichroism images from the surface of Fe_3O_4(100). Field of view: 50 µm.

INVITED PAPER

L1-07. Imaging non-Collinear Antiferromagnetic Textures via Single Spin Relaxometry. *A. Finco*[1] *1. Laboratoire Charles Coulomb, Université de Montpellier and CNRS, Montpellier, France*

Antiferromagnets attract a great interest for spintronics owing to the robustness of their magnetic textures and their fast dynamics. However, since they exhibit no net magnetization, antiferromagnets are challenging to work with. NV-center magnetometry, which provides a sensitivity of a few µT/$Hz^{-1/2}$ combined with a nanoscale spatial resolution, has emerged in the last years as a powerful technique to investigate them [1]. Here we introduce a new imaging mode of the NV-center magnetometer which does not rely on the measurement of the static magnetic stray field but on the detection of magnetic noise originating from spin waves inside the non-collinear antiferromagnetic textures of interest. The presence of magnetic noise accelerates the NV spin relaxation. As a consequence, the emitted photoluminescence is reduced, allowing a simple detection of the noise sources [2]. We demonstrate this new technique on synthetic antiferromagnets (SAF) [3] consisting of two ferromagnetic Co layers antiferromagnetically coupled through a Ru/Pt spacer. We first image domain walls and prove that we perform noise-based imaging by measuring a shorter NV spin relaxation time above an antiferromagnetic domain than above a domain wall. Calculations of the spin waves dispersion both in the antiferromagnetic domains and in the domains walls as well as maps of simulated magnetic noise intensity enable us to conclude that the noise which we probe arises from spin waves channelled in the domain walls. Going further, we tune the composition of the SAF stacks in order to stabilize spin spirals or antiferromagnetic skyrmions. In both cases, our relaxometry-based technique is able to image the non-collinear structures, demonstrating its efficiency and opening new avenues of exploration in the characterization of complex structures in magnetically-compensated materials. This work was performed in collaboration with the UMR CNRS/Thalès and the Center for Nanoscience and Nanotechnology (C2N) in Palaiseau, France. It has received funding from the European Union's Horizon 2020 research and innovation programme under the Marie Sklodowska-Curie grant agreement No 846597 and from the DARPA TEE Program.

[1] I. Gross et al, Nature, Vol 549, p 252 (2017) [2] A. Finco et al, arXiv:2006.13130 (2020) [3] W. Legrand et al, Nature Materials, Vol 19, p 34 (2020)

CONTRIBUTED PAPERS

L1-08. NV^- Center Magnetometry Using Sequential Bayesian Experiment Design. *S. Dushenko*[2,1], K. Ambal[3,4] and R.D. McMichael[2] *1. Institute for Research in Electronics and Applied Physics, University of Maryland, College Park, College Park, MD, United States; 2. Physical Measurement Laboratory, National Institute of Standards and Technology, Gaithersburg, MD, United States; 3. Institute for Research in Electronics and Applied Physics, University of Maryland, College Park/NIST, College Park, MD, United States; 4. Wichita State University, Wichita, KS, United States*

In wide-range magnetometry using optically detected magnetic resonance of NV^- centers, we demonstrate more than order-of-magnitude speedup with sequential Bayesian experimental design as compared with conventional frequency-swept measurements. The NV^- center is a quantum defect with spin 1 and coherence time up to several milliseconds at room temperature. Zeeman splitting of the NV^- energy levels allows detection of the magnetic field via photoluminescence. NV-center is an excellent platform for magnetometry with potential spatial resolution down to few nanometers and demonstrated sensitivity down to nT/$Hz^{1/2}$. We used a commercially available type IIa single crystal diamond grown by chemical vapor deposition (CVD). Green laser with 520 nm wavelength was used to optically

excite NV^- center, and a microstrip line was used to supply microwaves to manipulate spin state of the NV^- center. For each data point, photons were counted for 50 ms. Measurement of each data point was followed by 50 ms measurement of a reference data point with microwaves switched off. The combination of laser power, microwave power and counting time produced measurements with a signal-to-noise ratio on the order of 1. Moreover, the magnetic field was slightly misaligned from the NV^- center axis to produce a three-dip signal. Such experimental setup showcased ability of sequential Bayesian experiment design to locate and measure complex multiple-peak signal even in extremely noisy data and showed its broad dynamical range for sensitivity. Using the measurement described above, we compare conventional magnetic field measurements of fluorescence that use pre-determined sweeps of the microwave frequency with the measurement using a Bayesian inference methodology. In sequential Bayesian experiment design, the frequency of each measurement is determined in real-time from utility predictions based on the accumulated experimental data. We report more than order-of-magnitude speedup in magnetic field and hyperfine splitting determination with sequential Bayesian experimental design, compared with the conventional NV^- magnetometry measurement.

L1-09. Antiferromagnetic Spin Cycloidal Orders Imaged With a Commercial Scanning Nitrogen-Vacancy Magnetometer. *H. Zhong*[1], A. Stark[1], F. Favaro[1] and P. Maletinsky[1] *1. Qnami AG, Muttenz, Switzerland*

Antiferromagnetic thin films attract significant interest for future low-power spintronic devices. They are largely insensitive to external magnetic fields, exhibit domains with negligible cross-talk and can be switched at THz frequencies [1]. Furthermore, in multiferroics where antiferromagnetism can coexist with ferroelectricity, it is possible to control the magnetic state electrically - a particularly appealing feature for future device applications. In this talk, we show how the Qnami ProteusQ^{TM} -- a commercial room temperature scanning nitrogen-vacancy magnetometer (SNVM) -- can be used to quantitatively image antiferromagnetic spin textures with proven DC field sensitivity ≤ 2 μT/√Hz. We image the spin cycloid of a multiferroic bismuth ferrite ($BiFeO_3$) thin film and extract a period of about 103 nm, indicative of a type II spin cycloid. [2] In addition, we take advantage of the quantitative nature of SNVM to extract an average magnetic moment density of 0.08 ±0.02 μ_B /Fe in the $BiFeO_3$ film. These findings agree well with reported vibrating sample magnetometer results (M_S = 0.06 μ_B /Fe) on similar, strained $BiFeO_3$ thin films. [3] Our results shed light on future design requirements for reconfigurable nanoscale spin textures in such multiferroic systems.

[1] V. Baltz, *et al.*, Rev. Mod. Phys. 90, 015005 (2018) [2] A. Haykal, *et al.*, Nat. Commun. 11, 1704 (2020) [3] W Eerenstein, *et al.*, Science 307, 1203a (2005)

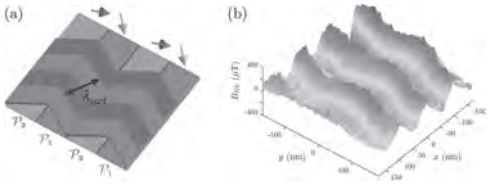

Figure: (a) Schematic antiferromagnetic spin cycloids in alternating ferroelectric domains with a surface propagation wavelength of λ_{surf}, (b) Quantitative SNVM results on 40 nm thick epitaxially grown $BiFeO_3$ thin film with tensile strength of ~ +0.5%.

L1-10. Magnetic Singularities Topological Charge Experimentally Revealed via Soft X-Ray Tomography. *A. Hierro-Rodriguez*[1,2], C. Quiros[1,2], A. Sorrentino[3], L. Alvarez Prado[1,2], J. Martín[1,2], J. Alameda[1,2], S. McVitie[4], E. Pereiro[3], M. Velez[1,2] and S. Ferrer[3] *1. Physics, Universidad de Oviedo, Oviedo, Spain; 2. CINN (CSIC-Universidad de Oviedo), El Entrego, Spain; 3. Experiments, CELLS, ALBA Synchrotron, Cerdanyola del Valles, Spain; 4. School of Physics and Astronomy, University of Glasgow, Glasgow, United Kingdom*

Future perspectives in Spintronics and 3D Nanomagnetism are related to the exploration and comprehension of topologically protected magnetization configurations which can be key for applications as well as bring novel interesting phenomena [1-3]. However, these topologically non-trivial textures are fully three-dimensional in nature, which requires for their study adequate experimental methods. In this framework, X-ray tomography-based approaches with high lateral resolution and large penetration depth are an excellent choice [4,5]. Here we have experimentally demonstrated the capabilities of magnetic soft X-ray transmission tomography by reconstructing the complex magnetization of a $Ni_{80}Fe_{20}/NdCo_5/Ni_{80}Fe_{20}$ heterostructure [6]. The system presents weak perpendicular magnetic anisotropy allowing for the formation of stripe domains and supporting magnetic non-trivial topological configurations [7,8]. After reconstruction, a Bloch point and a Meron-like texture have been identified, and the experimental volume-resolved topological charge map has been computed allowing to get further insight on the formed singularities. The results show the potential of the technique as a unique tool for experimental magnetic 3D characterization of arbitrary systems and heterostructures which could be of great interest for Spintronics, 3D Nanomagnetism and the broader magnetism community. Authors acknowledge the support from Generalitat de Catalunya (Spain), Spanish MICINN (FIS2016-76058, PID2019-104604RB (AEI/FEDER, UE)). A. Hierro-Rodriguez and S. McVitie acknowledge the support from the European Commission under the Marie-Sklodowska-Curie Actions H2020-MSCA-IF-2016-746958.

[1] A. Fert, V. Cros and J. Sampaio, Nature Nanotechnology 8, (2013) 152-156. [2] A. Fernandez-Pacheco, R. Streubel, O. Fruchart, R. Hertel, P. Fischer and R.P. Cowburn, Nature Communications 8, (2017) 15756. [3] D. Sánz-Hernández, A. Hierro-Rodríguez, C. Donnelly, J. Pablo-Navarro, A. Sorrentino, E. Pereiro, C. Magén, S. McVitie, J.M. de Teresa, S. Ferrer, P. Fischer and A. Fernández-Pacheco, arXiv:2001.07130, ACS Nano (accepted). [4] C. Donnelly, M. Guizar-Sicarios, V. Scagnoli, S. Gliga, M. Holler, J. Raabe and L.J. Heyderman, Nature 547, (2017) 328-331. [5] A. Hierro-Rodriguez, D. Gursoy, C. Phatak, C. Quiros, A. Sorrentino, L.M. Alvarez-Prado, M. Velez, J.I. Martin, J.M. Alameda, E. Pereiro and S. Ferrer, J. Synchrotron Radiat. 25, (2018) 1144-1152. [6] A. Hierro-Rodríguez, C. Quirós, A. Sorrentino, L.M. Álvarez-Prado, J.I. Martín, J.M. Alameda, S. McVitie, E. Pereiro, M. Vélez and S. Ferrer, arXiv:1907.01261. [7] C. Blanco-Roldan, C. Quiros, A. Sorrentino, A. Hierro-Rodriguez, L.M. Alvarez-Prado, R. Valcarcel, M.Duch, N. Torras, J. Esteve, J.I. Martin, M. Velez, J.M. Alameda, E. Pereiro and S. Ferrer, Nature Communications 6, (2015) 8196. [8] A. Hierro-Rodriguez, C. Quiros, A. Sorrentino, C. Blanco-Roldan, L.M. Alvarez-Prado, J.I. Martin, J.M. Alameda, E. Pereiro, M. Velez and S. Ferrer, Phys. Rev. B 95, (2017) 014430.

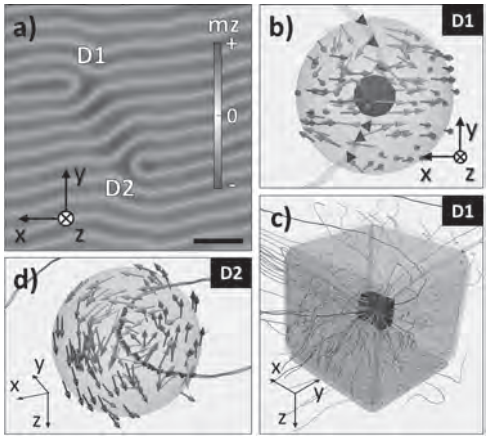

Fig. 1 a) Reconstructed mz magnetization slice showing stripe dislocations D1 and D2 (scale bar 520 nm). b) Magnetization configuration of the Bloch point at dislocation D1. c) Streamlines of the "emergent" field generated by the Bloch point singularity. d) Magnetization of the Meron-like texture at dislocation D2.

L1-11. Field Dependence Chirality in Ferromagnetic Multilayers Probed by Dichroism in x-ray Resonant Magnetic Scattering.
E.O. Burgos Parra[3,1], W. Legrand[1], S. Flewett[2], F. Ajejas[1], C. Leveille[3], Y. Sassi[1], P. Gargiani[4], M. Valvidares[4], N. Reyren[1], V. Cros[1] and N. Jaouen[3] *1. Unite Mixte de Physique CNRS/Thales, Palaiseau, France; 2. Pontificia Universidad Catolica de Valparaiso Facultad de Ciencias, Valparaiso, Chile; 3. Synchrotron SOLEIL, Gif-sur-Yvette, France; 4. Sincrotron ALBA, Barcelona, Spain*

Chiral magnetic structures induced by Dzyaloshinskii-Moriya interaction (DMI) [1] have been proposed as the cornerstone of new technology applications such as high-density data storage devices or neuromorphic computing [2], due their room temperature stability and efficient current induced motion. Recent studies of the amplitude of magnetic satellites of a crystal Bragg peak by Zhang *et al*. [3] showed that x-ray resonant magnetic scattering (XRMS) is a powerful tool to access to the relevant topological parameters of these magnetic structures. In this work, we use small angle reflectivity XRMS to reveal directly the chiral properties of FM multilayers with tailored magnetic chiralities driven by spin-orbit-related effects at interfaces [4,5]. We show that it can straightforwardly and unambiguously determine the main characteristics of chiral magnetic distributions in perpendicularly magnetized multilayers [4]: its chiral nature, the quantitative winding sense (clockwise or counterclockwise), and its type, *i.e.* Néel (cycloidal) or Bloch (helical). Moreover we prove that this approach combined with micromagnetic simulations reveals hybrid chiral spin texture in multilayers [5]. Finally, we studied the in plane field dependence intensity of the dichroism and the appearance of second order diffraction peaks, usually forbidden on these systems. An asymmetric change of the intensity of the magnetic asymmetry lobes and a hysteretic behavior of these ones with the external field suggest a complex interplay between the hybrid domain wall state existing in these systems and DMI fields. European Union Grant FLAG-ERA SoGraph (ANR-15-GRFL-0005), French ANR grant TOPSKY (ANR-17-CE24-0025), DARPA TEE program grant (MIPR#HR0011831554) and EU grant SKYTOP (H2020 FET Proactive 824123) are acknowledged for their financial support.

References [1] I. Dzyaloshinskii, J. of Phys. and Chem. of Solids 4, 241 (1958), T. Moriya, Phys. Rev. 120, 91 (1960) [2] A. Fert, N. Reyren and V. Cros, Nat. Rev. Mat. 2, 17031 (2017) [3] S. L. Zhang, G. van der Laan, and T. Hesjedal, Nat. Commun. 8, 14619 (2017) [4] J.-Y. Chauleau *et al.*, Phys. Rev. Lett. 120, 037202 (2018) [5] W. Legrand *et al.*, Sci. Adv. 4, eaat45 (2018)

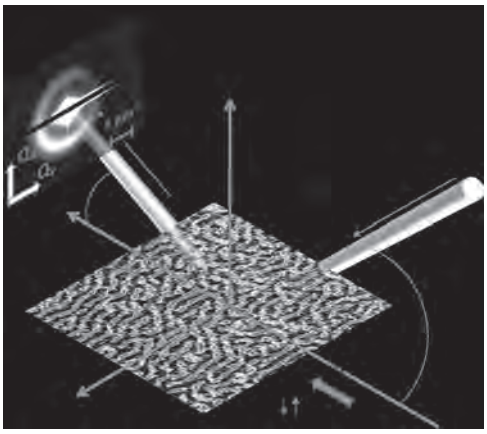

Schematic of the experimental setup. The specular reflection of circular polarised x-rays is captured by a CCD camera.

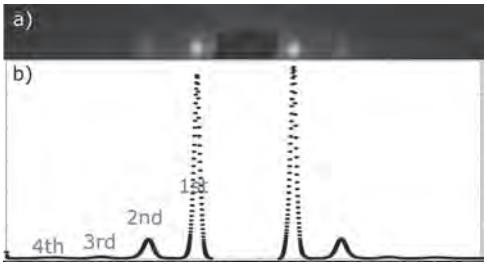

Sum of two XRMS patterns, one for each circular polarization (left and right), at a fixed in plane external field. (b) After a background substraction is performed for each polarization, each column of the CCD camera is averaged and plotted. 1st, 2nd, 2rd and 4th peaks are observed.

L1-12. Imaging Shape and Voltage Control of Spin Textures in Ferroic Heterostructures.
R.V. Chopdekar[1] *1. Advanced Light Source, E O Lawrence Berkeley National Laboratory, Berkeley, CA, United States*

Complex oxides offer possibilities to engineer and control spin textures via their many degrees of freedom and sensitivity to epitaxial strain, and have been proposed for use in energy efficient magneto-electric spin-orbit logic architectures.[1] Additionally, recent interest in antiferromagnetic spintronics has surged due to the possibility of obtaining ultrafast magnetization dynamics with no stray field[2]. However, lack of stray field makes imaging of antiferromagnetic domain structure difficult though conventional magnetic imaging techniques. This talk will discuss the use of X-ray photoemission electron microscopy (PEEM) with both x-ray linear and circular dichroism to spatially and chemically resolve the shape and voltage-controlled ferroic order in heterostructures containing antiferromagnetic (AFM), ferroelectric(FE), and ferromagnetic (FM) layers of including $(La,Sr)FeO_3$[3,4], Ni/CoFeB/PMN-PT[5], and CoFe/$(La,Bi)FeO_3$[6]. Dimensional confinement can be used to tailor the easy axis spin orientation in $(La,Sr)FeO_3$, as edge-induced anisotropy in microstructures can induce nearly-single domain structures in wires,[3] and in the limit of few unit-cell thick layers, the antiferromagnetic spin axis lies in the plane of the film in contrast to thicker layers where the spin axis cants out of plane.[4] By changing the ratio of Ni to CoFeB in artificial multiferroic heterostructures, the ground state domain configuration and magneto-electric coupling behavior are strongly modified, and this coupling can be visualized *in situ* with PEEM.[5] Furthermore, we show that the energy barrier for magneto-electric switching energy density can be scaled through careful engineering in a $BiFeO_3$-based system towards 10 $\mu J\ cm^{-2}$ at a switching field of 200 mV.[6] Thus, coupling at these interfaces allows for mutual control of the domain structure via a variety of pathways, including shape anisotropy and magneto-electric interactions, and thus offers additional degrees of freedom towards low-energy AFM-based spintronics.

1. S. Manipatruni et al, Nature 565 35 (2018). 2. V. Baltz et al, Rev. Mod. Phys 90, 015005 (2018). 3. A. D. Bang, RVC et al, Appl. Phys. Lett 115 112403 (2019). 4. M.S. Lee, RVC et al, J. Appl. Phys 127, 203901 (2020). 5. Z. Xiao, RVC et al, ACS Appl. Mat. 12, 6752 (2020). 6. B. Prasad, RVC et al, Adv. Mat. 2001943 (2020).

L1-13. Direct Observation of Temperature Dependent Vortex Dynamics in a $La_{0.7}Sr_{0.3}MnO_3$ Micromagnet. E. Digernes[2], *J. Leliaert*[1], M. Weigand[3], E. Folven[2] and B. Van Waeyenberge[1] *1. Dept. of Solid State Sciences, Universiteit Gent, Gent, Belgium; 2. Department of Electronic Systems, Norges teknisk-naturvitenskapelige universitet, Trondheim, Norway; 3. Helmholtz-Zentrum Berlin fur Materialien und Energie GmbH, Berlin, Germany*

Although it is well documented that the vortex core in a micromagnet can switch polarisation in response to magnetic field pulses[1], the temperature dependence of this process has not yet been addressed by experiments. Using scanning transmission x-ray microscopy, we investigate the magnetic vortex dynamics in a $La_{0.7}Sr_{0.3}MnO_3$ microplatelet at temperatures ranging from 150 K up to T_C at 350 K[2]. The time-resolved images reveal qualitatively different dynamic regimes as function of temperature and applied field, as the relative strengths of the micromagnetic energy terms strongly vary over this temperature range. By explicitly accounting for the temperature dependence of the magnetic parameters in our micromagnetic simulations[3], we found an excellent agreement with the experiments over the full measurement range. In line with previous models, the simulations reveal that the vortex core switches polarisation when it reaches a critical velocity[4] that mainly depends on the strength of the exchange interaction. It is therefore strongly temperature dependent, thus explaining our observation of the different dynamical regimes

[1] B. Van Waeyenberge, A. Puzic, H. Stoll, et al., Nature Vol. 444, p.461 (2006). [2] E. Digernes, J. Leliaert, M. Weigand, et al., *submitted manuscript* [3] A. Vansteenkiste, J. Leliaert, M. Dvornik, et al., AIP Adv. Vol.4, p.107133 (2014). [4] K. Y. Guslienko, K.-S. Lee, and S.-K. Kim, Phys. Rev. Lett. Vol. 100, p. 027203 (2008)

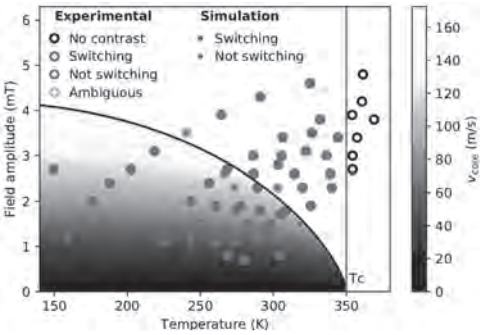

Classification of dynamics for experimental data points (edge color) and simulations (center color). Background is estimated maximum vortex core velocity for excitations up to the critical field (solid black line).

L1-14. Fiber-Optic Magnetic Vector Gradient Imaging With Fluorescent Defects in Diamond. *S.M. Blakley*[1,2], I.V. Fedotov[3,4], J. Becker[1] and A.M. Zheltikov[1,3] *1. Department of Physics & Astronomy, Texas A&M University, College Station, TX, United States; 2. Physical Measurement Laboratory, National Institute of Standards and Technology, Gaithersburg, MD, United States; 3. Physics Department, Lomonosov Moscow State University, Moscow, Russian Federation; 4. Russian Quantum Center, Skolkovo, Russian Federation*

Fluorescent defects in diamond present a versatile platform for compact quantum magnetometers, [1] and optical fiber technology enables *in situ* laser excitation and signal collection from these sensors. [2-4] The advent of microstructured fibers has allowed novel analytical techniques employing differential magnetic field measurements, common-mode noise rejection, [5] and high-resolution magnetic field imaging [6] to be used in environments without easy optical access. In this work, we demonstrate a microresolution stereomagnetometer probe by attaching a high nitrogen–vacancy (NV) concentration microdiamond to the tip of a dual-core photonic-crystal fiber (PCF) and simultaneously interrogate two regions of the diamond separated by the 6 μm core-to-core distance (Fig. 1 (a)). This probe was then used to characterize the magnetic field emanating from a 40 μm diameter current carrying wire in the presence of a large static bias solenoid by extracting the center wavelength of each peak in the optically detected magnetic resonance (ODMR) spectrum of the diamond fluorescence recollected by the PCF. [5] The magnitude and direction of the inhomogeneous wire field source was discriminated from a homogeneous background bias field with a magnitude more than 1000 fold larger than the localized wire field (Fig. 1 (b)). This stereomagnetometer was found to have a shot-noise limited sensitivity of 2 nT/√Hz and a 6 μm spatial resolution while imaging the vector field around the wire. [5]

[1] L. Bougas, A. Wilzewski, Y. Dumeige, et al., Micromachines 9 (6), 276 (2018) [2] Y. Ruan, D. A. Simpson, J. Jeske, et al., Scientific Reports 8 (1), 1268 (2018) [3] S. M. Blakley, I. V. Fedotov, S. Ya. Kilin, et al., Optics Letters 40, 3727-3730 (2015) [4] S. M. Blakley, I. V. Fedotov, L. V. Amitonova, et al., Optics Letters 41, 2057-2060 (2016) [5] S. M. Blakley, I. V. Fedotov, J. Becker, et al., Applied Physics Letters 113 (1), 011112 (2018) [6] I. V. Fedotov, S. M. Blakley, E. E. Serebryannikov, et al., Optics Letters 41, 472-475 (2016)

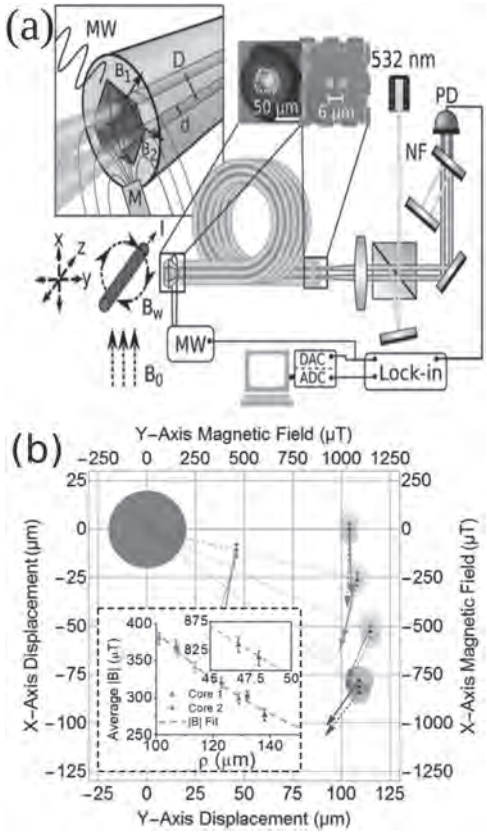

Fig. 1: (a) Experimental apparatus for the photonic crystal fiber stereomagnetometer. 4 μm diameter fiber cores separated by 6 μm (dashed red inset) interrogate NV diamond (middle inset) in microwave field (left inset). Fluorescence signal recollected by fiber imaged onto photodiode for lock-in detection. Current (I) generates inhomogeneous field (B_w) against bias field (B_0) background. (b) Magnetic field vectors (colored arrows) and location of measurement points from both cores (colored circles) around wire (grey disk). Wire field magnitude as a function of radial displacement (inset figure). [5]

Session L2
VOLTAGE-CONTROLLED MAGNETIC ANISOTROPY AND SWITCHING

Takayuki Nozaki, Chair
Natinaol Institute of Advanced Industrial Science and Technology, Tsukuba, Japan

INVITED PAPER

L2-01. Voltage Control of Magnetism Enabled by Resistive Switching. *P. Salev*[1], L. Fratino[2], D.Y. Sasaki[3], R. Berkoun[2], J. del Valle[4], Y. Kalcheim[1], Y. Takamura[3], M. Rozenberg[2] and I.K. Schuller[1] *1. University of California San Diego, La Jolla, CA, United States; 2. Laboratoire de Physique des Solides, Orsay, France; 3. University of California Davis, Davis, CA, United States; 4. Universite de Geneve, Geneva, Switzerland*

Application of a strong electrical stimulus, voltage or current, can drive metal-insulator transition in colossal magneto-resistance manganites, which produces concurrent resistive and magnetic switching. In (Ls,Sr) MnO_3 (LSMO), the resistive switching manifests as an N-type negative differential resistance in the I-V characteristics (Fig. 1a). We found that the switching does not occur uniformly throughout the device. Instead, a special out-of-equilibrium phase separation is favored: above a voltage threshold, a transverse insulating domain nucleates in the device center and acts as a barrier for the current flow. Because of the coupling between electronic and magnetic properties, inducing an insulating barrier allows turning on and off the ferromagnetism locally using a global voltage bias applied to the whole device. This produces an unusual ferromagnetic/paramagnetic/ferromagnetic (FM/PM/FM) configuration (Fig. 1b), which has a strong impact on the magnetic anisotropy. Before the PM domain nucleation, the device hysteresis loops have almost ideal square shape (Fig. 1c, blue line). After the PM domain nucleation, the remanence in the hysteresis deceases nearly to zero while the saturation field triples (Fig. 1c, red line). Effectively, the application of voltage switches the direction along the device length from an easy into a hard magnetic anisotropy axis. Our results present an original concept of employing resistive switching as a viable strategy to achieve voltage control of magnetism, a long-standing goal of spintronics. This research was supported by the Office of Basic Energy Science, U.S. Department of Energy, BES-DMS funded by the Department of Energy's Office of Basic Energy Science, DMR under grant DE FG02 87ER-45332.

[1] M. Tokunaga, Y. Tokunaga, and T. Tamegai, Phys. Rev. Lett. 93, 037203 (2004) [2] T. Wu and J. F. Mitchell, Appl. Phys. Lett. 86, 252505 (2005) [3] S. Balevicius, et. al., Appl. Phys. Lett. 90, 212503 (2007)

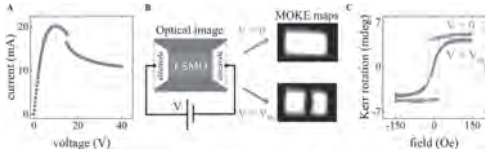

Fig. 1. A, Voltage-controlled I-V of an LSMO device showing an N-type negative differential resistance during the resistive switching. B, LSMO device optical image and two MOKE amplitude maps showing the voltage-driven formation of a PM domain. C, MOKE hysteresis loops recorded under different applied voltages illustrating the magnetic anisotropy change driven by the resistive switching.

CONTRIBUTED PAPERS

L2-02. Voltage-Induced Ferromagnetism in Diamagnetic FeS_2. J. Walter[1,2], B. Voigt[1], E. Day-Roberts[1], K. Heltemes[2], R. Fernandes[1], T. Birol[1] and *C. Leighton*[1] *1. University of Minnesota, Minneapolis, MN, United States; 2. Augsburg University, Minneapolis, MN, United States*

Increasingly impressive demonstrations of voltage-controlled magnetism have been achieved recently, highlighting the potential for low-power data processing and storage devices. Magnetoionic approaches appear particularly promising, electrolyte- and ionic-conductor-based devices being shown capable of on/off voltage control of ferromagnetism and voltage tuning of magnetic anisotropy [1-3]. A clear limitation, however, is that such demonstrations involve either electrically tuning a known ferromagnet, or electrically inducing ferromagnetism from another magnetic state, *e.g.*, antiferromagnetic. In this work, we report proof-of-principle that ferromagnetism can be voltage-induced even from a *diamagnetic*, *i.e.*, *zero-spin* state, suggesting that useful magnetic phases could be electrically-induced in "non-magnetic" materials [4]. We use ionic-liquid-gated diamagnetic semiconducting FeS_2 as a model system, showing that as little as +1 V gate bias induces a highly reversible insulator-metal transition, driven by electrostatic inversion of the surface from a *p*-type semiconductor to an *n*-type metal. Anomalous Hall effect measurements then reveal the onset of robust electrically-tunable surface ferromagnetism at Curie temperatures up to 25 K, with intriguing high temperature spin correlations. Density-functional-theory-based modelling explains the induced magnetism in terms of Stoner-type ferromagnetism induced solely *via* filling of a narrow Fe e_g band. Work supported primarily by the NSF MRSEC.

[1] Navarro-Senent, Quintana, Menendez, Pellicer, Sort, APL Mater. 7, 030701 (2019) [2] Molinari, Hahn, Kruk, Adv. Mater. 31, 1806662 (2019) [3] Leighton, Nat. Mater. 18, 13, (2019) [4] Walter, Voigt, Day-Roberts, Heltemes, Fernandes, Birol and Leighton, in press (2020)

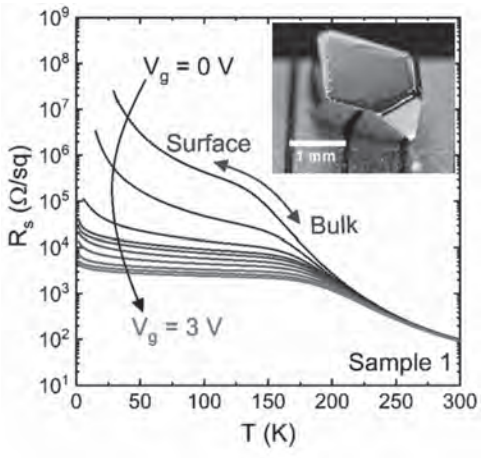

Fig. 1: Sheet resistance *vs.* temperature at multiple gate voltages in an ionic-liquid-gated FeS_2 single crystal (inset).

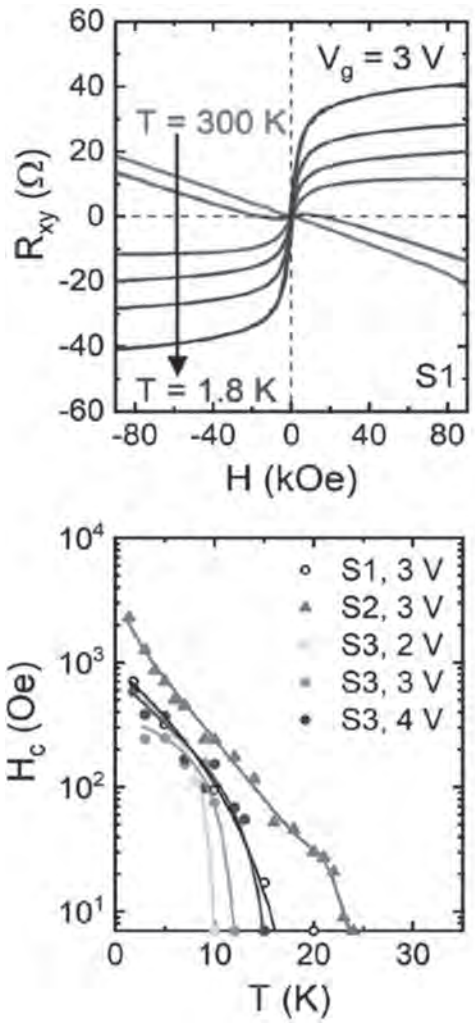

Fig. 2: Transverse (Hall) resistance *vs.* applied field and temperature at gate voltage of 3 V (top) and coercivity *vs.* temperature at different gate voltages in multiple samples (S1-S3) (bottom).

L2-03. Inverse of Voltage Controlled Magnetic Anisotropy (VCMA) Effect. *A. Shukla*[1], A. Chouhan[1], R. Pandey[1], R. Maripeddi[1], T. Yamamoto[2], H. Kubota[2], A. Fukushima[2], S. Yuasa[2], T. Nozaki[2] and A. Tulapurkar[1] *1. Electrical Engineering, Indian Institute of Technology Bombay, Mumbai, India; 2. Sangyo Gijutsu Sogo Kenkyujo Tsukuba Chuo, Tsukuba, Japan*

Manipulating magnetization of ferromagnetic material with small amount of energy is of contemporary interest in field of Spintronics. There are various ways in which manipulation of magnetization can be done such as,1) Using spin polarized current [1] 2) Electric field controlled [2] 3) SAW based technique [3],4) Heat current controlled [4],among all currently available techniques Electric Field controlled is ultra-low power [5].All the effects in nature also have a reciprocal effect based on the Onsager reciprocity e.g. the inverse of spin transfer torque effect viz. spin pumping can be used for converting magnetization oscillations into spin current. Here we have experimentally demonstrated the Inverse of VCMA effect by which magnetization oscillations produce charge voltage. To demonstrate the inverse-VCMA effect [6],we fabricated a two port device as shown schematically in Fig.1 We deposited stack on Si/SiO2 substrate: Ta(5)/Ru(5)/Ta(5)/Ru(5)/Ta(9)/COFEB(1)/CoFe(0.2)/Ir(0.1)/MgO(2.4)/Ta(5)/Ru(7). We then fabricated tunnel junctions of dimension 3umx80um with contacts. A CPW was fabricated on the top, which was electrically insulated from the bottom pillar. The patterning of the device was done by e-beam lithography and Ar-ion milling. We measured the S-parameters of the device using a (VNA). The magnetic field was swept along different directions by varying θ and φ. The measurement of S_{21} signal corresponds to the direct VCMA effect. Applying signal to port 1 oscillates magnetization of FM by the VCMA effect and signal is induced in the port 2 by induction. The measurement of S_{12} corresponds to the inverse of VCMA effect as shown in Fig.2. On applying oscillating voltage to port 2, creates oscillating field on the FM.The oscillation of the magnetization of the FM induces voltage in the port 1 by the inverse-VCMA effect. Both the S_{12} & S_{21} signal are largest at the FMR frequency. We observed that the Onsager reciprocity relation $S_{12}(B)=S_{21}(-B)$ is satisfied. The angular dependence of the S-parameters confirmed that the signals arise from inverse VCMA effect. We would like to thank IIT Bombay NanoFabrication facility for support

[1] J.C.Slonczewski JMMM volume 159, Issues 1–2 (1996). [2] T. Maruyama, et.al., Nat. Nanotechnology. 2008, 406(2009). [3] Swapnil Bhuktare et.al., Appl. Phys.Lett. 114, 052402 (2019). [4] Arnab Bose et.al, PhysRevB.98.184412 (2018). [5] T. Nozaki et.al., Nat. Physics. 2298 (2012). [6] Ambika Shanker Shukla et.al. Science Advances (accepted) 2020.

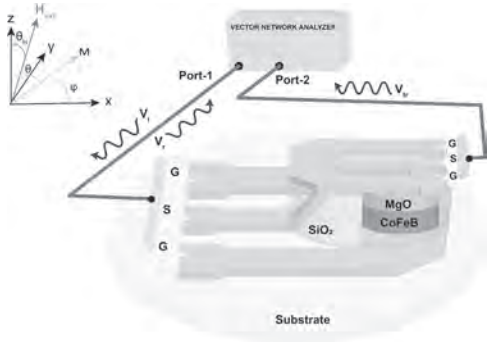

Schematic of the fabricated two port device

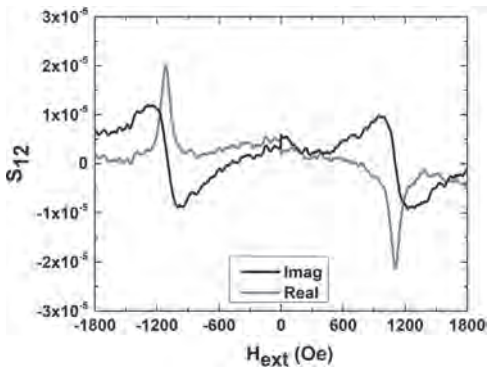

Angular dependance plot of S_{12} as a function of H_{ext}

L2-04. Optimization of the VCMA Driven Magnetization Reversal. *R. One*[1,2], H. Béa[2], C. Fillion[2], S. Mican[1], M. Joldos[3], B. Dieny[2], L. Buda-Prejbeanu[2] and C. Tiusan[1,3] *1. Faculty of Physics, Babes-Bolyai University, Cluj-Napoca, Romania; 2. Univ. Grenoble Alpes, CEA, CNRS, Grenoble INP, IRIG-SPINTEC, 38000 Grenoble, France; 3. Technical University of Cluj-Napoca, Cluj-Napoca, Romania*

Voltage controlled magnetic anisotropy (VCMA) became in the last ten years a subject of tremendous interest in the field of spintronics [1] due to its promising potential outcome: fast and low power consumption magnetization manipulation in magnetoresistive random access memories with enhanced storage density [2]. Our study, performed within a macrospin LLG simulation framework with key input parameters extracted from ab-initio calculations, reveals the full anatomy of the VCMA effect in magnetic nanostructures in which the magnetization can be controlled by purely precessional

switching. Our simulations emphasize the dependence of the switching probability and switching time on material and experiment parameters (e.g. surface anisotropy, Gilbert damping, electric and magnetic pulse shape and frequency) allowing thus predictive sets of parameters for optimum switching experiments in realistic devices. Following the conditions for the minimum electric field required to switch the magnetization, we demonstrate that a very interesting switching regime can be attained, where the fast precessional reversal does not anymore depend on the voltage pulse length. From an analysis of the energy landscape of the system, we discuss the physical origin of this critical regime and illustrate how it can be tuned via specific magnetic material parameters such as the Gilbert damping. Beyond the deep analysis of the toggling reversal induced by the electric field, our results identify an interesting paradigm: for voltage induced switching of perpendicularly magnetized magnetic nanostructures a large value of the Gilbert damping constant has a positive effect reinforcing control of the magnetization manipulation by electric field. Moreover, our study indicates that, for the development of voltage-torque MRAM devices in which both VCMA and spin-transfer-torque STT effects must be combined, an optimum value of Gilbert damping must be chosen in order to provide optimum device operation.

[1] H. Ohno et al, Nature 408(2000), no. 6815, 944–946. [2] T. Nozaki et al, Micromachines 2019, 10, 327.

L2-05. Impact of Ambient Temperature on the Switching Behavior of Voltage-Controlled Perpendicular Magnetic Tunnel Junction. *Y. Wu*[1,2], W. Kim[1], S. Van Beek[1], S. Couet[1], R. Carpenter[1], S. Rao[1], S. Kundu[1], F. Yasin[1], D. Crotti[1], J. Van Houdt[1,2], G. Groeseneken[1,2] and G.S. Kar[1]
1. imec, Leuven, Belgium; 2. ESAT, KULeuven, Leuven, Belgium

Voltage control of magnetic anisotropy (VCMA) offers a voltage-driven magnetization switching mechanism for high speed and ultra-low power applications [1]. The characteristics and performance of VCMA-MTJ devices at elevated temperatures are important not only for practical MRAM applications but also for scientific interests. Recent studies investigated the temperature (T) dependence of several magnetic properties [2]; however, no experimental study has been performed on the T-dependence of VCMA-induced switching. In this work, we use BEOL compatible MTJ devices with MgO/CoFeB(t)/Ta free layers to study the magnetic properties and switching behavior between 25°C and 125°C. First, we estimate T-dependence of $B_{k,eff}$ on devices with t = 1.5nm by switching magnetic field distribution [3]. From 25°C to 125°C, a 40% reduction in $B_{k,eff}$ is observed [Fig. 1(a)] as a consequence of a 10% decrease in M_S combined with an 18.5% decrease in interfacial anisotropy (K_i). Next, the VCMA effect is investigated. We quantify a 12% reduction in VCMA slope $dB_{k,eff}/dV$ [Fig. 1(b)], corresponding to a 17% reduction in VCMA coefficient (ξ). Since $B_{k,eff}$ is more sensitive to temperature than $dB_{k,eff}/dV$, lower switching voltages are expected at elevated temperatures. We validate it by studying the switching voltages of devices with t = 1.7nm. The switching speed (f_s) is measured at different pulse voltages, and the characteristic switching voltage (V_C) is deduced by acquiring the characteristic frequency $f = 2\gamma B_x$ [Fig. 2(a)] [4]. Finally, we observe that V_C decreases monotonically as a general behavior from multiple devices and B_x conditions [Fig. 2(b)], confirming the trend predicted by $V = B_{k,eff}/(dB_{k,eff}/dV)$. This work was supported by IMEC's Industrial Affiliation Program on MRAM devices.

[1] H. Noguchi et al., IEDM (2016) [2] J. G. Alzate et al., Appl. Phys. Lett. 104, 112410 (2014) [3] X. Feng et al., J. Appl. Phys. 95, 7043 (2004) [4] Y. C. Wu et al., AIP Adv. 10, 035123 (2020)

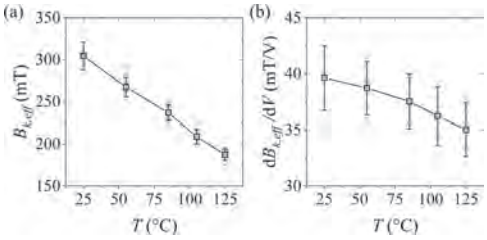

Fig. 1. *T*-dependence of (a) anisotropy field and (b) VCMA slope.

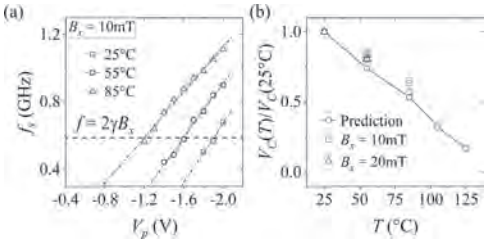

Fig. 2. (a) f_s as a function of pulse voltage with B_x = 10mT. Dashed line indicates the characteristic frequency $f = 2\gamma B_x$. Dotted lines represent linear dependence. (b) Normalized V_C as a function of temperature.

L2-06. Tuning Magnetic Anisotropy and Skyrmion Stability With Electric Field. *A. Fassatoui*[1], J. Peña Garcia[1], A. Mantel[2], L. Ranno[1], H. Béa[3], J. Vogel[1] and S. Pizzini[1] *1. Institut NEEL, Grenoble, France; 2. Laboratoire de Physique et Chimie des Nano-objets, Toulouse, France; 3. SPINtronique et Technologie des Composants, Grenoble, France*

Recently, we experimentally demonstrated that the nucleation and annihilation of μm-sized skyrmions in Pt/Co/AlOx trilayers can be controlled by tuning the perpendicular magnetic anisotropy with electric field gating [1]. Here, we show our present efforts to extend this concept to smaller skyrmions, down to 50 nm lateral size. Two trilayer systems, in which sub-100 nm skyrmions were observed at room temperature, were studied: Pt/Co/MgO [2] and Pt/Co/TbOx. The stacks were patterned by electron beam lithography and ion beam etching into stripes (1 – 50 μm width) then covered with a 10 nm thick ZrO_2 dielectric layer and a 6 nm thick Pt top electrode to form capacitor-like structures, Fig (a). Using Magnetic Force Microscopy, Fig (b-c), we show that in both stacks, starting from a stable skyrmion network, a positive electric field (EF) leads to the increase of the PMA and to the annihilation of the skyrmion phase. We attribute this to the EF-induced migration of oxygen towards the top Co interface. This result is confirmed by the variation of the hysteresis loops taken with polar Magneto-Optical Kerr Effect, Fig (d). This new state persists after removing the EF i.e. EF-gating leads to a non-volatile effect. In the Pt/Co/MgO trilayer, the application of a negative EF shows no effect on the magnetic anisotropy, preventing us to renucleate the skyrmions. This irreversible process is probably due to the stabilization of the stochiometric MgO phase induced by oxygen ion migration towards the Co/MgO interface when a positive gating is applied. On the contrary, for Pt/Co/TbOx trilayers, the application of a negative EF triggered the oxygen ion migration away from the top Co interface. This allows us to tune reversibly the magnetic anisotropy, and therefore to reproducibly nucleate and annihilate 50 nm size skyrmions. This is an easily integrable and energetically efficient solution that might ease the use of magnetic skyrmions as information carriers in future spintronic devices.

[1] Schott *et al.,* Nano Lett 17, 3006 (2017) [2] Boulle *et al.,* Nat Nano 11, 449 (2016)

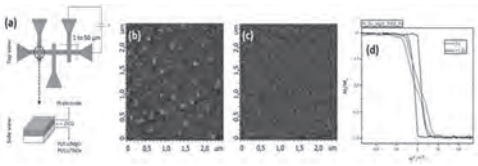

Fig: (a) Schematic representation of the device. MFM images of Pt/Co/MgO trilayers showing magnetic skyrmions (b) before (c) after applying a positive electric field. (d) PMOKE hysteresis loops of Pt/Co/MgO trilayers before and after EF gating.

L2-07. Hydroxide-Based Magneto-Ionics: Paramagnetic-to-Ferromagnetic Transition in Electrolyte-Gated α-$Co(OH)_2$.

A. Quintana-Puebla[1], A.A. Firme[2], C.J. Jensen[1] and K. Liu[1] *1. Physics Department, Georgetown University, Washington, DC, United States; 2. Physics and Astronomy, University of Wyoming, Laramie, WY, United States*

Magneto-ionics has emerged as a promising approach to manipulate magnetic properties in magnetic heterostructures, energy-efficiently. While this has led to exciting magneto-ionically controlled functionalities in primarily oxygen-based systems, such as perpendicular magnetic anisotropy, magnetization, exchange interaction, and superconductivity, there are challenges in oxygen-based magneto-ionics, in terms of switching speed and reversibility [1-3]. There have been keen interests in exploring other ionic systems which may overcome these issues [4]. Here we explore the use of α-$Co(OH)_2$ for hydroxide-based magneto-ionics, which undergoes a reversible paramagnet to ferromagnet transition under electrolyte gating. The α-$Co(OH)_2$ films are grown by electrochemical methods. Grazing incidence x-ray diffraction (XRD) confirmed the formation of α-$Co(OH)_2$ without traces of any other hydroxide or oxide phase. After voltage application in an electrolyte-gating configuration, a ferromagnetic signal can be induced in the paramagnetic as-grown sample under negative voltage due to the reduction of α-$Co(OH)_2$ into metallic Co (Fig. 1). Magneto-electric experiments revealed that the turn-on voltage, i.e. minimum voltage needed to generate the ferromagnetic response, is as low as -2V, among the lowest turns-on voltages reported for propylene carbonate gated experiments [5]. Its paramagnetic character can be fully recovered by reversing the applied voltage polarity. This reversible transition is due to the ionic diffusion of hydroxyl groups into the employed electrolyte. By tuning the voltage magnitude and sample area we demonstrate that the speed of the induced ionic effect can be drastically boosted, up to a factor 60 at -8V (Fig. 2). This work opens new avenues in exploring the benefits of layered materials and hydroxyl groups towards fast magneto-ionic processes. This work has been supported in part by the SRC/NIST SMART Center, the NSF (ECCS-1933527), NSF-REU (DMR-1659532) and NSF-MRI (DMR-1828420).

[1] U. Bauer *et al.*, Nat. Mater., 14, 174 (2015). [2] D. A. Gilbert *et al.*, Nat Commun 7, 12264, (2016). [3] P. D. Murray *et al.*, ACS Appl. Mater. Interfaces 12, 4741 (2020). [4] A. J. Tan *et al.*, Nat. Mater. 18, 35 (2019). [5] C. Navarro-Senent *et al*., APL Mater. 7, 030701 (2019).

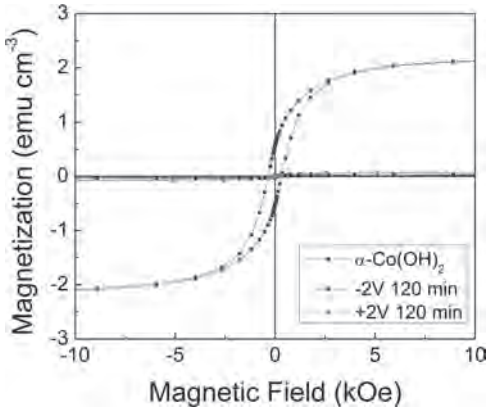

Fig. 1: Room temperature hysteresis loop for the as-grown sample (black), after a -2V (blue) electrolyte-gating, and a subsequent +2V (red) gating.

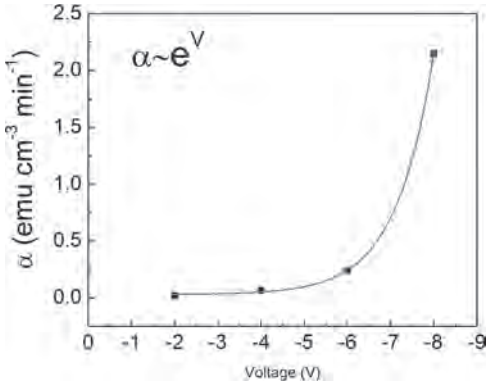

Fig. 2: Rate of magnetization change (α) as a function of the gating voltage.

L2-08. Magneto-Ionic Enhancement of Exchange Bias in MnN/CoFe.

C.J. Jensen[1], A. Quintana[1], P. Quarterman[2], A.J. Grutter[2] and K. Liu[1] *1. Physics, Georgetown University, Washington, DC, United States; 2. NIST Center for Neutron Research, Gaithersburg, MD, United States*

The magneto-ionic effect has shown promise as an effective approach to control magnetic properties through controlled motion of ionic species, which can be tailored under an applied electric field[1]. For example, magneto-ionic control of exchange bias, which is prominently used in spin valve type of devices, may lead to reduction in energy costs and the development of novel devices[2]. While early studies have primarily focused on oxygen-based systems, recent studies have featured alternative ionic species, such as hydrogen[3] and nitrogen[4]. Here, we have investigated the magneto-ionic control of exchange bias in MnN/CoFe films grown on a Ta seed layer. Upon field cooling the structure above the Néel temperature of MnN (T_N ~ 660K) in a 6.5 kOe field, a significant exchange bias of ~ 620 Oe is induced (Fig. 1). Polarized neutron reflectometry (PNR) shows that after field cooling nitrogen migrates into the Ta seed layer from MnN (Fig. 2). While the Ta seed layer enables the correct texture in MnN to produce substantial exchange bias, it also acts as a nitrogen getter material. Recent studies have shown that depletion of nitrogen in MnN leads to decreases in exchange bias[5, 6]. To take advantage of these findings, nitrogen was magneto-ionically driven from the Ta seed layer back into MnN by applying an electric field. PNR indicates that nitrogen indeed moves back into the MnN layer, manifested in small increases in the scattering length density in the interior of the MnN layer (Fig. 2). The increase in nitrogen content in MnN leads to an increase in exchange bias of ~ 30 Oe. These results indicate that small changes in nitrogen content can lead to significant changes in the exchange bias. This work has been supported by the NSF (ECCS- 1933527) and in part the nCORE-SMART Center (2018-NE-2861) through SRC/NIST.

[1] U. Bauer, et al., Nat. Mater. 14, 174 (2015). [2] D. A. Gilbert, et al., Nat. Commun. 7, 11050 (2016). [3] A. J. Tan, et al., Nat. Mater. 18, 35 (2019). [4] J. de Rojas, et al., arXiv:2003.11137 (2020). [5] P. Quarterman, et al., Phys. Rev. Mater. 3, 064413 (2019). [6] M. Dunz, et al., AIP Adv. 8, 056304 (2018).

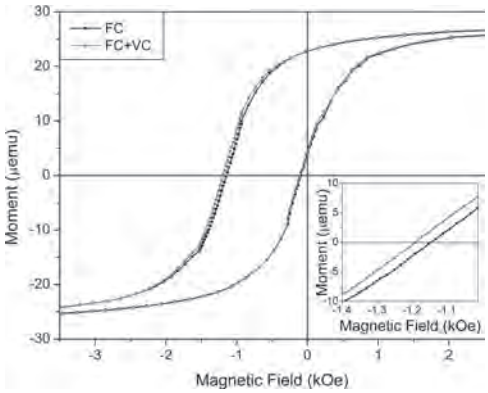

Fig. 1. Magnetometry of MnN/CoFe after field cooling (FC, black), and a subsequent voltage conditioning (FC+VC, red). Inset shows zoomed-in view of the descending-field branch.

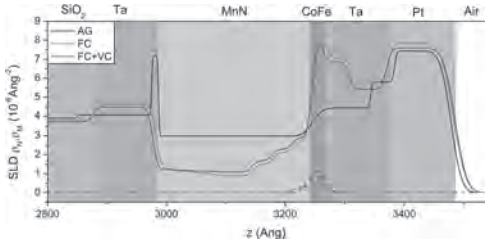

Fig. 2. Calculated nuclear (solid curves) and magnetic (dashed curves) scattering length densities of the MnN/CoFe system in the as-grown state (AG, black), field cooled (FC, red), and a subsequent voltage conditioned (FC+VC, blue) state.

L2-09. Superconductivity-Induced Change in Magnetic Anisotropy in Epitaxial Ferromagnet-Superconductor Hybrids With Spin-Orbit Interaction. *C. González-Ruano*[1*], D. Caso[1], L.G. Johnsen[2], C. Tiusan[3,4], M. Hehn[4], N. Banerjee[5], J. Linder[2] and F.G. Aliev[1] *1. Universidad Autonoma de Madrid, Madrid, Spain; 2. Center for Quantum Spintronics, Norwegian University of Science and Technology, Trondheim, Norway; 3. Center of Superconductivity Spintronics and Surface Science C4S, Technical University of Cluj-Napoca, Cluj-Napoca, Romania; 4. Institut Jean Lamour, Nancy Universite, Nancy, France; 5. Loughborough University, Epinal Way, Loughborough, United Kingdom*

Unlike the common expectation that superconducting spintronics and long-range triplet (LRT) proximity effects require complex ferromagnetic multilayers, relying on noncollinear/spiral magnetization or half-metals, we propose a new platform compatible with commercial spintronics. Recently, we have experimentally demonstrated that interfacial spin-orbit coupling (SOC) and symmetry-filtering in all-epitaxial V/MgO/Fe junctions, cooled below the critical temperature of vanadium, provide a thousand-fold increase in tunneling anisotropic magnetoresistance, supporting the LRT formation [1]. Here we report the converse effect: transformation of the magnetocrystalline anisotropy of a Fe(001) layer driven by the superconductivity of an underlying V layer through a spin-orbit coupled MgO interface [2]. We attribute this to an additional contribution to the free energy of the ferromagnet arising from the controlled generation of triplet Cooper pairs, which depends on the relative angle between the exchange field of the ferromagnet and the spin-orbit field. This observation offers the ability to fundamentally tune magnetic anisotropies using superconductivity - a key step in designing future cryogenic magnetic memories.

[1] I. Martínez et al; Phys. Rev. Appl. 13, 014030 (2020). [2] C. González-Ruano et al; accepted for publication as Rapid Communication in Phys. Rev. B, Cond Mat. ArXiv https://arxiv.org/abs/2006.02118

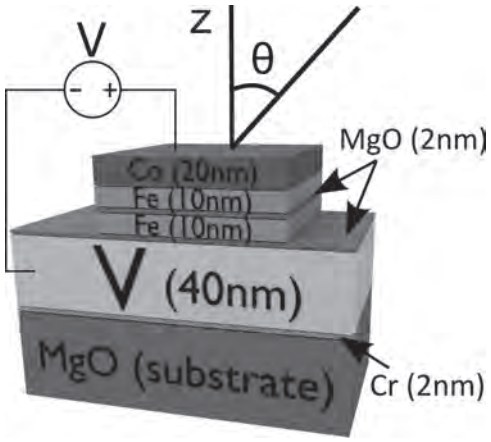

Fig.1: Sketch of the samples studied. The top part is a spin-valve device with FeCo as the hard layer and Fe as the soft one, interfaced with the MgO and the superconducting V.

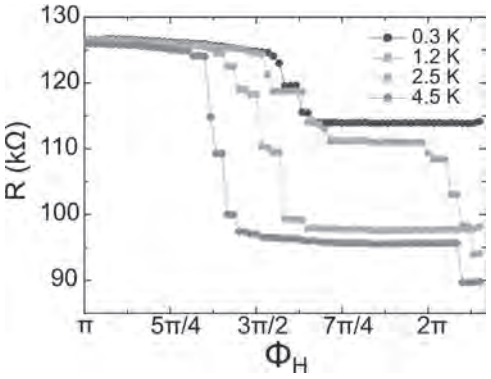

Fig.2: TMR experiments where the magnetic field is rotated in the in-plane direction of the samples, with |H|=70 Oe, for different temperatures, showing how new stable magnetic configurations arise under T=2 K. The changes in resistance values correspond to different magnetic states of the spin-valve: antiparallel (around 125 kΩ), 135 degrees (for the two low-temperature measurements, 115 kΩ), perpendicular in plane (100 kΩ) and parallel (90 kΩ, in the 4.5 K experiment).

* - *Best student presentation award finalist*

Session L3
MAGNETIZATION DYNAMICS AND DAMPING III (Poster Session)

Takeshi Kato, Chair
Nagoya University, Nagoya, Japan

L3-01. Fully-Vector Simulation Framework for the Investigation of Magnetisation Dynamics and Skyrmions. *J. O'Brien*[1] and P. Stamenov[1]
1. Physics, University of Dublin Trinity College, Dublin, Ireland

Atomistic simulations play a huge part in our understanding of static and dynamic magnetic states in current state-of-the-art research. Motivated by the recent interest in magnetic Heusler alloys, a model based on the LLG equation was developed for investigating magnetisation dynamics in near-compensated ferrimagnets. These materials, including Mn_2Ru_xGa (MRG), are predicted and often experimentally verified to possess key properties, including THz resonance frequencies and high spin-polarisation at the Fermi level [1, 2]. Another hot topic of study are magnetic skyrmions, topological defects in the spin texture of non-centrosymmetric crystals with chiral interactions. There is much interest in the dynamics of skyrmions, with fast skyrmionic magnetic storage one potential application [3, 4]. In this work, the stability of skyrmion states in a 1D ferrimagnet was investigated as a function of material parameters such as anisotropy and Dzyaloshinskii-Moriya interaction (DMI), see Fig. 1. Additionally, skyrmion propagation speed and breathing mode frequency [5] are investigated under the influence of an external magnetic field and/or spin-polarised current. The model has also been applied as a computationally efficient method to obtain magnon frequency dispersions. By applying a perturbing field pulse and taking the Fourier Transform of the resulting dynamics, the entire magnon dispersion can be obtained. A simple example for a 1D ferrimagnetic chain with Heisenberg exchange, DMI and uniaxial anisotropy is shown in Fig. 2. MRG shows compensation of its ferrimagnetic moment at room temperature and as a result is predicted to support sustained spin oscillations in the THz region [6]. Our simple model, once adjusted to accommodate the symmetry and dimensionality of the real material, will represent an efficient method to theoretically investigate the existence of such oscillations and of potential chiral ground states.

[1] H. Van Leuken and R.A. De Groot, Physical review letters., Vol. 74(7), p.1171 (1995) [2] S. Lenne et al., arXiv preprint arXiv:1903.04432. (2019) [3] W. Legrand et al., Nano letters., Vol. 17(4), pp.2703-2712 (2017) [4] A. Fert, N. Reyren and V. Cros, Nature Reviews Materials., Vol. 2(7), p.17031 (2017) [5] Y. Onose et al., Physical review letters., Vol. 109(3), p.037603 (2012) [6] R. E. Troncoso et al., Physical Review B., Vol. 99(5), p.054433 (2019)

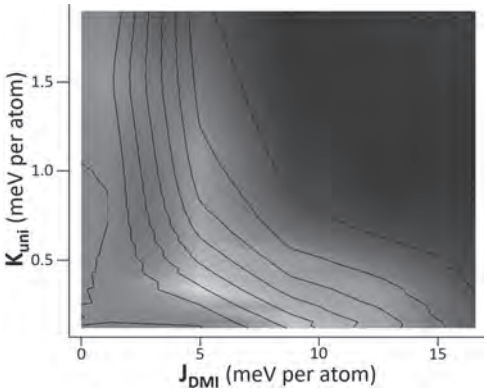

Fig. 1. Phase diagram showing skyrmion diameter as a function of DMI and uniaxial anisotropy strength (Heisenberg JH = 30.35 meV)

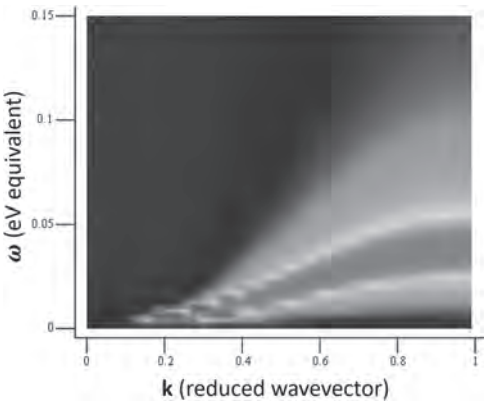

Fig. 2. An example magnon dispersion. Spatial symmetry is imposed by the perturbing field, such that magnons are created at the centre of the lattice and propagate outwards

L3-02. Utilizing Four-Node Tetrahedra-Shaped Hopfield Neural Network Configurations in the Local Magnetization Assessment of 3D Objects Exhibiting Hysteresis. *A. Adly*[1] and S. Abd-El-Hafiz[2] *1. Elect. Power Engineering Dept., Cairo University Faculty of Engineering, Cairo, Egypt; 2. Engineering Mathematics and Physics Dept., Cairo University Faculty of Engineering, Cairo, Egypt*

Assessment of local magnetization in 3D objects is indispensable to performance estimation of magnetic recording processes and electric power devices. It was shown that an elementary Stoner-Wohlfarth-like hysteresis operator may be constructed using two-node Hopfield neural network (HNN) having internal positive feedback [1]. The approach was further utilized to simulate vector hysteresis in arbitrary 2D geometries ([2, 3]). This paper presents an approach using which local magnetization in 3D objects exhibiting hysteresis may be assessed. It utilizes a four-node tetrahedron-shaped HNN (Fig. 1.a) with activation functions "f" constructed using a weighted superposition of a step and sigmoidal functions in accordance with the M-H curve squareness. Vector orientation of the activation function a neuron is

assumed to be along the unit vector e_v initiated from the tetrahedron center point to the vertex corresponding to that neuron (Fig. 1.b). Feedback k_{ij} between any two neurons is given by: $K_{ij}=k_{copl}$ (e_{vi}. e_{vj}), where k_{copl} is a constant identified by the material coercivity. Given an applied field H orientated along the unit vector e_H, activation function outputs of the tetrahedron HNN implicitly settles in accordance with the minimum of the energy E: $E=-\sum_{i=1\text{ to }4}(He_H.\ f\ e_{vi} + ½ \sum_{j=1\text{ to }4,\ j\neq i} k_{ij}\ fi\ fj)$. (1) Overall vector magnetization of the tetrahedron M e_M is given by: $M\ e_M = \sum_{i=1\text{ to }4} fi\ e_{vi}$. (2) Geometrical (shape) configuration of the tetrahedron affects the internal mutual node feedback factors and consequently the overall vector magnetization components. To demonstrate the applicability of the approach, an ellipsoid whose diameters were in the ratio of 2:1:1 was constructed using 120 tetrahedra. Main M-H curve of the material was assumed and corresponding activation function specifics and kcopl factor were consequently set (Figs. 1 and 2). More theoretical and computational details are given in the paper.

[1] A.A. Adly and S.K. Abd-El-Hafiz, Journal of Advanced Research, Vol. 4, p. 403 (2013). [2] A.A. Adly and S.K. Abd-El-Hafiz, Journal of the Applied Computational Electromagnetics Society, Vol. 31, p. 765 (2016). [3] A.A. Adly and S.K. Abd-El-Hafiz, Journal of Magnetism and Magnetic Materials, Vol. 434, p. 151 (2017).

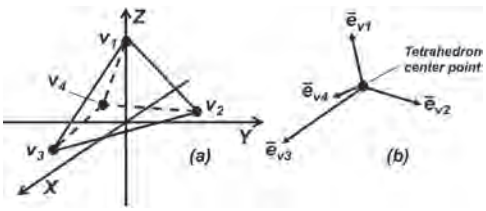

Fig. 1. (a) Tetrahedron HNN, and (b) the vector orienttion of its nodes.

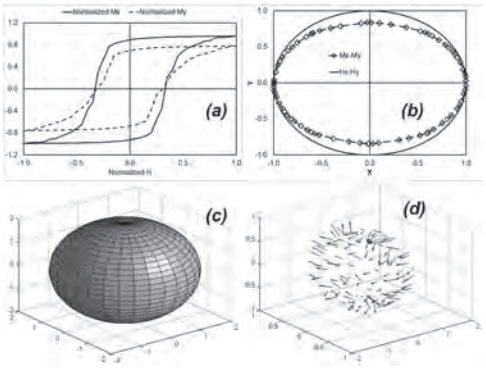

Fig. 2. (a) MH curves along x&y directns of the ellipsoid, (b) rotational MH curves in the x-y plane, (c) image of the ellipsoid under consideration, and (d) local magnetization vector plots in its 120 tetrahedral subregions.

L3-03. Discrete Magnetic Breathers in Monoaxial Chiral Helimagnet. *A. Ovchinnikov*[1], I. Bostrem[1], V. Sinitsyn[1], E. Ekomasov[3,4] and J. Kishine[2]
1. Institute Natural Sciences and Mathematics, Ural Federal Univeristy, Ekaterinburg, Russian Federation; 2. The Open University of Japan, Chiba, Japan; 3. Bashkir State University, Ufa, Russian Federation; 4. South Ural State University, Chelyabinsk, Russian Federation

We discuss localized spin modes in the model of monoaxial chiral helimagnet. Folllowing the idea suggested in Ref. [1] we address the so-called phase of forced ferromagnetism, where in the ground state all spins align with an external magnetic field applied along the chiral axis [2]. Our analysis shows that the intrinsic localized modes, or discrete breathers, exist and the Dzyaloshinskii-Moryia (DM) interaction does not hinder their emergence. We consider the spin Hamiltonian including the Heisenberg exchange coupling, the easy-plane anisotropy, the Zeeman coupling with an external magnetic field directed along the chiral axis, and the Dzyaloshinskii-Moryia interaction term along the chiral axis. It is supposed that the external field exceeds a critical value to stabilize the forced ferromagnetic phase. By using equations of motion for spin operators of a finite chain we find an approximate analytical solution of the discrete breather, establish necessary conditions for the breather frequency and the easy-plane anisotropy strength. The discrete breather accumulates not only magnon density but a topological charge. The topological charge depends on the balance between a scale of breather localization and a pitch of the spiral determined by the DM interaction. We calculate the energy of the discrete breather. It includes a part that may be obtained in the continuum limit and a pinning part that takes into account discreteness of the spin chain. The work is supported by the RFFI grant (project 20-02-00213)

[1] R.F. Wallis, D.L. Mills and A.D. Boardman, Physical Review B, Vol. 52, p. R3828, (1995). [2] J. Kishine, A.S. Ovchinnikov, Solid State Physics, Vol. 66, Pp. 1-130, (2015).

L3-04. Atomistic Spin-Lattice Dynamics on Model Hamiltonians in low-Dimensional Systems. *D. Thonig*[1], J. Hellsvik[4,5], M. Pereiro[2], J. Fransson[2] and A. Delin[3,2] *1. School of Science and Technology, Örebro University, Örebro, Sweden; 2. Department of Physics and Astronomy, Uppsala Universitet, Uppsala, Sweden; 3. Department of Applied Physics, School of Engineering Sciences, KTH Royal Institute of Technology, Kista, Sweden; 4. Nordic Institute for Theoretical Physics, Stockholm, Sweden; 5. Department of Physics, KTH Royal Institute of Technology, Stockholm, Sweden*

The understanding how magnons couple with phonons is of fundamental importance for magneto caloric, multiferroic, or spintronic applications. It is dominantly caused by distance dependent exchange between the magnetic moment [1], included e.g. in the *Ruderman–Kittel–Kasuya–Yosida* (RKKY)-like Heisenberg or dipole-dipole interaction. Both types of exchanges exhibit changes in the magnetic order, say from ferro to antiferromagnetic states, related to the crystal structure, which is affected by displacements and call for deeper studies, in particular on how angular momentum is transfered between magnon and phonon reservior. We report on an investigation of atomistic coupled spin-lattice dynamics by means of the Landau-Lifshitz-Gilbert and Newton equation. The exchange between the atomistic semi-classical magnetic moments, the finite displacements in the crystal lattice and the mixed terms of the Hamiltonian are approached by RKKY, the Levit-Fert type of anisotropic exchange, dipole-dipole as well as Born-Land'e exchange. The spin-lattice coupling is non-linear and directly included in the magnetic exchange couplings. For low dimensional systems like chains of atoms or small clusters, we focus on the evolution from disordered to ordered states in dependence on temperature, system size, exchange coupling strength and external magnetic field. It turns out that spin and displacements have a crucial influence on each other, especially near magnetic order transition. Transfer of angular momentum between magnons and phonons and the related time scales are resolved by correlation functions. Furthermore, we evaluate the validaty of the linearization of the spin-lattice coupling applied e.g. in Ref. [2], which in some limits breaks down.

[1] Y. Tokura, S. Seki, and N.Nagaosa, Rep. Prog. Phys. Vol. 77, p. 076501 (2014) [2] J. Hellsvik, D. Thonig, K. Modin et al., Phys. Rev. B, Vol. 99, p. 104302 (2019)

L3-05. Effect of Perpendicular Magnetic Field on Domain Wall Motion of Glass-Coated Magnetically Bistable Microwires With Different Anisotropy. *L. Fecova*[1,2], K. Richter[1,3] and R. Varga[2] *1. Department of Physics of Condensed Matters, Pavol Jozef Safarik University in Kosice Institute of Physics, Kosice, Slovakia; 2. Center for Progressive Materials, Pavol Jozef Safarik University in Kosice, Technology and Innovation Park, Kosice, Slovakia; 3. Institute of Materials Science, Kiel University, Kiel, Germany*

Fast domain wall motion is a required tool in modern magnetic sensors and spintronic devices. One of the materials characteristic by fast domain walls are amorphous magnetically bistable microwires. Their unique properties make them an ideal material to study the domain wall dynamics which

can be controlled by various parameters. One of them is a perpendicular magnetic field. Despite the cylindrical shape of the microwires, it has been presented that the domain wall velocity was increased in a perpendicular field of one direction and decreased in another one [1]. Additionally, it has been shown in a previous paper that by combining the perpendicular magnetic field and proper rotation of the microwire it is possible to enhance the domain wall velocity [2]. This is due to a gradient of a perpendicular magnetic anisotropy in a cross-section of the cylindrical microwires induced during fabrication (Fig. 1). In this work, we present the influence of the perpendicular magnetic field on the domain wall velocity in microwires with the different gradient of the perpendicular magnetic anisotropy in the cross-section. The gradient of the perpendicular magnetic anisotropy can be expressed as a ratio of the diameter of the metal core *d* to the total diameter of the microwire *D*. The higher the value of the ratio, the larger the effect of the perpendicular magnetic field. By preparing the microwires with a high *d/D* ratio, it is possible to fabricate materials strongly controlled by the perpendicular magnetic field. On the other hand, in the case of the microwires with a small *d/D* ratio, the effect of the perpendicular magnetic field is completely suppressed. Acknowledgement: This work was supported by Slovak Grant Agency VEGA 1/0053/19 and Slovak Grant Agency grant number APVV-16-0079.

[1] R. Varga et al, Physica Status Solidi A, Vol. 213, p. 356–362 (2016)
[2] L. Fecova, K. Richter and R. Varga, Acta Physica Polonica A, Vol. 137 (5), p. 849-851 (2020)

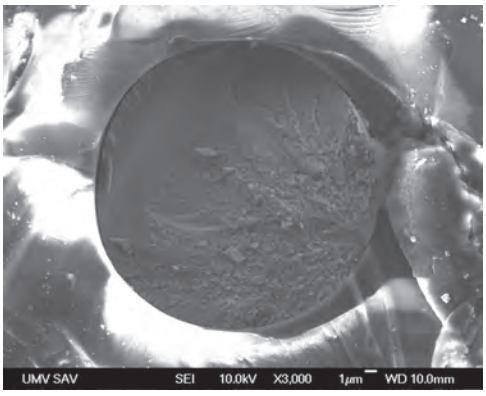

Fig. 1 SEM image of the microwire cross-section after annealing above crystallization temperature. The growth of crystals after annealing follows mechanical stresses in the cross-section of the microwire.

L3-06. Field Induced Uniaxial Anisotropy in Ferromagnetic Thin Films. *B. Nepal*[1], A. Pokhrel[1], M. Bruno[1], J. Cates[1], F. Brunson[1], D. Fox[1], A. Grice[1], J. Ingram[1], A. Leone[1], A. Lewis[1], C. Murray[1], L. Stoll[1], H. Trewin[1], T. Mewes[1], C. Mewes[1] and G. Mankey[1] *1. Physics and Astronomy, The University of Alabama, Tuscaloosa, AL, United States*

Thin films with high saturation magnetization deposited on semiconducting substrates have the potential to enable monolithic microwave integrated circuits (MMICs) operating at higher frequencies than conventional devices based on ferrites [1]. The ability to control the anisotropy in these films is a key requirement for use in high frequency devices. To demonstrate this ability, heterostructures of 2.5 nm Ru/50 nm FM/2.5 nm Ru, (FM = Co or $Fe_{60}Co_{40}$), were deposited by magnetron sputtering on native-oxide coated silicon substrates. The samples were deposited in the presence of a 20 mT in-plane bias field. The Ru underlayer is known to reduce the interfacial perpendicular anisotropy in transition metal films compared to SiO_2 [2] and the Ru overlayer protects the film from oxidizing in air. In addition to quasistatic magnetization reversal curves broadband ferromagnetic resonance measurements (FMR) and in-plane angle dependent FMR at 20GHz were used to determine the magnetic properties of the samples. This includes the saturation magnetization, the gyromagnetic ratio and the field induced in-plane anisotropy. We find that the bias field produces an easy axis along the bias field direction characterized by a uniaxial anisotropy field of 2.9 ± 0.1 mT for Co and 3.1 ± 0.1 mT for $Fe_{60}Co_{40}$. We also find a low effective damping parameter of 9.8×10^{-3} in Co and 3.4×10^{-3} in $Fe_{60}Co_{40}$.

1. Y. D. Zhang, S. H. Wang, J. I. Xiao et al., IEEE Trans. Mag. 37, 4 (2001).
2. J. B. Mohammado, G. Mankey, C. K. A. Mewes et al., J. Appl. Phys. 125, 023901 (2019).

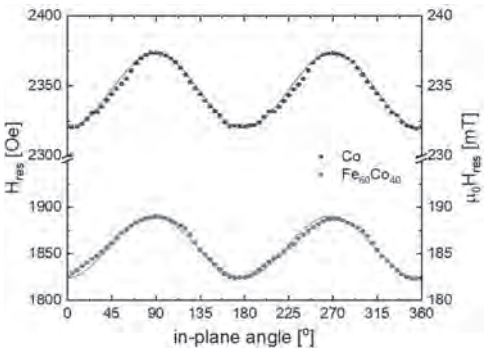

In-plane angle dependence of resonance field in Co and $Fe_{60}Co_{40}$ samples.

L3-07. Spin-Polarized Photocurrent in TbCo/FeCo Superlattice Observed via THz Time Domain Spectroscopy. *D. Khusyainov*[1], S.V. Ovcharenko[1], A. Buryakov[1], N. Tiercelin[2], V. Preobrajenski[3], E. Mishina[1] and A. Sigov[1] *1. Nanotechnology, MIREA Russian Technological University, Moscow, Russian Federation; 2. Universite de Lille, Lille, France; 3. Institut obsej fiziki imeni A M Prohorova RAN, Moscow, Russian Federation*

Recently, there has been a significant amount of interest in the areas of ultrafast magnetism and spintronics due to the search of faster methods to process and magnetically record information [1]. One of the most promising materials in the field of ultrafast magnetism and spintronics are heterostructures consisting of ferromagnetic and antiferromagnetic layers. In such structures, spin-polarized current can be excited by femtosecond laser pulses [2]. One example of such materials is an intermetallic superlattice of exchange-bonded nanolayers $TbCo_2$/FeCo, in which interlayer interaction shows ferrimagnetic pattern. Such structure possesses giant magnetostriction, a large coefficient of magnetomechanical coupling, controlled magnetic anisotropy and spin reorientation transitions, which can be generated by a magnetic field [3]. In this paper we investigated the spin-polarized photocurrent in a $TbCo_2$/FeCo superlattice by the THz time domain spectroscopy. The sample was grown on a SiO_2 substrate by cathode sputtering in magnetic field, which resulted in an in-plane anisotropy [4]. Optical pump beam illuminates the structure through the substrate and is focused on the superlattice. This allowed to excite spin-polarized currents in the superlattice, which generated an electromagnetic field in the THz range. The generated THz radiation was detected by electro-optical sampling [5]. The generation of THz radiation from a spintronic emitter based on $TbCo_2$/FeCo in the range from 0.1 to 3 THz was shown. The total phase change of the THz signal after switching the magnetization of the spintronic emitter was observed (Fig.1). The change of THz phase took place at the application of coercive field with the value ~ 10 mT. The work is supported by State Task for Universities FSFZ-0706-2020-0022 and RFBR (#18-52-16021)

1. Stanciu C. D. et al., Physical review letters, Vol. 99, p. 047601. (2007)
2. Huisman T. J. et al. Applied physics letters, Vol. 110, p. 072402.(2017)
3. A. Klimov et al, IEEE Trans. Magn., Vol. 42, p. 3090-3092 (2006). 4. N.Tiercelin et al. Journ of Mag. & Mag. Mat., Vol 249, p. 519-523 (2002).
5. Kovalev, S. P., G. Kh Kitaeva., JOSA B, Vol.30, p. 2650-2656 (2013)

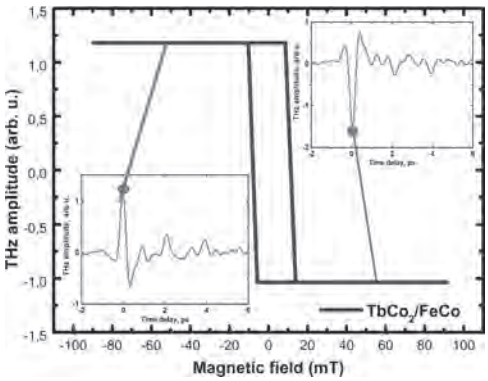

Fig. 1. Dependence of the THz emission amplitude on magnetic field applied in the easy axis direction. The insets show dependence of THz amplitude on time delay (the left one when the magnetic field is negative and the right one when magnetic field is positive).

L3-08. Influence of Induced Uniaxial Anisotropy in Silicon-Doped Yttrium Iron Garnet (YIG:Si) Film on Ultrafast Dynamics of Magnetization Excited by Femtosecond Laser Pulses. *S.V. Ovcharenko*[1], M.S. Gaponov[1] and E. Mishina[1] *1. Nanoelectronics, MIREA Rossijskij tehnologiceskij universitet, Moscow, Russian Federation*

With the development of the field of ultrafast magnetism [1], tremendous possibilities have been discovered for controlling magnetization without applying an external magnetic field. An excellent way to implement this control is through exposing to femtosecond laser pulses. This method demonstrates record-breaking low-power switching speeds for recording one bit of information [2]. Of particular relevance is the study of the possibility of ultrafast optical control of magnetization in dielectrics with small absorption in the spectral range of femtosecond lasers, due to the minimization of heat loss. The possibility of optical control of the magnetic order in YIG films with in plane magnetization was experimentally demonstrated [3]. Subsequently, all-optical switching was shown in Co-doped YIG films with cubic anisotropy [4]. However, the studies on photomagnetic method of recording information was very intensive in ninetieth, and its practical implementation using a CW laser was demonstrated in a silicon doped YIG single crystal [5]. Hence this material looks promising for ultrafast recording as well. In this work, we report the results of an experimental study of optically excited YIG:Si by femtosecond optical pump-probe technique. We reveal an influence of the strong anisotropy field on the spin precession parameters of this material. The azimuthal dependence of the amplitude of the spin precession is obtained. The maximum efficiency is observed when the external magnetic field is applied along the projection of the hard axis of the cubic magnetic anisotropy onto the film plane. A theoretical calculation of the magnetization dynamics based on the Landau-Lifshitz-Gilbert model. The work is supported by State Task for Universities (FSFZ-0706-2020-0022).

[1] E. Beaurepaire, J.-C. Merle, A. Daunois, and J.-Y. Bigot, Phys. Rev. Lett. 76, 4250 (1996). [2] A. V. Kimel and M. Li, Nat. Rev. Mater. 4, 189 (2019). 3 F. Hansteen, A. Kimel, A. Kirilyuk, and T. Rasing, Phys. Rev. B - Condens. Matter Mater. Phys. 73, 1 (2006). [4] A. Stupakiewicz, K. Szerenos, D. Afanasiev, A. Kirilyuk, and A. V. Kimel, Nature 542, 71 (2017). [5] V. Kovalenko, E.S.Kolezhuk, P.S.Kuts, Technical Physics Letters. 7(16):1012-1016 (1981)

L3-09. Time Dependence of Magnetic Moment of Strontium-Ferrite Powder Measured by Biaxial VSM. *T. Ahmed*[1], W.J. Geerts[1] and B. D.C.[1] *1. Material Science, Engineering and Commercialization, Texas State University System, San Marcos, TX, United States*

Strontium Ferrite magnetic nano-powder is being studied to be applied in magnetic 3D printer filament. Here we report on a study of the time dependence of its magnetic properties to better understand the permanent magnetic moment per unit volume of a nanocomposite containing the material [1,2,3]. Samples were made by loading up to 30 mg of OP-71 from Dowa Electronics Materials Company in a cylindrical custom design powder sample holder. Isotropic and anisotropic samples were made by loading the material in 0 field or in a field of 22,000 Oe. After loading the powder, the samples were compacted by compressing the powder along the cylindrical access. The typical samples were cylinders with a diameter of 2.5 mm and a length of 3 mm. The magnetic hysteresis curves of the samples were measured with a biaxial MicroSense Vibrating Sample Magnetometer (VSM) as a function of the field angle. For the isotropic samples, the average coercivity and the Mr/Ms were approximately constant as a function of the field angle for the Mx signal and were respectively 3402.35 Oe and 0.49. The shape of the M_x-hysteresis curves was independent of the field angle. For the anisotropic samples, the coercivities were around 3455 Oe (M_x curves). The Mr/Ms of the anisotropic samples depends on the field angle and varies from 0.41 along the hard axis to 0.64 along the easy axis. The coercivity of the My curves is around 4373 Oe. The coercivity of the anisotropic data seems to be larger than that of the isotropic sample due to the orientation of the crystallites. The time dependence of the M_x/M_s and M_y/M_s signals after a field step from saturation were measured for both the isotropic and anisotropic samples. The time derivative of the magnetization normalized on the Ms (S) depend on the field magnitude and shows a maximum. For the M_x signal this maximum coincides with the sample's coercivity. The S(H) for the anisotropic curve for the M_y signal is shifted to larger fields as shown in the graph below. This work was supported in part by NSF through an DMR-MRI Grant under Award 1726970.

[1] reference of strontium ferrite, maybe original philips patent. [2] R. Street, J. C. Wooley, Proc. Phys. Soc. London, Sect. A 62 (1949) 562. [3] L. Neel, Ann. Geophys. 5 (1949) 99.

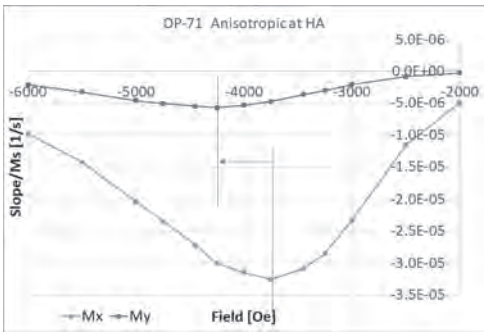

Fig. 1: Time dependence of anisotropic sample as a function of field.

L3-10. Effect of the Ga Composition on the Soft and High-Frequency Magnetic Properties of $Fe_{85.1-x}Ga_xB_{14.9}$ Thin Films. *S. Muramatsu*[1], T. Miyazaki[3] and Y. Endo[1,2] *1. Graduate School of Engineering, Tohoku University, Sendai, Japan; 2. Center for Science and Innovation in Spintronics, Tohoku University, Sendai, Japan; 3. Faculty of Engineering, Tohoku University, Sendai, Japan*

Recently, to achieve faster, smaller, and more energy efficient devices for information and communications technologies, much attention have been focused on Fe-Ga films. Until now, we investigated the magnetization dynamics of Fe-Ga polycrystalline films, and suggested that further study to appreciably reduce damping constant (α) for these highly magnetostrictive films are strongly desired from technological standpoints because of wide FMR widths and high α [(1)] for these films. Herein, to improve the soft magnetic properties and high-frequency magnetic properties of Fe-Ga films, we prepare 10-nm-thick B-doped Fe-Ga films with different Ga composition (x) and discuss the structures and magnetic properties of films in detail. As for static magnetic properties of every thin film, the uniaxial anisotropy appears and coercivity (H_c) are much lower than those of Fe-Ga films[(1)]. As shown in Fig. 1(a), the saturation magnetostriction (λ_s) increases for $x \leq 21.8$ at.%, decreases for 21.8 at.% $\leq x \leq$ 24.5 at.%, and further increases again for $x \geq 24.5$ at.%. Their values becomes approximately 49 - 67 ppm,

and are higher than that of amorphous $(Fe_{80}Ga_{20})_{0.85}B_{15}$ films (50 ppm)[2]. On the other hand, as for high-frequency magnetic properties of these films, the damping constant (α) increases slightly for $x \leq 20.8$ at.%, decreases for 20.8 at.% $\leq x \leq$ 24.5 at.%, and further increases for $x \geq 24.5$ at.% (Fig. 1(b)). This trend is similar to that of λ_s. The α values becomes 0.006 - 0.010 and are much lower than those of Fe-Ga binary alloys films [1], [3], which might be attribute to both the structural characteristics and the static magnetic properties. Therefore, these results demonstrate that B-doped Fe-Ga thin films possess good soft magnetic properties and high-frequency magnetic properties compared to the conventional Fe-Ga films.

(1)Y. Kawabe, Y. Endo and T. Miyazaki, T.Magn. Soc. Jpn. (Special Issues), 3, 34-38 (2019). (2)J. Lou, R. E. Insignares and Z. Cai, APPLIED PHYSICS LETTERS 91, 182504 (2007). (3)Daniel B. Gopman, Vimal Sampath and Hasnain Ahmad, IEEE TRANSACTIONS, VOL. 53, No.11, (2017).

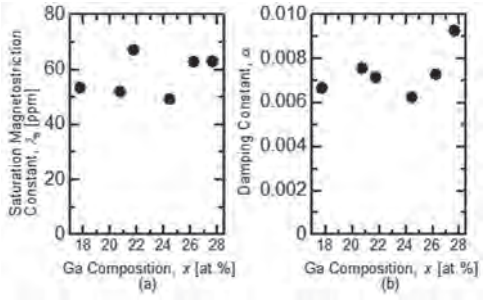

Fig.1 Change in magnetic properties of $Fe_{85.1-x}Ga_xB_{14.9}$ 10 nm thin films with Ga composition.

L3-11. Realization of Ferromagnetic Resonance in 1nm Co Ultrathin Film. *S. Yoshii*[1], R. Ohshima[1], Y. Ando[1], T. Shinjo[1] and M. Shiraishi[1]
1. Kyoto Daigaku, Kyoto, Japan

Physics in nanometer-thick metallic films has been attracting many researchers because of abundant spintronics nature. In ultrathin films, some physical properties, such as the spin-charge conversion [1] and ferromagnetism [2], are gate-tunable. To extend further potential of ultrathin metallic films in spintronics, we demonstrate ferromagnetic resonance (FMR) in a 1 nm-thick ultrathin Co film [3], which exhibits sufficiently small FMR resonance field and narrow FMR linewidth simultaneously, for future realization of tunable magnon excitation. We prepared SiO_2 (capping layer)/Co (t_{Co})/SiO_2 (Sample A), where t_{Co} was set to be 1, 2, 3 and 5 nm, and SiO_2 (capping layer)/Co (1 nm)/Ta (3 nm)/SiO_2 (Sample B). The Co was grown by using magnetron sputtering. The sample was placed in the center of an electron spin resonance (ESR) cavity (TE_{011}) and FMR spectra were measured. The external dc magnetic field (H_{ex}) and ac magnetic field ($\boldsymbol{h}_{rf}$) were applied along the in-plane direction of the film as shown in Fig. 1. Figure 2 shows comparison of the FMR spectra between Sample A (t_{Co} = 1 nm) and Sample B. Whereas the thickness of the Co of both samples are the same, the clear FMR signal was observed only from Sample B, where the half-width at half-maximum and the resonance field were comparable to that of the bulk Co system. The results directly indicate that the insertion of 3 nm-thick Ta plays a dominant role for generating FMR in the ultrathin Co film. Furthermore, the narrow linewidth and the low resonance field indicate that the ultrathin Co film simultaneously possesses uniform and strong magnetization, which has not been achieved previously [4,5]. The successful detection of FMR from ultrathin Co enables efficient magnon excitation that is gate-tunable. More detailed discussion will be given in the presentation.

[1] S. Dushenko, M. Shiraishi *et al.,* Nat. Commun. 9, 3118 (2018). [2] D. Chiba *et al.,* Nat. Mater. 10, 853 (2011). [3] S. Yoshii, M. Shiraishi *et al.*, submitted. [4] S. T. Purcell *et al*., J. Appl. Phys. 69, 5640 (1991) [5] R. *Gieniusz et* al., J. Magn. Magn. Mater. 272-276, E911 (2004)

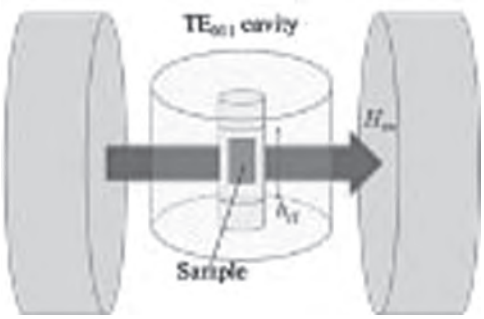

ESR measurement setup

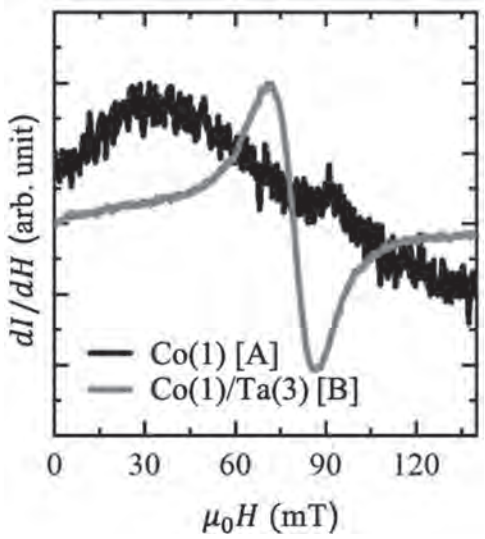

FMR signals of Sample A (t_{Co} = 1 nm, the solid black line) and Sample B (the solid red line)

L3-12. Ferromagnetic Resonance and Micromagnetic Simulations of FeSiB Amorphous Thin Films. *G. Soares*[1], F. Celegato[1], F. Garcia-Sanchez[2], G. Barrera[1], M. Pasquale[1] and P. Tiberto[1] *1. Istituto Nazionale di Ricerca Metrologica, Turin, Italy; 2. epartamento de Fisica Aplicada, Universidad de Salamanca, Salamanca, Spain*

The periodic structure of weak stripe domains in Fe based thin films has recently received renewed attention due to the possibility of propagation of spin waves for magnonics applications [1]. Fe based films with stripe domains have extensively been studied in the past decades [2,3]. Due to a weak out of plane (OOP) anisotropy associated to magnetostriction, these domains have a magnetization slightly tilted out-of-plane. Ferromagnetic resonance measurements were performed on selected amorphous FeSiB thin films having thickness of up to 230 nm as a function of their stress relieving annealing temperatures. The absorption spectra obtained with an in-plane external field show a double FMR peak structure that becomes a single uniaxial Kittel mode near saturation. The OOP anisotropy was characterized by the Kittel formula, and due to the in-plane stress-relief, the anisotropy field increases with increasing annealing temperatures; moreover, it was found to be quantitatively consistent with hysteresis loops measurements obtained by a Vibrating Sample Magnetometer [4]. The FMR linewidth analysis yielded an extremely low magnetic damping of 10^{-3}, which is of great interest for the propagation of spin waves. Micromagnetic simulations were then performed in order to verify the double peak structure and investigate spatially the respective modes.

[1] I. S. Camara et al. J. Condens. Matter 29 (2017) 465803 [2] O. Acher et al. J. Appl. Phys. 81 (8) (1997) 40058 [3] C. Zhou et al. J. Phys. D. Appl. Phys. 48 (2015) 265001 [4] M. Coïsson et al. J. Appl. Phys. 104 (2008) 03390

L3-13. Reconfigurable and Bias-Field-Free Microwave Properties in C-, L- and S-Shaped Nanomagnets. *K. Begari*[1] and A. Haldar[1] *1. Physics Department, Indian Institute of Technology Hyderabad, Hyderabad, India*

Self-biased nanomagnets (NMs) and their arrays with different remanent states associated with distinct dynamic responses are found to be promising for miniaturization of the microwave devices. However only a few nanostructures are reported so far with such functionality based on dipolar coupled nanopillars, nanowires, rhomboid shaped NMs, arrow-shaped NMs, and nanomagnetic multilayers [1-5]. Here, we present reconfigurable microwave properties based on C-, L- and S-shaped NMs that operate without any external bias field. Single layer arrays, isolated multilayers and networks of multilayers samples have been designed from these three type of NMs [6]. We have used micromagnetic simulation technique using OOMMF software to investigate magnetic and ferromagnetic resonance (FMR) properties. Shown in Fig. 1(a) are the arrays made from C, L and S-shaped nanomagnets which are labelled as CNM-A, LNM-A and SNM-A, respectively. When the initilization field (~ 2000 Oe) is applied along *y*-axis (*x*-axis) followed by removal of the field, we have obtained a remanent state which is denoted as Y-state (X-state). Figure 1(b) show the FMR spectra of the CNM-A, LNM-A, and SNM-A, for two different remanent states. We have identified different types of modes which are marked using two different symbols: triangle (localized at the arms of the NMs) and ● (central part of the NMs) and star (nodal lines near the central portion of the NMs). We have observed a frequency shift (●-labelled modes) of 700 MHz, 500 MHz and 300 MHz for CNM-A, LNM-A and SNM-A, respectively. The origin of the frequency shift has been attributed to the variation of the dipolar fields for two different remanent states. We have also investigated the multilayers of these nanostructures and we have found remarkably large frequency shifts (> 2.5 GHz) in the multilayers structures. In addition, the remanent states can be switched by using a sub-ns magnetic pulse which is suitable for ultrafast reconfiguration. The results have potential implications for the realization of reprogrammable microwave devices at nanoscale.

[1] R. Verba, G. Melkov, V. Tiberkevich, A. Slavin, Appl. Phys. Lett. 100, 192412 (2012). [2] G. Gubbiotti, P. Malagò, S. Fin, S. Tacchi, L. Giovannini, D. Bisero, M. Madami, G. Carlotti, J. Ding, A. O. Adeyeye, R. Zivieri, Phys Rev B 90, 024419 (2014). [3] J. Topp, D. Heitmann, M. P. Kostylev, D. Grundler, Phys. Rev. Lett. 104, 207205 (2010). [4] A. Haldar, A. O. Adeyeye, ACS Nano 10, 1690-1698 (2016). [5] B. Krishna, A. Haldar, J. Phys. D: Appl. Phys. 51, 275004 (2018). [6] K. Begari and A. Haldar, J. Phys. D: Appl. Phys. 52, 335003 (2019)

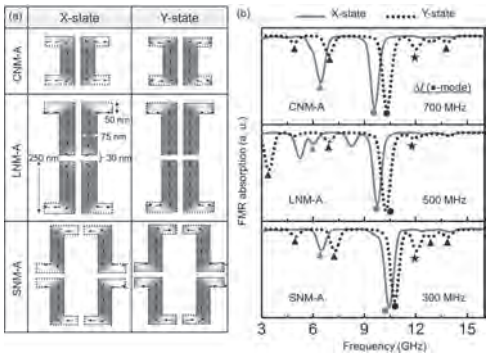

Figure 1. (a) Remanent magnetic configurations for the X-state and Y-states. (b) FMR spectra of single-layer arrays CNM-A, LNM-A, and SNM-A.

L3-14. Electromagnetic Wave Absorption and Resonance in Infinite Cobalt Nano-Prisms. *M. Aziz*[1] and C. McKeever[2] *1. Engineering, University of Exeter, Exeter, United Kingdom; 2. Physics, University of Exeter, Exeter, United Kingdom*

There is increased interest in conductive ferromagnetic materials and structures due to their higher moments and compatibility with semiconductor fabrication methods and technology. They offer enhancement in resonance frequencies and higher permeabilities in composites and nano-structures for applications in telecommunications and wave absorption [1,2]. The electromagnetic wave interaction with conductive ferromagnetic structures in these applications is complex due to coupling of both electric and magnetic fields with the magnetic material. This leads to non-uniform electromagnetic fields with different skin depths (both non-magnetic and magnetic). Early theoretical work focused on simple and saturated magnetic structures, excited in the linear region with uniform fields and involved solving the linearised system of Maxwell's equations and the Landau-Liftshitz equation for simplicity. This included planar structures [3], thin-films [4], and infinite cylinders [5]. Practical confined 2-D and 3-D magnetic structures found, for example, in composites have complex ground states and magnetic pinning, multi-layered with dielectrics, and experience non-uniform internal electromagnetic fields that yield complex precession and resonance modes that are not well understood. In this work, we solved the coupled system of Maxwell's and Landau-Lifshitz-Gilbert equations using a stable algorithm based on the finite-difference time-domain (FDTD) method to study the transient electromagnetic wave propagation and resonance in infinitely long cobalt nano-prisms with square cross-section of sides 50-1000 nm, excited by a 70 GHz plane wave [6]. The simulations revealed a curling exchange resonance mode excited by the induced axial current for prism sizes less than 100 nm. Larger prisms exhibited confined edge and corner resonance modes due to local power absorption and skin effects. The magnetic skin depth at resonance was estimated to be 50 nm from the calculated local power absorption spectra (see Fig. 1).

[1] Y. Shirakata; N. Hidaka, M. Ishitsuka, A. Teramoto, and T. Ohmi, IEEE Trans. Magn. 44, 2100 (2008). [2] Y-B. Feng, T. Qiu, C-Y. Shen, and X-Y. Li, IEEE Trans. Magn. 42, 363 (2006). [3] W. S. Ament and G. T. Rado, Phys. Rev. 97, 1558 (1955). [4] J. W. Hartwell, Proc. IEEE 56, 23 (1968). [5] L. Kraus, Czech. J. Phys. B 32, 1264 (1982). [6] M. M. Aziz and C. McKeever, Phys. Rev. Applied 13, 034073 (2020).

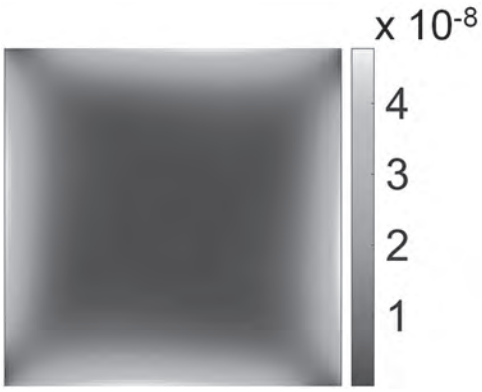

Fig. 1 Calculated local absorbed power in a 500 nm cobalt prism at the resonance frequency (intensity in W/m³).

L3-15. Optimization of Lumped Element Resonator via Total Capacitive Design and Coplanar Waveguide Configuration for Effective Magnon-Photon Coupling. *Y. Xiong*[1], Y. Li[2], T. Polakovic[2], R. Divan[2], J. Pearson[2], H. Qu[1], Z. Xiao[2,3], W. Kwok[2], W. Zhang[1] and V. Novosad[2]
1. Oakland University, Rochester, MI, United States; 2. Argonne National Laboratory, Lemont, IL, United States; 3. Northern Illinois University, DeKalb, IL, United States

We have investigated a magnetically sensitive lumped element resonator, which is capacitively-coupled to a coplanar waveguide transmission line that was fabricated by niobium nitride deposited on silicon substrate. The resonant frequencies f_r, quality factor Q of the resonators and the coupling strengths between the resonator and the transmission line can be tuned by varying the device geometries and dimensional parameters. Preliminary measurements of the resonator have been conducted at 1.5 K for optimal device performance. As a starting point, the relation between the dimension of the interdigitated electrodes of the resonator and the performance represented by the aforementioned parameters, were systematically studied. The position of the lumped element resonator relative to the transmission line, which is critical for the coupling efficiency, was also optimized through series structural design. The device demonstrates a resonant frequency of 4.05 GHz, with a coupling valley depth of 55 dB. The transmission characteristics were measured by connecting the device to a vector network analyzer and by applying a static magnetic field. Finite-element simulations show that the measured and simulated results, including the resonant frequencies and quality factor, were in good agreement.

Y. Li, *et al*. "Strong Coupling between Magnons and Microwave Photons in On-Chip Ferromagnetic-Superconductor Thin-Film Devices", *Phys. Rev. Lett.* 123, 107701 (2019)

Session L4
MAGNETO-ELASTIC AND MAGNETO-CALORIC MATERIALS III (Poster Session)

Brian Lejeune, Chair
Northeastern University, Boston, MA, United States

L4-01. The Effect of Mn Substitution by Co and Ni in Fe-Rich $(Mn,Fe)_2(P,Si)$. *A. Kiecana*[1], I. Batashev[1], A.I. Dugulan[1], N.v. van Dijk[1] and E. Brück[1] *1. Radiation, Science and Technology, Technische Universiteit Delft, Delft, Netherlands*

The use of magnetic cooling, which is based on the magnetocaloric effect (MCE), has emerged as a promising replacement for the conventional refrigeration technology. Among all known magnetocaloric materials, the $(Mn,Fe)_2(P,Si)$ family of compounds that crystallize in the hexagonal Fe_2P type of structure is considered as one of the most promising ones. Especially Mn-rich region of these materials has been extensively explored, since it was found that with additional amount of Mn it is feasible to obtain materials of a small hysteresis and exhibiting giant magnetocaloric effect in the room temperature region. Alternatively, it has been recently reported that compounds with additional Fe content might be also propitious due to larger magnetic moment. However, the thermal hysteresis originating from a first-order magnetic transition hampers practical application of these materials. The magnetocaloric properties and the structure of Fe-rich $(Mn,Fe)_2(P,Si)$ doped with Co and Ni ($Mn_{0.62-x}Fe_{1.33}Co_xP_{0.66}Si_{0.34}$ and $Mn_{0.62-x}Fe_{1.33}Ni_xP_{0.66}Si_{0.34}$) have been investigated. A decrease in thermal hysteresis, accompanied by a decrease in the Curie temperature (T_c) was observed upon Mn substitution by Co and Ni. A gradual decrease of the unit cell volume upon doping confirms substitutional effect of these elements, since Co and Ni have smaller radius than Mn. Moreover, a rapid increase of magnetization for a small doping of Co and Ni was revealed. An increase in Si content ($Mn_{0.56}Fe_{1.33}Co_{0.06}P_{0.66-x}Si_x$, $Mn_{0.58}Fe_{1.33}Ni_{0.04}P_{0.66-x}Si_x$) caused a further decrease in thermal hysteresis, accompanied by the increase in T_c to the desired temperature range for near room-temperature applications, while retaining a large MCE.

1. E. Brück, J. Phys. D. Appl. Phys., Vol. 38(23), pp. 381-391 (2005). 2. N. van Thang, N.H. van Dijk, E. Brück, Materials, Vol. 10(1), pp. 1–13 (2017). 3. Z.Q. Ou, N.H. Dung, L. Zhang, J. Alloys Compd., Vol. 730, pp. 392–398 (2018). 4. Z.Q. Ou, L. Zhang, N.H. Dung, J. Alloys Compd., Vol. 710, pp. 446–451 (2017).

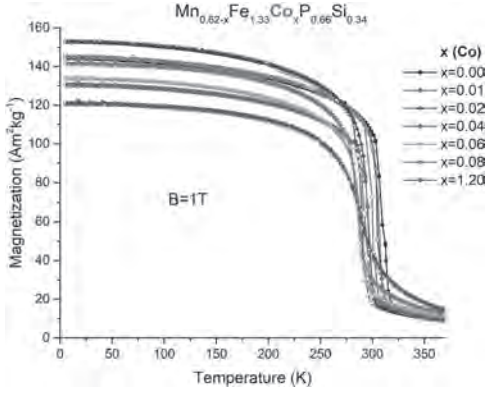

Fig. 1. Temperature dependence of the magnetization in the magnetic field of 1 T for $Mn_{0.62-x}Fe_{1.33}Co_xP_{0.66}Si_{0.34}$ upon heating and cooling.

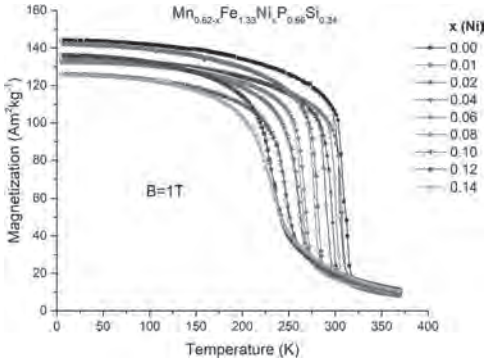

Fig. 2. Temperature dependence of the magnetization in the magnetic field of 1 T for $Mn_{0.62-x}Fe_{1.33}Ni_xP_{0.66}Si_{0.34}$ upon heating and cooling.

L4-02. Novel MnP Thin Films With Integrated Thermoelectric and Thermomagnetic Functionalities for Energy-Efficient Solid State Refrigeration. *C. Hung*[1], R.M. Madhogaria[1], A. Duong[2], R. Das[2], H. Pham[2], S. Cho[3], H. Srikanth[1] and M. Phan[1] *1. Physics, University of South Florida, Tampa, FL, United States; 2. Phenikaa Research and Technology Institute, Phenikaa University, Hanoi, Vietnam; 3. Department of Physics and Energy Harvest-Storage Research Center, University of Ulsan, Ulsan, The Republic of Korea*

A novel magnetic cooling device (MCD) that comprises thermoelectric (TE) and magnetocaloric (MC) materials is proposed, partially based on the previous work [1]. A sandwich structure, as shown in Fig. 1, has a MC material (MCM) in the center and two TE materials at the outer parts. The presence of the TE materials in the MCD guides the heat flow direction and enhances heat pulsation. In this case, the usage of a TE material that combines large TE with small MC responses within a similar temperature region enhances not only magnetic flux density but also heat exchange efficiency. In this study, we demonstrate that MnP thin films with integrated TE and MC functionalities are an excellent candidate for the proposed MCD. The MnP films were grown on Si substrates at 300, 400 and 500°C [2], and both the MC and TE effects were investigated systematically. The 400 °C sample shows the optimal TE and MC responses. A large TE effect is observed in the temperature region 250 – 400 K. The large power factor of 24.06 $\mu W\ m^{-1}\ K^{-2}$ is achieved at room temperature. In this temperature region, the film shows a small MC effect (~1.23 J/kgK at 5T) but a strong magnetic response that gives rise to the enhanced TE effect. These properties would enable the MCD to operate at high frequency.

[1] A. Kitanovski, and P. W. Egolf, Int. J. Refrig. 33.3,449464(2010). [2] A. T. Duong, T. M. H.Nguyen, D. L. Nguyen, R. Das, H. T. Nguyen, B. T. Phan, and S. Cho, J. Magn. Magn. Mater. 482,287291(2019).

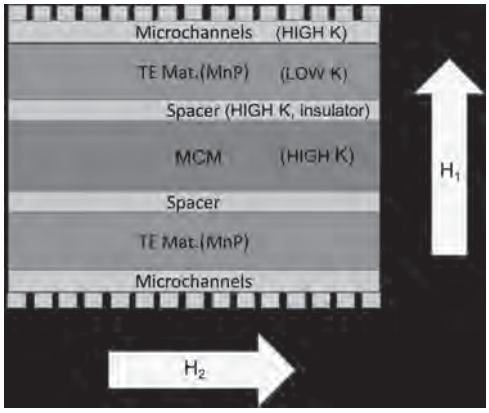

Fig. 1 A novel magnetocaloric-thermoelectric device designed as a layered structure.

L4-03. Structural and Magnetostrictive Properties of Fe-Ga-Tb Alloys: Density-Functional Theory Study. *M. Adelani*[1], S. Olive Méndez[1], F. Espinosa-Magaña[1] and M. Grijalva Castillo[1] *1. Material Physics, Centro de Investigacion en Materiales Avanzados, S.C., Chihuahua, Mexico*

In order to demonstrate that heavy rare-earth dopants with strong magnetocrystalline anisotropy can also induce giant magnetostriction in Galfenol, a heavy element Tb was selected as the third candidate to dope into $Fe_{81}Ga_{19}$ alloy. The lattice parameter, magnetic properties, magnetostriction, mechanical properties of Fe-Ga-Tb were investigated by Ab-initio method. Fe-Ga-Tb_x (x = 0, 0.78 and 1.85) were studied by the first-principle method using Vienna Ab initio Simulation Package (VASP). Our results show good qualitative agreement with experiment, in particular reproducing the lattice parameter, elastic constant and a high value of magnetostriction, which is yet to be reported using ab-initio. Doping of Tb with Fe-Ga improves the magnetostriction from the undoped value of 190 ppm (Fe-Ga) to 596 ppm (Fe-Ga-Tb). Our simulation also shows that all the composition study are mechanical stable and for the composition $Fe_{81}Ga_{19}$ and $Fe_{78.52}Ga_{19.63}Tb_{1.85}$ show the ductile nature, which is the characteristic of Galfenol system while for the composition $Fe_{79.38}Ga_{19.84}Tb_{0.78}$ exhibit brittle nature.

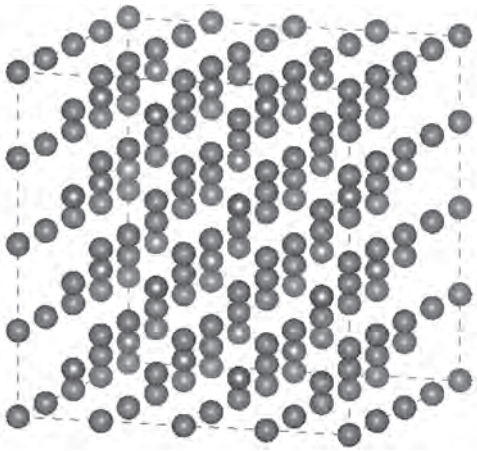

Figure 1: Crystal structure for the $Fe_{79.38}Ga_{19.84}Tb_{0.78}$ doped

L4-04. Structural and Magnetocaloric Properties $0.75La_{0.7}Ca_{0.3}MnO_3$/ $0.25La_{0.84}Sr_{0.16}MnO_3$ Nanocomposite. *P. Bisht*[1], M. .[1], A. Gaur[1] and R.N. Mahato[1] *1. School of Physical Sciences, Jawaharlal Nehru University, New Delhi, India*

The structural, magnetic and magnetocaloric properties of $0.75La_{0.7}Ca_{0.3}MnO_3$/ $0.25La_{0.84}Sr_{0.16}MnO_3$ nanocomposite material have been investigated. The parent nanocrystalline samples were prepared by sol-gel synthesis route. The crystal structure of the samples were analysed by Rietveld refinement of powder X-ray diffraction pattern [1]. The composite sample shows two structural phases, which corresponds to the both parent samples $La_{0.7}Ca_{0.3}MnO_3$ (Orthorhombic structure, Pbnm space group) and $La_{0.84}Sr_{0.16}MnO_3$ (Rhombohedral structure, space group) respectively. The Williamson-Hall method is used to evaluate the crystallite size and strain in the parent samples [2]. The values of crystallite size (D) and strain (ε) for $La_{0.7}Ca_{0.3}MnO_3$ (LC(3)) is 65 nm and 0.0009 respectively and for $La_{0.84}Sr_{0.16}MnO_3$ (LS(1)) is 37 nm and 0.0021. Homogeneity of the samples has been confirmed with scanning electron microscopy (SEM) images. The temperature dependent magnetization (M-T) data displays two successive transitions in composite sample at 155 K and 255 K that corresponds to the parent samples. M-T result is confirmed by using a numerical method expressed as a rule of mixtures sum. Fig.1 displays that for x = 0.6, our M-T data exactly coincides with the experimental magnetization data which means that there is no interaction between the particles of the composite sample. The maximum values of magnetic entropy change ($-\Delta S_M$) are observed to be 1.9 J/(kg-K) and 3.03 J/(kg-K) under a magnetic field change of 5 T for $La_{0.7}Ca_{0.3}MnO_3$ and $La_{0.84}Sr_{0.16}MnO_3$ respectively. The broadened temperature range is found in composite sample (LC-LS(3:1)), consequently the isothermal entropy change is reduced as shown in Fig. 1. An enhancement of 20% to 25% of relative cooling capacity is noticed in the composite sample as compared to the parent samples.

Reference: [1] H. M. Rietveld, J. Appl. Crystallogr. 2, 65 (1969) [2] P. Goel and K. L. Yadav, J. Mater. Sci. 4 2, 3928 (2007)

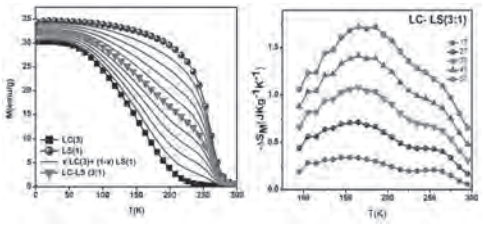

Fig. 1 (a)Magnetization vs. Temperature curve (b) Magntic entropy change ($-\Delta S_M$) vs. temperature at different applied fields for LC-LS(3:1) samples.

Sample	LC(1)	LS(3)	LC-LS(3:1)	
Space group	Pbnm	R3c	R3c	Pbnm
a (Å)	5.4658	5.50496	5.4800	5.4575
c (Å)	7.7156	5.50496	5.4800	7.7111
c (Å)	5.4817	13.35930	13.3586	5.5158
V (Å^3)	231.1741	350.628	347.4210	232.1221
χ^2	2.29	2.34	2.59	2.18
T_C(K)	155	255	-	-

Table 1 Lattice parameters, lattice volumes, convergence factors, Curie temperatures of $La_{0.7}Ca_{0.3}MnO_3$ (LC(1)), and $La_{0.84}Sr_{0.16}MnO_3$ (LS(3)) and composite (LC-LS(3:1))

L4-05. Thermoplastic Elastomers With Strontium Ferrite Particulate and Magnetic Annealing Used for Fused Deposition Modeling. *S. Ziemann*[1], N.A. Fischer[1], A. Robinson[1], T. Lee[1] and B. Nelson-Cheeseman[1] *1. Mechanical Engineering, University of Saint Thomas, Saint Paul, MN, United States*

Magnetorheological elastomers are smart materials that can deform and change shape based on the application of a magnetic field. These magnetic elastomers perform best in soft robotics and biomedical applications when they have increased anisotropy, or different properties along different axes. To increase this anisotropy, one can utilize hard magnetic particulate, magnetic annealing, and fused deposition modeling (FDM), also known

as 3D printing. Hard magnets can be oriented using an external alignment field, and strontium ferrite is specifically interesting because it costs less than other rare-earth magnets (or materials). FDM is usually a final step in creating anisotropy in a sample (1), and it allows magnetorheological elastomers components to be more accessible for other applications. Our thermoplastic magnetic elastomer composite is created using solvent-casting techniques with 15 vol% $SrFe_{12}O_{19}$ particulate. The material is then extruded into FDM filaments using a Filastuder. During the extrusion process, some filament is magnetically annealed in an axial applied field created by NdFeB magnets, while other filament extruded without magnetic annealing acts as the control. Mechanical stress vs. strain curves of the extruded filaments are acquired using an MTS tensile testing machine. Magnetic hysteresis loops are measured using a vibrating sample magnetometer (VSM). In order to determine the relative level of magnetic anisotropy within the samples due to these factors, hysteresis loops with the field applied parallel and perpendicular to the axis of extrusion are compared to one another. Magnetoactive testing is used to measure the mechanical deflection angle as a function of the strength of a transverse applied magnetic field. Understanding the mechanical, magnetic, and magnetoactive properties of this magnetorheological elastomer provides insight into how magnetic anisotropy can be controlled by a combination of hard magnetic particulate, magnetic annealing, and FDM for optimized performance.

1. Patton, et. al., "Manipulating magnetic anisotropy in fused filament fabricated parts via macroscopic shape, mesoscopic infill orientation, and infill percentage." *Additive Manufacturing*, Vol. 27, pp. 482-488 (2019).

L4-06. Large Magnetocaloric Effect due to Anhysteretic First-Order Transition in Pr_2in. *A. Biswas*[1], N.A. Zarkevich[1], A.K. Pathak[1,2], O. Dolotko[1], I.Z. Hlova[1], Y. Mudryk[1], A.V. Smirnov[1], D.D. Johnson[1,3] and V.K. Pecharsky[1,3] *1. Ames Laboratory, Ames, IA, United States; 2. SUNY Buffalo State College, Buffalo, NY, United States; 3. Department of Materials Science and Engineering, Iowa State University, Ames, IA, United States*

The design of the materials showing first-order magnetic transitions (FOMTs) with smallest possible thermomagnetic hysteresis stimulates considerable research interest because hysteresis can be detrimental for certain applications, such as solid-state caloric cooling [1]. The overwhelming majority of materials with a reasonably small hysteresis contain transition metals, and their behavior is closely associated with the itinerant-electron metamagnetism of the transition metals present in the system [2,3]. We observed anhysteretic FOMT in a lanthanide-based compound Pr_2In with the classical RKKY-type magnetic interaction between 4f electrons of trivalent Pr. Although such behavior is phenomenologically similar to Eu_2In, another lanthanide system showing hysteresis-free FOMT [4], the crystal structure and magnetic interactions in Eu_2In are markedly different from Pr_2In due to the presence of divalent Eu [4,5]. In the vicinity of ferromagnetic to paramagnetic transition temperature (T_C ~57 K) Pr_2In exhibits a large magnetic field-induced entropy change with the maximum value of $-\Delta S_M \sim 23$ J/kg K for $\Delta H = 50$ kOe, which is comparable to a number of other potential magnetocaloric materials in the temperature range of 40-80 K, reported in the literature [6]. The temperature and magnetic field dependence of ΔS_M can be expressed as $\Delta S_M \sim H^n$, where the local exponent *n* varies with both H and T, showing a clear maximum with $n>>2$, a characteristic feature of FOMT [7]. The observation of anhysteretic FOMT and a large MCE in Pr_2In with conventional RKKY-type magnetic exchange promises further advancements in developing novel functional caloric materials by manipulating electronic structure of 4f-based materials. Acknowledgement: This work was performed at Ames Laboratory and was supported by DMSE, BES, Office of Science of the U.S.DOE. Ames Laboratory is operated for U.S DOE by Iowa State University under Contract No. DE-AC02-07CH11358.

1. N. A. Zarkevich et al., Journal of Alloys and Compounds 802, 712-722 (2019). 2. F. X. Hu et al., Applied Physics Letters 78, 3675 (2001) 3. A. Fujita et al., Physical Review B 67, 104416 (2003) 4. F. Guillou et al., Nature Communications 9, 2925 (2018). 5. A. Biswas et al., Physical Review B 101, 224402 (2020). 6. L. Li et al., Journal of Alloys and Compounds 823, 153810 (2020). 7. J. Law et al., Nature Communication 9, 2680 (2018).

L4-07. Influence of Ni/Mn Concentration on the Magnetocaloric Effect in $Ni_{43+x}Mn_{46-x}Sn_{11}$ (x = 0; 1) Heusler Alloys. *S. Emelyanova*[1] and V. Marchenkov[1,2] *1. UB RAS, M.N. Mikheev Institute of Metal Physics, Ekaterinburg, Russian Federation; 2. Ural Federal University named after the first President of Russia B.N.Yeltsin, Ekaterinburg, Russian Federation*

Discovery of the giant magnetocaloric effect (MCE) in interrmetallic $Gd_5(Si_2Ge_2)$ [1] led to an increase the interest in the materials with large MCE due to the possibility of their practical application as a working body [2] in magnetic cooling devices. Recently so-called shape-memory ferromagnets based on Heusler alloys Ni-Mn-Z (Z = Ga, In, Sn, Sb) began to be considered as the promising materials. For example, for $Ni_{50}Mn_{35}Sn_{15}$ the value of $\Delta S = 14{,}2$ J/(kgK) at 187 K in a magnetic field of 50 kOe [3]. The aim of this work was to study the effect of variation in chemical composition (the relative concentration Ni/Mn) on the MCE in $Ni_{43+x}Mn_{46-x}Sn_{11}$ (x = 0; 1) Heusler alloys. Ingots were prepared by arc melting in an inert atmosphere and subsequently subjected to annealing at 1100 K for 24 h followed by furnace cooling. The elemental analysis and X-ray diffraction studies were performed. The magnetic and galvanomagnetic properties were measure at the Atomistitut, TU Wien using an MPMS XL7 (Quantum Design) SQUID magnetometer. The magnetic properties were measured in magnetic fields of up to 70 kOe in the temperatures range 150-330 K. As a result of this work it was established that the variation in the chemical composition does not lead to a significant change of the maximum value of the magnetocaloric effect ($\Delta S = 44$ J/(kgK) and 40 J/(kgK) for $Ni_{43}Mn_{46}Sn_{11}$ and $Ni_{44}Mn_{45}Sn_{11}$, respectively), but shift its maximum (≈ 32 K). It was found that in the investigated alloys a change in the relative concentration Ni/Mn (and hence the e/a) does not significantly influence on the value of Curie temperature T_C. The results of this work were obtained within the state assignment of the Ministry of Education and Science of the Russion Federation (theme "Spin" No. AAAA-A18-118020290104-2) and supported in part by RFBR grant (project No. 18-02-00739).

[1] V.K. Pecharsky, K.A. Gschneider, Physical Review Letters, Vol. 78, p. 4494 (1997) [2] V.K. Pecharsky, K.A. Gschneider, Journal of Magnetism and Magnetic Materials, Vol. 200, p. 44 (1999) [3] T. Krenke, E. Duman, M. Acet, E.F. Wassermann, X. Moya, L. Mañosa, A. Planes, Nature Materials, Vol. 4, p. 450 (2005)

L4-08. On the Synthesis and Magnetocaloric Behavior of the $Ni_{37.5}Co_{12.5}Mn_{35}Ti_{15}$ Quaternary Alloy. *M. López*[1], J. Zamora Mendieta[1], C.F. Sánchez Valdés[2] and J.L. Sánchez Llamazares[1] *1. División de materiales avanzados, Instituto Potosino de Investigacion Cientifica y Tecnologica AC, San Luis Potosi, Mexico; 2. División Multidisciplinaria, Universidad Autonoma de Ciudad Juarez, Juarez, Mexico*

The remarkable caloric effects around room temperature associated to the first-order martensitic-type transition found in the newly reported all-3d-metal Ni-Mn-Co-Ti alloys are a source of motivation for their investigation. In a recent work, it has been reported that $Ni_{37.5}Co_{12.5}Mn_{35}Ti_{15}$ melt-spun ribbons show one of the largest maximum magnetic entropy change for a magnetic field change of 2 T [1]. In the present study, we chosen the same alloy composition as a reference and fabricated melt-spun ribbons at a linear speed of the rotating copper wheel of 20 and 8 m/s; the structural transition, magnetic and magnetocaloric properties were studied for as-solidified and thermally annealed samples for 30 min. at temperatures between from 973 K to 1173 K. Ribbon samples undergo a martensitic transformation from a B2-type ferromagnetic austenite (AST) with a Curie temperature of 328 K to a 5M monoclinic martensite (MST), whereas SEM images evidenced that microstructure is formed by columnar in shape elongated grains with their major axis oriented along the thermal gradient during solidification. For thermally annealed samples, the temperature of the MST-AST transformation increases linearly with the heat treatment temperature. Magneto-structural transition for as-solidified ribbons obtained at 20 m/s occurs around room

temperature, but the reduction of the linear speed to 8 ms^{-1} shifts the structural transition to the paramagnetic region. For a magnetic field change of 2 T, as-solidified ribbons obtained at 20 m/s showed a maximum magnetic entropy change $|\Delta S_M|^{max}$ of 13.8 (9.5) $Jkg^{-1}K^{-1}$ for the MST-AST (AST-MST) transformation; this is below the reported in Ref. 1 (27.2 $Jkg^{-1}K^{-1}$) [1], a fact that is mainly explained because the samples show a well broader magnetostructural transition (and therefore a larger refrigerant capacity).

1. H. Neves Bez *et al.*, *Acta Mater.* 173 (2019) 225–230.

L4-09. Thermal Cycling Influence on the Thermomagnetic Properties of Ni-Mn-Sn Based Magnetic Shape Memory Alloys. A. Wederni[1], J. Saurina[1], M. Escoda[1], M. Ipatov[2], j. gonzalez[2] and *J. Suñol*[1] *1. Universitat de Girona, Girona, Spain; 2. University of Basque Country, San Sebastián, Spain*

In this work we analyze the influence of thermal cycling on the thermomagnetic behavior and microstructure of several magnetic shape memory alloys (Ga free Heusler Ni-Mn-Sn alloys with minor additions of Ti, Cu or Pd). The shape memory effect can be not only controlled by changing the temperature and/or the pressure, as it occurs in traditional shape memory alloys, but also by varying the magnetic field up to moderate field values [1]. These alloys have both magnetic and martensitic structural transformation. The hysteretic process and the magnetic response are usually analyzed in the literature during the first (or second) cycle [2]. Nevertheless, the applicability of these materials in magnetic refrigeration (due to the magnetocaloric effect) is based on the maintenance of this effect after cycling. Alloys with good thermal and structural stability are candidates for cycling applications. We have performed one hundred cooling-heating thermal cycles on several Ni-Mn-Sn based alloys doped with a fourth element. After cycling, both the microstructure (as determined by analysis of X-Ray diffraction patterns) and the thermal behavior (by differential scanning calorimetry) is found to be stable in all samples with one exception. In this case, after cycling it appears a pre-martensitic phase. Nevertheless, thermomagnetic analysis (vibrating sample magnetometry) show that magnetization and the magnetocaloric response were reduced at around 25%.

[1] J.D. Santos, T. Sánchez, P.Álvarez, M.L. Sánchez, J.L. Sánchez-Llamazares, B. Hernando, L. Escoda, J.J. Suñol, R. Varga, J. Appl. Phys. 103 (2008) 07B326 [2] H. Rekik; M. Krifa; T. Bachaga; L. Escoda; J. J. Suñol; M. Khitouni; M. Chmingui, International Journal of Advanced Manufacturing Technology 90 (2017) 291

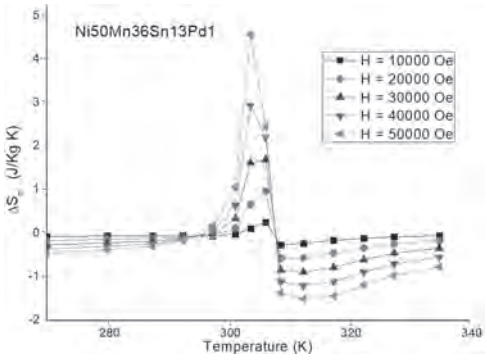

L4-10. Magnetic Annealing of Extruded Thermoplastic Magnetorheological Elastomers for 3D-Printing via FDM. *N.A. Fischer*[1], A. Robinson[1], T. Lee[1], T. Calascione[1], L.J. Koerner[2] and B. Nelson-Cheeseman[1] *1. Mechanical Engineering, University of Saint Thomas, Saint Paul, MN, United States; 2. Electrical & Computer Engineering, University of Saint Thomas, Saint Paul, MN, United States*

Magnetorheological elastomers (MREs) are magnetoactive smart materials that exhibit mechanical deformation in the presence of magnetic fields. The greatest MRE performance is seen from magnetic annealing, which creates high internal anisotropy. It is hypothesized that increased anisotropy from Fused Deposition Modeling (FDM, extrusion-based 3D-printing) could also increase MRE performance. Alignment of magnetic particulate within the material used in this process would further bolster the anisotropy and, thus likely, the magnetoactive response of the printed part. This work studies how different magnetic annealing setups can be applied to thermoplastic MRE extrusion geometries and how each setup effects resulting magnetoactive properties. Three different magnetic fields were used in the annealing process: no magnetic field (0M), stronger field (5M), and weaker field (3M). The magnetic annealing setup was composed of four stacks of NdFeB magnets arranged longitudinally around the extrusion path for an axial applied field. 0M had no magnets, 5M had 5 NdFeB magnets, and 3M had 3 NdFeB magnets each separated by a steel spacer acting as a saturated magnet. A map of each magnetic vector field was characterized in 3D using a gaussmeter mounted to a robotic arm. Despite the different number of rare-earth magnets, the non-zero fields had fairly minimal differences. Both non-zero magnetic annealing setups generated greater magnetoactive response in the final MRE than zero field (Fig 1). Between the two non-zero fields the stronger field gave the greatest response but was difficult to make samples with. This work demonstrates that both magnetic annealing setups can enhance performance over no magnetic field; while the preferred setup may depend on a compromise between enhanced performance with ease of extrusion.

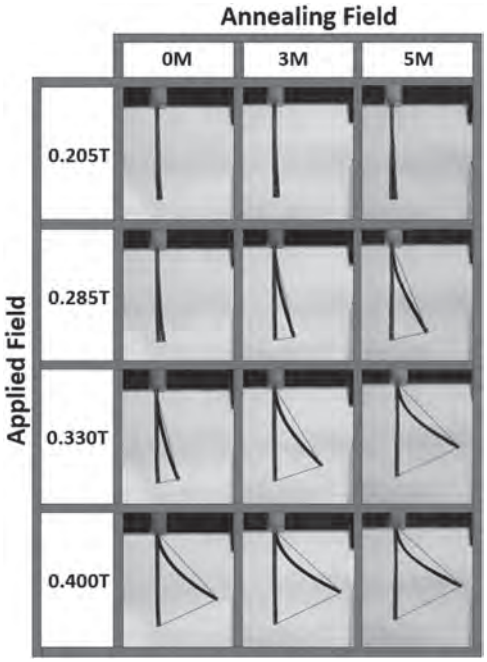

Figure 1: Deformation of each sample type under increasing transverse applied field along with an overlay of the sample at no magnetic field.

L4-11. Magnetic and Magnetocaloric Properties of Tb_5Si_4. *V. Khovaylo*[1,2], S.V. Taskaev[3,2], K. Skokov[4], M.N. Ulyanov[3], D. Bataev[3], M.Y. Bogush[3], D. Plakhotskiy[3], M. Kononova[1,3] and Z. Hu[5] *1. National University of Science and Technology MISiS, Moscow, Russian Federation; 2. National Research South Ural State University, Chelyabinsk, Russian Federation; 3. Department of Physics, Chelyabinsk State University, Chelyabinsk, Russian Federation; 4. Technische Universitat Darmstadt, Darmstadt, Germany; 5. University of Science and Technology Beijing, Beijing, China*

Considerable progress in the development of materials for room-temperature magnetic refrigeration has renewed interest to the materials which are perspective for cryogenic gases liquefactions. Numerous studies have identified a large variety of materials which exhibit a sizable magnetocaloric effect (MCE) in a temperature region of interest, from 15 to 150 K [1]. Almost all

these materials are rare-earth-based intermetallic compounds RTX, R_5T_4, R_3T, and RT_2 (R is a rare-earth metal, T is a 3*d* or 4*d* transition metal and X is the main group chemical element). Considering rapid development of superconducting magnets which can generate magnetic fields of 15 – 22 T, study of MCE in high magnetic fields is of considerable interest for the development of perspective technologies for cryogenic magnetic refrigeration. In this sense, there is a need to revisit magnetocaloric properties of the rare-earth-based intermetallic compounds and to study them in a wider range of applied magnetic fields. Among the rare-earth compounds, binary R_5T_4 systems have received smaller attention, as compared to intensively studied RTX or RT_2 systems [1]. For example, Tb_5Si_4 which order ferromagnetically at Curie temperature $T_C \sim 225$ K, undergoes another magnetic phase transition at lower temperatures [2,3]. Although magnetocaloric effect, specifically, isothermal magnetic entropy change, has been reported for Tb_5Si_4 in the vicinity of the Curie temperature T_C [4], no information is available in the literature on MCE around low-temperature magnetic phase transition of this materials. In order to better characterize magnetocaloric properties of Tb_5Si_4, we prepared polycrystalline sample of this compound and measured its structural and magnetic properties. The isothermal magnetic entropy change was calculated from the results of magnetic measurements performed in a wide temperature interval covering both T_C and the low-temperature magnetic transition at ~70 K. Direct measurement of MCE revealed that the adiabatic temperature change in Tb_5Si_4, reaches value up to 4 K, which is of interest for practical applications. The authors gratefully acknowledge for financial support RSF-Helmholtz project # 18-42-06201.

[1] H. Zhang, et al., Physica B 558, 65 (2019). [2] C. Ritter, L. Morellon, P. A. Algarabel, C. Magen, and M. R. Ibarra, Phys. Rev. B 65, 094405 (2002). [3] Y. I. Spichkin, V. K. Pecharsky, and K. A. Gschneidner, Jr., J. Appl. Phys. 89, 1738 (2001). [4] L. Morellon, C. Magen, P. A. Algarabel, M. R. Ibarra, and C. Ritter, Appl. Phys. Lett. 79, 1318 (2001).

L4-12. Thermal Switches in Solid State Magnetic Refrigeration: Conductivity Change Requirements and Effects. *D. Silva*[1], A. Pereira[1], J. Ventura[1], J. Araújo[1] and J. Oliveira[2] *1. IFIMUP, University of Porto, Porto, Portugal; 2. LAETA, University of Porto, Porto, Portugal*

The efficient use of energy has become a mainstay in the current world economic growth. The fact that approximately 30% of all energy consumed in the world is used in cooling and heating engines places refrigeration on the top of the priority lists of any modern economy [1]. In that respect, vapour compression is still the most used refrigeration technology, but requires bulky and noisy compressors. Alternative thermoelectric refrigerators are more compact and environmentally friendly, but at the cost of a much lower efficiency [2]. In a different rank, mainly due to its higher efficiency, is magnetic refrigeration (MR). With the discovery of the giant magnetocaloric effect by Percharsky and Gschneider, it is now possible to induce large temperature variations and develop MR applications near room temperature [3]. However, there are still obstacles to overcome, such as the use of moving parts and fluids that can easily reduce the working lifetime of the refrigerators. To solve these issues, the use of solid state thermal switches was proposed [4, 5]. Such thermal switches (TSs) are already used in space applications and cryogenics, although involving mechanical mechanisms. Even though some experimental results have been reported for Peltier based TSs, the performance of a fully solid state magnetic refrigerator making use of TSs has been addressed mostly by means of numerical simulations [4-6]. However, until now, the numerical studies always considered ideal TSs which behave as perfect insulators (k = 0) in the OFF state. In this work, we numerically searched for the most favourable thermal properties of non-ideal solid TSs. We based the TS properties on real materials, commonly used as thermal conductors, and simulated a percentage change of their conductivity (from 0% to 100%) for different operating frequencies (f) and working temperatures (T0). For each parameters combination, the temperature span between the hot and cold reservoirs was registered and mapped. Our results show that for high performance both thermal switches with near ideal behavior are required. However, for an intermediate performance, only one thermal switch with acceptable behavior is needed. We discuss all the possibilities.

[1] U. N. E. Programme, The importance of energy efficiency in the refrigeration, air-conditioning and heat pump sectors, Briefing note, 2018. [2] A. Majumdar, Nature Nanotechnology 4 (2009) 214. [3] V. K. Pecharsky et al., Physical Review Letters 78 (1997) 4494. [4] D. J. Silva et al., Applied Energy 93 (2012) 570. [5] D. J. Silva et al., Applied Energy 113 (2014) 1149. [6] D. J. Silva, et al., International Journal of Energy Research 43 (2018) 742.

L4-13. Optimization of Magnetic Refrigerant Capacity of Mn_5Ge_3 Alloy Near Room Temperature. *L. Bachhraj*[1], A. Rathi[1], A. Verma[1], B. Gahtori[1], R. Pant[1], P.D. Babu[2] and G. Basheed[1] *1. AcSIR, CSIR-National Physical Laboratory (NPL) Campus, New Delhi, India; 2. BARC campus, UGC-DAE Consortium for scientific research, Mumbai, India*

In search of potential replacement of highly expensive rare-earth metal (Gd) and its alloys [1-2] for environment friendly magnetic refrigeration technology [3] near room temperature, the earth-abundant Mn-based alloys, particularly Mn_5Ge_3 (T_C =297 K) [4], have got much attention with reasonably high relative cooling power (RCP). In this work, we undertake Mn_5Ge_3 alloy and optimize the synthesis, particularly excess Mn (to compensate evaporation loss) in arc melting method, followed by annealing conditions. The maximum magneto-caloric effect is observed for Mn_5Ge_3 alloy with ferromagnetic ordering at T_C = 299(2) K and M_S (at 5 K) =142 emu/g (by dc magnetization study) from arc melting synthesis with 5 % excess Mn and vacuum annealing at 800°C for 7 days. The magnetic ordering for optimized sample is further evaluated by detailed critical exponent study using modified Arrot plot (MAP) and scaling method gives second order phase transition at T_C = 297.5(1) K with exponents $\beta = 0.348(1)$ and $\gamma = 1.193(2)$, which lies in close proximity to 3D Heisenberg model. The magnetic isotherms are further employed to study the magneto-caloric effect. Using Maxwell equations, the change in magnetic entropy, $-\Delta S_{m|max}$ is calculated as 4.7 J/kgK at 5 T applied field; the field dependence of $-\Delta S_{m|max}$ follow power law behaviour, $-\Delta S_{m|max} \propto H^n$ with exponent, n = 0.62(1), in well consistent with n = 0.638 for 3D Heisenberg model. Finally, the material parameter for practical utilization in magnetic refrigeration i.e. $RCP = -\Delta S_{m|max} \times \delta T_{FWHM}$ is obtained as 450 J/kg for a field change of 5 T, which is significantly larger than earlier reported 388 J/kg for Mn_5Ge_3 synthesized with annealing at 750°C for 4 days. Although obtained RCP value is nearly 70 % that for the commonly used rare-earth Gd, importantly with production cost maximum 32 % only [see Table I] that makes Mn_5Ge_3 alloy highly promising for magnetic refrigeration application near room temperature

1. S. Y. Dankov, A. M. Tishin, V. K. Pecharsky, Phys. Rev. B 57, 3478 (1998) 2. S. Gorsse, B. Chevalier, and G. Orveillon, Applied Physics Letters 92, 122501 (2008) 3. C. Aprea, A. Greco, A. Maiorino, Journal of Physics: Conference Series 655, 012026 (2015) 4. T. Tolinski and K. Synoradzki, Intermetallic, vol. 47, pp. 1–5, (2014)

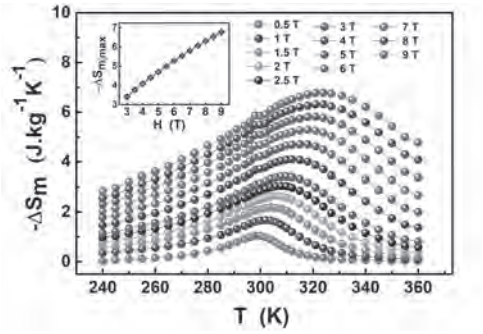

The temprature dependence of $-\Delta S_M$ in field range of 0.5-3T (ΔH =0.5T) & 4-9T (ΔH= 1T). The inset shows power law fit of $-\Delta S_{M|max}$ with applied field (in red)

Alloys & compound	T_C (K)	ΔS_m^{max} ($JKg^{-1}K^{-1}$)	ΔH (T)	RCP (JKg^{-1})	Cost per 100 gm (US dollar)	Reference
Gd	299 K	8	5	650	2976	[1]
$Gd_{68}Al_{16}Mn_{16}$	278 K	5.3	5	660	2389	[2]
Mn_5Ge_3	297 K	7.0	5	388	950	[4]
Mn_5Ge_3	299 K	4.7	5	450	950	This work

Comparison of magneto-caloric properties and material cost of Mn_5Ge_3 alloy with Gd based and other intermetallic system.

L4-14. A Study of Effect of Mechanical Preloads on Magnetorheological Elastomers Hysteresis Loop. *W.M. Kiarie*[1] and D.C. Jiles[2,1]
1. Materials Science and Engineering, Iowa State University, Ames, IA, United States; 2. Electrical and Computer Engineering, Iowa State University, Ames, IA, United States

In this work, an investigation of the effect of mechanical preloads on hysteresis loop of soft magnetorheological elastomers (MREs) was carried out. MREs are "smart" composite materials that consist of magnetic permeable particles in a non-magnetic elastomer[1]. When subjected to external magnetic field, a large deformational change occurs in the mechanical properties of these materials. Due to their coupled magnetomechanical response, MREs have been found suitable for a variety of engineering applications [2], [3]. Inspired by experimental work, we present a model of effect of mechanical preloads on magnetization response of MREs based on general continuum formulation[4]. Using the Jiles - Atherton (JA) model parameters calculated from experimental measurement, the hysteresis loop of isotropic MRE was numerically resolved, which was coupled to mechanical fields based on energetically constitutive model valid for finitely strained MREs [5]. Simulation analysis was performed for uniaxial stresses parallel to the direction of the applied magnetic field. For the applied tensile and compressive stresses as shown in Figs. 1 and 2, we observed a very small change in the magnetization of these materials. These results agree with the experimental work [6] whereby only a negligible change was observed in the magnetization response of MREs due to mechanical preloads. Although, greatly magnifying the magnetization curve we observe an increase/decrease in saturation magnetization with increase in the applied tensile/compressive stresses, respectively. Additionally, microscale modeling of the magnetization behavior of the isotropic MRE based on experimental results was performed. Considering the interaction of the magnetic particles, the magnetic and mechanical fields were resolved explicitly inside the composite material. Computational homogenization scheme was used to link the microscopic behavior to the effective macroscopic properties of the MRE. In principle, the predicted effective magnetization behavior was observed to agree with the measured hysteresis loop of MRE materials.

[1] M. R. Jolly, J. D. Carlson, and B. C. Muñoz, *Smart Mater. Struct.*, vol. 5, no. 5, pp. 607–614, 1996. [2] M. A. Cantera, M. Behrooz, and F. Gordaninejad, *Smart Mater. Struct.*, vol. 26, no. 2, 2017. [3] S. H. Kwon, J. H. Lee, and H. J. Choi, *Materials (Basel).*, vol. 11, no. 6, pp. 1–22, 2018. [4] B. Marvalova, "Modelling of Magnetosensitive Elastomers," *Model. Simul.*, 2008. [5] K. A. Kalina, P. Metsch, and M. Kästner, *Int. J. Solids Struct.*, vol. 102–103, pp. 286–296, 2016. [6] K. Danas, S. V. Kankanala, and N. Triantafyllidis, *J. Mech. Phys. Solids*, vol. 60, no. 1, pp. 120–138, 2012.

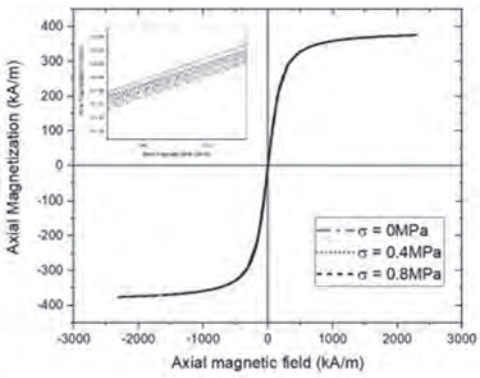

Modeled hysteresis loop for a point in the MRE under tensile stresses

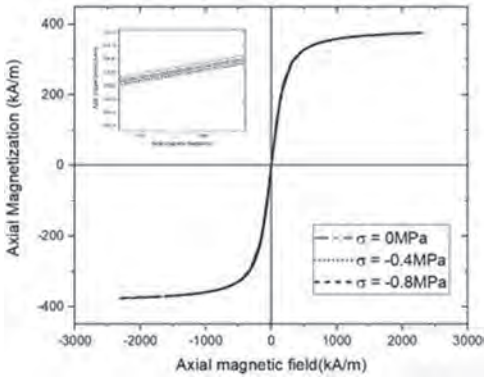

Modeled hysteresis loop for a point in the MRE under compressive stresses

L4-15. Withdrawn

L4-16. Effects of Particulate Size on the Magnetic and Magnetoactive Properties of an Extruded Magnetorheological Thermoplastic Elastomer. *A. Robinson*[1], N.A. Fischer[1], T. Lee[1], T.M. Calascione[1] and B. Nelson-Cheeseman[1] *1. Engineering, University of Saint Thomas, Saint Paul, MN, United States*

Magnetorheological elastomers (MREs) are a smart material with the ability to physically deform when in the presence of an applied magnetic field. Extruding MREs into filament allows for the use of FDM manufacturing. FDM has been shown to manipulate the mechanical and magnetic properties of polymer matrix composites, which in turn could fine-tune the magnetoactive responses of printed MREs. This project investigates how the magnetic and magnetoactive properties of composite materials made of thermoplastic polyurethane (TPU) and 15 vol% iron particulate are affected by the size of the particulate within the matrix. Two different sizes of iron particulate are tested: 100 mesh (<150 micron) and spherical carbonyl 1-3 micron. Varying particulate size is of interest for FDM 3D printing because of limitations due to small nozzle sizing. This means that larger particulate can cause more issues of clogging, though it is less expensive and more accessible than smaller particulate. After the composites were fabricated, the resulting magnetic properties were tested via a VSM. Hysteresis loops showed that the smaller particulate samples had a lower magnetic susceptibility than the larger particulate samples. That means the larger particulate will exhibit greater magnetization under the same applied field. The magnetoactive properties were tested by measuring the angle of deformation under various transverse applied magnetic field strengths (limit 0.4T). The magnetoactive properties of the filaments are shown visually in Figure 1 and quantitatively in Figure 2. In both, it can be clearly seen that the larger particulate samples respond with a greater angle of deformation at every tested applied field. In conclusion, larger particulate leads to greater magnetic susceptibility and magnetoactive deformation, but the smaller particulate does have a more desirable size and shape for FDM.

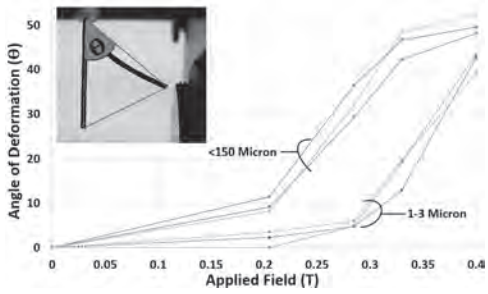

Figure 2: Angle of deformation (θ) vs applied field as a function of Fe particulate size (each in triplicate). Inset-a sample showing angle of deformation (θ).

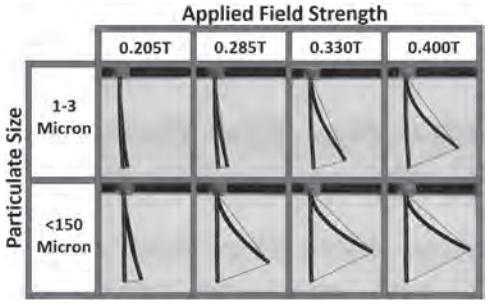

Figure 1: Samples of each particulate size showing the deformation due to the applied fields. Each 0T reference image was overlaid to show the total deformation from 0T.

L4-17. Withdrawn

Session S5
PHYSICS AND APPLICATIONS IN TRANSMISSION AND CONTROL OF SPIN-ORBIT TORQUES

Jonathan Sun, Chair
IBM T. J. Watson Research Center, Yorktown Heights, NY, United States

INVITED PAPERS

8:00

S5-01. Spin-Orbit Torque Induced Magnetization Switching Based on Topological Spin Textures and Magnons. *H. Yang*[1] *1. National University of Singapore, Singapore*

Spintronic research has recently focused on spin-orbit torques (SOTs) to alter the magnetic state. Layered topological materials such as topological insulators (TIs) and Weyl semimetals are a new class of quantum matters with large spin-orbit coupling, and probing the spin texture of these materials is of importance for functional devices. We reveal spin textures of such materials using a new kind of magneto-resistance, the bilinear magneto-electric resistance (BMR), which depends on the relative orientation of the current with respect to the magnetic field as well as the crystallographic axes [1,2]. We also directly visualize current-induced spin accumulation in topological insulators using photocurrent mapping [3]. Topological surface states (TSS) dominated spin orbit torques are identified in Bi_2Se_3 [4], and magnetization switching at room temperature using Bi_2Se_3 as a spin current source is demonstrated [5]. It is shown that TIs could give rise to a larger spin current generation efficiency and smaller switching current densities compared to that of heavy metals. Nevertheless, the resistive nature of TIs can cause serious current shunting issues, leading to a large power consumption. In order to tackle this issue, we propose two approaches. Weyl semimetals have emerged as potential alternatives to TIs. The nontrivial band structures of Weyl semimetals endow them with the potential for spin current generation. Unique advantages of Weyl semimetals over TIs are that Weyl semimetals have a much larger conductivity compared to TIs and they can generate a strong spin current from their bulk states. The Td-phase Weyl semimetal WTe_2 is chosen not only because its Weyl semimetal nature, which endows the potential for an interfacial Rashba-like effect and an intrinsic spin Hall effect, but also the atomically flat surfaces which can be produced with high quality, simplifying interfacial studies and facilitating device applications. Utilizing the magneto-optical Kerr microscopy, we show the current-driven magnetization switching in WTe_2/NiFe with a low current density and a low power [6]. The current shunting issue can be also overcome by the magnon-mediated spin torque as shown in Fig. 1, in which the angular momentum is carried by precessing spins rather than moving electrons. The electrical spin torque, involving moving charges suffers from unavoidable Joule heat and corresponding power dissipation, as well as a short spin propagation length. Magnon-torque-driven magnetization switching is demonstrated in the Bi_2Se_3/NiO/Py devices at room temperature [7]. By injecting the electric current to an adjacent Bi_2Se_3 layer, spin currents were converted to magnon torques through an antiferromagnetic insulator NiO. The presence of magnon torque is evident for larger values of the NiO-thickness where magnons are the only spin-angular-momentum carriers. The demonstration reveals that the magnon torque is sufficient to control the magnetization, which is comparable with previously observed electrical spin torque ratios of TIs [5]. Looking towards the future, we hope that these studies will spark more works on harnessing spin currents from topological materials and revealing interesting spin textures at topological material/magnet interfaces. All magnon-driven magnetization switching without involving electrical parts could be achieved in the near future. The results will invigorate magnon-based memory and logic devices, which is relevant to the energy-efficient control of spin devices.

[1] P. He et al., Nat. Phys. 14, 495 (2018) [2] P. He et al., Nat. Comm. 10, 1290 (2019) [3] Y. Liu et al., Nat. Comm. 9, 2492 (2018) [4] Y. Wang et al., Phys. Rev. Lett. 114, 257202 (2015) [5] Y. Wang et al., Nat. Comm. 8, 1364 (2017) [6] S. Shi et al., Nat. Nano. 14, 945 (2019) [7] Y. Wang et al., Science 366, 1125 (2019)

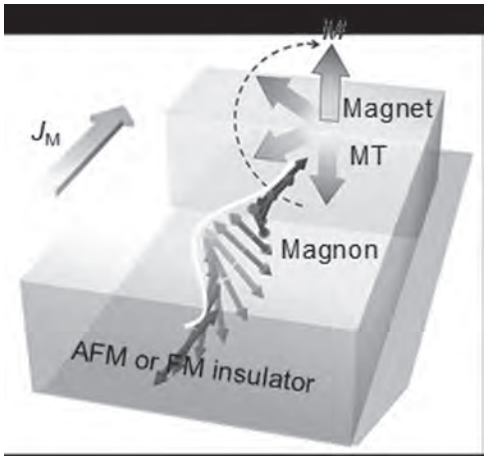

Fig. 1. Schematic of magnon current based magnetization switching.

8:36

S5-02. Magnetization Switching Utilizing Surface States in Topological Materials. *M. Wu*[1], P. Li[1], J. Kally[2], S. Zhang[3], T. Pillsbury[2], J. Ding[1], G. Csaba[4], J. Ding[3], S. Jiang[3], Y. Liu[5], R. Sinclair[5], C. Bi[6], A. DeMann[1], G. Rimal[7], W. Zhang[8], S. Field[1], J. Tang[7], W. Wang[6], O. Heinonen[3], V. Novosad[3], A. Hoffmann[3] and N. Samarth[2] *1. Colorado State University, Fort Collins, CO, United States; 2. Pennsylvania State University, University Park, PA, United States; 3. Argonne National Laboratory, Lemont, IL, United States; 4. Pazmany Peter Catholic University, Budapest, Hungary; 5. Stanford University, Stanford, CA, United States; 6. University of Arizona, Tucson, AZ, United States; 7. University of Wyoming, Laramie, WY, United States; 8. Oakland University, Rochester, MI, United States*

Due to the spin-momentum locking of its topological surface states, a topological insulator is expected to be able to produce a spin-orbit torque on a neighboring ferromagnet that is significantly stronger than what a heavy metal can produce. In fact, recent experiments have demonstrated efficient, spin-orbit torque-induced magnetization switching in topological insulator/ferromagnet bi-layers. However, the efficient switching in those experiments may not result from the surface states in the topological insulators. This is because the ferromagnets used were electrically conductive, while the proximity to a conductive ferromagnet can suppress the topological surface states as shown by very recent theoretical and experimental studies. In this talk we report bona fide topological surface state-driven magnetization switching. Our studies used a topological insulator/ferromagnet bi-layer where the ferromagnet is an insulator and the topological surface states are unspoiled or

preserved. The experiments used a $Bi_2Se_3/BaFe_{12}O_{19}$ heterostructure where Bi_2Se_3 is a topological insulator and $BaFe_{12}O_{19}$ is ferrimagnetic and has strong perpendicular anisotropy. We found that a charge current in Bi_2Se_3 can switch the magnetization in $BaFe_{12}O_{19}$ between the up and down states. When the magnetization is switched by a magnetic field, a charge current in Bi_2Se_3 can reduce the switching field by up to about 4000 Oe. The efficiency of the spin-orbit torque in assisting the switching increases with a decrease in temperature (T), and is two orders of magnitude higher at T=3 K than at T=300 K. Further, it is one order of magnitude higher than in $Pt/BaFe_{12}O_{19}$. The very strong effects at low T are associated with the presence of more pronounced topological surface states in Bi_2Se_3 due to enhanced surface state conductivity and reduced bulk state conductivity.

"Magnetization switching utilizing topological surface states," Peng Li, James Kally, Steven S.-L. Zhang, Timothy Pillsbury, Jinjun Ding, Gyorgy Csaba, Junjia Ding, Sam Jiang, Yunzhi Liu, Robert Sinclair, Chong Bi, August DeMann, Gaurab Rimal, Wei Zhang, Stuart B. Field, Jinke Tang, Weigang Wang, Olle G. Heinonen, Valentine Novosad, Axel Hoffmann, Nitin Samarth, and Mingzhong Wu, Science Advances 5, eaaw3415 (2019).

9:12

S5-03. Planar Hall Driven Spin Torque in a Ferromagnet/Nonmagnet/Ferromagnet System. *C. Safranski*[1], J. Xu[2], A.D. Kent[2] and J. Sun[1] *1. IBM T. J. Watson Research Center, Yorktown Heights, NY, United States; 2. Physics, Center for Quantum Phenomena, New York University, New York, NY, United States*

Transport current manipulation of magnetization based on spin-orbit effects aims to produce energy efficient nanomagnet devices. One area of investigation is the charge to spin current conversion in layers of magnetic and nonmagnetic materials. Typically studied materials have been mostly limited to the generation of in-plane polarized spin currents. We investigate spin currents produced by the planar Hall effect in Co/Ni multilayers, which carry a polarization dictated by the FM magnetization direction. We measure damping-like torques in FM/NM/FM systems via spin torque ferromagnetic resonance of patterned structures represented in Fig. 1(a). The slope of linewidth vs bias current is used to quantify the torques. The angular dependence of this slope, seen in Fig. 1(b), is consistent with the symmetry expected for torques produced by the planar Hall effect [1,2]. We find the magnitude of the spin-current thus generated to be comparable to that of the spin Hall effect in materials such as Pt. However, unlike the spin Hall effect, planar Hall can produce a partially out of plane spin polarization. Our results indicate that the planar Hall effect holds potential as a spin current source with a controllable polarization direction.

[1] *Phys. Rev. Appl.* 3, 044001 (2015), [2] *Nat. Nanotechnol.* 14, 27–30 (2019)

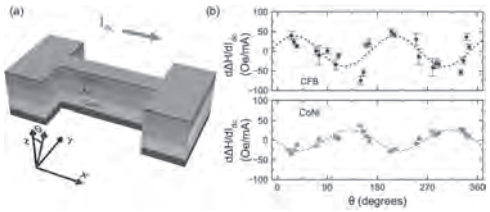

9:48

S5-04. Electrical Spin Current Generation in Ferromagnets and at Ferromagnetic Interfaces. *V. Amin*[1], P.M. Haney[2] and M.D. Stiles[2] *1. Physics, Indiana University Purdue University, Indianapolis, Indianapolis, IN, United States; 2. National Institute of Standards and Technology, Gaithersburg, MD, United States*

Electrical control of magnetization dynamics has widespread applications for information and communications technology. One way to manipulate a ferromagnet's magnetization in layered structures is to generate a spin current in a source layer that is absorbed by a nearby ferromagnetic layer, causing a transfer of spin angular momentum or spin torque. Under an applied electric field, both ferromagnetic and nonmagnetic layers generate spin currents. Generally, the spin torque occurs in a different layer than where the spin current was generated. However, for ferromagnetic metals with appreciable spin-orbit coupling, both can occur in the same layer. In these materials, conduction electrons can carry a substantial spin current flowing perpendicularly to the electric field with spin directions misaligned with the magnetization. When these symmetry-allowed spin currents flow into the layer boundaries, the resulting spin accumulations can exert substantial torques as measured through optical techniques such as polar MOKE [1]. Thus, ferromagnetic materials can be simultaneously the source and receiver of spin torques, suggesting a promising avenue to optimize electrical control of magnetization dynamics. In this talk, I discuss several mechanisms to electrically generate spin currents in ferromagnets and at ferromagnetic interfaces. Each mechanism can have a different dependence on magnetization direction, crystal structure, and/or disorder. While measurements of spin torques at layer boundaries provide evidence of spin current generation [1], disentangling contributions from spin currents and from other sources remains an open challenge. We present first principles transport calculations giving the strength and magnetization dependence of electrically generated spin currents via both intrinsic [2] and extrinsic [3] mechanisms. We find that in transition metal ferromagnets, both intrinsic and extrinsic mechanisms yield spin currents misaligned with the magnetization, with associated conductivities comparable to the spin Hall conductivity in Pt. Shedding light on these mechanisms could help optimize electrical control of magnetization dynamics with potential applications for information processing.

[1] W. Wang, T. Wang, V. P. Amin, Y. Wang, A. Radhakrishnan, A. Davidson, S. R. Allen, T. J. Silva, H. Ohldag, D. Balzar, B. L. Zink, P. M. Haney, J. Q. Xiao, D. G. Cahill, V. O. Lorenz, and X. Fan, Anomalous Spin-Orbit Torques in Magnetic Single-Layer Films, Nature Nanotechnology, 14, 819-824, 2019 [2] V. P. Amin, J. Li, M. D. Stiles, and P. M. Haney, Intrinsic Spin Currents in Ferromagnets, Phys. Rev. B 99, 220405(R), 2019 [3] V. P. Amin, J. Zemen, and M. D. Stiles, Interface generated spin currents, Phys. Rev. Lett. 121, 136805, 2018

10:24

S5-05. Metrology and Materials Optimization: Maximizing Spin Hall Ratio and Spin Torque Efficiency of Pt. *L. Zhu*[1], L. Zhu[2], S. Shi[1], D. Ralph[1] and R. Buhrman[1] *1. Cornell University, Ithaca, NY, United States; 2. Shaanxi Normal University, Xi'an, China*

Successful spin-orbit torque technologies require energy-efficient, high-endurance, and integration-friendly spin-current generators. From this point of view, the topological insulators BiSe and BiSb have possibly insurmountable challenges due to their high resistivities, pronounced roughness, poor chemical stability, and low melting/sublimation temperatures. Pt is advantageous except its low spin torque efficiency (ξ_{DL} =0.05-0.22, depending on the resistivity ρ). It is of great scientific and technological importance to advance the physics understanding of how, why, and to what limit ξ_{DL} can be enhanced. This talk will report on an unambiguous determination of the dominant mechanism of spin current generation in Pt [1], how the intrinsic spin Hall conductivity is affected by carrier lifetime, strain, interruption of crystal order [2,3], and how and to what limit θ_{SH} and ξ_{DL} of Pt can be

enhanced. Immediate benefits of these efforts include three optimal low-ρ high-θ_{SH} spin current generators (θ_{SH}≈0.8, ξ_{DL}=0.3-0.4) with the power consumption of only 1% of that for the BiSe device (ξ_{DL} =18.6, ρ=13000 μΩ cm). We find negligible Rashba-Edelstein effect in our samples. Finally, strategies for maximizing interfacial spin transmissivity, spin backflow and spin memory loss [4,5,6], will be discussed.

[1] Zhu et al., Sci. Adv. 5, eaav8025 (2019). [2] Zhu et al., Phys. Rev. Appl. 11, 061004 (2019). [3] Zhu, Buhrman, Phys. Rev. Appl. 12, 051002 (2019). [4] Zhu et al., PRL 123,057203 (2019). [5] Zhu et al., PRL 122,077201 (2019). [6] Zhu, Buhrman, Spin transparent magnetic interfaces enabled by insertion of a magnonic layer, (under review) (2020).

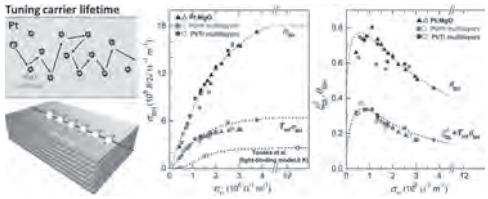

Characterestic variation of the intrinsic spin Hall conductivity of Pt with carrier lifetime, which predicts an theoretical upper limit of the spin Hall ratio and dampinglike torque efficiency in any approches that vary carrier lifetime by resistivity.

Session S6
NEXT GENERATION ARTIFICIAL SPIN ICE

Cristiano Nisoli, Chair
Los Alamos National Laboratory, Los Alamos, NM, United States

INVITED PAPERS

9:00

S6-01. Artificial Spin Ice, Vertex Frustration, and the Advantages of Intentional Design. *P. Schiffer*[1] *1. Yale University, New Haven, CT, United States*

Artificial spin ice consists of arrays of lithographically fabricated single-domain ferromagnetic elements, arranged in different geometries such that the magnetostatic interactions between the moments are frustrated. Because researchers can both design the lattice geometries and probe the individual moments, these systems open new windows to the study of frustrated systems in ways unavailable in natural materials. I will describe studies of artificial spin ice arrays that are intentionally designed to manifest novel forms of frustration. The primary focus will be on the so-called "vertex frustrated" lattices. These systems are frustrated in the sense that some local vertices are necessarily excited because of the lattice geometry, and there is a high degeneracy in the location of the excited local vertices. This novel form of frustrated system results in unusual collective behavior, including topological charges, strings of excitations that are topologically protected, and reduced dimensionality associated with the placement of the excited vertices. As a class of new frustration, they provide a playground in which new collective behavior is observed and novel dynamics can be explored, with implications for other frustrated and topologically complex systems. I will also discuss a quadrupolar artificial spin ice system in which the field-temperature phase diagram demonstrates phase coexistence in direct analogy to other important model magnetic systems. This work was supported by US Department of Energy, Office of Basic Energy Sciences, Materials Sciences and Engineering Division under Grant No. DE-SC0010778 and Grant No. DESC0020162. It was conducted with numerous collaborators, including: Alan Albrecht, Joseph T. Batley, Nicholas S. Bingham, Daniel Bromley, Francesco Caravelli, Isaac Carrasquillo, Gia-Wei Chern, Karin Dahmen, Ayhan Duzgun, Daniel Gardeazabal, Ian Gilbert, Yuyang Lao, Brian Le, Chris Leighton, Michael Manno, Cristiano Nisoli, Liam O'Brien, Jungsik Park, Hilal Saglam, Andreas Scholl, Mohammed Sheikh, Joseph Sklenar, Shayaan Subzwari, Justin D. Watts, Andreas Scholl, and Xiaoyu Zhang.

Gilbert *et al.*, Physics Today 69, 54 (2016), and Nature Physics 12,162 (2016); Nisoli *et al.,* Nature Physics 13, 200 (2017); Lao *et al.*, Nature Physics 14, 723 (2018); Sklenar *et al.,* Nature Physics 15, 191 (2019).

9:36

S6-02. Super-X-Magnetism: Investigation and Control of Ordering Processes in Artificial Spin Ice. *R. Stamps*[1] *1. Physics and Astronomy, University of Manitoba, Winnipeg, MB, Canada*

The interacting magnetic systems known as "Artificial Spin Ice" provide models of how interacting nanomagnetic particles can arrange themselves collectively into magnetically ordered states. As models for experiment, they allow for flexible adjustment of coupling parameters and geometric constraints on interactions. This flexibility facilitates their use in fundamental studies of ordering processes on mesoscopic length over a wide range of time scales [1]. We discuss the surprisingly wide variety of predicted and observed phenomena that can be realized with a simple two dimensional square lattice decorated by carefully arranged nanomagnets that are themselves ferromagnetic, and yet which collectively display behaviour that includes super- ferro, antiferro and paramagnetic orderings [2], as well as more complex and exotic zig-zag and super-vortex orderings. We identify in great detail mechanisms for mesoscopic domain growth mediated by nucleation of vertex structured 'domain walls' which exhibit coherent domain propagation [3]. In one geometry, seven types of mesoscopic domain-wall configurations are observed with non-trivial freezing behaviour [3].

1. R. Macedo, et al., *Phys. Rev. B,* 98 (2018).. 2. Y. Li, et al., *ACS Nano* 13, 2213 (2018). 3. G. W. Paterson, et al., *Phys. Rev. B*, 101, 144403 (2020).

10:12

S6-03. Frustrated Spin Architecture: From Macroscopically Degenerate Artificial Spin ice to Artificial Spin Glasses. *A. Farhan*[1] *1. Department of Applied Physics, Aalto University, Espoo, Finland*

Artificial spin ice [1] is a class of magnetic metamaterials consisting of coupled nanomagnets lithographically arranged onto a variety of lattices [2-4], leading to exotic emergent phenomena that are not only fascinating from a fundamental point of view, but also bear potential for future applications. Recently, by placing ultra-thin nanomagnets on pre-etched silicon substrates, we were able to create macroscopically degenerate artificial spin ice systems exhibiting emergent magnetic monopoles, which effectively behave as a plasma of magnetic charges [2]. This is done by a direct comparison of realspace observations with theoretical calculations based on Debye-Huckel theory. Utilizing a 3D spin architecture, combined with appropriate magnetic imaging, shows great promise not only in generating significant steps towards real-space observations of magnetic monopole currents or shedding light into the spin ice ground state, but will also lead to a whole new generation of artificial frustrated spin systems, exhibiting properties that cannot be realized by a simple 2D approach. Furthermore, first steps towards the realization of artificial spin glasses have been recently made [5,6], further confirming the importance of dimensionality as a crucial entity in achieving the first finite-temperature artificial spin glass system.

1. S.H. Skjærvø et al. Nat. Rev. Phys. (2020). 2. A. Farhan et al. Sci. Adv. 5, eaav 6380 (2019). 3. A. Farhan et al., Nature Comms. 8, 995 (2017). 4. A. Farhan et al. Nature Comms. 7, 1263 (2016). 5. M. Saccone et al. PRB 99, 224403 (2019). 6. M. Saccone et al. Nanoscale 12, 189 (2020).

10:48

S6-04. Spontaneous Superdomain Wall Fluctuations in a 2D Square Artificial Spin Ice. *S. Roy*[1], X. Chen[1,2], B. Farmer[2], J.S. Woods[2], S. Dhuey[3], W. Hu[4], C. Mazzoli[4], S. Wilkins[4], R.V. Chopdekar[1], A. Scholl[1], I.K. Robinson[5], L.E. DeLong[2] and J.T. Hastings[6] *1. Advanced Light Source, E O Lawrence Berkeley National Laboratory, Berkeley, CA, United States; 2. Dept. of Physics, University of Kentucky, Lexington, KY, United States; 3. Molecular Foundry, E O Lawrence Berkeley National Laboratory, Berkeley, CA, United States; 4. NSLSII, Brookhaven National Laboratory, Upton, NY, United States; 5. Condensed Matter Physics, Brookhaven National Laboratory, Upton, NY, United States; 6. Dept. Of Electrical and Computer Engg., University of Kentucky, Lexington, KY, United States*

Fluctuations and stochasticity are characteristics of material complexity that have been enduring themes in condensed matter and statistical physics research. Fluctuations are a fundamental component of phase transitions and critical phenomena in statistical mechanics, order parameter field theories in quantum criticality, etc. Artificial Spin Ices (ASI) can be tailored to achieve a phase transition. Under the assumption that nano-islands exhibit Ising-like character, the arrangement of mutually perpendicular nanomagnets over a square ASI results in an asymmetry in the inter-island interactions that, in principle, favors an antiferromagnetic ground state. In this work we fabricated a square ASI with the nano-island thickness controlled such that the sample exhibits a paramagnetic-to-antiferromagnetic (AF) phase transition near 330 K. The evolution of the AF order as a function of temperature was studied using resonant X-ray scattering [1]. We used coherent soft X-ray Photon Correlation Spectroscopy (XPCS) to study thermally induced spontaneous superdomain wall fluctuations. By analyzing the data within the framework of statistical mechanics, we demonstrated the existence different types of fluctuations and relaxation. We observed two distinct regimes of domain wall motion---a low temperature ballistic, and a high temperature diffusive type---as the sample goes through the antiferromagnetic phase transition. This work is supported by US DOE (Award# DE-SC0016519).

[1]. X. M. Chen, B. Farmer, et al., Phys. Rev. Lett. 123, 197202 (2019).

11:24

S6-05. Plasmon-Assisted Opto-Thermal Excitation of Nanomagnetic Arrays. *P. Vavassori*[1,2], N. Leo[1], M. Menniti[1], M. Pancaldi[3], P. Gypens[4] and J. Leliaert[4] *1. Nanomagnetism, CIC nanoGUNE, San Sebastian, Spain; 2. Ikerbasque, Bilbao, Spain; 3. Department of Physics, Stockholm University, Stockholm, Sweden; 4. Deptartment of Solid State Sciences, Gent University, Gent, Belgium*

Single-domain nanoscale magnets interacting via magnetostatic interactions are key metamaterials for low-power information processing [1] and to study novel frustrated phenomena in so-called artificial spin ices (ASIs) [2]. These magnetic metamaterials are fabricated using electron-beam nano-lithography where any desired two-dimensional arrangement of thin-film magnetic elements with dimensions of a few hundred nanometers can be designed. Their properties and functionality are determined by the capability to reverse the moment of each nanomagnet to minimize the mutual dipolar interactions, which happens more quickly at elevated temperatures. Over the years, different heating schemes have been employed to drive networks of interacting nanomagnets to an equilibrium state, ranging from thermal annealing of stable magnets to the fabrication of rapidly-fluctuating ultra-thin superparamagnetic elements. As of today, thermal excitation of artificial spin systems is achieved by thermal contact to a hot reservoir, either by heating the entire underlying substrate, or by an electrical current in a conductive wire nearby. All these approaches are energetically inefficient, spatially non-discriminative, and intrinsically slow, with time scales of seconds to hours [3,4], making it difficult to reach a true equilibrium state in extended frustrated nanomagnetic lattices. Furthermore, for implementation in devices of magnetic metamaterials, e.g. magnonic crystals and nanomagnetic logic circuits, global heating lacks the control, spatial discrimination, and speed required for integrated operation with CMOS technology. We propose and demonstrate an approach in which the nanomagnetic arrays are made of hybrid nanostructures that combine a plasmonic nanoheater with a magnetic element. We achieve the reliable and contactless plasmon-assisted optical heating of nanomagnets with a flexible control of length (down to the micrometer) and time (down to sub-ns) scales of the thermal excitation [5]. Furthermore, the polarization-dependent absorption cross section of elongated plasmonic elements enables selective heating of a desired subset of nanomagnets within the illuminated area depending on their in-plane orientation, which is not possible with conventional heating schemes. This enables deeper studies of equilibrium properties and emergent excitations in ASIs and provides the spatial discrimination and speed required for integration with CMOS technology. We have experimentally quantified the optical and magnetic properties of arrays of non-interacting single hybrid elements as well as vertex-like assemblies, and present strategies how to achieve efficient, fast, and selective control of the thermally-activated magnetic reversal by choice of hybrid nanostructure materials, internal structure and shape, together with laser wavelength, focal point size, pump power, polarization, and pulse duration [5]. Our results establish plasmon-assisted optical heating for contemporary thermalization schemes in ASIs and open a new path to the creation of new opto-thermally activated nanomagnet circuits for low-power computation.

[1] H. Arava et al., Phys. Rev. Applied Vol. 11, p. 054086 (2019) [2] R. F. Wang et al., Nature Vol. 439, p. 303 (2006) [3] S. Zhang et al., Nature Vol. 500, p. 553 (2013) [4] J. M. Porro, A. Bedoya-Pinto, A. Berger and P. Vavassori, New J. Phys. Vol.15, p. 055012 (2013) [5] M. Pancaldi, N. Leo, and P. Vavassori, Nanoscale Vol., p. (2019)

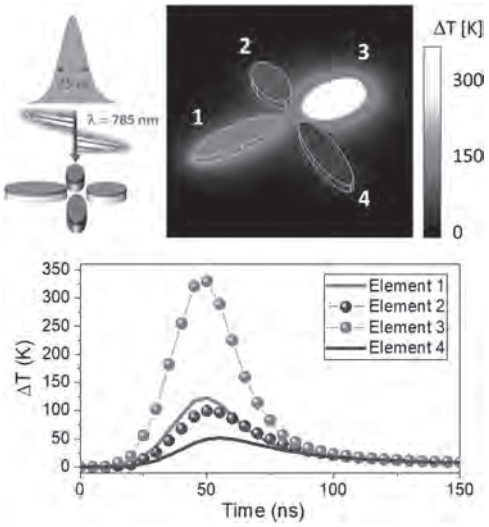

COMSOL simulation of the selective and fast (ns-range) plasmon-assisted optical heating of an individual nanostructure (element 3) belonging to a hybrid Au/Ni four-nanostructures vertex network using a 25 ns wide laser pulse of wavelength and linear polarization selected to excite a plasmon resonance in the desired nanostructure.

Session M1
ANTIFERROMAGNETIC SPINTRONICS III

Libor Smejkal, Chair
Johannes Gutenberg University of Mainz, Mainz, Germany

INVITED PAPER

M1-01. Large Spin-Orbit Torque Efficiency and Magnetic Symmetry Effect in the Antiferromagnet IrMn. J. Zhou[1], X. Shu[1] and *J. Chen*[1]
1. Materials Science and Engineering, National University of Singapore, Singapore

Current induced spin-orbit torque (SOT) has been extensively investigated as a promising mechanism to switch magnetization electrically, which potentially allows higher energy efficiency in information technologies [1]. Metallic antiferromagnets (AFM) have been demonstrated to be an efficient source of SOT [2]. However, the relationship between the magnetic structure and SOT of AFM has been frequently overlooked, which not only clouds the origin of SOT in AFM but also hampers the engineering efforts for application development. Here we demonstrate that the magnetic structure of AFM IrMn has a strong influence on its SOT generation [3-4]. We fabricate epitaxial IrMn thin films of three phases, which have distinct crystal and magnetic structures, as shown in Fig. 1(a) and 1(b). The magnetic structures of the three phases have been carefully studied using the neutron diffraction technique. Using spin-torque ferromagnetic resonance technique (ST-FMR) [Fig. 1(c)] and IrMn/permalloy (Py) bilayers, we show that the measured SOT efficiencies () of $L1_0$-IrMn, $L1_2$-$IrMn_3$ and γ-$IrMn_3$ are 0.61±0.01, 1.01±0.03 and 0.80±0.01, respectively, as displayed in Fig. 1(d). These values are substantially larger than that of the polycrystalline IrMn, which is only 0.083±0.002. By altering the direction of electric current in the crystal lattice of $L1_0$-IrMn, we observe a 4-fold rotation symmetry in both the SOT efficiency and the in-plane magnetic anisotropy, as shown in Fig. 1(e). Fig. 1(f) shows that 4-fold symmetry disappears when a thin Cu spacer is inserted between $L1_0$-IrMn and Py while the measured SOT efficiency decreases to 0.22±0.03. These results suggest a magnetic structure enhanced SOT efficiency in $L1_0$-IrMn, which consists of a large isotropic bulk contribution and a comparable anisotropic interfacial contribution [3]. Moreover, we observe an anomalous out-of-plane damping-like torque in both $L1_0$-IrMn and $L1_2$-$IrMn_3$ [4], as shown by the red curves in both Fig. 1(g) and 1(h). The microscopic origin of this torque appears to be an out-of-plane spin polarization. This is consistent with the intrinsic effects of the a laterally broken magnetic mirror symmetry () that is present commonly in both $L1_0$-IrMn and $L1_2$-$IrMn_3$. We attribute the absence of this anomalous SOT in γ-$IrMn_3$ to the lack of magnetic asymmetry due to a disordered magnetic structure.

[1] A. Manchon et al, Rev. Mod. Phys. 91, 035004 (2019). [2] W. Zhang et al, Phys. Rev. Lett. 113, 196602 (2014). [3] J. Zhou et al, Sci. Adv. 5, eaau6696 (2019). [4] J. Zhou et al, Phys. Rev. B 101, 184403 (2020).

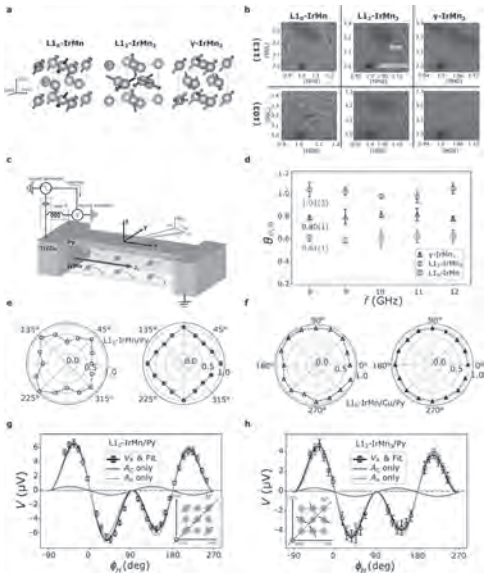

Fig. 1 (a) Unit cells of three phases of IrMn. Different types of spins are differentiated by colors. (b) Reciprocal space mappings of three phases of IrMn. (c) Schematic set-up of the spin-torque ferromagnetic resonance (ST-FMR) measurement. (d) Measured SOT efficiencies of three phases of IrMn in the frequency range of 8-12 GHz. (e) and (f) Normalized SOT efficiencies (hollow marker) and resonant field (solid marker) of $L1_0$-IrMn/Py and $L1_0$-IrMn/Cu/Py. (g) and (h) Components of the antisymmetric ST-FMR voltage (V_A) in $L1_0$-IrMn/Py and $L1_2$-$IrMn_3$.

CONTRIBUTED PAPERS

M1-02. Concurrent Magneto-Optical Imaging and Magneto-Transport Readout of Electrical Switching of Insulating Antiferromagnetic Thin Films. *F. Schreiber*[1*], L. Baldrati[1], C. Schmitt[1], R. Ramos[2], E. Saitoh[2,3], R. Lebrun[1,4] and M. Klaui[1,5] *1. Johannes Gutenberg Universität Mainz, Mainz, Germany; 2. Tohoku Daigaku, Sendai, Japan; 3. Tokyo Daigaku, Bunkyo-ku, Japan; 4. Unite Mixte de Physique CNRS/Thales, Palaiseau, France; 5. Johannes Gutenberg University Mainz Graduate School of Excellence Materials Science in Mainz, Mainz, Germany*

Electrical writing and readout of antiferromagnetic insulators is a key prerequisite in view of using this class of materials in applications. Only recently, this has been demonstrated in insulating AFM/heavy metal bilayers by utilizing the transverse spin Hall magnetoresistance effect (SMR) as the readout. In the electrical measurement, a steplike signal resulting from a magnetic SMR contribution was reported in NiO[1] and α-Fe_2O_3[2], while non-magnetic contributions due to artifacts in the heavy metal layer were found to mimic the signal expected from the magnetic switching.[3,4] These results have generated a debate on the magnitude of the magnetic contributions, the reliability of the SMR readout mechanism and even on the possibility of switching domains in AFMs electrically. In our work[5] we use a table-top approach to demonstrate stable and reversible current-induced switching of large-area antiferromagnetic domains in NiO/Pt by

direct imaging in a Kerr microscope.[6] Concurrent transport and magneto-optical imaging measurements allow us to correlate the AFM domain switching fraction and magneto-transport signal response. We establish a procedure to subtract the non-magnetic contributions and extract the magnetic SMR response from the transverse resistance signal. The disentanglement of magnetic and non-magnetic contributions clarifies the presence of a significant SMR response, associated with the switching of the antiferromagnetic domains. We thus highlight the possibility to deduce details of the antiferromagnetic switching from simple transport measurements.

[1] L. Baldrati, O. Gomonay, A. Ross, Phys. Rev. Lett. 123, 177201 (2019). [2] Y. Cheng, S. Yu, M. Zhu, Phys. Rev. Lett. 124, 027202 (2020). [3] A. Churikova, D. Bono, B. Neltner, Appl. Phys. Lett. 116, 022410 (2020). [4] C.C. Chiang, S.Y. Huang, D. Qu, Phys. Rev. Lett. 123, 227203 (2019). [5] F. Schreiber, L. Baldrati, C. Schmitt, Appl. Phys. Lett. 117, 082401 (2020). [6] J. Xu, C. Zhou, M. Jia, Phys. Rev. B 100, 134413 (2019).

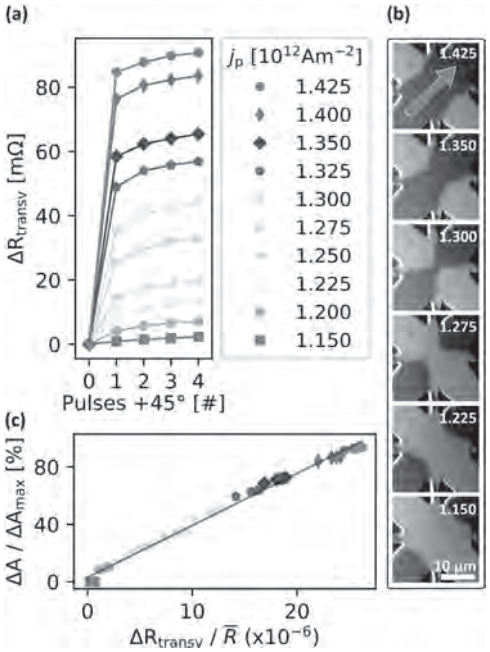

Fig. 1 Current-induced switching in NiO/Pt always starting with the same original state. (a) Electrical signal after subtraction of a linear non-magnetic contribution. (b) Domain structure for different current densities after the application of 15 pulses in the direction as indicated by the arrow. The scalebar provides the scale of all domain images. (c) Correlation of post-treated electrical signal and switching fraction calculated from the imaging. Adapted from Ref. [5].

M1-03. Nonlinear Optical Imaging of Current Induced Spin Switching in Antiferromagnetic Nickel Oxide/Platinum Devices. *J. Lee*[1], Y. Tang[2], A. Mei[3], D.G. Schlom[3], D. Ralph[2] and F. Rana[1] *1. Electrical and Computer Engineering, Cornell University, Ithaca, NY, United States; 2. Physics, Cornell University, Ithaca, NY, United States; 3. Material Science and Engineering, Cornell University, Ithaca, NY, United States*

Electrical switching of the Neel order in antiferromagnetic (AF) materials via spin transfer torque (STT) has attracted considerable attention [1,2]. Efficacy of STT in inducing AF switching has been questioned recently [3,4]. Table-top techniques that can image magnetic domains in AF materials and devices with sub-micron resolution are needed to better understand the physics associated with AF switching. In this paper, we show that scanning optical second harmonic generation (SHG) can be used to study spin switching in AF materials. SHG technique can image spin domains even when AF materials are covered with metallic spin Hall layers such as Pt (Fig.1). The SHG technique was applied to study spin switching in MgO/NiO(15 nm)/Pt(5 nm) devices in which the spin Hall effect in Pt is used to generate a spin torque. Although the measured changes in the transverse magnetoresistance upon applying current pulses in orthogonal directions (Fig.2a) was suggestive of spin switching in NiO, imaging using SHG revealed different results. We also developed a machine learning algorithm to determine the S/T domains from the SHG data. Our imaging results show that current induced spin switching involves both S and T domains, indicating that out-of-plane anisotropy is not enough to prevent the spins from reorienting out of a T-domain. Second, pattern of spin switching was most often seen to not correspond to the predictions of STT theories [1] and indicated that thermoelastic effects played an important role. This conclusion was confirmed by optically heating the device in a pattern similar to the one resulting from current flow and observing similar pattern changes in spin orientations. Third, switching was seen to be spatially very non-uniform and not all locations exhibited significant changes in their spin orientations. The contributions of various effects will be discussed in this talk. The research was funded by NSF DMR-1120296.

[1] X. Z. Chen, R. Zarzuela, Y. Tserkovnyak, Phys. Rev. Lett. 120, 207204 (2018) [2] T. Moriyama, K. Oda, T. Ono, Scientific Reports 8, 14167 (2018) [3] P. Zhang, J. Finley, L. Liu, Phys. Rev. Lett. 123, 247206 (2019) [4] C. Chiang, S. Y. Huang, C. L. Chien, Phys. Rev. Lett. 123, 227203 (2019) [5] L. Baldrati, O. Gomonay, M. Klaui, Phys. Rev. Lett. 123, 177201 (2019) [6] I. Sanger, V. V. Pavlov, M. Fiebig, Phys. Rev. B 74, 144401 (2006)

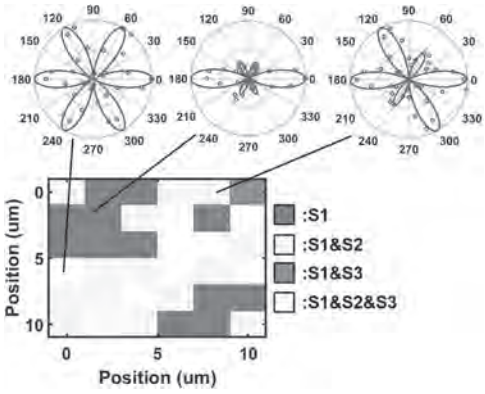

Fig.1: Spatial imaging of spin domains in NiO/Pt using second harmonic generation (SHG).

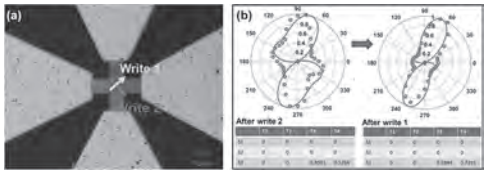

(a) A STT AF device using a 5nm thick Pt spin Hall layer to apply a spin torque on an epitaxially grown 15nm thick NiO layer. (b) The change of spin domains after the application of write 1 and write 2 currents.

M1-04. Atomistic Spin Dynamics Simulations of Iridium Manganese Alloys. *S. Jenkins*[1], R. Chantrell[1] and R.F. Evans[1] *1. Department of Physics, University of York, York, United Kingdom*

Antiferromagnets have gained significant interest in recent years due to their potential application in antiferromagnetic spintronic devices and neuromorphic computing where the antiferromagnet is the active element. A current problem in the development of such devices is a lack of understanding of the magnetic properties of antiferromagnets. Atomistic modelling is a powerful tool in understanding these properties as it has the ability to model the materials in atomistic detail but on a scale comparable to realistic device sizes. Here, an atomistic model [1] is used to model the technologically relevant anti-ferromagnetic material Iridium Manganese to calculate the ground state spin structure and magnetic anisotropy. Previously, only the properties of fully ordered Iridium Manganese alloys or disordered $IrMn_3$

have been investigated due to the complex material anisotropy of disordered crystal structures. Here, we have overcome this problem by modelling the anisotropy using the Néel pair anisotropy model which has the capability to accurately model any order or composition of IrMn [2]. Initially, the model was validated by comparing the results for ordered and disordered $IrMn_3$, against previous experimental and theoretical calculations. The properties of never before theoretically studied compositions and orders of IrMn were calculated with particular focus on the technologically relevant compositions close to $IrMn_4$ - $IrMn_5$ used in realistic devices. It was found that all the technologically relevant alloys of disordered IrMn have the same ground state structure. A full composition study of the fully ordered and fully disordered states was undertaken, and it was found that in both cases the Néel temperature increases as the Mn content is increased, stabilizing the spin structure. These findings are an important step towards understanding the fundamental properties of antiferromagnets for applications.

[1] R. F.L. Evans, et al, J Phys Cond. Matter, 26, (2014) [2] S. Jenkins, et al Physical Review B, 100, (2019)

M1-05. Optical Imaging of Antiferromagnetic Domains and Dynamics Switching in CoO Film by Magneto-Optical Birefringence Effect.
J. Xu[1], X. Zhang[2], J. Xia[2], C. Zhou[1], D. Shi[1], G. Chen[3], Y. Zhou[2] and Y. Wu[1] *1. Department of Physics and State Key Laboratory of Surface Physics, Fudan University, Shanghai, China; 2. School of Science and Engineering, The Chinese University of Hong Kong, Shenzhen, China; 3. Department of Physics, University of California Davis, Davis, CA, United States*

Spintronic devices based on antiferromagnetic (AFM) materials has drawn significant attention due to its potential for information storage with low power consumption and ultrafast switching speeds [1,2]. However, most experimental investigations on the switching of AFM spins relies on electrical detection means, like the anisotropic magnetoresistance, spin Hall magnetoresistance due to the difficulty of AFM spin detection. Recent works reported that the changes of electrical signals are not necessary correlated with the evolution of AFM domain states [3]. So, there is an urgent need to directly measure the AFM domain in real space during the spin switching process for further understanding the mechanism of AFM domain switching. In this contribution, we report the studies on the AFM domains in single crystal CoO thin films grown on MgO(001) substrates with the magneto-optical birefringence effect. The finite size effect of ordering temperature for ultrathin single crystal CoO film is revealed by the thickness and temperature dependent measurement of birefringence contrast. This effect is found to strongly depend on the photon energy of incident light. Moreover, we report the direct imaging on evolution of AFM domains under an external field in single-crystalline Fe/CoO bilayer. By manipulating the AFM spins with magnetic fields, we discovered that with the alternating fields, it is easier to overcome pinning energy barrier and the AFM domain switching process is dominated by domain wall motion, while for constant fields, domain nucleation dominates the switching process. We also confirmed the effect of alternating field on domain wall motion in AFM CoO film through micromagnetic simulations. Our studies demonstrate that the spin properties in AFM films under external fields can be measured in real time, which could be helpful for the development of AFM spintronics.

[1] T. Jungwirth, X. Marti, P. Wadley, and J. Wunderlich, Nat. Nanotechnol. 11, 231 (2016). [2] V. Baltz, A. Manchon, M. Tsoi, T. Moriyama, T. Ono, and Y. Tserkovnyak, Rev. Mod. Phys. 90, 015005 (2018). [3] C. C. Chiang, S. Y. Huang, D. Qu, P. H. Wu, and C. L. Chien, Phys. Rev. Lett. 123, 227203 (2019).

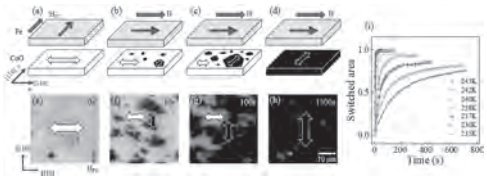

Figure 1. (a) Schematics of spin configurations in Fe/CoO bilayer after field cooling. (b)-(d) Schematics of time-dependent CoO AFM domain switching. (e)-(h) Time-dependent AFM domain evolution of Fe/CoO bilayer under a fixed field. (i) Temperature dependence of switched area of CoO domain as a function of time under a fixed field.

M1-06. Inertial Domain Wall Motion Driven by Staggered Spin-Orbit Fields in Layered Antiferromagnets.
R. Rama-Eiroa[1,2], P. Roy[3], J.M. González[2], K.Y. Guslienko[4,2], J. Wunderlich[5] and R.M. Otxoa[3,1] *1. Donostia International Physics Center, San Sebastian, Spain; 2. Materials Physics Department, Universidad del Pais Vasco - Campus Gipuzkoa, San Sebastián, Spain; 3. Hitachi Cambridge Laboratory, Cambridge, United Kingdom; 4. Ikerbasque, Bilbao, Spain; 5. Universitat Regensburg Fakultat fur Physik, Regensburg, Germany*

Magnetization switching plays a central role in the field of magnetism-based devices. A concrete example is the case of magnetic textures which play the role of carriers of information. A precise control of their mobility becomes crucial for potential applications such as racetrack memories [1], sensors [2], and logic-devices [3]. Both ferromagnets (FM) and antiferromagnets (AFM) can host multiple types of these textures. While FM have been investigated in depth, only recently a mechanism to excite AFM was proposed based on the fact that there are certain materials in which their magnetic sublattices form inversion partners, being possible to generate a current-induced Néel spin-orbit (SO) field [4]. With this objective in mind, we have evaluated the dynamics of a one-dimensional Néel-like DW in an embedded FM layer of the metallic layered Mn_2Au excited through the Néel SO field. To do this, we have combined atomistic spin dynamics simulations of the real crystalline structure together with an analytical model that combines the Lagrangian formalism with the collective coordinates approach. When theoretically formalizing the problem, complications arise to define an unique Néel order parameter due to the complexity of the system. To avoid this, we have introduced a pair of staggered AFM-coupled Néel vectors. Taking this into account, we have evaluated three consecutive correlated SO field-based regions: one of acceleration driven by a ramped stimulus, another of steady-steady at constant speed, and a friction-driven regime in the absence of external fields. Traces of the inertial dynamics of the magnetic texture and a great stability of the DW even at speeds very close to the maximum magnon group velocity of the medium have been observed. On the other hand, it has been possible to predict the distance traveled by the magnetic soliton in its friction-driven motion, which is of the order of 5-10 times greater than the DW width at rest for moderate fields of 10-60 mT. This opens up the possibility of exploiting the phenomenon of inertia to reduce the power consumption in those technological applications such as racetrack memories in which the position of the magnetic texture needs to be precisely determined.

[1] S. S. Parkin, M. Hayashi, and L. Thomas, Science, Vol. 320, p. 190-194 (2008) [2] R. Mattheis, S. Glathe, M. Diegel, et al., Journal of Applied Physics, Vol. 111, p. 113920 (2012) [3] P. Wadley, B. Howells, J. Zelezný, et al., Science, Vol. 351, p. 587-590 (2016) [4] J. Zelezný, H. Gao, K. Výborný, et al., Physical Review Letters, Vol. 113, p. 157201 (2014)

M1-07. Spin-Oribit Torques in Mn_2Au/HM Bilayers.
W. Fang[1] and K. Belashchenko[1] *1. Physics, University of Nebraska-Lincoln, Lincoln, NE, United States*

Antiferromagnets are promising materials for spintronic applications due to their unique features such as ultrafast spin dynamics and robustness against external magnetic fields. An efficient way to manipulate the antiferromagnetic

(AFM) order is to use spin-orbit torque (SOT), which utilizes the conversion of electric current to spin through the spin-orbit interaction. Current-induced switching of the AFM order has been demonstrated experimentally in several antiferromagnets including Mn_2Au. It has a broken sublattice inversion symmetry, which gives rise to opposite spin polarization on each sublattice under an electrical current. The staggered spin polarization results in a non-staggered field-like (FL) SOT, which is suitable for the switching of the AFM order. It is also possible to utilize the damping-like SOT originated from a spin current generated by a heavy metal (HM) layer adjacent to Mn_2Au. Here by using first-principles calculations, we calculate the SOTs of a Mn_2Au/HM bilayer, where HM is W or Pt. By expanding the SOT using vector spherical harmonics, layer-resolved angular dependence of SOT is obtained. For FL SOT, it has a large contribution from the Mn_2Au and a small contribution from the HM. For DL SOT, it has most of the contribution from the HM. FL SOT is non-staggered on each sublattice and it dominates the behavior of spin dynamics. DL SOT is staggered on each sublattice so that its net effect on spin dynamics is negligible.

INVITED PAPER

M1-08. Micromagnetic Modeling of Antiferromagnets. *G. Finocchio*[1], L. Sánchez-Tejerina[1], R. Tomasello[2], V. Puliafito[1], A. Giordano[1], F. Garesci[1] and M. Carpentieri[3] *1. Universita degli Studi di Messina, Messina, Italy; 2. Institute of Applied and Computational Mathematics, FORTH, Heraklion, Greece; 3. Politecnico di Bari, Bari, Italy*

Since the first experimental observation of electrical switching of antiferromagnet[1], the experiments on manipulation of antiferromagnetic order are exploded. However, the theoretical models are still very simplified (sigma model, macrospin approximation). This talk will discuss the recent developments of modeling antiferromagnets and ferromagnets considering a full numerical micromagnetic model. We benchmarked the approach with analytical theories for THz oscillator[2], domain wall and skyrmion dynamics[3], while predicting and describing some features for THz detectors, memories[4] and high speed DW motions [5]. Within this approach, it is possible to take into account three contributions for the exchange interactions (one homogeneous and two inhomogeneous) that are important to identify the two time scales of the antiferromagnetic dynamics. The first, at the THz range, that is related to relaxation processes from a misalignment of the antiferromagnetic state. The second one is related to the relaxation of domains and it is of the same order of the one of the ferromagnetic order. In the last part of the talk, It will discussed the origin of memristive behaviour [4] and the effect of grain sizes in the antiferomagnetic switching experiments.

1 P. Wadley, et al, Science, 351, 6273 (2016). 2 V. Puliafito, at al, Phys. Rev. B 99, 024405 (2019). 3 L. Sanchez-Tejerina, et al, Phys. Rev. B, 101, 014433, 2020. A. Salimath, et al Phys. Rev. B, 101, 024429, 2020. 4 S. Chen, G. Finocchio, et al, "Antiferromagnetic PtMn memory devices controlled by electric current" Nature Elettronics, 3, 92-98, 2020. 5 Heng-An Zhou, et al, "Compensated magnetic insulators for extremely fast spin-orbitronics", https://arxiv.org/abs/1912.01775.

CONTRIBUTED PAPERS

M1-09. Spin Flop and Crystalline Anisotropic Magnetoresistance in CuMnAs. *M. Wang*[1], C. Andrews[1], S. Reimers[1,2], O.J. Amin[1], P. Wadley[1], R.P. Campion[1], S.F. Poole[1], J. Felton[1], K.W. Edmonds[1], B.L. Gallagher[1], A.W. Rushforth[1], O. Makarovsky[1], K. Gas[3], M. Sawicki[3], D. Kriegner[4], J. Zubáč[4,5], K. Olejník[4], V. Novák[4], T. Jungwirth[4], M. Shahrokhvand[6], U. Zeitler[6], S.S. Dhesi[2] and F. Maccherozzi[2] *1. School of Physics and Astronomy, University of Nottingham, Nottingham, United Kingdom; 2. Diamond Light Source Ltd, Didcot, United Kingdom; 3. Institute of Physics, Polish Academy of Sciences, Warsaw, Poland; 4. Institute of Physics, Czech Academy of Science, Prague, Czechia; 5. Faculty of Mathematics and Physics, Univerzita Karlova Matematicko-fyzikalni fakulta, Praha, Czechia; 6. High Field Magnet Laboratory (HFML-EMFL), Radboud Universiteit, Nijmegen, Netherlands*

We report magnetic -field -induced rotation of the antiferromagnetic Néel vector in epitaxial CuMnAs thin films. Firstly, using soft x-ray magnetic linear dichroism spectroscopy and magnetometry, we demonstrate spin-flop switching and continuous spin reorientation in films with uniaxial and biaxial magnetic anisotropies, respectively, for applied magnetic fields of the order of 2 T. The remnant antiferromagnetic domain configurations are determined using x-ray photoemission electron microscopy. Next, we show that the Néel vector reorientations are manifested in the longitudinal and transverse anisotropic magnetoresistance. Dependency of the electrical resistance on the orientation of the Néel vector with respect to both the electrical current direction and the crystal symmetry are identified, including a weak 4th fourth-order term which is evident at high magnetic fields. The results provide characterization of key parameters including the anisotropic magnetoresistance coefficients, magnetocrystalline anisotropy, and spin-flop field in epitaxial films of tetragonal CuMnAs, a candidate material for antiferromagnetic spintronics.

1. M. Wang, C. Andrews, S. Reimers, et.al. Phys. Rev. B 101, 094429 (2020). 2. P. Wadley, B. Howells, J. Zelezny, et.al. Science 351, 587 (2016).

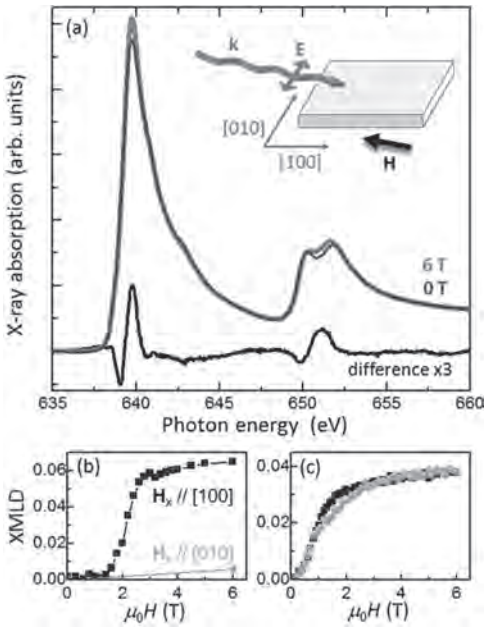

Fig.1 Spin-reorientation in antiferromagnetic CuMnAs using XMLD. (a) Mn *L* x-ray absorption spectra for 20 nm CuMnAs, in 0 and 6T field, and the difference, at 200 K. The x-ray incidence k and external magnetic field H are at 15° to the sample surface. (b,c) XMLD signal *vs*. magnetic field for b: 20 and c: 50 nm CuMnAs films.

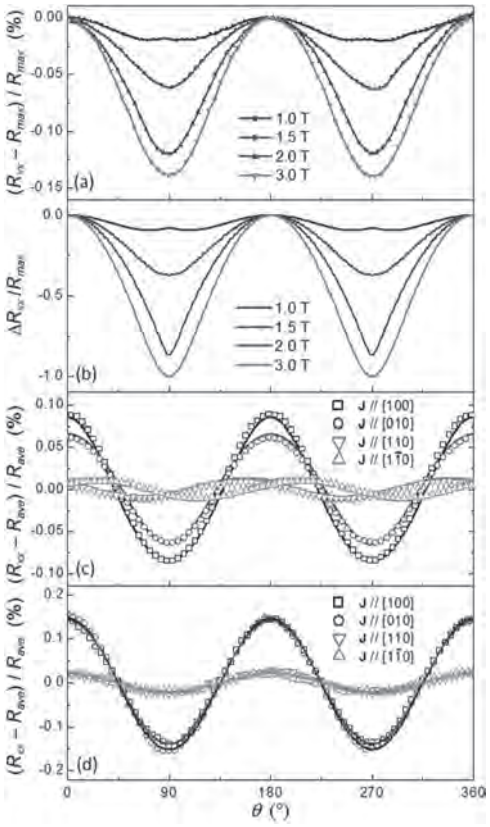

Fig.2 Resistance *vs.* angle between field and current directions, (a) for 10 nm CuMnAs, with current along the [010] direction and H = 1.0, 1.5, 2.0 and 3.0T at 4K. (b) Calculated AMR for uniaxial antiferromagnet with a Gaussian distribution of spin-flop fields centered on 1.6T. (c,d) for 10 and 50 nm CuMnAs, with magnetic field 5T at 4K. The lines are fitting results.

M1-10. Withdrawn

M1-11. Absence of Evidence of Electrical Switching of the Antiferromagnetic Néel Vector. *C. Chiang*[1], S. Huang[1], D. Qu[2], P. Wu[1] and C. Chien[1,3] *1. Department of Physics, National Taiwan University, Taipei, Taiwan; 2. Institute of Physics, Academia Sinica, Taipei, Taiwan; 3. Department of Physics and Astronomy, Johns Hopkins University, Baltimore, MD, United States*

Field-free switching of antiferromagnetic (AFM) Néel vector via spin-orbit torque (SOT) has attracted much attention. By applying a writing current in the AFM or the normal metal (NM)/AFM bilayer patterned multi-terminal structure, the measured resistance shows recurring signals due to supposedly electrical switching of the AFM Néel vector. However, in this work, we observe similar signals in such patterned structures, with and without the AFM layer [1], as shown in Fig. 1. The magnitude of the signals can be affected by different metals and substrates. When a large applied writing current density is beyond the Ohmic regime, there exist unintended anisotropic thermal gradients and voltages in the multi-terminal device. Also, large current densities cause electromigration and other irreversible effects. Therefore, the resistance difference may not be the conclusive evidence of the SOT switching of AFM Néel vector but the thermal artifacts of patterned structures on the substrate.

[1] C. C. Chiang, S. Y. Huang, D. Qu, P. H. Wu, and C. L. Chien, *Phys. Rev. Lett*., 123, 227203 (2019).

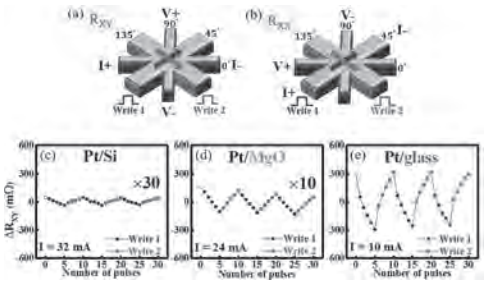

Fig. 1. Schematics of the eight-terminal patterned structure with the pulsed writing current along the 45° (write 1) and the 135° (write 2) lines for (a) planar Hall and (b) longitudinal resistance measurements. The values of ΔR_{XY} are determined after applying successive writing pulses current alternately along the 45° and the 135° lines for (c) Pt/Si, (d) Pt/MgO, and (e) Pt/glass.

M1-12. Zero Field Optic Mode Beyond 20 GHz in a Synthetic Antiferromagnet. *H.J. Waring*[1*], N. Johansson[1], I.J. Vera-Marun[2] and T. Thomson[1] *1. Computer Science, The University of Manchester, Manchester, United Kingdom; 2. Physics and Astronomy, The University of Manchester, Manchester, United Kingdom*

Antiferromagnets have considerable potential as spintronic materials [1]. Notably, they manifest resonant modes at frequencies higher than can be observed in conventional ferromagnetic materials. Synthetic Antiferromagnets (SAFs), engineered structures of antiferromagnetic (AF) RKKY exchange coupled ferromagnetic(FM)/non-magnetic(NM)/ferromagnetic trilayers, mimic the properties of single phase antiferromagnets whilst possessing greater compatibility with current device technologies such as those used for STT-MRAM production [2,3]. In addition to the conventional acoustic (Kittel) mode, SAFs also possess a higher order resonant (optic) mode [3]. The structure of a SAF is shown in Fig.1a. We report the dynamic properties of SAFs with structure Ta(2 nm)/CoFeB(5 nm)/Ru(t_{Ru})/CoFeB(5 nm)/Pt(4 nm) where t_{Ru} is the thickness of the Ru layer, acting as the NM spacer layer. The samples were fabricated using magnetron sputtering and characterized by X-ray Reflectivity (XRR) to measure layer thickness, vector Vibrating Sample Magnetometry (VSM) to verify AF interlayer coupling and a Vector Network Analyser – Ferromagnetic Resonance (VNA-FMR) setup to explore dynamic properties. Fig.1b shows the resonant dynamics of a single CoFeB layer and a CoFeB SAF. The data demonstrate the highest zero field frequencies observed in SAFs to date [4] with resonances of 18 GHz and 21 GHz at the 1st and 2nd instances of AF RKKY coupling respectively. A three part analytical model can reproduce the major features of the measured spectra.

[1] T. Jungwirth, X. Marti, P. Wadley et al., Nat. Nanotechnol., Vol. 11, p. 231–241 (2016) [2] R. Hao, L. Wang and T. Min, IEEE Trans. Magn., Vol. 55, p. 1-6 (2019) [3] S. Li, C. Wang, X. Chu et al., Adv. Funct. Mater., Vol. 26, p.3738-3744 (2016) [4] H. Waring, N.A.B. Johansson, I. Vera-Marun et al., Phys. Rev. Appl., Vol. 13, p. 034035 (2020)

** - Best student presentation award finalist*

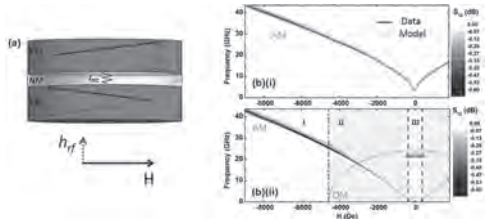

Fig.1 a) Schematic of the magnetic precession of a ferromagnetic (FM)/ non-magnetic (NM)/FM system due to a perturbation field h_{rf} when NM thickness promotes antiferromagnetic (AF) coupling. b) 2D map of the resonant spectra and modelling for (i) acoustic mode (AM) of single layer CoFeB and (ii) AM and optic mode (OM) of a synthetic antiferromagnet with interlayer coupling at the 2nd instance of AF RKKY coupling. Three magnetic states are highlighted: I) FM alignment II) Spin Flop III) AF alignment.

Session M2
COMPLEX OXIDES I

Cinthia Piamonteze, Co-Chair
Paul Scherrer Institut, Villigen, Switzerland
Peter Fischer, Co-Chair
Lawrence Berkeley National Laboratory, Berkeley, CA, United States

CONTRIBUTED PAPERS

M2-01. Interfacial Ferromagnetism and Structural Distortion in Ultrathin (111)-Oriented $LaNiO_3$. *M. Kane*[1,2], A. Vailionis[2], L.J. Riddiford[3,2], A. Mehta[4], A.T. N'Diaye[5], E. Arenholz[6] and Y. Suzuki[3,2] *1. Materials Science and Engineering, Stanford University, Stanford, CA, United States; 2. Geballe Laboratory for Advanced Materials, Stanford University, Stanford, CA, United States; 3. Applied Physics, Stanford University, Stanford, CA, United States; 4. Stanford Synchrotron Radiation Lightsource, Menlo Park, CA, United States; 5. E O Lawrence Berkeley National Laboratory, Berkeley, CA, United States; 6. Cornell High Energy Synchrotron Source, Ithaca, NY, United States*

$LaNiO_3$ (LNO) is unique among rare-earth nickelates in that it does not exhibit a temperature dependent metal-insulator transition or magnetic transition in the bulk. But in ultra-thin films of LNO, electronic and magnetic transitions emerge. Unique to films grown on (111)-oriented $LaAlO_3$, we observe evidence for a magnetic transition including the observation of the anomalous Hall effect and negative, hysteretic magnetoresistance in 8, 10, and 13 unit cell thick LNO films. These signatures of ferromagnetism imply that a ferromagnetic phase is present at the interface of the film and substrate where we observe a distortion of the unit cell and an increase in Ni^{2+} ions. Synchrotron x-ray diffraction data and dynamical x-ray diffraction analysis show an elongation of the lattice parameter spacing along the [111] direction to 2.4 Å near the film-substrate interface. This elongation also coincides with the onset of insulating behavior for films with thicknesses of 8 unit cells (d_{111}). For thicker films, the d_{111} spacing shrinks to 2.25 Å and the film exhibits bulk metallic behavior. We observe that the interfacial distortion is present in all our films and propose that it is distinct from strain accommodation in (001) films, where oxygen octahedra can more easily rotate to relieve strain. We also observe an increase in Ni^{2+} ions in thinner LNO(111) films from x-ray spectroscopy measurements, implying the presence of either oxygen vacancies or oxygen ligand holes that contribute to the insulating behavior observed at the film-substrate interface. Together these results imply that metallicity and magnetism in LNO films is governed by a balance among the charge, lattice and orbital degrees of freedom. Dept. of Energy, Director, Office of Science, Office of Basic Energy Sciences, Div. of Mat. Sci. and Eng., Contract No. DESC0008505 and NSF GRFP This research used resource of the Advanced Light Source, a U.S. DOE Office of Science User Facility under contract no. DE-AC02-05CH11231.

M2-02. Ferroelastic Nature and Ferromagnetism in Epitaxial $LaCoO_3$. *S. Yoon*[1], X. Gao[1], J. Ok[1], Z. Liao[1], M. Han[2], Y. Zhu[2], P. Ganesh[1], M. Chisholm[1], W. Choi[3] and H. Lee[1] *1. Oak Ridge National Laboratory, Oak Ridge, TN, United States; 2. Brookhaven National Laboratory, Upton, NY, United States; 3. Sungkyunkwan University, Suwon, The Republic of Korea*

Magnetism in strained $LaCoO_3$ (LCO) thin films has been an intriguing scientific subject for the last decade. While the bulk LCO is non-magnetic, strained LCO thin films exhibit robust ferromagnetism with a phase transition temperature (T_c) of 80 K.[1] Since this system is a representative example where epitaxial strain induces non-bulk magnetic properties, it has drawn lots of attentions in the field of magnetic oxide thin films. Despite extensive research over the past decade[2-6], the consensus on the origin of ferromagnetism has not yet to be achieved. A main challenge of this system is a complex microstructure inside the film; the existence of planar defects (seen as dark stripes in high-angle annular dark field scanning transmission electron microscopy (HAADF STEM) images) and their association with oxygen vacancies are important issues. Through the systematic STEM-based investigations, we verified that the planar defects always exist in epitaxial LCOs which undergo a ferroelastic response and the pristine planar defects do not involve oxygen vacancies. Furthermore, we have recently found that the compressed units sandwiched by the dark stripes are responsible for ferromagnetism in epitaxial LCOs. In this presentation, we will show that the ferroelastic nature of ferromagnetic structural units can account for many unusual magnetic properties of this system.

[1] D. Fuchs *et al. Phys. Rev. B* 75, 144402 (2007) [2] W. Choi *et al. Nano Lett.* 12, 4966 (2012) [3] N. Biskup *et al. Phys. Rev. Lett.* 112, 087202 (2014) [4] L. Qiao *et al. Nano Lett.* 15, 4677 (2015) [5] J. Fujioka *et al. Phys. Rev. Lett.* 111, 027206 (2013) [6] G. Sterbinsky *et al. Phys. Rev. Lett.* 120, 197201 (2018)

M2-03. Doping- and Strain-Dependent Electrochemical Control of Magnetism in Ion-Gel-Gated $La_{1-x}Sr_xCoO_{3-\delta}$ Films. *V. Chaturvedi*[1], W. Postiglione[1], B. Yu[2], W. Tabis[2,3], S. Hameed[2], N. Biniskos[2], H. Zhou[4], Z. Zhang[4], M. Greven[2] and C. Leighton[1] *1. Department of Chemical Engineering and Materials Science, University of Minnesota, Minneapolis, MN, United States; 2. School of Physics and Astronomy, University of Minnesota, Minneapolis, MN, United States; 3. Faculty of Physics and Applied Computer Science, AGH University of Science and Technology, Krakow, Poland; 4. Advanced Photon Source, Argonne National Laboratory, Lemont, IL, United States*

Electrolyte gating techniques involving ionic liquids/gels have proven remarkably powerful in controlling electronic, magnetic, and optical properties of materials. Both electrostatic and electrochemical approaches are possible [1], a striking example of the latter being the voltage-actuated perovskite (P) to brownmillerite (BM) transition in $SrCoO_{3-d}$ [2,3], which yields a ferromagnetic/antiferromagnetic transition. Here, we substantially expand on this topic through a detailed study of the ion-gel-gating-induced P to BM transition in $La_{1-x}Sr_xCoO_{3-\delta}$ across almost the entire phase diagram ($0 \leq x \leq 0.7$), considering also epitaxial strain. Building on our prior work [4-6], and using transport, magnetometry, and *operando* synchrotron X-ray diffraction, we first demonstrate that the P to BM transition can be electrically-actuated down to low x (Fig. 1(a)), where, critically, the films are air stable (unlike $SrCoO_3$) [7]. Detailed data on control of ferromagnetism and conductivity are thus obtained, including tuning of T_C over a 220 K window. We then show that the threshold voltage (V_{th}) for the P to BM transition and the reversibility window (V_{rev}) for the P phase systematically decrease with Sr-doping and tensile strain (Fig. 1(b)) [7]. We argue that this is due to thermodynamic rather than kinetic effects, related to decreases in the oxygen vacancy formation enthalpy with doping and tensile strain

[7]. These findings take us towards a global understanding of the electrochemical control of magnetism in this important model system. Work supported by NSF MRSEC and DOE Center for Quantum Materials.

[1] Leighton, Nat. Mat. 18, 13 (2018). [2] Lu *et al*., Nano Lett. 16, 1186 (2016). [3] Lu *et al*., Nature 546, 124 (2017). [4] Walter *et al*., ACS Nano 10, 7799 (2016). [5] Walter *et al*., Phys. Rev. Materials 1, 071403(R) (2017). [6] Walter *et al*., Phys. Rev. Materials 2, 111406(R) (2018). [7] Chaturvedi *et al*., in preparation (2020).

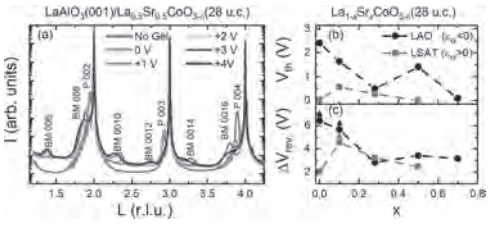

Fig. 1. (a) Operando synchrotron X-ray diffraction from a 28-unit-cell-thick $La_{0.5}Sr_{0.5}CoO_{3-\delta}$ film on $LaAlO_3$ at various gate biases at 150 K. Sr-doping (x) dependence of (b) the threshold voltage (V_{th}) for the P to BM transition and (c) the window of reversibility ($\Delta V_{rev.}$) for 28-unit-cell $La_{1-x}Sr_xCoO_{3-\delta}$ films on $LaAlO_3$ and LSAT substrates. ε_{xx} denotes in-plane biaxial strain.

M2-04. Strain and Thickness Dependent Magnetic Properties of Epitaxial $La_{0.7}Sr_{0.3}CoO_3/La_{0.7}Sr_{0.3}MnO_3$ Heterostructures. *M. Feng*[1], N. Ahlm[1], A.M. Kane[1], I. Chiu[2], D.Y. Sasaki[1], P. Shafer[3], A.T. N'Diaye[3], A. Mehta[4] and Y. Takamura[1] *1. Materials Science and Engineering, University of California, Davis, Davis, CA, United States; 2. Chemical Engineering, University of California, Davis, Davis, CA, United States; 3. Advanced Light Source, Lawrence Berkeley National Laboratory, Berkeley, CA, United States; 4. SLAC National Accelerator Laboratory, Menlo Park, CA, United States*

The emergent magnetic phenomena that arise due to electronic, spin, or lattice reconstruction at interfaces of perovskite oxide heterostructures motivate both fundamental research and the exploration of new device applications.[1] Lattice strain resulting from the lattice mismatch between the thin film and substrate can be an effective method to tune the interfacial characteristics and modify the magnetic properties of heterostructures.[2,3] In this work, we investigate the strain-related and thickness-dependent magnetic properties of $La_{0.7}Sr_{0.3}CoO_3$(LSCO)/$La0_{.7}Sr_{0.3}MnO_3$ (LSMO) heterostructures with LSCO thicknesses ranging from 2-12 nm and a constant LSMO thickness (6 nm) grown on $LaAlO_3$ (LAO) and $NdGaO_3$ (NGO) substrates. Both the LSCO and LSMO layers exist under in-plane compressive strain on LAO substrates, while on NGO substrates, the LSCO layer is under tensile strain and the LSMO layer is nearly un-strained. Bulk magnetometry reveals that the LSCO and LSMO layers are strongly magnetically coupled when grown on LAO substrates, as demonstrated by hysteresis loops with a single magnetic switching event with coercive fields similar to LSMO single layers regardless of LSCO layer thickness. In contrast, on NGO substrates this magnetic coupling is only observed in thinner bilayers (LSCO thickness < 6 nm). Bilayers with thicker LSCO layers exhibit hysteresis loops with distinct hard/soft switching events, and the soft layer experiences exchange bias from the underlying hard layer. Soft x-ray magnetic spectroscopy measurements reveal that the differing magnetic behavior is accompanied by changes in the Co ion valence states. On NGO substrates, magnetic coupling is characterized by magnetically active Co^{2+} ions in the LSCO layer, while thicker bilayers and all bilayers on LAO substrates have mixed valence Co^{3+}/Co^{4+} ions. These results suggest the complex interplay between the electronic, spin, and lattice degrees of freedom on perovskite oxides which can be used to control the functional properties of next generation magnetic random access memory and spintronic devices.

[1] M. Bibes, J. E. Villegas and A. Barthélèmy, *Advances in Physics*, Vol. 60, no. 1. p. 5–84 (2011) [2] J. P. Byers *et al.*, *J. Appl. Phys.*, Vol. 125, no. 8, p. 82518 (2019) [3] J. Zhang *et al.*, *ACS Appl. Mater. Interfaces*, Vol. 10, no. 47, p. 40951–40957 (2018)

M2-05. Study of Canonical Spin Glass Behavior in Co Doped $LaMnO_3$. *F.H. Bhat*[1,5], G.A. Khan[2], G. Kataria[3], R. Kumar[4], D. Sahdev[3] and M.A. Malik[5] *1. Physics, Islamic University of Science and Technology, Awantipora, India; 2. Physics, SP College, Cluster University Srinagar, Srinagar, India; 3. Quazartech, New Delhi, India; 4. Materials Science and Engineering, NIT, Hamirpur, Hamirpur, India; 5. Physics, University of Kashmir, Srinagar, India*

The manganites [1,2] and cobaltites [3-5] have been found to be depicting the spin-glass (SG) behaviour; arising out of randomly frozen state of the spins, below a critical temperature. A typical SG is characterized by the absence of long range ordering and magnetic frustration [6]. In $LaMn_{1-y}CoyO_3$ (y = 0.1 - 0.4) competing ferromagnetic (FM) and antiferromagnetic (AFM) interactions result in frustration consequently leading to SG state. In order to investigate the existence of SG behaviour in the present system susceptibility measurement in an *ac* field of 4 Oe and 0 Oe dc field has been performed at different frequencies. Temperature dependence of in-phase (χ'_{ac}) component of the *ac* susceptibility, show that the peak position which correspond to freezing temperature (T_f) moves toward higher temperatures and the magnitude of χ'_{ac} decreases as the frequency increases. This is a strong signature of the existence of SG behavior. The parameter called relative shift in freezing temperature (δT_f) per decade of frequency, suitable in characterizing a particular SG state [6, 7] is found to be δT_f = 0.008 for x = 0.1 and δT_f = 0.0053 for x = 0.4; in accordance with the one reported for canonical SG systems [3,6,10]. Temperature variation for out of phase component of ac susceptibility (χ_{ac}") show the existence of canonical SG state in both the samples, the prominent feature for which is the zero value of χ_{ac}" at temperatures larger than T_f and its finite value below T_f in both the samples. The frequency dependence of T_f is analyzed by using the Vogel-Fulcher (VF)- and Arrhenius –law [6], both of which prove the existence of canonical spin glass state in $LaMn_{1-x}Co_xO_3$ (x = 0.1 - 0.4).

1. I. O. Troyanchuk, L. S. Lobanovsky et al J. Magn. Magn.Mater. 210, 63 (2000). 2. X. L. Wang, M. James et al. Supercond. Sci. Technol. 15, 427-430 (2002) 3. N. Khan, A. Midya, P. Mandal and D. Prabhakaran J. App. Phys. 113, 183909 (2013). 4. V. Kumar, Y. Kumar, R. Kumar et al. *J.of App. Phys.* 113, 043918 (2013). 5. J. Wu and C. Leighton Phys. Rev. B 67, 174408 (2003). 6. J. A. Mydosh Spin glasses: an experimental introduction (1993 Taylor and Francis); 7. P. Bag, P. R. Baral, and R. Nath Phys. Rev. B 98, 144436 (2018). 8. C. A. M. Mulder, A. J.V. Duyneveldt, and J. A. Mydosh, Phys. Rev. B 25, 515 (1982).

M2-06. Versatile Magnetic Ordered Phases in $SrMnO_3$ Films and its co- Dependence on Structural Properties. *J.J. van Rijn*[1], A. Das[1], E. Vallabhaneni[1] and T. Banerjee[1] *1. Zernike Institute of Advanced Materials, University of Groningen, Groningen, Netherlands*

Antiferromagnetic (AF) spintronics has gained significant attention in recent years due to their fast magnetization dynamics and absence of stray field effects, enhancing prospects for potential applications. The highly correlated orbital, charge and spin degrees of freedom in manganite based oxide materials offer high tunability of magnetic properties through strain, temperature and magnetic field application. The ground-state G-type antiferromagnet, $SrMnO_3$, has been theoretically predicted to show a great variety of magnetic and electric properties, including multiple antiferromagnetic to ferromagnetic ordered states. Its strong co-dependence with structural characteristics such as epitaxial strain and off-stoichiometry even induces a highly polarized ferroelectric phase above the Néel temperature. Therefore, below the magnetic ordering temperature, a multiferroic phase is predicted. Such a vast range of possibilities ensures $SrMnO_3$ as an intriguing material of choice for studying the codependence of structure on magnetic ordering. In this work we demonstrate the tunability of magnetic interactions by altering growth conditions in Pulsed Laser Deposition such as oxygen pressure, temperature

and annealing strategy. $SrMnO_3$ thin films without and with a single $La_{0.67}Sr_{0.33}MnO_3$ overlayer are also studied. Structural characterization using diffraction techniques show clear $SrMnO_3$ peaks in 2θ scans and reciprocal space mapping, indicating fully strained epitaxial grown films. Bulk temperature dependent magnetization studies show both ferromagnetic and anti-ferromagnetic phases with temperature. To support the bulk magnetic observations, surface magnetic ordering of the deposited $SrMnO_3$ films is characterized using Spin Hall magnetoresistance as a probe, allowing for a distinction between antiferromagnetic and ferromagnetic ordering. A comprehensive overview of bulk and interface characterization establishes $SrMnO_3$ thin films as an interesting material choice for developing antiferromagnetic oxide based spintronics.

M2-07. Microstructure Analysis of Electrospun $La_{0.8}Sr_{0.2}MnO_3$ Nanowires Using Electron Microscopy and Electron Backscatter Diffraction (EBSD). *A. Koblischka-Veneva*[1,2], M.R. Koblischka[1,2], X. Zeng[2] and J. Schmauch[2] *1. Material Science, Shibaura Kogyo Daigaku, Koto-ku, Japan; 2. Experimental Physics, Universitat des Saarlandes Naturwissenschaftlich-Technische Fakultat, Saarbrucken, Germany*

The perovskite compound $La_{1-x}Sr_xMnO_3$ (LSMO) is known for the high spin-polarized currents, which makes it a material of great interest in spintronics [1]. The magnetoresistance (MR) observed was found to depend strongly on the microstructure, i.e., the grain boundaries (GBs) and the interfaces between the grains. By means of electrospinning, one can prepare long (up to 100 μm), free-standing LSMO nanowires. The diameter of the nanowires is in the 200 nm-range, and the individual nanowires are polycrystalline with a grain size of about 15-20 nm, which corresponds to the dimensions obtained via transmission electron microscopy (TEM). The microstructural properties of electrospun $La_{0.8}Sr_{0.2}MnO_3$ (LSMO) nanowires were investigated using SEM, TEM and electron backscatter diffraction (EBSD). By means of EBSD, it is possible to measure the crystallographic orientation of the LSMO grains within an individual nanowire. As the LSMO grains within the nanowires are in the 10-nm range, we employ here parts of the recently developed transmission-EBSD or transmission Kikuchi diffraction technique [2,3] in order to enhance the Kikuchi pattern quality to enable an automated mapping of the crystallographic data. The diffraction results demonstrate that the grain orientation is not random, but there is a texture induced by the shape of the polymer nanowire formed after the electrospinning step. Within an individual nanowire section, the dominating GBs are high-angle grain boundaries, which play an important role in the current flow through the sample (low- and high field magnetoresistance). The data obtained allow further an analysis of the grain shape aspect ratio, and elucidate the grain and grain boundary arrangement within electrospun LSMO nanowires. This work is supported by DFG-project Ko2323-8.

[1] J. Huang et al., ACS Appl. Mater. Interfaces 10, 42698 (2018) [2] P. W. Trimby, Ultramicroscopy 120, 16 (2012). [3] A. Koblischka-Veneva, M. R. Koblischka, J. Schmauch, *et al*., J. Microscopy 274, 123 (2019).

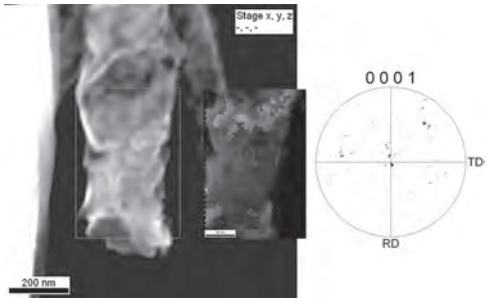

Fig.1 t-EBSD analysis of an individual section of a nanowire. (a) SEM image and crystallographic orientations determined by EBSD. (b) presents the EBSD-based pole figure in (1000)-direction.

M2-08. Surface Ferromagnetism in $Pr_{0.5}Ca_{0.5}MnO_3$ Nanoparticles as a Consequence of Local Imbalance Mn^{3+}:Mn^{4+} Ratio. D. Alshalawi[1], J. Alonso[1,2], *P. de la Presa*[1] and A. Hernando[1] *1. Instituto de Magnetismo Aplicado, Universidad Complutense de Madrid, Madrid, Spain; 2. Insitut of Materials Science of Madrid, Consejo Superior de Investigaciones Cientificas, Madrid, Spain*

Half-doped praseodymium manganites, $Pr_{0.5}Ca_{0.5}MnO_3$, nanoparticles synthesized by sol-gel method are annealed at different temperatures in order to obtain nanoparticles sizes ranging from 15 to 100 nm. HRTEM shows that the nanoparticles are very crystalline with no structural disorder at the surface. Rietveld powder diffraction profile determines that the samples have orthorhombic structure with space group Pnma and cell volume decreases with increasing particle size. The thermodiffraction patterns from 50 to 300 K indicate that the charge ordering (CO) is suppressed for the smallest particles, whereas the largest one still resembles the bulk. Hysteresis loops and ZFC-FC curves evince that, as the most of half-doped (Mn^{3+}:Mn^{4+} = 1) antiferromagnetic (AFM) charge-ordered manganites, ferromagnetism (FM) appears as particle size decreases. Hysteresis loops at FC procedure show a coercivity increase and a shift to negative field, confirming that both AFM and FM phases not only coexist but are also coupled. In addition, a spin glass behaviour is observed with glass temperature around 50 K. A possible origin of FM phase development is the lacking oxygen ligands at the surface that increases Mn^{3+} at expenses of Mn^{4+} in order to maintain the electronic neutrality. In this work, we show that Mn^{3+}:Mn^{4+} = 1 ratio is preserved in the whole crystalline particle with the exception of the surface, where this ratio changes to Mn^{3+}:Mn^{4+} >1. This Mn^{3+} excess makes double exchange $Mn^{3+}\rightarrow O^{2-}\rightarrow Mn^{4+}$ prevails over the super-exchange giving place to the FM interactions. We show that a "shell" thickness of only one-unit cell, with a_{cell} = 0.38 nm, is enough to explain the onset of FM at the surface, whereas the volume remains AFM. Furthermore, the FM to AFM ratio fits to the increase of surface to volume ratio with decreasing particle size.[1].

[1] H. D. Aliyu, J. M. Alonso, P de la Presa et al., *Chem Mater* 30, 7138-7145 (2018).

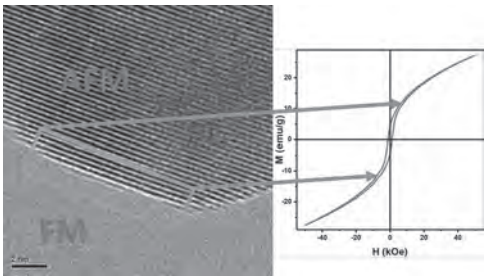

The atomic imbalance of Mn^{3+}:M^{4+} at the last atomic layer of the nanoparticle surface is responsible for the onset of FM in the AFM $Pr_{0.5}Ca_{0.5}MnO_3$

M2-09. Size Dependence of Charge Order and Magnetism in $Sm_{0.35}Ca_{0.65}MnO_3$ – Magnetization and Electron Paramagnetic Resonance Studies. *L.R. Goveas*[1], B. K.S.[2], A. K.N.[3] and S. Bhat[2] *1. Physics, St. Joseph's College (Autonomous), Bangalore, India; 2. Physics, Indian Institute of Science, Bangalore, India; 3. Physics, Dr. Ambedkar Institute of Technology, Bangalore, India*

We report a systematic tracking of the consequence of size reduction to nanoscale on charge order (CO) and magnetic properties of electron doped $Sm_{0.35}Ca_{0.65}MnO_3$ by magnetization and electron paramagnetic resonance (EPR) measurements. The bulk form of this system is charge ordered below 275 K and antiferromagnetic (AFM) below 130 K. The bulk sample and nanoparticles of various sizes (mean diameter ~ 15, 30, 60, 90 nm) were prepared by sol-gel method. Magnetic and X-band EPR measurements were carried out at temperatures from 10-300 K. Our studies show that the highly robust CO in the bulk gets weakened by size reduction and the nanoparticles exhibit ferromagnetic (FM) ordering[1]. Magnetization in the paramagnetic

region arising due to FM fluctuations caused by double exchange interaction is found to decrease as particle size decreases. However, at low temperature the trend of FM magnetization as a function of the size is found to be reversed as shown in Fig 1. Analysis of magnetic susceptibilities shows that magnetization in the FM phase is not due to the strengthening of double-exchange FM interactions but it is attributed to the dominance of surface effects. A detailed study on the EPR intensity, line width and g-factor reveals that in 15 nm particles though long range CO disappears, the signature of short range CO persists[2]. Line width variation indicating weakening of the AFM interactions and the development of the short-range FM phase are discussed based on Fig 2. As the particle size decreases the relative contribution of the surface ions increases. The prevalence of translational symmetry breaking, defects and surface imperfections lead to short range FM ordering in the system. We discuss the origin of these effects in terms of the presently existing models.

[1] S. S. Rao, S. Tripathi, D. Pandey, and S. V. Bhat, Phys. Rev. B 74, 144416 (2006) [2] S. Zhou, Y. Guo, J. Zhao, L. He, C. Wang, and L. Shi, J. Phys. Chem. C 115, 11500 (2011).

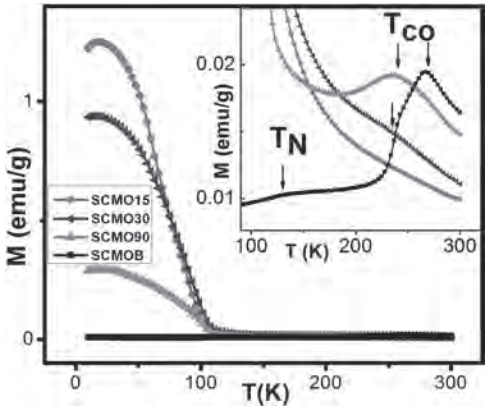

Fig1: Temperature dependence of magnetization

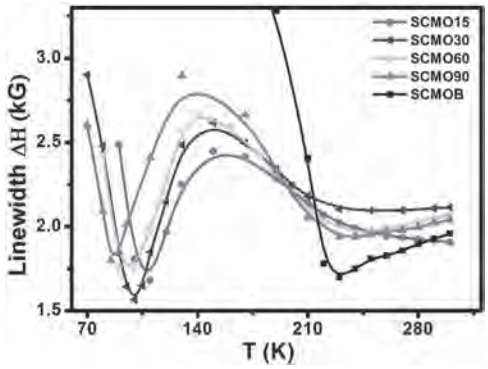

Fig 2:Temperature dependence of line width

INVITED PAPER

M2-10. Unusual Dynamical Properties of Oxide-Magnetic Heterostructures. *J. Ramirez*[1] *1. Department of Physics, Universidad de los Andes, Bogota, Colombia*

Electron-correlated oxide materials display a plethora of physics phenomena due to their multiples degrees of freedom. Transition-metal oxides, in particular, exhibit coincidental structural, magnetic, and metal-insulator transitions among others. When combined in proximity with single-metallic-ferromagnets, it is possible to enhance the magnetic control at the nanoscale [1]. Understanding the magnetic dynamics in such systems provides the means to untangle the underlying physical phenomena which govern these strongly correlated materials. Here we will present two examples of such systems studied by angular-dependent Ferromagnetic resonance as a function of temperature. In both cases, the magnetic dynamics is governed by the proximity of an oxide undergoing a structural transition with a ferromagnet, as in the case of VOx/Ni heterostructures [2], or in the case of La-Pr-Ca-Mn-O thin films, by their complex magnetic-electronic phase transitions [3]. FMR and micromagnetic simulations allowed us to trace back the details of the phase transitions and to map the changes in anisotropy and the magnetic domain reorganization. Work done in collaboration with Christian Wolowiec, Diego Carranza, Ali Basaran, Amlan Biswas, Michael Fitzsimmons, Arantxa Fraile Rodríguez, Javier Rodriguez-Alvarez, Amílcar Labarta, Xavier Batlle, and Ivan K. Schuller. Funded by the US DoE, Office of Basic Energy Sciences, under Award FG02-87ER-45332 and Colciencias under contract 137-2016. Spanish MINECO projects MAT2015-68772-P and PGC2018-097789-B-I00 and European Union FEDER funds.

[1] I. Valmianski, et al., in preparation. [2] J. G. Ramirez, et al., Phys. Rev. B 93, 1 (2016). [3] D. Carranza-Celis, et al., in preparation.

CONTRIBUTED PAPERS

M2-11. Withdrawn

M2-12. Magnetic-Domain-Wall-Induced Electrical Polarization in Rare-Earth Iron Garnet Systems: a First-Principle Study. *T. Bayaraa*[1], C. Xu[1], Y. Yang[2], H. Xiang[2] and L. Bellaiche[1] *1. Physics, University of Arkansas Fayetteville, Fayetteville, AR, United States; 2. State Key Laboratory of Surface Physics and Department of Physics, Fudan University, Shanghai, China*

Recently, there have been reports on observation of electrical polarization and/or giant magnetoelectric effect in epitaxial rare-earth iron garnet (RIG) films [1–5] but the mechanism behind it is still in dispute. First-principles methods are employed to understand the existence of such polarization in RIGs. In contrast with previous beliefs, it is found that its occurrence can be explained if the system adopts magnetic multidomains and does neither require local magnetic moments of the rare-earth ions nor non-collinear magnetism. Table I reports the predicted polarization of a studied RIG *multidomains* (with R=Gd) with DW in the middle of supercells when we consider or not *f*-electrons of the Gadolinium (G) ions as valence electrons, which we denote as the "with-f" *versus* the "without-f" cases, respectively. Within each supercell, the two magnetic domains have a magnetic configuration that is reversed with respect to each other. As one can see, domain walls (DW) in GIG gives rise to a polarization even without *f*-electrons. This is further confirmed by the prediction of polarization in Yttrium (IG) and Lutetium (IG) iron garnet systems having multidomains as well. Furthermore, we found that the microscopic mechanism responsible for this DW-induced-polarization originates from a magnetoelectric effect arising from ferromagnetic interactions between octahedral and tetrahedral Fe ions at the domain walls (note that this interaction is antiferromagnetic in bulk RIG). More precisely, this mechanism is a symmetric exchange-striction mechanism, which, for the electrical polarization, takes the analytical form of $P=\sum_{<i,j>} P_{es}^{ij} S_i \bullet S_j$, where the summation is over all the spin pairs and P_{es}^{ij} is the polarization coefficient vector associated with the <i,j> spin pair. Acknowledgments This work is supported by the Department of Energy, Office of Basic Energy Sciences, under Award No. DE-SC0002220

[1] A. S. Logginov, G. A. Meshkov, A. V. Nikolaev, and A. P. Pyatakov, JETP Lett. 86, 115 (2007). [2] G. V. Arzamastseva, A. M. Balbashov, F. V. Lisovskii, E. G. Mansvetova, A. G. Temiryazev, and M. P. Temiryazeva, J. Exp. Theor. Phys. 120, 687 (2015). [3] A. P. Pyatakov, A. K. Zvezdin, A. M. Vlasov, A. S. Sergeev, D. A. Sechin, E. P. Nikolaeva, A. V. Nikolaev, H. Chou, S. J. Sun, and L. E. Calvet, in *Ferroelectrics* (Taylor & Francis

Group, 2012), pp. 79–88. [4] V. Koronovskyy and Y. Vakyla, Electron. Mater. Lett. 11, 1028 (2015). [5] I. S. Veshchunov, S. V. Mironov, W. Magrini, V. S. Stolyarov, A. N. Rossolenko, V. A. Skidanov, J. B. Trebbia, A. I. Buzdin, P. Tamarat, and B. Lounis, Phys. Rev. Lett. 115, (2015).

	Supercell size		Polarization (C/m^2)
GIG	2x1x1	with f	-0.002133
		without f	-0.005117
	4x1x1	with f	-0.001100
		without f	-0.002553
LuIG	2x1x1	filled f-shell	-0.002458
YIG	2x1x1	empty f-shell	-0.002157

Polarization results of different supercells of RIG systems with DW at the center of the supercells

M2-13. Hidden Magnetoelectric Multipoles, and Anti-Magnetoelectric Effect in Fe_2O_3. *X.H. Verbeek*[1] and N.A. Spaldin[1] *1. Materials department, ETH Zurich, Zürich, Switzerland*

We present first-principles calculations of the magnetoelectric multipoles in Cr_2O_3 and its iron-based analogue, Fe_2O_3. Cr_2O_3 is the prototypical linear magnetoelectric material, in which an applied magnetic field induces a proportional electric polarization and vice versa, a process which can be understood in terms of the ferroic ordering of magnetoelectric multipoles[1]. Fe_2O_3 has the same structure as Cr_2O_3 but a different magnetic ordering which does not allow a linear magnetoelectric response. We used density functional theory with the LDA+U method in an extension[2] to the VASP code[3], to calculate the local magnetoelectric multipoles on the transition metal ions in both materials. In Cr_2O_3 we found local magnetoelectric monopoles and quadrupoles consistent with the established magnetoelectric effect. Surprisingly, our calculations revealed hidden magnetoelectric multipoles on the iron ions in Fe_2O_3, with the multipoles on adjacent ions having opposite sign consistent with the absence of a net magnetoelectric effect. We predict an *anti-magnetoelectric* effect in Fe_2O_3, in which pairs of spins cant in opposite directions under the application of an external electric field, to create an additional anti-ferromagnetic ordering along the axis of the applied field. We discuss possible consequences of this effect for bulk Fe_2O_3 and heterostructures of Fe_2O_3 and Cr_2O_3.

[1] N. A. Spaldin, M. Fiebig and M. Mostovoy, J. Phys.: Condens. Matter, Vol. 20, p. 434203 (2008) [2] F. Thöle and N. A. Spaldin, Phil. Trans. R. Soc. A, Vol. 376, p. 20170450 (2018) [3] G. Kresse, J Furthmüller, Phys. Rev. B, Vol. 54, p. 11169 (1996)

M2-14. Influence of the Oxide Termination and Polarization on the Interfacial Dzyaloshinskii-Moriya Interaction and the Perpendicular Magnetic Anisotropy in BTO/CoFeB/Pt System. *S. Tacchi*[1], W. Lin[2], B. Yang[3,4], A.P. Chen[5], X. Wu[2], R. Guo[2], S. Chen[2], Q. Xie[2], X. Shu[2], L. Liu[2], Y. Hui[2], G. Chow[2], Y.P. Feng[6,5], G. Carlotti[7], H. Yang[3,4] and J. Chen[2] *1. Istituto Officina dei Materiali, Sede Secondaria di Perugia, CNR, Consiglio Nazionale delle Ricerche, Perugia, Italy; 2. Department of materials science and engineering, National University of Singapore, Singapore; 3. Ningbo Institute of Materials Technology and Engineering, Chinese Academy of Sciences, Ningbo, China; 4. Center of Materials Science and Optoelectronics Engineering, University of Chinese Academy of Sciences, Beijing, China; 5. NUS Graduate School of Integrative Sciences and Engineering, National University of Singapore, Singapore; 6. Department of Physics, National University of Singapore, Singapore; 7. Department of Physics and Geology, Università degli Studi di Perugia, Perugia, Italy*

The interfacial Dzyaloshinskii-Moriya interaction (*i*-DMI), has attracted extensive attention due to its crucial role in the stabilization of chiral spin textures such as magnetic skyrmion lattices and chiral domain walls. Recently, a sizeable *i*-DMI has been found at the interface between an oxide layer and a ferromagnetic (FM) film[1]. Due to their versatility, oxide materials offer different degrees of freedom, which can be used to tailor the *i*-DMI. In this work we present a combined experimental and theoretical study of the *i*-DMI and the perpendicular magnetic anisotropy (PMA) at the oxide/FM interface in the $BaTiO_3$(BTO)/CoFeB/Pt system[2]. The *i*-DMI has been investigated by Brillouin light scattering (BLS), measuring the frequency difference Δf between counter-propagating Damon-Eshbach (DE) spin-waves, induced by the presence of *i*-DMI. BLS measurements were performed applying an in-plane magnetic field, and sweeping the in-plane wave-vector k along the perpendicular direction (DE geometry). Fig.1 shows the measured Δf values as a function of the spin-wave wave-vector k for the CoFeB/Pt films grown on TiO_2- and BaO-terminated BTO. The effective DMI constant D, determined by linear fit to the experimental data, is found to be 0.45±0.02 and 0.56±0.02 mJ/m^2, for TiO_2-BTO/CoFeB/Pt and BaO-BTO/CoFeB/Pt structures, respectively. Since the CoFeB/Pt interface gives the same contribution to the DMI of both systems, the different D values can be attributed to a larger DMI strength at the TiO_2-BTO/CoFeB interface. On the contrary, PMA, studied by superconducting quantum interference device magnetometry, is observed to be larger for the CoFeB films grown on a BaO-BTO substrate. Finally, we find that the ferroelectric polarization in the BTO film slightly affects both the *i*-DMI and the PMA. Using first principle calculations we show that these results can be ascribed to the different electronic states around the Fermi level at the oxide/FM interfaces. Financial support by the European Metrology Programme for Innovation and Research (EMPIR), under the Grant Agreement 17FUN08 TOPS is kindly acknowledged.

[1] M. Arora et al., Phys. Rev. B 101, 054421 (2020); H. T. Nembach et al., Phys. Rev. B 101, 020409 (2020). [2] W. Lin, et al. Phys. Rev. Lett. 124, 217202 (2020).

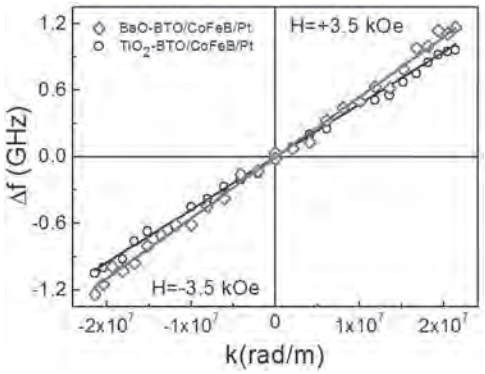

Measured (dots) frequency difference Δf as a function of k for the two investigated systems. The line is a linear best-fit.

M2-15. Tuning the Magnetic Anisotropy and Phase Transition in Superparamagnetic Cobalt Oxide Nanostructures Synthesized Through Novel Solution-Growth Technique. *N.N. Joshi*[1,2], V. Kochat[1] and S. S. A.[2] *1. Materials Science Centre, Indian Institute of Technology Kharagpur, Kharagpur, India; 2. Centre for Nano Science and Engineering, Indian Institute of Science, Bangalore, India*

In the present work, we show that the *in situ* growth of oriented nanometric aggregates of cobalt oxide can be explored to alter and tune magnetocrystaline anisotropy. As such, the impact of interparticle interaction on magnetic properties of the aggregates is studied. Mono-dispersed cobalt oxide (CoO) nanostructures were prepared through decomposition of metal-organic compound of cobalt (II) in an alcoholic solution under controlled microwave irradiation, below 150 °C. CoO nanostructures were effectively synthesized without the use of any surfactant. The structures were found to be inert to oxidation in ambient air for several months. We attribute the stability of CoO nanospheres to their dense packing, the driving force being, minimization of surface area and surface energy [1]. X-ray diffractometry (XRD)

measurements indicate the formation of well crystallized CoO nanoparticles, without the need for post-synthesis annealing. Deconvolution of the active modes in Raman spectra obtained at room temperature reveals the O_h symmetry in rock-salt CoO, induced by microwave-assisted synthesis route [2]. Its effect on magnetic characteristics of CoO is analyzed here. Field-dependent magnetization (MH) and temperature-dependent magnetization (MT) measurements show a phase transition from paramagnetic to superparamagnetic interactions in CoO nanostructures at around 10 K, at which the average particle size was estimated to be 9 nm. The nanostructures however do not exhibit a distinct antiferromagnetic transition around 300 K as the bulk sample [3], but instead show a hysteresis below a blocking temperature of ~10 K (Figure 1). This finding reveals the magnetic behavior of CoO nanostructures that opens new opportunities for future applications as anisotropy source for magnetic recording.

[1] M. Ibrahim Dar, S. Sampath and S. A. Shivashankar, Journal of Materials Chemistry., Vol. 22, p.22418 (2012) [2] A. V. Ravindra, B. C. Behera and W. Prellier, Journal of Applied Physics, Vol. 116, p.33912 (2014) [3] C.N.R. Rao and B. Raveau, Transition metal oxides, Wiley., (1995)

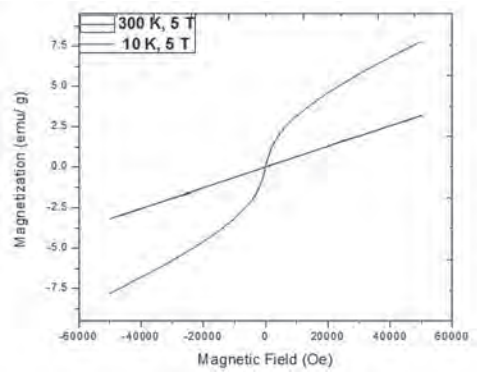

Fig. 1 Magnetization curves of CoO nanostructures measured at various temperatures (at 5 T)

M2-16. Withdrawn

Session M3
MAGNETIZATION DYNAMICS AND DAMPING IV: SPIN CURRENT, SPIN-TORQUE, SPIN TRANSPORT, VORTICES, SKYRMIONS AND DOMAIN WALLS

Igor Barsukov, Chair
University of California, Riverside, Riverside, CA, United States

CONTRIBUTED PAPERS

M3-01. Detection of in-Plane Magnetization Switching of $Ni_{80}Fe_{20}$ Layer by Spin Rectification Effect. *M. Aoki*[1], Y. Ando[1], R. Ohshima[1], E. Shigematsu[1], T. Shinjo[1] and M. Shiraishi[1] *1. Electronic Science and Engineering, Kyoto university, Nishikyo-ku, Kyoto, Japan*

Magnetization switching using spin orbit torque (SOT) [1] has been investigated intensively to realize the low power and high endurance magnetic memory. For the in-plane magnetization switching, fabrication of spin valves is generally required because the anomalous Hall effect is not applicable. Such an additional fabrication procedures impede the rapid development of material search for the materials that exhibit a large SOT. In this study we demonstrated SOT induced in-plane magnetization switching of a single $Ni_{80}Fe_{20}$ layer on platinum layer by using spin rectification effect (SRE). Under the microwave irradiation, dc voltage via SRE appears near the ferromagnetic resonance field, well known as the spin-torque FMR[2]. In contrast, non-zero dc voltage also appears around zero magnetic field due to the non-resonant SRE (nrSRE), whose voltage level corresponds to the magnetization direction [3]. We found that the nrSRE was drastically enhanced under the irradiation of microwave with a frequency lower than FMR condition. By using the enhanced nrSRE, we demonstrated a highly sensitive detection of in-plane magnetization switching even for a 100 nm-in-width Ni80Fe20 electrode. Figure 1 shows a schematic of the fabricated device. Firstly, a large magnetic field was applied along +y direction to initialize the magnetization direction. After removing the magnetic field, a low frequency microwave was applied to measure the initial DC voltage generated by the nrSRE. After stopping the microwave irradiation, a pulse current was applied into the Pt layer. Then, dc voltage induced by nrSRE was measured again to detect the magnetization reversal. Figure 2 shows the voltage difference between before and after application of the pulse current as a function of the pulse-current density. Clear voltage differences were obtained above 2.5×10^7 A/cm^2, indicating successful magnetization switching. In the presentation, we will discuss the origin of the enhanced nrSRE.

[1] L. Liu, C. -F. Pai, Y. Li, H. W. Tseng, D. C. Ralph and R. A. Buhrman, Science, Vol. 336, p.555 (2012) [2] L. Liu, T. Moriyama, D. C. Ralph and R. A. Buhrman, Phys. Rev. Lett., Vol. 106, p. 036601 (2011) [3] X. F. Zhu, M. Harder, J. Tayler, A. Wirthmann, B. Zhang, W. Li, Y. S. Gui and C. -M. Hu, Phys. Rev. B, vol. 83, p.140402 (2011)

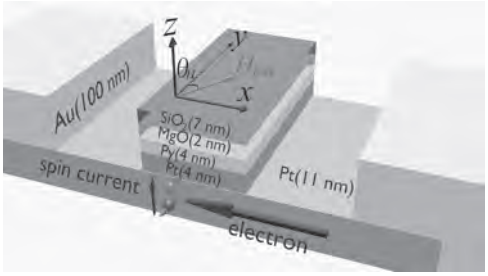

Fig.1. A schematic of device structure for demonstration of current induced magnetization switching.

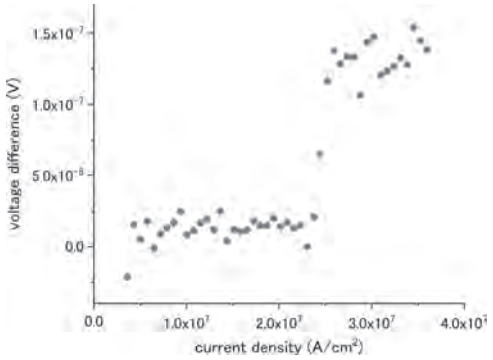

Fig.2. Voltage difference between before and after application of the pulse current as a function of dc charge current.

M3-02. Role of Crystalline and Damping Anisotropy to the Angular Dependences of Spin Rectification Effect in Single Crystal CoFe Film. *F. Zeng*[1], X. Shen[1], Y. Li[2], Z. Yuan[3], W. Zhang[2] and Y. Wu[1] *1. Fudan University, Shanghai, China; 2. Oakland University, Rochester, MI, United States; 3. Beijing Normal University, Beijing, China*

The electrical detection of ferromagnetic resonance through the spin rectification (SR) effect has inspired great interest to investigate the magnetization dynamics in the last two decades. Furthermore, a comprehensive understanding of SR is essential to study the spin pumping and spin Hall effects. Recently, the single crystalline $Co_{0.5}Fe_{0.5}$ (001) alloy film has attracted attention due to the giant damping anisotropy and current-orientation effect of anisotropic magnetoresistance [Phys. Rev. Lett. 122, 117203 (2019)]. In this experimental work, we studied the SR dependence on the magnetization and current orientations in the single crystalline $Co_{0.5}Fe_{0.5}$ (001) alloy film. We present the experimental evidence that the magnetization-orientation dependence of the SR signal in $Co_{0.5}Fe_{0.5}$ strongly differs from those reported in the polycrystalline films. The strong anisotropy ratio of the damping constant up to 520% is determined, which can induce the strong anisotropy of the resonant susceptibility driven by the microwave field. By considering the current-orientation dependent anisotropic magnetoresistance and the anisotropic susceptibility in single crystalline $Co_{0.5}Fe_{0.5}$, we explain such unusual angular dependent SR signal by the SR theory. Our measurements show the amplitude of the SR signal could have 13 times difference for the devices along the <110> and <100> directions, which introduces the crystalline symmetry as a new approach to engineer the microwave characteristics in microwave spintronics.

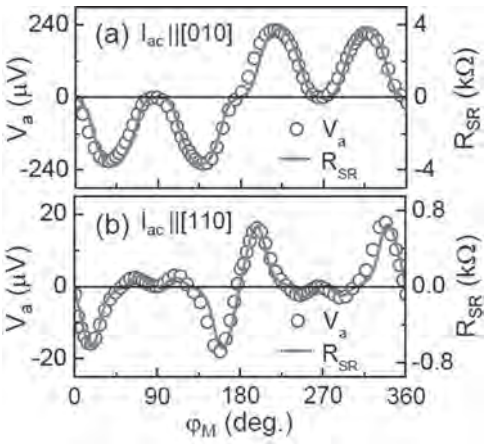

The SR voltage V_a as a function of φ_M with the microwave current along (a) [010] and (b) [110] for the Pt(3 nm)/MgO(6 nm)/FeCo(10 nm) sample. The lines are the calculated effective SR resistance R_{SR}.

M3-03. Phase-Resolved Electrical Detection of Strongly Coupled Magnon-Magnon Hybrid Device. *Y. Li*[1], C. Zhao[1], Z. Zhang[1], M. Vogel[1], Y. Xiong[2], J. Sklenar[3], R. Divan[4], J. Pearson[1], W. Zhang[2], A. Hoffmann[5] and V. Novosad[1] *1. Argonne National Laboratory Materials Science Division, Lemont, IL, United States; 2. Physics, Oakland University, Rochester, MI, United States; 3. Physics, Wayne State University, Detroit, MI, United States; 4. Center for Nanoscale Materials, Argonne National Laboratory, Lemont, IL, United States; 5. Materials Science Division, University of Illinois at Urbana-Champaign, Urbana, IL, United States*

Hybrid magnonic systems have recently attracted wide attentions due to due to rich potential applications in coherent information processing. One particularly interesting platform is the thin-film-based magnon-magnon hybrid system, which has been recently explored in magnetic bilayers [1-4]. Because magnon excitations are confined within the magnetic media, it is convenient to build up more compact hybrid platforms in micron scale compared with millimeter-scale microwave circuits. Furthermore, the abundant spintronic properties, such as spin-torque manipulation and spin pumping, can be used to control and engineer the hybrid dynamics especially for magnetic thin-film devices. In this work, we demonstrate electrical detection of strongly coupled magnon-magnon hybrid system in yttrium iron garnet/permalloy (YIG/Py) bilayer devices. Direct microwave current injection through the conductive Py layer drives the hybrid dynamics consisting of the uniform mode of Py and the first standing spin wave (n=1) mode of YIG, which are strongly coupled via interfacial exchange coupling. The hybrid dynamics is detected via the spin rectification signal from Py, which provides phase resolution of the coupled dynamics. For the Py-dominated mode we measure a constant phase evolution. For the YIG-dominated mode a π phase shift is measured across the avoided crossing, which agrees with theoretical prediction. In addition, the characterization of nonlocal devices consisting two Py devices on a YIG base device shows that the two Py devices are coupled by inductive coupling, allowing spin rectification measurements of the nonlocal Py device. Our results provide a new device platform for exploring hybrid magnonic dynamics and probing their phases, which are crucial for implementing coherent information processing with magnon excitations. Sample preparation and measurements were supported by the US Department of Energy, Basic Energy Sciences, Materials Science and Engineering Division. Use of the Center for Nanoscale Materials, an Office of Science user facility, was supported by the U.S. Department of Energy, Office of Science, Office of Basic Energy Sciences, under Contract No. DE-AC02-06CH11357.

[1] S. Klingler, et al., Phys. Rev. Lett. 120, 127201 (2018). [2] J. Chen, et al., Phys. Rev. Lett. 120, 217202 (2018). [3] H. Qin, et al., Sci. Rep. 8, 5755 (2018). [4] Y. Li, et al., Phys. Rev. Lett. 124, 117202 (2020)

M3-04. Picosecond Spin Orbit Torque Switching. *K. Jhuria*[1], J. Hohlfeld[1], A. Pattabi[2], E. Martin[1], A. Ygnacio Arriola Córdova[1,3], X. Shi[4], R. Lo Conte[2], S. Petit-Watelot[1], J. Rojas-Sanchez[1], G. Malinowski[1], S. Mangin[1], A. Lemaître[5], M. Hehn[1], J. Bokor[2,6], R. B. Wilson[4] and J. Gorchon[1] *1. Université de Lorraine, CNRS, IJL, Nancy, France; 2. Department of Electrical Engineering and Computer Sciences, University of California Berkeley, Berkeley, CA, United States; 3. Universidad Nacional de Ingenieria, Lima, Peru; 4. Department of Mechanical Engineering and Materials Science and Engineering Program, University of California Riverside, Riverside, CA, United States; 5. Centre de Nanoscience et de Nanotechnologies, Universite Paris-Saclay, Palaiseau, France; 6. Lawrence Berkeley National Laboratory, Berkeley, CA, United States*

Reducing energy dissipation while increasing speed in computation and memory is a long-standing challenge for spintronics research [1]. In the last 20 years, femtosecond lasers have emerged as a tool to control the magnetization in specific magnetic materials at the picosecond timescale [2]. However, the use of ultra-fast optics in integrated circuits and memories would require a major paradigm shift. An ultrafast electrical control of the magnetization [3] is far preferable for integrated systems. Here we demonstrate reliable and deterministic control of the out-of-plane magnetization of a 1 nm-thick Co layer with single 6 ps-wide electrical pulses that induce spin orbit torques on the magnetization. We can monitor the ultrafast magnetization dynamics due to the spin orbit torques with sub-picosecond resolution, thus far accessible only by numerical simulations. Due to the short duration of our pulses, we enter a counter-intuitive regime of switching where heat dissipation assists the reversal. Moreover, we estimate a low energy cost to switch the magnetization, below 50 pJ for our micrometer sized device. These experiments show that spintronic phenomena can be exploited on picosecond time-scales for full magnetic control and should launch a new regime of ultrafast spin torque studies and applications.

[1] Åkerman, J. Toward a universal memory. Science. 308, 508–510 (2005). [2] Kirilyuk, A., Kimel, A. V & Rasing, T. Ultrafast optical manipulation of magnetic order. Rev. Mod. Phys. 82, (2010). [3] Garello, K. et al. Ultrafast magnetization switching by spin-orbit torques. Appl. Phys. Lett. 105, 1–12 (2014).

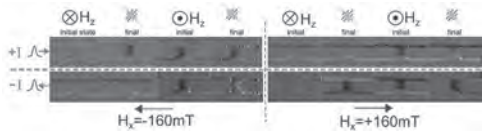

"Fig: Magneto-optical images of the switching of a 1nm Co film via 6ps wide electrical pulses, exploiting the spin Hall effect. Changing the in-plane magnetic field or current direction determines the final state of the magnet."

M3-05. Direct Imaging of the ac Component of Spin Pumping From Permalloy Into Uncompensated Antiferromagnetic Co Doped ZnO. S. Pile[1], M. Buchner[1], V. Ney[1], T. Schaffers[1], K. Lenz[2], R. Narkowicz[2], J. Lindner[2], H. Ohldag[3,4] and *A. Ney*[1] *1. Johannes Kepler Univ., Linz, Austria; 2. Helmholtz Center Dresden Rossendorf, Dresden Rossendorf, Germany; 3. Stanford Synchrotron Radiation Lightsource, Menlo Park, CA, United States; 4. University of California, Santa Cruz, Santa Cruz, CA, United States*

In spintronics the generation and manipulation of pure spin currents is in the focus of research activities. Amongst the utilized fundamental effects is spin pumping where a precessing magnetization of a ferromagnet being at ferromagnetic resonance (FMR) transfers angular momentum to an adjacent nonferromagnetic layer [1]. In that context, heterostructures of highly Co-doped ZnO (Co:ZnO) and Permalloy were investigated for their dynamic magnetic interactions due to spin pumping. The Co:ZnO is paramagnetic at room temperature and becomes an uncompensated antiferromagnet at low temperatures [2]. In a heterostructure with Permalloy (Py), an increase

in the Gilbert damping parameter at room temperature was found by multifrequency ferromagnetic resonance (FMR), indicating spin pumping [3]. In addition, temperature dependent FMR shows a maximum in magnetic damping close to the magnetic phase transition [3]. As direct evidence for spin pumping in the Py/Co:ZnO heterostructure the ac component of the pumped spin polarization is directly imaged with spatial resolution as well as element selectivity. The time-resolved detection in scanning transmission x-ray microscopy (STXM) allows to directly probe the spatial extent of the ac spin polarization in Co:ZnO which is generated by spin pumping from an adjacent Py microstrip at FMR. Using STXM-FMR, the dynamic out-of-plane component of the precessing magnetization can be measured. By that, the magnetic response of the driving ferromagnet Py and the pumped spin polarization inside the nonferromagnetic Co:ZnO can be probed directly and independently. We find a pumped ac spin polarization which is close to antiphase to the ferromagnet. Its spatial extent is not homogeneous and it extends laterally beyond the region of the ferromagnet [4]. Therefore the observations are better explained by a local spin pumping efficieny and a lateral propagation of the ac spin polarization in the nonferromagnet over the range of a few micrometers.

[1] Y. Tserkovnyak, A. Brataas, G. E. W. Bauer, Phys. Rev. Lett. 88 (2002) 117601 [2] V. Ney, B. Henne, J. Lumetzberger, F. Wilhelm, K. Ollefs, A. Rogalev, A. Kovacs, M. Kieschnick, A. Ney, Phys. Rev. B 94 (2016) 224405 [3] M. Buchner, J. Lumetzberger, V. Ney, T. Schaffers, N. Daffe, A. Ney, J. Appl. Phys. 127 (2020) 043901 [4] S. Pile, M. Buchner, V. Ney, T. Schaffers, K. Lenz, R. Narkowicz, J. Lindner, H. Ohldag, A. Ney, arXiv2005.08728

M3-06. Spin Pumping From $Ni_{80}Fe_{20}$ Into Monolayer Transition Metal Dichalcogenides. *H. Bangar*[1], R. Mudgal[1], A. Kumar[1], N. Chowdhury[1], S. Das[2] and P.K. Muduli[1] *1. Physics, Indian Institute of Technology Delhi, New Delhi, India; 2. Center for Applied Research in Electronics, Indian Institute of Technology Delhi, New Delhi, India*

Two-dimensional (2D) transition metal dichalcogenides (TMDs) have received considerable attention in recent years due to their unique properties and tremendous potential for device applications [1]. TMDs posses a direct bandgap [2] and a large spin-orbit coupling (SOC) strength [3] in the monolayer form, which makes them promising for spintronics. In the ferromagnetic resonance (FMR) condition, a ferromagnet (FM) acts as a source of spin angular momentum, and it leads to the pumping of pure spin current from FM to the non-magnetic layer (NM). In this work, we probe the efficiency of spin pumping from $Ni_{80}Fe_{20}$ (Py) into various monolayer TMDs (MoS_2, $MoSe_2$, WS_2, WSe_2) used as a spin sink. Py of different thickness was deposited using UHV magnetron sputtering on the commercially purchased monolayer TMD samples on the c-cut sapphire substrate. Spin pumping is studied using FMR setup for excitation frequency of 2-10 GHz. The FMR measurements clearly show enhanced damping in the case of tungsten (W) based TMD/Py samples (as shown in Fig.1). We calculated the spin mixing conductance ($g_{\uparrow\downarrow}$) and found it to be approximately four times in the case of WS_2/Py (7.28×10^{18} m^{-2}) as compared to MoS_2/Py (1.86×10^{18} m^{-2}) samples. The interfacial magnetic anisotropy energy density (K_S) is plotted with $g_{\uparrow\downarrow}$ (as shown in Fig.2), and it can be observed that K_S has a crucial role in the increased spin pumping. We attribute this to the d-d hybridization at the interface, which enhances interfacial SOC [4]. We have shown in this work that the spin pumping is much more significant in the case of W based TMD/Py samples because of their larger SOC strength. This work establishes a way to regulate spin pumping with the SOC strength, which can lead to advances in spintronics based devices.

[1] Y. P. Feng *et al.,* Wiley Interdiscip. Rev. Comput. Mol. Sci. 7, e1313 (2017). [2] K. F. Mak *et al.,* Phys. Rev. Lett. 105, 136805 (2010). [3] Z. Y. Zhu. *et al.,* Phys. Rev. B 84, 153402 (2011). [4] L. Zhu, *et al.,* Phys. Rev. Lett. 122, 077201 (2019).

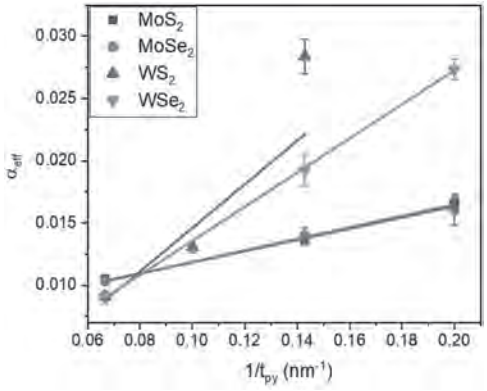

Fig.1: Gilbert damping parameter (α_{eff}) vs. inverse of Py thickness to determine spin mixing conductance ($g_{\uparrow\downarrow}$).

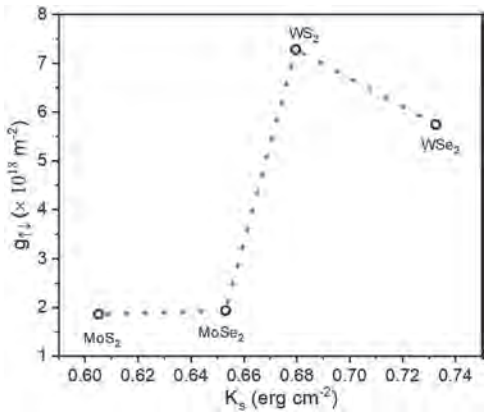

Fig.2: The plot between spin mixing conductance ($g_{\uparrow\downarrow}$) and interfacial magnetic anisotropy energy density (K_S) for various TMD/Py samples.

M3-07. Inversion of the Spin-Torque Effect via Resonant Magnon Scattering in Nanomagnets. *I. Barsukov*[1], H. Lee[2], A. Jara[2], Y. Chen[2], A. Gonçalves[2], C. Sha[2], J. Katine[3], R. Arias[4], B. Ivanov[5] and I. Krivorotov[2] *1. UC Riverside, Riverside, CA, United States; 2. UC Irvine, Irvine, CA, United States; 3. Western Digital, San Jose, CA, United States; 4. Universidad de Chile, Santiago, Chile; 5. National Academy of Sciences, Kyiv, Ukraine*

Nanoscale magnets are the building blocks of many existing and emergent spintronic applications, e.g. nonvolatile spin torque memory, spin torque oscillators, neuromorphic and probabilistic computing. Controlling magnetic damping in nanomagnets holds the key to improving the performance of future technologies. Here, we experimentally demonstrate and theoretically corroborate that a nanoscale ferromagnet can exhibit spin dynamics qualitatively different from those predicted by the harmonic oscillator model. Nonlinear contributions to the damping can be unusually strong, and the effective damping parameter itself can exhibit resonant dependence on field/frequency [1]. We carry out spin torque ferromagnetic resonance [2] on magnetic tunnel junction nanopillars with in-plane and out-of-plane magnetic anisotropy. We observe a discrete spin-wave spectrum in the geometrical confinement of the MTJ free layer. Its analysis uncovers a nonlinearity that has a strong impact on nanomagnet's response even at low excitation levels. The nonlinearity shows a distinct resonant enhancement at characteristic magnetic fields corresponding to the three-magnon scattering. We present evidence of processes in which two quanta of the lowest-energy mode merge into one quantum of higher-energy modes. Our work demonstrates that nonlinear damping in nanomagnets is qualitatively different from that in extended systems [1,3]. The observed resonant magnon scattering drastically alters the magnetization dynamics of a nanomagnet driven by spin torques. It reverses the effect of the spin torque on magnetic damping

and turns an anti-damping torque into a dissipation-enhancing torque. The discovery of this counter-intuitive effect advances our understanding of spin dynamics in nanoscale magnetic systems and has far-reaching implications for spin torque oscillators, spin torque memory, and other emergent spintronic technologies.

[1] I. Barsukov et al., Sci. Adv. 5, eaav6943 (2019) [2] A.M. Gonçalves et al., Appl. Phys. Lett. 103, 172406 (2013) [3] A. Navabi et al., Phys. Rev. Appl. 11, 034046 (2019)

M3-08. Controlling the Gyrotropic Critical Current by Resonant Excitation of the Higher Order Spin Wave Modes in Vortex-Based Magnetic Tunnel Junctions. *A. Jenkins*[1], L. San Emeterio Alvarez[1], S. Memshawy[2], B. Paolo[2], V. Cros[2], P. Freitas[1] and R. Ferreira[1]
1. Spintronics, International Iberian Nanotechnology Laboratory, Braga, Portugal; 2. Unite Mixte de Physique CNRS/Thales, Palaiseau, France

Vortex-based magnetic tunnel junctions (MTJs) are a rich dynamic system with a variety of different resonant modes, spanning a wide frequency spectrum from hundreds of MHz to tens of GHz [1, 2]. The diverse spectral properties of vortex-based MTJs makes them potential candidates for high frequency signal detectors [3, 4], with a dc rectification 'spin-diode' effect resulting when one of the resonant modes are excited with an rf current passing across the MTJ. In this study, we investigate the spin-wave modes present in a vortex-based MTJ, by analysis of the spin-diode rectification effect and by comparison with Fourier analysis of micromagnetic simulations. We demonstrate that the nature of the spin wave mode is strongly related to the position of the vortex core, varying from a pure azimuthal mode when the core is located at the centre of the MTJ, to a more standing wave edge mode when the core is strongly displaced to the edge. Furthermore, we demonstrate that the dominant excitation mechanism also changes depending upon core position, with the azimuthal mode being more sensitive to the field-like spin torque effect, and with the edge mode being more susceptible to the radial Oersted field. In addition to analysing the nature and the excitation scheme of these modes, we also show how their resonant excitation can lead to the modification of the critical current of the steady state excitation of the gyrotropic mode. The ability to control the gyrotropic mode via excitation of the higher order mode gives rise to a frequency down converter which can demodulate a signal with a carrier signal at 7.7 GHz with a modulation rate of 1 MHz. By harnessing the higher order spin wave modes present in vortex-based MTJs, new radio-frequency technologies such as signal detection and demodulation, which target GHz frequency bands can be envisaged. VC and PB acknowledge the ANR project "SPINNET" ANR-18-CE24-0012.

[1] K. Y. Guslienko, A. N. Slavin, V. Tiberkevich, and S. K. Kim, "Dynamic origin of azimuthal modes splitting in vortex-state magnetic dots," Phys. Rev. Lett., 101, 24, 1–4, 2008. [2] M. Kammerer et al., "Magnetic vortex core reversal by excitation of spin waves," Nat. Commun., 2, 1, 279, 2011. [3] - A. S Jenkins *et al.,* "Wideband High-Resolution Frequency-to-Resistance Converter Based on Nonhomogeneous Magnetic-State Transitions", Phys. Rev. Applied 13, 014046, (2020) [4] - A. S Jenkins *et al.,* "Spin-torque resonant expulsion of the vortex core for an efficient radiofrequency detection scheme", Nature Nanotechnology volume 11, 360–364, (2016)

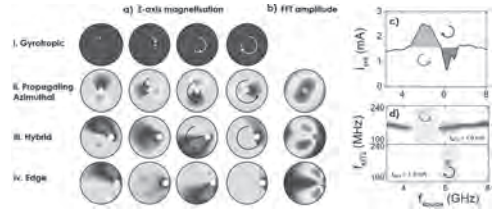

Figure 1. – a) Magnetisation along the z-axis at various timesteps and the b) equivalent FFT spatial analysis. C) Critical current for steady state gyrotropic motion as a function of the higher order mode excitation frequency and d) corresponding spectra at I_{MTJ} = 1.3 and 1.9 mA.

M3-09. Magnetization Dynamics of Helical and Skyrmion Phases in Bulk $Co_8Zn_8Mn_4$ at Room Temperature. *J. Soh*[1], D. Prabhakaran[2], A. Boothroyd[2] and D. Grundler[1,3] *1. Institute of Materials, Ecole Polytechnique Federale de Lausanne, Lausanne, Switzerland; 2. Department of Physics, University of Oxford, Oxford, United Kingdom; 3. Institute of Microengineering, Ecole Polytechnique Federale de Lausanne, Lausanne, Switzerland*

Recently, the $Co_8Zn_8Mn_4$ alloy was found to host the skyrmion crystal phase at room temperature [1,2]. Understanding the GHz spin dynamics and magnonic eigenmodes of this phase is key for developing room temperature applications in spintronics and magnonics. Here, we report the broadband microwave absorption spectroscopy measurement of bulk $Co_8Zn_8Mn_4$ crystal, mounted onto a coplanar waveguide (CPW). We have determined the resonance frequencies of the eigen-excitations of the various magnetic phases in $Co_8Zn_8Mn_4$ - at room temperature - including the helical, skyrmion crystal, conical and fully polarized magnetic order (Fig. 1 and Fig. 2). In particular, we found that the clockwise, counter-clockwise and breathing modes of the skyrmion crystal magnetic configuration resides between ~0.8 and 2.5(2) GHz. The frequencies of the modes depend on the orientation of the applied field with respect to the CPW and the long axis of the crystal. We account for the frequency variations by means of magnetic anisotropies. Furthermore, we augment our results with single crystal x-ray diffraction measurements and temperature-dependent magnetic susceptometry. We thank S. Watanabe, P. R. Baral and I. Zukovic for experimental support. The research was financially supported by the SNSF (grant no. 171003 - sinergia project Nanoskyrmionics) and the EPSRC (grant no. EP/M020517/1).

1. Y. Tokunaga, X. Z. Yu, J. S. White, et al. Nature Communication, Vol. 6 p. 7638 (2015) 2. K. Karube, J. S. White, N. Reynolds, et al. Nature Materials, Vol. 15, p. 4752 (2016)

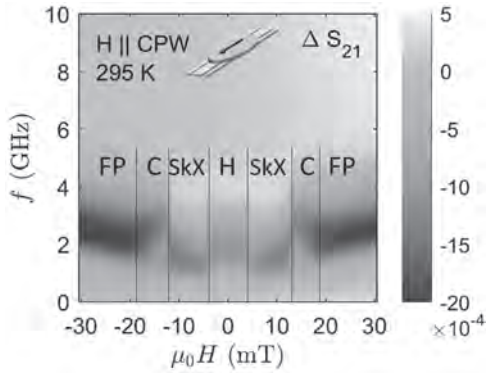

The spin-wave spectra of $Co_8Zn_8Mn_4$ in the various magnetization phases, including the helical (H), skyrmion crystal (SkX), conical (C) and fully polarized (FP) magnetization states. Here the external magnetic field was aligned along the length of the co-planar waveguide (CPW). By a detailed analysis of field-dependent spectra we extract two resonance frequencies of the skyrmion crystal dynamics which we attribute to the counter-clockwise and clockwise modes.

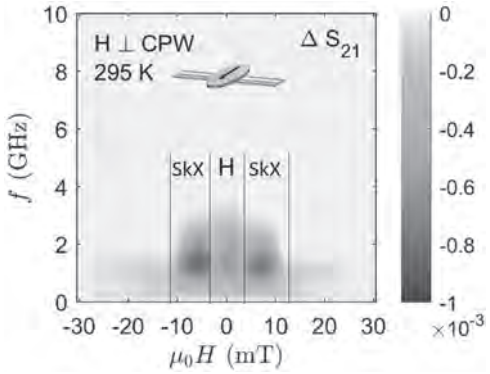

Broadband absorption spectroscopy with the external magnetic field aligned perpendicular to the length of the CPW. We resolve a single resonance frequency which we attribute to the breathing eigenmode of the skyrmion crystal dynamics.

M3-10. Deterministic Approach to Skyrmionic Dynamics at Nonzero Temperatures: Pinning Sites and Racetracks. *J. Castell-Queralt*[1], L. González-Gómez[1], N. del-Valle[1] and C. Navau[1] *1. Physics, Universitat Autonoma de Barcelona Facultat de Ciencies, Barcelona, Spain*

The finding of skyrmions at room temperature has boosted the potentiality of skyrmionic devices. From the theoretical point of view, the temperature in micromagnetic systems has been taken into account either using stochastic spin dynamics, the stochastic Landau-Lifshitz equation, or the Landau-Lifshitz-Block equation. Also, the rigid model has been used to describe the skyrmion dynamics taking into account thermal effects, using the stochastic Thiele equation [1]. Here we present a deterministic method to study the skyrmion dynamics [2], an approach in which the temporal motion of skyrmions can be studied without relying on repetition of stochastic simulations, but on solving once the associated deterministic Fokker-Planck equation. This is a substantial advance, since by finding and solving a single partial differential equation, one could obtain all the relevant probabilistic information of the system. Indeed, within the rigid approximation, the probability density for the presence of skyrmions under any external potential can be found at any time and position, and as a function of the temperature. This allows one to evaluate the probability of presence/survival trapping/escaping ... of skyrmions in many practical situations, which is a key information to ensure the viability of applications. In particular, the probability of trapping/escaping of a skyrmion that encounters a pinning site, and the probability of survival of a skyrmion along a track are presented as a function of temperature.

[1] D. Pinna, F. Abreu Araujo, J. Grollier, Phys. Rev. Applied., Vol. 9, (2018) [2] J. Castell-Queralt, L. González-Gómez, C. Navau. Phys. Rev. B 101, 140404 (R) (2020*)*

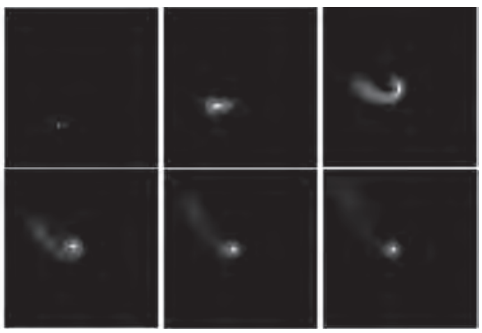

M3-11. Traveling Skyrmions in Chiral Antiferromagnets. *S. Komineas*[1,3] and N. Papanicolaou[2] *1. Department of Mathematics and Applied Mathematics, University of Crete, Heraklion, Greece; 2. Department of Physics, University of Crete, Heraklion, Greece; 3. Institute of Applied and Computational Mathematics, Idryma Technologias kai Ereunas, Heraklion, Greece*

Skyrmions in antiferromagnetic (AFM) materials with the Dzyaloshinskii-Moriya (DM) interaction are expected to exist for essentially the same reasons as in DM ferromagnets (FM). On the other hand, the dynamics of solitons in AFM is substantially different [1,2]. We give the fundamental formula and a corresponding argument to show that traveling solitary waves (such as skyrmions) are possible in an AFM in contrast to the dynamics observed in FM. The formula shows that the skyrmion number, known to be linked to the dynamics of topological solitons in FM, is, here, unrelated to the dynamical behavior. We calculate numerically the configuration of skyrmions in chiral antiferromagnets that are traveling as solitary waves. They are found to be elongated and they expand in size with the velocity (Fig. 1). The velocity takes values from zero up to a maximum value, which depends on a scaled DM parameter λ. The maximum skyrmion velocity is found analytically as a function of λ. The formula is based on a strong theoretical argument that links the breakdown of a traveling skyrmion with the DM parameter value $\lambda=2/\pi$ for the transition from the uniform to the spiral state. The energy and the linear momentum of an AFM skyrmion lead to a proper definition of its mass. We give the details of the energy-momentum dispersion of traveling skyrmions and explore their particle-like character based on exact relations. The traveling skyrmion behaves as a Newtonian particle for small velocities, while it presents relativistic behavior for velocities close to the critical. It is notable that the energy-momentum formula differs from the standard relativistic one by a constant shift of the energy. The solitonic and particle-like behavior of skyrmions in AFM is in stark contrast to the dynamical behavior of their FM counterparts [3]. We acknowledge support by the project ThunderSKY, funded by HFRI and GSRT, under Grant No. 871.

[1] E. G. Galkina and B. A. Ivanov, Low Temp. Phys. 44, 618 (2018) [2] H. Velkov, O. Gomonay, M. Beens, et al, New J. Phys. 18, 075016 (2016) [3] S. Komineas and N. Papanicolaou, SciPost Phys. 8, 086 (2020)

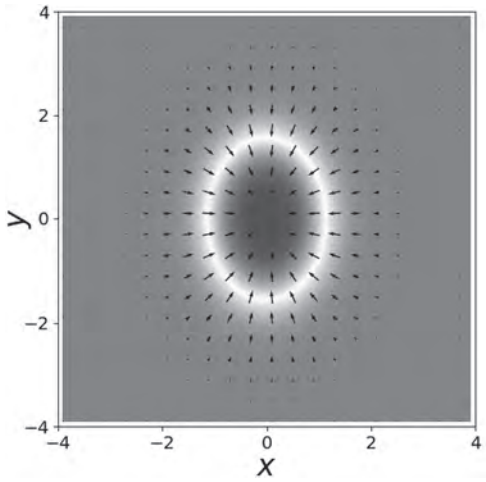

The Néel vector for a traveling AFM skyrmion with a large velocity (v=0.6 for λ=0.45). Vectors show the projection of the Néel vector on the plane and colors give the out-of-plane component (blue means negative and red means positive values).

M3-12. Inertial Dynamics of Magnetic Vortices. *M. Yoo*[1,2], F. Mineo[3,4] and J. Kim[1] *1. Centre de Nanosciences et de Nanotechnologies, Université Paris-Saclay, Palaiseau, France; 2. Laboratoire Matériaux Optiques, Photonique et Systèmes, CentraleSupélec, Université de Lorraine, Metz, France; 3. Max Planck Institute for the Science of Light, Erlangen, Germany; 4. Department of Physics, Friedrich-Alexander University of Erlangen-Nuremberg, Erlangen, Germany*

A common approach for describing the two-dimensional topological soliton dynamics in magnetic thin films, the so-called Thiele equation, relies on approximating the core as a rigid structure whose dynamics determines entirely the motion of the soliton [1]. However, it is well known that a magnetic soliton's motion should be accompanied by a deformation of its spatial profile, which arises from magnetization precession [2]. The deformation can result in nonlinear phenomena, such as Walker breakdown and vortex core reversal [3,4]. Interestingly, despite the large body of theoretical work on magnetic vortex and skyrmion dynamics to date, a consistent description of inertial effects and core deformation within the Thiele framework remains largely unexplored. Here, we present a model to account for the motion-induced inertia of magnetic vortices [5]. We describe an analytic model for the deformation of the core, based on Döring's kinetic field [2], then derive equations of motion of the deformation amplitudes that couple to the motion of the core. With the equations, complex inertial motion can be described. We define the effective inertial mass of the vortex core, then show that the mass depends on the core speed. The model provides a quantitative description of the inertial dynamics leading up to vortex core reversal, which is analogous to the Walker transition in domain wall dynamics. This work has supported by the Agence Nationale de la Recherche under contract no. ANR-17-CE24-0008 (CHIPMuNCS).

[1] A. A. Thiele, Physical Review Letters, Vol. 30, p.230 (1973). [2] W. Döring, Zeitschrift für Naturforschung A, Vol. 3a, p.373 (1948). [3] N. L. Schryer and L. R. Walker, Journal of Applied Physics, Vol. 45, p.5406 (1974). [4] B. Van Waeyenberge et al., Nature, Vol. 444, p.461 (2006). [5] M.-W. Yoo, F. Mineo, and J.-V. Kim, arXiv:2006.02866 (2020).

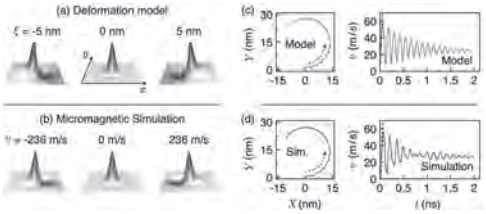

Fig. (a) Deformed vortex configurations calculated from the deformation model with the indicated deformation amplitude, ξ. (b) Deformation of the vortex obtained from a micromagnetic simulation at the indicated core velocity, *v*. (c) Calculated core trajectory (left) and time evolution of the velocity (right) from the analytical model during the inertial dynamics. (d) As in (c) but obtained from a micromagnetic simulation.

M3-13. Critical Depinning Dynamics of Domain Walls With Internal Degrees of Freedom. *A. Skaugen*[1,2] and L. Laurson[1,2] *1. Computational Physics Laboratory, Tampereen yliopisto, Tampere, Finland; 2. Helsinki Institute of Physics, Helsinki, Finland*

The bursty motion of magnetic domain walls (DWs) in disordered ferromagnets, known as Barkhausen noise, exhibits critical behavior in its depinning dynamics, giving rise to universal power laws [1]. For example, the average DW velocity V depends on the external magnetic field B as $(B-B_d)^\theta$ for a depinning field B_d and a critical exponent θ [2], and the distribution of velocity burst sizes S goes like $P(S) \sim S^{-\tau}$ for a critical exponent τ [3]. This is similar to many critical systems in statistical physics, ranging from earthquakes and geophysical flows [4] to dislocation avalanches in plastically deforming crystals [5]. However, current studies exploring the critical depinning dynamics of Barkhausen noise using micromagnetic modeling is severely limited by small system sizes [6]. We develop an effective model for the motion of domain walls in perpendicular magnetic anisotropy (PMA) thin films, by reducing the description of the magnet to a one-dimensional description of the DW, allowing access to large system sizes. For such Bloch-type DWs, the direction of in-plane magnetization is an important dynamical variable that leads to inertial effects in the DW dynamics, such as Walker Breakdown and the formation of Bloch lines (Fig. 1). We consider the critical depinning dynamics of such DWs in quenched disorder. For weak disorder strengths, the internal dynamics are suppressed, so the DW motion reduces to the quenched Edwards-Wilkinson (qEW) equation. With increasing disorder strength, the internal dynamics of the DW become increasingly important, leading to nucleation of Bloch lines. Using our effective model to access large system sizes, we characterize the critical exponents of the depinning problem, and explore the effect of internal dynamics and Bloch lines on the critical behavior.

[1]: S. Zapperi et. al., Phys. Rev. B, Vol. 58, p. 6353 (1998) [2]: R. D. Pardo et. al., Phys. Rev. B, Vol. 95, p. 184434 (2017) [3]: D. Spasojević et. al., Phys. Rev. E, Vol. 54, p. 2531 (1996) [4]: J. P. Sethna, K. A. Dahmen and C. R. Myers, Nature, Vol. 410, p. 242 (2001) [5]: See e.g., P. Moretti et. al., Phys. Rev. B, Vol. 69, p. 214103 (2004) [6]: T. Herranen and L. Laurson, Phys. Rev. Lett, Vol. 122, p. 117205 (2019)

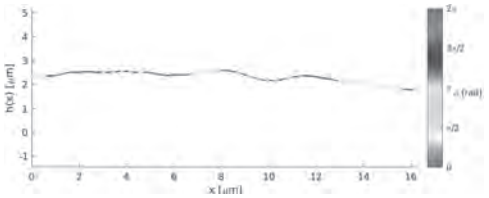

Fig. 1: An example DW configuration during critical relaxation, showing the DW height along the y direction as a function of x. Color indicates the direction of in-plane magnetization inside the DW, measured relative to the tangent vector. Note the abrupt flips between the 0 and π directions, indicating Bloch lines.

Session M4
SPIN CURRENTS II

Peng Li, Chair
Auburn University, Auburn, AL, United States

INVITED PAPER

M4-01. Giant Anomalous Nernst Effect in Topological Magnets.
A. Sakai[1,2], S. Minami[1,3], T. Koretsune[4], T. Chen[2], T. Higo[2], Y. Wang[2], T. Nomoto[5], M. Hirayama[6], S. Miwa[2,7], D. Nishio-Hamane[2], F. Ishii[3,6], R. Arita[5,6] and S. Nakatsuji[1,2] *1. Department of Physics, University of Tokyo, Tokyo, Japan; 2. Institute for Solid State Physics, University of Tokyo, Kashiwa, Japan; 3. Nanomaterials Research Institute, Kanazawa University, Kanazawa, Japan; 4. Department of Physics, Tohoku University, Sendai, Japan; 5. Department of Applied Physics, University of Tokyo, Tokyo, Japan; 6. Center for Emergent Matter Science (CEMS), RIKEN, Wako, Japan; 7. Trans-scale Quantum Science Institute, University of Tokyo, Tokyo, Japan*

The newly discovered topological magnets such as magnetic Weyl and nodal line semimetals feature characteristic band crossings in momentum space. Such materials may exhibit extraordinarily large transverse electric and thermoelectric responses arising from the Berry curvature — a fictitious magnetic field that is proportional to the inverse of the band gap. For example, the chiral antiferromagnet Mn_3Sn shows large anomalous Hall effect (AHE), anomalous Nernst effect (ANE), magneto-optical Kerr effect, and magnetic spin Hall effect, opening a new avenue for topological antiferromagnetic spintronics [1-6]. In particular, we highlight recent extensive studies on the giant anomalous Nernst effect (ANE) in the Weyl magnets such as Heusler ferromagnet Co_2MnGa [7]. The large ANE attracts a lot of attention as it is potentially useful for the energy harvesting technology; the transverse geometry of the Nernst effect may enable efficient, large-area and flexible coverage of a heat source. In this presentation, we focus on the most recently discovered topological magnets Fe_3X (X = Ga, Al) [8]. These materials show a large transverse thermoelectric coefficient of 5.2 A/(Km) at around 200 K and ANE of about 6 μV/K at room temperature. These phenomena have their roots in a nodal web -flat band structure made of interconnected nodal lines- near Fermi energy. We have also succeeded in fabricating thin films of these materials that exhibit a large ANE at zero field, suitable for designing low-cost, flexible microelectronic thermoelectric generators.

[1] S. Nakatsuji, N. Kiyohara, T. Higo, Nature 527, 212-215 (2015). [2] K. Kuroda, T. Tomita *et al*., Nature materials 16, 1090-1095 (2017). [3] M. Ikhlas, T. Tomita, T. Koretsune, M.-T. Suzuki, D. Nishio-Hamane, R. Arita, Y. Otani and S. Nakatsuji, Nature Physics 13, 1085-1090 (2017). [4] T. Higo *et al*., Nature Photonics 12, 73-78 (2018). [5] L. Šmejkal, Y. Mokrousov, B. Yan and A. H. MacDonald, Nat Phys. 14, 242–251(2018). [6] M. Kimata *et al*., Nature 565, 627–630 (2019). [7] A. Sakai, Y. P. Mizuta, A. A. Nugroho, R. Sihombing, T. Koretsune, M.-T. Suzuki, N. Takemori, R. Ishii, D. N.-Hamane, R. Arita, P. Goswami and S. Nakatsuji, Nature Physics, 14, 1119–1124 (2018). [8] A. Sakai, S. Minami, T. Koretsune, T. Chen, T. Higo, Y. Wang, T. Nomoto, M. Hirayama, S. Miwa, D. Nishio-Hamane, F. Ishii, R. Arita and S. Nakatsuji, Nature 581, 53–57 (2020).

CONTRIBUTED PAPERS

M4-02. Anomalous Nernst Effect in Iron- Based Sintered Alloys.
Y. Omori[1], Y. Iwasaki[1], R. Sawada[1], S. Kuroshima[1], M. Ishida[1] and A. Kirihara[1] *1. Nihon Denki Kabushiki Kaisha, Minato-ku, Japan*

Recently, the Anomalous Nernst Effect (ANE) is attractive as a thermoelectric conversion mechanism. An important characteristic of ANE is the transverse geometry of the thermoelectric conversion, which enables us to produce the thermoelectric module more simply and cheaper. However, the conversion efficiency of the ANE is still too small for applications compared to the traditional Seebeck Effect. It is necessary to explore more efficient and practical materials. In this research, we have studied the electromotive force of the ANE in iron based sintered alloys. Iron is one of the most common and cheap metal on the Earth. Also the sintering technique has advantage on mass production and processability. Firstly, we prepared Fe-Al alloys with different Al concentration by using Spark Plasma Sintering (SPS) technique. The electromotive force of the ANE S_{yx} has dramatically enhanced with increasing the ratio of Al and showed the maximum S_{yx}=4 μV/K when the ratio of Al is 25%. It is comparable for other researches on bulk single crystalline Fe_3Al [1]. Then we prepared $Fe_{75}X_{25}$ (X=B, Si, Ga) alloys for the comparison between the effects of different doping elements. They show similar enhancement of the ANE, but the effects were smaller than that of Al. Furthermore, to find more efficient ANE materials, we have tried to enhance the electromotive force of $Fe_{75}Al_{25}$ by adding other elements. We have successfully obtained S_{yx} = 5.6 μV/K in Fe-Al-Tb ternary alloy.

[1] A. Sakai, S. Minami, et al., Nature, Vol. 581, p.53–57 (2020)

M4-03. Interfacial Modulation of the Spin Pumping in YIG/Pt.
L. Liu[1], Y. Li[1], T. Feng[2], X. Wang[3], D. Wu[2], P. Gao[1] and *J. Li*[1] *1. Peking University, Beijing, China; 2. Nanjing University, Nanjing, China; 3. Hong Kong University of Science and Technology, Kowloon, Hong Kong*

Spin transfer across the interface of magnetic insulator/heavy metal is dominated by the magnetic state at interface. Utilizing aberration corrected scanning transmission electron microscopy and electron energy loss spectroscopy, we demonstrate the existence of metallic Fe^0 atoms at YIG/Pt interface. The observed spin pumping signal is linearly proportional to total Fe^0 magnetic moments at YIG/Pt interface, revealing the critical role of the interfacial magnetic moments on spin transfer. In addition, PtFe alloying might contribute to a new channel of spin sink at YIG/Pt interface.

Xingtao Jia, Kai Liu, Ke Xia and Gerrit E. W. Bauer, EPL, Vol.96, p.17005 (2011)

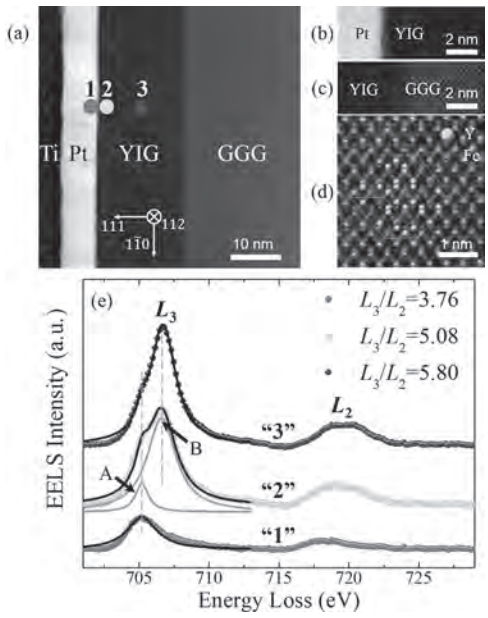

M4-04. Thoeretical Study on Anomalous Spin-Hall and Magnetic Spin-Hall Effect Induced by Anisotropic Spin-Flip Scattering on Ferromagnets. *Y. Yahagi*[1], J. Zelezny[2], D. Miura[1] and A. Sakuma[1]
1. Applied Physics, Tohoku Daigaku, Sendai, Japan; 2. Spintronics and Nanoelectronics, Fyzikalni ustav Akademie ved Ceske republiky, Praha, Czechia

Efficient spin generation methods like spin Hall effect (SHE) are being explored for the realization of next-generation spintronics devices[1]. SHE has been studied mainly in non-magnetic materials. However, because of the recent discoveries of various novel and promising effects in magnetic materials, such as anomalous spin-Hall effect (ASHE)[2,3], magnetic spin-Hall effect (MSHE)[4,5], and the spin-current driven by anisotropic magnetoresistance (AMR)[2,6], the spin-currents in magnetic materials have attracted much attention both from fundamental and applied viewpoints. Although the ASHE was initially thought to be a spin current driven by the anomalous Hall effect (AHE), some experimental results show an unaccountable spin current contribution that cannot be explained by AHE alone, and this is still an open question[7]. The theoretical studies of MSHE have so far assumed spin-independent scattering and focused largely on antiferromagnets. In ferromagnetic materials, the spin-dependent scattering can play an important role, however. In this study, we investigate the spin-dependent scattering mechanisms of ASHE and MSHE by using a microscopic model that assumes s-d scattering in 3d ferromagnetic metal (FM). The electrons in FM are described within the framework of the impurity Anderson model with spin splitting and spin-orbit coupling for 3d orbitals[8]. The spin-conductivities are calculated by using Kubo formula. We obtained both contributions of ASHE and MSHE (Fig.1) and showed that these phenomena are caused by anisotropic spin-flip scattering (Fig. 2). In particular, we found this mechanism of ASHE is different from that of conventional extrinsic SHE such as skew-scattering and side-jump. In the conference, we will present a complete expression of the magnetization direction dependence of these phenomena. In addition, we will discuss the effect of the crystal-field splitting.

[1] J. Sinova, S. O. Valenzuela, J. Wunderlich, et al., Rev. Mod. Phys., Vol. 87, p.1213 (2015), [2] T. Taniguchi, J. Grollier, and M. D. Stiles, Phys. Rev. Appl., Vol. 3, p.044001 (2015), [3] C. Qin, S. Chen, Y. Cai, et al., Phys. Rev. B, Vol. 96, p.134418 (2017), [4] J. Zelezny, Y. Zhang, C. Felser, and B. Yan, Phys. Rev. Lett., Vol. 119, p.187204 (2017), [5] M. Kimata, H. Chen, K. Kondou. et al., Nature, Vol 565, p.627 (2019), [6] C. Safranski, E. A. Montoya, and I. N. Krivorotov, Nature Nano., Vol. 14, p.27 (2019), [7] Y. Omori, E. Sagasta, Y. Niimi. et al., Phys. Rev. B, Vol. 99, p. 014403 (2019), [8] Y. Yahagi, D. Miura, and A. Sakuma, J. Phys. Soc. Jpn., Vol. 89, p.044714 (2020).

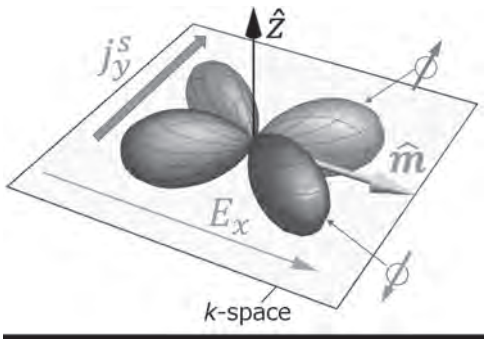

Momentum dependence of spin-flip scattering probability under the applied field.

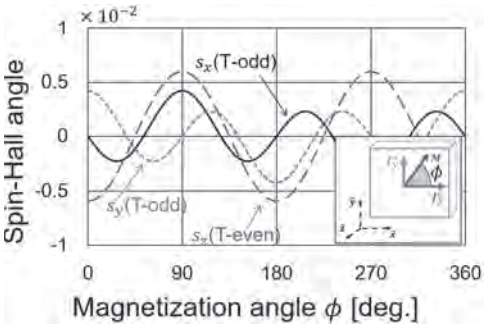

Spin-Hall angles as functions of magnetization angle. s_μ denotes spin-polarization component.

M4-05. Hidden (Staggered) Spin Hall Conductivity. *F. Xue*[1,2] and P.M. Haney[1] *1. Physical Measurement Lab, National Institute of Standards and Technology, Gaithersburg, MD, United States; 2. University of Maryland at College Park Institute for Research in Electronics and Applied Physics, College Park, MD, United States*

The intrinsic bulk spin Hall effect plays an important role in spintronics applications, such as spin-orbit torque-based memory. The bulk space group symmetry ultimately determines the form of spin current conductivity tensor under an applied electric field. The high symmetry normally present in heavy metals, such as Pt, only allows the electric-field-induced transverse spin current flow with spin polarization perpendicular to both electric field and spin current flow directions. Recent studies of spin Hall effects in semi-metallic transition metal dichalcogenides demonstrate the existence of additional spin conductivity tensor components when the crystal symmetry is reduced. In this paper we present an explicit first-principles method to compute the site-resolved spin current conductivity, which may be different from the bulk form. Because the local point group symmetry of individual atom is lower compared to the global space group symmetry, the unconventional spin current conductivity tensor component is staggered in the real-space, and hidden in the direct bulk spin Hall calculations. Our layer-resolved numerical study of 1T'-\ch{WTe2} shows a uniform conventional spin Hall conductivity tensor component σ^y_{xz} and a staggered unconventional component σ^z_{xz}. The magnitude of these two components, around 100 and 20 $\hbar/2e~(\rm \Omega\cdot cm)^{-1}$, are comparable to the spin-orbit torque exerted on adjacent ferromagnets. We present another example of orthorhombic PbTe in which both uniform and staggered spin current conductivity are one order larger. The position-dependent intrinsic spin current conductivity can broaden the applications of spin Hall effect.

M4-06. Enhanced Anomalous Nernst Effect in Ni / Pt Superlattice.
T. Seki[1,2], Y. Sakuraba[3,4], A. Miura[3], K. Masuda[3], M. Tsujikawa[5,2], K. Uchida[3,1], T. Kubota[1,2], Y. Miura[3], M. Shirai[5,2] and K. Takanashi[1,2]
1. Institute for Materials Research, Tohoku University, Sendai, Japan; 2. Center for Spintronics Research Network, Tohoku University, Sendai, Japan; 3. National Institute for Materials Science, Tsukuba, Japan; 4. PRESTO, Japan Science and Technology Agency, Saitama, Japan; 5. Research Institute of Electrical Communication, Tohoku University, Sendai, Japan

Spin caloritronics has attracted much attention not only for academic interests but also for practical applications because of the demand for a new route for high-efficient thermoelectric conversion. One of the thermoelectric phenomena in ferromagnets is the anomalous Nernst effect (ANE), in which the charge current appears in the cross-product direction of magnetization and a temperature gradient. A ferromagnet with a large anomalous Nernst coefficient (S^{ANE}) is the key for realizing the ANE-based thermoelectric conversion. Our group reported the enhancement of ANE in the metallic multilayers of Fe / Pt, Fe / Au, and Fe / Cu, indicating that the ANE is enhanced in alternately stacked ferromagnet / paramagnet multilayer films [Ref.1]. In this study, we focus on ferromagnetic Ni and paramagnetic Pt from the viewpoints of the characteristic electronic structure of Ni and the large spin-orbit interaction of Pt. We show the thermoelectric properties for the Ni / Pt (001) epitaxial superlattices with various Ni layer thicknesses (t). Ni / Pt layers were grown on $SrTiO_3$ (100) single crystal substrates employing a magnetron sputtering system, where the the Pt layer thickness was fixed at 1.0 nm. The deposition temperature was set at 400°C for the Ni and Pt layers. This deposition condition allows us to grow the Ni / Pt (001) epitaxial superlattices exhibiting perpendicular magnetization [Ref.2]. All the samples with t = 1.5 - 4.0 nm exhibit the large values of $S^{ANE} \geq 0.9$ μV K^{-1}, and the maximum $S^{ANE} = 1.14 \pm 0.05$ μV K^{-1} was obtained at t = 2.0 nm. This value is one order of magnitude larger than that for the bulk Ni [Ref.3]. We found that the enhanced ANE of the Ni / Pt (001) superlattices is attributable to the large transverse Peltier coefficient.

[1] K. Uchida *et al.*, *Phys. Rev. B,* 92, 094414 (2015). [2] T. Seki *et al.*, *Phys. Rev. Mater.,* 4, 064413-1-9 (2020). [3] A. Miura *et al.*, *Appl. Phys. Lett.,* 115, 222403 (2019).

M4-07. High-Quality Single Crystalline Europium Iron Garnet Films With Perpendicular Magnetic Anisotropy by Sputtering.
M. Guo[1], Y. Liu[1], C. Cheng[2], C. Wu[3], W. Chen[1], T. Chen[2], S. Zhou[4], C. Pai[2], S. Lee[5], M. Hong[2] and J. Kwo[1] *1. National Tsing Hua University, Hsinchu, Taiwan; 2. National Taiwan University, Taipei, Taiwan; 3. Max-Planck-Institut fur Chemische Physik fester Stoffe, Dresden, Germany; 4. Institut für Ionenstrahlphysik und Materialforschung, Forschungszentrum Dresden-Rossendorf e.V., Dresden, Germany; 5. Academia Sinica, Taipei, Taiwan*

The europium iron garnet (EuIG) thin films with strain-induced perpendicular magnetic anisotropy (PMA) were successfully grown on GGG(001) using off-axis sputtering technique. Our thin film samples exhibited an extremely smooth, particle free surface with root-mean-square roughness as low as 0.1 nm. High-resolution synchrotron radiation x-ray diffraction analysis revealed excellent crystallinity of the films and the reciprocal lattice mapping (RSM) showed the film is lattice matched to the substrate without strain relaxation. We were able to fine-tune the strength of PMA field ($H_\perp$), magnetization (M_S) and coercive field (H_C) of EuIG by slightly adjusting the Eu/Fe composition ratio via varying target-to-substrate longitudinal distance. The precise Eu/Fe ratio was determined using Rutherford backscattering spectrometry (RBS). The relative orientations of the magnetic moments of the cations were probed by x-ray magnetic circular dichroism (XMCD) measurement at *Eu* $M_{4,5}$ and *Fe* $L_{3,4}$ absorption edges. We also studied the spin Hall magnetoresistance (SMR) effect in the Pt/EuIG bi-layer samples and evaluated the spin mixing conductance. Finally, we demonstrated the current-induced switching in this structure with a low critical switching current density of 3.5×10^6 A/cm^2, showing great potential for low-dissipation spintronic devices constructed with strong spin-orbit-coupled materials and magnetic insulators.

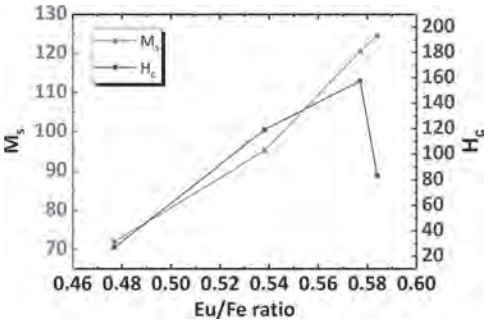

Plot of Eu: Fe composition versus M_s and H_c.

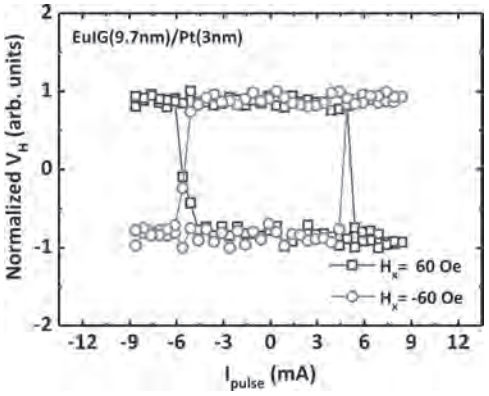

Current-induced magnetization switching of EuIG/Pt with a 60 Oe in-plane magnetic field applied on the x direction. The critical switching current density is 3.5×10^6 A/cm^2

M4-08. Thermomagnetic Control of Spintronic THz Emission Enabled by Ferrimagnets.
M. Fix[1], R. Schneider[2], J. Bensmann[2], S. Michaelis de Vasconcellos[2], R. Bratschitsch[2] and M. Albrecht[1] *1. Institute of Physics, University of Augsburg, Augsburg, Germany; 2. Institute of Physics and Center for Nanotechnology, University of Münster, Münster, Germany*

Bilayers of ferro-/ferrimagnetic (FM/FI) thin films and nonmagnetic metal (NM) layers have been shown to be THz emitters when excited by femtosecond laser pulses [1,2]. Amplitude and frequency of the emitted THz radiation can be tuned by varying the film thickness, the electrical conductivity, the magnetic properties of the FM/FI layer, and the spin-Hall angle Θ_{sh} of the NM layer [3]. In previous studies we showed that for FI rare earth-3d transition metal alloys mainly the electrons of the transition metal contribute to the spintronic THz emission [4,5]. Here we present a material system with two FI Gd_xFe_{100-x} layers where the relative orientation of the Fe magnetic moments can be set by temperature in the presence of an external magnetic field. [6] We demonstrate that, depending on the relative alignment of the Fe moments, the spintronic emitter system can be either in a high- (fig. 1a) or in a low-amplitude (fig. 1b) THz emitting state for temperatures below or above the FI compensation temperature T_{comp} of the $Gd_{30}Fe_{70}$ layer, respectively. Fig. 2 shows (a) the magnetic moment and (b) the emitted THz radiation in dependence on the temperature. NM layers with opposite spin Hall angles were used to further improve the efficiency. The study opens a route for a new type of a spintronic THz emitter system based on the FI properties of rare earth-3d transition metal alloys which allows switching of the emission state from high to low power by temperature.

[1] T. Kampfrath, M. Battiato, *et al.*, Nature Nanotechnology 8, 256 (2013). [2] T. J. Huisman, C. Ciccarelli, *et al.*, Applied Physics Letters 110, 72402 (2017). [3] T. Seifert, S. Jaiswal, *et al.*, Nature Photonics 10, 483 (2016). [4] R. Schneider, M. Fix, *et al.*, ACS Photonics 5, 3936 (2018).

[5] R. Schneider, M. Fix, *et al.*, Appl. Phys. Lett. 115, 152401 (2019).
[6] M. Fix, R. Schneider, *et al.*, Appl. Phys. Lett. 116, 12402 (2020).

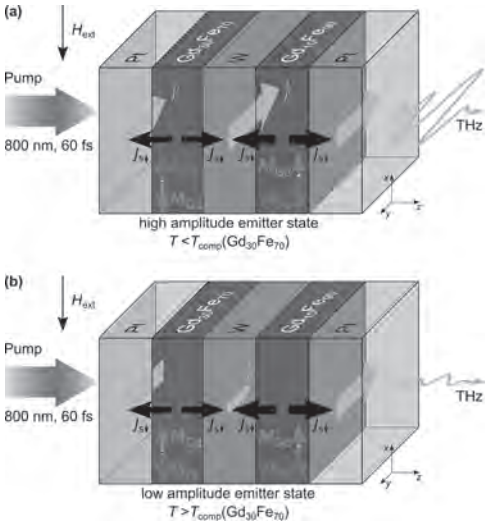

Fig. 1 Illustration of the layer stacking and THz excitation mechanism for the (a) high and (b) low amplitude emitter state. The excitation with a femtosecond laser pulse leads to the creation of spin currents J_s, caused mainly by Fe electrons of the ferrimagnetic Gd_xFe_{100-x} layers. In the Pt ($\Theta_{sh,Pt} > 0$) and W ($\Theta_{sh,W} < 0$) layers, the spin currents J_s are converted into transverse charge currents J_c, due to the inverse spin-Hall effect, that cause the emission of THz radiation.

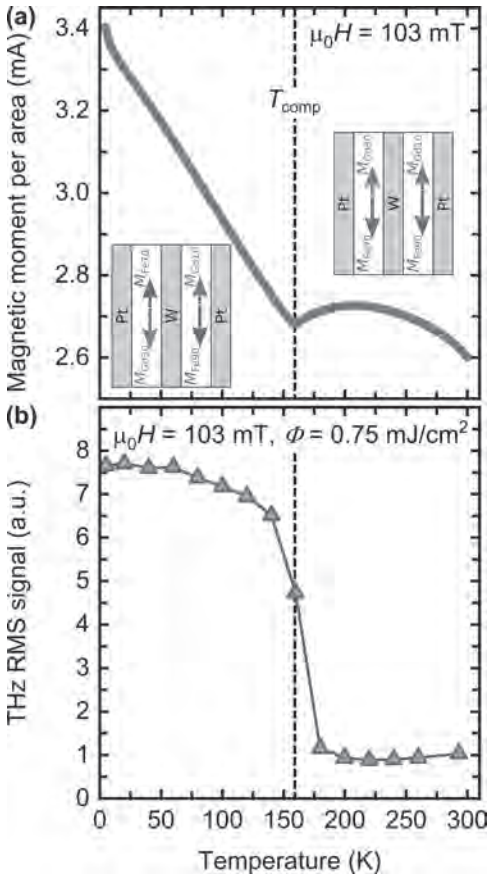

Fig. 2 (a) Magnetic moment and (b) THz RMS signal of a Pt/$Gd_{10}Fe_{90}$/W/$Gd_{30}Fe_{70}$/Pt sample measured for different temperatures. The minimum of the magnetization at 160 K and the strong reduction in the THz RMS signal can be attributed to the compensation temperature T_{comp} of the $Gd_{30}Fe_{70}$ layer.

M4-09. Coherent Long-Range Transfer of Angular Momentum Between Magnon Kittel Modes by Circularly Polarized Phonons.

K. An[1], A. Litvinenko[1], R. Kohno[1], v.v. naletov[2,1], G. de loubens[3], L. Vila[1], j. ben youssef[7], n. vukadinovic[4], G. Bauer[5], V. Tyberkevych[6], A.N. Slavin[6] and *O. Klein*[1] *1. SPINtronique et Technologie des Composants, Grenoble, France; 2. Kazanskij federal'nyj universitet, Kazan', Russian Federation; 3. Service de Physique de l'Etat Condense, Gif Sur Yvette, France; 4. Dassault Aviation, Saint-Cloud, France; 5. Tohoku Daigaku, Sendai, Japan; 6. Oakland University, Rochester, MI, United States; 7. Universite de Bretagne Occidentale, Brest, France*

We present experimental evidence for coherent long-distance transport of angular momentum inside a non-magnetic dielectric via the coupling to circularly polarized sound waves that exceeds previous benchmarks set by magnon diffusion by orders of magnitude. Most of the spintronics devices rely on the delocalized electrons in metals to carry the spin information, which induces loss by Joule heating. It turns out that insulating magnetic materials, such as yttrium iron garnet (YIG), also allow the spin to propagate between localized magnetic moments via propagating spin-waves which transmit information from an atomic site to the other without any Joule effect. In principle, the induced angular momentum can also pass through a non-magnetic insulators by coupling to circular vibrations of the crystal lattice called chiral phonons. But the extent to which these phonons can mediate spin currents in a circuit remains to be demonstrated. In a recent experiment [1], a collaboration lead by researchers at Spintec used a microwave field to excite a current of chiral phonons through a half-millimeter thick layer of non-magnetic gadolinium gallium garnet sandwiched between

two YIG films. By showing interference effects between the two magnetic layers, they demonstrated that circularly polarized acoustic phonons allow coherent transmission of spin information over millimeter distances. This work has since inspired theoretical work [2] showing the interest of using this discovery with an electric current which is more practical for powering spintronic devices.

[1] K. An, A. N. Litvinenko, R. Kohno, et al. Phys. Rev. B 101, 060407(R) – Published 21 February 2020; [2] Rückriegel, A. & Duine, R. A. Physical Review Letters, American Physical Society (APS), 2020, 124

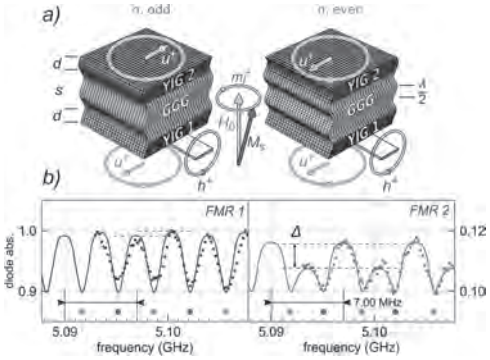

A) Schematic diagram of the dynamic coupling between two magnetic YIG layers: the magnetic precession m^+ generates a circular shear deformation u^+ of the crystal lattice that can be tuned into a coherent motion of all fields causing constructive or destructive interference patterns. B) The signature is a contrast Δ in the ferromagnetic resonance signal between tones separated by half a phonon wavelength. The orange/green dots indicate the spectral position of the even/odd acoustic resonances.

M4-10. Modulation of Magnon Spin Transport in a Magnetic Gate Transistor. K. Das[1], *F. Feringa*[1], M. Middelkamp[1], B. Van Wees[1] and I.J. Vera-Marun[2] *1. Rijksuniversiteit Groningen Faculty of Science and Engineering, Groningen, Netherlands; 2. The University of Manchester, Manchester, United Kingdom*

One of the major goals of magnon spintronics is the efficient generation and manipulation of the spin degree of freedom by using magnon spin currents [1]. In the ferrimagnetic insulator Yttrium Iron Garnet ($Y_3Fe_5O_{12}$, YIG) the spin current occurs via spin-waves or magnons. Magnons can be excited and detected electrically via the spin Hall effect (SHE) and the anomalous spin Hall effect (ASHE) and excited thermally via the spin Seebeck effect (SSE) in a nonlocal device geometry [2 - 4]. We demonstrate a modulation of up to 18% in the magnon spin transport in the magnetic insulator YIG using a common ferromagnetic metal (permalloy, Py) as a magnetic control gate [5]. A Py electrode, placed between two Pt injector and detector electrodes, acts as a magnetic gate in our prototypical magnon transistor device. By manipulating the magnetization direction of Py with respect to that of YIG, the transmission of magnons through the Py|YIG interface can be controlled, resulting in a modulation of the nonequilibrium magnon density in the YIG channel between the Pt injector and detector electrodes. Such a transistor operates in the absence of any electrical bias in the control gate, via the modulation of magnon absorption at the YIG|gate interface. This principle of operation, unexplored in previous magnon transistors [6], has the potential to implement nonvolatile memory and enable low-power programmable magnonics.

[1] A. A. Serga *et al.*, Journal of Physics D: Applied Physics, 43, 264002 (2010). [2] L. J. Cornelissen *et al.,* Nature Physics 11, 1022 (2015). [3] K. S. Das *et al.,* Phys. Rev. B 96, 220408(R) (2017). [4] K. S. Das *et al., Nano Letters* 2018 *18* (9), 5633-5639 [5] K. S. Das *et al.*, Phys. Rev. B 101, 054436 (2020) [6] L. J. Cornelissen *et al.,* Phys. Rev. Lett. 120, 097702 (2018).

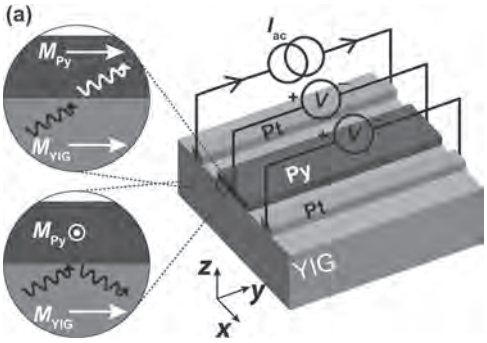

(a) Schematic illustration of the device geometry. The magnon-valve effect is depicted in the insets, where the transmission of magnons across the Py | YIG interface is dependent on the relative orientation of the Py (M_{Py}) and the YIG (M_{YIG}) magnetizations.

M4-11. Short-Range Study of Thermal Magnon Transport in Magnetic Garnets. *K. An*[1], R. Kohno[1], N. Thiery[1], D. Reitz[4], L. Vila[1], v.v. naletov[1,5], N. Beaulieu[2,3], j. ben youssef[2], G. de loubens[3], y. Tserkovnyak[4] and O. Klein[1] *1. Université Grenoble Alpes, CEA, CNRS, Grenoble INP, Spintec, Grenoble, France; 2. Laboratoire des Sciences et Techniques de l'Information de la Communication et de la Connaissance, Brest, France; 3. SPEC, CEA-Saclay, CNRS, Université Paris-Saclay, Gif-sur-Yvette, France; 4. University of California Los Angeles, Department of Physics and Astronomy, Los Angeles, CA, United States; 5. Kazan Federal University, Institute of Physics, Kazan, Russian Federation*

Conversion of heat into spin current has recently drawn a lot of attention due to its potential usage on heat recovery via the spin Seebeck effect (SSE) [1] as well as fundamental interests including generation of spin super currents [2] and Bose-Einstein condensation of magnons [3]. The underlying mechansim for SSE is understood as a combination of interfacial and bulk (intrinsic) contriubtion. The interfacial SSE is driven by the tempearture drop at the interface between metal and magnetic layer while the bulk SSE is driven by diffusive thermal magnons. In the nonlocal spin transport measurements, the long range exponential decay of thermally generated spin signal was explained solely by the intrinsic SSE [4] while there are several studies showing that there is another decay mechanism in subhundred nanometer scale [5-7]. Here, we study the spatial decay of thermally excited magnon currents inside a thin magnetic insulator by focusing on the short-range behavior in the nonlocal geometry. We compare SSE signal on the same device before and after adding a nonmagnetic Al capping layer. The Al capping alters the thermal profile significantly near the heat source, which results in that the nonequilibrium thermal magnon profile deviates from an exponential decay and shows two sign reversals within 1 μm from the heat source. From simulated temperature profiles, we find the vertical temperature gradient also reverses twice within the same length scale in the Al deposited case. The correlation suggests that thermal magnons behave locally at this length scale. Using a phenomenological spin transport model, we calculate the spatial profile of nonequilibrium spin density. The observed short-range behavior can be accounted if the relavant decay length is on the order of subhundred nanometers. Our result shows the existance of the shorter decay length in the nonlocal magnon transport experiments. This suggests that the long-range SSE signal in previous measurements should be attributed to magnons with lower energy.

[1] Boona, S. R., Myers, R. C., & Heremans, J. P. *Energy & Environmental Science*, *7*(3), 885-910 (2014) [2] Bozhko, D. A., Serga, A. A., Clausen, P. et al., *Nature Physics*, *12*(11), 1057-1062 (2016) [3] Tserkovnyak, Y., Bender, S. A., Duine, R. A. et al., *Physical Review B*, *93*(10), 100402 (2016) [4] Cornelissen, L. J., Liu, J., Duine, R. A. et al., *Nature Physics*, *11*(12), 1022-1026 (2015) [5] Kehlberger, A., Ritzmann, U., Hinzke, D. et al., *Physical review letters*, *115*(9), 096602 (2015) [6] Prakash, A., Flebus, B., Brangham, J. et al., P*hysical Review B*, *97*(2), 020408 (2018) [7] Jamison, J. S., Yang, Z., Giles, B. L. et al., *Physical Review B*, *100*(13), 134402 (2019)

M4-12. Thermoelectric Effects of Superconductor-Ferromagnetic Hybrids. *K. Blagg*[1], P. Allen[1], B. Lloyd[1], M.P. Lilly[2] and M. Singh[1]
1. Physics, Colorado School of Mines, Golden, CO, United States;
2. Sandia National Laboratories, Albuquerque, NM, United States

Usually negligible thermoelectric effects in superconductors can be increased using the simultaneous effects of spin splitting and spin filtering. These superconductor-ferromagnetic hybrids have been predicted to have thermal electric efficiencies (zT ~ 1.8) far exceeding any other cryogenic thermoelectric materials. Confirmation of these predictions requires controlled S-F interfaces, the generation of temperature gradients, and precise local cryogenic thermometry. S-F heterostructures have been fabricated using a combination of lithography, thermal evaporation, and magnetron sputtering, providing precise control over interfaces, materials, and geometries. Heaters and resistive thermometers, patterned via focused ion beam assisted platinum deposition have been calibrated and optimized for thermal transport measurements at cryogenic temperatures. Finally, the Seebeck coefficient of S-F heterostructures has been measured in the presence of a magnetic field. This measurement framework and measurement set the stage for additional studies of the effects of dimensionality, ferromagnet polarization, and interface quality.

P. Machon, M. Eschrig, and W. Belzig, "Nonlocal thermoelectric effects and nonlocal onsager relations in a three-terminal proximity-coupled superconductor-ferromagnet device," Phys. Rev. Lett., vol. 110, p. 47002, 2013.
P. Machon, M. Eschrig, and W. Belzig, "Giant thermoelectric effects in a proximity couple superconductor- ferromagnet device," New J. Phys., vol. 16, p. 073002, 2014.

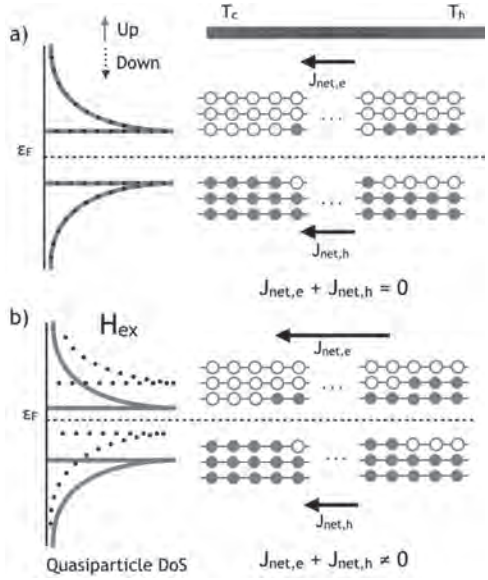

Left panel, - (a) quasiparticle density of states in the semiconductor model of superconductivity without and (b), with a magnetic field H_{ex}. Right panel - schematic representation of electron and hole occupations of spin up quasiparticle bands (solid line) shown in the left panel. Filled and empty circles represent electrons and holes respectively. For case (a), the spin down bands would look identical to the spin up but, for case (b), the occupations for the spin down bands would flip with respect to electrons and holes. In (a), the net electron and hole currents are equal leading to zero total current flowing in response to the thermal gradient. In (b), however, there are more electrons than holes, resulting in a total electronic current from T_h to T_c

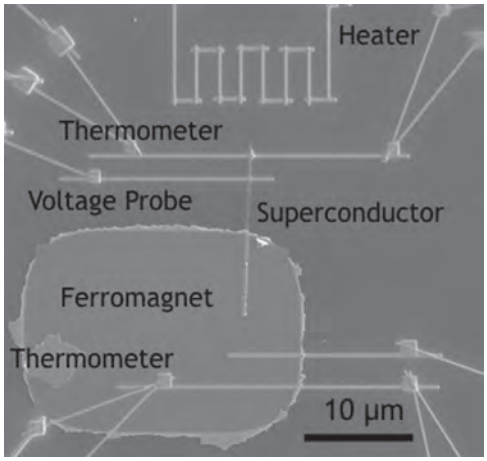

Electron Microscope image of experimental platform for the measurement of Seebeck coeffiecent in superconductor-ferromagnetic devices including: superconductor-ferromagnetic nanostructures, and FIB deposited local heaters and resistive thermometers.

Session M5
SKYRMIONS I
(Poster Session)

Nico Kerber, Co-Chair
Johannes Gutenberg University of Mainz, Mainz, Germany
Thomas Moore, Co-Chair
University of Leeds, Leeds, United Kingdom

M5-01. Skyrmion-Skyrmion Interaction in a Magnetic Film. *D. Capic*[1], D. Garanin[1] and E. Chudnovsky[1] *1. Physics, City University of New York, New York, NY, United States*

Interaction of two skyrmions stabilized by the ferromagnetic exchange, Dzyaloshinskii-Moriya interaction (DMI), and external magnetic field has been studied numerically on a 2D lattice of size large compared to the separation, d, between the skyrmions. We show that two skyrmions of the same chirality (determined by the symmetry of the crystal) repel. In accordance with earlier analytical results, their long-range pair interaction falls out with the separation as $\exp(-d/\delta_H)$, where δ_H is the magnetic screening length, independent of the DMI. The prefactor in this expression depends on the DMI that drives the repulsion. The latter results in the spiral motion of the two skyrmions around each other, with the separation between them growing logarithmically with time. When two skyrmions of the total topological charge $Q = 2$ are pushed close to each other, the discreteness of the atomic lattice makes them collapse into one skyrmion of charge $Q = 1$ below a critical separation. Experiment is proposed that would allow one to measure the interaction between two skyrmions by holding them in positions with two magnetic tips. Our findings should be of value for designing topologically protected magnetic memory based upon skyrmions.

D Capic, DA Garanin and EM Chudnovsky, Skyrmion-skyrmion interaction in a magnetic film, Journal of Physics: Condensed Matter, https://doi.org/10.1088/1361-648X/ab9bc8 (2020). (Accepted Manuscript)

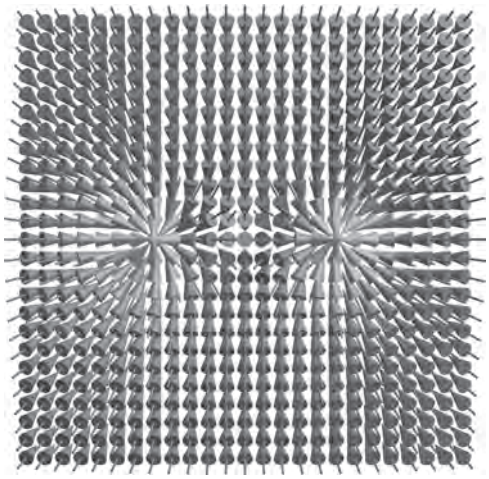

M5-02. XMCD-STXM Magnetic Imaging of Skyrmions With in-Situ Hall Transport Measurements in Pt/Co/Ir Multilayer Hall Discs. *A.J. Huxtable*[1], S. Finizio[2], K. Zeissler[1], E. Darwin[1], G. Burnell[1], M. Rosamond[1], E. Linfield[1], J. Raabe[2] and C.H. Marrows[1] *1. University of Leeds, Leeds, United Kingdom; 2. Paul Scherrer Institut, Villigen, Switzerland*

Transport measurements of skyrmions, and their interpretation by connection to the magnetic state at the time of measurement, are essential for their potential application in data storage. In-situ Hall transport measurements combined with XMCD-STXM imaging of the magnetic texture have been developed by Finizio et al. [1] and used in the investigation of the discrete hall resistivity contribution due to Néel skyrmions by Zeissler et al. [2]. Continued research into the skyrmion contribution to Hall resistivity is needed to explain the discrepancy in the size of the contribution observed in Ref. 2 compared to that predicted by theory [3, 4]. The magnetisation in 800 nm and 1 μm diameter Hall discs has been measured using combined XMCD-STXM imaging at the PolLux endstation at PSI [1]. The Hall devices are $[Pt/Co/Ir]_{xN}$ multilayers grown by DC magnetron sputtering on 200 nm Si_3N_4 membranes and patterned by electron beam lithography. The images were collected during in-situ Hall resistivity measurements in order to verify the texture of the magnetisation in the samples, yielding the images and Hall resistance data to be presented. The topology of the magnetisation of skyrmions is defined by the winding number, S, which takes an integer value dependent upon the number of topological 'twists' in magnetisation present in the multilayer disc. A major hysteresis loop for the saturated discs was measured allowing the out of plane magnetisation and Hall resistance of Skyrmions to be normalised. By performing the same measurements during minor hysteresis loops, in the presence of a skyrmion, one can plot R_H/R_{Hsat} and M_z/M_{sat}. We have shown that multilayer discs with three topologically equivalent (S=0) magnetisations have different overall Hall resistances (R_H).

[1] S. Finizio, K. Zeissler, G. Burnell et. al. *'In-situ Electrical Transport Measurements Combined with Scanning Transmission X-ray Microscopy',* Microscopy and Microanalysis, 24(S2), 76-77, 2018 [2] K. Zeissler, S.Finizio, K. Shahbazi et. al. '*Discrete Hall Resistivity contribution from Néel skyrmions in multilayer nanodiscs'*, Nature Nanotechnology 13, 1161 – 1166 (2018) [3] D. Maccariello, W. Legrand, N. Reyren et al. *'Electrical detection of single magnetic skyrmions in metallic multilayers at room temperature'*, Nature Nanotechnology, 13, 233–237 (2018) [4] M. Raju, A. Yagil, A. Soumyanarayanan et al. *'The evolution of skyrmions in Ir/Fe/Co/Pt multilayers and their topological Hall signature'*, Nature Communications, 10, 696 (2019)

M5-03. Withdrawn

M5-04. Magnetic Skyrmions and Phase Transitions in a Antiferromagnetic/Ferroelectric Bilayers. *I. Sharafullin*[1], A. Yuldasheva[1] and H.T. Diep[2] *1. Institute of Physics and Technology, Baskirskij Gosudarstvennyj Universitet, Ufa, Russian Federation; 2. Laboratory of Theoretical Physics and Modeling, Cergy Paris University, Paris, France*

Applications of skyrmions in spintronics have been largely discussed and their advantages compared to early magnetic devices such as magnetic bubbles have been pointed out in a recent review by W. Kang et al. [1]. Among the most important applications of skyrmions, let us mention skyrmion-based racetrack memory [2], skyrmion-based logic gates [3, 4], skyrmion-based transistor and skyrmion-based artificial synapse and neuron devices [5]. In this work we have studied the phase transition and ground state configurations in antiferromagnetic/ferroelectric bilayer formed by magnetic layer between ferroelectric layers by the use of Monte Carlo simulation and the steepest descent method. Antiferromagnetic film and ferroelectric films in this work were modeled as films of triangular lattice with respectively Heisenberg spins and polarizations. All interactions are limited to nearest neighbors (NN). We found the formation of a stable skyrmions in the ground state of bilayers with the triangular lattice at zero applied magnetic field in a region of interface magnetoelectric interaction (-1.0,-0.65) (meV). Very strong magnetoelectric interactions at the interface leads to the disappearance of the magnetic phase transition, unlike the case of simple cubic lattice where we observed very strong first-order phase transitions at large values of the interface magnetoelectric interaction. The existence of skyrmions at the magneto-ferroelectric interface in the ground state at zero magnetic field is very interesting and may have practical applications in digital technologies and spintronics. We found the formation of a perfect skyrmions lattice at acceptable values of magnetoelectric interaction. The skyrmions structure is stable in a large region of the external magnetic field. With a moderate increase in the magnetoelectric interaction parameter, the stability of the skyrmion lattice with respect to the magnitude of the applied magnetic field increases.

1. W.Kang, Y. Huang, X. Zhang, Y. Zhou and W. Zhao, Proceedings of the IEEE, Vol. 104, p. 2040 (2016) 2. S. S. P. Parkin, M. Hayashi and L. Thomas, Science, Vol. 320, p. 190 (2008) 3. X. Zhang, M. Ezawa and Y. Zhou, Scientific Reports, Vol. 5, p. 9400 (2015) 4. Y. Zhou, M.Ezawa, Nature communications, Vol. 5, p. 1 (2014) 5. S.Li, W. Kang, Y. Huang, X. Zhang X, Y. Zhou and W. Zhao, Nanotechnology, Vol. 28, p. 31LT01 (2017)

M5-05. Numerical Simulation of Magnetic Skyrmions on Flat Lattices. *V.Y. Kapitan*[1,2], E. Vasiliev[1,2], A. Perzhu[1,2], D. Kapitan[1,2], A. Rybin[1,2], A.O. Korol[1], K. Soldatov[1,2] and Y. Shevchenko[1,2] *1. Computer Systems, Dal'nevostocnyj federal'nyj universitet, Vladivostok, Russian Federation; 2. Institut prikladnoj matematiki DVO RAN, Vladivostok, Russian Federation*

Magnetic systems, in which due to competition between the direct Heisenberg exchange and the Dzyaloshinskii-Moriya interaction (DMI), magnetic vortex textures - skyrmions appear, were studied using the Metropolis algorithm. Skyrmions are attractive candidates as an information carrier in a new type of magnetic media - racetrack memory [1]. At the fundamental level, skyrmions are model systems for topologically protected spin textures and can be considered as an analog of topologically protected states, emphasizing the role of topology in the formation of complex states of condensed matter. Usually, skyrmions appear in noncentrosymmetric materials or interfaces. In contrast, a skyrmion phase was observed in the frustrated centrosymmetric triangular-lattice magnet Gd_2PdSi_3. The magnetic frustration helped stabilize the skyrmion phase in such systems [2]. In the abstract, the conditions for the nucleation and stable existence of magnetic skyrmions in two-dimensional magnetic films was considered in the frame of the classical Heisenberg model. We considered a triangular (6 nearest neighbors) flat lattice, as well as the case of 2 sublattices on a triangular one (3 neighbors with DMI and 3 without, taking into account direct exchange between all 6 neighbors). We compared it with results for spin systems on a square lattice (4 NN). To analyze the data obtained during the Monte Carlo simulation, a convolutional neural network were used for recognition of different phases of the spin system depends on various simulation parameters such as DMI, external magnetic field (B) and temperature (T). Based on these data, two types of phase diagrams (B,T) and (D,B) were built. As it is known, one of the features of the practical application of skyrmions that they are usually stable in a narrow region of low temperatures and external magnetic fields. Therefore, based on the data from the phase diagrams, we can select appropriate parameters that significantly affect the properties of the system and lead to the formation of various phases that provide different functionalities for use in spintronics. This work was supported by the state task of the MSHE of Russia No. 0657-2020-0005.

[1] A. Fert, V. Cros, J. Sampaio, Nature nanotechnology., Vol. 8 (3), pp. 152–156 (2013). [2] T. Kurumaji et al., Science., Vol. 365 (6456), pp. 914-918 (2019).

M5-06. Withdrawn

M5-07. Structural and Magnetic Properties of β-Mn Structured Cobalt-Zinc Thin Film Alloys. *M. Dearg*[1], A. Caruana[2], C. Kinane[2], G. Burnell[1], S. Langridge[2] and C.H. Marrows[1] *1. School of Physics and Astronomy, University of Leeds, Leeds, United Kingdom; 2. ISIS, Rutherford Appleton Laboratory, STFC, Oxon, United Kingdom*

Skyrmions, topologically protected particle-like vortices in the magnetization, hold potential as an energy efficient, high-density magnetic storage media due to their nanometric size and the low driving current densities [1]. The widely-studied B20 skyrmion materials (chiral cubic $P2_13$ space group) present a bottleneck to technological applications due to their below room-temperature transition [2]. However, CoZn alloys host a β-Mn phase [3], creating a structurally chiral cubic magnet which breaks spatial inversion symmetry. Such alloys can host Dzyaloshinkii-Moriya interaction (DMI) stabilised skyrmions at and above room temperature [4], making them a candidate for developing skyrmion technologies. To date these materials have primarily been studied as bulk crystals, but to realise technological applications it is necessary to produce thin films on planar substrates from which devices can be fabricated. We present the results of work to address this gap by growing thin films by co-sputtering of CoZn alloys from elemental targets, on Si/SiO_2 substrates at room-temperature. In their as-deposited form they are amorphous or nanocrystalline, lacking Bragg peaks in XRD or showing weak contributions from constituents' crystalline phases. After annealing at 400 °C for 48 hours, crystallites with the β-Mn structure form, as shown by the presence of Bragg reflections in XRD (Fig.1b) and further confirmed by TEM imaging (Fig.1c). Annealed samples also show an above room-temperature transition in the M(T) of almost 420 K (Fig.1a). Further, the results of a polarised neutron reflectometry (PNR) investigation on the magnetic depth profile are presented. These thin film alloys present with the β-Mn phase ($P4_132/P4_332$ space group), and thus possess an appropriate point group symmetry to give rise to a bulk DMI and are potential candidates for an above room-temperature thin film skyrmion material. This work was supported in part by the STFC ISIS Neutron and Muon Source.

[1] A. Fert, V. Cros & J. Sampiao, Nat. Nanotechnol. 8, 152-156 (2013) [2] N. Kanazawa, S. Seki & Y. Tokura, Adv. Mater. 29, 1603227 (2017). [3] K. H. J. Buschow et al., J. Magn. Magn. Mater. 38, 1 (1983). [4] Y. Tokunaga et al., Nature Commun. 6, 7638 (2015).

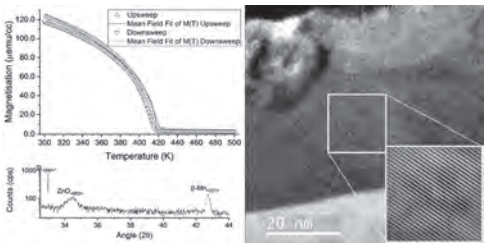

Fig.1. (a) M(T) of $Co_{47}Zn_{53}$ alloy, annealed at 400 °C for 48 hrs; (b) XRD of sample (a), identifying the (221) β-Mn phase; (c) TEM image of crystalline order in a Zn-rich sample under the same preparation conditions.

M5-08. Energetics, Equilibrium Shape, and Vorticity of Skyrmions and Antiskyrmions Stabilized by the Anisotropic Dzyaloshinskii-Moriya Interaction in Thin Films With C_{2v} Symmetry. *M.D. Kitcher*[1], M. De Graef[1] and V. Sokalski[1] *1. Materials Science & Engineering, Carnegie Mellon University, Pittsburgh, PA, United States*

When applied to C_{2V} ferromagnetic/heavy metal interfaces, Moriya's rules do not deterministically predict the orientation of interatomic DM vectors. Low-symmetry magnetic systems can exhibit both Rashba (D_R) and Dresselhaus (D_D) forms of the Dzyaloshinskii-Moryia interaction (DMI), as both spin-orbit couplings are generally present [1]. We assert that the spatial variation of the DM vectors—and thus that of the strength and direction of the effective DMI field—is determined by the DMI's character (i.e., $||D_D||/||D_R||$), as well as the unit cell's aspect ratio [2]. Overall, the DMI is thus nominally anisotropic and hybridized—potentially stabilizing antiskyrmions and Bloch-Néel (i.e. mixed) skyrmions [2-3]. Ascertaining the existence and tunability of [anti]skyrmions in such systems is of technological interest and would elucidate the nature of DMI [2]. Employing the Wulff construction [3], ξ-vector formalism [4], and an augmented wall energy that accounts for DMI character, this work models the equilibrium shape and wall magnetization profile of bubble domains and skyrmions in thin films with C_{2v} symmetry. We show that for sufficiently large DMI, square-shaped antiskyrmions are stable for certain DM vector orientations while lens- and oval-shaped mixed skyrmions are favored otherwise. A symmetry-breaking applied in-plane field stabilizes domain shapes resembling ovals and Reuleaux triangles. The impact of the unit cell's aspect ratio, the DM vector's orientation, and other material parameters on the shape of bubble domains and skyrmions are discussed. Moreover, our results reveal unusual relationships between faceting behavior and wall stiffness under rather reasonable conditions. Elucidating the interplay between the different effective fields present, we explore the validity of these results based on pedal plots, discontinuities in the magnetization profiles, and local extrema in the wall energy.

U. Güngördü et al., Physical Review B., 93, 064428 (2016) M. Hoffman et al., Nature Communications., 8, 308 (2017) J. P. Pellegren, D. Lau, and V. Sokalski, Physical Review Letters., 119, 027203 (2017) A. A. Wheeler, Journal of Statistical Physics., 95, 1245–1280 (1999)

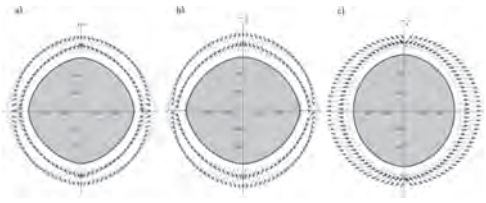

Fig. 1: Plots of energies (points), isolated wall magnetizations (outer arrows), Wulff equilibrium wall magnetizations (inner arrows), and equilibrium domain shape for DM vector orientations of (a) 0°, (b) 15° and (c) 90°.

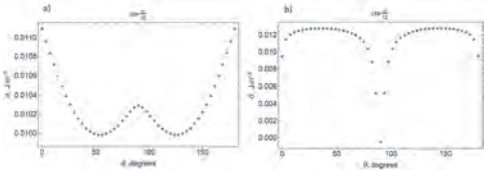

Fig. 2: Orientational dependence of (a) isolated wall energy and (b) stiffness for α = 15°

M5-09. Withdrawn

M5-10. Spin Transport Using a Magnetic Skyrmion Lattice. *D.I. King*[1], J. Tang[1] and J. Ackerman[2] *1. Physics and Astronomy, University of Wyoming, Laramie, WY, United States; 2. Chemical and Petroleum Engineering, University of Wyoming, Laramie, WY, United States*

Magnetic skyrmions are a topologically protected state in certain magnetic systems. Their topological properties make skyrmions stable and thus a possible basis for memory or energy storage spintronic devices. We present results for a transport device that uses a skyrmion lattice in the magnetic insulator Cu_2OSeO_3 as a precursor to an energy storage device. Data from the transport device and its fabrication are presented. Interestingly, spin transport in the skyrmion lattice is observed across the insulator over a long distance. The electronic transport data for several devices are then used to test the underlying elasticity theory for the skyrmion lattice[1].

1. H. Ochoa, S.K. Kim, and Y. Tserkovnyak, Physical Review B., Vol. 96, 020410(R) (2017)

M5-11. Skyrmions and Antiskyrmions From Current-Induced Boundary Instabilities. *S. Sandhoefner*[1], A.S. Raeliarijaona[1], R. Nepal[1], D. Snyder-Tinoco[2] and A.A. Kovalev[1] *1. Physics, University of Nebraska-Lincoln, Lincoln, NE, United States; 2. California State University San Bernardino, San Bernardino, CA, United States*

We study generation and dynamics of skyrmions and antiskyrmions using current-induced torques at edges of magnetic regions with DMI (Dzyaloshinskii-Moriya interaction). The generation of skyrmions and antiskyrmions can be interpreted as a current-induced Doppler shift acting on the magnons localized at the interface. These localized modes are analyzed by using the Bogoliubov-de-Gennes Hamiltonian written for magnons. We confirm our theoretical predictions using micromagnetics simulations where we observe that a current pulse closes the magnon band gap, leading to instabilities in the magnetic texture at the edge. From micromagnetic simulations, we observe that the closure of the magnon band gap effectively causes the system to form skyrmions and/or antiskyrmions, depending on the type of DMI present.

M5-12. Field and Temperature Dependence of the Skyrmion Lattice Phase and the Appearance of a Second Helical Phase in FeGe. *D. Burn*[1], S. Zhang[2,3], G. van der Laan[1] and T. Hesjedal[3] *1. Magnetic Spectroscopy Group, Diamond Light Source Ltd, Didcot, United Kingdom; 2. ShanghaiTech University School of Physical Science and Technology, Shanghai, China; 3. Department of Physics, University of Oxford, Oxford, United Kingdom*

FeGe is a noncentrosymmetric helimagnet exhibiting non-collinear spin textures. Below the ordering temperature, T_c, bulk FeGe has a well-established and rich magnetic phase diagram showing helical, conical, and skyrmion states [1]. The skyrmion pocket has a wide, layer thickness dependent, temperature vs. field window extending up to room temperature [2-4]. These features make FeGe of great interest due to the potential for novel room-temperature devices based on the manipulation of topological magnetic states. Here, we characterize the magnetic states in a thin membrane of FeGe

with small angle soft x-ray scattering as a function of both temperature and out-of-plane magnetic field. We reveal a hook-shaped dependence of the modulation vector on the applied field whilst traversing the skyrmion phase pocket. This dependence arises due to competition between changes in the skyrmion size and packing density that occur as a function of field [5]. In addition to the helical, conical, and skyrmion phases, we observe an additional helical phase which coexists beneath the skyrmion phase in the phase diagram, towards the higher field boundary of the helical phase. In contrast to the other phases this additional helical phase shows strong uniaxial preferential alignment of the modulation vector [6]. Our findings build upon other work on FeGe, strengthening the case that the room-temperature topological magnetic properties are of great interest for the development of novel technological devices. Our work shows how multiple coexisting phases can be simultaneously and uniquely identified, which will provide further opportunities for potential information processing and storage methodologies.

[1] A. Bauer *et.al. Springer Series in Materials Science* 228, 1 (2016). [2] X.Z. Yu *et.al. Nat. Mater.* 10, 106 (2011). [3] H. Wilhelm *et.al. J. Phys.: Condens. Matter* 24, 294204 (2012). [4] S. X. Huang *et.al. Phys. Rev. Lett.* 108, 267201 (2012). [5] D.M. Burn *et.al. Phys. Rev. B* 101, 014446 (2020). [6] D.M. Burn *et.al. Phys. Rev. B* 100, 184403 (2019).

M5-13. Stabilizing Skyrmions on Pt/Co/Ta Multilayers and Ordered Arrays of Nanodomes by FORC Hall Analysis. *J. Denardin*[1], D. Toneto[3], J.L. Palma[2], S. Oyarzun[1] and L. Dorneles[3] *1. Physics, Universidad de Santiago de Chile, Santiago de Chile, Chile; 2. Universidad Central de Chile, Santiago, Chile; 3. Physics, Universidade Federal de Santa Maria, Santa Maria, Brazil*

Magnetic skyrmions are non-trivial spin textures that resist external disturbances and are promising candidates for the next generation of magnetic recording devices [1,2]. However, a major challenge in the realization of devices based on skyrmions is the stabilization of ordered arrangements of these spin textures under ambient temperature and zero applied field conditions. Among the materials that have skyrmions, the multilayers of ferromagnetic materials (Co) interspersed with heavy metals (Pt and Ta), with strong spin-orbit coupling, have interesting properties, as they favor the Dzyaloshinskii-Moriya (DMI) interaction, which is an anti-symmetric exchange interaction that tilts the spins of neighboring layers and helps to stabilize skyrmions. In this work we study the formation and stabilization of magnetic skyrmions in Pt/Co/Ta films by a first order reversal curves (FORC) diagram analysis, obtained from Hall Effect measurements [3], as shown in Fig.1(b). The FORC diagram analysis was used to determine the magnetic fields to be applied to nucleate and stabilize skyrmions on the multilayers and on the nanodomes. We also demonstrate for the first time the formation and stabilization of magnetic skyrmions on arrays of self-assembled hexagonal nanodomes (Fig. 1(a)). Magnetic force microscopy (MFM) images of the arrays of nanodomes with 100 nm shows isolated skyrmions under an out-of-plane magnetic field of only 500 Oe, shown in Fig.1(c). At remanence, the special topography helps to stabilize the skyrmions in the hexagonal arrangement of the nanodomes. Micromagnetic simulations were compared with experiments to determine the correlation of the domain textures with the topography of the samples and with the applied field and magnetic parameters of the multilayers.

[1] R. Wiesendanger, Nat. Rev. Mater. 1, (2016). [2] Z. Hou, Q. Zhang, G. Xu, C. Gong, B. Ding, Y. Wang, H. Li, E. Liu, F. Xu, H. Zhang, Y. Yao, G. Wu, X.X. Zhang, and W. Wang, Nano Lett. 18, 1274 (2018). [3] D Toneto, R B da Silva, L S Dorneles, F Beron, S Oyarzun and J C Denardin, J. Phys. D: Appl. Phys. (2020). doi.org/10.1088/1361-6463/ab95be

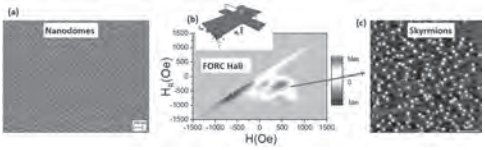

Fig.1: (a) SEM image of the array of nanodomes, (b) FORC Hall diagram of the Pt/Co/Ta multilayer depositted on 100 nm nanodomes, and (c) MFM image of nanodomes showing isolated magnetic skyrmions under an out-of plane magnetic field of 500 Oe.

M5-14. Magnetic Phase Diagram of Co Doped Cu_2OSeO_3: an AC Susceptibility Study. *U. Erugu*[1], D.I. King[1] and J. Tang[1] *1. Physics & Astronomy, University of Wyoming, Laramie, WY, United States*

Cu_2OSeO_3 is a magnetic insulator that hosts skyrmion lattice. Cobalt doped Cu_2OSeO_3 are investigated using dc and ac magnetometry and compared with its single crystalline parent compound. Chemical vapor transport method is employed to synthesize single crystals of Cu_2OSeO_3 while polycrystalline undoped and Co doped Cu_2OSeO_3 are prepared by solid state reaction method. The phase purity and grain size are confirmed by x-ray diffraction (XRD) and scanning electron microscopy (SEM). To construct the magnetic phase diagram, dc magnetization and ac magnetic susceptibility (χ_{ac}) measurements are performed while magnetic field is swept at desired temperatures. Our measurements show distinct features in χ_{ac} at magnetic phase transitions. The frequency dependency of some of these features may indicate the dissipation process at the magnetic phase transitions. The influence of grain size and interaction among grains on the magnetic phase diagram are studied. This work was supported by the National Science Foundation (DMR-1710512) and U.S. Department of Energy, Office of Science, Basic Energy Sciences (DE-SC0020074).

Session M6
STRUCTURED MATERIALS
(Poster Session)

Purnima Parvathy Balakrishnan, Chair
National Institute of Standards and Technology, Menlo Park, CA, United States

M6-01. Thermal Hysteresis of Thin Terbium (Tb) Films. *F.H. Sales*[1], J.J. Melo[1], A.L. Dantas[2], L.L. Oliveira[2] and A.S. Carriço[3] *1. Department of Physics, Federal Institute of Education, Science and Technology of Maranhão (IFMA), São Luís, Brazil; 2. Departament of Physics, University of State of Rio Grande do Norte (UERN), Natal, Brazil; 3. Departament of Physics, Federal University of Rio Grande do Norte (UFRN), Natal, Brazil*

A great deal of research report has recently been focused on studies of the impact of confinement on the equilibrium phases of magnetic systems with size comparable to fundamental magnetic lengths [1-5]. The magnetic states of helimagnetic rare-earth metals are likely to be particularly affected by confinement effects. [6-8]. We report an theoretical investigation of magnetic thermal hysteresis of terbium (Tb) nanolayers. For layer thicknesses of the order of a few helix periods, we find wide thermal hysteresis loops, spanning the temperature interval from below the Curie temperature up to the Neel temperature. The total change of magnetization in the thermal loops is tunable by external field strength of a few hundred Oersteds. We show that the thermal hysteresis is associated to the nucleation of alternate helix (AH) magnetic phases [9] in the heating and cooling branches of the loops (Figure 1). The reduction in the external field of 1 kOe to 100 Oe decreases the width of the thermal hysteresis curve (Figure 2). There is a temperature dependence of the turning angles of the AH phase of Tb. The alternate helix phase are made of units containing a finite number of hexagonal planes. These bulk magnetic phases observed on the thermal hysteresis curves consist of patterns made of a periodical repetition of units containing a finite number of planes along the b-axis. The overall magnetic pattern in both phases result from the balance between exchange, anisotropy and Zeeman energies.

[1] E.Weschke et al, Phys. Rev. Lett.93, 157204 (2004) [2] V. D. Mello, Ana L. Dantas and A. S. Carriço, Sol. Stat. Commun.140, 447 (2006) [3] Ana L. Dantas, R. E. Camley and A. S. Carriço, IEEE Trans. Magn. 42, 2942 (2006) [4] F. H. S. Sales, A. L. Dantas, and A. S. Carriço, Aip Advances 2, 032158 (2012) [5] F. H. S. Sales, A. L. Dantas, V. D. Mello, and A. S. Carriço, Journal of Materials Science 45, 5036 (2011) [6] Ana L. Dantas, R. E. Camley and A. S. Carriço, Phys. Rev.B75, 094436 (2007) [7] F. C. Medeiros Filho ; Mello, V. D. ; Dantas, Ana L. ; F. H. S. Sales ; Carriço, A. S.. J. Appl. Phys. (2011) [8] V. D. Mello, D. H. Anselmo, M. S. Vasconcelos, and N. S. Almeida, Solid State Commun. 268, 56–60 (2017) [9] F. H. S. Sales, A. L. Dantas, L. L. Oliveira and A. S. Carriço, Aip Advances 10, 015006 (2020)

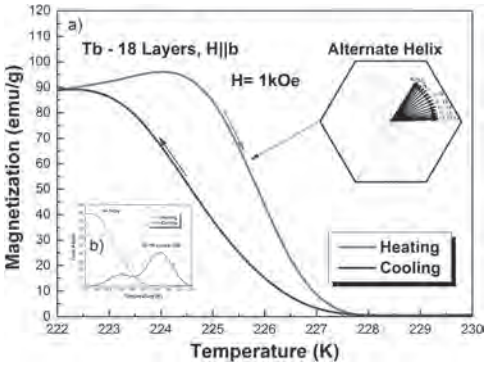

Thermal hysteresis of a 18-layer Tb film. (a) Temperature dependence of Magnetization and in the insets we show schematic representations of the alternating-helix phase in the 1.0 kOe isofield curve at a temperature of 225.5 K. and (b) Temperature dependence of average turn angle for H = 1.0 kOe. The red and blue continuos lines are for the heating (cooling) process.

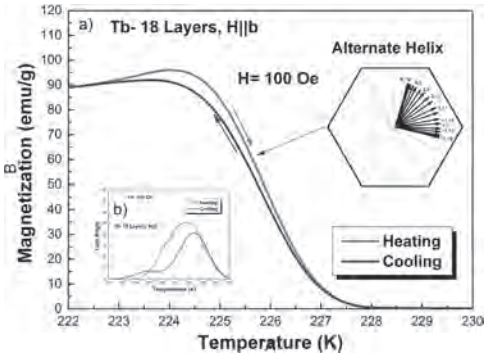

Temperature dependence of Thermal hysteresis of a 18-layer Tb film. (a) Magnetization and in the insets we show schematic representations of the alternating-helix phase in the 0.1 kOe isofield curve at a temperature of 225.5 K. and (b) Temperature dependence of average turn angle for H = 0.1 kOe. The red and blue continuos lines are for the heating (cooling) process.

M6-02. Kerr Microscopy Real-Time Imaging of the Magnetization Reversal Process in Kagome Artificial Spin ice. *D. Shi*[1] *1. physics department, Fudan University, Shanghai, China*

The magnetization reversal process in an interconnected kagome artificial spin ice has been investigated using high-resolution Kerr microscopy. The magnetization switching with two-dimensional system-size avalanches has been directly imaged for the applied field parallel to one of the sublattice branches, suggesting very low disorder in our sample. The discrete one-dimensional Dirac-string-like magnetization reversal is found for the field with a certain angle. The real-time imaging under the field suggests that the reversal of the third bars next to the reversed Dirac string can mediate the reversal of the neighboring Dirac string. The observed reversal behaviors can be understood by the ice rule, consistent with the micromagnetic simulation

results. Our studies demonstrate that Kerr microscopy can be applied to study the magnetization reversal process in artificial spin ice structures in real space and real time under an external magnetic field.

S. A. Daunheimer, O. Petrova, O. Tchernyshyov, and J.Cumings, Phys. Rev. Lett. 107, 167201 (2011). G. Chern, C. Reichhardt, and C. J. O. Reichhardt, New J. Phys.16, 063051 (2014). D. M. Burn, M. Chadha, and W. R. Branford, Phys. Rev. B. 92, 214425 (2015).

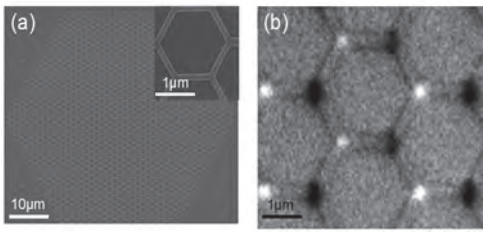

(a) SEM image of the interconnected kagome artificial spin ice structure. The inset shows a magnified view. (b)MFM image of the local structure.

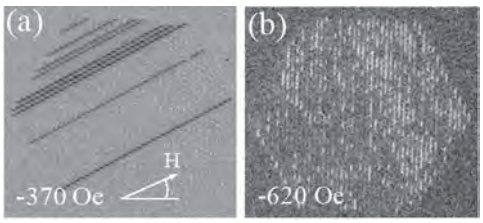

Selected sequential Kerr microscopy images during the magnetization reversal process. TheMx domain images (a)and My domain image (b) at different field strength

M6-03. Features of Magnetization Reversal of $Fe_{10}Ni_{90}$/Ti/(R-Co) (R = Gd, Dy) Films. *O.A. Adanakova*[1], E. Kudyukov[1], K. Balymov[1], A. Rusalina[1] and V. Vas'kovskiy[1,2] *1. Ural Federal University named after the first President of Russia B.N. Yeltsin, Ekaterinburg, Russian Federation; 2. M.N. Mikheev Institute of Metal Physics UB RAS, Ekaterinburg, Russian Federation*

Layers structuring is one of the effective methods of regulating the exchange interaction of heterogeneous magnetic layers, which, in turn, sets the specifics of the magnetization reversal of multilayered films, including the presence and the magnitude of the so-called exchange bias [1, 2]. This work is devoted to studying the features of the formation of interlayer interaction in the (Fe-Ni)/Ti/(R-Co) (R = Gd, Dy) film structures, where Fe-Ni is a polycrystalline ferromagnetic layer, R-Co is a structurally amorphous ferrimagnetic layer, and Ti is a paramagnetic spacer of variable thickness. The film samples were obtained on glass substrates by high-frequency ion-plasma sputtering of homogeneous (Fe-Ni, Ti) and mosaic (Gd-Co or Dy-Co) targets at the presence of an external magnetic field of 170 Oe. The nominal thicknesses of the Fe-Ni and R-Co layers were 50 and 110 nm, respectively. The thickness of the Ti spacer varied within $L = 0–1.3$ nm. The iron content in the ferromagnetic layers corresponded to 10 at.%. The concentration of rare-earth metal in the ferrimagnetic layers was 26–30 at.%. To analyze the magnetic properties, we used the measurements of hysteresis loops performed on a LakeShore 7407 VSM vibrating magnetometer. Figures 1 and 2 show the hysteresis loops $m(H)$ demonstrating the features of the magnetization reversal of individual layers in the considered film structures. It was found that at $L < 0.8$ nm, the joint magnetization reversal of the interacting layers, which is the result of a strong interlayer exchange coupling, takes place (Fig. 1(a), 2(a)). With an increase in L, the interlayer interaction weakens and the described peculiarity of the magnetization reversal process disappears (Fig. 1(b), 2(b)), however, for samples with Dy-Co, an exchange bias of the hysteresis loops of the Fe-Ni ferromagnetic layer begins to be observed. The work has been financially supported by the RSF grant, project no. 18-72-10044.

1. W. H. Meiklejohn and C. P. Bean, Phys. Rev. 102, 1413–1414 (1956). 2. F. Radu and H. Zabel, *Springer Tracts in Modern Physics* 227 (Springer, Berlin Heidelberg, 2008), pp. 97–184.

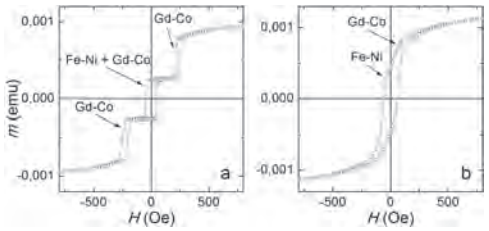

Fig. 1. Hysteresis loops measured at room temperature for the $Fe_{10}Ni_{90}$/Ti(*L*)/(Gd-Co) film samples with various *L*: without a spacer (a), 0.9 nm (b)

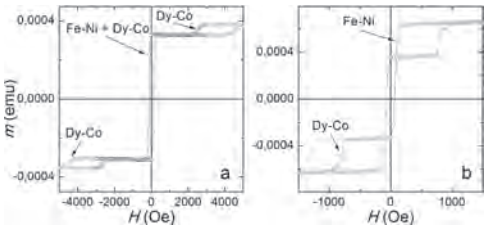

Fig. 2. Hysteresis loops measured at room temperature for the $Fe_{10}Ni_{90}$/Ti(*L*)/(Dy-Co) film samples with various *L*: without a spacer (a), 0.8 nm (b)

M6-04. The Structural, Magnetic, and Electrical Properties of Cubic Mn_3Ga. *H. Bang*[1] and M. Jung[1] *1. Sogang University, Mapo-gu, The Republic of Korea*

Manganese based Heusler materials has attached much attention due to its exotic properties. Mn_3Ga possesses a wide variety of properties depending on its crystalline structure. Magnetically, the tetragonal Mn_3Ga is a ferrimagnet, and the hexagonal and cubic Mn_3Ga are antiferromagnetic. The tetragonal Mn_3Ga has been extensively studied due to the high spin polarization, strong perpendicular magnetic anisotropy, and low saturation magnetization, which suit the need for spintronics applications. Recently, the cubic and hexagonal Mn_3Ga have received attention due to their interest in antiferromagnets. Especially, the cubic Mn_3Ga is theoretically predicted to be a half-metallic antiferromagnet. In the present work, we first report the experimental results on metastable cubic phase of Mn_3Ga thin films. The samples were deposited by RF magnetron sputtering on MgO(001) substrates. X-ray diffraction and transmission electron microcopy data show that the cubic phase Mn_3Ga is grown heteroepitaxially on the MgO substrate. The cubic Mn_3Ga exhibits antiferromagnetic magnetic ordering at the Neel temperature of $T_N \sim 420$ K. The electrical resistivity represents half-metallic behavior. These results are compared with simple metallic behavior of tetragonal Mn_3Ga with ferromagnetic order at $T_C \sim 820$ K.

M6-05. Fine-Tuned Perpendicular Magnetic Anisotropy of Co-Doped Mn_3Ga Thin Films. *W. Yoo*[1] and M. Jung[1] *1. Sogang University, Mapo-gu, The Republic of Korea*

Mn_3Ga has been proposed as a promising material for possible applications of spintronics because of high perpendicular magnetic anisotropy ($K_U \sim 1.0$ MJ/m^3), low saturation magnetization ($M_S \sim 0.1$ MA/m), high Curie temperature ($T_C \geq 700$ K), and high spin polarization ($P \sim 88$ %). To increase the prospect for the application, however, there are challenging issues to reduce its high its high coercivity ($H_C \sim 19$ kOe) and solve the problem related with lattice mismatch (~ 6%) between Mn_3Ga film and MgO substrate. Recently, transition metal doped Mn_3Ga has been investigated for tuning the electronic and magnetic properties while retaining their advantages. Among them, we focus on Co-doped Mn_3Ga ($Mn_{3-x}Co_xGa$) thin films showing a crystal

structure transition from tetragonal to cubic and simultaneously a magnetic change from ferrimagnetism with perpendicular magnetic anisotropy (PMA) to ferromagnetism with in-plane magnetic anisotropy (IMA). As finely tuning x, we could adjust the H_C and M_S values. At the critical composition of structural and magnetic transition, H_C is abruptly reduced to 1.2 kOe while retaining PMA and the lattice mismatch is lowered about 4.7%. These results are attributed to the decreasing ratio of Mn-Mn antiparallel coupling and the increasing ratio of Mn-Co parallel coupling, leading to a slight increment of saturation magnetization.

M6-06. Correlation of Strains and Interfacial DMI in Symmetric Epitaxial Pd/Co/Pd(111) Thin Films. *A.G. Kozlov*[1], N. Sarnavskii[1] and A. Davydenko[1] *1. School of natural sciences, Dal'nevostocnyj federal'nyj universitet, Vladivostok, Russian Federation*

In this work, we investigate the influence of interface parameters on the interfacial Dzyaloshinskii-Morya interaction (DMI) of symmetric Si(111)/Cu(2 nm)/Pd(d_{Pd1} 0-3 nm)/Co(0,7 nm)/Pd(d_{Pd2} 0-3 nm) epitaxial films with different thicknesses of Pd underlayer (d_{Pd1}) or top layer (d_{Pd2}). The lattice parameters of bulk Pd and Co materials are mismatched by about 9,7%, which leads to the appearance of significant elastic strains on the interfaces. Investigation of the DMI was performed by means of the observation of domain walls displacement in a combination of in-plane and out-of-plane magnetic fields using Kerr-microscope. H_{DMI} was determined by the minimum in the domain wall velocity dependencies on in-plane magnetic fields [1]. Lattice mismatch between the Pd underlayer and bulk Co is small at small thicknesses of Pd underlayer, but it rapidly increases with increase of the Pd thickness. Due to the small thickness of Co, the strains in Co layer at the upper interface do not completely disappear as shown in Fig.1. Based on the results of previous works [2, 3], we assume that the roughnesses of the top and bottom interfaces change insignificantly in the selected thickness range (d_{Pd} = 0-3 nm) therefore, we consider that the change in roughness does not responsible for the change in DMI field, as shown in Fig.2. The increasing strains asymmetry on the top and bottom interfaces contributes to a sharp increase in H_{DMI} at d_{Pd} thicknesses from 0.2 to 1 nm, after which it does not change significantly. In this way, H_{DMI} dependencies on d_{Pd1} correlates perfectly with the behavior of elastic strains on the top and bottom interfaces. Replacing the upper Co/Pd interface to Co/Cu leads to a significant decrease in investigating magnetic parameters, which indicates that the upper Co/Pd interface plays a important role in effective DMI in the investigated system. The reported study was partially funded by RFBR under the Research Projects No. 18-32-20057 and the Russian Ministry of Science and Higher Education (the state task 0657-2020-0013)

[1] S. G. Je et al. Phys. Rev. B 88, 214401 (2013) [2] A. V. Davydenko et al. *Phys. Rev. B* 95, 064430 (2017) [3] A.V. Davydenko et al. Appl. Surf. Sci. 384, 406 (2016)

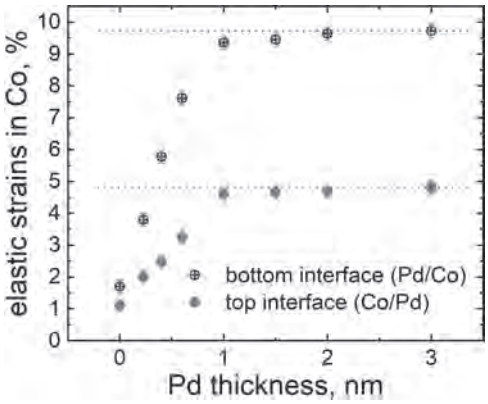

Fig.1. Dependencies of the strains in bottom Pd/Co and top Co/Pd interfaces on the Pd underlayer thickness

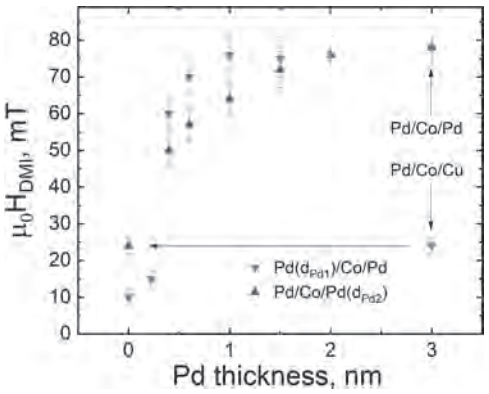

Fig.2. DMI-field as a function of the underlayer and top layer Pd thicknesses

M6-07. Above Room-Temperature Ferromagnetism in Wafer-Scale two-Dimensional van der Waals Fe_3GeTe_2 Tailored by Topological Insulator. *T. Nie*[1], H. Wang[1], Y. Liu[1], P. Wu[1] and W. Hou[1] *1. School of Microelectronics, Beihang University, Beijing, China*

Since the discovery of single-layer graphene in 2004, two-dimensional (2D) van der Waals (vdW) materials represented by it have demonstrated excellent electrical, magnetic, mechanical and optical physical properties under the structure of one or several layers of atomic thickness[1]. Based on these superior properties, 2D-layered vdW ferromagnetic materials have become the basis for constructing low-dimensional spintronics devices[2], in which Fe_3GeTe_2 (FGT)[3], $Cr_2Ge_2Te_6$[4] and CrI_3[5] as the main representative materials exhibit strong perpendicular magnetic anisotropy and other important characteristics in single layer. However, the Curie temperature (T_c) of above materials has not reached room temperature yet, which has greatly hinderer the subsequent development for device application. Therefore, recently researchers have been committed to explore 2D vdW ferromagnetic materials for room-temperature T_c in both theory and experiment. Here, we report that the interfacial engineering effect could effectively increase the T_c of the 2D vdW ferromagnetic material FGT from 230 K to 400 K, through heteroepitaxy with topological insulator of Bi_2Te_3. A theoretical calculation was further carried out to describe the magnetic properties by using first-principles calculations and the self-consistent Hubbard U approach (DFT+Uscf) together with the Monte Carlo (MC) simulations. After combination with Bi_2Te_3, the intralayer interactions in FGT was calculated to dramatically increase compared to that in pure FGT, well explaining the T_c enhancement. Our results may open up a new door to benefit the magnetic order in the 2D limit and realize spintronic devices based on 2D-layered vdW ferromagnetic materials with room temperature performances towards industrialization.

1. Geim, A. K.; Novoselov, K. S. The Rise of Graphene. *Nat. Mater.* 2007, *6* (3), 183–191. 2. Lin, X.; Yang, W.; Wang, K. L.; Zhao, W. Two-Dimensional Spintronics for Low-Power Electronics. *Nat. Electron.* 2019, *2* (7), 274–283. 3. Liu, S.; Yuan, X.; Zou, Y.; Sheng, Y.; Huang, C.; Zhang, E.; Ling, J.; Liu, Y.; Wang, W.; Zhang, C.; Zou, J.; Wang, K.; Xiu, F. Wafer-Scale Two-Dimensional Ferromagnetic Fe3GeTe2 Thin Films Grown by Molecular Beam Epitaxy. *npj 2D Mater. Appl.* 2017, *1* (1), 30. 4. Gong, C.; Li, L.; Li, Z.; Ji, H.; Stern, A.; Xia, Y.; Cao, T.; Bao, W.; Wang, C.; Wang, Y.; Qiu, Z. Q.; Cava, R. J.; Louie, S. G.; Xia, J.; Zhang, X. Discovery of Intrinsic Ferromagnetism in Two-Dimensional van Der Waals Crystals. *Nature* 2017, *546* (7657), 265–269. 5. Huang, B.; Clark, G.; Navarro-Moratalla, E.; Klein, D. R.; Cheng, R.; Seyler, K. L.; Zhong, D.; Schmidgall, E.; McGuire, M. A.; Cobden, D. H.; Yao, W.; Xiao, D.; Jarillo-Herrero, P.; Xu, X. Layer-Dependent Ferromagnetism in a van Der Waals Crystal down to the Monolayer Limit. *Nature* 2017, *546* (7657), 270–273.

M6-08. Growth-Field-Induced Magnetic Anisotropy in Sputtered Amorphous CoAlZr-SmCoTi Artificially Layered Structures. P. Rani[1], P.E. Jönsson[1] and *G. Andersson[1] 1. Department of Physics and Astronomy, Uppsala University, Uppsala, Sweden*

We have investigated amorphous CoAlZr-SmCoTi bilayers and multilayers deposited in an external magnetic field of around 0.1 T, applied along one edge of the square MgO substrate. This growth field induces a magnetic anisotropy in the layered structure, which may be useful in applications such as magnetism-based sensors, permanent magnets, spintronic and magnetic recording devices. Combining a hard magnetic rare-earth-transition metal alloy (SmCoTi) with a soft magnetic phase (CoAlZr) in a nanocomposite may enhance the ferromagnetic properties desirable for e.g. permanent magnet materials, while further decreasing the rare-earth content. In this study we investigated the impact of different interface densities, i.e. varying the number of CoAlZr-SmCoTi bilayer repetitions within a constant total film thickness of 20 nm. The samples had 1, 5 and 10 repetitions with individual layer thickness 10 nm, 2 nm and 1 nm, respectively, with the CoAlZr and SmCoTi layers equally thick in each case. Structural properties of the samples were investigated by GIXRD and XRR, confirming the samples to be amorphous with smooth interfaces. From MOKE and SQUID magnetometry, it was concluded that the interfaces are strongly coupled to each other in all the samples, and that the growth field imprints a uniaxial in-plane anisotropy in the samples (see figure 1). The coercivity is observed to increase with increasing interface density. The magnetic moment and element specific M-H loops of Co and Sm were investigated in detail using x-ray magnetic circular dichroism, which also showed that Ti remains non-magnetic.

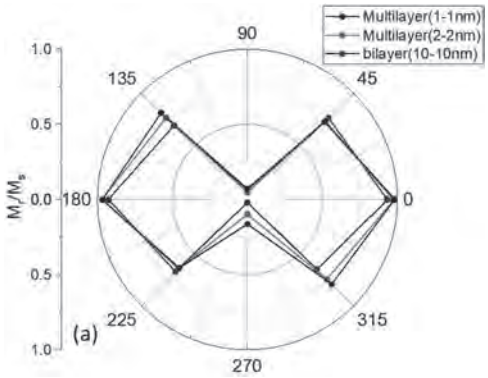

Fig. 1: In-plane polar plot of the normalized remanence M_r/M_s, as obtained from longitudinal MOKE at room temperature. The angle is defined with respect to one sample edge, with zero degrees along the direction of the growth field. All three samples have similar anisotropy.

M6-09. Investigation of Magnetic Anisotropy of Ultrathin Co Films Growth on Au(788) Vicinal Surface. *R.J. Rosa*[1], G. Gomes[2], R. Souza[1] and M. Martins[1] *1. Centro de Desenvolvimento da Tecnologia Nuclear, Belo Horizonte, Brazil; 2. Universidade Estadual de Montes Claros, Montes Claros, Brazil*

The origin of magnetic anisotropy in low-dimensional systems has been explored due to a series of promising questions raised in systematic studies [1]. Some of these questions are the relationship between the intrinsic anisotropy mechanism that contribute to in-plane magnetic anisotropy (IMA) and perpendicular magnetic anisotropy (PMA) [2]. In this work, we investigated the structural and magnetic properties of epitaxial ultrathin films of cobalt grown on the vicinal surface Au(788). The aim was to determine the influence of the regular arrangement of atomic steps, typical of a vicinal surface, on the magnetic anisotropy of the system Co/Au(788). The samples were prepared at room temperature under molecular beam epitaxy (MBE) conditions and characterized using the experimental techniques XPS, LEED, STM and MOKE. Initially a study of the magnetic anisotropy as a function of the Co film thickness was carried out by means of in situ MOKE measurements, in the polar and longitudinal geometries. The results showed that the easy axis of magnetization is out of plane for Co film thickness up to 13 ML of Co, when a spin reorientation transition takes place, causing the easy axis of magnetization to reorient to the plane of the film. From the values of the anisotropy field as a function of the thickness of the Co film on Au(788), it was determined the values of contributions to the effective magnetic anisotropy constant. The in-plane magnetic anisotropy of Co films with thickness of 15 and 20 ML coated with a protective layer of Au of 20 ML was characterized by ex situ LMOKE and VSM. The analysis of ex situ LMOKE measurements as a function of the orientation of applied external field (angle of rotation) indicates a uniaxial magnetic anisotropy in the plane of the film of Co/Au(788) for thickness greater than 13 ML, with easy axis of magnetization oriented along the direction parallel to the atomic steps of the Au(788) vicinal surface and hard axis oriented along the direction perpendicular to the atomic steps.

[1] T. Koide et al., Journal of Physics: Conference Series 502 (2014) 012002. [2] G. Shibata et al., Quantum Materials 3 (2018) 3.

M6-10. $NiCo_2O_4$ Thin Films Prepared by Reactive Molecular Beam Epitaxy and Annealing Under High-Pressure Oxygen Atmosphere. A. Tsujie[1], Y. Hara[1], T. Yanase[2], T. Shimada[2] and *T. Nagahama[2] 1. CSE, Hokkaido University, Sapporo, Japan; 2. Graduate School of Engineering, Hokkaido University, Sapporo, Japan*

The development of new oxide materials is an important issue for spintronics. Some properties such as half-metal properties expected to Fe_3O_4 [1] and perpendicular magnetic anisotropy observed in $CoFe_2O_4$ [2] are important for spintronics. Recently, $NiCo_2O_4$ (NCO) has attracted attention because of its electrical conductivity and perpendicular magnetic anisotropy [3]. In order to exhibit such characteristics, it is necessary to form a film in a high oxygen partial pressure, therefore PLD is mainly used for deposition. In this study, we conducted the fabrication of the films by the reactive MBE method in order to expand the choices of sample preparation and the possibility of new functions. In MBE, the oxygen partial pressure during the deposition is limited, therefore the oxygen partial pressure during the annealing is inevitable. The film was formed by a reactive MBE method at the substrate temperature of 373K, and the oxygen partial pressure of $4x10^{-4}$Pa, and then, it was transported to the load-lock chamber without breaking the vacuum. The thermal treatment was conducted at 773K in an oxygen partial pressure of $4x10^{-4}$ to 150 Pa. Fig. 1 shows the XRD profiles for each oxygen partial pressure. It was found that the crystal structure changed from rock-salt type to spinel with increasing oxygen partial pressure. These results were consistent with RHEED and STEM observations. In the cross-sectional STEM image, it was observed that the film was clearly divided into rock-salt and spinel-type domains. Fig. 2 shows the temperature dependence of electrical resistivity. The film formed at low oxygen partial pressure had high resistance. The films prepared at high oxygen partial pressure showed electrical conductivity, although, the temperature dependence was semiconductive. These results and the magnetic measurements imply that the rock-salt NCO is a nonmagnetic or antiferromagnetic insulator, and the spinel NCO is ferromagnetic or ferrimagnetic conductivity. The control of the two phases is key to obtain functional NCO films.

[1] A. Yanase and K. Siratori, J. Phys. Soc. Jpn. 53, 312 (1984). [2] T. Niizeki, Y. Utsumi, R. Aoyama, H. Yanagihara, J-I Inoue, Y. Yamasaki, H. Nakao, K. Koike, and E. Kita, Appl. Phys. Lett. 103, 162407 (2013). [3] A. Tsujie *et al.*, *Appl. Phys. Lett.* 116, 232404 (2020), and references therein.

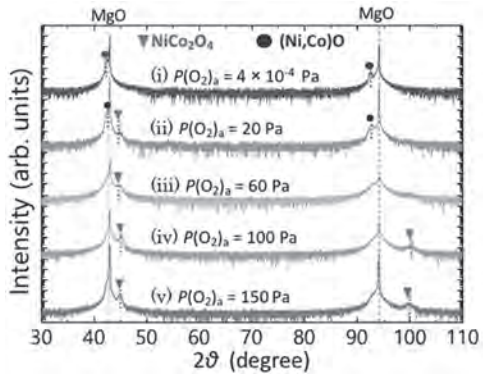

Fig.1 XRD 2θ/θ scans of the NCO films with various annealing O_2 pressure.

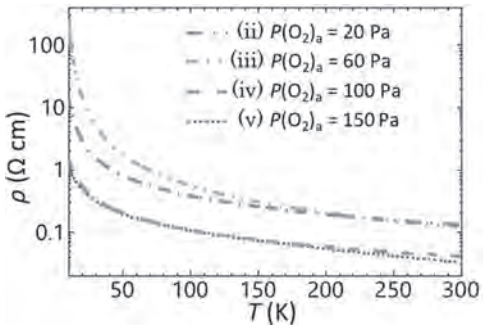

Fig.2 Temperature dependence of resistivity of NCO films annealed with various O_2 pressures.

M6-11. Tuning of Perpendicular Magnetic Anisotropy in $Ta/Co_xFe_{80-x}B_{20}/MgO$ With Varying Fe Content. *R.S. Yadav*[1], A. Kumar[1], K. Khan[1] and P.K. Muduli[1] *1. Department of Physics, Indian Institute of Technology Delhi, New Delhi, India*

Perpendicular magnetic anisotropy [PMA] in multilayers [1] plays a key role in various spintronic applications and is widely utilized in magnetic tunnel junctions [2] for high density applications. Recent studies suggest that the heavy metal (HM) having large spin-orbit coupling strength (SOC) can promote perpendicular magnetic anisotropy in the HM/FM/Oxide structures due to the interfacial magnetic anisotropy [3]. From the recent theoretical calculation, the origin of PMA in FM/Oxide heterostructures is attributed to the overlap between O-2p orbitals and transition metal 3d orbitals [4]. Hence, the ferromagnetic content is expected to play a crucial role in determining the PMA. Here, we studied the strength of PMA in $Ta/Co_xFe_{80-x}B_{20}/MgO$ heterostructures with varying Fe content for x=20 and 40. We use DC and RF magnetron sputtering for the deposition of Ta, CoFeB and MgO layers on the Silicon substrate. Here we have use the $Ta(5)/Co_xFe_{80-x}B_{20}(1.2)/MgO$ (2.5)/Ta (3) multilayers (nominal thickness in nm) with varying Fe content of x=20 and x=40. After deposition, the multilayers were annealed under high vacuum conditions at 300for one hour to enhance the perpendicular magnetic anisotropy [5]. The PMA properties can be investigated using out-of-plane M-H measurements, polar-magneto-optical Kerr effect (p-MOKE) measurements and anomalous Hall effect (AHE) measurement. Here, we have used p-MOKE and the AHE measurements for the study of PMA strength in our samples. The Hall effect in the ferromagnets consists of two terms, one is the ordinary Hall effect and another is the AHE. As shown in Fig. 1, the AHE measurement shows that the magnetization of the CoFeB (1.2 nm) layer stabilizes along the out-of-plane direction. We have found a squared shape of out-of-plane AHE hysteresis loops for Fe content x=40, which confirm the presence of larger PMA strength for x=40 compared to x=20 (as shown in Fig.1). This study provides a pathway to tune the PMA strength by varying FM content, which is useful for the storage devices.

[1] P.F. Carcia, et al, Appl. Phys. Lett., 47,178(1985) [2] S. Ikeda, et al. Nature Mater 9, 721–724 (2010). [3] M T Johnson. et al. Rep. Prog.59, 1409-1458, (1996) [4] H.X. Yang, et al., Phys. Rev.B 84, 054401 (2011). [5] Gweon, et al. Sci Rep 8, 1266 (2018)

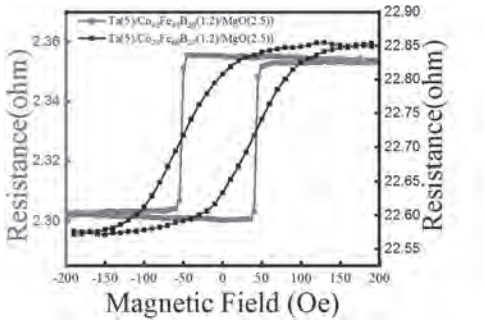

Figure1: Anomalous Hall resistance vs out-of-plane magnetic field

M6-12. From Bulk Frustrated Magnetism to Magnetic Long-Range Order in Thin Films of Double Perovskite Compound $BaTi_{1/2}Mn_{1/2}O_3$. *R.P. Amaral*[1], R.L. Serrano[1] and P. Schio[2] *1. Federal University of Uberlândia, Uberlândia, Brazil; 2. Laboratorio Nacional de Luz Sincrotron, Campinas, Brazil*

The disordered double perovskite $BaTi_{1/2}Mn_{1/2}O_3$ (BTMO) [1,2] presents a spin-glass ground state which stems from a disordered lattice of orphan spins and trimers [3]. Neutron diffraction measurements revealed no magnetic Bragg peaks down to 3.6 K [2], while no static magnetism was observed down to 19 mK with zero-field μ+ relaxation rate [3]. In the hexagonal 12R-type structure, the transition metals distribute themselves along corner- and face-shared octahedral sites following the distribution proposed in refs. [1,2]. All the physics investigated so far have been observed in polycrystalline bulk samples of BTMO. In this work, we show the preliminary investigation of thin-film samples of BTMO grown over $SrTiO_3$ (STO-[001]) substrate by using the pulsed laser deposition technique. The growing conditions were changed by varying the environment pressure, target/substrate distance, the substrate temperature, and laser fluence. We observed a weak ferromagnetic response in the magnetization data for all the measured temperatures (Fig. 1). The saturation moment increases with lowering the temperature. X-ray diffraction data shows that BTMO growths epitaxially on STO along the [001] direction. X-ray photoemission spectroscopy reveals that Mn occupies two different crystallographic sites, as observed in bulk samples. X-ray absorption spectroscopy data as a function of temperature and light polarization at the Mn $L_{2,3}$-edges qualitatively confirm a larger population of Mn_{4+} oxidation state coexisting with Mn^{3+} ions (Fig. 2). The Mn population ratio changes with the growing parameters. We discuss the magnetic ground state observed. We will also argue about the expected lattice strain field created on the thin films by the matching process to the substrate. The latter could be indeed responsible for the formation of different atomic stacking orders associated with twinning and (or) stacking faults, which could induce different BTMO polytypes.

[1] G. M. Keith, *et al.*, Chem. Mater. 16, 2007 (2004). [2] F. A. Garcia *et al*. Phys. Rev. B 91, 224416 (2015). [3] M. A. Cantarino *et al*. Phys. Rev. B 99, 054412 (2019).

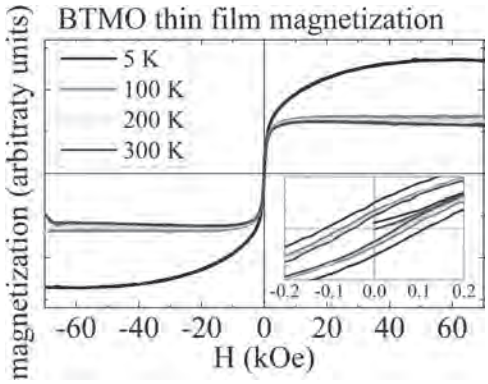

Magnetic field dependent magnetization data at 5, 100, 200 and 300 K. Saturation increases with lowering temperature.

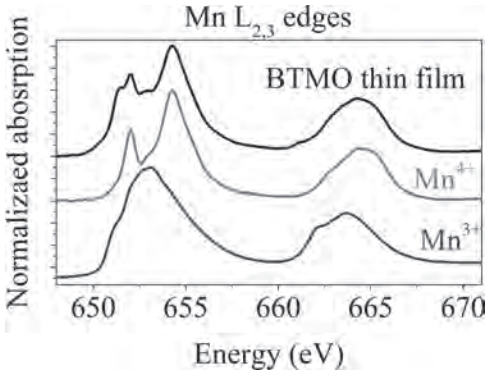

Mn $L_{2,3}$ absorption edges of BTMO thin film (black), BTMO bulk (red) and Mn_2O_3 (blue). Data was measures in Total Electron Yield mode in powder samples.

Session N1
SKYRMIONS II

Mathias Klaui, Co-Chair
Universität Mainz, Mainz, Germany
Guoqiang Yu, Co-Chair
Institute of Physics, Los Angeles, CA, United States

INVITED PAPER

N1-01. Chiral and Achiral Magnetic Spin Textures in Fe/Gd Multilayers. *S. Montoya*[1] *1. Naval Information Warfare Center Pacific, San Diego, CA, United States*

In recent years, topological materials have become very attractive due to their potential to realize a new generation of low dissipation, high sensitivity, high speed and low cost sensor and information technologies. For instance, the ability to design magnets that exhibit spin textures with local and/or global chiral order (e.g. chiral magnets) provides a pathway to build novel logic, memory and storage devices that exploit chiral domain walls [1] and/or skyrmions [2]. Commonly, chiral magnets are achieved by the presence of a sizeable Dzyaloshinskii-Moriya (DM) exchange interaction that arises in non-centrosymmetric bulk magnets or ferro(i)magnetic thin-film heterostructures with asymmetric interfaces that possess high-spin orbit coupling. The discovery, design and optimization of chiral magnets with tailored spin textures and properties continues to be a subject of intense research. In this talk, I will cover recent contributions to stabilize, design and manipulate chiral and achiral magnetic spin textures in Fe/Gd-based multilayers [3-7]. First, I will demonstrate that competing dipole and domain wall energy can result in the formation of sub-100-nm skyrmions, bi-skyrmions and bubbles in Fe/Gd multilayers with centrosymmetric symmetry [3-6]. Given the lack of DM interactions, skyrmions with two possible helicities are energetically favorable. Using transmission- and surface-sensitive microscopy techniques, I will show these dipole skyrmions possess a complex 3D hybrid structure with Bloch- and Néel-components. Dipole skyrmions befall a category of local chiral order and global achiral order. On the second part of my talk, I will focus on recent works exploring the domain states and electromagnetic properties of Fe/Gd-based multilayers modified to introduce weak DM interactions. By carefully designing the Fe/Gd-based multilayers, we can achieve a coexistence of opposite helicity chiral magnetic spin textures with unequal population distribution [7]. Figure 1 shows a post-processed LTEM image depicting the domain states with asymmetric population of left and right-chiral Block-lines. Unlike traditional field-reversal in achiral and chiral magnets, I will show the domain morphology in these Fe/Gd-based multilayers dramatically rearranges under applied perpendicular magnetic fields. Furthermore, I will demonstrate these field-dependent domain states result in novel transport signatures. Acknowledgment: This work was done in collaboration with J. A. Brock[1,2], J. J. Chess[3], S. Couture[1,2], J. C. T. Lee[3,4], H. Gulati[3], S. K. Sinha[5], P. Fischer[4], M.-Y. Im[4], S. D. Kevan[3,4], V. Lomakin[1,2], S. Roy[4], B. J. McMorran[3], and E. E. Fullerton[1,2],[1]Center for Memory and Recording Research, University of California San Diego, CA 92093, USA, [2]Department of Electrical and Computer Engineering, University of California San Diego, CA 92093, USA, [3]Department of Physics, University of Oregon, OR 97401, USA, [4]Center for X-ray Optics, Lawrence Berkeley National Laboratory, CA 94720, USA, [5]Department of Physics, University of California San Diego, CA 92093, USA, and was supported by the U.S. Office of Naval Research, ILIR program.

[1] G. Chen et al, Nat. Comm. 4, 2671 (2013). [2] A. Fert et al, Nat. Rev. Mater 2, 17031 (2017). [3] J. C. T. Lee *et al,* App. Phys. Lett. 109, 022402 (2016). [4] S. A. Montoya *et al,* Phys. Rev. B 95, 024415 (2017). [5] S. A. Montoya *et al,* Phys. Rev. B 98, 104432 (2018). [6] R. D. Desautels et al, Phys. Rev. Mater. 3, 104406 (2019). [7] S A Montoya *et al*, Preprint (2020).

Figure 1. Postprocessed LTEM image depicts the zero-field domain morphology of an [Fe/Gd/Fe/Pt/Ir]x40 multilayer at T = 160K. Right-chiral Bloch-lines appear as blue-hue lines and left-chiral Bloch-lines are shown as orange-hue lines, while the positive/negative perpendicular magnetization is depicted as gray/black features.

CONTRIBUTED PAPERS

N1-02. Skyrmion Breathing Modes in Synthetic Ferri- and Antiferromagnets. *M. Lonsky*[1] and A. Hoffmann[1] *1. Materials Science and Engineering, University of Illinois at Urbana-Champaign, Urbana, IL, United States*

Magnetic multilayers can combine strong spin-orbit interaction with lacking inversion symmetry, which may give rise to the presence of topologically nontrivial spin textures, so-called magnetic skyrmions. Recent studies have indicated strongly enhanced propagation velocities of skyrmions in antiferromagnets and compensated ferrimagnets [1]. At the same time, it is unclear how magnetic compensation may affect dynamic excitations of magnetic skyrmions, such as breathing modes, which entail an oscillation of the skyrmion size at GHz frequencies [2]. Here, we present comprehensive micromagnetic simulations of these resonance modes in synthetic ferri- and antiferromagnets that are excited by either out-of-plane radiofrequency magnetic fields or spin torques. The observed features in the calculated power spectra exhibit a systematic dependence on the strength of the RKKY-like antiferromagnetic coupling between the individual magnetic layers and are related to pure in-phase and anti-phase breathing modes as well as to hybridizations of breathing and spin wave modes that are characteristic for the considered circular-shaped geometry [3]. As a simplified classical analog, the coupled skyrmion breathing modes can be viewed as two harmonic oscillators that are connected by a spring. The experimental detection

of these resonant oscillation modes may provide a means for skyrmion sensing applications and for the general characterization of skyrmion states in multilayer stacks with antiferromagnetic interlayer exchange coupling. This work is supported by the Deutsche Forschungsgemeinschaft (DFG) through the research fellowship LO 2584/1-1.

[1] L. Caretta, M. Mann, F. Büttner, K. Ueda, B. Pfau, C. M. Günther, P. Hessing, A. Churikova, C. Klose, M. Schneider, D. Engel, C. Marcus, D. Bono, K. Bagschik, S. Eisebitt, and G. S. D. Beach, Nat. Nanotechnol. 13, 1154-1160 (2018) [2] M. Garst, J. Waizner, and D. Grundler, J. Phys. D: Appl. Phys. 50, 293002 (2017) [3] M. Lonsky, and A. Hoffmann, arXiv:2006.11318 (2020)

N1-03. Ferromagnetic Resonance of Skyrmions in Thin Film Multilayers. *T. Srivastava*[1,2], I. Ngouagnia[2], Y. Sassi[1], F. Ajejas[1], A. Vecchiola[1], K. Bouzehouane[1], N. Reyren[1], V. Cros[1], H. Hurdequint[2], J. Kim[3], T. Devolder[3] and G. de loubens[2] *1. Unité Mixte de Physique, CNRS, Thales, Université Paris-Saclay, 91767 Palaiseau, France; 2. SPEC, CEA-Saclay, CNRS, Université Paris-Saclay, 91191 Gif-sur-Yvette, France; 3. Centre for Nanoscience and Nanotechnology, CNRS, Université Paris-Saclay, 91120 Palaiseau, France*

The observation of magnetic skyrmions at room temperature has triggered extensive research to decipher their various static and dynamic properties for potential applications in memory and logic devices [1]. In the case of ultra-thin multilayer films consisting of heavy metal_(HM)/ferromagnet_(FM)/insulator_(I), skyrmions are primarily stabilized by interfacial Dzyaloshinskii-Moriya interaction in combination with: perpendicular anisotropy, dipolar, exchange and Zeeman energies, where each of these contributions can be finely tuned [2]. Owing to their non-trivial topology, skyrmions are theoretically shown to exhibit unique spectral signatures when excited by an RF magnetic field [3], opening up new prospects for skyrmion-based devices [4,5]. However, the experimental observation of their excitation modes is challenging due to usually elevated damping parameters and material inhomogeneities in sputtered HM/FM/I systems. Here we study the magnetization dynamics in a [Pt/CoFeB/AlOx]×20 multilayer deposited by sputtering. First, the system is optimized by tuning the Pt and CoFeB thicknesses to host magnetic skyrmions at room temperature, along with a minimized damping parameter $\alpha \sim 0.02$, measured by ferromagnetic resonance (FMR). The static magnetic domain configuration is observed by magnetic force microscopy where on sweeping the field from saturation (0.4 T) to zero, random skyrmion nucleation occurs forming a lattice structure which then breaks into a mixture of skyrmions and stripes at lower fields finally transforming into labyrinthine domains. The dynamic response of the system is measured by broadband FMR over a frequency range of 0.5-20 GHz, with an out-of-plane magnetic field swept over ± 0.6 T. The frequency-field dispersions show several resonant modes corresponding to the domain configurations observed by MFM at the respective applied fields. At fields above the saturation, the well-known Kittel mode is observed, pertaining to uniform precession. Below saturation, distinct modes arise in the resonance spectrum with both positive and negative dispersions, indicating the spectroscopic signatures corresponding to: randomly distributed skyrmions, skyrmion lattice, skyrmion-stripe mix, labyrinthine domains.

[1] A. Fert *et al.*, Nat. Rev. Mater. 2, 17031 (2017) [2] W. Legrand *et al.*, Sci Adv 4, 7, (2018) [3] J.-V. Kim, *et al.*, Phys. Rev. B 90, 064410 (2014) [4] G. Finocchio *et al.*, Appl. Phys. Lett. 107, 262401 (2015) [5] F. Garcia-Sanchez *et al.*, New J. Phys. 18, 075011 (2016)

N1-04. Skyrmion Generation by Ionic Liquid Gating in Ultra-Thin Films. *Y. Zhang*[1,2], G. Dubuis[1,2] and S. Granville[1,2] *1. Robinson Research Institute, Victoria University of Wellington, Wellington, New Zealand; 2. MacDiarmid Institute for Advanced Materials and Nanotechnology, Wellington, New Zealand*

Magnetic skyrmions are topologically protected whirling spin textures, which can be used as information carriers and have a potential application for spintronics, like skyrmion-based racetrack magnetic memory [1]. In thin films, skyrmions can be stabilized by the competition of different kind of interactions, like Heisenberg exchange interaction, magnetic anisotropy and Dzyaloshinskii-Moriya interaction (DMI). Recently, skyrmions have been generated by an electrical field applied on dielectric thin films [2-4]. But, to achieve a large gating effect, a high gate voltage must be applied. Ionic liquid gating using ionic liquids or ion gels has been demonstrated as a powerful method to effectively control the magnetic anisotropy with a low voltage since an ultra-high electric field is generated at the electric double layer interface between ions and electron conductors [5]. However, there is no evidence that shows skyrmions can be generated by ionic liquid gating. We have investigated the magnetic anisotropy and domain structures of $MgO/Mn_2CoAl/Pd$ ultra-thin films [6] at various gate voltages. This structure shows clear perpendicular magnetic anisotropy in its original state. By applying positive gate voltage $V_G = 1.5$ V, the coercive field can be slightly increased. On the other hand, the coercive field significantly shrinks after applying negative field, as shown in Fig. 1. Domain structures at various electric field were captured by magneto-optical Kerr microscopy at ambient temperature, as shown in Fig. 2. For the original state, the magnetization is still saturated at -1 mT due to the magnetic hysteresis. After applying $V_G = -1.5$ V, these uniformly ferromagnetic states are transformed to labyrinth domains. What's more, skyrmions with ~ 900 nm size can be induced at $V_G = -2.5$ V which can be ascribed to the voltage-induced reduction of effective perpendicular magnetic energy even though the DMI constant decreases as well.

1 A. Fert *et al.*, Nature Reviews Materials 2, 17031 (2017). 2 M. Schott *et al.*, Nano Letters, 17, 3006−3012 (2017). 3 T. Srivastava *et al.*, Nano Letters, 18, 4871−4877 (2018). 4 C. Ma *et al.*, Nano Letters, 19, 353−361 (2019). 5 C. N. Senent *et al.*, APL Materials 7, 030701 (2019). 6 B. M. Ludbrook *et al.*, Scientific Reports 7, 13620 (2017)

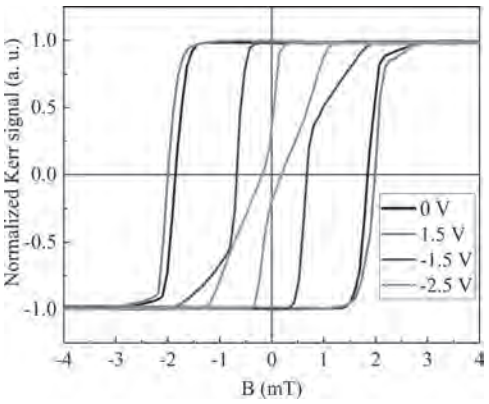

Fig. 1: Normalized Kerr signal as a function of out-of-plane field at various gate voltages for sample MgO(1.6 nm)/ Mn_2CoAl(2.6 nm)/ Pd(3.2 nm).

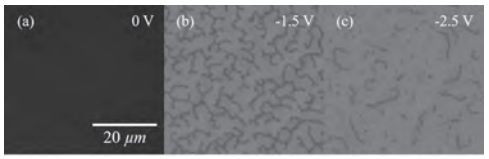

Fig. 2: MOKE images of domain structures of MgO/ Mn_2CoAl/ Pd trilayers captured with $H_z = -1$ mT at 0, -1.5, -2.5 V, respectively.

N1-05. Anisotropic Skyrmion Diffusion Controlled by Field-Induced Symmetry Breaking. *N. Kerber*[1,2], M. Weissenhofer[3], K. Raab[1], K. Litzius[1,4], J. Zázvorka[1,5], U. Nowak[3] and M. Klaui[1,2] *1. Institut für Physik, Johannes Gutenberg Universitat Mainz, Mainz, Germany; 2. Graduate School of Excellence Materials Science in Mainz, Mainz, Germany; 3. Fachbereich Phyisk, Universität Konstanz, Konstanz, Germany; 4. Department of Materials Science and Engineering, Massachusetts Institute of Technology, Cambridge, MA, United States; 5. Institute of Physics, Charles University, Prague, Czechia*

Thermally activated processes are intrinsic effects in every physical system and their understanding key to the underlaying dynamics of such systems. Using skyrmions, magnetic, topologically stabilized spin structures, we investigate the thermal diffusion dynamics in specifically tailored metal-multilayer. We find that for low pinning materials stacks, the thermal diffusion dominates the dynamics and allows for stable skyrmions at room temperature that move by thermal activation [1]. These stable Skyrmions allow for a wide range of possible applications in logic, data storage or Brownian token computing devices [2]. In Brownian circuits as well as other applications, the control of the skyrmion diffusion and the implementation of a certain control is necessary [3]. We show that by applying a magnetic in-plane field, the skyrmion diffusion becomes anisotropic with faster diffusion along the field direction and slower diffusion perpendicular to it [4]. We furthermore show that the absolute value of the applied field also controls the absolute values of the diffusion coefficients so that one can tune both the orientation of the diffusion and its strength. We can analytically and numerically explain the anisotropic diffusion due to an elliptical deformation of the skyrmions by the application of the in-plane field, which leads to a preferential diffusion axis [4].

[1] J. Zázvorka et al., Nat. Nanotech. 14, 658–661(2019). [2] F. Peper et al., ACM J. Emerg. Technol. Comput. Syst. 9, 3 (2013). [3] T. Nozaki et al., Appl. Phys. Lett. 114, 012402 (2019). [4] N. Kerber et al., arXiv:2004.07976 (2020).

N1-06. Skyrmion Dynamics in Tracks Patterned With Magnetic Anisotropy: Theory and Simulations. *S. Miki*[1,2], C. LIU[2,3], E. TAMURA[1,2], J. Cho[4], M. Goto[1,2], H. Nomura[1,2], R. NAKATANI[3] and Y. Suzuki[1,2] *1. Engineering and Science, Osaka Daigaku, Toyonaka, Japan; 2. The Center for Spintronics Research Network, Toyonaka, Japan; 3. Engineering, Osaka Daigaku, Suita, Japan; 4. Nanotechnology, Daegu Gyeongbuk Institute of Science and Technology, Daegu, The Republic of Korea*

Skyrmion has, in the last decade, attracted considerable attention for its application to novel devices. To realize the futuristic devices that will be using the skyrmion circuit, the tracks which guide the motion of skyrmions are needed. The tracks patterned with differences in the magnetic-anisotropy energy are well-paved without a potential pocket, whereas the tracks carved out of magnetic films have the potential pockets at corners due to the demagnetizing field[1]. This work aims to identify the forces acting between skyrmions and anisotropy walls of the tracks as a first step studying the dynamics of skyrmions in the tracks. The static force on a skyrmion can be expressed as minus the gradient of the potential energy caused by the magnetic-anisotropy undulation[2]. We find that the forces from the wall F_{wall} depend not only on the distance from the wall X but also on the shape of skyrmions with their radii R and domain wall widths w in Fig. 1[3]. We have also performed micromagnetic simulations where the Magnus force and the force by the magnetic-anisotropy gradient are taken into account. When these forces are in balance with F_{wall}, the values of F_{wall} are determined. The simulation results show good agreement with those calculated from the modeled skyrmions as Fig. 2[4]. The force F_{wall} has a characteristic X-dependence where a peak locates at the skyrmion radius, since the force stems mostly from the transition part of the magnetization overlapping the potential jump at X=0. The force also acts on the skyrmions that have crossed over the wall to push back them to tracks. The property might be useful to stabilize the skyrmion circuits. Another helpful feature is that the magnetic anisotropy wall does not give rise to additional friction. This research and development work was supported by the Center for Spintronics Research Network (CSRN), the ULVAC. Inc., and the MIC.

[1] Y. Jibiki *et al.*, arXiv: 1909.10130 (2019) [2] A.A. Thiele, Phys. Rev. Lett. 30, 230 (1973) [3] X.S. Wang, *et al*., Commun. Phys. 1, 31 (2018) [4] E. Tamura, *et al*., arXiv: 2005.04860 (2020)

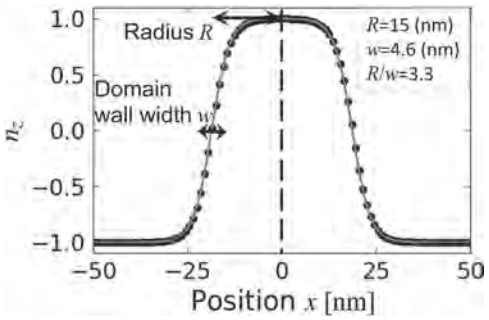

Fig. 1 The profile of a skyrmion. The dots represent the z component of the normalized magnetization obtained from the micromagnetic simulation and the curve shows the fitting function[3].

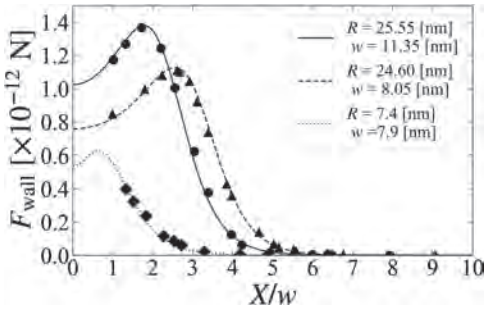

Fig. 2 The simulation (dots) and analytical results (curves) of the forces between 3 different skyrmions and walls. The curves are symmetric across X=0.

N1-07. Spin Dynamics of Skymion and Chiral Soliton Lattices in Cu_2OSeO_3 Locally Resolved by Scanning Brillouin Light Scattering. *P. Che*[1], T. Schönenberger[2], A. Kúkol'ová[1,3], A. Magrez[4], H. Berger[4], H.M. Rønnow[2] and D. Grundler[1,5] *1. Laboratory of Nanoscale Magnetic Materials and Magnonics, Institute of Materials (IMX), École Polytechnique Fédérale de Lausanne, Lausanne, Switzerland; 2. Laboratory for Quantum Magnetism, Institute of Physics, École Polytechnique Fédérale de Lausanne, Lausanne, Switzerland; 3. Laboratory of Semiconductor Materials, Institute of Materials (IMX), École Polytechnique Fédérale de Lausanne, Lausanne, Switzerland; 4. Crystal Growth Facility, Institut de Physique, École Polytechnique Fédérale de Lausanne, Lausanne, Switzerland; 5. Institute of Microengineering (IMT), École Polytechnique Fédérale de Lausanne, Lausanne, Switzerland*

Chiral magnets hosting non-collinear spin textures such as skyrmions[1] and chiral solitons lattices[2] provide novel functionality in magnonic because of the formation of bandgaps and minibands in the magnon band structures[3]. Collective excitations of magnons in bulk chiral magnets show complex resonances in the presence of multiple domains of different phases and boundary conditions. The understanding of the one-to-one correspondence between their magnonic properties and local magnetic configuration is fundamental for further design of skyrmion-based GHz devices. Here we report the local magnon modes detected by scanning Brillouin light scattering (BLS) technique in bulk Cu_2OSeO_3 (Fig. 1a) between about 10 and 60 K. Their characteristic field dependencies suggest a novel phase of a chiral soliton lattice (CSL) without additional stress applied (Fig. 1b). Pure skyrmion lattices and

a metastable skyrmion phase coexisting with other non-collinear spin structures were also identified. Our observations of locally excited magnons in Cu_2OSeO_3 deepen the understanding of the GHz dynamics of chiral magnets and pave the way for magnonic devices exploiting specific spin resonances of skyrmion hosting materials. We acknowledge the finical support from SNSF via Sinergia Network NanoSkyrmionics CRSII5 171003.

[1] S. Mühlbauer, B. Binz and F. Jonietz, etc. Science, 323, 915 (2009). [2] Y. Togawa, T. Koyama and K. Takayanagi, etc. Phys. Rev. Lett., 108, 107202 (2012). [3] M. Garst, J. Waizner and D. Grundler, J. Phys. D. Appl. Phys., 50, 293002 (2017).

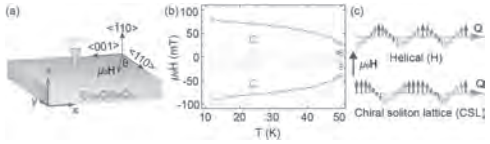

Figure 1. (a) Schematic diagram of the bulk-shape Cu_2OSeO_3 sample in a field *H*. The BLS laser is focused onto the upper surface. (b) Phase diagram obtained after zero field cooling and field *H* scanned from 140 mT to -140 mT applied along <110> direction. The phase boundaries (symbols) are extracted from the thermally excited magnons detected by BLS. The solid lines are guides to the eyes. Error bars indicate the step size of the magnetic field. (c) Sketch of the helical and chiral soliton lattice spin structure (colored arrows).

N1-08. Skyrmion Lattice Phases in Thin Film Multilayers.

J. Zázvorka[1,2], F. Dittrich[1], Y. Ge[1], N. Kerber[1,3], *K. Raab*[1], T. Winkler[1], K. Litzius[1,3], M. Veis[2], P. Virnau[1,3] and M. Klaui[1,3] *1. Institute of Physics, Johannes Gutenberg Universitat Mainz, Mainz, Germany; 2. Faculty of Mathematics and Physics, Univerzita Karlova, Praha, Czechia; 3. Johannes Gutenberg University Mainz Graduate School of Excellence Materials Science in Mainz, Mainz, Germany*

Phases of matter are ubiquitous with everyday examples including solids and liquids. In reduced dimensions, particular phases, such as the two-dimensional (2D) hexatic phase and corresponding phase transitions occur (*1-4*). A particularly exciting example of 2D ordered systems are skyrmion lattices (*5*), where in contrast to previously studied 2D colloid systems (*6*), the skyrmion size and density can be tuned by temperature and magnetic field (*7*). In this work we use a skyrmion lattice to study phase transitions in 2D *(8)*. We first show that we can drive the system from a liquid phase to a hexatic phase as deduced from the analysis of the hexatic order. The presence of a hexatic phase highlights the 2D nature of the system. Using coarse-grained molecular dynamics simulations of soft disks, we determine the skyrmion interaction potentials and we find that the simulations are able to reproduce the full two-dimensional phase behaviour. In particular by comparing the numerical simulations and the experimental results, we understand how the equilibration in the hexatic phase occurs on long timescales. This shows that not only the static behaviour of skyrmions is qualitatively well described in terms of a simple two-dimensional model system but skyrmion lattices are versatile two-dimensional model systems that allow for studying phases and phase transitions in reduced dimensions. Finally, as the next step, we investigate the effect of geometrical confinement and find a strong effect on the dynamics and ordering.

1. S. C. Kapfer, W. Krauth, *Phys. Rev. Lett.* 114, 035702 (2015). 2. Y. Nishikawa, K. Hukushima, W. Krauth, Phys. Rev. B 99, 064435 (2019). 3. M. Engel, J. Anderson, S. Glotzer, et al., Phys. Rev. E 87, 042134 (2013). 4. E. P. Bernard; W. Krauth, Phys. Rev. Lett. 107, 155704 (2011). 5. A. Fert, N. Reyren, V. Cros, *Nat. Rev. Mater.* 2, 17031 (2017). 6. K. Zahn, R. Lenke, G. Maret, *Phys. Rev. Lett.* 82, 2721–2724 (1999). 7. K. Everschor-Sitte, J. Masell, R. Reeve, M. Kläui, *J. Appl. Phys.* 124, 240901 (2018). 8. J. Zázvorka et al., arxiv:2004.09244

N1-09. Ultrafast Light-Induced Nucleation of Skyrmion Lattices.

P. Olleros-Rodríguez[1], M.S. Strungaru[2], S. Ruta[2], P.I. Gavriloaea[2], P. Perna[1], R. Chantrell[2] and O. Chubykalo-Fesenko[3] *1. IMDEA Nanoscience Institute, Madrid, Spain; 2. Physics, University of York, York, United Kingdom; 3. Materials Science Institute of Madrid (ICMM-CSIC), Madrid, Spain*

The use of magnetic skyrmions in technological applications is constrained by the ability to nucleate, stabilize and manipulate them[1]. Small skyrmions are frequently metastable states, so that at remanence either the saturated or the stripe domain states are present and the skyrmion nucleation is not easily accessible. Recent experiments have shown the feasibility of laser-induced nucleation of skyrmions by means of non-equilibrium ultrafast magnetisation dynamics processes [2]. This technique also opens the possibility of developing less-consuming and ultrafast skyrmionic memory or logic-gate devices. In the present work we explore the nucleation of magnetic skyrmions in realistically parametrised Pt/Co/Heavy-Metal magnetic trilayers via atomistic simulations using the software package Vampire[3]. Quasi-static simulations by increasing temperature above the Curie one and cooling the system down produce a stable state in the form of stripe domains. Next, we model the dynamics under ultrafast non-polarised femtosecond laser pulse varying the pulse duration and intensity. We present a state diagram of the magnetic states after the laser pulse action which shows the existence of small region of parameters where the final state is the skyrmion lattice. This region can be increased by application of static external field parallel or anti-parallel to the initial magnetic state. Our results unambiguously demonstrate the necessity of highly non-equilibrium dynamical path which could lead to the skyrmion lattice.

[1] A. Fert, N. Reyren, V. Cros, Nature Reviews Materials, Vol. 2(7), p. 17031 (2017) [2] S-G. Je, P. Vallobra, T. Srivastava, et al. Nano Letters, Vol. 18,p. 7362 (2018) [3] R.F.L. Evans, W.J. Fan, P. Chureemart, et al. Journal of Physics Condensed Matter, Vol. 26(10), p. 103202 (2014)

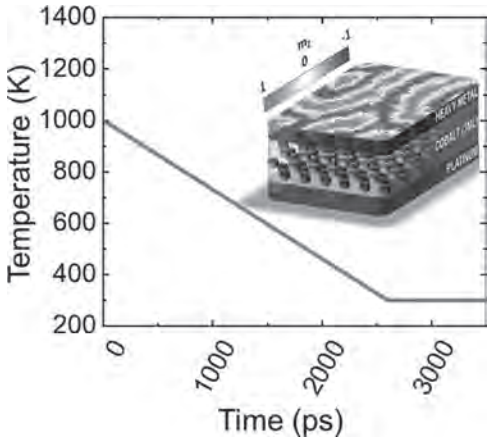

FIG.1. Temperature profile following a simulated slow field-cooling process. The final spin configuration reached is shown at the inset of the plot.

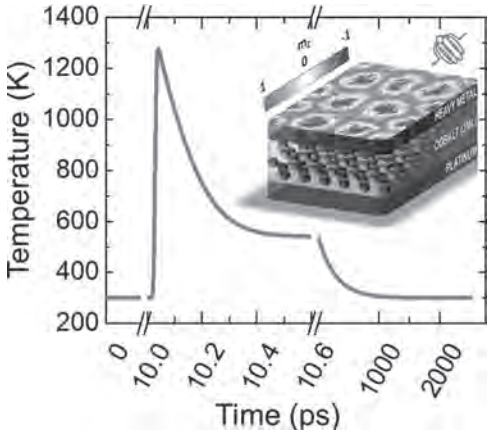

FIG.2. Tremperature profile arising after an ultrafast laser pulse is applied to the modelled system. The final skyrmion lattice nucleated at the end of the simulation can be seen in the inset.

N1-10. Skyrmion Racetracks Defined by Light-ion Irradiation and Current Induced Skyrmion Guiding at Room Temperature.
R. Juge[1], *K. Bairagi*[1], K. Rana[1], M. Sall[2], D. Mailly[3], D. Ravelosona[2], M. Belmeguenai[4], Y. Roussigné[4], S. Auffret[1], L. Buda-Prejbeanu[1], G. Gaudin[1] and O. Boulle[1] *1. CEA, CNRS, Grenoble INP, IRIG-SPINTEC, Universite Grenoble Alpes, Saint-Martin-d'Heres, France; 2. Spin-Ion Technologies, 10 Boulevard Thomas Gobert, 91120 Palaiseau, France; 3. CNRS, Université Paris-Sud, Université Paris-Saclay, 10 boulevard Thomas Gobert, Centre de Nanosciences et de Nanotechnologies, 91120 Palaiseau, France; 4. CNRS, Université Paris 13, Laboratoire des Sciences des Procedés et des Matériaux, 93430 Villetaneuse, France*

Magnetic skyrmions are localized chiral whirling of magnetization that hold great promise as nanoscale information carrier. Skyrmion racetrack memory and logic devices have recently been proposed where trains of skyrmions in tracks are manipulated by electrical current [1]. These devices require the controlled nucleation and current driven motion of skyrmions in narrow tracks. In particular, the skyrmion Hall effect (i.e. the skyrmion motion towards the track edge), is a critical issue as it can lead to the skyrmion annilation [2–5]. Here, we report on the controlled nucleation and current induced guiding of magnetic skyrmions along tracks defined by local He^+ ion irradiation on an ultrathin sputtered magnetic film at room temperature. A He^+ focused ion beam was used to define 150 nm wide tracks (red areas, Fig.1a) within a sputtered ultrathin Pt/Co/MgO film patterned into 3-µm-wide tracks [5,6]. Magnetometry and Brillouin Light Scattering measurements show that the He^+ ion irradiation results in a decrease of the perpendicular magnetic anisotropy as well as the Dzyaloshinskii-Moriya interaction. Under a small perpendicular magnetic field, this leads to the nucleation of skyrmion racetrack (Fig.1b), whose size and density can be tuned by the field amplitude. Experiments of current induced skyrmion motion, show that the skyrmions move along the He^+ ion defined tracks. Thus, the track acts as a local potential well that guides the skyrmion trajectory, which allows to suppress the skyrmion Hall effect. Our results are well substantiated by micromagnetic simulations using experimentally derived magnetic and transport parameters. These results open a new path to nucleate and guide skyrmions in racetrack memory and logic devices.

[1] A. Fert et al., Nat. Nanotechnol. 8, 152 (2013). [2] J. Sampaio et al., Nat. Nanotechnol. 8, 839 (2013). [3] W. Jiang et al., Nat. Phys. 13, 162 (2017). [4] S. Woo et al., Nat. Mater. 15, 501 (2016). [5] R. Juge et al., Phys. Rev. Appl. 12, 044007 (2019). [6] O. Boulle et al., Nat. Nanotechnol. 11, 449 (2016).

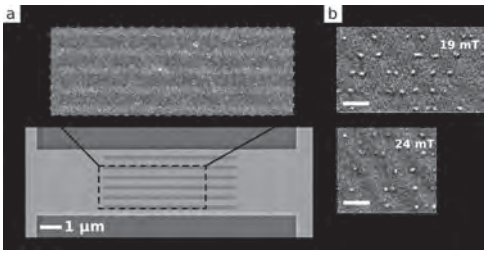

Figure 1: a) Bottom: SEM image of a 3-µm-wide Pt/Co/MgO track. The red lines indicate the irradiated patterns (6000×150 nm²). Top: AFM image after irradiation (Dose = 6 ion/nm²). b) MFM images showing the skyrmions along the track for $\mu_0 H$ = 19 mT and 24 mT (scale bar is 500 nm for both).

N1-11. Topology-Dependent Brownian Gyromotion of a Single Skyrmion.
L. Zhao[1,2], Z. Wang[1,2], X. Zhang[3], X. Liang[3], J. Xia[3], K. Wu[1,2], H. Zhou[1,2], Y. Dong[1,2], G. Yu[4], K. Wang[5], X. Liu[6], Y. Zhou[3] and W. Jiang[1,2] *1. State Key Laboratory of Low-Dimensional Quantum Physics and Department of Physics, Tsinghua University, Beijing, China; 2. Frontier Science Center for Quantum Information, Tsinghua University, Beijing, China; 3. School of Science and Engineering, The Chinese University of Hong Kong, Shenzhen, Shenzhen, China; 4. Beijing National Laboratory for Condensed Matter Physics, Institute of Physics, Chinese Academy of Sciences, Beijing, China; 5. University of California Los Angeles Department of Electrical Engineering, Los Angeles, CA, United States; 6. Department of Electrical and Computer Engineering, Shinshu University, Nagano, Japan*

Non-interacting particles exhibiting Brownian motion have been observed in many occasions of sciences, including spin textures in magnetic materials. Skyrmions are particle-like topological spin textures stabilized by the Dzyaloshinskii-Moriya interaction (DMI), with their topological properties being governed by the skyrmion number Q, which can also be thermally activated and behave like Brownian particles. In the present report, the Brownian dynamics of skyrmion is firstly discussed through performing micromagnetic simulation based on stochastic Landau-Lifshitz-Gilbert equation. More interestingly, a topology-dependent gyromotion from being clockwise (Q = +1) to counterclockwise (Q = -1) can be identified, as shown in Figs. 1(a) and 1(b), respectively. We subsequently utilized a polar magneto-optic Kerr effect (MOKE) microscopy to experimentally examine the Brownian motion of a single isolated skyrmion in the Ta/CoFeB/TaO_x multilayer. The diffusion coefficient of skyrmion is found to exhibit an exponential dependence on temperature, instead of simple linear temperature dependence as Einstein predicted, as shown in Fig.1(c). Further, a topology-dependent Brownian gyromotion is confirmed by revealing the clockwise and counterclockwise rotations for Q = +1 and Q = -1 skyrmions, as shown in Figs. 2(a) and 2(b), respectively. Average rotation angle $\langle\theta_{sr}\rangle$ is systematically calculated and shown in Fig.2(c), in which a clear difference in the whole temperature range can be seen. The experimental results are consistent with the analytical calculations from the stochastic Thiele equation, suggesting the Brownian gyromotion of a single skyrmion is captured.

[1] L. Zhao, Z. Wang, X. Zhang, Phys. Rev. Lett., (in press)

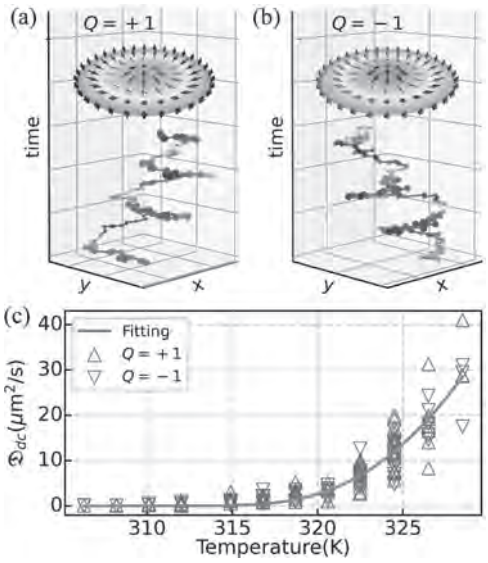

Fig.1 (a-b) Opposite gyromotion of skyrmions with opposite topological charges at finite temperatures. (c) Experimentally observed evolution of diffusion coefficient as a function of temperatures.

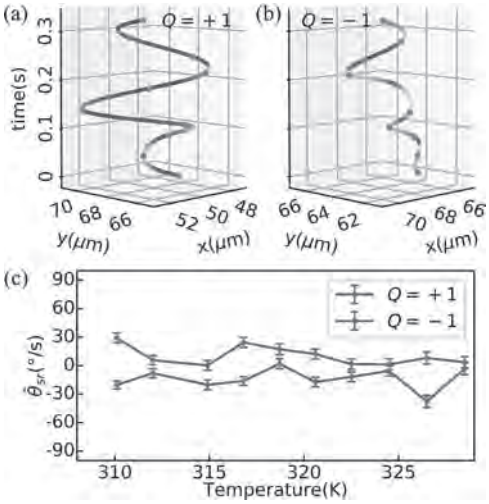

Fig.2 (a-b) Gyromotion of skyrmions at T = 328.5K. (c) Average rotation angle of skyrmions with opposite values of Q at different temperatures.

N1-12. Switching Fixed Magnetic Skyrmions in Continuous Film and Patterned Nanodots Using Voltage Control of Magnetic Anisotropy. *D. Bhattacharya*[1], S. Razavi[2], H. Wu[2], B. Dai[2], K. Wang[2] and J. Atulasimha[1] *1. Virginia Commonwealth University, Richmond, VA, United States; 2. University of California Los Angeles, Los Angeles, CA, United States*

Although current induced motion of magnetic skyrmions have been extensively studied in recent work [1-3], manipulation of magnetic skyrmions that are fixed in space can also be utilized to implement such devices. We have recently shown that, skyrmion core reversal and switching between ferromagnetic states via an intermediate skyrmion state can be achieved in the free layer of an MTJ using Voltage Control of Magnetic Anisotropy (VCMA) which could result in energy efficient memory devices with smaller footprint [4-5]. In this work, we demonstrate experimental evidence of voltage controlled switching of fixed skyrmions in both continuous film [6] and confined geometry. The continuous heterostructure film stack consists of IrMn/CoFeB/MgO layers. The exchange biased structure allows stabilization of skyrmions without any external magnetic field. Upon application of a voltage pulse, the perpendicular magnetic anisotropy (PMA) changes at the ferromagnet/oxide interface. When the PMA is increased by applying a negative voltage pulse, skyrmions are annihilated. On the other hand, skyrmions can be recreated using a positive voltage pulse. We will also present micromagnetic simulations which reveal the detailed magnetization dynamics of this switching. Next, we will show voltage control of skyrmions in patterned nanodots composed of Ta/CoFeB/MgO multilayers. The geometric confinement is expected to influence the switching dynamics as shown in Fig. 1 [4,5]. To systematically modulate the confinement strength, we fabricated nanodots of varying lateral dimensions. The magnetization configurations are imaged using Magnetic Force Microscopy (MFM). Preliminary result of MFM imaging of skyrmion states under 1300 mV applied voltage in a ~5 μm dot is shown in Fig. 2. We will present detailed analysis of the confinement effect on skyrmion switching using further in-situ MFM imaging and rigorous micromagnetic simulations and compare these observations with the switching in thin films. Acknowledgement: NSF CCF collaborative grants: 1909030 and 1909416.

[1] A. Fert et al, Skyrmions on the track, Nature Nanotechnology volume 8, pages152–156(2013) [2] K. Everschor-Sitte et al, Perspective: Magnetic skyrmions—Overview of recent progress in an active research field, Journal of Applied Physics 124, 240901 (2018) [3] G. Yu et al, Room-Temperature Skyrmion Shift Device for Memory Application, Nano Lett. 17, 1, 261–268 (2017) [4] D. Bhattacharya et al, Voltage controlled core reversal of fixed magnetic skyrmions without a magnetic field, Sci. Rep. 6, 31272 (2016) [5] D. Bhattacharya et al, Skyrmion-mediated voltage-controlled switching of ferromagnets for reliable and energy-efficient two-terminal memory, Applied Mater. & Interfaces 10 (20), 17455-17462 (2018). [6] D. Bhattacharya et al, Creation and annihilation of non-volatile fixed magnetic skyrmions using voltage control of magnetic anisotropy, Nature Electronics (2020)

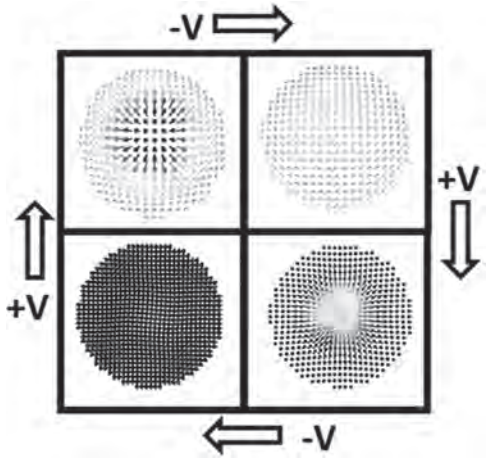

Micromagnetic simulation of Skyrmion reversal in a nanodot

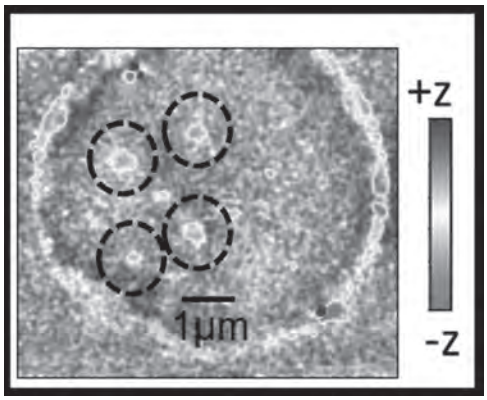

Skyrmions confined in a 5 μm dot, V=1300 mV

Session N2
SPIN WAVE II: MAGNONICS IN FERROMAGNETS AND ANTIFERROMAGNETS

Silvia Tacchi, Chair
CNR, Consiglio Nazionale delle Ricerche, Perugia, Italy

CONTRIBUTED PAPERS

N2-01. Theoretical Studies of Dipolar and Exchange Effects in Creating Magnetic Rogue Waves. *M. Copus*[1] and R. Camley[1] *1. Physics, University of Colorado at Colorado Springs, Colorado Springs, CO, United States*

Magnetic rogue waves, like ocean rogue waves, are large deviations from equilibrium which are localized in time and space. They can be created in thin magnetic films by a time-reversal process consisting of a recording step and a reconstruction step. During the recording step, an initial rogue wave is allowed to decay and the microwave fields at various sites are recorded. In reconstruction step, these fields are played backwards in time at the recording sites, ultimately recreating the initial rogue wave as seen in Fig. 1. This technique gives the ability to control the magnitude and position of the rogue waves, which may make them suitable for application in spin wave logic devices and for encryption and secure communications. We study the efficiency of constructing rogue waves. For a Permalloy film which is 30 nm thick, the peak to noise ratio (PNR) of the reconstructed rogue waves can vary by a factor of 5 depending on the location of sensors with respect to the magnetic field. This is caused by the emission of caustic beams as the initial wave evolves in time. The best location is with the sensors perpendicular to the applied field. We also study the relative importance of dipolar and exchange coupling in creating rogue waves. We explore a geometry of a square magnetic film (side length 300 nm) separated from a surrounding magnetic rim by a gap of 10 nm. This gap prevents exchange coupling between the two regions. The initial rogue wave, a small square (25 nm on a side) where the magnetization is raised out of plane by a maximum of 2 degrees, is established in the inner region, but all the recording sensors are in the outer region. It is clear in Fig. 2 that the system in the middle of the recording phase is dominated by short wavelength modes, where exchange is important. However, in the playback, it is the long wavelength dipolar fields which are important in reconstructing the rogue wave.

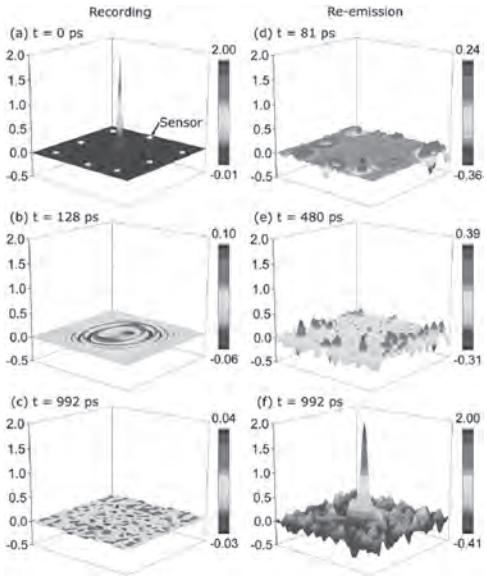

Fig 1. Illustration of the rogue wave recording (a) - (c) and reconstruction (d) - (f) process.

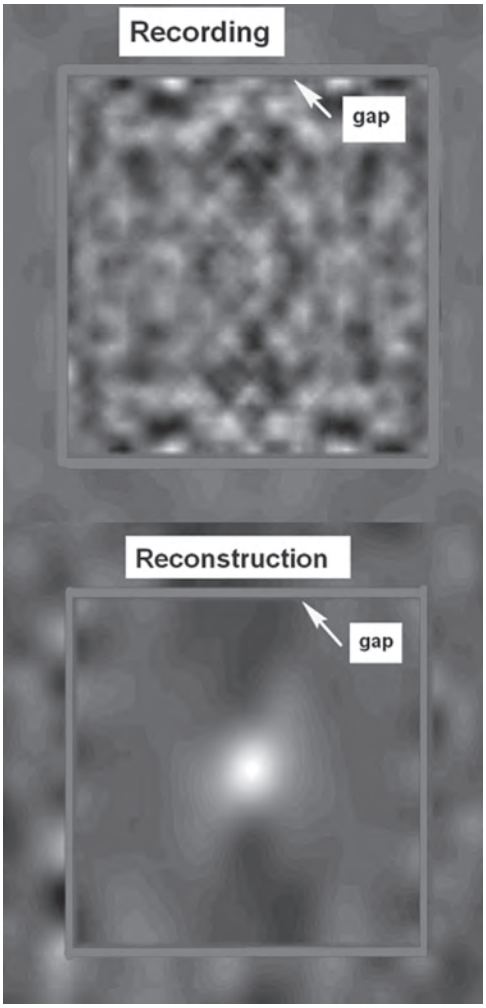

Fig. 2 Magnetic state during recording (top) and at the end of reconstruction process. We see a clean reconstructed peak in the center, despite the fact that all the sensors are located in the outer rim.

N2-02. Quantum Magnonics at the Edge of Space and Time.
G. Fabiani[1] and J. Mentink[1] *1. Institute for Molecules and Materials, Radboud University, Nijmegen, Netherlands*

Realizing magnon-based information transfer that exploits high-frequency magnons at the nanoscale is one of the holy grails for low-energy data processing. In principle, this regime can be accessed by magnons with wavelength as short as a few Angstrom. These magnons have the highest possible energy corresponding to the exchange interaction and therefore yield the edge of space and time of magnetism. It is well-known from Raman spectroscopy that pairs of such magnons can be excited in antiferromagnets and recently this has also been investigated in the time-domain [1-3]. However, the nonlocal spatial properties of these excitations, whose understanding is crucial for applications, have not been addressed yet. Moreover, the quasi-particle propagation relates to a fundamental problem of quantum many-body dynamics, namely the relation between propagation of information and evolution of the entanglement entropy. Rigorous theoretical results for this connection were so far limited to one-dimensional systems and it remains unclear if the same holds in higher dimensions. Beyond the limitations of existing theoretical methods, we adopt a machine learning inspired ansatz [4] to simulate the dynamics of the two-dimensional Heisenberg model [5-7], the minimal model for two-magnon physics. Despite the homogenous excitation, we find highly anisotropic spreading of spin correlations, which are qualitatively consistent with spin wave theory. Interestingly, at the smallest length and time scales, the spreading is even faster than expected from the highest magnon velocity of the system. Moreover, in contrast to what is known in one dimension, we show that the dynamics of entanglement is dominated by nearest neighbour correlations and is therefore essentially localized. We confirm this by demonstrating ultrafast coherent control of the entanglement oscillations. Hence, our results suggest that the quantum dynamics of antiferromagnets in two dimensions departs from the conventional quasi-particle picture. Our findings may have therefore profound impact on the fundamentals of nonequilibrium quantum many-body dynamics and on the future development of magnon-based information processing at the shortest space and time scales.

[1] J. Zhao et al, Phys. Rev. Lett. 93, 107203 (2004); [2] D. Bossini et al, Nature Communications 7, 10645 (2016); [3] D. Bossini et al, Phys. Rev. B 100, 024428 (2019); [4] G. Carleo and M. Troyer, Science 355, 602 (2017). [5] G. Fabiani and J.H. Mentink, SciPost Phys. 7, 004 (2019); [6] https://github.com/ultrafast-code/ULTRAFAST [7] G. Fabiani and J.H. Mentink, arXiv:1912.10845

N2-03. Magnonic Bending, Phase Shifting and Interferometry in a 2D Reconfigurable Nanodisk Crystal.
K. Stenning[1], J.C. Gartside[1], T. Dion[1,2], A. Vanstone[1], D. Arroo[2] and W. Branford[1] *1. Imperial College London, London, United Kingdom; 2. University College London, London, United Kingdom*

Strongly-interacting nanomagnetic systems are pivotal in novel technologies such as reconfigurable magnonics[1,2] and neuromorphic computation[3]. Controlling both magnetisation state and local coupling of neighbouring nanoelements allows vast reconfigurable functionality, a vital part of realising next generation devices. However, the extent of reconfigurability is often limited by a lack of local magnetisation control alongside an inability to redefine active and inactive elements in an array. Furthermore, shaping magnon pathways in two dimensions adds additional complexities in terms of power losses and changes in magnon frequency and phase[4]. A subset of nanomagnetic elements are circular-shaped nanomagnets (nanodisks) capable of supporting macrospin and vortex states[5] [Fig. 1] offering higher a density compared to nanowire-based designs. Macrospin states comprise all spins aligning along a freely rotating macrospin axis resulting in a net magnetisation and large dipolar field enabling strong coupling between neighbouring elements. Whereas vortex states comprise an independent in-plane chirality and out-of-plane polarity characterised by a low dipolar-field leakage due to the chiral flux-closure. Yet, means of complete state control on individual nanodisks in an array are lacking. To address these challenges, we propose a novel nanodisk-based magnonic crystal where leveraging the coupling behaviours of different nanodisk states is employed to attain reprogrammable waveguiding capable of bending and splitting magnons around a 2D network [Fig. 2], amplitude gating and phase-shifting of magnons. We then demonstrate the potential of nanodisk-based magnonics by the design of an all-magnonic interferometer performing XNOR logic functionality. State preparation is achieved through local spin manipulation via a high-moment magnetic force microscopy enabling control of vortex chirality, polarity and macrospin axis across a range of nanodisk dimensions.

1. Grundler, D., *Nature Physics*, *11*(6), pp.438-441. (2015) 2. Chumak, A.V., Vasyuchka, V.I., Serga, *et. al. Nature Physics*, *11*(6), pp.453-461. (2015) 3. Grollier, J., Querlioz, D., Camsari, *et. al*. *Nature Electronics*, pp.1-11. (2020) 4. Haldar, A., Kumar, D. and Adeyeye, A.O., *Nature nanotechnology*, *11*(5), pp.437-443. (2016) 5. Cowburn, R.P., Koltsov, D.K., Adeyeye, A.O., *et. al. Physical Review Letters*, *83*(5), p.1042. (1999)

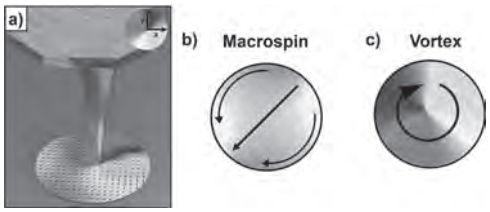

Fig 1. a) Schematic of nanodisk state preparation via a high-moment magnetic force microscopy tip. Metstable b) macrospin and c) vortex states present in nanodisks.

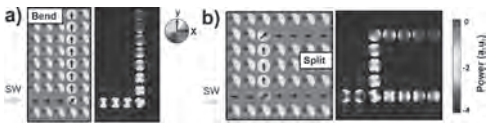

Fig. 2 Magnetisation and power profiles demonstrating a) bending and b) splitting of magnons across a 2D network.

INVITED PAPER

N2-04. Non-Hermitian Hybrid Magnonics. *X. Zhang*[1] *1. Argonne National Laboratory, Lemont, IL, United States*

Non-Hermitian physics[1] has been drawing intensive attentions and studied on many different physical platforms, including microwave, mechanical and integrated photonic systems. Very recently, hybrid magnonics, which studies strongly-coupled electromagnetic waves and spin waves—the collective excitation of magnetization, has been emerging as a promising candidate because of its unique properties. Hybrid magnonics exhibits great tunability and can intrinsically beak the time reversal symmetry (TRS). More importantly, unlike previous non-Hermitian systems that utilize a single degree of freedom, hybrid magnonics employs two different types of excitations. Therefore, different physical properties and tuning mechanisms can be combined to enable novel physics and functionalities. The great potential of hybrid magnonics for non-Hermitian physics has yet to be fully explored. As an example, we will show its unique applications in two different scenarios (Fig.1). First, hybrid magnonics can be used to study exceptional points (EPs)—singularities of eigen-energies in non-Hermitian systems—in higher dimensions.[2] Intriguing phenomena have been previously observed at or around EPs. However, previous demonstrations are limited to 0-dimensional points and 1-dimensional lines. The large tunability of hybrid magnonics allows us to construct a 4-dimensional synthetic space, in which we were able to demonstrate the first experimental observation of an exceptional surface and exceptional saddle point. Second, TRS plays a pivotal role in non-Hermitian physics. On a hybrid magnonic platform, we show that TRS can be broken even in the strong coupling regime by utilizing the chirality of microwave photons and magnons, and broadband nonreciprocal transmission can be obtained accordingly.[3] Our hybrid magnonics platform opens new opportunities for both fundamental research and practical applications of non-Hermitian physics.

[1] Ramy El-Ganainy et al, Nature Physics, Vol. 14, 11 (2018) [2] Xufeng Zhang, Kun Ding, Xianjing Zhou, Jing Xu, and Dafei Jin, Phys. Rev. Lett., Vol. 123, 237202 (2019) [3] Xufeng Zhang, Alexey Galda, Xu Han, Dafei Jin, and V. Vinokur, Phys. Rev. Applied, Vol. 13, 044039 (2020)

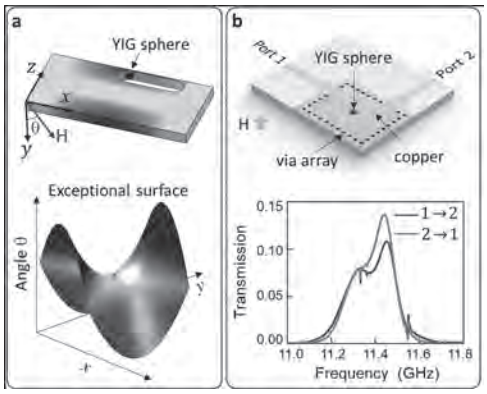

Fig.1 a. Experimental observation of an exceptional surface. b. Measurement of nonreciprocal transmission on a TRS-broking hybrid magnonic device. YIG: yttrium iron garnet.

CONTRIBUTED PAPERS

N2-05. Magnon Antibhunching in a Nanomagnet. *H. Yuan*[1] and R. Duine[1] *1. Institute for Theoretical Physics, Universiteit Utrecht, Utrecht, Netherlands*

We investigate the correlations of magnons inside a nanomagnet and identify an unconventional phase so-called magnon antibunching, i.e., where there is a large probability for occupation of the single-magnon state. This antibunched state is very different from magnons at thermal equilibrium and microwave-driven coherent magnons. We further obtain the steady state analytically and describe the magnon dynamics numerically, and ascertain the stability of such antibunched magnons over a large window of magnetic anisotropy, damping and temperature. This means that the antibunched magnon state is feasible in a wide class of low-damping magnetic nanoparticles. To detect this quantum effect, we propose to transfer the quantum information of magnons to photons by magnon-photon coupling and then measure the correlations of photons to retrieve the magnon correlations. Our findings may provide a promising platform to study quantum-classical transitions and for designing a single magnon source.

1. H. Y. Yuan and Rembert A. Duine, arXiv:2005.13637v1. 2. H. Y. Yuan, Peng Yan, Shasha Zheng et al., Phys. Rev. Lett. Vol. 124, p.053602 (2020). 3. H. Y. Yuan, Shasha Zheng, Z. Ficek et al., Phys. Rev. B Vol. 101, p.014419 (2020).

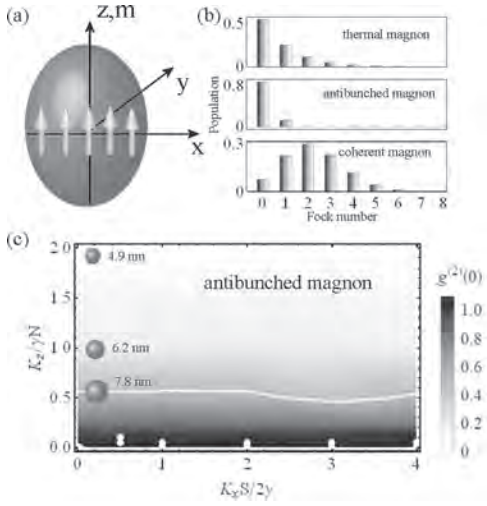

Fig. 1 (a) Schematic of a nanomagnetic particle magnetized along the *z* axis while the *x* axis is a hard axis. (b) Fock distribution of the thermal, antibunched and coherent magnons, respectively. (c) Phase diagram of the nanoparticle in the ($K_xS/2\gamma$, $K_z/\gamma N$)$ plane. The white line corresponds to the second-order auto-correlation function $g^{(2)}(0)=0.5$.

N2-06. Withdrawn

N2-07. Insight on the Time-Resolved Spin Wave Amplification in Nano-Magnonic Devices Using Spin-Orbit-Torque. *H. Merbouche*[1], B. Divinskiy[2], D. Gouéré[1], C. Calo[4], B. Paolo[3], V. Cros[1], A. Anane[1], V.E. Demidov[2] and S. Demokritov[2] *1. Unite Mixte de Physique CNRS/ Thales, Palaiseau, France; 2. Institue for Applied Physics, University of Muenster, Munster, Germany; 3. Thales Research and Technology France, Palaiseau, France; 4. III-V Lab, Palaiseau, France*

Spin wave (SW) based computing i.e. magnonics relies on propagating SW as information carriers. Being quasiparticles, magnons (the SW quanta) have a fine lifetime characterizing the exponential decay of the magnons population. Consequently, up to now, all magnonic devices operate within a short time-window. Finding a SW amplification paradigm is hence a prerequisite for the development of magnonics as a credible CMOS alternative. Two schemes are envisioned for SW amplification: Parametric pumping[1] and spin-orbit-torque (SOT)[2]. Here we will discuss SOT amplification in BiYIG/Pt bilayer[3]. By passing current in the Pt layer, the spin accumulation resulting from the spin-Hall effect induces a positive torque that compensate the Gilbert damping of BiYIG. At subcritical values, the current has a linear effect that decreases the losses of the system and leads to a lower effective damping. Once the current in the Pt layer reaches a threshold values, the vanishing effective damping allows for the onset of the auto-oscillation regime[4]. Coherent propagating spin waves are strongly scattered by auto-oscillations[5] leading to a strong decrease of their attenuation length[6]. Here we propose an amplification mechanism that circumvent this detrimental effect. We show using micro Brillouin light scattering spectroscopy (μ-BLS) on a 500 nm Pt/BiYIG waveguide that the precise timing of the dc current in the Pt layer with respect to the radiofrequency pulse in the strip antenna enables experimental observation of a lossless propagation of spin-waves. We take advantage of the strong BLS signal of BiYIG (nearly two orders of magnitude the one of YIG[3]) to extensively characterize the auto-oscillations non-linear dynamic regime in the presence of SOT. Work supported by ANR grant CE24-0021(MAESTRO).

[1] T. Brächer, P. Pirro, and B. Hillebrands, Phys. Rep. 699, 1 (2017) [2] V.E. Demidov, A. Anane, S.O. Demokritov, J. Appl. Phys. 127, 170901 (2020) [3]L. Soumah, A. Anane, Nat. Commun. 9, 3355 (2018) [4] M. Collet, G. de Loubens, and O. Klein, Nat. Commun. 7, 10377 (2016) [5] B. Divinskiy. O. Demokritov, and V.E. Demidov, Nat. Commun. 10, 5211 (2019) [6] M. Evelt, V.E. Demidov, M. Collet, Appl. Phys. Lett. 108, 172406 (2016)

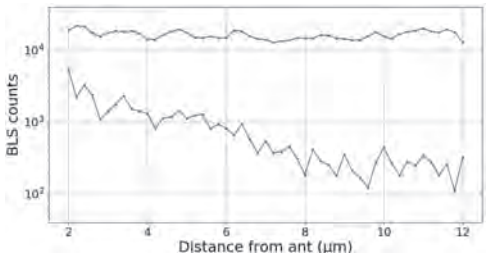

μ-BLS amplitude of two rf-excited SWs (4.925 GHz) propagating during a pulse of SOT in a BiYIG/Pt bilayer versus the propagation distance. The blue curve corresponds to a sub-threshold dc current where an attenuation length of 10.5μm can still be observed. The red curve is measured with a dc current 20% above the critical current and does not show any decay over the investigated length. Note the natural decay with no current applied is 1.7μm.

N2-08. Controlling of Nonlinear Relaxation of Quantized Magnons in Nano-Devices. *M. Mohseni*[1], Q. Wang[2], B. Heinz[1], M. Kewenig[1], M. Schneider[1], F. Kohl[1], B. Lägel[1], A. Chumak[2] and P. Pirro[1] *1. Physics, Technische Universitat Kaiserslautern, Kaiserslautern, Germany; 2. Physics, Universitat Wien, Wien, Austria*

The use of spin waves (SWs) and their quanta, the magnons opens many opportunities in wave-based and unconventional data processing units [1]. Owing to their low magnetic losses, yttrium iron garnet (YIG) films are known as the most promising hosts for SWs. For the realization of the SW based devices, downscaling YIG films to nanometer sizes is a necessary task. In principle, downscaling leads to a strong quantization of the energy levels, and consequently, to the appearance of distinct SW bands in the magnon spectrum [2,3]. This strong quantization opens up new avenues to design data processing devices using nonlinear effects. However, such mechanisms are not well investigated in nanoscaled YIG magnonic conduits. Here, we use space- and time-resolved micro-focused Brillouin light scattering spectroscopy and micromagnetic simulations to investigate the nonlinear relaxation of strongly driven SWs based on the second order Suhl instability process in YIG nano-conduits. We show that the nonlinear magnon relaxation in this highly quantized system possesses intermodal features, i.e. magnons scatter to higher-order quantized modes through a cascade of scattering events. We demonstrate that this type of scattering saturates on a time scale of approximately 4 ns, and meditates the decay rate of the resonantly driven magnons. We further show how to control such intermodal dissipation processes by quantization of the magnon band in single-mode devices, where this phenomenon approaches its fundamental limit [4].

[1] A.V. Chumak, *et al,* Nat. Phy. 11 453–461 (2015) [2] Q. Wang, *et al,* Phys. Rev. Lett. 122, 247202 (2019) [3] M. Mohseni, *et al,* Phys. Rev. Lett. 122, 197201 (2019) [4] M. Mohseni, *et al,* arXiv:2006.03400 (2020)

N2-09. Enhancement of the Spin Mixing Conductance at YIG/Pt Interfaces by Electrical Annealing. *R. Kohno*[1], N. Thiery[1], K. An[1], P. Noël[1], L. Vila[1], v.v. naletov[1,4], N. Beaulieu[2,3], j. ben youssef[3], G. de loubens[2] and O. Klein[1] *1. Universite Grenoble Alpes, CEA, CNRS, Spintec, Grenoble, France; 2. SPEC, CEA-Saclay, CNRS, Universite Paris-Saclay, Gif-sur-Yvette, France; 3. LabSTICC, CNRS, Université de Bretagne Occidentale, Brest, France; 4. Institute of Physics, Kazan Federal University, Kazan, Russian Federation*

We report the evolution of spin conductivity at the YIG/Pt interface when the Pt is subject to an electrical current annealing. By injecting a large current density ($12 \times 10^{11} A/m^2$) into Pt nanostrips and reaching a local temperature of 550 K, we observe a clear increase of the spin density emitted and probed

at the YIG interface in three different measurements: spin Hall magnetoresistance, spin pumping and non-local magnon transport. As shown in Fig.1, the amplitude of FMR spectra by spin pumping enhances gradually in applying local Joule heating, leading to double the efficiency of spin transmmision by one-hour annealing. On the other hand the FWHM of the spectra remains the same over the whole annealing process (inset of Fig.1), indicating no farther extra damping at the YIG/Pt interface[1] appearing and relaxation processes occuring mainly in extended YIG films beside the strip. Fig.2 shows the non-local magnon transport signals mostly excited by spin orbit torque (SOT) (corresponding to the 1st hamonic signal in ref. [2] and Σ signal in ref. [3]). The non-local voltage enhances by 3 times by one strip annealing (either the injector or detector) and by 9 times by both strips annealing. Finally we estimated that the spin mixing conductance of evaporated Pt on YIG is increased from 0.8 to 1.9×10^{18} m^{-2}. To sum up, the local annealing allows achieving spin mixing conductance of evaporated Pt on YIG similar quality to sputtered one and is of particular interest for very thin YIG films where chemical etching of the interface has to be avoided.

[1]: O. Mosendz, V. Vlaminck, J. Pearson, *et. al*., Physical Review B 82, 214403 (2010). [2]: L. Cornelissen, J. Liu, R. Duine,*et. al*., Nature Physics 11, 1022 (2015). [3]: N. Thiery, A. Draveny, V. Naletov, *et. al*., Physical Review B 97, 060409 (2018)

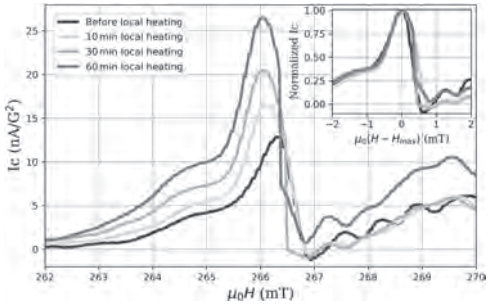

Fig.1: Spin pumping signal by injecting a current density Jc=12×10^{11} A/m^2 into the Pt for three different annealing time. The inset represents the normalized spin pumping spectra.

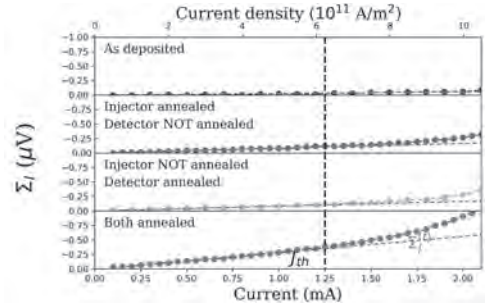

Fig.2: Non-local SOT related magnon transport signals (Σ). The first panel (top) shows the signal directly after the nanofabrication. The second and the third panel represent the signals with one-hour annealing at either the injector strip or the detector strip. In the last panel (bottom), both the injector and detector are annealed.

N2-10. Spin-Transport and Spin-Dynamics in Ultra-low Damping Insulating Antiferromagnets. A. Ross[1,2], *I. Boventer*[3], O. Gomonay[1], L. Baldrati[1], V. Baltz[4], U. Ebels[4], A.L. Barra[5], A. Anane[3], A. Qaiumzadeh[6], A. Brataas[6], P. Kläui[1,2] and R. Lebrun[3] *1. Institute for Physics, Johannes Gutenberg University Mainz, Mainz, Germany; 2. Graduate School of Excellence Materials Science in Mainz, Mainz, Germany; 3. Unité Mixte de Physique CNRS/Thalès, Palaiseau, France; 4. Université Grenoble Alpes CNRS/CEA, Grenoble INP, SPINTEC, Grenoble, France; 5. Laboratoire National des Champs Magnétiques Intenses, CNRS-UGA-UPS-INSA-EMFL, FR, Grenoble, France; 6. Center for Quantum Spintronics, Department of Physics, Norwegian University of Science and Technology, Trondheim, Norway*

Antiferromagnetically ordered materials are the most common class of magnetic materials with several crucial advantages over ferromagnetic systems. In contrast to the latter, antiferromagnets are stable in external fields and can be operated at THz frequencies. Recent works highlighted how insulating antiferromagnets could be integrated into ultrafast spintronic and magnonic devices[1,2]. However, spin-transport and spin-pumping effects have until now only been observed at low temperature and in easy-axis antiferromagnets[3–6]. In my talk, I will first discuss how easy-plane antiferromagnets can propagate spin-information through current induced pairs of linearly polarized antiferromagnetic magnons[7]. These magnon pairs carry an effective spin-angular momentum parallel to the Néel vector with a decay length determined by their dephasing length. In the antiferromagnet hematite α-Fe_2O_3, this process allows for the propagation of spin-information over long-distances at room temperature due to the low magnetic damping and magnon modes close in energy. The dephasing length can reach a few micrometers, of similar order as the magnon spin-diffusion length. These results show that easy-plane antiferromagnets can be as promising as easy-axis antiferromagnets. Then, I will discuss how the presence of bulk and interfacial symmetry breaking in antiferromagnets can enhance both their response to microwave cavity field and their spin-pumping response[8]. This class of compounds will enable the integration of antiferromagnetic materials into spintronic and spin-cavitronic devices.

[1] V. Baltz et al., Rev. Mod. Phys. 90, 015005 (2018). [2] T. Jungwirth et al., Nat. Nanotechnol. 11, 231 (2016). [3] R. Lebrun et al., Nature 561, pp. 222-225 (2018). [4] P. Vaidya et al., Science 368, pp.160-165 (2020). [5] J. Li et al., Nature 578, pp. 70–74 (2020). [6] A. Ross et al, Nano Lett. 20, pp. 306-313 (2020). [7] R. Lebrun et al., arXiv:2005.14414 (2020). [8] I. Boventer et al., in preparation (2020).

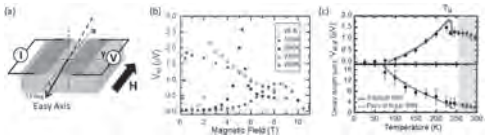

Figure 1 Spin-transport through the Morin transition (T_M) (a) Schematic of the nonlocal devices with two electrically isolated Pt wires. (b) Temperature dependence of the nonlocal spin-signals for a magnetic field parallel to the platinum stripes. (c) Top: The spin signal approaches zero at low temperature, indicating a diffusive regime. Bottom: Spin-wave decay length (spin diffusion length λ for $T < T_M$ and dephasing length L for $T > T_M$) as a function of temperature. (The fits correspond to a model with a magnon transport based on elliptically polarized spin-waves (SWs) and on pairs of linearly polarized spin-waves).

N2-11. Optically Inspired Nanomagnonics With Patterned Spin Textures in Synthetic Antiferromagnets. *E. Albisetti*[1], S. Tacchi[2], R. Silvani[3], G. Scaramuzzi[1], S. Finizio[4], S. Wintz[4], C. Rinaldi[1], M. Cantoni[1], J. Raabe[4], G. Carlotti[3], R. Bertacco[1], E. Riedo[5] and D. Petti[1]
1. Dipartimento di Fisica, Politecnico di Milano, Milano, Italy; 2. CNR-IOM, Perugia, Italy; 3. Università di Perugia, Perugia, Italy; 4. Paul Scherrer Institut, Villigen, Switzerland; 5. New York University Tandon School of Engineering, Brooklyn, NY, United States

Spin waves represent a promising avenue for implementing unconventional wave-based computing platforms. However, combining controlled generation, manipulation and long-distance propagation of submicrometric wavelength spin waves is an outstanding challenge. Recently, nanoscale spin textures such as structured domains, domain walls and vortices, have raised interest as versatile active components in magnonic devices. In this framework, we demonstrated that nanopatterning spin textures via thermally assisted magnetic scanning probe lithography (tam-SPL) [1] allows the stabilization, in exchange bias systems, of 2D domains with arbitrary shape and spin configuration, 1D domain walls and 0D magnetic solitons such as vortices with tailored topology and position [2]. Here, first we show the channeling and steering of spin-waves in arbitrarily shaped nanomagnonic waveguides based on straight and curved domain walls, and a prototypic nanomagnonic circuit comprising two converging waveguides, allowing for the tunable spatial superposition and interference of confined spin-wave modes [3]. Then, we present an optically inspired platform for controlling the generation, propagation, and interference of short-wavelength spin waves, using nanopatterned spin textures in synthetic antiferromagnets, at remanence [4]. We demonstrate the spatial engineering of spin-wave wavefronts, the directional emission and focusing of spin-wave beams, and the generation of robust interference patterns which span multiple times the wavelength. Furthermore, we show that SAF allows to combine concepts borrowed from optics, with phenomena naturally arising from the nonreciprocal spin wave dispersion, such as resilience to spurious back reflections. The ability to control magnons via nanopatterned spin-textures at remanence opens up a range of new possibilities for developing energy-efficient unconventional computing concepts.

[1] E. Albisetti, D. Petti, M. Pancaldi et al., *Nat. Nanotechnol*. Vol. 11, p. 545 (2016). [2] E. Albisetti, A. Calò, M. Spieser et al., *Appl. Phys. Lett.* Vol. 113, p. 162401 (2018). [3] E. Albisetti, D. Petti, G. Sala et al., *Commun. Phys.* Vol. 1, p. 56 (2018). [4] E. Albisetti, S. Tacchi, R. Silvani et al., *Adv. Mater.* Vol. 32, p. 1906439 (2020).

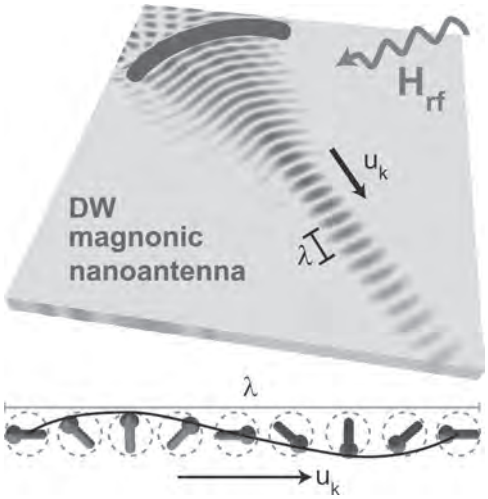

Fig. 1. Simulations of the emission of a focused directional spin-wave beam by a domain wall nanoantenna.

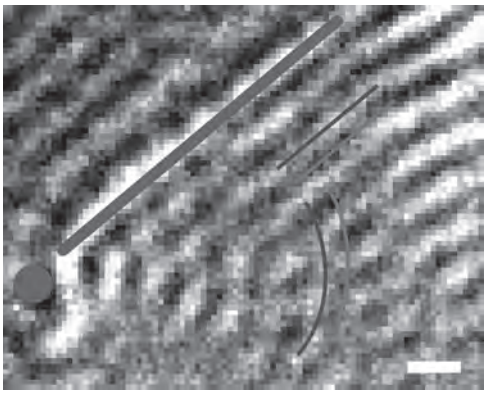

Fig. 2. X-Ray Microscopy image of the interference of radial wavefronts emitted by a vortex and planar wavefronts emitted from a domain wall. Scale bar 500 nm.

N2-12. Antiferromagnetic Spin Wave Propagation on Nonuniform Magnetic Backgrounds. *M. Hu*[1,2], M. Hoefer[1], E. Iacocca[3] and M.J. Donahue[4] *1. Applied Mathematics, University of Colorado Boulder, Boulder, CO, United States; 2. Applied and Computational Mathematics Division, National Institute of Standards and Technology, Boulder, CO, United States; 3. Mathematics, Physics and Electrical Engineering, Northumbria University, Newcastle upon Tyne, United Kingdom; 4. Applied and Computational Mathematics Division, National Institute of Standards and Technology, Gaithersburg, MD, United States*

Antiferromagnets (AFMs) have become the focus of intense research for potentially novel spintronic applications[1]. AFMs have been theoretically proposed to be ideal candidates to support spatially-coherent textured states, that may transport angular momentum over long distance, often called spin superfluids[2,3,4]. The stability of these states hinges upon the structure of the dispersion for excited spin waves. Here, we introduce the spin hydrodynamic equations for AFMs, modeled as two exchange-coupled spin sublattices[5], each dynamically described by a Landau-Lifshitz (LL) equation in the continuum approximation. We include an external magnetic field, the nearest-neighbor inter-lattice exchange interaction, and an easy-plane anisotropy field. Spin hydrodynamics[6] are exactly represented in terms of the spin densities, the perpendicular magnetization component, and the spin velocities, the azimuthal phase gradients, for each spin sublattice. We have identified two distinct classes of spin textures that can be identified as hydrodynamic states[6]: 1) The phase-locked state in which the spins from the two sublattices maintain a constant π phase difference; this state has previously been referred to as a spin superfluid[2]; 2) The polarization state in which the dynamics are governed by oscillating relative phases. This decomposition in terms of the total and relative phase dynamics has been effective in the study of the coupled two-component Bose-Einstein condensates[7]. For the phase-locked state, we verify that the spin dispersion is a gapped mode spectrum[2] and the state exhibits modulational instability at large enough total spin velocity[2,6]. We further study the stability properties of the polarization state by determining dispersion relations for spin wave propagation. Our results suggest that this newly identified state may be favorably excited in long-range spin transport experiments under appropriate conditions.

[1] V. Baltz, et al., Reviews of Modern Physics, Vol. 90, No. 1, p.015005 (2018). [2] E. B. Sonin, Physical Review B, Vol. 99, No. 10, p.104423 (2019). [3] S. Takei and Y. Tserkovnyak, Physical review letters, Vol. 112, No. 22, p.227201 (2014). [4] W. Yuan, Wei, et al., Science Advances, Vol. 4, No. 4, p. eaat1098 (2018). [5] V. Puliafito, et al., Physical Review B Vol. 99, No. 2, p.024405 (2019). [6] E. Iacocca, T. J. Silva and M. A. Hoefer, Physical Review Letters, Vol. 118, No. 1, p.017203 (2017). [7] A. M. Kamchatnov, et al., Physical Review A, Vol. 89, No. 3, p.033618 (2014).

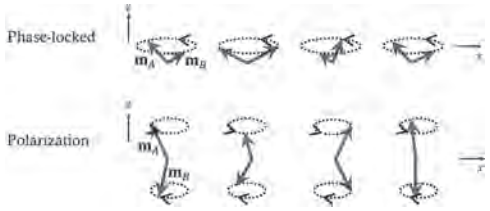

Fig. 1: (top) Phase-locked state; (bottom) Polarization state. The dotted circles represent temporal precession. The spatial precession is illustrated left to right at a fixed time.

N2-13. Withdrawn

N2-14. Simulating Spin Wave Noise in Synthetic Antiferromagnetic Textures. *J. Kim*[1], J. Adam[1], A. Finco[2] and V. Jacques[2] *1. Centre de Nanosciences et de Nanotechnologies, CNRS, Université Paris-Saclay, Palaiseau, France; 2. Laboratoire Charles Coulomb, CNRS, Université de Montpellier, Montpellier, France*

Synthetic antiferromagnets (SAFs) comprise coupled ultrathin ferromagnetic films with a variety of ground states that can be stabilized at room temperature by tuning the magnetic parameters such as the effective anisotropy, interlayer exchange, and Dzyaloshinskii-Moriya interactions. As a result, nonuniform spin textures such as domain walls, spin spirals, and skyrmions can be stabilized under zero applied fields [1], which can be detected using quantum spin sensing [2]. Here, we present results of micromagnetics simulations in which we examined the spin wave dispersion associated with localized modes of domain walls, spin spirals, and skyrmions in such SAF structures. For domain walls and spin spirals, the combination of dipole-dipole and Dzyaloshinskii-Moriya interaction results in spectra with frequency-wave vector nonreciprocity (Fig. 1), which results from asymmetries in the micromagnetic ground state. Skyrmion breathing modes are found to be in the low GHz range, which differs from their counterparts in confined ferromagnetic systems. We also discuss a numerical spectroscopic technique to estimate the magnetic noise at the electron spin resonance frequency for nitrogen-vacancy center measurements, which relies on estimating the magnetic susceptibility by computing the transient response to driving fields that are harmonic in time but random in space. Good agreement is found with recent experimental results [2]. This work was supported by the Agence Nationale de la Recherche under contract no. ANR-17-CE24-0025 (TOPSKY).

[1] W. Legrand et al., Nature Materials, Vol 19, p. 34 (2020). [2] A. Finco et al., arXiv:2006.13130 (2020).

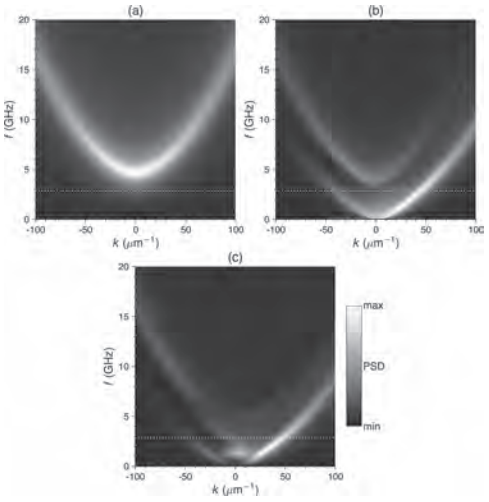

Fig. 1. Simulated spin wave dispersion relation in different ground states of a synthetic antiferromagnet: (a) Uniform state, (b) domain wall, (c) spin spiral. The dashed line indicates the electron spin resonance frequency of the nitrogen-vacancy defect.

Session N3
MAGNETIC RECORDING VIA OPTICAL, HEAT AND MAGNETIC EXCITATION I (Poster Session)

Yassine Quessab, Co-Chair
New York University, New York, NY, United States
Stephanie Hernandez, Co-Chair
Seagate Technology, Minneapolis, MN, United States

N3-01. Medium H_k Structure Effects in Microwave Assisted Magnetic Recording. K. Kurihara[1], *T. Tanaka*[1], X. Ya[1], Y. Kanai[2] and K. Matsuyama[1] *1. ISEE, Kyushu University, Fukuoka, Japan; 2. Department of Engineering, Niigata Institute of Technology, Kashiwazaki, Japan*

Microwave-assisted magnetic recording (MAMR)[1] has potential application in high density recording. Recent researches proposed notched structure media[2] which extracts the effects of microwave assistance in magnetization reversals. In this study, the effects of microwave assisted magnetization reversals for the notched structure media and that for conventional gradient media were estimated and its recording characteristics were compared through micromagnetic simulations. Field distributions of a 30-nm-track-wide single pole type head with a spin torque oscillator were computed by FEM methods. 4 layered media with 2-2-2-6 nm in thickness were assumed. Notched media have notch type layer H_k structure that the high H_k layer exists at the top surface, while the top layer is low H_k for the conventional gradient media. The switchable maximum H_k[3] ($H_{k.max}$) was estimated from footprint calculations considering the variety of the interlayer exchange constants and layer H_k ratios. The calculation revealed that $H_{k.max}$ for MAMR in the gradient media are slightly higher than those in the notched media. However, notched media showed higher MAMR H_k gains which is defined by ($H_{k.max}$ for MAMR)/($H_{k.max}$ for non-MAMR). The calculation also showed that H_k for the second layer from the top surface has impact to determine $H_{k.max}$. Fig. 1(a) and 1(b) show SNRs and MWWs, respectively, for the selected parameter sets which showed relatively higher $H_{k.max}$ and MAMR H_k gains for the footprint calculations. Recording characteristics were estimated with decreasing the averaged medium H_k ($H_{k.ave}$) because $H_{k.ave}$ for the selected parameter sets are too high to obtain preferable SNRs. The average grain size of these media are detemined to be from 4.6 nm to 8 nm to retain thermal stability index (K_uV/k_BT) ~ 60. The highest SNRs are 18 dB regardless of the medium H_k structures but MWWs for the notched media tends to be narrower than those for the gradient media, which implies notched structures are superior as MAMR media.

[1] J.-G. Zhu, X. Zhu, and Y. Tang, IEEE Trans. Magn. 44, 125 (2008). [2] X. Bai and J.G. Zhu, AIP Advances 8, 056508 (2018). [3] M. Shiimoto, M. Igarashi, M. Sugiyama, Y. Nishida, I. Tagawa, IEEE, Trans. Magn., 49, 3636(2013).

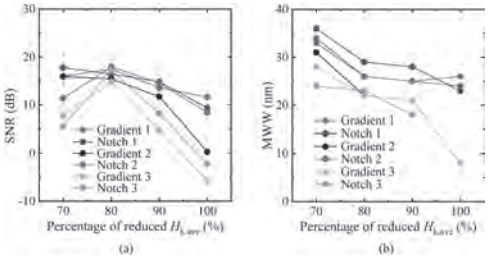

Fig. 1(a) SNRs and 1(b) MWWs for selected parameter sets of the gradient media and notched media.

N3-02. Optimisation of Dual Structure Recording Media. *S. Greaves*[1] and Y. Kanai[2] *1. RIEC, Tohoku Daigaku, Sendai, Japan; 2. Niigata Koka Daigaku, Kashiwazaki, Japan*

Earlier work described microwave-assisted magnetic recording on dual structure media, in which a spin torque oscillator (STO) was used to select the structure on which to write [1]. In this work we discuss further improvements to the recording system that allow for higher density storage. A new write head design with a STO tilted at 15° to the vertical axis was used. Tilting the STO was necessary to allow the free layer of the STO to oscillate in the large magnetic field within the head gap. The recording structures were changed from exchange-coupled composite (ECC) to "notched"' structures [2]. The notched structures each consisted of three magnetic layers: a hard layer with high K_u, a soft layer with low K_u, and a cap layer with intermediate K_u. The average grain pitch was reduced from 9 nm in the previous work to 7 nm and the average grain size was 6 nm. A schematic of the medium design and layer thicknesses is shown in fig. 1. The K_u of each layer and the vertical exchange coupling between layers within the same structure was chosen to maximise the effective head field gradient, which reached 2.88 kOe/nm in RL1 and 3.68 kOe/nm in RL2. Tracks were written on RL1 and RL2 using STOs with widths of 36 nm and 18 nm, respectively. A wider STO was necessary to write on RL1 as it was further from the write head and the field from the STO was otherwise insufficient. Fig. 2 shows the SNR of written tracks as a function of linear recording density. The recording performance of RL1 was further optimised by introducing antiferromagnetic exchange coupling between RL1 and RL2 ($J_{1,2}$) to mitigate the effect of the magnetostatic field. In-plane exchange coupling of $A = 0.073$ erg/cm^2 was also found to improve the SNR of RL1. A grain switching probability model was used to write long bit sequences and calculate the bit error rate of each structure. From this the user areal density of RL1 and RL2 was 0.69 Tbit/in^2 for RL1 and 2.29 Tbit/in^2 for RL2, giving a total user areal density of about 3 Tbit/in^2.

[1] S. J. Greaves, K. S. Chan and Y. Kanai, IEEE Trans. Magn. 55, 6701509, (2019). [2] X. Bai and J. G. Zhu, IEEE Trans. Magn. 53, 3001405, (2017).

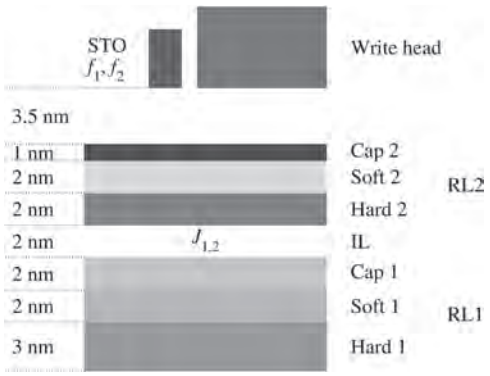

Fig. 1 Schematic of recording medium with two recording structures.

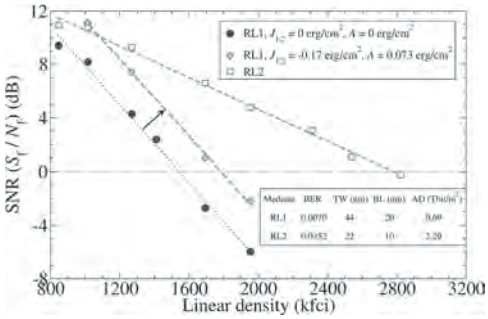

Fig. 2 SNR vs. linear density for RL1 and RL2 and estimates of the user areal density (AD) for each structure. BER = bit error rate, TW = track width, BL = bit length.

N3-03. Separate Quantitative Evaluation of Perpendicular Magnetic Anisotropy for Disorder and Order Portion in FePt Granular Films.

T. Saito[1], K. Tham[2], R. Kushibiki[2], T. Ogawa[1] and S. Saito[1] *1. Tohoku Daigaku Daigakuin Kogaku Kenkyuka Kogakubu, Sendai, Japan; 2. Tanaka Kikinzoku Kogyo Kabushiki Kaisha, Chiyoda-ku, Japan*

High perpendicular magnetic anisotropy ($K_u^{pep.}$) $L1_0$ FePt based granular media is eagerly required for HAMR media[1,2]. Although a structural inhomogeneity brought by the size effect and/or a randomly crystalline orientation of magnetic grains[4] existed, a correlation between the structural inhomogeneity and $K_u^{pep.}$ for the films had not been sufficiently clarified yet. In this presentation, a precise evaluation of thickness dependences of degree of order and $K_u^{pep.}$ was carried out for the granular films with various grain boundary materials (GBMs: C, B_2O_3, SnO, WO_3, Nb_2O_5, TiO_2, MnO, Y_2O_3, MgO). Fig. 1 shows dependence of the torque coefficient of twofold components (l_{20}) against a magnetic moment angle derived from 90 kOe torque curves for typical granular films with B_2O_3, SnO, and C GBMs on the film thickness (d_{mag}). l_{20} changes proportionally to d_{mag} below 7.5 nm in the SnO- and C-GBM films and below 5 nm in the B_2O_3-GBM film. The magnitude of gradients depended on GBMs. Note that there were the intersections of the fitted lines with the d_{mag} axis. Fig. 2 shows integral intensity of FePt (110) and (220) diffractions (I_{110} and I_{220}) observed in in-plane XRD profile plotted against d_{mag} for the typical SnO-GBM film. Here, I_{110} and I_{220} are superlattice and fundamental lines, respectively. Focusing on the extrapolated linear lines, I_{110} had the intersection with the d_{mag} axis while I_{220} crossed the origin coordinate, which suggested that a disorder portion was existed. I_{110} and I_{220} increased linearly with d_{mag} from 2 to 5 nm, which meant that there was a portion with constant degree of order (S_{in}). Based on these results, a separate evaluation of the volume, degree of order, and magnetic properties for the portions with disorder and order in the FePt granular films was enabled; the volume thicknesses of the disorder portions were 0.82, 0.98, 0.11 nm, and S_{in} and K_u^{pep} (erg/cm^3) for the portion with constant degree of order were (0.74, 9.8×10^6), (0.99, 2.3×10^7), and (0.97, 2.1×10^7) for the B_2O_3-, SnO-, and C-GBM films, respectively.

B. Lim et al., *J. Appl. Phys.*, vol. 103, p. 07E143-1 (2008) D. Weller et al., *Phys. Status Solidi* A, vol. 210, p. 1245 (2013) H. Sepehri-Amin et al., *Scripta Materialia*, vol. 130, p.247 (2017) B. Varaprasad et al., *IEEE Trans. Magn*. vol. 51, Art. no. 3200904 (2015)

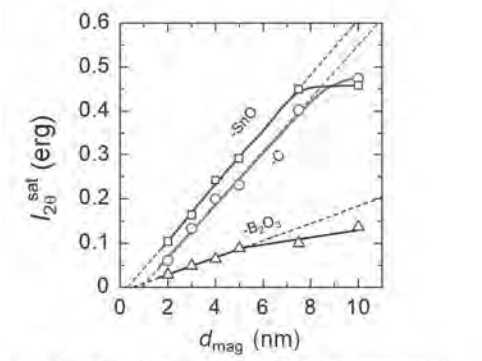

Fig. 1. Dependence of the torque coefficient of twofold components (l_{20}) for typical granular films with B_2O_3, SnO, and C on the film thickness (d_{mag}).

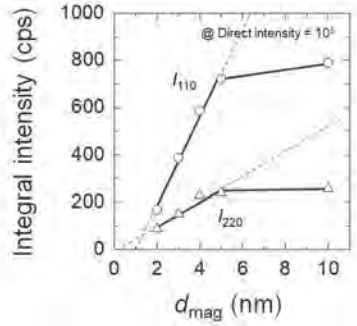

Fig. 2. Integral intensity of $L1_0$ FePt phase derived from in-plane XRD plotted against d_{mag} for the typical granular film with SnO.

N3-04. Incoherent Magnetization Switching Within a Fept-$L1_0$ Grain.

Y. Yan[1] and J. Zhu[1] *1. Electrical and Computer Engineering, Carnegie Mellon University, Pittsburgh, PA, United States*

In a $L1_0$ ordered FePt grain, Fe and Pt monolayers alternate along the ordering direction. Studies have shown that induced magnetic moment from the Pt monolayers is less than 10% of the total magnetic moment and the Fe-Pt and Pt-Pt exchange coupling is significantly weaker than that of Fe-Fe bonds [1][2]. Magnetization temperature dependence should be dominated by Fe monolayers, especially near Curie temperature. Based on such a physical picture, each $L1_0$ ordered FePt grain is modeled as a chain of exchange coupled macro-spins with each macro-spin representing a single Fe monolayer. Doubtlessly, this model specifically takes into account of the atomic structure and atomic exchange interactions that are specific to $L1_0$ ordering. Using this new model, systematic micromagnetic modeling has been performed to study magnetization switching of the $L1_0$ FePt grains in granular thin-film media during heat-assisted magnetic recording process as well as magnetization switching characteristics at room temperature. The study found that multiple oppositely magnetized domains within a FePt grain can be formed during the recording process. In the transition centers, significant percentages of grains, 20%~60% depending on recording conditions, can have domain walls stably remain within the grains. This mechanism enables grains in transition centers to have fractional magnetization, reducing the number of grains across the track width required for a desired SNR. On the other hand, the effective activation volume is much smaller than that of the grain volume due to the alternating Fe and Pt monolayers, limiting the grain diameter from reduction, a widely-accepted direction for increasing linear density. The results seemly provide an explanation for the current success of HAMR in achieving high track densities while facing challenges in increasing linear density capability.

[1] Antoniak C, Lindner J, Fauth K, et al. Physical Review B, 2010, 82(6): 064403. [2] Mryasov O N, Nowak U, Guslienko K Y, et al. EPL (Europhysics Letters), 2005, 69(5): 805.

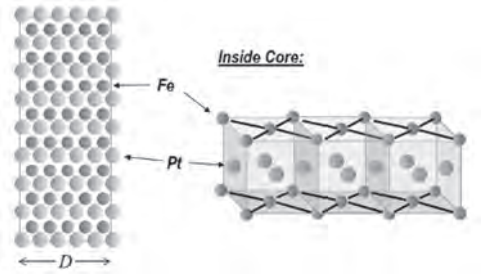

Fig.1 Illustration of atomic structure in a $L1_0$ ordered FePt grain.

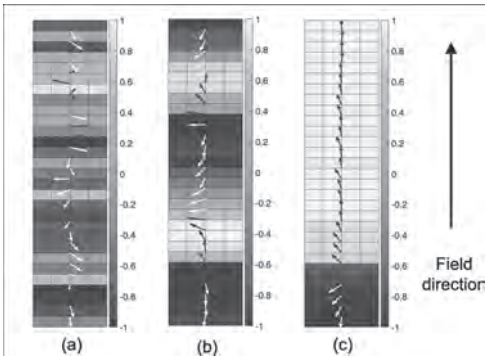

Fig.2 Grain (30 Fe-monolayers) magnetization state during the cooling in HAMR: (a) Slightly below T_c: each Fe monolayer acts rather independently; (b) Forming well-defined domains slightly above recording temperature; (c) A domain wall remains within a grain in the transition center after recording.

N3-05. Multiscale Micromagnetic-Atomistic Modelling of the Effects of MgO/CoFeB Interfacial Anisotropy, Dzyaloshinskii-Moriya Interactions, and Spin Transfer Torque in HDD TMR Reader. S. Jenkins[1], A. Dobrynin[2], K. McNeill[2], R. Chantrell[1] and *R.F. Evans*[1] *1. Physics, University of York, York, United Kingdom; 2. Research and Development, Seagate Technology (Ireland), Derry, United Kingdom*

Finite difference multiscale micromagnetic – atomistic HDD reader model has been developed, allowing to simulate realistic device designs, while benefiting from atomic scale resolution in the most critical parts, such as tunnelling barrier or interface between ferromagnetic and antiferromagnetic layers. The model features LLG and LLB solvers for dynamics calculations, with consistent time steps for the atomistic and micromagnetic regions; constrained Monte-Carlo solvers for modelling of equilibrium properties, such as temperature dependence of magnetization and magnetocrystalline anisotropy. In this presentation we will demonstrate some of the model's capabilities by considering effects of perpendicular anisotropy at the reference layer CoFeB / tunnel barrier MgO / free layer CoFe interfaces, as well as Dzyaloshinskii-Moriya interactions (DMI) arising at the same interfaces. Furthermore, effects of spin transfer torque (STT), introduced in the model via Slonczewski formalism are considered. First we compare fully atomistic, fully micromagnetic, and multiscale atomistic-micromagnetic models of a limited size trilayer, consisting of a CoFe pinned layer, antiferromagnetically coupled to a CoFeB reference layer via RKKY exchange coupling through a thin Ru layer (forming a synthetic antiferromagnet structure), and a free layer, separated from RL by an MgO tunnelling barrier. In-plane and out-of-plane field sweeps are used to characterize magnetic behaviour and to obtain the spin valve's transfer curves, and FMR spectra are used to characterize layers' anisotropy and magnetic noise, induced by thermal fluctuations. Then we present results of a full multiscale reader model, where the benefits of having an atomistic region around the tunnelling barrier are used to realistically simulate temperature dependent effects of interfacial anisotropy, DMI, and STT on the reader's performance.

N3-06. Iterative Detection With Multilayer Perceptron for Bit-Patterned Media Recording. *S. Jeong*[1] and J. Lee[1] *1. School of Electronic Engineering, Soongsil University, Seoul, The Republic of Korea*

Bit-patterned media recording (BPMR) is a promising candidate for the next generation of magnetic storage system to achieve areal density beyond one terabit per square inch [1]. For increasing a density of BPMR, the bit islands must be close to each other. However, we have faced the problem of intersymbol interference (ISI) and intertrack interference (ITI) that severely degrade the performance of BPMR system [2]. In this paper, we propose iterative detection with multilayer perceptron (MLP) for BPMR to improve bit error rate (BER) performance. Fig. 1 shows the block diagram of proposed iterative detection scheme that consists of partial response maximum likelihood (PRML) and MLP. The PRML detector is used to reduce ISI and ITI and the MLP is utilized to improve the system performance. After data is passed through BPMR channel, the proposed detection process is as follows. (1) First, we apply the MLP comprised of three hidden layer. The MLP output are fed to equalizer and SOVA and exploited as extrinsic information. (2) The received data with scaled down MLP output are equalized by 2D minimum mean square error (MMSE) equalizer. (3) When the branch metric of Viterbi detector is calculated, the equalizer output are used to reduce the impact of ISI, and the scaled down MLP output are used to reduce the impact of ITI. Then, the Viterbi output are sent to the MLP. (4) In iterative detection process, the MLP delivers the output only to the Viterbi detector, and the Viterbi detector delivers the output only to the MLP. And, Viterbi detector outputs the estimated data. Fig. 2 illustrates the BER performance of the proposed detection scheme according to the number of iteration at 3 terabit per square inch. At the BER of 10^{-4}, the performance of proposed scheme at 1st iteration shows best performance.

[1] H. J. Richter *et al*, IEEE Trans. Magn., Vol. 42, pp. 2255-2260, (2006)
[2] W. Chang and J. R. Cruz, IEEE Trans. Magn., Vol. 46, pp. 3899-3908, (2010)

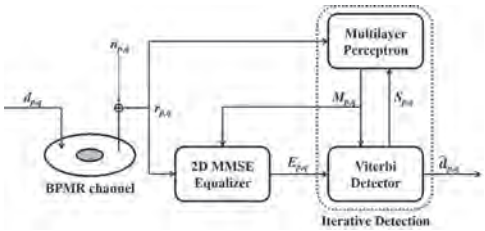

Fig. 1. Block diagram of the proposed iterative detection scheme.

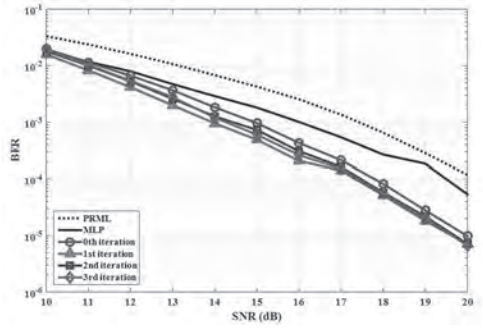

Fig. 2. BER performance of the proposed iterative detection scheme.

N3-07. Constrained Codes for Single-Reader/Two-Track Reading Technique in Bit-Patterned Magnetic Recording Systems. *S. Sokjabok*[1], M. Mattayakan[1], C. Buajong[1], S. Koonkarnkhai[2], P. Kovintavewat[2] and c. warisarn[1] *1. College of Advanced Manufacturing Innovation (AMI), King Mongkut's Institute of Technology Ladkrabang, 1 Soi Chalongkrung 1, Ladkrabang, Bangkok 10520, Thailand., Bangkok, Thailand; 2. Data Storage Technology Research Center, Nakhon Pathom Rajabhat University (NPRU), Nakhon Pathom 73000, Thailand., Nakhon Pathom, Thailand*

A reduction in the track width of magnetic recording systems results in a welcome increase in areal density (AD), but also in the unfortunate appearance of extreme inter-track interference (ITI) that can severely deteriorate system performance [1]. To deal with this problem, we propose to use a single-reader/two-track reading (SRTR) technique in a bit-patterned magnetic recording (BPMR) system where a single reader was used to read the desired parallel-track that was arranged as in the staggered structure [2]. Then, the received readback signal was sampled using the over-sampling technique as shown in Fig. 1. The data sequences that were obtained from the over-sampling process is then easily operated using one-dimensional (1D) equalization and detection schemes [3]. Moreover, we also present the rate-3/4 and -5/6 constrained codes for the SRTR BPMR system with the new criteria for encoding the user data bit. The error percentages of all considered data patterns i.e., $2^4 = 16$ and $2^6 = 64$ possible patterns for the rate-3/4 and -5/6 constrained codes, respectively, are first investigated as shown in Fig. 2. Then, the selected patterns which provide the lowest error percentage will be then given as the codeword. For instance, the first 32 patterns that give the lowest error percentage will be select as codewords for the rate-5/6 coded system as depicted in Fig. 2. Furthermore, the specified constraints at the boundaries between each codeword can be mitigated using the proposed sub-codeword which depends on its prior transmitted codeword. Besides, the decoding process can be easily operated under both the Euclidean distance and max-min based on Boolean logic functions [4] methods. The computer simulation results show that the effect of severe ITI can be mitigated through the use of our proposed coding schemes when compared with uncoded-, coded-SRTR, and conventional recording systems at the same considered user densities.

[1] S. Nabavi, B. V. K. V. Kumar, and J.-G. Zhu, IEEE Trans. Magn., Vol. 43, p.2274–2276 (2007) [2] C. Buajong and C. Warisarn, IEEE iEECON., p.1–4, (2017) [3] J. Moon and W. Zeng, IEEE Trans. Magn., Vol. 31, p.1083–1088 (1995) [4] N. Duric and M. Despotovic, in Proc. EUROCON., p.490–493 (2005)

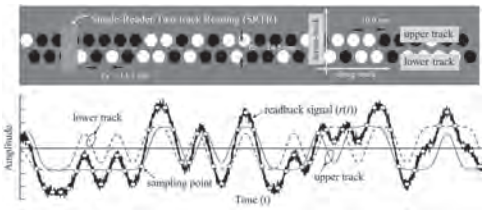

Fig.1 Staggered bit-patterned media with an SRTR technique and its related readback signal under an AD of 3.0 Tb/in^2.

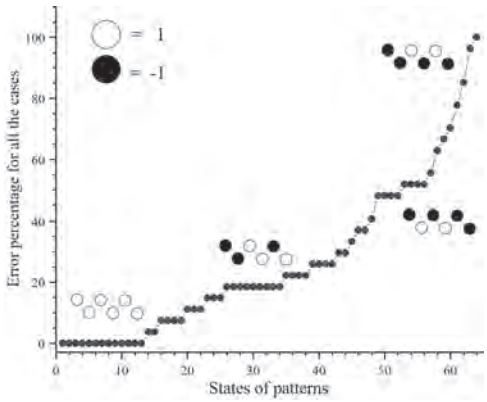

Fig.2 An error percentage of all possible 64 staggered data patterns in the rate-5/6 coded system.

N3-08. Soft-Information Flipper Based on Long-Short Term Memory Networks for Ultra-High Density Magnetic Recording. *N. Rueangnetr*[1], L.M. Myint[2] and c. warisarn[1] *1. College of Advanced Manufacturing Innovation, King Mongkut's Institute of Technology Ladkrabang, KMITL, Bangkok, Thailand; 2. Faculty of Engineering, King Mongkut's Institute of Technology Ladkrabang Faculty of Engineering, King Mongkut's Institute of Technology Ladkrabang, KMITL, Bangkok, Thailand*

An inter-track interference (ITI) effect can severely degrade the performance of ultra-high density magnetic recording systems such as bit-patterned media recording (BPMR) [1]. The two-dimensional (2D) modulation code can protect the severe ITI [2] which can efficiently improve the overall system performance: however, it cannot offer performance gain over the conventional system when the recording system must encounter with severe ITI from its sidetracks. Then, the flipping technique [3] was proposed to deal with that ITI sidetrack effect using the normalized soft-information values to be as bit-flipping criteria, which can efficiently improve the overall system performance. However, we found that those normalized values are difficult to confirm where is the optimal threshold value in the bit-flipping process. Therefore, this paper proposes a soft-information flipper based on long-short term memory (LSTM) networks [4] to deal with the mentioned shortcoming, which leads to improving the bit-error rate (BER) performance of three-track/three-head (3T/3H) BPMR system. Here, we directly map the soft-information, e.g., the datasets that were obtained from the 2D soft-output Viterbi algorithm (SOVA), $s_{l,k}$ with the hard-information that are achieved from encoding process, $x_{l,k}$ as shown in Fig. 1. Simulation results indicate that, at the same user density (UD), the proposed system (areal density (AD) = 3 Tb/in^2) provides BER performance gain over the conventional uncoded (AD = 2.5 Tb/in^2), coded [2], and normalization threshold systems (AD = 3 Tb/in^2) [3] as shown in Fig. 2. Moreover, the results also reveal that the proposed system is more robust to the media noise than the other systems.

[1] Y. Shiroishi et al., IEEE Trans. Magn., vol. 45, no. 10, pp. 3816-3822 (2009). [2] C. Warisarn, A. Arrayangkool, and P. Kovintavewat, IEICE Trans. Electron. vol. E98-C, no.6, pp. 528-533 (2015). [3] C. Warisarn, W. Busyatras, and L. M. M. Myint, AIP Advances., vol. 8, pp. 056509 (2018). [4] S. Hochreiter and J. Schmidhuber, Neural Computation, vol. 9, no. 8, pp. 1735–1780 (1997).

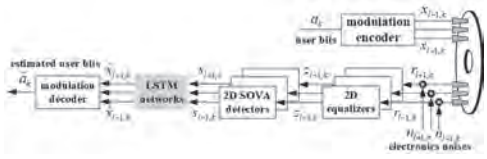

Fig. 1. A 3T/3H BPMR channel model with the rate-5/6 2D modulation code that performs together with the proposed soft-information flipper based on LSTM networks.

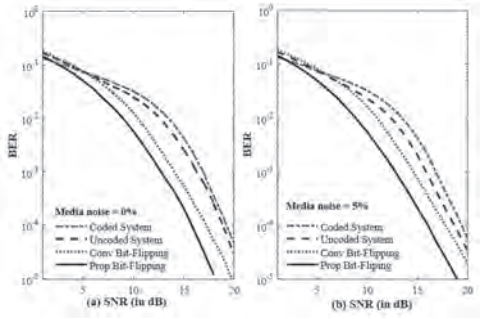

Fig. 2. BER performances of several systems (a) without and (b) with 5% media noise under different ADs (same UD = 2.5 Tb/in^2).

N3-09. A Simple Skew-Angle Detection and Alleviation Method Based on Readback Signal in Bit-Patterned Magnetic Recording Systems.
S. Koonkarnkhai[1], c. warisarn[2] and P. Kovintavewat[1] *1. Nakhon Pathom Rajabhat University, Nakhon Pathom, Thailand; 2. King Mongkut's Institute of Technology Ladkrabang, Bangkok, Thailand*

A skew angle (SA) is one of the main problems inevitable in the read/write processes of ultra-high density bit-patterned magnetic recording (BPMR) system [1], which can change the comparative place of the read/write elements on the slider [2]. However, the difference of SA depends on a zone of a magenetic medium, i.e., inner, middle, or outer diameter, varying between 25 – 35 degrees [3]. A large SA causes an increase in side reading and writing, resulting in reducing an expected areal density (AD) and increasing errors in the data detection process. Typically, the SA approach zero degrees is essential for BPMR systems. In practice, an actuation mechanism is used to mitigate this SA effect [2, 3]. Fig. 1 shows the impulse responses of upper, center, and lower tracks at 0˚ and 30˚ SA at an AD of 3 Tb/in^2. Clearly, unlike at 30˚ SA, the impulse response of the upper and lower tracks are similar at 0˚ SA. In this study, a binary input sequence $a_{j,k}$ is sent to the BPMR channel, representing by a 3×3 channel matrix with coefficients $\{h_{i,j}\}$ for -1 ≤ $\{i, j\}$ ≤ 1. At the receiver, the readback signal is fed to an one-dimensional (1D) equalizer and followed by a two-dimensional (2D) Viterbi detector to obtain an estimated input sequence. The 3×3 target matrix with coefficients $\{g_{i,j}\}$ for -1 ≤ $\{i, j\}$ ≤ 1 and its compatible 1D equalizer are designed based on a minimum mean-squared error approach [4]. Fig. 2 shows the SA profiles of the channel coefficient $h_{-1,0}$ and the target coefficient $g_{-1,0}$ at 3, 3.5, and 4 Tb/in^2 for different SAs. Apparently, we found that there is a relationship between $h_{-1,0}$ and $g_{-1,0}$. Therefore, we propose a simple SA detection and alleviation method by using $g_{-1,0}$ to approximate the SA experienced in the system. Then, a pair of suitable 2D target and 1D equalizer associated with the estimated SA is employed in data detection process. Results indicate that the proposed method can detect the SA and help improve the BPMR system performance.

[1] Y. Shiroishi, K. Fukuda, I. Tagawa, and et al., IEEE Trans. Magn., Vol. 45, pp. 2816 – 3822 (2009) [2] Z. He, and et al., Microsyst Technol Vol. 21, pp. 131–137 (2015) [3] Z. M. He, E. H. Ong, and G. X. Guo, J Appl Phys AIP, Vol. 91, pp. 8709–8711 (2002) [4] J. Moon and W. Zeng, IEEE Trans. Magn., Vol. 31, pp. 1083–1088 (1995)

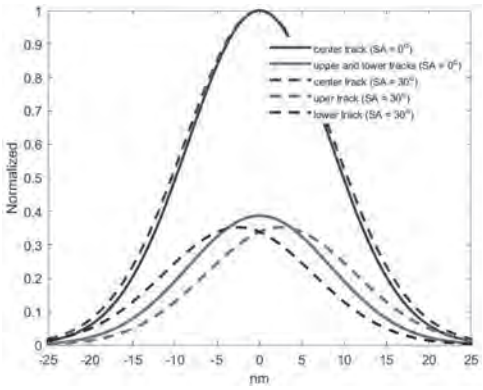

Fig. 1: The impulse responses of the upper, center, and lower tracks for various SAs.

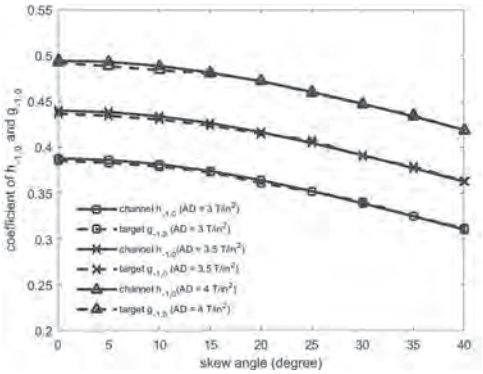

Fig. 2: The SA profile with respect to different channel and target coefficients.

N3-10. Viscoelastic Effects of Thermal Decomposed Lubricants on the Head-Disk Interface in Heat-Assisted Magnetic Recording.
H. Son[1] and *P. Chung*[1] *1. Department of Energy Engineering, Inje University, Gimhae, The Republic of Korea*

Magnetic recording system is currently evolving with the new recording techniques such as heat-assisted magnetic recording (HAMR) to drastically increase the areal density of the magnetic layer, while the thermal stability issues still exist on the lubricant layer. Specifically, lubricant molecules can cause the unexpected situations including the evaporation and contamination of the head and other components since the molecules can be chemically decomposed due to the cyclic thermal stresses with extremely high temperature [1,2]. Along with the thermal degradation, the contact between the slider and the disk causes the elongational stress on the intervening polymeric lubricant film so that the lubricant molecule can be mechanically decomposed as well as the anchored molecules can be also decoupled from the carbon overcoat [3]. Therefore, it is critically important to understand the molecular scale effects of the non-equilibrium perturbation on the decomposition and decoupling of the lubricants under the high temperature conditions to develop the sustainable lubricant materials for the HAMR systems. We investigated the thermal lubricant decomposition and the layer decoupling under the vertically elongational forces applied to the functional oligomeric film, which is similar as the contacting behavior between the head and the disk, by modeling the confined PFPE films with the static bottom and moving top substrates. To precisely estimate the thermos-mechanical molecular decomposition and decoupling phenomena, we utilized the full atomistic molecular dynamics, which fundamentally catches the intramolecular and intermolecular binding characteristics. We performed the coarse-grained non-equilibrium molecular dynamics with the deformation similar as the extensional flow experiment using atomic force microscopy (Fig. 1) to investigate the the viscoelastic properties of the lubricants as a function

of a fragmented molecules, which is correlated to the thermos-mechanical conditions. We also provide a nanostructural analysis of the lubricant layer for the future development of the HDI systems.

1. B. Marchon and Y. Saito, IEEE Trans. Magn., 48, 4471 (2012). 2. D. Pan, A. Ovcharenko, J.-P. Peng, and H. Jiang, *IEEE Trans. Magn.*, 50, 3302005 (2014). 3. J.A. Odell, A.J. Muller, K.A. Narh, and A. Keller, Macromolecules, 23, 3092 (1990). 4. Q. Guo, S. Izumisawa, M.S. Jhon, and Y.-T. Hsia, *IEEE Trans. Magn.*, 44, 3698 (2008).

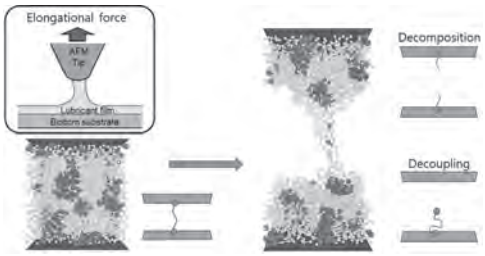

Fig.1. The elongational stress on the confined PFPE Zdol and the schematic description of the decomposition and the decoupling.

N3-11. Withdrawn

N3-12. The Influence of Finite-Size Effects on the Curie Temperature of $L1_0$-FePt. *B.T. Nguyen*[1], S. Ruta[1], O. Hovorka[2], R.F. Evans[1] and R. Chantrell[1] *1. Physics, University of York, York, United Kingdom; 2. Engineering and Physical Sciences, University of Southampton, Southampton, United Kingdom*

$L1_0$-phase Iron Platinum ($L1_0$-FePt) has been widely studied [1] for application in Heat-Assisted Magnetic Recording (HAMR). An important aspect for successful HAMR media is controlling the Curie temperature dispersion, which for $L1_0$-FePt a strong dependence on finite-size effects is reported [2] [3]. This poses a serious problem as the inevitable grain size distribution causes a Curie temperature (T_c) distribution which potentially limits recording density. We employed an atomistic model based on the VAMPIRE code [4] to study finite-size effects in $L1_0$-FePt grains using nearest-neighbour Heisenberg Hamiltonian exchange. Our grains had variable surface geometries (cylindrical, parallelepiped, and randomly-generated shape) and sizes (1 to 10nm). Importantly, our model gives access to the magnetisation properties of each atomic layer of the grains which provides insights into the magnetisation profile along a specific dimension. We hypothesised a correlation between the T_c distribution of $L1_0$-FePt and the percentage of atomistic bond loss on the grain surface as a function of grain size. Our result establishes a size threshold at 2.5nm below which the impact of finite-size effects starts to permeate into the centre of the grain and contributes to the overall drop of the grain T_c [Fig.1]. The magnetisation profile [Fig.2] further illustrates this. In larger grains surface disorder (lower magnetisation) is seen to penetrate only a few layers, whilst in smaller grains surface effects begin to dominate. Consequently, the grain T_c profile was also found to follow a similar trend. Our findings are consistent with semi-analytical mean-field calculations and have been extended to incorporate different crystal structures, which strongly suggests that if using a suitable correlation factor the T_c distribution of a generic material can be correlated to the percentage of atomistic bond loss on the surface as a universal parameter.

[1]: D. Weller et al., *Journal of Vacuum Science & Technology B*, 34, 060801 (2016) [2]: O. Hovorka et al., *Applied Physics Letters*, 101, 052406 (2012) [3]: A. Lyberatos et al., *Journal of Applied Physics* 114, 233904 (2013) [4]: R. F. L. Evans et al., *Journal of Physics: Condensed Matter*, 26, 103202 (2014). More information about VAMPIRE can be found at: http://vampire.york.ac.uk/features/

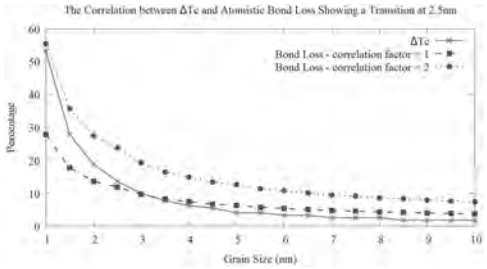

Fig 1: At 2.5nm, ΔT_c is seen to transit between the 2 limits of atomistic bond loss where surface effect fully confines (correlation factor=1) or fully permeates into grain centre (correlation factor=2)

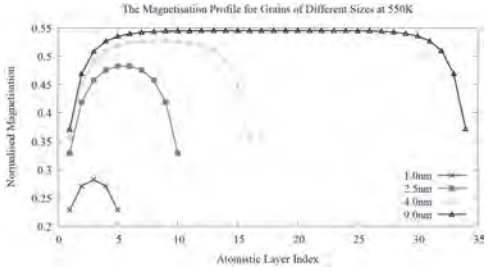

Fig 2: The magnetisation profile at 550K showing the dominance of surface disorder in smaller grains

N3-13. Curvature Change of Heat Assisted Magnetic Recording Patterns With Different Bit Lengths. *K. Xue*[1] and R. Victora[1] *1. Electrical and Computer Engineering, University of Minnesota, Minneapolis, MN, United States*

Heat assisted magnetic recording (HAMR) has become a very promising candidate for next-generation information storage technology. As recording bit lengths decrease down near ten nanometers in order to further increase the storage density, the recording performance (mainly the signal to noise ratio) cannot satisfy demands. In this study, a new method to characterize the recording pattern quality has been proposed in order to better understand the observed change in performance and help provide improved HAMR designs. In this method, for a given bit length (21nm, 15nm, and 10.5nm), more than 100 recording bit patterns are written micromagnetically, summed and averaged, generating a pattern contour with a crescent shape (Figure 1). This shape is due to the circular shape of the moving heating spot. A single tone binary sequence is used. Thermal Exchange-Coupled Composite media is used, where a moderate anisotropy material serves as the writing layer and an FePt layer serves as the storage layer [1]. By fitting the convex arm of the contour to a parabolic function, the curvature of the contour can be quantified (Figure 2): 10.5nm: 0.0184 (DC) and 0.0178(AC); 15nm: 0.0198 (DC) and 0.0189(AC); 21nm: 0.0222 (DC) and 0.0204(AC) (nm^{-1}). The results show that smaller bit length gives a contour with lower curvature, which means that the recording patterns are less affected by the heat spot shape, less overlapping with each other and better separated. AC-erased media show even smaller curvatures than their DC-erased counterparts, suggesting that AC-erased media could provide better performance.

[1] Z. Liu and R. Victora, IEEE Transactions on Magnetics, Vol. 52, No. 7, p. 1-4(2016)

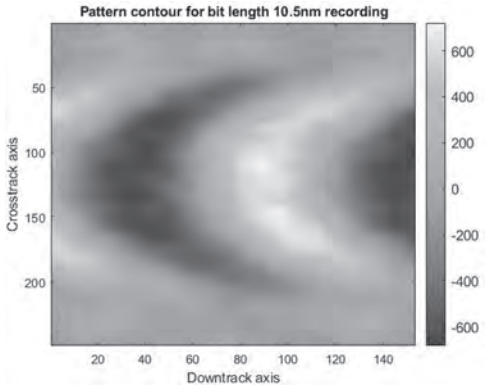

Fig. 1 Pattern contour of the 10.5nm bit length recording. Media are AC-erased. Totally 128 bits are summed and averaged.

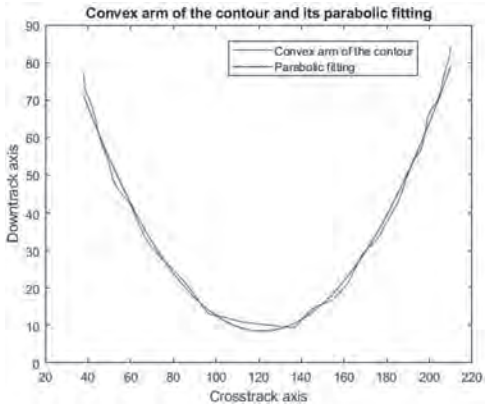

Fig. 2 Convex arm of the contour and its parabolic curve fitting. The contour is rotated 90 degrees counter-clockwise.

N3-14. Effects of Thermo-Mechanical Contact on Ferromagnetic Thin Film of PMR (Perpendicular Magnetic Recording) Media. *C. Yeo*[1], M. He[1], J. Lee[1], M. Choi[3], Y. Hong[3], J. You[2], D. Purani[4], J. Lee[5] and H. Won[3] *1. Department of Mechanical Engineering, Texas Tech University, Lubbock, TX, United States; 2. School of Engineering, University of Saint Thomas, Saint Paul, MN, United States; 3. Department of Electrical and Computer Engineering, The University of Alabama, Tuscaloosa, AL, United States; 4. Head Disk Interface Group, Seagate Technology, Shakopee, MN, United States; 5. Hysitron Nanomechanical Test Instruments, Bruker Corporation, Eden Prairie, MN, United States*

We used the nanoscratch method to study the response of perpendicular recording media (Co-Cr-Pt magnetic layer) to thermal-mechanical contact. Nanoscratched and non-scratched areas are characterized for magnetic and physical (morphological) properties at elevated temperatures by atomic force microscopy (AFM) and magnetic force microscopy (MFM). The figure below shows a 2T patterned MFM image and phase angle, i.e., the magnetic signal of recording media. The magnetic signal is not distorted. In the non-contact surface area far from the nanoscratch, the magnetic signal (strength) was gradually weakened with increasing annealing temperature to 300 °C due to the thermal agitation of magnetic spins. Still, the area close to the scratch center recovers the magnetic signal at elevated temperatures, indicating a partial recovery of ferromagnetism of an unscratched area. On the other hand, for the nanoscratched area, the magnetic signal at high local stressed zone was completely lost and did not recover after heating the film at 100 °C. Regarding the nanoscratch morphology, the as-scratch depth is about 8 nm at 25 °C. Surprisingly, the scratch is recovered to a depth of 1 - 2 nm at a temperature between 100 and 300 °C. This is attributed to the oxidation of the fresh surface (scratch) of the magnetic film. However, the scratch deepens at 400 - 600 °C so that the scratch depth is 8 nm, which is the same as the as-scratched depth. The deepening process at 400 - 600 °C is attributed to the evaporation of PtO_2. We have proposed the mechanism of scratch recovering and deepening and also stress distribution caused by nanoscratch. The results of this study may help design future HAMR media to secure long term reliability of HDD.

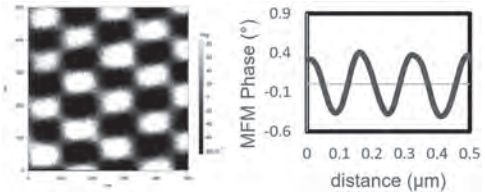

Fig. 1. 2T patterned MFM image and its phase angle.

Session N4
MAGNETIC TUNNEL JUNCTION AND RELATED EFFECTS, VOLTAGE CONTROLLED MAGNETISM (Poster Session)

Joseph Prestigiacomo, Chair
Naval Research Lab, Washington, DC, United States

N4-01. Compact Model of Nanometer STT-MTJ Device With Scale Effect. *M. Wang*[1] and Y. Jiang[1] *1. Jiangnan University, Wuxi, China*

The emergence and growing maturity of spintronics presents new ideas and methods for low-power design. Spin-transfer torque magnetic tunnel junction (STT-MTJ) device is one of the spintronic applications for future promising non-volatile memory. In this paper, a compact model for STT-MTJ device in nanoscale is presented. The scale effect of the device is included in the model. Firstly, by analyzing the influence of the device scale on the device properties, the scale effect of the MTJ device is presented. Secondly, the thermal stability factor is trimmed to reflect the influence of the scale effect of the device. In this way, the compact model is presented for the nanometer MTJ device with obvious scale effect. For the compact model, the simulation is conducted at different process nodes to reflect the influence of the scale effect. The simulation results involve resistance, thermal stability, switching time and other characteristics. At the same time, the write error rate is also presented. Figure 1 shows the dynamic properties of the z-axis component with three different device sizes. It can be seen that a larger diameter corresponds to a larger switching time. Figure 2(a) and Figure 2(b) shows the error rates of writing "1" and writing "0" with different voltage and different size, separately. As the voltage or device size increases, the write error rate decreases.

[1] Roberto Carboni, Elena Vernocchi and Manzar Siddik, IEEE Transactions on Electron Devices., Vol. 66, p.4176-4180 (2019). [2] Yue Zhang, Weisheng Zhao and Yahya Lakys, IEEE Transactions on Electron Devices., Vol. 59, p.819-824 (2012).

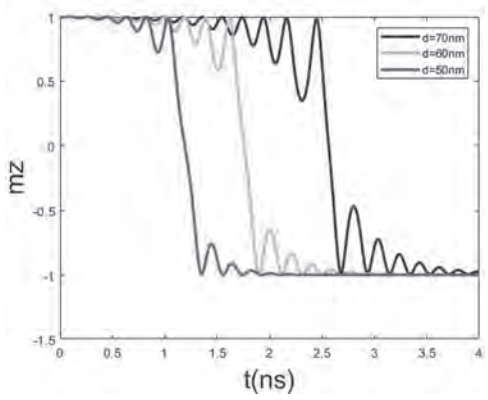

Fig.1 Dynamic properties of the z-axis magnetization vector with different device sizes.

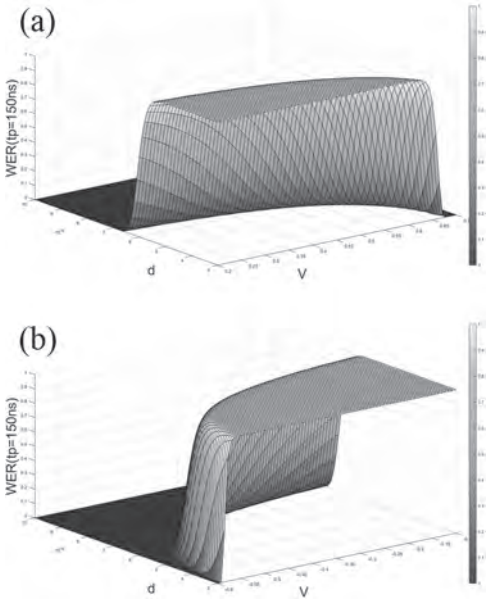

Fig.2 (a) The error rate of writing "1" with different voltages and different sizes. Fig.2 (b) The error rate of writing "0" with different voltages and different sizes.

N4-02. Low Resistivity Spin Orbit Torque Wiring With WCu Composite Material. *E. Komura*[1], Y. Shiokawa[1], Y. Ishitani[1], K. Hamanaka[1], K. Suda[1], A. Tsumita[1], Y. Kakinuma[1], Y. Terasaki[1] and T. Sasaki[1] *1. TDK Corporation, Ichikawa, Japan*

Recently, spin current type magnetic memory (SC memory) with Spin Orbit Torque (SOT) has attracted much attention because of the potential for high speed non-volatile memory. We have already reported that this SC memory with β-W SOT wiring had high write endurance up to 10^{12}[1] and low write error rate (WER) under 10^{-7}[2]. However, an issue is clarified that the SOT wiring is attacked by Joule heating due to high resistivity of β-W. In this presentation, we proposed low resistivity SOT wiring of WCu composite material and achieved small switching current density as same as β-W SOT wiring. We fabricated the Magnetic Tummel Junction (MTJ)device of top pinned type on SOT wiring, Sub. / SOT wiring / CoFeB-based Free layer / tunnel barrier / CoFeB-based SAF-pinned layer / IrMn / Capping. We prepared three kinds of SOT wiring as β-W, WCu-1(low Cu composition), and WCu-2 (high Cu composition). The shape of the MTJ was ellipse of 80 nm × 250 nm and long axis of MTJ was orthogonal to the direction of write current, generally called as Type-Y. SOT wiring was designed of 380nm length, 250nm width. The resistivity of β-W, WCu-1, and WCu-2 were obtained of 570μΩcm, 400 μΩcm, and 380 μΩcm, respectively. The increase of Cu composition could decrease the resistivity. Fig.1 shows the relationship between switching current density and pulse. In spite of including Cu in β-W, the switching current density could remain low as same as β-W. This Cu composition for reduction of resistivity could help to avoid the thermal attack by Joule heating.

[1] Y. Shiokawa, et al, AIP Advances 9, 035236 (2019) [2] Y. Shiokawa, et al, IEDM special MRAM poster session, 07 (2019)

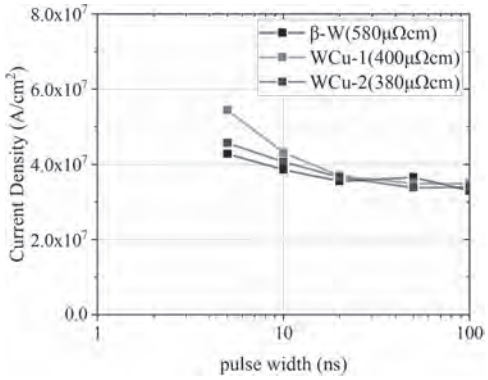

Fig.1 Relationship between current density and pulse width with β-W, WCu-1, and WCu-2 as WCu composite material.

N4-03. Measurement of Anisotropy Field Under External Perpendicular Magnetic Field in FeCoB and FeB Nanomagnets. Study of PMA Features in a Nanomagnet. *V. Zayets*[1] *1. Research Institute for Advanced Electronics and Photonics, National Institute of Advanced Industrial Science and Technology (AIST), Tsukuba, Japan*

A FeCoB nanomagnet with perpendicular magnetic anisotropy (PMA) is important as a storage element for Magnetic Random Access memory (MRAM), because of their single-domain magnetic state and a high-thermal stability. In order to achieve a required high- performance of MRAM, both the enhancement of the PMA and a high-controllability of PMA are required. A parameter, which characterizes the PMA strength in a nanomagnet, is the anisotropy field H_{anis}. The H_{anis} is the magnetic field, which is applied in-plane and therefore perpendicularly to the easy axis of a nanomagnet and at which initially-perpendicular magnetization turns completely to the in-plane direction. A half of product of H_{anis} and nanomagnet magnetization is a common estimate of the PMA energy [1]. We measure the H_{anis} as a function of a perpendicularly- applied external magnetic field H_z using a Hall setup. In-plane magnetic field H_x and H_z were applied simultaneously. Under a fixed H_z, the H_x was scanned. Measured in-plane component of magnetization M_x changes linearly with respect to H_x (at least in region $-0.7\ H_{anis} < H_x < 0.7\ H_{anis}$). From the slope of the measured linear dependence, the H_{anis} is evaluated. Figure 1 shows the measured H_{anis} vs H_z for a magnetically-softer FeB nanomagnet (H_c=70 Oe) and magnetically-harder FeCoB nanomagnet (H_c=560 Oe). In both nanomagnets, the dependence becomes linear at H_z >3 kG as it is predicted theoretically. From the slop of the linear dependence the strength of the Spin-Orbit interaction at nanomagnet interface is estimated. The dependence at smaller H_z gives an estimate of the intrinsic magnetic field, which always exists along nanomagnet magnetization, and the demagnetization field.

[1] M.T. Johnson, P.J.H. Bloemen, F.J.A. Den Broeder, and J.J. De Vries, Reports Prog. Phys. Vol. 59, p.1409 (1996).

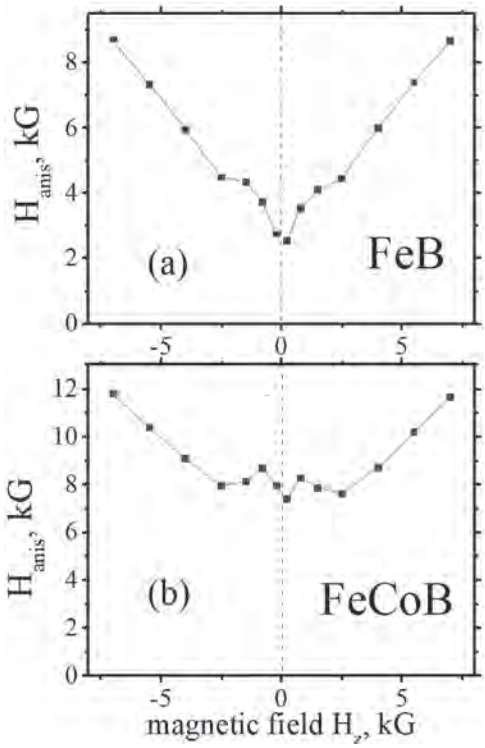

Fig.1 Anisotropy field H_{anis} as a function of external magnetic field H_z applied perpendicularly to interface and along the magnetization. (a) magnetically-softer FeB nanomagnet. (b) magnetically-harder FeCoB nanomagnet

N4-04. Developing a Vampire Model for TAMR. *B.W. Wilson*[1], J.N. Scott[1], W. Hendren[1] and R. Bowman[1] *1. Queen's University Belfast, Belfast, United Kingdom*

To increase the areal density of hard disk drives (HDD) requires both the writability of smaller bits and the ability to read these bits. This can only be achieved by reducing the size of conventional tunnelling magnetoresistance (TMR) sensors. A possible solution is tunnel anisotropic magnetoresistance (TAMR), which arises due to a change of density of states at the Fermi level when a magnetic (sub)lattice rotates with respect to the crystal field. It is particularly present in materials which possess large spin-orbit (SO) interactions such as CoPt [1] Very large TAMR signals have been observed at low temperatures consisting of an IrMn based magnetic tunnel junction (MTJ) [2]. Optimisation of this structure to achieve TAMR at room temperature could potentially remove the requirement for a second ferromagnetic electrode and thus reduce the size of the sensor. The atomistic spin simulation package, VAMPIRE [3], is used in conjunction with SQUID and vibrating sample magnetometry (VSM) to investigate the bilayer system of $Ni_{80}Fe_{20}$/ $Co_{70}Fe_{30}$ deposited via magnetron sputtering, in order to optimise the ferromagnetic layer of the MTJ. Simulation parameters are achieved directly from experiment and supplied to the model. Integration of simulation and experiment in this manner can yield insight into the magnetisation dynamics on the atomic scale and guide experimental development. The inclusion of the thin layer of $Co_{70}Fe_{30}$ within simulations of a permalloy thin film has been found to enhance the coercive field of ferromagnetic layer of the MTJ. Experimental confirmation of this result will provide the basis for layer by layer optimisation of the TAMR structure which will pave the way in the advancement of data storage.

[1] - B. G. Park et al., Phys. Rev. Letts 100, 087204 (2008) [2] - B. G. Park et al., Nature Mat. 10, 347 (2011) [3] - R. F. L. Evans et al., Appl. Phys. Lett. 104, 082410 (2014)

N4-05. Withdrawn

N4-06. Reversible Voltage Control of Magnetism via Lithium Ion Migration in a Battery-Inspired Magneto-Ionic Heterostructure.
M. Ameziane[1], R. Mansell[1] and S. van Dijken[1] *1. Applied Physics, Aalto University, Espoo, Finland*

Control of magnetism via electric fields is relevant for the development of energy-efficient memory and logic devices. One possible mechanism utilizes electric-field-driven migration of ions into or away from a magnetic film. This approach, known as magneto-ionics, often relies on the redistribution of oxygen ions [1], but extensions to other ionic species are possible. For instance, a reversible modulation of magnetic properties has been realized with lithium ions recently [2-5]. Inspired by solid-state lithium-ion battery architectures, we report on reversible voltage control of magnetization in a 10-nm-thick $Co_{40}Fe_{40}B_{20}$ (CoFeB) film at room temperature. In our magneto-ionic heterostructure (Fig. 1a), the CoFeB layer is gated by lithium phosphorous oxynitride (LiPON), a popular solid-state lithium-ion conductor, in a patterned crossbar geometry. Lithium cobalt oxide (LCO) is used as a storage layer for lithium ions on top of LiPON. The magneto-ionic structures are fabricated by magnetron sputtering through metal shadow masks and their magnetic properties are investigated by magneto-optical Kerr effect (MOKE) microscopy under *in-operando* conditions. Using cyclic voltammetry, we demonstrate the onset of electrochemical activity at small bias voltages (Fig. 1b), in agreement with COMSOL simulations. The application of a positive voltage to the top gate significantly reduces the magnetization of the CoFeB film (Fig. 1c). The original magnetization recovers completely under negative bias. Reversible switching between high and low magnetization states extends over many cycles (Fig. 1d). We attribute the electric-field-driven magnetic effects to lithium ion migration into (positive bias) and out of (negative voltage) the CoFeB layer. The dependence of magnetization control on the film thickness and the ferromagnetic material will be discussed.

[1] U. Bauer, L. Yao, A. J. Tan, Nat Mater., Vol. 14, p. 174-181 (2015). [2] S. Dasgupta, B. Das, M. Knapp, Adv. Mater., Vol. 26, p. 4639-4644 (2014). [3] Q. Zhang, X. Luo, L. Wang, Nano Lett., Vol. 16, p. 583-587 (2015). [4] G. Wei, L. Wei, D. Wang, Appl. Phys. Lett., Vol. 110, p. 062404 (2017). [5] D. Pravarthana, B. Wang, Z. Mustafa, Phys. Rev. Appl., Vol. 12, p. 054065 (2019).

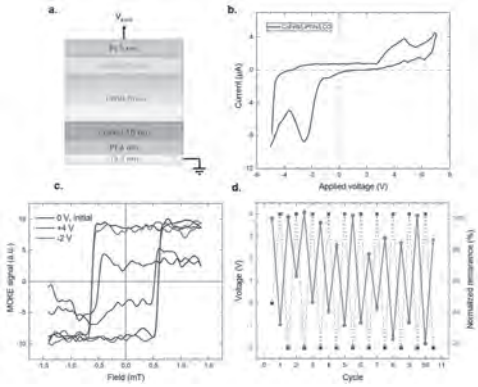

(a) Schematic of the magneto-ionic structure. (b) A cyclic voltammogram of the crossbar junction. (c) In-plane MOKE loops of the CoFeB film at 0 V (black) and after biasing the structure for 2 minutes at +4 V (blue) and -2 V (red). (d) Modulation of the remanent magnetization upon repeated biasing at +4 V and -2 V.

N4-07. The Voltage-Controlled Magnetic Anisotropy Effect Under High Electric Field.
B. Zhou[1], M. Xu[1], P. Khanal[1], Y. Zhang[1] and W. Wang[1] *1. Physics, The University of Arizona, Tucson, AZ, United States*

The discovery of voltage-controlled magnetic anisotropy (VCMA) effect in perpendicular magnetic tunneling junction (pMTJ) has attracted considerable interests for low-power and high-speed memory applications. In a recent DFT study [1], the VCMA effect is expected to diverge from commonly observed linear PMA vs E-field relation and exhibit nonlinearity under high E-field. However, the limitations of established methods make high E-field unattainable. A modified TMR method is performed in this work. By using pulsed voltage, on-time can be reduced by at least 2 orders of magnitude, which increases the MTJ breakdown voltage and allows for higher E-field (>800mV/nm). Unexpected magnetoresistance independent of relative FM spin alignment was discovered and attributed to impurity-assisted tunneling. Efforts were made to exclude it from conventional TMR and a nonlinear E-field dependence of PMA can be observed under high bias. Electron doping with different metals as buffer and insertion is carried out and their influence is reported and compared with DFT study.

[1] J. Zhang et al., Phys. Rev. B 96, 014435 (2017).

N4-08. Nonvolatile Voltage Controlled Molecular Spin State Switching for Memory Applications.
G. Hao[1,2], A. Mosey[3], X. Jiang[1], R.V. Chopdekar[2], R. Cheng[3], X. Xu[1], A. Marshall[4] and *A.T. N'Diaye*[2] *1. Department of Physics and Astronomy, University of Nebraska-Lincoln, Lincoln, NE, United States; 2. Advanced Light Source, Lawrence Berkeley National Laboratory, Berkeley, CA, United States; 3. Physics Department, Indiana University Purdue University at Indianapolis, Indianapolis, IN, United States; 4. Department of Electrical Engineering, University of Texas at Dallas, Austin, TX, United States*

As the expectations for novel printable electronics grows, the design of flexible and high-density nonvolatile memory devices remains a high-stakes target. Molecular materials systems have highly tunable electronic properties which do not rely on long range crystallographic order, but on short range chemical order, and are therefore ideally suited as printable functional materials. Among the such materials, spin crossover (SCO) materials are known for their two spin states with distinct electronic and magnetic properties. They can be designed to show bistability at various temperatures including room temperature and the spin crossover transition can be tuned induced and influenced by various external stimuli. Molecular systems have the very real possibility of providing a room temperature device on a length scale less than 10 nm while delivering low power GHz nonvolatile local magneto-electric logic or memory operations. As magneto-electric coupling has now been demonstrated, printable molecular spintronics is a very real possibility. In this contribution we will discuss how $[Fe\{H_2B(pz)_2\}_2(bipy)]$, where pz = tris(pyrazol-1-yl)- borohydride and bipy = 2,2'-bipyridine, can be locked in the low spin (LS) state by a dielectric substrate and excited into the high spin (HS) state at room temperature by an X-ray fluence and then relaxed back to the low spin state either thermally [1] or through magnetic field switching [2]. Coupling to ferroelectric materials, enables voltage controlled isothermal reversible switching of the spin state is accompanied by a resistance change, and is seen to be nonvolatile, i.e., retained in the absence of an applied electric field [3]. We will furthermore use x-ray photoelectron microscopy (PEEM) to map out the local distribution of the spin state. This allows us to formulate goals materials design to enable reliable spin-crossover devices.

[1] X. Zhang, P. S. Costa, J. Hooper, D. P. Miller, A. T. N'Diaye, S. Beniwal, X. Jiang, Y. Yin, P. Rosa, L. Routaboul, M. Gonidec, L. Poggini, P. Braunstein, B. Doudin, X. Xu, A. Enders, E. Zurek, and P. A. Dowben, Adv. Mater. 29, 1702257 (2017). [2] X. Zhang, A. T. N'Diaye, X. Jiang, X. Zhang, Y. Yin, X. Chen, X. Hong, X. Xu, and P. A. Dowben, Chem. Commun. 54, 944 (2018). [3] G. Hao, A. Mosey, X. Jiang, A. J. Yost, K. R. Sapkota, G. T. Wang, X. Zhang, J. Zhang, A. T. N'Diaye, R. Cheng, X. Xu and P. A. Dowben, Appl. Phys. Lett. 114, 032901 (2019)

Session N5
NOVEL SENSORS II
(Poster Session)

Jeffrey McCord, Chair
CAU Kiel, Kiel, Germany

N5-01. Application of 90-Degree Configuration MTJ With PMA Pinned Layer and in-Plane Sensing Layer on Large Area Biosensors. *C. Lee*[1], D. Su[3], J. Wang[2] and C. Lai[1] *1. Department of Materials Science and Engineering, National Tsing Hua University, Hsinchu, Taiwan; 2. Department of Electrical and Computer Engineering, University of Minnesota, Minneapolis, MN, United States; 3. Department of Chemical Engineering and Materials Science, University of Minnesota, Minneapolis, MN, United States*

Spintronics sensors have been used for bio-sensing purpose for years[1]. In giant magnetoresistive (GMR) biosensors, it is easy to obtain a linear response by taking the advantage of shape anisotropy if the stripes are patterned with a moderate aspect ratio. However, the non-uniform signal of magnetic nanoparticles (MNP) and the small sensing area lower the sensor performance[2]. A large area sensor was demonstrated[3] and modeled to address these concerns[4]. However, the lack of the linearity restricts the sensor application. In this work, we propose a new approach to achieve linear response in large-area MTJs for bio-sensing. By using MTJs composed of a pinned layer (PL) with perpendicular magnetic anisotropy (PMA) and a sensing layer (SL) with an in-plane magnetic anisotropy (IMA), a bias-free biosensor with linear response can be obtained. Since shape anisotropy does not play any role in this method, the area and the shape of the sensing element are not restricted. Consequently, sensing area can be effectively increased while maintaining linearity. The feasibility of the CoFeB/MgO based biosensing scheme is demonstrated by OOMMF [8] on 100x100 nm^2 element. Fig. 1(a) is the simulated MH loops of CoFeB SL with various number of MNPs for 1.7nm CoFeB and the calculated sensor signal vs. MNP concentration in a field range of ± 100 Oe is plotted in Fig.1(b). This result does demonstrate the feasibility of 90-degree configuration MTJs with PMA PL and IMA SL for bio-sensing. In summary, a 90-degree configuration MTJ sensor with PMA PL and in-plane SL is proposed for biosensing. Since the linear output is contributed by the cross anisotropy between PMA PL and in-plane SL, this method could be extended to a large-area sensing element. Most importantly, this idea combines all the advantages of currently used biosensors such as large detection area, uniform signal, and linear output without the need of external bias field.

1. Baselt, D.R., et al., *A biosensor based on magnetoresistance technology.* Biosensors and Bioelectronics, 1998. 13(7): p. 731-739. 2. Klein, T., et al., *Comparative analysis of several GMR strip sensor configurations for biological applications.* Sensors and Actuators A: Physical, 2014. 216: p. 349-354. 3. Srinivasan, B., et al., *A Detection System Based on Giant Magnetoresistive Sensors and High-Moment Magnetic Nanoparticles Demonstrates Zeptomole Sensitivity: Potential for Personalized Medicine.* Angewandte Chemie International Edition, 2009. 48(15): p. 2764-2767. 4. Su, D., K. Wu, and J.-P. Wang, *Large-area GMR bio-sensors based on reverse nucleation switching mechanism.* Journal of Magnetism and Magnetic Materials, 2019. 473: p. 484-489. 5. Porter, M.D.a.d., *The Object Oriented MicroMagnetic Framework (Oommf) Project at ITL/NIST. The OOMMF code is Available at http://math.nist. gov/oommf.*

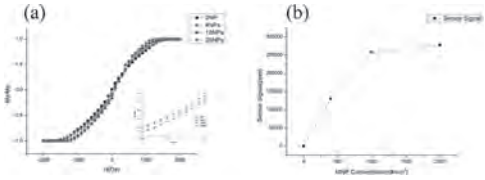

Fig. 1. (a) Simulated MH loops of 1.7nm CoFeB with nanoparticles. (b) Sensor signal vs. nanoparticle concentration.

N5-02. Serial Magnetic Tunnel Junctions Based Sensor for Non-destructive Flux Leakage Testing. *Z. Jin*[1], M. Mohd Noor Sam[1,2], M. Oogane[1,3] and Y. Ando[1,4] *1. Applied Physics, Tohoku university, Sendai, Japan; 2. Graduate Program in Spintronics, Tohoku University, Sendai, Japan; 3. Center for Science and Innovation in Spintronics (Core Research Cluster), Organization for Advanced Studies, Tohoku university, Sendai, Japan; 4. Center for Spintronics Research Network, Tohoku university, Sendai, Japan*

Because of high sensitivity, excellent scalability, and low power consumption, magnetic tunnel junctions (MTJs) based sensors have been widely used in various industrial fields [1]. In the magnetic flux leakage testing (MFL) field, it is required to use high-sensitivity sensors to detect small changes in the inhomogeneous magnetic field. In a previous study, serial MTJs based sensors were successfully introduced to detect surface cracks in electromagnetic NDT [2]. In this study, we modify serial MTJs based sensors with a good response for external fields and demonstrate the sensor can identify a fractured steel bar in MFL testing. The MTJ films were prepared by the sputtering system and the MTJ devices were micro-fabricated by photolithography and argon ion milling. The free-layer pattern with a rectangular shape was chosen due to the suitable shape anisotropy. The two-step field annealing was adopted, which leads to the easy axis of the free layer is perpendicular to that of the pinned layer, and improves the linearity of the sensor. After fabrication, MTJ devices were connected in a full-bridge circuit, and the transfer curve and noise were measured for determining detectivity. Figure 1 shows that the sensor exhibits a linear response for an external field, and presents a low detectivity in the range of -8 to 8 Oe. Moreover, the fractured and intact steel bars were detected by using flux leakage testing with the sensor. Figure 2 shows the measurement results present that the fractured steel bar can be successfully inspected by using the TMR senor. Furthermore, the location of the defect can be estimated from the output, which suggests the developed MTJs based sensor is applicable in the MFL testing.

[1] L. Jogschies et al., *Sensors*, vol. 15, no. 11, pp. 28665, (2015) [2] Z. Jin, M. Oogane, K. Fujiwara et al., *Journal of Applied Physics*, vol. 122, no. 17, p. 174502, (2017)

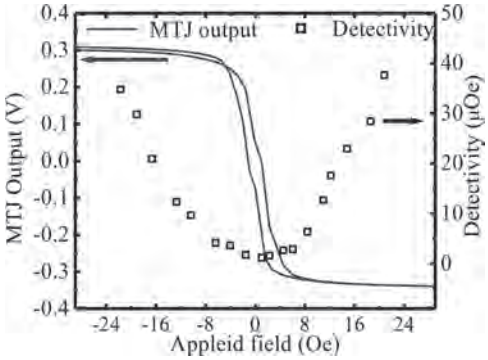

Fig.1 MTJ bridge-circuit response to an applied field, and the dependence of detectivity on the applied field.

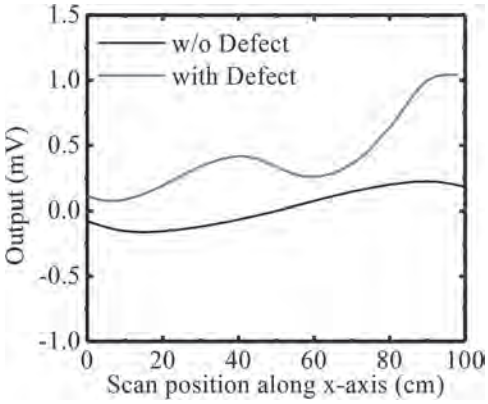

Fig.2 MFL testing result by using the MTJs based sensor at lift-off of 10 cm.

N5-03. Sensing Scheme Design and High-Moment Magnetic Nanoparticles for Next-Generation Giant Magnetoresistance-Based Biosensors. *D. Su*[1], K. Wu[2] and J. Wang[2] *1. Chemical Engineering and Materials Science, University of Minnesota, Minneapolis, MN, United States; 2. Electrical and Computer Engineering, University of Minnesota, Minneapolis, MN, United States*

Over the past few years, giant magnetoresistance (GMR) sensors have been widely employed for bioassays. Our recent research on the wash-free detection of influenza A virus on a portable handheld device has demonstrated its comparable sensitivity to the Enzyme linked immunosorbent assay (ELIZA), which is the golden standard for immunoassays [1]. Stripe-shaped GMR biosensors with large aspect ratios have been widely used to achieve linear response curves. However, the effective sensing area is significantly reduced by the narrow GMR sensing stripes that are in sub-micron range. The GMR sensor signal is also reported to be highly dependent on the position of the MNPs [2] landing on the stripes. To increase the effective sensing area, large-area GMR biosensors based on reverse nucleation mechanism were proposed and demonstrated [3-5]. The sensor designs proposed here are 40 μm × 80 μm in length, resulting in a sensing area 30 times larger than the stripe-shaped sensors. As the MNPs bind to the sensor surface, localized magnetization reversal sites occur in the free layer of the GMR sensor (Figure 1). It was shown that by transforming a 20 nm × 4 μm stripe into a 4 μm × 4 μm square, the sensor signal increased by over 20 times. The large-area sensor signal also exhibits a linear response to the number of MNPs regardless of the position of the MNPs. In addition, we propose using high-moment MNPs such as FeCo, FePt, and Fe_4N as magnetic tags in GMR biosensing. Nowadays, iron oxide MNPs (γ-Fe_2O_3) are widely used as tags/contrasts/carriers for magnetic biosensing/imaging/drug delivery, due to high biocompatibility and low cost. γ-Fe_4N shows at least 3 times higher saturation magnetization than iron oxide MNPs, which, as a result, gives rise to the stronger magnetic signals [5]. With proper surface chemical modifications, our proposed physicochemically stable and non-toxic γ-Fe_4N MNPs could replace the iron oxide MNPs in GMR-based biosensing and achieve higher sensitivity.

[1] D. Su, K. Wu, and V. D. Krishna, Frontiers in Micorbiology, vol. 21, p. 1077 (2019) [2] T. Klein, Y. Wang, and L. Tu, Sensors and Actuators A-Physical, Vol. 216, p. 349 (2014). [3] D. Su, K. Wu and J-P Wang, Journal of Magnetism and Magnetic Materials, Vol. 473, p. 484 (2019) [4] Y. Feng, J. Liu, and T. Klein, Journal of Applied Physics, Vol. 122, p. 123901 (2017) [5] arXiv preprint arXiv:1910.06842.

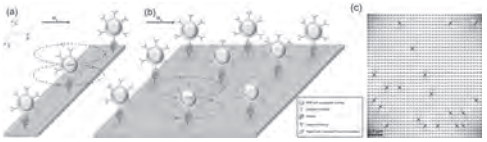

Figure 1. Detection schemese of (a) Stripe-shaped GMR sensor and (b) large-area GMR sensor with localized reverse nucleation sites. (c) OOMMF simulation results of reverse nucleation sites in a 4 μm × 4 μm large-area GMR sensor.

N5-04. Design and Performance of GMR Line Devices for High Sensitive Magnetic Sensor Applications. *N. Fukatani*[1], M. Ichimura[1] and J. Hayakawa[1] *1. Center for Exploratory Research, Hitachi Ltd., Tokyo, Japan*

In recent years, giant magnetoresistance (GMR) devices have been used in many applications due to their small size, high sensitivity, low power consumption, and low cost[1, 2]. For a high sensitive magnetic sensor application, the device resistance is required to be varied linearly over a wide magnetic field range. A high aspect ratio of the GMR line device is useful for the wide range high linearity of the MR curve. However, the high aspect ratio reduces MR ratio because the exchange bias for minor axis direction in the GMR line is suppressed due to the strong shape anisotropy in the pinned layer. In this study, we investigated the correlation between GMR device performance and GMR device design including aspect ratios and line patterns for magnetic sensor applications. The GMR stack is composed of Si/SiO sub.//seed layer/IrMn(6)/CoFe(1.6)/ Ru(0.85)/CoFe(1.6)/Cu(2.5)/ CoFe(1)/NiFe(3.5)/capping layer (all thickness in nm). The pinned layers were magnetized for minor axis direction in GMR lines. Figures 1 (a)-(c) shows a schematic, cross sectional and top view of scanning electron microscope (SEM) images of the GMR device, respectively. The GMR device has ten GMR lines in the parallel configuration. The line length (L) was fixed at 100 μm. The line width (W)was varied from 300 nm to 2 μm and the space width (S) was varied from 400 nm to 1.5 μm. Figure 2 (a) shows S dependence of MR ratio at each aspect ratio of the GMR line. For S = 1.5 μm, the MR ratio strongly decreased as increasing the aspect ratio. On the other hand, the MR ratio increased as decreasing S, especially at the high aspect ratio as shown Figs. 2(b) and 2(c), because the exchange bias at the pinned layer is stabilized due to the dipole interaction between the GMR lines. Optimization of GMR device design enables to realize the high performance of magnetic sensor.

[1] A. Bernieri, G. Betta, L. Ferrigno, and M. Laracca, IEEE Sens. J. 13, 4513 (2013). [2] L. Jogschies, D. Klaas, R. Kruppe, J. Rittinger, P. Taptimthong, A. Wienecke, L. Rissing, and M. C. Wurz, IEEE Sens. J. 15, 28665 (2015).

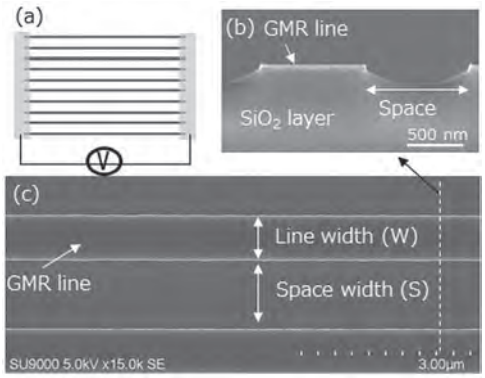

Fig. 1 (a) A schematic, (b) cross sectional and (c) top view of SEM images of the GMR device.

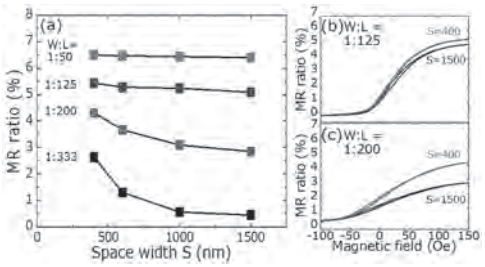

Fig. 2 (a) Aspect ratio and space width dependence of he MR ratio of the GMR devices. (b), (c) The representative MR curves.

N5-05. Ultrasensitive Anomalous Hall Effect Sensor Based on CoFeB With Compensated in-Plane and Perpendicular Magnetic Anisotropies. *Y. Zhang*[1], K. Wang[1] and G. Xiao[1] *1. Physics, Brown University, Providence, RI, United States*

The anomalous Hall Effect (AHE) in ferromagnetic metals and alloys have been widely studied as a potential candidate for magnetic sensing applications, due to the relative easiness of fabrication, broad frequency response and lower intrinsic noise. Nevertheless, AHE sensor suffers from relatively low sensitivity in comparison with semiconductor Hall sensor. In this work, we have demonstrated that sensitivity of AHE sensor based on Ta/CoFeB/MgO/Ta multi-layer structure can be greatly enhanced, through engineering of magnetic anisotropy. Near the spin-reorientation transition of CoFeB layer, ultra-high sensitivity comparable with semiconductor Hall sensor and zero hysteresis can be achieved. We have performed temperature-dependent measurements to investigate the tunable magnetic anisotropy's effect. Both 1/*f* noise and sensitivity have a strong temperature dependence. Moreover, the scaling relations between 1/*f* noise and sensitivity change dramatically as temperature changes, showing different noise originations depending on magnetic anisotropies. The best magnetic field detectability of our AHE sensor reaches 70 nT/rtHz at 1 Hz and 2 nT/rtHz at 10 kHz. Our work shows that AHE sensors are suitable for ultra-small magnetic field sensing applications. The work was supported by National Science Foundation (NSF) under Grant No. OMA-1936221. Y.Z. acknowledges support from Fermilab-Graduate Instrumentation Research Award from DOE grant number DE-AC05-00OR22725

N5-06. Vibrational Electromagnetic Energy Harvester and GMI Accelerometer Combined Device. *J.J. Beato-López*[1,3], I. Royo[1], J. Algueta-Miguel[1,2] and C. Gómez-Polo[1,3] *1. Universidad Publica de Navarra, Pamplona, Spain; 2. Institute of Smart Cities, Universidad Pública de Navarra, Pamplona, Spain; 3. Institute for Advanced Materials and Mathematics, INAMAT2, Universidad Pública de Navarra, Pamplona, Spain*

The characterization of mechanical vibrations is mandatory to prevent or identify damages in structures, machinery and industrial mechanisms among other fields [1]. In parallel, the development of vibrational energy harvesters has become a relevant issue due to the possibility of generating electric power from the residual vibrational energy, quite common in that kinds of systems [2]. These two aspects are simultaneously addressed in this work by the design of a single combined device formed by an electromagnetic harvester and a non-contact magnetic linear accelerometer, permitting the energy generation and simultaneous characterization of low frequency vibrating systems. The device is composed of an electromagnetic harvester with a cylindrical frame (height 62 mm, inner diameter 15 mm) and a coil (1000 turns) to collect the electromotive force. The magnetic levitation system is composed of different NdFeB magnets, with two fixed at the extremes of the frame and a magnet inertial mass levitating freely when vibration occurs. At resonance (10 Hz) maximum electrical power of 1.4 mW at 0.5 g was observed. The magnetic accelerometer is based on the GMI effect [3], that is, huge changes in impedance as a consequence of the variations of the effective magnetic field, in this case, in an amorphous wire ($Co_{66}Fe_{12}Si_{13}B_{15}Cr_4$, 3 cm in length, 90 μm diameter). Its response (f_{GMI} = 300 kHz) was examined, under sinusoidal vibration (f_{VIB} = 10-40 Hz) of a simple ferrite magnet and for a complex magnetic system, namely the electromagnetic harvester. In both cases, the magnetic system periodic motion generates an amplitude modulated (AM) signal output, being its amplitude proportional to mechanical vibration amplitude (or acceleration). Results show the possibility of the potential design of an almost self-autonomous single combined device to simultaneously generate electrical energy and characterize low frequency vibrations.

[1] A. Fauziyah, T. R. Sulistomo, M. N. Farid, and D. Arifianto, *J. Phys.: Conf. Ser.*, vol. 1075, p. 012011, Aug. 2018, doi: 10.1088/1742-6596/1075/1/012011. [2] R. L. Harne and K. W. Wang, *Smart Mater. Struct.*, vol. 22, no. 2, p. 023001, Jan. 2013, doi: 10.1088/0964-1726/22/2/023001. [3] M.-H. Phan and H.-X. Peng, *Progress in Materials Science*, vol. 53, no. 2, pp. 323–420, Feb. 2008, doi: 10.1016/j.pmatsci.2007.05.003.

N5-07. Development of Highly Sensitive MI Element by Controlling Anisotropy and Noise Analysis of MI Element. *J. Ma*[1] and T. Uchiyama[1] *1. Department of Electrical Engineering, Graduate School of Engineering, Nagoya University, Nagoya, Japan*

The MI element used in this study is composed of a pickup coil and a tension-annealed CoFeSiB amorphous wire which is almost zero magnetostriction, made by rotating submerged spinning method [1]. The amorphous wires are 30um diameters and anneaed at 475°C under tension of 3kg/mm^2, 4kg/mm^2, 8kg/mm^2, 64kg/mm^2. Fig. 1(a) shows impedance of a-wire depending on applied magnetic field. The rising time of excitation pulse is 10 ns which is corresponded to 50 MHz sine wave. The induced voltage in pick up coil can be estimated based on non-diagonal impedance theory [2]. As illustrated in Fig. 1(b), sensitivity of MI element increases with the ratio of impedance change and anisotropy field (ΔZ/Hk). The theoretical model shows same effect as measurement results. It is possible to increase sensitivity of MI element by controlling anisotropy. The noise of MI sensor is considered to be mainly due to circuit noise, fluctuation of wire magnetic moment (thermal magnetic noise), and irreversible movement of domain wall trapped by impurities and scratches on wire surface. First is thermal magnetic noise (B_n). We have calculated thermal magnetic noise of amorphous wire by considering BH loop loss, and using general theory of fluctuation with frequency range lower than infrared region. Fig. 2(a) illustrates relationship between magnetic thermal magnetic noise and anisotropy field (Hk). The thermal noise of MI element increases with anisotropy. Next, we will discuss about magnetic noise (e_w) due to domain wall trapped by scratches and scratches on wire surface. As illustrated in Fig. 2(b), e_w decreases when anisotropy field increases. According to fitting result, noise due to trapped domain walls is linearly proportional to the -0.25 power of anisotropy field. It is considered that magnetic noise increases with the number of domain walls. According to these results, we can reduce magnetic noise of amorphous wire by controlling anisotropy field and improving structure of amorphous wire.

[1] K. Mohri, T. Uchiyama, L. V. Panina, M. Yamamoto, and K. Bushida, J. Sensors, vol. 2015, 2015, Art. no. 718069. [2] S. Sandacci, D. Makhnovskiy, L. Panina, K. Mohri, and Y. Honkura, IEEE Trans. Magn., vol. 40, no.6, pp. 18- 23, (2008).

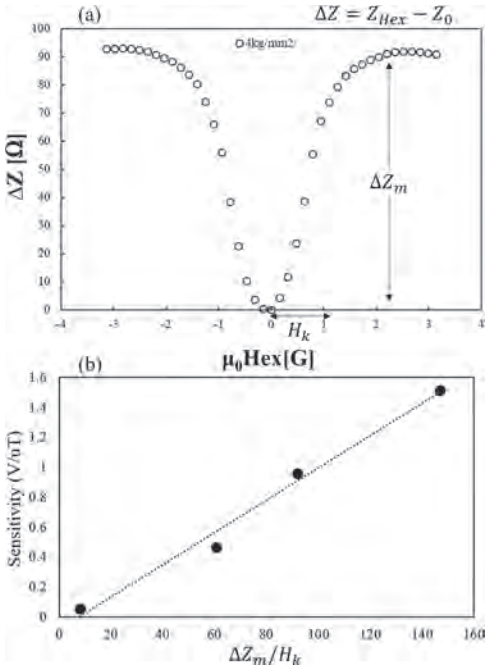

Fig. 1 (a) Impedance of a-wire depending on applied magnetic field. (b) Sensitivity of MI element vs ΔZ/Hk.

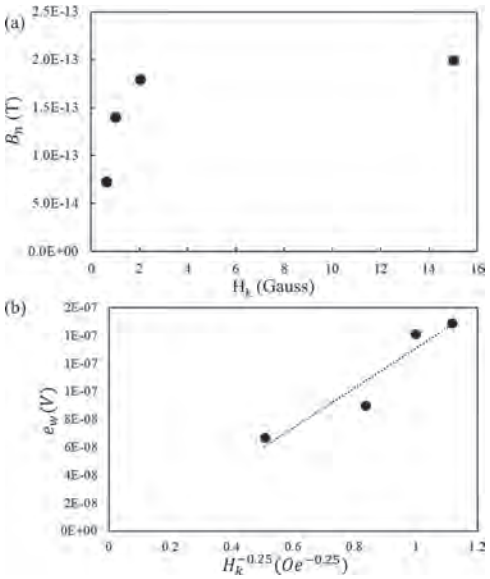

Fig. 2 (a) Magnetic noise due to thermal fluctuation of magnetic moment. (b) Estimated noise due to irreversible domain wall motion.

N5-08. Withdrawn

N5-09. New Aspects on the Performance of a Fundamental Mode Orthogonal Fluxgate Magnetometer Based on Amorphous Wire Cores.
M. Tibu[1], S. Corodeanu[1], C. Hlenschi[1,2], H. Chiriac[1] and N. Lupu[1] *1. MDM, Institutul National de Cercetare-Dezvoltare pentru Fizica Tehnica, Iasi, Romania; 2. Physics, A. I. Cuza University of Iasi, Ïasi, Romania*

The performance of a fundamental mode orthogonal fluxgate magnetometer based on amorphous wires produced at INCDFT-IFT Iasi is presented. Our efforts are concentrated on reducing the sensor noise (magnetic noise + noise of the electronics) and in the same time increasing the sensitivity in order to achieve a maximum signal to noise ratio. The characteristics and performances of the sensor are strongly affected by the excitation parameters [1,2]. It is well known that DC bias diminish the magnetic noise of the sensor core (especially in the 1/f region) when working in fundamental mode, but in the same time it strongly affects the sensitivity [3]. By tuning the DC bias current and the AC amplitude of the excitation current we found the optimum excitation conditions as a compromise between noise and sensitivity (fig 1). For cores made by as cast amorphous wires (120 microns in diameter) ($Co_{68.15}Fe_{4.35}Si_{12.5}B_{15}$), the best results concerning the signal to noise ratio (fig 2) were achieved using 40 mA DC bias current and 50 mA_{pp} AC amplitude. The equivalent magnetic noise estimated using the power spectral density (PSD) is decreased in this conditions to 25pT/√Hz at 1Hz and respectively 13pT//√Hz at 10 Hz. The sensitivity of the sensor for which we achieved maximum signal to noise ratio was 9.5 μV/nT. The performance of the sensor can be further improved by using annealed core and well adapted excitation parameters. Acknowledgements: Work supported by the Nucleu Programme (Project PN 19 28 01 01) and Contract No. 11PFE/16.10.2018 financed by the Romanian Ministry of Education and Research.

[1] I. Sasada "Symmetric response obtained with an orthogonal fluxgate operating in fundamental mode" IEEE Trans. Magn., vol. 38, no. 5 pp.3377-3379, Sept. 2002 [2] E. Paperno "Suppresion of magnetic noise in the fundamental-mode orthogonal fluxgate" Sens. Actuators, A, Phys., Vol. 116 Nr. 3 pp. 405-409, Oct. 2004. [3] M. Butta, I. Sasada and M. Janosek, "Sources of noise in magnetometer based on orthogonal fluxgate operated in fundamental mode" IEEE Trans. Mag. Vol. 48, Nr. 4 pp. 1508-1511, Apr. 2012.

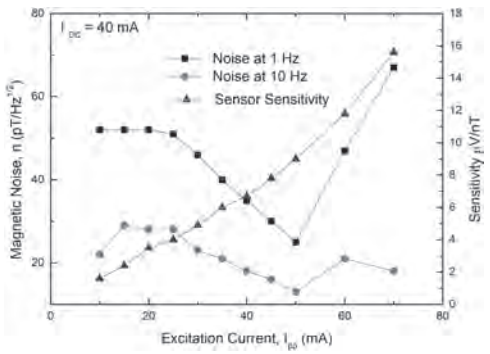

Fig.1. Equivalent magnetic noise and sensitivity dependences on the excitation current for a DC bias of 40 mA.

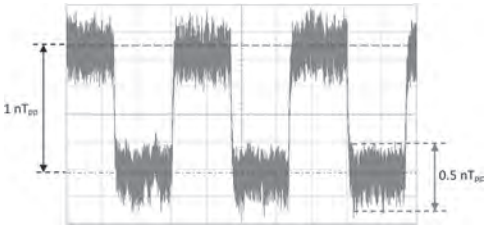

Fig.2. Sensor response for 1nT_{pp} square shape (0.3Hz) applied magnetic field (Measured in magnetic shielded environment).

N5-10. On Reduction of the Magnetic Noise Limits of Orthogonal Fluxgate Sensor. *M. Dressler*[1], M. Butta[1] and M. Janosek[1] *1. Department of Measurement, Czech Technical University in Prague Faculty of Electrical Engineering, Prague, Czechia*

The ongoing progress in preparing new sensors based on magnetic microwires orthogonal fluxgate operated with DC bias [1], reaching noise below pT level, puts intense demands on its conditioning cirucit parameters. As we have previously shown [2], we have been able to create magnetometer with 1 pT/√Hz at 1 Hz with a unit consisting of multichannel DDS, stable current excitation and two independent sensor inputs working in open loop. The noise limiting factor of our setup was mainly the pickup preamplifier and also its low CMMR of coupled excitation feed-through and environment EMI. The sensor is formed by 4-wire U-shape core from Unitika microwires prepared using flipped current Joule annealing [3]. We have replaced the former preamplifier, which was built around LT6234 as a simple difference amplifier with considerable low input impedance, by incorporating JFET differential amplifier with LSK389 matched low noise transistor pair. Also, we reduced pickup coil turns to half. As a result, not only the effective impedance of the pickup coil is lower, but it also reduces its capacitive coupling to core wires, in addition to better CMMR. Therefore it reduces the excitation feed-through and allows us to use higher gain to minimize noise contribution of the following stages. The new preamplifier gain is 34 (previously 30), but with higher input impedance. Thanks to negligible loading of pickup coil and higher Q-factor of the tuned resonant circuit, we have obtained sensitivity above 1 MV/T at a resonance frequency, as shown in Fig. 1. By utilizing unit both input channels with an independent signal path to perform cross-spectrum analysis on a single sensor in the former case and on two sensors with shared excitation in the latter case (shown in Fig. 2), we have also verified that the achieved noise parameters are neither further limited by preamplifier input noise nor excitation current noise [4]. We conclude that at least in the 1/f region, we observe the magnetic noise of the sensor, which we reduced to about 0.7 pT@1Hz and 3 pT@0.1Hz. This work was supported by the Grant Agency of the Czech Technical University in Prague, grant No. SGS20/182/OHK3/3T/13.

[1] I. Sasada, Journal of Applied Physics, vol. 91, no. 10, pp. 7789, May 2002. [2] M. Butta, and B.P. Schutte, IEEE Transactions on Magnetics, Vol. 55, Iss. 7, 2019. [3] M. Janosek, M. Butta, M. Dressler, et al., IEEE Transactions on Instrumentation and Measurement, vol. 69, no. 5, pp. 2552-2560, May 2020 [4] M. Butta, S. Yamashita, and I. Sasada, IEEE Transactions on Magnetics, vol. 47, no. 10, pp. 3748-3751, 2011.

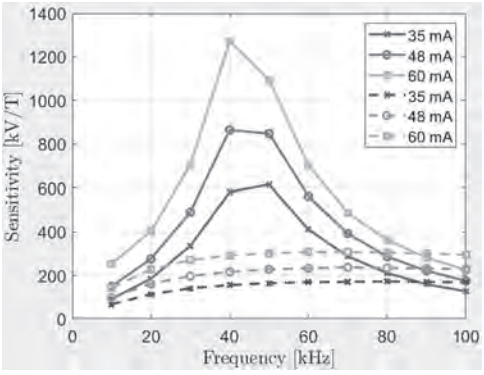

Fig. 1. Sensor sensitivity frequency dependence with the old unit (dashed) and new unit (solid) with the JFET stage

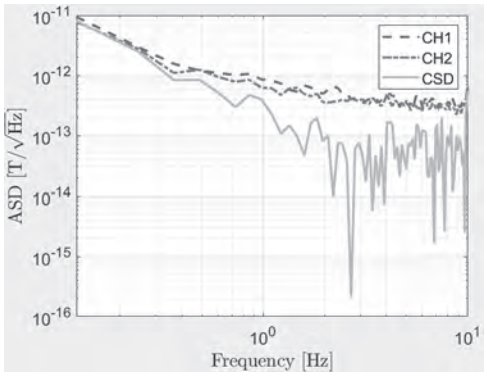

Noise density of two independent sensors and their cross-spectrum.

N5-11. Distributed Magnetic Sensor Using Reflection Coefficients From Both Ends of Single Magnetic Coaxial Cable. *K. Takenaka*[1] and N. Noguchi[1] *1. Yokogawa Denki Kabushiki Kaisha, Musashino, Japan*

Facilities in many plants are aging after many years of operation. Nondestructive testing (NDT) is a key technology to evaluate the properties of materials without causing damage. The distributed magnetic sensor is required for wide area and spatially continuous magnetic field measurement along any profile of measuring object. A distributed magnetic sensor using Faraday rotation with an optical fiber was proposed [1]. And a distributed magnetic sensor by magneto-impedance (MI) effect with time domain reflectometry (TDR) was developed for high sensitivity on the order of μT [2]. This paper presents a distributed magnetic sensor using the forward and reverse reflection coefficients S_{11} and S_{22} from both ends of single magnetic coaxial cable. The method using reflection coefficients includes novel features such as: (1) improvement of Signal-Noise ratio (SNR) for equivalent measurement time, (2) cancellation of the time fluctuation by jitter [3-4]. Furthermore, the attenuation of a signal wave could be compensated by synthesizing the reflected waves from both ends. Figure 1 shows the experimental set-up of the distributed magnetic sensor. The magnetic coaxial cable features 78-Permalloy wire as the inner conductor to induce an MI effect. A reflected wave is delayed and attenuated depending on the position of a miniature coil within a range of 20 mm to 180 mm when the magnetic field of 1.5 mT is applied as shown in figure 2 (a) and (b). It is confirmed that SNR of a reflected wave with vector network analyzer is improved by 21.3 dB compare to an oscilloscope. A signal wave is less affected by the attenuation along the length of the cable as shown in figure 2 (c) and improved by 19.0 dB at the position of 180 mm by synthesizing the reflected waves. This sensor could be used in the future for inspection systems that continuously monitor for defects due to its flexibility and high sensitivity.

[1] J. N. Ross, “Measurement of magnetic field by polarisation optical time-domain reflectometry,” *Electronics Letters*, 17 (17), 596, 1981 [2] K. Takenaka, “Magnetic Fiber Sensing by Magneto-Impedance Effect with Time-Domain-Reflectometry”, *Transducers 2019*, Berlin, Germany, June 23-27, 2019 [3] M. Engl, et al., “Comparison of Time Domain Package Characterization Techniques using TDR and VNA,” *2004 Electronics Packaging Technology Conference*, 2004 [4] “Comparison of Measurement Performance between Vector Network Analyzer and TDR Oscilloscope,” *Keysight Technologies White Paper*, 5990-5446EN, July 2014

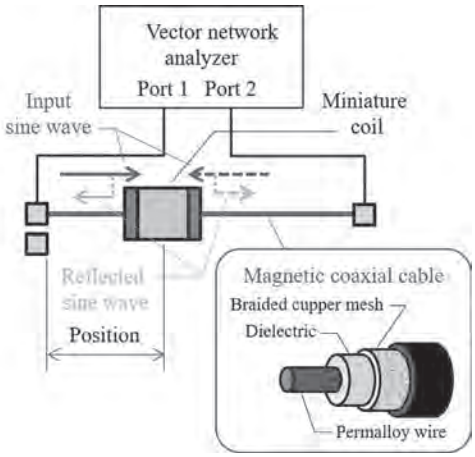

Figure 1: Schematic view of distributed magnetic sensor.

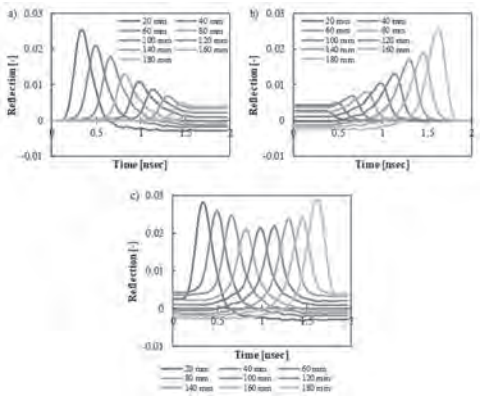

Figure 2: (a) A reflected wave from the input end; (b) A reflected wave from the output end is moved symmetrically around the center position of the cable; (c) A signal wave by synthesizing the reflected waves in (a) and (b).

N5-12. Smartphone-Based Indoor Localization Using Permanent Magnets and Artificial Intelligence for Pattern Recognition. *E. Fisher*[1,2], a. ivry[1,3], R. Alimi[1] and E. Weiss[1] *1. Soreq Nuclear Research Center, Yavne, Israel; 2. Jerusalem College of Technology, Yerushalayim, Israel; 3. Technion Israel Institute of Technology, Haifa, Israel*

Smartphone-based indoor localization methods are frequently employed for position estimation of users inside enclosures like malls, conferences, and crowded venues. Existing solutions extensively use wireless technologies, like Wi-Fi, Bluetooth, and magnetic sensing. However, these approaches depend on the presence of active beacons and suitable mapping surveys of the deployed areas, which render them highly sensitive to the local ambient field clutters. Thus, current localization systems often underperform. We embed small-volume and large-moment magnets in pre-known locations and arrange them in specific geometric forms. Each constellation of magnets creates a super-structure pattern of supervised magnetic signatures. These signatures constitute an unambiguous magnetic environment with respect to the moving sensor carrier. The localization algorithm learns the unique patterns of the scattered magnets during training and detects them from ongoing streaming of data during localization. Our work innovates regarding two essential features: first, instead of relying on active magnetic transmitters, we deploy passive permanent magnets that do not require power supply. Second, we perform localization based on smartphone motion rather than on static positioning of the magnetometer. Therefore, we present a novel and unique dynamic indoor localization method combined with artificial intelligence (AI) techniques for post processing. Experiments describe an enclosure that embeds 3 permanent magnets arranged in a row. The user strolls with a smartphone in-pocket and records 40 minutes of magnetic measurements (Fig. 1). Six pre-trained AI models were applied to this data in real-time (Fig. 2). The best result was obtained by the long short-term memory (LSTM) architecture leading to localization accuracy of 93% and resolution of 0.5 meters.

Suining He, Kang G Shin. "Geomagnetism for Smartphone-Based Indoor Localization: Challenges, Advances, and Comparisons". *ACM Comput. Surv.* 50, 6, Article 97 (2018) Kosuke Watanabe, Kei Hiroi, Takeshi Kamiyama. "A Smartphone 3D Positioning Method using a Spinning Magnet Marker" Journal of Information Processing Vol.27 10–24 (2019)

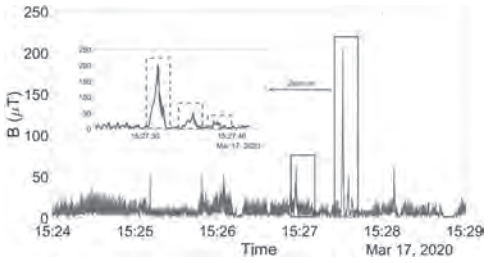

Norm value of three-axial magnetic signals recorded in real-time with a smartphone. Solid rectangles confine measurements of three magnets positioned in a row. Dashed rectangles confine the signature of each magnet.

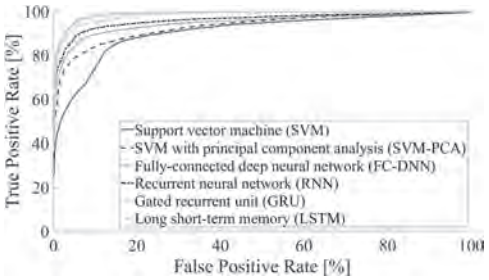

Localization performance of six AI methods.

N5-13. Printed Magnetic Needle Probes Sensor. *S. Nguedjang Kouakeuo*[1,3], Y. Tene Deffo[1], B. Ducharne[2], L. Morel[3], M. Raulet[3], P. Tsafack[1], J. Garcia-Bravo[4] and B. Newell[4] *1. Faculty of Engineering and Technology, University of Buea, Buea, Cameroon; 2. Laboratoire de Génie Electrique et Ferroélectricité, INSA de Lyon, Villeurbanne, France; 3. Laboratoire Ampère, Université de Lyon, Villeurbanne, France; 4. School of Engineering Technology, Purdue University, West Lafayette, IN, United States*

The magnetic needle probes (MNP) is a sensor used to locally characterize the magnetic state of a ferromagnetic component. This method has a rich conceptual history, but it has never been used in the industrial field [1] [2]. There are mainly two reasons for this: instrumentation limitations and inappropriate sizes of sensors' geometries. The first limitation has been overcome in the last 20 years due to large improvements in both the analog and digital electronic fields. In this study, the second limitation, size/geometry is addressed by printing the magnetic needle probe using conductive ink directly on the ferromagnetic specimen to be controlled. The resulting sensor exhibits a drastic volume reduction. Such improvements allow measurement of the magnetic state of a previously inaccessible magnetic lamination through a magnetic laminated core. This opens up the possibility of measuring in situ magnetic behavior and monitoring many electromagnetic devices such as electric transformers, AC/DC electric motors, or even real-time electromagnetic non-destructive testing of ferromagnetic steel components [3]. Over the past few years, simulation approaches including space discretization methods: finite elements, finite differences, and boundary elements have been proposed to describe the internal behavior of magnetic lamination stacks but experimental results validating these simulations could

not be realized due to the aforementioned limitations [4][6]. The printed magnetic needle probe method (PMNP) described in this paper can be used to collect such local information and to validate homogenization methods. Experimental validations are proposed by comparing the sum of the laminations magnetic induction, they are individually measured with the PMNP method to calculate the average induction obtained from a surrounding coil.

[1] Y. A. Tene et al., IEEE Transaction on Magnetics, vol. 55, iss. 7, 2019. [2] T. Yamaguchi et al., Journal of Physique IV, vol. 8, p. 717–20, 1998. [3] S.H. Nguedjang Kouakeuo et al., Journal of Magnetism and Magnetic Materials, Vol. 505, 166767, 2020. [4] M. A. Raulet et al., IEEE Transactions on Magnetics, Vol. 40, iss 2, pp. 872-875, (2004). [5] B. Ducharne et al., Journal of Applied Physics, vol. 117, iss. 24, (2015). [6] B. Ducharne et al., The European Physical Journal Plus, 135:325, (2020).

N5-14. High-Sensitive Symmetric Response Magnetoresistance Sensor With Magnetic Field Concentrator Using Anti-Phase AC Modulation Bridge. *S. Shirotori*[1], A. Kikitsu[1], Y. Higashi[1], Y. Kurosaki[1] and H. Iwasaki[1] *1. Kabushiki Kaisha Toshiba Kenkyu Kaihatsu Center, Kawasaki, Japan*

High-sensitive Magneto-resistance (MR) sensors have attracted much attention as an Internet of Things sensor [1], [2]. To improve the sensitivity, it is important to reduce 1 / *f* noise. An AC modulation system using a modulation coil was reported for a solution of reducing the 1 / *f* noise [3]. However, its noise level was high for the high-sensitive MR sensors. In the previous work, we have proposed a new high-sensitive sensor which is referred to a symmetric response magnetoresistance (SRMR) sensor for reducing the 1 / *f* noise [4]. It used giant magnetoresistance (GMR) elements with symmetric response and an anti-phase AC modulation bridge. In this paper, a magnetic field concentrator (MFC) is applied to the GMR elements in order to increase the sensitivity. Figure 1 (a) shows a schematic view of the GMR unit. The GMR unit is placed in a gap of two MFC units made of NiFe. Figure 2 shows a Input-referred output voltage spectral density as a function of frequency. It is found that the detectivity is 150 pT at 60 Hz. This number is about 1/3 of that of the conventional linear-response measurements by a bias magnetic field [5]. When the full bridge is applied to this system, detectivity of about 75 pT is expected. Figure 2 also shows an increase in the noise level near the modulated frequency. Origin of this noise is not clear now. Detailed of this noise and perspective for picotesla detection will be presented. This work was supported by the Cabinet Office (CAO), Crossministerial Strategic Innovation Promotion Program (SIP), “An intelligent knowledge processing infrastructure, integrating physical and virtual domains” (funding agency: NEDO).

[1] C. Zheng et al.: IEEE Trans. Magn., 55, 0800130, 2019 [2] K. Fujiwara et al., Appl. Phys. Express, 11, 023001, 2018 [3] K. Tsukada et al., AIP Advances, 7, 056670, 2017 [4] S. Shirotori et. al., Abstract of Intermag2020, 2020 [5] R. Lambrton et. Al., IEEE Trans. Magn., 43, 2, pp. 645-650, 2007

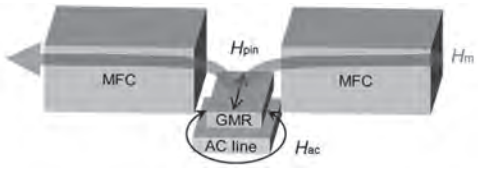

Schematic diagram of SRMR sensor. An AC line is placed under a line-shape GMR element to apply an AC magnetic field (H_{ac}). A magnetic field to be measured (H_m) is amplified through MFC.

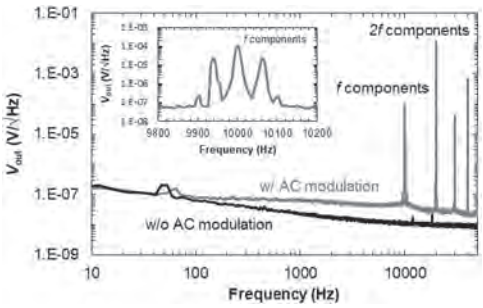

Input-referred output voltage spectral density (V_{out}) as a function of frequency. The red line shows the case of AC modulation, where H_{ac}, and H_m were set to 0.06 mT (10 kHz), and 1 mT (60 Hz), respectively.

N5-15. Generation of Eddy Current at Localized Region Using Magnetic Focusing Probe for Eddy Current Testing. *K. Sakai*[1], T. Kiwa[1] and K. Tsukada[1] *1. Graduate School of Interdisciplinary Science and Engineering in Health Systems, Okayama University, Okayama, Japan*

The eddy current testing is one of the non-destructive testing methods and widely used in the industrial field to evaluate the defect and material properties. However, the evaluation of the defect and material properties at the edge of measurement sample using the eddy current testing is difficult to perform because the distribution of eddy current near the edge changes. Consequently, the magnetic field generated from the sample is affected by the change of eddy current distribution. This is the so-called edge effect and makes it difficult to detect the magnetic field which is related to the defect or material properties. In this study, to avoid the change of eddy current distribution near the edge, a new measurement probe which can focus the applied magnetic field at the localized region was developed and the validity of reducing the edge effect using the developed probe was investigated by measuring the defect and the difference of hardness near the edge of a steel plate. To focus the applied magnetic field, an induction coil was wound around one end of a composite made of a soft magnetic material and rubber. As the composite has high permeability and the resistivity is more than 10^{10} Ωm, the skin effect is reduced and the AC magnetic field passes through inside the composite. Moreover, the other end of composite was processed like a needle so that the tip of the needle is 1 × 1 mm^2. This enables the area of applied magnetic field under the composite becomes small. For the detection of magnetic field from the sample, a magnetoresistive sensor was used and this sensor was placed between two composites. The developed measurement probe could reduce the region where the eddy current was generated. This improvement enabled to reduce the edge effect compared to the conventional measurement probe and the defect and the difference of hardness was clearly visualized even at 5 mm from the edge of the steel plate. This result can be useful for evaluating the practical product in which the edge effect occurs due to its complicated shape with many edges.

[1] J. García-Martín, J. Gómez-Gil and E. Vázquez-Sánchez, “Non-Destructive Techniques Based on Eddy Current Testing”, *Sensors*, Vol. 11, 2525-2565 (2011) [2] K. Tsukada, Y. Haga, K. Morita, N. Song, K. Sakai, T. Kiwa, Weiying Cheng, “Detection of Inner Corrosion of Steel Construction Using Magnetic Resistance Sensor and Magnetic Spectroscopy Analysis”, *IEEE Trans. Magn.*, Vol. 52, 7, 6201504 (2016) [3] K. Sakai, T. Ito, T. Kiwa, and K. Tsukada, “Evaluation of Hardened and Non-hardened Regions Using Eddy Current Testing”, *Electromagnetic Non-Destructive Evaluation (XXI)*, Vol. 43, pp. 1-8 (2018)

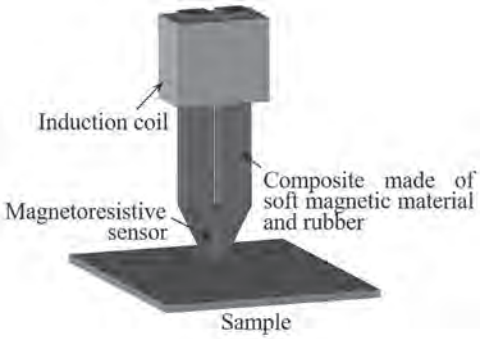

Fig. 1 Configuration of the developed measurement probe.

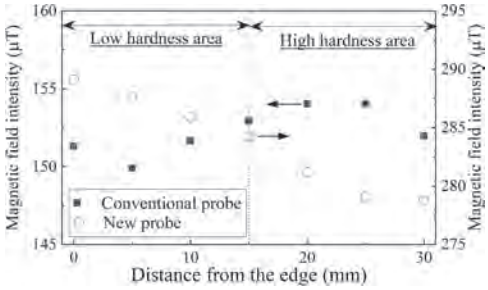

Fig.2 Magnetic field change near the edge of steel plate. The steel plate had different hardness near the edge.

N5-16. The Einstein-de Haas Effect in Yttrium Iron Garnet at 3 MHz.

K. Mori[1], *M. Dunsmore*[1], J.E. Losby[1,2], D. Jenson[1], M. Belov[2] and M.R. Freeman[1] *1. Physics, University of Alberta, Edmonton, AB, Canada; 2. National Research Council Canada Nanotechnology Research Centre, Edmonton, AB, Canada*

The classical Einstein-de Haas (EdH) effect [1] is a AC mechanical torque arising from a time rate of change of net magnetization, and represents the intrinsic relationship between magnetism and mechanical angular momentum. Nanofabrication of torque sensing devices is opening new avenues for exploration and applications of the EdH effect. The scale-up of mechanical resonance frequencies with continued miniaturization enhances EdH torques, which increase linearly with drive frequency, relative to frequency-independent magnetic cross-product torques. Previously, miniaturized EdH experiments have been performed at the microscale using mechanical modes in the audio frequency range (13 kHz). The present work brings the measurements to radio frequencies. Single-crystal Yttrium Iron Garnet (YIG) disks with magnetic vortex ground states are mounted on nanomechanical resonators having fundamental torsional modes close to 3 MHz. For DC bias fields below about 200 A/m the maximum cross-product torques, historically an important source of systematic error in EdH experiments, remain smaller than the EdH torques [3]; no control of the field geometry to null cross-product torques is required. Quadrature lock-in measurements allow cross-product and EdH torque signals to be recorded simultaneously, owing to a 90° relative phase shift arising between the driving torques, and referenced to the phase of the driving field. The simultaneous measurement scheme enables determination of the magnetomechanical ratio, g′, without requiring separate experimental inputs. Results from measurements around the full vortex hysteresis loop, and comparisons with micromagnetic simulations of cross-product and EdH torques, also will be presented and discussed.

[1] A. Einstein and W.J. de Haas, Proceedings - KNAW 18, 696 (1915). [2] T.M. Wallis, J. Moreland, and P. Kabos, Appl. Phys. Lett. 89, 122502 (2006) [3] K. Mori, M.G. Dunsmore, and M.R. Freeman, arXiv:2005.08406 [cond-mat.mes-hall] (2020)

Session S7
NEW APPROACHES FOR INFORMATION PROCESSING COUPLING SPINTRONICS AND MAGNONICS

Tamalika Banerjee, Chair
University of Groningen, Groningen, Netherlands

INVITED PAPERS

3:00

S7-01. Towards Magnonic Devices Based on Voltage-Controlled Magnetic Anisotropy. *B. Rana[1] 1. Center for Emergent Matter Science, RIKEN, Wako, Japan*

The modern electronic devices suffer from unescapably increasing rates of Joule heating and power consumption in spite of significant technological advances in miniaturization and operational speed. As an alternative, charge-neutral information carrier may be used. Hence, spin waves (SWs), i.e., the collective precessional motion of localized electronic spins in ordered magnetic materials, were proposed as a promising alternative system for encoding and carrying information. In order to surpass the operational speed, efficiency, functionality and integration density of current electronic devices, the magnonic devices should be preferably operated by electric-field induced methods. Recently, voltage-controlled magnetic anisotropy (VCMA) has emerged as a novel means to control the spins by electric-field. The interfaces between 3*d* transition ferromagnetic metals and nonmagnetic insulators (i.e., oxides) possess perpendicular magnetic anisotropy (PMA) due to the hybridization of 3*d* orbitals of ferromagnets and 2*p* orbitals of O (Fig. 1(a)). The relative change in the electronic occupation state in 3*d* orbitals of ferromagnets under the application of electric field at ferromagnet/oxide interface modifies the interfacial orbital hybridization and controls the interfacial spin properties through relativistic spin-orbit coupling of ferromagnets [1] (Fig. 1(b)). A typical magnonic device consist of four basic elements: a SW waveguide, a microwave source for SW excitation, a SW detector, and some functional elements for manipulation of SW properties. In my talk I will briefly discuss the recent progress in the development of magnonic devices by utilizing VCMA [2]. In particular, I will talk about the excitation, channeling and manipulations of SWs by VCMA. The VCMA can excite ferromagnetic resonance and SWs (Fig. 2(a)) at low power consumption as compared to the charge current induced Oersted field excitation [3]. The localized nature of electric field also makes VCMA a suitable alternative method for the development of nanoscale magnonic devices [4]. After excitation the SWs should be guided through channels so that they can reach to the targeted positions on the waveguide. SWs can be guided through virtual nanochannels, which can be created and reconfigured by applying VCMA [5] (Fig. 2(b)). The experimentally measured frequency versus wavevector dispersion character of the SWs propagating through VCMA-induced parallel nanochannels reveals the presence of two types of SW modes with a frequency gap between their dispersion curves, which can even be tuned by gate voltage. The SW properties such as resonance frequency, group velocity and decay length can be controlled by VCMA while propagating underneath a metal gate electrode [6]. Various magnonic logic gates [5] and reconfigurable magnonic crystals [7] can even be developed by utilizing VCMA. Another important aspect is that the damping constant of ultrathin ferromagnetic films can be tuned by electric field. However, the modulation of damping constant shows a nontrivial dependence with the gate voltage (Fig. 2(c)) originated from the electric field modulation of Rashba SOC present at ferromagnet/oxide interface [8]. Interestingly, the engineering of underlying and top oxide materials properties of ultrathin ferromagnetic films can increase the device functionality significantly.

[1] K. Nakamura, R. Shimabukuro, Y. Fujiwara *et al. Phys. Rev. Lett.* 102, 187201 (2009). [2] B. Rana and Y. Otani, *Commun. Phys.* 2, 90 (2019). [3] T. Nozaki, Y. Shiota, S. Miwa *et al., Nat. Phys.* 8, 491 (2012). [4] B. Rana, Y. Fukuma, K. Miura *et al. Appl. Phys. Lett.* 111, 052404 (2017). [5] B. Rana and Y. Otani, *Phys. Rev. Applied* 9, 014033 (2018). [6] B. Rana, S. Choudhury, K. Miura *et al. Phys. Rev. B* 100, 224412 (2019). [7] Q. Wang, A. V. Chumak, L. Jin *et al. Phys. Rev. B* 95, 134433 (2017). [8] B. Rana, C. A. Akosa, K. Miura *et al. Phys. Rev. Applied* (in press).

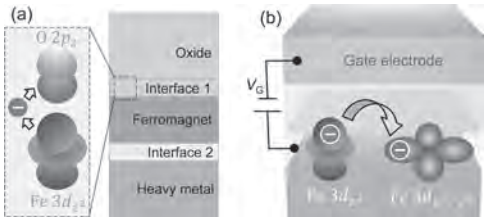

(a) Schematic diagram shows the origin of perpendicular magnetic anisotropy at ferromagnet/oxide interface. (b) The schematic illustration shows the mechanism of VCMA.

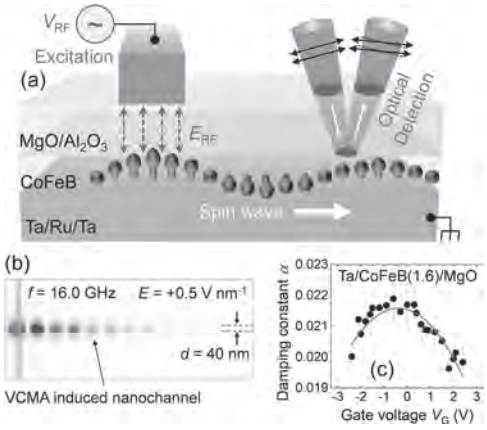

(a) Schematic diagram shows the excitation of propagating spin waves by VCMA and detection by magneto-optical Kerr effect (MOKE). (b) Simulation result shows the propagation of SW through a VCMA induced nanochannel. (c) Nonlinear variation of damping constant in ultrathin CoFeB film by electric field.

3:36

S7-02. Mechanisms of the Voltage Control of Magnetic Anisotropy at Magnetic Metal/Oxide Interfaces. *F. Ibrahim*[1], A. Hallal[1], H. Yang[1,2], B. Dieny[1] and M. Chshiev[1] *1. Univ. Grenoble Alpes, CEA, CNRS, SPINTEC, F-38000 Grenoble, France, Grenoble, France; 2. Key Laboratory of Magnetic Materials and Devices, Ningbo Institute of Materials Technology and Engineering, Chinese Academy of Sciences, Ningbo 315201, China, Ningbo, China*

Using electric fields rather than currents is proposed as an alternative way for magnetization manipulation where a reduction in the energy dissipation by a factor of 100 is anticipated. The electric field control of perpendicular magnetic anisotropy (PMA) has been intensively investigated in ferromagnet/oxide interfaces and a mature understanding of this effect is building up to clarify the mechanisms underlying this effect. We have employed first-principles calculations to unveil and describe the mechanisms behind the voltage control of magnetic anisotropy effect (VCMA), namely the (i) charge-mediated [1] and (ii) ionic-migration [2] induced VCMA was addressed in Fe/MgO interfaces. In the charge-mediated VCMA, we elucidate this effect in relation to the intrinsic electric dipole at the Fe/MgO interface, which has been observed and quantified. The increase (decrease) of PMA under an electric field is associated with a decrease (increase) of the interfacial electric dipole field which spontaneously exists even without application of any electrical field. Moreover, our on-site projected PMA analysis reveals that even if the electric field is screened on a very short Thomas-Fermi length (1–2 Å) in the metallic electrode, its influence extends beyond the interfacial Fe layer. In particular, we show that the main contribution to the PMA variation arises from the second Fe layer, a behavior which is understood in view of orbital hybridizations. However, the range of the VCMA efficiency is found to be of the order of tenths fJ/(V.m). In the ionic-migration mediated VCMA, a characteristic dependence of the effect on oxygen migration at Fe/MgO interfaces was revealed. The VCMA efficiency as a function of the migrated O-atoms concentration exhibits an exponential variation of the form, with P, and W respectively being the percentage of migrating oxygen atoms, VCMA efficiency maximum and newly introduced characteristic concentration of migrating ions. Interestingly, depending on the range of variation of the applied voltage, two regimes associated with reversible or irreversible ions displacement are predicted to occur, yielding different VCMA response. In the irreversible case, O-migration mediated VCMA can reach thousands of fJ/(V.m) consistent with the experimental observations. Based on our findings, one can distinguish from the order of magnitude of the VCMA driving mechanism: an effect of several tens of fJ/(V.m) is likely associated to charge-mediated effect combined with slight reversible oxygen displacements whereas an effect of the order of thousands of fJ/(V.m) is more likely associated with irreversible oxygen ionic migration.

[1] F. Ibrahim et al., Phys. Rev. B 93, 014429 (2016). [2] F. Ibrahim et al., Phys. Rev. B 98, 214441 (2018).

4:12

S7-03. Designing Ferroelectric-Gated Mott Transistors via Interfacial Charge Engineering. *X. Hong*[1] *1. Department of Physics and Astronomy, University of Nebraska-Lincoln, Lincoln, NE, United States*

Ferroelectric field effect transistors (FeFETs) built upon Mott insulator channel materials have been intensively investigated over the last two decades for developing nonvolatile memory and low power logic applications with sub-nanometer size scaling limit. However, the intrinsically high carrier density of the Mott channel (10^{21}-10^{23}/cm^3) also imposes significant challenges in achieving substantial modulation of the channel conduction. Previous studies have focused on engineering either the film thickness or charge mobility of the Mott channel, while only moderate resistance switching ratio has been achieved via a solid state gate. In this talk, I'll discuss how we exploit the interfacial charge transfer effect between two correlated oxides to realize a giant enhancement of the ferroelectric field effect in Mott-FeFETs. We work with prototype Mott-FeFETs based on epitaxial oxide heterostructures composed of ferroelectric $Pb(Zr,Ti)O_3$ and rare earth nickelate $RNiO_3$ (R = La, Nd, Sm). For devices with 1-5 nm single layer $RNiO_3$ channels, the room temperature resistance switching ratio $(R_{off}-R_{on})/R_{on}$ increases exponentially with decreasing channel thickness till it reaches the electrical dead layer thickness. Inserting a (La,Sr)MnO_3 (LSMO) buffer layer has led to more than two orders of magnitude enhancement in the resistance switching ratio compared with the single layer channel devices with the same channel thickness. A record high nonvolatile resistance ON-OFF ratio (>50) has been achieved in ultrathin $RNiO_3$/LSMO channels at 300 K, where the $RNiO_3$ layer is scaled below the dead layer thickness. Systematic studies of the layer thickness dependence of the field effect show that the LSMO buffer layer not only tailors the carrier density profile in $RNiO_3$ through interfacial charge transfer, but also provides an extended screening layer that reduces the depolarization effect in the ferroelectric gate. Our study points to an effective strategy for building high density, low power nanoelectronic and spintronic applications via functional complex oxide heterointerfaces. This work was supported by NSF through Grant No. DMR-1710461 and Nebraska MRSEC Grant No. DMR-1420645, DOE BES under Award No. DE-SC0016153, and SRC under GRC Task Number 2831.001.

4:48

S7-04. Potential of $SrTiO_3$-Based 2DEG for Spin-Charge Interconversion. *A. Barthelemy*[1] *1. Unite Mixte de Physique CNRS/Thales, Palaiseau, France*

Classical spintronics traditionally relied on ferromagnetic metals as spin generators and detectors. A new approach called spin-orbitronics exploits the interplay between charge and spin currents enabled by the spin-orbit coupling in non-magnetic systems. We studied the potential of the bidimensional electron gases (2DEG) that forms at the interface between $LaAlO_3$ and $SrTiO_3$ [1] or by deposition of Al on $SrTiO_3$ [2] for spin-current to charge-current conversion through the inverse Edelstein effect [2, 3]. The sizeable Rashba spin-orbit coupling of the gas allows to obtain a very efficient conversion characterized by an Inverse Edelstein effect length, l_{IEE}, larger than the one measured for the topological insulator a-Sn or at Bi/Ag interfaces [4]. This conversion efficiency can be highly modulated by a gate voltage. We used angle-resolved photoemission spectroscopy and semi-classical Boltzmann transport theory to map this peculiar gate dependence and linked it to the band structure [2]. Moreover, we exploited electric-field induced ferroelectricity in $SrTiO_3$ to manipulate the spin-orbit properties of a 2DEG and convert spin currents into either positive or negative charge currents in a non-volatile manner [5]. This suggest that oxide interfaces [6] have a strong potential for spin-based information readout in novel memory such as the magneto-electric spin-orbit transistor proposed by Intel [7].

[1] E. Lesne et al., Nat. Comm. 5, 4291 (2014) ; D. C. Vaz et al., Adv. mat. 29, 1700486 (2017). [2]; D. C. Vaz et al., Nat. Mat.. 18, 1187 (2019) [3] E. Lesne et al., Nat. Mat. 15, 1261 (2016) [4] J.-C. Rojas-Sánchez et al., Nat. Comm. 4, 2944 (2013) ; PRL 116, 096602 (2016). [5] P. Noel et al., Nature, 580, 483 (2020) [6] J. Varignon et al., Nat. Phys. 14, 322 (2018) [7] S. Manipatruni et al., Nature 565, 35 (2019)

5:24

S7-05. Controlling Magnetic Anisotropy by Rashba and Other Spin-Orbit Couplings. *J. Ieda*[1] *1. Advanced Science Research Center, Japan Atomic Energy Agency, Tokai, Japan*

The control of the magnetism of ultra-thin ferromagnetic layers using an electric field would lead to many technologically important applications. To date, while it is usually assumed the changes in the magnetic anisotropy, leading to such a control, arises from surface charge doping of the magnetic layer, a number of key experiments cannot be understood within such a scenario. Much studied is the fact that, for nonmagnetic metals or semiconductors, a large surface electric field gives rise to a Rashba spin-orbit coupling which leads to a spin-splitting of the conduction electrons. Here we develop a simple analytic theory for the existence and electrical control of the magnetic anisotropy based upon the Rashba spin-orbit interaction and the Stoner model of magnetism [1]. We show that the competition between the Rashba spin-orbit fields and the exchange interaction leads to a very large magnetic anisotropy arising from the internal electric fields which exist at, e.g., ferromagnetic/metal and ferromagnetic/oxide insulator interfaces but modified by the addition of an applied electric field. This different path to an electrically induced anisotropy energy can explain the electric field, thickness, and material dependence reported in many experiments. The concept can be extended to noncentrosymmetric antiferromagnets [2] and multilayered van der Waals materials [3]. This work was done in collaboration with S. E. Barnes, S. Maekawa, H. Matsuoka, M. Nakano, and Y. Iwasa.

[1] S. E. Barnes, J. Ieda, and S. Maekawa, Scientific Reports 4, 4105 (2014). [2] J. Ieda, S.E. Barnes, and S. Maekawa Journal of the Physical Society of Japan 87, 053703 (2018). [3] H. Matsuoka, S. E. Barnes, J. Ieda, et al. (submitted).

Session O1
2D MAGNETIC MATERIALS

Yasuhiro Niimi, Chair
Osaka University, Osaka, Japan

INVITED PAPER

O1-01. Spin Transport and Spin-Orbit Proximity Phenomena in van der Waals Heterostructures. *J.F. Sierra*[1], L. Benítez[1,3], W.F. Savero Torres[1], M. Costache[1] and S.O. Valenzuela[1,2] *1. Catalan Institute of Nanoscience and Nanotechnology (ICN2), CSIC and The Barcelona Institute of Science and Technology (BIST), Bellaterra, Spain; 2. Institució Catalana de Recerca i Estudis Avançats (ICREA), Barcelona, Spain; 3. Universitat Autònoma de Barcelona, Barcelona, Spain*

In recent years, spin-based technologies, in which particle spin is utilized for information processing, have become promising for "beyond-CMOS" solid-state devices. Graphene and other layered materials have rapidly established themselves as intriguing building blocks for spintronics applications [1]. Because of the graphene intrinsic low spin-orbit interaction, spins can flow snugly through its crystal lattice over long distances, resulting in an ideal spin communication channel. At the same time, the graphene's low spin-orbit interaction inhibits spin manipulation, which is the cornerstone for successfully implementing spin-based devices. Nevertheless, this bottleneck can be overcome by combing graphene with other layered materials in artificial van der Waals heterostructures. In this talk, I will present a set of experiments where we study the spin-relaxation in graphene-transition metal dichalcogenides heterostructures [2]. In such engineered van der Waals systems, spin-orbit coupling in graphene is enhanced by proximity-induced effects. As a consequence, the spin dynamics becomes anisotropic [2, 3], with a spin relaxation that depends on the spin orientation. Interestingly, these systems can be also exploited for efficient spin-charge interconversion driven by the spin Hall effect and the inverse spin galvanic effect at room temperature, with conversion efficiencies tailored by electrostatic gating [4].

1. W. Han *et al*., *Nature Nanotechnology* 9, 794 (2014). 2. L. A. Benítez, J. F. Sierra *et al*., *Nature Physics* 14, 303 (2018). 3. L. A. Benítez, J. F. Sierra *et al*., *APL Materials* 7, 120701 (2019). 4. L. A. Benítez, W. Savero Torres, J. F. Sierra, *et al*., *Nature Materials* 19, 170 (2020).

CONTRIBUTED PAPERS

O1-02. Room-Temperature Ferromagnetism in $CrTe_2$ Thin Flakes Imaged by Single Spin Magnetometry. *F. Fabre*[1], A. Purbawati[2], A. Finco[1], A. Haykal[1], S. Chouaieb[1], N. Rougemaille[2], J. Coraux[2], I. Philip[1] and V. Jacques[1] *1. Laboratoire Charles Coulomb, Montpellier, France; 2. Institut NEEL, Grenoble, France*

Even if magnetic van der Waals crystals where known since decades, two-dimensional (2D) magnetism has been obtained experimentally only a few years ago[1]. Since its discovery in $Cr_2Ge_2Te_6$ and CrI_3, an intense research effort has started, triggered by their high potential in studying 2D magnetic states[2-4]. A wide range of new physical properties emerging from the reduced dimensionality can be explored and exploited like the control of magnetic properties through gating. New devices based on van der Waals magnetic heterostructures have been proposed, such as spin-filter magnetic tunnel junctions based on CrI_3 heterostructures, showing a tunneling magnetoresistance higher than their counterparts based on conventionally grown magnetic thin films. The potential of 2D magnets in topological spintronics is also under investigation, with for example recent works on the stabilization of skyrmions in Fe_3GeTe_2. However, in order to use van der Waals magnets as building blocks for relevant spintronics devices, a magnetic material with a Curie temperature (T_C) above room temperature is required. Unfortunately, most of the available van der Waals magnets have a low intrinsic T_C. Even though a 2D magnetic state at room temperature can be achieved through gating for example, it remains a challenging task and only few materials are reported to have a T_C above 300K down to the monolayer limit, like $MnSe_x$, VSe_2 and more recently for few-layers $CrTe_2$[5]. Here, we report our work on $CrTe_2$ from bulk to 40nm thin mechanically exfoliated flakes using Nitrogen-Vacancy (NV) magnetometry, a well-suited technique for the study of 2D magnets[6]. We find an in-plane ferromagnetic order at room temperature and we extract a value for the saturation magnetization Ms of 24.5 ± 3.0 kAm^{-1} at room temperature.

[1] N. Samarth, Nature 546, 216 (2017) [2] K. S. Burchet al., Nature 563, 47 (2018) [3] X. Z. Cheng Gong, Science 363, 6428 (2019) [4] M. Gibertini et al., Nature Nanotechnology 14, 408 (2019) [5] A. Purbawati et al., ACS Appl. Mater. Interfaces (2020) [6] L. Thiel et al., Science 364, 973 (2019)

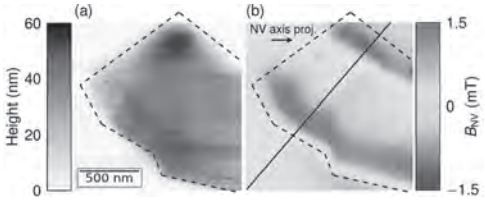

(a) AFM image of a 40 nm-thick CrTe2 flake. (b) Map of the magnetic stray field produced by the flake shown in panel (a). Only the component of the field along the NV quantization axis B_{NV} is measured, in the presence of a bias field of 3 mT.

O1-03. Complex Spin Dynamics in Layered $CrBr_3$. *S. Siddiqui*[3], J. Sklenar[2], D. Lebedev[1], J.T. Gish[1], M. Hersam[1] and A. Hoffmann[3] *1. Department of Materials Science and Engineering, Northwestern University, Evanston, IL, United States; 2. Department of Physics and Astrnomy, Wayne State University, Detroit, MI, United States; 3. Department of Materials Science and Engineering, University of Illinois at Urbana-Champaign College of Engineering, Urbana, IL, United States*

Spin dynamics in magnetic materials is of interest for a range of applications including embedded memory [1] and logic-in-memory computation [2]. Layered magnetic materials, because of their unique crystal structures and weak interlayer coupling, give rise to unconventional spin dynamics and electrically accessible resonance frequencies even in the antiferromagnetic states. Towards this end, we investigated the rich spin dynamics in a layered $CrBr_3$ crystal using magnetic resonance phenomena. Compared to the other chromium trihalides (i.e., CrX_3, X = Cl, I), $CrBr_3$ possesses unique magnetic properties such as strong ferromagnetic intralayer exchange interaction and weaker interlayer ferromagnetic coupling due to competing ferromagnetic and antiferromagnetic exchange interactions at low temperature [3]. Here, we show that magnetic excitation for the in-plane and out-of-plane directions of $CrBr_3$ give rise to distinct magnon modes. In particular, we have applied radio-frequency (RF) inductive magnetic fields to measure the resonant modes in the crystal using transmission measurements where the crystal *c* axis is normal to the coplanar waveguide plane. Magnetic resonance

is measured at 1.6 K by fixing the excitation frequency of the RF field and slowly varying the static magnetic field in the in-plane and out-of-plane directions. With the out-of-plane magnetic field, only one resonance mode (Kittel mode) is observed. However, we have identified three different modes in the $CrBr_3$ crystal when the applied field is in-plane. To help explain the origin of different modes, we use micromagnetic simulations that include different anisotropy energies and intralayer & interlayer exchange energies. Our study shows that broadband microwave transmission spectroscopy can reveal the intricate spin dynamics phenomena in layered magnetic materials that originate from the interplay of intralayer and interlayer exchange energies.

[1] Memory with a spin. Nature Nanotech, vol.10, p. 185 (2015). [2] S. A. Siddiqui, S. Dutta, A. Tang et al., Nano Lett., vol. 20, p. 1033 (2020). [3] E. J. Samuelsen, R. Silberglitt, G. Shirane et al., Phys. Rev. B, vol. 3, p. 157 (1971).

O1-04. Manipulation of the van der Waals Magnet $Cr_2Ge_2Te_6$ by Spin-Orbit Torques. *V. Gupta*[1], T.M. Cham[1], G.M. Stiehl[1], A. Bose[1], J.A. Mittelstaedt[1], K. Kang[1], S. Jiang[1], K. Mak[1], J. Shan[1], R. Buhrman[1] and D. Ralph[1,2] *1. Cornell University, Ithaca, NY, United States; 2. Kavli Institute at Cornell, Ithaca, NY, United States*

The discovery of intrinsic magnetism in 2D materials has opened an exciting new platform for spintronics, allowing fundamental studies of efficient mechanisms for electrically controlling magnetic materials. In this work we show that the magnetization orientation of the semiconducting vdW magnet $Cr_2Ge_2Te_6$ (CGT) can be detected electrically and can be manipulated efficiently by current-induced spin-orbit torques from heavy-metals like Pt and Ta. We provide a direct quantitative measurement of these torques in CGT/Pt. Our results indicate that the interfacial spin-current transparency in these devices is similar to metallic-ferromagnet/Pt samples but is higher than in oxide-ferromagnet/Pt structures and that the interlayer exchange coupling in multilayer CGT is strong enough so that all layers reorient in response to the spin-orbit torque. We also characterize strong magnetothermal signals arising from the interplay between thermal gradients and magnon spin currents in these devices, as detected by the spin-Seebeck effect. These results demonstrate the promise of semiconducting vdW magnets in 2D material-based spin-orbitronic and magneto-thermal devices

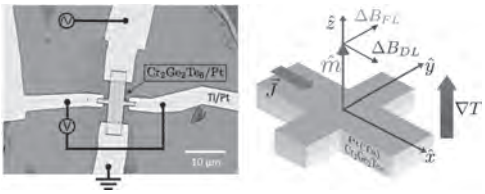

***(left)* Optical image of $Cr_2Ge_2Te_6$/Pt heterostructure patterned into a Hall bar geometry for transport measurements. *(right)* Schematic illustrating the orientation of effective fields due to current-induced damping like torque ΔB_{DL} and field-like torque ΔB_{FL} The injected current also generates an out-of-plane thermal gradient resulting in large magnetothermal signals.**

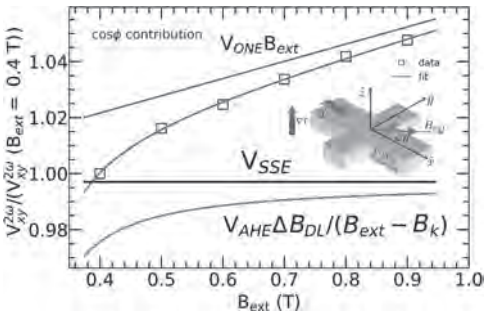

$\cos\varphi_B$ contribution of the measured second harmonic Hall voltage as a function of an externally applied in-plane field for a CGT/Pt sample. The data are fit to spin-Seebeck (black), ordinary Nernst effect (red) and damping-like torque (red) contributions. The green and red curves are offset by V_{SSE} for comparison. After subtraction of the thermoelectric signals, anti-damping spin torque efficiency of $\xi_{DL} = 0.25 \pm 0.09$ is obtained.

O1-05. Distinct Magneto-Raman Signatures of Spin-Flip Phase Transitions in CrI_3. *A. McCreary*[1], T.T. Mai[1,2], F. Utermohlen[2], J.R. Simpson[1,3], K. Garrity[1], X. Feng[2], D.L. Shcherbakov[2], Y. Zhu[4], J. Hu[5], D. Weber[2], K. Watanabe[6], T.T. taniguchi.takashi@nims.go.jp[6], J. Goldberger[2], Z. Mao[4], C. Lau[2], Y. Lu[2], N. Trivedi[2], R. Valdes Aguilar[2] and A.R. Hight Walker[1] *1. National Institute of Standards and Technology, Gaithersburg, MD, United States; 2. The Ohio State University, Columbus, OH, United States; 3. Towson University, Towson, MD, United States; 4. Pennsylvania State University, University Park, PA, United States; 5. University of Arkansas Fayetteville, Fayetteville, AR, United States; 6. National Institute for Materials Science, Ibaraki, Japan*

Recent observations of long-ranged magnetic ordering in van der Waals bonded, layered magnetic materials down to the single layer limit has led to a plethora of research dedicated to the study of two-dimensional (2D) magnets, with plenty of opportunities to investigate fundamental physics and potential quantum applications. With these materials, the properties are typically strongly correlated to the number of layers, with new physics occurring in the few-layer (~few nm) regime. In this sense, common techniques used to measure magnetic behaviors such as neutron scattering and SQUID are at a disadvantage due to sample size requirements. On the other hand, Raman spectroscopy, which has diffraction-limited spatial resolution, is a powerful, non-destructive optical method to probe magnetism in 2D layered materials through inelastic scattering as a function of temperature, laser energy, polarization, and magnetic field. One material of particular interest is chromium tri-iodide (CrI_3), a ferromagnet at bulk thicknesses below the Curie temperature but with the remarkable property of layered antiferromagnetism in thin multilayers. Here, we will report on a magneto-Raman spectroscopy study on multi-layered CrI_3 [1], focusing on two new features in the spectra which appear at temperatures below the magnetic ordering temperature and were previously assigned to high frequency magnons. We observe a striking evolution of the Raman spectra with increasing magnetic field applied perpendicular to the atomic layers in which clear, sudden changes in intensities of the modes are attributed to the interlayer ordering changing from antiferromagnetic to ferromagnetic at a critical magnetic field. In addition, through DFT-calculations and symmetry arguments, we conclude that the new modes are not magnons as previously believed, but instead are zone-folded phonons.

[1] A. McCreary *et al.* arXiv:1910.01237.

O1-06. Topological Surface States-Caused Large Damping Enhancement in Dirac Semimetal-Ferromagnetic Metal Layered Structures. *J. Ding*[1], C. Liu[1], R. Yu[1,2], U. Erugu[3], J. Tang[3], H. Ding[2], H. Chen[1,4] and M. Wu[1] *1. Department of Physics, Colorado State University, Fort Collins, CO, United States; 2. National Laboratory of Solid State Microstructures and Department of Physics, Nanjing University, Nanjing, China; 3. Department of Physics and Astronomy, University of Wyoming, Laramie, WY, United States; 4. School of Advanced Materials Discovery, Colorado State University, Fort Collins, CO, United States*

Spin pumping refers to the transfer of spins from precessional moments in a ferromagnet to a non-magnetic material. In a ferromagnetic/non-magnetic bi-layered system, spin pumping manifests itself as a damping enhancement in the ferromagnetic layer and a spin current in the non-magnetic layer. This effect can be strong if the non-magnetic layer is a heavy metal thin film, because such a film can work as a spin sink and produce a very weak spin backflow. The effect can be even stronger if the non-magnetic component is a topological insulator, because it can efficiently convert a spin current to a charge current and thereby serve as a very efficient spin absorber, due to the spin-momentum locking of the topological surface states (TSS). In principle, TSS should also be present in other topological materials, such as Dirac or Weyl semimetals. These TSS are also expected to exhibit spin-momentum locking, but their interplays with magnetism are largely unexplored. This presentation reports strong damping enhancement in a ferromagnetic NiFe thin film due to a neighboring α-Sn thin film. Multiple evidences suggest that the damping enhancement is associated with TSS in the topological Dirac semimetal (TDS) phase of α-Sn. The TDS α-Sn films are realized on InSb substrates. The measurements used α-Sn(6nm)/Ag(2nm)/NiFe(20nm) layered structures where Ag works as a spacer to physically separate α-Sn and NiFe. Ferromagnetic resonance studies show that the damping in these structures is ~4.8 bigger than in the bare NiFe film. Control measurements indicate that this damping enhancement is mostly due to the TSS in the α-Sn, rather than the bulk of the α-Sn film or the Ag spacer; it is absent in β-Sn(6nm)/Ag(2nm)/NiFe(20nm) where the Sn film is topologically trivial. This work demonstrates that TDS may be as promising as topological insulators in terms of spintronics applications.

O1-07. Weak Antilocalization and Anisotropic Magnetoresistance in Topological $Bi_2Te_xSe_{3-x}$ Thin Films. *G.M. Stephen*[1], O. Vail[2], J. Lu[3], P. Taylor[2] and A.L. Friedman[1] *1. Laboratory for Physical Sciences, College Park, MD, United States; 2. Army Research Lab, Adelphi, MD, United States; 3. Materials Science and Engineering, University of Virginia, Charlottesville, VA, United States*

Topological materials, such as the quintessential topological insulators in the Bi_2X_3 family (X = O, S, Se, Te), are extremely promising for beyond Moore's Law computing applications where alternative state variables and energy efficiency are prized. It is essential to understand how the topological nature of these materials changes with growth conditions and, more specifically, chalcogen content. In this study, we investigate the evolution of the magnetoresistance of $Bi_2Se_{3-x}Te_x$ for varying chalcogen ratios as a function of both temperature and angle of applied field. Weak antilocalization (WAL), an indicator of topological surface states, is observed to weaken with Te substitution. We also demonstrate that the anisotropy of the WAL follows the Tkachov-Hankiewicz model of magnetoconductance in topological insulators rather than a more trivial sinθ dependence. This model, which is a generalization of the Hikami-Larkin-Nagaoka model, allows for measurement of both coherence length and skin depth of the conducting surface states. The measured skin depth is on the order on the roughness of the samples, indicating that the roughness of films is detrimental to the surface states and a major hurdle for practical applications.

G.M. Stephen, O.A. Vail, J. Lu, *et. al*, Sci. Rep. 10 (2020) 4845

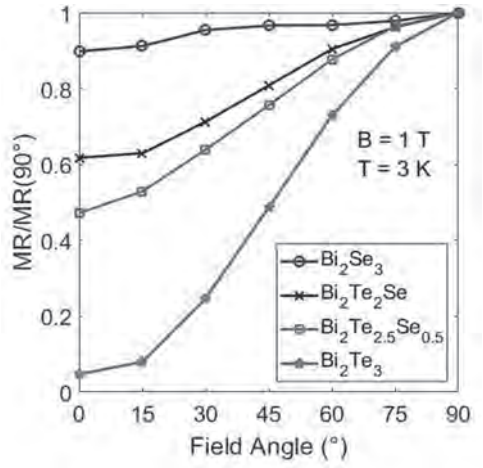

INVITED PAPER

O1-08. Spin-to-Charge Conversion in van der Waals Heterostructures. *S. Chenattukuzhiyil*[1] *1. CIC nanoGUNE, San Sebastian, Spain*

Graphene has been known as an excellent material for long-distance spin transport due to its weak spin-orbit coupling (SOC). However, the same reason makes graphene an adverse candidate for different spintronics applications in which strong SOC is required, such as the Datta and Das spin transistor proposal or spin-charge interconversions. It has recently been predicted theoretically that SOC can be induced in graphene so that spin-orbit phenomena such as spin Hall effect (SHE) or Rashba-Edelstein effect can be obtained. In our work, by using van der Waals heterostructure-based lateral spin valves, we experimentally demonstrate spin-to-charge conversion (SCC) due to SHE in graphene via spin-orbit proximity with MoS_2, a transition metal dichalcogenide (TMD)[1]. The combination of long-distance spin transport and large spin-to-charge conversion in a van der Waals heterostructure gives rise to a hitherto unreported efficiency for the spin-to-charge voltage output. We performed similar experiments in graphene in proximity with WSe_2[2]. Here we observed gate-tunable SHE with SCC efficiency larger than in some of the best SCC materials such as topological insulators. Similarly, we observed efficient SHE in graphene combined with an insulator, $Bi2O_3$[3]. Here, the SHE can be due to extrinsic mechanisms such as skew scattering in graphene decorated with adatoms. Using a similar approach, we observed large multidirectional SCC in Weyl semimetal $MoTe_2$[2]. Here, due to the low symmetry of $MoTe_2$ crystal, we detect, along with the conventional SCC, an unconventional SCC where the spin polarization and the charge current are parallel. Our finding enables the simultaneous conversion of spin currents with any in-plane spin polarization in one single experimental configuration. All in all, these exceptional effects obtained by the unique properties of 2D materials open exciting opportunities in a variety of future spintronic applications.

1. C. K. Safeer, et al. Nano Letters, 19, 2, 1074-1082 (2019). 2. F. Herling, et al. APL Materials 8, 071103 (2020). 3. C. K. Safeer, et al. Nano Letters, 20, 6, 4573-4579 (2020). 4. C. K. Safeer, et al. Nano Letters, 19, 12, 8758-8766 (2019).

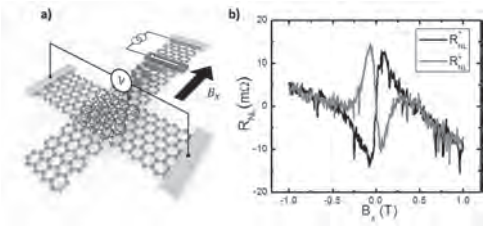

a) Sketch of the measurement configuration of inverse SHE in graphene proximitized with MoS_2. Nonlocal spin-to-charge conversion voltage is measured across the graphene/MoS_2 stripe by applying a charge current between Co electrode and graphene. The magnetic field is applied along the in-plane hard axis direction creating spin precession in graphene channel. b) Antisymmetric Hanle spin precession curves obtained using the experimental configuration described in panel a, for the initial positive (black) and negative (red) easy axis magnetization directions of the Co electrodes.

CONTRIBUTED PAPERS

O1-09. Electric-Field Control of Spin-Orbit Torque and Magnetic Anisotropy in Topological Insulator Heterostructures. *T. Chiba*[1] and T. Komine[2] *1. National Institute of Technology, Fukushima College, Iwaki, Japan; 2. Faculty of Engineering, Ibaraki University, Hitachi, Japan*

Electric-field control of magnetization is essential for the next-generation spintronic technologies such as nonvolatile magnetic memory. In particular, the voltage-control of the magnetic anisotropy (VCMA) in ferromagnets promises an energy-efficient reversal of magnetization based on the clocking scheme, which earlier has been demonstrated by using a pulsed voltage in magnetic tunnel junction (MTJ). However, the VCMA method in MTJ still requires a high gate voltage and a constant-bias magnetic field, which is a disadvantage for practical applications. In contrast, as another important method for magnetization reversal, current-induced spin-orbit torque (SOT) in topological insulator (TI) based magnetic heterostructures has been studied in recent experiments [1], which succeeded in reducing the switching power consumption by current pulse injected parallel to a bias magnetic field [2]. In this research, inspired by the VCMA and SOT approaches for magnetization control, we combine them and present two distinct clocking methods for the magnetization switching in TI based magnetic heterostructures. First, we analytically formulate the uniaxial magnetic anisotropy in magnetic TIs as a function of the Fermi energy. Next, as shown in Fig. 1, we propose a transistor-like device with the functionality of a nonvolatile magnetic memory adopting the VCMA writhing method that require no external magnetic fields and the anomalous-Hall-effect based readout scheme. For the magnetization reversal, the estimated source-drain current density and gate voltage are the orders of 10^4 - 10^5 A/cm^2 and 0.1V, respectively, which are much smaller than those of traditional heavy-metal/ferromagnet heterostructures as well as the MTJs. We also discuss the possibility of using the proposed method for magnetization reversal in TI/ferromagnetic-insulator bilayers with magnetic proximity at the interface.

[1] Y. Fan *et al.*, Nat. Nanotechnol. 11, 352 (2016). [2] K. Yasuda *et al.*, Phys. Rev. Lett. 119, 137204 (2017).

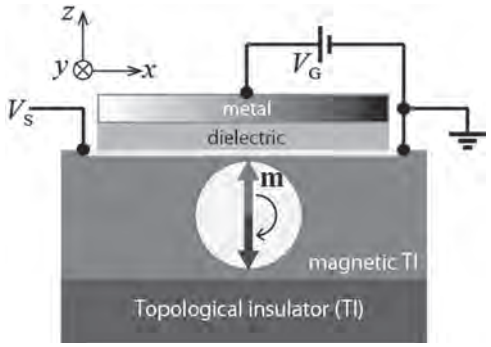

FIG. 1. Schematic geometry (side view) of field-effect transistor (FET)-like device. *m* denotes magnetization vector.

O1-10. Temperature- and Magnetic Field-Dependent Raman Spectroscopy of Layered, Antiferromagnetic $FePS_3$. *J.R. Simpson*[1,2], A. McCreary[2], T.T. Mai[2], C. Dennis[3], R. Valdes Aguilar[4] and A.R. Hight Walker[2] *1. Physics, Astronomy, and Geosciences, Towson University, Towson, MD, United States; 2. Physical Measurement Laboratory, National Institute of Standards and Technology, Gaithersburg, MD, United States; 3. Materials Measurement Laboratory, National Institute of Standards and Technology, Gaithersburg, MD, United States; 4. Physics, The Ohio State University, Columbus, OH, United States*

The recent discovery that van der Waals-bonded magnetic materials retain long range magnetic ordering down to a single layer[1,2] stimulates a thorough Raman spectroscopic study of one such material, $FePS_3$, a large spin ($S = 2$) Mott insulator where the Fe atoms form a honeycomb lattice. Bulk $FePS_3$ was shown to be a quasi-2D Ising antiferromagnet, with additional features in the Raman spectra emerging below the Neel temperature ($T_N \sim 120$ K). Using temperature- and magnetic field-dependent Raman spectroscopy as an optical probe of magnetic structure, we demonstrate[3] that one of these Raman-active modes (ψ_4) below T_N is a magnon with a frequency of ~ 3.7 THz (~122 cm^{-1}). Contrary to previous work[4], which interpreted this feature as a phonon, our Raman data[3] shows the expected frequency shifting and splitting of the magnon as a function of temperature and magnetic field, respectively, were we find the *g*-factor ~2. Other Raman-active modes emerging below T_N are attributed to zone-folded phonons in the antiferromagnetic state. The anomalous temperature dependence of these modes along with an analysis of temperature-dependent magnetization data, suggests a persistence of short-range magnetic order above T_N.

[1] C. Gong, L. Li, Z. Li, *et al*., Nature 546, 265 (2017). [2] B. Huang, G. Clark, E. Navarro-Moratalla, *et al*., Nature 546, 270 (2017). [3] A. McCreary, J. R. Simpson, T. T. Mai, *et al.*, Phys. Rev. B 101, 064416 (2020). [4] J.-U. Lee, S. Lee, S. H. Ryoo, *et al.*, Nano Lett. 16, 7433 (2016).

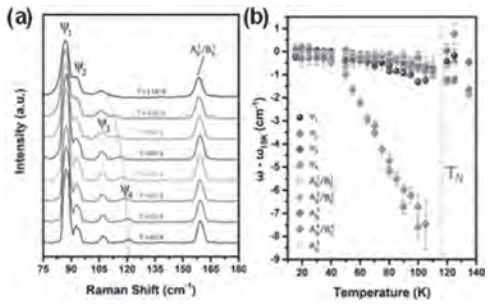

Fig. 1. (a) Temperature-dependent Raman spectra of $FePS_3$ around and below T_N (dashed vertical line). (b) Relative peak frequencies, ω(T) - ω(15K) as a function of temperature. Below T_N, magnon mode ψ_4 increases in frequency (hardens) significantly (~ 8 cm^{-1}) with decreasing temperature, while other Raman-active modes only slightly harden (~ 1 to 2 cm^{-1}), consistent with typical lattice anharmonicity. Several modes exhibit an anomaly in peak frequency around T_N.[3]

O1-11. Spin Hall Effect in Paramagnetic Kagome-Lattice Semimetal $Co_3Sn_2S_2$. *Y. Lau*[1,2], K. Fujiwara[1], J. Ikeda[1], T. Seki[1,2], A. Tsukazaki[1,2] and K. Takanashi[1,2] *1. Institute for Materials Research (IMR), Tohoku University, Sendai, Japan; 2. Center for Spintronics Research Network, Tohoku University, Sendai, Japan*

Ferromagnetic shandite $Co_3Sn_2S_2$(CSS) has recently been identified as an exotic magnetic Weyl semimetal[1,2]. Giant intrinsic anomalous Hall effect[3] and anomalous Nernst effect[4] were found in ferromagnetic CSS, owing to its unique topologically non-trivial band structure protected by the time-reversal symmetry. The relatively low Curie temperature T_C ~ 180K of the ferromagnetic CSS, however, hinders the prospect of exploiting its topological properties for many practical applications. Meanwhile, only few studies[5] have been devoted for exploring the usefulness of CSS in the paramagnetic state, e.g. at room temperature. Here, we examine the potential of the paramagnetic CSS as a spin current source at room temperature via the spin Hall effect(SHE). High-quality encapsulated CSS films of varying thicknesses were grown on Al_2O_3(0001) substrates by magnetron co-sputtering followed by high temperature annealing, as described in our previous work[6]. The SiO_2 encapsulating layer was then dry-etched *ex situ* using Ar ion milling, followed by ion beam sputtering deposition of either Cu(1.8)/$Co_{20}Fe_{60}B_{20}$(2)/AlO_x(3) or AlO_x(3) structures (thicknesses in nanometers). We carried out harmonic Hall measurement and spin-torque ferromagnetic resonance line-shape analysis on the former heterostructures with CoFeB for independent spin-orbit torque quantification. The latter structures without CoFeB served as references. The two experiments yield consistent estimation of the damping-like spin Hall efficiency, ξ_{DL}. Considering the current distribution within the heterostructure, we obtain ξ_{DL} ~ +0.11 for paramagnetic CSS at room temperature, corresponding to a spin Hall conductivity of ~340 (hbar/2e) $\Omega^{-1}cm^{-1}$. Possible correlation between the observed SHC and the presence of avoided linear crossing in the band structure of paramagnetic CSS (corresponding to the Weyl nodes for the ferromagnetic CSS) will be discussed. This work was partly supported by the Grant-in-Aid for Scientific Research (S) (Grant No. JP18H05246) and Grant-in-Aid for Early-Career Scientists (Grant No. JP20K15156) from JSPS KAKENHI, Japan.

1. D.F. Liu *et al.*, *Science* 365, 1282-1285 (2019) 2. N. Morali *et al.*, *Science* 365, 1286-1291 (2019) 3. E. Liu *et al.*, *Nat. Phys.* 14, 1125-1131(2018) 4. S.N. Guin *et al.*, *Adv. Mater.* 31, 1806622 (2019) 5. G. Li *et al.*, *Sci. Adv.* 5, eaaw9867(2019) 6. K. Fujiwara *et al.*, *Jpn. J. Appl. Phys.* 58, 050912 (2019)

O1-12. Ferromagnetism and Giant Magnetoresistance in Zinc-Blende FeAs/InAs Superlattice Structures. *L. Anh*[2,3], T. Hayakawa[1], Y. Nakagawa[4], H. Shinya[5,6], T. Fukushima[7,8], H. Katayama-Yoshida[9], Y. Iwasa[4,10] and M. Tanaka[1,9] *1. Dept. of Electrical Engineering and Information Systems, The University of Tokyo, Tokyo, Japan; 2. Institute of Engineering Innovation, The University of Tokyo, Tokyo, Japan; 3. JST, PRESTO, Saitama, Japan; 4. QPEC & Dept. of Applied Physics, The University of Tokyo, Tokyo, Japan; 5. Research Institute of Electrical Communication, Tohoku University, Sendai, Japan; 6. Center for Spintronics Research Network (CSRN), Tohoku University, Sendai, Japan; 7. Institute for Solid State Physics, The University of Tokyo, Chiba, Japan; 8. Center for Spintronics Research Network (CSRN), Osaka University, Osaka, Japan; 9. Center for Spintronics Research Network (CSRN), The University of Tokyo, Tokyo, Japan; 10. RIKEN Center for Emergent Matter Science (CEMS), Tokyo, Japan*

Material structures containing tetrahedral FeAs bonds, depending on their density and geometrical distribution, can host several competing quantum ground states ranging from superconductivity to ferromagnetism. In Fe-based superconductors where the FeAs bonds are confined in 2D monolayers (MLs), the magnetic ground state of the Fe spins is antiferromagnetic[1]. On the other hand, in Fe-based ferromagnetic semiconductors such as (In,Fe)As where the FeAs bonds are distributed randomly in a three-dimensional (3D) InAs matrix, the Fe spins are coupled ferromagnetically via interactions with electron carriers[2]. Here we examine structures of quasi two-dimensional (2D) layers of tetrahedral FeAs bonds embedded with a regular interval in a semiconductor InAs matrix, which resemble the crystal structure of Fe-based superconductors. The samples were grown by low-temperature molecular beam epitaxy on InAs (001) or semi-insulating GaAs (001) substrates. Lattice images by scanning transmission electron microscopy (STEM) reveal that the zinc-blende structure of the host InAs is well maintained, and the Fe atoms are mainly confined within a thickness of 2-3 MLs (Fig. 1a). We study magnetic and transport properties of a series of FeAs/InAs superlattices (thickness is fixed at 12 nm) containing (1ML of FeAs / t ML of InAs) x N periods (t = 20, 10, 7, 5; N = 1, 3, 5, 7) (the inset of Fig. 1(b)). All the samples exhibit intrinsic ferromagnetism, and the T_C value changes rapidly as t^{-3} (Fig 1b). Furthermore, extremely large magnetoresistance (MR) (~500%, Fig. 1c) are observed, whose origin can be attributed to the giant MR occurring in these multilayer structures. These interesting features indicate that the FeAs/InAs superlattice structures are promising for functional spintronic devices[3]. This work was partly supported by Grants-in-Aid for Scientific Research (17H04922, 18H05345, 19H05602, 19K21961), CREST program (JPMJCR1777) and PRESTO program (JPMJPR19LB) of JST, and Spin-RNJ.

[1] H. Hosono *et al. Materials Today* 21, 278-302 (2018). [2] P. N. Hai, L. D. Anh *et al.*, Appl. Phys. Lett. 101, 182403 (2012). [3] L. D. Anh *et al*, ArXiv:2005.10181 (2020).

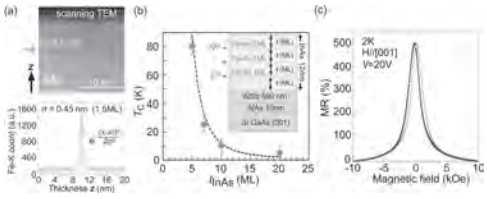

(a) STEM lattice image of 1ML FeAs in InAs (top), and the Fe distribution along the growth direction z (bottom). (b) T_C of FeAs/InAs superlattices as a function of t (inset: sample structure). (c) Giant MR in the sample with t = 5 and N = 7.

O1-13. Proximity-Induced Spin Hall Effect in Graphene/WSe_2 van der Waals Heterostructures With Tunable, Highly Efficient Spin-to-Charge Conversion. *F. Herling*[1,2], S. Chenattukuzhiyil[1], J. Ingla-Aynés[1], N. Ontoso[1], L.E. Hueso[1,3] and F. Casanova[1,3] *1. CIC nanoGUNE, San Sebastian, Spain; 2. QuESTech, Horizon 2020 ITN, Marie Sklodowska-Curie Action (No 766025), Grenoble, France; 3. IKERBASQUE, Basque Foundation for Science, Bilbao, Spain*

The proximity effect in two-dimensional materials opens ways to achieve important functions for future spintronic devices. In van der Waals heterostructures (vdWHs), transition metal dichalcogenides (TMD) can be used to enhance the spin-orbit coupling of graphene leading to highly efficient spin-to-charge conversion (SCC) by spin Hall effect (SHE) that is predicted to be controllable by a gate voltage. Here, we report for the first time the observation of the SHE in graphene proximitized with WSe_2 in a vdWHs. These kind of vdWHs are a promising platform to study a variety of spin-dependent phenomena [1,2]. By Hanle precession measurements, we quantify the spin transport and SCC parameters from 10 K up to room temperature. Exceptional for graphene/TMD devices, the sole mechanism is the SHE for all measurements and no Rashba-Edelstein effect is observable. Importantly, we are able to amplify and turn off the SCC by applying a back-gate voltage, demonstrating the long-awaited milestone of an electrically-tunable SHE. The amplified SCC shows a high efficiency, measured with an unprecedented SCC length of larger than 20 nm, defined as the product of the spin Hall angle (Θ_{SH}) and the spin diffusion length (λ_s). These results show the capability of two-dimensional materials to advance towards the implementation of novel spin-based devices and future applications.

[1] W. Yan et al., Nat. Commun. 7, 13372 (2016). [2] C. K. Safeer et al., Nano Lett. 19, 1074–1082 (2019).

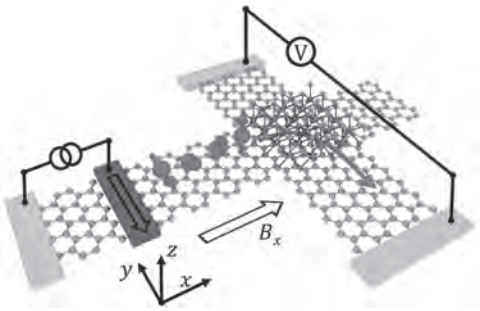

Fig. 1: Non-local configuration for the Hanle precession measurement in the van der Waals heterostructure of graphene and WSe_2. The spin injection via an applied charge current through a ferromagnetic electrode, the precession of the spin polarization by an applied magnetic field and the spin-to-charge conversion is sketched.

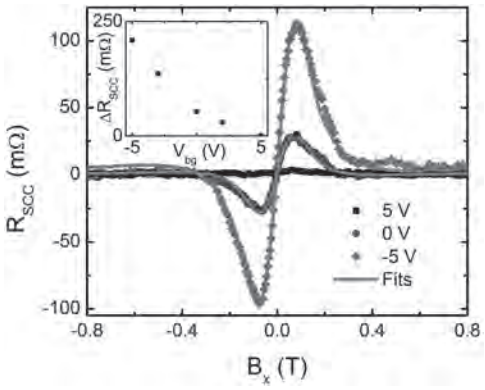

Fig. 2: Net antisymmetric Hanle signals (R_{SCC} is the signal due to spin-to-charge conversion calculated from the non-local resistance difference for both magnetization directions of the ferromagnetic electrode) measured at different back-gate voltages and 100 K. The scatter plots are the experimental data, the red solid lines are fits of the 1D diffusion equation to the data.

O1-14. Coexistance of Quantum Oscillation and Magnetic Hysteresis in $CeTe_3$ Thin Films. *M. Watanabe*[1], S. Lee[1], T. Asano[1], T. Ibe[1], M. Tokuda[1], H. Taniguchi[1], D. Ueta[2], Y. Okada[2], K. Kobayashi[1,3] and Y. Niimi[1,4] *1. Graduate School of Science, Osaka University, Toyonaka, Japan; 2. Okinawa Institute of Science and Technology Graduate University, Kunigami-gun, Japan; 3. Institute for Physics of Intelligence and Department of Physics, The University of Tokyo, Bunkyo-ku, Japan; 4. Center for Spintronics Researh Network, Osaka University, Toyonaka, Japan*

Recently, van-der-Waals (vdW) magnets have attracted much attention and been researched extensively [1]. The present study aims to elucidate the magnetic properties of a vdW magnet, namely $CeTe_3$. $CeTe_3$ is a cleavable magnetic material in the family of rare earth tritellurides. Its crystal structure consists of a CeTe slab, separated by two Te layers. The material undergoes two magnetic phase transitions at $T_{N1} = 3$ K and $T_{N2} = 1.2$ K. For bulk $CeTe_3$, the first transition is understood to be to an antiferromagnetic (AFM) state with an in-plane easy axis [2, 3]. The second transition is known to be to a different AFM state with still an in-plane easy axis, but a nonparallel axis to the first AFM state [4]. However, details of these AFM states are still unknown, and thin film transport measurements have not been performed yet. In this work, we have performed magnetoresistance measurements from 0.4 to 4 K on 40 nm $CeTe_3$ thin film devices [5]. Figure 1 shows magnetoresistance at different temperatures. We have observed a clear Shubnikov-de-Haas oscillation from well above T_{N1}, which has never been reported so far. Such a large oscillation implies a highly two-dimensional (2D) nature of the electrical conduction. Moreover, we have observed a unique hysteresis and peak structure below T_{N1} which is retained even below T_{N2}, as shown in Fig. 2. This implies a possible canting of the magnetic moments along the stacking direction induced through the thin film fabrication. Further studies could lead to understanding the possible enhancement of perpendicular magnetic anisotropy in magnetic thin films. Moreover, the coexistence of quantum oscillation and magnetic hysteresis is extremely unique, and the material would pave the way for understanding the interaction between magnetic moments and highly 2D conduction electrons.

[1] Y. Deng *et al*., Nature 563, 94 (2018) [2] Y. Iyeiri *et al*., Phys. Rev. B 67, 144417 (2003). [3] K. Deguchi *et al*., J. Phys.: Conf. Ser. 150, 042023 (2009). [4] D. A. Zocco *et al*., Phys. Rev. B 79, 134428 (2009). [5] M. Watanabe *et al*., arXiv: 2006.14955.

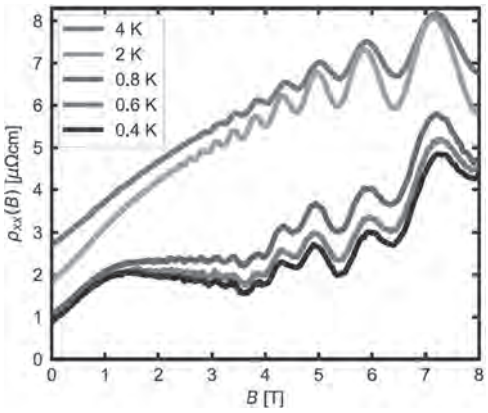

Fig.1 : Shubnikov-de-Haas oscillation observed in the $CeTe_3$ thin film.

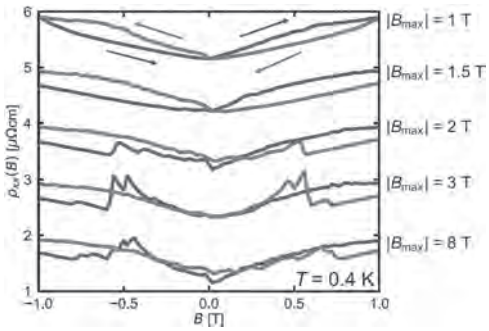

Fig.2 : Magnetoresistance at 0.4 K. A hysteresis is observed, and a peak structure emerges as we increase the maximum applied field $|B_{max}|$.

Session O2
MRAM AND MAGNETIC TUNNEL JUNCTIONS

Takayuki Nozaki, Co-Chair
Natinaol Institute of Advanced Industrial Science and Technology, Tsukuba, Japan
Kevin Garello, Co-Chair
SPINTEC, Grenoble Cedex, France

INVITED PAPER

O2-01. Technologies for Commercial MRAM Products and Radiation Hard Applicability. *F.B. Mancoff*[1], S. Ikegawa[1], J. Janesky[1], S. Aggarwal[1], S. Alam[1], H. Almasi[1], M. DeHerrera[1], B. Hughes[1], H. Lee[1], K. Nagel[1], G. Shimon[1], J. Sun[1], J. Yang-Scharlotta[2], A. Narasimham[2] and S. Guertin[2] *1. Everspin Technologies, Inc., Chandler, AZ, United States; 2. Jet Propulsion Laboratory, California Institute of Technology, Pasadena, CA, United States*

Compared to traditional semiconductor memories, magnetoresistive random access memory (MRAM) can potentially offer improvements in operating speed, endurance, system power, and resistance to radiation damage. The first MRAM introduced commercially was field-switched or "Toggle" MRAM, in 2006, which Everspin followed with a complete family of products spanning 128kb to 32Mb densities. A decade later, Everspin introduced the industry's first production spin-transfer torque (STT) MRAM offering higher density (256Mb) and lower power. In 2019-2020, multiple companies introduced commercial embedded STT-MRAM products [1], and Everspin initiated production of a 1Gb standalone discrete memory [2], the industry's highest density commercial device. In this talk, we will review the technologies needed to achieve functioning STT-MRAM arrays for commercial production, including reliability performance such as cycling endurance and data retention. For example, Figure 1 shows an example of the STT switching error rate curves from the 1Gb array as a function of applied voltage bias. The switching distributions for antiparallel (AP) to parallel (P) and for P to AP writing are both shown on a normal quantile plot across temperatures from -35°C to 110°C. The well-behaved switching distributions are highly linear to more than 4σ and show a wide operating range. We also discuss considerations in future scaling of STT-MRAM in key areas such as data retention, switching current density, switching efficiency, and endurance. For many space, telecommunications, and defense applications, the use of DRAM, SRAM, and FLASH is limited by radiation-induced errors due to disruption of the stored electron charge state in these memories. MRAM storage uses the electron spin and is not susceptible to radiation. Toggle MRAM is already used with radiation-hardened front-end semiconductor circuitry in high radiation environments, and STT-MRAM promises higher density for these applications. By measuring individual magnetic tunnel junctions with perpendicular magnetic anisotropy (pMTJs) with no underlying transistors, the fundamental limits of STT-MRAM to radiation can be explored. For example, Montoya *et al*. [3] measured a high degree of immunity of individual pMTJs to ionizing gamma and neutron radiation, while Wang *et al.* [4] examined the effects of swift heavy ions on pMTJ films and large patterned bits. We report measurements of pMTJs over a range of bit size and with no underlying transistor before and after exposure to total ionizing dose (TID) gamma radiation of up to 7 Mrad(Si) at JPL's HDR Co-60 source, including no significant change to the magnetic field and spin-torque voltage induced switching. Figure 2(a) shows the resistance of the pMTJs measured in the low-resistance state with the x-axis (y-axis) showing values before (after) the radiation exposure. The measurements fall closely along the diagonal, indicating no significant change after exposure. Figure 2(b) shows no significant change to the magnetic field switching coercivity Hc measured post-exposure vs. pre-exposure. We also examined the spin-torque switching and breakdown of the pMTJs in response to 50 ns voltage pulses with almost no measured difference due to the radiation. Finally, we will examine radiation exposure measurements of Everspin's 256Mb commercial STT-MRAM product dies, which indicated a high degree of radiation resistance of the MRAM cells to both heavy ions and TID effects [5,6]. This lack of significant radiation-induced effects to the pMTJs at high doses makes STT-MRAM promising as an alternative to DRAM, SRAM, and FLASH for applications requiring high immunity to radiation damage.

[1] S. Ikegawa, F. B. Mancoff, J. Janesky, and S. Aggarwal, "Magnetoresistive Random Access Memory: Present and Future", IEEE. Trans. Elec. Dev. 67(4), 1407 (2020); doi: 10.1109/TED.2020.2965403. [2] S. Aggarwal *et al.*, "Demonstration of a reliable 1 Gb standalone spin-transfer torque MRAM for industrial applications," in IEDM Tech. Dig., Dec. 2019, pp. 2.1.1-2.1.4; doi: 10.1109/IEDM19573.2019.8993516. [3] E. A. Montoya *et al.*, "Immunity of nanoscale magnetic tunnel junctions to ionizing radiation", arXiv:1909.11360v1. [4] B. Wang *et al.*, "Radiation impact of swift heavy ion beams on double-interface CoFeB/MgO magnetic tunnel junctions", Appl. Phys. Lett. 116, 172401 (2020); doi: 10.1063/1.5145124. [5] R. R. Katti *et al.*, "Heavy ion bit response and analysis of 256 Megabit non-volatile spin-torque-transfer magnetoresistive random access memory (STT-MRAM)," IEEE Radiation Effects Data Workshop (REDW), (2018); doi: 10.1109/NSREC.2018.8584321. [6] S. M. Guertin, J. Yang-Scharlotta, and R. Some, "Evaluating Memory Array Radiation Performance in Commercial DDR2 and MRAM Devices", Conference on Radiation Effects on Components and Systems (2018, Gothenburg, Sweden).

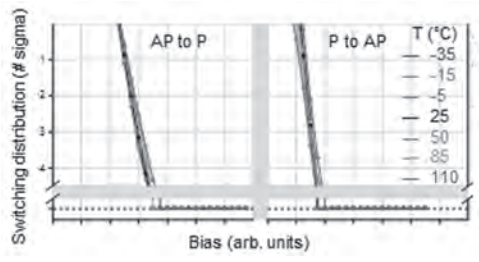

Fig. 1. STT write distributions in both transition directions in a 1Gb die measured across temperatures from -35°C to 110°C.

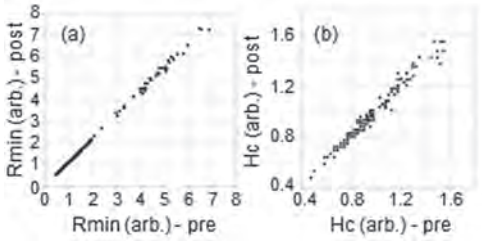

Fig. 2. pMTJ resistance Rmin (a) and magnetic field switching coercivity Hc (b) measured post vs. pre exposure to 7 Mrad(Si) gamma radiation.

CONTRIBUTED PAPERS

O2-02. Simplified Double Magnetic Tunnel Junction With Switchable Assistance Layer for Improved STT-MRAM Performance. *D. Sanchez Hazen*[1], S. Auffret[1], I. Joumard[1], L. Vila[1], L. Buda-Prejbeanu[1], R. Sousa[1], L. Prejbeanu[1] and B. Dieny[1] *1. SPINtronique et Technologie des Composants, Grenoble, France*

The use of double magnetic tunnel junctions (DMTJ) is a well-known strategy to enhance STT-MRAM efficiency by increasing thermal stability (Δ) while reducing the critical switching current (Ic). In these structures, the Storage layer (SL) is sandwiched between two tunnel barriers, each with its corresponding fixed polarizer. For the case of perpendicular DMTJ, the SL Δ is increased due to the two interfacial anisotropy contributions arising from both magnetic metal-oxide interfaces. If the top (TP) and bottom (BP) polarizers are set antiparallel, the Ic is found both theoretically [1] and experimentally [2] to be reduced due to additive spin-transfer torques. Another feature of DMTJ is the possibility of switching one of the polarizers, allowing to tune the STT depending on the polarizers parallel (Read Mode) or antiparallel (Write Mode) configuration [3]. Fig.1 (a) and (b) show the structure of such p-DMTJ with switchable TP and the two operation modes, where the polarizers are coupled to a hard Co/Pt synthetic antiferromagnetic multilayer (SAF). In this study, we investigate the possibility of replacing the TP SAF by a single magnetic layer realizing a p-DMTJ structure as depicted in Fig.1.(c). The structure proposed comprises a SAF based BP acting also as a fixed reference layer, a composite SL and the top free polarizer called assistance layer (ASL). The ASL is designed to have an out-of-plane anisotropy and a coercivity lower than that of the SL. In standby, the magnetic coupling between the SL and the ASL sets the magnetization of these two layers in parallel configuration, reinforcing the Δ of the SL. During write, the ASL acts as a polarizer inducing an additional STT, thus reducing the Ic. To investigate this concept, we fabricated, characterized and modeled these devices to understand the ASL working conditions. We demonstrate an increase by a factor of 5 in the figure of merit Δ/Ic of these structures compared to conventional MTJ stack for STT-MRAM with double barriers and a non-magnetic ASL Fig.2.

[1] Daniel C. Worledge, IEEE MAGNETICS LETTERS, Volume 8 (2017) [2] G. Hu, J. H. Lee, J. J. Nowak, IEEE International Electron Devices Meeting (IEDM), (2015) [3] P.-Y. Clément, C. Baraduc, M. Chshiev, B. Diény, IEEE 6th International Memory Workshop (IMW), (2014) [4] K. Nishioka, H. Honjo, S. Ikeda, Symposium on VLSI Technology Digest of Technical Papers, (2019)

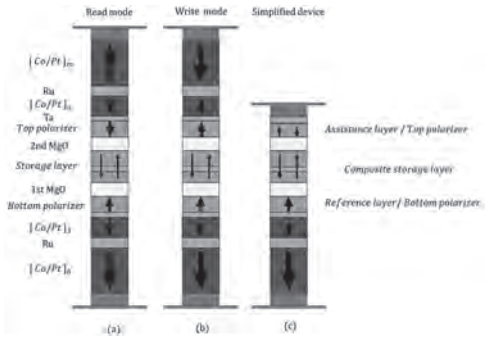

Fig.1: Conventional DMTJ in (a) writing mode and (b) reading mode. Simplified DMTJ with an ASL (c).

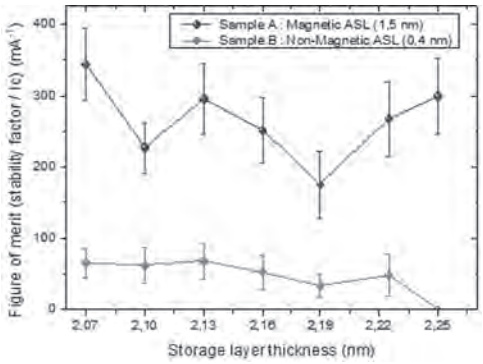

Fig. 2: Figure of merit extracted from measurements of a sample with magnetic-ASL and Non-magnetic ASL.

O2-03. Effect of Surface Modification Treatment on top Pinned MTJ With Perpendicular Easy Axis. *H. Honjo*[1], M. Yasuhira[1], S. Ikeda[1] and T. Endoh[1] *1. Center for Innovative Integrated Electronic Systems, Tohoku University, Sendai, Japan*

CoFeB-MgO-based magnetic tunnel junctions (MTJs) with perpendicular magnetic anisotropy (PMA) (p-MTJs) [1-3] have become the de-facto standard of current STT-MRAM. In the STT-MRAM, the bottom pinned structure [4,5], and in the SOT-MRAM, the top pinned structure has been employed [6,7]. The bottom pinned structure exhibits high PMA, whereas the top pinned structure is difficult to obtain a high PMA of Co/Pt due to the unavailability of a thick buffer layer under Co/Pt. In the bottom pinned p-MTJs, as the Pt buffer layer thickness increases, the PMA of Co/Pt increases [8]. However, Pt thickness cannot exceed 2 nm to obtain sufficient magnetic coupling between ferromagnetic layers [9]. Therefore, there is a trade-off between PMA and magnetic coupling in the top pinned structure. To overcome this trade-off, we developed a high PMA Co/Pt pinned layer for top pinned p-MTJs, using surface modification treatment (SMT). In Stack A without SMT, Pt seed layer (SL) thickness varied from 0.5 to 2.5 nm. In Stack A with SMT, a 6 nm-thick Pt SL was exposed to Ar ion plasma. After SMT, the residual Pt SL thickness was varied from 0.5 to 2.5 nm. We also prepared top pinned p-MTJs (Stack B) with a synthetic ferrimagnetic structure with and without SMT (Fig.2(a)). Annealing temperature is 300, 350, and 400°C for 1 h. In Stack A with SMT, the values of magnetic anisotropy energy density Keff*t are larger than those without SMT (Fig.1). In Stack B with SMT, TMR ratio increases up to 400°C, whereas in Stack B without SMT, TMR ratio degrades at 400°C (Fig.2(b)). The employment of SMT is very effective for achieving both higher perpendicular anisotropy and robustness against annealing for top pinned structure. This work is supported by CIES's Industrial Affiliation on STT MRAM program, CIES Consortium, JST-OPERA, and CAO-SIP.

[1] S. Ikeda et al., Nature Mater. 9, 721 (2010). [2] H. Sato et al., Appl. Phys. Lett. 101, 022414 (2012). [3] H. Sato et al., IEEE Trans. Magn. 49, 4437 (2013). [4] H. Honjo et al., J. Appl. Phys., 126, 113902 (2019). [5] K. Nishioka et al., IEEE Trans Electron Devices 67, 995 (2020). [6] H. Honjo et al., IEDM, 28.5.1. (2019). [7] M. Natsui et al., VLSI, CM2.2 (2020). [8] H. Honjo et., al, VLSI, T160 (2015). [9] H. Honjo et., al, IEEE Trans. Magn. 50, 1401904 (2014).

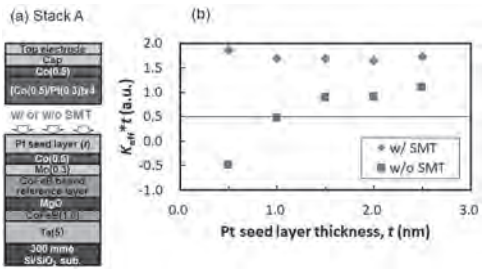

Fig. 1 (a) Stack structure schematic and (b) Pt seed layer thickness dependence of Keff*t for Stack A w/ and w/o SMT annealed at 400 °C for 1 h.

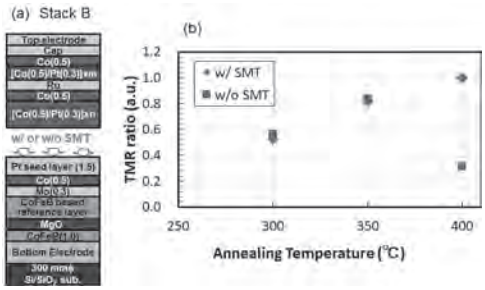

Fig. 2 (a) Stack structure schematic and (b) annealing temperature dependence of TMR ratio for Stack B w/ and w/o SMT.

O2-04. Back-Hopping in Spin-Transfer-Torque Switching of Perpendicularly Magnetized Tunnel Junctions. *T. Devolder*[3], O. Bultynck[1,2], P. Bouquin[3,1], V. Nguyen[1], S. Rao[1], D. Wan[1], B. Sorée[1,2], I. Radu[1], G.S. Kar[1] and S. Couet[1] *1. IMEC, Leuven, Belgium; 2. KUL, Leuven, Belgium; 3. Université Paris-Saclay, Palaiseau, France*

A major obstacle to reliable and fast STT-induced switching is a counter-intuitive phenomenon: the back-hopping (BH). We generally expect that the switching probability should always increase with the applied voltage. However the contrary can sometimes occur: in many instances, the MTJ resistance can back-hop to its original state after the apparent successful switching of the FL magnetization, as in the STT loop in Figure 1 at large positive voltage bias. We analyze the BH phenomenon in STT induced switching of perpendicularly magnetized tunnel junctions mimicking state-of-the art STTMRAM cells. The analysis is based on single-shot nanosecond time-resolved conductance measurements of the pulse-induced BH. The protocol allows to assign the conductance dynamics to the sole magnetization dynamics by avoiding the contributions from the bias dependence of the conductance and from current-induced heating. Studying several material variants reveals that the back-hopping is a feature of the nominally fixed system of the tunnel junction. This rules out earlier proposed scenarios based on the switching back of the free layer as a result of some anomalous voltage dependence of the STT acting on the free layer. The back-hopping is found (figure) to proceed by two sequential switching events that lead to a final state P' of conductance close to --but distinct from-- that of the conventional parallel state. The P' state does not exist at remanence. It generally relaxes to the conventional antiparallel state if the current is removed. The P' state involves a switching of the sole spin-polarizing part of the fixed layers, i.e. the barrier-facing part of the fixed layers. The analysis of our several material variants indicates that back-hopping occurs only when the spin-polarizing layer is too weakly coupled to the rest of the fixed system. This provides mitigation strategies of back-hopping for next generation STTMRAMs.

T. Devolder et al, arXiv:2006.05108.

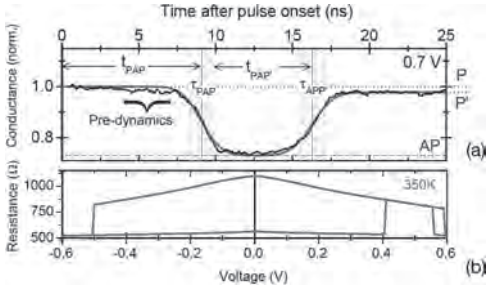

Fig. 1: (a) Representative single shot response with 3 GHz bandwidth with the definition of the P to AP and AP to P' switching times and their transition times. (b) Typical STT loop at high voltage bias and elevated temperatures.

O2-05. Impact of $Fe_{80}B_{20}$ Insertion on the Properties of Dual-MgO Perpendicular Magnetic Tunnel Junctions. *E. Liu*[1], T. Lee[2] and H. Yang[1] *1. National University of Singapore, Singapore; 2. Globalfoundries Inc Singapore, Singapore*

Magnetic tunnel junctions (MTJs) with perpendicular magnetic anisotropy (PMA) have been studied in the recent decades as the crucial element for next generation memory applications [1]. As the data-storage layer in MTJs, the dual-MgO free layers (FLs) with a structure as MgO/CoFeB/spacer/CoFeB/MgO have been under intense development to provide high PMA and low damping after annealing, which guarantees the high thermal stability and low switching current in MTJ devices [2]. The previous efforts for the optimization of dual-MgO FLs include the engineering of non-magnetic spacer [3-5] and boron composition [6]. As a novel approach, we explore the impact of $Fe_{80}B_{20}$ inserted at both $Co_{20}Fe_{60}B_{20}$/MgO interfaces of dual-MgO FLs under different annealing conditions in bottom-pinned MTJs. Current-in-plane tunnelling measurements are carried out to characterize magnetotransport properties of the MTJs. Conventional magnetometry measurements and ferromagnetic resonance are conducted to estimate the PMA and the Gilbert damping of dual-MgO FLs as a function of the $Fe_{80}B_{20}$ thickness and annealing temperatures. With ultrathin $Fe_{80}B_{20}$ (0.2 - 0.4 nm) inserted at the bottom interface, the tunnel magneto-resistance (TMR) can be maintained with a lower resistance-area (RA) product, while the top-FeB insertion results in a more RA drop with a similar TMR (Fig. 1(a)). The PMA of dual-MgO FLs with FeB inserted at the bottom interface shows a larger improvement than its top FeB insertion counterpart, even after 400 °C annealing (Fig. 1(b,c)). At the same time, the ultrathin FeB insertion at either interface reduces the damping constant in the FL (Fig. 1(d,e)). By optimizing the FeB insertion layer thickness and location, dual-MgO FLs with an unchanged TMR, higher effective anisotropy and lower damping can be achieved. This study demonstrates a novel approach to tune properties of dual-MgO FLs up to 400 °C annealing, which enables MTJ stacks for various applications.

[1] Ikeda S, *et al.* 2010 Nat. Mater. 9 721–4 [2] Sato H, *et al.* 2014 Appl. Phys. Lett. 105 062403 [3] Liu T, *et al.* 2015 Sci. Rep. 4 5895 [4] Couet S, *et al.* 2016 IEEE Magn. Lett. 7 3103004 [5] Chatterjee J, *et al.* 2017 Appl. Phys. Lett. 110 202401 [6] Honjo H, *et al.* 2016 IEEE Trans. Magn. 52 1–4

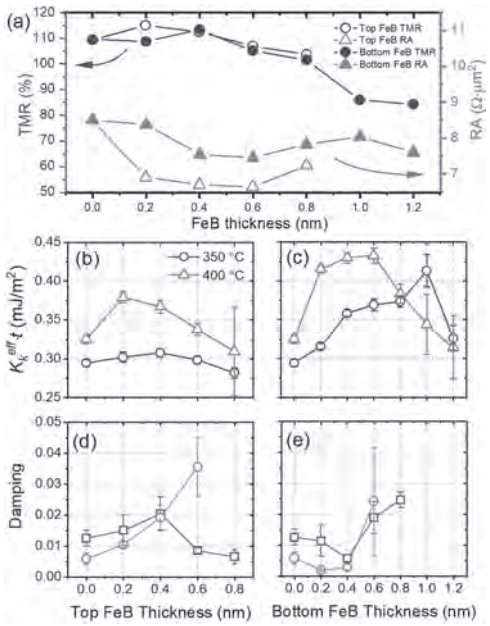

Fig.1 (a) Effect of FeB insertion on TMR and RA after 350 °C annealing. (b) and (d) show the impact from FeB insertion at the top CoFeB/MgO interface on PMA and damping, respectively, while (c) and (e) show the impact from the bottom interface.

O2-06. Enhancement of Magnetic Interaction and Magnetic Anisotropy in MTJ With Multiple CoFeB/MgO Interfaces for High Thermal Stability. *K. Nishioka*[1], H. Honjo[1], M. Yasuhira[1], S. Ikeda[1,2] and T. Endoh[1,3] *1. Center for Innovative Integrated Electronic Systems, Tohoku Daigaku, Sendai, Japan; 2. Center for Spintronics Integrated Systems, Tohoku University, Sendai, Japan; 3. Graduate school of Engineering, Tohoku University, Sendai, Japan*

Development of CoFeB/MgO based magnetic tunneling junction with perpendicular magnetic anisotropy (PMA) (p-MTJ) [1] has greatly contributed to realize the mass production of STT-MRAM. The higher thermal stability factor (Δ) is required for further scaling down of MTJ. In order to achieve high Δ, double and quad CoFeB/MgO interfaces p- MTJs have been proposed [2-4]. Single thin nonmagnetic layer (e.g., Ta, W, MgO, etc.) is inserted in the free layer to obtain high PMA (Stack A in Fig.1) [2]. In addition, enhancement of magnetic coupling (J_{cpl}) between free layer 1 and free layer 2 is also important to increase Δ, because Δ does not increase when the magnets behave magnetically independently without J_{cpl}. Previous study showed an enhancement of PMA in double interface p-MTJ by inserting a thin ferromagnetic layer sandwiched by two nonmagnetic layers in the free layer [5] (we call as "ferromagnetic bridge layer (FBL)"). However, J_{cpl} for the free layer with FBL was not considered. In this study, we investigated $K_{eff}t^*$ and J_{cpl} for the free layer with FBL in the double interface p-MTJ and simulated its impact on Δ. We prepared two types of stack with single insertion layer (Stack A) and FBL (Stack B). All stacks were deposited by DC/RF magnetron sputtering system, and then annealed at 400°C for 1h. Figures1-2 show experimental results of total insertion layer thickness (t) dependence of J_{cpl} and $K_{eff}t^*$. Stack B with FBL showed higher $K_{eff}t^*$ than Stack A with single insertion layer in all t range, while keeping higher J_{cpl} when t was up to 0.5 nm because each insertion layer thickness is much thinner than single insertion layer. This could result in higher Δ in Stack B with FBL because Δ is proportional to $K_{eff}t^*$ and effective free layer volume. Detailed simulation method and results will be presented. The FBL structure is an important technology to achieve high values both in J_{cpl} and $K_{eff}t^*$, which result in high Δ for double and quad CoFeB/MgO interfaces MTJ. This work is supported by CIES's Industrial Affiliation on STT MRAM program, CIES Consortium, JST-OPERA, and CAO-SIP.

[1] S. Ikeda et al., Nat. Mater. 9, 721 (2010). [2] H. Sato et al., Appl. Phys. Lett. 101, 022414 (2012). [3] H. Honjo et al., Dig. Tech. Pap. Symp. VLSI Technology, 2015, T160. [4] K. Nishioka et at., IEEE Trans. Electron Devices 67, 995 (2020). [5] J. Chatterjee at al., Phys Rev. Appl 12, 044043 (2019). [6] G. D. Chaves-O'Flynn et al., Phys. Rev. Appl. 4, 024010 (2015).

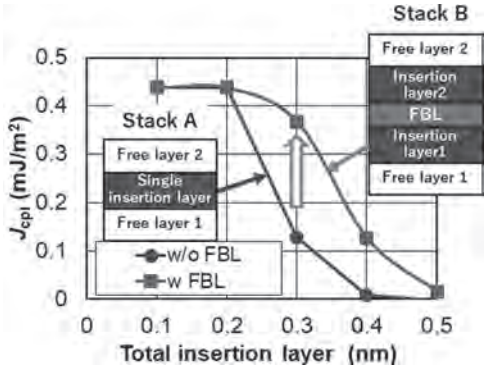

Fig.1 total non-magnetic insertion layer thickness dependence of J_{cpl}

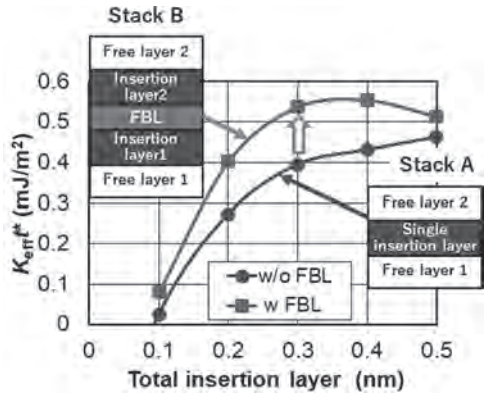

Fig.2 total non-magnetic insertion layer thickness dependence of $K_{eff}t^*$

O2-07. Thermal Stability and Magnetization Switching of Exchanged Coupled Composite Free Layer of Perpendicular Magnetic Tunnel Junction. *I. Volvach*[1], E. Fullerton[3] and V. Lomakin[2] *1. Material Science and Engineering, University of California San Diego, La Jolla, CA, United States; 2. Electrical & Computer Engineering, University of California San Diego, La Jolla, CA, United States; 3. Center for Memory and Recording Research, University of California San Diego, La Jolla, CA, United States*

Magnetic random access memory (MRAM) devices are envisioned as a major candidate for future memory technologies. Using an exchange coupled composite free layer (ECC FL) for perpendicular magnetic tunnel junction can improve the operation as predicted by a two-spin model [1]. Here, we show that ECC FL leads to significant reduction of the switching current and increase of the efficiency defined as the ratio between the energy barrier and switching current for device sizes (20-50nm) when the magnetization dynamics can be non-uniform. The results are obtained via the micromagnetic simulations performed with the micromagnetic simulator FastMag [2]. Figure 1 shows the thermal stability factor Δ and switching current density J_{c0} as a function of the surface exchange energy density J_{ex} for different anisotropy ratios γ between the ECC sublayers (i.e. FL_{soft} and FL_{hard}). of the ECC FL. The thermal stability factor increases with J_{ex} (Fig. 1a). The switching current density J_{c0} has an optimal value of the J_{ex} at which it is minimal (Fig. 1b). The reduction of J_{c0} is greater for greater γ and it can be reduced more than half as compared to a regular FL. The corresponding efficiency exhibits the maximal improvement of over 1.65 as compared to a regular FL. The mechanism leading to these improvements is that the switching of the softer layer assists in the switching of the harder layer. It is important that the reference layer is next to the softer layer. We find that

the devices of a smaller size need to have a significantly greater surface coupling strength to achieve optimal operation. Support from the Semiconductor Research Corporation is greatly acknowledged.

[1] I. Yulaev, M. V. Lubarda, S. Mangin, V. Lomakin, E. E. Fullerton, APL 99 (13), 132502 (2011). [2] R. Chang, S. Li, M. V. Lubarda, B. Livshitz, and V. Lomakin, J Appl Phys 109 (3), 07D358 (2011).

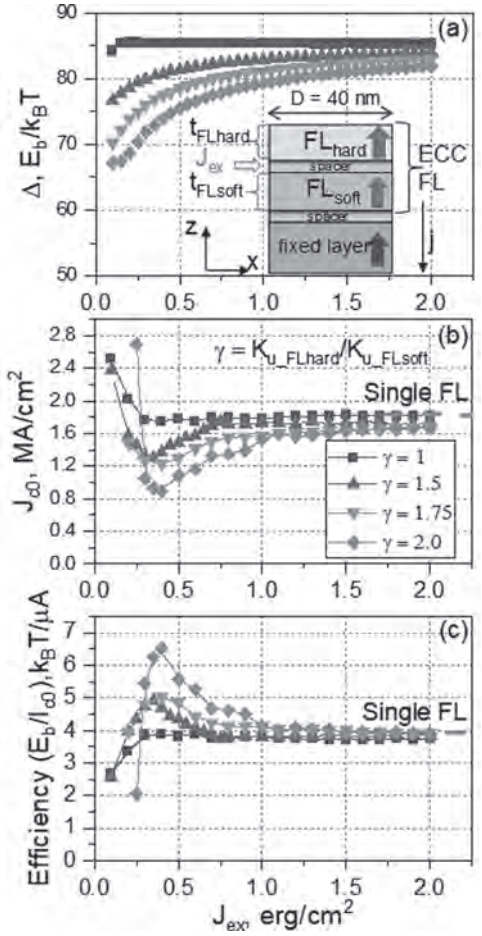

Fig.1. (a) Δ (b) J_{c0} (c) *Efficiency* vs. exchange coupling constant J_{ex} with $M_{sFLhard} = M_{sFLsoft}$ = 960 emu/cc, $K_{uFLhard}/K_{uFLsoft} = \gamma$, $A_{ex} = 10^{-6}$ erg/cm, α=0.008, $t_{FLhard} = t_{FLsoft}$ = 1.2 nm, t_{spacer} = 1.0 nm*

O2-08. Withdrawn

O2-09. Resolution of Non-Destructive Imaging for Buried Interfaces.

A. Hirohata[1], B. Aditya[2], J. Wu[2], M. Ota[3] and K. Elphick[1] *1. Electronics Engineering, University of York, York, United Kingdom; 2. City University of Hong Kong, Kowloon, Hong Kong; 3. Nagaoka Gijutsu Kagaku Daigaku Denki Denshi Joho Kogaku Katei Denki Denshi Joho Kogaku Senko, Nagaoka, Japan*

Non-destructive imaging for buried interfaces has been recently developed by decelerating electron-beam energy in scanning electron microscope (SEM) [1]. This imaging technique has proven to be very useful to identify the contaminations formed in a magnetic tunnel junctions (MTJs), which reduce their tunnelling magnetoresistance (TMR) ratios. For example, in a Heusler-alloy MTJ, residual resist has been found to react with Al during Al-O sputtering for the isolatation of the top and bottom electrodes. By reducing the Al-O sputtering power, the yield of the MTJs has been reported to be improved over 70% [2]. In order to further evaluate the resolution of this technique, we prepared a new set of samples with elevating capping layers in this study. The samples, consisting of Ta (5)/(Ru (5)/)W or Pt (0.5)/Ta (5~60) (thickness in nm), were deposited on Si substrates using a high target utilisation sputtering system. Here, the heavy metal layer of W or Pt were intrinsically dispersed as nano-particles. Their diameters were evaluated by imaging with the non-destructive technique, confirming the resolution. The penetration depth of the electron beam in SEM with different energy was estimated using CASINO programme [3]. The electron beam at 4.7 keV is found to reach the interface between Pt and Ta for the case of the 60 nm thick Ta capping layer and to generate back scattered electrons (BSE). The electron beam at 5.0 keV, on the other hand, is found to reach the bottom Pt (or W) interface and to generate BSE. By subtracting these images, the distribution of the Pt nano-particles can be assessed. The corresponding SEM image taken by the subtraction of these acceleration voltages can resolve the Pt nano-particles with 10 nm diameter. For the case of the 5 nm thick Ta capping layer, 2 nm resolution is achieved. Such resolution can be useful for the evaluation of buried MTJs with a few 10 nm diameter. We will further improve the resolution by optimising the imaging conditions, so that we will be able to image smaller MTJs. This work is partially supported by EPSRC-JSPS Core-to-Core programme (EP/M02458X/1) and JST CREST (JPMJCR17J5).

[1] A. Hirohata *et al.*, *Nat. Commun.* 7, 12701 (2016). [2] E. Jackson *et al.*, *Sci. Rep.* 8, 7585 (2018). [3] D. Drouin *et al.*, *Scanning* 29, 92 (2007).

O2-10. Perpendicular Magnetic Anisotropy in Cu_2Sb-Type (Mn-Cr) AlGe Films: Layer Thickness and Adjacent Layer Dependence.

T. Kubota[1,2], K. Ito[1,2], R.Y. Umetsu[1,2], M. Mizuguchi[1,2] and K. Takanashi[1,2] *1. Institute for Materials Research, Tohoku Daigaku, Sendai, Japan; 2. Center for Spintronics Research Network, Tohoku Daigaku, Sendai, Japan*

The Cu_2Sb-type MnAlGe and (Mn-Cr)AlGe are materials showing uniaxial magnetocrystalline anisotropy and relatively small saturation magnetization, M_s (~ 300 emu/cm^3) [1,2], which are attractive for application to the magnetization switching layer of spin-transfer-torque and spin-orbit-torque magnetoresistive random access memories, MRAMs. Perpendicularly magnetized (001)-textured (Mn-Cr)AlGe films with a thickness of 100 nm were successfully fabricated onto thermally oxidized silicon (Si, SiO_2) substrates in our previous work [2], however, the thickness should be reduced for practical applications such as MRAMs. In this study the layer thickness and the adjacent layer dependence of magnetic properties have been investigated for MnAlGe and (Mn-Cr)AlGe films. The samples were fabricated using a magnetron sputtering machine with the stacking structure as follows: Si, SiO_2 sub. | buffer layers | MnAlGe or (Mn-Cr)AlGe *t* | MgO 1.5 nm | Ta 5 nm, where *t* is the layer thickness changing from 5 to 100 nm. For the buffer layers, "no buffer" or Ta 5 nm | CoFeBTa 1 nm | MgO 1.5 nm was used. From x-ray diffraction measurements, the MnAlGe and (Mn-Cr) AlGe layers exhibited no diffraction peak for the as-deposited states, while (001)-texture was confirmed after *ex situ* annealing at 300 – 500 °C. The magnetic dead layer thicknesses, t_{dead}, were evaluated from the *t* dependence of areal magnetization. The t_{dead} was 1.7 nm for MnAlGe films onto no buffer. On the other hand, for the Ta | CoFeBTa | MgO buffer samples, the values were 2.9 and 3.5 nm for MnAlGe and (Mn-Cr)AlGe, respectively, which are about double compared to that of no buffer sample, and suggesting that the dead layer originates from the MgO interfaces. From magnetization curve measurements, perpendicular magnetization was clearly confirmed for *t* down to 5 nm for both MnAlGe and (Mn-Cr)AlGe films as shown in Fig. 1. The perpendicular magnetic anisotropy energy, K_u, exhibits no dependence on *t* down to 10 nm, while the K_u decreased at *t* of 5 nm. The finite dead layer is a reason for the degraded K_u, which should be improved for enhancement of K_u in thinner samples in future.

[1] K. Shibata *et al.*, J. Phys. Soc. Jpn. 35, 448 (1973). [2] T. Kubota *et al.*, Appl. Phys. Express 12, 103002 (2019).

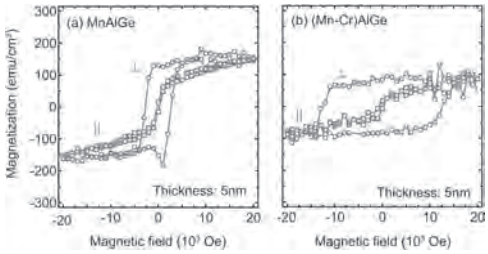

Magnetization curves of 5-nm-thick (a) MnAlGe and (b) (Mn-Cr)AlGe films deposited onto MgO buffer.

O2-11. Variation of Energy Barrier With Temperature in X/1X-nm Shape-Anisotropy Magnetic Tunnel Junctions. *J. Igarashi*[1], B. Jinnai[2], V. Desbuis[3], S. Mangin[3], S. Fukami[1,4] and H. Ohno[1,4] *1. Laboratory for Nanoelectronics and Spintronics, Research Institute of Electrical Communication, Tohoku University, Sendai, Japan; 2. WPI Advanced Institute for Materials Research, Tohoku University, Sendai, Japan; 3. Institut Jean Lamour, Université de Lorraine, Nancy, France; 4. Center for Science and Innovation in Spintronics, Tohoku University, Sendai, Japan*

Shape-anisotropy magnetic tunnel junction (MTJ)[1] enables to shrink MTJ size down to X/1X nm while keeping high thermal stability factor Δ ($\equiv E/k_BT$, where E is the energy barrier between the two magnetization states, k_B is the Boltzmann constant, and T is the temperature)[1,2]. For fundamental and application points of view, it is important to evaluate E at high temperature. Whereas the temperature dependence of E is reported for the conventional interfacial-anisotropy MTJs[3], that of the shape-anisotropy MTJ has not been studied to date. In this study, we investigate the temperature dependence of E in the CoFeB/MgO-based shape-anisotropy MTJs at various temperatures to understand the physics governing the temperature dependence of E. Figure 1(a) shows the switching probability as a function of the pulse magnetic field H_{pulse} at various temperatures for an MTJ with a diameter D = 5.8 nm. Solid lines are fitted curves. Fig. 1(b) shows the temperature dependence of D obtained from the fitting for MTJs with D = 5.8, 8.4, and 11.9 nm. We note that MTJs studied here are designed not to have too high Δ so that the properties are clearly changed within the temperature range we can access in our setup. We then evaluated the scaling relationship between the temperature dependence of E ($= \Delta k_BT$) and spontaneous magnetization M_S. The relationship enables one to design the MTJ dimensions (D and free-layer thickness t) to achieve high Δ at arbitrary temperatures. From this analysis, we discuss a window of shape-anisotropy MTJ to design devices beyond 20 nm for high-temperature applications. This work was supported in part by JST-OPERA JPMJOP1611, Core-to-Core Program of JSPS, Cooperative Research Projects of RIEC, JSPS KAKENHI JP19J12926 and JP19K04486, DIARE of Tohoku University, and JSPS Bilateral Joint Research Program. J.I. acknowledges financial support from GP-Spin of Tohoku University and JST-OPERA.

[1] K. Watanabe et al., Nature Commun. 9, 663 (2018). [2] N. Perrissin et al., Nanoscale 10, 12187 (2018). [3] Y. Takeuchi et al., Appl. Phys. Lett. 107, 152405 (2015).

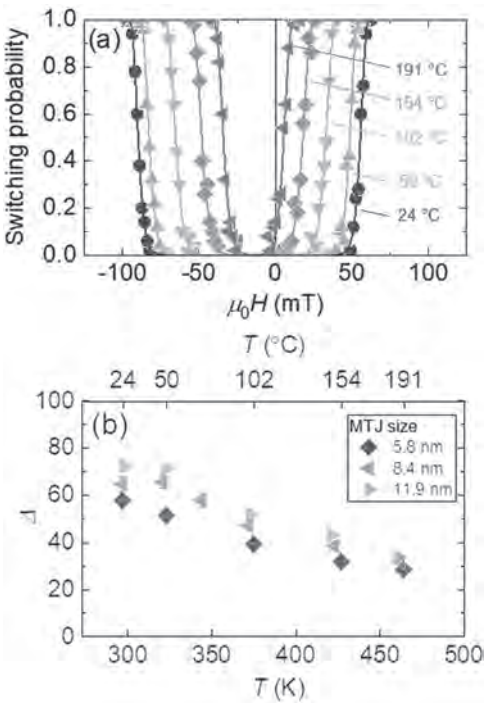

Fig. 1 (a) Switching probability measured under application of H_{pulse} with pulse duration of 1 s for D = 5.8 nm at various temperatures. (b) Temperature dependence of Δ for D = 5.8, 8.4, and 11.9 nm.

O2-12. Combined Effects of Stray Field and Dzyaloshinskii–Moriya Interaction on Magnetic Tunnel Junction With Stepped and Pillar Structures. *C. Cheng*[1], K. Chen[1], J. Wei[2], Y. Hsin[2], S. Sheu[2] and Y. Tseng[1] *1. National Chiao Tung University, Hsinchu, Taiwan; 2. Industrial Technology Research Institute, Hsinchu, Taiwan*

It is a matter of debate whether a pillar or a stepped structure better retains magnetic tunnel junctions' (MTJs) performance while scaling down. In this work we use micromagnetic simulation to model the scaling effects on the free-layer's stray-field (H_{stray}) for the two MTJ structures. The model was built on an MTJ containing a synthetic ferromagnetic (*SyF*) layer (free-layer/MgO/reference-layer) and a synthetic antiferromagnetic (*SyAF*) layer (reference-layer/Ru/hard-layer). Approximate H_{stray} strength is obtained in both structures with a free-layer of ~ 100nm. However, upon size reduction the H_{stray} raises significantly in the pillar structure, but it appears less responsive in the stepped structure. This trend is shared by experimental results with the MTJ reduced from 130 to 80 nm. We are suggested that the stepped structure is a more promising candidate on mitigating H_{stray} in pursuit of high density MRAM [1]. The combined effects of H_{stray} and Dzyaloshinskii–Moriya interaction (*DMI*) on switching current density (J_c) were also calculated for a 30 nm free-layer MTJ. The in-plane H_{stray} appears to interact with the *DMI* in a complementary or a competing manner, depending on the sign of the *DMI* and initial switching state (parallel or antiparallel) of the MTJ. The stepped structure is able to reduce J_c more effectively than the pillar case. This is due to strong mediation from the *Ruderman-Kittel-Kasuya-Yosida (RKKY) interaction of the SyAF* layer in the stepped structure.

[1]. S. Bandiera, S. Bandiera, R. C. Sousa, et al., *IEEE Magn. Lett.* 1, 3000204 (2010).

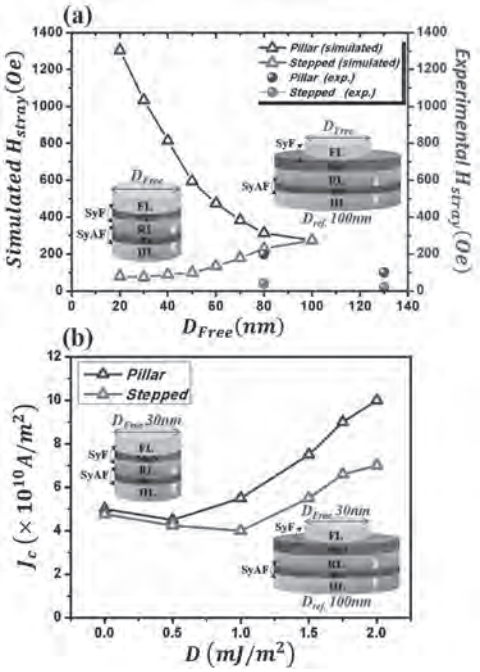

Fig. 1: (a) simulated H_{stray} (open symbols, units on left y-axis) and experimental H_{stray} (filled symbols, units on right y-axis) for stepped and pillar MTJs, with variable free-layer dimension (D_{free}). For pillar structure the reference layer is fixed to 100 nm. (b) simulated J_c as a function of the *DMI* strength for stepped and pillar MTJs with the free layer both fixed to 30 nm. H_{stray} effect (both in-plane and out-of-plane) of a 30 nm free-layer was added to interact with the *DMI* to obtain J_c.

O2-13. Investigation of Acoustic Wave Induced FMR Assisted Spin Toque Switching of MTJs With Lateral Anisotropy Variation.
W. Misba[1], M. Rajib[1], D. Bhattacharya[1] and J. Atulasimha[1] *1. Virginia Commonwealth University, Richmond, VA, United States*

Surface acoustic wave (SAW) can induce ferromagnetic resonance (FMR) [1] in the magnetostrictive soft layer of a magnetic tunnel junction (MTJ) that can be leveraged for magnetization reversal with reduced STT current [2]. However, in realistic scenarios, the MTJ soft layer can have inhomogeneity in its lateral anisotropy due to the intrinsic anisotropy variation, edge modification, roughness and thickness variation [3]. Consequently, different regions of magnetizations precess non-uniformly under the excitation of SAW and this incoherent precession become more prominent in the presence of thermal noise (see Fig.1 for 1 ns and 0.92 ns snapshots at T=0 K and T=300 K respectively for inhomogeneous anisotropy distribution). Such incoherency is detrimental as it can reduce the net magnetization deflection to a much lower value and thereby prove ineffective in reducing the STT current needed to switch the magnetization. Remarkably, magnetization precessions in different regions are found to be in phase even though they are precessing in non-uniform cones and the resulting high net magnetization deflection contributes to decrease the STT current required for magnetization reversal. In addition, such magnetization reversal is attained with SAW induced stress amplitude that is much lower than the total anisotropic barrier. This work points to the energy efficiency of the SAW assisted STT scheme and the potential for scalability below lateral dimension ~ 50 nm, which is technologically significant for STT-RAM application. It also shows the robustness of the scheme in realistic scenarios with thermal noise and material inhomogeneity. Finally, we will present some experimental results to demonstrate the effect of ferromagnetic resonance on ~ 100 nm magnetostrictive nanomagnets driven to FMR by SAW where the lateral anisotropy variation would be inherently present due to lithography and fabrication imperfection. ACKNOWLEDGEMENT: NSF SHF grant 1815033 and VMEC Seed grant.

[1]. M. Weiler, L. Dreher and C. Heeg, Phys. Rev. Lett. Vol. 106, p. 117601 (2011) [2]. A. Roe, D. Bhattacharya and J. Atulasimha, Appl. Phys. Lett. Vol. 115, p. 112405 (2019) [3]. W. A. Misba, M. M. Rajib and D. Bhattacharya, arXiv:2003.12903 (2020)

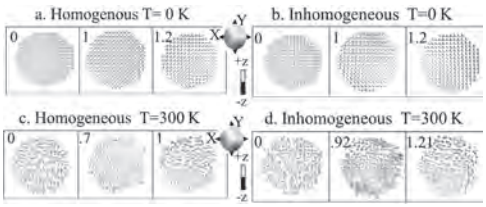

Fig. 1: Micromagnetic spin configurations at different times (shown in left corner in ns) under the SAW excitation applied at t=0 ns for homogeneous anisotropy at a. T=0 K and c. T=300 K and for inhomogeneous anisotropy at b. T=0 K and d. T=300 K.

O2-14. Evaluation of Read Disturbance Reduction Effect by Bi-Directional Read on Ferromagnetic Material Properties of SOT-MRAM.
Y. Kishi[1], K. Tabata[1], M. Ke[1] and T. Kawahara[1] *1. Department of Electrical Engineering, Faculty of Engineering, Tokyo University of Science, Katsushika-ku, Japan*

Spin-orbit torque (SOT) -MRAM is characterized by its fast write operation, and decoupled read and write current paths that enable separate optimization for the two operations [1]. While SOT-MRAM has shown promise as a memory that can eliminate a trade-off between read and write, we previously reported that there is a trade-off [2]. To resolve this issue, we proposed a stabilized structure with a bi-directional read path (Fig. 1(a)) and demonstrated that high read reliability is possible [2]. In this paper, we propose two new layouts and schematics for this stabilized structure: a single bit line type and a double bit line type (Fig. 1(b)). Both circuits perform a write operation when WW is ON, and a bi-directional read operation when RW is ON (Fig. 1(a)). Our evaluation shows that a single bit line type achieves higher integration density and is suitable for bi-directional read. To determine if SOT-MRAM can be stabilized accurately, when the ferromagnetic layers of MTJ are made of iron, permalloy, and cobalt, which are the main ferromagnetic materials, with different easy axis types of magnetization, we evaluated reduction effects using an LLG simulator. Specifically, we compared magnetization reversal probability for conventional and stabilized structure. Results showed that read disturbance was reduced by more than ten times for all three materials (Fig. 2). Iron and cobalt were ten times more effective, and permalloy was 45 times more effective. When we compare these material parameters, the coercive force of permalloy is small, and when it is small, conventional SOT-MRAM receives more read disturbance due to magnetization reversal stemming from spin current generated by the spin Hall effect. This is the cause of reduction effect difference. This work was partly supported by JSPS KAKENHI Grant Number JP19K04536.

[1] Y. Kim et al., DOI: 10.1109/TED.2014.2377721, IEEE Transactions on Electron Devices, Vol. 62, No. 2, pp. 561-567 (2015) [2] H. Kazama and T. Kawahara, DOI: 10.1109/INTMAG.2017.8007571, IEEE International Magnetics Conference (2017)

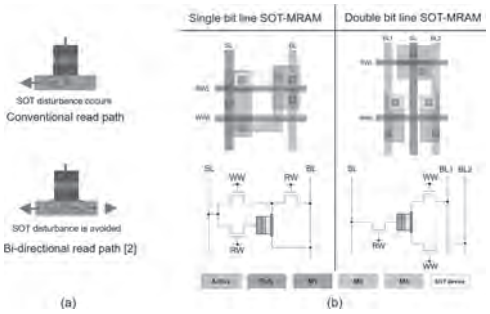

Fig. 1 (a) Read path of conventional and stabilized structure (bi-directional read) of SOT-MRAM device [2]. (b) Two proposed layouts and schematics of stabilized SOT-MRAM memory cell.

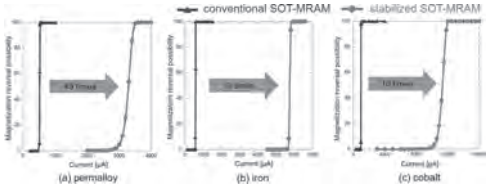

Fig. 2 Magnetization reversal probabilities for read current of conventional and stabilized (bi-directional read) SOT-MRAM for read times of 5 ns. Ferromagnetic layers of MTJ are (a) permalloy, (b) iron, and (c) cobalt.

O2-15. Multilevel Magnetization Switching of Magnetic Tunnel Junctions Induced by Spin-Orbit Torque. *J. Lourembam*[1], L. Huang[1], B. Chen[2], J. Qiu[1], H. Chung[1], Q. Yap[1], S. Lee Koon Yap[3], S. Wong[3] and S. Lim[1] *1. Electronic Materials, Institute of Materials Research and Engineering, Singapore, Singapore; 2. Institute of High Performance Computing, Singapore, Singapore; 3. Institute of Materials Research and Engineering, Singapore, Singapore*

Magnetization switching of magnetic tunnel junctions (MTJs) via spin-orbit torque (SOT) is gaining interest in cache memory applications due to its benefits in lowering power consumption. Although SOT switching of perpendicular MTJs offers better scalability, in practice the requirement of an external magnetic field to assist SOT switching is a fundamental bottleneck. Meanwhile, in-plane (IP) MTJs, fabricated in the form of an ellipse, have been demonstrated to switch by SOT without an external field. Here, the easy axis of the elliptical MTJ is perpendicular to the charge flow in the spin-hall channel, and the magnetization trajectory is argued to undergo several precessions before magnetization flip similar to spin-transfer torque switching. [1] However, in this work we experimentally show that these IP-SOT MTJs, can in fact switch as fast as 400 ps, shorter than the precessional trajectory. The IP MTJs, which implements Pt/CoFeB/MgO as the free layer, are fabricated on a 200 mm wafer using stepper lithography and ion-beam etching. Interestingly, by applying asymmetric SOT pulse segments at substantially small voltage steps, we found that a significant number of MTJs demonstrated multilevel resistance states. While multilevel states have been reported in antiferromagnet/ferromagnet structures, the underlying mechanism arising from variation in exchange bias is not applicable in our case. [2] Using micromagnetic simulations, we formulate that the existence of meta-stable domain states inside the MTJ free-layer is a likely explanation in our case. In addition, we also probe the role of CoFeB thickness, aspect ratio, and switching probabilities of these devices. Multilevel resistance states in SOT devices could find potential in neuromorphic circuits.

[1] S. Fukami et.al. Nat. Nanotechnol. 11, 621 (2016). [2] A. Kurenkov et.al. Appl. Phys. Lett. 110, 092410 (2017).

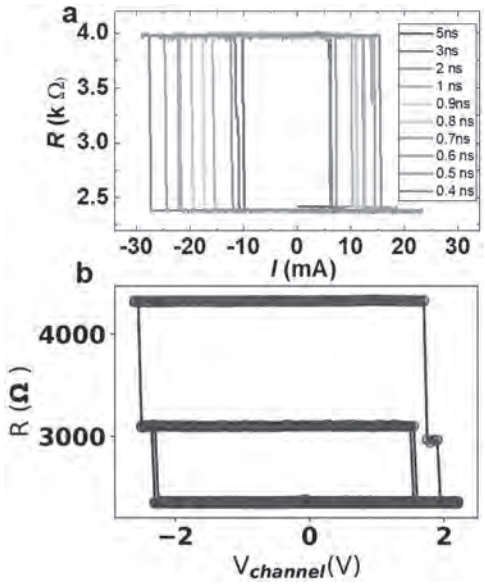

Fig. a Demonstration ultrafast SOT switching on an IP MTJ using pulse widths 0.4 ns to 5 ns. b Multilevel memory states using asymmetric SOT pulse segments.

O2-16. Effect of Edge Roughness in Spin-Orbit Torque Magnetoresistive Random-Access Memory With Damping Constant Variation. *J. Byun*[1], D. Kang[1] and M. Shin[1] *1. School of Electrical Engineering, Korea Advanced Institute of Science and Technology, Daejeon, The Republic of Korea*

Magnetic tunnel junction (MTJ) is known to suffer from critical dimension variations during manufacturing process [1] and the deformation affect the switching behavior of spin transfer torque-magnetic random access memory (STT-MRAM). However, the effect of shape deformation of MTJ on the SOT-MRAM is not yet elucidated to the best our knowledge. We present a micromagnetic simulation study of shape deformation due to edge roughness effect in the spin orbit torque-magnetic random access memory (SOT-MRAM). The two different write schemes for deterministic switching, magnetic field induced SOT write scheme and SOT-STT hybrid write scheme, are studied and compared in this work. Randomly deformed MTJs were generated according to the roughness generation model [2] as shown in Fig. 1. The simulation was performed by using object oriented micromagnetic framework [3]. From Fig. 2, the deformation can cause switching back behavior in the devices if the SOT-magnetic field write scheme with low Gilbert damping constant (α) is used. High α of 0.09 is required to achieve 100% switching probability. However, the SOT-STT hybrid write scheme shows 100% switching probability at relatively low $\alpha = 0.02$. This is because the perpendicular STT suppresses the precession towards upper hemisphere. As the α increases, the switching time is enhanced for the SOT-magnetic field write scheme and the device variations are lowered. On the other hand, the switching speed of SOT-STT write scheme is almost independent of α. It is because the intermediate state of the SOT-STT write scheme is in close proximity to the x-y plane. The STT competes with the damping towards the initial state and this damping increases with the higher α. In conclusion, we found that under the edge roughness effect, MTJ with high α material is effectively switched by the SOT-magnetic field write scheme, while SOT-STT enhances the switching behavior for the device with low damping constant material.

[1] K. Lee, J. H. Bak and Y.J. Kim, in 2019 IEEE International Electron Devices Meeting (IEDM), San Francisco, CA, USA (2019) [2] H. Jung and M. Shin, IEEE Transactions on electron devices, Vol. 60, p. 1861 - 1866 (2013) [3] R. McMichael and M. Donahue, National Institute of Standards and Technology, Gaithersburg, MD, USA, Interagency Report NISTIR 6376 (1999)

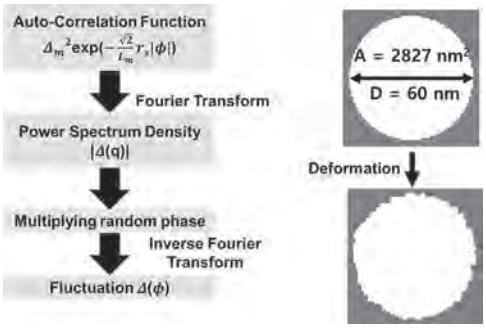

Fig. 1: Deformation process of MTJ, 1000 samples were generated having ±5% of area difference within 3sigma distributions.

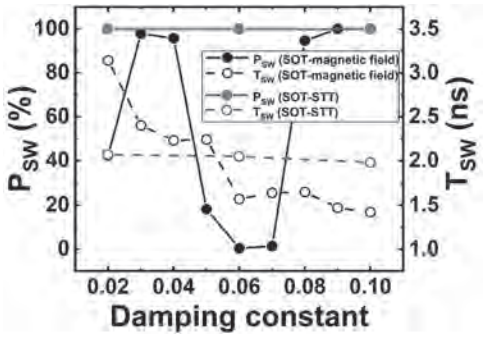

Fig. 2: Switching probability (P_{SW}) and switching time (T_{SW}) with damping constant α variation.

Session O3
SKYRMIONS AND BEYOND

Haifeng Du, Co-Chair
High Magnetic Field Laboratory of Chinese Academy of Sciences, Hefei, China
Yizhou Liu, Co-Chair
Rikagaku Kenkyujo Sohatsu Bussei Kagaku Kenkyu Center, Tianjin, China

INVITED PAPER

O3-01. Beyond Skyrmions: Alternative Magnetic Quasiparticles. *B. Göbel*[1,2], I. Mertig[1] and O. Tretiakov[3] *1. Martin-Luther-Universitat Halle-Wittenberg, Halle, Germany; 2. Max Planck Institute of Microstructure Physics, Halle, Germany; 3. School of Physics, University of New South Wales, Sydney, NSW, Australia*

Magnetic skyrmions have attracted enormous research interest since their discovery a decade ago. Especially the non-trivial real-space topology of these nano-whirls leads to fundamentally interesting and technologically relevant effects – the skyrmion Hall effect of the texture and the topological Hall effect of the electrons. Furthermore, it grants skyrmions in a ferromagnetic surrounding great stability even at small sizes, making skyrmions aspirants to become the carriers of information in the future. Still, the utilization of skyrmions in spintronic devices has not been achieved yet, among others, due to shortcomings in their current-driven motion. In this talk, we present recent trends in the field of topological spin textures that go beyond skyrmions [1]. The majority of these objects can be considered the combination of multiple skyrmions or the skyrmion analogues in different magnetic surroundings, as well as three-dimensional generalizations. We classify the alternative magnetic quasiparticles – some of them observed experimentally, others theoretical predictions – and present the most relevant and auspicious advantages of this emerging field. A special focus is on magnetic antiskyrmions [2], bimerons [3], antiferromagnetic skyrmions [4] and hopfions [5]. These objects (shown in Fig. 1) exhibit advantageous emergent electrodynamic effects compared to skyrmions, either due to their lower symmetry or due to a compensated topological charge.

[1] B. Göbel, I. Mertig, O. Tretiakov "Beyond skyrmions: Review and perspectives of alternative magnetic quasiparticles" arXiv preprint: 2005.01390 [2] J. Jena*, B. Göbel*, T. Ma, V. Kumar, R. Saha, I. Mertig, C. Felser, S. Parkin. "Elliptical Bloch skyrmion chiral twins in an antiskyrmion system" *Nature Communications* 11, 1115 (2020). [3] B. Göbel, A. Mook, J. Henk, I. Mertig, O. Tretiakov. "Magnetic bimerons as skyrmion analogues in in-plane magnets" *Phys. Rev. B*. 99, 060407(R) (2019). [4] B. Göbel, A. Mook, J. Henk, I. Mertig, "Antiferromagnetic skyrmion crystals: Generation, topological Hall, and topological spin Hall effect" *Phys. Rev. B*. 96, 060406(R) (2017). [5] B. Göbel, C. Akosa, G. Tatara, I. Mertig. "Topological Hall signatures of magnetic hopfions" *Phys. Rev. Research* 2, 013315 (2020).

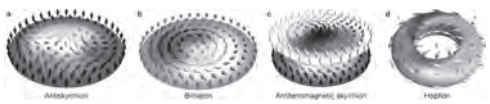

Fig. 1. (a) Magnetic antiskyrmion, (b) magnetic bimeron, (c) antiferromagnetic skyrmion, (d) magnetic hopfion. The arrows correspond to magnetic moments whose color is determined by their orientation.

CONTRIBUTED PAPERS

O3-02. Topological Half-Skyrmions and Bimerons in an Antiferromagnetic Insulator at Room Temperature. *H. Jani*[1] and P. Radaelli[2] *1. Physics, National University of Singapore, Singapore; 2. Physics, University of Oxford, Oxford, United Kingdom*

In the quest for post-CMOS technologies, ferromagnetic skyrmions and their anti-particles have shown great promise as topologically protected[1–6] solitonic information carriers in memory-in-logic or neuromorphic devices[1,7–9]. However, the presence of dipolar fields in ferromagnets, restricting the formation of ultra-small topological textures[2–4,6,7,10], and the deleterious skyrmion Hall effect when driven by spin torques[7,8,10] have thus far inhibited their practical implementations. Antiferromagnetic analogues, which are predicted to demonstrate relativistic dynamics, fast deflection-free motion and size scaling have recently come into intense focus[7,11–17], but their experimental realizations in natural antiferromagnetic systems are yet to emerge. Here, we demonstrate a family of topological antiferromagnetic spin-textures in α-Fe_2O_3 – an earth-abundant oxide insulator – capped with a Pt over-layer. By exploiting a first-order analogue of the Kibble-Zurek mechanism[18,19], we stabilize exotic merons-antimerons (half-skyrmions[6]), and bimerons[14,20], which can be erased by magnetic fields and re-generated by temperature cycling. These structures have characteristic sizes in the range ~100 nm that can be chemically controlled via precise tuning of the exchange and anisotropy, with pathway to further scaling. Driven by current-based spin torques from the heavy-metal over-layer, some of these AFM textures could emerge as prime candidates for low-energy antiferromagnetic spintronics at room temperature[1,7-9,21]. This paper can be accessed at the Arxiv Link: https://arxiv.org/abs/2006.12699

1 Christian, H. B. et al. The 2020 skyrmionics roadmap. Journal of Physics D: Applied Physics (2020). 2 Kurumaji, T. et al. Skyrmion lattice with a giant topological hall effect in a frustrated triangular-lattice magnet. Science 365, 914–918 (2019). 3 Woo, S. et al. Observation of room-temperature magnetic skyrmions and their current-driven dynamics in ultrathin metallic ferromagnets. Nature Materials 15, 501–506 (2016). 4 Soumyanarayanan, A. et al. Tunable room-temperature magnetic skyrmions in Ir/Fe/Co/Pt multi-layers. Nature Materials 16, 898–904 (2017). 5 Nayak, A. K. et al. Magnetic antiskyrmions above room temperature in tetragonal heusler materials. Nature 548, 561–566 (2017). 6 Yu, X. Z. et al. Transformation between meron and skyrmion topological spin textures in a chiral magnet. Nature 564, 95–98 (2018). 7 Büttner, F., Lemesh, I. & Beach, G. S. D. Theory of isolated magnetic skyrmions: From fundamentals to room temperature applications. Scientific Reports 8, 4464 (2018). 8 Zhang, X. et al. Skyrmion-electronics: writing, deleting, reading and processing magnetic skyrmions toward spintronic applications. Journal of Physics: Condensed Matter 32, 143001 (2020). 9 Grollier, J. et al. Neuromorphic spintronics. Nature Electronics (2020). 10 Litzius, K. et al. Skyrmion hall effect revealed by direct time-resolved x-ray microscopy. Nature Physics 13, 170–175 (2017). 11 Barker, J. & Tretiakov, O. A. Static and dynamical properties of antiferromagnetic skyrmions in the presence of applied current and temperature. Physical Review Letters 116, 147203 (2016). 12 Baltz, V. et al. Antiferromagnetic spintronics. Rev. Mod. Phys. 90, 015005 (2018). 13 Zhang, X., Zhou, Y. & Ezawa, M. Magnetic bilayer-skyrmions without skyrmion hall effect. Nature Communications

7, 10293 (2016). 14 Shen, L. et al. Current-induced dynamics and chaos of antiferromagnetic bimerons. Physical Review Letters 124, 037202 (2020). 15 Caretta, L. et al. Fast current-driven domain walls and small skyrmions in a compensated ferrimagnet. Nature Nanotechnology 13, 1154–1160 (2018). 16 Dohi, T., DuttaGupta, S., Fukami, S. & Ohno, H. Formation and current-induced motion of synthetic antiferromagnetic skyrmion bubbles. Nature Communications 10, 5153 (2019). 17 Legrand, W. et al. Room-temperature stabilization of antiferromagnetic skyrmions in synthetic antiferromagnets. Nature Materials 19, 34–42 (2020). 18 Kibble, T. W. B. Topology of cosmic domains and strings. J. Phys. A: Math. Gen. 9, 1387–1398 (1976). 19 Zurek, W. H. Cosmological experiments in superfluid helium? Nature 317, 505–508 (1985). 20 Göbel, B., Mook, A., Henk, J., Mertig, I. & Tretiakov, O. A. Magnetic bimerons as skyrmion analogues in in-plane magnets. Physical Review B 99, 060407 (2019). 21 Liang, X. et al. Antiferromagnetic skyrmion-based logic gates controlled by electric currents and fields. arXiv preprint arXiv:1909.10709 (2019).

O3-03. Three-Dimensional Dynamics of a Magnetic Hopfion.
Y. Liu[1,2], W. Hou[3], X. Han[1] and J. Zang[3] *1. Beijing National Laboratory of Condensed Matter Physics, Institute of Physics, Chinese Academy of Sciences, Beijing, China; 2. Center for Emergent Matter Science, RIKEN, Wako, Japan; 3. Department of Physics and Astronomy, University of New Hampshire, Durham, NH, United States*

Magnetic hopfions are three-dimensional (3D) topological spin textures characterized by the Hopf invariant. As manifesting by their 3D real-space topologies, magnetic hopfions may exhibit interesting dynamics. Here, we study the current-induced dynamics of a magnetic hopfion with unit Hopf invariant in a 3D frustrated magnetic system. Attributed to the spin Berry phase and symmetry of the hopfion, the phase space entangles multiple collective coordinates, thus the hopfion exhibits rich dynamics including longitudinal motion along the current direction, transverse motion perpendicular to the current direction, rotational motion, and dilation. A current within the torus-midplane of hopfion mainly drives a longitudinal motion of hopfion associated with transverse motions and rotations. While a current perpendicular to the torus-midplane of hopfion drives a longitudinal motion of hopfion associated with rotation and dilation. The characteristics of hopfion dynamics, including the hopfion Hall angles, the rotation directions, and the dilation factor, are determined by the ratio between the nonadiabatic spin transfer torque parameter and the damping parameter. The 3D hopfion dynamics can be well captured by a collective coordinate based analysis. Such peculiar 3D dynamics of magnetic hopfion could shed light on understanding the universal physics of hopfions in different systems and boost the prosperous development of 3D spintronics.

INVITED PAPER

O3-04. Chirality in Action: From Antiferromagnets to Novel Chiral Particles. *Y. Mokrousov*[1,2] *1. Forschungszentrum Julich GmbH, Julich, Germany; 2. Johannes Gutenberg Universitat Mainz, Mainz, Germany*

In the field of spintronics, antiferromagnetic (AFM) materials steadily move to the center of attention. In my talk I will show that spin chirality (SC), which is inherent to many AFM materials, can serve as a new type of emergent variable in magnetic materials, getting a handle on which can provide a way to material realization of novel phenomena. I will demonstrate that the SC is ultimately responsible not only for the "topological" Hall effect of chiral AFMs, but it also mediates chiral light-matter interaction, giving rise to topological magneto-optical effects in AFMs [1]. Further, I will show that the Berry phase effects mediated by SC in AFMs give rise to novel exchange interactions among spins which pave a way towards the realization of novel three-dimensional spin textures such as hopfions [2]. I will also make it clear that the discussed phenomena are inherent to a wide class of collinear ferromagnets and AFMs subject to thermal fluctuations. Finally, based on our recent findings that predict and classify the SC-sensitive contributions to magneto-transport in skyrmions and domain walls [3], I will provide a classification of transport phenomena occurring in frustrated magnets based on the flavors of crystal and magnetic chirality [4], briefly discussing possible applications of uncovered effects in the realm of spintronics.

[1] Feng et al., Nature Comm. 11, 118 (2020) [2] Grytsiuk et al., Nature Comm. 11, 511 (2020) [3] Lux et al., Phys. Rev. Lett. 124, 096602 (2020) [4] Kipp et al., arXiv:2007.01529 (2020)

CONTRIBUTED PAPERS

O3-05. Electric-Field Switching of Magnetic Topological Charge in Type-I Multiferroics. *C. Xu*[1], P. Chen[1], H. Tan[2], Y. Yang[3], H. Xiang[4] and L. Bellaiche[1] *1. University of Arkansas Fayetteville, Fayetteville, AR, United States; 2. Max Planck-Institute of Microstructure Physics, Halle, Germany; 3. Nanjing University, Nanjing, China; 4. Fudan University, Shanghai, China*

Applying electric field to control magnetic properties would be a very convenient and energy-efficient way for spintronics devices. However, the control of magnetic characteristics by electric fields is not straightforward, due to the time-reversal symmetry of magnetism versus spatial inversion symmetry of electricity. Such fundamental difficulty makes it challenging to modify the topology of magnetic skyrmionic states with electric field. Here, we propose a novel mechanism that realizes the electric-field (E) switching of magnetic topological charge (Q) in a controllable and reversible fashion, through the mediation of electric polarization (P) and Dzyaloshinskii-Moriya interaction (D). Such mechanism is coined here EPDQ. Its validity is demonstrated in a multiferroic VOI_2 monolayer, which is predicted to host magnetic bimerons. The change in magnetic anisotropy is found to play a crucial role in realizing EPDQ process and its microscopic origin is discussed. Our study thus provides a new approach toward the highly-desired electric-field control of magnetism.

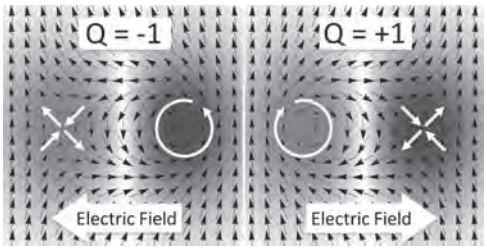

O3-06. Stabilization of Zero Field Skyrmions in Synthetic Antiferromagnetic Multilayers. *M. Sim*[2,1], D. Thian[2], M. Ramu[2], X. Chen[2], S. Goolaup[2], C. Li[2], H. Tan[2], N. Lim Chee Beng[2], S. Lee Koon Yap[2], P. Ho[2] and A. Soumyanarayanan[2,1] *1. Department of Physics, National University of Singapore, Singapore; 2. Institute of Materials Research and Engineering, Agency for Science, Technology and Research (A*STAR), Singapore, Singapore*

Magnetic skyrmions (Sk) are topologically protected spin structures that can exist at room temperature (RT) in multilayer (ML) magnetic films [1,2]. Their stability and ease of electrical manipulation by spin-orbit torque suggest tremendous applications in next-generation memory and computing devices but a key impediment is its transverse deflection via skyrmion Hall effect (SkHE) [3]. It was predicted that anti-ferromagnetic (AF) coupled Sk do not exhibit SkHE [4] but, conclusive experimental verifications of AF Sk in ML systems remain elusive. In this work, we demonstrate the field-free stabilization of AF Sk at RT mediated by a Ir heavy metal spacer between ferromagnetic (FM) Ir/Fe/Co/Pt MLs (Fig.1a-b inset). By tuning the spacer thickness, the oscillatory Ruderman–Kittel–Kasuya–Yoshida

coupling energy fosters AF and FM coupled MLs (Fig.1a-b). Micromagnetic simulation suggests that AF spin textures in AF MLs stabilizes at zero field (ZF), supporting experimental observations (Fig.1a inset), while predicting magnetic textures uncoupling across layers at higher fields. Next, we present definitive evidence of AF and FM character of spin textures in both AF and FM coupled MLs by magnetic force microscopy (MFM) analysis. Inferring from the relative amplitudes of MFM phase contrast, we find stronger stray fields from FM coupled ML textures than AF coupled ML (Fig.1c). Notably, the detection of AF stray fields suggest an incomplete compensation of field in the near range. The field dependent evolution of phase contrast was also investigated alongside simulations. Larger phase contrast was detected for uncoupled Sk as compared to AF Sk, indicating that stray field increases slightly as the AF textures switches from AF to uncoupled regime with applied fields. We demonstrate a tunable synthetic AF ML platform for hosting field-free AF Sk and presents the most convincing evidence yet of the AF nature of ZF Sk in the said system.

1. A. Fert *et al.*, Magnetic skyrmions: advances in physics and potential applications. Nat. Rev. mater. 2, 17031 (2017). 2. Anjan Soumyanarayanan *et al.*, Tunable room-temperature magnetic skyrmions in Ir/Fe/Co/Pt multilayers. Nat. Mater. 16, 898 (2017). 3. A. K. C. Tan*, Pin Ho* *et al.*, Visualizing the Strongly Reshaped Skyrmion Hall Effect in Multilayer Nanowire Devices (2020, In Prep). 4. X. Zhang *et al.*, Magnetic bilayer-skyrmions without skyrmion Hall effect. Nat. Comm. 7, 10293 (2016).

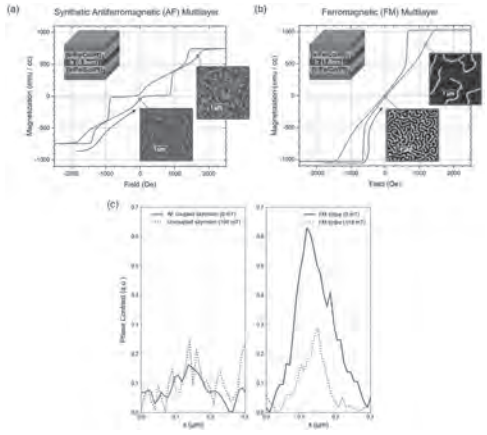

Fig.1: Out-of-plane hysteresis loops of the (a) AF and (b) FM coupled MLs. Inset: schematics of the ML and MFM images of magnetic textures at zero and high field. (c) Representative phase contrast profile of AF (red) and FM (blue) textures at zero (solid) and high (dotted) field shown in (a)-(b).

O3-07. Skyrmions in Synthetic Antiferromagnets and Their Current Induced Nucleation. R. Juge[5], N. Sisodia[5], V. Pham[5], Q. Zhang[5], K. Rana[5], L. Aballe[1], M. Foerster[1], r. Belkhou[4], M. Belmeguenai[2], G. Gaudin[5], J. Gräfe[3], M. Weigand[3] and *O. Boulle[5] 1. Sincrotron ALBA, Barcelona, Spain; 2. Laboratoire des Sciences des Procedes et des Materiaux, Villetaneuse, France; 3. Max-Planck-Institute Stuttgart, Stuttgart, Germany; 4. Synchrotron SOLEIL, Gif-sur-Yvette, France; 5. Spintec, Univ. Grenoble Alpes, CNRS, CEA, Grenoble, France*

Magnetic skyrmions are nanoscale whirling spin configurations. Their small size, topological protection and the fact than they can be manipulated by small in-plane current densities have opened a new paradigm to manipulate magnetisation at the nanoscale. Recently, antiferromagnetic (AF) skyrmions have attracted a large attention [1–7]: their vanishing magnetic moment would allow the stabilization of nm scale skyrmions at room temperature and their zero net topological charge eliminates the unwanted transverse velocity related to the skyrmion Hall effect [8,9], thereby ensuring a straight skyrmion trajectory with enhanced mobility [3,5,6,7]. Here we report on the observation of antiferromagnetic skyrmions in compensated synthetic antiferromagnetic (SAF) multilayers at room temperature and zero external magnetic field as well as their reproducible current induced nucleation. SAF based on (Pt/Co/Ru//Pt/Co/NiFe) multilayers with vanishing magnetization were grown using magnetron sputtering. Using X-ray microscopy XMCD-PEEM and STXM, we observe chiral Néel domain walls as well as AF skyrmions at zero external field and room temperature, with an average diameters of 180 nm. The results are well substantiated by micromagnetic simulations and analytical models using experimental parameters, which confirm the AF skyrmion spin texture and allow the identification of the physical mechanisms that control the AF skyrmion size and stability. We also demonstrate the current-induced nucleation/annihilation of AF skyrmions with diameters in the 100 nm range induced by the local injection of ns-long pulses at zero field. Time resolved pump-probe STXM experiments reveal that the nucleation occurs within the first ns of the current pulse injection. Our results pave the way for the current-induced manipulation of AF skyrmions in technology-relevant sputtered magnetic tracks.

[1] T. Dohi *et al.*, Nat. Commun. 10, 1 (2019). [2] W. Legrand *et al.*, Nat. Mater. 1 (2019). [3] R. Tomasello *et al.*, J. Phys. Appl. Phys. 50, 325302 (2017). [4] J. Barker *et al.*, Phys. Rev. Lett. 116, 147203 (2016). [5] L. Šmejkal *et al.*, Nat. Phys. 14, 242 (2018). [6] X. Zhang *et al.*, Nat. Commun. 7, 10293 (2016). [7] J. Barker *et al.*, Phys Rev Lett 116, 147203 (2016). [8] W. Jiang *et al.*, Nat. Phys. 13, 162 (2017). [9] R. Juge *et al.*, Phys Rev Appl. 12, 44007 (2019).

O3-08. Stabilisation of Skyrmions in an Antiferromagnet at Room Temperature Using Exchange Bias. K. Rana[2], *R. Lopes Seeger[2]*, S. Ruiz-Gomez[1], R. Juge[2], Q. Zhang[2], S. Auffret[2], M. Foerster[1], L. Aballe[1], G. Gaudin[2], V. Baltz[2] and O. Boulle[2] *1. Sincrotron ALBA, Barcelona, Spain; 2. Spintec, Univ. Grenoble Alpes CNRS CEA, Grenoble, France*

Magnetic skyrmions are topological spin textures holding great potential as nanoscale information carriers. Recently, skyrmions have been predicted in antiferromagnets, with key advantages over their ferromagnetic analogs [1,2]; they produce no dipolar fields, making them stable at the nanometer scale in zero external magnetic field; they are robust against perturbation due to magnetic fields, which is beneficial for data retention; they exhibit zero net topological charge [1,3], thus eliminating the unwanted transverse velocity related to the skyrmion Hall effect, [4,5], thereby ensuring a straight skyrmion trajectory with enhanced mobility [1]. Here we show that skyrmions can be stabilized at zero field and room temperature in an IrMn thin film exchange-coupled to a ferromagnetic layer. A Ta/Cu/IrMn(5)/Pt(0.5)/Co(0.3)/NiFe(0.9)/Al (nm) stack was deposited by magnetron sputtering on a Si substrate and annealed at 250°C for 30 minutes under a perpendicular magnetic field to achieve exchange bias (see Fig.1a). Using the high-spatial-resolution magnetic microscopy technique X-PEEM, we observe that exchange bias allows the stabilization of magnetic skyrmions at zero field and room temperature in the Co/NiFe (see Fig.1b, Fe edge). X-PEEM image of the uncompensated Mn spin at the IrMn interface show that these skyrmions are replicated within the IrMn layer (see Fig1c, Mn edge). This result opens up a path for logic and memory devices based on skyrmion manipulation in antiferromagnets.

[1] J. Barker *et al.*, Phys Rev Lett 116, 147203 (2016). [2] O. Gomonay *et al.*, Nat. Phys. 14, 213 (2018). [3] L. Šmejkal *et al.*, Nat. Phys. 14, 242 (2018). [4] W. Jiang *et al.*, Nat. Phys. 13, 162 (2017). [5] R. Juge *et al.*, Phys Rev Appl. 12, 44007 (2019).

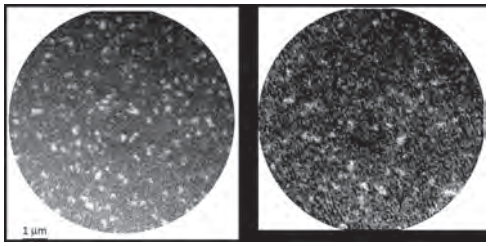

Fig. 1 a. Kerr signal as a function of the magnetic field applied perpendicularly to the film plane. b-c. XMCD-PEEM images at zero field and room temperature at the Fe L3 edge (b) and at the Mn L3 edge (c).

O3-09. Magnonic Quadrupole Topological Insulator in Antiskyrmion Crystals. T. Hirosawa[1], *S.A. Diaz*[2], J. Klinovaja[2] and D. Loss[2] *1. Physics, University of Tokyo, Tokyo, Japan; 2. Physics, Universitat Basel, Basel, Switzerland*

When the crystalline symmetries that protect a higher-order topological phase are not preserved at the boundaries of the sample, gapless hinge modes or in-gap corner states cannot be stabilized. Therefore, careful engineering of the sample termination is required. Similarly, magnetic textures, whose quantum fluctuations determine the supported magnonic excitations, tend to relax to new configurations that may also break crystalline symmetries when boundaries are introduced. Here we uncover that antiskyrmion crystals provide an experimentally accessible platform to realize a magnonic quadrupole topological insulator, whose hallmark signatures are robust magnonic corner states. Furthermore, we show that tuning an applied magnetic field can trigger the self-assembly of antiskyrmions carrying a fractional topological charge along the sample edges. Crucially, these fractional antiskyrmions restore the symmetries needed to enforce the emergence of the magnonic corner states. Using the machinery of nested Wilson loops, adapted to magnonic systems supported by noncollinear magnetic textures, we demonstrate the quantization of the bulk quadrupole moment, edge dipole moments, and corner charges.

[1] T. Hirosawa, S. A. Díaz, J. Klinovaja, and D. Loss, arXiv:2005.05884

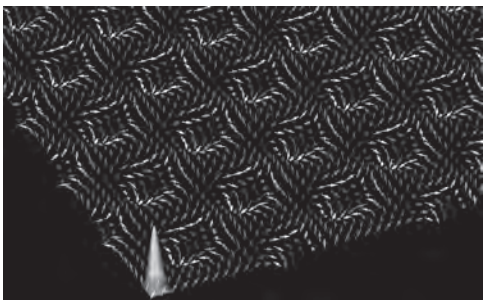

Fig. 1. Antiskyrmion crystals support topological magnonic corner states. Magnetic texture of an antiskyrmion crystal in the vicinity of a sample corner. Fractional antiskyrmions that self-assemble along the sample edge allow the emergence of a topological magnonic state whose probability amplitude (depicted in yellow) is corner-localized.

O3-10. Withdrawn

O3-11. Tuning Zero-Field Magnetic Skyrmions in all-Light-Metals Multilayers. *R. Lo Conte*[1,2], A.K. Nandy[3], G. Chen[4], A. Fernandes Cauduro[5], A. Maity[3], C. Ophus[5], Z. Chen[6], A.T. N'Diaye[7], K. Liu[6,4], A.K. Schmid[5] and R. Wiesendanger[1] *1. Department of Physics, University of Hamburg, Hamburg, Germany; 2. Department of Materials Science and Engineering, University of California Berkeley, Berkeley, CA, United States; 3. School of Physical Sciences, National Institute of Science Education and Research, Jatni, India; 4. Department of Physics, University of California Davis, Davis, CA, United States; 5. Molecular Foundry, E O Lawrence Berkeley National Laboratory, Berkeley, CA, United States; 6. Department of Physics, Georgetown University, Washington, DC, United States; 7. Advanced Light Source, E O Lawrence Berkeley National Laboratory, Berkeley, CA, United States*

Magnetic skyrmions [1,2], topologically protected magnetic quasi-particles, are at the core of many recently proposed spintronic devices. Most of the materials systems shown hosting magnetic skyrmions at room temperature [3-5] are characterized by [heavy metals]\ferromagnet interfaces to generate a strong Dzyaloshinskii-Moriya interaction (DMI) and need an external magnetic field to stabilize the skyrmions. From an application point of view, both the use of heavy metals and the need for an external magnetic field are limitations. The former are usually rare, which makes them expensive; the latter is not compatible with nanoelectronics due to scalability issues. Accordingly, it is highly desirable to have a robust and tunable protocol to build systems made only with light metals which can host magnetic skyrmions in zero external magnetic field. Here we report [6] the observation of isolated magnetic skyrmions at room temperature and zero magnetic field, stabilized through interlayer exchange coupling [7,8] between a *reference* magnet and a *free* magnet (Fig. 1). In our stack, both magnets and the non-magnetic spacer in between are made out of 3d transition metals, and by carefully changing the thickness of the spacer we can tune the size of the observed skyrmions, whose 3D spin-texture is directly imaged by spin-polarized low energy electron microscopy. In addition, via density functional theory calculations we gain a deeper understanding on the origin of the DMI in such systems, allowing us to extract the strength of the DMI, which compares well with experimental results. Our findings open up the possibility to develop cheap skyrmion-based spintronic devices suitable for general-use applications which go beyond modern nanoelectronics.

[1] A. Bogdanov and A. Hubert, J. Magn. Magn. Mater. 138, 255 (1994). [2] N. Romming et *al.*, Science 341, 636 (2013). [3] C. Moreau-Luchaire et *al.*, Nat. Nanotechnol. 11, 444 (2016). [4] S. Woo et *al.*, Nat. Mater. 15, 501 (2016). [5] A. Soumyanarayanan et *al.*, Nat. Mater. 16, 898 (2017). [6] R. Lo Conte et al., Nano Lett. (2020), https://pubs.acs.org/doi/10.1021/acs.nanolett.0c00137. [7] G. Chen et *al.*, *Appl. Phys. Lett.* 106, 242404 (2015). [8] A. K. Nandy et *al.*, *Phys. Rev. Lett.* 116, 177202 (2016).

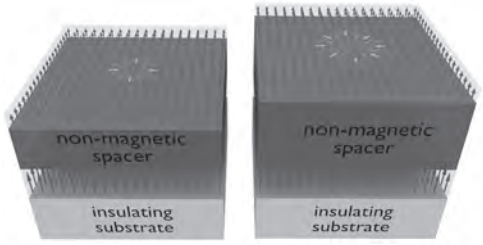

Schematic of the studied multilayers, consisting of two magnetic layers with a non-magnetic spacer in between, deposited on top of an insulating substrate. The *reference* magnet at the bottom is used to generate an effective field acting on the *free* magnet at the top. For different thicknesses of the spacer, skyrmions with different sizes are stabilized, without the application of any external magnetic field.

O3-12. Observation of Opposite Topological Charges in Single D_{2d} Heusler Compound. *J. Jena*[2*], B. Göbel[2], T. Ma[2], V. Kumar[1], R. Saha[2], I. Mertig[3], C. Felser[1] and S.S. Parkin[2,3] *1. Max Planck Institute for Chemical Physics of Solids, Dresden, Germany; 2. NISE, Max Planck Institute of Microstructure Physics, Halle, Germany; 3. Institute of Physics, Martin Luther University, Halle, Germany*

Magnetic skyrmions and antiskyrmions are topologically protected non-collinear spin textures. They have opposite topological charges of +1 and – 1 owing the differently winding of the in-plane spin component about a fixed direction of the core[1]. The existence of them in a material system mostly depends on the symmetry of the underlying crystal structure. For example, cubic B20 compounds host Bloch skyrmion of isotropic spin texture[2], whereas D_{2d} symmetry compounds have anisotropic spin texture named 'antiskyrmion'[3,4]. Antiskyrmions comprise of alternating chiral boundaries of helicoids and cycloids. They found in two varieties of shape, namely round and square-shaped antiskyrmion[5]. Here for the first time, using the Lorentz microscopy technique, we have discovered elliptical shape skyrmions in the same material which comprises of Bloch walls only[5]. We named them as "elliptical Bloch skyrmions". The elliptical skyrmion's major axis is oriented along the helical propagation directions, [100] and [010], and have opposite chiralities. They are found as spare and lattice states. Interestingly, both topological structure phases can also be stabilized in zero biased fields and below, over wide temperature ranges. It is found that in D_{2d} long-range dipole-dipole interactions play a significant rule for the stabilization of those different opposite topological spin textures. Micromagnetic simulations also confirms these nano-objects. Antiskyrmions are mostly found in room temperature and above, and in lower temperatures, elliptical Bloch skyrmion is observed. At a critical temperature of 268 K, both these nano-objects are stabilized. We also performed experiment at room temperature on the nano-stripes. The transformation and density variation of antiskyrmions and elliptical Bloch skyrmions occur here that depend on the degree of tilting[6]. Notably, those nano-objects in the nano-tracks produce as a single chain form in the middle of the track even without giving an in-plane field that was indeed needed in the broad width lamellae. The novel and unanticipated finding of opposite topological charges of 1in one material system make the family of D_{2d} material exceptional.

1. A. Bogdanov, U. Roeßler and K.-H. Mueller, Phys. Rev. B, 66, 214410 (2002) 2. S. Muehlbauer, B. Binz and C. Pfleiderer, Science, 323, 915-919 (2009) 3. A. K. Nayak, V. Kumar and S. S. P. Parkin, Nature, 548, 561 (2017) 4. J. Jena, R. Stinshoff and S. S. P. Parkin, Nano Lett., 20, 59–65 (2019) 5. J. Jena, B. Goebel and S. S. P. Parkin, Nat. Commun., 11, 1115 (2020) 6. J Jena, B. Goebel and S. S. P. Parkin, Submitted., XX,XXX (2020)

O3-13. Micromagnetic Simulations of Skyrmionic Bubbles in the Van Der Waals Structure Fe_3GeTe_2. *M. Grelier*[1], Y. Sassi[1], B. Dlubak[1], M. Martin[1], P. Seneor[1], V. Cros[1], N. Reyren[1] and A. Fert[1] *1. Unité Mixte de Physique, CNRS, Thales, Université Paris-Saclay, Palaiseau, France*

Recently, two-dimensional van der Waals (vdW) systems with a ferromagnetic behavior were found [1], [2], [3], [4], representing exciting opportunities for magneto-optics and magneto-electric applications. In those materials, the long-range magnetic order exists despite the thermal fluctuations of the Mermin-Wagner theorem because of a strong magnetic anisotropy. The compound Fe_3GeTe_2 (FGT) stands as a promising candidate among the vdW structures due to the tunability of its ferromagnetism under an electric field, allowing to rise the Curie temperature above 300 K [5]. In recent experiments by Park et al. on non-oxidized multilayer of FGT [6], Bloch skyrmions were observed using Differential Phase Contrast Microscopy and Lorentz Transmission Electron Microscopy and their stability cannot be explained by the existence of a chiral interaction such as Dzyaloshinskii–Moriya interaction (DMI), forbidden by the centrosymmetric structure of FGT. In this work, we numerically study the magnetic textures hosted by FGT using the micromagnetic solver Mumax3 [7] and axisymmetric simulations [8] to apprehend the phenomena at play. We demonstrate the existence of small hybrid magnetic textures, composed of Bloch skyrmionic bubbles in the middle of the structure with Néel "caps" close to the interface. These bubbles are stable in FGT for a range of external magnetic field and take sizes in the range of 20 nm for perpendicular fields in the range of a few 10 of mT comparable with the experimental observations. We would like to acknowledge S.Woo, X. Yu, A. Hassan and M. Chsiev for fruitful discussions. The ANR grant TOPSky TOPSKY (ANR-17-CE24-0025), the FLAGERA 2019 SOgraphMEM and the EU grant SKYTOP (H2020 FET Proactive 824123) are acknowledged for their financial support.

[1] Cheng Gong et al., *Nature* 546, no. 7657 (June 2017): 265–69. [2] Shengwei Jiang, Jie Shan, and Kin Fai Mak, *Nature Materials* 17, no. 5 (May 2018): 406–10. [3] Jie Liu et al., *AIP Advances* 8, no. 5 (May 2018): 055316. [4] Bevin Huang et al., *Nature* 546, no. 7657 (June 2017): 270–73. [5] Yujun Deng et al., *Nature* 563, no. 7729 (November 2018): 94–99. [6] Park, Tae-Eon, et al., *arXiv preprint arXiv:1907.01425* (2019). [7] Arne Vansteenkiste et al., *AIP Advances* 4, no. 10 (October 2014): 107133. [8] William Legrand et al., *Physical Review Applied* 10, no. 6 (December 2018): 064042.

** - Best student presentation award finalist*

Session O4
SPIN HALL AND RELATED EFFECTS I

Vlad E. Demidov, Co-Chair
University of Muenster, Muenster, Germany
Francisco J. T. Gonçalves, Co-Chair
HZDR- Helmholtz Zentrum Dresden Rossendorf, Dresden, Germany

CONTRIBUTED PAPERS

O4-01. Giant Transition-State Enhancement of Quasiparticle Spin-Hall Effect in an Exchange-Spin-Split Superconductor Detected by non-Local Magnon Spin-Transport. *K. Jeon*[1], J. Jeon[1], X. Zhou[1], A. Migliorini[1], J. Yoon[1] and S.S. Parkin[1] *1. Max Planck Institute of Microstructure Physics, Halle (Saale), Germany*

Non-equilibrium phenomena of quasiparticles (QPs) in a spin-split superconductor (SC) rely on the mutual coupling between different non-equilibrium imbalances of spin, charge, heat, and spin-heat [1]. Although recent experiments and theories have shown a variety of exotic transport properties in SC-based devices with either Zeeman or exchange spin splitting [1], how QP interplays with magnon spin currents [2] remains elusive. Here, using non-local magnon spin-transport devices [3] where a singlet SC (Nb) on top of a ferrimagnetic insulator ($Y_3Fe_5O_{12}$) serves as a magnon spin detector, we demonstrate that the conversion efficiency of magnon spin to QP charge via inverse spin-Hall effect (iSHE) in such an exchange-spin-split SC [4] can be greatly enhanced by up to 3 orders of magnitude compared with that in the normal state, particularly when its interface superconducting gap matches the magnon spin accumulation. Through systematic measurements with varying the current density and SC thickness, we identify that superconducting coherence peaks and exchange spin-splitting of the QP density-of-states, yielding a larger spin excitation while retaining a modest QP charge-imbalance relaxation, are responsible for the giant QP iSHE. Our results provide a new device concept in which the non-local voltage created from long-rage magnon-carried spin is orders of magnitude controllable by turning the superconductivity on and off [5].

[1] F. S. Bergeret, M. Silaev, P. Virtanen, and T. T. Heikkilä, Rev. Mod. Phys. 90, 041001 (2018). [2] L. J. Cornelissen, J. Liu, R. A. Duine, J. Ben Youssef, and B. J. van Wees, Nat. Phys. 11, 1022 (2015). [3] A. V. Chumak, V. I. Vasyuchka, A. A. Serga, and B. Hillebrands, Nat. Phys. 11, 453 (2015). [4] M. Silaev, P. Virtanen, F. S. Bergeret, and T. T. Heikkilä, Phys. Rev. Lett. 114, 167002 (2015) [5] K.-R. Jeon, J.-C. Jeon, X. Zhou, A. Migliorini, J. Yoon and S. S. P. Parkin, arXiv:2004.09467 (2020).

O4-02. Strong Interfacial Exchange Field in a Heavy Metal/ Ferromagnetic Insulator System Determined by Spin Hall Magnetoresistance. *J. Gomez-Perez*[1], X. Zhang[2,3], F. Calavalle[1], M. Ilyn[3], C. González-Orellana[3], M. Gobbi[1,4], C. Rogero[2,3], A. Chuvilin[1,4], V. Golovach[2,4], L.E. Hueso[1,4], F. Bergeret[2,4] and F. Casanova[1,4] *1. CIC nanoGUNE BRTA, Donostia-San Sebastián, Spain; 2. Donostia International Physics Center, San Sebastian, Spain; 3. Centro de Fisica de Materiales, San Sebastian, Spain; 4. Ikerbasque, Basque Foundation for Science, Bilbao, Spain*

Spin-dependent scattering transport at heavy metal (HM)/magnetic insulator (MI) interface can be described in terms of three parameters: the spin-sink conductance G_s and the real and imaginary part of the spin-mixing conductance, $G_{\uparrow\downarrow}=G_r+iG_i$ [1,2]. Each parameter is relevant for different spin-dependent phenomena. For instance, G_s originates from spin-flip processes and therefore is the leading parameter in electrical biasing of magnons [3], whereas G_r accounts for the spin-transfer (Slonczewski) torque to the magnetization and plays a fundamental role in spin-pumping experiments [4]. On the other hand, G_i quantifies the interfacial exchange field, which induces a field-like torque in the conduction electrons of the HM and is important for example in spin-splitting field experiments in superconductivity [5]. These conductances are broadly studied in ferrimagnetic insulators, where usually the contribution of G_r is much larger than that of G_i [6], leading to only a few reports on the exchange field at HM/MI interfaces [7]. In this work [8], we study the three spin conductance terms by spin Hall magnetoresistance (SMR) in a new system: a ferromagnetic insulator (FMI) such as EuS. By SMR measurements as a function of the temperature, and taking advantage of the newly developed microscopic theory for SMR [2], we can extract relevant microscopic parameters such as the exchange interaction between the 1*s* electrons in Pt and the localized magnetic moments in EuS (J_{int}~18 meV) [8]. An interfacial exchange field of the order of 1 meV (~15 T) acting upon the conduction electrons of Pt can be estimated from G_i, which is at least three times larger than G_r below the Curie temperature [8]. Our work provides an easy method to quantify this interfacial spin-splitting field, which is of interest in different areas of Condensed Matter Physics, such as proximity effects in superconducting hybrid systems.

[1] T.-Y. Chen *et al.*, Phys Rev. B 87, 144411 (2013) [2] X.-P. Zhang *et al.*, Nano Lett. 19, 6330 (2019) [3] L. J. Cornelissen *et al.*, Nat. Phys. 11, 1022 (2015). [4] M. Weiler *et. al.*, Phys. Rev. Lett., 111, 176601 (2013) [5] B. Li *et al.*, Phys. Rev. Lett. 110, 097001 (2013). [6] X. Jia *et al*., Europhysics Lett. 96, 17005 (2011). [7] N. Vlietstra *et al.*, Appl. Phys. Lett. 103, 032401 (2013); T. Kosub *et al.*, Appl. Phys. Lett. 113, 222409 (2018). [8] J. M. Gomez-Perez *et al*., arXiv:2004.12009 (2020)

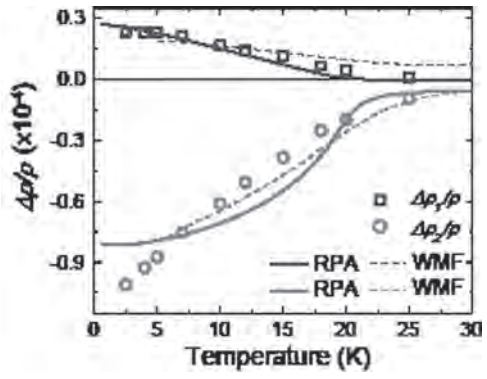

Temperature dependence of the normalized SMR amplitudes $\Delta\rho_1/\rho$ and $\Delta\rho_2/\rho$. The open dots represent the experimental data and the solid (dashed) lines are the amplitudes obtained with the microscopic theory [2].

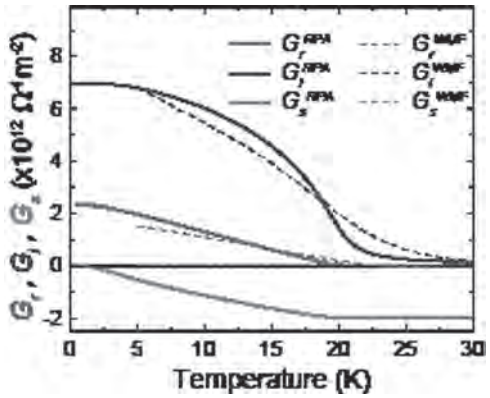

Temperature dependence of the G_r, G_i, and G_s. The values are calculated from the best fits of microscopic theory.

O4-03. Spin Transport in $La_{0.67}Sr_{0.33}MnO3/YBa_2Cu_3O_{7-\delta}$ Bilayers.
J. Wisser[1] and Y. Suzuki[1] *1. Applied Physics, Stanford University, Stanford, CA, United States*

Relatively little work has been done to date to understand the transport of spin waves generated via ferromagnetic resonance (FMR) in anisotropic high-temperature superconductors. To this end, we have fabricated bilayers of yttrium barium copper oxide (YBCO) with the half-metallic ferromagnet lanthanum strontium manganite (LSMO) via pulsed laser deposition on $(LaAlO_3)_{0.3}(Sr_2TaAlO_6)_{0.7}$ (LSAT) (001) substrates. We fix the LSMO thickness at 30 nm and vary the YBCO thickness from 2-17 nm. We have verified that the YBCO superconducts with T_c varying from 55-88 K depending on YBCO thickness (with a minimum thickness of 5 nm required for superconductivity). Since the variation in T_c with thickness is not as strong in single YBCO layers grown on LSAT substrates we believe that the magnetic exchange field from the LSMO, rather than a epitaxial strain effect, is the governing factor for T_c. To characterize spin wave transport, we performed FMR measurements on the bilayers as a function of temperature and YBCO thickness. We find that the resonance linewidth of bare LSMO increases with decreasing temperature, which is attributed to an increased contribution from two-magnon scattering at lower temperatures. Additionally, with the addition of 17 nm of YBCO, we see a near doubling of the FMR linewidth at all temperatures. Although more work needs to be done to fully characterize the system, these results possibly point to spin wave dissipation in the YBCO layer, which has not previously been observed.

O4-04. Dephasing of Transverse Spin Current in Ferrimagnetic Alloys.
Y. Lim[1], B. Khodadadi[1], J. Li[2], D. Viehland[2], A. Manchon[3,4] and S. Emori[1] *1. Physics, Virginia Polytechnic Institute and State University, Blacksburg, VA, United States; 2. Materials Science and Engineering, Virginia Polytechnic Institute and State University, Blacksburg, VA, United States; 3. Physical Science and Engineering Division, King Abdullah University of Science and Technology, Thuwal, Saudi Arabia; 4. CNRS, CINaM, Aix-Marseille Universite, Marseille, France*

It has been predicted that the coherence length of transverse spin current in antiferromagnetic and ferrimagnetic metals can be much longer than ≈1 nm in typical ferromagnets. A recent experiment qualitatively reports a spin coherence length of >10 nm in ferrimagnetic CoTb alloys [1], although this is rather surprising given the strong spin-orbit coupling in CoTb. Here, we quantitatively determine how far a spin current remains coherent in ferrimagnetic CoGd [2], which possesses much weaker spin-orbit coupling than CoTb. In our sample structures of $Ni_{80}Fe_{20}(7)/Cu(4)/Co_{100-x}Gd_x(t)$ (unit: nm), a coherent spin current is pumped from the $Ni_{80}Fe_{20}$ spin source to the $Co_{100-x}Gd_x$ spin sink via ferromagnetic resonance spin pumping. The decoherence of spin current in the spin sink is measured by non-local damping enhancement $\Delta\alpha$ of the spin source. The spin sink thickness dependence of $\Delta\alpha$, combined with a modified drift-diffusion model that accounts for spin dephasing [3,4], reveals the spin coherence length (Fig. 1). By studying different compositions of $Co_{100-x}Gd_x$ spin sinks, we observe a peak in the spin coherence length of ≈5-6 nm near the magnetic compensation region (Fig. 2). Our study confirms the suppression of spin dephasing enabled by antiferromagnetic order and demonstrates a new approach to understand spin transport for antiferromagnetic spintronics.

[1] J. Yu et al., Nature Materials., Vol.18, 29–34 (2019). [2] Y. Lim et al., arXiv:2001.06918 (2020) [3] T. Taniguchi et al., Applied Physics Express., Vol.1, 31302 (2008). [4] K.W. Kim, Physical Review B, Vol.99, 224415 (2019).

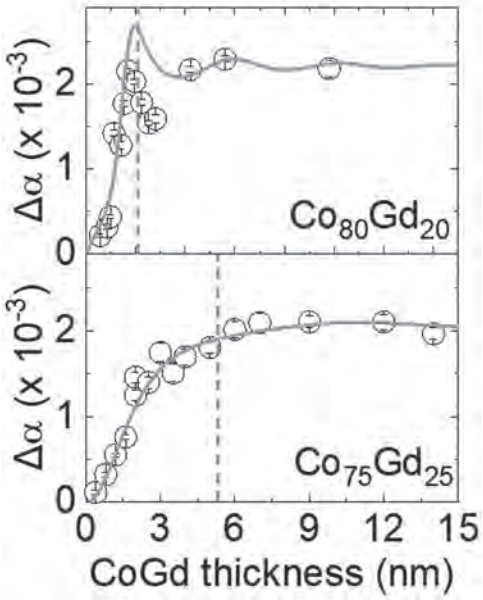

Enhanced Gilbert damping ($\Delta\alpha$) of $Ni_{80}Fe_{20}$ spin source layer versus $Co_{80}Gd_{20}$ and $Co_{75}Gd_{25}$ spin sink layer thickness. For each composition, the modified drift-diffusion model fit is shown as the solid curve, and the spin coherence length is marked as the vertical dashed line.

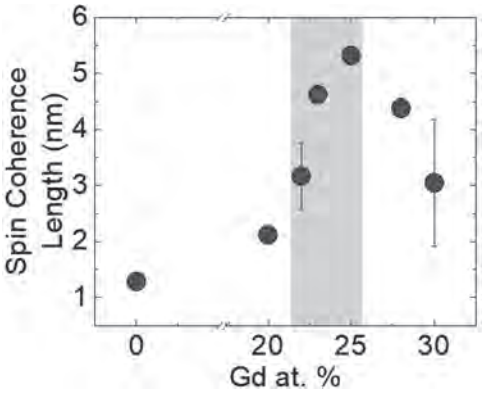

Spin coherence length versus CoGd spin sink composition (Gd atomic percent). The shaded region indicates the window of composition corresponding to magnetic compensation.

O4-05. Charge-to-Spin Conversion Efficiency in Ferromagnetic Nanowires by Spin Torque Ferromagnetic Resonance: Reconciling Lineshape and Linewidth Analysis Methods.
J. Xu[1] and A.D. Kent[1] *1. physics department, New York University, New York, NY, United States*

Spin orbit torques (SOTs) are being actively considered for use in the next generation memory devices for magnetization switching, spin oscillators and racetrack memories, including those using magnetic skyrmions. SOTs

are fundamentally based on charge-to-spin conversion by the spin-Hall or Rashba effect. Taking advantage of the spin current, the torques can be used to switch magnetic insulators or the free layer of magnetic tunnel junctions with high energy efficiency. Therefore, it is important to accurately measure the charge-to-spin conversion efficiency. SOTs are principally of interest in nanostructured samples, samples with minimum dimension less than a micron. However, the magnitude and form of the torques are most often characterized in micron scale samples, using spin torque ferromagnetic resonance (ST-FMR), a technique that involves analyzing the resonance linewidth [1] or lineshape [2]. On microstructures, these two analysis methods are quite consistent. Here we present ST-FMR results on permalloy $Ni_{80}Fe_{20}$ nanowires --- with widths varying from 150 to 800 nm --- that show that the standard model used to analyze the resonance linewidth and lineshape give different results [3]. Fig. 1 a-c show examples of ST-FMR spectra. Fig. 1d shows the efficiency of nanowires with different width, which shows greatly enhanced efficiency when the lineshape method is used. We present a ST-FMR model that properly accounts for the sample shape. It shows a much better consistency between the two methods, as illustrated in Fig. 2. Micromagnetic simulations are used to verify the model. These results and the more accurate nanowire model presented are of importance for characterizing and optimizing charge-to-spin conversion efficiencies in nanostructures.

[1] S. Petit *et al.,* Physical Review Letters 98, 077203 (2007) [2] L. Liu *et al.*, Physics Review Letters 106, 036601 (2011). [3] J.-W. Xu *et al.,* arXiv:2004.03784(2020). [to appear in Physical Review Applied]

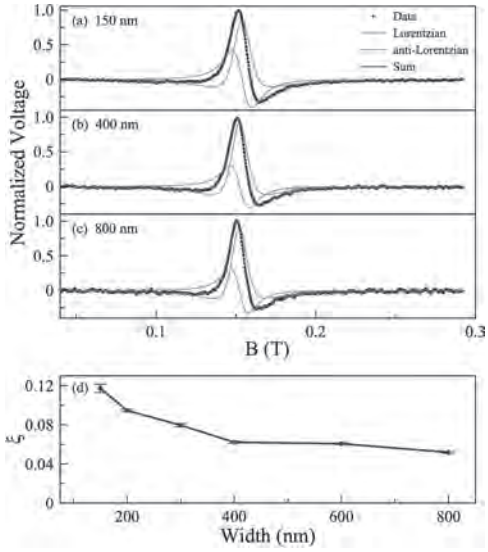

Figure 1. (a)-(c) Examples of ST-FMR spectra on different width nanowires. (d) Charge-to-spin conversion efficiency vs. wire width determined using the film model lineshape analysis method.

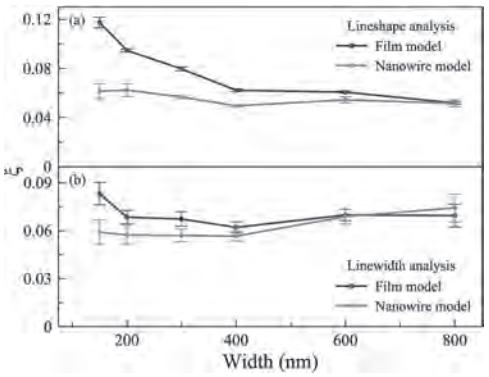

Figure 2. A comparison of charge-to-spin conversion efficiency on nanowires with different widths using the film model and nanowire model for (a) the lineshape analysis method and (b) the linewidth analysis method.

O4-06. Modulation of Spin Sink Efficiency Using Magnetic Phase Transition on NiFe/Dy System. *K. Yamanoi*[1], Y. Sakakibara[1], J. Fujimoto[2], M. Matsuo[2,3] and Y. Nozaki[1,4] *1. Department of Physics, Keio University, Yokohama, Japan; 2. Kavli Institute for Theoretical Sciences, University of Chinese Academy of Sciences School of Computer and Control Engineering, Beijing, China; 3. RIKEN Noshinkei Kagaku Kenkyu Center, Wako, Japan; 4. Center for Spintronics Research Network, Kanagawa, Japan*

A spin pumping (SP) effect that generates a spin current at an interface between ferromagnetic and nonmagnetic materials has been widely investigated for developing spintronic devices. The magnitude of the SP effect depends on the spin sink efficiency in the nonmagnetic materials which is proportional to the transverse spin susceptibility χ [1, 2]. Recently, the modulation of *c* has been reported at a magnetic phase transition from paramagnetic (PM) to ferromagnetic (FM) or antiferromagnetic (AFM) phases [2, 3]. In this study, we investigate the spin sink efficiency in Dy thin film which shows magnetic phase transitions from PM to AFM phases followed by an additional FM phase. From the temperature dependence of the SP effect in the NiFe/Dy bilayer, we found that the value of c was strongly suppressed when a noncollinear AFM phase appeared. 50-nm-thick Dy film was sputtered on a Si substrate at 620 K. Figure 1 shows the magnetization of the Dy film as a function of temperature measured while applying an external field of 200 mT. The transitions from FM to AFM and from AFM to PM appear at T_C = 130 K and T_N = 178 K, respectively. To evaluate the spin sink efficiency in the Dy film, we measured a difference in the Gilbert damping constant Dα between NiFe monolayer and NiFe/Dy bilayers by means of vector network analyzer-ferromagnetic resonance spectroscopy. From the theoretical work, it was predicted that the value of χ of the nonmagnetic materials in the bilayer was in proportion to $\Delta\alpha$ which gives the spin sink efficiency. Figure 2 shows the temperature dependence of $\Delta\alpha$. As shown in Fig. 2, a local maximum of $\Delta\alpha$ owing to a growth of magnetization fluctuation appears at T_N. Interestingly, $\Delta\alpha$ was remarkably reduced at the AFM phase followed by a rapid increase at T_c. The result implies that spin relaxation in Dy can be suppressed at the AFM phase. Our finding is helpful to realize a long-distance propagation of exchange spin current in the magnonic devices.

[1] Y. Ohnuma, et., al. PRB 89, 174417 (2014). [2] Z. Qiu, et., al. Nature comm. 7, 12670 (2016). [3] O. Gladii, et., al. APEX. 12, 023001 (2019).

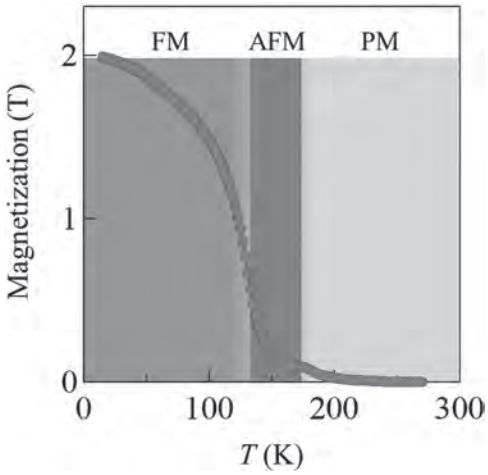

Fig. 1 Magnetization of 50 nm-thick Dy film as Δα function of temperature under an external magnetic field with 200 mT.

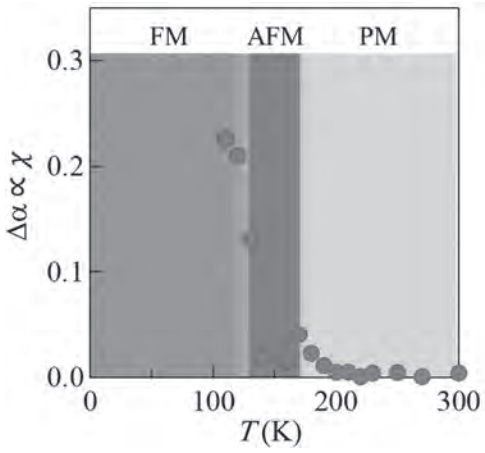

Fig. 2 Temperature dependence of the spin sink efficiency in Dy film.

INVITED PAPER

O4-07. Molecular Spintronics Utilizing a Novel Metal-Organic Interface. *S. Miwa*[1] *1. The Institute for Solid State Physics (ISSP), The University of Tokyo, Kashiwa, Japan*

Spintronics research has been developed utilizing symmetry at an interface. For instance, a finite spin-orbit torque associated with spin-accumulation induced by spin-Hall effect can be obtained at a ferromagnet-nonmagnet interface. Besides, perpendicular magnetic anisotropy and its electric-field-induced change appear at a ferromagnet-dielectric interface. For both cases, relatively simple materials such as Fe and Pt have been employed. Recently, novel materials have been employed in the emerging spintronics researches. One example is a quantum material, which has a non-trivial electronic structure due to topology, e.g. a topological insulator [1] and a Weyl magnet [2]. The other one is a functional organic molecule. Specifically, a metal-organic interface has been highlighted in recent years [3]. In this talk, we focus on the latter. Molecular magnetism has attracted attention in the fields of spintronics and quantum information processing. Moreover, the electronic structure of a complex molecule can be controlled via hybridization with a metallic film. Therefore, by using such an interesting system, a novel spintronic function would be exhibited. In this talk, we show the various spintronics phenomena utilizing the metal-organic interface. First, we show an epitaxial-like multilayer system consisting of metals and phthalocyanine molecules. Specifically, we have fabricated tunnel junction based on an Fe(001)/Co-phthalocyanine (CoPc)/MgO(001) multilayer, which has comparable voltage endurance to an Fe/MgO based junction [4]. Moreover, we find that the CoPc molecule induces a large built-in electric field over 3 V/nm and changes perpendicular magnetic anisotropy energy in the system [5]. Then we show the transport properties of Pt/Fe-phthalocyanine (FePc) bilayer system. The Pt/FePc shows a magnetoresistance which has the same symmetry as the spin-Hall magnetoresistance. The results show that it is feasible to conduct spin-transfer from metal to magnetic molecules [6]. Finally, we show a sizable and tunable spin-to-charge current conversion, that is, inverse Rashba-Edelstein effect at Cu/Pb-phthalocyanine (PbPc) interface [7]. The maximum conversion efficiency, the Edelstein length, at the Cu/PbPc interface is ~0.4 nm which is as large as the largest Rashba spin splitting reported for the Ag/Bi interface [8]. This is a work in collaboration with E. Minamitani of IMS, A. Hirohata of University of York, J. Nitta, M. Kohda, and H. Gamou of Tohoku University, K. Kondou of Riken, S. Sakamoto, Y. Otani, H. Isshiki, S. Takizawa, Y. Sugimoto, and A. Shotari of The University of Tokyo, Y. Suzuki, K. Shimose, and T. Kawabe of Osaka University, T. Nakamura, Y. Kotani, and K. Toyoki of JASRI.

[1] A. R. Mellnik *et al.*, Nature Vol. 511, p.449 (2014) [2] H. Tsai, S. Miwa, S. Nakatsuji *et al.*, Nature Vol. 580, p.608 (2020) [3] M. Cinchetti *et al.*, Nat. Mater. Vol. 16, p.507 (2017) [4] T. Kawabe, S. Miwa *et al.*, Appl. Phys. Express Vol. 11, p.013201 (2018) [5] S. Sakamoto, S. Miwa *et al.*, unpublished [6] H. Gamou, J. Nitta, S. Miwa *et al.*, Nano Lett. Vol. 20, p.75 (2020) [7] H. Isshiki, S. Miwa, Y. Otani *et al.*, Nano Lett. Vol. 19, p.7119 (2019) [8] J. C. Rojas Sánchez *et al.*, Nat. Commun. Vol. 4, p.2944 (2013)

CONTRIBUTED PAPERS

O4-08. Enhancement of Spin Hall Effect in Ta_xW_{1-x} Alloys. *L. Qian*[1], K. Wang[1], Y. Zheng[2] and G. Xiao[1] *1. Physics, Brown University, Providence, RI, United States; 2. Northeastern University, Boston, MA, United States*

Alloying has been demonstrated as an effective method to tune spin Hall angles (SHAs) in recent studies. Ta_xW_{1-x} is an attractive alloying system to study, with the large spin Hall angle in both β-W and β-Ta. Theoretical studies have also predicted enhancement in SHA of Ta_xW_{1-x}. In this work, we performed a systematic study on the giant spin Hall effect (GSHE) in Ta_xW_{1-x} alloys. We fabricated α- and β-Ta_xW_{1-x} in the full composition range of $x = 0$ to 1 at varying thicknesses from 3.0 nm to 28.5 nm. The phase diagram of the alloy is determined based on X-ray diffraction and transmission electron microscopy. Through magneto-transport measurement and macrospin model analysis, we observed enhancement in SHAs of both α- and β-Ta_xW_{1-x}. The SHA in α-Ta_xW_{1-x} ranges from -0.06 to -0.23, which is significantly larger than that in α-Ta and α-W. In β-$Ta_{0.25}W_{0.75}$, we achieved the largest SHA of -0.59 at the thickness of 5.3 nm, which doubles the SHA in β-W and is a five-fold enhancement over the SHA of β-Ta, at comparable thicknesses. Moreover, a linear correlation between the parameters of SHA and resistivity is observed in the Ta_xW_{1-x} system, providing strong evidence that the GSHE is caused by the intrinsic mechanism and/or side-jump scattering.

O4-09. Large Spin Hall Effect in non-Equilibrium Cu-Based Binary Alloys Beyond Solubility Limit. *H. Masuda*[1], R. Modak[2], T. Seki[1,2], K. Uchida[1,2], Y. Lau[1,3], Y. Sakuraba[2,4], R. Iguchi[2] and K. Takanashi[1,3] *1. Institute for Materials Research, Tohoku university, Sendai, Japan; 2. National Institute for Materials Science, Tsukuba, Japan; 3. Center for Spintronics Research Network, Tohoku University, Sendai, Japan; 4. JST PRESTO, Saitama, Japan*

High-efficient conversion between charge current (J_c) and spin current (J_s) is the key for developing spintronic devices. A way for the conversion from J_c to J_s is to exploit the spin Hall effect (SHE), in which the conversion efficiency is given by the spin Hall angle (α_{SH}). Thus, materials showing large α_{SH} is indispensable. Aside from the use of elemental nonmagnetic materials

such as Pt, Ta, and W, element doping or alloying is a promising way to develop a spin Hall material. Cu-Ir [Ref.1-4] is interesting because it shows SHE of $\alpha_{SH} \sim 2.1$ % at the Ir concentration from 1% to 12% [Ref.1] although neither Cu nor Ir exhibits remarkable SHE. In addition, Cu-based spin Hall materials are advantageous for practical applications because of their compatibility to the standard integrated circuit interconnection technology. In spite of the attracting features, the comprehensive study on SHE for the Cu-based binary alloys is limited. In this study, we comprehensively carried out a study on the SHE of Cu-Ir binary alloys in a wide range of the composition by exploiting the spin Peltier effect (SPE) measured from the thermal imaging for a composition-spread film [Ref.5]. The formation of solid solutions was confirmed from X-ray diffraction, showing the Vegard's law for all the composition. The temperature modulation due to the SPE (ΔT^{SPE}) and the spatial distribution of ΔT^{SPE} were visualized by the active infrared emission microscopy called the lock-in thermography. We have found that the optimum Ir concentration for enhancing SHE of Cu-Ir is around 25 at.%, which is beyond the solubility limit and is out of thermodynamically stable composition in the bulk phase diagram. We evaluated α_{SH} of the $Cu_{76}Ir_{24}$ alloy using the harmonic Hall voltage measurements, and obtained $\alpha_{SH} = 6.29\pm 0.19$ %. This large α_{SH} suggests that the non-equilibrium Cu-Ir alloy is a candidate of spin Hall material.

[1] Y. Niimi *et al.*, *Phys. Rev. Lett.* 106, 126601 (2011). [2] M. Yamanouchi *et al.*, *Appl. Phys. Lett.* 102, 212408 (2013). [3] J. Cramer *et al.*, *Nano Lett.* 18, 1064 (2018). [4] H. Masuda *et al.*, *Phys. Rev. B* 101, 224413 (2020). [5] K. Uchida *et al.*, *Sci. Rep.* 8, 16067 (2018).

O4-10. Observation of Inverse Spin Hall Effect at CoFeB/C_{60} Interface.

P. Sharangi[1], B.B. Singh[1] and S. Bedanta[1] *1. School of Physical Science, National Institute of Science Education and Research, Bhubaneswar, India*

Generation and manipulation of pure spin current play an important role in fabrication of power efficient spintronics devices[1]. Spin pumping is very efficient way of creation of pure spin current in ferromagnetic (FM)/nonmagnetic (NM) system by microwave excitation which can be converted into a voltage by inverse spin Hall effect (ISHE) Various materials possessing high spin orbit coupling (SOC) like Pt, Ta, W, Bi_2Se_3 etc., have been utilized for efficient spin to charge conversion[2,3]. However, these are limited by very small spin diffusion length (λ_{sd} ~10 nm). In this context organic semiconductors (OSC) e.g. C_{60} are emerging as a potential candidate due to large value of λ_{sd}. The low value of SOC in OSC limits them for efficient spin to charge conversion. However, when the OSC is deposited on a substrate the structural distortion may exhibit enhancement of SOC. Here we report simultaneous observation of spin pumping and ISHE measurements in the CoFeB/C_{60} bilayers by ferromagnetic resonance (FMR) in the frequency range 6 – 17 GHz. During the measurement the sample was kept on the wide coplanar waveguide (CPW) in the flip-chip manner. Angle dependent ISHE measurements have been performed at fixed frequency of 7 GHz and 11 mW power by using a nanovoltmeter at the two edges of the sample. Figure1 shows dc voltage (V_{meas}) and FMR signal versus applied magnetic field (H) plot. At 180-degree ISHE signal is reversed as the magnetic field direction is reversed, which indicates that signal is not coming from any artefacts and it is due to spin pumping. Also, we have calculated the spin Hall angle for CoFeB/C_{60} bilayer system is 0.04 which is higher than the reported value.

1. Y. Tserkovnyak, A. Brataas, *et al.*, *Rev. Mod. Phys.* 77, 13751421 (2005) 2. B. B. Singh *et al.*, *physica status solidi (RRL) Rapid Research Letters* 13, 1800492 (2019) 3. B. B. Singh *et. al., Phys. Rev. Appl*. 13, 044020 (2020)

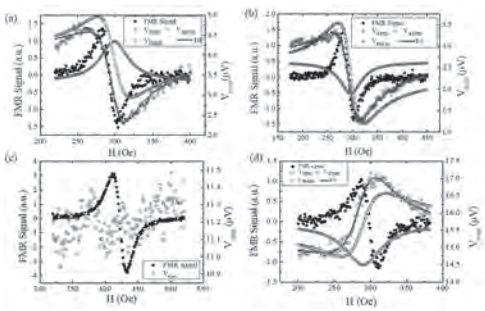

Fig 1: V_{meas} (blue open circle) and FMR signal (black solid circle) versus applied magnetic field (H) for the sample at (a) 0°, (b) 30°, (c) 90° and (d) 180° angles. Solid lines are best fits using Lorentzian function to evaluate symmetric (V_{sym}) and antisymmetric (V_{asym}) components from the V_{meas}.

O4-11. Inverse Spin Hall Effect in Sputtered MoS_2/CoFeB Bilayers.

A. Mishra[1], V. Thiruvengadam[1], K. Roy[1], P. Gupta[1], B.B. Singh[1] and S. Bedanta[1] *1. National Institute of Science Education and Research, Bhubaneswar, India*

2D-transition metal dichalcogenides (TMD) are known to have high spin-orbit coupling, an essential property for spintronic applications [1,2]. TMD materials with this property can replace the heavy metals for next generation spintronic devices. In this context MoS_2 has been of great interest in recent years due to its unique electrical and optoelectronics properties. It can be fabricated in very thin layers due to weak Van der waals forces, which makes it suitable to investigate interface dominated Rashba and Edelstein effects. However, fabrication of MoS_2 by chemical or exfoliation methods makes it difficult for spintronics applications. In this work, we demonstrate inverse spin Hall effect in MoS_2(t)/CoFeB(10nm)/MgO(2nm) heterostructures where 't' varies from 7 to 30nm. The heterostructure was fabricated by RF and DC sputtering of MoS_2 and CoFeB, respectively, on thermally oxidized Si substrate. MgO capping layer was deposited by thermal evaporation. Here the spin current was generated from CoFeB and injected into MoS_2 layer via spin pumping using ferromagnetic resonance (FMR). The resulting spin to charge conversion at interface was measured using nanovoltmeter. Various spin rectification effects were separated by performing angle dependent measurements [3]. For the sample with MoS_2(30nm), a spin pumping voltage of -1.6 mV was measured which was dominant over the rectification effects. The spin mixing conductance value was found to be ~ 3.72×10^{18} m^{-2} which is comparable to that of MoS_2 and Pt obtained from literature. Figure 1 shows the measured voltage signal for the sample Si/SiO_2/MoS_2(30nm)/CoFeB(10nm)/MgO(2nm). In order to understand the origin of this voltage, power and frequency dependent measurements were also performed. The linear increase in the symmetric component of dc voltage with the microwave power further indicated spin pumping [4].

[1] Qing Hua, Kourosh Kalantar-Zadeh, Andras Kis, Jonathan N. Coleman and Michael S. Strano Nature Nanotechnology, 7, 699–712 (2012) [2] Zehua Hu, Zhangting Wu, Cheng Han, Jun He, Zhenhua Ni and Wei Chen, Chemical Society Reviews, 47, 3100-3128, (2018) [3] Braj B. Singh, Sukanta K. Jena, Manisha Samanta, Kanishka Biswas, Biswarup Satpati and Subhankar Bedanta, Phys. Status Solidi RRL, Volume 13, Issue 3,1800492 (2019) [4] K. Ando, S. Takahashi, J. Ieda, Y. Kajiwara, H. Nakayama, T. Yoshino, K. Harii, Y. Fujikawa, S. Maekawa and E. Saitoh, J. Appl. Phys.109, 103913 (2011).

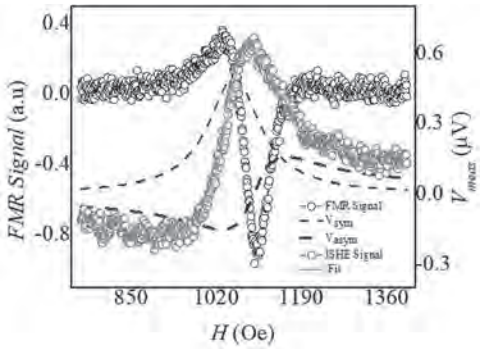

Fig. 1 : FMR spectra and spin pumping voltage (V_{meas}) measured at = 39° with applied dc magnetic field (H).

O4-12. Direct Observation of Spin Accumulation in Cu Induced by Spin Pumping. J. Ding[2], W. Zhang[1,2], M. Jungfleisch[3,2], J. Pearson[2], *H. Ohldag*[4,5], V. Novosad[2] and A. Hoffmann[6,2] *1. Oakland University, Rochester, MI, United States; 2. Argonne National Laboratory Materials Science Division, Lemont, IL, United States; 3. University of Delaware, Newark, DE, United States; 4. E O Lawrence Berkeley National Laboratory, Berkeley, CA, United States; 5. University of California Santa Cruz Division of Physical and Biological Sciences, Santa Cruz, CA, United States; 6. University of Illinois at Urbana-Champaign, Urbana, IL, United States*

Pure spin currents have been ubiquitous in contemporary spintronics research. Despite its pro- found physical and technological significance, the detection of pure spin current has largely remained indirect, which is usually achieved by probing spin-transfer torque effects or spin-to-charge conversions. By using scanning transmission X-ray microscopy, we report the direct detection and spatial mapping of spin accumulation in a nonmagnetic Cu layer without any direct charge current injection. Such a pure spin current is induced by spin pumping from a NiFe layer and is not accompanied by concomitant charge motion. The observed frequency dependence indicates that the signal is dominated by a coherent, pure spin current, but the magnitude of the spin accumulation suggests also possible additional thermal contributions. Our technique takes advantage of the X-ray magnetic circular dichroism and the synchronization of microwave with X-ray pulses, which together provide a high sensitivity for probing transient magnetic moment. From the detected X-ray signals, we observe two distinct resonance modes induced by spin pumping, which, based on micromagnetic simulations, we attribute to non-linear microwave excitations. Our result provides a new pathway for detecting pure spin currents that originate from many spintronics phenomena, such as spin Hall and spin Seebeck effects, and which can be applied to both metal and insulator spin current sources [1]. Work at Argonne, including experimental design and measurement, sample fabrication, data analysis, and manuscript preparation, was supported by the U.S. Department of Energy (DOE), Office of Science, Basic Energy Sciences, Materials Science and Engineering Division under Contract No. DE-AC02-06CH11357. Use of the Stanford Synchrotron Radiation Light source, SLAC National Accelerator Laboratory, is supported by the U.S. Department of Energy, Office of Science, Office of Basic Energy Sciences under Contract No. DE-AC02-76SF00515. W.Z. acknowledges the DOE visiting Faculty Program.

1.) "Direct Observation of spin accumulation in Cu induced by spin pumping" J. Ding, W. Zhang, B. Jungfleisch, J.E. Pearson, H. Ohldag, V. Novosad, A. Hoffmann, Phys. Rev. Res vol 2(1), p. 013262 (2020)

Session O5
MAGNETIC MICROSCOPY AND IMAGING II (Poster Session)

Agustina Asenjo, Chair
ICMM-CSIC, Madrid, Spain

O5-01. Nucleation of Magnetic Singularities at Interfaces in Ferro/Ferrimagnetic Multilayers Studied by Magnetic Force Microscopy and X-ray Magnetic Tomography. *J. Hermosa*[1,2], A. Hierro-Rodriguez[1,2], C. Quiros[1,2], L. Alvarez Prado[1,2], R. Valcarcel[3], A. Sorrentino[3], E. Pereiro[3], J. Martín[1,2], M. Velez[1,2] and S. Ferrer[3] *1. Physics Dept., Universidad de Oviedo, Oviedo, Spain; 2. CINN (CSIC – Universidad de Oviedo), El Entrego, Spain; 3. ALBA Synchrotron, Cerdanyola del Vallès, Spain*

Rare Earth (RE)-Transition Metal (TM) alloys and bilayers in which there is a large antiferromagnetic (AF) coupling between the RE and TM have recently attracted large attention due to their potential interest for very fast domain wall (DW) motion, opening new possibilities for applications [1,2]. We investigated the magnetic singularities (walls, Bloch points, merons…) occurring at the interfaces in ferri/ferrro/ferri magnetic trilayers based on Gd_xCo_{1-x}/NdCo/Gd_yCo_{1-y} combinations. By appropriate tuning of the composition [1], the upper GdCo layer will couple AF with the central NdCo layer (that has weak perpendicular anisotropy) whereas the bottom GdCo will exhibit ferromagnetic coupling. Magnetic force microscopy (MFM) of a 40 nm Gd_xCo_{1-x}/80 nm NdCo/ 40 nm Gd_yCo_{1-y} trilayer shows the typical stripe domains of weak perpendicular anisotropy materials. These stripes are bent into chevron patterns and a proliferation of free disclinations at the corners with enhanced magnetic contrast is also observed. Magnetic transmission X-ray microscopy (MTXM) [3] at the Mistral beamline of the ALBA synchrotron images tuned at the Gd absorption edge reveal different shades of grey in the dichroic contrast within the stripe domain pattern, that indicate a complex magnetization configuration across the multilayer thickness. Also, micromagnetic simulations suggest the presence of magnetic singularities at the ferri/ferro interface with effective AF coupling. Thus, we have performed vector tomography measurements using our method described in [4] to obtain the full 3D magnetic configuration. The different kinds of magnetic singularities observed in the sample and their topology will be discussed in detail. Work supported by Spanish MICINN (FIS2016-76058, PID2019-104604RB (AEI/FEDER, UE)), A.H.-R. acknowledges support from Marie Sklodowska-Curie grant (H2020-MSCA-IF-2016-746958).

[1] C. Blanco-Roldán, *et al.*, Phys. Rev. B 92 224433 (2015) [2] A. Hierro-Rodriguez *et al.*, Phys. Rev. B 95 014430 (2017) [3] C. Blanco-Roldán, *et al.*, Nat. Comm. 6 8196 (2015) [4] A. Hierro-Rodriguez, *et al.*, J. Synchrotron Rad. 25 1144 (2018)

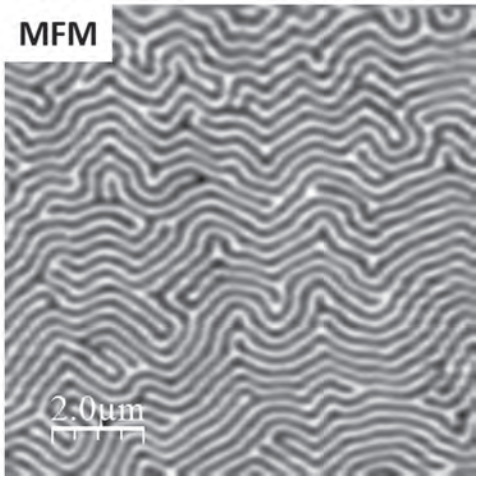

Fig. 1. Chevron stripe patterns in 40 nm GdCo/80 nm NdCo/40 nm GdCo' trilayer by MFM

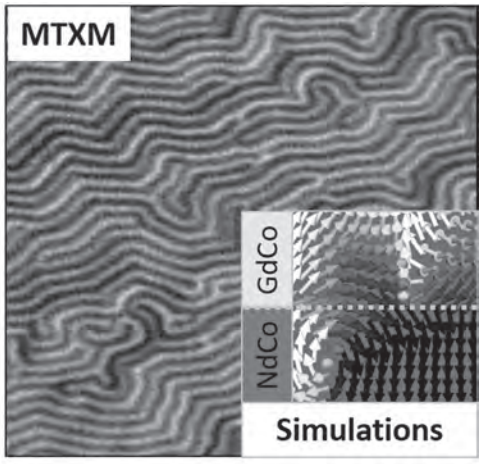

Fig. 2. MTXM (top view) of the same trilayer. Inset is a detail of the cross section of a magnetic singularity localized at the GdCo/NdCo interface with effective AF coupling (dashed line), obtained by micromagnetic simulations.

O5-02. Nucleation and Current-Induced Bubble Structures Motion in PMA Multilayers. *J. Marqués Marchán*[1], M. Pérez-Carmona[1], J. Prieto[2] and A. Asenjo[1] *1. Instituto de Ciencia de Materiales de Madrid (ICMM), Consejo Superior de Investigaciones Cientificas, Madrid, Spain; 2. Instituto de Sistemas Optoelectrónicos y Microtecnología (ISOM), Universidad Politecnica de Madrid, Madrid, Spain*

Perpendicular Magnetic Anisotropy (PMA) multilayers have been intensely studied in the past due to their applications in magnetic recording [1]. More recently, this kind of materials has renewed its interest due to the discovery of the DMI (Dzyaloshinskii-Moriya Interaction) that appears in the interfaces

of ferromagnetic and heavy metals multilayers [2]. DMI interaction promotes the development of exotic configurations so called "skyrmions" and bubbles of great interest in spintronics [3]. In this work, CoPt nanostructures with different shapes and sizes are fabricated by electron beam lithography. The CoPt multilayers are grown by sputtering over Si/SiO_2 substrates. Apart from the macroscopic characterization of the CoPt thin films, the nanostructures have been studied by AFM (Atomic Force Microscopy) and MFM (Magnetic Force Microscopy). The goal of this work is to control the nucleation, motion and annihilation of the magnetic bubbles by applying external magnetic fields and current. Nanometer size magnetic bubbles are created in these PMA multilayer nanostructures as demonstrated by the MFM imaging experiments. Besides the MFM imaging in remanent state, a Variable Field MFM system has been used to obtain images under in-plane or out of plane magnetic fields [4]. By applying an *in-situ* out of plane magnetic field in the VF-MFM system, we are able to control the density of bubbles due to their annihilation. The shape and the size of the bubbles is also analyzed as well as the dependence with the geometry of the nanostructures.

[1] A. Kirilyuk et al., Journal of Magnetism and Magnetic Materials, Vol. 171, p.45-63 (1997) [2] T. Moriya, Physical Review, Vol. 120(1), p.91-98 (1960) [3] J. Sampaio et al., Nature Nanotechnology, Vol. 8, p.839-844 (2013) [4] M. Jaafar et al., Ultramicroscopy, Vol. 109(6), p.693-699 (2009)

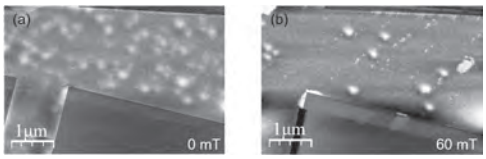

Figure 1. MFM images in remanence of a selected area of a nanostructure (a) after the nucleation of the bubbles and (b) after applying a perpendicular field of 60 mT antiparallel to the bubble magnetic moment.

O5-03. Withdrawn

O5-04. Magnetic Stray Field Sensing With Spin Defects in Silicon Carbide. *M. Bejarano*[1], F.J. Gonçalves[1], M. Hollenbach[1,2], T. Hache[1,3], Y. Berencén[1], G.V. Astakhov[1] and H. Schultheiss[1] *1. Helmholtz-Zentrum Dresden-Rossendorf, Dresden, Germany; 2. Technische Universitat Dresden, Dresden, Germany; 3. Technische Universitat Chemnitz, Chemnitz, Germany*

Magnetometry based on the electron spin has gathered attention in the past decades as a means for imaging and resolving nano-sized complex spin textures in a highly sensitive and non-perturbative way. While the nitrogen-vacancy (NV) center spin in diamond is certainly the most known and mature system for atomic-scale sensing of magnetic fields, silicon vacancy (V_{Si}) centers in the silicon carbide (SiC) matrix have recently surged as an alternative system due to its competitive optical and electrical properties and its potential for integrated and scalable quantum photonic chips [1]. V_{Si} centers in SiC have been employed for sensing uniform magnetic fields across a SiC substrate with sub-millitesla resolution [2,3]. In this work, we use an ensemble of V_{Si} centers as a room-temperature nanoscale sensor of static stray fields generated by magnetic nanostructures patterned on top of a SiC substrate. We use optically detected magnetic resonance (ODMR) to measure the impact of the stray fields on the intrinsic V_{Si} resonance frequencies. We observe a spatially dependent frequency shift of the V_{Si} resonances which enables us to determine the field contribution from the magnetic element in its close vicinity. Our studies show a way to exploit nanoscale stray fields to selectively address V_{Si} centers in SiC.

[1] S. Castelleto, A. Boretti, J. Phys. Photonics 2, 022002 (2020) [2] H. Kraus et. al., Sci. Rep. 4, 5303 (2014) [3] D. Simin, et. al., Phys. Rev. Applied 4, 014009 (2015)

O5-05. Magneto-Optical Investigation of Scattering by Superparamagnetic Nanoparticles Using Multi-Harmonic Analysis. C. Patterson[2], *M. Syed*[1], N. Fried[1] and T. Li[1] *1. Physics & Optical Engineering, Rose-Hulman Institute of Technology, Terre Haute, IN, United States; 2. Physics, University of Michigan, Ann Arbor, MI, United States*

Superparamagnetic nanoparticles (SNPs) are widely used in biomedical applications like imaging, magnetic hyperthermia, drug delivery, etc. [1-3]. We present a continuation of our study of dilute aqueous suspensions of single-domain magnetite nanoparticles using an AC Faraday rotation setup [4-5]. Our previous results focused on analyzing the first and higher odd harmonics of the magnetic field frequency using the Fourier components of the theoretical signal determined by a nonlinear, Langevin-like magnetization. With this procedure, we determined the average particle magnetic moment μ, particle number density *n*, and Verdet constant of the sample. In this study, we investigate the leading even harmonic (2f) signal to analyze scattering, and thereby investigate the process of cluster formation. This signal is independent of the polarization state of the incident light, and therefore is not relatable to Faraday rotation. The evidence of clustering/chain formation along with the geometric shadowing effect may explain the evolution of the scattering response as a function of field frequency and amplitude [6-7]. Investigation of clusters in SNPs is critical to establish their effective moment and size as a function of magnetic field profile. This analysis can provide a consistency check on the odd harmonic analysis, in addition to providing a physical picture of the underlying process of cluster formation. The setup employs a stabilized He-Ne laser (633 nm) along with an AC magnetic field (800-1600 Hz) that enables lock-in detection. We have measured the scattering response of magnetite nanoparticles that vary in size from 15 to 25 nm. In addition, two different types of SNPs with the same core diameter (20 nm) but different functionalization layers (carboxyl and PEG) are also investigated. We hope to elucidate the role of nanoparticle size (core and hydrodynamic), particle concentration, and magnetic field profile (intensity and frequency) in the formation dynamics of clusters. To explain the change in light intensity as a function of magnetic field, we have developed a model that employs a field-dependent cross-section which we hope to relate to cluster size

[1] Rudolf Hergt, Silvio Dutz, and Matthias Zeisberger, Nanotechnology, vol. 21, (2010). [2] Satoshi Ota, Tsutomu Yamada, and Yasushi Takemura, J. Appl. Phys., 117, 17D713 (2015). [3] Y. Xiao and J. Du, J. Mater. Chem. B, vol. 8, 3, 354–367, (2020) [4] Vandendriessche S., Brullot W., and Verbiest TAppl. Phys. Lett., vol. 102, (2013). [5] Cody Patterson, Maarij Syed, Yashushi Takemaura, JMMM, 451, 248-253 (2018) [6] Jian Li, Huang, Xiao Liu, Rong li Gao, Physics Letters A, 372, 6952–6955 (2008). [7] Corneliu Rablau, Prem Vaishnava, and Ratna Naik, Physical review E 78, 051502 (2008)

O5-06. Characterizing Tunable Nanoparticle Systems for Thermometry. *T.Q. Bui*[1], A.J. Biacchi[1], A.R. Hight Walker[1], B. Correa[1], C. Dennis[1] and S. Woods[1] *1. National Institute of Standards and Technology, Gaithersburg, MD, United States*

Magnetic nanoparticle (MNP) thermometry is a promising approach for non-invasive and remote temperature sensing for fundamental and applied sciences. However, the small thermosensitivity (temperature-dependent magnetization) of conventional single-phase MNPs near room temperature limit the requisite sensitivity needed for practical utility. Cation-substituted magnetite and bimagnetic (core/shell) nanoparticles with tunable thermosensitivity[1,2] and operating temperature ranges represent potential routes to overcome these limitations. Here we present results on the temperature-dependent AC magnetization of synthesized cobalt-doped ferrite and bimagnetic MNPs, and we demonstrate the feasibility of engineered material composition and structure towards the realization of a highly sensitive MNP thermometer. We report progress towards a bimagnetic nanoparticle system, by first characterizing the magnetic properties of the synthesized cobalt-doped ferrite "core" of the core/shell system. We measure the temperature-dependent DC and AC (770 Hz) magnetization for our synthesized

cobalt-doped ferrite MNPs in comparison with a commercial MNP sample near room temperature and demonstrate the capability to tune the former's magnetization curves. The commercial sample displayed a linear magnetization with temperature whereas the synthesized cobalt-doped ferrites (9.5 nm in Fig. 1 and 7.5 nm in Fig. 2) displayed nonlinear behavior. For the commercial sample, the temperature-dependent magnetization displays the expected negative, linear slope. On the other hand, cobalt-doped ferrite MNPs display nonlinear curvature, and a remarkable change in the sign of the temperature-dependent magnetization slope upon increasing the particle size from 7.5 nm to 9.5 nm. The sign of the curvature was further verified by DC magnetization measurements (insets in Figs. 1 and 2) over the temperature range of 275 to 305 K. Our preliminary results reveal that cobalt-doped ferrite nanoparticles warrant further development and engineering as the basis for bimagnetic MNPs, with the anticipation that the thermosensitivity of the completed core/shell topology would be significantly better over a tunable temperature range.

[1] Anderson & Camley. *Phys. Rev. B*, 94, 134432, p. 1-8 (2016). [2] Polishchuk et al. *Nanoscale Res. Lett.*. 13 (245), p. 1-7 (2018).

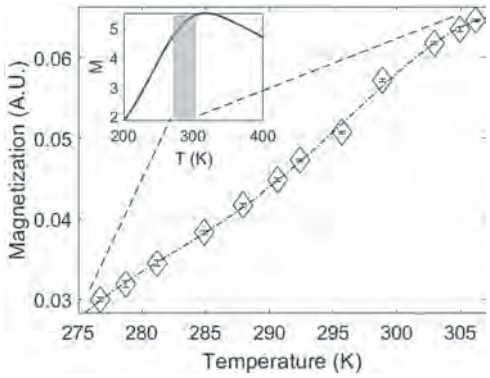

Fig. 1: 9.5 nm MNP

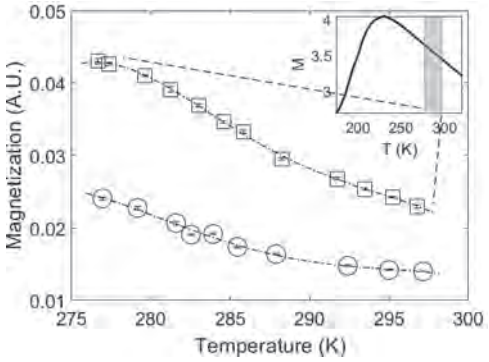

Fig. 2: 7.5 nm MNP

O5-07. A Description of Laser Impacts on Magnetic Properties for GO Electrical Steels Under Surface Treatment With Short and Ultra-Short Pulses. *M. Nesser*[1], O. Maloberti[2,1], E. Salloum[1], J. Dupuy[3], J. Birat[4], C. Pineau[4], S. Panier[1], J. Fortin[1,2] and P. Dassonvalle[5,2] *1. LTI Laboratory, Amiens, France; 2. ESIEE Amiens, Amiens, France; 3. Multitel, Mons, Belgium; 4. Instituts de Recherche Technologique Materiaux Metallurgie Procedes, Metz, France; 5. MIS, Amiens, France*

Grain-oriented electrical steel sheets constitute the main core of electrical power transformers and generators. Manufacturers seek to improve the performance of these magnetic components and to save energy. Using the technique of domains'refinement by local laser treatment on the surface of grain-oriented electrical sheets showed effective results on the reduction of iron losses [1] [2]. The ultimate goal of this study is to understand and control the loss reduction effect in grain-oriented silicon iron sheets while maintaining a good permeability performance. To do so, materials were submitted to laser treatments with different pulse durations: short and ultra-short pulses. Each treatment corresponds to different effects on the sheet surface leading to different impacts on the magnetic properties [3]. We measured the power loss of treated samples with a Single Sheet Tester. Results show an average power loss reduction of 20% at the peak induction level 1.5T for frequency 50Hz using a laser treatment with short and ultra-short pulses. Applying either a dynamical model [4] or the power loss separation principle of Bertotti [5], we identify the magnetic properties and loss coefficients, study its dependencies on the laser energetic parameters and separate the different physical origins of magnetic modifications. As already suggested in previous work, we confirm that some laser configurations with ultra-short pulses give different behaviors comparing to a long pulse [3]. An estimation model of the groove depth and affected zone as a function of laser's energy density is also presented. This makes it possible to correlate lasers' impacts (groove depth, affected zone …) to magnetic properties and at the end to determine the range of acceptable values for the laser parameters that should optimize the magnetic parameters and ensure an improvement in the permeability and core loss of the sheets. Finally, to visualize the domain refinement and infer any walls mobility enhancement resulting from the laser treatments with different pulse durations, we also present the surface magnetic images collected with a Magnetic Force Microscope (MFM) and a magnetic field camera system using a Magneto-Optical Interferential Film.

[1] I. Petryshynets, F. Kovac, V. Puchy, M. Sebek, J. Fuzer, P. Kollar, AIP Advances, Vol. 8 p. 047604 (2018) [2]Y. Huang, W. Ming, M. Li, Y. Liu, J. Guo, J. Li, X. Shao, S. Wang, international journal of advanced manufacturing technology, Vol. 70 p. 1 (2014) [3] M. Nesser, O. Maloberti, J. Dupuy, E. Salloum, S. Panier, J. Fortin, P. Dassonvalle, Journal of magnetism and magnetic materials, Vol. 504, p.166696 (2020) [4] O. Maloberti, G. Meunier, A. Kedous Lebouc, IEEE Transactions on Magnetics, Vol. 44 (2008) [5] G. Bertotti, IEEE transactions on magnetics, Vol. 24, p. 621 (1988)

O5-08. Evidence of the Interfacial Dzyaloshinskii-Moriya Interaction in $Ni_{80}Fe_{20}$/Graphene Using Bragg-MOKE. *N. Bansal*[1], N. Chowdhury[1], A. Kumar[1], S. Das[2] and P.K. Muduli[1] *1. Physics, Indian Institute of Technology Delhi, New Delhi, India; 2. Centre for Applied Research in Electronics (CARE), Indian Institute of Technology Delhi, New Delhi, India*

The Dzyaloshinskii-Moriya interaction (DMI) plays a crucial role in the stabilization of chiral spin textures [1]. Interfacial DMI (iDMI) induced by a lack of inversion symmetry and strong spin orbit coupling at the interface of Ferromagnet/Heavy Metal (FM/HM) heterostructures provides various opportunities for future spintronic devices. Recently, iDMI in a thin film of NiFe/Graphene (NiFe/Gr) heterostructures has been detected using Brillouin light scattering [2] and using spin-polarized electron microscopy [3]. In this study, we propose a simple method of measuring DMI by using the Bragg magneto-optical Kerr effect (MOKE). We observe an asymmetric shift in the hysteresis loop, which is proportional to the strength of iDMI [4]. Here, we utilize Bragg-MOKE in longitudinal mode to which occurs when a broad polarized beam is incident on a periodic array of the magnetic features with size comparable to the wavelength of laser. We have investigated the hysteresis loop shift for 1st and 2nd order of diffraction in off-specular geometry for both patterned graphene (Gr/NiFe(10nm)/Ta) and reference (NiFe(10nm)/Ta). We used triangular pattern (Fig. 1) as proposed in Ref [4]. We found a shift in hysteresis loop for the Gr/NiFe/Ta sample (Fig. 2), which likely due to the presence of iDMI that was previously measured using BLS [2]. Hence, the Bragg-MOKE technique can be a potential technique for rapid quantification of iDMI in magnetic heterostructures. We will also present variable field magnetic force microscopy (MFM) and micromagnetic simulations to support these results.

1. M. Bode, *et al.,* Nature 447, 190 (2007). 2. A. Kumar, *et al*. Phys. Rev. *B* 99.3,035402 (2019). 3. H. Yang, *et al*. Nat. Mater. 17, 605 (2018). 4. D-S Han, *et al*. Nano Lett. 16, 4438 (2016).

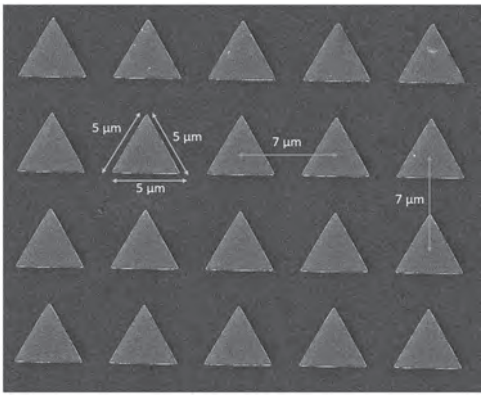

Figure 1. FESEM image of an array of equilateral triangular (vertex 5 µm & periodicity 7 µm) fabricated using e-beam.

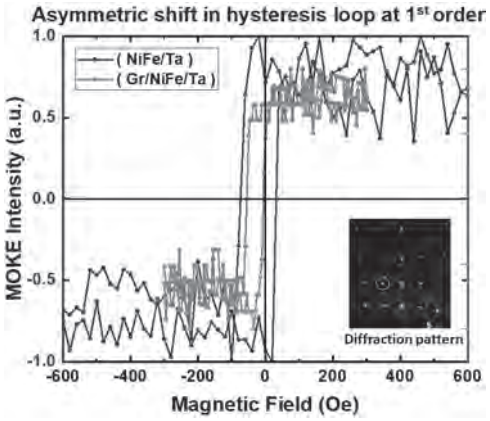

Figure 2 The hysteresis loop for the reference (NiFe/Ta) & for the graphene sample (Gr/NiFe/Ta) measured for 1st order of Bragg MOKE diffraction pattern (inset) showing the asymmetric shift in hysteresis.

O5-09. Effect of Ti as an Under and Spacer-Layer on the Perpendicular Magnetic Anisotropy of Tb-Fe Thin Film. *A.K. Sahoo*[2], J.A. Chelvane[1] and J.R. Mohanty[2] *1. Defence Metallurgical Research Laboratory, Hyderabad 500058, India, Hyderabad, India; 2. Nanomagnetism and Microscopy Laboratory, Department of Physics, Indian Institute of Technology Hyderabad, Kandi, Sangareddy 502285, Telangana, India, Hyderabad, India*

The perpendicular magnetic media has the potential to improve data storage beyond 1 Tb/in^2. Improving data density is a major challenge in data recording industries due to its sustainability and performance issues [1]. In the present study, by employing Ti as under-layer (UL) and spacer-layer (SL) the bulk perpendicular magnetic anisotropy (PMA) of Tb-Fe thin films is found to be improved considerably. 100 nm thick Tb-Fe film devoid of UL exhibited a maze-like domain pattern with strong out-of-plane (OOP) contrast. With 10 nm thin Ti UL, the domain width, and the OOP contrast of Tb-Fe (100 nm) film were found to improve considerably (fig. 1). Accordingly, the coercive field for Tb-Fe film with Ti UL was doubled when compared with the bare Tb-Fe film. The possible reason for the enhancement in OOP properties could be due to the lateral extent of *d-d* hybridization that exists at the interface. Similarly, PMA and domain areal density also increased by placing a 2 nm thin Ti SL: Tb-Fe (100 nm) / Ti (2 nm) / Tb-Fe (100 nm) (fig. 1). Here, we observed a large dipolar coupling that exists between the top and bottom Tb-Fe layers. The H_c of about 0.5 T observed for bare Tb-Fe (200 nm), was found to increase to about 1 T for the Tb-Fe films with Ti SL. Interestingly, Tb-Fe film with SL exhibited a hybrid domain pattern probably due to the bottom Tb-Fe layer. Thus, Ti when used either as UL or SL improved the OOP magnetic properties of Tb-Fe thin films considerably. The fundamental observation and understanding will have a significant impact on perpendicular media which may also useful in other areas of spintronic applications.

1. K. Tang, et. al, IEEE transactions on magnetics, Vol. 45 p. 786-792 (2009).

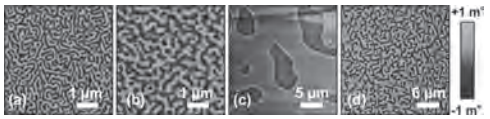

Fig. 1: MFM images of various films, (a) bare Tb-Fe film (100 nm), (b) Tb-Fe film (100 nm) with UL of 10 nm, (c) bare Tb-Fe film (200 nm), (d) bare Tb-Fe film (200 nm) with SL of 2 nm.

Session O6
MICROMAGNETIC MODELLING I
(Poster Session)

Harald Oezelt, Chair
Danube University Krems, Wr. Neustadt, Austria

O6-01. Scalable Space and Time Hierarchical Dipole-Dipole Interactions in the VAMPIRE Code. S. Jenkins[1], A. Meo[1] and *R.F. Evans*[1]
1. Physics, University of York, York, United Kingdom

Atomistic spin models [1] provide a natural bridge between electronic and micromagnetic length scales, where the magnetic properties are described by localised atomic spins within the Heisenberg model. The model parameters can be calculated *ab-initio* but the macroscopic magnetization dynamics and properties can also be simulated. While powerful, atomistic models are computationally expensive. A particular difficulty is the calculation of long-range dipole-dipole interactions, arising from the stray magnetic fields of localised atomic moments and causes complex magnetisation structures, such as magnetic vortices or Skyrmions. The dipole -dipole interactions are typically solved using a Fast-Fourier-Transform (FFT) [2] or the Fast Multipole Method (FMM) [3]. However, for atomistic simulations the continuum approximation does not accurately reflect the local dipole-dipole interactions at the atomic level and leads to systematic errors in the calculation of the dipole field. A brute force atomistic dipole-dipole approach is infeasible for the time (nanosecond+) and length (100 nm+) scales needed to extract useful data. Here we present modifications to the VAMPIRE software package [1] to include accurate and scalable calculations of dipole-dipole interactions for improved performance and scalability on ARCHER, the UK national supercomputer. We have developed a space-time hierarchical calculation of the dipole field calculation with order *NlogN* scalability with problem size, a comparison to the brute force tensor approach [4] is shown in Fig. 1. Our novel approach combines exact near-field computation of the dipole field with an *M*-Level hierarchical representation of the far-field dipole field [5]. The method is hierarchical in time and space, since the far-field time-evolution of the magnetization is much slower than the near-field which changes on the femtosecond timescale. Our improved algorithm enables the inclusion of accurate dipole-dipole interactions in atomistic simulations for large system sizes in the micrometre range for the first time.

[1] R. F. L. Evans *et al,* J. Phys.: Condens. Matter 26, 103202 (2014) [2] S. Yuan and H. Bertram, IEEE Trans. Mag. 28, 2031 (1992) [3] G. Brown et al, IEEE Trans. Mag. 40 2146 (2004) [4] G.J. Bowden et al., J. Phys. Condens. Matter 28, 066001 (2016) [5] J.J. Miles and B.K. Middleton, J. Magn. Magn. Mater. 95, 99 (1991)

O6-02. Micromagnetic Modeling Magnetization Excitation by a Resonance. *V. Teplov*[1], V. Bessonov[1], S. Batalov[1] and A. Telegin[1] *1. Institute of Metallurgy UB RAS, Yekaterinburg, Russian Federation*

With the development of electronic low-dimension systems, numerical modeling has become a powerful method for studying and predicting the physical properties of materials. To model dynamic magnetic systems the micromagnetic approach [1] and the methods of GPU acceleration of calculations on the video core of the system [2] are successfully applied. In our work, this approach is used to simulate the effect of nonlinear autoresonant excitation [3, 4] of nanoscale films of yttrium iron garnet (YIG) by a weak external magnetic field. The proposed analytical equations for autoresonance do not take into account a number of important real conditions, for example: attenuation, three-dimensional geometry of the sample, dipole – dipole interaction of spins, surface anisotropy, etc., which does not allow one to directly verify the theoretical model in practice. The aim of the work was to find the conditions for the excitation of autoresonance in a film with some real physical parameters using micromagnetic simulation in the MUMAX3 software. As a planar model, a YIG film with a size of 1600 × 1600 × 160 nm was chosen. The film thickness was taken to satisfy the conditions of a single-mode spin wave excitation and proximity to real planar samples. During simulations the sample was separated into rectangular elements in the form of cells, the interactions between them were calculated by using the Landau-Lifshitz equation. Since the YIG has the minimum level of attenuation of the magnetic subsystem, the damping parameter was excluded at this stage. Then the sample saturated along the axis of easy magnetization by H = 20 kOe was excited by a weak perpendicular pump field *h* with an amplitude of about 1 Oe. As a result, the stable nonlinear regime of excitation of magnetic oscillations of high magnitude in the film by a chirp rate of the pump field frequency was obtained in in the MUMAX3 simulations for the first time - the autoresonance effect. For the modelled YIG film the optimal chirp rate was a 4.3×10^16 s^(– 2). Finally, the full conditions for the autoresonance excitation of magnetization in the quasi-three-dimensional magnetic film by numerical methods were defined. Supported by the RFBR grant No. 19-32-90014.

1 A. Vansteenkiste, J. Leliaert, M. Dvornik, M. Helsen, F. Garcia-Sanchez // AIP Advances. 2014. Vol. 4. P. 107133. 2 V. S. Teplov, V. D. Bessonov. Resource and Mechanics of materials and structures. 2018. V. 6. P. 222—228. 3. S.V. Batalov, A. G. Shagalov. Physics of Metals and Metallography, 2010. Vol 109, N1, P. 3-8. 4 S,V. Batalov, A. G. Shagalov.. Physics of Metals and Metallography, 2013, Vol 114, N 2, P. 115–119

O6-03. Skyrmions in Nanodiscs of Co/Pt and the Effect of Inter-Skyrmionic Dipolar Interactions on Their Stability in Nanostructure. *Y. Kumar*[1], H. Saren[1] and P. Das[1] *1. Physics, Indian Institute of Technology Delhi, New Delhi, India*

Magnetic skyrmions are nontrivial topological object, that can originate from the interplay between various types of interactions, such as magneto-static, anisotropy, exchange interaction, and most importantly Dzyaloshinskii-Moriya (DMI)[1,2]. As a different strategy to stabilize these nontrivial structures at room temperature using an alternate top-down approach, there is an ongoing interest in the skyrmions in predefined nanostrutucres[3,4]. Detailed studies of stabilization and field evolution of individual skyrmions at room temperature in nanostructures is important for the development of this parallel field of research for any potential applications. Also, it is essential to have a proper understanding of the effect of the magnetostatic interactions between skyrmions[5,6,7]. In this work, we report the results of detailed investigation of skyrmions, which are stabilized in individual nanostructures of thin films of Co/Pt with DMI energy of 3 mJ/m^2. Using micromagnetic simulation we aim to understand how individual skyrmions get nucleated and annihilated in presence of external field. Such detailed information are usually obscured in the investigations of large arrays. From the field-dependent hysteresis of magnetization and the corresponding values of skyrmion numbers, we identify a clear signature of nucleation and annihilation of skyrmions (Fig.1). We have also investigated the effect of inter-skyrmionic magnetostatic interaction on their nucleation and annihilation mechanism in arrays of such Co/Pt nanodiscs. Our results show an important role of the interactions on the nucleation and annihilation of skyrmions with different interdiscs separation. These results suggest possibilities of tuning the skyrmionic behavior in nanostructures by their geometry which may be helpful to understand the behavior of skyrmions in general such as in continuous films.

[1] J. Iwasaki, M. Mochizuki, and N. Nagaosa, Nat. Nanotechnol. 8, 742 (2013). [2] J. Sampaio, V. Cros, S. Rohart, A. Thiaville, and A. Fert, Nat. Nanotechnol. 8, 839 (2013). [3] L. Sun et al, Phys. Rev. Lett. 110, 167201 (2013). [4] D. A. Gilbert et al., Nature Comm. 6, 8462 (2015). [5] R. V. Verba et al., Phys. Rev. B 101, 064429 (2020). [6]B. Goebel, J. Henk and I. Mertig, Sci. Rep.9, 9521 (2019). [7]M. A. Castro, D. Mancilla-Almonacid, J. A. Valdivia and S. Allende, J. Phys. Cond. Mat. 32, 175801 (2020).

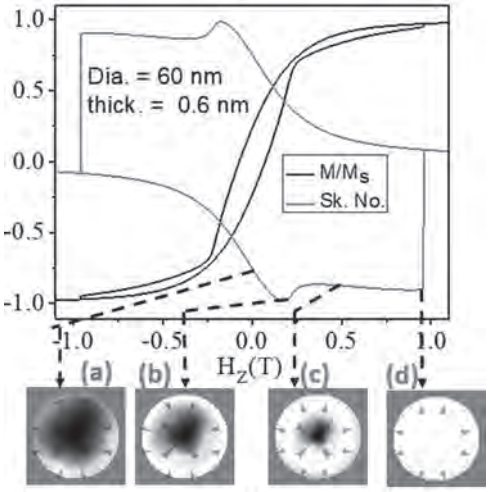

Fig. 1. M-H (black) and evolution of Skyrmion no. as a function of external field (red) for a single Co/Pt nanodisc.

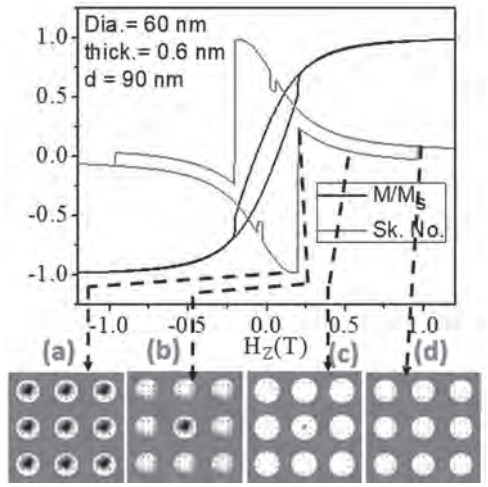

Fig. 2. M-H (black) and evolution of Skyrmion no. as a function of external field (red) in an array of 3 X 3 skyrmions, where d is the inter-disc separation. The data shows the role of magnetostatic interaction between skyrmions in an array.

O6-04. Possible Realization of Double Spin Vortex State in Hollow Submicron Particles. *N. Hirano*[1], E. Nomura[1], M. Chiba[1], H. Magara[2], T. Sato[2], Z. Akase[2] and S. Kobayashi[1] *1. Faculty of Science and Engineering, Iwate University, Morioka, Japan; 2. Institute of Multidisciplinary Research for Advanced Materials, Tohoku University, Sendai, Japan*

Spherical nanoparticles with hollow structure have received much attention because of their unique magnetic features reflecting their large surface area [1,2]. Recent works suggested the formation of a spin vortex for hollow spherical submicron Fe_3O_4 particles, whose stability is enhanced with increasing the diameter [3]. In this work, the formation mechanism of spin vortexes have been studied for a hollow submicron sphere using micromagnetic simulations, where possible realization of a double vortex reflecting the hollow structure was revealed. The magnetization reversal and magnetic configurations under magnetic fields along the [100] or [111] axis were studied using OOMMF for a single hollow Fe_3O_4 spherical particle with the varying diameter (d = 300 - 700 nm) and inner/outer diameter ratio (γ = 0 - 0.75). Electron holography was also performed for 400- nm hollow spheres to directly characterize a magnetic state. Figure 1 shows a typical example of the M-H curves for a hollow sphere (d = 300 nm, γ = 0.5). Before entering a single vortex state (phase IV) typically observed in a solid sphere, two types of vortex structures are formed for a hollow sphere, associated with multi-step magnetization changes. We find that as the magnetic field is reduced from high fields, a clockwise and anti-clockwise vortices are formed at the ends of the sphere (phase II) and then transform into a single vortex with cores displaced by changing a magnetic field (phase III). The formation of such double vortices can be due to reduced Zeeman energy by spins at and around the equatorial plane of the sphere. With increasing d or γ, a field range, where the phases II and III are stabilized, expands for both [100] and [111] field orientations. Magnetic phase images obtained by electron holography revealed no significant stray field around the hollow sphere in zero fields, being consistent with the formation of a spin vortex.

1] H. Khurashid et al., Scientific Reports 5, 15054 (2015) 2] Y. Liang et al., Colloids and Surfaces A 530 191-199 (2017) 3] M. Chiba et al., Journal of Magnetism and Magnetic Materials 512 167012 (2020)

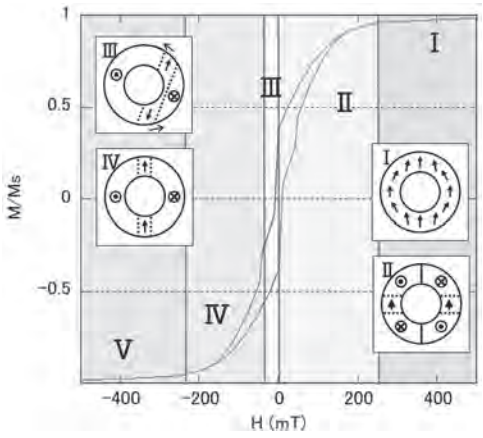

M-H curve for a hollow sphere with d = 300 nm and γ = 0.5. Spin maps in the states I - IV are schematically shown.

O6-05. Stress-Induced Modification of Gyration Eigen-Frequencies in Stacked Double-Vortex Structures. *V. Iurchuk*[1], A. Kákay[1] and A. Deac[1] *1. Institute of Ion Beam Physics and Materials Research, Helmholtz-Zentrum Dresden-Rossendorf, Dresden, Germany*

The ground state of nanoscale circular magnetic disks of certain geometric aspect ratios is a spontaneously forming stable vortex configuration with circulating in-plane magnetization and a vortex core pointing out-of-plane. Resonantly exciting the vortex core via either an rf magnetic field or an rf spin-polarized current yields a gyrotropic motion around its equilibrium position, characterised by a specific eigen-frequency, which depends on the material parameters and the disk geometry [1]. Such oscillations, which can be read out via periodic magnetoresistance changes, generate rf signals with high quality factors (>10000) in the sub-GHz bandwidth [2,3]. While all these features make vortex-based nano-oscillators interesting as nanoscale rf sources, the major drawback remains their low frequency tunability associated with the linear characteristics of the gyrotropic mode. Here, we investigate, by micromagnetic simulations, the role of magnetostriction in improving the tunability of vortex nano-oscillators. Specifically, we consider a double-disk structure comprising magnetostrictive (CoFe) and non-magnetostrictive (Py) layers separated vertically by a non-magnetic (NM) spacer. We show that, when the two vortices have different eigen-frequencies and the magnetostatic coupling between them is sufficiently strong, the stress-induced magnetoelastic anisotropy can lead to the synchronized gyration of the two vortex cores (Fig. 1). The stress-induced transition from double-frequency

to single-frequency dynamics is mostly controlled by the polarization of the vortices and the magnetostatic coupling strength (i.e. spacer thickness). These findings offer a frequency tunability of vortex-based oscillators via mechanical stress, which can be generated and controlled electrically, for example, using piezoelectric substrates [4]. Funding from the EU Horizon 2020 project No. 737038 (TRANSPIRE) is acknowledged.

[1] K. Yu. Guslienko, et al, J. Appl. Phys. 91, 8037 (2002). [2] A. Dussaux, et al, Nat. Commun. 1, 1 (2010). [3] N. Locatelli, et al, Appl. Phys. Lett. 98, 062501 (2011). [4] M. Filianina, et al, Appl. Phys. Lett. 115, 062404 (2019).

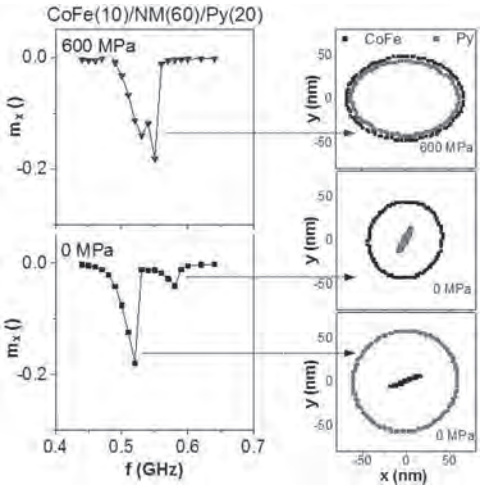

Fig. 1. Simulated FMR spectra for the CoFe(10nm)\NM(60nm)\ Py(20nm) double-vortex structure (diameter is 300 nm) at zero stress and 600 MPa uniaxial stress, and corresponding resonant trajectories of the vortex cores in CoFe and Py layers. The dynamics was excited by a sinusoidal rf magnetic field with 1 mT amplitude.

O6-06. Vortex-Induced Topological Rearrangements in Permalloy Antidot Films. *V.V. Zverev*[1,2] and I.M. Izmozherov[1,2] *1. Department of Theoretical Physics and Applied Mathematics, Ural Federal University named after the first President of Russia B N Yeltsin, Institute of Physics and Technology, Ekaterinburg, Russian Federation; 2. M N Miheev Institute of Metal Physics, Institut fiziki metallov imeni M N Miheeva Ural'skogo otdelenia Rossijskoj akademii nauk, Ekaterinburg, Russian Federation*

Ferromagnetic films with antidot arrays can be used for various purposes, including high-density magnetic recording and information processing. Numerous studies have examined global characteristics of these artificial structures and possibilities of controlled switching between global magnetic configurations [1-3]. A more ambitious task is to control the states of stable topological structures located near individual holes (antidots). In this work, we present numerical simulations of magnetization topological rearrangements in films of various thickness containing a domain wall (DW) and a square antidot array. The simulations were performed using *mumax3* solver [4]. To visualize the magnetization topological structure we employed an approach based on the calculation of topological charges of two types [5]. The DW movement leads to multiple events of birth and annihilation of vortex-antivortex pairs. As in the case of homogeneous magnetic materials this system is characterised by unstable behaviour and irregular dynamics [5]. We classify the emerging topological structures and find that not only local topological solitons, but also the holes became carriers of the topological charge (Fig. 1). A type of topological charge translocation was discovered to depend on film thickness and array geometric parameters.

[1] D.H.Y. Tse, S.J. Steinmuller, T. Trypiniotis et al. Phys. Rev. B, Vol. 79, 054426 (2009) [2] B. Van de Wiele, A. Manzin, A. Vansteenkiste, et al, J. Appl. Phys., Vol. 111, 053915 (2012) [3] R. Streubel, F. Kronast, U.K. Roessler et al. Phys. Rev. B, Vol. 92, 104431 (2015) [4] A. Vansteenkiste, J. Leliaert, M. Dvornik et al. AIP Advances, Vol. 4, 107133 (2014) [5] V.V. Zverev, I.M. Izmozherov, B.N. Filippov. Phys. Solid State, Vol. 60, p. 299 (2018)

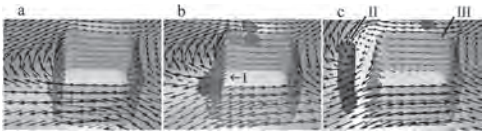

Fig. 1. (a) A hole in the antidot array. (b) Nucleation of the vortex-antivortex pair (I) near the hole. (c) A linear vortex (II) between the boundary surfaces of the film and the hole (III) embedded in the antivortex configuration of the magnetization field.

O6-07. Withdrawn

O6-08. Spatial Magnetization Modes in Spin Hall Driven Oscillators. *E. Zhang*[1] and J. Zhu[1] *1. Electrical and Computer Engineering, Carnegie Mellon University, Pittsburgh, PA, United States*

Transverse injection of pure spin current utilizing spin Hall effect(SHE) has been used for magnetization switching of in-plane MTJs, for propelling domain wall motion in perpendicular spin logic devices, and for exciting ferromagnetic resonance.[1-3] In particular, the transverse spin injection geometry enables a type of spin torque oscillators(STO) that can be used to apply a very localized ac magnetic field at nano-scale with a dc current.[4] Such capability may facilitate the creation of nanodevices needing a localized magnetic field at the GHz regime. In this paper, we present a systematic micromagnetic study on the dynamics and spatial incoherent modes of magnetization oscillation in these STOs as excited by the transverse spin injection utilizing SHE. Fig.1(b) shows a sketch of an elliptically shaped STO with a heavy normal metal wire underneath. And Fig.1(a) shows the calculated oscillation frequency as a function of applied field for an STO with 120x80 nm^2 in two in-plane dimensions. Permalloy of Ms=800 emu/cm^3 is assumed for the oscillation layer. The spin polarization direction of the injected spin current is opposite to the field direction along the length of the ellipse. The Kittel formula is used to fit the calculated data, and an excellent agreement is obtained with a planar demagnetization factor p = 0.8. Considering that the stray field generated by the magnetization oscillation will be in proportion to the oscillator thickness, calculations were performed for STOs over a broad range of thicknesses. Fig.2 shows the spatial oscillation modes for two oscillators with different thicknesses, δ=4nm (a)(c) and δ=8nm (b)(d). It should be noted that the magnetization oscillation amplitude is always the greatest at the two ends of the elliptical-shaped oscillator. For thinner oscillators, the magnetization at the two ends oscillate coherently whereas for thicker oscillators, 180° phase difference between the oscillation at two ends is observed. In the talk, the spatial incoherent modes will be analyzed in detail.

[1] L. Liu, C.-F. Pai, D. C. Ralph and R. A. Buhrman, Phys. Rev. Lett. 109, 186602 (2012). [2] D.M. Bromberg, M.T. Moneck, V.M. Sokalski, J. Zhu, L. Pileggi, J.-G. Zhu, IEDM 2014 Proceedings, IEDM14-792 (2014). [3] B. Divinskiy, V. E. Demidov, S. Urazhdin, R Freeman, A. B. Rinkevich and S. O. Demokritov, Adv. Mater. 30, 1802837 (2018). [4] E. Chen, J. Xu, J. Zhu, and V. Chen, IEEE International Midwest Symposium on Circuits and Systems (MWSCAS), Springfield, MA, Aug. (2020).

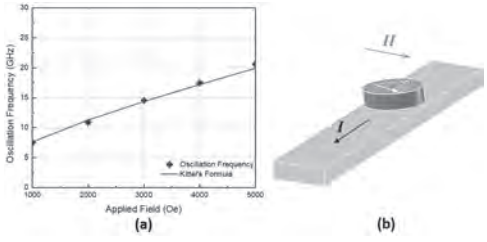

Fig.1 (a) The oscillation frequency dependency on the applied field.

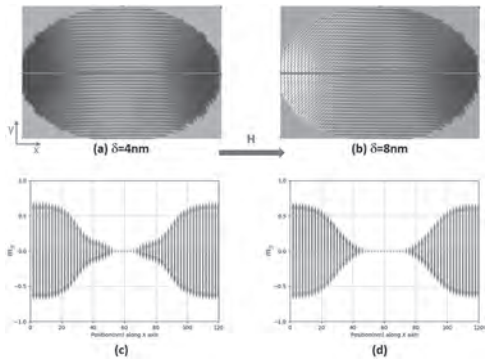

Fig.2 (a) coherent oscillation. (b) incoherent oscillation. (c-d) The m_y distribution along the solid red midline for (a) and (b).

O6-09. Spin Waves Transport in the 3D Magnonic Waveguides.
A.A. Martyshkin[1], E. Beginin[1] and A. Sadovnikov[1] *1. Saratovskij nacional'nyj issledovatel'skij gosudarstvennyj universitet imeni N G Cernysevskogo, Saratov, Russian Federation*

Development of the theory of ferromagnetic materials and the improvement of the manufacturing process for the production of thin ferrite films made it possible to design micro- and nanostructured surfaces that are suitable for studying spin waves (SWs). One of the key problems in creating spin-wave devices is associated with the attenuation of magnetostatic spin waves. A magnetic dielectric, yttrium iron garnet (YIG), has the smallest dynamic attenuation, which makes it possible to have an SW propagation length sufficient to create various magnon devices. Studies of the characteristics and control methods of spin-wave transport in various magnetic waveguide systems are of great interest, since magnetic oscillations in such structures propogates in the GHz and THz ranges and are a promising object for data transmission and processing [1]. Based on YIG microwaveguides, it is possible to create devices for processing signals — magnon networks in which logical operations are based on the principles of spin-wave interference [2]. In this work, using numerical and experimental studies, the possibility of transmitting a spin wave signal in a structure with a three-dimensional topology formed by magnetic orthogonally articulated sections is shown (Fig. 1). The mechanisms of formation of the multimode composition of the spin-wave signal in areas of irregular structure with violation of translational symmetry are revealed. It is shown that the proposed structure makes it possible to transmit SW signals in an irregular structure in the propagation mode of a surface magnetostatic wave in a wide frequency range. The proposed mechanism for transmitting the spin-wave angular momentum allows us to improve the devices operating on the principles of magnon logic by increasing the density of the functional nodes of the magnon network. The proposed structure can serve as a building block in multi-level integrated magnon networks by transmitting a signal between layers, while performing the functions of a frequency filter. Numerical simulation based on the micromagnetic calculation was supported by the Russian Foundation for Basic Research (18-29-27026)

Chumak A. V., Vasyuchka V. I., Serga A. A., Nature Physics, Vol. 11, p. 453, (2015) Sadovnikov A. V., and Davies S., Grishin S. V., Appl. Phys. Lett., Vol. 106, p.192406, (2015)

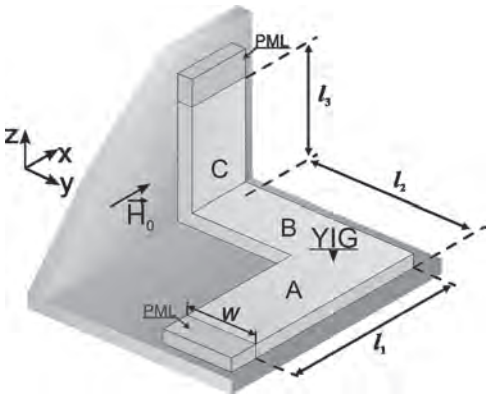

Fig.1 Schematical view of the structure under study

O6-10. Shape-Related Effects on Ferromagnetic Nanoparticles: a Micromagnetic Approach for Highly Diluted and Highly Ordered Systems.
R. Delgado-Garcia[1], G. Rodriguez-Rodriguez[1], A. López-Ortega[1] and J. Colino[1] *1. Applied Physics, Universidad de Castilla-La Mancha, Toledo, Spain*

Recent improvements in nanoparticle synthesis have allowed the application of magnetic nanoparticles (MNPs) in many fields where particle size control is key, such as data storage, spintronics or biomedicine, in which drug delivery and cancer treatment using hyperthermia stand out. In MNP systems, shape can trigger magnetostatic anisotropy effects induced by the demagnetizing factor. This feature is most notorious in highly degenerated systems on which shape anisotropy can be induced to alter properties like coercive field and remanence of non-interacting MNPs. In addition, magnetostatic dipolar interactions between MNPs can be tuned in disordered and crystalline structures by adding non-magnetic coatings, which can also control the lattice parameter, in a core-shell scheme, thus affecting the effective anisotropy of the system. This work focuses on the angular study of magnetization reversal processes in quasi-spherical (ε~1) single MNPs with different shapes and magnetic properties. Simulations show different hysteresis loops for different sphericalnesses of the MNPs, which can be related to the presence of different magnetization pinning events at the sharp edges of less spherical MNPs[Fig. 1]. Moreover, the effect of dipolar interactions has been tested out with simulations of the remanent state in MNP superlattices with simple, body-centered and face-centered cubic arrangements[Fig. 2].

D.L. Huber, small., Vol. 1(5), p.482-501 (2005) D. Kim et al., Journal of Magnetism and Magnetic Materials., Vol. 320(19), p.2390-2396 (2008) Q. Li et al., Scientific Reports., Vol. 7, p.9894 (2017) D. Peddis et al., Chemistry of Materials., Vol. 25(10), p.2005-2013 (2013) A. Vansteenkiste et al., AIP Advances, Vol. 4, p.107133 (2014)

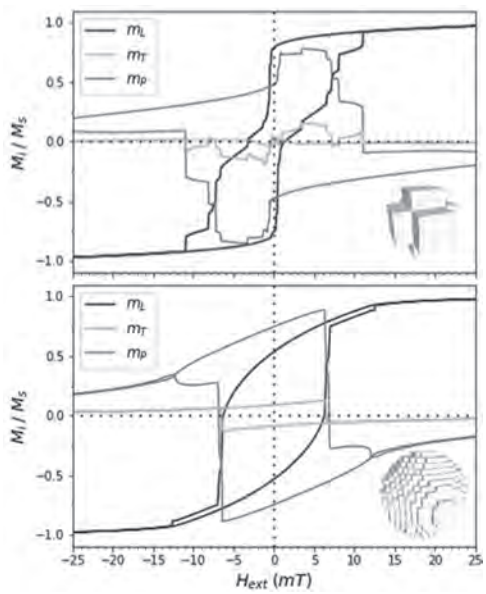

Fig. 1. Hysteresis loops of randomly oriented non-interacting MNPs with Stoner-Wohlfarth behavior with different shapes.

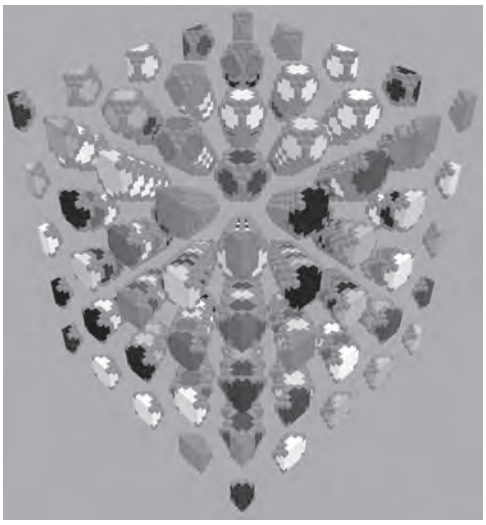

Fig. 2. MNPs ordered in a body-centered cubic (bcc) superlattice.

O6-11. The Analysis of Magnetite Nanoparticles Allowed to Warm Through Superparamagnetic Transition. *D. McPherson*[1] and K. Chesnel[1] *1. Physics and Astronomy, Brigham Young University, Provo, UT, United States*

Magnetic nanoparticles (NPs) have a wide range of applications, from engineering to medicine. Understanding the properties of magnetic nanoparticles provides insight that enhance and expand their use. There are a number of computational methods that are employed to study magnetic NPs in order to determine their magnetic behavior in various field and temperature environments, such as the dynamics of the magnetic fluctuations throughout the superparamagnetic blocking transition. I will present on analysis of these magnetic dynamics for magnetite (Fe_3O_4) nanoparticles. These NPs have been previously characterized through: electron imaging and magnetonetry [1], x-ray magnetic circular dichroism (XMCD) [2], and x-ray resonant magnetic scattering (XRMS) [3]. Here we are using coherent x-ray resonant magnetic scattering (C-XRMS) [4, 5] to access the dynamics of magnetic fluctuations. The data was collected at the SLAC synchrotron facility from assemblies of 11 nm magnetite NPs. In this experiment, series of C-XRMS speckle patterns are collected at subsequent times and cross-correlated, to follow the dynamics of fluctuations. I will compare two separate methods of correlation: the standard punctual photon correlation method [6], and a two-dimensional spatial correlation method using spatial features in the speckle patterns [7, 8].

[1] Chesnel, K, et al., Journal of Physics: Conference Series., Vol. 521, p. 012004 (2014) [2] Cai, Y. P., et al., Journal of Applied Physics., Vol. 115, no. 17 (2014) [3] Chesnel, Karine, et al., Magnetochemistry., Vol. 4, no. 4, p. 42. (2018) [4] Chesnel, K., et al., Physical Review B., Vol. 66, no. 17 (2002) [5] Mangin, S., et al.. Physical Review B., Vol. 78, no. 2 (2008) [6] Wiseman, Paul W., and Jeffrey A. Squier., Multiphoton Microscopy in the Biomedical Sciences., Vol 200 (2001) [7] Chesnel, K., et al., Physical Review B., Vol. 78, no. 13 (2008) [8] Chesnel, Karine, et al., Nature Communications., Vol. 7, no. 1 (2016)

O6-12. Asymmetry Induced Inhomogeneous Magnetization Reversal in Hemispherical Shells. *A. Mary*[1] and S. Thomas[1] *1. Department of Physics, Cochin University of Science and Technology, Cochin 682022, India*

Inhomogeneous magnetic phases like magnetic vortex are expected to open up a wide range of opportunities both from a fundamental and technological perspective. Asymmetric nanostructures offer alternative data storage possibilities by suggesting a control over the vortex formation and thereby chirality [1-3]. Asymmetry introduced in the geometry also has a strong impact on magnetization reversal. Increased coercivity, remanence, and switching field distribution with the degree of asymmetry establishes the existence of an induced anisotropy, which in turn could even destabilize the magnetic vortex depending on the degree of asymmetry in a particular geometry [4]. Following these ideas, in this work, we investigate how the asymmetry modifies the magnetization reversal in hemispherical shells. We address this issue by breaking the symmetry of non-interacting hemispherical cap structures through a thickness modulation inclined at an angle with the symmetry plane and by analyzing the magnetization reversal mechanism for varying thicknesses. Micromagnetic simulations indicate that the asymmetric nanocaps reverse through the propagation of a curling state, while in the symmetric caps, magnetization reversal happens via coherent rotation. With an increase in thickness, the field at which curling state nucleates, shifts towards a higher applied field. The non-uniform magnetization reversal is apparently due to the altered energy contributions resulting from the asymmetry introduced in the nanocaps.

[1] M. Schneider, H. Hoffmann, and J. Zweck, Appl. Phys. Lett., Vol. 79, p.3113 (2001) [2] D. B. Gopman, Y. P. Kabanov, J. Cui, *et al*., Appl. Phys. Lett., Vol. 109, p.082407 (2016) [3] J. Rothman, M. Kläui, L. Lopez-Diaz, *et al.,* Phys. Rev. Lett., Vol. 86, p.1098 (2001) [4] K. M. Wu, J. F. Wang, Y. H. Wu, *et al.,* J. Appl. Phys., Vol. 103, p.07F314 (2008)

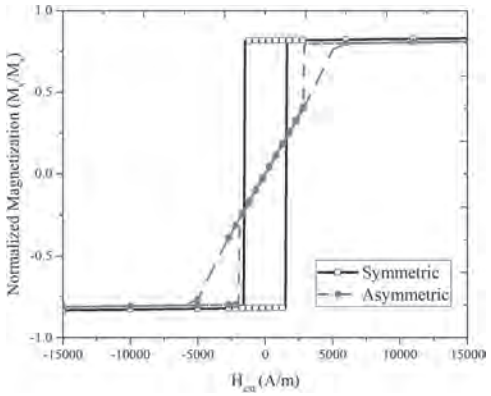

Fig.1: Simulated hysteresis loops for symmetric and asymmetric nanocaps with diameter 100 nm and thickness 10 nm. Square loops account for the magnetization reversal via coherent rotation in symmetric caps. Hysteresis loops for asymmetric caps of diameter 100 nm show negligible remanence and coercivity.

O6-13. Withdrawn

O6-14. Switching in Square Ferromagnetic Nanodot. *P. Eroshenko*[2], S. Komogortsev[2] and V.A. Fel'k[1] *1. Sibirskij gosudarstvennyj universitet nauki i tehnologij imeni akademika M F Resetneva, Krasnoarsk, Russian Federation; 2. Kirensky Institute of Physics, Federal Research Center KSC SB RAS, Krasnoyarsk, Russian Federation*

Magnetization patterns and reversal modes are the key points in applications of magnetic nanoparticles. Using numerical simulation with OOMMF tool, we have investigated magnetic reversal in plate-like magnetite nanoelements of square and cylindrical shape. Magnetocrystalline anisotropy was off (that is acceptable for polycrystalline or amorphous elements) or set to be equal the constant of magnetite. The field was applied in the plane and for square element – along the side of the square. Element size changing from 50 to 600 nm results in uniform magnetization pattern changes to the buckling one. The coercive force shows qualitatively different behavior with lateral size changing for square and the cylindrical dots. For square dot the overlap of some critical size results in skipping up of coercivity, which is accompanied by switching from the uniform rotation to the mixed uniform and buckling-type reversal. For the cylindrical dot the coercivity monotonously reduced with nanoelement size. Numerical data help us to understand some magnetic properties of magnetite nanocrystals, which were fabricated by chemical deposition. Magnetization distribution in maghemite square-shaped nano-plates would be close to the uniform, as far as the size of square is about 9 nm lower than the exchange length. The Stoner – Wohlfarth model for predicts coercivity much bigger then experimental value. In-plane anisotropy of coercivity follows the Stoner-Wohlfarth model well, for field orientations not along diagonals of the square. Since in the experiment we deals with an array of randomly oriented particles, it should to be expected that the average coercivity field will be several times lower than the maximum one predicted by the Stoner-Wohlfarth model. Support by Russian Foundation for Basic Research, Government of Krasnoyarsk Territory, Krasnoyarsk Region Science and Technology Support Fund to the research project number 18-42-240006 is acknowledged.

O6-15. Phase-Field Simulation of Domain Evolution and Magnetization Switching Mechanism Near the Ferromagnetic Morphotropic Phase Boundary. *C. Hu*[1], Z. Zhang[1], T. Yang[2], W. Li[1] and L. Chen[2] *1. Liaocheng University, Liaocheng, China; 2. The Pennsylvania State University, University Park, PA, US, University Park, PA, United States*

The morphotropic phase boundary (MPB), separating two ferroic phases with rhombohedral and tetragonal crystal symmetries, has been utilized extensively in ferroelectrics because it can lead to high-performance piezoelectricity. Recently, a parallel ferromagnetic MPB was experimentally reported and was suggested that the optimal point for magneto-mechanical applications might lies on the rhombohedral side. However, the insight of the domain structures and switching mechanism near ferromagnetic MPB is still unclear. In this work, phase-field micromagnetic microelastic modeling was employed to simulate the domain formation and magnetization switching around the rhombohedral side of ferromagnetic MPB. The results show that four kinds of domains of the rhombohedral phase automatically form twins of either 110 or 100 boundaries with 71 degree and 109 degree domain walls after a process of nucleation and growth. The rhombohedral domain evolution and phase volume fraction under the external field of 120 kA/m along different directions are investigated. In ferromagnetics subject to an alternating magnetic field, domain magnetization switches to cause a magnetization hysteresis loop and an associated butterfly magnetostriction loop with the alternating magnetic field.

[1] S. Yang, H. Bao and C. Zhou, Phys. Rev. Lett., 104(19), 719-726 (2010). [2] B. Richard, W. Manfred and C. James., Phys. Rev. Lett., 111(1), 429-440 (2013). [3] T. Y. Ma, X. Liu, X. Pan, Appl. Phys. Lett., 105, 192407 (2014). [4] C. C. Hu, T. N. Yang and L. Q. Chen. Appl. Phys. Lett., 108, 141908 (2016). [5] F. Li, D. B. Lin and Z. B. Chen, Nat. Mater., 17:349-354 (2018). [6] C. C. Hu, Z. Zhang and L. Q. Chen. Appl. Phys. Lett., 115, 1624028 (2019). [7] W. F. Rao, Y. C. Xu and C. C. Hu, Acta Mater, 171, 240-252 (2020).

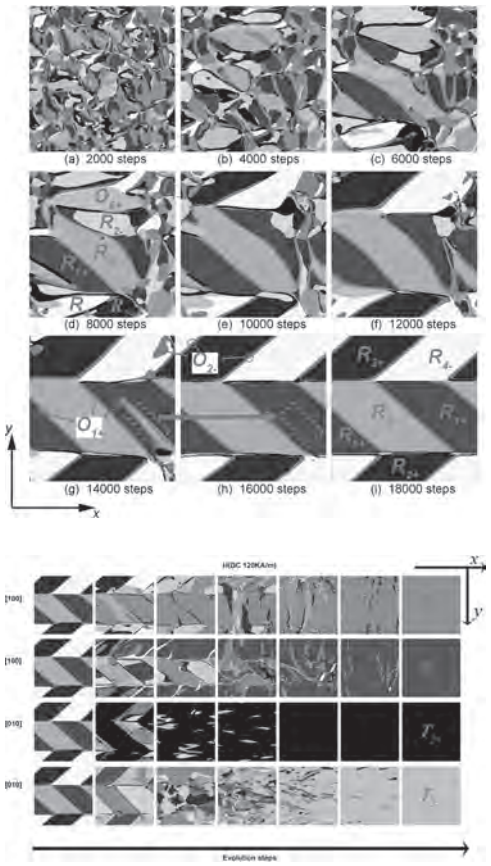

O6-16. Withdrawn

O6-17. Micromagnetic Simulations of the Quasi-Static Properties of Dissimilar Bilayers. *A. Pokhrel*[1], B. Nepal[1], U. Karki[1], A. Sapkota[1], A. Rai[1], T. Mewes[1] and C. Mewes[1] *1. Physics and Astronomy, The University of Alabama System, Tuscaloosa, AL, United States*

Achieving a strong perpendicular magnetic anisotropy is of great importance for materials intended for use in spintronics devices. Perpendicular anisotropy in magnetic multilayers arises from the broken symmetry at the interfaces due to the enhanced orbital and spin moments relative to the bulk system[1]. In order to accurately describe the quasi-static properties of these materials using a macrospin approach, the inclusion of both second-order (K_2) fourth-order (K_4) uniaxial anisotropies is essential. Beik Mohammadi et al[2] have shown that lateral inhomogeneities of the second-order uniaxial anisotropy in thin films with perpendicular uniaxial anisotropy can give rise to higher-order anisotropy contributions. Here, we report on the study of the layer to layer variation of the second-order perpendicular anisotropy in magnetic bilayers and its influence on the quasi-static properties. We analyze the results of micromagnetic simulations[3] in magnetic bilayers using a macrospin model. We show that in order to describe the micromagnetic simulation data using macrospin model, one requires a fourth-order uniaxial anisotropy contribution although the underlaying micromagnetic model does not include such term. Quasi-static calculations show that the fourth-order uniaxial anisotropy is caused by the deviation of the magnetization from the applied field direction.

1. J. M. Shaw, H. T. Nembach and T. J. Silva, Physical Review B 87 (5), 054416 (2013). 2. J. Mohammadi, K. Cole, T. Mewes and C. Mewes, Physical

Review B 97 (1), 014434 (2018). 3. T. Mewes, C. Mewes, MATLAB based micromagnetics code M3, (2018). URL http://magneticslab.ua.edu/micromagnetics-code.html

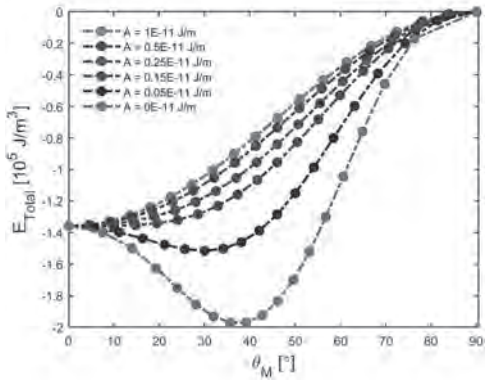

Fig.1 Energy landscape for different exchange constants in bilayer system

O6-18. Micromagnetic Modelling of Stripe Domains in Thin Films With a Columnar Microstructure. *E. Dengina*[1], A. Bolyachkin[1], N. Kulesh[1] and V. Vas'kovskiy[1,2] *1. Ural Federal University, Ekaterinburg, Russian Federation; 2. Insitute of Metal Physics UB RAS, Ekaterinburg, Russian Federation*

Magnetic films with a columnar microstructure are media in which nanosized magnetic columns passing through the full thickness of the film are surrounded by regions with lower, or even zero, magnetization [1]. Such films with prominent perpendicular magnetic anisotropy are used for information recording and usually made of CoCr, CoCrPt, FeFt, *etc*. [2]. The columnar microstructure was also found in rare-earth-transition metal amorphous films, that in some cases demonstrate stripe domain pattern. It is sensitive to microstructural and micromagnetic features that are emphasized and studied in some theoretical works [3]. However, it was investigated mainly for uniform films and practically important case of films with columnar microstructure was not studied yet. To elucidate this, we have performed a micromagnetic modelling of columnar films with stripe domain patterns. Micromagnetic model was created using Matlab and Mumax3 software packages. In the first one the microstructure is constructed using Voronoi tessellation based on a distorted hexagonal grid of points and subsequent homothety of the obtained polyhedra (fig.1, on the right). Periodic boundary conditions were taken into account. The magnetization reversal was carried out in Mumax3, and as a result, hysteresis loops and micromagnetic configurations of the films were obtained. The dependences of the stripe width, remanence and saturation field on the parameters inherent in the model (column size, film thickness, and phase volume ratio) were determined. In addition, the effect of a decrease in the exchange coupling between columns and surrounding matrix on the magnetic structure was investigated. The micromagnetic model was tested on La-Co films. Parameters of stripe domains (fig. 1, on the left) and hysteresis properties, obtained for them, were close to the experimental data. This work was supported by the Russian Science Foundation (Project No 18-72-10044).

1. G. M. Chow *et al* (Eds.). Nanostructured Films and Coatings, p. 86 (2000). 2. B.S.D.Ch.S. Varaprasad *et al*. IEEE Transactions on Magnetics, Vol. 51(11), 7117424 (2015). 3. F. Virot, L. Favre *et al*. J. Phys. D: Appl. Phys., Vol. 45, 405003 (2012).

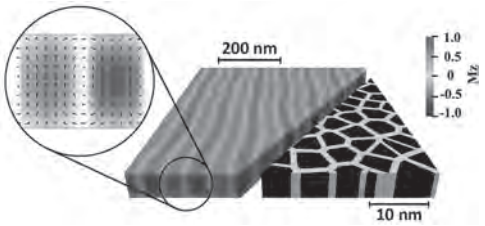

Fig.1. Magnetic stripe structure obtained by micromagnetic simulation (on the left) and a part of zoomed columnar microstructure of the film (on the right).

Session O7
SPIN WAVE III: CONTROLLING SPIN WAVE DYNAMICS (Poster Session)

Maciej Dabrowski, Co-Chair
University of Exeter, Exeter, United Kingdom
Juan Gabriel Ramirez, Co-Chair
Universidad de los Andes, Bogotá, Colombia

O7-01. Systematic Micromagnetic Study of the Band Structure of One-Dimensional Artificial Magnonic Crystals in Presence of Interfacial Dzyaloshinskii-Moriya Interaction. *R. Silvani*[1,2], S. Tacchi[3], M. Kuepferling[1] and G. Carlotti[2] *1. Istituto Nazionale di Ricerca Metrologica, Torino, Italy; 2. Universita degli Studi di Perugia Dipartimento di Fisica e Geologia, Perugia, Italy; 3. Istituto Officina dei Materiali Consiglio Nazionale delle Ricerche, Trieste, Italy*

We study the effect of the Dzyaloshinskii-Moriya interaction (DMI) in magnetic thin films with periodically varied properties[1,2], known as magnonic crystals (MCs), by micromagnetic simulations based on the software MuMax3. Two one-dimensional MCs are considered (Fig. 1), both with the same periodicity $p=300$ *nm*, saturation magnetization $M_s=730$ *kA/*m and exchange stiffness $A=10$ *pJ/m,* but different implementation of the DMI modulation. In the first case, the sample is a thin ferromagnetic film (thickness $t=2$ *nm)* on top of a regular array of parallel heavy metal nanostripes (width $w=150$ *nm*), equally separated, with an edge-to-edge distance $d=150$ *nm*. In the second case, a continuous heavy metal substrate supports an array of magnetic nanostripes (width $w=150$ *nm*) with variable thickness ($t_1=2$ *nm* and $t_2=4$ *nm*). The modification of the magnonic band structure of both MCs is studied by a systematic variation of the DMI strength D in the range between *0* and *2 mJ/m*^{2}. Fig.2 reports the spin wave (SW) dispersion relation of the first kind of MC calculated for different values of D. We show that for small values of D (in the range *0.1-0.6 mJ/m*^{2}) the folding of the branches permits to access the dispersion curves by Brillouin light scattering (BLS) in a much larger wavevector range than usually accessible in continuous films. Consequently, since the frequency non-reciprocity increases almost linearly with the modulus of the k-vector of the SWs (i.e. with the quantum number of the band structure), these results pave the way to extend the sensitivity of BLS experiments to values of the DMI constant D smaller than those usually measurable by BLS in plane films. For large values of D (in the range *0.7-2.0 mJ/m*^{2}) instead, it is found that the lower bands become flat, reflecting the localized character of the corresponding magnonic modes. Financial support from the EMPIR programme 17FUN08-TOPS, co-financed by the Participating States and from the European Union's Horizon 2020 program, is kindly acknowledged.

1. R. A. Gallardo et all., Phys. Rev. Lett. 122, 067204 (2019) 2. M. Mruczkiewicz et all, Phys. Rev. 94, 024434 (2016)

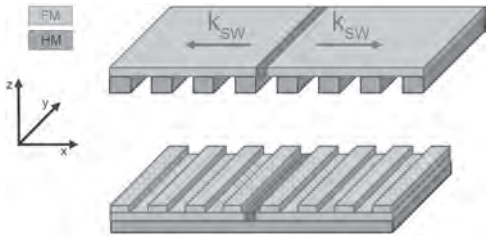

Fig.1 Sketch of the two MCs considered, consisting of a ferromagnetic film (FM) and heavy metal (HM) substrate, with the excitation line in red

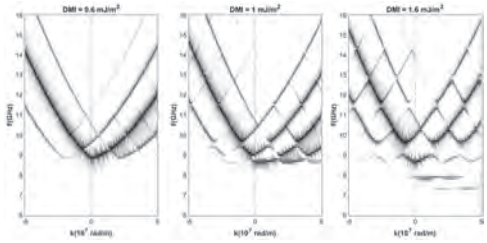

Fig.2 The simulated dispersion curves of the spin waves for three different values of D

O7-02. Effect of the Interfacial Dzyaloshinskii-Moriya Interaction on Spin Waves Eigenmodes of Elliptical CoB Dots Magnetized in-Plane. M. Alunni[1], R. Silvani[1,2], S. Tacchi[3] and *G. Carlotti*[1] *1. Dept of Physics and Geology, Universita degli Studi di Perugia, Perugia, Italy; 2. Istituto Nazionale di Ricerca Metrologica, Torino, Italy; 3. Istituto Officina dei Materiali del CNR (CNR-IOM), Perugia, Italy*

There is currently a great interest to understand the effect of the Dzyaloshinskii-Moriya interaction (DMI) on the dynamic properties of layered and/or laterally confined nanostructures. In this work we analize the characteristics of spin waves eigenmodes in isolated elliptical dots of CoB, magnetized in-plane, 1.5 nm thick and with lateral dimensions of 100 x 50, 200 x100 and 300 x150 nm^2, in presence of a sizeable interfacial DMI provided by a heavy-metal substrate. By micromagnetic simulations based on the GPU-accelerated software MuMax3, we show that the eigenmodes spectrum of the above mentioned nanostructures is appreciably modified by the DMI-induced non-reciprocity in spin-waves propagation: the frequencies of the eigenmodes are red-shifted and their spatial profiles appreciable altered due to the lack of stationary character in the direction orthogonal to the magnetization direction. As a consequence, one finds a modification of the expected cross-section of the different modes in either ferromagnetic resonance or Brillouin light scattering experiments, enabling one to detect modes that would remain invisible without DMI. This is illustrated in Fig. 1 where one can see that the number of visible modes and their spatial profiles appreciably evolve when the value of the DMI constant D is lifted from zero to 2 mJ/m^2. Moreover, if one further increases the value of D the fundamental eigenmode of the nanostructures becomes soft, reflecting the transition of the ground state from a uniform state to a chiral one. Finally, we discuss the possibility of using the above-mentioned modifications of the eigenmodes spectrum, to achieve a quantitative estimation of the DMI constant in nanostructured samples. Financial support from the EMPIR programme 17FUN08-TOPS, co-financed by the Participating States and from the European Union's Horizon 2020 research and innovation program, is kindly acknowledged.

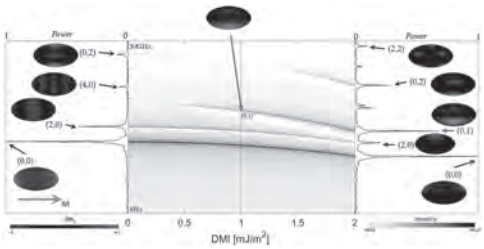

Evolution of the frequencies of the spin waves eigenmodes of a CoB elliptical dot of dimensions 100 nm x 50 nm x 1.5 nm as a function of the strength of the DMI constant D. The left and right panels show the eigenmode spectra at D=0 and D=2 mJ/m², respectively.

O7-03. Spin Wave Resonance Properties of Magnetic Squares With Different Aspect Ratios Based on $Co_{90}Fe_{10}$. *X. Ya*[1], K. Kurihara[1], T. Tanaka[1] and K. Matsuyama[1] *1. ISEE, Kyushu University, Fukuoka, Japan*

The geometrically confined standing spin wave resonance (SSWR) has attracted intense research interests as a fundamental physics and practical applications[1][2]. The magnetostatic surface wave (MSSW) mode has been reported owning large signal and long attenuation length[3]. In order to generate MSSW along the length direction of magnetic square, bias field or magnetic anisotropy field is required in the width direction to overcome the demagnetizing field. In this research, we deposited $Co_{90}Fe_{10}$ films containing 4-fold in plane anisotropy and studied SSWR properties of fabricated magnetic squares. 40-nm-thick $Co_{90}Fe_{10}$ film was deposited on MgO (001) substrate by sputtering method. The angular dependence of the squareness are plotted as fig. 1(a), which show 4-fold in plane anisotropy (an easy axis corresponds to MgO[011]) at 400°C. The corresponding XRD shown in Fig. 1(b) translates the film deposited at 400°C is well crystallized. The magnetic squares were fabricated by lithography techniques, where the lateral coordinates were defined to coincide with the anisotropy directions. 100-nm-thick SiO_2 layer was deposited on the squares and Grand-Signal-Grand coplanar waveguide (CPW) was fabricated on the SiO_2 layer (Fig. 2(a)). The dependence of SSWR frequency on H_b applied in the easy and the hard axes for different L were shown in Fig. 2(b) and (c). The SSWR frequencies discontinuously decrease with the decrease of H_b and multiple SSWR frequencies were observed when H_b is weak. Micromagnetic simulation explains the reason that the discontinuous change in SSWR frequency come from the change in the order of SSWR and different orders of SSWR coexist at weak H_b. In the case of H_b applied in the hard axis, the SSWR frequency decreases with decreasing H_b when H_b is stronger than the marked thresholds. However, when H_b is weaker than the thresholds, SSWR frequency increases with decrease in H_b, represent that the magnetization leans to the easy axis because of weak H_b.

[1] C. Mathieu, J. Jorzick, A. Frank, S. O. Demokritov, A. N. Slavin, and B.Hillebrands, Phys. Rev. Lett. 81, 3968 (1998). [2] Z. K. Wang, M. H. Kuok, S. C. Ng, D. L. Lockwood, M. G. Cottam, K.Nielsch, R. B. Wehrspohn, and U. Gosele, Phys. Rev. Lett. 89, 027201(2002). [3] K.-S. Lee and S.-K. Kim, J. Appl. Phys. 104, 053909 (2008).

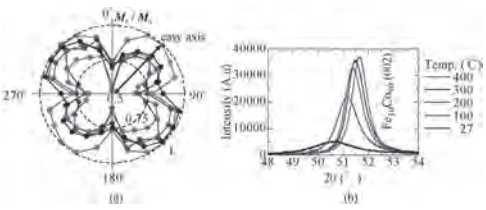

Fig. 1. (a) Squareness and (b) XRD diagrams for the film deposited at various temperature.

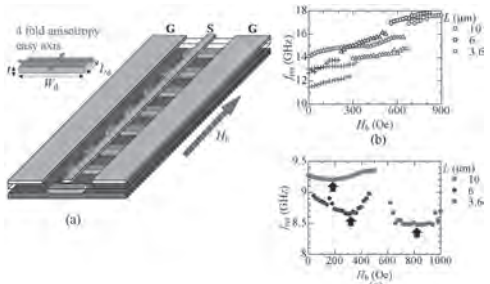

Fig. 2. (a)Schematic of a CPW on magnetic square, (b) dependence of resonance frequency on the magnetic field applied in the easy axis and (c) that in the hard axis.

O7-04. Withdrawn

O7-05. Spin Waves in Cylindrical Nanowires in the Vortex State. *D. Caso*[1], C. Bran[2], M. Vazquez[2], K.Y. Guslienko[3,4] and F.G. Aliev[1] *1. Condensed Matter Physics, Universidad Autonoma de Madrid, Madrid, Spain; 2. Instituto de Ciencia de Materiales de Madrid, ES, Madrid, Spain; 3. Material Physics, Universidad del Pais Vasco, Bilbao, Spain; 4. Ikerbasque, Bilbao, Spain*

Magnetic nanowires (NW, both single and in arrays) have recently received considerable attention due to their potential applications in magnetic storage technology. While their static magnetic properties have been well investigated, their magnetization dynamics have received less attention [1,2]. Due to their reduced dimensions, the possibility to control spin wave (SW) confinement and the possibility to couple to the magnetization textures with non-trivial topologies designates NWs as good candidates to next generation information technologies. Here we present experimental studies of broadband ferromagnetic resonance of hexagonally ordered arrays of Fe28Co63Cu10 NWs with 120 nm diameter, 300 nm lattice constant and about of 25-micron length. Microwave permeability investigated with DC and microwave fields perpendicular to the nanowire axis shows enhanced losses in the 1-4 GHz frequency range below 2 kOe. In order to understand this behavior, we have simulated SWs in a 1-5 micron long and 120nm diameter NW array. We observed the formation of a single vortex state in short NWs, broken for the NWs longer than 2 microns, where only vortices localized at the NW ends are visible. For 1-micron long NW the vortex state is formed in the perpendicular field range close to the one where the extra losses are detected experimentally. We have also carried out a detailed investigation of how the excited SW modes depend on the NW length, as well as its evolution as a function of the distance from the NW end and the product of vortex polarity and vortex chirality. Our simulations are able to distinguish between two different types of the SW modes: a lower frequency mode localized close to the NW ends and higher frequency delocalized modes, which are approximately described as plane waves with a finite pinning at the NW ends. The simulation results are in qualitative agreement with the analytical model based on the generalized Thiele equation for the vortex core string. The model accounts for the exchange and non-local magnetostatic interactions.

[1] C. Bran, E. Berganza, J.A. Fernandez-Roldan, ACS Nano., Vol. 12, p.5932−5939 (2018) [2] J.A. Fernandez-Roldan, R.P. del Real, C. Bran, Nanoscale., Vol. 10, p.5923-5927 (2018)

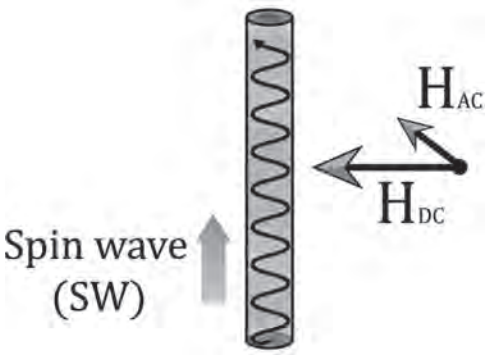

Fig. 1. Sketch of a cylindrical NW with DC and AC magnetic fields applied in the transverse direction.

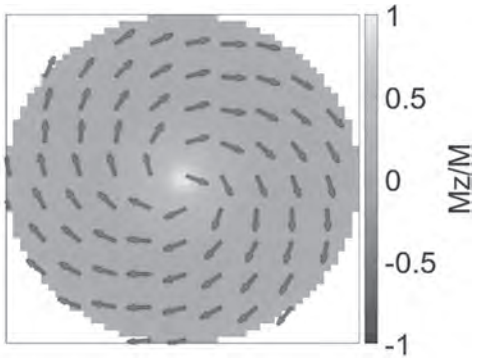

Fig. 2. Magnetization distribution at the ends of the NW showing a vortex state.

O7-06. Terahertz Magnonics in 2D Chromium Trihalides With Atomically-Engineered Dzyaloshinskii–Moriya Interaction.
R.M. de Menezes[1,2], D. Sabani[1], C. Bacaksiz[1], C. de Souza Silva[2] and M.V. Milošević[1] *1. Physics, Universiteit Antwerpen, Antwerpen, Belgium; 2. Physics, Universidade Federal de Pernambuco, Recife, Brazil*

Two-dimensional (2D) magnetic materials, such as chromium trihalides and manganese dichalcogenides, have recently drawn immense attention of both theoretical and experimental research, due to both fundamental significance and promising technological applications. Particularly, some chromium trihalides have been shown able to host terahertz spin-waves (SW) [1] and are promising candidates for ultra-fast information transport and processing based on magnons. In this work we investigated the spin-wave propagation in the presence of strategically-placed defects (halide vacancies) in the honeycomb structure of chromium trihalides. We performed Density Functional Theory (DFT) calculations to obtain the magnetic parameters of the considered structures, followed by spin-dynamics simulations of the SW propagation. We reveal that the lattice defects host strong Dzyaloshinskii–Moriya interaction (DMI), so that a designed pattern of defects can serve as a spin-wave guide. We show the spectra of spin-waves propagating across periodic defect lines that prove such structures can work as a magnonic crystal [2] for terahertz SWs, exhibiting key features such as band gaps where SWs are not allowed to propagate. Such broad degree of manipulations available in 2D materials therefore suggests these systems as a front-runner for terahertz magnonics, applicable in cutting-edge devices.

[1] W. Jin, H. Kim, Z. Ye, et al. Nature communications, 9, 5122 (2018). [2] A. V. Chumak, A. A. Serga, and B. Hillebrands. Journal of Physics D: Applied Physics, 50, 244001 (2017).

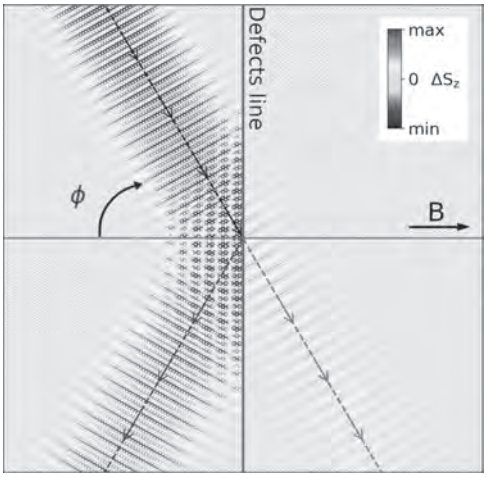

Fig.1 Example (snapshot) of spin-wave reflection by a line of vacancies in $CrBr_3$.

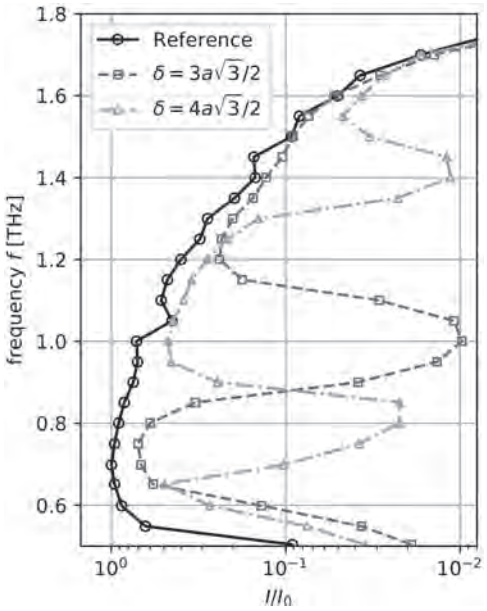

Fig.2 Normalized spin-wave transmission spectra for the magnonic crystal created by defect lines in $CrBr_3$, for two different separations δ between the lines, in comparison with the reference wave guide.

O7-07. Strain-Induced Spin-Wave Transport in 3D Magnonic Structures Based on YIG/PZT and YIG/GaAs Multilayers.
A. Sadovnikov[1], E. Beginin[1], A. Grachev[1], S. Sheshukova[1], A. Stognij[3] and S. Nikitov[1,2] *1. nonlinear physics, Saratovskij nacional'nyj issledovatel'skij gosudarstvennyj universitet imeni N G Cernysevskogo, Saratov, Russian Federation; 2. FGBUN Institut radiotehniki i elektroniki imeni V A Kotel'nikova Rossijskoj akademii nauk, Moskva, Russian Federation; 3. NPC Belarus Material science, Minsk, Belarus*

The progress in modern information technologies induced a lot of research directed towards the use of spin waves(SWs) in ferromagnetic and antiferromagnetic films for signal processing at microwave and terahertz frequencies. The most intriguing feature of SWs is the possibility to carry the information signal without the transmission of a charge current [1,2,3]. Recent theoretical and experimental studies suggest that strain can be used to engineer energy-efficient complicated 2D and 3D piezoelectric material and heterostructures [3,4]. The combination of strain tuning and SW coupling can underlie a new branch of magnonics -- magnon straintronics [5-7]. Here we demonstrate the voltage-driven and laser induced nonreciprocity of spin

waves in the ferromagnetic-semiconductor and ferromagnetic-piezoelectric structure. Surface SWs in yttrium iron garnet (YIG) film grown at the top of n-type gallium arsenide (GaAs) and periodically etched PZT (lead zirconate titanate) substrate were studied by means of Brillouin light-scattering (BLS) spectroscopy. We demonstrate the experimental observations of the strain-mediated SW coupling phenomena in the asymmetric adjacent magnonic crystals, adjacent magnetic array of YIG stripes, which demonstrates the collective spin-wave phenomena[8]. The voltage-controlled spin-wave transport along bilateral magnonic stripes (BMSs) was demonstrated (Fig.1). BMSs distinguish itself as an ideal platform for magnonics in three key aspects: (i) dual tunability with both the magnetic and electric field; (ii) it supports large SW propagation distances, which is appropriate for interference of SW in magnonic logic applications; (iii) it is versatile magnonic component with the voltage-controlled frequency-selective characteristics. We also show that the spin-wave dispersion can be modified in a controlled manner by illumination of the semiconductor substrate with the infrared laser radiation (Fig.2). This may be the first experimental step in integrated semiconductor magnonics on the base of YIG/GaAs structures. This work was supported by the grant of Russian Science Foundation (# 20-79-10191).

1. V. V. Kruglyak, S. O. Demokritov, and D. Grundler, J. Phys. D 43, p. 264001 (2010). 2. D. Sander, S.O. Valenzuela, D. Makarov et al, J. of Phys.D: Appl. Phys. Vol. 50, p. 363001 (2017) 3. A. V. Chumak, et.al. Nat. Phys. 11, p. 453 (2015). 4. Y. K. Fetisov and G. Srinivasan, Appl. Phys. Lett. 88, p. 143503 (2006). 5. A. V. Sadovnikov, Phys. Rev. Lett. 120, p. 257203 (2018) 6. A. V. Sadovnikov, et. al., Phys. Rev. B 99, p. 054424 (2019). 7. A. V. Sadovnikov et. al. IEEE Magnetics Letters. Vol. 10. 5506405 (2019) 8. A.V. Sadovnikov, A.A. Grachev, V.A. Gubanov, et al Appl. Phys. Lett. 112, 142402 (2018).

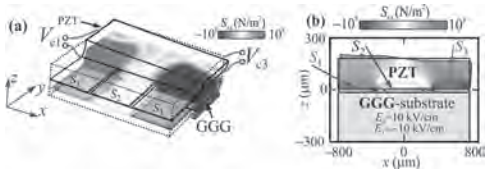

Magnonic bilateral structure (a) and strain profile (b)

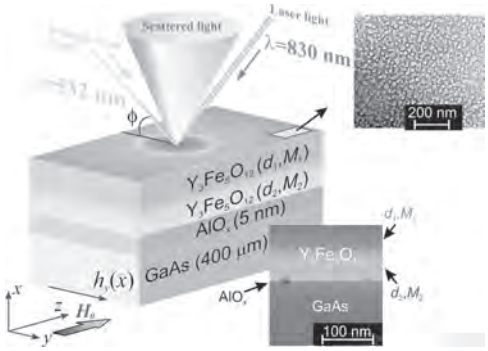

YIG/GaAs structure and scheme of BLS experiment

O7-08. Non-Reciprocal Spin Wave Propagation in Magnetic Bilayer Structures. *O. Gladii*[1], R. Salikhov[1], O. Hellwig[1,2], J. Lindner[1] and H. Schultheiss[1] *1. Institute of Ion Beam Physics and Materials Research, Helmholtz-Zentrum Dresden-Rossendorf, Dresden, Germany; 2. Physics, Technische Universitat Chemnitz, Chemnitz, Germany*

One of the peculiar features of spin waves is their non-reciprocal dispersion relation, meaning the modification of the transport characteristics of spin waves upon reversal of their propagation direction. The non-reciprocity of Magnetostatic Surface Spin Waves (MSSW) can be caused by various factors, such as surface anisotropy [1], interfacial Dzyaloshinskii-Moriya interaction [2] or inhomogeneous saturation magnetization across the film thickness [3]. Recently, it has been shown that a strong non-reciprocal propagation can be induced by the dynamic dipole-dipole interaction between two magnetic layers in spin-valve-like structures, for which the relative magnetization orientation in remanence is stabilized in antiparallel configuration [4]. In the present work we investigate the frequency non-reciprocity in ferromagnetic bilayer systems, where a nonmagnetic thin Ru interlayer is used to achieve antiferromagnetic alignment at zero field. Using conventional Brillouin light scattering, we perform systematic measurements of the frequency non-reciprocity as a function of an external magnetic field. As expected [4], for antiparallel alignment of the magnetic moments in the two layers we observe a large frequency non-reciprocity up to a few GHz, which vanishes when the relative magnetization orientation switches to the parallel configuration. Moreover, a non-monotonous dependence of the frequency non-reciprocity is found in the transition from the antiparallel to the parallel orientation, where the maximum of the frequency shift corresponds to the spin-flop phase. By varying the parameters of the bilayer structures, the non-reciprocal propagation at the spin-flop transition is studied. We demonstrate that by adjusting the strength of the exchange coupling between the two ferromagnetic layers via the appropriate choice of the stack parameters, one can precisely control the non-reciprocal propagation of spin waves via the field-driven magnetization reorientation.

[1] O. Gladii et al., Phys. Rev. B 93, 054430 (2016) [2] H. Nembach et al., Nature Phys 11, 825 (2015) [3] R. A. Gallardo et al, New J. Phys. 21, 033026 (2019) [4] R. A. Gallardo et al., Phys. Rev. Appl. 12, 034012 (2019)

O7-09. Spin Wave Spectral Probing of Possible Micro-States in Building Block of Macroscopically Degenerate Artificial Spin Ice. *N. Arora*[1] and P. Das[1] *1. Department of Physics, Indian Institute of Technology Delhi, New Delhi, India*

Square Artificial Spin Ices (S-ASI)[1-3] are the 2-dimensional realization of the standard 3-dimensional spin ice material of the type $Dy_2Ti_2O_7$ (pyrochlore compound), with the alluring possibility of studying geometric frustration in a controlled way. In addition to the frustration, these kinds of structures enable the investigation of a variety of fascinating phenomena such as frustration, emergent magnetic monopoles, collective magnetization dynamics of interacting spins, and phase transition, etc. Recently, there is a focus on the understanding of dynamical behavior of spins or spin wave (sw) modes in such dipolar coupled systems. Detailed understanding of such behavior may be of importance to the applications in magnonics[4,5]. Here, we have investigated the sw modes of strongly dipolar coupled, highly anisotropic nanoislands forming S-ASI system using micro-magnetic simulation in MUMAX3 in combination with MATLAB coding. For the same, we have systematically scrutinized the sw spectra of the building block of S-ASI which is a square ring-like structure of highly shape anisotropic nanoislands of permalloy[6,7]. The evolution of the spectra as a function of no. of rings of up to four rings forming a S-ASI with closed edges exhibit a direct relation between the sw modes and the micro-states of the system. The study reveals that a single ring-type structure can alone be adequately used to understand the sw modes of S-ASI as well as it's behavior in the presence of an external bias field. All the ring-type structures studied show ubiquitous switching identifier mode at approximately 14 GHz. Detailed analysis of the spin wave propagation modes in the building block as well as individual vertices of S-ASI structure will be discussed in this work.

[1] P.W. Anderson, Phys. Rev., Vol. 102, p.1008 (1956). [2] C. Castelnovo *et al.,* Nature, Vol. 451, p.42–45 (2008). [3] L. Balents, Nature Vol. 464, p.199–208 (2010). [4] E. Iacocca *et al.,* Phys. Rev. B, Vol. 93, p.134420 (2016). [5] S. Mamica *et al.,* Adv. Cond. Matter Phys., Vol. 2012 (2012). [6] N. Keswani and P. Das, AIP Adv., Vol. 8, p.101501 (2018). [7] N. Keswani *et al.,* Appl. Phys. Lett., Vol 116, p. 102401 (2020).

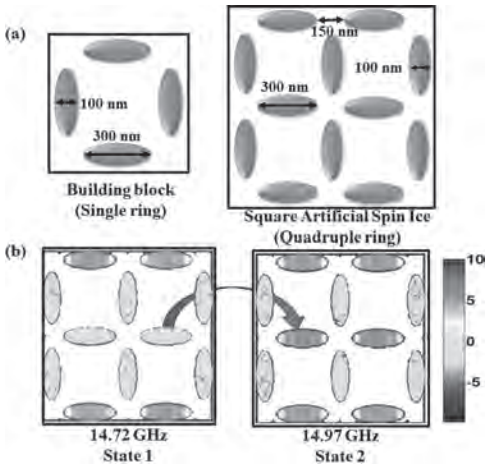

Figure 1: (a) Schematic representation of the single ring and S-ASI (b) Spectral probing of magnetization switching at the vertex represented via power amplitude profile.

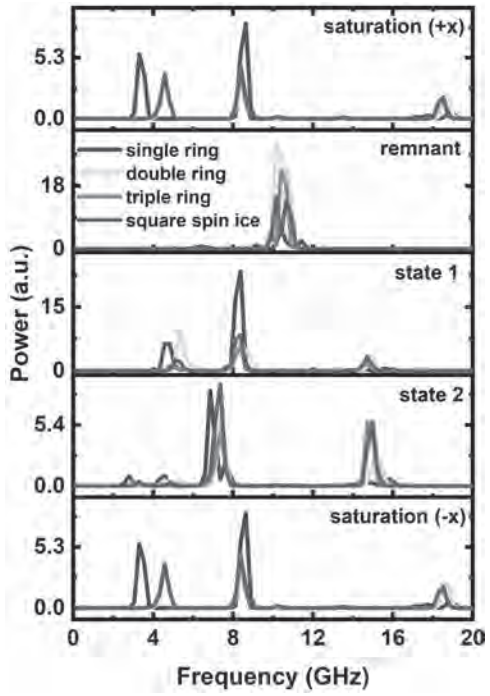

Figure 2: Spin wave mode spectra of the ring-type structures at the evolved microstates during the external bias field sweep in the range of ± 300 mT. Here, states 1 and 2 correspond to the micromagnetic configuration after first and second switching.

O7-10. The Formation of Waveguide Channels for Spin Waves in a Three-Dimensional Magnon Network Based on Multilayer Magnonic Crystall Arrays. *S. Odintsov*[1], S. Sheshukova[1], S. Nikitov[2] and A. Sadovnikov[1] *1. Saratovskij nacional'nyj issledovatel'skij gosudarstvennyj universitet imeni N G Cernysevskogo, Saratov, Russian Federation; 2. FGBUN Institut radiotehniki i elektroniki imeni V A Kotel'nikova Rossijskoj akademii nauk, Moscow, Russian Federation*

Recently, of great interest is the study of spin-wave transport in yttrium iron garnet (YIG) films with a thickness of 20 nm to 10 μm in the gigahertz and sub-gigahertz frequencies[1,2].The control of lateral spin-wave transport is the basis for the functioning of such elements of magnon networks as spin-wave couplers which allow spatial-frequency signal selection[3]. The creation of systems with spatial-frequency selection of the spin-wave signal in three-dimensional topologies of magnon networks will increase the density of magnon elements and compensate for the damping effect in the lateral directions by transmitting the signal between different layers of the three-dimensional structure. Figure 1 shows a schematic view of the structure under study based on two films of yttrium iron garnet (YIG), on a gallium gadolinium garnet (GGG) substrate, separated by a gap of g in the direction of the z axis. A system of waveguides (S_1,S_2, S_3 and S_4) of equal width $w = 200$ μm, S_1 and S_2 are oriented parallel to each other, S_3 and S_4 are formed from the YIG film is placed above them. The thickness of YIG films was $t = 10$ μm. The length of the coupled region is $L = 4$ mm. This work presents the results of a study of the propagation of spin waves in the three-dimensional topology of a magnon network formed by a magnetized magnonic crystall structure. Using Mandelstam-Brillouin spectroscopy with layer-by-layer visualization of the stationary spatial distribution of dynamic magnetization, the possibility of transmitting the angular torsion moment in the lateral and vertical directions and spatial-frequency selection of the spin-wave signal is demonstrated. Using the micromagnetic simulation, the features of the formation of collimated spin-wave beams based on the obtained dispersion characteristics and mode decomposition of a signal propagating at the band gap frequencies of studied structure are revealed. It is shown that the proposed structure can be used as an element for spatial-frequency selection of a microwave signal in three-dimensional topologies of magnon networks. This work was supported by RFBR (19-37-90079, 18-29-27026)

1. P. A. Grünberg, "Nobel lecture: From spin waves to giant magnetoresistance and beyond," Rev. Mod. Phys., vol. 80, pp. 1531–1540 (2008) 2. V. V. Kruglyak, S. O. Demokritov, and D. Grundler J.Phys. D: Appl. Phys., vol. 43, p. 264001 (2010). 3. S. A. Odintsov, A. V. Sadovnikov, and A. A. Grachev, JETP Letters, vol. 104, pp. 563–567 (2017)

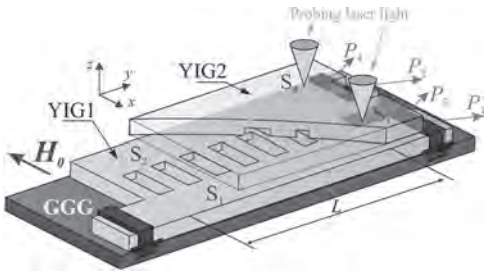

Schematic representation of structure under study

O7-11. Strain-Tuned Reconfigurable Spin-Wave Transport in Magnonic Crystal/Piezoelectric Structure. *A. Grachev*[1], E. Beginin[1] and A. Sadovnikov[1] *1. Saratov State University, Saratov, Russian Federation*

A promising area for overcoming the limitations of semiconductor technologies may be straintronics, a new area in condensed matter physics which use an elastic strains and physical effects induced by mechanical deformations in ferromagnetic structures to implement a new generation of information, sensor, and energy-efficient technologies [1]. Ferrite films of yttrium iron garnet (YIG), exhibiting record low damping values of spin waves (SW), are used as medias suitable for these purposes. Recent theoretical and experimental studies show that deformation can be used to create energy-efficient complex two-dimensional and three-dimensional piezoelectric materials and heterostructures based on semiconductors [2], ferroelectrics [3], piezoelectric crystals or ceramics [4] It was also shown that it is possible to induce a frequency shift of the ferromagnetic resonance due to the influence of the conversion of the electric field to the magnetic field [5]. Here, we report the effect of electrical field control of the SW spectra in magnonic crystal (MC) with piezoelectric layer. Using numerical sumulations and experimental techniques, we revealed the mechanisms of guiding of SWs by elastic strains localized in the region of maximums of the electric field. It is possible to effectively control the properties of the propagating spin waves and the spatial distribution of the dynamic magnetization intensity in the multilayered structure. A sketch of the tested device is shown in Fig. 1. The width of

the MC was 200 μm. MC was fabricated from the monocrystalline ferromagnetic 10 μm-thick YIG film with a saturation magnetization of M_s = 139 G on 500 μm-thick gallium gadolinium garnet substrate. The length of the groove in the x-direction was 100 μm. 1 μm-thick titanium electrode is placed on the upper surface of the piezoelectric ceramic layer of lead zirconate titanate (PZT) with dimensions 500 x 3000 x 200 μm^3, which does not have a significant effect on the propagation of SW in MC. The calculations were supported by Russian Foundation for Basic Research (# 19-37-90145, #18-29-27026), the fabrication of the multiferroic structure was supported by Russian Science Foundation (# 20-79-10191).

A.V. Sadovnikov et. al. Phys. Rev. Letters, Vol. 120, p. 257203 (2018). A.A. Shevyrin et. al. Phys. Rev. Lett. Vol. 117, p. 017702 (2016). S. Liu and R. E. Cohen, Phys. Rev. Lett. Vol. 119, p.207601 (2017). A.V. Sadovnikov et. al. IEEE Magnetics Letters, Vol. 10, p. 1-4, (2019). Y. K. Fetisov and G. Srinivasan, Appl. Phys. Lett. Vol. 93, p. 033508 (2008).

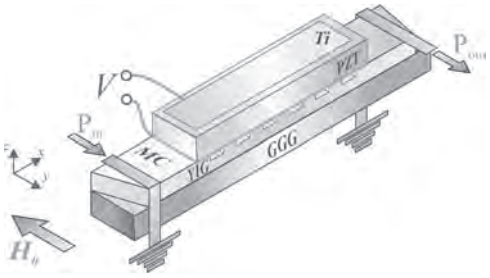

Scheme of the considered structure.

O7-12. The Edge Effect on the Magnetic Skyrmion Motion Driving by Spin Wave. *T. Huang*[1], K. Wu[1], Y. Lin[1], W. Peng[1], P. Chen[1] and M. Chen[1]
1. National Applied Research Laboratories, Hsinchu, Taiwan

The edge roughness and shape of the magnetic structure may scatter and reflect the spin waves during the spin waves propagate in a magnetic medium. The edge roughness and shape of the magnetic structure may also affect the magnetic skyrmion motion, while spin waves drive the magnetic skyrmion movement. Therefore, this study aims to explore the boundary influence on the magnetic skyrmion motion driving by spin wave. The magnetic nanostructure utilizes a vertically anisotropic Pt/Co thin film as the material. Figure 1(a) is a schematic diagram of the nanostructure. A pulsed spin-polarized current is injected at the quarter position of the magnetic ribbon to produce a magnetic skyrmion. It is important for a good reliability of magnetic storage medium, we wait 10 ns to let the skyrmion reaches a steady motion. Figure 1(b) shows the dimensions of magnetic skyrmions with different widths and thicknesses. The diameters of the magnetic skyrmions vary with the widths of the structures. The thickness of the structure does not change significantly. Figure 2 shows the relationship between the notch width of the magnetic ribbon and the position of the magnetic skyrmion after 10 ns later. The velocities of magnetic skyrmion motions significantly reduced as the notch widths become longer.

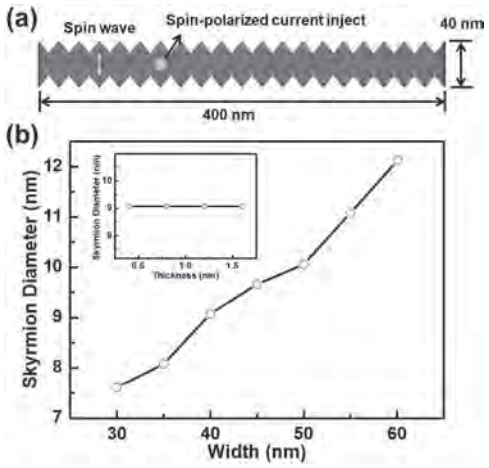

Fig. 1. (a) The schematic diagram of the magnetic structure. (b) The sizes of magnetic skyrmions in different structural widths. The inserted figure is the sizes of magnetic skyrmions in different thicknesses.

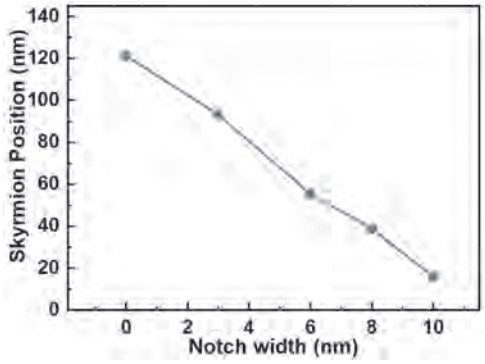

Fig. 2. The relationship between the notch width and the position of the magnetic skyrmions. The spin wave amplitude is 2.5k Gauss and the frequency is 100 GHz. The position of the magnetic skyrmions are measured after 10 ns.

O7-13. Interferometric Properties in Standing Spin Wave Resonance of $Co_{90}Fe_{10}$ and the Application as an Integrated Phase Comparator. *X. Ya*[1], K. Kurihara[1], T. Tanaka[1] and K. Matsuyama[1] *1. ISEE, Kyushu University, Fukuoka, Japan*

Standing spin waves (SSWs) have been attracting intense research interest[1] [2]. The SSW resonance (SSWR) is one of the most power efficient excitation mode and various aspects as magnetic quanta have been reported[3]. In this study, we experimentally study the SSWR properties in a magnetic strip and demonstrate the practical application as an integrated phase comparator. 40-nm-thick $Co_{90}Fe_{10}$ film containing 4-fold in plane anisotropy is deposited on MgO (001) at 400°C. The magnetic strip is fabricated by lithography techniques, where the lateral coordinates are defined to coincide with the anisotropy directions. 100-nm-thick SiO_2 layer is deposited on the strip and two spin wave generators, G_A and G_B, and a hairpin shape inductive output voltage detector(DE) are fabricated on the SiO_2 layer (Fig. 1(a)). The S_{21} is measured by VNA at H_b ranged from 800 Oe to -800 Oe. Fig. 1 (b) shows the dependence of SSWR frequency on H_b in the case of the phase lag between G_A to G_B is 0. The SSWR frequency continuously decreases with the decrease of H_b from 800 Oe to -110 Oe, while the resonance frequency abruptly jumps up to 12 GHz due to the magnetization reversal at H_b = -110 Oe. The SSWR at zero bias is 10.5 GHz, which is higher than Py and YIG films. The normalized output voltage intensity are shown in Figs. 2 as a function of the phase lags at 2 different frequencies when H_b = 400 Oe. At 13.5 GHz, the induced output voltage becomes the maximum when the phase lag is 0, while becomes the minimum when the phase lag is p. Micromagnetic

simulation explain that the high output voltage comes from the 9th order of SSWR. The relation between the output voltage and the phase lag reverses at 15.6 GHz, and the same results are observed at different H_b from 600 to 0 Oe. These results experimentally demonstrates SSW application as an integrated phase comparator, and the demonstrated operations are also available as logic functions.

[1] T. Schneider, A. A. Serga, B. Leven, and B. Hillebrands, Appl. Phys. Lett., vol. 92, pp. 022505-1-3 (2008). [2] X. Ya, H. Chen, S. Oyabu, B. Peng, H. Otsuki, T. Tanaka, and K. Matsuyama, J. Appl. Phys., vol. 117, pp. 17A719-1-3 (2015). [3]C. Mathieu, J. Jorzick, A. Frank, S. O. Demokritov, A. N. Slavin and B. Hillebrands, Phys. Rev. Lett., 81, 3968 (1998).

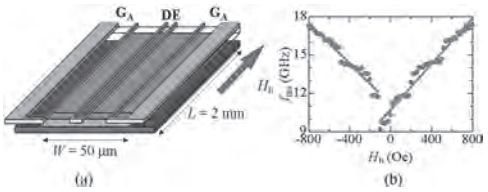

Fig. 1. (a) Schematic of a designed phase comparator, (b) The dependence of SSWR on H_b.

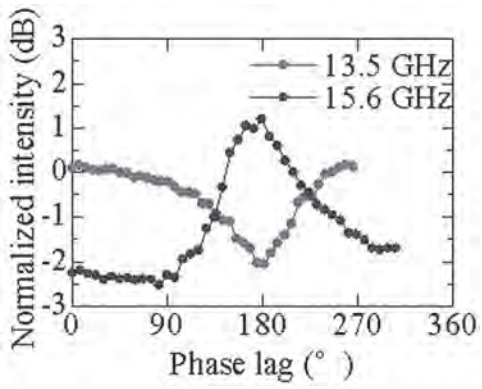

Fig. 2 The dependences of normalized output voltage intensity on phase lag.

O7-14. Compressed Sensing for Time- and Space-Resolved Spin-Wave Propagation. *R. Kainuma*[1], K. Matsumoto[1,2] and T. Satoh[1] *1. Department of Physics, Tokyo Institute of Technology, Meguro-ku, Japan; 2. Department of Physics, Kyushu University, Fukuoka, Japan*

Spin-waves (magnons) in insulators are desirable information career because it can transport through crystals avoiding Joule heating. Recent studies have achieved all-optical magnon excitation and detection using pump-probe magneto-optical imaging techniques [1, 2], and ultrafast magnetic dynamics have been investigated. Experiments with a high-frequency resolution are needed to study the dynamics in detail. To perform the well-known Fourier analysis, a large number of equally spaced samplings in the time domain must be performed. However, we found a possibility to extract information on all modes of the spin-wave from a small number of samples by applying compressed sensing, which is an achievement of computer science [3]. In this study, a technique for adding a compressed sensing technique to the time-resolved pump-probe imaging method was investigated. We used micromagnetic simulations (MuMax3) [4] to mimic the data of spatiotemporal waveform of spin-wave which is excited in a ferromagnetic thin film with uniaxial anisotropy in the perpendicular direction. Such spin-wave has already been well known as backward volume magnetostatic wave and its dispersion relation has been studied. The simulated spatiotemporal waveform was randomly sampled in the temporal direction to create irregularly deficient waveform as shown in Fig.1. To analyze this missing waveform, we applied the least absolute shrinkage and selection operator (LASSO), and, as a result, we were able to estimate a dispersion relation with sufficient frequency resolution. As shown in Fig.2, the results were in good agreement with theoretical curve. This result indicates that we can reduce the number of samples required for the time-resolved pump-probe imaging method. From another point of view, it would be possible to perform experiments with the same measurement time and even higher frequency resolution.

T. Satoh et al., Nat. Photonics 6, 662 (2012). Y. Hashimoto et al., Nat. Commun. 8, 15859 (2017). E. J. Candès and T. Tao, IEEE Trans. Inf. Theory 52, 5406 (2006). A. Vansteenkiste et al., AIP Adv. 4, 107133 (2014).

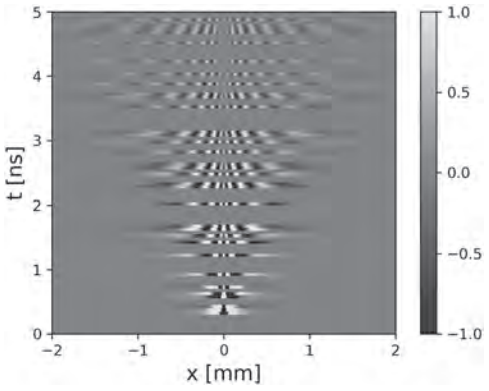

A part of the irregularly deficient waveform. The waveform was made up to 50 ns, but a range of up to 5 ns is drawn.

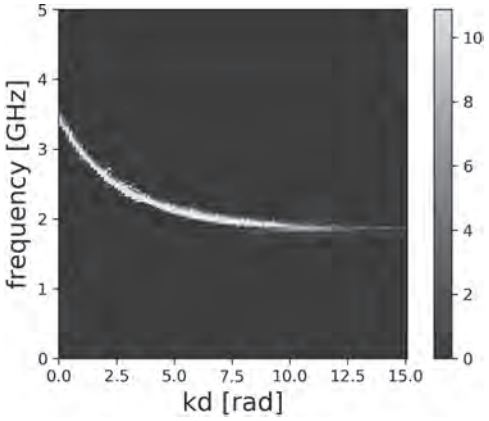

Dispersion relation estimated with LASSO and theoretical curve (red dashed line). The horizontal axis represents the wavenumber of magnons multiplied by the thickness of the film.

O7-15. Modification of Magnon Threshold and Characteristics Using a Secondary Signal and Phase Noise. *A. Venugopal*[1] and R. Victora[1] *1. Department of Electrical Engineering and Computer Science, University of Minnesota, Minneapolis, MN, United States*

Non-linear parametric excitation phenomena of magnons, with their interesting properties, can be utilized to realize magnonic devices for futuristic computation [1,2] and processing of microwave signals [3]. However, for robust device-design, much more remains to be understood regarding the effects of noise on magnons. The modification of the parametric resonance effects, in the presence of an additional signal, is a problem of both theoretical as well as practical interest. We use micromagnetics to model an yttrium iron garnet film of dimensions 5.1 μm x 100 μm x 1250 μm, employing 128x128x1 cells. A parallel-pumping configuration that scatters magnons largely in a plane perpendicular to the bias-field is used, allowing the use of a 2D simulation paradigm [3]. Saturation magnetization of 145 emu/cm^3, exchange constant 3.77e-7 ergs/cm, and intrinsic-damping 0.0007 along with 2D periodic boundary conditions and thermal-fields (300 K) are used. A bias field of 200 Oe and a primary frequency of 6 GHz are used. The secondary signal is polarized parallel to the bias-field. Introduction of a secondary signal is found to limit the non-linearity by increasing the threshold-field. This effect, as shown in Fig. 1, is found to dominate at a frequency that

corresponds to the relaxation rate of the longitudinal magnetization. Oscillatory behavior of the threshold with secondary frequency is noticeable especially for higher frequencies. These features have been explained analytically and are physically brought about by the modification of the relative phase of the magnons with respect to the microwave photons. The magnon modes that are dominant differ from the original 3 GHz modes by integer multiples of alf the secondary frequency. The variation in the number of such modes w.r.t secondary frequency is also studied. We also examine phase noise and find that it affects the magnon instability by reducing the non-linearity and growth rate of magnons as shown in Fig. 2.

1. A. Chumak, A. Serga, B. Hillebrands, *Nat. Comm.* 5, 4700, 2014. 2. A. Khitun, M. Bao, K. L. Wang, *J. Phys. D: Appl. Phys.* 43, 264005, 2010. 3. A. Venugopal, T. Qu and R. H. Victora, *IEEE Trans. Microw. Theory and Techn*., vol. 68, no. 2, pp. 602-610, Feb. 2020.

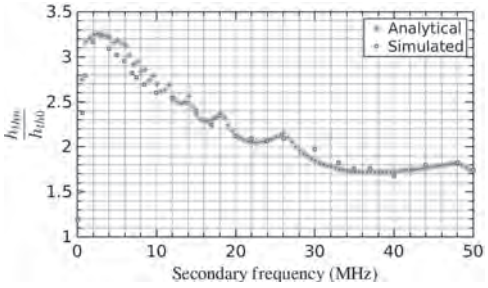

Fig. 1. Threshold field, h_{thn}, with secondary (h_{th0} : without) w.r.t primary signal of 6 GHz is determined as the secondary signal frequency is varied.

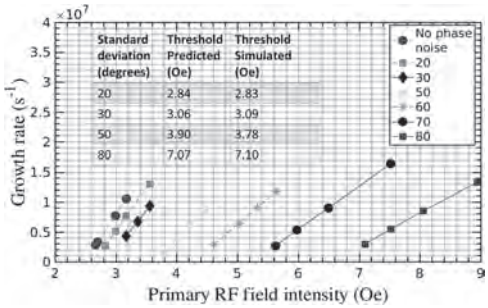

Fig. 2. Increase in standard-deviation of noise increases the threshold and reduces the growth rate of magnons.

O7-16. Sub-GHz Resonant Magnetoelastic Coupling in Epitaxial Fe Thin Films. J. Duquesne[1], *P. Rovillain*[1], C. Hepburn[1], M. Eddrief[1], P. Atkinson[1], A. Anane[2] and M. Marangolo[1] *1. Institut des NanoSciences de Paris, Sorbonne Université, CNRS, UMR7588, F-75005 Paris, France, Paris, France; 2. Unité Mixte de Physique CNRS, Thales, Université Paris-Saclay, F-91767 Palaiseau, France, Palaiseau, France*

New fascinating phenomena involving coupled spin waves and phonons are observed at the magneto-elastic resonance: magnetic field dependent spin Seebeck effect [1], acoustically-assisted spin pumping [2, 3] and magnetization swiching [4, 5]. In this context, it has been shown that an efficient mean to excite phonons is by surface acoustic waves (SAW). The integration of SAW-FMR (ferromagnetic resonance) mechanism in spintronic and magnonic devices are claimed to operate with very low power. However, most ferromagnetic materials have precession frequencies well above 5 GHz, i.e. above the highest frequency reached by today's SAW technologies. This restricts the research on SAW-FMR to low magnetization and/or low magnetic anisotropy materials, such as (Ga,Mn)As or (GaMn)(As,P), Ni, and YIG. Here, we show that thin films of Fe epitaxially grown on GaAs(001), a spintronic and magnonic compatible magnetoelastic and piezoelectric heterostucture, give the opportunity to obtain SAW-FMR, at room temperature, below 1 GHz despite the high Fe magnetization. This is obtained by exploiting the softening of the magnetic stiffness when the field is applied along a hard axis, at moderate intensity (60 mT). Slight variations of the magnetic field direction, less than 0.1 deg off, increase dramatically magnetization precession frequency leading to off-resonance interaction and suppressing SAW attenuation. The observed phenomena are described by adopting a very simple magnetization dynamics model that catches the physics of the interaction. The observation of resonant, low frequency and highly directional magnetoelastic coupling in Fe suggests that SAW mature technology offers the opportunity to magnonics and spintronics to handle magnetization precession in a remote way, without using any dissipative electron current. [6]

[1] Takashi Kikkawa, et al., Phys. Rev. Lett. 117, 207203, (2016) [2] M. Weiler, et al. Phys. Rev. Lett. 108, 176601, (2012) [3] Ken ichi Uchida, et al., Solid State Communications 198, 26, (2014) [4] L. Thevenard, et al. Phys. Rev. B 93, 134430, (2016) [5] P. Kuszewski, et al. Journal of Physics: Condensed Matter 30, 244003 (2018) [6] J.-Y. Duquesne, P. Rovillain, et al. *Phys. Rev. Appl.* 12, 024042 (2019)

Session P1
BIOMEDICAL APPLICATIONS III - IMAGING AND DIAGNOSTIC SENSING

Pilar Marin, Co-Chair
Universidad Complutense de Madrid, Madrid, Spain
Jonathan Leliaert, Co-Chair
Ghent University, Ghent, Belgium

INVITED PAPER

P1-01. Controlling Exotic Molecular Spins Toward Next-Generation MRI Probes. *J. Zadrozny*[1], T. Ozvat[1], A. Campanella[1], M. Broussard[1] and M. Mignard[1] *1. Chemistry, Colorado State University, Fort Collins, CO, United States*

Proton magnetic resonance imaging (^{1}H-MRI) is one of the most powerful noninvasive biomedical imaging techniques to date. Conventional ^{1}H-MRI can deliver pictures of exquisite anatomical detail, which is revolutionary in terms of its window into the body. A clear next step would be the delivery of novel MRI methods and molecular imaging probes to enable a window into the physiological chemistry of the body. The chemistry of the body governs nearly all function and dysfunction. Hence, the ability to noninvasively detect said chemistry would revolutionize diagnostic possibilities. We will present two efforts in our lab to develop novel molecular probes for chemical sensitivity. Notably, our efforts focus on magnetic species that are relatively exotic to the commonly used Gd^{3+} contrast agents: Cobalt-59 nuclear spins and high-spin metal ions (Fig. 1). Our first effort is directed at understanding the temperature-sensitivity of the Cobalt-59 nuclear magnetic resonance (NMR) signal in highly stable Co(III) complexes. Molecules containing the Cobalt-59 nucleus were recognized in 1980 as effective NMR thermometers owing to a highly sensitive chemical shift.[1] Indeed, the chemical shifts for Cobalt-59-containing molecules exhibit two orders of magnitude higher sensitivities (on the order of 1-3 ppm/°C) than traditional ^{1}H signals (0.01 ppm/°C).[2] If translated into an applicable chemical probe, Cobalt-59 NMR probes could thus facilitate novel imaging techniques for, e.g., monitoring thermal ablation of tumors[3] or thermal drug delivery.[4] Yet, the exact design parameters to deliver molecular ^{59}Co thermometers with even higher sensitivity (for higher-resolution imaging) are lacking. We will present novel results from our efforts to understand and control temperature sensitivity by molecular design.[5,6] A second effort in our group to be presented is developing metal complexes for an imaging scheme that uses the electron analog of nuclear magnetic resonance: electron paramagnetic resonance imaging (EPRI). EPRI is capable of delivering local chemical information, including pH and oxygen content.[7] Given the inherent tunability of the chemical properties of unpaired electrons, the potential exists for far more areas of chemical sensitivity relative to nuclei. Hence, merging EPRI with the anatomical detail of ^{1}H-MRI could provide revolutionary new imaging techniques. A key challenge to doing so, however, is the fact that conventional EPRI molecular imaging probes (organic radicals) would use high-frequency microwaves for function in a typical 1.5 T MRI scanner. High-frequency microwaves are absorbed by water, which would heat and injure tissue. Molecules containing high-spin metal ions, owing to a unique electronic feature called zero-field splitting, may surmount this challenge. However, to fully realize this potential, significant insight is necessary in controlling the properties of metal ions under the action of low-frequency microwaves. In the second part of the presentation, we will touch on our efforts in this area.

[1] G. C. Levy, T. J. Bailey and D. A. Wright, J. Magn. Reson. Vol. 37, p. 353–356 (1980). [2] J. C. Hindman, J. Chem. Phys. Vol. 44, p. 4582–4592 (1966). [3] M. Ahmed, L. Solbiati and C. L. Brace et al., J. Vasc. Interv. Radiol. Vol. 25, p. 1691-1705.e4 (2014). [4] N. Hijnen, N.; S. Langereis and H. Grüll, Adv. Drug Deliv. Rev. Vol. 72, p. 65–81 (2014). [5] T. M. Ozvat, M. E. Peña and J. M. Zadrozny, Chem. Sci. Vol. 10, p. 6727–6734 (2019). [6] T. M. Ozvat, G. E. Sterbinsky and A. J. Campanella et al., Dalton Trans. Advance Article [DOI: 10.1039/D0DT01391A] (2020). [7] *In Vivo EPR (ESR)*; L. J. Berliner, Ed.; Springer US: Boston, MA (2003).

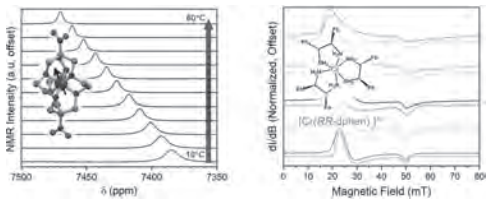

Fig. 1. In this presentation, we will present two different efforts in our group to produce novel MR imaging probes of local chemical environments. Left: variable-temperature Cobalt-59 NMR properties will be discussed in the context of preparing new MR thermometers. Right: the low-frequency EPR analyses of high-spin metal complexes will be discussed in the context of novel imaging modalities.

CONTRIBUTED PAPERS

P1-02. Superparamagnetic Particles as MRI Temperature Contrast Agent. J.H. Hankiewicz[1], J. Stroud[1], R. Camley[1], S.E. Russek[2], D. Lachowicz[3], A. Kmita[3], M. Gajewska[3], E. Trynkiewicz[3], R. Wirecka[3], M. Przybylski[3], G. Parigi[4] and *Z. Celinski*[1] *1. Center for BioFrontiers, Universityof Colorado, Colorado Springs, CO, United States; 2. National Institute of Standards and Technology, Boulder, CO, United States; 3. Academic Centre for Materials and Nanotechnology, AGH University of Science and Technology, Krakow, Poland; 4. University of Florence, Florence, Italy*

A method of MRI temperature contrast developed by our group [1-5], which employs temperature dependent local field inhomogeneities due to a presence of micrometer sized magnetic particles and corresponding changes in image intensity (T_2* contrast), faces limitations due to particle size. For human applications, large particles cannot be used as they face problems with delivery and secretion. Smaller particles are required. However, spin transverse relaxation process for such particles is no longer governed by a static dephasing regime and T_2* temperature dependent inhomogeneity contributions vanish due to averaging by spin motion. On the other hand, the superparamagnetic particles could provide contrast mechanisms if a nuclear relaxation would be temperature dependent. To test this hypothesis, we used Mn-Zn ferrite superparamagnetic particles with an average size of 7.8 ± 2.1 nm. We studied their superparamagnetic properties using SQUID magnetometer (see Fig.1). In addition to blocking temperature near 100 K, mass magnetization in strong magnetic fields is temperature dependent (not shown). Particles with a 2 mM concentration were embedded in agar gel for NMR and MRI measurements at temperature 5 - 50 °C. At 3.0 T, NMR results show that T_1 is temperature independent, while observed NMR linewidth decreases from 130 Hz to 70 Hz and T_2 increases from 1.3 ms to 2.8 ms. Fig. 2 shows changing intensity of T_2 weighted MR image of the phantom during laser heating. Such MRI image not only allowed to determine

the change of the local temperature of the tissue mimicking phantom but also a spatial resolution with which temperature can be determined. These experiments providing the new contrasting mechanism necessary for temperature determination during MRI guide ablation surgeries.

1) J.H. Hankiewicz et al., Nature Communications, 7, 12415 (2016) 2) J. H. Hankiewicz et al., AIP Advances 7, 056703 (2017) 3) N. A. Alghamdi et al., Phys. Rev. Applied, 9, 054030 (2018) 4) J. H. Hankiewicz et al., J. Magn. Magn. Mater., 469, 550-557 (2019) 5) N. A. Alghamdi et al. J. Magn. Magn. Mater., 497, 165981, (2020)

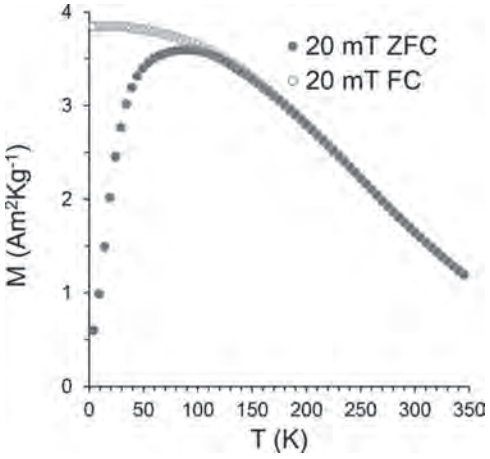

Fig. 1 Mass magnetization vs. temperature measured at 20 Oe.

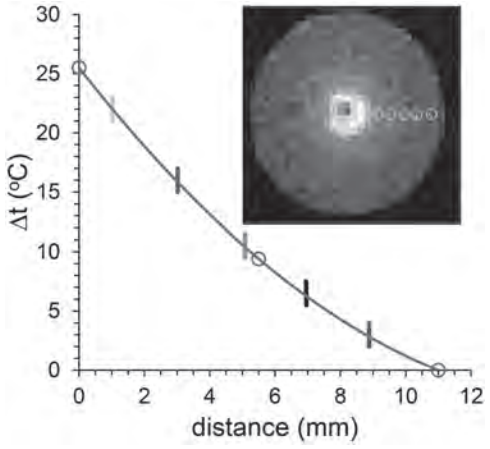

Fig. 2 Insite shows an image of the phantom during the laser heating. The temperature change vs. position as determined by local MRI image brightness. Circular data points indicate temperature determined by the sensors.

P1-03. Development of Biocompatible Ferrite Particles for Magnetic Resonance Imaging. *J. Stroud*[1], J.H. Hankiewicz[2], N. Alghamdi[1], T. Read[2], P. Bilski[3], K. Klodowski[4], J. Brown[5], M. Przybylski[6,7] and Z. Celinski[1] *1. Physics, University of Colorado at Colorado Springs, Colorado Springs, CO, United States; 2. Biofrontiers, University of Colorado at Colorado Springs, Colorado Springs, CO, United States; 3. Physics, Uniwersytet im Adama Mickiewicza w Poznaniu, Poznan, Poland; 4. Medical Physics and Biophysics, Akademia Gorniczo-Hutnicza imienia Stanislawa Staszica w Krakowie, Krakow, Poland; 5. Skaggs School of Pharmacy and Pharmaceutical Sciences, University of Colorado Denver - Anschutz Medical Campus, Aurora, CO, United States; 6. Academic Centre for Materials and Nanotechnology, Akademia Gorniczo-Hutnicza imienia Stanislawa Staszica w Krakowie, Krakow, Poland; 7. Physics and Applied Computer Science, Akademia Gorniczo-Hutnicza imienia Stanislawa Staszica w Krakowie, Krakow, Poland*

Magnetic nanoparticles have recently garnered interest for applications as MRI temperature contrast agents for Magnetic Resonance Imaging Thermometry (tMRI)[1]. Magnetic materials which can be used to noninvasively monitor body temperature would be greatly beneficial both for diagnostic purposes as well as MRI guided thermal procedures such as laser ablation of tumors. However, materials studied previously [1,2] are toxic. In this work we present an MRI thermometry study of MgZn ferrite microparticles. Such materials where shown in an earlier study to be less toxic than previously studied ferrites [3]. MgZn ferrites were prepared using a standard ceramic method and size distribution analysis was carried out using Scanning Electron Microscopy (SEM). Proton NMR linewidth, T_1, and T_2 relaxation times where measured of solutions containing MgZn microparticles ata 3T. T_2* weighted images were acquired in a high magnetic field of 3T and low magnetic fieeld of 0.2T scanners (Figure 1) to investigate temperature dependent contrast in images. In addition, tests of particle stability in solution where carried out and Inductively Coupled Plasma Mass Spectroscopy (ICP-MS) was used to determine dissolution of Mg and Fe in aqueous solutions of MgZn particles. results show that MgZn particles are promising compounds for tMRI as images show show strong dependence of image brightness vs temperature. (Figure 2). MgZn compounds have shown a lesserdegree of toxicity putting us closer to the ability to use ferrite particles as tMRI contrast agents in a clinical setting.

[1] J. Hankiewicz, Z. Celinski, and K. Stupic, Nat. Commun, 7 (2016) [2] J. Hankiewicz, J. Stoll, and J. Stroud, J. Magnet. Magnet. Mater., 469, pp. 550-557, (2019) [3] N. Alghamdi, J. Stroud, and M. Przybylski, Structural, Magnetic and Toxicity Studies of Ferrite particles for Magnetic Resonance Imaging Thermometry, J. Magnetism and Magnetic Materials. 497, (2019)

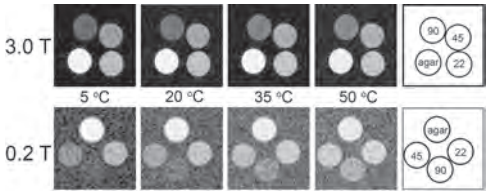

Fig 1. Comparison of T_2* weighted images taken at applied fields of 0.2T and 3T

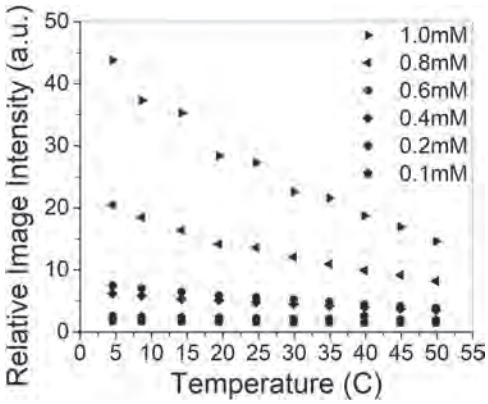

Fig 2. Relative Image Intensity of MRI images acquired at 3T for various concentrations of particles

P1-04. Signal to Noise Ratio of Single Domain Nanomagnet Amplification of Nuclear Magnetic Resonance Signals at Ambient Temperature. *M. Rajib*[1], T. Kaisar[1], M. Barbic[2], H. ElBidweihy[3] and J. Atulasimha[1] *1. Mechanical and Nuclear Engineering Department, Virginia Commonwealth University, Richmond, VA, United States; 2. Applied Physics and Instrumentation Group, Howard Hughes Medical Institute, Janelia Research Campus, Ashburn, VA, United States; 3. Electrical and Computer Engineering, United States Naval Academy, Annapolis, MD, United States*

Traditional inductive methods used for Magnetic Resonance Imaging (MRI) suffer from significant challenges due to the low signal-to-noise ratio (SNR) arising from the weak nuclear magnetic moment of protons when they precess about a large magnetic field at room temperature [1]. In an attempt to amplify the magnetic flux, it has been proposed to use magnetic nanoparticles of various geometrical shapes that are inserted into an NMR inductive coil [1-3]. Thus, the magnetic flux due to the response of the ensemble of proton spins to the RF field can be significantly enhanced as these nanoparticles have high transverse magnetic susceptibility under appropriate DC bias conditions. Prior work did not consider random thermal magnetization fluctuations in such nanomagnets that affect the SNR. In this work, we simulated the magnetization dynamics of a single-domain ellipsoidal nanomagnet driven by an AC field (H_{AC}) along the easy axis for different bias fields (H_{DC}) along the hard axis of the nanomagnet (Fig 1a). Importantly, our simulation also included the effect of room temperature thermal noise as shown in Fig 2. For $H_{DC} = h_c$, the energy profile is nearly flat (Fig 1b) that leads to the maximum magnetization amplification (Fig 1c) in response to the driving AC field that mimics the field due to proton spins precessing at nuclear magnetic resonance (NMR) frequency. However, the flat energy profile also increases the random magnetization fluctuations due to the thermal noise (Fig 2). Nevertheless, the SNRs for h=0, $0.5h_c$, $0.75h_c$, $1.0h_c$ and $1.5h_c$ are 0.003, 0.29, 0.63, 0.7 and 0.23 respectively showing $h = h_c$ provides the highest SNR. However, these are considering a single nanomagnet only. We will further investigate improvement of NMR detection SNR as a function of the coil-filling factor (millions of magnetic nanoparticles), nanoparticle shape, applied NMR polarizing field, and narrow band filtering to increase the SNR > 1000.

1. M. Barbic, A. Scherer, Solid State Nuclear Magnetic Resonance 28, 91 (2005). 2. M. Barbic, H. Elbidweihy, Journal of applied physics 120, 104506 (2016). 3. H.Elbidweihy, R. Smith and M. Barbic, AIP Advances 9, 045031 (2019).

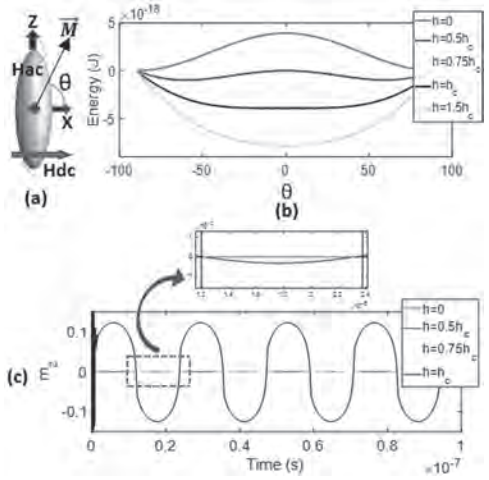

Figure 1: (a) Nanomagnet with AC field along the easy (Z) axis and dc bias field along the hard axis (X). (b) Energy plot as a function of θ and for various DC fields. (c) Non-thermal oscillation for different values of DC fields.

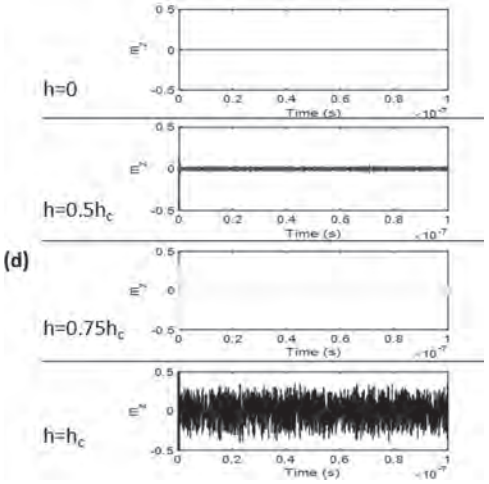

Figure 2: Thermal oscillation for different values of DC fields.

P1-05. Rapid Diagnostic Tests With Magnetic Particles as Mediators for Inductive Sensing. M. Salvador[1,2], Á. Gallo-Cordova[3], A. Moyano[1,4], J.C. Martínez-García[1], M.P. Morales[3] and *M. Rivas*[1] *1. Department of Physics, Universidad de Oviedo, Gijon, Spain; 2. Istituto di Struttura della Materia - Consiglio Nazionale delle Ricerche (CNR, Rome, Italy; 3. Instituto de Ciencia de Materiales de Madrid, Madrid, Spain; 4. Department of Physical and Analyticl Chemistry, University of Oviedo, Gijon, Spain*

In the last months, due to the COVID-19 pandemic, we have become familiar with the expression "rapid tests" referred to fast and easy-to-use bioanalytical devices to detect viral proteins or antibodies generated by the patient's immune system in response to the infection. World Health Organization (WHO) highly encourages the research into their performance and utility for disease surveillance [1]. The rapid tests are based on the lateral flow immunoassay (LFIA) technique. In it, the target molecule is specifically tagged with fluorescent enzymes or particles to make it visible. There are limitations of LFIA related to the biomarker usefulness and the recognition molecules' effectivity, which are being overcome (for COVID-19 as for other diseases) by the intense investigation in molecular biology and immunology. One crucial aspect in which magnetism can contribute is magnetic nanotags for magnetic detection [2]. This is the motivation of this work, and the question to answer is how magnetic particles can optimize the LFIA combined with

an inductive sensor. We have proved the viability of the inductive sensing of magnetic LFIA to quantify prostatic cancer biomarkers [3] and toxic biogenic amines [4]. The most critical parameters are the particle magnetic moment and initial permeability at the working frequency. To assess the possibility of controlling these variables, we studied the influence of the nanoparticles' magnetic core size. We synthesized magnetite nanoparticles (5 to 23 nm in size) by thermal decomposition. They were coated with dimercaptosuccinic acid and functionalized with neutravidin [5]. We tested them with a biotin-binding in lateral flow strips. They were characterized and calibrated in the sensing device. Our study concludes that superparamagnetism is essential for this application because it keeps high values of the initial magnetic permeability up to radio frequencies. Then, the agglomeration of superparamagnetic particles helps to achieve significant magnetic moments per biomolecule. Both together, large initial permeability and magnetic moment, optimize the performance of magnetic LFIA.

[1] https://www.who.int/news-room/commentaries/detail/advice-on-the-use-of-point-of-care-immunodiagnostic-tests-for-covid-19 [2] A. Moyano, E. Serrano-Pertierra, M. Salvador, et al., *Diagnostics*, 2020, 10, 288. [3] D. Lago-Cachón, M. Oliveira-Rodríguez, M. Rivas, et al., IEEE Magn. Lett., 2017, 8, 1. [4] A. Moyano, M. Salvador, J. C. Martínez-García, et al., Anal. Bioanal. Chem, 2019, 411, 6615. [5] G. Salas, C. Casado, F. J. Teran, et al., J. Mat. Chem., 2012, 22, 21065; R. Mejías, L. Gutiérrez, G. Salas, et al., J. Control. Release, 2013, 171, 225.

P1-06. Real-Time Tracking of Coronavirus Progress Using Magnetic Sensing and Machine Learning. *K. Hwang*[1], V. Ortiz Jimenez[1], Y. Pham[1], B. Muchharla[1], O. Thiabgoh[1], T. Eggers[1] and M. Phan[1] *1. University of South Florida, Tampa, FL, United States*

Common symptoms of Corona virus 2019 (COVID-19) include: (i) shortness of breath or difficulty breathing, (ii) cough and (iii) fever. Current detectors provide limited information and possess lengthy processing time, or are physically contacted to patients. Therefore, there is an urgent need for developing contactless devices that enable early and fast detection of COVID-19 and track their growth rates in real time. In this study, we have integrated an ultra-sensitive magnetic sensor technology [1] with machine learning to develop an innovative, contactless diagnostic device that can sense the breathing symptoms of COVID-19 at multiple stages of disease progress and provide crucial information on the growth rate by patient of this deadly virus. We add predictive analytics, with the help of machine learning, to provide a good understanding of what can and cannot be said about a patient's health condition status and a possible treatment plan, based on the available data. Figure 1a shows a tested person's characteristic breathing pattern and how his breathing amplitude varies within 60 seconds. This "shortness of breath" feature (at 35th s and 50th s) is not detectable using a commercially available respiratory monitor. The sensor also provides an accurate measure on strength of his breath at multiple stages, as shown in Figure 1b for the normal breath – Stage I, the deepest breath – Stage II, and the intermediate/random breath – Stage III.

[1] O. Thiabgoh, T. Eggers, and M. H. Phan, A new contactless magneto-LC resonance technology for real time respiratory motion monitoring, *Sensors and Actuators A* 265, 120 (2017).

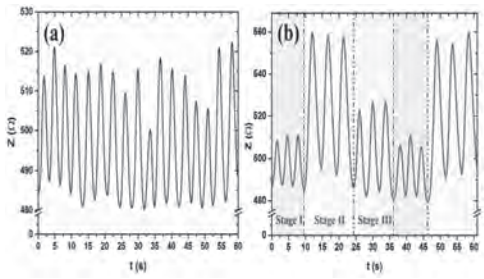

INVITED PAPER

P1-07. Issues of Magnetic Particle Transport Over Patterned Magnetic Thin Film Systems for lab-on-Chips. *A. Ehresmann*[1,2] *1. Faculty of Mathematics and Sciences, Institute of Physics, University of Kassel, Kassel, Germany; 2. Center for Interdisciplinary Nanostructure Science and Technology (CINSaT), University of Kassel, Kassel, Germany*

Ferromagnetic and superparamagnetic micro- und nano-particles (MPs) are regarded as key components for lab-on-chip or micro-total analysis devices in biotechnological applications. A controlled transport of many individual receptor-molecule-functionalized MPs in liquids will enable to extract biomolecules from body fluids, to enhance diffusion of diluted analyte molecules towards receptor molecules, to clean liquid samples from unwanted and detector-signal disturbing ingredients, and to accumulate MPs loaded with analyte molecules in a certain chip area. One key issue in such a device is the full control over MP motion in the liquid environment without agglomeration or surface sticking. The use of engineered local magnetic field landscapes (MFL, static stray fields from magnetic domains or micro magnets varying laterally over (sub)micron distances) superposed by a dynamically varying external magnetic field has proven to enable a controlled transversal motion along predefined tracks. Whereas this strategy has been realized by a variety of techniques generating the necessary dynamic MFLs [1 and references therein] several further aspects relevant to include MPs in a lab-on-chip device must be considered. A selection of these aspects will be discussed in the presentation. 1) In lab-on-chip devices it is advantageous to realize a controlled two- or even three-dimensional transport of MPs to direct the particles to a defined chip area and not only a transport on essentially one-dimensional tracks. Examples will be shown how such a 2D transport can be achieved over magnetically patterned continuous layer systems. Moreover it will be shown that patterned continuous magnetic thin film systems deposited on strained layers can be used to fabricate particle tracks through and on confined channels [2]. 2) If a detection of analytes shall be performed through MP dimer formation via analyte bridges a defined approach between two potentially binding MPs has to be ensured. Here the transfer of principles known from ray optics for directing the MP transport may be a solution. A lens-like magnetic pattern element [3] focussing the MP trajectories into a limited surface area is able to increase the particle density in this area and will, therefore, lead to an increased probability for building analyte bridges. 3) When an MP transport is achieved by dynamic MFLs created by a magnetically patterned substrate or topographic micromagnets with superposed varying external field one essential parameter is the distance between particle and surface. This distance determines the hydrodynamic drag and therefore equilibrium velocities and it influences the acting magnetic driving forces. The equilibrium distance is determined by a delicate balance of the relevant interactions, mainly between the electrostatic repulsion and the magnetic attraction between MPs and substrate and it may change as a function of position within the trajectory. The electrostatic repulsion is largely determined by the ionic strength of the surrounding liquid, which for realistic biological samples differs from the one of deionized water. Experiments will be shown where the influence of a changing pH-value on the MP transport characteristics and on particle sticking at the surface will be demonstrated. 4) If a sensitive detection of single or few analyte molecules shall be performed by MP surface immobilization via analyte bridges each surface segment of the MP should see the substrate surface. Therefore a controlled rotation over or an MP rolling across the surface is necessary. Here MPs with anisotropic magnetic characteristics must be used, like Janus-type particles. Results of investigations on the motion characteristics of well-known spherical Janus particles (polymer spheres covered by magnetic layer hemispheres) will be shown and it will be shown how geometrically more complex MPs can be formed using nanoimprint techniques [4].

[1] A. Ehresmann, I. Koch and D. Holzinger, Sensors 15, 28854 (2015) [2] Timo Ueltzhoeffer, Robert Streubel, Iris Koch et al., ACS Nano 10, 8491 (2016) [3] M. Urbaniak, D. Holzinger, A. Ehresmann et al., Biomicrofluidics 12, 044117 (2018) [4] U.M. Ha, B. Kaban, A. Tomita et al., Applied Nanoscience 8,1161–1169 (2018)

CONTRIBUTED PAPERS

P1-08. Quantitative Demultiplexing Magnetically Enriched Biological Tissues. *M. Zamani Kouhpanji*[1] and B. Stadler[1] *1. Electrical and Computer Engineering, University of Minnesota, Minneapolis, MN, United States*

Magnetic nanowires (MNWs) rank among the most promising multifunctional magnetic nanomaterials for biomedical applications, especially biolabeling, owing to their nontoxicity and remote excitation using a single magnetic source[1]. Until recently, the first-order reversal curve (FORC)[2] technique has been broadly used to study the demultiplexing capability of the MNWs for biolabeling applications. However, since FORC measurements require huge numbers of data points, this technique is very slow which makes it inapplicable for clinical use[3]. For this reason, we recently developed a new framework for the quantitative demultiplexing of magnetically enriched biological tissues using the projection method[4]. This method projects the FORC heat-maps onto the reversal field (H_r) axis, P_{Hr} in Eq. (1), to determine the irreversible switching field (ISF) distribution of the MNWs as a unique signature for demultiplexing. Moreover, since the ISF distribution can be determined using only few points next to the upper branch of the hysteresis loop, it is significantly faster than full FORC measurements without the need for complex and destructive data processing. (1) The location of the P_{Hr} peaks determines the coercivity (H_c) and its broadening/width is correlated to the interaction fields (H_u) of the MNWs. As proof of concept, several types of MNWs were electrodeposited into polycarbonate templates. Several combinations of the MNWs were prepared and their ISF distributions were measured using the projection method. We also measured their other magnetic signatures (coercivity distribution (P_{Hc}) and interaction field distribution (P_{Hu}) using FORC) to evaluate these measurements' reliability for quantitative demultiplexing. Figure 1 shows a few of the ISF distributions measured on the combinations. In this presentation, it will be explained how to tune the aforementioned parameters of MNWs to achieve the most reliable quantitative paradigm for demultiplexing MNWs combinations using their ISF distribution. We also show a demultiplexing framework that is able to predict the MNWs in the combinations even though their ISF distributions have partial overlaps, something that cannot be accomplished using most demultiplexing measurements.

1 M. R. Zamani Kouhpanji and B. J. H. Stadler, *Sensors*, 2020, 20, 2554. 2 M. R. Zamani Kouhpanji and B. J. H. Stadler, *Nano Express*, 2020, 1, 010017. 3 M. R. Zamani Kouhpanji, J. Um and B. J. H. Stadler, *ACS Appl. Nano Mater.*, 2020, 3, 3080–3087. 4 M. R. Zamani Kouhpanji and B. J. H. Stadler, *RSC Adv.*, 2020, 10, 13286–13292.

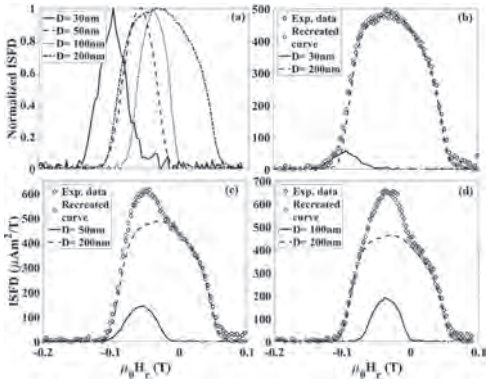

P1-09. Withdrawn

Session P2
MAGNETIC RECORDING VIA OPTICAL, HEAT AND MAGNETIC EXCITATION II

Simon Greaves, Chair
Tohoku University, Sendai, Japan

INVITED PAPER

P2-01. Resolving the Role of Magnetic Circular Dichroism in Multishot Helicity-Dependent all-Optical Switching. *Y. Quessab*[2,1], M. Deb[2,3], J. Gorchon[2], M. Hehn[2], G. Malinowski[2] and S. Mangin[2] *1. Department of Physics, New York University, New York, NY, United States; 2. Institut Jean-Lamour, CNRS UMR 7198, Universite de Lorraine, Nancy, France; 3. Institut fur Physik und Astronomie, Universitat Potsdam, Potsdam, Germany*

The ultrafast optical control of the magnetic order rapidly emerged as a promising approach in ultrafast magnetism. Yet, more than a decade after the discovery of complete and deterministic magnetization switching induced by femtosecond circularly polarized laser pulses[1], many fundamental questions remain unanswered. In particular, the issue of the relative contribution of pure thermal or nonthermal effects induced by the laser pulses is crucial for the understanding of the magnetization reversal mechanism. Several theoretical models have been developed for multipulse all-optical helicity-dependent switching (AO-HDS) without reaching a consensus. Using circular polarization, transfer of light angular momentum and the emergence of an effective magnetic field via the inverse Faraday effect (IFE), a nonthermal optomagnetic effect, may occur[2]. In contrast, it has been argued that AO-HDS could originate from a purely heating mechanism[3]. In this case, the asymmetry would arise from the difference in light absorption between left- and right-circular polarization due to the magnetic circular dichroism (MCD). By conducting helicity-dependent ultrafast magnetization dynamics in a CoTb ferrimagnetic alloy that exhibits AO-HDS, we are able to quantitatively determine the MCD and resolve its role in the switching mechanism[4]. We find a MCD of ~1% from time-resolved Kerr effect measurements (Fig. 1a). Unequivocal interpretation of the sign of the dichroism is provided by performing AOS and, for the first time in a ferrimagnet, fs laser-induced domain wall motion experiments (Figs 2a-2b). We demonstrate that AOS occurs when the magnetization is initially in the most absorbent state, according to the light helicity. Moreover, we evidence that the MCD creates a thermal gradient that drives a domain wall toward hotter regions. Our experimental results are in agreement with the purely thermal models of AOS reported in the literature.

[1] C. D. Stanciu *et al.*, PRL 99, 047601 (2007) [2] T. D. Cornelissen *et al.*, APL 108, 142405 (2016) [3] J. Gorchon *et al.*, PRB 94, 020409(R) (2016) [4] Y. Quessab *et al.*, PRB 100, 024425 (2019)

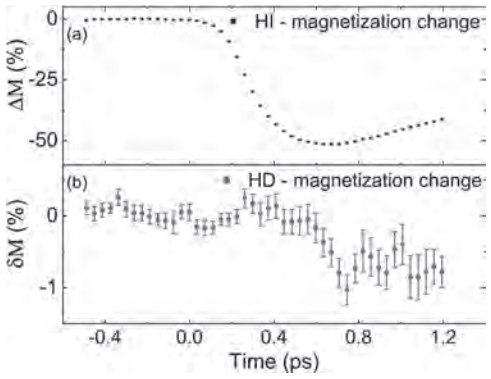

Fig1: (a) Helicity-independent and (b) helicity-dependent (proportional to MCD) magnetization change extracted from ultrafast magnetization dynamics induced by circularly polarized light

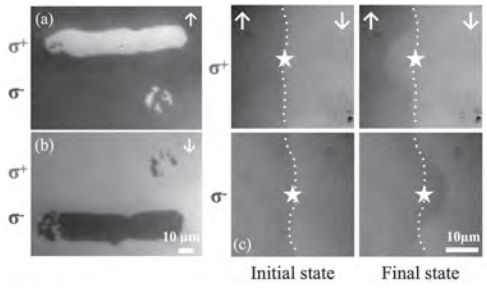

Fig2: Magneto-optical Kerr images showing (a-b) AO-HDS and (c) helicity-dependent laser-induced domain wall motion.

CONTRIBUTED PAPERS

P2-02. Templated Growth of $L1_0$-FePt for HAMR Media. *B. Zhou*[2,1], C. Xu[2,1], B. Varaprasad[2,3], D.E. Laughlin[2,1] and J. Zhu[2,3] *1. Materials Science and Engineering, Carnegie Mellon University, Pittsburgh, PA, United States; 2. The Data Storage Systems Center, Carnegie Mellon University, Pittsburgh, PA, United States; 3. Electrical and Computer Engineering, Carnegie Mellon University, Pittsburgh, PA, United States*

Granular $L1_0$-FePt thin film deposited on (002) textured MgO underlayers have come long way in the support of the present HAMR media areal density capability. However, further reduction of the center-to-center pitch distance between adjacent grains below 6nm is meeting the nucleation density limit of this media/underlayer material combination [1]. Here, we present a novel fabrication method utilizing metal-oxide/nitride materials systems with two-phase separation to develop a pre-defined and robust oxide/nitride template to increase the nucleation density and the columnar growth of $L1_0$-ordered FePt grains. The template is directly formed on top of MgO underlayer by co-sputtering metal and oxide/nitride materials, resulting in metal particles embedded in the oxide/nitride matrix. This is followed by the selective etching of the metal nanoparticles from the matrix [2]. Experimental demonstration shows that FePt can be backfilled into the "craters"

left by the metal nanoparticles with the correct texture on the MgO underlayer. By comparing the mean pitch distance of FePt grains without and with template layer in Fig. 1, it is shown that the nucleation density of FePt grains is determined by the areal density of the "craters" formed in Au-SiO_2 template layer. With the help of such a fabrication method, the material choices for further reducing the pitch distance of the FePt grains in HAMR media are expanded. The several combinations of various matrix materials forming the template and their results on nucleation and growth of FePt will be presented and discussed.

[1] I. Suzuki, J. Wang, Y. Takahashi, K. Hono, Journal of Magnetism and Magnetic Materials, Vol. 500, 166418 (2020) [2] B. Zhou, C.c. Xu, B. S. D. C. S. Varaprasad, D. Laughlin, J. Zhu, 2019 MMM conference (2019)

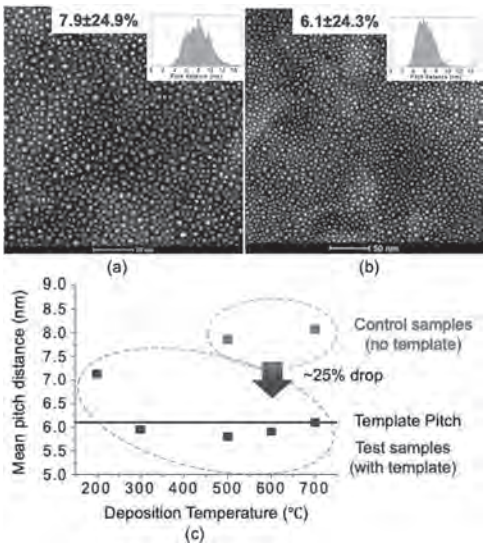

The HADDF image of FePt grains at nucleation stage deposited on MgO underlayer at 700 °C (a) without and (b) with prefabricated template layer. Film stack: Sub. | Ta (4) | Cr (40) | MgO (8) | (template) (2) | FePt (1) with thickness in nm. The template refers to the layer of Au – 35 vol.% SiO_2 co-sputtered on MgO underlayer. (c) describes the mean pitch distance of FePt grains as a function a deposition temperature from 200 °C to 700 °C for the samples with the same film stack without (red marks) and with (blue marks) the pre-fabricated template layer. The black line describes the mean pitch distance of the template layer.

P2-03. Analysis of Adjacent Track Erasure for the HAMR Media.
N.A. Natekar[1] and R. Victora[1] *1. Electrical Engineering, University of Minnesota, Minneapolis, MN, United States*

Writing tracks narrowly spaced in the crosstrack direction appears to increase the User Areal Density (UAD), but can lead to erasure of the adjacent tracks. This phenomena is called Adjacent Track Erasure (ATE). Our research aims to establish the numerical extent of ATE and introduce efforts to reduce this ATE for different HAMR media. This research can help increase the HAMR storage density by making HAMR media resistant to ATE. The ATE in HAMR is limited to tracks immediately adjacent to the track being overwritten [1]. For a single write, we have previously found that the optimum track spacing between these tracks to maximize the UAD for a noise free reader is 70% of the heat spot FWHM [2]. By implementing micromagnetic simulations, we find the single layer FePt media is more susceptible to ATE as its thickness decreases. The 3nm-6nm high temperature Thermal ECC media [3] has a slightly higher ATE susceptibility compared to the 9nm single layer FePt media. In contrast the 3nm-6nm low temperature Thermal ECC media [4] has a significantly higher ATE susceptibility (Table 1). To reduce the ATE, we change the applied field angle and introduce exchange coupling between grains of the media. The single layer FePt media ATE is impervious to the applied field angle although the ATE reduces as the field angle reduces for the high temperature Thermal ECC media. The ATE reduces for the single layer FePt media and the high temperature Thermal media with optimized exchange coupling (IGC) values. The ATE for the single layer FePt and high temperature Thermal ECC media using these optimization techniques is shown in Fig. 2. Both these optimization techniques however do not sufficiently improve the ATE susceptibility for the low temperature Thermal ECC media. We believe the ATE is proportional to the thermal stability factor at a temperature just below the write temperature. This hypothesis correctly predicts the ATE in the single layer FePt media assuming coherent rotation. For Thermal ECC media, other mathematical techniques that capture incoherent rotation can be used to verify this hypothesis.

[1] S. Kalarickal, A. Tsoukatos, S. Hernandez, C. Hardie and E. Gage, "Adjacent Track Interference in Heat-Assisted Magnetic Recording: Impact and Implications," in IEEE Transactions on Magnetics, vol. 55, no. 7, pp. 1-4, July 2019 [2] Z.Liu, Y.Jiao and R.H. Victora, "Composite media for high density heat assisted magnetic recording", Appl. Phys. Lett. 108, 232402(2016) [3] Z.Liu & R.H.Victora (2016). "Composite structure with superparamagnetic writing layer for heat-assisted magnetic recording", IEEE Transactions on Magnetics, vol. 52, no. 7, pp. 1-4, July 2016 [4] N.A. Natekar, W.Tipcharoen & R.H.Victora, "Composite media with reduced write temperature for heat assisted magnetic recording", Journal of Magnetism and Magnetic Materials 486 (2019) 165253

Structure (HAMR Media)	Media thickness	RW ≈ 15nm	RW ≈ 25nm
Single Layer FePt	6nm	-0.30 dB	-0.42 dB
Single Layer FePt	7.5nm	-0.27 dB	-0.38 dB
Single Layer FePt	9nm	-0.08 dB	-0.23 dB
High temperature Thermal ECC T_c (write layer) = 900K; T_c (storage layer) = 700K	3nm (write layer) 6nm (storage layer)	-0.19 dB	-0.25 dB
Low temperature Thermal ECC T_c (write layer) = 600K; T_c (storage layer) = 500K	3nm (write layer) 6nm (storage layer)	-0.50 dB	-0.46 dB

ATE for different HAMR media

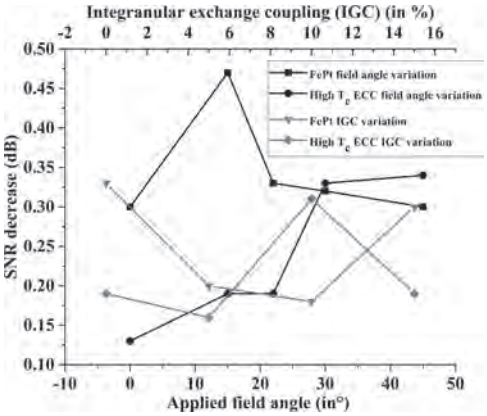

ATE improvement for HAMR media of varying intergranular exchange coupling and applied field angle

P2-04. Rotated Read Head for High Density Heat-Assisted Shingled Magnetic Recording.
W. Hsu[1] and R. Victora[1] *1. Electrical and Computer Engineering, University of Minnesota, Minneapolis, MN, United States*

Heat-assisted magnetic recording (HAMR) is the most promising candidate for next generation data storage. Previous study suggests that user areal density in HAMR with composite media can reach up to 4.7 Tb/in^2 [1]. On the other hand, shingled magnetic recording has been adopted to keep the growth in user areal density for current state-of-art perpendicular magnetic recording. In this work, Heat-assisted Shingled Magnetic Recording (HSMR) is studied. It is known that adjacent track erasure can degrade signal-to-noise ratio (SNR) in conventional HAMR especially when the number of adjacent track write increases [2]. In HSMR, since there will be only one adjacent track write due to the shingled-style writing, HSMR should have better performance than conventional HAMR under the same cross-track density. As a consequence of transition curvature in HAMR [3],

the shape of the remaining track after shingled writing is a half arc (Fig. 1). Thus, the read head should also be rotated by a certain angle (θ) to capture the effect from the arc shape of the transition. Table 1 shows the SNR for different track pitch and rotation angle of the read head for a heat spot with peak temperature of 850 K and full width at half maximum (FWHM) of 30 nm. It can be seen that SNR is enhanced by around 1 dB if the read head is rotated an optimal amount. Bit error rate is then calculated with a 1-D equalizer and an improved Viterbi detector [4]. It is shown that for a three-read head arrays, the user areal density can approach up to 5 Tb/in^2.

[1] Z. Liu, Y. Jiao, and R.H. Victora, Applied Physics Letters 108, 232402 (2016) [2] S. Kalarickal, A. Tsoukatos, S. Hernandez, C. Hardie, and E. Gage, IEEE Transactions on Magnetics 1 (2019) [3] J.-G.J. Zhu and H. Li, IEEE Transactions on Magnetics 53, 1 (2017) [4] Y. Wang, M.F. Erden, and R.H. Victora, IEEE Magnetics Letters 3, (2012)

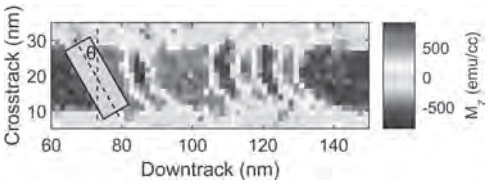

Schematic of recording pattern with a rotated read head sensor (rectangle region).

Track Pitch (nm)	Rotation angle (°)	SNR (dB)
18	0	8.7515
18	75	10.34
21	0	10.40
21	60	11.15

SNR for different track pitch and rotation angle of the read head for FHWM of 30 nm.

P2-05. Models of Advanced Recording Systems (MARS) - a Multi-Timescale Micromagnetic Code for Granular Film Simulations. *S.E. Rannala*[1], A. Meo[2], S. Ruta[1], R. Chantrell[1], P. Chureemart[2] and J. Chureemart[2] *1. Physics, University of York, York, United Kingdom; 2. Physics, Mahasarakham University, Mahasarakham, Thailand*

Micromagnetic modelling enables the accurate simulation of large magnetic systems with a significantly reduced computational cost compared to atomistic simulations. Through micromagnetic modelling it is possible to simulate systems consisting of thousands of grains over a range of timescales from nanoseconds to years. Here we present an open-source multi-timescale micromagnetic code, called MARS, consisting of the key solvers Landau-Lifshitz-Gilbert (LLG), Landau-Lifshitz-Bloch (LLB) and Kinetic Monte Carlo (kMC). The included solvers have been rigorously tested and are bundled into an overarching solver class to enable the creation of simulations which can utilise any of the available solvers at run-time. This combination of solvers also enables multi-timescale simulations with dynamic switching between solvers for specified timescales. The granular systems used are generated via a Voronoi construction and can consist of multiple or single layers. Each layer is assigned its own material with separate material configuration files. MARS is designed to use atomistic parameterisation for the material parameter inputs, obtained from software such as VAMPIRE [1]. MARS includes numerous bundled simulation types including but not limited to: FORC, FMR, HAMR writing. Fig.1 shows the result of a HAMR writing simulation of a pseudorandom bit sequence via the LLB solver followed by the read back of the system after a week via the kMC solver. Such simulations provide an easy method to test a system's suitability for data writing and long term storage. A detailed model of the HAMR write head is provided including custom field and temperature profiles, skew angle and near-field transducer to write head spacing.

[1] R. Evans, W. Fan and P. Chureemart, et al. Journal of Physics: Condensed Matter, Vol. 26, p103202 (2014)

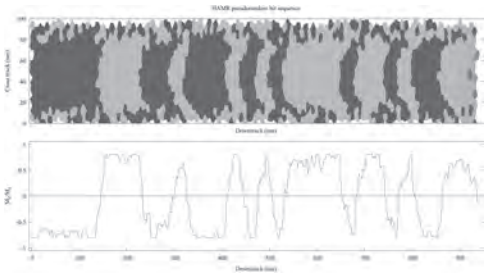

HAMR write/read simulation of a pseudorandom bit sequence performed using MARS via the LLB and kMC solvers. Upper part shows magnetisation of the grains. The lower part shows the obtained readback signal.

P2-06. Hypersonic Heat-Induced Flows of Magnons Induced by Femtosecond Laser Pulses. *S. Ruta*[1], Z. Fu[1,2], T. Ostler[3], A. Kimel[4] and R. Chantrell[1] *1. University of York, York, United Kingdom; 2. Tongji University, Shanghai, China; 3. Sheffield Hallam University, Sheffield, United Kingdom; 4. Radboud Universiteit, Nijmegen, Netherlands*

Understanding the fundamental physics of energy transfer in spin textures via magnon flows and domain wall motion is crucial for the development of future, low-power technological applications. In the research community, controlling magnetisation dynamics using femtosecond laser pulse excitation (all-optical switching) has been intensely investigated as an energy-efficient method. In this work, we present via numerical methods the presence of ultrafast pure magnonic currents on the sub-picosecond time scale due to local spin temperature imbalances. The magnons propagate ballistically and have a critical role in deterministic switching of the bilayer systems and ferrimagnetic alloys, but on a localised level. During the ultrafast laser pulse, the electrons heat up rapidly and cool down in a few ps, leading to a change in the spin system configuration, which can be described by the spin temperature. To quantity the magnon propagation, we constructed a bilayer system with different spin temperature. The high energy magnons from the hot regions will cross the interface and propagate into the cold region. The propagation is visualised in figure 1, where the high energy magnons (represented by the low magnetisation value) are formed at the interface (fig 1a) and then propagate (fig 1b) into the cold region, with a speed of propagation in the order of km/s. To calculate the magnon propagation we used the expression for the energy flux vector: [dm(r)/dt]x[m(r)] where m(r) is the net magnetisation as a function of position r. The maximum change in the expression is correlated with the front of magnon propagation. This result shows ultrafast transport of magnons due to inhomogeneous spin temperature as present in ultrafast laser experiments.

[1] G.-M. Choi, C.-H. Moon, B.-C. Min, K.-J. Lee, and D. G. Cahill, Nature Physics 11, 576 (2015). [2] K. Uchida, S. Takahashi, K. Harii, J. Ieda, W. Koshibae, K. Ando, S. Maekawa, and E. Saitoh, Nature 455, 778 (2008). [3] D. Hinzke and U. Nowak, Physical Review Letters 107, 027205 (2011).

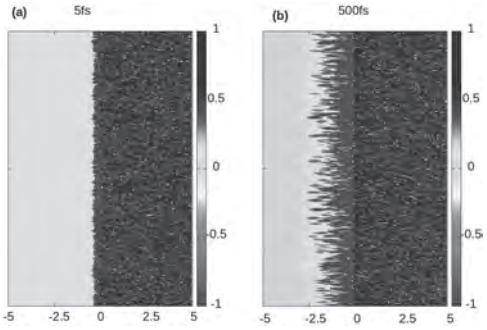

Magnetisation map of the bilayer system at 5fs and 500 fs. The system is divided along X-direction into two regions with the interface at x=0. The left side is equilibrated at 0K and the right side at 100K. The evolution of Z-component of magnetisation is shown as a colour map, where green corresponds to the equilibrium value of each region individually, and red and blue corresponds to increase and decrease of the magnetization with respect to the equilibrium value.

P2-07. Energy Barrier Calculations in Multispin Systems for Magnetic Recording Purposes. *P.I. Gavriloaea*[1], S. Ruta[1] and R. Chantrell[1]
1. Department of Physics, University of York, York, United Kingdom

The data storage industry is currently migrating to Heat Assisted Magnetic Recording (HAMR) technology for the next generations of hard drives. HAMR allows the use of high anisotropy media by introducing laser pulses to lower the coercivity to writable levels at elevated temperatures. However, the long-term stability of written data remains a problem, especially when it may be subjected to high temperatures during the writing or rewriting of neighbouring tracks. A simple model is desirable for the evaluation of energy barriers for complex media. Concerning the long term and controlled stability of the recorded information, we developed a numerical model which allows us to perform energy barrier calculations for multispin systems. Our work is based on the Lagrange multiplier method of finding points of extremum for functions subject to equality constraints. While this approach has been previously used in conjunction with the Landau-Lifshitz-Gilbert equation [1-2], we were able to integrate the Lagrange optimisation strategy in a direct minimisation tool. Making use of our model, we investigate several spin chain systems, mapping the minimum energy paths (MEPs) and extracting the corresponding energy barriers, while characterising the specific reversal mechanisms, ranging from the extremes of coherent rotation and domain wall formation (see Fig.1). Furthermore we use our description to explore the exchange spring behaviour and the reduction of the switching field and energy barrier via the hard/soft coupling [3].

[1] D.A. Garanin and H. Kachkachi, Phys. Rev. Lett. 90, 65504,(2003). [2] R. Yanes, O. Chubykalo-Fesenko, H. Kachkachi, Phys. Rev. B 76, 064416 (2007) [3] K. Yu. Guslienko, O. Chubykalo-Fesenko, O. Mryasov, Phys. Rev. B 70, 104405 (2004)

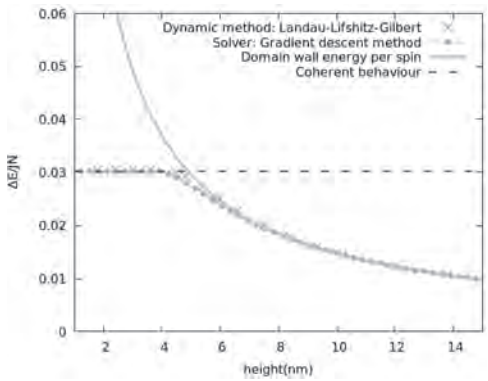

Fig.1 FePt example:dashed line – single domain energy barrier; dotted line & starred points - energy barrier vs grain height; solid line – domain wall energy: $4(0.5J/K)^{1/2}$. All values on the y axis have been normalised to the exchange constant J and the number of spins N in the system.

P2-08. Tuneable, Perpendicular Synthetic Ferrimagnets With Negative Remanence. *J.N. Scott*[1], W. Hendren[1], R. Bowman[1], R. Hicken[2], M. Dabrowski[2], D. Burn[3], A. Frisk[3] and G. van der Laan[3] *1. Queen's University Belfast, Belfast, United Kingdom; 2. University of Exeter, Exeter, United Kingdom; 3. Diamond Light Source Ltd, Didcot, United Kingdom*

Synthetic ferrimagnets (SFM), two ferromagnetic layers with different magnetic moments, exchange-coupled via the RKKY interaction across a non-magnetic spacer layer, are of particular interest as a feasible media for all optical magnetic switching [1,2]. We present a series of compensating Ni_3Pt/Ir/Co SFMs fabricated via magnetron sputtering and exhibiting perpendicular magnetic anisotropy. Design of the magnetic properties of these SFM structures requires knowledge and control of the magnetisation, M(T), and anisotropy, K(T), of the individual ferromagnetic layers, and the strength of the exchange coupling between them, $J_{ij}(T)$. This can be achieved in the Ni_3Pt/Ir/Co system by varying the deposition temperature [3] and layer thicknesses, providing a tuneable structure with which to investigate the effect of M(T), K(T) and $J_{ij}(T)$ on reversal mechanisms within SFM materials. Distinct magnetic species in each layer of the SFM structure also allows for element specific characterisation via x-ray magnetic circular dichroism (XMCD), which is used in conjunction with SQUID magnetometry. Magneto optical Kerr effect (MOKE) microscopy has been employed to explore the domain structure in these materials and initial experiments have revealed that it is possible to switch the layers by application of optical laser pulses under only a small applied field. We demonstrate our ability to engineer the magnetic properties of these SFM structures, including control of the magnetic compensation point, T_{comp}, and regions of negative remanent magnetisation where the moment aligns opposite to that of the applied field [4].

[1] S. Mangin et al, Nature Materials 13, 286 (2014) [2] R. F. L. Evans et al, Appl. Phys. Lett. 104, 082410 (2014) [3] D. Vasumathi et al, JMMM 223, 221-232 (2001) [4] K. Takanashi et al, Appl. Phys. Lett. 63, 1585 (1993)

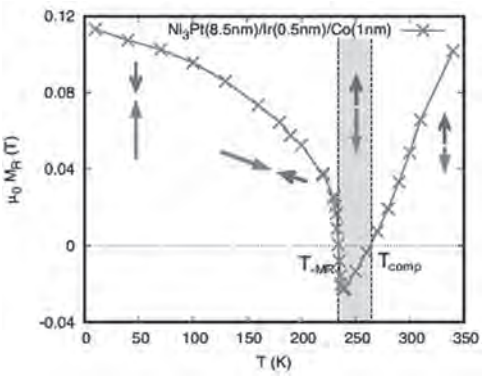

Remanent magnetisation as a function of temperature of a Ni_3Pt(8.5nm)/Ir(0.5nm)/Co(1nm) SFM with arrows depicting the alignment of the Co (blue) and Ni_3Pt (Red) layers and noting the positions of the magnetisation compensation point, T_{comp} and T_{-MR}, the onset temperature of negative remanent magnetisation.

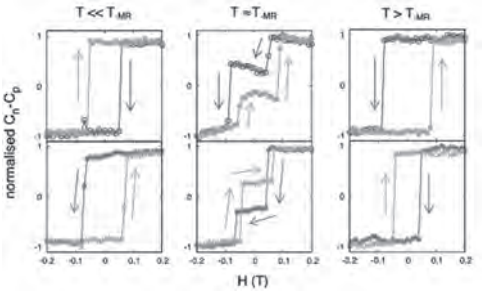

Element specific XMCD hysteresis loops of a Ni_3Pt(8.5nm)/Ir(0.5nm)/Co(1nm) SFM recorded at temperatures $T < T_{-MR}$ (~200K), $T \sim T_{-MR}$ (~220K) and $T > T_{-MR}$ (~250K), with Co (blue) loops shown on top and Ni (red) shown below. Arrows show the direction of the field sweep.

INVITED PAPER

P2-09. Integration of Single-Shot all-Optical Switching Tb/Co Multilayer-Based Electrodes Within Perpendicular Magnetic Tunnel Junctions. L. Avilés Félix[1], A. Olivier[1], Q. Li[2], C. Davies[2,3], L. Alvaro-Gomez[1], M. Rubio-Roy[1], S. Auffret[1], A. Kirilyuk[3], A. Kimel[2], T. Rasing[2], R. Sousa[1], L. Buda-Prejbeanu[1], B. Dieny[1] and *L. Prejbeanu*[1] *1. Spintec, Univ Grenoble Alpes, CEA, CNRS, Grenoble INP, IRIG-SPINTEC, Grenoble, France; 2. Radboud University, Institute for Molecules and Materials, Nijmegen, Netherlands; 3. FELIX Laboratory, Radboud University, Nijmegen, Netherlands*

Since the observation of all-optical switching of magnetization in the ferrimagnetic alloy GdFeCo using femtosecond laser pulses, there has been a significant interest in exploiting this switching process for data recording [1]. The ultrafast speed of the magnetization switching allows to push the writing speeds of magnetic memories towards THz frequencies. A first approach for the exploitation of all-optical switching in spintronic devices was explored by Chen *et al*. [2] on optically switchable GdFeCo layer integrated within a microsized magnetic tunnel junction pillar. In this talk we will discuss the recent advances on the development of perpendicular magnetic tunnel junctions incorporating [Tb/Co]-CoFeB electrodes whose magnetization can be optically controlled via helicity-independent single-shot switching. The ultrafast optical control of the magnetization in this system gives rise to capabilities to be exploited as a storage layer in a magnetic tunnel junction. Within our results we will highlight a first evidence of helicity-independent all-optical switching in a [Co/Tb] multilayered-based system coupled to CoFeB layers with both ps- and fs-long single laser pulses. We also explore the magneto-optical properties of multilayers and their thermal stability upon different annealing temperatures. The magneto optical response and the perpendicular magnetic anisotropy of our system was achieved even after annealing at 250°C. The laser pulse duration and fluence dependence for the CoFeB/$[Tb/Co]_5$ electrodes were explored using single 70fs and 7ps laser pulses with fluences F = 3.1, 3.5 and 4.0mJ/cm^2. As can be seen from Fig.1, images obtained for a laser pulse duration D = 7ps and 70fs, a clear magnetization reversal can be achieved for F = 3.5mJ/cm^2. Results also determined that reducing the pulse duration to 70fs, the fluence required to induce thermal demagnetization on the sample increases. Our all-optical switching electrodes FeCoB/Ta/$[Tb/Co]_N$ were finally integrated into a magnetic tunnel junction. Electrical evaluation of nanopatterned AOS-MTJ showed TMR ratios up to 36 % depending on the diameter of the junctions and on the number of repetitions of the [Tb/Co] bilayers. The full structure of the junctions consist of: Ta(30Å)/FeCoB(11Å)/MgO(23Å)/FeCoB(13Å)/Ta(2Å)/$[Tb(9.5Å)/Co(12.5Å)]_5$. The TMR values distribution of hundreds of MTJ with different diameters is shown in Fig. 2a. The maximum TMR ratio (36 %) was observed for a 200 nm-diameter junction with a minimum resistance of 6 kΩ. Fig. 2b shows the corresponding Resistance loop extracted from the 200 nm-diameter (yellow) distribution of Fig. 2a. To our knowledge, we are presenting the first study that reports the helicity-independent all-optical switching in a Co/Tb multilayered-based system. The integration of optically switchable electrodes within magnetic tunnel junctions is a key step towards future spintronic technologies. In this direction, the research presented here, related to the nanofabrication of high TMR ratio-magnetic tunnel junction using [Co/Tb]-CoFeB electrodes, are a contribution that can lead to substantial advances in hybrid spintronic-photonic devices and contribute to the development of magnetic tunnel junctions with new functionalities, particularly the ability to control the magnetization of the storage layer with ultrafast laser pulses. This research has received funding from the European Union's Horizon 2020 research and innovation program under FET-Open Grant Agreement No. 713481 SPICE.

1. A. V. Kimel et al. Nat. Mater. 13 225 (2014) 2. J. Y. Chen *et al*. Phys. Rev. Appl. 7 021001 (2017) 3. L. Avilés-Félix *et al*. Sci. Rep. 10 5211 (2020). 4. L. Avilés-Félix, *et al*. AIP Advances 9, 125328 (2019) 5. A. Olivier *et al*. Accepted in IOP Nanotechnology (2020)

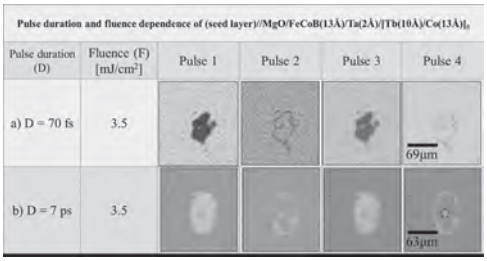

Fig 1. Magneto-optical images demonstrating the pulse duration of the magnetization reversal. Images were taken after the incidence of single a) 70 fs and b) 7 ps laser pulses with a fluence F = 3.5 mJ/cm^2. Purple dashed circle indicates the region which showed clear thermal demagnetization after the pulse.

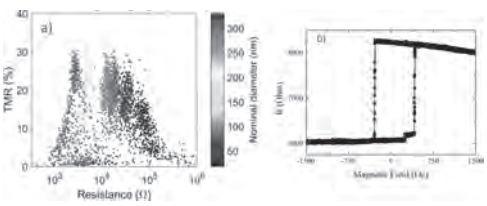

Fig 2. a) TMR distribution of the nanopatterned junction for different diameters. b) Resistance loop of a 200 nm-diameter with a TMR ratio of 36 %.

CONTRIBUTED PAPERS

P2-10. Layer-Selective Magnetization Reversal and Optical Switching in Ni_3Pt/Ir/Co Synthetic Ferrimagnets. *M. Dabrowski*[1], J.N. Scott[2], W. Hendren[2], A. Frisk[3], D. Burn[3], D. Newman[1], C. Klewe[4], A.T. N'Diaye[4], P. Shafer[4], P.S. Keatley[1], T. Hesjedal[5], G. van der Laan[3], R. Bowman[2] and R. Hicken[1] *1. Department of Physics and Astronomy, University of Exeter, Exeter, United Kingdom; 2. School of Mathematics and Physics, Queen's University Belfast, Belfast, United Kingdom; 3. Magnetic Spectroscopy Group, Diamond Light Source Ltd, Didcot, United Kingdom; 4. Advanced Light Source, Lawrence Berkeley National Laboratory, Berkeley, CA, United States; 5. Department of Physics, University of Oxford, Oxford, United Kingdom*

Synthetic ferrimagnets and antiferromagnets with perpendicular anisotropy have attracted great interest as they allow for stabilization of room-temperature skyrmions [1], fast domain wall motion [2], and all-optical switching of magnetization [3]. Here we study Ni_3Pt/Ir/Co structures in the vicinity of the compensation point temperature T_M, where the magnetizations of the two layers have the same magnitude and are anti-parallel to each other. By measuring element-specific hysteresis loops using x-ray magnetic circular dichroism (XMCD) and wide-field magneto-optical Kerr effect (MOKE) microscopy, we explore the magnetization reversal and domain structure of the Ni_3Pt and Co layers (Fig. 1). We show that the change of the magnetic state upon increasing the temperature through the compensation point is a continuous transition, associated with formation of a domain structure at remanence. Furthermore, we show that increasing the magnetic field sweep rate between saturation and remanence changes the mechanism of the magnetization reversal from propagation of domain walls to nucleation of reverse domains. Finally, we demonstrate how the layers can be switched by optical laser pulses, with the assistance of a small external magnetic field (down to 1 mT). The Ni_3Pt/Ir/Co structures are promising candidates for all-optical control of magnetism in rare-earth-free synthetic ferrimagnets.

[1] W. Legrand et al., Nature Materials 19, 34-42 (2020). [2] S.-H. Yang et al., Nature Nanotechnology 10, 221-226 (2015). [3] J. W. Liao et al., Advanced Science 1901876 (2019).

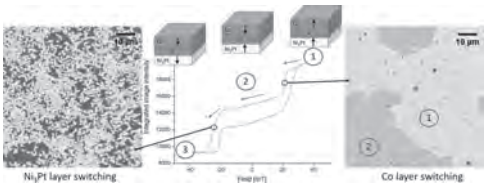

Fig. 1. Wide-field Kerr microscopy of a Ni_3Pt/Ir/Co structure in a polar geometry. The different domain structure of the Co and Ni_3Pt layers allows the magnetization reversal of these layers to be distinguished.

P2-11. Chemical Order-Disorder Transitions in Intermetallic Alloys for High-Density Magnetic Recording. *N.I. Polushkin*[1], T.B. Moeller[2], S.A. Bunyaev[3], A.V. Bondarenko[3], M. He[4], M.V. Shugaev[4], J. Boneberg[2] and G.N. Kakazei[3] *1. Institut fiziki mikrostruktur Rossijskoj akademii nauk, Niznij Novgorod, Russian Federation; 2. Physics, Universitat Konstanz, Konstanz, Germany; 3. Institute of Physics for Advanced Materials, Nanotechnology and Photonics (IFIMUP)/Departamento de Física e Astronomia, Universidade do Porto, Porto, Portugal; 4. Materials Science and Engineering, University of Virginia, Charlottesville, VA, United States*

Today magnetic recording is still the leading technology for mass data storage with data densities beyond 1 Tbit/in^2. Pushing the recording density in the terabit regime requires new storage materials, novel recording schemes, and media designs. We propose an approach to magnetic recording upon the basis of thermally induced chemical order-disorder transitions (CODTs) in alloys of transition metals, which exhibit disorder-induced ferromagnetism. [1,2] Here we report on our simulations of CODTs and demonstrate that nanosecond laser irradiation concentrated within a nanoscale spot on the sample surface is able to induce the reversible transitions in Fe-rich Fe_xAl_{1-x} alloys. Figure 1 shows a design of magnetic recording media which can be realized upon that basis by using near-field optical effects and special tools, e.g., a near-field transducer (NFT) [3]. It is crucial for this approach that the bits can be written as *erasable* nanoscale entities in which the magnitude of magnetization differs from that of encompassing matrix. Therefore, contrary to the existing magnetic memories, the information here can be encoded in not the polarity of magnetization but in its magnitude. As a result, difficult problems in current magnetic recording technologies, e.g., thermal upsets of magnetization and cross-talks between adjacent bits, can be circumvented by using the approach we propose. This work was supported by RFBR (grant #18-02-00827_a), DFG through the SFB 767 at the University of Konstanz, by NECL and FCT support through Project Nos. NORTE-01-0145-FEDER-022096, PTDC/FIS-MAC/31302/2017, and by EXPL/IF/00541/2015, and by NSF (project TG-DMR110090).

[1] J. Ehrler, M. He, M.V. Shugaev, *et al*., Laser-rewriteable ferromagnetism at thin-film surfaces. *ACS Appl. Mater. Interfaces*, Vol.10 (17), p.15232 (2018) [2] N. I. Polushkin, V. Oliveira, R. Vilar, *et al*., Phase-change magnetic memory: rewritable ferromagnetism by laser quenching of chemical disorder in $Fe_{60}Al_{40}$ alloy, *Phys. Rev. Appl.,* Vol.10 (2), 024023 (2018) [3] W. Challener, C. Peng, A. Itagi, *et al*., Heat-assisted magnetic recording by a near-field transducer with efficient optical energy transfer. *Nat. Photon.*, Vol. 3 (4), p. 220 (2009)

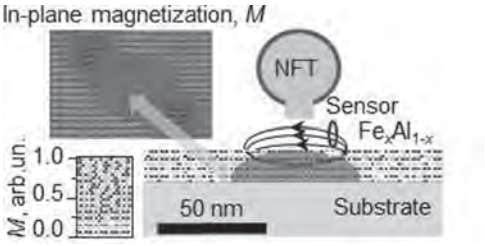

Fig.1. Design of magnetic recording media based on CODTs. Information bits are nanoscale regions with a reduced magnitude of the magnetization written with near-field optical effects [3]. The written information can be read out by detection of the stray field. In the upper left corner, the simulated distribution of magnetization in the written bit is shown.

Session P3
MICROMAGNETIC MODELLING II

Ali Ghoreyshi, Chair
Seagate Technology, Sain Louis Park, MN, United States

INVITED PAPER

P3-01. Macromagnetic Simulations by Micromagnetic Superposition.
H. Oezelt[1], M. Gusenbauer[1], P. Zhao[2], T.G. Woodcock[2] and T. Schrefl[1]
1. Department for Integrated Sensor Systems, Danube University Krems, Wr. Neustadt, Austria; 2. Institute for Metallic Materials, IFW Dresden, Dresden, Germany

Micromagnetic simulations are typically limited to a few micrometers due to the high demand on computing resources. But in applications and experiments the specimen size is usually orders of magnitude larger. While the micromagnetic simulations reproduce trends nicely, the absolute value of the results differ from the experiments [1]. Often the size limitation in the simulations is the reason for this deviation. Normally this is overcome either by artificial scaling [2] or by a reduced-order model [3]. In this work we introduce a type of reduced-order model to bridge the length scale from micromagnetism to experiments. In contrast to the work of Blank [4], we also consider the microstructural features of the magnet. We subdivide the computation of a large sample, e.g. from experimental measurements, into multiple independent feasible-sized subsets. For each subset, the nucleation field is either calculated by micromagnetic simulation or predicted by a trained machine learning model [5] (Fig. 1). The subsets along with their microstructure and nucleation fields are fed into a newly developed python code to spatially reassemble the entire sample and compute the overall hysteresis (Fig. 2). To take the microstructure into account, each subset is further discretized in cubic elements with their own anisotropic easy axis. In each calculation step, the magnetostatic field and the exchange field of the entire sample is calculated based on the magnetic moments of these elements. The two field contributions and an increasing external field are summed up to a total field. Taking this total field into account, we compute the reversible rotations with the Stoner-Wohlfarth model and use the prestored nucleation fields to irreversibly switch the respective subset. We gratefully acknowledge the financial support of the Austrian Science Fund (FWF), Project: I 3288-N36 and the German Research Foundation (DFG), Project:326646134.

[1] X. Tang, et al., Acta Mater. 144, 884-895 (2018) [2] S. Bance, et al., Acta Mater. 131, 48-56 (2017) [3] L. Exl, et al., J. Phys. Mater. 2, 014001 (2019) [4] R. Blank, J. Magn. Magn. Mater. 101, 1-3, 317-322 (1991) [5] M. Gusenbauer, et al., accepted npj Comput. Mater., (2020)

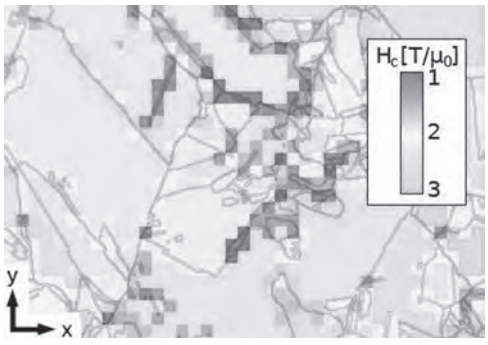

Fig. 1: Local nucleation fields for subsets (color coded squares) of magnetic sample with microstructure shown in background.

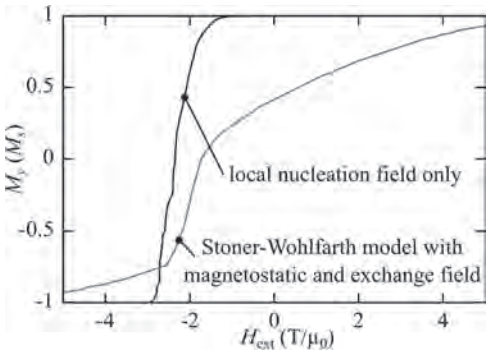

Fig. 2: By applying the Stoner-Wohlfarth model and including the magnetostatic and the exchange field, a realistic hysteresis curve of a 180x120 µm² thin film sample was calculated.

CONTRIBUTED PAPERS

P3-02. High Order Methods for Computing the Demagnetization Tensor for Periodic Boundaries.
M.J. Donahue[1] and D.G. Porter[1]
1. Information Technology Laboratory, National Institute of Standards and Technology, Gaithersburg, MD, United States

In finite-difference micromagnetics the self-magnetostatic field is computed via the demagnetization tensor N, where $H(r_2) = -N(r_2-r_1)\, M(r_1)$. For simulations with periodic boundary conditions, N is replaced with the periodic variant N^{PBC}, which is the infinite sum of the non-periodic tensor offset by periodic dimension width W, $N^{PBC}(r)=\sum_{k=-\infty}^{\infty} N(r+kW)$. Truncating the sum at k=±M yields a poor approximation to N^{PBC} because the convergence rate is only $O(1/M^2)$ (Fig. 1). This can be improved to $O(1/M^4)$ by replacing the summation tails with an integral of the dipole approximation [1], but even so roughly 200 terms are needed to obtain single precision accuracy. This work studies high-order approximations to N^{PBC} using the Euler-Maclaurin formula [2]: $N^{PBC}(r) = \sum_{k=-M}^{M} N(r+kW) + (\int_{-\infty}^{-MW} + \int_{MW}^{\infty}) F(r+sW)\, ds + (F(r-MW)-F(r+MW))/2 + \sum_{k=2}^{P} B_k/k!\, (F^{(k-1)}(r-MW) - F^{(k-1)}(r+MW))$ where B_k are Bernoulli numbers and F is a high-order asymptotic approximate to N. High accuracy in N^{PBC} can be obtained with M as small as 5 or 10. This improvement is especially pertinent for 2D PBC, where the truncation convergence drops from $O(1/M^2)$ to $O(1/M)$, and the number of N images within distance MW increases from O(M) to $O(M^2)$. The Euler-Maclaurin formula requires integrals and derivatives of F. F has the form $\sum_{ijkn} c_{ijkn}\, x^i y^j z^k / R^n$, and can be represented as a list of quintuples, (c,i,j,k,n). Derivatives of F have the same form and can be computed via a simple rule, admitting implementation as a handful of routines operating on quintuples rather than hard-coded explicit formulae. Integrals of F can be handled similarly. The result is a compact code that is simple to write and maintain that allows run-time selection of method order. The last is important because optimal method order and cut-off value M vary with discretization cell aspect ratio. The presentation will detail N^{PBC} error estimates for 1D and 2D PBC, method order and cut-off value M selection, and estimated computation times.

[1] K.M. Lebecki, M.J. Donahue, and M.W. Gutowski, *Journal of Physics D-Applied Physics*, Vol. 41, p. 175005 (2008). [2] *NIST Digital Library of Mathematical Functions*. http://dlmf.nist.gov/, Release 1.0.27, Eq. 2.10.1. F. W. J. Olver, A. B. Olde Daalhuis, et al., eds.

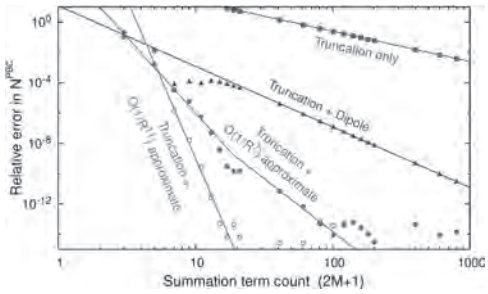

Relative error in N^{PBC} for a sample with discretization cell geometry 2×3×1 and a 1D periodic window width W=20. The top curve (filled squares) is error when the PBC sum is truncated at ±M. The lower curves show error improvement using higher order approximates.

P3-03. Micromagnetic Exchange Field Calculations for Unstructured Meshes. *E.B. Poulsen*[1], A.R. Insinga[1] and R. Bjørk[1] *1. Department of Energy Conversion and Storage, Technical University of Denmark (DTU), Kgs. Lyngby, Denmark*

Micromagnetic simulations are employed for predicting the behavior of magnetic materials from their microscopic properties, using the Landau-Lifshitz-Gilbert Equation $dM/dt = -\gamma M \times H_{eff} - \gamma \alpha (M \times (M \times H_{eff})) / M_s$, with magnetization M, gyromagnetic ratio γ, dampening coefficient α and effective field H_{eff}, $H_{eff} = H_{exch} + H_{dem} + H_{ext} + H_{anis}$. Here H_{exch} is the exchange field, H_{dem} the demagnetization field, H_{ext} an applied field and H_{anis} the anisotropy field. By far the most time consuming part of these calculations consists of calculating the demagnetization field, H_{dem}. Standard approaches compute H_{dem} as the convolution of magnetization with the dipolar interaction kernel using fast-Fourier transforms[1][2][3]. The framework MagTense[4], by contrast, calculates the demagnetization field analytically from a mesh of computational elements, which can be prisms[5] or tetrahedrons[6], as shown in Fig. 1. Such unstructured grids present new challenges for computing the differential operator in the exchange field H_{exch}. Here we investigate differential operators on general unstructured polyhedral meshes[7] and apply them to the micromagnetics standard problems[8] using MagTense. Specifically, we employ a weighted least squares interpolation[9] and a potentially novel method for calculating the Laplacian directly. The results are analyzed in terms of accuracy and speed and compared to those obtained with prism meshes.

[1] M.J. Donahue and D.G. Porter, Interagency Report NISTIR 6376, National Institute of Standards and Technology, Gaithersburg, MD (1999) [2] A. Vansteenkiste and B. Van de Wiele, Journal of Magnetism and Magnetic Materials 323, (21), 2585 - 2591, (2011) [3] A. Kakay, E. Westphal and R. Hertel, IEEE Transactions on Magnetics 46, (6), 2303-2306, (2010) [4] K.K. Nielsen and R. Bjørk, https://doi.org/10.11581/DTU:00000071 (2019) [5] A. Smith, K.K. Nielsen and D.V. Christensen, J. Appl. Phys. 107 (10), 103910 1-8, (2010) [6] K. K. Nielsen, A. R. Insinga and R. Bjørk, IEEE Magnetics Letters 10, 1-5, (2019) [7] E. Sozer, C. Brehm and C.C. Kiris, Gradient Calculation Methods on Arbitrary Polyhedral Unstructured Meshes for Cell-Centered CFD Solvers, 52nd Aerospace Sciences Meeting (2014) [8] https://www.ctcms.nist.gov/~rdm/mumag.org.html (Visited June 26, 2020) [9] D. Pérez-Grande, O. Gonzalez-Martinez and P. Fajardo, Applied Sciences 6 (2016)

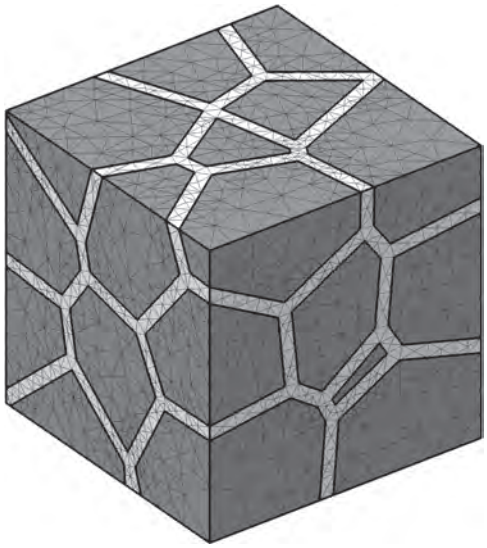

Fig. 1: An example tetrahedral meshed grain structure. Colored tiles represent the grains and white tiles represent the inter-grain phase. The resolution can be altered to resolve the same structure with more or fewer tiles.

P3-04. Coarse-Graining in Micromagnetic Simulations of Dynamic Hysteresis Loops. *R. Behbahani*[1,2], M.L. Plumer[1] and I. Saika-Voivod[1,2] *1. Physics and Physical Oceanography, Memorial University of Newfoundland, St. John's, NL, Canada; 2. Applied Mathematics, Western University, London, ON, Canada*

We use micromagnetic simulations based on the stochastic Landau–Lifshitz–Gilbert equation to calculate dynamic magnetic hysteresis loops at finite temperatures that are invariant with simulation cell size. As a test case, we simulate a magnetite nanorod, the building block of magnetic nanoparticles that have been employed in preclinical studies of hyperthermia [1]. With the goal to effectively simulate loops for large iron-oxide-based systems at relatively slow sweep rates on the order of 1 Oe/ns or less, we modify and employ a previously derived renormalization group (RG) approach for coarse-graining [2]. The scaling algorithm is shown to produce nearly identical loops over several decades in the model cell volume [3]. We also demonstrate sweep-rate scaling involving the Gilbert damping parameter that allows orders of magnitude speed-up of the loop calculations.

[1] C. L. Dennis et al., Nanotechnology Vol. 20, p.395103 (2009) [2] G. Grinstein and R. H. Koch, Phys. Rev. Lett. Vol. 90, No. 20, p.207201 (2003) [3] R. Behbahani, M. L. Plumer and I. Saika-Voivod, J. Phys. Condens. Matter, Vol. 32, No.35LT01 (2020)

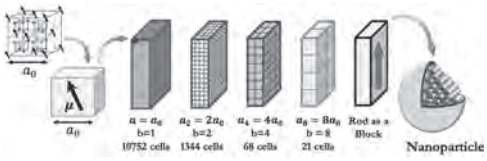

Fig. 1) Coarse-grained modelling of a magnetite nanorod. The smallest micromagnetic cell models the atomic spins within a cubic unit cell of length a_0 = 0.839 nm with a single magnetic moment. Our goal is to model the system using a smaller number of larger cells (of length $a_b = ba_0$ for b > 1) with appropriately scaled exchange and anisotropy parameters. Nanoparticles comprise nanorods [1].

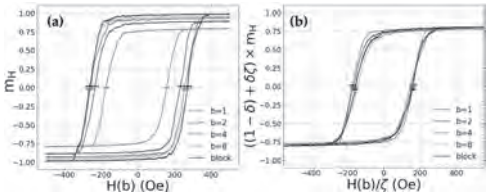

Fig. 2) Application of RG coarse-graining to nanorod MH loops at T = 310 K and sweep rate of 2.5 Oe/ns. (a) Changing cell length ($a_b = ba_0$) without changing magnetic parameters. (b) Exchange constant and uniaxial anisotropy energy density are scaled according to Grinstein and Koch [2], and m and H are scaled according to the modification in Ref. [3] with δ= 0.511, Δt = 1 fs for all simulations. Horizontal error bars shown for H_C represent one standard error and are vertically displaced to avoid overlap. Uncertainty in H_C is approximately 7 to 13%.

P3-05. High-Performance Micromagnetics on GPUs for Batched Simulations. *X. Wang*[1] and V. Lomakin[1] *1. University of California San Diego, La Jolla, CA, United States*

An important task in micromagnetics is performing a large ensemble of simulations of a structure with only one or a few changed parameters. An example is computing write error rates in magnetic random-access memories (MRAM), where simulations are needed for different stochastic thermal fields. Such computations, which are done by multiple runs on a single or multiple computing devices. have various numerical overheads related to preprocessing, matrix operations, and excessive data storage. We demonstrate a computational approach for performing a large batch of repetitive micromagnetic simulations on a Graphics Processing Unit (GPU) simultaneously. This batched approach has the following benefits: (i) it utilizes GPUs much more efficiently than the traditional approach of running multiple simulations, including much increased speed and reduced memory consumption, (ii) it hides various numerical overheads, such as preprocessing as well as matrix and time stepping operations, (iii) it makes obtaining results and post-processing much more efficient by allowing computing only required properties, e.g. ensemble averages or switching counts. We extended our FEM based micromagnetic framework FastMag to implement the batched approach in all code components, including pre-processing, matrix operations (Fig. 1a), time stepping with adaptivity to step, order, and decisions of a stopping evens per instance (Fig. 1b). Figure 2 shows major improvements of the computational time and memory consumption for switching simulations of an MRAM cell using three 100-instance batch scenarios on an Nvidia GTX1080 GPU: sequential launching of 100 instances, simulating a 100 x 100 array of sufficiently separated cells (to prevent the strong magnetostatic coupling), batched approach. This work was supported as part of the Quantum Materials for Energy Efficient Neuromorphic Computing, an EFRC funded by the U.S. DOE, Office of Science.

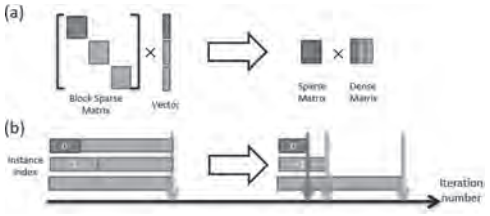

Fig.1: (a) data re-use by replacing several sparse matrices – vector product by a sparse – dense matrix product; (b) stopping of simulations independently per each batch realization.

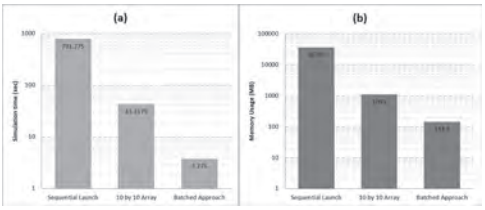

Fig.2: (a) Computational time and (b) memory consumption.

P3-06. Introducing Flatspin: Enabling Large Scale Dynamical Artificial Spin Ice Simulations. J.H. Jensen[1], *A. Strømberg*[2], O. Lykkebø[1], A. Penty[1], M. Själander[1], E. Folven[2] and G. Tufte[1] *1. Department of Computer Science, Norges teknisk-naturvitenskapelige universitet, Trondheim, Norway; 2. Department of Electronic Systems, Norges teknisk-naturvitenskapelige universitet, Trondheim, Norway*

We introduce flatspin, a novel simulator for artificial spin ices (ASI), i.e., ensembles of dipole coupled nanomagnets arranged in a deliberately constructed geometry. Understanding the complex behavior of these systems has provided insight into a wide range of phenomena [4]. Modeling the dynamics of ASI and their connection to the specific design has been paramount to the progression of ASI research [5]. However, conventional modeling techniques are often either too computationally costly or do not provide enough insight into the dynamics of the ASI. Monte Carlo methods approximating each magnet as a single dipole are useful in the search for low-energy configurations [1, 6], but capturing state transitions and dynamics observed in real systems is challenging. On the other hand, high-fidelity micromagnetic simulations are restricted to a small number of nanomagnets due to the computational cost. With the relatively small systems available through this approach, it is difficult to capture large-scale emergent behavior, e.g. [6]. With flatspin, we offer a different approach to the challenge of modeling, and aim to capture large-scale ASI behaviors. At the heart of flatspin lies a robust magnetic dipole model and a switching criteria based on a generalized Stoner-Wohlfarth model. GPU acceleration together with a model optimized for speed enables flatspin to simulate realistic dynamics of millions of magnets within practical time frames. We demonstrate the versatility of flatspin by modeling a diverse set of established experimental results. Reproduced results include emergent fine-scale patterns in kagome ASI [3], large-scale domain sizes in square ASI [6], and different magnetic ordering of square and pinwheel ASI [2] (see Fig. 1). Furthermore, magnetization details of pinwheel ASI during field-driven reversal have been reproduced, for the first time, by a dipole model. With its capability to model ASI dynamics at unprecedented speeds, we believe flatspin will be an asset to the ASI community.

[1] X. Ke, J. Li, C. Nisoli et al., Physical Review Letters., Vol. 101(3), p.037205 (2008) [2] R. Macêdo, G. M. Macauley, F. S. Nascimento et al., Physical Review B., Vol. 98(1), p. 014437 (2018) [3] E. Mengotti, L. J. Heyderman, A. F. Rodríguez et al., Nature Physics., Vol. 7(1), p.68 (2011) [4] S. H. Skjærvø, C. H. Marrows, R. L. Stamps et al., Nature Reviews Physics., Vol. 2(1), p.13–28 (2020) [5] R. L. Stamps, Nature Physics., Vol. 10(9), p.623–624 (2014) [6] S. Zhang, I. Gilbert, C. Nisoli, Nature., Vol. 500(7464), p.553–557 (2013)

Magnetization maps of square (right) and pinwheel (left) ASI. Each pixel represents the net magnetization of eight magnets, highlighted in insets. Note that white indicates no net magnetization (the eight moments cancel).

P3-07. Magnetic Barkhausen Noise: a Simulation Tool. *P. Fagan*[1,2], B. Ducharne[2], L. DANIEL[3] and A. SKARLATOS[1] *1. CEA – DISC, CEA-LIST, CEA Saclay DIGITEO LABS, Gif-sur-yvette, France; 2. Institut National des Sciences Appliquees de Lyon, Villeurbanne, France; 3. Université Paris-Saclay, CentraleSupélec, CNRS, Group of Electrical Engineering-Paris (GeePs), Gif-sur-yvette, France*

Non-destructive magnetic controls are increasing in the industrial field. In this domain, the expectation for simulation tools able to anticipate the magnetic signature, improve the understanding and avoid fastidious and uncertain experimental pre-characterization is high. Among different methods, the magnetic Barkhausen noise (MBN) control is probably the most popular [1]. MBN raw signal is stochastic, not reproducible and complex to exploit. MBN_{energy}, which is obtained by integrating the square of the MBN voltage signal with respect to the time axis is a much more stable indicator [2][3]. Although the so-called MBN_{energy} is not, strictly speaking, an energy, it is connected to the domain wall motion and their kinetic energy. By plotting MBN_{energy} as a function of H (the tangent surface excitation field) hysteresis cycles are observed. After rescaling MBN_{energy} on B (the induction field), $B(H)$ and $MBN_{energy}(H)$ hysteresis cycles look similar for high magnetocrystalline anisotropy energy material, i.e. when domain wall contribution dominates magnetization rotation during the magnetization process. In this study, a multiscale model [4] is used to simulate an anhysteretic behavior limited to the domain wall contribution. By using, this anhysteretic contribution in the Jiles-Atherton model and running an inverse procedure [5][6], a MBN envelop very close to the experimental ones can be obtained. By modulating the amplitude of an alternating, high frequency signal using this envelop, an accurate simulation of the raw Barkhausen noise is obtained.

[1] B. Ducharne et al., IEEE Trans. Magn., Vol. 54, Iss. 11, 6202606 (2018). [2] B. Ducharne et al., J. Magn. Magn. Mater., Vol. 432, pp. 231-238 (2017). [3] B. Gupta et al., J. Magn. Magn. Mater., Vol. 498, 166102 (2020). [4] L. Daniel et al., Arch. Appl. Mech., Vol. 84, pp. 1307-1323 (2014). [5] J.V. Leite et al., IEEE Trans. Magn., Vol. 39, n° 3, pp. 1397-1400 (2003). [6] B. Zhang et al., IEEE Trans. Magn., Vol. 54, Iss. 11, 7301605 (2018).

P3-08. Thermal Activation Barriers for Creation and Annihilation of Magnetic Droplet Solitons in the Presence of Spin Transfer Torque. *G.D. Chaves*[1] and D.L. Stein[2,3] *1. Department of Thin Films, Polska Akademia Nauk Instytut Fizyki Molekularnej, Poznan, Poland; 2. Department of Physics and Courant Institute of Mathematical Sciences, New York University, New York, NY, United States; 3. Santa Fe Institute, Santa Fe, NM, United States*

Droplet solitons are magnetization fluctuations that preserve their shape as they precess with uniform frequency ω=0. They satisfy a delicate balance between anisotropy and exchange interactions, and decay in the presence of dissipation. To prevent this, a spin polarized current σ can be applied via a nanocontact of radius ρ*. The magnitude of the current can be increased to induce switching between uniform precession at the ferromagnetic resonance frequency (ω=1), and a stable precession at a frequency larger than the Zeeman frequency (ω=0, in zero applied field). In the absence of dissipation, conservative solitons of frequency ω_0 are described by a function $\Theta(\rho;\omega_0)$, where Θ is the angle of the magnetization with the easy axis and ρ is the distance to the center of the nanocontact[1]. We introduce an effective energy ξ that quantifies the work done (against damping and spin torque) to create a fluctuation of arbitrary shape Θ(ρ). We show that, for specific values of σ, some conservative soliton solutions are saddles of ξ. This allows us to calculate activation barriers Δξ between uniform precession at the ferromagnetic resonance and stable solitons. We present results of Δξ as a function of σ for a variety of nanocontact radii ρ* and spin-torque anisotropy parameters ν. We present micromagnetic simulations with a modified Spin-Transfer-Torque extension in OOMMF which uses the effective energy ξ introduced here. In this way, the difference of energies between transition states and metastable configurations can be used to estimate annihilation rates of droplet solitons.

[1] Gabriel D. Chaves-O'Flynn and D. L. Stein, Phys. Rev. B 101, 184421 (2020) [2] M. A. Hoefer, T. J. Silva, and M. W. Keller, Phys. Rev. B 82, 054432 (2010).

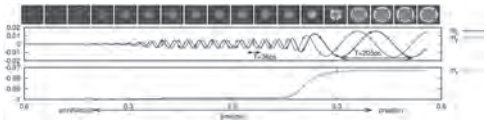

Micromagnetic OOMMF simulations showing evolution of the magnetization starting from the transition state. Depending of the strength of the current the magnetization relaxes into the uniform magnetization (from the center to the left), or to a stable droplet soliton (from the center to the right). Image taken from Ref [1].

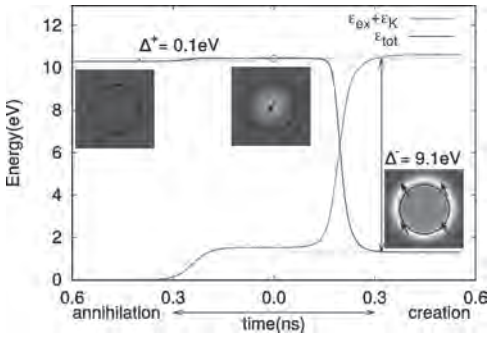

Evolution of the effective energy from OOMMF simulations starting from the transition state. The activation barriers can be measured by subtracting the energy of the final state (left and right) from the saddle state (center). Image published in Ref [1].

P3-09. Theoretical Study of Current Induced Domain Wall Motion in Magnetic Nanotubes With Azimuthal Magnetization. *J. Hurst*[1], A. De Riz[1], O. Fruchart[1], J. Toussaint[2] and D. Gusakova[1] *1. Univ. Grenoble Alpes, CNRS, CEA, Grenoble INP**, Spintec, F-38000, Grenoble, France, Grenoble, France; 2. Univ. Grenoble Alpes, CNRS, Institut NEEL, Grenoble, France*

While magnetic nanowires and to a lesser extent nanotubes have been synthesized and investigated for three decades, it is only recently that their properties are being monitored at the scale of single objects, such as for instance domain wall motion. In particular, a peculiar class of domains were observed in nanotubes – domains with azimuthal (flux-closure) magnetization [1] (CoNiB, 400nm diameter). The azimuthal magnetization even in long tubes is related to magnetic anisotropy of the material itself, either through intergranular interface anisotropy or magneto-elastic coupling (inverse magnetostriction). Interestingly, this may opens the possibility of moving walls with only electric currents via the Oersted field. We explored the current-induced dynamics of such walls with theory and numerics, considering both the effect of the Oersted field and spin-torque-induced effects (STT) [2]. We derive a phase diagram predicting the stable azimuthal domains versus the anisotropy strength and the tube geometry, see Fig. 1. In addition, we similarly predict the type of stable walls, either Néel or Bloch, pictured in Fig. 2, resulting from the competition between the curvature induced exchange energy, the demagnetization energy and the anisotropy energy. We show the existence of STT and/or Oersted dominated regime for both domain wall structures and we report large domain wall speeds reaching potentially 800 m/s, before of the occurrence of a so-called Walker breakdown. We show how the domain wall speed and the walker field depend on the anisotropy and the geometrical parameter of the magnetic tubes. Our study may guide the experimental realization of magnetic tubes, targeting the optimal parameters to get the desired properties.

[1] M.Staño, O. Fruchart, Magnetic Nanowires and Nanotubes, Handbook of Magnetic Materials, Elsevier, v. 27, pp.155-267 (2018). [2] J. Hurst, A. De Riz, O. Fruchart, J. C. Toussaint and D. Gusakova, Theoretical study of

current induced domain wall motion in magnetic nanotubes with azimuthal magnetization, (to be submitted). [3] Alouges, F. Kritsikis, E. Steiner, J.-C. Toussaint, A convergent and precise finite element scheme for Landau–Lifschitz–Gilbert equation. *Numer. Math.* 128, 407–430 (2014).

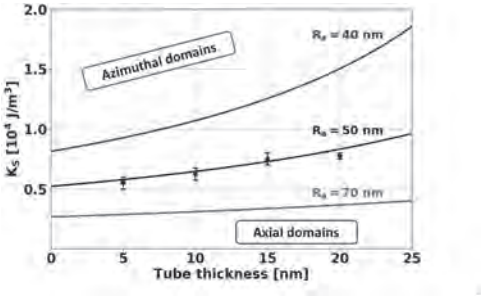

Fig. 1: Threshold values of the anisotropy strength separating axial monodomain (below the curve) from azimuthal monodomain (above the curve) as a function of the tube thickness for three different external tube radius. The markers indicate an estimation of the threshold anisotropy value obtained with feeLLGood simulations [3].

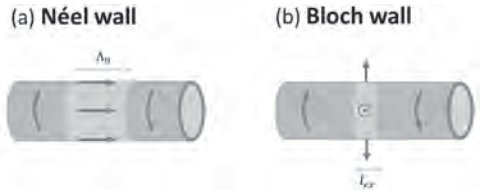

Fig. 2: Sketch of Néel (a) and Bloch (b) walls in magnetic nanotubes with azimuthal magnetization.

P3-10. Exchange Explosions of Topological Edge Defects in a Square Micromagnet. *S. Slöetjes*[1], E. Folven[2] and J.K. Grepstad[2] *1. Physics and Astronomy, Uppsala Universitet, Uppsala, Sweden; 2. Department of Electronic Systems, Norges teknisk-naturvitenskapelige universitet, Trondheim, Norway*

The magnetodynamic properties of a square thin-film micromagnet (2μm×2μm×16nm) with a flux-closure magnetic ground state were investigated by micromagnetic simulations. The system was excited with an applied magnetic field, displacing the vortex core sufficiently far from its equilibrium position to result in a nonlinear relaxation upon removal of the field. We focus on the edge defects that are created in the process of the vortex core displacement, and carry a half-integer winding number. The edge topological defects are seen to perform quasi-periodic exchange explosions and a resulting emission of short-wavelength spin waves upon travelling back to the equilibrium position. The exchange explosions of the edge topological defects are investigated and explained in terms of vortex/antivortex creation and the formation of a Bloch point. This finding could prove useful to the development of nanoscale devices for periodic generation of high-frequency microwave radiation.

1. S. D. Slöetjes, E. Folven, and J. K. Grepstad, Physical Review B Vol. 101, p. 014450 (2020) 2. R. Hertel, and C. M. Schneider, Physical Review Letters Vol. 97, p. 177202 (2006) 3. M. Noske et al., Physical Review B Vol. 91, p. 014414 (2015) 4. S. D. Slöetjes et al., Applied Physics Letters Vol. 112, p. 042401 (2018)

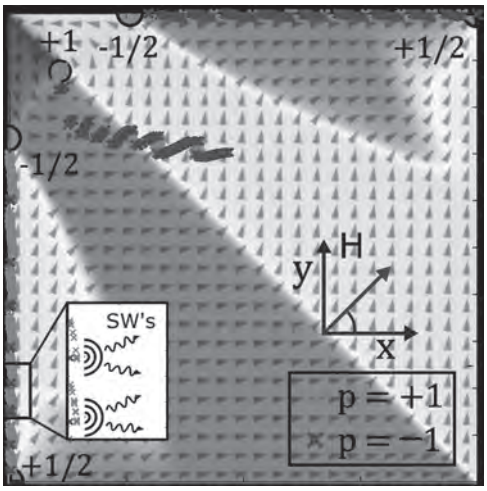

The emission of spin waves and accompanied changes in the edge and bulk defect core polarities upon travelling back to equilibrium.

P3-11. Exploring Coercivity as a Function of Boundary Conditions in Simulated Nanochessboard Colonies: Free Surface, Semi-Infinite Single Crystal, and Intra-Colony Conditions. *A. Savovici*[1], Y. Jin[2], W.A. Soffa[1] and J.A. Floro[1] *1. Materials Science Department, University of Virginia, Charlottesville, VA, United States; 2. Materials Science Department, Michigan Technological University, Houghton, MI, United States*

The nanochessboard is a fascinating microstructure in which to investigate exchange-coupled ferromagnetism. We have produced Co-Pt alloys with 60 at %Pt in which nanorods of the magnetically hard L10 phase are enmeshed within a magnetically soft, ordered L12 matrix. The L10 & L12 nanorods self-assemble by cooling through the eutectoid and arrange into quasi-periodic tiles with coherent interfaces – allowing unimpeded exchange coupling to occur. Our previous micromagnetic simulations have shown that the nanochessboard exhibits non-monotonic changes in coercivity as the tiling lengthscales vary due to competing exchange interactions between the phases[1]. Our micromagnetic simulations can be used to answer another pertinent question: what are the effects of boundary conditions on magnetization reversal? Crystal symmetry dictates that chessboard colonies align along one of the three equivalent [100] directions of the original parent crystal. The boundaries of each colony will support uncompensated poles due to the discontinuities in magnetic easy axes, leading to demagnetizing fields that reduce the coercivity. We are simulating three scenarios to explore the effect of colony structure on chessboard coercivity: (1) two-dimensional periodic boundary conditions in the plane of the chessboard tiling, which approximates a semi-infinite single crystal; (2) fully free boundary conditions, that treat a colony as a free-standing particle with no surface compensation; and (3) a simplified "mean-field" approach that sandwiches a chessboard colony within a uniform ferromagnetic medium. The chessboards are simulated using the OOMMF (Objected Oriented Micromagnetic Framework) package. To better compare with our experiments, our ultimate goal is to simulate first order reversal curves (FORCs). Chessboard FORCs tend to show complex features whose origins are still not understood. Support of the National Science Foundation through grant DMR-1709914 is gratefully acknowledged.

1. Geng LD, Soffa WA, Floro JA, Jin YM. Exchange coupling effects in Co-Pt nanochessboards. *J Appl Phys*. 2018;123(9):0-7.

P3-12. Magnetization Reversal of FePt Thin Films: Experiments and Simulations. *A. Román*[1], J. Gómez[2], A. Butera[2], K. Bouzehouane[3,4], C. García[5] and L. Steren[1] *1. Laboratorio de Nanoestructuras Magnéticas y Dispositivos, Instituto de Nanociencia y Nanotecnologia CNEA-CONICET, San Martin, Argentina; 2. Centro Atomico Bariloche, Bariloche, Argentina; 3. Unité Mixte de Physique CNRS/Thales, Palaiseau, France; 4. Univ. Paris-Sud/Université Paris-Saclay, Palaiseau, France; 5. Universidad Técnica Federico Santa María, Departamento de Física & Centro Científico Tecnológico de Valparaíso-CCTVal, Valparaiso, Chile*

Thin films with stripe domains configuration have been extensively investigated because of their intriguing behavior. This configuration results from the competition between perpendicular and shape anisotropies measured by the quality ratio $Q = K/2\pi M_s^2$. For $Q<1$ two situations can occur depending on the films thickness: above a critical value, *tc*, the system develops stripe domains while for $t<tc$ the magnetization lies in the plane of the films. The thicker films exhibit a rotational anisotropy, i.e. a uniaxial in-plane anisotropy whose axis is parallel to that of the applied magnetic field [1-3]. In this work, we present an analysis of the magnetization reversal in FePt films grown by sputtering on silicon substrates. The films thickness was varied from 10nm to 60nm in order to examine the magnetic properties below and over the critical thickness. The magnetic properties were studied by magnetometry and Magnetic Force Microscopy experiments. Magnetization loops and MFM images were simulated using Mumax3 software [4]. For the thinner films, the coercive field (Fig. 1) follows the angular dependence described by Kondorsky for magnetization reversal driven by domain-wall motion [5]. By micromagnetic simulations we investigated the formation of the domains and the domain wall motion during the magnetization reversal. Coercive field angular dependence for the thicker films (Fig. 2) was fitted by a sine-law, associated to coherent rotation, with a finite value for the hard-axis. Our simulation results indicate that the magnetization reversal within each stripe occurs by coherent rotation. In summary, we determined the magnetization switching mechanisms for FePt films by experiments and simulations, contributing to the comprehension of this phenomenon.

[1] S. Fin, R.Tomasello and A. Rettori, Phys. Rev. B., Vol. 92, p. 224411(2015) [2] I.S. Camara, S.Tacchi and M. Marangolo, J. Phys.: Condens. Matter., vol. 29, p. 465803 (2017) [3] J.M. Guzman, N. Álvarez and A. Butera, J. Magn. Magn. Mater., vol. 347, p. 61 (2013) [4] A. Vansteenkiste, J. Leliaert and B. Van Waeyenberge, AIP Adv., vol. 4, p. 107133 (2014) [5] K. R. Coffey, T. Thomson, and J. Thiele, J. Appl. Phys., vol. 92, p. 4553(2002)

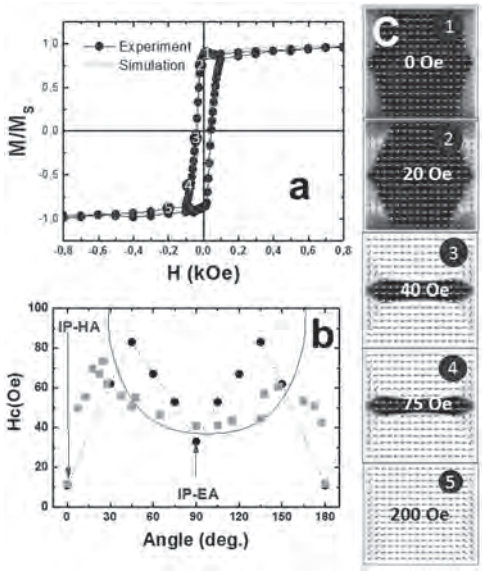

Fig.1: 12nm FePt thin film: (a) Simulated and experimental hysteresis loops (b) Coercive field angular dependence (c) Simulated domain configuration

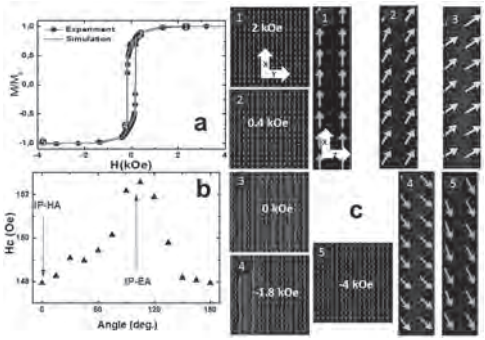

Fig.2: 40nm FePt thin film: (a) Simulated and experimental hysteresis loops (b) Coercive field angular dependence (c) Simulated domain configuration

Session P4
ANTIFERROMAGNETIC SPINTRONICS IV
(Poster Session)

Romain Lebrun, Chair
Unité Mixte de Physique CNRS/Thales, Palaiseau, France

P4-01. Withdrawn

P4-02. Withdrawn

P4-03. Spatial Oscillations of the Spin Transfer Torque in Ferrimagnetic MTJs From First Principles. *M.T. Stamenova*[1], P.S. Stamenov[1], Q. Sun[2], N. Kioussis[2] and S. Sanvito[1] *1. School of Physics and CRANN, University of Dublin Trinity College, Dublin, Ireland; 2. W. M. Keck Computational Materials Theory Center, California State University, Northridge, Northridge, CA, United States*

While ubiquitous in bulk resonance devices, ferrimagnets are just beginning to make their way into spintronic devices, as both insulating and metallic components. Here we report on first principles calculations of spin-transfer torque (STT) in epitaxial magnetic tunnel junctions (MTJs) based on ferrimagnetic tetragonal Mn_3Ga [1] electrodes, both as analyser in a Fe/MgO stack, and also in an analogous stack with Mn_3Ga electrode (insead of Fe) as polariser. Solving self-consistently the ballistic transport problem for the non-equilibrium spin density [2,3] in a scattering region extended to over 8 nm into the Mn_3Ga electrode, we find a long-range spatial oscillation of the STT decaying on a length scale of a few nm (Fig. 1), both in linear response and for finite bias. The STT oscillation is robust against variations in the stack geometry: the barrier thickness and the interface spacing affect only the amplitude and phase of the spatial oscillation, the chief frequency is largely determined by the lattice constant of Mn_3Ga. This oscillatory behaviour of the linear-response STT is understood from the bulk electronic structure of Mn_3Ga and Fe, and the spin-filtering properties of the MgO barrier. Comparison to a fully Mn_3Ga-based stack shows similar STT oscillations but a significant enhancement of the TMR effect (Fig. 2), both at the Fermi level (for the thinner barrier) and at around 0.15 eV above the Fermi level. In view of this bias asymmetry, more effort is to be invested in Fermi-level engineering of ferrimagnetic electrodes, by means of both composition and strain.

[1] K. Rode, N. Baadji, D. Betto, et al. Phys. Rev. B, vol. 87, p. 184429 (2013). [2] M. Stamenova, I. Rungger, S. Sanvito, et al. Phys. Rev. B, vol. 95, p. 060403(R) (2017). [3] I. Rungger, A. Droghetti and M. Stamenova, Non-equilibrium Green's functions methods for spin transport and dynamics. In: Andreoni W., Yip S. (eds) Handbook of Materials Modeling, Springer (2018).

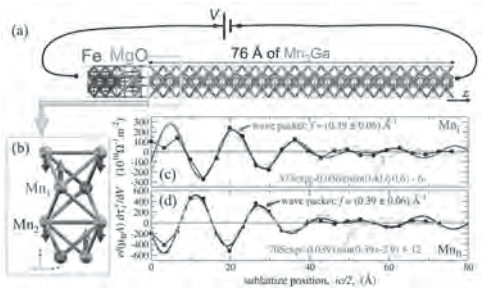

Fig. 1: (a) Schematic of the Fe/MgO/Mn_3Ga junction studied, (b) the unit cell of tetragonal Mn_3Ga depicting also the magnetic moments localised on the Mn_1 and Mn_2 magnetic sublattices. Shown in the graphs are atomically-resolved linear-response STT on Mn_1 and Mn_2, panels (c,d) respectively, starting from the MgO interface. The structures are periodic in the x-y plane.

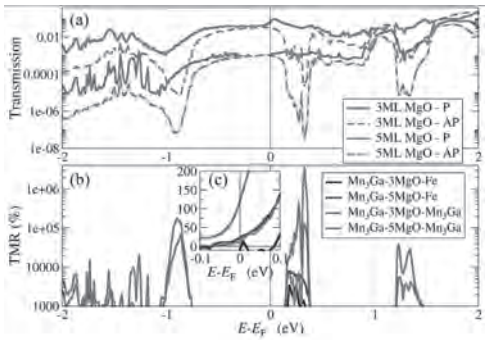

Fig. 2: Energy-resolved transmission coefficients for the different spin orientations at the interface (a) and TMR (b) for two different barrier thicknesses of Mn_3Ga/MgO/Mn_3Ga stacks, in (b) also is comparison to the Fe-polariser stack. The inset (c) is a zoom around the Fermi level.

P4-04. Withdrawn

P4-05. Sputtering Growth of Non-Collinear Antiferromagnetic Mn_3Sn Thin Films. *V. Kalappattil*[1], G. Street[1] and M. Wu[1] *1. Department of Physics, Colorado State University, Fort Collins, CO, United States*

Recent years have witnessed a rapidly growing interest in non-collinear antiferromagnet Mn_3X materials (X=Sn, Ge, or Ga) – a subgroup of topological Weyl semimetals. Experimentally, recent work has shown that, despite zero magnetization, Mn_3X exhibits strong anomalous Hall, magneto-optical Kerr, and magnetic spin Hall effects.[1-3] On the theory side, several new phenomena have been recently predicted to exist in Mn_3X, including an unusual spin Hall effect, a strong spin Nernst effect, and electric manipulation of antiferromagnetic ordering.[3-6] Inspired by those exciting phenomena, there have been efforts in the sputtering growth of Mn_3X thin films,[7,8] but it has proven challenging to fabricate Mn_3X films with smooth surfaces and properties comparable to the bulk properties. This work demonstrates sputtering growth

of Mn_3Sn films with smooth surfaces, right stoichiometry, and expected magnetic and transport properties. Specifically, [11-20] oriented Mn_3Sn films were grown on Al_2O_3 [1-102] substrates via co-sputtering of Mn and Sn targets; the co-sputtering enabled precise control of the stoichiometry. It's found that a substrate temperature of ~400 °C is crucial for obtaining high crystallinity without impurity phase; substrate cleaning prior to the sputtering and film annealing after the sputtering strongly affects film surface smoothness. 50-nm-thick films showed a surface roughness of 0.74 nm, much smaller than the values reported previously;[8] only [11-20] and [22-40] peaks in the X-ray diffraction spectrum; an atomic ratio of Mn:Sn=3.07:1.00, which is slightly higher than 3:1, as desired; a weak ferromagnetic response at room temperature, with 0.021 μ_B per formula unit, which is smaller than previously reported values for thin films;[7,8] an antiferromagnetic-to-ferromagnetic transition at 42-62 K, which is consistent with that in the bulk crystals (50 K); and an anomalous Hall resistivity of ~0.7 μΩ.cm. This work demonstrates the feasibility of the use of sputtering to grow high-quality Mn_3X thin films for the development of Mn_3X-based spintronic devices.

1. S. Nakatsuji, et al. Nature 527, 212 (2015). 2. T.Higo, et al. Nature Photonics 12, 73 (2018). 3. M.Kimata, et al. Nature (London) 565, 627 (2019). 4. G-Y. Guo and T-C. Wang, Phys. Rev. B 96, 224415 (2017). 5. H. Fujita, et al. Rapid Research Letters, 11, 1600360 (2017). 6. J. Liu and L. Balents, Phys. Rev. Lett. 119, 087202 (2017). 7. A. Markou, et al. Phys. Rev. Mater. 2, 051001(R) (2018). 8. Y. You, et al. Adv. Electron. Mater. 5, 1800818 (2019).

P4-06. Electrical Switching of Hall Resistance in Noncollinear Antiferromagnetic Antiperovskite Nitrides. *K. Matsuura*[1], T. Hajiri[1], K. Sonoda[1], S. Ishino[1] and H. Asano[1] *1. Nagoya Daigaku, Nagoya, Japan*

Recently, noncollinear antiferromagnets (AFMs) have become one of the most fascinating classes among AFMs, because they exhibit various peculiar magnetotransport properties include the anomalous Hall effect (AHE). [1] The theoretical study shows that the noncollinear AFM Néel vector can be manipulated by spin current with a realistic current density of 10^7 A/cm^2[2]. The antiperovskite manganese nitride Mn_3GaN (MGN) is a good platform to investigate the electrical current manipulation of noncollinear AFMs. In MGN, the Mn atoms form a kagome lattice in the (111) plane. The Neel temperature is reported to be above 380 K[3], which are relatively high for this class of materials. In this presentation, we show the spin-torque switching of noncollinear AFM MGN/Pt bilayers at room temperature[4] as well as AHE. MGN (001) films were prepared on MgO (001) substrates by reactive magnetron sputtering. The AHE versus magnetic field curve for MGN films are shown in Fig. 1. The AHE loop is observed with the same coercive field as the out of plane magnetization curves for MGN films. Therefore, the AHE loops shows the electrical detection of the magnetization for MGN films. The change in the Hall resistivity as a function of current density for MGN(20 nm)/Pt(3 nm) bilayers is shown in Fig. 2. Hall resistivity changes sharply and a clear hysteresis loop is observed at 300 K without an external magnetic field. The change of Hall resistivity is the same as AHE loop shown in Fig. 1, indicating the electrical write–read operation of noncollinear AFM Néel vector. The critical current density is estimated to be 3.6×10^6 A/cm^2, which is one to two orders of magnitude smaller than that for typical FM/HM bilayers[5] and the threshold current for collinear AFMs NiO/Pt spin-torque switching.[6] These results open the pathway to the efficient control of the noncollinear AFM order.

[1] S. Nakatsuji, N. Kiyohara, and T.Higo, Nature 527, 212-215(2015). [2] Y. Yamane, O. Gomonay, and J. Sinova, Phys. Rev. B 100, 054415 (2019). [3] W. J. Feng, D. Li, Y. F. Dend, and Q. Zhang *et al*., J. Mater. Sci. 45, 2770 (2010). [4] T. Hajiri, S. Ishino, and K. Matsuura *et al*., Appl. Phys. Lett. 115, 052403 (2019). [5] L. Liu, O. J. Lee, and T. J. Gudmundsen *et al*., Phys. Rev. Lett. 109, 096602 (2012). [6] X. Z. Chen, R. Zarzuela, and J. Zhang *et al*., Phys. Rev. Lett. 120, 207204 (2018).

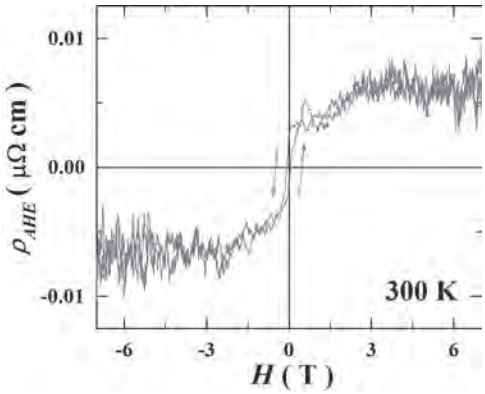

The AHE vs. magnetic field curve for Mn_3GaN films. (300 K)

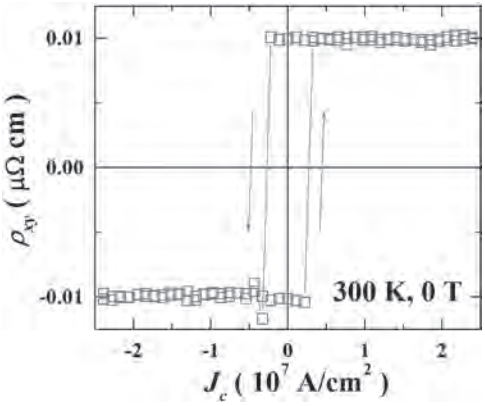

Hall resistance vs. current density for Mn_3GaN/Pt bilayers. (300 K, 0 T)

P4-07. Quantifying Current-Induced Torques Leading to Néel Vector Switching in CoO/Pt Bilayers. L. Baldrati[1], *C. Schmitt*[1], O. Gomonay[1], R. Lebrun[1], R. Ramos[2], E. Saitoh[2,3], J. Sinova[1,4] and M. Klaui[1,5] *1. Johannes Gutenberg Universitat Mainz, Mainz, Germany; 2. Tohoku Daigaku, Sendai, Japan; 3. Tokyo Daigaku, Bunkyo-ku, Japan; 4. Akademie ved Ceske republiky, Praha, Czechia; 5. Johannes Gutenberg University Mainz Graduate School of Excellence Materials Science in Mainz, Mainz, Germany*

Antiferromagnets (AFMs) are promising spintronic materials compared to ferromagnets, since they potentially enable faster operation, enhanced stability with respect to interfering magnetic fields and higher bit packing density due to the absence of stray fields [1]. However, the use of AFMs in applications requires efficient electrical reading and writing of information. While current-induced switching in NiO/Pt thin film systems has been shown, with various mechanisms proposed [2-4], key information such as the absolute torque strength is missing. Studying MgO//CoO(001)/Pt entails a number of advantages: due to the compressive strain by the substrate, a fourfold in-plane magnetic anisotropy of the CoO layer with two easy axes in the (001) plane is favored and the spin flop field is accessible [5]. Such anisotropy is ideal for applications where the orientation of the Néel order *n* is read by spin Hall magnetoresistance (SMR) [6,7]. To study current-induced switching, we used 8-arms Hall stars devices with the pulsing arms oriented along the [110] and [-110] easy axes directions (Fig. 1a). Initially *n* is aligned along [110]. When current pulses are applied along the contacts 3-2 (initial state $n \parallel j_{pulse}$), the transverse resistance drops after the first pulse, indicating a current-induced 90° *n* rotation (Fig. 1b). Performing a MR scan with field along 4-1 afterwards (Fig. 1c) yields a field-induced spin flop transition of *n* back to the initial state (Fig. 1d). By applying current pulses and magnetic fields, we can quantify the current field equivalence of the current-induced torques on the reorientation of *n* in the CoO, showing that, for the switching of AFMS, currents are much more efficient than magnetic fields.

[1] V. Baltz et al., Rev. Mod. Phys., 90, 015005 (2018). [2] X. Z. Chen et al., PRL, 120, 207204 (2018). [3] L. Baldrati et al., PRL, 123, 177201 (2019). [4] P. Zhang et al., PRL 123, 247206 (2019). [5] L. Baldrati et al., ArXiv:2003.05923 (2020). [6] H. Nakayama et al., PRL, 110, 206601 (2013). [7] L. Baldrati et al., PRB, 98, 024422 (2018).

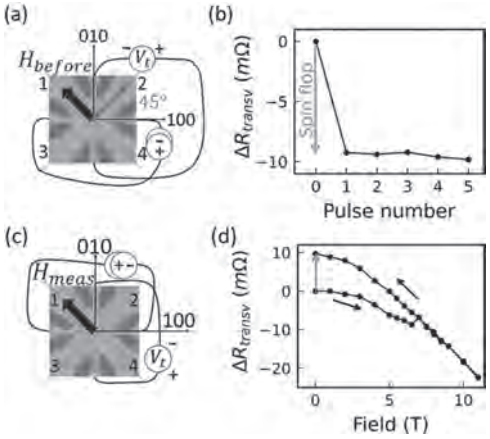

Fig.1 (a) Connection scheme for the current induced switching. We set a well-defined starting state by orienting *n* in the 3-2 direction. (b) Current-induced spin flop transition of *n*. (c) Connection scheme for the field-induced switching. (d) Field-induced spin flop, resetting *n*.

P4-08. Antiferromagnetic Moments Switching Induced by a Topological Insulator. *X. Chen*[1], C. Song[1], X. Kou[2] and F. Pan[1] *1. Tsinghua University, Beijing, China; 2. Shanghai Tech University, Shanghai, China*

Electrical manipulation of antiferromagnetic (AFM) moments is at the heart of AFM spintronics. However, previous studies show a large discrepancy on the origin of current induced switching of AFM moments. Here we investigate the current-induced switching of the AFM moments in AFM/topological insulator (TI) heterostructures, which is used to verify the unique role of spin orbit torque. Moreover, the low threshold current density via TI show great potential for AFM magnetoresistive random-access memory with ultralow power consumption. Our results provide a direct avenue towards applicable topological AFM devices.

P4-09. Magnon Landau Levels and Topological Spin Responses in Antiferromagnets. A.A. Kovalev[1] and *B. Li*[1] *1. University of Nebraska-Lincoln, Lincoln, NE, United States*

We predict staggered-field-stabilized collinear, spiral, cone, skrymion crystal (SkX), and square crystal (SC) of vortices and antivortices phases in antiferromagnets (see figure). In SkX and SC phases, magnons experience emergent gauge fields, which leads to magnon-mediated topological spin responses. The underlying physics can be qualitatively understood by considering magnon Landau levels induced by the fictitious magnetic flux. In the long wavelength limit, the unevenly spaced energy bands can be described by the relativistic Klein-Gordon equation. As we propose, these Landau levels can be also realized in antiferromagnetic magnonic topological insulator where the fictitious flux is induced by inhomogeneous DMI. A smoking gun experiment observing the Hofstadter's butterfly of magnons in AFM could establish the connection between emergent electromagnetism and topological properties of antiferromagnetic magnons.

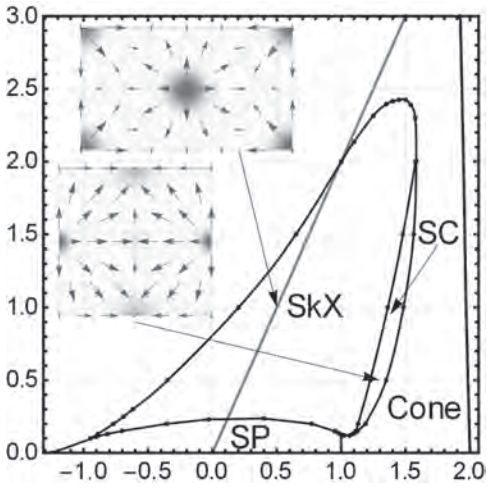

Zero temperature phase diagram of AFM with DMI. The axes correspond to the dimensionless staggered magnetic field and dimensionless effective anisotropy. The gray line separates the aligned and the tilted regions of the FM phase. This phase is taken over by the hexagonal skyrmion lattice (SkX), spiral (SP), cone phase, and the square crystal of vortices and antivortices (SC). The upper inset shows a hexagonal lattice unit cell with a skyrmion in the center. The lower inset shows a square crystal unit cell with AFM antimeron in the center. Red and yellow correspond to positive topological charge density and blue corresponds to the negative topological charge density.

P4-10. Withdrawn

P4-11. Spin-Transfer Torque Oscillator Based on Composite Synthetic Antiferromagnets. *I. Volvach*[1], A.D. Kent[3], E. Fullerton[4] and V. Lomakin[2] *1. Material Science and Engineering, University of California San Diego, La Jolla, CA, United States; 2. Electrical & Computer Engineering, University of California San Diego, La Jolla, CA, United States; 3. Department of Physics, New York University, New York, NY, United States; 4. Center for Memory and Recording Research, University of California San Diego, La Jolla, CA, United States*

We present a spin-transfer torque oscillator (STO) based on composite (hard-soft) synthetic antiferromagnets (CSAFs) with perpendicular uniaxial magnetic anisotropy energy density. The CSAF STO can operate with and without an applied field and generates strong oscillations in a broad frequency range from tens to hundreds GHz with precessions mostly generated by the soft layer. The STO is comprises of a cylindrical cross – section stack of diameter *D* (Fig.1), including a reference layer and a free layer composed of SAF layers (FL_{soft} and FL_{hard}). FL_{hard} is much harder than FL_{soft} and the sub-layers are exchange coupled with surface exchange energy density J_{AF}. The results are obtained via micromagnetic simulations with the FastMag[1] simulator. Fig.1 shows the precession frequency of the FL_{soft} as a function of the applied current density *J* for weak and strong J_{AF}. The precession frequency of FL_{soft} is proportional to J_{AF} and *J* and it can be tuned in a broad range of frequencies up to 200 GHz. Fig.2 shows the time dependence of the magnetization components for FL_{soft} and FL_{hard}. Both z-components are in the same direction while the in-plane components are opposite. The precession direction sense is clockwise for both layers, but the precession is dominated by the soft layer, i.e. the device generates a strong oscillating magnetic field. The operation mechanism is based on the exchange field due to the AF coupling, which is similar to AF STO[2]. However, CSAF STO offers a great flexibility in tuning the parameters and practicality in the material choice. It can be used to generate electric signal or for microwave assisted magnetic recording, This work was supported by the

Quantum-Materials for Energy Efficient Neuromorphic-Computing(Q-MEEN-C), an Energy Frontier Research Center funded by the U.S. DOE, under Award No. DE-SC0019273.

[1] R. Chang, S. Li, M. V. Lubarda, B. Livshitz, and V. Lomakin, J Appl Phys 109 (3), 07D358 (2011). [2] V. Puliafito, R. Khymyn, M. Carpentieri, B. Azzerboni,1 V. Tiberkevich, A. Slavin, and G. Finocchio, PRB 99, 024405 (2019).

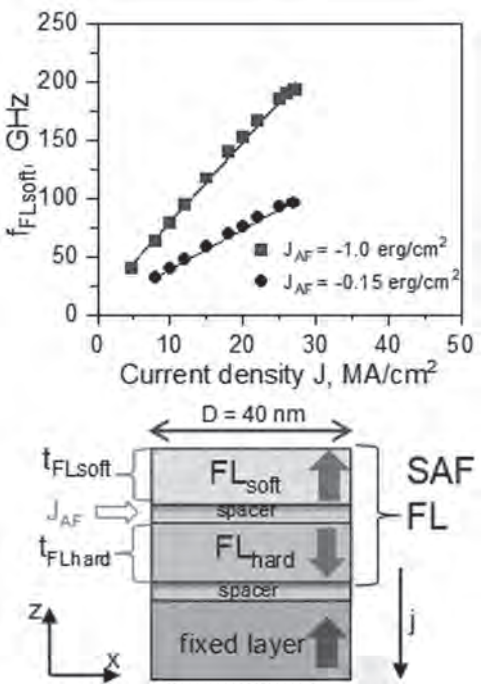

Fig. 1. Precession frequency of FL_{soft} vs. applied current density J for different J_{AF} with $M_{sFLsoft}$=$M_{sFLhard}$=960 emu/cc, $K_{uFLsoft}$= 3.055 Merg/cc, $K_{uFLhard}$= 9.165 Merg/cc, α=0.008, t_{FLhard}=t_{FLsoft} =1.2 nm, t_{spacer} =1.0 nm.

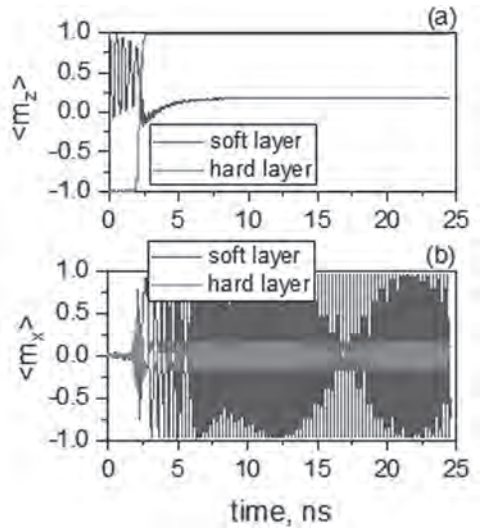

Fig. 2. (a) Average normalized magnetization m_z and (b) m_x vs. time for J_{AF}= -0.15 erg/cm². An applied current density was J = 20 MA/cm².

P4-12. Current Induced out-of-Plane Spin Accumulation on $IrMn_3$(001) Antiferromagnet. Y. Liu[1], Y. Liu[1], P. He[1], K. Teo[1], T. Phung[2], S. Yang[2] and *H. Yang[1] 1. National University of Singapore, Singapore; 2. IBM Research - Almaden, San Jose, CA, United States*

Recent experimental breakthrough on manipulating the spin textures via spin Hall effect paved the way of applying antiferromagnets (AFs) beyond their passive role on providing an exchange bias field. Though the field-free switching has been achieved in AF/FM systems, the roles of the antiferromagnets on the magnetization switching are still in debate [1-4]. In addition, the anisotropic spin Hall physics in AFs has not yet been clearly understood. Thus, visualizing the anisotropic current induced spin textures is of great importance to provide a detailed understanding of anisotropic spin Hall phenomena and its application towards the efficient magnetization switching in antiferromagnetic systems. In this work, we spatially image the current induced spin accumulation in $IrMn_3$ antiferromagnets upon injecting currents along different crystallographic directions by scanning photovoltage microscopy [5]. In contrast to the conventional spin Hall effect in which the spins lie in-plane at the top surface of devices, we observe significant out-of-plane spin accumulation on the device surface in $IrMn_3$ (001) as shown in Fig. 1, while the out-of-plane spin accumulation is negligible in $IrMn_3$ (111). The spin accumulation in $IrMn_3$ (001) depends on the current flow in different crystallographic directions, which is not the case for $IrMn_3$ (111). The out-of-plane spin accumulation shows the maximum with currents applying along the [-110] direction (θ = 0°). In contrast, the out-of-plane spins accumulate only along the edges of the channel in (111)-oriented $IrMn_3$. The maximum spin Hall angle of $IrMn_3$ (001) and $IrMn_3$ (111) are determined to be 0.083 and 0.018, respectively. Our results show the great potential of using (001)-$IrMn_3$ to achieve field-free magnetization switching in AF/FM bilayer systems.

[1] Y.-W. Oh *et al.*, Nat. Nanotech. 11, 878 (2016) [2] S. Fukami *et al.*, Nat. Mater. 15, 535 (2016) [3] A. van den Brink *et al.*, Nat. Commun. 7, 10854 (2016) [4] Y.-C. Lau *et al.*, Nat. Nanotech. 11, 758 (2016) [5] Y. Liu *et al.*, Phys. Rev. Applied 12, 064046 (2019)

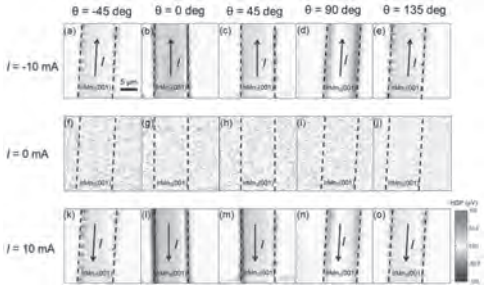

Fig. 1. Two-dimensional helicity dependent photovoltage (HDP) data in (001)-oriented $IrMn_3$ under various currents. θ = 0° corresponds to the bias current applied through the [-110] direction in (001)-plane of $IrMn_3$. Black dashed lines indicate the edges of the device while black arrows indicate the current direction.

P4-13. Spin Transport Experiments in the Easy-Plane Phase of the Antiferromagnetic Insulator Hematite. *T. Wimmer*[1,2], J. Gueckelhorn[1,2], M. Opel[1], S. Geprägs[1], H. Huebl[1,2], R. Gross[1,2] and M. Althammer[1,2] *1. Magnetism and Spintronics Group, Walther-Meissner-Institut, Garching, Germany; 2. Physik Department, Technische Universität München, Garching, Germany*

Spin transport via antiferromagnetic magnons represents a promising route towards the implementation of novel spintronic devices [1,2,3]. Remarkably, the two exchange-coupled magnetic sublattices in antiferromagnets inherently exhibit two magnon modes with opposite circular polarizations, giving rise to the simultaneous existence of both up- and down-spin excitations [3,4]. Recent experiments have shown that these degenerate modes can transport spin information over μm lengthscales [1,2]. In such experiments,

a pure spin current is injected into the antiferromagnetic insulator using a Pt electrode employing the spin Hall effect. The flow of spin current can then be electrically detected with a second Pt strip utilizing the inverse spin Hall effect, which transforms the spin current back into a charge current at the Pt detector. Here, we investigate the spin current transport in the antiferromagnetic insulator hematite (α-Fe_2O_3) by electrically exciting and detecting magnons via the (inverse) spin Hall effect. For the electrical magnon transport experiments, we use a 15 nm thin hematite layer grown via laser-MBE on a (0001)-oriented sapphire substrate. On top of the hematite layer we deposit and pattern Pt strips with a separation of several 100 nm via electron beam lithography and lift-off techniques. In our experiments, we restrict ourselves to the antiferromagnetic easy-plane phase of the hematite layer. We discuss the obtained temperature and external magnetic field dependence in our thin hematite layer with respect to the role of the magnon modes in the easy-plane antiferromagnet. Finally, we compare our extracted spin transport parameters to recent experiments [1,2,3] on all-electrical magnon transport in hematite thin films. We gratefully acknowledge the financial support of the German Research Foundation via Germany's Excellence Strategy (Grant No. EXC-2111-390814868) and project AL2110/2-1.

[1] R. Lebrun, A. Ross, M. Kläui *et al.*, Nature 561, 222-225 (2018). [2] A. Ross, R. Lebrun, M. Kläui *et al.*, Nano Letters 20, 306-313 (2020). [3] J. Han, P. Zhang. L. Liu *et al.*, Nature Nanotechnology, 1748-3395 (2020) [4] S. M. Rezende, A. Azevedo and R. L. Rodríguez-Suárez, Journal of Applied Physics 126, 151101 (2019).

P4-14. Withdrawn

Session P5
MULTIFERROIC MATERIALS AND HETERO-STRUCTURES II (Poster Session)

Ales Hrabec, Chair
ETH Zurich, Villigen, Switzerland

P5-01. Application of Bayesian Optimization to Ferroic Materials Development. *A.R. Will-Cole*[2], A.G. Kusne[1], P. Tonner[1], X. Liang[2], C. Dong[2], Y. Wei[2], H. Chen[2] and N.X. Sun[2] *1. National Institute of Standards and Technology, Gaithersburg, MD, United States; 2. Electrical Engineering, Northeastern University, Boston, MA, United States*

Bayesian optimization (BO) is a well-developed machine learning algorithm for black box optimization. In BO a predictive model, here a Gaussian process regression, is implemented to predict the black box function and the uncertainty of the predictive model is evaluated as predicted variance, then an acquisition function defined by the surrogate predictive model decides where to sample next. In this study we applied this technique to known ferroic materials such as ferromagnetic $(Fe_{100-y}Ga_y)_{1-x}B_x$ (x=0–21 & y=9–17) and ferromagnetic $(Co_{0.5}Fe_{0.5})_{1-x}C_x$ (x=0–16) to provide proof of concept of how BO can be used to optimize properties such as magnetostriction and ferromagnetic resonance (FMR) linewidth with fewer samples required than traditional experimental approaches.[1,2] Additionally, we applied this technique to optimize thin films of ferromagnetic $(Fe_{100-y}Ga_y)_{1-x}C_x$ (x=1–26 and y=2–18) and ferroelectric $(HfO_2)_{1-x}Y_x$ (x=0–15). For each of these systems, we applied BO through building a predictive model with the GPy library (https://sheffieldml.github.io/GPy/) and evaluating the next experiment to sample with the GPyOpt library (https://github.com/SheffieldML/GPyOpt), both in python.

[1] J. Lou *et al*. Appl. Phys. Lett. 91, 182504 (2007). [2] J. Wang *et al.* Phys. Rev. Applied 12, 034011 (2019)

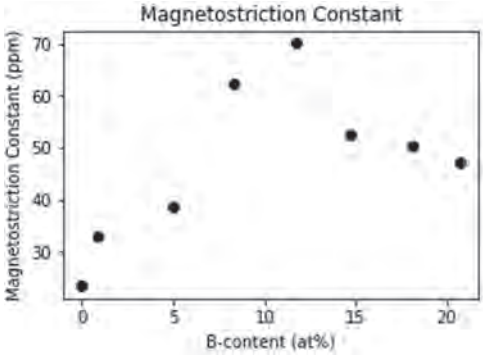

This plot shows the B-content of $(Fe_{100-y}Ga_y)_{1-x}B_x$ alloy versus the corresponding Magnetostrictive constant. This experimental data required a minimum of 8 experiments to determine the overall structure-property relationship.

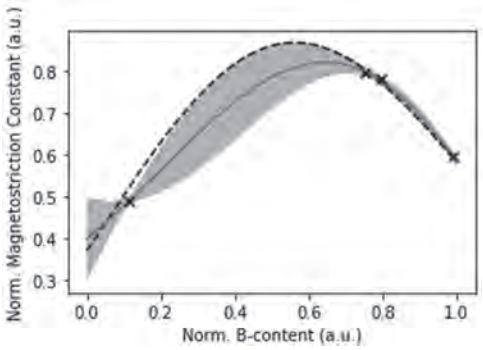

This plot displays similarly captured behavior from the previous figure, but with just 4 experiments implementing the Bayesian optimization method – with fewer experiment samples we are able to determine the optimal boron dopant concentration to enhance the Magnetostrictive response. This displays proof of concept for one-variable-at-a-time (OVAT) variation. However, this method can easily be applied to a larger dimensional case varying conditions such as stoichiometry, doping concentration, and temperature processing to quickly identify optimal processing conditions or structure.

P5-02. Free Layer Magnetic Anisotropy Control in the Multiferroic Tunnel Junction: a Computational Study on Materials Interfaces. *A.P. Chen*[1,2], W. Lin[2], J. Chen[2] and Y.P. Feng[2] *1. Case Western Reserve University, Cleveland, OH, United States; 2. National University of Singapore, Singapore*

The $BaTiO_3$ (BTO)/CoFe multiferroic material interface is an example of an interface which displays voltage-controlled magnetic anisotropy (VCMA), a valuable property in the operation of multiferroic tunnel junctions in an STT-MRAM device. Through first principles calculations, it is possible to predict trends in film magnetic anisotropy energy (MAE) and enumerate the individual physical mechanisms contributing to ferroelectric control of MAE in the CoFe film. For CoFe of up to 2 atomic layers on BTO, MAE can be modulated by ferroelectric switching through Fe-O orbital interations in BaO-terminated interfaces, and Ti-Fe orbital interactions in TiO_2-terminated interfaces. A difference in interface termination produces a difference of MAE in CoFe films of up to 9 atomic layers. The inclusion of a 5*d* transition metal capping layer (Hf, Ta, W, Re, Os, Ir, Pt, or Au) on top of the CoFe layer exerts a significant effect on both MAE and the ferroelectric switching effect, in particular inducing a discernible ferroelectric switching control even in thicker CoFe films. This points to the additional, if counterintuitive, contribution of CoFe 3*d* top interface (or surface) states and their interactions with partially filled 5*d* orbitals of the capping layer atoms.

A. P. Chen and Y. P. Feng, ACS Appl. Mater. Interfaces., Vol. 12, p25383-25389 (2020) A. P. Chen, W. Lin, J.-S. Chen, and Y. P. Feng, in preparation.

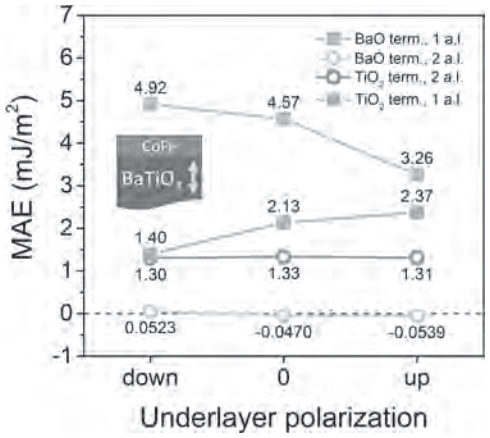

Fig. 1. MAE of 1 atomic layer of Fe and 2 atomic layers of CoFe on upward, zero, and downward polarized BTO, given a fully-relaxed atomic structure of BaO- and TiO_2-terminated interfaces.

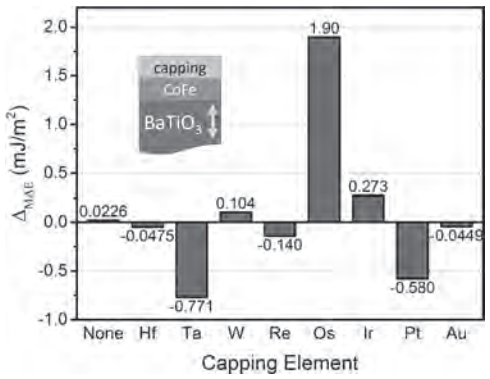

Fig. 2. Change in MAE (Δ_{MAE}) of BTO/CoFe and BTO/CoFe/(Hf, Ta, W, Re, Os, Ir, Pt, or Au) during a downward to upward ferroelectric polarization switching process.

P5-03. New Optical Approach for Development of Straintronics.

A. Telegin[1], V.A. Bessonova[1], Y.P. Sukhorukov[1] and A.P. Nossov[1]
1. magnetic semiconductors, M.N. Miheev Institute of Metal Physics UB of RAS, Yekaterinburg, Russian Federation

The interaction between strain and spins has received intensive attention due to its abundant physical phenomena and huge technological impact. For example, straintronics demonstrates a fundamentally new way to control electronics at nanoscale [1]. Straintronics usually explores the change of electronic states of magnetics via magnetic/electric-field-induced mechanical deformations and vice versa. On the other hand, magneto-optical (MO) properties of magnetics are known to be highly sensitive to external fields and stresses [2]. To explore the coupling between straintronics and optics, we have studied the influence of a magnetic field on the MO properties of a ferrimagnetic spinel single crystals of $CoFe_2O_4$ with high magnetostriction (about 600×10^{-6}). Surprisingly strong influence of an external magnetic field on the absorption (up to tens of percent) and reflection of natural light is found for $CoFe_2O_4$ [3,4]. The estimated contribution of Faraday rotation in the observed effects is quite small [5]. It is revealed the relationship between the magnetoelastic properties of the spinel and magnetoabsorption (MA) in the IR range. For example, there is a similarity of the field behavior of MA and magnetostriction at different orientations of magnetization with respect to the crystal axes. It is also observed that in the $CoFe_2O_4$ magnetostriction gives an abnormally large (about 50%) contribution to the magnetic anisotropy constant K_1 [6]. A few mechanisms of MA of light in the spinel connected with the magnetic-field-induced mechanical deformation are proposed. The effect of the magnetic field on the optical properties of $CoFe_2O_4$ seems to be indirect: the magnetic field strongly affects the crystal lattice, which in turn leads to the changes in the absorption and reflection spectra. The new mechanism of MO effects observed in the $CoFe_2O_4$ paves the way towards new optical approach for development of straintronics called as a strain-magnetooptics. *Supported by the program No. AAAA-A18-118020290104-2 "Spin" and the program No. 18-10-2-37 in part.*

1. Roy K., Bandyopadhyay S., Atulasimha J., Appl. Phys. Lett., 99, 063108 (2011). 2. Telegin A.V., Sukhorukov Yu.P. et al. JMMM, 383, 104 (2015). 3. Sukhorukov Yu.P., TeleginA.V., Bebenin N.G., et al. Sol. State Comm., 263, 27 (2017). 4. Sukhorukov Yu.P., TeleginA.V., Bebenin N.G., et al. JETP Letters, 108, 482018 (2018). 5. Telegin A.V., Sukhorukov Yu.P., Bessonov V.D., Naumov S.V. Tech. Phys. Lett., 45, 601 (2019).

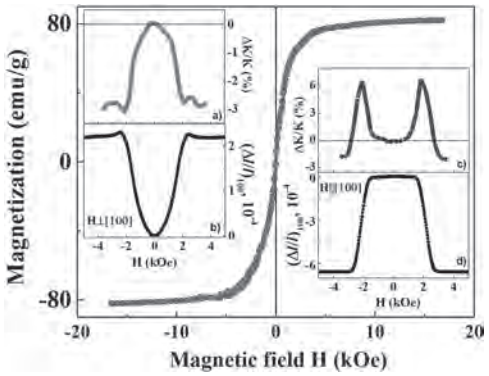

Field dependences of magnetization of $CoFe_2O_4$ at H||[100]. In the insets, ones of the magnetostriction $(\Delta l/l)_{100}$ and the magnetoabsorption ΔK/K at λ=2.7 μm.

P5-04. Magnetic Structure at Perovskite/Antiperovskite Interface.

J. Zemen[1] and O. Heczko[2,1] *1. Faculty of Electrical Engineering, Czech Technical University in Prague, Praha, Czechia; 2. Magnetic Measurement and Materials, Institute of Physics CAS, Prague, Czechia*

Mn-based antiperovskite nitrides with a formula unit Mn_3AN (A = Ga, Sn, In, Ni, Zn,…) show potential for a wide range of applications including spintronics [1,2,3] and solid-state cooling [4,5,6]. The functionality is mainly derived from the frustrated exchange interactions in the triangular antiferromagnetic (AF) structure and its response to symmetry lowering caused by biaxiail strain [3,5] or by an adjacent layer with ferroelectric polarization [7]. Using density functional theory (DFT) and linear response approximation of the permitivity tensor as implemented in the VASP package we simulate the non-collinear magnetic structure in a thin film of Mn_3NiN and Mn_3SnN deposited on ferroelectric perovskite $BaTiO_3$. We find local deviations from the triangular magnetic order of the bulk system. Following predictions of magneto-optical Kerr effect (MOKE) in bulk antiperovskite nitrides [8], we simulate the MOKE spectra of bulk Mn_3NiN assuming the magnetic structure obtained for the $Mn_3NiN/BaTiO_3$ bilayer earlier. Our results can be compared directly with measured MOKE data in order to identify the desirable magnetic structure in thin film samples.

[1] T. Higo et al. Nature photonics, 12.2, 73 (2018). [2] S. Nakatsuji et al., Nature 580, 608 (2020). [3] D. Boldin, J. Zemen et al. ACS Appl. Mater. Interfaces, 10, 18863 (2018). [4] D. Matsunami et al. Nature Materials, 14, 73–78 (2015). [5] J. Zemen et al. Phys. Rev. B, 95, 184438 (2017). [6] D. Boldrin J. Zemen et al. Phys. Rev. X 8, 041035 (2018). [7] D.F. Shao, et al. Phys. Rev. Materials 3.2, 024405 (2019). [8] Y. Mokousov et al.: Phys. Rev. B, 99, 104428 (2019).

P5-05. The Role of Electroacoustic Magnons in Enhancing Magnetoelectric Responses. *S. Sayedaghaee*[1,2], C. Paillard[3], S. Prosandeev[1], B. Xu[4] and L. Bellaiche[1] *1. Physics Department and Institute for Nanoscience and Engineering, University of Arkansas Fayetteville, Fayetteville, AR, United States; 2. Microelectronics-Photonics Program, University of Arkansas Fayetteville, Fayetteville, AR, United States; 3. CentraleSupélec, Structures Proprietes et Modelisation des Solides, Gif-sur-Yvette, France; 4. School of Physical Science and Technology, Soochow University, Suzhou, China*

Recently, the cross-coupling between magnetic and ferroelectric ordering in multiferroic materials known as magnetoelectric (ME) effect is paving the way towards designing novel devices. Here we develop an analytical model to gain microscopic insights into the quadratic magnetoelectric responses, specifically the second harmonic generation in the electrical polarization due to an applied magnetic field. The model is then verified using numerical experiments based on a first-principle built effective Hamiltonian and subsequent atomistic Molecular Dynamics (MD) simulations [1]. Our theoretical and numerical results highlight two mechanisms acting in the quadratic magnetoelectic response of a single phase multiferroic such as $BiFeO_3$: (1) a direct coupling between microscopic electric dipoles and spins (electromagnonic in nature), and (2) a 3-body coupling between electric dipoles, strain, and spins, resulting from the combined action of magnetostriction and piezoelectricity. The latter, when strain resonances are induced, leads to the emergence of new quasi-particles, coined electroacoustic magnons [2], and are unambiguously detected in our MD simulations. Two components of the quadratic ME response of $BiFeO_3$, $\beta(0,\omega)$ and $\beta(\omega,\omega)$, are computed when the homogeneous strain of the supercell is not allowed to change (clamped) and relaxed to change (unclamped) during the simulations. Remarkably, and as predicted by our model [3], the first component of the ME response, $\beta(0,\omega)$, experiences resonances when the frequency of applied magnetic field corresponds to the frequencies associated with electroacoustic magnons (Fig. 1). The second component, $\beta(\omega,\omega)$, experiences resonances when the applied frequency corresponds to the frequencies associated with electroacoustic magnons as well as *half* of those frequencies (Fig. 2). As a result, electroacoustic magnons can enhance the ME response of multiferroics through strain engineering (e. g. by altering the size or shape of the material) and open opportunities for designing more advanced sensors, actuators, and memory devices. This study is mostly financially supported by DARPA for the simulations and ARO for the analytical model.

[1] S. Prosandeev, D. Wang, W. Ren, J. Íñiguez, and L. Bellaiche, Advanced Functional Materials 23, 234 (2013) [2] S. O. Sayedaghaee, B. Xu, S. Prosandeev, C. Paillard, and L. Bellaiche, Phys. Rev. Lett. 122, 097601 (2019) [3] S. O. Sayedaghaee, C. Paillard, S. Prosandeev, B. Xu, and L. Bellaiche, Npj Computational Materials 6, 1 (2020)

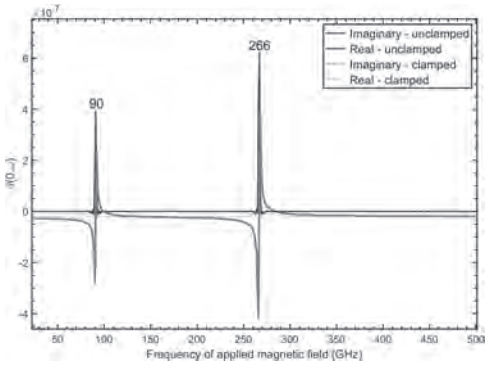

Fig. 1. $\beta(0,\omega)$, vs. ω

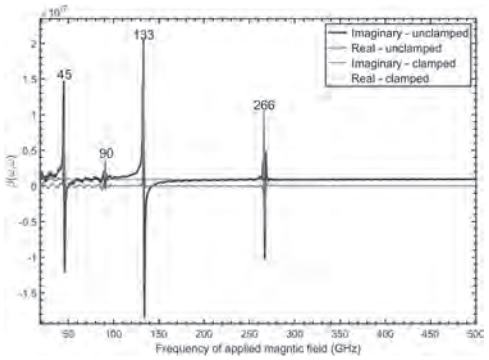

Fig. 2. $\beta(\omega,\omega)$, vs. ω

P5-06. Magnetoelectric Coupling and Decoupling in Multiferroic Hexagonal $YbFeO_3$ Thin Films. *X. Li*[1], Y. Yun[1] and X. Xu[1,2] *1. Department of Physics and Astronomy, University of Nebraska, Lincoln, Lincoln, NE, United States; 2. Nebraska Center for Materials and Nanoscience, University of Nebraska, Lincoln, Lincoln, NE, United States*

The coupling between ferroelectric and magnetic orders is an enduring experimental challenge with fundamental importance to elucidate the nature of magnetoelectric (ME) effects in multiferroic materials. In this work, we have studied the response of magnetization to ferroelectric switching in thin-film hexagonal $YbFeO_3$, an improper multiferroic which is a fruitful platform for investigating the ME coupling in single-phase materials. The bulk ME decoupling and potential domain-wall ME coupling were revealed using X-ray magnetic circular dichroism (XMCD) measurements with in-situ ferroelectric polarization switching. Our Landau theory analysis suggests that the bulk ME-coupled ferroelectric switching path has an higher energy barrier than that of the ME-decoupled path; this extra barrier energy is also too high to reduce by the magneto-static energy in the process of breaking single magnetic domains into multi-domains. In addition, the reduction of magnetization around the ferroelectric domain walls predicted by the Landau theory, may induce the domain-wall ME coupling in which he magnetization is correlated with the density of ferroelectric domain walls. These results provide important experimental evidences and theoretical insights to the rich possibilities of ME couplings in hexagonal ferrites.

1] J.F. Scott, Room-temperature multiferroic magnetoelectrics, NPG Asia Materials, 5 (2013) e72-e72. [2] S. Fusil, V. Garcia, A. Barthelemy, M. Bibes, Magnetoelectric Devices for Spintronics, Annual Review of Materials Research, 44 (2014) 91-116. [3] P. Mandal, M.J. Pitcher, J. Alaria, H. Niu, P. Borisov, P. Stamenov, J.B. Claridge, M.J. Rosseinsky, Designing switchable polarization and magnetization at room temperature in an oxide, Nature, 525 (2015) 363-366. [4] N.A. Spaldin, R. Ramesh, Advances in magnetoelectric multiferroics, Nat. Mater., 18 (2019) 203-212. [5] S.-W. Cheong, Topological domains/domain walls and broken symmetries in multiferroics, National Science Review, 6 (2015) 624-626. [6] S. Dong, J.M. Liu, S.W. Cheong, Z.F. Ren, Multiferroic materials and magnetoelectric physics: symmetry, entanglement, excitation, and topology, Adv Phys, 64 (2015) 519-626. [7] M. Fiebig, T. Lottermoser, D. Meier, M. Trassin, The evolution of multiferroics, Nature Reviews Materials, 1 (2016). [8] H. Das, A.L. Wysocki, Y. Geng, W. Wu, C.J. Fennie, Bulk magnetoelectricity in the hexagonal manganites and ferrites, Nature communications, 5 (2014) 2998. [9] S. Artyukhin, K.T. Delaney, N.A. Spaldin, M. Mostovoy, Landau theory of topological defects in multiferroic hexagonal manganites, Nat. Mater., 13 (2014) 42-49. [10] W. Wang, J. Zhao, W. Wang, Z. Gai, N. Balke, M. Chi, H.N. Lee, W. Tian, L. Zhu, X. Cheng, D.J. Keavney, J. Yi, T.Z. Ward, P.C. Snijders, H.M. Christen, W. Wu, J. Shen, X. Xu, Room-temperature multiferroic hexagonal $LuFeO_3$ films, Phys Rev Lett, 110 (2013) 237601. [11] X. Xu, W. Wang, Multiferroic hexagonal ferrites (h-$RFeO_3$, R = Y, Dy-Lu): a brief experimental review, Modern Physics Letters B, 28 (2014) 1430008. [12] S. Cao, K. Sinha, X. Zhang, X. Zhang, X. Wang, Y. Yin, A.T. N'Diaye, J. Wang, D.J. Keavney, T.R. Paudel, Y. Liu, X. Cheng, E.Y. Tsymbal, P.A. Dowben, X. Xu, Electronic structure and direct observation of

ferrimagnetism in multiferroic hexagonal $YbFeO_3$, Physical Review B, 95 (2017). [13] W. Wang, J.A. Mundy, C.M. Brooks, J.A. Moyer, M.E. Holtz, D.A. Muller, D.G. Schlom, W. Wu, Visualizing weak ferromagnetic domains in multiferroic hexagonal ferrite thin film, Physical Review B, 95 (2017). [14] K. Sinha, H.H. Wang, X. Wang, L.Y. Zhou, Y.W. Yin, W.B. Wang, X.M. Cheng, D.J. Keavney, H.B. Cao, Y.H. Liu, X.F. Wu, X.S. Xu, Tuning the Neel Temperature of Hexagonal Ferrites by Structural Distortion, Phys Rev Lett, 121 (2018). [15] K. Du, B. Gao, Y.Z. Wang, X.H. Xu, J. Kim, R.W. Hu, F.T. Huang, S.W. Cheong, Vortex ferroelectric domains, large-loop weak ferromagnetic domains, and their decoupling in hexagonal (Lu, Sc)FeO_3, Npj Quantum Mater, 3 (2018). [16] Y. Geng, N. Lee, Y.J. Choi, S.W. Cheong, W. Wu, Collective magnetism at multiferroic vortex domain walls, Nano Lett, 12 (2012) 6055-6059. [17] J.A. Moyer, R. Misra, J.A. Mundy, C.M. Brooks, J.T. Heron, D.A. Muller, D.G. Schlom, P. Schiffer, Intrinsic magnetic properties of hexagonal $LuFeO_3$ and the effects of nonstoichiometry, APL Materials, 2 (2014) 012106. [18] M.E. Holtz, K. Shayovalov, J.A. Mundy, C.S. Chang, Z.W. Yan, E. Bourret, D.A. Muller, D. Meier, A. Cano, Topological Defects in Hexagonal Manganites: Inner Structure and Emergent Electrostatics, Nano Lett, 17 (2017) 5883-5890. [19] T. Matsumoto, R. Ishikawa, T. Tohei, H. Kimura, Q. Yao, H. Zhao, X. Wang, D. Chen, Z. Cheng, N. Shibata, Y. Ikuhara, Multivariate statistical characterization of charged and uncharged domain walls in multiferroic hexagonal YMnO3 single crystal visualized by a spherical aberration-corrected STEM, Nano Lett, 13 (2013) 4594-4601. [20] Y.K. Jeong, J.H. Lee, S.J. Ahn, S.W. Song, H.M. Jang, H. Choi, J.F. Scott, Structurally tailored hexagonal ferroelectricity and multiferroism in epitaxial $YbFeO_3$ thin-film heterostructures, J Am Chem Soc, 134 (2012) 1450-1453. [21] Y.N. Geng, H. Das, A.L. Wysocki, X.Y. Wang, S.W. Cheong, M. Mostovoy, C.J. Fennie, W.D. Wu, Direct visualization of magnetoelectric domains, Nature materials, 13 (2014) 163-167.

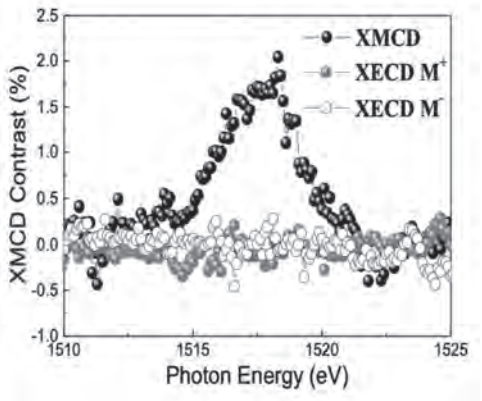

XMCD contrasts of the remnant magnetization (measured under zero magnetic field after application of ± 18 kOe magnetic field) and X-ray electric circular dichroism (XECD) contrasts between FE polarization up and down under magnetic field +18 kOe (XECD M^+) and -18 kOe (XECD M^-) at Yb M_5 edge.

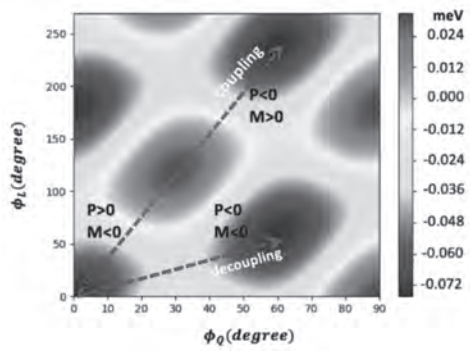

Energy landscape with Φ_Q and Φ_L as coordinates, where Q is fixed at 0.33 Å.

P5-07. Microscopic Theory of Spin Driven Electric Polarization in Lacunar Spinels GaV_4S_8 and $GaMo_4S_8$. *S.A. Nikolaev*[1] and I. Solovyev[2] *1. Tokyo Kogyo Daigaku, Meguro-ku, Japan; 2. Busshitsu Zairyo Kenkyu Kiko Kokusai Nanoarchitectonics Kenkyu Kyoten, Tsukuba, Japan*

Being studied mostly in nonpolar chiral structures, skyrmions in polar crystals are of great interest owing to their interplay with electric polarization, giving rise to fascinating multiferroic properties. Recently, skyrmion lattices have been reported in lacunar spinel GaV_4S_8 [1], where a complex phase diagram comprising paramagnetic, ferromagnetic, skyrmion, and cycloidal states has been demonstrated, and the spin-driven excess polarization was assigned in each magnetic phase with a total value of ~100 μC/m^2 [2]. The existence of multiple ferroelectric phases in GaV_4S_8 indicates an intricate interplay between charge, spin, and lattice degrees of freedom, making their theoretical description extremely important. In our studies, we present the microscopic theory of spin-driven electric polarization P in GaV_4S_8 and $GaMo_4S_8$ [3,4]. To this end, we extend the theory of superexchange for magnetic interactions to deal with the change of electric polarization depending on the relative direction of spins in each bond. Based on realistic Hubbard-type models derived for the magnetically active molecular orbitals formed in the V_4 and Mo_4 tetrahedra, we show that (i) although a skyrmion layer in these materials is mainly formed by the in-plane magnetic interactions, the spin-excess polarization perpendicular to the rhombohedral z axis is given by the interlayer electron transfer and originates from strongly competing isotropic and antisymmetric contributions; (ii) P arises from the stacking misalignment of such layers in the perpendicular direction, which is inherent to the lacunar spinel structure; (iii) while the interorbital Hund's coupling is small, it is one of the key parameter responsible for P in lacunar spinels; (iv) an importnat aspect of multiferroicity in $GaMo_4S_8$, which can also potentially host skyrmionic states, is strong exchange anisotropy; and (v) the direction of rhombohedral distortions leads to opposite signs of P in GaV_4S_8 and $GaMo_4S_8$.

[1] I. Kézsmárki, S. Bordács, P. Milde et. al, Nat. Mater., Vol. 14, 1116 (2015). [2] E. Ruff, S. Widmann, P. Lunkenheimer et. al, Sci. Adv., Vol. 10, e1500916 (2015). [3] S. A. Nikolaev and I. V. Solovyev, Phys. Rev. B, Vol. 99, 100401(R) (2019). [4] S. A. Nikolaev and I. V. Solovyev, Phys. Rev. B 102 014414 (2020).

P5-08. Withdrawn

P5-09. Morphotropic $BiFeO_3$-$PbTiO_3$: Effect of La^{3+} Substitution. *R. Payyadi Porayil*[1], A. Swain[1], V. Subramanian[1] and M. Rao[1] *1. Indian Institute of Technology, Madras, Chennai, India*

A multiferroic $BiFeO_3$–$PbTiO_3$ at MPB was substituted with ions (La^{3+}) in the A-site. It was found that the ferroelectric and weak-ferromagnetic orders are strongly correlated to the structures thus evolved. Effect of the substituent in improving the weak-magnetic moment was also observed.

Here, the substitution led to the weakening of the cycloidal effect on the canted spins and thus released the ferromagnetic interaction. $BiFeO_3$ is a single phase multiferroic with distorted rhombohedral perovskite structure. The resident antiferromagnetism is accompanied by a weak Dzyaloshinskii–Moriya (DM)-type interaction. However, the canted moments, in general, are modified by the spin cycloid. Substitutions are often presented as a major improvement mechanism.[1][2][3] The compositions with $BiFeO_3$:$PbTiO_3$ ratio in and around 50:50, in the highly desirable morphotropic phase boundary (MPB), can favour the weakening of the cycloidal effect. The substitution of La^{3+} for Bi^{3+}, in general, stabilizes the formation of $BiFeO_3$ and favours magneto-electric aspects of the solution.[4][5] A series of solutions with $BiFeO_3$:$PbTiO_3$ ratio 55:45 and La^{3+} % ranging from 10 to 30 (w. r. t. Bi) were chosen for the studies. A transition from cubic-like rhombohedral + tetragonal (*R*3*c* +*P*4*mm*) phase to rhombohedral (*R*3*c*) with increasing La^{3+} substitution was observed. For a poled sample, two tetragonal peaks, $(002)_T$ and $(200)_T$, replaced the $(200)_R$ pseudo-cubic rhombohedral peak. Hysteresis loops, with no ideal desired saturation, were observed. A coherent increase in the ferroelectric performance with La^{3+} substitution was visible (Fig.1). Piezo coefficient (d_{33}) also raises from 20-25 pC/N to 40-45 pC/N. The samples showed weak ferromagnetic loops at 300 K. The effect of La substitution in improving the net moment was visible (Fig. 2). The cycloidal moments contributed to the linear variation in higher field, whereas the canted moments gave the hysteresis-like behavior in the lower field. The spiral spins on the moments were partially disturbed and disappeared. Here, the substitution of La^{3+} led to the partial destruction of the cycloidal AFM and thus released the weak DM-type interaction.[6][7]

[1] J. Yang, Q. He and P. Yu, Annual Review of Materials Research., Vol. 25, p.249 (2015) [2] T. Leist, T. Granzow, W. Jo, Journal of Applied Physics., Vol. 108, p.014103 (2010) [3] V. F. Freitas, G. S. Dias and O. A. Protzek, Journal of Advanced Ceramics., Vol. 2(2), p.103 (2013) [4] B. Narayan, J. S. Malhotra and R. Pandey, Nature Materials., Vol. 17, p.427 (2018) [5] T. Leist, W. Jo and T. Comyn, Japanese Journal of Applied Physics., Vol. 48, p.120205 (2009) [6] W.-M. Zhu, H.-Y. Guo and Z.-G. Ye, Physical Review B, Vol. 78, p.014401 (2008) [7] K. K. Mishra, A. T. Satya and A. Bharathi, Journal of Applied Physics., Vol. 110, p.123529 (2011)

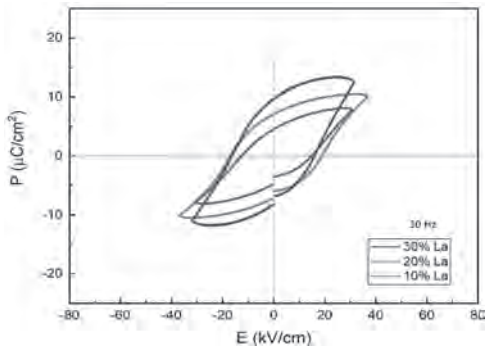

Fig.1.

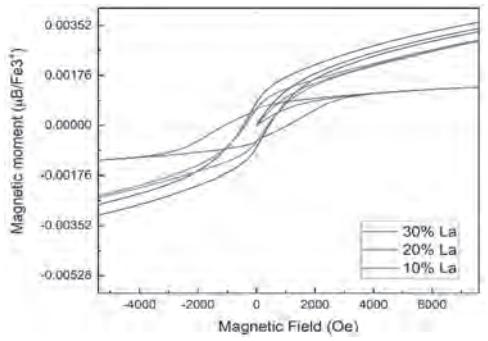

Fig. 2. Substituent improving the weak moment.

P5-10. Jahn-Teller Distortions in $(Co_{1-x}Cu_x)Cr_2O_4$ (x = 0.5, 0.25) Nanoparticles: Structural, Magnetic and Electronic Properties.

P. Mohanty[1], C. Sheppard[1], B. Doyle[1], E. Carleschi[1] and A. Prinsloo[1]
1. Physics, University of Johannesburg, Auckland Park, South Africa

The normal spinel ferrimagnet $CoCr_2O_4$ with $T_C \approx 93$–97 K [1–3] demonstrates multiferroic properties due to a spiral ordering at 26 K [2–4]. In addition, a lock-in transition appears at 15 K [3]. Structurally, $CoCr_2O_4$ retains the cubic phase down to 11 K [4]. In contrary, the normal spinel $CuCr_2O_4$ only crystallizes into the cubic phase above 853 K [1]. The tetrahedral crystal field around Cu^{2+} in the cubic phase causes fully occupied low energy *e* levels and triply degenerate t_2 levels that leads to a cooperative lattice distortion from cubic to tetragonal symmetry below 853 K with a disputed ambient temperature structure [1]. Jahn-Teller (JT) activity of the Cu elevates the frustration in the Cr^{3+} sublattice [1]. Neutron diffraction studies confirm the magnetic structure of $CuCr_2O_4$ consisting of two canted Cr^{3+} sublattices with a net magnetic moment and a Cu^{2+} sublattice that couples antiferromagnetically to the net moment of the Cr^{3+} sublattices below 135 K [1]. Compression of CuO_4 tetrahedra towards a square planar configuration accounts for the tetragonal to orthorhombic phase transition at ~ 130 K [1]. Looking at such strong links between the distinct degrees of freedom motivates exploring new classes of multifunctional systems specifically at the nanoscale [5, 6]. In this direction, current work focuses on the modification of structural and magnetic properties upon substituting Cu at the Co site in $CoCr_2O_4$. In order to do so, $(Co_{1-x}Cu_x)Cr_2O_4$ (x = 0.5, 0.25) nanoparticles were synthesized through sol-gel techniques. XRD reveals the cubic structure at ambient temperature for x = 0.25 and 0.5, with average crystallite sizes of ~21 nm and ~13 nm, respectively. JT distortion becomes prominent for x = 0.75. The temperature dependent magnetization studies reveal the T_C remains similar for both the samples: 101.6(4) K for x = 0.5 and 100.2(3) K for x = 0.25. However, the feature related to T_S has been enhanced for x = 0.25, whereas it becomes suppressed for x = 0.5. Hysteresis loops measured at low temperature show enhanced constriction for x = 0.25 quite distinct from both chromites. Changes in the valence band and core level electronic structure from XPS support these observations.

[1] M. R. Suchomel, D. P. Shoemaker, and L. Ribaud, *Phys. Rev. B* 86 (2012) 054406. [2] Y. Yamasaki, S. Miyasaka, Y. Kaneko, J.-P. He, T. Arima, and Y. Tokura, *Phys. Rev. Lett.* 96 (2006) 207204. [3] K. Tomiyasu, J. Fukunaga, and H. Suzuki, *Phys. Rev. B* 70 (2004) 214434. [4] G. Lawes, B. Melot, K. Page, C. Ederer, M. A. Hayward, Th. Proffen, and R. Seshadri, *Phys. Rev. B* 74 (2006) 024413. [5] P. Mohanty, C.J. Sheppard, A.R.E. Prinsloo, W.D. Roos, L. Olivi, and G. Aquilanti, *J. Mag. Mag. Mat.* 451 (2018) 20. [6] P. Mohanty, S. Chowdhury, R.J. Choudhary, A. Gome, V.R. Reddy, G.R. Umapathy, S. Ojha, E. Carleschi, B.P. Doyle, A.R.E. Prinsloo, and C.J. Sheppard, *Nanotechnology* 31 (2020) 285708.

P5-11. Materials Characterization and Multiferroic Properties Optimization of Magnetoelectric Composites Based on Sintered Cobalt Ferrite/Barium Titanate Nanoparticles.

F. Safi Samghabadi[1], M. Khodadadi[1,2], L. Chang[3,2] and D. Litvinov[3,1] *1. Materials Science and Engineering, University of Houston, Houston, TX, United States; 2. Center for Integrated Bio and Nano Systems, University of Houston, Houston, TX, United States; 3. Electrical and Computer Engineering, University of Houston, Houston, TX, United States*

Magnetoelectric materials with exceptional properties emerging from the coupling between the magnetic and electric ferroic orders bring about functionalities that can be exploited in fields such as sensors, energy harvesters, MERAM, antenna, and biomedical [1,2]. Multi-phase ME composites that are composed of a ferromagnetic/piezoelectric junction can be fabricated in versatile connectivity configurations with a wide choice of materials and microstructure [3,4]. The extrinsic ME effect in these composites occurs due to the generation of magnetostriction in the ferromagnetic phase and its transfer via the interface to the piezoelectric one, which induces a voltage. Cobalt ferrite as a ferrimagnet and barium titanate as a piezoelectric are promising candidates for the preparation of nanostructured ME materials due to their outstanding magnetic and electric properties, respectively [5].

We report synthesis, characterization, and optimization of CoFe2O4-BaTiO3 composite using commercial nanoparticle precursors. The dry ball milling followed by high-temperature annealing of pressed powder was used as a low cost and highly reproducible synthesis method. We have investigated the structural, electric, magnetic, and magnetoelectrical properties of CFO-BTO composites prepared and electrically poled with two different types of BTO nanoparticles: 50 nm (cubic) and 200 nm (tetragonal) in conjunction with CFO nanoparticles of about 30 nm. The transformation of non-piezoelectric cubic BTO to piezoelectric tetragonal one after sintering at temperatures higher than Curie point was confirmed utilizing XRD. The maximum obtained ME coefficient (3.7 mV/Oe.cm for 50 nm BTO) is higher than the reported values for core-shell structures [6]. The hypothesis is that the smaller BTO nanoparticles can form shell-like structures around CFO nanoparticles and enhance the interface and resistivity of the samples. This enhancement results in a more efficient poling process and an improved ME coupling. The ME analysis has confirmed the dependence of the coupling coefficient on the size and fraction of BTO nanoparticles in the composite.

1. Cheng, Y., Peng, B. and Hu, Z., Physics Letters A vol. 382 3018–3025 (2018). 2. Spaldin, N. A., Cheong, S.-W. & Ramesh, R, Physics Today vol. 63 38–43 (2010). 3. Andrew, J. S., Starr, J. D. & Budi, M. A. K, Scripta Materialia vol. 74 38–43 (2014). 4. Ortega, N., Kumar, A., Scott, J. F. & Katiyar, R. S, Journal of Physics: Condensed Matter vol. 27 504002 (2015). 5. Baji, A., Mai, Y.-W., Yimnirun, R. & Unruan, S, RSC Adv. vol. 4 55217–55223 (2014). 6. Duong, G. V., Groessinger, R. & Turtelli, R. S, IEEE Transactions on Magnetics vol. 42 3611–3613 (2006).

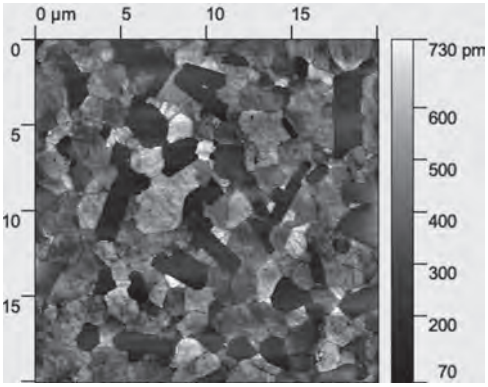

Fig 1. PFM amplitude of CFO:BTO (50 nm):30-70% composite

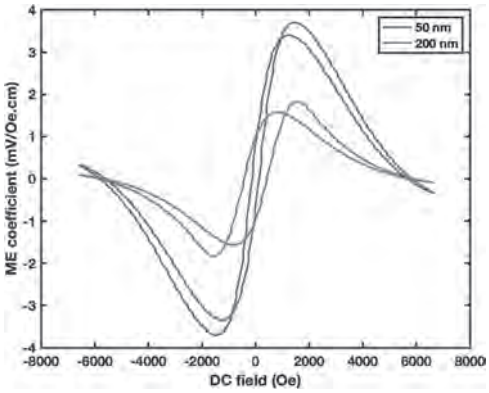

Fig. 2 ME coefficient vs dc bias for CFO-BTO:25-75% composite

P5-12. Study of Ferromagnetic Resonance of Micro and Nano Size Barium Ferrite Powders. W. Quan[1] and *M.N. Afsar*[1] *1. Tufts University, Medford, MA, United States*

Complex dielectric and magnetic properties of micro- and nano-size hexagonal ferrites have been studied. Two different measurement techniques as shown in Fig. 1 have been applied to characterize the samples in the broad frequency range from 1.7 GHz to 120 GHz. It was observed that the constitutive material properties, namely permittivity and permeability, as well as the ferromagnetic resonance frequency of the samples vary with the change in particle dimensions. Based on the results of these measurements, a model for calculating the ferromagnetic resonance frequency of ferrite powders has been derived, which takes into account the size and shape of the particles in the sample. Since the properties have been found to be size dependent, it is important that the measurement set-up is accurate enough to detect these differences. In the past, the powder samples have been diluted with conductive materials or epoxy to fabricate a solid sample for measurements. The procedure followed in this study does not use any such additive. Therefore, the properties of the samples can be determined precisely. The results presented in Fig. 2 reveal that the ferromagnetic resonance frequency of the ferrite samples varies with the particle size. Therefore, the material can be tuned to resonate at different frequencies by changing the size of the particles. The resonance observed in the case of nanoparticles is much sharper than that observed for bulk samples or samples containing micro-sized particles. Absolutely no resonance was observed in case of samples that did not contain the proper phase of barium hexaferrite. The techniques developed in this study can be used for non-destructive testing to check if the desired phase has been achieved or not. Accurate characterization would allow scientists to utilize nanomaterials to their full potential and achieve high performance in diverse applications.

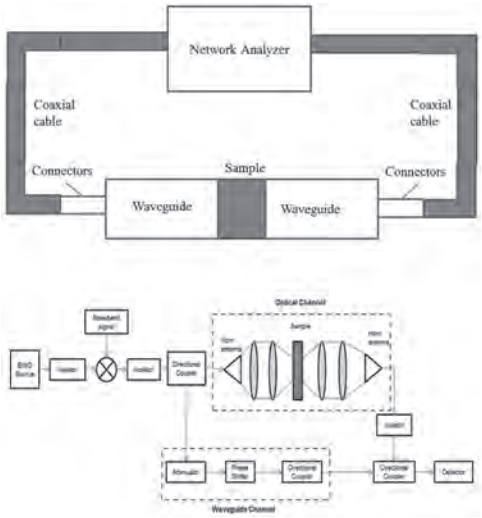

Fig. 1. Block diagram of the VNA measurement setup and Spectrometer for measuring the transmission characteristics of the material at millimeter wave frequencies.

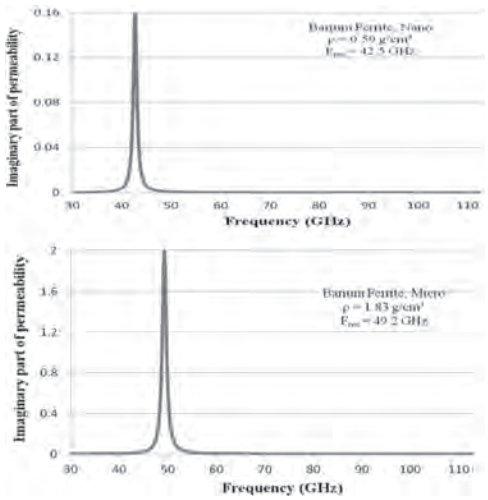

Fig 2. Imaginary parts of permeability for Barium nano-ferrite powder and micro-ferrite powder measured in the millimeter wave frequency range.

P5-13. Withdrawn

P5-14. Controlling Magnetic Properties of Epitaxial Nanocomposite Thin Films Through Ionic Liquid Gating. S. Ning[1], *E. Cho*[1] and C. Ross[1]
1. Department of Materials Science and Engineering, Massachusetts Institute of Technology, Cambridge, MA, United States

Voltage control of the structure, magnetic and electronic properties of materials enables the realization of new types of nonvolatile magnetoelectric memory devices. Here, we investigate the effect of ionic liquid gating on the magnetic properties of self-assembled heterostructure films consisting of nanoscale $Co_yFe_{3-y}O_4$ (CFO) spinel pillars embedded in a $SrCo_{1-x}Fe_xO_{3-\delta}$ (SCFO) perovskite (P) or brownmillerite (BM) matrix, over a range of compositions x and y. These self-assembled nanocomposites are grown by pulsed laser deposition on $SrTiO_3$ substrates using $SrCoO_{3-\delta}$-$SrFeO_{3-\delta}$, $SrCoO_{3-\delta}$-Fe_3O_4, or $SrFeO_{3-\delta}$-Co_3O_4 pairs of targets. We first describe the growth kinetics of these nanocomposites, focusing on how the oxygen pressure affects the distribution of Co and Fe between the two phases and the formation of P vs. BM structure for the matrix. Unusually, at high oxygen pressures, the two-phase structure can grow from the codeposition of $SrCoO_{3-\delta}$ and $SrFeO_{3-\delta}$, attributed to depletion of the Sr in the film. The pillar CFO magnetism depends on y, e.g. ferrimagnetic with room temperature saturation magnetization Ms ~300 kA/m for y=1 and paramagnetic for y=0. The matrix SCFO with the BM phase has antiferromagnetic ordering irrespective of x, while the magnetism of the P phase depends strongly on x and can exhibit a room temperature Ms ~100 kA/m for x=0.5 but almost no moment for x=0 and x=1 [1]. With the gating voltage of -3V/+3V, the lattice parameter of matrix SCFO changes ±3% and induces strain transfer around ±1% to the pillar phase (Fig. 1). In particular, for x=0.5 and y=0 (Fig. 2), the negative gating inserts oxygens into the BM phase and changes it into a P phase showing ferromagnetism. Our study clarifies the manipulation of the magnetism of composite materials through an electrochemical process, expanding the applications of magnetoelectric coupling.

[1] S. Ning, Q. Zhang and C. A. Ross, ACS Nano, https://dx.doi.org/10.1021/acsnano.0c03750 (2020)

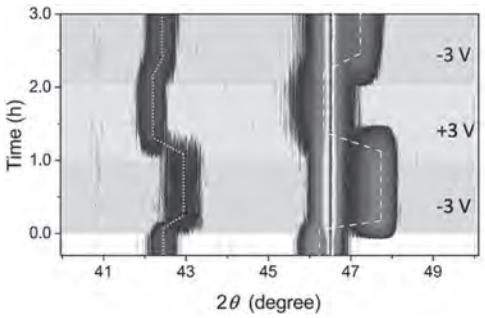

In situ XRD of SCFO-Co_3O_4 nanocomposite around the (002) peak of $SrTiO_3$. The line on the left corresponds to Co_3O_4, and the line on the rights correspond to SCFO.

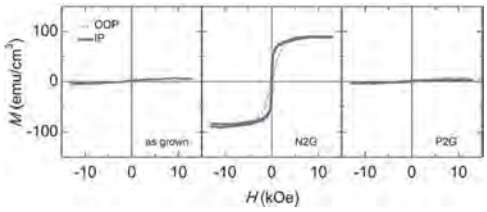

Room temperature magnetic hysteresis loops of as grown, -2V gated, and +2V gated nanocomposite. Magnetization is normalized by the total volume.

Session P6
SPIN HALL AND RELATED EFFECTS II
(Poster Session)

Shu Zhang, Co-Chair
University of California, Los Angeles, Los Angeles, CA, United States
Tao Zhu, Co-Chair
Institute of Physics, Chinese Academy of Sciences, Beijing, China

P6-01. Large Field Like Torque in Amorphous Ru2Sn3 Originated From Intrinsic Spin Hall Effect. *T. Peterson*[1], M. DC[2], Y. Fan[1], J. Chen[1], D. Zhang[1], H. Li[1], P. Swatek[1] and J. Wang[1] *1. University of Minnesota, Minneapolis, MN, United States; 2. Stanford University, Stanford, CA, United States*

We report large field-like torques with non-negligible damping-like torques in sputtered, amorphous Ru_2Sn_3 thin films. We confirm the amorphous structure of the films with high resolution tunneling electron microscopy and the 2:3 composition with Rutherford backscattering techniques. Through the second harmonic Hall measurement we can extract and characterize the damping-like (DL) and field-like (FL) SOTs originating in the Ru_2Sn_3 films. We find room temperature a DL torque efficiency of 0.14 ± 0.008 and 0.07 ± 0.012 and a FL torque efficiency of -0.03 ± 0.006 and -0.20 ± 0.009 for 4 and 10 nm Ru_2Sn_3 films respectively. By analyzing the resistivity dependence of the spin torque efficiencies, we extracted the contributions from the intrinsic and extrinsic spin Hall effects. The FL torques show dominant contributions from the intrinsic spin Hall effect with intrinsic spin conductivity up to -240 ± 19 $(\Omega cm)^{-1}$ while the DL torques show dominate contributions from the extrinsic spin hall effects with sum of the skew scattering and side jump up to -175 ± 19 μΩcm. We performed macro-spin calculations of the LLGS equation to simulate switching a perpendicular magnetic layer including both the DL and FL torques generated from our Ru_2Sn_3 SOT channel. We find the inclusion of FL toques three times greater than the DL can reduce the critical current required for switching and the switching time by almost 50% compared to the DL torque only case.

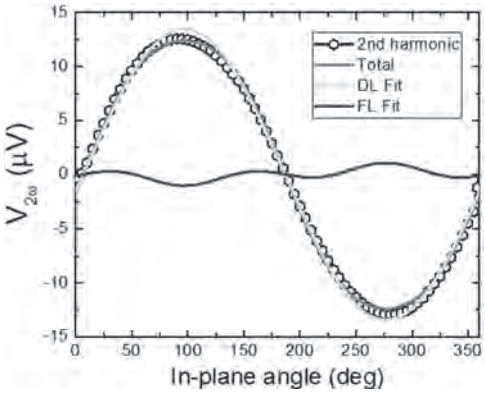

Fig. 1. The second harmonic Hall voltage for the 10 nm sample rotated in a 1500 Oe external field at 300 K fitted to extract the DL and FL torque contributions.

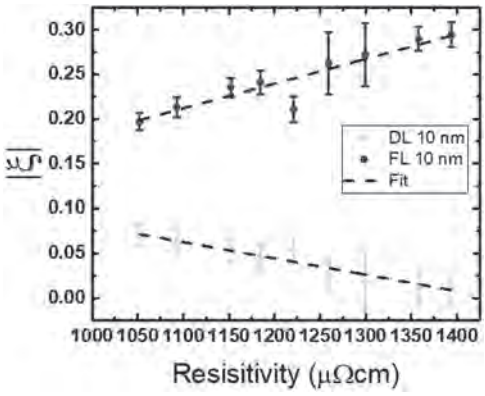

Fig. 2. Relation between magnitude DL and FL torque efficiencies and the resistivity of the 10 nm Ru2Sn3 sample.

P6-02. Spin Pumping and Anti-Damping in Trilayer Structures. *P. Gupta*[1], A. Kumar[1], K. Khan[1], N. Chowdhury[1] and P.K. Muduli[1] *1. Department of Physics, Indian Institute of Technology Delhi, New Delhi, India*

Spin pumping [1] in a ferromagnet (FM)/ non-magnetic (NM) thin films plays an important role in spin to charge conversion and defining various applications in microwave and THz spintronic devices [2]. In a FM/NM bilayer structure, the spin pumping enhances the phenomenological Gilbert damping coefficient (α) of the FM layer [3]. On the other hand, a NM/FM/NM trilayer heterostructure offers two FM/NM interfaces, which results in a larger spin pumping as compared to the bilayer counterpart. In this work, we have studied the spin pumping in NiFe (10 nm)/Pt (t_{Pt}), Pt (t_{Pt})/NiFe (10 nm)/Pt (2 nm) and IrMn (t_{IrMn})/NiFe (10 nm)/Pt (2 nm) heterostructures by systematically varying the thickness of the underlayer and top-layer. Here, the trilayer heterostructures were grown using DC magnetron sputtering at ultra-high vacuum conditions. Ferromagnetic resonance (FMR) spectroscopy [4] was performed for a frequency range of 3-8 GHz to study the dependence of the NM layer thickness on effective Gilbert damping constant (α_{eff}). In NiFe/Pt bilayer system, maximum spin pumping/enhancement in Gilbert damping is observed when the thickness of Pt layer is greater than diffusion length ($t_{Pt} > \lambda$) as shown in Fig.1 (a). However, even larger α_{eff} is observed for Pt on both sides of NiFe. Hence, both underlayer and top layer Pt thin films contribute equally to enhance the spin pumping from NiFe layer. In the case of IrMn/NiFe/Pt, up to a thickness of ~ 1 nm of IrMn layer, we observe a decrease in α_{eff} shown in Fig.1 (c). This decrease in α_{eff} is an anti-damping effect [5] arising either due to underlayer microstructures or some Néel ordering at the NiFe/IrMn interface. For IrMn thickness larger than 1.8 nm, a small contribution of spin pumping is observed from IrMn layer as well. Our results suggest that IrMn underlayer acts as a bad spin sink material and does not enhance the spin pumping. This study also shows a potential method of using different underlayer in NM/FM/NM trilayer structures to obtain a tunable Gilbert damping.

1. Y. Tserkovnyak, A. Brataas, G.E.W. Bauer, Phys. Rev. Lett. 88, 117601 (2002). 2. L.Bocklage, Phys. Rev. Lett. 118, 257202(2017). 3. T.L. Gilbert, Phys. Rev. 100, 1243 (1955). 4. C. Kittel, Phys. Rev. 73, 155 (1948). 5. N. Behera, S. Chaudhary, D.K. Pandya, Sci. Rep. 6, 19488 (2016).

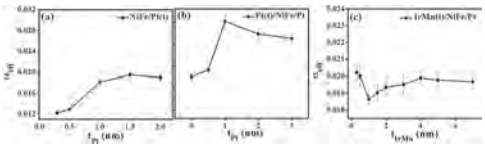

Figure 1 (a) Variation of α_{eff} with thickness of top-Pt layer, (b) Variation of α_{eff} with thickness of underneath-Pt layer, (c) Variation of α_{eff} with thickness of underneath-IrMn layer.

P6-03. Unusual Electronic Transport Properties of Sputter-Deposited $Co_{25}Fe_{75}$ /Pt Based Heterostructured Thin Film Sample. *H. Saren*[1], Y. Kumar[1], A. Deka[2], Y. Fukuma[2], H. Asada[3] and P. Das[1] *1. Physics, Indian Institute of Technology Delhi, New Delhi, India; 2. Computer Science and Electronics, Kyushu Institute of Technology, Iizuka, Japan, Iizuka, Japan; 3. Graduate School of Science and Engineering, Yamaguchi University, Ube, Japan*

Spin-orbit coupling (SOC) and symmetry breaking, which may be due to the interface between a thin film of a ferromagnet and a heavy metals aid to the development of Dzyaloshinskii-Moriya interaction (DMI) [1,2], favoring the formation of a chiral arrangement of spin configurations. Electrical detection and manipulation are the key requirements for any potential exploitation of these materials and that demands proper understanding of the transport behavior of charge carriers in these materials. Different feature such as topological Hall effect[3,4], narrow band noise[5] unusual magneto resistance[6] in electronic transport measurements are observed owing to interactions between conduction electrons and different magnetic states and their dynamics, revealing intriguing underlying physics. In this work, we have performed electronic transport (Hall, magnetoresistance, noise fluctuation spectroscopy) measurements for CoFe/Pt-based thin film sample. A characteristic peak in Hall resistance is reproducibly observed during up and down sweep of the magnetic field as shown in Fig.1. Temperature dependent Hall effect measurements reveal that such peak shifts towards higher value with decreasing temperature as shown in the inset of Fig.1. The dynamics of charge carriers as measured using noise fluctuation spectroscopy technique at varying field as shown in Fig.2 shows systematic and reproducible variations across H_{peak}. Particularly, electronic fluctuations are found to increase at around these fields. The results demonstrate an interesting correlation between the interface induced magnetic states and the carrier dynamics.

[1] I. Dzyaloshinsky, J. Phys. Chem. Solids 4, 241 (1958). [2] T. Moriya, Phys. Rev. 120, 91 (1960). [3] A. Neubauer, *et al.*, Phys. Rev. Lett. 102, (2009). [4] D. Liang, *et al*., Nat. Commun. 6, 8217 (2015). [5] T. Sato, *et al.*, Phys. Rev. B 100, (2019). [6] K. Meng, *et al*., Sci. Rep. 6, 20522 (2016).

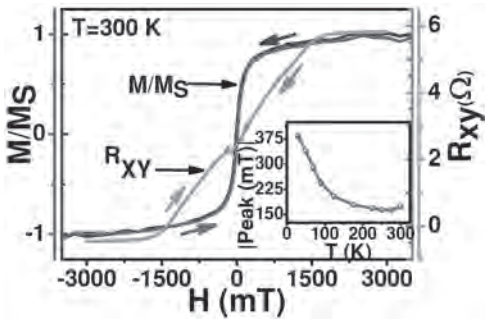

Fig. 1 Hall resistance and its temperature dependent behavior.

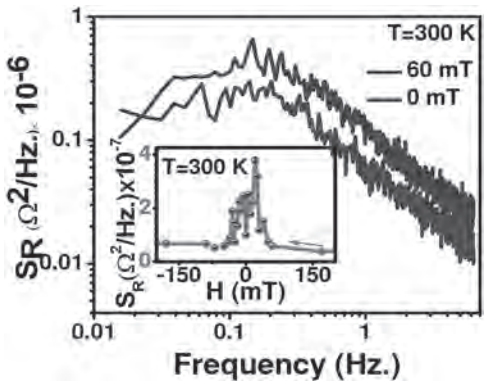

Fig. 2 Representative noise spectra at 0 and 60 mT field and variation of noise power measured at 1 Hz as a function applied magnetic field.

P6-04. Angle Dependent Magnetoresistance in EuO_{1-x} Thin Films. *N. Shrestha*[1] and J. Tang[1] *1. Department of Physics and Astronomy, University of Wyoming, Laramie, WY, United States*

At present significant research effort is being placed in the study of ferromagnetic thin films and 2-dimensional electron gas (2DEG) system for electronic and spintronic applications. We have prepared thin films EuO_{1-x} on Si (001) substrate by pulsed laser deposition (PLD) using europium (Eu) metal as a target in order to examine its spin-dependent transport. The magnetic and transport properties of the films have been studied as function of temperature and field. The magnetic data shows enhancement in the Curie temperature from 70K to 140K, which is characteristics of oxygen deficient samples. And the transport measurement reveals the metal-insulator transition known to be associated with the ferromagnetic ordering of EuO. We present the magnetoresistance of EuO_{1-x} thin films when a magnetic field (B) is applied in three mutually orthogonal orientations. With current flowing in the x-direction and z being normal to the film plane, we found that the resistance changes when B is rotated in the y-z and x-z plane. However, the resistance changes little when B is rotated in the x-y plane. Although the result may in principle be explained in terms of shape anisotropy, other mechanisms are being examined. There is an enhancement in the magnetic anisotropy from the transport measurements, which is much larger than that obtained from magnetic bulk measurement, which may result from strong spin-orbit coupling in EuO_{1-x}.

P6-05. Withdrawn

P6-06. Spin-Orbit Torque Induced Switching in CoFeB and β-W Bilayer With a 1 nm Ta Insert Layer. *S. Allen*[2], A.J. Narasimham[1], M. Zhu[3], A. Diebold[3], V.P. LaBella[3] and P. Dhagat[2] *1. College of Nanoscale Science and Engineering, State University of New York, Albany, NY, United States; 2. Electrical Engineering, Oregon State University, Corvallis, OR, United States; 3. SUNY PI, State University of New York, Albany, NY, United States*

Strong spin-orbit coupling in Tungsten (W) allows for it to be considered for use as a third terminal for spin orbit torque (SOT) switching of a magnetic tunnel junction (MTJ) and thereby, enable independent control of read and write currents in the device [1–3]. In this work, we study SOT switching in Hall-bar structures patterned from a stack of β-W (5 nm)/Ta (1 nm)/CoFeB (1 nm)/MgO (1.6 nm)/Ta (cap layer) on Si/SiO2 substrates. The beta phase of tungsten is chosen as it exhibits larger spin orbit effects than the alpha phase [2,4]. The 1 nm Ta insert layer between β-W and CoFeB/MgO/Ta preserves the perpendicular magnetic anisotropy at the MgO/CoFeB interface, necessary for thermal stability and efficient scaling of SOT-MTJ devices [5]. The Hall-bar structures are fabricated as 5 μm by 20 μm in dimensions. Anomalous Hall voltage measurements are conducted to confirm perpendicular magnetic anisotropy in the stack (Fig. 1a). To demonstrate spin orbit torque

switching, a direct current (along X-axis) is swept while measuring the Hall voltage (along Y axis) under a constant external in-plane (along X-axis) magnetic field (Fig. 1b). At an optimum in-plane current, due to sufficient spin orbit torque from the β-W/Ta layer, the magnetization of CoFeB is seen to switch as noted from the discontinuous change in the Hall voltage, which is proportional to the Z-component of magnetization [6]. The presentation will discuss in detail in-plane direct-current induced switching under varying external in-plane magnetic fields, as well as damping-like and field-like spin-orbit effective-fields obtained from alternating-current induced second harmonic-Hall measurements.

1. A. D. Kent and D. C. Worledge, Nat. Nanotechnol., 10,187–191, 2015. 2. C-F. Pai et al., Appl. Phys. Lett., 101, 122404, 2012. 3. P. Debashis, T.Y.T Hung and Z. Chen, NPJ 2D Mater., 4, 18, 2020. 4. E. Derunova et al., Sci. Adv., 5, eaav8575, 2019. 5. W. Kim et al., 2011 International Electron Devices Meeting, Washington, DC, 2011, 24.1.1–24.1.4. 6. A. J. Narasimham et al., AIP Adv., 4, 117139, 2014.

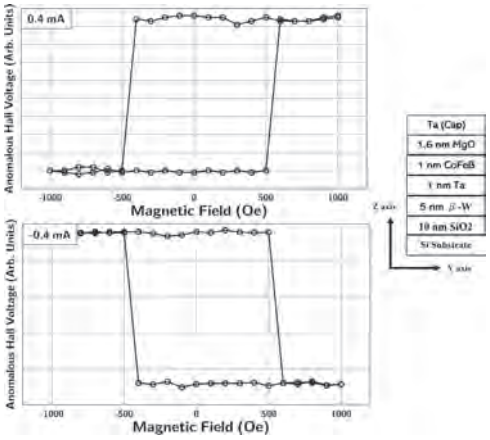

Fig. 1a: Anomalous Hall voltage vs. external magnetic field (along Z-axis). A constant in-plane current of ±0.4 mA is applied as shown in the inset.

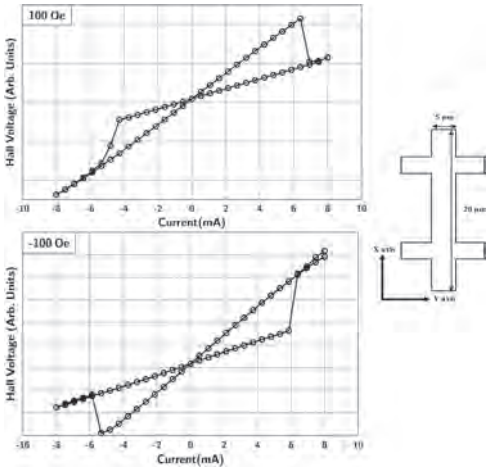

Fig. 1b: Hall voltage vs. In-plane current (along X-axis). A constant external in-plane magnetic field (along X-axis) of ±100 Oe is applied as shown in the inset. The change in switching symmetry with the direction of the external field is consistent with spin Hall effect switching.

P6-07. Study of Magnetic Field Dependence of Hall Effect in FeB and FeCoB Nanomagnets. an Evidence of Contribution of Inverse Spin Hall Effect. *V. Zayets*[1] and A.S. Mishchenko[2] *1. Research Institute for Advanced Electronics and Photonics, National Institute of Advanced Industrial Science and Technology (AIST), Tsukuba, Japan; 2. Center for Emergent Matter Science, RIKEN, Wako, Japan*

We measured the Hall effect (HE) in a ferromagnetic nanomagnet with a strong perpendicular magnetic anisotropy (PMA), in which the local magnetic moments are very stable and well- aligned along the easy axis of the nanomagnet. The adopted mechanisms of HE predict linear plus a constant dependence on the external field originating from the ordinary and anomalous Hall effects, respectively. Our measurement revealed an extra non- linear contribution indicating an additional contribution to HE, which was suggested to be the Inverse Spin Hall effect (ISHE). The ISHE describes the fact that an electrical current is created perpendicularly to the flow of the spin- polarized current. The ISHE requires existence of the spin-polarized electrons. In a ferromagnetic metal the electron gas is spin- polarized even in equilibrium and any electrical current in a ferromagnetic metal is spin- polarized. As a result, any electrical current in a ferromagnetic metal must always experience the ISHE and there must be a flow of the Hall current perpendicularly to the bias current. There are several methods to change the number of spin- polarized electron in a ferromagnetic metal and therefore the magnitude of the ISHE. E.g. the spin polarization can arise due to the influence of an external magnetic field, the mechanism considered by Landau and Lifshitz a long time ago[1]. The Hall angle α_{HE} can be presented as $\alpha_{HE} = \alpha_{OHE}$ H+ $\alpha_{AHE} + \alpha_{ISHE}$ P_S(H) where the non-linear dependence of spin polarization P_S on magnetic field is calculated as[2] $P_S(H)=(P_{S,0}+H/H_S)/(1+H/H_S)$ where $P_{S,0}$ is the spin polarization at H=0. H_S is the scaling magnetic field. Figure 1 shows that the fit of the experimental data with the above relation is excellent proving the importance of the ISHE contribution to the HE in a ferromagnetic metal.

[1] L. D. Landau and E. M. Lifshitz, Phys. Z. Sowjetunion. Vol. 8, p.153 (1935). [2] V. Zayets, J. Magn. Magn. Mater. Vol. 356, p. 52 (2014).

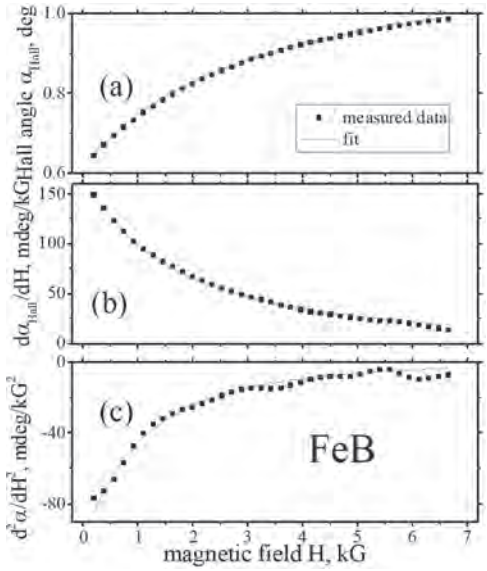

Fig.1. Comparison of experimental data (circles) and theoretical fit (lines): (a) Hall angle α_{HE} (b) first derivative, and (c) second derivative of α_{HE}.

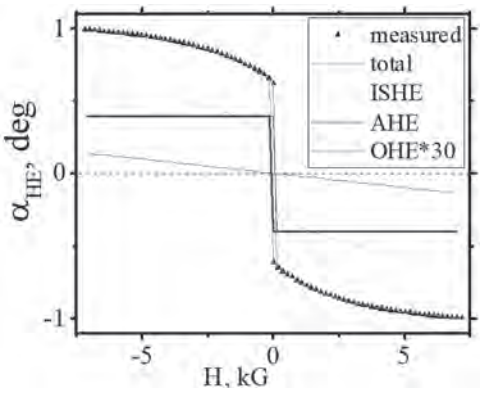

Fig.2 Decomposing of measured Hall angle into 3 contributions.

P6-08. Enhancements of the Spin Seebeck Effect Owing to the Bismuth-Substitution in Thermoelectric Generators Comprising an LPE Bi-Substituted YIG Film. *M. Imamura*[1], H. Asada[2], D. Tashima[1] and J. Kitagawa[1] *1. Fukuoka Inst. of Tech., Fukuoka, Japan; 2. Yamaguchi Univ., Ube, Japan*

A spin-thermoelectric generator is composed of a thin paramagnetic metal (PM) layer, ferrimagnetic insulator (FMI) and PM/FMI bilayer interface. To raise the spin thermoelectric voltage V_{STE}, studies for improving the characteristics of each part have been done.[1-3] We took notice of the bismuth-substitution for yttrium to increase the spin pumping at the PM/FMI interface,[2,4] and tested the Bi-substituted YIG films grown by liquid phase epitaxy (LPE). LPE Bi-substituted YIG films exhibit a large growth-induced magnetic anisotropy perpendicular to the film surface,[5] and the in-plane *M-H* properties vary due to this anisotropy. Figure 1 shows the normalized *M-H* and V_{STE}-*H* curves concerning $Y_{3-x}Bi_xFe_5O_{12}$ films. It is confirmed that the V_{STE}-*H* curve agrees well with the *M-H* curve indicating V_{STE} strongly depends on the magnetic properties of FMI's. Figure 2 shows the dependence of the spin Seebeck coefficient S_{SSE} on the Bi-concentration *x*. S_{SSE} increases very clearly with increasing *x*, and the S_{SSE} value for x=1.3 is about 1.5 times that of x=0 in our measurements. It has been suggested that the mixing of the 6p orbitals of Bi ions with the O 2p orbitals increases the effective spin-orbit coupling of Fe^{3+} ions.[6] We presume that this physical situation increases the damping constant $\alpha_{Bi:YIG}$ and, as a result, the spin mixing conductance g_r at the PM/FMI interface becomes large. We have obtained the high V_{STE} value of 80μV (S_{SSE}=3.2μV/K) with a generator comprising the $Y_{2.35}Bi_{0.65}Fe_5O_{12}$ film in the condition of l_d=5mm, t_{Pt}=4nm and ΔT=25K. To obtain higher V_{STE} values, the issue of a heat-flow in the STE generator is important from its structural viewpoint. [The ref. paper #3 ([3]M. Imamura *et al.*, Electr Eng Japan, Vol. 208, No. 3-4 (Wiley Online Library 2019)) can be referred by putting the paper title "Spin-thermoelectric voltage in longitudinal SSE elements incorporating LPE YIG films and polycrystalline YIG slabs with an ultrathin Pt layer" into Google's search window.]

[1] K. Uchida, H. Adachi and T. Kikkawa, Proc. IEEE, Vol. 104, p.1946 (2016) [2] M. Ishida, JJAP, Vol. 87, p.11 (2018) in Japanese [3] M. Imamura, H. Asada and D. Tashima, Electr Eng Japan, Vol. 208, No. 3-4, p.10 (Wiley Online 2019) [4] H. Asada, A. Kuwahara and N. Sakata, JAP, Vol. 117, p.17C724 (2015) [5] P. Hansen, K. Witter and W. Tolksdorf, Phys. Rev. B, Vol. 27, p.6608 (1983) [6] P. Hansen and J. P. Krumme, Thin Solid Films, Vol. 114, p.69 (1984)

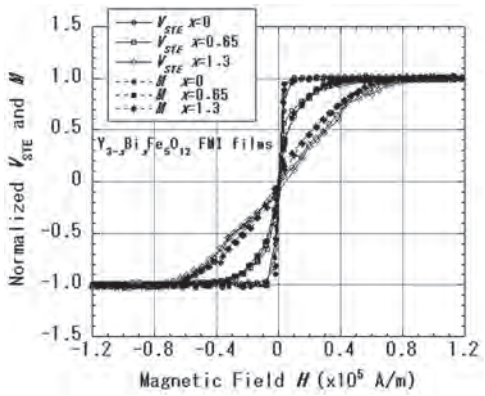

Fig. 1. Comparison between the normalized V_{STE}-*H* and *M-H* curves: l_d=5 mm; t_{Pt}=4 nm.

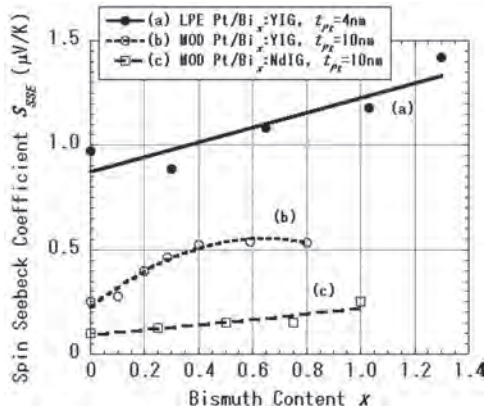

Fig. 2. The dependence of S_{SSE} on Bi-content (a) Our measurements, (b) Ishida,[2] (c) Asada *et al.*.[4]

P6-09. Spin Transport Property in Thermally-Evaporated Pigment-Red Films by Using a Dynamical Spin Injection Method. K. Nishida[1], Y. Teki[1] and *E. Shikoh*[1] *1. Osaka City University, Osaka, Japan*

Carbon-based molecular materials attract attention for the wide possibility of spintronic applications because of the small spin-orbit interaction and various spin-related functionalities. To develop molecular spintronic devices, improvement of the physical durability is an indispensable issue. In this study, the spin transport property in pigment-red (perylene-3,4,9,10-tetracarboxylic dianhydride: PTCDA) films was investigated which is known as one robust molecular material. Pd/PTCDA/$Ni_{80}Fe_{20}$ trilayer samples were formed as follows: On a Si/SiO_2 substrate, a Pd layer (the thickness of 10 nm) was formed by using an EB deposition under a vacuum of $<10^{-6}$ Pa. Next, under the same vacuum condition, PTCDA molecules were thermally evaporated. The PTCDA layer thickness was varied between 0 to 60 nm. Finally, a $Ni_{80}Fe_{20}$ layer (25 nm) was formed by using an EB deposition under the same vacuum condition. To prevent the samples during the $Ni_{80}Fe_{20}$ deposition, the sample substrate temperature was kept at 271 K. The ferromagnetic resonance (FMR) of $Ni_{80}Fe_{20}$ films was excited with a conventional ESR system. Output voltages from the samples with a Pd layer were observed under the FMR of the $Ni_{80}Fe_{20}$ film, and the voltage sign was inverted at the magnetization reversal of the $Ni_{80}Fe_{20}$ film. The output voltage was increased with increasing the microwave power of the ESR system. Meanwhile, tiny output voltages from the samples with a Cu layer instead of the Pd layer were observed under the FMR of the $Ni_{80}Fe_{20}$ film. These indicate that the output voltage observed from the samples with the Pd is mainly due to the inverse spin-Hall effect in the Pd layer. That is, spin

transport in evaporated PTCDA films was achieved at room temperature, and it is confirmed that a PTCDA film is useful not only as a robust protection layer material but also as a spintronic material [1].

[1] K. Nishida, Y. Teki, and E. Shikoh, Solid State Commun., Vol. 312, p.113898 (2020).

P6-10. Spin Injection Into Vanadium Dioxide Films From a Typical Ferromagnetic Metal, Across the Metal-Insulator Transition of the Vanadium Dioxide Films. *K. Tamura*[1], T. Kanki[2], S. Shirai[1], H. Tanaka[2], Y. Teki[1] and E. Shikoh[1] *1. Osaka City University, Osaka, Japan; 2. Osaka University, Osaka, Japan*

A vanadium dioxide (VO_2) film shows metal-insulator transition (MIT) with the crystal structure change induced by changing the environmental temperature [1]. Recently, the spin injection into a VO_2 film from a ferrimagnetic insulator YIG film by using the spin-pumping was achieved across the MIT temperature [2]. For the practical use, however, to prepare the YIG films with good quality is needed and is basically hard. In this study, a typical ferromagnetic metal $Ni_{80}Fe_{20}$ was utilized as a simply available good spin injector. $VO_2/Ni_{80}Fe_{20}$ bilayer junctions were prepared on TiO_2 substrates and the temperature dependence of electromotive force properties generated in the $VO_2/Ni_{80}Fe_{20}$ bilayer junctions under the ferromagnetic resonance (FMR) of the $Ni_{80}Fe_{20}$ layer was evaluated. The electrical resistance of the VO_2 films at 280 K was 1000 times larger than at 300 K corresponding to the MIT of the VO_2 films. Meanwhile, the detected electromotive forces in the bilayer samples under the FMR show almost constant value in the temperature range between 280 and 300 K. This behavior was not explained only with the temperature dependence of the electromotive force property generated in the $Ni_{80}Fe_{20}$ film itself under the FMR [3], but also with the generated electromotive forces due to the inverse spin-Hall effect (ISHE) in VO_2 films under the FMR of the $Ni_{80}Fe_{20}$ film. That is, we successfully demonstrated the spin injection from a typical ferromagnetic metal $Ni_{80}Fe_{20}$ film into a VO_2 film, across the MIT temperature of the VO_2 films.

[1] H. Takami, T. Kanki, H. Tanaka, et al., Appl. Phys. Exp., Vol.3, p.063201 (2010). [2] T.S. Safi, et al., Nat. Commun., Vol.11, p.476 (2020). [3] A. Tsukahara, E. Shikoh, et al., Phys. Rev. B, Vol.89, p.235317 (2014).

P6-11. Flat and Highly (100) Texture of MgO Tunnel Barrier and W/Hf Thickness Ratio Dependence in MgO/CoFeB/(W/Hf)-Multilayer Large Spin Hall Effect Electrode System. *Y. Saito*[1], N. Tezuka[2], S. Ikeda[1] and T. Endoh[1] *1. Center for Innovative Integrated Electronic Systems, Tohoku University, Sendai, Japan; 2. Department of Materials Science, Graduate School of Engineering, Tohoku University, Sendai, Japan*

Current-induced spin-orbit torque (SOT) originating from the spin-Hall effect (SHE) in heavy metal/ferromagnet (HM/FM) systems has attracted attention due to their potential application in the efficient manipulation of magnetization of nano magnets in SOT-MRAM [1], skyrmion and domain wall devices. For the application to a large-scale integration, the efficient SOT operation (high spin Hall angle $|\theta_{SH}|$) in low resistivity (ρ_{xx}) HM is necessary [2-4]. Due to the extensive efforts, the $|\theta_{SH}|$ becomes larger day by day, however, almost all HMs with large magnitude of $|\theta_{SH}|$ have a very high ρ_{xx}. The magnitude of $|\theta_{SH}|$ for both intrinsic and extrinsic (side jump mechanism) terms is proportional to the magnitude of ρ_{xx} value ($|\theta_{SH}| \sim \sigma_{SH}\,\rho_{xx}$) [5, 6], where σ_{SH} is spin Hall conductivity. Therefore, increase in the magnitude of σ_{SH} would be important from the application point of view. Recently, we observed large magnitude of σ_{SH} and enhancement of perpendicular magnetic anisotropy in MgO/CoFeB/(W/Hf)-multilayer system compared to MgO/CoFeB/β-W system [4]. In this paper, we prepared MgO/CoFeB/(W/Hf)-multilayer systems with various W/Hf thickness ratios and investigated the W/Hf thickness ratio dependence of θ_{SH}, σ_{SH}, ρ_{xx}, and (100) texture of MgO tunnel barrier in the MgO/CoFeB/(W/Hf)-multilayer systems. These systems were patterned into the microscale Hall bar by photolithography and Ar ion milling, and annealed at 573 K. SHE in MgO/CoFeB/(W/Hf)-multilayer systems by means of spin Hall magnetoresistance (SMR) was studied. The analysis based on the drift diffusion model reveals that the magnitude of σ_{SH} monotonically increases with increasing W/Hf thickness ratio (Fig. 1). Spin diffusion length (λ) for (W/Hf)-multilayer is shorter than the estimated value of β-W (Fig. 1), which would be related to the increase in the interfacial scattering of multilayer system. In this presentation, we will report the details of SMR, $\theta_{SH,}$ λ and the film structure including the (100) texture of MgO tunnel barrier. This work was supported by the JST OPERA (JPMJOP1611) and JSPS KAKENHI (19H00844).

[1] H. Honjo et al., IEDM Tech. Dig. 28.5 (2019). [2] Y. Saito et al., Appl. Phys. Exp. 12, 053008 (2019). [3] Y. Saito et al., AIP Advances, 9, 125312 (2019). [4] Y. Saito et al., Appl. Phys. Lett. 116, 132401/1-5 (2020). [5] C. Zhang et al., Appl. Phys. Lett. 109, 192405 (2016). [6] L. Wang et al., Phys. Rev. Lett. 116, 196602 (2016).

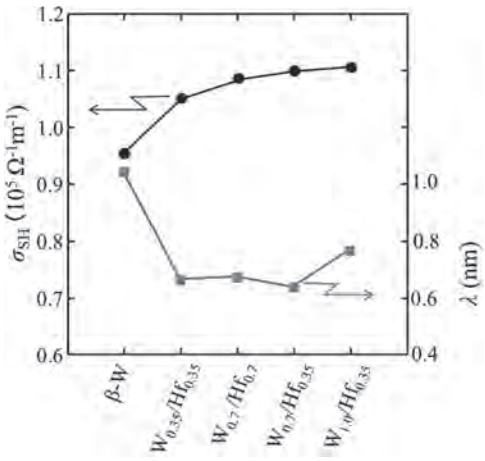

Estimated magnitude of the σ_{SH} and λ in MgO/CoFeB/β-W and MgO/CoFeB/(W/Hf) multilayer systems

P6-12. Influence of Ferromagnetic-Layer Thickness on Dynamical Spin Injection. *S. Obinata*[1], K. Miyazaki[1], K. Ohnishi[1] and T. Kimura[1] *1. Dept of Physics, Kyushu University, Fukuoka, Japan*

Dynamical spin injection based on ferromagnetic resonance (FMR) has been intensively investigated owing to its simple structure. When the FMR is excited in ferromagnetic-metal (FM)/nonmagnetic-metal (NM) bilayer thin films, the spin current flows from FM layer into NM layer. Although the mechanism of the dynamical spin injection is mainly explained by spin pumping, FMR-heating could be a possible reason for the spin injection [1]. Spin-Torque FMR (ST-FMR) is widely utilized to characterize the spin injection property where symmetric voltage changes are known to be induced by inverse spin hall effect (ISHE) due to the spin injection. However, recent study pointed out that the AMR and other spurious effect also produce the symmetric voltage change [2]. In order to improve these unfavorable situations, we developed a new structure for the precise evaluation of the ST-FMR and investigated the thickness dependence of FM layer on the ISHE voltage. Figure 1 shows the schematic illustration of the sample structure developed for the precise ST-FMR measurement. CoFeB(5~20nm)/Pt(10nm) bilayer films have been prepared by magnetron sputtering on Si-sub, and the top layer of Cu(100nm) is prepared by Joule evaporation. Note is that the thick Cu capping layer enable to exclude the AMR contribution in the ST-FMR signal. Figure 2 shows the spectra of Pt/CoFeB/Cu for various CoFeB thicknesses at. These spectra seems completely symmetric and can be understood by the ISHE voltage. We find that the voltage change due to ISHE is proportional to the thickness of CoFeB. Since the spin pumping is known as the interfacial effect, the obtained result suggests the importance of the FMR heating in the dynamical spin injection. We also have conducted same experiment using W, and Ta, and obtain similar tendency for the thickness dependence of CoFeB on ISHE.

[1] K.Yamanoi et al., Physical Review Applied 8,054031(2017). [2] Yin Zhang et al., Physical Review B 99, 064424 (2019).

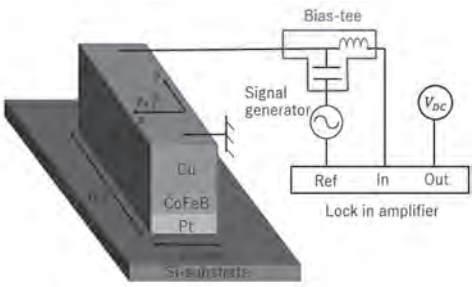

Fig.1 Schematic illustration of measurement system.

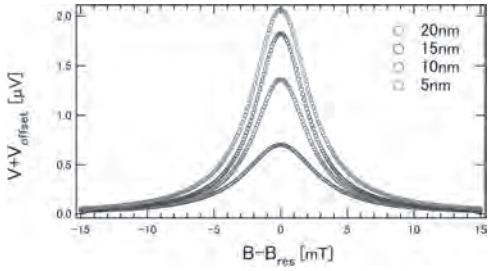

Figure.2 ST-FMR spectra of Pt/CFB(5~20nm)/Cu with 11GHz rf current.

P6-13. Optical Method of Determining Spin Diffusion Length of Ferromagnetic Metals. *K. Ko*[1] and G. Choi[1,2] *1. Department of Energy Science, Sungkyunkwan University, Suwon, The Republic of Korea; 2. Center for Integrated Nanostructure Physics, Institute for Basic Science (IBS), Suwon, The Republic of Korea*

Spin diffusion length is a characteristic length that describes the spatial decay of the spin polarization. We demonstrate an optical method of determining the spin diffusion length of ferromagnetic metal. We optically induced the spin transport from ferromagnetic metal to nonmagnetic metal via ultrafast demagnetization of the ferromagnetic metal. The spin accumulation on nonmagnetic metal is measured by magneto-optical Kerr effect. The ultrafast demagnetization and the spin transport are analyzed based on the theory that the spin is generated by electron-magnon scattering in the bulk of ferromagnetic metal, then it diffuses to the NM. We perform two independent approaches to figure out the spin diffusion length: the quantitative analysis and the relative analysis of the spin accumulation. First, we quantitatively compare the Kerr rotation and the spin accumulation on nonmagnetic metal at a fixed thickness of ferromagnetic metal. Second, we measured the spin accumulation on nonmagnetic metal varying the thickness of ferromagnetic metal. Both methods give consistent results for the spin diffusion length. From our methods, we determine the spin diffusion length of 7.0, 4.6, and 3.3 nm for the ferromagnetic metal of Fe, Co, and Ni, respectively.

K.-H. Ko and G.-M. Choi*, Journal of Magnetism and Magnetic Materials, Vol. 510, 166945 (2020).

P6-14. Voltage Control of Magnetic Proximity Effect and Anomalous Hall Effect in $CoFe_2O_4$/Pt Bilayer by Ionic Liquid Gating. *S. Nodo*[1], S. Ono[2], T. Yanase[3], T. Shimada[3] and T. Nagahama[3] *1. Hokkaido University, Graduate School of Chemical Sciences and Engineering, Sapporo, Japan; 2. Central Research Institute of Electric Power Industry, Yokosuka, Japan; 3. Hokkaido University, Graduate School of Engineering, Sapporo, Japan*

Recently, the magnetic proximity effect (MPE) in HM/FMI has attracted attention as the spin manipulation method of nonmagnetic materials. In the Platinum, ferromagnetism via MPE is easily induced because it has the DOS nearly Stoner criterion[1]. Previously, other methods to be induced ferromagnetism in Pt have been reported such as quantum size effect[2] and ionic gating[3]. In this study, we report the control of the MPE in Pt by using ionic gate technique[3, 4] The film was grown on an MgO (001) substrate by reactive molecular beam epitaxy method. The film structure was MgO (001) /NiO (5 nm) /$CoFe_2O_4$ (50 nm) /Pt (2.5 - 12 nm). The $CoFe_2O_4$/Pt film was patterned into 100-μm-wide Hall bars by using a standard photolithography system. The Ionic Liquid, $[EMI]^+[TFSI]^-$ gel sheet (TA210 : EMI-TFSI = 1 : 1) was put on the Hall bars directly. Figure 1 shows the gate voltage dependence of resistance of $CoFe_2O_4$/Pt (2.5 nm) by ionic gating. The electric resistance varied by -5% - +10% in ±2V, which suggested that the carrier density of Platinum was modified by the applied gate voltage. Figure 2 shows Hall resistivity in $CoFe_2O_4$/Pt with various gate voltage at room temperature. The Hall resistivity showed hysteretic signal which means ferromagnetism was induced in Pt layer due to MPE[5]. Furthermore, the magnitude of anomalous Hall effect was significantly changed by applying a gate voltage, implying the induced ferromagnetism was modified through modulation of carrier density[6].

[1] A. H. MacDonald *et al.*, *Phys. Rev. B* 23, 6377 (1981). [2] M. A. Garcia *et al., Chem. Mater.*19, 4, 889-893(2007). [3] S. Shimizu *et al.*, *Phys. Rev. Lett.* 111, 216803 (2013). [4] S. Dushenko *et al.*, *Nat. Commun.* 9, 3118 (2018). [5] W. Amamou *et al., Phys. Rev. Mater.* 2, 011401 (2018). [6] S. Nodo *et al., Appl. Phys. Express* 13, 063004 (2020).

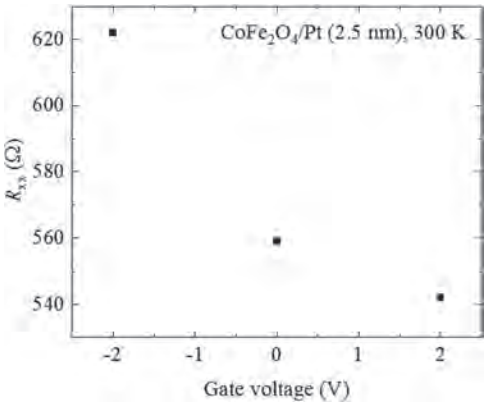

Figure 1 Gate voltage variation of the electrical resistance for $CoFe_2O_4$/Pt(2.5 nm) at 300 K.

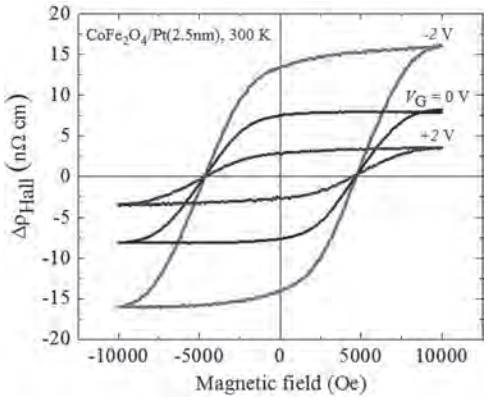

Figure 2 Gate voltage variation of Hall resistivity for $CoFe_2O_4$/Pt (2.5 nm) at room temperature.

P6-15. Effects of a Molecular Interfaces on the Spin Hall Magnetoresistance for YIG/Pt and YIG/Ta. *S. Alotibi*[1] *1. University of Leeds, Leeds, United Kingdom*

5d metals are used in electronic architectures because of their high spin-orbit coupling (SOC) leading to efficient spin ↔ electric conversion and strong magnetic interactions. When C_{60} is grown on a metal, the electronic structure is altered due to hybridisation and charge transfer. Previously, it has been shown that this can lead to the emergence of spin ordering [1]. This

interfacial effect is also critical in spin filtering and spin transport effects [2]. The spin Hall magnetoresistance for Pt/C_{60} and Ta/C_{60} at room temperature are up to a factor 6 higher than for the pristine metals, with the spin Hall angle increased by 20-60%. At low fields of 1-30 mT, there is an anisotropic magnetoresistance, increased up to 700% at room temperature by C_{60}. This is correlated with non-collinear Density Functional Theory simulations showing changes in the acquired magnetic moment of transport electrons via SOC. Given the dielectric properties of molecules, this opens the possibility of gating the effective SOC of metals, with applications for spin transfer torque memories and pure spin current dynamic circuits. According to our density functional theory (DFT) calculations for Pt/C_{60}, 0.18-0.24electrons per C_{60} molecule are transferred, and the first molecular layer is metallised. This reduces the electron surface scattering, improving the residual resistance ratio (RRR) –Figs. b. Our Ta wires have a resistivity and a negative temperature coefficient consistent with a sputtered b-Ta phase [3]. Opposite to Pt, C_{60} increases the resistivity of Ta –see Fig. b. The SHMR saturates once the applied field saturates the magnetisation out-of-plane, at 0.1-0.15 T for a YIG film 170 nm thick at 290 K, and no higher than 0.5 T for any measured condition. However, above this field range, other contributions such as Koehler MR, localisation and the Hanle effect can result in significant linear and parabolic contributions to the MR that would artificially enhance the SHMR ratio and q_{SH} (Fig. c) [4]. In YIG/Ta(4nm), where C_{60} increases the resistance rather than reducing it, both the SHMR up to 0.15 T and the polynomial MR at higher fields are enhanced (Fig. d)

1. F. Al ma'mari, *et al*., Nature. 524, 69—73 (2015) 2. M. Cinchetti, *et al*., Nature materials. 16, 507 (2017) 3. M. Grosser and U. Schmid, Thin Solid Films 517, 4493 (2009). 4. S. Velez *et al.*, Physical Review Letters 116, 016603 (2016).

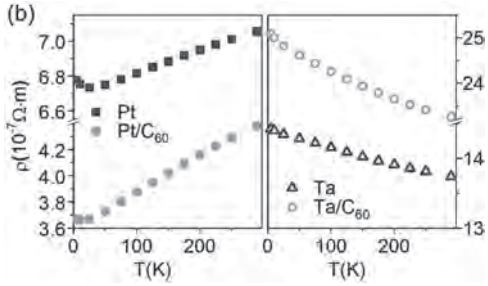

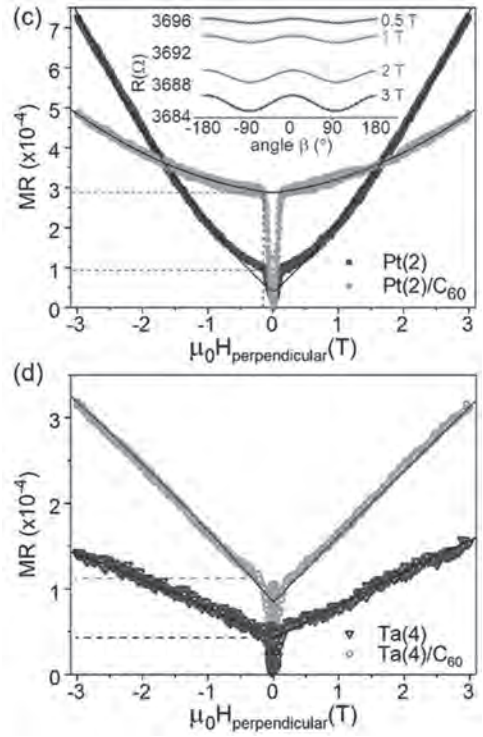

P6-16. Negative Spin Hall Angle and Large Spin-Charge Conversion in Thermally-Evaporated Chromium Thin Films. *S.M. Bleser*[1], R.W. Greening[1], M. Roos[1], X. Fan[1] and B.L. Zink[1] *1. Physics and Astronomy, University of Denver, Denver, CO, United States*

Continued progress toward both fundamental knowledge and industrial applications of spintronics relies on improved materials for converting charge to spin and vice-versa. Inexpensive metals, compared to the platinum that is most commonly used, are of particular interest. In this work, we have experimentally demonstrated effective spin-to-charge conversion in thermally evaporated chromium (Cr) thin films using the longitudinal spin Seebeck effect (LSSE). We thermally deposited Cr with thicknesses from 2 nm to 12 nm onto bulk polycrystalline yttrium-iron-garnet (YIG) substrates. As shown in Fig. 1, with a thermal difference of approximately 40 K across the structure, we measure large LSSE voltages in both evaporated Cr and sputtered Pt with the same nominal 10 nm thickness. The LSSE signal for evaporated Cr/YIG shows the opposite sign, and larger total thermal voltage than Pt. As shown in Fig. 2, the resistivity of the evaporated Cr is high, and comparable to beta W in an at similar thickness [2]. This is not uncommon for Cr films [3]. Models used in [1], suggests the actual spin conversion is most likely low in the thermally evaporated Cr samples due to either poor spin mixing conductance or a spin Hall angle smaller than observed sputtered Cr; however, the LSSE voltages are still significant due to large charge resistivity and under optimal conditions the spin-charge conversion could be more effective than previous studies on sputtered Cr [1].

[1] Qu, *et al* PRB 92, 020418 (2015) [2] Hao, et al APL 106, 182403 (2015) [3] Boekelheide, et al PRB 80, 134426 (2009) Funding Acknowledgement: NSF DMR 2004646

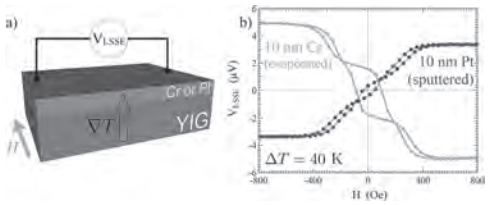

FIG 1: a) In the experimental setup, (Cr, Pt)/YIG samples were subjected to a thermal gradient in the z-direction and a transverse magnetic field which resulted in an observable longitudinal voltage across the samples via LSSE. b) Longitudinal spin Seebeck voltage plotted against magnetic field for a 10 nm Cr sample and a 10 nm Pt sample at a temperature difference of 40 K.

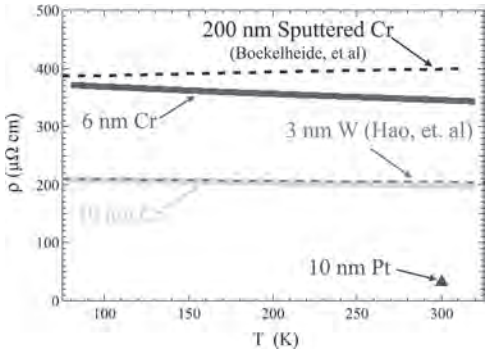

FIG 2: Resistivity vs temperature for 10 nm Cr/YIG and 6 nm Cr/YIG samples from 320 K to 78 K. The 10 nm Cr sample had similar resistivity to that of a 3 nm W sample [2] at nearly all temperatures. The 6 nm Cr sample had comparable resistivity at low temperatures to a 200 nm sputtered Cr sample [1], but had opposite behavior.

Session S8
NOVEL APPROACHES TO THE EXCITATION AND CONTROL OF NANO-SCALE PROPAGATING SPIN WAVES

Johan Åkerman, Chair
University of Gothenburg, Göteborg, Sweden

INVITED PAPERS

9:00

S8-01. Control of Nonlinear Damping and Excitation of Spin Waves by Spin-Orbit Torque in Systems With Perpendicular Magnetic Anisotropy. *V.E. Demidov*[1], B. Divinskiy[1], M. Evelt[1], S. Demokritov[1], S. Urazhdin[2], L. Soumah[3], V. Cros[3], j. ben youssef[4], G. de loubens[5], O. Klein[6], B. Paolo[3] and A. Anane[3] *1. Westfalische Wilhelms-Universitat Munster, Munster, Germany; 2. Emory University, Atlanta, GA, United States; 3. Unite Mixte CNRS/Thales, Palaiseau, France; 4. Universite de Bretagne Occidentale, Brest, France; 5. SPEC, CEA-Saclay, CNRS, Université Paris-Saclay, Gif-sur-Yvette, France; 6. SPINTEC, CEA-Grenoble, CNRS and Université Grenoble Alpes, Grenoble, France*

A large spin-Hall effect (SHE) exhibited by materials with strong spin-orbit interaction results in the generation of significant pure spin currents, enabling the implementation of a variety of efficient active magnetic nanodevices. These applications take advantage of the compensation of the natural magnetic damping by the antidamping effect of spin current. The antidamping torque is proportional to spin current, at small currents resulting in a linear decrease of the net effective damping. However, the amplitude of the dominant dynamical mode significantly increases when the damping compensation point is approached, leading to the onset of strong nonlinear relaxation into other spin-wave modes, which can be described as amplitude-dependent nonlinear damping. Starting with the first experiments on the interaction of pure spin currents with the magnetization, this mechanism has become recognized as the main culprit generally preventing complete damping compensation and excitation of coherent magnetization auto-oscillations in spatially extended magnetic systems. The adverse effects of nonlinear damping can be reduced by using the mechanism of frequency-selective radiative losses. However, this mechanism requires the localization of the injection of spin current to a small nano-scale region of the magnetic system, which limits the achievable dynamical coherence and the possibilities for the magnonic device integration. Here, we demonstrate a novel approach minimizing the nonlinear damping without constraining the geometry or the efficiency of spin current-driven nanostructures. We show experimentally and by micromagnetic simulations that the nonlinear spin wave coupling is determined by the ellipticity of magnetization precession, which is controlled by the magnetic anisotropy. We achieve almost circular precession by tailoring the perpendicular magnetic anisotropy (PMA) of the magnetic film to compensate the dipolar anisotropy, resulting in suppression of nonlinear damping, and enabling coherent magnetization dynamics driven by the injection of spin current generated by the spin Hall effect into an extended magnetic region. In particular, we show that this approach allows one to excite coherent magnetization auto-oscillations in a relatively large CoNi disk subjected to the uniform injection of the spin current, which cannot be achieved in a similar disk made of Permalloy (Py) without PMA (Fig. 1). Moreover, we show that the same approach enables excitation of highly coherent magnetization dynamics in a large area of an extended Bi-substituted film of Yttrium Iron Garnet (YIG) exhibiting PMA (Fig. 2). In this system, current-driven magnetic auto-oscillations can additionally radiate propagating spin waves with nanometer-range wavelengths. Our findings open a route for the implementation of spin-Hall oscillators capable of generating microwave signals with technologically relevant power levels and coherence, circumventing the challenges of phase locking a large number of oscillators with nano-scale dimensions. They also provide a route for the implementation of spatially extended excitation and amplification of coherent propagating spin waves. The proposed approach can also facilitate the experimental realization of spin current-driven Bose-Einstein condensation of magnons, which has not been achieved so far due to the detrimental effects of nonlinear damping.

V. E. Demidov, et al. Phys. Rev. Lett. 107, 107204 (2011). V. E. Demidov et al., Nature Mater. 11, 1028 (2012). V. E. Demidov et al., Phys. Rep. 673, 1 (2017). V. E. Demidov et al., Nature Commun. 8, 1579 (2017). M. Evelt et al., Phys. Rev. Appl. 10, 041002 (2018). B. Divinskiy et al., Nature Commun. 10, 5211 (2019). V. E. Demidov, et al., J. Appl. Phys. 127, 170901 (2020).

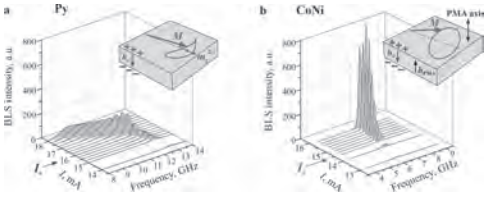

Fig. 1 Measured spectra of current-driven magnetic oscillations for (a) Py and (b) CoNi samples. Ic marks the critical current, at which the spin current is expected to completely compensate the natural linear magnetic damping. Insets illustrate peculiarities of magnetization precession in the two systems.

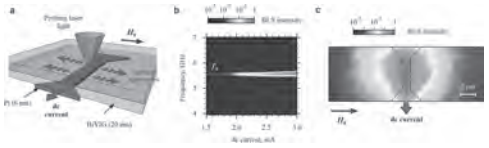

Fig. 2 (a) Experimental layout. (b) Measured spectra of current-induced magnetization auto-oscillations. (c) Measured spatial map of the spin-wave intensity.

9:36

S8-02. Robust Voltage-Control of Damping, Threshold Current, and Frequency in Spin Hall Nano-Oscillators. *H. Fulara*[1], M. Zahedinejad[1], R. Khymyn[1], M. Dvornik[1], S. Fukami[2], S. Kanai[2], H. Ohno[2] and J. Åkerman[1] *1. Physics, University of Gothenburg, Gothenburg, Sweden; 2. Laboratory for Nanoelectronics and Spintronics, Research Institute of Electrical Communication, Tohoku University, Sendai, Japan*

Spin Hall nano-oscillators (SHNOs) [1-4] are promising spintronic devices for high-quality microwave signal generation and ultra-fast neuromorphic computing as they exhibit wide frequency tunability [2], CMOS integration compatibility [3] and robust mutual synchronization both in long chains [2] and two-dimensional arrays [6]. Recently, we demonstrated how the presence of perpendicular magnetic anisotropy (PMA) in such SHNOs can raise the frequency of spin-wave (SW) auto-oscillations well above the SW bandgap, resulting in the straightforward generation of spin-orbit torque driven propa-

gating SWs [4]. While the propagating SWs could be tuned with both current and external magnetic field, neither of them will serve as an ideal approach for an energy-efficient data transfer and non-conventional wave-based computing. Besides, the current tunability of SHNOs is not a conducive approach for individual oscillator control desired to perform cognitive tasks in synchronized networks e.g. oscillator-based neuromorphic computing [6]. It would, therefore, be highly advantageous if an energy-efficient approach, such as electrostatic gating, could be used to control the excitation of propagating SWs as this would not only make SHNOs amenable to nanomagnonic circuits but also enable complex neuromorphic tasks using mutually synchronized SHNO networks [5, 6]. Here we demonstrate electrostatically gated nano-constriction based W(5nm)/CoFeB(1.7nm)/MgO(2nm) SHNOs in which the voltage-induced changes in PMA tunes the auto-oscillation frequency (12 MHz/V) such that the SW confinement in the gated constriction region is considerably modified. Figure 1(a) displays a scanning electron micrograph (SEM) image of such an electrically gated 150 nm constriction width SHNO device and a material stack, displaying layer order and thicknesses, is shown in Fig 1 (b). High-frequency auto-oscillation measurements, as shown in Fig. 1(c-d), show a significant variation in threshold current and auto-oscillation frequency as the gate voltage (V_G) changes from -2 V to +2V. Our detailed analysis based on spin-torque ferromagnetic resonance (ST-FMR) in conjunction with micromagnetic simulations unveils that the strong voltage-induced tunabilities in both threshold current and frequency are caused by the interplay between a moderate voltage control of the PMA and the specific geometry of nano-constriction SHNOs resulting in a large 42% variation of effective damping, as shown in Fig 1(e). Our demonstration introduces an energy-efficient approach to critically control effective damping and therefore the SW propagation in SHNOs. The energy-efficient fine individual oscillator control in mutually synchronized SHNO networks is also an important step to scale the neuromorphic computing to large dynamical neural networks.

[1] V. E. Demidov, S. Urazhdin, H. Ulrichs, V. Tiberkevich, A. Slavin, D. Baither, G. Schmitz, and S. O. Demokritov, Nature Mater. 11, 1028-1031 (2012). [2] A. A. Awad, P. Dürrenfeld, A. Houshang, M. Dvornik, E. Iacocca, R. K. Dumas, J. Åkerman, Nat. Phys. 13, 292-299 (2017). [3] M. Zahedinejad, H. Mazraati, H. Fulara, J. Yue, S. Jiang, A. A. Awad, J. Åkerman, Appl. Phys. Lett. 112, 132404 (2018). [4] H. Fulara, M. Zahedinejad, R. Khymyn, A. A. Awad, S. Muralidhar, M. Dvornik, J. Åkerman, Sci. Adv. 5, eaax8467 (2019). [5] M. Romera, P. Talatchian, S. Tsunegi, F. A. Araujo, V. Cros, P. Bortolotti, J. Trastoy, K. Yakushiji, A. Fukushima, H. Kubota, S. Yuasa, M. Ernoult, D. Vodenicarevic, T. Hirtzlin, N. Locatelli, D. Querlioz, J. Grollier, Nature 563, 230–234 (2018). [6] M. Zahedinejad, A. A. Awad, S. Muralidhar, R. Khymyn, H. Fulara, H. Mazraati, M. Dvornik, J. Åkerman, Nat. Nanotechnol. 15, 47–52 (2020).

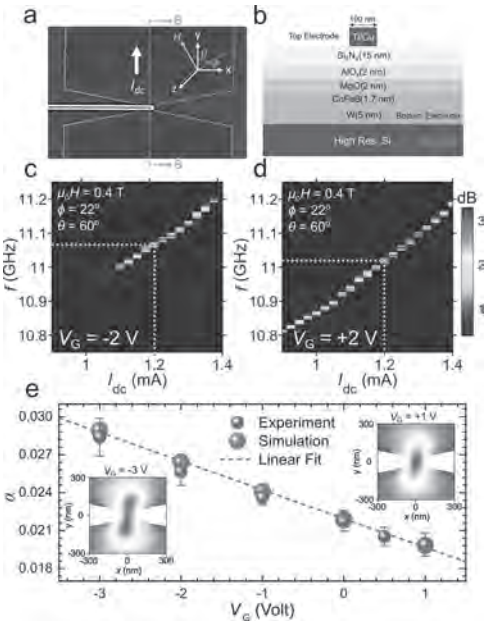

Fig. 1(a) SEM image of a gated SHNO device of width 150 nm. (b) Material stack with individual layers along the current direction. Power spectral densities (PSDs) of auto-oscillations as a function of drive current for two different gate voltages (c) V_G = -2 V, (d) V_G = +2 V. (e) Effective damping constant α vs. gate voltage obtained from the experiment (cyan) and simulation (red) displaying an excellent agreement. Spatial mode profile at V_G = +1 V (right inset) exhibiting stronger localization compared to the one at V_G = -3 V (left inset).

10:12

S8-03. Spin-Wave Data Processing in YIG Nanostructures. *A. Chumak*[1]
1. Faculty of Physics, University of Vienna, Vienna, Austria

Spin waves, and their quanta magnons, are of great interest as potential data carriers in future low-energy computing devices [1]. The phase of a spin wave provides an additional degree of freedom, while the scalability of structures and wavelengths down to the nanometer regime [2, 3] are further advantages. In my talk, the following recent achievements in the direction of magnon-based data processing will be addressed. *Spin-wave properties in nanostructures.* Over the recent years, significant progress towards the miniaturization of the magnonic elements below 100 nm lateral sizes took place. In particular, spin waves are investigated in yttrium iron garnet (YIG) waveguides with a thickness of 39 nm and widths ranging down to 50 nm [2], i.e., with an aspect ratio thickness over width approaching unity, using Brillouin-Light-Scattering (BLS) spectroscopy. The experimental results are verified by analytc theory and micromagnetic simulations. A critical width is found, below which the exchange interaction suppresses the dipolar pinning phenomenon. *Propagating spin waves in 50 nm wide waveguides.* The feasibility of the magnonics essentially relies on the scalability to the nanoscale and proof that coherent spin waves can propagate in these structures. A study of the propagating spin-wave dynamics in individual YIG conduits with lateral dimensions down to 50 nm – see Fig. 1a [3]. Space and time-resolved micro-focused BLS spectroscopy is used to extract the exchange constant and directly measure the spin-wave decay length and group velocity. This experimental proof of propagating spin waves in nano-sized conduits demonstrates the fundamental feasibility of a nano-scaled magnonics. *Realization of the nano-scale directional coupler.* Recently, a set of magnonic data processing units was demonstrated [1]. Nowadays, the challenge is the realization of an integrated magnonic circuit [4-6]. In the talk, the experimental realization of a nanoscale magnonic directional coupler will be presented [5]. A SEM image of the structure fabricated from an 85 nm thick YIG is shown in Fig. 1b. The two spin-wave waveguides, each

of 350 nm width, are separated by a gap of 320 nm. A U-shaped antenna is used to excite spin waves and space-resolved BLS spectroscopy is exploited for detection. It is shown experimentally [4] and numerically [5] that the data is coded into the spin-wave amplitude is guided towards one of its two outputs depending on the signal frequency, magnitude, and on the magnetic field. By controlling these degrees of freedom, the multi-functionality and reconfigurability of the device is achieved. The nonlinear switching of the output by changing the spin-wave amplitude is demonstrated in Fig. 1d. Particularly, this ability opens a path for the realization of all-magnon integrated circuits. *Numerical investigations of an integrated magnonic circuit in a form of half-adder.* In the final part of my talk, an integrated magnonic circuit at the example of a magnonic half-adder will be presented [6]. Its key element is a nonlinear directional coupler serving as a combined XOR and AND logic gate that utilizes the dependence of the spin-wave dispersion on its amplitude. The circuit constitutes of only three planar nano-waveguides and processes all information within the magnon domain – Fig. 1c. Benchmarking of the proposed device is performed showing the potential for sub-aJ energy consumption per operation. This research has been supported by ERC StG 678309 MagnonCircuits.

[1] A. V. Chumak, V. I. Vasyuchka, A. A. Serga, and B. Hillebrands, Magnon spintronics, Nat. Phys. 11, 453 (2015). [2] Q. Wang, B. Heinz, R. Verba, et al., Spin pinning and spin-wave dispersion in nanoscopic ferromagnetic waveguides, Phys. Rev. Lett. 122, 247202 (2019). [3] B. Heinz, T. Brächer, M. Schneider, et al., Propagation of coherent spin waves in individual nano-sized yttrium iron garnet magnonic conduits, Nano Letters 20, 6, 4220 (2020). [4] Q. Wang, M. Kewenig, M. Schneider, et al., Realization of a nanoscale magnonic directional coupler for all-magnon circuits, e-print arXiv: arXiv:1905.12353 (2019). [5] Q. Wang, P. Pirro, R. Verba, et al., Reconfigurable nano-scale spin-wave directional coupler, Sci. Adv. 4, e1701517 (2018). [6] Q. Wang, R. Verba, T. Brächer, et al., Integrated magnonic half-adder, e-print arXiv: 1902.02855 (2019).

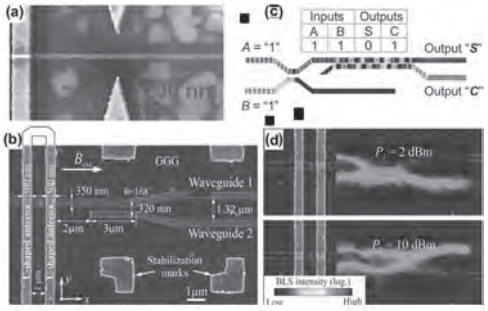

Figure 1: ***(a) SEM picture of a YIG spin wave waveguide of width 40 nm and a microstrip antenna for spin wave excitation. (b) SEM image of the directional coupler with the U-shaped antenna. (c) Magnonic half-adder design and operational principle for the "1"-"1" logic input combination. The colour encodes the spin wave amplitude. (d) Nonlinear functionality of the coupler. Two-dimensional BLS maps of the spin wave intensity for different input powers.***

10:48

S8-04. Magnetic Excitations in a two-Dimensional Honeycomb Magnet CrI_3. *L. Zhao*[1] *1. Physics, University of Michigan, Ann Arbor, MI, United States*

Two-dimensional (2D) honeycomb ferromagnets are predicted to host massless Dirac magnons because of the two equivalent magnetic sites per unit cell of the honeycomb lattice, mimicking Dirac electrons in graphene. More interestingly, the introduction of the next-nearest-neighbor Dzyaloshinskii-Moriya interaction breaks the sublattice equivalency and suggests the emergence of topological magnons in these honeycomb ferromagnets. in this talk, i will present polarization-resolved Raman spectroscopy studies on magnetic excitations in a honeycomb ferromagnet CrI3, as a function of temperature, layer number, and magnetic eld.

1. *Phys. Rev. X* 10, 011075 (2020) 2. *PNAS* 116, 11131 (2019) 3. *Nature Communications* 9, 5122 (2018)

11:24

S8-05. Spin Textures as Coherent Excitation Sources for Ultrashort Spin Waves. *S. Wintz*[1,2] *1. Max-Planck-Institut für Intelligente Systeme, Stuttgart, Germany; 2. Paul Scherrer Institut, Villigen PSI, Switzerland*

Excitations of ordered spin systems are known as spin waves [Fig. 1(a)], with the 'magnon' being their fundamental unit of quantization [1]. In the framework of *magnonics*, spin waves are proposed as signal carrier for future spintronic information processing devices, with the potential to outperform present charge-based technologies in terms of energy efficiency and device miniaturization [2]. Yet a successful implementation of magnonic technology will require the usage and control of spin waves with nanoscale wavelengths. For the coherent excitation of spin-wave signals, typically patterned metallic conductors are used. Alternating charge currents flowing in such antennas result in spatially inhomogenous oersted fields that excite spin waves in an adjacent magnetic medium. While this method is well applicable down to the micrometer wavelength regime, it fails to work for nanoscale spin waves: The critical patterning size employed (e.g. the width of a stripline antenna) limits the minimum wavelength that can be efficiently excited [3]. At the same time, nanoscale patterned antennas are difficult to impedance match for high-frequency microwave transmission. Other coherent spin-wave generation mechanisms such as spin-transfer torques in point contacts or spin-orbit torques in geometric constrictions suffer from similar constraints. An approach overcoming these constraints is to exploit static or dynamic inhomogeneous fields originating from the magnetic medium itself, e.g. [4]. In particular, we will show that the nanoscale cores of vortex spin textures [Fig. 1(b)] can be driven to efficiently excite coherent spin waves with ~100 nm wavelengths in a synthetic antiferomagnet (Co/Ru/NiFe) as it was directly imaged by time-resolved scanning transmission x-ray microscopy (TR-STXM) [5]. It was found that the resulting wavelength is tunable by the excitation frequency and that the corresponding dispersion can be gapless, linear and strongly non-reciprocal [5]. This concept can be transferred to single ferromagnetic layers (NiFe) of intermediate thickness (~100 nm), which allow for higher operation frequencies (~10 GHz) and sub-100 nm wavelengths [cf. Fig. 1(c)][6]. Here, a strong intermode hybridization causes an inhomogeneous thickness mode profile and regions with anti-larmor precession sense of magnetization [6]. A vortex core always acts as point source for isotropically propagating waves. Therefore the emitted spin-wave signal will decay with the distance from the core even in the absence of any intrinsic magnetic damping. This situation can be avoided when a uniaxial magnetic anisotropy is introduced to a vortex pair in a synthetic antiferromagnet (NiFe/Ru/CoFeB), thereby causing in each layer the formation of two uniform domains of opposite orientation and a sharp 180° domain wall in between [7]. Similarly to a vortex core, such localized domain walls can act as natural spin-wave antennas, yet emitting directional plane waves that are not anymore subject to geometrically-induced signal decay. Moreover, for frequencies below the anisotropy-determined spin-wave frequency gap of the domains, one-dimensional signals can be confined to the domain wall itself that can be therefore utilized as an efficient waveguide for spin waves [Fig. 1(d)]. Another way to increase the propagation length of spin-wave signals is to exploit materials with a lower intrinsic magnetic damping than that of the metallic systems described. We will show that TR-STXM can also be applied to single-crystalline thin films of the ferrimagnetic insulator YIG [Fig. 2] [8]. Using a NiFe vortex structure as spin-wave transducer, it is possible to excite coherent ~100 nm wavelength spin waves in YIG, the extended propagation of which was directly observed [8].

References: [1] F. Bloch, Z. Phys. 61, 206 (1930). [2] A. Chumak *et al.,* Nat. Phys. (2015). [3] A. G. Gurevich and G. A. Melkov, New York CRC (1996). [4] H. Yu *et al.*, Nat. Comm. 4, 2702 (2013). ---- [5] S. Wintz *et al.*, Nat. Nanotech. 11, 453 (2016). [6] V. Sluka *et al.,* Nat. Nanotech. 14, 328 (2019). [7] G. Dieterle *et al.,* Phys. Rev. Lett. 122, 117202 (2019). [8] J. Förster *et al.,* Phys. Rev. B 100, 214416 (2019).

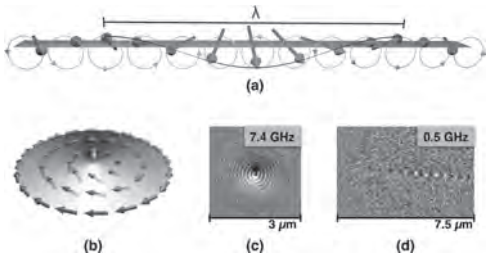

Figure 1: (a) Propagating spin wave [5]. (b) Spin vortex [5]. (c) Spin-wave emission from a vortex core (TR-STXM) [7]. (d) Domain wall as 1D spin-wave channel (TR-STXM) [6].

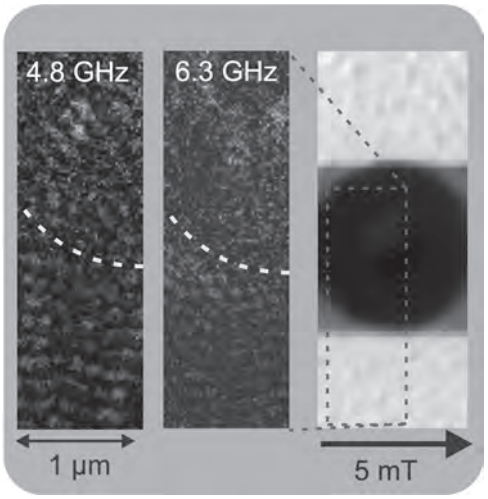

Fig. 2: Spin waves in YIG (TR-STXM) [8].

Session Q1
HARD MAGNETIC MATERIALS: RARE-EARTH-FREE

Jeotikanta Mohapatra, Chair
University of Texas at Arlington, Arlington, TX, United States

CONTRIBUTED PAPERS

Q1-01. First-Principles Investigation of the Impact of Chemical Order on the Magneto-Crystalline Anisotropy in $L1_0$ FeNi (Tetrataenite).
A. Izardar[1] and C. Ederer[1] *1. Eidgenossische Technische Hochschule Zurich, Zurich, Switzerland*

The volatility in price and uncertainty in supply of the rare earth elements makes it highly desirable to find alternatives to rare-earth based magnets, in order to meet the increasing global demand for permanent magnets. One interesting candidate in this quest is the chemically-ordered $L1_0$ phase of $Fe_{50}Ni_{50}$ (tetrataenite) found in iron meteorites. While the laboratory synthesis of the ordered phase is very difficult due to the slow diffusion of atoms at the rather low order-disorder transition temperature, several attempts have been made to achieve samples with a high degree of chemical order. Nevertheless, synthesis of a fully ordered system remains challenging. Using first-principles-based density-functional theory calculations in combination with Monte Carlo (MC) simulations, we investigate the interplay between the degree of chemical order and the magnetic properties of $L1_0$ FeNi [1]. Our calculations demonstrate a strong effect of the magnetic order on the chemical order-disorder transition temperature, and a strong effect of the chemical order on the magnetic transition temperature, in agreement with previous studies. Furthermore, we investigate the dependence of the magneto-crystalline anisotropy on the chemical long range order. Our results indicate that the anisotropy does not decrease significantly as long as the deviations from perfect order are not too large. Moreover, we also find that a slight disorder in the alloy can in principle result in an even higher anisotropy than for the fully ordered structure. We further analyze the correlation between the magneto-crystalline anisotropy and the orbital magnetic moment anisotropy. This allows us to study the effect of the local chemical environment on both quantities, potentially enabling further optimization of the magneto-crystalline anisotropy with respect to both long-range order and stoichiometric composition.

1. A. Izardar, C. Ederer, Phys. Rev. Materials, Vol. 4, p.054418 (2020)

Q1-02. Extrusion Based 3D Printing of Partially Transformed $Fe_{16}N_2$/Fe Flakes Into Permanent Magnet.
O. Zirhli[1], N. Gunduz Akdogan[2], Y.N. Odeh[3], I. Misirlioglu[1], E. Devlin[4] and O. Akdogan[5] *1. Materials Science and Nano Engineering, Sabanci Universitesi, Istanbul, Turkey; 2. Ship Construction, Piri Reis Universitesi, Istanbul, Turkey; 3. Faculty of Engineering and Natural Sciences, Bahcesehir Universitesi, Istanbul, Turkey; 4. Institute of Nanoscience and Nanotechnology, Ethniko Kentro Ereunas Physikon Epistemon 'Demokritos' Tomeas Epistemes Ylikon, Athens, Greece; 5. Mechatronics Engineering, Bahcesehir Universitesi, Istanbul, Turkey*

Rare-earth based alloys dominate the global magnet industry because of their high magnetic properties. Since 2010, researcher focus was shifted towards rare-earth free magnets. BCT phase α"-$Fe_{16}N_2$ compound has promising giant saturation magnetization that may exceed rare-earth based magnets. Moreover, the abundancy of iron and nitrogen makes $Fe_{16}N_2$ compound an ideal rare-earth free magnet. In this study, a low-cost and low temperature (< 473 K) synthesis method was established to obtain the α"-$Fe_{16}N_2$ BCT phase. This method could be scaled up to produce $Fe_{16}N_2$ powders on an industrial scale. The morphology of the starting Fe powder was chosen to be in flake shape (Figure 1a) to maximize the nitrogenization of the powders due to the high surface area. Iron flakes were synthesized from irregularly shaped iron powder by employing surfactant-assisted high energy ball milling. Then, iron flakes were reduced and thermally cleaned at 673 K with Ar/H_2 gas mixture, followed by a low-temperature nitridation process under ammonia (NH_3) gas. Examination of X-ray diffraction and Mössbauer analysis revealed that up to 50% of the powder was transformed into α"-$Fe_{16}N_2$ BCT phase (Figure 1b). Since the $Fe_{16}N_2$ compound is stable up to 495 K, classical magnet production route, which includes sintering at high temperature, cannot be used to produce permanent magnets. Ergo, extrusion-based 3D-printing method is utilized, a composite $Fe_{16}N_2$-SU8 (photoresist) permanent magnet was successfully prototyped. This work was supported by TUBITAK project: 217M322.

O. Zirhli, N. G. Akdogan, Y. N. Odeh, I. B. Misirlioglu, E. Devlin, O. Akdogan, Advanced Engineering Materials., (2020)

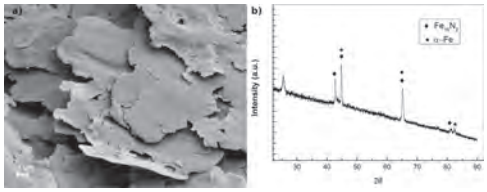

Fig. 1 a) SEM image of $Fe_{16}N_2$ showing the flake structure. b) XRD measurement of $Fe_{16}N_2$ flakes, nitrided at 463 K.

Q1-03. Withdrawn

INVITED PAPER

Q1-04. Novel Database Driven Method for Discovering New Co-Based Ferromagnets.
J.K. Byland[1], S. Ding[1], Y. Shi[1], R. Mata[1], P. Klavins[1] and V. Taufour[1] *1. Physics and Astronomy, University of California, Davis, Davis, CA, United States*

There exists a wide array of uses for ferromagnetic materials with easy-axis magnetic anisotropy, including motors, magnetic imaging devices, and acoustic devices. As most of the highest quality permanent magnets are financially and environmentally costly, the search for alternative magnetic materials is ongoing and paramount. Magnetic elements are rare, and the best way to predict novel magnetic materials is to constrain a search to analyzing the magnetic properties of compounds containing iron, cobalt, and manganese. However, while many databases exist for the purposes of analyzing structural properties of compounds, any such database of magnetic materials that exists is either outdated or incomplete. The magnetic properties of 10,760 compounds containing the element cobalt are being gathered through a literature search, with the goal to eventually complete the entire list, as well as those of iron and manganese compounds. As of now, a total of 1,282 ferromagnetic compounds have been found and catalogued. Structure types, lattice parameters, cobalt percentage, and lattice angles of each compound

were also collected; the shortest cobalt-cobalt bond lengths within the crystal lattice were calculated; and data trends were analyzed to predict novel ferromagnetic and anisotropic compounds. From this data, a previously unstudied member of the Cu_2MnAl family was confirmed to be ferromagnetic with a Curie temperature above room temperature. Currently, compounds in the $MgZn_2$, $La_6Co_{11}Ga_3$, and Mg_3Cd families are being studied to check for ferromagnetism and uniaxial anisotropy. The research was supported by the Critical Materials Institute, an Energy Innovation Hub funded by the U.S. Department of Energy, Office of Energy Efficiency and Renewable Energy, Advanced Manufacturing Office.

CONTRIBUTED PAPERS

Q1-05. Investigation of Magnetic and Electromagnetic Properties of Cobalt Substituted M-Type Barium Hexaferrite in X-Band. *K. Rana*[1], V. Gupta[2], M. Tomar[2] and A. Thakur[1,3] *1. Innovative Science Research Society, Shimla, India; 2. Department of Physics & Astrophysics, University of Delhi, New Delhi, India; 3. Nanotechnology, Amity University Gurgaon, Gurgaon, India*

In the present investigation, the magnetic and electromagnetic character of cobalt substituted M-type barium hexaferrite with composition $BaCo_x$-$Fe_{12-x}O_{19}$ (x = 0.0 to1.0 in the steps of 0.2) by co-precipitation method has been studied. After the appropriate heat treatments, the structural, magnetic and electromagnetic properties at X band ranging from 8-12 GHz are thoroughly examined. XRD confirmed the formation of M phase and revealed that with an increase in the content of cobalt ions the average crystallite size is found to be increased from 28 to 45 nm whereas the morphology examined from FESEM and TEM confirmed the formation of high quality and densely packed nano ferrites. From all the six samples the composition $BaCo_{0.8}Fe_{11.2}O_{19}$ exhibit remarkable magnetic and electromagnetic properties and found to be one of the best compositions. For this particular composition very higher value of coercivity of the order of 3789 Oe along with good saturation magnetisation value of 65 emu/g is observed. Similar kinds of results are observed form electromagnetic properties of the same composition. Again the composition $BaCo_{0.8}Fe_{11.2}O_{19}$ showed some excellent and sustainable values of complex permittivity and tangent losses i.e 11, 0.024 and 0.035. So based on the magnetic and electromagnetic performances, the composition BaCo0.8Fe11.2O19 may emerge as an ideal candidate for high-speed recording, permanent magnet applications, microwave absorption at high-frequency applications ranges from 8-12 GHz and many more.

Robert C Puller, Progress in Material Science., 57, 1191-1334 (2012). K. Kumar and D. Pandey, Physical Review B., 96, 024102 (2017). H. Lou, S. Sun, X. Lu, C. He, Y. Pan, Q. Song, W. Xuejin, W. Jianjiang, J Mater Sci: Mater Electron., 27, 11231–11240 (2016). A. Baykal, I. A. Auwal, S. Guner, H. Sozeri, J. Magn. Magn Mater. 430, 29-35 (2017). S Kumar, M K Manglam, S Supriya and H Kumar et.al., J Magn. Magn. Mater., 473, 312-319 (2019).

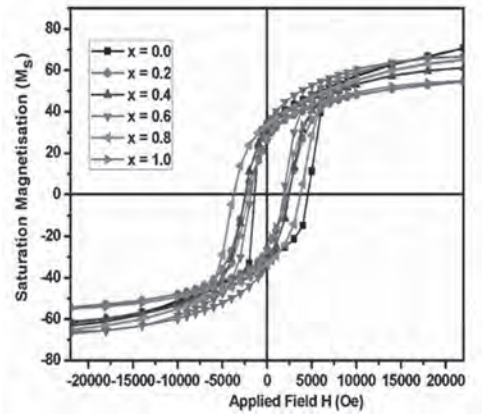

Fig.1 M-H loops of for pure BaM and Cobalt substituted BaM sintered at 900°C.

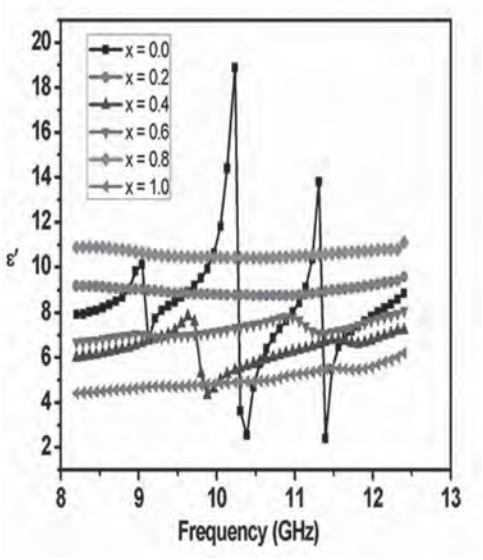

Fig.2 Real part of permittivity with frequency for pure BaM and Cobalt substituted BaM sintered at 900°C.

Q1-06. Formation and Magnetic Properties of τ-MnAlC Synthesized by Spark Plasma Sintering Process. F. Maccari[1], A. Aubert[1], *S. Ener*[1], I. Radulov[1], K. Skokov[1] and O. Gutfleisch[1] *1. Technische Universitat Darmstadt Fachbereich Material- und Geowissenschaften, Darmstadt, Germany*

The increasing demand of permanent magnets (PM) based technology going along with the limitation of global supply of rare-earths (RE) elements drives the development of RE-free PM [1]. Based on the material requirements regarding magnetic properties, costs and criticality, Mn-Al(-C) alloys have been pointed as candidates for PM applications. The hard magnetic properties originate from the metastable τ-phase which is usually formed during annealing from the parent high temperature ε-phase [2,3]. However, the annealing parameters have to be optimized in order to avoid the decomposition of the ferromagnetic phase into the nonmagnetic stable phases in the Mn-Al system. In this context, the Spark Plasma Sintering (SPS) can be a useful technique to optimize this process by combining uniaxial pressure and fast heating/cooling rates due to efficient Joule heating, caused by direct current pulses, and possible side effects related to electric field/current [4]. In this study, we investigate the transformation from ε- to τ-$Mn_{54}Al_{44}C_2$ using the SPS and compared the results with conventional annealing. The ε- to τ-phase transformation has been done by SPS at different temperatures (400, 450, 500 and 550°C) and different times (5 and 15 min). A pure

τ-MnAlC is obtained at 500°C/5min (Figure 1 (a)). Below this temperature there is still presence of ε-MnAlC and above we observe the formation of undesired β-phase. On the other hand, conventional heat treatment shows a full transformation at 500°C only after 30 min. Magnetic properties are dependent on the phase formation (Figure 1 (b)), but similar coercivity and saturation magnetization are obtained for the pure τ-MnAlC formed either by SPS or by conventional annealing. However, the SPS method allows to significantly shorter the time necessary to complete the transformation and limits the grain growth.

[1] K.P. Skokov, O. Gutfleisch, Scripta Mater., 154 289 (2018) [2] V. Øygarden et al., J. Alloys Compd. 779 776 (2019) [3] H. Jian et al., J. Alloys Compd. 622 524 (2015) [4] O. Guillon et al., Adv. Eng. Mater., 16 830 (2014)

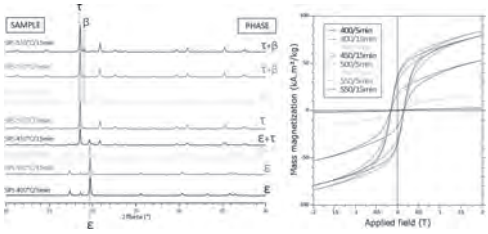

Figure 1. (a) XRD patterns and (b) hysteresis loops of MnAlC annealed by SPS.

Q1-07. Recent Progress in the Development of MnAl-C Magnets.

T.G. Woodcock[1] *1. Leibniz IFW Dresden, Dresden, Germany*

MnAl-C magnets, based on the τ-phase, contain no critical elements and have the potential to achieve energy products which would enable them to replace isotropic Nd-Fe-B bonded magnets, thus contributing to the long-term sustainability of rare earth magnet production. The τ-phase is thermodynamically metastable and is formed from the hexagonal precursor phase, ε. The phase transformation mechanism is of interest because it determines the population of defects in the product τ-phase. The various proposed transformation mechanisms will be reviewed here. The stability of the τ-phase can be greatly improved by the addition of C. The solubility of C in the relevant phases, along with the phase equilibria will be discussed. Detailed knowledge of the intrinsic magnetic properties of the τ-phase are useful both for estimating the upper limits of the extrinsic properties and as input for first principles calculations and micromagnetic models. Recent measurements of the intrinsic properties will be summarised and typical values will be given. The best extrinsic magnetic properties in MnAl-C to date were achieved more than 40 years ago in commercially produced, extruded materials. Since then, a number of alternative processing routes have been explored and these will be compared and contrasted here. The reported energy products of all MnAl-C materials fall short of the upper limits, estimated from the intrinsic properties of the τ-phase and therefore further improvements are possible. The extruded MnAl-C materials contain a range of defects, which potentially interact with magnetic domain walls. Understanding both this interaction and the formation mechanisms of the defects is the key to developing enhanced processing routes which deliver materials with higher energy product. Various insights from the characterisation of these defects on different length scales will be discussed.

Q1-08. Rare-Earth-Free MnAl-C-Ni Permanent Magnets With State-of-the-Art Properties, Produced by Extrusion of Milled Powder.

L. Feng[1,2], J. Freudenberger[1,3], T. Mix[1], K. Nielsch[1,2] and T.G. Woodcock[1]
1. Leibniz IFW Dresden, Dresden, Germany; 2. Institute of Materials Science, Technische Universitat Dresden, Dresden, Germany; 3. Institute of Materials Science, Technische Universitat Bergakademie Freiberg, Freiberg, Germany

The intrinsic magnetic properties of the τ-phase in MnAl-C alloys show its strong potential as a rare earth free permanent magnet. Until now the best magnetic properties were achieved through hot extrusion using bulk material or gas-atomised powders. In the current work, crushed and milled powders were used for the hot extrusion to make bulk MnAl-C magnets. A material with energy product, $(BH)_{max}$ = 46 kJ/m^3 was obtained, which is comparable to state-of-the-art values. Samples were made with various different parameters and new insights into the role of the microstructure in determining the magnetic properties were gained by characterising these materials. The samples were characterised using magnetometry, scanning electron microscopy, electron backscatter diffraction and x-ray diffraction. After extrusion, non-recrystallized grains with hierarchical true twins were observed, which are thought to be deleterious to both coercivity and loop squareness. Milling the powders and using higher extrusion temperature both hinder the formation of these non-recrystallized grains. The texture of the extruded samples was a broad <001> fibre. Higher extrusion temperature and quicker extrusion speed decreased the degree of texture of the extruded sample, as a result, the remanence also decreased. As a result of the axial symmetry of the extrusion process, the edge of the extruded samples was found to have higher coercivity, remanence, squareness and $(BH)_{max}$ than the centre. This detailed characterisation will be used to guide future processing routes, enabling the production of materials with properties beyond the state of the art.

Q1-09. Novel Ferrite Materials Possessing Record Magnetic Hardness.

E. Gorbachev[4,2], L.A. Trusov[1], A.E. Sleptsova[4], E.S. Kozlyakova[3], L.N. Alyabyeva[5], M.A. Karpov[1], B.P. Gorshunov[5], A.S. Prokhorov[5,6] and P.E. Kazin[1] *1. Department of Chemistry, Moskovskij gosudarstvennyj universitet imeni M V Lomonosova, Moscow, Russian Federation; 2. Energy Storage, Skolkovskij institut nauki i tehnologij, Skolkovo, Russian Federation; 3. Department of Physics, Moskovskij gosudarstvennyj universitet imeni M V Lomonosova, Moscow, Russian Federation; 4. Department of Materials Science, Moskovskij gosudarstvennyj universitet imeni M V Lomonosova, Moscow, Russian Federation; 5. Moskovskij fiziko-tehniceskij institut, Dolgoprudnyj, Russian Federation; 6. Institut obsej fiziki imeni A M Prohorova RAN, Moscow, Russian Federation*

Hard magnetic ferrites have broad applications ranging from permanent magnets and data storage media to high-frequency devices. The only known ferrite material exhibiting giant coercivity over 20 kOe at room temperatures is epsilon-iron oxide (ε-Fe_2O_3). In addition, it displays sub-THz natural ferromagnetic resonance (NFMR) frequency of 182 GHz. The Rh-doping of the material leads to an increase in both the NFMR up to 209 GHz and the coercivity up to 27 kOe [1]. However, since ε-Fe_2O_3 is a metastable polymorph and its production as a pure phase is quite complex, it still has not been applied in industry. Recently we have reported [2] an effective method for production of single-domain M-type hexaferrite particles with composition of $Sr_{0.67}Ca_{0.33}Fe_8Al_4O_{19}$, which demonstrated coercivity of 21.3 kOe and saturation magnetization of 15 emu/g, which is close to ε-Fe_2O_3. The proposed preparation technique is based on citrate-nitrate auto-combustion method; therefore, it is simple, economical, and readily scalable, and it can be efficiently integrated into modern ferrite technology. Herein, we show that further increase of Al substitution degree leads to significant improvement of coercivity (up to 36 kOe) and NFMR frequency (up to 250 GHz), which are record-high values for ferrites to date [3]. Furthermore, we discuss temperature dependence of the magnetic and microwave properties, crystal and magnetic structures of the ultra-hard magnetic hexaferrites $Sr_{1-x/12}Ca_{x/12}Fe_{12-x}Al_xO_{19}$ (x = 3 – 5.5) in a range of 4.2 – 700 K. Temperature dependencies of both NFMR and coercivity have a maximum shifted

to low temperatures with increase of aluminium content. For x = 5.5 the compound coercivity is raised from 36 kOe at 300 K up to 41 kOe at 180 K. Furthermore, we developed a technique for preparation of dense ceramics with single-domain grains and studied their room temperature magnetic properties and NFMR. The obtained ceramic materials possess coercivity higher than 18 kOe at specific density of 67 - 95%. NFMR frequency of the ceramics is 200 GHz, which is 20% blue-shifted compared to that of a powder sample. The ferrite ceramics with a coercivity of more than 10 kOe and sub-terahertz absorption were obtained for the first time. The work was supported by RFBR grant No. 20-02-00887.

[1] A. Namai, et al, Nature Communications, Vol. 3, p. 1035, (2012). [2] L.A. Trusov, E.A. Gorbachev, et al, Chemical Communications, Vol. 54, p. 479-482 (2018). [3] E.A. Gorbachev, L.A. Trusov, et al, Materials Today, Vol. 32, p. 13-18 (2020).

INVITED PAPER

Q1-10. Modern FORC Data Analysis and Interpretation Approaches.
J. Gräfe[1], *F. Gross*[1], J.C. Martínez-García[2], E. Goering[1] and M. Rivas[2]
1. Max-Planck-Institut fur Intelligente Systeme, Stuttgart, Germany;
2. Universidad de Oviedo, Gijon, Spain

First-order reversal-curves (FORCs) are a powerful tool, which is increasingly used in material science and nano-magnetism as well as ferroelectricity, geology, archeology, and for spin-transition materials [1-4]. Ideally, it can access microscopic distributions of interaction and coercive fields without the need for lateral resolution [5]. Unfortunately, the reliable data analysis and interpretation poses a major challenge. This is why FORC is often seen as a magnetic fingerprint instead of a measurement method yielding quantitative information. To push past these limitations, we present a fast and user-independent analysis algorithm and possibilities to interpret the resulting FORC diagrams beyond the Preisach model. We present a new evaluation approach which exploits the diversity of Fourier space to not only speed up the calculation by a factor of 1000 but also move away from the conventional smoothing factor towards real field resolution. By comparing the baseline resolution of the new and the old algorithm we are able to deduce an analytical equation which converts the smoothing factor into field resolution making the old and new algorithm comparable. We find excellent agreement not only for various systems of increasing complexity but also over a large range of smoothing factors. The achieved speed up enables us to calculate a large number of first-order reversal-curve diagrams with increasing smoothing factor allowing for an autocorrelation approach to find a hard criterion for the optimum smoothing factor. This previously computational prohibitive evaluation of first-order reversal-curves solves the problem of over- and undersmoothing by increasing general readability and preventing information destruction. However, these measured FORC densities are not always straightforward to interpret, especially if the system is interaction dominated and the Preisach-like interpretation of the FORC density breaks down. To understand additional features arising from the interactions in the system, we purposely designed permalloy microstructures which violate the Mayergoyz criteria [7]. These artificial systems allow us to isolate the origin of an additional interaction peak in the FORC density. Modeling the system as a superposition of dipoles allows us to extract interaction strength parameters from this static simulation. Additionally, we suggest a linear relation between integrated interaction peak volume and interaction strength within the system. The presented correlation could be used to investigate the interaction behavior of samples as a function of structural parameters within a series of FORC measurements. This is an important step towards a more quantitative understanding of FORCs which violate the Mayergoyz criteria and away from a fingerprint interpretation.

[1] J. Gräfe, Phys. Rev. B, 93 (2016) 014406 [2] F. Groß, Phys. Rev. B, 99 (2019) 064401 [3] C.-I. Dobrota, J. Appl. Phys., 113 (2013) 043928 [4] C. R. Pike, Phys. Rev. B, 71 (2005) 134407 [5] J. Gräfe, Rev. Sci. Instr., 85 (2014) 023901 [6] D. Cimpoesu, J. Appl. Phys., 125 (2019) 023906 [7] I. D. Mayergoyz, Phys. Rev. Lett., 56 (1986) 1518

CONTRIBUTED PAPERS

Q1-11. Hard Magnetic Properties of $FeCoNiAlCu_XTi_X$ Based High Entropy Alloys.
S. Na[1], P.K. Lambert[1] and N.J. Jones[1] *1. Physical Metallurgy and Fire Performance Branch, Naval Surface Warfare Center, Carderock Division, West Bethesda, MD, United States*

Alnico permanent magnets contain a number of major alloying additions such as Fe, Co, and Ni, along with some other minor elemental additions; this alloying convention is similar to the high entropy alloys (HEAs) concept [1]. In this paper, we investigate the hard magnetic properties of FeCoNiAl-based HEAs with additions of Cu/Ti. Additions of both Cu and Ti to an equimolar FeCoNiAl alloy are more effective at enhancing coercivity compared to Cu only, but they also decrease the saturation magnetization and remanence (Figure 1). By changing the Fe/Co amounts, however, we can regain some of these properties. $Fe_2CoNiAlCu_{0.4}Ti_{0.4}$ shows promising hard magnetic properties as an isotropic, cast magnet, with a coercivity (H_C) of 1.1 kOe and maximum energy product, $(BH)_{max}$, of 2.06 MGOe, which is slightly better than the performance of isotropic, cast Alnico 2 magnets [2]. The thermal stability is also sufficient to be used at temperatures over 200 °C. The drastic change in H_C might be strongly associated with spinodal decomposition at annealing temperatures of ~650-700 °C for all samples (Figure 2).

[1] D. B. Miracle and O. N. Senkov, Acta Mater. Vol. 122, p.448 (2017). [2] https://en.wikipedia.org/wiki/Alnico.

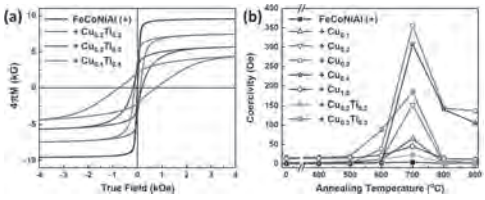

Figure 1. (a) Demagnetization-corrected magnetic hysteresis loops of high entropy alloys (HEAs) with varying Cu_XTi_X additions to an equimolar FeCoNiAl base, optimally annealed at a temperature of 700 °C (after prior sequential anneals at 400, 500, 600 °C), and (b) the coercivity values as a function of sequential annealing temperatures with Cu and/or Ti additions to the FeCoNiAl alloy. NOTE: H_c for + $Cu_{0.4}Ti_{0.4}$ is included in Figure 2(a).

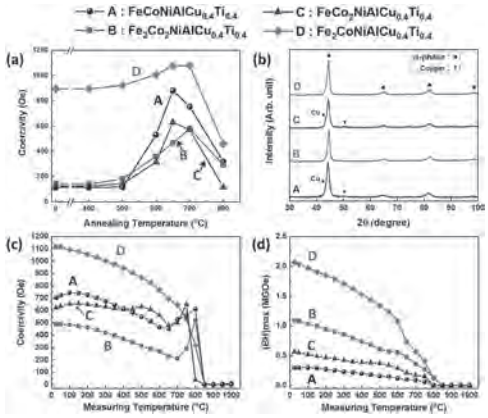

Figure 2. Magnetic and structural properties of four different HEAs with $Cu_{0.4}Ti_{0.4}$ additions; A – $FeCoNiAlCu_{0.4}Ti_{0.4}$, B – $Fe_2Co_2NiAlCu_{0.4}Ti_{0.4}$, C – $FeCo_2NiAlCu_{0.4}Ti_{0.4}$, and D – $Fe_2CoNiAlCu_{0.4}Ti_{0.4}$; (a) Coercivity measured at RT as a function of sequencial annealing temperatures, (b) X-ray powder diffraction patterns of the samples prepared from each as-cast HEA, (c) temperature dependence of coercivity and (d) temperature dependence of $(BH)_{max}$ for the HEAs annealed at 650 °C.

Q1-12. Sub-20nm Rare-Earth Free Ferrimagnetic Films Fabricated by Reactive Sputtering. *W. Zhou*[1], T. Hartnett[2], P. Balachandran[2] and J. Poon[1] *1. Physics, University of Virginia, Charlottesville, VA, United States; 2. Material science, University of Virginia, Charlottesville, VA, United States*

The magnetic skyrmion is a candidate for informational carries of high-density data storage due to its abilities to be small, stable, and controllable by electric current[1]. Most reported room-temperature skyrmions in ferromagnetic multilayers have large sizes (50nm-1μm) due to the large saturation magnetization and stray field[2,3]. Those skyrmions are not suitable to get high density for applications. Theoretical work shows several ferrimagnetic materials were located in magnetic parameters space for holding ultrasmall skyrmions at room temperature (RT)[3]. The decay of interfacial Dzyaloshinskii–Moriya interaction[4] and spin-orbit torques[5] from the interface limit the thickness of magnetic layers. A recent simulation and experiment has found small (10–30nm) skyrmions in 6nm GdCo thin films at RT[6,7]. However, this rare-earth transition-metal amorphous thin film has poor thermal stability. Mn4N is a rare earth free ferrimagnetic material with stronger thermal stability and is a promising material for RT ultrasmall skyrmion due to its comparable magnetic properties with CoGd thin film[8,9]. But to date, sub-20nm Mn4N films have only been reported by few groups by using molecular beam epitaxy[9], which is not suitable for mass production. Here, by using reactive sputtering, we successfully deposited 15nm Mn4N films on pretreated MgO substrates with low saturation magnetization (Ms= 40 emu/cc), low magnetic anisotropy energy (0.7 Merg/cc) and a Mr/Ms ratio of 0.7, which is suitable for ultrasmall skyrmion at room-temperature. Ab inito density functional theory (DFT) calculations were performed to show the effect of crystalline structure on magnetic properties of Mn4N thin film.

[1] Fert, A., et al. Magnetic skyrmions: advances in physics and potential applications. Nat Rev Mater 2, 17031 (2017). [2] Jiang, W. et al. Skyrmions in magnetic multilayers, Phys Rep 704(2017) 1-49 [3] Büttner, F., et al. Theory of isolated magnetic skyrmions: From fundamentals to room temperature applications. Sci Rep 8, 4464 (2018). [4] Ma, X. et al. Interfacial control of Dzyaloshinskii-Moriya interaction in heavy metal/ferromagnetic metal thin film heterostructures. Phys. Rev. B 94, 180408(R) (2016). [5] Ramaswamy, R. et al. Recent advances in spin-orbit torques: Moving towards device applications, Applied Physics Reviews 5, 031107 [6] Caretta, L. et al. Fast current-driven domain walls and small skyrmions in a compensated ferrimagnet. Nature Nanotech 13, 1154–1160 (2018). [7] Ma, C.T., Xie, Y., Sheng, H. et al. Robust Formation of Ultrasmall Room-Temperature Neél Skyrmions in Amorphous Ferrimagnets from Atomistic Simulations. Sci Rep 9, 9964 (2019). [8] Isogami, S. et al Contributions of magnetic structure and nitrogen to perpendicular magnetocrystalline anisotropy in antiperovskite ε–Mn4N. Phys. Rev. Materials 4, 014406 [9] Gushi, T. et al. Large Current Driven Domain Wall Mobility and Gate Tuning of Coercivity in Ferrimagnetic Mn4N Thin Films. Nano Lett. 2019, 19, 12, 8716–8723

Session Q2
MAGNETIZATION DYNAMICS AND DAMPING V: MAGNETIZATION DYNAMICS

Benjamin Ducharne, Chair
Institut National des Sciences Appliquees de Lyon, Villeurbanne, France

CONTRIBUTED PAPERS

Q2-01. Resonant Coupling Between Magnetic Layers by Acoustic Phonons. *K. An*[1], R. Kohno[1], A. Litvinenko[1], v.v. naletov[1,7], L. Vila[1], G. de loubens[2], j. ben youssef[3], n. vukadinovic[4], G. Bauer[5], A.N. Slavin[6], V. Tyberkevych[6] and O. Klein[1] *1. Univ. Grenoble Alpes, CEA, CNRS, Grenoble INP, INAC-Spintec, Grenoble, France; 2. SPEC, CEA-Saclay, CNRS, Université Paris-Saclay, Gif-sur-Yvette, France; 3. LabSTICC, CNRS, Université de Bretagne Occidentale, Brest, France; 4. Dassault Aviation, Saint-Cloud, France; 5. Institute for Materials Research and WPI-AIMR and CSRN, Tohoku University, Sendai, Japan; 6. Department of Physics, Oakland University, Rochester, MI, United States; 7. Kazan Federal University Institute of Physics, Tatarstan, Kazan, Russian Federation*

The coherent transfer of information between different waveform is an important ingredient of information technology as it allows transport of quantum states without loss of frequency or phase. An efficient hybridization, though, requires to reach the strong coupling regime, where the interaction rate between two collective states becomes larger than their relaxation rates. This has revived interest for insulating magnetic garnets with low magnetic and acoustic dampings. It was recently shown that the circularly polarized phonons in dielectric crystals can transfer angular momentum over millimeters due to the strong magnon phonon coupling in a dielectric spin valve system, which is composed of two yittrium iron garnet (YIG) layers on both sides of gadolium gallium garnet substrate [1]. The evidence of this coupling is the emergence of a bright and a dark collective states that can be revealed through an interference pattern in the ferromagnetic resonance signal. In this work, we will focus on the collective behavior when the splitting between two Kittel modes is within the coupling strength. We tune the splitting either i) by varying the polar angle of an external magnetic field or ii) by applying a temperature gradient along the stack direction. We describe their mutual coupling as provided by a dissipative cavity, which represents the nearly degenerate standing acoustic shear wave mode that resonates across the whole crystal thickness. The reactive part of this mutual coupling is responsible for the usual level repulsion between the two modes. The contrast between the bright and dark states enhances as the splitting between two Kittel modes reduces. However, when the zero detuning becomes degenerate with an acoustic resonance, the dissipative part dominates over the reactive part and it leads to partial level attraction between the two collective modes. From the experimentally measured voltage contrast between two frequency tones, we extract a qualitative behavior of the coupling strength as a function of detuning, which reproduces the reactive and dissipative part of the phonon mediated coupling. We show that our results can be explained by three coupled oscillator model.

[1] K. An, A. N. Litvinenko, R. Kohno et al., *Physical Review B* 101.6 060407 (2020)

Q2-02. Parametric Amplification of Magnons in Synthetic Antiferromagnets. *A. Kamimaki*[1,2], S. Iihama[2,3], K. Suzuki[2,3], N. Yoshinaga[4,2] and S. Mizukami[2,3] *1. Department of Applied Physics, Tohoku University, Sendai, Japan; 2. WPI-AIMR, Tohoku University, Sendai, Japan; 3. CSRN, Tohoku University, Sendai, Japan; 4. MathAM-OIL, AIST, Sendai, Japan*

Non-linear interactions related to magnons are expected to be applied to advanced computing devices [1,2]. Synthetic antiferromagnets (SAFs) are candidate materials to observe non-linear magnon interactions because they have two fundamental magnon modes, that are the acoustic (AC) and optical (OP) modes [3]. However, there are no reports whether the AC and OP mode can interact with each other. Here, we report parametric amplification of the AC mode by the OP mode in SAFs using time-resolved magneto-optical Kerr effect (TRMOKE) technique [4]. SAF films, Si/SiO_2 (subs.)/ $Ta(3)/Co_{20}Fe_{60}B_{20}(3)/Ru(0.4)/Co_{20}Fe_{60}B_{20}(3)/Ta(3)$ (thickness is in nm), was prepared by a sputtering. Fig. 1(a) shows the TRMOKE data with various pump laser power P_{pump} at the critical magnetic field angle $\theta_{H,c}$. At this angle, $2f_{AC} = f_{OP}$ is satisfied, where f_{AC} and f_{OP} are the frequency of the AC and OP mode, respectively. $\Delta\theta_K$ and Δt are the change in the Kerr rotation angle and the pump-probe delay time, respectively. In case of P_{pump} > 5 mW, the temporal amplification of the magnetization precession was observed (dashed curves). Fig. 1(b) shows the θ_H dependence of the peak intensity of the FFT spectrum at the P_{pump} = 10 mW for the AC and OP mode, respectively. At around $\theta_H = 45° \sim \theta_{H,c}$, the intensity of the AC mode rapidly enhanced. This indicates the non-linear interaction between the AC and OP modes is allowed for SAFs. The threshold of the OP mode to the amplification will be also discussed. This work was partially supported by KAKENHI (Nos. 26103004 and 19K15430). A.K. thanks to GP-Spin at Tohoku University.

[1] S. Manipatruni *et al*., Nat. Phys. 14, 338 (2018). [2] J. Torrejon *et al*., Nature 547, 428 (2017). [3] A. Kamimaki *et al*., Appl. Phys. Lett. 115, 132402 (2019). [4] A. Kamimaki *et al*., Phys. Rev. Appl. 13, 044036 (2020).

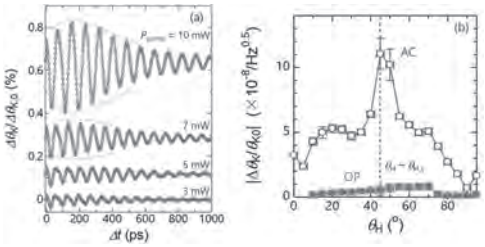

Fig. 1 (a) The TRMOKE results at the critical magnetic field angle $\theta_{H,c}$, with different pump power P_{pump} = 3, 5, 7, and 10 mW. At P_{pump} > 5 mW, temporal amplification of the magnetization presession was observed (dashed curves). (b) The θ_H dependence of FFT power density for acoustic (AC) and optical (OP) mode. Dashed line shows the $\theta_{H,c}$ where the peak of the AC mode remarkably enhanced.

Q2-03. Latent State in Time-Resolved Nonlinear Magnon Scattering in Thin Films. *T. Qu*[1], A. Hamill[1], A. Venugopal[1], J.J. Etheridge[1], P.A. Crowell[1] and R. Victora[1] *1. University of Minnesota, Minneapolis, MN, United States*

The physics of nonlinear magnon scattering has been exploited in nonlinear microwave devices for wireless and satellite communication applications. The latent state, which is the time delay in the magnon response to a microwave pulse, is required to be reduced for rapid information transfer. We have studied the latent state in time-resolved nonlinear magnon scattering in thin films, in both theory and experiment. The experiment is performed using phase-sensitive time-resolved heterodyne ferromagnetic resonance. The theory is a hybrid time-resolved model which uses an analytical equation of motion based on the Holstein-Primakoff transformation, and realistic micromagnetic simulation. From the experiment in Fig. 1(a), we find the latent state is extraordinarily sensitive to the power. When the power is near the threshold, the lifetime t_0 of the latent state is of order ten microseconds. At high powers, t_0 decreases sharply to a hundred nanosecond. Our simulation shows consistent behavior of the latent state in the same dynamic power range in Fig. 1(b). From capturing the time-resolved magnon number of all the existing modes, we find that the origin of the latent state is the magnon redistribution: the k=0 mode takes time to scatter into non-uniform magnum modes k≠0. The power controls the scattering rate from k=0 to k≠0, where the rate is time dependent on the magnon number. We thank DARPA, XSEDE, and the SMART center (funded by SRC and NIST) for support of this project.

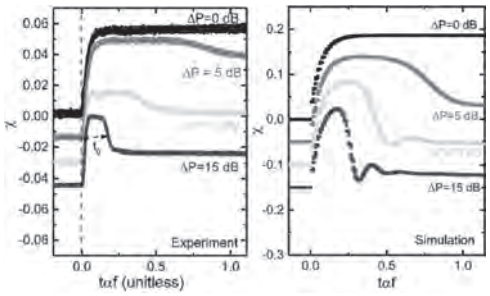

Fig. (a) Experimental measurement of susceptibility at different microwave powers for a frequency of 2.0 GHz. The x-axis is a dimensionless time tαf where t is the real time, α is the damping constant (α=6×10⁻³) and f is the microwave frequency. The susceptibility shows latent states, where t_0 indicates the lifetime of the latent states. ΔP is the increase of power amplitude, using the power at the linear region as the baseline (the black line). Fig. (b) Corresponding simulated susceptibility at varying microwave powers at the same frequency. The varying powers are in the same dynamic range as the experiment in Fig. (a).

Q2-04. Discrepancy Between Constraining and Effective Fields in Ab-Initio Spin Dynamics. *S. Streib*[1], V. Borisov[1], M. Pereiro[1], A. Bergman[1], E. Sjöqvist[1], A. Delin[2,3], O. Eriksson[1,4] and D. Thonig[4,1] *1. Department of Physics and Astronomy, Uppsala University, Uppsala, Sweden; 2. Department of Applied Physics, KTH Royal Institute of Technology, Stockholm, Sweden; 3. Swedish e-Science Research Center (SeRC), KTH Royal Institute of Technology, Stockholm, Sweden; 4. School of Science and Technology, Örebro University, Örebro, Sweden*

The aim of ab-initio spin dynamics is to go beyond the limitations of standard atomistic spin dynamics, which is based on a mapping of the original electronic Hamiltonian to an effective spin Hamiltonian. This spin Hamiltonian assumes constant magnetic moment lengths and constant interaction parameters and is therefore only valid in the magnetic ground-state configuration. Recent studies [1] have shown that non-collinearity in the magnetic state reduces the spin-spin interaction and gives improved accuracy compared to experiment. However, the proposed method in Ref. [1] is not applicable for the general case and reveals limitations of the above mentioned mapping [2]. In ab-initio spin dynamics the magnetic moment lengths and the quasi-classical torques acting on the atomic magnetic moments are calculated from a quasi-equilibrium electronic ground state within the adiabatic approximation [3], where constraining fields are required to stabilize non-collinear magnetic moment configurations [4]. The constraining field has therefore to cancel the internal effective magnetic field, which is expected to be minus the gradient of the energy with respect to the magnetization. In practical calculations the constraints on the moment directions are often only implemented approximately without constraining fields, which can introduce serious errors [5]. We present surprising numerical results from constrained density functional (cDFT) calculations which demonstrate that the constraining field and the effective field obtained from the energy gradient are not exactly opposite, as would be expected [4]. Furthermore, we provide a theoretical explanation of this discrepancy based on a theorem that relates the constraining field and the energy gradient: the constraining field theorem. We argue that in the case of cDFT the correct effective magnetic field is actually given by the energy gradient and not by the constraining field.

[1] Szilva et al., Phys. Rev. Lett. 111, 127204 (2013). [2] Szilva et al., Phys. Rev. B 96, 144413 (2017). [3] Antropov et al., Phys. Rev. Lett. 75, 729 (1995). [4] Stocks et al., Philos. Mag. B 78, 665 (1998). [5] Singer et al., Phys. Rev. B 71, 214435 (2005).

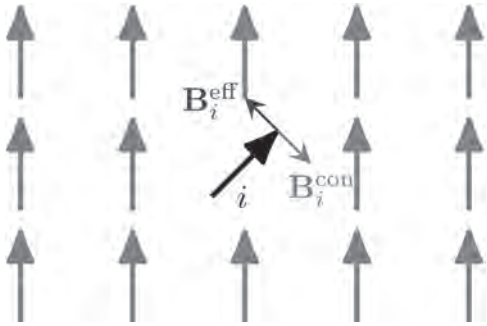

Effective and constraining fields acting on a magnetic moment.

Q2-05. Fractional Equation for the Anomalous Magnetic Diffusion in Ferromagnetic Materials. *B. Ducharne*[1], Y. Tene Deffo[2], P. Tsafack[2], B. Zhang[3] and G. Sebald[4] *1. Laboratoire de Génie Electrique et Ferroélectricité – INSA de Lyon, Villeurbanne, France; 2. Faculty of Engineering and Technology, University of Buea, Buea, Cameroon; 3. Green Manufacturing R&D Laboratory, School of Mechanical, Electrical and Information Engineering, Shandong University, Weihai, China; 4. ELyTMaX UMI 3757, CNRS – Université de Lyon – Tohoku University, International Joint Unit, Tohoku University, Sendai, Japan*

Ferromagnetic materials are used in a wide range of electromagnetic applications (energy converters, sensors, inductances …). In this domain, we observed a growing interest in the development of simulation tools reducing the experimental campaigns and improving the knowledge and the performances. Accurate simulation results can only be obtained by coupling precise electromagnetic equations to the exact material laws (hysteresis, saturation, frequency dependence) [1]-[3]. Under the influence of an external magnetic excitation, the local magnetic state through the ferromagnetic specimen is ruled by the combination of both the magnetic domain kinetics and the external magnetic field diffusion. The usual methods for the simulation of the magnetic behavior are all based on the separation of the magnetic contributions, where the microscopic Eddy currents due to the domain wall motions and the macroscopic ones due to the extern magnetic field variations are considered separately [4]. This separation remains artificial, since practically both losses mechanisms occurs simultaneously and interact on each other [5]. In this study, an alternative solution is proposed through the resolution of an anomalous fractional magnetic field diffusion (1, 2 or 3D depending on the experimental situation). The fractional order constitutes an additional degree of freedom in the simulation scheme [6]-[8]. It is identified through comparisons to experimental results. By adjusting precisely this

order, very accurate local and global simulation results can be obtained on a very broad frequency bandwidth. It allows to predict precisely the dynamic magnetic behavior of classic ferromagnetic components.

[1] B. Zhang et al., IEEE Transaction on Magnetics, vol. 54, iss. 11 (2018) [2] B. Zhang et al., IEEE Transaction on Magnetics, Vol. 54, iss. 3, (2017). [3] B. Gupta et al., IEEE Transaction on Magnetics, Vol. 54, Iss. 3, (2018). [4] G. Bertotti, IEEE Transaction on Magnetics, vol. 24, iss. 1, pp. 621-630, (1980). [5] M. A. Raulet et al., IEEE Transactions on Magnetics, Vol. 40, iss 2, pp. 872-875, (2004). [6] B. Ducharne et al., International journal of dynamics and control, vol. 6, pp. 89-96, (2018). [7] B. Ducharne et al., Journal of Applied Physics, vol. 117, iss. 24, (2015). [8] B. Ducharne et al., The European Physical Journal Plus, 135:325, (2020).

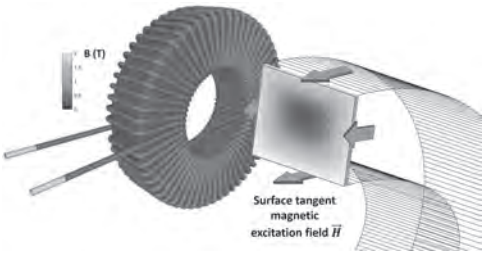

Q2-06. Withdrawn

INVITED PAPER

Q2-07. Magnon Mediated Coherent Information Manipulation and Processing. *C.A. Trevillian*[1] and V. Tyberkevych[1] *1. Physics, Oakland University, Rochester, MI, United States*

Coherent manipulation of quantum information is pivotal for real quantum computing applications. Promising approaches employ hybrid quantum systems based on coupled superconducting qubits and resonators and magnetic elements [1-6], where strong coupling rates (exceeding 100 MHz) are easily reached. An advantage of magnetic elements is that their resonance frequencies are tunable in a wide range by a bias magnetic field. However, all previous studies in this area focus on quasi-static systems where magnetic resonance frequency is constant during the signal lifetime. Here, we propose a new method of coherent information manipulation in hybrid magnetic/superconducting systems based on dynamic control of the magnetic element at timescales comparable or less than characteristic coherence times. This method opens new possibilities for quantum information transduction, processing, and entanglement generation, that are not possible to realize in static hybrid systems. Fig. 1 shows a simple example of how to coherently transfer information from one superconducting resonator P_1 to another P_2 using intermediate magnetic resonator P_m, where the resonance frequency is rapidly swept across the resonance frequencies of resonators $P_{1,2}$ with ramp rate $\rho = d\omega_m/dt = 2\pi\times 2.5$ MHz/ns. As one can see, such "passage" results in almost complete information transfer to the P_2 resonator. Notably, the population of the magnetic resonator P_m stays low (< 0.2) during the whole process (see bottom of Fig. 1), which explains the weak sensitivity of this process to magnetic damping. Dynamically changing the resonant magnon frequency can be used for information transfer between disparate systems, creating quantum gates, and realizing quantum data exchange between two elements. This dynamic frequency change may perform information processing and can be used to study fundamental properties of magnons, such as if we do 50% information transfer, thereby generating magnon-mediated quantum entanglement.

[1] H. Huebl, C. W. Zollitsch, J. Lotze, et al., Phys. Rev. Lett., vol. 111, no. 127003, 2013. [2] Y. Tabuchi, S. Ishino, T. Ishikawa, et al., Phys. Rev. Lett, vol. 113, no. 083603, 2014. [3] X. Zhang, C.-L. Zou, L. Jiang, and H. X. Tang, Phys. Rev. Lett., vol. 113, no. 156401, 2014. [4] Y. Tabuchi, S. Ishino, A. Noguchi, et al., Science, vol. 349, no. 6246, pp. 405-408, 2015. [5] Y. Li, T. Polakovic, Y.-L. Wang, et al., Phys. Rev. Lett., vol. 123, no. 107701, 2019. [6] J. Hou and L. Liu, Phys. Rev. Lett., vol. 123, no. 107702, 2019.

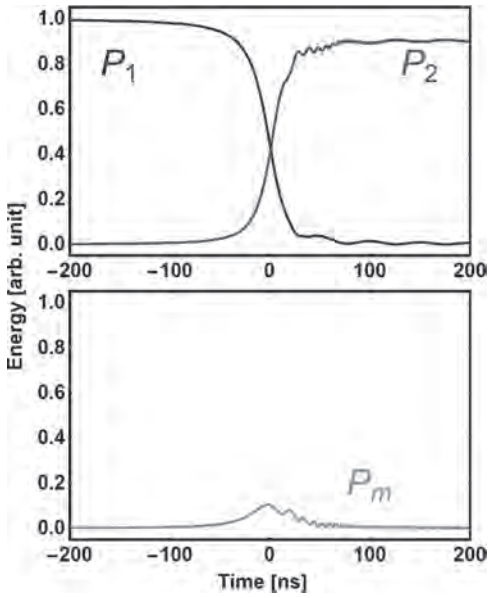

Fig. 1. Temporal profiles of populations of two superconducting resonators $P_{1,2}$ (top) coupled to magnetic resonator P_m (bottom) during the fast (ramp rate $\rho/2\pi = 2.5$ MHz/ns) tuning process of the magnetic resonance frequency.

CONTRIBUTED PAPERS

Q2-08. Spin Dynamics and Relaxation in Thin Film La0.7Sr0.3MnO3/SrTiO3: ac Magnetic Susceptibility and Magnetic Viscosity Investigations. *N. Mottaghi*[1], M.S. Seehra[1], J. Shi[3], M. Jain[2] and M.B. Holcomb[1] *1. Physics and Astronomy, West Virginia University, Morgantown, WV, United States; 2. Institute of Materials Science & Department of Physics, University of Connecticut, Storrs, Storrs, CT, United States; 3. Department of Materials Science and Engineering, University of Connecticut, Storrs, CT, United States*

Recently we studied magnetic inhomogeneity effects in magnetocaloric properties of a 7.6 nm $La_{0.7}Sr_{0.3}MnO_3$ (LSMO) thin film to understand the nature of magnetic phases transitions[1]. We proved this sample has two main magnetic phase transitions: superparamagnetic ferromagnetic and ferromagnetic-paramagnetic phases transitions, at T = 240 K (= T_B) and T = 270 K (= T_C), respectively. Here we want to understand the spin dynamics and relaxation in this sample. Analysis of the results from our investigations of the temperature dependence of ac susceptibilities (χ' and χ'') and magnetic viscosity in a 7.6 nm thin film of $La_{0.7}Sr_{0.3}MnO_3$ grown on $SrTiO_3$ (001) substrate are presented. The Curie temperature (T_C) of this film is magnetic field (H) dependent varying as: $[T_C(H)-T_C(0)] \sim H^n$, $n \sim 0.15$. Temperature dependence of χ' and χ'' measured at ac frequencies f_m in the range of 0.1 to 10 kHz shows a broad peak near 230 K associated with the blocking temperature of spin clusters present in the 1.4 nm surface layer and a frequency dependent peak near 270 K associated with T_C (Fig. 1). The mean relaxation time τ determined from the Cole-Cole analysis of and is shown to fit the Vogel-Fulcher law: $\tau = \tau_0 \exp[\Delta E / k_B(T-T_0)]$, with T_B = 245 K, $\Delta E / k_B$ = 270 K = T_C, and $\tau = 1.2\ 10^{-9}$ (s) (Fig. 2). Magnetic viscosity S (measured in H = 0 for a sample cooled in H = 50 Oe) determined from the fit to the magnetization: $M(t) = M(0) - S \ln t$, with time t up to 2 hours, shows a

peak at 230 K above which the *M* (2 hrs) switches to negative values for temperatures up to $T_C(0)$. It is argued that this negative magnetization results from interaction between the superparamagnetic like spin clusters and the ferromagnetic phase.

[1] N. Mottaghi, R.B. Trappen, S.Y. Sarraf, M.S. Seehra, and M.B. Holcomb, J. Alloys Compd. 154200 (2020).

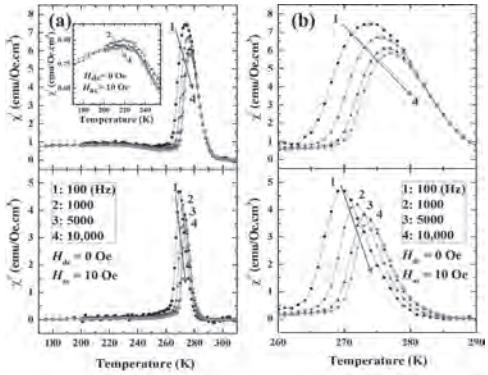

FIG. 1. (Left figure) Experimental χ' and χ'' vs temperature for the 7.6 nm LSMO/STO sample at four frequencies. (Right figure) high temperature zoom in of the χ' and χ'' vs temperature at different frequencies.

FIG. 1. (Left figure) Experimental χ' and χ'' vs temperature for the 7.6 nm LSMO/STO sample at four frequencies. (Right figure) high temperature zoom in of the χ' and χ'' vs temperature at different frequencies.

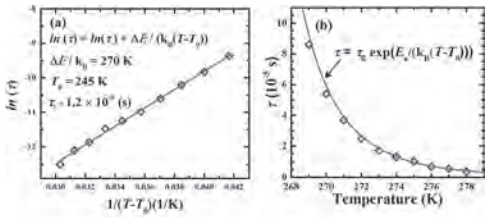

FIG. 2. (a) The best-fit line of $ln(\tau)$ versus $1/(T-T_0)$ to the Vogel-Fulcher law to determine the $\Delta E/k_B T$ and τ_0. (b) Shows how the calculated values of τ is following the Vogel-Fulcher law.

FIG. 2. (a) The best-fit line of *ln* (τ) versus $1/(T-T_0)$ to the Vogel-Fulcher law to determine the $\Delta E / k_B T$ and τ_0. (b) Shows how the calculated values of τ is the following the Vogel-Fulcher law.

Q2-09. Thermodynamics of Interacting Magnetic Nanoparticles.
P. Torche[1], D. Serantes[2], D. Baldomir[2], K. Livesey[3], O. Chubykalo-Fesenko[4], S. Ruta[5], R. Chantrell[5] and *O. Hovorka*[1] *1. University of Southampton, Southampton, United Kingdom; 2. University of Santiago de Compostela, Santiago de Compostela, Spain; 3. University of Colorado at Colorado Springs, Colorado Springs, CO, United States; 4. Instituto de Ciencia de Materiales de Madrid, Madrid, Spain; 5. University of York, York, United Kingdom*

We address the issue of quantifying the heat produced by a single magnetic nanoparticle (MP) embedded within an interacting MP cluster. This is relevant for MP hyperthermia considered as a modality for enhancing cancer therapies, where recent experiments raised questions whether it is the net heating effect of the entire MP aggregate that leads to tumor death, or the local heat distribution across it [1]. Thus, it becomes necessary to understand the distribution of heat production across a MP aggregate inside a living cell. In this work we apply the non-equilibrium stochastic thermodynamics combined with the Néel-Arrhenius transition state theory to systems of interacting Stoner-Wohlfarth MPs [2]. We show that it is possible to associate the expressions for entropy production with the individual MPs within an interacting assembly, which in turn allows computing the single particle heat across the assembly. Our calculations suggest that dipolar interactions lead to a significant heat distribution across a particle system, often varying by as much as 50% - 100% of the mean heat practically measurable from the full hysteresis loop area. This could lead to considerable local heating produced inside cancer cells while the net temperature effect remains small, corroborating the earlier experimental findings. We also show that due to the presence of dipolar interactions between the MPs, the area of the hysteresis sub-loops corresponding to individual MPs does not represent the particle heat, and performing explicit calculations based on evaluating the entropy, such as developed in this work, is necessary [3].

[1] M. Creixell et al., ACS Nano 5, 7124 (2011). [2] U. Seifert, Rep. Prog. Phys. 75, 126001 (2012). [3] P. Torche et al., Phys. Rev. B 100, 125431 (2020).

Q2-10. Disentangling Local Heat Contributions in Interacting Magnetic Nanoparticles.
C. Munoz-Menendez[1,2], *D. Serantes*[1,2], O. Chubykalo-Fesenko[3], S. Ruta[4], O. Hovorka[5], P. Nieves[6], K. Livesey[7], D. Baldomir[1,2] and R. Chantrell[4] *1. Applied Physics, Universidade de Santiago de Compostela, Santiago de Compostela, Spain; 2. Instituto de Investigacións Tecnolóxicas, Universidade de Santiago de Compostela, Santiago de Compostela, Spain; 3. Instituto de Ciencia de Materiales de Madrid, Madrid, Spain; 4. Physics, University of York, York, United Kingdom; 5. University of Southampton Faculty of Engineering and the Environment, Southampton, United Kingdom; 6. Technical University of Ostrava, Ostrava-Poruba, Czechia; 7. University of Colorado at Colorado Springs, Colorado Springs, CO, United States*

Accurate knowledge of the heat released by nanomagnets when subjected to an alternating magnetic field is critical for diverse applications, from catalysis to magnetogenetics. A fundamental and unsolved problem remains: if the nanomagnets are interacting with each other, how can we determine the individual heat released? A common approach is to evaluate the hysteresis loops of each nanomagnet [1,2] and then estimate the heat as proportional to the hysteresis loop area. In this talk we highlight that such an approach is incorrect, as interacting particles perform work on each other and thus the usual heat/area relation cannot be applied. This is evidenced, for example, by the simple fact that individual particles may display "inverted" hysteresis cycles [3,4], that would wrongly imply absorption of energy. Thus, how can the local heat distribution be estimated? (see figure) We present here a magneto-thermodynamics model that allows one to disentangle heat from work in individual particles under interacting conditions. Thus, accurate knowledge of the heating performance of individual nanomagnets can be achieved. Focusing on usual magnetic fluid hyperthermia conditions for illustrative purposes, our results show that heat is released not only when a particle's magnetization switches but also when a neighboring one switches, due to the sudden change in the effective magnetic field. Remarkably, our results indicate that the heat released by both types of processes can be comparable. These completely unexpected results bring fundamentally new understanding to magneto-thermodynamics phenomena and emphasize a need for fresh approaches when investigating applications that rely on heating.

[1] C. Munoz-Menendez, I. Conde-Leboran, D. Baldomir, et al. Phys. Chem. Chem. Phys. 17, 27812 (2015) [2] R. P. Tan, J. Carrey, and M. Respaud, Phys. Rev. B 90, 214421(2014) [3] J. Yang, J. Kim, J. Lee, et al. Phys. Rev. B 78, 094415 (2008) [4] S. Gu, W. He, M. Zhang, et al. Sci. Rep. 4, 6267 (2014)

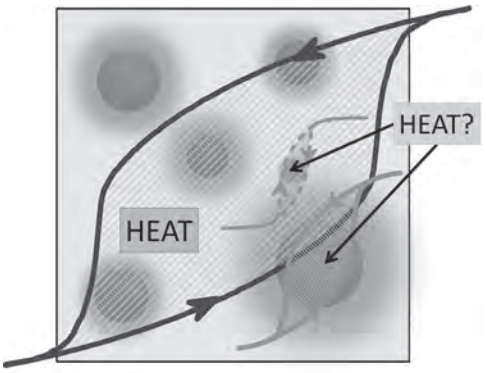

Schematic of the problem posed: how to estimate the heat of individual nanoparticles, given that it is not equal to the local hysteresis loops?

Q2-11. Tuning the Dynamics in Fe_3O_4 Nanoparticles for Hyperthermia Optimization. *H. Chen*[1], D. Billington[2], E. Riordan[2], J. Blomgren[3], S. Giblin[2], C. Johansson[3] and S. Majetich[1] *1. Physics, Carnegie Mellon University, Pittsburgh, PA, United States; 2. Cardiff University, Cardiff, United Kingdom; 3. RISE Research Institutes of Sweden, Göteborg, Sweden*

Iron oxide nanoparticles (NP) are under investigation for many biomedical applications [1], including magnetic hyperthermia. The heating efficiency of magnetic hyperthermia depends on how well the single excitation frequency matches the Néel and Brownian relaxation frequencies of the NPs. We directly measured the magnetostatic interaction induced frequency distribution with a custom-built AC susceptometer [2]. Our results show that both the peak and amplitude of this distribution can be tuned by addition of a small DC field, thus enabling a better match to the AC excitation field frequency. We measured the AC magnetic susceptibility (ACS) of 10.7±1.2 nm Fe_3O_4 NPs dispersed in eicosane (0.15 vol%). The ZFC-FC curve shows a blocking temperature (T_B) of ~ 105 K, and the greatest response of the real (χ') and imaginary (χ'') parts of the ACS was found between 110 and 150 K. Fig. 1 shows the imaginary component of the ACS as a function of frequency, for H_{DC} = 0, at different temperatures. The imaginary part shows a very broad peak at 110K. At higher temperatures the dispersive peak sharpens and the peak shifts to higher frequencies. Both the breadth of the peak and its shift with temperature show that magnetostatic interactions affect high frequency response even for dilute samples. We extended our ACS measurement at 140 K with additional DC fields, ranging from 0 to 4mT. Fig.2 shows the non-monotonical trend of the imaginary part of the ACS at various DC magnetic fields. Below 1.25 mT the peak frequency decreases and the amplitude increases with increasing DC fields. At and above 1.25 mT these trends reverse. The dissipation at 100 kHz increases by a factor of 3.8 between 0 and 1.25 mT. The peak DC field is comparable to the average magnetostatic interaction field. Applying the DC field overcomes part of the spin freezing and enables a larger fraction of the spins to contribute to the dissipation. This methodology can be extended to polydisperse NPs at higher concentrations at body temperature.

[1] Q.A. Pankhurst, et al., J. Phys. D Appl. Phys. 36, R167 (2003).
[2] E. Riordan, et al., Review of Scientific Instruments 90, 073908 (2019).

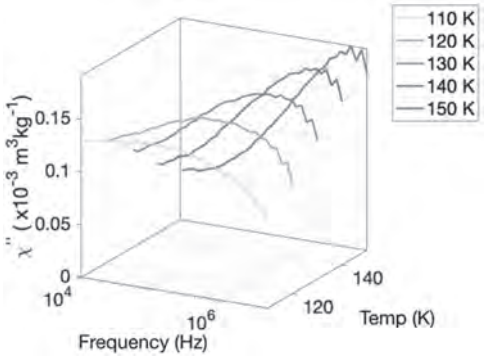

AC susceptibility of the imaginary (χ'') part versus frequency.

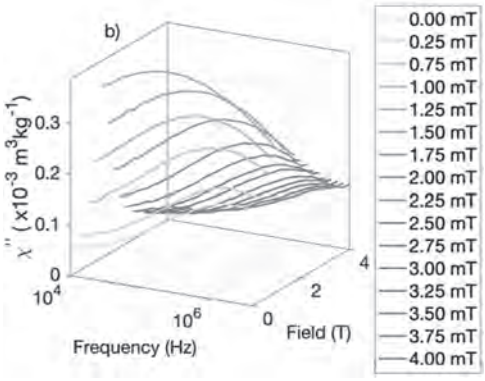

Imaginary susceptibility (χ'') versus frequency at 140 K at different DC fields parallel to the AC fields.

Session Q3
NEUROMORPHIC COMPUTING WITH SPIN-TORQUE OSCILLATORS

Danijela Marković, Chair
CNRS, University of Paris-Sud, Paris, France

CONTRIBUTED PAPERS

Q3-01. Dynamic Effects of Exchange Inertia in Artificial Neural Networks Based on Antiferromagnetic Oscillators. *H. Bradley*[1] and V. Tyberkevych[1] *1. Department of Physics, Oakland University, Rochester, MI, United States*

Antiferromagnetic (AFM) spin Hall oscillators driven by a sub-threshold spin current produce ultra-short (~ 5 ps) spikes in response to a weak external stimulus and can be used as ultra-fast artificial neurons [1, 2]. One of specific features of AFM oscillators is the effective inertia that originates from exchange coupling between two AFM magnetic sublattices and manifests itself, for instance, in hysteretic behavior of the threshold generation current [3]. Here, we theoretically investigate influence of the exchange inertia on the dynamics of AFM-based artificial neural networks. The exchange inertia leads to delay of the spike generated by an AFM neuron relative to the input stimulus signal. The delay time depends on the coupling strength between AFM neurons and can vary from ~ 10 ps to several 100s ps. This effect can be used to create a tunable periodic spike generator by coupling several AFM neurons in a ring structure, in which output of one neuron serves as an input for the next neuron. The exchange inertia can also be used to create an "inhibitor" neuromorphic circuit, in which propagation of a spike is suppressed in the presence of another ("inhibiting") signal. The inhibitor works by splitting the signal path in two branches and controlling the delay time in one branch by the inhibiting signal. In the presence of the inhibiting signal, the spikes in two branches arrive at the output neuron at different times and do not induce an output spike. It should be noted, that such "inhibitor" circuit is impossible to realize with inertia-less integrate-and-fire neurons. Combining the inhibitor circuit with a ring structure allows one to realize a controllable neuromorphic memory loop (see example simulations in Fig. 1). These and other examples demonstrate that exchange inertia effects can be utilised to achieve new functionalities of AFM-based artificial neural networks.

[1] R. Khymyn, I. Lisenkov, J. Voorheis, et al., Sci. Rep. 8, 15727 (2018). [2] O. Sulymenko, O. Prokopenko, I. Lisenkov, et al., J. Appl. Phys. 124, 152115 (2018). [3] R. Khymyn, I. Lisenkov, V. Tiberkevich, et al., Sci. Rep. 7, 43705 (2017).

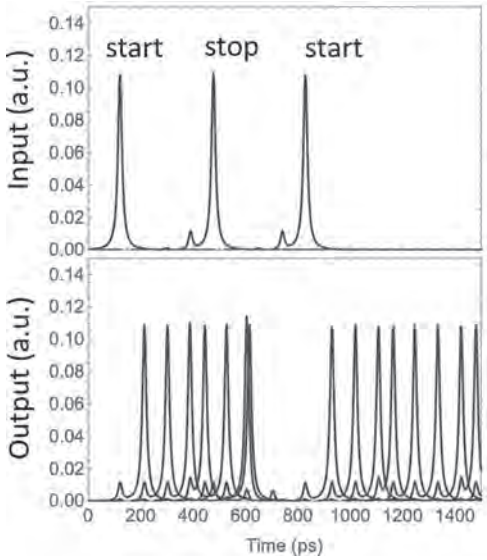

Example simulations of a controllable memory loop based on AFM neurons. Top: time profile of input signal with two "start" spikes (at 100 ps and 800 ps) and one "stop" spike (at 500 ps). Bottom: output spike sequence generated by the memory loop.

Q3-02. Memristive Functionality of a Thin-Film Ferromagnet/Antiferromagnet Bilayer. *S. Ivanov*[1] and S. Urazhdin[1] *1. Department of Physics, Emory University, Atlanta, GA, United States*

Memristors – two-terminal circuit elements whose resistance is ideally proportional to the integral of input over time – enable the implementation of synapses in artificial neural networks. However, "ideal" memristive functionality has not been yet achieved. We experimentally demonstrate the possibility to implement almost ideal memristors using thin-film ferromagnet/antiferromagnet (F/AF) bilayers, where frustrated exchange interaction at the F/AF interface results in the correlated spin liquid state of the AF characterized by viscous magnetization dynamics [1]. We utilize a bilayer formed by a 10 nm-thick F Permalloy (Py) and an 8 nm-thick AF NiO film. External magnetic field H serves as the driving input in our demonstration. The angle of magnetization rotation is proportional to the integral of the field over time, which is converted into resistance variations by anisotropic magnetoresistance (AMR). The resulting magnetoelectronic hysteresis loop is consistent with that expected for an ideal memristor. Analysis of the time-domain response shows deviations from ideal behaviors, which are associated with the inhomogeneity of viscous dynamical properties. We also discuss how the demonstrated memristive functionality can be achieved with current-driven nanostructures by utilizing spin torque [2]. The demonstrated memristors are amenable to downscaling and should exhibit high endurance, making them particularly attractive for neuromorphic applications.

1. S. Urazhdin, W. Li and L. Novozhilova, JMMM, Vol. 476, pp.75-85 (2019) 2. G.X. Chen, S. Ivanov, and S. Urazhdin, arXiv:2006.07996 (2020)

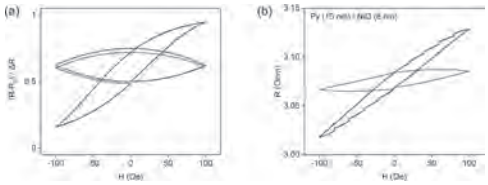

Memristive functionality of an F/AF bilayer device: (a) simulation of magnetization dynamics with the viscous contribution in AF dynamics, (b) experimental demonstration. Black lines correspond to the state of the system during application of magnetic field, red lines – final state of the system after turning the field off, blue line – calculated integral of the applied periodic field.

Q3-03. Ideal Memristor Based on Viscous Magnetization Dynamics Driven by Spin Torque. *G. Chen*[1], S. Ivanov[1] and S. Urazhdin[1] *1. physics, Emory University, Atlanta, GA, United States*

Memristors are circuit elements whose resistance is ideally proportional to the total charge that passes through them, which can provide synaptic functionality in artificial neural networks. Many implementations of generalized memristors – devices whose resistance depends on their electronic history – have been explored, but ideal memristor functionality has not yet been achieved. We utilize analytical arguments and numerical simulations to show that ideal memristors can be realized using spin transfer torque (STT)-driven viscous magnetization dynamics. The latter can be achieved in the spin liquid state of thin-film F/AF heterostructures resulting from frustrated exchange interaction [1]. We show that the magnetization dynamics can be efficiently driven by STT, despite large damping associated with viscous dynamics. For a magnetic system with negligible in-plane anisotropy and large damping, magnetization response to current pulses with varied duration Δt and amplitude I_0 depends only on the total pulse charge Q [Fig.1], consistent with ideal memristive behaviors. Additionally, we show that current-induced Joule heating can serve as an extra state control variable, resulting in the dependence of current-driven resistance variation on the relative timing of the current pulses [Fig.2]. This additional second-order memristive functionality [2] provides natural implementation for the spike-timing dependent plasticity in spintronic neuromorphic network with non-overlapping spikes. Our work thus opens a new route for the development of advanced spintronic neuromorphic hardware.

[1] Urazhdin, Sergei, Weijie Li, and Lydia Novozhilova. "Magnetic freezing transition in a CoO/Permalloy bilayer revealed by transverse ac susceptibility." *Journal of Magnetism and Magnetic Materials* 476 (2019): 75-85. [2] Kim, Sungho, et al. "Experimental demonstration of a second-order memristor and its ability to biorealistically implement synaptic plasticity." *Nano letters* 15.3 (2015): 2203-2211.

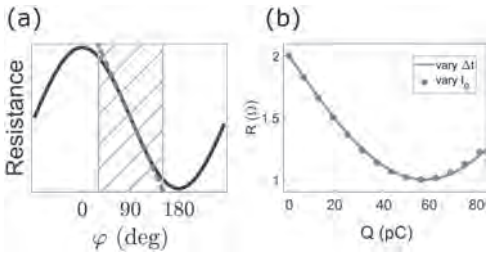

Fig.1 (a) Expected angular range of nearly ideal memristive behaviors. (b) Dependence of resistance variation on the total charge $Q = I_0 * \Delta t$ of the current pulses with varied amplitude I_0 at fixed duration Δt and varied Δt at fixed I_0.

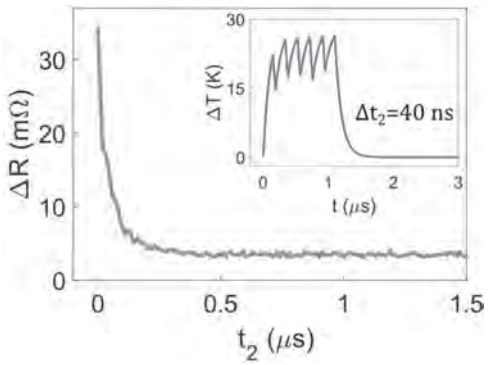

Fig.2 Dependence of the resistance change driven by five 150 ns-long pulses on the delay Δt_2 between the pulses. Inset: T vs t for Δt_2 = 40 ns.

INVITED PAPER

Q3-04. 2D Mutually Synchronized Spin Hall Nano-Oscillator Networks for Neuromorphic Computing. M. Zahedinejad[1], A.A. Awad[1], S. Muralidhar[1], A. Houshang[1], R. Khymyn[1], H. Fulara[1], M. Dvornik[1] and *J. Åkerman*[1] *1. Department of Physics, University of Gothenburg, Goteborg, Sweden*

Mutually synchronized spin-torque nano-oscillators (STNOs) are one of the promising platforms for bioinspired computing and microwave signal generation [1]. Using STNOs one can achieve 90% recognition rate in spoken vowels [2]. However, in order to do more complex tasks, larger-scale synchronized oscillators are needed, something that is not easily done with the STNOs demonstrated so far. In my talk, I will describe a different type of spin current-driven device called spin Hall nano-oscillators (SHNOs), which can generate microwave frequencies over a very wide frequency range [3]. The SHNOs are based on 50 – 120 nm wide nano-constrictions in Pt(5)/Hf(0.5)/NiFe(3) trilayers (all numbers in nm). When multiple nano-constrictions are fabricated close to each other (300 – 1200 nm separation) they can mutually synchronize and chains of up to nine nano-constrictions have been demonstrated to exhibit complete synchronization [4]. For the first time, we can now also synchronize two-dimensional SHNO arrays with as many as 8 x 8 = 64 SHNOs [5]. The mutual synchronization is observed both electrically and using scanning micro-BLS microscopy. Both the output power and linewidth of the microwave signal improves substantially with increasing number of mutually synchronized SHNOs, such that quality factors of about 170,000 can be reached. Following the approach of Romera et al, we also demonstrate neuromorphic computing using a 4 x 4 SHNO array with two injected microwave signals as inputs. Given their high operating frequency (~10 GHz), easy fabrication, and highly robust synchronization properties, nano-constriction SHNO arrays are likely the most promising candidates for neuromorphic computing based on oscillator networks.

[1] Torrejon J., et al. Neuromorphic computing with nanoscale spintronic oscillators. Nature 547, 428 (2017) [2] Torrejon J., et al. Vowel recognition with four coupled spin-torque nano-oscillators. Nature 563, 230 (2018) [3] Chen T., et al. Spin-torque and spin-Hall nano-oscillators. Proc. IEEE 104, 1919 (2016) [4] Awad A. A. et al. Long-range mutual synchronization of spin Hall nano-oscillators. Nature Physics 13, 292 (2017) [5] Zahedinejad M., et al. Two-dimensional mutually synchronized spin Hall nano-oscillator arrays for neuromorphic computing. Nature Nanotechnology 15, 47 (2020)

CONTRIBUTED PAPERS

Q3-05. Withdrawn

Q3-06. Radio-Frequency Synapses for Neural Networks Made of Spin-Torque Nano-Oscillators. *N. Leroux*[1], D. Marković[1], J. Laydevant[1], M. Ernoult[1,3], J. Trastoy[1], E. Martin[1], T. Petrisor[1], L. Martins[2], A. Jenkins[2], R. Ferreira[2], D. Querlioz[3], A. Mizrahi[1] and J. Grollier[1] *1. Unite Mixte de Physique CNRS/Thales, Palaiseau, France; 2. International Iberian Nanotechnology Laboratory, Braga, Portugal; 3. Centre de Nanosciences et de Nanotechnologies, Orsay, France*

Spin Torque Nano-Oscillators are magnetic devices that use tunnel magnetoresistance to emit microwaves. They hold great promise for neuromorphic computing [1], as we can use their non-linear dynamic to emulate neurons and they can be integrated by millions in CMOS chips. In previous works, it has been shown that their transient or coupled dynamics can be used to perform pattern recognition [2], [3]. In order to build deep neural networks [4] it is now crucial to find a way to interconnect different layers of neurons with artificial tunable synapses. Here we present an architecture using spintronic resonators to weight the microwave encoded signals of artificial RF spintronic nano-neurons. These synaptic resonators leverage the spin-diode effect [5,6]. The resistance of the devices oscillates at the same frequency as the signal they receive. The rectified voltages are proportional to the power of the microwaves and depend strongly on the frequency mismatch between the signal and the resonance frequency of the device. Hence to tune these resonance frequencies is analog to tune the synaptic weights. And because of the frequency selectivity of our resonators, each of them rectifies only the signal of its corresponding neuron. We use an analytical model and dynamical simulations to show that a chain of spintronic resonators wired in series, rectifying different microwave signals, is equivalent to the key operation of neural networks, called Multiply-And-Accumulate (MAC), despite the nonlinearity of these components. We also demonstrate experimentally with Magnetic Tunnel Junctions as resonators and several RF generators, the validity of this MAC operation. Finally, we simulate a full network with spintronic oscillators and resonators to test our architecture. We manage to achieve state-of-the-art recognition on a handwritten digit dataset. These are encouraging results for high density hardware neural network, as it is the first demonstration of a fully-spintronic radio-frequency neural network.

[1] J. Grollier, D. Querlioz and M. D. Stiles, Proceedings of the IEEE, Vol. 104, p. 2024-2039 (2016) [2] J. Torrejon, M. Riou et al, Nature, Vol. 547, p. 428 (2017) [3] M. Romera, P. Talatchian, S. Tsunegi et al, Nature, Vol. 563 (7730), p. 230-234 (2018) [4] Yann LeCun et al, Nature, Vol. 521, p. 436-44 (2015) [5] C. Wang, Y.-T. Cui et al, Phys. Rev. B Vol. 79, p. 224416 (2009) [6] D. Marković, N. Leroux, A. Mizrahi, et al, Phys. Rev. Appl, Vol. 13 (4), p. 044050 (2020)

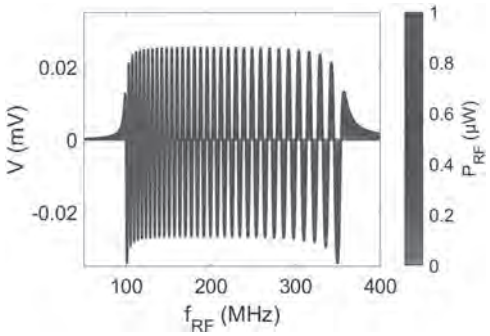

Fig.1 simulation of the voltage rectified by a 64 spintronic resonators chain with a microwave signal.

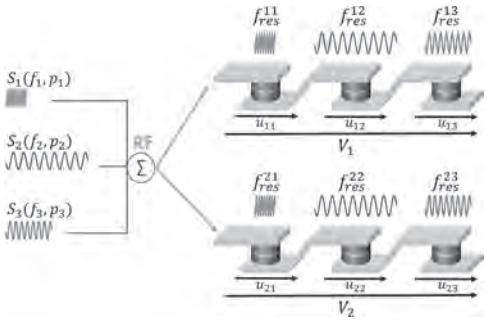

Fig.2 several signals are summed and send to different chains of resonators to implement a MAC operation.

Q3-07. Uniform Mode Spin Hall Nano-Oscillator Array Based Scalable Learning of Classification Tasks Using Different Machine Learning Datasets. *U. Singh*[1], S. Kumar[2], N. Garg[3], P.K. Muduli[3] and D. Bhowmik[2] *1. Department of Electronics and Communication Engineering, Delhi Technological University, Delhi, India; 2. Department of Electrical Engineering, Indian Institute of Technology Delhi, New Delhi, India; 3. Department of Physics, Indian Institute of Technology Delhi, New Delhi, India*

A system of magnetic Vortex Oscillators (VO) has recently been experimentally trained to classify vowel-sounds [1]. But Uniform Mode Nano-Oscillator (UMNO) can be used instead of VO to scale up such a neuromorphic system since UMNO can be much smaller in size than VO [1,2,3]. Classification tasks on more complex Machine Learning (ML) datasets than vowel-sound, e.g. MNIST dataset of handwritten digits (MNIST has higher dimensional input and more output-classes than vowel-sound dataset) can be learned with such a scaled-up-system [1,4]. This brings it closer to real applications. Here, we have carried out simulation-based device-system co-study of an array of such UMNO-s to demonstrate learning of classification for different ML data-sets: MNIST [4], Fisher's Iris (flower-type) [5] and Wisconsin Breast Cancer (WBC) data-set [6]. First, we model a heavy metal/ ferromagnetic metal heterostructure based spin Hall nanooscillator of diameter 75 nm using micromagnetic package *mumax3* (Fig. 1a) [7]. Upon applying in-plane current of current density greater than 7.5 x 10^{11} A/m^2 through it, the magnetization inside the ferromagnetic layer exhibits a sustained uniform mode oscillation at a frequency range of 6–7 GHz (Fig. 1b), which is one order higher than the frequency range of VO [1]. Next, for each of the above mentioned data-sets, we compress the features for each input data-sample to two frequencies (f_A,f_B) in the GHz-range. Through Neighborhood Component Analysis [8], we ensure that (f_A,f_B) form clusters corresponding to the different output labels of the data (Fig. 2a: MNIST). Then we match the characteristic frequencies of our UMNOs to those frequency clusters [1] by modulating the currents that excite the oscillation following the device-characteristic in Fig. 1b. Thus we achieve learning (specific oscillators synchronize based on the output-class of the input) and report high classification accuracy for the data-sets: 85% for MNIST, 91% for Iris and 96 % for WBC (Fig. 2b).

[1] M. Romera, P. Talatchian, S. Tsunegi *et al.,* Nature, Vol. 563, pp. 230–234 (2018). [2] K. L. Metlov and K. Y. Guslienko, Journal of Magnetism and Magetic Materials, Vol. 242–245, Part 2, pp. 1015–1017 (2002). [3] M. Gajek, J. J. Nowak, J. Z. Sun *et al.* Applied Physics Letters, Vol. 100, no. 132408 (2012). [4] Y. LeCun, L. Bottou, Y. Bengio *et al.* Proceedings of the IEEE, Vol. 86, pp. 2278–2324 (1998). [5] R. A. Fisher, Annual Eugenics, Vol. 7, pp. 179–188 (1936). [6] W. N. Street, W. H. Wolberg and O. L. Mangasarian, IS&T/SPIE International Symposium on Electronic Imaging: Science and Technology, Vol. 1905, pp. 861–870 (1993). [7] T. Taniguchi, H. Arai, H. Kubota *et al.*, IEEE Transactions on Magnetics, Vol. 50, No. 1 (2014). [8] J. Goldberger, G. E. Hinton, S. T. Roweis *et al.* Proceedings in Neural Information Proceedings Systems 17 (2004).

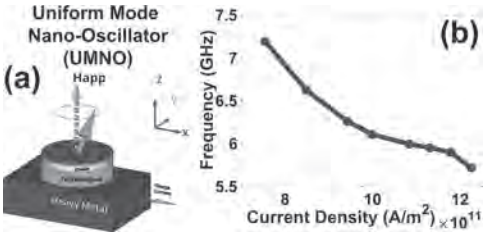

Fig. 1: (a) schematic of UMNO (b) Its frequency of oscillation vs. current density plot

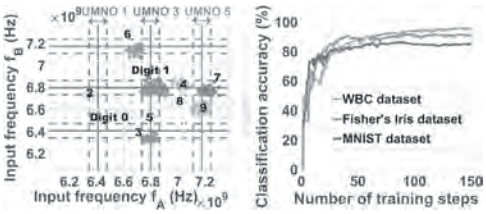

Fig. 2: (a) Synchronization pattern of five UMNOs to classify images for 10 digits (0–9) in MNIST (b) Classification accuracy for MNIST, Iris and WBC datasets

Session Q4
SPIN CURRENTS III

Lijun Zhu, Co-Chair
Cornell University, Ithaca, NY, United States
Shilei Zhang, Co-Chair
ShanghaiTech University School of Physical Science and Technology, Shanghai, China

INVITED PAPER

Q4-01. Domain Wall Based Spin-Hall Nano-Oscillators.
H. Schultheiss[1,2], T. Hache[1], N. Sato[1], L. Körber[1,2], N. Puwenberg[3], T. Mühl[3], A.A. Awad[4], S.S. Arekapudi[5], F.J. Gonçalves[1], O. Hellwig[1,5] and J. Fassbender[1,2] *1. Institute for Ion Beam Physics and Materials Research, Helmholtz-Zentrum Dresden-Rossendorf, Dresden, Germany; 2. Technische Universitat Dresden Fakultat Mathematik und Naturwissenschaften, Dresden, Germany; 3. Leibniz-Institut fur Festkorper- und Werkstoffforschung Dresden eV, Dresden, Germany; 4. Department of Physics, Goteborgs universitet Naturvetenskapliga Fakulteten, Goteborg, Sweden; 5. Technische Universitat Chemnitz, Chemnitz, Germany*

In the last decade, two revolutionary concepts emerged in nano-magnetism from research for advanced information processing and storage technologies. The first suggests the use of magnetic domain walls (DWs) in ferromagnetic nanowires to permanently store information in DW racetrack memories. The second proposes a hardware realisation of neuromorphic computing in nano-magnets using nonlinear magnetic oscillations in the GHz range. Both ideas originate from the transfer of angular momentum from conduction electrons to localised spins in ferromagnets, either to push data encoded in DWs along nanowires or to sustain magnetic oscillations in artificial neurones. Even though both concepts share a common ground, they live on very different time scales which rendered them incompatible so far. Here, we bridge both ideas by demonstrating the excitation of magnetic auto-oscillations inside nano-scale DWs [1] using pure spin currents originating from the spin-Hall effect. While the auto-oscillations are in a domain wall are shown for a bilayer from a heavy metal (HM) and a ferromagnet (FM) we also demonstrated the realization of a bipolar spin-Hall Nano-oscillator using a FM/HM/FM trilayer system [2].

[1] N. Sato, K. Schultheiss, L. Körber, N. Puwenberg, T. Mühl, A. A. Awad, S. S. P. K. Arekapudi, O. Hellwig, J. Fassbender, and H. Schultheiss, Phys. Rev. Lett. 123, 057204 (2019). [2] T. Hache, Y. Li, T. Weinhold, B. Scheumann, F. J. T. Gonçalves, O. Hellwig, J. Fassbender, and H. Schultheiss, Appl. Phys. Lett. 116, 192405 (2020).

CONTRIBUTED PAPERS

Q4-02. Role of Dirac Nodal Lines and Strain on the Spin Hall Conductivity of Epitaxial IrO_2 Thin Films.
A. Bose[1], J.N. Nelson[2], X.S. Zhang[1], R. Jain[2], D.G. Schlom[3], D. Ralph[2], D.A. Muller[1], K.M. Shen[2] and R. Buhrman[1] *1. AEP, Cornell University, Cornell University, Ithaca, NY, US, Ithaca, NY, United States; 2. Department of Physics, Cornell University, Cornell University, Cornell University, Ithaca, NY, US, Ithaca, NY, United States; 3. Department of Materials Science and Engineering, Cornell University, Cornell University, Ithaca, NY, US, Ithaca, NY, United States*

After the discovery of the giant spin Hall effect (SHE) in certain heavy metals [1], topological materials have drawn considerable attraction [2-3]. In this work, we report crystal orientation-dependent large spin Hall conductivity (SHC) in epitaxially grown IrO_2 thin film [4]. IrO_2 is predicted to host Dirac nodal lines (DNL) in the band structure [5], which could lead to a large SHC. Our ARPES studies show the presence of DNL in (001) IrO_2 films [6] that exhibit exceptionally high damping like torque efficiency ranging from 0.45 at 293 K to 0.65 at 30 K which sets the lower bounds of SHC to be 1900 μΩ-cm and 3750 μΩ-cm respectively [4], ten times higher and opposite than the available theoretical prediction [5]. In contrast, anisotropic strain breaks the symmetry of (110) film and opens a gap in the band anti-crossing due to the strain effect which deteriorates the SHC substantially. We also report the SHC varying from dirty metal regime to clean metal regime as IrO2 conductivity increases from (001) to (110) films. This work establishes the correlation of the presence of DNL and strain on the SHC.

[1] L. Liu et. al. *Science* 336, 555 (2012) [2] A. R. Mellnik et. al. *Nature* (London) 511, 449 (2014) [3] Y. Fan et. al. *Nature Mater*. 13, 699 (2014) [4] A. Bose et. al. arXiv:2006.04365 [5] Y. San et. al. *Phys. Rev. B*. 95, 235104 (2017) [6] J. N. Nelson et. al. *Phys. Rev. Mater.* 3, 064205 (2017)

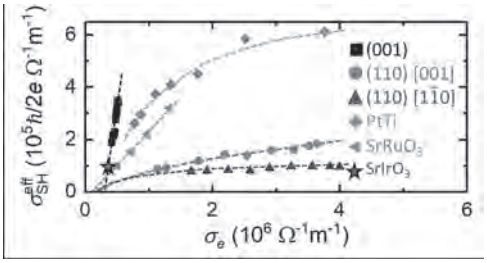

Comparison of SHC with the electrical conductivity of various planes and directions of IrO_2 with other materials such as Pt-Ti alloys, SrRuO3 and SrIrO3

Q4-03. Artificial Enhancement of the Spin Hall Angle of Ge Using the Interdiffusion of Atoms in $Co_2FeAl_{0.5}Si_{0.5}$/*n*-Ge Heterostructures.
S. Kaneta-Takada[1], M. Yamada[2], S. Sato[1], S. Arai[1], L. Anh[1,3], K. Hamaya[2] and S. Ohya[3,4] *1. Department of Electrical Engineering and Information Systems, The University of Tokyo, Bunkyo-ku, Japan; 2. Graduate School of Engineering Science, Osaka University, Toyonaka, Japan; 3. Institute of Engineering Innovation, The University of Tokyo, Bunkyo-ku, Japan; 4. Center for Spintronics Research Network (CSRN), The University of Tokyo, Bunkyo-ku, Japan*

Realizing efficient spin-charge conversion is an important issue in spintronics, especially for the development of low-power-consumption magnetization switching. A spin-charge conversion is generally induced in a nonmagnetic (NM) layer by the inverse spin Hall effect. The spin-charge conversion efficiency, so-called the spin Hall angle θ_{SHE}, is limited by the spin-orbit interaction of the NM layer. Thus, artificially enhancing the θ_{SHE} to greater than its intrinsic value is difficult. Here, using spin pumping measurements on all-epitaxial single-crystalline heterostructures composed of ferromagnetic (FM) $Co_2FeAl_{0.5}Si_{0.5}$ (CFAS) and an NM *n*-type Ge, we demonstrate that the θ_{SHE} can be strongly enhanced by annealing the sample and the resulting interdiffusion of the atoms within only ~3.7 nm around the CFAS/*n*-Ge interface. The magnitude of the electromotive force was significantly different between the as-grown and

annealed samples as shown in Fig. 1. From these results, θ_{SHE} is estimated to be 0.0058–0.0079 for the as-grown sample and 0.015–0.019 for the annealed one at 70–300 K (Fig. 2), which is much larger than the intrinsic value of the θ_{SHE} reported for Ge (0.00096–0.002) [1-3] and is comparable to θ_{SHE} values reported for Pt. This enhancement is attributed to strong scattering of the spin current in the intermixed layer formed at the interface by annealing. Our results indicate that the θ_{SHE} is strongly influenced by the atomic structure of the FM/NM interface, which suggests a new and efficient method to control spin-charge conversion by precise control of the FM/NM interface [4]. This work was partly supported by Grants-in-Aid for Scientific Research (No.18H03860, 19H05616), CREST of JST (No. JPMJCR1777), and the Spintronics Research Network of Japan (Spin-RNJ).

[1] M. Koike *et al*., Appl. Phys. Express 6, 023001 (2013). [2] A. Jain *et al*., Phys. Rev. Lett. 109, 106603 (2012). [3] J. C. Rojas-Sánchez *et al*., Phys. Rev. B 88, 064403 (2013). [4] S. Kaneta-Takada *et al.*, submitted (2020).

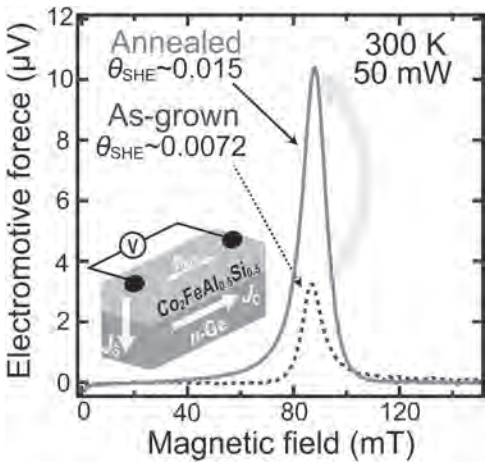

Fig.1. Magnetic field dependencies of the electromotive force at 300 K measured for the as-grown and annealed samples.

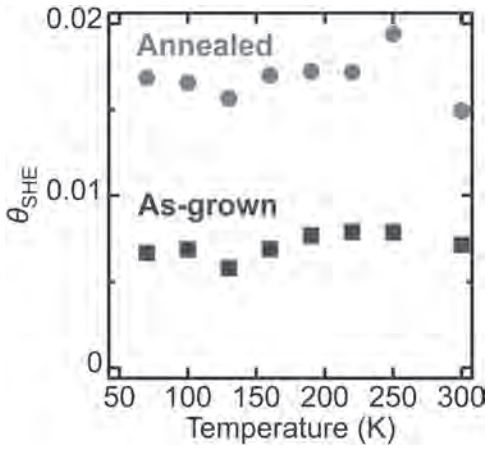

Fig.2. Temperature dependence of the θ_{SHE} of the as-grown and annealed samples.

Q4-04. Agility of Spin Hall Nano-Oscillators Measured Using Time-Resolved Micro-BLS. *F.J. Gonçalves*[1], T. Hache[1], C. McKeefry[1], O. Hellwig[1,2], J. Fassbender[1] and H. Schultheiss[1] *1. Institute of Ion Beam Physics and Materials Research, Helmholtz-Zentrum Dresden - Rossendorf, Dresden, Germany; 2. Physics, Technische Universitat Chemnitz, Chemnitz, Germany*

Spin Hall nano-oscillators (SHNOs) have the unique ability to convert a direct current input to microwave signals by means of spin Hall effect and spin orbit torque [1]. The generated microwave signals depend on several factors inherent to having a flow of direct current such as the current density, Oersted fields, Joule heating and naturally the magnetic state in a given device geometry. In addition, other factors such as frequency locking or synchronisation onto an external microwave source can contribute to the microwave output of a given SHNO [2-5]. The interplay of all these factors affects the agility of the magnetisation auto-oscillations of an SHNO. We report the study of SHNOs while subject to current pulses as well as RF pulses, measured using time resolved micro-focused Brillouin light scattering (micro-BLS). The SHNOs under test consist of a double-disk constriction of NiFe(5 nm)/Pt(7 nm). First, we discuss how few-nanosecond pulses can still efficiently induce magnetisation auto-oscillations, thereby demonstrating that both the onset and outset of the auto-oscillations occur within a sub-nanosecond timescale. Then, we proceed to showing how auto-oscillations can be affected by external microwave pulses. Various degrees of enhancement (injection-locking) or suppression of the auto-oscillation signal can be achieved by choice of the frequency and the amplitude of the external microwave signal. The knowledge of the agility or the response to either intended or unwanted parasitic external excitations is paramount for SHNOs to be able to operate on very short time-scale with well defined responses in, for example, the context neuromorphic computing [6].

[1] Demidov, V. E. et al., Nature Materials, 11(12), 1028–1031 (2012). [2] Demidov, V. E. et al., Nature Communications, 5(1), 3179 (2014). [3] Sato, N. et al. Physical Review Letters, 123(5), 057204 (2019). [4] Hache, T. et al., Applied Physics Letters, 116(19), 192405 (2020). [5] Hache, T. et al., Applied Physics Letters, 114(10), 102403 (2019). [6] Zahedinejad, M. et al., Nature Nanotechnology, 15(1), 47–52 (2020).

Q4-05. Spin-Orbit Magnetic State Readout in Scaled Ferromagnetic/Heavy Metal Nanostructures. *I. Groen*[1], V. Pham[1], S. Manipatruni[3], W. Choi[1], D. Nikonov[3], E. Sagasta[1], C. Lin[3], T. Gosavi[3], A. Marty[2], L.E. Hueso[1], I. Young[3] and F. Casanova[1] *1. Nanodevices, CIC nanoGUNE BRTA, San sebastian, Spain; 2. 2D and Semiconductor Spintronics, SPINTEC, CEA-INAC/CNRS/Univ. Grenoble, Grenoble, France; 3. Components Research, Intel Corp., Hillsboro, OR, United States*

The efficient detection of a magnetic state at nanoscale dimensions is important for the development of spin logic devices. Magnetoresistance effects can be used to detect magnetic states, but they cannot produce sufficiently large signals when the dimensions of the devices are reduced to the nanoscale, nor do they generate an electromotive force that can be used to drive a circuit element for logic device applications.[1] In this work[2], we report a favorable scaling law for the detection of an in-plane magnetic state of a magnet by using the inverse spin Hall effect in cobalt–iron/platinum ($Co_{50}Fe_{50}$/Pt) nanostructure devices. By reducing the dimensions of the device, we obtain a large spin Hall signal of 0.4 Ω (0.3 Ω) at 10 K (room temperature) (see figure 1a), and quantify an effective spin-to-charge conversion rate for the ferromagnetic/heavy metal nanostructure system (see figure 1b). Finally, we predict that this spin-orbit detection of magnetic states could be used to drive spin logic circuits

[1] S. Manipatruni, D.E. Nikonov, C.C. Lin, *et al*., Nature 565, 35–42 (2019). [2] V.T. Pham*, I. Groen*, S. Manipatruni *et al*., Nat.Electron. 3, 309-315 (2020)

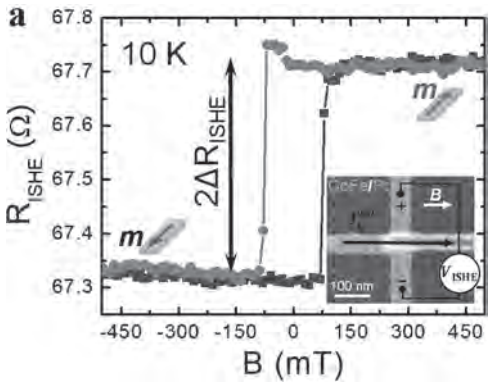

Fig 1a: The magnetic field dependence of the transverse resistance ($R_{ISHE} = V_{ISHE}/ I_c^{app}$) for a minaturizated $Co_{50}Fe_{50}$/Pt nanostructure device at 10 K measured by the configuration shown in the inset. The blue squares and red circles are the trace and retrace of the magnetic field, respectively. The spin Hall signal ($2\Delta R_{ISHE}$), in this devices is 0.4 Ω.

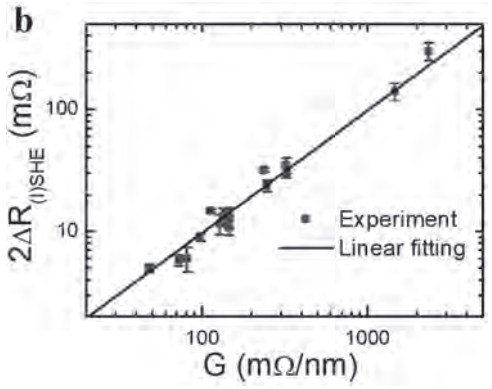

Fig. 1b: The measured spin Hall signals ($2\Delta R_{ISHE}$) at room temperature for $Co_{50}Fe_{50}$/Pt nanostructure devices with different electrode dimensions and resistivities as a function of a "geometrical" factor G [=1/ ($t_{CoFe}/\rho_{CoFe} + t_{Pt}/\rho_t$) w_{Pt}, where t_x, ρ_x and w_x are the thickness, resistivity and width, respectively and x indicates the CoFe and Pt electrodes; blue solid squares]. The black solid line is a linear fit to $2\Delta R_{ISHE} = G$ x $2\lambda_{eff}$ with a slope that correspond to two times the efficiency factor λ_{eff} which for $Co_{50}Fe_{50}$/Pt systems is (0.05±0.01) nm.

Q4-06. Spin Hall Angle Control by Doping Element Into Pt Host.

H. Li[1], *H. Yuasa*[1], T. Yamauchi[1] and Y. Kurokawa[1] *1. Faculty of information Science and Electrical Engineering, Kyushu University, Fukuoka, Japan*

Since it is important to find materials with large spin Hall angles for utilizing spintronic devices, various materials have been reported, e. g. Ir–O, Pt-Cu, $Ta_{50}W_{50}$, and BiSb [1-4]. We investigated the composition effect on spin Seebeck coefficient in YIG/Pt-based alloy systematically, where Pt-based alloy is $Pt_{1-X}Ru_X$, $Pt_{1-X}Cu_X$, and $Pt_{1-X}(Cu_{0.5}Ru_{0.5})_X$. The additive elements of Cu and Ru have equally small spin Hall angles in the single state, whereas they have the different atom sizes. In all systems the composition of around 50 at% showed the maximum spin Seebeck coefficient, from which we estimated spin Hall angles [5, 6]. As a result, the spin Hall angle was increased from 0.1 to 0.19, 0.25, 0.34 by changing Pt to Pt-Ru, Pt-RuCu, and Pt-Cu. It means that additive Cu is more effective on spin Hall angle improvement than additive Ru although their own original spin Hall angles are comparably small. X-ray diffraction analysis revealed that Cu and/or Ru doping in Pt host decreased the unit cell size, and there is an obvious relation between the lattice constant and the spin Hall angle as shown in Fig. 1(a). Since the resistivity dependence on lattice constant exhibit the similar tendency in Fig. 1(b), it suggests that the unit cell size modification in heavy metal Pt layer increases the electron scattering including spin-dependent scattering, leading the extrinsic spin Hall angle enhancement.

[1] K. Fujiwara, Y. Fukuma, J. Matsuno, H. Idzuchi, Y. Niimi, Y. Otani, and H. Takagi, Nat. Commun. 4, 1 (2013). [2] R. Ramaswamy, Y. Wang, M. Elyasi, M. Motapothula, T. Venkatesan, X. Qiu, and H. Yang, Phys. Rev. Appl. 8, 024034 (2017). [3] H. Yuasa, F. Nakata, R.Nakamura and Y. Kurokawa, J. Phys. D: Appl. Phys. 51, 134002 (2018). [4] N. H. D. Khang, Y. Ueda and P. N. Hai, Nat. Mater. 17, 808 (2018). [5] K. Tian and A. Tiwari, Sci. Rep. 9, 1 (2019). [6] H. Li, Y. Kurokawa, T. Niimura, T. Yamauchi, and H. Yuasa, Jpn. J. Appl. Phys. 59, 073001 (2020).

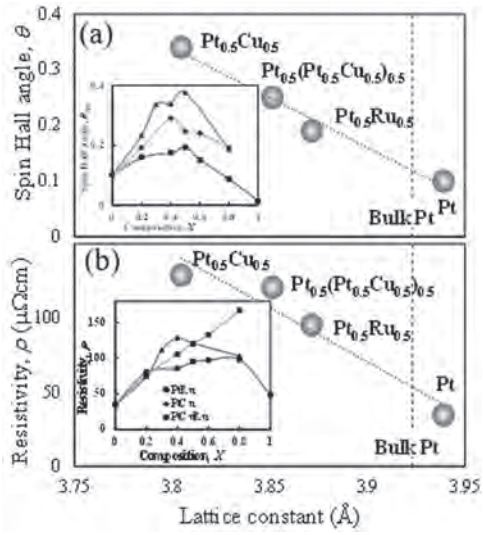

Fig. 1 Resistivity (a) and spin Hall angle (b) dependence on lattice constant of Pt-based alloy. Insets are resistivity and spin Hall angle as a function of composition, *X*.

Q4-07. Current-Induced Switching From the Spin Hall Effect of BiTe.

T. Chen[1], C. Peng[1], H. Yen[1] and C. Pai[1] *1. National Taiwan University, Taipei, Taiwan*

Topological insulators (TIs) have gained many attractions due to its extremely large spin-orbit torque (SOT) efficiency [1]. Unlike conventional heavy metals (HMs) like Ta [2], W [3], and Pt [4] which the SOT efficiencies typically range from 0.1 to 0.3, the TIs can possess SOT efficiency larger than 1. Many works report that this large SOT efficiency in TIs is due to its topologically-protected surface state (TSS), which provides strong spin momentum locking and thus can be effectively used to realize high SOT efficiency [5]. Although the TIs are the potential candidate to replace the HMs into the magnetic random access memory (MRAM) device, the complicate fabrication process for such materials systems in a well-texture crystalline phase is still a challenging task. In this work, we use conventional magnetron sputtering to deposit Bi_xTe_{1-x}/ferromagnet heterostructures. To estimate the DL-SOT efficiency, we perform the harmonic voltage measurement [6] and the hysteresis loop shift measurement [7]. The DL-SOT efficiency from the sputtered chalcogenide can reach values greater than 100% at room temperature even without the TSS, and it is originated from the bulk spin-orbit interactions of such non-epitaxial heterostructures. The current-induced SOT switching in these Bi_xTe_{1-x}-based heterostructures with thermally stable ferromagnetic layers is also demonstrated, which indicates that such non-epitaxial chalcogenide materials can be potential efficient SOT sources in future SOT magnetic memory devices.

[1] Y. Wang, P. Deorani, K. Banerjee, N. Koirala, M. Brahlek, S. Oh, and H. Yang, Phys. Rev. Lett. 114, 257202 (2015). [2] L. Q. Liu, C.-F. Pai, Y. Li, H. W. Tseng, D. C. Ralph, and R. A. Buhrman, Science 336, 555 (2012). [3] C.-F. Pai, L. Q. Liu, Y. Li, H. W. Tseng, D. C. Ralph, and R. A. Buhrman,

Appl. Phys. Lett. 101, 122404 (2012). [4] L. Q. Liu, T. Moriyama, D. C. Ralph, and R. A. Buhrman, Phys. Rev. Lett. 106, 036601 (2011). [5] J. E. Moore, Nature 464, 194 (2010). [6] J. Kim, J. Sinha, M. Hayashi, M. Yamanouchi, S. Fukami, T. Suzuki, S. Mitani, and H. Ohno, Nat. Mater. 12, 240 (2012). [7] C. F. Pai, M. Mann, A. J. Tan, and G. S. D. Beach, Phys. Rev. B 93, 144409 (2016).

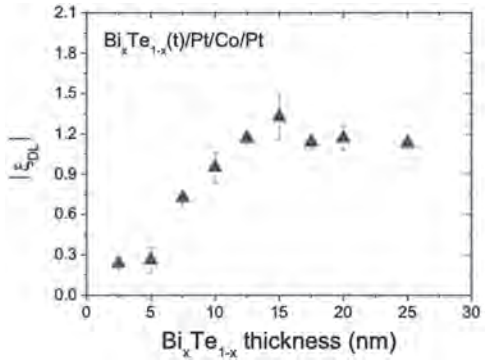

Figure1. Bi_xTe_{1-x} thickness dependence of DL-SOT efficiency for Bi_xTe_{1-x}-based heterostructures.

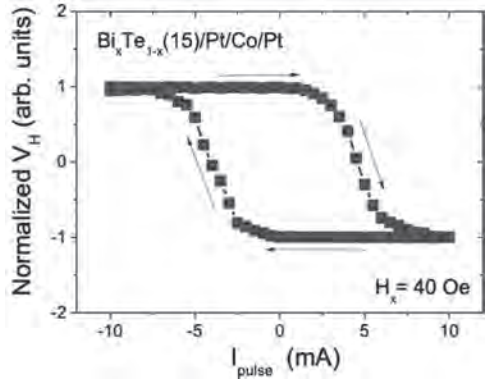

Figure 2. Representative current-induced switching loops of Bi_xTe_{1-x}(15)/Pt/Co/Pt Hall bar device.

Q4-08. Large Improvement on Spin-Orbit Torque Switching Efficiency in Pt-Cu Alloy. *C. Hu*[1] and C. Pai[1] *1. Materials Science and Engineering, National Taiwan University, Taipei, Taiwan*

Spin-orbit torque (SOT) provides a way to effectively manipulate magnetization in nanoscale, and plays a key role in spin-orbit torque magnetic random-access memories (SOT-MRAM), which is an attractive candidate in future memories industries due to its fast operation speed and energy efficiency. To make SOT-MRAM more competitive than other emerging memories, a material system simultaneously with large SOT switching efficiency, good thermal stability, and low power consumption is significant to ensure the performance, endurance, energy efficiency of the memory device, respectively. In this research, we report a significant improvement in the spin-orbit torque switching efficiency of Pt-Cu alloy in Pt_xCu_{1-x}/Co/MgO magnetic heterostructure with perpendicular magnetic anisotropy (PMA). The largest damping-like spin-orbit torque (DL-SOT) efficiency of Pt-Cu alloy, as determined by hysteresis loop shift measurements, is about 0.44, which is almost three times the value from pure Pt based on our control experiments. Moreover, we then confirm the large DL-SOT efficiency of Pt-Cu alloy by current-induced magnetization switching measurements. The thermal stability of the Co layer is unaffected under alloying of the Pt layer. A lower critical switching current density in Pt-Cu-based devices is reached by proper alloying due to the simultaneous enhancement of spin-orbit torque efficiency and reduction of coercivity of the Co layer. The lowest critical switching current density in the Pt-Cu alloy layer is about 2.4×10^6 A/cm^2, which is much lower than 3.4×10^7 A/cm^2 of pure Pt in our control experiments. Furthermore, due to large DL-SOT efficiency and moderate resistivity of Pt-Cu alloy, the power consumption reduces from 1.6×10^{13} mW/cm^3 (pure Pt) to 4.6×10^{11} mW/cm^3 (Pt-Cu alloy). Due to the observed large DL-SOT efficiency, low power consumption, and moderate thermal stability in Pt_xCu_{1-x}/Co/MgO magnetic heterostructure, Pt-Cu alloy is suggested to be an attractive SOT source for the future SOT-MRAM applications.

Miron, I. M., Garello, K., Gaudin, G., Nature, 476.7359, p.189-193. (2011) Liu, L., Lee, O. J., Gudmundsen, T. J., Physical Review Letters, 109, 096602. (2012) Pai, C. F., Mann, M., Tan, A. J., Physical Review B, 93, 144409. (2016)

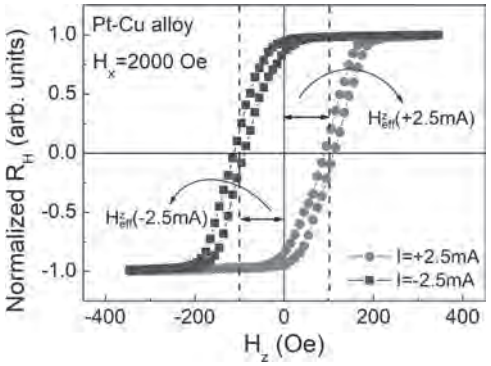

representative hysteresis loop shift results of a $Pt_{0.57}Cu_{0.43}$-based device

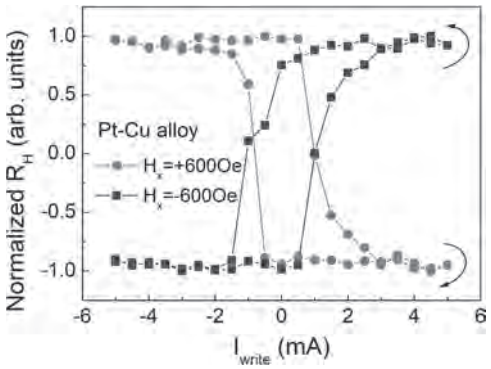

representative current-induced magnetization loops of a $Pt_{0.57}Cu_{0.43}$-based device

Q4-09. Manipulation of Coupling and Magnon Transport in Magnetic Metal-Insulator Hybrid Structures. *Y. Fan*[1], P. Quarterman[2], J. Finley[1], J. Han[1], P. Zhang[1], J.T. Hou[1], M.D. Stiles[3], A.J. Grutter[2] and L. Liu[1] *1. EECS, Massachusetts Institute of Technology, Cambridge, MA, United States; 2. NIST Center for Neutron Research, National Institute of Standards and Technology, Gaithersburg, MD, United States; 3. Physical Measurement Laboratory, National Institute of Standards and Technology, Gaithersburg, MD, United States*

Ferromagnetic metals and insulators are widely used for generation, control, and detection of magnon spin signals. Most magnonic structures are based primarily on either magnetic insulators or ferromagnetic metals, while heterostructures integrating both are less explored. Here, by introducing a Pt/yttrium iron garnet (YIG)/permalloy (Py) hybrid structure grown on Si substrate, we studied the magnetic coupling and magnon transmission across the interface of the two magnetic layers [1]. Interestingly, we found the YIG and the Py layers show antiferromagnetic coupling when external field is small, and the two layers align to the same direction only when the in-pane field is above 150 mT, as evidenced by both vibrating-sample magnetometry and polarized neutron reflectometry measurements. More importantly, the parallel and antiparallel magnetization configurations in this YIG/Py structure

could be utilized to control magnon spin flow in spin-pumping and spin Seebeck experiments. In Figure 1(a) and 1(b), we schematically illustrate the effect of magnetization configuration (antiparallel vs parallel) on the magnon current transmission efficiency across the two magnetic layers' interface. In the spin-pumping experiment, as plotted in Figure 1(c), we demonstrate that a magnon spin-valve device with an ON/OFF ratio of ~130% can be realized out of this multilayer structure at room temperature. Owing to the efficient control of magnon current and the compatibility with Si technology, the Pt/YIG/Py hybrid structure could potentially find applications in magnon-based logic and memory devices.

[1] Yabin Fan, P. Quaterman *et al.*, Phys. Rev. Appl. 13, 061002 (2020).

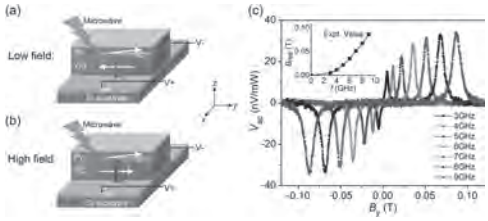

Fig. 1. Schematic of the Py spin-pumping process when the Py and the YIG magnetization are in the antiparallel (a) and parallel (b) configurations under the low-field and high-field regimes, respectively. (c) Spin-pumping voltages measured from the ISHE in the Pt layer when the Py magnetization is excited to ferromagnetic resonance by external rf field in the Si/Pt(10)/YIG(40)/Py(20)/Ru(3) (unit in nm) hybrid structure. Inset: resonance field versus frequency.

Q4-10. Spintronic GdFe/Pt THz Emitters. *R. Schneider*[1], M. Fix[2], J. Bensmann[1], S. Michaelis de Vasconcellos[1], M. Albrecht[2] and R. Bratschitsch[1] *1. Institute of Physics and Center for Nanotechnology, University of Münster, Münster, Germany; 2. Institute of Physics, University of Augsburg, Augsburg, Germany*

Spintronic THz emitters have attracted a lot of attention due to their high power, broadband and gapless emission as well as easy fabrication and handling [1, 2]. However, the microscopic mechanism governing the THz emission, especially for complex magnetic layers, is presently not fully understood and limits their optimization. We perform a systematic study of the THz emission of a series of spintronic bilayers based on thin films of platinum (Pt) and ferrimagnetic gadolinium-iron (Gd_xFe_{1-x}) alloys, covering the entire concentration range of Gd ($0 \le x \le 1$). We find that the THz emission amplitude is closely governed by the in-plane magnetization of the samples and dominated by the 3d electrons of iron, which is in agreement with previously investigated THz emitters based on terbium-iron alloys [3, 4]. As a consequence, samples below and above the magnetic compensation point show inverted THz waveforms (fig. 1). Furthermore, we model the composition-dependent THz amplitudes considering the iron content, the THz electrical conductivity as well as the alignment of the magnetic moments, which is approximated by the ratio of the in-plane magnetization in the THz emission experiment and the saturation magnetization. The model yields excellent agreement up to a Gd content $x \le 0.4$ for all applied external magnetic fields and is even valid close to the magnetic compensation point (fig. 2). Our systematic study reveals design rules for optimized spintronic THz emitters and demonstrates that time resolved THz emission spectroscopy is a powerful tool for gaining deep insights into complex magnetic systems und ultrafast spin transport processes.

[1] T. Seifert, S. Jaiswal, U. Martens, *et al.*, Nature Photonics 10, 483 (2016)
[2] D. Yang, J. Liang, C. Zhou, *et al.*, Adv. Optical Mater. 4, 1944 (2016)
[3] R. Schneider, M. Fix, R. Heming, *et al.*, ACS Photonics 5, 3936 (2018)
[4] R. Schneider, M. Fix, J. Bensmann, *et al.*, Appl. Phys. Lett. 115, 152401 (2019)

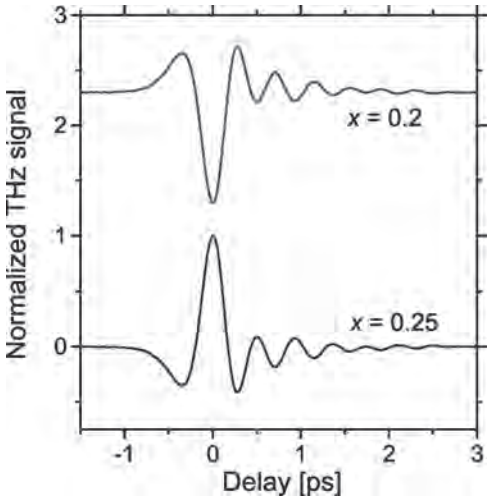

Figure 1: Measured transient THz electric fields for $Gd_{0.2}Fe_{0.8}$/Pt (green) and $Gd_{0.25}Fe_{0.75}$/Pt (blue). The THz waveform for $Gd_{0.25}Fe_{0.75}$/Pt is inverted compared to $Gd_{0.2}Fe_{0.8}$/Pt.

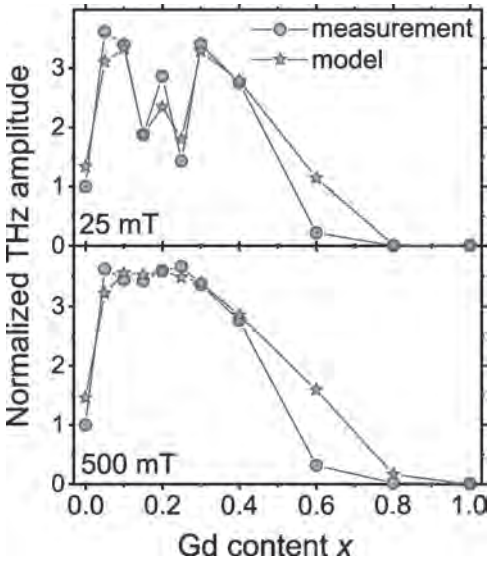

Figure 2: Measured (blue circles) and modeled (red stars) THz amplitudes as a function of the Gd content *x* for an externally applied in-plane field of 25 mT (upper graph) and 500 mT (lower graph).

Q4-11. Room-Temperature non-Volatile Ferroelectric Control of Spin Hall Effect in the Semiconductor GeTe. S. Varotto[1], L. Nessi[1], S. Cecchi[2], J. Slawinska[3], P. Noël[5], S. Petrò[1], A. Novati[1], M. Cantoni[1], M. Costa[7], R. Calarco[8], M. Buongiorno Nardelli[3], M. Bibes[6], S. Picozzi[4], J. Attané[5], L. Vila[5], R. Bertacco[1] and *C. Rinaldi*[1] *1. Physics, Politecnico di Milano, Milano, Italy; 2. Epitaxy, Paul-Drude-Institut fur Festkorperelektronik, Berlin, Germany; 3. Physics, University of North Texas, Denton, TX, United States; 4. Consiglio Nazionale delle Ricerche - CNR-SPIN, Chieti, Italy; 5. Grenoble Alpes, CEA, CNRS Grenoble INPUniversity, Grenoble, France; 6. CNRS Thales, Thales, France; 7. Physics, Fluminense Federal University, Rio de Janeiro, Brazil; 8. Consiglio Nazionale delle Ricerche, CNR-IMM, Roma, Italy*

Semiconductor spintronics has traditionally suffered the need for suitable spin injectors and detectors. The typical solution of combining ferromagnets with semiconductors collided with materials compatibility and found the major obstacle of the impedance mismatch issue. In this context, the recently discovered class of ferroelectric Rashba semiconductors (FERSC) is

emerging as an exciting road for the development of semiconductor devices operating based on spin and integrating a memory function. Indeed, FERSC are relativistic semiconductors whose bulk spin texture is intimately linked to the direction of the ferroelectric polarization; thus, the spin degrees of freedom could be controlled by the electric field in a non-volatile way [1, 2]. While the properties of FERSC could allow for the integration of spin generation, manipulation, and detection in one semiconductor, their potential has not yet been explored. Here we demonstrate a switchable spin-to-charge conversion in GeTe thin films at room temperature. First, we show that the polar distortion can survive the p-type doping of GeTe. Robust control of the ferroelectric polarization through electrical gating is achieved. Then, by spin pumping experiments in Fe/GeTe heterostructures [3, 4], we demonstrate the ferroelectric control of the spin-to-charge conversion, whose efficiency is comparable to that of reference heavy metals like Pt. First-principle calculations suggest spin Hall effect [5] as the leading mechanism for such interconversion and reveal that the sign of the spin Hall conductivity can be inverted by the electric polarization. While the non-volatile control of spin-to-charge conversion has been recently shown in 2DEG generated in ferroelectric $SrTiO_3$ [6], GeTe offers a different spin-charge interconversion mechanism that relies on its robust bulk band structure, room-temperature operations, endurance, CMOS compatibility, low voltage operations as well as fast ferroelectric switching. These results indicate novel opportunities to design all-in-one spintronics devices that could perform non-volatile logic-in-memory operations without the use of magnetic fields. Acknowledgments. CR acknowledges the project TWEET, grant no. 2017YCTB59 by MIUR.

[1] D. Di Sante *et al.*, Adv. Mater., 25, 509 (2013). [2] C. Rinaldi *et al.*, Nano Letters, 18, 2751 (2018). [3] C. Rinaldi *et al.*, APL Mater. 4, 032501 (2016). [4] J. Slawinska *et al.*, Physical Review B 99 075306 (2019). [5] H. Wang *et al.,* npj Comput. Mater. 6, 7 (2020). [6] P. Nõel *et al.*, Nature 580, 483-486 (2020).

Session Q5
BIOMEDICAL APPLICATIONS IV
(Poster Session)

Horia Chiriac, Chair
National Institute of Research and Development for Technical Physics, Iasi, Romania

Q5-01. Investigation of a Coupled Elasto-Magnetic Discs for Low Reynolds Number Pumps. *E.L. Martin*[1], M.T. Bryan[2], A. Pac[1], A.D. Gilbert[1] and F. Ogrin[1] *1. The College of Engineering, Mathematics and Physical Sciences, University of Exeter, Exeter, United Kingdom; 2. Department of Electronic Engineering, University of London Royal Holloway, Egham, United Kingdom*

The focus of lab-on-a-chip technology centers on small, low power devices that can be integrated on a microscopic scale to perform laboratory functions within one unit or "chip". In order to achieve this, one has to understand how to transfer fluid at this scale. Due to the low Reynolds number limit, such devices need to break time-reversible symmetry to produce a net flow. There has been a degree of interest and research into using magnetic materials to achieve this. In this work, we propose a new model employing ferromagnetic elements for construction of a practical microfluidic pump. The design is based on a repeated chain of magnetic discs connected together via links with hinges at the centers of the discs, which allow the discs to rotate (Fig 1a). While the model is based on that of ferromagnetic swimmers[1]. The device is surrounded by fluid and is activated by an external AC magnetic field. The magnetic and elastic forces in this device can work together against the fluidic forces to create a time-irreversible movement, which results in a net flow. While magnetisation of all the discs are oriented in the same direction, the relative rotational stiffness of the discs (or hinge stiffness) is varied to produce a lag in the response to the magnetic torque. This collective effect is similar to that of a metachronal wave, which is ultimately responsible for the flow. We found that if both discs had the same rotational stiffness, then no flow was produced. Depending on the chosen frequency, there is an optimal rotation stiffness of the two discs where a maximum flow rate is achieved. We observed as the frequency increases so does the flow, until the frequency is too large for the discs to turn to their maximum angle before the direction of the magnetic field reverses. To conclude, we demonstrated that an elasto-magnetic device can produce a net flow at low Reynolds number. The flow direction can be controlled by altering the frequency of the driving magnetic field or by using different rotational stiffness. These results could lead to new types of ferromagnetic pumping devices.

[1] A. D. Gilbert, et al., Q. J. Mech. Appl. Math., 64, 239 (2011).

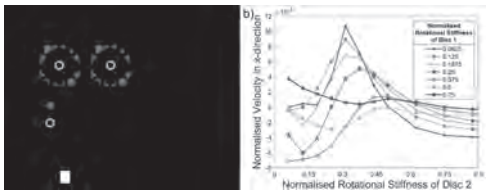

Fig. 1. (a) A diagram representing the model setup; (b) The dependence of the fluid velocity on the rotational stiffness of the discs.

Q5-02. Optimization of Transcranial Magnetic Stimulator Coil Using Stream Function for Reducing the Influence of Individual Variabilities of Head Geometry. *S. Liu*[1], H. Yoshioka[1], A. Kuwahata[1] and M. Sekino[1] *1. Department of Electrical Engineering and Information Systems, Graduate School of Engineering, The University of Tokyo, Bunkyo-ku, Japan*

Introduction: Transcranial magnetic stimulation (TMS) is an emerging method for depression and neuropathic pain therapy with a painless and noninvasive neuromodulation function [1]. The winding path of the TMS coil can be realized in several ways [2]. For instance, the H1 coil is designed for deep brain stimulation [3], the "hat-like" coil is designed to suppress temperature rise during stimulation [4], and the fdTMS coil comprehensively considers energy, depth, and focality [5]. However, a practical TMS coil satisfying both high energy efficiency and robustness against individual variabilities in head shape has not yet been realized. Purpose: To optimize an energy-efficient TMS coil that is robust against individual differences in head shape. Methods: The optimization scheme is shown in Fig. 1. Multiple MRI anatomical images are used to optimize the shape to facilitate fitting of the scalp at the target stimulation position. Subsequently, the winding path of this shape is optimized through the following steps. First, the forward model $E=A\Psi$ for the scalar stream function Ψ and target-induced electric field E is established. Second, the Tikhonov regularization is used to solve the stream function Ψ numerically, given E. Finally, the coil winding path is extracted from the contour lines of Ψ [4]. This coil was compared with two commercial TMS coils by simulating the eddy current distribution in the digital brain model. Result: The results are shown in Fig. 2. Under the same energy consumption condition, compared with planar fig-8 and butterfly coils, this "head-fit" coil has stimulus area increases of 87% and 67%, respectively, with the corresponding efficiency drops of only 2% and 3%. The expansion of the stimulation area indicates that stimulation to the target area can be ensured even with a slight movement of the head during ~30min treatment. Furthermore, considering the shape of the scalp of different subjects facilitates close fitting of the head. Conclusion: Our method allows the design of TMS coils suitable for practical TMS therapy.

[1] J. P. Lefaucheur *et al.*, "Evidence-based guidelines on the therapeutic use of repetitive transcranial magnetic stimulation (rTMS)," *Clin. Neurophysiol.*, vol. 125, no. 11. Elsevier Ireland Ltd, pp. 2150–2206, 2014. [2] Z. De Deng, S. H. Lisanby, and A. V. Peterchev, "Electric field depth-focality tradeoff in transcranial magnetic stimulation: Simulation comparison of 50 coil designs," *Brain Stimul.*, vol. 6, no. 1, pp. 1–13, Jan. 2013. [3] H. M. Gellersen and K. K. Kedzior, "Antidepressant outcomes of high-frequency repetitive transcranial magnetic stimulation (rTMS) with F8-coil and deep transcranial magnetic stimulation (DTMS) with H1-coil in major depression: a systematic review and meta-analysis," *BMC Psychiatry*, vol. 19, no. 1, pp. 139, 2019. [4] L. M. Koponen, J. O. Nieminen, and R. J. Ilmoniemi, "Coil optimisation for transcranial magnetic stimulation in realistic head geometry," *Brain Stimul.*, vol. 10, no. 4, pp. 795–805, 2017. [5] L. J. Gomez, S. M. Goetz, and A. V. Peterchev, "Design of transcranial magnetic stimulation coils with optimal trade-off between depth, focality, and energy," *J. Neural Eng.*, vol. 15, no. 4, pp. 1–31, 2018. [6] G. N. Peeren, "Stream function approach for determining optimal surface currents," *J. Comput. Phys.*, vol. 191, no. 1, pp. 305–321, 2003.

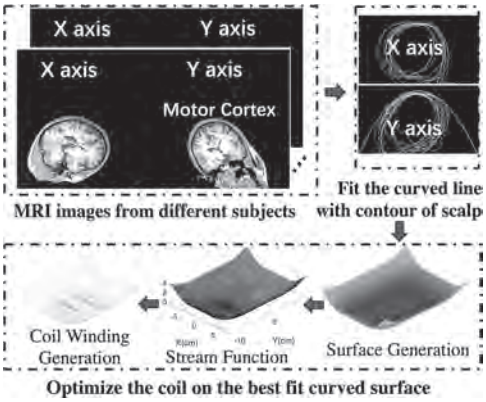

Schematic for the optimization of the TMS coils using stream function

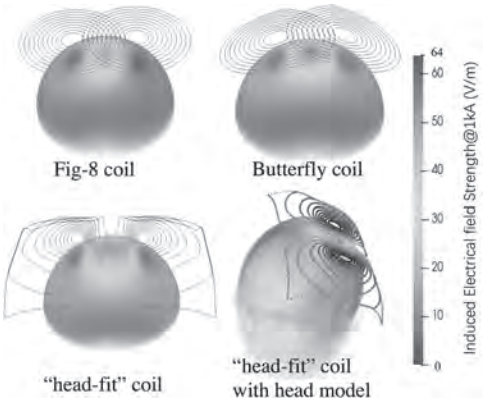

Simulation result on the hemisphere model for the fig-8 coil, butterfly coil, and the "head-fit" coil @ 1 kA

Q5-03. Fe-Cr-Nb-B Magnetic Particles and STEM Cells, Triggers for Cancer Cells Apoptosis by Magneto-Mechanical Actuation. *H. Chiriac*[1], A. Minuti[1,2], C. Stavila[1,2], L. Labusca[1], D. Herea[1] and N. Lupu[1] *1. Magnetic Materials and Devices, National Institute of Research and Development for Technical Physics, Iasi, Romania; 2. Faculty of Physics, "Alexandru Ioan Cuza" University, Iasi, Romania*

Recently, we have introduced a new type of magnetic particles (MPs), prepared by wet milling of superferromagnetic Fe-Cr-Nb-B precursor glassy ribbons, for cancer treatment by magneto-mechanical actuation in low magnetic fields (1÷20 Oe) [1]. In this work we studied the possibility of using adipose derived stem cells (ADSCs) for the transport of Fe-Cr-Nb-B MPs to areas with MG-63 human osteosarcoma (HOS), and the effect of MPs incorporated into ADSCs on the viability of HOS following the magneto-mechanical actuation of MPs with dimensions between 5 and 100 nm. The viability tests performed 24 hours after the magneto-mechanical actuation by MTT assay indicated values of 24÷25% for HOS and up to 10% for ADSCs. We also investigated the capacity of ADSCs to incorporate Fe-Cr-Nb-B MPs, and we found that large amounts of MPs were ingested as confirmed by a colorimetric ferrozine-based assay that quantitatively evaluates the Fe content in cells. We used a time-lapse cell imaging method to record the cellular migration of ADSCs loaded with MPs towards tumor cells *in vitro*. The recorded films demonstrated that MPs-loaded ADSCs were able to target osteosarcoma cells. We performed *in vitro* tests, where ADSCs were incubated with Fe-Cr-Nb-B MPs, then transferred onto an osteosarcoma cell culture and exposed to the rotating magnetic field. Magneto-mechanical actuation led to the destruction of ADSCs and to the release of MPs on HOS culture, which incorporated the released MPs. By magneto-mechanic actuation, the HOS viability dropped down to 21÷22%. The irregular shape of the MPs combined with their rotational motion in the rotating magnetic field produce irreversible damages on the cells membranes and organelles, and, subsequently, the cells death. *Work supported by the Nucleu Programme (Project PN 19 28 01 01) and Contract No. 11PFE/16.10.2018 financed by the Romanian Ministry of Education and Research.)*

[1] H. Chiriac, E. Radu, M. Tibu, *et al.*, *Sci. Rep.* 8 (2018) 11538.

Q5-04. Co/Pd-Based Synthetic Antiferromagnetic Multi-Stacks for Biomedical Applications. *G. Varvaro*[1], S. Laureti[1], M. Hassan[1,3], D. Peddis[2,1], G. Barucca[3], P. Mengucci[3], A. Gerardino[4], E. Giovine[4], O. Lik[5] and M. Albrecht[5] *1. Institute of Structure of Matter, Consiglio Nazionale delle Ricerche, Roma, Italy; 2. DCCI, Universita degli Studi di Genova, Genova, Italy; 3. SIMAU, Universita Politecnica delle Marche, Ancona, Italy; 4. Istituto di Fotonica e Nanotecnologie, Consiglio Nazionale delle Ricerche, Roma, Italy; 5. Institute of Physics, Universitat Augsburg, Augsburg, Germany*

Mesoscale magnetic particles (from few nanometers to microns) are a major class of materials with the potential to revolutionize current clinical diagnostic and therapeutic techniques. They are commonly fabricated by bottom-up chemical methods; however, recent studies have demonstrated that top-down approaches based on techniques developed for micro/nano electronics can be used to fabricate monodisperse magnetic micro/nanoparticles with a complex structure and shape that are hard to obtain by means of chemical routes [1,2]. In this work, thin film stacks consisting of multiple repeats M of single $[Co/Pd]_N/Ru/[Co/Pd]_N$ units with antiferromagnetic coupling and perpendicular magnetic anisotropy were investigated and exploited as a potential starting material to fabricate free-standing synthetic antiferromagnetic microdisks [3]. For this purpose, films were directly grown on a sacrificial optical resist layer (AZ5214) spinned on a thermally oxidized Si substrate, which would serve to obtain free-standing particles after its dissolution. Furthermore, the film stack is sandwiched between two Au layers to allow further bio-functionalization. The samples fulfill all the key criteria required for biomedical applications up to M = 6, i.e., zero remanence, zero field susceptibility at small fields and sharp switching to saturation, together with the ability to vary the total magnetic moment (by changing the number of repetitions of the multi-stack) without significantly affecting any other magnetic features (Figure 1 left). Moreover, the samples show a strong perpendicular magnetic anisotropy, which is required for applications relying on the transduction of a mechanical force through the particles under an external magnetic field, such as the mechanical cell disruption, which is nowadays considered as promising alternative to the more investigated magnetic hyperthermia approach for cancer treatment [4]. Preliminary results on microdisks (M = 5, diameter: 2 μm, pitch: 4 μm) obtained from the continuous multistacks by combing electron beam lithography and Ar ion milling are also discussed (Figure 1 right).

[1] T. Vemulkar et al., Appl. Phys. Lett., Vol. 110, p. 042402 (2017) [2] J.G. Gibbs et al., Nanoscale, Vol. 6, p. 9457 (2014) [3] G. Varvaro et al., Nanoscale, Vol. 11, p. 21891 (2019) [4] Y. Cheng et al., J. Contr. Rel., Vol. 223, p. 75 (2016)

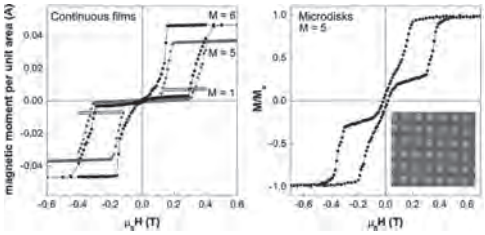

Figure 1. Room temperature out-of-plane hysteresis loops of SAF multistacks.

Q5-05. Withdrawn

Q5-06. A Two-Dimensional Magnetic Gripper Robot Driven by a Triad of Electromagnetic Coils. *H. Lee*[1], D. Yang[1], K. Lee[1] and S. Jeon[1]
1. Mechanical and Automotive Engineering, Kongju National University, Gongju, The Republic of Korea

Magnetically actuated micro- or milli-scale gripper robots have been widely studied as a promising means to manipulate a variety of small objects, such as biological cells, medical drugs, and other functional materials, in an untethered and uncontaminated manner [1-3]. In this research, we propose a magnetic gripper robot (MGR) composed of a simple flexible body with three permanent magnets inserted into different parts of the body (Fig. 1). A cube magnet is fixed into the base of the flexible body, whereas two freely rotatable cylindrical magnets are inserted into each gripper arm of the body. Without an external magnetic field, the two cylindrical magnets in the gripper arm tend to align in the same lateral direction, which can make the MGR form a closed posture due to the attractive magnetic force. Under a specific magnetic field, on the other hand, the two magnets may align into a vertical direction parallel to the fixed magnet, in which the MGR can make an open posture due to the repulsive magnetic force. In this research, we derived an equation that can calculate the equilibrium postures of the MGR's magnets under an external magnetic field and the corresponding structural deformation of the flexible body by using the MGR's magnetic and elastic potential energy (Fig. 1). From this equation, we could establish a method to generate the MGR's gripper motions and its two-dimensional (2D) translational motion at the same time by using an efficient coil system comprised of only a triad of electromagnetic coils (TEC) shown in Fig. 2a [4]. We then fabricated a prototype MGR and a TEC to demonstrate the proposed MGR's gripper motions such as the pick-and-place motions shown in Fig. 2. The results showed that the proposed MGR could play a role as an effective untethered gripper which can be utilized for various biomedical purposes such as cell manipulation, drug delivery, biopsy, etc.

[1] T. R. Ger, H. T. Huang, W. Y. Chen, and M. F. Lai, Lab on a Chip, Vol. 13, p. 2364-2369 (2013) [2] E. Diller and M. Sitti, Advanced Functional Materials, Vol. 24, p. 4397-4404 (2014) [3] T. Xu, J. Zhang, M. Salehizadeh, O. Onaizah, E. Diller, Science Robotics, Vol. 4 (2019) [4] H. J. Lee and S. M. Jeon, AIP Advances, Vol. 10 (2020)

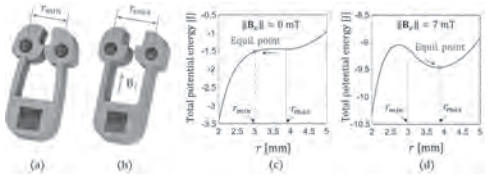

Fig. 1 Schematic views of the proposed MGR's (a) closed and (b) open equilibrium postures. (c) and (d) show examples of the two postures' potential energy calculated using the prototype MGR shown in Fig. 2.

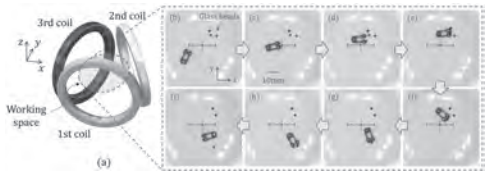

Fig. 2 (a) Schematic view of the TEC. (b)-(i) Sequential images of a prototype MGR's pick-and-place motions in a horizontal plane.

Q5-07. Influence of Magnetic Nanoparticles on Cells of Ehrlich Ascites Carcinoma. *S. Stolyar*[1,3], O. Kryukova[1], R. Yaroslavtsev[1,3] and N. Latyshev[2] *1. Krasnoyarsk Scientific Center, Krasnoyarsk, Russian Federation; 2. Siberian Federal University, Krasnoarsk, Russian Federation; 3. Kirensky Institute of Physics, Krasnoyarsk, Russian Federation*

Due to the biological compatibility of iron, nanoparticles of oxides (oxyhydroxides) based on it are used in various biomedical applications: preparations for iron anemia, contrast agents for magnetic resonance imaging, drug delivery. Magnetic iron oxide nanoparticles can affect the phagocytic activity of macrophages, the yield of nitric oxide (NO) and reactive oxygen species [1]. Nitric oxide is capable of both stimulating the growth of tumor cells and exerting a cytotoxic effect [2]. NO in cells and tissues can form paramagnetic dinitrosyl iron complexes (DNIC), which are reliably recorded by EPR. Nanoparticles were synthesized by precipitation with a solution of ammonium hydroxide under conditions of ultrasonic cavitation. The results of a high-resolution transmission electron microscopy study of iron oxide nanoparticles are shown in Figure 1. The average particle size is ~ 2 nm. According to the diffraction image, the nanoparticles are ferrihydrite. Figure 2 shows the spectra of ferromagnetic resonance measured in the temperature range from 120 to 360 K. The values of the resonance fields of the FMR monotonically increased from 3320 Oe to 3380 Oe in the studied temperature range. To assess the biological activity of the nanoparticles, incubation of Ehrlich ascites carcinoma (EAC) cells with nanoparticles was performed and the EPR spectra of the samples were analyzed. The death of EAC cells is associated with an increase in the NO concentration. A unique feature of EAC cells is that they are capable of producing nitric oxide, which is associated with their defense mechanisms from the immune system [3]. The cultivation of EAC cells with magnetic particles increases the yield of nitric oxide NO. Higher concentrations of NO and reactive nitrogen species (RNS) lead to reactions that cause DNA damage and the activation of various transcription factors. Due to this, for example, p53 protein expression can increase, causing cell death.

1. Zhaoming Guo, Ye Liu, Hao Zhou. Colloids and Surfaces B: Biointerfaces, V.184, pp.1–36 (2019) 2. Vanin A.F., Chetverikov A.G. Biophysics, V.13, p. 608-615 (1968) 3. A. Aikemu, X. Xiaerfuding, C. Shiwenhui, Oharmacogn Mag., V. 9, p. 187–191 (2013)

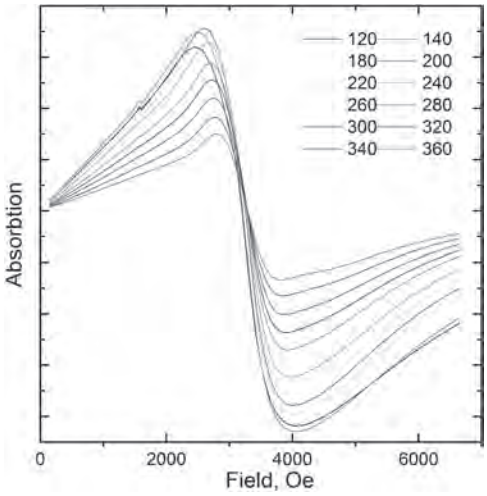

Q5-08. Towards Next-Generation Nerve Repair: Effects of Static Magnetic Field on Neurite Extensions. *X. Zhang*[1], C. Mills[2], Y. Hua[2], R. Koppes[2], R. Pérez del Real[3], M. Vazquez[3], A. Koppes[2] and L. Lewis[1,2]
1. Mechanical and Industrial Engineering, Northeastern University, Boston, MA, United States; 2. Chemical Engineering, Northeastern University, Boston, MA, United States; 3. Instituto de Ciencia de Materiales de Madrid, CSIC, Madrid, Spain

Injuries to the peripheral nervous system, which is a network of nerves that connect the brain and spinal cord to the entire human body, affect millions of people worldwide each year[1]. Modern nerve repair often relies on nerve regeneration, which is sensitive to topographical, chemical, and electromagnetic stimuli. This current work considers the effect of passive and directed static magnetic fields, a stimulus that has not been extensively explored, on neurite outgrowth. Magnetic stimulation was applied to neuron cells, using an apparatus developed with Ansys simulation software (Electromagnetics Suite)[2], to deliver a quasi-uniform magnetic field of up to 500 G (0.05 T) near the cell growth area. This apparatus employed a pair of axially magnetized Nd-Fe-B magnets joined by two electrical steel flux closure paths and was placed ~1 mm below cell culture well plates, Fig. 1. The magnetic field magnitude and direction near the neurons were varied by adjusting the inter-magnet distance within the apparatus. Dorsal root ganglia (DRG) neurons were cultured for three consecutive days, with one hour of magnetic field exposure per day, under controlled conditions in an incubator. Neurite outgrowth of stimulated DRGs, with a minimum of six replicates, was compared with that of unstimulated controls, for three separate experiments. Preliminary results were dramatic: data derived from immunocytochemistry and image analysis with MATLAB revealed that the magnetic field application increased the overall neurite outgrowth volume by up to 152% (± 115%) compared to unstimulated controls, Fig. 2. Future investigations involve employment of meshes of magnetized glass-coated amorphous magnetic microwires[3] as a cell growth substrate, providing a potentially enhanced magnetic field effect combined with topographical guidance to further enhance neurite extensions. Acknowledgments: Fulbright Scholar Program, i-Link A20074 (CSIC) project, Northeastern University, and ICMM/CSIC, Spain

1. A.N. Koppes, et al., J. neural eng., vol.11(4), 046002 (2014) 2. Ansys® Electromagnetics Suite, Release 17.2.0, ANSYS, Inc. 3. M. Vázquez, Handbook of Magnetism and Advanced Magnetic Materials, John Wiley, vol.4, p.2192-2222 (2007)

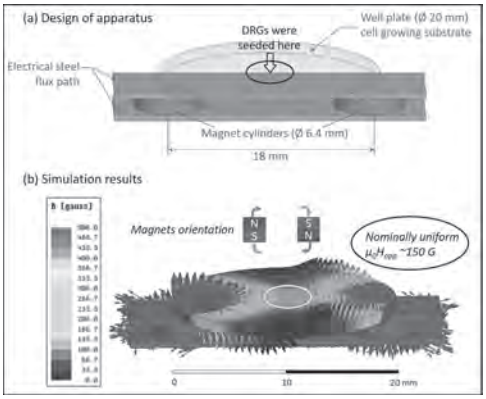

Fig.1. (a) The magnetic apparatus constructed to apply magnetic fields to neurons; (b) simulation of B-field induced by the apparatus

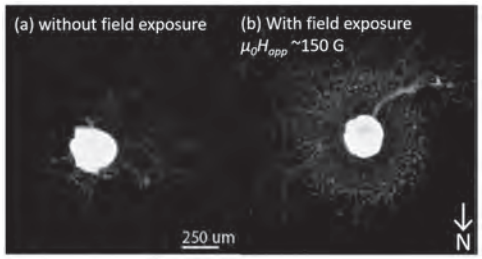

Fig. 2. Representative immunofluorescent images show that magnetic field stimulation promotes the overall neurite outgrowth.

Q5-09. Study on the Acid-Base Balance in Blood Under Pulsed Magnetic Field Using Magnetic Beads. *S. Bang*[1] and H. Lee[1] *1. Oriental Biomedical Engineering, Sangji University, Wonju, The Republic of Korea*

The blood's acid-base balance is precisely controlled because even a minor deviation from the normal range can severely affect many organs. Due to Warburg effect, in tumor cells, an imbalance between oxygen supply and consumption, and accumulation of lactate cause increasing the concentration of H+. As a consequence, intracellular pH decreases, resulting in acidity. Since the pulsed magnetic field (PMF) influences human physiology, many studies have been reported its effect on anti-nociception as well as improvement of blood circulation[1-2]. Our study has tried to investigate the influence of PMF on blood's acid-base balance in microvascular channels. In addition, the applicability of PMF to H+ pump inhibitor in tumor cells was evaluated using negatively- charged magnetic beads(MB). Tert-butyl hydroperoxide (tBHP) was used to oxidizing agents, in order to make acidic environment similar to tumor cells. All experiments were done with red blood cells(RBCs) and plasma suspension with hematocrit (Ht) of 45%. Our PMF stimulator has the maximum intensity of 0.27T at a transition time of 102 μs with pulse intervals of 1Hz. The changes in pH of blood and the number of RBCs with MB attached were examined before and after PMF stimulus. The blood treated with tBHP on RBCs is more acidic than that of normal blood, but it was observed that the pH is restored after PMF stimulus. Also it was confirmed that MB adheres more to the RBCs after PMF stimulus, which could be inferred that PMF stimulus not only increases the zeta potential, but also reduces the H+ in the blood by combining MB with plasma cations. Further study needs to optimize PMF stimulation conditions such as pulse shape, duration, or repetition rate for fast homeostasis recovery in acid-base unbalanced blood.

[1] N. M. Shupak, F. S. Prato & A. W. Thomas, Neurosci. Lett. Vol. 363, p.157–162(2004). [2] J. Mok, S. Han, & H. Lee, AIP Advances, 10(1), 015005 (2020).

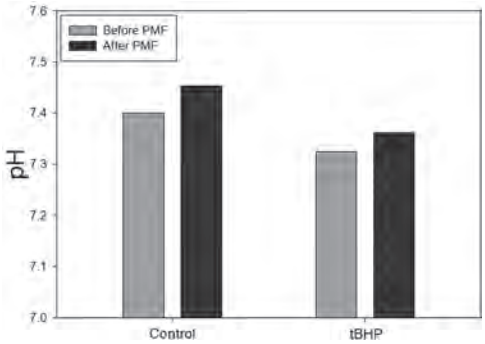

The change of pH on PMF stimulus and tBHP treated blood.

Q5-10. Withdrawn

Q5-11. High Throughput Magnetic Single-Cell Sorting Using Spin Orbit Torque. *V.M. Estrada*[1], R. Zheng[1], G. Carman[1] and A. Sepulveda[1]
1. Mechanical Engineering, University of California Los Angeles, Los Angeles, CA, United States

Cell Sorting has become an indispensable technique for a variety of biological and biomedical applications. Moreover, with the development of fields such as personalized medicine and new breakthroughs in cancer treatments, cell sorting devices that have high throughput and single-cell manipulation capabilities are needed now more than ever[1]. Magnetically activated cell sorting (MACS) has quickly become one of the most widely used techniques due to its extremely high performance in throughput and ease of use, unfortunately these systems lack the much needed single-cell resolution that modern biomedical problems require. To address this, there has been much research and development aimed at creating MACS devices in the microfluidic regime where microscale fabrication can allow for single-cell sorting mechanisms to be implemented. In addition to increased resolution, these microfluidic MACS devices have other benefits that include low cost, the ability to run fast low volume experiments, and the ability to capture and release cells while simultaneously culturing them within a device. In this paper we present a novel method of capturing and releasing magnetically activated cells using Spin Orbit Torque (SOT) to change the magnetization of micromagnet structures patterned within a microfluidic channel. SOT has been shown to be a reliable and fast method of manipulating the magnetization of magnetic memory devices[2] and for this reason it was chosen as the method of operation. This device is a significant improvement on current cell sorting technologies because it has both single cell manipulation capabilities and high throughput whereas most current cell sorting technologies suffer a tradeoff between these two properties. This paper includes both modeling and experimental data to verify the theoretical mechanism proposed.

[1] X. Wang, S. Chen, D. Sun. *Lab on a Chip.*, Vol. 11, p. 3656 (2011) [2] W. Kwak, J. Kwon, B. K. Cho. *Scientific Reports*.,Vol 8 (2018)

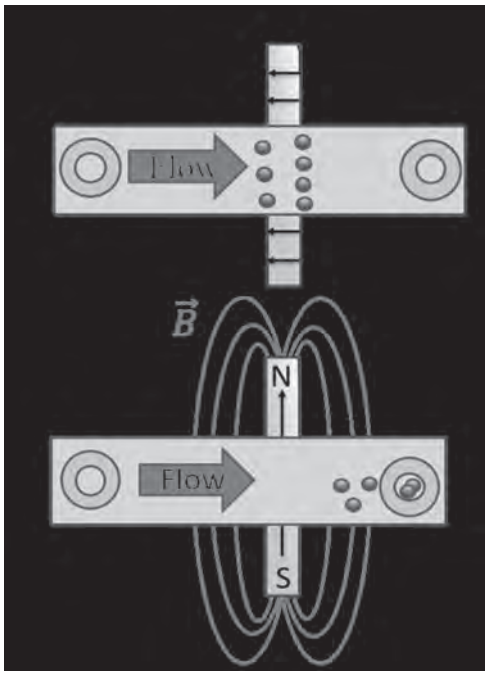

Figure 1. Top view of the Mechanism. a) Capture mode. b) Release Mode.

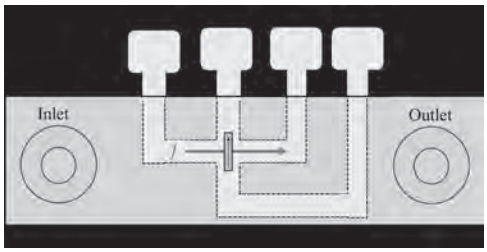

Figure 2. Proposed SOT switching mechanism. Two intersecting tantalum wires provide the SOT required to switch the magnet into the capture or release state.

Q5-12. Portable Magnetic Particle Spectroscopy (MPS) Device for Future Rapid, One-Step and Wash-Free Bioassays. *V.K. Chugh*[1], K. Wu[1], A. Nair[1], A. di Girolamo[1], N. Seekaew[2], L. Nguyen[2], R. Saha[1], W. Davies[3], V. D Krishna[4], D. Su[5], M. C-J. Cheeran[4] and J. Wang[1]
1. Department of Electrical and Computer Engineering, University of Minnesota, Minneapolis, MN, United States; 2. Department of Mechanical Engineering, University of Minnesota, Minneapolis, MN, United States; 3. Department of Computer Science and Engineering, University of Minnesota, Minneapolis, MN, United States; 4. Department of Veterinary Population Medicine, University of Minnesota, Minneapolis, MN, United States; 5. Department of Chemical Engineering and Material Science, University of Minnesota, Minneapolis, MN, United States

The dynamic magnetic responses of magnetic nanoparticles (MNPs) under an external magnetic field have been long studied for different diagnostic applications such as immunoassays and imaging[1]–[3]. In this modality of the magnetic particle spectroscopy (MPS) platform, as shown in Fig. 1, the external sinusoidal field is applied to the MNP suspension and their magnetization responses are recorded in the form of higher harmonics which can be utilized to monitor the presence of specific biomarkers from biofluids[4]–[6]. Herein, we present the development of a highly sensitive, wash-free, and portable MPS device for the detection of biomarkers. This paper reports the circuit and mechanical designs of the handheld MPS platform. Using a streptavidin–biotin binding system as a model, we demonstrated the feasibility of using this MPS system to monitor molecular interactions with MNPs and to quantify biomarkers from biofluid samples. Our results show that the developed MPS platform allows rapid, wash-free, volumetric bioassays and is suitable for future point-of-care, sensitive, and versatile diagnosis. The MPS handheld device has dimensions of 15.5 cm × 6.4 cm × 6 cm and operates on an off-the-shelf 24V-5A rated DC power supply. It communicates wirelessly to smartphones via Bluetooth V5.0. User interfaces for both Android as well as IOS systems have been developed to provide step-by-step self-test instructions, store past testing results, and update electronic health records (EHR).

[1] K. Wu, D. Su, J. Liu, R. Saha, and J.-P. Wang, "Magnetic nanoparticles in nanomedicine: a review of recent advances," *Nanotechnology*, vol. 30, no. 50, p. 502003, 2019. [2] M. Colombo *et al.*, "Biological applications of magnetic nanoparticles," *Chem. Soc. Rev.*, vol. 41, no. 11, pp. 4306–4334, 2012. [3] P. Srivastava, P. K. Sharma, A. Muheem, and M. H. Warsi, "Magnetic nanoparticles: A review on stratagems of fabrication and its biomedical applications," *Recent Pat. Drug Deliv. Formul.*, vol. 11, pp. 101–113, 2017. [4] H. Khurshid, Y. Shi, B. L. Berwin, and J. B. Weaver, "Evaluating blood clot progression using magnetic particle spectroscopy," *Med. Phys.*, vol. 45, no. 7, pp. 3258–3263, 2018. [5] K. Wu, D. Su, R. Saha, D. Wong, and J.-P. Wang, "Magnetic particle spectroscopy-based bioassays: methods, applications, advances, and future opportunities," *J. Phys. Appl. Phys.*, vol. 52, p. 173001, 2019. [6] S. Draack *et al.*, "Multiparametric Magnetic Particle Spectroscopy of CoFe2O4 Nanoparticles in Viscous Media," *J. Phys. Chem. C*, vol. 123, no. 11, pp. 6787–6801, 2019.

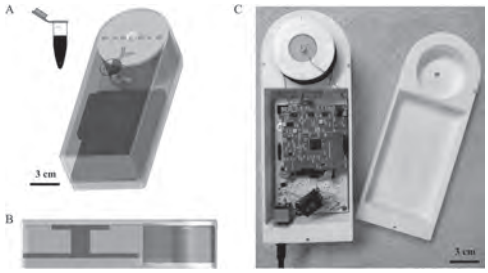

Fig.1: 3D models of A) front view, B) side view of the developed MPS handheld system. C) the final assembled system with coils and plastic vial containing MNPs inserted. The shell as well as the 3 coil molds (2 excitation coils and 1 pick-up coil) are 3-D printed for cost-efficiency.

Session Q6
COMPLEX OXIDES II
(Poster Session)

Suzanne G.E. te Velthuis, Chair
Argonne National Laboratory, Argonne, IL, United States

Q6-01. Direct Observation of Double Exchange in Ferromagnetic $La_{0.7}Sr_{0.3}CoO_3$ by Broadband Ellipsometry. *A. Dubroka[1] 1. Condensed matter, IQVIA Spain, Brno, Czechia*

We present results of our broadband ellipsometry measurements of the optical response of ferromagnetic $La_{0.7}Sr_{0.3}CoO_3$. Our data [1] show that the ferromagnetic transition is accompanied by a transfer of optical spectral weight from an absorption band centered at 1.5 eV to a narrow component of the Drude-like peak, see the Figure. The associated reduction of the intra-band kinetic energy is significantly larger than k_BT_c, confirming that the double exchange plays a major role in the ferromagnetism of doped cobaltites. In conjunction with results of recent theoretical studies, the temperature dependence of the Drude-like peak suggests that the double exchange is mediated by t_{2g} orbitals.

[1] P. Friš, D. Munzar, O. Caha, and A. Dubroka, Phys. Rev. B 97, 045137 (2018).

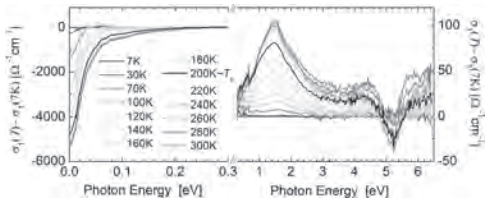

Fig. 1 The real part of the optical conductivity of La0.7Sr0.3CoO3 deposited on LSAT. The left and right panel displays the difference conductivity with respect to 7 K.

Q6-02. Characterization of $La_xSr_{1-x}FeO_3/SrTiO_3$ Superlattices Grown by Pulsed Laser Deposition. *M. Kiaba[1], T. Číž[1], O. Caha[1], G. Koster[2] and A. Dubroka[1] 1. Department of Condensed Matter Physics, Masaryk University, Brno, Czechia; 2. Universiteit Twente Faculteit Technische Natuurwetenschappen, Enschede, Netherlands*

We report on deposition and structural characterization of superlattices of antiferromagnetic $La_{1-x}Sr_xFeO_3$ and $SrTiO_3$ with x=0 and 0.67. Superlattices were grown by pulsed laser deposition with various numbers of monolayers n=1,2 and 3 of the individual materials, including symmetrical and asymmetrical combinations. The superlattices were deposited on SrTiO3 substrate with single TiO termination and Their total thickness is about 8nm ± 1nm. The thickness of the individual layers was in situ controlled by reflection high-energy electron diffraction (RHEED) in order to ensure that each layer had an integer number of monolayers. Figure 1 shows the evolution of RHEED intensity during the deposition of an asymmetrical superlattice with 1 monolayer of $LaFeO_3$ and 2 monolayers of $SrTiO_3$. Surface characterization of films was made by atomic force microscopy where atomically flat surface with vicinal steps was observed and a typical AFM image is shown in Figure 2. The structural quality of films was also examined by X-ray diffraction. The in-plain position of the diffraction peaks shows that our films are pseudomorphic and from the out-of-plain position we determined lattice parameters of films. We also observed the out-of-plain diffraction from the superlattice periodicity demonstrating the very high structural quality of our superlattices. Preliminary transport and magnetic characterization of the superlattices will be presented.

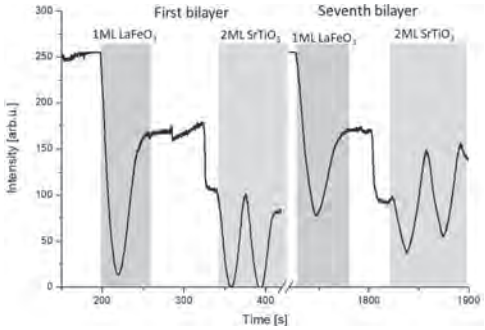

Fig. 1 RHEED intensity during the deposition of the first and seventh bilayer.

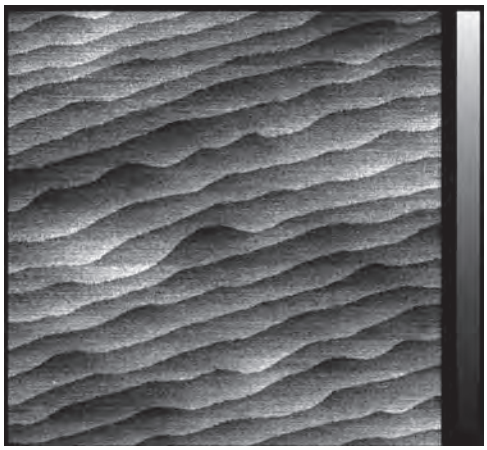

Fig. 2 AFM image of the surface of the superlattice from figure 1 showing vicinal steps.

Q6-03. Withdrawn

Q6-04. Magnetic Anisotropy and Spin Scattering in $(La_{2/3}Sr_{1/3})MnO_3/CaRuO_3$ Bilayers. *P.P. Balakrishnan[1,2] and Y. Suzuki[1] 1. Geballe Laboratory for Advanced Materials, Stanford University, Stanford, CA, United States; 2. NIST Center for Neutron Research, National Institute of Standards and Technology, Gaithersburg, MD, United States*

Complex oxide perovskites are attractive for spintronics applications due to the ease of integration into functional devices through epitaxial, isostructural growth. However, this epitaxial integration may cause unexpected changes and interfacial phenomena. Here, we report on modifications to the magnetic properties of ferromagnetic $(La_{2/3}Sr_{1/3})MnO_3$ (LSMO) films on LSAT substrates by an epitaxial layer of $CaRuO_3$ (CRO). Using ferromagnetic resonance (FMR) as a sensitive magnetic probe, we find that the presence of CRO can modify the magnetic anisotropy of the LSMO. By increasing CRO thickness, we find a reduction of the out-of-plane anisotropy and simultaneous rotation of the easy axis within the plane, from the <110> to <100>

axes (see Fig. 1a). The anisotropy strength determined by FMR disagrees with bulk SQUID magnetometry. This is consistent with a depth-dependent structural change, such as oxygen octahedral rotations imposed on rhombohedral LSMO [1] by orthorhombic CRO. FMR is also used to study spin pumping across this LSMO/CRO interface. Spin pumping manifests as an increase in Gilbert damping with CRO thickness. The frequency dependence of the FMR linewidth with an in-plane field indicates two-magnon scattering is significant. By varying the field direction in-plane, we find the in-plane anisotropy of the FMR linewidth – and therefore strength of two-magnon scattering – increases as a function of increasing CRO thickness (see Fig. 1b). These results suggest that while LSMO and CRO remain promising candidates for efficient pure spin current generation and detection, respectively, the epitaxial integration of perovskites for spintronics applications will cause additional changes which must be accounted for.

[1] Z. Liao, M. Huijben, Z. Zhong et al., Nature Materials, Vol. 15, p.425 (2016) [2] H. K. Lee, I. Barsukov, A. G. Swartz et al., AIP Advances, Vol. 6, p.055212 (2016)

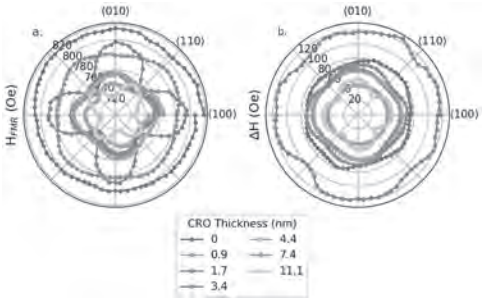

Resonant field (a) and linewidth (b) of x nm CRO / 22 nm LSMO extracted from FMR peaks at 5 GHz, vs. in-plane field direction. (a) 4-fold symmetry reflects the in-plane cubic magnetic anisotropy, which starts slightly negative (blue), decreases (red), increases (green) and switches sign (yellow). H_{FMR} is minimal along the easy axis. (b) 4-fold symmetry indicates two-magnon scattering from crystalline defects within or at the interface of LSMO [2].

Q6-05. High-Frequency Magnetotransport in $La_{1-x}Sr_xMnO_3$ (x = 0.12-0.20). U. Chaudhuri[1] and *R. Mahendiran*[1] *1. Physics, National University of Singapore, Singapore*

In manganites, a large intra-atomic exchange coupling aligns e_g electron spin (S = ½) of Mn^{3+} : ($t_{2g}^3e_g^1$) ion parallel to the localized t_{2g} spin (S = 3/2) of the same ion. Since electrical conduction in these manganites is due to thermally activated hopping of e_g electron along the Mn^{3+} : ($t_{2g}^3e_g^1$) -O^{2-}- Mn^{4+} : ($t_{2g}^3e_g^0$) network in the background localized t_{2g}^3 spins, it is of scientific curiosity to understand how oscillating electric current affects the electrical resistivity and magnetoresistance(*MR*) of these oxides[1]. Dc voltage at a frequency of 9.8 GHz was detected in $La_{0.7}Sr_{0.3}MnO_3$ during ferromagnetic resonance when the thin film sample was subjected to microwave irradiation inside a resonant cavity [2]. Instead of using resonant cavity, we studied room-temperature magnetoresistance (*MR)* in $La_{1-x}Sr_xMnO_3$ (x = 0.20,0.18,0.12) series by passing alternating current (*ac*) of frequencies, f =30 MHz to 3000 MHz using a radio-frequency impedance analyzer and sweeping an applied magnetic field along the direction of current from -3kOe to 3kOe. Ferromagnetic Curie temperatures of x=0.20, 0.18, and 0.12 are 306 K, 292 K, and 240 K, respectively. As illustrated in Fig.1, at f =30 MHz all the compounds showed negative *MR* with x = 0.20 showing a maximum change of 1.53% for x = 0.2 at 3 kOe. As the frequency of current was increased the single peak at low frequencies for x = 0.20 evolved into double peaks about 0 Oe while for x = 0.18 and x = 0.12 the line shape response contained an admixture of Lorentzian absorptive and dispersive features. At 3000 MHz the maximum *ac* MR are 49.01%, 17.60% and 1.62% for the three samples respectively. The maximum positive *MR* in these compounds always occurs at higher magnetic fields with increasing frequency of the current. Our analysis indicates that high-frequency magnetoresistance is due to a change in magnetic permeability of the sample caused by ferromagnetic and paramagnetic resonance in these samples. R. M. acknowledges the Ministry of Education, Singapore for supporting this work (Grant no. R144-000-404-114).

[1] R. Mahendiran et al., Phys. Rev. B, 53, 3348 (1996). [2] V. A. Atsarkin et al., Phys. Rev. B. 82, 144414 (2010).

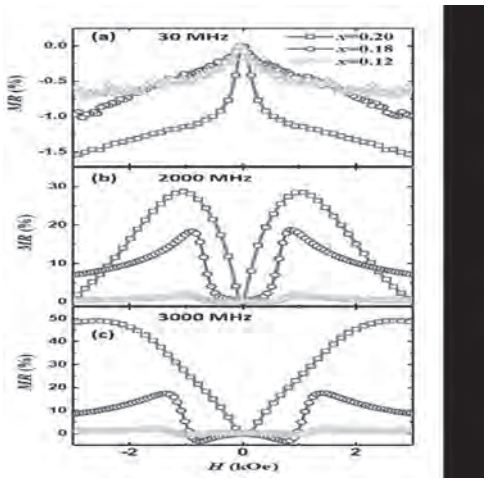

Fig. 1. *Ac MR* of $La_{1-x}Sr_xMnO_3$ for x = 0.20 (squares),0.18 (circles), and 0.12(triangles) with *ac* frequencies of (a) 30MHz, (b) 2000 MHz and (c) 3000 MHz.

Q6-06. Magnetic and Electron Paramagnetic Resonance Studies of Charge Ordered $R_{0.5}Ca_{0.5}MnO_3$ (R = Pr, Bi) Manganites. *A. K.N.*[1] and S. Bhat[2] *1. Physics, Dr. Ambedkar Institute of Technology, Bangalore, India; 2. Physics, Indian Institute of Science, Bangalore, India*

Rare earth managnites with general formula R_{1-x} A_x MnO_3 (where R = rare earth cat ion such as La^{3+}, Pr^{3+}, etc and A = alkaline earth cation such as Ca^{2+}, Sr^{2+}, etc) have complex phase diagram which consist of paramagnetic, ferromagnetic insulator, ferromagnetic metallic, charge order insulator phases etc. Charge ordering is one of the fascinating properties exhibited by manganites. The charge order in $Bi_{0.5}Ca_{0.5}MnO_3$ is robust and the retention of CO even at nanoscale [1] in contrast with rare earth based CO systems. In this paper we report the magnetization and electron paramagnetic resonance(EPR) studies of charge ordered $R_{0.5}Ca_{0.5}MnO_3$ (R = Pr, Bi) manganites. $Pr_{0.5}Ca_{0.5}MnO_3$ (PCMO) and $Bi_{0.5}Ca_{0.5}MnO_3$ (BCMO) manganites were prepared by solid state reaction method. A commercial SQUID magnetometer was used to study the dc- magnetization in the temperature range of 10 -300 K. The EMR experiments were carried out using a commercial X-band (frequency ~ 9.4 GHz) spectrometer in the temperature range 4 K – 300 K. Marked differences are found when the magnetic and EPR properties of rare earth(PCMO) and bismuth based managnites(BCMO) are compared. Temperature dependence of magnetization shows that in BCMO system the separation between the two transitions, i.e. T_{CO} and T_N is much larger compared to that in the PCMO system. In PCMO the two transitions being close to each other are strongly coupled whereas in BCMO system the two transitions are weakly coupled and therefore are less influenced by each other. Temperature dependence of EPR parameters viz. the linewidth, the intensity and the resonance fields of PCMO and BCMO manganites are studied and compared. The temperature dependent resonance field of PCMO and BCMO samples are seen to be opposite to each other. PCMO sample shows the resonannce field behavior similar to other charge ordered manganites [2], i.e., it, decreases with the decrease in temperature where as the resonance field of BCMO increases with decrease in temperature. The opposite behavior of resonance field could be due to the different magnetic structure present in the BCMO manganite.

[1] S. S. Rao and S. V. Bhat, Journal of Nanoscience and Nanotechnology, 7, 2025 (2007) [2]. Janhavi P. Joshi, A. K. Sood, S. V. Bhat, Sachin Parashar, A. R. Raju, and C. N. R. Rao, Phys.Rev. B, 65, 024410, (2001).

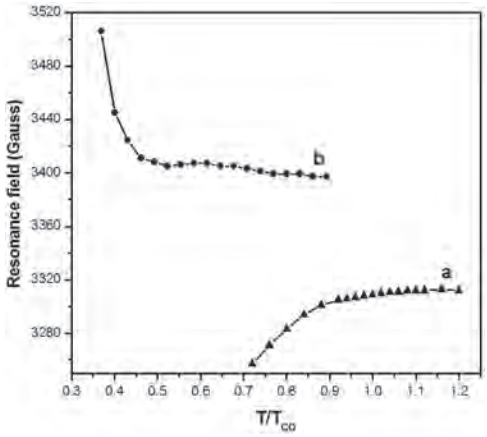

Temperature dependence of resonance field for (a) $Pr_{0.5}Ca_{0.5}MnO_3$ and (b) $Bi_{0.5}Ca_{0.5}MnO_3$

Q6-07. Phases Competition in Half-Doped $La_{0.5-x}Dy_xCa_{0.5-y}Sr_yMnO_3$ Films. *Y. Tang*[1], A. Zhang[1], X. Wu[2] and Z. Zhai[3] *1. Hohai University, Nanjing, China; 2. Nanjing University, Nanjing, China; 3. Huaiyin Normal University, Huai'an, China*

The semi-doped $La_{0.5}Ca_{0.5}MnO_3$ (LCMO50) with x=0.5 exhibits the phenomenon of ferromagnetic (FM) and charge-ordered (CO) antiferromagnetic (AFM) competition, where the subtle balance between the phases can be tuned by magnetic fields, electrical currents, X-rays, laser excitation, epitaxial strain, high pressure or surface effects. It is found that magnetic and electric properties could be controlled by A-site disordering in our previous work (*Ceramics International* 46 (2020) 10598–10602). In present work, high-quality $La_{0.5-x}Dy_xCa_{0.5-y}Sr_yMnO_3$ ($0\leq x\leq 0.2$) (LDCSMO) thin films with different thicknesses were deposited on $SrTiO_3$ (STO) substrates. The influence of the lattice structure and magnetoelectric properties of the LDCSMO thin film epitaxially grown on the STO substrate were studied. In-plane tensile strain is produced in LDCSMO films on the STO substrate, which is manipulated by changing the film thickness. Magnetic results show that the Curie temperature of the thin film sample is significantly lower than that of the bulk material, indicating that there are other phases in the sample besides the ferromagnetic phase. X-ray diffraction and Raman spectra at different temperature were combined to explore the structural distortion performed by the tensile strain. Besides, a "dead layer" was found at the interface between the STO substrate and the LDCSMO film through simulation using the distorted wave Born approximation. The co-existing of magnetic phases was understood by considering the structural distortion and the "dead layer" at the interfaces.

Q6-08. Structural and Magneto Transport Properties of Ruddlesden – Propper $La_{2-2x}Sr_{2+2x}Mn_2O_7$ ($0.42\leq x\leq 0.52$) Layered Manganites. *A.K. Saw*[1], S. Gupta[2], V.K. Pecharsky[2] and V. Dayal[1] *1. Department of Physics, Maharaja Institute of Technology Mysore, Mandya, India; 2. Division of Materials Science and Engineering, Ames Laboratory, US Dept. of Energy, Ammes, IA, United States*

The La-based double layered (DL) managnites $La_{2-2x}Sr_{2+2x}Mn_2O_7$ have gained importance due to colossal magnetoresistance (CMR) [1] analogous to 3D perovskite manganite. However, In incongruity with the three-dimensional (3D) half doped perovskite manganites ($La_{0.5}Sr_{0.5}MnO_3$), which shows charge exchange (CE) spin/charge ordering (CO) [2], the A-type of antiferromagnetic (AFM) state is dominant in Ruddlesden –Propper half doped bilayered manganites ($La_1Sr_2Mn_20_7$) [3]. The MR observed in the layered system is much higher than observed in 3D perovskites manganites because of the high spin polarisation of conduction electron. This abstract reports on the structural and magneto-transport properties of $La_{2-2x}Sr_{2+2x}Mn_2O_7$ ($0.42\leq x\leq 0.52$) synthesized by solid state reaction method. The Rietveld refined X-ray diffraction pattern suggests that the samples crystallizes into tetragonal structure (I4/mmm) without any trace of impurity phase. The temperature dependent resistivity plot of the samples in the magnetic field 0-5T is shown in Fig 1. At 0T, the samples $0.42\leq x\leq 0.48$ show insulator to metal (T_{MI}) transition and later a resistivity mimima (T_{min}) with the lowering of temperature, whereas x=0.50 and 0.52 shows CO with trace of metal-insulator transition. The application of magnetic field reduces the resistivity to a large order and T_{MI} shifts towards the higher temperature side suppressing the resistivity minima. This can be understood due to reduction of the spin fluctuation by the field [4]. The resistivity of the samples increases with Sr subsitution upto x=0.48, and later decreases for higher Sr substitution, which may be due to phase transformation from canted AFM to the CO insulator [5]. The conduction mechanism at high temperature follows hopping polaron model. At 5K and 8T, $0.46\leq x\leq 0.50$, shows nearly similar MR (58%) and decreases for (x=0.42, 0.52). MR is dominated by the spin-polarised tunnelling across the interface or grain separated by the insulating barrier. We intend to study the magnetic behaviour of all the samples. This work is supported by UGC-DAE-CSR, Indore (grant No. CSR-IC/CRS-89), Ames Lab and MRF(MITM)

1. Moritomo Y., Asamitsu A., Tokura Y., Nature, 380, 141.(1996) 2. C. N. R. Rao and B. Raveau, Colossal Magnetoresistance, Charge Ordering and Related Properties of Manganese Oxides, edited by (World Scientific, Singapore, (1998). 3. M. Kubota, H. Yoshizawa, Y. Moritomo, Y. Endoh, J. Phys. Soc. Jpn. 68, 2202 (1999). 4. C. Zener, Phys. Rev. 82 403 (1951) 5. Mitchell J F, Ling C D, Millburn Medarde M J. Appl. Phys. 89, 6618 (2001)

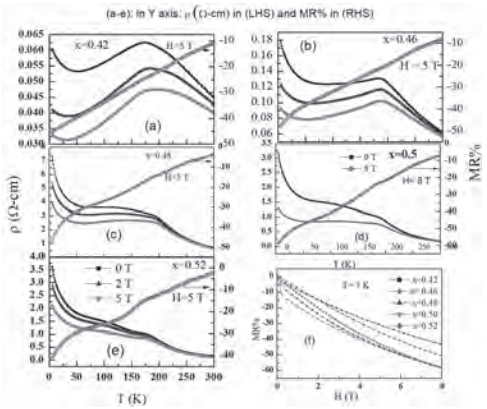

Fig 1. (a-e) ρ vs.T. curves at different magnetic field (H) and (f) MR % Vs T ; MR % vs H at 5K (0-8T)

Q6-09. Adjustment of Electromagnetic Properties in $SrRuO_3$ via Ru Content. *Z. Zhang*[1], X. Yang[1], F. Duan[1], Y. Wang[1], T. Zhang[1], Y. Sun[1], A. Zhang[2] and X. Wu[1] *1. Department of physics, Nanjing University, Nanjing, China; 2. College of Science, Hohai University, Nanjing, China*

Material magnetism may be adjusted by the adjacent magnetic ions, such as Ru^{3+}. It is well known that the RuO_2 is a volatile mater, which is very difficult to be controlled in synthesizing $SrRuO_3$ by solid station reactions. We here report a thoroughly study of the structure, electro-transport and magnetic properties of poly-crystallized $SrRu_xO_3$ (the nominal composition of x=0.9, 0.95, 1, 1.05, 1.1), which is synthesized by solid-state reaction. Based on the phase determinations that there is about 5% Ru content loss during the reaction, and the grain size increases with increasing the Ru content. Results further show that $SrRu_xO_3$ remains the single phase equivalent to that of $SrRuO_3$, i.e., the orthorhombic crystal structure with space group Pnma. Structural distortion of $SrRu_xO_3$ is also determined due to the Ru defects, which varying with Ru content. A semiconducting behavior with $x\leq 1$, and a Fermi Liquid behavior with x>1 are observed based on the temperature dependence of resistivity. Further, the magnetic Curie temperature, T_c, varies slightly. Hysteresis loop at 10K shows that as x increases the saturated magnetic moment increases from 21.02 to 29.82 (emu/g), and the coercivity decreases from 5100 to 910 (Oe). To conclude, certain amount of Ru rich before the solid-state reaction can lead to the produced poly stoichiometric

close to $SrRuO_3$, and leads to less defects and better electromagnetic properties. These results are also confirmed by first principle calculations.

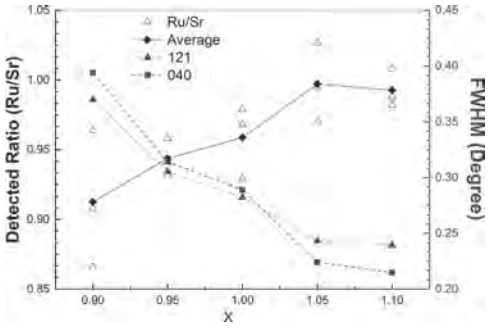

FIG. 1. The EDS detected Ru/Sr ratio (left) and FWHM (right) of (121) and (040) peaks form XRD results as a function of Ru content x

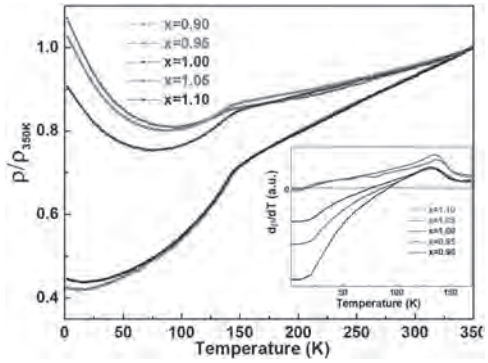

FIG. 2. The temperature-dependent relative resistivity ρ/ρ_{350K} for $SrRu_xO_3$ (0.9≤x≤1.1). The inset shows the dρ/dT vs the Temperature curve.

Q6-10. Magnetic Anisotropy and Dzyaloshinskii-Moriya Interaction in Perovskite $SrRuO_3/SrTiO_3$ Oxide Heterostructues. *Z. Li*[1], W. Mi[1] and H. Bai[1] *1. Tianjin University, Tianjin, China*

It is significant to modulate the magnetic anisotropy and Dzyaloshinskii-Moriya interaction (DMI) in perovskite-type oxides heterostructures toward the multifunctional spintronic devices[1,2]. Herewith, the magnetic properties of $SrRuO_3$ (SRO) /$SrTiO_3$ (STO) heterostructures are modulated by different SRO atomic layers (ALs) and interfacial oxidizations. In Fig. 1, as the SRO AL increases from 3 to 9, the SRO/STO heterostructures remain the perpendicular magnetic anisotropy (PMA), where PMA shows an oscillating characteristic due to the oscillation of the in-plane $d_x2_{-y}2$ and out-of-plane $d_{xz}+d_{yz}+d_z2$ orbitals. The DMI increases at underoxidized interface but significantly decreases at overoxidized interface, which can be attributed to the different contributions of layer-resolved *E*soc. This work is supported by National Natural Science Foundation of China (51871161). It is also supported by High Performance Computing Center of Tianjin University, China.

[1] A. Hallal, H. X. Yang, B. Dieny, and M. Chshiev, Anatomy of perpendicular magnetic anisotropy in Fe/MgO magnetic tunnel junctions: first-principles insight. *Phys. Rev. B* 88, 184423 (2013). [2] H. X. Yang, A. Thiaville, S. Rohart, A. Fert and M. Chshiev, Anatomy of Dzyaloshinskii-Moriya interaction at Co/Pt interfaces. *Phys. Rev. Lett.* 115, 267210 (2015).

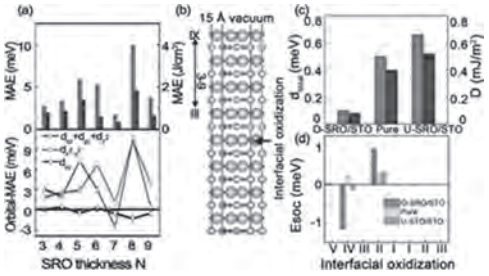

Magnetic anisotropy energy and Dzyaloshinskii-Moriya interaction of SRO/STO heterostructures with different SRO ALs and interfacial oxidizations.

Q6-11. Observation of Room Temperature Magnetoresistance in Graphene / $CoFe_2O_4$ Nanocomposite. *S. Roy*[1,2], I. S.[1], F. Francis[1], V. G. V.[1] and A. Subramanian[1] *1. Centre for Nano and Soft Matter Sciences, Bangalore, India; 2. Manipal Academy of Higher Education, Manipal, India*

The considerable spin diffusion length and high electron mobility of graphene at room temperature makes it a suitable candidate to improve the spin transport properties of magnetic semiconductors when incorporated in a suitable stoichiometry. Here, we report observation of room temperature magnetoresistance properties of reduced graphene oxide (rGO) / cobalt ferrite (CFO) nanocomposite, which were synthesized by chemical methods followed by mixing in different ratios. The structural properties and morphology of rGO-CFO mixed states have been investigated from the x-ray diffraction and TEM imaging. The Raman spectroscopy shows the presence of various vibrational bands of CFO in addition to the D and G bands at ~ 1354 and 1591 cm^{-1} respectively, which indicates the formation of rGO. The magnetic field dependent electrical resistivity shows a decrease in resistivity with the increase in magnetic field from 0 to 0.5 T, representing a negative magnetoresistance in our samples. The highest MR of around – 1.4 % was observed in the 1:1 ratio CFO and rGO nanocomposite, whereas the samples with 2:1 and 3:1 ratio show the MR of maximum value about 1%. In the rGO-CFO nanocomposite, the charge transport takes place mainly through the rGO flakes due to the insulating nature of the CFO nanoparticles. However, the ferromagnetic moments of the CFO nanoparticles induce electron-spin scattering during the charge transport. The reduction in electron-spin scattering due to the parallel alignment of the magnetic moments results in negative magnetoresistance in our sample. The alignment of ferromagnetic moments under the external magnetic field has been further confirmed from the observation of the magnetocapacitance effect of CFO nanoparticles. Our results show the possibility to utilize the wide band gap magnetic oxides for room temperature magnetotransport applications when incorporated with the 2D materials like graphene.

Q6-12. Withdrawn

Q6-13. Withdrawn

Session R1
DOMAIN WALLS

Liza Herrera Diez, Co-Chair
CNRS, University of Paris-Sud, Orsay, France
Reinoud Lavrijsen, Co-Chair
TU Eindhoven, Eindhoven, Netherlands

INVITED PAPER

R1-01. Interactions Between Spin Wave and Magnetic Domain Structures. *L. Liu*[1] *1. Massachusetts Institute of Technology, Cambridge, MA, United States*

Spin waves are considered as promising candidate for realizing compact wave-based computing. Recently quite a lot of research efforts have been spent to explore the interactions between spin wave and magnetic domain structures, with the goal of realizing efficient modulation of spin wave propagation. Particularly, spin wave transmission along or across the wall between different magnetic domains have been studied experimentally, numerically and analytically. In this talk, I will describe our recent experimental activities on investigating the mutual interactions between magnetic domain wall and spin wave, where magnetic domain walls manipulate the phase and magnitude of spin wave (Fig. 1), and a strong spin wave in turn moves the position of magnetic domain walls (Fig. 2) [1]. These mutual interactions can potentially provide the possibility of realizing all-magnon spintronic devices.

1. J. Han, et al, "Mutual control of coherent spin waves and magnetic domain walls in a magnonic device", Science 366, 1121 (2019)

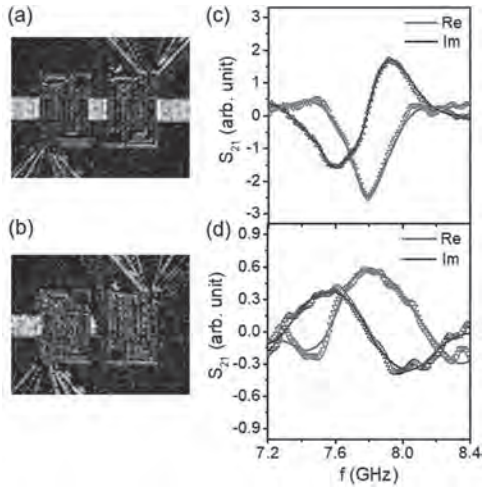

MOKE image and transmission coefficient (S21) of spin wave with [(a) and (c)], and without [(b) and (d)] a domain wall.

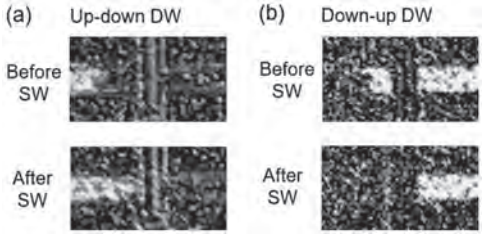

Magnetic domain switching induced by spin wave. (a) and (b) MOKE images showing the movement of the up-down and down-up domain walls under zero dc magnetic field by applying microwave at resonant frequency.

CONTRIBUTED PAPERS

R1-02. Magnetic Domain Formation and Shift in Magnetic Nanowire Memory Element With U-Shaped Writer Observed by Magneto-Optical Kerr Microscopy. Y. Hori[1], M. Endo[1], N. Ishii[1] and *Y. Miyamoto*[1] *1. Science & Technology Research Labs., NHK (Japan Broadcasting Corp.), Setagaya-ku, Japan*

Future large-capacity memories [1] and spatial light modulators [2] based on fast current-driven domain wall (DW) motion in magnetic nanowires (NWs) have been proposed. We have also proposed a magnetic nanowire memory [3] for future 3D-video storage. Although a Hall bar is usually used as a "domain wall writer" for NW experiments, by considering storage application, the formation of narrow magnetic domains (MDs), which correspond to recorded bits, is required. As shown in Fig.1, for our NW memory, we adopted a U-shaped writer consisting of two metal wires aligned in parallel. The resultant magnetic field, generated at the gap between a pair of antiparallel wires in the U-shaped writer, could achieve local magnetic reversal in the NW. We estimated the magnetic reversal by the U-shaped writer using the Landau–Lifshitz–Gilbert (LLG) equation. The MDs appeared to form in the NW just beneath the gap of the U-shaped writer, making them suitable for memory application. Consequently, we prototyped an NW memory element equipped with the U-shaped writer. Pt(3)/$[Co(0.3)/Tb(0.6)]_5$ and Si_3N_4(18) thin films (units in nm) were used as the layers of the magnetic NW and the insulation layer between the NW and writer, respectively. The U-shaped writer was patterned from an Au(100) thin film. Fig.2(a) shows a microscopy image of the fabricated element and the configuration of the evaluation system. Two pulse generators were connected to the element for independent MD formation and shifting. A pulse current of 3.1×10^7A/cm^2 with a pulse width of 3μs was applied to the writer, while the shift current was 1.6×10^7A/cm^2 with a pulse width of 500ns, as shown in the timing charts in Fig.2(b). We succeeded in observing the formation of successive MDs and their shift along the NW by magneto-optical Kerr microscopy (MOKE) as shown in Fig.2(c). These results suggest that binary information can be stored in this memory by using the U-shaped writer.

[1] S. S. P. Parkin *et al*., Science, Vol. 320, p. 190 (2008) [2] K. Aoshima *et al*., Journal of Display Technology, Vol. 12, p. 1212 (2016) [3] Y. Miyamoto *et al*., Joint MMM-Intermag 2019, GN-01 (2019)

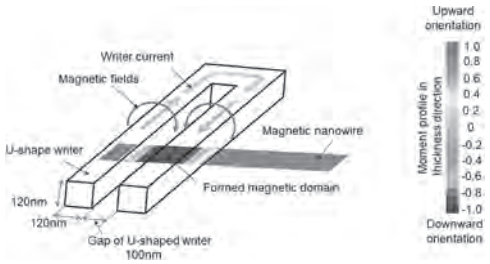

Fig.1 LLG simulation of magnetic domain formation in a magnetic nanowire by using a U-shaped writer.

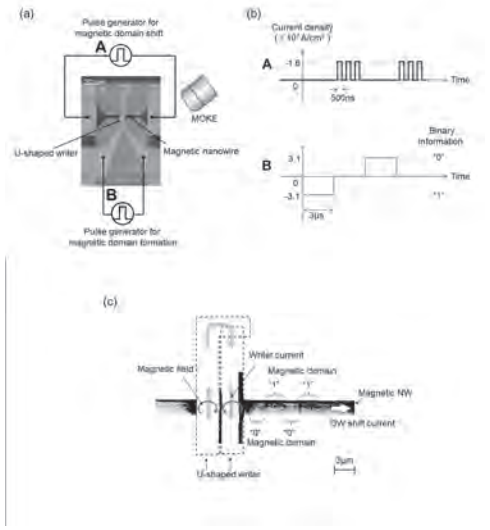

Fig.2(a) Microscopy image of specimen NW memory element and measurement system, (b) timing charts of pulse generator for MD formation and shift, (c) magneto-optical Kerr Effect (MOKE) image.

R1-03. Withdrawn

R1-04. Domain Wall Dynamics in Junctions of Bi-Ring Structures. *G. Venkat*[1], T.J. Hayward[1], A. Strømberg[2], I.T. Vidamour[1], E. Folven[2] and D. Allwood[1] *1. Materials Science and engineering, The University of Sheffield, Sheffield, United Kingdom; 2. Electronic Systems, Norges teknisk-naturvitenskapelige universitet, Trondheim, Norway*

Magnetic domain walls (DWs) in ferromagnetic nanowires are candidates for both Boolean [1–3] and non-Boolean computing architectures such as neuromorphic/stochastic computing [4]. In this context, interconnected nanorings are particularly interesting as they show emergent behaviour which make them interesting for reservoir computing [5-6]. Since these approaches use magnetic DW motion for logic operations, it is crucial to understand the dynamics of DWs in these structures for device realisation. We used micromagnetic simulations (using MuMax3 [7]) to simulate DWs passing through junctions of 2 μm diameter, 5 nm-thick Permalloy bi-ring structures with different ring widths and degrees of ring overlap. An example structure is shown in the inset of Fig. 1. The system was initialized with DWs in the upper and lower halves of the left and right ring. A rotating field was then applied to move the DWs towards the junction following previous experimental approaches [8]. The field amplitude was varied to record the depinning field H_{DP} when the DWs separated from the junction. The variation of H_{DP} for different overlap and wire widths is shown in Fig. 1. A minimum in H_{DP} is observed for most widths indicating that competing mechanisms are involved in the depinning mechanism. In order to better understand these competing mechanisms, we look at the magnetic energy density [7] E=-½M.B_{eff} (1) for a wire width of 100 nm with 12 (Fig. 2a) and 100 nm (Fig. 2b) overlap. In Fig. 2 (a), the DWs form a 'diamond' state which forms an energy minima requiring a high H_{DP} to depin the DW. For the largest overlap in Fig. 2 (b), the DWs get 'pinned' before and after the junction and a high H_{DP} is required to overcome this pinned energy threshold. Thus the intermediate overlap states (of 25 & 50 nm) require lower H_{DP} due to competition between these states. We expect that the understanding of these dynamics is crucial for the development of ring based computing applications.

[1] S. S. P. Parkin, M. Hayashi, L. Thomas, Science 320, 190 (2008). [2] D. A. Allwood et. al., Science 309, 1688 (2005). [3] K. A. Omari et. al., Adv. Func. Mater. 29, 1807282 (2019). [4] J. Grollier, et. al., Nat. Electron. 1-11 (2020). [5] R. Dawidek et al., MMM conference (2017). [6] R. Dawidek et al., submitted [7] A. Vansteenkiste et. al., AIP Adv. 4 (10), 107133 (2014). [8] M. Negoita et. al., J. Appl. Phys. 114.1, 013904 (2013).

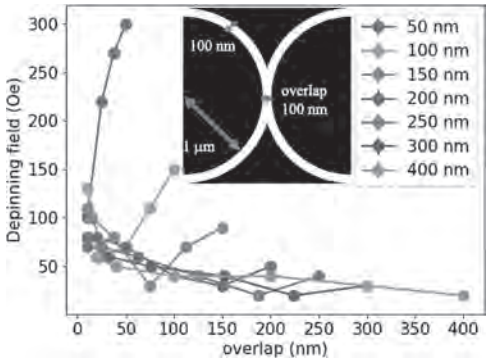

Fig. 1: The variation of the depinning field with junction overlap for different ring widths. The inset shows the simulated structure.

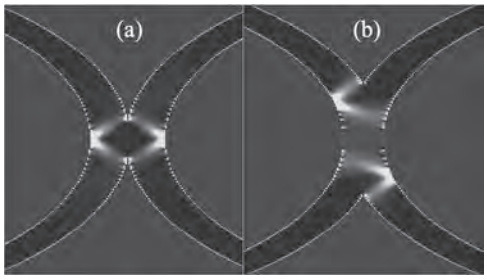

Fig. 2: The energy density for the (a) 12 nm and (b) 100 nm overlap cases for the 100 nm ring width case showing the different DW states.

R1-05. Direct Imaging of Chiral Domain Walls due to the Dzyaloshinskii-Moriya Interaction in Ferrimagnetic Alloys at Different Temperatures. *B. Seng*[1,2], D. Schönke[1], R.M. Reeve[1,3], J. Yeste[1], N. Kerber[1,3], D. Lacour[2], F. Kammerbauer[1], J. Bello[2], M. Hehn[2], S. Mangin[2] and P. Kläui[1,3] *1. Institut für Physik, Johannes Gutenberg-Universität Mainz, 55099 Mainz, Germany; 2. Institut Jean Lamour, UMR CNRS 7198, Université de Lorraine, 54506 Vandoeuvre-lès-Nancy, France; 3. Graduate School of Excellence Materials Science in Mainz, 55128 Mainz, Germany*

Magnetic skyrmions are topological spin textures that can be stabilized by the Dzyaloshinskii-Moriya interaction [1,2]. There are particularly suitable for next generation spintronics devices, like the skyrmion-based racetrack memory [3]. Recent studies confirmed their current-driven skyrmion dynamics in ultrathin ferromagnets via spin-orbit torques [4], where the chirality and spin texture of the skyrmions are key. However, the topological Magnus effect leads to a transverse motion of ferromagnetic skyrmions due to their non-zero topological charge [5], which is disadvantageous for devices. Antiferromagnetically exchange-coupled skyrmions or compensated ferrimagnets could suppress this effect owing to an overall zero topological charge [6]. Especially at the angular momentum compensation

temperature skyrmion propagation is predicted to be collinear with the current [7]. Here we explore a GdFeCo-based ferrimagnet system with perpendicular magnetic anisotropy. We demonstrate that in this system chiral worm domains as well as magnetic skyrmions can be observed using scanning electron microscopy with polarization analysis (SEMPA) (Figure 1). The high spatial resolution magnetic imaging technique reveals the domain wall spin structure as a function of temperature, with the observed structures found to be pure Néel-type spin textures, which is promising for devices. From the images we extract the domain wall width, which allows us to calculate the exchange stiffness for the system across the full temperature range.

[1] I. Dzyaloshinsky, J. Phys. Chem. Solids 4, 241 (1958) [2] T. Moriya, Phys. Rev. 120, 91 (1960) [3] R. Tomasello *et al.*, Sci. Rep. 4, 6784 (2015) [4] S. Woo *et al.*, Nat. Mater. 15, 501 (2016) [5] K. Litzius *et al.*, Nat. Phys. 13, 170 (2017) [6] Y. Hirata *et al.*, Nat. Nanotechnol. 14, 232 (2019) [7] J. Barker *et al.*, Phys. Rev. Lett. 116, 147203 (2016)

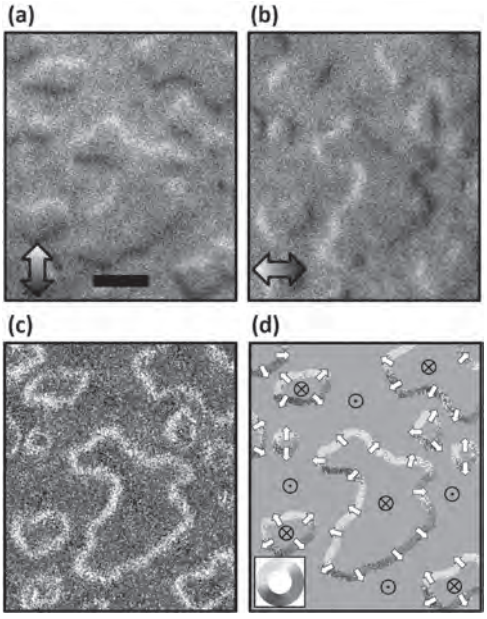

Spin textures in Ta/Ir/Fe/GdFeCo/Pt at 296 K with SEMPA (a) Vertical and (b) horizontal in-plane component of the spin polarization. The direction of magnetization is indicated by the double arrows. The scale bar indicates 1 µm. (c) Reconstruction of the absolute in-plane magnetization intensity. The white contrast indicates the saturated magnetization. (d) Color-coded direction of the in-plane magnetization in the domain walls as indicated in the color wheel.

R1-06. Modelling of Magneto-Thermoelectric Response From a Domain Wall. *E. Saugar*[4], T. Ostler[1], C. Barton[2], R. Puttock[2], P. Klapetek[3], O. Kazakova[2] and O. Chubykalo-Fesenko[4] *1. Materials and Engineering Research Institute, Sheffield Hallam University, Sheffield, United Kingdom; 2. National Physical Laboratory, Hampton Rd, Teddington, Middlesex TW11 0LW, United Kingdom; 3. Czech Metrology Institute, Okruzni 31, 638 00 Brno, Czechia; 4. Instituto de Ciencia de Materiales de Madrid, CSIC, Madrid, Spain*

Thermal magnetometry is a novel rapidly developing tool which makes use of the fact that thermoelectrical response of a nanostructure depends on its magnetic state. The use of nanometric local heat spots, e.g. from an actively and controllably heated scanning probe, with localized thermal gradients allows a nanoscale magnetization mapping of localized spin textures such as pinned domain walls [1]. The measured voltage is a convolution of magnetization and temperature distribution in the presence of several spin-caloritronic effects and thus its interpretation is not straightforward. Here, we model the thermoelectric response of Néel and Bloch domain walls in FeCoB nanostripes with or without a lithographed notch. The heat distribution is modelled by solving the Poisson heat equation for different positions of the heated probe across and along the stripe. Thermal modelling is used as an input for large scale thermal micromagnetics using the Landau-Lifshitz-Bloch approach [2]. Our modelling shows that at room temperature both Néel and Bloch domain walls represent energetically stable configurations, pinned at the notch. The presence of localized a asymmetric heat source forces the domain wall to widen and curve. Additionally, Bloch structures appear locally inside the Néel domain wall. With the aim to understand different responses, we model separately electric response of both domain walls in the presence of anomalous Nernst (ANE), perpendicular and parallel Seebeck (SE) effects and study their symmetry. The comparison with recent experiment demonstrates that only the response of the Neel domain wall under the action of both ANE and SE is compatible with the symmetry of the experimentally measured voltage.

[1] P. Krzysteczko et al Phys. Rev. B 95, 220410(R) (2017) [2] O. Chubykalo-Fesenko et al, Phys. Rev. B 74, 094436 (2006)

R1-07. Surface Acoustic Wave Assisted Depinning of Magnetic Domain Walls. *A. Adhikari*[1], E. Gilroy[2], T.J. Hayward[2] and S. Adenwalla[1] *1. Physics and Astronomy, University of Nebraska-Lincoln, Lincoln, NE, United States; 2. Department of Materials Science and Engineering, University of sheffield, Sheffield S1 3JD, United Kingdom*

The pinning of magnetic domain walls (DWs) results in reduced velocities and non-deterministic motion, both undesirable effects in the evolution of domain wall based memories. Perpendicular anisotropy materials possess the desired narrow width and high stability, but the narrow width make them more susceptible to pinning barriers. We investigate the effects of high frequency strain on the depinning and motion of DWs in perpendicular magnetic anisotropy films, multilayer of Co/Pt, patterned into micron wide stripes between a pair of identical inter-digital transducers (IDTs). The IDTs generate high frequency (114.8 MHz) standing surface acoustic waves (SAW), and a magneto-optical Kerr effect microscope measures the motion of DWs as a function of time, magnetic field and SAW amplitude. Initial measurements of DW movement under magnetic field pulses of variable width and height identify the location, characteristic depinning time (τ), pinning potential and critical field of highly reproducible strong pinning sites. SAW substantially assist the depinning of DW even from deep pinning potentials, providing a low power, remote depinning boost corresponding to a 4-9-fold increase in depinning probability. Acknowledgement This work was supported by NSF (DMR-1409622) and NSF Nebraska MRSEC (DMR-1420645). The research was performed in part in the Nebraska Nanoscale Facility: National Nanotechnology Coordinated Infrastructure and the Nebraska Center for Materials and Nanoscience, which are supported by the National Science Foundation under Award ECCS: 1542182, and the Nebraska Research Initiative.

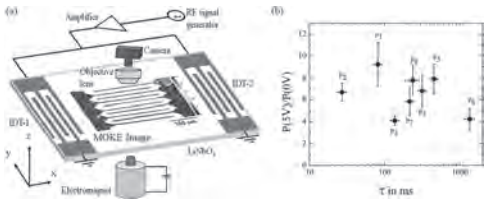

Figure 1. (a) Schematic of the magnetic stripes, IDTs, MOKE microscope and rf electronics. The magnetic stripes and IDTs consist of Co/Pt multilayers on 128 Y cut $LiNbO_3$. The MOKE image of the stripes shows up (red) and down (blue) magnetic domains. (b) Ratios of depinning probability with and without SAW for 8 pinning sites (P_i, i=1-8) on 3 different stripes as a function of the characteristic depinning time (τ), which is a measure of pinning strength.

R1-08. Experimental Observation and Control of Coupled Chiral Domain Walls in Synthetic Antiferromagnets Using in-Situ Lorentz Transmission Electron Microscopy. *N. Pandey*[1], M.P. Li[1], M. De Graef[1] and V. Sokalski[1] *1. Carnegie Mellon University, Pittsburgh, PA, United States*

We present Ir-based Synthetic Antiferromagnets (SAFs) composed of asymmetric building blocks of Pt/$[CoNi]_x$/Ir (PCI) and Ir/$[CoNi]_x$/Pt (ICP). The number of repeats 'x' and thickness of the Ir spacer layer allow, respectively, for simultaneous control of the interfacial Dzyaloshinskii-Moriya interaction (iDMI).[1] and interlayer exchange coupling (IEC).[2] CoNi layers show strong iDMI that reverses in sign when Pt and Ir stacking sequence are reversed (PCI or ICP), which induces Néel (over Bloch) DWs of opposite chirality. Using Lorentz Transmission Electron Microscopy (LTEM), we explore configurations of coupled SAF DWs with different magnitudes and sign of iDMI. We demonstrate conditions to directly observe these DWs with LTEM and study their "untangling" under in-situ perpendicular magnetic field (see Fig 1). Possible 1D excitations confined to the SAF DWs in these films are presented and compared to micromagnetic and LTEM simulations. The prospects for thin film SAFs with DMI will be discussed in the context of domain wall devices, where high velocity and a low critical current are desirable.

1. Lau, D., et al. "Disentangling Factors Governing Dzyaloshinskii Domain-Wall Creep in Co/Ni Thin Films Using PtxIr1−x Seed Layers." *Physical Review B*, vol. 98, no. 18, 2018, doi:10.1103/physrevb.98.184410. 2. Prudnikov, Aleksandr, et al. "Simultaneous Control of Interlayer Exchange Coupling and the Interfacial Dzyaloshinskii–Moriya Interaction in Ru-Based Synthetic Antiferromagnets." *IEEE Magnetics Letters*, vol. 10, 2019, pp. 1–4., doi:10.1109/lmag.2018.2882163.

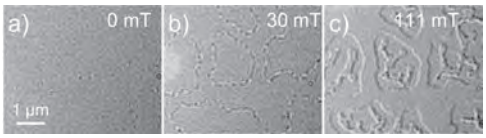

Fig 1. Observation of "Untangling" of Synthetic Antiferromagnet domain walls with application of in-situ perpendicular magnetic field in a Lorentz TEM
Configuration: Ta(30)/Pt(30)/$[Co(2)/Ni(6)]_6$/Co(2)/Ir(4)/Co(2)/ $[Co(2)/Ni(6)]_6$/Pt(30), thicknesses in parenthesis (Angstroms)

R1-09. Domain Wall Tilt and Enhancement of the Walker Limit in Stripes With Dzyaloshinskii-Moriya Interaction and Perpendicular Anisotropy. *O. Pylypovskyi*[1], V. Kravchuk[2,3], O. Volkov[1], J. Fassbender[1], D. Sheka[4] and D. Makarov[1] *1. Helmholtz-Zentrum Dresden-Rossendorf e.V., Dresden, Germany; 2. Karlsruher Institut fur Technologie, Karlsruhe, Germany; 3. Institut teoreticnoi fiziki imeni M M Bogolubova Nacional'na akademia nauk Ukraini, Kyiv, Ukraine; 4. Taras Shevchenko National University of Kyiv, Kyiv, Ukraine*

The efficiency of manipulation of domain walls and skyrmions in ferromagnetic racetracks with perpendicular anisotropy determines perspectives of development of data storage and logic devices relying on spintronic and spin-orbitronic concepts [1, 2]. The domain wall dynamics is dependent on its orientation with respect to the racetrack axis. In-plane fields [3], edge roughness [4] and current [5] result in the domain wall tilt in samples, possessing Dzyaloshinskii-Moriya interaction (DMI). Here, we show theoretically, that the tilt can appear in equilibrium and describe the domain wall dynamics under the action of external field. We consider a thin biaxial stripe with DMI of interfacial type [6]. The main easy axis of anisotropy is perpendicular to the plane, and the direction of the second easy axis lies in the stripe plane under the angle α to the stripe axis. While the shape anisotropy results in $\alpha = 0$, a general case $\alpha \neq 0$ can appear under the influence of other effects, e.g crystalline structure [7]. While the second easy axis defines the preferable in-plane magnetization within the domain wall, the DMI forces the domain wall being perpendicular to the magnetization gradient. The competition between these two energy contributions and the domain wall tension results in the unidirectional tilt of the whole domain wall. If the DMI is weak enough, there is an additional metastable domain wall state, tilted into the opposite direction. The symmetry break is observed not only for static magnetization texture, but also in the domain wall dynamics under the action of external magnetic field. The domain wall reveals fast and slow motion regimes for the opposite signs of A. The maximum of the Walker field and Walker velicities is determined by the angle A of the second easy axis anisotropy and does not coincide with a shape-induced anisotropy direction A=0. The domain wall possesses the switch of the magnetization direction inside the domain wall in the slow motion regime, which results in the faster motion.

[1] K.-S. Ryu, L. Thomas, S.-H. Yang et al., Nat. Nanotech., Vol. 8, 527 (2013) [2] O. Pylypovskyi, D. Sheka, V. Kravchuk et al., Sci. Rep. Vol. 6, 23316 (2016) [3] C. Muratov, V. Slastikov, A. Kolesnikov et al., Phys. Rev. B. Vol. 96, 134417 (2017) [4] E. Martinez, S. Emori, N. Perez et al. J. Appl. Phys. Vol. 115, 213909 (2014) [5] O. Boulle, S. Rohart, L. Buda-Prejbeanu et al., Phys. Rev. Lett. Vol. 111, 217203 (2013) [6] O. Pylypovskyi, V. Kravchuk, O. Volkov et al., J. Phys. D. (2020), DOI:10.1088/1361-6463/ab95bd [7] M. Heide, G. Bihlmayer, S. Blügel, Pys. Rev. B, Vol. 78, p. 140403 (2008).

R1-10. Chiral Magnetic Domain Walls Dynamics in Creep Regime. *C. Nguiepe Segnou*[1], M. Belmeguenai[2], S. Eimer[1], Y. Roussigne[2], S. Cherif[2], A. Stashkevich[2], T. Devolder[1] and J. Adam[1] *1. C2N, Paris-Saclay University, Palaiseau, France; 2. Universite Sorbonne Paris Nord Institut Galilee, Villetaneuse, France*

Chiral magnetic domain walls stabilised by the interfacial Dzyaloshinskii-Moriya interaction are of great technological interest since the latter favors a given Néel wall with fast current-driven domain wall propagation [1]. We study experimentally by Kerr microscopy, numerically and analytically chiral magnetic domain wall motion in the creep regime under easy-axis driving fields in materials with a perpendicular magnetic anisotropy with an in plane magnetic field. We study two samples: one asymmetric [Pt(3nm)/Co(0.6nm)/Ta(3nm)] and one symmetric [Pt(3nm)/Co(0.6nm)/Pt(3nm)]. Brillouin light scattering has been used to determine the DMi constant: $D = -1.2 mJ/m^2$ and $D = 0$ mJ/m^2 in the asymmetric and symmetric case respectively. As expected from the DMi constant measured by BLS, the DW velocity curves as a function of the in-plane magnetic field are qualitatively different. In the asymmetric system, we could not reach a minimum of the velocity v within our experimental in plane field range (Fig 1a), consistently with the DM field = 220 mT estimated from the BLS measurements. For the symmetric system, a slight asymmetry is observed with a minimum around $\mu_0 H_{ip} = 0$ mT (Fig 1c). We detail the creep regime analysis by studying the evolution of the depinning field from the creep regime to the flow regime for different $\mu_0 H_{ip}$ by studying the linear variation of $\ln(v)$ vs $(\mu_0 H_z)^{-1/4}$. In the asymmetric case the slope is constant (Fig 1b) unlike in the symmetric case (Fig 1d): when $|\mu_0 H_{ip}| < 50$ mT the DW goes from left-handed Néel to Bloch to right-handed Néel wall and the slope varies while for larger fields the slope is constant. We can extrapolate the evolution of the depinning field which is strongly influenced by the in-plane biasing field. In the asymmetric system, we observe an excess of velocity with respect to the creep law close to the depinning field (Fig 1d, explained by the increase of the size of the deterministic relaxation close to the depinning transition [2]. The stronger the DMi field, the more this excess of velocity occurs at larger out-of-plane field values.

[1] A. Thiaville, *et al.* EPL 100, 57002 (2012) [2] N. B. Caballero, *et al.*, Phys. Rev. B 96, 224422 (2017).

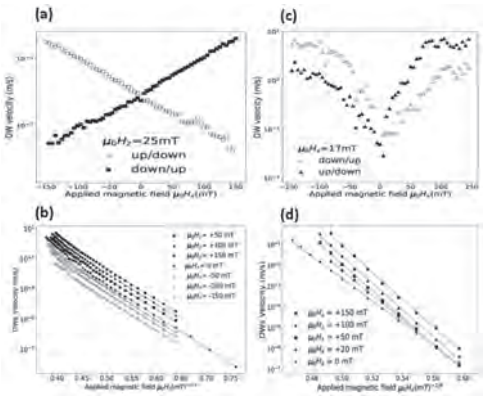

Figure 1: DW velocity vs in-plane field for Pt/Co/Ta (a), and for Pt/Co/Pt (c). DW velocity vs out-of-plane field Pt/Co/Ta (b), and for Pt/Co/Pt (d).

R1-11. Current Induced Domain Wall Motion at the Magnetic Compensation Point in Manganese Nickel Nitride (MnNiN) Thin Films. *S. Ghosh*[1,2], T. Komori[2], A. Hallal[1], T. Hirose[2], J. Peña Garcia[3], H. Okuno[4], J. Vogel[3], M. Chshiev[1], J. Attané[1], T. Suemasu[2], L. Vila[1] and S. Pizzini[3] *1. Grenoble Alpes University, CEA, CNRS, Grenoble INP, IRIG-Spintec, Grenoble, France; 2. University of Tsukuba, Graduate School of Pure and Applied Sciences, Tsukuba, Japan; 3. Grenoble Alpes University, CNRS, Institut Néel, Grenoble, France; 4. Grenoble Alpes University, CEA, IRIG-MEM, Grenoble, France*

Spintronics has developed into a growing field with the fabrication of magnetic memories and logic devices. Domain wall motion is a major part of the research in spintronics where spin polarized current is used to move the domain walls by two mechanisms spin tranfer torque(STT) and spin orbit torque(SOT). Compensated ferrimagnets have been in focus recently for their ability to reach the magnetic and angular compensation points. At the angular compensation point, the precessional motion of the local magnetic moment becomes negligible which massively enhances the domain wall velocity near this point[1,2]. In our previous studies, we had shown epitaxially grown ferrimagnet Manganese Nitride(Mn_4N) having an anti-perovskite crystal structure with Mn atoms at the corner and the face centre sites while Nitrogen atom in the centre[3]. It has a very low magnetization (71kA/m) and a high perpendicular magnetic anisotropy(PMA) with mm sized domains[3]. Such small magnetization and high PMA is necessary for faster domain wall motion. Such properties led us to observe a very high domain wall velocity of 900 m/s at $1.2*10^{12}$ A/m^2 [4] using pure STT. Here we report an even larger domain wall velocity of more than 2000 m/s at $1.16*10^{12}$ A/m^2 using pure adiabatic STT near the magnetic and angular compensation point in epitaxially grown Ni substituted Mn_4N nanowires (MnNiN). We also show a very small thresold current density of $1*10^{11}$ A/m^2. This high speed is comparable to the best velocities obtained by SOT with the assitance of an external in-plane field. In our case, such domain wall velocity is achieved without any external in-plane field, with the sole action of pure current in this single layer system. Addtionally, we also show a reversal in the direction of the domain wall motion after the magnetic compensation point, where the domain walls move in the same direction as the current. We discuss this reversal of the domain wall motion phenomena with the help of DFT calculations.

1. K.J. Kim, S.K. Kim, Y Hirata, Nature Materials., Vol 16, p1187 (2017) 2. L. Caretta, M. Mann, F. Buttner, Nature Nanotechnology., Vol 13, p1154 (2018) 3. T. Gushi, L. Vila, O. Fruchart., Jpn J. Appl. Phys. Vol 57, p120310 (2018) 4. T. Gushi, M. J. Klug, J.P. Garcia, Nano Letters, Vol 19, p8716 (2019)

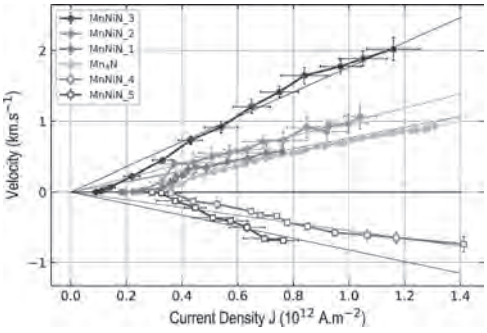

Fig. 1 Current density versus domain wall velocity curves showing the velocites obtained from different Ni concentrations before and after the compensation points at room temperature.

R1-12. Directional Growth of Dendritic Domains in Co/Ni/Pt Multilayers - Significance of Domain Wall Steady-State Dynamics and Dispersive Stiffness. *J.A. Brock*[1], M.D. Kitcher[2], R. Medapalli[1], V. Sokalski[2] and E. Fullerton[1] *1. Center for Memory and Recording Research, University of California San Diego, La Jolla, CA, United States; 2. Materials Science and Engineering Department, Carnegie Mellon University, Pittsburgh, PA, United States*

The interfacial Dzyaloshinskii-Moriya interaction (iDMI) attracts significant attention due to its potential applications in efficient spintronic devices. While the impacts of symmetry-breaking in-plane magnetic fields on the growth of large circular domains in systems with iDMI have been studied extensively, the behavior of dendritic domains hasn't. We present an experimental study of $[Co(0.7\text{ nm})/Ni(0.5\text{ nm})/Pt(0.7\text{ nm})]_{xN}$ ($1 \le N \le 5$) multilayers designed to have asymmetric Pt/Co and Ni/Pt interfaces and perpendicular anisotropy. MOKE images reveal that for $N \ge 3$, reversal in perpendicular fields occurs via dendrites and that when a constant in-plane magnetic field is applied, the growth directionality is strongly linked to the field direction and strength. At low fields, growth is roughly perpendicular to the field (Fig. 1a). The growth direction subsequently becomes more collinear with increasing in-plane field strength, first in the field direction (Fig. 1b) and then antiparallel above a critical field (Fig. 1c). The experimental directionalities shown in Fig. 2 are not predicted from the elastic energy creep framework commonly applied to circular domains in the presence of iDMI [1, 2]. However, the field-like torque arising from the propagation field can impose a steady-state wall profile that deviates significantly from the static case [3]. Furthermore, recent work indicates that the stiffness, compared to the domain wall energy, can better capture the creep elastic energy scale and trends in the domain propagation direction [4]. Integrating these two treatments into a creep model, we find that the calculated velocities agree well with the experimentally observed field-dependent propagation trends (Fig. 2).

[1] S.-G. Je *et al.*, Phys. Rev. B 88 (2013). [2] A. Hrabec *et al.*, Phys. Rev. B 90, 020402(R) (2014). [3] L. Sanchez-Terjerina *et al.*, J. Magn. Magn. Mater. 423, 405 (2017). [4] J.P. Pellegren *et al*., Phys. Rev. B 119, 027203 (2017).

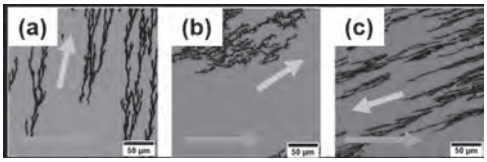

Figure 1: Polar MOKE images of domain growth in the $[Co/Ni/Pt]_3$ sample in response to perpendicular field pulses applied in static in-plane fields of (a) +40 mT, (b) +120 mT, and (c) +200 mT. The blue arrows show the in-plane field direction.

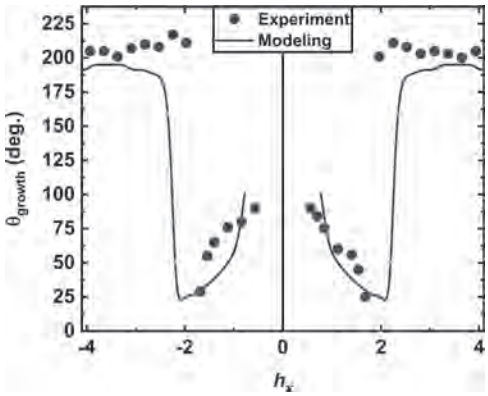

Figure 2: The favored growth direction θ_{growth} (relative to the in-plane field direction) of domains in a $[Co/Ni/Pt]_3$ sample as a function of reduced in-plane field strength h_x as observed experimentally and compared to a steady-state dynamic-stiffness-creep model.

R1-13. Creating 3D Nanomagnetic Circuits for Spintronics Applications. *F. Meng*[3], C. Donnelly[3], C. Abert[4], S. Holmes[1], Z. Xiao[2], J. Liao[3], D. Suess[4] and A. Fernandez-Pacheco[5] *1. University College London, London, United Kingdom; 2. Engineering, University of Cambridge, Cambridge, United Kingdom; 3. Physics, University of Cambridge, Cambridge, United Kingdom; 4. Physics, Universitat Wien, Wien, Austria; 5. Physics, University of Glasgow, Glasgow, United Kingdom*

Bringing nanomagnetism into the third dimension is of growing interest due to the many advantages that 3D structures provide. The possibility for larger volumes and higher surface-to-volume ratios, as well as the introduction of new topologies, chirality and curvature into the structure, lead to numerous opportunities for new physics and applications.[1] Combining this promising field of 3D nanomagnetism with the well-established field of spintronics offers huge opportunities, a key example being the proposal to use 3D nanomagnets in a 3D racetrack architecture that promises the delivery of non-volatile and ultra-high-density information storage[2]. However, the integration of 3D nanomagnets into 2D microelectronics is challenging and has so far impeded the realisation of technological applications such as sensing, computing or memory. Now, with 3D Nano-printing capabilities, we have developed a method to integrate complex 3D magnetic nanostructures [3] into 2D microelectronic circuits and to measure the magneto-transport properties of our 3D nanomagnetic structures. Here, we demonstrate the direct integration of a complex 3D magnetic nanostructure in a microelectronic circuit (Figure 1). In particular, we exploit the recent advances of Focused Electron Beam Induced Deposition, a 3D nano-printing technique, to directly print a high-quality 3D Cobalt nanobridge on pre-synthesized electrical contacts. This 3D nanomagnetic circuit allows for the determination of the bridge's magnetic and transport properties by performing magnetotransport measurements for different geometries of the field with respect to the 3D nanostructure (Figure 2). In addition, we infer the field-induced switching process of the 3D nanostructure from the transport measurement, that includes the nucleation, propagation and pinning of domain walls. [4]. This methodology can be extended to more complicated geometries and materials, and so this work represents the first step towards the realisation of 3D nanomagnetic devices and will facilitate further exploration of 3D nanomagnetism for both fundamental and device-based studies.

1 A. Fernandez-Pacheco, R.Streubel, O. Fruchart, Nature Communications., Vol. 8, p.15756 (2017) 2 S. Parkin, M. Hayashi, L.Thomas, Science., Vol. 320, p.190 (2008) 3 L.Skoric, D. Sanz-hernandez, F. Meng., Vol. 20, p.184 (2020) 4 F.Meng, C. Donnelly, C. Abert (In preparation).

Fig.1 Direct fabrication and measurent of the Co nanobridge

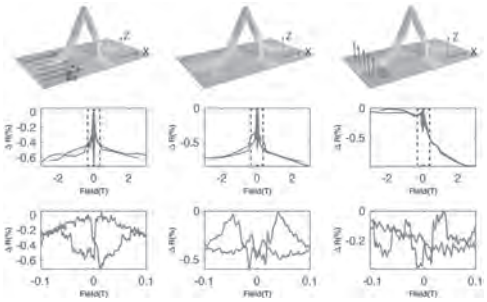

Fig.2 MR measurements for B applied in different directions

Session R2
DOMAIN WALLS AND THE DZYALOSHINSKII-MORIYA INTERACTION II

Damien McGrouther, Chair
University of Glasgow, Glasgow, United Kingdom

INVITED PAPER

R2-01. Ultrafast Domain Wall Dynamics in Metallic and Insulating Ferrimagnets. *L. Caretta*[1,2], S. Kim[3], K. Lee[4], C. Ross[5] and G. Beach[5]
1. Materials Science and Engineering, University of California Berkeley, Berkeley, CA, United States; 2. Materials Sciences Division, E O Lawrence Berkeley National Laboratory, Berkeley, CA, United States; 3. Department of Physics and Astronomy, University of Missouri, Columbia, MO, United States; 4. Department of Materials Science and Engineering, Korea University, Seongbuk-gu, The Republic of Korea; 5. Materials Science and Engineering, Massachusetts Institute of Technology, Cambridge, MA, United States

A promising approach is to encode bits of information for next-generation memory and logic is by using solitons, such as chiral domain walls (DW) or topological skyrmions, which can be translated by currents across race-track-like wire devices[1,2]. One technological and scientific challenge is to stabilize small spin textures and to move them efficiently with high velocities, which is critical for dense, fast memory. However, despite over a decade of research on ferromagnetic materials, current-driven spin texture dynamics faced a "speed limit" of a few hundred m/s, and room-temperature-stable magnetic skyrmions were an order of magnitude too large to be useful in any competitive technologies. These problems were rooted in two fundamental characteristics of ferromagnets: large stray fields, which limit spin texture size[3] (packing density), and precessional dynamics, which limit speed[4]. By using a broader class of multi-sublattice magnetic materials, namely compensated metallic and insulating ferrimagnets, fundamental limits plaguing ferromagnets can be overcome. Here, we engineer compensated chiral ferrimagnets with reduced magnetisation and angular momentum, realizing order-of-magnitude improvements in both bit size and speed[5]. By using ferrimagnetic Pt/$Gd_{44}Co_{56}$/TaOx films with a sizeable Dzyaloshinskii–Moriya interaction (DMI), we realize a current-driven DW motion with a speed of 1.3 km s^{-1} near the angular momentum compensation temperature and room-temperature-stable skyrmions with minimum diameters close to 10 nm near the magnetic compensation temperature (Figure 1). Both the size and dynamics of the ferrimagnet are in excellent agreement with a simplified effective ferromagnet theory. In addition to metallic systems, a broader, ubiquitous class of materials – ferrimagnetic insulating garnets – have been extensively studied for their technologically-desired magnetooptical and spintronic properties. Their low damping and ferrimagnetic dynamics also make them ripe candidates for ultrafast DW motion. Although spin-orbit effects and spin-transport phenomenon from adjacent heavy metal layers have been used to manipulate the magnetisation in this class of materials[6], the DMI and chiral spin textures had not been discovered. Here, we discover chiral magnetism that allows for pure spin-current-driven chiral DW motion in iron garnet films and elucidate the origins of the chiral exchange interaction in these films. Moreover, by exploiting reduced angular momentum and low-dissipation in ferrimagnetic insulators, we drive DWs to their relativistic limit using pure spin currents from the spin Hall effect of Pt, achieving record velocities in excess of 4300 m/s, within ~10% of the relativistic limit (Figure 2). We observe key signatures of relativistic motion including Lorentz contraction and velocity saturation. The experimental results are well-explained through analytical and atomistic modeling. More broadly, these observations provide critical insight into the fundamental limits of the dynamics of magnetic solitons and establish a readily-accessible experimental framework to study relativistic solitonic physics. Technologically, this work shows that high-speed, high-density spintronic devices based on current-driven spin textures can be realized using materials in which magnetisation and angular momentum are compensated.

1. Parkin, S. S. P., Hayashi, M. & Thomas, L. *Science* 320, 190–4 (2008). 2. Fert, A., Cros, V. & Sampaio, J. *Nat. Nanotechnol.* 8, 152–156 (2013). 3. Büttner, F., Lemesh, I. & Beach, G. S. D. *Sci. Rep.* 8, 4464 (2018). 4. Kim, K.-J. J. *et al*. *Nat. Mater.* 16, 1187–1192 (2017). 5. Caretta, L. *et al. Nat. Nanotechnol.* 13, 1154–1160 (2018). 6. Avci, C. O. *et al*. *Nat. Mater.* 16, 309–314 (2017).

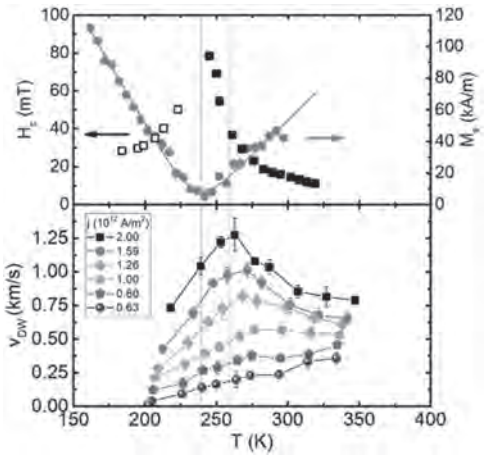

Coercivity (H_c), magnetization (M_s) as a function of temperature (T) and domain wall velocity (v_{DW}) as a function of temperature (T) for various current densities (j) in Pt/$Gd_{44}Co_{56}$/TaOx. The tan vertical line indicates magnetic compensation, while the green vertical line indicates angular momentum compensation.

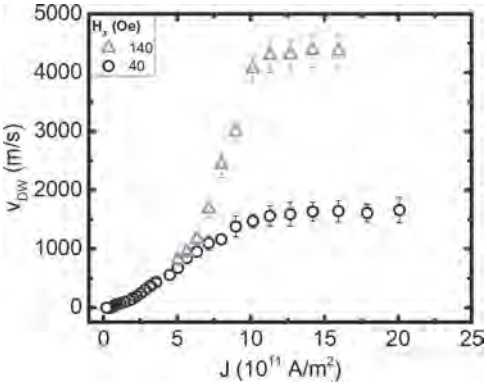

Domain wall velocity v_{DW} as a function of current density J in a low-damping iron garnet/Pt heterostructure for various in-plane fields H_x

CONTRIBUTED PAPERS

R2-02. Interface Engineering to Control the Dzyaloshinskii-Moriya Interaction in Ferrimagnetic GdCo: *ab Initio* Calculations.
M. Morshed[1], K. Khoo[2], Y. Quessab[3], J. Xu[3], R. Laskowski[2], P. Balachandran[4,5], A.D. Kent[3] and A.W. Ghosh[1,6] *1. Department of Electrical and Computer Engineering, University of Virginia, Charlottesville, VA, United States; 2. Institute of High Performance Computing, Agency for Science, Technology and Research, Singapore, Singapore; 3. Center for Quantum Phenomena, Department of Physics, New York University, New York, NY, United States; 4. Department of Materials Science and Engineering, University of Virginia, Charlottesville, VA, United States; 5. Department of Mechanical and Aerospace Engineering, University of Virginia, Charlottesville, VA, United States; 6. Department of Physics, University of Virginia, Charlottesville, VA, United States*

The interfacial Dzyaloshinskii-Moriya Interaction (DMI), an anti-symmetric exchange originating from strong spin-orbit coupling (SOC) in systems with broken inversion symmetry, plays a critical role in stabilizing chiral spin textures such as magnetic skyrmions. Magnetic skyrmions with their non-trivial properties have recently emerged as a potential candidate for next-generation spintronics applications such as race-track memory and logic devices [1, 2]. Recently, ferrimagnetic materials have been found to be more attractive for hosting stable ultra-small skyrmions at room temperature than conventional ferromagnets, due to their low saturation magnetization, low stray field, and fast spin dynamics [3, 4]. However, to manipulate skyrmions properties, controlling the DMI is essential. Herein, we present a systematic analysis of the DMI variation in compensated ferrimagnetic Pt/GdCo/$Pt_{1-x}W_x$ multilayer as a function of Tungsten (W) composition (x) using Density Functional Theory (DFT). We find that a small amount of W (~10%) is sufficient to give rise to a non-zero DMI by breaking the inversion symmetry of Pt/GdCo/Pt. We also find that our calculated DMI increases as the W composition increases, but saturates at higher W composition, in agreement with experiment [5]. We show that the vanishing of spin-orbit coupling (SOC) energy to the adjacent metal layers of the top interface, and the simultaneous constancy of the bottom interface are responsible for such a saturating behavior of the DMI. Additionally, we investigate Pt/GdCo/X, where X=Ta, W, Ir to demonstrate the effect of capping layer heavy metals on the DMI. Our results predict that W in the capping layer favors a higher value of the DMI than Ta and Ir. Our results open up exciting combinatorial possibilities for controlling the DMI in ferrimagnets to nucleate and manipulate ultrasmall high-speed skyrmions.

[1] A. Fert, N. Reyren and V. Cros, Nat. Rev. Mater., 2, 1-15 (2017) [2] H. Vakili, Y. Xie and A. W. Ghosh, arXiv (2020), 2001.00729 [3] L. Caretta, M. Mann and F. Büttner, Nat. Nanotechnol., 13, 1154-1160 (2018) [4] S. J. Poon and C. T. Ma, J. Supercond. Novel Magn., 33, 269-273 (2020) [5] Y. Quessab, J. Xu, C. T. Ma, Sci. Rep., 10, 1-8 (2020)

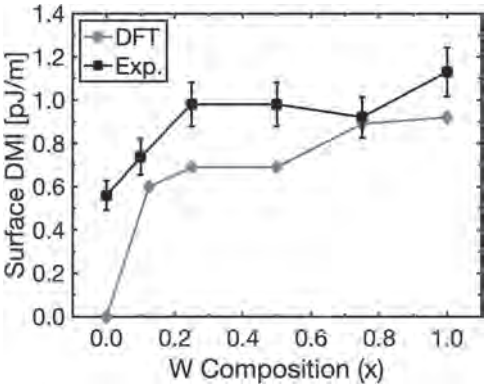

Fig. 1 Surface DMI as a function of W composition (x) in Pt/GdCo/$Pt_{1-x}W_x$ structure. In the experiment [5], the DMI at x=0 is associated with asymmetries introduced in the film deposition.

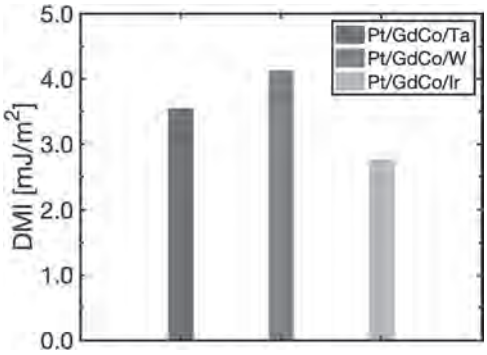

Fig. 2 Calculated DMI in Pt/GdCo/X, where X=Ta, W, Ir.

R2-03. Tunable Magnetic Anisotropy and Dzyaloshinskii-Moriya Interaction at Cobalt/Diamond Interfaces.
J. Jiang[1], J. Liang[2], Q. Cui[2], Z. Wang[2], W. Mi[1] and H. Yang[2,3] *1. Tianjin University, Tianjin, China; 2. Ningbo Institute of Industrial Technology Chinese Academy of Sciences, Ningbo, China; 3. Center of Materials Science and Optoelectronics Engineering, University of Chinese Academy of Sciences, Beijing, China*

The interfacial Dzyaloshinskii-Moriya interaction (DMI) has been recognized to play a key role in the formation of exotic chiral magnetic textures[1]. Here, the interfacial DMI and magnetic anisotropy of Co(0001)/diamond(111) interfaces are investigated by first-principles calculations. Significant DMI with clockwise chirality is generated at the Co/diamond interface. The overall DMI strength of Co film decreases by boron doped diamond (B-Dia), while the DMI chirality turns into anticlockwise by nitrogen doped diamond (N-Dia). Large perpendicular magnetic anisotropy (PMA) appears at both Co/diamond and Co/B-Dia interfaces, while that at the Co/N-Dia interface is weakened. The DMI and PMA can be ascribed to the occupations of *d* orbitals of interfacial Co atomic layers. This work was supported by the National Natural Science Foundation of China (51871161 and 11874059), Key Research Program of Frontier Sciences, CAS, Grant NO. ZDBS-LY-7021, Zhejiang Province Natural Science Foundation of China (LR19A040002).

[1] A. Fert, N. Reyren, and V. Cros, Magnetic skyrmions: advances in physics and potential applications. Nat. Rev. Mater. 2, 17031 (2017).

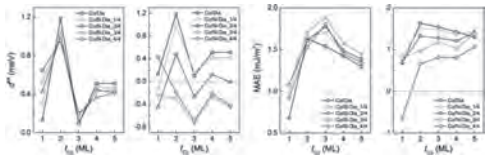

Calculated DMI and magnetic anisotropy energy as functions of Co atomic layer number and doping concentration at the Co/diamond interfaces.

R2-04. Withdrawn

R2-05. Interplay Between Spin-Orbit Torque and Dzyaloshinskii-Moriya Interactions in Thin Amorphous Ferrimagnetic Films.
Y. Quessab[1], J. Xu[1], N.N. Statuto[1] and A.D. Kent[1] *1. Department of Physics, New York University, New York, NY, United States*

In ferrimagnetic films spin-orbit torque (SOT) has been used for current-induced magnetization switching[1] but also domain wall[2] and skyrmion motion[3]. Ferrimagnets with interfacial Dzyaloshinskii-Moriya interaction (DMI) are attractive materials due to their low stray field and fast spin dynamics which can lead to ultrasmall[2] and fast skyrmions. Yet, so far, the reported skyrmion velocities[3] are much lower than of domain walls[2]. The current-induced dynamics of DMI skyrmions is intrinsically related to the charge-spin conversion efficiency. Here we investigate the DMI and SOT in CoGd ferrimagnetic thin films, in which we previously showed that we can tune the DMI in a range that allows sub-100 nm skyrmion formation[4]. DMI and SOT both arise from interfacial effects. It is thus important to understand the interplay between these two effects to achieve efficient and fast skyrmion motion. For this purpose, we studied Pt/Co_xGd_{1-x}/(Ir, W or Ta) films as a function of the cap layer to systematically vary the DMI and spin-Hall efficiency (SHE). We performed SOT magnetization switching experiments that we correlate to the measurements of DMI energy and SHE. Figure 1 shows an example of SOT switching phase diagram. The switching current density for different field values and cap layer is summarized in Fig. 2(a). W and Ta capping, which induce the largest net DMI, provide the lowest switching current density, thus the most efficient switching. However, Pt/CoGd/Ir requires a smaller in-plane field to achieve full magnetization switching. In the low field region, the films capped by W and Ta exhibit a metastable state [Fig. 2(b)] composed of skyrmion bubbles as suggested by micromagnetic simulations. Our results provide insight into achieving energy-efficient and fast skyrmion devices.

[1] S.-G. Je *et al.*, APL 112, 062401 (2018) [2] L. Caretta *et al.*, Nature Nanotechnology 13, 1154 – 1160 (2018) [3] S. Woo *et al.*, Nature Communications 9, 959 (2018). [4] Y. Quessab *et al.*, Scientific Reports 10, 7447 (2020)

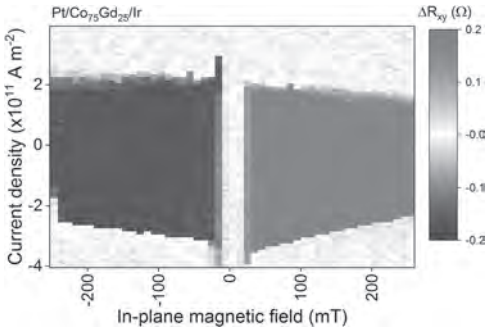

Figure 1: SOT switching phase diagram of $Pt/Co_{75}Gd_{25}/Ir$.

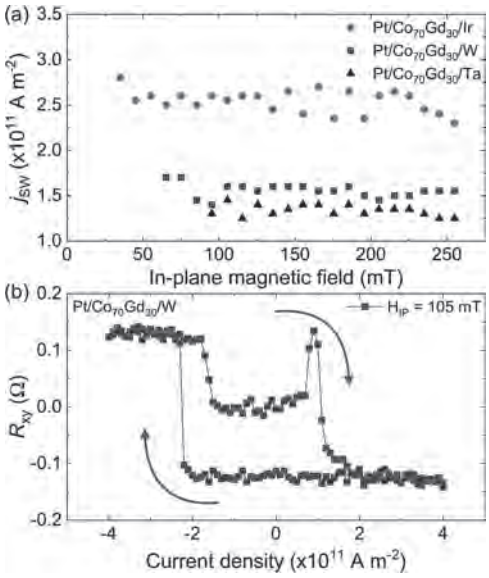

Figure 2: (a) Switching current density for different capping layers. (b) Switching hysteresis loop of $Pt/Co_{70}Gd_{30}/W$ showing an intermediate metastable state.

R2-06. Universal High-Speed Dynamics of Distorted Bubble Skyrmions in an Uncompensated Amorphous Ferrimagnet. *K. Litzius*[1], F. Buettner[1], A. Wittmann[1], W. Zhou[2], C. Ma[2], J. Gräfe[3], N. Träger[3], S. Finizio[4], Y. Quessab[5], D. Suzuki[1], L. Caretta[1], M. Huang[1], S. Sheffels[1], S. Huang[1], H. Nembach[6], G.A. Riley[6], J. M. Shaw[6], M. Valvidares[7], P. Gargiani[7], G. Schütz[3], A.D. Kent[5], J. Poon[2] and G. Beach[1] *1. Massachusetts Institute of Technology, Cambridge, MA, United States; 2. University of Virginia, Charlottesville, VA, United States; 3. Max Planck Institute for Intelligent Systems, Stuttgart, Germany; 4. Paul Scherrer Institut, Villigen, Switzerland; 5. Department of Physics, New York University, New York, NY, United States; 6. National Institute of Standards and Technology, Gaithersburg, MD, United States; 7. ALBA Synchrotron Light Source, Barcelona, Spain*

Magnetic skyrmions are topologically stabilized spin configurations that, like domain walls (DWs), can react to external stimuli by collective displacement, which is both physically intriguing and bears promises to realize next generation non-volatile data storage technologies. [1] However, skyrmions in ferromagnets are challenging to implement in wire devices due to their movement at an angle to the current direction (skyrmion Hall effect) and comparably low speeds. [2] Antiferromagnetically coupled systems with compensated angular momentum (such as compensated ferrimagnets and natural antiferromagnets) can reduce this skyrmion Hall effect to zero and provide high speed dynamics to move spin structures at unprecedented speeds, thus making them promising candidates for spintronic devices. [3,4] Besides the compensation of perpendicular motion of skyrmions with respect to the drive, the predictability and thus the study of the stochasticity of their trajectories is also of major importance for applications. Most notably, the models describing rigid, circular bubble domains and skyrmions differ significantly from those for straight 180° DWs, leading to different speed predictions for skyrmions and DWs at a given drive. [5] However, DWs and skyrmions are often not perfectly straight or circular, making predictions potentially difficult as it is not always clear which model describes a given deformed skyrmion with the highest accuracy. Here, we study how deformed DWs and bubble skyrmions move in uncompensated ferrimagnetic Pt/CoGd/W in response to current pulses. We find that all 1D spin textures as well as all fully enclosed spin textures, reach speeds >500 m/s and display identical dynamics (Fig. 1), independent of their exact shape. While high speeds are indeed reached, the predicted differences between skyrmion and

DW dynamics could not be observed. We attribute this deviation from the commonly used model to significant deformations of the skyrmions during their motion.

[1] K. Everschor-Sitte *et al.*, *Journal of Applied Physics* 124, 240901 (2018). [2] W. Jiang *et al.*, *Physics Reports* 704, 1-49 (2017). [3] S. Woo *et al.*, *Nature Communications* 9, 959 (2018). [4] L. Caretta *et al.*, *Nature Nanotechnology* 13, 1154 (2018). [5] F. Büttner, I. Lemesh & G. S. D. Beach, *Scientific Reports* 8, 4464 (2018).

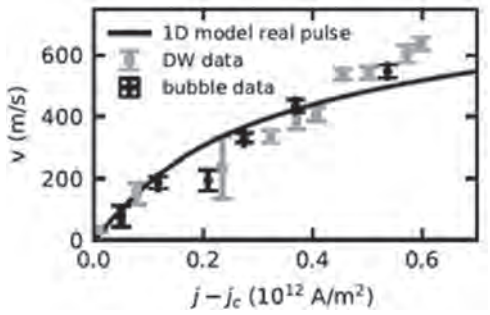

Fig. 1: Speed comparison of magnetic skyrmion bubble and DWs in the same material. Both saturate and follow the 1D-DW model.

R2-07. MnGa/Co_2MnSi Bilayer for Spin-Orbit Torque Magnetization Switching. *M. Yamanouchi*[1], K. Jono[2], F. Shimohashi[2] and T. Uemura[2]
1. Research Institute for Electronic Science, Hokkaido University, Sapporo, Japan; 2. Division of Electronics for Informatics, Graduate School of Information Science and Technology, Hokkaido University, Sapporo, Japan

Spintronics devises using spin-orbit torque (SOT) magnetization switching is attractive for low-power and high-speed electronics. MnGa/Co_2MnSi bilayer is promising for realizing such devises because of a relatively large perpendicular magnetic anisotropy with low magnetization of MnGa and half-metallicity of Co_2MnSi (CMS) [1]. Here, we report SOT and SOT magnetization switching in MnGa/CMS/Ta structures. Stacking structures consisting of, from the substrate side, MgO(10)/NiAl(5)/MnGa(2,3)/CMS(0,1)/Ta(5)/MgO(2) were deposited on a (001) MgO single-crystal substrate (numbers in parentheses are nominal thicknesses in nm). The films were processed into Hall devices with a 5-μm-wide channel. Measurements of transverse resistance reflecting the anomalous Hall effect showed all films had perpendicular magnetization. Moreover, magnetization and polar Kerr signal measurements showed MnGa and CMS were antiferromagnetically coupled each other. We examined SOT magnetization switching under in-plane magnetic field (parallel to channel direction) $\mu_0 H_x$ in the MnGa(2)/CMS/Ta and MnGa(2)/Ta devices. Clear magnetization switching was observed for both devices and the switching current for the MnGa/CMS/Ta device was about half of that for the MnGa/Ta device. The directions of current and $\mu_0 H_x$ inducing magnetization switching were consistent with those expected from the switching by the SOT originating from the spin Hall effect in the Ta layer. We also evaluated the effective magnetic field $\mu_0 H_{\mathrm{eff}}$ originating from the SOT in the MnGa(3)/CMS/Ta and MnGa(3)/Ta devices by examining interaction between domain walls and the SOT [2]. The value of $\mu_0 H_{\mathrm{eff}}$ was ~5 times larger for the MnGa/CMS/Ta device than that for the MnGa/Ta device at 12 mA and $\mu_0 H_x$ = 0.45 T. These results indicate that MnGa/CMS bilayer structure is effective for enhancing efficiency of generating SOT and reducing switching current. The reduction of magnetization by the antiferromagnetic coupling can contribute to the enhancement. This work was supported in part by Japan Society for the Promotion of Science KAKENHI (Grant No. 20H02174 and 20H02598), the Center for Spintronics Research Network, and Hitachi Metals-Materials Science Foundation.

[1] S. Mao *et al*., Sci. Rep. 7, 43064 (2017). [2] M. Yamanouchi *et al*., Jpn. J. Appl. Phys. 58, 100903 (2019).

R2-08. In Pursuit of the Anisotropic Dzyaloshinskii-Moriya Interaction: Structural and Magnetic Characterization of Uniaxial Pt/Co-Based C_{2V} Thin Films. *M.D. Kitcher*[1], T. Mewes[2], C. Mewes[2], M. De Graef[1] and V. Sokalski[1] *1. Materials Science & Engineering, Carnegie Mellon University, Pittsburgh, PA, United States; 2. Physics and Astronomy, University of Alabama, Tuscaloosa, AL, United States*

Antiskyrmions and other unconventional topological excitations can potentially be supported by low-symmetry ferromagnet--heavy metal (FM-HM) thin films by the Dresselhaus-type anisotropic Dzyaloshinskii-Moriya interaction (aDMI) arising at the FM-HM interfaces. This work presents the potential of C_{2V} Ag/Pt/Co-based films to exhibit aDMI and stabilize new chiral magnetic textures. X-ray diffraction 2θ-ω scans of Ag/Pt/Co/Pt films grown epitaxially on Si(110) single crystal substrates show that Co grows predominantly with (10.0) hexagonal closed-packed (hcp) orientation, deviating from the (110)-oriented face-centered cubic (fcc) structure of Ag and Pt. These findings were corroborated by selected area electron diffraction patterns and further supported by a strong in-plane uniaxial anisotropy measured along the hcp c-axis by alternating gradient field magnetometry. Crosstie domain walls in these films were directly observed by Lorentz transmission electron microscopy, which are also predicted from micromagnetic simulations. The materials system introduced above creates the previously unexplored situation where an in-plane easy axis is coupled with a strong (potentially anisotropic) DMI, which may lead to interesting spin configurations. However, to break the z-mirror plane [v1] and create a non-zero DMI, we fabricate thinner Ag/Pt/$[Co/Ni]_x$/Pt films. X-ray diffraction analysis suggest that the hcp structure is preserved throughout the Ni layers. Structural and magnetic observations of this lower symmetry film stack are compared to micromagnetic simulations and discussed in the context of C_{2V} films potentially exhibiting Dresselhaus-type aDMI and hosting antiskyrmions.

1. U. Güngördü et al., Physical Review B., 93, 064428 (2016) 2. M. Hoffman et al., Nature Communications., 8, 308 (2017)

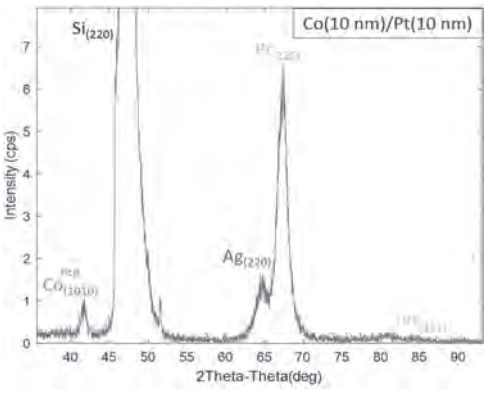

Fig. 1: X-ray diffraction 2θ-ω scan of Co(10 nm) sample showing the Co(10.0) peaks indicative of a dominant (10.0)-oriented hcp-Co phase in spite of the (110)-oriented fcc structure of the Ag and Pt layers, represented by the (220) peaks.

Fig. 2: (a) LTEM image of a saw-tooth domain (b) Induction map showing the in-plane magnetization profile of the leftmost section of the domain as calculate using the transport-of-intensity equations formalism.

R2-09. The Effects of Disorder on Hysteresis Loops in Chiral Magnets.
V. Nehruji[1], M. Beg[1], H. Fangohr[1,2], T. Hesjedal[3], T. Lancaster[4], P. Hatton[4] and O. Hovorka[1] *1. University of Southampton, Southampton, United Kingdom; 2. European XFEL GmbH, Schenefeld, Germany; 3. Oxford University, Oxford, United Kingdom; 4. Durham University, Durham, United Kingdom*

We investigate the effect of the distribution of pinning sites on the magnetization behavior in systems with Dzyaloshinskii–Moriya interaction (DMI). We consider the standard classical spin Hamiltonian with Heisenberg exchange, DMI, uniaxial anisotropy statistically varying across the lattice sites, and the Zeeman energy. The statistical variation of the anisotropy constants follows from a spatial Gaussian distribution with non-zero mean and standard deviation σ, and serves as a way to model the structural disorder in the sample. First, we discuss the reduction of the model to a lattice resolved mean-field theory and the development of energy minimisation algorithm for solving it. This approach allows to compute systematically and efficiently the magnetisation versus field, $M(H)$, dependence for variable σ and temperature, and can be used for computing qualitative thermodynamic phase diagrams to explore material behaviour and to guide the computationally costly Monte-Carlo simulations. We show that as the σ increases, relative to the strength of exchange interaction and DMI, the nature of the reversal modes observed along a typical $M(H)$ hysteresis loop changes in a certain temperature window. Namely, in 'clean' systems with small σ, the reversal proceeds first through the appearance of skyrmion lattices at low external fields, while in 'dirty' systems with large σ the reversal is through the nucleation of individual or small groups of skyrmions. We systematically quantify this effect and discuss its broader implications for applications.

R2-10. Tuning Spin-Orbit Torques Across the Phase Transition in VO_2/NiFe Heterostructures.
J. Kim[1], K. Lee[1], J. Cramer[1], D. Han[2], P. Salev[3], P.N. Lapa[3], N.M. Vargas[3], I.K. Schuller[3], G. Jakob[1] and M. Klaui[1] *1. Institute of Physics, Johannes Gutenberg University, Mainz, Germany; 2. Korea Institute of Science and Technology, Seol, The Republic of Korea; 3. Department of Physics, University of California San Diego, La Jolla, CA, United States*

The emergence of spin-orbit torque as a promising research topic has motivated large interest in material systems with easily tunable spin-orbit torques. Here, we investigate spin-orbit torques in a VO_2 / NiFe heterostructure using spin-torque ferromagnetic resonance (ST-FMR). VO_2 undergoes a prominent (IMT) insulator-metal transition (accompanied by a monoclinic-to-rutile phase transition) in a narrow temperature range. This makes it an ideal candidate to investigate how spin-orbit torque generation in NiFe is affected by the electrical/structural phase transition in VO_2. Fig. 1 shows the two to four orders of magnitude hysteretic resistance changes of sputter-deposited VO_2 films in the temperature range 320 – 370 K [1]. The lower resistance change in thinner films is caused by the increased disorder. Using DC-modulated ST-FMR technique [2], changes in the ferromagnetic resonance linewidth and damping-like spin-orbit torques in VO_2/NiFe heterostructures are measured as shown in Fig. 2. The change in the FMR linewidth per unit current, $\Delta W/I_{DC}$, and its sign, change with temperature, across the VO_2 phase transition. The large change (±100%) of the damping modulation demonstrates efficient tunability of the magnitude and sign of spin-orbit torques in the VO_2/NiFe heterostructure and calls out for further investigation of spin-orbit torques in materials which undergo phase transitions. This research is supported by the Deutsche Forschungsgemeinschaft (DFG, German Research Foundation) TRR 173 – 268565370 and at UCSD by the Office of Basic Energy Science, U.S. Department of Energy, BES-DMS funded by the Department of Energy's Office of Basic Energy Science, DMR under grant DE FG02 87ER-45332.

[1] J. del Valle, P. Salev, F. Tesler *et al.,* Nature, Vol. 569, p.388 (2019) [2] L. Liu, T. Moriyama, D. C. Ralph *et al.*, Phys. Rev. Lett. Vol.106, p.036601 (2011)

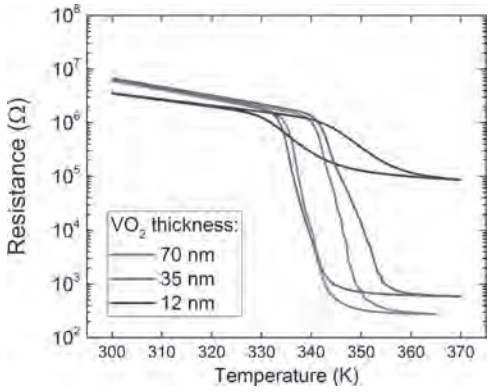

Fig. 1: Resistance of as-deposited 15, 35 and 70 nm VO_2 films across the insulator-metal transitions in the temperature range 300 – 370 K

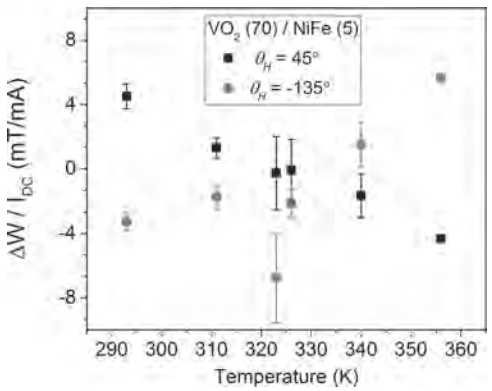

Fig. 2: Changes in the FMR linewidth W over applied dc current I_{DC} in VO_2 (70) / NiFe (5, thickness in nm) heterostructure across VO_2 phase transition

R2-11. Engineering Chiral Magnetic Textures in W/Co/AuPt Thin Films.
J. Peña Garcia[3], L. Camosi[2], A. Fassatoui[3], S. Pizzini[3], O. Fruchart[4], A. Thiaville[1], S. Rohart[1], F. Genuzio[5], T. Onur Mentes[5], A. Locatelli[5] and J. Vogel[3] *1. Laboratoire de Physique des Solides, Orsay, France; 2. Institut Catala de Nanociencia i Nanotecnologia, Bellaterra, Spain; 3. Institut NEEL, Grenoble, France; 4. SPINtronique et Technologie des Composants, Grenoble, France; 5. Elettra Sincrotrone Trieste SCpA, Trieste, Italy*

Topological magnetic textures such as skyrmions have been extensively studied during the last decade due to their potential application in spintronics devices. In ultrathin films systems, a key parameter to stabilize chiral topological magnetic textures is the Dzyaloshinskii-Moriya interaction (DMI), obtained at the interfaces between ferromagnetic layers and heavy-metals, promoting a unique chirality of the magnetic texture. In this work, we focus on an ultra-thin epitaxial W/Co(0.6-1nm)/$Au_{1-x}Pt_x$ trilayer, a model system exhibiting perpendicular magnetic anisotropy and interface DMI. Moreover, due to the strained epitaxial growth of Co(0001) on W(110) giving rise into a C_{2v} crystal symmetry at the W/Co interface. This symmetry results into a biaxial magnetic anisotropy, with an in-plane easy axis along the W[-110] direction, and into an anisotropic DMI [1]. The balance between the in-plane anisotropy and the DMI leads to an anisotropic domain wall configuration along the easy- and hard in-plane axis (Fig 1). This is confirmed experimentally by our X-ray magnetic circular dichroism photoemission electron microscopy (XMCD-PEEM) experiments [2]. Chiral stripe-domains mostly oriented along the in-plane hard-axis are observed as a consequence of the lower energy for domain walls oriented along this axis, with respect to the in-plane easy axis [2]. Another example is shown in Fig. 2a, where the stripe-domains are transformed into elliptical skyrmions when a weak out-of-plane magnetic field is applied, which is confirmed by micromagnetic

simulations (Fig 2b). In this presentation, we will show the effect of different Pt-to-Au composition on the magnetic properties such as the perpendicular magnetic anisotropy and the anisotropic DMI by Brillouin light spectroscopy.. Finally, we will show the observation by XMCD-PEEM of different chiral magnetic textures in sub-micron circular and elliptical dots, and discuss under which conditions these textures can be stabilized

[1] L. Camosi, S. Rohart, ... J.Vogel. Physical Review B, 95, 214422 (2017)
[2] L. Camosi, J.Peña Garcia, ... J. Vogel, in preparation

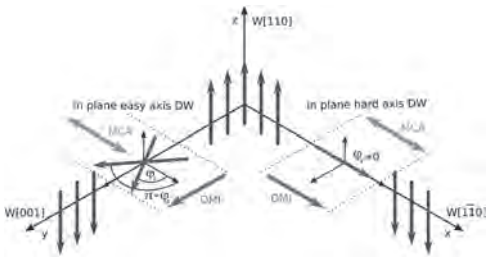

Sketch of the possible configurations for domain walls oriented along the main in-plane axes.

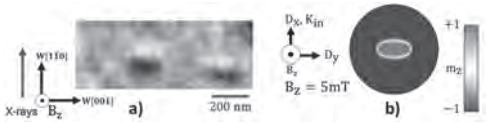

a) XMCD-PEEM image of an elliptical Skyrmion. The Skyrmion is elongated along the W[001] direction, hard-in plane axis.b) Micromagnetic simulation of a).

Session R3
MRAM, MAGNETIC LOGIC, AND RELATED DEVICES

Liliana D. Buda-Prejbeanu, Co-Chair
CEA, Paris, France
Lauren Garten, Co-Chair
Naval Research Lab, Washington, DC, United States

INVITED PAPER

R3-01. Current-Driven Magnetic Domain-Wall Logic. *Z. Luo*[1], A. Hrabec[1], T. Dao[1], G. Sala[1], S. Finizio[2], J. Feng[1], S. Mayr[1], J. Raabe[2], P. Gambardella[1] and L. Heyderman[1] *1. ETH Zurich, Zurich, Switzerland; 2. Paul Scherrer Institut, Villigen, Switzerland*

Development of complementary metal–oxide–semiconductor (CMOS) logic is expected to approach its fundamental limit as the scaling down of the CMOS technology is reaching an end. As a route to extend the technology roadmap beyond traditional CMOS logic, novel spin-based logic architectures are being developed to provide nonvolatile data retention, near-zero leakage, and scalability. In particular, architectures based on magnetic domain walls (DWs) take the advantage of the fast motion, high density, non-volatility and flexible design of DWs to process and store information [1,2]. Such schemes have so far relied on DW manipulation and clocking using an external magnetic field, which hinders their implementation in dense, large-scale chips. Here we demonstrate a method for performing all-electric logic operations and cascading using DW racetracks [3]. Our concept for the magnetic DW logic is based on efficient DW motion induced by spin-orbit torques (SOTs) [4] and recently developed chiral coupling between adjacent magnets where the magnetic anisotropy competes with the interfacial Dzyaloshinskii–Moriya interaction (DMI) [5,6]. First we created a DW inverter, the essential basic building block for all implementations of Boolean logic, by embedding a narrow in-plane magnetized region in a racetrack with out-of-plane magnetization and demonstrate the operation of the DW inversion on application of an electric current (Fig. 1a). Building on the principles used to construct the DW inverter, we then fabricated reconfigurable NAND and NOR logic gates, making our concept for current-driven DW logic functionally complete. Finally, we cascaded several NAND gates to build XOR and full adder gates, demonstrating electrical control of magnetic data and device interconnection in logic circuits (Fig. 1b). Our work provides a viable platform for scalable all-electric magnetic logic, paving the way for memory-in-logic applications.

[1] Allwood, D. A. et al. Science 309, 1688–1692 (2005). [2] Parkin, S. & Yang, S.-H. Nature Nanotechnol. 10, 195–198 (2015). [3] Luo, Z. et al. Nature 579, 214-218 (2020). [4] Manchon, A. et al. Rev. Mod. Phys. 91, 035004 (2019). [5] Luo, Z. et al. Science 363, 1435 (2019). [6] Dao, P. D. et al. Nano Lett. 19, 5930-5937 (2019).

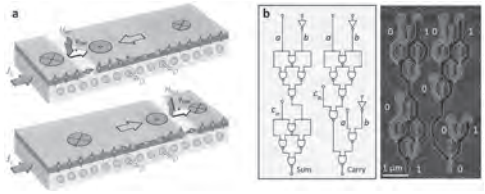

Fig. 1. Current-driven magnetic DW logic. (a) Schematic showing current-driven DW inversion, occurring as the DW moves across the in-plane region. After selective oxidization, the magnetizations of neighboring OOP (oxidized; red-shaded) and IP (unoxidized; blue-shaded) regions align with a left-handed chirality in Pt/Co/AlOx. The white-shaded region is the DW, and the directions of the effective field induced by the SOTs, H_{SOT}, and the DW velocity, v_{DW}, are indicated with arrows. (b) Full adder gate. Left, logic-circuit diagram of the full adder with input operands of a ='0', b ='1' and a carry bit of c_{in} ='1'. Right, magnetic force microscopy (MFM) image of the full adder magnetic circuit. The bright and dark areas in the device regions correspond to up and down magnetization, respectively.

CONTRIBUTED PAPERS

R3-02. Threshold Logic With Current-Driven Magnetic Domain Walls. *X. Hu*[1], B.A. Hill[1], F. Garcia-Sanchez[2] and J.S. Friedman[1] *1. Electrical & Computer Engineering, The University of Texas at Dallas, Richardson, TX, United States; 2. Universidad de Salamanca, Salamanca, Spain*

Threshold logic [1] efficiently implements complex logical functions within a single gate, but its widespread adoption has been impeded by insufficient nonlinearity in conventional transistors. The recent experimental demonstration of cascaded logic gates with current-driven magnetic domain walls [2] operates based on the nonlinearity intrinsic to anisotropic systems, thus naturally enabling threshold logic gates. However, these logic gates are described in [2] as reconfigurable NAND and NOR gates, rather than as three-input minority threshold logic gates. We therefore propose a novel domain wall threshold logic (DWTL) paradigm that enables circuits that are simpler and more efficient than can be achieved with the reconfigurable gates of [2]. Similar to [2], magnetic domains magnetized in the $+z$ ($-z$) direction represent logic '1' ('0'), and each in-plane region causes magnetization reversal due to chiral coupling resulting from the interfacial DMI. As demonstrated in [2], DWTL gates produce an output domain that is the inversion of the majority of the inputs. That is, this logic gate performs the minority threshold function, which is significantly more logically expressive than NAND or NOR. By leveraging this minority gate behavior, the one-bit full adder of Fig. 1 can be realized with three logic gates, 80% fewer than the 15 required in [2]. We also propose DWTL functions with logical expressivity increased further by using more than three inputs, and with inputs that have non-uniform impacts on the output magnetization. As shown in Fig. 2a, a four-input DWTL gate can be realized in which one input has twice the width of the other three; therefore, this wider input will have roughly twice the impact

on the output magnetization. DWTL gates with greater logical expressivity further reduce the number of devices required to perform logical operations, such as in the three-bit DWTL full adder of Fig. 2b that requires only two gates per bit (87% reduction).

[1] D. Hampel and R. O. Winder, IEEE Spectrum, Vol. 8, pp. 32-39 (1971)
[2] Z. Luo, A. Hrabec, T. P. Dao, *et al*., Nature, Vol 579, pp. 214-218 (2020)

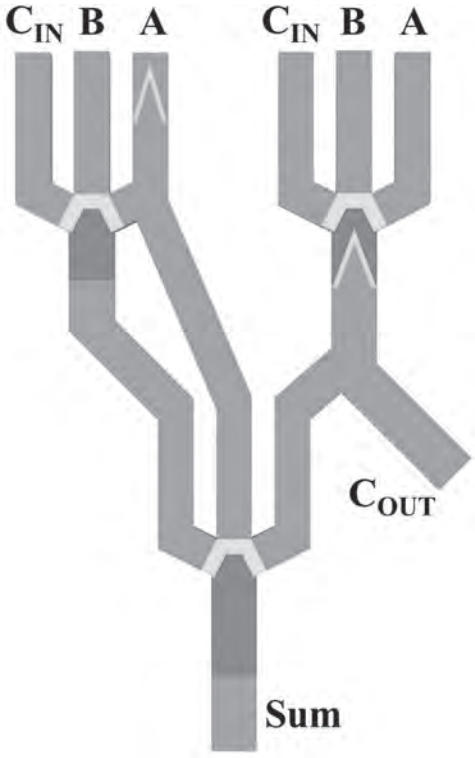

Fig. 1. One-bit full adder implemented with only three DWTL minority gates.

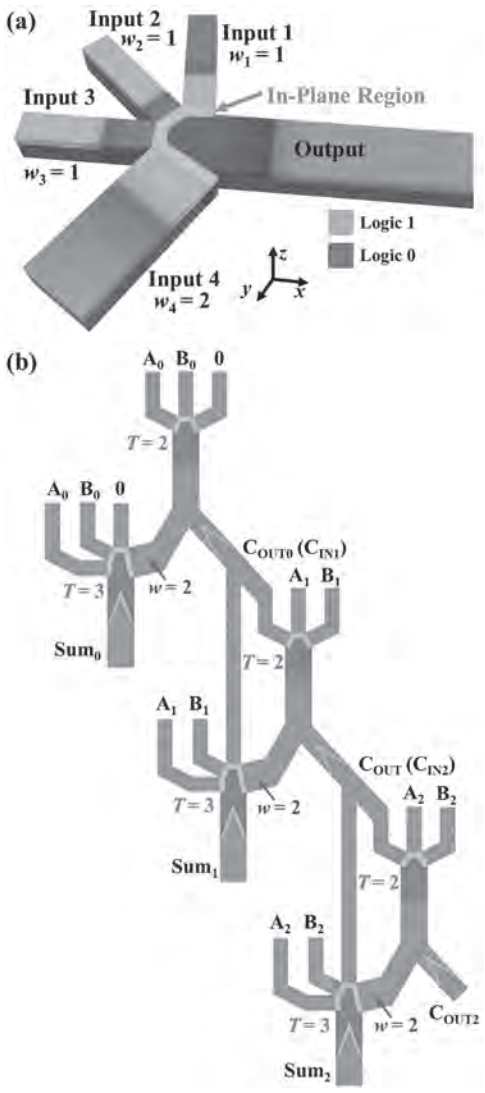

Fig. 2. a) Four-input DWTL gate in which three inputs have weight w=1, and one input has w=2. b) Three-bit full adder with only two DWTL gates per bit (six total).

R3-03. Speed Enhancement of Magnetic Logic-Memory Device by Insulator-to-Metal Transition. *Y. Pu*[1] and X. Zhang[1] *1. Materials Science and Engineering, Tsinghua University, Beijing, China*

In conventional computers, CMOS logic circuits require frequent communication with external nonvolatile memories, causing the memory wall problem [1]. Luo et al [2] proposed a magnetic logic-memory device by use of the anomalous Hall effect (AHE) in magnetic materials and the negative differential resistance (NDR) in semiconductors [3], which can potentially bridge this gap. However, its high-frequency performance, especially the switching time of NDR in logic operations, is not well studied. Here, our investigation shows that the switching time of the NDR in logic operations is ~300 ns and limited by the NDR's internal turn-on properties. To improve the frequency performance, we propose a novel magnetic logic-memory device by coupling the AHE in Ta/CoFeB/MgO multilayers and the insulator-to-metal transition (IMT) in VO_2 [4][5]. The VO_2 thin films (35 nm in thickness) are grown on (0001)-Al_2O_3 substrates, and the two-terminal VO_2 device (length = 3μm, width = 5μm) is fabricated. Due to IMT, an abrupt change in resistivity is observed when the current reaches critical current (0.21mA). The imbalance of the spin-polarized electron current caused by AHE in CoFeB can be enlarged by IMT in VO_2, resulting in a large magnetism

controlled current bifurcation. All four basic Boolean logic operations including AND, NAND, OR and NOR, could be realized at room temperature with high output ratio (>10^3 %) and low magnetic field (<20 mT). The switching time and energy consumption of our device is 7.5 ns and 6.3 pJ, much better than the device based on the NDR (~300 ns and 350 pJ).

[1] T. Ikenaga, T. Ogura. Ieee Transactions on Computers. Vol. 47(7), p.788 (1998). [2] Z. Luo, Z. Lu, C. Xiong, et al. Advanced Materials. Vol. 29, p.1605027 (2017). [3] L. Chua, Yu Juebang, Yu Youying. IEEE Transactions on Circuits and Systems. Vol. 32(1), p.46 (1985). [4] T. M. Rice, H. Launois, J. P. Pouget. Physical Review Letters. Vol. 73(22), p.3042 (1994). [5] W. A. Vitale, E. A. Casu, A. Biswas, et al. Scientific Reports. Vol. 7, p.10 (2017).

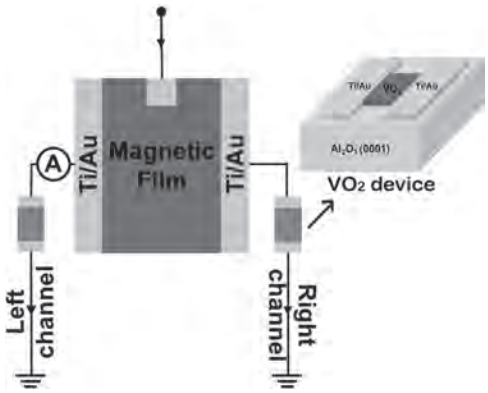

Schematics of the structure of our magnetic logic-memory device. Magnetization of magnetic film and the channel current are logic input and output, respectively. The Schematic of a two-terminal VO_2 device is indicated in the inset.

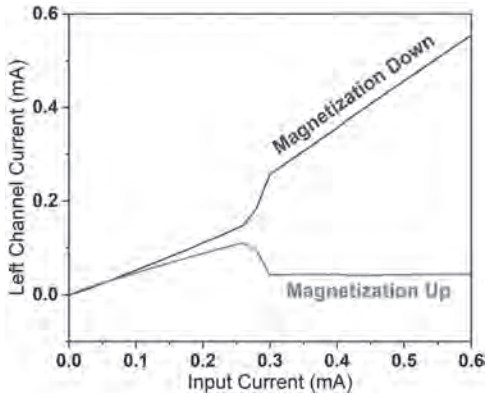

Left channel current of magnetization down and up.

R3-04. Walker-Like Domain Wall Motion in STTMRAM Cells: Evidence and Consequences for the Write Error Rate. P. Bouquin[2,1], J. Kim[1], O. Bultynck[2], S. Rao[2], S. Couet[2], G.S. Kar[2] and *T. Devolder*[1]
1. Université Paris-Saclay, Palaiseau, France; 2. IMEC, Leuven, Belgium

The understanding of magnetization reversal in STTMRAM cells is of considerable interest. We use time-resolved conductance measurement, micromagnetic simulations and modeling to study it. The samples are fabricated from proprietary supersoft free layers of high volume and low moment. The experiments reveal the oscillatory nature of the conductivity signature of the switching (see figure). Modeling indicates that the conductance oscillations arise from the domain wall motion that happens in the so-called precessional regime above the Walker breakdown, when the domain wall propagation involves back-and-forth motions on top of a global drift. We first extend a collective coordinate model, taking into account the position of the wall and the tilt of the in-plane component of the magnetization within the wall. The mean wall velocity and its oscillations can be understood from the continuous exchange of energy between these two degrees of freedom, and the work supplied by the STT. In discs of diameters 70-100nm, experiments identify several distinct switching paths that occur stochastically and lead to distinct switching durations, while in disks of diameter 40 nm much less variability is found. Micromagnetics is used to understand these switching paths. For disks with 40 nm of diameter, the wall sweeps through the disk in an almost monotonous manner regardless of the wall state (Bloch, Néel or more complex). Conversely at larger diameters, the manner in which the wall crosses the disk depends on the wall state, and sets the variability of the transition time during the switching. The wall oscillation and its advance are essentially stopped if and only if a Bloch line is nucleated from the edge of the wall. This leads to switching times that are usually long compared to the standard deviation; this is one of the main mechanisms determining the write error rate in the ultrafast switching regime. Our model is finally used to design sample specifications with shall lead to rather reproducible propagation times, of direct interest for magnetic memories.

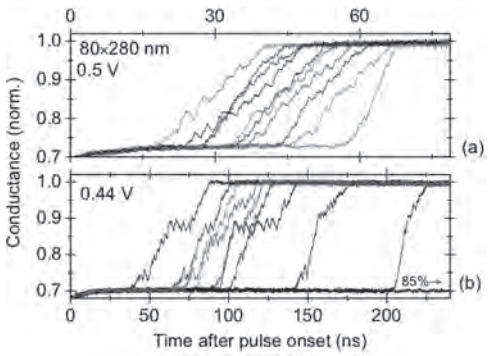

Figure 1: Conductance signatures of various STT induced switching events as a result of voltage pulses on a rectangular device. Notice the pronounced oscillations.

R3-05. Micromagnetic Instabilities Associated With Domain Wall Dynamics in Perpendicular Magnetized Magnetic Tunnel Junction Nanopillars. *N.N. Statuto*[1], J. Beik Mohammadi[2] and A.D. Kent[1] *1. Physics Department, Center for Quantum Phenomena, New York University, New York, NY, United States; 2. Department of Physics, Loyola University New Orleans, New Orleans, LA, United States*

Magnetoresistive random access memories (MRAM) based on spin-transfer torque are a scalable low-power nonvolatile memory solution being actively developed by industry, where a perpendicularly magnetized thin disk is reversed by a spin polarized current. During the switching process domain walls (DWs) can form [1-4] and understanding their dynamics in a disk geometry becomes of great interest. Here we show that DW surface tension always leads to oscillatory DW motion and instabilities that affect the switching dynamics. In a disk, a DW generally takes a circular form to minimize the sum of the surface and volume energies of the reversed domain, with the domain boundary perpendicular to the element boundary [1]. In a collective coordinate model the domain wall has two degrees of freedom, its position relative to the center of the disk q and the angle of the spins relative to the normal to the DW Φ. Here, Φ=0 is a Neel and Φ=90 deg. is a Bloch DW. We analyze the dynamics with micromagnetic and the collective coordinate model. Fig. 1a shows micromagnetic simulations of the evolution of the average perpendicular magnetization (m_z) with fixed initial DW position q, such that m_z<0, and different initial angles Φ, with no field or current applied. Whereas both Neel and Bloch DWs states relax towards a reversed state (m_z=-1), an intermediate initial angle DWs (Φ=45 deg) switches. Fig. 1b shows the (q,Φ) phase diagram indicating that the dynamics of domains close to the disk center is sensitive to small changes in the initial phase. Fig. 2 shows the same phase diagram as in Fig. 1b, now driven by a fixed spin-polarized J/Jc= 0.1. The results from both relaxation and switching simulations indicate that the DW phase Φ plays a critical role

in the dynamics. A collective coordinate model will be presented which captures aspects of these instabilities and illustrates their physical origin.

[1] G. Chaves-O'Flynn et al., Phys. Rev. Appl. 4, 024010 (2015) [2] T. Devolder et al., Phys. Rev. B 93, 024420 (2016) [3] P. Bouquin et al., Appl. Phys. Lett. 113, 222408 (2018) [4] J. B. Mohammadi et al., arXiv:2003.13875 (2020)

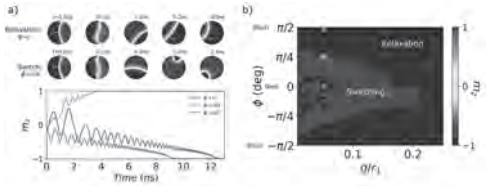

FIG. 1 a) Time evolution of mz for different Φ. b) (q,Φ) Relaxation phase diagram. The colored dots show the parameters in panel a.

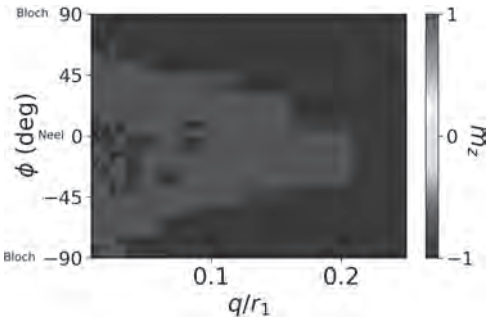

FIG. 2 Relaxation phase diagram for the parameters q and Φ when a spin current of J/Jc= 0.1.

R3-06. Spintronic Control of Magnetostatically Coupled dot Assemblies. *S. Jeon*[1], H. Chen[1] and S. Majetich[1] *1. Physics, Carnegie Mellon University, Pittsburgh, PA, United States*

Magnetostatically coupled monodomain patterns have been studied for use as cellular automata and logic gates [1, 2]. Here the external magnetic field clocked switching is deterministic, and the magneto-optic Kerr (MOKE) effect microscopy or magnetic force microscopy (MFM) characterization only detects slow dynamics. We investigate similar systems, but with the use of spintronics for fast, all-electronic control and measurement. This is relevant both for low power magnetic logic, and for detection of fast dynamics in coupled superparamagnets that could be used in reservoir computing. We have demonstrated the ability to deterministically switch the state of a magnetic tunnel junction (MTJ) using spin orbit torque (SOT) [3], and this is used to switch the control dot at the beginning of the coupled patterns (Fig.1a). We have also detected magnetization changes in patterned nanodot MTJs using tunnel magnetoresistance (TMR) and a conductive atomic force microscopy (C-AFM) probe tip [4], and this is used to detect the dot magnetization at different locations. The dots were patterned by E-beam lithography from an MTJ thin film stack with a 3 nm thick CoFeB free layer. Fig.1b shows the schematic for a control dot and a neighboring secondary dot. Mumax3 simulations were conducted to match the magnetic field generated by the control dot with the coercive field of the secondary dot to facilitate the signal processing in magnetically coupled dots [5]. Fig.2 shows the magnetic field profile along +x direction. Inside the secondary dot, the magnetic field ranged from 2 to 15 mT, comparable to the 8 mT coercive field of the secondary dot, as shown in the Fig.2 inset. This ensures us that we could propagate a signal inside magnetically coupled dots. C-AFM measurements test the predicted switching and propagation along the nanodot chain of Fig.1.

1. R. P. Cowburn and M. E. Welland, Science 287 1466 (2000). 2. A. Imre, et al., Science 311 205 (2006). 3. M. Bapna, et al., Phys. Rev. Applied 10, 024013 (2018). 4. B.Parks, et al., Phys. Rev. Applied 13, 014063 (2020). 5. A. Vansteenkiste et al., AIP Adv. 4, 107133 (2014).

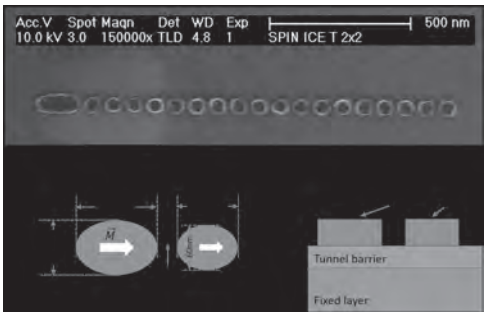

Fig.1 a) SEM of patterned thin file stack. b) Schematic of two magnetostactically coupled dots.

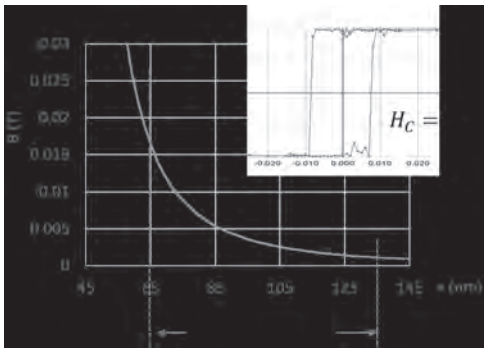

Fig.2 Magnetic field profile generated by the control dot, inset with the hysteresis loop of the secondary dot at room temperature.

R3-07. Data Transmission in an Insulator Utilizing Rotational Magnetization Wave. *A. Shadman*[1] and J. Zhu[1] *1. Electrical and Computer Engineering, Carnegie Mellon University, Pittsburgh, PA, United States*

In the racetrack or similar technologies, information (bit) stored in the direction of the magnetic moment of domains placed next to each other in a wire is shifted when electrical current passes along or parallel to the wire. While using electrons as 'carrier', these technologies sometimes lack the deterministic motion of the bits causing data integrity issues [1]. In this work, we are proposing a more deterministic, 'carrier' free transmission of data in an insulating ferromagnetic wire where the data is encoded in the oscillation frequencies of magnetic moments. Fig. 1 shows the schematic view of the device, including a thin transmission strip made of soft magnetic material. An Antiferromagnet (AF)/Ferromagnet (F) coupled perpendicular spin torque oscillator (STO) [2] is used to generate the full 360° in-plane magnetization rotation in a small confined region of the transmission strip that is also the free layer of the STO. This precession at STO end generates a traveling rotational magnetization wave along the wire, as seen in Fig. 1. While the spatial wavelength is increasing with distance, the rotational frequency along the wire remains constant, which is a key for our data transmission method. By changing the current amplitude according to the transmission bits, STO frequency can be tuned. Even at 800 nm away from the STO end (Fig. 2), the variation of the rotational frequency with time matches the variation of input STO frequency (or the input current pulse), affirming reliable data transmission. For this micromagnetic simulation, archetypal values for F such as α = 0.01 and Ms = 800 emu/cc are considered. 1 μm wire with a width of 10 nm and thickness of 2 nm is discretized using a grid size of 4nm x 2nm x 2nm.

[1] Foerster M. et al., Domain Wall Memory Device (2016). In: Xu Y., Awschalom D., Nitta J. (eds) Handbook of Spintronics. Springer, Dordrecht [2] J.-G. Zhu, A. Shadman, IEEE Trans. Magn., vol. 55, no. 3, 2019.

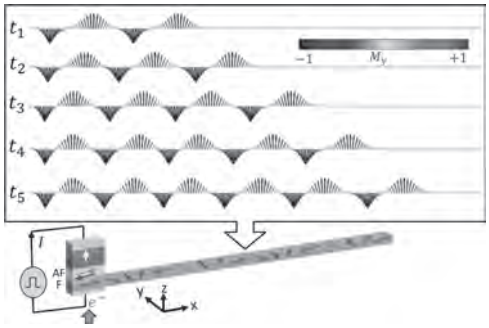

Fig. 1. DC current, I is applied to the AF/F coupled STO. Snapshot of in-plane magnetization orientation along the wire is shown at different time stamps, signaling traveling rotational magnetization wave.

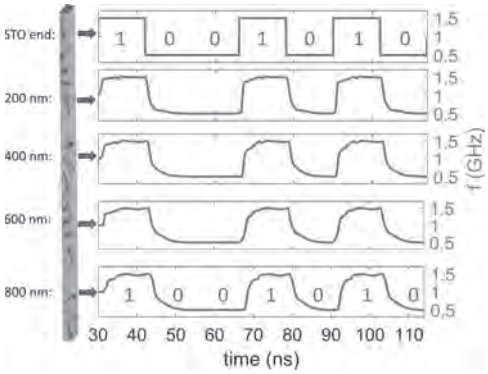

Fig. 2. Data modulated current pulse applied to STO generates a data proportional oscillation frequency profile at STO end. 1.5 GHz (0.5 GHz) is used to represent bit '1' ('0'). Bit duration is 12 ns. Frequency variation w.r.t time matches that of input data even at 800 nm.

R3-08. The Influence of a Thermal Noise on the Accuracy of a Spectrum Analyzer Based on a Spin Torque Nano-Oscillator. *S. Louis*[1], A. Litvinenko[2], V. Iurchuk[2], P. Sethi[2], P. Elphick[3], V. Tyberkevych[4], P. Artemchuk[4], A. Jenkins[5], R. Ferreira[5], B. Dieny[2], U. Ebels[2] and A.N. Slavin[4] *1. Electrical and Computer Engineering, Oakland University, Rochester, MI, United States; 2. CEA, CNRS, INAC, SPINTEC – University Grenoble Alpes, Grenoble, France; 3. KOSTAL of America, Troy, MI, United States; 4. Physics, Oakland University, Rochester, MI, United States; 5. International Iberian Nanotechnology Laboratory, Braga, Portugal*

It has been shown both theoretically [1] and experimentally [2] that a spectrum analyzer based on an externally driven spin torque nano-oscillator (STNOs) can perform high-speed, wide-band spectrum analysis in a microwave frequency band. In such a spectrum analyzer, an STNO generates a signal whose frequency is tuned in a linear manner over a scanning bandwidth Δf. Theoretical estimations show that when employing an STNO in spectrum analysis, the following can be achieved: a Δf of 10 GHz, a linear scanning rate $\rho=\Delta f/T$ (where T is the scanning period) of up to 2 GHz/ns, all in a frequency range of operation between 200 MHz and 70 GHz [3]. The fast speed of frequency analysis in a STNO-based spectrum analyzer can be achieved mainly due to the nano-scale size of the STNO, and the consequent ns characteristic scanning times. At a sufficiently large scanning rate ρ, the accuracy of the frequency determination ΔF (defined as the minimum separation required to distinguish two neighboring frequencies) of an STNO-based spectrum analyzer is fundamentally limited by the bandwidth theorem. In contrast, at low scanning rates, this accuracy is limited by the STNO generation linewidth [4], which is determined by the thermal (or random-walk) noise that is causing the jitter of the STNO generation frequency. Fig. 1 shows the frequency accuracy ΔF as a function of the scanning rate ρ for the STNO-based spectrum analyzer [2], where the gray solid line is the result of numerical modeling, dash-dotted line is a result of the experimental measurement [2], and dashed line shows the limit due to the "bandwidth" theorem. It is evident that at sufficiently large scanning rate, ΔF approaches the fundamental limit $\Delta F = 1/T$, whereas at smaller ρ the ΔF is limited by the magnitude of the STNO linewidth.

[1] S. Louis, *et al*., Appl. Phys. Lett., 113, p. 112401, (2018). [2] A. Litvinenko, et al., "Experimental demonstration of a rapid sweep-tuned spectrum analyzer with temporal resolution based on a spin-torque nano-oscillator," arXiv preprint arXiv:2004.03508, (2020). [3] S. Louis, "Development of a spectrum analyzer using a spin torque nano-oscillator," Ph.D. dissertation, Department of Electrical and Computer Engineering, Oakland University, (2020). [4] Joo-Von Kim, *et al*., Phys. Rev. Lett. 100, 017207 (2008).

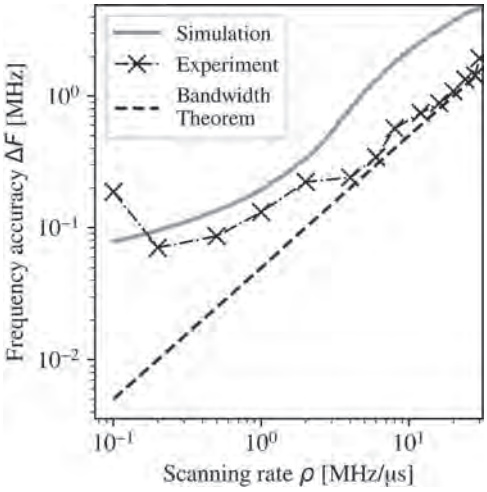

Figure 1: Frequency resolution of spectrum analysis with respect to tuning speed. Dashed line shows theoretical best resolution, and black crosses show experimental results from [2]. The solid gray line shows numerical simulation for STNOs with a linewidth of 50 kHz.

R3-09. Entropy-Reduced Retention Times in Magnetic Memory Elements: a Case of the Meyer-Neldel Compensation Rule. *L. Desplat*[1,2] and J. Kim[2] *1. Institut de Physique et de Chimie des Matériaux de Strasbourg, CNRS, Université de Strasbourg, Strasbourg, France; 2. Centre de Nanosciences et de Nanotechnologies, CNRS, Université Paris-Saclay, Palaiseau, France*

The Meyer-Neldel (MN) rule, also known as entropy-enthalpy compensation, is a peculiar phenomenon that has been reported across diverse fields of the natural sciences, in semiconductors, chemical reactions, biology, etc [1]. In magnetism, it was very recently observed in the decay of the skyrmion lattice [2]. Consider a family of thermally activated processes whose rates k obey an Arrhenius-type law, i.e., $k = f_0 \exp(-\beta\Delta E)$, in which ΔE is the internal energy barrier, $\beta = (k_B T)^{-1}$ is Boltzmann's factor, and f_0 is the Arrhenius prefactor — the so-called "attempt frequency". If the Meyer-Neldel rule applies, the prefactor scales like an exponential of the energy barrier. In this work, we compute the mean waiting time between thermally activated magnetization reversals in a nanodisk, with parameters that resemble that of a free CoFeB layer, as used in magnetic random access memories [3]. We use two independent approaches, namely Langer's theory [4] and forward flux sampling [5]. By varying the perpendicular anisotropy, and the interfacial Dzyaloshinkii-Moriya interaction (DMI), we find that the Arrhenius prefactor can take extreme, seemingly non-physical values up to 10^{21} Hz, which is orders of magnitude beyond the typically assumed value of 10^9 Hz, and vary drastically as a function of material parameters. We show that it behaves like an exponential of the energy barrier, ΔE, which stems from a linear variation of the activation entropy, ΔS, with the energy barrier, thereby demonstrating a new case of the Meyer-Neldel rule (Fig. 1). Our results show that the Arrhenius prefactor is not an attempt frequency, because it also

contains an important entropic contribution which cannot be neglected in complex systems. This suggests that modelling information retention times with a barrier-independent prefactor in magnetic storage elements is not justified [6].

[1] A. Yelon, B. Movaghar, and R. Crandall, Reports on Progress in Physics, Vol. 69, p.1145 (2006) [2] J. Wild, T. N. Meier, S. Pollath et al., Science Advances, Vol. 3, p. e1701704 (2017) [3] J. Sampaio, A. Khvalkovskiy, M. Kuteifan et al., Applied Physics Letters, Vol. 108, p.112403 (2016) [4] J. S. Langer, Annals of Physics, Vol. 54, p. 258 (1969) [5] R. J. Allen, P. B. Warren, and P. R. ten Wolde, Physical Review Letters, Vol. 94, p. 018104 (2005) [6] L. Desplat and J.-V. Kim, submitted (2020)

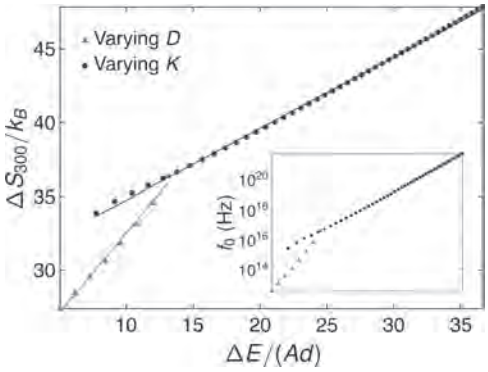

Fig. 1. Activation entropy at T = 300 K as a function of the activation energy normalized by the exchange constant, A, and film thickness d, for variations of the DMI, D, and of the anisotropy, K. The inset shows the corresponding variation of f_0 for α = 0.5 with the same horizontal scale.

R3-10. An Eigenvalue-Based Framework for the Magnetization Switching by Spin Torque. *Z. Lin*[1], I. Volvach[1] and V. Lomakin[2]
1. Materials Science and Engineering, University of California San Diego, La Jolla, CA, United States; 2. Department of Electrical and Computer Engineering, University of California San Diego, La Jolla, CA, United States

Understanding the magnetization dynamics driven by spin transfer torque (STT) and Spin Hall effect (SHE) is important for designing magnetic devices. We show that the dynamics can be predicted based on only a few resonant modes of the linearized Landau-Lifshitz-Gilbert (LLG) equation. The approach is based on obtaining the resonant modes and frequencies of the system driven by STT or SHE as a perturbation based on the modes of the system without STT or SHE [1], all done with the finite element method [2]. This approach allows obtaining the critical switching current (Jc0) much faster and much more reliably than the brute-force time domain LLG modeling. The approach can reliably predict the switching time for a given current and the switching current for a given pulse shape. The approach allows explaining the nature of the STT and SHE switching, including uniform, domain wall, and bubble-like switching; e.g. different currents may lead to the excitation of different modes with different switching mechanisms. Additionally, the presented approach can help understand the switching dynamics driven by higher-order resonant modes, which is important for large-current pulse excitations. Moreover, the approach explains why the extraction of Jc0 based on an extrapolation from finite time pulses to the infinite time can be unreliable and misleading. The solver is integrated with the FastMag simulator framework [2] and is accelerated by Graphics Processing Unit (GPU) and multi-core CPU computing. We carried out numerical experiments to show the validity of simulation results and to study various cases (see Table 1 and Fig. 1). This work was supported as part of the Quantum Materials for Energy Efficient Neuromorphic Computing, an EFRC funded by the U.S. DOE, Office of Science.

[1] d'Aquino Massimiliano, et al. *Journal of Computational Physics*, *228*(17), pp.6130-6149 (2009). [2] R. Chang, et al. *Journal of Applied Physics*, 109(7), p.07D358 (2011).

Critical current (uA)	D = 20 nm, α = 0.001	D = 40 nm, α = 0.008	D = 80nm, α = 0.1
Time domain linear fitting	5.322e-7	1.466e-5	6.126e-4
Resonant solver prediction	5.491e-7	1.480e-5	6.304e-4

Table 1. **Jc0 predictions for MRAM disc of different diameters (D) and damping factors (α). Magnetic material parameters are Ms = 1000emu/cc, Ku = 8e6erg/cc, and easy axis is (0, 0, 1).**

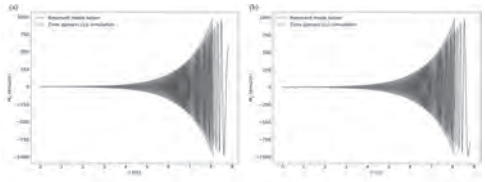

Fig. 1. **In-plane average magnetization time evolution of an MRAM disc with STT: D = 20nm, α = 0.001, I = 5e-6μA and same magnetic material parameters in Table 1. Results show that the resonant mode based solver has good agreement with results based on time domain LLG.**

R3-11. Development of the Metastable Electrode Materials for the Huge Tunnel Magnetoresistance Effect. *T. Ichinose*[1], J. Ikeda[1,2], Y. Onodera[1,2], K. Suzuki[1,3] and S. Mizukami[1,4] *1. WPI-AIMR, Tohoku University, Sendai, Japan; 2. Department of Applied Physics, Tohoku University, Sendai, Japan; 3. CSRN, Tohoku University, Sendai, Japan; 4. CSIS and CSRN, Tohoku University, Sendai, Japan*

Realization of the large tunnel magnetoresistance (TMR) ratio is the key issue for the high-performance spintronic applications. Recently, the magnetic tunnel junctions (MTJs) with the metastable bcc CoMn electrodes have been developed, which exhibited the large TMR ratios of 240% (600%) at 300 K (10 K). [1, 2] Since the metastable CoMn have not been fully investigated, the CoMn based MTJs may possess the unknown factors giving rise to the high TMR ratios. In this work, the effect of Fe substitution into the CoMn electrodes on the TMR properties was investigated. [3] The MTJ structures composed of MgO (001) sub./ Cr(40)/ CoMnFe(10)/ MgO(2.4)/ CoMnFe(4)/ IrMn(10)/ Ru(7) (thickness in nanometer) were prepared by DC/RF magnetron sputtering techniques. The post-annealing at 523 K – 698 K under a magnetic field of 5 kOe was carried out. The structural and magnetic properties were investigated by the X-ray diffraction (XRD) and the vibrating sample magnetometry (VSM). The transport properties were measured by the 4-probe system and physical property measurement system (PPMS). The XRD 2θ/ω profiles revealed that the crystal structures of the CoMnFe epitaxial films were bcc although the thermodynamically stable phase of bulk CoMnFe was hcp or fcc. [4] Since the magnetic moment of Mn could ferromagnetically couple with the magnetic moments of Co and Fe in the bcc CoMnFe, the large magnetization of 1600 emu/cm^3 could be observed. These results indicated the CoMnFe/MgO MTJs would show the coherent tunneling due to the bcc structure of CoMnFe. In fact, the CoMnFe MTJs exhibited the large TMR ratios of 320% at 300 K, which increased with decrease in temperature; the TMR ratio at 10 K reached to 930%. It is worth noting that the TMR ratios of CoMnFe MTJs at low temperature were comparable to CoFeB MTJs which exhibited the highest TMR ratio at room temperature to date, [5] indicating the potentials of the CoMn based electrodes to realize the large TMR ratio. The understanding for the mechanism of the large TMR ratios in the CoMn based MTJs could open the way for the material design for the next generation MTJs. This work was supported in part by JST CREST (No. JPMJCR17J5).

[1] K. Kunimatsu et al., Jpn. J. Appl. Phys. 58, 080908(R) (2019). [2] K. Kunimatsu et al., submitted. [3] T. Ichinose et al., in preparation. [4] M. Matsui et al., J. Phys. Soc. Jpn. 35, 419 (1973). [5] S. Ikeda et al., Appl. Phys. Lett. 93, 082508 (2008).

R3-12. Enhancement of Magnetoresistance Characteristics of Ge-Rich $Co_2Fe(Ga,Ge)$-Based Current-Perpendicular-to-Plane Giant Magnetoresistance Devices. *K. Nakada*[1], Y. Chikaso[2], T. Tanimoto[2], M. Inoue[2], K. Inubushi[1] and T. Uemura[2] *1. Advanced Products Development Center, Technology & Intellectual Property HQ, TDK Corporation, Ichikawa, Japan; 2. Grad. School of Information Science and Technology, Hokkaido University, Sapporo, Japan*

Current-perpendicular-to-plane (CPP) giant magnetoresistance (GMR) devices using Co-based Heusler alloys (Co_2YZ, where Y is usually a transition metal and Z is a main group element) have attracted much interest as reading heads for next-generation hard disk drives [1-5]. To take full advantage of the half-metallic character of Co-based Heusler alloys, it is important to suppress the antisite of Co atoms, where Co atoms replace Y or Z site [6]. To do this increasing Y or Z composition in Co_2YZ is highly effective, and we recently demonstrated the enhancement of MR ratios in off-stoichiometric Mn-rich Co_2MnSi-based MTJs [7] and CPP-GMR devices [4]. In this study we systematically investigated the Ge-composition dependence of MR ratios in $Co_2Fe(Ga,Ge)$ (CFGG)-based CPP-GMR devices, and achieved the highest MR ratios of 88% at room temperature. We prepared CFGG-based CPP-GMR devices with various Ge composition α in $Co_2Fe_{1.03}Ga_{0.41}Ge_{\alpha}$ electrodes ranging from 0.56 to 1.25. The layer structures of the fabricated CPP spin valves were as follows: (from the substrate side) MgO (10 nm)/ $Co_{50}Fe_{50}$ (10)/Ag (100)/CFGG lower electrode (10)/NiAl (0.21)/Ag (5)/NiAl (0.21)/CFGG upper electrode (8)/Ru (5), grown on MgO(001) substrates. Ultrathin (0.21 nm) NiAl layers were aimed to enhancing the MR ratio [3]. Just after the deposition of CFGG upper electrodes, the layer structure was *in-situ* annealed at 550°C. We fabricated CPP spin valves with the nominal junction sizes ranging from 70 × 120 nm to 400 × 640 nm by using EB lithography and Ar ion milling. The MR characteristics were measured using a dc four-probe method at 290 K. We observed the MR ratio enhanced from 21% to 88% as α increased from 0.56 (Ge-stoichiometric CFGG) to 1.25 (Ge-rich CFGG). To the best of our knowledge, the MR ratio of 88% is the highest value ever reported among CPP-CMR devices. This result suggests that Ge-rich CFGG is effective in improving the half-metallic character of CFGG possibly due to the suppression of Co antisite with the increase of Ge composition.

[1] Y. Sakuraba *et al*., Appl. Phys. Lett. 101, 252408 (2012). [2] H. Narisawa *et al*., Appl. Phys. Express 8, 063008 (2015). [3] Y. Du *et al*., Appl. Phys. Lett. 107, 112405 (2015). [4] M. Inoue *et al*., Appl. Phys. Lett. 111, 082403 (2017). [5] J. W. Jung *et al*., Appl. Phys. Lett. 108, 102408 (2016). [6] S. Picozzi *et al*., Phys. Rev. B 69, 094423 (2004). [7] H.-x. Liu *et al*., Appl. Phys. Lett. 101, 132418 (2012).

R3-13. Current-in-Plane Spin-Valve Magnetoresistance in Ferromagnetic Semiconductor (Ga,Fe)Sb Heterostructures With High Curie Temperature. *K. Takase*[1], L. Anh[2,3], K. Takiguchi[1] and M. Tanaka[1,4] *1. Department of Electrical Engineering and Information Systems, The University of Tokyo, Bunkyo-ku, Japan; 2. Institute of Engineering Innovation, The University of Tokyo, Bunkyo-ku, Japan; 3. PRESTO, JST, Kawaguchi, Japan; 4. Center for Spintronics Research Network (CSRN), The University of Tokyo, Bunkyo-ku, Japan*

Ferromagnetic semiconductors (FMSs) which show both ferromagnetic and semiconducting characteristics are promising materials for spintronics applications. Recently, we have successfully grown Fe-doped FMSs; p-type (Ga,Fe)Sb with Curie temperature (T_C) ≈ 340 K[2] and n-type (In,Fe)Sb with T_C ≈ 335 K[3], which are promising for devices operating at room temperature. One of the important steps towards practical applications is to realize spin-valve effects in heterostructures containing Fe-doped FMSs. In this work, we demonstrate spin-valve magnetoresistance (MR) in all-semiconductor heterostructures containing Fe-doped FMS (Ga,Fe)Sb layers with T_C ≈ 260 K. The samples examined here consist of $(Ga_{0.75},Fe_{0.25})Sb$ (40 nm) / InAs (thickness t_{InAs} = 0, 3, 6, 9 nm) / $(Ga_{0.8},Fe_{0.2})Sb$ (40 nm) grown by low temperature molecular beam epitaxy (LT-MBE) [Fig. 1(a) and (b)]. In these structures, electrical current flows mainly in InAs due to the high resistivity of (Ga,Fe)Sb layers at low temperature (≤ 20 K)[4]. A clear spin-valve effect with an MR ratio of ~ 1.6% with an open minor loop is observed in the structure with t_{InAs} = 3 nm at 3.7 K [Fig. 2], whose peaks (≈ ±0.1 T) correspond to the coercive forces in the magnetization characteristics of the (Ga,Fe)Sb layers obtained with superconducting quantum interference device (SQUID) magnetometry and anomalous Hall effect (AHE) measurements. We found that the spin-valve MR (MR_{SV}) increases (from 0.03 to 1.6%) with decreasing t_{InAs} (from 9 to 3 nm), which reflects the enhancement of spin-dependent scattering at the InAs/(Ga,Fe)Sb interfaces. This demonstration is the first important step towards device application of these promising high-T_C FMSs.

[1] L. Chen *et al*, Nano Lett., Vol. 11, p.2584 (2011). [2] N. T. Tu, *et al*, Appl. Phys. Lett., Vol. 108, p.192401(2016). [3] N. T. Tu, *et al*, Appl. Phys. Express, Vol. 11, p.063005(2018). [4] N. T. Tu, *et al*., Phys. Rev. B, Vol. 92, p.144403 (2015). [5] K. Sriharsha, *et al*., APL Mater., Vol. 7, p.021105 (2019).

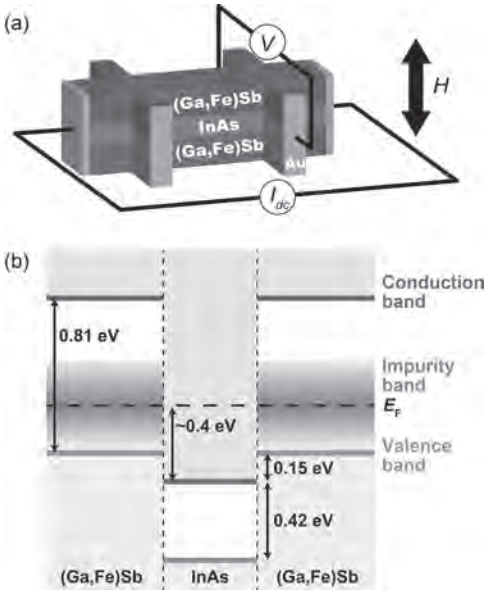

Fig. 1. (a) Schematic device structure and measurement configuration of the Hall bar devices with size of 100 × 400 μm². (b) Schematic band alignment. The Fermi level E_F is pinned at 0.2 – 0.3 eV above the valence band top of the (Ga,Fe)Sb[5].

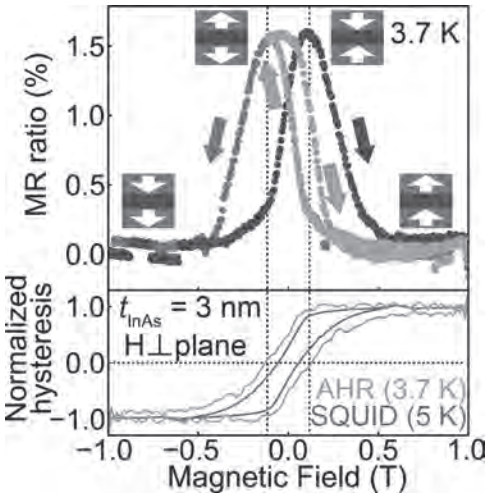

Fig. 2. MR curve of the sample with t_{InAs} = 3 nm measured at 3.7 K and corresponding magnetization hystereses obtained with SQUID magnetometry and AHE. The red and blue curves are major loops with magnetic-field sweeping directions of + to − and − to +, respectively. Green curves show a minor loop.

R3-14. Perpendicular Magnetized Spin-Valves on Flexible Substrates. a Comparative Study Between Transfer-and-Bond Approaches and Direct Deposition on Flexible Substrates. *G. Varvaro*[1], M. Hassan[1,2], S. Laureti[1], G. Barucca[2], C. Rinaldi[3], F. Fagiani[3], N. Schmidt[4] and M. Albrecht[4] *1. Institute of Structure of Matter, Consiglio Nazionale delle Ricerche, Roma, Italy; 2. SIMAU, University Polytechnic Marche, Ancona, Italy; 3. Dept. of Physics, Politecnico di Milano, Milano, Italy; 4. Institute of Physics, Universitat Augsburg, Augsburg, Germany*

Flexible spintronic devices have received a great deal of attention over the past few years thanks to the wide number of advantages (lightness, flexibility, shapeability, wearability and low cost) with respect to the conventional rigid counterpart [1]. While the progress and development of longitudinal magnetized devices on non-planar substrates has been remarkable over the last years, to the best of our knowledge, no studies are reported about magneto-resistive systems with perpendicular magnetic anisotropy on flexible substrates, despite such systems are of great relevance with regards to non-volatile memories and sensing applications. The stringent constrains required to obtain high-quality systems including suitable substrates and/or buffer layers with a specific crystallographic orientation, a very smooth surface and in some cases high temperatures, make the fabrication of such structures on flexible substrates a main challenge, as all those features are not compatible with polymeric flexible substrates. In this work, different strategies including transfer-and-bond approaches exploiting low-adhesion and sacrificial layers/substrates and the direct deposition on flexible substrates are investigated and compared. As an illustrative case, the different approaches were applied to the fabrication of perpendicular magnetized [Co/Pd]-based GMR spin valves, consisting of a fully compensated [Co/Pd]/Ru/[Co/Pd] synthetic antiferromagnet (SAF) [2] reference and a [Co/Pd] free multilayer (Figure 1). The high complexity of the chosen system in terms of number of interfaces whose quality strongly affects the final properties of the heterostructure (i.e. anisotropy of the Co/Pd multilayer, efficiency of the interlayer coupling in the SAF reference layer and GMR ratio) makes such a system a perfect candidate to test and demonstrate the potential of the proposed strategies.

[1] M Melzer et al. J. Phys. D: Appl. Phys., Vol. 53, p. 083002 (2020) [2] G. Varvaro et al., Nanoscale, Vol. 11, p. 21891 (2019)

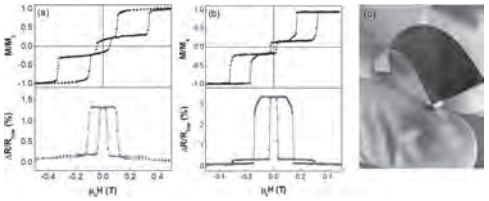

Figure 1. (a,b) Representative room temperature out-of-plane hysteresis loop and corresponding magneto-resistance response of SAF-based spin-valve on large area flexible substrates obtained by using (a) transfer-and-bond approaches and (b) direct deposition of flexible tapes. (c) Representative picture of the large-area flexible spin-valve.

Session R4
SPIN HALL AND RELATED EFFECTS III

Hidekazu Kurebayashi, Chair
University College London, London, United Kingdom

CONTRIBUTED PAPERS

R4-01. Robust two-Terminal Spin-Valve Effect From Chirality-Induced Spin Selectivity. *T. Liu*[1], X. Wang[2,4], H. Wang[2], G. Shi[3], F. Gao[3], H. Feng[3], H. Deng[1], L. Hu[1], E. Lochner[1], P. Schlottmann[1], S. von Molnar[1], Y. Li[3], J. Zhao[2] and P. Xiong[1] *1. Physics, Florida State University, Tallahassee, FL, United States; 2. State Key Laboratory of Superlattices and Microstructures, Institute of Semiconductors Chinese Academy of Sciences, Beijing, China; 3. Beijing National Laboratory for Condensed Matter Physics, Institute of Physics, Beijing, China; 4. College of Applied Sciences, Beijing University of Technology, Beijing, China*

Chirality-induced spin selectivity (CISS), with which structural chirality leads to different electric conductivities for electrons of opposite spins, is of significant current interest for its underlying physics and device potentials.[1] The spin filtering effect has been reported for a number of chiral molecules, however, the microscopic origin and transport mechanisms remain controversial. In particular, the Onsager relation is expected to preclude linear-response detection of CISS by a ferromagnet in a two-terminal spin valve device. Here, we report observation of CISS in vertical heterojunctions of (Ga,Mn)As/AHPA-L molecules/Au. The robust CISS effect in such devices enables a detailed examination of its bias dependence, which shows the presence of both linear- and nonlinear-response magnetoconductance. The experiment directly verifies spin filtering by the AHPA-L molecules and spin detection by the (Ga,Mn)As. The results constitute definitive signature of CISS-induced two-terminal spin-valve effect, in apparent violation of the Onsager reciprocity. As a new twist in spintronics, the CISS effect on semiconductors has the potential of facilitating spin injection into GaAs at room temperature without the use of any ferromagnet. *This work is supported by NSF grant DMR-1905843.*

[1] R. Naaman and D.H. Waldeck, Annu. Rev. Phys. Chem. 66, 263 (2015).

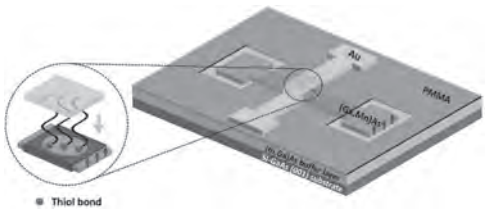

Fig. 1 Schematic diagram of a device of Au/chiral molecules/(Ga,Mn) As vertical junction.

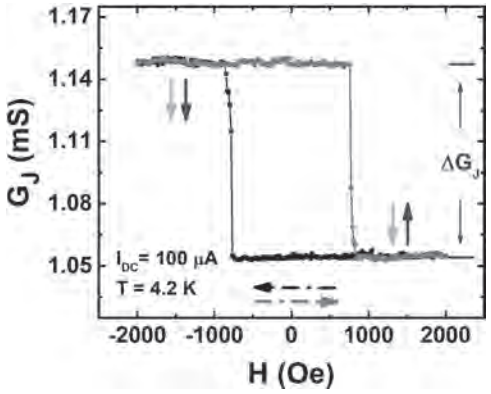

Fig. 2 Junction conductance versus perpendicular magnetic field measured at a DC bias of 100 μA.

R4-02. Room Temperature Gate Tunable Spin-to-Charge Conversion in $LaCrO_3/SrTiO_3$ Heterostructures. S. Yang[1], A. Al-Tawhid[1], E. Vetter[1], D. Kumah[1] and *D. Sun*[1] *1. Department of Physics, North Carolina State University, Raleigh, NC, United States*

The recent emergence of novel spintronics studies focuses on the generation, transmission, and control of a pure spin current through spin-orbit effects by converting the pure spin current into the charge current or vice versa. The emergence of novel electronic and magnetic phenomena at the interfaces between polar and non-polar crystalline transition metal complex oxides such as high mobility two-dimensional electron gases (2DEG) provides an ideal platform for the design of spin-to-charge (StC) convertors. At these interfaces, an interface-driven spin-orbit coupling mechanism - the Rashba effect - shows great promise due to its unprecedented StC interconversion efficiency, so-called inverse Rashba-Edelstein effect (IREE). Here we report a new type of 2DEG formed at the interface between the antiferromagnetic $LaCrO_3$ and insulating $SrTiO_3$ heterostructure with efficient StC conversion efficiency. The measured IREE length is up to 0.3 nm which can be modulated by a gate voltage. The frequency and field orientation dependence of IREE response are both consistent with the spin pumping model, from which the spin relaxation time (~30ps) is derived. Our findings launch a new class of oxide-based 2DEGs for future spin orbitronic applications. Device preparation was partially supported by ECCS-1933297 and NC State-Nagoya Collaboration Grant. Sample growth was supported by NSF DMR-1751455.

R4-03. Independent Geometrical Control of Spin and Charge Resistances in Curved Spintronics. K. Das[1], D. Makarov[2], P. Gentile[3,4], M. Cuoco[3,4], B. Van Wees[1], C. Ortix[5,4] and *I.J. Vera-Marun[6] 1. Physics of Nanodevices, Zernike Institute for Advanced Materials, Rijksuniversiteit Groningen, Groningen, Netherlands; 2. Institute of Ion Beam Physics and Materials Research, Helmholtz-Zentrum Dresden-Rossendorf, Dresden, Germany; 3. CNR-SPIN, c/o Universita degli Studi di Salerno, Fisciano, Italy; 4. Dipartimento di Fisica "E. R. Caianiello", Universita degli Studi di Salerno, Fisciano, Italy; 5. Institute for Theoretical Physics, Center for Extreme Matter and Emergent Phenomena, Universiteit Utrecht, Utrecht, Netherlands; 6. Department of Physics and Astronomy, The University of Manchester, Manchester, United Kingdom*

Spintronic devices operating with pure spin currents represent a new paradigm in nanoelectronics, with higher energy efficiency and lower dissipation as compared to charge currents. This technology, however, will be viable only if the amount of spin current in a nanochannel can be tuned while guaranteeing electrical compatibility with other device elements, to which it should be integrated in high-density three-dimensional architectures. Here, we address these two crucial milestones and demonstrate that pure spin currents can effectively propagate in metallic nanochannels with a three-dimensional curved geometry [1]. We report the first measurements of pure spin currents in curved metallic channels. The curved channel is realized by e-beam evaporation of aluminium thin films over predefined profiles in the form of focussed ion beam-etched trenches (Fig. 1). Remarkably, the geometric design of the nanochannels can be used to reach an independent tuning of spin transport and charge transport characteristics. These results put the foundation for the design of efficient pure spin current based electronics, which can be integrated in complex three-dimensional architectures.

[1] Das, K. S. *et al., Nano Letters,* Vol. 19, p. 6839–6844 (2019)

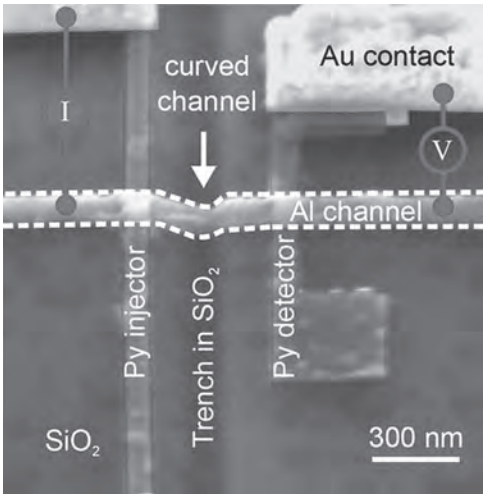

Fig. 1. Scanning electron microscopy image of a spin valve device with a curved Al channel across a trench. The electrical connections for nonlocal spin valve measurements are also depicted.

R4-04. Simultaneous Observation of Anti-Damping and Inverse Spin Hall Effect in $La_{0.67}Sr_{0.33}MnO_3$/Pt Bilayers. *P. Gupta*[1], B.B. Singh[1], K. Roy[1], A. Sarkar[2], M. Waschk[2], T. Brueckel[2] and S. Bedanta[1] *1. Laboratory for Nanomagnetism and Magnetic Materials (LNMM), School Of Physical Sciences, National Institute of Science Education and Research, Jatni- 752050, India; 2. Forschungszentrum Jülich GmbH, Jülich Centre for Neutron Science (JCNS-2) and Peter Grünberg Institut (PGI-4), Jarafit-52425, Germany*

Manganites have shown potential in spintronics due to their low damping and insulating characteristics. Here, we studied the damping properties of $La_{0.67}Sr_{0.33}MnO_3$/Pt bilayer samples which are prepared using oxide molecular beam epitaxy. We have observed decrease in damping coefficient (α) with increase in Pt thickness. Further, we investigated inverse spin Hall effect (ISHE) and observed that ISHE signal gets enhanced with Pt thickness. We observed maximum spin pumping voltage of 20.05 μV for the sample with Pt thickness of 3 nm. We have evaluated spin Hall angle for these samples. Introduction: Pure spin current based devices are potential for faster and low power consumption [1]. Generation of pure spin current has been demonstrated by ferromagnetic resonance (FMR) through spin pumping mechanism [2]. This pure spin current can loss their spin angular momentum in the presence of high spin orbit coupling (SOC) material e.g. Pt, W, Ta. The loss of spin angular momentum can develop voltage by asymmetric scattering of spins, which is known as inverse spin Hall effect (ISHE) [3]. So far studies have been concentrated mostly on Pt and FM metals [4]. However, magnetic oxides are less explored. $La_{0.67}Sr_{0.33}MnO_3$ (LSMO) is well known FM oxide for exhibiting high Curie temperature (T_C=350 K) and nearly 100% spin polarization (in bulk) [5]. In this work, in order to get high spin Hall angle, high resistive Pt film is grown on LSMO thin film. Experimental details: LSMO (20 nm)/Pt (t_{Pt} = 0, 3 and 10 nm) bilayer samples have been prepared on $SrTiO_3$(001) substrate using an oxygen plasma assisted molecular beam epitaxy system. ISHE measurements are performed using home modified coplanar wave-guide (CPW) based ferromagnetic resonance (FMR) spectroscopy [6]. Results: We have studied the static and dynamic properties of the LSMO/Pt systems. A decrease in α has been observed with increase in Pt thickness. We performed angle dependent ISHE at frequency of 7 GHz. From angle dependent ISHE measurement spin Hall angle were calculated 0.033 and 0.014 for samples with 3 and 10 nm of Pt, respectively.

[1]. C. Chappert, A. Fert, and F. N. Van Dau, Nature Materials 6, 813 (2007). [2]. O. Mosendz, J. Pearson, F. Fradin, Phys. Rev. Lett. 104, 046601 (2010). [3]. J. Hirsch, Phys. Rev. Lett. 83, 1834 (1999). [4]. J.-C. Rojas-Sanchez, N. Reyren, P. Laczkowski, Phys. Rev. Lett. 112, 106602 (2014). [5]. J.-H. Park, E. Vescovo, H.-J. Kim, Nature 392, 794 (1998). [6]. B. B. Singh, S. K. Jena, M. Samanta, Phys. Status Solidi Rapid Res. Lett. 13, 1800492 (2019).

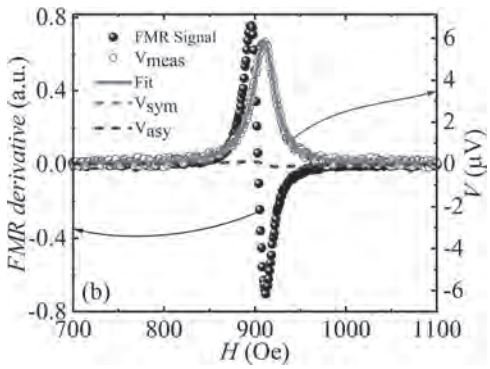

ISHE signal corresponding to FMR signal for S3.

R4-05. Impact of Symmetry on Anisotropic Magnetoresistance in Textured Ferromagnetic Thin Films. *A. Philippi-Kobs*[1,2], A. Farhadi[2], L. Matheis[2], D. Lott[3], A. Chuvilin[4,5] and H. Oepen[2] *1. Deutsches Elektronen-Synchrotron DESY, Hamburg, Germany; 2. Universitat Hamburg, Hamburg, Germany; 3. Helmholtz-Zentrum Geesthacht, Geesthacht, Germany; 4. CIC nanoGUNE, San Sebastian, Spain; 5. Ikerbasque, Bilbao, Spain*

Generally, crystalline texture and interfaces are neglected in the analysis of the anisotropic magnetoresistance (AMR) behavior of polycrystalline ferromagnetic thin film systems. This led to the misinterpretations of MR data for decades, especially since the advent of newly found spin-orbitronic effects like the spin Hall magnetoresistance (SMR), which occurs in bilayers consisting of an insulating ferrimagnet and a heavy paramagnet, in recent years [1,2]. Frequent attempts exist to study the SMR effect in all-metallic layered structures (stacking of ferromagnetic and paramagnetic layers), where the shunting through the ferromagnetic layer has to be considered

for a proper correction for AMR effects [3,4]. In a combined theoretical and experimental study, we revealed the nature of the AMR effect in all-metallic layered structures originating from crystalline texture and interfaces [5]. By symmetry considerations we captured the general AMR features and experimentally verified the newly found AMR expression containing second order (proportional to $\cos^2\theta$ where θ is the angle between magnetization orientation and film normal) and higher order terms ($\cos^{2n}\theta$). We show that the anisotropic interface magnetoresistance discovered by us [6,7] and the geometrical size effect (caused by crystalline texture) [8,9] are mere features of the general expression for AMR. Further, a proper quantification of the interfacial MR contributions reveals that they contradict the SMR behavior confirming the dominant role of AMR in all-metallic systems.

[1] H. Nakayama et al., Phys. Rev. Lett. 110, 206601 (2013), [2] Y.-T. Chen et al., J. Phys. Cond. Mat. 28, 103004 (2016), [3] A. Kobs, A. Frauen, H. P. Oepen, Phys. Rev. B 90, 016401 (2014), [4] A. Kobs and H. P. Oepen, Phys. Rev. B 93, 014426 (2016), [5] A. Philippi-Kobs et al, Phys. Rev. Lett. 123, 137201 (2019), [6] A. Kobs et al., Phys. Rev. Lett. 106, 217207 (2011), [7] A. Kobs et al., Philos. Mag. 92, 2835 (2012), [8] T. T. Chen and V. A. Marsocci, J. Appl. Phys. 43, 1554 (1972), [9] W. Gil et al., Phys.Rev. B 72, 134401 (2005).

R4-06. Spin Seebeck Effect and Anomalous Nernst Effect in Ferrimagnetic TbCo Alloys. *A. Yagmur*[1], S. Sumi[1], H. Awano[1] and K. Tanabe[1] *1. Toyota Technological Institute, Nagoya, Japan*

Since the first observation of spin Seebeck effect (SSE), many researchers interest in clarifying the mechanism of spin-thermoelectric effect and improving its efficiency [1]. Most studies of the spin-to-charge current conversion are focused on non-magnetic materials. Recently, magnetic materials attract the researcher's interest as a spin-to-charge current converter since magnetic materials reveal not only anomalous Nernst effect (ANE) [2]. It is believed the combination of the SSE and ANE may increase the spin-thermoelectric devices. In this study, we investigate the SSE and ANE in $Tb_xCo_{(100-x)}$/Cu/YIG devices and report the influence of direction of TbCo magnetization, Co moments and Tb moments on the SSE and ANE. The TbCo alloy is a ferrimagnetic material, where the magnetic moment of Co is antiparallel to that of Tb [3]. We can fabricate Tb-rich films, where net magnetization is parallel to the moment of the Tb metal, and Co-rich films, where the Co moments mainly contributes net magnetization, by controlling the composition of the alloy. We found that the amplitude and sign of the SSE voltage signals are not affected significantly by changing direction of TbCo magnetization, Tb and Co moments. On the other hand, the sign of ANE voltage signal for the Tb-rich device is opposite in sign to the Co-rich devices.

[1] Uchida, K. *et al. Nature* 455, 778–781 (2008). [2] Miao, B. F., Huang, S. Y., Qu, D. & Chien, C. L. *Phys. Rev. Lett.* 111, 066602 (2013). [3] Buschow, K. H. J. *J. Appl. Phys.* 51, 2795–2798 (1980).

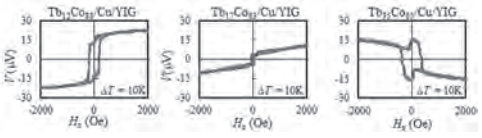

R4-07. Wave-Diffusion Approach to Spin Current Dynamics in Magnetic Multilayers Driven by THz Fields. *M. Burgard*[1], D.M. Nenno[2] and H. Schneider[1] *1. Physics, Technische Universitat Kaiserslautern, Kaiserslautern, Germany; 2. Harvard University John A Paulson School of Engineering and Applied Sciences, Cambridge, MA, United States*

Recent developments in spintronic Terahertz emitter design have yielded broadband pulses up to 30 THz and beyond [1]. While the THz pulse generation in magnetic multilayers amounts to a down-conversion of optical photons, we investigate here the same magnetic multilayer structures but focus on the electron dynamics driven by externally controlled Terahertz pulses, see Fig. 1. Our theoretical approach to spin-dependent high-frequency electron transport is based on the wave-diffusion equations for spin-densities and currents [2], which results from a microscopic Boltzmann transport model. Starting from a consistent microscopic model of the interaction of THz pulses with carriers in metals we derive macroscopic equations for the density and current dynamics in ferromagnet-metal heterostructures, which take into account the effects of both the transverse and longitudinal electric fields (including screening). From the frequency and position dependent spin currents and densities, as shown in Fig. 2, we determine the absorption and transmission of the layers.

[1] T. Seifert, et al., Nature Photon 10, 483 (2016). [2] Y.-H. Zhu, B. Hillebrands, and H. C. Schneider, Phys. Rev. B 78, 054429 (2008).

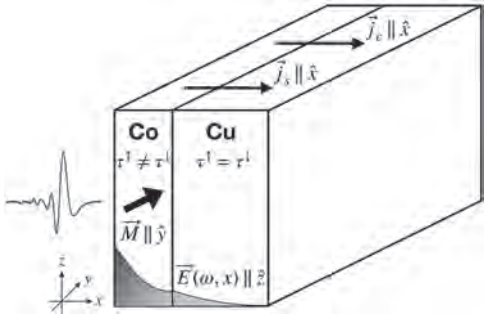

Sketch of numerical setup. Time-dependent spin-resolved currents and charge densities driven by THz excitation are calculated for a bilayer structure, including internal electric fields.

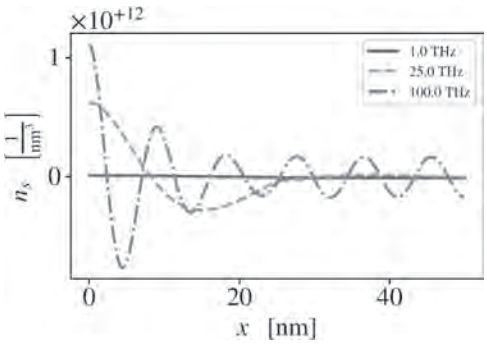

Spin-density in the Cu part of the bilayer shown in Fig. 1 for different driving frequencies.

R4-08. Influence of Carriers in Spin Pumping in Organic Semiconductors. *C. Nicolaides*[1] and T. Trypiniotis[1] *1. Physics, Panepistemio Kyprou Schole Thetikon kai Epharmosmenon Epistemon, Nicosia, Cyprus*

Conductive polymers have recently been attracting particular attention in spintronics due their low cost, ease of processing and flexible molecular structure. In general, these materials consist of elements with small atomic numbers and exhibit weak spin-orbit and hyperfine interaction. As a result, long spin diffusion length (1) and large spin relaxation time is exhibited making semiconductor polymers candidate materials for spintronic devices as spin conveyers. Organic semiconductors have as main charge carriers polarons and bipolarons and the spin properties interplay between these carriers remain elusive. In this context, we report an experimental demonstration of spin transport at room temperature in PEDOT:PSS (poly(3,4-ethylenedioxythiophene) polystyrene sulfonate) films. We have employed spin pumping under ferromagnetic resonance in a microwave cavity for a series of PEDOT:PSS/NiFe heterostructures with varying PEDOT:PSS conductivity. An overall conductivity change of 7 orders has been achieved by changing the ratio between PEDOT and PSS and by chemically doped or

dedoped the polymer. The evolution of the polaron/bipolaron concentration as a function of conductivity was investigated by means of EPR. The generated spin current is detected via the inverse spin-Hall effect which converts it to a measurable charge current. The combined data provide clear evidence that the polaron/bipolaron concentration is the regulator of inverse spin-Hall effect voltage.

1. S.-J. Wang, et al., Nat. Electron., Vol. 2, p. 98–107 (2019).

R4-09. Microwave and Thermally Driven Spin Currents in $Tm_3Fe_5O_{12}$/Pt With Perpendicular Magnetic Anisotropy. *G.L. da Silva Vilela*[1,2], J.E. Abrao[3], E. Santos[3], Y. Yao[4,5], J.B. Mendes[6], R.L. Rodríguez-Suárez[7], W. Han[4,5], S.M. Rezende[3], A. Azevedo[3] and J.S. Moodera[2,8] *1. Física de Materiais, Universidade de Pernambuco Escola Politecnica de Pernambuco, Recife, Brazil; 2. Plasma Science and Fusion Center, and Francis Bitter Magnet Laboratory, Massachusetts Institute of Technology, Cambridge, MA, United States; 3. Departamento de Física, Universidade Federal de Pernambuco, Recife, Brazil; 4. International Center for Quantum Materials, Peking University, Beijing, China; 5. Collaborative Innovation Center of Quantum Matter, Beijing, China; 6. Departamento de Física, Universidade Federal de Vicosa, Viçosa, Brazil; 7. Facultad de Física, Pontificia Universidad Catolica de Chile, Santiago, Chile; 8. Department of Physics, Massachusetts Institute of Technology, Cambridge, MA, United States*

Ferrimagnetic insulator garnet films play an important role in magnon spintronics where magnon-mediated spin currents are used to carry, transport, and process information. This wave-based computing technologies lead to energetically more efficient devices and allows a decrease in the footprint of computing elements [1]. When a magnetic insulator (MI) film is combined with a non-magnetic (NM) spin current detector material like platinum, it is possible to electrically control the MI's magnetization via the spin-orbit torque (SOT) effect. If the MI presents a perpendicular magnetic anisotropy (PMA), the electrical current density required to switch the magnetization is lower, and the process is faster. This makes the magnetoresistive random access memories based on SOT (SOT-MRAM) challenge the MRAMs based on the spin-transfer torque effect (STT-MRAM) [2]. Moreover, ferrimagnetic garnets with PMA enables high-speed domain-wall (DW) motion that also can be driven by electrical currents via SOT and are ideal materials for developing efficient DW racetrack memories [3]. Thulium iron garnet (TIG – $Tm_3Fe_5O_{12}$) is a good candidate due to its high critical temperature of 549 K, a Gilbert damping of 10^{-2}, and negative magnetostriction constant that favors the control of the PMA [4]. When combined with Pt, TIG/Pt is a reach system for the study of spin waves and the observation of spin-orbit effects. We investigate the generation and detection of magnon-based spin currents driven by microwaves and heat currents via the spin pumping (SPE) and spin Seebeck (SSE) effects in TIG(60 nm)/Pt(4 nm), at room temperature. The TIG film was deposited over GGG ($Gd_3Ga_5O_{12}$) substrate using the sputtering technique and presented a flat surface with an RMS roughness of 0.1 nm. The magnetization saturation was ~ 100 emu/cm^3, and the Gilbert damping parameter was 0.02. The results showed an effective spin-to-charge conversion via the inverse spin Hall effect (ISHE). It made it possible to detect a micro-voltage at the edges of the Pt film and confirmed high spin transparency of the interface TIG/Pt. The spin Seebeck coefficient was 0.54 μV/K, whereas the ratio between the microwave-driven voltage and the microwave power was 4μV/W.

[1] A. V. Chumak et al., Nature Physics, Vol. 11, p. 453 (2015). [2] M. Cubukcu et al., IEEE Transactions on Magnetics, Vol. 54, p. 1 (2018). [3] S. Vélez et al., Nature Communications, Vol. 10, p. 4750 (2019). [4] G. Vilela et. al., Journal of Applied Physics, Vol. 127, p. 115302 (2020).

INVITED PAPER

R4-10. Non-Volatile Electric Control of Spin–Charge Conversion in a SrTiO3 Rashba System. *P. Noël*[1,4], F. Trier[2], L. Vincente Arche[2], J. Bréhin[2], D. Vaz[3,2], V. Garcia[2], S. Fusil[2], A. Barthelemy[2], L. Vila[4], M. Bibes[2] and J. Attané[4] *1. DMATL, Eidgenossische Technische Hochschule Zurich, Zurich, Switzerland; 2. Unité Mixte de Physique, CNRS, Thales, Université Paris-Saclay, Palaiseau, France, Palaiseau, France; 3. CIC nanoGUNE, San Sebastian, Spain; 4. SPINtronique et Technologie des Composants, Grenoble, France*

Spintronics has traditionally relied on ferromagnetic materials to provide non-volatility and to generate and detect spin currents. However, magnetization reversal by spin transfer and spin orbit torques is a power-consuming process. This is driving research on multiferroics to achieve low-power electric-field control of the magnetization, but practical materials are scarce and magnetoelectric switching remains difficult to control. In this presentation we will focus on an alternative strategy: use ferroelectricity to obtain the remanent control of the spin-charge interconversion. At the interface between a ferroelectric and an ultrathin spin orbit coupling (SOC) systems -such as 2DEG- electrons are accumulated or depleted depending on the polarization direction. This modifies the electric field in the interface region, and in the ideal case changes its sign. If a Rashba state is present in the SOC system at the interface with the ferroelectric, reversing the sign of the local electric field reverses the chirality of the spin textures in both split Fermi contours as depicted in figure 1. This mechanism offers the possibility to design a wealth of devices such as bipolar memories and can also be the basis of logic devices akin to the magnetoelectric spin–orbit device proposed by Intel A highly efficient conversion was evidenced in the two-dimensional electron gas (2DEG) obtained at the interface between $SrTiO_3$ (STO) and $LaAlO_3$ (LAO). Moreover, thanks to the high dielectric constant of STO at cryogenic temperature the spin current generation and detection can be tuned using gate voltage [1,2]. A similar 2DEG can be obtained by depositing a thin layer of a reducing metal as Al on top of STO alleviating the need for the high-temperature growth of crystalline LAO and allowing the modulation of the carrier density through the adjustment of the Al thickness. In this system the gate tunability of the spin to charge conversion and its link to the bandstructure of STO was evidenced [3]. But despite the possibility to tune the conversion using gate voltage in STO based Rashba system, the remanent control of the 2DEG was still not achieved. While STO is not a ferroelectric it is possible to induce ferroelectricity in STO based structure either by doping it with Calcium [4] or by applying high electric field. In this presentation we will evidence that it is possible to control the 2DEG carrier density and the sign of the spin to charge conversion in a remanent way in ferroelectric-like STO based structures [5]. After applying a high enough electric field to induce a ferroelectric state in STO It is possible to modulate the sign of the conversation with positive and negative voltage pulses as depicted in figure 2.

[1] E. Lesne, Y. Fu, S. Oyarzun *et al.,* Nature Materials 15,1261–1266(2016) [2] F. Trier, D.C. Vaz, P. Noël et al., Nano Lett. 20, 1, 395–401 (2020) [3] D. C. Vaz,P. Noël, A. Johansson et al., Nature Materials 18, 1187–1193(2019) [4] J. Bréhin, F. Trier, P. Noël et al., Phys. Rev. Materials 4, 041)002(R) (2020) [5] P. Noël, F. Trier, L. M. Vicente Arche et al., Nature 580, 483–486(2020)

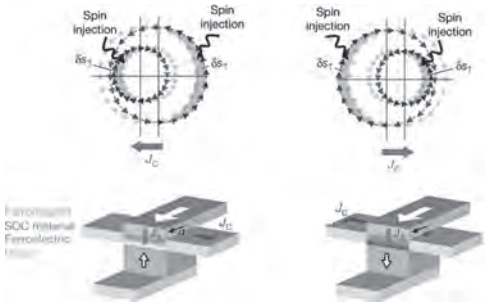

Non-volatile device operated by ferroelectricity and Rashba SOC. Through the inverse Edelstein effect a charge current J_C is generated by the conversion of a spin current J_S injected from the ferromagnet. The sign of J_C changes with the direction of the ferroelectric polarization.

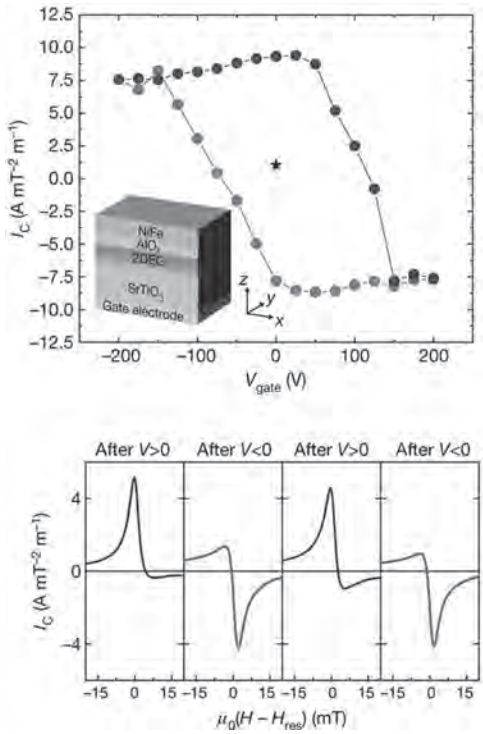

Gate-voltage dependence of the normalized current produced by the inverse Edelstein effect. Spin to charge current conversion can be remanently controlled after applying positive or negative voltage pulses of ±200 V.

CONTRIBUTED PAPERS

R4-11. Spin Pumping From Acoustically Driven Parametric Spin Waves in a Hybrid Magnon-Phonon Resonator. *N. Polzikova*[1], S. Alekseev[1], V. Luzanov[2], A. Raevskiy[2] and S. Nikitov[1] *1. Kotelnikov Institute of Radio Engineering and Electronics of Russian Academy of Sciences, Moscow, Russian Federation; 2. Fryazino branch Kotelnikov Institute of Radio Engineering and Electronics of Russian Academy of Sciences, Fryazino, Russian Federation*

Significant interest in acoustically driven spin waves (ADSW) is due to the possibility of their use in low power consumption microwave spintronic and magnonic devices. Linear and parametric excitation of ADSW was demonstrated in various hybrid magnon-phonon structures containing piezoelectric and ferro (ferri) magnetic layers. In our previous works [1-3], we have demonstrated the piezoelectric excitation of linear ADSW in the gigahertz frequency range and their detection by the combination of spin pumping and inverse spin Hall effect (ISHE) in the spintronic hybrid High overtone Bulk Acoustic wave Resonator (HBAR) with the structure ZnO – YIG– GGG–YIG – Pt (Fig.1). Here, we report on the first observation of parametric ADSW excitation using an analogous HBAR. For investigation of parametric ADSW the spin pumping effect and its detection via the dc ISHE voltage U_{ISHE} in a YIG/Pt system are also used. The pump frequency f_p, power P, and magnetic field H dependences of the U_{ISHE} are studied. Figure 2 shows dependence $U_{ISHE}(H, f)$ versus magnetic field and frequency. The maximum of $U_{ISHE}(H, f_p)$ is observed at $H=H_c\approx190$ Oe, at which $f_p/2=f_{FMR}(H_c)$ and under the condition $f_p=f_n$ were f_n - HBAR resonant frequencies, $f_{FMR}(H)$ – ferromagnetic resonance frequency according to the Kittel's formula. Note that when the field direction is reversed, the voltage value changes sign, which is typical for ISHE symmetry. For comparison, the region of linear resonance excitation of ADSW at the same frequency is located at higher fields: H_{FMR}=530 Oe. The power and field dependences $U_{ISHE}(P,H)$ measurements give the threshold values in the range 0.4 – 0.8 mW which is consistent with the theoretical estimations [4]. This work was carried out in the framework of the State task 0030-2019-0013 "Spintronics" and with partial support of the RFBR No. 20-07-01075.

1. N. I. Polzikova, S. G. Alekseev, I. I. Pyataikin, et al, AIP Advances, p. 056306 (2016) 2. N. I. Polzikova, S. G. Alekseev, I. I. Pyataikin, et al, AIP Advances, Vol.8, p.056128 (2018) 3. N. I. Polzikova, S. G. Alekseev, V. A. Luzanov, et al., J. Magn. and Magn. Mater., Vol. 479, p. 38 (2019) 4. C. W. Haas, J. Phys. Chem. Solids, Vol.27, p.1687 (1966)

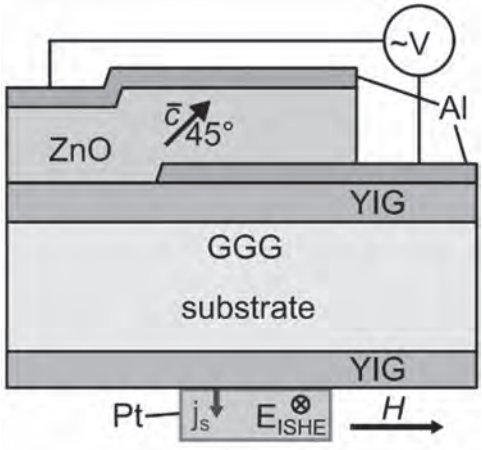

Fig.1. Schematic of hybrid HBAR for acoustic spin pumping. The rf voltage V is applied across the piezoelectric transducer sandwiched between thin-film Al electrodes. The transducer launches and detects a bulk shear acoustic waves, which propagate vertically.

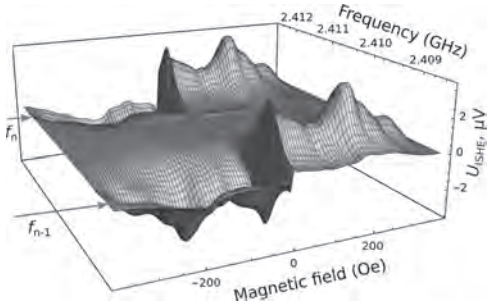

Fig.2. 3D image of voltage U_{ISHE} in Pt layer versus frequency and field. The red arrows indicate the resonant frequencies of HBAR.

R4-12. Monte Carlo Simulation of Ultrafast Nonequilibrium Spin and Charge Transport in Iron. *J. Briones*[1], H. Schneider[1] and B. Rethfeld[1]
1. Department of Physics and Research Center OPTIMAS, University of Kaiserslautern, Kaiserslautern, Germany

Ultrashort laser pulses in magnetic materials and ferromagnet-metal heterostructures drive complicated dynamics that may result in ultrafast demagnetization as well as ballistic to diffusive transport of highly excited electrons [1,2,3]. We focus here exclusively on the spin-dependent transport of electrons excited to states far above the Fermi energy. We have adapted the asymptotic-trajectory Monte Carlo technique [4] to trace the spatio-temporal dynamics of electrons excited by an ultrashort laser pulse in ferromagnetic metals, and apply our approach to the case of iron. In particular, we resolve the change of electronic energy induced by various scattering processes. Our model takes into account electron-ion scattering, electron impact ionization and, in a phenomenological way, the contribution of spin flips. This approach directly yields a space-time picture of electron cascade processes and allows us analyze the influence of secondary-electron generation on the transport characteristics of high-energy electrons in the linear excitation regime. The Figure shows as an example the time evolution of the parameter that characterizes the particle transport [2,3]: The hot electron dynamics is initially ballistic (= 2), then superdiffusive (> 1) and finally diffusive (= 1). The secondary electrons keep the system noticeably longer in the superdiffusive regime.

[1] D. Rudolf, et al, Nat. Commun. 3, 1037 (2012). [2] M. Battiato, K. Carva, and P. M. Oppeneer, Phys. Rev. Lett. 105, 027203 (2010). [3] D. M. Nenno, B. Rethfeld, and H. C. Schneider, Phys. Rev. B 98, 224416 (2018). [4] K. Huthmacher et al., Physica A 429, 241-251 (2015).

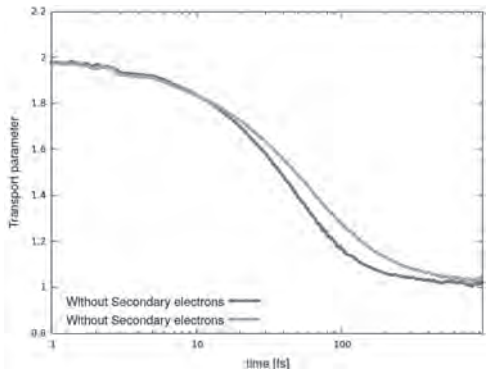

Time dependence of transport parameter: ballistic (=2), superdiffusive (>1) or diffusive (=1).

Session R5
SOFT MAGNETIC MATERIALS
(Poster Session)

Arkady Zhukov, Co-Chair
Basque Foundation for Science, San Sebastian, Spain
Gaoyuan Ouyang, Co-Chair
Iowa State University, Ames, IA, United States

R5-01. Magnetic Correlations and Coercivity in Nanocrystalline Alloys With Grain-Size Distribution. *A. Bolyachkin*[1], E. Dengina[1] and S. Komogortsev[2] *1. Ural Federal University, Yekaterinburg, Russian Federation; 2. Kirensky Institute of Physics, Federal Research Center KSC SB RAS, Krasnoyarsk, Russian Federation*

Some nanocrystalline alloys are prospective soft magnetic materials due to extremely low coercivity that can be achieved if their mean grain size D is less then basic exchange length [1]. Below this limit coercivity H_c varies drastically with D. Well-known experimental correlation $H_c \propto D^6$ is explained using random magnetic anisotropy model [2]. For such steep power-law dependence, a grain-size distribution should have a significant effect on the $H_c(D)$. This work presents the study of this possibility using computer modeling [3]. A polycrystalline alloy was simulated as an ensemble of close packed polyhedra with lognormally distributed sizes. Such ensembles were generated by radical 3D Voronoi tessellation taking into account periodic boundary conditions. It was assumed that each polyhedron (grain) has a uniform magnetization changing by the coherent rotation. Exchange interaction between neighboring grains was simulated in a direct Heisenberg-like form. The uniaxial magnetic anisotropy with randomly oriented easy magnetization axes among grains was considered. Equilibrium micromagnetic structures of ensembles were obtained by reiterative energy minimization. Major hysteresis loops of the monodisperse ensemble and a series of polydisperse ones with different reduced grain size standard deviations σ/D were calculated. The sharp power-law dependence of coercivity $H_c \propto D^6$ was observed in simulations for the monodisperse ensemble. However, coercivities of all polydisperse ensembles followed the power law D^n with exponents n lower than 6. The dependence of the exponent on the reduced grain size standard deviation was extracted. It sharply decreased first and then it changed gradually reaching values of about $n = 3$ with increasing σ/D. The correlation analysis of obtained micromagnetic structures was performed for polydisperse ensembles to reveal the underlying physics of these results observed previously in [3].

[1] K. Suzuki and J.M. Cadogan, Phys. Rev. B, Vol. 58, p. 2730 (1998). [2] G. Herzer, IEEE Trans. Magn., Vol. 26 p. 1397 (1990). [3] A.S. Bolyachkin and S.V. Komogortsev, Scr. Mater., Vol. 152, p. 55 (2018).

R5-02. Magnetic Critical Behavior, Hall Effect, and Magnetic Interactions in $Fe_{73.5-x}Cr_xCu_1Nb_3Si_{13.5}B_9$ Metallic Glasses on the Road to Percolation. *A. Rosales-Rivera*[1], N.A. Salazar-Henao[1], R. Gonzalez-Sánchez[1], J. López Tabares[1], A.A. Velazques-Salazar[1] and F.D. Saccone[2] *1. Laboratorio de Magnetismo y Materiales Avanzados, Universidad Nacional de Colombia, Sede Manizales, Manizales, Colombia; 2. Departamento de Física, Facultad de Ingeniería, Universidad de Buenos Aires, Buenos Aires, DC, Argentina*

A study of the magnetic critical behavior and Hall effect, and magnetic interactions is presented for $Fe_{73.5-x}Cr_xCu_1Nb_3Si_{13.5}B_9$ metallic glasses on the road to percolation ($x_p \approx 24$ at.% Cr) [1]. The samples under study were prepared as amorphous ribbons from $Fe_{73.5-x}Cr_xCu_1Nb_3Si_{13.5}B_9$ with $10 \le x \le 20$ at. % ingot alloys by means of the melt-spinning technique. The amorphous structural state of each sample was confirmed using X-ray diffraction with CuKa radiation. The critical behavior is studied by determining the critical exponents for the zero-field magnetization (β), zero-field isothermal susceptibility (γ), critical isotherm (δ), and critical temperature T_C, from magnetization measurements using the Kouvel-Fisher method [2]. The obtained (β, γ, δ) values indicate that the universality class of these metallic glasses is consistent with the mean-field model with long-range interactions. The critical temperature, T_C, quasi-linearly decreases with the increase of Cr content. This behavior indicates that the exchange interaction weakens with the increase of Cr content. The Hall effect measurements were carried out in the field range $-10 < H < 10$ kOe for several *DC* electrical currents applied to the samples at room temperature. These measurements reveal an ordinary and extraordinary contribution to the Hall effect and a positive Hall constant. From the ordinary contribution to the Hall effect, we obtained the following physical parameters: ordinary Hall coefficient, resistivity, concentration and drift velocity of charge carriers, besides mean free path of charge carriers and relaxation time. An analysis of the physical parameters previously mentioned and of their dependence on Cr concentration is presented. Special attention is given to exchange interaction and spin-orbit interaction that might be active in these materials, and their possible effects on the (β, γ, δ) values are analyzed.

1. M.S. Mahmud, "Magnetic behavior of $Fe_{73.5-x}Cr_xCu_1Nb_3Si_{13.5}B_9$ amorphous alloys at low temperature", J. Mat. Sci. & Eng., A1, 58-63 (2011). 2. J.S. Kouvel, M.E. Fisher, Phys. Rev. 136 (1964) 1626, https://doi.org/10.1103/ PhysRev. 136.A1626.

R5-03. Electronic Structure of Amorphous Fe-P-C-Ge Soft Magnet. J. Han[1], M. Choi[2], H. Won[2], *H.C. Yim*[1] and Y. Hong[2] *1. Physics, Sookmyung Women's University, Yongsan-gu, The Republic of Korea; 2. Electrical & Computer Engineering, The University of Alabama College of Arts and Sciences, Tuscaloosa, AL, United States*

Amorphous soft magnet Fe-P-C has been developed to lower core loss and coercivity and also increase saturation magnetization (M_s). By rapidly quenching of melt and annealing of $Fe_{80}P_{13}C_7$ at 300 °C, M_s of 1.22 T was achieved [1], while M_s of 1.51 and 1.53 T [2] are realized from arc-melted and re-melted and J-quenched $Fe_{80}P_{13}C_7$ alloys, respectively. When Fe concentration increases to 82 ($Fe_{82}P_{12}C_6$) from 80 ($Fe_{80}P_{13}C_7$), M_s increased to 1.56 T [2]. Both C and P have negative contribution to the total magnetic moment [3, 4] but more from C. Zhang et al. calculated magnetic moments of $Fe_{80}P_{13}C_7$, which includes 100 atoms, and found magnetic moments of 1.85 μ_B for Fe, -0.0595 μ_B for P, and -0.1085 μ_B for C (147.267 μ_B /100 atoms) [4]. To further increase M_s of amorphous Fe-P-C alloy, we have replaced part of P in Fe-P-C with Ge and fabricated $Fe_{80}P_{13-x}C_7Ge_x$ (x = 0, 2, 4) glass ribbons by rapidly quenching. The M_s increased to 1.62 T (x = 4) from 1.46 T (x = 0). To investigate the enhancement of magnetization with Ge replacement, we have performed first-principles calculations based on the density functional theory (DFT) using VASP package [5]. A mixture of Fe, P, C, and Ge atoms in the total of 100 atoms was heated up to 3000 K within 12×10^{-12} sec using *ab initio* molecular dynamics. The atoms are randomly distributed in a box (100-atom cuboid cell) in Fig.1, where a and b axes are equal, but c axis is shorter than a (= b). We have relaxed the cuboid cell until the lowest system (free) energy is reached. Then, $a = b$ and c are

determined. Electronic structures of three amorphous alloys ($Fe_{80}P_{13-x}C_7Ge_x$; x = 0, 2, 4) were calculated. The calculated results are in agreement with experimental measurements as summarized in Table 1. It was found that P replacement with Ge remarkably enhances M_s of Fe-P-C system. This enhancement mechanism is under investigation. This work was supported in part by the National Science Foundation IUCRC under Grant No. 1650564

[1] H. Fujimori, T. Masumoto, Y. Obi, and M. Kikuchi, "On the Magnetization Process in an Iron-Phosphorus-Carbon Amorphous Ferromagnet," Japan. J. Appl. Phys. 13, 1889 (1974) [2] Q. Li, J.F. Li, P. Gong, K.F. Yao, J.G. Gao, and H.X. Li, "Formation of bulk magnetic ternary $Fe_{80}P_{13}C_7$ glassy alloy," Intermetallics 26, 62 (2012) [3] H. Wang, T. Hu, and T. Zhang, "Atomic, electronic and magnetic properties of $Fe_{80}P_{11}C_9$ amorphous alloy: A first-principles study," Physica B, 411, 161(2013). [4] W. Zhang, Q. Li, and H. Duan, "Study of the effects of metalloid elements (P, C, B) on Fe-based amorphous alloys by ab initio molecular dynamics simulations," J. Appl. Phys. 117, 104901 (2015) [5] P. Blaha, et al., WIEN2k, Inst. F. Materials Chemistry TU Vienna, 2001

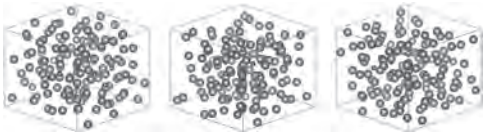

Fig. 1. Amorphous 100-atom cuboid cell: (a) $Fe_{80}P_{13}C_7$, (b) $Fe_{80}P_{11}C_7Ge_2$, and (c) $Fe_{80}P_9C_7Ge_4$

		$Fe_{80}P_{13}C_7$	$Fe_{80}P_{11}C_7Ge_2$	$Fe_{80}P_9C_7Ge_4$
Relaxed volume dimension	$a = b$(Å)	11.039	11.066	11.092
	c(Å)	9.200	9.222	9.241
	V(Å^3)	1121.108	1129.293	1137.189
Magnetic moment (μ_B/cuboid cell)		150.183	157.693	162.229
Saturation Magnetization (T)	Cal.	1.57	1.63	1.67
	Exp.	1.46	1.57	1.62

Table 1. Relaxed volume dimension, magnetic moment, and saturation magnetization for amorphous $Fe_{80}P_{13-x}C_7Ge_x$ (x = 0, 2, 4)

R5-04. Simulation of Magnetic Field Modulation of Magnetic Flux Concentrator. *J. Peng*[1,2], F. Jin[1,2], L. Xu[1,2], J. Jiang[1,2], B. Yang[1,2], K. Dong[1,2], W. Mo[1,2] and J. Song[1,2] *1. School of Automation, China University of Geosciences, Wuhan, China; 2. Hubei key Laboratory of Advanced Control and Intelligent Automation for Complex Systems, Wuhan, China*

Magnetic sensors based on the giant magnetic impedance effect (GMI) have become a hotspot in the development of high-performance magnetic sensors due to their miniaturization, high sensitivity, and fast response. However, low frequency 1/f noise and other issues have seriously troubled the development of GMI magnetic sensors. Due to the fact that its noise sources have not yet been unified, it is increasingly difficult to optimize 1/f noise by means such as improving circuit structure and improving material quality. The magnetic field modulation technology based on the idea of dynamic shunt has achieved good results in improving the effect of 1/f noise on MTJ magnetic sensors[1]. This technology is mainly realized through the function of the magnetic flux concentrator(MFC) to modulate the magnetic field. Therefore, this paper studies the relationship between MFC parameters and the function of modulating the magnetic field to be measured. The effect of MFC on the amplitude of the measured magnetic field is studied with COMSOL software in this paper[2]. As can be seen from Figure 1, when a trapezoidal MFC with larger bottom-top ratio and longer height is close to the point to be measured, it has a better amplification effect on the magnetic field of the point to be measured. Figure 2 shows a structure with a frequency modulation of the magnetic field to be measured. The cantilever beam is driven by piezoelectric material to achieve periodic MFC vibration. The curves of Modulated magnetic field versus drive signal under different frequencies are obtained by simulation. Through the magnetic field modulation technology, the frequency of the signal to be measured is modulated to a high frequency for detection, so as to avoid the influence of 1/f noise and achieve the purpose of optimizing the signal to be measured.

[1] J. Hu, et al, Sensors, Vol.19, No.20, p.4475 (2019) [2] Predrag M., et al, Sensors and Actuators A: Physical, Vol.97-98, p.10-14 (2002)

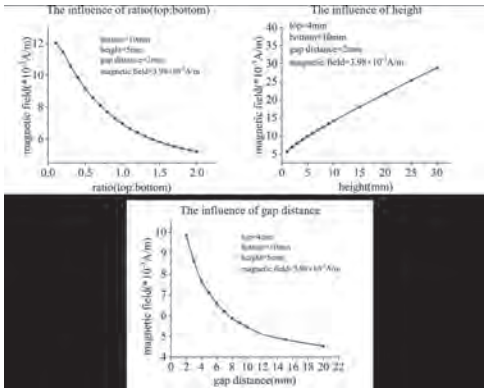

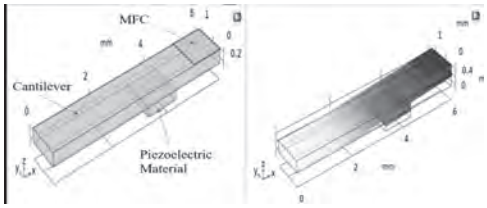

R5-05. Mild Electro-Mechanical Processing of Water-Quenched Amorphous Microwires for Property Improvements. *A. Valeriano Inchausti*[1], X. Zhang[2], A. Jacas[1], R. Pérez del Real[1], M. Butta[3,1], L. Lewis[2,1] and M. Vazquez[1] *1. Materials for Emergent Technologies, Instituto de Ciencia de Materiales de Madrid, Madrid, Spain; 2. Northeastern University College of Engineering, Boston, MA, United States; 3. Ceske vysoke uceni technicke v Praze Fakulta elektrotechnicka, Praha, Czechia*

The rapidly solidification techniques to fabricate amorphous microwires generate strong mechanical stresses which, coupled to magnetostriction, determine their magnetic properties in competition with exchange interaction plus shape anisotropy energy terms [1]. However, most technological applications employing amorphous microwires rely on the quality of their geometrical and compositional homogeneity [2]. In this concern, small variations of the fabrication parameters can result in inhomogeneities that degrade the magnetic properties. Thus, in this work a novel mild electromechanical treatment is demonstrated to improve their morphology without damaging their structural and magnetic properties. Amorphous microwires with zero-magnetostriction composition (130 mm diameter) were prepared by in-rotating-water-quenching technique. The microwiresshow a natural curvature owing to that of the rotating drum (0.8 m diameter) as well as kind of undulating morphologydue to quench instabilities arising from the conditions such as the pressure of the ejecting gas, the drum rotation velocity and the melt ejection temperature. The as-quenched wires were subjected to an electromechanical annealing that passes an electrical current through the microwire (maximum current density of 50MA/m^2) for ~140 seconds in a vertical configuration under constant tensile stress (maximum of 130MPa). The structural and magnetic changes induced by the electromechanical treatmentswere assessed by differentprobes. After annealing, the microwires showed a nicely straight shape, losing both natural and undulating morphology (Fig. 1). In addition, the samples were confirmed to be amorphous, with partly relaxed structure, and maintained ultrasoft character with a coercivity of about 130 mOe (Fig. 2). This mild electromechanical annealing is demonstrated to be successful for the precise control over the morphology, structure and magnetism of amorphous microwires to optimize their technological applicability.

Vazquez, M. - Advanced Magnetic Microwires, in Handbook of magnetism and advanced magnetic materials. Ed. H. Kronmüller & S. Parkin, John Wiley & Sons, Cambridge, Vol. 4, pp. 2183-2223. (2007). Butta, M.,

Vazquez, M., Perez del Real, R. - Dependence of the noise of an orthogonal fluxgate on the composition of its amorphous wire-core. AIP Advances, 10, 025114 (2020)

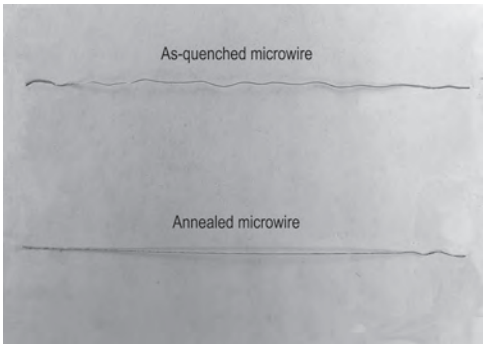

Images of the microwire in as-cast and after annealing (current density of 47 MA/m^2).

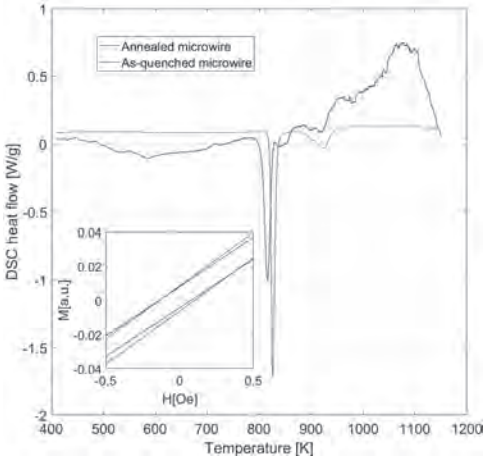

DSC for as-quenched and annealed microwire. The inset shows a zoom into the corresponding low-field hysteresis loops.

R5-06. Tensile, Torsion and Bending Stresses Modulation of Co-Based Microwire's Domain Structure and Magnetoimpedance Effect.
Y. Wang[1], F. Qin[1], T. Feng[1], D. Estevez[1] and H. Peng[1] *1. Zhejiang University, Hangzhou, China*

The Co-based amorphous microwires have a complex domain structure consisting of the circular domain in the outer shell and the axial domain in the inner core. Owing to the magnetic structure, we find that the microwires show a peculiar magnetoimpedance (MI) curve transition from several hundred MHz to several GHz and it can be modulated by applied stress in different forms. This also suggests that the change of magnetic domain could be characterized by frequency-impedance spectrum. The microwires employed in this experiment have a nominal composition of Co68.7Fe4Si11B13Ni1Mo2.3, fabricated by a modified Taylor–Ulitovskiy method. Different types of stress annealing were adopted to the microwires. to construct different domain morphologies, including torsion annealing (T), tension annealing (S) and bending annealing (B). The hysteresis loops (Fig.1) show that different types of stress annealing have different effects on the magnetic properties of microwires. The torsion annealing (Fig.1(a)) can reduce the coercivity, the tension annealing (Fig. 1(b)) can increase the permeability of the microwires, while the bending annealing (Fig. 1(c)) can worsen the magnetic properties. Further, through the impedance spectrum, we can identify the changes of the magnetic structure in microwires more specifically. The tiny magnetic field can induce ferromagnetic resonance (FMR) in axial domains and will not cause a violent rotation of the domain. As such, there are both ferromagnetic resonance and natural resonance (NR) in the microwires. The FMR peak can indicate the state of axial domains, and NR indicates the state of domains with large angles deviating from the axial direction. The T group samples (Fig. 2(a)) shows torsion annealing can strengthen axial domain and circumferential domain; but when the torsion angle is large enough, the effect of stress will contribute more to circumferential domain. The S group samples (Fig. 2(b)) shows the tension annealing can significantly increase the axial domain when the tensile stress is large enough. The B group samples (Fig. 2(c)) shows the bending annealing can increase the disorder of domain direction, which is consistent with the hysteresis loop.

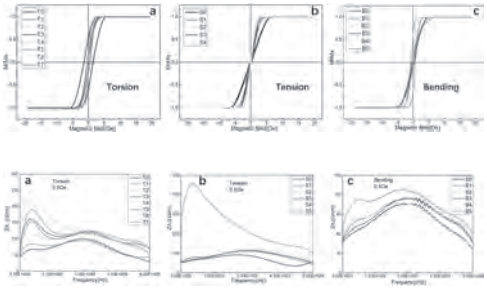

R5-07. On the Path to New Magnetic Cores: Electromagnetic Simulations of Amorphous Magnetic Microwires for Inductive Applications.
C. Johnson[1], *X. Zhang*[2], R. Pérez del Real[3], S. Pakdelian[4], M. Vazquez[3], L. Lewis[2,5] and B. Lehman[1] *1. Electrical and Computer Engineering, Northeastern University, Boston, MA, United States; 2. Mechanical and Industrial Engineering, Northeastern University, Boston, MA, United States; 3. Instituto de Ciencia de Materiales de Madrid, CSIC, Madrid, Spain; 4. Electrical and Computer Engineering, University of Massachusetts Lowell, Lowell, MA, United States; 5. Chemical Engineering, Northeastern University, Boston, MA, United States*

The advancement of next-generation power electronic devices with improved energy efficiency and compact sizes requires the development of new types of soft magnetic cores. Recently, water-quenched Fe(Co)SiB-based amorphous magnetic microwires (~100 microns in diameter) have been assessed to show improved soft magnetic properties and unique magnetic anisotropies relative to conventional core materials[1]. Here, we present electromagnetic simulation results that confirm an improved magnetization alignment and amplified core inductance in amorphous magnetic microwires as compared to those of benchmark core materials. Preliminary electromagnetic simulations were performed using Ansys software (Electromagnetics Suite 17.2)[2] based on two simplified models of 1) a regular inductor and 2) an air-gapped toroidal core inductor. As seen in Fig. 1, each model incorporates a cylindrical magnetic core element of 100 microns in diameter surrounded by a single-turn copper winding that carries an alternating current at a frequency, f=100 kHz. To guarantee model convergence, it was necessary to employ an exaggerated AC peak magnitude of I_{peak} =100 A. These models consider core elements of the amorphous Fe(Co)SiB microwire specified using its experimentally determined magnetic responses, and additionally, of two benchmark core materials – soft ferrite (MnZn type) and Metglas (2605SA1). Simulation results indicate that the microwire core exhibits a higher degree of magnetization alignment along its length under the electromagnetic field created by the loop current, relative to those of the other two cores, Fig. 2. The microwire core also exhibits increased inductance by as much as 20% compared to the other two materials. These results demonstrate that the amorphous magnetic microwires have intriguing potential as core materials for inductive applications. Acknowledgments: NSF S-POWER Program (DUE-1564653), the Fulbright Scholar Program, i-Link A20074 (CSIC) project

1. M. Vázquez, Handbook of Magnetism and Advanced Magnetic Materials, John Wiley, vol.4, p.2192-2222 (2007) 2. Ansys® Electromagnetics Suite, Release 17.2.0, ANSYS, Inc.

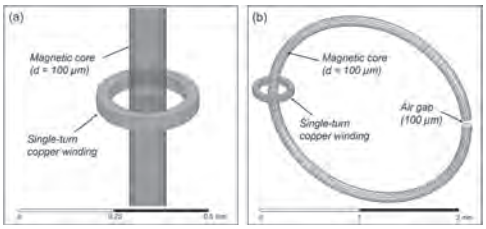

Fig. 1. Two simplified models were considered in this study: (a) regular inductor and (b) air-gapped toroidal core inductor

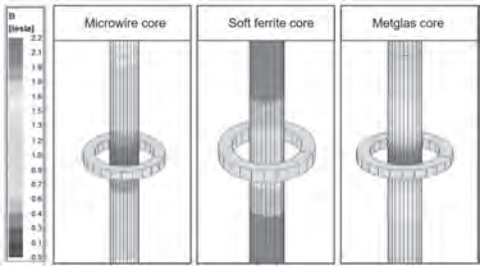

Fig. 2. A comparison of magnetic inductions of the three cores under the electromagnetic field created by the loop current (regular inductor model)

R5-08. Influence of Stress Relief on the Domain Wall Velocity of Rapidly Quenched Amorphous Submicron Wires. S. Corodeanu[1], C. Hlenschi[1], C. Rotarescu[1], H. Chiriac[1], N. Lupu[1] and *T. Óvári[1] 1. Department of Magnetic Materials and Devices, National Institute of Research and Development for Technical Physics, Iasi, Romania*

$Fe_{77.5}Si_{7.5}B_{15}$ and $(Co_{0.94}F_{0.06})_{72.5}Si_{12.5}B_{15}$ amorphous glass-coated submicron wires and nanowires with diameters from 100 to 900 nm were prepared by rapid quenching from the melt [1]. They are magnetically bistable, featuring a rectangular hysteresis loop, with magnetization reversal being achieved through the fast displacement of a 180-degree domain wall. We investigate the effect of stress relief annealing on domain wall velocity for amorphous FeSiB and CoFeSiB samples with the magnetostriction of 25 x 10^{-6} and -1 x 10^{-7}, respectively. Samples have been furnace annealed for 1h in vacuum at 200°C and 350°C, respectively, to partially relieve internal stresses induced during preparation. The field dependence of domain wall velocity has been measured using a technique developed specifically for such thin wires [2]. Fig. 1 shows the field dependence of domain wall velocity for an FeSiB sample with 340 nm in diameter, with annealing temperature as a parameter. Domain wall velocity increases monotonically with temperature, reaching from 1000 m/s to nearly 2200 m/s after annealing at 350°C. Fig. 2 shows the same dependence for a CoFeSiB sample with 770 nm in diameter, similarly with annealing temperature as a parameter. In this case, velocity decreases with annealing temperature, although the measured values are larger: from over 4500 m/s in as-cast state down to around 2500 m/s after annealing at 350°C. The results have been explained based on the dominant type of magnetic anisotropy in each case (magnetoelastic for the Fe-based sample and shape anisotropy for the Co-based one), and its changes with stress relief. Stress relief annealing can be used to fine-tune the domain wall velocity in amorphous cylindrical submicron wires, which is key for their future applications. Work supported by the Nucleu Programme (Project PN 19 28 01 01) and Contract No. 11PFE/16.10.2018 financed by the Romanian Ministry of Education and Research.

[1] T.-A. Óvári, N. Lupu and H. Chiriac, in Magnetic Nano- and Microwires, M. Vázquez (Ed.), Woodhead Publishing, Cambridge, 199 (2015). [2] S. Corodeanu, H. Chiriac and T.-A. Óvári, Rev. Sci. Instrum., Vol. 82, 094701 (2011).

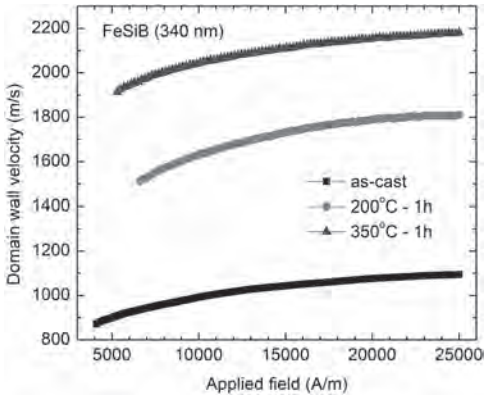

Fig. 1. Domain wall velocity vs. applied field for an FeSiB amorphous submicron wire, with the annealing temperature as a parameter.

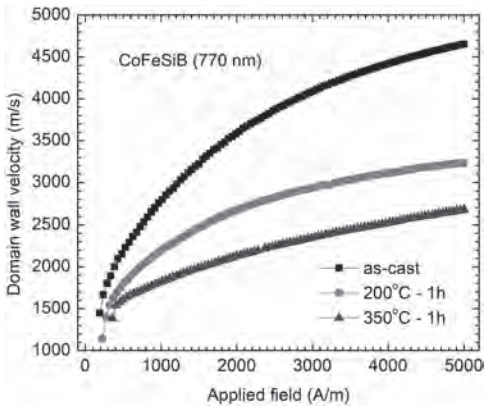

Fig. 2. Domain wall velocity vs. applied field for a CoFeSiB amorphous submicron wire, with the annealing temperature as a parameter.

R5-09. High-Induction FeCo Films: Green Synthesis and Magnetic Properties. *E. Denisova*[1,2], L. Chekanova[1], S. Komogortsev[1,2], I. Nemtsev[3] and R. Iskhakov[1] *1. Kirensky Institute of Physics Federal Research Center KSC SB RAS, Krasnoyarsk, Russian Federation; 2. Siberian Federal University, Krasnoyarsk, Russian Federation; 3. Federal Research Center "Krasnoyarsk Science Center of the Siberian Branch of the Russian Academy of Sciences", Krasnoyarsk, Russian Federation*

Alloys of Fe and Co constitute an important class of soft magnetic materials with a wide and important range of technological applications where high magnetic flux densities are required. Although there are many methods available for the preparation of CoFe films, such as sputtering, ion beam deposition, electrodeposition and so on [1–2]. Electroless plating shows low cost and no size or shape limit for the preparation of nano-scale films [3]. However, traditional reducing agents (hypophosphite or borohydride) are often toxic. In this paper, economic and green approach was explored to prepare FeCo films by using different types of carbohydrates as reducers and dispersers. The saturation magnetizations, local magnetic anisotropy field and coercivities of FeCo film plated, under various processing conditions have been investigated to optimize soft magnetic properties. The FeCo films were prepared by electroless reduction of metals from aqueous solutions of the corresponding salts. We used several types of carbohydrates as reducing agents: arabinogalactan, corn starch and sucrose. XRD analysis revealed the $Fe_{1-x}Co_x$ films exhibited a bcc structure even for samples with very high content of Co (x~0.85). The average crystallite size for the all types of reducing agents was in rage 10-27 nm. The local anisotropy field value of FeCo alloys increases with a decrease in Fe content for all reducing agent types and was in range 0.3-2 kOe. The coercivity values range from 8 up to 22 Oe for films produced with carbohydrates. Nonlinearity in the saturation magnetization M_s dependencies on Fe content are expected for

any type of the FeCo films [4]. Maximum of M_s magnitude is reached for films with 70% iron. The produced FeCo films demonstrated significantly better M_s values, compared to those for the sample preparing with conventional reducing agent. The M_s value for film reducing with hypophosphite does not exceed 190 emu/g due to phosphorus contaminations. In cases FeCo films reduced with carbohydrates the M_s values are 205, 235 and 240 emu/g for arabinogalactan, starch and sucrose respectively. So, a simple, eco-friendly and efficient route for obtaining high-induction FeCo films has been explored.

1. S. Amsarajan, B. R. Jagirdar, *J. of Alloys and Compounds,* Vol. 816, p.152632 (2020) 2. T.Yanai, K. Shiraishi, and Y. Watanabe, *J. Appl. Phys*., Vol.117, p.17A925 (2015) 3. K. Sun, K. Wang, Yu T, Liu X, *Int. J. Hydrogen energ., Vol* 44, p 1328 (2019) 4. Ferromagnetism, by R. M. Bozorth, pp. 992. Wiley-VCH (1993)

R5-10. Research on Core Loss of Soft Magnetic Composites Based on 3D Modeling. *Y. Yang*[1], Y. Wang[1] and C. Liu[1] *1. Hebei University of Technology, Tianjin, China*

Soft magnetic composite (SMC) material is a relatively new kind soft magnetic material which is made by ferromagnetic particle and enclosed by electric insulation layer. Due to the existence of the insulation layer and small size particle, the eddy current loss of SMC material is very low, and thus the high frequency core loss is lower than that of silicon steel sheets[1]. While during the manufacturing process, the electric insulation layer may be destroyed and thus the eddy current will be induced which makes it difficult to calculate the eddy current loss [2]. In this paper, the eddy current loss is s divided into inter-particle eddy current loss and intra-particle eddy current loss. Intra-particle eddy current loss is considered by modeling only one particle of SMC in the frequency domain using homogenization method [3]. The inter-particle eddy current loss is very complex at the microscopic level and difficult to simulate. Therefore, the overall effect of inter-particle eddy current is considered at the macro-scale by modeling the actual sample and using measured conductivity of the sample. Fig.1 shows the established SMC models, including SMC sample model and SMC particle model. Then the iron losses at different frequencies are measured, and the iron loss at low frequency is used to calculate the hysteresis loss. Finally, iron losses are calculated and they are compared with measured results to verify the proposed model. Fig. 2 shows the comparison of calculated iron losses of the model proposed in this paper with the existing model. As shown, the calculated iron losses agree well with the measured ones below 3k Hz and the method proposed in this paper is more accurate compared to existing model.

[1] C.C. Liu, J.G. Zhu, Y.H. Wang and et al. “Comparative Study of Small Electrical Machines With Soft Magnetic Composite Cores”, IEEE transactions on industrial electronics, Volume: 64, Issue: 2, Feb. 2017. [2] C. Appino, O. Bottauscio, O. d. l. Barriere, F. Fiorillo, A. Manzin, and C. Ragusa, “Computation of Eddy Current Losses in Soft Magnetic Composites,” IEEE Transactions on Magnetics, vol. 48, no. 11, pp. 3470-3473, 2012. [3] Gao Y, Fujiki T, Dozono H, et al. Modeling of Magnetic Characteristics of Soft Magnetic Composite Using Magnetic Field Analysis[J]. IEEE Transactions on Magnetics, 2018, 54(3):1-4.

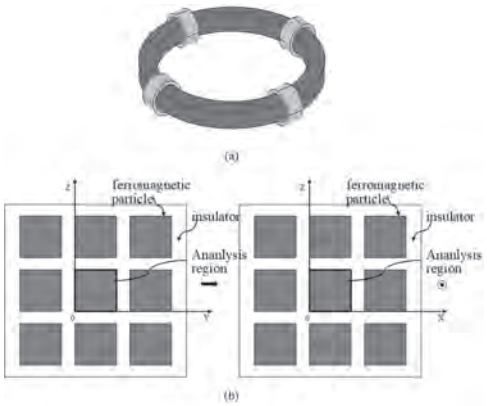

Fig.1. 3D models of SMC (a) SMC sample model (b) SMC particles model

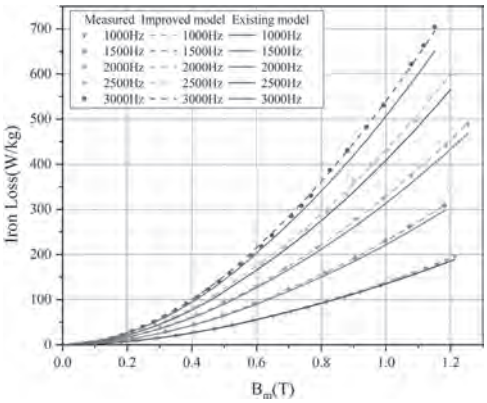

Fig.2. Comparison of calculated iron losses of the model proposed in this paper with the existing model

R5-11. Comparative Analysis of High-Frequency Magnetic Properties of C-Type Amorphous and Nanocrystalline at Different Air Gap. Y. Li[1], *H. Liu*[1], H. Sun[1] and Z. Wan[1] *1. State Key Laboratory of Reliability and Intelligence of Electrical Equipment, Hebei University of Technology, Tianjin, China*

Air-gaps are placed in magnetic core structures for the following important reasons: (a) to support a high magneto-motive force, (b) to reduce the slope of the B–H curve, which increases the saturation field intensity, (c) to avoid core saturation due to currents with large amplitudes[1]. The air gap will change the magnetic characteristics of the core. Therefore, accurate measurement of the magnetic properties of the core with an air gap is significant to electrical equipment optimization. In this paper, the dynamic magnetic characteristics of the amorphous (AMCC016B) and nanocrystalline (F3CC0125) materials are measured under different air gap lengths (0-3mm) and different frequencies (1-20kHz) basing on a test system that can accurately change the C-core air gap. The experimental results are shown in Fig. 1. The effect of the air gap on both materials is similar. That is, the core loss gradually increases with the increasing of the air gap length at the same magnetic density and frequency. Finally, by analyzing the experimental data, it is found that when the air gap length is small and the magnetic density is low, the effect of the air gap on the core loss is negligible, as shown in Fig. 2. By comparing the experimental data of amorphous and nanocrystalline materials under the same operating conditions, it is found that the greater the permeability μ is, the greater the effect of the air gap on the magnetic properties of the materials is. The conclusion of this article provides theoretical guidance for the optimal design of magnetic components, and more details will be shown in the full text.

[1] A. Ayachit and M. K. Kazimierczuk, Iet Circuits Devices & Systems, Vol.11, p.209-215 (2017). [2] S. Zurek, IEEE Transactions on Magnetics,

Vol.48, p.1520–1523(2012). [3] Y. Wang, G. Calderonlopez, and A. J. Forsyth, IEEE Transactions on Power Electronics, Vol.32, p.4683-4690(2017).

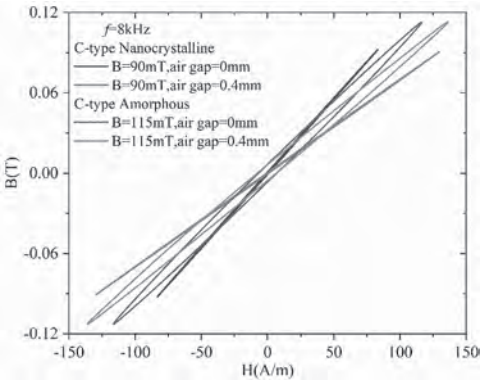

Fig. 1 Hysteresis loops of amorphous and nanocrystals materials at different magnetic densities and different air gaps at specific frequencies

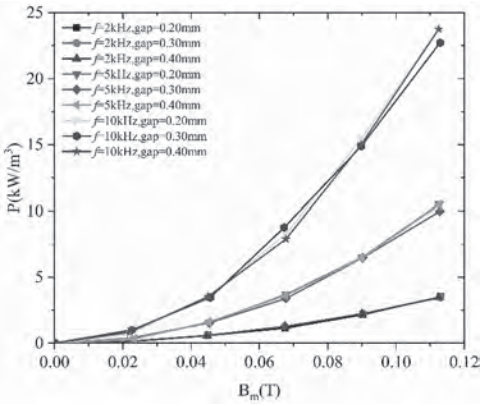

Fig. 2 Loss of amorphous materials under different air gaps at different frequencies and different magnetic densities

R5-12. Magnetic and Magnetocaloric Properties of the Nanocrystalline $Pr_{0.7}Ba_{0.2}Ca_{0.1}MnO_3$ Sample. M. .[1], *P. Bisht*[1], A. Kumar[1] and R.N. Mahato[1] *1. School Of Physical Sciences, Jawaharlal Nehru University, New Delhi, India*

Nowadays, magnetic refrigeration (MR) technology is considered as an alternative to the conventional vapor pressure cycle, due to its environmental-friendly nature and higher cooling efficiency [1]. The basic principle of the MR technology is the magnetocaloric effect (MCE) which can be defined as the change in entropy of a magnetic material on applying the magnetic field. MCE is characterized by the isothermal magnetic entropy change (ΔS_M) and the relative cooling power (RCP). Thus, it is of great importance to search the magnetic materials which can possibly exhibit large values of magnetic entropy change close to the room temperature at lower applied fields. In the present work, we have synthesized the nanocrystalline $Pr_{0.7}Ba_{0.2}Ca_{0.1}MnO_3$ sample using the sol-gel method. The Rietveld refinement of the X-ray diffraction pattern (recorded at room temperature) confirmed the formation of the orthorhombic crystal structure with pbnm space group. The temperature dependent magnetization M(T) measurements suggested that the sample undergo paramagnetic (PM) to ferromagnetic (FM) phase transition and the Curie temperature was found to be ~ 128 K. The field dependence of magnetization M(H) data at 2 K showed the formation of hysteresis loop which indicates the presence of FM behavior in the sample at lower temperatures and the linear behavior of M(H) at 300 K confirms the PM nature of the sample. The slopes of the Arrott plots for the present sample are positive describing the second-order of magnetic phase transition (SOMPT), as per the Banerjee criterion [2]. The maximum value of magnetic entropy change and RCP were found to be ~2.3 J $kg^{-1}K^{-1}$ and 230 Jkg^{-1} for a field change of 5 T (Fig. 1). The phenomenological universal curves were constructed and the rescaled ΔS_M curves (shown in Fig. 1) were found to collapse into one the universal curve confirming the SOMPT for the present sample. The relatively large values of $|\Delta S_M|$ and RCP make the present compound promising for magnetic refrigeration technology.

[1] I. Hussain, S. N. Khan, E. J. Kim, S. E. Jeon, and B. H. Koo, Ceram. Int. 44, 2892 (2018). [2] S.K. Banerjee, Phys. Rev. Lett. 12, 1 (1964).

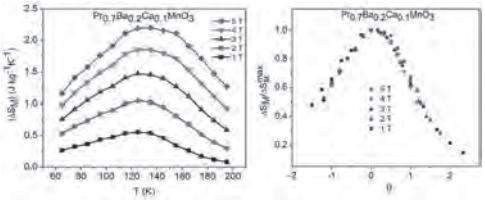

Fig. 1 Temperature dependence of magnetic entropy change for the nanocrystalline $Pr_{0.7}Ba_{0.2}Ca_{0.1}MnO_3$ sample at different fields and rescaled magnetic entropy chnage curves as a function of rescaled temperature.

R5-13. Synthesis and Characterization of Fe_3O_4-HfO_2 Nanoparticles by Magnetization and Hyperfine Interactions Measurements. *I.T. Matos*[1], T.S. Sales[1], G. Cabrera-Pasca[2], A. Burimova[1], R.N. Saxena[1], L.F. Pereira[1], L. Otubo[1] and A.W. Carbonari[1] *1. Instituto de Pesquisas Energéticas e Nucleares, IPEN-CNEN/SP, São Paulo, Brazil; 2. Universidade Federal de Pará, Abaetetuba, PA, Brasil, Pará, Brazil*

Nanoparticles (NPs) that combine biocompatibility and enhanced physical characteristics for biomedical applications are currently an area of intense scientific research. Hafnium oxide NPs is an innovative approach in the anticancer treatment by radiotherapy due to their low toxicity and enhancement of local dose in the tumor reducing the total radiation dose for the patient [1]. The combination of this amazing property with the excellent magnetic hyperthermia performance of Fe_3O_4 NPs can produce a promising nanomaterial for cancer therapy. In the present work, we have synthesized NPs samples of Fe_3O_4 doped with 10%Hf and HfO_2 doped with 10% Fe by chemical procedures. The samples had their morphological, structural, and magnetic properties characterized by some results being displayed in Fig. 1. The crystal structure of the samples was characterized by X-ray Diffraction (XRD), whose results present a single phase. Transmission Electron Microscopy (TEM) images show spherical and hexagonal NPs with an average size of 12 nm as displayed in Fig. 2. The magnetic property was investigated by magnetization measurement. The results from the temperature dependence of ZFC-FC magnetization show a large peak in the ZFC curve corresponding to a broad distribution of blocking temperatures as shown in Fig. 1(b). Fortunately, when irradiated with neutrons in a research reactor, the nuclear reaction $^{180}Hf(n,\gamma)^{181}Hf$ yields the probe nucleus $^{181}Hf(^{181}Ta)$ used by the perturbed angular correlations (PAC) technique to measure hyperfine interactions. Both samples show electric quadrupole interaction characteristics of the HfO_2 phase indicating that the Fe replaces Hf in HfO_2 NPs, but rather than substituting Fe, Hf form HfO_2 NPs diluted in Fe_3O_4 NPs. Moreover, a pure time-dependent magnetic dipole interaction below 300 K was observed for Fe_3O_4 NPs mixed with 10% of HfO^2.

References: [1] J.A. Fild et al Chemosphere, Vol. 84, p. 1401-1407 (2011).

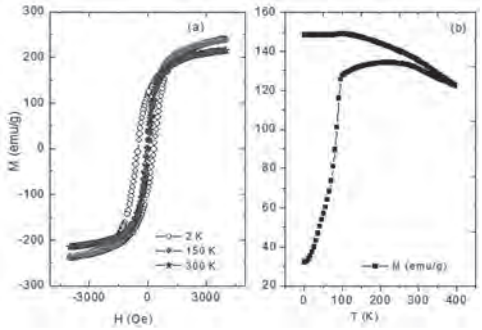

Fig. 1: Results for Fe_3O_4-HfO_2 NPs (a) Magnetic measurement, ZFC and FC magnetization curves, were carried out for the sample doped with Hf between 2-300K with an applied field of 500Oe and (b) M x H measurements at different temperatures.

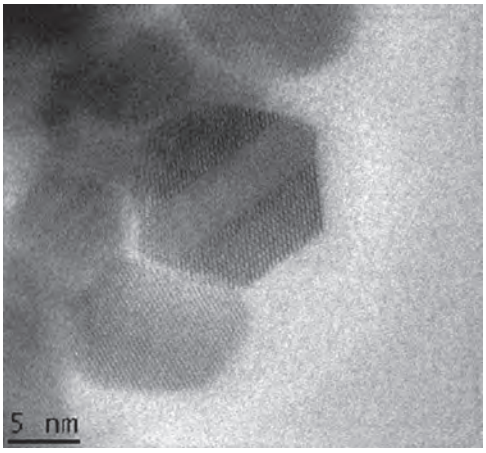

Fig. 2: TEM image showing spherical and hexagonal NPs ascribed to Fe_3O_4 and HfO_2, respectively.

R5-14. Effect of v-Doping on the Magnetic Transition of Fe-Rich $(Mn,Fe)_{1.9}(P,Si)$ Compounds. *O. Hamutu*[1], N.v. van Dijk[1] and E. Brück[1]
1. Technische Universiteit Delft Faculteit Technische Natuurwetenschappen, Delft, Netherlands

In MnFePSi compounds, Fe-rich samples show a higher saturation magnetization than Mn-rich samples [1][2]. In this work, the effects of V doping on structure, impurity, and magnetocaloric effects of Fe-rich $Mn_{0.6}Fe_{1.3-x}P_{0.36}Si_{0.34}V_x$ (x = 0, 0.01, 0.02, 0.03, and 0.04) compound are studied. Melt spinning is adopted in the preparation of samples. Melt spinning can better control the formation of impurities and the required raw materials, like Fe_2P and MnP, are relatively cheaper. According to the XRD results, the V-doped samples all crystallize in the hexagonal Fe_2P structure, containing a small amount (less than 1%) of the $(Fe, Mn)_3Si$ phase. The Curie temperature of the compounds gradually decreases with V content, from 330 K at x = 0 to 189 K at x = 0.04. For an increasing V content the hysteresis increases and the maximum isothermal magnetic entropy change decreases. The n-value is used to define the type of magnetic phase transition. The magnetic entropy change scales with the magnetic field as $\Delta S_M \propto H^n$ in the vicinity of the phase transition. The index of the magnetic field can be expressed as $n=(\mathrm{d}\ \ln|\Delta S_M|)/(\mathrm{d}\ \ln H)$ [3][4]. If the maximum n-value is greater than 2, the material behavior corresponds to a first-order phase transition, and if it is less than 2, it corresponds to a second-order phase transition. Compared with the Arrott plot, using the n-value gives more accurate results to define the nature of the magnetic phase transition. With the introduction of V, the maximum n-value near the phase transition is found to be greater than 2 for all doped samples, while for the non-doped sample $n \approx 1.56$. This means that V doping gradually adjusts the compounds from second-order into first-order magnetic phase transition materials.

1. Z.Q. Ou, L. Zhang, N.H. Dung, Journal of Alloys & Compounds, 710, 446-451 (2017) 2. J. V. Leitao, M. V. D. Haar, A. Lefering, Journal of Magnetism & Magnetic Materials, 344(oct.), 49-54 (2013) 3. L. J. Yan, F. Victorino, Nature Communications, 9:2680 (2018) 4. C. Bean & D. Rodbell, Physical Review, 126, 104–115 (1962)

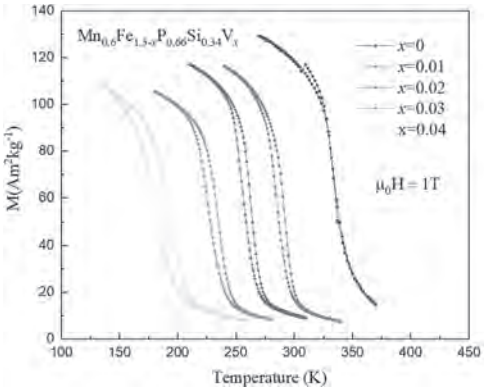

Fig. 1 Temperature dependence of the magnetization of $Mn_{0.6}Fe_{1.3-x}P_{0.36}Si_{0.34}V_x$ compounds

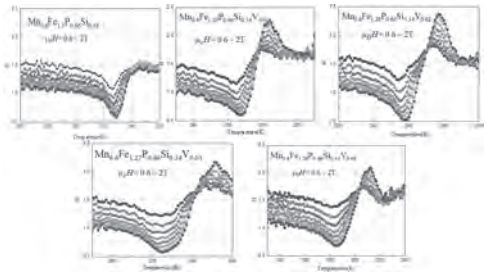

Fig. 2 n-value of $Mn_{0.6}Fe_{1.3-x}P_{0.36}Si_{0.34}V_x$ compounds

R5-15. Eddy Current Loss Reduction in Axial-Flux Motors Using 3D Printing. *H. Pyo*[1], S. Yang[1] and W. Kim[1] *1. Electrical Engineering, Gachon University, Seongnam, The Republic of Korea*

Axial-flux permanent magnet synchronous motors (AFPMSMs) have higher torque densities than the conventional radial-flux permanent magnet synchronous motors (RFPMSMs). However, RFPMSMs have the advantage of lower eddy current losses in the core, owing to the use of electrical steel plates that can be stacked. Therefore, most studies on reducing the eddy current losses of the existing AFPMSMs cores have focused on reducing the eddy current loss by using a soft magnetic composite (SMC) material or rolling an amorphous electrical steel plate [1]-[3]. The method proposed for reducing the eddy current loss of AFPMSMs in this paper uses 3D printing technology to insert a 3D-printed SMC core into the stator shape of a motor. A 3D-printed shape design that reduced eddy current loss among core loss components using 3D-Printed SMC material, which is currently under development, was analyzed. In the case of the AFPMSM proposed in the paper, the eddy current loss was reduced by inserting a slit structure into the stator core of the proposed motor as air insulation, as in the principle of laminating the core in order to reduce the eddy current loss in RFPMSM. Figure 1 shows the theoretical conventional AFPMSM and proposed AFPMSM eddy current loss loop. As a result, it was confirmed through finite element analysis (FEA) analysis that the actual eddy current loss was reduced by up to 37.6%, when compared to that of the previous models. Figure 2 shows eddy current loss loops through FEA. Moreover, while reducing the eddy current loss, seven models that satisfied the target specifications were derived. Finally, when comparing the core loss of the proposed model and the model designed with AFPMSM as a high performance electrical steel plate with low core loss, the feasibility was verified through the FEA that there is no difference in core loss.

[1] B. Scheerlinck, H. De Gersem, P. Sergeant, "3-D Eddy current and fringing-flux distribution in an axial-flux permanent-magnet synchronous machine with stator in laminated iron or SMC", *IEEE Transactions on Magnetics*, vol. 51, Nov 2015. [2] Xiaoguang Wang, Sheng Zhou, Lei Wu, Meng Zhao, Cangxian Hu, "Iron Loss and Thermal Analysis of High Speed PM motor Using Soft Magnetic Composite Material", *Electrical Machines and Systems (ICEMS) 2019 22nd International Conference on*, pp. 1-4, 2019. [3] X. Sun, Y. Shen, S. Wang, G. Lei, Z. Yang, S. Han, "Core Losses Analysis of a Novel 16/10 Segmented Rotor Switched Reluctance BSG Motor for HEVs Using Nonlinear Lumped Parameter Equivalent Circuit Model," *IEEE/ASME Transactions on Mechatronics,* vol. 23, no. 2, pp.747-757, April. 2018

Theoretical conventional AFPMSM and proposed AFPMSM eddy current loss loop

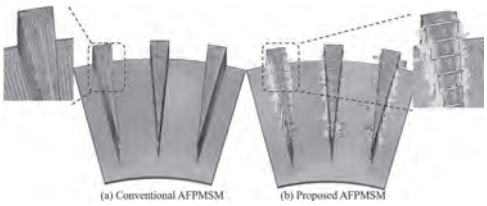

Eddy current loss loops through FEA

R5-16. Neutron Diffraction Studies of the $(Cr_{84}Re_{16})_{100-x}V_x$ Alloy System. *S. Jacobs*[1], A. Prinsloo[1], A. Venter[2], Z. Sentsho[2], A. Studer[3] and C. Sheppard[1] *1. Physics, University of Johannesburg, Auckland Park, South Africa; 2. South African Nuclear Energy Corporation Ltd, Pretoria, South Africa; 3. Australian Nuclear Science and Technology Organisation, Kirrawee, NSW, Australia*

Temperature dependence of electrical resistivity as well as neutron diffraction measurements of $(Cr_{84}Re_{16})_{100-x}V_x$ alloys with x = 0, 4.2, 5.5 and 6.2 are reported here. Previous studies probing the quantum critical behaviour (QCB) in the $(Cr_{84}Re_{16})_{100-x}V_x$ alloy system revealed prominent anomalies in physical properties close to the previously defined critical concentration of $x_c \approx 10.5$ [1]. One of the key indicators of critical behaviour is the Sommerfeld coefficient, γ [2,3]. γ is obtained by fitting the low temperature specific heat (C_p) data to the equation $C_p = \gamma T + \beta T^3$ [3], where the first and second terms are the electronic and lattice contributions to specific heat respectively [4]. For the $(Cr_{84}Re_{16})_{100-x}V_x$ alloy system, γ(x) showed a broad deep minimum at $x \approx 4.4$ and a continuous decrease through x = 10.5 [1]. The latter anomaly was associated with the onset of QCB, but the anomaly at $x \approx$ 4.4 had to be probed further. It was proposed that the minimum corresponds to the transition from the commensurate spin-density-wave (CSDW) phase to the incommensurate (I) SDW phase upon increasing x. There is a larger gap in the electronic spectrum in the CSDW phase than in the ISDW phase [5]. In the CSDW phase, there is perfect nesting of the electron and hole Fermi sheets which leads to stronger reduction of density of states at the Fermi level. This hypothesis has now been further investigated with neutron powder diffraction (NPD) that provides information directly from the reciprocal lattice to facilitate identification of the magnetic order. Results indicate that the base alloy with x = 0 is in the CSDW state as expected and the x = 4.2, 5.5 and 6.2 alloys display ISDW trends. An additional magnetic peak associated with the Cr_2O_3 phase was also identified in the $(Cr_{84}Re_{16})_{100-x}V_x$ alloys using NPD. Quantification analyses revealed that the Cr_2O_3 content was less than 2 wt.% in all of the samples.

1. B.S. Jacobs, A.R.E. Prinsloo, C.J. Sheppard and A.M. Strydom, J. Appl. Phys., Vol. 113, p.17E126 (2013) 2. L. Reddy, H.L. Alberts, A.M. Strydom, A.R.E. Prinsloo and A.M. Venter, J. Appl. Phys., Vol. 103, p.07C903 (2008) 3. J. Takeuchi, H. Sasakura and Y. Masuda, J. Phys. Soc. Jpn., Vol. 49, p.508 (1980) 4. T. Mamiya and Y. Masuda, J. Phys. Soc. Jpn., Vol. 40, p.390 (1976) 5. E. Fawcett, H.L. Alberts, V.Y. Galkin, D.R. Noakes and J.V. Yakhmi, Rev. Mod. Phys., Vol. 66, p.25 (1994)

R5-17. Spin Glass Behaviour in $(Cr_{84}Re_{16})_{100-x}Mn_x$ Alloys. *S. Jacobs*[1], C. Sheppard[1], P. de Camargo[2] and A. Prinsloo[1] *1. Physics, University of Johannesburg, Auckland Park, South Africa; 2. Physics, Universidade Federal de Sao Carlos, Sao Carlos, Brazil*

The effect of Mn doping of a $Cr_{84}Re_{16}$ alloy are reported, as well as the possible existence of a spin glass (SG) state which were investigated using electrical resistivity and magnetisation measurements. Mn is an electron donor resulting in a concomitant increase in the size of the electron sheet and a subsequent increase in Néel temperature, T_N [1]. The temperature dependence of magnetisation, $M(T)$, for the $(Cr_{84}Re_{16})_{100-x}Mn_x$ alloys with x = 0.4, 0.6 and 3.1 showed bifurcation of the $M(T)$ data at the pinning temperature, T_p, in the zero field cooled (ZFC) and field cooled (FC) curves. The splitting of the ZFC and FC curves is not in itself a signature of SG but is an indication of magnetic anisotropy in the system [2]. In the $(Cr_{84}Re_{16})_{100-x}Mn_x$ alloy system, there is a sharp increase in magnetisation on increasing T after ZFC. A prominent peak is observed close to 40 K above which the behaviour is identical to that observed in the FC state as shown in the figure for the x = 0.4 alloy. Other signatures associated with canonical SG namely the time dependence of isothermal remanent magnetisation (IRM) and the increase of magnetic stiffness upon increasing the wait time in thermoremanent magnetisation (TRM) were also observed in the $(Cr_{84}Re_{16})_{100-x}Mn_x$ alloys [3]. The frequency dependence of the real component of AC-susceptibility shows the SG characteristic cusp close to T_p [4]. However, there is no dependence of the maximum value of cusp or the temperature corresponding to the cusp on frequency which is contrary to the SG state [5]. As only some of the SG signatures were observed in the $(Cr_{84}Re_{16})_{100-x}Mn_x$ alloy system, it cannot be categorised as canonical SG. These alloys can be classified as a new type of SG with frustration of itinerant spins at the interfaces between antiferromagnetic (AFM) domains established around each Mn local magnetic moment.

[1] E. Fawcett, H.L. Alberts, V.Y. Galkin, D.R. Noakes and J.V. Yakhmi, Rev. Mod. Phys., Vol. 66, p.25 (1994) [2] P.A. Joy, P.S. Anil Kumar and S.K. Date, J. Phys. Condens. Matter., Vol. 10, p.11049 (1998) [3] B. Li, H.L. Alberts, A.M. Strydom, B.M. Wu, A.R.E. Prinsloo and Zh.J. Chen, J. Magn. Magn. Mater., Vol. 321, p.61 (2009) [4] C.A.M. Mulder, A.J. Van Duyneveldt and J.A. Mydosh, Phys. Rev. B., Vol. 25, p.515 (1982) [5] J.A. Mydosh, "Spin glasses: an experimental introduction", Taylor and Francis, London (1993)

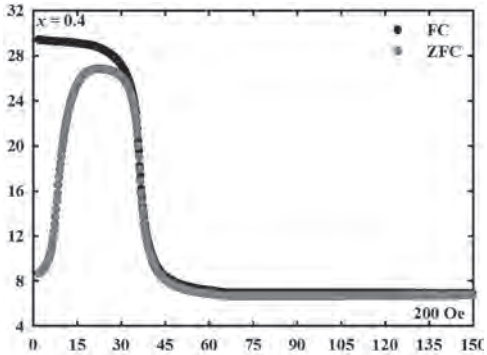

Fig.1: Zero field cooled (ZFC) and field cooled (FC) curves for the x = 0.4 alloy at 200 Oe.

- A -

Ababei, G. (H1-01) . . . 211
Aballe, L. (O3-07) . . . 439
Aballe, L. (O3-08) . . . 439
Abd-El-Hafiz, S. (L3-02) . . . 334
Abdulla, R. (I5-06) . . . 265
Abe, T. (D3-07) . . . 98
Abert, C. (B1-02) . . . 33
Abert, C. (B1-05) . . . 34
Abert, C. (R1-13) . . . 543
Abrao, J.E. (R4-09) . . . 561
Achilli, S. (K2-08) . . . 306
Ackerman, J. (M5-10) . . . 379
Adachi, T. (J1-04) . . . 270
Adachi, Y. (G2-13) . . . 188
Adam, J. (E4-11) . . . 132
Adam, J. (N2-14) . . . 399
Adam, J. (R1-10) . . . 541
Adanakova, O.A. (M6-03) . . . 382
Adelani, M. (L4-03) . . . 342
Adenwalla, S. (R1-07) . . . 540
Adeyemo, D. (I1-06) . . . 240
Adeyeye, A. (B1-10) . . . 36
Adeyeye, A. (I2-07) . . . 246
Adhikari, A. (R1-07) . . . 540
Aditya, B. (O2-09) . . . 432
Adly, A. (L3-02) . . . 334
Aeschlimann, M. (E1-07) . . . 114
Aeschlimann, M. (G3-03) . . . 190
Aeschlimann, M. (G3-04) . . . 191
Aeschlimann, M. (G3-11) . . . 194
Affronte, M. (B2-02) . . . 40
Affronte, M. (D2-05) . . . 92
Afsar, M.N. (C1-06) . . . 57
Afsar, M.N. (P5-12) . . . 494
Afuwape, O.F. (K5-06) . . . 320
Agarwal, N. (G3-06) . . . 191
Aggarwal, S. (O2-01) . . . 428
Agladze, N. (S4-02) . . . 236
Aguilà, D. (D2-03) . . . 91
Aguilera, E. (A4-11) . . . 24
Ahadi, K. (J5-01) . . . 288
Ahlm, N. (M2-04) . . . 360
Ahmad, T. (C2-06) . . . 64
Ahmadzadeh, M. (D4-14) . . . 104
Ahmed, T. (L3-09) . . . 337
Ahmed, T.N. (G2-12) . . . 187
Ahn, H. (G6-02) . . . 206
Ahrens, V. (E5-02) . . . 135
Ait-Oukaci, K. (E4-11) . . . 132
Aizawa, Y. (H4-04) . . . 229
Ajan, A. (A3-11) . . . 18
Ajejas, F. (E5-08) . . . 137
Ajejas, F. (I3-09) . . . 255
Ajejas, F. (I3-10) . . . 256
Ajejas, F. (L1-11) . . . 327
Ajejas, F. (N1-03) . . . 388
Akamatsu, S. (F3-06) . . . 154
Akase, Z. (O6-04) . . . 453
Akashi, N. (B3-10) . . . 49
Akashi, T. (L1-04) . . . 324
Akdogan, O. (B2-06) . . . 42
Akdogan, O. (F4-05) . . . 160
Akdogan, O. (K5-02) . . . 318
Akdogan, O. (Q1-02) . . . 508
Åkerman, J. (Q3-04) . . . 519
Åkerman, J. (S8-02) . . . 504
Akinola, O.G. (A5-01) . . . 28
Akinola, O.G. (A5-02) . . . 29
Akinola, O.G. (A5-03) . . . 29
Akinola, O.G. (A5-05) . . . 31
Akiyama, Y. (J1-09) . . . 272
Aktas, S. (E2-10) . . . 120
Al-Dujaili, M. (I5-06) . . . 265
Al-Mahdawi, M. (F3-07) . . . 155
Al-Tawhid, A. (R4-02) . . . 558
Alam, S. (O2-01) . . . 428
Alameda, J. (L1-10) . . . 326
Alario-Franco, M. (J3-08) . . . 279
Albertini, F. (F2-15) . . . 149
Albino, A. (F5-07) . . . 166
Albisetti, E. (N2-11) . . . 398
Albrecht, M. (D1-04) . . . 84
Albrecht, M. (M4-08) . . . 373
Albrecht, M. (Q4-10) . . . 526
Albrecht, M. (Q5-04) . . . 529
Albrecht, M. (R3-14) . . . 557
Aldea, R. (A2-10) . . . 11
Aldosary, M. (S4-02) . . . 236
Alekseev, S. (R4-11) . . . 562
Aleshkevych, P. (E5-10) . . . 137
Alexanian, Y. (A2-03) . . . 8
Alff, L. (H3-14) . . . 227
Alghamdi, N. (P1-03) . . . 468
Alghamdi, S. (D1-07) . . . 86
Algueta-Miguel, J. (N5-06) . . . 412
Ali, M. (D1-07) . . . 86
Ali, M. (H1-15) . . . 217
Ali, M. (J5-05) . . . 289
Aliev, F.G. (L2-09) . . . 333
Aliev, F.G. (O7-05) . . . 460
Alimi, R. (F4-07) . . . 161
Alimi, R. (N5-12) . . . 415
Alkhatib, S. (K5-02) . . . 318
Allen, P. (M4-12) . . . 376
Allen, S. (P6-06) . . . 497
Allende, S. (C5-05) . . . 80
Allende, S. (E5-01) . . . 135
Allodi, G. (F2-15) . . . 149
Allodi, G. (F5-07) . . . 166
Allwood, D. (A5-04) . . . 30
Allwood, D. (G4-07) . . . 199
Allwood, D. (R1-04) . . . 539
Almasi, H. (O2-01) . . . 428
Alonso, J. (M2-08) . . . 361
Alonso, M. (D1-12) . . . 88
Alonso, P. (D2-03) . . . 91
Alotaibi, S. (E2-10) . . . 120
Alotibi, S. (P6-15) . . . 501
Alshalawi, D. (M2-08) . . . 361
Alshammari, H.A. (B2-06) . . . 42
Alshammari, K.N. (H1-15) . . . 217
Althammer, M. (P4-13) . . . 487
Alunni, M. (O7-02) . . . 459
Alvarez Prado, L. (L1-10) . . . 326
Alvarez Prado, L. (O5-01) . . . 448
Alvaro-Gomez, L. (P2-09) . . . 476
Alyabyeva, L.N. (Q1-09) . . . 510
Alyami, M. (H1-15) . . . 217
Amara, S. (C5-08) . . . 82
Amaral, R.P. (M6-12) . . . 385
Ambal, K. (L1-08) . . . 325
Amelin, K. (A2-03) . . . 8
Ameziane, M. (N4-06) . . . 409
Amin, O.J. (G1-10) . . . 180
Amin, O.J. (J6-07) . . . 294
Amin, O.J. (M1-09) . . . 356
Amin, V. (S5-04) . . . 349
An, K. (M4-09) . . . 374
An, K. (M4-11) . . . 375
An, K. (N2-09) . . . 396
An, K. (Q2-01) . . . 513
Anane, A. (C1-10) . . . 59
Anane, A. (K1-07) . . . 299
Anane, A. (N2-07) . . . 396
Anane, A. (N2-10) . . . 397
Anane, A. (O7-16) . . . 466
Anane, A. (S8-01) . . . 504
Ander Arregi Uribeetxebarria, J. (G3-06) . . . 191
Ander Arregi Uribeetxebarria, J. (H5-01) . . . 232
Anderson, C.R. (K3-03) . . . 309
Anderson, C.R. (K4-10) . . . 316
Andersson, G. (H3-03) . . . 224
Andersson, G. (I2-11) . . . 247
Andersson, G. (M6-08) . . . 384
Ando, Y. (E1-11) . . . 115
Ando, Y. (F3-06) . . . 154
Ando, Y. (F3-07) . . . 155
Ando, Y. (J4-07) . . . 285
Ando, Y. (L3-11) . . . 338
Ando, Y. (M3-01) . . . 365
Ando, Y. (N5-02) . . . 410
Andreev, A.V. (H2-12) . . . 222
Andrew, J. (E2-08) . . . 120
Andrews, C. (M1-09) . . . 356
Andrieu, S. (E1-13) . . . 116
Andrieu, S. (G3-02) . . . 190
Andriushchenko, P. (A2-04) . . . 9
Anh, L. (K2-10) . . . 306
Anh, L. (O1-12) . . . 425
Anh, L. (Q4-03) . . . 522
Anh, L. (R3-13) . . . 556
Anton, E.M. (D1-11) . . . 88
Antonio Coaquira, J.A. (C1-08) . . . 58
Antonov, G. (C5-04) . . . 80
Aoki, M. (M3-01) . . . 365
Appino, C. (J2-03) . . . 273
Arabski, J. (D1-08) . . . 86
Arabski, J. (F1-10) . . . 143
Arackal, S. (C1-13) . . . 60
Aragon, F.H. (C1-08) . . . 58
Arai, S. (Q4-03) . . . 522

Araújo, J. (L4-12) . . . 345
Arauzo, A. (B2-03) . . . 41
Arava, H. (B1-05) . . . 34
Archilla, D. (E2-13) . . . 121
Archilla, D. (H1-08) . . . 214
Arekapudi, S.S. (Q4-01) . . . 522
Arena, D.A. (E2-02) . . . 117
Arena, D.A. (I4-13) . . . 262
Arenholz, E. (A3-08) . . . 16
Arenholz, E. (M2-01) . . . 359
Argo, J. (G5-11) . . . 205
Arias, R. (M3-07) . . . 367
Arita, R. (M4-01) . . . 371
Aromi, G. (D2-03) . . . 91
Arora, N. (O7-09) . . . 462
Arras, R. (H2-02) . . . 219
Arras, R. (K1-05) . . . 298
Arroo, D. (C4-01) . . . 74
Arroo, D. (N2-03) . . . 394
Artemchuk, P. (R3-08) . . . 554
Arzhnikov, A. (J3-11) . . . 280
Asada, H. (P6-03) . . . 497
Asada, H. (P6-08) . . . 499
Asami, K. (D3-01) . . . 96
Asano, H. (F5-05) . . . 165
Asano, H. (I3-07) . . . 254
Asano, H. (P4-06) . . . 485
Asano, T. (O1-14) . . . 426
Aseguinolaza, I.R. (A4-18) . . . 27
Asenjo, A. (G2-04) . . . 184
Asenjo, A. (L1-01) . . . 323
Asenjo, A. (L1-03) . . . 323
Asenjo, A. (O5-02) . . . 448
Ashby, P. (A1-06) . . . 5
Ashok Krishnaswamy, S. (H3-02) . . . 223
Ashok, S. (G3-03) . . . 190
Ashok, S. (G3-11) . . . 194
Askey, J. (B1-15) . . . 39
Askey, J. (C4-10) . . . 77
Aslam, Z. (D1-07) . . . 86
Assaf, B. (I4-09) . . . 261
Astakhov, G.V. (O5-04) . . . 449
Ataca, C. (E1-03) . . . 112
Atcheson, G. (E1-02) . . . 111
Atcheson, G. (E3-07) . . . 125
Atcheson, G. (E3-08) . . . 126
Atcheson, G. (I2-06) . . . 246
Atcitty, S. (J2-06) . . . 275
Atkinson, P. (O7-16) . . . 466
Attané, J. (Q4-11) . . . 526
Attané, J. (R1-11) . . . 542
Attané, J. (R4-10) . . . 561
Atulasimha, J. (N1-12) . . . 392
Atulasimha, J. (O2-13) . . . 434
Atulasimha, J. (P1-04) . . . 469
Atzori, M. (D2-01) . . . 90
Atzori, M. (F5-07) . . . 166
Aubert, A. (Q1-06) . . . 509
Auffret, S. (B3-09) . . . 49
Auffret, S. (G4-02) . . . 197
Auffret, S. (I3-11) . . . 256
Auffret, S. (N1-10) . . . 391
Auffret, S. (O2-02) . . . 429
Auffret, S. (O3-08) . . . 439
Auffret, S. (P2-09) . . . 476
Augusto, P.A. (B2-14) . . . 45
Augusto, P.A. (C3-09) . . . 70
Autieri, C. (E5-10) . . . 137
Avedissian, G. (D1-08) . . . 86
Avedissian, G. (F1-10) . . . 143
Avilés Félix, L. (P2-09) . . . 476
Avraham, N. (S1-01) . . . 105
Awad, A.A. (Q3-04) . . . 519
Awad, A.A. (Q4-01) . . . 522
Awano, H. (F1-08) . . . 142
Awano, H. (R4-06) . . . 560
Aydil, E.S. (E2-03) . . . 118
Azevedo, A. (R4-09) . . . 561
Aziz, M. (I5-06) . . . 265
Aziz, M. (L3-14) . . . 339

- B -

B. Wilson, R. (G3-01) . . . 190
B. Wilson, R. (M3-04) . . . 366
Babu, P.D. (L4-13) . . . 345
Bac, S. (I4-09) . . . 261
Bacaksiz, C. (O7-06) . . . 461
Bachhraj, L. (L4-13) . . . 345
Bachmaier, A. (H1-06) . . . 213
Back, C. (G3-06) . . . 191
Bacova, M. (J1-03) . . . 269
Badawy, G. (K3-06) . . . 311
Baenitz, M. (B4-01) . . . 51
Baez Flores, G.G. (J4-12) . . . 287
Bagschik, K. (G3-05) . . . 191
Bai, H. (K1-02) . . . 297
Bai, H. (Q6-10) . . . 537
Bai, Y. (G3-10) . . . 193
Bailleul, M. (E4-11) . . . 132
Bairagi, K. (N1-10) . . . 391
Baker, A. (C2-05) . . . 64
Baker, A. (I2-01) . . . 243
Baker, A. (K2-06) . . . 305
Bakkers, E.P. (K3-06) . . . 311
Bakuzis, A.F. (C1-08) . . . 58
Balachandran, P. (A3-04) . . . 14
Balachandran, P. (E5-06) . . . 136
Balachandran, P. (J5-13) . . . 291
Balachandran, P. (Q1-12) . . . 512
Balachandran, P. (R2-02) . . . 545
Balaev, D. (C4-02) . . . 74
Balakrishnan, G. (E5-14) . . . 139
Balakrishnan, G. (I3-01) . . . 251
Balakrishnan, P.P. (Q6-04) . . . 534
Balasubramanian, B. (E2-06) . . . 119
Balasubramanian, B. (E2-12) . . . 121
Balcells, L. (D1-12) . . . 88
Baldomir, D. (Q2-09) . . . 516
Baldomir, D. (Q2-10) . . . 516
Baldrati, L. (G1-11) . . . 181
Baldrati, L. (M1-02) . . . 353
Baldrati, L. (N2-10) . . . 397
Baldrati, L. (P4-07) . . . 485
Balli, M. (F2-02) . . . 145
Ballou, R. (A2-03) . . . 8
Baltz, V. (N2-10) . . . 397
Baltz, V. (O3-08) . . . 439
Balymov, K. (M6-03) . . . 382
Bana, H. (K2-08) . . . 306
Bandurin, D. (K3-03) . . . 309
Banerjee, C. (I2-06) . . . 246
Banerjee, N. (L2-09) . . . 333
Banerjee, R. (J2-07) . . . 275
Banerjee, S.K. (E5-05) . . . 136
Banerjee, T. (G1-06) . . . 179
Banerjee, T. (I4-04) . . . 258
Banerjee, T. (M2-06) . . . 360
Bang, H. (M6-04) . . . 382
Bang, S. (Q5-09) . . . 531
Bang, T. (D3-03) . . . 96
Bang, T. (G6-06) . . . 207
Bangar, H. (M3-06) . . . 367
Bannenberg, L.J. (D2-14) . . . 94
Bansal, N. (O5-08) . . . 450
Baraduc, C. (I3-11) . . . 256
Barandiarán, J. (A4-05) . . . 22
Barbic, M. (P1-04) . . . 469
Barbosa, D. (B2-14) . . . 45
Barbosa, D. (C3-09) . . . 70
Barick, k. (K5-05) . . . 319
Baron, M.S. (J1-02) . . . 268
Barra, A.L. (N2-10) . . . 397
Barral, M. (K2-13) . . . 307
Barral, M.A. (I4-07) . . . 259
Barrera, G. (J1-05) . . . 270
Barrera, G. (L3-12) . . . 338
Barriga-Castro, E. (H5-03) . . . 233
Barrio, M.A. (F1-01) . . . 140
Barrios, L. (D2-03) . . . 91
Barsukov, I. (M3-07) . . . 367
Barthelemy, A. (K1-07) . . . 299
Barthelemy, A. (R4-10) . . . 561
Barthelemy, A. (S7-04) . . . 419
Bartolome, E. (B2-03) . . . 41
Bartolome, E. (B2-04) . . . 41
Bartolome, F. (B2-03) . . . 41
Bartolome, F. (B2-04) . . . 41
Bartolome, J. (B2-03) . . . 41
Bartolome, J. (B2-04) . . . 41
Barton, C. (L1-01) . . . 323
Barton, C. (R1-06) . . . 540
Barton, L.X. (G1-10) . . . 180
Barua, R. (F2-12) . . . 148
Barucca, G. (Q5-04) . . . 529
Barucca, G. (R3-14) . . . 557
Bas, D.A. (I2-02) . . . 243
Basheed, G. (F4-02) . . . 159
Basheed, G. (L4-13) . . . 345
Bashtovoi, V. (F4-03) . . . 159
Batabyal, R. (S1-01) . . . 105
Bataev, D. (F2-14) . . . 149

Bataev, D. (L4-11) . . . 344
Batalov, S. (O6-02) . . . 452
Batashev, I. (A4-03) . . . 21
Batashev, I. (L4-01) . . . 341
Batley, J. (E2-03) . . . 118
Battiato, M. (K3-02) . . . 308
Bauer, G. (J5-11) . . . 291
Bauer, G. (M4-09) . . . 374
Bauer, G. (Q2-01) . . . 513
Bauer, J. (F1-04) . . . 141
Bauer, J. (K2-04) . . . 304
Baumgaertl, K. (A1-07) . . . 5
Baumgaertl, K. (E4-05) . . . 129
Baumgarten, D. (S3-03) . . . 175
Bayaraa, T. (M2-12) . . . 362
Béa, H. (I3-11) . . . 256
Béa, H. (L2-04) . . . 330
Béa, H. (L2-06) . . . 331
Beach, G. (C1-02) . . . 54
Beach, G. (G1-02) . . . 178
Beach, G. (G1-05) . . . 179
Beach, G. (R2-01) . . . 544
Beach, G. (R2-06) . . . 546
Beato-López, J.J. (N5-06) . . . 412
Beatty, J. (G5-13) . . . 205
Beatty, J. (K5-04) . . . 319
Beauchamp, M. (I1-05) . . . 240
Beaulieu, N. (M4-11) . . . 375
Beaulieu, N. (N2-09) . . . 396
Beaurepaire, E. (D1-08) . . . 86
Becherer, M. (E5-02) . . . 135
Becker, J. (L1-14) . . . 328
Becker, S. (G1-11) . . . 181
Beckmann, B. (F2-03) . . . 146
Beckmann, B. (F2-16) . . . 150
Bedanta, S. (A4-14) . . . 25
Bedanta, S. (D1-02) . . . 83
Bedanta, S. (J5-12) . . . 291
Bedanta, S. (O4-10) . . . 446
Bedanta, S. (O4-11) . . . 446
Bedanta, S. (R4-04) . . . 559
Beg, M. (D1-07) . . . 86
Beg, M. (R2-09) . . . 548
Begari, K. (L3-13) . . . 339
Beginin, E. (O6-09) . . . 455
Beginin, E. (O7-07) . . . 461
Beginin, E. (O7-11) . . . 463
Behbahani, R. (P3-04) . . . 479
Beidenkopf, H. (S1-01) . . . 105
Beik Mohammadi, J. (R3-05) . . . 552
Bejarano, M. (O5-04) . . . 449
Belashchenko, K. (J4-12) . . . 287
Belashchenko, K. (M1-07) . . . 355
Belcher, C. (J2-06) . . . 275
Belduque, M.C. (G2-12) . . . 187
Belin, N. (F3-02) . . . 153
Belkhou, r. (O3-07) . . . 439
Bellaiche, L. (H2-02) . . . 219
Bellaiche, L. (M2-12) . . . 362
Bellaiche, L. (O3-05) . . . 438
Bellaiche, L. (P5-05) . . . 491
Belliard, L. (K1-09) . . . 300
Belliot, P. (F3-02) . . . 153
Bello, J. (R1-05) . . . 539
Belmeguenai, M. (I3-06) . . . 254
Belmeguenai, M. (I3-11) . . . 256
Belmeguenai, M. (N1-10) . . . 391
Belmeguenai, M. (O3-07) . . . 439
Belmeguenai, M. (R1-10) . . . 541
Belov, M. (G2-11) . . . 187
Belov, M. (N5-16) . . . 417
ben youssef, j. (M4-09) . . . 374
ben youssef, j. (M4-11) . . . 375
ben youssef, j. (N2-09) . . . 396
ben youssef, j. (Q2-01) . . . 513
ben youssef, j. (S8-01) . . . 504
Ben, T. (I1-09) . . . 241
Ben, T. (J2-01) . . . 273
Benguettat-El Mokhtari, I. (I3-11) . . . 256
Benítez, L. (O1-01) . . . 421
Benito, L. (H1-15) . . . 217
Bennett, C.H. (A5-01) . . . 28
Bennett, C.H. (A5-02) . . . 29
Bennett, C.H. (A5-03) . . . 29
Bennett, C.H. (A5-05) . . . 31
Bennett, C.H. (A5-06) . . . 31
Bensmann, J. (M4-08) . . . 373
Bensmann, J. (Q4-10) . . . 526
Bentley, P. (G5-03) . . . 201
Bentley, P. (L1-06) . . . 325
Berencén, Y. (O5-04) . . . 449
Berganza, E. (G2-04) . . . 184
Berganza, E. (L1-03) . . . 323
Bergbreiter, S. (A1-08) . . . 5
Berger, H. (N1-07) . . . 389
Berger, K. (J3-09) . . . 279
Bergeret, F. (O4-02) . . . 442
Bergman, A. (D2-10) . . . 93
Bergman, A. (E2-02) . . . 117
Bergman, A. (Q2-04) . . . 514
Beritta, M. (I2-11) . . . 247
Berkoun, R. (L2-01) . . . 329
Berkowski, M. (F2-07) . . . 147
Berntsen, M. (G3-05) . . . 191
Bertacco, R. (N2-11) . . . 398
Bertacco, R. (Q4-11) . . . 526
Bertram, F. (C1-11) . . . 59
Bertran, F. (E1-13) . . . 116
Bertran, F. (G3-02) . . . 190
Besbas, J. (I2-06) . . . 246
Bessonov, S. (E5-03) . . . 135
Bessonov, V. (O6-02) . . . 452
Bessonova, V.A. (P5-03) . . . 490
Betto, D. (B2-04) . . . 41
Betto, D. (E1-02) . . . 111
Bharati, B. (I4-11) . . . 261
Bhaskar, U. (E4-11) . . . 132
Bhat, F.H. (M2-05) . . . 360
Bhat, N. (C1-13) . . . 60
Bhat, S. (M2-09) . . . 361
Bhat, S. (Q6-06) . . . 535
Bhat, V.S. (E4-05) . . . 129
Bhattacharrya, S. (D2-04) . . . 91
Bhattacharya, A. (G1-13) . . . 182
Bhattacharya, D. (N1-12) . . . 392
Bhattacharya, D. (O2-13) . . . 434
Bhobe, P. (K2-02) . . . 303
Bhowmik, D. (Q3-07) . . . 520
Bi, C. (S1-04) . . . 106
Bi, C. (S5-02) . . . 348
Bi, L. (I2-10) . . . 247
Bi, L. (I2-12) . . . 248
Bi, Z. (G1-12) . . . 181
Biacchi, A.J. (H1-14) . . . 217
Biacchi, A.J. (O5-06) . . . 449
Bibes, M. (Q4-11) . . . 526
Bibes, M. (R4-10) . . . 561
Bilardello, D. (I2-14) . . . 249
Billington, D. (Q2-11) . . . 517
Bilski, P. (P1-03) . . . 468
Biniskos, N. (M2-03) . . . 359
Birat, J. (O5-07) . . . 450
Birch, M.T. (I3-01) . . . 251
Bird, J. (F4-13) . . . 163
Bird, J. (G6-06) . . . 207
Bird, T. (E2-10) . . . 120
Bird, T. (G5-03) . . . 201
Birge, N.O. (G1-02) . . . 178
Birge, N.O. (G1-05) . . . 179
Birol, T. (L2-02) . . . 329
Birowska, M. (I2-09) . . . 247
Bisht, P. (L4-04) . . . 342
Bisht, P. (R5-12) . . . 569
Biswas, A. (F2-12) . . . 148
Biswas, A. (L4-06) . . . 343
Bjørk, R. (P3-03) . . . 479
Björling, A. (J6-07) . . . 294
Blagg, K. (M4-12) . . . 376
Blakley, S.M. (L1-14) . . . 328
Bleser, S.M. (P6-16) . . . 502
Blomgren, J. (Q2-11) . . . 517
Blon, T. (C4-08) . . . 76
Bloom, B. (I2-13) . . . 249
Bloom, R.P. (G4-01) . . . 196
Bluegel, S. (F1-01) . . . 140
Blyakhman, F.A. (J1-07) . . . 271
Boes, A. (K5-07) . . . 320
Bogush, M.Y. (D4-01) . . . 100
Bogush, M.Y. (L4-11) . . . 344
Bohannon, N.J. (E2-08) . . . 120
Bokor, J. (G3-12) . . . 194
Bokor, J. (M3-04) . . . 366
Boldrey, J. (K5-07) . . . 320
Bolyachkin, A. (O6-18) . . . 458
Bolyachkin, A. (R5-01) . . . 564
Bondarenko, A.V. (P2-11) . . . 477
Boneberg, J. (P2-11) . . . 477
Bonizzoni, C. (B2-02) . . . 40
Bonnin, A. (J1-04) . . . 270
Boothroyd, A. (M3-09) . . . 368
Borchers, J.A. (E2-02) . . . 117
Borchers, J.A. (F1-04) . . . 141
Borchers, J.A. (K2-04) . . . 304

Borisov, V. (D2-10) . . . 93
Borisov, V. (Q2-04) . . . 514
Borland, A. (G4-05) . . . 198
Borme, J. (B3-03) . . . 46
Bortolotti, P. (B3-05) . . . 48
Bortolotti, P. (B3-06) . . . 48
Bortolotti, P. (C1-10) . . . 59
Bortolotti, P. (F3-08) . . . 155
Bosch-Santos, B. (D4-08) . . . 102
Bose, A. (O1-04) . . . 422
Bose, A. (Q4-02) . . . 522
Bostrem, I. (L3-03) . . . 335
Bouchenoire, L. (S2-03) . . . 108
Bouda, N. (G6-01) . . . 206
Boulle, O. (I3-06) . . . 254
Boulle, O. (N1-10) . . . 391
Boulle, O. (O3-07) . . . 439
Boulle, O. (O3-08) . . . 439
Bouma, D. (H1-12) . . . 216
Bouma, D. (J4-03) . . . 283
Bouma, D. (J4-11) . . . 287
Bouquin, P. (O2-04) . . . 430
Bouquin, P. (R3-04) . . . 552
Bourdon, C. (J1-04) . . . 270
Bouzehouane, K. (E5-08) . . . 137
Bouzehouane, K. (I3-09) . . . 255
Bouzehouane, K. (I3-10) . . . 256
Bouzehouane, K. (N1-03) . . . 388
Bouzehouane, K. (P3-12) . . . 483
Boventer, I. (K1-07) . . . 299
Boventer, I. (N2-10) . . . 397
Bowman, R. (A3-10) . . . 17
Bowman, R. (N4-04) . . . 408
Bowman, R. (P2-08) . . . 475
Bowman, R. (P2-10) . . . 477
Bozhko, D.A. (E4-12) . . . 132
Bradley, H. (Q3-01) . . . 518
Bradlyn, B. (S1-03) . . . 105
Braganca, P.M. (C5-03) . . . 80
Brahlek, M. (H2-09) . . . 221
Bramley, F. (D1-11) . . . 88
Bran, C. (A1-03) . . . 3
Bran, C. (O7-05) . . . 460
Brandon, F. (G1-13) . . . 182
Branford, W. (C4-01) . . . 74
Branford, W. (N2-03) . . . 394
Brangham, J. (F1-06) . . . 142
Brataas, A. (G1-08) . . . 179
Brataas, A. (G1-11) . . . 181
Brataas, A. (N2-10) . . . 397
Bratschitsch, R. (M4-08) . . . 373
Bratschitsch, R. (Q4-10) . . . 526
Bréhin, J. (R4-10) . . . 561
Breitbach, D. (E4-12) . . . 132
Brems, S. (K2-08) . . . 306
Breth, L. (B1-13) . . . 38
Brigner, W.H. (A5-01) . . . 28
Brigner, W.H. (A5-03) . . . 29
Brigner, W.H. (A5-06) . . . 31
Briones, J. (G3-11) . . . 194
Briones, J. (R4-12) . . . 563
Brock, J.A. (R1-12) . . . 542
Bromley, D. (K3-05) . . . 310
Brookes, N.B. (E1-02) . . . 111
Broussard, M. (P1-01) . . . 467
Brouwer, E. (C2-06) . . . 64
Brown, H. (C3-11) . . . 71
Brown, J. (P1-03) . . . 468
Brück, E. (A4-03) . . . 21
Brück, E. (A4-06) . . . 22
Brück, E. (L4-01) . . . 341
Brück, E. (R5-14) . . . 570
Bruckner, F. (B1-02) . . . 33
Brueckel, T. (R4-04) . . . 559
Brueckl, H. (B1-13) . . . 38
Brunn, O. (A2-05) . . . 9
Bruno, M. (L3-06) . . . 336
Brunson, F. (L3-06) . . . 336
Brus, P. (K4-03) . . . 313
Bryan, M.T. (A1-04) . . . 4
Bryan, M.T. (Q5-01) . . . 528
Buajong, C. (N3-07) . . . 403
Bublikov, K. (L1-02) . . . 323
Buchanan, K. (A4-13) . . . 25
Büchner, B. (J5-07) . . . 290
Buchner, M. (C1-07) . . . 57
Buchner, M. (E4-03) . . . 128
Buchner, M. (M3-05) . . . 366
Buckley, R.G. (J5-09) . . . 290
Buda-Prejbeanu, L. (C5-05) . . . 80
Buda-Prejbeanu, L. (G4-02) . . . 197
Buda-Prejbeanu, L. (I3-06) . . . 254
Buda-Prejbeanu, L. (L2-04) . . . 330
Buda-Prejbeanu, L. (N1-10) . . . 391
Buda-Prejbeanu, L. (O2-02) . . . 429
Buda-Prejbeanu, L. (P2-09) . . . 476
Budhathoki, S. (A3-03) . . . 14
Budhathoki, S. (A3-09) . . . 17
Budhathoki, S. (E1-06) . . . 113
Budzinauskas, K. (A2-10) . . . 11
Buettner, F. (R2-06) . . . 546
Buhrman, R. (J4-10) . . . 286
Buhrman, R. (O1-04) . . . 422
Buhrman, R. (Q4-02) . . . 522
Buhrman, R. (S5-05) . . . 349
Bui, T.Q. (H1-14) . . . 217
Bui, T.Q. (O5-06) . . . 449
Bukin, N. (I3-01) . . . 251
Bultynck, O. (O2-04) . . . 430
Bultynck, O. (R3-04) . . . 552
Bulut, G. (K5-02) . . . 318
Bunyaev, S.A. (P2-11) . . . 477
Buongiorno Nardelli, M. (Q4-11) . . . 526
Burema, A. (I4-04) . . . 258
Burgard, M. (R4-07) . . . 560
Burgos Parra, E.O. (L1-11) . . . 327
Burimova, A. (D4-08) . . . 102
Burimova, A. (F5-06) . . . 166
Burimova, A. (F5-11) . . . 168
Burimova, A. (R5-13) . . . 569
Burkov, A. (J5-03) . . . 288
Burkov, A. (S1-02) . . . 105
Burn, D. (E4-01) . . . 127
Burn, D. (M5-12) . . . 379
Burn, D. (P2-08) . . . 475
Burn, D. (P2-10) . . . 477
Burnell, G. (J5-05) . . . 289
Burnell, G. (M5-02) . . . 377
Burnell, G. (M5-07) . . . 378
Buryakov, A. (L3-07) . . . 336
Butera, A. (P3-12) . . . 483
Butler, T.J. (I3-02) . . . 251
Butler, W.H. (E1-06) . . . 113
Butta, M. (N5-10) . . . 414
Butta, M. (R5-05) . . . 565
Buzdakov, A. (E4-10) . . . 131
Buzi, E. (F4-09) . . . 161
Buznikov, N.A. (J1-07) . . . 271
Bykovetz, N. (D2-13) . . . 94
Byland, J.K. (Q1-04) . . . 508
Byun, J. (O2-16) . . . 435

- C -

C-J. Cheeran, M. (Q5-12) . . . 532
Cabanova, K. (C3-13) . . . 72
Cabrera-Pasca, G. (D4-08) . . . 102
Cabrera-Pasca, G. (F5-06) . . . 166
Cabrera-Pasca, G. (F5-11) . . . 168
Cabrera-Pasca, G. (R5-13) . . . 569
Caha, O. (Q6-02) . . . 534
Cahaya, A. (J5-11) . . . 291
Cahill, D. (D2-16) . . . 95
Cailing, H. (C1-09) . . . 58
Caisse, C. (G2-05) . . . 184
Calarco, R. (Q4-11) . . . 526
Calascione, T. (A1-10) . . . 7
Calascione, T. (C4-09) . . . 77
Calascione, T. (L4-10) . . . 344
Calascione, T.M. (L4-16) . . . 346
Calavalle, F. (O4-02) . . . 442
Calo, C. (N2-07) . . . 396
Calvo, M. (K4-09) . . . 315
Cambel, V. (L1-02) . . . 323
Camley, R. (D1-10) . . . 87
Camley, R. (E4-04) . . . 128
Camley, R. (E4-10) . . . 131
Camley, R. (I5-05) . . . 265
Camley, R. (N2-01) . . . 393
Camley, R. (P1-02) . . . 467
Camosi, L. (R2-11) . . . 548
Campanella, A. (P1-01) . . . 467
Campbell, A.R. (H3-13) . . . 227
Campion, R.P. (G1-10) . . . 180
Campion, R.P. (J3-03) . . . 277
Campion, R.P. (J6-07) . . . 294
Campion, R.P. (M1-09) . . . 356
Campos, A.C. (D4-08) . . . 102
Canals, B. (A2-05) . . . 9
Canals, B. (A2-08) . . . 10
Cannamela, M. (C4-11) . . . 77
Canon Bermudez, G. (F3-12) . . . 157

Cantoni, M. (N2-11) . . . 398
Cantoni, M. (Q4-11) . . . 526
Caouette-Mansour, M. (C5-03) . . . 80
Caouette-Mansour, M. (E3-05) . . . 125
Capic, D. (M5-01) . . . 377
Capotondi, F. (G3-05) . . . 191
Capotondi, F. (G3-08) . . . 192
Car, D. (K3-06) . . . 311
Carbonari, A.W. (D4-08) . . . 102
Carbonari, A.W. (F5-06) . . . 166
Carbonari, A.W. (F5-11) . . . 168
Carbonari, A.W. (R5-13) . . . 569
Carbone, D. (J6-07) . . . 294
Caretta, L. (R2-01) . . . 544
Caretta, L. (R2-06) . . . 546
Caretta, L.M. (C1-02) . . . 54
Carey, M. (G4-05) . . . 198
Carleschi, E. (P5-10) . . . 493
Carley, R. (G3-06) . . . 191
Carlotti, G. (M2-14) . . . 363
Carlotti, G. (N2-11) . . . 398
Carlotti, G. (O7-01) . . . 459
Carlotti, G. (O7-02) . . . 459
Carman, G. (Q5-11) . . . 532
Carmona, I.C. (J1-02) . . . 268
Carmona, I.C. (K5-11) . . . 321
Carneiro, E. (H3-03) . . . 224
Carpenter, R. (L2-05) . . . 331
Carpentieri, M. (M1-08) . . . 356
Carrétero, C. (C1-10) . . . 59
Carrétero, C. (K1-07) . . . 299
Carretta, S. (B2-03) . . . 41
Carretta, S. (D2-01) . . . 90
Carretta, S. (D2-02) . . . 90
Carretta, S. (D2-03) . . . 91
Carretta, S. (F5-07) . . . 166
Carretta, S. (G2-01) . . . 183
Carriço, A.S. (M6-01) . . . 381
Caruana, A. (E1-10) . . . 115
Caruana, A. (E4-14) . . . 134
Caruana, A. (M5-07) . . . 378
Casanova, F. (K4-09) . . . 315
Casanova, F. (O1-13) . . . 426
Casanova, F. (O4-02) . . . 442
Casanova, F. (Q4-05) . . . 523
Cascales Sandoval, M. (F1-03) . . . 141
Caso, D. (L2-09) . . . 333
Caso, D. (O7-05) . . . 460
Castell-Queralt, J. (M3-10) . . . 369
Castelo-Grande, T. (B2-14) . . . 45
Castelo-Grande, T. (C3-09) . . . 70
Castro, M. (C5-05) . . . 80
Cates, J. (L3-06) . . . 336
Cavazzini, G. (F2-15) . . . 149
Cavill, S. (H1-15) . . . 217
Cazayous, M. (K1-09) . . . 300
Ceballos, A. (A1-06) . . . 5
Cebollada, F. (D1-12) . . . 88
Cebollada, F. (F2-18) . . . 150
Cebollada, F. (H1-05) . . . 213
Cecchi, S. (Q4-11) . . . 526
Celegato, F. (J1-05) . . . 270
Celegato, F. (L3-12) . . . 338
Celinski, Z. (H4-02) . . . 228
Celinski, Z. (I5-05) . . . 265
Celinski, Z. (P1-02) . . . 467
Celinski, Z. (P1-03) . . . 468
Cespedes, O. (D1-07) . . . 86
Chai, J. (K3-02) . . . 308
Chai, Y. (A1-06) . . . 5
Chakraborti, H. (B1-14) . . . 38
Chalise, A. (K5-04) . . . 319
Cham, T.M. (O1-04) . . . 422
Chan, J. (I4-14) . . . 262
Chan, K. (G5-03) . . . 201
Chang-Sheng, W. (G6-11) . . . 209
Chang, A. (K4-05) . . . 314
Chang, C. (C2-10) . . . 66
Chang, C. (F5-10) . . . 167
Chang, C. (I4-03) . . . 258
Chang, H.W. (F6-05) . . . 171
Chang, H.W. (F6-06) . . . 172
Chang, L. (P5-11) . . . 493
Chang, W. (F6-05) . . . 171
Chang, W. (F6-06) . . . 172
Chang, Y. (J4-06) . . . 284
Channagoudra, G. (B4-04) . . . 51
Chantrell, R. (D1-06) . . . 85
Chantrell, R. (G3-13) . . . 195
Chantrell, R. (M1-04) . . . 354
Chantrell, R. (N1-09) . . . 390
Chantrell, R. (N3-05) . . . 402
Chantrell, R. (N3-12) . . . 405
Chantrell, R. (P2-05) . . . 474
Chantrell, R. (P2-06) . . . 474
Chantrell, R. (P2-07) . . . 475
Chantrell, R. (Q2-09) . . . 516
Chantrell, R. (Q2-10) . . . 516
Chao, C. (K3-08) . . . 312
Charlier, J. (K4-03) . . . 313
Charlton, T.R. (D2-06) . . . 93
Chatterjee, J. (G3-12) . . . 194
Chatterjee, R. (C1-03) . . . 55
Chatterjee, R. (C4-03) . . . 74
Chaturvedi, V. (M2-03) . . . 359
Chaudhary, V. (J2-07) . . . 275
Chaudhuri, U. (E1-08) . . . 114
Chaudhuri, U. (Q6-05) . . . 535
Chauhan, N. (B1-14) . . . 38
Chavent, A. (G4-02) . . . 197
Chaves, G.D. (P3-08) . . . 481
Che, P. (N1-07) . . . 389
Cheekati, S.K. (B2-10) . . . 43
Cheekati, S.K. (F4-06) . . . 160
Cheema, S. (J4-11) . . . 287
Chekanova, L. (G6-12) . . . 210
Chekanova, L. (R5-09) . . . 567
Chelvane, J.A. (D1-02) . . . 83
Chelvane, J.A. (E5-12) . . . 138
Chelvane, J.A. (O5-09) . . . 451
Chen, A.P. (M2-14) . . . 363
Chen, A.P. (P5-02) . . . 489
Chen, B. (F3-11) . . . 156
Chen, B. (O2-15) . . . 435
Chen, D. (F6-02) . . . 170
Chen, F. (J2-01) . . . 273
Chen, G. (D1-03) . . . 84
Chen, G. (F1-01) . . . 140
Chen, G. (I3-08) . . . 255
Chen, G. (M1-05) . . . 355
Chen, G. (O3-11) . . . 440
Chen, G. (Q3-03) . . . 519
Chen, H. (D2-08) . . . 93
Chen, H. (F3-11) . . . 156
Chen, H. (G2-03) . . . 183
Chen, H. (G4-06) . . . 199
Chen, H. (O1-06) . . . 423
Chen, H. (P5-01) . . . 489
Chen, H. (Q2-11) . . . 517
Chen, H. (R3-06) . . . 553
Chen, J. (K4-14) . . . 317
Chen, J. (M1-01) . . . 353
Chen, J. (M2-14) . . . 363
Chen, J. (P5-02) . . . 489
Chen, J. (P6-01) . . . 496
Chen, K. (C3-03) . . . 68
Chen, K. (O2-12) . . . 433
Chen, L. (I1-09) . . . 241
Chen, L. (J2-01) . . . 273
Chen, L. (O6-15) . . . 457
Chen, M. (C4-07) . . . 76
Chen, M. (O7-12) . . . 464
Chen, P. (C4-07) . . . 76
Chen, P. (O3-05) . . . 438
Chen, P. (O7-12) . . . 464
Chen, S. (M2-14) . . . 363
Chen, T. (J4-06) . . . 284
Chen, T. (M4-01) . . . 371
Chen, T. (M4-07) . . . 373
Chen, T. (Q4-07) . . . 524
Chen, W. (K5-04) . . . 319
Chen, W. (M4-07) . . . 373
Chen, X. (A1-04) . . . 4
Chen, X. (O3-06) . . . 438
Chen, X. (P4-08) . . . 486
Chen, X. (S6-04) . . . 352
Chen, Y. (C1-04) . . . 56
Chen, Y. (F4-08) . . . 161
Chen, Y. (G2-05) . . . 184
Chen, Y. (I2-10) . . . 247
Chen, Y. (K2-05) . . . 304
Chen, Y. (M3-07) . . . 367
Chen, Y.P. (C5-01) . . . 79
Chen, Y.P. (G5-10) . . . 204
Chen, Z. (O3-11) . . . 440
Chenattukuzhiyil, S. (O1-08) . . . 423
Chenattukuzhiyil, S. (O1-13) . . . 426
Cheng, C. (M4-07) . . . 373
Cheng, C. (O2-12) . . . 433
Cheng, E. (J1-01) . . . 268
Cheng, H. (K1-01) . . . 297
Cheng, L. (K3-02) . . . 308
Cheng, M. (K3-02) . . . 308

Cheng, R. (G1-12) . . . 181
Cheng, R. (G5-08) . . . 203
Cheng, R. (J6-03) . . . 293
Cheng, R. (N4-08) . . . 409
Cheng, R. (S4-02) . . . 236
Cheng, W. (I5-09) . . . 267
Cheng, X. (A4-13) . . . 25
Cheng, X. (G2-03) . . . 183
Cheng, X. (K3-02) . . . 308
Cheng, Y. (F1-06) . . . 142
Cheng, Y. (G1-04) . . . 178
Cheng, Y. (J6-04) . . . 293
Cheol Hong, S. (D4-10) . . . 102
Cheol Hong, S. (D4-11) . . . 103
Chérif, S. (I3-11) . . . 256
Cherif, S. (R1-10) . . . 541
Cherifi-Hertel, S. (K1-05) . . . 298
Chernenko, V. (A4-05) . . . 22
Chesnel, K. (D1-14) . . . 89
Chesnel, K. (E2-04) . . . 118
Chesnel, K. (E2-05) . . . 119
Chesnel, K. (O6-11) . . . 456
Chi, D. (K3-02) . . . 308
Chia, E. (K3-02) . . . 308
Chiang, C. (M1-11) . . . 357
Chiba, M. (O6-04) . . . 453
Chiba, T. (K4-08) . . . 315
Chiba, T. (O1-09) . . . 424
Chicco, S. (F2-15) . . . 149
Chicco, S. (F5-07) . . . 166
Chien, C. (M1-11) . . . 357
Chiesa, A. (D2-02) . . . 90
Chiesa, A. (D2-03) . . . 91
Chiesa, A. (F5-07) . . . 166
Chiesa, A. (G2-01) . . . 183
Chikara, S. (K1-01) . . . 297
Chikaso, Y. (R3-12) . . . 556
Chikina, I. (B2-13) . . . 44
Childress, L. (C5-03) . . . 80
Childress, L. (E3-05) . . . 125
Chioar, I. (B1-12) . . . 37
Chioar, I. (I2-11) . . . 247
Chiocchetta, A. (A2-10) . . . 11
Chiriac, H. (H1-01) . . . 211
Chiriac, H. (N5-09) . . . 413
Chiriac, H. (Q5-03) . . . 529
Chiriac, H. (R5-08) . . . 567
Chisholm, M. (M2-02) . . . 359
Chistyakov, V. (J5-08) . . . 290
Chistyakov, V. (K4-13) . . . 317
Chiu, C. (F6-06) . . . 172
Chiu, I. (H2-01) . . . 219
Chiu, I. (M2-04) . . . 360
Cho, E. (P5-14) . . . 495
Cho, H. (D3-03) . . . 96
Cho, H. (G6-06) . . . 207
Cho, J. (N1-06) . . . 389
Cho, S. (I4-06) . . . 259
Cho, S. (L4-02) . . . 341
Choi, E. (H2-09) . . . 221
Choi, G. (G3-09) . . . 193
Choi, G. (J4-04) . . . 283
Choi, G. (P6-13) . . . 501
Choi, H. (F5-02) . . . 164
Choi, H. (F5-08) . . . 167
Choi, H. (H4-07) . . . 230
Choi, J. (C4-05) . . . 75
Choi, J. (D3-03) . . . 96
Choi, J. (F4-13) . . . 163
Choi, J. (G6-06) . . . 207
Choi, M. (N3-14) . . . 406
Choi, M. (R5-03) . . . 564
Choi, W. (M2-02) . . . 359
Choi, W. (Q4-05) . . . 523
Choi, Y. (H2-09) . . . 221
Chopdekar, R.V. (B1-05) . . . 34
Chopdekar, R.V. (B1-06) . . . 34
Chopdekar, R.V. (G1-04) . . . 178
Chopdekar, R.V. (H2-09) . . . 221
Chopdekar, R.V. (L1-12) . . . 327
Chopdekar, R.V. (N4-08) . . . 409
Chopdekar, R.V. (S6-04) . . . 352
Chopin, C. (F3-02) . . . 153
Chopin, C. (F3-09) . . . 156
Chouaieb, S. (I3-06) . . . 254
Chouaieb, S. (O1-02) . . . 421
Choudhary, R. (C2-02) . . . 62
Choudhary, R. (D2-11) . . . 94
Chouhan, A. (L2-03) . . . 330
Chow, G. (M2-14) . . . 363
Chowdhury, N. (M3-06) . . . 367
Chowdhury, N. (O5-08) . . . 450
Chowdhury, N. (P6-02) . . . 496
Chshiev, M. (R1-11) . . . 542
Chshiev, M. (S7-02) . . . 419
Chuang, T. (J4-09) . . . 286
Chubykalo-Fesenko, O. (A1-03) . . . 3
Chubykalo-Fesenko, O. (G3-13) . . . 195
Chubykalo-Fesenko, O. (L1-03) . . . 323
Chubykalo-Fesenko, O. (N1-09) . . . 390
Chubykalo-Fesenko, O. (Q2-09) . . . 516
Chubykalo-Fesenko, O. (Q2-10) . . . 516
Chubykalo-Fesenko, O. (R1-06) . . . 540
Chudnovsky, E. (M5-01) . . . 377
Chugh, V.K. (Q5-12) . . . 532
Chumak, A. (E4-12) . . . 132
Chumak, A. (N2-08) . . . 396
Chumak, A. (S8-03) . . . 505
Chung, H. (O2-15) . . . 435
Chung, P. (N3-10) . . . 404
Chureemart, J. (P2-05) . . . 474
Chureemart, P. (P2-05) . . . 474
Churikova, A. (G1-02) . . . 178
Churikova, A. (G1-05) . . . 179
Chuvilin, A. (K4-09) . . . 315
Chuvilin, A. (O4-02) . . . 442
Chuvilin, A. (R4-05) . . . 559
Cibiel, G. (B3-05) . . . 48
Ciuciulkaite, A. (B1-12) . . . 37
Ciuciulkaite, A. (I2-11) . . . 247
Číž, T. (Q6-02) . . . 534
Clark, A.T. (A4-13) . . . 25
Clark, A.T. (G2-03) . . . 183
Clavel, M. (A3-04) . . . 14
Clavel, M. (A3-05) . . . 15
Clements, E. (I4-06) . . . 259
Clifford, D. (F2-12) . . . 148
Coene, A. (S3-04) . . . 175
Coey, M. (E1-02) . . . 111
Coey, M. (E3-08) . . . 126
Coey, M. (I2-06) . . . 246
Coey, M. (J1-04) . . . 270
Cogulu, E. (G1-04) . . . 178
Coh, S. (G3-01) . . . 190
Coïsson, M. (J1-05) . . . 270
Colbois, J. (A2-09) . . . 10
Cole-Piepke, K. (J3-04) . . . 278
Coleman, C. (D2-04) . . . 91
Colino, J. (O6-10) . . . 455
Colis, S. (E3-08) . . . 126
Collette, D. (D1-03) . . . 84
Collin, S. (E5-08) . . . 137
Collin, S. (I3-09) . . . 255
Collin, S. (I3-10) . . . 256
Colson, D. (K1-09) . . . 300
Constable, E. (A2-03) . . . 8
Cooper, J.F. (G4-07) . . . 199
Copus, M. (E4-10) . . . 131
Copus, M. (N2-01) . . . 393
Coraux, J. (O1-02) . . . 421
Corbae, P. (H1-12) . . . 216
Corbae, P. (J4-03) . . . 283
Corodeanu, S. (N5-09) . . . 413
Corodeanu, S. (R5-08) . . . 567
Correa, B. (H1-14) . . . 217
Correa, B. (O5-06) . . . 449
Corte-León, H. (L1-01) . . . 323
Cortés-Ortuño, D. (I3-01) . . . 251
Costa, M. (Q4-11) . . . 526
Costache, M. (O1-01) . . . 421
Couet, S. (E3-01) . . . 123
Couet, S. (L2-05) . . . 331
Couet, S. (O2-04) . . . 430
Couet, S. (R3-04) . . . 552
Couture, P. (I5-05) . . . 265
Cowburn, R. (F1-03) . . . 141
Cox, C. (E1-10) . . . 115
Cox, C. (E4-14) . . . 134
Cramer, J. (G3-08) . . . 192
Cramer, J. (R2-10) . . . 548
cropper, m. (E1-10) . . . 115
cropper, m. (E4-14) . . . 134
Cros, V. (B3-05) . . . 48
Cros, V. (B3-06) . . . 48
Cros, V. (B3-10) . . . 49
Cros, V. (C1-10) . . . 59
Cros, V. (E5-08) . . . 137
Cros, V. (F3-08) . . . 155
Cros, V. (I3-09) . . . 255
Cros, V. (I3-10) . . . 256
Cros, V. (L1-11) . . . 327
Cros, V. (M3-08) . . . 368
Cros, V. (N1-03) . . . 388

Cros, V. (N2-07) . . . 396
Cros, V. (O3-13) . . . 441
Cros, V. (S8-01) . . . 504
Crotti, D. (L2-05) . . . 331
Crowell, P.A. (A3-12) . . . 18
Crowell, P.A. (K3-05) . . . 310
Crowell, P.A. (K3-06) . . . 311
Crowell, P.A. (Q2-03) . . . 514
Csaba, G. (S5-02) . . . 348
Cugat, O. (S3-02) . . . 174
Cugini, F. (F2-15) . . . 149
Cui, C. (A5-01) . . . 28
Cui, C. (A5-05) . . . 31
Cui, Q. (E1-12) . . . 116
Cui, Q. (R2-03) . . . 545
Cui, W. (C3-08) . . . 70
Cuoco, M. (R4-03) . . . 559
Curcio, A. (J1-06) . . . 271
Cuya Huaman, J. (C3-01) . . . 67

- D -

D Krishna, V. (Q5-12) . . . 532
D.C., B. (L3-09) . . . 337
da Silva Vilela, G.L. (R4-09) . . . 561
Dabrowski, M. (P2-08) . . . 475
Dabrowski, M. (P2-10) . . . 477
Daffe, N. (C1-07) . . . 57
Dai, B. (I3-05) . . . 253
Dai, B. (N1-12) . . . 392
Dalgliesh, R.M. (D2-14) . . . 94
Danailov, M. (G3-05) . . . 191
Dang, T. (A4-13) . . . 25
DAngelo, C. (C3-11) . . . 71
DANIEL, L. (P3-07) . . . 481
Dantas, A.L. (M6-01) . . . 381
Dao, T. (R3-01) . . . 550
Darwin, E. (M5-02) . . . 377
Das Gupta, K. (B1-14) . . . 38
Das, A. (G1-06) . . . 179
Das, A. (M2-06) . . . 360
Das, B. (E2-03) . . . 118
Das, G. (H1-11) . . . 215
Das, K. (M4-10) . . . 375
Das, K. (R4-03) . . . 559
Das, P. (B1-14) . . . 38
Das, P. (O6-03) . . . 452
Das, P. (O7-09) . . . 462
Das, P. (P6-03) . . . 497
Das, R. (E1-08) . . . 114
Das, R. (I4-06) . . . 259
Das, R. (L4-02) . . . 341
Das, S. (M3-06) . . . 367
Das, S. (O5-08) . . . 450
Dasari, S. (J2-07) . . . 275
Dassonvalle, P. (O5-07) . . . 450
David, P. (I3-06) . . . 254
Davies, C. (I2-11) . . . 247
Davies, C. (P2-09) . . . 476
Davies, W. (Q5-12) . . . 532
Davydenko, A. (M6-06) . . . 383
Dawidek, R. (G4-07) . . . 199
Day-Roberts, E. (L2-02) . . . 329
Dayal, V. (B4-04) . . . 51
Dayal, V. (Q6-08) . . . 536
DC, M. (P6-01) . . . 496
DC, M. (S1-04) . . . 106
De Biasi, E. (J1-08) . . . 271
De Brion, S. (A2-03) . . . 8
de Camargo, P. (R5-17) . . . 571
de Coster, G. (K4-05) . . . 314
De Graef, M. (I3-03) . . . 252
De Graef, M. (M5-08) . . . 379
De Graef, M. (R1-08) . . . 541
De Graef, M. (R2-08) . . . 547
de Juan, F. (K4-09) . . . 315
de la Barrière, O. (J2-03) . . . 273
de la Presa, P. (E2-13) . . . 121
de la Presa, P. (M2-08) . . . 361
de loubens, G. (M4-09) . . . 374
de loubens, G. (M4-11) . . . 375
de loubens, G. (N1-03) . . . 388
de loubens, G. (N2-09) . . . 396
de loubens, G. (Q2-01) . . . 513
de loubens, G. (S8-01) . . . 504
de Melo, C. (G3-02) . . . 190
de Menezes, R.M. (O7-06) . . . 461
De Renzi, R. (F5-07) . . . 166
De Riz, A. (P3-09) . . . 481
de Souza Silva, C. (O7-06) . . . 461
de Teresa, J. (A1-02) . . . 2
de Teresa, J. (E2-01) . . . 117
de Teresa, J. (L1-03) . . . 323
Deac, A. (E3-08) . . . 126
Deac, A. (O6-05) . . . 453
Dearg, M. (J5-05) . . . 289
Dearg, M. (M5-07) . . . 378
Deb, M. (P2-01) . . . 472
Debray, J. (A2-03) . . . 8
Decorse, C. (A2-03) . . . 8
Deepchand, V. (D4-02) . . . 100
Deffenbaugh, M. (F4-09) . . . 161
DeHerrera, M. (O2-01) . . . 428
Deka, A. (P6-03) . . . 497
Del Rose, T. (J5-14) . . . 292
del Valle, J. (L2-01) . . . 329
del-Valle, N. (M3-10) . . . 369
Delaney, R. (J2-06) . . . 275
Delattre, G. (S3-02) . . . 174
Delczeg-Czirjak, E.K. (E1-07) . . . 114
Delgado-Garcia, R. (O6-10) . . . 455
Delin, A. (D2-10) . . . 93
Delin, A. (E2-02) . . . 117
Delin, A. (L3-04) . . . 335
Delin, A. (Q2-04) . . . 514
DeLong, L.E. (S6-04) . . . 352
DeMann, A. (S5-02) . . . 348
Demidov, V.E. (N2-07) . . . 396
Demidov, V.E. (S8-01) . . . 504
Demin, G.D. (G6-05) . . . 207
Demokritov, S. (N2-07) . . . 396
Demokritov, S. (S8-01) . . . 504
Denardin, J. (M5-13) . . . 380
Deng, H. (R4-01) . . . 558
Deng, L. (I2-10) . . . 247
Deng, L. (I2-12) . . . 248
Dengina, E. (O6-18) . . . 458
Dengina, E. (R5-01) . . . 564
Denisova, E. (G6-12) . . . 210
Denisova, E. (R5-09) . . . 567
Denneulin, T. (I3-06) . . . 254
Dennis, C. (H1-14) . . . 217
Dennis, C. (O1-10) . . . 424
Dennis, C. (O5-06) . . . 449
Derlet, P. (B1-05) . . . 34
Desautels, R. (H2-09) . . . 221
Desbuis, V. (O2-11) . . . 433
Desplat, L. (R3-09) . . . 554
Dev, A.A. (J1-04) . . . 270
Dev, K. (J2-05) . . . 274
Dev, P. (E2-12) . . . 121
Devillers, T. (S3-02) . . . 174
Devlin, E. (Q1-02) . . . 508
Devolder, T. (E4-11) . . . 132
Devolder, T. (N1-03) . . . 388
Devolder, T. (O2-04) . . . 430
Devolder, T. (R1-10) . . . 541
Devolder, T. (R3-04) . . . 552
Dhagat, P. (C4-11) . . . 77
Dhagat, P. (P6-06) . . . 497
Dhesi, S.S. (G1-10) . . . 180
Dhesi, S.S. (G4-07) . . . 199
Dhesi, S.S. (J6-07) . . . 294
Dhesi, S.S. (M1-09) . . . 356
Dhuey, S. (S6-04) . . . 352
di Girolamo, A. (Q5-12) . . . 532
Di Napoli, S.M. (I4-07) . . . 259
Diamond, S. (S3-01) . . . 174
Diao, Z. (G2-11) . . . 187
Díaz-García, Á. (F2-08) . . . 147
Diaz, S.A. (O3-09) . . . 440
Diduszko, R. (F2-07) . . . 147
Diebold, A. (P6-06) . . . 497
Dieckow, K. (G2-12) . . . 187
Diehl, O. (C2-06) . . . 64
Diehl, S. (A2-10) . . . 11
Dieny, B. (B3-09) . . . 49
Dieny, B. (C5-05) . . . 80
Dieny, B. (G4-02) . . . 197
Dieny, B. (L2-04) . . . 330
Dieny, B. (O2-02) . . . 429
Dieny, B. (P2-09) . . . 476
Dieny, B. (R3-08) . . . 554
Dieny, B. (S7-02) . . . 419
Diep, H.T. (M5-04) . . . 378
Digernes, E. (L1-13) . . . 328
Dimitrov, D. (F2-02) . . . 145
Ding, H. (F1-01) . . . 140
Ding, H. (O1-06) . . . 423
Ding, J. (O1-06) . . . 423
Ding, J. (O4-12) . . . 447
Ding, J. (S5-02) . . . 348

Ding, S. (Q1-04) 508
Dinulovic, D. (I1-02) 238
Dion, T. (N2-03) 394
Dittrich, F. (N1-08) 390
Divan, R. (L3-15) 340
Divan, R. (M3-03) 366
Divinskiy, B. (N2-07) 396
Divinskiy, B. (S8-01) 504
Djemia, P. (K1-09) 300
Djuzhev, N.A. (G6-05) 207
Dlubak, B. (K4-03) 313
Dlubak, B. (O3-13) 441
Doan-Nguyen, V. (G5-11) 205
Dobrowolska, M. (I4-09) 261
Dobrynin, A. (N3-05) 402
Dohi, T. (J6-12) 296
Doi, M. (H3-10) 226
Dolotko, O. (L4-06) 343
Domac, B.H. (K5-02) 318
Domozhirova, A. (J5-08) 290
Domozhirova, A. (K4-13) 317
Donahue, M.J. (N2-12) 398
Donahue, M.J. (P3-02) 478
Dong, C. (P5-01) 489
Dong, K. (R5-04) 565
Dong, Y. (H4-07) 230
Dong, Y. (N1-11) 391
Dongquoc, V. (G6-02) 206
Donnelly, C. (A1-02) 2
Donnelly, C. (A1-09) 6
Donnelly, C. (R1-13) 543
Dorjsuren, T. (D4-11) 103
Dorneles, L. (M5-13) 380
Dou, Y. (I5-02) 264
Doudin, B. (E3-08) 126
Doudin, B. (J1-04) 270
Douine, B. (J3-09) 279
Doyle, B. (P5-10) 493
Drechsler, S. (A2-01) 8
Dressler, M. (N5-10) 414
Driesen, B. (G5-05) 202
Du, Y. (D3-04) 97
Duan, F. (Q6-09) 536
Duan, H. (I2-10) 247
Dubois, S. (K4-03) 313
Dubowik, J. (E4-02) 127
Dubroka, A. (Q6-01) 534
Dubroka, A. (Q6-02) 534
Dubs, C. (E4-12) 132
Dubuis, G. (I3-02) 251
Dubuis, G. (N1-04) 388
Ducharne, B. (G2-10) 186
Ducharne, B. (N5-13) 415
Ducharne, B. (P3-07) 481
Ducharne, B. (Q2-05) 514
Dufouleur, J. (J5-07) 290
Dugulan, A.I. (L4-01) 341
Duine, R. (A4-11) 24
Duine, R. (G1-11) 181
Duine, R. (N2-05) 395
Dunin-Borkowski, R. (I3-06) 254
Dunne, P. (E3-08) 126
Dunne, P. (J1-04) 270
Dunsmore, M. (G2-11) 187
Dunsmore, M. (N5-16) 417
Duong, A. (I4-06) 259
Duong, A. (L4-02) 341
Duong, D. (K2-07) 305
Dupuy, J. (O5-07) 450
Duquesne, J. (E4-09) 131
Duquesne, J. (O7-16) 466
Durr, H. (G3-06) 191
Dushenko, S. (L1-08) 325
Dutton, S. (A4-04) 21
Dvornik, M. (Q3-04) 519
Dvornik, M. (S8-02) 504
Dwivedi, J. (H1-11) 215
Dzubinska, A. (A4-01) 20

- E -

E. Van Kuiken, B. (G3-06) 191
Ebels, U. (B3-05) 48
Ebels, U. (B3-06) 48
Ebels, U. (B3-09) 49
Ebels, U. (C5-05) 80
Ebels, U. (F3-08) 155
Ebels, U. (N2-10) 397
Ebels, U. (R3-08) 554
Eckert, J. (K1-01) 297
Eddrief, M. (O7-16) 466
Ederer, C. (Q1-01) 508
Ederer, J. (C3-13) 72
Edmonds, K.W. (G1-10) 180
Edmonds, K.W. (J3-03) 277
Edmonds, K.W. (J6-07) 294
Edmonds, K.W. (M1-09) 356
Edwards, A.J. (G4-03) 197
Eggers, T. (K2-07) 305
Eggers, T. (P1-06) 470
Ehresmann, A. (P1-07) 470
Eimer, S. (R1-10) 541
Ekomasov, A. (C5-04) 80
Ekomasov, E. (C5-04) 80
Ekomasov, E. (L3-03) 335
El Hadri, M. (F2-01) 145
ElBidweihy, H. (I1-05) 240
ElBidweihy, H. (P1-04) 469
Elkins, J. (G5-13) 205
Elkins, J. (K5-04) 319
Ellis, M.O. (A5-04) 30
Ellis, M.O. (G3-13) 195
Elphick, K. (O2-09) 432
Elphick, P. (R3-08) 554
Emelyanova, S. (L4-07) 343
Emori, S. (A3-01) 13
Emori, S. (A3-02) 13
Emori, S. (A3-04) 14
Emori, S. (A3-05) 15
Emori, S. (A3-08) 16
Emori, S. (O4-04) 443
Endo, M. (R1-02) 538
Endo, Y. (L3-10) 337
Endoh, T. (O2-03) 429
Endoh, T. (O2-06) 431
Endoh, T. (P6-11) 500
Ener, S. (F2-03) 146
Ener, S. (H3-09) 226
Ener, S. (Q1-06) 509
Enokido, Y. (C2-09) 66
Ensslin, K. (K4-09) 315
Erickson, M.J. (K3-05) 310
Erickson, T. (K2-13) 307
Eriksson, O. (D2-10) 93
Eriksson, O. (E1-07) 114
Eriksson, O. (E2-02) 117
Eriksson, O. (Q2-04) 514
Ernoult, M. (Q3-06) 520
Eroshenko, P. (O6-14) 457
Ersan, F. (E1-03) 112
Erugu, U. (M5-14) 380
Erugu, U. (O1-06) 423
Escobar-Steinvall, S. (A1-07) 5
Escoda, M. (L4-09) 344
Espinosa-Magaña, F. (L4-03) 342
Espinosa, A. (J1-06) 271
Estevez, D. (R5-06) 566
Estrada, V.M. (I2-03) 244
Estrada, V.M. (Q5-11) 532
Etheridge, J.J. (Q2-03) 514
Evans, R.F. (D1-06) 85
Evans, R.F. (G3-13) 195
Evans, R.F. (L1-06) 325
Evans, R.F. (M1-04) 354
Evans, R.F. (N3-05) 402
Evans, R.F. (N3-12) 405
Evans, R.F. (O6-01) 452
Evelt, M. (S8-01) 504
Everschor-Sitte, K. (A5-07) 32

- F -

Fabbrici, S. (F2-15) 149
Fabiani, G. (N2-02) 394
Fabre, F. (I3-06) 254
Fabre, F. (O1-02) 421
Fagan, P. (P3-07) 481
Fagiani, F. (R3-14) 557
Fähler, S. (I1-01) 238
Fähler, S. (K1-03) 298
Fakhrul, T. (C1-02) 54
Falus, P. (D2-14) 94
Fan, R. (I3-01) 251
Fan, X. (H5-08) 235
Fan, X. (P6-16) 502
Fan, Y. (G1-12) 181
Fan, Y. (K2-04) 304
Fan, Y. (P6-01) 496
Fan, Y. (Q4-09) 525
Fang, W. (M1-07) 355
Fangohr, H. (D1-07) 86

Fangohr, H. (I3-01) . . . 251
Fangohr, H. (R2-09) . . . 548
Farhadi, A. (R4-05) . . . 559
Farhan, A. (S6-03) . . . 351
Fariborzi, H. (C5-08) . . . 82
Farmer, B. (S6-04) . . . 352
Farmer, T. (H2-09) . . . 221
Faske, T. (F2-04) . . . 146
Fassatoui, A. (L2-06) . . . 331
Fassatoui, A. (R2-11) . . . 548
Fassbender, J. (B3-02) . . . 46
Fassbender, J. (E4-06) . . . 129
Fassbender, J. (F3-12) . . . 157
Fassbender, J. (J6-05) . . . 294
Fassbender, J. (Q4-01) . . . 522
Fassbender, J. (Q4-04) . . . 523
Fassbender, J. (R1-09) . . . 541
Fast, K. (G2-11) . . . 187
Faupel, F. (F3-11) . . . 156
Favaro, F. (L1-09) . . . 326
Fecova, L. (L3-05) . . . 335
Fedor, J. (L1-02) . . . 323
Fedotov, I.V. (L1-14) . . . 328
Feilhauer, J. (L1-02) . . . 323
Fel'k, V.A. (O6-14) . . . 457
Felser, C. (E1-01) . . . 111
Felser, C. (J5-02) . . . 288
Felser, C. (O3-12) . . . 441
Felser, C. (S1-01) . . . 105
Felton, J. (M1-09) . . . 356
Feng, H. (R4-01) . . . 558
Feng, J. (R3-01) . . . 550
Feng, L. (Q1-08) . . . 510
Feng, M. (M2-04) . . . 360
Feng, T. (M4-03) . . . 371
Feng, T. (R5-06) . . . 566
Feng, X. (O1-05) . . . 422
Feng, Y. (C3-08) . . . 70
Feng, Y.P. (M2-14) . . . 363
Feng, Y.P. (P5-02) . . . 489
Feringa, F. (M4-10) . . . 375
Fermon, C. (F3-02) . . . 153
Fermon, C. (F3-08) . . . 155
Fermon, C. (F3-09) . . . 156
Fernandes Cauduro, A. (F1-01) . . . 140
Fernandes Cauduro, A. (O3-11) . . . 440
Fernandes, R. (L2-02) . . . 329
Fernandez- Roldan, J.A. (L1-03) . . . 323
Fernandez-Pacheco, A. (A1-02) . . . 2
Fernandez-Pacheco, A. (A1-09) . . . 6
Fernandez-Pacheco, A. (F1-03) . . . 141
Fernandez-Pacheco, A. (R1-13) . . . 543
Fernandez-Roldan, J. (A1-03) . . . 3
Ferrara, E. (J2-03) . . . 273
Ferrari, V. (K2-13) . . . 307
Ferreira, A. (G5-03) . . . 201
Ferreira, R. (B3-03) . . . 46
Ferreira, R. (B3-04) . . . 47
Ferreira, R. (B3-05) . . . 48
Ferreira, R. (B3-06) . . . 48
Ferreira, R. (B3-09) . . . 49
Ferreira, R. (M3-08) . . . 368
Ferreira, R. (Q3-06) . . . 520
Ferreira, R. (R3-08) . . . 554
Ferreira, W. (D4-08) . . . 102
Ferreira, W. (F5-06) . . . 166
Ferrer, S. (A1-02) . . . 2
Ferrer, S. (L1-10) . . . 326
Ferrer, S. (O5-01) . . . 448
Fert, A. (E5-08) . . . 137
Fert, A. (I3-09) . . . 255
Fert, A. (I3-10) . . . 256
Fert, A. (O3-13) . . . 441
feuchtwanger, J.F. (A4-05) . . . 22
Field, S. (S5-02) . . . 348
Filianina, M. (J4-05) . . . 284
Fillion, C. (I3-11) . . . 256
Fillion, C. (L2-04) . . . 330
Finco, A. (I3-06) . . . 254
Finco, A. (L1-07) . . . 325
Finco, A. (N2-14) . . . 399
Finco, A. (O1-02) . . . 421
Finizio, S. (M5-02) . . . 377
Finizio, S. (N2-11) . . . 398
Finizio, S. (R2-06) . . . 546
Finizio, S. (R3-01) . . . 550
Fink-Finowicki, J. (F2-07) . . . 147
Finley, J. (G1-12) . . . 181
Finley, J. (Q4-09) . . . 525
Finocchio, G. (M1-08) . . . 356
Fiorillo, F. (J2-03) . . . 273
Firme, A.A. (L2-07) . . . 332
Fischbacher, J. (B1-13) . . . 38
Fischer, N.A. (A1-10) . . . 7
Fischer, N.A. (C4-09) . . . 77
Fischer, N.A. (L4-05) . . . 342
Fischer, N.A. (L4-10) . . . 344
Fischer, N.A. (L4-16) . . . 346
Fischer, P. (A1-02) . . . 2
Fischer, P. (A1-06) . . . 5
Fisher, E. (F4-07) . . . 161
Fisher, E. (N5-12) . . . 415
Fix, M. (M4-08) . . . 373
Fix, M. (Q4-10) . . . 526
Flacke, L. (E4-10) . . . 131
Flahaut, E. (D2-04) . . . 91
Flajšman, L. (A2-08) . . . 10
Flewett, S. (L1-11) . . . 327
Floro, J.A. (P3-11) . . . 482
Fnaiech, E.A. (I5-03) . . . 264
Foerster, M. (O3-07) . . . 439
Foerster, M. (O3-08) . . . 439
Folkes, P. (K4-05) . . . 314
Folven, E. (L1-13) . . . 328
Folven, E. (P3-06) . . . 480
Folven, E. (P3-10) . . . 482
Folven, E. (R1-04) . . . 539
Fontcuberta-Morral, A. (A1-07) . . . 5
Forrer, D. (B2-04) . . . 41
Forrest, T. (H1-15) . . . 217
Förster, J. (E4-02) . . . 127
Förster, J. (E4-03) . . . 128
Förster, J. (E4-07) . . . 130
Forth, J. (A1-06) . . . 5
Fortin, J. (O5-07) . . . 450
Fortunato, N. (F2-03) . . . 146
Fortune, Z. (A1-08) . . . 5
Fouquet, P. (D2-14) . . . 94
Fournier, P. (F2-02) . . . 145
Fowley, C. (E3-08) . . . 126
Fox, D. (L3-06) . . . 336
Fraerman, A.A. (A4-02) . . . 20
França, E. (K1-14) . . . 302
Francis, F. (Q6-11) . . . 537
Franco Jr, A. (K1-14) . . . 302
Franco, V. (A4-09) . . . 24
Franco, V. (E1-03) . . . 112
Franco, V. (E1-06) . . . 113
Franco, V. (F2-08) . . . 147
Fransson, J. (L3-04) . . . 335
Fratesi, G. (K2-08) . . . 306
Fratino, L. (L2-01) . . . 329
Freeland, J.W. (G2-03) . . . 183
Freeland, J.W. (H2-09) . . . 221
Freeman, M.R. (G2-11) . . . 187
Freeman, M.R. (N5-16) . . . 417
Freimuth, F. (G3-08) . . . 192
Freitas, P. (B3-04) . . . 47
Freitas, P. (M3-08) . . . 368
Freitas, R.S. (D4-08) . . . 102
Freudenberger, J. (Q1-08) . . . 510
Fridman, Y. (F5-01) . . . 164
Fried, N. (O5-05) . . . 449
Friedman, A.L. (O1-07) . . . 423
Friedman, J.S. (A5-01) . . . 28
Friedman, J.S. (A5-02) . . . 29
Friedman, J.S. (A5-03) . . . 29
Friedman, J.S. (A5-05) . . . 31
Friedman, J.S. (A5-06) . . . 31
Friedman, J.S. (G4-03) . . . 197
Friedman, J.S. (R3-02) . . . 550
Fries, M. (A4-07) . . . 23
Frisk, A. (P2-08) . . . 475
Frisk, A. (P2-10) . . . 477
Frömter, R. (G3-05) . . . 191
Fruchart, O. (I3-06) . . . 254
Fruchart, O. (P3-09) . . . 481
Fruchart, O. (R2-11) . . . 548
Fry, P.W. (G4-07) . . . 199
Fu, C. (J5-02) . . . 288
Fu, L. (G1-12) . . . 181
Fu, M. (A2-06) . . . 9
Fu, X. (G2-07) . . . 185
Fu, Y. (I5-02) . . . 264
Fu, Z. (P2-06) . . . 474
Fuchs, C. (H1-12) . . . 216
Fuchs, C. (J4-03) . . . 283
Fujimoto, J. (O4-06) . . . 444
Fujita, Y. (K3-04) . . . 310
Fujiwara, K. (O1-11) . . . 425
Fujiwara, S. (K5-10) . . . 321
Fukami, S. (E3-02) . . . 124
Fukami, S. (J6-09) . . . 295

Fukami, S. (J6-12) . . . 296
Fukami, S. (O2-11) . . . 433
Fukami, S. (S8-02) . . . 504
Fukatani, N. (N5-04) . . . 411
Fukuma, Y. (P6-03) . . . 497
Fukumoto, H. (C3-01) . . . 67
Fukushima, A. (B3-05) . . . 48
Fukushima, A. (B3-10) . . . 49
Fukushima, A. (L2-03) . . . 330
Fukushima, T. (O1-12) . . . 425
Fukutani, K. (I4-05) . . . 258
Fulara, H. (Q3-04) . . . 519
Fulara, H. (S8-02) . . . 504
Fullerton, E. (D1-14) . . . 89
Fullerton, E. (F2-01) . . . 145
Fullerton, E. (O2-07) . . . 431
Fullerton, E. (P4-11) . . . 486
Fullerton, E. (R1-12) . . . 542
Furdyna, J. (I4-09) . . . 261
Furtado, J. (F4-04) . . . 160
Furukawa, N. (F5-12) . . . 168
Furukawa, Y. (B4-01) . . . 51
Furuya, K. (E3-02) . . . 124
Fusil, S. (K1-07) . . . 299
Fusil, S. (R4-10) . . . 561

- G -

G. V., V. (Q6-11) . . . 537
G.Saiz, P. (K1-10) . . . 300
Gaderbauer, W. (C1-07) . . . 57
Gahtori, B. (L4-13) . . . 345
Gajewska, M. (P1-02) . . . 467
Galais, Y. (K1-09) . . . 300
Galbiati, M. (K4-03) . . . 313
Galdun, L. (G6-09) . . . 209
Galdun, L. (H5-03) . . . 233
Galik, J. (J1-03) . . . 269
Gallagher, B.L. (J3-03) . . . 277
Gallagher, B.L. (M1-09) . . . 356
Galliou, S. (B3-05) . . . 48
Gallo-Cordova, Á. (P1-05) . . . 469
Gambardella, P. (E3-01) . . . 123
Gambardella, P. (R3-01) . . . 550
Gamcova, J. (J1-03) . . . 269
Gammer, C. (H1-06) . . . 213
Gandha, K. (C2-08) . . . 65
Ganesh, P. (M2-02) . . . 359
Gangopadhyay, S. (J5-13) . . . 291
Gao, F. (R4-01) . . . 558
Gao, L. (H4-08) . . . 231
Gao, P. (M4-03) . . . 371
Gao, Q. (E1-04) . . . 113
Gao, X. (H2-09) . . . 221
Gao, X. (M2-02) . . . 359
Gaponov, M.S. (L3-08) . . . 337
Garanin, D. (M5-01) . . . 377
García-Arribas, A. (L1-03) . . . 323
Garcia-Bravo, J. (N5-13) . . . 415
Garcia-Sanchez, F. (A5-01) . . . 28
Garcia-Sanchez, F. (A5-03) . . . 29
Garcia-Sanchez, F. (A5-06) . . . 31
Garcia-Sanchez, F. (L3-12) . . . 338
Garcia-Sanchez, F. (R3-02) . . . 550
García, C. (P3-12) . . . 483
Garcia, F. (C1-08) . . . 58
Garcia, L.M. (B2-04) . . . 41
Garcia, V. (K1-07) . . . 299
Garcia, V. (R4-10) . . . 561
Garello, K. (E3-01) . . . 123
Garesci, F. (M1-08) . . . 356
Garg, N. (Q3-07) . . . 520
Gargiani, P. (J5-12) . . . 291
Gargiani, P. (L1-11) . . . 327
Gargiani, P. (R2-06) . . . 546
Garlatti, E. (B2-03) . . . 41
Garlatti, E. (D2-01) . . . 90
Garlatti, E. (F5-07) . . . 166
Garlatti, E. (G2-01) . . . 183
Garrity, K. (G5-11) . . . 205
Garrity, K. (O1-05) . . . 422
Garshev, A.V. (A4-17) . . . 27
Gartside, J.C. (C4-01) . . . 74
Gartside, J.C. (N2-03) . . . 394
Gary, D. (F4-04) . . . 160
Gas, K. (M1-09) . . . 356
Gassmann, J. (C2-06) . . . 64
Gassmann, J. (C2-07) . . . 65
Gaudin, G. (I3-06) . . . 254
Gaudin, G. (N1-10) . . . 391
Gaudin, G. (O3-07) . . . 439
Gaudin, G. (O3-08) . . . 439
Gault, B. (H3-09) . . . 226
Gaur, A. (L4-04) . . . 342
Gaur, A.B. (S3-01) . . . 174
Gavriloaea, P.I. (N1-09) . . . 390
Gavriloaea, P.I. (P2-07) . . . 475
Gavrilova, M.A. (D4-01) . . . 100
Gawryluk, D. (F2-07) . . . 147
Gay, J. (A1-07) . . . 5
Gayles, J. (E1-01) . . . 111
Gazibegovic, S. (K3-06) . . . 311
Ge, J. (F3-12) . . . 157
Ge, Y. (N1-08) . . . 390
Gebara, P. (F2-08) . . . 147
Geerts, W.J. (G2-12) . . . 187
Geerts, W.J. (L3-09) . . . 337
Gentile, P. (R4-03) . . . 559
Gentillon, A. (F1-11) . . . 144
Gentry, C. (E1-07) . . . 114
Genuzio, F. (R2-11) . . . 548
George, T.F. (G3-10) . . . 193
Georgieva, Z. (I2-13) . . . 249
Geprägs, S. (P4-13) . . . 487
Gerardino, A. (Q5-04) . . . 529
Gerasimenko, A. (E5-07) . . . 136
Gerasimova, N. (G3-06) . . . 191
Gercsi, Z. (E1-02) . . . 111
Gerevenkov, P. (A3-13) . . . 18
Germov, A.Y. (H2-12) . . . 222
Gerrity, M. (E1-07) . . . 114
Ghirri, A. (B2-02) . . . 40
Ghirri, A. (D2-05) . . . 92
Ghosh, A.W. (R2-02) . . . 545
Ghosh, S. (H2-04) . . . 220
Ghosh, S. (R1-11) . . . 542
Giacchetti, L. (J1-04) . . . 270
Gibbons, J. (J6-12) . . . 296
Giblin, S. (Q2-11) . . . 517
Gilbert, A.D. (Q5-01) . . . 528
Gilbert, M. (S1-03) . . . 105
Gilroy, E. (R1-07) . . . 540
Giordano, A. (M1-08) . . . 356
Giordano, M. (A1-07) . . . 5
Giovine, E. (Q5-04) . . . 529
Giraud, R. (J5-07) . . . 290
Gish, J.T. (O1-03) . . . 421
Gladii, O. (O7-08) . . . 462
Gliga, S. (B1-01) . . . 33
Glowinski, H. (E4-02) . . . 127
Gnoli, L. (E5-02) . . . 135
Gobbi, M. (O4-02) . . . 442
Gobbo, J. (J4-01) . . . 282
Göbel, B. (O3-01) . . . 437
Göbel, B. (O3-12) . . . 441
Godel, F. (K4-03) . . . 313
Goennenwein, S. (E1-01) . . . 111
Goering, E. (Q1-10) . . . 511
Goh, K. (K3-02) . . . 308
Goiriena-Goikoetxea, M. (L1-03) . . . 323
Gokhale, V.J. (G2-07) . . . 185
Goldberger, J. (J4-01) . . . 282
Goldberger, J. (O1-05) . . . 422
Goldman, S. (H4-02) . . . 228
Golovach, V. (O4-02) . . . 442
Golubeva, E. (F3-01) . . . 152
Golubeva, E. (F3-11) . . . 156
Gomes, G. (M6-09) . . . 384
Gomez-Perez, J. (O4-02) . . . 442
Gómez-Polo, C. (N5-06) . . . 412
Gómez, J. (P3-12) . . . 483
Gomonay, O. (G1-09) . . . 180
Gomonay, O. (G1-11) . . . 181
Gomonay, O. (J6-07) . . . 294
Gomonay, O. (N2-10) . . . 397
Gomonay, O. (P4-07) . . . 485
Gonçalves, A. (M3-07) . . . 367
Gonçalves, F.J. (B3-02) . . . 46
Gonçalves, F.J. (E4-10) . . . 131
Gonçalves, F.J. (O5-04) . . . 449
Gonçalves, F.J. (Q4-01) . . . 522
Gonçalves, F.J. (Q4-04) . . . 523
Gonçalves, V. (F5-06) . . . 166
Gong, C. (E1-09) . . . 115
Gong, S. (E1-09) . . . 115
González-Gómez, L. (M3-10) . . . 369
González-Orellana, C. (O4-02) . . . 442
González-Ruano, C. (L2-09)* . . . 333
Gonzalez-Sánchez, R. (R5-02) . . . 564
gonzalez, j. (L4-09) . . . 344
González, J.M. (D1-12) . . . 88
González, J.M. (F2-18) . . . 150

González, J.M. (H1-05) 213
González, J.M. (M1-06) 355
Goodway, C. (D2-14) 94
Goolaup, S. (O3-06) 438
Gorbachev, E. (Q1-09) 510
Gorchon, J. (G3-02) 190
Gorchon, J. (M3-04) 366
Gorchon, J. (P2-01) 472
Gorman, J.J. (G2-07) 185
Gorshunov, B.P. (Q1-09) 510
Gort, R. (G3-06) 191
Gosavi, T. (Q4-05) 523
Goss, G. (K5-07) 320
Gosteau, J. (H2-02) 219
Gotić, M. (F4-12) 162
Goto, M. (C5-06) 81
Goto, M. (N1-06) 389
Goto, S. (I4-15) 263
Gottschall, T. (F2-03) 146
Gottschall, T. (F2-04) 146
Gottschall, T. (F2-16) 150
Gouéré, D. (C1-10) 59
Gouéré, D. (N2-07) 396
Gourdon, C. (E4-09) 131
Goveas, L.R. (M2-09) 361
Grachev, A. (O7-07) 461
Grachev, A. (O7-11) 463
Graef, M.D. (A3-06) 15
Gräfe, J. (E4-02) 127
Gräfe, J. (E4-07) 130
Gräfe, J. (I3-01) 251
Gräfe, J. (I3-05) 253
Gräfe, J. (O3-07) 439
Gräfe, J. (Q1-10) 511
Gräfe, J. (R2-06) 546
Graham, A. (G5-03) 201
Granville, S. (D1-11) 88
Granville, S. (I3-02) 251
Granville, S. (N1-04) 388
Grassi, M.G. (E4-11) 132
Grave, D. (G1-11) 181
Gray, B. (A3-08) 16
Greaves, S. (N3-02) 400
Greening, R.W. (H5-08) 235
Greening, R.W. (P6-16) 502
Greer, J.A. (G1-02) 178
Greer, J.A. (G1-05) 179
Grefe, S.E. (J5-06) 289
Grelier, M. (O3-13) 441
Grenèche, J. (F4-12) 162
Grepstad, J.K. (P3-10) 482
Gretton, J. (G5-01) 200
Greven, M. (M2-03) 359
Grice, A. (L3-06) 336
Grigoras, M. (H1-01) 211
Grigorieva, I. (K3-03) 309
Grigorieva, I. (K4-10) 316
Grijalva Castillo, M. (L4-03) 342
Grillo, V. (S2-05) 109
Grimaldi, E. (E3-01) 123
Griner, D. (E2-04) 118
Griner, D. (E2-05) 119
Grizzle, A. (C3-11) 71
Grizzle, A. (F4-01) 159
Groen, I. (Q4-05) 523
Groeseneken, G. (L2-05) 331
Grollier, J. (B3-06) 48
Grollier, J. (B3-10) 49
Grollier, J. (Q3-06) 520
Gross, F. (E4-02) 127
Gross, F. (E4-07) 130
Gross, F. (I3-01) 251
Gross, F. (I3-05) 253
Gross, F. (Q1-10) 511
Gross, R. (P4-13) 487
Grübel, G. (G3-05) 191
Grundler, D. (A1-07) 5
Grundler, D. (E4-05) 129
Grundler, D. (M3-09) 368
Grundler, D. (N1-07) 389
Gruner, M. (F2-15) 149
Gruszecki, P. (E4-02) 127
Grutter, A.J. (F1-04) 141
Grutter, A.J. (K2-04) 304
Grutter, A.J. (L2-08) 332
Grutter, A.J. (Q4-09) 525
Grutter, A.J. (S2-04) 109
Gu, J. (K1-01) 297
Guarochico Moreira, V. (K3-03) 309
Guarochico-Moreira, V.H. (K4-10) 316
Gueckelhorn, J. (P4-13) 487
Guenzing, D. (H3-14) 227
Guertin, S. (O2-01) 428
Gueye, P. (H1-08) 214
Gueye, P. (H1-09) 215
Guidi, T. (B2-03) 41
Guidi, T. (D2-01) 90
Guidi, T. (G2-01) 183
Guillemard, C. (E1-13) 116
Guillemard, C. (G3-02) 190
Guin, S. (J5-02) 288
Gumerov, A. (C5-04) 80
Gunduz Akdogan, N. (B2-06) 42
Gunduz Akdogan, N. (F4-05) 160
Gunduz Akdogan, N. (K5-02) 318
Gunduz Akdogan, N. (Q1-02) 508
Guo, E. (T1-03) 1
Guo, G. (D4-04) 101
Guo, M. (M4-07) 373
Guo, R. (M2-14) 363
Guo, S. (C4-08) 76
Guo, Y. (F3-11) 156
Gupta, A. (E1-03) 112
Gupta, A. (E1-06) 113
Gupta, A. (H1-11) 215
Gupta, A. (I4-12) 262
Gupta, J. (K5-05) 319
Gupta, M. (H1-11) 215
Gupta, P. (O4-11) 446
Gupta, P. (P6-02) 496
Gupta, P. (R4-04) 559
Gupta, R. (I4-12) 262
Gupta, S. (B4-04) 51
Gupta, S. (F2-12) 148
Gupta, S. (Q6-08) 536
Gupta, V. (O1-04) 422
Gupta, V. (Q1-05) 509
Guragain, D. (H4-05) 230
Gürel, B.D. (F4-05) 160
Gusakova, D. (P3-09) 481
Gusenbauer, M. (P3-01) 478
Guslienko, K.Y. (L1-03) 323
Guslienko, K.Y. (M1-06) 355
Guslienko, K.Y. (O7-05) 460
Gutfleisch, O. (A4-07) 23
Gutfleisch, O. (A4-08) 23
Gutfleisch, O. (C2-06) 64
Gutfleisch, O. (C2-07) 65
Gutfleisch, O. (F2-03) 146
Gutfleisch, O. (F2-04) 146
Gutfleisch, O. (F2-16) 150
Gutfleisch, O. (H3-09) 226
Gutfleisch, O. (Q1-06) 509
Gutierrez, J. (K1-10) 300
Gutt, C. (G3-08) 192
Gypens, P. (S6-05) 352

- H -

Hache, T. (B3-02) 46
Hache, T. (O5-04) 449
Hache, T. (Q4-01) 522
Hache, T. (Q4-04) 523
Hadimani, R.L. (F2-12) 148
Hadimani, R.L. (J1-01) 268
Hadimani, R.L. (J1-02) 268
Hadimani, R.L. (K5-11) 321
Hadjipanayis, G.C. (D4-02) 100
Hajiri, T. (F5-05) 165
Hajiri, T. (I3-07) 254
Hajiri, T. (P4-06) 485
Haldar, A. (L3-13) 339
Hall, A. (E5-14) 139
Hallal, A. (R1-11) 542
Hallal, A. (S7-02) 419
Hamada, S. (K5-08) 321
Hamanaka, K. (N4-02) 407
Hamasaki, A. (C3-06) 69
Hamaya, K. (K3-04) 310
Hamaya, K. (Q4-03) 522
Hameed, S. (M2-03) 359
Hamill, A. (Q2-03) 514
Hammel, P. (B3-08) 49
Hammel, P. (F1-06) 142
Hamrle, J. (E1-11) 115
Hamutu, O. (R5-14) 570
Han, D. (J4-05) 284
Han, D. (R2-10) 548
Han, J. (D4-12) 103
Han, J. (G1-12) 181
Han, J. (G6-10) 209
Han, J. (I2-01)* 243

Han, J. (Q4-09) . . . 525
Han, J. (R5-03) . . . 564
Han, M. (M2-02) . . . 359
Han, W. (R4-09) . . . 561
Han, X. (O3-03) . . . 438
Hanajiri, T. (B1-14) . . . 38
Haney, P.M. (M4-05) . . . 372
Haney, P.M. (S5-04) . . . 349
Hanke, J. (J4-05) . . . 284
Hankiewicz, J.H. (P1-02) . . . 467
Hankiewicz, J.H. (P1-03) . . . 468
Hanley, T. (G2-08) . . . 186
Hannachi, E. (J3-09) . . . 279
Hansen, T. (A4-05) . . . 22
Hao, G. (N4-08) . . . 409
Hara, R. (H4-04) . . . 229
Hara, S. (F6-03) . . . 170
Hara, Y. (M6-10) . . . 384
Haran, K.S. (D3-03) . . . 96
Harikumar, P. (H5-07) . . . 234
Harmon, B. (G5-02) . . . 200
Harrington, S. (K4-05) . . . 314
Harris, V. (C1-04) . . . 56
Harris, V. (G2-05) . . . 184
Harrison, R. (E2-04) . . . 118
Harrison, R. (E2-05) . . . 119
Hartnett, T. (A3-04) . . . 14
Hartnett, T. (J5-13) . . . 291
Hartnett, T. (Q1-12) . . . 512
Hashizume, H. (I5-09) . . . 267
Haskel, D. (H2-09) . . . 221
Haslinger, M.J. (B1-13) . . . 38
haspot, V. (K1-07) . . . 299
Hassan, M. (Q5-04) . . . 529
Hassan, M. (R3-14) . . . 557
Hassan, N. (A5-01) . . . 28
Hassan, N. (A5-03) . . . 29
Hassan, N. (A5-05) . . . 31
Hassan, N. (A5-06) . . . 31
Hassan, P. (K5-05) . . . 319
Hastings, J.T. (S6-04) . . . 352
Hatton, P. (I3-01) . . . 251
Hatton, P. (R2-09) . . . 548
Haug, M. (I1-02) . . . 238
Hauser, A.J. (A3-03) . . . 14
Hauser, A.J. (A3-09) . . . 17
Hayakawa, J. (N5-04) . . . 411
Hayakawa, T. (O1-12) . . . 425
Hayashi, K. (H5-04) . . . 233
Hayashida, M. (I4-15) . . . 263
Haykal, A. (I3-06) . . . 254
Haykal, A. (O1-02) . . . 421
Hayward, T.J. (A1-04) . . . 4
Hayward, T.J. (A5-04) . . . 30
Hayward, T.J. (G4-07) . . . 199
Hayward, T.J. (R1-04) . . . 539
Hayward, T.J. (R1-07) . . . 540
He, L. (E1-04) . . . 113
He, M. (N3-14) . . . 406
He, M. (P2-11) . . . 477
He, P. (P4-12) . . . 487
He, S. (D3-05) . . . 97
He, S. (F4-04) . . . 160
He, Z. (J2-04) . . . 274
Heczko, O. (P5-04) . . . 490
Hehn, M. (E4-11) . . . 132
Hehn, M. (L2-09) . . . 333
Hehn, M. (M3-04) . . . 366
Hehn, M. (P2-01) . . . 472
Hehn, M. (R1-05) . . . 539
Heigl, M. (D1-04) . . . 84
Heinonen, O. (B1-01) . . . 33
Heinonen, O. (J5-03) . . . 288
Heinonen, O. (S1-02) . . . 105
Heinonen, O. (S5-02) . . . 348
Heinz, B. (N2-08) . . . 396
Heinze, L. (A2-01) . . . 8
Heischmidt, B. (K3-06) . . . 311
Heistracher, P. (B1-02) . . . 33
Held, K. (K3-02) . . . 308
Hellbrück, L. (E1-07) . . . 114
Hellman, F. (A1-06) . . . 5
Hellman, F. (H1-12) . . . 216
Hellman, F. (J4-03) . . . 283
Hellman, F. (J4-11) . . . 287
Hellsvik, J. (L3-04) . . . 335
Hellwig, O. (B3-02) . . . 46
Hellwig, O. (F1-11) . . . 144
Hellwig, O. (O7-08) . . . 462
Hellwig, O. (Q4-01) . . . 522
Hellwig, O. (Q4-04) . . . 523
Helms, B. (A1-06) . . . 5
Heltemes, K. (L2-02) . . . 329
Hemme, P. (K1-09) . . . 300
Hendren, W. (A3-10) . . . 17
Hendren, W. (N4-04) . . . 408
Hendren, W. (P2-08) . . . 475
Hendren, W. (P2-10) . . . 477
Henry, Y. (E4-11) . . . 132
Henschel, M. (C4-08) . . . 76
Hepburn, C. (O7-16) . . . 466
Herea, D. (Q5-03) . . . 529
Heremans, J. (A3-04) . . . 14
Herling, F. (K4-09) . . . 315
Herling, F. (O1-13) . . . 426
Hermans, T.M. (E3-08) . . . 126
Hermans, T.M. (J1-04) . . . 270
Hermosa, G.C. (C3-03) . . . 68
Hermosa, G.C. (K2-05) . . . 304
Hermosa, J. (O5-01) . . . 448
Hernández García, L. (C3-09) . . . 70
Hernández, L. (B2-14) . . . 45
Hernandez, L.A. (H5-08) . . . 235
Hernando, A. (E2-13) . . . 121
Hernando, A. (M2-08) . . . 361
Herrero-Albillos, J. (B2-04) . . . 41
Herrero-Martin, J. (B2-04) . . . 41
Herrero, A. (A4-17) . . . 27
Herrero, A. (A4-18) . . . 27
Hersam, M. (O1-03) . . . 421
Hesjedal, T. (E4-01) . . . 127
Hesjedal, T. (M5-12) . . . 379
Hesjedal, T. (P2-10) . . . 477
Hesjedal, T. (R2-09) . . . 548
Hesjedal, T. (S2-01) . . . 108
Heyderman, L. (A2-09) . . . 10
Heyderman, L. (B1-05) . . . 34
Heyderman, L. (G3-07) . . . 192
Heyderman, L. (R3-01) . . . 550
Hicken, R. (P2-08) . . . 475
Hicken, R. (P2-10) . . . 477
Hickey, B. (D1-07) . . . 86
Hierro-Rodriguez, A. (A1-02) . . . 2
Hierro-Rodriguez, A. (L1-10) . . . 326
Hierro-Rodriguez, A. (O5-01) . . . 448
Higashi, Y. (N5-14) . . . 416
Hight Walker, A. (G5-11) . . . 205
Hight Walker, A.R. (H1-14) . . . 217
Hight Walker, A.R. (O1-05) . . . 422
Hight Walker, A.R. (O1-10) . . . 424
Hight Walker, A.R. (O5-06) . . . 449
Higo, T. (M4-01) . . . 371
Hill, B.A. (R3-02) . . . 550
Hillebrands, B. (E4-12) . . . 132
Hillier, A. (J3-08) . . . 279
Himel, M. (F2-05) . . . 146
Hindmarch, A. (S2-03) . . . 108
Hinokihara, T. (C2-01) . . . 62
Hirano, N. (O6-04) . . . 453
Hirayama, M. (M4-01) . . . 371
Hirohata, A. (O2-09) . . . 432
Hirosawa, S. (H3-10) . . . 226
Hirosawa, T. (O3-09) . . . 440
Hirose, T. (R1-11) . . . 542
Hitosugi, T. (I4-05) . . . 258
Hjörvarsson, B. (B1-04) . . . 34
Hjörvarsson, B. (B1-12) . . . 37
Hjörvarsson, B. (C4-06) . . . 75
Hlawacek, G. (E3-08) . . . 126
Hlenschi, C. (N5-09) . . . 413
Hlenschi, C. (R5-08) . . . 567
Hlova, I.Z. (L4-06) . . . 343
Ho, P. (O3-06) . . . 438
Hoefer, J. (G3-03) . . . 190
Hoefer, J. (G3-11) . . . 194
Hoefer, M. (N2-12) . . . 398
Hoffmann, A. (G1-13) . . . 182
Hoffmann, A. (J6-12) . . . 296
Hoffmann, A. (M3-03) . . . 366
Hoffmann, A. (N1-02) . . . 387
Hoffmann, A. (O1-03) . . . 421
Hoffmann, A. (O4-12) . . . 447
Hoffmann, A. (S1-03) . . . 105
Hoffmann, A. (S5-02) . . . 348
Hoffmann, M. (F1-01) . . . 140
Hofherr, M. (E1-07) . . . 114
Hofhuis, K. (A2-09) . . . 10
Hofhuis, K. (B1-02) . . . 33
Hofhuis, K. (B1-05) . . . 34
Hohlfeld, J. (M3-04) . . . 366
Holcomb, M.B. (Q2-08) . . . 515
Hollenbach, M. (O5-04) . . . 449
Holmes-Hewett, W. (D1-11) . . . 88

Holmes-Hewett, W. (I4-14) 262
Holmes-Hewett, W. (J5-09) 290
Holmes, S. (R1-13) 543
Holt, S.J. (E5-14) 139
Hon, K. (C5-06) 81
Hong, D. (G1-13) 182
Hong, J. (C5-07) 81
Hong, M. (M4-07) 373
Hong, X. (S7-03) 419
Hong, Y. (N3-14) 406
Hong, Y. (R5-03) 564
Honjo, H. (O2-03) 429
Honjo, H. (O2-06) 431
Hono, K. (H3-02) 223
Hono, K. (H3-10) 226
Hontecillas, I. (D1-05) 85
Hori, Y. (R1-02) 538
Horn, A. (G2-05) 184
Hosokai, Y. (K5-08) 321
Hotta, T. (K2-10) 306
Hou, J.T. (Q4-09) 525
Hou, V.D. (S1-04) 106
Hou, W. (M6-07) 383
Hou, W. (O3-03) 438
Houshang, A. (Q3-04) 519
Hovorka, O. (I3-01) 251
Hovorka, O. (N3-12) 405
Hovorka, O. (Q2-09) 516
Hovorka, O. (Q2-10) 516
Hovorka, O. (R2-09) 548
Howe, B.M. (A3-08) 16
Howells, B. (J3-03) 277
Howlader, C.Q. (G2-12) 187
Hoyt, M. (J2-06) 275
Hrabec, A. (A2-09) 10
Hrabec, A. (B1-05) 34
Hrabec, A. (R3-01) 550
Hsin, Y. (O2-12) 433
Hsu, C. (J4-03) 283
Hsu, C. (J4-11) 287
Hsu, T. (G5-04) 201
Hsu, W. (F6-06) 172
Hsu, W. (P2-04) 473
Hu, C. (O6-15) 457
Hu, C. (Q4-08) 525
Hu, J. (O1-05) 422
Hu, L. (R4-01) 558
Hu, M. (N2-12) 398
Hu, W. (S6-04) 352
Hu, X. (A5-01) 28
Hu, X. (A5-02) 29
Hu, X. (A5-03) 29
Hu, X. (A5-06) 31
Hu, X. (R3-02) 550
Hu, Z. (E4-13) 133
Hu, Z. (F2-14) 149
Hu, Z. (L4-11) 344
Hua, Y. (Q5-08) 531
Huang, B. (K3-08) 312
Huang, J.A. (J5-08) 290
Huang, J.A. (K4-13) 317
Huang, L. (O2-15) 435
Huang, M. (R2-06) 546
Huang, N. (C3-14) 73
Huang, Q. (F6-02) 170
Huang, S. (C1-02) 54
Huang, S. (I4-13) 262
Huang, S. (J4-09) 286
Huang, S. (M1-11) 357
Huang, S. (R2-06) 546
Huang, T. (C4-07) 76
Huang, T. (O7-12) 464
Huang, Y. (B1-05) 34
Huang, Z. (E3-04) 125
Huang, Z. (I2-13) 249
Hubert, O. (F4-04) 160
Hubert, O. (I5-03) 264
Hudait, M. (A3-04) 14
Hudait, M. (A3-05) 15
Huebl, H. (J4-07) 285
Huebl, H. (P4-13) 487
Hueso, L.E. (K4-09) 315
Hueso, L.E. (O1-13) 426
Hueso, L.E. (O4-02) 442
Hueso, L.E. (Q4-05) 523
Hug, H.J. (D1-04) 84
Hughes, B. (O2-01) 428
Hui, Y. (M2-14) 363
Hula, T. (E4-06) 129
Hula, T. (E4-10) 131
Hung, C. (I4-06) 259
Hung, C. (L4-02) 341
Hunt, D. (K2-13) 307
Hunt, M.O. (B1-15) 39
Hunt, M.O. (C4-10) 77
Hurdequint, H. (N1-03) 388
Hurst, J. (P3-09) 481
Huxtable, A.J. (M5-02) 377
Huy, P. (I4-06) 259
Hwang, J. (J6-04) 293
Hwang, K. (P1-06) 470

- I -

Iacocca, E. (B1-01) 33
Iacocca, E. (N2-12) 398
Ibarra, M. (C5-05) 80
Ibe, T. (O1-14) 426
Ibrahim, F. (S7-02) 419
Ichimura, M. (N5-04) 411
Ichimura, T. (I4-15) 263
Ichinose, T. (R3-11) 555
Ichiyanagi, Y. (K5-08) 321
Idrobo, J. (S2-05) 109
Idzuchi, H. (C5-01) 79
Idzuchi, H. (G5-10) 204
Ieda, J. (J6-09) 295
Ieda, J. (S7-05) 420
Igarashi, J. (O2-11) 433
Iglesias, R. (B2-14) 45
Iguchi, R. (O4-09) 445
Iihama, S. (C5-01) 79
Iihama, S. (E3-02) 124
Iihama, S. (E3-03) 124
Iihama, S. (J4-02) 282
Iihama, S. (Q2-02) 513
Ikeda, J. (O1-11) 425
Ikeda, J. (R3-11) 555
Ikeda, S. (O2-03) 429
Ikeda, S. (O2-06) 431
Ikeda, S. (P6-11) 500
Ikegawa, S. (O2-01) 428
Ilyn, M. (O4-02) 442
Imamura, H. (H1-03) 211
Imamura, M. (P6-08) 499
Inaba, N. (F6-03) 170
Inada, K. (D3-07) 98
Inagaki, Y. (B4-01) 51
Incorvia, J.C. (A5-01) 28
Incorvia, J.C. (A5-02) 29
Incorvia, J.C. (A5-03) 29
Incorvia, J.C. (A5-05) 31
Incorvia, J.C. (A5-06) 31
Ingla-Aynés, J. (K4-09) 315
Ingla-Aynés, J. (O1-13) 426
Ingram, J. (L3-06) 336
Inoue, M. (R3-12) 556
Insinga, A.R. (P3-03) 479
Inubushi, K. (R3-12) 556
Inyang, O.A. (S2-03) 108
Ipatov, M. (L4-09) 344
Irkhin, V. (H5-02) 232
Irkhin, V. (H5-05) 234
Isaeva, A. (J5-07) 290
Ishibashi, K. (E3-02) 124
Ishida, M. (M4-02) 371
Ishii, F. (M4-01) 371
Ishii, N. (R1-02) 538
Ishino, S. (P4-06) 485
Ishitani, Y. (N4-02) 407
Iskhakov, R. (C4-02) 74
Iskhakov, R. (G6-12) 210
Iskhakov, R. (R5-09) 567
Islam, R. (E5-10) 137
Itakura, M. (F6-03) 170
Ito, K. (I4-15) 263
Ito, K. (O2-10) 432
Iurchuk, V. (B3-09) 49
Iurchuk, V. (O6-05) 453
Iurchuk, V. (R3-08) 554
Ivanov, B. (M3-07) 367
Ivanov, S. (Q3-02) 518
Ivanov, S. (Q3-03) 519
ivry, a. (N5-12) 415
Iwanowski, P. (F2-07) 147
Iwasa, Y. (O1-12) 425
Iwasaki, H. (N5-14) 416
Iwasaki, Y. (M4-02) 371
Iwata, S. (A3-07) 16
Izardar, A. (Q1-01) 508
Izmozherov, I.M. (O6-06) 454
Izquierdo, M. (G3-06) 191

- J -

J, S. (E2-14) . . . 122
J. Konno, T. (I4-15) . . . 263
Jaafar, M. (G2-04) . . . 184
Jaafar, M. (L1-01) . . . 323
Jaafar, M. (L1-03) . . . 323
Jacas, A. (R5-05) . . . 565
Jacobs, S. (H2-05) . . . 220
Jacobs, S. (R5-16) . . . 571
Jacobs, S. (R5-17) . . . 571
Jacques, V. (I3-06) . . . 254
Jacques, V. (N2-14) . . . 399
Jacques, V. (O1-02) . . . 421
Jadaun, P. (E5-05) . . . 136
Jaeschke-Ubiergo, R. (E5-01) . . . 135
Jain, M. (A4-10) . . . 24
Jain, M. (Q2-08) . . . 515
Jain, R. (Q4-02) . . . 522
Jaiswal, S. (J4-05) . . . 284
Jakob, G. (G1-11) . . . 181
Jakob, G. (J4-05) . . . 284
Jakob, G. (R2-10) . . . 548
Jakubowski, M. (E5-10) . . . 137
Jamone, L. (B2-01) . . . 40
Jandl, S. (F2-02) . . . 145
Janesky, J. (O2-01) . . . 428
Jang, G. (F4-13) . . . 163
Jang, H. (G3-12) . . . 194
Jangid, R. (G2-02) . . . 183
Jani, H. (G1-07) . . . 179
Jani, H. (O3-02) . . . 437
Janiš, V. (D2-09) . . . 93
Janolin, P. (H2-08) . . . 221
Janos, P. (C3-13) . . . 72
Janosek, M. (N5-10) . . . 414
Jansen, R. (K3-04) . . . 310
Jaouen, N. (F1-03) . . . 141
Jaouen, N. (L1-11) . . . 327
Jara, A. (M3-07) . . . 367
Jaufenthaler, A. (S3-03) . . . 175
Jayaraman, T.V. (J2-08) . . . 276
Jedryka, E. (I4-10) . . . 261
Jena, J. (O3-12)* . . . 441
Jena, S.K. (E5-10) . . . 137
Jenkins, A. (B3-03) . . . 46
Jenkins, A. (B3-04) . . . 47
Jenkins, A. (B3-09) . . . 49
Jenkins, A. (M3-08) . . . 368
Jenkins, A. (Q3-06) . . . 520
Jenkins, A. (R3-08) . . . 554
Jenkins, S. (D1-06) . . . 85
Jenkins, S. (M1-04) . . . 354
Jenkins, S. (N3-05) . . . 402
Jenkins, S. (O6-01) . . . 452
Jensen, C.J. (L2-07) . . . 332
Jensen, C.J. (L2-08) . . . 332
Jensen, J.H. (P3-06) . . . 480
Jenson, D. (N5-16) . . . 417
Jeon, H. (A3-08) . . . 16
Jeon, J. (O4-01) . . . 442
Jeon, K. (O4-01) . . . 442
Jeon, S. (D3-08) . . . 98
Jeon, S. (Q5-06) . . . 530
Jeon, S. (R3-06) . . . 553
Jeong, J. (G6-02) . . . 206
Jeong, S. (N3-06) . . . 402
Jeyadevan, B. (C3-01) . . . 67
Jha, A. (E3-07) . . . 125
Jhuria, K. (M3-04) . . . 366
Ji, Y. (K3-07) . . . 311
Jia, H. (F1-01) . . . 140
Jiang-Wei, L. (A5-01) . . . 28
Jiang, D.Y. (B1-06) . . . 34
Jiang, J. (G5-09) . . . 204
Jiang, J. (R2-03) . . . 545
Jiang, J. (R5-04) . . . 565
Jiang, S. (G1-13) . . . 182
Jiang, S. (O1-04) . . . 422
Jiang, S. (S5-02) . . . 348
Jiang, W. (N1-11) . . . 391
Jiang, X. (N4-08) . . . 409
Jiang, Y. (A1-06) . . . 5
Jiang, Y. (N4-01) . . . 407
Jiang, Z. (A3-04) . . . 14
Jike, K. (I2-04) . . . 244
Jiles, D.C. (A4-12) . . . 24
Jiles, D.C. (K5-06) . . . 320
Jiles, D.C. (K5-07) . . . 320
Jiles, D.C. (L4-14) . . . 346
Jimenez, A. (H1-02) . . . 211
Jin, C. (K1-02) . . . 297
Jin, F. (R5-04) . . . 565
Jin, M. (K5-04) . . . 319
Jin, Y. (P3-11) . . . 482
Jin, Z. (F3-07) . . . 155
Jin, Z. (N5-02) . . . 410
Jing, C. (G2-07) . . . 185
Jinnai, B. (O2-11) . . . 433
Jiraskova, Y. (C3-13) . . . 72
Johansson, C. (Q2-11) . . . 517
Johansson, N. (M1-12) . . . 357
Johnsen, L.G. (L2-09) . . . 333
Johnson, C. (R5-07) . . . 566
Johnson, D.D. (L4-06) . . . 343
Joldos, M. (L2-04) . . . 330
Jones, L. (S2-05) . . . 109
Jones, N.J. (Q1-11) . . . 511
Jono, K. (R2-07) . . . 547
Jönsson, P.E. (B1-12) . . . 37
Jönsson, P.E. (H3-03) . . . 224
Jönsson, P.E. (M6-08) . . . 384
Joseph, N. (D4-07) . . . 101
Joseyphus, R.J. (E2-14) . . . 122
Joshi, N.N. (M2-15) . . . 363
Jotta Garcia, M. (B3-06) . . . 48
Jotta Garcia, M. (F3-08) . . . 155
Joumard, I. (G4-02) . . . 197
Joumard, I. (I3-11) . . . 256
Joumard, I. (O2-02) . . . 429
Jovičević Klug, M. (F3-01) . . . 152
Juang, J. (F2-02) . . . 145
Juge, R. (N1-10) . . . 391
Juge, R. (O3-07) . . . 439
Juge, R. (O3-08) . . . 439
Jung, M. (M6-04) . . . 382
Jung, M. (M6-05) . . . 382
Jungfleisch, M. (B1-11) . . . 37
Jungfleisch, M. (O4-12) . . . 447
Jungwirth, T. (J6-07) . . . 294
Jungwirth, T. (M1-09) . . . 356
Jurkin, T. (F4-12) . . . 162

- K -

K R S, P. (H2-08) . . . 221
K, A. (A4-01) . . . 20
K.N., A. (M2-09) . . . 361
K.N., A. (Q6-06) . . . 535
K.S., B. (M2-09) . . . 361
Kačmarčík, J. (G6-09) . . . 209
Kahmei, R.R. (C1-13) . . . 60
Kainuma, R. (O7-14) . . . 465
Kaisar, T. (P1-04) . . . 469
Kaiser, M. (B2-07) . . . 42
Kákay, A. (A1-05) . . . 4
Kákay, A. (E4-06) . . . 129
Kákay, A. (E4-10) . . . 131
Kákay, A. (O6-05) . . . 453
Kakazei, G.N. (P2-11) . . . 477
Kakinuma, Y. (N4-02) . . . 407
Kalappattil, V. (G5-07) . . . 203
Kalappattil, V. (K2-07) . . . 305
Kalappattil, V. (P4-05) . . . 484
Kalashnikova, A. (A3-13) . . . 18
Kalcheim, Y. (L2-01) . . . 329
Kalkan, B. (H2-03) . . . 219
Kally, J. (S5-02) . . . 348
Kalpana, G. (E1-05) . . . 113
Kaltenbrunner, M. (F3-12) . . . 157
Kalvig, R. (I4-10) . . . 261
Kambayashi, M. (H3-10) . . . 226
Kamboj, I. (E2-03) . . . 118
Kamimaki, A. (B3-10) . . . 49
Kamimaki, A. (Q2-02) . . . 513
Kamiya, N. (A3-07) . . . 16
Kammerbauer, F. (R1-05) . . . 539
Kanai, S. (E3-02) . . . 124
Kanai, S. (J6-09) . . . 295
Kanai, S. (S8-02) . . . 504
Kanai, Y. (N3-01) . . . 400
Kanai, Y. (N3-02) . . . 400
Kanareykin, A. (G2-07) . . . 185
Kane, A.M. (M2-04) . . . 360
Kane, M. (M2-01) . . . 359
Kaneta-Takada, S. (Q4-03) . . . 522
Kang, D. (O2-16) . . . 435
Kang, K. (D2-16) . . . 95
Kang, K. (G3-09) . . . 193
Kang, K. (O1-04) . . . 422
Kanki, T. (P6-10) . . . 500
Kantorovich, S. (A4-15) . . . 26

Kantorovich, S. (B2-07) 42
Kantorovich, S. (K2-12) 307
Kao, C. (G5-04) 201
Kao, I. (J4-01) 282
Kapaklis, V. (B1-04) 34
Kapaklis, V. (B1-12) 37
Kapaklis, V. (C4-06) 75
Kapaklis, V. (I2-11) 247
Kapitan, D. (A2-04) 9
Kapitan, D. (D1-13) 89
Kapitan, D. (M5-05) 378
Kapitan, V.Y. (A2-04) 9
Kapitan, V.Y. (D1-13) 89
Kapitan, V.Y. (M5-05) 378
Kapteyn, H. (E1-07) 114
Kar, G.S. (E3-01) 123
Kar, G.S. (L2-05) 331
Kar, G.S. (O2-04) 430
Kar, G.S. (R3-04) 552
Karaiskaj, D. (I4-13) 262
Karel, J. (H1-12) 216
Karel, J. (J4-03) 283
Karel, J. (J4-11) 287
Karimeddiny, S. (J4-10) 286
Karki, U. (E1-03) 112
Karki, U. (O6-17) 457
Karpenkov, A.Y. (F2-04) 146
Karpov, M.A. (Q1-09) 510
Karumuri, S. (K2-10) 306
Kashyap, A. (B4-06) 52
Kashyap, A. (B4-08) 53
Kashyap, A. (C3-02) 67
Kassem, M. (L1-04) 324
Kataria, G. (M2-05) 360
Katayama-Yoshida, H. (O1-12) 425
Katayanagi, H. (K5-08) 321
Katine, J. (G4-05) 198
Katine, J. (M3-07) 367
Kato, F. (H1-04) 212
Kato, F. (I1-07) 241
Kato, H. (D3-01) 96
Kato, H. (F5-05) 165
Kato, H. (F6-03) 170
Kato, H. (F6-04) 171
Kato, T. (A3-07) 16
Katoch, J. (J4-01) 282
Katsuki, A. (C3-06) 69
Katz, M.B. (G2-07) 185
Kaul, S. (K1-12) 301
Kaun, C. (K3-08) 312
Kav, A. (G2-11) 187
Kavand, M. (S4-02) 236
Kawahara, T. (O2-14) 434
Kay, A. (G1-11) 181
Kaynar, M. (H2-03) 219
Kazakova, O. (L1-01) 323
Kazakova, O. (R1-06) 540
Kazin, P.E. (Q1-09) 510
KC, S. (A3-03) 14
KC, S. (A3-09) 17
KC, S. (E1-03) 112
KC, S. (E1-06) 113
Ke, L. (G5-02) 200
Ke, M. (O2-14) 434
Keatley, P.S. (H1-15) 217
Keatley, P.S. (P2-10) 477
Keavney, D. (D1-14) 89
Kelly, N. (A4-04) 21
Kent, A.D. (G1-04) 178
Kent, A.D. (O4-05) 443
Kent, A.D. (P4-11) 486
Kent, A.D. (R2-02) 545
Kent, A.D. (R2-05) 546
Kent, A.D. (R2-06) 546
Kent, A.D. (R3-05) 552
Kent, A.D. (S5-03) 349
Kent, N. (A1-06) 5
Kepaptsoglou, D. (E2-10) 120
Kerber, N. (G3-08) 192
Kerber, N. (N1-05) 389
Kerber, N. (N1-08) 390
Kerber, N. (R1-05) 539
Keskinbora, K. (E4-07) 130
Keswani, N. (B1-14) 38
Kewenig, M. (N2-08) 396
Khadka, D. (I4-13) 262
Khalili Amiri, P. (E4-13) 133
Khalili Amiri, P. (G4-05) 198
Khan, G.A. (M2-05) 360
Khan, K. (M6-11) 385
Khan, K. (P6-02) 496
Khan, M. (F2-05) 146
Khanal, P. (N4-07) 409
Khanduri, H. (F4-02) 159
Khatri, Y. (B4-08) 53
Khodadadi, B. (O4-04) 443
Khodadadi, M. (P5-11) 493
Khokhlov, N. (A3-13) 18
Khomskii, D. (A2-10) 11
Khoo, K. (R2-02) 545
Khovaylo, V. (F2-14) 149
Khovaylo, V. (L4-11) 344
Khusyainov, D. (L3-07) 336
Khymyn, R. (Q3-04) 519
Khymyn, R. (S8-02) 504
Kiaba, M. (Q6-02) 534
Kiarie, W.M. (A4-12) 24
Kiarie, W.M. (L4-14) 346
Kiecana, A. (L4-01) 341
Kikitsu, A. (N5-14) 416
Kim, B. (D3-08) 98
Kim, C. (F5-02) 164
Kim, C. (F5-08) 167
Kim, D. (F6-07) 172
Kim, G. (F5-04) 165
Kim, J. (M3-12) 370
Kim, J. (N1-03) 388
Kim, J. (N2-14) 399
Kim, J. (R2-10) 548
Kim, J. (R3-04) 552
Kim, J. (R3-09) 554
Kim, K. (J4-04) 283
Kim, M. (F3-07) 155
Kim, P. (A1-06) 5
Kim, S. (F6-07) 172
Kim, S. (G1-01) 177
Kim, S. (R2-01) 544
Kim, W. (L2-05) 331
Kim, W. (R5-15) 570
Kim, Y. (F3-07) 155
Kimel, A. (I2-11) 247
Kimel, A. (P2-06) 474
Kimel, A. (P2-09) 476
Kimura, K. (A2-06) 9
Kimura, T. (P6-12) 500
Kinane, C. (M5-07) 378
Kinane, C. (S2-03) 108
King, D.I. (M5-10) 379
King, D.I. (M5-14) 380
Kioussis, N. (P4-03) 484
Kirby, B. (F1-04) 141
Kirby, B. (J5-01) 288
Kirihara, A. (M4-02) 371
Kirilyuk, A. (I2-11) 247
Kirilyuk, A. (P2-09) 476
Kirimura, M. (J1-09) 272
Kirk, E. (G3-07) 192
Kishi, Y. (O2-14) 434
Kishine, J. (L3-03) 335
Kiskinova, M. (G3-05) 191
Kitagawa, J. (P6-08) 499
Kitamoto, Y. (C2-09) 66
Kitcher, M.D. (M5-08) 379
Kitcher, M.D. (R1-12) 542
Kitcher, M.D. (R2-08) 547
Kiwa, T. (N5-15) 416
Kiwi, M. (D1-01) 83
Kiwi, M. (K2-06) 305
Klapetek, P. (R1-06) 540
Klaui, M. (G1-11) 181
Klaui, M. (G3-08) 192
Klaui, M. (J4-05) 284
Klaui, M. (L1-05) 324
Klaui, M. (M1-02) 353
Klaui, M. (N1-05) 389
Klaui, M. (N1-08) 390
Klaui, M. (P4-07) 485
Klaui, M. (R2-10) 548
Kläui, P. (N2-10) 397
Kläui, P. (R1-05) 539
Kläui, P. (S4-04) 237
Klavins, P. (Q1-04) 508
Kleibert, A. (B1-05) 34
Kleibert, A. (I2-11) 247
Klein, O. (M4-09) 374
Klein, O. (M4-11) 375
Klein, O. (N2-09) 396
Klein, O. (Q2-01) 513
Klein, O. (S8-01) 504
Kleiner, R. (E2-01) 117

Klevets, P. (F5-01) . . . 164
Klewe, C. (A3-08) . . . 16
Klewe, C. (P2-10) . . . 477
Klič, A. (D2-09) . . . 93
Klinovaja, J. (O3-09) . . . 440
Klodowski, K. (P1-03) . . . 468
Kmita, A. (P1-02) . . . 467
Knopke, C. (S3-01) . . . 174
Ko, K. (P6-13) . . . 501
Kobayashi, K. (G5-05) . . . 202
Kobayashi, K. (O1-14) . . . 426
Kobayashi, S. (C4-05) . . . 75
Kobayashi, S. (H3-02) . . . 223
Kobayashi, S. (O6-04) . . . 453
Koblischka-Veneva, A. (J3-09) . . . 279
Koblischka-Veneva, A. (M2-07) . . . 361
Koblischka, M.R. (J3-09) . . . 279
Koblischka, M.R. (M2-07) . . . 361
Kochat, V. (M2-15) . . . 363
Koda, A. (C2-09) . . . 66
Koelle, D. (E2-01) . . . 117
Koenig, A. (J3-04) . . . 278
Koerner, L.J. (L4-10) . . . 344
Koganezawa, T. (I4-15) . . . 263
Kohl, F. (N2-08) . . . 396
Kohno, R. (M4-09) . . . 374
Kohno, R. (M4-11) . . . 375
Kohno, R. (N2-09) . . . 396
Kohno, R. (Q2-01) . . . 513
Koike, K. (F6-03) . . . 170
Koike, K. (F6-04) . . . 171
Koike, Y. (J4-02) . . . 282
Kolesnikov, A. (E5-07) . . . 136
Kolesnikov, A. (E5-13) . . . 138
Kolezhuk, A. (F5-03) . . . 165
Komine, T. (K4-08) . . . 315
Komine, T. (O1-09) . . . 424
Komineas, S. (M3-11) . . . 369
Komissinskiy, P. (H3-14) . . . 227
Komogortsev, S. (C4-02) . . . 74
Komogortsev, S. (O6-14) . . . 457
Komogortsev, S. (R5-01) . . . 564
Komogortsev, S. (R5-09) . . . 567
Komori, M. (D3-01) . . . 96
Komori, S. (K4-04) . . . 314
Komori, T. (R1-11) . . . 542
Kompouras, K. (E1-07) . . . 114
Komura, E. (N4-02) . . . 407
Kondo, K. (K4-04) . . . 314
Kondo, K. (K4-12) . . . 316
Kononenko, D. (J6-05) . . . 294
Kononova, M. (F2-14) . . . 149
Kononova, M. (L4-11) . . . 344
Konopelnyk, Y. (F2-07) . . . 147
Kons, C. (E2-02) . . . 117
Koo, B. (B4-01) . . . 51
Koo, T. (F3-07) . . . 155
Koomson, V. (C1-06) . . . 57
Koonkarnkhai, S. (N3-07) . . . 403
Koonkarnkhai, S. (N3-09) . . . 404
Koppes, A. (Q5-08) . . . 531
Koppes, R. (Q5-08) . . . 531
Koraltan, S. (B1-02) . . . 33
Koraltan, S. (B1-05) . . . 34
Körber, L. (E4-06) . . . 129
Körber, L. (Q4-01) . . . 522
Korenistov, P. (H5-02) . . . 232
Koretsune, T. (M4-01) . . . 371
Korol, A.O. (D1-13) . . . 89
Korol, A.O. (M5-05) . . . 378
Korostynski, C. (E2-03) . . . 118
Kortright, J. (E2-04) . . . 118
Kosaka, T. (I1-03) . . . 239
Koster, G. (Q6-02) . . . 534
Kotter, S. (E2-05) . . . 119
Kou, X. (P4-08) . . . 486
Kovac, J. (H5-03) . . . 233
Kovalev, A.A. (M5-11) . . . 379
Kovalev, A.A. (P4-09) . . . 486
Kovintavewat, P. (N3-07) . . . 403
Kovintavewat, P. (N3-09) . . . 404
Kozlov, A.G. (M6-06) . . . 383
Kozlyakova, E.S. (Q1-09) . . . 510
Kraimia, M. (E4-09) . . . 131
Král, D. (E1-11) . . . 115
Krasikov, A. (C4-02) . . . 74
Kravchuk, V. (R1-09) . . . 541
Kravtsov, E. (D1-09) . . . 87
Krawczyk, M. (E4-02) . . . 127
Krawczyk, M. (E4-07) . . . 130
Krenkel, E. (K1-01) . . . 297
Krenn, H. (H1-06) . . . 213
Kriegner, D. (E1-01) . . . 111
Kriegner, D. (J6-07) . . . 294
Kriegner, D. (M1-09) . . . 356
Krivorotov, I. (M3-07) . . . 367
Krizakova, V. (E3-01) . . . 123
Krizek, F. (G1-10) . . . 180
Krizek, F. (J6-07) . . . 294
Kröger, R. (E2-10) . . . 120
Kronast, F. (F1-02) . . . 140
Kronast, F. (G1-11) . . . 181
Krycka, K.L. (E2-02) . . . 117
Kryukova, O. (Q5-07) . . . 530
Ksenzov, D. (G3-08) . . . 192
Kubo, Y. (F6-04) . . . 171
Kubomura, K.H. (H4-04) . . . 229
Kubota, H. (B3-05) . . . 48
Kubota, H. (B3-10) . . . 49
Kubota, H. (F3-08) . . . 155
Kubota, H. (L2-03) . . . 330
Kubota, T. (E1-11) . . . 115
Kubota, T. (M4-06) . . . 373
Kubota, T. (O2-10) . . . 432
Kuchi, R. (F6-07) . . . 172
Kudinoor, A.S. (E4-04) . . . 128
Kudryavtsev, R. (C5-04) . . . 80
Kudyukov, E. (D1-09) . . . 87
Kudyukov, E. (M6-03) . . . 382
Kuepferling, M. (O7-01) . . . 459
Kúkol'ová, A. (N1-07) . . . 389
Kukreja, R. (G2-02) . . . 183
Kulesh, N. (O6-18) . . . 458
Kumah, D. (R4-02) . . . 558
Kumar Nag, P. (S1-01) . . . 105
Kumar, A. (M3-06) . . . 367
Kumar, A. (M6-11) . . . 385
Kumar, A. (O5-08) . . . 450
Kumar, A. (P6-02) . . . 496
Kumar, A. (R5-12) . . . 569
Kumar, D. (F1-09) . . . 143
Kumar, D. (F2-06) . . . 147
Kumar, N. (J5-04) . . . 289
Kumar, P. (C4-12) . . . 78
Kumar, P. (F4-02) . . . 159
Kumar, R. (I3-11) . . . 256
Kumar, R. (M2-05) . . . 360
Kumar, S. (B1-14) . . . 38
Kumar, S. (C1-03) . . . 55
Kumar, S. (D3-09) . . . 99
Kumar, S. (I4-12) . . . 262
Kumar, S. (Q3-07) . . . 520
Kumar, V. (O3-12) . . . 441
Kumar, Y. (O6-03) . . . 452
Kumar, Y. (P6-03) . . . 497
Kumatani, A. (C5-01) . . . 79
Kumbhare, D. (J1-02) . . . 268
Kunchur, N. (J5-07) . . . 290
Kundu, S. (L2-05) . . . 331
Kundys, B. (E3-08) . . . 126
Kunstmann, J. (I2-09) . . . 247
Kuo, M. (I4-03) . . . 258
Küpper, K. (C1-11) . . . 59
Kura, H. (I4-15) . . . 263
Kurahashi, M. (L1-06) . . . 325
Kurian, J. (E3-08) . . . 126
Kurihara, K. (N3-01) . . . 400
Kurihara, K. (O7-03) . . . 460
Kurihara, K. (O7-13) . . . 464
Kurlyandskaya, G.V. (J1-07) . . . 271
Kurokawa, Y. (Q4-06) . . . 524
Kurosaki, Y. (N5-14) . . . 416
Kuroshima, S. (M4-02) . . . 371
Kurta, R. (G3-06) . . . 191
Kurzmann, A. (K4-09) . . . 315
Kuschel, T. (C1-11) . . . 59
Kuschel, T. (E1-11) . . . 115
Kuschel, T. (F1-05) . . . 142
Kushibiki, R. (N3-03) . . . 401
Kusne, A.G. (P5-01) . . . 489
Kuswik, P. (E4-02) . . . 127
Kuszewski, P. (E4-09) . . . 131
Kuttner, C. (J1-06) . . . 271
Kuwabiraki, Y. (C5-06) . . . 81
Kuwahara, M. (I3-07) . . . 254
Kuwahata, A. (Q5-02) . . . 528
Kuznetsov, M.A. (A4-02) . . . 20
Kuzovnikova, L. (G6-12) . . . 210
Kvashnin, Y. (D2-10) . . . 93
Kvashnin, Y. (E1-07) . . . 114

Kwo, J. (M4-07) 373
Kwok, W. (L3-15) 340
Kyle, S. (G4-07) 199
Kyle, S.J. (A5-04) 30

- L -

LaBella, V.P. (P6-06) 497
Labracherie, V. (J5-07) 290
Labusca, L. (Q5-03) 529
Lachowicz, D. (P1-02) 467
Lacour, D. (E4-11) 132
Lacour, D. (G3-08) 192
Lacour, D. (R1-05) 539
Ladak, S. (B1-15) 39
Ladak, S. (C4-10) 77
Ladygina, V. (C4-02) 74
Lägel, B. (E4-12) 132
Lägel, B. (N2-08) 396
Lai, C. (N5-01) 410
Lai, H. (F5-10) 167
Lai, H. (J5-06) 289
Lambert, P.K. (Q1-11) 511
Lammel, M. (E1-01) 111
Lan, Q. (F6-02) 170
Lancaster, T. (R2-09) 548
Landeros, P. (A1-05) 4
Langbein, W. (C4-10) 77
Langridge, S. (M5-07) 378
Lapa, P.N. (H2-01) 219
Lapa, P.N. (R2-10) 548
Lari, L. (E2-10) 120
Lasheras, A. (K1-10) 300
Laskowski, R. (R2-02) 545
Latyshev, N. (Q5-07) 530
Lau, C. (O1-05) 422
Lau, J.W. (G2-07) 185
Lau, Y. (O1-11) 425
Lau, Y. (O4-09) 445
Laughlin, D.E. (P2-02) 472
Laur, V. (C1-01) 54
Laurenson, A. (I3-01) 251
Laureti, S. (Q5-04) 529
Laureti, S. (R3-14) 557
Laurson, L. (M3-13) 370
Lavernia, E. (J2-06) 275
Law, J. (E1-03) 112
Law, J. (E1-06) 113
Law, J. (F2-08) 147
Law, K. (A3-03) 14
Law, K. (A3-09) 17
Laydevant, J. (Q3-06) 520
Lazpita, P. (A4-05) 22
Le Denmat, S. (I3-06) 254
Le Fevre, P. (E1-13) 116
Le Guyader, L. (G3-06) 191
Le, M. (A2-01) 8
Leary, A. (J3-04) 278
Lebedev, D. (O1-03) 421
Lebourgeois, R. (C1-01) 54
Lebrun, R. (B3-06) 48
Lebrun, R. (C1-10) 59
Lebrun, R. (G1-11) 181
Lebrun, R. (M1-02) 353
Lebrun, R. (N2-10) 397
Lebrun, R. (P4-07) 485
LeClair, P. (A3-09) 17
LeClair, P. (E1-03) 112
LeClair, P. (E1-06) 113
Lee Koon Yap, S. (O2-15) 435
Lee Koon Yap, S. (O3-06) 438
Lee, C. (N5-01) 410
Lee, C. (S1-04) 106
Lee, D. (J4-04) 283
Lee, H. (D3-08) 98
Lee, H. (H2-09) 221
Lee, H. (J4-04) 283
Lee, H. (M2-02) 359
Lee, H. (M3-07) 367
Lee, H. (O2-01) 428
Lee, H. (Q5-06) 530
Lee, H. (Q5-09) 531
Lee, I. (B3-08) 49
Lee, J. (G6-06) 207
Lee, J. (M1-03) 354
Lee, J. (N3-06) 402
Lee, J. (N3-14) 406
Lee, J.R. (K2-06) 305
Lee, K. (J4-04) 283
Lee, K. (J4-05) 284
Lee, K. (Q5-06) 530
Lee, K. (R2-01) 544
Lee, K. (R2-10) 548
Lee, M. (H2-01) 219
Lee, M.S. (B1-06) 34
Lee, S. (A3-12) 18
lee, s. (J4-04) 283
Lee, S. (J4-09) 286
Lee, S. (M4-07) 373
Lee, S. (O1-14) 426
Lee, T. (A1-10) 7
Lee, T. (L4-05) 342
Lee, T. (L4-10) 344
Lee, T. (L4-16) 346
Lee, T. (O2-05) 430
Lee, Y. (F6-06) 172
Lee, Y. (G5-02) 200
Lee, Y. (G5-04) 201
Lees, M. (E5-14) 139
Legrand, W. (E5-08) 137
Legrand, W. (I3-09) 255
Legrand, W. (I3-10) 256
Legrand, W. (L1-11) 327
Lehman, B. (R5-07) 566
Leighton, C. (E2-03) 118
Leighton, C. (K3-05) 310
Leighton, C. (L2-02) 329
Leighton, C. (M2-03) 359
Leistner, K. (C4-08) 76
Leistner, K. (K1-03) 298
Lejeune, B. (H1-08) 214
Leliaert, J. (L1-13) 328
Leliaert, J. (S3-04) 175
Leliaert, J. (S6-05) 352
Lelièvre-Berna, E. (D2-14) 94
Lemaître, A. (E4-09) 131
Lemaître, A. (M3-04) 366
Lendinez, S. (B1-11) 37
Lenne, S. (E3-07) 125
Lenz, K. (C1-07) 57
Lenz, K. (E4-03) 128
Lenz, K. (M3-05) 366
Leo, N. (B1-02) 33
Leo, N. (B1-05) 34
Leo, N. (S6-05) 352
Leon, A.O. (J5-11) 291
Leone, A. (L3-06) 336
Leonov, A.O. (D2-14) 94
Lepalovskij, V. (D1-09) 87
Lere-Adams, A.J. (D4-14) 104
Leroux, N. (Q3-06) 520
Leveille, C. (L1-11) 327
Lewinska, S. (E5-10) 137
Lewis, A. (L3-06) 336
Lewis, L. (H1-02) 211
Lewis, L. (H1-08) 214
Lewis, L. (Q5-08) 531
Lewis, L. (R5-05) 565
Lewis, L. (R5-07) 566
Li, B. (P4-09) 486
Li, C. (G1-08) 179
Li, C. (I1-06) 240
Li, C. (O3-06) 438
Li, G. (I5-07) 266
Li, H. (H5-04) 233
Li, H. (P6-01) 496
Li, H. (Q4-06) 524
Li, J. (A4-13) 25
Li, J. (D3-05) 97
Li, J. (G1-08) 179
Li, J. (G2-02) 183
Li, J. (I5-07) 266
Li, J. (J5-04) 289
Li, J. (M4-03) 371
Li, J. (O4-04) 443
Li, J. (S4-02) 236
Li, L. (J3-10) 280
Li, M.P. (A3-06) 15
Li, M.P. (I3-03) 252
Li, M.P. (R1-08) 541
Li, P. (S1-04) 106
Li, P. (S5-02) 348
Li, Q. (A3-08) 16
Li, Q. (C1-04) 56
Li, Q. (G2-05) 184
Li, Q. (P2-09) 476
Li, R. (J5-03) 288
Li, S. (C5-07) 81
Li, T. (O5-05) 449
Li, W. (O6-15) 457
Li, X. (I3-05) 253
Li, X. (P5-06) 491

Li, X. (S1-04) . . . 106
Li, Y. (B3-02) . . . 46
Li, Y. (F4-08) . . . 161
Li, Y. (G5-08) . . . 203
Li, Y. (I5-02) . . . 264
Li, Y. (I5-08) . . . 266
Li, Y. (L3-15) . . . 340
Li, Y. (M3-02) . . . 365
Li, Y. (M3-03) . . . 366
Li, Y. (M4-03) . . . 371
Li, Y. (R4-01) . . . 558
Li, Y. (R5-11) . . . 568
Li, Z. (Q6-10) . . . 537
liang, J. (E1-12) . . . 116
Liang, J. (R2-03) . . . 545
Liang, X. (N1-11) . . . 391
Liang, X. (P5-01) . . . 489
Liao, C. (K2-05) . . . 304
Liao, J. (R1-13) . . . 543
Liao, Z. (M2-02) . . . 359
Lichtenstein, A. (G3-06) . . . 191
Liebl, M. (S3-03) . . . 175
Liensberger, L. (E4-10) . . . 131
Liensberger, L. (J4-07) . . . 285
Lik, O. (Q5-04) . . . 529
Lilly, M.P. (M4-12) . . . 376
Lim Chee Beng, N. (O3-06) . . . 438
Lim, M. (J4-04) . . . 283
Lim, S. (O2-15) . . . 435
Lim, Y. (A3-04) . . . 14
Lim, Y. (O4-04) . . . 443
Lima Jr., E. (J1-08) . . . 271
Lin, C. (Q4-05) . . . 523
Lin, G. (F6-05) . . . 171
Lin, J. (E2-01) . . . 117
Lin, J. (K5-01) . . . 318
Lin, K. (G5-04) . . . 201
Lin, P. (K2-08) . . . 306
Lin, S. (S1-04) . . . 106
Lin, W. (M2-14) . . . 363
Lin, W. (P5-02) . . . 489
Lin, Y. (C4-07) . . . 76
Lin, Y. (O7-12) . . . 464
Lin, Z. (D4-09) . . . 102
Lin, Z. (F6-08) . . . 172
Lin, Z. (J3-05) . . . 278
Lin, Z. (R3-10) . . . 555
Linder, J. (L2-09) . . . 333
Lindgren, B. (I2-11) . . . 247
Lindner, J. (E3-08) . . . 126
Lindner, J. (E4-03) . . . 128
Lindner, J. (M3-05) . . . 366
Lindner, J. (O7-08) . . . 462
Linfield, E. (M5-02) . . . 377
Lipp, V. (G3-05) . . . 191
Lisenkov, I. (I2-02) . . . 243
Lisiecki, F. (E4-02) . . . 127
Litvinenko, A. (B3-09) . . . 49
Litvinenko, A. (C5-05) . . . 80
Litvinenko, A. (M4-09) . . . 374
Litvinenko, A. (Q2-01) . . . 513
Litvinenko, A. (R3-08) . . . 554
Litvinov, D. (P5-11) . . . 493
Litzius, K. (G3-08) . . . 192
Litzius, K. (N1-05) . . . 389
Litzius, K. (N1-08) . . . 390
Litzius, K. (R2-06) . . . 546
Liu, A. (G2-07) . . . 185
Liu, C. (A3-11) . . . 18
Liu, C. (C1-09) . . . 58
Liu, C. (G1-13) . . . 182
LIU, C. (N1-06) . . . 389
Liu, C. (O1-06) . . . 423
Liu, C. (R5-10) . . . 568
Liu, E. (O2-05) . . . 430
Liu, E. (S1-01) . . . 105
liu, f. (I2-13) . . . 249
Liu, H. (I4-13) . . . 262
Liu, H. (I5-08) . . . 266
Liu, H. (R5-11) . . . 568
Liu, J. (D4-04) . . . 101
Liu, K. (F1-01) . . . 140
Liu, K. (I3-08) . . . 255
Liu, K. (L2-07) . . . 332
Liu, K. (L2-08) . . . 332
Liu, K. (O3-11) . . . 440
Liu, L. (G1-12) . . . 181
Liu, L. (K2-04) . . . 304
Liu, L. (M2-14) . . . 363
Liu, L. (M4-03) . . . 371
Liu, L. (Q4-09) . . . 525
Liu, L. (R1-01) . . . 538
Liu, M. (G5-07) . . . 203
Liu, M. (K2-07) . . . 305
Liu, P. (G5-13) . . . 205
Liu, P. (G6-10) . . . 209
Liu, P. (K5-04) . . . 319
Liu, Q. (I2-10) . . . 247
Liu, S. (G6-10) . . . 209
Liu, S. (G6-11) . . . 209
Liu, S. (I2-12) . . . 248
Liu, S. (Q5-02) . . . 528
Liu, T. (R4-01) . . . 558
Liu, W. (A1-04) . . . 4
Liu, W. (F2-16) . . . 150
Liu, X. (A1-06) . . . 5
Liu, X. (C2-03) . . . 63
Liu, X. (C2-08) . . . 65
Liu, X. (H3-04) . . . 224
Liu, X. (I4-09) . . . 261
Liu, X. (N1-11) . . . 391
Liu, Y. (J4-06) . . . 284
Liu, Y. (M4-07) . . . 373
Liu, Y. (M6-07) . . . 383
Liu, Y. (O3-03) . . . 438
Liu, Y. (P4-12) . . . 487
Liu, Y. (S5-02) . . . 348
Livesey, K. (D1-10) . . . 87
Livesey, K. (E4-04) . . . 128
Livesey, K. (I5-05) . . . 265
Livesey, K. (Q2-09) . . . 516
Livesey, K. (Q2-10) . . . 516
Liz-Marzán, L. (J1-06) . . . 271
Llacsahuanga Allcca, A.E. (G5-10) . . . 204
Llois, A.M. (I4-07) . . . 259
Lloyd, B. (M4-12) . . . 376
Lo Conte, R. (F1-01) . . . 140
Lo Conte, R. (M3-04) . . . 366
Lo Conte, R. (O3-11) . . . 440
Lo, T. (J4-06) . . . 284
Lobo-Checa, J. (B2-04) . . . 41
Locatelli, A. (R2-11) . . . 548
Lochner, E. (R4-01) . . . 558
Lograsso, T.A. (D2-14) . . . 94
Lohmann, M. (S4-02) . . . 236
Loidl, A. (A2-10) . . . 11
Lomakin, V. (O2-07) . . . 431
Lomakin, V. (P3-05) . . . 480
Lomakin, V. (P4-11) . . . 486
Lomakin, V. (R3-10) . . . 555
Lone, A. (C5-08) . . . 82
Lonsky, M. (N1-02) . . . 387
Loomis, L. (G4-03) . . . 197
Lopes Seeger, R. (O3-08) . . . 439
Lopes, A. (K1-10) . . . 300
Lopez Dominguez, V. (E4-13) . . . 133
Lopez Dominguez, V. (G4-05) . . . 198
López Paz, S.A. (J3-08) . . . 279
López Tabares, J. (R5-02) . . . 564
López-Ortega, A. (O6-10) . . . 455
Lopez-Quintas, I. (G3-08) . . . 192
López, M. (L4-08) . . . 343
Losby, J.E. (G2-11) . . . 187
Losby, J.E. (N5-16) . . . 417
Loss, D. (O3-09) . . . 440
Lostun, M. (H1-01) . . . 211
Lott, D. (R4-05) . . . 559
Loudon, J. (I3-01) . . . 251
Louis, S. (B3-09) . . . 49
Louis, S. (R3-08) . . . 554
Lourembam, J. (O2-15) . . . 435
Lovery, B. (I3-11) . . . 256
Lu, J. (O1-07) . . . 423
Lu, X. (E1-04) . . . 113
Lu, Y. (O1-05) . . . 422
Lu, Z. (C3-14) . . . 73
Luber, E. (G2-11) . . . 187
Luders, U. (H2-08) . . . 221
Luengo, Y. (F2-18) . . . 150
Luis, F. (D2-03) . . . 91
Lujan, D. (I3-05) . . . 253
Lumetzberger, J. (C1-07) . . . 57
Luna, C. (H5-03) . . . 233
Lunacek, J. (C3-13) . . . 72
Lunghi, A. (D2-01) . . . 90
Luo, Y. (G1-13) . . . 182
Luo, Z. (A2-09) . . . 10
Luo, Z. (G3-07) . . . 192
Luo, Z. (J6-11) . . . 296
Luo, Z. (R3-01) . . . 550
Lupu, N. (H1-01) . . . 211
Lupu, N. (N5-09) . . . 413
Lupu, N. (Q5-03) . . . 529

Lupu, N. (R5-08) . . . 567
Luzanov, V. (R4-11) . . . 562
Lv, Y. (G4-01) . . . 196
Lv, Y. (H4-01) . . . 228
Lv, Y. (K2-04) . . . 304
Lyakh, A.S. (F5-09) . . . 167
Lykkebø, O. (P3-06) . . . 480
Lynnyk, A. (E5-10) . . . 137

- M -

M. (L4-04) . . . 342
M. (R5-12) . . . 569
M. Shaw, J. (C1-02) . . . 54
M. Shaw, J. (C1-12) . . . 60
M. Shaw, J. (E1-07) . . . 114
M. Shaw, J. (R2-06) . . . 546
Ma, B. (D4-04) . . . 101
Ma, C. (R2-06) . . . 546
Ma, J. (N5-07) . . . 412
Ma, T. (O3-12) . . . 441
Ma, Y. (K2-13) . . . 307
Maat, S. (I5-05) . . . 265
Maazaz, Z. (I5-03) . . . 264
Macaluso, E. (D2-02) . . . 90
Macaluso, E. (D2-03) . . . 91
Maccari, F. (H3-09) . . . 226
Maccari, F. (Q1-06) . . . 509
Maccherozzi, F. (G1-10) . . . 180
Maccherozzi, F. (G4-07) . . . 199
Maccherozzi, F. (H1-15) . . . 217
Maccherozzi, F. (J6-07) . . . 294
Maccherozzi, F. (M1-09) . . . 356
Macedo, R. (E4-04) . . . 128
Machado, F. (K1-14) . . . 302
Madhogaria, R.M. (L4-02) . . . 341
Magara, H. (O6-04) . . . 453
Magen, C. (A1-02) . . . 2
Magen, C. (D1-12) . . . 88
Magen, C. (E2-01) . . . 117
Magén, C. (L1-03) . . . 323
Magni, A. (J2-03) . . . 273
Magno, J.F. (D4-08) . . . 102
Magrez, A. (N1-07) . . . 389
Mahajan, R. (C3-02) . . . 67
Mahat, R. (E1-03) . . . 112
Mahat, R. (E1-06) . . . 113
Mahato, R.N. (L4-04) . . . 342
Mahato, R.N. (R5-12) . . . 569
Mahendiran, R. (E1-08) . . . 114
Mahendiran, R. (Q6-05) . . . 535
Mai, T.T. (G5-11) . . . 205
Mai, T.T. (O1-05) . . . 422
Mai, T.T. (O1-10) . . . 424
Mailly, D. (N1-10) . . . 391
Maity, A. (O3-11) . . . 440
Majetich, S. (G4-04) . . . 197
Majetich, S. (G4-06) . . . 199
Majetich, S. (Q2-11) . . . 517
Majetich, S. (R3-06) . . . 553
Major, M. (H3-14) . . . 227
Mak, K. (O1-04) . . . 422
Makarov, A. (D1-13) . . . 89
Makarov, D. (A1-05) . . . 4
Makarov, D. (F3-12) . . . 157
Makarov, D. (I4-01) . . . 257
Makarov, D. (J6-05) . . . 294
Makarov, D. (R1-09) . . . 541
Makarov, D. (R4-03) . . . 559
Makarova, K. (D1-13) . . . 89
Makarovsky, O. (M1-09) . . . 356
Malaviya, D. (F2-05) . . . 146
Maletinsky, P. (L1-09) . . . 326
Malik, M.A. (M2-05) . . . 360
Malinowski, G. (G3-02) . . . 190
Malinowski, G. (M3-04) . . . 366
Malinowski, G. (P2-01) . . . 472
Mallah, T. (D2-05) . . . 92
Mallick, D. (C3-10) . . . 71
Mallick, D. (K1-06) . . . 298
Maloberti, O. (O5-07) . . . 450
Mamiya, H. (C3-01) . . . 67
Manchanda, P. (E2-12) . . . 121
Manchon, A. (O4-04) . . . 443
Manchon, A. (S4-01) . . . 236
Mancilla, D. (C5-05) . . . 80
Mancilla, D. (E5-01) . . . 135
Mancoff, F.B. (O2-01) . . . 428
Mandru, A. (D1-04) . . . 84
Mandrus, D. (C3-14) . . . 73
Manfredda, M. (G3-05) . . . 191
Manfrinetti, P. (A4-18) . . . 27
Mangin, P. (J1-04) . . . 270
Mangin, S. (F2-01) . . . 145
Mangin, S. (G3-02) . . . 190
Mangin, S. (M3-04) . . . 366
Mangin, S. (O2-11) . . . 433
Mangin, S. (P2-01) . . . 472
Mangin, S. (R1-05) . . . 539
Manipatruni, S. (Q4-05) . . . 523
Mankey, G. (L3-06) . . . 336
Manna, P.K. (D1-02) . . . 83
Mansell, R. (F1-02) . . . 140
Mansell, R. (F1-03) . . . 141
Mansell, R. (N4-06) . . . 409
Mansouri Tehrani, A. (H2-07) . . . 221
Mansouri, S. (F2-02) . . . 145
Mansueto, M. (G4-02) . . . 197
Mantel, A. (L2-06) . . . 331
Mao, Z. (O1-05) . . . 422
Marangolo, M. (O7-16) . . . 466
Marchenkov, V. (H5-02) . . . 232
Marchenkov, V. (H5-05) . . . 234
Marchenkov, V. (J5-08) . . . 290
Marchenkov, V. (K4-13) . . . 317
Marchenkov, V. (L4-07) . . . 343
Marchfield, D. (A4-13) . . . 25
Marchi, F. (S3-02) . . . 174
Marciesky, M. (I2-13) . . . 249
Marcos, J. (B2-14) . . . 45
Margaillan, F. (E4-09) . . . 131
Marić, I. (F4-12) . . . 162
Marin, J.M. (K1-14) . . . 302
Marin, P. (E2-13) . . . 121
Marin, P. (H1-08) . . . 214
Marin, P. (H1-09) . . . 215
Marinella, M.J. (A5-01) . . . 28
Marinella, M.J. (A5-02) . . . 29
Marinella, M.J. (A5-03) . . . 29
Marinella, M.J. (A5-05) . . . 31
Marinella, M.J. (A5-06) . . . 31
Maripeddi, R. (L2-03) . . . 330
Markou, A. (E1-01) . . . 111
Marković, D. (Q3-06) . . . 520
Marqués Marchán, J. (O5-02) . . . 448
Marrows, C.H. (J5-05) . . . 289
Marrows, C.H. (M5-02) . . . 377
Marrows, C.H. (M5-07) . . . 378
Marshall, A. (N4-08) . . . 409
Marshall, R.A. (J3-03) . . . 277
Martin, E. (M3-04) . . . 366
Martin, E. (Q3-06) . . . 520
Martin, E.L. (Q5-01) . . . 528
Martin, I. (S1-02) . . . 105
Martín, J. (L1-10) . . . 326
Martín, J. (O5-01) . . . 448
Martin, M. (K4-03) . . . 313
Martin, M. (O3-13) . . . 441
Martínez Criado, G. (H1-05) . . . 213
Martínez-García, J.C. (P1-05) . . . 469
Martínez-García, J.C. (Q1-10) . . . 511
Martinez-Perez, M. (E2-01) . . . 117
Martínez, B. (D1-12) . . . 88
Martínez, J. (D2-03) . . . 91
Martinez, Y. (B2-07) . . . 42
Martino, L. (J2-03) . . . 273
Martins, L. (B3-03) . . . 46
Martins, L. (Q3-06) . . . 520
Martins, M. (M6-09) . . . 384
Marty, A. (Q4-05) . . . 523
Martyshkin, A.A. (O6-09) . . . 455
Mary, A. (O6-12) . . . 456
Mascaraque, A. (F1-01) . . . 140
Mason, J. (B1-06) . . . 34
Mason, N. (S1-03) . . . 105
Masuda, H. (O4-09) . . . 445
Masuda, K. (M4-06) . . . 373
Mata, R. (Q1-04) . . . 508
Mathaudhu, S. (G3-01) . . . 190
Matheis, L. (R4-05) . . . 559
Mathias, S. (E1-07) . . . 114
Matos, I.T. (F5-11) . . . 168
Matos, I.T. (R5-13) . . . 569
Matsui, N. (I1-03) . . . 239
Matsuki, H. (D3-07) . . . 98
Matsuki, H. (D3-10) . . . 99
Matsumori, H. (I1-03) . . . 239
Matsumoto, K. (F1-08) . . . 142
Matsumoto, K. (O7-14) . . . 465
Matsumoto, Y. (A2-06) . . . 9
Matsuo, M. (O4-06) . . . 444
Matsuura, K. (F5-05) . . . 165

Matsuura, K. (P4-06) . . . 485
Matsuyama, K. (N3-01) . . . 400
Matsuyama, K. (O7-03) . . . 460
Matsuyama, K. (O7-13) . . . 464
Mattayakan, M. (N3-07) . . . 403
Mattevi, C. (K4-03) . . . 313
Matyushov, A. (F3-11) . . . 156
Matyushov, A. (I2-02) . . . 243
May, A. (B1-15) . . . 39
Mayoh, D. (E5-14) . . . 139
Mayr, S. (E4-03) . . . 128
Mayr, S. (R3-01) . . . 550
Maziewski, A. (E5-10) . . . 137
Mazza, A.R. (D2-06) . . . 93
Mazzoli, C. (S6-04) . . . 352
Mccall, S. (C2-05) . . . 64
Mccall, S. (I2-01) . . . 243
McCloy, J. (D4-14) . . . 104
McCollum, E. (A3-11) . . . 18
McCord, J. (F3-01) . . . 152
McCord, J. (F3-11) . . . 156
McCreary, A. (G5-11) . . . 205
McCreary, A. (O1-05) . . . 422
McCreary, A. (O1-10) . . . 424
McCullian, B. (B3-08) . . . 49
McDonald, N.R. (G4-03) . . . 197
McDonough, C. (K5-01) . . . 318
McGhie, H. (F1-11) . . . 144
McGrath, B.R. (D1-10) . . . 87
McKeefry, C. (Q4-04) . . . 523
McKeever, C. (L3-14) . . . 339
McMaster, M.R. (A3-10) . . . 17
McMichael, R.D. (L1-08) . . . 325
McNeill, K. (N3-05) . . . 402
McNulty, J. (D1-11) . . . 88
McPhearson, D. (E2-04) . . . 118
McPherson, D. (O6-11) . . . 456
McVitie, S. (A1-02) . . . 2
McVitie, S. (L1-10) . . . 326
Medapalli, R. (R1-12) . . . 542
Mehta, A. (M2-01) . . . 359
Mehta, A. (M2-04) . . . 360
Mehta, J. (G2-02) . . . 183
Mehta, U.M. (J1-01) . . . 268
Mei, A. (M1-03) . . . 354
Mello, A. (C1-08) . . . 58
Melo, J.J. (M6-01) . . . 381
Memshawy, S. (M3-08) . . . 368
Mendawar, B. (A5-02) . . . 29
Mendes, J.B. (R4-09) . . . 561
Mendisch, S. (E5-02) . . . 135
Mendoza-Reséndez, R. (H5-03) . . . 233
Meng, C. (G6-11) . . . 209
Meng, F. (A1-09) . . . 6
Meng, F. (R1-13) . . . 543
Meng, K. (K2-13) . . . 307
Mengucci, P. (Q5-04) . . . 529
Menniti, M. (B1-02) . . . 33
Menniti, M. (S6-05) . . . 352
Mentink, J. (N2-02) . . . 394
Meny, C. (D1-08) . . . 86
Meny, C. (F1-10) . . . 143
Meo, A. (O6-01) . . . 452
Meo, A. (P2-05) . . . 474
Merbouche, H. (C1-10) . . . 59
Merbouche, H. (K1-07) . . . 299
Merbouche, H. (N2-07) . . . 396
Mercadier, L. (G3-06) . . . 191
Merchán, L. (B2-14) . . . 45
Mercurio, G. (G3-06) . . . 191
Mertig, I. (O3-01) . . . 437
Mertig, I. (O3-12) . . . 441
Mesa, J. (H1-02) . . . 211
Mewes, C. (A3-03) . . . 14
Mewes, C. (A3-04) . . . 14
Mewes, C. (A3-06) . . . 15
Mewes, C. (A3-09) . . . 17
Mewes, C. (I3-03) . . . 252
Mewes, C. (J3-04) . . . 278
Mewes, C. (L3-06) . . . 336
Mewes, C. (O6-17) . . . 457
Mewes, C. (R2-08) . . . 547
Mewes, T. (A3-03) . . . 14
Mewes, T. (A3-04) . . . 14
Mewes, T. (A3-05) . . . 15
Mewes, T. (A3-06) . . . 15
Mewes, T. (A3-09) . . . 17
Mewes, T. (I3-03) . . . 252
Mewes, T. (J3-04) . . . 278
Mewes, T. (L3-06) . . . 336
Mewes, T. (O6-17) . . . 457
Mewes, T. (R2-08) . . . 547
Meyers, D. (I5-05) . . . 265
Mi, W. (G5-09) . . . 204
Mi, W. (I4-02) . . . 257
Mi, W. (Q6-10) . . . 537
Mi, W. (R2-03) . . . 545
Mican, S. (L2-04) . . . 330
Michaelis de Vasconcellos, S. (M4-08) . . . 373
Michaelis de Vasconcellos, S. (Q4-10) . . . 526
Michel, E.G. (F1-01) . . . 140
Michez, L. (I4-10) . . . 261
Middelkamp, M. (M4-10) . . . 375
Migliorini, A. (O4-01) . . . 442
Mignard, M. (P1-01) . . . 467
Miki, S. (N1-06) . . . 389
Mila, F. (A2-09) . . . 10
Milinska, E. (E5-10) . . . 137
Milkovic, O. (H5-03) . . . 233
Miller, J. (I4-14) . . . 262
Mills, C. (Q5-08) . . . 531
Mills, S.C. (E2-08) . . . 120
Milošević, M.V. (O7-06) . . . 461
Min, B. (J4-04) . . . 283
Mina, M. (G6-01) . . . 206
Mina, M. (I2-16) . . . 250
Minami, S. (M4-01) . . . 371
Mineo, F. (M3-12) . . . 370
Minikayev, R. (E5-10) . . . 137
Minuti, A. (Q5-03) . . . 529
Misba, W. (O2-13) . . . 434
Mishchenko, A.S. (P6-07) . . . 498
Mishina, E. (L3-07) . . . 336
Mishina, E. (L3-08) . . . 337
Mishra, A. (H1-11) . . . 215
Mishra, A. (O4-11) . . . 446
Mishra, K. (I2-11) . . . 247
Mishra, S.R. (H4-05) . . . 230
Misirlioglu, I. (Q1-02) . . . 508
Mitobe, K. (K5-03) . . . 318
Mitrofanov, A. (K3-01) . . . 308
Mittelstaedt, J.A. (J4-10) . . . 286
Mittelstaedt, J.A. (O1-04) . . . 422
Mitteramskogler, T. (B1-13) . . . 38
Miura, A. (M4-06) . . . 373
Miura, D. (M4-04) . . . 372
Miura, Y. (M4-06) . . . 373
Miwa, S. (M4-01) . . . 371
Miwa, S. (O4-07) . . . 445
Mix, T. (Q1-08) . . . 510
Miyahara, S. (D3-07) . . . 98
Miyahara, S. (D3-10) . . . 99
Miyamoto, Y. (R1-02) . . . 538
Miyamura, H. (C3-01) . . . 67
Miyashita, S. (C2-01) . . . 62
Miyazaki, K. (P6-12) . . . 500
Miyazaki, T. (I1-03) . . . 239
Miyazaki, T. (L3-10) . . . 337
Miyazaki, Y. (F5-12) . . . 168
Miyazaki, Y. (H5-04) . . . 233
Miyazawa, Y. (I2-04) . . . 244
Mizrahi, A. (Q3-06) . . . 520
Mizuguchi, M. (I4-15) . . . 263
Mizuguchi, M. (O2-10) . . . 432
Mizukami, S. (C5-01) . . . 79
Mizukami, S. (E3-02) . . . 124
Mizukami, S. (E3-03) . . . 124
Mizukami, S. (J4-02) . . . 282
Mizukami, S. (Q2-02) . . . 513
Mizukami, S. (R3-11) . . . 555
Mizuno, Y. (F6-04) . . . 171
Mizutani, D. (I1-03) . . . 239
Mo, C. (F6-06) . . . 172
Mo, W. (R5-04) . . . 565
Modak, R. (O4-09) . . . 445
Moeller, T.B. (P2-11) . . . 477
Mohan, R. (G3-01) . . . 190
Mohanty, H.N. (E5-12) . . . 138
Mohanty, J.R. (E5-12) . . . 138
Mohanty, J.R. (O5-09) . . . 451
Mohanty, P. (H2-05) . . . 220
Mohanty, P. (P5-10) . . . 493
Mohapatra, J. (G5-13) . . . 205
Mohapatra, J. (K5-04) . . . 319
Mohd Noor Sam, M. (N5-02) . . . 410
Mohelsky, I. (H5-01) . . . 232
Mohseni, M. (N2-08) . . . 396
Mokrousov, Y. (G3-08) . . . 192
Mokrousov, Y. (J4-05) . . . 284
Mokrousov, Y. (O3-04) . . . 438
Mole, R. (A2-01) . . . 8
Molina-Luna, L. (H3-14) . . . 227
Molodtsov, S. (G3-06) . . . 191

Momose, S. (I3-07) 254
Mondelli, C. (A4-05) 22
Monson, T. (J2-06) 275
Monteblanco, E. (F3-02) 153
Monton, C. (K2-06) 305
Montoya, I. (D1-01) 83
Montoya, S. (N1-01) 387
Moodera, J.S. (R4-09) 561
Moody, S. (I3-01) 251
Moore, T. (H1-15) 217
Moorsom, T. (D1-07) 86
Morales, I. (E2-13) 121
Morales, M.P. (F2-18) 150
Morales, M.P. (P1-05) 469
Morales, R. (D1-01) 83
Morali, N. (S1-01) 105
Morel, L. (N5-13) 415
Moreno-Ramírez, L.M. (A4-09) 24
Mori, K. (N5-16) 417
Morishima, K. (K4-12) 316
Moro, M.V. (C1-07) 57
Moro, M.V. (I2-11) 247
Morozkin, A.V. (A4-17) 27
Morrison, K. (E1-10) 115
Morrison, K. (E4-14) 134
Morshed, M. (R2-02) 545
Mosey, A. (N4-08) 409
Moskalev, M. (D1-09) 87
Mostarac, D. (A4-15) 26
Mottaghi, N. (Q2-08) 515
Moulin, J. (F3-02) 153
Moulin, J. (F3-08) 155
Moyano, A. (P1-05) 469
Mucha, N. (F1-09) 143
Mucha, N. (F2-06) 147
Muchharla, B. (G5-07) 203
Muchharla, B. (K2-07) 305
Muchharla, B. (P1-06) 470
Mudgal, R. (M3-06) 367
Mudryk, Y. (F2-12) 148
Mudryk, Y. (J5-14) 292
Mudryk, Y. (L4-06) 343
Muduli, P.K. (M3-06) 367
Muduli, P.K. (M6-11) 385
Muduli, P.K. (O5-08) 450
Muduli, P.K. (P6-02) 496
Muduli, P.K. (Q3-07) 520
Mueller, B. (E2-01) 117
Mugarza, A. (B2-04) 41
Mühl, T. (Q4-01) 522
Mukharjee, P.K. (B4-01) 51
Müller, C. (F3-01) 152
Muller, D.A. (Q4-02) 522
Müller, L. (G3-05) 191
Munoz-Menendez, C. (Q2-10) 516
Muñoz-Noval, A. (J1-06) 271
Muraca, D. (C1-08) 58
Murakami, M. (G3-10) 193
Muralidhar, S. (Q3-04) 519
Muramatsu, S. (L3-10) 337
Murnane, M. (E1-07) 114
Murray, C. (L3-06) 336
Muscas, G. (B1-12) 37
Muscas, G. (H3-03) 224
Musembi, R.J. (B4-06) 52
Musiienko-Shmarova, H. (E4-12) 132
Muthui, Z.W. (B4-06) 52
Muzzio, R. (J4-01) 282
Mwabora, J.M. (B4-06) 52
Myint, B. (B1-09) 35
Myint, L.M. (N3-08) 403

- N -

N'Diaye, A.T. (G2-02) 183
N'Diaye, A.T. (M2-01) 359
N'Diaye, A.T. (M2-04) 360
N'Diaye, A.T. (N4-08) 409
N'Diaye, A.T. (O3-11) 440
N'Diaye, A.T. (P2-10) 477
Na, S. (Q1-11) 511
Nagahama, T. (M6-10) 384
Nagahama, T. (P6-14) 501
Nagashima, Y. (H5-04) 233
Nagatana, M. (I2-04) 244
Nagel, K. (O2-01) 428
Nagel, U. (A2-03) 8
Nah, J. (F4-13) 163
Nahar, R. (A3-09) 17
Nahir, K. (F4-07) 161
Nair, A. (Q5-12) 532
Nair, M.N. (K2-08) 306
Nakada, K. (R3-12) 556
Nakagawa, H. (K5-10) 321
Nakagawa, Y. (O1-12) 425
Nakajima, K. (B3-10) 49
Nakajima, Y. (B1-14) 38
Nakamura, H. (L1-04) 324
Nakamura, S. (A2-06) 9
Nakamura, S. (F5-05) 165
Nakano, S. (K4-01) 313
NAKATANI, R. (C5-06) 81
NAKATANI, R. (N1-06) 389
Nakatsuji, S. (A2-06) 9
Nakatsuji, S. (M4-01) 371
Nakatsuji, S. (S1-05) 106
Nakayama, H. (H4-04) 229
naletov, v.v. (M4-09) 374
naletov, v.v. (M4-11) 375
naletov, v.v. (N2-09) 396
naletov, v.v. (Q2-01) 513
Nalevanko, S. (G6-09) 209
Namai, A. (C1-05) 56
Namai, A. (I2-05) 245
Nandy, A.K. (O3-11) 440
Narasimham, A. (O2-01) 428
Narasimham, A.J. (P6-06) 497
Narkowicz, R. (E4-03) 128
Narkowicz, R. (M3-05) 366
Nartu, M.S. (J2-07) 275
Natali, F. (D1-11) 88
Natali, F. (I4-14) 262
Natekar, N.A. (P2-03) 473
Natera Cordero, N. (K3-03) 309
Natera Cordero, N. (K4-10) 316
Nath, R. (B4-01) 51
Naumov, S.V. (J5-08) 290
Navarro, E. (D1-12) 88
Navarro, E. (F2-18) 150
Navarro, E. (H1-05) 213
Navarro, E. (H1-08) 214
Navarro, E. (H1-09) 215
Navas, D. (B1-08) 35
Navau, C. (M3-10) 369
Nayak, S. (D1-02) 83
Ncube, S. (D2-04) 91
Need, R. (J5-01) 288
Nefedev, K. (A2-04) 9
Negi, D. (S2-05) 109
Nehruji, V. (R2-09) 548
Nelson-Cheeseman, B. (A1-10) 7
Nelson-Cheeseman, B. (C4-09) 77
Nelson-Cheeseman, B. (L4-05) 342
Nelson-Cheeseman, B. (L4-10) 344
Nelson-Cheeseman, B. (L4-16) 346
Nelson, J.N. (Q4-02) 522
Nembach, H. (C1-02) 54
Nembach, H. (C1-12) 60
Nembach, H. (E1-07) 114
Nembach, H. (R2-06) 546
Nemtsev, I. (G6-12) 210
Nemtsev, I. (R5-09) 567
Nenno, D.M. (R4-07) 560
Nepal, B. (A3-03) 14
Nepal, B. (L3-06) 336
Nepal, B. (O6-17) 457
Nepal, R. (M5-11) 379
Nesser, M. (O5-07) 450
Nessi, L. (Q4-11) 526
Neu, V. (C4-08) 76
Neu, V. (L1-01) 323
Newbold, B. (E2-04) 118
Newbold, B. (E2-05) 119
Newell, B. (N5-13) 415
Newhouse-Illige, T. (G1-02) 178
Newhouse-Illige, T. (G1-05) 179
Newman, D. (P2-10) 477
Ney, A. (C1-07) 57
Ney, A. (E4-03) 128
Ney, A. (M3-05) 366
Ney, V. (C1-07) 57
Ney, V. (E4-03) 128
Ney, V. (M3-05) 366
Ng, V. (B1-09) 35
Ng, V. (E2-07) 119
Ngo, S. (C1-12) 60
Ngouagnia, I. (N1-03) 388
Nguedjang Kouakeuo, S. (N5-13) 415
Nguiepe Segnou, C. (R1-10) 541
Nguyen, B.T. (N3-12) 405
Nguyen, H. (K4-01) 313
Nguyen, L. (Q5-12) 532

Nguyen, M. (E2-03) . . . 118
Nguyen, V. (O2-04) . . . 430
Ni, X. (I2-13) . . . 249
Nichols, J. (H2-09) . . . 221
Nicholson, B. (S2-03) . . . 108
Nicolaides, C. (R4-08) . . . 560
Nie, R. (J6-11) . . . 296
Nie, T. (M6-07) . . . 383
Nielsch, K. (K1-03) . . . 298
Nielsch, K. (Q1-08) . . . 510
Nien, C. (S1-04) . . . 106
Nieves, P. (Q2-10) . . . 516
Niimi, Y. (G5-05) . . . 202
Niimi, Y. (O1-14) . . . 426
Nikitov, S. (E5-07) . . . 136
Nikitov, S. (O7-07) . . . 461
Nikitov, S. (O7-10) . . . 463
Nikitov, S. (R4-11) . . . 562
Nikolaev, S.A. (B4-02) . . . 51
Nikolaev, S.A. (P5-07) . . . 492
Nikonov, D. (Q4-05) . . . 523
Ning, S. (P5-14) . . . 495
Niraula, G. (C1-08) . . . 58
Nishida, K. (P6-09) . . . 499
Nishimoto, S. (A2-01) . . . 8
Nishino, M. (C2-01) . . . 62
Nishio-Hamane, D. (H3-08) . . . 225
Nishio-Hamane, D. (M4-01) . . . 371
Nishio, T. (I4-15) . . . 263
Nishioka, K. (O2-06) . . . 431
Nlebedim, I.C. (B2-09) . . . 43
Nlebedim, I.C. (C2-03) . . . 63
Nlebedim, I.C. (C2-08) . . . 65
Nlebedim, I.C. (H3-04) . . . 224
Nodo, S. (P6-14) . . . 501
Noebe, R. (J3-04) . . . 278
Noël, P. (N2-09) . . . 396
Noël, P. (Q4-11) . . . 526
Noël, P. (R4-10) . . . 561
Nogovitsyna, T. (E5-03) . . . 135
Noguchi, N. (N5-11) . . . 414
Noh, M. (C3-05) . . . 69
Noky, J. (E1-01) . . . 111
Nomoto, T. (M4-01) . . . 371
Nomura, E. (O6-04) . . . 453
Nomura, H. (C5-06) . . . 81
Nomura, H. (N1-06) . . . 389
Nordström, L. (D2-10) . . . 93
Nossov, A.P. (P5-03) . . . 490
Nouailhetas, Q. (J3-09) . . . 279
Novák, V. (G1-10) . . . 180
Novák, V. (J6-07) . . . 294
Novák, V. (M1-09) . . . 356
Novati, A. (Q4-11) . . . 526
Novosad, V. (L3-15) . . . 340
Novosad, V. (M3-03) . . . 366
Novosad, V. (O4-12) . . . 447
Novosad, V. (S5-02) . . . 348
Nowak, U. (N1-05) . . . 389
Nozaki, T. (L2-03) . . . 330
Nozaki, Y. (C5-02) . . . 79
Nozaki, Y. (E4-08) . . . 130
Nozaki, Y. (O4-06) . . . 444
Nozawa, K. (H4-03) . . . 229
Ntallis, N. (B2-05) . . . 41
Ntallis, N. (B2-13) . . . 44
Ntallis, N. (E2-02) . . . 117
Nunez, A. (A4-11) . . . 24
Núñez, A. (E5-01) . . . 135

- O -

O'Brien, J. (L3-01) . . . 334
O'Brien, L. (K3-05) . . . 310
Obinata, S. (P6-12) . . . 500
Och, M. (K4-03) . . . 313
Ochirkhuyag, T. (D4-10) . . . 102
Odeh, Y.N. (Q1-02) . . . 508
Odintsov, S. (O7-10) . . . 463
Odkhuu, D. (D4-10) . . . 102
Odkhuu, D. (D4-11) . . . 103
Oepen, H. (G3-05) . . . 191
Oepen, H. (R4-05) . . . 559
Oezelt, H. (P3-01) . . . 478
Ogata, K. (I2-05) . . . 245
Ogawa, D. (H3-10) . . . 226
Ogawa, T. (N3-03) . . . 401
Ogawa, Y. (H3-08) . . . 225
Ogloblichev, V.V. (H2-12) . . . 222
Ognev, A. (E5-07) . . . 136
Ognev, A. (E5-13) . . . 138
Ogrin, F. (I3-01) . . . 251
Ogrin, F. (Q5-01) . . . 528
Oh, J. (J4-04) . . . 283
Oh, J. (S1-03) . . . 105
Ohashi, K. (F6-03) . . . 170
Ohkoshi, S. (C1-05) . . . 56
Ohkoshi, S. (I2-05) . . . 245
Ohkubo, T. (H3-02) . . . 223
Ohkubo, T. (H3-10) . . . 226
Ohldag, H. (G1-04) . . . 178
Ohldag, H. (M3-05) . . . 366
Ohldag, H. (O4-12) . . . 447
Ohmer, D. (A4-07) . . . 23
Ohmer, D. (A4-08) . . . 23
Ohmer, D. (H3-14) . . . 227
Ohnishi, K. (P6-12) . . . 500
Ohno, H. (B1-14) . . . 38
Ohno, H. (J6-09) . . . 295
Ohno, H. (O2-11) . . . 433
Ohno, H. (S8-02) . . . 504
Ohno, Y. (B1-14) . . . 38
Ohshima, R. (J4-07) . . . 285
Ohshima, R. (L3-11) . . . 338
Ohshima, R. (M3-01) . . . 365
Ohta, H. (F6-03) . . . 170
Ohta, T. (G5-05) . . . 202
Ohya, S. (Q4-03) . . . 522
Ok, J. (H2-09) . . . 221
Ok, J. (M2-02) . . . 359
Okada, Y. (G5-05) . . . 202
Okada, Y. (O1-14) . . . 426
Okamoto, S. (H2-09) . . . 221
Okano, G. (C5-02) . . . 79
Okawauchi, Y. (I1-03) . . . 239
Okita, C. (F6-03) . . . 170
Okita, K. (H4-03) . . . 229
Okubo, S. (F6-03) . . . 170
Okuno, H. (R1-11) . . . 542
Oleaga, A. (A4-17) . . . 27
Oleaga, A. (A4-18) . . . 27
Olejník, K. (M1-09) . . . 356
Olive Méndez, S. (L4-03) . . . 342
Oliveira, J. (L4-12) . . . 345
Oliveira, L.L. (M6-01) . . . 381
Olivier, A. (P2-09) . . . 476
Ollefs, K. (H3-14) . . . 227
Olleros-Rodríguez, P. (N1-09) . . . 390
Omori, Y. (M4-02) . . . 371
One, R. (L2-04) . . . 330
Ono, K. (H1-03) . . . 211
Ono, S. (P6-14) . . . 501
Onodera, Y. (R3-11) . . . 555
Ontoso, N. (K4-09) . . . 315
Ontoso, N. (O1-13) . . . 426
Onur Mentes, T. (R2-11) . . . 548
Oogane, M. (F3-06) . . . 154
Oogane, M. (F3-07) . . . 155
Oogane, M. (N5-02) . . . 410
Opel, M. (P4-13) . . . 487
Opelt, K. (C2-06) . . . 64
Ophus, C. (F1-01) . . . 140
Ophus, C. (O3-11) . . . 440
Oppeneer, P.M. (I2-11) . . . 247
Orlandi, F. (F2-15) . . . 149
Ortega, D. (S3-05) . . . 176
Ortega, J. (S3-05) . . . 176
Ortix, C. (R4-03) . . . 559
Ortiz Jimenez, V. (G5-07) . . . 203
Ortiz Jimenez, V. (K2-07) . . . 305
Ortiz Jimenez, V. (P1-06) . . . 470
Ortiz, V.H. (G3-01) . . . 190
Oshima, D. (A3-07) . . . 16
Ostler, T. (P2-06) . . . 474
Ostler, T. (R1-06) . . . 540
Östman, E. (B1-12) . . . 37
Ota, M. (O2-09) . . . 432
Otani, Y. (S4-05) . . . 237
Otubo, L. (F5-11) . . . 168
Otubo, L. (R5-13) . . . 569
Otxoa, R.M. (M1-06) . . . 355
Ou, J. (C3-04) . . . 68
Ouaddi, A. (F4-04) . . . 160
Óvári, T. (R5-08) . . . 567
Ovcharenko, S.V. (L3-07) . . . 336
Ovcharenko, S.V. (L3-08) . . . 337
Ovchinnikov, A. (L3-03) . . . 335
Oyanagi, K. (C4-05) . . . 75
Oyarzun, S. (M5-13) . . . 380

Ozawa, T. (I4-05) 258
Özcan, S. (H2-03) 219
Ozeki, S. (C3-06) 69
Ozvat, T. (P1-01) 467

- P -

P S, A.K. (H5-06) 234
P, M. (H5-06) 234
P.D, B. (K1-12) 301
Pablo Navarro, J. (A1-02) 2
Pablo Navarro, J. (E2-01) 117
Pablo-Navarro, J. (L1-03) 323
Pac, A. (Q5-01) 528
Pagan, J.D. (K5-01) 318
Page, M. (I2-02) 243
Pahari, R. (E2-06) 119
Pahari, R. (E2-12) 121
Pai, C. (J4-06) 284
Pai, C. (M4-07) 373
Pai, C. (Q4-07) 524
Pai, C. (Q4-08) 525
Paillard, C. (H2-02) 219
Paillard, C. (P5-05) 491
Pakdelian, S. (R5-07) 566
Palanisamy, D. (H3-09) 226
Palma, J.L. (M5-13) 380
Palmstrom, C. (K4-05) 314
Palomares, F. (D1-12) 88
Palomares, F. (F2-18) 150
Palomares, F. (H1-05) 213
Pan, F. (P4-08) 486
Pan, H. (G4-06) 199
Pan, X. (G5-10) 204
Pancaldi, M. (B1-02) 33
Pancaldi, M. (S6-05) 352
Pandey, A. (A2-11) 12
Pandey, A. (I4-12) 262
Pandey, D. (B4-07) 53
Pandey, E. (A4-14) 25
Pandey, N. (R1-08) 541
Pandey, R. (L2-03) 330
Pandurangi, A.K. (J1-01) 268
Panier, S. (O5-07) 450
Panighel, M. (B2-04) 41
pannetier-lecoeur, M. (F3-02) 153
pannetier-lecoeur, M. (F3-08) 155
pannetier-lecoeur, M. (F3-09) 156
Pant, R. (F4-02) 159
Pant, R. (L4-13) 345
Paolo, B. (M3-08) 368
Paolo, B. (N2-07) 396
Paolo, B. (S8-01) 504
Papaefthimiou, V. (D1-08) 86
Papanicolaou, N. (M3-11) 369
Pappas, C. (D2-14) 94
Pappas, S.D. (B1-12) 37
Paranthaman, P. (B2-09) 43
Parchenko, S. (B1-05) 34
Parchenko, S. (I2-11) 247
Parigi, G. (P1-02) 467
Park, G. (E1-01) 111
Park, S. (C3-05) 69
Park, Y. (C3-05) 69
Parkes, M. (D1-14) 89
Parkin, S.S. (J6-02) 293
Parkin, S.S. (O3-12) 441
Parkin, S.S. (O4-01) 442
Parks, B. (G4-06) 199
Parthasarathy, A. (B2-12) 44
Paschen, S. (J5-06) 289
Pashenkin, I.Y. (A4-02) 20
Pasquale, M. (A5-01) 28
Pasquale, M. (L3-12) 338
Paszkowicz, W. (E5-10) 137
Patel, D.K. (A1-08) 5
Patel, S.K. (J3-02) 277
Pathak, A.K. (F2-05) 146
Pathak, A.K. (J5-14) 292
Pathak, A.K. (L4-06) 343
Pathak, P. (C3-10) 71
Pathak, P. (K1-06) 298
Pathak, S. (F4-02) 159
Pattabi, A. (M3-04) 366
Pattanaik, M.S. (B2-10) 43
Pattanaik, M.S. (F4-06) 160
Patterson, C. (O5-05) 449
Paudyal, D. (C2-02) 62
Paudyal, D. (D2-11) 94
Paul, A.A. (J2-08) 276
Paul, E. (F3-09) 156
Payyadi Porayil, R. (P5-09) 492
Pearce, C. (J2-06) 275
Pearson, J. (G1-13) 182
Pearson, J. (J6-12) 296
Pearson, J. (L3-15) 340
Pearson, J. (M3-03) 366
Pearson, J. (O4-12) 447
Pecharsky, V.K. (B4-04) 51
Pecharsky, V.K. (F2-12) 148
Pecharsky, V.K. (J5-14) 292
Pecharsky, V.K. (L4-06) 343
Pecharsky, V.K. (Q6-08) 536
Peddis, D. (B2-13) 44
Peddis, D. (Q5-04) 529
Pedersoli, E. (G3-05) 191
Pedersoli, E. (G3-08) 192
Pei, R. (H4-08) 231
Pelekhov, D. (F1-06) 142
Peña Garcia, J. (L2-06) 331
Peña Garcia, J. (R1-11) 542
Peña Garcia, J. (R2-11) 548
Peng, C. (Q4-07) 524
Peng, H. (R5-06) 566
Peng, J. (R5-04) 565
Peng, W. (C4-07) 76
Peng, W. (O7-12) 464
Penty, A. (P3-06) 480
Pereira, A. (L4-12) 345
Pereira, L.F. (D4-08) 102
Pereira, L.F. (F5-06) 166
Pereira, L.F. (F5-11) 168
Pereira, L.F. (R5-13) 569
Pereira, L.M. (K2-08) 306
Pereiro, E. (A1-02) 2
Pereiro, E. (L1-10) 326
Pereiro, E. (O5-01) 448
Pereiro, M. (D2-10) 93
Pereiro, M. (E2-02) 117
Pereiro, M. (L3-04) 335
Pereiro, M. (Q2-04) 514
Perevozchikova, Y.A. (H5-02) 232
Perevozchikova, Y.A. (H5-05) 234
Pérez del Real, R. (A1-03) 3
Pérez del Real, R. (H1-02) 211
Pérez del Real, R. (H1-08) 214
Pérez del Real, R. (Q5-08) 531
Pérez del Real, R. (R5-05) 565
Pérez del Real, R. (R5-07) 566
Pérez-Carmona, M. (O5-02) 448
Pérez-Checa, A. (A4-05) 22
Peria, W. (A3-12) 18
Perna, P. (N1-09) 390
Perrin, B. (K1-09) 300
Perrin, Y. (A2-05) 9
Perzhu, A. (M5-05) 378
Peterson, T. (P6-01) 496
Petit-Watelot, S. (E1-13) 116
Petit-Watelot, S. (G3-02) 190
Petit-Watelot, S. (M3-04) 366
Petit, D. (F1-03) 141
Petit, M. (I4-10) 261
Petiziol, F. (D2-02) 90
Petrenko, O. (E5-14) 139
Petrisor, T. (Q3-06) 520
Petrò, S. (Q4-11) 526
Petroff, F. (K4-03) 313
Pétrot, R. (S3-02) 174
Petti, D. (N2-11) 398
Pfeuffer, L. (F2-03) 146
Pfeuffer, L. (F2-04) 146
Pfeuffer, L. (F2-16) 150
Pham, H. (L4-02) 341
Pham, H.N. (J4-08) 285
Pham, H.N. (K4-01) 313
Pham, V. (K4-09) 315
Pham, V. (O3-07) 439
Pham, V. (Q4-05) 523
Pham, Y. (G5-07) 203
Pham, Y. (K2-07) 305
Pham, Y. (P1-06) 470
Phan, M. (E2-02) 117
Phan, M. (G5-07) 203
Phan, M. (I4-06) 259
Phan, M. (K2-03) 304
Phan, M. (K2-07) 305
Phan, M. (L4-02) 341
Phan, M. (P1-06) 470
Phase, D. (I4-12) 262
Philip, I. (O1-02) 421
Philippi-Kobs, A. (G3-05) 191
Philippi-Kobs, A. (R4-05) 559

Phung, T. (P4-12) . . . 487
Phuoc, C. (G6-02) . . . 206
Piantek, M. (B2-04) . . . 41
Picozzi, S. (Q4-11) . . . 526
Pietruczik, A. (E5-10) . . . 137
Pile, S. (C1-07) . . . 57
Pile, S. (E4-03) . . . 128
Pile, S. (M3-05) . . . 366
Pillsbury, T. (S5-02) . . . 348
Pineau, C. (O5-07) . . . 450
Pioro-Ladrière, M. (C5-03) . . . 80
Piovano, A. (E4-14) . . . 134
Pirro, P. (E4-12) . . . 132
Pirro, P. (N2-08) . . . 396
Pištora, J. (E1-11) . . . 115
Pizzini, S. (E5-08) . . . 137
Pizzini, S. (L2-06) . . . 331
Pizzini, S. (R1-11) . . . 542
Pizzini, S. (R2-11) . . . 548
Plakhotskiy, D. (F2-14) . . . 149
Plakhotskiy, D. (L4-11) . . . 344
Plumer, M.L. (P3-04) . . . 479
Podgornykh, S.M. (J5-08) . . . 290
Pohlit, M. (B1-12) . . . 37
Pohlmann, T. (C1-11) . . . 59
Pokharel Madhogaria, R. (I4-06) . . . 259
Pokhrel, A. (A3-06) . . . 15
Pokhrel, A. (I3-03) . . . 252
Pokhrel, A. (L3-06) . . . 336
Pokhrel, A. (O6-17) . . . 457
Polakovic, T. (L3-15) . . . 340
Polat, Ö. (H5-01) . . . 232
Polčak, J. (H5-01) . . . 232
Polewczyk, V. (F2-01) . . . 145
Poli, E. (D1-07) . . . 86
Polley, D. (G3-12) . . . 194
Polushkin, N.I. (A4-02) . . . 20
Polushkin, N.I. (P2-11) . . . 477
Polzikova, N. (R4-11) . . . 562
Poole, S.F. (M1-09) . . . 356
Poon, J. (Q1-12) . . . 512
Poon, J. (R2-06) . . . 546
Popescu, H. (I3-01) . . . 251
Porro, J. (A4-05) . . . 22
Porter, D.G. (P3-02) . . . 478
Porter, Z. (J5-01) . . . 288
Postiglione, W. (M2-03) . . . 359
Postnikov, E. (F4-03) . . . 159
Potapov, A.M. (H2-12) . . . 222
Poudel, T.P. (H4-05) . . . 230
Poulsen, E.B. (P3-03) . . . 479
Povzner, A. (E5-03) . . . 135
Prabhakaran, D. (M3-09) . . . 368
Prabhu Gaunkar, N. (G6-01) . . . 206
Prabhu Gaunkar, N. (I2-16) . . . 250
Prakash, R. (E1-05) . . . 113
Pratt, A. (E2-10) . . . 120
Pratt, A. (G5-03) . . . 201
Pratt, A. (L1-06) . . . 325
Prejbeanu, L. (B3-09) . . . 49
Prejbeanu, L. (G4-02) . . . 197
Prejbeanu, L. (O2-02) . . . 429
Prejbeanu, L. (P2-09) . . . 476
Preobrajenski, V. (L3-07) . . . 336
Pribiag, V.S. (K3-06) . . . 311
Prida, V.M. (H5-03) . . . 233
Prieto, J. (O5-02) . . . 448
Primetzhofer, D. (C1-07) . . . 57
Primetzhofer, D. (H3-03) . . . 224
Prinsloo, A. (D2-04) . . . 91
Prinsloo, A. (H2-05) . . . 220
Prinsloo, A. (P5-10) . . . 493
Prinsloo, A. (R5-16) . . . 571
Prinsloo, A. (R5-17) . . . 571
Prokhorov, A.S. (Q1-09) . . . 510
Prosandeev, S. (P5-05) . . . 491
Provino, A. (A4-18) . . . 27
Prudnikov, P.V. (F5-09) . . . 167
Prudnikov, V.V. (F5-09) . . . 167
Przybylski, M. (P1-02) . . . 467
Przybylski, M. (P1-03) . . . 468
Pu, Y. (R3-03) . . . 551
Puliafito, V. (M1-08) . . . 356
Purani, D. (N3-14) . . . 406
Purbawati, A. (O1-02) . . . 421
Pustak, A. (F4-12) . . . 162
Puttock, R. (L1-01) . . . 323
Puttock, R. (R1-06) . . . 540
Puwenberg, N. (Q4-01) . . . 522
Puzniak, R. (E5-10) . . . 137
Puzniak, R. (F2-07) . . . 147
Pylypovskyi, O. (A1-05) . . . 4
Pylypovskyi, O. (J6-05) . . . 294
Pylypovskyi, O. (R1-09) . . . 541
Pyo, H. (R5-15) . . . 570

- Q -

Qaiumzadeh, A. (G1-11) . . . 181
Qaiumzadeh, A. (N2-10) . . . 397
Qi, S. (G5-09) . . . 204
Qian, K. (C1-04) . . . 56
Qian, L. (O4-08) . . . 445
Qian, Z. (F3-11) . . . 156
Qiang, B. (F5-05) . . . 165
Qiang, B. (I3-07) . . . 254
Qin, F. (R5-06) . . . 566
Qin, J. (I2-10) . . . 247
Qin, J. (I2-12) . . . 248
Qiu, J. (C3-04) . . . 68
Qiu, J. (F4-10) . . . 162
Qiu, J. (O2-15) . . . 435
Qiu, Z.Q. (A3-08) . . . 16
Qiu, Z.Q. (S2-02) . . . 108
Qu, d. (I2-01) . . . 243
Qu, D. (J4-09) . . . 286
Qu, D. (M1-11) . . . 357
Qu, H. (L3-15) . . . 340
Qu, T. (Q2-03) . . . 514
Quan, L. (D3-04) . . . 97
Quan, W. (C1-06) . . . 57
Quan, W. (P5-12) . . . 494
Quarterman, P. (F1-04) . . . 141
Quarterman, P. (K2-04) . . . 304
Quarterman, P. (L2-08) . . . 332
Quarterman, P. (Q4-09) . . . 525
Querlioz, D. (Q3-06) . . . 520
Quessab, Y. (P2-01) . . . 472
Quessab, Y. (R2-02) . . . 545
Quessab, Y. (R2-05) . . . 546
Quessab, Y. (R2-06) . . . 546
Quintana-Puebla, A. (L2-07) . . . 332
Quintana, A. (I3-08) . . . 255
Quintana, A. (L2-08) . . . 332
Quiros, C. (L1-10) . . . 326
Quiros, C. (O5-01) . . . 448

- R -

Raab, K. (N1-05) . . . 389
Raab, K. (N1-08) . . . 390
Raabe, D. (H3-09) . . . 226
Raabe, J. (M5-02) . . . 377
Raabe, J. (N2-11) . . . 398
Raabe, J. (R3-01) . . . 550
Rackham, J. (E2-04) . . . 118
Rackham, J. (E2-05) . . . 119
Radaelli, P. (O3-02) . . . 437
Radelytskyi, I. (F2-07) . . . 147
Radomski, A. (I1-06) . . . 240
Radon, P. (S3-04) . . . 175
Radousky, H. (C2-05) . . . 64
Radu, C. (I2-14) . . . 249
Radu, I. (O2-04) . . . 430
Radulov, I. (H3-14) . . . 227
Radulov, I. (Q1-06) . . . 509
Raeliarijaona, A.S. (M5-11) . . . 379
Raevskiy, A. (R4-11) . . . 562
Ragusa, C. (J2-03) . . . 273
Rahimi, M. (J5-11) . . . 291
Rai, A. (A3-04) . . . 14
Rai, A. (A3-05) . . . 15
Rai, A. (A3-06) . . . 15
Rai, A. (A3-09) . . . 17
Rai, A. (I3-03) . . . 252
Rai, A. (O6-17) . . . 457
Rai, B.K. (H4-05) . . . 230
Raikher, Y. (A4-16) . . . 26
Rajan, A. (J4-05) . . . 284
Rajib, M. (O2-13) . . . 434
Rajib, M. (P1-04) . . . 469
Rakheja, S. (B2-12) . . . 44
Ralph, D. (J4-10) . . . 286
Ralph, D. (M1-03) . . . 354
Ralph, D. (O1-04) . . . 422
Ralph, D. (Q4-02) . . . 522
Ralph, D. (S5-05) . . . 349
Rama-Eiroa, R. (M1-06) . . . 355
Ramamoorthi, N. (A4-01) . . . 20
Ramanujan, R. (B2-10) . . . 43
Ramanujan, R. (F4-06) . . . 160

Ramanujan, R. (J2-07) 275
Ramirez, J. (M2-10) 362
Ramos, A. (G5-13) 205
Ramos, R. (M1-02) 353
Ramos, R. (P4-07) 485
Ramu, M. (O3-06) 438
Rana, B. (S7-01) 418
Rana, F. (M1-03) 354
Rana, K. (I3-06) 254
Rana, K. (N1-10) 391
Rana, K. (O3-07) 439
Rana, K. (O3-08) 439
Rana, K. (Q1-05) 509
Rancan, M. (B2-03) 41
Ranchal, R. (D1-05) 85
Rani, P. (H3-03) 224
Rani, P. (M6-08) 384
Ranjit, S. (A3-03) 14
Ranjit, S. (A3-09) 17
Ranjith, K. (B4-01) 51
Rannala, S.E. (P2-05) 474
Ranno, L. (I3-11) 256
Ranno, L. (L2-06) 331
Rao, M. (P5-09) 492
Rao, S. (L2-05) 331
Rao, S. (O2-04) 430
Rao, S. (R3-04) 552
Rappe, A. (E1-09) 115
Rasing, T. (P2-09) 476
Rastogi, A. (H2-09) 221
Rastogi, P. (K5-06) 320
RATH, C. (I4-11) 261
Rathi, A. (L4-13) 345
Ratkovski, D.R. (K1-14) 302
Raulet, M. (N5-13) 415
Ravelosona, D. (N1-10) 391
Razavi, S. (I3-05) 253
Razavi, S. (N1-12) 392
Read, T. (P1-03) 468
Reddy, V. (H1-11) 215
Reddy, V.R. (J2-05) 274
Redondo, C. (D1-01) 83
Reeve, R.M. (L1-05) 324
Reeve, R.M. (R1-05) 539
Register, L.F. (E5-05) 136
Regmi, S. (E1-03) 112
Reguera, J. (J1-06) 271
Reichlova, H. (E1-01) 111
Reid, A. (E2-04) 118
Reid, A. (E2-05) 119
Reiffers, M. (A4-01) 20
Reiffers, M. (G6-09) 209
Reijonen, J. (C2-07) 65
Reimers, S. (G1-10) 180
Reimers, S. (J6-07) 294
Reimers, S. (M1-09) 356
Reitz, D. (G1-08) 179
Reitz, D. (M4-11) 375
Reks, A. (F4-03) 159
Rethfeld, B. (G3-03) 190
Rethfeld, B. (G3-11) 194
Rethfeld, B. (R4-12) 563
Retterer, S. (B1-06) 34
Reynolds, N.D. (H1-12) 216
Reyren, N. (E5-08) 137
Reyren, N. (I3-09) 255
Reyren, N. (I3-10) 256
Reyren, N. (L1-11) 327
Reyren, N. (N1-03) 388
Reyren, N. (O3-13) 441
Rezende, S.M. (R4-09) 561
Richards, C. (F1-11) 144
Richardson, R. (C3-14) 73
Richter, K. (L3-05) 335
Rico, J. (B2-14) 45
Riddiford, L.J. (A3-02) 13
Riddiford, L.J. (M2-01) 359
Riedo, E. (N2-11) 398
Riegg, S. (C2-07) 65
Riente, F. (E5-02) 135
Riepp, M. (G3-05) 191
Righi, L. (F2-15) 149
Riley, G.A. (C1-02) 54
Riley, G.A. (C1-12) 60
Riley, G.A. (R2-06) 546
Rimal, G. (S5-02) 348
Rimmler, B. (J6-02) 293
Rinaldi, C. (N2-11) 398
Rinaldi, C. (Q4-11) 526
Rinaldi, C. (R3-14) 557
Rinaldi, M. (F3-11) 156
Riordan, E. (Q2-11) 517
Ritzinger, P. (E1-01) 111
Rivas, M. (P1-05) 469
Rivas, M. (Q1-10) 511
Robert, J. (A2-03) 8
Robertson, M. (F1-01) 140
Robinson, A. (C4-09) 77
Robinson, A. (L4-05) 342
Robinson, A. (L4-10) 344
Robinson, A. (L4-16) 346
Robinson, I.K. (S6-04) 352
Robinson, T. (I5-05) 265
Robles, J. (E2-02) 117
Robredo, I. (K4-09) 315
Rode, K. (E1-02) 111
Rode, K. (E3-07) 125
Rode, K. (I2-06) 246
Rodewald, J. (C1-11) 59
Rodionova, V. (H1-07) 214
Rodrigues, P.S. (F5-11) 168
Rodriguez-Rodriguez, G. (O6-10) 455
Rodríguez-Suárez, R.L. (R4-09) 561
Roessler, U. (A2-01) 8
Roessler, U. (J6-05) 294
Rogero, C. (O4-02) 442
Rogers, M.D. (D1-07) 86
Rohart, S. (R2-11) 548
Rojas-Sanchez, J. (M3-04) 366
Roldán-Molina, A. (A4-11) 24
Román, A. (P3-12) 483
Romera, M. (B3-06) 48
Rønnow, H.M. (N1-07) 389
Rõõm, T. (A2-03) 8
Roos, M. (H5-08) 235
Roos, M. (P6-16) 502
Rosa, R.J. (M6-09) 384
Rosales-Rivera, A. (R5-02) 564
Rosamond, M. (M5-02) 377
Roschewsky, N. (J4-03) 283
Roschewsky, N. (J4-11) 287
Roseker, W. (G3-05) 191
Rosenberg, E. (C1-02) 54
Rosenberg, E.R. (C1-12) 60
Rosenberg, M. (K2-12) 307
Ross, A. (G1-11) 181
Ross, A. (N2-10) 397
Ross, C. (C1-02) 54
Ross, C. (C1-12) 60
Ross, C. (F1-04) 141
Ross, C. (K2-04) 304
Ross, C. (P5-14) 495
Ross, C. (R2-01) 544
Rossa, J.D. (C2-06) 64
Rotarescu, C. (R5-08) 567
Rothschild, A. (G1-11) 181
Rotunno, E. (S2-05) 109
Roubeau, O. (D2-03) 91
Rougemaille, N. (A2-05) 9
Rougemaille, N. (A2-08) 10
Rougemaille, N. (O1-02) 421
Roussigné, Y. (I3-11) 256
Roussigné, Y. (N1-10) 391
Roussigne, Y. (R1-10) 541
Rovillain, P. (K1-09) 300
Rovillain, P. (O7-16) 466
Rowan-Robinson, R. (C4-06) 75
Rowan-Robinson, R. (I2-11) 247
Rowan-Robinson, R. (S2-03) 108
Roy, K. (O4-11) 446
Roy, K. (R4-04) 559
Roy, M. (F1-09) 143
Roy, P. (M1-06) 355
Roy, S. (Q6-11) 537
Roy, S. (S6-04) 352
Royo, I. (N5-06) 412
Rozenberg, M. (L2-01) 329
Ruan, X. (J5-10) 290
Ruane, W. (F1-06) 142
Rubia-Rodríguez, I. (S3-05) 176
Rubín, J. (B2-03) 41
Rubín, J. (B2-04) 41
Rubin, M. (D2-03) 91
Rubio-Roy, M. (P2-09) 476
Rubiola, E. (B3-05) 48
Ruck, B. (D1-11) 88
Ruck, B. (I4-14) 262
Ruck, B. (J5-09) 290
Rueangnetr, N. (N3-08) 403
Ruffolo, B. (C5-03) 80
Ruffolo, B. (E3-05) 125
Ruiz-Gomez, S. (O3-08) 439
Ruiz, A. (D1-12) 88

Rule, K.C. (A2-01) . . . 8
Ruo Roch, M. (E5-02) . . . 135
Rupert, T. (J2-06) . . . 275
Rusalina, A. (M6-03) . . . 382
Rushforth, A.W. (A3-13) . . . 18
Rushforth, A.W. (G1-10) . . . 180
Rushforth, A.W. (J3-03) . . . 277
Rushforth, A.W. (M1-09) . . . 356
Russek, S.E. (P1-02) . . . 467
Russell, T. (A1-06) . . . 5
Rusz, J. (S2-05) . . . 109
Ruta, S. (G3-13) . . . 195
Ruta, S. (N1-09) . . . 390
Ruta, S. (N3-12) . . . 405
Ruta, S. (P2-05) . . . 474
Ruta, S. (P2-06) . . . 474
Ruta, S. (P2-07) . . . 475
Ruta, S. (Q2-09) . . . 516
Ruta, S. (Q2-10) . . . 516
Ruwisch, K. (C1-11) . . . 59
Ryapolov, P. (F4-03) . . . 159
Ryba, T. (G6-09) . . . 209
Rybin, A. (A2-04) . . . 9
Rybin, A. (D1-13) . . . 89
Rybin, A. (M5-05) . . . 378

- S -

S, L. (K1-12) . . . 301
S, S. (A4-01) . . . 20
S, S. (K1-12) . . . 301
S. A., S. (M2-15) . . . 363
S., I. (Q6-11) . . . 537
Sabani, D. (O7-06) . . . 461
Saccone, F.D. (R5-02) . . . 564
Saccone, M.D. (B1-15) . . . 39
Sacuto, A. (K1-09) . . . 300
Sadílek, J. (A2-08) . . . 10
Sadohara, A. (C3-06) . . . 69
Sadovnikov, A. (E5-07) . . . 136
Sadovnikov, A. (O6-09) . . . 455
Sadovnikov, A. (O7-07) . . . 461
Sadovnikov, A. (O7-10) . . . 463
Sadovnikov, A. (O7-11) . . . 463
Sadykov, R. (D2-14) . . . 94
Safeer, C. (K4-09) . . . 315
Safi Samghabadi, F. (P5-11) . . . 493
Safi, T.S. (G1-12) . . . 181
Safranski, C. (S5-03) . . . 349
Safronov, A.P. (J1-07) . . . 271
Sagasta, E. (Q4-05) . . . 523
Saglam, H. (J6-12) . . . 296
Saglam, H. (S1-03) . . . 105
Saha, R. (O3-12) . . . 441
Saha, R. (Q5-12) . . . 532
Saha, S. (G3-07) . . . 192
Sahasrabudhe, A. (A2-10) . . . 11
Sahdev, D. (M2-05) . . . 360
Sahoo, A.K. (E5-12) . . . 138
Sahoo, A.K. (O5-09) . . . 451
Sahu, P. (K4-14) . . . 317
Sai, R. (C1-13) . . . 60
Sai, R. (I2-04) . . . 244
Saied, J. (C1-01) . . . 54
Saika-Voivod, I. (P3-04) . . . 479
Saito, G. (H3-10) . . . 226
Saito, H. (K3-04) . . . 310
Saito, S. (N3-03) . . . 401
Saito, T. (D4-13) . . . 103
Saito, T. (H3-05) . . . 224
Saito, T. (H3-08) . . . 225
Saito, T. (N3-03) . . . 401
Saito, Y. (F6-03) . . . 170
Saito, Y. (P6-11) . . . 500
Saitoh, E. (M1-02) . . . 353
Saitoh, E. (P4-07) . . . 485
Sakai, A. (A2-06) . . . 9
Sakai, A. (M4-01) . . . 371
Sakai, K. (G5-05) . . . 202
Sakai, K. (N5-15) . . . 416
Sakai, N. (D3-01) . . . 96
Sakai, T. (A2-07) . . . 10
Sakakibara, M. (G2-13) . . . 188
Sakakibara, T. (A2-06) . . . 9
Sakakibara, Y. (O4-06) . . . 444
Sakuma, A. (M4-04) . . . 372
Sakuraba, Y. (M4-06) . . . 373
Sakuraba, Y. (O4-09) . . . 445
Sala, G. (E3-01) . . . 123
Sala, G. (R3-01) . . . 550
Salahuddin, S. (J4-03) . . . 283
Salahuddin, S. (J4-11) . . . 287
Salazar-Henao, N.A. (R5-02) . . . 564
Salazar, A. (A4-17) . . . 27
Salazar, A. (A4-18) . . . 27
Salazar, D. (H3-07) . . . 225
Sales, F.H. (M6-01) . . . 381
Sales, T.S. (D4-08) . . . 102
Sales, T.S. (F5-06) . . . 166
Sales, T.S. (F5-11) . . . 168
Sales, T.S. (R5-13) . . . 569
Salev, P. (L2-01) . . . 329
Salev, P. (R2-10) . . . 548
Salikhov, R. (O7-08) . . . 462
Sall, M. (N1-10) . . . 391
Salloum, E. (O5-07) . . . 450
Salvador, M. (P1-05) . . . 469
Samanta, T. (K2-02) . . . 303
Samardak, A. (E5-07) . . . 136
Samardak, A.S. (E5-07) . . . 136
Samardak, A.S. (E5-13) . . . 138
Samarth, N. (S5-02) . . . 348
Sambi, M. (B2-03) . . . 41
Sambi, M. (B2-04) . . . 41
Samsonov, K. (C5-04) . . . 80
San Emeterio Alvarez, L. (B3-04) . . . 47
San Emeterio Alvarez, L. (M3-08) . . . 368
Sanchez Hazen, D. (O2-02) . . . 429
Sánchez Llamazares, J.L. (L4-08) . . . 343
Sánchez Valdés, C.F. (L4-08) . . . 343
Sánchez-Agudo, M. (H1-05) . . . 213
Sánchez-Tejerina, L. (M1-08) . . . 356
Sanchez, J. (H1-09) . . . 215
Sánchez, P.A. (A4-15) . . . 26
Sánchez, P.A. (A4-16) . . . 26
Sandeman, K.G. (F2-10) . . . 148
Sandhoefner, S. (M5-11) . . . 379
Sankey, J. (C5-03) . . . 80
Sankey, J. (E3-05) . . . 125
Sanli, U. (E4-07) . . . 130
Sannidhi, A. (G2-08) . . . 186
Santana, A. (S3-05) . . . 176
Santini, P. (D2-01) . . . 90
Santini, P. (D2-02) . . . 90
Santini, P. (G2-01) . . . 183
Santos, E. (R4-09) . . . 561
Sanvito, S. (D2-01) . . . 90
Sanvito, S. (P4-03) . . . 484
Sanyal, B. (H2-04) . . . 220
Sanz-Hernandez, D. (A1-02) . . . 2
Sanz-Hernandez, D. (A1-09) . . . 6
Sapkota, A. (A3-03) . . . 14
Sapkota, A. (A3-04) . . . 14
Sapkota, A. (A3-06) . . . 15
Sapkota, A. (I3-03) . . . 252
Sapkota, A. (O6-17) . . . 457
Sapozhnikov, M.V. (A4-02) . . . 20
Saren, H. (O6-03) . . . 452
Saren, H. (P6-03) . . . 497
Sari, D. (J3-08) . . . 279
Sarkar, A. (B2-09) . . . 43
Sarkar, A. (C2-03) . . . 63
Sarkar, A. (R4-04) . . . 559
Sarnavskii, N. (M6-06) . . . 383
Sasaki, D.Y. (B1-06) . . . 34
Sasaki, D.Y. (L2-01) . . . 329
Sasaki, D.Y. (M2-04) . . . 360
Sasaki, S. (D3-10) . . . 99
Sasaki, S. (G5-01) . . . 200
Sasaki, T. (N4-02) . . . 407
Sassi, Y. (E5-08) . . . 137
Sassi, Y. (I3-09) . . . 255
Sassi, Y. (I3-10) . . . 256
Sassi, Y. (L1-11) . . . 327
Sassi, Y. (N1-03) . . . 388
Sassi, Y. (O3-13) . . . 441
sato, f. (D3-07) . . . 98
sato, f. (D3-10) . . . 99
Sato, F. (J1-09) . . . 272
Sato, H. (F6-04) . . . 171
Sato, H. (H1-04) . . . 212
Sato, H. (I1-07) . . . 241
Sato, N. (Q4-01) . . . 522
Sato, S. (Q4-03) . . . 522
Sato, T. (O6-04) . . . 453
Satoh, T. (O7-14) . . . 465
Sauer, V. (G2-11) . . . 187
Saugar, E. (R1-06) . . . 540
Saurina, J. (L4-09) . . . 344
Sauter, R. (E4-07) . . . 130
Savero Torres, W.F. (O1-01) . . . 421
Savovici, A. (P3-11) . . . 482

Saw, A.K. (Q6-08) . . . 536
Sawa, T. (D3-10) . . . 99
Sawada, R. (M4-02) . . . 371
Sawicki, M. (M1-09) . . . 356
Saxena, R.N. (D4-08) . . . 102
Saxena, R.N. (F5-06) . . . 166
Saxena, R.N. (F5-11) . . . 168
Saxena, R.N. (R5-13) . . . 569
Sayed, S. (J4-11) . . . 287
Sayedaghaee, S. (P5-05) . . . 491
Scagnoli, V. (G3-07) . . . 192
Scalise, L. (F5-06) . . . 166
Scaramuzzi, G. (N2-11) . . . 398
Schaefer, L. (H3-09) . . . 226
Schäfer, R. (K1-03) . . . 298
Schaffers, T. (E4-03) . . . 128
Schaffers, T. (M3-05) . . . 366
Schanilec, V. (A2-05) . . . 9
Schánilec, V. (A2-08) . . . 10
Scheibel, F. (F2-03) . . . 146
Scheibel, F. (F2-04) . . . 146
Scheibel, F. (F2-16) . . . 150
Scherz, A. (G3-05) . . . 191
Scherz, A. (G3-06) . . . 191
Scheumann, B. (B3-02) . . . 46
Schier, P. (S3-03) . . . 175
Schiewitz, D. (F3-01) . . . 152
Schiffer, P. (S6-01) . . . 351
Schio, P. (M6-12) . . . 385
Schlagel, D.L. (D2-14) . . . 94
Schlappa, J. (G3-06) . . . 191
Schleife, A. (D2-16) . . . 95
Schlenhoff, A. (I3-04) . . . 253
Schliep, K.B. (G2-07) . . . 185
Schlitz, R. (E1-01) . . . 111
Schlom, D.G. (M1-03) . . . 354
Schlom, D.G. (Q4-02) . . . 522
Schlottmann, P. (R4-01) . . . 558
Schmauch, J. (M2-07) . . . 361
Schmid, A.K. (F1-01) . . . 140
Schmid, A.K. (I3-08) . . . 255
Schmid, A.K. (O3-11) . . . 440
Schmidt, A. (B2-07) . . . 42
Schmidt, N. (R3-14) . . . 557
Schmitt, C. (M1-02) . . . 353
Schmitt, C. (P4-07) . . . 485
Schneider, H. (G3-03) . . . 190
Schneider, H. (R4-07) . . . 560
Schneider, H. (R4-12) . . . 563
Schneider, M. (E4-12) . . . 132
Schneider, M. (N2-08) . . . 396
Schneider, R. (M4-08) . . . 373
Schneider, R. (Q4-10) . . . 526
Schneider, S. (K1-03) . . . 298
Scholl, A. (S6-04) . . . 352
Schönenberger, T. (N1-07) . . . 389
Schönfeldt, M. (C2-06) . . . 64
Schönke, D. (L1-05) . . . 324
Schönke, D. (R1-05) . . . 539
Schotter, J. (B1-13) . . . 38
Schrefl, T. (B1-13) . . . 38
Schrefl, T. (P3-01) . . . 478
Schreiber, F. (M1-02)* . . . 353
Schrittwieser, S. (B1-13) . . . 38
Schuller, I.K. (D1-01) . . . 83
Schuller, I.K. (H2-01) . . . 219
Schuller, I.K. (K2-06) . . . 305
Schuller, I.K. (L2-01) . . . 329
Schuller, I.K. (R2-10) . . . 548
Schultheiss, H. (B3-02) . . . 46
Schultheiss, H. (E4-06) . . . 129
Schultheiss, H. (E4-10) . . . 131
Schultheiss, H. (O5-04) . . . 449
Schultheiss, H. (O7-08) . . . 462
Schultheiss, H. (Q4-01) . . . 522
Schultheiss, H. (Q4-04) . . . 523
Schultheiss, K. (E4-06) . . . 129
Schultheiss, K. (E4-10) . . . 131
Schütz, G. (I3-01) . . . 251
Schütz, G. (R2-06) . . . 546
Scipioni, L. (G1-02) . . . 178
Scipioni, L. (G1-05) . . . 179
Scott, B. (K1-01) . . . 297
Scott, E. (J5-02) . . . 288
Scott, J.N. (A3-10) . . . 17
Scott, J.N. (N4-04) . . . 408
Scott, J.N. (P2-08) . . . 475
Scott, J.N. (P2-10) . . . 477
Sebald, G. (Q2-05) . . . 514
Sedona, F. (B2-03) . . . 41
Sedona, F. (B2-04) . . . 41
Seehra, M.S. (Q2-08) . . . 515
Seekaew, N. (Q5-12) . . . 532
Seibel, C. (G3-03) . . . 190
Seibel, C. (G3-11) . . . 194
Seki, T. (M4-06) . . . 373
Seki, T. (O1-11) . . . 425
Seki, T. (O4-09) . . . 445
Sekiguchi, F. (A2-10) . . . 11
Sekino, M. (Q5-02) . . . 528
Sellmyer, D.J. (B4-08) . . . 53
Sellmyer, D.J. (E2-06) . . . 119
Sellmyer, D.J. (E2-12) . . . 121
Semiannikova, A. (H5-02) . . . 232
Semiannikova, A. (H5-05) . . . 234
Seneor, P. (K4-03) . . . 313
Seneor, P. (O3-13) . . . 441
Seng, B. (G3-08) . . . 192
Seng, B. (R1-05) . . . 539
Sentsho, Z. (R5-16) . . . 571
Seo, J. (F5-02) . . . 164
Seo, J. (F5-08) . . . 167
Seo, S. (F4-13) . . . 163
Sepehri Amin, H. (H3-02) . . . 223
Sepehri Amin, H. (H3-10) . . . 226
Sepulveda, A. (I2-03) . . . 244
Sepulveda, A. (Q5-11) . . . 532
Serantes, D. (Q2-09) . . . 516
Serantes, D. (Q2-10) . . . 516
Seren, H.R. (F4-09) . . . 161
Serga, A.A. (E4-12) . . . 132
Serrano, A. (H1-09) . . . 215
Serrano, R.L. (M6-12) . . . 385
Sert, E. (H2-03) . . . 219
Servet, B. (K4-03) . . . 313
Sese, J. (E2-01) . . . 117
Sessoli, R. (D2-01) . . . 90
Sessoli, R. (F5-07) . . . 166
Sethi, P. (B3-09) . . . 49
Sethi, P. (R3-08) . . . 554
Sha, C. (M3-07) . . . 367
Sha, Y. (J2-04) . . . 274
Shadman, A. (R3-07) . . . 553
Shafer, P. (A3-08) . . . 16
Shafer, P. (C1-11) . . . 59
Shafer, P. (M2-04) . . . 360
Shafer, P. (P2-10) . . . 477
Shah, P.J. (I2-02) . . . 243
Shahrokhvand, M. (M1-09) . . . 356
Shaib, A. (I4-14) . . . 262
Shaikh, M. (H2-04) . . . 220
Shaji, S. (F2-06) . . . 147
Shan, J. (O1-04) . . . 422
Shao, Y. (E4-13) . . . 133
Shao, Y. (G4-05) . . . 198
Sharafullin, I. (M5-04) . . . 378
Sharangi, P. (A4-14) . . . 25
Sharangi, P. (J5-12) . . . 291
Sharangi, P. (O4-10) . . . 446
Sharma, P. (C4-03) . . . 74
Sharma, S. (H3-14) . . . 227
Sharma, S.K. (C1-08) . . . 58
Shcherbakov, D.L. (O1-05) . . . 422
Shcherbinin, S.V. (J1-07) . . . 271
Sheffels, S. (R2-06) . . . 546
Sheka, D. (A1-05) . . . 4
Sheka, D. (J6-05) . . . 294
Sheka, D. (R1-09) . . . 541
Shen, K.M. (Q4-02) . . . 522
Shen, Q. (A4-03) . . . 21
Shen, X. (K3-07) . . . 311
Shen, X. (M3-02) . . . 365
Shepard, A. (G1-02) . . . 178
Shepard, A. (G1-05) . . . 179
Shepeta, N. (G6-12) . . . 210
Sheppard, C. (D2-04) . . . 91
Sheppard, C. (H2-05) . . . 220
Sheppard, C. (P5-10) . . . 493
Sheppard, C. (R5-16) . . . 571
Sheppard, C. (R5-17) . . . 571
Sheridan, R.S. (H3-13) . . . 227
Sherwin, M. (S4-02) . . . 236
Sheshukova, S. (O7-07) . . . 461
Sheshukova, S. (O7-10) . . . 463
Sheu, S. (O2-12) . . . 433
Shevchenko, Y. (D1-13) . . . 89
Shevchenko, Y. (M5-05) . . . 378
Shi, D. (F6-02) . . . 170
Shi, D. (M1-05) . . . 355
Shi, D. (M6-02) . . . 381
Shi, G. (R4-01) . . . 558
Shi, J. (A4-10) . . . 24
Shi, J. (G1-08) . . . 179

*Best student presentation award finalist

Shi, J. (Q2-08) . . . 515
Shi, J. (S4-02) . . . 236
Shi, S. (A1-06) . . . 5
Shi, S. (S5-05) . . . 349
Shi, X. (I4-02) . . . 257
Shi, X. (M3-04) . . . 366
Shi, Y. (F6-02) . . . 170
Shi, Y. (Q1-04) . . . 508
Shigematsu, E. (J4-07) . . . 285
Shigematsu, E. (M3-01) . . . 365
Shikin, V.S. (B2-13) . . . 44
Shikoh, E. (P6-09) . . . 499
Shikoh, E. (P6-10) . . . 500
Shim, J.S. (S1-03) . . . 105
Shima, T. (H3-10) . . . 226
Shimada, T. (M6-10) . . . 384
Shimada, T. (P6-14) . . . 501
Shimada, Y. (I4-15) . . . 263
Shimizu, R. (I4-05) . . . 258
Shimohashi, F. (R2-07) . . . 547
Shimon, G. (O2-01) . . . 428
Shimura, M. (C5-01) . . . 79
Shin, J. (D3-08) . . . 98
Shin, K. (D3-03) . . . 96
Shin, K. (G6-06) . . . 207
Shin, M. (O2-16) . . . 435
Shinjo, T. (J4-07) . . . 285
Shinjo, T. (L3-11) . . . 338
Shinjo, T. (M3-01) . . . 365
Shinnoh, T. (G2-13) . . . 188
Shinya, H. (O1-12) . . . 425
Shiokawa, Y. (N4-02) . . . 407
Shirai, M. (M4-06) . . . 373
Shirai, S. (P6-10) . . . 500
Shiraishi, M. (J4-07) . . . 285
Shiraishi, M. (L3-11) . . . 338
Shiraishi, M. (M3-01) . . . 365
Shirokura, T. (J4-08) . . . 285
Shirotori, S. (N5-14) . . . 416
Shivashankar, S. (C1-13) . . . 60
Shoshi, A. (B1-13) . . . 38
Shoup, J. (I4-13) . . . 262
Shousha, M. (I1-02) . . . 238
Shrestha, N. (P6-04) . . . 497
Shu, X. (M1-01) . . . 353
Shu, X. (M2-14) . . . 363
Shuang, X. (I2-10) . . . 247
Shugaev, M.V. (P2-11) . . . 477
Shukla, A. (L2-03) . . . 330
Si, Q. (J5-06) . . . 289
Sichelschmidt, J. (B4-01) . . . 51
Siddiqui, S. (O1-03) . . . 421
Sidi El Valli, A. (B3-09) . . . 49
Sierra, J.F. (O1-01) . . . 421
Siewierska, K.E. (E1-02) . . . 111
Siewierska, K.E. (I2-06) . . . 246
Sigov, A. (L3-07) . . . 336
Sikola, T. (A2-08) . . . 10
Sikola, T. (H5-01) . . . 232
Silber, R. (E1-11) . . . 115
Silva, D. (L4-12) . . . 345
Silva, T. (E1-07) . . . 114
Silvani, R. (N2-11) . . . 398
Silvani, R. (O7-01) . . . 459
Silvani, R. (O7-02) . . . 459
Sim, M. (O3-06) . . . 438
Simensen, H.T. (G1-08) . . . 179
Simonet, V. (A2-03) . . . 8
Simpson, J. (G5-11) . . . 205
Simpson, J.R. (O1-05) . . . 422
Simpson, J.R. (O1-10) . . . 424
Sinaga, S. (G4-05) . . . 198
Sinclair, R. (S5-02) . . . 348
Singh, A. (F4-02) . . . 159
Singh, B.B. (A4-14) . . . 25
Singh, B.B. (D1-02) . . . 83
Singh, B.B. (O4-10) . . . 446
Singh, B.B. (O4-11) . . . 446
Singh, B.B. (R4-04) . . . 559
Singh, K. (F4-02) . . . 159
Singh, M. (M4-12) . . . 376
Singh, N. (B1-10) . . . 36
Singh, P. (B4-07) . . . 53
Singh, S. (B3-08) . . . 49
Singh, S. (J4-01) . . . 282
Singh, U. (Q3-07) . . . 520
Singleton, J. (K1-01) . . . 297
Sinitsyn, V. (L3-03) . . . 335
Sinova, J. (G1-11) . . . 181
Sinova, J. (P4-07) . . . 485
Sisodia, N. (O3-07) . . . 439
Själander, M. (P3-06) . . . 480
Sjöqvist, E. (D2-10) . . . 93
Sjöqvist, E. (E2-02) . . . 117
Sjöqvist, E. (Q2-04) . . . 514
SKARLATOS, A. (P3-07) . . . 481
Skaugen, A. (M3-13) . . . 370
Skjærvø, S.H. (B1-05) . . . 34
Sklenar, J. (G5-06) . . . 203
Sklenar, J. (M3-03) . . . 366
Sklenar, J. (O1-03) . . . 421
Sklenar, J. (S1-03) . . . 105
Skokov, K. (C2-07) . . . 65
Skokov, K. (F2-03) . . . 146
Skokov, K. (F2-04) . . . 146
Skokov, K. (F2-14) . . . 149
Skokov, K. (F2-16) . . . 150
Skokov, K. (H3-09) . . . 226
Skokov, K. (H3-14) . . . 227
Skokov, K. (L4-11) . . . 344
Skokov, K. (Q1-06) . . . 509
Skomski, R. (B4-08) . . . 53
Skomski, R. (E2-06) . . . 119
Skomski, R. (E2-12) . . . 121
Skoric, L. (A1-09) . . . 6
Skoropata, E. (D2-06) . . . 93
Skoropata, E. (H2-09) . . . 221
Skourski, Y. (B4-01) . . . 51
Skovdal, B. (C4-06) . . . 75
Slanovc, F. (B1-02) . . . 33
Slavin, A.N. (B3-09) . . . 49
Slavin, A.N. (E4-12) . . . 132
Slavin, A.N. (M4-09) . . . 374
Slavin, A.N. (Q2-01) . . . 513
Slavin, A.N. (R3-08) . . . 554
Slawinska, J. (Q4-11) . . . 526
Sleptsova, A.E. (Q1-09) . . . 510
Slimani, Y. (J3-09) . . . 279
Slöetjes, S. (B1-04) . . . 34
Slöetjes, S. (P3-10) . . . 482
Slovinska, L. (J1-03) . . . 269
Smirnov, A.V. (L4-06) . . . 343
Smirnov, D. (C3-14) . . . 73
Smith-Gray, N. (D4-14) . . . 104
Smith, A.R. (K2-13) . . . 307
Smith, D. (E2-05) . . . 119
Smith, D.A. (A3-04) . . . 14
Smith, D.A. (A3-05) . . . 15
Smythe, N. (K1-01) . . . 297
Snyder-Tinoco, D. (M5-11) . . . 379
Snyder, M. (I2-15) . . . 249
Soares, G. (L3-12) . . . 338
Soffa, W.A. (P3-11) . . . 482
Soh, J. (M3-09) . . . 368
Soh, Y. (J5-04) . . . 289
Sohn, C. (H2-09) . . . 221
Sokalski, V. (A3-06) . . . 15
Sokalski, V. (I3-03) . . . 252
Sokalski, V. (M5-08) . . . 379
Sokalski, V. (R1-08) . . . 541
Sokalski, V. (R1-12) . . . 542
Sokalski, V. (R2-08) . . . 547
Sokjabok, S. (N3-07) . . . 403
Sokolov, E. (F4-03) . . . 159
Sola, A. (J2-03) . . . 273
Soldatov, I. (E5-13) . . . 138
Soldatov, I. (K1-03) . . . 298
Soldatov, K. (D1-13) . . . 89
Soldatov, K. (M5-05) . . . 378
Solheid, P. (I2-14) . . . 249
Solignac, A. (F3-02) . . . 153
Solignac, A. (F3-08) . . . 155
Solignac, A. (F3-09) . . . 156
Solovyev, I. (B4-02) . . . 51
Solovyev, I. (P5-07) . . . 492
Soltys, J. (L1-02) . . . 323
Solyom, A. (C5-03) . . . 80
Solyom, A. (E3-05) . . . 125
Solzi, M. (F2-15) . . . 149
Son, H. (N3-10) . . . 404
Song, C. (P4-08) . . . 486
Song, J. (K3-02) . . . 308
Song, J. (R5-04) . . . 565
Sonoda, K. (P4-06) . . . 485
Sorace, L. (F5-07) . . . 166
Sorée, B. (O2-04) . . . 430
Sorrenti, A. (J1-04) . . . 270
Sorrentino, A. (A1-02) . . . 2
Sorrentino, A. (L1-10) . . . 326
Sorrentino, A. (O5-01) . . . 448
Soumah, L. (S8-01) . . . 504
Soumyanarayanan, A. (O3-06) . . . 438
Sousa, R. (B3-09) . . . 49

*Best student presentation award finalist

Sousa, R. (G4-02) . . . 197
Sousa, R. (O2-02) . . . 429
Sousa, R. (P2-09) . . . 476
Souza, R. (M6-09) . . . 384
Sozinov, A. (A4-05) . . . 22
Spaldin, N.A. (H2-07) . . . 221
Spaldin, N.A. (M2-13) . . . 363
Spatarelu, C. (S3-01) . . . 174
Spetzler, B. (F3-11) . . . 156
Spiesser, A.M. (K3-04) . . . 310
Srikanth, H. (E2-02) . . . 117
Srikanth, H. (I4-06) . . . 259
Srikanth, H. (L4-02) . . . 341
Srinivasan, K. (A3-11) . . . 18
Srinivasan, K. (I2-14) . . . 249
Srivastava, A. (A3-04) . . . 14
Srivastava, A. (J3-04) . . . 278
Srivastava, T. (N1-03) . . . 388
Stadler, B. (I2-14) . . . 249
Stadler, B. (P1-08) . . . 471
Stadtmüller, B. (G3-03) . . . 190
Stadtmüller, B. (G3-11) . . . 194
Stamenov, P. (L3-01) . . . 334
Stamenov, P.S. (E3-07) . . . 125
Stamenov, P.S. (G2-14) . . . 188
Stamenov, P.S. (I2-06) . . . 246
Stamenov, P.S. (P4-03) . . . 484
Stamenova, M.T. (P4-03) . . . 484
Stamps, R. (S6-02) . . . 351
Stanescu, S. (F1-03) . . . 141
Stankiewicz, A. (F3-05) . . . 153
Stansill, S. (D1-07) . . . 86
Stark, A. (L1-09) . . . 326
Starr, N.E. (E2-08) . . . 120
Stashkevich, A. (I3-11) . . . 256
Stashkevich, A. (R1-10) . . . 541
Stasiak, J. (C4-11) . . . 77
Statuto, N.N. (G1-04) . . . 178
Statuto, N.N. (R2-05) . . . 546
Statuto, N.N. (R3-05) . . . 552
Stavila, C. (Q5-03) . . . 529
Stavrou, E. (C2-05) . . . 64
Steadman, P. (I3-01) . . . 251
Stebliy, M. (E5-07) . . . 136
Stebliy, M. (E5-13) . . . 138
Štefanić, G. (F4-12) . . . 162
Stein, A. (B1-12) . . . 37
Stein, D.L. (P3-08) . . . 481
Steinhoff, U. (S3-03) . . . 175
Steinhoff, U. (S3-04) . . . 175
Steinke, N. (G4-07) . . . 199
Stejskal, O. (E1-11) . . . 115
Stemmer, S. (J5-01) . . . 288
Stenning, K. (C4-01) . . . 74
Stenning, K. (N2-03) . . . 394
Stepanov, S. (C5-04) . . . 80
Stephan, O. (S3-02) . . . 174
Stephen, G.M. (O1-07) . . . 423
Steren, L. (P3-12) . . . 483
Stevens, T. (J2-06) . . . 275
Stewart, A. (A3-09) . . . 17
Stiehl, G.M. (O1-04) . . . 422
Stiehl, M. (G3-03) . . . 190
Stiehl, M. (G3-11) . . . 194
Stienen, S. (E4-03) . . . 128
Stiles, M.D. (Q4-09) . . . 525
Stiles, M.D. (S5-04) . . . 349
Stoeckl, P. (D4-05) . . . 101
Stoeffler, D. (E4-11) . . . 132
Stognij, A. (O7-07) . . . 461
Stoian, G. (H1-01) . . . 211
Stolbov, O. (A4-16) . . . 26
Stoll, H. (L1-05) . . . 324
Stoll, L. (L3-06) . . . 336
Stolyar, S. (C4-02) . . . 74
Stolyar, S. (Q5-07) . . . 530
Stopfel, H. (B1-12) . . . 37
Stopfel, H. (C4-06) . . . 75
Stopfel, H. (H3-03) . . . 224
Strandqvist, N. (C4-06) . . . 75
Stransky, M. (G3-05) . . . 191
Street, G. (P4-05) . . . 484
Streib, S. (Q2-04) . . . 514
Strelkov, N. (C5-05) . . . 80
Streltsov, S. (B4-02) . . . 51
Streubel, R. (A1-06) . . . 5
Strømberg, A. (P3-06) . . . 480
Strømberg, A. (R1-04) . . . 539
Stroud, J. (P1-02) . . . 467
Stroud, J. (P1-03) . . . 468
Strungaru, M.S. (G3-13) . . . 195
Strungaru, M.S. (N1-09) . . . 390
Stückler, M. (H1-06) . . . 213
Studer, A. (R5-16) . . . 571
Su, D. (N5-01) . . . 410
Su, D. (N5-03) . . . 411
Su, D. (Q5-12) . . . 532
Subramanian, A. (J2-05) . . . 274
Subramanian, A. (Q6-11) . . . 537
Subramanian, V. (P5-09) . . . 492
Suda, K. (N4-02) . . . 407
Suellow, S. (A2-01) . . . 8
Suemasu, T. (R1-11) . . . 542
Suess, D. (B1-02) . . . 33
Suess, D. (B1-05) . . . 34
Suess, D. (D1-04) . . . 84
Suess, D. (R1-13) . . . 543
Sugai, M. (K5-10) . . . 321
Sugawara, A. (L1-04) . . . 324
Suh, P. (C3-12) . . . 72
Sukhorukov, Y.P. (P5-03) . . . 490
Sulla, I. (J1-03) . . . 269
Sumi, S. (F1-08) . . . 142
Sumi, S. (R4-06) . . . 560
Sun, A. (C2-10) . . . 66
Sun, A. (C3-03) . . . 68
Sun, A. (I4-03) . . . 258
Sun, A. (K2-05) . . . 304
Sun, D. (E3-04) . . . 125
Sun, D. (I2-13) . . . 249
Sun, D. (R4-02) . . . 558
Sun, G. (F5-02) . . . 164
Sun, G. (F5-08) . . . 167
Sun, H. (I5-08) . . . 266
Sun, H. (K3-02) . . . 308
Sun, H. (R5-11) . . . 568
Sun, J. (B3-01) . . . 46
Sun, J. (O2-01) . . . 428
Sun, J. (S5-03) . . . 349
Sun, N.X. (F3-11) . . . 156
Sun, N.X. (I2-02) . . . 243
Sun, N.X. (P5-01) . . . 489
Sun, Q. (G1-08) . . . 179
Sun, Q. (P4-03) . . . 484
Sun, X. (L1-06) . . . 325
Sun, Y. (E1-01) . . . 111
Sun, Y. (G3-01) . . . 190
Sun, Y. (Q6-09) . . . 536
Sun, Y. (S1-01) . . . 105
Sunmola, I. (G4-05) . . . 198
Suñol, J. (L4-09) . . . 344
Sushruth, M. (E4-11) . . . 132
Suzuki, D. (R2-06) . . . 546
Suzuki, K. (C3-01) . . . 67
Suzuki, K. (Q2-02) . . . 513
Suzuki, K. (R3-11) . . . 555
Suzuki, T. (F6-03) . . . 170
Suzuki, Y. (A3-02) . . . 13
Suzuki, Y. (A3-08) . . . 16
Suzuki, Y. (C5-06) . . . 81
Suzuki, Y. (M2-01) . . . 359
Suzuki, Y. (N1-06) . . . 389
Suzuki, Y. (O4-03) . . . 443
Suzuki, Y. (Q6-04) . . . 534
Suzuki, Y. (S1-04) . . . 106
Sveklo, I. (E5-10) . . . 137
Swain, A. (P5-09) . . . 492
Swatek, P. (D4-05) . . . 101
Swatek, P. (P6-01) . . . 496
Swekis, P. (E1-01) . . . 111
Syed, M. (O5-05) . . . 449
Syromyatnikov, A.V. (K1-11) . . . 300
Szabo, P. (H5-03) . . . 233
Szymczak, H. (F2-07) . . . 147

- T -

Tabata, K. (O2-14) . . . 434
Tabata, Y. (L1-04) . . . 324
Tabis, W. (M2-03) . . . 359
Tacchi, S. (M2-14) . . . 363
Tacchi, S. (N2-11) . . . 398
Tacchi, S. (O7-01) . . . 459
Tacchi, S. (O7-02) . . . 459
Taghipour Kaffash, M. (B1-11) . . . 37
Takahashi, A. (I2-04) . . . 244
Takahashi, K. (F6-04) . . . 171
Takahashi, S. (K4-08) . . . 315
Takahashi, Y. (H3-01) . . . 223
Takahashi, Y. (H3-10) . . . 226
Takamura, Y. (B1-06) . . . 34
Takamura, Y. (H2-01) . . . 219

Takamura, Y. (L2-01) . . . 329
Takamura, Y. (M2-04) . . . 360
Takanashi, K. (I4-15) . . . 263
Takanashi, K. (M4-06) . . . 373
Takanashi, K. (O1-11) . . . 425
Takanashi, K. (O2-10) . . . 432
Takanashi, K. (O4-09) . . . 445
Takase, K. (K2-10) . . . 306
Takase, K. (R3-13) . . . 556
Takenaka, K. (N5-11) . . . 414
Takeuchi, I. (A3-12) . . . 18
Takeuchi, Y. (C3-06) . . . 69
Takeuchi, Y. (E3-02) . . . 124
Takeuchi, Y. (J6-09) . . . 295
Takiguchi, K. (K2-10) . . . 306
Takiguchi, K. (R3-13) . . . 556
Talapatra, A. (B1-10) . . . 36
Talapatra, A. (I2-07) . . . 246
Talatchian, P. (B3-06) . . . 48
Tamazawa, Y. (H3-10) . . . 226
TAMURA, E. (N1-06) . . . 389
Tamura, K. (P6-10) . . . 500
Tan, A. (J5-07) . . . 290
Tan, H. (O3-05) . . . 438
Tan, H. (O3-06) . . . 438
Tanabe, K. (F1-08) . . . 142
Tanabe, K. (R4-06) . . . 560
Tanaka, D. (C2-09) . . . 66
Tanaka, H. (H4-04) . . . 229
Tanaka, H. (P6-10) . . . 500
Tanaka, M. (K2-10) . . . 306
Tanaka, M. (O1-12) . . . 425
Tanaka, M. (R3-13) . . . 556
Tanaka, S. (I2-04) . . . 244
Tanaka, T. (N3-01) . . . 400
Tanaka, T. (O7-03) . . . 460
Tanaka, T. (O7-13) . . . 464
Tang, J. (M5-10) . . . 379
Tang, J. (M5-14) . . . 380
Tang, J. (O1-06) . . . 423
Tang, J. (P6-04) . . . 497
Tang, J. (S5-02) . . . 348
Tang, N. (A2-06) . . . 9
Tang, W. (C2-08) . . . 65
Tang, X. (H3-02) . . . 223
Tang, Y. (K3-08) . . . 312
Tang, Y. (M1-03) . . . 354
Tang, Y. (Q6-07) . . . 536
Tanigaki, K. (G5-10) . . . 204
Taniguchi, H. (G5-05) . . . 202
Taniguchi, H. (O1-14) . . . 426
Taniguchi, T. (B3-10) . . . 49
taniguchi.takashi@nims.go.jp, T.T. (O1-05) . . . 422
Tanimoto, T. (R3-12) . . . 556
Tantillo, A.N. (F2-10) . . . 148
Tashima, D. (P6-08) . . . 499
Taskaev, S.V. (D4-01) . . . 100
Taskaev, S.V. (F2-14) . . . 149
Taskaev, S.V. (L4-11) . . . 344
Tate, J. (G2-12) . . . 187
Tateno, S. (E4-08) . . . 130
Taubel, A. (F2-03) . . . 146
Taubel, A. (F2-04) . . . 146
Taubel, A. (F2-16) . . . 150
Taufour, V. (Q1-04) . . . 508
Taylor, J.M. (J3-03) . . . 277
Taylor, P. (K4-05) . . . 314
Taylor, P. (O1-07) . . . 423
te Velthuis, S.G. (T1-01) . . . 1
Teichert, N. (E1-02) . . . 111
Teichert, N. (E3-08) . . . 126
Teichert, N. (I2-06) . . . 246
Teichmann, M. (G3-06) . . . 191
Teki, Y. (P6-09) . . . 499
Teki, Y. (P6-10) . . . 500
Telegin, A. (O6-02) . . . 452
Telegin, A. (P5-03) . . . 490
Temple, R. (H1-15) . . . 217
Tene Deffo, Y. (G2-10) . . . 186
Tene Deffo, Y. (N5-13) . . . 415
Tene Deffo, Y. (Q2-05) . . . 514
Tengdin, P.M. (E1-07) . . . 114
Teo, K. (P4-12) . . . 487
Teobaldi, G. (D1-07) . . . 86
Teplov, V. (O6-02) . . . 452
Terasaki, Y. (N4-02) . . . 407
Terrones, M. (G5-07) . . . 203
Terrones, M. (K2-07) . . . 305
Tesi, L. (D2-01) . . . 90
Tezuka, N. (P6-11) . . . 500
Thakur, A. (Q1-05) . . . 509
Tham, K. (N3-03) . . . 401
Thapaliya, T.R. (I4-13) . . . 262
Thatcher, H. (A1-10) . . . 7
Thatcher, H. (C4-09) . . . 77
Theh, W. (G6-01) . . . 206
Theh, W. (I2-16) . . . 250
Thevenard, L. (E4-09) . . . 131
Thi, T. (G6-02) . . . 206
Thiabgoh, O. (P1-06) . . . 470
Thian, D. (O3-06) . . . 438
Thiaville, A. (R2-11) . . . 548
Thibault, J. (G2-11) . . . 187
Thiem, C.D. (G4-03) . . . 197
Thien, J. (C1-11) . . . 59
Thiery, N. (M4-11) . . . 375
Thiery, N. (N2-09) . . . 396
Thirunavukkuarasu, K. (C3-14) . . . 73
Thiruvengadam, V. (D1-02) . . . 83
Thiruvengadam, V. (O4-11) . . . 446
Thomas, A. (E1-01) . . . 111
Thomas, S. (D4-07) . . . 101
Thomas, S. (O6-12) . . . 456
Thompson, G. (J3-04) . . . 278
Thomson, T. (M1-12) . . . 357
Thonig, D. (D2-10) . . . 93
Thonig, D. (E1-07) . . . 114
Thonig, D. (E2-02) . . . 117
Thonig, D. (L3-04) . . . 335
Thonig, D. (Q2-04) . . . 514
Thunström, P. (D2-10) . . . 93
Thuss, R. (C2-05) . . . 64
Tiberto, P. (J1-05) . . . 270
Tiberto, P. (L3-12) . . . 338
Tibu, M. (N5-09) . . . 413
Tiercelin, N. (L3-07) . . . 336
Timco, G. (G2-01) . . . 183
Timirgazin, M. (J3-11) . . . 280
Tiusan, C. (L2-04) . . . 330
Tiusan, C. (L2-09) . . . 333
Tiwari, P. (K1-15) . . . 302
Tobik, J. (L1-02) . . . 323
Todd, P. (G2-08) . . . 186
Toga, Y. (C2-04) . . . 63
Togashi, N. (I3-07) . . . 254
Toh, A.K. (E2-07) . . . 119
Tokac, M. (S2-03) . . . 108
Tokuda, M. (O1-14) . . . 426
Tomar, M. (Q1-05) . . . 509
Tomasello, R. (M1-08) . . . 356
Tomilo, A. (J6-05) . . . 294
Ton That, L. (H4-03) . . . 229
Ton That, L. (K5-03) . . . 318
Toneto, D. (M5-13) . . . 380
Tonner, P. (P5-01) . . . 489
Tonyushkin, A. (K5-01) . . . 318
Torche, P. (Q2-09) . . . 516
Torres, F. (D1-01) . . . 83
Torres, F. (K2-06) . . . 305
Toscano Figueroa, J.C. (K3-03) . . . 309
Toscano Figueroa, J.C. (K4-10) . . . 316
Tosoni, O. (C2-07) . . . 65
Toussaint, J. (P3-09) . . . 481
Tozman, P. (H3-02) . . . 223
Trabada, D.G. (B1-08) . . . 35
Träger, N. (E4-02) . . . 127
Träger, N. (E4-07) . . . 130
Träger, N. (I3-01) . . . 251
Träger, N. (R2-06) . . . 546
Tran, L.T. (C2-10) . . . 66
Tran, L.T. (I4-03) . . . 258
Transtrum, M. (E2-04) . . . 118
Transtrum, M. (E2-05) . . . 119
Trastoy, J. (Q3-06) . . . 520
Tretiakov, O. (O3-01) . . . 437
Trevillian, C.A. (Q2-07) . . . 515
Trewin, H. (L3-06) . . . 336
Trier, F. (R4-10) . . . 561
Trivedi, N. (O1-05) . . . 422
Trodahl, H. (D1-11) . . . 88
Trodahl, H. (I4-14) . . . 262
Trodahl, H. (J5-09) . . . 290
Trohidou, K.N. (B2-05) . . . 41
Trohidou, K.N. (B2-13) . . . 44
Troksa, A. (I2-01) . . . 243
Trusov, L.A. (Q1-09) . . . 510
Trynkiewicz, E. (P1-02) . . . 467
Trypiniotis, T. (R4-08) . . . 560
Tsafack, P. (G2-10) . . . 186
Tsafack, P. (N5-13) . . . 415
Tsafack, P. (Q2-05) . . . 514
Tsai, T. (G5-04) . . . 201
Tsai, T. (J4-06) . . . 284

*Best student presentation award finalist

Tsai, W. (S1-04) . . . 106
Tsai, Y. (K2-05) . . . 304
Tseng, Y. (O2-12) . . . 433
Tserkovnyak, y. (G1-08) . . . 179
Tserkovnyak, y. (M4-11) . . . 375
Tsirlin, A. (B4-01) . . . 51
Tsuchiura, H. (F6-04) . . . 171
Tsujie, A. (M6-10) . . . 384
Tsujikawa, M. (M4-06) . . . 373
Tsukada, K. (N5-15) . . . 416
Tsukahara, H. (H1-03) . . . 211
Tsukazaki, A. (O1-11) . . . 425
Tsumita, A. (N4-02) . . . 407
Tsunegi, S. (B3-05) . . . 48
Tsunegi, S. (B3-10) . . . 49
Tsunegi, S. (F3-08) . . . 155
Tsunoda, M. (F3-06) . . . 154
Tsurkan, V. (A2-10) . . . 11
Tu, C. (F3-11) . . . 156
Tu, J. (J5-10) . . . 290
Tufaile, A. (I2-15) . . . 249
Tufaile, A.P. (I2-15) . . . 249
Tufte, G. (P3-06) . . . 480
Tulapurkar, A. (L2-03) . . . 330
Tummalapalli, S. (I4-08) . . . 260
Tung, Y. (G5-04) . . . 201
Tuo, F. (K4-01) . . . 313
Turenne, D. (G3-06) . . . 191
Turnbull, L. (I3-01) . . . 251
Tweddle, D. (J3-04) . . . 278
Twitchett-Harrison, A. (I3-01) . . . 251
Tyagi, P. (C3-11) . . . 71
Tyagi, P. (C3-12) . . . 72
Tyagi, P. (F4-01) . . . 159
Tyberkevych, V. (B3-09) . . . 49
Tyberkevych, V. (E4-12) . . . 132
Tyberkevych, V. (M4-09) . . . 374
Tyberkevych, V. (Q2-01) . . . 513
Tyberkevych, V. (Q2-07) . . . 515
Tyberkevych, V. (Q3-01) . . . 518
Tyberkevych, V. (R3-08) . . . 554
Tzitzios, V. (D4-02) . . . 100

- U -

U D, R. (A4-01) . . . 20
Ucar, H. (C2-02) . . . 62
Uchida, K. (M4-06) . . . 373
Uchida, K. (O4-09) . . . 445
Uchiyama, T. (N5-07) . . . 412
Uehara, G. (G2-13) . . . 188
Uemura, T. (R2-07) . . . 547
Uemura, T. (R3-12) . . . 556
Ueno, S. (K5-10) . . . 321
Ueta, D. (O1-14) . . . 426
Uhlir, V. (A2-05) . . . 9
Uhlir, V. (A2-08) . . . 10
Uhlir, V. (G3-06) . . . 191
Uhm, Y. (F5-02) . . . 164
Uhm, Y. (F5-08) . . . 167
Ukai, T. (B1-14) . . . 38
Ullah, A. (E2-06) . . . 119
Ullah, A. (E2-12) . . . 121
Ullakko, K. (A4-05) . . . 22
Ulloa, C. (G1-11) . . . 181
Ullstad, F. (I4-14) . . . 262
Ulyanov, M.N. (D4-01) . . . 100
Ulyanov, M.N. (F2-14) . . . 149
Ulyanov, M.N. (L4-11) . . . 344
Umeda, Y. (C2-09) . . . 66
Umetsu, R.Y. (O2-10) . . . 432
Ummelen, F. (F1-03) . . . 141
Ünlü, C. (H2-03) . . . 219
Urazhdin, S. (D1-03) . . . 84
Urazhdin, S. (K3-01) . . . 308
Urazhdin, S. (Q3-02) . . . 518
Urazhdin, S. (Q3-03) . . . 519
Urazhdin, S. (S8-01) . . . 504
Urdiroz, U. (D1-12) . . . 88
Urdiroz, U. (F2-18) . . . 150
Urdiroz, U. (H1-05) . . . 213
Urs, N. (F3-01) . . . 152
Usui, A. (K5-08) . . . 321
Utermohlen, F. (O1-05) . . . 422
Utesov, O.I. (K1-11) . . . 300
Uysal, I.E. (C2-01) . . . 62

- V -

Vail, O. (K4-05) . . . 314
Vail, O. (O1-07) . . . 423
Vailionis, A. (M2-01) . . . 359
Valcarcel, R. (O5-01) . . . 448
Valdes Aguilar, R. (G5-11) . . . 205
Valdes Aguilar, R. (O1-05) . . . 422
Valdes Aguilar, R. (O1-10) . . . 424
Valdés, D.P. (J1-08) . . . 271
Valencia, S. (F1-02) . . . 140
Valenzuela, S.O. (O1-01) . . . 421
Valeriano Inchausti, A. (R5-05) . . . 565
Vallabhaneni, E. (G1-06) . . . 179
Vallabhaneni, E. (M2-06) . . . 360
Valmispild, V. (G3-06) . . . 191
Valvidares, M. (J5-12) . . . 291
Valvidares, M. (L1-11) . . . 327
Valvidares, M. (R2-06) . . . 546
van Aken, P. (S2-05) . . . 109
Van Beek, S. (L2-05) . . . 331
Van de Walle, A. (J1-06) . . . 271
van den Berg, A. (B1-15) . . . 39
van den Brink, J. (J6-05) . . . 294
van der Laan, G. (E4-01) . . . 127
van der Laan, G. (M5-12) . . . 379
van der Laan, G. (P2-08) . . . 475
van der Laan, G. (P2-10) . . . 477
van der Laan, G. (S2-01) . . . 108
van Dijk, N.v. (A4-03) . . . 21
van Dijk, N.v. (A4-06) . . . 22
van Dijk, N.v. (L4-01) . . . 341
van Dijk, N.v. (R5-14) . . . 570
van Dijken, S. (F1-02) . . . 140
van Dijken, S. (N4-06) . . . 409
Van Houdt, J. (L2-05) . . . 331
van Loosdrecht, P.H. (A2-10) . . . 11
van Rijn, J.J. (I4-04) . . . 258
van Rijn, J.J. (M2-06) . . . 360
Van Waeyenberge, B. (L1-13) . . . 328
Van Wees, B. (M4-10) . . . 375
Van Wees, B. (R4-03) . . . 559
Vanderelli, T.A. (I2-15) . . . 249
Vanstone, A. (C4-01) . . . 74
Vanstone, A. (N2-03) . . . 394
Varaprasad, B. (P2-02) . . . 472
Varga, R. (G6-09) . . . 209
Varga, R. (H5-03) . . . 233
Varga, R. (J1-03) . . . 269
Varga, R. (L3-05) . . . 335
Vargas, N.M. (K2-06) . . . 305
Vargas, N.M. (R2-10) . . . 548
Varlamov, A.A. (B2-13) . . . 44
Varma, K. (H2-08) . . . 221
Varma, V.B. (B2-10) . . . 43
Varma, V.B. (F4-06) . . . 160
Varotto, S. (Q4-11) . . . 526
Varvaro, G. (Q5-04) . . . 529
Varvaro, G. (R3-14) . . . 557
Vas'kovskiy, V. (D1-09) . . . 87
Vas'kovskiy, V. (M6-03) . . . 382
Vas'kovskiy, V. (O6-18) . . . 458
VASHISHT, G. (J2-05) . . . 274
Vasilakaki, M. (B2-05) . . . 41
Vasilakaki, M. (B2-13) . . . 44
Vasilaki, E. (A5-04) . . . 30
Vasilaki, E. (G4-07) . . . 199
Vasiliev, E. (A2-04) . . . 9
Vasiliev, E. (D1-13) . . . 89
Vasiliev, E. (M5-05) . . . 378
Vaskivskyi, I. (G3-06) . . . 191
Vaughan, M. (J5-05) . . . 289
Vavassori, P. (B1-02) . . . 33
Vavassori, P. (S6-05) . . . 352
Vaz, D. (R4-10) . . . 561
Vazquez, M. (A1-03) . . . 3
Vazquez, M. (B1-08) . . . 35
Vazquez, M. (H1-02) . . . 211
Vazquez, M. (H1-08) . . . 214
Vazquez, M. (O7-05) . . . 460
Vazquez, M. (Q5-08) . . . 531
Vazquez, M. (R5-05) . . . 565
Vazquez, M. (R5-07) . . . 566
Vecchiola, A. (E5-08) . . . 137
Vecchiola, A. (I3-09) . . . 255
Vecchiola, A. (N1-03) . . . 388
Vedmedenko, E.Y. (B1-03) . . . 33
Vedmedenko, E.Y. (F1-03) . . . 141
Vega, V. (H5-03) . . . 233
Veintemillas-Verdaguer, S. (F2-18) . . . 150
Veis, M. (E1-11) . . . 115
Veis, M. (N1-08) . . . 390
Velasquez, A. (A5-03) . . . 29
Velazques-Salazar, A.A. (R5-02) . . . 564

Velez-Fort, E. (B2-04) 41
Velez, C. (A1-08) 5
Velez, M. (L1-10) 326
Velez, M. (O5-01) 448
Venkat, G. (E4-14) 134
Venkat, G. (R1-04) 539
Venkatesan, M. (E3-08) 126
Venkatesan, T. (G1-07) 179
Venter, A. (R5-16) 571
Ventura, J. (B3-03) 46
Ventura, J. (L4-12) 345
Venugopal, A. (O7-15) 465
Venugopal, A. (Q2-03) 514
Vera-Marun, I.J. (K3-03) 309
Vera-Marun, I.J. (K4-10) 316
Vera-Marun, I.J. (M1-12) 357
Vera-Marun, I.J. (M4-10) 375
Vera-Marun, I.J. (R4-03) 559
Verba, R.V. (E4-06) 129
Verbeek, X.H. (M2-13) 363
Verdier, M. (S3-02) 174
Verezhak, J. (I3-01) 251
Vergniory, M. (K4-09) 315
Verkhovskii, S.V. (H2-12) 222
Verma, A. (L4-13) 345
Verma, V. (D3-09) 99
Verma, V.K. (C4-12) 78
Versteeg, R.B. (A2-10) 11
Vetrova, I. (L1-02) 323
Vetter, E. (E3-04) 125
Vetter, E. (I2-13) 249
Vetter, E. (R4-02) 558
Vezzoni, V. (F2-15) 149
Victora, R. (N3-13) 405
Victora, R. (O7-15) 465
Victora, R. (P2-03) 473
Victora, R. (P2-04) 473
Victora, R. (Q2-03) 514
Vidal-Silva, N. (A4-11) 24
Vidamour, I.T. (G4-07) 199
Vidamour, I.T. (R1-04) 539
Viehland, D. (A3-04) 14
Viehland, D. (O4-04) 443
Vieille, V. (S3-02) 174
Viet, D. (G6-02) 206
Vila, L. (B3-09) 49
Vila, L. (G4-02) 197
Vila, L. (M4-09) 374
Vila, L. (M4-11) 375
Vila, L. (N2-09) 396
Vila, L. (O2-02) 429
Vila, L. (Q2-01) 513
Vila, L. (Q4-11) 526
Vila, L. (R1-11) 542
Vila, L. (R4-10) 561
Villalba, P. (B1-02) 33
Villarreal, R. (K2-08) 306
Vincente Arche, L. (R4-10) 561
Virnau, P. (N1-08) 390
Vogel, J. (L2-06) 331
Vogel, J. (R1-11) 542
Vogel, J. (R2-11) 548
Vogel, M. (M3-03) 366
Vogler, C. (B1-02) 33
Vogler, C. (B1-05) 34
Vogler, C. (D1-04) 84
Voigt, B. (L2-02) 329
Volkov, A. (E5-03) 135
Volkov, O. (A1-01) 2
Volkov, O. (R1-09) 541
Volvach, I. (O2-07) 431
Volvach, I. (P4-11) 486
Volvach, I. (R3-10) 555
von Molnar, S. (R4-01) 558
Voneshen, D. (D2-01) 90
Voneshen, D. (E4-14) 134
Vreeland, E. (J2-06) 275
Vuichard, M. (A1-07) 5
vukadinovic, n. (M4-09) 374
vukadinovic, n. (Q2-01) 513
Vyborny, K. (E1-01) 111

- W -

Wada, S. (I3-07) 254
Wadley, P. (G1-10) 180
Wadley, P. (J6-07) 294
Wadley, P. (M1-09) 356
Wagner, J. (G3-05) 191
Waki, T. (L1-04) 324
Waldeck, D. (I2-13) 249
Walia, R. (D3-09) 99
Walker, C.S. (D1-14) 89
Walter, J. (L2-02) 329
Wan, D. (O2-04) 430
Wan, Z. (I5-08) 266
Wan, Z. (R5-11) 568
Wang, A. (C3-05) 69
Wang, C. (G6-10) 209
Wang, D. (A1-06) 5
Wang, D. (F3-11) 156
Wang, D. (H2-04) 220
Wang, F. (D4-09) 102
Wang, F. (F6-08) 172
Wang, H. (M6-07) 383
Wang, H. (R4-01) 558
Wang, J. (D4-04) 101
Wang, J. (D4-05) 101
Wang, J. (G4-01) 196
Wang, J. (H4-01) 228
Wang, J. (I4-09) 261
Wang, J. (K2-04) 304
Wang, J. (K4-14) 317
Wang, J. (N5-01) 410
Wang, J. (N5-03) 411
Wang, J. (P6-01) 496
Wang, J. (Q5-12) 532
Wang, K. (F3-10) 156
Wang, K. (I3-05) 253
Wang, K. (N1-11) 391
Wang, K. (N1-12) 392
Wang, K. (N5-05) 412
Wang, K. (O4-08) 445
Wang, M. (F5-10) 167
Wang, M. (J3-03) 277
Wang, M. (M1-09) 356
Wang, M. (N4-01) 407
Wang, P. (K1-02) 297
Wang, Q. (N2-08) 396
Wang, S. (K2-05) 304
Wang, S. (K3-02) 308
Wang, S. (S1-04) 106
Wang, W. (N4-07) 409
Wang, W. (S4-03) 236
Wang, W. (S5-02) 348
Wang, X. (A2-09) 10
Wang, X. (G2-03) 183
Wang, X. (K3-02) 308
Wang, X. (M4-03) 371
Wang, X. (P3-05) 480
Wang, X. (R4-01) 558
Wang, Y. (C1-09) 58
Wang, Y. (G2-03) 183
Wang, Y. (G6-08) 208
Wang, Y. (I1-04) 239
Wang, Y. (I1-09) 241
Wang, Y. (J5-04) 289
Wang, Y. (M4-01) 371
Wang, Y. (Q6-09) 536
Wang, Y. (R5-06) 566
Wang, Y. (R5-10) 568
Wang, Z. (A2-03) 8
Wang, Z. (A2-10) 11
Wang, Z. (C3-04) 68
Wang, Z. (N1-11) 391
Wang, Z. (R2-03) 545
Ward, T.Z. (D2-06) 93
Waring, H.J. (M1-12)* 357
Warisarn, C. (N3-07) 403
Warisarn, C. (N3-08) 403
Warisarn, C. (N3-09) 404
Waschk, M. (R4-04) 559
Watanabe, K. (I2-04) 244
Watanabe, K. (O1-05) 422
Watanabe, M. (O1-14) 426
Watanabe, S. (E4-05) 129
Watson, A. (G1-06) 179
Watzman, S. (J5-02) 288
Wawro, A. (E5-10) 137
Weber, D. (O1-05) 422
Weber, F. (D2-14) 94
Weber, M. (G3-03) 190
Weber, S. (G3-03) 190
Weber, S. (G3-11) 194
Wederni, A. (L4-09) 344
Wei, J. (J4-06) 284
Wei, J. (O2-12) 433
Wei, P. (S4-02) 236
Wei, Y. (P5-01) 489
Weigand, M. (E4-02) 127
Weigand, M. (E4-03) 128
Weigand, M. (E4-07) 130

*Best student presentation award finalist

Weigand, M. (I3-01) . . . 251
Weigand, M. (L1-13) . . . 328
Weigand, M. (O3-07) . . . 439
Weiler, M. (E4-10) . . . 131
Weiler, M. (J4-07) . . . 285
Weinhold, T. (B3-02) . . . 46
Weiss, E. (F4-07) . . . 161
Weiss, E. (N5-12) . . . 415
Weiss, J. (D1-08) . . . 86
Weiss, J. (F1-10) . . . 143
Weissenhofer, M. (N1-05) . . . 389
Weissitsch, L. (H1-06) . . . 213
Welbourne, A. (A5-04) . . . 30
Weschke, E. (C1-11) . . . 59
White, S. (F1-06) . . . 142
Wiekhorst, F. (S3-03) . . . 175
Wiekhorst, F. (S3-04) . . . 175
Wiesendanger, R. (F1-01) . . . 140
Wiesendanger, R. (O3-11) . . . 440
Wilhelm, C. (J1-06) . . . 271
Wilkins, S. (S6-04) . . . 352
Will-Cole, A. (F3-11) . . . 156
Will-Cole, A.R. (P5-01) . . . 489
Willey, T.M. (K2-06) . . . 305
Wilson, B.W. (N4-04) . . . 408
Wilson, C. (S4-02) . . . 236
Wilson, M. (I3-01) . . . 251
Wilson, S. (J5-01) . . . 288
Wimberger, S. (D2-02) . . . 90
Wimmer, T. (P4-13) . . . 487
Wines, D. (E1-03) . . . 112
Winkler, T. (N1-08) . . . 390
Winpenny, R.E. (G2-01) . . . 183
Wintz, S. (E4-03) . . . 128
Wintz, S. (N2-11) . . . 398
Wintz, S. (S8-05) . . . 506
Wintz, S. (T1-02) . . . 1
Wirecka, R. (P1-02) . . . 467
Wisser, J. (A3-02) . . . 13
Wisser, J. (O4-03) . . . 443
Wittmann, A. (G1-02) . . . 178
Wittmann, A. (G1-05) . . . 179
Wittmann, A. (R2-06) . . . 546
Wittrock, S. (B3-05) . . . 48
Wittrock, S. (B3-06) . . . 48
Wittrock, S. (F3-08) . . . 155
Wojcik, M. (I4-10) . . . 261
Wolf, T. (D2-14) . . . 94
Wollschläger, J. (C1-11) . . . 59
Wolter, A. (A2-01) . . . 8
Wolter, A. (J5-07) . . . 290
Won, H. (N3-14) . . . 406
Won, H. (R5-03) . . . 564
Wong, S. (O2-15) . . . 435
Wong, Y. (F6-05) . . . 171
Wong, Y. (F6-06) . . . 172
Woo, J. (G6-06) . . . 207
Woodcock, T.G. (P3-01) . . . 478
Woodcock, T.G. (Q1-07) . . . 510
Woodcock, T.G. (Q1-08) . . . 510
Woods, J.S. (S6-04) . . . 352
Woods, S. (H1-14) . . . 217
Woods, S. (O5-06) . . . 449
Woollett, N. (C2-05) . . . 64
Wright, A.J. (K3-05) . . . 310
Wu, C. (M4-07) . . . 373
Wu, D. (M4-03) . . . 371
Wu, G. (F1-06) . . . 142
Wu, H. (I3-05) . . . 253
Wu, H. (K2-05) . . . 304
Wu, H. (N1-12) . . . 392
Wu, J. (O2-09) . . . 432
Wu, K. (C4-07) . . . 76
Wu, K. (N1-11) . . . 391
Wu, K. (N5-03) . . . 411
Wu, K. (O7-12) . . . 464
Wu, K. (Q5-12) . . . 532
Wu, M. (A3-11) . . . 18
Wu, M. (O1-06) . . . 423
Wu, M. (P4-05) . . . 484
Wu, M. (S5-02) . . . 348
Wu, P. (M1-11) . . . 357
Wu, P. (M6-07) . . . 383
Wu, S. (A3-05) . . . 15
Wu, S. (C1-09) . . . 58
Wu, W. (G5-04) . . . 201
Wu, X. (G3-10) . . . 193
Wu, X. (M2-14) . . . 363
Wu, X. (Q6-07) . . . 536
Wu, X. (Q6-09) . . . 536
Wu, Y. (H1-13) . . . 216
Wu, Y. (J6-11) . . . 296
Wu, Y. (K3-02) . . . 308
Wu, Y. (L2-05) . . . 331
Wu, Y. (M1-05) . . . 355
Wu, Y. (M3-02) . . . 365
Wunderlich, J. (M1-06) . . . 355
Wurster, S. (H1-06) . . . 213
Wytko, J. (D1-08) . . . 86
Wytko, J. (F1-10) . . . 143

- X -

Xia, J. (M1-05) . . . 355
Xia, J. (N1-11) . . . 391
Xia, Y. (J3-05) . . . 278
Xiang, H. (M2-12) . . . 362
Xiang, H. (O3-05) . . . 438
Xiang, J. (G1-12) . . . 181
Xiao, D. (I3-03) . . . 252
Xiao, G. (F3-10) . . . 156
Xiao, G. (N5-05) . . . 412
Xiao, G. (O4-08) . . . 445
Xiao, J.Q. (G2-03) . . . 183
Xiao, Y. (F2-01) . . . 145
Xiao, Z. (L3-15) . . . 340
Xiao, Z. (R1-13) . . . 543
Xie, D. (C3-04) . . . 68
Xie, D. (F4-10) . . . 162
Xie, Q. (M2-14) . . . 363
Xing, M. (G5-13) . . . 205
Xing, M. (K5-04) . . . 319
Xiong, H. (I1-09) . . . 241
Xiong, P. (R4-01) . . . 558
Xiong, Y. (E3-04) . . . 125
Xiong, Y. (J5-04) . . . 289
Xiong, Y. (L3-15) . . . 340
Xiong, Y. (M3-03) . . . 366
Xu, B. (A4-07) . . . 23
Xu, B. (A4-08) . . . 23
Xu, B. (H3-14) . . . 227
Xu, B. (P5-05) . . . 491
Xu, C. (M2-12) . . . 362
Xu, C. (O3-05) . . . 438
Xu, C. (P2-02) . . . 472
Xu, J. (M1-05) . . . 355
Xu, J. (O4-05) . . . 443
Xu, J. (R2-02) . . . 545
Xu, J. (R2-05) . . . 546
Xu, J. (S5-03) . . . 349
Xu, L. (R5-04) . . . 565
Xu, M. (N4-07) . . . 409
Xu, Q. (C3-04) . . . 68
Xu, Q. (G6-10) . . . 209
Xu, Q. (S1-01) . . . 105
Xu, X. (N4-08) . . . 409
Xu, X. (P5-06) . . . 491
Xu, Y. (E1-04) . . . 113
Xu, Y. (J5-10) . . . 290
Xu, Y. (J6-11) . . . 296
Xue, F. (M4-05) . . . 372
Xue, F. (S1-04) . . . 106
Xue, K. (N3-13) . . . 405

- Y -

Ya, X. (N3-01) . . . 400
Ya, X. (O7-03) . . . 460
Ya, X. (O7-13) . . . 464
Yabukami, S. (H4-03) . . . 229
Yabukami, S. (K5-03) . . . 318
Yadav, R.S. (M6-11) . . . 385
Yadav, V.K. (C3-10) . . . 71
Yagmur, A. (R4-06) . . . 560
Yahagi, Y. (M4-04) . . . 372
Yakushiji, K. (B3-05) . . . 48
Yakushiji, K. (F3-08) . . . 155
Yamada, M. (Q4-03) . . . 522
Yamada, S. (K3-04) . . . 310
Yamaguchi, M. (I2-04) . . . 244
Yamamoto, D. (F5-12) . . . 168
Yamamoto, T. (L2-03) . . . 330
Yamamoto, Y. (K5-03) . . . 318
Yamane, Y. (J6-09) . . . 295
Yamanoi, K. (O4-06) . . . 444
Yamanouchi, M. (R2-07) . . . 547
Yamauchi, T. (Q4-06) . . . 524
Yamauchi, Y. (L1-06) . . . 325
yan, B. (S1-01) . . . 105
Yan, J. (D2-09) . . . 93
yan, J. (J4-01) . . . 282

Yan, R. (J2-01) . . . 273
Yan, W. (I2-12) . . . 248
Yan, Y. (N3-04) . . . 401
Yanagihara, H. (I4-15) . . . 263
Yanase, T. (M6-10) . . . 384
Yanase, T. (P6-14) . . . 501
Yang-Scharlotta, J. (O2-01) . . . 428
Yang, B. (M2-14) . . . 363
Yang, B. (R5-04) . . . 565
Yang, C. (G5-04) . . . 201
Yang, D. (Q5-06) . . . 530
Yang, F. (F1-06) . . . 142
Yang, F. (G1-04) . . . 178
Yang, F. (J6-04) . . . 293
Yang, F. (K2-13) . . . 307
Yang, H. (E1-12) . . . 116
Yang, H. (K3-02) . . . 308
Yang, H. (M2-14) . . . 363
Yang, H. (O2-05) . . . 430
Yang, H. (P4-12) . . . 487
Yang, H. (R2-03) . . . 545
Yang, H. (S5-01) . . . 348
Yang, H. (S7-02) . . . 419
Yang, J. (D4-09) . . . 102
Yang, J. (F6-08) . . . 172
Yang, J. (G6-08) . . . 208
Yang, J. (G6-11) . . . 209
Yang, J. (J3-05) . . . 278
Yang, K. (D2-16) . . . 95
Yang, M. (A3-08) . . . 16
Yang, M. (K3-02) . . . 308
Yang, S. (J4-06) . . . 284
Yang, S. (P4-12) . . . 487
Yang, S. (R4-02) . . . 558
Yang, S. (R5-15) . . . 570
Yang, T. (O6-15) . . . 457
Yang, W. (K3-02) . . . 308
Yang, X. (Q6-09) . . . 536
Yang, Y. (G6-10) . . . 209
Yang, Y. (I2-12) . . . 248
Yang, Y. (J6-11) . . . 296
Yang, Y. (M2-12) . . . 362
Yang, Y. (O3-05) . . . 438
Yang, Y. (R5-10) . . . 568
Yang, Z. (K3-06) . . . 311
Yao, A. (H1-04) . . . 212
Yao, A. (I1-07) . . . 241
Yao, Y. (R4-09) . . . 561
Yap, Q. (O2-15) . . . 435
Yapaskurt, V.O. (A4-17) . . . 27
Yarigina, E. (F5-01) . . . 164
Yaroslavtsev, A. (G3-06) . . . 191
Yaroslavtsev, R. (C4-02) . . . 74
Yaroslavtsev, R. (Q5-07) . . . 530
Yasin, F. (E3-01) . . . 123
Yasin, F. (L2-05) . . . 331
Yasuhira, M. (O2-03) . . . 429
Yasuhira, M. (O2-06) . . . 431
Yee, S. (I1-05) . . . 240
Yen, H. (Q4-07) . . . 524
Yeng, I. (H1-13) . . . 216
Yeo, C. (N3-14) . . . 406
Yershov, K. (J6-05) . . . 294
Yeste, J. (R1-05) . . . 539
Ygnacio Arriola Córdova, A. (M3-04) . . . 366
Yi, D. (S1-04) . . . 106
Yi, M. (A4-07) . . . 23
Yi, M. (A4-08) . . . 23
Yi, Q. (I1-09) . . . 241
Yim, H.C. (D4-12) . . . 103
Yim, H.C. (R5-03) . . . 564
Yokosawa, M. (D3-07) . . . 98
Yoo, M. (M3-12) . . . 370
Yoo, W. (M6-05) . . . 382
Yoon, J. (J6-09) . . . 295
Yoon, J. (O4-01) . . . 442
Yoon, S. (H4-05) . . . 230
Yoon, S. (M2-02) . . . 359
Yoshii, S. (L3-11) . . . 338
Yoshikiyo, M. (C1-05) . . . 56
Yoshikiyo, M. (I2-05) . . . 245
Yoshinaga, N. (Q2-02) . . . 513
Yoshioka, H. (Q5-02) . . . 528
Yoshioka, T. (F6-04) . . . 171
You, J. (N3-14) . . . 406
You, L. (C5-07) . . . 81
You, X. (A4-06) . . . 22
Young, I. (Q4-05) . . . 523
Yu, B. (M2-03) . . . 359
Yu, C. (C1-04) . . . 56
Yu, G. (N1-11) . . . 391
Yu, H. (A3-12) . . . 18
Yu, H. (H1-13) . . . 216
Yu, H. (I4-08) . . . 260
Yu, K. (I5-07) . . . 266
Yu, R. (O1-06) . . . 423
Yu, S. (G1-04) . . . 178
Yu, S. (J6-04) . . . 293
Yuan, H. (N2-05) . . . 395
Yuan, W. (S4-02) . . . 236
Yuan, Z. (M3-02) . . . 365
Yuasa, H. (Q4-06) . . . 524
Yuasa, S. (B3-05) . . . 48
Yuasa, S. (B3-10) . . . 49
Yuasa, S. (F3-08) . . . 155
Yuasa, S. (K3-04) . . . 310
Yuasa, S. (L2-03) . . . 330
Yuldasheva, A. (M5-04) . . . 378
Yun, Y. (P5-06) . . . 491

- Z -

Zabel, H. (G3-08) . . . 192
Zadrozny, J. (P1-01) . . . 467
Zaeimbashi, M. (F3-11) . . . 156
Zahedinejad, M. (Q3-04) . . . 519
Zahedinejad, M. (S8-02) . . . 504
Zálešák, J. (H1-06) . . . 213
Zamani Kouhpanji, M. (P1-08) . . . 471
Zamora Mendieta, J. (L4-08) . . . 343
Zanfrognini, M. (S2-05) . . . 109
Zang, J. (O3-03) . . . 438
Zapf, V. (K1-01) . . . 297
Zarkevich, N.A. (L4-06) . . . 343
Zatko, V. (K4-03) . . . 313
Zavertanyi, T. (F5-03) . . . 165
Zayets, V. (N4-03) . . . 408
Zayets, V. (P6-07) . . . 498
Zázvorka, J. (N1-05) . . . 389
Zázvorka, J. (N1-08) . . . 390
Zehner, J. (K1-03) . . . 298
Zeiger, P. (S2-05) . . . 109
Zeissler, K. (M5-02) . . . 377
Zeitler, U. (M1-09) . . . 356
Zelent, M. (E4-07) . . . 130
Zelezny, J. (M4-04) . . . 372
Zemen, J. (P5-04) . . . 490
Zeng, C. (F4-08) . . . 161
Zeng, F. (M3-02) . . . 365
Zeng, X. (M2-07) . . . 361
Zha, L. (D4-09) . . . 102
Zha, L. (F6-08) . . . 172
Zhai, Z. (Q6-07) . . . 536
Zhang, A. (Q6-07) . . . 536
Zhang, A. (Q6-09) . . . 536
Zhang, B. (I1-06) . . . 240
Zhang, B. (Q2-05) . . . 514
Zhang, C. (B3-08) . . . 49
Zhang, D. (I5-07) . . . 266
Zhang, D. (P6-01) . . . 496
Zhang, E. (O6-08) . . . 454
Zhang, F. (A4-06) . . . 22
Zhang, F. (G5-07) . . . 203
Zhang, F. (J2-04) . . . 274
Zhang, F. (K2-07) . . . 305
Zhang, G. (G3-10) . . . 193
Zhang, H. (F2-03) . . . 146
Zhang, H. (H3-14) . . . 227
ZHANG, H. (H4-08) . . . 231
Zhang, H. (J6-03) . . . 293
Zhang, J. (C5-07) . . . 81
Zhang, J.C. (G5-03) . . . 201
Zhang, K. (D3-04) . . . 97
zhang, K. (I5-02) . . . 264
Zhang, P. (G1-12) . . . 181
Zhang, P. (I3-05) . . . 253
Zhang, P. (Q4-09) . . . 525
Zhang, Q. (J6-11) . . . 296
Zhang, Q. (O3-07) . . . 439
Zhang, Q. (O3-08) . . . 439
Zhang, S. (C3-08) . . . 70
Zhang, S. (C5-07) . . . 81
Zhang, S. (E4-01) . . . 127
Zhang, S. (G1-13) . . . 182
Zhang, S. (J5-03) . . . 288
Zhang, S. (M5-12) . . . 379
Zhang, S. (S1-02) . . . 105
Zhang, S. (S2-01) . . . 108
Zhang, S. (S5-02) . . . 348
Zhang, T. (Q6-09) . . . 536
Zhang, W. (E3-04) . . . 125
Zhang, W. (G3-02) . . . 190

*Best student presentation award finalist

Zhang, W. (G5-06) 203
Zhang, W. (L3-15) 340
Zhang, W. (M3-02) 365
Zhang, W. (M3-03) 366
Zhang, W. (O4-12) 447
Zhang, W. (S5-02) 348
Zhang, X. (E1-09) 115
Zhang, X. (G6-10) 209
Zhang, X. (H1-02) 211
Zhang, X. (J6-11) 296
Zhang, X. (K1-01) 297
Zhang, X. (M1-05) 355
Zhang, X. (N1-11) 391
Zhang, X. (N2-04) 395
Zhang, X. (O4-02) 442
Zhang, X. (Q5-08) 531
Zhang, X. (R3-03) 551
Zhang, X. (R5-05) 565
Zhang, X. (R5-07) 566
Zhang, X.S. (Q4-02) 522
Zhang, Y. (F3-10) 156
Zhang, Y. (I3-02) 251
Zhang, Y. (N1-04) 388
Zhang, Y. (N4-07) 409
Zhang, Y. (N5-05) 412
Zhang, Z. (M2-03) 359
Zhang, Z. (M3-03) 366
Zhang, Z. (O6-15) 457
Zhang, Z. (Q6-09) 536
Zhao, C. (M3-03) 366
Zhao, H. (H2-02) 219
Zhao, J. (R4-01) 558
Zhao, L. (N1-11) 391
Zhao, L. (S8-04) 506
Zhao, P. (P3-01) 478
Zhao, X. (D1-04) 84
Zhao, Y. (G2-07) 185
Zheltikov, A.M. (L1-14) 328
Zheng, B. (J2-06) 275
Zheng, R. (I2-03) 244
Zheng, R. (Q5-11) 532
Zheng, T. (I1-04) 239
Zheng, X. (A3-02) 13
Zheng, Y. (O4-08) 445
Zhong, H. (L1-09) 326
Zhou, B. (N4-07) 409
Zhou, B. (P2-02) 472
Zhou, C. (M1-05) 355
Zhou, G. (J2-04) 274
Zhou, H. (M2-03) 359
Zhou, H. (N1-11) 391
Zhou, J. (F3-11) 156
Zhou, J. (G3-07) 192
Zhou, J. (M1-01) 353
Zhou, P. (G4-03) 197
Zhou, S. (M4-07) 373
Zhou, W. (Q1-12) 512
Zhou, W. (R2-06) 546
Zhou, X. (O4-01) 442
Zhou, Y. (F1-02) 140
Zhou, Y. (J2-06) 275
Zhou, Y. (M1-05) 355
Zhou, Y. (N1-11) 391
Zhu, J. (D3-05) 97
Zhu, J. (K3-02) 308
Zhu, J. (N3-04) 401
Zhu, J. (O6-08) 454
Zhu, J. (P2-02) 472
Zhu, J. (R3-07) 553
Zhu, L. (S5-05) 349
Zhu, M. (J6-04) 293
Zhu, M. (P6-06) 497
Zhu, X. (D3-04) 97
Zhu, Y. (G2-07) 185
Zhu, Y. (M2-02) 359
Zhu, Y. (O1-05) 422
Ziaja, B. (G3-05) 191
Ziemann, S. (L4-05) 342
Zimmermann, B. (F1-01) 140
Zink, B.L. (H5-08) 235
Zink, B.L. (P6-16) 502
Zink, B.R. (H4-01) 228
Zintler, A. (H3-14) 227
Zirhli, O. (K5-02) 318
Zirhli, O. (Q1-02) 508
Zivotsky, O. (C3-13) 72
Zubáč, J. (M1-09) 356
Zuo, L. (J2-04) 274
Zusin, D. (E1-07) 114
Zverev, V.V. (O6-06) 454
Zvezdin, K. (C5-04) 80
Zysler, R.D. (J1-08) 271